

Dissertation zur Erlangung des Doktorgrades
der Fakultät für Chemie und Pharmazie
der Ludwig-Maximilians-Universität München

**Rational development of stabilized cyclic
disulfide redox probes and bioreductive
prodrugs to target dithiol oxidoreductases**

Jan Gabriel Felber

aus

Augsburg, Deutschland

2022

Erklärung

Diese Dissertation wurde im Sinne von §7 der Promotionsordnung vom 28. November 2011 von Herrn Dr. Oliver Thorn-Seshold betreut.

Eidesstattliche Versicherung

Diese Dissertation wurde eigenständig und ohne unerlaubte Hilfe erarbeitet.

München, den 14. Februar 2023

.....
Jan Gabriel Felber

Dissertation eingereicht am 15. Dezember 2022

1. Gutachter	Dr. Oliver Thorn-Seshold
2. Gutachter	Prof. Dr. Ivan Huc

Mündliche Prüfung am 27. Januar 2023

Abstract

Countless biological processes allow cells to develop, survive, and proliferate. Among these, tightly balanced regulatory enzymatic pathways that can respond rapidly to external impacts maintain dynamic physiological homeostasis. More specifically, redox homeostasis broadly affects cellular metabolism and proliferation, with major contributions by thiol/disulfide oxidoreductase systems, in particular, the Thioredoxin Reductase-Thioredoxin (TrxR/Trx) and the Glutathione Reductase-Glutathione-Glutaredoxin (GR/GSH/Grx) systems. These cascades drive vital cellular functions in many ways through signaling, regulating other proteins' activity by *redox switches*, and by stoichiometric reductant transfers in metabolism and antioxidant systems. Increasing evidence argues that there is a persistent alteration of the redox environment in certain pathological states, such as cancer, that heavily involve the Trx system: upregulation and/or overactivity of the Trx system may support or drive cancer progression, making both TrxR and Trx promising targets for anti-cancer drug development.

Understanding the biochemical mechanisms and connections between certain redox cascades requires research tools that interact with them. The *state-of-the-art* genetic tools are mostly ratiometric reporters that measure reduced:oxidized ratios of selected redox pairs or the general thiol pool. However, the precise cellular roles of the central oxidoreductase systems, including TrxR and Trx, remain inaccessible due to the lack of probes to selectively measure turnover by either of these proteins. However, such probes would allow measuring their effective reductive activity apart from expression levels in native systems, including in cells, animals, or patient samples. They are also of high interest to identify chemical inhibitors for TrxR/Trx in cells and to validate their potential use as anti-cancer agents (to date, there is no selective cellular Trx inhibitor, and most known TrxR inhibitors were not comprehensively evaluated considering selectivity and potential off-targets). However, small molecule redox imaging tools are underdeveloped: their protein specificity, spectral properties, and applicability remain poorly precedented.

This work aimed to address this opportunity gap and develop novel, small molecule diagnostic and therapeutic tools to selectively target the Trx system based on a modular *trigger-cargo* design: artificial cyclic disulfide substrates (*trigger*) for oxidoreductases are tethered to molecular agents (*cargo*) such that the cargo's activity is masked and is re-established only through reduction by a target protein. The rational design of these novel reduction sensors to target the cell's strongest disulfide-reducing enzymes was driven by the following principles: (i) cyclic disulfide triggers with stabilized ring systems were used to gain low reduction potentials that should resist reduction except by the strongest cellular reductases, such as Trx; and (ii) the cyclic topology also offers the potential for kinetic reversibility that should select for dithiol-type redox proteins over the cellular *monothiol background*.

Creating imaging agents based on such two-component designs to selectively measure redox protein activity in native cells required to combine the correct trigger reducibility, probe activation kinetics, and imaging modalities and to consider the overall molecular architecture. The major prior art in this field has applied cyclic 5-membered disulfides (1,2-dithiolanes) as substrates for TrxR in a similar way to create such tools. However, this motif was described elsewhere as thermodynamically unstable and was due to widely used for dynamic covalent cascade reactions. By comparing a novel 1,2-dithiolane-based

probe to the *state-of-the-art* probes, including commercial TrxR sensors, by screening a conclusive assay panel of cellular TrxR modulations, I clarified that 1,2-dithiolanes are not selective substrates for TrxR in biological settings (**Nat Commun 2022**).

Instead, aiming for more stable ring systems and thus more robust redox probes, during this work, I developed bicyclic 6-membered disulfides (piperidine-fused 1,2-dithianes) with remarkably low reduction potentials. I showed that molecular probes using them as reduction sensors can be mostly processed by thioredoxins while being stable against reduction by GSH. The thermodynamically stabilized decalin-like *topology* of the *cis*-annelated 1,2-dithianes requires particularly strong reductants to be cleaved. They also select for dithiol-type redox proteins, like Trx, based on kinetic reversibility and offer fast cyclization due to the preorganization by annelation (**JACS 2021**). This work further expanded the system's modularity with structural cores based on piperazine-fused 1,2-dithianes with the two amines allowing independent derivatization. Diagnostic tools using them as reduction sensors proved equally robust but with highly improved activation kinetics and were thus cellularly activated. Cellular studies evolved that they are substrates for both Trxs and their protein cousins Grxs, so measuring the cellular *dithiol protein pool* rather than solely Trx activity (**ChemRxiv 2023**).

Finally, a trigger based on a slightly adapted reduction sensor, a desymmetrized 1,2-thiaselenane, was designed for selective reduction by TrxR's selenol/thiol active site, then combined with a precipitating large Stokes' shift fluorophore and a solubilizing group, to evolve the first selective probe **RX1** to measure cellular TrxR activity, which even allowed high-throughput inhibitor screening (**Chem 2022**).

The central principle of this work was further advanced to therapeutic prodrugs based on the duocarmycin cargo (CBI) with tunable potency (**JACS Au 2022**) that can be used to create *off-to-on* therapeutic prodrugs. Such CBI prodrugs employing stabilized 1,2-dichalcogenide triggers proved to be cytotoxins that depend on Trx system activity in cells. They could further be exploited for cell-line-dependent reductase activity profiling by screening their *redox activation indices*, the reduction-dependent part of total prodrug activation, in 177 cell lines. Beyond that, these prodrugs were well-tolerated in animals and showed anti-cancer efficacy *in vivo* in two distinct mouse tumor models (**BioRxiv 2022**).

Taken together, I introduced unique monothiol-resistant reducible motifs to target the cellular Trx system with chemocompatible units for each for TrxR and Trx/Grx, where the cyclic nature of the dichalcogenides avoids activation by GSH. By using them with distinct molecular cargos, I developed novel selective fluorescent reporter probes; and introduced a new class of bioreductive therapeutic constructs based on a common modular design. These were either applied to selectively measure cellular reductase activity or to deliver cytotoxic anti-cancer agents *in vivo*. Ongoing work aims to differentiate between the two major redox effector proteins Trx and Grx, requiring additional layers of selectivity that may be addressed by tuned molecular recognition. The flexible use of various molecular cargos allows harnessing the same cellular redox machinery by either probes or prodrugs. This allows predictive conclusions from diagnostics to be directly translated into therapy and offers great potential for future adaptation to other enzyme classes and therapeutic venues.

Kurzzusammenfassung

Die zelluläre Redox-Homöostase hängt von Thiol/Disulfid-Oxidoreduktasen ab, die den Stoffwechsel, die Proliferation und die antioxidative Antwort von Zellen beeinflussen. Die wichtigsten Netzwerke sind die Thioredoxin Reduktase-Thioredoxin (TrxR/Trx) und Glutathion Reduktase-Glutathion-Glutaredoxin (GR/GSH/Grx) Systeme, die über *Redox-Schalter* in Substratproteinen lebenswichtige zelluläre Funktionen steuern und so an der Redox-Regulation und -Signalübertragung beteiligt sind. Persistente Veränderungen des Redoxmilieus in pathologischen Zuständen, wie z. B. bei Krebs, sind in hohem Maße mit dem Trx-System verbunden. Eine Hochregulierung und/oder Überaktivität des Trx-Systems, die bei vielen Krebsarten auftreten, unterstützt zudem das Fortschreiten des Krebswachstums, was TrxR/Trx zu vielversprechenden Zielproteinen für die Entwicklung neuer Krebsmedikamente macht.

Um die biochemischen Prozesse dahinter zu erforschen, sind spezielle Techniken zur Visualisierung und Messung enzymatischer Aktivität nötig. Die hierzu geeigneten, meist genetischen Sensoren messen *ratiometrisch* das Verhältnis reduzierter/oxidierter Spezies in zellulärem Umfeld oder spezifisch ausgewählte Redoxpaare. Die weitere Erforschung der exakten Funktion von TrxR/Trx und deren Substrate ist jedoch durch mangelnde Nachweismethoden limitiert. Diese sind außerdem zur Validierung chemischer Hemmstoffe für TrxR/Trx in Zellen und deren potenziellen Verwendung als Krebsmittel von großem Interesse. Bislang gibt es keinen selektiven zellulären Trx-Inhibitor und potenzielle Off-Target-Effekte der bekannten TrxR-Inhibitoren wurden nicht abschließend bewertet.

Ziel dieser Arbeit ist die Entwicklung niedermolekularer, diagnostischer und therapeutischer Werkzeuge, die selektiv auf das Trx-System abzielen und auf einem modularen *Trigger-Cargo-Design* basieren. Hierzu werden zyklische Disulfid-Substrate (*Trigger*) für Oxidoreduktasen so mit molekularen Wirkstoffen (*Cargo*) verknüpft, dass dabei die Wirkstoffaktivität maskiert, und erst nach Reduktion durch ein Zielprotein wiederhergestellt wird. Diese neuartigen, synthetischen Reduktionssensoren basieren auf den folgenden Grundprinzipien: (i) Zyklische Disulfide sind thermodynamisch stabilisiert und können nur durch die stärksten Reduktasen gespalten werden; und (ii) die zyklische Topologie ermöglicht die kinetische Reversibilität der zwei Thiol-Disulfid-Austauschreaktionen, die eine erste Reaktion mit Monothiolen, wie z. B. *GSH*, sofort umkehrt und so eine vollständige Reduktion verhindert.

Die meisten früheren Arbeiten auf diesem Gebiet verwendeten ein zyklisches, fünfgliedriges Disulfid (1,2-Dithiolan) als Substrat für TrxR. Das gleiche Strukturmotiv wurde jedoch an anderer Stelle als thermodynamisch instabil beschrieben und aufgrund dieser Eigenschaft explizit für dynamische Kaskadenreaktionen verwendet. Deshalb vergleicht diese Arbeit zu Beginn einen neuen 1,2-Dithiolan-basierten fluorogenen Indikator mit bestehenden, z. T. kommerziellen, Redox-Sonden für TrxR in einer Reihe von Zellkultur-Experimenten unter Modulation der zellulären TrxR-Aktivität und stellt so einen Widerspruch in der Literatur klar: 1,2-Dithiolane eignen sich nicht als selektive Substrate für TrxR, da sie labil sowohl gegen die Reduktion durch andere Redoxproteine, als auch gegen den *Monothiol-Hintergrund* in Zellen sind (**Nat. Commun. 2022**).

Als alternatives Strukturmotiv wird in dieser Arbeit ein bizyklisches sechsgliedriges Disulfid (anneliertes 1,2-Dithian) etabliert. Durch sein niedriges Reduktionspotenzial, also seine hohe Resistenz gegen

Reduktion, werden molekulare Sonden basierend auf diesem 1,2-Dithian als Reduktionssensor fast ausschließlich von Trx aktiviert, nicht aber von TrxR oder GSH (**JACS 2021**). Dieses Kernmotiv bestimmt dabei die Reduzierbarkeit, und damit die Enzymspezifität, durch seine zyklische Natur und die Annelierung, auch unter Verwendung unterschiedlicher Farb-/Wirkstoffe. Auf dieser Grundlage konnte die molekulare Struktur durch einen weiteren Modifikationspunkt für die flexible Verwendung weiterer funktioneller Einheiten ergänzt werden. Obwohl zelluläre Studien ergaben, dass diese neuartigen 1,2-Dithian-Einheiten in Zellen sowohl Trx als auch das strukturell verwandte Grx adressieren, sind die daraus resultierenden diagnostischen Moleküle wertvoll, um den katalytischen Umsatz zellulärer *Dithiol-Reduktasen*, der sogenannten Trx-Superfamilie, selektiv anzuzeigen (**ChemRxiv 2023**).

Begünstigt durch das modulare Moleküldesign stellt diese Arbeit zudem das erste Reportersystem **RX1** zum selektiven Nachweis der TrxR-Aktivität in Zellen vor. Es basiert auf der Verwendung eines zyklischen, unsymmetrischen Selenenylsulfid-Sensors (1,2-Thiaselenan), der selektiv von dem einzigartigen Selenolat der TrxR angegriffen wird, und dadurch letztlich nur von TrxR reduziert werden kann. **RX1** eignete sich zudem für eine Hochdurchsatz-Validierung bestehender TrxR-Inhibitoren und unterstreicht dadurch den kommerziellen Nutzen derartiger Diagnostika (**Chem 2022**).

Das zentrale *Trigger-Cargo*-Konzept dieser Arbeit wurde für therapeutische Zwecke weiterentwickelt und nutzt dabei den einzigartigen Wirkmechanismus der Duocarmycin-Naturstoffklasse (CBI) (**JACS Au 2022**) zur Entwicklung reduktiv aktivierbarer Therapeutika. CBI-Prodrugs basierend auf stabilisierten Redox-Schaltern (1,2-Dithiane für Trx; 1,2-Thiaselenan für TrxR) reagierten signifikant auf TrxR-Modulation in Zellen. Sie wurden darüber hinaus durch das Referenzieren ihrer Aktivität gegenüber nicht-reduzierbaren Kontrollmoleküle für die Erstellung zelllinienabhängiger Profile der Reduktaseaktivität in 177 Zelllinien genutzt. Schließlich waren diese neuen Krebsmittel im Tiermodell gut verträglich und zeigten in zwei verschiedenen Mausmodellen eine krebshemmende Wirkung (**BioRxiv 2022**).

Zusammenfassend präsentiert diese Dissertation monothiol-resistente reduzierbare Trigger-Einheiten für das zelluläre Trx-System zur Entwicklung neuartiger, selektiver Reporter-Sonden, sowie eine neue Klasse reduktiv aktivierbarer Krebsmittel auf Basis eines adaptierbaren *Trigger-Cargo*-Designs. Diese fanden entweder zur selektiven Messung zellulärer Proteinaktivität oder zum Einsatz als Antikrebsmittel Verwendung. Es wurden chemokompatible Motive sowohl für TrxR als auch für Trx/Grx identifiziert, wobei deren zyklische Natur eine Aktivierung durch GSH verhindert. Eine weitere Differenzierung zwischen den beiden Redox-Proteinen Trx und Grx und anderen Proteinen der Trx-Superfamilie erfordert eine zusätzliche Ebene der Selektierung, z. B. durch molekulare Erkennung, und ist Gegenstand laufender Arbeiten.

Die flexible Verwendung verschiedener molekularer Wirkstoffe ermöglicht dabei die „Pipeline-Entwicklung“ von Diagnostika und Therapeutika, die von der zellulären Redox-Maschinerie analog umgesetzt werden, und dadurch Schlussfolgerungen aus der Diagnostik direkt auf eine Therapie übertragbar machen. Dies birgt großes Potenzial für künftige Entwicklungen bei einer potenziellen Übertragung des modularen Konzepts auf andere Enzymklassen und therapeutische Einsatzgebiete.

Parts of this work have been published in peer-reviewed journals:

- (1) **Jan G. Felber**, Lena Poczka, Karoline C. Scholzen, Lukas Zeisel, Martin S. Maier, Sander Busker, Ulrike Theisen, Christina Brandstädter, Katja Becker, Elias S. J. Arnér, Julia Thorn-Seshold, Oliver Thorn-Seshold. *Cyclic 5-membered disulfides are not selective for thioredoxin reductase, but are opened nonspecifically*. **Nature Communications** **2022**, *13*, 1754 (<https://doi.org/10.1038/s41467-022-29136-4>).
- (2) **Jan G. Felber**, Lukas Zeisel, Lena Poczka, Karoline C. Scholzen, Sander Busker, Martin S. Maier, Ulrike Theisen, Christina Brandstädter, Katja Becker, Elias S. J. Arnér, Julia Thorn-Seshold, Oliver Thorn-Seshold. *Selective, Modular Probes for Thioredoxins enabled by rational Tuning of a Unique Disulfide Structure Motif*. **Journal of the American Chemical Society** **2021**, *143*, 8791-8803 (<https://doi.org/10.1021/jacs.1c03234>).
- (3) Lukas Zeisel, **Jan G. Felber**, Karoline C. Scholzen, Lena Poczka, Dorian Cheff, Martin S. Maier, Qing Cheng, Min Shen, Matthew D. Hall, Elias S. J. Arnér, Julia Thorn-Seshold, Oliver Thorn-Seshold. *Selective cellular probes for mammalian thioredoxin reductase TrxR1: Rational design of RX1, a modular 1,2-thiaselenane redox probe*. **Chem** **2022**, *8*, 1493-1517 (<https://doi.org/10.1016/j.chempr.2022.03.010>).
- (4) **Jan G. Felber**, Oliver Thorn-Seshold. *40 Years of Duocarmycins: A Graphical Structure/Function Review of Their Chemical Evolution, from SAR to Prodrugs and ADCs*. **JACS Au** **2022**, *2*, 2636-2644 (<https://doi.org/10.1021/jacsau.2c00448>).

Parts of this work have been filed as international patent applications:

- (5) Oliver Thorn-Seshold, Julia Thorn-Seshold, **Jan G. Felber**, Lukas Zeisel. *Disulfide-based prodrug compounds*. PCT patent application: **WO 2022/200347 A1**.
- (6) Oliver Thorn-Seshold, Lukas Zeisel, **Jan G. Felber**. *Dichalcogenide prodrugs*. PCT patent application: **WO 2022/214598 A1**.

Parts of this work was deposited on a preprint server while being under scientific review:

- (7) **Jan G. Felber**, Annabel Kitowski, Lukas Zeisel, Martin S. Maier, Constanze Heise, Julia Thorn-Seshold, Oliver Thorn-Seshold. *Cyclic dichalcogenides extend the reach of bioreductive prodrugs to harness the thioredoxin system: applications to seco-duocarmycins*. **BioRxiv** **2022** (<https://doi.org/10.1101/2022.11.11.516112>).
- (8) **Jan G. Felber**[#], Lukas Zeisel[#], Karoline C. Scholzen, Carina Schmitt, Alexander J. Wiegand, Leonid Komissarov, Elias S. J. Arnér, Oliver Thorn-Seshold. *Bifunctional, piperazine-fused cyclic disulfides for oxidoreductase-activated cellular proagents*. **ChemRxiv** **2023** (<https://doi.org/10.26434/chemrxiv-2023-tm21m>).

[#]these authors contributed equally as first authors

Table of contents

1 Introduction.....	10
1.1 Chalcogen Redox Biology	10
1.1.1 Thiol and selenol redox biochemistry	10
1.1.2 Disulfide redox systems.....	12
1.1.3 Structure-function-relationship for dithiol-type redox effector proteins.....	17
1.2 The role of redox regulation in health and disease	20
1.2.1 Tumor biology from a redox perspective	20
1.2.2 Therapeutic potential for the TrxR/Trx couple as a drug target	22
1.3 Probing the cellular disulfide redox state	24
1.3.1 Genetic engineering for redox-responsive fluorescent proteins	25
1.3.2 Small molecule turn-on fluorescence probes.....	26
1.4 Thiol-mediated uptake and its connection to cellular redox systems	30
2 Aims and objectives of this research	32
3 Results and Discussion	35
3.1 Development of selective chemotypes to target the Trx system.....	35
3.1.1 The controversial use of 1,2-dithiolanes in chemical biology probes	35
3.1.2 Identification of a Trx-specific chemotype by rational design	51
3.1.3 Development of a cellular 1,2-thiaselenane probe for TrxR	68
3.1.4 Bifunctional cleavable 1,2-dithiane linkers for chemical biology	97
3.2 Redox-targeted therapeutic prodrugs for anti-cancer use.....	111
3.2.1 A searchable database and graphical review of the duocarmycin cytotoxins	111
3.2.2 Duocarmycin-based therapeutic prodrugs targeting the Trx system.....	122
3.2.3 Fused cyclic disulfide probes and prodrugs for use in diagnostics and therapeutics	138
3.2.4 Cyclic dichalcogenide probes and prodrugs for use in diagnostics and therapeutics.....	152
4 Research summary.....	165
5 Ongoing work and Future perspectives	167
5.1 Towards selective imaging agents for cellular redox function	167
5.1.1 Screening for chemical recognition elements for redox effector proteins.....	167
5.1.2 Using chemical proteomics for validation of chemical recognition motifs.....	169
5.1.3 The “perfect” cellular Trx1 probe design of the future	170
5.2 Improving the imaging modalities of fluorescent redox reporter probes.....	171
5.2.1 Over and beyond the visible spectrum for in vivo imaging of redox function.....	171
5.2.2 The use of chromophores for optoacoustic in vivo imaging of redox states.....	172
5.2.3 Cyclic disulfide-based FRET probes expand the portfolio of redox probes.....	172

5.3 Characterising chronic hypoxic states with small molecule redox sensors.....	173
5.4 Cyclic disulfide linkers for tandem activation of antibody-drug conjugates.....	174
6 Acknowledgements.....	176
7 Abbreviations.....	178
8 References.....	181
9 Appendix.....	191
9.1 Supporting Information to the publications presented in this doctoral thesis.....	191
9.1.1 Supporting Information to chapter 3.1.1: Paper 1: 1,2-dithiolane probes.....	191
9.1.2 Supporting Information to chapter 3.1.2: Paper 2: piperidine-fused 1,2-dithianes for Trx.230	
9.1.3 Supporting Information to chapter 3.1.3: Paper 3: 1,2-thiaselenane probes for TrxR.....	313
9.1.4 Supporting Information to chapter 3.1.4: Paper 4: bifunctional cyclic disulfide linker.....	411
9.1.5 Supporting Information to chapter 3.2.1: Paper 5: 40 years of duocarmycins.....	515
9.1.6 Supporting Information to chapter 3.2.2: Paper 6: bioreductive 1,2-dithiane prodrugs.....	538
9.2 Additional experimental sections.....	616
9.2.1 Experimental Part for chapter 5.2.2: Chemical proteomics probes for cysteine profiling..	616
9.2.2 Experimental Part for chapter 5.4: A new disulfide linker for ADCs.....	631

1 Introduction

Redox reactions are chemical transformations that transfer electrons between reaction partners. In biological systems, numerous enzymes harvest a small set of redox-active cofactors like nicotinamides (NADPH) or flavins (FAD) as freely diffusing electron carriers to perform reductions/oxidations in proteins with a variety of chemistries. However, the chemical nature of the cofactor does not determine the biological transformation; enzymes perform specific redox transitions in cells that instead exploit amino acids as redox-active sites.

Cysteines (Cys) and selenocysteine (Sec - found only rarely in the proteome) are of the most important residues among the canonical amino acid side chains and are highly redox-active. Biology exploits the intrinsically reversible redox properties of protein cysteines for redox reactions, as well as for redox-based regulation of protein activity, in diverse ways.¹ Cys also features a wealth of chemistry that is not connected to its dynamic redox capabilities: it is the strongest protein nucleophile and is found as the catalytic residue crucial for various enzymes' activity. It also is a good ligand for metals that themselves act as active sites. However, this thesis focuses on (seleno)cysteine redox biochemistries.

The chemical environment of thiols/selenols and (cyclic) disulfides in proteins is what determines their reactivity. Redox proteins rely on their active sites' tertiary structure that can allow very distinct reactivities even when similar redox-active residues are involved. For example, the small redox protein thioredoxin (Trx) shares a conserved active site with two cysteines required to reduce disulfides with the related protein disulfide isomerase (PDI).^{2,3} However, influenced by the proteins' distinct shapes, these two proteins show vastly different reactivities and functions in cells. Understanding the structural features that dictate these redox properties requires to consider a chemical space that has rarely been looked at in biology from an organic chemist's perspective: structurally tuned cyclic dichalcogenides. New exploratory chemical developments are waiting to mimic the reactivities of protein disulfides. Subject of this thesis is to explore novel structural features by studying the interaction of synthetic dichalcogenide biomimics with oxidoreductases in biological settings.

1.1 Chalcogen Redox Biology

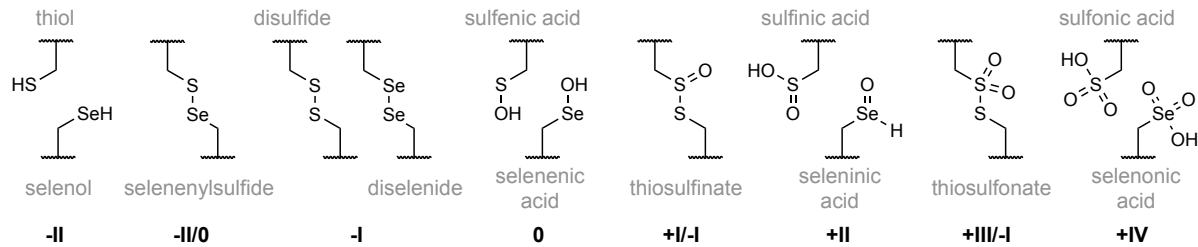
A small set of redox-active cofactors play roles as simple electron transmitters; whereas cysteine (Cys) and selenocysteine (Sec) are the key canonical amino acid residues that allow building intrinsically redox-active proteins since they can cycle between multiple oxidation states. Indeed, many processes in redox biology rely on thiol- or selenol-mediated redox reactions between redox-active proteins.

1.1.1 Thiol and selenol redox biochemistry

Chalcogen oxidation status. Protein cysteines are primarily found as free thiols (oxidation state -II) or as disulfides that are formed between two cysteine residues (oxidation state -I). Besides the thiol/selenol (-II) and dichalcogenide (-I) states, in biology, organochalcogens may also be present in a variety of higher oxidation states (**Figure 1a**).⁴ Sulfenic/selenenic acids (0) are formed by mono-oxidation and may e.g. be reduced by thiols under elimination of H₂O to form disulfides/selenenylsulfides.⁵ Thiosulfonates (+I/-I) and thiosulfonates (+III/-I) with mixed oxidation states

are oxidized disulfide analogs with various intermediary biological functions. Higher oxidation state sulfinic/seleninic (+II) and sulfonic/selenonic acids (+IV) are formed by overoxidation of redox-active sites and are mostly protein silencing modifications.⁶

a organochalcogen oxidation states



b thiol-mediated disulfide reduction

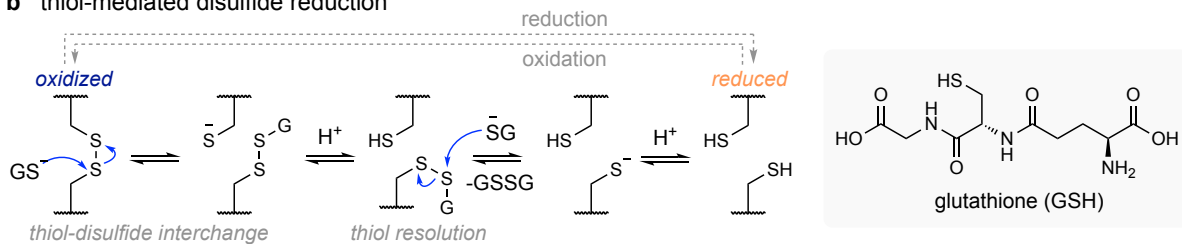


Figure 1 (a) Oxidation states of thiols/selenols and dichalcogenides.⁴ (b) Thiol-mediated disulfide reduction mechanism: two consecutive thiol-disulfide interchange reactions lead to the net reduction of a disulfide by GSH.

Thiol-disulfide interchange. Disulfides (termed: *oxidized*) may be cleaved, resulting in two free thiol cysteine residues (termed: *reduced*). Typically, this 2-step process (**Figure 1b**) involves a nucleophilic attack by a thiolate that cleaves the disulfide, releases one of the initial sulfurs as a thiolate, and forms an intermediary mixed disulfide (termed: *thiol-disulfide interchange*). Next, another nucleophilic attack by another thiolate liberates the second initial sulfur residue (termed: *thiol resolution*).⁷ (Selenolates, found in selenol/thiol active sites, may also participate in such a reduction, usually as the initial rather than resolving nucleophile.) A prominent thiol nucleophile in biology is the redox-active peptide glutathione (GSH), which acts as a versatile redox cofactor together with its oxidized counterpart glutathione disulfide (GSSG). GSH is present at millimolar levels in cells and can perform net reductions of protein disulfides (**Figure 1b**).

How does nature use disulfides? Structural disulfide bonds can be formed between cysteine residues of different subunits or secondary structures (to stabilize tertiary protein structures) or between proteins (forming oligomeric structures).^{8,9} However, some disulfides between protein subunits may be formed or cleaved reversibly, particularly to induce conformational changes that regulate protein function (termed: *redox switch*). Nature uses such *redox switches* between active and inactive forms of enzymes as a way to reversibly post-translationally regulate enzyme stability and activity.¹⁰ One example is the transcription factor activator protein-1 (AP-1), a heterodimeric protein complex containing two the components Fos and Jun (**Figure 2**). These are two inter-coiled helices that bind noncovalently by leucine-leucine interactions (leucine zipper) to form the DNA-binding module. However, upon formation of an inter-subunit disulfide bond, AP-1 undergoes a conformational rearrangement that prevents DNA binding (*off-state*). Reduction of the disulfide restores its DNA-binding module and re-initiates transcription (*on-state*).

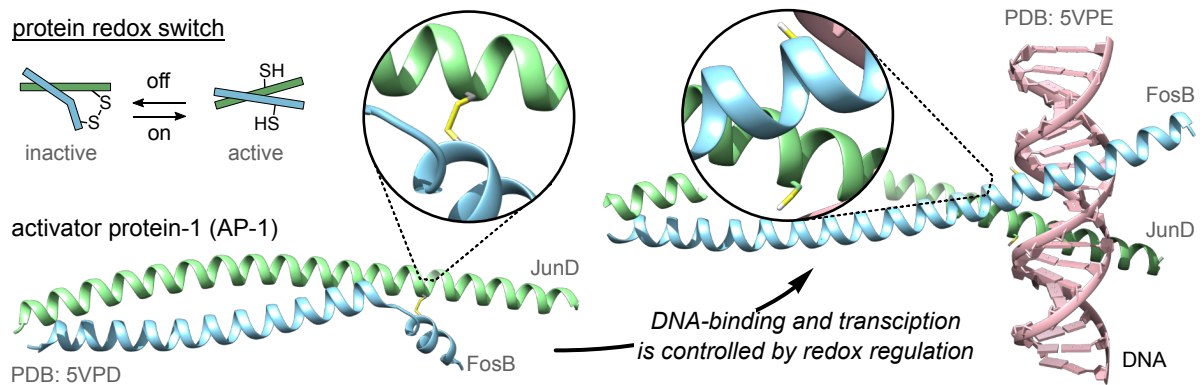


Figure 2 Example of a thiol/disulfide-mediated redox switch. Binding of the transcription factor activator protein-1 (AP-1) to DNA is enabled by reduction (PDB: 5VPD, 5VPE).¹³ Heterodimeric AP-1 consists of Fos/Jun subunits.

A known pathway where AP-1 activity is modulated by reduction is through the multifunctional protein apurinic endonuclease 1 (APE1),¹¹ also known as redox factor 1 (Ref-1) that is ultimately recovered by the redox effector protein thioredoxin (Trx).¹² Disulfide reduction can also influence protein activity directly. Besides providing H₂-equivalents for reduction of other substrates, reducing a disulfide may liberate catalytic cysteine residues, unblock access to a catalytic site, or any combination of these.¹⁴ One example is given by ribonucleotide reductase (RNR), an enzyme that catalyzes the reduction of ribonucleotides (NTPs) to deoxyribonucleotides (dNTPs). During each cycle, a stable disulfide is formed between the two active site cysteines and blocks the binding site. Reduction of RNR by Trx not only transfers the H₂-equivalent required for NTP reduction but also re-opens the binding site, ready for another cycle.^{15–17}

1.1.2 Disulfide redox systems

A short summary will now be given of the redox systems that act as central players in driving stoichiometric redox reactions, as well as in regulating redox-controlled proteins and pathways.¹⁸ For clarity, this summary is focused on the human isoforms of redox proteins and enzymes.

The glutathione system (Figure 3a)

GR: The nicotinamide redox cofactor NADPH is the major source of reducing equivalents in the cell. Only two oxidoreductase enzymes exploit NADPH to act as an electron relay for reduction of disulfide bonds: glutathione disulfide reductase (GR) and thioredoxin reductase (TrxR). Both are homodimeric flavoproteins with a conserved CVNVGC dithiol active site that additionally contains FAD as a prosthetic group for transfer of the H₂-equivalent. GR is a highly specific enzyme for the reduction of GSSG to GSH and is conserved across all kingdoms.¹⁹ It is central for cellular antioxidant systems, which use GSH as a versatile redox adaptor in diverse ways (**Figure 3a**).²⁰ The major ones are listed below.

GPx: GSH is required for recovery of active glutathione peroxidase (GPx) enzymes that are responsible for reduction/detoxification of hydroperoxides in the cell.²¹ Most GPxs have a Sec as their active site, which is mono-oxidized by hydroperoxides to give the corresponding selenenic acid. Then, an attack by a first GSH molecule gives the intermediary selenenylsulfide, which is resolved by a second GSH molecule to recover the active Sec center.²⁰ GPx1-3 transform H₂O₂ and other organic hydroperoxides

in different cell types and cellular localizations, e.g. GPx1 in erythrocytes prevents hemoglobin from oxidative breakdown.²² The membrane-located GPx4 is responsible for reduction of lipid peroxides in the plasma membrane and has been identified as the gatekeeping enzyme for ferroptosis, a non-apoptotic cell death pathway characterized by iron-dependent lipid peroxidation.²³

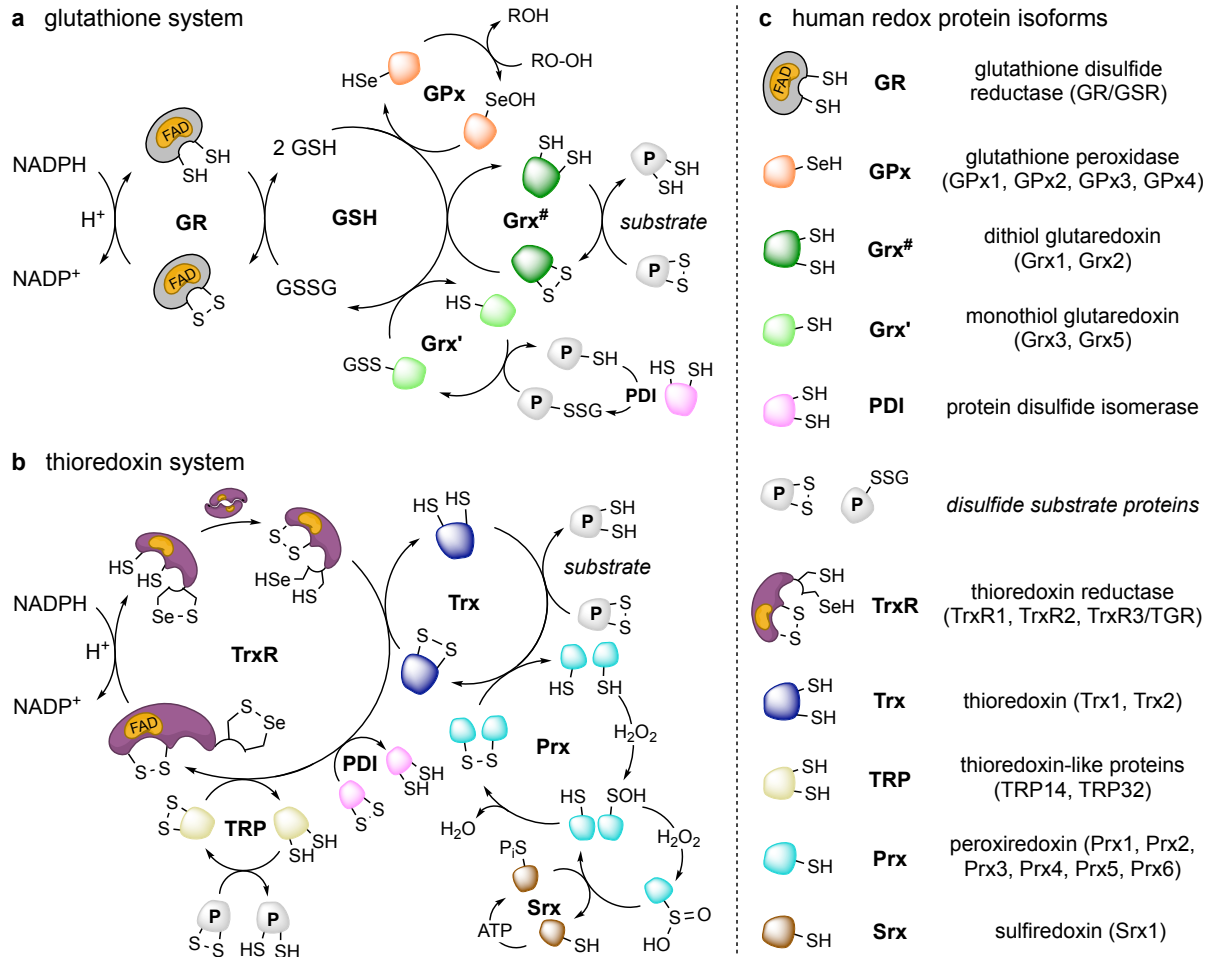


Figure 3 (a) The glutathione redox system and its substrates. (b) The thioredoxin system and its link to peroxiredoxin activity. (c) Human redox protein isoforms: **GR/GSR**: dimeric flavoenzyme with FAD cofactor. **GPx**: mono-Sec glutathione peroxidase. **Grx1**: cytosolic dithiol-type redox effector protein. **Grx2**: mitochondrial dithiol-type, iron-sulfur core. **Grx3**: monothiol-type, also protein kinase C-interacting cousin of thioredoxin (PICOT) or Trx-like protein 2, iron-sulfur core. **Grx5**: mitochondrial monothiol-type. **PDI**: dithiol-type protein disulfide isomerase. **TrxR1**: cytosolic, dimeric flavoenzyme with FAD cofactor. **TrxR2**: mitochondrial. **TrxR3/TGR**: mixed: thioredoxin-glutathione reductase. **Trx1**: dithiol-type redox effector protein. **Trx2**: mitochondrial. **TRP14**: Trx domain-containing protein 17. **TRP32**: Trx-like protein 1. **Prx**: peroxide acceptors. **Srx1**: ATP-dependent Prx-sulfenic acid reductase.

Dithiol Grx: Dithiol glutaredoxins (Grxs) are central for redox regulation with various disulfide protein substrates, such as RNR (shared substrate with Trx) and phosphoadenylylsulfate reductase (PAPS).^{24,25} Dithiol Grx1 and its mitochondrial counterpart Grx2 are strongly reducing redox effector proteins that contain the *Trx-fold* motif and so are part of the Trx-superfamily (see below). However, Grxs are unique due to their high specificity for interacting with GSH, GSSG, or GSS-Pr_R (glutathionylated proteins); and they contain a conserved CPYC active site.^{20,26} Dithiol Grxs are reduced by GSH through two consecutive thiol-disulfide interchanges (see **Figure 1b**).²⁷ Additionally, Grx2 activity relies on a [Fe₂S₂]-cluster between two monomers to form an active dimeric complex that is further stabilized by two additional GSH molecules to act as redox cofactors in iron homeostasis.²⁵

Monothiol Grx: Monothiol Grx3 and mitochondrial Grx5 with their CGFS-active site are responsible for the regulated deglutathionylation of protein thiols, a common post-translational modification (PTM) to modulate their function/activity or prevent other irreversible PTMs on cysteines.^{28,29} Their reduced state is recovered by a single GSH.²⁵

PDI: Protein disulfide isomerases (PDI) are multifunctional oxidoreductases of the Trx-superfamily that are also involved in protein S-deglutathionylation but are, more broadly, needed for isomerization of protein disulfide bonds as required during protein folding in the ER.^{30,31} Interestingly, the dimeric PDI complex can catalyze both the reduction and the oxidation of protein disulfides/dithiol species³².

The thioredoxin system (Figure 3b)

TrxR: Thioredoxin reductase (TrxR) is a high-turnover redox enzyme that primarily reduces the redox effector protein Trx but also operates on other proteins of the Trx-superfamily. TrxR shares most of its structural core with GR (the NADPH-binding N-terminal redox-active site (CVNVGC) with FAD as a prosthetic group), but TrxRs are extended at the C-terminus by a short, flexible amino acid chain containing a unique peripheric vicinal Cys-Sec redox-active site (described as a flexible arm). It uses this C-terminal site to perform reduction, leaving an intermediary cyclic selenenylsulfide. However, TrxR forms a homodimeric species, which transfers reduction equivalents from NADPH in the buried N-terminal active site of one unit to the C-terminal site of the other to restore activity.^{33–35} The cytosolic TrxR1 and the mitochondrial TrxR2 are ubiquitous, while the third, tissue-specific human isoform TrxR3 (also called thioredoxin-glutathione reductase – TGR) is a mixed oxidoreductase with both TrxR- and Grx-domains.^{36,37} TrxR together with its effector Trx (termed: *thioredoxin system*) (**Figure 3b**) offers a pathway for redox regulation that operates separately to the glutathione system,³⁸ although both systems are interlinked at several points and also can function as backup systems for each other (see below).^{39–41}

Trx: Thioredoxin (Trx) is a ubiquitous, small redox effector protein of 12 kDa that was first described in 1964 as the hydrogen donor for RNR.^{42,43} Its highly conserved molecular architecture (termed: *Trx-fold*) consists of 4-5 central β -sheets surrounded by 3-4 α -helices ($[\beta_1\alpha_1]\beta_2\alpha_2\beta_3-\alpha_3-\beta_4\beta_5\alpha_4$) (see **Figure 4c**) and is also found in several other redox effector proteins, such as thioredoxin-related proteins (TRPs), Grxs, PDIs, glutathione S-transferases (GSTs) and GPxs (termed: the *Trx-superfamily*).⁴⁴ Trx1 is found in the cytosol, whereas the human mitochondrial redox environment is controlled by Trx2. Beyond reducing RNR, Trx drives antioxidant activity since it is the direct reducing agent for peroxiredoxins (Prx) and methionine sulfoxide reductase (MSR)); and it functions as a multivalent regulator in redox signaling targeting a variety of other proteins⁴⁵, such as apoptosis signaling-regulating kinase 1⁴⁶ (ASK1), nuclear factor kappa B (NF- κ B)^{47,48}, the nuclear factor erythroid 2-related factor 2 (Nrf2), the hypoxia-inducing factor 1 alpha (HIF-1 α)⁴⁹, the transcription factor p53 and activator protein-1 (AP-1) via redox-factor 1 (Ref-1/APE1) reduction^{12,50,51} (see **chapter 1.1.1**). It has to be noted that Trx1 and Grx1 share several protein targets, explaining the partial redundancy of Trx and Grx systems.^{10,52}

TRP: Thioredoxin-related proteins (TRPs) (also referred to as Trx-like or Trx-domain-containing proteins) are a heterogeneous group of proteins that contain at least one Trx-fold and show oxidoreductase activity. While these proteins may also be recycled through reduction by TrxR, they display different substrate specificities depending on their cellular compartments. Thioredoxin-related protein of 14 kDa (TRP14) has been described to have very similar properties as Trx1 but interestingly does not share most of its protein targets and acts as an independent modulator for redox regulation.^{53–55} Thioredoxin-related protein of 32 kDa (TRP32 – also referred to as thioredoxin-like protein 1, Tx11) was shown to regulate 26 S proteasome via interaction with its substrate-recruiting factor eEF1A1⁵⁶ and to reduce oxidized phosphatase of regenerating liver (PRL), an inducing factor for cancer metastasis.⁵⁷

The peroxiredoxin system (Figure 3b)

Prx: Peroxiredoxins (Prx) reduce H₂O₂ to H₂O. Prxs are highly abundant (up to 1 % of all soluble cellular proteins) and there are six human isoforms (Prx1-6) with different cellular localization.⁵⁸ Prxs only contain one redox-active cysteine that is oxidized by reaction with H₂O₂ at very high rates to its sulfenic acid form. Then, nucleophilic attack of an active site thiol from a different Prx monomer eliminates H₂O forming a stable interprotein disulfide bond (leading to homodimerization/oligomerization), though this is then re-reduced by Trx (**Figure 3b**). Prx also acts in cellular detoxification with other substrates as peroxynitrites and organic hydroperoxides.^{59,60} Hyperoxidation of Prx active site thiols gives sulfinic or sulfonic acids that can no longer be recovered by Prx dimerization and Trx reduction and, therefore, are inactivated for redox regulation. However, the sulfinic acid active Prxs were found to be re-established by a different, unusual redox mechanism: sulfiredoxin (Srx) contains a phosphorylated redox-active cysteine that transfers its phosphate to Prx sulfinic acids activating them for nucleophilic attack of another Prx-thiol to give a thiosulfinate intermediate. Interprotein Prx thiosulfates are recycled by sequential thiol-mediated reduction to recover the active Prxs.⁶¹ Besides that, Srx has also been shown to be an active component in protein deglutathionylation.⁶²

Compartmentalization. Mammalian cells are tightly organized in compartments with very distinct redox environments but these are poorly understood. Broad statements about "reducing" or "oxidizing" compartments do not explain activity or inactivity of precise redox couples. Understanding the compartmentalization of redox activity will instead require non-trivial subcellular detection and differentiation of protein function that is only recently becoming a subject of ongoing research (see **chapter 1.3**). Interesting examples are extracellular dithiol proteins that were previously thought to be predominantly maintained in the oxidized state with poor catalytic activity.⁶³ Evidence now suggests that the cell membrane contains protein systems for redox regulation and signaling that function autonomously to the cytoplasmic redox pool⁶⁴, which would also match observations about the role of transmembrane thiol-mediated uptake cascades^{65,66} (see **chapter 1.4**).

A summary and overview of all major human redox-active proteins/enzymes of the GSH and Trx redox systems and some of their downstream effectors are shown in **Table 1**. It links to the UniProt ID, the gene code, and the PDB code for further details on protein function, expression, and structure.

Table 1 Major human redox proteins with their redox-active site (seleno)cysteines. AA: amino acids; kDa: molecular weight; UniProt ID (beta.uniprot.org); gene code (ncbi.nlm.nih.gov); PDB code (rcsb.org). Mitochondrial protein isoforms* labeled. Dithiol redox effector proteins are highlighted in yellow.^{60,67}

	redox-active site	AA	kDa	UniProt ID	Gene	PDB
GR	TC ¹⁰² VNVGC ¹⁰⁷ V	479	52	P00390-2	GSR	1GRA, 2GRT
GPx1	SLU ⁴⁹ GT	203	22	P07203	GPX1	2F8A
GPx2	SLU ⁴⁰ GT	190	22	P18283	GPX2	2HE3
GPx3	SYU ⁷³ GL	226	26	P22352	GPX3	2R37
GPx4	SQU ⁷³ GK	197	22	P36969	GPX4	6ELW
Grx1	TC ²³ PYC ²⁶ R	106	12	P35754	GLRX	4RQR
Grx2*	SC ⁷⁷ SYC ⁸⁰ T	164	18	Q9NS18	GLRX2	2FLS, 2HT9
Grx3	RC ¹⁵⁹ GFSK and KC ²⁶¹ GFSK	335	37	O76003	GLRX3	2WZ9, 2YAN
Grx5*	QC ⁶⁷ GFSN	157	17	Q86SX6	GLRX5	2WUL
PDI	WC ⁵³ GHC ⁵⁶ K and WC ³⁹⁷ GHC ⁴⁰⁰ K	508	57	P07237	P4HB	4EL1
TrxR1	TC ⁵⁹ VNVGC ⁶⁴ I and GC ⁴⁹⁷ U ⁴⁹⁸ G	499	55	Q16881-5	TXNRD1	3QFB, 2ZZC, 2CFY, 2J3N
TrxR2*	TC ⁸⁵ VNVGC ⁹¹ I and GC ⁵²² U ⁵²³ G	524	57	Q9NNW7	TXNRD2	
TrxR3	TC ²⁰² VNVGC ²⁰⁸ I and GC ⁶⁴¹ U ⁶⁴² G	643	71	Q86VQ6	TXNRD3	3H8Q
Trx1	TWC ³² GPC ³⁵ KM	105	12	P10599	TXN	1ERT, 1ERU
Trx2*	QWC ⁹⁰ GPC ⁹³ KI	166	18	Q99757	TXN2	1W4V, 1W89
TRP14	SWC ⁴³ PDC ⁴⁶ VQ	123	14	Q9BRA2	TXNDC17	1WOU
TRP32	RG ³⁴ GPC ³⁷ LR	289	32	O43396	TXNL1	1GH2
Prx1	FVC ⁵² PT	199	22	Q06830	PRDX1	2RII
Prx2	FVC ⁵¹ PT	198	22	P32119	PRDX2	7KIZ, 7KJ0
Prx3*	FVC ¹⁰⁸ PT	256	28	P30048	PRDX3	5JCG
Prx4	FVC ¹²⁴ PT	271	31	Q13162	PRDX4	3TJF
Prx5*	PGC ¹⁰⁰ SK	214	22	P30044	PRDX5	1HD2
Prx6	PVC ²⁷ TT	224	25	P30041	PRDX6	1PRX
Srx1	GGC ⁹⁹ HR	137	14	Q9BVN0	SRXN1	1XW3

1.1.3 Structure-function-relationship for dithiol-type redox effector proteins

To sum up the “central dogma” of cellular redox regulation in this chemical space: reduction reactions are driven by NADPH consumption through the flavoenzymes GR and TrxR and so transfer reducing equivalents to various redox effector proteins/enzymes that then perform a wide range of cellular reductions. The central nodes in redox regulation are the dithiol active site (CXXC) proteins Trxs, Grxs, TRPs, and PDIs of the Trx-superfamily (highlighted in **Table 1**; termed: *redox effector proteins*).

This heterogenous group of proteins shares similar protein domains but with very distinct reduction properties and target substrate scopes. Some of the structural features affecting their reactivity are discussed in the following.

Reduction potential. The reduction potential of a specific redox protein pair ($P(SH)_2/PS_2$) is a common entry point to discuss the “reducing power” of a protein reductant (**Figure 4a**), and values are often compared to the thiol/disulfide-pair 2GSH/GSSG (-0.24 V at pH 7).^{2,68,69} Reduction of disulfide-type proteins involves additional acid-base equilibria and is therefore highly pH-dependent (see pH-dependent Nernst’s equation – **Figure 4a**). Note that reduction potentials for the redox proteins Trx, TRP14, TRP32, dithiol Grx[#], monothiol Grx^{*}, and PDI reported in the literature are also highly dependent on the specific experimental settings applied to determine them. **Figure 4a**, therefore, gives literature ranges of reduction potentials for each redox effector protein pair. This shows two main features: (i) Proteins sharing the Trx-fold may have very different reduction potentials, from highly reducing (Trx: -0.27 to -0.22 V;^{2,70–72} TRP14/TRP32: -0.26 to -0.25 ^{55,56}; Grx[#]: -0.24 to -0.22)^{2,70} to weakly reducing (Grx^{*}: -0.20 to -0.18 ^{2,70}; PDI: -0.18 to -0.16)^{2,73} or even oxidizing (*E.coli* DsbA: -0.11 to -0.09)²; and (ii) the reduction potential of some redox effector proteins is comparable to that of GSH, even if many of their substrates are not reducible by GSH. Aiming to understand these trends, prior work has outlined the following points that may affect the “reducing power” and substrate specificity differences within the Trx superfamily:

Steric tension. Ring strain in a cyclic disulfide system can be estimated from the geometrical parameters S-S bond distance, CSS/SSC bond angles, and most importantly, the dihedral CSSC torsion angle. These are well studied in small molecule settings: depending on ring size, small alicyclic disulfides may suffer from considerable ring tension that favors their reduced state (4-, 5-, and 7-membered); or else may have thermodynamically preferred cyclic disulfide forms (6-membered disulfides) - one reason why 1,2-dithiothreitol (DTT) is a strong reducing agent for disulfides.⁷⁴ Bond distances and bond angles of unstrained linear/6-membered cyclic disulfides (2.04 Å, 100°) and torsion angles of linear disulfides (90°) and 1,2-dithianes (60°) are preferred configurations that minimize lone-pair repulsion.^{65,75} However, no large deviations from these preferred S-S bond distances, CSS/SSC bond angles, or dihedral CSSC torsion angles was identified for any of the oxidized Trx-fold proteins looking at the crystallographic data.⁷⁶ This argues that their differences in “reducing power” are not explained by ring strain in their macrocyclic disulfides.

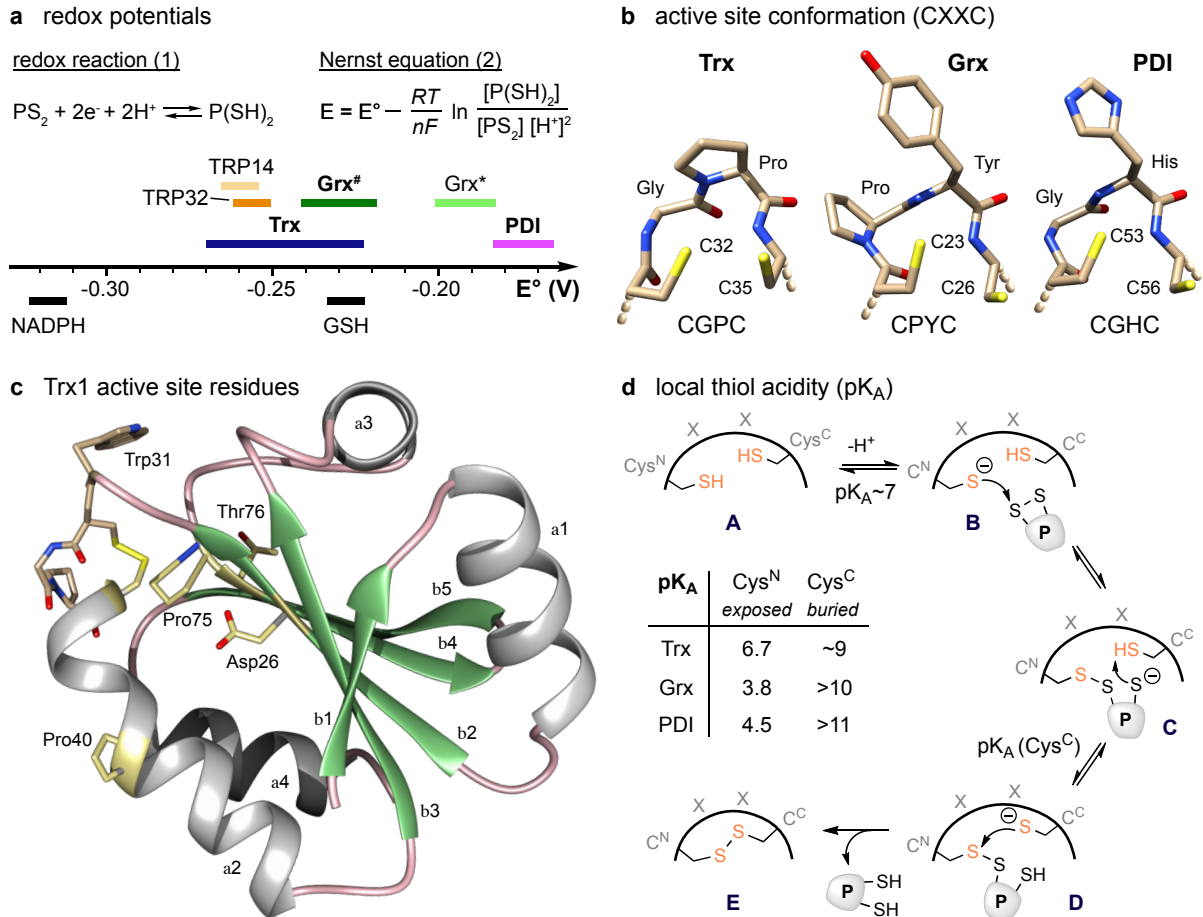


Figure 4 Redox properties of Trx-fold proteins. (a) Calculation of reduction potentials for redox proteins using the pH-dependent Nernst equation; and experimental reduction potential ranges for redox effector proteins. (b) CXXC active site conformations for prototype proteins Trxs, Grxs, and PDIs. (c) Trx1 active site's functional residues. (d) Mechanism of reduction for dithiol-type redox effector proteins: pK_A values for the exposed *N*-terminal thiol (Cys^N) and the buried C-terminal thiol (Cys^C).

CXXC motif. Redox effector proteins share a conserved CXXC redox-active motif (Figure 4b). The nature of the two XX residues is one obvious sequence-based difference between the protein classes: Trxs/TRP32 (Gly-Pro), TRP14 (Pro-Asp), and Grx1 (Pro-Tyr) all share a functional proline that geometrically pre-organizes both cysteines and decreases rotatory degrees of freedom, while PDI (Gly-His) and Grx2 (Ser-Tyr), both with high reduction potentials, lack this residue. Following this idea, a Trx P34H mutant (mimicking PDI's active site) or P34S/T indeed significantly increased reduction potential leading to decreased "reducing power," as slower reactions with disulfide substrates were observed.⁷⁷⁻⁸¹ On the other hand, isolated octapeptides containing the active site sequences of Trx, Grx, and PDI did not reflect the trend in redox properties observed for the native proteins and were all found to provide a *fragment-based* reduction potential of ca. -0.20 V.⁸² In summary, the nature of the CXXC motif is one major determinant of low reduction potentials across the different proteins,² but its differences become apparent only in the folded protein context.^{3,76}

Tertiary structure and amino acid residues. Each of the redox effector proteins contains important amino acid residues close to the active site that are key to substrate specificity and activity. Grxs have a binding affinity to GSH/GSSG that is directed by local side chains, as excellently reviewed by Deponte.²⁰ This part will focus on the tertiary structure and important amino acids in Trx proteins (e.g. Trx1, shown in **Figure 4c**). Besides the active site Pro34, Trx contains two additional important proline residues. The conserved Pro40 introduces a kink in the α_2 -helix that separates the CGPC active site from the rest of the helix.⁴⁴ Mutation of Pro40 leads to destabilization of the overall protein structure.^{83,84} Pro75 is positioned on the opposite site of the active site stabilizing this crucial region through hydrogen bonding with the conserved Thr76.⁸⁵ Mutation of Pro75 leads to inefficient reduction catalysis. Trp31, located directly before the active site, forms van der Waals contacts with the opposite residues, plays important roles for protein stability, and may contribute to substrate recognition.^{44,86} Finally, charged residues may contribute to the acid-base equilibria that are key to the catalytic mechanism. Particularly, Asp26 was initially attributed to deprotonate Cys^C and influence protein catalysis,^{85,87} though Trx function was recently shown to be unaffected by Asp26 replacement,⁸⁸ so its role is controversial.⁴⁴

Thiol pK_A and XX backbone. The multi-step mechanism established for reduction of target proteins (or probes) by a redox effector is shown in **Figure 4d**. The N-proximal cysteines (Cys^N) of such proteins are often solvent exposed and exhibit lower pK_A values as compared to the C-proximal cysteines (Cys^C) that are buried in the secondary structure of the protein and have a higher pK_A (**A**). As Cys^N is the stronger nucleophile, target protein disulfides are attacked by the Cys^N thiolate (**B**) to give a mixed disulfide intermediate (**C**). After deprotonation of Cys^C, (e.g. by the released target protein's thiolate) the resulting Cys^C thiolate (**D**) resolves the mixed disulfide to give the reduced target protein and oxidized effector (**E**). Ultimately, both cysteine acidities have strong influence on the protein's ability to reduce by establishing kinetic barriers to reduction processes, even if they are thermodynamically favored.⁸⁹ Interestingly, the highly reducing Trx proteins have moderate pK_A's (~6.7), while low pK_A's were found for dithiol Grxs[#] (~3.8) and PDIs (~4.5), so that lowering pK_A does negatively correlate with "reducing power".^{3,76} Thiol acidity (pK_A) can be strongly influenced by the protein's microenvironment that may provide residues to stabilize the charged thiolate form. This includes ionic interactions with charged side chains, hydrogen bonding, desolvation, and helix-dipole effects. Instead, charged side chains, like Asp26 for Trx, are now understood to play a minor role in discriminating the pK_A values of active site cysteines of a CXXC protein. The number of hydrogen bonds with amide backbones instead correlated with the thiol's pK_A.^{90,91} The more direct hydrogen bonds, the lower the pK_A of the respective Cys^N. Mutagenesis studies have additionally supported this influence of the XX residues on the thiol-acidity.^{79,91-93} Overall, the various effects on protein thiol pK_A values do also not conclusively explain differences between the redox effector proteins.

Electrostatic complementarity. Several examples of protein substrates are known, where the thermodynamics favor a disulfide reduction process while it is kinetically hindered. This argues that redox pathways are based on substrate specificity with redox effector proteins and are not primarily determined by reduction potential differences. Recently, shared substrates of Trxs and Grxs have been used as model systems to study the nature of protein-specificity; the distribution of charged/uncharged

amino acids and the overall electrostatics of the proteins' surfaces were important factors, with complementarity in these aspects identified as a major driving force for specific interactions.^{41,94,95}

Conclusions. For decades, cellular disulfide reduction cascades were simplistically assumed to follow thermodynamic paths. However, redox regulation based on the distinct redox effector proteins of the Trx-superfamily is by far more complex. Differences in (sub)cellular function and substrate specificity of Trxs, Grxs, TRPs, and PDIs cannot be attributed to reduction potential or macrocyclic ring tensions. Several lines of evidence support the central role of the differential CXXC active site motifs, not only in steric pre-organization of the dithiol but also highly influencing the reduction kinetics. The degree of hydrogen bonding of the CXXC amide backbone has been found to determine the active site thiols' acidity and reaction rates. While conserved side chain amino acids may be crucial for the catalytic protein function of each member, differences between the effector proteins could not be correlated to conserved sites. Electrostatic complementarity and protein-protein binding between the effector and the substrate may also be major determinants for substrate specificity and redox activity. Thus, many key aspects that allow understanding of their cellular redox activity remain unknown.

1.2 The role of redox regulation in health and disease

The following chapter discusses cellular redox regulation in the context of disease, particularly cancer, and outlines potential therapeutic implications and target strategies within redox systems with a focus on the TrxR/Trx couple.

1.2.1 Tumor biology from a redox perspective

Due to protein dysfunction or dysregulation, some cells may collectively proliferate uncontrollably, form solid tumors, aggressively invade distant tissues, heavily damage their surroundings and, ultimately, the host organism. These disease states are loosely summarized under the term *cancer* and are prominent causes of death in the human population.^{96,97} A number of acquired capabilities of these cancerous cells are crucial preconditions for cancer progression and are known as *hallmarks of cancer* (**Figure 5**): being independent of external growth factors (1: *self-sufficiency in growth signals*), resistant to external growth suppressors (2: *insensitivity to anti-growth signals*) and resilient to programmed cell death (3: *evading apoptosis*); being able to continuously reproduce (4: *limitless replicative potential*) while perpetually recruiting oxygen/nutrient supply (5: *sustained angiogenesis*); and having the ability to spread and colonize distant tissues (6: *tissue invasion and metastasis*).⁹⁸ More recently, having the capacity to reprogram energy metabolism in cells (7: *deregulated energetics*) and to avoid recognition by immune (killer) cells (8: *evading immune destruction*) have been added to this list of classic hallmarks. Induced inflammatory conditions (a: *tumor-promoting inflammation*) and higher rates of mutagenesis through a breakdown in the genomic maintenance machinery (b: *genome instability and mutation*) are also considered as further layers of enabling characteristics for cancer progression.⁹⁹

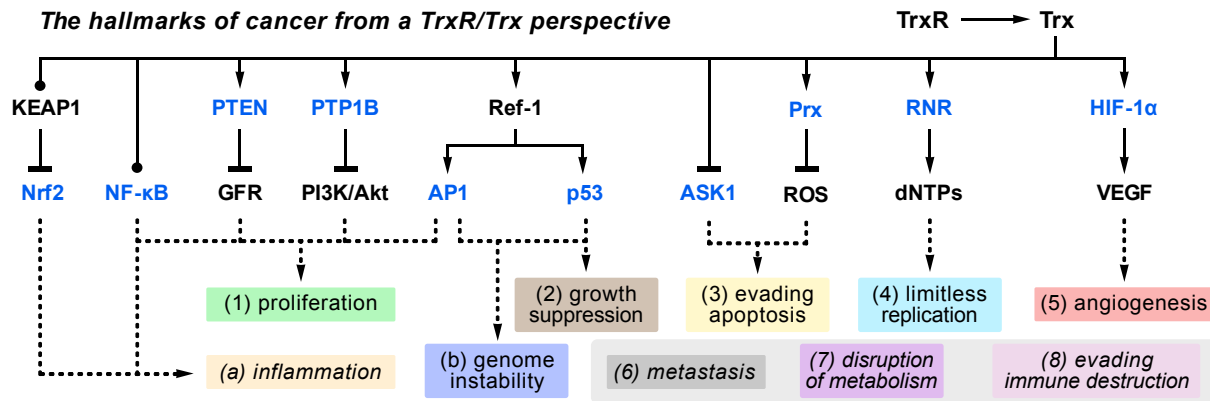


Figure 5 The *hallmarks of cancer* from a TrxR/Trx perspective. Trx is a multivalent regulator of cellular transcription factors and affects various other signaling pathways (see **chapter 1.1.2**) that are correlated to cancer progression.

The versatile pathways for redox regulation and signaling are involved in most, if not all, of these *hallmarks of cancer*: with both cancer-promoting, as well as cancer-impeding effects. Dansen *et al.* explicitly looked into each of the hallmarks *from a redox perspective*, outlining several examples of redox-controlled factors impacting cell cycle initiation, apoptosis, and angiogenesis.¹⁰⁰ The Trx system, and specifically the cytosolic redox effector Trx1, has been reported with many implications for these *hallmarks of cancer*.¹⁰¹ Likely in connection to this, Trx seems to be upregulated in many cancer types^{102–106}, although it remains difficult to compare the relative importance of each of the cellular processes influenced by Trx (or TrxR) for cancer (**Figure 5**). Specific examples of Trx1 activity on cancer progression, including potentially counteracting effects, are its impacts on: **NF-κB**⁴⁸ influencing tumoral growth¹⁰⁷ and inflammatory response^{47,108}; on **Nrf2**¹⁰⁹ enabling many cellular processes including metabolism¹¹⁰ and inflammation¹¹¹; on **p53**⁵¹, promoting growth suppression and genomic integrity¹¹²; on **AP-1**, with both oncogenic and anti-oncogenic downstream effects¹¹³; on HIF-1α, where the activating effect of reduced Trx leads to increased tumor vascularization through vascular endothelial growth factor (VEGF) production⁴⁹; on **ASK1**, that is inhibited by reduced Trx to prevent apoptosis.¹¹⁴ Trx1 also indirectly impacts many cancer-associated pathways. Some examples where reduced Trx is also implicated in promoting cancer survival and progression are: recovery of **Prxs** by reduced Trx enables detoxification of O₂^{•-} and H₂O₂ (general apoptosis inducer¹¹⁵) in cancer cells; Trx provides the reducing equivalents for **RNR** for the synthesis of dNTPs required for unlimited replication (see **chapter 1.1.1**)¹¹⁶; and self-sufficiency of tumor growth mediated through the growth factor receptor tyrosine kinase (EGFR) signaling pathway can be promoted by reduced Trx, since it counteracts EGFR inhibition by the oxidised forms of the suppressing factors **PTP1B** and **PTEN**, leading to enhanced pathway activation of the PI3K-Akt proliferative response.^{100,117}

More generally, there are many implications of redox regulation on cancer cell metabolism and cancer progression: sometimes with counteracting impulses and many with complex interactions. Nonetheless, it becomes increasingly evident that redox systems such as the Trx system play a central role in cancer development.^{101,118} Also, beyond the cancer context, often similar redox dysregulation patterns are being recognized in a number of other diseases like rheumatoid arthritis, neurodegenerative diseases, inflammation, or viral infections.¹¹⁹

1.2.2 Therapeutic potential for the TrxR/Trx couple as a drug target

With many roles assigned to the Trx system in cancerous and other diseased states, targeting the Trx system for therapeutic purposes is considered a promising avenue for drug development in cancer, inflammation, and beyond. This chapter will summarize different approaches to targeting Trx either directly, or else through inhibiting its unique upstream reductase TrxR by small molecules (**Figure 6a**).

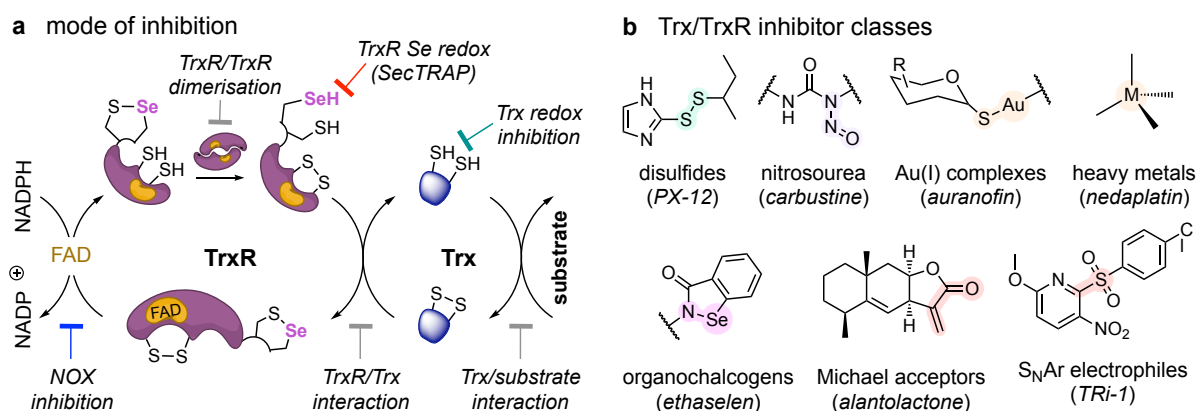


Figure 6 Therapeutic potential and mode of actions of potential anti-cancer agents targeting the TrxR/Trx redox couple. (a) Mechanism of inhibition at different steps of the catalytic thioredoxin redox cascade. (b) Chemotypes used for inhibition of the thioredoxin system.

Targeting the redox effector Trx selectively by small molecule-based inhibition is challenging. Its active site has similarity to that of Grxs and other members of the Trx-superfamily, and it has a broad substrate scope with low substrate specificities, which is associated with a relatively featureless surface lacking a traditional binding site for small molecules. To date, no *selective* inhibitor for Trx1 or other isoforms is known. 1-methylpropyl-2-imidazolyl disulfide (PX-12) was shown to inhibit Trx1-related enzymatic activity by modulating its active site¹²⁰ and entered phase II clinical trials as an anti-cancer agent, though without observing therapeutic benefit.^{121,122} Based on its simple disulfide molecular design (**Figure 6b**), PX-12 is likely to interact with multiple off-target cysteines making its potential for selectivity in cells or *in vivo* questionable.^{123,124}

Recovery of reduced (active) Trx is also decreased by inhibition of TrxR. Potential therapeutics to do this can operate through a diverse set of molecular mechanisms (**Figure 6b**): (i) TrxR is strongly inhibited by nitrosoureas, such as carmustine, by reaction of its N-terminal active site cysteines with reactive electrophilic degradation products formed *in situ*. However, they also broadly inhibit all other members of the glutathione reductase (GR) family, as well as other proteins with reactive cysteines.^{116,125} Most other target strategies for TrxR exploit its unique selenocysteine reactivity using metals or other electrophiles: (ii) Thio-gold (I) complexes, such as auranofin, are a class of TrxR inhibitors that particularly target selenocysteine nucleophiles due to the strong affinity of the soft Lewis base Se to the soft acid Au(I).¹²⁶ Auranofin is clinically used as an anti-rheumatic agent, although with a mostly unknown mechanism of action *in vivo*¹²⁷ having TrxR as only one of its primary cellular targets.^{128,129} Following the same logic, complexes of other metals such as Pt, Ru, Ir, Fe, Pd, and Ag, or semi-metal species based on As¹³⁰, have been tuned to inhibit TrxR by Sec complexation, with varying potencies and off-target profiles.¹³¹ (iii) Synthetic organic molecules containing selenophilic

chalcogens like Te¹³² or Se (Ethselen¹³³) are also reported to react with the Sec⁴⁹⁸ residue in TrxR, presumably leading to stable dichalcogenide adducts; although confusingly, the structurally similar Ebselen, another prominent organoselenium anti-cancer agent, was reported to interact with the TrxR/Trx system without inhibition.¹³⁴ (iv) Targeting the surface-exposed nucleophilic selenocysteine with covalently alkylating organic electrophiles is the mechanism underlying a number of small molecules. Especially natural products bearing Michael acceptors are numerous reported in this respect.¹³⁵ Instead, to gain better selectivity over off-target cysteines, TrxR inhibitors based on tuned S_NAr electrophiles have recently been developed, such as 2-sulfonylpyridine TRI-1¹³⁶ and the dichloropyrazine-3-one TRI-3¹³⁷, which are to date the most selective cellular inhibitors for TrxR.¹³⁸

It is important to note that covalent inhibition of TrxR at its catalytic Sec⁴⁹⁸ has two independent effects. First, it blocks the reduction of Trx, and decreasing levels of reduced Trx affect multiple downstream substrates (see **chapter 1.2.1**). Second, although Sec alkylation irreversibly inactivates the C-terminal active site function (that directly reduces the enzyme's targets), the N-terminal active site will still turnover electrons from NADPH, shuttle them onto other electron acceptors and so gain function of a NADPH oxidase (NOX).¹³⁶ Such Sec-blocked TrxR enzymes have been named more comprehensively as "Selenium-compromised Thioredoxin Reductase-derived Apoptotic Proteins" (SecTRAPs) and can themselves actively induce cell death unrelated to its native reducing capabilities, validating a separate mechanism to cause the anti-cancer effects of covalent TrxR inhibition.¹³⁹

Alternative concepts for TrxR/Trx functional inhibition remain essentially unexplored. For example, selective inhibition of the protein-protein interaction between TrxR and Trx remains unknown, although this would allow suppressing of Trx reduction over others. Blocking defined interactions between Trx and a specific substrate would be another promising, yet so far unaddressed, and challenging, mechanism of functional inhibition. Finally, selective inhibition of TrxR/TrxR homodimerization would not only decrease Trx reduction but also likely cause a SecTRAP effect. All these approaches remain unexplored, although the molecular and structural details of the TrxR/Trx couple are well-studied.³⁴

In summary, because of the broad substrate scope of Trx and its versatile involvements in most of the hallmarks of cancer, the irreversible inhibition of its activity may result in a complex mixture of counteracting biological effects. Nevertheless, targeting the TrxR/Trx redox couple for anti-cancer drug development is considered a promising avenue, and several of the small molecule inhibitors have been extensively studied in cells, *in vivo*, and even in patients. However, to date, no therapeutic agent with the TrxR/Trx being its primary target and mode of anti-cancer efficacy has been approved for cancer therapy. Notably, the dithiol/selenolthiol selectivity of most of the small molecule inhibitors of either TrxR or Trx remains poor, and current drugs are known or are likely to affect a large number of potentially catalytically active off-target cysteines. Future research should aim to identify new ways of selective chemical inhibition to minimize these off-target effects which likely requires selective cellular tools to measure their protein activity in native systems.

1.3 Probing the cellular disulfide redox state

With an increasing focus on precisely defined interactions between redox-active proteins, it becomes clear that tools for qualitative and quantitative and spatiotemporal monitoring of these systems are required. Prior art approaches have been conceptually limited in many respects. For example, determining whole-cell ratios of individual species was based on destructive methods where sample preparation was prone to parasitic oxidation; thus, cellular levels of oxidized GSSG had been heavily overestimated.^{69,140} Moreover, there are problems in the description and interpretation of such measurements in the literature: The terms *cellular redox "state," "environment," "balance," "equilibrium,"* or *"homeostasis"*^{141–143} are frequently, sometimes interchangeably, used often without precisely defining the actual classes of redox-active species and/or redox couples being referred to (**Figure 7a**). Furthermore, these terms wrongly suggest that cellular redox systems are collectively maintained at equilibrium and that exogenous perturbations such as by *"reactive oxygen/nitrogen species (ROS/RNS)"* or *"oxidative stress"* globally affect these overall equilibria. In reality, individual redox pairs have distinct functions and chemical natures (see **chapter 1.1.2**), and most, if not all, interacting couples are independently and kinetically regulated far beyond thermodynamic equilibria.¹⁴⁴ It must also be noted that the terms *ROS/RNS* are mostly used without precise definitions or specifications of their mechanistic relevance and are, therefore, subject to controversial views in the field.^{145,146}

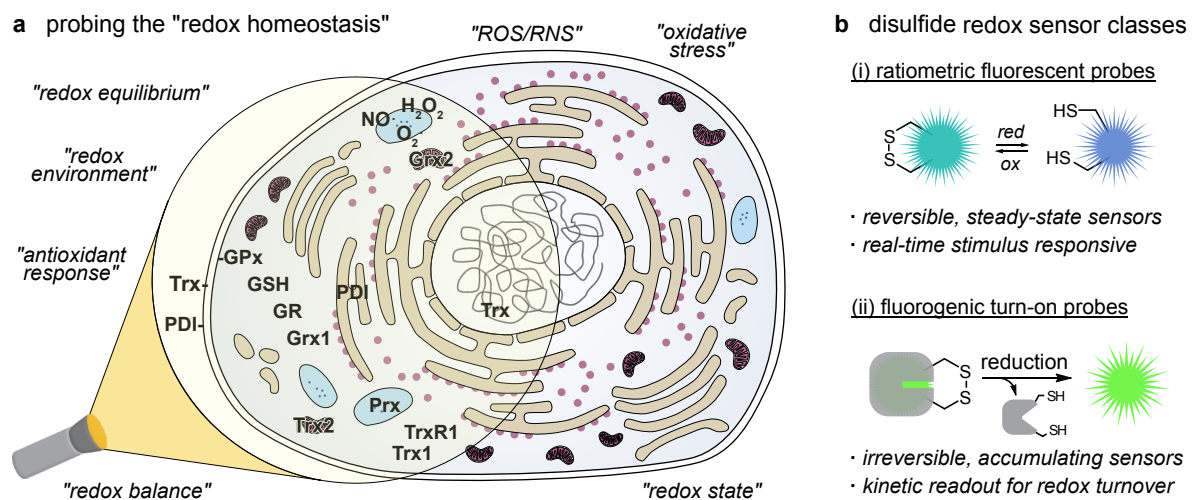


Figure 7 Probing the cellular "redox homeostasis" (a) Several terms are used to describe the cellular states of redox-active species. Imaging tools are required for each individual redox couple. (b) Fluorescent imaging agents for disulfide redox couples are either based on (i) ratiometric two-state or (ii) on fluorogenic turn-on probes.

Aiming to instead probe specific thiol/disulfide redox couples while avoiding to perturb the native environment, several fluorescence-based imaging techniques have been implemented. Most such redox probes were created utilizing disulfide substrate mimics for thiol/disulfide redox-active proteins, whereby reduction to the corresponding dithiol results in a measurable change in spectral properties. These probes fit into two classes: (i) reversible steady-state sensors that are usually based on fluorescent proteins, with two spectral states depending on a disulfide/dithiol motifs' redox state, and that can be used for ratiometric imaging of reduced:oxidized ratios; or (ii) irreversible fluorogenic turn-on probes, usually based on small, artificial disulfides linked to inactivated fluorophores, such that reduction irreversibly liberates the dye leading to accumulation of fluorescence over time (**Figure 7b**).

1.3.1 Genetic engineering for redox-responsive fluorescent proteins

Analogues of green fluorescent protein (GFP), originally isolated from the jellyfish *Aequorea victoria*, are widely used as fluorescent tools for molecular biology.¹⁴⁷ Its fluorescence is based on the 4-(*p*-hydroxybenzylidene)imidazolidin-5-one (HBI) chromophore in its anionic phenolate form that is surrounded by a shielding barrel of 11 β -sheets.¹⁴⁸ The groups of Winther and Remington independently created the reduction/oxidation-responsive GFP analogs rxYFP and roGFP by engineering unnatural cysteine sites that can form an interstrand disulfide bond upon oxidation.^{149,150} These artificial constructs can reversibly cycle between disulfide and dithiol states with measurable differences in spectral properties of the chromophore between the two states. **Figure 8** shows the excitation spectra for the reduced and oxidized states (**Figure 8a**) and the structural and mechanistic details of roGFP2 (**Figure 8b**). Knowing that deprotonation of the phenol by H147 is crucial for fluorescence, in both cases, cysteine insertion (S148C) created the desired redox-responsive effect: disulfide reduction leads to a conformational change that increases the distance between H147 and the phenol, and by that prevents deprotonation in the reduced state, whereas the oxidized state is mostly deprotonated (**Figure 8c**). The EGFP-derived derivative roGFP2 exhibits particularly favorable properties for ratiometric measurements due to its high dynamic range.¹⁵⁰

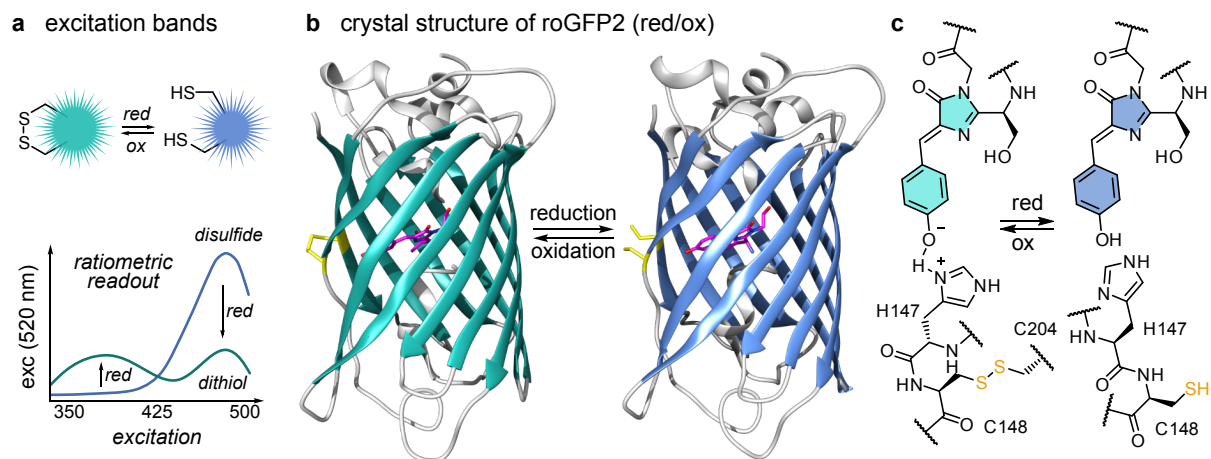


Figure 8 Redox-responsive fluorescent proteins. (a) Excitation spectra (emission at 520 nm) for reduced/oxidized roGFPs. (b) Crystal structures of roGFP2 (PDB: 1JC0 and 1JC1). (c) Molecular mechanism leading to redox-state-dependent fluorescence properties.^{144,151}

When introduced into cells, these disulfide FPs predominantly reflect the cellular GSH/GSSG redox couple, albeit with very slow equilibration rates (several hours) and midpoint potentials of -260 mV to -290 mV. The applicability of the first redox-responsive FPs was limited by kinetics and, therefore, mainly used to explore the steady-state redox conditions related to the glutathione system in different compartments.¹⁴⁴ The cytosolic and mitochondrial environments were consistently found to be highly reducing^{150,152–154}, whereas expression in the ER led to fully oxidized FPs.^{153,155}

In recent years, an extensive range of redox-responsive FPs has been developed to overcome these kinetic limitations, target other redox couples, or focus on different redox balances: (i) The concept of redox-relay constructs was guided by the observation of a faster response of roFPs in the presence of Grx. Thus, by *covalently* linking roFP and Grx domains gave such constructs where the Grx rapidly

performs the GSH/GSSG equilibration and transmits the signal to the roFP. Both rxYFP and roGFP2 have been used as templates for Grx fusions, creating e.g. Grx1-roGFP2 that allows measuring of cellular GSH levels in real-time with high specificity.^{152,156} Extending the redox-relay instead to oxidizing species also succeeded with the H₂O₂-sensing fusion proteins of the HyPer family,¹⁵⁷ that are well reviewed elsewhere.^{158,159} (ii) Redox-responsive FPs like roGFP2 were surprisingly unaffected by dithiol proteins of the Trx family, and it was assumed that roGFP reduction by e.g. Trx was hindered through steric repulsion.¹⁴⁴ Recently, an adapted rxRFP covalently linked to Trx1 (TrxRFP1) was published, aiming to more specifically detect the redox status of Trx. Its sensor domain is primarily reduced by TrxR1, with little crosstalk to GSH or other Trx-like proteins, and the new fusion protein could also be used simultaneously with Grx1-roGFP2.¹⁶⁰ (iii) By rationally increasing the roFP midpoint potentials by up to 60 mV, more precise measurements in oxidizing environments are also accessible.¹⁶¹

Genetic engineering has been very successful in developing ratiometric two-state sensing systems that give precise information of steady-state ratios at a certain time or location and that can be followed in real-time as they change in response to external stimuli. Coupling the redox-responsive FPs to Trx/Grx domains created redox-relay probes that are helping to characterize redox pathways and their independent responses to internal or external stimuli. However, such probes are not well suited to characterize the *turnover* or *activity* of the cell's Trx or Grx effectors; and such ratiometric approaches would not reveal useful information about their upstream reductants (TrxR/GR) either. These enzymes do not feature a steady-state reduced:oxidized balance but are continuously re-primed for reduction. They can also not serve as tools for measuring redox states in native cells or native tissues, as genetic engineering is required. For these purposes, small molecule probes are better fitted.

1.3.2 Small molecule turn-on fluorescence probes

Although most redox protein substrates are protein disulfides, chemical development has pursued fluorogenic turn-on probes utilizing artificial disulfide substrate units in the hope of identifying oxidoreductase-selective substrate motifs. These probes' disulfides are usually tethered to an inactivated fluorescent dye, such that reduction of the disulfide leads to fragmentation and then liberation of the dye, and this either accumulates fluorescence directly, or it stops FRET-based fluorescence quenching (**Figure 9a**). Multiple designs are summarized in **Table 2**, with a focus on the reducible motifs and the fluorophores that were applied. Several chemical design criteria are important: target selectivity is largely directed by choice of the reducible trigger unit that must resist cellular levels of monothiols (50 mM "overall thiols" out of which 5 mM GSH), including resisting catalyzed mono-glutathionylation while still being activatable by their cellular redox protein targets. Furthermore, off-target activation must be prevented by avoiding (bio)chemical instability e.g. unspecific/catalyzed hydrolysis. This may be achieved by preferably using carbamates when acylating key functional units rather than carbonates and esters. Finally, probe performance overall also relies on large fluorescence turn-on ratios and low background fluorescence of intact constructs. For imaging in cells or even *in vivo*, excitation/emission windows, as well as the dye's brightness, must also be suited and well-chosen. Key factors of prior work are discussed in the following section.

Fluorophore choice. Fluorescent dyes often consist of large aromatic systems that contain electron-donating and/or -accepting groups (*push-pull-systems*). Fluorogenic systems are commonly created when key functional units (e.g. electron-donating phenols or anilines) are masked by acylation, which makes them more electron-withdrawing and often leads to changes in fluorescence properties. Reducible dichalcogenide units may be attached to these acylating units such that their cleavage initiates an intramolecular fragmentation reaction that deacylates the key functional unit. Such designs give reduction-responsive probes, whereby reduction re-establishes fluorescence (**Figure 9a**). Quenching depends on the fluorophore's functional groups and the masking method for them: acylated naphthalenes (Cho **2010**)^{162,163}, naphthalimides^{164–169}, oxazines^{170,171}, hemicyanins¹⁷², or coumarins¹⁷³ have rather different degrees of quenching. Alternatively, using acylation to lock a non-fluorescent *spiro*-form of xanthenes (rhodamines, fluoresceins, rhodols) is particularly beneficial since large fluorescence turn-on ratios can be achieved after deacylation. However, mono-*O*-acylation of ordinary fluorescein with a linear disulfide unit giving a GSH-responsive probe reduced emission only by a factor of ca. 50%, giving a molecular probe with poor turn-on ratio (Kim **2014**¹⁷⁴). In contrast, a rhodamine-based cellular probe with two linear disulfide units attached on both sides of the xanthene showed true off-to-on fluorescence after monothiol challenge (Chmielewski **2008**¹⁷⁵). Recently, mono-*O/N*-substituted xanthenes (e.g. *O*-alkyl-rhodols) have become preferred for true off-to-on probes, such as the diselenide fluorogenic probe derived from a seminaphthorhodafleur scaffold (Strongin **2020**¹⁷⁶).

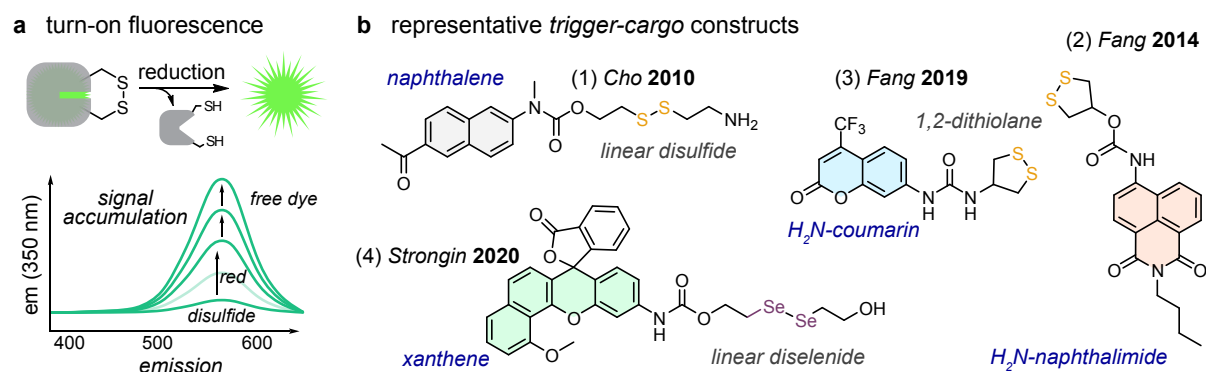


Figure 9 Small molecule redox probes. (a) Turn-on fluorescence: emission spectra with increasing portions of a fluorophore. (b) *Trigger-cargo* constructs: (1) Cho **2010**: Linear disulfide GSH-probe¹⁶²; (2) Fang **2014**: first cyclic disulfide-based probe TRFS-green¹⁶⁶; (3) Fang **2019**: non-releasing, direct reduction-sensing probe Fast-TRFS¹⁷⁷; (4) Strongin **2020**: first diselenide as the reducible motif.¹⁷⁶ Probe designs (1)-(4) are highlighted in **Table 2**.

Trigger choice. Most reduction-responsive probes (summarized in **Table 2**) contain linear disulfide units as reducible sites that are structurally derived from GSSG with similar reduction potentials to that of the GSH/GSSG couple.¹⁷⁸ As a result, linear disulfide units are intrinsically unstable to monothiol reductants and are, therefore, mostly reported as GSH sensors (or, more transparently, understood as “overall cellular thiol” sensors). While redox effector proteins, such as Trx, can be faster reducing than monothiols *in vitro*¹⁶⁶, monothiol levels in cellular environments are $\sim 10^3$ -fold higher, which prevents linear disulfides from selectively reporting on specific redox players. Kinetic selectivity for Trxs and related proteins has only been claimed for linear disulfide probes when drastically altering cellular compartmentalization may have reduced GSH exposure, e.g. by attachment of directing groups for mitochondrial¹⁶⁶ or membrane-associated¹⁶⁷ redox systems or by using charged molecular cargoes.¹⁷¹

Table 2 Small molecule redox probes sorted by year of publication. (a) *Trigger-cargo* constructs categorized by target, reducible motif, and molecular cargo. (b) *Fluorophore-quencher* constructs used as reduction-responsive FRET probes or similar bifunctional conjugates. Molecular designs shown in **Figure 8b** are highlighted in yellow.

a small molecule trigger-cargo-constructs							
	publication	year	group	target	moiety	cargo	
1	JACS	2006	Wender ¹⁷⁹	thiols	linear disulfide	luciferin	
2	JACS	2007	Chang ¹⁸⁰	thiols	naphtho-1,8-disulfide	fluorescein	
3	Org. Lett.	2008	Chmielewski ¹⁷⁵	GSH	linear disulfide	rhodamine	
4	Chem. Comm.	2010	Zhuang ¹⁶⁴	thiols	linear disulfide	H ₂ N-naphthalimide	
5	JACS	2010	Cho ¹⁶²	GSH	linear disulfide	H ₂ N-acetylnaphthalene	
6	JACS	2011	Cho ¹⁸¹	GSH	linear disulfide	H ₂ N-benzothiazolyl-naphthalene-(PPh ₃ ⁺)	
7	Org. Lett.	2012	Reddie ¹⁸²	GSH	linear disulfide	3-benzothiazolyl-thiocoumarin	
8	JACS	2012	Kim ¹⁶⁵	GSH	linear disulfide	H ₂ N-naphthalimide-(galactoside)	
9	JACS	2012	Kim ¹⁶⁶	Trx2	linear disulfide	H ₂ N-naphthalimide-(PPh ₃ ⁺)	
10	JACS	2014	Kim ¹⁶⁷	Trx	linear disulfide	H ₂ N-naphthalimide-(C ₁₂ H ₂₅)	
11	RSC Adv.	2014	Kim ¹⁷⁴	Trx	linear disulfide	fluorescein	
12	JACS	2014	Fang ¹⁶⁸	TrxR	1,2-dithiolane	H ₂ N-naphthalimide	
13	Chem. Comm.	2016	Fang ¹⁶⁹	TrxR2	1,2-dithiolane	H ₂ N-naphthalimide-(PPh ₃ ⁺)	
14	Chem. Comm.	2016	Fang ¹⁷⁰	TrxR	1,2-dithiolane	H ₂ N-oxazine (Nile blue)	
15	Anal. Chem.	2017	Tang ¹⁷²	H ₂ Se	1,2-dithiane	H ₂ N-hemicyanine	
16	Nat. Commun.	2019	Fang ¹⁷⁷	TrxR	1,2-dithiolane	H ₂ N-coumarin	
17	Anal. Chem.	2019	Fang ¹⁷¹	Trx	linear disulfide	H ₂ N-oxazine (Nile blue)	
18	Nature Nano.	2019	Krishnan ¹⁸³	thiols	linear disulfide	fluorescein	
19	Chem. Eur. J.	2019	Lukesh ¹⁷³	H ₂ S	linear thiaselenane	HO-coumarin	
20	Spectrochim.	2020	Yin ¹⁸⁴	H ₂ S	dipyridyl disulfide	dicyanoisophorone	
21	Chem. Comm.	2020	Fang ¹⁶³	TrxR	1,2-dithiolane	H ₂ N-acetylnaphthalene	
22	ANIE	2020	Strongin ¹⁷⁶	TrxR2	linear diselenide	seminaphthorhodafluor	
b small molecule fluorophore-quencher-constructs							
	publication	year	group	target	moiety	residue 1	residue 2
23	JACS	2004	Schneider ¹⁸⁵	thiols	linear disulfide	carbostyryl	terbium
24	Anal. Chem.	2007	Karuso ¹⁸⁶	GSH	linear disulfide	fluorescein	fluorescein
25	Anal. Biochem.	2006	Sem ¹⁸⁷	thiols	linear disulfide	rhodamine	fluorescein
26	JOC	2011	Yu ¹⁸⁸	thiols	linear disulfide	coumarin	porphyrin
27	Sci. Rep.	2014	Zhao ¹⁸⁹	thiols	linear disulfide	coumarin	pyridine
28	ChemBioChem	2019	Beharry ¹⁹⁰	thiols	linear disulfide	porphyrin	BHQ-3

Only very recently have alternative substrate units, such as cyclic disulfides and diselenides, been considered, aiming at selective targeting of redox proteins by substrate preference. Cyclic 5-membered (1,2-dithiolane) and 6-membered (1,2-dithiane) disulfides have long been known to possess lower reduction potentials and mechanistic preference for dithiol reductants.^{191,192} Over one series of studies, 1,2-dithiolane was reported to be a selective substrate unit for probing TrxR in the cytosol^{168,170,177} or in mitochondria¹⁶⁹ but neglected previous reports on thermodynamic lability of such strained cyclic dichalcogenides. So far, the very few 1,2-dithiane probes were not evaluated for the Grx/Trx systems but were instead only challenged with H₂Se *in vitro* and evaluated for such Se-metabolite turnover in cells, leaving potential use for specific cellular turnover out of focus.¹⁷² Alternative approaches have utilized linear diselenides to target TrxR¹⁷⁶ (*Strongin 2020*), whereas an interesting linear selenenylsulfide with a desymmetrized bond (Se-S), was reported to respond to H₂S with preference over GSH (while being intrinsically irreversibly cleaved), again without checking for Grx/Trx-related activation.¹⁷³ Overall, cyclic disulfides recently gained increasing attention for use as reduction sensors but were, so far, were not comprehensively screened for targeting dithiol-type proteins.

Fluorophore-quencher constructs. As an alternative approach to *trigger-cargo* constructs, several studies have also utilized small molecule designs, where a fluorescent dye is conjugated to a quenching chromophore via a reducible disulfide-containing linker. Thereby, after excitation, energy is transferred emission-free to the quencher only if it stays in proximity to the dye (FRET: Förstner resonance energy transfer). A turn-on in fluorescence results from a reduction by spatial detachment and “liberation” of the fluorophore from its quencher unit. Multiple combinations of dyes^{186–190} and even related techniques (e.g. masked luminescence¹⁸⁵) have been reported. However, so far, only linear disulfides have been used as reducible linkers, and the few examples shown in **Table 2b** leave space for future developments exploring alternative reduction sensing units, including cyclic disulfides.

Overall, by design, small molecule turnover probes are modular and therefore flexibly applicable for different purposes while not requiring genetic engineering. Probing cellular redox using a set of selective, orthogonal probes for redox players would enable further understanding of their role in cellular processes. It may also elucidate unknown redox interconnections and downstream protein targets. When applying such probes in cells, upon internal/external stimuli, or in disease models, they may be used to further understand the role of redox and its regulation in health and disease and to identify novel targets for future therapeutic efforts. Genetic and chemical tools may even be used simultaneously to examine different types of redox behaviors and combine results from them to develop a more conclusive picture.

1.4 Thiol-mediated uptake and its connection to cellular redox systems

For most therapeutic purposes, fast, reliable, and non-damaging delivery of small molecules, peptides, proteins, or particles into cells is required.^{193,194} Cellular membranes are impermeable for large organic molecules, (bio)nanoparticles, and other macromolecular constructs; they may be permeable to small organic molecules by passive diffusion, depending on their polarity.

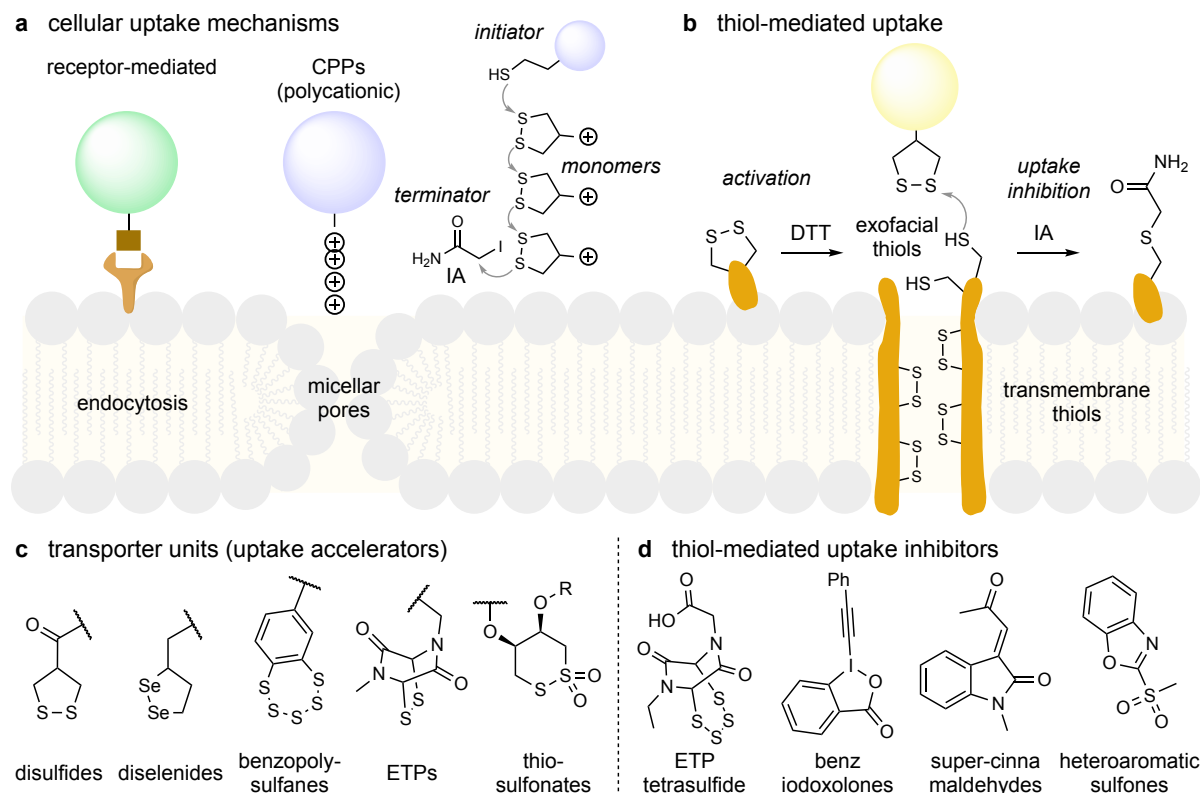


Figure 10 Cellular uptake mechanisms. (a) Receptor-mediated endocytosis, cell-penetrating peptides (CPPs), and (b) thiol-mediated uptake as selected cellular uptake mechanisms. (c) Molecular units with transporter properties for thiol-mediated uptake. (d) Thiol-reactive agents active identified as thiol-mediated uptake inhibitors.

Transmembrane delivery of chemical/biological agents or particles may instead be enabled by active cellular uptake. Several uptake mechanisms are known, out of which receptor-mediated endocytosis is the most prominent^{195,196} (**Figure 10a**), but others are more amenable to small molecule approaches. For example, cellular uptake can be accelerated through the triggered formation of micellar pores by e.g. using polycationic small peptide chains (termed: *cell-penetrating peptides*: CPP) attached to cargo proteins or drugs.^{197–199} Interestingly, in the context of strained disulfides, ring-opening polymerization of 1,2-dithiolanes was used to establish such a polycationic anchor *in situ*:^{200–204} the CPP analog was built from a thiol initiator (with a molecular cargo), oligomerizing a cyclic disulfide monomer decorated with a cationic backbone, capped by a thiol-reactive terminator (**Figure 10a**) and the poly(disulfide) tail was later cleaved off intracellularly, to release the cargo in the cytosol.²⁰⁵

Thiol-mediated uptake. A distinct uptake mechanism was proposed based on the simple observation that cellular uptake is accelerated if molecular cargos are decorated with oligochalcogenides capable of dynamic covalent exchange.^{66,206} This process was found to be unaffected by endocytosis inhibitors but heavily suppressed by irreversible thiol-reactive reagents.²⁰⁷ (**Figure 10b**) These findings indicated

that uptake is enabled by dynamic covalent interaction of exofacial and transmembrane thiols²⁰⁸ with the oligochalcogenides on the cargo's surface.⁶⁵ Enhanced uptake was shown for cargos as diverse as small molecules, nucleic acids,²⁰⁹ peptides,²¹⁰ liposomes,²¹¹ and even protein-coated quantum dots.²¹² Thiol-mediated uptake has also been correlated to the uptake of toxins and viral particles.^{206,213–215}

Uptake accelerators and inhibitors. The thiol-mediated mechanism is thought to rely on dynamic covalent (de)polymerization with transmembrane thiols,^{208,216} but its molecular details are hardly understood. 1,2-dithiolanes²¹⁷, 1,2-diselenolanes²¹⁸, benzopolysulfanes^{219,220}, and epidithiodiketopiperazine (ETP)^{75,221,222} are all suitable to accelerate cellular uptake (**Figure 10c**). It is assumed that the tendency for ring-opening polymerization that is related to the ring strains of these cyclic polychalcogenides leads to thiol-mediated uptake activity.^{207,217} Inhibition of thiol-mediated uptake may be used to intentionally suppress cell entry through this mechanism as a therapeutic approach. Molecules with known thiol reactivity were screened to identify lead structures for thiol-mediated uptake inhibition.^{223–225} Interestingly, small molecule analogs of 1,2-dithiolanes, benzopolysulfanes, or ETPs were each most effective in inhibiting the uptake of their counterpart oligochalcogenide-bearing cargos. Notably, uptake inhibitors can also function via irreversible alkylation of surface thiols (**Figure 10d**).

Uptake mediators. The characterization of which exofacial cysteines mediate thiol-mediated uptake is challenging due to the dynamic nature of these interactions. However, the transferrin receptor (TFRC), a receptor that also modulates endocytosis²²⁶, has been identified as one such host protein for thiol-mediated uptake by interacting with 1,2-dithiolane units.^{65,208} TMEM16F, a Ca²⁺-activated scramblase for the exchange of phospholipids²²⁷, is also thought to passage transporter-decorated cargos by interaction with cysteines along its transmembrane helices. Further potential hosts include EGFR²²⁸ and the ion channels CLIC1, TRPA1 and Ca_v1.1.⁶⁵ Interestingly, CLIC1 has a Grx-like redox-active site and oxidoreductase activity that regulates its ion channel activity.²²⁹

In contrast to the rather reducing cytosolic redox environment, it was long thought that the lack of reductants available to the extracellular space would result in most surface thiols remaining oxidized.⁶³ However, the role of redox control systems outside/across the cell membrane is increasingly understood to modulate signaling and cell-cell interaction and may also be involved in cellular uptake. Examples are known of redox proteins that are translocated or secreted to the cell surface^{230–232} where they organize a functionally independent membrane-associated redox system⁶⁴; for example, exofacial redox effector proteins modulate several transmembrane proteins, such as the cell adhesion protein integrin^{233,234} and the ion channel TRPC5²³⁵, and exofacial PDI isoforms function as reducing factors rather than isomerases²³⁶ and modulate the cell entry of the HIV viral particle.^{214,237}

It should also be noted that the concept of thiol-mediated uptake may be relevant in the context of small molecule redox probe development (see **chapter 1.3.2**). Redox probe and prodrug designs that are based on dichalcogenides which are *also* known to be highly active transporters for thiol-mediated uptake, due to their kinetic lability and tendency for ring-opening polymerization, will have potential interactions with thiol-uptake transporter proteins and potentially distinct uptake rates and reactions at the cell surface that distort experimental results must be considered (see **chapter 3.1.1**)

2 Aims and objectives of this research

Conserved, highly specialized enzymes of the oxidoreductase cascades exploit thiol/disulfide reactions to control cellular redox homeostasis, signaling, and metabolism. The GR/GSH/Grx and the TrxR/Trx redox systems are the central thiol/disulfide nodes. They act as backup systems for each other and share some, but not all, of their substrates while their substrate overlap remains hardly known.

Particularly, the Trx system is heavily involved during the dysregulation of redox pathways in pathological states, making both TrxR and Trx promising targets for anti-cancer drug development and beyond. However, their relative importance for supporting or driving the *acquired capabilities* of cancer cells (*hallmarks of cancer*) remains unclear. Increasing evidence argues that Trx expression is upregulated in many cancer types. However, we lack the molecular or genetic tools to measure the catalytic activity of Trx in cells and/or in tumor microenvironments or to compare its level and/or its activity to other oxidoreductases.

The currently available genetic tools are *radiometric tools* that measure cellular redox poise rather than protein turnover/activity, and that are unsuitable for diagnostic use with patient samples. Small-molecule imaging tools are still underdeveloped with respect to protein specificity, spectral properties, and applicability. Lastly, decades of development of small molecule inhibitors for the TrxR/Trx couple have evolved chemical motifs with a variety of molecular mechanisms, often intended for anti-cancer use. However, no Trx inhibitor has proven to be reliable and selective in cells against other redox effectors; and there has been no systematic comparison of the performance and off-target effects of various chemical classes of TrxR inhibitors. Both failings are directly due to the lack of molecular tools to selectively quantify and validate redox activity in complex cellular or *in vivo* settings.

In this work, I aimed to tackle several of these areas by developing synthetic organic dichalcogenides as artificial substrates for selected members of these oxidoreductase systems. I intended to advance the current state of redox tools and prodrugs by employing these artificial dichalcogenides as *trigger units* linked to arbitrary *cargo units* (payloads), such that trigger processing by redox proteins will release and activate the cargo. By extending the structural chemical space of triggers and cargos, this approach should deliver selective agents that are activated through reduction by either TrxR or Trx with low background from the cellularly highly abundant GSH, aiming at the following goals: (i) small molecules that can be used across many different cell lines and tissue types without needing genetic engineering; (ii) fluorogenic turnover probes that accumulate a reporter signal to integrate protein activity over time, and may even be used for subcellular visualization; (iii) modular probe designs that explicitly work towards real-time multiplexed imaging of several oxidoreductases, by easily permitting the use of a range of orthogonal fluorophores; (iv) in particular, selective cell-free or cellular probes for either TrxR or Trx that can be used to cross-validate chemical inhibitors, and to identify new molecular motifs for selective inhibition; and lastly, (v) modularity of the *trigger-cargo* design, allowing to release many cargo types (including cytotoxic drugs), so that if e.g. protein overactivity is found to be correlated to diseased states, it can be harnessed for therapeutic purposes by a corresponding approach.

Previous designs based on *trigger-cargo* constructs have primarily used linear dichalcogenides as trigger motifs, yet these are irreversibly kinetically labile. Cyclic dichalcogenides instead offer the possibility for kinetic reversibility and thus may be able to differentiate between mild and strong reductants (e.g. monothiol vs. dithiol-type proteins). The only extensive previous work on cyclic dichalcogenides proposed 5-membered disulfides (1,2-dithiolanes) as units for selective reduction by TrxR in cells, offering fluorogenic and therapeutic constructs. However, the same trigger motif was also described elsewhere as highly labile and prone to ring-opening polymerization, making it a warhead for thiol-mediated uptake based on dynamic covalent reactions on cell surfaces.

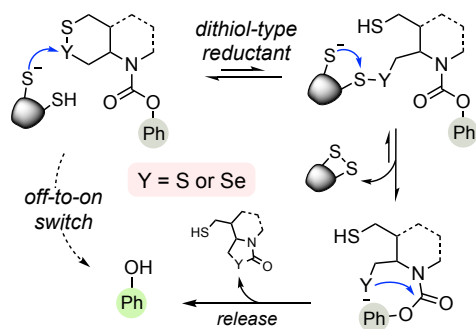
In this work, I wanted to establish a standardized workflow to screen the reduction of linear vs. 5-, 6- and 7-membered cyclic disulfides, to test their kinetic lability, and clarify the literature disagreement about 1,2-dithiolanes' potential as TrxR substrates (**chapter 3.1.1**). I also wanted to create and screen structurally novel cyclic 6-membered disulfides (1,2-dithianes) for reduction by the TrxR/Trx couple and related redox proteins. With this, I wanted to contribute crucial steps towards a cellular probe for Trx1 that is selective over its structurally related cousins Grx1 and TRP14 and, in turn, could identify novel chemical inhibition motifs for this almost untargeted biological space (**chapter 3.1.2**).

In another part of this work, I introduce novel heterocyclic structures like cyclic 6-membered selenenylsulfides (1,2-thiaselenanes) intended for selective reduction by the unique Cys⁴⁹⁷Sec⁴⁹⁸ redox-active site found in TrxR1 (that I helped to develop) and outlined their potential use for validating cellular TrxR inhibitors aimed at anti-cancer use (**chapter 3.1.3**). I also explore how bifunctional fused 1,2-dithiane motifs that are operated by the thioredoxin system may be used not only for imaging redox activity or for releasing cancer-targeted therapeutics but may be applicable as bifunctional molecular linkers for tunable cellular cleavage, or even in materials sciences (**chapter 3.1.4**).

Since both TrxR and Trx are promising targets in the context of cancer, I also wanted to apply artificial dichalcogenide constructs for therapeutic purposes beyond the concept of irreversible chemical inhibition. DNA-alkylating agents of the duocarmycin class are cytotoxins with tunable cellular potency that can offer anti-cancer efficacy. An excursus within this thesis introduces their fascinating molecular mechanism and describes the structural evolution of duocarmycin-type agents intended for clinical uses (**chapter 3.2.1**). I wanted to exploit the modularity of the *trigger-cargo* design to create a series of duocarmycin prodrugs actuated by the thioredoxin system based on the same logic: cumulative activation of bioactivity by reduction (**chapter 3.2.2**). With these, I wanted to evaluate redox activity across multiple cell lines as well as their anti-cancer efficacy in animal models.

This led me to outline the patentable space and commercial interest around novel motifs for *trigger-cargo* constructs targeting the Trx system for diagnosis and therapy, far beyond those that are the subject of this thesis (**chapters 3.2.3 and 3.2.4**). Taken together, this work is also a strong development towards a semi-empirical "pipeline" for modular redox prodrugs: first looking at redox activity in cancer cells using fluorogenic probes, then taking the trigger(s) that offer disease-selective cargo release and adapting them instead to release therapeutic drugs.

This doctoral thesis presents molecular probes and prodrugs based on *trigger-cargo* constructs that are activated through reduction (**Figure 11a**). These probes and prodrugs, and control compounds have a **general nomenclature system** (**Figure 11c**) describing their important structural features to allow systematic and meaningful use of molecule names (e.g. **Figure 11b**) throughout the thesis.

a activation mechanism

b representative examples

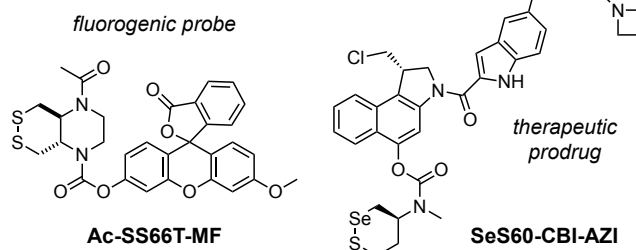
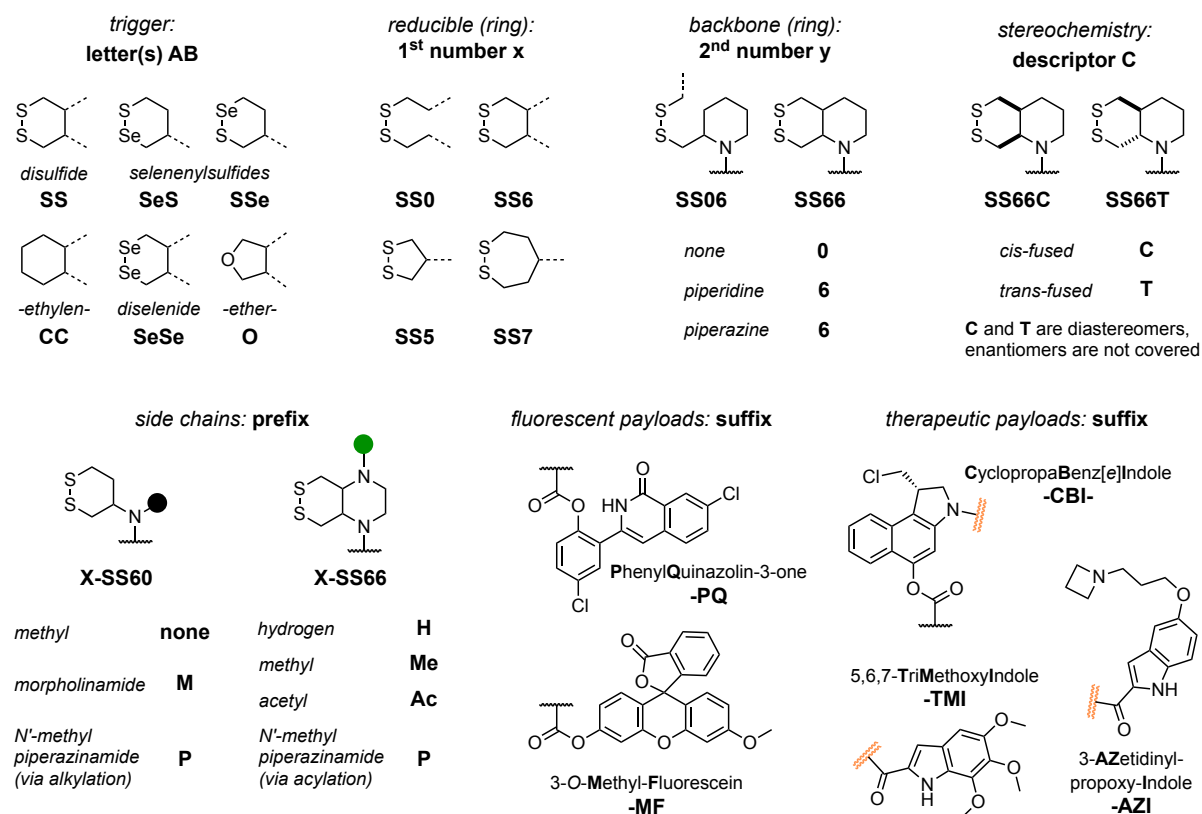
 prototype nomenclature: **prefix-ABxyC-suffix**

c nomenclature: prefix-ABxyC-suffix


Figure 11 Common nomenclature for redox probes and prodrugs based on *trigger-cargo* constructs presented in this doctoral thesis. (a) A general mechanism for reduction triggered activation of inactive phenolic cargos by dithiol-type reductants. (b) Representative examples of fluorogenic probes and prodrugs are presented in this doctoral thesis. (c) Nomenclature according to “**prefix-ABxyC-suffix**” representing the reducible dichalcogenide and non-reducible control motifs (letter/s **AB**), the reducible motif’s topology (1st number), the backbones’ topologies (2nd number) and differentiating the diastereomeric isomers (descriptor) of fused bicyclics. Prefixes are used for chains and suffixes to describe the nature of fluorescent and therapeutic cargos.

3 Results and Discussion

3.1 Development of selective chemotypes to target the Trx system

3.1.1 The controversial use of 1,2-dithiolanes in chemical biology probes

This chapter was published as follows:

Journal	Nature Communications 2022 , 13, 1754.
Title	<i>Cyclic 5-membered disulfides are not selective for thioredoxin reductase, but are opened nonspecifically</i>
Author List	Jan G. Felber [#] , Lena Poczka, Karoline C. Scholzen, Lukas Zeisel, Martin S. Maier, Sander Busker, Ulrike Theisen, Christina Brandstädter, Katja Becker, Elias S. J. Arnér, Julia Thorn-Seshold, Oliver Thorn-Seshold* #first author; *corresponding author
Publication date	Apr 1 st , 2022
Available at	https://www.nature.com/articles/s41467-022-29136-4

Author contributions and collaborations

(1) Work performed in the Thorn-Seshold group, LMU Munich:

I performed synthesis and analysis of the major 1,2-dithiolane-based probe **SS50-PQ** described in this work (**Fig. 2**) and chemoreductant, cell-free biochemical studies and cellular studies (**Fig. 3 and 4**). I also performed literature analysis (**Fig. 1**), data assembly and visualization (**Fig. 5 and 6**), and conceptually analyzed the scientific outcome of the results.

Lena Poczka performed microscopy-based fluorescence imaging, single-cell statistics using flow cytometry (**Fig. 4**), cellular inhibitor studies (**Fig. 5**), and cell-free, enzyme-free *in vitro* polymerization assays (**Fig. 6**). **Lukas Zeisel** performed synthesis and analysis of the TrxR-selective reference compound RX1. **Martin S. Maier** performed synthesis and analysis of the literature-known reference compounds TRFS-green and Fast-TRFS and the reference compound Linear-TRFS (**Fig. 6**). **Julia Thorn-Seshold** supervised cell biology and coordinated data assembly. **Oliver Thorn-Seshold** designed the concept and experiments, supervised all other experiments, coordinated data assembly, and wrote the manuscript.

(2) Collaboration with the Becker group, Justus-Liebig University, Giessen: **Christina Brandstädter** provided human TrxR1 isolated from primary tissues. **Katja Becker** supervised specificity screenings.

(3) Collaboration with the Arnér group, Karolinska Institutet (KI), Stockholm: **Karoline C. Scholzen** performed biochemical screenings (**Fig. 3**), cellular inhibitor and knockout studies (**Fig. 5**). **Sander Busker** performed initial screenings. **Elias S. J. Arnér** supervised biochemistry/cell biology.

(4) Collaboration with the Zoological Institute, TU Braunschweig: **Ulrike Theisen** performed and analyzed zebrafish embryo studies (**Fig. 4**).

Background

I had started the redox program by creating a series of fluorogenic probes based on the precipitating dye hydroxyphenyl-quinazolin-3-one (HPQ) that employed the linear disulfide **SS00**, the cyclic disulfides **SS50** (1,2-dithiolane), **SS60** (1,2-dithiane) and **SS7** (1,2,5-dithiazepane) together with a non-reducible control (**Figure 12a,b**). Fundamental reactivity differences between the simple trigger units were observed. Not only were their reducibilities, activation kinetics, and redox resistance properties vastly different, but especially the chemical instability of **SS50** during synthesis and in solution was surprising. We screened previous work on this simple motif, which is similar to the cellular cofactor lipoic acid. We found reports describing its unfavorable ring strain, its relatively high reduction potential - even comparable to that of linear disulfides - and its fast kinetics for thiol-disulfide interchange reactions.¹⁹² Moreover, this motif was shown to undergo proximity-driven ring-opening polymerization (ROP) to form long chains of linear disulfide polymers via dynamic covalent reactions.²³⁸ Matile *et al.* exploited these properties, using 1,2-dithiolane handles covalently attached to small molecules or even large biomolecules, for thiol-mediated uptake by dynamic covalent reaction cascades with surface/membrane thiols (see **chapter 1.4**). In contrast, Fang *et al.* used the very same motif 1,2-dithiolane as a reducible unit in a similar way as we had intended to create off-to-on fluorogenic probes designed to selectively target TrxR.¹⁶⁸

Summary

1,2-dithiolane cannot at the same time be kinetically labile, thiol-reactive, and prone to dynamic polymerization; while also being selectively reduced by the unique redox-active site Cys⁴⁹⁷Sec⁴⁹⁸ of TrxR and not being touched by GSH, other redox proteins, and surface thiols. In this work, we aimed to solve this fundamental disagreement using our 1,2-dithiolane probe **SS50-PQ** against the prior-art 1,2-dithiolane probes **TRFS-green**¹⁶⁸ and **Fast-TRFS**¹⁷⁷ (**Figure 12c**), alongside the TrxR probe **RX1**.

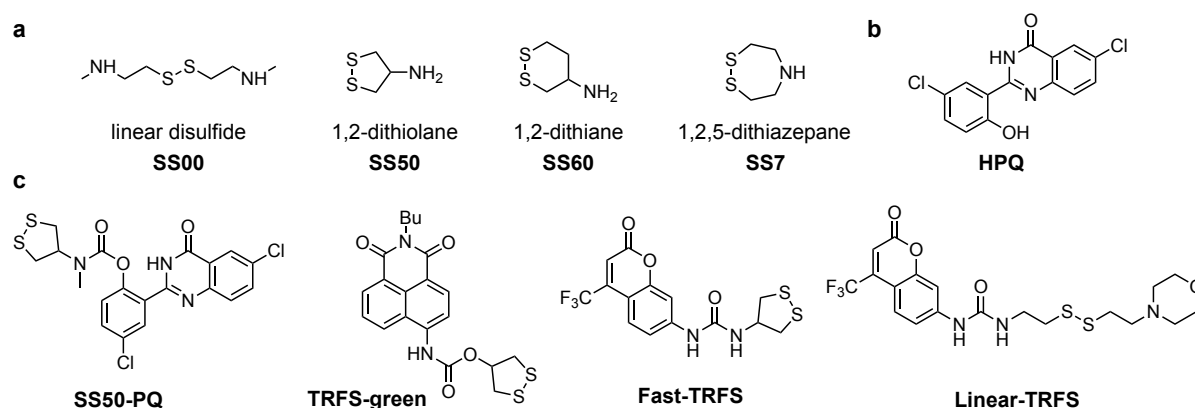


Figure 12 Structure overview of (a) linear vs. cyclic disulfides, (b) the precipitating fluorophore hydroxyphenyl-quinazolin-3-one (HPQ), and (c) the molecular probes used in this study.

In simple reduction assays, I found that 1,2-dithiolane probes are reduced non-specifically by GSH, Trx1/2, TrxR1, Grx1/2, and TRP14 (**Fig. 3**), arguing that 1,2-dithiolanes' reduction is not TrxR-selective in cell-free settings. I also characterized the unusual cellular activation properties of our novel 1,2-dithiolane probe **SS50-PQ** which is based on the release of the HPQ solid-state fluorophore. Upon








reduction, solid needles were observed intracellularly that can be traced on a subcellular level and quantified using flow cytometry (**Fig. 4**). We established a conclusive panel of cellular assays to test TrxR-dependency of the activation of the 1,2-dithiolane probes (**Fig. 5**). We used (a) selenium starvation/saturation in cell culture medium to prevent/ensure incorporation of TrxR's active site selenol; (b) $\text{Na}_3\text{PO}_3\text{S}$ for chemical inhibition of selenocysteine biosynthesis; (c) a stable genetic TrxR1 knockout cell line; and (d,e) co-treatments with two $\text{S}_\text{N}\text{Ar}$ -type chemical inhibitors for TrxR, as well as the Au(I)-based therapeutic auranofin. With this panel, we screened the dependency of **SS50-PQ** and **TRFS-green** signal upon the activity of selenium-containing TrxR and simultaneously controlled using our linear disulfide-based **SS00-PQ** (mainly not TrxR-dependent) and our own TrxR-selective cellular reporter **RX1** (see **chapter 3.1.3**).

Both 1,2-dithiolane probes are unaffected by Se-modulation and chemical inhibition and are activated in TrxR1-knockout cells, arguing against recent literature reports on this topic by Fang *et al.* We studied how chemical inhibitors, especially those based on thiol-reactive warheads, must be used and interpreted with caution, in order to identify why misinterpretations may have arisen. We suspected that any simple thiol-reactive groups will also block surface/membrane thiols and thus interfere with thiol-mediated uptake mechanisms which are likely key for 1,2-dithiolane probes' cellular signals, such that their fluorescence is diminished even without ever affecting TrxR intracellularly.

Lastly, we were cautious observing ultra-fast activation kinetics on cells for 1,2-dithiolane **Fast-TRFS**, which relies on a reducible, but non-releasing mechanism. Knowing the drastically environment-sensitive fluorescence of coumarin-based dyes, we asked the questions: can non-reductive ROP be a valid mechanism for opening the 1,2-dithiolane motif and giving fluorescence? And can partitioning of the probe into membrane phases drive this non-reductive signal generation? These questions are unique to the **Fast-TRFS** probe due to its unusual quenching mechanism. Whereas a linearisation of **SS50-PQ** would result in a non-fluorescent polymer, the linearization of **Fast-TRFS** would be directly measurable. A simple experiment using lecithin-derived lipid vesicles in an aqueous solution supported our ROP hypothesis: We measured quantitative partitioning-based "activation" of **Fast-TRFS** fluorescence, *in the absence of any reductant*, that is dependent only on the vesicle and probe concentration, and that reaches the same fluorescence as a linearized reference **Linear-TRFS** (**Fig. 6**).

In this study, we thus demonstrated that 1,2-dithiolanes are highly reactive to various reductants and that fluorogenic probes based on this warhead are not selective reporters for TrxR in cellular settings. We concluded that 1,2-dithiolane is better seen as a motif for thiol-mediated uptake of small molecules and large constructs, so assays using thiol-reactive chemical inhibitors, which potentially interfere with surface/membrane thiols, must be interpreted with caution.

Cyclic 5-membered disulfides are not selective substrates of thioredoxin reductase, but are opened nonspecifically

Jan G. Felber ¹, Lena Poczka¹, Karoline C. Scholzen ², Lukas Zeisel ¹, Martin S. Maier¹, Sander Busker^{2,6}, Ulrike Theisen ³, Christina Brandstädter⁴, Katja Becker⁴, Elias S. J. Arnér ^{2,5}, Julia Thorn-Seshold ¹ & Oliver Thorn-Seshold ¹✉

The cyclic five-membered disulfide 1,2-dithiolane has been widely used in chemical biology and in redox probes. Contradictory reports have described it either as nonspecifically reduced in cells, or else as a highly specific substrate for thioredoxin reductase (TrxR). Here we show that 1,2-dithiolane probes, such as “TRFS” probes, are nonspecifically reduced by thiol reductants and redox-active proteins, and their cellular performance is barely affected by TrxR inhibition or knockout. Therefore, results of cellular imaging or inhibitor screening using 1,2-dithiolanes should not be interpreted as reflecting TrxR activity, and previous studies may need re-evaluation. To understand 1,2-dithiolanes’ complex behaviour, probe localisation, environment-dependent fluorescence, reduction-independent ring-opening polymerisation, and thiol-dependent cellular uptake must all be considered; particular caution is needed when co-applying thiophilic inhibitors. We present a general approach controlling against assay misinterpretation with reducible probes, to ensure future TrxR-targeted designs are robustly evaluated for selectivity, and to better orient future research.

¹Department of Pharmacy, Ludwig-Maximilians University Munich, Butenandtstr. 5-13, 81377 Munich, Germany. ²Department of Medical Biochemistry, Karolinska Institutet, Solnavägen 9, 171 77 Stockholm, Sweden. ³Zoological Institute, Cellular and Molecular Neurobiology, TU Braunschweig, Spielmannstr. 7, 38106 Braunschweig, Germany. ⁴Interdisciplinary Research Centre (IFZ), Justus-Liebig University Giessen, Heinrich-Buff-Ring 26-32, 35392 Giessen, Germany. ⁵Department of Selenoprotein Research, National Institute of Oncology, 1122 Budapest, Hungary. ⁶Present address: Pelago Bioscience AB, 171 48 Solna, Sweden. ✉email: oliver.thorn-seshold@cup.lmu.de

Specific dithiol/disulfide-exchange reactions underlie a great number of crucial pathways in biology. Often, these are coordinated through conserved, highly specialised networks of oxidoreductases¹. The thioredoxin reductase–thioredoxin (TrxR–Trx) system, and the glutathione reductase–glutathione–glutaredoxin (GR–GSH–Grx) system, are central “nodes” in these networks. TrxR (nM cellular concentration) passes reducing equivalents from NADPH to Trx-fold effector proteins (μM). Similarly, GR (nM) passes reducing equivalents from NADPH to the redox-active peptide GSH (mM), that can directly function as a cellular reductant or be further shuttled to effector Grx proteins (μM). These systems drive hundreds of redox reactions vital to cellular metabolism, and also regulate protein activity, protein–protein interactions, and protein localisation by reversible dithiol/disulfide-type reactions². Their complex homeostasis³ is dysregulated in many diseases, particularly in autoimmune disorders and cancer⁴, making Trx and TrxR promising therapeutic targets⁵. Designing selective probes or substrates that report on their activities or target these redox nodes, would enable a broad range of applications in both basic biological and applied biomedical research, and is, therefore, a subject of intense development both through genetic engineering and chemical biology approaches^{6,7}.

Disulfides are the typical native substrates of these redox systems, and both linear and cyclic disulfides have been exploited as artificial substrates in biophysics, materials chemistry and chemical biology. Driven by the high intracellular concentration of thiols (ca. 50 mM total, ca. 5 mM GSH) compared to low concentrations in blood or in the extracellular space, linear disulfides undergo irreversible and nonspecific thiol–disulfide interchange and reduction in cells (Fig. 1a)^{8,9}. Linear disulfides are thus used for nonspecific intracellular release and/or activation of appended cargos, exploiting the cellular thiol pool.

By contrast, cyclic disulfides can exhibit very different kinetics and thermodynamics of thiol–disulfide interchange or reduction,

so they may have different specificities. Cyclic disulfides are found in nature, perhaps most remarkably in the epidithiodiketopiperazine class of natural products (ETPs)^{10–12}. ETPs such as gliotoxin (Fig. 1b) and chaetocin feature a near-planar diketopiperazine that is 1,4-bridged by a disulfide with a CSSC dihedral angle of 0° , which is high in energy compared to unstrained linear disulfides (90°) or 6-membered alicyclic disulfides (60°). ETPs were initially reported to inhibit a range of enzymes and cause a variety of cellular effects, but these poorly reproducible bioactivities are now understood as nonspecific reactivity of their highly strained disulfide¹³.

A particularly important cyclic disulfide which remains less clearly analysed is the 5-membered 1,2-dithiolane (Fig. 1c). This motif underlies the key cellular redox cofactor lipoic acid; it is also found in several natural products^{14,15}, and it has emerged as a motif of general interest within the last decade^{16–18}. The strained 1,2-dithiolane is kinetically labile to thiol–disulfide interchange¹⁹, which likely underpins its role as a redox cofactor. The disulfide’s opening/reduction kinetics have made it the focus of numerous chemical biology approaches, although these have been predicated on two mutually contradictory views of its cellular behaviour: which we aim to examine and resolve in this paper.

Following one view, 1,2-dithiolane has been cast as an easily, nonspecifically, and irreversibly opened and/or reduced motif²⁰. Whitesides’ systematic disulfide investigations highlighted that its strained CSSC dihedral angle of ca. 30° destabilises it by more than 8 kJ/mol relative to linear disulfides, and that its reduction potential (ca. -240 to -270 mV) is not significantly below that of linear disulfides (ca. -230 mV). In the 1950s, Fava observed that 1,2-dithiolane undergoes thiol–disulfide interchange with alkyl thiols ca. 5000 times faster than do linear aliphatic disulfides²¹. Creighton reported that its reduction by the vicinal dithiol dithiothreitol (DTT) is over 100 times faster still²², and Whitesides showed that this rate is only 100-fold slower than the diffusion limit in DMSO²³. With favourable thermodynamics and

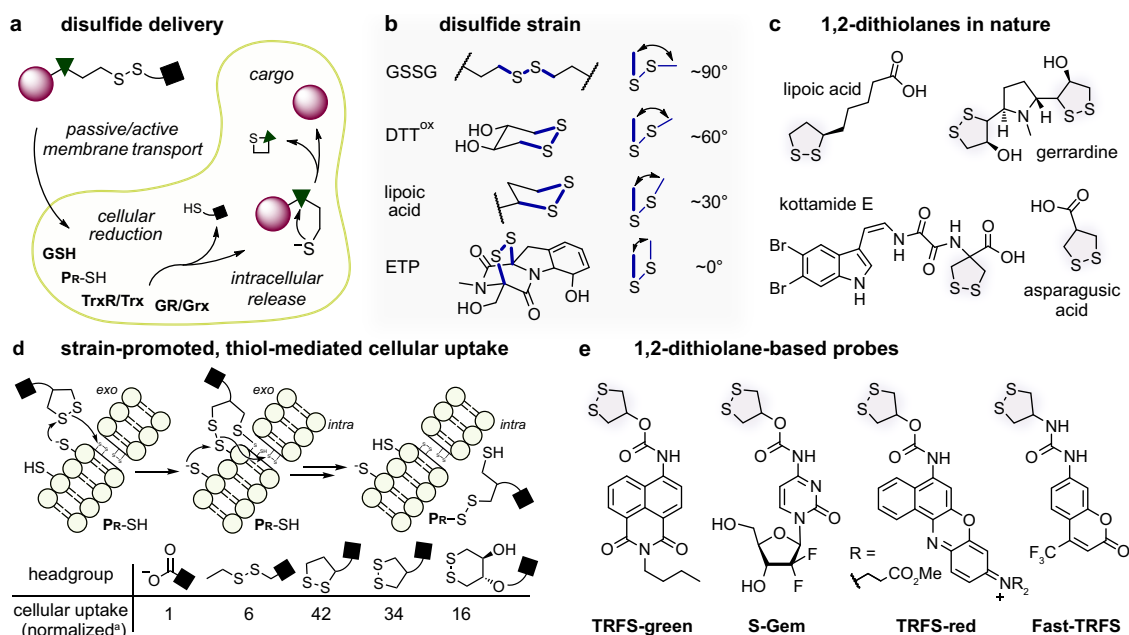


Fig. 1 1,2-dithiolanes in chemical biology. **a** Linear disulfide-based cellular delivery: irreversible cleavage of linear disulfides after cell entry leads to intracellular cargo release (Pr-SH: intracellular protein thiol). **b** From linear, to cyclic 6-membered, to increasingly ring-strained 5-membered disulfides, to ETPs. **c** Strained 1,2-dithiolanes in natural products. **d** Fast, irreversible and nonspecific thiol–disulfide interchange of 1,2-dithiolanes by exofacial thiols, followed by dynamic transmembrane exchange cascades, enhances cellular uptake and intracellular delivery. [²: data from Matile et al.³⁰]. **e** Some of the 1,2-dithiolane-based “TRFS” probes and prodrugs that have been reported as selective cellular substrates of thioredoxin reductase [TRFS = “Thioredoxin Reductase Fluorogenic Substrate”^{16,18,45}].

high kinetic lability, 1,2-dithiolanes readily polymerise by nucleophile-catalysed ring-opening polymerisation, in particular in the presence of thiols^{24,25}. Matile showed that the sterically less shielded 1,2-dithiolanes in asparagusic acid derivatives (two primary thiols) polymerise even more easily than do lipoic acid derivatives²⁶, giving them valuable applications e.g. in “SOSIPs” exploiting proximity-induced-polymerisation²⁷.

The intrinsic lability of 1,2-dithiolanes has also been extensively applied for thiol-mediated cellular uptake systems. Promoted by strain, 1,2-dithiolanes are attacked by cell surface thiols, then are internalised through a series of dynamic covalent reactions first with membrane thiols and later with intracellular thiols²⁸. Attaching these strained disulfides to a molecular cargo thus drastically enhances its cellular uptake rate (Fig. 1d; overview in Supplementary Fig. 2a)^{26,29–35}. It will be important to note that this process may be strongly affected by treatment with thiol-reactive species: cellular uptake rates are decreased many-fold by thiol-reactive electrophiles or oxidants; or instead enhanced by reducing agents^{30,36,37}. Studying the role of membrane thiols in this process, and their connection to the intracellular redox environment, is also an expanding topic^{38–42}. Other recent studies further demonstrate that 1,2-dithiolanes undergo fast strain-driven cross-linking or polymerisation, initiated either by thiols or by other nucleophiles^{43,44}.

In contrast however, 1,2-dithiolanes have also been reported as reduction-sensing units with a remarkable selectivity for TrxR. The fluorogenic TRFS-probes^{16,18,45,46} and prodrugs¹⁷ have been widely used for cellular studies, commercialised, and reviewed^{47–51} (Fig. 1e; overview in Supplementary Fig. 2b). These probes have since been used in biology to study the role of TrxR in Parkinson’s disease⁵² and stroke⁴⁶, and have been employed for mechanistic validation of putative TrxR inhibitors during cellular screening approaches¹⁸.

Which is the real situation? 1,2-dithiolane cannot be both highly and nonspecifically reactive, yet also TrxR-selective in the cellular setting. To develop a systematic understanding of redox biology, it is necessary to clarify such fundamental disagreements, and reveal why such contradictory interpretations could arise.

Towards this goal, we have investigated the environment-insensitive 1,2-dithiolane-based reduction-sensing probe **SS50-PQ** and systematically compared its performance to the prominent 1,2-dithiolane-based compound **TRFS-green**. We show that (a) 5-membered cyclic disulfides employed in these probes are nonspecifically reduced by a broad range of monothiols, dithiols, proteins and enzymes, and that (b) their cellular fluorogenicity is substantially independent of TrxR. We also show that (c) 1,2-dithiolane-based compound **Fast-T RFS** is fluorogenic even without cells and without TrxR, and that its fluorogenicity is consistent with reduction-independent, hydrophobicity-driven partitioning followed by catalytic ring-opening polymerisation. In the year after the preprint of this paper was posted, both **TRFS-green** and **Fast-TRFS** were re-evaluated by the same authors, now finding that they do indeed react at least with Grx, Trx, and GSH⁵³. These revised reports are coherent with the much stronger conclusions we derive in this paper: that not only the **TRFS** probes, but indeed any 1,2-dithiolane probes, cannot be simplistically interpreted as cellular reporters for TrxR, Trx, Grx, GSH, or any combination of such species: the highly strained disulfide makes cellular readouts essentially not interpretable, and the compounds should not be used as probes in this manner.

Taken together, we and increasingly others are concluding that 1,2-dithiolane-based compounds cannot be selective cellular probes of TrxR. We signal to the community that previous studies interpreting the cellular performance of TRFS probes as TrxR

reporters^{16–18,45,46,52} will benefit from stringent re-evaluation, and the interpretations will probably be found to be wrong. We also signal to the community that the cellular performance of strained disulfide probes are probably best understood as nonspecifically monitoring thiol-mediated uptake rates, with the caveat that they are cellularly activatable by such a broad range of species and even non-reductive processes, that to interpret their cellular behaviour in terms of specific actors is also likely to be wrong. This does not prevent them from being legitimately applicable for enhanced delivery and nonspecific activation of trigger-cargo-systems, which opens up promising avenues for chemical biology. We also outline a strategy to control against assay misinterpretations with reducible probes, to promote progress towards a robust and useful toolset of probes for redox biology.

Results

Probe design. We aimed to explore the properties of 1,2-dithiolanes using an environment-independent reduction-activated probe. Reduction-activated probes and prodrugs are typically trigger-cargo designs, where a reduction-sensitive trigger is connected to the cargo while masking a key functional group. Trigger reduction then results in a fragmentation reaction that restores activity by unmasking that key functional group. This concept has been used for a range of imaging agent^{54,55} and drug^{56–58} cargos.

The TRFS probes are also designed as trigger-cargo constructs with 1,2-dithiolane as the redox sensor, attached to aniline fluorophores through a carbamate (**TRFS-red**, **TRFS-green**; Fig. 1e) or urea (**Fast-TRFS**; Fig. 1e). For the carbamate probes, disulfide reduction and thiol cyclisation slowly releases the active aniline fluorophore; though the urea probe operates without aniline unmasking, and its fluorescence turn-on mechanism is not fully understood. Generally, most trigger-cargo disulfide probes employ aniline rather than phenol cargos (Supplementary Fig. 2b). While aniline carbamates have high hydrolytic stability¹⁸, phenol-releasing designs would in many ways be more attractive targets, due to a large scope of potential cargos and to their improved release kinetics. Therefore, to test the reduction selectivity of 1,2-dithiolane with a rapidly-responding probe—and at the same time to establish a modular design that allows delivering a wide range of agents in the future—we created the phenol-releasing probe **SS50-PQ** (Fig. 2a).

The **SS50-PQ** design has several advantages. As a tertiary carbamate, this probe cannot decompose by E_{1cB} elimination^{59,60}, avoiding the instability¹⁸ that has blocked previous phenol-releasing 1,2-dithiolane probes. The choice of a 2-(2'-hydroxyphenyl)-4(3H)-quinazolinone (**PQ-OH**) as the cargo, ensures a fully off-to-on signal readout for carbamate cleavage. This is because only **PQ-OH**, but not **SS50-PQ**, can exhibit large-Stokes-shift ES IPT-based fluorescence due to intramolecular transfer of the phenolic hydrogen (ex/em 360/530 nm). Mechanistically, **PQ-OH** is released after cyclisation of the thiolate resulting from thiol-disulfide interchange or reduction expels the electron-poor phenolate (Fig. 2a); **PQ-OH** then precipitates upon reaching its low aqueous solubility limit (ca. 0.5 μM) activating its ES IPT fluorescence that is only visible in the solid state^{61,62}. Therefore, fluorescence is unambiguously due to cyclisation-mediated cargo release; and as a solid-state fluorophore, it is not subject to environment-dependent effects. With the additional benefit of its large Stokes shift, this fully off-to-on system gives excellent signal-to-background fluorescence ratios of typically >100 without needing background subtraction, making it a sensitive and easily interpreted sensor of dithiolane cleavage.

Probe synthesis. 1,2-dithiolane **6** was prepared using an approach initially reported by Raines⁶³ followed by *N*-

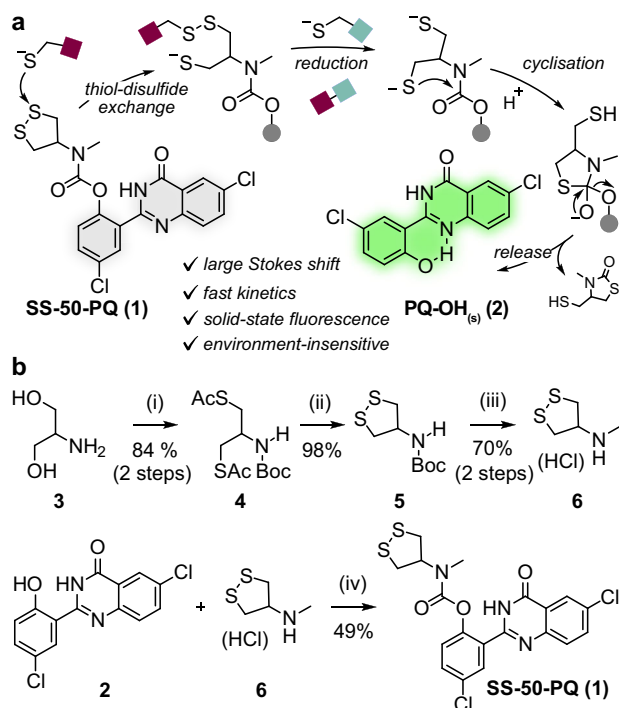


Fig. 2 1,2-dithiolane probe design and synthesis. **a** After opening or reduction of the 1,2-dithiolane in **SS50-PQ**, thiolate cyclisation releases the precipitating phenol **PQ-OH** that gives ESIP-T-based fluorescence in the solid state. **b** Synthesis of **SS50-PQ**: (i) Boc_2O , NEt_3 , dioxane/ H_2O , r.t., 15 h (96%); then either MsCl , py , DCM followed by KSac , acetone, 60°C , 2 h (89%), or HSac , PPh_3 , DIAD , THF , 0°C to r.t., 15 h (88%). (ii) KOH , MeOH , open to air, r.t., 15 h (98%). (iii) MeI , NaH , DMF , 0°C to r.t., 0.5 h (70%). (iv) **PQ-OH**, triphosgene, NEt_3 , DCM , 0°C to r.t., 1 h; then **6**, NEt_3 , DCM , 0°C to r.t., 1 h (49%).

methylation and Boc-deprotection (Fig. 2b). All intermediates containing the 5-membered cyclic disulfide showed degradation upon standing, presumably producing linear polydisulfide oligomers (see Supplementary Information). This occurred even without clear stimuli (e.g., stirring in dichloromethane). The cyclic monomer could typically be recovered by stirring in dilute solution, although isolating the monomer from this solution while avoiding re-polymerisation was not straightforward. The *N*-methylation step suffered particularly from polymerisation, until we found that the monomeric product could be extracted from methanol by hexane washes (see Supplementary Information). The final fluorogenic probe **SS50-PQ** was assembled by carbamate coupling with **PQ-OH**.

1,2-dithiolane is unstable in probes. Polymerisation was also observed for probe stock solutions in DMSO. Their maximal fluorescence, determined in a standardised reducibility test (aqueous buffer, pH 7.4, 10 eq of the quantitative disulfide reductant tris(carboxyethyl) phosphine, TCEP) decreased over time. We understood this as a consequence of polymerisation, since the hydrophobic, polymeric degradation products would have decreased accessibility to solvated reductants. Fresh probe stocks were, therefore, prepared immediately for each assay from powdered solid, then assayed for quality by comparison of the maximum TCEP-driven fluorescence to calibrations established by precipitating the theoretical amount of **PQ-OH**. Only stocks yielding TCEP-driven signals within 10% of the calibration intensity were used in assays. In fact, we re-prepared **SS50-PQ** five times during this research to maintain high-quality stocks.

1,2-dithiolane is nonspecifically reduced by various thiols. A disulfide trigger can only be enzyme-selective in the cellular context, if it resists signal generation from thiol-disulfide interchange or reduction by the cellular monothiol background (ca. 50 mM, of which ca. 5 mM GSH^{64–66}). Hence, we began testing the potential for selectivity by performing cell-free incubations of **SS50-PQ** (10 μM) with GSH.

Probe “sensitivity or resistance” to challenge by a species, is often reported based on measurement at a single challenge concentration at a single timepoint. However, this simplification can misrepresent the situation by “hiding” signal that increases after a certain lag time. To provide a characterisation of probe resistance to monothiols, we titrated GSH over a wide concentration range (0.01 to 10 mM) and collected timecourse fluorescence data (Fig. 3a). For meaningful representation, we normalised the signals at each timepoint against the maximum possible fluorescence value at that timepoint (from the TCEP control: see Fig. 3a). This normalisation is important because it separates the upstream kinetics of reduction, from the potentially slower downstream kinetics of fragmentation which otherwise can obscure sensitivity to reduction; so it allows direct comparison of experiments relative to their theoretical maxima, and can be generally recommended. We also compared dose-response curves from various endpoint times (Supplementary Fig. 3) to ensure that any presented curve is representative of the probe’s general behaviour.

We observed strong, fast probe response to even subphysiological GSH levels. The GSH concentrations causing half-maximal fluorescence (“ $\text{EC}_{50}^{\text{GSH}}$ ”) were $\lesssim 1$ mM (Fig. 3a; Supplementary Fig. 3). This indicates that 1,2-dithiolane probes can be rapidly and fully reduced by cellular GSH concentrations, even without enzyme catalysis involved.

We also screened other monothiol reductants, e.g., cysteine (Cys), *N*-acetylcysteine (NAC), *N,N*-dimethyl-cysteamine (MEDA), and cysteamine (CA) and found fast probe activation (Fig. 3b) with similar concentrations and kinetics compared to GSH. This suggests that 1,2-dithiolane is generally instable to monothiols, so that probes derived from it will be rapidly activated by the intracellular thiol background. Matching expectations from Creighton²² and Whitesides²³, the probe was quantitatively and rapidly triggered by equimolar amounts of vicinal dithiol DTT. We controlled for release by mechanisms other than interchange/reduction-triggered cyclisation, using serine (Ser) and glutathione disulfide (GSSG). The probe was entirely stable to non-reductive degradation by e.g. aminolysis, highlighting the stability of the tertiary phenolic carbamate, and supporting that interchange/reduction is its pathway for signal generation (Fig. 3b).

In summary, these assays show that 1,2-dithiolanes do not resist uncatalysed thiol-disulfide interchange and/or reduction even by monothiols and even at subphysiological concentrations, making them unlikely to be enzyme-selective in the cellular context.

1,2-dithiolanes are nonspecifically reduced by redox-active proteins and enzymes. We next tested probe reduction by redox proteins from the Trx/TrxR and Grx/GSH/GR systems. Each protein has multiple isoforms, as has been excellently reviewed⁶⁷. We employed recombinant human Trx1 and Trx2; the thioredoxin-related protein TRP14, which features a vicinal dithiol/disulfide redox-active site that is similarly recovered by TrxR1; the oxidoreductases TrxR1, TrxR2 and GR; and human vicinal dithiol glutaredoxins Grx1 and Grx2. Both Trxs and Grxs have orders of magnitude higher cellular concentrations (ca. 10 μM) than their upstream TrxR and GR partners (ca. 20 nM), so we reflected these concentrations in our assays.

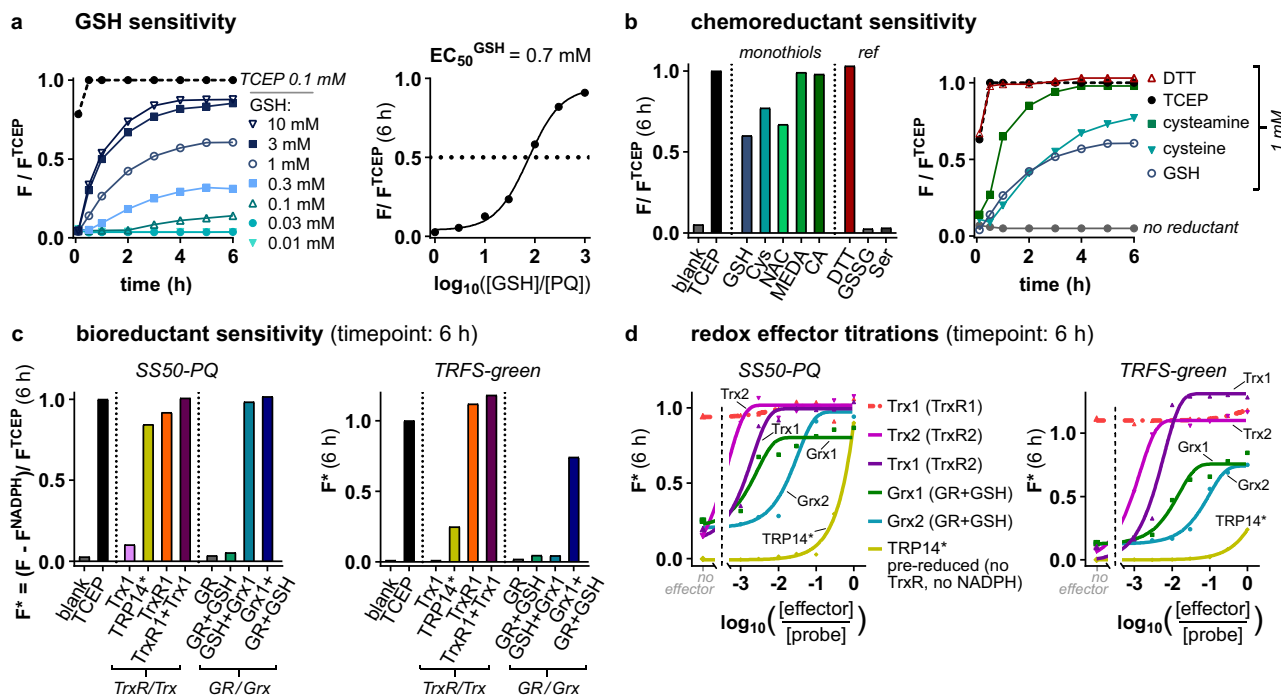


Fig. 3 1,2-dithiolane probes are activated by a range of chemical and biological reductants. **a** GSH challenge. Fluorescence timecourses of **SS50-PQ** exposed to GSH, and the corresponding dose-response plot ($t = 6$ h at 37°C). **b** Chemical reductant assays. Normalised signal from **SS50-PQ** challenged with monothiols (GSH, cysteamine (CA), and mercaptoethyl-dimethylamine (MEDA) each at 1 mM), dithiol (1 mM dithiothreitol (DTT)), non-reductants (GSH disulfide (GSSG) and serine (Ser) each at 1 mM), or tris(2-carboxyethyl)phosphine (TCEP) ($100\ \mu\text{M}$); showing all endpoint results (6 h at 37°C) and selected kinetics. **c** Redox enzyme assays. Normalised signal from **SS50-PQ** and **TRFS-green** challenged with TrxR/Trx or GR/GSH/Grx network proteins (20 nM TrxR1/GR, $10\ \mu\text{M}$ Trx1/Grx1/TRP14*, $100\ \mu\text{M}$ GSH as indicated; $100\ \mu\text{M}$ NADPH in all TrxR/GR assays). **d** Dose-response plots for redox effector proteins (20 nM TrxR1/TrxR2/GR, 0.03 – $10\ \mu\text{M}$ Trx1/Grx1/TRP14*, $100\ \mu\text{M}$ GSH as indicated; $100\ \mu\text{M}$ NADPH in all TrxR/GR assays). (**a**–**d**: data are for single representative examples from either 2 (**b**) or 3 (**a**, **c**, **d**) independent experiments; probes at $10\ \mu\text{M}$ in aqueous TE-buffer; notation TRP14* indicates pre-reduced TRP14 (see “Methods”).

We had hypothesised that the reducible trigger of a trigger-cargo probe is the key determinant of its reactivity and selectivity, so that results from the fast-response, environment-independent 1,2-dithiolane **SS50-PQ** should be valid for any cargo-releasing 1,2-dithiolane probes (Supplementary Note 1). To test this, we synthesised the 1,2-dithiolane **TRFS-green**¹⁶, which has ca. 200-fold slower kinetics of releasing its aniline cargo following TCEP reduction than does **SS50-PQ** for releasing its phenol (Supplementary Fig. 5); and we challenged both **SS50-PQ** and **TRFS-green** with proteins from these redox systems (note: **TRFS-green** also suffers environment-dependency of fluorescence signal, discussed in Supplementary Note 4). To study whether probes were reduced by the effectors Trx or Grx, and/or by direct reaction with the upstream reductants TrxR or GR, we compared assays using both effectors and upstream reductants, against assays employing only upstream reductants or only effectors (TrxR/GR assays included NADPH; GR + Grx assays included $100\ \mu\text{M}$ GSH for Grx reduction; see Supplementary Information).

Both 1,2-dithiolane probes were nonspecifically reduced, with Trx1, Trx2, TRP14, Grx1, Grx2 and TrxR1, all giving high rates of conversion as compared to the TCEP benchmark (Fig. 3c). Only the mitochondrial TrxR2 isoform and the GSSG-specific enzyme GR gave no signal (Supplementary Figs. 4, 5). Timecourse measurements and redox effector dose–response plots showed that the Trx system and the Grx-coupled GSH system (TrxR/Trx and GR/GSH/Grx; Fig. 3d, Supplementary Figs. 5–7) have identical activation profiles for both 1,2-dithiolane-based probes regardless of their cargos’ leaving group character or release kinetics.

Taken together, the 1,2-dithiolane probes are nonselectively and nonenzymatically triggered by GSH and other monothiols at

subphysiological concentrations, as well as by a broad range of dithiol/disulfide-type proteins and enzymes. The systematic variation and titration of chemo- and bioreductants, and the examination of both timecourse and endpoint data, show that 1,2-dithiolanes are not TrxR-selective substrates in cell-free settings.

General cellular and in vivo performance of the phenolate-releasing SS50-PQ probe design. To use **SS50-PQ** to report on 1,2-dithiolane performance in general, relies on showing the technical suitability of its phenolic 2-mercapto-secondary amine carbamate design, to act as a robust reporter for redox performance of its trigger, in a variety of settings. Before tackling cellular selectivity, we therefore tested its general biological performance.

We applied **SS50-PQ** in HeLa cervical cancer, A549 lung cancer, Jurkat T-cell lymphoma, and mouse embryonic fibroblast (MEF) cell lines. All cell lines rapidly generated well-defined fluorescent precipitates of **PQ-OH**. Fluorescence plate reader quantification showed a nearly linear (Fig. 4a), concentration-dependent (Fig. 4b) increase of signal, indicating that no saturation effects are operative (compare to **TRFS-green**, which saturates at $10\ \mu\text{M}$: discussed in Supplementary Fig. 8). The solid precipitates of **PQ-OH** were intracellularly localised and visible in most cells (Fig. 4c; Supplementary Movie 1).

Because microscopy can misrepresent population-level response, we used flow cytometry to collect single-cell-resolved statistics of probe activation. Though this is unusual for chemical probes, it is possible with **SS50-PQ** because the solid **PQ-OH**

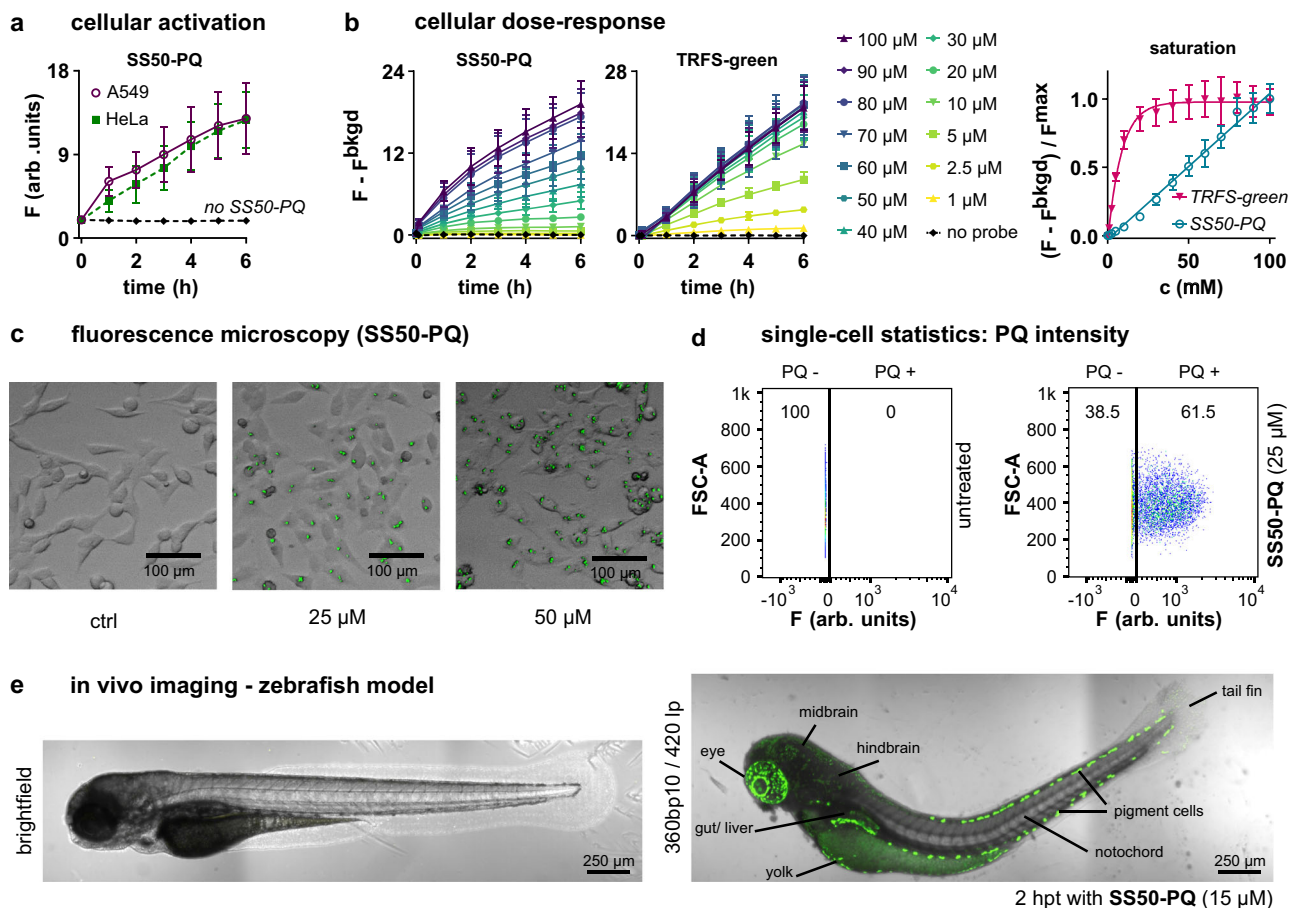


Fig. 4 The phenolic carbamate design of SS50-PQ gives reliable performance across biological assays. **a** Cellular fluorescence timecourses of SS50-PQ in HeLa and A549 cells (50 μM probe). **b** Dose-dependency of cellular fluorescence timecourses with SS50-PQ, as compared to TRFS-green (HeLa cells). (**a, b**: data as mean ± SD of ≥3 independent experiments). **c** Microscopy of SS50-PQ-treated HeLa cells shows fluorescent intracellular solid precipitates of released PQ-OH (representative images from 3 independent experiments with similar results). **d** Flow cytometry-based single-cell statistics of cellular fluorescence after SS50-PQ treatment (25 μM; Jurkat T-cells). (**c, d**: representative examples of ≥3 independent experiments with similar results). **e** Fluorescence imaging of embryonic zebrafish before and after SS50-PQ treatment (representative example of 3 independent experiments). (**c, e**: brightfield transmission image in greyscale, fluorescence superimposed in green).

precipitate is cellularly retained during fixation. These data showed a monomodal fluorescence intensity distribution with ca. >60% of cells exhibiting strong PQ-OH fluorescence (Fig. 4d, Supplementary Fig. 14).

We finally applied SS50-PQ in vivo, to stringently test three goals for its general design: (a) zero signal background, due to mechanistic quenching in the probe and to the high Stokes shift of the released fluorophore; (b) no spontaneous cargo release, due to the hydrolytic robustness of the tertiary carbamate; and (c) cellular retention of PQ-OH precipitates; which combine to enable high-spatial-resolution imaging in vivo. We incubated zebrafish zygotes and embryos up to 3 days post fertilisation (dpf) with SS50-PQ during live epifluorescence and confocal microscopy imaging (Fig. 4e, Supplementary Figs. 17, 18). Probe activation began within two hours, with interesting cell-type-specificity of the marked cells (which we do not believe is connected to differences in TrxR activity). All three probe-design goals were achieved, so that high-contrast images were obtained without background manipulation, and with precise resolution: which marks the redox probe design we report as valuable for future adaptations with other triggers.

1,2-dithiolane probes are not cellular reporters of TrxR. We then tested the TrxR-specificity of cellular activation of both 1,2-

dithiolane probes, using the TrxR-independent linear disulfide SS00-PQ⁹ and the strongly TrxR-dependent selenenylsulfide-containing RX1⁶⁸ as references to indicate the expected outcomes of selectivity-testing cellular experiments.

Cells cultured without selenium supplementation do not fully incorporate Sec in TrxR, lowering cellular TrxR activity⁶⁹. However, Na₂SeO₃ starvation or supplementation did not significantly affect SS50-PQ or TRFS-green signal (Fig. 5a, Supplementary Fig. 8a). Another method to modulate TrxR activity is to supply thiophosphate, which promotes cysteine insertion at Sec-encoding UGA codons during selenoprotein synthesis⁶⁹. Again, we saw no effects on SS50-PQ or TRFS-green signal timecourses (Fig. 5b, Supplementary Fig. 8b). These results mirror those for the TrxR-independent probe SS00-PQ.

Next, we more stringently evaluated TrxR1-dependency comparing a TrxR1 knockout MEF cell line (TrxR1^{-/-})⁷⁰ to its parental cell line (TrxR1^{fl/fl}) and using its vector-based TrxR1-knock-in line⁷¹ TrxR1^{2ATG} as an additional control. Knockout did not affect signal from SS50-PQ (or SS00-PQ), and only reduced that of TRFS-green by ca. 40% (Fig. 5c, Supplementary Fig. 8c), in assays that are otherwise entirely kinetically intercomparable (same cell count, parental cell line, timecourse, assay plate etc). This indicates that the dithiolane probes are indeed not effective reporters of TrxR activity in cells, as non-TrxR signal activation proceeds at highly comparable rates (see

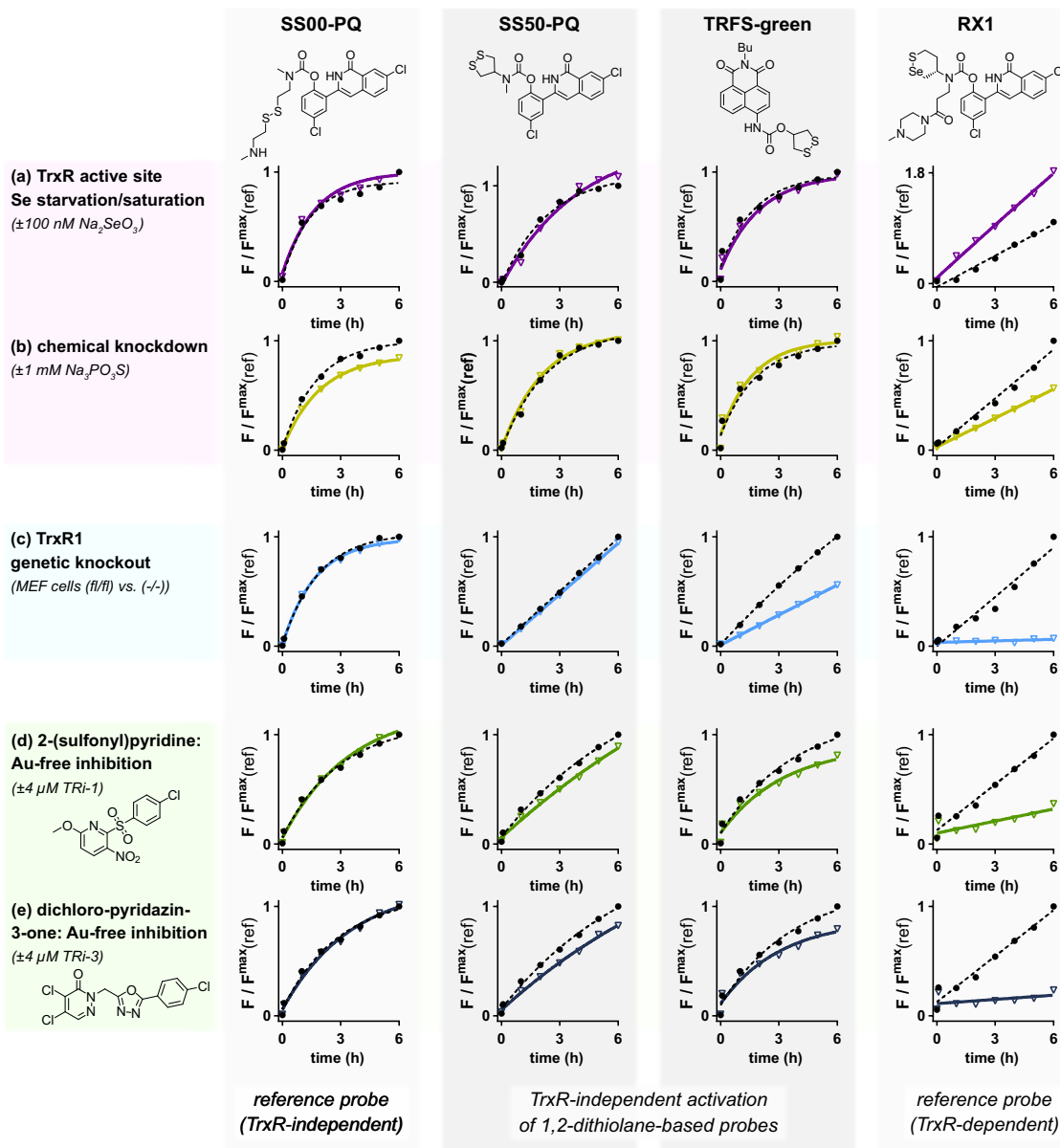


Fig. 5 Cellular signal from 1,2-dithiolane probes does not report on TrxR. **a–e** Cellular fluorescence timecourse studies of **SS50-PQ** and **TRFS-green**, with the TrxR-independent **SS00-PQ** and the TrxR-dependent **RX1** as benchmarks for assay outcomes. **a** A549 cells starved of, or supplemented with, selenium (as Na_2SeO_3) (probes at 100 μM ; full data in Supplementary Fig. 8a). A549 cells treated with $\text{Na}_3\text{PO}_3\text{S}$ (probes at 100 μM ; full data in Supplementary Fig. 8b). **c** TrxR1-knockout (–/–) and –wildtype (fl/fl) MEF cells (probes at 100 μM ; full data in Supplementary Fig. 8c). **d, e** A549 cells pre-incubated for 2 h with the gold-free TrxR inhibitors TRI-1 and TRI-3 (probes at 50 μM ; full data in Supplementary Fig. 10–13). (**a–e**: data shown as mean from 3 independent experiments; full representations in Supplementary Information). Note: plots on the same graphs are run under identical conditions except for the indicated variable (TrxR knockout/presence, etc.) so are kinetically comparable).

Supplementary Note 1 and discussion at Supplementary Fig. 8). The benchmark TrxR-selective **RX1** probe was instead silent in knockout cells (further evaluations in ref. 68).

Literature claims for cellular TrxR-selectivity of probes have substantially relied on chemical inhibitor treatments that suppress their cellular activation. We first tested the recently-developed TrxR inhibitors TRI-1 and TRI-3⁷². **SS50-PQ** or **TRFS-green** had similar signal in cells pre-incubated with TRIs as in untreated controls: behaviour characteristic for the TrxR-independent **SS00-PQ**, but unlike the strongly suppressed benchmark **RX1** (Fig. 5d, e, Supplementary Figs. 10–12). These results were independent of the pre-incubation time, and of whether results were acquired as population-average timecourses or as single-cell-resolved statistics (Supplementary Figs. 14, 15).

Therefore, neither TrxR suppression nor TrxR knockout greatly alter the cellular activation of **SS50-PQ** or **TRFS-green**. Taken together with the cell-free results showing rapid and nonspecific activation of the 1,2-dithiolane probe by a range of cellular thiols, we conclude that cellular activation of 1,2-dithiolane probes does not meaningfully report on TrxR activity.

Auranofin assays can be misleadingly interpreted with 1,2-dithiolane probes. Some previous studies of 1,2-dithiolane probes have claimed excellent cellular TrxR selectivity on the basis that treating cells with the thiophilic gold complex auranofin (AF; Supplementary Fig. 12) dose-dependently reduces fluorescence signals as compared to untreated controls⁵². AF is

popularly used as an inhibitor of TrxR; and it binds TrxR in cell-free assays as well as in cells. However, AF is a broadly “potent thiol-reactive species”⁷³ with at least 20 other known thiol protein targets, and is likely to bind many more depending on target exposure⁷⁴.

Notably, AF is a particularly strong binder of membrane thiols, possibly driven by its lipophilicity as well as the immediate exposure of these thiols to extracellularly-administered AF⁷⁵. Given the extensive research showing e.g., 40-fold enhancement³⁰ of cellular uptake by reaction of free membrane thiols⁷⁶ with strained disulfides, we hypothesised that inhibition of dithiolane probe signal with AF treatment might simply report on uptake inhibition, rather than relating to the portion of AF which may bind to TrxR. Matching these expectations, cells pretreated with AF (0.1–4 μ M) gave decreased processing of dithiolane probes but not of linear benchmark **SS00-PQ**, seen by both single-cell (Supplementary Figs. 10–13) and population average (Supplementary Figs. 14, 15) measurements.

As the dithiolanes are neither cell-free- nor cellularly-selective reporters of TrxR, this matches emerging literature to suggest that auranofin (or indeed, any other likely membrane-thiol-reactive species) in cellular studies do not test putative reductant-selectivity of 1,2-dithiolane probes (or other compounds liable for thiol-based uptake)²⁸. In future work, it would be beneficial to take precautions e.g. cell-free controls testing AF-probe interactions (see Supplementary Fig. 9, with nonstrained reference **SS66C-PQ**), and comparisons to heavy-metal-free inhibitors, to check intracellular targets of strained disulfides without relying on auranofin (see Supplementary Note 2).

The tendency of 1,2-dithiolanes to oligomerise can also be misinterpreted as probe activation. We had seen during synthesis and handling that the 1,2-dithiolane probes and intermediates suffer from concentration-dependent, non-reductive ring-opening polymerisation (ROP), as has been extensively studied by Whitesides^{24,25}, and applied by Matile in SOSIPs²⁷. Polydisulfides of **SS50-PQ** are fully nonfluorescent, since the ESIPIT responsible for their fluorescence cannot take place without a phenolic hydrogen: thus ROP cannot trigger misinterpretable signal generation in **SS50-PQ**. As **PQ-OH** is a solid-state fluorophore, its fluorescence is also environment-independent. However, neither is true for prior art 1,2-dithiolane probes. *N*-acylated 8-aminonaphthylimide (**TRFS-green**) and 4-aminocoumarin (**Fast-TRFS**) both contain environment-sensitive fluorophores which are not fully fluorescence-quenched either in the *N*-acylated probe or in their reduction intermediates. As we had already shown the cellular non-selectivity of **TRFS-green** experimentally (discussions at Supplementary Fig. 3; and 8, and Supplementary Note 4), we now tested **Fast-TRFS** to see if ROP might operate and cause misinterpretation of its performance.

Fast-TRFS is a 1,2-dithiolane-based probe that does not release a cargo upon reduction (Fig. 6a)¹⁸. Due to partial PET-quenching from the strained 1,2-dithiolane, **Fast-TRFS** has weak fluorescence, that is partially enhanced in apolar media. Its fluorescent reduction product **dithiol-TRFS** does not have PET quenching (Fig. 6a), and its fluorescence is again much stronger in apolar media.

We asked the questions: Can non-reductive strain-promoted ROP of **Fast-TRFS** lead to signal generation under typical assay conditions? If so, can it have previously been misinterpreted as reporting on intracellular probe reduction?

Cellular assays where a relatively large surface area of lipid membrane is accessible, present a very different environment than cell-free assays in homogenous aqueous media. For hydrophobic species, and particularly for environment-sensitive fluorophores, we reasoned that this difference might be

significant. Therefore, we considered small lipid/phospholipid vesicle suspensions as a useful cell-free model to capture some aspects of inhomogenous cell-assay environments, and to test the behaviour of environment-sensitive compounds, without the complexity of cellular reductants (Fig. 6b).

Our first hypothesis was that hydrophobic **Fast-TRFS** may concentrate from aqueous media into high-surface-area apolar environments, thus initiating concentration-dependent, strain-promoted ROP of its dithiolane, giving polymer **PolyLinear-TRFS** (Fig. 6c). This is conceptually similar to Matile’s SOSIPs, which exploit π -stacking of species similar to **TRFS-green** to raise local concentrations of 1,2-dithiolanes and so initiate polymerisation²⁷: except that the organising principle in our hypothesis is based on partitioning out of an aqueous phase. We expected that the rate of at-membrane polymerisation of **Fast-TRFS** would depend on the available membrane surface area: i.e., the higher the vesicle concentration, the faster that ROP would proceed.

Our second hypothesis was that the fluorescence of the non-strained ROP polydisulfide product **PolyLinear-TRFS** would mimic that of non-strained monodisulfide analogues like **Linear-TRFS** (Fig. 6a): i.e., it would be more fluorescent than **Fast-TRFS** since no more PET quenching would operate. We expected that **Linear-TRFS** would also increase in fluorescence intensity with higher lipid vesicle concentration, until reaching a limit where all **Linear-TRFS** would be extracted into the lipid phase. We noted that the **PolyLinear-TRFS** would be much more hydrophobic than the morpholine **Linear-TRFS** and so might be more fluorescent in low- or zero-lipid systems, through a combination of more efficient extraction, plus the possibility of self-aggregation to exclude water and maximise fluorescence. The key prediction arising, is that the fluorescence observed during any fluorogenic ROP of **Fast-TRFS** into **PolyLinear-TRFS** should approach a similar limit as would be seen almost immediately with **Linear-TRFS**, as long as the lipid content is high enough. Relatedly, assuming **Linear-** and **Fast-TRFS** would initially partition similarly into lipid phases, we expected that in a vesicle concentration range where lipid content limits **Linear-TRFS** fluorescence, the rate of fluorescence increase of **Fast-TRFS** would also be vesicle-limited.

To test these experimentally, we synthesised **Fast-TRFS**¹⁸ and the water-soluble analogue **Linear-TRFS** (see Supplementary Information). We prepared a vesicle suspension stock by sonicating commercial soybean lecithin (ca. 60% phospholipid, 35% lipid, with no known reductants or TrxR or NADPH) in water^{77,78}, then incubated stock dilutions with **Fast-TRFS** and **Linear-TRFS**.

In brief, these incubations showed strong vesicle-dependent fluorogenicity of **Fast-TRFS** in the absence of any reductant, which within an hour reached the same fluorescence values as quantitative reduction with TCEP. The data were consistent to all predictions arising from the hypotheses of non-reductive signal generation by partitioning-and-ROP-based fluorogenicity. This argues that cellular assays of environment-dependent 1,2-dithiolane probes may have suffered particular problems of misinterpretation:

At <1%wt vesicles, the lipid content controlled **Linear-TRFS** fluorescence, which plateaued after <5 min regardless of vesicle concentration, coherent with a fast extraction equilibrium into a fluorescence-enhancing apolar environment (Fig. 6d). In the first 5 min, a fast increase in **Fast-TRFS** fluorescence also reached a lipid-content-dependent value, also coherent with fast extraction of the intact dithiolane to initial equilibrium in lipid, though with its environment-dependent fluorescence increase being smaller. Then, however, fluorescence of **Fast-TRFS** continued to increase, at slower rates that were also dependent on lipid content:

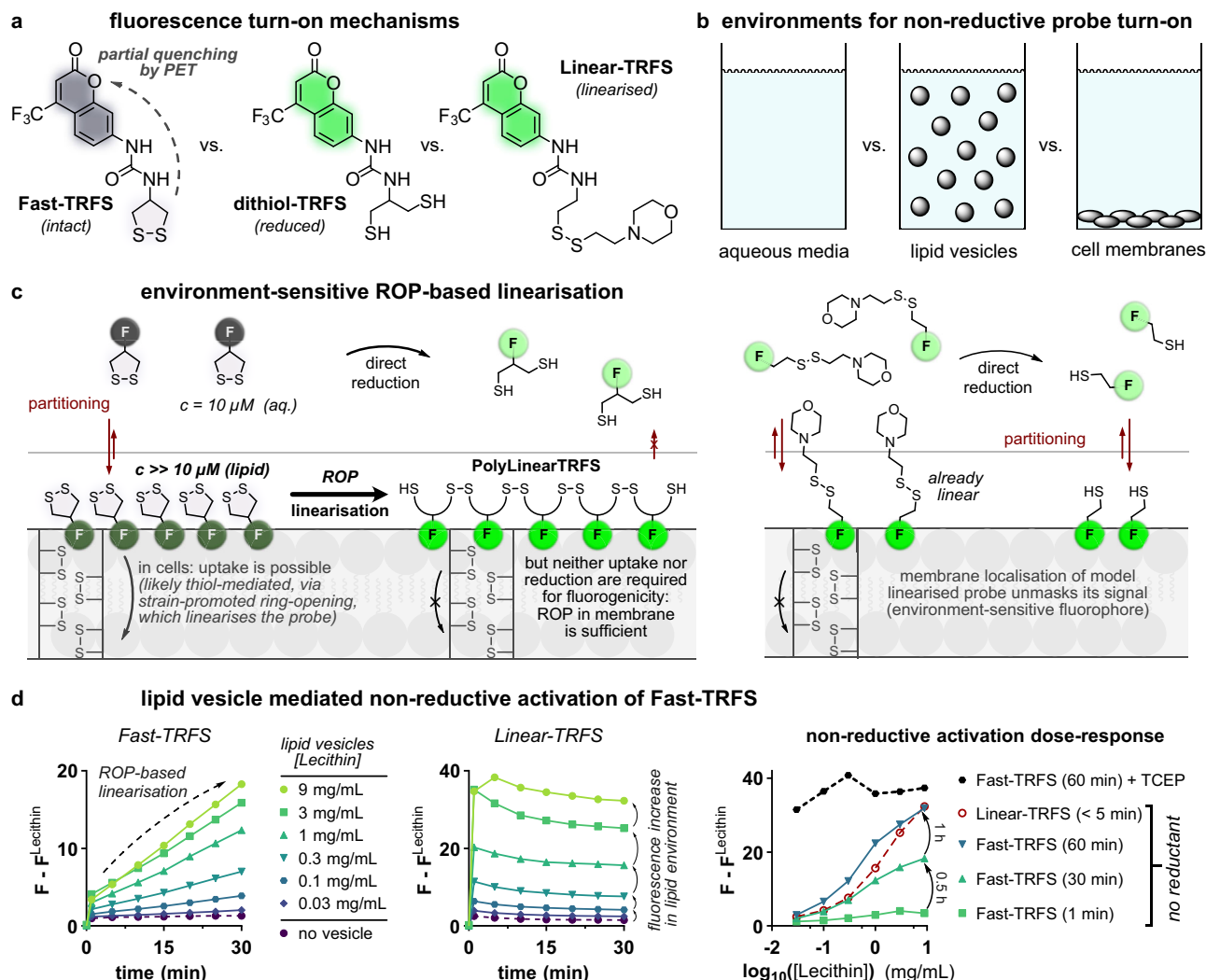


Fig. 6 The fluorescence of non-cargo-releasing 1,2-dithiolane Fast-TRFS activates in the absence of TrxR and of reductants, after partitioning into membranes: coherent with strain-promoted oligomerisation and environment-dependent fluorescence. **a** Weak, environment-dependently fluorescent Fast-TRFS¹⁸; and strong environment-dependently fluorescent compounds dithiol-TRFS (its reduction product) and Linear-TRFS (a reference compound). **b** The inhomogenous media of cellular assays may be closer modelled with lipid vesicle suspensions than as an all-aqueous system. **c** Extractive concentration of Fast-TRFS into lipid membranes may drive concentration-dependent, strain-promoted ring-opening polymerisation (ROP) to nonstrained polydisulfide PolyLinearTRFS, whose fluorescence may mimic that of nonstrained monodisulfide Linear-TRFS. Thus, ROP may be a non-reductive mechanism for fluorescence turn-on of Fast-TRFS. **d** Fast-TRFS and Linear-TRFS (each 10 μ M) incubated with lecithin vesicles. After 60 min, TCEP (0.1 mM) was added to benchmark complete reduction. (Representative example from 2 independent experiments; full data in Supplementary Fig. 16).

coherent with slower fluorogenic oligomerisation of Fast-TRFS, for which the available lipid volume plays the role of catalyst loading. In just one hour, the Fast-TRFS signal in the presence of 0.9%wt vesicles but without reductants, reached the same fluorescence plateau as established by adding 10 eq. of TCEP, which pleasingly was the same signal as seen within ≤ 5 min of mixing Linear-TRFS with 0.9%wt vesicles (Fig. 6d).

These data are fully coherent with our hypotheses of Fast-TRFS undergoing non-reductive ROP to PolyLinear-TRFS in inhomogenous media, that can easily reach maximum theoretical fluorescence values. We also noted that addition of TCEP to Linear-TRFS (giving the monothiol) did not change its fluorescence (Supplementary Fig. 16b). Thus, in the inhomogenous-media settings of cellular or lysate assays, Fast-TRFS likely cannot distinguish reduction to Dithiol-TRFS, from thiol-disulfide exchange to a monothiol product, or from non-reductive ROP to PolyLinear-TRFS. Fast-TRFS signal is likely to be dominated just by the environment-dependency of

fluorescence that each of these three species displays. While these cell-free data do not test the fate of Fast-TRFS in the cellular setting, we feel that it is likely that confounding factors operating in simple models will be even more problematic in complex ones (see Supplementary Note 3).

In summary, we believe that this hitherto-unreported reduction-independent fluorogenicity of the 1,2-dithiolane probe, combined with the orthogonal demonstrations of cell-free and cellular nonspecificity shown for the robustly-interpretable SS50-PQ as well as for TRFS-green, argue convincingly that 1,2-dithiolane-based probes should not be interpreted as being selective reporters for any specific reductase in lysates, cells or in vivo.

Discussion

Dithiol/disulfide-exchange reactions are central to biology, and engineered disulfides exploiting these reaction manifolds are

finding applications from chemical biology probes to biophysics and materials chemistry. Linear disulfides have been known for decades as substrates for nonspecific thiol attack/reduction, and often used for intracellular release of cargos. 1,2-dithiolanes have emerged as substrates of interest in chemical biology^{16–18}, although it has remained contentious whether their reduction is nonspecific, or is selectively performed by TrxR. We answered this question by studying the biochemical and biological performance of the 1,2-dithiolane-based redox probe **SS50-PQ**, where the disulfide was integrated in a stable, modular design, with a release-activated fluorogenic cargo, that we could even use in flow cytometry studies and for cell-resolved imaging in live embryos. We used nonselective linear disulfide **SS00-PQ** and TrxR-selective probe **RX1** as negative and positive benchmarks in our assays; and to show the general applicability of the results, we also performed comparisons to the known 1,2-dithiolane probes **TRFS-green** and **Fast-TRFS**, introducing further compounds (**Linear-TRFS** and **SS66C-PQ**) as needed to study aspects of the fluorophores.

We have demonstrated the nonspecific cleavage of 1,2-dithiolane probes through a rigorous methodology of reductant titrations; cell-free enzyme screenings; and cellular knockout/knock-down/knock-in, activity suppression, and electrophilic inhibitor experiments, which we believe will be a valuable methods addition to the literature. While the probes can indeed be rapidly opened by TrxR¹⁹, they are opened just as rapidly by nearly every other reducing thiol species we tested (Fig. 3, Supplementary Fig. 7), most of which are expressed at much higher concentrations in cells. We conclude that in cells, they do not selectively report on TrxR. We also conclude that this is an intrinsic feature of the 1,2-dithiolane motif itself, independent of the cargo to which it is attached and of the chemical manner of the attachment (Fig. 5). This is coherent with recent reports stating that **TRFS-green** and **Fast-TRFS** are cellularly reducible by Trx and Grx⁵³, although our assays support a much stronger statement: that nonspecific, and very likely cell-surface, reduction by thiols - and not reaction with any limited set of intracellular reductases - is likely responsible for cellular signals from 1,2-dithiolane probes.

We have revealed features of previous probes and experimental designs which may have been misleadingly interpreted in the field as showing TrxR-selectivity. These include: (1) environment-dependent fluorogenicity of intact probes (Supplementary Note 4); (2) concentration-dependent, strain-promoted, non-reductive oligomerisation of 1,2-dithiolane probes which in the case of **Fast-TRFS** fully unquenches its fluorescent signal upon concentration into lipid membrane environments (Fig. 6 and Supplementary Note 3); (3) thiol-coordinating or thiol-alkylating reagents such as auranofin may suppress cellular signal generation by blocking thiol-mediated, strain-promoted cellular uptake.

Taken together, we conclude that 1,2-dithiolane is an easily and nonspecifically thiol-opened/-reduced motif which is not a TrxR-selective substrate in cells; and that 1,2-dithiolane-based probes are not selective TrxR reporters in cellular settings.

We note however, that there may be immediate rewards if the growing literature of 1,2-dithiolane-based probes is re-evaluated⁵³. This would (i) maintain a clear literature; (ii) avoid that nonspecific electrophilic pan-assay interference compounds which suppress dithiolane probe signal by blocking thiol-mediated uptake are falsely identified as TrxR-substrate hits (PAINS: see Supplementary Note 1); and could perhaps (iii) allow 1,2-dithiolane-derived prodrugs instead to find uses as modular systems for thiol-mediated cellular uptake and activation, impacting research in cell penetration and assisted uptake (discussion in Supplementary Note 2).

Diversifying trigger structures to reach redox substrates that are selective for key oxidoreductases remains a central goal for

research in the field. By identifying and avoiding problematic and nonselective substrate types such as 1,2-dithiolane, chemical development may instead be oriented towards selective and robust redox chemotypes for bioreductive probe and prodrug research. Indeed, novel reducible motifs with chemotype-based selectivity, as in the recent Trx-selective **SS60-PQ**⁹ and the TrxR-reporting probe **RX1**⁶⁸, are just now emerging. The modular reduction-triggered phenolic carbamate system we developed for this work already ensures valuable performance in biology, through its zero signal background, excellent hydrolytic robustness, and retained cell-marking signal, which combine to offer high-spatial-resolution imaging and cell-resolved statistics (Fig. 4). As selective reduction-sensing units for e.g. for GR, TrxR or Trx are identified, installing them as trigger motifs in this modular system would retain these beneficial features: giving powerful and useful probes for redox biology that can at last allow researchers to unveil the dynamics of these major dithiol/disulfide-type enzyme systems within cells. Such probes are already being reported and further developments will be communicated in due course.

Methods

For detailed experimental protocols and further information on all 'Methods', see Supplementary Information.

Probe synthesis and characterisation. Reactions and characterisations were performed by default with non-degassed solvents, reagents and building blocks, that were purchased from standard commercial sources. Anhydrous solvents obtained in septum-capped bottles and analytical grade or higher quality solvents were used without purification. Industrial grade solvents were distilled prior to use. Unless otherwise stated, reactions were performed at room temperature without precautions regarding air or moisture and were stirred using magnetic Teflon®-coated stir bars. Air or moisture sensitive reactions were conducted in dry Schlenk glassware. Flash column chromatography was performed on Geduran® Si 60 silica gel from Merck GmbH, Darmstadt (Germany) or using a Biotage® Select automated column chromatography system with manufacturer's cartridges from Biotage GmbH, Uppsala (Sweden). Thin layer chromatography to monitor reactions and determine R_f-values was performed on silica coated aluminium sheets with fluorescent indicator (TLC Si 60 F254 from Merck GmbH, Darmstadt, Germany) with visualisation by UV irradiation (254 nm/360 nm) or staining with KMnO₄ solution (3.0 g KMnO₄, 20 g K₂CO₃, 0.30 g KOH, 0.30 L H₂O).

General fluorescence assay methods. Fluorescence readout of cell-free activity and/or cell assays was performed either using a FluoStar Omega plate reader from BMG Labtech, Ortenburg (Germany) (ex/em 355bp/520lp or 440bp/520lp) using Omega Software version 5.50 R3 from BMG Labtech, Ortenburg (Germany) or a Tecan Infinite M200 plate reader with integrated software from Tecan, Maennedorf (Switzerland) (ex/em 355bp/520lp or 440bp/520lp) recording fluorescence intensity. Reduction-mediated activation of **SS50-PQ** releases the water-insoluble dye **PQ-OH**_(s) with precipitation-based induction of ESIP_T-based fluorescence (typically monitored with ex/em 355bp/520lp). Reduction-mediated activation of **TRFS-green** releases 1-butyl-6-amino-naphthalimide (typically monitored with ex/em 445bp/520lp). For **TRFS-green**, subtraction of background fluorescence was conducted as indicated in the Supplementary Information. We noted that upon standing, dithiolane probe stocks showed decreasing capacity to generate fluorescence in reductant assays. Consequently, stocks were prepared freshly for all assays. All reactions were incubated at 37 °C and 100% humidity. Timecourse measurements were conducted to determine kinetics of reduction-mediated release. Data were typically interpreted by normalising the absolute, time-dependent fluorescence intensity F(t) to the peak theoretical signal observed in a maximum-fluorescence experiment using 100 μM of TCEP (F_{TCEP}(t)) to remove the influence of cyclisation/release/precipitation kinetics from analysis. For cell-free bioreductant assays, F(t) was pre-corrected by subtracting the absolute time-dependent background fluorescence F_{NADPH}(t) caused by auto-fluorescence of reduced β-NADPH in the assay. Dose–response curves were fitted using GraphPad Prism version 8.0.2. from GraphPad Software, San Diego (USA).

Cell-free chemoreductant assays. In a black 96-well plate with black bottom, 80 μL of a diluted solution (12.5 μM in aq. TE, pH 7.4, 1.25% DMSO) of **SS50-PQ** (final concentration 10 μM) was mixed with a solution of selected chemical reductants (20 μL of a solution (50 μM to 50 mM in aq. TE, pH 7.4). Reductants used include tris(carboxyethyl)phosphine (TCEP) at 100 μM final concentration, and dithiothreitol (reduced, DTT), glutathione (reduced, GSH), glutathione disulfide (oxidized, GSSG), cysteine (Cys), serine (Ser), mercaptoethyl-dimethylamine

(MEDA), cysteamine (CA) and N-acetylcysteine (NAC) all at 1 mM final concentration for single-concentration profiling; or e.g. 10 μ M, 30 μ M, 100 μ M, 300 μ M, 1 mM, 3 mM and 10 mM reductant for dose-response characterisation.

Cell-free inhibition experiments. 80 μ L of a diluted solution (62.5 μ M in aq. TE, pH 7.4, 1.25% DMSO) of **SS50-PQ** (final concentration 25 μ M or 50 μ M as indicated) was pre-treated with 2-((4-chlorophenyl)sulfonyl)-6-methoxy-3-nitropyridine (TRi-1), 4,5-dichloro-2-((5-(4-chlorophenyl)-1,3,4-oxadiazol-2-yl)methyl)pyridazin-3(2H)-one (TRi-3)⁷⁹ (from DMSO stock solutions) or aurano-fin (AF) (from ethanol stock solutions) with final inhibitor concentrations from 0.1 μ M to 4.5 μ M.

Cell-free bioreductant assays. In a black 96-well plate with black bottom, 50 μ L of a diluted solution (20 μ M in aq. TE, pH 7.4, 2% DMSO) of **SS50-PQ** or **TRFS-green** (final concentration 10 μ M) was mixed with 40 μ L of the selected oxidoreductase (TrxR1, TrxR2, GR to reach final concentrations of 20 nM) and/or its native substrate (Trx1, Trx2, TRP14, Grx1, Grx2 to reach final concentrations of 10 nM to 10 μ M respectively), including 100 μ M final concentration of GSH for the GR-GSH-Grx system assays. The reaction was started by addition of 10 μ L of a solution of β -NADPH (1 mM in aq. TE, pH 7.4, reaching 100 μ M final concentration). Human recombinant thioredoxin (Trx1 and Trx2) (lyophilized), human recombinant glutaredoxin (Grx1 and Grx2) (lyophilized from 10 μ L TE-buffer, pH 7.5), human recombinant thioredoxin-related protein of 14 kDa (TRP14), human thioredoxin reductases (TrxR1 and TrxR2) (1.5 mg/mL in 50% glycerol/TE buffer, pH 7.5) and human recombinant glutathione reductase (GR) (100 μ M in 50% glycerol/TE buffer, pH 7.5) were obtained from IMCO Corp., Stockholm (Sweden) or produced and purified as previously described^{80,81}.

Cell-free environment-dependent polymerisation assay. Commercial α -lecithin (CAS 8002-43-5, Sigma-Aldrich P5638) was hydrated with ultrapure water (Milli-Q, Reptile Bioscience Ltd., Boston, MA) to a final concentration of 9 mg/mL. The suspension was gently vortexed to achieve a homogeneous phase, which was then subjected to one freeze/thaw cycle. The stock solution was extruded 21 times through a polycarbonate membrane with a pore diameter of 400 nm, using a Mini Extruder (Avanti Polar Lipids, Inc., Alabama, United States) according to Fromherz et al.⁷⁷. The vesicle stock was then diluted to the indicated concentrations and treated with DMSO stock solutions of **Fast-TRFS** and **Linear-TRFS** to final probe concentrations of 10 μ M or 100 μ M with maximum 1% DMSO. 1-octadecanethiol (RSH) was optionally spiked at catalytic (0.05 eq) or excess (1.5 eq vs. probe concentration) amounts. Fluorescence intensity (355bp10/460bp20) was recorded over time and compared to an untreated reference experiment (vesicle scattering background). The potential for further fluorescence increase mediated by reduction of intact monomolecular dithiolane was tested by subsequent treatment of the system with excess TCEP (0.1 mM, i.e. 1-10 eq).

General cell culture. Cells were grown at 37 °C under 5% CO₂ atmosphere and cell growth was confirmed using a Nikon Eclipse Ti microscope (Nikon Corp., Minato (Japan)). HeLa (DSMZ; ACC57), A549 (DSMZ; ACC107) and Jurkat (ATCC; TIB-152) cell lines were purchased from the German Collection of Microorganisms and Cell Cultures. Parent ("fl/fl"), TrxR1 knockout ("^{-/-}", ko) and Sec-TrxR1 reconstituted ("2ATG") mouse embryonic fibroblasts (MEF) were a kind gift from Marcus Conrad (ko; MEFs isolated from conditional TrxR1 knockout mouse embryos were immortalized by lentiviral transduction. In vitro deletion of TrxR1 was achieved by Tat-Cre induced recombination and verified by PCR and Immunoblotting for TrxR1⁷⁰. 2ATG: lentiviral transgenic stable expression of Tmxr4^{4985Sec} on the ko line⁷¹). All cell lines are tested regularly for mycoplasma contamination and only mycoplasma negative cells are used in assays. HeLa, A549 or MEF cells were grown in Dulbecco's modified Eagle's medium (DMEM: glucose (4.5 g/L), glutamine, pyruvate, phenol red, NaHCO₃ (2.7 g/L); PAN Biotech, Aidenbach (Germany)). Jurkat cells were grown in RPMI-1640 medium (glutamine, sodium bicarbonate; Merck KGaA, Darmstadt (Germany)). Media were supplemented with 10% heat-inactivated fetal bovine serum, penicillin (100 U/mL), streptomycin (100 μ g/mL) and optionally with Na₂SeO₃ (0–100 nM) or Na₃PO₄S (0–1.2 mM). PBS Dulbecco buffer (Merck GmbH, Darmstadt (Germany)) was used for washing and resuspending steps; TrypLETM Express (gibco Life Technologies Inc., Massachusetts (USA)) was used for trypsinisation.

Cellular activation/inhibition assays. Cells were seeded in 96-well plates (F-Bottom, black, Fluotrack, high binding; Greiner bio-one GmbH, Kremstünster (Austria)) in 100 μ L medium. Medium was treated with **SS50-PQ**, **TRFS-green**, **SS00-PQ**⁹ or **RX1**⁶⁸ (from stock solutions in 100% DMSO) to reach final concentrations of 1 μ M to 100 μ M at maximum final levels of 1% DMSO. For inhibition experiments, cells were pre-treated with TrxR inhibitors TRi-1 and TRi-3⁷⁹ (from DMSO stock solutions) and AF (from ethanolic stock solution), 2 h, 3 h or 15 h before probe treatment. Treated cell plates were incubated at 37 °C under 5% CO₂ atmosphere. Kinetics of cellular processing were determined by timecourse fluorescence measurements, performed as in the cell-free assays, with optional background-corrected fluorescence intensity $F(t) - F_{\text{Background}}(t)$ where indicated, as needed.

Fluorescence microscopy. Intracellular PQ-OH_(s) precipitation was confirmed using a Nikon Eclipse Ti2 upright microscope from Nikon Instruments Europe BV, Amsterdam (Netherlands) (ex/em 355bp50/410lp; or transmitted light, as appropriate). Images were processed using Fiji version 1.51 (ImageJ). Confocal time lapse microscopy was performed on live HeLa cells seeded in 8-well slides (ibiTreat μ ibidi slides, ibidi GmbH, Martinsried (Germany)). Slides were placed on the motorized stage of a Leica SP8 laser-scanning confocal microscope (Wetzlar, Germany), treated with **SS50-PQ** at 50 μ M on the stage and immediately imaged for one hour with ex/em 405laser/530bp20, collecting fluorescence and brightfield images.

Flow cytometry-based single-cell statistics. After treatment, cells were harvested and stained with a fixable viability dye according to the manufacturer's recommendations (zombie NIR™ Fixable Viability Kit, BioLegend). Cells were fixed in 4% paraformaldehyde (PFA) in PBS for 30 min and either stored in PBS or immediately resuspended in a wash buffer containing PBS with 1% bovine serum albumin (BSA) and 1 mM EDTA. Flow cytometry was conducted at the BioMedical Centre Core Facility of the LMU Munich on a BD LSRFortessa (BD Bioscience, Heidelberg (Germany)) using the integrated BD FACS Diva software v.8.0.1. The following excitation/detection settings were used: zombie (ex/em 647laser/780bp60) and PQ fluorescence (ex/em 355laser/530bp30). Data were processed using FlowJo v.10.7.1 (BD Biosciences). An unstained sample was used to exclude cell debris and doublets. Zombie dye was used to exclude dead cells. PQ-positive gate was set so that 0% of cells were PQ-positive in an unstained sample. Cell debris, singlets, Zombie and PQ gates were set on an appropriate sample in each experiment and applied to all samples. Gating strategy is shown in Supplementary Fig. 6.

In vivo activation experiments. *Danio rerio* embryos (8 hpf or 3 dpf, sex undetermined) were housed in groups of 20–40 individuals in a fish facility (Aquaneering) maintaining approx. 700 mS, pH 6.9–7.1 and 28 °C with a 14/10 h light/dark cycle as outlined by common zebrafish handling guidelines. All experiments used fertilized eggs from *ab* wild-type parents, grown in 30% Danieau medium (0.12 mM MgSO₄, 0.21 mM KCl, 0.18 mM Ca(NO₃)₂, 17.4 mM NaCl, 1.5 mM HEPES, pH 7.2) at 28 °C with a 14/10 h light/dark cycle. Where reported, to suppress melanin pigmentation, 150 μ M phenylthiourea (PTU) was added to the 30% Danieau medium at 8–10 hpf. All procedures involving animals were carried out according to EU guidelines and German legislation (EU Directive 2010_63, licence number AZ 325.1.53/56.1-TU-BS). As all zebrafish embryos in this study were analysed at ages below 5 dpf, no approval by an ethics board was required. The study adhered to ARRIVE guidelines. **SS50-PQ** stocks (10 mM in DMSO) were warmed to 37 °C before use. 5 μ M, 15 μ M and 45 μ M dilutions were freshly prepared in 30% Danieau supplemented with DMSO to 1% (final concentration). At 8 hpf or 3 dpf, embryos were transferred to each well of a 6 well plate, and the 30% Danieau medium exchanged for the test dilutions (5 mL per well). Embryos were incubated at 28 °C until the formation of solid green-fluorescent particles was observed. Signal development was initially monitored on a stereofluorescence microscope (Leica M205FA or MDG41, from Leica Microsystems, Wetzlar, Germany) equipped with a UV filter (ex/em 360bp40/420lp) and acquired using Las X software v. 5.0.3. (Leica Microsystems, Wetzlar (Germany)). Then, for confocal imaging, the embryos were embedded in lateral position in 1.2% ultra-low gelling agarose (type IX-A), overlaid with the test solution. The embryos were transferred to a Zeiss Airyscan confocal microscope (Carl Zeiss, Jena (Germany)), with a Life Imaging Services heating chamber set to 28 °C. Whole embryos were recorded using a \times 10 objective and the 405 nm diode for excitation, with image acquisition controlled by Zen Black software v.2.5. (Carl Zeiss, Jena (Germany)), and subsequent tile/grid stitching in Fiji version 1.51 (ImageJ).

Statistics. Sample size and a description of the statistical parameters including central tendency, variation or estimates of uncertainty is provided in Figure legends. Representative experiments are shown where appropriate and indicated accordingly.

Reporting summary. Further information on research design is available in the Nature Research Reporting Summary linked to this article.

Data availability

All data generated or analysed during this study are included in this article and its Supplementary Information files, including the Source Data file (raw data for Figs. 3–6 and Supplementary Figs. 3–16). These and all data of this study can also be obtained from the authors upon request. None of these datasets are resources of public interest and therefore are not archived publicly in other forms. Source data are provided with this paper.

Received: 12 January 2021; Accepted: 1 March 2022;
Published online: 01 April 2022

References

1. Arnér, E. S. J. & Holmgren, A. Physiological functions of thioredoxin and thioredoxin reductase. *Eur. J. Biochem.* **267**, 6102–6109 (2000).
2. Jones, D. P. & Sies, H. The redox code. *Antioxid. Redox Signal.* **23**, 734–746 (2015).
3. Turanov, A. A. et al. Mammalian thioredoxin reductase 1: roles in redox homeostasis and characterization of cellular targets. *Biochemical J.* **430**, 285–293 (2010).
4. Arnér, E. S. J. & Holmgren, A. The thioredoxin system in cancer. *Semin. Cancer Biol.* **16**, 420–426 (2006).
5. Arnér, E. S. J. in *Oxidative Stress* 639–667 (Elsevier, 2020).
6. Hanson, G. T. et al. Investigating mitochondrial redox potential with redox-sensitive green fluorescent protein indicators*. *J. Biol. Chem.* **279**, 13044–13053 (2004).
7. Schwarzländer, M., Dick, T. P., Meyer, A. J. & Morgan, B. Dissecting redox biology using fluorescent protein sensors. *Antioxid. Redox Signal.* **24**, 680–712 (2016).
8. Lee, M. H. et al. Disulfide-cleavage-triggered chemosensors and their biological applications. *Chem. Rev.* **113**, 5071–5109 (2013).
9. Felber, J. G. et al. Selective, modular probes for thioredoxins enabled by rational tuning of a unique disulfide structure motif. *J. Am. Chem. Soc.* **143**, 8791–8803 (2021).
10. Welch, T. R. & Williams, R. M. Epidithiodioxopiperazines: occurrence, synthesis and biogenesis. *Nat. Prod. Rep.* **31**, 1376–1404 (2014).
11. Takahashi, M. et al. Inhibition of histone H3K9 methyltransferases by gliotoxin and related epipolythiodioxopiperazines. *J. Antibiotics* **65**, 263–265 (2012).
12. Zong, L. et al. Epidithiodiketopiperazines: strain-promoted thiol-mediated cellular uptake at the highest tension. *ACS Cent. Sci.* **3**, 449–453 (2017).
13. Cherblanc, F. L., Chapman, K. L., Brown, R. & Fuchter, M. J. Chaetocin is a nonspecific inhibitor of histone lysine methyltransferases. *Nat. Chem. Biol.* **9**, 136–137 (2013).
14. Appleton, D. R. & Copp, B. R. Kottamide E, the first example of a natural product bearing the amino acid 4-amino-1,2-dithiolane-4-carboxylic acid (Adt). *Tetrahedron Lett.* **44**, 8963–8965 (2003).
15. Kato, A., Okada, M. & Hashimoto, Y. Occurrence of gerrardine in cassipourea guianensis. *J. Nat. Prod.* **47**, 706–707 (1984).
16. Zhang, L. et al. Highly selective off-on fluorescent probe for imaging thioredoxin reductase in living cells. *J. Am. Chem. Soc.* **136**, 226–233 (2014).
17. Li, X. et al. Selective activation of a prodrug by thioredoxin reductase providing a strategy to target cancer cells. *Angew. Chem. Int. Ed.* **57**, 6141–6145 (2018).
18. Li, X. et al. A fast and specific fluorescent probe for thioredoxin reductase that works via disulfide bond cleavage. *Nat. Commun.* **10**, 1–12 (2019).
19. Lothrop, A. P., Ruggles, E. L. & Hondal, R. J. No selenium required: reactions catalyzed by mammalian thioredoxin reductase that are independent of a selenocysteine residue. *Biochemistry* **48**, 6213–6223 (2009).
20. Lüttringhaus, A. & Brechlin, A. Cyclische disulfide, III. cis- und trans-2,3-dithia-decalin. *Chem. Ber.* **92**, 2271–2277 (1959).
21. Fava, A., Ilceto, A. & Camera, E. Kinetics of the thiol-disulfide exchange. *J. Am. Chem. Soc.* **79**, 833–838 (1957).
22. Creighton, T. E. Interactions between cysteine residues as probes of protein conformation: The disulfide bond between Cys-14 and Cys-38 of the pancreatic trypsin inhibitor. *J. Mol. Biol.* **96**, 767–776 (1975).
23. Singh, R. & Whitesides, G. M. Degenerate intermolecular thiolate-disulfide interchange involving cyclic five-membered disulfides is faster by approximately 103 than that involving six- or seven-membered disulfides. *J. Am. Chem. Soc.* **112**, 6304–6309 (1990).
24. Singh, R. & Whitesides, G. M. in *Sulphur-Containing Functional Groups* 633–658, <http://doi.wiley.com/10.1002/9780470034408.ch13> (Wiley, 1993).
25. Burns, J. A. & Whitesides, G. M. Predicting the stability of cyclic disulfides by molecular modeling: effective concentrations in thiol-disulfide interchange and the design of strongly reducing dithiols. *J. Am. Chem. Soc.* **112**, 6296–6303 (1990).
26. Laurent, Q., Sakai, N. & Matile, S. The opening of 1,2-dithiolanes and 1,2-diselenolanes: regioselectivity, rearrangements, and consequences for poly(disulfide)s, cellular uptake and pyruvate dehydrogenase complexes. *Helvetica Chim. Acta* **102**, e1800209 (2019).
27. Sakai, N. et al. Self-organizing surface-initiated polymerization: facile access to complex functional systems. *J. Am. Chem. Soc.* **133**, 15224–15227 (2011).
28. Laurent, Q. et al. Thiol-mediated uptake. *JACS Au* **1**, 710–728 (2021).
29. Abegg, D. et al. Strained cyclic disulfides enable cellular uptake by reacting with the transferrin receptor. *J. Am. Chem. Soc.* **139**, 231–238 (2017).
30. Gasparini, G., Sargsyan, G., Bang, E.-K., Sakai, N. & Matile, S. Ring tension applied to thiol-mediated cellular uptake. *Angew. Chem. Int. Ed.* **54**, 7328–7331 (2015).
31. Chuard, N. et al. Strain-promoted thiol-mediated cellular uptake of giant substrates: liposomes and polymersomes. *Angew. Chem. Int. Ed.* **56**, 2947–2950 (2017).
32. Carmine, A., Domoto, Y., Sakai, N. & Matile, S. Comparison of lipoic and asparagusic acid for surface-initiated disulfide-exchange polymerization. *Chem. Eur. J.* **19**, 11558–11563 (2013).
33. Chuard, N. et al. Diselenolane-mediated cellular uptake. *Chem. Sci.* **9**, 1860–1866 (2018).
34. Schneider, A. F. L., Kithil, M., Cardoso, M. C., Lehmann, M. & Hackenberger, C. P. R. Cellular uptake of large biomolecules enabled by cell-surface-reactive cell-penetrating peptide additives. *Nat. Chem.* **13**, 530–539 (2021).
35. Li, T. et al. Biscysteine-bearing peptide probes to reveal extracellular thiol–disulfide exchange reactions promoting cellular uptake. *Anal. Chem.* **89**, 8501–8508 (2017).
36. Cheng, Y. et al. Inhibitors of thiol-mediated uptake. *Chem. Sci.* <https://doi.org/10.1039/D0SC05447J> (2021).
37. Lim, B. et al. Inhibition of thiol-mediated uptake with irreversible covalent inhibitors. *Helvetica Chim. Acta* **104**, e2100085 (2021).
38. Gao, W., Li, T., Wang, J., Zhao, Y. & Wu, C. Thioether-bonded fluorescent probes for deciphering thiol-mediated exchange reactions on the cell surface. *Anal. Chem.* **89**, 937–944 (2017).
39. Kosower, N. S., Kosower, E. M., Zipser, Y., Faltin, Z. & Shomrat, R. Dynamic changes of red cell membrane thiol groups followed by bimane fluorescent labeling. *Biochim. Biophys. Acta* **640**, 748–759 (1981).
40. Torres, A. G. & Gait, M. J. Exploiting cell surface thiols to enhance cellular uptake. *Trends Biotechnol.* **30**, 185–190 (2012).
41. Xu, X., Chiu, J., Chen, S. & Fang, C. Pathophysiological roles of cell surface and extracellular protein disulfide isomerase and their molecular mechanisms. *Br. J. Pharm.* **178**, 2911–2930 (2021).
42. Mukherjee, T., Kanvah, S., Klymchenko, A. S. & Collot, M. Probing variations of reduction activity at the plasma membrane using a targeted ratiometric FRET probe. *ACS Appl. Mater. Interfaces* **13**, 40315–40324 (2021).
43. Barcan, G. A., Zhang, X. & Waymouth, R. M. Structurally dynamic hydrogels derived from 1,2-Dithiolanes. *J. Am. Chem. Soc.* **137**, 5650–5653 (2015).
44. Scheutz, G. M. et al. Harnessing strained disulfides for photocurable adaptable hydrogels. *Macromolecules* **53**, 4038–4046 (2020).
45. Ma, H., Zhang, J., Zhang, Z., Liu, Y. & Fang, J. A fast response and red emission probe for mammalian thioredoxin reductase. *Chem. Commun.* **52**, 12060–12063 (2016).
46. Zhao, J. et al. Loss of thioredoxin reductase function in a mouse stroke model disclosed by a two-photon fluorescent probe. *Chem. Commun.* **56**, 14075–14078 (2020).
47. Zhang, J., Li, X., Han, X., Liu, R. & Fang, J. Targeting the thioredoxin system for cancer therapy. *Trends Pharmacol. Sci.* **38**, 794–808 (2017).
48. Zhang, B., Liu, Y., Li, X., Xu, J. & Fang, J. Small molecules to target the selenoprotein thioredoxin reductase. *Chem. Asian J.* **13**, 3593–3600 (2018).
49. Zhang, J. et al. Small molecule inhibitors of mammalian thioredoxin reductase as potential anticancer agents: an update. *Medicinal Res. Rev.* **39**, 5–39 (2019).
50. Zhang, J., Duan, D., Osama, A. & Fang, J. Natural molecules targeting thioredoxin system and their therapeutic potentials. *Antioxid. Redox Signal.* <https://doi.org/10.1089/ars.2020.8213> (2020).
51. Zhang, B. et al. Thioredoxin reductase inhibitors: a patent review. *Expert Opin. Therapeutic Pat.* **27**, 547–556 (2017).
52. Liu, Y. et al. A small molecule probe reveals declined mitochondrial thioredoxin reductase activity in a Parkinson’s disease model. *Chem. Commun.* **52**, 2296–2299 (2016).
53. Zhao, Y. et al. A fluorescent probe to detect quick disulfide reductase activity in bacteria. *Antioxidants* **11**, 377 <https://doi.org/10.3390/antiox11020377> (2022).
54. Hong, K.-H., Kim, D. I., Kwon, H. & Kim, H.-J. A fluoresceinylcarbonate-based fluorescent probe for the sensitive detection of biothiols in a HEPES buffer and its cellular expression. *RSC Adv.* **4**, 978–982 (2014).
55. Lim, C. S. et al. Ratiometric detection of mitochondrial thiols with a two-photon fluorescent probe. *J. Am. Chem. Soc.* **133**, 11132–11135 (2011).
56. Vrudhula, V. M., MacMaster, J. F., Li, Z., Kerr, D. E. & Senter, P. D. Reductively activated disulfide prodrugs of paclitaxel. *Bioorg. Med. Chem. Lett.* **12**, 3591–3594 (2002).
57. Henne, W. A., Doorneweerd, D. D., Hilgenbrink, A. R., Kularatne, S. A. & Low, P. S. Synthesis and activity of a folate peptide camptothecin prodrug. *Bioorg. Med. Chem. Lett.* **16**, 5350–5355 (2006).
58. Lee, S. H. & Kohn, H. Cyclic disulfide C(8) iminoporphyrin: nucleophilic activation of a porphyrin. *J. Am. Chem. Soc.* **126**, 4281–4292 (2004).
59. Ghosh, A. K. & Brindisi, M. Organic carbamates in drug design and medicinal chemistry. *J. Medicinal Chem.* **58**, 2895–2940 (2015).
60. Vacondio, F., Silva, C., Mor, M. & Testa, B. Qualitative structure-metabolism relationships in the hydrolysis of carbamates. *Drug Metab. Rev.* **42**, 551–589 (2010).

61. Machida, T., Dutt, S. & Winssinger, N. Allosterically regulated phosphatase activity from peptide-PNA conjugates folded through hybridization. *Angew. Chem. Int. Ed.* **55**, 8595–8598 (2016).
62. Rando, G., Winssinger, N. & Lindberg, E. & Anzola, M. New compounds and uses thereof for detection of target molecules in a sample. <https://patents.google.com/patent/US20190315713A1/en> (US 2019/0315713 A1).
63. Lukesh, J. C., Palte, M. J. & Raines, R. T. A potent, versatile disulfide-reducing agent from aspartic acid. *J. Am. Chem. Soc.* **134**, 4057–4059 (2012).
64. Wu, G., Fang, Y.-Z., Yang, S., Lupton, J. R. & Turner, N. D. Glutathione metabolism and its implications for health. *J. Nutr.* **134**, 489–492 (2004).
65. Griffith, O. W. Biologic and pharmacologic regulation of mammalian glutathione synthesis. *Free Radic. Biol. Med.* **27**, 922–935 (1999).
66. Jones, D. P. in *Methods in Enzymology* (eds. Sies, H. & Packer, L.) Vol. 348, 93–112, [https://doi.org/10.1016/S0076-6879\(02\)48630-2](https://doi.org/10.1016/S0076-6879(02)48630-2) (Academic Press, 2002).
67. Fridovich, I. Antioxidant Enzymes. in *Redox Biochemistry* 49–134 (Wiley, 2007). <https://doi.org/10.1002/9780470177334.ch3>.
68. Zeisel, L. *et al.* Selective cellular probes for mammalian thioredoxin reductase TrxR1: rational design of RX1, a modular 1,2-thiaselenane redox probe. *Chem*, in press: <https://doi.org/10.1016/j.chempr.2022.03.010> (2022).
69. Peng, X., Xu, J. & Arner, E. S. J. Thiophosphate and selenite conversely modulate cell death induced by glutathione depletion or cisplatin: effects related to activity and Sec contents of thioredoxin reductase. *Biochem. J.* **447**, 167–174 (2012).
70. Mandal, P. K. *et al.* Loss of thioredoxin reductase 1 renders tumors highly susceptible to pharmacologic glutathione deprivation. *Cancer Res.* **70**, 9505–9514 (2010).
71. Mandal, P. K. Complex Redundancy between the Mammalian Thioredoxin and Glutathione Systems in Cell Proliferation and Tumorigenesis, https://edoc.ub.uni-muenchen.de/11958/1/Mandal_Pankaj_Kumar.pdf (Ludwig-Maximilian-University Munich, 2009).
72. Stafford, W. C. *et al.* Irreversible inhibition of cytosolic thioredoxin reductase 1 as a mechanistic basis for anticancer therapy. *Sci. Transl. Med.* **10**, eaaf7444 (2018).
73. Cassini, A. & Messori, L. Molecular mechanisms and proposed targets for selected anticancer gold compounds. *Curr. Top. Med. Chem.* **11**, 2647–2660 (2011).
74. Saei, A. A. *et al.* Comprehensive chemical proteomics for target deconvolution of the redox active drug auranofin. *Redox Biol.* **32**, 101491 (2020).
75. Snyder, R. M., Mirabelli, C. K. & Crooke, S. T. Cellular interactions of auranofin and a related gold complex with raw 264.7 macrophages. *Biochem. Pharmacol.* **36**, 647–654 (1987).
76. Gasparini, G., Bang, E.-K., Montenegro, J. & Matile, S. Cellular uptake: lessons from supramolecular organic chemistry. *Chem. Commun.* **51**, 10389–10402 (2015).
77. Fromherz, P. & Ruppel, D. Lipid vesicle formation: the transition from open disks to closed shells. *FEBS Lett.* **179**, 155–159 (1985).
78. Blaschke, B. M., Böhm, P., Drieschner, S., Nickel, B. & Garrido, J. A. Lipid monolayer formation and lipid exchange monitored by a graphene field-effect transistor. *Langmuir* **34**, 4224–4233 (2018).
79. Busker, S. *et al.* Irreversible TrxR1 inhibitors block STAT3 activity and induce cancer cell death. *Sci. Adv.* **6**, eaax7945 (2020).
80. Dóka, É. *et al.* A novel persulfide detection method reveals protein persulfide- and polysulfide-reducing functions of thioredoxin and glutathione systems. *Sci. Adv.* **2**, e1500968 (2016).
81. Pader, I. *et al.* Thioredoxin-related protein of 14 kDa is an efficient L-cystine reductase and S-denitrosylase. *Proc. Natl Acad. Sci. USA* **111**, 6964–6969 (2014).

Acknowledgements

This research was supported by funds from the German Research Foundation (DFG: SFB 1032 project B09 number 201269156, SFB TRR 152 project P24 number 239283807, SPP 1926 project number 426018126, and Emmy Noether grant 400324123 to O.T.-S.; SPP 1710 project BE 1540/23-2 to K.B. (now transferred to Stefan Rahlfs)); LMUExcellent (Junior Researcher Fund to O.T.-S.); the Munich Centre for NanoScience initiative

(CeNS, to O.T.-S.); and from Karolinska Institutet, The Knut and Alice Wallenberg Foundations, The Swedish Cancer Society, The Swedish Research Council and the Hungarian Thematic Excellence Programme (TKP2020-NKA-26) to E.S.J.A. J.G.F. thanks the Studienstiftung des deutschen Volkes for support through a PhD scholarship; L.Z. thanks the Fonds der Chemischen Industrie for support through a PhD scholarship; L.P. thanks the GRK 2338 for support through a PhD scholarship; J.T.-S. thanks the Joachim Herz Foundation for fellowship support. We thank Martina Ober (LMU) for extensive help preparing vesicles; Marcus Conrad (Helmholtz Centre, Munich) for MEF and knockout MEF cell lines; Hartmann Harz and Christoph Jung (LMU microscopy platforms) for assistance with microscopy facilities; and Matt Fuchter (ICL), Kate Carroll (Scripps), Rob Hondal (UVM), Stefan Matile (Uni Geneva), and the attendees of the SPP 1710 Thiol-Based Redox Switches conferences in 2019 and 2021 for their supportive and collegial discussions.

Author contributions

J.G.F. performed synthesis, chemical analysis, chemoreductant and enzymatic cell-free studies, cellular studies, and coordinated data assembly. L.P. and K.C.S. performed enzymatic specificity screenings, cellular inhibitor studies and FACS-based single-cell statistics. S.B. and C.B. performed enzymatic specificity screenings. U.T. performed zebrafish embryo studies. L.Z. and M.S.M. performed synthesis and analysis. K.B. and E.S.J.A. supervised enzymatic specificity screenings. J.T.-S. performed cellular studies, supervised cell biology and coordinated data assembly. O.T.-S. designed the concept and experiments, supervised all other experiments, coordinated data assembly and wrote the manuscript, with input from all co-authors.

Funding

Open Access funding enabled and organized by Projekt DEAL.

Competing interests

J.G.F., L.Z., and O.T.-S. are inventors on patent application EP21167187.0 filed by the LMU Munich in 2021 covering the structure of compound **RX1** which is used as a control in this paper. All authors declare no other competing interests.

Additional information

Supplementary information The online version contains supplementary material available at <https://doi.org/10.1038/s41467-022-29136-4>.

Correspondence and requests for materials should be addressed to Oliver Thorn-Seshold.

Peer review information *Nature Communications* thanks Kate Carroll and the other, anonymous, reviewer(s) for their contribution to the peer review of this work. Peer reviewer reports are available.

Reprints and permission information is available at <http://www.nature.com/reprints>

Publisher's note Springer Nature remains neutral with regard to jurisdictional claims in published maps and institutional affiliations.



Open Access This article is licensed under a Creative Commons Attribution 4.0 International License, which permits use, sharing, adaptation, distribution and reproduction in any medium or format, as long as you give appropriate credit to the original author(s) and the source, provide a link to the Creative Commons license, and indicate if changes were made. The images or other third party material in this article are included in the article's Creative Commons license, unless indicated otherwise in a credit line to the material. If material is not included in the article's Creative Commons license and your intended use is not permitted by statutory regulation or exceeds the permitted use, you will need to obtain permission directly from the copyright holder. To view a copy of this license, visit <http://creativecommons.org/licenses/by/4.0/>.

© The Author(s) 2022

3.1.2 Identification of a Trx-specific chemotype by rational design

This chapter was published as follows:

Journal	Journal of the American Chemical Society 2021 , <i>143</i> , 8791-8803.
Title	<i>Selective, Modular Probes for Thioredoxins enabled by rational Tuning of a Unique Disulfide Structure Motif</i>
Author List	Jan G. Felber [#] , Lukas Zeisel, Lena Poczka, Karoline C. Scholzen, Sander Busker, Martin S. Maier, Ulrike Theisen, Christina Brandstädter, Katja Becker, Elias S. J. Arnér, Julia Thorn-Seshold, Oliver Thorn-Seshold* [#] first author; *corresponding author
Publication date	June 1 st , 2021
Available at	https://pubs.acs.org/doi/10.1021/jacs.1c03234

Author contributions and collaboration

(1) Work performed in the Thorn-Seshold group, LMU Munich:

I developed the synthetic strategies for diastereomerically pure access of piperidine-fused 1,2-dithianes, performed synthesis, chemical and photophysical analysis of the disulfide precursors **SS00**, **SS06**, **SS50**, **SS60**, **SS66C**, **SS66T**, and **SS7** and the disulfide-based fluorogenic probes described in this work (**Fig. 3 and 4**). The evaluation also involved redox potential measurements (**Fig. 5**), chemoreductant (**Fig. 6**), and biochemical studies (**Fig. 7**). I further coordinated data assembly and visualization, conceptually analyzed the scientific outcome, and wrote the manuscript.

Lukas Zeisel performed synthesis and analysis and performed biochemical assays (**Fig. 7**). **Lena Poczka** performed cellular studies (results not contained in the publication). **Martin S. Maier** improved several steps towards the diastereomerically pure syntheses of piperidine-fused 1,2-dithianes and performed synthesis and analysis of the **SS00_M** precursors and **SS60-MR**. **Julia Thorn-Seshold** supervised cellular studies (results not contained in the publication). **Oliver Thorn-Seshold** designed the concept and experiments, coordinated data assembly, and wrote the manuscript.

(2) Collaboration with the Becker group, Justus-Liebig University, Giessen: **Christina Brandstädter** provided human TrxR1 isolated from primary tissues and performed initial enzymatic specificity assays. **Katja Becker** supervised biochemical studies.

(3) Collaboration with the Arnér group, Karolinska Institutet (KI), Stockholm: **Karoline C. Scholzen** performed enzymatic specificity screenings (**Fig. 7**). **Sander Busker** performed initial screenings. **Elias S. J. Arnér** supervised biochemical studies.

(4) Collaboration with the Zoological Institute, TU Braunschweig: **Ulrike Theisen** performed zebrafish embryo studies (results not contained in the publication).

Background

Cyclic disulfides (compared to linear topologies) can be thermodynamically stabilized and offer the potential for kinetic reversibility during thiol-disulfide interchange or reduction. I had established a robust fluorogenic probe design based on the precipitating dye HPQ (**chapter 3.1.1**) and shown that probes based on labile cyclic 5-membered disulfides are non-selectively reduced. However, cyclic 6-membered disulfides are highly stable ring systems with low ring strain and low reduction potentials. Whitesides *et al.* reported reduction properties of a large range of cyclic disulfides and supported that annelation of 1,2-dithianes by a second ring is a valid strategy to further stabilize the ring system since this can give the lowest reduction potential known for any disulfide ($E^\circ < -0.3$ V).¹⁹² We noted that while previous fluorogenic probe designs had failed to selectively target the cell's strongest dithiol reductant Thioredoxin (Trx) ($E^\circ \sim -0.3$ V), they had only used redox sensing units with much higher reduction potentials, such as linear disulfides¹⁷⁴, that were simply processed by weaker but more highly concentrated reductants such as GSH (ca. -0.22 V).

Summary

In this work, we rationalized that the reduction potential of cyclic disulfides is one major determinant of their reducibility by proteins. We analyzed the major redox effector proteins' active site and found that the cell's strongest reductants are proteins with a dithiol-type redox-active site (CXXC motif) (**Fig. 1**, see also **chapter 1.1.3**). We also rationalized that a disulfide's resistance to the cellular *monothiol background*, primarily of GSH, is dictated by its topology: whereas linear disulfides are cleaved irreversibly by a single thiol-disulfide interchange step, cyclic disulfides may rapidly (intramolecularly) expel nucleophiles after a first interchange, and likely require dithiol-type reductants with competitively low reduction potentials to drive full reduction (**Fig. 2**). Therefore, we hypothesized that stable cyclic disulfide triggers might be reducible only by such strongly reducing redox effector proteins.

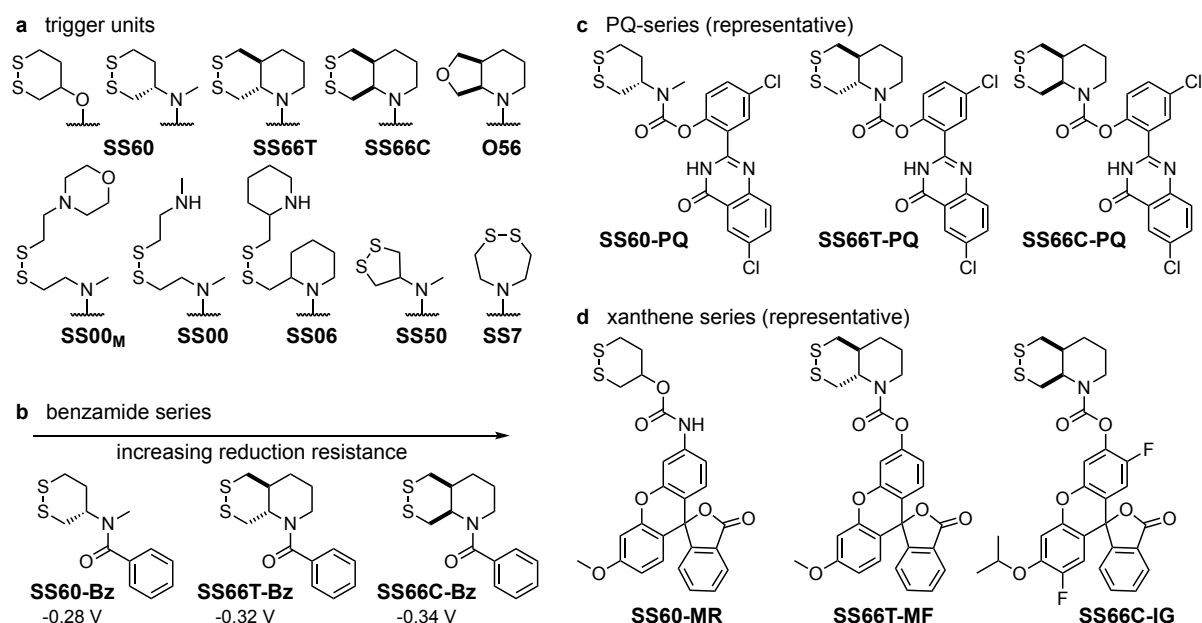


Figure 13 (a) Overview of trigger motifs used in this study. (b) Lowering the reduction potential of 1,2-dithianes by annelation. Representative examples of the (c) PQ-series and (d) xanthene-based series of fluorogenic probes.

To experimentally test these rationales, I built a probe palette based on two novel, annelated cyclic 6-membered disulfide triggers - the *trans*-fused **SS66T** and the *cis*-fused **SS66C** (**Figure 13a**) - for which I developed diastereomerically pure syntheses (**Fig. 4**). I also included cyclic trigger controls (non-annelated **SS60**, and destabilized **SS50** and **SS7**) and topology controls (simple linear **SS00**, preorganized linear **SS06**) to complete the *trigger* palette. Then, following two orthogonal methods to create off-to-on fluorogenic systems (**Figure 13c,d**: precipitating HPQ for H-bond formation or mono-*O*-alkylated xanthenes for $sp^3 \rightarrow sp^2$ transition), I used four different fluorophores as *cargos* to create a series of 20 fluorogenic probes and controls (**Fig. 3**).

Before testing probe kinetics, I investigated the reduction potentials and structures of the novel annelated disulfides using reducible but non-releasing disulfide benzamides. I could verify by equilibration assays that their E° were indeed remarkably low (**SS66T**: -0.32 V, **SS66C**: -0.34 V; **Fig. 5**, **Figure 13b**). Then, when testing our series of fluorogenic probes, I observed that cyclic 6-membered disulfide-based probes gave signal only with strong dithiol-based reductants, such as dithiothreitol (DTT), qualitatively separating them from linear and cyclic 5-membered disulfides, which were labile to monothiol reductants. Despite very different cargo expulsion kinetics between HPQ and the xanthene dyes, consistent kinetic enhancement was observed for annelated trigger units vs. their non-annelated counterparts (**SS66C** vs. **SS60**; **SS06** vs. **SS00**). Surprisingly, the *trans*-fused 1,2-dithiane **SS66T** was labile to reduction by GSH, which we interpreted as a result of unfavoured reversibility (**Fig. 6**).

Finally, I challenged the probes with full oxidoreductase systems. I developed a standardized screening based on a constant supply of NADPH (100 μ M), constant low concentrations of the reductase enzymes (GR and TrxR at 20 nM), with the redox cofactor GSH at 100 μ M only for the GR/GSH/Grx system and titration orders of magnitude in the concentration of the redox effector proteins Trx, Grx and TRP14 (from 10 nM to 10 μ M). These experiments showed that probes based on **SS66C** and **SS60** were reduced primarily by Trxs, much more than by their protein cousins Grx and TRP14, and in contrast to the linear and cyclic 5-membered disulfide probes that are non-specifically reduced by all reductants independent of their appended reporter dyes. By titrating the redox effector proteins, I was also able to quantitatively compare their dose-response characteristics and finally separate *trigger*- from *cargo*-dependent reactivity features (**Fig. 7**).

In this study, I thus verified our fundamental rationale of matching chemocompatible, artificial cyclic disulfide substrates to cellular oxidoreductases based on their thermodynamic stability and kinetic reversibility. I identified piperidine-fused 1,2-dithianes as the first motif to selectively target Trx, the cell's strongest reductant, and validated its properties using two orthogonal fluorogenic systems.

Covert Art graphic

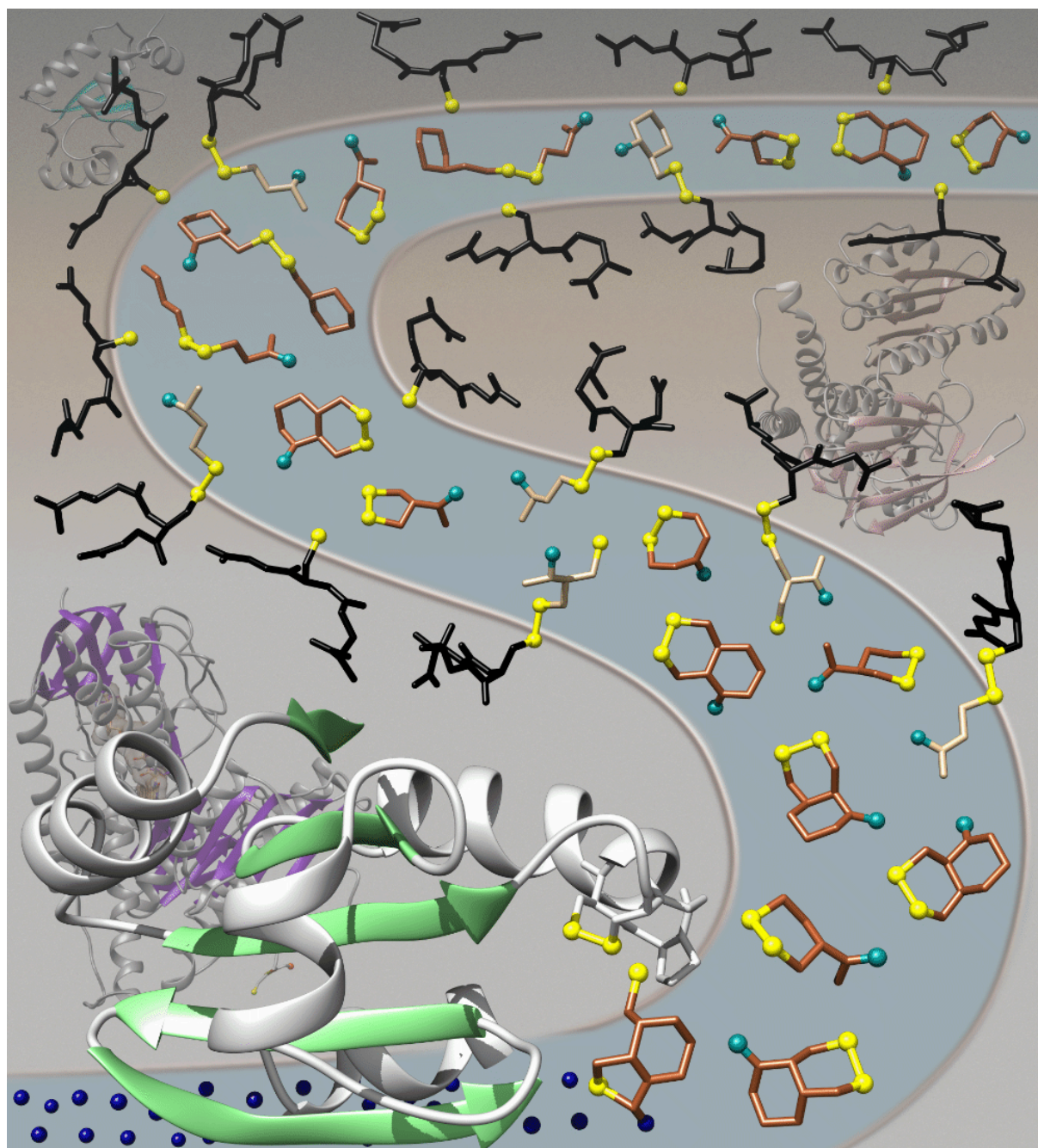


Figure 14 Graphical representation of the scientific outcome of this study. This graphic was created as a potential Cover Art graphic for publication in *the Journal of American Chemical Society* and was not published with the original article. It shows *trigger-cargo* constructs (in brown/yellow) with various disulfide-based reducible motifs carrying molecular cargos on their way toward their cellular targets. Linear or cyclic 5-membered disulfide constructs get “fished” out by the monothiol gatekeeper GSH (in black), and only constructs based on cyclic 6-membered disulfides reach their cellular target, the redox effector protein Thioredoxin (in gray/green), that accumulates released molecular cargos (blue) at the location of its activity. Close behind, its upstream reductase (grey/purple) enables the continuous reductive activity of Trx without touching the trigger-cargo-constructs.

Selective, Modular Probes for Thioredoxins Enabled by Rational Tuning of a Unique Disulfide Structure Motif

Jan G. Felber, Lukas Zeisel, Lena Poczka, Karoline Scholzen, Sander Busker, Martin S. Maier, Ulrike Theisen, Christina Brandstädter, Katja Becker, Elias S. J. Arnér, Julia Thorn-Seshold, and Oliver Thorn-Seshold*



Cite This: *J. Am. Chem. Soc.* 2021, 143, 8791–8803



Read Online

ACCESS |



Metrics & More

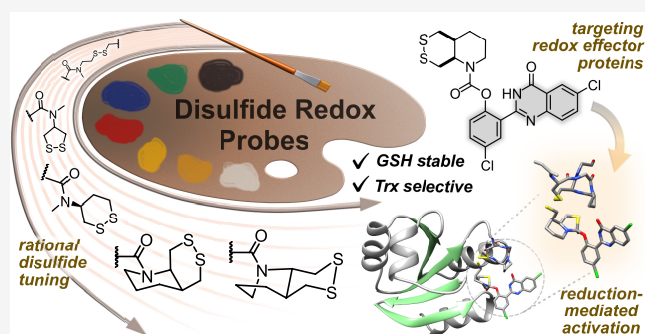


Article Recommendations



Supporting Information

ABSTRACT: Specialized cellular networks of oxidoreductases coordinate the dithiol/disulfide-exchange reactions that control metabolism, protein regulation, and redox homeostasis. For probes to be selective for redox enzymes and effector proteins (nM to μ M concentrations), they must also be able to resist non-specific triggering by the ca. 50 mM background of non-catalytic cellular monothiols. However, no such selective reduction-sensing systems have yet been established. Here, we used rational structural design to independently vary thermodynamic and kinetic aspects of disulfide stability, creating a series of unusual disulfide reduction trigger units designed for stability to monothiols. We integrated the motifs into modular series of fluorogenic probes that release and activate an arbitrary chemical cargo upon reduction, and compared their performance to that of the literature-known disulfides. The probes were comprehensively screened for biological stability and selectivity against a range of redox effector proteins and enzymes. This design process delivered the first disulfide probes with excellent stability to monothiols yet high selectivity for the key redox-active protein effector, thioredoxin. We anticipate that further applications of these novel disulfide triggers will deliver unique probes targeting cellular thioredoxins. We also anticipate that further tuning following this design paradigm will enable redox probes for other important dithiol-manifold redox proteins, that will be useful in revealing the hitherto hidden dynamics of endogenous cellular redox systems.



1. INTRODUCTION

Controlled dithiol/disulfide-exchange reactions are essential to cellular metabolism, protein folding, protein regulation, and diverse aspects in cellular homeostasis and stress response.^{1,2} Two ubiquitous networks are particularly important: the thioredoxin (Trx)–thioredoxin reductase (TrxR) system and the glutaredoxin (Grx)–glutathione (GSH)–glutathione reductase (GR) systems (Figure 1a).^{3,4} These systems are driven by catalytically active enzymes, GR and isozymes of TrxR (low nM cellular concentrations), which pass reducing equivalents from NADPH into a wide range of dithiol/disulfide-type reactions via effector proteins, especially several isozymes of Trx and Grx (μ M); in the case of GR, this transfer goes over the redox-active peptide GSH (mM concentration).^{5,6} The networks are interlinked and can function as backup systems for each other.^{4,7} The Trx and Grx systems catalyze two-electron dithiol/disulfide-exchange reactions proceeding via polar ionic mechanisms with high substrate specificities and precise biological control.^{8,9} Their scope of substrates is controlled by chemocompatibility as well as protein–substrate binding, and the relative turnover rates of each step in these

redox networks are tightly regulated by reaction kinetics and compartmentalization.¹⁰

The biochemistry and isoforms of the Trx and GSH/Grx networks have been excellently reviewed;¹¹ relevant aspects are summarized here. (i) TrxRs and GRs use similar FAD-containing domains to harvest electrons from NADPH, passing them to similar structurally restricted dithiol/disulfide active sites (CVNVC motif).¹² Mammalian TrxR also has a C-terminal selenolthiol/selenenylsulfide active site (CU motif) on a flexible surface-exposed loop, to relay electrons from the NADPH-driven dithiol site onto its substrates.¹³ These include Trxs and related redox proteins, e.g., TRP14 (also known as TXNDC17), though it can also reduce non-physiological small molecules (Figure 1b).^{14,15} Due to its rare selenolthiol, TrxR has unusual redox properties compared to dithiols: with both

Received: March 26, 2021

Published: June 1, 2021



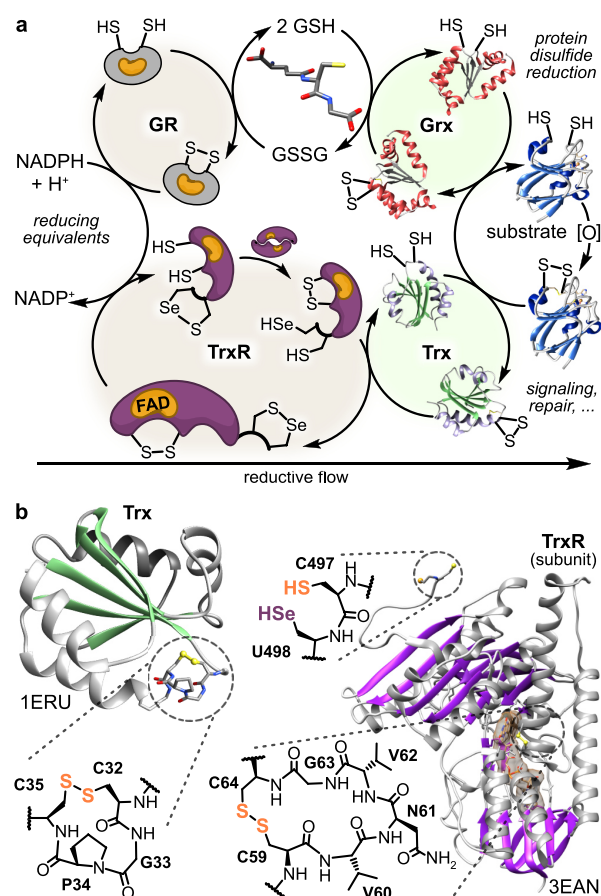


Figure 1. Key players in dithiol/disulfide homeostasis. (a) NADPH-driven cellular signal transduction and redox repair through the GSH/Grx and Trx and TrxR systems. (b) Active-site structures of Trx¹⁸ and TrxR.^{12,14,19,20} pre-organized cyclic dichalcogenides.

enhanced reaction kinetics and lowered reduction potential.¹⁶ GR is unusual in that it is highly specific for the small molecule glutathione disulfide (GSSG), so offering little scope for other substrates. (ii) Trxs and dithiol Grxs (includes Grx1 and Grx2) are dithiol/disulfide redox-active proteins with surface-exposed dithiol redox-active sites (CxxC motifs) that recognize and reduce a variety of protein substrates in pro- and eukaryotic organisms (Figure 1b). Trxs have lower reduction potentials and are reduced by selenolthiol TrxR; Grxs have higher reduction potentials and use monothiol GSH for their reduction.¹⁷

In all these enzymes, the spatial pre-organization and flexibility of the dichalcogenide redox-active sites are key to their kinetics and thermodynamics (mirroring what is known for small-molecule reductants).²¹ These factors, plus others such as protein recognition, redox potentials, and non-equilibrium metabolic flows, contribute to their substrate scopes in cells—though our understanding of the determinants for cellular activities of these enzymes remains poor.²²

The lack of techniques to measure or respond to the turnover dynamics of these redox proteins *in situ* greatly limits our understanding of redox biology, because it is turnover dynamics that are key to understanding network function and homeostasis.² So far, the best-developed probes for use in redox biology are genetically engineered ratiometric fluorescent sensors of redox-active protein or small-molecule redox poise.^{23–26} These give specific, spatiotemporally resolved

readouts for the reduced-to-oxidized state ratio of the target species. However, as ratiometric readouts of redox state, they do not reveal turnover dynamics. Also, genetic approaches are monitoring-only systems that cannot respond to redox reactions with an action, such as delivering a therapeutic cargo.

To quantify turnover, selective turn-on probes are needed, whereby enzymatic turnover events can be measured by integrating cumulative and irreversible signal accumulation in the form of an activated probe. In this context, small-molecule probes that employ disulfide-based trigger–cargo designs (Figure S1) are promising alternatives to protein sensors, and are potentially chemocompatible with the redox enzymes. Such probes are ideally created so that their cargo is deactivated in the oxidized state, while reduction irreversibly activates the cargo, resulting in a signal. Typically, activation proceeds by a fragmentation reaction, exposing a key structural element on the cargo, often simply by cleaving it from the trigger. This is a conceptually simple design, and it is additionally attractive because, unlike genetic probes, it can act upon a stimulus: modular designs can enable not only probes for detection and quantification of enzyme activity but also prodrugs delivering drug cargos conditional upon this activity.

In the thiol redox context, trigger–cargo designs have been used to release a range of cargo types upon reduction, including phenol- and aniline-type fluorophores and drugs (Figure S1a,b). For such designs to be selective, a probe must only commit to the *first irreversible step* on the pathway to turn-on after it reacts with the targeted enzyme—and not with any undesired species (reducing or otherwise). Therefore, while analyzing thiol/disulfide exchanges in light of equilibrium thermodynamic parameters (e.g., reduction potential E°) is generally informative, to design selective cumulative-release probes for enzyme turnover requires considering the kinetics and reversibility of each step in the reaction sequence. These, in turn, depend on the chemistry of the redox trigger and its reaction with target enzymes and reductants. For this analysis, we must distinguish the reaction of a disulfide with a single thiolate to liberate a thiolate, which we refer to as *exchange*, from the net reduction of a disulfide to liberate two thiolates by two stepwise exchanges, which we will refer to as *reduction*.

Linear disulfides are the most-used redox triggers in cargo-releasing designs (Figure S1a,b).²⁷ However, linear disulfides cannot selectively detect or respond to enzyme activities in the cellular context.^{28–30} This is because thiol–disulfide exchange at either sulfur irreversibly and non-selectively commits linear disulfides to turn-on (Figure 2a), and the rapidity of even uncatalyzed exchange with the high intracellular monothiol concentrations (ca. 5 mM GSH, ca. 50 mM protein thiols (PrSH)) causes a high degree of monothiol-based cargo release that likely drowns out enzyme-specific components.²⁸ Therefore, at best, linear disulfides report non-specifically on initial thiol–disulfide exchange rates.³¹

Cyclic disulfide redox triggers of type A (Figure 2b) instead allow kinetic reversibility in both exchange steps: their first irreversible step is the actual cargo release itself (k_{rel}). Reversion to the cyclic disulfide A after exchange to B or D (k_{T1} or k_{G1} in Figure 2b) is a unimolecular reaction that may be kinetically rapid (intramolecular cyclization that can also be pre-organized) as well as thermodynamically favored by enthalpic (pre-organized disulfide geometry) and entropic effects (molecular cleavage). These factors can be amenable to tuning by structural design of the disulfide trigger. However,

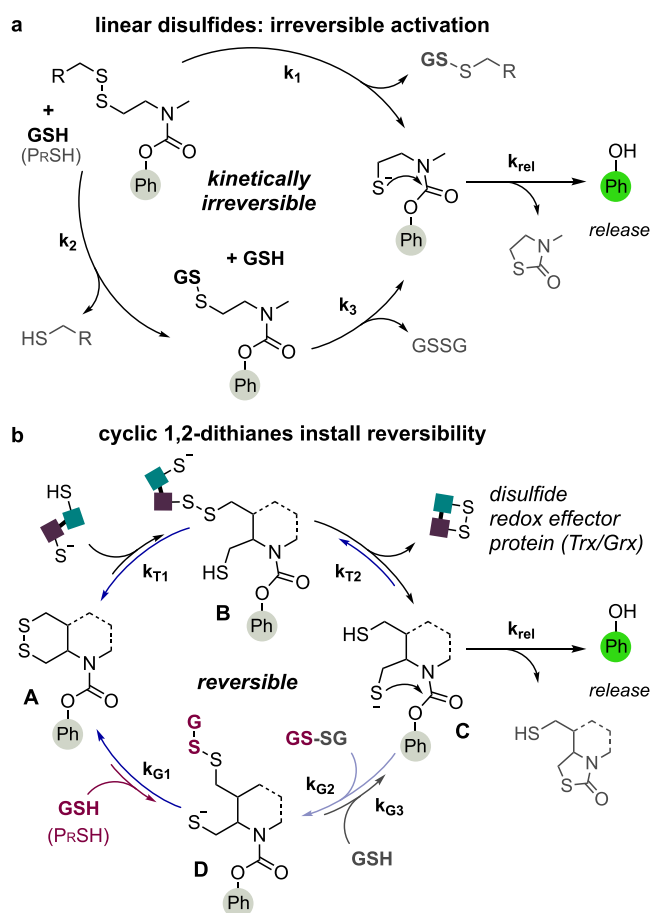


Figure 2. Mechanistic aspects of (a) irreversible monothiol reduction of linear disulfide-type reduction-sensing units and (b) thermodynamically reversible dithiol reduction of cyclic disulfide systems as part of irreversible release probes.

for dithiol proteins, completing the reduction (B to C) is a pre-organized, unimolecular reaction that reductases are evolved to perform, and which could therefore be competitive to or faster than k_{T1} . By contrast, the reaction of D to C is both bimolecular and not kinetically favored, so reversion by k_{G1} is the most probable fate of D under monothiol challenge. Therefore, A should be much more rapidly reduced to the signal-generating intermediate C by dithiol proteins than by monothiol background. Reversion of C to A is also well known: it underlies the use of dithiothreitol (DTT) as a rapid, stoichiometric, non-specific reductant particularly of linear disulfides GSSG, PrSSG, and PrSSPr (k_{G2} in Figure 2b); this pathway could also prove relevant in suppressing signal generation by monothiol challenge. Therefore, we concluded that stably pre-organized cyclic disulfides A would be suitable starting points for triggers in enzyme-selective probes (Figure 2b), and we determined to explore their synthesis and use.

Cyclic disulfide trigger substrates for trigger–cargo probes have been sparsely reported, and structures that are known have rarely been assessed for redox selectivity and kinetic performance. The most studied are strained cyclic 6-membered disulfide epidithiodiketopiperazines (ETPs), but their strain-promoted reactivity with monothiols is non-specific and significant, so they are not suitable for selective probes.³² Moderately strained 5-membered cyclic disulfides (1,2-dithiolanes) had been reported to be selectively reduced by

TrxR and were applied in the fluorogenic “TRFS” probes^{33–35} and prodrugs.³⁶ However, 1,2-dithiolanes undergo strain-promoted, kinetically irreversible, facile, and non-specific exchange with cell-surface monothiols,^{37,38} as known from disulfide-mediated cellular uptake studies.^{39–41} Our work confirmed that 1,2-dithiolane probes are, correspondingly, non-specifically activated by monothiols.³¹

To resist monothiol reduction by minimizing the concentration of C under monothiol challenge requires a high reversion rate k_{G1} (and optionally k_{G2}) compared to k_{G3} . We thus focused on unstrained cyclic disulfides, which are in fact the most poorly explored as triggers of irreversibly activated redox probes (Figure S1c,d, and further discussion in the Supporting Information). The few notable studies concern the 6-membered cyclic disulfide 1,2-dithiane. As far as we know, only three concepts of 1,2-dithiane designs intended to release a general molecular cargo after reduction by biological species have been disclosed. First, Butora used DTT phosphoesters to release phosphate cargos after reduction, which was stated to occur by reaction with GSH;^{30,42} this approach was since used by, e.g., Urata.⁴³ Second, Xu and Tang used an aniline carbamate of DTT to release aniline cargos after reduction, which was stated to occur by reaction with H_2Se ;⁴⁴ Fang also applied this approach, but contradicting Butora, stated that neither TrxR nor GSH caused release.³⁵ Third, Ziv disclosed phenolic carbamate prodrugs of 4-amino-1,2-dithiane, intended to release the phenol cargo after reduction, though this was only described as occurring through the “ambient reductive environment” of the cell.^{45,46} Relatedly, Kohn worked on 6-membered cyclic disulfide derivatives of porfiro-mycin and mitomycin, though not releasing a cargo;^{47,48} like Butora, their reports cited non-specific dithiane exchange/reduction by monothiols (Figure S1c,d).

We consider these reports both contradictory and limited in their assessment of which cellular reductants are, or are not, effective for exchange/reduction of 1,2-dithiane-based trigger–cargo probes: so we set out to assess this comprehensively.

We also believed that tuning rates throughout the turn-on process would prove critical for achieving protein selectivity. Particularly, we wished to explore pre-organization by annelating the cyclic disulfide triggers (dotted ring in Figure 2b). This modification adds minimal steric pressure at the redox-active -SS- site, so it might not suppress enzyme docking, but it could bring two favorable effects into play: (i) increasing thiol cyclization rate of C (k_{rel}), to accelerate signal generation without changing the reductant selectivity profile, and so improve probe performance (N.B.: k_{rel} is equally increased by both *cis*- and *trans*-annelation); (ii) stabilizing the cyclic disulfide A, to increase k_{T1} and k_{G1} and so potentially change the selectivity profile (N.B.: these effects *should* depend on the *cis*-/*trans*-stereochemistry). Such annelated disulfides have not yet been reported, so we wished to develop scalable and convenient syntheses, enabling their general application to redox research.

Lastly, we noted that, according to our proposed mechanism, as long as hydrolytic cargo release is blocked, the choice of cargo only influences k_{rel} and *should not* affect a probe’s reductant selectivity. We were therefore curious to use the same trigger with different cargos, to test the bioreductant selectivities, and to rationally tune probe performance.

In this work we address the lack of information on cyclic disulfide suitability for probes. We test our design principles by stepwise exploration of the features predicted to determine

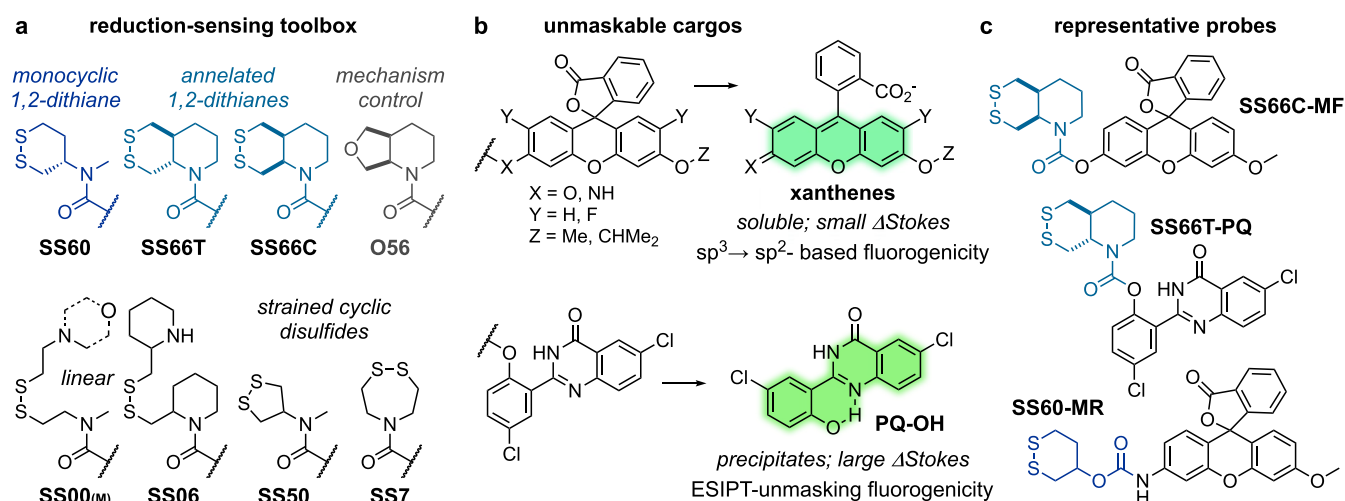


Figure 3. Trigger-and-cargo design for redox probes. (a) Stable cyclic disulfide-based reduction sensors and their control and comparison systems. (b) Complete off \rightarrow on fluorogenic cargos based on phenol mono-unmasking. (c) Representatives of the 20 fluorogenic probes used in this study, derived by trigger-cargo combinations.

cargo release selectivity and rate. We scalably synthesize novel cyclic disulfide-based triggers and apply them in robust, irreversible-release probes suitable for generalized cargos. We comprehensively evaluate the probes' selectivity for key redox-active proteins and their resistance to a high monothiol background, also benchmarking previously reported but poorly characterized disulfides. This will reveal the potential of pre-organized disulfides as enzyme-selective reduction sensors and identify a promising Trx-selective probe design.

2. RESULTS AND DISCUSSION

2.1. Trigger Design. We designed a broad panel of disulfide-based redox triggers for this study (Figure 3a). To avoid unspecific monothiol-triggered cargo release, we used stable cyclic 6-membered disulfide triggers: most simply, disulfide trigger SS60. To study how pre-organizing annelation affects both cargo release and selectivity profiles, we designed *cis*- and *trans*-fused triggers SS66C and SS66T. As linear disulfide controls, we used simple trigger SS00²⁷ and annelated SS06 (which, when compared, should test for pre-organization only of cargo release k_{rel}). Where needed, we compare the results with those of the strained and/or polymerizable monocyclic disulfide controls SS50^{31,33} and SS7.⁴⁹ This broad panel of disulfide structure motifs would allow us to compare reductant selectivity and cargo release rates, across stable or pre-organized or strained, cyclic or linear disulfide redox probes, on a level that to our knowledge has not yet been attempted. Lastly, we introduced O56 as a similarly polar but non-reducible negative control trigger to check stringently for stability against non-reductive chemical or enzymatic release of probe cargos.

2.2. Probe Design Considerations. To create modular probe designs, we chose to work primarily with phenolic fluorophores. Anilines are simpler to adapt into fluorogenic probes, as acylation usually substantially suppresses fluorescence (though only in special cases does it do so completely), and since acylated anilines have good hydrolytic stability.³⁵ Aniline carbamates are well represented in trigger-probe designs. However, the poor leaving-group nature of anilides results in slow cargo release for 5-*exo*-trig thiol cyclization, with physiological half-lives of >3 h, even under fully reduced

conditions.³⁵ Alternative anilide designs such as amides and ureas are not cleavable and so do not represent modular response systems as we sought.^{35,50}

By comparison, phenol-releasing systems could benefit from superior leaving-group nature to improve release kinetics. Several phenolic systems featuring true off-to-on fluorogenicity are known, and phenols are found as key activity-determining groups in a broad range of diagnostic or therapeutic cargos, meaning that modular designs in this work could be extended into a useful series of probes and prodrugs. Stability against non-reductive hydrolysis is the major challenge for most phenols. For example, disulfide-trigger phenolic esters and carbonates have been reported,^{51,52} but non-reductive phenol release by spontaneous and enzymatic hydrolysis is certain to prevent them achieving any selectivity in biological settings. Phenolic carbamates have previously been reported to be unstable.³⁵ However, we interpreted this instability as the spontaneous E_{1cB} elimination pathway that affects primary carbamates,⁵³ so we designed all triggers for secondary carbamate linkages to avoid this (Figure 3a),^{54,55} guided by precepts from our earlier work.^{31,56}

2.3. Cargo Choice and Use. We selected two major series of fluorescent cargos to be masked by mono-*O*-carbamylation (Figure 3b), requiring that this should entirely suppress their fluorescence by mechanism-based quenching. (i) We used xanthene-based mono-*O*-alkylated fluorescein MF-OH⁵⁷ and its acidified photostable congener IG-OH⁵⁸ (as its *iPr* might resist nucleophilic attack better than MF-OH's methyl). Their mono-*O*-carbamylation mechanistically quenches fluorescence by locking the central carbon as sp^3 , so destroying conjugation. Conjugation is restored by cleaving the carbamate substrate (simplifying kinetics compared to typical double-substrate probes such as fluorescein diacetate), giving soluble, biocompatible, bright fluorophores (ex/em 485/515 nm). (ii) We also used the precipitating fluorophore PQ-OH,^{59,60} whose high-quantum-yield, large-Stokes-shift fluorescence (ex/em 360/520 nm) depends on excited-state intramolecular proton transfer (ESIPT) of the phenolic hydrogen. Carbamylating the phenol entirely and mechanistically abolishes ESIPT fluorescence of the probe. The electron-withdrawn PQ should also have fast release. To compare our phenolic designs to

prior art in aniline disulfide redox probes, we also prepared 3-*O*-methyl-rhodol MR-NH₂ for kinetic comparisons.⁶¹ Thus, all our probes feature a true off-to-on mechanistic switch of signal upon disulfide trigger cleavage, thereby maximizing their signal-to-noise ratio and simplifying analysis (details in Figure S2).

We combined triggers freely with cargos to create a panel of probes for analysis. We name the resulting probes by the combination used; e.g., in Figure 3c, SS66C-MF is an SS66C-trigger MF-OH-releasing probe, etc. (further details and discussion in the Supporting Information).

2.4. Diastereomerically Pure Synthesis of Annelated SS66 Disulfides. The simpler disulfide redox triggers were accessed straightforwardly. Monocyclic disulfide SS60 was obtained using the approach reported by Raines⁶² to give the protected primary amine, then by *N*-methylation and deprotection to prepare the novel secondary amine SS60. Known polymerization-prone^{38,63} unstable cyclic disulfides SS50 and SS7 were accessed from aminopropanediol³¹ and from a nitrogen mustard precursor,⁴⁹ respectively, as described. Symmetric linear disulfides SS00 and SS06 were accessed by oxidative dimerization of the respective thiols; as far as we know, cyclization-pre-organized linear disulfides like SS06 have not been studied before (Figure 3a). The secondary amine of these symmetric disulfides proved inconvenient for yields and purification, with double-reaction side products being formed during later carbamate coupling. Unsymmetric linear disulfides of the SS00 type are rarely reported in the literature, and we found no convenient methods to synthesize them. We developed a versatile batch synthesis strategy for unsymmetric linear disulfides by coupling easily prepared, isolable precursors (one primary *S*-acetyl and one primary *S*-tosyl), achieving high chemoselectivity and isolating the unsymmetric morpholino-substituted SS00M (Figure 3a) in good yields. For details, see the Supporting Information.

The bicyclic redox triggers were more challenging (Figure 4). We first focused on the *cis*-fused SS66C system, setting the stereochemistry by heterogeneous hydrogenation of pyridine 1. Boc-protection to amine 2 and then ester reduction gave *cis*-diol 3, which we could not, however, convert into a bicyclic disulfide. During Mitsunobu reaction with thioacetic acid under Raines's conditions,⁶² no bis(thioacetate) but rather undesired *cis*-ether 5 was isolated, with X-ray confirming its structure. Fortunately, 5 provided ideal non-reducible hydrolysis controls, as the O56 series. Other strategies to activate the hydroxy groups for *S*-nucleophile substitution were unsuccessful; e.g., attempted bis(sulfonylation)s gave intramolecularly cyclized carbamates, e.g., 4, as known for Boc-/Cbz-methanol-piperidines.^{64–66} To avoid carbamate cyclizations, we switched to PMB for the *N*-protecting group. Diastereomerically pure *N*-PMB-diol 10 was accessed in decent yield by hydrogenation of 1, ester reduction to 9, and *N*-alkylation. It was crucial to reduce the esters before nitrogen protection, to avoid partial *cis*–*trans*-isomerization at the diester stage. Mesylation of diol 10 and nucleophilic substitution with KSac gave bis-(thioacetate) 11, and tandem basic acetate cleavage/oxidation gave novel annelated disulfide 12. PMB was deprotected without reductive or oxidative conditions by using 2-chloroethyl chloroformate (ACE-Cl),⁶⁷ giving the precursor to all SS66C probes (Figure 4).

For the *trans*-fused SS66T, we took a route exploiting the previous setbacks to our advantage. First, we could use basic *cis*–*trans*-epimerization to recycle *cis*-diester 2, after some trials

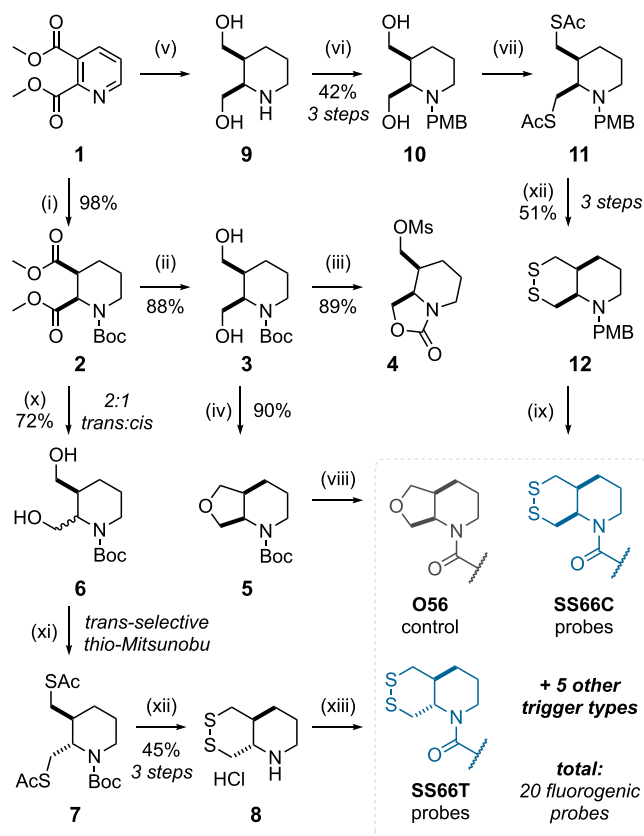


Figure 4. Diastereomerically pure syntheses of SS66T- and SS66C-series bicyclic disulfide redox probes. Reagents and conditions: (i) (1) H₂, H₂SO₄, Pd/C, MeOH, 80 bar, r.t., 15 h; (2) Boc₂O, NEt₃, dioxane/H₂O, r.t., 15 h (98%). (ii) LiAlH₄, Et₂O, 0 °C to r.t., 3 h (88%). (iii) MsCl, DCM, NEt₃, r.t., 15 h (89%). (iv) *Cis*-selective tetrahydrofuran formation: (1) PPh₃, DIAD, HSac, THF, r.t., 15 h (90%); (2) HCl, MeOH, 80 °C, 4 h (quant.). (v) (1) H₂, H₂SO₄, Pd/C, MeOH, 80 bar, r.t., 15 h; (2) LiAlH₄, THF, 0 °C to r.t., 3 h. (vi) PMB-Cl, K₂CO₃, EtOH, r.t., 15 h (v–vi: 42% over 3 steps). (vii) (1) MsCl, NEt₃, DCM, r.t., 1 h; (2) KSac, DMF, r.t., 15 h. (viii) KOH, MeOH, r.t., 15 h (vii–viii: 51% over 3 steps). (ix) (1) ACE-Cl, DCE, 80 °C, 5 h; (2) MeOH, 80 °C, 2 h; (3) carbamate coupling. (x) (1) NaOMe, MeOH, r.t., 1 h; then AcOH (2:1 *trans*:*cis*); (2) LiAlH₄, Et₂O, 0 °C to r.t., 2 h. (72% over 2 steps). (xi) *Trans*-selective bis(thioacetylation): HSac, PPh₃, DIAD, THF, r.t., 15 h. (xii) (1) KOH, MeOH, r.t., 15 h; (2) HCl, r.t., 4 h (xi–xii: 45% over 3 steps). (xiii) Carbamate coupling.

reaching an inseparable 2:1 *trans*:*cis* epimerized mixture by NaOMe treatment and then quenching by AcOH. Ester reduction gave 2:1 *cis*:*trans*-diol 6, still unseparated. Then, we could selectively destroy the residual *cis* while carrying the *trans* through its next step of thio-Mitsunobu reaction: *trans*-diol 6 converted smoothly to the *trans*-bis(thioacetate) 7, while *cis*-diol 6 converted to *cis*-ether 5, separable by chromatography. Thioester hydrolysis of 7, dithiol oxidation, and deprotection gave diastereomerically pure *trans*-8, the key SS66T precursor, in decent yields (Figure 4). (This also suggested that the *cis*-fused system's greater tendency to 5-exo-tet cyclization than the *trans* might be reflected in a greater kinetic and/or thermodynamic stability of its *cis*-disulfide, which we soon examined, as described below.)

Deprotected secondary amines of the disulfide triggers were reacted with *O*-chloroformates of phenolic fluorophores to deliver 19 fluorogenic MF, IG, and PQ series probes (Figure

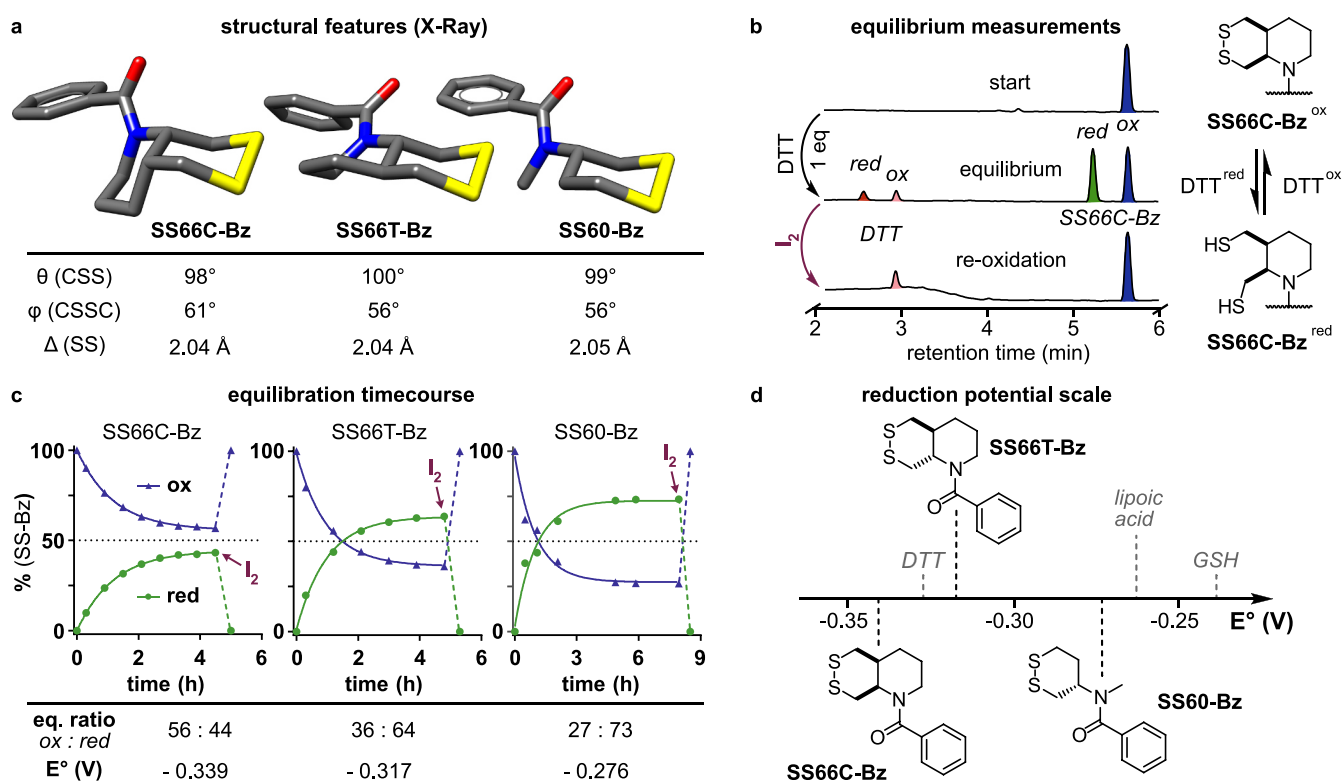


Figure 5. Redox thermodynamics of cyclic 6-membered disulfide triggers. (a) Single-crystal X-ray structures of 1,2-dithianes: CSS bond angles θ ; CSSC dihedral angles φ ; disulfide bond distance Δ . (b) HPLC-based E° measurement protocol. Disulfides are equilibrated against DTT^{red} , and then dithiols are quantitatively re-oxidized by iodine as a control. (c) HPLC time courses, equilibrium ratios, and resulting disulfide E° values. (d) Graphical depiction of E° for this study's 1,2-dithianes against known (bio)reductants.¹¹

4) and one MR reference compound.⁶⁸ These were all colorless and non-fluorescent both as solids and in solution, as expected for their mechanistically quenched emission. To assess disulfide thermodynamics, we also benzoylated the amines to give “SS-Bz” compounds that mimic the geometry of the triggers in the carbamate probes but can be reversibly equilibrated as well as crystallized (see below).

2.5. Thermodynamic Analyses: Redox Potentials Are Lowest for Annelated Cyclic Disulfides (SS66). Redox potentials depend on structural/geometric features that (de)stabilize the disulfide relative to the dithiol. Bond distance (SS), bond angle (CSS/SSC), and dihedral angle (CSSC),⁴⁰ together with strain factors, typically affect disulfide stability. We could acquire X-ray structures of all three SS-Bz 1,2-dithianes (Figure 5a), showing their disulfide rings in chairlike conformations with minimal eclipsing and CSSC dihedral angles close to that of the model 1,2-dithiane DTT^{ox} (56°).⁶⁹ But, while a double-chair conformation was found for SS66C-Bz (similar to a *cis*-decalin), against our expectations SS66T-Bz formed a more strained boat-chair system unlike a *trans*-decalin (for further discussion, see Raines⁷⁰ and references therein, and Supporting Information).

We then experimentally examined the thermodynamic reduction potential E° of the cyclic disulfides. We had anticipated that thermodynamic stability (low E°) would be important to resist reduction by monothiol and so to achieve selectivity for dithiol species. Whitesides calculated and experimentally determined E° values of uncommon disulfides in the 1980s–90s.^{63,71} The lowest E° values they reported were indeed for 2,3-dithiadecalin-type disulfides,⁷² which under non-standard conditions (50:50 buffer:cosolvent) were -0.35

V (*trans*) and -0.34 V (*cis*). This extraordinary stability compared to linear disulfides (E° ca. -0.22 V)⁶³ was promising for our aims in this study. However, while we expected the E° of the tetrahedral amine triggers SS66T and SS66C to match these, we believed that the restrained geometries of the carbamates would modify the probes' potentials. To mimic these while avoiding the influence of kinetic considerations that also determine irreversible probe performance (trigger reduction and thiol cyclization rates), we again used the reversible SS-Bz series; these also allowed us to benchmark our reduction potentials under normalized conditions.

To determine reduction potentials, we equilibrated the SS-Bz series against chemocompatible reductant standards, analyzing oxidized:reduced compound ratios by HPLC. We did this similarly to methods used by Raines⁶² and others^{63,73} though with three additional features. First, the benzamide is a convenient UV-active tag for HPLC signal integration. Second, we detected oxidized:reduced ratios for both benzamide probe and reductant standard (e.g., DTT); this controls for parasitic oxidation by adventitious oxygen (which would be reflected by an increasing total of oxidized species). Third, we performed time course measurements to follow the progress of equilibration, and upon reaching stable plateaus we controlled for reversibility by re-oxidizing all dithiols to disulfides using I_2 (Figure 5b). This controls for polymerization of strained disulfides, which risks being misinterpreted. By titrating reductants, we determined reduction potentials of -0.276 V for SS60-Bz, -0.317 V for SS66T-Bz, and -0.339 V for SS66C-Bz (Figure 5c,d), whereas the strained analogues SS50-Bz and SS7-Bz were not equilibrating systems. We estimate ± 0.01 V precision in our experiment. The lower reduction

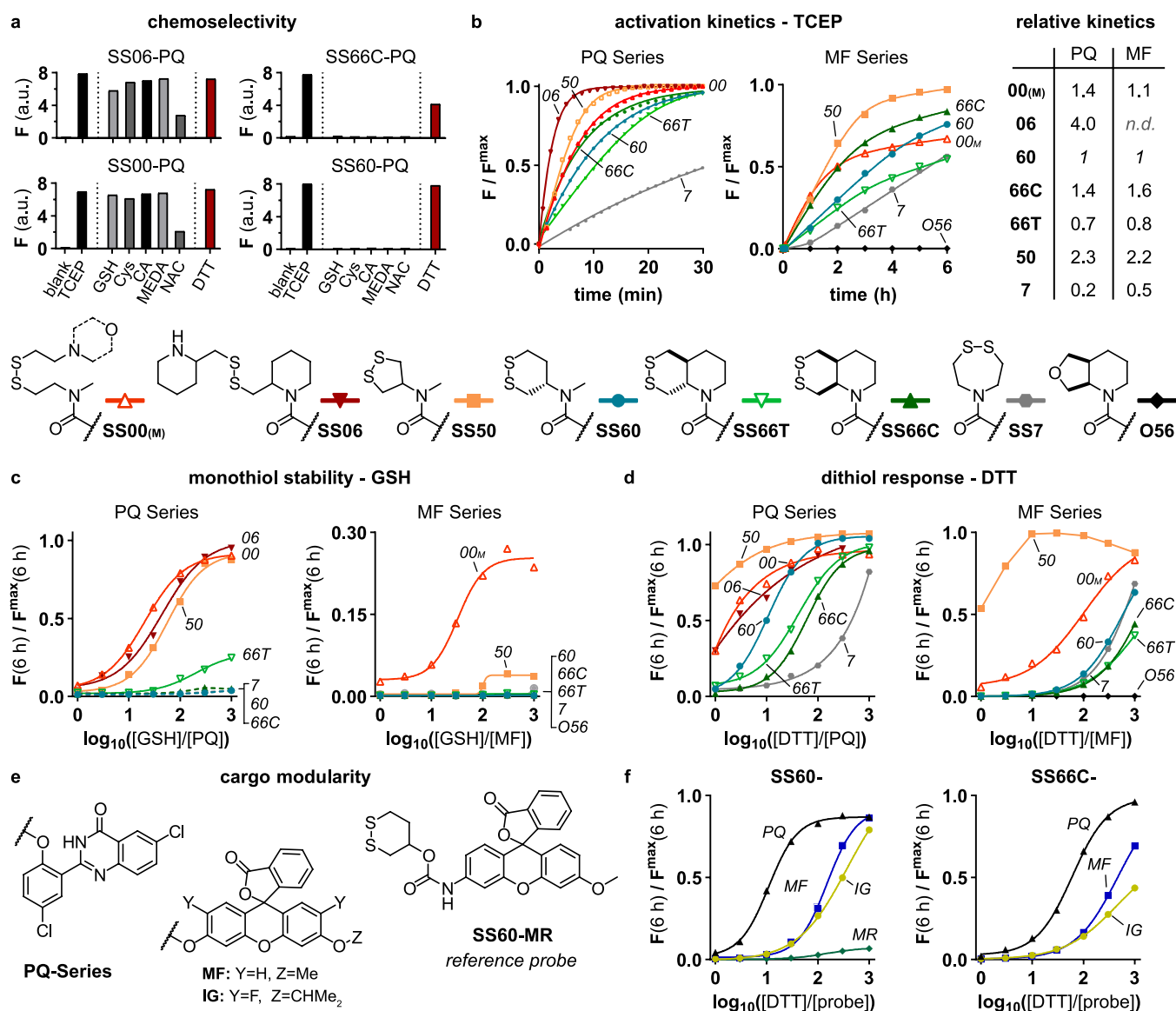


Figure 6. Reductant-resistance profiling and cargo-release kinetics. (a) Fluorescence response of representative linear and 1,2-dithiane probes to monothiol reductants (1 mM), benchmarked to quantitative reductant TCEP (100 μ M) and to dithiol DTT (1 mM); $t = 2$ h. (b) Probe activation kinetics with TCEP (100 μ M). (c) GSH challenge titrations (0.01–10 mM GSH, 10 μ M probe, $t = 6$ h data). (d) Dithiol challenge titrations (0.01–10 mM DTT, 10 μ M probe, $t = 6$ h data). (e, f) Modular probe design allows comparing cargo release kinetics.

potentials of the annelated SS66 compared to the monocyclic SS60 matched expectations. Potentially due to the benzamide strain, SS66T-Bz indeed had 0.02 V higher E° than SS66C-Bz. While Whitesides gave a 0.01 V lower potential for the *trans*-2,3-dithiadecalin,⁶³ this may only hold true for the SS66 amines (Figure S5d; see also Supporting Information).

2.6. Kinetic Analyses: Cyclic 6-Membered Disulfides Resist GSH Reduction but Are Triggered by Vicinal Dithiols. We now turned to the PQ- and MF/IG-based fluorogenic probes, to test their activation by, or resistance to, small-molecule reductants.

Calibrations on the cargos MF-OH, IG-OH, and PQ-OH confirmed large linear concentration/signal ranges (20 nM–30 μ M for xanthenes, >1 μ M for PQ-OH; Figure S2a,b). Assays of the probes' fluorogenic character highlighted their true off-to-on fluorescence switching, based on complete mechanistic quenching in the intact probes (Figure S2c). Throughout the reductant challenge assays, we controlled

against fluorophore release by non-reductive degradation mechanisms (such as carbamate hydrolysis, or carbamate thiolytic by thiol reductants) using the O56 probe series. Matching our design requirements, the O56 series showed in all cases that the secondary amine carbamates were entirely robust, thereby solving the problems with prior phenolic carbamates³⁵ and indicating that disulfide reduction and intramolecular thiol cyclization would be the only pathway for signal generation with our disulfide probe series.

First, to report selectively on enzyme activity, a probe must resist reduction by the cellular monothiol background (ca. 50 mM, of which up to 5 mM GSH).¹¹ We therefore began by incubating probes with monothiols (1 mM) to profile their monothiol resistance. Linear SS00 and SS06 probes and strained 5-membered cyclic SS50 probes were rapidly triggered by all monothiols: GSH, cysteine, cysteamine (CA), *N,N*-dimethyl cysteamine (MEDA), and *N*-acetylcysteine (NAC). In contrast, 1,2-dithiane SS60, SS66C, and SS66T as well as 7-

membered cyclic SS7 probes resisted monothiol reduction (Figure 6a, Figures S4 and S5 for PQ series, Figure S6 for MF series, and Figure S7 for IG and MR series).

Next, we examined the kinetic performance of each probe, using the rapid and quantitative disulfide reducing agent tris(2-carboxyethyl)phosphine (TCEP). In these settings where no dithiol re-oxidation is possible (cf. k_{T2} and k_{G2} , Figure 2), probe signal generation depends on the rates of reduction by the phosphine, 5-*exo*-trig thiol cyclization, and cargo expulsion. Under such special conditions, the cargo nature rather than the disulfide structure became the major determinant of signal kinetics (Figure 6b; PQ-OH release approximately 10 times faster than that of MF-OH). While some reports claim that distal cargos substantially affect the reductant selectivity profile,⁷⁴ we attribute the faster release of PQ-OH than MF-OH simply to its better leaving-group character.

Pleasingly, the relative rates of probes *within* each series were almost identical for the MF as for the PQ series (Figure 6b; fits in Figure S3), revealing trigger-based performance features. (1) While annulations have been used for amine cyclization promotion,^{56,75} this has not yet been studied for thiols. The ca. 3-fold rate enhancement of annulation in the linear disulfides was significant (SS06 > SS00, also suggesting that their thiol cyclization is more rate-determining than their phosphine reduction). Annulation in the 1,2-dithianes was interesting; while the *cis*-fused SS66C was faster than SS60 as expected, the *trans*-fused SS66T was slower than SS60. (2) Thiol cyclization/cargo elimination (C → PhOH, Figure 2) occurs on a scale of minutes. As intramolecular thiol–disulfide exchanges (B → A, B → C, and D → A) typically take <10 ms,⁷⁶ we propose that “on-reductant” cyclization of the exchange intermediates B and D to release PhOH before their full reduction to C (Figure 2) is not a major contributor to cargo release. (3) The rates of bisthiolate cyclization (from SS50) were twice those of the corresponding monothiolate (SS00), a satisfying match to theory, though the SS7 probes were sluggish and behaved irreproducibly. (We believe oligomerization of SS7^{37,63,71} causes its poor performance, paralleling the behavior of polymerizable³¹ SS50 probes. Additionally, neither SS7-Bz nor SS50-Bz performed reliably in the equilibration/reoxidation assay. So, while we carried these probes through all assays, we focus on interpreting only the reliable 1,2-dithiane and linear disulfide results; see Supporting Information.)

We next aimed to profile GSH sensitivity more meaningfully than by single-concentration assays, to reach results predictively applicable to diverse settings. Therefore, we titrated the probes with GSH over a wide concentration range (0.01–10 mM GSH, 10 μ M probe) to build logarithmic dose–response curves profiling GSH sensitivity with long-term challenge (fluorescence at $t = 6$ h; Figure 6c, Figures S4–S7). These showed that linear disulfide (SS00/SS06) and 5-membered cyclic SS50-type probes are indeed quantitatively activated by physiological GSH concentrations (Figure 6c). The novel 1,2-dithiane probes, however, gave either zero response to GSH up to 10 mM (SS66C, SS60) or else very low signal from 1 to 3 mM GSH (SS66T; Figure 6c). As the 1,2-dithiane probes are monothiol-resistant, this indicated they might have potential for protein-selective monitoring.

We then explored a simple model system for vicinal dithiol reactivity using DTT. Vicinal dithiols reduce cyclic disulfide triggers via a net bimolecular pathway, in contrast to monothiols (net trimolecular; Figure 2). We hoped that this

mechanistic difference would allow monothiol-stable cyclic disulfide probes to be selectively activated by vicinal dithiols.

Dose–response titrations showed that the GSH-resistant SS60, SS66T, and SS66C cyclic disulfide probes were indeed fully activated by DTT (Figure 6d). The linear and SS50 probes were quantitatively triggered by even equimolar DTT, and the control OS6 probes were again fully resistant (Figures S4–S7). Pleasingly, the ordering of DTT resistance (SS00/SS06 < SS60 < SS66T/SS66C) was common to all cargos, again supporting the modularity of the probes’ design.

As for the monothiols, we noted apparent differences of probe sensitivity to DTT depending on the cargo nature, but again we attribute this to leaving-group kinetics (PQ-OH ca. 10-fold faster-releasing than MF-OH/IG-OH; we had expected that the acidification of IG-OH would make it a faster cargo than MF-OH⁷⁷ but we did not see this; Figure 6e,f, Figures S4–S7). The design control probe SS60-MR had poor activation (ca. 5% at 10 mM DTT at 6 h, Figure 6f), highlighting a general benefit of our phenol-releasing design over standard aniline-releasing probes (further detailed evaluation in the Supporting Information).

Taken together, this systematic comparison strongly showed that only 6-membered disulfides resist uncatalyzed reduction by monothiols at physiological concentrations, but that such motifs can still be reduced by vicinal dithiols. To the best of our knowledge, dose–response assays evaluating, e.g., GSH and DTT stability across wide concentration ranges to test for trigger reductant preferences have not been used in this field before, nor have previous reports established trigger or cargo selectivities on the basis of independently varying both triggers and cargos within the same probe series. In our opinion, both would be useful additions to the toolbox of standard assays for cumulative-release turnover probes.

2.7. Cyclic 6-Membered Disulfides Are Selectively Reduced by Trx Rather than by Other Oxidoreductases.

Having established the selectivity of the 6-membered cyclic disulfide probes for reduction by vicinal dithiols and their resistance to monothiols, we next proceeded to profile the probes’ reduction by biological vicinal dithiol/disulfide-type proteins, focusing on the main components of the TrxR/Trx and GR/GSH/Grx systems. In cells, the effector proteins Trx and Grx (ca. 10 μ M each) have orders of magnitude higher cellular concentrations than their upstream reductases TrxR and GR (ca. 20 nM each). To design cell-free assays to predict cellular enzyme selectivities, we ensured that the assays were performed (a) with cellular reductant concentrations, (b) using the catalytically powered redox systems rather than only pre-reduced effector proteins, and (c) examining a range of protein isoforms, both isolated from primary tissues as well as recombinantly expressed. The last point is particularly relevant for TrxR since the key selenocysteine (Sec, U) residue in its active site is highly present in isolates of native enzymes⁷⁸ or recombinant forms made with novel production methodologies (up to 100% Sec contents),⁷⁹ which we employed in this study, rather than the ca. 30% Sec content from standard expression methods.⁸⁰ Accordingly, our tests used recombinant human TrxRs, both cytosolic TrxR1 and mitochondrial TrxR2; recombinant human Trxs, both cytosolic Trx1 and mitochondrial Trx2; and as a comparison, recombinant human thioredoxin-related protein TRP14,⁸¹ which also features a vicinal dithiol/disulfide active site that is reduced by TrxR. Grx variants were examined using recombinant human vicinal

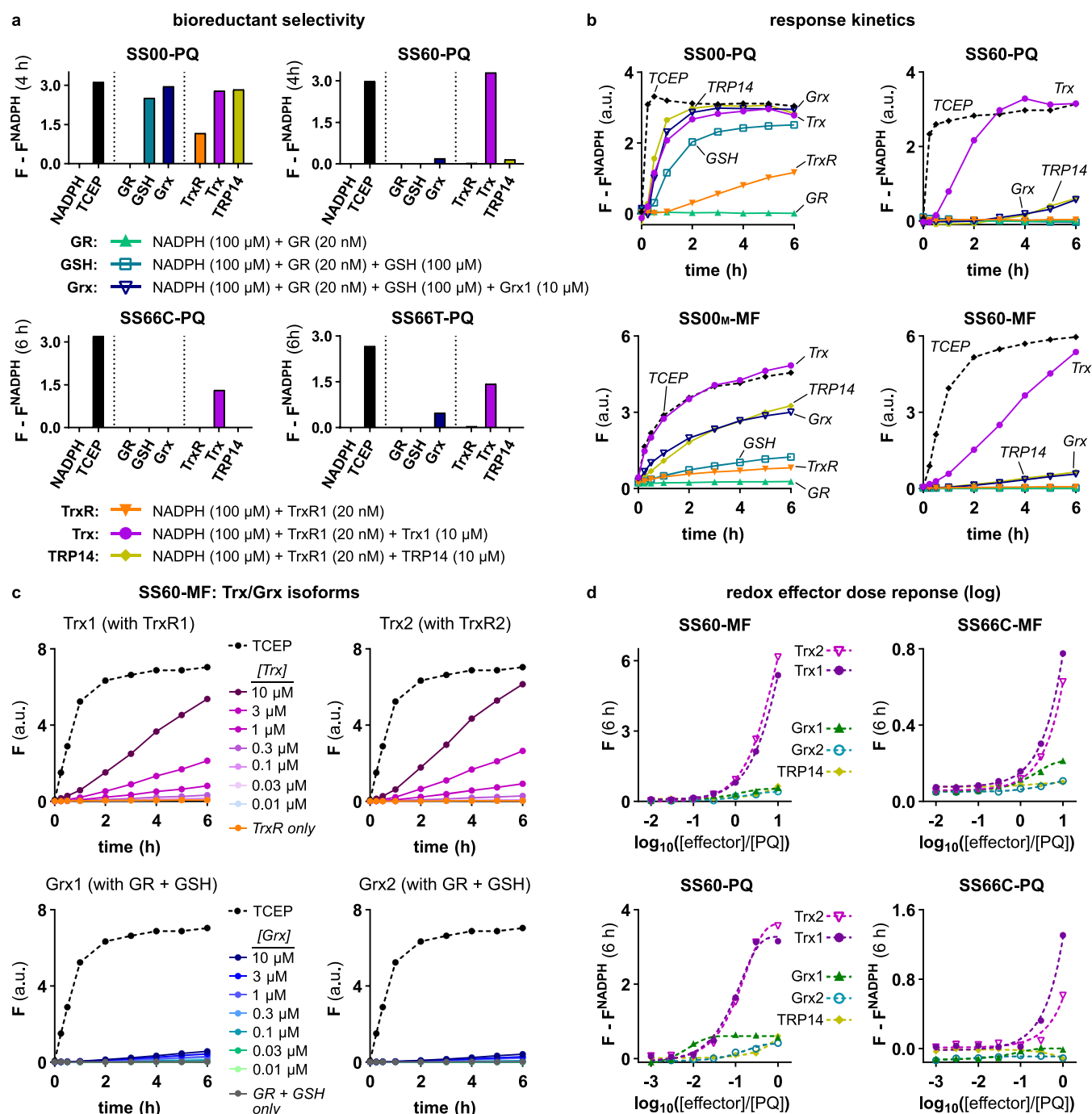


Figure 7. Cyclic 6-membered disulfides are Trx-selective substrates. (a) Bioreductant selectivity (single-concentration profiling; $t = 4$ h and $t = 6$ h; see also Figures S8 and S9). (b) Response kinetics of SS60-PQ (10 μ M) and SS60-MF (1 μ M) compared to their linear disulfide analogues. (c) Kinetic response of SS60-MF (1 μ M) to titrated redox effectors Trx1, Trx2, Grx1, and Grx2. (d) Dose-response profiles of the 1,2-dithiane probes to redox effector proteins ($t = 6$ h). See Supporting Information for details (Figures S8–S13).

dithiol glutaredoxins Grx1 and Grx2 together with human recombinant GR.

We evaluated all probes in fluorescence time courses. To conclude on whether probes were reduced by the effectors Trx and Grx, and/or by direct reaction with the upstream reductants TrxR and GR, we compared assays using both effectors and upstream reductants against assays with only upstream reductants, controlling against the effectors only. We also confirmed these interpretations by titrating effectors (e.g., Trx1) in the presence of a fixed concentration of upstream reductants (e.g., TrxR1) or *vice versa*. To our knowledge, this

approach has not been reported with other compounds described as redox turnover probes, but it proved to be a powerful technique to illustrate probe selectivities. All assays were performed with NADPH; GR assays optionally included a low concentration of GSH to allow Grx reduction without significantly reducing probe directly; see Supporting Information for further details.

The 6-membered cyclic disulfide probes based on SS60, SS66C, and SS66T were selectively activated by thioredoxins Trx1 and Trx2 (Figure 7a), with the SS60 series the most sensitive. The SS66C series had the highest Trx selectivity,

with almost zero detected signal under challenge by the Grx+GSH+GR and TrxR+TRP14 cascades over 4 or 6 h, respectively (Figure 7b,c, Figures S8–S13). Both Trx1 and Trx2 dose-dependently activated the dithiane probes, though pleasingly, under relevant concentrations, these probes were non-responsive to any of the TrxR isoforms in the absence of the effector Trx. It is notable that the 1,2-dithiane-type probes were not affected by the Trx-analogue vicinal dithiol protein TRP14, which likely reflects the different active-site structure and/or electrostatic surface charge of TRP14 compared to either Trx1 or Trx2.⁸² We note that the general order of Trx selectivity in the dithiane series ($SS66C \gtrsim SS60 > SS66T$) matches the order of stability against the supraphysiological monothiol levels (e.g., GSH at 10 mM, Figure 6c), supporting the earlier interpretation of structural influences on the relative kinetic instability of the *trans*-fused system. Matching expectations, linear disulfide reference probes **SS00(M)** were activated completely non-specifically by Trx1, Trx2, TRP14, Grx1, Grx2, and TrxR1 (Figure 7a,b, Figures S8, S10, and S11) in addition to the monothiols previously shown. This highlights the importance of the dithiane for achieving Trx selectivity (Figure 2). The signal kinetics for all **PQ** probes were again faster than for the corresponding **MF** probes (Figures S8–S13).

We again performed dose–response titrations to test the sensitivity profiles of all probes to varying concentrations of the redox-active proteins, which should be a useful predictive tool to estimate performance in complex applications. Figure 7d shows these dose–response plots for the two major dithiane triggers, the more-Trx-sensitive **SS60** and the most-Trx-selective **SS66C**, as applied to both **PQ** and **MF** probes (other probes in Figures S8–S13). This highlights the highly preferred processing of the novel dithiane probes by the Trx isoforms, regardless of their cargo (Figure 7d)—an excellent result for the mechanism-based design.

In summary, this systematic exploration of disulfide probe reductive triggering has relied on time course rather than endpoint data, and featured systematic variations and titrations of all reducing species. The results indicate that *regardless of the cargos with which they are used*, the hitherto-reported linear and cyclic 5-membered disulfide triggers do not withstand non-selective and non-enzymatic triggering by GSH, monothiols, and a range of cellular reductants, and are therefore non-selective reduction sensors. In contrast, the new 6-membered cyclic disulfide probes display excellent selectivity and steep dose–response curves for reduction by vicinal dithiols, particularly by Trx1 and Trx2. **SS60** and **SS66C** were thus identified as promising disulfide motifs for sensitive, modular probes selectively reduced by thioredoxins.

3. CONCLUSIONS

Specific dithiol–disulfide-type reactions underlie a multitude of biological pathways, and engineered disulfides are recently finding applications from probes in chemical biology to uses in biophysics and materials chemistry. Linear disulfides have been used for decades as non-specifically and irreversibly intracellularly cleaved substrates, often for intracellular release of appended cargos. While strained cyclic disulfides have found several applications, it has remained unproven whether *any* disulfide could be used reliably for creating robust, modular, enzyme-selective small-molecule probes.³¹ The challenge posed has been to unite (i) a broadly applicable, robust design that is suitable for efficiently releasing arbitrary cargos (toward

both probes and prodrugs) with (ii) a disulfide/dithiol-type redox trigger that resists the high cellular background of monothiols yet can be triggered by specific redox-active dithiol-type enzymes.

In this work we used mechanism-based analysis to design novel disulfide-based trigger–cargo probes which unite both features. The 6-membered cyclic disulfide probes characterized here feature rational tuning of thermodynamic and kinetic parameters of disulfide reduction as well as of cargo release, to achieve higher stability to the monothiol background than any probes previously reported. The trigger motifs were synthesized scalably, with the novel bicyclic disulfide structures being accessed by divergent diastereomerically pure routes, and then integrated into modular phenol-releasing probes which feature stability to cleavage by non-reductive mechanisms. These probes have been evaluated through a rigorous methodology combining time course and dose–response screening of chemical and biological reductants. The disulfides we report, and the probe designs we apply them to, fill a gap in the literature by being the first systematic exploration of the synthesis and reductant selectivity of non-strained and non-polymerizing disulfides, with the outlook toward adapting these modular phenol-releasing designs for a range of purposes. Pleasingly, the design logic of achieving selectivity by matching probe energetics and mechanism to those of the desired reducing species was supported by the selectivity in reduction of the 6-membered disulfides by the vicinal dithiol Trx, but not by the other redox-active enzymes analyzed here.

Further developing the Trx-selective 1,2-dithiane chemotypes for cellular monitoring of endogenous Trx is a major aim of our ongoing research. This faces challenges including (1) ensuring reduction is competitive with native Trx substrates, to reach high turnover or signal in the cellular context, and (2) favoring the post-reduction cyclization k_{rel} relative to the re-oxidation pathways (particularly k_{G2} ; Figure 2), to maximize the proportion of Trx-reduced probe which releases its cargo. These are non-trivial challenges. We also expect that tuning the probes' intracellular localization will prove crucial for performance.

Diversifying disulfide trigger structures to address other key oxidoreductases is another goal of our research. The scope of redox biology would be greatly expanded by developing probes that are GSSG-competitive substrates of GR, or Trx-competitive substrates of TrxR. This would allow researchers to tap into the turnover dynamics that drive the major dithiol/disulfide-manifold processes throughout the cell. This work has demonstrated that disulfides are a still-untapped well of potential for redox probes. We therefore hope that further developments of probes with increased selectivity for specific redox enzymes will facilitate progress in the many areas and applications of research in redox biology.

■ ASSOCIATED CONTENT

Supporting Information

The Supporting Information is available free of charge at <https://pubs.acs.org/doi/10.1021/jacs.1c03234>.

Synthesis, analysis, and biochemistry, including Figures S1–S13 (PDF)

Accession Codes

CCDC 2072438–2072442 contain the supplementary crystallographic data for this paper. These data can be obtained free of charge via www.ccdc.cam.ac.uk/data_request/cif, or by

emailing data_request@ccdc.cam.ac.uk, or by contacting The Cambridge Crystallographic Data Centre, 12 Union Road, Cambridge CB2 1EZ, UK; fax: +44 1223 336033.

AUTHOR INFORMATION

Corresponding Author

Oliver Thorn-Seshold – Department of Pharmacy, Ludwig Maximilians University Munich, 81377 Munich, Germany; orcid.org/0000-0003-3981-651X; Email: oliver.thorn-seshold@cup.lmu.de

Authors

Jan G. Felber – Department of Pharmacy, Ludwig Maximilians University Munich, 81377 Munich, Germany; orcid.org/0000-0002-5010-9624

Lukas Zeisel – Department of Pharmacy, Ludwig Maximilians University Munich, 81377 Munich, Germany; orcid.org/0000-0001-7813-7099

Lena Poczka – Department of Pharmacy, Ludwig Maximilians University Munich, 81377 Munich, Germany

Karoline Scholzen – Department of Medical Biochemistry, Karolinska Institutet, 17177 Stockholm, Sweden

Sander Busker – Department of Medical Biochemistry, Karolinska Institutet, 17177 Stockholm, Sweden; orcid.org/0000-0002-7069-3864

Martin S. Maier – Department of Pharmacy, Ludwig Maximilians University Munich, 81377 Munich, Germany; orcid.org/0000-0002-0409-0539

Ulrike Theisen – Institute of Pharmacology and Toxicology, Medical Center, University of Rostock, 18057 Rostock, Germany

Christina Brandstädter – Interdisciplinary Research Centre (IFZ), Justus Liebig University Giessen, 35392 Giessen, Germany

Katja Becker – Interdisciplinary Research Centre (IFZ), Justus Liebig University Giessen, 35392 Giessen, Germany; orcid.org/0000-0003-4673-3675

Elias S. J. Arnér – Department of Medical Biochemistry, Karolinska Institutet, 17177 Stockholm, Sweden; Department of Selenoprotein Research, National Institute of Oncology, 1122 Budapest, Hungary; orcid.org/0000-0002-4807-6114

Julia Thorn-Seshold – Department of Pharmacy, Ludwig Maximilians University Munich, 81377 Munich, Germany; orcid.org/0000-0002-4879-4159

Complete contact information is available at: <https://pubs.acs.org/10.1021/jacs.1c03234>

Funding

This research was supported by funds from the German Research Foundation (DFG: SFB 1032 project B09 number 201269156, SFB TRR 152 project P24 number 239283807, SPP 1926 project number 426018126, and Emmy Noether grant 400324123 to O.T.-S.; SPP 1710 project BE 1540/23-2 to K.B. (now transferred to Stefan Rahlfs)); LMUExcellent (Junior Researcher Fund to O.T.-S.); the Munich Centre for NanoScience initiative (CeNS) to O.T.-S.; and from Karolinska Institutet, The Knut and Alice Wallenberg Foundations, The Swedish Cancer Society, The Swedish Research Council, Cayman Biomedical Research Institute (CABRI), and the Hungarian Thematic Excellence Programme (TKP2020-NKA-26) to E.S.J.A. J.G.F. thanks the Studienstiftung des deutschen Volkes for support through a Ph.D.

scholarship; L.Z. thanks the Fonds der Chemischen Industrie (FCI) for support through a Ph.D. scholarship; L.P. thanks the GRK 2338 for support through a Ph.D. scholarship; J.T.-S. thanks the Joachim Herz Foundation for fellowship support.

Notes

The authors declare the following competing financial interest(s): J.G.F., L.Z., J.T.-S., and O.T.-S. are inventors on a patent application filed by the LMU Munich in 2021 covering compound structures reported in this paper.

ACKNOWLEDGMENTS

We thank Peter Mayer (LMU) for X-ray crystallography; Qing Cheng (KI) for production and purification of recombinant enzymes; Paula Ruppel, Christina Wichmann, and Julia Rauh (LMU) for synthetic assistance; Reviewer 2 for the helpful comments regarding the sources of artifactual signal; and Matt Fuchter (ICL), Klaus T. Wanner (LMU), Kate Carroll (Scripps), and the attendees of the SPP 1710 conference Thiol-Based Redox Switches in 2019, for their supportive and collegial discussions.

DEDICATION

This paper is dedicated to George Whitesides, who so greatly contributed to setting thiol/disulfide redox chemistry on secure theoretical and practical foundations.

REFERENCES

- (1) Herrmann, J. M.; Dick, T. P. Redox Biology on the Rise. *Biol. Chem.* **2012**, 393 (9), 999–1004.
- (2) Jones, D. P.; Sies, H. The Redox Code. *Antioxid. Redox Signaling* **2015**, 23 (9), 734–746.
- (3) Arnér, E. S. J.; Holmgren, A. Physiological Functions of Thioredoxin and Thioredoxin Reductase. *Eur. J. Biochem.* **2000**, 267 (20), 6102–6109.
- (4) Miller, C. G.; Holmgren, A.; Arnér, E. S. J.; Schmidt, E. E. NADPH-Dependent and -Independent Disulfide Reductase Systems. *Free Radical Biol. Med.* **2018**, 127, 248–261.
- (5) Pillay, C. S.; Hofmeyr, J.-H. S.; Rohwer, J. M. The Logic of Kinetic Regulation in the Thioredoxin System. *BMC Syst. Biol.* **2011**, 5 (1), 15.
- (6) Deponete, M. Glutathione Catalysis and the Reaction Mechanisms of Glutathione-Dependent Enzymes. *Biochim. Biophys. Acta, Gen. Subj.* **2013**, 1830 (5), 3217–3266.
- (7) Lu, J.; Holmgren, A. The Thioredoxin Antioxidant System. *Free Radical Biol. Med.* **2014**, 66, 75–87.
- (8) Fernandes, A. P.; Holmgren, A. Glutaredoxins: Glutathione-Dependent Redox Enzymes with Functions Far Beyond a Simple Thioredoxin Backup System. *Antioxid. Redox Signaling* **2004**, 6 (1), 63–74.
- (9) Holmgren, A.; Johansson, C.; Berndt, C.; Lönn, M. E.; Hudemann, C.; Lillig, C. H. Thiol Redox Control via Thioredoxin and Glutaredoxin Systems. *Biochem. Soc. Trans.* **2005**, 33 (6), 1375.
- (10) Hanschmann, E.-M.; Godoy, J. R.; Berndt, C.; Hudemann, C.; Lillig, C. H. Thioredoxins, Glutaredoxins, and Peroxiredoxins—Molecular Mechanisms and Health Significance: From Cofactors to Antioxidants to Redox Signaling. *Antioxid. Redox Signaling* **2013**, 19 (13), 1539–1605.
- (11) Fridovich, I.; Poole, L. B.; Holmgren, A.; Lou, M. F.; David, S. S.; Osborne, R. L.; Dawson, J. H.; Copley, S. D.; Kadokura, H.; Beckwith, J.; Gilbert, H. F.; Ragsdale, S. W.; Gladyshev, V. N.; Becker, D.; Dickmann, M.; Banerjee, R. *Antioxidant Enzymes. Redox Biochemistry*; John Wiley & Sons, Inc.: Hoboken, NJ, 2008; pp 49–134.
- (12) Cheng, Q.; Sandalova, T.; Lindqvist, Y.; Arnér, E. S. J. Crystal Structure and Catalysis of the Selenoprotein Thioredoxin Reductase 1. *J. Biol. Chem.* **2009**, 284 (6), 3998–4008.

- (13) Fritz-Wolf, K.; Urig, S.; Becker, K. The Structure of Human Thioredoxin Reductase 1 Provides Insights into C-Terminal Rearrangements During Catalysis. *J. Mol. Biol.* **2007**, *370* (1), 116–127.
- (14) Gromer, S.; Johansson, L.; Bauer, H.; Arscott, L. D.; Rauch, S.; Ballou, D. P.; Williams, C. H.; Schirmer, R. H.; Arner, E. S. J. Active Sites of Thioredoxin Reductases: Why Selenoproteins? *Proc. Natl. Acad. Sci. U. S. A.* **2003**, *100* (22), 12618–12623.
- (15) Arnér, E. S. J. Focus on Mammalian Thioredoxin Reductases — Important Selenoproteins with Versatile Functions. *Biochim. Biophys. Acta, Gen. Subj.* **2009**, *1790* (6), 495–526.
- (16) Maroney, M. J.; Hondal, R. J. Selenium versus Sulfur: Reversibility of Chemical Reactions and Resistance to Permanent Oxidation in Proteins and Nucleic Acids. *Free Radical Biol. Med.* **2018**, *127*, 228–237.
- (17) Sagemark, J.; Elgán, T. H.; Bürglin, T. R.; Johansson, C.; Holmgren, A.; Berndt, K. D. Redox Properties and Evolution of Human Glutaredoxins. *Proteins: Struct., Funct., Genet.* **2007**, *68* (4), 879–892.
- (18) Weichsel, A.; Gasdaska, J. R.; Powis, G.; Montfort, W. R. Crystal Structures of Reduced, Oxidized, and Mutated Human Thioredoxins: Evidence for a Regulatory Homodimer. *Structure* **1996**, *4* (6), 735–751.
- (19) Johansson, L.; Arscott, L. D.; Ballou, D. P.; Williams, C. H., Jr.; Arnér, E. S. J. Studies of an Active Site Mutant of the Selenoprotein Thioredoxin Reductase: The Ser-Cys-Cys-Ser Motif of the Insect Orthologue Is Not Sufficient to Replace the Cys-Sec Dyad in the Mammalian Enzyme. *Free Radical Biol. Med.* **2006**, *41* (4), 649–656.
- (20) Fritz-Wolf, K.; Kehr, S.; Stumpf, M.; Rahlfs, S.; Becker, K. Crystal Structure of the Human Thioredoxin Reductase–Thioredoxin Complex. *Nat. Commun.* **2011**, *2* (383), 1–8.
- (21) Pan, J. L.; Bardwell, J. C. A. The Origami of Thioredoxin-like Folds. *Protein Sci.* **2006**, *15* (10), 2217–2227.
- (22) Palde, P. B.; Carroll, K. S. A Universal Entropy-Driven Mechanism for Thioredoxin–Target Recognition. *Proc. Natl. Acad. Sci. U. S. A.* **2015**, *112* (26), 7960–7965.
- (23) Meyer, A. J.; Dick, T. P. Fluorescent Protein-Based Redox Probes. *Antioxid. Redox Signaling* **2010**, *13* (5), 621–650.
- (24) Lukyanov, K. A.; Belousov, V. V. Genetically Encoded Fluorescent Redox Sensors. *Biochim. Biophys. Acta, Gen. Subj.* **2014**, *1840* (2), 745–756.
- (25) Schwarzländer, M.; Dick, T. P.; Meyer, A. J.; Morgan, B. Dissecting Redox Biology Using Fluorescent Protein Sensors. *Antioxid. Redox Signaling* **2016**, *24* (13), 680–712.
- (26) Sallin, O.; Reymond, L.; Gondrand, C.; Raith, F.; Koch, B.; Johansson, K. Semisynthetic Biosensors for Mapping Cellular Concentrations of Nicotinamide Adenine Dinucleotides. *eLife* **2018**, *7*, e32638.
- (27) Lee, M. H.; Yang, Z.; Lim, C. W.; Lee, Y. H.; Dongbang, S.; Kang, C.; Kim, J. S. Disulfide-Cleavage-Triggered Chemosensors and Their Biological Applications. *Chem. Rev.* **2013**, *113* (7), 5071–5109.
- (28) Pires, M. M.; Chmielewski, J. Fluorescence Imaging of Cellular Glutathione Using a Latent Rhodamine. *Org. Lett.* **2008**, *10* (5), 837–840.
- (29) Lim, C. S.; Masanta, G.; Kim, H. J.; Han, J. H.; Kim, H. M.; Cho, B. R. Ratiometric Detection of Mitochondrial Thiols with a Two-Photon Fluorescent Probe. *J. Am. Chem. Soc.* **2011**, *133* (29), 11132–11135.
- (30) Butora, G.; Qi, N.; Fu, W.; Nguyen, T.; Huang, H.-C.; Davies, I. W. Cyclic-Disulfide-Based Prodrugs for Cytosol-Specific Drug Delivery. *Angew. Chem., Int. Ed.* **2014**, *53* (51), 14046–14050.
- (31) Felber, J. G.; Poczka, L.; Busker, S.; Theisen, U.; Zeisel, L.; Maier, M. S.; Brandstätter, C.; Scholzen, K.; Becker, K.; Arnér, E. S. J.; Ahlfeld, J.; Thorn-Seshold, O. Cyclic 5-Membered Disulfides Are Not Selective Substrates of Thioredoxin Reductase, but Are Opened Nonspecifically by Thiols. *ChemRxiv* **2020**, DOI: 10.26434/chemrxiv.13483155.v1 (accessed May 9, 2021).
- (32) Cherblanc, F. L.; Chapman, K. L.; Brown, R.; Fuchter, M. J. Chaetocin Is a Nonspecific Inhibitor of Histone Lysine Methyltransferases. *Nat. Chem. Biol.* **2013**, *9*, 136–137.
- (33) Zhang, L.; Duan, D.; Liu, Y.; Ge, C.; Cui, X.; Sun, J.; Fang, J. Highly Selective Off–On Fluorescent Probe for Imaging Thioredoxin Reductase in Living Cells. *J. Am. Chem. Soc.* **2014**, *136* (1), 226–233.
- (34) Ma, H.; Zhang, J.; Zhang, Z.; Liu, Y.; Fang, J. A Fast Response and Red Emission Probe for Mammalian Thioredoxin Reductase. *Chem. Commun.* **2016**, *52* (81), 12060–12063.
- (35) Li, X.; Zhang, B.; Yan, C.; Li, J.; Wang, S.; Wei, X.; Jiang, X.; Zhou, P.; Fang, J. A Fast and Specific Fluorescent Probe for Thioredoxin Reductase That Works via Disulphide Bond Cleavage. *Nat. Commun.* **2019**, *10* (2745), 1–12.
- (36) Li, X.; Hou, Y.; Meng, X.; Ge, C.; Ma, H.; Li, J.; Fang, J. Selective Activation of a Prodrug by Thioredoxin Reductase Providing a Strategy to Target Cancer Cells. *Angew. Chem., Int. Ed.* **2018**, *57* (21), 6141–6145.
- (37) Houk, J.; Whitesides, G. M. Structure-Reactivity Relations for Thiol-Disulfide Interchange. *J. Am. Chem. Soc.* **1987**, *109* (22), 6825–6836.
- (38) Singh, R.; Whitesides, G. M. Degenerate Intermolecular Thiolate-Disulfide Interchange Involving Cyclic Five-Membered Disulfides Is Faster by Approximately 103 than That Involving Six- or Seven-Membered Disulfides. *J. Am. Chem. Soc.* **1990**, *112* (17), 6304–6309.
- (39) Abegg, D.; Gasparini, G.; Hoch, D. G.; Shuster, A.; Bartolami, E.; Matile, S.; Adibekian, A. Strained Cyclic Disulfides Enable Cellular Uptake by Reacting with the Transferrin Receptor. *J. Am. Chem. Soc.* **2017**, *139* (1), 231–238.
- (40) Gasparini, G.; Sargsyan, G.; Bang, E.-K.; Sakai, N.; Matile, S. Ring Tension Applied to Thiol-Mediated Cellular Uptake. *Angew. Chem., Int. Ed.* **2015**, *54* (25), 7328–7331.
- (41) Cheng, Y.; Pham, A.-T.; Kato, T.; Lim, B.; Moreau, D.; López-Andarias, J.; Zong, L.; Sakai, N.; Matile, S. Inhibitors of Thiol-Mediated Uptake. *Chem. Sci.* **2021**, *12*, 626.
- (42) Butora, G. Nucleoside Kinase Bypass Compositions and Methods. WO2014088923A1, 2014.
- (43) Hayashi, J.; Samezawa, Y.; Ochi, Y.; Wada, S.; Urata, H. Syntheses of Prodrug-Type Phosphotriester Oligonucleotides Responsive to Intracellular Reducing Environment for Improvement of Cell Membrane Permeability and Nuclease Resistance. *Bioorg. Med. Chem. Lett.* **2017**, *27* (14), 3135–3138.
- (44) Kong, F.; Zhao, Y.; Liang, Z.; Liu, X.; Pan, X.; Luan, D.; Xu, K.; Tang, B. Highly Selective Fluorescent Probe for Imaging H₂ Se in Living Cells and in Vivo Based on the Disulfide Bond. *Anal. Chem.* **2017**, *89* (1), 688–693.
- (45) Ziv, I. Compounds and Methods for Trans-Membrane Delivery of Molecules. US9687556B2, 2017.
- (46) Ziv, I. Pro-Drugs and Related Methods. WO2017017669A1, 2017.
- (47) Na, Y.; Kohn, H. Quinone-Cyclized Porfiromycins. *Heterocycles* **2001**, *55* (7), 1347–1364.
- (48) Lee, S. H.; Kohn, H. Cyclic Disulfide C(8) Iminoporfiromycin: Nucleophilic Activation of a Porfiromycin. *J. Am. Chem. Soc.* **2004**, *126* (13), 4281–4292.
- (49) Ollivier, N.; Dheur, J.; Mhida, R.; Blanpain, A.; Melnyk, O. Bis(2-Sulfanylethyl)Amino Native Peptide Ligation. *Org. Lett.* **2010**, *12* (22), 5238–5241.
- (50) Zhu, B.; Zhang, X.; Li, Y.; Wang, P.; Zhang, H.; Zhuang, X. A Colorimetric and Ratiometric Fluorescent Probe for Thiols and Its Bioimaging Applications. *Chem. Commun.* **2010**, *46* (31), 5710.
- (51) Hong, K.-H.; Kim, D. I.; Kwon, H.; Kim, H.-J. A Fluoresceinylcarbonate-Based Fluorescent Probe for the Sensitive Detection of Biothiols in a HEPES Buffer and Its Cellular Expression. *RSC Adv.* **2014**, *4* (2), 978–982.
- (52) Dan, K.; Veetil, A. T.; Chakraborty, K.; Krishnan, Y. DNA Nanodevices Map Enzymatic Activity in Organelles. *Nat. Nanotechnol.* **2019**, *14* (3), 252–259.

- (53) Mata, G.; do Rosário, V. E.; Iley, J.; Constantino, L.; Moreira, R. A Carbamate-Based Approach to Primaquine Prodrugs: Antimalarial Activity, Chemical Stability and Enzymatic Activation. *Bioorg. Med. Chem.* **2012**, *20* (2), 886–892.
- (54) Ghosh, A. K.; Brindisi, M. Organic Carbamates in Drug Design and Medicinal Chemistry. *J. Med. Chem.* **2015**, *58* (7), 2895–2940.
- (55) Vacondio, F.; Silva, C.; Mor, M.; Testa, B. Qualitative Structure-Metabolism Relationships in the Hydrolysis of Carbamates. *Drug Metab. Rev.* **2010**, *42* (4), 551–589.
- (56) Thorn-Seshold, O.; Vargas-Sanchez, M.; McKeon, S.; Hasserodt, J. A Robust, High-Sensitivity Stealth Probe for Peptidases. *Chem. Commun.* **2012**, *48* (50), 6253–6255.
- (57) Tian, L.; Yang, Y.; Wysocki, L. M.; Arnold, A. C.; Hu, A.; Ravichandran, B.; Sternson, S. M.; Looger, L. L.; Lavis, L. D. Selective Esterase-Ester Pair for Targeting Small Molecules with Cellular Specificity. *Proc. Natl. Acad. Sci. U. S. A.* **2012**, *109* (13), 4756–4761.
- (58) Orte, A.; Crovetto, L.; Talavera, E. M.; Boens, N.; Alvarez-Pez, J. M. Absorption and Emission Study of 2',7'-Difluorofluorescein and Its Excited-State Buffer-Mediated Proton Exchange Reactions. *J. Phys. Chem. A* **2005**, *109* (5), 734–747.
- (59) Machida, T.; Dutt, S.; Winssinger, N. Allosterically Regulated Phosphatase Activity from Peptide-PNA Conjugates Folded Through Hybridization. *Angew. Chem., Int. Ed.* **2016**, *55* (30), 8595–8598.
- (60) Rando, G.; Winssinger, N.; Lindberg, E.; Anzola, M. New Compounds and Uses Thereof for Detection of Target Molecules in a Sample. US 2019/0315713 A1.
- (61) Fu, Q.; Li, H.; Duan, D.; Wang, C.; Shen, S.; Ma, H.; Liu, Z. External-Radiation-Induced Local Hydroxylation Enables Remote Release of Functional Molecules in Tumors. *Angew. Chem., Int. Ed.* **2020**, *59* (48), 21546–21552.
- (62) Lukesh, J. C.; Palte, M. J.; Raines, R. T. A Potent, Versatile Disulfide-Reducing Agent from Aspartic Acid. *J. Am. Chem. Soc.* **2012**, *134* (9), 4057–4059.
- (63) Lees, W. J.; Whitesides, G. M. Equilibrium Constants for Thiol-Disulfide Interchange Reactions: A Coherent, Corrected Set. *J. Org. Chem.* **1993**, *58* (3), 642–647.
- (64) Chênevert, R.; Dickman, M. Enzymatic Route to Chiral, Nonracemic Cis-2,6- and Cis,Cis-2,4,6-Substituted Piperidines. Synthesis of (+)-Dihydropinidine and Dendrobate Alkaloid (+)-241D. *J. Org. Chem.* **1996**, *61* (10), 3332–3341.
- (65) Le Corre, L.; Kizirian, J.-C.; Levraud, C.; Boucher, J.-L.; Bonnet, V.; Dhimane, H. Diastereoselective Functionalizations of Enecarbamates Derived from Pipecolic Acid towards 5-Guanidinopipicolates as Arginine Mimetics. *Org. Biomol. Chem.* **2008**, *6* (18), 3388–3398.
- (66) Vartak, A. P.; Gabriela Deaciu, A.; Dwozkin, L. P.; Crooks, P. A. Quinolobane: A Water-Soluble Lobelane Analogue and Inhibitor of VMAT2. *Bioorg. Med. Chem. Lett.* **2010**, *20* (12), 3584–3587.
- (67) Yang, B. V.; O'Rourke, D.; Li, J. Mild and Selective Debenzylation of Tertiary Amines Using α -Chloroethyl Chloroformate. *Synlett* **1993**, *1993* (03), 195–196.
- (68) Thorn-Seshold, O.; Felber, J.; Thorn-Seshold, J.; Zeisel, L. Disulfide-Based Prodrug Compounds. EP1163944.8.
- (69) Capasso, S.; Zagari, A. 1,2-Dithiane-4,5-Diol. *Acta Crystallogr., Sect. B: Struct. Crystallogr. Cryst. Chem.* **1981**, *37* (7), 1437–1439.
- (70) Kilgore, H. R.; Raines, R. T. Disulfide Chromophores Arise from Stereoelectronic Effects. *J. Phys. Chem. B* **2020**, *124* (19), 3931–3935.
- (71) Burns, J. A.; Whitesides, G. M. Predicting the Stability of Cyclic Disulfides by Molecular Modeling: Effective Concentrations in Thiol-Disulfide Interchange and the Design of Strongly Reducing Dithiols. *J. Am. Chem. Soc.* **1990**, *112* (17), 6296–6303.
- (72) Lüttringhaus, A.; Brechlin, A. Cyclische Disulfide, III. cis- und trans-2,3-Dithia-decalin. *Chem. Ber.* **1959**, *92* (9), 2271–2277.
- (73) Rothwarf, D. M.; Scheraga, H. A. Equilibrium and Kinetic Constants for the Thiol-Disulfide Interchange Reaction between Glutathione and Dithiothreitol. *Proc. Natl. Acad. Sci. U. S. A.* **1992**, *89* (17), 7944–7948.
- (74) Jia, H.; Hu, G.; Shi, D.; Gan, L.; Zhang, H.; Yao, X.; Fang, J. Fluorophore-Dependent Cleavage of Disulfide Bond Leading to a Highly Selective Fluorescent Probe of Thioredoxin. *Anal. Chem.* **2019**, *91* (13), 8524–8531.
- (75) Dal Corso, A.; Borlandelli, V.; Corno, C.; Perego, P.; Belvisi, L.; Pignataro, L.; Gennari, C. Fast Cyclization of a Proline-Derived Self-Immolative Spacer Improves the Efficacy of Carbamate Prodrugs. *Angew. Chem., Int. Ed.* **2020**, *59* (10), 4176–4181.
- (76) Laurent, Q.; Sakai, N.; Matile, S. The Opening of 1,2-Dithiolanes and 1,2-Diselenolanes: Regioselectivity, Rearrangements, and Consequences for Poly(Disulfide)s, Cellular Uptake and Pyruvate Dehydrogenase Complexes. *Helv. Chim. Acta* **2019**, *102* (2), e1800209.
- (77) Chyan, W.; Kilgore, H. R.; Gold, B.; Raines, R. T. Electronic and Steric Optimization of Fluorogenic Probes for Biomolecular Imaging. *J. Org. Chem.* **2017**, *82* (8), 4297–4304.
- (78) Cheng, Q.; Arnér, E. S. J. Selenocysteine Insertion at a Predefined UAG Codon in a Release Factor 1 (RF1)-Depleted Escherichia Coli Host Strain Bypasses Species Barriers in Recombinant Selenoprotein Translation. *J. Biol. Chem.* **2017**, *292* (13), 5476–5487.
- (79) Cheng, Q.; Arnér, E. S. J. Overexpression of Recombinant Selenoproteins in E. Coli. In *Selenoproteins*; Chavatte, L., Ed.; Methods in Molecular Biology; Springer: New York, 2018; Vol. 1661, pp 231–240. DOI: 10.1007/978-1-4939-7258-6_17.
- (80) Lacey, B. M.; Eckenroth, B. E.; Flemer, S.; Hondal, R. J. Selenium in Thioredoxin Reductase: A Mechanistic Perspective. *Biochemistry* **2008**, *47* (48), 12810–12821.
- (81) Espinosa, B.; Arnér, E. S. J. Thioredoxin-Related Protein of 14 kDa as a Modulator of Redox Signalling Pathways: TRP14 in Redox Signalling. *Br. J. Pharmacol.* **2019**, *176* (4), 544–553.
- (82) Woo, J. R.; Kim, S. J.; Jeong, W.; Cho, Y. H.; Lee, S. C.; Chung, Y. J.; Rhee, S. G.; Ryu, S. E. Structural Basis of Cellular Redox Regulation by Human TRP14. *J. Biol. Chem.* **2004**, *279* (46), 48120–48125.

3.1.3 Development of a cellular 1,2-thiaselenane probe for TrxR

This chapter was published as follows:

Journal	Chem 2022 , 8, 1493-1517. (highlighted in: R. Hondal. Redox Biology 2022 , 54, 102376; L. Zeisel. Chem 2022 , 8, 1167; and Payne et al. Chem 2022 , 8, 1175).
Title	<i>Selective cellular probes for mammalian thioredoxin reductase TrxR1: Rational design of RX1, a modular 1,2-thiaselenane redox probe</i>
Author List	Lukas Zeisel [#] , Jan G. Felber , Karoline C. Scholzen, Lena Poczka, Dorian Cheff, Martin S. Maier, Qing Cheng, Min Shen, Matthew D. Hall, Elias S. J. Arnér, Julia Thorn-Seshold, Oliver Thorn-Seshold* [#] first author; *corresponding author
Publication date	Apr 14 th , 2022
Available at	https://www.cell.com/chem/fulltext/S2451-9294(22)00147-4

Author contributions and collaborations

(1) Work performed in the Thorn-Seshold group, LMU Munich:

Lukas Zeisel developed the synthetic access to desymmetrized 1,2-thiaselenane regioisomers and performed synthesis and analysis of the fluorogenic probes described in this work (**Fig. 3**). He further performed chemoreductant, enzymatic cell-free studies (**Fig. 4**), mechanistic analysis (**Fig. 1 and 2**), informatics (**Fig. 6**), coordinated data assembly and visualization (**Fig. 5,6**), conceptually analyzed the scientific outcome, and wrote the manuscript.

I performed synthesis and analysis of the solubilized fluorogenic probes containing morpholinamides (**M**) and piperazinamides (**P**) as part of a general solubilization effort within our set of redox probes (**Fig. 3**). I further performed chemoreductant and enzymatic specificity screening (**Fig. 4**).

Lena Poczka performed cellular studies (**Fig. 5**). **Martin S. Maier** performed synthesis and analysis. **Julia Thorn-Seshold** supervised cell biology. **Oliver Thorn-Seshold** designed the concept and experiments, performed informatics, coordinated data assembly, and wrote the manuscript.

(2) Collaboration with the Arnér group, Karolinska Institutet (KI), Stockholm: **Karoline C. Scholzen** performed biochemical screenings (**Fig. 4**), cellular inhibitor, and knockout studies (**Fig. 5**). **Qing Cheng** expressed and purified recombinant TrxR, Trx, and related redox proteins. **Min Shen** performed informatics. **Elias S. J. Arnér** supervised biochemical studies and cell biology.

(3) Collaboration with the National Center for Advancing Translational Sciences (NCATS), National Institutes of Health (NIH), Rockville (USA): **Dorian Chef** performed the high-throughput LOPAC screen (**Fig. 6**). **Matthew D. Hall** supervised LOPAC screening.

Background

Cyclic 5-membered disulfides (1,2-dithiolanes) were reported as selective sensors for reduction by TrxR, despite their kinetic lability and tendency for ring-opening linearisation being long known. Based on our cell-free and cellular evaluation, we had concluded that 1,2-dithiolanes are not suitable to selectively report on TrxR activity in cells (see **chapter 3.1.1**). Separately, we had developed the first molecular motif to target thioredoxins based on cyclic 6-membered disulfides as artificial substrates by rational design (see **chapter 3.1.2**). It is because of its highly stabilized ring system, extremely low reduction potential, and intrinsic reversibility that the *cis*-fused 1,2-dithiane motif **SS66C** was a “chemocompatible” fit to vicinal dithiol-type proteins like Trx.

Summary

Following these rationales, we now designed novel cyclic dichalcogenide reduction sensing units to target the unusual Cys⁴⁹⁷Sec⁴⁹⁸ active site found in TrxR: using desymmetrized cyclic 6-membered selenenylsulfides (1,2-thiaselenanes). We expected the cyclic topology to avoid nonspecific triggering by monothiols like GSH, while again, vicinal dichalcogenide-type cellular reductants would be required (**Fig. 1**). By installing the Se atom within the reducible trigger, we further hoped for drastic kinetic effects to favoring selenolates over thiolates as incoming nucleophiles when attacking at the Se atom. While a selenolate attack would form diselenide intermediates with lifetimes that allow subsequent resolution and cargo expulsion, a selenenylsulfide formed after a thiolate attack would be more rapidly reversed, potentially even from vicinal dithiols and not only from monothiols (**Fig. 2**). In other words: 1,2-thiaselenanes could require a vicinal dichalcogenide-type redox-active site with a selenolate as the initial nucleophile. Mammalian TrxRs are the only mammalian enzyme with that structural motif.

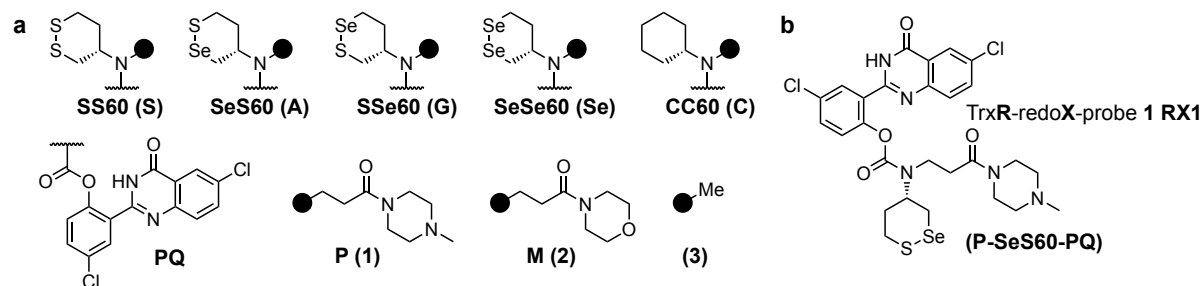


Figure 15 (a) Structure overview of *trigger*, *cargo*, and side chain motifs used in this study. (b) Molecular design of the selective cellular TrxR1 reporter probe RX1.

To experimentally test our design logic and its applicability when used in fluorogenic imaging agents, we synthesized the two regioisomers 1,2-thiaselenane-4-amine (**SeS60, A**) and 1,2-thiaselenane-5-amine (**SSe60, G**) as trigger precursors. We introduced morpholinamide (**M**) and *N*-methyl piperazinamide (**P**) sidechains assuming that additional solubilization of the otherwise rather lipophilic constructs would be required (**Figure 15a**). We assembled a series of 12 fluorogenic probes based on the precipitating dye hydroxyphenyl-quinazolin-3-one (HPQ) employing the new trigger motifs, their parent disulfides (**SS60, S**), and diselenides (**SeSe60, Se**), and a non-reducible control (**CC60, C**) (**Fig. 3**). Biochemical assays revealed the following mechanistic features (**Fig. 4**): (i) the Se-proximal probes (**SeS60**) completely resisted signal generation through reduction by GSH, whereas its Se-distal

regioisomers (**SSe60**) were labile to monothiol triggering; (ii) rapid and quantitative turnover by TrxR1 was observed for both 1,2-thiaselenanes with selenolate nucleophile being crucial, as controlled using TrxR2 (no Sec) or the respective TrxR1^{U498C} mutant; (iii) other cellular monoselenol redox enzymes like GPx gave no activation; and (iv) activation of 1,2-thiaselenane probes by strong dithiol-type reductants like Trx was possible, but with orders of magnitude lower sensitivities.

Previous fluorogenic probe designs (**chapter 3.1.2**) had shown poor cellular activation, presumably due to their lipophilic character and, subsequently, low bioavailability. Here, we observed similar results for the simple non-solubilized probes (e.g. **SeS60-PQ**) but when we attached side chain motifs introducing non-basic polarity (**M**) or a distal basic amine (**P**), we saw good dose-dependent cellular activation (**Fig. 5**). The level of activation for **P-SSe60-PQ (G1)** was comparable to that found for the linear disulfide control probe **SS00-PQ**, which we interpreted as the result of cellular processing by GSH and other protein monothiols. In contrast, **P-SeS60-PQ** gave a lower absolute signal with a strong dependence on supplementation with Na₂SeO₃ in the cell culture medium. We aimed to investigate the mechanism of cellular activation and used the selective inhibitors TRi-1 and TRi-3, both based on tuned S_NAr-type electrophilicity which differentiates selenolate nucleophiles from thiolates.¹³⁶ We saw strong suppression of cellular signals for **P-SeS60-PQ** upon inhibitor treatment and also observed no activation in cells with a genetic knockout of cytosolic TrxR1 making it the first true cellular reporter for TrxR1 activity (**Fig. 5**).

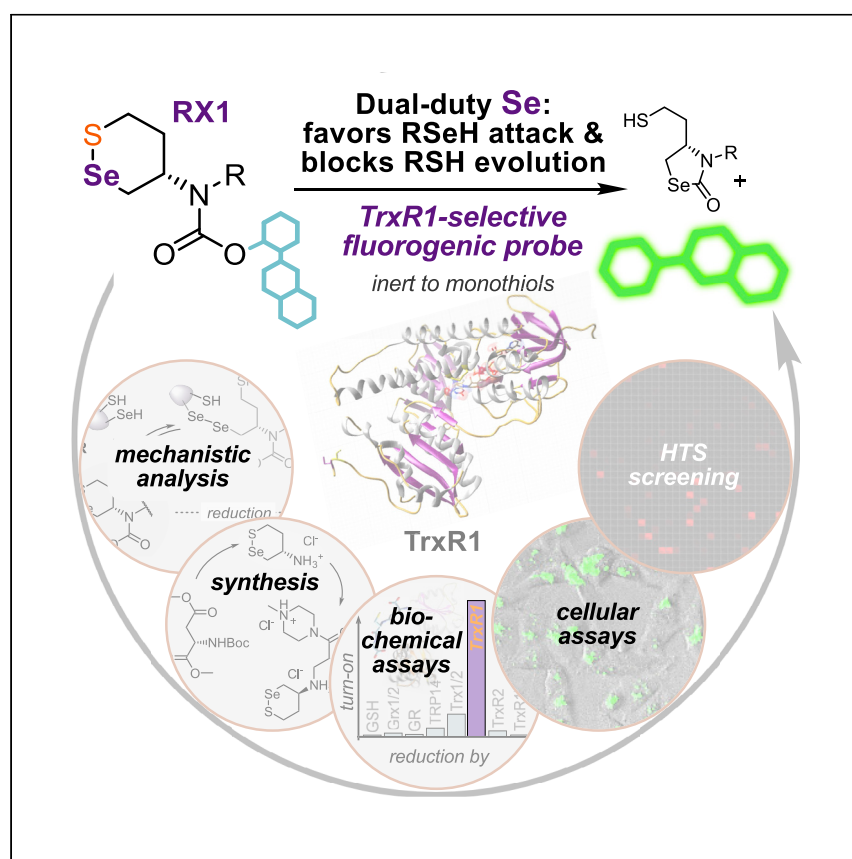
We called the “star compound” TrxR-redox-probe-1 (**RX1**), which combined all structural design features of previous efforts (**Figure 15b**): (i) a stabilized cyclic dichalcogenide allowing kinetic reversibility; (ii) a unique reduction sensitive unit with the Se atom placed at the correct position to prevent monothiol processing, that is still “chemocompatible” with the Cys⁴⁹⁷Sec⁴⁹⁸ redox-active site found in TrxR; (iii) an environment-insensitive cumulative reporter dye that is based on solid-state large Stokes shift fluorescence orthogonal to e.g. GFP imaging; and (iv) a distal basic amine enabling sufficient cellular delivery and bioavailability.

To demonstrate our new probe’s applicability for the discovery of cellular inhibitors for TrxR, we performed a pilot high-throughput screen using the Library of Pharmaceutically Active Compounds (LOPAC₁₂₈₀). **RX1** showed excellent assay properties, and we identified a number of qualified hits that we validated against a very expensive previous cell-free (purified enzyme) screen performed by our collaborators.²³⁹ In this way, we could classify inhibitors by chemotype, when looking at their relative performance in cells as compared to their previous cell-free inhibition. We found that primarily inhibitors based on fine-tuned S_NAr-type electrophiles are reliable both cell-free and in cells (**Fig. 6**).

Taken together, these results show how the rational chemical design of a fluorogenic probe requiring various well-chosen design features can deliver a selective cellular reporter for a redox enzyme that is also a promising drug target for cancer research. We believe that **RX1** will function as a useful research tool for the validation of biochemical mechanisms and the discovery of new classes of cellular inhibitors that may be used for cancer therapy in the future.

Article

Selective cellular probes for mammalian thioredoxin reductase TrxR1: Rational design of RX1, a modular 1,2-thiaselenane redox probe



Lukas Zeisel, Jan G. Felber, Karoline C. Scholzen, ..., Elias S.J. Arnér, Julia Thorn-Seshold, Oliver Thorn-Seshold

oliver.thorn-seshold@cup.lmu.de

Highlights

Rational design of TrxR-selective, monothiol-resistant selenenylsulfide probe RX1

RX1 reveals cellular TrxR expression and activity in live cells

High-throughput screen for cellularly effective TrxR inhibitors shows S_NAr privileged

Dual-duty selenium recruits TrxR but blocks monothiois; regioisomer shows role of pathway

Quantifying the activity of cellular redox processes is crucial for understanding their physiological roles and targeting their dysregulation in pathologies. We report RX1, the first cellularly selective probe for thioredoxin reductase 1 (TrxR1)—a central node of cellular redox. A reactivity-based approach selectively targets TrxR's active site selenolthiol yet resists one million times higher concentrations of monothiois. RX1 sets the stage for *in vivo* imaging of TrxR1 activity in health and disease and will drive and reorient TrxR1-inhibitor drug design.



Zeisel et al., Chem 8, 1493–1517
May 12, 2022 Published by Elsevier Inc.
<https://doi.org/10.1016/j.chempr.2022.03.010>



Article

Selective cellular probes for mammalian thioredoxin reductase TrxR1: Rational design of RX1, a modular 1,2-thiaselenane redox probe

Lukas Zeisel,¹ Jan G. Felber,¹ Karoline C. Scholzen,² Lena Poczka,¹ Dorian Cheff,³ Martin S. Maier,¹ Qing Cheng,² Min Shen,³ Matthew D. Hall,³ Elias S.J. Arnér,^{2,4} Julia Thorn-Seshold,¹ and Oliver Thorn-Seshold^{1,5,*}

SUMMARY

Quantifying the activity of key cellular redox players is crucial for understanding physiological homeostasis and for targeting their perturbed states in pathologies, including cancer and inflammatory diseases. However, cellularly selective probes for oxidoreductase turnover are sorely lacking. We rationally developed the first probes that selectively target the mammalian selenoprotein thioredoxin reductase (TrxR) by using a cyclic selenenylsulfide oriented to harness TrxR's unique selenolthiol chemistry while resisting the cellular monothiol background. Lead probe RX1 had excellent TrxR1-selective performance in cells, cross-validated through the use of knockout, selenium starvation, knockin, and chemical inhibitors. Its background-free fluorogenicity enabled us to perform the first quantitative high-throughput live-cell screen for TrxR1 inhibitors, which indicated that tempered S_NAr electrophiles may be more selective TrxR drugs than the classical electrophiles used hitherto. The RX1 design thus sets the stage for *in vivo* imaging of the activity of this key oxidoreductase in health and disease and can also drive TrxR1-inhibitor drug design.

INTRODUCTION

The thioredoxin reductase-thioredoxin (TrxR-Trx) system and the glutathione reductase-glutathione-glutaredoxin (GR-GSH-Grx) system are the two highly evolutionarily conserved “central nodes” of redox biology, which are of fundamental importance across all eukaryotes (Figure 1A).^{1,2} They drive and buffer a range of biological redox reactions that are crucial to metabolism, protein folding, signaling, protein regulation, and many aspects of cellular homeostasis and stress responses.^{3,4} These systems are driven by reducing equivalents harvested from NADPH through the enzymes TrxR and GR, then distributed by downstream effector proteins, mainly isoenzymes of Trx and Grx, into various manifolds of dithiol/disulfide-type reactions. For all these redox enzymes, both chemocompatibility and protein-substrate binding determine their substrate scopes; these combine with subcellular compartmentalization of the isoforms and substrates in each cascade to allow sophisticated regulation and spatial organization of redox reactions in cells.⁵

Due to the fundamental importance of redox networks across biology, developing techniques to monitor and respond to their dynamics is critical for understanding cellular physiology. Biological approaches to monitor redox biochemistry include

The bigger picture

Redox reactions are key to biology at all levels. To understand redox in health and during stress responses and to target the dysregulated redox that is a hallmark of disease, we need tools that report non-invasively on the activity of the key oxidoreductases. However, we lack these tools, and fulfilling the need to selectively target individual oxidoreductases out of manifolds that perform similar chemistries is challenging. Here, we rationally developed RX1: the first chemical probe that is selectively activated in cells by the key mammalian selenoenzyme, thioredoxin reductase (TrxR). This enabled us to perform the first high-throughput live-cell screen for TrxR1 inhibitors—a drug class of intense interest as therapeutics for autoimmune/inflammatory disease and cancer—and allowed critical re-evaluation of commonly used electrophilic warheads. RX1 thus sets the stage for *in vivo* imaging of TrxR1 activity in health and disease, and it can also drive TrxR1-inhibitor drug design. Finally, the thermodynamic and kinetic considerations behind RX1's selectivity will also rationally guide the design of probes for other key players in redox biology.



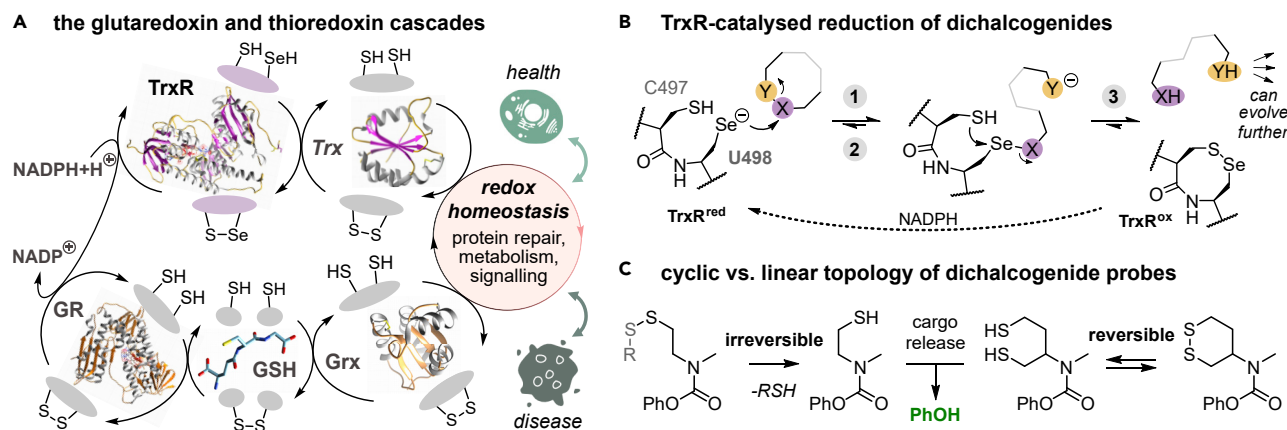


Figure 1. Mechanistic considerations toward designing TrxR-selective probes

(A) Simplified view of the central dithiol/disulfide-type redox cascades of cell biology.

(B) Reaction mechanism for TrxR reducing a generalized dichalcogenide XY, using its C-terminal Sec-Cys active site. Initial exchange (1) gives an intermediate that can either evolve backward by reforming the dichalcogenide (2) or else evolve forward by full reduction (3) to the dichalcogenol. Recovery of TrxR by NADPH makes this a non-equilibrium process.

(C) Topology considerations: linear topology dichalcogenides are irreversibly committed to cargo release after monothiol exchange, whereas the exchange and reduction steps for cyclic topology dichalcogenides are reversible (full mechanism in Figure S3).

redox-responsive ratiometric fluorescent protein fusions. These are well established for imaging redox poise (the balance between reduced and oxidized fusion protein) and include sensors for Grxs and Trxs.^{6–8} However, they do not reveal the turnovers these species undergo, which are integral to a network understanding of redox homeostasis. In addition, since TrxR and GR are NADPH-driven enzymes, ratiometric monitoring of their redox poise is not informative about their biology, which depends on turnover. Measuring mRNA or protein expression levels are also insufficient to understand cellular redox systems since reaction rates through networks are dynamically controlled on many levels, e.g., by protein binding partners, post-translational modifications, subcellular localization, and throttling flow from upstream reductants (or to downstream electron acceptors). Molecular probes that selectively report on the activity of individual redox-active proteins within the TrxR/Trx and GR/GSH/Grx networks would be ideal tools for studying redox biology: but no such probes exist.

Here, we sought to develop TrxR-selective molecular probes that noninvasively report TrxR activity in live cells. We focused on chemical designs to monitor enzymatic turnover by irreversible accumulation of signals in the form of an activated probe. We additionally required the probes to be modular, i.e., the same approach should be applicable to activating arbitrary cargoes, including drugs. This is of particular interest since redox dysregulation, including upregulation of TrxR activity and expression, is correlated to disease progression, severity, and resistance to conventional therapeutics, in a range of pathologies.⁹ These include nearly all solid tumors (hypoxia-induced gene expression shifts), as well as autoimmune and inflammatory conditions (redox signaling and microenvironment effects).¹⁰ Developing modular strategies to activate imaging agents (for diagnostics) and drugs (for redox-targeted therapeutics) could therefore be a powerful approach not just for understanding but also for usefully responding to cellular redox activity in health and in disease.

The challenge for small-molecule probes of dithiol/disulfide-type oxidoreductases is to distinguish selectively between proteins that perform similar chemistries. The

¹Department of Pharmacy, Ludwig Maximilians University of Munich, Butenandtstr. 5–13, Munich 81377, Germany

²Division of Biochemistry, Department of Medical Biochemistry and Biophysics, Karolinska Institutet, Solnavägen 9, Stockholm 17177, Sweden

³National Center for Advancing Translational Sciences, National Institutes of Health, 9800 Medical Center Drive, Rockville, MD 20850, USA

⁴Department of Selenoprotein Research, National Institute of Oncology, Budapest 1122, Hungary

⁵Lead contact

*Correspondence: oliver.thorn-seshold@cup.lmu.de
<https://doi.org/10.1016/j.chempr.2022.03.010>

TrxR and GR systems that are the major mammalian dithiol/disulfide reductants (Figure 1A) have been well reviewed.⁵ In brief, (1) TrxRs and GRs are low-expression enzymes (ca. 20 nM cellular concentration) that harvest electrons from NADPH to dithiol/disulfide active sites (CVNVGC motif).¹¹ GR has high specificity for reducing glutathione disulfide (GSSG) and little activity on other species. The major TrxRs in mammals are cytosolic TrxR1 and mitochondrial TrxR2. They have a broader substrate scope than GR due to their additional C-terminal selenolthiol/selenenylsulfide active site (CU motif) located on an exposed flexible tail, which relays electrons from the NADPH-driven dithiol site to substrates. TrxR's native substrates include disulfide Trxs and TRP14; diverse small molecules can also be reduced (Figure 1B).^{12,13} The rare selenolthiol of TrxR endows it with distinctive redox properties compared with dithiol proteins, including enhanced reaction kinetics, lowered reduction potential, and resistance to permanently function-suppressing oxidation.^{14,15} (2) Trxs and dithiol Grxs are proteins with exposed dithiol/disulfide redox-active sites (CxxC motif) that reduce a broad scope of substrates, including disulfides; they have moderate expression levels (up to ca. 10 μ M). Trxs have lower reduction potentials and are reduced by TrxR; Grxs have higher reduction potentials and use monothiol GSH (ca. 1–8 mM in the cytosol) for recovery via a net trimolecular reaction.¹⁶

Chemocompatible disulfide-based probes have long been explored as reporters for dithiol-type enzymes.¹⁷ Disulfide trigger-cargo constructs are a conceptually simple, modular turn-on design for probes (Figure 1C). Ideally, the trigger is attached to the cargo to mask a key structural element, such that (1) the intact probe is fully deactivated (e.g., optically silent), but (2) trigger reduction causes a cascade that irreversibly restores activity by unmasking (e.g., fluorogenesis), often by simply liberating the cargo (Figure S1C). Analyzing disulfide trigger-cargo probes' performance shows that both disulfide topology (linear or cyclic), as well as geometry (strained or stabilized), are key to cellular performance since they determine a probe's sensitivity to monothiols.¹⁷ Monothiols are highly concentrated in cells, with 1–8 mM GSH, and an even larger pool of protein thiols (PRSH).^{18,19} To report selectively on redox-active dithiol/disulfide proteins, probes must resist attack by this monothiol background.

However, any thiol/disulfide exchange reaction upon linear topology disulfides irreversibly commits a probe to cargo release (Figures 1C and S3A). This makes linear topology probes nonspecifically labile to cellular monothiols,^{20–22} preventing them from being enzyme-selective reporters in the cellular context.²³ Although some reports have used linear disulfide probes (Figure S1A), we believed that selective reporters would require a different design.¹⁷

Cyclic topology disulfide probes can resist triggering by monothiols in two ways. They can reform the disulfide after the initial thiol-disulfide exchange by expelling the attacking monothiol, or after reduction to the dithiol, they can be re-oxidized by other disulfides in their environment, both of which prevent them from committing to cargo release (Figure S3B; full discussion in Felber et al.²³). The geometry of the cyclic disulfide is critical for these reactions and so determines the cellular performance of such probes. Strained cyclic disulfides were characterized by Whitesides in the 1990s.^{24–26} They are kinetically labile, being rapidly and nonspecifically opened by monothiols, and the opening is irreversible since the disulfide strain disfavors reclosure. Thus, in the cellular context, cyclic 7-membered,¹⁷ ETP-type-6-membered,²⁷ and cyclic 5-membered disulfides^{23,28} cannot be selective substrates for dithiol proteins. Although probes based on cyclic 5-membered disulfides have

been published and commercialized as TrxR selective (Figure S1A),^{29–31} their unselectivity and kinetic problems have been demonstrated (Figures S1B and S1C).^{23,28,32–35} Alicyclic 6-membered disulfides (1,2-dithianes), however, are unstrained and are stable against monothiols. Monocyclic and annelated bicyclic 1,2-dithianes were recently used as reductive triggers that resist GSH²² and TrxR³¹ yet can be harnessed in probes that are selective for Trx (Figure S1C; Note S1).¹⁷

Here, we wished to leverage these design principles to develop modular probes that resist the cellular monothiol background but would report selectively on TrxR1 activity in live cells. Analyzing thermodynamics, kinetics, and reaction pathways led us to design novel cyclic 6-membered selenenylsulfides as reduction triggers. We developed scalable syntheses for a palette of cumulative-release fluorogenic probes with a modular design. A range of cell-free and cellular assays, including genetic knockout, knockin, chemical inhibition, selenium supplementation, and depletion studies, confirmed their outstanding selectivity for reporting on cellular TrxR1. The solubilized probe **RX1**, for TrxR1-redox-probe **1**, is a particularly rapid and stable cellular fluorescence imaging reporter of TrxR1 activity. We could apply **RX1** to enable the first high-throughput selective cellular screening for TrxR inhibitors, which indicated S_NAr-based inhibitors may be favored chemotypes for future development. **RX1** offers a flexible platform for TrxR1 imaging and further development of TrxR probes and prodrugs, and the analysis guiding its development can light a path for other key redox-active enzymes.

RESULTS

Design for cellular selectivity: Cyclic 6-membered dichalcogenide triggers

We wished to design (nondisulfide) dichalcogenide triggers that would react selectively with TrxR's unique selenolthiol motif and give rapid cargo release even with nM TrxR, without releasing cargo with other cellular reductants—whether μ M vicinal dithiols or mM monothiols.

Since we were designing irreversible-release probes, we first considered kinetic aspects of the path to cargo release as relevant to selectivity. We consider that the same topology restrictions apply as in the disulfide series,¹⁷ i.e., that linear dichalcogenides are likely to be nonselective due to the irreversibility of triggering under monothiol challenge. We note that two linear (nondisulfide) dichalcogenide-trigger probes have been published as selective (Figure S1A),^{36,37} but according to our analysis, selectivity in the cellular context was not shown (Note S2). We instead proceeded with cyclic topology designs. We also considered that the same geometric factors would apply as for disulfides, ruling out strained dichalcogenides from being cellularly selective. In support of this view, Matile has shown the lability of cyclic 5-membered diselenide probes³⁴ to nonspecific thiol exchange, mirroring that of the corresponding disulfides (Figure S1B).

We therefore expected that only cyclic 6-membered dichalcogenides might avoid kinetically irreversible, nonspecific triggering in cells, by ensuring that monothiol attack has the potential to be reversible (discussion in Felber et al.¹⁷). However, this is only a partial solution. Ensuring that highly reducing dithiol proteins, e.g., Trx and Grx (10 μ M) or GSH (up to 8 mM) do not catalyze cargo release, while only ca. 20 nM TrxR can do so, cannot be feasible by considering thermodynamics alone (e.g., Trx-reducible 1,2-dithianes resist TrxR; see Note S3). Ensuring this requires specificity either in binding or in the pathway to cargo release, and since TrxR's CU active site is on an unstructured tail, we focused instead on pathways.

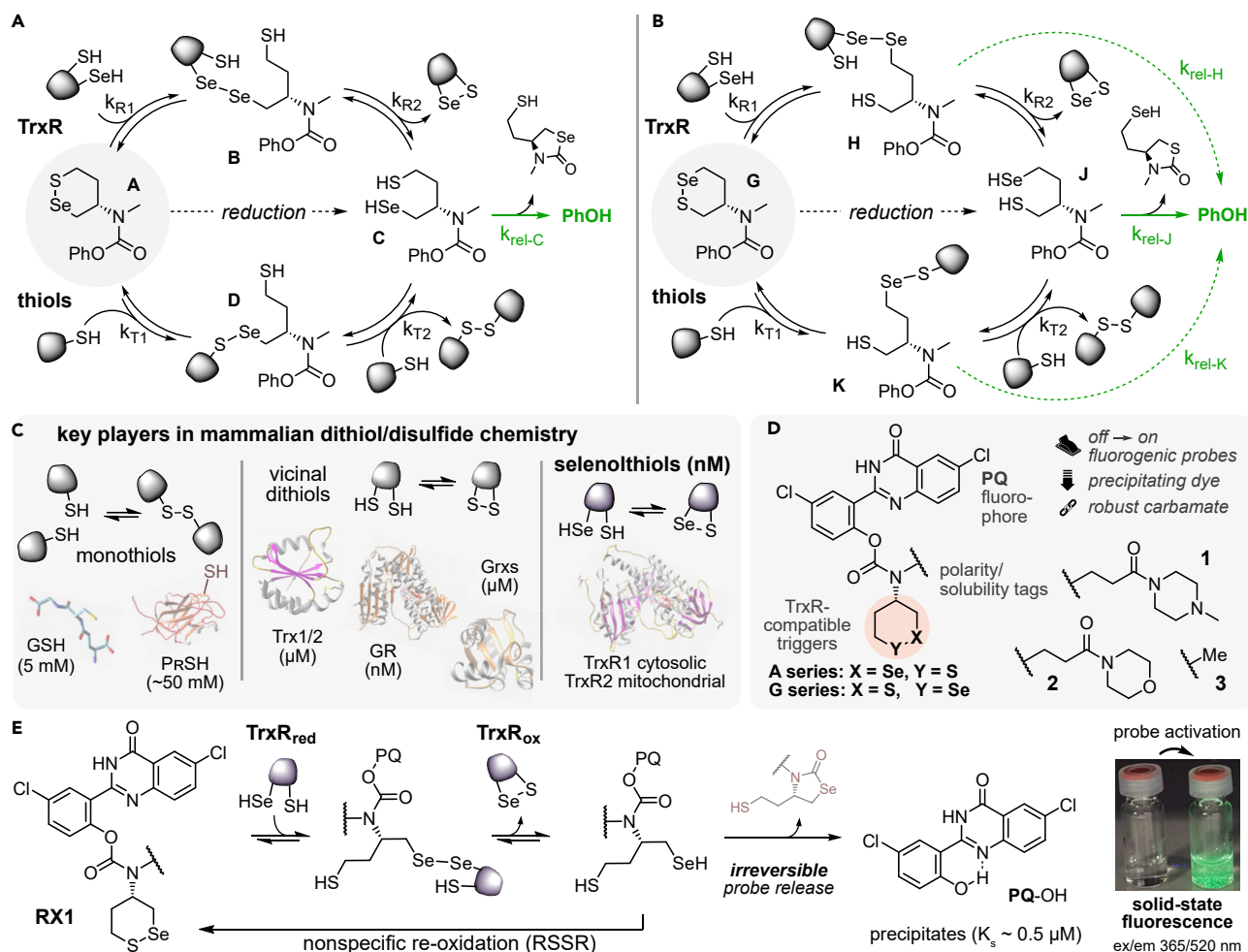


Figure 2. Selenenylsulfides A, designed for TrxR selectivity, and thermodynamically identical regioisomers G, designed for nonselectivity (A and B) Probes of type A (includes RX1) are predicted to avoid monothiol-based signal generation, whereas regioisomeric control probes of type G are predicted to be monothiol-labile (full mechanism in Figure S4). (C) Some chemocompatible cellular reductants that a TrxR-selective probe must resist. (D) Modular trigger-cargo design for fluorogenic probes with freely adjustable polarity. (E) Signal activation pathway for RX1.

Design for cellular TrxR selectivity: An oriented selenenylsulfide trigger

Analyzing reductive release pathways identified four key design aspects, which convinced us that probes based on a desymmetrized cyclic selenenylsulfide trigger A represent a unique TrxR-selective solution (Figure 2A; see also Figure S4 and Note S3). It also suggests that the thermodynamically identical regioisomer G (Figure 2B) ought not be TrxR selective, thus giving highly stringent controls for our postulated specificity mechanism.

Selectivity aspect 1 (attack kinetics): Selenenylsulfides should be rapidly attacked at Se by TrxR selenolate

Nucleophilic attack on a selenenylsulfide at Se is much more kinetically favored than at S (closest data³⁸ suggest by a factor of 10^4), and experimentally, this fixes the initial attack site exclusively at the selenium regardless of whether thiolates (undesired) or selenolates (desired) are the attacking species.^{38–40} Then, several factors combine such that the rates of attack by selenol species are likely to be rapid in an absolute

sense and to be many orders of magnitude faster than the rates of attack by thiol species (k_{R1} versus k_{T1}). In general, selenolates are ca. 100 times as nucleophilic as thiolates; this is associated with their greater polarizability.³⁸ Furthermore, both species must be deprotonated to attack, and while selenols are deprotonated at physiological pH (pK_a ca. 5; that of RSeH in TrxR is still lower⁴¹), thiols are mainly not (pK_a ca. 8),^{34,38} and this further widens the gap in their reactivities toward selenenylsulfides. Although there are no strictly corresponding data for thiol attack on selenenylsulfides, the fact that selenolate attack at Se on selenenylsulfides proceeds ca. 10^7 -fold faster than thiol attack on disulfides under physiological conditions gives confidence in a biologically important rate of attack by TrxR at Se of a cyclic selenenylsulfide.

Selectivity aspect 2 (intermediate thermodynamics): A selenenylsulfide's attack intermediate should keep the attacking nucleophile bound to Se and not to S

The initial kinetic products of exchange with symmetrical cyclic dichalcogenides can rearrange intramolecularly within milliseconds to form the thermodynamic products.³⁴ However, the thermodynamic preference for exchange intermediates to remain bound to Se rather than migrate to be bound to S is strong regardless of the attacking nucleophile.⁴⁰ For selenolate attack, a proximally *N*-acylated linear diselenide intermediate has E° ca. 270 mV lower than the alternative linear selenenylsulfide (ca. -550 ³⁹ versus -280 mV), so the diselenide should remain the favored intermediate (e.g., B rather than E in Figure S4A). For thiolate attack, linear selenenylsulfides have E° ca. 70 mV lower than the alternative disulfide (ca. -280 versus -210 mV),⁴² also favoring the Se-bound intermediate (e.g., D rather than F in Figure S4A). Thus, the kinetically favored attack at Se (see aspect 1) also gives the thermodynamic intermediates, and these are the only intermediates relevant to probe evolution (B and D for probes of type A; H and K for probes of type G; Figures 2A and 2B), which simplifies the pathways to cargo release (cf. Figure S4).

Instructively too, initial attack by TrxR should be much more thermodynamically favored than attack by thiols. The E° values for the intermediates can be compared with the ca. -364 mV for intact cyclic selenenylsulfide triggers from Iwaoka's elegant study (Figure S1D).⁴⁰ Thus, the stability of linear diselenide intermediates B and H (from TrxR selenol attack; -550 mV) better offsets the energetic penalty of opening the cyclic selenenylsulfide than can linear selenenylsulfide intermediates D and K (from thiol attack; ca. -280 mV).

Selectivity aspect 3: A correctly oriented selenenylsulfide's intermediate should avoid cargo release before full reduction and have high monothiol resistance

Although thiol attack is much less kinetically and thermodynamically favored than selenolate attack (see aspects 1 and 2), we anticipated that some monothiol exchange of A \rightarrow D would be unavoidable because of the high cellular thiol concentration (Figure 2C), so it is crucial to assess the fate of D as well as B. We estimated that rates of cargo release directly from D (or B) by 6-*exo-trig* "on-reductant" cyclization of its thiol should be insignificant, particularly compared with those for 5-*exo-trig* cyclization of the likely deprotonated and more nucleophilic selenolate in fully reduced C. Thus, we expected that A would significantly release cargo only if it was fully reduced to C, so we considered the relative tendencies of B and D to evolve to C.

TrxR completes this full reduction (B \rightarrow C) in a unimolecular step that is structurally preorganized for productive completion by closing the enzyme's cyclic selenenylsulfide, and for B, this involves kinetically very favorable TrxR thiolate⁴¹ attack

onto the proximal Se of its diselenide.³⁸ Thus, we expect a large fraction of the TrxR attack intermediate **B** to evolve fully to signal-generating **C**. By contrast, for monothiols to complete the reduction (**D**→**C**) before **D** retro-reacts to return **A** (by fast³⁴ intramolecular attack of the pendant thiol of **D** at Se of its selenenylsulfide), an intermolecular reaction with a second equivalent of RSH is required, and crucially, this reaction must occur at the 10⁴-fold kinetically disfavored sulfur site of the selenenylsulfide^{38–40} (because attack at the favored Se simply “cycles” the monothiol: the second RSH replaces the first without causing intermediate **D** to evolve⁴³). This means that the selenium in **A** not only recruits the desired reductant TrxR but also does “dual duty” by acting as a sink for parasitic monothiol reactivity. (In a supraphysiological, extreme scenario, even if the concentration of challenger monothiol would be so high as to match the “effective local thiol concentration” represented by **D**’s own pendant thiol, only 0.01% of **D** would evolve productively to signal-generating **C** before competing intramolecular reclosure returns **A**.) Thus, while we expected overall very strong kinetics for TrxR-induced full reduction of **A** to **C**, we anticipated that **D**’s strongly disfavored monothiol evolution would combine with **A**’s lower monothiol sensitivity to give overall excellent monothiol resistance (Figure 2A).

A mechanistic test of the importance of controlling the fate of the pendant thiol in the exchange intermediate is provided by regioisomer **G**. This has identical thermodynamic and kinetic susceptibilities to TrxR/monothiol attack as **A**. However, exchange intermediates **H** and **K** do allow the intermediate to undergo fast 5-exo-trig thiol cyclization, permitting “on-reductant release” (k_{rel-K}) without full reduction to **J**. Full reduction by the preorganized TrxR is likely to be much faster than on-reductant cyclization, so we expected the k_{rel-H} pathway to play little role in TrxR-based cargo release. (This is revisited in the section “RX1 reports sensitively on TrxR1 activity; analogous disulfide probes do not.”) However, for monothiol challenge intermediate **K** (which is similarly hindered from full reduction like **D**), we expected that this new productive route for intramolecular evolution of the thiol would result in significantly more unwanted cargo release after the unavoidable initial exchange with the monothiol background (Figure 2B).

Selectivity aspect 4: Cargo release after reduction

Reduced **C** or **J** are small flexible reductants⁴⁰ that are likely to reduce accessible disulfides in their environment (**C**→**D**) instead of cyclizing to release cargo. Still, as **C** (selenolate) is likely to cyclize faster than **J** (thiol), we anticipated that **A** could be better than **G** for signal generation after full reduction in the cellular setting, where disulfides offer a return pathway.

Taken together, these four aspects informed our hypotheses that probes of type **A** (which includes the RX1 probe) will be (1) more rapidly attacked by TrxR than by thiols, (2) more efficiently reduced through to **C** by TrxR than by thiols, (3) resistant to on-reductant signal generation by (mono)thiols, and (4) rapidly cyclized after reduction to **C**. In contrast, though probes of type **G** will share features (1–2), they (3) should be labile to thiols, thus acting as stringent control for our mechanism-based design.

Design for high-value probes: Modular cargo-trigger integration for performance

We designed selenenylsulfide-based probes that use carbamate cyclization to release phenolic cargoes (Figure 2D). This is a modular system that can be applied to any phenol-type cargoes, including drugs. The phenolic carbamate system offers

a range of desirable features, reviewed elsewhere;^{17,44} important aspects are as follows: (1) Phenolates are good leaving groups that give fast cargo release that is orders of magnitude faster¹⁷ than with the more frequently used aniline carbamates.³¹ (2) Though primary amine phenolic carbamates are so unstable due to E1cB elimination that they are usually discarded³¹ (half-life \sim seconds⁴⁵), secondary amine carbamates avoid E1cB and such probes are very robust to spontaneous hydrolysis (only ca. 1% in 3 weeks).⁴⁴ (3) Masking the hydroxyl of many phenols blocks their activities, so this system allows true off-to-on performance (zero activity before release) with a range of cargoes. For example, phenol *O*-unmasking is required for activation of masked fluoresceins,¹⁷ indigo-type chromophores,⁴⁶ luciferins,⁴⁷ and bioactivity in many series of drugs (irinotecan⁴⁸ and duocarmycin⁴⁹). Thus, it should be possible to extend this work's modular design to probes with diverse imaging modalities and to many prodrug types.

We selected Haugland's precipitating fluorophore PQ-OH (Figures 2D, 2E, and S6)⁵⁰ as our proof-of-concept fluorogenic phenolic cargo. Acylating its phenol completely mechanistically quenches its high-quantum-yield, environment-independent, large-Stokes-shift fluorescence (ex/em 360/520 nm), since this depends on excited-state intramolecular proton transfer (ESIPT) of the phenolic hydrogen. Therefore, PQ-releasing probes can operate as true turn-on systems, with zero self-background and excellent signal-to-noise ratios, typically above 300 even without background signal subtraction. There are many further advantages⁵¹ and a few drawbacks to PQ-OH for cell-free and cellular proof-of-concept studies (see Note S4).

PQ probes with *N*-methylated triggers proved to have low solubility and irreproducible results above 25 μ M in an aqueous buffer with 1% DMSO. To address the challenge of the flat hydrophobic PQ without switching cargoes, we used a basic *N*-methylpiperazinamide and a neutral morpholinamide as solubilizing *N*-alkyl sidechains to minimally crowd the redox-active site while being tracelessly removed upon cyclization (Figure 2D). The reproducibility of the resulting probes was greatly improved by their solubility, so we denoted the sidechains as 1 (piperazinamide, preferred; reliable to >250 μ M), 2 (morpholinamide), or 3 (methyl). The modularity of this design ensures that any trigger can be fitted with any solubilizing sidechain and any phenolic cargo. We freely combined triggers and sidechains to create PQ-releasing probes, which we name by the letter of the trigger (e.g., A) combined with the number of the sidechain (e.g., 2), thus, e.g., A2 (Figures 2D and 3C).

As well as the A-type selenenylsulfides and their G-type design controls, we also designed hydrolytic, kinetic/thermodynamic, and mechanistic controls: reaching a panel of eleven cyclic probes and one linear probe (Figures 3C and S5). We used an isosteric cyclohexane "trigger" as a nonreducible control for spontaneous or enzymatic hydrolysis, or aminolysis/thiolysis, of the carbamate (C type); this is important when applying mM concentrations of thiolates (that might intermolecularly attack carbamates, confounding the desired reduction). We used a cyclic disulfide (S type) and a cyclic diselenide (Se3) as reducible controls with different thermodynamic and kinetic sensitivity profiles, which we anticipated would make them not TrxR selective. Linear disulfide SS00¹⁷ (Figure S5) was a mechanistic control since according to our hypotheses it ought to access the irreversible pathway and so be thiol-labile (see Note S2).

Synthesis of RX1

We prepared the key selenenylsulfide building blocks in a straightforward, divergent manner from bis-mesylate 1 (Figure 3A), which can easily be accessed from aspartic

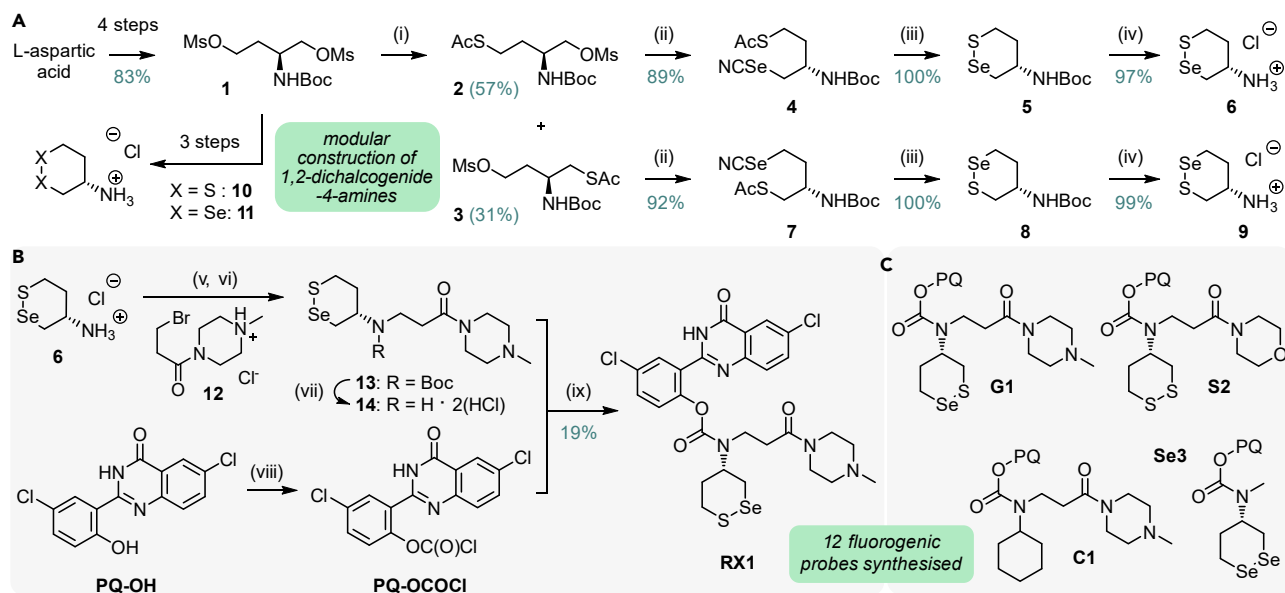


Figure 3. Synthesis of triggers and probes

(A) Divergent synthesis of amino-1,2-thiaselenane triggers: (i) KSAc, 18-crown-6, DMF, 15 h, room temperature (RT); (ii) NaI, 18-crown-6, KSeCN, THF, 10 h, 50°C; (iii) KOH, MeOH/THF, 1 min, RT; (iv) HCl, dioxane/DCM, 11 h, RT.

(B) Representative probe synthesis, shown for RX1: (v) NEt₃, MeOH, 1 h, MW 120°C; (vi) Boc₂O, NEt₃, DCM, 15 h, RT; (vii) HCl, dioxane/DCM, 11 h, RT; (viii) triphosgene, DIPEA, DCM, 2 h, 0°C → RT; (ix) DIPEA, DCM, 4 h, 0°C → RT.

(C) Representative PQ probes (full list in Figure S5).

acid.⁵² Reaction with 1 equiv of potassium thioacetate afforded a mixture of mono-substitution products 2 and 3, with a small preference for 2. These regioisomers were separated by chromatography. Treatment with potassium selenocyanate followed by thioester cleavage directly resulted in the formation of the cyclic dichalcogenides 5 and 8 by expulsion of cyanide. Boc-deprotection then gave the amine hydrochlorides 6 and 9. In parallel to our work, Iwaoka elegantly reported the synthesis of compounds 6 and 9 via a similar approach but used non-commercial PMBSeH as the selenium source.⁴⁰ In comparison, our synthesis offers more atom economy, reduced step count, fewer chromatographic separations, and more rapid access to the final compounds, although these differences are not crucial. To obtain the control Se and S series dichalcogenides (Figure 3A), bis-mesylate 1 was either treated with excess potassium thioacetate⁵² and KOH/air, or excess KSeCN and KOH, followed by Boc-deprotection to form disulfide 10 or diselenide 11, respectively. The symmetrical linear disulfide SS00 was accessed from commercial cystamine. We diversified these trigger building blocks by installing the sidechains, giving secondary amines. Finally, deprotection and coupling with chloroformate PQ-OCOCI⁴⁵ (Figure 3B) yielded a panel of twelve PQ probes (Figures 3C and S5): the A-type and G-type cyclic selenenylsulfides RX1, A2–A3, and G1–G3 as candidates/controls for TrxR-selective probes; the cyclic diselenide Se3 and cyclic disulfides S1–S3 as well as the linear disulfide SS00 as reduction-responsive controls; and the non-reducible cyclohexyl probe C1 as a control for non-reductive activation. All probes were nonfluorescent as solids and in solution. (Further details and discussion of synthesis are given in Note S7 and Figures S7 and S8.)

HPLC analysis of cargo release supports the mechanistic design behind RX1

To test the 5-exo-trig cyclization mechanism of Figures 2A and 2B, we performed an HPLC-MS study of tris(2-carboxyethyl)phosphine (TCEP)-mediated probe activation. This is critical since alternative postreductive release mechanisms could give

different kinetics and selectivity. For example, 3-*exo-tet* cyclization releasing an *N*-methyl probe carbamate via thiirane or selenirane formation (similarly to a report by Melnyk⁵³ with a half-life of ca. 4.5 h), followed by fast E1cB, could also be postulated as a mechanism. We also wished to test whether the triggers resist parasitic reactions, such as TCEP deselenization,⁵⁴ which would otherwise complicate cell-free benchmarking.

In the TCEP challenge, **RX1** reacted fully to selenocarbamate and **PQ-OH**. **G1** reacted similarly, although more slowly, to give the thiocarbamate and **PQ-OH**, potentially reflecting the desired difference in C/J cyclization kinetics (section “selectivity aspect 4: cargo release after reduction”). The 5- rather than 6-*exo-trig* cyclization is supported in two ways: (1) The **RX1** cyclization byproduct was found as the monomer, while the **G1** byproduct was a monooxidized dimer matching interpretation as an easily formed and highly stable linear diselenide. (2) Equimolar selenolate alkylators almost entirely blocked **PQ-OH** release from **RX1**, but only slightly reduced **PQ-OH** release from **G1**. This latter observation crucially suggests that on-reductant cyclization (which also proceeds from an intermediate with engaged selenium) may be significant for **G1** but not **RX1**: so matching design aspect 3. The controls ran as expected: **SS00** reacted fully to thiocarbamate and **PQ-OH**, while **C1** remained intact (for a full discussion, see [supplemental information](#) section “mechanistic analysis of probe activation,” [Figures S32–S37](#), and [Note S5](#).)

In summary, the HPLC studies showed that reductive release is fast and operates by 5-*exo-trig* cyclization according to the proposed mechanism, that deselenization is not a complicating factor, and that on-reductant cyclization may be speedy (**G1**) or absent (**RX1**). As on-reductant cyclization can be key for probes to resist (**RX1**), or succumb to (**G1**), monothiol-exchange-based triggering, we expected this to determine their reduction selectivity in cells.

RX1 is extremely stable against monothiol challenge

To report on a protein selectively in cellular settings, a trigger must be completely resistant to reduction by the mM cellular monothiol background.¹⁸ Resistance or sensitivity to a reductant is best addressed by dose-response functions over time. Therefore, to best characterize the response to reductant challenges, we titrated the reductants up to supraphysiological concentrations and collected full time course rather than endpoint data.^{17,23}

We began with GSH challenge tests. Over 6 h, **A**-type probes showed zero fluorescence response to 10 mM GSH, indicating outstanding monothiol resistance ([Figures 4A, S9](#), and [S10](#)). The thermodynamically identical **G**-type controls were GSH-labile (3 mM GSH activated to ca. 25%, [Figures S9](#) and [S10](#)), supporting our pathway-based design ([Figure 2B](#)). Dose-response plots of GSH resistance with the 6-h time point data ([Figures 4B](#) and [S10](#)) highlight the GSH-robustness of all **A**-type probes and the partial GSH lability of **G**-type pathway controls. The comparison probe types behaved as expected: we had hoped that cyclic disulfides **S1–S2**, analogously to previously reported vicinal-dithiol-selective probe **S3**,¹⁷ would be monothiol resistant (i.e., no destabilization by the solubilizer sidechains); they indeed resisted GSH up to 10 mM ([Figures S9](#) and [S10](#)). In comparison with these, linear disulfide **SS00** is a mechanistic control for the need for a cyclic dichalcogenide topology ([Figure 1C](#)); its sensitivity to monothiol-based release was striking (nearly full activation by 1 mM GSH; [Figures 4A](#) and [S9](#)). The cyclic diselenide **Se3** was nonreactive ([Figure S9](#)), suggesting that selenium is tolerated at both positions of the reduction-based probes without Se-oxidation-mediated release mechanisms (see [Note S2](#)). The zero-level fluorescence seen with **RX1** (and **Se3**) under

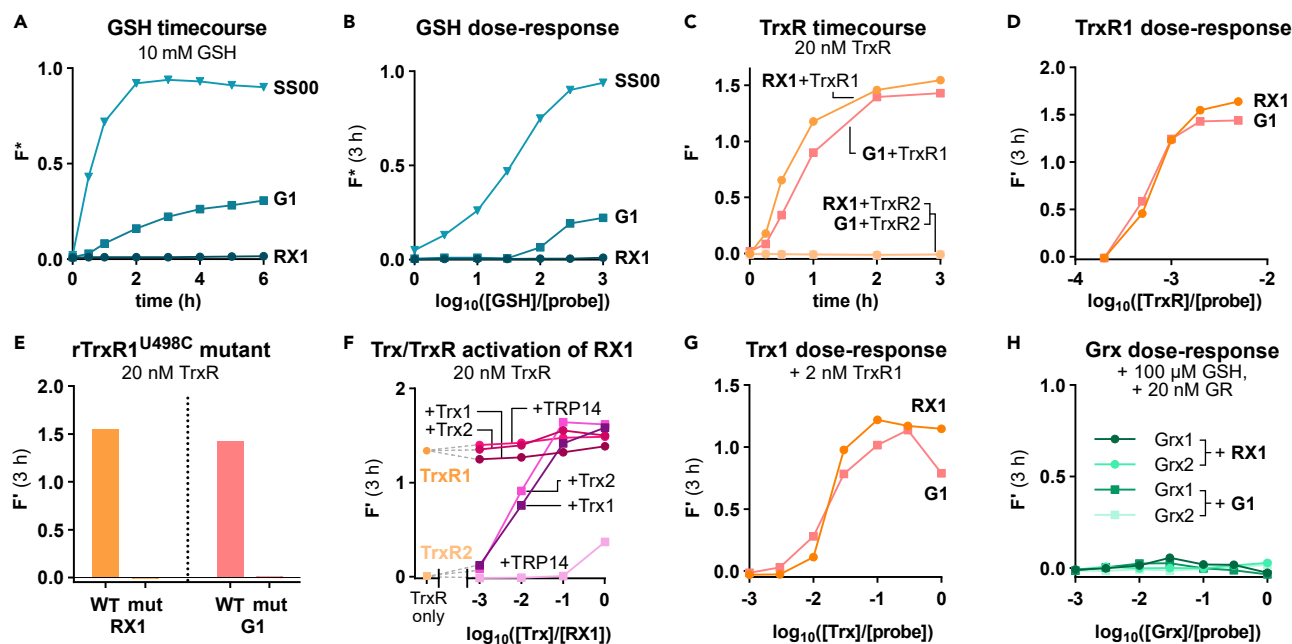


Figure 4. In vitro characterization of TrxR-selective RX1 versus comparison probes

(A and B) Selected GSH-resistance time courses, and GSH dose response (0.01–10 mM GSH).

(C) Selected TrxR1-activation time courses (20 nM TrxR1 and TrxR2).

(D) TrxR1 dose response.

(E) Selenenylsulfide probe activation by wild-type TrxR (Sec-Cys) compared with Cys-Cys mutant rTrxR1^{U498C}.

(F) Dose-response titrations with vicinal dithiols Trx1, Trx2, and TRP14 (0.01–10 μM) in the presence of 20 nM TrxR.

(G) Trx1 dose-response (0.01–10 μM) titrations in the presence of 2 nM TrxR.

(H) Dose-response (0.01–10 μM) profiles to the GR/GSH/Grx cascade (20 nM GR, 100 μM GSH).

All probes used at 10 μM in TE buffer. TCEP (10 equiv, 100 μM) was used as a reference for fast, quantitative probe reduction and activation; F^* in enzyme-free assays is the relative fluorescence signal compared with full activation ($F^* = F/F^{\text{TCEP}}$). NADPH (200 μM) was applied as native upstream component for enzymatic assays; F' in enzymatic assays is F^* additionally corrected for NADPH autofluorescence; see also [supplemental information](#).

a 1,000-fold challenge by GSH also qualifies the secondary amine phenolic carbamate design as exceptionally stable to monothiolysis, hydrolysis, and aminolysis.

RX1 reports sensitively on TrxR1 activity; analogous disulfide probes do not

We next tested the probes against a range of purified recombinant reducing enzymes in cell-free assays, including TrxRs as well as nontargeted Trxs, Grxs, GR, TRP14, and GPx1. The source and production methods are relevant for TrxRs since the key selenocysteine (U498) residue in their active sites that is predominant in native enzymes⁵⁵ is typically not incorporated via standard recombinant expression systems.⁵⁶ Therefore, we used human cytosolic TrxR1 and human mitochondrial TrxR2 produced with recent recombinant production methodologies that approach 100% CU active site content.⁵⁷ To stringently test the validity of our design for selenothiol-dependent activation, we also used the U498C point mutant of rat TrxR1 (rTrxR1^{U498C}).⁵⁸

The selenenylsulfide probes showed strong signal responses to TrxR1. RX1 at 10 μM was strongly activated by 20 nM TrxR1 with a half-time to maximal signal of ca. 30 min (Figure 4C), contrasting with its total stability to one million times higher concentrations of GSH over 6 h. RX1 responded well to TrxR1 down to the subphysiological concentration of 5 nM (Figure 4D). As this cell-free assay underestimates probe sensitivity to low concentrations of TrxR (see Note S5), this was encouraging for cellular use. TrxR1-turn-on kinetics and response profiles were similarly good for

all other cyclic selenenylsulfide probes (A2–A3 and G1–G3) (Figure S13). This unity of TrxR1-selective performance despite the structural diversity of the probes matched our hypothesis that the cyclic selenenylsulfide is responsible for reactivity and that the solubilizing motif can be exchanged without altering the triggers' redox activity. An important result for selectivity, which completes the k_{rel} -H discussion (see "design" section), is that the rates of probe activation by TrxR1 were essentially identical between the A-type and G-type triggers (Figure S13). If on-TrxR cyclization (Figures 2A and 2B) were significant for probe release, the G-type probes would be significantly faster than the A-type in releasing cargo. However, the data rather support that TrxR1 indeed fully reduces the cyclic selenenylsulfide probes to C/J, before they cyclize: full reduction by TrxR is faster than cyclization.

Disulfide controls S1–S3 were nearly inert to TrxR1 (Figure S13), though piperazinamide sidechain 1 gave faster reaction speeds compared with less soluble methyl and morpholinamide sidechains, presumably due to hydrophobic adsorptive loss²³ of the intact probes as well as local pH modulation. This effect was often seen later with A- and G-type probes and supported the choice of piperazinamides as the standard sidechain ("1") for the probes. Diselenide control Se3 was completely nonresponsive to TrxR1, as it later proved to be to all other reductants except for DTT (Figures S9 and S12).

Of the selenenylsulfides, only RX1 and G1 were reduced by mitochondrial TrxR2, matching the trend of greater reactivity for the piperazinamides, and only at high TrxR2 (50–100 nM; Figures 4C and S13). Some TrxR2 response was expected, as it has the same Sec-Cys motif as TrxR1, but this mirrors ample literature precedents of TrxR2 being slower to process small-molecule substrates than TrxR1.⁵⁹ Since cytosolic TrxR1 has many-fold higher total expression in cells; we, therefore, expected the faster-reactive TrxR1 to be the dominant cellular reductant for our selenenylsulfide probes.

RX1's "selenium required" mechanism reports selectively on intact TrxR1

Next, we wished to test our hypothesis that the selenenylsulfides should interact selectively with mammalian TrxR based on the TrxR selenolthiol. TrxR has two redox-active sites, with the NADPH-driven N-terminal Cys-Cys shuttling electrons to the C-terminal Sec-Cys. As Hondal et al. have shown in their paper "no selenium required,"³² many compounds that had been assumed to require a selenol for reactivity can be similarly processed by a C-terminal Cys-Cys mutant TrxR^{U498C}, or are better or exclusively processed by the N-terminal dithiol site. We compared probe activation by wild-type TrxR (Sec-Cys) with Cys-Cys mutant rTrxR1^{U498C}. The mutant no longer reduced either the A- or G-type probes, while its reduction of standard substrates DTNB (5,5'-dithiobis-(2-nitrobenzoic acid)) and juglone was unimpeded (Figures 4E and S14). This supports that both A- and G-selenenylsulfide probes do indeed require native mammalian TrxR's C-terminal selenolthiol for efficient reduction, matching our pathway designs.

RX1 resists reduction by monoselenol enzymes such as GPx1

With excellent monothiol resistance, and strong processing by selenolthiol TrxR1 rather than its dithiol mutant, it remained an open question whether physiological concentrations of other selenol-bearing proteins would also be capable of probe triggering, which is important for enzymatic selectivity. There are only 25 selenoproteins in the human proteome; only a few of these have ubiquitous expression at substantial concentrations, and nearly all of those have monoselenol active sites (not selenolthiols). The highest-concentration ubiquitous selenoproteins are the monoselenol glutathione peroxidases GPx1 and GPx4 (see Note S6).¹⁰ We challenged RX1 and G1 with GPx1 up to a supraphysiological 1 μ M concentration,

and no probe activation was detected over 6 h (Figure S15). This was an encouraging step for the possibility of cyclic selenenylsulfides acting as TrxR-selective probes.

RX1 is far more sensitive to TrxR than to dithiol oxidoreductases

Having tested the major biological monothiol, monoselenol, and selenolthiol reductants, we finally examined the effect of vicinal dithiols on probe activation. We began by screening the probes' dose-response to dithiothreitol (DTT), a nonphysiological vicinal dithiol that is ca. 50 mV more reducing than Trx1 but reproduces some aspects of its behavior and so can be helpful to study dithiol reactivity.¹⁷ Excess DTT triggered all A- and G-type selenenylsulfide probes. Although selenenylsulfides are more thermodynamically resistant to reduction than disulfides, their reaction with DTT was more rapid and more sensitive than that of the corresponding S1–S3 series (Figure S11). This is a reminder of the importance of kinetics to probe release, as the greater electrophilicity of Se in selenenylsulfides than S in disulfides determined the assay outcomes.

We then tested Trxs, titrating them to a physiological 10 μ M in the presence of a 10 μ M probe. These assays require TrxR and NADPH to reduce Trx from the nonreactive, oxidized, stored state, and to re-reduce it after each oxidation by probe or by molecular O₂ in the nondegassed assay buffer. RX1 is already fully and rapidly activated by 20 nM TrxR1 alone (Figure 4C), so, unsurprisingly, titrating in Trx1/2 or other Trx-fold proteins such as TRP14 did not reveal extra processing by those species (cf. TrxR1 data in Figure 4F). To study direct probe reduction by Trx only, we instead used concentrations of TrxR1 and TrxR2 that gave insignificant direct activation of RX1 and observed half-maximal probe activation with ca. 0.1–0.2 μ M of Trx1 or Trx2 regardless of which TrxR was chosen (TrxR2 data in Figures 4F, S17, and S19; TrxR1 data in Figures 4G and S22). This represents a ca. 50-fold lower sensitivity to Trx than to TrxR1, under continually re-reduced conditions. The TrxR-resistant disulfide comparison probes S1–S3 were activated by Trx as expected,¹⁷ with half-maximal activation around 0.3 μ M Trx (Figures S16–S20).

Finally, we tested alternative redox-active dithiol proteins. We first profiled dose-response to Grx1 and Grx2, the other major vicinal dithiol protein redox effectors, applied as part of the full GR-GSH-Grx cascades (Figures 4H, S23, and S24). Both RX1 and G1 fully resisted up to 10 μ M Grx1/Grx2 over 3 h (including 20 nM GR, 200 μ M NADPH, and 100 μ M GSH for Grx reduction). This is a significant result. Although the Grxs are vicinal dithiol redox enzymes similar to the Trxs, they are more RSSG selective. Therefore, the cyclic probes should resist Grx processing in as much as they resist monothiol exchange (note too that although GR is NADPH driven, it has very high specificity for GSSG, so it is not expected to directly reduce the probes). We also examined the TrxR-reduced redox-active vicinal dithiol TRP14, finding that the probes resisted it up to 3–10 μ M (Figures 4F, S18, and S21). These results show that the probes are not sensitive to all vicinal dithiol proteins *per se* but have a specific sensitivity to the highly reducing Trxs, at least in cell-free conditions. While it would have been best for our TrxR-reporter goal if Trxs were incapable of probe reduction, sensitivity can be expected in a cell-free assay where excess NADPH and the absence of other oxidants and binding partners offer no alternative pathway except probe reduction. However, in cells, Trx as an effector protein has many binding partners that recognize and oxidize its Trx fold, while NADPH-powered TrxR binds fewer substrates (mainly Trx, also TRP14, and potentially Grx2).^{13,60,61} This gave hope that if Trx in cells were substantially engaged with preferred protein substrates, then RX1's extraordinary kinetics of turnover by TrxR1, combined with its total stability to GSH, might give it functional TrxR1-selectivity in cells. In line with this understanding, previous research on Trx has identified

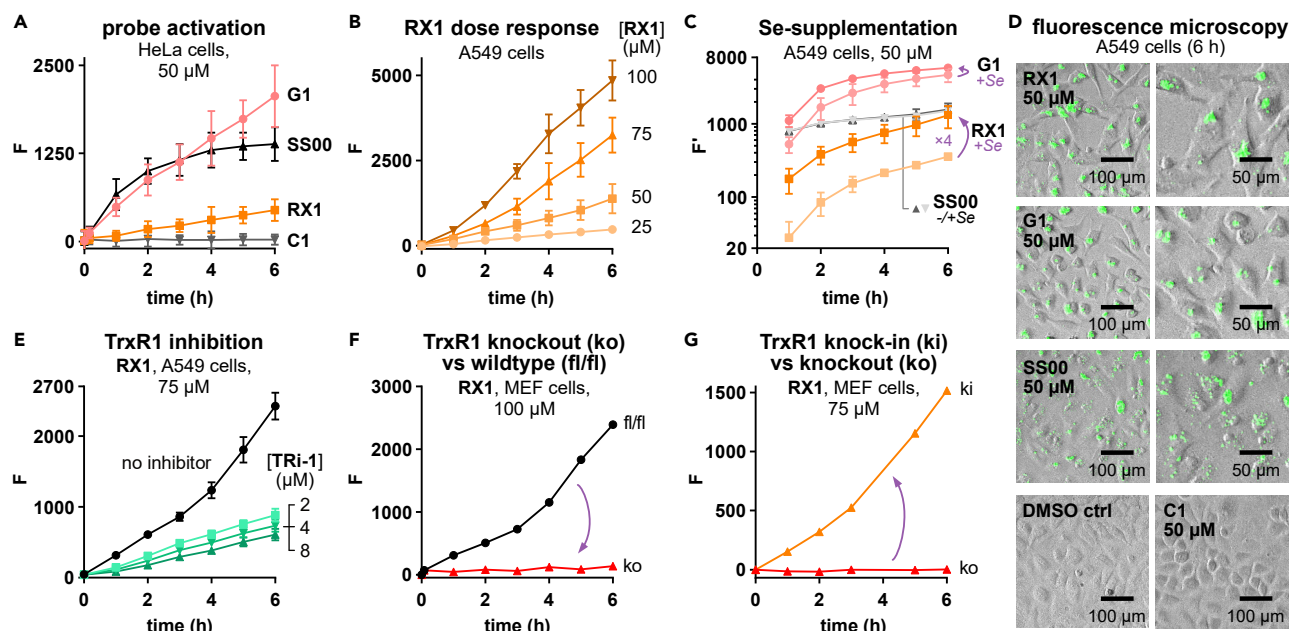


Figure 5. Cellular evaluation of TrxR selectivity of RX1

(A and B) fluorescence activation in HeLa and A549 cell lines.

(C) Cellular RX1 signal depends on selenium starvation/supplementation, while comparison probes SS00 and G1 do not.

(D) Fluorescence microscopy images showing the cell-marking performance of the PQ probes. Overlay of PQ-OH fluorescence (green) on brightfield images.

(E) Cellular RX1 signal is efficiently suppressed by the TrxR inhibitor, TRI-1.

(F and G) Genetic knockout of TrxR1 entirely suppresses signal generation by RX1, whereas reconstitution of TrxR1 expression restores RX1 activation (MEF [TrxR1^{ko}/TrxR1^{ki}] cell lines).

F is the raw fluorescence signal minus the signal of DMSO-only controls (platereader assay; 20,000 cells per well, three wells per data point); F' (in C) is the raw signal minus its time-zero value, i.e., $F'(0) \equiv 0$ by definition (hence timepoint zero is not shown), which gives a more sensitive comparison of conditions. Data in (A)–(C) and (E) are represented as mean \pm SD from three independent experiments (error bars are not shown in cases where errors are too small to be visible outside the data point); data in (F) and (G) are from one experiment representative of three independent experiments; see also [supplemental information](#).

cyclic dichalcogenide probe chemotypes that were highly sensitive to purified Trx (but not to TrxR) in cell-free settings yet were unexpectedly inactive in cellular settings despite the high cellular concentrations of this universal reductant.¹⁷

RX1 is a cellularly active fluorogenic reporter

By now we had shown that, in line with our pathway hypothesis, RX1 was monothiol resistant and could therefore be a protein-selective probe, while its regioisomeric control G1 had some lability to physiological GSH concentrations. Under cell-free conditions, both RX1 and G1 were rapidly activated by TrxR1, dependent upon its selenolthiol active site, and had minor sensitivity to TrxR2; both were sensitive to fully reduced Trx but almost entirely nonresponsive to the alternative vicinal dithiol Trx-related protein TRP14 and were inert to GR/Grx. We now entered cell-based assays, aiming to test the probes' TrxR dependency indicated in the cell-free assays as well as their potential for functional TrxR1 selectivity in the cellular context by elucidating the cellular mechanism of activation of these compounds (see [supplemental information](#) for assay conditions, processing methods, full data for all probes, and accompanying discussions; and [Note S5](#) for discussion of fluorescence normalization).

Signal from the selenenylsulfide probes was strong in different cell lines (Figures 5A, 5B, and S25), dose dependent (Figure 5B), stable over long time courses, and not due to

direct carbamate cleavage (C1; Figure 5A). The potentially TrxR-selective RX1 was predictably slower to generate a signal than nonselective disulfide SS00 or GSH-sensitive G1. Fluorescence imaging showed near-ubiquitous turn-on of RX1 with PQ-OH fluorophore being cellularly retained for hours (Figures 5D and S28).

RX1 is a cellularly selective reporter for TrxR1

We then performed several orthogonal tests to determine whether cellular activation of the RX1 probe is indeed TrxR selective.

Cells cultured without selenium supplementation do not fully incorporate Sec in TrxR but instead incorporate Cys, so lowering the cellular concentration of the selenolthiol form of TrxR.⁶² RX1 signal was four times higher in cells supplemented with selenium than without (Figure 5C), whereas SS00 and G1 were essentially unaffected. This is consistent with an interpretation that RX1 activation in cells depends on native TrxR, while the mechanistic control G1 (just like nonselective SS00) is not selective in the cellular context for TrxR (presumably, the residual GSH lability of G1 allows it to be activated by the monothiol background; Figure 4B).

We next explored how chemical inhibition of TrxR affects signal generation. We relied on the metal-free compounds TRi-1 and TRi-3, which are inhibitors with good cellular TrxR selectivity,⁶³ rather than the common thiophilic gold complex auranofin, which has potential pitfalls²³ (see Note S1 and Figure S2). Cellular RX1 signal was strongly inhibited by acute TRi treatment, with just 2 μ M TRi-1 reducing signal by 66%, whereas G1 signal was only reduced by 15% and SS00 signal was unaffected by this treatment (Figures 5E and S26). TRi-3 dose dependently reproduced the same inhibitory effects. This supports the idea that cellular RX1 activation is highly dependent on the activity of the TRi-1/3 target TrxR, whereas activation of its regioisomer G1 is largely TrxR independent.

Finally, we stringently evaluated RX1's TrxR1 dependency by using TrxR1-knockout (ko) cells (mouse embryonic fibroblasts [MEFs]),⁶⁴ which we compared against their corresponding wild-type control (fl/fl). This knockout upregulates compensatory thiol-based reductive pathways to survive (e.g., the GSH system), with Trx being mainly reduced instead by Grx2.^{65,66} Therefore, we expected that the only circumstances under which we would see zero signal for a hitherto cellularly active probe dependent on Se-containing TrxR1 would be if that probe was exclusively activated by TrxR1 in the cellular context. The TrxR1^{ko} MEFs showed zero RX1 activation, while the corresponding wild type gave a strong signal (Figure 5F). As the mitochondrial TrxR2 is still functional in the knockout, this strongly suggests that the cellular RX1 signal reports essentially on cytosolic TrxR1 at least in this cell line. Signal from mechanistic control G1 was suppressed by ca. 60% though not abolished in the KO cells (Figure S27A), again matching expectations that G1 cannot be fully TrxR1 selective in cells. To obtain still stronger proof of mechanism, we tested TrxR1-knockin (ki) to the MEF TrxR1-knockout background.⁶⁵ This fully restored the strong, dose-dependent RX1 signal generation (Figures 5G and S27B).

Taken together, the data strongly support that RX1 is exclusively activated in cells by TrxR1. RX1 is therefore the first validated probe design that can selectively and meaningfully report on the activity of mammalian TrxR1 non-invasively in live cells.

RX1 enables quantitative high-throughput cellular screening for TrxR1 inhibitors

Inhibitors of TrxR1 hold promise as therapeutics for treating cancer, autoimmune, and inflammatory diseases. The chalcophilic gold complex auranofin (Ridaura) is

one effective though poorly selective TrxR inhibitor, clinically used against the autoimmune inflammatory disease, rheumatoid arthritis. It and many analog complexes have reached late-stage clinical trials in cancer, motivated by tumoral upregulation and reliance upon redox systems.⁶⁷ Other TrxR inhibitor classes include redox-active species and organic electrophiles (Figure S2). Until now, TrxR1 assays to guide inhibitor development were enzymatic ("cell-free") or utilized cell lysates. The technical and cost challenges of expressing and purifying mTrxR with near-quantitative selenium incorporation on a sufficient scale for large screening have limited enzymatic TrxR screening: only one high-throughput screen (HTS) has been reported.^{63,68} Enzymatic or lysate assay hits can be irrelevant in cells (poor permeability, bio-localization, or target specificity), report artifactual hits (e.g., fluorescence quenching or aggregation), and can identify promiscuous compounds that are unlikely to be useful in biology, rather than selective compounds. Biochemical assays cannot identify compounds that are biotransformed into active inhibitors: a field that is recently emerging for selenoprotein targeting.⁶⁹

Cellular HTS can be far simpler and cheaper to perform, and it allows screening of different cell lines, toward therapeutic TrxR inhibitors effective in target cells (with varied expression levels of TrxR and of likely off-target thiol/selenol species), while controlling for drug-relevant performance issues such as upregulated electrophile detoxification and drug efflux pumping, and cell-type-dependent uptake. If a selective probe/readout is used, the data can also be more likely to emphasize selectivity over nonspecific reactivity, making it more actionable in drug development. An HTS-suitable probe must be TrxR selective, but it must also pass many additional criteria for automatic operation, including (1) broad dynamic range (negligible background and cellular crosstalk, high signal-to-noise); (2) broad linear range (for quantitative use); (3) minimal count of error-prone steps (no additional reagents or handling); (4) no manual tailoring of conditions or processing by compound classes; and (5) high-quality data: stable signal, with high precision (small deviations) and high accuracy (confidence of TrxR quantification, minimum interference from test compounds) (see "high-throughput screening" in the supplemental information).

The stability and constant environment of RX1's signal (crystallizing fluorophore, protected from interferences), its low background (ESIPT-quenched probe) and low crosstalk (high Stokes shift), and its ability to directly generate a readout were promising features. We therefore set out to develop the first cellular quantitative HTS (qHTS) assay for TrxR1 inhibitors by using RX1 and performing pilot screening with the 1,280-compound Library of Pharmaceutically Active Compounds (LOPAC)₁₂₈₀.⁷⁰ LOPAC is intended to cover drugs and drug-like scaffolds with much comparative data available for target selectivity, potency, and cellular and *in vivo* bioactivity without a focus on any particular mechanism of action. The LOPAC library was used in the only previously reported qHTS enzymatic TrxR assay (in 2011), and there is an 82% overlap in composition between the 2011 and 2021 versions.⁶⁸

Cellular screening using RX1, optimized for HTS with 1,536-well plates (assay volume 6 μ L, 500 cells/well) over 4 h run time (Table S1), reproduced the strong performance seen in 96-well format (Figures 4 and 5). Untreated versus no-cell controls gave a 7-fold raw signal to background ratio [S:B] without background compensation, with a high Z' value of 0.64, suitable for HTS (Figure 6A). RX1 signal was linear over the assay time and linearly reflected turnover rate (varied RX1 concentration or cell count; Figure 6B). Pre-incubating cells for 1 h with reference inhibitors prior to RX1 gave concentration-dependent inhibition consistent with reported values (Figure 6C).

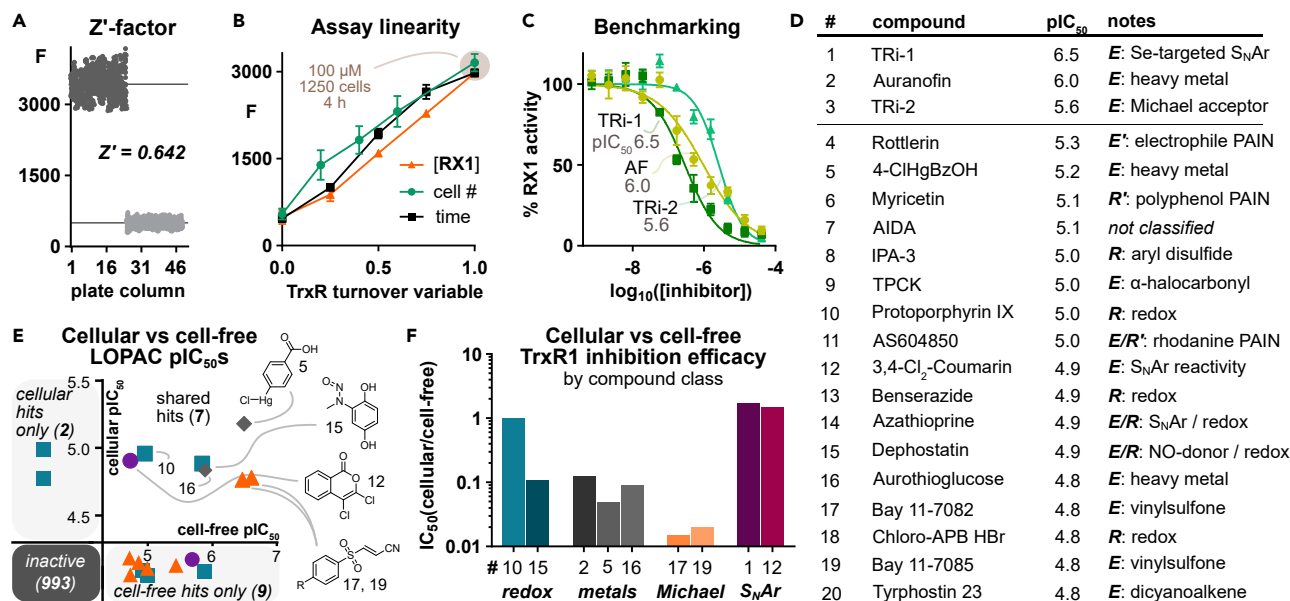


Figure 6. A high-throughput screen with RX1 quantifies cellular TrxR inhibition by pharmaceutically active compounds

(A) Wide assay dynamic range and excellent data precision lead to an outstanding Z' value (cells versus no cells controls).

(B) The signal-turnover relationship of RX1 is linear over the whole dynamic range (parameters varied: incubation time, RX1 concentration, cell count; standard parameter values normalized to 1).

(C) Dose-response plots obtained in 6 μ L automatic RX1 HTS for reference inhibitors.

(D) Potencies for all 18 hits from LOPAC₁₂₈₀ RX1 qHTS plus TRI-1 and TRI-2, annotated for reactivity and compound class (E, electrophile; R, redox active; all structures in Figure S30; pIC₅₀ = log₁₀(IC₅₀ [M])).

(E) Potency distribution among compounds tested in current cellular as well as previous cell-free qHTS.

(F) Ratios of cellular to cell-free potencies of shared hits suggest that S_NAr-based TrxR inhibitors may translate well through development.

Data in (B) and (C) are shown as mean \pm SD from three independent experiments. See also Figures S30 and S31.

A LOPAC₁₂₈₀ screen using this assay protocol performed well ($Z' = 0.63$, S:B 7:1; Figure S29). Compounds with apparent toxicity within the assay time were excluded by a separate viability counterassay. Moderate cutoff criteria (IC₅₀ < 20 μ M and curve form; see Data S1) gave a <1.5% hit rate (18 of 1,278 compounds, plus TRI-1 and TRI-2; Figures 6D and S30). None of the LOPAC₁₂₈₀ compounds were expected to have truly TrxR-selective inhibitory activity in cells: the panel simply serves to demonstrate HTS assay performance, likely to hit rates in larger-scale screening, and to identify trends among hit classes. Pleasingly, the hit rate was manageably low, and the hits were indeed likely selenol-reactive species: 3 heavy metal complexes, 13 organic electrophiles or redox-active species, and a known TrxR-inhibiting porphyrin, which may act via redox.⁶⁸ Encouragingly, only one non-obvious hit was present, the glutamate receptor ligand AIDA (Figure S30). pIC₅₀ values also followed likely cellular reactivity: lipophilic vinylsulfones BAY 11-7085 (methyl) and BAY 11-7082 (*tert*-butyl) had identical pIC₅₀ despite a difference of ca. 1.1 in their LogP; pIC₅₀ for the permeability-limited drug aurothioglucose was 10-fold lower than for its ester prodrug auranofin, etc. (Figures 6D and S30). Matching expectations, with the exception of auranofin, none of these species approached the potency of TRI-1.⁶⁴

RX1 enables comparison of cellular to cell-free potencies, which may direct the development of effective and cellularly selective TrxR1 inhibitors

One opportunity afforded by RX1-enabled cellular screening is to compare, for the first time, cell-free to cellular TrxR inhibition across a range of species to assess trends for cellularly useful or less-useful inhibitors. 1,047 LOPAC compounds were

assessed across both the screens,⁶⁸ of which 1,011 generated robust enough data quality for comparisons (Table S2; supplemental information section "LOPAC HTS-screen using RX1, and comparison to prior art enzymatic screen"). Of these, 993 compounds were inactive in both assays, and 7 were active in both (Figure S31). This 99% overlap of conclusive results between RX1 and the purified enzyme screen speaks strongly to the precision of the cellular RX1 assay. Only 2 compounds, IPA-3 and chloro-APB, were active in the cellular screen despite inactivity in the enzymatic assay: and these are catechol-like species with plausible redox activity in cells (Figure S30). To us, this indicates that the cellular RX1 assay has excellent robustness against false positives. Given that hits were classed up to 20 μM , while RX1 relies on precipitation of $>1 \mu\text{M}$ of a flat aryl fluorophore for signal generation, we feared false positive inhibition from the many LOPAC pan-assay interference (PAINS) compounds that have aggregation effects, or could alkylate the reduced intermediate C (Figure 2A). However, not even powerful cellular PAINS rottlerin, rhodanine, and myricetin⁷¹ gave apparent potencies above 3% of that of the reference inhibitor TRi-1 (Figure 6D). Finally, 9 compounds were inactive in the RX1 assay despite activity in the enzymatic screen. These were also redox-actives and electrophiles (catechols, α -haloketone, nitrosyl donor, Michael acceptors, wortmannin), which may indicate filtering of low-quality hits by the more stringent cellular assay (Table S3 and Data S1).

Interestingly, the ratios of cell-free to cellular potencies of the shared hits clustered with their reactivity (Figures 6E and 6F). The $S_{\text{N}}\text{Ar}$ -reactive species had near-identical cell-free and cellular potencies; heavy metals and nitrosylating agent Dephostatin had >10 -fold potency loss in cells, and Michael system electrophiles up to ~ 100 -fold potency loss. The on-target potency of irreversibly reactive compounds in cellular assays is strongly ruled by their biolocalization and reaction rates with off-target species. We expect that our data comparison (Figures 6F and S31) reflects the degree of undesirable drug loss to off-targets according to compound class, and we propose that the superior cellular translation of the selenophilic tempered $S_{\text{N}}\text{Ar}$ electrophiles suggests how drug development can pursue both effective and selective inhibitors of this key oxidoreductase.

In conclusion, these strong results give confidence that cellular qHTS with RX1 is a valid and valuable TrxR inhibitor screening strategy, promising that focused libraries can be used with cell lines of choice to guide the development of cellularly acting TrxR inhibitors. We suggest that tempered $S_{\text{N}}\text{Ar}$ electrophiles would be a good starting point for such developments. Certainly, quantitative, robust, and selective cellular TrxR probes, with the HTS compatibility and high data quality that RX1 has shown across these assays, will be vital to guide progress in this new territory of redox-targeting drugs.

DISCUSSION

TrxR's position as a central redox node in diverse physiological processes drives the hitherto-unmet need for precise, selective molecular probes to characterize and decrypt its activity in cell biology and in physiological responses to stress. Furthermore, the significant and potentially unique dysregulation of cellular redox systems in pathology, notably of the Trx system, opens exciting vistas toward using TrxR-selective probes as tools both to study and ultimately to diagnose pathologies featuring redox dysregulation, such as autoimmune diseases and cancer. Finally, if such molecular probes are also modular designs, they offer to meet the full spectrum of needs in translational chemical biology: from redox-triggered diagnostics of

diverse modalities (that are predictive of arbitrary cargo release), to the redox-triggered prodrugs that may allow targeting bioactivity selectively to the identified pathological tissues.

RX1 is a rationally designed modular probe for TrxR1

The selenenylsulfide-based probe **RX1** exploits a “selenium-required”-mechanism-based design to perform as the first TrxR1-selective, modular, cargo-releasing cellular probe system. The cyclic topology of the stabilized selenenylsulfide substrates, and the mechanistic bias of the 5-*exo-trig* selenolate cyclization, are both required for this performance. Its design is robust, yet its high selectivity for mammalian TrxR1 is accompanied by fast kinetics of processing and cargo release. Its true off-to-on optical performance (zero pre-activation background, to bright and photo-stable environment-independent fluorescence) and its cell-retained localization permit cell-resolved imaging with excellent signal-to-noise ratios. **RX1** will thus be directly useful for redox biology studies quantifying TrxR1 activity in physiology and disease. Moreover, its high-quality performance in high-throughput screening can earn it a crucial place in development pipelines for selective cellular inhibitors of TrxR1: a goal of significant pharmaceutical interest, and one which we believe will more broadly enlighten the field toward the scope for high-selectivity inhibitors, whether tempered electrophiles or noncovalents.

RX1's modularity is extensible toward other redox probes and prodrugs

The modularity of **RX1** also suits it for flexible adaptation to TrxR1-triggered release of a range of cargoes, far beyond the fluorogenic **RX1** probe for cell culture. The use of a traceless solubilizer sidechain to ensure reliable and cargo-independent solubility is explicitly intended to favor just such adaptation. The design is suited for translation to any molecular cargo with unmaskable activity: of which the fluorogenic, indigogenic, or bioluminogenic probe possibilities in the section “[design for high-value probes: modular cargo-trigger integration for performance](#),” and the accompanying drug-releasing prodrug possibilities, are just a small selection. Particularly given the strong pharmaceutical interest in TrxR-targeted and redox-activated drugs in the inflammation, immunity, and cancer therapy fields,¹⁰ it will be exciting to test whether redox-responsive prodrug designs based around **RX1**-like selenenylsulfides can harness pathologically dysregulated TrxR1 activity to target drugs to diseased tissues. We also anticipate that improved **RX1** analogs can be rationally designed to retain its specificity while installing enhanced reaction kinetics, alternative cargo delivery scope, and maximizing its still-untested resistance to *in vivo* metabolism-based cargo release mechanisms, which will further promote its utility in biological and therapeutic applications. We thus expect that the **RX1** system will impact both redox biology quantification or mapping studies, as well as translational research and therapy of locally redox-dysregulated pathologies such as cancer, inflammation, and autoimmune disorders.

Rigorous selectivity testing, as for RX1, is crucial for progress in redox research

The development and use of chemical probes for redox biology has been hampered by several systematic problems.⁷² Only very few redox-active trigger chemotypes have been explored; in our field, this lack of diversity is exacerbated by the overwhelming use of linear disulfides in probes (Figure S1). The rational mechanism-based design of new redox-active motifs that are chemocompatible with the major biological redox systems, is urgently needed to drive innovation and research across the field. A second problem is the lack of clarity about what molecular information the known redox chemotypes do, or do not, provide. We believe that high-quality

chemotypes should exhibit logical structure-activity relationships: for redox just as much as is accepted for ligand binding. A third problem is that redox selectivity testing is rarely as thorough as it could be. Selectivity for a desired target is often claimed without clearly describing and controlling for alternative cellular reductants in plausible conditions and without using orthogonal assays to quantify what *percentage* of cellular activation should be attributed to the target species. The combination of these problems has resulted in a large number of redox probe reports claiming selectivity for various species, with even the same redox-active motifs being claimed as selective for a range of different redox species (Figure S1), occasionally without or against supporting data or rationale.^{23,32}

We also intended this probe research to test how such systematic problems may be overcome with chemistry. The two cyclic selenenylsulfide cores are new chemical species that open up broad possibilities for probe adaptations, which are easily accessible through their operationally simple, divergent, gram-scale syntheses. The exploration of the solubilizer sidechains, and the comparisons to related probe structures, confirms the rule of structure-activity relationships from cell-free to cellular applications. The battery of cell-free and cellular tests we have employed have stringently assayed all key aspects of redox probe performance, in particular to validate **RX1**'s TrxR1 selectivity. The comprehensive cell-free characterizations, using key redox-active species and proteins in their full interacting systems, tested several key features that cellular assays later confirmed by orthogonal measurements. **RX1**'s cell-free resistance to physiological levels of monothiols over hours was indeed shown to depend on mechanism, since its thermodynamically identical but mechanistically differentiated **G1** analog is GSH-labile. The cell-free selenolthiol selectivity of **RX1** was demonstrated by its non-response to the TrxR^{U498C} mutant, which until now was assumed to be similarly reactive to most small-molecule redox substrates, including all that contain selenium.³² The cellular counterpoint of these assays has been the validation of TrxR1 as the only relevant cellular target of **RX1**, by three independent biological and chemical methods (knockout/knockin, chemical inhibition, and selenium starvation). The comparison to the performance of mixed-mode **G1** (processed by both TrxR and thiols, as revealed by all three methods) further substantiated **RX1**'s cellular selectivity and provides a comprehensive and quantitative basis for reporting **RX1** as a TrxR1-selective probe.

Rational designs for selective, modular reagents for redox biology

The use of chemical diversity, i.e., regioisomeric as well as disulfide and diselenide probes, as mechanistic, thermodynamic, and hydrolytic controls, has thus been a key element in testing and rationalizing **RX1**'s selenolthiol selectivity. More broadly, the rationally designed panel of selenium-containing motifs we present here complements the all-sulfur series we have reported^{17,23} to allow functional comparison and selectivity screening across a total of >40 biocompatible dichalcogenide redox probes, with a level of intercomparability and rigor that to our knowledge has not yet been attempted. It was our aim to increase the breadth and depth of this body of data, and particularly to provide explicit mechanistic descriptions (Figures S3 and S4) of how these small-molecule probes have been designed for selectivity despite lacking the protein recognition features upon which genetic approaches can rely. Our hope is that by doing so, this research will both inspire new chemical approaches in the still-untapped field of redox chemical biology and will also open doors for a range of powerful biological studies: revealing the key cellular redox networks in action and addressing them through therapeutics targeted by the physiology and the pathology of TrxR1.

EXPERIMENTAL PROCEDURES

Resource availability

Lead contact

Further information and requests for resources should be directed to and will be fulfilled by the lead contact, Oliver Thorn-Seshold (oliver.thorn-seshold@cup.lmu.de).

Materials availability

All materials generated in this study are available from the lead contact on request. The authors will supply RX1 entirely free of obligations for any reasonable research requests; requesting scientists should please take charge of shipping fees and organization.

Data and code availability

All data relevant to this paper has been provided in the [supplemental information](#) and [Data S1](#); any additional information required to reanalyze the data reported in this paper is available from the lead contact upon request.

Handling and application of RX1 in cell-free and cellular settings

General notes

- RX1 can best be stored long-term at room temperature as solid, dissolved when needed, and if solutions are kept at room temperature then use within 2 months for best results. Alternatively, DMSO stocks (1–10 mM) are stable to repeated freeze/thaw cycles, long-term storage at 4°C, and exposure to air. To confirm that the probe is intact, dilute a stock into aqueous buffer (final 1% DMSO, ca. 100 μ M); if PQ-OH fluorescence is absent then the stock is usable, or if PQ-OH fluorescence is significant, discard the stock.
- Fluorescence response upon activation has a lag time since PQ-OH requires a minimum threshold concentration, at which kinetically irreversible precipitation of the insoluble fluorophore occurs. The fluorophore is best excited between 340 and 390 nm and best emits at 530–560 nm.
- To establish a baseline for quantitative probe activation (= max fluorescence signal), RX1 can be fully reduced within <15 min with a 20-fold excess of the strong reductant TCEP. This can also be used to confirm stock quality (reaches expected fluorescence).
- pH can be adjusted depending on the selected buffer system (optimal window: pH 7–8). Outside this range, fluorophore release and signal appearance are somewhat slower.

Typical experiment 1: In vitro enzyme-activity assay

A black 96-well plate with a black bottom was charged with 40 μ L of the reductant (TrxR final concentrations of 2–50 nM in TE buffer [50 mM Tris-HCl, 1 mM EDTA, pH 7.5]) and/or the corresponding native substrate (Trxs in TE, final concentrations of 0.01–10 μ M). Next, 50- μ L RX1 solution (at 20 μ M in TE buffer/2% DMSO) was added and the reaction was started by the addition and mixing of 10 μ L of NADPH (1 mM) giving a final assay concentration of 10 μ M RX1 in 1% DMSO with 100 μ M NADPH. A first measurement (time point zero) was conducted immediately. The PQ-OH release kinetics were monitored at set time points (1, 15, and 30 min and 1–6 h). TCEP (40 μ L, 5 mM in TE, 20 equiv, final concentration of 200 μ M) was added for the control of maximum activation.

Typical experiment 2: Cellular activation of RX1 including TrxR inhibition

Cells were seeded in black 96-well plates with transparent bottom (10,000–20,000 cells per well, total volume 100 μ L) and incubated at 37°C (5% CO₂, 0.1%–21% O₂) for 24–96 h. Cells were treated with a solution of RX1 (50–100 μ M) and incubated

at 37°C for 6–9 h. For all tests DMSO was used at 1% as a cosolvent. Time course measurements were conducted with a plate reader detecting fluorescence intensity $F(t)$ ($\lambda_{\text{ex}} = 355 \text{ nm}$, $\lambda_{\text{em}} = 520 \text{ nm}$). For inhibition experiments, cells were pre-treated with TrxR inhibitors 3 h prior to probe treatment, although optimization can be needed according to the nature of the inhibitor and the cell line.

SUPPLEMENTAL INFORMATION

Supplemental information can be found online at <https://doi.org/10.1016/j.chempr.2022.03.010>.

ACKNOWLEDGMENTS

This research was supported by funds from the German Research Foundation (DFG: SFB 1032 project B09 number 201269156, SFB TRR 152 project P24 number 239283807, SPP 1926 project number 426018126, and Emmy Noether grant 400324123), LMUExcellent (Junior Researcher Fund), and the Munich Centre for NanoScience initiative (CeNS) to O.T.-S.; from Karolinska Institutet, the Knut and Alice Wallenberg Foundations (KAW 2015.0063 and KAW 2019.0059), the Swedish Cancer Society (CAN 2018/333 and 19 0330 Pj), the Swedish Research Council (2017-01872), the Hungarian Thematic Excellence Programme (TKP2020-NKA-26), the Hungarian National Research, Development and Innovation Office (ED_18-1-2019-0025), the Hungarian National Laboratories Excellence program (under the National Tumor Biology Laboratory project, NLP-17), and the Hungarian Ministry of Human Capacities (ÁEEK/41872-16/2020) to E.S.J.A.; and the Intramural Research Program of the National Institutes of Health (NIH), National Center for Advancing Translational Sciences (NCATS) to M.D.H.

L.Z. thanks the Fonds der Chemischen Industrie for generous financial support through a Kekulé fellowship. J.G.F. thanks the Studienstiftung des deutschen Volkes for support through a PhD scholarship. L.P. thanks the GRK 2338 for support through a PhD scholarship. J.T.-S. thanks the Joachim Herz Foundation for fellowship support. We thank Marcus Conrad (Helmholtz Centre, Munich, DE) for MEF and knockout MEF cell lines. We thank the attendees of the SPP 1710 conference Thiol-Based Redox Switches in 2019, in particular Christopher Lillig (Greifswald, DE), as well as Robert Hondal (Vermont, USA), for their supportive, collegial, and helpfully challenging discussions.

This paper is dedicated to Yasuteru Urano, whose rigorous and far-reaching developments toward translational applications of chemical biology probes are inspiring to us and to the field.

AUTHOR CONTRIBUTIONS

L.Z. performed synthesis, chemical analysis, chemoreductant and enzymatic cell-free studies, and informatics; coordinated data assembly; and wrote the manuscript. J.G.F. performed synthesis, chemical analysis, and chemoreductant and enzymatic cell-free studies. K.C.S. performed enzymatic specificity screenings and cellular studies. L.P. performed cellular studies. D.C. performed the LOPAC screening. M.S.M. performed synthesis and analysis. Q.C. expressed and purified recombinant TrxR and Trx isoenzymes. M.S. performed informatics. M.D.H. supervised LOPAC screening. E.S.J.A. supervised enzymatic specificity screenings and cellular studies and helped in interpretations of results and writing of the manuscript. J.T.-S. performed cellular studies and supervised cell biology. O.T.-S. designed the concept

and experiments, performed informatics, supervised all other experiments, coordinated data assembly, and wrote the manuscript.

DECLARATION OF INTERESTS

L.Z., J.G.F., and O.T.-S. are inventors on patent application EP21167187.0 covering compound structures reported in this paper. The authors declare no competing financial interests.

Received: January 24, 2022

Revised: February 28, 2022

Accepted: March 3, 2022

Published: April 14, 2022

REFERENCES

1. Arnér, E.S.J., and Holmgren, A. (2000). Physiological functions of thioredoxin and thioredoxin reductase. *Eur. J. Biochem.* 267, 6102–6109. <https://doi.org/10.1046/j.1432-1327.2000.01701.x>.
2. Miller, C.G., Holmgren, A., Arnér, E.S.J., and Schmidt, E.E. (2018). NADPH-dependent and -independent disulfide reductase systems. *Free Radic. Biol. Med.* 127, 248–261. <https://doi.org/10.1016/j.freeradbiomed.2018.03.051>.
3. Herrmann, J.M., and Dick, T.P. (2012). Redox biology on the rise. *Biol. Chem.* 393, 999–1004. <https://doi.org/10.1515/hsz-2012-0111>.
4. Jones, D.P., and Sies, H. (2015). The redox code. *Antioxid. Redox Signal.* 23, 734–746. <https://doi.org/10.1089/ars.2015.6247>.
5. Fridovich, I., Poole, L.B., Holmgren, A., Lou, M.F., Gladyshev, V.N., David, S.S., Osborne, R.L., Dawson, J.H., Copley, S.D., Kadokura, H., et al. (2007). Antioxidant enzymes. In *Redox Biochemistry* (John Wiley & Sons), pp. 49–134.
6. Meyer, A.J., and Dick, T.P. (2010). Fluorescent protein-based redox probes. *Antioxid. Redox Signal.* 13, 621–650. <https://doi.org/10.1089/ars.2009.2948>.
7. Lukyanov, K.A., and Belousov, V.V. (2014). Genetically encoded fluorescent redox sensors. *Biochim. Biophys. Acta* 1840, 745–756. <https://doi.org/10.1016/j.bbagen.2013.05.030>.
8. Schwarzländer, M., Dick, T.P., Meyer, A.J., and Morgan, B. (2016). Dissecting redox biology using fluorescent protein sensors. *Antioxid. Redox Signal.* 24, 680–712. <https://doi.org/10.1089/ars.2015.6266>.
9. Yoo, M.-H., Xu, X.-M., Carlson, B.A., Patterson, A.D., Gladyshev, V.N., and Hatfield, D.L. (2007). Targeting thioredoxin reductase 1 reduction in cancer cells inhibits self-sufficient growth and DNA replication. *PLoS One* 2, e1112. <https://doi.org/10.1371/journal.pone.0001112>.
10. Labunsky, V.M., Hatfield, D.L., and Gladyshev, V.N. (2014). Selenoproteins: Molecular pathways and physiological roles. *Physiol. Rev.* 94, 739–777. <https://doi.org/10.1152/physrev.00039.2013>.
11. Cheng, Q., Sandalova, T., Lindqvist, Y., and Arnér, E.S.J. (2009). Crystal structure and catalysis of the selenoprotein thioredoxin reductase 1. *J. Biol. Chem.* 284, 3998–4008. <https://doi.org/10.1074/jbc.M807068200>.
12. Gromer, S., Johansson, L., Bauer, H., Arscott, L.D., Rauch, S., Ballou, D.P., et al. (2003). Active sites of thioredoxin reductases: Why selenoproteins? *Proc. Natl. Acad. Sci. USA* 100, 12618–12623. <https://doi.org/10.1073/pnas.2134510100>.
13. Arnér, E.S.J. (2009). Focus on mammalian thioredoxin reductases – Important selenoproteins with versatile functions. *Biochim. Biophys. Acta* 1790, 495–526. <https://doi.org/10.1016/j.bbagen.2009.01.014>.
14. Maroney, M.J., and Hondal, R.J. (2018). Selenium versus sulfur: Reversibility of chemical reactions and resistance to permanent oxidation in proteins and nucleic acids. *Free Radic. Biol. Med.* 127, 228–237. <https://doi.org/10.1016/j.freeradbiomed.2018.03.035>.
15. Reich, H.J., and Hondal, R.J. (2016). Why nature chose selenium. *ACS Chem. Biol.* 11, 821–841. <https://doi.org/10.1021/acscchembio.6b00031>.
16. Sagemark, J., Elgán, T.H., Bürklin, T.R., Johansson, C., Holmgren, A., and Berndt, K.D. (2007). Redox properties and evolution of human glutaredoxins. *Proteins* 68, 879–892. <https://doi.org/10.1002/prot.21416>.
17. Felber, J.G., Zeisel, L., Pocзка, L., Scholzen, K., Busker, S., Maier, M.S., Theisen, U., Brandstädter, C., Becker, K., Arnér, E.S.J., et al. (2021). Selective, modular probes for thioredoxins enabled by rational tuning of a unique disulfide structure motif. *J. Am. Chem. Soc.* 143, 8791–8803. <https://doi.org/10.1021/jacs.1c03234>.
18. Griffith, O.W. (1999). Biologic and pharmacologic regulation of mammalian glutathione synthesis. *Free Radic. Biol. Med.* 27, 922–935. [https://doi.org/10.1016/S0891-5849\(99\)00176-8](https://doi.org/10.1016/S0891-5849(99)00176-8).
19. Hansen, R.E., Roth, D., and Winther, J.R. (2009). Quantifying the global cellular thiol-disulfide status. *Proc. Natl. Acad. Sci. U. S. A.* 106, 422–427. <https://doi.org/10.1073/pnas.0812149106>.
20. Pires, M.M., and Chmielewski, J. (2008). Fluorescence imaging of cellular glutathione using a latent rhodamine. *Org. Lett.* 10, 837–840. <https://doi.org/10.1021/ol702769n>.
21. Lim, C.S., Masanta, G., Kim, H.J., Han, J.H., Kim, H.M., and Cho, B.R. (2011). Ratiometric detection of mitochondrial thiols with a two-photon fluorescent probe. *J. Am. Chem. Soc.* 133, 11132–11135. <https://doi.org/10.1021/ja205081s>.
22. Butora, G., Qi, N., Fu, W., Nguyen, T., Huang, H.C., and Davies, I.W. (2014). Cyclic-disulfide-based prodrugs for cytosol-specific drug delivery. *Angew. Chem. Int. Ed.* 53, 14046–14050. <https://doi.org/10.1002/anie.201407130>.
23. Felber, J.G., Pocзка, L., Scholzen, K.C., Zeisel, L., Maier, M.S., Busker, S., et al. (2022). Cyclic 5-membered disulfides are not selective substrates of thioredoxin reductase, but are opened nonspecifically. *Nat. Commun.* <https://doi.org/10.1038/s41467-022-29136-4>.
24. Burns, J.A., and Whitesides, G.M. (1990). Predicting the stability of cyclic disulfides by molecular modeling: Effective concentrations in thiol-disulfide interchange and the design of strongly reducing dithiols. *J. Am. Chem. Soc.* 112, 6296–6303. <https://doi.org/10.1021/ja00173a017>.
25. Houk, J., and Whitesides, G.M. (1987). Structure-reactivity relations for thiol-disulfide interchange. *J. Am. Chem. Soc.* 109, 6825–6836. <https://doi.org/10.1021/ja00256a040>.
26. Lees, W.J., and Whitesides, G.M. (1993). Equilibrium constants for thiol-disulfide interchange reactions: A coherent, corrected set. *J. Org. Chem.* 58, 642–647. <https://doi.org/10.1021/jo00055a016>.
27. Cherblanc, F.L., Chapman, K.L., Brown, R., and Fuchter, M.J. (2013). Chaetocin is a nonspecific inhibitor of histone lysine methyltransferases. *Nat. Chem. Biol.* 9, 136–137. <https://doi.org/10.1038/nchembio.1187>.
28. Zong, L., Bartolami, E., Abegg, D., Adibekian, A., Sakai, N., and Matile, S. (2017). Epidithiodiketopiperazines: Strain-promoted thiol-mediated cellular uptake at the highest tension. *ACS Cent. Sci.* 3, 449–453. <https://doi.org/10.1021/acscentsci.7b00080>.
29. Zhang, L., Duan, D., Liu, Y., Ge, C., Cui, X., Sun, J., and Fang, J. (2014). Highly selective off-on fluorescent probe for imaging thioredoxin reductase in living cells. *J. Am. Chem. Soc.* 136, 226–233. <https://doi.org/10.1021/ja408792k>.

30. Ma, H., Zhang, J., Zhang, Z., Liu, Y., and Fang, J. (2016). A fast response and red emission probe for mammalian thioredoxin reductase. *Chem. Commun.* 52, 12060–12063. <https://doi.org/10.1039/C6CC04984B>.
31. Li, X., Zhang, B., Yan, C., Li, J., Wang, S., Wei, X., Jiang, X., Zhou, P., and Fang, J. (2019). A fast and specific fluorescent probe for thioredoxin reductase that works via disulphide bond cleavage. *Nat. Commun.* 10, 2745. <https://doi.org/10.1038/s41467-019-10807-8>.
32. Lothrop, A.P., Ruggles, E.L., and Hondal, R.J. (2009). No selenium required: Reactions catalyzed by mammalian thioredoxin reductase that are independent of a selenocysteine residue. *Biochemistry* 48, 6213–6223. <https://doi.org/10.1021/bi802146w>.
33. Singh, R., and Whitesides, G.M. (1990). Degenerate intermolecular thiolate-disulfide interchange involving cyclic five-membered disulfides is faster by $\sim 10^3$ than that involving six- or seven-membered disulfides. *J. Am. Chem. Soc.* 112, 6304–6309. <https://doi.org/10.1021/ja00173a018>.
34. Laurent, Q., Sakai, N., and Matile, S. (2019). The opening of 1,2-dithiolanes and 1,2-diselenolanes: Regioselectivity, rearrangements, and consequences for poly(disulfide)s, cellular uptake and pyruvate dehydrogenase complexes. *Helv. Chim. Acta* 102, e1800209. <https://doi.org/10.1002/hlca.201800209>.
35. Abegg, D., Gasparini, G., Hoch, D.G., Shuster, A., Bartolami, E., Matile, S., and Adibekian, A. (2017). Strained cyclic disulfides enable cellular uptake by reacting with the transferrin receptor. *J. Am. Chem. Soc.* 139, 231–238. <https://doi.org/10.1021/jacs.6b09643>.
36. Suarez, S.I., Ambrose, R., Kalk, M.A., and Lukesh, J.C., III. (2019). Selenosulfides tethered to gem-dimethyl esters: A robust and highly versatile framework for H₂S probe development. *Chem. Eur. J.* 25, 15736–15740. <https://doi.org/10.1002/chem.201904133>.
37. Mafireyi, T.J., Laws, M., Bassett, J.W., Cassidy, P.B., Escobedo, J.O., and Strongin, R.M. (2020). A diselenide turn-on fluorescent probe for the detection of thioredoxin reductase. *Angew. Chem. Int. Ed.* 59, 15147–15151. <https://doi.org/10.1002/anie.202004094>.
38. Steinmann, D., Nauser, T., and Koppenol, W.H. (2010). Selenium and sulfur in exchange reactions: A comparative study. *J. Org. Chem.* 75, 6696–6699. <https://doi.org/10.1021/jo1011569>.
39. Bachrach, S.M., Walker, C.J., Lee, F., and Royce, S. (2007). Effect of ring strain on nucleophilic substitution at selenium: A computational study of cyclic diselenides and selenenyl sulfides. *J. Org. Chem.* 72, 5174–5182. <https://doi.org/10.1021/jo070578s>.
40. Arai, K., Matsunaga, T., Ueno, H., Akahoshi, N., Sato, Y., Chakrabarty, G., et al. (2019). Modeling thioredoxin reductase-like activity with cyclic selenenyl sulfides: Participation of an NH \cdots Se hydrogen bond through stabilization of the mixed Se–S intermediate. *Chem. Eur. J.* 25, 12751–12760. <https://doi.org/10.1002/chem.201902230>.
41. Wessjohann, L.A., Schneider, A., Abbas, M., and Brandt, W. (2007). Selenium in chemistry and biochemistry in comparison to sulfur. *Biol. Chem.* 388, 997–1006. <https://doi.org/10.1515/BC.2007.138>.
42. Hamsath, A., and Xian, M. (2020). Chemistry and chemical biology of selenenyl sulfides and thioseleninic acids. *Antioxid. Redox Signal.* 33, 1143–1157. <https://doi.org/10.1089/ars.2020.8083>.
43. Sarma, B.K., and Mughesh, G. (2005). Glutathione peroxidase (GPx)-like antioxidant activity of the organoselenium drug ebbselen: Unexpected complications with thiol exchange reactions. *J. Am. Chem. Soc.* 127, 11477–11485. <https://doi.org/10.1021/ja052794t>.
44. Thorn-Seshold, O., Vargas-Sanchez, M., McKeon, S., and Hasserodt, J. (2012). A robust, high-sensitivity stealth probe for peptidases. *Chem. Commun.* 48, 6253–6255. <https://doi.org/10.1039/C2CC32227G>.
45. Mata, G., do Rosário, V.E., Iley, J., Constantino, L., and Moreira, R. (2012). A carbamate-based approach to primaquine prodrugs: Antimalarial activity, chemical stability and enzymatic activation. *Bioorg. Med. Chem.* 20, 886–892. <https://doi.org/10.1016/j.bmc.2011.11.059>.
46. Kiernan, J.A. (2007). Indigogenic substrates for detection and localization of enzymes. *Biotech. Histochem.* 82, 73–103. <https://doi.org/10.1080/10520290701375278>.
47. Kaskova, Z.M., Tsarkova, A.S., and Yampolsky, I.V. (2016). 1001 lights: Luciferins, luciferases, their mechanisms of action and applications in chemical analysis, biology and medicine. *Chem. Soc. Rev.* 45, 6048–6077. <https://doi.org/10.1039/C6CS00296J>.
48. Sharma, A., Arambula, J.F., Koo, S., Kumar, R., Singh, H., Sessler, J.L., and Kim, J.S. (2019). Hypoxia-targeted drug delivery. *Chem. Soc. Rev.* 48, 771–813. <https://doi.org/10.1039/C8CS00304A>.
49. Twum, E.A., Nathubhai, A., Wood, P.J., Lloyd, M.D., Thompson, A.S., and Threadgill, M.D. (2015). Initial development of a cytotoxic amino-seco-CBI warhead for delivery by prodrug systems. *Bioorg. Med. Chem.* 23, 3481–3489. <https://doi.org/10.1016/j.bmc.2015.04.034>.
50. Huang, Z., Terpetschnig, E., You, W., and Haugland, R.P. (1992). 2-(2'-Phosphoryloxyphenyl)-4(3H)-quinazolinone derivatives as fluorogenic precipitating substrates of phosphatases. *Anal. Biochem.* 207, 32–39. [https://doi.org/10.1016/0003-2697\(92\)90495-S](https://doi.org/10.1016/0003-2697(92)90495-S).
51. Prost, M., Canaple, L., Samarut, J., and Hasserodt, J. (2014). Tagging live cells that express specific peptidase activity with solid-state fluorescence. *ChemBioChem* 15, 1413–1417. <https://doi.org/10.1002/cbic.201402091>.
52. Lukesh, J.C., Palte, M.J., and Raines, R.T. (2012). A potent, versatile disulfide-reducing agent from aspartic acid. *J. Am. Chem. Soc.* 134, 4057–4059. <https://doi.org/10.1021/ja211931f>.
53. Diemer, V., Ollivier, N., Leclercq, B., Drobecq, H., Vicogne, J., Agouridas, V., and Melnyk, O. (2020). A cysteine selenosulfide redox switch for protein chemical synthesis. *Nat. Commun.* 11, 2558. <https://doi.org/10.1038/s41467-020-16359-6>.
54. Metanis, N., Keinan, E., and Dawson, P.E. (2010). Traceless ligation of cysteine peptides using selective deselenization. *Angew. Chem. Int. Ed.* 49, 7049–7053. <https://doi.org/10.1002/anie.201001900>.
55. Lu, J., Zhong, L., Lönn, M.E., Burk, R.F., Hill, K.E., and Holmgren, A. (2009). Penultimate selenocysteine residue replaced by cysteine in thioredoxin reductase from selenium-deficient rat liver. *FASEB J.* 23, 2394–2402. <https://doi.org/10.1096/fj.08-127662>.
56. Cheng, Q., and Arnér, E.S.J. (2018). Overexpression of recombinant selenoproteins in *E. coli*. In *Selenoproteins: Methods and Protocols*, L. Chavatte, ed. (Springer), pp. 231–240. https://doi.org/10.1007/978-1-4939-7258-6_17.
57. Cheng, Q., and Arnér, E.S.J. (2017). Selenocysteine insertion at a predefined UAG codon in a release factor 1 (RF1)-depleted *Escherichia coli* host strain bypasses species barriers in recombinant selenoprotein translation. *J. Biol. Chem.* 292, 5476–5487. <https://doi.org/10.1074/jbc.M117.776310>.
58. Cheng, Q., Antholine, W.E., Myers, J.M., Kalyanaraman, B., Arnér, E.S.J., and Myers, C.R. (2010). The selenium-independent inherent pro-oxidant NADPH oxidase activity of mammalian thioredoxin reductase and its selenium-dependent direct peroxidase activities. *J. Biol. Chem.* 285, 21708–21723. <https://doi.org/10.1074/jbc.M110.117259>.
59. Rackham, O., Shearwood, A.-M.J., Thyer, R., McNamara, E., Davies, S.M.K., Callus, B.A., et al. (2011). Substrate and inhibitor specificities differ between human cytosolic and mitochondrial thioredoxin reductases: Implications for development of specific inhibitors. *Free Radic. Biol. Med.* 50, 689–699. <https://doi.org/10.1016/j.freeradbiomed.2010.12.015>.
60. Espinosa, B., and Arnér, E.S.J. (2019). Thioredoxin-related protein of 14 kDa as a modulator of redox signalling pathways. *Br. J. Pharmacol.* 176, 544–553. <https://doi.org/10.1111/bph.14479>.
61. Johansson, C., Lillig, C.H., and Holmgren, A. (2004). Human mitochondrial glutaredoxin reduces S-glutathionylated proteins with high affinity accepting electrons from either glutathione or thioredoxin reductase. *J. Biol. Chem.* 279, 7537–7543. <https://doi.org/10.1074/jbc.M312719200>.
62. Peng, X., Xu, J., and Arnér, E.S.J. (2012). Thiophosphate and selenite conversely modulate cell death induced by glutathione depletion or cisplatin: Effects related to activity and Sec contents of thioredoxin reductase. *Biochem. J.* 447, 167–174. <https://doi.org/10.1042/BJ20120683>.
63. Stafford, W.C., Peng, X., Olofsson, M.H., Zhang, X., Luci, D.K., Lu, L., Cheng, Q., Trésaugues, L., Dexheimer, T.S., Coussens, N.P., et al. (2018). Irreversible inhibition of cytosolic thioredoxin reductase 1 as a mechanistic basis for anticancer therapy. *Sci. Transl. Med.* 10, eaaf7444. <https://doi.org/10.1126/scitranslmed.aaf7444>.

64. Mandal, P.K., Seiler, A., Perisic, T., Kölle, P., Banjac Canak, A., Förster, H., Weiss, N., Kremmer, E., Lieberman, M.W., Bannai, S., et al. (2010). System x_c^- and thioredoxin reductase 1 cooperatively rescue glutathione deficiency. *J. Biol. Chem.* **285**, 22244–22253. <https://doi.org/10.1074/jbc.M110.121327>.
65. Peng, X., Mandal, P.K., Kaminsky, V.O., Lindqvist, A., Conrad, M., and Arnér, E.S.J. (2014). Sec-containing TrxR1 is essential for self-sufficiency of cells by control of glucose-derived H_2O_2 . *Cell Death Dis.* **5**, e1235. <https://doi.org/10.1038/cddis.2014.209>.
66. Peng, X., Giménez-Cassina, A., Petrus, P., Conrad, M., Rydén, M., and Arnér, E.S.J. (2016). Thioredoxin reductase 1 suppresses adipocyte differentiation and insulin responsiveness. *Sci. Rep.* **6**, 28080. <https://doi.org/10.1038/srep28080>.
67. Abdalbari, F.H., and Telleria, C.M. (2021). The gold complex auranofin: New perspectives for cancer therapy. *Discov. Oncol.* **12**, 42. <https://doi.org/10.1007/s12672-021-00439-0>.
68. Prast-Nielsen, S., Dexheimer, T.S., Schultz, L., Stafford, W.C., Cheng, Q., Xu, J., Jadhav, A., Arnér, E.S.J., and Simeonov, A. (2011). Inhibition of thioredoxin reductase 1 by porphyrins and other small molecules identified by a high-throughput screening assay. *Free Radic. Biol. Med.* **50**, 1114–1123. <https://doi.org/10.1016/j.freeradbiomed.2011.01.020>.
69. Eaton, J.K., Furst, L., Ruberto, R.A., Moosmayer, D., Hilpmann, A., Ryan, M.J., Zimmermann, K., Cai, L.L., Niehues, M., Badock, V., et al. (2020). Selective covalent targeting of GPX4 using masked nitrile-oxide electrophiles. *Nat. Chem. Biol.* **16**, 497–506. <https://doi.org/10.1038/s41589-020-0501-5>.
70. Choudhary, S., Malik, Y.S., and Tomar, S. (2020). Identification of SARS-CoV-2 cell entry inhibitors by drug repurposing using in silico structure-based virtual screening approach. *Front. Immunol.* **11**, 1664. <https://doi.org/10.3389/fimmu.2020.01664>.
71. Plemper, R.K., and Cox, R.M. (2018). Biology must develop herd immunity against bad-actor molecules. *PLoS Pathog.* **14**, e1007038. <https://doi.org/10.1371/journal.ppat.1007038>.
72. Forman, H.J., Augusto, O., Brigelius-Flohe, R., Dennery, P.A., Kalyanaram, B., Ischiropoulos, H., et al. (2015). Even free radicals should follow some rules: A guide to free radical research terminology and methodology. *Free Radic. Biol. Med.* **78**, 233–235. <https://doi.org/10.1016/j.freeradbiomed.2014.10.504>.

3.1.4 Bifunctional cleavable 1,2-dithiane linkers for chemical biology

This chapter was deposited on a preprint server and is currently under review:

Repository intended	ChemRxiv 2023 .
Title	<i>Bifunctional, piperazine-fused cyclic disulfides for oxidoreductase-activated cellular proagents</i>
Author List	Jan G. Felber [#] , Lukas Zeisel [#] , Karoline C. Scholzen, Carina Schmitt, Alexander J. Wiegand, Leonid Komissarov, Elias S. J. Arnér, Oliver Thorn-Seshold* [#] these authors contributed equally as first authors; *corresponding author
Publication date	Jan 9 th , 2023
Available at	https://doi.org/10.26434/chemrxiv-2023-tm21m

Author contributions and collaborations

(1) Work performed in the Thorn-Seshold group, LMU Munich:

I performed synthesis and analysis of the fluorogenic probes described in this work and developed strategies for functional diversification (**Fig. 4 and 8**). I further performed chemoreductant and enzymatic screenings, mechanistic analysis (**Fig. 5, 6, and 7**), cellular studies (**Fig. 7**), and some DFT-based calculations of thermodynamic stabilities (**Fig. 3**). **Lukas Zeisel** developed the synthetic access to diastereomerically pure piperazine-fused 1,2-dithianes and 1,2-diselenanes and performed synthesis and analysis of the fluorogenic probes described in this work (**Fig. 2 and 4**). He further performed chemoreductant assays and mechanistic analysis (**Fig. 3, 5 and 6**). He and I contributed equally to the design of the experiments, data assembly and visualization, conceptual analysis of the scientific outcomes, and to writing the manuscript.

Carina Schmitt performed synthesis and analysis of the initial synthetic route towards *trans*-piperazine-fused 1,2-dithianes. **Alexander J. Wiegand** performed synthesis and analysis of desymmetrized bifunctional SS66C-type linkers and of the diversified **X-SS66C-MF** probe platform (**Fig. 8**). **Oliver Thorn-Seshold** designed the concept and experiments, coordinated data assembly, and wrote the manuscript.

(2) Collaboration with the Arnér group, Karolinska Institutet (KI), Stockholm: **Karoline C. Scholzen** performed biochemical screenings, cellular inhibitor and knockout studies (**Fig. 7**). **Elias S. J. Arnér** supervised biochemical studies and cell biology.

(3) Collaboration with the Center of Molecular Modeling (CMM), Ghent University, Ghent: **Leonid Komissarov** performed the other DFT-based calculations on thermodynamic parameters of bicyclic dichalcogenides (**Fig. 3**).

Background

Our previous works developing selective reporters for vicinal dithiol-type bioreductants, like Trx, based on *trigger-cargo* constructs, evolved 6-membered cyclic dichalcogenide reducible units that offer stabilized thermodynamics and kinetic reversibility to resist triggering by relatively concentrated monothiols while still sensing dithiols. We had identified the piperidine-fused 1,2-dithiane **SS66C** as being chemocompatible to Trxs and stable to GSH, in contrast to its diastereomer **SS66T** (see **chapter 3.1.2**), and the Se-proximal 1,2-thiaselenane **SeS60** as chemocompatible to TrxR and stable to GSH in contrast to its GSH-labile Se-distal regioisomer **SSe60**. Whereas the precise combination of reduction and cyclization kinetics, chemical and photophysical properties of the fluorescent cargo, and solubilization by appropriate side chains had resulted in **RX1** as the first selective probe for TrxR1 activity in cells (see **chapter 3.1.3**), we were disappointed that probes using the **SS66C**-type sensor showed very slow cyclization kinetics when using standard phenolic cargos like 3-O-methylfluoresceins (**MF**) and gave poor results (no activation under typical conditions) in cellular settings.

Summary

This work aimed to develop vicinal dithiol-targeted fluorogenic probes that are quantifiably processed in cells by adapting the **SS66**-type design. We had previously noted a strong kinetic enhancement of signal generation when attaching a distal basic amine side chain (**P-SS60** vs. **SS60**) and some enhancement of cargo expulsion kinetics by annelation (**SS66C** vs. **SS60**). We now hypothesized that a condensed molecular design, with a second basic nitrogen in the annelating ring (a piperazine-fused 1,2-dithiane), would retain the thermodynamic stability and selectivity profiles of **SS60** (**Figure 16a**) while enhancing signal generation rates so that cellular processing might be resolved.

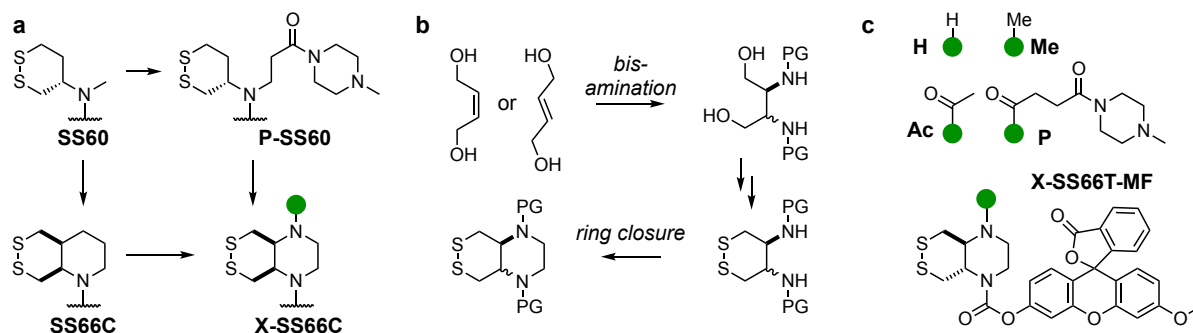


Figure 16 (a) Structure evolution aiming to enhance cyclization/cargo expulsion kinetics. (b) Synthetic access to piperazine-fused 1,2-dithiane precursors. (c) Fluorogenic probe prototype with optional derivatization by alkylation or acylation.

To access these novel, densely heteroatom-functionalized structures, we first applied similar methods as in our previous papers, resulting in a 13-step synthetic route with good yields, but needing various poorly scalable purifications. However, two recent publications on diastereodivergent bis-amination of alkenes²⁴⁰ and on the use of 5-vinyl-thianthrenium as a bis-electrophile for ring closing formation of piperazines from 1,2-diamines²⁴¹ enabled us to adapt the initial synthetic route. We ultimately developed a sequence of only 6 synthetic steps, using only one chromatographic purification to prepare both *cis*- and *trans*-fused piperazine 1,2-dithianes as pure diastereomers (**Fig. 2**, summary in **Figure 16b**).

We confirmed that the novel piperazine-fused 1,2-dithianes retained their extremely low reduction potentials when evaluated through equilibration with DTT, and we used DFT-based calculations to explore the thermodynamic and geometric effects from substitutions at either of the two nitrogen atoms (**Fig. 3**). We then experimentally evaluated the second nitrogen's influence as a secondary (**H**) or tertiary (**Me**) or acylated (**Ac**) amine or when installing a distal basic amine (**P**). For this, we chose the soluble 3-O-methylfluorescein (**MF**) as fluorogenic cargo (**Fig. 4, Figure 16c**). We analyzed the kinetics of cargo expulsion upon fast and quantitative reduction by TCEP and found that all probes based on the novel piperazine-fused design were at least 20× faster to cyclize than previous probes (**Fig. 5, see chapter 3.2.1**). We next examined the kinetics of reversible reduction and found that, as expected, the 6-membered cyclic topologies dictated the differentiation between monothiol and dithiol-type reductants. Again, the *trans*-fused bicyclic trigger was labile to GSH, which validated our initial findings on diastereomer-derived specificity between **SS66C** and **SS66T** (**Fig. 6**).

The main goal of this work was to develop molecular constructs based on the bicyclic **SS66**-type design that enter cells, are bioavailable in the cytosol, and are processed by the cellular redox machinery. We were pleased to see that all novel fluorogenic probes gave signal upon treatment to cells in a dose- and time-dependent manner. We observed ca. 10× higher intensities for **SS66T**-based constructs than **SS66C** probes (**Fig. 7b**). We suggested that these bifunctional piperazine-fused 1,2-dithianes can serve as a cleavable motif for various chemical biology approaches, with the following properties: high chemical robustness, fast cleavage kinetics, orthogonal chemistries, and defined reducibility/resistance profiles. To underline this, we showed that an arbitrary “standard” phenolic cargo can be liberated with fast kinetics by reduction and that, depending on its stereochemistry, low (**SS66C**) or high (**SS66T**) amounts can be delivered in a biological setting, with low/zero extracellular background activation.

Biochemical evaluation verified that **SS66C**-based constructs showed selective response to the two major vicinal dithiol-type redox effectors Trx and Grx. In contrast, **SS66T** probes were susceptible to reduction by most redox proteins (TrxR, Trx, Grx, TRP14) and even GSH (**Fig. 7a**). While options for direct inhibition of the redox effector proteins Trx or Grx were unavailable, we again tested cellular responses when interfering with the Trx system by TrxR activity modulation (Se starvation and chemical inhibition or genetic knockout of TrxR1). We found that cellular processing of **SS66C**-type probes was correlated to TrxR activity with about 50% signal reduction, whereas probes of the **SS66T** series were not: but instead showed signal suppression after chemical depletion of cellular GSH (**Fig. 7**).

Taken together, vicinal dithiol-type proteins of the Trx superfamily (Trxs and Grxs) are capable of effectively reducing our tuned **SS66C**-based designs in cells. We rationalized that relative processing rates between these effectors, guided by previous results on cell-free or cellularly selective processing by Trx (see **chapter 3.1.2**), may be exploited as an additional layer of selectivity for future designs using non-covalent interactions to enhance the protein affinity of the small molecule probes.

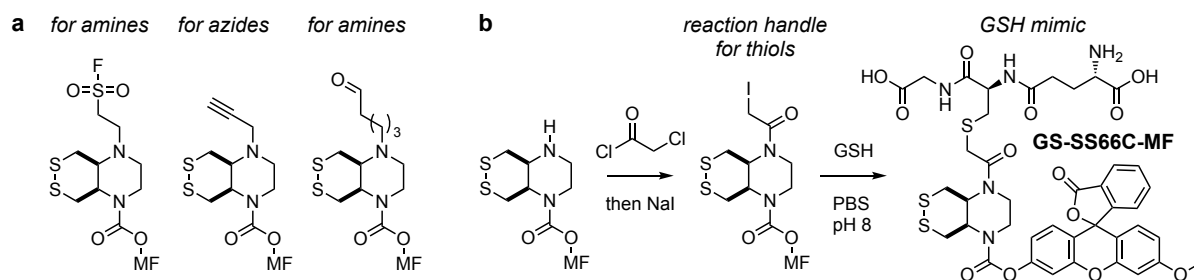


Figure 17 (a) Reaction handles for flexible derivatization of the **SS66C**-core. (a) Using thiol-reactive diversification for the assembly of the prototype GSH-mimic probe **GS-SS66C-MF**.

To work toward installing such interactions with late-stage flexible derivatization, we attached reaction handles based on iodoacetamide (for thiols), alkynes (for azides via CuAAC), sulfonylfluorides (for amines via SuFEx), aldehydes (for amines via reductive amination), and NHS esters (for amines via amide coupling) (**Fig. 8**, **Figure 17a**). In one particular example, we then used our iodoacetamide derivatization handle to install a non-reducing GSH mimic, hoping to test for increased protein affinity for GSH-binding Grxs over Trxs (**Figure 17b**), and calculated the kinetic preference for Grxs of our new **GS-SS66C-MF** construct in a proof-of-principle experiment. Achieving good non-covalent binding by attaching small binding motifs is non-trivial and requires extensive screening in combination with detailed analysis of both on- and off-target protein surfaces. We believe that this is a valid avenue for developing two future orthogonal probes that discriminate Trxs and Grxs in a cellular setting (see **chapter 5.1.1**).

We also offer outlook applications for the somewhat GSH-labile **SS66T**, noting that constructs in chemical biology or medicinal chemistry often consist of two or more covalently linked components to enable cellular entry and sometimes localization or targeting of the whole construct: but that often, their intracellular separation may be desired. This is especially the case for antibody-drug conjugates (ADCs). Here, our cleavable disulfide **SS66T** could act as a linker to replace other, less reliable units based on hydrolysis or proteolysis. We also envision these linkers can find applications far beyond cell biology/drug delivery, e.g. as protein purification handles or for solid phase peptide/protein syntheses, wherever fast and reliable liberation of a construct upon disulfide reduction is desirable.

Bifunctional, piperazine-fused cyclic disulfides for oxidoreductase-activated cellular proagents

Lukas Zeisel^{1,‡}, Jan G. Felber^{1,‡}, Karoline C. Scholzen², Carina Schmitt¹, Alexander J. Wiegand¹, Leonid Komissarov³, Elias S.J. Arnér^{2,4}, Oliver Thorn-Seshold^{1,*}

¹ Department of Pharmacy, Ludwig Maximilians University Munich, Butenandtstr. 5-13, 81377 Munich.

² Division of Biochemistry, Department of Medical Biochemistry and Biophysics, Karolinska Institutet, SE-171 77 Stockholm, Sweden

³ Center for Molecular Modeling (CMM), Ghent University, Technologiepark-Zwijnaarde 46, 9052 Ghent, Belgium.

⁴ Department of Selenoprotein Research, National Institute of Oncology, 1122 Budapest, Hungary.

[‡]The two first authors contributed equally to this work. *Corresponding author.

ABSTRACT: We report piperazine-fused six-membered-cyclic dichalcogenides as rapid-response redox sensors for probes, prodrugs, and bifunctional conjugates that interface with cellular thiol/disulfide redox biology. By combining the thermodynamic stability of 1,2-dithianes with unprecedentedly rapid kinetics of self-immolation after reduction, these motifs are uniquely reliable and flexible reduction-based sensors for live cell applications. We synthesise four *cis*- and *trans*-piperazine-fused cyclic disulfides and diselenides by scalable, diastereomerically pure, six-step synthetic routes with just one chromatographic purification. Fluorogenic probes using these redox-active diamines are >100-fold faster activated than the previously known monoamines, which now allowed us to deconvolute the kinetics of the reduction and the cyclisation steps during activation. The diastereomers have remarkably different reductant specificity. In particular, the *cis*-fused disulfides are only activated by strong vicinal dithiol reductants, while *trans*-fused disulfides are activated even by monothiols like GSH. Thus, although both disulfides are good substrates for glutaredoxins and thioredoxins in cell-free assays, upon cellular applications the *cis*-disulfide probes substantially report on oxidoreductase activity in the thioredoxin system (the *trans*-disulfides remain promiscuously reactive). Finally, we showcase efficient late-stage synthetic diversification of the piperazine-disulfides, promising their broad applicability as cleavable bifunctional cores for redox probes and prodrugs, for solid phase synthesis, and as linkers for antibody-drug conjugates.

1. INTRODUCTION

Biological research relies on chemical tools with selective reactivity profiles that can be used in living cells. Redox biology remains under-supplied with high-quality chemical tools, particularly in the context of thiol/disulfide redox manifolds: which are used in hundreds of protein networks not only to shuttle electrons but also to modulate protein shape or activity, to control protein-protein interactions, or to trigger or block signaling. The highly conserved, upstream oxidoreductases that supply reducing equivalents for these many reaction manifolds are attractive targets as the "central nodes of thiol/disulfide redox biology": particularly the dithiol-type redoxins, including the thioredoxin/thioredoxin reductase system (Trx/TrxR), the glutaredoxin/glutathione/glutathione reductase system (Grx/GSH/GR), and a handful of related proteins.¹⁻³

There are tremendous untapped opportunities for small molecule approaches that are chemocompatible with these dithiol/disulfide chemistries (or even selectively address certain oxidoreductases), and that work effectively and non-invasively in live cells. Such reagents may drive basic research into biological redox dynamics and regulation, support translational medicine with redox- or metabolically-gated diagnostics and therapeutics, or contribute in many other ways to the broader field of chemical biology. A selective reagent platform for the selenol/thiol enzyme TrxR1 was recently developed, relying on the unusual reactivity of its rare active-site selenocysteine.⁴ However, there remain no cellularly-effective reagent systems that selectively address dithiol reductases like Trxs and Grxs; and despite some efforts,^{5,6} even inhibitors that could be

selective for these proteins in the cellular context⁷ are not known, regardless of their prominence as cancer-relevant targets⁸.

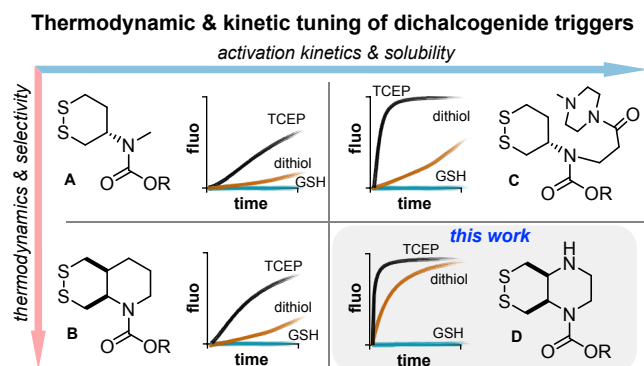


Fig 1 Thermodynamic and kinetic tuning of cyclic dichalcogenide chemistry. We combined the previous designs to establish a condensed molecular core that also enables further derivatisation.

The chemical challenge for targeting these central dithiol reductases is to develop artificial disulfide-type substrates with fast on-target reactivity in cells, yet without broad lability to other (di)thiol proteins or to concentrated monothiols such as GSH. Recently, guided by Whitesides' studies on disulfide thermodynamics,⁹ we identified monothiol-resistant cyclic disulfide monoamines **SS60** and **SS66C** as dithiol protein substrates that even offer good selectivity for reduction by Trxs in cell-free assays (**Fig 1A,B**). Their cyclic topology is crucial to dithiol protein selectivity, as it requires full reduction before triggering probe activation;⁹ the kinetic and

thermodynamic stabilisation of the 6-membered disulfide were also expected to promote their cellular selectivity by resisting activation from less strongly reducing downstream reductases or GSH. Unfortunately, when these substrates were incorporated into fluorogenic probes, their cargo release kinetics were poor; and they proved to be inactive in cells.¹⁰ This is not surprising since, to be active, their post-reduction dithiol intermediate must cyclise and irreversibly expel a leaving group *before* it is simply re-oxidised by reducing any disulfide in its surroundings: and this dithiol intermediate's similarity to the powerful reductant DTT, that is known to rapidly reduce very many cellular disulfides, suggests that it would need exceptional cyclisation rates to effectively out-compete cellular re-oxidation. We tested using an *N*-methylpiperazinamide (**P**) group to enhance activation kinetics, hoping that local basicity could keep the thiolate deprotonated and so enhance cyclisation. The resulting **P-SS60** (**Fig 1C**) had remarkably faster cell-free activation but still remained cellularly silent.⁴ Likely, its post-reduction thiolate cyclisation was still slower than re-oxidation in the cellular environment, or it was too poor a substrate for its target dithiol proteins - or both.

In this work, we wanted to tackle both these potential problems, to develop cellularly-activated proagents triggered by dithiol-type redox effector proteins. We aimed to combine the cyclisation preorganisation delivered by **SS66**-type fused 1,2-dithianes with a nearby amine as in **P-SS60** for local basicity while maintaining the thermodynamic and kinetic disulfide stability that seems to favour

their being selective for the powerful Trx/Grx-type dithiol proteins. Condensing these features, we designed *cis*- and *trans*-piperazine-fused cyclic disulfides and diselenides (**Fig 1D**) as a densely-functionalised new class of redox substrate for diverse cellular uses. We aimed to employ them in probes achieving high chemical robustness, fast reduction and cleavage kinetics, and strong dithiol protein selectivity in live cells; we also wanted to explore whether their diamine structure would permit flexible chemical diversification so that they might be broadly applicable well beyond enzyme probes: e.g. as robust but quickly reversible linkers for ADCs or protein purification. Lastly, if the cellular activity were obtained without incurring broad reductant lability, we aimed to test if tuning structural features could enhance processing by selected dithiol proteins as an opening step towards the not only rapid but also highly selective redox probes of the future.

2. RESULTS

2.1 Syntheses of dichalcogenide piperazine redox substrates

Since cargo release, reduction potentials, and reductant sensitivity of annelated dithianes are strongly affected by *cis*- or *trans*-fusion of the bicyclic system; we desired diastereomerically pure synthetic routes that also avoid epimerisation at any of the synthetic steps (from e.g. strong base conditions).⁹ We also aimed at scalable synthetic routes that could provide all four disulfide and diselenide piperazines from one starting material type.

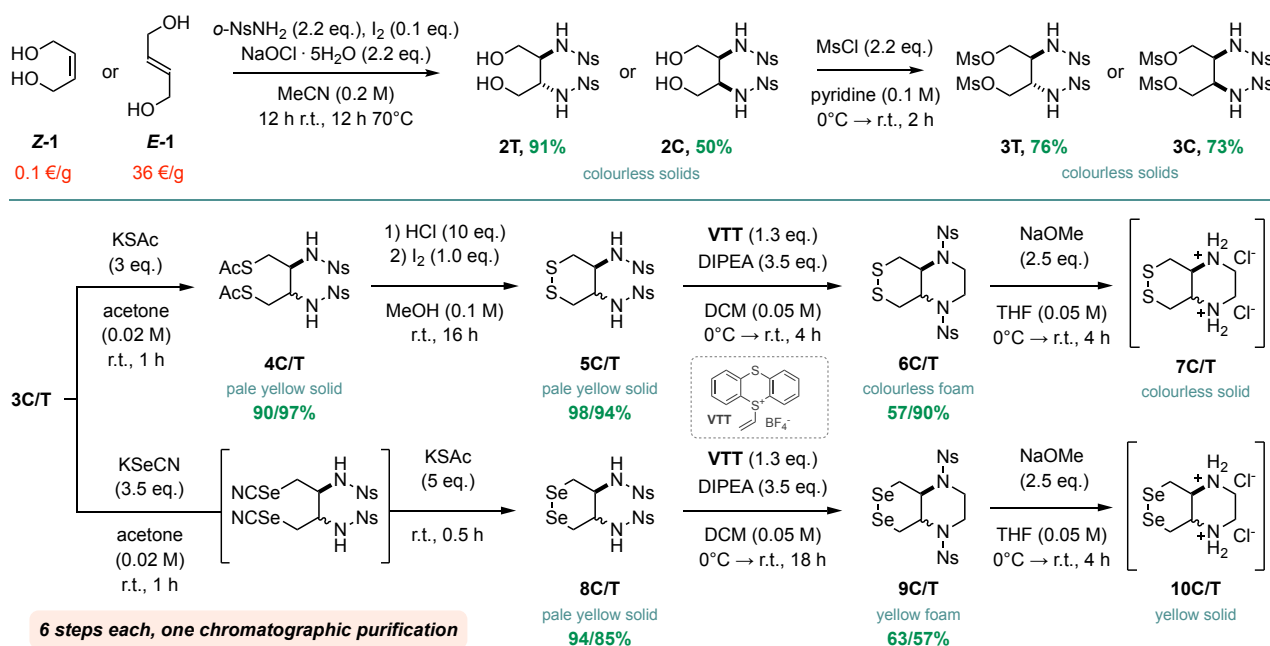


Fig 2 Scalable, modular synthetic procedure for dichalcogenide-fused piperazines.

1,4-dithioerythritol and 1,4-dithiothreitol are alluring starting materials for *cis* and *trans* disulfide piperazines respectively: after oxidation to the dithianes (**DTE^{ox}/DTT^{ox}**), they would only require converting the diol to a piperazine. Unfortunately, **DTE^{ox}/DTT^{ox}** mesylates and triflates were unsuccessful in C-N bond formation regardless of the *N*-nucleophile used (**DEX/DTX**, **Fig S1**). *Cis*-butene-diol **Z-1** is also a cheap

feedstock, whose 1,4-diol promises straightforward chalcogen introduction^{4,10} but whose alkene may allow alternative 2,3-diamine installations. After 1,4-diol protection, we set up *trans* stereochemistry by epoxidation and basic nucleophilic ring opening, or else *cis* stereochemistry by Upjohn bishydroxylation (**26T/C**, **Fig S1**). We aminated 2,3-diols **26T/C** to the 1,4-dihydroxybutane-2,3-diamines **29T/C** in 4 steps. First, we tested

installing the chalcogens before piperazine formation; in the sulfur series, 1,2-dithiane-4,5-diamines were easily accessed (e.g. **36T/C**), but subsequent reductive amination with glyoxal to assemble the piperazine gave only a complex mixture of species, including the pyrazine formed by oxidation. We then tested forming the piperazine *before* the dichalcogenide: first condensing the open-chain 2,3-diamine with dimethyl oxalate and reducing to the piperazine¹¹ (e.g. **31**→**39**→**40**, **Fig S1**), then deprotecting the 1,4-diol and introducing the chalcogens, to give bicyclic dithiane target **7T** in 13 steps overall with an overall yield of 6% (**Fig S1**).

Unsatisfied by the high step-count and time-cost of that route, we then tested direct olefin (di-)amination, as pioneered by Sharpless and recently refined by Okumura¹² (**Fig S1**). To our delight, iodine-catalysed 1,2-anti-diamination of starting butenols **Z-1** and **E-1** provided nosyl-protected 1,4-dihydroxybutane-2,3-diamines **2T/C** as pure diastereomers in good to excellent yield without chromatography (**Fig 2**), cutting 6 steps from the previous route. Diol mesylation gave **3T/C** in excellent purity and good yields by simple precipitation, ready to transform into the 1,2-dithianes and 1,2-diselenanes by using appropriate chalcogen sources (**Fig 2**).

Sulfur was smoothly introduced by treating **3T/C** with KSAC; acidic cleavage of bis(thioester) **4** then oxidation gave protected dithiane-2,3-diamine **5** in near-quantitative yield, again isolated purely by precipitation. (Basic thioester cleavage should be avoided since rapid intramolecular S_NAr onto the nosyl groups gives the aryl thioethers). Now, **5** faced the challenge of annelating the piperazine, which had failed for **36T/C** by e.g. reductive amination. Bis-alkylations of **5** e.g. using 1,2-dihaloethanes did not give good conversion. However, bis-electrophile methodologies from Aggarwal (diphenylsulfonium)^{13,14} and Ritter (vinyl thianthrenium "VTT")¹⁵ offered alternatives. Diphenylsulfoniums did not perform well with our substrates, but VTT gave the piperazines **6T/C** in good yields with purification just over a short silica plug, removing thianthrene as the only reaction byproduct (**Fig 2**). We avoided Fukuyama nosyl deprotection with thiol reagents¹⁶ due to the risk of dithiane reduction then S_NAr; but NaOMe deprotection ran smoothly, and purification by precipitation as the di-hydrochloride gave **7T/C** in excellent yield (63 wt% alongside 2.5 equiv. NaCl, **Fig 2**).

For the selenium introduction, we avoided taking an analogous route to that for sulfur since selenoesters are notoriously unstable¹⁷. Se could be instead introduced to dimesylates **3T/C** by KSeCN. However, to minimise exposure to selenium species, we aimed to convert the bis-selenocyanates to diselenanes **8** in a one-pot procedure. Again, to avoid intramolecular S_NAr reaction onto the nosyl groups, we did not wish to unmask the selenolates, so avoided O-nucleophiles that would perform S_N2 at carbon (RSeCN). Instead, we chose KSAC as a chalcophilic nucleophile for deprotection: transiently forming an activated R-SeSAC species that then undergoes intramolecular Se-Se bond formation, presumably via hypervalent selenium. To our delight, the formation of diselenanes **8T/C** was fast and visible by eye (evolution of a bright yellow colour). From here, the procedures matched that for the dithianes, with VTT to form the piperazines **9T/C** from the 2,3-nosylamide, then basic solvolytic deprotection, with purification by precipitation, to give piperazine-diselenanes

10T/C. Interestingly, during the piperazine annelation, both **9C** and **9T** significantly degraded to insoluble solids: presumably ring-opened oligodiselenides, promoted by the strain introduced by the bis(sulfonamide) bicycle; whereas **10T/C** appeared stable.

In summary, we developed a scalable and efficient sequence towards piperazine-annelated 1,2-dithianes (**SS66C**, **SS66T**) and 1,2-diselenanes (**SeSe66C**, **SeSe66T**). The syntheses provide all four dichalcogenides in 6 steps, as pure diastereomers, on a gram scale, and require only one chromatographic purification (**Fig 2**).

2.2 Thermodynamic features of the piperazine-bicycles

We wanted to find out how functional groups near the dichalcogenide affect the thermodynamic stability of the piperazine-annelated systems. In particular, we wanted to compare their performance against that of the corresponding piperidine-annelated systems (**Fig 1B**), to test for influences of their second ring nitrogen: e.g. i) nitrogen lone pair electronics, and bond angle preferences that may distort the annelating ring geometry; ii) the influence of a local basic amine that may lower the local pK_a; or iii) the influence of substituents at the amine that may influence CSSC/CSeSeC-dihedral angles and SS/SeSe bond distance. We determined the reduction potentials of piperazine dithianes **7T/C** by known methods¹⁰, using HPLC to measure reduced-to-oxidised equilibria of model benzamides **H-SS66C-Bz** and **H-SS66T-Bz** against dithiothreitol (DTT; E° -327 mV¹⁸). Notably, equilibria were reached 10× faster than for piperidine dithianes **SS66C/T-Bz**, although the endpoints were similar: with **H-SS66C-Bz** (-335 mV) harder to reduce than **H-SS66T-Bz** (-317 mV), similar to previous findings^{9,10} (**Fig 3a**, **Fig S3**).

a experimental reduction potential

	C-C	C-N	N-N
E° [V]	Whitesides 1993	Thorn-Seshold 2021	this work
<i>cis</i>	-0.34	-0.339	-0.343
<i>trans</i>	-0.35	-0.317	-0.305

b DFT calculations

	ox	red		
E [kJ/mol]	oxidized	reduced	ΔE (E^{red}-E^{ox})	
	E ^{rel} [kJ/mol]	E ^{rel} [kJ/mol]	[kJ/mol]	
C-C	<i>cis</i>	31	5	-26
	<i>trans</i>	23	0	-23
C-N	<i>cis</i>	63	23	-40
	<i>trans</i>	32	0	-32
N-N	<i>cis</i>	60	22	-38
	<i>trans</i>	35	0	-35

Fig 3 Thermodynamics of bicyclic 1,2-dithianes. (a) Experimental reduction potentials^{9,10,18} determined by HPLC equilibration against DTT (E° = -0.327 V) (see **Fig S3**). (b) DFT calculation of energetic minima - examples for C-C, C-Ac, and H-Ac substitution (see **Fig S4**).

Density functional theory (DFT)-based calculations using the B3LYP functional¹⁹ were performed to look for systematic trends in how annelation influences (i) the relative energies of *cis/trans* diastereoisomers; (ii) ring tension, revealed by SS/SeSe distance and dihedral angles (Table S2); and (iii) the energy gain/penalty upon reduction of the dichalcogenides (Fig 3b). To that end, energetic minima of oxidized and reduced SS66C/T and SeSe66C/T species were compared while varying groups in the annelating ring (-CH₂-, -NH-, -NMe-, -NAc-, or -N(CO₂Me)-; see Table S1). We were pleased to see that the second, optionally substituted nitrogen atom did not drastically destabilize the bicyclic dichalcogenides. Unsurprisingly, the reduction of SS66 was much more favourable than that of SeSe66 (Fig S4); but other trends were much smaller, and overall, these calculations did not suggest very different reduction thermodynamics as compared to previous piperidine SS66 systems (Tables S1-S2, Fig S4).

2.3 Redox probes: diversified design and synthesis

To test the kinetic properties of these piperazine dichalcogenides in probes, we incorporated them into fluorogenic probes based on *O*-methylfluorescein (MF). As previously established, MF probes are locked as nonconjugated nonfluorescent lactones, so this design allows true off-to-on activation of fluorescence after a reduction-cyclisation-expulsion cascade (Fig 4a).^{10,20}

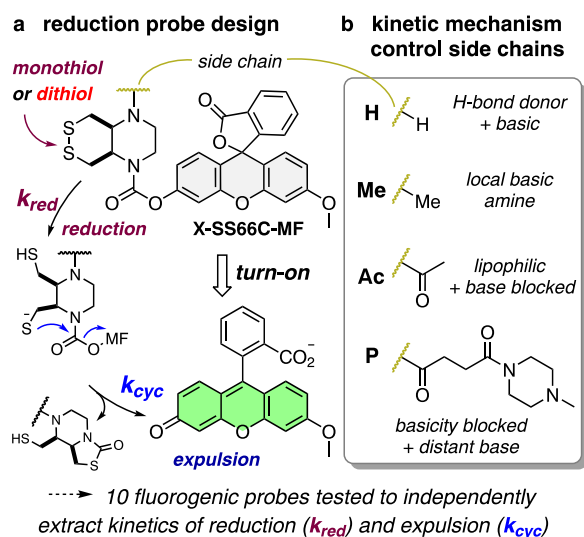


Fig 4 (a) Probes based on carbamates between triggers and 3-*O*-methylfluorescein (MF) as a fluorogenic cargo that are activated after reduction (k_{red}) and cargo expulsion (k_{cyc}) steps that re-establish MF's xantheno-based fluorescence.

A major advantage of the piperazines is the potential for diversifying e.g. H-SS66C/T probes at the final step of the synthesis, by reactions with the free amine. We now used derivatisations to showcase the modularity of this platform, ultimately preparing a probe library of 16 piperazine dithianes and four additional controls (Fig S2). At this stage, we examined the two parent H-SS66C/T-MF probes alongside derivatives with three types of sidechain, intended to test the effects of acylation and alkylation on probe performance: methyl (Me-, local basic amine, sp³), acetyl (Ac-, abasic, ~sp²) and succinamidyl-

(*N*-methyl)piperazine (P-, ~sp², distant basic amine) (Fig 4b, Fig S2). We did not derivatise the SeSe66-MF probes, fearing their potential for problematic linearisation as observed during synthesis. All derivatives were accessed in a single step from the free amine precursors in good yields (see Supporting Information). Controls with a non-reducible piperazine-cyclohexane (H-CC66-MF) or a P-derivatised monocyclic dithiane trigger (P-SS60-MF) were also synthesised following similar methods (Fig S2).

2.4 Kinetic analysis of reduction-based performance

We aimed to understand the structural influences on the two consecutive kinetic steps involved in the probes' generation of fluorescent signal: (i) reduction (k_{red}); and (ii) cyclisation/cargo expulsion (k_{cyc}) (Fig 4a). To separate these steps, we first analysed signal generation kinetics upon reaction with the fast and irreversible reducing agent TCEP (tris(2-carboxyethyl) phosphine): allowing us to extract pseudo-1st-order kinetics of the k_{cyc} step since in our assay conditions, cyclisation and expulsion were rate-limiting (increasing TCEP concentrations did not accelerate fluorescence turn-on; Fig S5). We then used this rate to deconvolute reductant-specific k_{red} values from the overall signal generation rates measured with biologically relevant monothiol- and dithiol-reductants GSH and DTT (Fig S5).

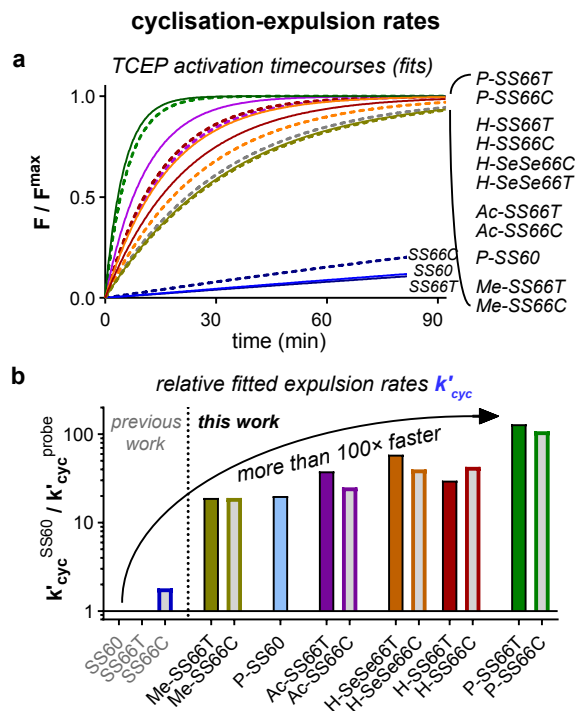


Fig 5 Post-reduction cyclisation kinetics. (a) TCEP-mediated activation is fast and irreversible, allowing to fit fluorescence with pseudo-1st-order kinetics reflecting cyclisation/expulsion rates. (b) The piperazine-annelated redox triggers give up to >100x faster cyclisation/expulsion kinetics than previous¹⁰ triggers (see Fig S6).

The piperazine-fused disulfide probes had vastly faster TCEP-triggered signal generation rates (Fig 5a; Fig S6) than prior simple dithiane SS60-MF and piperidine-dithianes SS66C/T-MF (Fig

1A,B), which had all had slow activation kinetics that was intrinsically limited by their small k_{cyc} (taking several hours to approach full activation even with a large excess of the quantitative irreversible TCEP)¹⁰. For the piperazines, even when releasing the electron-rich MF phenolate, **P-SS66T/C** showed an exceptional half-time of < 5 min, indicating >100× faster k_{cyc} than **SS66C/T** or **SS60** probes (all with MF cargo).

k_{cyc} values for *trans* and *cis* diastereomers of each trigger were closely similar, which is coherent with the assumption that TCEP reduction is both fast and irreversible. However, several trends are apparent when comparing trigger types. The side chain on the piperazines affects k_{cyc} , with **Me** (20×) < **Ac** (30×) < **H** (ca. 50×) < **P** (ca. 110×) (**Fig 5b**; k_{cyc} values are given relative to that for monocyclic **SS60**). Since the bicyclic piperidines **SS66T/C** also had relative rates of just ca. 1-2×, these enhanced rates should *not* be attributed to the triggers' bicyclic structure causing classic Thorpe-Ingold preorganisation. Instead, a large kinetic enhancement can be expected from adding a local basic amine (since **P-SS60** gives ca. 20× enhancement over **SS60**) or from having the second piperazine nitrogen in the ring (e.g. **Ac-SS66T/C** ca. 20× faster than **SS66T/C**), and these effects are somewhat additive (**P-SS66T/C** >100× faster than **SS66C/T**).

We next assayed reduction kinetics with monothiol and dithiols, titrating the cellular monothiol reductant GSH (ca. 5 mM in cytoplasm) and the artificial dithiol reductant DTT (that serves as a cheap model for dithiol proteins) at increasing concentrations and collecting timecourse data (**Fig 6a,b**). DTT gave strong signal generation for all compounds, with 10 mM DTT giving nearly identical signal generation speed as 100 μM TCEP. By contrast, GSH only reduced **SS66T**-type probes: all **SS66C** probes, plus **P-SS60**, **SeSe66T**, and **SeSe66C**, were fully inert to GSH up to 10 mM (**Fig 6c, Fig S7**). Unlike the dithianes, **H-SeSe66C** was more slowly activated by DTT than *trans*-fused **H-SeSe66T**.

To compare reduction rates numerically, we considered data where reduction (**Fig S6b**) is orders of magnitude slower than cyclisation; here, the initial signal generation rates (normalised for reductant concentration) approach a maximum k'_{red} at low reductant concentration, which is a lower bound for the true reduction rate per unit of reductant (**Fig 6c, Fig S8**).

The main feature of interest is that the *cis*-annelated dithianes are remarkably monothiol-resistant, while their *trans*-diastereoisomers are moderately (**Me/H-SS66T**) or even highly (**P-SS66T**) sensitive. We find the *cis*-dithianes' resistance particularly remarkable considering their highly increased cyclisation kinetics compared to previous constructs, which might otherwise have been thought to make them more generally labile. The three last assay types show that the *cis*- and *trans*-diastereomers have very similar thermodynamic reduction potentials (**Fig 3**) and cyclisation rates (**Fig 5**): it is rather their apparent reduction rates k'_{red} that distinguish them (**Fig 6**). Noting that these k'_{red} values also reflect the reversibility of the thiol-disulfide exchange (and/or full reduction) steps, one possible explanation for the different monothiol lability/resistance of the **T/C** isomers (a difference that is consistent across so many fluorogenic probes), is that the *trans* diastereomer has a unique kinetic inhibition of retro-reaction after thiol-disulfide exchange

(and/or full reduction), potentially by relaxation of a more strained mono/bis-*N*-acylated piperazine ring geometry. Though other factors are also possible, a systematic exploration of the reasons for **T**-instability is best left to future investigations.

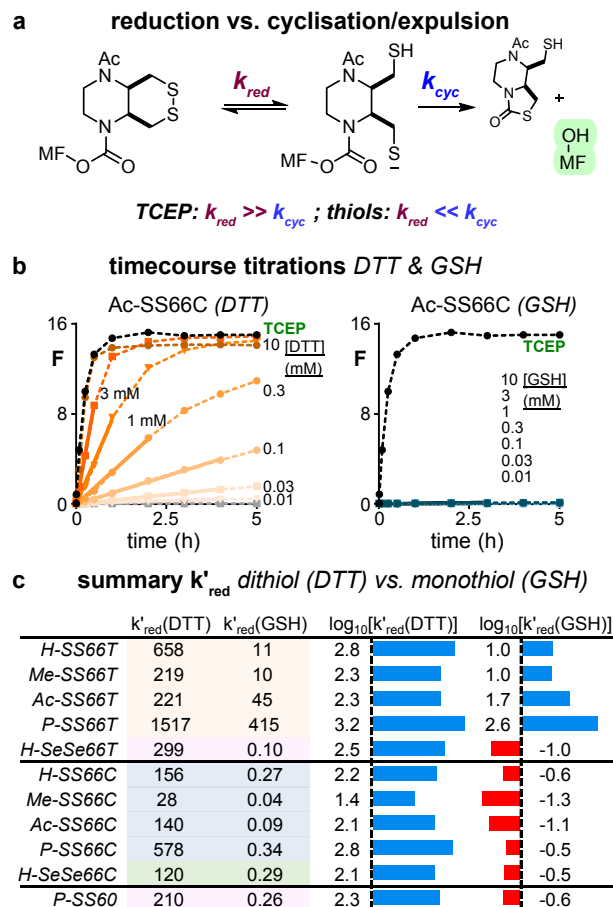


Fig 6 Evaluation of monothiol vs. dithiol reduction kinetics. (a) Simplified mechanism of dithiol- vs monothiol-based **Ac-SS66C-MF** probe activation. (b) Dose response timecourses for DTT and GSH (0.01-10 mM) reduction of **Ac-SS66C-MF**. (c) Reduction rate constants k'_{red} for dithiol and monothiol reduction.

2.5 Artificial oxidoreductase substrate character

Building upon the chemical characterisation of fluorogenic disulfide piperazines, we next were interested in assessing their reactivity in biochemical assays with redox-active proteins and enzymes (**Fig 7a**). Generally, and independent of the substitution and diastereomer, disulfide conjugates were activated well within the thioredoxin and glutaredoxin systems and did not notably react with the upstream reductases TrxR1, TrxR2, or GR.

The key observations we had made during chemical characterisation applied nonetheless, with substitution at the idle nitrogen determining release kinetics and (to some degree) enzyme promiscuity along **Me**<**H**<**Ac**<**P**. Concerning diastereomerism, **SS66T** conjugates' reduction (and thus activation) rates were significantly higher than for **SS66Cs** and thus resulted in faster activation regardless of the enzymatic system used. Adding to the significant background reactivity with GSH as

part of the GR-GSH-Grx system, higher reduction rates of the *trans*-trigger unit appears to render the *trans*-fused probes more promiscuous than their *cis*-counterparts (Fig S9-S10): **SS66T** probes were readily activated by glutaredoxins, thioredoxins, and even TRP14. In contrast, **SS66C** probes were unreactive with GSH and TRP14, while being readily activated by Trx1/2 and by Grx1/2, albeit at somewhat different rates.

Diselenanes **SeSe66T** and **C** both reacted with the Trx- and Grx-systems, but to a significantly lesser degree than their sulfur-counterparts – both in terms of slower kinetics and lower absolute fluorescence; though we remain cautious about interpreting the results for diselenane probes (discussion at Fig S11).

2.6 Piperazine-dithiane probes are active in live cells

Having determined the *in vitro* selectivity profiles for these piperazine-fused dichalcogen probes, we next turned to cellular assays. At this point, we abandoned diselenane-based probes after initial experiments (Fig S12) due to recurring issues with compound degradation and polymerisation: exclusion criteria for meaningful cellular assays.

We were delighted to observe efficient and dose-dependant activation for **SS66T** probes in A549 cells (1-100 μ M, Fig 5b, Fig S12); activation kinetics and absolute fluorescent signal generation were again determined by the side chain (Me<H<Ac<P). We assessed the role of the thioredoxin system in this signal generation by variation of selenium supply (starvation or supplementation, to decrease or promote synthesis of full-length active seleno-TrxR); by TrxR1 chemical inhibition (using inhibitor TRi-1²¹); or by TrxR1 genetic knockout (from a mouse embryonic fibroblast (MEF) cell line, annotated "fl/fl" for MEF cells expressing TrxR1, "-/-" for the TrxR1 knockout^{22,23}). Matching expectations of promiscuity from the cell-free GSH titrations, probe activation was unchanged by all three modulations, showing it was independent of thioredoxin system activity. However, inhibition of GSH-biosynthesis by buthionine-sulfoximine (BSO) reduced activation of **H-SS66T** by almost 50% (Figures S13-15). Together with chemical and enzymatic *in vitro* activity assays, this suggests that **SS66T**s function as probes for cellular thiol activity, strongly involving GSH, but at this stage, we cannot exclude roles for redox effector proteins and other protein thiols.

SS66C-based probes were also reliably and dose-dependently activated in A549 cells (Fig 5c, Fig S12), but in contrast to their *trans*-counterparts, they provided ca. 10-fold less fluorescent signal. This was not unexpected, as *in vitro* results (Fig 5a) indicated monothiol-resistance, thus excluding a major portion of active thiols that likely contribute to the activation of **SS66T**s. To our delight, the three orthogonal methods of modulating thioredoxin system activity all strongly affected **SS66C** activation. Based on earlier *in vitro* assays, we attribute this to modulating the effector protein thioredoxin (Fig 5c, Fig S14-16). BSO also causes a notable but smaller effect on **SS66C** activation; since **SS66C** resists direct GSH challenge, we suggest that this effect proceeds through the Grxs that use GSH for recovery. Thus, we propose that all **C**-type probes report on both Trx and Grx activity but are unaffected by cellular monothiols.

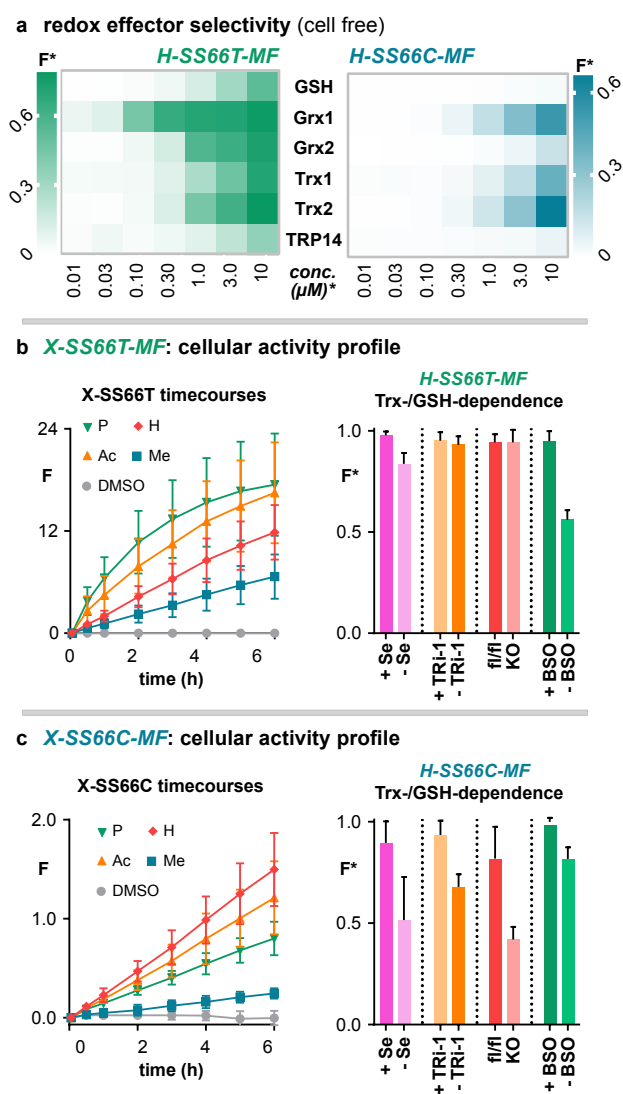


Fig 7 Biochemical and cellular evaluation. (a) **SS66C/T** piperazine probes are artificial substrates for Grx and Trx. Low turnover with TRP14, TrxR or GR. *For GSH, concentrations are given in mM. (b,c) Probes based on **SS66T** are strongly activated in A549 cells, whereas **SS66C**s shows 10× lower signal. Dose-dependent linear signal increases over time suggest intracellular turnover. Cellular manipulations of the Trx/TrxR system (\pm Se, \pm TrxR inhibitor TRi-1, TrxR ko vs. wt) gives a significant effect only with **SS66C**-type probes. [F(t) is raw fluorescence intensity; F* is an F(endpoint) value normalised to compare between conditions, defined in cell-free assays as $F^* = [F(3\text{h}) - F_{\text{blank}}(t_0)]/F_{\text{TCEP-max}}$ and in cellular assays as $F^* = [F(6\text{h}) - F(t_0)]/F_{\text{max}}$ where F_{max} is the largest raw F(6h) replicate value; see Supporting Information Parts 4-5 for details.]

In summary, we identified the first dithiane-based fluorogenic probes that report strongly on cellular redox activity. This advance was enabled by the development of the piperazine-disulfide motif, which provides orders of magnitudes faster probe activation kinetics than literature precedents. We believe that particularly the speed of cyclisation (k_{cyc}) is key for cellular performance, as it determines the efficiency of irreversible fluorophore release and accumulation. Previously known dithiane probes had >100-fold

with iodoacetamide probe **16**, with the reaction in aqueous buffer at pH 7.4, giving full conversion to **GS-SS66C-MF (17)** within minutes (**Fig 7b**). In line with the monothiol-stability we established earlier for the SS66C, this establishes another synthetic modality which the dithiane-core is robust to.

We compared model probe **17**'s activation by Trx1 and Grx1 as compared to **H-**, **Ac-** and **P-SS66C-MF**; and identified only a small kinetic Grx1-preference for the **GS-SS66C-MF** probe. Even though this effect was minor, this result is encouraging for the idea of directing redoxin selectivity through introduction of affinity/electrostatic complementarity fragments.

3. SUMMARY AND OUTLOOK

Our previous efforts towards reducible triggers for applications to thiol/disulfide redox biology focused on thermodynamically stable cyclic dichalcogenides that were mechanistically designed to resist monothiol reduction. We had identified *cis*-piperidine-fused 1,2-dithianes as motifs selectively operated by thioredoxins. However, the activation of their fluorogenic probes in cells was poor, which we attributed to slow cyclisation kinetics (k_{cyc}).

In this study, we have improved these cyclisation and cargo expulsion kinetics to achieve workable cellular tools. We assumed that by accelerating cyclisation kinetics, faster turnover would result that could overcome the challenges of cellular release, and that this need not compromise its reductant selectivity profile which would still be predetermined by its topology and geometry. We used disulfide piperazines as a condensed design that combines a cyclic disulfide's redox properties with a basic or derivatisable amine within the bicyclic system to achieve this enhancement: all dichalcogenide piperazine probes were activated at least 20× faster than the previous examples. Building on this assay, we then used titrations with monothiol- (GSH) and dithiol-type (DTT) reductants to extract apparent overall rate constants for the reversible reduction steps (k'_{red}), which had, to the best of our knowledge, not been done for reducible probes so far. The *cis*-fused isomers retained full resistance to reduction by monothiols, while the *trans*-fused isomers were rapidly responsive to both monothiols and dithiols. We also saw that the dichalcogenide piperazines' redox profiles are determined by diastereomerism, and independent of *N*-substitution.

We tested the probes' responses to the GR/GSH/Grx and the TrxR/Trx systems, i.e. the two prominent oxidoreductase systems present in cells. *In vitro*, biochemical assays with isolated proteins showed selective activation of the *cis*-fused series by Trxs and Grxs, but promiscuous reactivity for the *trans*-fused isomers. In cells, and for the first time for any dithiane-based redox probes, we saw dose-dependent activation. The *trans*-fused probe series was activated at high rates and signal intensities; signal generation was independent of modulation of the cellular Trx/TrxR system but responsive to chemical inhibition of GSH biosynthesis. The *cis*-fused probes were activated at lower rates, but this was coherent with their selectivity for dithiol-type proteins, which we validated by the dependence of cellular activation on Trx system activity.

In a conceptual sense, we envision disulfide piperazines as flexibly applicable tools for chemical biology. The modular nature of this

system offers the arbitrary choice of a "cargo", e.g. a diagnostic, therapeutic, or other functional agents. For example, similarly to our recent report of thioredoxin-system-targeted bioreductive prodrugs,³² a **SS66C**-bifunctional linker could be used to gate drug release to redox activity (e.g. releasing duocarmycin-type DNA alkylators³³). Importantly, the cellular performance, degree of activation, and speed of release will be inherited from one cargo construct to any other since these are defined by the disulfide piperazine chosen. The bifunctionality of disulfide piperazines also offers flexible derivatisation at the second nitrogen for, e.g. tuning probes' physicochemical properties or targeting biolocalisation.³⁴

Finally, in a practical sense, to promote the applications of disulfide piperazines, the streamlined 6-step protocol we report that rapidly accesses these piperazines as pure diastereomers on gram-scale will be important; as will the versatile diversification possibilities that they offer e.g. via orthogonal clickable handles. Due to their ease of functionalisation, their stability against non-reductive cleavage, and their remarkably fast reductive cleavage rates, disulfide piperazines may well establish themselves as broadly applicable bifunctional units for redox chemical biology in cells and beyond.

ASSOCIATED CONTENT

Supporting Information

Synthesis, analysis, biochemical evaluations (PDF).

AUTHOR INFORMATION

Corresponding Author

* oliver.thorn-seshold@cup.lmu.de

Author Contributions

L.Z. performed synthesis and analysis, chemoreductant assays, and mechanistic analysis. J.G.F. performed synthesis and analysis, performed chemoreductant, enzymatic specificity screening and DFT-based calculations. L.Z. and J.G.F. contributed equally to the design of the experiments, data assembly and visualisation, conceptual analysis of the scientific outcomes, and writing the manuscript, and declare equal shared first authorship. K.C.S. performed biochemical screenings and cellular inhibition and knockout studies. C.S. and A.J.W. performed synthesis and analysis. L.K. performed DFT-based calculations. E.S.J.A. supervised biochemical studies and cell biology. O. T.-S. designed the concept and experiments, coordinated data assembly, and wrote the manuscript with input from all co-authors.

Funding Statement

This research was supported by funds from the German Research Foundation (DFG: SFB 1032 project B09 number 201269156, SFB TRR 152 project P24 number 239283807, SPP 1926 project number 426018126, and Emmy Noether grant 400324123), and the Munich Centre for NanoScience initiative (CeNS) to O.T.-S.; from Karolinska Institutet, the Knut and Alice Wallenberg Foundations (KAW 2015.0063 and KAW 2019.0059), the Swedish Cancer Society (CAN 2018/333 and 19 0330 Pj), the Swedish Research Council (2017-01872), the Hungarian Thematic Excellence Programme (TKP2020-NKA-26), the

Hungarian National Research, Development and Innovation Office (ED_18-1-2019-0025), the Hungarian National Laboratories Excellence program (under the National Tumor Biology Laboratory project, NLP-17), and the Hungarian Ministry of Human Capacities (A' EEK/41872-16/2020) to E.S.J.A. L.K. has received funding from the European Union's Horizon 2020 research and innovation programme (Grant agreement No 814143).

L.Z. thanks the Fonds der Chemischen Industrie for generous funding through a Kekulé fellowship. J.G.F. thanks the Studienstiftung des deutschen Volkes for support through a PhD scholarship.

ACKNOWLEDGMENTS

We are very grateful to Prof. Tobias Ritter for providing a generous sample of VTT, and the helpful discussions on the reagents' reactivity. We thank Markus Müller for mechanism and kinetics discussion; and Paula Ruppel and Jannick Gehring for synthetic assistance. We also thank Software for Chemistry & Materials B.V. (SCM), Amsterdam for providing us the Amsterdam Modeling Suite (AMS) software for DFT calculations. We thank Marcus Conrad (Helmholtz Centre, Munich) for MEF TrxR1 knockout cell lines.

REFERENCES

- (1) Arnér, E. S. J.; Holmgren, A. Physiological Functions of Thioredoxin and Thioredoxin Reductase. *Eur. J. Biochem.* 2000, 267 (20), 6102–6109. <https://doi.org/10.1046/j.1432-1327.2000.01701.x>.
- (2) Fernandes, A. P.; Holmgren, A. Glutaredoxins: Glutathione-Dependent Redox Enzymes with Functions Far beyond a Simple Thioredoxin Backup System. *Antioxid. Redox Signal.* 2004, 6 (1), 63–74. <https://doi.org/10.1089/152308604771978354>.
- (3) Jones, D. P.; Sies, H. The Redox Code. *Antioxid. Redox Signal.* 2015, 23 (9), 734–746. <https://doi.org/10.1089/ars.2015.6247>.
- (4) Zeisel, L.; Felber, J. G.; Scholzen, K. C.; Poczka, L.; Cheff, D.; Maier, M. S.; Cheng, Q.; Shen, M.; Hall, M. D.; Arnér, E. S. J.; Thorn-Seshold, J.; Thorn-Seshold, O. Selective Cellular Probes for Mammalian Thioredoxin Reductase TrxR1: Rational Design of RX1, a Modular 1,2-Thiaselenane Redox Probe. *Chem* 2022, 8 (5), 1493–1517. <https://doi.org/10.1016/j.chempr.2022.03.010>.
- (5) Powis, G.; Kirkpatrick, D. L.; Angulo, M.; Baker, A. Thioredoxin Redox Control of Cell Growth and Death and the Effects of Inhibitors. *Chem. Biol. Interact.* 1998, 111–112, 23–34. [https://doi.org/10.1016/S0009-2797\(97\)00148-8](https://doi.org/10.1016/S0009-2797(97)00148-8).
- (6) Baker, A. F.; Dragovich, T.; Tate, W. R.; Ramanathan, R. K.; Roe, D.; Hsu, C.-H.; Kirkpatrick, D. L.; Powis, G. The Antitumor Thioredoxin-1 Inhibitor PX-12 (1-Methylpropyl 2-Imidazolyl Disulfide) Decreases Thioredoxin-1 and VEGF Levels in Cancer Patient Plasma. *J. Lab. Clin. Med.* 2006, 147 (2), 83–90. <https://doi.org/10.1016/j.lab.2005.09.001>.
- (7) Kirkpatrick, D. L.; Kuperus, M.; Dowdeswell, M.; Potier, N.; Donald, L. J.; Kunkel, M.; Berggren, M.; Angulo, M.; Powis, G. Mechanisms of Inhibition of the Thioredoxin Growth Factor System by Antitumor 2-Imidazolyl Disulfides. *Biochem. Pharmacol.* 1998, 55 (7), 987–994. [https://doi.org/10.1016/S0006-2952\(97\)00597-2](https://doi.org/10.1016/S0006-2952(97)00597-2).
- (8) Ramanathan, R. K.; Kirkpatrick, D. L.; Belani, C. P.; Friedland, D.; Green, S. B.; Chow, H.-H. S.; Cordova, C. A.; Stratton, S. P.; Sharlow, E. R.; Baker, A.; Dragovich, T. A Phase I Pharmacokinetic and Pharmacodynamic Study of PX-12, a Novel Inhibitor of Thioredoxin-1, in Patients with Advanced Solid Tumors. *Clin. Cancer Res.* 2007, 13 (7), 2109–2114. <https://doi.org/10.1158/1078-0432.CCR-06-2250>.
- (9) Lees, W. J.; Whitesides, G. M. Equilibrium Constants for Thiol-Disulfide Interchange Reactions: A Coherent, Corrected Set. *J. Org. Chem.* 1993, 58 (3), 642–647. <https://doi.org/10.1021/jo00055a016>.
- (10) Felber, J. G.; Zeisel, L.; Poczka, L.; Scholzen, K.; Busker, S.; Maier, M. S.; Theisen, U.; Brandstädter, C.; Becker, K.; Arnér, E. S. J.; Thorn-Seshold, J.; Thorn-Seshold, O. Selective, Modular Probes for Thioredoxins Enabled by Rational Tuning of a Unique Disulfide Structure Motif. *J. Am. Chem. Soc.* 2021, 143 (23), 8791–8803. <https://doi.org/10.1021/jacs.1c03234>.
- (11) Oishi, T.; Hirama, M. Synthesis of Chiral 2,3-Disubstituted 1,4-Diazabicyclo [2.2.2] Octane. New Ligand for the Osmium-Catalyzed Asymmetric Dihydroxylation of Olefins. *Tetrahedron Lett.* 1992, 33 (5), 639–642. [https://doi.org/10.1016/S0040-4039\(00\)92331-1](https://doi.org/10.1016/S0040-4039(00)92331-1).
- (12) Minakata, S.; Miwa, H.; Yamamoto, K.; Hirayama, A.; Okumura, S. Diastereodivergent Intermolecular 1,2-Diamination of Unactivated Alkenes Enabled by Iodine Catalysis. *J. Am. Chem. Soc.* 2021, 143 (11), 4112–4118. <https://doi.org/10.1021/jacs.1c00228>.
- (13) Yar, M.; McGarrigle, E. M.; Aggarwal, V. K. An Annulation Reaction for the Synthesis of Morpholines, Thiomorpholines, and Piperazines from β -Heteroatom Amino Compounds and Vinyl Sulfonium Salts. *Angew. Chem. Int. Ed.* 2008, 47 (20), 3784–3786. <https://doi.org/10.1002/anie.200800373>.
- (14) Yar, M.; McGarrigle, E. M.; Aggarwal, V. K. Bromoethylsulfonium Salt—A More Effective Annulation Agent for the Synthesis of 6- and 7-Membered 1,4-Heterocyclic Compounds. *Org. Lett.* 2009, 11 (2), 257–260. <https://doi.org/10.1021/ol8023727>.
- (15) Juliá, F.; Yan, J.; Paulus, F.; Ritter, T. Vinyl Thianthrenium Tetrafluoroborate: A Practical and Versatile Vinylating Reagent Made from Ethylene. *J. Am. Chem. Soc.* 2021, *jacs.1c06632*. <https://doi.org/10.1021/jacs.1c06632>.
- (16) Kan, T.; Fukuyama, T. Ns Strategies: A Highly Versatile Synthetic Method for Amines. *Chem. Commun.* 2004, No. 4, 353. <https://doi.org/10.1039/b311203a>.
- (17) Zeisel, L.; Maier, M. S.; Thorn-Seshold, O. Regioselective, Efficient and Scalable Syntheses of 1,2-Thiaselenanes. *ChemRxiv* 2022. <https://doi.org/10.26434/chemrxiv-2022-99slz>.
- (18) Lukesh, J. C.; Palte, M. J.; Raines, R. T. A Potent, Versatile Disulfide-Reducing Agent from Aspartic Acid. *J. Am. Chem. Soc.* 2012, 134 (9), 4057–4059. <https://doi.org/10.1021/ja211931f>.
- (19) Stephens, P. J.; Devlin, F. J.; Chabalowski, C. F.; Frisch, M. J. Ab Initio Calculation of Vibrational Absorption and Circular Dichroism Spectra Using Density Functional Force Fields. *J. Phys. Chem.* 1994, 98 (45), 11623–11627. <https://doi.org/10.1021/j100096a001>.
- (20) Felber, J. G.; Poczka, L.; Scholzen, K. C.; Zeisel, L.; Maier, M. S.; Busker, S.; Theisen, U.; Brandstädter, C.; Becker, K.; Arnér, E. S. J.; Thorn-Seshold, J.; Thorn-Seshold, O. Cyclic 5-Membered Disulfides Are Not Selective Substrates of Thioredoxin Reductase, but Are Opened Nonspecifically. *Nat. Commun.* 2022, 13 (1), 1754. <https://doi.org/10.1038/s41467-022-29136-4>.
- (21) Stafford, W. C.; Peng, X.; Olofsson, M. H.; Zhang, X.; Luci, D. K.; Lu, L.; Cheng, Q.; Trésaugues, L.; Dexheimer, T. S.; Coussens, N. P.; Augsten, M.; Ahlén, H.-S. M.; Orwar, O.; Östman, A.; Stone-Elander, S.; Maloney, D. J.; Jadhav, A.; Simeonov, A.; Linder, S.; Arnér, E. S. J. Irreversible Inhibition of Cytosolic Thioredoxin Reductase 1 as a Mechanistic Basis for Anticancer Therapy. *Sci. Transl. Med.* 2018, 10 (428), eaaf7444. <https://doi.org/10.1126/scitranslmed.aaf7444>.
- (22) Mandal, P. K. Complex Redundancy between the Mammalian Thioredoxin and Glutathione Systems in Cell Proliferation and Tumorigenesis, Ludwig-Maximilian-University Munich, Munich, 2009. https://edoc.ub.uni-muenchen.de/11958/1/Mandal_Pankaj_Kumar.pdf (accessed 2021-08-19).
- (23) Mandal, P. K.; Schneider, M.; Kolle, P.; Kuhlencordt, P.; Forster, H.; Beck, H.; Bornkamm, G. W.; Conrad, M. Loss of Thioredoxin Reductase 1 Renders Tumors Highly Susceptible to Pharmacologic Glutathione Deprivation. *Cancer Res.* 2010, 70 (22), 9505–9514. <https://doi.org/10.1158/0008-5472.can-10-1509>.
- (24) Hoyle, C. E.; Bowman, C. N. Thiol–Ene Click Chemistry. *Angew. Chem. Int. Ed.* 2010, 49 (9), 1540–1573. <https://doi.org/10.1002/anie.200903924>.

- (25) Hoogenboom, R. Thiol–Yne Chemistry: A Powerful Tool for Creating Highly Functional Materials. *Angew. Chem. Int. Ed.* 2010, 49 (20), 3415–3417. <https://doi.org/10.1002/anie.201000401>.
- (26) Meldal, M.; Tornøe, C. W. Cu-Catalyzed Azide–Alkyne Cycloaddition. *Chem. Rev.* 2008, 108 (8), 2952–3015. <https://doi.org/10.1021/cr0783479>.
- (27) Chen, Q.; Mayer, P.; Mayr, H. Ethenesulfonyl Fluoride: The Most Perfect Michael Acceptor Ever Found? *Angew. Chem. Int. Ed.* 2016, 55 (41), 12664–12667. <https://doi.org/10.1002/anie.201601875>.
- (28) Dong, J.; Krasnova, L.; Finn, M. G.; Sharpless, K. B. Sulfur(VI) Fluoride Exchange (SuFEx): Another Good Reaction for Click Chemistry. *Angew. Chem. Int. Ed.* 2014, 53 (36), 9430–9448. <https://doi.org/10.1002/anie.201309399>.
- (29) Barrow, A. S.; Smedley, C. J.; Zheng, Q.; Li, S.; Dong, J.; Moses, J. E. The Growing Applications of SuFEx Click Chemistry. *Chem. Soc. Rev.* 2019, 48 (17), 4731–4758. <https://doi.org/10.1039/C8CS00960K>.
- (30) Berndt, C.; Schwenn, J.-D.; Lillig, C. H. The Specificity of Thioredoxins and Glutaredoxins Is Determined by Electrostatic and Geometric Complementarity. *Chem. Sci.* 2015, 6 (12), 7049–7058. <https://doi.org/10.1039/C5SC01501D>.
- (31) Begas, P.; Liedgens, L.; Moseler, A.; Meyer, A. J.; Deponte, M. Glutaredoxin Catalysis Requires Two Distinct Glutathione Interaction Sites. *Nat. Commun.* 2017, 8 (1), 14835. <https://doi.org/10.1038/ncomms14835>.
- (32) Felber, J. G.; Kitowski, A.; Zeisel, L.; Maier, M. S.; Heise, C.; Thorn-Seshold, J.; Thorn-Seshold, O. Cyclic Dichalcogenides Extend the Reach of Bioreductive Prodrugs to Harness the Thioredoxin System: Applications to Seco-Duocarmycins. *bioRxiv* 2022. <https://doi.org/10.1101/2022.11.11.516112>.
- (33) Felber, J. G.; Thorn-Seshold, O. 40 Years of Duocarmycins: A Graphical Structure/Function Review of Their Chemical Evolution, from SAR to Prodrugs and ADCs. *JACS Au* 2022, 2 (12), 2636–2644. <https://doi.org/10.1021/jacsau.2c00448>.
- (34) Jia, S.; Lin, E.; Lim, I.; Mobley, E.; Guo, L.; Sletten, E. Water Soluble Chromenylium Dyes for Shortwave Infrared Imaging in Mice. *ChemRxiv* 2022. <https://doi.org/10.26434/chemrxiv-2022-h8rjb>.

3.2 Redox-targeted therapeutic prodrugs for anti-cancer use

3.2.1 A searchable database and graphical review of the duocarmycin cytotoxins

This chapter was published as follows:

Journal JACS Au **2022**, 2, 2636-2644. (*highlighted as ACS Editor's Choice article*)
Title *40 Years of Duocarmycins: A Graphical Structure/Function Review of Their Chemical Evolution, from SAR to Prodrugs and ADCs*
Author List **Jan G. Felber***, Oliver Thorn-Seshold*
*co-corresponding authors
Publication date Nov 15th, 2022
Available at <https://doi.org/10.1021/jacsau.2c00448>

Author contributions

I performed the Systematic Literature Review (SLR), structure-based analysis, categorization of literature reports, statistical evaluation, and meta-analysis. I designed the concept of a searchable graphical review of structural evolution based on chemical design features, performed visualization and graphic design, and wrote the manuscript.

Oliver Thorn-Seshold initiated, designed, and supervised work on prodrugs of the duocarmycin family, coordinated data assembly and visualization, and wrote the manuscript.

A0 Poster (available at <https://tinyurl.com/200carmycins>)

40 years of duocarmycins: a graphical structure/function review of their chemical evolution, from SAR to prodrugs and ADCs

Jan G. Felber and Oliver Thorn-Seshold; LMU Munich: <https://thornsehold.cup.uni-muenchen.de>

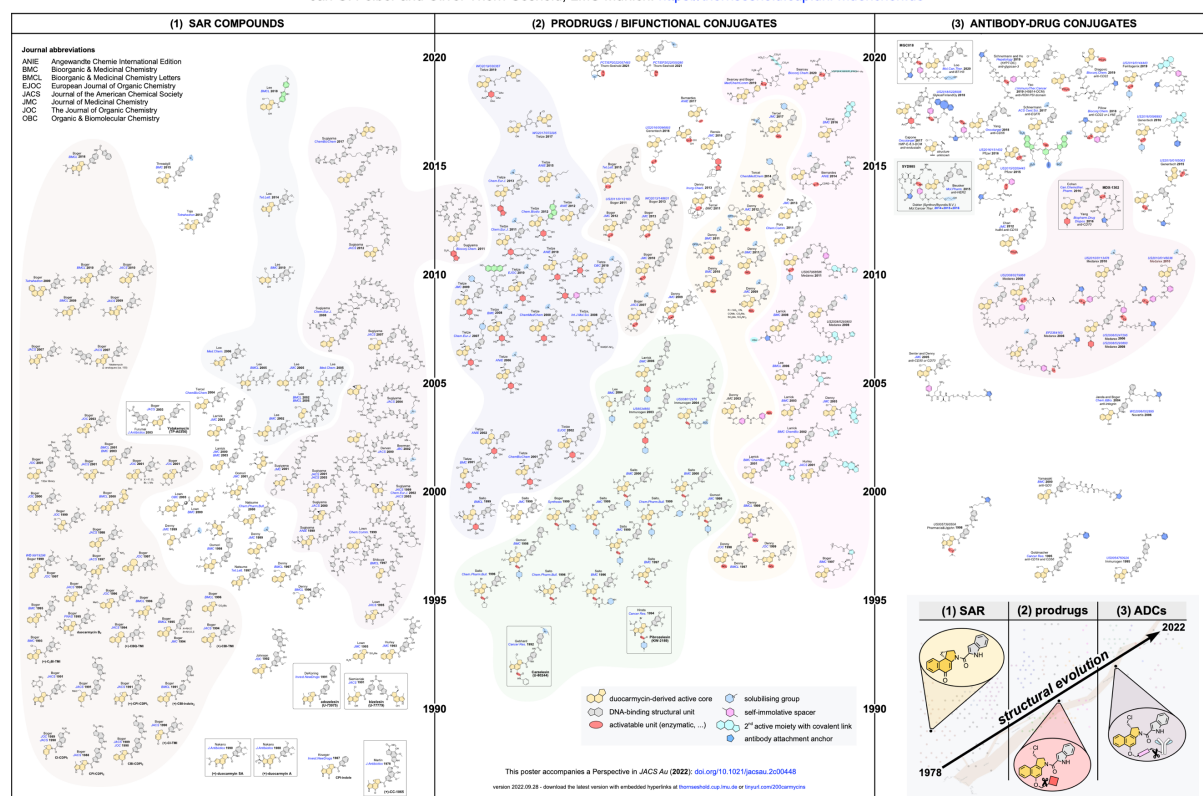


Figure 18 A0-poster with hyperlinked molecular structures representing the structural evolution of duocarmycin bioactives from 1978-2022, classed by (i) SAR, (ii) prodrugs, and (iii) ADCs.

Background

The work presented in this thesis has so far used fluorogenic imaging probes based on *trigger-cargo* constructs that liberate small-molecule dyes upon activation of their appended trigger units leading to an off-to-on switch of the dye's fluorescence. In the context of cancer prodrug development, we were looking for a small molecule therapeutic agent that can work through the same logic: an off-to-on switch of bioactivity triggered by molecular fragmentation following reduction.

Summary

The duocarmycin class of bioactives consists of highly potent, cytotoxic agents that function via DNA minor groove docking and then irreversible alkylation of DNA bases, leading to spontaneous base excision and cell death. The cyclopropane electrophilic site responsible for alkylation can be formed *in situ* by intramolecular cyclization from its inactive phenolic *seco*-precursor. Bioactivity can thus be masked by covalently binding the phenol to prevent cyclization until it is unmasked. We were fascinated by this unusual mechanism and by the evolution of structural chemical designs over the last 40 years.

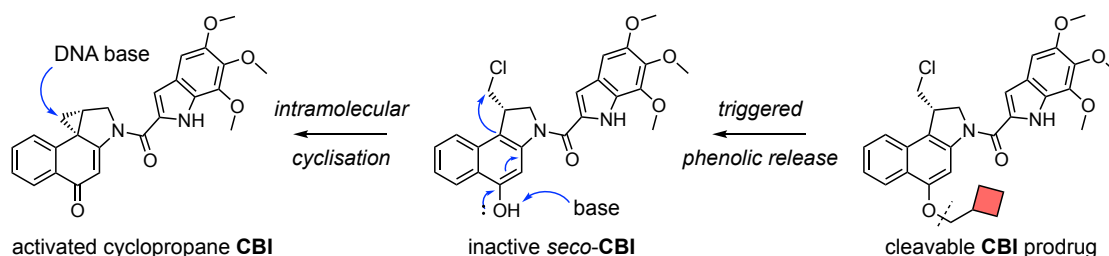


Figure 19 Duocarmycins: CBI prodrugs release *seco*-CBIs, that, upon cyclization, give the active CBI alkylators.

This work presents a Systematic Literature Review (SLR) on the duocarmycin family from its early discovery in 1978 to its versatile applications as highly flexible, tunable bioactives in large constructs, such as antibody-drug conjugates (ADCs). The main goal of this work was to provide an information-rich graphical overview of the key molecular design steps on a chronological development line, as structured by class of applications from (i) structure-activity-relationship (SAR) to (ii) prodrugs and (iii) ADCs. For this purpose, we presented an A0-poster with DOI-hyperlinked references (see **Figure 18**) for each of the >200 structures that can be used to easily trace back the original publications.

We complemented the searchable poster with a mini-review describing the past 40 years of structural evolution from a medicinal chemist's viewpoint. We explained the parameters behind the SLR (**Fig. 1**) and analyzed literature metrics of the 583 primary references we covered (**Fig. 2**) before describing the logic and structure of the A0-poster (**Fig. 3**). We then gave a single-figure summary of the key structural elements in duocarmycin SAR, prodrugs and ADCs, drawn from nearly 100 papers (**Fig. 4**). Lastly, we gave an outlook for the duocarmycins, with guiding principles for future developments (**Fig. 5**).

We hope the graphical representation and searchable character of this review will serve as a prototype for mini-reviews of molecular evolution within a series or as analogs to Njardarson's Top 200 posters. We further hope that future investigators interested in duocarmycins will benefit from the large body of references that are fast to browse and easy to access in such a format.

40 Years of Duocarmycins: A Graphical Structure/Function Review of Their Chemical Evolution, from SAR to Prodrugs and ADCs

Jan G. Felber* and Oliver Thorn-Seshold*



Cite This: *JACS Au* 2022, 2, 2636–2644



Read Online

ACCESS |

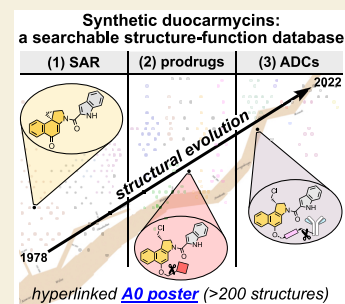
Metrics & More

Article Recommendations

Supporting Information

ABSTRACT: Synthetic analogues of the DNA-alkylating cytotoxins of the duocarmycin class have been extensively investigated in the past 40 years, driven by their high potency, their unusual mechanism of bioactivity, and the beautiful modularity of their structure–activity relationship (SAR). This Perspective analyzes how the molecular designs of synthetic duocarmycins have evolved: from (1) early SAR studies, through to modern applications for directed cancer therapy as (2) prodrugs and (3) antibody–drug conjugates in late-stage clinical development. Analyzing 583 primary research articles and patents from 1978 to 2022, we distill out a searchable A0-format “Minard map” poster of ca. 200 key structure/function-tuning steps tracing chemical developments across these three key areas. This structure-based overview showcases the ingenious approaches to tune and target bioactivity, that continue to drive development of the elegant and powerful duocarmycin platform.

KEYWORDS: duocarmycin, cancer prodrug, CC-1065, antibody–drug–conjugates (ADC), CBI therapeutics, structural evolution



1. INTRODUCTION

The natural products CC-1065 and duocarmycin SA are irreversible DNA alkylators that react after docking in the minor groove. Since their isolation from *Streptomyces* from 1978 onward,^{1,2} their picomolar cytotoxic potency has attracted continuous attention. Several total syntheses have been reported,^{3–5} and biochemical research has shown how

their site-selectivity of DNA alkylation depends on structural features and stereochemistry.^{6,7} Clinical drug⁸ and prodrug⁹ candidates for cancer treatment quickly advanced to phase I and II clinical trials.^{10–13} Even after initial trials were discontinued due to narrow therapeutic index or strong side effects, an entire “duocarmycin family” of synthetic analogues with a broad range of aims and applications have been pursued. This minireview aims to distill this diversity of duocarmycin development into a rapidly grasped, yet comprehensive, format.

Medicinal chemistry around duocarmycins has focused on three key areas (Figure 1). (1) SAR studies have explored the relationship of pharmacophore structure to DNA alkylation, and simplified synthetic analogues such as the cyclopropa-benz[e]indoles (CBIs)¹⁴ have been developed, to retain the parent functionality but with greater chemical tractability.¹⁵ (2) Prodrugs aiming to direct activity better toward target cancer cells have explored activatable alkylation motifs and bifunctional conjugates.¹⁶ (3) Antibody–drug conjugates (ADCs) have also been developed for improved targeting, and in this incarnation the first duocarmycin derivative was recently FDA-approved.¹⁷

In this Perspective we present a focused digest of the chemistry in these areas, collating most of the prolific research

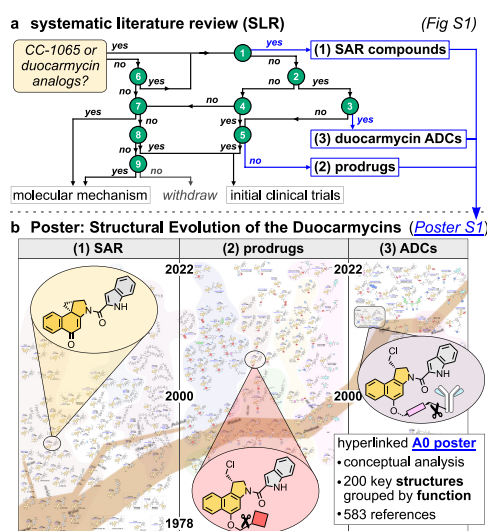


Figure 1. (a) 583 duocarmycin research reports were classified by a nine-point scheme, then structurally analyzed. (b) The A0-sized Poster S1 “Minard map” summarizes the structural evolution of >200 duocarmycin-derived agents from SAR to prodrugs and ADC.

Received: August 12, 2022

Revised: September 16, 2022

Accepted: September 27, 2022

Published: November 15, 2022



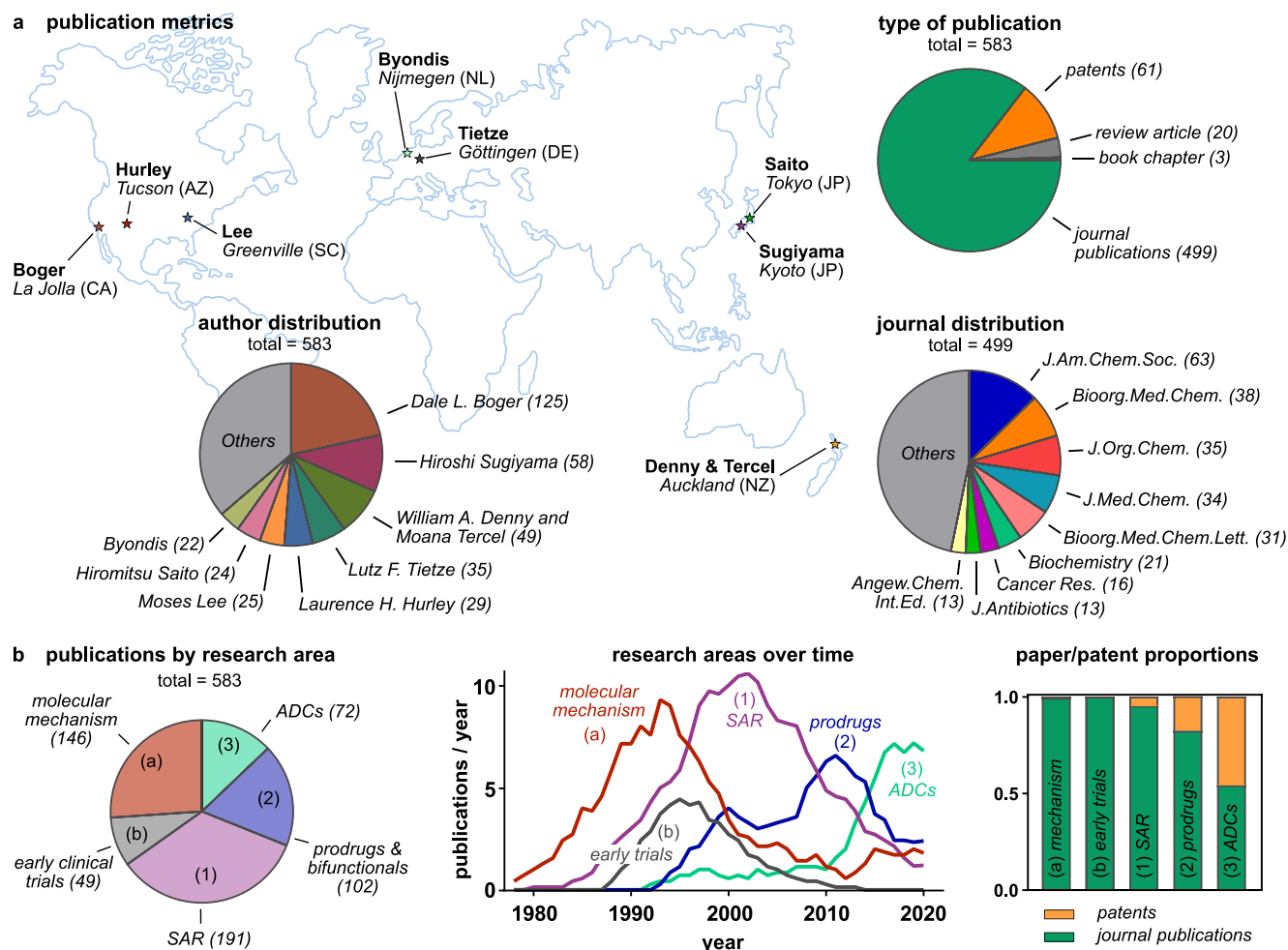


Figure 2. Literature metrics. (a) 583 primary research items from the duocarmycin literature database reviewed here. Charts show the major research groups (>20 publications) and journals (>10 publications). (b) The literature was grouped as: (a) natural products, biochemistry, and molecular mechanism of CC-1065 and close analogues; (b) initial clinical trial compounds; then the focus groups of this Perspective: (1) synthetic analogues and SAR; (2) prodrugs and bifunctional conjugates; (3) ADCs. Group histograms reveal the chronological progress of duocarmycin research. Paper/patent ratios may indicate perceived commercialisation chances.

on duocarmycins using a systematic literature review workflow (SLR;¹⁸ Figure 1a, details in Supporting Information), then graphically summarizing it for rapid analysis. We classify the SLR database according to research focus, use it for meta-analysis, and provide it for future researchers with an interest in the field to orient their molecular designs. We then provide a searchable, dynamic datafile in A0 poster format (Figure 1b; Poster S1) which groups and analyzes structural design features, with particular focus on duocarmycin family (1) SAR, (2) prodrugs and bifunctional conjugates, and (3) ADCs.

2. SYSTEMATIC LITERATURE REVIEW (SLR)

SLR¹⁸ was conducted to collate and group the vast majority of experimental literature concerning duocarmycins. Two groups with low structural diversity were split off: (a) reports of the isolation, characterization, and mechanism of action of natural products structurally related to CC-1065; and (b) reports of preclinical and clinical trials of early cancer drug candidates. Three groups with high structural diversity are analyzed here: (1) **SAR**: synthesis and cellular evaluation of derivatives in structure–activity-relationship (SAR) studies; (2) **Prodrugs**: synthesis, evaluation, and/or therapeutic use of prodrugs, mainly based on bioactivation of the *seco*-duocarmycin latent

alkylator functional unit, or of bifunctional small molecule conjugates bearing at least one (*seco*-)duocarmycin; (3) **ADCs**: synthesis, conjugation, and therapeutic efficacy of (multi)-functional ADCs incorporating a synthetic duocarmycin or its *seco*-precursor.

Literature screening was first done by Boolean keyword search initiated with, e.g., [“CC-1065” or “duocarmycin”] AND [“analog” or “prodrug” or “derivative”] then refined with more specific keywords (see Supporting Information). From this, the major academic groups or pharmaceutical companies in each area of research were identified. For each group, all references reporting duocarmycin family agents were manually collected and categorized. Lastly, selected recent reviews on specific topics within the field of duocarmycins^{16,17,19–24} were harvested for additional references. Thus, a comprehensive duocarmycin structural library was assembled, from 583 reports—mainly of primary research (Figure 2).

2.1. Literature Metrics

A bibliographic overview of this library is given in Figure 2. Of the 583 total research items, the vast majority were published in scientific journals (123 journals, 499 publications, 86%) covering all areas from basic biology, biochemistry, medicinal chemistry, and molecular sciences, to physical chemistry,

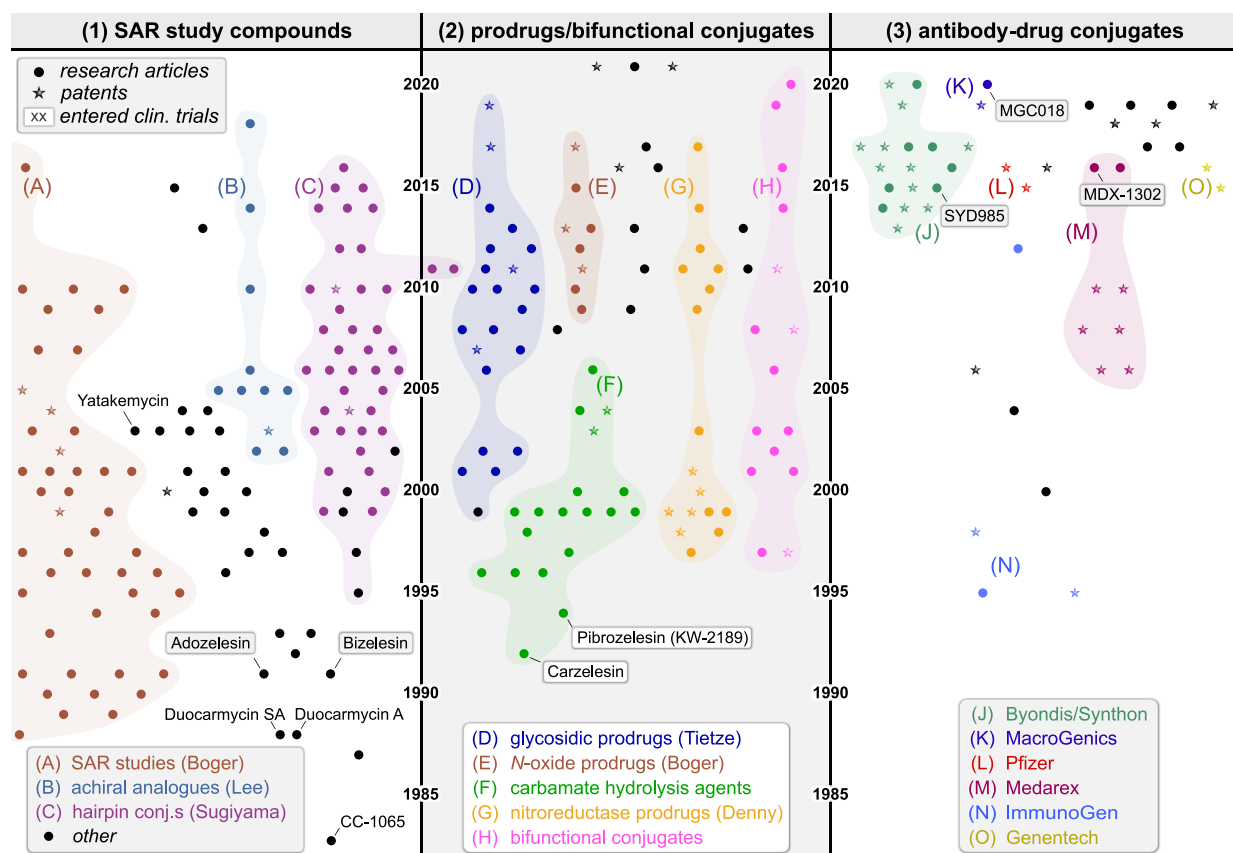


Figure 3. Structural developments of the duocarmycins (cartoon; all chemical structures in [Poster S1](#)). In Group 1 (SAR compounds), studies resolved the molecular motifs crucial for rational tuning of bioactivity. In Group 2 (Prodrugs), non-natural prodrugs (glycosides, nitroaryls, carbamates, *N*-oxides) and bifunctional conjugates expanded the scope of duocarmycins. In Group 3 (ADCs), industry has been a main driver of research.

theoretical chemistry, and preclinical or clinical oncology. Major progress in chemical design and SAR has been published in chemistry (*JACS* 63, *JOC* 35, *JMC* 33, *ANIE* 13, *Chem. Eur. J.* 11) and bioorganic chemistry journals (*BMC* 38, *BMCL* 31); isolation and mechanism reports cluster in *Biochemistry* (21) and *J. Antibiotics* (13); and clinical results in oncology journals (*Cancer Res.* 16, *Cancer Chemother. Pharmacol.* 11, *Mol. Cancer Ther.* 9). 61 patents or patent applications filed by academic groups and pharmaceutical companies also entered this library ([Figure 2a](#)).

2.2. Evolution of the Focus of Duocarmycin Research

The sequence of duocarmycin development is easily visible when analyzing the five report groups by date ([Figure 2b](#)). Isolation and early molecular mechanism studies (group a; 146 items) dominate the 1980s and 1990s and have been key for further molecular designs. Rapidly following initial cytotoxicity studies, small molecule drugs (adozelesin and bizelesin) and hydrolytic prodrugs (carzelesin and pibrozelesin) were taken into initial clinical anticancer trials, that were discontinued during the 2000s (group b; 49 items). Hurley (29), Krueger (17), and others were the major academic groups driving both these developments.

Exhaustive and creative structural variations during the 1990s and 2000s largely mapped the SAR in this molecular class (**Group 1, SAR:** 192 items) with major contributions by Boger (125), Sugiyama (58), and Lee (25). Innovation increasingly focused on targeting, with activatable prodrugs and bifunctional small molecule conjugates taking off during

the 2000s and 2010s (**Group 2, Prodrugs:** 102 items) led by Denny and Tercel (49), Tietze (35), Saito (23), and others. Finally, since the 2010s, conjugates of duocarmycins with monoclonal antibodies (**Group 3, ADCs:** 71 items) have opened up a new future for this class of bioactives. Combining the tunable potency and molecular flexibility of the duocarmycins, with the potential for enriched delivery to cancers, has led to a new wave of duocarmycin antibody–drug conjugates in clinical trials, driven by Byondis B.V. (22), Medarex Inc. (7), and others. With their increasing therapeutic relevance, the share of patents in the last two areas of research is also significantly higher ([Figure 2b](#)).

3. STRUCTURAL EVOLUTION OF DUOCARMYCIN ANALOGUES

The structural evolution of duocarmycins across these groups can also be best understood along a time axis, that resolves both the stepwise and disruptive innovations that have driven this field from 1978 to 2022. [Figure 3](#) is a cartoon representation showing a data point for each research item in the three focus groups (circle: journal; star: patent); the A0-size [Poster S1 in the Supporting Information](#) maps these data points one-to-one onto representative chemical structures from each research item, color-coded for functionality, and DOI-hyperlinked for access to the original papers. We also encourage interested chemists to print a copy for easy reference.

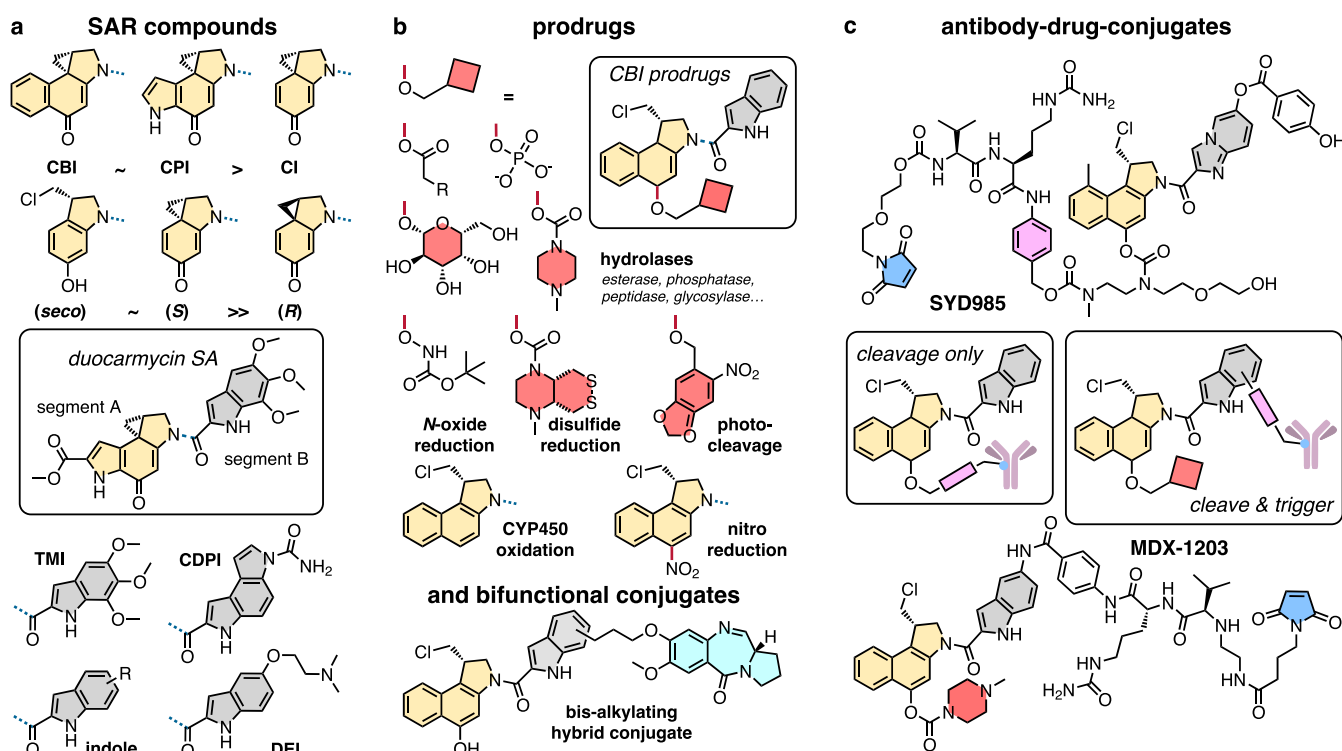


Figure 4. Structural elements of duocarmycin therapeutics. (a) SAR analysis: variations of segments A and B. (b) Activatable prodrugs: strategies to trigger bioactivity. (c) Antibody–drug conjugates: CBI-ADCs including clinical candidates SYD985 and MDX-1302. See also [Poster S1](#).

3.1. Group 1: SAR Compounds

The lead natural product CC-1065 was isolated in 1978,¹ and its first total synthesis was reported in 1988, laying the grounds for much synthetic development.³ During the 1990s and 2000s, systematic variations of both the core alkylator motif (“segment A”, typically an activated cyclopropane) and the DNA-docking motif (“segment B”) led to our current understanding of the structural features that need to be arranged for DNA association and sequence-selective alkylation (succinctly described by Hurley⁷).

Many heterocyclic systems beyond the native cyclopropa-[e]pyrroloindole (CPI) of duocarmycin SA²⁵ can serve as segment A. Much research has focused on the chemically tractable CBI, with optional substitutions;¹⁴ cyclopropaindole²⁶ (CI) and others²⁷ also alkylate DNA with the reactivity trend (CBI ~ CPI > CI) (Figure 4a).

The activated cyclopropane electrophile must be in its native (S)-configuration for DNA alkylation,^{28,29} but high potency can be maintained with “proagent” *seco*-variants, that use *in situ* intramolecular Winstein spirocyclization to unfurl their activated cyclopropane, relying on the *para*-phenol.³⁰ Good leaving groups (-Cl, -Br, -OMs)^{9,31} and several alternatives to the dihydroindole (5-, 6-, 7-membered rings)³² are all tolerated. Alternatively, masking this phenol suppresses spirocyclization:³³ a disruptive step that opened the door for rational tuning of prodrug candidates in later years (see below). The group of Lee also introduced achiral *seco*-variants that are similarly reactive, but structurally simpler and more accessible.^{34,35}

Segment B heterocycles have mainly clustered around indole-based rings that strengthen DNA binding. Stepwise simplification of the native dimeric segment B (in CC-1065) gave variously the deoxygenated CDPI dimer,³⁶ 3,4,5-trimethoxyindole (TMI),²⁹ and monoalkoxylated (DEI),³⁷ or

even simple mono/oligoindoles; and other heterocycles³⁸ can also be used. These do impact DNA binding, alkylation site-selectivity, and potency; but overall, the tolerance for segment B variance is high (Figure 4a).

Assembling the A and B segments has also received attention. A remarkable class of hairpin duocarmycin conjugates was driven by Lown and Sugiyama in the 2000s.³⁹ Using synthetic oligo-pyrroles/imidazoles from the minor-groove binder distamycin A as segment B binding domains gave potent duocarmycin analogues allowing sequence-selective alkylation in specific areas of DNA.^{40,41} “Standard” duocarmycins consist of segments A and B linked by an amide bond: but the natural product Yatakemycin^{42,43} has revealed that multiple B segments may be used, and randomly shuffled around without losing bioactivity.⁴⁴ Dimeric bisalkylators with two A segments, allowing interstrand DNA cross-linking, also give extremely high potency.^{45,46}

3.2. Group 2: Activatable Prodrugs and Bifunctionals

Early trials already exploited duocarmycin prodrugs where *seco*-duocarmycin bioactivity was to be triggered *in situ* by unmasking a *para*-phenol, to avoid parasitic loss of a preformed cyclopropane *en route* to target tissues. These carbamate hydrolysis designs (Carzelesin,^{47,48} Pibrozolesin/KW-2189^{9,49}) were discontinued in clinical trials due to side effects and low therapeutic index.^{13,50} Follow-up work mined esters, solubilized carbamates, phosphates, and others as other hydrolytic activation methods (Figure 4b),^{51–56} although none of these promise any greater mechanistic selectivity for cancer, since the activating hydrolases are ubiquitously expressed.

Key steps toward cancer-selective prodrugs were initiated by the lab of Denny in the late 1990s. They introduced nitro-*seco*-CBIs that can be irreversibly reduced to the amino-*seco*-CBI in the low-oxygen conditions found in solid tumors. These

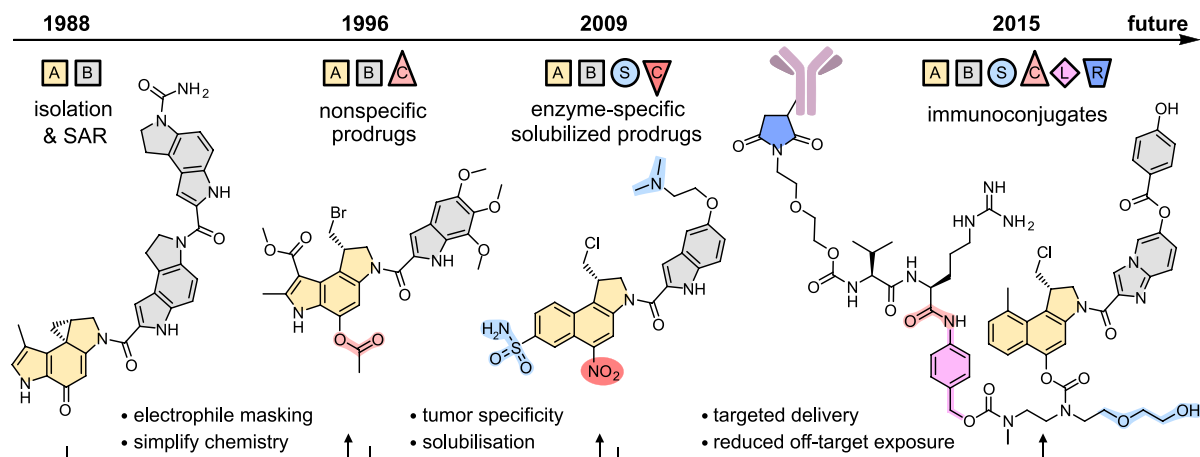


Figure 5. Color-coded highlights of the disruptive chemical steps that have led the duocarmycins from isolation to the clinic (see also Poster S1). (Key: A,B = A-,B-segments. C = intracellular cleavage site. S = solubilizer. L = self-immolative spacer. R = reactive group for antibody conjugation.)

amines then undergo Winstein cyclization becoming DNA-alkylators (Figure 4b).^{57–59} In the early 2000s, Tietze developed glycosidic prodrugs that can be built modularly, aiming at antitumor uses relying on glycosidases.^{37,60,61} Adopting novel chemistries in the 2010s, Boger introduced *O*-amino-*N*-acyl-*seco*-CBIs that are also subject to bioreductive activation.^{62–64} The field of masked *seco*-CBIs has by now exploited the full arsenal of chemical biology, passing through reducible Co-complexes,⁶⁵ Fe(II)-reactive peroxides,⁶⁶ photo-activated designs,^{67,68} and oxidizable naphthalenes.⁶⁹ Recently, cyclic dithalogenides (that resist monothiol exchange, but can be reductively activated by specific oxidoreductases such as thioredoxin) have joined this panoply of prodrugs.^{70,71} Finally, bifunctional conjugates of duocarmycins with other pharmaceuticals (glucuronide,⁷² biotin,⁷³ antibiotics,⁷⁴ pyrrolobenzodiazepine (Figure 4b),^{75,76} albumin,⁷⁷ peptides⁷⁸) show the wide applicability and adaptability of this unique class of bioactives.

3.3. Group 3: Antibody–Drug Conjugates (ADCs)

Monoclonal antibodies against cancer-selective biomarkers have the potential to deliver high-potency cytotoxic cancer drugs to tumors in a targeted and therapeutically effective manner. The duocarmycins' outstanding potency has motivated much ADC research, with two general designs emerging. Type A designs mask the *seco*-duocarmycin phenol with a linker conjugated to the antibody: allowing spirocyclization-based activation after linker cleavage. Intracellular cleavage of these linkers (dipeptides like ValCit that are prone to lysosomal proteolysis; hydrolyzable phosphates; reducible disulfides) can directly liberate the key Winstein cyclization phenol, but additional self-immolative spacers, that undergo cyclization or elimination cascades to liberate this phenol, are common.^{79–83} Type B designs attach a phenolic prodrug of the duocarmycin, via a peripheral site, to the antibody: permitting an extra layer of prodrug-based selectivity if prerelease activation can be avoided (Figure 4c). ADCs of Type B are less clearly reported, and many are IP-protected by pharmaceutical companies.^{84–87}

The late-2000s rebirth of preclinical/clinical development in the duocarmycin class has essentially been driven by these ADCs, with a variety of designs achieving *in vivo* efficacy in mouse cancer models.^{56,88–92} Beyond the choice of biomarker and payload, ADC development must balance factors from

conjugation site, degree of labeling, and linker nature,^{93,94} through to chemical conjugation method, making refinement of ADCs more complex than that of prodrugs.⁹⁵ Nevertheless, the ADCs SYD985, MGC018, and MDX-1203 all reached clinical trials with promising results and high efficacy.^{96–98} While MDX-1203 was halted due to insufficient improvement of therapeutic benefit compared to alternative therapeutics, SYD985 was recently given fast-track approval as a follow-up or cotreatment for patients with HER2-positive metastatic breast cancer.⁹⁹ This is the first duocarmycin approved for clinical use; its success will spur the developments of the future (Figure 5).

3.4. Guiding Principles for Future Developments

Predicting the future of drug development is a challenge, but this structure/function-based Perspective highlights trends that can drive the duocarmycins' next decades. First, duocarmycins will remain high-value targets in cancer therapy. If their bioactivity can be directed, then their outstanding potency and their binding-triggered covalent-reactive mechanism, promise high efficacy with limited resistance in a broad scope of indications. Second, progress will continue to rely on disruptive innovations in duocarmycin chemistry. Key strategies so far include (i) SAR simplification for synthetic access, (ii) protecting the cyclopropane warhead by forming it *in situ*, (iii) chemical mechanisms for tumor-selective prodrug activation, and (iv) antibody-based mechanisms for tumor-selective prodrug delivery. Solubilization and self-immolative spacers have also proven critical. It is perhaps no accident that the first duocarmycin to be clinically successful had built in nearly all these strategies (Figure 5). We see much potential for new therapeutics that also harness these strategies but tackle other indications with different target expression profiles and biodistribution needs. We also believe that finding sufficiently selective yet sufficiently high-turnover chemical mechanisms for tumor-specific activation would revolutionize both ADC and small molecule prodrug applications, and we await developments in this still-underexplored chemical space.

4. CONCLUSIONS

Duocarmycins have undergone great efforts toward developing targeted cancer therapeutics. A careful understanding of their unusual mechanism of bioactivity, leveraging spirocyclization and docking for high-potency site-selective DNA alkylation,

has enabled many creative approaches using the duocarmycins as a modular bioactive platform. Here we have provided a structured literature review tracking the chemical developments of the last 40 years, that have led from isolation to basic understanding, early trials and setbacks, re-engineering, and ultimately a first clinical anticancer agent.

We hope this concise overview will promote a structure/function-based understanding, allowing rational design and use of duocarmycin-based bioactives. It also follows the didactic tradition of Njardarson's Posters¹⁰⁰ with the A0-size [Poster S1](#), that can be printed and hung up in hallways for graphical overview and discussions, or used digitally for easy followup of its 200 embedded key structures (DOI hyperlinks).

The modularity of duocarmycin bioactivity should encourage researchers to design in structural features *à la carte*. A structure-based overview to guide the choice and understanding of these features, with easy direction to the corresponding references, may be very helpful for gaining a *coup d'oeil* when entering new scientific territory: particularly where the frontiers of research are increasingly interdisciplinary. We can still expect much from the duocarmycins; and we hope this Perspective and its Poster bring a graphic understanding of how to design, incorporate, and exploit this powerful molecular class.

■ ASSOCIATED CONTENT

SI Supporting Information

The Supporting Information is available free of charge at <https://pubs.acs.org/doi/10.1021/jacsau.2c00448>.

Details of how the SLR has been performed, including grouped lists of the major contributors to SAR/prodrug/ADC research, and containing the hyperlinked full-format bibliography of the 583 references in the SLR, organized by theme (PDF)

Poster S1 (>200 structures with hyperlinked references) (PDF)

ChemDraw file corresponding to the Poster, which contains all the duocarmycin structures without hyperlinks in CDX format for use/reuse of structures by copy-paste, or for mining the structures by SMILES (CDX) ~600-work literature citation database provided as an RIS that can be imported into any reference manager software with one double-click, to make all the duocarmycin citations available (ZIP)

■ AUTHOR INFORMATION

Corresponding Authors

Jan G. Felber – Department of Pharmacy, Ludwig-Maximilians University of Munich, D-81377 Munich, Germany; orcid.org/0000-0002-5010-9624; Email: jan.felber@cup.lmu.de

Oliver Thorn-Seshold – Department of Pharmacy, Ludwig-Maximilians University of Munich, D-81377 Munich, Germany; orcid.org/0000-0003-3981-651X; Email: oliver.thorn-seshold@cup.lmu.de

Complete contact information is available at: <https://pubs.acs.org/doi/10.1021/jacsau.2c00448>

Author Contributions

CRedit: **Jan Gabriel Felber** conceptualization, data curation, investigation, methodology, software, validation, visualization,

writing-original draft, writing-review & editing; **Oliver Thorn-Seshold** conceptualization, supervision, visualization, writing-original draft, writing-review & editing.

Notes

The authors declare no competing financial interest.

■ ACKNOWLEDGMENTS

We thank Julia Schulz (Institute for Machine Tools and Industrial Management, TU Munich) for conceptual input concerning structured literature review, Dale Boger (Scripps) for references and kind discussion, Marc-André Kasper (Tubulis GmbH, Martinsried) for collegial discussion about the therapeutic impact of antibody-drug-conjugates.

■ ABBREVIATIONS

CBI, cyclopropabenz[e]indole; CDPI, 3-carbamoyl-1,2-dihydro-3H-pyrrolo[3,2-e]indole-7-carboxylate; CPI, cyclopropa[e]pyrroloindole; Cl, cyclopropaindole; DEI, *N,N*-dimethylaminoethoxyindole; TMI, 3,4,5-trimethoxyindole

■ REFERENCES

- (1) Hanka, L. J.; Dietz, A.; Gerpeide, S. A.; Kuentzel, S. L.; Martin, D. G. CC-1065 (NSC-298223), A New Antitumor Antibiotic. Production, In Vitro Biological Activity, Microbiological Assays and Taxonomy of the Producing Microorganism. *J. Antibiot.* **1978**, *31* (12), 1211–1217.
- (2) Takahashi, I.; Takahashi, K.-I.; Ichimura, M.; Morimoto, M.; Asano, K.; Kawamoto, I.; Tomita, F.; Nakano, H. Duocarmycin A, a New Antitumor Antibiotic from *Streptomyces*. *J. Antibiot.* **1988**, *41* (12), 1915–1917.
- (3) Boger, D. L.; Coleman, R. S. Total Synthesis of (+)-CC-1065 and Ent-(−)-CC-1065. *J. Am. Chem. Soc.* **1988**, *110* (4), 1321–1323.
- (4) Boger, D. L.; Machiya, K.; Hertzog, D. L.; Kitos, P. A.; Holmes, D. Total Synthesis and Preliminary Evaluation of (+)- and Ent-(−)-Duocarmycin SA. *J. Am. Chem. Soc.* **1993**, *115* (20), 9025–9036.
- (5) Okano, K.; Tokuyama, H.; Fukuyama, T. Total Synthesis of (+)-Yatakemycin. *J. Am. Chem. Soc.* **2006**, *128* (22), 7136–7137.
- (6) Hurley, L. H.; Reynolds, V. L.; Swenson, D. H.; Petzold, G. L.; Scahill, T. A. Reaction of the Antitumor Antibiotic CC-1065 with DNA: Structure of a DNA Adduct with DNA Sequence Specificity. *Science* **1984**, *226* (4676), 843–844.
- (7) Hurley, L. H.; Lee, C. S.; McGovern, J. P.; Warpehoski, M. A.; Mitchell, M. A.; Kelly, R. C.; Aristoff, P. A. Molecular Basis for Sequence-Specific DNA Alkylation by CC-1065. *Biochemistry* **1988**, *27* (10), 3886–3892.
- (8) Bhuyan, B. K.; Smith, K. S.; Adams, E. G.; Wallace, T. L.; Von Hoff, D. D.; Li, L. H. Adozelesin, a Potent New Alkylating Agent: Cell-Killing Kinetics and Cell-Cycle Effects. *Cancer Chemother. Pharmacol.* **1992**, *30* (5), 348–354.
- (9) Kobayashi, E.; Okamoto, A.; Asada, M.; Okabe, M.; Nagamura, S.; Asai, A.; Saito, H.; Gomi, K.; Hirata, T. Characteristics of Antitumor Activity of KW-2189, a Novel Water-Soluble Derivative of Duocarmycin, against Murine and Human Tumors. *Cancer Res.* **1994**, *54*, 2404–2410.
- (10) Shamdas, G. J.; Alberts, D. S.; Modiano, M.; Wiggins, C.; Power, J.; Kasunic, D. A.; Elfring, G. L.; Earhart, R. H. Phase I Study of Adozelesin (U-73,975) in Patients with Solid Tumors. *Anti-Cancer Drugs* **1994**, *5*, 10–14.
- (11) Alberts, S. R.; Erlichman, C.; Reid, J. M.; Sloan, J. A.; Ames, M. M.; Richardson, R. L.; Goldberg, R. M. Phase I Study of the Duocarmycin Semisynthetic Derivative KW-2189 given Daily for Five Days Every Six Weeks. *Clin. Cancer Res.* **1998**, *4*, 2111–2117.
- (12) Cristofanilli, M.; Bryan, W. J.; Miller, L. L.; Chang, A. Y.-C.; Gradishar, W. J.; Kufe, D. W.; Hortobagyi, G. N. Phase II Study of Adozelesin in Untreated Metastatic Breast Cancer. *Anti-Cancer Drugs* **1998**, *9*, 779–782.

- (13) Markovic, S. N.; Suman, V. J.; Vukov, A. M.; Fitch, T. R.; Hillman, D. W.; Adjei, A. A.; Alberts, S. R.; Kaur, J. S.; Braich, T. A.; Leitch, J. M.; Creagan, E. T. Phase II Trial of KW2189 in Patients With Advanced Malignant Melanoma. *Am. J. Clin. Oncol.* **2002**, *25* (3), 308–312.
- (14) Boger, D. L.; Ishizaki, T.; Zarrinmayeh, H.; Kitos, P. A.; Suntornwat, O. A Potent, Simple Derivative of an Analog of the CC-1065 Alkylation Subunit. *Bioorg. Med. Chem. Lett.* **1991**, *1* (1), 55–58.
- (15) MacMillan, K. S.; Boger, D. L. Fundamental Relationships between Structure, Reactivity, and Biological Activity for the Duocarmycins and CC-1065. *J. Med. Chem.* **2009**, *52* (19), 5771–5780.
- (16) Jukes, Z.; Morais, G. R.; Loadman, P. M.; Pors, K. How Can the Potential of the Duocarmycins Be Unlocked for Cancer Therapy? *Drug Discovery Today* **2021**, *26* (2), 577–584.
- (17) Yao, H.-P.; Zhao, H.; Hudson, R.; Tong, X.-M.; Wang, M.-H. Duocarmycin-Based Antibody–Drug Conjugates as an Emerging Biotherapeutic Entity for Targeted Cancer Therapy: Pharmaceutical Strategy and Clinical Progress. *Drug Discovery Today* **2021**, *26* (8), 1857–1874.
- (18) Boell, S. K. Cecez-Kecmanovic Dubravka. On Being “Systematic” in Literature Reviews in IS. *Journal of Information Technology* **2015**, *30* (2), 161–173.
- (19) Ghosh, N.; Sheldrake, H.; Searcey, M.; Pors, K. Chemical and Biological Explorations of the Family of CC-1065 and the Duocarmycin Natural Products. *Curr. Top. Med. Chem.* **2009**, *9* (16), 1494–1524.
- (20) Patil, P.; Satam, V.; Lee, M. A Short Review on the Synthetic Strategies of Duocarmycin Analogs That Are Powerful DNA Alkylating Agents. *Anti-Cancer Agents in Med. Chem.* **2015**, *15* (5), 616–630.
- (21) Searcey, M. Duocarmycins - Natures Prodrugs? *Curr. Pharm. Des.* **2002**, *8* (15), 1375–1389.
- (22) Cacciari, B.; Romagnoli, R.; Baraldi, P. G.; Ros, T. D.; Spalluto, G. CC-1065 and the Duocarmycins: Recent Developments. *Exp. Op. Ther. Patents* **2000**, *10* (12), 1853–1871.
- (23) Tietze, L. F.; Krewer, B. Antibody-Directed Enzyme Prodrug Therapy: A Promising Approach for a Selective Treatment of Cancer Based on Prodrugs and Monoclonal Antibodies. *Curr. Biol. Drug Des.* **2009**, *74* (3), 205–211.
- (24) F. Tietze, L.; Schmuck, K. Prodrugs for Targeted Tumor Therapies: Recent Developments in ADEPT, GDEPT and PMT. *Curr. Pharm. Des.* **2011**, *17* (32), 3527–3547.
- (25) Boger, D. L.; Coleman, R. S. Total Synthesis of (+)-N2-(Phenylsulfonyl)-CPI, (+)-CC-1065, (+)-CC-1065, Ent(-)-CC-1065, and the Precise, Functional Agents (+)-CPI-CDPI2, (+)-CPI-CDPI2, and (-)-CPI-CDPI2 [(+)-(-3bR*,4aS*)-, (+)-(-3bR,4aS)-, and (-)-(-3bS,4aR)-Deoxy-CC-1065]. *J. Am. Chem. Soc.* **1988**, *110* (14), 4796–4807.
- (26) Boger, D. L.; Zarrinmayeh, H.; Munk, S. A.; Kitos, P. A.; Suntornwat, O. Demonstration of a Pronounced Effect of Non-covalent Binding Selectivity on the (+)-CC-1065 DNA Alkylation and Identification of the Pharmacophore of the Alkylation Subunit. *Proc. Natl. Acad. Sci. U.S.A.* **1991**, *88* (4), 1431–1435.
- (27) Boger, D. L.; Garbaccio, R. M.; Jin, Q. Synthesis and Evaluation of CC-1065 and Duocarmycin Analogues Incorporating the Iso-CI and Iso-CBI Alkylation Subunits: Impact of Relocation of the C-4 Carbonyl. *J. Org. Chem.* **1997**, *62* (25), 8875–8891.
- (28) Boger, D. L.; Yun, W.; Terashima, S.; Fukuda, Y.; Nakatani, K.; Kitos, P. A.; Jin, Q. DNA Alkylation Properties of the Duocarmycins: (+)-Duocarmycin A, Epi-(+)-Duocarmycin A, Ent(-)-Duocarmycin A and E&Ent(-)-Duocarmycin A. *Bioorg. Med. Chem. Lett.* **1992**, *2* (7), 759–765.
- (29) Boger, D. L.; Yun, W. CBI-TMI: Synthesis and Evaluation of a Key Analog of the Duocarmycins. Validation of a Direct Relationship between Chemical Solvolytic Stability and Cytotoxic Potency and Confirmation of the Structural Features Responsible for the Distinguishing Behavior of Enantiomeric Pairs of Agents. *J. Am. Chem. Soc.* **1994**, *116* (18), 7996–8006.
- (30) Baird, R.; Winstein, S. Neighboring Carbon and Hydrogen. Li. Dienones from Ar1[UNK]-3 Participation. Isolation and Behavior of Spiro(2,5)Octa-1,4-Diene-3-One. *J. Am. Chem. Soc.* **1963**, *85*, 567.
- (31) Boger, D. L.; Munk, S. A.; Zarrinmayeh, H. (+)-CC-1065 DNA Alkylation: Key Studies Demonstrating a Noncovalent Binding Selectivity Contribution to the Alkylation Selectivity. *J. Am. Chem. Soc.* **1991**, *113* (10), 3980–3983.
- (32) Boger, D. L.; Hertzog, D. L.; Bollinger, B.; Johnson, D. S.; Cai, H.; Goldberg, J.; Turnbull, P. Duocarmycin SA Shortened, Simplified, and Extended Agents: A Systematic Examination of the Role of the DNA Binding Subunit. *J. Am. Chem. Soc.* **1997**, *119* (21), 4977–4986.
- (33) Tietze, L. F.; Lieb, M.; Herzig, T.; Haunert, F.; Schubert, I. A Strategy for Tumor-Selective Chemotherapy by Enzymatic Liberation of Seco-Duocarmycin SA-Derivatives from Nontoxic Prodrugs. *Bioorg. Med. Chem.* **2001**, *9* (7), 1929–1939.
- (34) Daniell, K.; Stewart, M.; Madsen, E.; Le, M.; Handl, H.; Brooks, N.; Kiakos, K.; Hartley, J. A.; Lee, M. Design, Synthesis, and Biological Evaluation of Achiral Analogs of Duocarmycin SA. *Bioorg. Med. Chem. Lett.* **2005**, *15* (1), 177–180.
- (35) Sato, A.; McNulty, L.; Cox, K.; Kim, S.; Scott, A.; Daniell, K.; Summerville, K.; Price, C.; Hudson, S.; Kiakos, K.; Hartley, J. A.; Asao, T.; Lee, M. A Novel Class of In Vivo Active Anticancer Agents: Achiral Seco -Amino- and Seco -Hydroxycyclopropylbenz[e]Indolone (Seco -CBI) Analogues of the Duocarmycins and CC-1065. *J. Med. Chem.* **2005**, *48* (11), 3903–3918.
- (36) Boger, D. L.; Ishizaki, T.; Wysocki, R. J.; Munk, S. A.; Kitos, P. A.; Suntornwat, O. Total Synthesis and Evaluation of (+)-N-(Tert-Butoxycarbonyl)-CBI, (+)-CBI-CDPI1, and (+)-CBI-CDPI2: CC-1065 Functional Agents Incorporating the Equivalent 1,2,9,9a-Tetrahydrocyclopropa[1,2-c]Benz[1,2-e]Indol-4-One (CBI) Left-Hand Subunit. *J. Am. Chem. Soc.* **1989**, *111* (16), 6461–6463.
- (37) Tietze, L. F.; Major, F.; Schubert, I. Antitumor Agents: Development of Highly Potent Glycosidic Duocarmycin Analogues for Selective Cancer Therapy. *Angew. Chem., Int. Ed.* **2006**, *45* (39), 6574–6577.
- (38) Boger, D. L.; Yun, W.; Han, N. 1,2,9,9a-Tetrahydrocyclopropa-[c]Benz[e]Indol-4-One (CBI) Analogs of CC-1065 and the Duocarmycins: Synthesis and Evaluation. *Bioorg. Med. Chem.* **1995**, *3* (11), 1429–1453.
- (39) Fregeau, N. L.; Wang, Y.; Pon, R. T.; Wylie, W. A.; Lown, J. W. Characterization of a CPI-Lexitropsin Conjugate-Oligonucleotide Covalent Complex by 1H NMR and Restrained Molecular Dynamics Simulation. *J. Am. Chem. Soc.* **1995**, *117* (35), 8917–8925.
- (40) Bando, T.; Narita, A.; Asada, K.; Ayame, H.; Sugiyama, H. Enantioselective DNA Alkylation by a Pyrrole–Imidazole S -CBI Conjugate. *J. Am. Chem. Soc.* **2004**, *126* (29), 8948–8955.
- (41) Tao, Z.-F.; Fujiwara, T.; Saito, I.; Sugiyama, H. Rational Design of Sequence-Specific DNA Alkylating Agents Based on Duocarmycin A and Pyrrole–Imidazole Hairpin Polyamides. *J. Am. Chem. Soc.* **1999**, *121* (21), 4961–4967.
- (42) Igarashi, Y.; Futamata, K.; Fujita, T.; Sekine, A.; Senda, H.; Naoki, H.; Furumai, T. Yatakemycin, a Novel Antifungal Antibiotic Produced by Streptomyces Sp. TP-A0356. *J. Antibiot.* **2003**, *56* (2), 107–113.
- (43) Tichenor, M. S.; Kastrinsky, D. B.; Boger, D. L. Total Synthesis, Structure Revision, and Absolute Configuration of (+)-Yatakemycin. *J. Am. Chem. Soc.* **2004**, *126* (27), 8396–8398.
- (44) Tichenor, M. S.; MacMillan, K. S.; Trzupke, J. D.; Rayl, T. J.; Hwang, I.; Boger, D. L. Systematic Exploration of the Structural Features of Yatakemycin Impacting DNA Alkylation and Biological Activity. *J. Am. Chem. Soc.* **2007**, *129* (35), 10858–10869.
- (45) Fukuda, Y.; Seto, S.; Furuta, H.; Ebisu, H.; Oomori, Y.; Terashima, S. The Novel Cyclopropapyrroloindole(CPI) Bisalkylators Bearing 3,3'-(1,4-Phenylene)Diacyloyl Group as a Linker. *Bioorg. Med. Chem. Lett.* **1998**, *8* (15), 2003–2004.
- (46) Bando, T.; Iida, H.; Saito, I.; Sugiyama, H. Sequence-Specific DNA Interstrand Cross-Linking by Imidazole–Pyrrole CPI Conjugate. *J. Am. Chem. Soc.* **2001**, *123* (21), 5158–5159.

- (47) Li, L. H.; DeKoning, T. F.; Kelly, R. C.; Krueger, W. C.; McGovern, J. P.; Padbury, G. E.; Petzold, G. L.; Wallace, T. L.; Ouding, R. J.; Prairie, M. D.; Gebhard, I. Cytotoxicity and Antitumor Activity of Carzelesin, a Prodrug Cyclopropylpyrroloindole Analogue. *Cancer Res.* **1992**, *52*, 4904–4913.
- (48) van Tellingen, O.; Nooijen, W. J.; Schaaf, L. J.; Henrar, R. E. C.; Beijnen, J. H. Comparative Pharmacology of the Novel Cyclopropylpyrroloindole-Prodrug Carzelesin in Mice, Rats, and Humans. *Cancer Res.* **1998**, *58*, 2410–2416.
- (49) Ogasawara, H.; Nishio, K.; Takeda, Y.; Ohmori, T.; Kubota, N.; Funayama, Y.; Ohira, T.; Kuraishi, Y.; Isogai, Y.; Saijo, N. A Novel Antitumor Antibiotic, KW-2189 Is Activated by Carboxyl Esterase and Induces DNA Strand Breaks in Human Small Cell Lung Cancer Cells. *Jpn. J. Cancer Res.* **1994**, *85*, 418–425.
- (50) Pavlidis, N.; Aamdal, S.; Awada, A.; Calvert, H.; Fumoleau, P.; Sorio, R.; Punt, C.; Verweij, J.; van Oosterom, A.; Morant, R.; Wanders, J.; Hanauske, A.-R. Carzelesin Phase II Study in Advanced Breast, Ovarian, Colorectal, Gastric, Head and Neck Cancer, Non-Hodgkin's Lymphoma and Malignant Melanoma: A Study of the EORTC Early Clinical Studies Group (ECSG). *Cancer Chemother. Pharmacol.* **2000**, *46* (2), 167–171.
- (51) Boger, D. L. CBI Prodrug Analogs of CC-1065 and the Duocarmycins. *Synthesis* **1999**, *1999* (S1), 1505–1509.
- (52) Nagamura, S.; Kanda, Y.; Kobayashi, E.; Gomi, K.; Saito, H. Synthesis and Antitumor Activity of Duocarmycin Derivatives. *Chem. Pharm. Bull.* **1995**, *43* (9), 1530–1535.
- (53) Wang, Y.; Li, L.; Tian, Z.; Jiang, W.; Larrick, J. W. Synthesis and Antitumor Activity of CBI-Bearing Ester and Carbamate Prodrugs of CC-1065 Analogue. *Bioorg. Med. Chem.* **2006**, *14* (23), 7854–7861.
- (54) Junutula, J. R.; Smith, S. W.; Borkin, D.; Degrado, S. Isoquinolidinobenzodiazepine (ICQ) - 1-(Chloromethyl)-2,3-Dihydro-1H-Benzo[8e]indole (CBI) Dimers. WO2018/071455A1, April 19, 2018.
- (55) Zhao, R. Y.; Chari, R. V. J. Prodrugs of CC-1065 Analogs. US007655660B2, June 29, 2004.
- (56) Zhao, R. Y.; Erickson, H. K.; Leece, B. A.; Reid, E. E.; Goldmacher, V. S.; Lambert, J. M.; Chari, R. V. J. Synthesis and Biological Evaluation of Antibody Conjugates of Phosphate Prodrugs of Cytotoxic DNA Alkylators for the Targeted Treatment of Cancer. *J. Med. Chem.* **2012**, *55* (2), 766–782.
- (57) Atwell, G. J.; Wilson, W. R.; Denny, W. A. Synthesis and Cytotoxicity of Amino Analogues of the Potent DNA Alkylating Agent Seco-CBI-TMI. *Bioorg. Med. Chem. Lett.* **1997**, *7* (12), 1493–1496.
- (58) Hay, M. P.; Sykes, B. M.; Denny, W. A.; Wilson, W. R. A 2-Nitroimidazole Carbamate Prodrug of 5-Amino-1-(Chloromethyl)-3-[(5,6,7-Trimethoxyindol-2-yl)Carbonyl]-1,2-Dihydro-3H-Benz[e]-Indole (Amino-Seco-CBI-TMI) for Use with ADEPT and GDEPT. *Bioorg. Med. Chem. Lett.* **1999**, *9*, 2237–2242.
- (59) Tercel, M.; Atwell, G. J.; Yang, S.; Ashoorzadeh, A.; Stevenson, R. J.; Botting, K. J.; Gu, Y.; Mehta, S. Y.; Denny, W. A.; Wilson, W. R.; Pruijn, F. B. Selective Treatment of Hypoxic Tumor Cells In Vivo: Phosphate Pre-Prodrugs of Nitro Analogues of the Duocarmycins. *Angew. Chem., Int. Ed.* **2011**, *50* (11), 2606–2609.
- (60) Tietze, L. F.; von Hof, J. M.; Müller, M.; Krewer, B.; Schuberth, I. Glycosidic Prodrugs of Highly Potent Bifunctional Duocarmycin Derivatives for Selective Treatment of Cancer. *Angew. Chem., Int. Ed.* **2010**, *49* (40), 7336–7339.
- (61) Tietze, L. F.; Schuster, H. J.; Krewer, B.; Schuberth, I. Synthesis and Biological Studies of Different Duocarmycin Based Glycosidic Prodrugs for Their Use in the Antibody-Directed Enzyme Prodrug Therapy. *J. Med. Chem.* **2009**, *52* (2), 537–543.
- (62) Lajiness, J. P.; Robertson, W. M.; Dunwiddie, I.; Broward, M. A.; Vielhauer, G. A.; Weir, S. J.; Boger, D. L. Design, Synthesis, and Evaluation of Duocarmycin O -Amino Phenol Prodrugs Subject to Tunable Reductive Activation. *J. Med. Chem.* **2010**, *53* (21), 7731–7738.
- (63) Vielhauer, G. A.; Swink, M.; Parelkar, N. K.; Lajiness, J. P.; Wolfe, A. L.; Boger, D. Evaluation of a Reductively Activated Duocarmycin Prodrug against Murine and Human Solid Cancers. *Cancer Biol. & Ther.* **2013**, *14* (6), 527–536.
- (64) Wolfe, A. L.; Duncan, K. K.; Parelkar, N. K.; Brown, D.; Vielhauer, G. A.; Boger, D. L. Efficacious Cyclic N -Acyl O -Amino Phenol Duocarmycin Prodrugs. *J. Med. Chem.* **2013**, *56* (10), 4104–4115.
- (65) Lu, G.-L.; Stevenson, R. J.; Chang, J. Y.-C.; Brothers, P. J.; Ware, D. C.; Wilson, W. R.; Denny, W. A.; Tercel, M. N-Alkylated Cyclen Cobalt(III) Complexes of 1-(Chloromethyl)-3-(5,6,7-Trimethoxyindol-2-ylcarbonyl)-2,3-Dihydro-1H-Pyrrolo[3,2-f]Quinolin-5-Ol DNA Alkylating Agent as Hypoxia-Activated Prodrugs. *Bioorg. Med. Chem.* **2011**, *19* (16), 4861–4867.
- (66) Spangler, B.; Fontaine, S. D.; Shi, Y.; Sambucetti, L.; Mattis, A. N.; Hann, B.; Wells, J. A.; Renslo, A. R. A Novel Tumor-Activated Prodrug Strategy Targeting Ferrous Iron Is Effective in Multiple Preclinical Cancer Models. *J. Med. Chem.* **2016**, *59* (24), 11161–11170.
- (67) Tietze, L. F.; Müller, M.; Duefert, S.-C.; Schmuck, K.; Schuberth, I. Photoactivatable Prodrugs of Highly Potent Duocarmycin Analogues for a Selective Cancer Therapy. *Chem.—Eur. J.* **2013**, *19* (5), 1726–1731.
- (68) Nani, R. R.; Gorke, A. P.; Nagaya, T.; Yamamoto, T.; Ivanic, J.; Kobayashi, H.; Schnermann, M. J. In Vivo Activation of Duocarmycin–Antibody Conjugates by Near-Infrared Light. *ACS Cent. Sci.* **2017**, *3* (4), 329–337.
- (69) Pors, K.; Loadman, P. M.; Shnyder, S. D.; Sutherland, M.; Sheldrake, H. M.; Guino, M.; Kiakos, K.; Hartley, J. A.; Searcey, M.; Patterson, L. H. Modification of the Duocarmycin Pharmacophore Enables CYP1A1 Targeting for Biological Activity. *Chem. Commun.* **2011**, *47* (44), 12062.
- (70) Thorn-Seshold, O.; Felber, J.; Thorn-Seshold, J.; Zeisel, L. Disulfide-Based Prodrug Compounds. PCT/EP2022/057483, 2021.
- (71) Thorn-Seshold, O.; Zeisel, L.; Felber, J. G. Dichalcogenide Prodrugs. PCT/EP2022/059280, 2021.
- (72) Wang, Y.; Yuan, H.; Wright, S. C.; Wang, H.; Larrick, J. W. Synthesis and Preliminary Cytotoxicity Study of Glucuronide Derivatives of CC-1065 Analogues. *Bioorg. Med. Chem.* **2003**, *11* (7), 1569–1575.
- (73) Wang, Y.; Yuan, H.; Wright, S. C.; Wang, H.; Larrick, J. W. Synthesis and Cytotoxicity of a Biotinylated CC-1065 Analogue. *BMC Chem. Bio.* **2002**, *2*, 1–4.
- (74) Wang, Y.; Yuan, H.; Wright, S. C.; Wang, H.; Larrick, J. W. Synthesis and Preliminary Cytotoxicity Study of a Cephalosporin-CC-1065 Analogue Prodrug. *BMC Chem. Bio.* **2001**, *1*, 4–8.
- (75) Zhou, Q.; Duan, W.; Simmons, D.; Shayo, Y.; Raymond, M. A.; Dorr, R. T.; Hurley, L. H. Design and Synthesis of a Novel DNA–DNA Interstrand Adenine–Guanine Cross-Linking Agent. *J. Am. Chem. Soc.* **2001**, *123* (20), 4865–4866.
- (76) Purnell, B.; Sato, A.; O'Kelley, A.; Price, C.; Summerville, K.; Hudson, S.; O'Hare, C.; Kiakos, K.; Asao, T.; Lee, M.; Hartley, J. A. DNA Interstrand Crosslinking Agents: Synthesis, DNA Interactions, and Cytotoxicity of Dimeric Achiral Seco-Amino-CBI and Conjugates of Achiral Seco-Amino-CBI with Pyrrolobenzodiazepine (PBD). *Bioorg. Med. Chem. Lett.* **2006**, *16* (21), 5677–5681.
- (77) Wang, Y.; Jiang, J.; Jiang, X.; Cai, S.; Han, H.; Li, L.; Tian, Z.; Jiang, W.; Zhang, Z.; Xiao, Y.; Wright, S. C.; Larrick, J. W. Synthesis and Antitumor Activity Evaluations of Albumin-Binding Prodrugs of CC-1065 Analog. *Bioorg. Med. Chem.* **2008**, *16* (13), 6552–6559.
- (78) Krall, N.; Pretto, F.; Decurtins, W.; Bernardes, G. J. L.; Supuran, C. T.; Neri, D. A Small-Molecule Drug Conjugate for the Treatment of Carbonic Anhydrase IX Expressing Tumors. *Angew. Chem., Int. Ed.* **2014**, *53* (16), 4231–4235.
- (79) Gangwar, S.; Sufi, B. Cytotoxic Compounds and Conjugates with Cleavable Substrates. US 20060247295A1, November 2, 2006.
- (80) Boyd, S. E.; Chen, L.; Gangwar, S.; Guerlavais, V.; Horgan, K.; Sufi, B.; Huang, H.; King, D. J.; Pan, C.; Cardarelli, J. M. Antibody-

Drug Conjugates and Methods of Use. US20080279868A1, November 13, 2008.

(81) Maderna, A.; Doroski, M. D.; Chen, Z.; Risley, H. L.; Casavant, J. M.; O'Donnell, C. J.; Porte, A. M.; Subramanyam, C. Bifunctional Cytotoxic Agents. US20150209445A1, July 30, 2015.

(82) Maderna, A.; Subramanyam, C.; Tume, L. N.; Chen, Z.; Casavant, J. M. Bifunctional Cytotoxic Agents Containing the CTI Pharmacophore. WO 2016/151432A1, September 29, 2016.

(83) Beusker, P. H.; Coumans, R. G. E.; Elgersma, R. C.; Menge, W. M. P. B.; Joosten, A. F.; Spijker, H. J.; de Groot, F. M. H. Novel Conjugates of CC-1065 Analogs and Bifunctional Linkers. US20130224227A1, August 29, 2013.

(84) Janda, K. D.; Wirsching, P.; Boger, D. L. Compositions and Methods for Delivery of Antitumor Agents. WO2006/002895A2, January 12, 2006.

(85) Chen, L.; Gangwar, S.; Guerlavais, V.; Lonberg, N.; Zhang, Q. Chemical Linkers with Single Amino Acids and Conjugates Thereof. US20100113476A1, May 6, 2010.

(86) Jackson, P. M. J.; Thurston, D. E.; Rahman, K. M. Asymmetric Conjugate Compounds. US20190144443A1, May 16, 2019.

(87) Helin, J.; Saarinen, J.; Satomaa, T.; Ekholm, F. S. Saccharide Derivative of a Toxic Payload and Antibody Conjugates Thereof. US20180228906A1, August 16, 2018.

(88) Dokter, W.; Ubink, R.; van der Lee, M.; van der Vleuten, M.; van Achterberg, T.; Jacobs, D.; Loosveld, E.; van den Dobbels, D.; Egging, D.; Mattaar, E.; Groothuis, P.; Beusker, P.; Coumans, R.; Elgersma, R.; Menge, W.; Joosten, J.; Spijker, H.; Huijbregts, T.; de Groot, V.; Eppink, M.; de Roo, G.; Verheijden, G.; Timmers, M. Preclinical Profile of the HER2-Targeting ADC SYD983/SYD985: Introduction of a New Duocarmycin-Based Linker-Drug Platform. *Mol. Cancer Ther.* **2014**, *13* (11), 2618–2629.

(89) Yu, L.; Lu, Y.; Yao, Y.; Liu, Y.; Wang, Y.; Lai, Q.; Zhang, R.; Li, W.; Wang, R.; Fu, Y.; Tao, Y.; Yi, S.; Gou, L.; Chen, L.; Yang, J. Promiximab-Duocarmycin, a New CD56 Antibody-Drug Conjugates, Is Highly Efficacious in Small Cell Lung Cancer Xenograft Models. *Oncotarget* **2018**, *9* (4), 5197–5207.

(90) Fu, Y.; Urban, D. J.; Nani, R. R.; Zhang, Y.-F.; Li, N.; Fu, H.; Shah, H.; Gorka, A. P.; Guha, R.; Chen, L.; Hall, M. D.; Schnermann, M. J.; Ho, M. Glypican-3-Specific Antibody Drug Conjugates Targeting Hepatocellular Carcinoma. *Hepatology* **2019**, *70* (2), 563–576.

(91) Scribner, J. A.; Brown, J. G.; Son, T.; Chiechi, M.; Li, P.; Sharma, S.; Li, H.; De Costa, A.; Li, Y.; Chen, Y.; Easton, A.; Yee-Toy, N. C.; Chen, F. Z.; Gorlatov, S.; Barat, B.; Huang, L.; Wolff, C. R.; Hooley, J.; Hotaling, T. E.; Gaynutdinov, T.; Ciccarone, V.; Tamura, J.; Koenig, S.; Moore, P. A.; Bonvini, E.; Loo, D. Preclinical Development of MGC018, a Duocarmycin-Based Antibody-Drug Conjugate Targeting B7-H3 for Solid Cancer. *Mol. Cancer Ther.* **2020**, *19* (11), 2235–2244.

(92) Tong, X.-M.; Feng, L.; Suthe, S. R.; Weng, T.-H.; Hu, C.-Y.; Liu, Y.-Z.; Wu, Z.-G.; Wang, M.-H.; Yao, H.-P. Therapeutic Efficacy of a Novel Humanized Antibody-Drug Conjugate Recognizing Plexin-Semaphorin-Integrin Domain in the RON Receptor for Targeted Cancer Therapy. *J. Immunotherapy Cancer* **2019**, *7* (1), 250.

(93) McCombs, J. R.; Owen, S. C. Antibody Drug Conjugates: Design and Selection of Linker, Payload and Conjugation Chemistry. *AAPS* **2015**, *17* (2), 339–351.

(94) Peters, C.; Brown, S. Antibody-Drug Conjugates as Novel Anti-Cancer Chemotherapeutics. *Bioscience Reports* **2015**, *35* (4), e00225.

(95) Kasper, M.; Stengl, A.; Ochtrop, P.; Gerlach, M.; Stoschek, T.; Schumacher, D.; Helma, J.; Penkert, M.; Krause, E.; Leonhardt, H.; Hackenberger, C. P. R. Ethynylphosphonamidates for the Rapid and Cysteine-Selective Generation of Efficacious Antibody-Drug Conjugates. *Angew. Chem., Int. Ed.* **2019**, *58* (34), 11631–11636.

(96) Banerji, U.; van Herpen, C. M. L.; Saura, C.; Thistlethwaite, F.; Lord, S.; Moreno, V.; Macpherson, I. R.; Boni, V.; Rolfo, C.; de Vries, E. G. E.; Rottey, S.; Geenen, J.; Eskens, F.; Gil-Martin, M.; Mommers, E. C.; Koper, N. P.; Aftimos, P. Trastuzumab Duocarmazine in

Locally Advanced and Metastatic Solid Tumours and HER2-Expressing Breast Cancer: A Phase 1 Dose-Escalation and Dose-Expansion Study. *Lancet Oncology* **2019**, *20* (8), 1124–1135.

(97) Owonikoko, T. K.; Hussain, A.; Stadler, W. M.; Smith, D. C.; Kluger, H.; Molina, A. M.; Gulati, P.; Shah, A.; Ahlers, C. M.; Cardarelli, P. M.; Cohen, L. J. First-in-Human Multicenter Phase I Study of BMS-936561 (MDX-1203), an Antibody-Drug Conjugate Targeting CD70. *Cancer Chemother. Pharmacol.* **2016**, *77* (1), 155–162.

(98) Jang, S.; Powderly, J. D.; Spira, A. I.; Bakkacha, O.; Loo, D.; Bohac, G. C.; Sharma, M. Phase 1 Dose Escalation Study of MGC018, an Anti-B7-H3 Antibody-Drug Conjugate (ADC), in Patients with Advanced Solid Tumors. *J. Clin. Onc.* **2021**, *39* (15_suppl), 2631–2631.

(99) FDA Updates. Fast Track Designation Granted for Breast Cancer Treatment. *Oncology Times* **2018**, *40* (5), 16.

(100) McGrath, N. A.; Brichacek, M.; Njardarson, J. T. A Graphical Journey of Innovative Organic Architectures That Have Improved Our Lives. *J. Chem. Educ.* **2010**, *87* (12), 1348–1349.

Recommended by ACS

The Time and Place for Nature in Drug Discovery

Robert J. Young, Herbert Waldmann, *et al.*

OCTOBER 14, 2022
JACS AU

READ 

Bridging Known and Unknown Unknowns: From Natural Products and Their Mimics to Unmet Needs in Neuroscience

Stephen F. Martin.

AUGUST 12, 2022
ACCOUNTS OF CHEMICAL RESEARCH

READ 

Deep Learning Promotes the Screening of Natural Products with Potential Microtubule Inhibition Activity

Xiao-Nan Jia, Feng Gao, *et al.*

AUGUST 05, 2022
ACS OMEGA

READ 

General Synthetic Approach to Diverse Taxane Cores

Melecio A. Perea, Richmond Sarpong, *et al.*

NOVEMBER 08, 2022
JOURNAL OF THE AMERICAN CHEMICAL SOCIETY

READ 

Get More Suggestions >

3.2.2 Duocarmycin-based therapeutic prodrugs targeting the Trx system

This chapter was deposited on a preprint server and is currently in revisions at ACS Central Science:

Deposit	BioRxiv 2022 .
Title	<i>Cyclic dichalcogenides extend the reach of bioreductive prodrugs to harness the thioredoxin system: applications to seco-duocarmycins</i>
Author List	Jan G. Felber [#] , Annabel Kitowski, Lukas Zeisel, Martin S. Maier, Constanze Heise, Julia Thorn-Seshold, Oliver Thorn-Seshold* #first author; *corresponding author
Publication date	Nov 11 th , 2022
Available at	https://www.biorxiv.org/content/10.1101/2022.11.11.516112v1

Author contributions

I developed the synthetic procedures for prodrug assembly and for the novel azetidiny l indole building block (**AZI**) and performed synthesis and analysis of the reducible prodrugs presented in this work (**Fig. 4**). My evaluations also involved HPLC-based reduction assays (**Fig. 5**) and initial cellular cytotoxicity assays (**Fig. 6**). I further coordinated external screening, performed data analysis of the results from the Proliferator-140 and the NCI-60 screens (**Fig. 8 and 9**), coordinated data assembly and visualization, conceptualized the scientific outcome, and wrote the manuscript.

Annabel Kitowski performed HPLC-based reduction assays (**Fig. 5**), cellular cytotoxicity assays in regular cell culture (**Fig. 6**), and using genetic knockout cell lines (**Fig. 7**), designed and coordinated external screening and *in vivo* studies, performed data analysis and data assembly.

Lukas Zeisel developed the synthetic access to the 1,2-thiaselenane, and piperazine-fused 1,2-dithiane trigger units and performed synthesis and analysis (**Fig. 3**). **Martin S. Maier** performed synthesis and analysis of the **SS00_M** precursors and the prodrugs **P-SS60-CBI-TMI** and **P-CC60-CBI-TMI**.

Constanze Heise performed cellular cytotoxicity assays (**Fig. 6 and 7**). **Julia Thorn-Seshold** designed, coordinated, and analyzed *in vivo* studies and performed data assembly.

Oliver Thorn-Seshold designed the concept and experiments, performed screening data analysis, coordinated data assembly, and wrote the manuscript.

Summary

After 40 years of research, the duocarmycin class (also called CBIs) has evolved into a powerful platform for medicinal chemistry. Intrigued by their unique mechanism of action and tunability of bioactivity (see **chapter 3.2.1**), we now aimed to create off-to-on cytotoxic prodrugs by attaching bio-reducible groups to its phenol. By that, we specifically aimed to develop a novel class of bio-reductive prodrugs operated by the Trx system in cells and *in vivo* (**Fig. 1**).

We had previously validated molecular triggers compatible with the redox effector protein Trx and its upstream reductase TrxR, in combination with fluorogenic cargos (see **chapters 3.1.2 - 3.1.4**). To transfer our probe concept to activatable prodrugs, I conjugated these or similar cyclic dichalcogenides to *seco*-CBIs. Following our central ideas of the thermodynamic stability and kinetic reversibility that cyclic dichalcogenides offer, we hoped that such prodrugs would show long-term GSH stability and activation that correlates to cellular Trx redox activity.

We designed CBI-based prodrugs using either the classic indole derivative 5,6,7-trimethoxyindole (**TMI**) or else the novel synthetic azetidiny-propoxy-indole (**AZI**) (**Fig. 2**). We selected the following trigger units to create a palette of 10 reduction-responsive prodrugs: piperazine-fused 1,2-dithianes **Me-SS66T**, **Me-SS66C**, and **P-SS66C**, 1,2-dithianes **SS60** and **P-SS60** and 1,2-thiaselenane **SeS60**, plus “upper-limit” hydrolyzable methyl carbonate (**MC**), non-specifically reducible linear disulfide (**SS00_M**), and “lower-limit” non-reducible **O56** and **P-CC60** carbamates (**Fig. 3+4**).

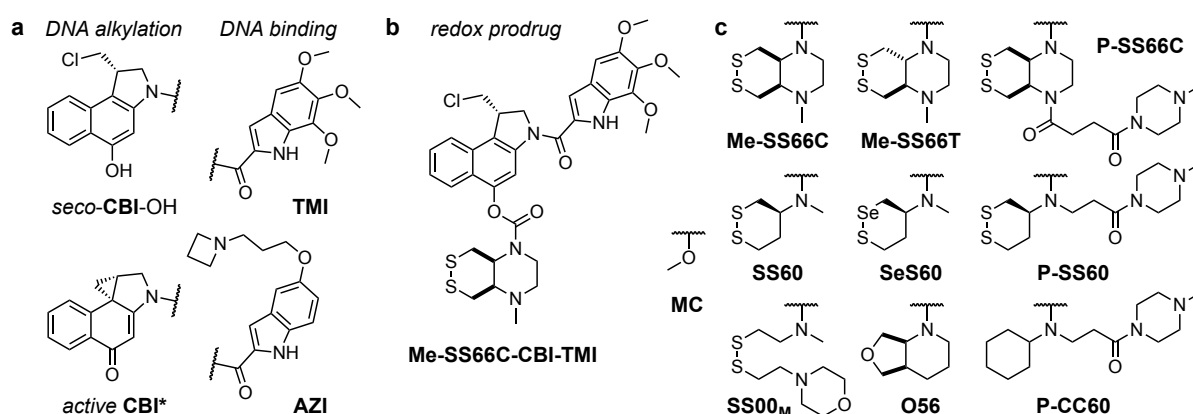


Figure 20 (a) CBI core and side chain indole motifs and (b) representative redox prodrug (**Me-SS66C-CBI-TMI**) structures; (c) reduction trigger and control units used in this study.

We verified the reduction-mediated fragmentation mechanism by detecting the cascade fragments upon release of the active DNA-alkylator with HPLC/MS (**Fig. 5**). We performed cellular proliferation assays in HeLa and A549 cells that situated the upper and lower limits of our series between ester- and carbamate-based CBI prodrugs known from the literature (**Table 1**). We consistently observed an order of cellular potencies in the TMI- and AZI-based prodrug series that we interpreted as directed by trigger choice (decreasing potency: **MC** > **SS00_M** > **SS66T** > **SS66C** \approx **SS60** > **P-CC60**) matching previous findings of cellular processing rates for each of the units (**Fig. 6**). Characteristic potency differences of 1,2-dithiane prodrugs between the two cell lines already indicated a correlation of activity with the cellular redox systems (e.g. TrxR1 is overexpressed in A549 cells). To verify that cellular activation is

tied to the Trx system, we performed cytotoxicity studies in cells with a genetic knockout of TrxR1. For 1,2-dithiane probes, we consistently saw higher potencies in the parental compared to the knockout cells, while control prodrugs, including **SS00M**, gave identical results in both cell lines (**Fig. 7**).

Screening for *cellular Trx redox activity* (i.e., a combination of TrxR/Trx expressions and activities) was previously inaccessible. With these Trx-dependent prodrugs, we intended to use automated potency screening over a large number of standard cancer cells to reveal trends. The first screen we performed (Proliferator-140) gave high-quality results in 140 cell lines for the two redox activatable prodrugs, **P-SS66C-CBI-TMI** and **P-SS60-CBI-TMI**, that we compared to their non-activatable control **P-CC60-CBI-TMI**. We defined the *reductive activation index* to quantify the proportion of reductive vs. hydrolytic activation and used it to group cell lines according to their indices that we interpreted as indicators for their cellular Trx redox state (**Fig. 8**). A second screen by the US National Cancer Institute (NCI-60) was performed for **P-SS66C-**, **Me-SS66C-**, **Me-SS66T-**, **P-SS60-CBI-**, and **P-CC60-CBI-TMI**, with different experimental settings, but broadly reproducing the results of the reductive activation index across the 19 overlapping cell lines for the two overlapping prodrugs, while providing data for 36 new cell lines and two additional prodrugs (**Fig. 9**).

We had aimed to develop these prodrugs as anti-cancer agents *in vivo*, which required us to test their tolerance profiles in an animal model. We performed an HPLC-based plasma PK analysis in mice, then several maximum-tolerated-dose and repeated-dosing studies to evaluate which of the prodrug candidates were suitable for *in vivo* use (**Table 2**). We found that prodrugs of the solubilized TMI-series were well-tolerated at repeated dosing of 3 mg/kg once or twice per week.

Stringently testing anti-cancer efficacy of an activatable prodrug is a non-trivial task in a complex animal model and requires conditions including that: (i) mice have to develop a well-defined tumor; (ii) they must survive for several weeks with the growing tumor; and (iii) the tumors need to be responsive to treatment with a well-chosen control that sets the window for therapeutic efficacy of novel prodrug candidates. With our redox prodrugs, we hoped that reductive activation would primarily occur under tumoral conditions with an altered redox state, while the general prodrug robustness would prevent the release of the cytotoxin in other tissues. We performed efficacy studies using 4T1 (breast cancer) and Bx-PC3 (pancreatic cancer) tumors in two *in vivo* models. We observed anti-cancer efficacy in both models using prodrugs based on **P-SS60**, which was just as effective in suppressing tumor growth as the approved cancer therapeutic irinotecan (**Fig. 10**).

To conclude, we successfully transferred the concept of reduction-triggered switch-on agents of molecular cargos from fluorogenic probes to cytotoxic prodrugs. We built two series of novel duocarmycin prodrugs and validated their reduction-mediated, tunable potencies in 177 cell lines in three different laboratories. We used the *reductive activation indices* to characterize cellular redox states of standard cancer cell lines and showed anti-cancer efficacy of well-tolerated 1,2-dithiane prodrugs *in vivo*. We believe that the prodrug design presented in this work provides a valid general tool for molecular tuning of bioactives based on reducible trigger units.

Cyclic dichalcogenides extend the reach of bioreductive prodrugs to harness thiol/disulfide oxidoreductases: applications to *seco*-duocarmycins targeting the thioredoxin system

Jan G. Felber, Annabel Kitowski, Lukas Zeisel, Martin S. Maier, Constanze Heise, Julia Thorn-Seshold, Oliver Thorn-Seshold*

Department of Pharmacy, Ludwig-Maximilians University Munich, Butenandtstr. 5-13, 81377 Munich, DE; *oliver.thorn-seshold@cup.lmu.de

ABSTRACT: Small molecule prodrug approaches that can activate cancer therapeutics selectively in tumors are urgently needed. Here, we developed the first antitumor prodrugs designed for activation by thiol-manifold oxidoreductases, targeting the thioredoxin (Trx) system. The Trx system is a critical cellular redox axis that is tightly linked to dysregulated redox/metabolic states in cancer, yet it cannot be addressed by current bioreductive prodrugs, which mainly cluster around oxidised nitrogen species. We instead harnessed Trx/TrxR-specific artificial dichalcogenides to gate the bioactivity of a series of 10 "off-to-on" reduction-activated duocarmycin prodrugs. The prodrugs were tested for cell-free and cellular activity dependent on reducing enzyme systems in 177 cell lines, to establish broad trends for redox-based cellular bioactivity of the dichalcogenides. They were well tolerated *in vivo* in mice, indicating low systemic release of their duocarmycin cargo, and *in vivo* anti-tumor efficacy trials in mouse models of breast and pancreatic cancer gave promising initial results indicating effective tumoral drug release, presumably by *in situ* bioreductive activation. This work therefore presents a chemically novel class of bioreductive prodrugs against a previously unaddressed reductase chemotype, validates its ability to access *in vivo* compatible small-molecule prodrugs even of potentially cumulative toxins, and so introduces carefully tuned dichalcogenides as a platform strategy for specific bioreduction-based release.

1. INTRODUCTION

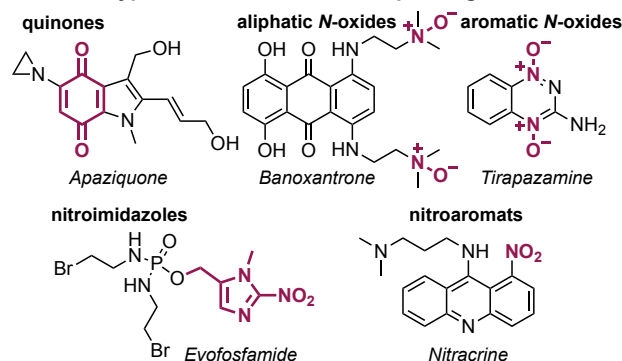
Classic cancer chemotherapy, treating tumors with cytotoxic drugs against ubiquitous critical biological targets (DNA integrity, cell division, etc.), incurs severe systemic side effects from unspecific drug distribution to healthy tissues whose function also depends on these targets. Prodrug concepts can deliver an additional layer of control over drug activity beyond simple biodistribution, and tumor-preferential mechanisms for drug unmasking – e.g. small molecule¹ or antibody-directed² approaches – are intensively pursued.

Bioreductive prodrugs are enzymatically unmasked *in situ* by reduction³. Reductive processes are especially prominent in hypoxic environments, such as tumors, since re-oxidation of metastable intermediates is hindered. Thus, bioreductive prodrugs are sometimes termed "hypoxia-activated". They are in active development, and several reached phase III clinical trials. However, only a small biological target space and a correspondingly restricted small chemical space have been explored for bioreductive prodrugs, which is a missed opportunity for innovative therapeutics (Fig 1a). The first class developed were natural product quinones, activated by ubiquitous quinone reductases, such as the mitomycins and their synthetic analogues (e.g. apaziquone⁴). Later, oxidised nitrogen species that can be reduced by a broader range of enzyme classes came to dominate designs: including (i) aliphatic *N*-oxides that are reduced to basic amines, which can trigger DNA binding (AQ4N/banoxantrone⁵); (ii) aromatic *N*-oxides that are reduced to bioactive nitrogenous bases (tirapazamine⁶); (iii) nitroaryls, that after reduction can eliminate a drug (TH-302/Evofosfamide⁷), or nucleophilically assist reaction mechanisms (PR-104⁸), or dock to targets (nitracrine⁹) (Fig 1a). However, no cancer prodrug using these oxidised nitrogen chemotypes and their targets has been approved;¹⁰ and novel, modular strategies to bioreductively activate drugs specifically inside tumors are required.

The thioredoxin system, composed of the thioredoxins (Trxs) and their NADPH-dependent reductases (TrxRs), are enzymatic reductants that are central to redox homeostasis, cellular metabolism, DNA synthesis, protein folding, and antioxidant response.¹¹ Overactivity of the thioredoxin system is strongly

implicated in cancer progression¹² and Trx expression is often upregulated in tumors.¹³ This may offer a unique point of chemical attack: Trx is the cell's strongest dithiol-based reductant, so reduction-resistant substrates, that are selectively but only slowly activated by Trx under physiological conditions, might be faster activated by Trx in diseased tissues. However, bioreductive prodrug approaches for the Trx system have not yet been designed.

a chemotypes used for bioreductive prodrugs



b this work: new chemical space for bioreduction

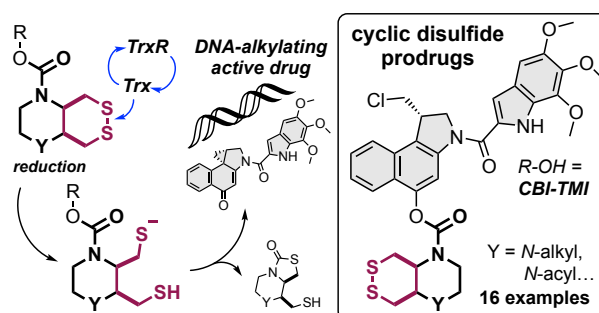


Figure 1: Bioreductive prodrugs. (a) Chemotypes used for bioreductive clinical prodrugs: i) aliphatic *N*-oxides, ii) aromatic *N*-oxides, iii) nitroimidazoles and nitroaromats. (b) Bicyclic disulfides targeting the Trx/TrxR system: one of the new motifs for bioreductive prodrug development introduced in this paper.

Chemically, Trx/TrxR are dithiol/selenolthiol reductases that can address protein as well as small molecule disulfides. The biological target space tested by (any) disulfide-based prodrugs has remained limited, as essentially only GSH-labile nonspecific linear disulfides¹⁴ and 1,2-dithiolanes^{15,16} have been examined. Recently, we have developed sets of 6-membered cyclic dichalcogenides with unique reduction-resisting properties as well as reductase selectivity profiles.^{17–19} Stabilised disulfides in these series were selectively activated by Trxs, with excellent resistance to even thousand-fold higher levels of GSH and monothiols,¹⁷ and bifunctional bicyclic disulfides permitted drastic enhancement of their reductive activation kinetics.¹⁹ Cyclic selenenylsulfides instead had a selenium-preferring, regioisomer-dependent activation mechanism making them excellently selective substrates for TrxR1 in live cells.¹⁸ These bioreductive motifs were validated in fluorogenic probes in acute applications (minutes to hours) in cell culture. However, it is unknown whether such designs can be useful for long-term redox-selective drug delivery, particularly in the context of cancer for which their Trx/TrxR targets' biology is most relevant (**Fig 1b**), since *in vivo* uses are more stringent: e.g. requiring them to also resist activation by hydrolytic or oxidative metabolism in the long-term.

The duocarmycins are DNA alkylators with high potency across a broad range of cell lines,²⁰ that have excellent characteristics as

modular payloads for cytotoxic anticancer prodrugs.²¹ Their key motif is an activated cyclopropane electrophile, which can be generated *in situ* from a biologically inactive *seco*-precursor by unmasking a phenol or aniline that then spontaneously undergoes phenylogous cyclisation (**Fig 2**).²² Due to this elegant off-to-on bioactivity switch, synthetic *seco*-duocarmycin-type prodrugs have been broadly developed as stimulus-responsive proagents, often harnessing the simpler **CBI**^{23,24} alkylator and the minimal **TMI**²⁵ DNA binder motifs.²⁵ Hydrolase-unmaskable phenolic substrates such as esters, carbamates^{26,27} and glycosides^{28,29} have been broadly applied. Bioreductive substrates aiming at increased tumor-specificity have also been tested, including nitro-*seco*-CBIs as aniline precursors^{30,31} and *N*-acyl-*O*-amines as phenol precursors.^{32,33} The modular “puzzle” design of *seco*-duocarmycins, combining a DNA binder with an electrophile segment and its unmaskable trigger, sets up a platform approach for prodrug development (**Fig 2b**).

Aiming to test the potential of Trx/TrxR-responsive cyclic dichalcogenides as trigger units that may open new chemical space as well as target spaces for bioreductive prodrugs, we now design and test a suite of ten redox-responsive **CBI**-based therapeutic prodrugs based on cyclic dichalcogenides (**Fig 2**).

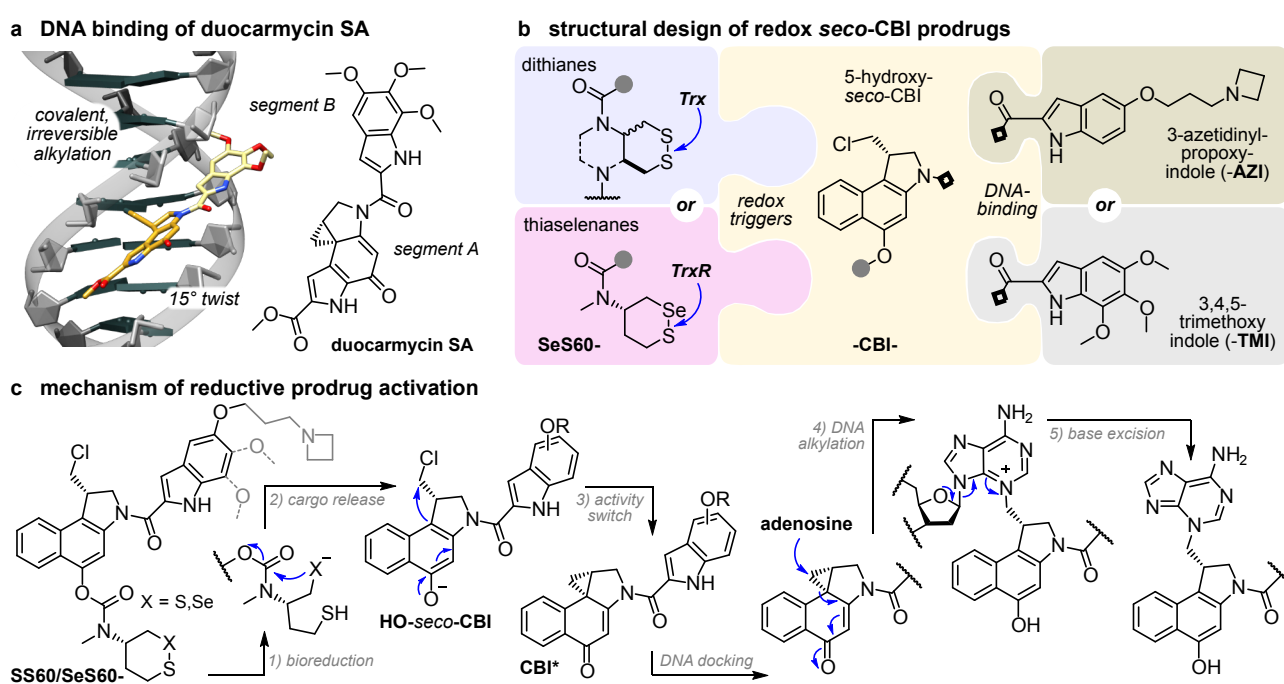


Figure 2: *seco*-duocarmycin prodrug design and mechanism of activation. (a) DNA docking by duocarmycin SA with a 15° amide twist that initiates DNA alkylation (PDB: 1DSM). (b) Our three-part bioreductive prodrug design: (i) an enzyme-selective dithiane/thiaselenane masks (ii) the *seco*-CBI phenol to which (iii) an indole segment is attached for DNA binding and/or solubility. Prodrugs are named by parts, e.g. **SeS60-CBI-AZI** (thiaselenane trigger **SeS60**, **-CBI**-, and 3-azetidyl-propoxy-indole **AZI**). (c) Reductive activation: (1) enzymatic bioreduction; (2) the reduced chalcogenide cyclises to expel the **CBI** phenolic leaving group; (3) bioactivity switch: intramolecular Winstein cyclisation creates the activated cyclopropane; (4) DNA docking leads to DNA alkylation and (5) base excision, irreversible DNA damage, and apoptosis³⁴.

2. RESULTS AND DISCUSSION

2.1 Modular design logic for dichalcogenide prodrugs

We aimed at modular prodrug designs, separating the Trx/TrxR-bioreducible trigger module from its duocarmycin cargo module. This design also separates the functional steps responsible for bioactivity (**Fig 2c**): (1) bioreduction of the trigger by dithiol or

selenolthiol reductases e.g. Trx¹⁷ or TrxR¹⁸; (2) 5-exo-trig cyclisation by the trigger to release the (biologically inactive) duocarmycin phenolic cargo; (3) 1,4-nucleophilic Winstein cyclisation³⁵ creates the activated cyclopropane **CBI***; (4) **CBI*** docks in the DNA minor groove while twisting its aryl-aryl plane, and the now more activated cyclopropane irreversibly alkylates adenosine at the N3-position;³⁶

(5) the quaternised purine base is spontaneously excised, causing DNA damage and ultimately cell death.

We expected that varying trigger and cargo motifs would clarify the separate contributions of reduction and of drug sensitivity to the overall prodrug efficacy, thus setting a rational basis both for further tuning of dichalcogenide triggers, as well as for their adaptation to alternative bioactive cargos³⁷. This is because, in our model (**Fig 2c**), the trigger mainly determines the rate or degree of cargo release, by controlling reduction and cyclisation rates (steps 1-2); whereas the cargo mainly determines the expected potency for a particular degree of drug release, by controlling the speed of cyclopropane formation and likelihood of DNA binding/alkylation (steps 3-4).

We therefore planned to use a range of dichalcogenide redox triggers (e.g. dithiane **SS60**-) to covalently mask hydroxy-*seco*-CBI (-CBI-) by a stable tertiary carbamate linkage,^{38,39} while varying the DNA-binding indoles that complete the duocarmycins to modulate the ADME/potency of the prodrug/drug (e.g. -AZI). The assembled prodrugs would then be named as the combination of these abbreviations: e.g. **SS60-CBI-AZI** (**Fig 2c**).

2.2 Choice of modules for dichalcogenide prodrugs

Choosing trigger motifs with the right redox selectivity profile and cargo release kinetics is key to success of the prodrug design. Our redox trigger choices were based on results from short-term assays relying on phenol-releasing fluorogenic probes (**Fig 3**). Cyclic 6-membered disulfides (**SS60** or its faster-activated, solubilised analogue **P-SS60**) were used as slowly/moderately-reduced Trx-selective substrates (minor crosstalk to dithiol Grx is expected¹⁷). Their unstrained *cis*-annelated-piperazinyl bicyclic congeners (**P-SS66C**, **Me-SS66C**) have much faster, though less selective, Trx reductive activation (more crosstalk to dithiol Grx); strained *trans*-annelated congeners (**Me-SS66T**) are likewise rapidly activated by reductases, but are also moderately labile to monothiols such as GSH so were expected to produce more unspecifically toxic prodrugs. Separately to these Trx-targeted triggers, we included the specifically TrxR1-activated cyclic 6-membered selenenylsulfide **SeS60**, to probe the performance and selectivity possible by targeting the regulator (rather than effector) of the thioredoxin system (**Fig 3**).

To benchmark the performance of these redox-activated triggers and to separate the contributions of reductive vs non-reductive activation (hydrolytic, oxidative, etc.), we designed "upper limit" and "lower limit" reference triggers. At the extreme end of unspecificity, we used linear disulfides (e.g. **SS00_M**) which are unselectively reduced by any biological thiol,¹⁷ as well as a rapidly and unspecifically hydrolase-cleavable carbonate (**MC**), to test the potency expected for the fully released drug cargos and so to estimate the degree of release from the hopefully redox-selective triggers. To understand the degree of *non-reductive* drug release which contributes to the prodrugs' overall cytotoxicity, we would compare the cytotoxicity from a non-reducible isosteric carbamate (**O56**) or a solubilised analogue (**P-CC60**), to a more-resistant ether (**OBn**; **Fig 3**). An overview of the redox and control triggers is given at **Fig S1** where their performance features are detailed.

To complete the prodrugs, we equipped hydroxy-*seco*-CBI with two types of "segment B" indole (**Fig 2b**). For a benchmark that can be compared to literature results, we used the classic trimethoxyindole **TMI** residue, as found in the original natural products duocarmycin SA/A.²² The lipophilic **CBI-TMI** tends to aggregate, so this cargo was only employed with the solubilised trigger motifs. To evolve the properties of synthetic duocarmycins,

we also designed a novel abiotic segment B, 3-azetidiny-propoxy-indole (**AZI**), which is the first azetidine used on a duocarmycin. Our hopes were that the basic amine would (i) add solubility so that non-solubilised triggers (e.g. **SS60**, **SeS60**) could be incorporated into useful and bioavailable **AZI** prodrugs; and also (ii) increase DNA association by Coulombic interactions, and so raise potency. These two features are known from e.g. dimethylamine-substituted B segments ("DEI").²⁸ However, our design also aimed to (iii) avoid undesirable metabolic attack/demethylation *in vivo*, which we expected might be useful for its *in vivo* performance. For an overview of all the resulting prodrug combinations, see the discussion at **Fig S3**.

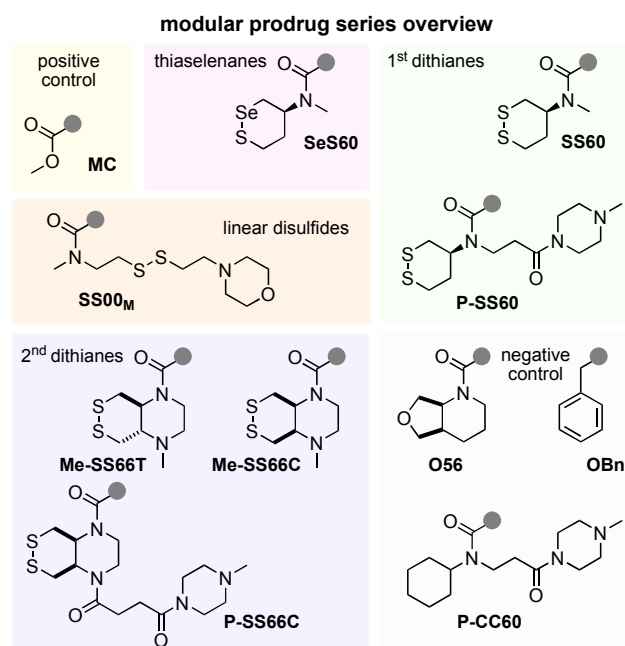


Figure 3: Redox triggers for modular prodrugs. 1st generation Trx-triggers **SS60** and solubilised **P-SS60**;¹⁷ 2nd generation solubilised bicyclic Trx-triggers **Me-SS66T**, **Me-SS66C** and **P-SS66C**;¹⁹ TrxR-trigger **SeS60**¹⁸. "Upper limit" control triggers: very labile **MC**, monothiol-labile **SS00_M**. "Lower limit" control triggers: hydrolysis benchmarks **O-56** and **P-CC60**, and carbamate stability test **OBn**.

2.3 Prodrug assembly by a versatile 2-step approach that avoids dangerously toxic intermediates

Commercial *O*-benzyl-*N*-Boc-(*S*)-*seco*-CBI (**BnO-CBI-Boc**) **1** served as a synthetic starting point (**Fig 4**). While the prodrug retrosynthesis is straightforward, we wished to avoid handling any directly potent DNA alkylators during synthesis, i.e. we aimed to avoid free 5-hydroxy-CBI-indoles that are otherwise the most easily diversified synthetic intermediates: so we wanted to install the triggers before coupling to the indoles. We performed *O*-debenzylation by mild heterogeneous hydrogenation on Pd/C using aq. NH₄HCO₂ as the hydrogen source, as reported by Major²⁸, to avoid the unwanted naphthalene hydrogenation and dechlorination seen with H₂ (g). The phenolic chloroformate produced by reaction with *in situ* generated phosgene was carbamylated^{17,18} with the eight trigger secondary amines giving good to excellent yields of trigger-CBI intermediates (e.g. trigger **H-SS66C-H** (**2**) giving intermediate **H-SS66C-CBI-Boc** (**3**), **Fig 4**). The bisamine SS66-type triggers could then be additionally functionalised by reductive amination (e.g. with formaldehyde

giving **Me-SS66-CBI-Boc** species) or acylation (e.g. with acid anhydride **4**⁴⁰ giving **P-SS66-CBI-Boc** species). The indolecarboxylic acid segments had then to be coupled. **TMI-OH** is commercial; we prepared **AZI-OH** by a 4-step literature procedure⁴¹ that we adapted into a 3-step sequence, using Mitsunobu-type *O*-alkylation of a 5-hydroxy-1*H*-indole-2-carboxylic ester with commercial 3-azetidyl-propan-1-ol.⁴² Finally, the trigger-CBI intermediates were *N*-Boc-protected with HCl in organic solutions⁴³, with TFA or with BF₃·OEt₂²⁹, then coupled either to **AZI-OH** with similar conditions as reported by Tercel³¹ or else to the acid chloride **TMI-Cl**⁴⁴, giving the sixteen prodrugs and controls used in this study (Fig S3) with moderate overall yields (Fig S2). Note that even traces of residual **CBI-OH**, **CBI*** cyclopropane, or easily cleaved CBI byproducts, must be avoided for cellular and *in vivo* testing: their much higher potency can overpower the true performance of the major species prodrugs.

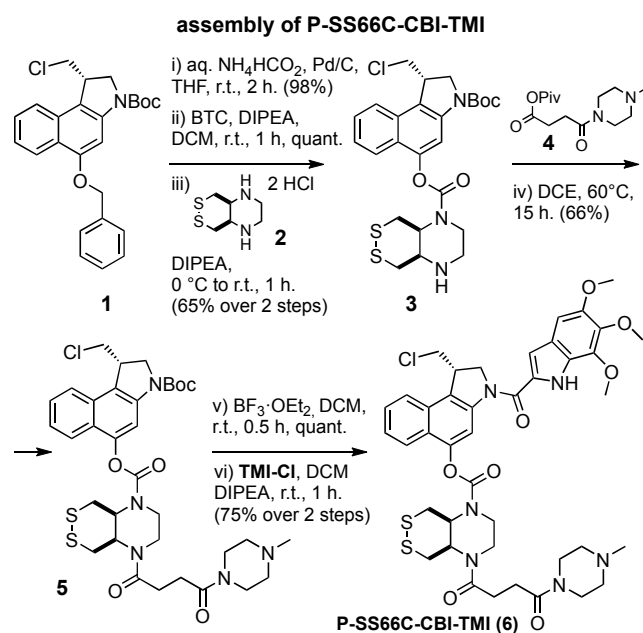


Figure 4: Modular *seco*-CBI prodrug synthesis. Synthesis of representative prodrug **P-SS66C-CBI-TMI** from commercial **BnO-CBI-Boc 1** (full synthesis overview in Fig S2-S3).

2.4 The prodrugs are not activated by monothiois, so may be specifically reducible by disulfide reductases in cells

The cyclic dichalcogenide redox triggers were previously shown to resist activation by monothiois such as glutathione (GSH), but to allow reduction/cyclisation-based release of phenolic fluorophore cargos when treated with disulfide reductase enzymes (e.g. Trx, and/or TrxR, Grx, etc.).^{17,18} These performance features had not been tested with naphthols, so we used HPLC to test them and show their reduction-based activation sequence (Fig 2c and Fig S4-S6).

In brief, treatment with the quantitative reductant TCEP triggered a reaction cascade matching the activation sequence we expected (Fig 2c): dichalcogenides are reduced to dichalcogenols, that cyclise giving the naphthol cargos (plus thiol trigger byproduct) that evolve to the activated cyclopropanes (Fig 5). Also matching expectations, the redox triggers which previously resisted monothiol-reductant-based release of phenolic cargos (**SS/SeS60** and **SS66C** types) likewise gave no detectable release of 5-hydroxy-*seco*-CBI or cyclopropane CBI* when challenged with 5 mM GSH

(50 eq.) over 24 h, though partial activation by GSH was indicated for the strained **SS66T** (Fig S6). The reference compounds performed as expected, either being sensitive to GSH (linear disulfide **SS00_M**) or else resistant to all reduction conditions (non-chalcogenide **O56** or solubilised **P-CC60**).

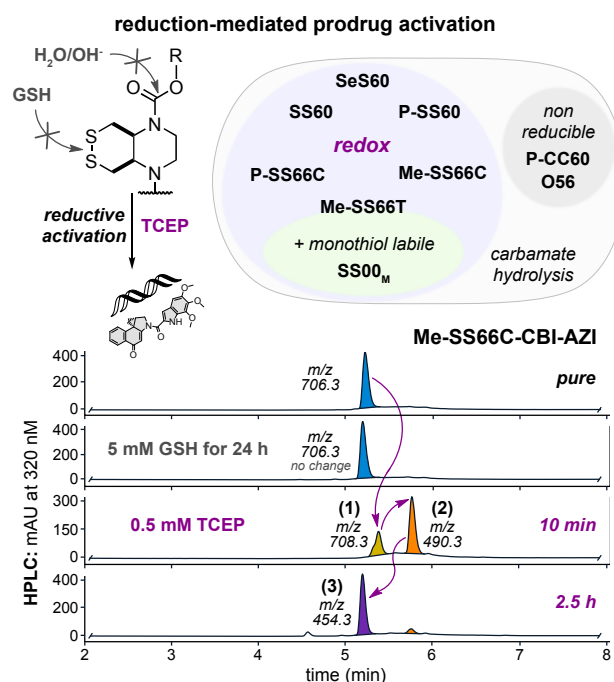


Figure 5: Reduction-triggered prodrug activation. HPLC-MS analysis of activation of **Me-SS66C-CBI-AZI**: (1) TCEP reduction gives the dithiol, (2) the phenolate is expelled, (3) Winstein cyclisation gives the activated cyclopropane (see Fig S4-S6).

Taken together, this indicated that the (**P/Me**)-**SS60**, -**SeS60**, -**SS66C** prodrugs would indeed be monothiol-resistant, giving potential for them to act as prodrugs that are selectively activated by dithiol reductases of the Trx system in cells; and that the reference prodrugs could be used as intended, to estimate the high potency expected if activated by all thiol reductants (**SS00_M**), or the low potency expected if only activated by non-reductive mechanisms, e.g. hydrolysis (**O56**, **P-CC60**) (Fig 5).

2.5 Tunable reduction-based activity allows rational selection of reducible motifs for future *in vivo* applications

While cell lines vary in their intrinsic sensitivity to duocarmycin drugs, the *relative* toxicity of duocarmycin-type *prodrugs*, within any single cell type, should reflect their degrees of cellular activation. We were particularly interested in "low potency" prodrugs, with low activation in usual cell cultures. As a counterexample, prodrugs that are fully activated in all cell types will have high cell culture potencies, like their free duocarmycin cargo: but they are also likely to be activated in all tissues during systemic treatment *in vivo*, so causing dose- and therapy-limiting toxic side-effects.^{45,46} Instead, a prodrug that is little activated in most or all 2D cell cultures (lower potency than its free cargo) may escape such broad activation *in vivo* and be well-tolerated; and if it is distributed to tumors with a suitable bioreduction profile, it may be selectively activated there: so delivering therapeutic benefits. Comparing the relative potencies of duocarmycin prodrugs across cell cultures may give valuable indications about their likely tolerance in therapeutic settings.

For example, free CBIs (cellular IC_{50} ca. 5-30 pM^{24}) and hydroxy-*seco*-CBIs (5-50 $pM^{34,47}$) have low tolerated dosages *in vivo*; but their prodrugs are increasingly tolerated, as their cellular activation is reduced from high (esters for esterases: 100-500 pM^{26}), to moderate (tertiary carbamates for oxidative and/or peptidolytic processing: 50-300 nM^{26}), to low (glycosides for glycosidases: 5-10 μM^{28}). Amino-*seco*-CBIs are less efficient alkylators than the phenols (100-500 pM^{30}); their prodrugs can also be tuned for low nonspecific release (nitro prodrugs for metabolic reduction: 5-50 μM^{31}). **Table 1** summarises these approximate average IC_{50} s over a range of cell lines, highlighting how duocarmycin prodrug potency can be tuned over ca. 7 orders of magnitude by the choice of bioactivation strategy.

Table 1: Benchmark potencies of CBI prodrug classes in cell culture. Averaged literature potencies for CBIs and their prodrugs, to put the potencies of the tertiary carbamate redox prodrugs of this work into perspective. Recall that potency maximisation within the redox prodrug series is *opposed* to the aim of this work (section 2.5).

relative cellular potencies of CBI-based agents				
literature			this work: redox prodrugs	
	pIC_{50}	rel. potency	pIC_{50}	rel. potency
activated CBI*	11	100,000	labile carbonate hydrolysis (MC)	9, 1,000
HO- <i>seco</i> -CBI	10.7	50,000	unspecific thiol reduction (SS00 _M)	8, 100
H ₂ N- <i>seco</i> -CBI	9.7	5,000	TrxR-mediated activation (SeS60)	7.5, 30
esters	9.5	3,000	resistant dithianes (SS60/SS66C)	6.5-8, 3-100
carbamates	6	1	stable carbamate hydrolysis (P-CC60)	6, 1
glycosides	4.3	0.02	stable ether (OBn)	5.5, 0.3
nitro-CBIs	4	0.01		

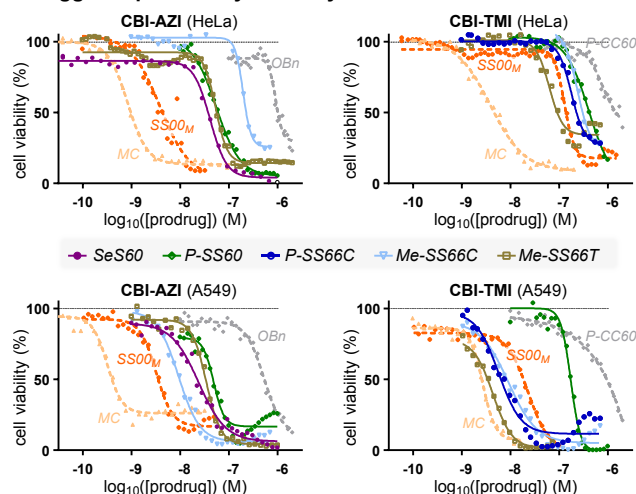
$pIC_{50} = -\log_{10}(IC_{50})$ (M); potencies referenced to carbamate hydrolysis as 1
 literature estimates are geometric averages from different cell lines and compounds

We wished to understand the degree of bioreduction-mediated activation across the series of novel dichalcogenide prodrugs by studying their cellular potencies relative to "minimum/maximum-potency" reference compounds. Our redox-activatable prodrugs are tertiary carbamates, which will have some activation by hydrolysis, as well as by bioreduction. We thus expected their cell culture potencies to fall between a minimum for the non-reducible hydrolysis-only carbamates **OS6** and **P-CC60** (ideally: low potency, anticipating low systemic release), and a maximum for the rapidly enzyme-hydrolysed carbonate **MC** (bioreductive activation unlikely to be faster than this): within which range, variations of potency would report on their relative reductive stability or lability. We also tested nonspecifically-reducible linear disulfide **SS00_M** prodrugs, to probe our expectation that only the monothiol-resistant dichalcogenides such as those we recently introduced^{17,18} can access a different performance space than prior, linear disulfides.

We used A549 lung cancer and HeLa cervical cancer cell lines for initial screening of the prodrugs. These had a >1000-fold range of potencies: rapidly hydrolysed **MC** set an enzymolytic maximum (IC_{50} ca. 0.5 nM; **Fig 6a**) that can be approached by linear disulfide **SS00_M** (nonspecific redox activation by thiols), while the non-reducible carbamates set a hydrolysis-only minimum (ca. 300 nM for **OS6-CBI-AZI**, >1 μM for **P-CC60-CBI-TMI**) that was similar to ether **OBn-CBI-AZI** (>1 μM). We thus estimated that the tertiary carbamate design, with its excellent cell culture stability, offers a

window of up to 1000-fold toxicity enhancement for the dichalcogenide prodrugs according to how much reductive release they undergo (**Fig 6a**). (The 3-10 \times higher potency and better reproducibility of our novel, solubilised **AZI**- as compared to **TMI**-series prodrugs are additional positive features).

a trigger-dependent cytotoxicity



prodrug		IC_{50} (nM): HeLa		IC_{50} (HeLa)/ IC_{50} (A549)	
CBI-AZI					
1	MC	0.8	1.6	0.5	
2	SS00 _M	6.9	4.1	1.7	
3	SeS60	49	60	0.8	
4	Me-SS66T	49	51	1.0	
5	Me-SS66C	400	12	33	
6	SS60	96	120	0.8	
7	P-SS60	890	100	8.9	
8	OS6	460	410	1.1	
9	OBn	750	420	1.8	
CBI-TMI					
10	MC	4.3	2.9	1.5	
11	SS00 _M	125	35	3.6	
12	Me-SS66T	59	5.9	10	
13	Me-SS66C	220	17	13	
14	P-SS60	420	180	2.3	
15	P-SS66C	200	12	17	
16	P-CC60	1,250	1,700	0.7	

Figure 6: Trigger-dependent cellular cytotoxicity. (a-b) Potency in A549 / HeLa cells. Note e.g. consistent 13-to-30-fold greater toxicities in HeLa than in A549 cells for **SS66C** triggers (**AZI** or **TMI** cargos, **P**- or **Me**- substituents) (see also **Table S1** and **Fig S7-S8**).

The toxicities of the novel cyclic dichalcogenide prodrugs (**Fig 6b**) revealed increasing redox-based release in the order **SS60**~**SS66C** (Trx-activated) < **SS66T** (Trx-activated plus some monothiol sensitivity) < **SeS60** (TrxR-activated with high turnover) < **SS00_M** (monothiol-activated limit): matching the order in acute assays of their corresponding fluorogenic probes^{17,18}. This supports our hypothesis that engineered dichalcogenides can resist non-specific thiol-mediated release even in long-term assays (IC_{50} s below **SS00_M**). We consider that by avoiding substantial activation in usual cellular conditions (ca. 30-300-fold less release than references **MC/SS00_M**), they keep alive the possibility of enhanced release selectively in tumors, as long as their bioreduction sensitivity

profile suits the potentially increased expression and/or activity of reductases in tumor environments.

2.6 Redox activation is tied to thioredoxin system activity

Testing whether the cellular activation of the prodrugs is due to their intended target, thioredoxin, is a non-trivial task: since there are no stable Trx knockouts, nor are pharmacologically clean cellular Trx inhibitors available. A TrxR1 knockout (ko) in mouse embryonic fibroblast (MEF) cells is however accessible. We compared its prodrug sensitivity to that of its parental line⁴⁸ (wt), on the basis that TrxR1-ko should leave most Trx1 in its oxidised state (only a fraction of it can be maintained in the reduced state by alternative reductants such as Grx2)⁴⁹, so prodrugs relying on the cytosolic thioredoxin system (Trx1/TrxR1) for most of their bioreductive activation in long-term assays will have lower potency in TrxR1-ko cells.

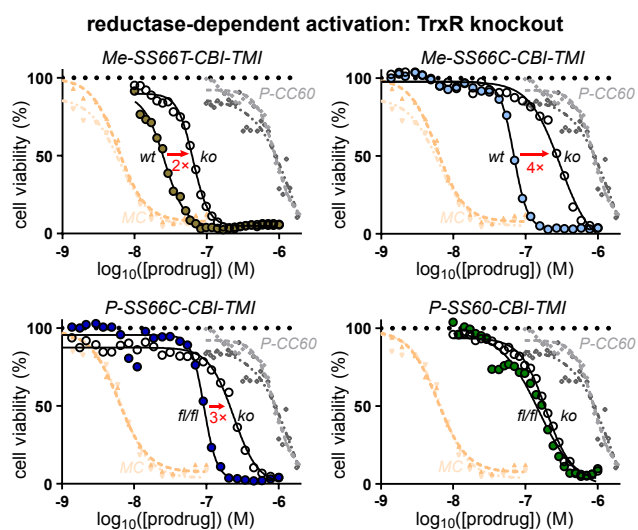


Figure 7: Target-dependent cellular cytotoxicity. Comparing prodrug toxicities in intact (*wt*) vs TrxR1-knockout (*ko*) MEF cells, to test whether the major cellular activation route is rate-limited by the cytosolic thioredoxin couple (TrxR1/Trx1). That is indicated for bicyclic **-SS66C** and **-SS66T**, but not monocyclic **-SS60** (see also **Table S1** and **Fig S9**).

The overall MEF potency trends were similar as in HeLa/AS49 cells (pIC_{50} : MC > MeSS66T > Me-SS66C \approx P-SS66C > P-SS60 > P-CC60; **Fig 5c** and **Fig S10**). Excitingly, all five prodrugs based on the bicyclic **SS66**-type trigger, which have the lowest reduction potential of the disulfide series, were many fold less potent against TrxR1-ko than wt cells (**Fig 7**). This is consistent with reductive processing of **SS66** strongly requiring thioredoxin system activity. That is not an obvious result: since, the multi-day assay provides plenty of time for dithiol reductases outside the TrxR1/Trx1 system (e.g. Grxs) to perform reductive activation instead. Indeed, the three less-stabilised monocyclic **SS60**-type prodrugs showed no such fold-change of potency (see **Table S1** and **Fig S9**), suggesting that in long term assays, cellular activation of simple dithianes can proceed through multiple redox paths. We also find it satisfying that there is such a clear division between the **SS66** and **SS60** structural classes. No matter which cargo (**AZI** or **TMI**) and what variable substituents (**P**- or **Me**- type) are employed, it is the core chemical nature of the redox trigger that dictates cellular performance. Although some redox papers have resisted the idea that SAR rules operate for reducible probes¹⁶, just as they do for drugs, we believe that such

consistent patterns will continue to emerge and to enlighten the field, wherever design and testing are performed comprehensively.

Taken together, these assays had validated the hypothesis of tunable redox-based cellular activation of dichalcogenide prodrugs. Consistent with our aims, the **SS66**-type strongly depend on a specific, key enzyme pair: the thioredoxin system; even in long-term assays (**Fig 7**). This validates the first bioreductive prodrug design capable of selectively targeting a disulfide reductase in cells.

2.7 Profiling thioredoxin- and redox-activated prodrugs in 176 cancer cell lines suggests their *in vivo* potential

We wished to study the *in vivo* suitability of the dichalcogenide strategies, while benchmarking the performance of the different triggers in a thorough and reproducible manner that can be used to guide rational future design of other prodrug families. We therefore planned to screen the prodrugs' redox-dependent bioactivity across large numbers of validated cancer cell lines with standard and objective assay conditions.

We initially focused on **P-SS66C** (reducible by thioredoxin) and **P-SS60** (reducible by thioredoxin and unknown other actors). Both will also undergo non-reductive release by carbamate cleavage (hydrolases and/or oxidative metabolism), at rates that are likely to vary with cell type. Other factors depending on cell type include intrinsic cellular sensitivity to the duocarmycin cargo, and cell entry rate and degree of accumulation of the prodrug. To control for all these cell-line-dependent features, we included the closely similar but non-reducible carbamate analogue, **P-CC60**. We think this is a vitally important step. Rather than focusing on the *absolute* potencies of a redox prodrug in a certain cell line, we could then examine the *fold difference* of potency between reducible **P-SS66C** or **P-SS60** vs. non-reducible **P-CC60**, to focus on the degree of bioreductive processing that the prodrugs undergo in cell culture (see below).

Note that while expression of some reductases have been measured on mRNA and protein levels, their actual *activity* levels are unknown in clinically relevant samples (e.g. patient tumors) as well as simple cell lines - due to the lack of suitable tools to quantify them. Thus, we were also interested to explore if expression patterns might or might not correlate to drug potency profiles (see below).

We obtained a first high-throughput automated screen of the antiproliferative potencies of reducible **P-SS66C-CBI-TMI** and **P-SS60-CBI-TMI** alongside **P-CC60-CBI-TMI** as a hydrolysis-only reference, over a panel of 140 standard cancer cell lines with diverse tissue origins (skin, ovary, lung, colon, breast, pancreas, prostate, kidney, brain, etc), run by commercial provider Reaction Biology ("ProliFiler-140" screen). The topoisomerase inhibitor doxorubicin served as a benchmark for assay validation, and to illustrate trends in cell line drug sensitivity. Incubations were performed for 72 hours before automated viability readout with CellTiterGlo[®] (**Fig 8**).

All 140 cell lines gave well-formed and complete sigmoidal dose-response curves with steep and uniform Hill slopes, consistent with excellent assay technical performance, including compounds being well soluble at all concentrations (selection in **Fig 8a**, full data in **Table S2** and **Fig S10**). Antiproliferative IC_{50} values range from ca. 1-100 nM for reducible **P-SS60** and **P-SS66C**, and ca. 10-1000 nM for non-reducible **P-CC60** (**Fig 8b**). Prodrug potencies correlated slightly to those of doxorubicin (**Fig 8b**), but much better to **P-CC60** (**Fig 8c**), matching expectations from their overall similar structures and shared mechanism of action. Noteworthy, **P-SS60** potency correlated more tightly than **P-SS66C** to that of **P-CC60**

(green vs. blue data, **Fig 8c**). This difference now gave broad support to the indication from the single cell line TrxR knockout assay

(**Fig 7**), that their bioreductive activating mechanisms in long term assays are substantially differentiated.

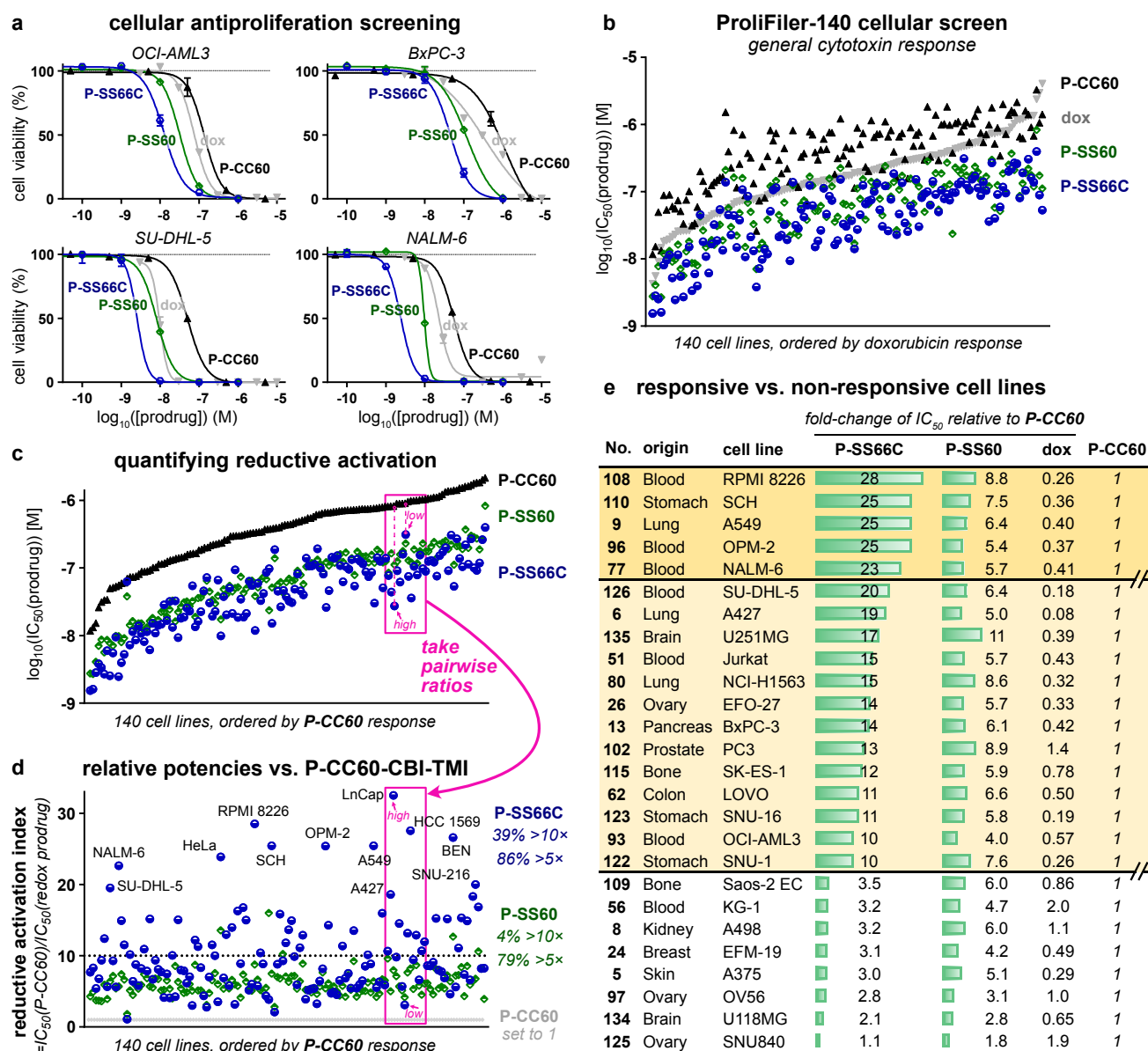


Figure 8: Screening bioreductive activity patterns for P-SS66C-CBI-TMI and P-SS60-CBI-TMI redox prodrugs, by benchmarking against hydrolysis control P-CC60-CBI-TMI, across 140 cancer cell lines ("Prolifer-140"). (a) Sample cell lines, of the 140 tested (see too **Table S2** and **Fig S10-S11**). (b) Rank ordering by sensitivity to the mechanistically unrelated drug doxorubicin. (c) Rank ordering by sensitivity to hydrolysis control P-CC60. (d) IC_{50} s as ratios relative to that of P-CC60 hydrolysis control. (e) Sets of cell lines suggest different redox activity patterns.

Matching our model, the potencies of reducible P-SS60 and P-SS66C were greater than of non-reducible P-CC60 within each one of the 140 cell lines, even though their absolute potencies vary over more than 100-fold between the different cell lines. This supports P-CC60 being a suitable predictor of minimal, purely non-reductive release levels in any given cell line: compared to which, any additional reductive release is reflected in increased potency of the reducible prodrugs (**Fig 8a,c**).

This additional reductive release is, in our opinion, the most important data delivered by the screening. To analyse it, we define a prodrug's "reductive activation index" in a given cell line to reflect how many fold more potent it is than the hydrolytic control: i.e. $\text{index} = IC_{50}(P-CC60)/IC_{50}(\text{prodrug})$ (**Fig 8d**). This is a

qualitative indicator of how much reductive activation a prodrug experiences, benchmarked to unknown but variable level of hydrolytic cleavage, in a given cell line.

Trends emerge when the reductive index is viewed across so many cell lines (selection in **Fig 8e**, full list in **Table S2**): (1) The index of P-SS66C is variable with some cell lines reaching up to 30-fold; and there is no relation between which cell lines have a high index, and which are most sensitive to P-SS66C in an absolute sense (**Fig 8d**). This contrasts to P-SS60 whose index remains in a narrow band between 5 and 8 over nearly all cell types. **Fig 7** had indicated that TrxR1 activity strongly impacts the bioreductive activation of P-SS66C, but not of P-SS60. Thus, it is tempting to interpret the index of P-SS66C as reporting substantially on

variations of specific TrxR1 activity, and to see the index of **P-SS60** as reporting on other bioreductive actors which seem more constant. (2) The cell lines can be grouped by suggestive trends in the reductive index. For example: (i) *high index for P-SS66C but not P-SS60* (Fig 8e, top bracket): suggesting cell lines where comparatively high reductive activity driven by TrxR1 could be harnessed with novel bioreductive prodrug strategies such as the modular Trx/TrxR-dichalcogenides we present; (ii) *index for P-SS60 is similar to that of P-SS66C* (Fig 8e, middle bracket): suggesting significant disulfide bioreduction activity outside the Trx1/TrxR1 couple, that may be exploitable by future prodrugs tuned towards other reductases e.g. Grxs; or, (iii) *low indices for both redox prodrugs* (Fig 8e, bottom bracket): bioreduction is outweighed by other cleavage mechanisms, so dichalcogenide prodrugs may be unsuitable for addressing these cell types.

We also used this large dataset to check for biological features that might correlate usefully to reductive activation. First, we tested whether reductive performance was clustered according to the tissue of origin of the cell lines: which could be suggestive of e.g. cancer indications that might be promising for selective targeting by reductive prodrugs. However, the tissue of origin played no role in either the reductive index or the absolute potency of the compounds tested (Fig S11). Second, we wished to examine if prodrug potency correlated to gene transcript levels, which could have suggested biomarkers predictive for response to redox prodrugs, thus orienting their therapeutic opportunities. However, mRNA transcript analysis did not give confidently interpretable results, and we believe that direct (e.g. fluorogenic) protein activity probes would be better prodrug predictors (see Table S2).

We next wished to test the reproducibility and validity of these results by standardised screening in a different lab and location, while scrutinising in more detail the bicyclic **SS66** structure which had indicated tantalising TrxR/Trx-selectivity. We obtained a second high-throughput automated screen of antiproliferative potencies through the non-commercial NCI Developmental Therapeutics Program (DTP), over the NCI-60 standardised human tumor cell line panel.⁵⁰ 19 of the NCI cell lines overlap with the Prolifer-140 screen so could be used for benchmarking, though differences in assay setup, run time, and readout introduce systematic shifts in absolute potencies. In a series of **-CBI-TMI** prodrugs, we newly tested **Me-SS66C-** and its more reduction-prone diastereomer **Me-SS66T-** (basic amines at the redox site), in comparison to previously tested **P-SS66C-**, **P-SS60-**, and non-reducible **P-CC60-** (all amides; Fig 3).

The new prodrugs showed dramatically how stereochemistry can rule reductive lability. *Trans*-dithiane **Me-SS66T** was consistently far more potent than any other drug, with a mean reductive index ca. 70; while *cis*-dithiane **Me-SS66C** was roughly similar in potency to **P-SS60** with mean index ca. 7 (Fig 9a).

The benchmarking results of reductive index matched between NCI and Prolifer screens: e.g. (1) variable **P-SS66C** index (average 14, maximum 30), but with nearly all **P-SS60** index in a narrow range around 6-8 (Fig 9a); and (2) no trends from the cell lines' tissue of origin (Table S3). As expected, the *absolute* potencies of a prodrug in a given cell line differed between the screens (Prolifer: average 4-fold higher, standard deviation 3.2-fold). Pleasingly though, despite these differences, the reductive index was well conserved between the screens (Fig 9b), particularly for **P-SS66C** (average 1.8-fold higher, standard deviation 1.1-fold) (Table S4). This suggests that the index

reports reproducible aspects of reductive release, which in turn supports that the results of these screens (NCI-60: tested more prodrugs, Prolifer: tested more cell lines) can be combined: building an unprecedented, predictive, modular overview of trigger- and cell line-dependent bioreductive performance for novel dichalcogenide bioreductive prodrugs.

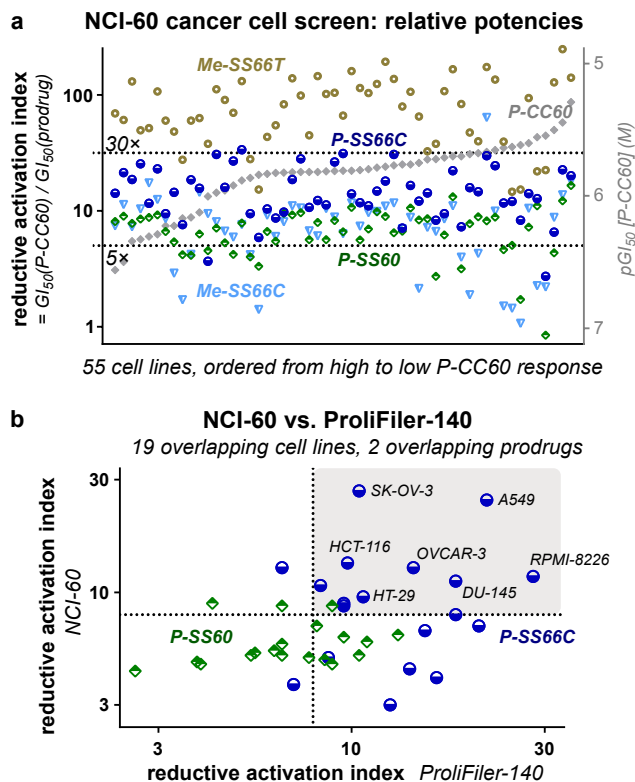


Figure 9: Independent screen of bioreductive activity for all redox prodrugs across the standard "NCI-60" panel. (a) Selected NCI results (full data in Table S3). (b) NCI-60 and Prolifer screens give similar reductive activation indices (details in Table S4).

We again took advantage of the large screening data to test for potential correlations between drug potency and easily measurable biomarkers: here, proteomics-based protein expression levels. Neither absolute potencies nor the reductive indices were well correlated to the expression of any specific reductases (including Trx1, TrxR1, etc; Fig S12). Considering the many layers of post-translational regulation of redox activity, we find this unsurprising. We argue further, that such a lack of mRNA and protein level correlations probably highlights a need for the redox field to avoid considering gene/protein expression levels as suitable data to propose pathological mechanisms or therapeutic opportunities - these may be better argued by analysing activity (note at Fig S12).

Taken together, these first-ever high-throughput screens for reductase-targeting disulfide prodrugs showed outstanding performance features. Referencing analysis to the key hydrolytic control factors out variable aspects of cell entry, non-reductive prodrug activation, and intrinsic cell line sensitivity, to show how redox SAR robustly predicts prodrug performance in these long-term assays, across 176 cell lines from many tissue types of origin. The reductive activation indices are reproducible in different labs and setups; they follow clear trends across cell lines; and above all they match the molecular understanding gained from simple cell-free and cellular assays¹⁷ of how the trigger structures (*trans*- or *cis*-

fused, monocyclic or bicyclic) influence acute kinetic lability and reductase promiscuity. The modular tertiary carbamate design is crucial for reaching this intercomparability of results; and combines with the choice of the unmaskable, irreversibly DNA-alkylating cargo **CBI** as cargo, to ensure robust and reproducible data quality can be obtained by machine screens. This sets solid foundations for rational design or selection, and stringent validation, of reducible dichalcogenides as redox prodrug triggers in future work, even on vastly different cargos: which has been one goal of our methodological research.

The second goal of these screens was to test if any reducible triggers generally displayed the moderately activation-resisting performance that we sought, for systemically well-tolerated prodrugs, with potential for stronger tumoral bioreductive activation, towards anticancer use *in vivo*. **Me-SS66C**, **P-SS60** and **P-SS66C** appeared suitable for this (indices usually ca. 5-20).

It is important to clarify that although this screening identified some cancer cell lines with low nanomolar sensitivity to duocarmycin prodrugs in general (e.g. SK-MEL-28), this study did not aim to perform therapeutic assays by implanting such cargo-sensitive cell lines *in vivo*. In our opinion, such assays do not deliver useful information, since they are biased to 'succeed' in a way that is not replicable in uncontrolled clinical settings (cf. **section 2.9**). By focusing instead on the properties conferred by the *triggers*, we hoped to identify modular motifs that would be generally tolerated for high repeated dose administration, no matter the cargo. We therefore moved on to test these prodrugs *in vivo* in mice.

2.8 *In vivo* pharmacokinetics and prodrug tolerance

We first examined the *in vivo* pharmacokinetics of representative compound **SS60-CBI-AZI** in Balb/c mice after i.v. administration at 5 mg/kg (3 animals per timepoint, four timepoints from 5-90 minutes post injection). Compound plasma half-life was ca. 20 min, by HPLC-MS/MS (**Fig S13a**). Matching expectations for a low-release prodrug, no released **HO-CBI-AZI**, or activated cyclopropane, or adducts, were detected. This gave confidence that the redox prodrugs might give low systemic exposure of the activated CBI, and therefore be tolerable *in vivo*.

To test if low prodrug activation could enable *in vivo* use, we performed dosing and toxicity studies in Balb/c mice, comparing the toxicity and the tolerated dosing of low-reducible **SS60-CBI-AZI** or substantially-reducible **SeS60-CBI-AZI** and to non-reducible carbamate **O56-CBI-AZI**. Single dose toxicity was studied over the range 0.1-10 mg/kg. Dosing at ≤ 3 mg/kg was typically tolerated, which should be compared to the toxicity limit for fully activatable duocarmycins: typically ca. 0.1 mg/kg for *total, cumulative* dose.⁴⁵ However, 10 mg/kg of any **AZI** carbamate was lethal in the week following treatment, though the ether control was not lethal at this dose and not even body weight variations were noted for it: suggesting that at this dose, even hydrolytic carbamate release passes the threshold for toxicity.

The potential for toxicity under low repeated dosing was then studied, comparing **SS60-** and **SeS60-** to **O56-CBI-AZI** (injections once per week over three weeks; 7 animals per condition). No adverse bodyweight losses were seen, but two toxicity features were identified. First, liver damage was indicated by statistically significant, ca. 10% increases of liver weight for the reducible probes, often with increased alanine aminotransferase levels and decreased alkaline phosphatase levels (liver damage markers); these changes were much lower for hydrolytic **O56**.

Second, anemia was indicated by statistically significant decreases of typically 4-12% in hemoglobin, hematocrit, and red blood cell count, for all **CBIs** (**Fig S13b**). All other organ weights and gross pathology features were normal. Given the small statistical power of the assay, these results should be taken cautiously; but they are consistent with the liver as a site of primarily reductive activation of the monocyclic dichalcogenides.

Next, a moderate repeated dosing study in Balb/c mice (three animals per group) tested the importance of solubilising the prodrugs. For example, we have seen elsewhere that a solubilising piperazinamide **P-** sidechain near the dichalcogenide greatly increases reproducibility of cellular results¹⁸. Now *in vivo*, **P-SS60-CBI-TMI** was tolerated at once weekly 3 mg/kg dosing in all animals over 3 injections, without adverse effects at the end of observation 2 weeks later. By contrast, at 3 mg/kg, the still monobasic but less soluble analogues **SS60-CBI-AZI** and **SeS60-CBI-AZI** lead to significant loss of body weight (**Fig S13c**) with visible adverse effects at the injection site potentially arising from local aggregation or precipitation, since they were avoided by lower dosing at e.g. 1 mg/kg. This suggested solubilisation near the reducible trigger could indeed be beneficial for tolerability.

A larger study was run in fifty athymic nu/nu NMRI mice (ten animals per group), inoculated with BxPc3 pancreatic cancer cells since the study had been intended as a therapeutic efficacy trial (see **section 2.9**). Similarly solubilised **SS66C** derivatives were now included. In this study, the tumor growth rates in all animals were much lower than in any previous or subsequent trials (**Fig S14c**): so, we could only extract data about drug tolerability, not antitumor efficacy. Still, the study confirmed that the solubilised **P-SS60-**, **Me-SS66C-**, and **P-SS66C-** prodrugs of **-CBI-TMI**, and the corresponding carbamate hydrolysis control **P-CC60-CBI-TMI**, were tolerated with twice weekly injections at 3 mg/kg, over a course of five injections, in all animals: since no distinct differences of body weight or animal health were seen as compared to the vehicle control (**Fig S14a**).

Table 2 Tolerability for repeated dose administration *in vivo*. The table summarizes dosages that are well-tolerated under weekly or twice-weekly administration, as tested in multiple study settings (PK: pharmacokinetics; MTD: maximum tolerated dose).

<i>in vivo</i> tolerability under repeated dosing (mouse)			
prodrug	studies	dose recommended (mg/kg)	
SS60-CBI-AZI	PK, MTD	0.3-1	<i>adverse effects</i>
SeS60-CBI-AZI	MTD	0.3-1	<i>adverse effects</i>
O56-CBI-AZI	MTD	1	
P-SS60-CBI-AZI	MTD, efficacy	3	<i>well tolerated</i>
P-SS60-CBI-TMI	MTD, efficacy	3	<i>well tolerated</i>
P-SS66C-CBI-TMI	MTD, efficacy	3	<i>well tolerated</i>
Me-SS66C-CBI-TMI	MTD, efficacy	3	<i>well tolerated</i>
Me-SS66T-CBI-TMI	MTD, efficacy	3	<i>well tolerated</i>
P-CC60-CBI-TMI	MTD, efficacy	3	<i>well tolerated</i>

Finally, another large study intended for antitumor efficacy also had to be examined only in terms of tolerability. This assay in immunocompetent Balb/c mice (ten animals per group), inoculated with 4T1 murine breast cancer cells, also treated animals with reducible **P-SS60-**, **Me-SS66C-**, **P-SS66C-CBI-TMI**, or carbamate control **P-CC60-CBI-TMI** (3 mg/kg), once or twice per week. Here, tumors grew well in all groups, but since even the technical positive control irinotecan failed to slow

tumor growth (Fig S14d), no efficacy conclusions could be drawn. Repeated dosing at 3 mg/kg was however tolerated also in this mouse strain, again in mice bearing the additional burden of tumors (Fig S14b). This excellent tolerability supported our aim to develop solubilised, low-release, reducible carbamate prodrugs for *in vivo* use with duocarmycin-type cargos.

2.9 Dichalcogenide CBI prodrugs show anticancer efficacy in murine cancer models

We then moved to *in vivo* anticancer efficacy trials of these prodrugs. We anticipated that the *in vivo* growth environments significantly regulate the tumoral redox/metabolic biochemistries which can activate the prodrugs: so, we did not expect cell lines' reductive index from 2D cell culture to be reproduced *in vivo*, but selected tumor models for their technical reproducibility and for their value as biologically meaningful or medically relevant models (Fig 10a). As one model, we chose the syngeneic murine breast cancer 4T1, implanted orthotopically (at the native tissue site) into the fat pad of immunocompetent Balb/c mice (i.e. offering a realistic immune system and tumor microenvironment). This model gives rapid, aggressive tumor growth.⁵¹ As a second model, we chose to xenograft human BxPC-3 pancreatic adenocarcinoma cells into immunodeficient hosts. This is a slower-growing model, with low metastasis, that can be more resistant to traditional antimitotic therapy.^{52,53} Mice were implanted, randomized once tumors reached 100-150 mm³ volume, and treated once or twice weekly with prodrug or control compounds typically at 3 mg/kg (8-12 animals per condition, Fig 10a). Tumors were measured by caliper during the assay and weighed at termination.

The 4T1 efficacy study compared reducible **P-SS60-CBI-TMI** to non-reducible **P-CC60-CBI-TMI** (3 mg/kg). This time, the technical positive control irinotecan showed the expected tumor-slowng effect. Both reducible prodrugs and non-reducible control delayed tumor growth in the first week of treatment. However, only the reducible prodrugs maintained statistically significant tumor suppression until study termination (Fig 10b,d and Fig S15). Although other interpretations are possible, this is highly suggestive that reductive activation in tumors indeed delivers CBI at effective tumor-suppressing levels, that are also significantly above those provided by systemic or tumoral carbamate hydrolysis.

Finally, we tested **P-SS60-CBI-TMI** in the slower-growing pancreatic cancer model BxPC-3 in athymic NMRI mice (8 animals per group). The response to once weekly **P-SS60** treatment (3 mg/kg) was outstanding, almost identically tumor-suppressive as the technical control irinotecan (10 mg/kg), with consistent ca. 70% tumor growth rate suppression over four weeks, and high statistical significance (Fig 10c,e and Fig S15). As the **P-CC60** non-reductive control had not been included, we cannot estimate how much of the therapeutically beneficial effect in this model stems from reductive or non-reductive CBI release: but at least in cell culture, BxPC-3 had reductive release six-fold higher than the non-reductive level alone (Fig 8e), so we expect that similarly, tumoral reductive release may be a significant factor.

After these promising studies showing efficacy and supporting the importance of reductive release, the critical question is now: is reductive CBI release higher in tumors than in healthy tissues? This cannot be answered from efficacy data alone, since acute tumoral response to CBI is different from that of healthy tissues; and exposure to released CBI cargo is also challenging to track in

tissue by typical HPLC methods, due to its low (~subnanomolar) levels that irreversibly alkylate DNA. To tackle this question and thus to estimate the potential of these dichalcogenide strategies to provide tumor-selective drug delivery, we have now begun a new *in vivo* assay program, with a different set of bioreductive prodrugs that allow sensitive tracking and quantification of release. Results will be reported in due course.

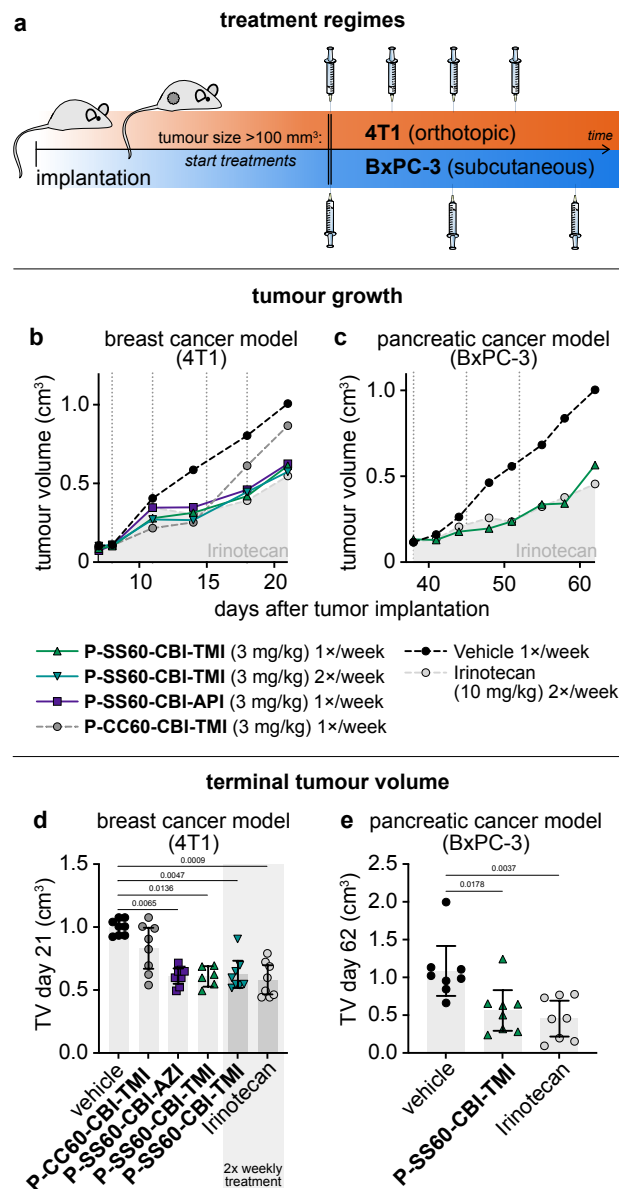


Figure 10: *in vivo* anticancer efficacy. (a) Designs for mouse anticancer efficacy assays: murine breast cancer (4T1) implanted orthotopically in the mammary fat pad of immunocompetent Balb/c mice; human pancreatic cancer (BxPC-3) implanted subcutaneously in athymic nu/nu NMRI mice. (b,c) Tumor volume (TV) over the course of the studies (median values). (d,e) TV at study termination (raw values with means; days 21 and 62 respectively; *p*-values from Kruskal-Wallis test indicated where *p* < 0.05). See also Fig S15.

3. SUMMARY AND CONCLUSIONS

We have developed a novel, modular chemical space of bioreductive dichalcogenide prodrugs, for the as-yet unaddressed target space of disulfide reductases such as the thioredoxin system

(Fig 1). The ten redox-sensitive triggers and controls allowed us to resolve contributions of reductive vs. non-reductive prodrug activation, and the 16 prodrugs (including a novel CBI azetidone) allowed us to test a modular "redox SAR"-based design hypothesis, relying on minimal and maximal activation controls (Fig 2-4). We have confirmed their reductive activation mechanisms (Fig 5) and used cellular knockout assays to quantify triggers that can reach up to $\geq 80\%$ cellular selectivity for activation by the thioredoxin system (Fig 6-7). Two independent, automated, high-throughput cellular screens in 176 cancer cell lines confirmed the redox SAR principle of rationally tuned prodrug potency; they deliver an unprecedentedly comprehensive body of data which we argue indicates actual disulfide reductase activity, as distinct from reductase gene expression or protein levels, across this broad range of cell types (Fig 8-9). Several of the solubilised prodrugs were well tolerated *in vivo* over multiple trials, supporting their design principle of high metabolic and hydrolytic robustness which we believe is a prerequisite for effective tumor-selective reductive release. Tolerability is a stringent hurdle for duocarmycin prodrugs, due to their severe, cumulative toxicity; so, this success is encouraging for future applications (Table 2).

Most importantly, *all these aspects*, from synthesis to systemic robustness *in vivo*, are modular features of the dichalcogenide prodrug strategy: so, the same principles and performance can be expected from *any* cargo that is used with this (stabilised dichalcogenide plus tertiary carbamate) prodrug approach.

By combining tolerability with efficacy, this first set of CBI prodrugs also indicates that using the dichalcogenide prodrug strategy (even with the historically difficult-to-tame CBI cargo) can be a promising route for *in vivo* anticancer applications. In particular, piperazinamide **P-SS60-CBI-TMI** gave high antitumor efficacy in the relatively resistant BxPC-3 pancreatic cancer model, on the same level as a 3-fold higher dose of FDA-approved irinotecan; and it likewise gave good efficacy in the aggressive syngeneic 4T1 breast cancer model (Fig 10).

More broadly, we expect that while the tolerability is a general feature of the redox prodrug platform which can benefit any chemical cargo or animal model, efficacy within the tolerability window will only be reliably achieved by matching the choices of model, redox trigger, and cargo type. This multi-variable problem requires a much deeper knowledge level around disulfide manifold bioreduction than currently available. However, by separating the features of prodrug performance that are based on redox reactivity of the trigger, from those that are based on trigger hydrolysis, as well as separating the model-dependent and cargo-dependent contributions to results, the systematic modular approach we present makes significant advances towards reaching this level.

The ideal goal for redox prodrugs is to develop a platform approach that can maximise the ratio of drug exposure in tumoral vs. in healthy tissues, rather than relying only on differences of their intrinsic sensitivities to a given cargo. Testing this exposure ratio, with directly quantifiable redox reporter prodrugs based around another cargo than the CBIs, is our aim in ongoing work.

Quantifying exposure with reporters, and developing increasingly effective prodrug-based therapeutics, are mutually reinforcing advances for testing the potential of bioreductive prodrugs. We believe that both will be required, over multiple interleaved cycles of refinement, in order to face this multi-variable problem with a quantitative, SAR-based understanding. We

anticipate that the systematic body of predictive data in this study, which complements previous *in vitro* development steps,¹⁶⁻¹⁸ should prove vital to enable and orient such *in vivo* followup cycles; and we believe that direct reporter methods will at last start to reveal the selectivity that engineered, synthetic dichalcogenide redox substrates can deliver by harnessing oxidoreductase-based release in the disulfide/dithiol manifold.

That challenge should not be underestimated: bioreductive release prodrug systems based on oxidised nitrogen species have taken several *decades* to reach their current, and still incomplete, level of predictive or SAR-based understanding.^{3,31} However, we believe that by emphasising a high volume of comparative SAR-based data, this work will help quantitative *in vivo* investigations to succeed rather more rapidly.

A reliable, actionable understanding of the disease indications in which redox dysregulation can be exploited, and to what degree it may provide selective therapeutic benefits, would resolve several decades of tantalising observations and theoretical deadlock. These dichalcogenides are bringing a new biochemical target space into play: time will tell if they can be used as straightforwardly as in this study, i.e. modularly retrofitting existing cargos to turn them into powerful bioreductive diagnostics and prodrugs.

AUTHOR INFORMATION

Corresponding Author

*oliver.thorn-seshold@cup.lmu.de

ORCID*s*

Jan G. Felber:	0000-0002-5010-9624
Annabel Kitowski	0000-0002-8001-5928
Lukas Zeisel:	0000-0001-7813-7099
Martin S. Maier:	0000-0002-0409-0539
Julia Thorn-Seshold:	0000-0002-4879-4159
Oliver Thorn-Seshold:	0000-0003-3981-651X

Funding

This research was supported by funds from the German Research Foundation (DFG: SFB 1032 project B09 number 201269156, SFB TRR 152 project P24 number 239283807, SPP 1926 project number 426018126, and Emmy Noether grant 400324123 to O.T.-S.); LMUExcellent (Junior Researcher Fund to O.T.-S.); the Munich Centre for NanoScience initiative (CeNS to O.T.-S.); and Federal Ministry of Education and Research GO-Bio 161B0632 to O.T.-S. and J.T.-S..

Notes

J.G.F., L.Z., J.T.-S. and O.T.-S. are inventors on patent applications PCT/EP2022/057483 and PCT/EP2022/059280 filed by the Ludwig-Maximilians-University (LMU) Munich in 2021, covering compound structures reported in this paper. The authors declare no competing financial interests.

Where quantities are averaged over non-comparable conditions, the geometric mean (logarithmic) is used. For example, IC₅₀ values 0.25 nM and 1 nM in two cell lines are averaged to 0.5 nM to give a single indicative value; *idem* for mean reductive index values over e.g. 55 NCI cell lines.

Author Contributions

J.G.F. performed synthesis, analysis, cell-free prodrug activation and cellular assays; coordinated screening, analysed

screening data, performed data assembly. A.K. performed cell-free prodrug activation, cellular assays, coordinated screening and *in vivo* studies, and performed data analysis. L.Z. and M.S.M. performed synthesis and analysis. C.H. performed cell-free prodrug activation and cellular assays. J.T.-S. designed, coordinated, and analysed *in vivo* studies, and performed data assembly. O.T.-S. designed the concept and experiments, supervised experiments, performed screening data analysis, and coordinated data assembly. J.G.F. and O.T.-S. wrote the manuscript with input from all co-authors.

Acknowledgements

J.G.F. thanks the Studienstiftung des deutschen Volkes for support through a PhD scholarship; L.Z. thanks the Fonds der Chemischen Industrie (FCI) for support through a PhD scholarship; J.T.-S. thanks the Joachim Herz Foundation for fellowship support. We thank the NCI DTP for NCI60 screening; Ramon Messeguer at Leitat for initial *in vivo* proof of concept studies; Diana Behrens and team at EPO Berlin for followup *in vivo* studies; Anna Kondratiuk, Yuliia Holota, Sergey Zozulya and the other team members at Bienta (Kyiv, Ukraine) for *in vivo* PK and initial MTD studies; Bettina Stahnke and Philipp Metzger and team at Reaction Biology for further *in vivo* studies.

REFERENCES

- Quinney, S. K.; Sanghani, S. P.; Davis, W. L.; Hurley, T. D.; Sun, Z.; Murry, D. J.; Bosron, W. F. Hydrolysis of Capecitabine to 5'-Deoxy-5-Fluorocytidine by Human Carboxylesterases and Inhibition by Loperamide. *J. Pharmacol. Exp. Ther.* **2005**, *313* (3), 1011–1016. <https://doi.org/10.1124/jpet.104.081265>.
- Peters, C.; Brown, S. Antibody–Drug Conjugates as Novel Anti-Cancer Chemotherapeutics. *Biosci. Rep.* **2015**, *35* (4), e00225. <https://doi.org/10.1042/BSR20150089>.
- Seddon, B.; Kelland, L. R.; Workman, P. Bioreductive Prodrugs for Cancer Therapy. In *Suicide Gene Therapy: Methods and Reviews*; Springer, C. J., Ed.; Methods in Molecular Medicine; Humana Press: Totowa, NJ, 2004; pp 515–542. <https://doi.org/10.1385/1-59259-429-8-515>.
- Phillips, R. M.; Hendriks, H. R.; Peters, G. J.; on behalf of the EORTC-Pharmacology and Molecular Mechanism Group. EO9 (Apaziquone): From the Clinic to the Laboratory and Back Again: Preclinical and Clinical History of EO9. *British Journal of Pharmacology* **2013**, *168* (1), 11–18. <https://doi.org/10.1111/j.1476-5381.2012.01996.x>.
- Furman, R. R.; Bartlett, N. L.; Wong, A. F.; McCulloch, L. M.; Lam, G. N.; Rosenthal, T.; Flinn, I.; Leonard, J. P. B. Anoxantrone (AQ4N), a Tissue Targeted Prodrug: Results of a Phase I Study in Lymphomas. *Blood* **2006**, *108* (11), 2429. <https://doi.org/10.1182/blood.V108.11.2429.2429>.
- Hay, M. P.; Hicks, K. O.; Pchalek, K.; Lee, H. H.; Blaser, A.; Puijn, F. B.; Anderson, R. F.; Shinde, S. S.; Wilson, W. R.; Denny, W. A. Tricyclic [1,2,4]Triazine 1,4-Dioxides As Hypoxia Selective Cytotoxins. *J. Med. Chem.* **2008**, *51* (21), 6853–6865. <https://doi.org/10.1021/jm800967h>.
- Sun, J. D.; Liu, Q.; Wang, J.; Ahluwalia, D.; Ferraro, D.; Wang, Y.; Duan, J.-X.; Ammons, W. S.; Curd, J. G.; Matteucci, M. D.; Hart, C. P. Selective Tumor Hypoxia Targeting by Hypoxia-Activated Prodrug TH-302 Inhibits Tumor Growth in Preclinical Models of Cancer. *Clin. Cancer Res.* **2012**, *18* (3), 758–770. <https://doi.org/10.1158/1078-0432.CCR-11-1980>.
- McKeage, M. J.; Jameson, M. B.; Ramanathan, R. K.; Rajendran, J.; Gu, Y.; Wilson, W. R.; Melink, T. J.; Tchekmedyan, N. S. PR-104 a Bioreductive Pre-Prodrug Combined with Gemcitabine or Docetaxel in a Phase Ib Study of Patients with Advanced Solid Tumours. *BMC Cancer* **2012**, *12* (1), 496. <https://doi.org/10.1186/1471-2407-12-496>.
- Wilson, W. R.; Denny, W. A.; Twigden, S. J.; Baguley, B. C.; Probert, J. C. Selective Toxicity of Nitracrine to Hypoxic Mammalian Cells. *Br. J. Cancer* **1984**, *49* (2), 215–223. <https://doi.org/10.1038/bjc.1984.34>.
- Spiegelberg, L.; Houben, R.; Niemans, R.; de Ruysscher, D.; Yaromina, A.; Theys, J.; Guise, C. P.; Smill, J. B.; Patterson, A. V.; Lambin, P.; Dubois, L. J. Hypoxia-Activated Prodrugs and (Lack of) Clinical Progress: The Need for Hypoxia-Based Biomarker Patient Selection in Phase III Clinical Trials. *Clin. Trans. Rad. Oncol.* **2019**, *15*, 62–69. <https://doi.org/10.1016/j.ctro.2019.01.005>.
- Holmgren, A.; Lu, J. Thioredoxin and Thioredoxin Reductase: Current Research with Special Reference to Human Disease. *Biochemical and Biophysical Research Communications* **2010**, *396* (1), 120–124. <https://doi.org/10.1016/j.bbrc.2010.03.083>.
- Arnér, E. S. J. Perspectives of TrxR1-Based Cancer Therapies. In *Oxidative Stress*; Elsevier, 2020; pp 639–667.
- Powis, G.; Kirkpatrick, D. L. Thioredoxin Signaling as a Target for Cancer Therapy. *Current Opinion in Pharmacology* **2007**, *7* (4), 392–397. <https://doi.org/10.1016/j.coph.2007.04.003>.
- Henne, W. A.; Doorneweer, D. D.; Hilgenbrink, A. R.; Kularatne, S. A.; Low, P. S. Synthesis and Activity of a Folate Peptide Camptothecin Prodrug. *Bioorganic & Medicinal Chemistry Letters* **2006**, *16* (20), 5350–5355. <https://doi.org/10.1016/j.bmcl.2006.07.076>.
- Li, X.; Hou, Y.; Meng, X.; Ge, C.; Ma, H.; Li, J.; Fang, J. Selective Activation of a Prodrug by Thioredoxin Reductase Providing a Strategy to Target Cancer Cells. *Angew. Chem. Int. Ed.* **2018**, *57* (21), 6141–6145. <https://doi.org/10.1002/anie.201801058>.
- Felber, J. G.; Poczka, L.; Scholzen, K. C.; Zeisel, L.; Maier, M. S.; Busker, S.; Theisen, U.; Brandstädter, C.; Becker, K.; Arnér, E. S. J.; Thorn-Seshold, J.; Thorn-Seshold, O. Cyclic 5-Membered Disulfides Are Not Selective Substrates of Thioredoxin Reductase, but Are Opened Nonspecifically. *Nat. Commun.* **2022**, *13* (1), 1754. <https://doi.org/10.1038/s41467-022-29136-4>.
- Felber, J. G.; Zeisel, L.; Poczka, L.; Scholzen, K.; Busker, S.; Maier, M. S.; Theisen, U.; Brandstädter, C.; Becker, K.; Arnér, E. S. J.; Thorn-Seshold, J.; Thorn-Seshold, O. Selective, Modular Probes for Thioredoxins Enabled by Rational Tuning of a Unique Disulfide Structure Motif. *J. Am. Chem. Soc.* **2021**, *143* (23), 8791–8803. <https://doi.org/10.1021/jacs.1c03234>.
- Zeisel, L.; Felber, J. G.; Scholzen, K. C.; Poczka, L.; Cheff, D.; Maier, M. S.; Cheng, Q.; Shen, M.; Hall, M. D.; Arnér, E. S. J.; Thorn-Seshold, J.; Thorn-Seshold, O. Selective Cellular Probes for Mammalian Thioredoxin Reductase TrxR1: Rational Design of RX1, a Modular 1,2-Thiaselenane Redox Probe. *Chem* **2022**, *8* (5), 1493–1517. <https://doi.org/10.1016/j.chempr.2022.03.010>.
- Zeisel, L.; Felber, J. G.; Thorn-Seshold, O. A Bifunctional Dichalcogenide-Fused Piperazine Platform for Tunable Thiol-Mediated Cellular Activation of Proagents. *in preparation* **2022**.
- Li, L. H.; Swenson, D. H.; Schpok, S. L. F.; Kuentzel, S. L.; Dayton, B. D.; Krueger, W. C. CC-1065 (NSC-298223), a Novel Antitumor Agent That Interacts Strongly with Double-Stranded DNA. *Cancer Res.* **1982**, *42*, 999–1994.
- Felber, J. G.; Thorn-Seshold, O. 40 Years of Duocarmycins: A Graphical Structure/Function Review of Their Chemical Evolution, from SAR to Prodrugs and ADCs. *JACS Au* **2022**. <https://doi.org/10.1021/jacsau.2c00448>.
- Boger, D. L.; Hertzog, D. L.; Bollinger, B.; Johnson, D. S.; Cai, H.; Goldberg, J.; Turnbull, P. Duocarmycin SA Shortened, Simplified, and Extended Agents: A Systematic Examination of the Role of the DNA Binding Subunit. *J. Am. Chem. Soc.* **1997**, *119* (21), 4977–4986. <https://doi.org/10.1021/ja9637208>.
- Boger, D. L.; Ishizaki, T.; Kitos, P. A.; Suntornwat, O. Synthesis of N-(Tert-Butyloxycarbonyl)-CBI, CBI, CBI-CDPI1, and CBI-CDPI2: Enhanced Functional Analogs of CC-1065 Incorporating the 1,2,9,9a-Tetrahydrocyclopropa[c]Benz[e]Indol-4-One (CBI) Left-Hand Subunit. *J. Org. Chem.* **1990**, *55* (23), 5823–5832. <https://doi.org/10.1021/jo00310a013>.
- Boger, D. L.; Yun, W.; Han, N. 1,2,9,9a-Tetrahydrocyclopropa[c]Benz[e]Indol-4-One (CBI) Analogs of CC-1065 and the Duocarmycins: Synthesis and Evaluation. *Bioorg. Med. Chem.* **1995**, *3* (11), 1429–1453. [https://doi.org/10.1016/0968-0896\(95\)00130-9](https://doi.org/10.1016/0968-0896(95)00130-9).
- Boger, D. L.; Yun, W. CBI-TMI: Synthesis and Evaluation of a Key Analog of the Duocarmycins. Validation of a Direct Relationship between Chemical Solvolytic Stability and Cytotoxic Potency and Confirmation of the Structural Features Responsible for the Distinguishing Behavior of Enantiomeric Pairs of Agents. *J. Am. Chem. Soc.* **1994**, *116* (18), 7996–8006. <https://doi.org/10.1021/ja00097a006>.
- Nagamura, S.; Kobayashi, E.; Gomi, K.; Saito, H. Synthesis and Antitumor Activity of Duocarmycin Derivatives: A-Ring Pyrrole Analogues of Duocarmycin B2. *Bioorg. Med. Chem.* **1996**, *4* (8), 1379–1391. [https://doi.org/10.1016/0968-0896\(96\)00132-0](https://doi.org/10.1016/0968-0896(96)00132-0).

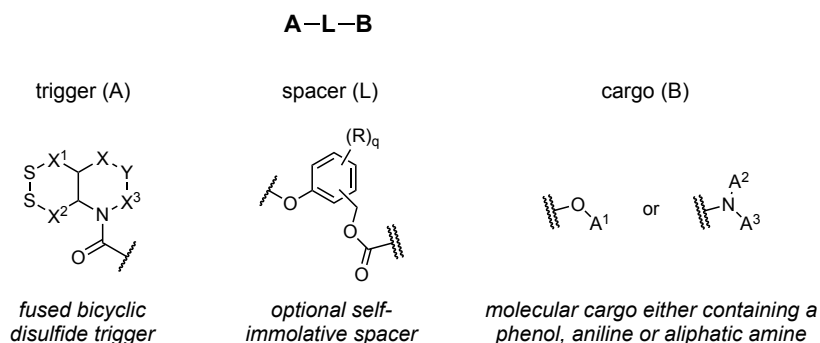
- (27) Boger, D. L. CBI Prodrug Analogs of CC-1065 and the Duocarmycins. *Synthesis* **1999**, 1999 (S1), 1505–1509. <https://doi.org/10.1055/s-1999-3658>.
- (28) Tietze, L. F.; Major, F.; Schuberth, I. Antitumor Agents: Development of Highly Potent Glycosidic Duocarmycin Analogues for Selective Cancer Therapy. *Angew. Chem. Int. Ed.* **2006**, *45* (39), 6574–6577. <https://doi.org/10.1002/anie.200600936>.
- (29) Tietze, L. F.; von Hof, J. M.; Müller, M.; Krewer, B.; Schuberth, I. Glycosidic Prodrugs of Highly Potent Bifunctional Duocarmycin Derivatives for Selective Treatment of Cancer. *Angew. Chem. Int. Ed.* **2010**, *49* (40), 7336–7339. <https://doi.org/10.1002/anie.201002502>.
- (30) Atwell, G. J.; Milbank, J. J. B.; Wilson, W. R.; Hogg, A.; Denny, W. A. 5-Amino-1-(Chloromethyl)-1,2-Dihydro-3H-Benz[e]Indoles: Relationships between Structure and Cytotoxicity for Analogues Bearing Different DNA Minor Groove Binding Subunits. *J. Med. Chem.* **1999**, *42* (17), 3400–3411. <https://doi.org/10.1021/jm990136b>.
- (31) Tercel, M.; Atwell, G. J.; Yang, S.; Ashoorzadeh, A.; Stevenson, R. J.; Botting, K. J.; Gu, Y.; Mehta, S. Y.; Denny, W. A.; Wilson, W. R.; Pruijn, F. B. Selective Treatment of Hypoxic Tumor Cells In Vivo: Phosphate Pre-Prodrugs of Nitro Analogues of the Duocarmycins. *Angew. Chem. Int. Ed.* **2011**, *50* (11), 2606–2609. <https://doi.org/10.1002/anie.201004456>.
- (32) Jin, W.; Trzupke, J. D.; Rayl, T. J.; Broward, M. A.; Vielhauer, G. A.; Weir, S. J.; Hwang, I.; Boger, D. L. A Unique Class of Duocarmycin and CC-1065 Analogues Subject to Reductive Activation. *J. Am. Chem. Soc.* **2007**, *129* (49), 15391–15397. <https://doi.org/10.1021/ja075398e>.
- (33) Boger, D. L. CBI Derivatives Subject to Reductive Activation. US 20110112163A1, May 12, 2011.
- (34) Boger, D. L.; Johnson, D. S. CC-1065 and the Duocarmycins: Understanding Their Biological Function through Mechanistic Studies. *Angew. Chem. Int. Ed.* **1996**, *35* (1314), 1438–1474. <https://doi.org/10.1002/anie.199614381>.
- (35) Baird, R.; Winstein, S. Neighboring Carbon and Hydrogen. II. Dienones from Ar1-3 Participation. Isolation and Behavior of Spiro(2,5)Octa-1,4-Diene-3-One. *J. Am. Chem. Soc.* **1963**, *85*, 12. <https://doi.org/10.1021/ja00888a020>.
- (36) Boger, D. L.; Johnson, D. S.; Yun, W.; Tarby, C. M. Molecular Basis for Sequence Selective DNA Alkylation by (+)- and Ent(-)-CC-L065 and Related Agents: Alkylation Site Models That Accommodate the Offset AT-Rich Adenine N3 Alkylation Selectivity. *Bioorg. Med. Chem.* **1994**, *2* (2), 115–135. [https://doi.org/10.1016/s0968-0896\(00\)82007-6](https://doi.org/10.1016/s0968-0896(00)82007-6).
- (37) Kitowski, A.; Zeisel, L.; Thorn-Seshold, O. Use of HPLC-MS/MS for Detection of in Vivo Compatible SN-38 Redox Prodrugs. **2022**.
- (38) Ogasawara, H.; Nishio, K.; Takeda, Y.; Ohmori, T.; Kubota, N.; Funayama, Y.; Ohira, T.; Kuraishi, Y.; Isogai, Y.; Saijo, N. A Novel Antitumor Antibiotic, KW-2189 Is Activated by Carboxyl Esterase and Induces DNA Strand Breaks in Human Small Cell Lung Cancer Cells. *Jpn. J. Cancer Res.* **1994**, *85*, 418–425. <https://doi.org/10.1111/j.1349-7006.1994.tb02375.x>.
- (39) Dittert, L. W.; Higuchi, T. Rates of Hydrolysis of Carbamate and Carbonate Esters in Alkaline Solution. *Journal of Pharmaceutical Sciences* **1963**, *52* (9), 852–857. <https://doi.org/10.1002/jps.2600520908>.
- (40) Jarho, E. M.; Wallén, E. A. A.; Christiaans, J. A. M.; Forsberg, M. M.; Venäläinen, J. I.; Männistö, P. T.; Gynther, J.; Poso, A. Dicarboxylic Acid Azacycle L-Prolyl-Pyrrolidine Amides as Prolyl Oligopeptidase Inhibitors and Three-Dimensional Quantitative Structure–Activity Relationship of the Enzyme–Inhibitor Interactions. *J. Med. Chem.* **2005**, *48* (15), 4772–4782. <https://doi.org/10.1021/jm0500020>.
- (41) Frecentese, F.; Fiorino, F.; Perissutti, E.; Severino, B.; Magli, E.; Esposito, A.; De Angelis, F.; Massarelli, P.; Nencini, C.; Viti, B.; Santagada, V.; Caliendo, G. Efficient Microwave Combinatorial Synthesis of Novel Indolic Arylpiperazine Derivatives as Serotonergic Ligands. *Eur. J. Med. Chem.* **2010**, *45* (2), 752–759. <https://doi.org/10.1016/j.ejmech.2009.11.023>.
- (42) Hennequin, L. F. A.; Ple, P.; Stokes, E. S. E.; McKerrecher, D. Quinazoline Derivatives as Angiogenesis Inhibitors. EP 1154774B1, June 22, 2005.
- (43) Giddens, A. C.; Lee, H. H.; Lu, G.-L.; Miller, C. K.; Guo, J.; Lewis Phillips, G. D.; Pillow, T. H.; Tercel, M. Analogues of DNA Minor Groove Cross-Linking Agents Incorporating AminoCBI, an Amino Derivative of the Duocarmycins: Synthesis, Cytotoxicity, and Potential as Payloads for Antibody–Drug Conjugates. *Bioorg. Med. Chem.* **2016**, *24* (22), 6075–6081. <https://doi.org/10.1016/j.bmc.2016.09.068>.
- (44) Butkevich, A. N.; Bossi, M. L.; Lukinavičius, G.; Hell, S. W. Triarylmethane Fluorophores Resistant to Oxidative Photobleaching. *J. Am. Chem. Soc.* **2019**, *141* (2), 981–989. <https://doi.org/10.1021/jacs.8b11036>.
- (45) Li, L. H.; DeKoning, T. F.; Kelly, R. C.; Krueger, W. C.; McGovern, J. P.; Padbury, G. E.; Petzold, G. L.; Wallace, T. L.; Ouding, R. J.; Prairie, M. D.; Gebhard, I. Cytotoxicity and Antitumor Activity of Carzelesin, a Prodrug Cyclopropylpyrroloindole Analogue. *Cancer Res.* **1992**, *52*, 4904–4913.
- (46) Wang, Y.; Li, L.; Tian, Z.; Jiang, W.; Larrick, J. W. Synthesis and Antitumor Activity of CBI-Bearing Ester and Carbamate Prodrugs of CC-1065 Analogue. *Bioorg. Med. Chem.* **2006**, *14* (23), 7854–7861. <https://doi.org/10.1016/j.bmc.2006.07.062>.
- (47) Sato, A.; McNulty, L.; Cox, K.; Kim, S.; Scott, A.; Daniell, K.; Summerville, K.; Price, C.; Hudson, S.; Kiakos, K.; Hartley, J. A.; Asao, T.; Lee, M. A Novel Class of in Vivo Active Anticancer Agents: Achiral *Seco*-Amino- and *Seco*-Hydroxycyclopropylbenz [e]Indolone (*Seco*-CBI) Analogues of the Duocarmycins and CC-1065. *J. Med. Chem.* **2005**, *48* (11), 3903–3918. <https://doi.org/10.1021/jm050179u>.
- (48) Mandal, P. K.; Schneider, M.; Kölle, P.; Kuhlencordt, P.; Förster, H.; Beck, H.; Bornkamm, G. W.; Conrad, M. Loss of Thioredoxin Reductase 1 Renders Tumors Highly Susceptible to Pharmacologic Glutathione Deprivation. *Cancer Res.* **2010**, *70* (22), 9505–9514. <https://doi.org/10.1158/0008-5472.CAN-10-1509>.
- (49) Du, Y.; Zhang, H.; Lu, J.; Holmgren, A. Glutathione and Glutaredoxin Act as a Backup of Human Thioredoxin Reductase 1 to Reduce Thioredoxin 1 Preventing Cell Death by Aurothioglucose. *J. Biol. Chem.* **2012**, *287* (45), 38210–38219. <https://doi.org/10.1074/jbc.M112.392225>.
- (50) Shoemaker, R. H. The NCI60 Human Tumour Cell Line Anticancer Drug Screen. *Nature Reviews Cancer* **2006**, *6* (10), 813–823. <https://doi.org/10.1038/nrc1951>.
- (51) Pulaski, B. A.; Ostrand-Rosenberg, S. Mouse 4T1 Breast Tumor Model. *Current Protocols in Immunology* **2000**, *39* (1), 20.2.1–20.2.16. <https://doi.org/10.1002/0471142735.im2002s39>.
- (52) Tan, M. H.; Nowak, N. J.; Loor, R.; Ochi, H.; Sandberg, A. A.; Lopez, C.; Pickren, J. W.; Berjian, R.; Douglass, H. O.; Chu, T. M. Characterization of a New Primary Human Pancreatic Tumor Line. *Cancer Investigation* **1986**, *4* (1), 15–23. <https://doi.org/10.3109/07357908609039823>.
- (53) Deer, E. L.; González-Hernández, J.; Coursen, J. D.; Shea, J. E.; Ngatia, J.; Scaife, C. L.; Firpo, M. A.; Mulvihill, S. J. Phenotype and Genotype of Pancreatic Cancer Cell Lines. *Pancreas* **2010**, *39* (4), 425–435. <https://doi.org/10.1097/MPA.0b013e3181c15963>.

3.2.3 Fused cyclic disulfide probes and prodrugs for use in diagnostics and therapeutics

This chapter was published as an international PCT patent application through the EPO/WIPO.

Agency	World Intellectual Property Organization
Title	<i>Disulfide-based prodrug compounds</i>
Publication Number	WO 2022/200347 A1
Applicant	Ludwig-Maximilians-Universität München
Inventors	Oliver Thorn-Seshold, Julia Thorn-Seshold, Jan G. Felber , Lukas Zeisel
Agent	Vossius & Partner Patentanwälte mbH, München
Priority Filing	Mar 22 th , 2021
Publication date	Sep 29 th , 2022
Full Text at	https://patentscope.wipo.int/search/de/detail.jsf?docId=WO2022200347

General structure of the patented chemical space



Description of the chemical space

The patent application *disulfide-based prodrug compounds* covers *trigger-cargo* construct structures of the general formula **A–L–B**, where **A** is a reducible trigger unit based on a bicyclic disulfide; **L** is either a direct bond or else a self-immolative spacer; and **B** is a molecular cargo containing a phenol, aniline or aliphatic amine, where the trigger/linker is covalently attached *via* the cargo's oxygen/nitrogen atom.

The simplest possible trigger structures (**A**) are **SS66C** and **SS66T** (see **chapter 3.1.2**), where $X^1=X^2=X^3=X=Y=CH_2$. The general formula of **A** is described in the patent to cover the following structural variations: (i) X^1 and X^2 can be chosen such that any fused 1,2-dithiane or 1,2-dithiepane is covered; (ii) Y and X^3 can be chosen such that 5-, 6- or 7-membered annelating ring systems are covered; (iii) X can be chosen such that pyrrolidines/piperidines/azepanes or imidazolidines/piperazines/1,4-diazepanes are covered; (iv) the second nitrogen atom in the ring can optionally be substituted by alkylation, acylation or sulfonylation with small solubilization handles or targeting groups including elongated morpholinamides (**M**) or *N*¹-methylpiperazinamides (**P**). By varying these different parameters, the trigger units **Me-SS66C**, **Me-SS66T**, **P-SS66C**, **Ac-SS66C**, etc., that are used for the solubilization of molecular probes and prodrugs are covered (see **chapter 3.1.4**).

While phenolic cargos can be released by reduction in direct conjugates of **A** and **B**, a molecular spacer **L** must be used for the liberation of amine cargos and can also be used for phenols. For the spacer, the benzyl alcohol position must be in 1,2- or 1,4-position to the phenol, and the choice of $(R)_q$ tunes the rate of elimination upon the liberation of the spacer's phenol.

Molecular cargos are suitable as **B** if they contain a phenol, aniline, or aliphatic amine, and covalent attachments at the oxygen/nitrogen modulate their spectral properties (dyes) or bioactivities (drugs). Several mechanisms are known where such modulation can be exploited to create activatable diagnostic tools or therapeutic or theranostic prodrugs that are the subject to this patent application.

Summary

During our research on reducible *trigger-cargo* constructs that are operated by the cellular thiol/disulfide redox systems, we identified fused bicyclic 1,2-dithianes as lead structures (**SS66**-type). We applied these trigger units to fluorescent phenolic cargos where covalent attachment abolishes their fluorescence and allows to the creation of fluorogenic probes that are activated upon reduction of the 1,2-dithiane (see **chapter 3.1.2**). We also found that similar probes based on piperazine-fused 1,2-dithianes allow reduction-initiated fragmentation with much faster kinetics and cellular processing and turnover (see **chapter 3.1.4**). We finally employed these trigger units to create a novel class of bioreductive prodrugs based on the highly potent cytotoxic duocarmycin payload (see **chapter 3.2.2**).

This patent application aimed to cover the chemical space around reducible *trigger-cargo* constructs based on fused bicyclic disulfides in a very general way. As we had shown their utility for three very distinct molecular cargos using various examples, we envisioned that they are generally applicable to activate a large body of potential diagnostic, therapeutic, or theranostic agents upon reduction.

We drew the general formula of a trigger-cargo-construct **A-L-B** with the aim to (i) cover a large space of potential fused bicyclic disulfide structures within the patentable space (the simple 1,2-dithiane trigger **SS60** had already been covered elsewhere²⁴²), including a second nitrogen atom in the backbone ring and potential further substitutions; and (ii) to allow a large number of potential molecular cargos: for diagnostics including xanthenes, coumarins, phenothiazines, luciferins; and for therapeutic purposes including topoisomerase inhibitors (camptothecin), DNA intercalators (doxorubicin) and alkylators (chlorambucil) and antimetotics (Monomethyl Auristatin E). We provided a panel of illustrative embodiments of potential conjugates to emphasize the design flexibility and general applicability of the concept and 22 synthesized and characterized illustrative examples to show synthetic accessibility and feasibility of probes and prodrugs of the formula **A-L-B**. The patent application also claims the general manufacturing of the fused bicyclic disulfide trigger units (**A**) and the full constructs (**A-L-B**) that we described providing generally applicable experimental conditions.

The invention presented in this patent application relates to probes and prodrugs that can release their active components in the presence of a thiol/disulfide bioreductant. Under certain pathological conditions, such as neoplastic disorders, atherosclerosis, an autoimmune disorder, an inflammatory disease, ischemia, reperfusion injury, and in particular, cancerous states, the cellular redox homeostasis may be significantly dysregulated. The patent application, therefore, claims the use of probes and prodrugs of the formula **A-L-B** to be used as diagnostics or therapeutic/theranostic agents to diagnose, treat or prevent such a diseased state. It further covers the use of a second pharmaceutically active compound that can disrupt the tissue vasculature, typically a microtubule-depolymerising agent, to intentionally initiate such dysregulated redox states (hypoxic vascular shutdown and/or reperfusion injury) and maximize the diagnostic/therapeutic benefit of the compounds of the invention.

By expanding the concept of reducible probes and prodrugs and outlining a general design with various potential trigger and cargo choices, we think this provides a promising common ground for future developments that is of commercial interest.

Disulfide-based prodrug compounds

Technical Field

The present application relates to a compound having the formula (I). The compound having the formula (I) is capable of releasing a molecular cargo in the presence of a reductant and is thus suitable for treating, ameliorating, preventing or diagnosing a disorder selected from a neoplastic disorder; atherosclerosis; an autoimmune disorder; an inflammatory disease; a chronic inflammatory autoimmune disease; ischaemia; and reperfusion injury.

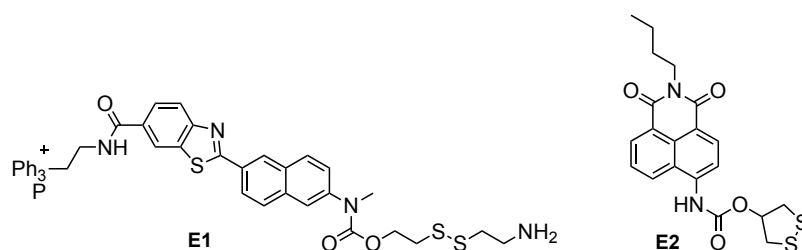
In particular, the molecular cargo can be a therapeutic or diagnostic agent. In particular, the reductant can be a biological disulfide reductase or its effector disulfide protein which may be catalytically active. The invention further relates to a pharmaceutical or diagnostic composition comprising the same.

Prior Art

Dithiol/disulfide-exchange redox reactions are critical in a great number of biological pathways. Often, these are coordinated through conserved, specialised networks of oxidoreductases that perform redox reactions upon or using disulfides and/or thiols. The thioredoxin reductase – thioredoxin (TrxR–Trx) system, and the glutathione reductase – glutathione – glutaredoxin (GR–GSH–Grx) system, are two of the central redox systems; other key reductive enzymes/proteins include but are not limited to peroxiredoxins, glutathione peroxidases, glutathione-S-transferases, methionine sulfoxide reductase, and protein disulfide isomerases (PDIs).²⁴³ Such redox systems drive reactions vital to cellular metabolism, and can also regulate protein activity, protein–protein interactions, and protein localisation by reversible dithiol/disulfide-type reactions.²⁴⁴

To better investigate and understand biological processes, it is of great interest to develop specific methods to image or quantify the activity of biological species, or otherwise to respond to their activity. Therefore it was an object of the present invention to provide compounds which have high selectivity for an oxidoreductase or its redox effector protein and which can be reduced by the disulfide reductive activity of that enzyme and thus release a molecular cargo. This has been a longstanding goal of research in the field of cellular dithiol/disulfide-exchange redox reactions. In this field, a significant challenge for chemical probe development is to ensure that a probe is specific for being reduced by the targeted species, and is not significantly reduced by any other reducing species in the cell. Therefore, to selectively probe one of the species TrxR, GR, Trx, or Grx, a compound must not be activated by any of the others or by GSH. This is difficult because these reductants can perform similar chemical reactions, and because the most active of these reductants have the lowest cellular concentrations (TrxR and GR have nM cellular concentrations; Trx and Grx have μ M concentrations) while the least active reductant GSH is the most concentrated (mM).

These reducing species all act upon disulfides, so most reduction-activated chemical probes in the prior art have used disulfides as reduction-sensing motifs. Probes based on linear disulfides (such as **E1**) have been extensively reported, but it has been shown since decades that these disulfides are nonspecifically reduced by thiols including by GSH.^{181,245} Therefore, linear disulfides are not suitable as selective probes in a cellular context. Recently, there has been limited development of probes using cyclic disulfides as reduction-sensing motifs. For example, Fang and coworkers have developed several so-called "TRFS" probes and prodrugs (such as **E2**)¹⁶⁸ based on a cyclic five-membered disulfide motif; most of these release a cargo after reduction of the disulfide. However, it has been shown that this type of disulfide too is nonspecifically reduced by monothiols including by GSH, and therefore that five-membered cyclic disulfides are not suitable as the basis for oxidoreductase-selective probes in a cellular context (see **chapter 3.1.1**).

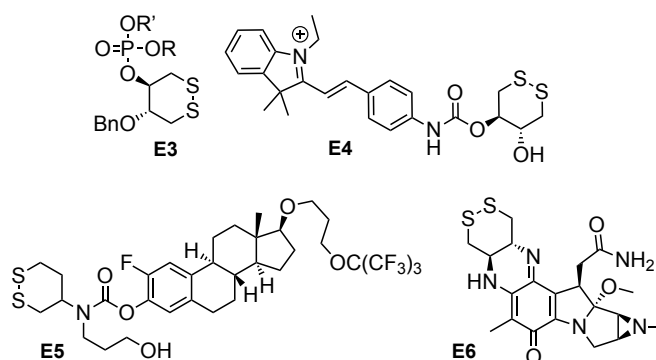


As far as we are aware, only three concepts have been disclosed of probe or prodrug designs based on cyclic six-membered disulfides that are intended to release a general molecular cargo after reduction inside cells.

Firstly, in 2014, Butora disclosed a six-membered cyclic disulfide **E3** capable of releasing a phosphate molecular cargo (R'O)(RO)P(O)OH after reduction. **E3** was applied to cells, and the report stated that release was effected by intracellular GSH.^{245,246} The approach has since been used by e.g. Hayashi in 2017.²⁴⁷

Secondly, in 2017, Kong et al. reported a six-membered cyclic disulfide **E4** intended to release an aniline molecular cargo after reduction. **E4** was applied to cells, and the report stated that release was effected by intracellular H₂Se.¹⁷² A similar concept was used by Li et al. in 2019 in a six-membered cyclic disulfide probe intended to release a different aniline cargo (molecule TRFS7 in their report) but the report stated that "the 1,2-dithianes cannot be reduced by either TrxR or GSH"; a related six-membered cyclic disulfide probe (molecule TRFS8 in their report) featuring a urea linkage was not intended to release a molecular cargo and indeed did not release it.¹⁷⁷

Thirdly, in 2017, Ziv disclosed prodrugs where a 4-amino-1,2-dithiane is linked to a phenolic molecular cargo as the carbamate, so as to release the phenol following reduction which was ascribed to occur through the "ambient reductive environment" of the cell although no cellular reductive species were demonstrated. An example of this is shown as molecule **E5**.^{248,249} Somewhat relatedly, Kohn has worked on six-membered cyclic disulfide derivatives, although not intended to release a cargo. In 2004, Kohn published the molecule **E6**.²⁵⁰ In this molecule three of the atoms in the piperazine-like ring that is annelated to the cyclic disulfide are sp²-configured, which rigidifies the system and prevents it from adopting a decalin-like geometry that would stabilise the disulfide. Notably, **E6** was reported to be transthiolated by "an intracellular thiol or albumin" (i.e. by a monothiol) then to subsequently undergo a cyclisation that results in the attached mitomycin moiety becoming reactive. In 2005, Lee et al. published a related mitomycin derivative containing a six-membered cyclic disulfide that likewise did not release a molecular cargo after activation.²⁵¹



Therefore the relevant prior art in disulfides capable of releasing a molecular cargo after reduction contains (i) linear and cyclic five-membered disulfide designs that are unstable to monothiols such as GSH and therefore in a cellular context cannot be selective for a particular reductant; and (ii) monocyclic six-membered disulfide designs such as **E3**, **E4**, and **E5**, for which the literature is contradictory about what the relevant cellular reductant is (suggesting it is respectively GSH, H₂Se, or an undefined ambient reductive environment, or alternatively stating that GSH cannot reduce the cyclic six-membered disulfide). The example of the geometrically strained six-membered disulfide **E6**, or the strained cyclic five-membered disulfides such as **E2** (discussed in [chapter 3.1.1](#)) shows that destabilisation of the disulfide enhances its reactivity to reductants, which makes the disulfides sensitive to monothiols including GSH (and therefore in a cellular context they cannot be selective for a particular reductant).

Therefore there remain numerous unsolved challenges, including to: (i) design cyclic disulfide-based probe or prodrug systems that release a molecular cargo and that feature optimised disulfide ring geometries that stabilise the disulfide; and to (ii) design disulfide-based probe or prodrug systems that release a molecular cargo and that are selective for a particular cellular reductant, i.e. are shown to resist reduction by other major cellular reductants (e.g. GSH, TrxR, Trx, Grx, GR etc as appropriate).

Under pathological conditions, homeostasis in these redox systems and in their target proteins is significantly dysregulated. This has been particularly shown in diseases such as cancer, inflammatory diseases such as autoimmune disorders, under acute stress such as reperfusion injury, and under other chronic conditions such as cardiovascular disease.^{252,253} Such dysregulation has also been studied in the context of disease-associated biomarkers, such as hypoxia. Hypoxia is a pathology-associated feature, prevalent in cancer and inflammation, that is tightly correlated with significant biochemical changes including oxidoreductase dysregulation, many of which rely on the hypoxia-dependent

transcription factor HIF-1. Oxidoreductase dysregulation may be reflected in a combination of changes to their expression level, enzymatic activity, redox poise (the ratio of oxidised to reduced form of the oxidoreductase), localisation, and/or other parameters. For example, under pathological conditions, the TrxR—Trx and GR—GSH—Grx systems act as repair systems, counteracting acute cellular damage by oxidants, and re-normalising redox imbalances e.g. from oxygen depletion (hypoxia) or from the switching of metabolic pathways due to cellular stress (e.g. the Warburg Effect in cancer)^{101,254}; therefore cells affected by pathologies that require such repair and renormalisation are often found to upregulate expression levels and activity of these oxidoreductase systems, and shift their redox poise.²⁵⁵ This dysregulation has been particularly studied in the context of cancer, where for the example of Trx it has been shown that cycling hypoxia, which is a hallmark of most tumors, upregulates Trx expression levels;²⁵⁶ that Trx overexpression contributes to hallmarks of cancer including increased proliferation and angiogenesis, and evasion of apoptosis;²⁵⁷ and that Trx overexpression in tumors contributes to chemoresistance and is associated to poor patient survival.²⁵⁸ Dysregulated function is also particularly studied in the context of inflammatory diseases, since many central players in inflammation (NFκB, TNF-α, Keap1, Nrf2) are regulated by these oxidoreductases, and processes from inflammasome activation to immune cell chemotaxis have also been shown to depend on these oxidoreductases.^{259,260}

The disease-correlated nature of these dysregulated states of oxidoreductases - particularly of Trx, TrxR, and PDIs - makes them promising targets for diagnostic or therapeutic applications using diagnostic or therapeutic drugs that target these oxidoreductases. For example, the TrxR-inhibiting drug auranofin is FDA-approved for use in the inflammatory disease, rheumatoid arthritis.^{101,243} In this context, a probe or prodrug system to release a molecular cargo, that is selectively triggered by one of these oxidoreductases, would be very valuable. Similarly, substantial efforts have been made to use the disease-correlated feature, hypoxia, both as a diagnostic marker and for therapeutic exploitation, for example by using diagnostic and therapeutic drugs that target hypoxia, which has been extensively reviewed.²⁶¹

Therefore it was a further object of the present invention to provide compounds which may have high selectivity for a oxidoreductase in a pathologically dysregulated state, and can be reduced by the disulfide reductive activity of that oxidoreductase or its effector proteins and thus release a molecular cargo after reduction. It was a further object of the present invention to provide compounds which may have high selectivity for pathologically dysregulated redox states and/or for cells in hypoxia and/or cells with an activated hypoxic response pathway.

It was a further object of the present invention to provide compounds which are also useful, e.g. in a diagnostic or therapeutic capacity, in that they are efficiently activated upon delivery into cells so releasing a molecular cargo, in which case the delivery into the cell is intended to be the process that gives selectivity for the targeted cells or tissues.

In conclusion therefore, the objects of the present invention were to provide compounds which are capable of releasing a molecular cargo after reductive activation, and which

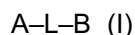
- (A) are suitable for diagnosing, quantifying, or responding to disulfide reductive activity; and/or
- (B) are suitable for diagnosing, treating, ameliorating or preventing a disorder associated with disulfide reductive activity; and/or
- (C) are suitable for diagnosing, treating, ameliorating or preventing a disorder selected from a neoplastic disorder; atherosclerosis; an autoimmune disorder; an inflammatory disease; a chronic inflammatory autoimmune disease; ischaemia; and reperfusion injury, particularly cancer; and/or
- (D) are suitable for diagnosing, treating, ameliorating or preventing a disorder associated with a dysregulated redox state and/or with hypoxia and/or with activation of the hypoxic response pathway; and/or
- (E) are useful because they are efficiently activated upon delivery into cells.

Note that it is possible, and in many cases it is desirable, that one or more of these objectives should be fulfilled by the same compound; for example, a single compound of the invention may fulfil objectives A and E simultaneously; while another compound of the invention may fulfil objectives A, B, C and D simultaneously, etc.

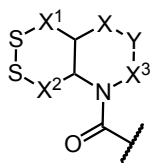
Summary of the Invention

The present invention relates to the following items:

1. A compound having the formula (I)



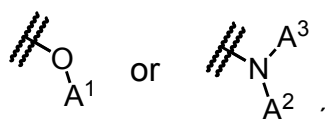
wherein



A is represented by;

denotes the attachment point of A to L;

L is a bond or a self-immolative spacer;



B is represented by



denotes the attachment point of B to L;

A¹ is selected such that A¹-OH is a therapeutic, diagnostic or theranostic agent which contains an -OH group that is attached to a 5- or 6-membered aromatic or heteroaromatic ring;

A² and A³ are independently selected such that A²-NH-A³ is a therapeutic, diagnostic or theranostic agent which contains an -NH₂ or -NH- moiety;

X is selected from -N(R^a)-, -N(R^b)- and -CR^c₂-;

X¹ is -(CR^d₂)_m-;

X² is -(CR^e₂)_n-;

X³ is -CR^f₂-;

Y is -(CR^g₂)_p-;

W is independently selected from -OH, -N(R^h)(Rⁱ), -C(O)-heterocyclic group, or -heterocyclic group, wherein the heterocyclic group is selected from azetidiny, pyrrolidiny, piperidiny, piperaziny, N'-(C₁₋₄-alkyl)piperaziny, or morpholino, and wherein if W is -heterocyclic group then the heterocyclic group is attached to the -C₁₋₄-alkyl or -(C₂₋₄-alkylene)- group via the N atom, or if W is -C(O)-heterocyclic group then the heterocyclic group is attached to the C(O) moiety via the N atom;

R^a is selected from -H, -C₁₋₄-alkyl, -C(O)-C₁₋₄-alkyl, -C(O)-O-C₁₋₄-alkyl, -C(O)-N(C₁₋₄-alkyl)₂, -S(O)₂-C₁₋₄-alkyl, and -(C₂₋₄-alkylene)-O-(C₁₋₄-alkyl), wherein -C₁₋₄-alkyl or -(C₂₋₄-alkylene)- can be optionally substituted by W;

R^b is an acyl group of a mono-peptide selected from -proteinogenic amino acids attached via a carboxy group;

R^c groups are independently selected from -H and -C₁₋₄-alkyl;

R^d groups are independently selected from -H and -C₁₋₄-alkyl;

R^e groups are independently selected from -H and -C₁₋₄-alkyl;

R^f groups are independently selected from -H and -C₁₋₄-alkyl;

R^g groups are independently selected from -H and -C₁₋₄-alkyl;

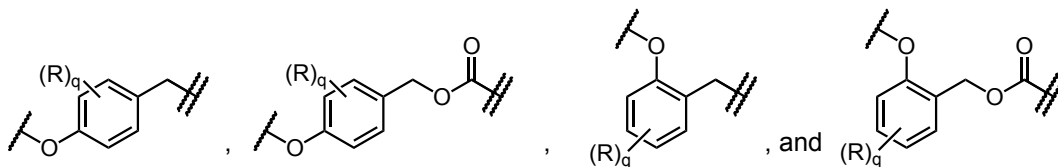
R^h is independently selected from -H, -C₁₋₄-alkyl and -CH₂CH₂OH;

Rⁱ is independently selected from -H, -C₁₋₄-alkyl and -CH₂CH₂OH;

m is 0, 1 or 2;

- n is 1 or 2, provided that m+n is 2 or 3;
 p is 0, 1, or 2, provided that when X = -N(R^a)- or -N(R^b)- then p = 1 or 2;
 or any pharmaceutically acceptable salt, solvate or ester thereof.

2. The compound according to item 1, wherein L is a bond.
 3. The compound according to item 1, wherein L is a self-immolative spacer selected from



wherein

denotes the attachment point to A;

denotes the attachment point to B;

R is independently selected from halogen, -O(R^r), -N(R^s)(R^t), -NO₂, -CN, and a heterocyclic group selected from azetidiny, pyrrolidiny, piperidiny or morpholino, wherein the heterocyclic group is attached to the phenyl ring *via* the N atom;

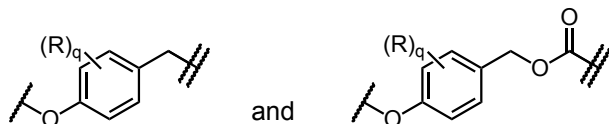
q is 0, 1, 2, 3 or 4;

R^r is independently selected from -H, -C₁₋₄-alkyl and -(C₂₋₄-alkylene)-O-(C₁₋₄-alkyl), wherein -C₁₋₄-alkyl or -(C₂₋₄-alkylene)- can be optionally substituted by W;

R^s is independently selected from -H, -C(O)-C₁₋₄-alkyl and -C₁₋₄-alkyl; and

R^t is independently selected from -H, -C(O)-C₁₋₄-alkyl and -C₁₋₄-alkyl.

4. The compound according to item 3, wherein L is a self-immolative spacer selected from



wherein R and q are as defined in item 3.

5. The compound according to any one of items 1 to 4, wherein X¹ and X² are -CH₂-.
 6. The compound according to any one of items 1 to 5, wherein A¹-OH or A²-NH-A³ is selected from a diagnostically acceptable dye, a therapeutically acceptable DNA-alkylating agent, a therapeutically acceptable tubulin-inhibiting agent, and a therapeutically acceptable DNA-intercalating agent.

7. The compound according to any one of items 1 to 6, wherein A¹-OH or A²-NH-A³ is selected from 10-hydroxycamptothecin, 10-hydroxybelotecan, 10-hydroxygimatecan, 10-hydroxy-CKD-602, 10-hydroxy-BNP-1350, 10-hydroxy-sinotecan, topotecan, 7-ethyl-10-hydroxy-camptothecin (SN-38), 10-hydroxy-20-acetoxy-camptothecin, pyrrolbenzodiazepine, methotrexate, duocarmycin, CC-1065, doxorubicin, epirubicin, daunorubicin, pirarubicin, carminomycin, doxorubicin-*N,O*-acetal, 4-(bis(2-chloroethyl)amino)phenol, 4-(bis(2-bromoethylamino)phenol, 4-(bis(2-mesyethyl)amino)phenol, 4-((2-chloroethyl-2'-mesylethyl)amino)phenol, (S)-(1-(chloromethyl)-5-hydroxy-1,2-dihydro-3H-benzo[e]indol-3-yl)(5,6,7-trimethoxy-1H-indol-2-yl)methanone, (S)-(5-(3-(azetidin-1-yl)propoxy)-1H-indol-2-yl)(1-(chloromethyl)-5-hydroxy-1,2-dihydro-3H-benzo[e]indol-3-yl)methanone, 5-hydroxy-seco-cyclopropabenzaindoles, 5-hydroxy-seco-(2-methyl-cyclopropa)benzaindoles, 5-hydroxy-seco-cyclopropamethoxybenzaindoles, 5-amino-seco-cyclopropabenzaindoles, etoposide, teniposide, GL331, NPF, TOP53, NK611, tubulysin A, tubulysin B, tubulysin C, tubulysin G, tubulysin I, monomethyl auristatin E, monomethyl auristatin F, dolastatin 10, dolastatin 15, symprostastin 1, symprostastin 3, narciclasine, pancratistatin, 2-epi-narciclasine, narciprimine, calicheamicin α1, calicheamicin β1, calicheamicin γ1, calicheamicin δ1, calicheamicin ε, calicheamicin θ, calicheamicin T, diclofenac, aceclofenac, mefenamic acid, clonixin, piroxicam, meloxicam, tenoxicam, lornoxicam, baricitinib,

filgotinib, tofacitinib, upadacitinib, ruxolitinib, peficitinib, decemotinib, solcitinib, itacitinib, fostamatinib, SHR0302, leuco-methylene blue, leuco-methyl methylene blue, leuco-dimethyl methylene blue, leuco-toluidine blue, leuco-Azure A, leuco-Azure B, leuco-Azure C, leuco-Thionin, leuco-methylene violet, leuco-new methylene blue, leuco-Nile blue A, leuco-brilliant cresyl blue, firefly luciferin (D-Luciferin), umbelliferone, 4-trifluoromethylumbelliferone, 6,8-difluoro-4-methylumbelliferone, 7-hydroxycoumarin-3-carboxylic acid, 6,8-difluoro-7-hydroxy-5-methylcoumarin (DiFMU), 7-amino-4-methylcoumarin, 7-amino-4-chloromethylcoumarin, 3-O-methylfluorescein, 3-O-ethyl-5-carboxyfluorescein, 2,7-difluoro-3-O-methylfluorescein, 3-N-acetyl-rhodamine, 3-N-acetyl-dimethylsilarhodamine, 2,7-dibromo-3-N-acetyl-dimethylcarborhodamine, 3-N-acetyl-6-carboxyrhodamine, 2,7-difluoro-3-N-acetyl-rhodol, 3-O-(N,N-dimethyl-2-aminoethyl)-6-carboxyfluorescein, 2,7-dichloro-3-O-(N,N-dimethyl-2-aminoethyl)fluorescein, blackberry quencher (BBQ), black hole quencher 3 (BHQ3), 2-(2-hydroxyphenyl)quinazolin-4-one, 6-chloro-2-(5-chloro-2-hydroxyphenyl)quinazolin-4-one, and 6-bromo-2-(5-bromo-2-hydroxyphenyl)quinazolin-4-one, preferably A¹-OH or A²-NH-A³ is selected from 10-hydroxycamptothecin, 10-hydroxybelotecan, 10-hydroxygimatecan, 10-hydroxy-CKD-602, 10-hydroxy-BNP-1350, 10-hydroxy-sinotecan, topotecan, 7-ethyl-10-hydroxy-camptothecin (SN-38), 10-hydroxy-20-acetoxy-camptothecin, pyrrolbenzodiazepine, methotrexate, duocarmycin, CC-1065, doxorubicin, epirubicin, daunorubicin, pirarubicin, carminomycin, doxorubicin-N,O-acetal, 4-(bis(2-chloroethyl)amino)phenol, 4-(bis(2-bromoethylamino)phenol, 4-(bis(2-mesyethyl)amino)phenol, 4-((2-chloroethyl-2'-mesylethyl)amino)phenol, 5-hydroxy-seco-cyclopropabenzaindoles, 5-hydroxy-seco-(2-methyl-cyclopropa)benzaindoles, 5-hydroxy-seco-cyclopropamethoxybenzaindoles, 5-amino-seco-cyclopropabenzaindoles, etoposide, teniposide, GL331, NPF, TOP53, NK611, tubulysin A, tubulysin B, tubulysin C, tubulysin G, tubulysin I, monomethyl auristatin E, monomethyl auristatin F, dolastatin 10, dolastatin 15, symplostatin 1, symplostatin 3, narciclasine, pancratistatin, 2-epi-narciclasine, narciprimine, calicheamicin α 1, calicheamicin β 1, calicheamicin γ 1, calicheamicin δ 1, calicheamicin ϵ , calicheamicin θ , calicheamicin T, diclofenac, aceclofenac, mefenamic acid, clonixin, piroxicam, meloxicam, tenoxicam, lornoxicam, baricitinib, filgotinib, tofacitinib, upadacitinib, ruxolitinib, peficitinib, decemotinib, solcitinib, itacitinib, fostamatinib, SHR0302, leuco-methylene blue, leuco-methyl methylene blue, leuco-dimethyl methylene blue, leuco-toluidine blue, leuco-Azure A, leuco-Azure B, leuco-Azure C, leuco-Thionin, leuco-methylene violet, leuco-new methylene blue, leuco-Nile blue A, leuco-brilliant cresyl blue, firefly luciferin (D-Luciferin), umbelliferone, 4-trifluoromethylumbelliferone, 6,8-difluoro-4-methylumbelliferone, 7-hydroxycoumarin-3-carboxylic acid, 6,8-difluoro-7-hydroxy-5-methylcoumarin (DiFMU), 7-amino-4-methylcoumarin, 7-amino-4-chloromethylcoumarin, 3-O-methylfluorescein, 3-O-ethyl-5-carboxyfluorescein, 2,7-difluoro-3-O-methylfluorescein, 3-N-acetyl-rhodamine, 3-N-acetyl-dimethylsilarhodamine, 2,7-dibromo-3-N-acetyl-dimethylcarborhodamine, 3-N-acetyl-6-carboxyrhodamine, 2,7-difluoro-3-N-acetyl-rhodol, 3-O-(N,N-dimethyl-2-aminoethyl)-6-carboxyfluorescein, 2,7-dichloro-3-O-(N,N-dimethyl-2-aminoethyl)fluorescein, blackberry quencher (BBQ), black hole quencher 3 (BHQ3), 2-(2-hydroxyphenyl)quinazolin-4-one, 6-chloro-2-(5-chloro-2-hydroxyphenyl)quinazolin-4-one, and 6-bromo-2-(5-bromo-2-hydroxyphenyl)quinazolin-4-one.

8. A pharmaceutical or diagnostic composition comprising the compound according to any one of items 1 to 7, or a pharmaceutically acceptable salt, solvate, or ester thereof, and optionally a pharmaceutically acceptable carrier or excipient.

9. The pharmaceutical or diagnostic composition according to item 8, further comprising a second pharmaceutically active agent selected from a vascular disrupting agent, a cytotoxic chemotherapeutic agent and an immunomodulator.

10. The pharmaceutical or diagnostic composition according to item 9, wherein the second pharmaceutically active agent is selected from combretastatin A-4 (CA4), 3'-aminocombretastatin A-4, BNC105, ABT-751, ZD6126, combretastatin A-1, or prodrugs of the same (which includes but is not limited to combretastatin A-4 phosphate (CA4P), 3'-aminocombretastatin A-4 3'-serinamide (ombrabulin), combretastatin A-1 bisphosphate (CA1P), and BNC105 phosphate (BNC105P)), and pharmaceutically acceptable salts, solvates or esters of the same.

11. A compound according to any one of items 1 to 7, or a pharmaceutically acceptable salt, solvate, or ester thereof, for use in medicine.

12. A compound according to any one of items 1 to 7, or a pharmaceutically acceptable salt, solvate, or ester thereof, for use in the treatment, amelioration, prevention or diagnosis of a disorder selected from a neoplastic disorder; atherosclerosis; an autoimmune disorder; an inflammatory disease; a chronic inflammatory autoimmune disease; ischaemia; and reperfusion injury.

13. The compound for use according to item 12, wherein the neoplastic disorder is cancer which is preferably selected from acoustic neuroma, adenocarcinoma, angiosarcoma, basal cell carcinoma, bile duct carcinoma, bladder carcinoma, breast cancer, bronchogenic carcinoma, cervical cancer, chondrosarcoma, chordoma, choriocarcinoma, craniopharyngioma, cystadenocarcinoma, embryonal carcinoma, endotheliosarcoma, ependymoma, epithelial carcinoma, Ewing's tumor, fibrosarcoma, hemangioblastoma, leiomyosarcoma, liposarcoma, Merkel cell carcinoma, melanoma, mesothelioma, myelodysplastic syndrome, myxosarcoma, oligodendroglioma, osteogenic sarcoma, ovarian cancer, pancreatic cancer, papillary adenocarcinomas, papillary carcinoma, pinealoma, prostate cancer, renal cell carcinoma, retinoblastoma, rhabdomyosarcoma, sebaceous gland carcinoma, seminoma, squamous cell carcinoma, sweat gland carcinoma, synovioma, testicular tumor, Wilms' tumor, adrenocortical carcinoma, urothelial carcinoma, gallbladder cancer, parathyroid cancer, Kaposi sarcoma, colon carcinoma, gastrointestinal stromal tumor, anal cancer, rectal cancer, small intestine cancer, brain tumor, glioma, glioblastoma, astrocytoma, neuroblastoma, medullary carcinoma, medulloblastoma, meningioma, leukemias including acute myeloid leukemia, multiple myeloma, acute lymphoblastic leukemia, liver cancer including hepatoma and hepatocellular carcinoma, lung carcinoma, non-small-cell lung cancer, small cell lung carcinoma, lymphangioendotheliosarcoma, lymphangiosarcoma, primary CNS lymphoma, non-Hodgkin lymphoma, and classical Hodgkin's lymphoma, preferably colon cancer, rectal cancer, small intestine cancer, brain tumor, leukemia, liver cancer, lung cancer, lymphoma, basal cell carcinoma, breast cancer, cervical cancer, melanoma, ovarian cancer, pancreatic cancer, and squamous cell carcinoma.

14. Use of a compound according to any one of items 1 to 7, or a pharmaceutically acceptable salt, solvate, or ester thereof, for the manufacture of a medicament for the treatment, amelioration, prevention or diagnosis of a disorder selected from a neoplastic disorder; atherosclerosis; an autoimmune disorder; an inflammatory disease; a chronic inflammatory autoimmune disease; ischaemia; and reperfusion injury.

15. Use of a compound according to item 14, or a pharmaceutically acceptable salt, solvate, or ester thereof, wherein the neoplastic disorder is cancer which is preferably selected from acoustic neuroma, adenocarcinoma, angiosarcoma, basal cell carcinoma, bile duct carcinoma, bladder carcinoma, breast cancer, bronchogenic carcinoma, cervical cancer, chondrosarcoma, chordoma, choriocarcinoma, craniopharyngioma, cystadenocarcinoma, embryonal carcinoma, endotheliosarcoma, ependymoma, epithelial carcinoma, Ewing's tumor, fibrosarcoma, hemangioblastoma, leiomyosarcoma, liposarcoma, Merkel cell carcinoma, melanoma, mesothelioma, myelodysplastic syndrome, myxosarcoma, oligodendroglioma, osteogenic sarcoma, ovarian cancer, pancreatic cancer, papillary adenocarcinomas, papillary carcinoma, pinealoma, prostate cancer, renal cell carcinoma, retinoblastoma, rhabdomyosarcoma, sebaceous gland carcinoma, seminoma, squamous cell carcinoma, sweat gland carcinoma, synovioma, testicular tumor, Wilms' tumor, adrenocortical carcinoma, urothelial carcinoma, gallbladder cancer, parathyroid cancer, Kaposi sarcoma, colon carcinoma, gastrointestinal stromal tumor, anal cancer, rectal cancer, small intestine cancer, brain tumor, glioma, glioblastoma, astrocytoma, neuroblastoma, medullary carcinoma, medulloblastoma, meningioma, leukemias including acute myeloid leukemia, multiple myeloma, acute lymphoblastic leukemia, liver cancer including hepatoma and hepatocellular carcinoma, lung carcinoma, non-small-cell lung cancer, small cell lung carcinoma, lymphangioendotheliosarcoma, lymphangiosarcoma, primary CNS lymphoma, non-Hodgkin lymphoma, and classical Hodgkin's lymphoma, preferably colon cancer, rectal cancer, small intestine cancer, brain tumor, leukemia, liver cancer, lung cancer, lymphoma, basal cell carcinoma, breast cancer, cervical cancer, melanoma, ovarian cancer, pancreatic cancer, and squamous cell carcinoma.

16. A method of treating, ameliorating, preventing or diagnosing a disorder selected from a neoplastic disorder; atherosclerosis; an autoimmune disorder; an inflammatory disease; a chronic inflammatory autoimmune disease; ischaemia; and reperfusion injury, wherein an effective amount of a compound according to any one of items 1 to 7, or a pharmaceutically acceptable salt, solvate, or ester thereof, is administered to a patient in need thereof.

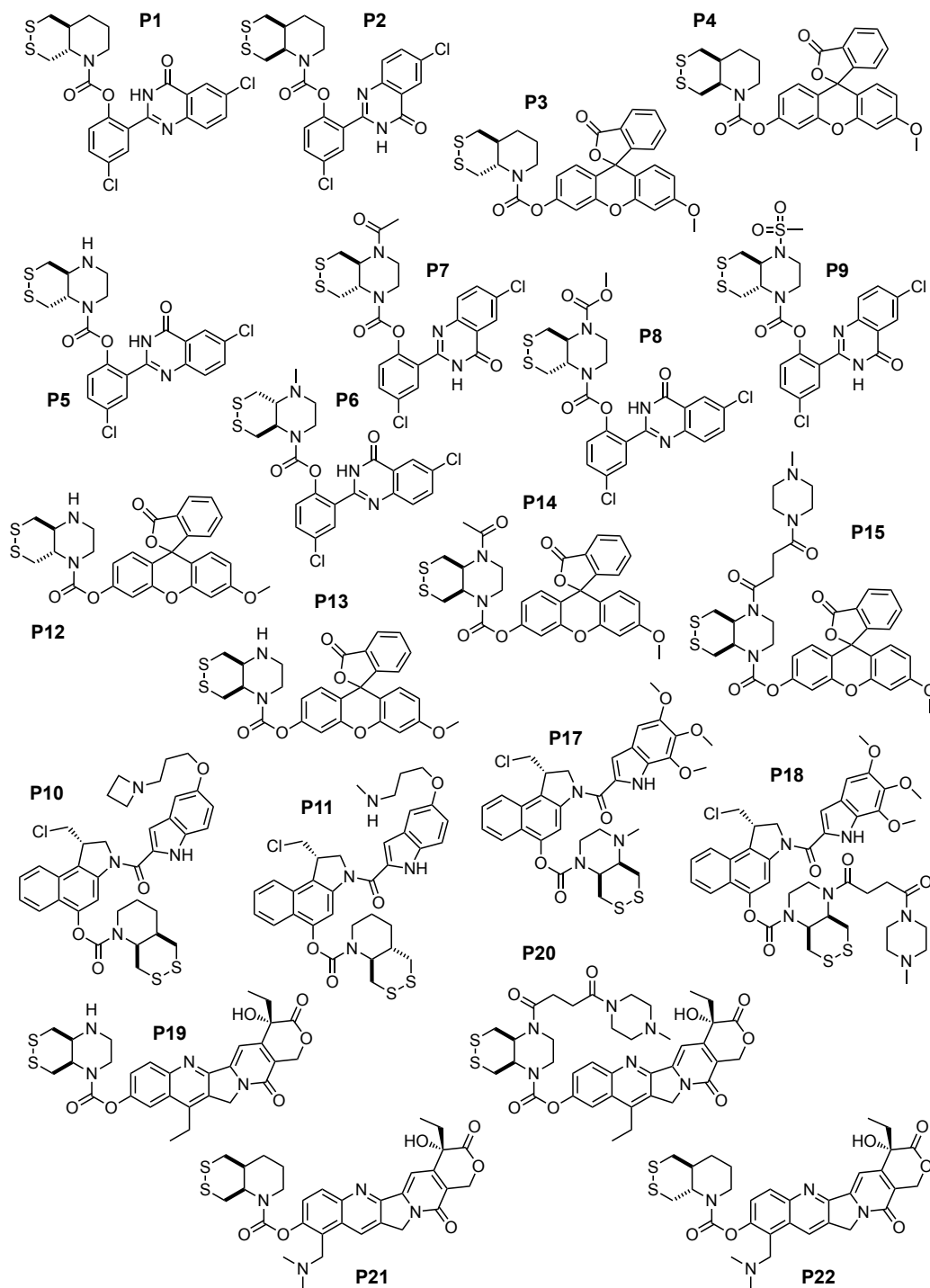
17. A method according to item 16, wherein the neoplastic disorder is cancer which is preferably selected from acoustic neuroma, adenocarcinoma, angiosarcoma, basal cell carcinoma, bile duct carcinoma, bladder carcinoma, breast cancer, bronchogenic carcinoma, cervical cancer, chondrosarcoma, chordoma, choriocarcinoma, craniopharyngioma, cystadenocarcinoma, embryonal carcinoma, endotheliosarcoma, ependymoma, epithelial carcinoma, Ewing's tumor, fibrosarcoma, hemangioblastoma, leiomyosarcoma, liposarcoma, Merkel cell carcinoma, melanoma, mesothelioma, myelodysplastic syndrome, myxosarcoma, oligodendroglioma, osteogenic sarcoma, ovarian cancer,

pancreatic cancer, papillary adenocarcinomas, papillary carcinoma, pinealoma, prostate cancer, renal cell carcinoma, retinoblastoma, rhabdomyosarcoma, sebaceous gland carcinoma, seminoma, squamous cell carcinoma, sweat gland carcinoma, synovioma, testicular tumor, Wilms' tumor, adrenocortical carcinoma, urothelial carcinoma, gallbladder cancer, parathyroid cancer, Kaposi sarcoma, colon carcinoma, gastrointestinal stromal tumor, anal cancer, rectal cancer, small intestine cancer, brain tumor, glioma, glioblastoma, astrocytoma, neuroblastoma, medullary carcinoma, medulloblastoma, meningioma, leukemias including acute myeloid leukemia, multiple myeloma, acute lymphoblastic leukemia, liver cancer including hepatoma and hepatocellular carcinoma, lung carcinoma, non-small-cell lung cancer, small cell lung carcinoma, lymphangioendotheliosarcoma, lymphangiosarcoma, primary CNS lymphoma, non-Hodgkin lymphoma, and classical Hodgkin's lymphoma, preferably colon cancer, rectal cancer, small intestine cancer, brain tumor, leukemia, liver cancer, lung cancer, lymphoma, basal cell carcinoma, breast cancer, cervical cancer, melanoma, ovarian cancer, pancreatic cancer, and squamous cell carcinoma.

18. A method of predicting the suitability of a compound having the formula (I) as defined in any one of items 1 to 7, or a pharmaceutically acceptable salt, solvate, or ester thereof, for treating a patient who is suffering from a disorder selected from a neoplastic disorder; atherosclerosis; an autoimmune disorder; an inflammatory disease; a chronic inflammatory autoimmune disease; ischaemia; and reperfusion injury, wherein the method comprises:

- (i) obtaining a sample from the patient;
- (ii) contacting the sample with a compound having the formula (I) as defined in any one of items 1 to 7, or a pharmaceutically acceptable salt, solvate, or ester thereof, wherein A^1 is selected such that A^1-OH is a diagnostic or theranostic agent or A^2 and A^3 are independently selected such that A^2-NH-A^3 is a diagnostic or theranostic agent; and
- (iii) detecting the presence or absence of A^1-OH or A^2-NH-A^3 .

Illustrative embodiments of the compound having formula (I) also include



It is understood that all combinations of the above definitions and preferred definitions are envisaged by the present inventors.

The examples **1-15** include the following therapeutic designs:

1 releases a DNA-alkylating nitrogen mustard cargo subunit of a type which is of interest especially for cancer therapy. The released bis(2-haloethyl)aniline species will feature similar activity to PR-104's bioactive alkylating metabolite PR-104M whereas the intact species **1** will not be as potently alkylating as the released cargo, since unmasking the electron-donating phenol in *para* to the aniline nitrogen increases electronic density and alkylating reactivity (similar principles are known for PR-104 and a range of related prodrugs).²⁶² Note that a range of leaving groups (halogens -Cl, -Br, -I or other leaving groups such as -OS(O)₂CH₃) can be used as the halogen substituents of the 2-haloethyl groups without

compromising functionality, and/or an aniline nitrogen (requiring the use of a spacer subunit) could be used instead of the phenolic hydroxyl as the unmasked group of the cargo, while remaining within the scope of a compound having the formula (I).

4 and **9** are similar to compound **P4** in that they release cargo subunits that are analogues of 5-hydroxy-*seco*-cyclopropabenzaindole, which (when their phenolic hydroxyl is unmasked) can then undergo Winstein cyclisation to the active DNA-alkylating cyclopropabenzaindoles (CBIs), which are of interest especially for cancer therapy, whereas no Winstein cyclisation can take place until the phenol is unmasked. In this way only the released cargo (and not the proagents) will be bioactive (similar principles are known for a range of related prodrugs).²⁶³ Note that a range of analogues of 5-hydroxy- or 5-amino-*seco*-cyclopropabenzaindoles or related cargos with various substitution motifs (such as the inclusion of the dimethylamino substituent on **9** to enhance solubility and DNA-binding potency) could be used, while remaining within the scope of a compound having the formula (I).

11 releases a cargo subunit that is the Amaryllidaceae-type alkaloid pancratistatin. Amaryllidaceae-type alkaloids (such as pancratistatin or narciclasine) are metabolism-affecting drugs that have shown utility in disease indications featuring metabolic deregulation, from cancer to chronic inflammation.^{264,265} The cargo release process (following triggering of the disulfide trigger subunit of **11**) removes steric hindrance and so allows binding of the lycorane to its molecular target, such that only the released cargo is bioactive. Note that a range of lycorane-type alkaloids with various substitution motifs could be used, while remaining within the scope of a compound having the formula (I).

14 releases a cargo subunit that is SN-38, the active metabolite of the camptothecin class topoisomerase inhibitor irinotecan, a class which also contains the agent topotecan. As known for irinotecan, blocking the phenol removes bioactivity of the proagent so **14** will be biologically inactive except if triggered to release cargo; note that a range of similar cargo structures (e.g. modifying the ethyl group at the 7-position, or introduction of solubility and potency enhancing groups such as (dimethylamino)methyl as seen in topotecan) could be used, as is known for a range of related prodrugs,²⁶² while remaining within the scope of a compound having the formula (I).

It is illustrated by **1**, **4**, **9**, **11** and **14** that a broad range of bioactive phenolic cargos with a range of different bioactivity mechanisms and disease indication scopes can therefore be used, including with extensive structural substitutions, within the scope of the invention to deliver cargo-release-based activation of proagent bioactivity, i.e. functional prodrugs dependent upon triggering of the key disulfide of a compound having the formula (I).

13 releases an amine cargo subunit that is a tubulin-inhibiting auristatin derivative, of particular interest for cancer therapy and for neoangiogenic vasculopathies. A range of auristatins (and related peptide tubulin binders such as dolastatins and tubulysins) have been used in prodrugs where bioactivity is suppressed by conjugation of the agent to a large but cleavable trigger and/or trigger+spacer subunit,²⁶⁶ then restored upon its removal. Note that a range of such agents with various substitution patterns (including monomethyl auristatin E, monomethyl auristatin F, dolastatin or symprostatin) could be used; and/or that beyond the 3-fluoro-4-hydroxybenzyl alcohol spacer depicted in **13**, a range of spacers could instead be used, while remaining within the scope of a compound having the formula (I), to activate cytotoxic activity upon triggering of the proagent.

15 releases an amine cargo subunit that is of the anthracycline class of topoisomerase-inhibitors. This class includes doxorubicin, daunorubicin and idarubicin, and is of particular interest for cancer therapy. Basicity of the aliphatic amine of doxorubicin and its analogues is important for bioactivity; its carbamylation in **15** blocks bioactivity, but bioactivity can be restored by disulfide triggering followed by spacer-mediated release of the doxorubicin analogue.²⁶⁶ Note that a range of related cargos with various substitution motifs and/or related spacers could instead be used, while remaining within the scope of a compound having the formula (I), to activate cytotoxic activity upon triggering of the proagent.

It is illustrated by **13** and **15** that a broad range of bioactive amine cargos with different bioactivity mechanisms and disease indication scopes can therefore be used in conjunction with a range of spacers, each with optional extensive structural substitutions, while remaining within the scope of the invention to deliver cargo-release-based activation of proagent bioactivity, i.e. functional prodrugs dependent upon triggering of the key disulfide of a compound having the formula (I).

The examples **1-15** include the following diagnostic designs:

2 releases a fluorescent precipitating phenolic cargo subunit with large Stokes shift and green emission; **3**, **7** and **10** release fluorescent phenolic cargos with small Stokes shifts and UV, cyan, or orange emission; all the proagents **2**, **3**, **7** and **10** are nonfluorescent due to masking of the phenol groups

(either due to blocking excited-state intramolecular proton transfer in **2**, or reducing electron-donating capacity in **3**, or blocking the opening of the spirolactone in **7** and **10**); and all these designs provide a signal turn-on upon cargo release stimulated by triggering of the trigger subunits (and similar principles are known for a range of related probe cargos;²⁶⁷ they are thus diagnostic fluorescence probes that may be useful in a variety of diagnostic purposes. It is also illustrated that spacer subunits can be optionally included (**7**), and that a range of cargos [e.g. **2** (2-hydroxyphenyl)quinazolin-4(3*H*)-one), **3** (coumarin), **7** and **10** (xanthene fluorophores of the fluorescein type)] with a range of structures and diagnostic properties are possible while remaining within the scope of a compound having the formula (I).

5 releases a phenolic cargo subunit that is D-luciferin, the substrate of firefly luciferase enzyme, whereas the intact probe **5** is too bulky to be a substrate of luciferase. Therefore **5** is a disulfide-reduction-triggered diagnostic luminescence probe allowing detection by bioluminescence in the presence of luciferase, which may be useful as a diagnostic for reductive probe turnover with ultra-low background signal (high sensitivity). Note that a range of luciferins for different luciferases and with different structural modifications are known and could also be used as cargo subunits²⁶⁸ while remaining within the scope of a compound having the formula (I).

8 releases a phenolic cargo subunit that is a functional analogue of Black Hole Quencher 3 (BHQ3) which has fluorescence quenching and photoacoustic signal generation properties.²⁷⁰ The proagent **8** is non-signal-generating and non-quenching due to masking of the key electron-donating phenol group, while the released cargo has no masking of the phenol and therefore has fluorescence quenching and photoacoustic signal generation activity, thus **8** functions as a multimodal diagnostic proagent. Note that similar unmasking-based activity turn-on principles are known for a range of related compounds including other quenchers, which could also be used as cargo subunits while remaining within the scope of a compound having the formula (I).

12 releases a spacer-cargo system that fragments to release an aniline cargo subunit that is a silarhodamine derivative which has fluorescence and photoacoustic signal generation properties.¹ The proagent **12** is non-signal-generating and non-fluorescent due to the masking of the amine group by carbamylation, while the released cargo silarhodamine is active in both diagnostic modalities. Note that a range of related or analogous cargos with various substitution motifs (such as a range of aniline-based fluorophores or photoacoustics dyes, including rhodols and rhodamines) could also be used as cargo subunits along the same design principles while remaining within the scope of a compound having the formula (I).

It is illustrated by **2**, **3**, **5**, **7**, **8**, **10** and **12** that a broad range of diagnostically active phenol or amine cargos, enabling a range of structures and diagnostic detection methods, can therefore be used, including with extensive structural substitutions, within the scope of the invention, to deliver cargo-release-based activation of proagent diagnostic activity, i.e. functional diagnostic probes dependent upon triggering of the key disulfide of a compound having the formula (I).

The examples **1-15** also include the theranostic design **6** that releases a cargo subunit that is *leuco*-methylene blue, a reduced form of the theranostic compound methylene blue which after release in biological media is spontaneously converted to methylene blue (similar principles are known for a range of related prodrugs). Methylene blue can be useful therapeutically including as a photosensitiser in photodynamic therapy (e.g. of the autoimmune disorder psoriasis, or of cancers) and/or as a redox-active selective toxin (e.g. against malaria parasite); as well as diagnostically (e.g. as a fluorescent agent or a photoacoustic dye); therefore being capable of theranostic activity.²⁷² Note that a range of functionally and structurally related compounds (e.g. phenoxazines) can also be used as cargo subunits in theranostics following the same design principles while remaining within the scope of a compound having the formula (I).

Various modifications and variations of the invention will be apparent to those skilled in the art without departing from the scope of the invention. Although the invention has been described in connection with specific preferred embodiments, it should be understood that the invention as claimed should not be unduly limited to such specific embodiments. Indeed, various modifications of the described modes for carrying out the invention which are obvious to those skilled in the relevant fields are intended to be covered by the present invention.

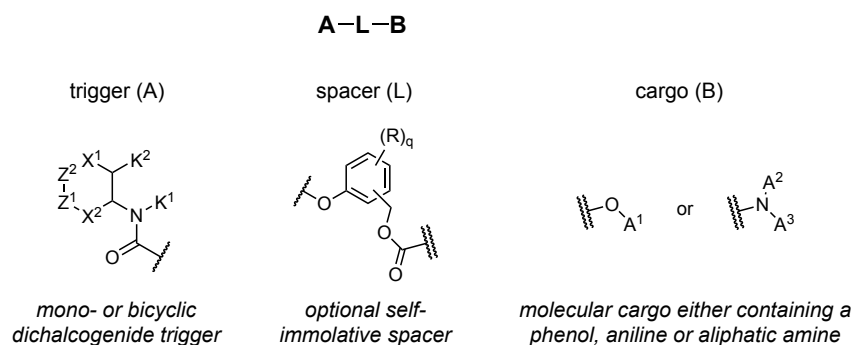
For the full text including Claims, Detailed Description of the Invention, Examples, Figures and General Principles, see the full published patent application (142 pages) available online at <https://patentscope.wipo.int/search/de/detail.jsf?docId=WO2022200347>.

3.2.4 Cyclic dichalcogenide probes and prodrugs for use in diagnostics and therapeutics

This chapter was published as an international PCT patent application through the EPO/WIPO.

Agency	World Intellectual Property Organization
Title	<i>Dichalcogenide prodrugs</i>
Publication Number	WO 2022/214598 A1
Applicant	Ludwig-Maximilians-Universität München
Inventors	Oliver Thorn-Seshold, Lukas Zeisel, Jan G. Felber
Agent	Vossius & Partner Patentanwälte mbH, München
Priority Filing	Apr 7 th , 2021
Publication date	Oct 13 th , 2022
Full text at	https://patentscope.wipo.int/search/de/detail.jsf?docId=WO2022214598

Structure of the patented chemical space



Description of the chemical space

The patent application *dichalcogenide prodrugs* covers *trigger-cargo* constructs of the general formula **A-L-B**, where **A** is a reducible trigger unit based on a mono- or bicyclic selenenylsulfide or diselenide; **L** is a bond or self-immolative spacer; and **B** is a molecular cargo containing a phenol, aniline or aliphatic amine, where the trigger/linker is covalently attached *via* the cargo's oxygen/nitrogen atom.

The simplest possible trigger structures (**A**) are the **SeS60** and **SSe60** units (see **chapter 3.1.3**), where $Z^1=S$; $Z^2=Se$ or $Z^1=Se$; $Z^2=S$ and $K^1=CH_3$; $K^2=H$. The general formula of **A** is described in the patent to cover the following structural variations: (i) Z^1 and Z^2 ; X^1 and X^2 can be chosen such that any optionally substituted 1,2-thiaselenane, 1,2-diselenane, 1,2-thiaselenepane or 1,2-diselenepane is covered; (ii) K^1 and K^2 can be chosen such that monocyclic dichalcogenides with optional amine substitution by alkylation with small solubilization handles or targeting groups are covered; (iii) K^1 and K^2 can also be linked and chosen such that bicyclic ring system with fused 5-, 6- or 7-membered saturated heterocycles are covered; (iv) the optional second nitrogen atom in the backbone ring can also be substituted by alkylation, acylation or sulfonylation with elongated side chains. By varying these different parameters, the trigger units **H-SeSe66C** and **H-SeSe66T** are also covered (see **chapter 3.1.4**).

While phenolic cargos can be released by reduction in direct conjugates of **A** and **B**, a molecular spacer **L** must be used for the liberation of amine cargos and can be used for phenols. Rationally choosing $(R)_q$ tunes the spacer elimination and fragmentation rate.

Molecular cargos are suitable as **B** if they contain a phenol, aniline, or aliphatic amine, and covalent attachments at the oxygen/nitrogen modulate their spectral properties (dyes) or bioactivities (drugs). Several mechanisms are known where such modulation can be exploited to create activatable diagnostic tools or therapeutic or theranostic prodrugs that are the subject to this patent application.

Summary

Probes and prodrugs based on fused bicyclic 1,2-dithianes target vicinal dithiol-type bioreductants (see **chapter 3.1.2**), which we exploited to develop diagnostic imaging agents, reducible linkers (see **chapter 3.1.4**) and bioreductive prodrugs for the Trx system (see **chapter 3.2.2**). We covered the chemical space around fused bicyclic disulfide units for use in diagnostic or therapeutic applications in a first patent application (see **chapter 3.2.3**). Based on a similar rationale but slightly adapted chemical design, we used desymmetrized cyclic dichalcogenides, namely 1,2-thiaselenane **SeS60**, as chemocompatible trigger units for selective reduction by the unique Cys⁴⁹⁷Sec⁴⁹⁸ redox-active site found in TrxR. We validated the first selective diagnostic tool for TrxR in cells, which is based on a fluorogenic **SeS60**-type probe, and performed a pilot high-throughput screen to unravel new chemical inhibitors (see **chapter 3.1.3**). Both the diagnosis of TrxR-related redox states and the development of potential anti-cancer agents based on TrxR inhibition are of high commercial relevance.

This second patent application is structurally and conceptually similar to *disulfide-based prodrug compounds* (see **chapter 3.2.3**) but now aimed to cover the chemical space around reducible *trigger-cargo* constructs based on mono- or bicyclic dichalcogenides with at least one Se atom. We envisioned that these alternative motifs are generally applicable to activate a large body of potential diagnostic, therapeutic, or theranostic agents upon reduction.

We copied the general formula **A-L-B** from our first patent application with the aim to (i) cover a large proportion around potential mono- and fused bicyclic dichalcogenide structures within the patentable space, including further substitutions at either of the potential nitrogen atoms in the backbone; and (ii) to allow multiple molecular cargos for diagnostic or therapeutic purposes (see **chapter 3.2.3**). We provided a panel of illustrative embodiments of potential constructs to emphasize the flexible combinations of trigger and cargos and another set of 8 illustrative examples that we experimentally evaluated to show synthetic accessibility of probes and prodrugs of the formula **A-L-B**.

The invention presented in this patent application relates to probes and prodrugs that specifically release their active components in the presence of TrxR. Under certain pathological conditions or disease states, cellular homeostasis, including its TrxR activity, may be dysregulated. The patent application claims the use of probes and prodrugs of the formula **A-L-B** as diagnostics or therapeutic/theranostic agents to diagnose, treat or prevent such a diseased state. It further covers the structure, manufacturing, and use of prodrugs or selective cellular imaging agents, such as **RX1**, that can be used for high-throughput screening to characterize existing and novel TrxR inhibitors in cellular settings. We think that the first selective fluorogenic probe and related constructs provide a promising tool for future developments that is of high commercial interest.

Dichalcogenide prodrugs

Technical Field

The present application relates to a compound having the formula (I). The compound having the formula (I) is capable of releasing a molecular cargo in the presence of a reductant and is thus suitable for diagnosing or quantifying the presence or activity of the reductant; and for treating, ameliorating, preventing or diagnosing a disorder selected from a neoplastic disorder; atherosclerosis; an autoimmune disorder; an inflammatory disease; a chronic inflammatory autoimmune disease; ischaemia; and reperfusion injury.

In particular, the molecular cargo can be a therapeutic or diagnostic agent. In particular, the reductant can be a biological oxidoreductase and/or its redox effector protein which may be catalytically active. The invention further relates to a pharmaceutical or diagnostic composition comprising the same.

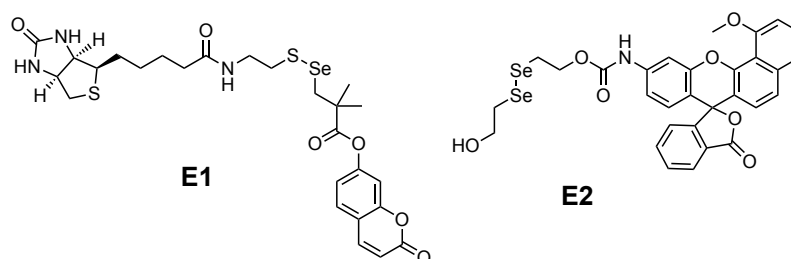
Prior Art

Dithiol/disulfide-exchange redox reactions are critical in a great number of biological pathways. Often, these are coordinated through conserved, specialised networks of oxidoreductases that perform redox reactions upon or using disulfides and/or thiols. The thioredoxin reductase – thioredoxin (TrxR–Trx) system, and the glutathione reductase – glutathione – glutaredoxin (GR–GSH–Grx) system, are two of the central redox systems; other key reductive enzymes/proteins include but are not limited to peroxiredoxins, glutathione peroxidases, glutathione-S-transferases, methionine sulfoxide reductase, and protein disulfide isomerases (PDIs).²⁴³ Such redox systems drive reactions vital to cellular metabolism, and can also regulate protein activity, protein–protein interactions, and protein localisation by reversible dithiol/disulfide-type reactions.²⁴⁴

To better investigate and understand biological processes, it is of great interest to develop specific methods to image or quantify the activity of biological species, or otherwise to respond to their activity. Therefore, it was an object of the present invention to provide compounds which have high selectivity for an oxidoreductase or redox effector protein, and which can be reduced by the disulfide reductive activity of that enzyme and thus release a molecular cargo. This has been a longstanding goal of research in the field of cellular dithiol/disulfide-exchange redox reactions. In this field, a significant challenge for chemical probe development is to ensure that a probe is specific for being reduced by the targeted species and is not significantly reduced by any other reducing species in the cell. Therefore, to selectively probe one of the species TrxR, GR, Trx, or Grx, a compound must not be activated by any of the others or by GSH. This is difficult because these reductants can perform similar chemical reactions, and because the most active of these reductants have the lowest cellular concentrations (TrxR and GR have nM cellular concentrations; Trx and Grx have μ M concentrations) while the least active reductant GSH is the most concentrated (mM).

These reducing species all act upon disulfides, so most reduction-activated chemical probes in the prior art have used disulfides as reduction-sensing motifs. Such disulfides have been reviewed elsewhere (see **chapter 3.1.1.** and **3.1.2.**).

Probes based on dichalcogenides other than disulfides (such as selenenylsulfides –RSeSR–, and diselenides –RSeSeR–) are very rare in the literature. The reports that exist do not teach towards features that determine their reductant selectivity, and the performance reported for the compounds that do exist is often contradictory or inconclusive. The prior art in cargo-releasing dichalcogenide reduction probes are **E1-E2**:

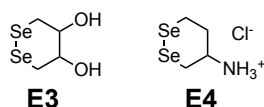


Suarez *et al.* reported linear selenenylsulfide-based reductively-activated fluorogenic probe **E1**.¹⁷³ This probe was stated to be a biological sensor for H₂S, developed to have "remarkable reactivity and selectivity" for H₂S. **E1** was not tested against any redox enzymes or proteins, nor were controls run for

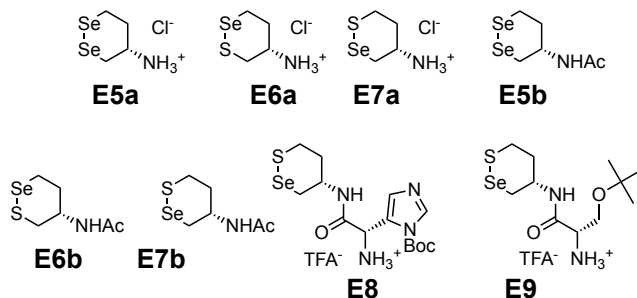
thiolysis of the phenolic ester by 50 μM Na_2S . The report also teaches a linear topology of the selenenylsulfide.

Mafireyi *et al.* reported linear diselenide-based reductively-activated fluor

ogenic probe **E2**.¹⁷⁶ This is an aniline carbamate linear diselenide (therefore will have slow rates of cyclisation-driven release due to the poor leaving-group nature of the aniline). While it was claimed as selective for TrxR1, no other redox proteins were actually tested; and in fact a low concentration of GSH gave strong signal turn-on within 20 minutes (**Fig S1e** in that paper). Therefore this report does not teach towards cyclic dichalcogenides; also it does not teach towards phenol-releasing probes; and it does not teach about stability against GSH or how to ensure it.



The molecules **E3** and **E4** were reported by Li¹⁷⁷ and were investigated for their reduction in an *in vitro* screen to provide a far-limit case as part of investigations into interactions between disulfides and TrxR. It was reported that **E4** was resistant to TrxR, and that **E3** was processed by TrxR, therefore the report teaches that there is no clear relationship between structure and capacity to act as a TrxR substrate in a cell-free setting ("the reduction... is a little bit complicated"). The molecules **E3-E4** are completely reversibly reducible/oxidisable, and therefore do not indicate how an irreversibly-triggered molecule would perform in this assay; also there is no suggestion that such six-membered cyclic diselenides could be applied in cells for any purpose. This report also mentions that phenol-releasing carbamates (TRFS2 in that report) "hydrolyzed spontaneously in aqueous buffer,".



Cyclic 6-membered selenenylsulfides that are known in the literature are reported by Arai *et al.*,²⁷³ including the interrelated series of molecules **E6a**, **E6b**, **E7a**, **E7b**, **E8**, **E9**, as well as diselenides **E5a**, **E5b**. These molecules were intended as *mimics* of the SecCys active site of mammalian TrxR, that could be studied by chemical methods to gain understanding of the mechanism by which TrxR operates as an enzyme. Again it will be noted that the molecules are completely reversibly reducible/oxidisable.

Therefore there remain numerous unsolved challenges, including to: (i) determine what, if any, utility dichalcogenide species other than disulfides can have in a biological setting; (ii) design probe or prodrug systems that release a molecular cargo upon reductive triggering and are selective for being triggered by a particular cellular reductant, i.e. are shown to resist reduction by the other major cellular reductants (e.g. GSH, TrxR, Trx, Grx, or GR etc. as appropriate); (iii) ensuring that the probe/prodrug design is hydrolytically stable; and (iv) designing probe or prodrug systems that release a molecular cargo upon reductive triggering and are selective for being triggered under pathological conditions. If these challenges can be solved, highly valuable probes or prodrugs to report on the activity of those reductants, or to respond to this activity by releasing a drug, would be created.

Under pathological conditions, homeostasis in these redox systems and in their target proteins is significantly dysregulated. This has been particularly shown in diseases such as cancer, inflammatory diseases such as autoimmune disorders, under acute stress such as reperfusion injury, and under other chronic conditions such as cardiovascular disease.^{252,253} Such dysregulation has also been studied in the context of disease-associated biomarkers, such as hypoxia. Hypoxia is a pathology-associated feature, prevalent in cancer and inflammation, that is tightly correlated with significant biochemical changes including oxidoreductase dysregulation, many of which rely on the hypoxia-dependent transcription factor HIF-1. Oxidoreductase or redox effector protein dysregulation may be reflected in a combination of changes to their expression level, enzymatic activity, redox poise (the ratio of oxidised to reduced form of the oxidoreductase or redox effector protein), localisation, and/or other parameters.

For example, under pathological conditions, the TrxR—Trx and GR—GSH—Grx systems act as repair systems, counteracting acute cellular damage by oxidants, and re-normalising redox imbalances e.g. from oxygen depletion (hypoxia) or from the switching of metabolic pathways due to cellular stress (e.g. the Warburg Effect in cancer;^{101,254} therefore cells affected by pathologies that require such repair and renormalisation are often found to upregulate expression levels and activity of these oxidoreductase and redox effector protein systems, and shift their redox poise.²⁵⁵ This dysregulation has been particularly studied in the context of cancer, where for the example of Trx it has been shown that cycling hypoxia, which is a hallmark of most tumors, upregulates Trx expression levels²⁵⁶ that Trx overexpression contributes to hallmarks of cancer including increased proliferation and angiogenesis, and evasion of apoptosis²⁵⁷ and that Trx overexpression in tumors contributes to chemoresistance and is associated to poor patient survival.²⁵⁸ Dysregulated function is also particularly studied in the context of inflammatory diseases, since many central players in inflammation (NFκB, TNF-α, Keap1, Nrf2) are regulated by these oxidoreductases or redox effector proteins, and processes from inflammasome activation to immune cell chemotaxis have also been shown to depend on these oxidoreductases or redox effector proteins.^{259,260}

The disease-correlated nature of these dysregulated states of oxidoreductases and redox effector proteins - particularly of Trx, TrxR, and PDIs - makes them promising targets for diagnostic or therapeutic applications using diagnostic or therapeutic drugs that target these oxidoreductases or redox effector proteins. For example, the TrxR-inhibiting drug auranofin is FDA-approved for use in the inflammatory disease, rheumatoid arthritis.^{101,243} In this context, a probe or prodrug system to release a molecular cargo, that is selectively triggered by one of these oxidoreductases or redox effector proteins, would be very valuable. Similarly, substantial efforts have been made to use the disease-correlated feature, hypoxia, both as a diagnostic marker and for therapeutic exploitation, for example by using diagnostic and therapeutic drugs that target hypoxia, which has been extensively reviewed.^{261,274}

Therefore, it was a further object of the present invention to provide compounds which may have high selectivity for an oxidoreductase or redox effector protein in a pathologically dysregulated state, and can be reduced by the disulfide reductive activity of that oxidoreductase or effector protein and thus release a molecular cargo after reduction. It was a further object of the present invention to provide compounds which may have high selectivity for pathologically dysregulated redox states and/or for cells in hypoxia and/or cells with an activated hypoxic response pathway.

In conclusion therefore, objects of the present invention were to provide compounds which are capable of releasing a molecular cargo after reductive activation, and which

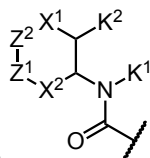
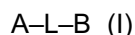
- (A) are suitable for diagnosing, quantifying, or responding to reductive activity of one or more selected oxidoreductases or redox effector proteins; and/or
- (B) are suitable for diagnosing, treating, ameliorating or preventing a disorder associated with redox activity; and/or
- (C) are suitable for diagnosing, treating, ameliorating or preventing a disorder selected from a neoplastic disorder; atherosclerosis; an autoimmune disorder; an inflammatory disease; a chronic inflammatory autoimmune disease; ischaemia; and reperfusion injury, particularly cancer; and/or
- (D) are suitable for diagnosing, treating, ameliorating or preventing a disorder associated with a dysregulated redox state and/or with hypoxia and/or with activation of the hypoxic response pathway.

Note that it is possible, and in many cases it is desirable, that one or more of these objectives should be fulfilled by the same compound; for example, a single compound of the invention may fulfil objectives A and B simultaneously; while another compound of the invention may fulfil objectives A, B, C and D simultaneously, etc.

Summary of the Invention

The invention is summarized in the following items:

1. A compound having the formula (I)

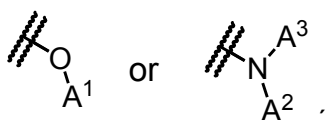


wherein

A is represented by

 denotes the attachment point of A to L;

L is a bond or a self-immolative spacer;



B is represented by



denotes the attachment point of B to L;

A¹ is selected such that A¹-OH is a therapeutic, diagnostic or theranostic agent which contains an -OH group that is attached to a 5- or 6-membered aromatic or heteroaromatic ring;

A² and A³ are independently selected such that A²-NH-A³ is a therapeutic, diagnostic or theranostic agent which contains an -NH₂ or -NH- moiety;

K¹ is selected from -C₁₋₄-alkyl optionally substituted by W¹;

K² is selected from -H, -O-R^j, and -O-R^k; or

K¹ and K² are bonded together and K¹ and K² represent -X³-Y-X-, wherein X³ is bonded to N and X is bonded to C;

X is selected from -N(R^a)-, -N(R^b)-, -CR^c₂- and -O-;

X¹ is -(CR^d)_m-;

X² is -(CR^e)_n-;

X³ is -CR^f₂-;

Y is -(CR^g)_p-;

Z¹ and Z² are independently selected from S or Se such that either Z¹ is Se and Z² is S, or Z¹ is S and Z² is Se, or Z¹ and Z² are both Se;

W is independently from -OH, -C(O)-N(R^h)(Rⁱ), -N(R^h)(Rⁱ), -PR^x₃⁺, -C(O)-4-(morpholine), -C(O)-1-(piperazine), -C(O)-1-(4-methylpiperazine), -C(O)-1-(4-ethylpiperazine), and a heterocyclic group selected from azetidin-1-yl, pyrrolidin-1-yl, piperidin-1-yl, piperazin-1-yl, 4-methylpiperazin-1-yl, 4-ethylpiperazin-1-yl, 4-(2-hydroxyethyl)piperazin-1-yl, or morpholino, wherein that heterocyclic group is attached to the -C₁₋₄-alkyl or -(C₂₋₄-alkylene)- group via the N atom;

W¹ is independently selected from -OH, -C(O)-N(R^h)(Rⁱ), -N(R^h)(Rⁱ), -PR^x₃⁺, -C(O)-4-(morpholine), -C(O)-1-(piperazine), -C(O)-1-(4-methylpiperazine), -C(O)-1-(4-ethylpiperazine), and a heterocyclic group selected from azetidin-1-yl, pyrrolidin-1-yl, piperidin-1-yl, piperazin-1-yl, 4-methylpiperazin-1-yl, 4-ethylpiperazin-1-yl, 4-(2-hydroxyethyl)piperazin-1-yl, or morpholino, wherein that heterocyclic group is attached to the -C₁₋₄-alkyl or -(C₂₋₄-alkylene)- group via the N atom;

R^a is selected from $-H$, $-C_{1-4}\text{-alkyl}$, $-C(O)-C_{1-4}\text{-alkyl}$, $-C(O)-O-C_{1-4}\text{-alkyl}$, $-C(O)-N(C_{1-4}\text{-alkyl})_2$, $-S(O)_2-C_{1-4}\text{-alkyl}$, and $-(C_{2-4}\text{-alkylene})-O-(C_{1-4}\text{-alkyl})$, wherein $-C_{1-4}\text{-alkyl}$ or $-(C_{2-4}\text{-alkylene})-$ can be optionally substituted by W ;

R^b is an acyl group of a mono-peptide selected from $-$ proteinogenic amino acids attached via a carboxy group;

R^c groups are independently selected from $-H$ and $-C_{1-4}\text{-alkyl}$;

R^d groups are independently selected from $-H$ and $-C_{1-4}\text{-alkyl}$;

R^e groups are independently selected from $-H$ and $-C_{1-4}\text{-alkyl}$;

R^f groups are independently selected from $-H$ and $-C_{1-4}\text{-alkyl}$;

R^g groups are independently selected from $-H$ and $-C_{1-4}\text{-alkyl}$;

R^h is independently selected from $-H$, $-C_{1-4}\text{-alkyl}$ and $-CH_2CH_2OH$;

R^i is independently selected from $-H$, $-C_{1-4}\text{-alkyl}$ and $-CH_2CH_2OH$;

R^j is selected from $-H$, $-C_{1-4}\text{-alkyl}$, $-C(O)-C_{1-4}\text{-alkyl}$, $-C(O)-O-C_{1-4}\text{-alkyl}$, $-C(O)-N(C_{1-4}\text{-alkyl})_2$, $-S(O)_2-C_{1-4}\text{-alkyl}$, and $-(C_{2-4}\text{-alkylene})-O-(C_{1-4}\text{-alkyl})$, wherein $-C_{1-4}\text{-alkyl}$ or $-(C_{2-4}\text{-alkylene})-$ can be optionally substituted by W^1 ,

R^k is an acyl group of a mono-peptide selected from $-$ proteinogenic amino acids attached via a carboxy group;

R^x groups are independently selected from phenyl- and 4-methoxyphenyl-;

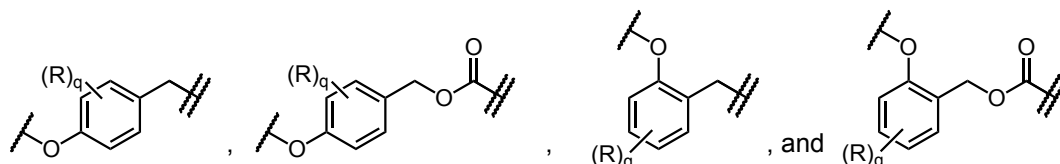
m is 0, 1 or 2;

n is 1 or 2, provided that $m+n$ is 2 or 3;

p is 0, 1, or 2, provided that when K^1 and K^2 are bonded together and K^1 and K^2 represent $-X^3-$ $Y-X-$ and X represents $-N(R^a)-$ or $-N(R^b)-$, then $p = 1$ or 2 ;

or any pharmaceutically acceptable salt, solvate or ester thereof.

- The compound according to item 1, wherein either Z^1 is Se and Z^2 is S, or Z^1 is S and Z^2 is Se.
- The compound according to item 1 or 2, wherein L is a bond.
- The compound according to item 1 or 2, wherein L is a self-immolative spacer selected from



wherein

denotes the attachment point to A;

denotes the attachment point to B;

R is independently selected from halogen, $-O(R^r)$, $-N(R^s)(R^t)$, $-NO_2$, $-CN$, and a heterocyclic group selected from azetidiny, pyrrolidiny, piperidiny or morpholino, wherein the heterocyclic group is attached to the phenyl ring *via* the N atom;

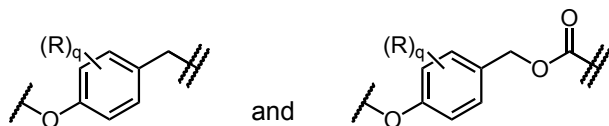
q is 0, 1, 2, 3 or 4;

R^r is independently selected from $-H$, $-C_{1-4}\text{-alkyl}$ and $-(C_{2-4}\text{-alkylene})-O-(C_{1-4}\text{-alkyl})$, wherein $-C_{1-4}\text{-alkyl}$ or $-(C_{2-4}\text{-alkylene})-$ can be optionally substituted by W ;

R^s is independently selected from $-H$, $-C(O)-C_{1-4}\text{-alkyl}$ and $-C_{1-4}\text{-alkyl}$; and

R^t is independently selected from $-H$, $-C(O)-C_{1-4}\text{-alkyl}$ and $-C_{1-4}\text{-alkyl}$.

- The compound according to item 4, wherein L is a self-immolative spacer selected from



wherein R and q are as defined in item 4.

6. The compound according to any one of items 1 to 5, wherein X^1 and X^2 are $-\text{CH}_2-$.
7. The compound according to any one of items 1 to 6, wherein K^1 and K^2 are bonded together and K^1 and K^2 represent $-\text{X}^3-\text{Y}-\text{X}-$.
8. The compound according to any one of items 1 to 6, wherein K^1 is $-\text{C}_{1-4}$ -alkyl optionally substituted by W^1 and K^2 is $-\text{H}$, $-\text{O}-\text{R}^j$ or $-\text{O}-\text{R}^k$.
9. The compound according to any one of items 1 to 8, wherein A^1-OH or $\text{A}^2-\text{NH}-\text{A}^3$ is selected from a diagnostically acceptable dye, a therapeutically acceptable DNA-alkylating agent, a therapeutically acceptable tubulin-inhibiting agent, and a therapeutically acceptable topoisomerase-inhibiting agent.
10. The compound according to any one of items 1 to 9, wherein A^1-OH or $\text{A}^2-\text{NH}-\text{A}^3$ is selected from 10-hydroxycamptothecin, 10-hydroxybelotecan, 10-hydroxygimatecan, 10-hydroxy-CKD-602, 10-hydroxy-BNP-1350, 10-hydroxy-sinotecan, topotecan, 7-ethyl-10-hydroxy-camptothecin (SN-38), 10-hydroxy-20-acetoxy-camptothecin, pyrrolbenzodiazepine, methotrexate, duocarmycin, CC-1065, doxorubicin, epirubicin, daunorubicin, pirarubicin, carminomycin, doxorubicin-*N,O*-acetal, 4-(bis(2-chloroethyl)amino)phenol, 4-(bis(2-bromoethyl)amino)phenol, 4-(bis(2-mesyethyl)amino)phenol, 4-((2-chloroethyl-2'-mesylethyl)amino)phenol, 5-hydroxy-seco-cyclopropabenzaindoles, 5-hydroxy-seco-(2-methyl-cyclopropa)benzaindoles, 5-hydroxy-seco-cyclopropamethoxybenzaindoles, 5-amino-seco-cyclopropabenzaindoles, etoposide, teniposide, GL331, NPF, TOP53, NK611, tubulysin A, tubulysin B, tubulysin C, tubulysin G, tubulysin I, monomethyl auristatin E, monomethyl auristatin F, dolastatin 10, dolastatin 15, symplostastin 1, symplostastin 3, narciclasine, pancratistatin, 2-epi-narciclasine, narciprimine, calicheamicin $\alpha 1$, calicheamicin $\beta 1$, calicheamicin $\gamma 1$, calicheamicin $\delta 1$, calicheamicin ϵ , calicheamicin θ , calicheamicin T, diclofenac, aceclofenac, mefenamic acid, clonixin, piroxicam, meloxicam, tenoxicam, lornoxicam, baricitinib, filgotinib, tofacitinib, upadacitinib, ruxolitinib, peficitinib, decemotinib, solcitinib, itacitinib, fostamatinib, SHR0302, leuco-methylene blue, leuco-methyl methylene blue, leuco-dimethyl methylene blue, leuco-toluidine blue, leuco-Azure A, leuco-Azure B, leuco-Azure C, leuco-Thionin, leuco-methylene violet, leuco-new methylene blue, leuco-Nile blue A, leuco-brilliant cresyl blue, firefly luciferin (D-Luciferin), umbelliferone, 4-trifluoromethylumbelliferone, 6,8-difluoro-4-methylumbelliferone, 7-hydroxycoumarin-3-carboxylic acid, 6,8-difluoro-7-hydroxy-5-methylcoumarin (DiFMU), 7-amino-4-methylcoumarin, 7-amino-4-chloromethylcoumarin, 3-O-methylfluorescein, 3-O-ethyl-5-carboxyfluorescein, 2,7-difluoro-3-O-methylfluorescein, 3-*N*-acetyl-rhodamine, 3-*N*-acetyl-dimethylsilarhodamine, 2,7-dibromo-3-*N*-acetyl-dimethylcarborhodamine, 3-*N*-acetyl-6-carboxyrhodamine, 2,7-difluoro-3-*N*-acetyl-rhodol, 3-O-(*N,N*-dimethyl-2-aminoethyl)-6-carboxyfluorescein, 2,7-dichloro-3-O-(*N,N*-dimethyl-2-aminoethyl)fluorescein, blackberry quencher (BBQ), black hole quencher 3 (BHQ3), 2-(2-hydroxyphenyl)quinazolin-4-one, 6-chloro-2-(5-chloro-2-hydroxyphenyl)quinazolin-4-one, and 6-bromo-2-(5-bromo-2-hydroxyphenyl)quinazolin-4-one.
11. A pharmaceutical or diagnostic composition comprising the compound according to any one of items 1 to 10, or a pharmaceutically acceptable salt, solvate, or ester thereof, and optionally a pharmaceutically acceptable carrier or excipient.
12. The pharmaceutical or diagnostic composition according to item 11, further comprising a second pharmaceutically active agent selected from a vascular disrupting agent, a cytotoxic chemotherapeutic agent and an immunomodulator.
13. The pharmaceutical or diagnostic composition according to item 12, wherein the second pharmaceutically active agent is selected from combretastatin A-4 (CA4), 3'-aminocombretastatin A-4, BNC105, ABT-751, ZD6126, combretastatin A-1, or prodrugs of the same (which includes but is not limited to combretastatin A-4 phosphate (CA4P), 3'-aminocombretastatin A-4 3'-serinamide (ombrabulin), combretastatin A-1 bisphosphate (CA1P), and BNC105 phosphate (BNC105P)), and pharmaceutically acceptable salts, solvates or esters of the same.
14. A compound according to any one of items 1 to 10, or a pharmaceutically acceptable salt, solvate, or ester thereof, for use in medicine.

15. A compound according to any one of items 1 to 10, or a pharmaceutically acceptable salt, solvate, or ester thereof, for use in the treatment, amelioration, prevention or diagnosis of a disorder selected from a neoplastic disorder; atherosclerosis; an autoimmune disorder; an inflammatory disease; a chronic inflammatory autoimmune disease; ischaemia; and reperfusion injury.

16. The compound for use according to item 15, wherein the neoplastic disorder is cancer which is preferably selected from acoustic neuroma, adenocarcinoma, angiosarcoma, basal cell carcinoma, bile duct carcinoma, bladder carcinoma, breast cancer, bronchogenic carcinoma, cervical cancer, chondrosarcoma, chordoma, choriocarcinoma, craniopharyngioma, cystadenocarcinoma, embryonal carcinoma, endotheliosarcoma, ependymoma, epithelial carcinoma, Ewing's tumor, fibrosarcoma, hemangioblastoma, leiomyosarcoma, liposarcoma, Merkel cell carcinoma, melanoma, mesothelioma, myelodysplastic syndrome, myxosarcoma, oligodendroglioma, osteogenic sarcoma, ovarian cancer, pancreatic cancer, papillary adenocarcinomas, papillary carcinoma, pinealoma, prostate cancer, renal cell carcinoma, retinoblastoma, rhabdomyosarcoma, sebaceous gland carcinoma, seminoma, squamous cell carcinoma, sweat gland carcinoma, synovioma, testicular tumor, Wilms' tumor, adrenocortical carcinoma, urothelial carcinoma, gallbladder cancer, parathyroid cancer, Kaposi sarcoma, colon carcinoma, gastrointestinal stromal tumor, anal cancer, rectal cancer, small intestine cancer, brain tumor, glioma, glioblastoma, astrocytoma, neuroblastoma, medullary carcinoma, medulloblastoma, meningioma, leukemias including acute myeloid leukemia, multiple myeloma, acute lymphoblastic leukemia, liver cancer including hepatoma and hepatocellular carcinoma, lung carcinoma, non-small-cell lung cancer, small cell lung carcinoma, lymphangioendotheliosarcoma, lymphangiosarcoma, primary CNS lymphoma, non-Hodgkin lymphoma, and classical Hodgkin's lymphoma, preferably colon cancer, rectal cancer, small intestine cancer, brain tumor, leukemia, liver cancer, lung cancer, lymphoma, basal cell carcinoma, breast cancer, cervical cancer, melanoma, ovarian cancer, pancreatic cancer, and squamous cell carcinoma.

17. Use of a compound according to any one of items 1 to 10, or a pharmaceutically acceptable salt, solvate, or ester thereof, for the manufacture of a medicament for the treatment, amelioration, prevention or diagnosis of a disorder selected from a neoplastic disorder; atherosclerosis; an autoimmune disorder; an inflammatory disease; a chronic inflammatory autoimmune disease; ischaemia; and reperfusion injury.

18. Use of a compound according to item 17, or a pharmaceutically acceptable salt, solvate, or ester thereof, wherein the neoplastic disorder is cancer which is preferably selected from acoustic neuroma, adenocarcinoma, angiosarcoma, basal cell carcinoma, bile duct carcinoma, bladder carcinoma, breast cancer, bronchogenic carcinoma, cervical cancer, chondrosarcoma, chordoma, choriocarcinoma, craniopharyngioma, cystadenocarcinoma, embryonal carcinoma, endotheliosarcoma, ependymoma, epithelial carcinoma, Ewing's tumor, fibrosarcoma, hemangioblastoma, leiomyosarcoma, liposarcoma, Merkel cell carcinoma, melanoma, mesothelioma, myelodysplastic syndrome, myxosarcoma, oligodendroglioma, osteogenic sarcoma, ovarian cancer, pancreatic cancer, papillary adenocarcinomas, papillary carcinoma, pinealoma, prostate cancer, renal cell carcinoma, retinoblastoma, rhabdomyosarcoma, sebaceous gland carcinoma, seminoma, squamous cell carcinoma, sweat gland carcinoma, synovioma, testicular tumor, Wilms' tumor, adrenocortical carcinoma, urothelial carcinoma, gallbladder cancer, parathyroid cancer, Kaposi sarcoma, colon carcinoma, gastrointestinal stromal tumor, anal cancer, rectal cancer, small intestine cancer, brain tumor, glioma, glioblastoma, astrocytoma, neuroblastoma, medullary carcinoma, medulloblastoma, meningioma, leukemias including acute myeloid leukemia, multiple myeloma, acute lymphoblastic leukemia, liver cancer including hepatoma and hepatocellular carcinoma, lung carcinoma, non-small-cell lung cancer, small cell lung carcinoma, lymphangioendotheliosarcoma, lymphangiosarcoma, primary CNS lymphoma, non-Hodgkin lymphoma, and classical Hodgkin's lymphoma, preferably colon cancer, rectal cancer, small intestine cancer, brain tumor, leukemia, liver cancer, lung cancer, lymphoma, basal cell carcinoma, breast cancer, cervical cancer, melanoma, ovarian cancer, pancreatic cancer, and squamous cell carcinoma.

19. A method of treating, ameliorating, preventing or diagnosing a disorder selected from a neoplastic disorder; atherosclerosis; an autoimmune disorder; an inflammatory disease; a chronic inflammatory autoimmune disease; ischaemia; and reperfusion injury, wherein an effective amount of a compound according to any one of items 1 to 10, or a pharmaceutically acceptable salt, solvate, or ester thereof, is administered to a patient in need thereof.

20. A method according to item 19, wherein the neoplastic disorder is cancer which is preferably selected from acoustic neuroma, adenocarcinoma, angiosarcoma, basal cell carcinoma, bile duct carcinoma, bladder carcinoma, breast cancer, bronchogenic carcinoma, cervical cancer,

chondrosarcoma, chordoma, choriocarcinoma, craniopharyngioma, cystadenocarcinoma, embryonal carcinoma, endotheliosarcoma, ependymoma, epithelial carcinoma, Ewing's tumor, fibrosarcoma, hemangioblastoma, leiomyosarcoma, liposarcoma, Merkel cell carcinoma, melanoma, mesothelioma, myelodysplastic syndrome, myxosarcoma, oligodendroglioma, osteogenic sarcoma, ovarian cancer, pancreatic cancer, papillary adenocarcinomas, papillary carcinoma, pinealoma, prostate cancer, renal cell carcinoma, retinoblastoma, rhabdomyosarcoma, sebaceous gland carcinoma, seminoma, squamous cell carcinoma, sweat gland carcinoma, synovioma, testicular tumor, Wilms' tumor, adrenocortical carcinoma, urothelial carcinoma, gallbladder cancer, parathyroid cancer, Kaposi sarcoma, colon carcinoma, gastrointestinal stromal tumor, anal cancer, rectal cancer, small intestine cancer, brain tumor, glioma, glioblastoma, astrocytoma, neuroblastoma, medullary carcinoma, medulloblastoma, meningioma, leukemias including acute myeloid leukemia, multiple myeloma, acute lymphoblastic leukemia, liver cancer including hepatoma and hepatocellular carcinoma, lung carcinoma, non-small-cell lung cancer, small cell lung carcinoma, lymphoendotheliosarcoma, lymphangiosarcoma, primary CNS lymphoma, non-Hodgkin lymphoma, and classical Hodgkin's lymphoma, preferably colon cancer, rectal cancer, small intestine cancer, brain tumor, leukemia, liver cancer, lung cancer, lymphoma, basal cell carcinoma, breast cancer, cervical cancer, melanoma, ovarian cancer, pancreatic cancer, and squamous cell carcinoma.

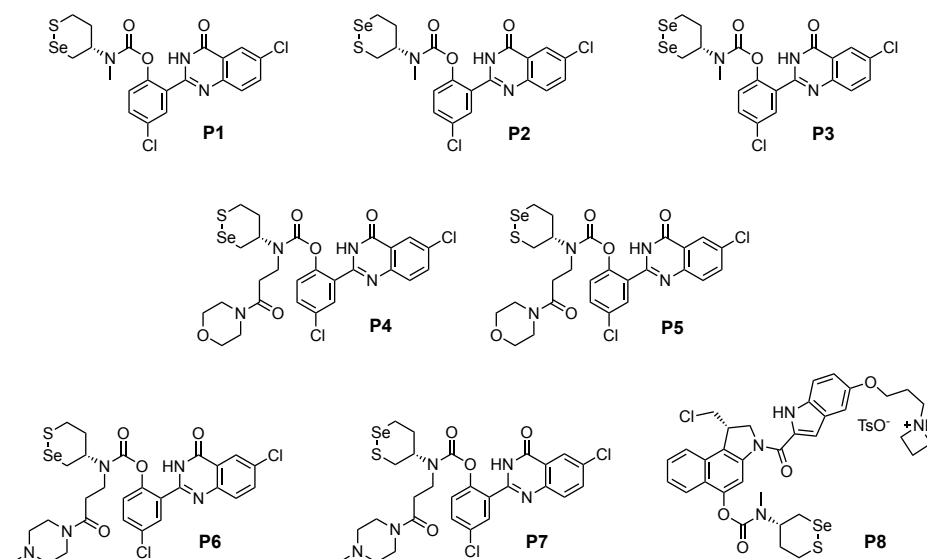
21. A method of predicting the suitability of a compound having the formula (I) as defined in any one of items 1 to 10, or a pharmaceutically acceptable salt, solvate, or ester thereof, for treating a patient who is suffering from a disorder selected from a neoplastic disorder; atherosclerosis; an autoimmune disorder; an inflammatory disease; a chronic inflammatory autoimmune disease; ischaemia; and reperfusion injury, wherein the method comprises:

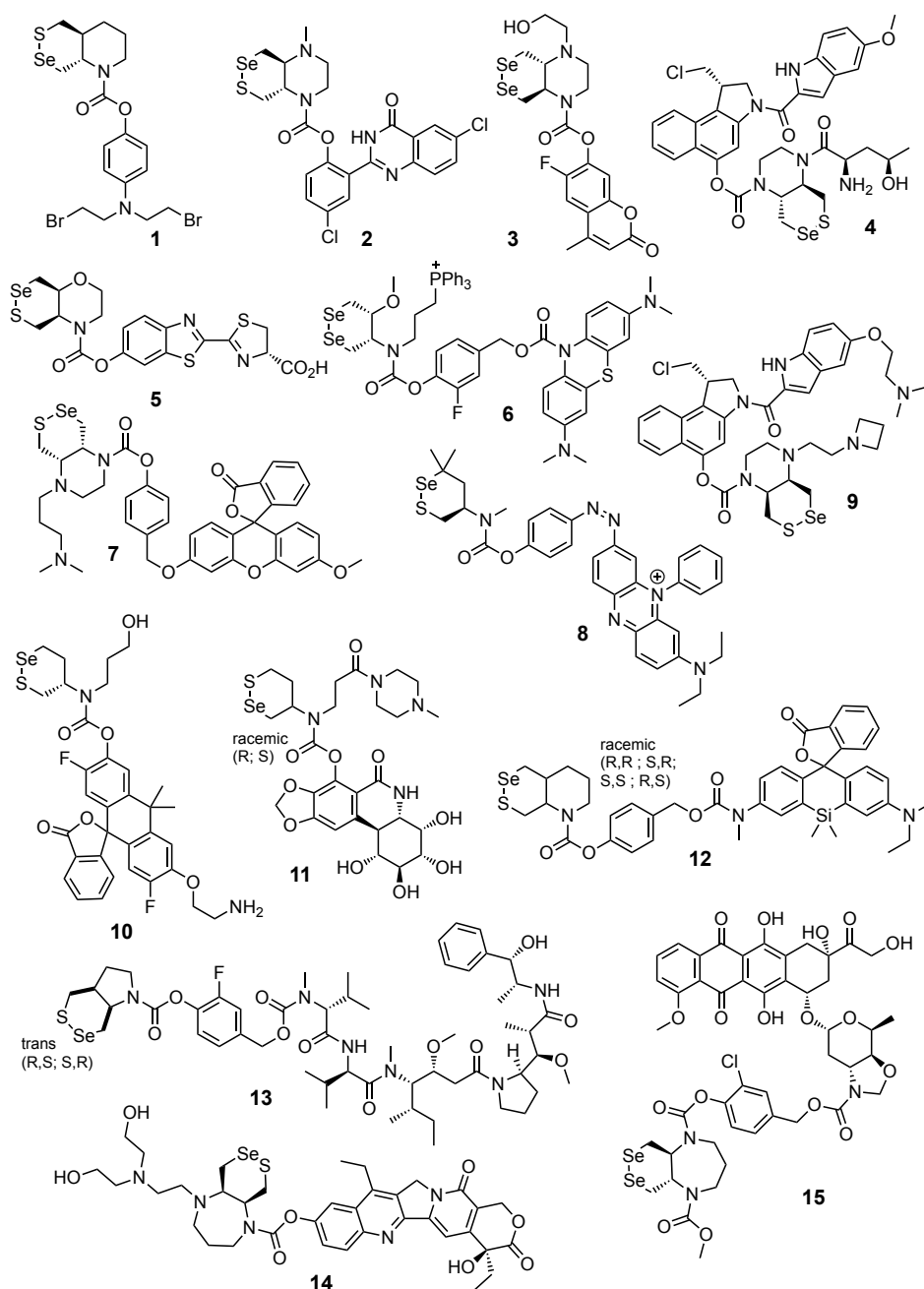
- (i) obtaining a sample from the patient;
- (ii) contacting the sample with a compound having the formula (I) as defined in any one of items 1 to 10, or a pharmaceutically acceptable salt, solvate, or ester thereof, wherein A^1 is selected such that A^1-OH is a diagnostic or theranostic agent or A^2 and A^3 are independently selected such that A^2-NH-A^3 is a diagnostic or theranostic agent; and
- (iii) detecting the presence or absence of A^1-OH or A^2-NH-A^3 .

22. A method of determining an inhibitory activity of a candidate inhibitor or candidate drug upon an oxidoreductase and/or a redox effector protein, wherein the method comprises:

- (i) contacting a compound having the formula (I) as defined in any one of items 1 to 8, or a pharmaceutically acceptable salt, solvate, or ester thereof, wherein A^1 is selected such that A^1-OH is a diagnostic or theranostic agent or A^2 and A^3 are independently selected such that A^2-NH-A^3 is a diagnostic or theranostic agent, with the oxidoreductase and/or the redox effector protein as well as the candidate inhibitor or candidate drug; and
- (ii) detecting the presence or absence of A^1-OH or A^2-NH-A^3 .

Illustrative embodiments of the compound having the formula (I) include





It is understood that all combinations of the above definitions and preferred definitions are envisaged by the present inventors.

In the following, examples of preferred compounds having the formula (I) are described, to illustrate some of the ways in which conjugation of a cargo H-B as the compound A-L-B masks its diagnostic and/or therapeutic activity, until the cargo is released following reduction.

These examples include the following therapeutic designs:

1 releases a DNA-alkylating nitrogen mustard cargo subunit of a type which is of interest especially for cancer therapy. The released bis(2-haloethyl)aniline species will feature similar activity to PR-104's bioactive alkylating metabolite PR-104M whereas the intact species **1** will not be as potently alkylating as the released cargo, since unmasking the electron-donating phenol in *para* to the aniline nitrogen increases electronic density and alkylating reactivity (similar principles are known for PR-104 and a range of related prodrugs.²⁶² Note that a range of leaving groups (halogens -Cl, -Br, -I or other leaving groups such as -OS(O)₂CH₃) can be used as the halogen substituents of the 2-haloethyl groups without compromising functionality, and/or an aniline nitrogen (requiring the use of a spacer subunit) could be

used instead of the phenolic hydroxyl as the unmasked group of the cargo, while remaining within the scope of a compound having the formula (I).

4 and **9** are similar to compound **P8** in that they release cargo subunits that are analogues of 5-hydroxy-*seco*-cyclopropabenzaindole, which (when their phenolic hydroxyl is unmasked) can then undergo Winstein cyclisation to the active DNA-alkylating cyclopropabenzaindoles (CBIs), which are of interest especially for cancer therapy, whereas no Winstein cyclisation can take place until the phenol is unmasked. In this way only the released cargo (and not the proagents) will be bioactive (similar principles are known for a range of related prodrugs.²⁶³ Note that a range of analogues of 5-hydroxy- or 5-amino-*seco*-cyclopropabenzaindoles or related cargos with various substitution motifs (such as the inclusion of the dimethylamino substituent on **9** to enhance solubility and DNA-binding potency) could be used, while remaining within the scope of a compound having the formula (I).

11 releases a cargo subunit that is the Amaryllidaceae-type alkaloid pancratistatin. Amaryllidaceae-type alkaloids (such as pancratistatin or narciclasine) are metabolism-affecting drugs that have shown utility in disease indications featuring metabolic deregulation, from cancer to chronic inflammation.^{264,265} The cargo release process (following triggering of the dichalcogenide trigger subunit of **11**) removes steric hindrance and so allows binding of the lycorane to its molecular target, such that only the released cargo is bioactive. Note that a range of lycorane-type alkaloids with various substitution motifs could be used, while remaining within the scope of a compound having the formula (I).

14 releases a cargo subunit that is SN-38, the active metabolite of the camptothecin class topoisomerase inhibitor irinotecan, a class which also contains the agent topotecan. As known for irinotecan, blocking the phenol removes bioactivity of the proagent so **14** will be biologically inactive except if triggered to release cargo; note that a range of similar cargo structures (e.g. modifying the ethyl group at the 7-position, or introduction of solubility and potency enhancing groups such as (dimethylamino)methyl as seen in topotecan) could be used, as is known for a range of related prodrugs,²⁶² while remaining within the scope of a compound having the formula (I).

It is illustrated by **1**, **4**, **9**, **11** and **14** that a broad range of bioactive phenolic cargos with a range of different bioactivity mechanisms and disease indication scopes can therefore be used, including with extensive structural substitutions, within the scope of the invention to deliver cargo-release-based activation of proagent bioactivity, i.e. functional prodrugs dependent upon triggering of the key selenenylsulfide of a compound having the formula (I).

13 releases an amine cargo subunit that is a tubulin-inhibiting auristatin derivative, of particular interest for cancer therapy and for neoangiogenic vasculopathies. A range of auristatins (and related peptide tubulin binders such as dolastatins and tubulysins) have been used in prodrugs where bioactivity is suppressed by conjugation of the agent to a large but cleavable trigger and/or trigger+spacer subunit,²⁶⁶ then restored upon its removal. Note that a range of such agents with various substitution patterns (including monomethyl auristatin E, monomethyl auristatin F, dolastatin or symprostatin) could be used; and/or that beyond the 3-fluoro-4-hydroxybenzyl alcohol spacer depicted in **13**, a range of spacers could instead be used, while remaining within the scope of a compound having the formula (I), to activate cytotoxic activity upon triggering of the proagent.

15 releases an amine cargo subunit that is of the anthracycline class of topoisomerase-inhibitors. This class includes doxorubicin, daunorubicin and idarubicin, and is of particular interest for cancer therapy. Basicity of the aliphatic amine of doxorubicin and its analogues is important for bioactivity; its carbamylation in **15** blocks bioactivity, but bioactivity can be restored by diselenide triggering followed by spacer-mediated release of the doxorubicin analogue.²⁶⁶ Note that a range of related cargos with various substitution motifs and/or related spacers could instead be used, while remaining within the scope of a compound having the formula (I), to activate cytotoxic activity upon triggering of the proagent.

It is illustrated by **13** and **15** that a broad range of bioactive amine cargos with different bioactivity mechanisms and disease indication scopes can therefore be used in conjunction with a range of spacers, each with optional extensive structural substitutions, while remaining within the scope of the invention to deliver cargo-release-based activation of proagent bioactivity, i.e. functional prodrugs dependent upon triggering of the key dichalcogenide of a compound having the formula (I).

These examples include the following diagnostic designs:

2 releases a fluorescent precipitating phenolic cargo subunit with large Stokes shift and green emission; **3**, **7** and **10** release fluorescent phenolic cargos with small Stokes shifts and UV, cyan, or orange emission; all the proagents **2**, **3**, **7** and **10** are nonfluorescent due to masking of the phenol groups (either due to blocking excited-state intramolecular proton transfer in **2**, or reducing electron-donating

capacity in **3**, or blocking the opening of the spirolactone in **7** and **10**); and all these designs provide a signal turn-on upon cargo release stimulated by triggering of the trigger subunits (and similar principles are known for a range of related probe cargos;²⁶⁷ they are thus diagnostic fluorescence probes that may be useful in a variety of diagnostic purposes. It is also illustrated that spacer subunits can be optionally included (**7**), and that a range of cargos [e.g. **2** (2-hydroxyphenyl)quinazolin-4(3*H*)-one), **3** (coumarin), **7** and **10** (xanthene fluorophores of the fluorescein type)] with a range of structures and diagnostic properties are possible while remaining within the scope of a compound having the formula (I).

5 releases a phenolic cargo subunit that is D-luciferin, the substrate of firefly luciferase enzyme, whereas the intact probe **5** is too bulky to be a substrate of luciferase. Therefore **5** is a dichalcogenide-reduction-triggered diagnostic luminescence probe allowing detection by bioluminescence in the presence of luciferase, which may be useful as a diagnostic for reductive probe turnover with ultra-low background signal (high sensitivity). Note that a range of luciferins for different luciferases and with different structural modifications are known and could also be used as cargo subunits²⁶⁸ while remaining within the scope of a compound having the formula (I).

8 releases a phenolic cargo subunit that is a functional analogue of Black Hole Quencher 3 (BHQ3) which has fluorescence quenching and photoacoustic signal generation properties.²⁷⁰ The proagent **8** is non-signal-generating and non-quenching due to masking of the key electron-donating phenol group, while the released cargo has no masking of the phenol and therefore has fluorescence quenching and photoacoustic signal generation activity, thus **8** functions as a multimodal diagnostic proagent. Note that similar unmasking-based activity turn-on principles are known for a range of related compounds including other quenchers, which could also be used as cargo subunits while remaining within the scope of a compound having the formula (I). **12** releases a spacer-cargo system that fragments to release an aniline cargo subunit that is a silarhodamine derivative which has fluorescence and photoacoustic signal generation properties.²⁷¹ The proagent **12** is non-signal-generating and non-fluorescent due to the masking of the amine group by carbamylation, while the released cargo silarhodamine is active in both diagnostic modalities. Note that a range of related or analogous cargos with various substitution motifs (such as a range of aniline-based fluorophores or photoacoustics dyes, including rhodols and rhodamines) could also be used as cargo subunits along the same design principles while remaining within the scope of a compound having the formula (I).

It is illustrated by **2**, **3**, **5**, **7**, **8**, **10** and **12** that a broad range of diagnostically active phenol or amine cargos, enabling a range of structures and diagnostic detection methods, can therefore be used, including with extensive structural substitutions, within the scope of the invention, to deliver cargo-release-based activation of proagent diagnostic activity, i.e. functional diagnostic probes dependent upon triggering of the key dichalcogenide of a compound having the formula (I).

These examples also include the theranostic design **6** that releases a cargo subunit that is *leuco*-methylene blue, a reduced form of the theranostic compound methylene blue which after release in biological media is spontaneously converted to methylene blue (similar principles are known for a range of related prodrugs). Methylene blue can be useful therapeutically including as a photosensitiser in photodynamic therapy (e.g. of the autoimmune disorder psoriasis, or of cancers) and/or as a redox-active selective toxin (e.g. against malaria parasite); as well as diagnostically (e.g. as a fluorescent agent or a photoacoustic dye); therefore being capable of theranostic activity.²⁷² Note that a range of functionally and structurally related compounds (e.g. phenoxazines) can also be used as cargo subunits in theranostics following the same design principles while remaining within the scope of a compound having the formula (I).

Various modifications and variations of the invention will be apparent to those skilled in the art without departing from the scope of the invention. Although the invention has been described in connection with specific preferred embodiments, it should be understood that the invention as claimed should not be unduly limited to such specific embodiments. Indeed, various modifications of the described modes for carrying out the invention which are obvious to those skilled in the relevant fields are intended to be covered by the present invention.

For the full text including Claims, Detailed Description of the Invention, Examples, Figures and General Principles, see the full published patent application (113 pages) available online at <https://patentscope.wipo.int/search/de/detail.jsf?docId=WO2022214598>.

4 Research summary

The TrxR/Trx and the GR/GSH/Grx oxidoreductase systems are the major pathways for thiol/disulfide-based control of vital redox-mediated functions and are involved in many cellular processes in health and disease. The precise analysis of their cellular roles remains inaccessible due to the lack of probes to, e.g., measure expression vs. activity in native systems. TrxR and Trx are also promising targets for anti-cancer drug development, as the cellular redox state is often dysregulated under diseased states, particularly cancer. Selective molecular imaging probes for these proteins are, thus, also of high interest to identify and validate chemical inhibitors in complex biological systems.

This doctoral thesis investigated the use of artificial dichalcogenide trigger units to report on the activity of vicinal dithiol-type redox proteins, such as TrxR, Trx, or Grx. These reduction sensors were validated in *trigger-cargo* constructs with a range of molecular cargos, from fluorophores to therapeutics with masked activity, that were switched upon reduction of the dichalcogenides via triggered fragmentation.

Results presented in this doctoral thesis

I have demonstrated that probes based on 5-membered cyclic disulfides (1,2-dithiolanes), just like those based on linear disulfides, are non-specifically operated by the highly abundant redox cofactor GSH and most redox proteins, so that both motifs are unsuitable for creating selective probes that resist the ca. 50 mM monothiol background in cells. The results presented in **chapter 3.1.1** clarified a fundamental disagreement in the literature by showing that 1,2-dithiolanes are not selective motifs to report on TrxR activity in cells but rather are non-specifically reduced by most thiols and are prone to ring-opening polymerization supporting their use instead as thiol-mediated uptake motifs.

This work has rationalized and validated a central idea: (i) disulfide structures with cyclic topologies and stabilized ring systems require the strongest cellular redox proteins for reduction due to their low reduction potentials; and (ii) cyclic systems offer kinetic reversibility of thiol/disulfide-interchange reactions, that selects for vicinal dithiol-type reductants over monothiols like GSH. I have demonstrated this key rationale by using mono- and bicyclic 1,2-dithianes with stabilized energetics and showed that these motifs are specifically operated by Trx over most other reductants and redox proteins (**chapter 3.1.2**).

Following these central principles, I presented a condensed chemical design of piperazine-fused 1,2-dithianes as reduction sensing units with the following improved features: (i) enhanced cargo expulsion kinetics with identical reductant-specificities, and (ii) flexible derivatization based on reactive side chain handles for amines, thiols, or alkylazides that allows screening for molecular recognition elements (**chapter 3.1.4**).

Another part of this work evaluated a novel desymmetrized dichalcogenide (1,2-thiaselenane) based on the same principles but with a design logic adapted to target the unusual Cys⁴⁹⁷Sec⁴⁹⁸ redox-active site found exclusively in TrxR. This revealed a regioisomer-dependent mechanism whereby the Se-proximal redox probe **RX1** proved highly resistant to GSH reduction while also reporting rapidly and selectively on TrxR1 activity in cells (**chapter 3.1.3**).

This work also intended to transfer the underlying concept of validated reducible cyclic dichalcogenide trigger units from fluorogenic probes to therapeutic prodrugs based on the same activation mechanism. I presented a graphical structure/function review of the chemical evolution of the highly potent cytotoxic duocarmycins, with tunable potencies that perfectly matched our requirements to serve as such an off-to-on therapeutic platform (**chapter 3.2.1**). With a set of 16 CBI prodrug and control molecules, I demonstrated the following features: (i) potency can be tuned by trigger choice matching their performance in fluorogenic probes; (ii) reductive prodrug activation in cells is tied to the TrxR/Trx redox couple and can be used to characterize Trx states in various standard cancer cell lines; and (iii) a novel class of bio-reductive prodrugs based on 1,2-dithiane can be used in animal models to treat cancer and observe anti-cancer efficacy (**chapter 3.2.2**).

General conclusion

The toolbox of reducible cyclic dichalcogenides had remained vastly underdeveloped in the prior art. This work sets common grounds for the principal idea: only cyclic dichalcogenides with stabilized ring systems resist reduction by monothiols; and so may be able to serve as reliable artificial substrates that are selective for cellular thiol/disulfide oxidoreductases. Over this thesis, several new heterocyclic moieties (fused 1,2-dithianes, 1,2-thiaselenanes, or fused 1,2-diselenides) were added to this toolbox.

The small-molecule constructs presented in this thesis complement several of the existing tools to measure, disrupt or interact with the thiol/disulfide redox cascades. Selective fluorogenic reporters can now employ the two novel dichalcogenide chemotypes shown here, either 1,2-thiaselenane to target TrxR, or else 1,2-dithianes to target cellular dithiol redox effectors (primarily Trx), and both can be applied in native cellular systems or *in vivo*. The selenenylsulfide probe **RX1**, the first probe to selectively measure TrxR1 activity in cells, has proven suitable for all cell biology assays we have run with it (including high-throughput screening to classify target binding by chemical inhibitors and validate/refute candidate inhibitors for TrxR). Adapting the disulfide probes to differentiate cleanly between redox effector proteins of the Trx superfamily is a non-trivial task requiring additional molecular recognition layers beyond the use of the “chemocompatible” trigger unit and is subject to ongoing work.

Overall, these accumulative imaging agents are valid to measure protein activity under normal or dysregulated conditions without genetic engineering required. The reducible design is modular so that orthogonal dyes can, in principle, be used for multiplexed imaging of several proteins. By masking cytotoxic drugs instead, the therapeutic benefit can be accrued dependent on redox protein activity. Diagnostic and therapeutic efforts might also be coupled: if a diagnostic tool with a particular trigger senses redox overactivity under a pathological state, one can then employ a therapeutic prodrug with the same trigger for treatment. I believe that the dichalcogenide tuning and the probes and prodrugs presented in this doctoral thesis represent only a portion of the potential space for future developments based on the general ideas of this work.

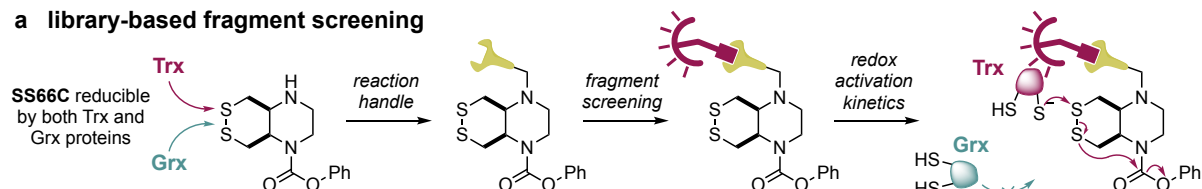
5 Ongoing work and Future perspectives

5.1 Towards selective imaging agents for cellular redox function

5.1.1 Screening for chemical recognition elements for redox effector proteins

The results presented in this work have evolved artificial disulfide substrates for vicinal dithiol-type redox proteins of the Trx-superfamily (see **chapter 1.1.3**) based on stabilized ring systems and kinetic reversibility. We found that *cis*-fused 1,2-dithianes of the **SS66C** class resist interaction with the highly abundant *monothiol background* in biology, while their *trans*-fused diastereomers **SS66T** are susceptible to reduction by monothiols like GSH (see **chapter 3.1.2**). Our condensed structural design contains an additional nitrogen in the backbone ring that helped to strongly enhance fragmentation kinetics while keeping its reductant resistance profile. Side chain attachments by alkylation or acylation did not affect these properties and gave fluorogenic probes with good cellular turnover. However, cell-free enzymatic specificity assays revealed that **SS66C** could, besides our primary target Trx1, also be reduced by its Grx protein cousins, and its cellular turnover was only partially suppressed by modulation of the Trx system (see **chapter 3.1.4**). When employed in our cytotoxic prodrugs, we found that potency in TrxR knockout cells did not reflect our non-reducible control and led to the conclusion that remaining activation had occurred by bioreductants other than Trx (see **chapter 3.2.2**). This indicated that, so far, our artificial substrate was part of the shared substrate scope between Trx and Grx proteins, which function as a backup system for each other.⁴⁰

a library-based fragment screening



b experimental setup for high turnover screenings

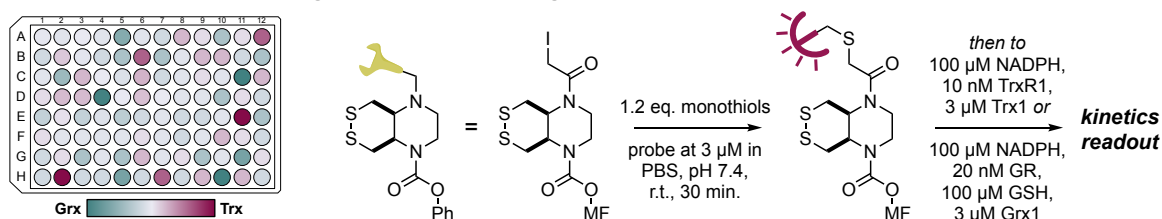


Figure 21 Fragment-based screening for redox effector protein recognition elements. (a) The general concept of a two-step diversification of *trigger-cargo* constructs with molecular fragments to recruit protein reductants based on molecular recognition or electrostatic complementarity. (b) Experimental setup for a thiol-library diversification screening using the iodoacetamide probe **IA-SS66C-MF**.

One of the primary goals of this research is the development of a selective small-molecule reporter for each of the redox proteins, including Trxs and Grxs. With a “chemocompatible” fit for these proteins, the first and crucial performance feature of artificial substrate triggers has been reached: the cyclic topology dictates a preference for dithiol-type proteins and prevents reduction by the monothiol background. To differentiate between proteins of the Trx superfamily, future designs need to get to a second layer of selectivity e.g. by exploiting non-covalent protein affinity. In principle, only weak binding

is required, which brings protein and substrate in proximity while rejecting its competing protein cousin. With our Grx-aimed probe **GS-SS66C-MF** we have already advanced the first step in this direction by attaching a non-reducible GSH mimic, hoping for affinity through electrostatic complementarity with Grx surface charges⁹⁴ (see **chapter 3.1.4**).

Thrilled by these initial steps and the flexibility of our robust molecular design, future efforts should follow this idea and expand the portfolio of potential recognition elements for either of the protein targets. This requires a detailed analysis of the protein surface structures and, most probably, extensive fragment-based screening. I propose that a high-throughput diversification approach is suitable that relies on the attachment of a single reactive handle to fluorogenic constructs, such as **SS66C-MF**, and *in situ* fragment labeling (**Figure 21a**). Potential readouts would be the cell-free enzyme kinetics experiment or even a cellular experiment using cells with genetic knockouts, for e.g. TrxR1 or Grx1/2. We have exemplified such an approach by introducing reactive anchor units for thiols (iodoacetamide), amines (aldehyde, sulfonyl fluoride, or NHS ester), or alkylazides (propargylamine) with rapid, quantitative, and orthogonal chemistries (see **chapter 3.1.4**).

Thiols. We experimentally validated that the covalent attachment to the platform probe **IA-SS66C-MF** of even ca. 350 Da monothiols (GSH) can be achieved in aqueous buffered solution at 37°C: i.e., at the same assay conditions that are used for specificity screenings. Instead of isolating each of the new probes, I assume that a fragment-based screening of a thiol-reagent library can be performed in a 96-well format (**Figure 21b**) due to the following features: (i) the reducible core resists monothiols, and potentially undesired activation would be detected; (ii) the diversification reaction is fast and quantitative, so no purification is required; (iii) the high sensitivity of the fluorescent cargo allows to use the probe at comparably low concentrations of 1-3 μM ; and (iv) residual monothiol reagent should not significantly interfere with reactions of protein effectors (or cells) that are added later. However, there is a limited number of free thiol reagents with diverse backbones that are commercially available. The thiols that are ready-to-use have very different polarities and are potentially oxidized in stocks, both of which could disturb assay results. I propose that a thiol-based fragment screening could best rely on a diversification based on small peptide oligomers with exactly one defined cysteine (exemplified by GSH) aiming for structural diversity within the canonical amino acid space. These thiol reagents are easily accessible by solid-phase peptide synthesis.

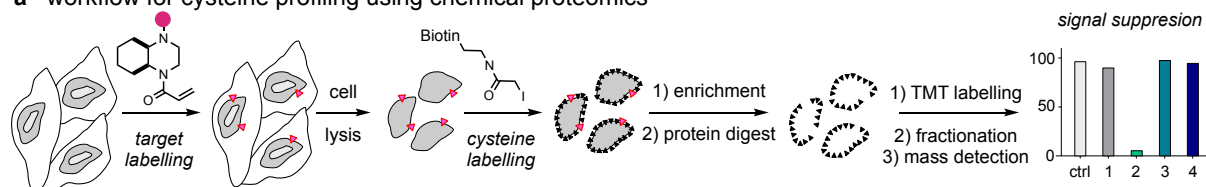
Amines and Others. Diversification can also be performed using alternative reactive handles for, e.g., amines. Advantageously, amine-containing fragment libraries are widely accessible and offer high structural diversity. If the reaction conditions for covalent attachment of fragments are not compatible with the experimental conditions for specificity readouts, I propose to adapt the approach by replacing the 3-O-methyl-fluorescein we used as our sensitive fluorogenic cargo instead by a surface-bound, immobilized fluorescein, with attachment at this 3-O-alkyl site, to allow washing between the diversification and the screening steps and to further increase the sensitivity of the assay setup.

5.1.2 Using chemical proteomics for validation of chemical recognition motifs

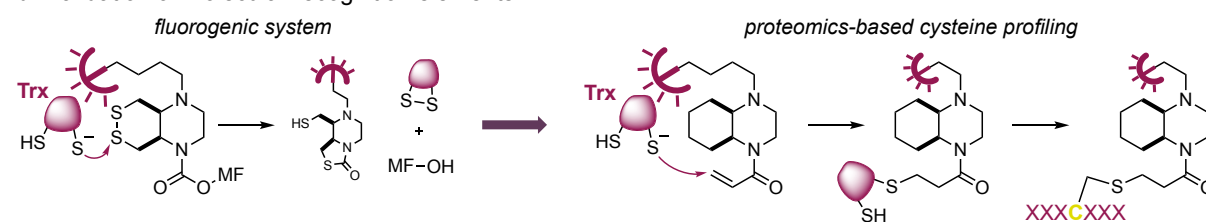
Potential “recognition hits,” as described in **chapter 5.1.1**, would have to be tested by cleanly preparing and isolating the probes containing the “hit motifs” and screening their properties in biologically more complex experiments. This includes not only cell-free evaluations but also cellular studies under modulation of the potential reductant target species. However, the experimental setups presented in this doctoral thesis (see **chapters 3.1.1 - 3.1.4**) represent only one approach to look for structure-based affinity/reactivity differentiation and are limited to specific examples within the redox proteome. They cannot cheaply be adapted to other proteins, and they lack the ability to identify off-target interactions. Ideally, methods that could precisely quantify effects from increased or decreased affinity toward *many* redox proteins (beyond just the specific Trx or Grx isoforms tested here) in their native biological environments could also be employed: such as chemical proteomics.

Our probes should be operated on by cysteine-containing proteins undergoing covalent but reversible interactions. An adapted design could trace which protein cysteine thiolates are most brought into contact with such probes by bearing the same “hit motifs” but adding irreversible Cys-reactive warheads, such as acrylamide electrophiles. Then, cysteine profiling could be performed using conventional chemical proteomics^{275,276} to evaluate the protein directing ability of the “hit motifs”: (i) treatment of native cells with cysteine-labeling covalent probes; (ii) cell lysis and labeling of residual accessible cysteine residues in the proteome with biotin-based tags; (iii) biotinylated protein enrichment and protein digest; and (iv) mass spectrometry-based analysis of peptide fragments to identify signal suppression by the treatment as compared to control experiments (**Figure 22a,b**).

a workflow for cysteine profiling using chemical proteomics



b validation of molecular recognition elements



c first series of small fragment proteomics probes

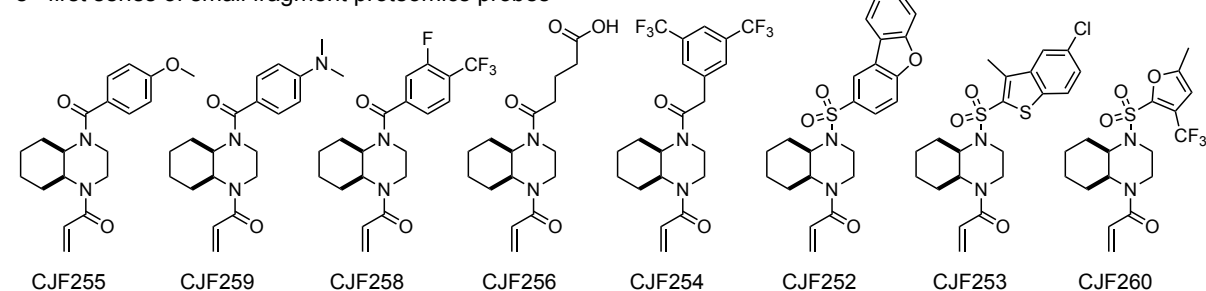


Figure 22 (a) General workflow for cysteine profiling using chemical proteomics. (b) From fluorogenic systems to proteomics probes validating “hit elements” for redox proteins. (c) A first set of small fragment-based probes.

Following these lines, I suggest replacing the original **SS66C** core with a non-reducible **CC66C** mimic and the fluorescent cargo with a cysteine labeling acrylamide, such that the electrophilic site is as close to the original disulfide as possible (**Figure 22b**). Attaching the very same “hit motifs” identified with the fluorogenic platform would deliver a palette of probes to verify molecular recognition in native cellular environments while covering the whole redox proteome; and allowing to precisely quantify ratios between single redox proteins.

Alternatively, this approach theoretically allows to directly screen for novel recognition elements by installing potential “hit motifs” by alkylation, acylation, or even sulfonylation on the alkylator core (within the proteomics field, this is sometimes referred to as “fragment screening”). As proof of principle, I have prepared a small library of such probes for cysteine profiling using chemical proteomics based on the **CC66C**-acrylamide precursor (**Figure 22c**). I prepared these probes in a 4-step sequence, offering structural diversity (see **Appendix 7.2.1**). I treated cells with them and followed the preparation protocol for proteomics analysis while being at the Cravatt laboratory at Scripps Research, San Diego (USA). However, such a low-throughput approach may be unsuitable for exploring unknown chemical space and unlikely to identify binding motifs quickly. It is limited by the number of potential motifs to screen, as each compound must be isolated, and sample preparation (5 days with max. eight compounds), mass spectrometry, and analysis are time-consuming and expensive when performed on a large scale.

The mass spectrometry analysis and protein quantifications have not yet been performed, so conclusions cannot yet be drawn, but I believe that these concepts and experimental settings may, in principle, be suitable to identify and validate small- to medium-size molecular recognition elements for differentiation of redox effector proteins of the Trx-superfamily based on non-covalent binding and/or electrostatic complementarity. I propose that by adding such elements to our simple *trigger-cargo* constructs employing the **SS66C** motif, we can deliver fluorogenic probes that can act as selective cellular reporter units for single redox effector proteins in complex biological settings.

5.1.3 The “perfect” cellular Trx1 probe design of the future

One of the major ongoing efforts from this work is to develop small-molecule imaging agents for measuring the activity of Trx1 in native cells that ideally can be imaged orthogonally to the TrxR1 probe **RX1**. The structural features that should be combined to create the “perfect” cellular Trx1 probe of the future may include: (i) the redox trigger should be a structural analog of **SS66C**; its thermodynamics could even be further stabilized by e.g. attaching one/more sulfur-geminal methyl groups to the 1,2-dithiane; (ii) a fragment-based recognition element for the protein surface of Trx should be covalently attached to improve protein active site residence likelihood; and (iii) xanthene-based fluorescent cargos are preferred due to real off-to-on character and orthogonality to the **RX1** fluorophore HPQ. However, free **MF-OH** is highly membrane-permeable. Intracellular localization and single-cell quantification require a xanthene-based design that is intracellularly trapped upon release., so: (iv) polarity, total size, and potential intracellular targeting of the probe may be further tuned by sidechain attachments. I am confident that all these properties can be reached by rational chemical design while exploiting the modularity of the system to deliver a probe that reports selectively on Trx1 activity in cells.

5.2 Improving the imaging modalities of fluorescent redox reporter probes

5.2.1 Over and beyond the visible spectrum for *in vivo* imaging of redox function

Fluorogenic probes presented in this doctoral thesis are based on two specific phenolic dyes that are suitable for creating off-to-on fluorogenic probes by masking the phenol. The solid-state fluorescence of the **PQ-OH** dye is based on an unusual excited-state intramolecular proton transfer (ESIPT) mechanism that results in a large Stokes shift of >150 nm. This property makes the imaging orthogonal to most standard dyes in the visible region but requires the use of UV-light for irradiation in living systems, which is problematic. A large number of fluorescent dyes that are excited, and emit, in the visible spectrum, are suitable for use in fluorogenic probes based on triggered fragmentation reactions.^{277,278} This includes hydroxycoumarins²⁷⁹, fluoresceins, carbo- or silicon-fluoresceins^{280,281}, seminaphthorhodols^{176,282} and even amine dyes like (silicon-)rhodamines²⁸³ or norcyanines^{284,285} that can be released directly or via self-immolative linker fragmentations (**Figure 23**).

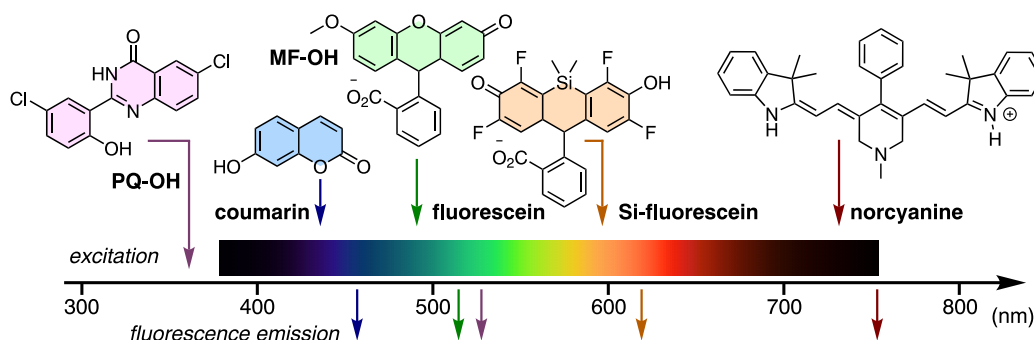


Figure 23 Representative dyes suitable for use in fluorogenic probes covering the visible spectrum.

The major advantage of our reduction-triggered fluorogenic probe design is its modularity, which allows the flexible use of various fluorescent dyes as cargos. We rationalized in this work that trigger reduction dictates the activation profiles, while the cargo mainly influences the speed of cyclization and expulsion. Selecting the right molecular cargo depends on the intended use: for many cellular applications, the unusual **PQ-OH** is an excellent choice (see **chapter 3.1.3**); for others, more sensitive red-shifted dyes allowing imaging with less phototoxicity, or that are orthogonal to widely used GFP, would be better. The carbo-fluorescein Virginia Orange²⁸¹ and its silicon variant Maryland Red²⁸⁰ are impressive examples of fine-tuned fluorescent dyes that are first-class alternative xanthene cargos with similar off-to-on properties as **MF-OH**.

Stimulus-responsive molecular probes for true *in vivo* fluorescence imaging require fluorescent cargos that are excited at the far end of the visible spectrum or beyond. Only near-infrared (NIR) light has sufficient penetration depths in tissues to measure fluorescent readout in living animals.²⁸⁶ Remarkable dyes based on stabilized heptamethine cyanines with excitation/emission far in the NIR region and a reliable switch-on mechanism induced by molecular fragmentation have been recently developed.²⁸⁵ I suppose that the use of such dyes in combination with the right reducible trigger unit would be suitable for *in vivo* redox imaging through tissues in living animals.

5.2.2 The use of chromophores for optoacoustic in vivo imaging of redox states

Tissue penetrating fluorescence imaging requires excitation/emission in the far red or NIR region, but typically quantum yields of these fluorophores are very low ($\ll 10\%$) due to internal conversion. However, the energy loss due to internal conversion can also be detected since thermo-elastic expansion can result in a pressure wave (optoacoustic effect). Excitation pulsing with kilohertz frequencies can be detected as ultrasound, giving images from living tissue with excellent penetration depths.²⁸⁷ Particularly, dyes with extremely low or zero fluorescence quantum yields are potentially good chromophores for optoacoustic imaging (**Figure 24a**).

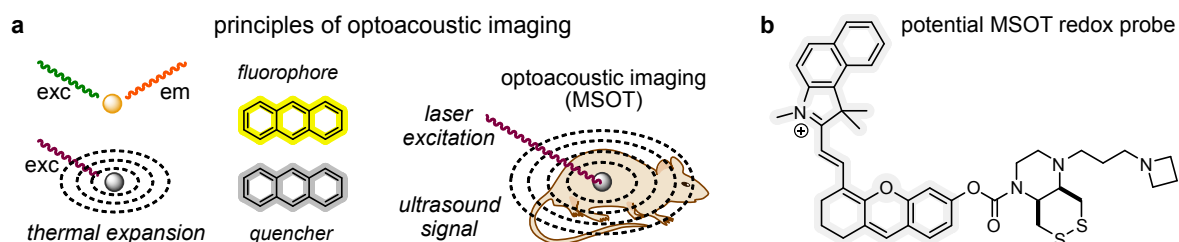


Figure 24 Optoacoustic imaging. (a) Molecular quenchers are contrast agents for MSOT that are used to target and image tissues in living animals. (b) Potential structure of a reducible MSOT probe.

The multispectral optoacoustic tomography (MSOT) technique has mainly relied on either the endogenous chromophore hemoglobin or very classical exogenous chromophores such as methylene blue²⁸⁸ or indocyanine green (ICG),²⁸⁹ as anatomical contrast agents. Instead, dyes that are activated by enzymes *in vivo* through fragmentation mechanisms²⁹⁰ could act as molecular probes to image tissue redox activity in living animals: and *trigger-cargo* constructs using our reducible trigger units to mask such activatable MSOT chromophores might be a robust point of entry for such probes (**Figure 24b**).

5.2.3 Cyclic disulfide-based FRET probes expand the portfolio of redox probes

Other than re-establishing fluorescence by unmasking crucial structural features of dyes, previously reported thiol probes have also relied on cleaving bivalent *donor-acceptor* constructs, where masking/activation is based on FRET between these two units.²⁹¹ This area of probe development has not yet advanced to test trigger units that resist GSH reduction (see **chapter 1.3.2**). Now that we have expanded the toolbox with bifunctional cyclic disulfide units that are operated selectively by cellular vicinal dithiol-type proteins, new possibilities are available. **Figure 25** shows two potential molecular designs that either (a) rely on a *donor-acceptor* (fluorescein-Cy 3) pair to use as a FRET probe for fluorescence imaging,²⁹² or else (b) use the molecular quencher BHQ-3 together with the red fluorophore protoporphyrin IX as an off-to-on FRET design.¹⁹⁰

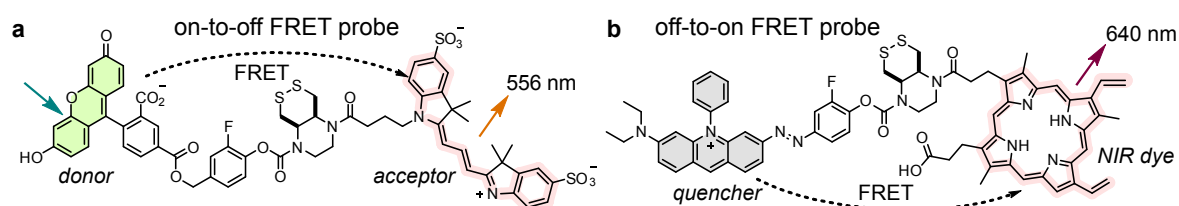
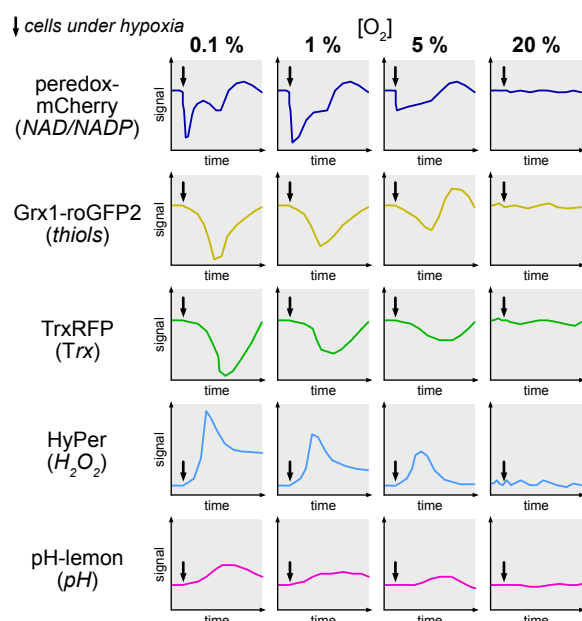


Figure 25 Potential bivalent imaging agents based on FRET as (a) on-to-off or (b) off-to-on designs.

5.3 Characterising chronic hypoxic states with small molecule redox sensors

Ratiometric tools for cellular redox poise are based on the genetic encoding of fluorescent proteins responsive to reversible thiol/disulfide redox, including Grx1-roGFP2¹⁵² (general thiol state), TrxRFP¹⁶⁰ (Trx protein redox relay), HyPer¹⁵⁷ (H₂O₂ sensing redox relay) and peredox-mCherry²⁹³ (for NAD(P)⁺/NAD(P)H ratios). These tools must first be encoded by transient transfection; and then show a response to external stimuli. In contrast, we have provided multiple novel small molecules reporting on thiol/disulfide states, including **H-SS66T-MF** (general thiol/GSH), **Ac-SS66C-MF** (dithiol-type proteins), and **RX1** (TrxR1 activity) that are turn-on probes and give cumulative signal upon treatment.

a ratiometric genetic tools for acute hypoxia



b turn-on small molecule tools for chronic hypoxia

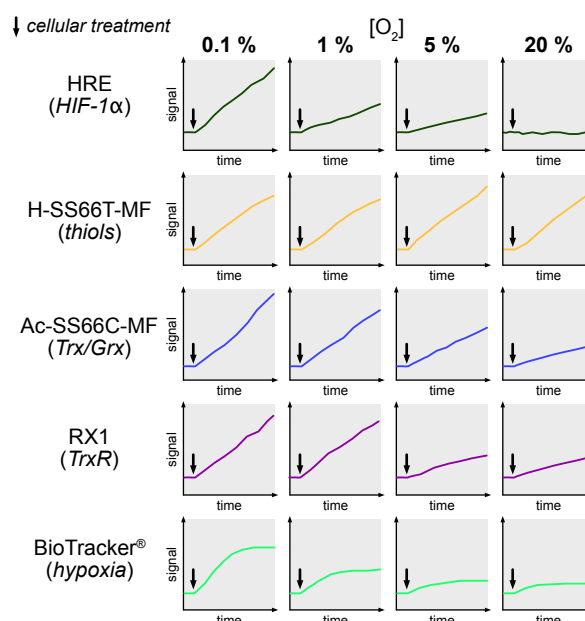


Figure 26 Applying small molecule redox sensors for measuring hypoxic states in cells (**mock results**). (a) Characterization of cellular redox response to acute hypoxia using ratiometric genetic tools (note: pH-Lemon²⁹⁴ used for cellular pH). (b) Characterization of chronic/cyclic hypoxia by using (small molecule) turn-on probes.

Cells respond to chronic oxygen deficiency (hypoxia, e.g. within most solid tumors) through altered redox regulation/signaling that is related to a persistent genetic switch.²⁹⁵ Selective tools to measure the distinct cellular redox pairs would be powerful to characterize these responses on a protein level in live cells. I suggest that experiments comparing ratiometric genetic tool response to that of our cumulative probes may evaluate distinct hypoxic states in cells (**Figure 26**). Ratiometric tools (a) respond reversibly in real-time and indicate short-term changes within single redox pairs or overall thiol states. In contrast, after incubating cells under hypoxia for at least 48 h to induce the genetic switch (b: made visible by a "hypoxia-responsive element: luciferase" (HRE-Luc) reporter gene²⁹⁶), cells could then be treated with our chemical probes to measure changes in overall thiol, Trx/Grx or TrxR activity under chronic hypoxia, which we expect to offer different information compared to commercial small molecule "hypoxia probes" (e.g. BioTracker[®]) that report on molecular oxygen concentration. So far, such a clear differentiation of thiol redox states responding to acute vs. chronic hypoxia lacks the molecular tools to measure them. Particularly in the context of cancer, where upregulated TrxR/Trx activity is linked a genetic switch, such thiol states may be ultimately exploited for therapeutic purposes.

5.4 Cyclic disulfide linkers for tandem activation of antibody-drug conjugates

The duocarmycin class of cytotoxins offers great incentives to use rationally tuned prodrugs to deliver them to their target tissue while reducing exposure of healthy tissues (see **chapter 3.2.1**). Although we have designed reductively activated cytotoxic prodrugs based on the CBI core (see **chapter 3.2.2**), they may be challenging to progress further (since no small molecule duocarmycin prodrug has yet been approved, despite many trials). However, the first duocarmycin agent for anti-cancer use has recently been FDA fast-track-designated for anti-cancer use in patients: the antibody-drug conjugate (ADC) SYD985.²⁹⁷ (**Figure 27a**). ADCs are large bivalent constructs that function as therapeutics according to the following general principles: (i) monoclonal antibodies (mAb) for surface-exposed antigens of cancer-associated cell types are used for targeting and cellular delivery via receptor-mediated endocytosis; (ii) the antibody is decorated with (optionally masked) therapeutic payloads by covalent attachment to cysteines or lysines (*labeling motifs highlighted in green*); (iii) to ensure the intracellular release of the active agent, cleavable linker units are required (*red*): the valine-citrulline (VC) dipeptide linker is widely used with site-specific proteolysis by cathepsins (lysosomal proteases) to liberate drug payloads;²⁹⁸ and (iv) solubilization handles are often required to prevent payload aggregation (*blue*).

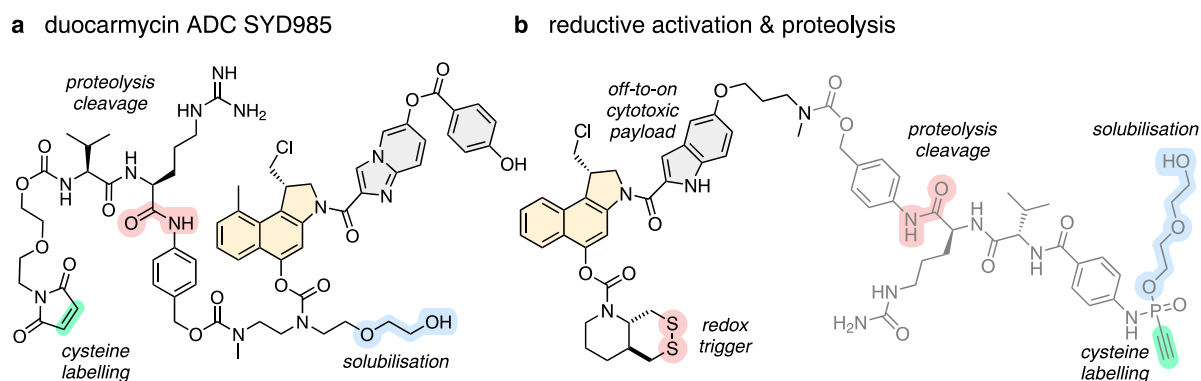


Figure 27 Design of redox-activated duocarmycin-ADCs. (a) Structural features of the ADC SYD985. (b) Design of a dual activation duocarmycin-ADC based on proteolysis and reduction.

We envisioned that bioreductive duocarmycin prodrug ADCs could provide an additional layer of selectivity to protect healthy tissues against drug exposure arising from extracellular release, using our disulfides as a reliable intracellular activation mechanism. Two conceptually different ADC designs are used in general: (i) cleavage of the covalent link between antibody and payload is triggered independently from fragmentations that re-establish bioactivity, or (ii) cleavage of the linker simultaneously results in activation of the drug's activity.

A first design we are pursuing (**Figure 27b**) is where the cleavage of the payload from the antibody does not directly establish its bioactivity but an additional intracellular activation step is required. To achieve this goal, we planned to attach the redox trigger **SS66T** to create an off-to-on potency switch that would slowly activate the payload in the target cells. We would then also require VC linkers for proteolysis-based intracellular release and a reactive warhead for ADC coupling that is e.g. based on cysteine-selective ethynylphosphonamidate (P5) chemistry.²⁹⁹ As a proof-of-principle, we prepared the simple amine precursor **SS66T-CBI-NHPI** (see **Appendix 7.3.2**) that was structurally derived from our

prodrug **SS60-CB-AZI** (Figure 27b, see *chapter 3.2.2*) and can be further elongated with commercial VC precursors in one synthetic step. I think that this first design is a good starting point that allows the flexible use of various redox triggers and relies on well-established cleavage and coupling sites.

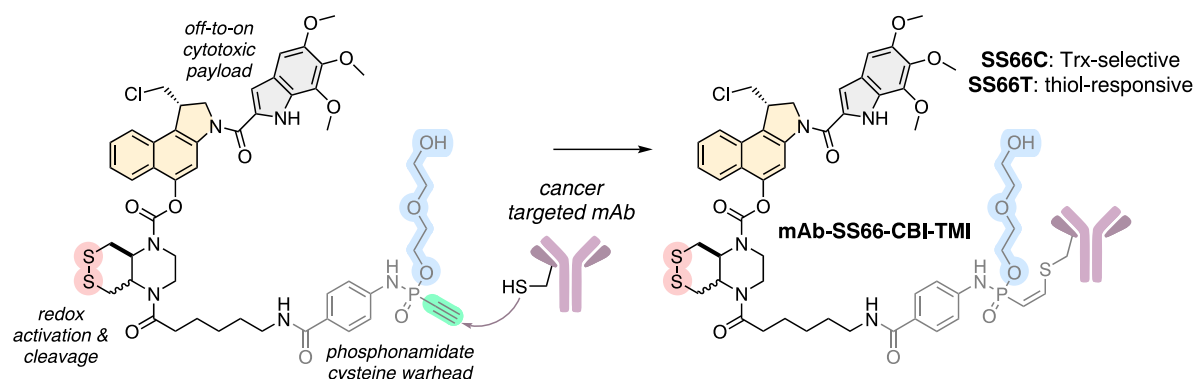


Figure 28 Potential structure of a one-step tandem-cleavable bioreductive duocarmycin-ADC based on bifunctional piperazine-fused 1,2-dithianes.

Cleavable linkers in ADCs must be extracellularly robust and give reliable enzymatic activation in cells after cell entry. However, peptide-based linkers may be sensitive to extracellular esterase cleavage^{300,301}, and novel linker chemistries are of high interest.³⁰² I propose to employ our piperazine-fused 1,2-dithianes and exploit their utility as bifunctional reductively cleavable linker units (see *chapter 3.1.4*) by replacing the potentially unstable VC linker with the **SS66C** core. The resulting condensed ADC precursor design is shown in **Figure 28**. Again, as a proof of principle, I have prepared the amine precursors employing the GSH-labile **SS66T**, the slow-releasing **SS66C**, and their non-reducing **CC66** control motif (see *chapter 7.2.2*).

I think that in these ways, the implementation of bioreductive gating designs in ADCs is a promising avenue towards reductively activated anti-cancer agents with improved therapeutic indices, and their evaluation is the subject of ongoing work. Not only could stabilized cyclic disulfides be valid trigger units with reliable and fast activation kinetics to replace linear disulfides in ADC designs. They could also be great to replace the VC cleavable linker with excellent extracellular robustness and alternative intracellular cleavage kinetics. The high modularity of our design also allows modifications at late stages of development, which could contribute valuable options for ADC work with duocarmycins and beyond.

6 Acknowledgements

First, I want to thank my supervisor and scientific mentor, Dr. Oliver Thorn-Seshold, for guiding me through my PhD time: for drawing a scientific rationale around such a simple chemical design to create such a broad and challenging project and allowing me to independently develop versatile paths in different directions that finally built such a conclusive picture of scientific outcomes. Thank you for entrusting me with one of the group's first independent research programs from the very beginning while throwing me "*ins kalte Wasser*" and for building such a great *team redox* around me.

I want to thank Prof. Ivan Huc for reviewing my doctoral thesis as a 2nd referee and Prof. Franz Bracher, Prof. Thomas Carell, Prof. Oliver Trapp, and Prof. Elias Arnér for being part of my scientific committee.

I am so grateful to Prof. Elias Arnér for establishing such a strong collaboration around my doctoral project and for complementing our joint publications with his broad *redox expertise* and such a precise view. Particularly, I want to thank Prof. Arnér for joining my PhD defense in person all over from Sweden after we had not met in person during the first two years of collaboration during the pandemic. And for bringing Karo into the project: It was really a pleasure to work with you, to exchange ideas and strategies, and accompany your development to the most reliable collaborator that one could wish for.

I had the honor to share most of the ups and downs of my PhD time and projects with Lukas, a great chemist, excellent colleague, and great friend. I am very thankful that we had the chance to create so many of the advances within our project from scratch while running up some peak, paddling down some river, fighting some glacier's ice, or enjoying some tasty brew. Thank you for always supporting the overall idea, making this a true teamwork effort, and driving me to overachiever skills. I deeply wish you the very best for your future, and I am confident that you will land your PhD impressively.

I want to thank (Papa) Li for laying the ground in the group that I could build on; for always being supportive and funny while emptying your own plate of ****, to thank Adi, the man, for challenging my organic chemistry conscience and Alex for your dirty humor cheering up even the darkest pandemic days. I want to thank Markus for his calm and straight thinking, calming down my inner restlessness and for always giving me the worst shot in exchange for his *mikrigen Baum*; Ben for showing me the world out there with all the famous chemists and for keeping the minimum order, time- and process-management and Philipp for his patience, his faith for horrible music and for being Philipp Mauker.

I want to thank Annabel for her tireless efforts supporting the redox translation, Lena for venturing into such a different field and making such a big impact during her time with us, and Martin Maier for showing me how you do organic chemistry after I had already done it for so many years. I want to thank Julia, Carina, Michaela, Elena Fajardo-Ruiz, Franzi, Constanze, Petar, Elena Longhi, Martin Reynders, Kasia, Nynke, and Yelena for building such a supportive environment during all these years. I thank my interns, Chrissi, Vicky, Paula, Julia, and Alex, for helping me out in the lab. I wish you the best for your future.

During my time at LMU Munich, our group was supported by the groups of Prof. Klaus Wanner and Prof. Daniel Merk. I am very grateful for all the practical aid, and I want specifically to thank Jörg Pabel for his help and patience during my laboratory teaching times. Furthermore, I am grateful to Lars

Acknowledgements

Allmendinger, Claudia Glas, Werner Spahl, Peter Mayer, and Claudia Ober for the endless efforts characterizing the hundreds of new compounds that I could publish during my time. I want to recognize Sandra Hemmers, Cornelia Hanich-Depner, Thuc Huong Kuno, and Christin Scharping for professionally supporting my time at LMU and Michi Geyer, Heidi Buchholz, Armin Andres, and Ronald Schürer for so many days of practical help.

From the beginning, the Centre of Nanoscience (CeNS) has supported the group with an excellent program surrounding the scientific communities in Munich, and I want to thank Susanne Hennig for organizing initiatives like the *Nano Innovation Award 2021*, which gave me the chance to present my work to a broader audience. I also want to thank Natalia Berryman from *Vossius* for guiding me to write my own patent application without having any law background. Finally, I want to recognize Mark-André Kasper from *Tubulis* for working with me toward a new generation of redox ADCs and showing some of the reality of drug development.

During my PhD time, I was supported through a scholarship by the *Studienstiftung des deutschen Volkes* that provided me excellent opportunities to meet doctorates from other areas, develop my personal skillset beyond science, and be part of a great network all over the country. I want to acknowledge Peter Antes for his continuous support and Prof. Christian Pfeleiderer for his external guidance.

At the end of my PhD time, I had the chance to realize an unprecedented PhD exchange to work at The Scripps Research Institute in San Diego. I am so grateful to Prof. Ben Cravatt for accepting me as such a visiting researcher and giving me a perfect short-term project that enabled me to advance into the exciting area of chemical proteomics. I am so thankful to David Remillard, who guided me into these new topics and showed me such a calm and efficient way of doing science. I also want to thank Kim Masuda and Margaret Hellwarth for making this exchange possible and Michael Schafroth, Chris Reinhardt, Wieland Goetzke, Martin Jäger, Garret Lindsey, Hayden Sharma, and Yijun Xiong for making my time in California such a pleasant experience.

I want to thank Vinc and Jan for their true friendship and support during the PhD years and the input from their lives keeping me on track. I also want to acknowledge my roommates Andi, Sophia, and Rike at Thalkichner WG, who withstood my presence during stressful times and created a diverting home experience. I want to thank my parents Angelika and Sascha, my brother Tilman and my grandmothers Gabi and Anne for their honest support for a thing that we mostly could not even talk about and that sometimes must have looked like an impasse from the outside.

Lastly, I want to thank Julia, who was truly committed to supporting my path in science with all her patience, capabilities, and creativity. Thank you for taking up so much useless scientific fun-facts from endless “*did you actually know that...*” conversations and for being with me.

7 Abbreviations

Concepts

(HR)MS	(high resolution) mass spectrometry
(m)RNA	(messenger) ribonucleic acid
ADC	antibody-drug conjugate
BHQ	Black Hole Quencher
BW	body weight
COSY	correlated spectroscopy
CPP	Cell-penetrating peptides
CuAAC	Copper-catalyzed azide-alkyne cycloaddition
DFT	density functional theory
DNA	deoxyribonucleic acid
dNTP	deoxyribonucleotide
DOI	Digital Object Identifier
EI	electron (impact) ionisation
ER	endoplasmic reticulum
ESI	electron spray ionization
ESIPT	excited-state intramolecular proton transfer
FACS	fluorescence-activated cell sorting (flow cytometry)
FCC	flash column chromatography
FRET	Förstner resonance energy transfer
HPLC	high performance liquid chromatography
HRE	hypoxia-responsive element
HSQC	heteronuclear multiple bond correlation
HTS	high throughput screening
HyPer	Hydrogen Peroxide Sensor
LC(MS)	liquid chromatography (mass spectrometry)
mAb	monoclonal antibody
MEF	mouse embryonic fibroblast
MQ water	MilliQ millipore filtered water
MSOT	multispectral optoacoustic tomography
MTD	maximum tolerated dosing
NIR	near infrared
NMR	nuclear magnetic resonance
PAINS	pan-assay interference compounds
PCR	polymer chain reaction
PET	photoinduced electron transfer
PK	pharmacokinetics
RNS	reactive nitrogen species
ROP	ring-opening polymerization
ROS	reactive oxygen species
RSS	reactive sulfur species
RX1	TrxR-redox-probe 1
SAR	structure-activity relationship
SecTRAP	Selenium-compromised TrxR-derived apoptotic proteins
SLR	Systematic Literature Review
SOSIP	Self-organizing surface-initiated polymerization
SuFEx	Sulfur(VI) fluoride exchange
TLC	thin layer chromatography
TMT	tandem mass tag
TRFS	Thioredoxin Reductase fluorogenic substrate
TV	tumor volume
VC / ValCit	valine-citrulline
ZPE	zero point vibrational energy

Chemical abbreviations

AA	amino acid
Asn (N)	asparagine
Asp (D)	aspartic acid
Cys (C)	cysteine
Gly (G)	glycine
His (H)	histidine
Pro (P)	proline
Sec (U)	selenocysteine
Ser (S)	serine
Thr (T)	threonine
Trp (W)	Tryptophan
Tyr (Y)	tyrosine
Val (V)	valine
PG	protecting group
Me	methyl
Et	ethyl
Pr / <i>i</i> Pr	propyl/isopropyl
Ac	acetyl
Ph	phenyl
Bn	benzyl
Bz	benzoyl
Ar	aryl/aromatic
Ms	mesyl: methanesulfonyl
Ts	tosyl: 4-toluenesulfonyl
Tf	triflyl: trifluoromethanesulfonyl
Ns	nosyl: nitrophenylsulfonyl
PMB	<i>para</i> -methoxybenzyl
Boc	<i>tert</i> -butyloxycarbonyl
Fmoc	fluorenylmethyloxycarbonyl
AU / a.u.	arbitrary units
C _{Ar} (H)	aromatic carbon/hydrogen
dpf	days post fertilization
E°	(standard) reduction potential
EC ₅₀ / IC ₅₀	half maximum effective/ /inhibitory concentration
em	emission
eq./equiv.	equivalents
exc / ex	excitation
F	(raw) fluorescence intensity
GI	growth inhibition
hpt	hours post treatment
r.t. / RT	room temperature
R _f	retention factor
r _{fx}	reflux
S/N	signal to noise
SD	standard deviation
S _N Ar	nucleophilic aromatic substitution
UV	ultraviolet
w/o	without
wt / ko / ki	wildtype / knockout / knockin
ΔStokes	Stokes shift

Abbreviations

Chemicals / Reagents (1/2)

ACE-CI	2-chloroethyl chloroformate
AF	auranofin
ATP	adenosine triphosphate
AZI	3-azetidiny-5-propoxy-indole
BCA	bicinchoninic acid
BSO	buthioninsulfoximin
BTC	triphosgene
CA	cysteamine
CA4P	combretastatin A-1 bisphosphate
CBI	cyclopropabenz[e]indole
CDPI	3-carbamoyl-1,2-dihydro-3 <i>H</i> -pyrrolo [3,2,e]indole-7-carboxylate
CI	cyclopropaindole
CPI	cyclopropapyrrolo[e]indole
DBU	diazabicycloundecene
DCM	dichloromethane / methylenechloride
DDQ	1,2-dichloro-5,6-dicyano-1,4-benzoquinone
DEI	<i>N,N</i> -dimethylaminoethoxyindole
DIAD	diisopropylazodicarboxylate
DIPEA	<i>N,N</i> -diisopropylethylamine
DMEM	Dulbecco's modified Eagle's medium
DMF	dimethylformamide
DMSO	dimethylsulfoxide
DNCB	1-chloro-2,4-dinitrobenzol
dox	doxorubicin
DTE	1,4-dithioerythritol
DTNB	5,5'-dithio-bis-(2-nitrobenzoic acid)
DTT	1,4-dithiothreitol
EDCI	1-Ethyl-3-(3-dimethylaminopropyl)carbodiimide
EDTA	ethylenediaminetetraacetic acid
ESF	ethenesulfonyl fluoride
ETP	epidithiodiketopiperazine
FA	formic acid
FAD	flavin adenine dinucleotide
FBS	fetal bovine serum
GSH	glutathione
GSSG	glutathione disulfide
HBI	4-(<i>p</i> -hydroxybenzylidene)imidazolidin-5-one
HPQ/PQ- OH	6-chloro-2-(5-chloro-2-hydroxyphenyl) quinazolin-4(3 <i>H</i>)-one
IA	iodoacetamide
ICG	indocyanine green
IG(-OH)	(2',7'-difluoro-3'-hydroxy-6'-isopropoxy-3 <i>H</i> -spiro [isobenzofuran-1,9'-xanthen]-3-one)
MEDA	<i>N,N</i> -dimethyl-cysteamine
MF-OH	3'-hydroxy-6'-methoxy-3 <i>H</i> -spiro [isobenzofuran-1,9'-xanthen]-3-one
MR(-NH ₂)	3'-amino-6'-methoxy-3 <i>H</i> -spiro [isobenzofuran-1,9'-xanthen]-3-one
NAC	<i>N</i> -acetyl cysteine
NADH	nicotinamide adenosine dinucleotide
NADPH	nicotinamide adenosine dinucleotide phosphate

Proteins / Enzymes

AP-1	activating-protein 1
APE1	apurinic endonuclease 1
ASK1	apoptosis signaling-regulating kinase 1
BSA	bovine serum albumin
CLIC1	chloride intracellular channel protein 1
CYP450	Cytochrome P450
DsbA	bacterial thiol disulfide oxidoreductase A
EGFP	enhanced green fluorescent protein
EGFR	epidermal growth factor receptor tyrosine kinase
FP	fluorescent protein
GFP	green fluorescent protein
GPx	glutathione peroxidase
GR/GSR	glutathione disulfide reductase
Grx	glutaredoxin
GSS-P _R	glutathionylated protein
GST	glutathione S-transferase
HIF-1 α	hypoxia-inducing factor 1 alpha
HIV	human immunodeficiency virus
KEAP1	Kelch-like ECH-associated protein 1
MSR	methionine sulfoxide reductase
MST1 / MSP	macrophage-stimulating (protein) 1
NF- κ B	nuclear factor kappa B
NOX	NADPH oxidase
Nrf2	nuclear factor erythroid 2-related factor 2
Nrx	nucleoredoxin
PDI	protein disulfide isomerase
PI3K/Akt	phosphatidylinositol 3-kinase / protein kinase B
PICOT	protein kinase C-interacting cousin of thioredoxin
PR	3'-5'-adenosine diphosphate reductase
PRL	phosphatase of regenerating liver
PR-SH	protein thiol
Prx	peroxiredoxin
PTEN	phosphatase and tensin homolog
PTP1B	protein-tyrosine phosphatase 1B
Ref-1	redox-factor 1
RNR	ribonucleotide reductase
roGFP	redox sensitive green fluorescent protein
rxRFP	redox-sensitive red fluorescent protein
rxYFP	redox-sensitive yellow fluorescent protein
SOD	superoxide dismutase
Srx	sulfiredoxin
TFRC	transferrin receptor
TGR	thioredoxin glutathione reductase
TMEM16F	transmembrane protein 16 F
TNF- α	tumor necrosis factor-alpha
TRP	thioredoxin related protein
TRPA1	transient receptor potential cation channel A1
TRPC5	short transient receptor potential channel 5
Trx	thioredoxin
TrxR	thioredoxin reductase
Txl	thioredoxin-like protein
VEGF	Vascular endothelial growth factor

Abbreviations

Chemicals / Reagents (2/2)

NHS	<i>N</i> -hydroxysuccinimide
PAPS	3'-phosphoadenosine-5'-phosphosulfate
PBS	phosphate-buffered saline
PEG	polyethyleneglycol
PFA	paraformaldehyde
p-TSA	<i>para</i> -toluenesulfonic acid
PX-12	1-methyl-2-imidazolyl disulfide
RPMI	Roswell Park memorial institute medium
SN-38	7-ethyl-10-hydroxy-camptothecin
TCEP	tris(2-carboxyethyl)phosphine
TE	trisaminomethane(tris)/EDTA buffer
TFA	trifluoroacetic acid
TFAA	trifluoroacetic anhydride
THF	tetrahydrofuran
TMI	5,6,7-trimethoxyindole
TRi-1	2-((4-chlorophenyl)sulfonyl)-6-methoxy-3-nitropyridine
TRi-3	4,5-dichloro-2-((5-(4-chlorophenyl)-1,3,4-oxadiazol-2-yl)methyl)
TSTU	<i>N'</i> -tetramethyl- <i>O</i> -(<i>N</i> -succinimidyl)uronium tetrafluoroborate
VTT	5-vinyl-5 <i>H</i> -thianthren-5-ium tetrafluoroborate

Institutions

ACS	American Chemical Society, Washington (USA)
ANIE	Angewandte Chemie - International Edition
ATCC	American Type Culture Collection, Manassas (USA)
BMC	Bioorganic Medicinal Chemistry
BMCL	Bioorganic Medicinal Chemistry Letters
CCDC	Cambridge Crystallographic Data Centre, Cambridge (UK)
CeNS	Centre of Nanoscience, Munich (GER)
DSMZ	Deutsche Sammlung von Mikroorganismen und Zellkulturen, Brunswick (GER)
EPO	European Patent Office, Munich (GER)
FDA	Food and Drug Administration, Silver Spring (USA)
IFZ	Interdisciplinary Research Centre, Giessen (GER)
JACS	Journal of the American Chemical Society
JMC	Journal of Medicinal Chemistry
JOC	The Journal of Organic Chemistry
LMU	Ludwig-Maximilians-Universität, Munich (GER)
LOPAC	Library of Pharmaceutically Active Compounds
NCATS	National Center for Advancing Translational Sciences, Bethesda (USA)
NCI	National Cancer Institute, Bethesda (USA)
NIH	National Institute of Health, Bethesda (USA)
NMRI	Naval Medical Research Institute, Bethesda (USA)
PCT	Patent Cooperation Treaty
PDB	protein database
TU	Technical University
UniProt	Universal Protein Resource
WIPO	World Intellectual Property Organization, Geneva (CH)

8 References

- (1) Arnér, E. S. J. Selenoproteins - What Unique Properties Can Arise with Selenocysteine in Place of Cysteine? *Exp. Cell Res.* **2010**, *316* (8), 1296–1303. <https://doi.org/10.1016/j.yexcr.2010.02.032>.
- (2) Chivers, P. T.; Prehoda, K. E.; Raines, R. T. The CXXC Motif: A Rheostat in the Active Site. *Biochemistry* **1997**, *36* (14), 4061–4066. <https://doi.org/10.1021/bi9628580>.
- (3) Sousa, S. F.; Neves, R. P. P.; Waheed, S. O.; Fernandes, P. A.; Ramos, M. J. Structural and Mechanistic Aspects of S-S Bonds in the Thioredoxin-like Family of Proteins. *Biol. Chem.* **2019**, *400* (5), 575–587. <https://doi.org/10.1515/hsz-2018-0319>.
- (4) Reddie, K. G.; Carroll, K. S. Expanding the Functional Diversity of Proteins through Cysteine Oxidation. *Curr. Opin. in Chem. Biol.* **2008**, *12* (6), 746–754. <https://doi.org/10.1016/j.cbpa.2008.07.028>.
- (5) Gupta, V.; Carroll, K. S. Sulfenic Acid Chemistry, Detection and Cellular Lifetime. *BBA - General Subjects* **2014**, *1840* (2), 847–875. <https://doi.org/10.1016/j.bbagen.2013.05.040>.
- (6) Nagy, P.; Winterbourn, C. C. Redox Chemistry of Biological Thiols. In *Advances in Molecular Toxicology*; Elsevier, 2010; Vol. 4, pp 183–222. [https://doi.org/10.1016/S1872-0854\(10\)04006-3](https://doi.org/10.1016/S1872-0854(10)04006-3).
- (7) Hudson, D. A.; Gannon, S. A.; Thorpe, C. Oxidative Protein Folding: From Thiol–Disulfide Exchange Reactions to the Redox Poise of the Endoplasmic Reticulum. *Free Rad. Biol. Med.* **2015**, *80*, 171–182. <https://doi.org/10.1016/j.freeradbiomed.2014.07.037>.
- (8) Wiedemann, C.; Kumar, A.; Lang, A.; Ohlenschläger, O. Cysteines and Disulfide Bonds as Structure-Forming Units: Insights From Different Domains of Life and the Potential for Characterization by NMR. *Front. Chem.* **2020**, *8*.
- (9) Nagy, P. Kinetics and Mechanisms of Thiol–Disulfide Exchange Covering Direct Substitution and Thiol Oxidation-Mediated Pathways. *Antioxidants & Redox Signalling* **2013**, *18* (13), 1623–1641. <https://doi.org/10.1089/ars.2012.4973>.
- (10) Meyer, Y.; Buchanan, B. B.; Vignols, F.; Reichheld, J.-P. Thioredoxins and Glutaredoxins: Unifying Elements in Redox Biology. *Annual Review of Genetics* **2009**, *43* (1), 335–367. <https://doi.org/10.1146/annurev-genet-102108-134201>.
- (11) Thakur, S.; Sarkar, B.; Cholia, R. P.; Gautam, N.; Dhiman, M.; Mantha, A. K. APE1/Ref-1 as an Emerging Therapeutic Target for Various Human Diseases: Phytochemical Modulation of Its Functions. *Exp. Mol. Med.* **2014**, *46* (7), e106–e106. <https://doi.org/10.1038/emmm.2014.42>.
- (12) Hirota, K.; Matsui, M.; Iwata, S.; Nishiyama, A.; Mori, K.; Yodoi, J. AP-1 Transcriptional Activity Is Regulated by a Direct Association between Thioredoxin and Ref-1. *Proc. Natl. Acad. Sci. U.S.A.* **1997**, *94* (8), 3633–3638. <https://doi.org/10.1073/pnas.94.8.3633>.
- (13) Yin, Z.; Machius, M.; Nestler, E. J.; Rudenko, G. Activator Protein-1: Redox Switch Controlling Structure and DNA-Binding. *Nucl. Acid Res.* **2017**, *45* (19), 11425–11436. <https://doi.org/10.1093/nar/gkx795>.
- (14) Schmidt, B.; Ho, L.; Hogg, P. J. Allosteric Disulfide Bonds. *Biochemistry* **2006**, *45* (24), 7429–7433. <https://doi.org/10.1021/bi0603064>.
- (15) Uhlin, U.; Eklund, H. Structure of Ribonucleotide Reductase Protein R1. *Nature* **1994**, *370* (6490), 533–539. <https://doi.org/10.1038/370533a0>.
- (16) Brignole, E. J.; Tsai, K.-L.; Chittuluru, J.; Li, H.; Aye, Y.; Penczek, P. A.; Stubbe, J.; Drennan, C. L.; Asturias, F. 3.3-Å Resolution Cryo-EM Structure of Human Ribonucleotide Reductase with Substrate and Allosteric Regulators Bound. *eLife* **2018**, *7*, e31502. <https://doi.org/10.7554/eLife.31502>.
- (17) Minnihan, E. C.; Nocera, D. G.; Stubbe, J. Reversible, Long-Range Radical Transfer in E. Coli Class Ia Ribonucleotide Reductase. *Acc. Chem. Res.* **2013**, *46* (11), 2524–2535. <https://doi.org/10.1021/ar4000407>.
- (18) Holmgren, A.; Johansson, C.; Berndt, C.; Lönn, M. E.; Hudemann, C.; Lillig, C. H. Thiol Redox Control via Thioredoxin and Glutaredoxin Systems. *Biochemical Society Transactions* **2005**, *33* (6), 1375. <https://doi.org/10.1042/BST20051375>.
- (19) Schulz, G. E.; Schirmer, R. H.; Sachsenheimer, W.; Pai, E. F. The Structure of the Flavoenzyme Glutathione Reductase. *Nature* **1978**, *273* (5658), 120–124. <https://doi.org/10.1038/273120a0>.
- (20) Deponte, M. Glutathione Catalysis and the Reaction Mechanisms of Glutathione-Dependent Enzymes. *BBA - General Subjects* **2013**, *1830* (5), 3217–3266. <https://doi.org/10.1016/j.bbagen.2012.09.018>.
- (21) Ladenstein, R.; Epp, O.; Bartels, K.; Jones, A.; Huber, R.; Wendel, A. Structure Analysis and Molecular Model of the Selenoenzyme Glutathione Peroxidase at 2.8 Å Resolution. *J. Mol. Biol.* **1979**, *134* (2), 199–218. [https://doi.org/10.1016/0022-2836\(79\)90032-9](https://doi.org/10.1016/0022-2836(79)90032-9).
- (22) Mills, G. C. Hemoglobin Catabolism. I. Glutathione Peroxidase, an Erythrocyte Enzyme Which Protects Hemoglobin from Oxidative Breakdown. *J. Biol. Chem.* **1957**, *229* (1), 189–197. [https://doi.org/10.1016/S0021-9258\(18\)70608-X](https://doi.org/10.1016/S0021-9258(18)70608-X).
- (23) Seibt, T. M.; Proneth, B.; Conrad, M. Role of GPX4 in Ferroptosis and Its Pharmacological Implication. *Free Rad. Biol. Med.* **2019**, *133*, 144–152. <https://doi.org/10.1016/j.freeradbiomed.2018.09.014>.
- (24) Sagemark, J.; Elgan, T. H.; Burglin, T. R.; Johansson, C.; Holmgren, A.; Berndt, K. D. Redox Properties and Evolution of Human Glutaredoxins. *Proteins: Structure, Function, and Bioinformatics* **2007**, *68* (4), 879–892.
- (25) Lillig, C. H.; Berndt, C. Glutaredoxins in Thiol/Disulfide Exchange. *Antioxidants & Redox Signaling* **2013**, *18* (13), 1654–1665. <https://doi.org/10.1089/ars.2012.5007>.
- (26) Begas, P.; Liedgens, L.; Moseler, A.; Meyer, A. J.; Deponte, M. Glutaredoxin Catalysis Requires Two Distinct Glutathione Interaction Sites. *Nat. Commun.* **2017**, *8* (1), 14835. <https://doi.org/10.1038/ncomms14835>.
- (27) Iversen, R.; Andersen, P. A.; Jensen, K. S.; Winther, J. R.; Sigurskjold, B. W. Thiol–Disulfide Exchange between Glutaredoxin and Glutathione. *Biochemistry* **2010**, *49* (4), 810–820. <https://doi.org/10.1021/bi9015956>.
- (28) Wang, J.; Boja, E. S.; Tan, W.; Tekle, E.; Fales, H. M.; English, S.; Mieval, J. J.; Chock, P. B. Reversible Glutathionylation Regulates Actin Polymerization in A431 Cells. *J. Biol. Chem.* **2001**, *276* (51), 47763–47766. <https://doi.org/10.1074/jbc.C100415200>.
- (29) Xiong, Y.; Manevich, Y.; Tew, K. D.; Townsend, D. M. S-Glutathionylation of Protein Disulfide Isomerase Regulates Estrogen Receptor Stability and Function. *International Journal of Cell Biology* **2012**, *2012*, e273549. <https://doi.org/10.1155/2012/273549>.
- (30) Appenzeller-Herzog, C.; Ellgaard, L. In Vivo Reduction-Oxidation State of Protein Disulfide Isomerase: The Two Active Sites Independently Occur in the Reduced and Oxidized Forms. *Antioxidants & Redox Signaling* **2008**, *10* (1), 55–64. <https://doi.org/10.1089/ars.2007.1837>.
- (31) Freedman, R. B.; Brockway, B. E.; Nigel, L. Protein Disulfide-Isomerase and the Formation of Native Disulfide Bonds. *Biochemical Society Transactions* **1984**, *12* (6), 929–932. <https://doi.org/10.1042/bst10120929>.
- (32) Wilkinson, B.; Gilbert, H. F. Protein Disulfide Isomerase. *BBA - General Subjects* **2004**, *1699* (1–2), 35–44. [https://doi.org/10.1016/S1570-9639\(04\)00063-9](https://doi.org/10.1016/S1570-9639(04)00063-9).
- (33) Zhong, L.; Arnér, E. S. J.; Holmgren, A. Structure and Mechanism of Mammalian Thioredoxin Reductase: The Active Site Is a Redox-Active Selenothiol/Selenenylsulfide Formed from the Conserved Cysteine-Selenocysteine Sequence.

References

- Proceedings of the National Academy of Sciences* **2000**, *97* (11), 5854–5859. <https://doi.org/10.1073/pnas.100114897>.
- (34) Fritz-Wolf, K.; Kehr, S.; Stumpf, M.; Rahlfs, S.; Becker, K. Crystal Structure of the Human Thioredoxin Reductase–Thioredoxin Complex. *Nat. Commun.* **2011**, *2* (383), 1–8. <https://doi.org/10.1038/ncomms1382>.
- (35) Cheng, Q.; Sandalova, T.; Lindqvist, Y.; Arnér, E. S. J. Crystal Structure and Catalysis of the Selenoprotein Thioredoxin Reductase 1. *J. Biol. Chem.* **2009**, *284* (6), 3998–4008. <https://doi.org/10.1074/jbc.M807068200>.
- (36) Lu, J.; Holmgren, A. Selenoproteins. *J. Biol. Chem.* **2009**, *284* (2), 723–727. <https://doi.org/10.1074/jbc.R800045200>.
- (37) Arnér, E. S. J. Focus on Mammalian Thioredoxin Reductases — Important Selenoproteins with Versatile Functions. *Biochimica et Biophysica Acta - General Subjects* **2009**, *1790* (6), 495–526. <https://doi.org/10.1016/j.bbagen.2009.01.014>.
- (38) Lu, J.; Holmgren, A. The Thioredoxin Antioxidant System. *Free Radical Biology and Medicine* **2014**, *66*, 75–87. <https://doi.org/10.1016/j.freeradbiomed.2013.07.036>.
- (39) Mandal, P. K. Complex Redundancy between the Mammalian Thioredoxin and Glutathione Systems in Cell Proliferation and Tumorigenesis, Ludwig-Maximilian-University Munich, Munich, 2009. https://edoc.ub.uni-muenchen.de/11958/1/Mandal_Pankaj_Kumar.pdf (accessed 2021-08-19).
- (40) Du, Y.; Zhang, H.; Lu, J.; Holmgren, A. Glutathione and Glutaredoxin Act as a Backup of Human Thioredoxin Reductase 1 to Reduce Thioredoxin 1 Preventing Cell Death by Aurothioglucose. *J. Biol. Chem.* **2012**, *287* (45), 38210–38219. <https://doi.org/10.1074/jbc.M112.392225>.
- (41) Fernandes, A. P.; Holmgren, A. Glutaredoxins: Glutathione-Dependent Redox Enzymes with Functions Far Beyond a Simple Thioredoxin Backup System. *Antioxidants & Redox Signaling* **2004**, *6* (1), 63–74. <https://doi.org/10.1089/152308604771978354>.
- (42) Laurent, T. C.; Moore, E. C.; Reichard, P. Enzymatic Synthesis of Deoxyribonucleotides. *J. Biol. Chem.* **1964**, *239* (10), 3436–3444. [https://doi.org/10.1016/S0021-9258\(18\)97742-2](https://doi.org/10.1016/S0021-9258(18)97742-2).
- (43) Holmgren, A. Thioredoxin. *Ann. Rev. Biochem.* **1985**, *54*, 237–271.
- (44) Collet, J.-F.; Messens, J. Structure, Function, and Mechanism of Thioredoxin Proteins. *Antioxidants & Redox Signaling* **2010**, *13* (8), 1205–1216. <https://doi.org/10.1089/ars.2010.3114>.
- (45) Lillig, C. H.; Holmgren, A. Thioredoxin and Related Molecules—From Biology to Health and Disease. *Antioxidants & Redox Signaling* **2007**, *9* (1), 25–47. <https://doi.org/10.1089/ars.2007.9.25>.
- (46) Matsuzawa, A.; Ichijo, H. Redox Control of Cell Fate by MAP Kinase: Physiological Roles of ASK1-MAP Kinase Pathway in Stress Signaling. *BBA - General Subjects* **2008**, *1780* (11), 1325–1336. <https://doi.org/10.1016/j.bbagen.2007.12.011>.
- (47) Muri, J.; Thut, H.; Feng, Q.; Kopf, M. Thioredoxin-1 Distinctly Promotes NF- κ B Target DNA Binding and NLRP3 Inflammasome Activation Independently of Txnip. *eLife* **2020**, *9*, e53627. <https://doi.org/10.7554/eLife.53627>.
- (48) Matthews, J. R.; Wakasugi, N.; Virelizier, J.-L.; Yodoi, J.; Hay, R. T. Thioredoxin Regulates the DNA Binding Activity of by Reduction of a Disulphide Bond Involving Cysteine 62. *Nucl. Acid Res.* **1992**, *20* (15), 11.
- (49) Welsh, S. J.; Bellamy, W. T.; Briehl, M. M.; Powis, G. The Redox Protein Thioredoxin-1 (Trx1) Increases Hypoxia-Inducible Factor 1 α Protein Expression: Trx1 Overexpression Results in Increased Vascular Endothelial Growth Factor Production and Enhanced Tumor Angiogenesis. *Cancer Res.* **2002**, *62*, 5089.
- (50) Xanthoudakis, S.; Curran, T. Identification and Characterization of Ref-1, a Nuclear Protein That Facilitates AP-1 DNA-Binding Activity. *The EMBO Journal* **1992**, *11* (2), 653–665. <https://doi.org/10.1002/j.1460-2075.1992.tb05097.x>.
- (51) Ueno, M.; Masutani, H.; Arai, R. J.; Yamauchi, A.; Hirota, K.; Sakai, T.; Inamoto, T.; Yamaoka, Y.; Yodoi, J.; Nikaido, T. Thioredoxin-Dependent Redox Regulation of P53-Mediated P21 Activation. *J. Biol. Chem.* **1999**, *274* (50), 35809–35815. <https://doi.org/10.1074/jbc.274.50.35809>.
- (52) López-Grueso, M.; González-Ojeda, R.; Requejo-Aguilar, R.; McDonagh, B.; Fuentes-Almagro, C.; Muntané, J.; Bárcena, J. A.; Padilla, C. Thioredoxin and Glutaredoxin Regulate Metabolism through Different Multiplex Thiol Switches. *Redox Biology* **2019**, *21*, 101049. <https://doi.org/10.1016/j.redox.2018.11.007>.
- (53) Woo, J. R.; Kim, S. J.; Jeong, W.; Cho, Y. H.; Lee, S. C.; Chung, Y. J.; Rhee, S. G.; Ryu, S. E. Structural Basis of Cellular Redox Regulation by Human TRP14. *J. Biol. Chem.* **2004**, *279* (46), 48120–48125. <https://doi.org/10.1074/jbc.M407079200>.
- (54) Espinosa, B.; Arnér, E. S. J. Thioredoxin-Related Protein of 14 kDa as a Modulator of Redox Signalling Pathways: TRP14 in Redox Signalling. *British J. Pharmacol.* **2019**, *176* (4), 544–553. <https://doi.org/10.1111/bph.14479>.
- (55) Jeong, W.; Jung, Y.; Kim, H.; Park, S. J.; Rhee, S. G. Thioredoxin-Related Protein 14, a New Member of the Thioredoxin Family with Disulfide Reductase Activity: Implication in the Redox Regulation of TNF- α Signaling. *Free Rad. Biol. Med.* **2009**, *47* (9), 1294–1303. <https://doi.org/10.1016/j.freeradbiomed.2009.07.021>.
- (56) Andersen, K. M.; Madsen, L.; Prag, S.; Johnsen, A. H.; Semple, C. A.; Hendil, K. B.; Hartmann-Petersen, R. Thioredoxin Txn1/TRP32 Is a Redox-Active Cofactor of the 26 S Proteasome. *J. Biol. Chem.* **2009**, *284* (22), 15246–15254. <https://doi.org/10.1074/jbc.M900016200>.
- (57) Ishii, T.; Funato, Y.; Miki, H. Thioredoxin-Related Protein 32 (TRP32) Specifically Reduces Oxidized Phosphatase of Regenerating Liver (PRL). *J. Biol. Chem.* **2013**, *288* (10), 7263–7270. <https://doi.org/10.1074/jbc.M112.418004>.
- (58) Rhee, S. G. Overview on Peroxiredoxin. *Molecules and Cells* **2016**, *39* (1), 1–5. <https://doi.org/10.14348/molcells.2016.2368>.
- (59) Espinosa-Diez, C.; Miguel, V.; Mennerich, D.; Kietzmann, T.; Sánchez-Pérez, P.; Cadenas, S.; Lamas, S. Antioxidant Responses and Cellular Adjustments to Oxidative Stress. *Redox Biology* **2015**, *6*, 183–197. <https://doi.org/10.1016/j.redox.2015.07.008>.
- (60) Hanschmann, E.-M.; Godoy, J. R.; Berndt, C.; Hudemann, C.; Lillig, C. H. Thioredoxins, Glutaredoxins, and Peroxiredoxins - Molecular Mechanisms and Health Significance: From Cofactors to Antioxidants to Redox Signaling. *Antioxidants & Redox Signaling* **2013**, *19* (13), 1539–1605. <https://doi.org/10.1089/ars.2012.4599>.
- (61) Rhee, S. G.; Jeong, W.; Chang, T.-S.; Woo, H. A. Sulfiredoxin, the Cysteine Sulfenic Acid Reductase Specific to 2-Cys Peroxiredoxin: Its Discovery, Mechanism of Action, and Biological Significance. *Kidney International* **2007**, *72*, S3–S8. <https://doi.org/10.1038/sj.ki.5002380>.
- (62) Jeong, W.; Bae, S. H.; Toledano, M. B.; Rhee, S. G. Role of Sulfiredoxin as a Regulator of Peroxiredoxin Function and Regulation of Its Expression. *Free Rad. Biol. Med.* **2012**, *53* (3), 447–456. <https://doi.org/10.1016/j.freeradbiomed.2012.05.020>.
- (63) Banerjee, R. Redox Outside the Box: Linking Extracellular Redox Remodeling with Intracellular Redox Metabolism. *J. Biol. Chem.* **2012**, *287* (7), 4397–4402. <https://doi.org/10.1074/jbc.R111.287995>.
- (64) Lorenzen, I.; Eble, J. A.; Hanschmann, E.-M. Thiol Switches in Membrane Proteins - Extracellular Redox Regulation in Cell Biology. *Biol. Chem.* **2021**, *402* (3), 253–269. <https://doi.org/10.1515/hsz-2020-0266>.
- (65) Laurent, Q.; Martinent, R.; Lim, B.; Pham, A.-T.; Kato, T.; López-Andarias, J.; Sakai, N.; Matile, S. Thiol-Mediated

References

- Uptake. *JACS Au* **2021**, *1* (6), 710–728. <https://doi.org/10.1021/jacsau.1c00128>.
- (66) Torres, A. G.; Gait, M. J. Exploiting Cell Surface Thiols to Enhance Cellular Uptake. *Trends in Biotechnology* **2012**, *30* (4), 185–190. <https://doi.org/10.1016/j.tibtech.2011.12.002>.
- (67) Dammeyer, P.; Arnér, E. S. J. Human Protein Atlas of Redox Systems - What Can Be Learnt? *BBA - General Subjects* **2011**, *1810* (1), 111–138. <https://doi.org/10.1016/j.bbagen.2010.07.004>.
- (68) Jones, D. P. Redox Potential of GSH/GSSG Couple: Assay and Biological Significance. In *Methods in Enzymology*; Sies, H., Packer, L., Eds.; Protein Sensors and Reactive Oxygen Species - Part B: Thiol Enzymes and Proteins; Academic Press, 2002; Vol. 348, pp 93–112. [https://doi.org/10.1016/S0076-6879\(02\)48630-2](https://doi.org/10.1016/S0076-6879(02)48630-2).
- (69) Flohé, L. The Fairytale of the GSSG/GSH Redox Potential. *BBA - General Subjects* **2013**, *1830* (5), 3139–3142. <https://doi.org/10.1016/j.bbagen.2012.10.020>.
- (70) Åslund, F.; Berndt, K. D.; Holmgren, A. Redox Potentials of Glutaredoxins and Other Thiol-Disulfide Oxidoreductases of the Thioredoxin Superfamily Determined by Direct Protein-Protein Redox Equilibria. *J. Biol. Chem.* **1997**, *272* (49), 30780–30786. <https://doi.org/10.1074/jbc.272.49.30780>.
- (71) Watson, W. H.; Pohl, J.; Montfort, W. R.; Stuchlik, O.; Reed, M. S.; Powis, G.; Jones, D. P. Redox Potential of Human Thioredoxin 1 and Identification of a Second Dithiol/Disulfide Motif. *J. Biol. Chem.* **2003**, *278* (35), 33408–33415. <https://doi.org/10.1074/jbc.M211107200>.
- (72) Mössner, E.; Huber-Wunderlich, M.; Rietsch, A.; Beckwith, J.; Glockshuber, R.; Åslund, F. Importance of Redox Potential for the in Vivo Function of the Cytoplasmic Disulfide Reductant Thioredoxin from *Escherichia Coli* *. *J. Biol. Chem.* **1999**, *274* (36), 25254–25259. <https://doi.org/10.1074/jbc.274.36.25254>.
- (73) Lundström, J.; Holmgren, A. Determination of the Reduction-Oxidation Potential of the Thioredoxin-like Domains of Protein Disulfide-Isomerase from the Equilibrium with Glutathione and Thioredoxin. *Biochemistry* **1993**, *32* (26), 6649–6655. <https://doi.org/10.1021/bi00077a018>.
- (74) Cleland, W. W. Dithiothreitol, a New Protective Reagent for SH Groups. *Biochemistry* **1964**, *3* (4), 480–482. <https://doi.org/10.1021/bi00892a002>.
- (75) Zong, L.; Bartolami, E.; Abegg, D.; Adibekian, A.; Sakai, N.; Matile, S. Epidithiodiketopiperazines: Strain-Promoted Thiol-Mediated Cellular Uptake at the Highest Tension. *ACS Cent. Sci.* **2017**, *3* (5), 449–453. <https://doi.org/10.1021/acscentsci.7b00080>.
- (76) Carvalho, A. P.; Fernandes, P. A.; Ramos, M. J. Similarities and Differences in the Thioredoxin Superfamily. *Progress in Biophysics and Molecular Biology* **2006**, *91* (3), 229–248. <https://doi.org/10.1016/j.pbiomolbio.2005.06.012>.
- (77) Krause, G.; Lundström, J.; Barea, J. L.; Pueyo de la Cuesta, C.; Holmgren, A. Mimicking the Active Site of Protein Disulfide-Isomerase by Substitution of Proline 34 in *Escherichia Coli* Thioredoxin. *J. Biol. Chem.* **1991**, *266* (15), 9494–9500. [https://doi.org/10.1016/S0021-9258\(18\)92848-6](https://doi.org/10.1016/S0021-9258(18)92848-6).
- (78) Lundström, J.; Krause, G.; Holmgren, A. A Pro to His Mutation in Active Site of Thioredoxin Increases Its Disulfide-Isomerase Activity 10-Fold. New Refolding Systems for Reduced or Randomly Oxidized Ribonuclease. *J. Biol. Chem.* **1992**, *267* (13), 9047–9052. [https://doi.org/10.1016/S0021-9258\(19\)50386-6](https://doi.org/10.1016/S0021-9258(19)50386-6).
- (79) Mössner, E.; Huber-Wunderlich, M.; Glockshuber, R. Characterization of *Escherichia Coli* Thioredoxin Variants Mimicking the Active-Sites of Other Thiol/Disulfide Oxidoreductases. *Prot. Sci.* **1998**, *7* (5), 1233–1244.
- (80) Gleason, F. K.; Lim, C. J.; Gerami-Nejad, M.; Fuchs, J. A. Characterization of *Escherichia Coli* Thioredoxins with Altered Active Site Residues. *Biochemistry* **1990**, *29* (15), 3701–3709. <https://doi.org/10.1021/bi00467a016>.
- (81) Roos, G.; Garcia-Pino, A.; Van Belle, K.; Brosens, E.; Wahni, K.; Vandebussche, G.; Wyns, L.; Loris, R.; Messens, J. The Conserved Active Site Proline Determines the Reducing Power of *Staphylococcus Aureus* Thioredoxin. *J. Mol. Biol.* **2007**, *368* (3), 800–811. <https://doi.org/10.1016/j.jmb.2007.02.045>.
- (82) Siedler, F.; Rudolph-Boehner, S.; Doi, M.; Musiol, H. J.; Moroder, L. Redox Potentials of Active-Site Bis(Cysteiny)l Fragments of Thiol-Protein Oxidoreductases. *Biochemistry* **1993**, *32* (29), 7488–7495. <https://doi.org/10.1021/bi00080a021>.
- (83) Chakrabarti, A.; Srivastava, S.; Swaminathan, C. P.; Surolia, A.; Varadarajan, R. Thermodynamics of Replacing an α -Helical Pro Residue in the P40S Mutant of *Escherichia Coli* Thioredoxin. *Prot. Sci.* **1999**, *8* (11), 2455–2459. <https://doi.org/10.1110/ps.8.11.2455>.
- (84) de Lamotte-Guéry, F.; Pruvost, C.; Minard, P.; Delsuc, M. A.; Miginiac-Maslow, M.; Schmitter, J. M.; Stein, M.; Decottignies, P. Structural and Functional Roles of a Conserved Proline Residue in the Alpha2 Helix of *Escherichia Coli* Thioredoxin. *Protein Engineering, Design and Selection* **1997**, *10* (12), 1425–1432. <https://doi.org/10.1093/protein/10.12.1425>.
- (85) Gleason, F. K. Mutation of Conserved Residues in *Escherichia Coli* Thioredoxin: Effects on Stability and Function. *Prot. Sci.* **1992**, *1* (5), 609–616. <https://doi.org/10.1002/pro.5560010507>.
- (86) Garcia-Pino, A.; Martínez-Rodríguez, S.; Wahni, K.; Wyns, L.; Loris, R.; Messens, J. Coupling of Domain Swapping to Kinetic Stability in a Thioredoxin Mutant. *J. Mol. Biol.* **2009**, *385* (5), 1590–1599. <https://doi.org/10.1016/j.jmb.2008.11.040>.
- (87) Chivers, P. T.; Raines, R. T. General Acid/Base Catalysis in the Active Site of *Escherichia Coli* Thioredoxin. *Biochemistry* **1997**, *36* (50), 15810–15816. <https://doi.org/10.1021/bi9715041>.
- (88) Roos, G.; Foloppe, N.; Van Laer, K.; Wyns, L.; Nilsson, L.; Geerlings, P.; Messens, J. How Thioredoxin Dissociates Its Mixed Disulfide. *PLoS Comput Biol* **2009**, *5* (8), e1000461. <https://doi.org/10.1371/journal.pcbi.1000461>.
- (89) Jensen, K. S.; Hansen, R. E.; Winther, J. R. Kinetic and Thermodynamic Aspects of Cellular Thiol-Disulfide Redox Regulation. *Antioxidants & Redox Signaling* **2009**, *11* (5), 1047–1058. <https://doi.org/10.1089/ars.2008.2297>.
- (90) Roos, G.; Foloppe, N.; Messens, J. Understanding the pK_a of Redox Cysteines: The Key Role of Hydrogen Bonding. *Antioxidants & Redox Signaling* **2013**, *18* (1), 94–127. <https://doi.org/10.1089/ars.2012.4521>.
- (91) Foloppe, N.; Nilsson, L. The Glutaredoxin -C-P-Y-C- Motif: Influence of Peripheral Residues. *Structure* **2004**, *12* (2), 289–300. <https://doi.org/10.1021/bi0001501>.
- (92) Huber-Wunderlich, M.; Glockshuber, R. A Single Dipeptide Sequence Modulates the Redox Properties of a Whole Enzyme Family. *Folding and Design* **1998**, *3* (3), 161–171. [https://doi.org/10.1016/S1359-0278\(98\)00024-8](https://doi.org/10.1016/S1359-0278(98)00024-8).
- (93) Dillet, V.; Dyson, H. J.; Bashford, D. Calculations of Electrostatic Interactions and PKas in the Active Site of *Escherichia Coli* Thioredoxin. *Biochemistry* **1998**, *37* (28), 10298–10306. <https://doi.org/10.1021/bi980333x>.
- (94) Berndt, C.; Schwenn, J.-D.; Lillig, C. H. The Specificity of Thioredoxins and Glutaredoxins Is Determined by Electrostatic and Geometric Complementarity. *Chem. Sci.* **2015**, *6* (12), 7049–7058. <https://doi.org/10.1039/C5SC01501D>.
- (95) Kim, S. J.; Woo, J. R.; Hwang, Y. S.; Jeong, D. G.; Shin, D. H.; Kim, K.; Ryu, S. E. The Tetrameric Structure of *Haemophilus Influenza* Hybrid Prx5 Reveals Interactions between Electron Donor and Acceptor Proteins. *J. Biol. Chem.* **2003**, *278* (12), 10790–10798. <https://doi.org/10.1074/jbc.M209553200>.
- (96) Alberts, B. *Essentials of Cell Biology - Chapter 20: Cell Communications. Tissues, Stem Cells and Cancer*, 4th ed.; Garland Science, Taylor & Francis Group, 2014.

References

- (97) What Is Cancer? The Definition of Cancer. *National Institute of Health (NIH) - National Cancer Institute (NCI)*.
- (98) Hanahan, D.; Weinberg, R. A. The Hallmarks of Cancer. *Cell* **2000**, *100* (1), 57–70. [https://doi.org/10.1016/S0092-8674\(00\)81683-9](https://doi.org/10.1016/S0092-8674(00)81683-9).
- (99) Hanahan, D.; Weinberg, R. A. Hallmarks of Cancer: The Next Generation. *Cell* **2011**, *144* (5), 646–674. <https://doi.org/10.1016/j.cell.2011.02.013>.
- (100) Hornsveld, M.; Dansen, T. B. The Hallmarks of Cancer from a Redox Perspective. *Antioxidants & Redox Signaling* **2016**, *25* (6), 300–325. <https://doi.org/10.1089/ars.2015.6580>.
- (101) Arnér, E. S. J.; Holmgren, A. The Thioredoxin System in Cancer. *Seminars in Cancer Biology* **2006**, *16* (6), 420–426. <https://doi.org/10.1016/j.semcancer.2006.10.009>.
- (102) Kim, H. J.; Chae, H.-Z.; Kim, Y.-J.; Kim, Y. H.; Hwang, T.-S.; Park, E.-M.; Park, Y.-M. Preferential Elevation of Prx I and Trx Expression in Lung Cancer Cells Following Hypoxia and in Human Lung Cancer Tissues. *Cell Biol. Toxicol.* **2003**, *19* (5), 285–298. <https://doi.org/10.1023/B:CBTO.0000004952.07979.3d>.
- (103) Hedley, D.; Pintilie, M.; Woo, J.; Nicklee, T.; Morrison, A.; Birlle, D.; Fyles, A.; Milosevic, M.; Hill, R. Up-Regulation of the Redox Mediators Thioredoxin and Apurinic/Apyrimidinic Excision (APE)/Ref-1 in Hypoxic Microregions of Invasive Cervical Carcinomas, Mapped Using Multispectral, Wide-Field Fluorescence Image Analysis. *The American Journal of Pathology* **2004**, *164* (2), 557–565. [https://doi.org/10.1016/S0002-9440\(10\)63145-8](https://doi.org/10.1016/S0002-9440(10)63145-8).
- (104) Raffel, J.; Bhattacharyya, A. K.; Gallegos, A.; Cui, H.; Einspahr, J. G.; Alberts, D. S.; Powis, G. Increased Expression of Thioredoxin-1 in Human Colorectal Cancer Is Associated with Decreased Patient Survival. *Journal of Laboratory and Clinical Medicine* **2003**, *142* (1), 46–51. [https://doi.org/10.1016/S0022-2143\(03\)00068-4](https://doi.org/10.1016/S0022-2143(03)00068-4).
- (105) Grogan, T. M.; Fenoglio-Prieser, C.; Zeheb, R.; Bellamy, W.; Frutiger, Y.; Vela, E.; Stemmerman, G.; Macdonald, J.; Richter, L.; Gallegos, A.; Powis, G. Thioredoxin, a Putative Oncogene Product, Is Overexpressed in Gastric Carcinoma and Associated with Increased Proliferation and Increased Cell Survival. *Human Pathology* **2000**, *31* (4), 475–481. <https://doi.org/10.1053/hp.2000.6546>.
- (106) Cha, M.-K.; Suh, K.-H.; Kim, I.-H. Overexpression of Peroxiredoxin I and Thioredoxin1 in Human Breast Carcinoma. *J. Exp. Clin. Cancer Res.* **2009**, *28* (1), 93. <https://doi.org/10.1186/1756-9966-28-93>.
- (107) Hoesel, B.; Schmid, J. A. The Complexity of NF-KB Signaling in Inflammation and Cancer. *Mol. Cancer* **2013**, *12* (1), 86. <https://doi.org/10.1186/1476-4598-12-86>.
- (108) Liu, T.; Zhang, L.; Joo, D.; Sun, S.-C. NF-KB Signaling in Inflammation. *Sig. Transduct. Target Ther.* **2017**, *2* (1), 1–9. <https://doi.org/10.1038/sigtrans.2017.23>.
- (109) Cebula, M.; Schmidt, E. E.; Arnér, E. S. J. TrxR1 as a Potent Regulator of the Nrf2-Keap1 Response System. *Antioxidants & Redox Signaling* **2015**, *23* (10), 823–853. <https://doi.org/10.1089/ars.2015.6378>.
- (110) He, F.; Ru, X.; Wen, T. NRF2, a Transcription Factor for Stress Response and Beyond. *International Journal of Molecular Sciences* **2020**, *21* (13), 4777. <https://doi.org/10.3390/ijms21134777>.
- (111) Ahmed, S. M. U.; Luo, L.; Namani, A.; Wang, X. J.; Tang, X. Nrf2 Signaling Pathway: Pivotal Roles in Inflammation. *BBA - General Subjects* **2017**, *1863* (2), 585–597. <https://doi.org/10.1016/j.bbadis.2016.11.005>.
- (112) Marei, H. E.; Althani, A.; Affi, N.; Hasan, A.; Caceci, T.; Pozzoli, G.; Morrione, A.; Giordano, A.; Cenciarelli, C. P53 Signaling in Cancer Progression and Therapy. *Cancer Cell International* **2021**, *21* (1), 703. <https://doi.org/10.1186/s12935-021-02396-8>.
- (113) Eferl, R.; Wagner, E. F. AP-1: A Double-Edged Sword in Tumorigenesis. *Nat. Rev. Cancer* **2003**, *3* (11), 859–868. <https://doi.org/10.1038/nrc1209>.
- (114) Lu, J.; Holmgren, A. Thioredoxin System in Cell Death Progression. *Antioxidants & Redox Signaling* **2012**, *17* (12), 1738–1747. <https://doi.org/10.1089/ars.2012.4650>.
- (115) Nordberg, J.; Arnér, E. S. J. Reactive Oxygen Species, Antioxidants, and the Mammalian Thioredoxin System. *Free Rad. Biol. Med.* **2001**, *31* (11), 26.
- (116) Gromer, S.; Urig, S.; Becker, K. The Thioredoxin System? From Science to Clinic. *Med. Res. Rev.* **2004**, *24* (1), 40–89. <https://doi.org/10.1002/med.10051>.
- (117) Dagnell, M.; Frijhoff, J.; Pader, I.; Augsten, M.; Boivin, B.; Xu, J.; Mandal, P. K.; Tonks, N. K.; Hellberg, C.; Conrad, M.; Arnér, E. S. J.; Östman, A. Selective Activation of Oxidized PTP1B by the Thioredoxin System Modulates PDGF- β Receptor Tyrosine Kinase Signaling. *Proc. Natl. Acad. Sci. U.S.A.* **2013**, *110* (33), 13398–13403. <https://doi.org/10.1073/pnas.1302891110>.
- (118) Yoo, M.-H.; Xu, X.-M.; Carlson, B. A.; Gladyshev, V. N.; Hatfield, D. L. Thioredoxin Reductase 1 Deficiency Reverses Tumor Phenotype and Tumorigenicity of Lung Carcinoma Cells. *J. Biol. Chem.* **2006**, *281* (19), 13005–13008. <https://doi.org/10.1074/jbc.C600012200>.
- (119) Holmgren, A.; Lu, J. Thioredoxin and Thioredoxin Reductase: Current Research with Special Reference to Human Disease. *Biochem. Biophys. Res. Comm.* **2010**, *396* (1), 120–124. <https://doi.org/10.1016/j.bbrc.2010.03.083>.
- (120) Kirkpatrick, D. L.; Kuperus, M.; Dowdeswell, M.; Potier, N.; Donald, L. J.; Kunkel, M.; Berggren, M.; Angulo, M.; Powis, G. Mechanisms of Inhibition of the Thioredoxin Growth Factor System by Antitumor 2-Imidazolyl Disulfides. *Biochemical Pharmacology* **1998**, *55* (7), 987–994. [https://doi.org/10.1016/S0006-2952\(97\)00597-2](https://doi.org/10.1016/S0006-2952(97)00597-2).
- (121) Ramanathan, R. K.; Stephenson, J. J.; Weiss, G. J.; Pestano, L. A.; Lowe, A.; Hiscox, A.; Leos, R. A.; Martin, J. C.; Kirkpatrick, L.; Richards, D. A. A Phase I Trial of PX-12, a Small-Molecule Inhibitor of Thioredoxin-1, Administered as a 72-Hour Infusion Every 21 Days in Patients with Advanced Cancers Refractory to Standard Therapy. *Invest. New Drugs* **2012**, *30* (4), 1591–1596. <https://doi.org/10.1007/s10637-011-9739-9>.
- (122) Ramanathan, R. K.; Abbruzzese, J.; Dragovich, T.; Kirkpatrick, L.; Guillen, J. M.; Baker, A. F.; Pestano, L. A.; Green, S.; Von Hoff, D. D. A Randomized Phase II Study of PX-12, an Inhibitor of Thioredoxin in Patients with Advanced Cancer of the Pancreas Following Progression after a Gemcitabine-Containing Combination. *Cancer Chemother Pharmacol* **2011**, *67* (3), 503–509. <https://doi.org/10.1007/s00280-010-1343-8>.
- (123) Baker, A. F.; Dragovich, T.; Tate, W. R.; Kirkpatrick, L.; Powis, G. Pharmacodynamic Proteomic Studies of the Thioredoxin-1 Inhibitor PX-12 in Mice and Patients. *Cancer Res.* **2004**, *64* (7), Supplement.
- (124) Mao, Z.; Yang, X.; Mizutani, S.; Huang, Y.; Zhang, Z.; Shinmori, H.; Gao, K.; Yao, J. Hydrogen Sulfide Mediates Tumor Cell Resistance to Thioredoxin Inhibitor. *Front. Oncol.* **2020**, *10*, 252. <https://doi.org/10.3389/fonc.2020.00252>.
- (125) Schallreuter, K. U.; Gleason, F. K.; Wood, J. M. The Mechanism of Action of the Nitrosourea Anti-Tumor Drugs on Thioredoxin Reductase, Glutathione Reductase and Ribonucleotide Reductase. *BBA - General Subjects* **1990**, *1054* (1), 14–20. [https://doi.org/10.1016/0167-4889\(90\)90199-N](https://doi.org/10.1016/0167-4889(90)90199-N).
- (126) Casini, A.; Messori, L. Molecular Mechanisms and Proposed Targets for Selected Anticancer Gold Compounds. *Curr. Top. Med. Chem.* **2011**, *11* (21), 2647–2660. <https://doi.org/10.2174/156802611798040732>.
- (127) Furst, D. E. Mechanism of Action, Pharmacology, Clinical Efficacy and Side Effects of Auranofin: An Orally Administered Organic Gold Compound for the Treatment of Rheumatoid Arthritis. *Pharmacotherapy* **1983**, *3* (5), 284–296. <https://doi.org/10.1002/j.1875-9114.1983.tb03277.x>.
- (128) Zhang, X.; Selvaraju, K.; Saei, A. A.; D'Arcy, P.; Zubarev, R. A.; Arnér, E. S. J.; Linder, S. Repurposing of Auranofin: Thioredoxin Reductase Remains a Primary Target of the

References

- Drug. *Biochimie* **2019**, *162*, 46–54. <https://doi.org/10.1016/j.biochi.2019.03.015>. (143)
- (129) Saei, A. A.; Gullberg, H.; Sabatier, P.; Beusch, C. M.; Johansson, K.; Lundgren, B.; Arvidsson, P. I.; Arnér, E. S. J.; Zubarev, R. A. Comprehensive Chemical Proteomics for Target Deconvolution of the Redox Active Drug Auranofin. *Redox Biology* **2020**, *32*, 101491. <https://doi.org/10.1016/j.redox.2020.101491>.
- (130) Lu, J.; Chew, E.-H.; Holmgren, A. Targeting Thioredoxin Reductase Is a Basis for Cancer Therapy by Arsenic Trioxide. *Proc. Natl. Acad. Sci. U.S.A.* **2007**, *104* (30), 12288–12293. <https://doi.org/10.1073/pnas.0701549104>.
- (131) Cheng, Y.; Qi, Y. Current Progresses in Metal-Based Anticancer Complexes as Mammalian TrxR Inhibitors. *Anti-Cancer Agents in Med. Chem.* **2017**, *17* (8). <https://doi.org/10.2174/1871520617666170213150217>.
- (132) Engman, L.; Al-Maharik, N.; McNaughton, M.; Birmingham, A.; Powis, G. Thioredoxin Reductase and Cancer Cell Growth Inhibition by Organotellurium Antioxidants. *Anti-Cancer Drugs* **2003**, *14* (2), 153–161. <https://doi.org/10.1097/00001813-200302000-00009>.
- (133) Wang, L.; Yang, Z.; Fu, J.; Yin, H.; Xiong, K.; Tan, Q.; Jin, H.; Li, J.; Wang, T.; Tang, W.; Yin, J.; Cai, G.; Liu, M.; Kehr, S.; Becker, K.; Zeng, H. Ethaselen: A Potent Mammalian Thioredoxin Reductase 1 Inhibitor and Novel Organoselenium Anticancer Agent. *Free Rad. Biol. Med.* **2012**, *52* (5), 898–908. <https://doi.org/10.1016/j.freeradbiomed.2011.11.034>.
- (134) Zhao, R.; Masayasu, H.; Holmgren, A. Ebselen: A Substrate for Human Thioredoxin Reductase Strongly Stimulating Its Hydroperoxide Reductase Activity and a Superfast Thioredoxin Oxidant. *Proc. Natl. Acad. Sci. U.S.A.* **2002**, *99* (13), 8579–8584. <https://doi.org/10.1073/pnas.122061399>.
- (135) Zhang, J.; Zhang, B.; Li, X.; Han, X.; Liu, R.; Fang, J. Small Molecule Inhibitors of Mammalian Thioredoxin Reductase as Potential Anticancer Agents: An Update. *Med. Res. Rev.* **2019**, *39* (1), 5–39. <https://doi.org/10.1002/med.21507>.
- (136) Stafford, W. C.; Peng, X.; Olofsson, M. H.; Zhang, X.; Luci, D. K.; Lu, L.; Cheng, Q.; Trésaugues, L.; Dexheimer, T. S.; Coussens, N. P.; Augsten, M.; Ahlzén, H.-S. M.; Orwar, O.; Östman, A.; Stone-Elander, S.; Maloney, D. J.; Jadhav, A.; Simeonov, A.; Linder, S.; Arnér, E. S. J. Irreversible Inhibition of Cytosolic Thioredoxin Reductase 1 as a Mechanistic Basis for Anticancer Therapy. *Sci. Transl. Med.* **2018**, *10* (428), eaaf7444. <https://doi.org/10.1126/scitranslmed.aaf7444>.
- (137) Busker, S.; Qian, W.; Haraldsson, M.; Espinosa, B.; Johansson, L.; Attarha, S.; Kolosenko, I.; Liu, J.; Dagnell, M.; Grandér, D.; Arnér, E. S. J.; Tamm, K. P.; Page, B. D. G. Irreversible TrxR1 Inhibitors Block STAT3 Activity and Induce Cancer Cell Death. *Sci. Adv.* **2020**, *6* (12), eaax7945. <https://doi.org/10.1126/sciadv.aax7945>.
- (138) Sabatier, P.; Beusch, C. M.; Gencheva, R.; Cheng, Q.; Zubarev, R.; Arnér, E. S. J. Comprehensive Chemical Proteomics Analyses Reveal That the New TRi-1 and TRi-2 Compounds Are More Specific Thioredoxin Reductase 1 Inhibitors than Auranofin. *Redox Biology* **2021**, *48*, 102184. <https://doi.org/10.1016/j.redox.2021.102184>.
- (139) Anestål, K.; Prast-Nielsen, S.; Cenas, N.; Arnér, E. S. J. Cell Death by SecTRAPs: Thioredoxin Reductase as a Prooxidant Killer of Cells. *PLoS ONE* **2008**, *3* (4), e1846. <https://doi.org/10.1371/journal.pone.0001846>.
- (140) Aquilano, K.; Baldelli, S.; Ciriolo, M. R. Glutathione: New Roles in Redox Signaling for an Old Antioxidant. *Front. Pharmacol.* **2014**, *5*.
- (141) Ursini, F.; Maiorino, M.; Forman, H. J. Redox Homeostasis: The Golden Mean of Healthy Living. *Redox Biology* **2016**, *8*, 205–215. <https://doi.org/10.1016/j.redox.2016.01.010>.
- (142) Le Gal, K.; Schmidt, E. E.; Sayin, V. I. Cellular Redox Homeostasis. *Antioxidants* **2021**, *10* (9), 1377. <https://doi.org/10.3390/antiox10091377>.
- (143) Tretter, V.; Hochreiter, B.; Zach, M. L.; Krenn, K.; Klein, K. U. Understanding Cellular Redox Homeostasis: A Challenge for Precision Medicine. *International Journal of Molecular Sciences* **2021**, *23* (1), 106. <https://doi.org/10.3390/ijms23010106>.
- (144) Meyer, A. J.; Dick, T. P. Fluorescent Protein-Based Redox Probes. *Antioxidants & Redox Signaling* **2010**, *13* (5), 621–650. <https://doi.org/10.1089/ars.2009.2948>.
- (145) Herrmann, J. M.; Dick, T. P. Redox Biology on the Rise. *Biol. Chem.* **2012**, *393* (9), 999–1004. <https://doi.org/10.1515/hsz-2012-0111>.
- (146) Murphy, M. P.; Holmgren, A.; Larsson, N.-G.; Halliwell, B.; Chang, C. J.; Kalyanaram, B.; Rhee, S. G.; Thornalley, P. J.; Partridge, L.; Gems, D.; Nyström, T.; Belousov, V.; Schumacker, P. T.; Winterbourn, C. C. Unraveling the Biological Roles of Reactive Oxygen Species. *Cell Metabolism* **2011**, *13* (4), 361–366. <https://doi.org/10.1016/j.cmet.2011.03.010>.
- (147) Örmö, M.; Cubitt, A. B.; Kallio, K.; Gross, L. A.; Tsien, R. Y.; Remington, S. J. Crystal Structure of the Aequorea Victoria Green Fluorescent Protein. *Science* **1996**, *273* (5280), 1392–1395. <https://doi.org/10.1126/science.273.5280.1392>.
- (148) Yang, F.; Moss, L. G.; Phillips, G. N. The Molecular Structure of Green Fluorescent Protein. *Nat. Biotechnol.* **1996**, *14* (10), 1246–1251. <https://doi.org/10.1038/nbt1096-1246>.
- (149) Ostergaard, H.; Henriksen, A.; Hansen, F. G.; Winther, J. R. Shedding Light on Disulfide Bond Formation: Engineering a Redox Switch in Green Fluorescent Protein. *The EMBO Journal* **2001**, *20* (21), 5853–5862. <https://doi.org/10.1093/emboj/20.21.5853>.
- (150) Hanson, G. T.; Aggeler, R.; Oglesbee, D.; Cannon, M.; Capaldi, R. A.; Tsien, R. Y.; Remington, S. J. Investigating Mitochondrial Redox Potential with Redox-Sensitive Green Fluorescent Protein Indicators. *J. Biol. Chem.* **2004**, *279* (13), 13044–13053. <https://doi.org/10.1074/jbc.M312846200>.
- (151) Campbell, B. C.; Petsko, G. A.; Liu, C. F. Crystal Structure of Green Fluorescent Protein Clover and Design of Clover-Based Redox Sensors. *Structure* **2018**, *26* (2), 225–237.e3. <https://doi.org/10.1016/j.str.2017.12.006>.
- (152) Gutscher, M.; Pauleau, A.-L.; Marty, L.; Brach, T.; Wabnitz, G. H.; Samstag, Y.; Meyer, A. J.; Dick, T. P. Real-Time Imaging of the Intracellular Glutathione Redox Potential. *Nat. Methods* **2008**, *5* (6), 553–559. <https://doi.org/10.1038/nmeth.1212>.
- (153) Schwarzer, C.; Illek, B.; Suh, J. H.; Remington, S. J.; Fischer, H.; Machen, T. E. Organelle Redox of CF and CFTR-Corrected Airway Epithelia. *Free Rad. Biol. Med.* **2007**, *43* (2), 300–316. <https://doi.org/10.1016/j.freeradbiomed.2007.04.015>.
- (154) Chi, A. Y.; Waypa, G. B.; Mungai, P. T.; Schumacker, P. T. Prolonged Hypoxia Increases ROS Signaling and RhoA Activation in Pulmonary Artery Smooth Muscle and Endothelial Cells. *Antioxidants & Redox Signaling* **2010**, *12* (5), 603–610. <https://doi.org/10.1089/ars.2009.2861>.
- (155) Merksamer, P. I.; Trusina, A.; Papa, F. R. Real-Time Redox Measurements during Endoplasmic Reticulum Stress Reveal Interlinked Protein Folding Functions. *Cell* **2008**, *135* (5), 933–947. <https://doi.org/10.1016/j.cell.2008.10.011>.
- (156) Björnberg, O.; Ostergaard, H.; Winther, J. R. Mechanistic Insight Provided by Glutaredoxin within a Fusion to Redox-Sensitive Yellow Fluorescent Protein. *Biochemistry* **2006**, *45* (7), 2362–2371. <https://doi.org/10.1021/bi0522495>.
- (157) Belousov, V. V.; Fradkov, A. F.; Lukyanov, K. A.; Staroverov, D. B.; Shakhbazov, K. S.; Tersikh, A. V.; Lukyanov, S. Genetically Encoded Fluorescent Indicator for Intracellular Hydrogen Peroxide. *Nat. Methods* **2006**, *3* (4), 281–286. <https://doi.org/10.1038/nmeth866>.
- (158) Bilan, D. S.; Belousov, V. V. HyPer Family Probes: State of the Art. *Antioxidants & Redox Signaling* **2016**, *24* (13), 731–751. <https://doi.org/10.1089/ars.2015.6586>.

References

- (159) Bilan, D. S.; Belousov, V. V. New Tools for Redox Biology: From Imaging to Manipulation. *Free Rad. Biol. Med.* **2017**, *109*, 167–188. <https://doi.org/10.1016/j.freeradbiomed.2016.12.004>.
- (160) Fan, Y.; Makar, M.; Wang, M. X.; Ai, H. Monitoring Thioredoxin Redox with a Genetically Encoded Red Fluorescent Biosensor. *Nat Chem Biol* **2017**, *13* (9), 1045–1052. <https://doi.org/10.1038/nchembio.2417>.
- (161) Aller, I.; Rouhier, N.; Meyer, A. Development of RoGFP2-Derived Redox Probes for Measurement of the Glutathione Redox Potential in the Cytosol of Severely Glutathione-Deficient Rml1 Seedlings. *Frontiers in Plant Science* **2013**, *4*.
- (162) Lee, J. H.; Lim, C. S.; Tian, Y. S.; Han, J. H.; Cho, B. R. A Two-Photon Fluorescent Probe for Thiols in Live Cells and Tissues. *J. Am. Chem. Soc.* **2010**, *132* (4), 1216–1217. <https://doi.org/10.1021/ja9090676>.
- (163) Zhao, J.; Qu, Y.; Gao, H.; Zhong, M.; Li, X.; Zhang, F.; Chen, Y.; Gan, L.; Hu, G.; Zhang, H.; Zhang, S.; Fang, J. Loss of Thioredoxin Reductase Function in a Mouse Stroke Model Disclosed by a Two-Photon Fluorescent Probe. *Chem. Commun.* **2020**, *56* (90), 14075–14078. <https://doi.org/10.1039/D0CC05900E>.
- (164) Zhu, B.; Zhang, X.; Li, Y.; Wang, P.; Zhang, H.; Zhuang, X. A Colorimetric and Ratiometric Fluorescent Probe for Thiols and Its Bioimaging Applications. *Chemical Communications* **2010**, *46* (31), 5710. <https://doi.org/10.1039/c0cc00477d>.
- (165) Lee, M. H.; Han, J. H.; Kwon, P.-S.; Bhuniya, S.; Kim, J. Y.; Sessler, J. L.; Kang, C.; Kim, J. S. Hepatocyte-Targeting Single Galactose-Appended Naphthalimide: A Tool for Intracellular Thiol Imaging in Vivo. *J. Am. Chem. Soc.* **2012**, *134* (2), 1316–1322. <https://doi.org/10.1021/ja210065g>.
- (166) Lee, M. H.; Han, J. H.; Lee, J.-H.; Choi, H. G.; Kang, C.; Kim, J. S. Mitochondrial Thioredoxin-Responding Off-On Fluorescent Probe. *Journal of the American Chemical Society* **2012**, *134* (41), 17314–17319. <https://doi.org/10.1021/ja308446y>.
- (167) Lee, M. H.; Jeon, H. M.; Han, J. H.; Park, N.; Kang, C.; Sessler, J. L.; Kim, J. S. Toward a Chemical Marker for Inflammatory Disease: A Fluorescent Probe for Membrane-Localized Thioredoxin. *J. Am. Chem. Soc.* **2014**, *136* (23), 8430–8437. <https://doi.org/10.1021/ja503356q>.
- (168) Zhang, L.; Duan, D.; Liu, Y.; Ge, C.; Cui, X.; Sun, J.; Fang, J. Highly Selective Off-On Fluorescent Probe for Imaging Thioredoxin Reductase in Living Cells. *J. Am. Chem. Soc.* **2014**, *136* (1), 226–233. <https://doi.org/10.1021/ja408792k>.
- (169) Liu, Y.; Ma, H.; Zhang, L.; Cui, Y.; Liu, X.; Fang, J. A Small Molecule Probe Reveals Declined Mitochondrial Thioredoxin Reductase Activity in a Parkinson's Disease Model. *Chem. Commun.* **2016**, *52* (11), 2296–2299. <https://doi.org/10.1039/C5CC09998F>.
- (170) Ma, H.; Zhang, J.; Zhang, Z.; Liu, Y.; Fang, J. A Fast Response and Red Emission Probe for Mammalian Thioredoxin Reductase. *Chem. Commun.* **2016**, *52* (81), 12060–12063. <https://doi.org/10.1039/C6CC04984B>.
- (171) Jia, H.; Hu, G.; Shi, D.; Gan, L.; Zhang, H.; Yao, X.; Fang, J. Fluorophore-Dependent Cleavage of Disulfide Bond Leading to a Highly Selective Fluorescent Probe of Thioredoxin. *Anal. Chem.* **2019**, *91* (13), 8524–8531. <https://doi.org/10.1021/acs.analchem.9b01779>.
- (172) Kong, F.; Zhao, Y.; Liang, Z.; Liu, X.; Pan, X.; Luan, D.; Xu, K.; Tang, B. Highly Selective Fluorescent Probe for Imaging H₂Se in Living Cells and in Vivo Based on the Disulfide Bond. *Anal. Chem.* **2017**, *89* (1), 688–693. <https://doi.org/10.1021/acs.analchem.6b03136>.
- (173) Suarez, S. I.; Ambrose, R.; Kalk, M. A.; Lukesh, J. C. Selenosulfides Tethered to Gem-Dimethyl Esters: A Robust and Highly Versatile Framework for H₂S Probe Development. *Chem. Eur. J.* **2019**, *25* (69), 15736–15740. <https://doi.org/10.1002/chem.201904133>.
- (174) Hong, K.-H.; Kim, D. I.; Kwon, H.; Kim, H.-J. A Fluoresceinylcarbonate-Based Fluorescent Probe for the Sensitive Detection of Biothiols in a HEPES Buffer and Its Cellular Expression. *RSC Advances* **2014**, *4* (2), 978–982. <https://doi.org/10.1039/C3RA42935K>.
- (175) Pires, M. M.; Chmielewski, J. Fluorescence Imaging of Cellular Glutathione Using a Latent Rhodamine. *Organic Letters* **2008**, *10* (5), 837–840. <https://doi.org/10.1021/ol702769n>.
- (176) Mafireyi, T. J.; Laws, M.; Bassett, J. W.; Cassidy, P. B.; Escobedo, J. O.; Strongin, R. M. A Diselenide Turn-On Fluorescent Probe for the Detection of Thioredoxin Reductase. *Angew. Chem. Int. Ed.* **2020**, *59* (35), 15147–15151. <https://doi.org/10.1002/anie.202004094>.
- (177) Li, X.; Zhang, B.; Yan, C.; Li, J.; Wang, S.; Wei, X.; Jiang, X.; Zhou, P.; Fang, J. A Fast and Specific Fluorescent Probe for Thioredoxin Reductase That Works via Disulphide Bond Cleavage. *Nat. Commun.* **2019**, *10* (2745), 1–12. <https://doi.org/10.1038/s41467-019-10807-8>.
- (178) Lamoureux, G. V.; Whitesides, G. M. Synthesis of Dithiols as Reducing Agents for Disulfides in Neutral Aqueous Solution and Comparison of Reduction Potentials. *J. Org. Chem.* **1993**, *58* (3), 633–641. <https://doi.org/10.1021/jo00055a015>.
- (179) Jones, L. R.; Goun, E. A.; Shinde, R.; Rothbard, J. B.; Contag, C. H.; Wender, P. A. Releasable Luciferin-Transporter Conjugates: Tools for the Real-Time Analysis of Cellular Uptake and Release. *J. Am. Chem. Soc.* **2006**, *128* (20), 6526–6527. <https://doi.org/10.1021/ja0586283>.
- (180) Miller, E. W.; Bian, S. X.; Chang, C. J. A Fluorescent Sensor for Imaging Reversible Redox Cycles in Living Cells. *J. Am. Chem. Soc.* **2007**, *129* (12), 3458–3459. <https://doi.org/10.1021/ja0668973>.
- (181) Lim, C. S.; Masanta, G.; Kim, H. J.; Han, J. H.; Kim, H. M.; Cho, B. R. Ratiometric Detection of Mitochondrial Thiols with a Two-Photon Fluorescent Probe. *Journal of the American Chemical Society* **2011**, *133* (29), 11132–11135. <https://doi.org/10.1021/ja205081s>.
- (182) Reddie, K. G.; Humphries, W. H.; Bain, C. P.; Payne, C. K.; Kemp, M. L.; Murthy, N. Fluorescent Coumarin Thiols Measure Biological Redox Couples. *Org. Lett.* **2012**, *14* (3), 680–683. <https://doi.org/10.1021/ol203105c>.
- (183) Dan, K.; Veetil, A. T.; Chakraborty, K.; Krishnan, Y. DNA Nanodevices Map Enzymatic Activity in Organelles. *Nature Nanotechnology* **2019**, *14* (3), 252–259. <https://doi.org/10.1038/s41565-019-0365-6>.
- (184) Wu, Q.; Huo, F.; Wang, J.; Yin, C. Fluorescent Probe for Detecting Hydrogen Sulfide Based on Disulfide Nucleophilic Substitution-Addition. *Spectrochimica Acta Part A: Molecular and Biomolecular Spectroscopy* **2020**, *238*, 118437. <https://doi.org/10.1016/j.saa.2020.118437>.
- (185) Lee, K.; Dzubeck, V.; Latshaw, L.; Schneider, J. P. De Novo Designed Peptidic Redox Potential Probe: Linking Sensitized Emission to Disulfide Bond Formation. *J. Am. Chem. Soc.* **2004**, *126* (42), 13616–13617. <https://doi.org/10.1021/ja047300r>.
- (186) Piggott, A. M.; Karuso, P. Fluorometric Assay for the Determination of Glutathione Reductase Activity. *Anal. Chem.* **2007**, *79* (22), 8769–8773. <https://doi.org/10.1021/ac071518p>.
- (187) Pullela, P. K.; Chiku, T.; Carvan, M. J.; Sem, D. S. Fluorescence-Based Detection of Thiols in Vitro and in Vivo Using Dithiol Probes. *Analytical Biochemistry* **2006**, *352* (2), 265–273. <https://doi.org/10.1016/j.ab.2006.01.047>.
- (188) Cao, X.; Lin, W.; Yu, Q. A Ratiometric Fluorescent Probe for Thiols Based on a Tetrakis(4-Hydroxyphenyl)Porphyrin-Coumarin Scaffold. *J. Org. Chem.* **2011**, *76* (18), 7423–7430. <https://doi.org/10.1021/jo201199k>.
- (189) Ang, C. Y.; Tan, S. Y.; Lu, Y.; Bai, L.; Li, M.; Li, P.; Zhang, Q.; Selvan, S. T.; Zhao, Y. “Turn-on” Fluorescence

References

- Probe Integrated Polymer Nanoparticles for Sensing Biological Thiol Molecules. *Sci. Rep.* **2014**, *8*.
- (190) Gharibi, N.; Kailass, K.; Beharry, A. A. Exploiting the Cellular Redox-Control System for Activatable Photodynamic Therapy. *ChemBioChem* **2019**, *20* (3), 345–349. <https://doi.org/10.1002/cbic.201800585>.
- (191) Burns, J. A.; Whitesides, G. M. Predicting the Stability of Cyclic Disulfides by Molecular Modeling: Effective Concentrations in Thiol-Disulfide Interchange and the Design of Strongly Reducing Dithiols. *J. Am. Chem. Soc.* **1990**, *112* (17), 6296–6303. <https://doi.org/10.1021/ja00173a017>.
- (192) Lees, W. J.; Whitesides, G. M. Equilibrium Constants for Thiol-Disulfide Interchange Reactions: A Coherent, Corrected Set. *J. Org. Chem.* **1993**, *58* (3), 642–647. <https://doi.org/10.1021/jo00055a016>.
- (193) Yang, N. J.; Hinner, M. J. Getting Across the Cell Membrane: An Overview for Small Molecules, Peptides, and Proteins. *Methods Mol. Biol.* **2015**, *1266*, 29–53. https://doi.org/10.1007/978-1-4939-2272-7_3.
- (194) Gasparini, G.; Bang, E.-K.; Montenegro, J.; Matile, S. Cellular Uptake: Lessons from Supramolecular Organic Chemistry. *Chem. Commun.* **2015**, *51* (52), 10389–10402. <https://doi.org/10.1039/C5CC03472H>.
- (195) Gao, H.; Shi, W.; Freund, L. B. Mechanics of Receptor-Mediated Endocytosis. *Proc. Natl. Acad. Sci. U.S.A.* **2005**, *102* (27), 9469–9474. <https://doi.org/10.1073/pnas.0503879102>.
- (196) Iversen, T.-G.; Skotland, T.; Sandvig, K. Endocytosis and Intracellular Transport of Nanoparticles: Present Knowledge and Need for Future Studies. *Nano Today* **2011**, *6* (2), 176–185. <https://doi.org/10.1016/j.nantod.2011.02.003>.
- (197) Heitz, F.; Morris, M. C.; Divita, G. Twenty Years of Cell-Penetrating Peptides: From Molecular Mechanisms to Therapeutics. *British J. Pharmacol.* **2009**, *157* (2), 195–206. <https://doi.org/10.1111/j.1476-5381.2009.00057.x>.
- (198) Schneider, A. F. L.; Kithil, M.; Cardoso, M. C.; Lehmann, M.; Hackenberger, C. P. R. Cellular Uptake of Large Biomolecules Enabled by Cell-Surface-Reactive Cell-Penetrating Peptide Additives. *Nat. Chem.* **2021**, *13* (6), 530–539. <https://doi.org/10.1038/s41557-021-00661-x>.
- (199) Schneider, A. F. L.; Wallabregue, A. L. D.; Franz, L.; Hackenberger, C. P. R. Targeted Subcellular Protein Delivery Using Cleavable Cyclic Cell-Penetrating Peptides. *Bioconjugate Chem.* **2019**, *30* (2), 400–404. <https://doi.org/10.1021/acs.bioconjchem.8b00855>.
- (200) Bang, E.-K.; Gasparini, G.; Molinard, G.; Roux, A.; Sakai, N.; Matile, S. Substrate-Initiated Synthesis of Cell-Penetrating Poly(Disulfide)s. *J. Am. Chem. Soc.* **2013**, *135* (6), 2088–2091. <https://doi.org/10.1021/ja311961k>.
- (201) Carmine, A.; Domoto, Y.; Sakai, N.; Matile, S. Comparison of Lipoic and Asparagusic Acid for Surface-Initiated Disulfide-Exchange Polymerization. *Chem. Eur. J.* **2013**, *19* (35), 11558–11563. <https://doi.org/10.1002/chem.201301567>.
- (202) Fu, J.; Yu, C.; Li, L.; Yao, S. Q. Intracellular Delivery of Functional Proteins and Native Drugs by Cell-Penetrating Poly(Disulfide)s. *J. Am. Chem. Soc.* **2015**, *137* (37), 12153–12160. <https://doi.org/10.1021/jacs.5b08130>.
- (203) Du, S.; Liew, S. S.; Li, L.; Yao, S. Q. Bypassing Endocytosis: Direct Cytosolic Delivery of Proteins. *J. Am. Chem. Soc.* **2018**, *140* (47), 15986–15996. <https://doi.org/10.1021/jacs.8b06584>.
- (204) Yuan, P.; Mao, X.; Wu, X.; Liew, S. S.; Li, L.; Yao, S. Q. Mitochondria-Targeting, Intracellular Delivery of Native Proteins Using Biodegradable Silica Nanoparticles. *Angew. Chem. Int. Ed.* **2019**, *58* (23), 7657–7661. <https://doi.org/10.1002/anie.201901699>.
- (205) Pulcu, G. S.; Galenkamp, N. S.; Qing, Y.; Gasparini, G.; Mikhailova, E.; Matile, S.; Bayley, H. Single-Molecule Kinetics of Growth and Degradation of Cell-Penetrating Poly(Disulfide)s. *J. Am. Chem. Soc.* **2019**, *141* (32), 12444–12447. <https://doi.org/10.1021/jacs.9b00387>.
- (206) Feener, E. P.; Shen, W. C.; Ryser, H. J. Cleavage of Disulfide Bonds in Endocytosed Macromolecules. A Processing Not Associated with Lysosomes or Endosomes. *J. Biol. Chem.* **1990**, *265* (31), 18780–18785. [https://doi.org/10.1016/S0021-9258\(17\)30580-X](https://doi.org/10.1016/S0021-9258(17)30580-X).
- (207) Gasparini, G.; Sargsyan, G.; Bang, E.-K.; Sakai, N.; Matile, S. Ring Tension Applied to Thiol-Mediated Cellular Uptake. *Angew. Chem. Int. Ed.* **2015**, *54* (25), 7328–7331. <https://doi.org/10.1002/anie.201502358>.
- (208) Abegg, D.; Gasparini, G.; Hoch, D. G.; Shuster, A.; Bartolami, E.; Matile, S.; Adibekian, A. Strained Cyclic Disulfides Enable Cellular Uptake by Reacting with the Transferrin Receptor. *J. Am. Chem. Soc.* **2017**, *139* (1), 231–238. <https://doi.org/10.1021/jacs.6b09643>.
- (209) Shu, Z.; Tanaka, I.; Ota, A.; Fushihara, D.; Abe, N.; Kawaguchi, S.; Nakamoto, K.; Tomoike, F.; Tada, S.; Ito, Y.; Kimura, Y.; Abe, H. Disulfide-Unit Conjugation Enables Ultrafast Cytosolic Internalization of Antisense DNA and siRNA. *Angew. Chem. Int. Ed.* **2019**, *58* (20), 6611–6615. <https://doi.org/10.1002/anie.201900993>.
- (210) Tirla, A.; Rivera-Fuentes, P. Peptide Targeting of an Intracellular Receptor of the Secretory Pathway. *Biochemistry* **2019**, *58* (9), 1184–1187. <https://doi.org/10.1021/acs.biochem.9b00029>.
- (211) Chuard, N.; Gasparini, G.; Moreau, D.; Lörcher, S.; Palivan, C.; Meier, W.; Sakai, N.; Matile, S. Strain-Promoted Thiol-Mediated Cellular Uptake of Giant Substrates: Liposomes and Polymersomes. *Angew. Chem. Int. Ed.* **2017**, *56* (11), 2947–2950. <https://doi.org/10.1002/anie.201611772>.
- (212) Bartolami, E.; Basagiannis, D.; Zong, L.; Martinent, R.; Okamoto, Y.; Laurent, Q.; Ward, T. R.; Gonzalez-Gaitan, M.; Sakai, N.; Matile, S. Diselenolane-Mediated Cellular Uptake: Efficient Cytosolic Delivery of Probes, Peptides, Proteins, Artificial Metalloenzymes and Protein-Coated Quantum Dots. *Chem. Eur. J.* **2019**, *25* (16), 4047–4051. <https://doi.org/10.1002/chem.201805900>.
- (213) Ryser, H. J.; Mandel, R.; Ghani, F. Cell Surface Sulfhydryls Are Required for the Cytotoxicity of Diphtheria Toxin but Not of Ricin in Chinese Hamster Ovary Cells. *J. Biol. Chem.* **1991**, *266* (28), 18439–18442. [https://doi.org/10.1016/S0021-9258\(18\)55080-8](https://doi.org/10.1016/S0021-9258(18)55080-8).
- (214) Ryser, H. J.-P.; Flückiger, R. Keynote Review: Progress in Targeting HIV-1 Entry. *Drug Discovery Today* **2005**, *10* (16), 1085–1094. [https://doi.org/10.1016/S1359-6446\(05\)03550-6](https://doi.org/10.1016/S1359-6446(05)03550-6).
- (215) Falnes, P. Ø.; Olsnes, S. Cell-Mediated Reduction and Incomplete Membrane Translocation of Diphtheria Toxin Mutants with Internal Disulfides in the A Fragment. *J. Biol. Chem.* **1995**, *270* (35), 20787–20793. <https://doi.org/10.1074/jbc.270.35.20787>.
- (216) Laurent, Q.; Sakai, N.; Matile, S. The Opening of 1,2-Dithiolanes and 1,2-Diselenolanes: Regioselectivity, Rearrangements, and Consequences for Poly(Disulfide)s, Cellular Uptake and Pyruvate Dehydrogenase Complexes. *Helvetica Chimica Acta* **2019**, *102* (2), e1800209. <https://doi.org/10.1002/hlca.201800209>.
- (217) Martinent, R.; Laurent, Q.; Sakai, N.; Matile, S. Cellular Uptake Mediated by Cyclic Oligochalcogenides. *CHIMIA* **2019**, *73* (4), 304–307. <https://doi.org/10.2533/chimia.2019.304>.
- (218) Chuard, N.; Poblador-Bahamonde, A. I.; Zong, L.; Bartolami, E.; Hildebrandt, J.; Weigand, W.; Sakai, N.; Matile, S. Diselenolane-Mediated Cellular Uptake. *Chem. Sci.* **2018**, *9* (7), 1860–1866. <https://doi.org/10.1039/C7SC05151D>.
- (219) López-Andarias, J.; Saabach, J.; Moreau, D.; Cheng, Y.; Derivery, E.; Laurent, Q.; González-Gaitán, M.; Winssinger, N.; Sakai, N.; Matile, S. Cell-Penetrating Streptavidin: A General Tool for Bifunctional Delivery with Spatiotemporal Control, Mediated by Transport Systems Such as Adaptive Benzopolysulfane Networks. *J. Am. Chem. Soc.* **2020**, *142* (10), 4784–4792. <https://doi.org/10.1021/jacs.9b13621>.
- (220) Cheng, Y.; Zong, L.; López-Andarias, J.; Bartolami, E.; Okamoto, Y.; Ward, T. R.; Sakai, N.; Matile, S. Cell-

References

- Penetrating Dynamic - Covalent Benzopolysulfane Networks. *Angew. Chem. Int. Ed.* **2019**, *58* (28), 9522–9526. <https://doi.org/10.1002/anie.201905003>.
- (221) Welch, T. R.; Williams, R. M. Epidithiodioxopiperazines. Occurrence, Synthesis and Biogenesis. *Nat. Prod. Rep.* **2014**, *31* (10), 1376–1404. <https://doi.org/10.1039/C3NP70097F>.
- (222) Koning, N. R.; Sundin, A. P.; Strand, D. Total Synthesis of (–)-Glonitrin A and B Enabled by an Asymmetric Oxidative Sulfenylation of Triketopiperazines. *J. Am. Chem. Soc.* **2021**, *143* (50), 21218–21222. <https://doi.org/10.1021/jacs.1c10364>.
- (223) Cheng, Y.; Pham, A.-T.; Kato, T.; Lim, B.; Moreau, D.; López-Andarias, J.; Zong, L.; Sakai, N.; Matile, S. Inhibitors of Thiol-Mediated Uptake. *Chem. Sci.* **2021**, *12* (2), 626–631. <https://doi.org/10.1039/D0SC05447J>.
- (224) Lim, B.; Cheng, Y.; Kato, T.; Pham, A.-T.; Le Du, E.; Mishra, A. K.; Grinhagena, E.; Moreau, D.; Sakai, N.; Waser, J.; Matile, S. Inhibition of Thiol-Mediated Uptake with Irreversible Covalent Inhibitors. *Helvetica Chimica Acta* **2021**, *104* (8), e2100085. <https://doi.org/10.1002/hlca.202100085>.
- (225) Kato, T.; Lim, B.; Cheng, Y.; Pham, A.-T.; Maynard, J.; Moreau, D.; Poblador-Bahamonde, A. I.; Sakai, N.; Matile, S. Cyclic Thiosulfonates for Thiol-Mediated Uptake: Cascade Exchangers, Transporters, Inhibitors. *JACS Au* **2022**, *2* (4), 839–852. <https://doi.org/10.1021/jacsau.1c00573>.
- (226) Daniels, T. R.; Delgado, T.; Helguera, G.; Penichet, M. L. The Transferrin Receptor Part II: Targeted Delivery of Therapeutic Agents into Cancer Cells. *Clinical Immunology* **2006**, *121* (2), 159–176. <https://doi.org/10.1016/j.clim.2006.06.006>.
- (227) Alviaña, C.; Lim, N. K.; Clerico Mosina, V.; Oostergetel, G. T.; Dutzler, R.; Paulino, C. Cryo-EM Structures and Functional Characterization of the Murine Lipid Scramblase TMEM16F. *eLife* **2019**, *8*, e44365. <https://doi.org/10.7554/eLife.44365>.
- (228) Mansour, T. S.; Potluri, V.; Palapati, R. R.; Basetti, V.; Keesara, M.; Moghudula, A. G.; Maiti, P. Lead Generation of 1,2-Dithiolanes as Exon 19 and Exon 21 Mutant EGFR Tyrosine Kinase Inhibitors. *Bioorg. Med. Chem. Lett.* **2019**, *29* (12), 1435–1439. <https://doi.org/10.1016/j.bmcl.2019.04.029>.
- (229) Al Khamici, H.; Brown, L. J.; Hossain, K. R.; Hudson, A. L.; Sinclair-Burton, A. A.; Ng, J. P. M.; Daniel, E. L.; Hare, J. E.; Cornell, B. A.; Curmi, P. M. G.; Davey, M. W.; Valenzuela, S. M. Members of the Chloride Intracellular Ion Channel Protein Family Demonstrate Glutaredoxin-Like Enzymatic Activity. *PLoS ONE* **2015**, *10* (1), e115699. <https://doi.org/10.1371/journal.pone.0115699>.
- (230) Nakamura, H.; Masutani, H.; Yodoi, J. Extracellular Thioredoxin and Thioredoxin-Binding Protein 2 in Control of Cancer. *Seminars in Cancer Biology* **2006**, *16* (6), 444–451. <https://doi.org/10.1016/j.semcancer.2006.09.001>.
- (231) Schwertassek, U.; Weingarten, L.; Dick, T. P. Identification of Redox-Active Cell-Surface Proteins by Mechanism-Based Kinetic Trapping. *Science Signaling* **2007**, *2007* (417). <https://doi.org/10.1126/stke.4172007p8>.
- (232) Matsuo, Y. Introducing Thioredoxin-Related Transmembrane Proteins: Emerging Roles of Human TMX and Clinical Implications. *Antioxidants & Redox Signaling* **2022**, *36* (13–15), 984–1000. <https://doi.org/10.1089/ars.2021.0187>.
- (233) Yan, B.; Smith, J. W. A Redox Site Involved in Integrin Activation. *J. Biol. Chem.* **2000**, *275* (51), 39964–39972. <https://doi.org/10.1074/jbc.M007041200>.
- (234) Bergerhausen, L.; Grosche, J.; Meißner, J.; Hecker, C.; Caliendo, M. F.; Westerhausen, C.; Kamenac, A.; Rezaei, M.; Mörgelin, M.; Poschmann, G.; Vestweber, D.; Hanschmann, E.-M.; Eble, J. A. Extracellular Redox Regulation of A7β Integrin-Mediated Cell Migration Is Signaled via a Dominant Thiol-Switch. *Antioxidants* **2020**, *9* (3), 227. <https://doi.org/10.3390/antiox9030227>.
- (235) Xu, S.-Z.; Sukumar, P.; Zeng, F.; Li, J.; Jairaman, A.; English, A.; Naylor, J.; Ciurtin, C.; Majeed, Y.; Milligan, C. J.; Bahnasi, Y. M.; Al-Shawaf, E.; Porter, K. E.; Jiang, L.-H.; Emery, P.; Sivaprasadarao, A.; Beech, D. J. TRPC Channel Activation by Extracellular Thioredoxin. *Nature* **2008**, *451* (7174), 69–72. <https://doi.org/10.1038/nature06414>.
- (236) Jiang, X.-M.; Fitzgerald, M.; Grant, C. M.; Hogg, P. J. Redox Control of Exofacial Protein Thiols/Disulfides by Protein Disulfide Isomerase. *J. Biol. Chem.* **1999**, *274* (4), 2416–2423. <https://doi.org/10.1074/jbc.274.4.2416>.
- (237) Matthias, L. J.; Hogg, P. J. Redox Control on the Cell Surface: Implications for HIV-1 Entry. *Antioxidants & Redox Signaling* **2003**, *5* (1), 133–138. <https://doi.org/10.1089/152308603321223621>.
- (238) Singh, R.; Whitesides, G. M. Comparisons of Rate Constants for Thiolate-Disulfide Interchange in Water and in Polar Aprotic Solvents Using Dynamic Proton NMR Line Shape Analysis. *Journal of the American Chemical Society* **1990**, *112* (3), 1190–1197. <https://doi.org/10.1021/ja00159a046>.
- (239) Prast-Nielsen, S.; Dexheimer, T. S.; Schultz, L.; Stafford, W. C.; Cheng, Q.; Xu, J.; Jadhav, A.; Arnér, E. S. J.; Simeonov, A. Inhibition of Thioredoxin Reductase 1 by Porphyrins and Other Small Molecules Identified by a High-Throughput Screening Assay. *Free Rad. Biol. Med.* **2011**, *50* (9), 1114–1123. <https://doi.org/10.1016/j.freeradbiomed.2011.01.020>.
- (240) Minakata, S.; Miwa, H.; Yamamoto, K.; Hirayama, A.; Okumura, S. Diastereodivergent Intermolecular 1,2-Diamination of Unactivated Alkenes Enabled by Iodine Catalysis. *J. Am. Chem. Soc.* **2021**, *143* (11), 4112–4118. <https://doi.org/10.1021/jacs.1c00228>.
- (241) Juliá, F.; Yan, J.; Paulus, F.; Ritter, T. Vinyl Thianthrenium Tetrafluoroborate: A Practical and Versatile Vinylating Reagent Made from Ethylene. *J. Am. Chem. Soc.* **2021**, *143* (33), 12992–12998. <https://doi.org/10.1021/jacs.1c06632>.
- (242) Raines, R. T.; Lukesh, J. C. Dithioamine Reducing Agents. US 2013/0211055 A1, August 15, 2013.
- (243) Lee, S.; Kim, S. M.; Lee, R. T. Thioredoxin and Thioredoxin Target Proteins: From Molecular Mechanisms to Functional Significance. *Antioxidants & Redox Signaling* **2013**, *18* (10), 1165–1207. <https://doi.org/10.1089/ars.2011.4322>.
- (244) Jones, D. P.; Sies, H. The Redox Code. *Antioxidants & Redox Signaling* **2015**, *23* (9), 734–746. <https://doi.org/10.1089/ars.2015.6247>.
- (245) Butora, G.; Qi, N.; Fu, W.; Nguyen, T.; Huang, H.-C.; Davies, I. W. Cyclic-Disulfide-Based Prodrugs for Cytosol-Specific Drug Delivery. *Angew. Chem. Int. Ed.* **2014**, *53* (51), 14046–14050. <https://doi.org/10.1002/anie.201407130>.
- (246) Butora, G. Nucleoside Kinase Bypass Compositions and Methods. WO 2014/088923 A1, 2014.
- (247) Hayashi, J.; Samezawa, Y.; Ochi, Y.; Wada, S.; Urato, H. Syntheses of Prodrug-Type Phosphotriester Oligonucleotides Responsive to Intracellular Reducing Environment for Improvement of Cell Membrane Permeability and Nuclease Resistance. *Bioorg. Med. Chem. Lett.* **2017**, *27*, 3135–3138.
- (248) Ziv, I. Pro-Drugs and Related Methods. WO 2017/017669 A1, 2017.
- (249) Ziv, I. Compounds and Methods for Trans-Membrane Delivery of Molecules. US 2017/0037401 A1, 2017.
- (250) Lee, S. H.; Kohn, H. Cyclic Disulfide C(8) Iminoporphiromycin: Nucleophilic Activation of a Porphiromycin. *J. Am. Chem. Soc.* **2004**, *126* (13), 4281–4292. <https://doi.org/10.1021/ja030577r>.
- (251) Lee, S. H.; Kohn, H. 7-N,7'-N'-(1'',2''-Dithianyl-3'',6''-Dimethylenyl)Bismitomycin C: Synthesis and Nucleophilic Activation of a Dimeric Mitomycin. *Org. Biomol. Chem.* **2005**, *3* (3), 471–482. <https://doi.org/10.1039/B414806A>.

References

- (252) Mohammadi, F.; Soltani, A.; Ghahremanloo, A.; Javid, H.; Hashemy, S. I. The Thioredoxin System and Cancer Therapy: A Review. *Cancer Chemother. Pharmacol.* **2019**, *84* (5), 925–935. <https://doi.org/10.1007/s00280-019-03912-4>.
- (253) Whayne, T. F.; Parinandi, N.; Maulik, N. Thioredoxins in Cardiovascular Disease. *Can. J. Physiol. Pharmacol.* **2015**, *93* (11), 903–911. <https://doi.org/10.1139/cjpp-2015-0105>.
- (254) Karlenius, T. C.; Tonissen, K. F. Thioredoxin and Cancer: A Role for Thioredoxin in All States of Tumor Oxygenation. *Cancers* **2010**, *2* (2), 209–232. <https://doi.org/10.3390/cancers2020209>.
- (255) Jiang, J.; Auchinclove, C.; Fisher, K.; Campbell, C. J. Quantitative Measurement of Redox Potential in Hypoxic Cells Using SERS Nanosensors. *Nanoscale* **2014**, *6* (20), 12104–12110. <https://doi.org/10.1039/C4NR01263A>.
- (256) Karlenius, T. C.; Shah, F.; Di Trapani, G.; Clarke, F. M.; Tonissen, K. F. Cycling Hypoxia Up-Regulates Thioredoxin Levels in Human MDA-MB-231 Breast Cancer Cells. *Biochemical and Biophysical Research Communications* **2012**, *419* (2), 350–355. <https://doi.org/10.1016/j.bbrc.2012.02.027>.
- (257) Powis, G.; Kirkpatrick, D. L. Thioredoxin Signaling as a Target for Cancer Therapy. *Curr. Opin. Pharmacol.* **2007**, *7* (4), 392–397. <https://doi.org/10.1016/j.coph.2007.04.003>.
- (258) Biaglow, J. E.; Miller, R. A. The Thioredoxin Reductase/Thioredoxin System: Novel Redox Targets for Cancer Therapy. *Cancer Biology & Therapy* **2005**, *4* (1), 13–20. <https://doi.org/10.4161/cbt.4.1.1434>.
- (259) Bertini, R.; Zack Howard, O. M.; Dong, H.-F.; Oppenheim, J. J.; Bizzarri, C.; Sergi, R.; Caselli, G.; Pagliei, S.; Romines, B.; Wilshire, J. A.; Mengozzi, M.; Nakamura, H.; Yodoi, J.; Pekkari, K.; Gurunath, R.; Holmgren, A.; Herzenberg, L. A.; Herzenberg, L. A.; Ghezzi, P. Thioredoxin, a Redox Enzyme Released in Infection and Inflammation, Is a Unique Chemoattractant for Neutrophils, Monocytes, and T Cells. *J. Exp. Med.* **1999**, *189* (11), 1783–1789. <https://doi.org/10.1084/jem.189.11.1783>.
- (260) Yoshihara, E.; Masaki, S.; Matsuo, Y.; Chen, Z.; Tian, H.; Yodoi, J. Thioredoxin/Txnip: Redoxosome, as a Redox Switch for the Pathogenesis of Diseases. *Front. Immunol.* **2014**, *4*. <https://doi.org/10.3389/fimmu.2013.00514>.
- (261) Phillips, R. M. Targeting the Hypoxic Fraction of Tumours Using Hypoxia-Activated Prodrugs. *Cancer Chemother. Pharmacol.* **2016**, *77* (3), 441–457. <https://doi.org/10.1007/s00280-015-2920-7>.
- (262) Sharma, A.; Arambula, J. F.; Koo, S.; Kumar, R.; Singh, H.; Sessler, J. L.; Kim, J. S. Hypoxia-Targeted Drug Delivery. *Chem. Soc. Rev.* **2019**, *48* (3), 771–813. <https://doi.org/10.1039/C8CS00304A>.
- (263) Twum, E. A.; Nathubhai, A.; Wood, P. J.; Lloyd, M. D.; Thompson, A. S.; Threadgill, M. D. Initial Development of a Cytotoxic Amino-Seco-CBI Warhead for Delivery by Prodrug Systems. *Bioorg. Med. Chem.* **2015**, *23* (13), 3481–3489. <https://doi.org/10.1016/j.bmc.2015.04.034>.
- (264) McNulty, J.; Nair, J. J.; Griffin, C.; Pandey, S. Synthesis and Biological Evaluation of Fully Functionalized Seco - Pancreatistatin Analogues. *J. Nat. Prod.* **2008**, *71* (3), 357–363. <https://doi.org/10.1021/np0705460>.
- (265) Lubahn, C.; Schaller, J. A.; Shewmacker, E.; Wood, C.; Bellinger, D. L.; Byron, D.; Melody, N.; Pettit, G. R.; Lorton, D. Preclinical Efficacy of Sodium Narcistatin to Reduce Inflammation and Joint Destruction in Rats with Adjuvant-Induced Arthritis. *Rheumatology International* **2012**, *32* (12), 3751–3760. <https://doi.org/10.1007/s00296-011-2217-z>.
- (266) Singh, Y.; Palombo, M.; Sinko, P. Recent Trends in Targeted Anticancer Prodrug and Conjugate Design. *Curr. Med. Chem.* **2008**, *15* (18), 1802–1826. <https://doi.org/10.2174/092986708785132997>.
- (267) Thorn-Seshold, O.; Vargas-Sanchez, M.; McKeon, S.; Hasserodt, J. A Robust, High-Sensitivity Stealth Probe for Peptidases. *Chem. Commun.* **2012**, *48* (50), 6253–6255. <https://doi.org/10.1039/c2cc32227g>.
- (268) Kaskova, Z. M.; Tsarkova, A. S.; Yampolsky, I. V. 1001 Lights: Luciferins, Luciferases, Their Mechanisms of Action and Applications in Chemical Analysis, Biology and Medicine. *Chem. Soc. Rev.* **2016**, *45* (21), 6048–6077. <https://doi.org/10.1039/C6CS00296J>.
- (269) Kaskova, Z. M.; Tsarkova, A. S.; Yampolsky, I. V. 1001 Lights: Luciferins, Luciferases, Their Mechanisms of Action and Applications in Chemical Analysis, Biology and Medicine. *Chem. Soc. Rev.* **2016**, *45* (21), 6048–6077. <https://doi.org/10.1039/C6CS00296J>.
- (270) Chevalier, A.; Massif, C.; Renard, P.-Y.; Romieu, A. Bioconjugatable Azo-Based Dark-Quencher Dyes: Synthesis and Application to Protease-Activatable Far-Red Fluorescent Probes. *Chem. Eur. J.* **2013**, *19* (5), 1686–1699. <https://doi.org/10.1002/chem.201203427>.
- (271) Myochin, T.; Hanaoka, K.; Iwaki, S.; Ueno, T.; Komatsu, T.; Terai, T.; Nagano, T.; Urano, Y. Development of a Series of Near-Infrared Dark Quenchers Based on Si-Rhodamines and Their Application to Fluorescent Probes. *J. Am. Chem. Soc.* **2015**, *137* (14), 4759–4765. <https://doi.org/10.1021/jacs.5b00246>.
- (272) Schirmer, R. H.; Adler, H.; Pickhardt, M.; Mandelkow, E. "Lest We Forget You — Methylene Blue ..." *Neurobiology of Aging* **2011**, *32* (12), 2325.e7–2325.e16. <https://doi.org/10.1016/j.neurobiolaging.2010.12.012>.
- (273) Arai, K.; Matsunaga, T.; Ueno, H.; Akahoshi, N.; Sato, Y.; Chakrabarty, G.; Mughes, G.; Iwaoka, M. Modeling Thioredoxin Reductase-Like Activity with Cyclic Selenenyl Sulfides: Participation of an NH...Se Hydrogen Bond through Stabilization of the Mixed Se-S Intermediate. *Chem. Eur. J.* **2019**, *25* (55), 12751–12760. <https://doi.org/10.1002/chem.201902230>.
- (274) Airley, R. E.; Monaghan, J. E.; Stratford, I. J. Hypoxia and Disease: Opportunities for Novel Diagnostic and Therapeutic Prodrug Strategies. *Pharmaceutical Journal* **2000**, *264*, 666–673.
- (275) Vinogradova, E. V.; Zhang, X.; Remillard, D.; Lazar, D. C.; Suci, R. M.; Wang, Y.; Bianco, G.; Yamashita, Y.; Crowley, V. M.; Schafroth, M. A.; Yokoyama, M.; Konrad, D. B.; Lum, K. M.; Simon, G. M.; Kemper, E. K.; Lazear, M. R.; Yin, S.; Blewett, M. M.; Dix, M. M.; Nguyen, N.; Shokhirev, M. N.; Chin, E. N.; Lairson, L. L.; Melillo, B.; Schreiber, S. L.; Forli, S.; Tejaro, J. R.; Cravatt, B. F. An Activity-Guided Map of Electrophile-Cysteine Interactions in Primary Human T Cells. *Cell* **2020**, *182* (4), 1009–1026.e29. <https://doi.org/10.1016/j.cell.2020.07.001>.
- (276) Tao, Y.; Remillard, D.; Vinogradova, E. V.; Yokoyama, M.; Banchenko, S.; Schwefel, D.; Melillo, B.; Schreiber, S. L.; Zhang, X.; Cravatt, B. F. Targeted Protein Degradation by Electrophilic PROTACs That Stereoselectively and Site-Specifically Engage DCAF1. *J. Am. Chem. Soc.* **2022**, *144* (40), 18688–18699. <https://doi.org/10.1021/jacs.2c08964>.
- (277) Chyan, W.; Raines, R. T. Enzyme-Activated Fluorogenic Probes for Live-Cell and *in Vivo* Imaging. *ACS Chem. Biol.* **2018**, *13* (7), 1810–1823. <https://doi.org/10.1021/acscchembio.8b00371>.
- (278) Grimm, J. B.; Heckman, L. M.; Lavis, L. D. The Chemistry of Small-Molecule Fluorogenic Probes. In *Progress in Molecular Biology and Translational Science*; Elsevier, 2013; Vol. 113, pp 1–34. <https://doi.org/10.1016/B978-0-12-386932-6.00001-6>.
- (279) Fang, Y.; Luo, F.; Cao, Z.; Peng, C.; Dehaen, W. Umbelliferone-Based Fluorescent Probe for Selective Recognition of Hydrogen Sulfide and Its Bioimaging in Living Cells and Zebrafish. *Chemosensors* **2022**, *10* (10), 427. <https://doi.org/10.3390/chemosensors10100427>.
- (280) Grimm, J. B.; Brown, T. A.; Tkachuk, A. N.; Lavis, L. D. General Synthetic Method for Si-Fluoreceins and Si-Rhodamines. *ACS Cent. Sci.* **2017**, *3* (9), 975–985. <https://doi.org/10.1021/acscentsci.7b00247>.
- (281) Grimm, J. B.; Gruber, T. D.; Ortiz, G.; Brown, T. A.; Lavis, L. D. Virginia Orange: A Versatile, Red-Shifted Fluorescein Scaffold for Single- and Dual-Input

References

- Fluorogenic Probes. *Bioconjugate Chem.* **2016**, *27* (2), 474–480. <https://doi.org/10.1021/acs.bioconjchem.5b00566>.
- (282) Jia, X.; Li, X.; Geng, X.; Nie, C.; Zhang, P.; Wei, C.; Li, X. A Seminaaphthorhodafuor-Based near-Infrared Fluorescent Probe for Hydrazine and Its Bioimaging in Living Systems. *Spectrochimica Acta Part A: Molecular and Biomolecular Spectroscopy* **2019**, *223*, 117307. <https://doi.org/10.1016/j.saa.2019.117307>.
- (283) Tachibana, R.; Kamiya, M.; Suzuki, S.; Morokuma, K.; Nanjo, A.; Urano, Y. Molecular Design Strategy of Fluorogenic Probes Based on Quantum Chemical Prediction of Intramolecular Spirocyclization. *Commun. Chem.* **2020**, *3* (1), 1–8. <https://doi.org/10.1038/s42004-020-0326-x>.
- (284) Usama, S. M.; Marker, S. C.; Caldwell, D. R.; Patel, N. L.; Feng, Y.; Kalen, J. D.; St. Croix, B.; Schnermann, M. J. Targeted Fluorogenic Cyanine Carbamates Enable In Vivo Analysis of Antibody–Drug Conjugate Linker Chemistry. *J. Am. Chem. Soc.* **2021**, *143* (51), 21667–21675. <https://doi.org/10.1021/jacs.1c10482>.
- (285) Usama, S. M.; Inagaki, F.; Kobayashi, H.; Schnermann, M. J. Norcyanine–Carbamates Are Versatile Near-Infrared Fluorogenic Probes. *J. Am. Chem. Soc.* **2021**, *143* (15), 5674–5679. <https://doi.org/10.1021/jacs.1c02112>.
- (286) Cilliers, C.; Nessler, I.; Christodolu, N.; Thurber, G. M. Tracking Antibody Distribution with Near-Infrared Fluorescent Dyes: Impact of Dye Structure and Degree of Labeling on Plasma Clearance. *Mol. Pharmaceutics* **2017**, *14* (5), 1623–1633. <https://doi.org/10.1021/acs.molpharmaceut.6b01091>.
- (287) MacCuaig, W. M.; Jones, M. A.; Abeyakoon, O.; McNally, L. R. Development of Multispectral Optoacoustic Tomography as a Clinically Translatable Modality for Cancer Imaging. *Radiology: Imaging Cancer* **2020**, *2* (6), e200066. <https://doi.org/10.1148/rycan.2020200066>.
- (288) Chen, Z.; Chattaraj, R.; Pulsipher, K. W.; Karmacharya, M. B.; Hammer, D. A.; Lee, D.; Sehgal, C. M. Photoacoustic and Ultrasound Dual-Mode Imaging via Functionalization of Recombinant Protein-Stabilized Microbubbles with Methylene Blue. *ACS Appl. Bio Mater.* **2019**, *2* (9), 4020–4026. <https://doi.org/10.1021/acsabm.9b00545>.
- (289) Beziere, N.; Lozano, N.; Nunes, A.; Salichs, J.; Queiros, D.; Kostarelos, K.; Ntziachristos, V. Dynamic Imaging of PEGylated Indocyanine Green (ICG) Liposomes within the Tumor Microenvironment Using Multi-Spectral Optoacoustic Tomography (MSOT). *Biomaterials* **2015**, *37*, 415–424. <https://doi.org/10.1016/j.biomaterials.2014.10.014>.
- (290) Wu, Y.; Huang, S.; Wang, J.; Sun, L.; Zeng, F.; Wu, S. Activatable Probes for Diagnosing and Positioning Liver Injury and Metastatic Tumors by Multispectral Optoacoustic Tomography. *Nat. Commun.* **2018**, *9* (1), 3983. <https://doi.org/10.1038/s41467-018-06499-1>.
- (291) Wu, L.; Huang, C.; Emery, B. P.; Sedgwick, A. C.; Bull, S. D.; He, X.-P.; Tian, H.; Yoon, J.; Sessler, J. L.; James, T. D. Förster Resonance Energy Transfer (FRET)-Based Small-Molecule Sensors and Imaging Agents. *Chem. Soc. Rev.* **2020**, *49* (15), 5110–5139. <https://doi.org/10.1039/C9CS00318E>.
- (292) Aron, A. T.; Loehr, M. O.; Bogena, J.; Chang, C. J. An Endoperoxide Reactivity-Based FRET Probe for Ratiometric Fluorescence Imaging of Labile Iron Pools in Living Cells. *J. Am. Chem. Soc.* **2016**, *138* (43), 14338–14346. <https://doi.org/10.1021/jacs.6b08016>.
- (293) Smith, E. N.; Schwarzländer, M.; Ratcliffe, R. G.; Kruger, N. J. Shining a Light on NAD- and NADP-Based Metabolism in Plants. *Trends in Plant Science* **2021**, *26* (10), 1072–1086. <https://doi.org/10.1016/j.tplants.2021.06.010>.
- (294) Burgstaller, S.; Bischof, H.; Gensch, T.; Stryeck, S.; Gottschalk, B.; Ramadani-Muja, J.; Eroglu, E.; Rost, R.; Balfanz, S.; Baumann, A.; Waldeck-Weiermair, M.; Hay, J. C.; Madl, T.; Graier, W. F.; Malli, R. PH-Lemon, a Fluorescent Protein-Based PH Reporter for Acidic Compartments. *ACS Sensors* **2019**, *4* (4), 883–891. <https://doi.org/10.1021/acssensors.8b01599>.
- (295) Koh, M. Y.; Lemos, R.; Liu, X.; Powis, G. The Hypoxia-Associated Factor Switches Cells from HIF-1 α - to HIF-2 α -Dependent Signaling Promoting Stem Cell Characteristics, Aggressive Tumor Growth and Invasion. *Cancer Res.* **2011**, *71* (11), 4015–4027. <https://doi.org/10.1158/0008-5472.CAN-10-4142>.
- (296) Doran, D. M.; Kulkarni-Datar, K.; Cool, D. R.; Brown, T. L. Hypoxia Activates Constitutive Luciferase Reporter Constructs. *Biochimie* **2011**, *93* (2), 361–368. <https://doi.org/10.1016/j.biochi.2010.10.009>.
- (297) Menderes, G.; Bonazzoli, E.; Bellone, S.; Black, J.; Predolini, F.; Pettinella, F.; Masserdotti, A.; Zammataro, L.; Altwerger, G.; Buza, N.; Hui, P.; Wong, S.; Litkouhi, B.; Ratner, E.; Silasi, D.-A.; Azodi, M.; Schwartz, P. E.; Santin, A. D. SYD985, a Novel Duocarmycin-Based HER2-Targeting Antibody–Drug Conjugate, Shows Antitumor Activity in Uterine and Ovarian Carcinomas with HER2/Neu Expression. *Clin. Cancer Res.* **2017**, *23* (19), 5836–5845. <https://doi.org/10.1158/1078-0432.CCR-16-2862>.
- (298) Dubowchik, G. M.; Firestone, R. A.; Padilla, L.; Willner, D.; Hofstead, S. J.; Mosure, K.; Knipe, J. O.; Lasch, S. J.; Trail, P. A. Cathepsin B-Labile Dipeptide Linkers for Lysosomal Release of Doxorubicin from Internalizing Immunoconjugates: Model Studies of Enzymatic Drug Release and Antigen-Specific In Vitro Anticancer Activity. *Bioconjugate Chem.* **2002**, *13* (4), 855–869. <https://doi.org/10.1021/bc025536j>.
- (299) Kasper, M.; Stengl, A.; Ochtrup, P.; Gerlach, M.; Stoschek, T.; Schumacher, D.; Helma, J.; Penkert, M.; Krause, E.; Leonhardt, H.; Hackenberger, C. P. R. Ethynylphosphonamidates for the Rapid and Cysteine-Selective Generation of Efficacious Antibody–Drug Conjugates. *Angew. Chem. Int. Ed.* **2019**, *58* (34), 11631–11636. <https://doi.org/10.1002/anie.201904193>.
- (300) Dorywalska, M.; Dushin, R.; Moine, L.; Farias, S. E.; Zhou, D.; Navaratnam, T.; Lui, V.; Hasa-Moreno, A.; Casas, M. G.; Tran, T.-T.; Delaria, K.; Liu, S.-H.; Foletti, D.; O'Donnell, C. J.; Pons, J.; Shelton, D. L.; Rajpal, A.; Strop, P. Molecular Basis of Valine-Citrulline-PABC Linker Instability in Site-Specific ADCs and Its Mitigation by Linker Design. *Mol. Cancer Ther.* **2016**, *15* (5), 958–970. <https://doi.org/10.1158/1535-7163.MCT-15-1004>.
- (301) Chuprakov, S.; Ogunkoya, A. O.; Barfield, R. M.; Bauzon, M.; Hickle, C.; Kim, Y. C.; Yeo, D.; Zhang, F.; Rabuka, D.; Drake, P. M. Tandem-Cleavage Linkers Improve the In Vivo Stability and Tolerability of Antibody–Drug Conjugates. *Bioconjugate Chem.* **2021**, *32* (4), 746–754. <https://doi.org/10.1021/acs.bioconjchem.1c00029>.
- (302) Su, Z.; Xiao, D.; Xie, F.; Liu, L.; Wang, Y.; Fan, S.; Zhou, X.; Li, S. Antibody–Drug Conjugates: Recent Advances in Linker Chemistry. *Acta Pharmaceutica Sinica B* **2021**, *11* (12), 3889–3907. <https://doi.org/10.1016/j.apsb.2021.03.042>.

9 Appendix

9.1 Supporting Information to the publications presented in this doctoral thesis

9.1.1 Supporting Information to chapter 3.1.1: Paper 1: 1,2-dithiolane probes

Supporting Information to: **Jan G. Felber**, Lena Poczka, Karoline C. Scholzen, Lukas Zeisel, Martin S. Maier, Sander Busker, Ulrike Theisen, Christina Brandstädter, Katja Becker, Elias S. J. Arnér, Julia Thorn-Seshold, Oliver Thorn-Seshold. *Cyclic 5-membered disulfides are not selective for thioredoxin reductase, but are opened nonspecifically*. *Nature Communications* **2022**, 13, 1754. (39 pages)

9.1.2 Supporting Information to chapter 3.1.2: Paper 2: piperidine-fused 1,2-dithianes for Trx

Supporting Information to: **Jan G. Felber**, Lukas Zeisel, Lena Poczka, Karoline C. Scholzen, Sander Busker, Martin S. Maier, Ulrike Theisen, Christina Brandstädter, Katja Becker, Elias S. J. Arnér, Julia Thorn-Seshold, Oliver Thorn-Seshold. *Selective, Modular Probes for Thioredoxins enabled by rational Tuning of a Unique Disulfide Structure Motif*. *Journal of the American Chemical Society* **2021**, 143, 8791-8803. (83 pages)

9.1.3 Supporting Information to chapter 3.1.3: Paper 3: 1,2-thiaselenane probes for TrxR

Supporting Information to: Lukas Zeisel, **Jan G. Felber**, Karoline C. Scholzen, Lena Poczka, Dorian Cheff, Martin S. Maier, Qing Cheng, Min Shen, Matthew D. Hall, Elias S. J. Arnér, Julia Thorn-Seshold, Oliver Thorn-Seshold. *Selective cellular probes for mammalian thioredoxin reductase TrxR1: Rational design of RX1, a modular 1,2-thiaselenane redox probe*. *Chem* **2022**, 8, 1493-1517. (98 pages)

9.1.4 Supporting Information to chapter 3.1.4: Paper 4: bifunctional cyclic disulfide linker

Supporting Information to: **Jan G. Felber**[#], Lukas Zeisel[#], Karoline C. Scholzen, Carina Schmitt, Alexander J. Wiegand, Leonid Komissarov, Elias S. J. Arnér, Oliver Thorn-Seshold. *Bifunctional, piperazine-fused cyclic disulfides for oxidoreductase-activated cellular proagents*. *ChemRxiv* **2023**. (104 pages)

[#]these authors contributed equally as first authors

9.1.5 Supporting Information to chapter 3.2.1: Paper 5: 40 years of duocarmycins

Supporting Information to: **Jan G. Felber**, Oliver Thorn-Seshold. *40 Years of Duocarmycins: A Graphical Structure/Function Review of Their Chemical Evolution, from SAR to Prodrugs and ADCs*. *JACS Au* **2022**, 2, 2636-2644. (23 pages)

9.1.6 Supporting Information to chapter 3.2.2: Paper 6: bioreductive 1,2-dithiane prodrugs

Supporting Information to: **Jan G. Felber**, Annabel Kitowski, Lukas Zeisel, Martin S. Maier, Constanze Heise, Julia Thorn-Seshold, Oliver Thorn-Seshold. *Cyclic dichalcogenides extend the reach of bioreductive prodrugs to harness the thioredoxin system: applications to seco-duocarmycins*. *BioRxiv* **2022**. (77 pages)

Supplementary Information to:

Cyclic 5-membered disulfides are not selective substrates of thioredoxin reductase, but are opened nonspecifically

Jan G. Felber¹, Lena Poczka¹, Karoline C. Scholzen², Lukas Zeisel¹, Martin S. Maier¹, Sander Busker^{2,#}, Ulrike Theisen³, Christina Brandstädter⁴, Katja Becker⁴, Elías S. J. Arnér^{2,5}, Julia Thorn-Seshold¹, Oliver Thorn-Seshold^{1,*}¹ Department of Pharmacy, Ludwig-Maximilians University Munich, Butenandtstr. 5-13, 81377 München, DE.² Department of Medical Biochemistry, Karolinska Institutet, Solnavägen 9, 17177 Stockholm, SE.³ Zoological Institute, Cellular and Molecular Neurobiology, TU Braunschweig, Spielmannstr. 7, 38106 Braunschweig, DE.⁴ Interdisciplinary Research Centre (IFZ), Justus-Liebig University Giessen, Heinrich-Buff-Ring 26-32, 35392 Giessen, DE.⁵ Department of Selenoprotein Research, National Institute of Oncology, 1122 Budapest, HU.

Present affiliation: Pelago Bioscience AB, 171 48 Solna, Sweden.

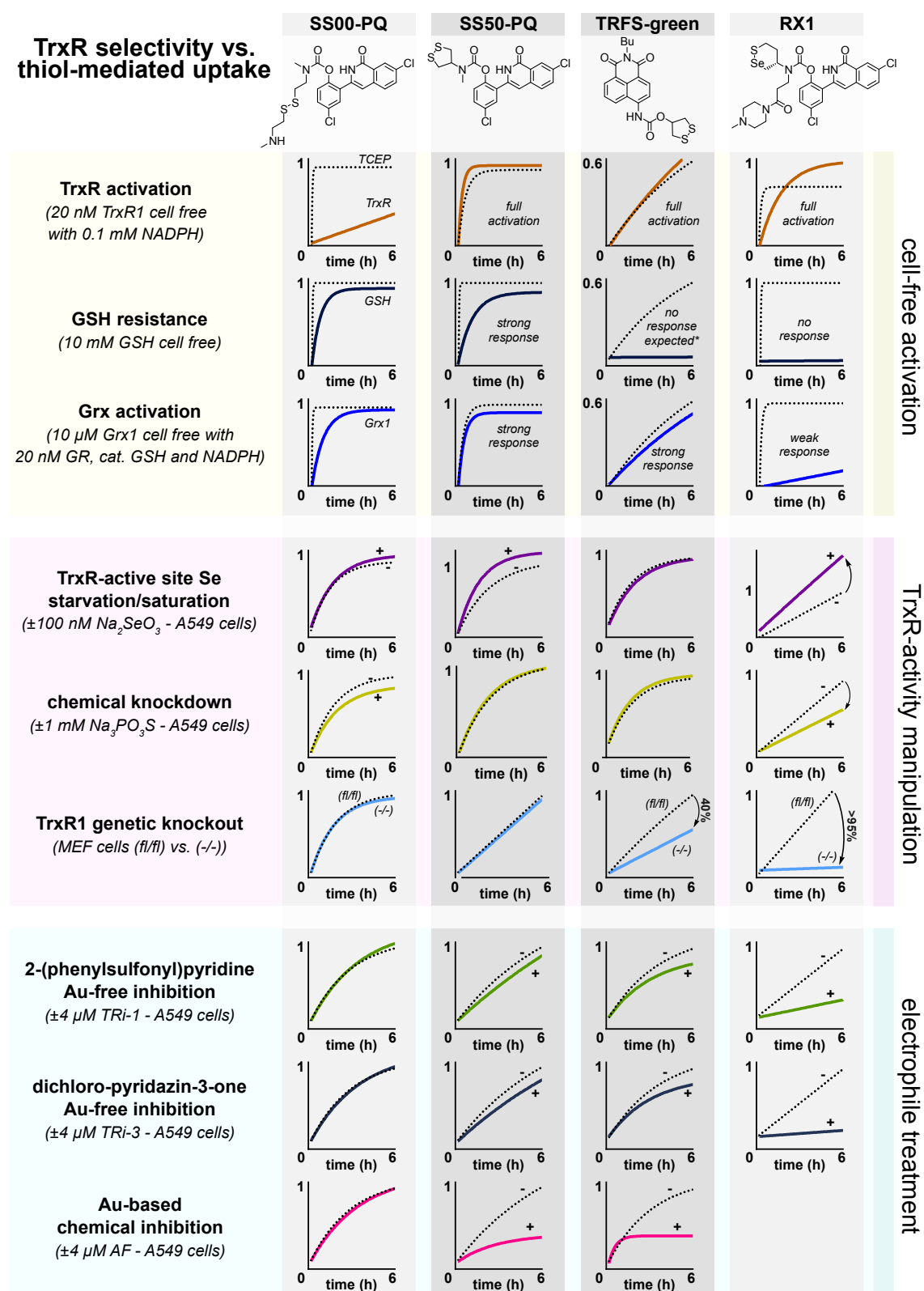
* Correspondence to: oliver.thorn-seshold@cup.lmu.de

Table of contents

1	Supplementary Discussion	S2
1.1	Summary: TrxR selectivity vs. thiol-mediated uptake	S2
1.2	1,2-dithiolane-based probe strategies	S3
1.3	Cell-free evaluation of reduction-mediated release: methods	S4
1.4	Cell-free enzyme specificity/activity studies.....	S5
1.5	Cellular TrxR suppression, knockdown, knockout and knockin.....	S8
1.6	Supplementary Note 1: 1,2-dithiolanes; and PAINS	S9
1.7	Cell-free and cellular studies with electrophilic inhibitors	S12
1.8	Supplementary Note 2: Auranofin's polypharmacology	S17
1.9	Lipid vesicle-mediated ROP of Fast-TRFS.....	S19
1.10	Supplementary Note 3: Fast-TRFS' TrxR-independent fluorogenicity	S20
1.11	Supplementary Note 4: TRFS-green's TrxR-independent fluorogenicity	S21
1.12	In vivo animal model, zebrafish: results and impact	S22
1.13	Supplementary Movie Caption.....	S24
2	Supplementary methods	S24
2.1	Methods for in vitro evaluation.....	S24
2.2	Cell culture methods.....	S25
2.3	Methods for in vivo animal model	S26
2.4	Laboratory techniques	S27
3	Synthetic Procedures	S28
4	NMR Spectra	S33
5	Supplementary References	S39

1 Supplementary Discussion

1.1 Summary: TrxR selectivity vs. thiol-mediated uptake



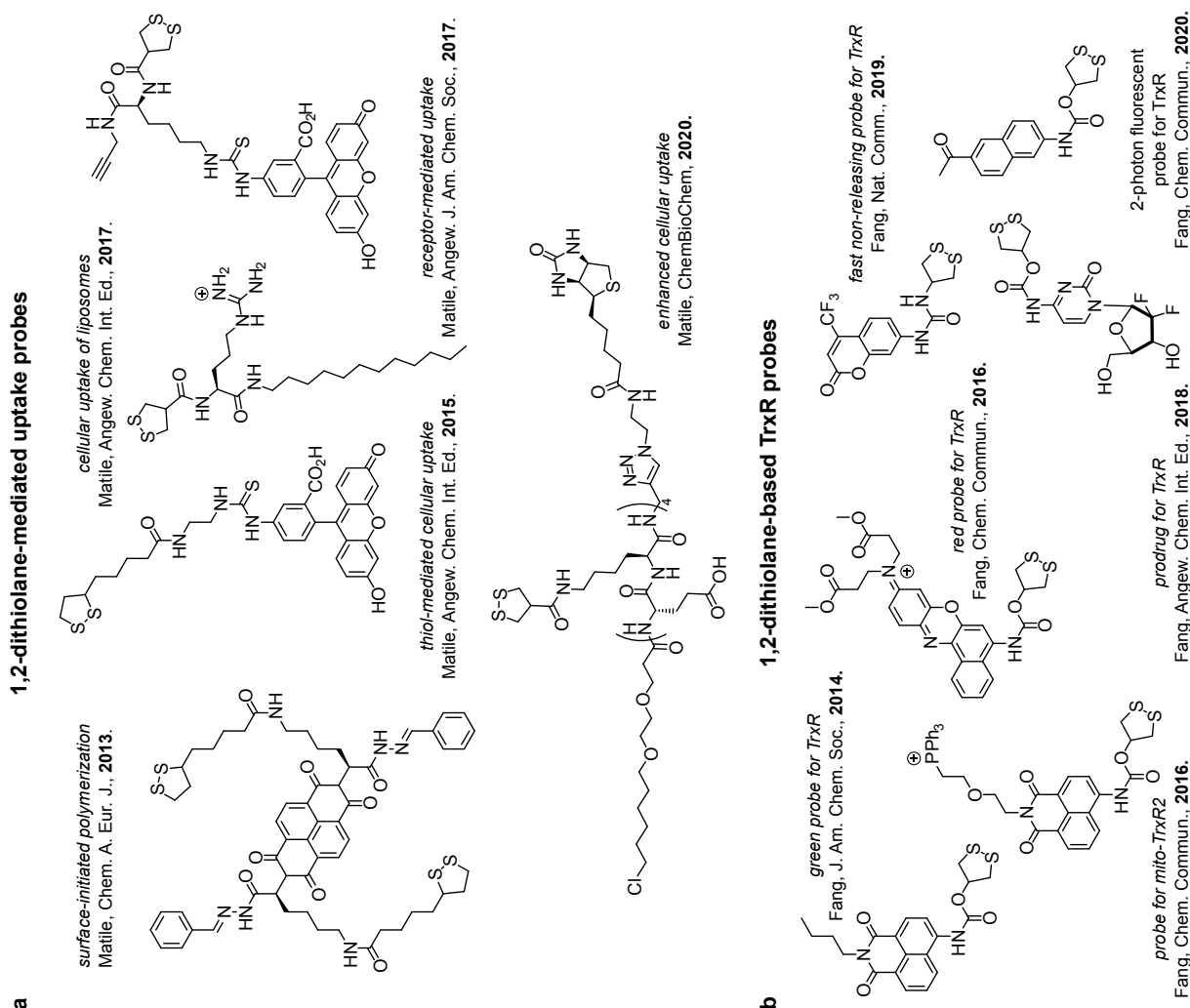
Supplementary Figure 1 Overview of major experimental results related to TrxR-(non)selectivity of 1,2-dithiolane-based probes cross-evaluated with TrxR-independent **SS00-PQ** and TrxR-dependent **RX1** in cell-free (at 10 μM) and in cellular settings (at 50 μM).

Discussion of Results Overview

Several features are apparent in **Supplementary Figure 1**, as discussed in the main text. Noteworthy, the strong cell-free responses with **SS50-PQ** show its nonselectivity for TrxR, while cellular TrxR activity manipulation experiments show that its processing is substantially independent of TrxR, leading to the conclusion that its pattern of cellular results in the electrophile treatments cannot be interpreted as TrxR selectivity. Therefore, **TRFS-green** which reproduces this identical pattern of cellular results in the electrophile treatments, and shows zero to low sensitivity to TrxR activity manipulation, and strong response to Grx in the cell-free assay, should not be interpreted as TrxR-selective either. This highlights the general sensitivity of 1,2-dithiolane towards a broad range of thiol reductants as well as confounding influences (see also vesicle experiments). Results for **RX1²**, a redox probe which displays excellent cellular TrxR-selectivity, are provided for comparison to illustrate trends that would be expected for a TrxR-selective compound. The strong effects of auranofin on the non-TrxR-selective **SS50-PQ** and **TRFS-green** can be coherently interpreted as deriving from the effects of auranofin upon its targets other than TrxR, of which membrane thiol blocking is one. A dependency of cellular signal of the dithiolane-based cyclisation-driven release probes upon membrane thiol mediated, strain-promoted cellular uptake, is expected (see e.g. **Supplementary Figure 2**); consistent with this, **SS00-PQ** which does not benefit from strain-promoted thiol-mediated uptake is unaffected by auranofin.

*For the **TRFS-green** GSH data, see **Supplementary Figure 3c**.

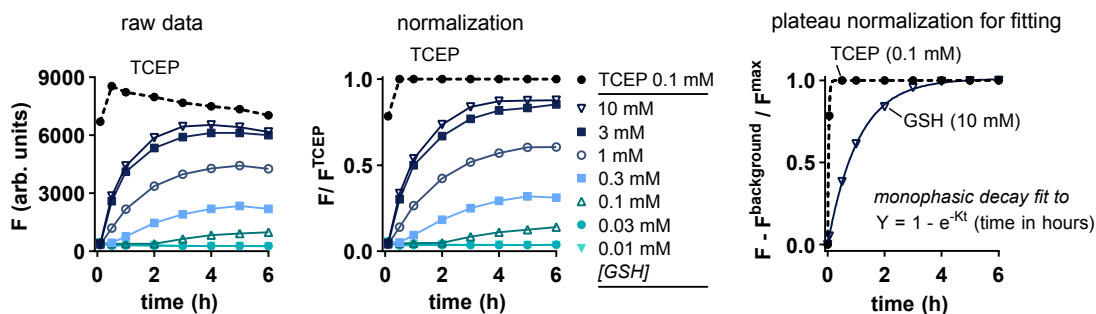
1.2 1,2-dithiolane-based probe strategies



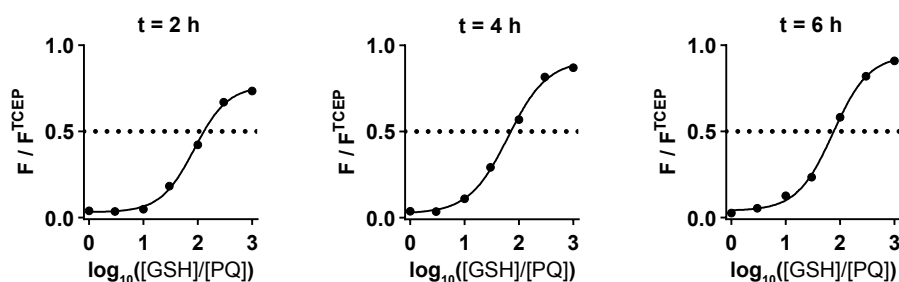
Supplementary Figure 2 1,2-dithiolane-based probe strategies: recent examples from the literature. (a) 1,2-dithiolanes are used by Matile³⁻⁷ for strain-promoted thiol-mediated cellular uptake initiated by exofacial thiols, as well as for ring-opening polymerization (ROP) initiated by thiols or other nucleophiles; (b) 1,2-dithiolane is employed by Fang⁸⁻¹³ as a reduction-sensing motif in cyclisation-driven release probes **TRFS-green**, **TRFS-red**, **mito-TRFS** and **TP-TRFS** and the prodrug **S-Gem** for TrxR activity, as well as in the dithiolane-opening-triggered fluorogenic probe **Fast-TRFS**.

1.3 Cell-free evaluation of reduction-mediated release: methods

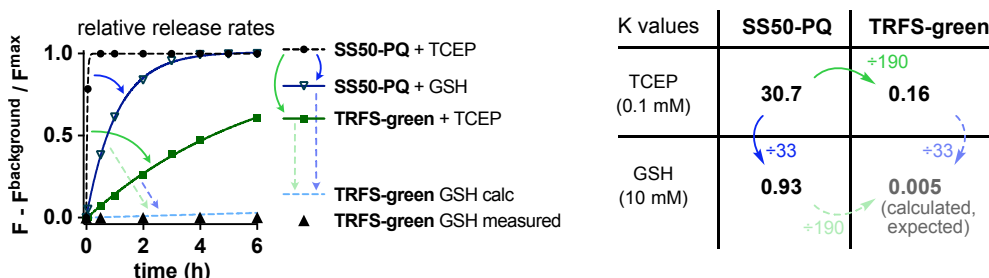
a calculation of normalized fluorescence increase



b calculation of GSH dose-reponse



c calculation of release rates for SS50-PQ and TRFS-green



Supplementary Fig 3 Methods used in evaluation of *in vitro* performance of probes during reductant challenge. Example for **SS50-PQ** (10 μ M) challenged with the monothiol reductant *L*-glutathione (GSH), monitoring reduction-mediated release of solid fluorescent **PQ-OH**. (a) Calculation of normalized fluorescence increase from raw fluorescence data recorded on a platereader (ex/em 355bp10/520lp) by reference to an experiment with maximum expected signal (TCEP at 100 μ M). Only for the expected rate calculation in **Supplementary Figure 3c**, was the plateau of the GSH series adjusted to 1.0, for exponential fitting (assumes TCEP reduction near-instantaneous, so rate reports on cyclisation-elimination). (b) Dose-response curves for **SS50-PQ** upon challenge with GSH are very similar no matter what timepoint of data is used ($t = 2$ h, 4 h, 6 h): which is associated to the rapidity of post-reductive cyclisation-elimination of **SS50-PQ**. *Representative example out of 3 independent experiments.* (c) **TRFS-green** gives no significant fluorescence under GSH challenge in these assay conditions. However, it is ca. 190-fold slower to generate signal when treated with excess TCEP, than is **SS50-PQ**. Assuming that their reduction & cyclisation kinetics are identical, we interpret this as the expectedly slower kinetics of anilide vs phenolate leaving-group expulsion. Noting that GSH challenge of a 1,2-dithiolane is 33-fold slower to generate signal than TCEP challenge (**SS50-PQ** data), we can calculate the expected rate of signal generation under GSH challenge of **TRFS-green** either from its own TCEP rate, or from **SS50-PQ**'s GSH rate: but we arrive at a K-value of 0.005 regardless of which route is taken, which speaks to the accuracy of our rate assumptions.

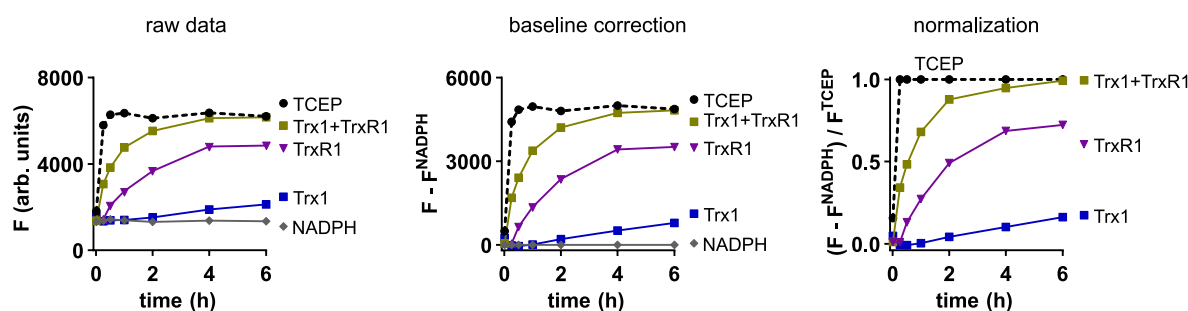
The key outcome of this calculation is that no significant signal generation by **TRFS-green** can be expected in only 6 h of cell-free GSH challenge in homogenous media - *not because it is GSH-resistant*, but because its post-reduction kinetics are so slow that 6 h is insufficient to see much outcome. Contrasting this slow release rate to its instantaneous fluorogenicity in cellular experiments (e.g. early timepoints of **Supplementary Figure 11b**) supports that **TRFS-green** in cellular settings substantially gives signal through environment-dependent fluorogenicity of the trigger-cargo pair (whether as intact probe, or as e.g. a membrane-thiol-exchange adduct), and not through the very slow anilide elimination: therefore interpreting its fluorogenicity as reporting on post-reduction-elimination is therefore dangerous. It is an instructive exercise to calculate just what fraction of the reaction speed of 10-fold excess of TCEP that any given reductant (such as a 500-fold lower concentration of TrxR) would have to give, in

order to drive this slow probe to display any significant fluorescence increase, *unless effects such as environment-dependent fluorogenicity dominate the readout.*

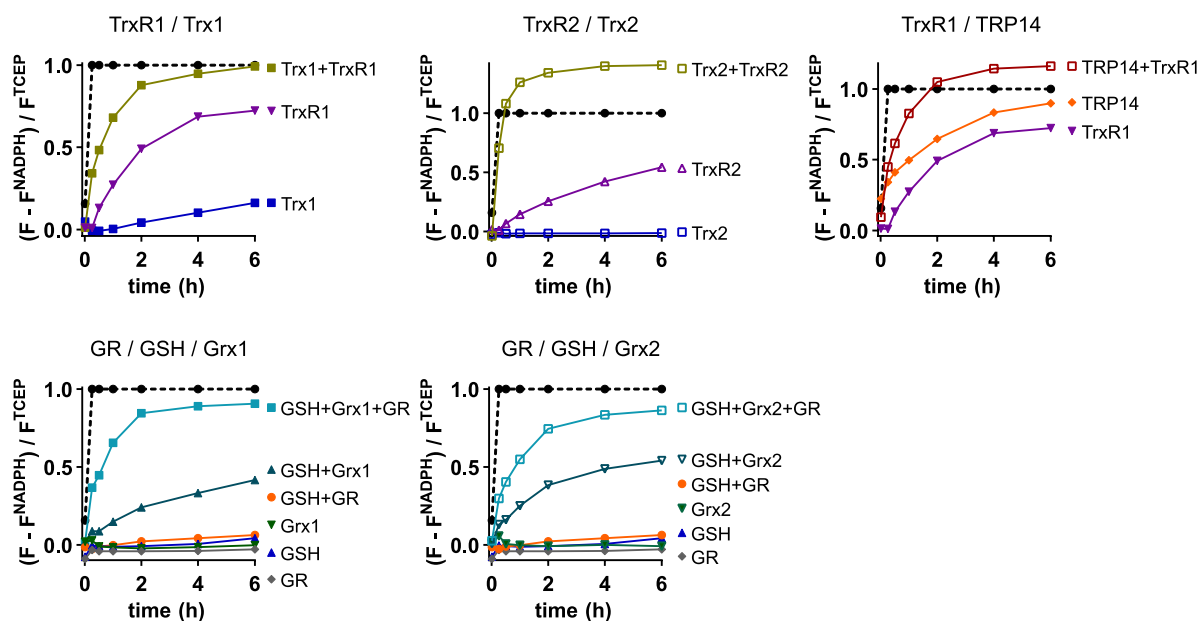
Further discussions of rates relevant to signal generation are to be found in Felber *et al.*¹⁴

1.4 Cell-free enzyme specificity/activity studies

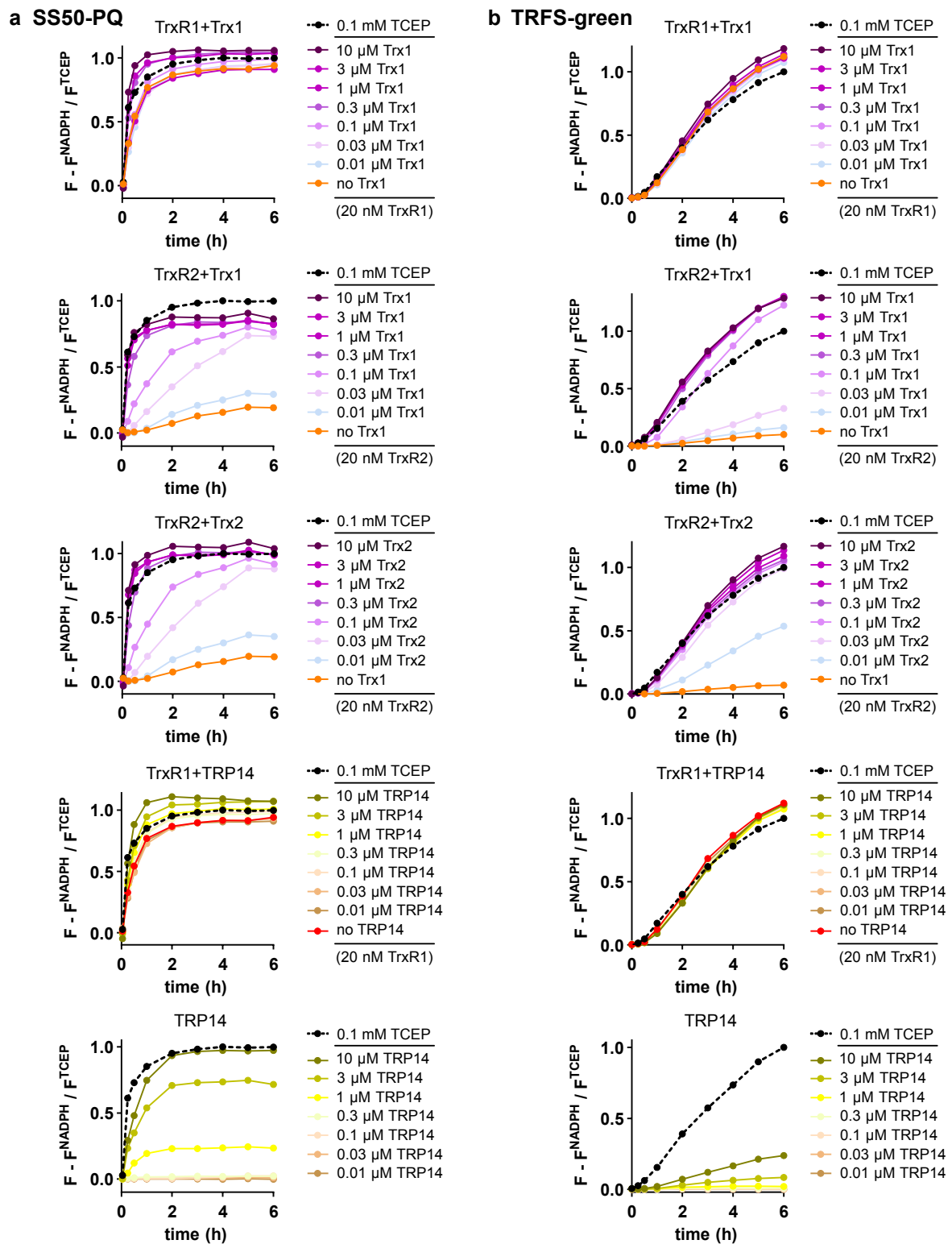
a calculation of normalized fluorescence increase



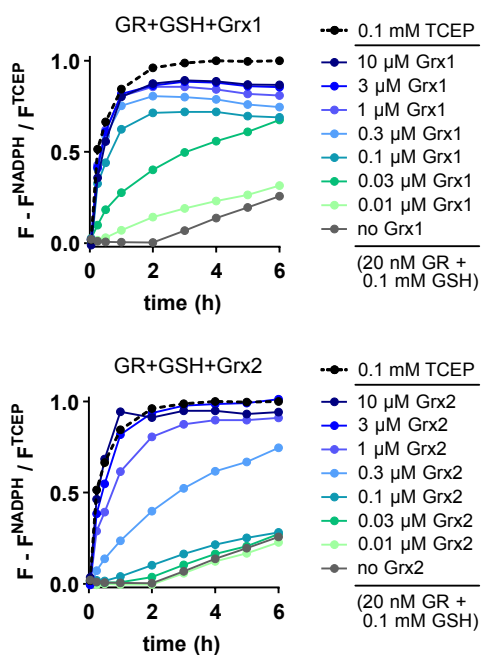
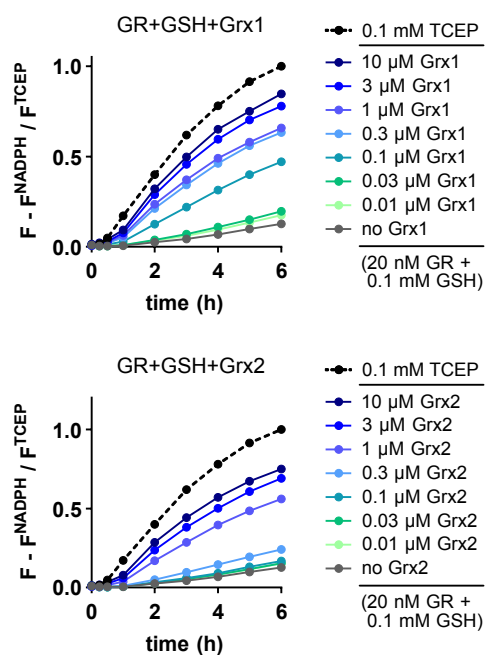
b probe activation by various redox cascades



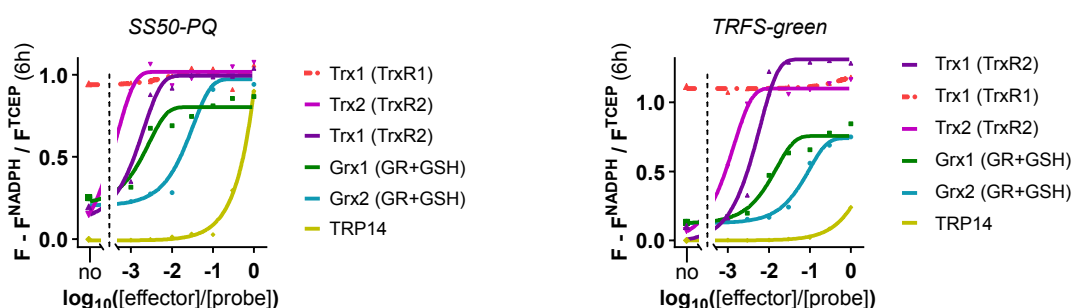
Supplementary Fig 4 Methods used in evaluation of *in vitro* performance of probes when treated with purified enzymes. Example for **SS50-PQ** (10 μ M) treated with various members of different redox cascades, monitoring reduction-mediated release of solid fluorescent **PQ-OH**. (a) Example enzyme activity assay: calculation of normalized fluorescence increase from raw fluorescence data recorded on a platerreader (ex/em 355bp10/520lp), corrected for the baseline autofluorescence of reduced β -NADPH, and normalised to a reference experiment with maximum expected signal (TCEP at 100 μ M); (b) Resulting normalised data for probe activation by various members of the different redox cascades: (1) TrxR1 (20 nM), Trx1 (10 μ M), TrxR1+Trx1; (2) TrxR2 (20 nM), Trx2 (10 μ M), TrxR2+Trx2; (3) TrxR1 (20 nM), TRP14 (10 μ M), TrxR1+TRP14; (4) GR (20 nM), GSH (10 μ M), Grx1 (10 μ M), GR+GSH, GR+Grx1, GSH+Grx1, GR+GSH+Grx1; (5) GR (20 nM), GSH (10 μ M), Grx2 (10 μ M), GR+GSH, GR+Grx2, GSH+Grx1, GR+GSH+Grx2. *Representative examples of 3 independent experiments.*



Supplementary Fig 5 Redox-effector protein titrations of the Trx-system challenging (a) **SS50-PQ** and (b) **TRFS-green** (10 μM). TrxR1 or TrxR2 (both at 20 nM) were employed with $\beta\text{-NADPH}$ (100 μM) to recycle the redox effector proteins Trx1, Trx2 or TRP14 (from 0.01 μM to 10 μM); the "no Trx" results show that TrxR2 alone at this concentration is ineffective in reducing the probes, while significant direct reduction by TrxR1 at this concentration occurs that overlays the Trx-mediated reduction. Raw fluorescence data recorded on a platerreader (ex/em 355bp10/520lp or 440bp10/520lp) is represented corrected by the basal fluorescence caused by autofluorescence of reduced $\beta\text{-NADPH}$ if applicable and normalized to a reference experiment with maximum expected signal (TCEP at 100 μM). *Representative example out of 3 independent experiments.*

a SS50-PQ

b TRFS-green


Supplementary Fig 6 Redox-effector protein titrations of the Grx-system challenging (a) **SS50-PQ** and (b) **TRFS-green** (10 μM). GR (at 20 nM) was employed with $\beta\text{-NADPH}$ (100 μM) and used to recycle low concentrations of GSH (0.1 mM) and finally the redox effector proteins Grx1 or Grx2 (from 0.01 μM to 10 μM). Raw fluorescence data recorded on a platereader (ex/em 355bp10/520lp or 440bp10/520lp) is represented corrected by the basal fluorescence caused by autofluorescence of reduced $\beta\text{-NADPH}$ if applicable and normalized to a reference experiment with maximum expected signal (TCEP at 100 μM). *Representative example out of 3 independent experiments.*

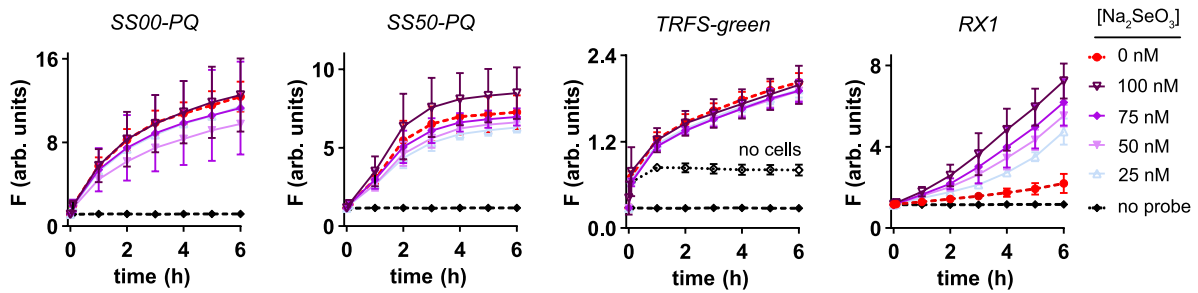
redox effector protein - dose-reponse


EC_{50} (nM)	Trx1 (TrxR2)	Trx2 (TrxR2)	Grx1 (GR+GSH)	Grx2 (GR+GSH)	TRP14*
SS50-PQ	1.4	0.3	1.9	22.9	9,016
TRFS-green	4.2	1.0	10.7	67.5	> 10,000

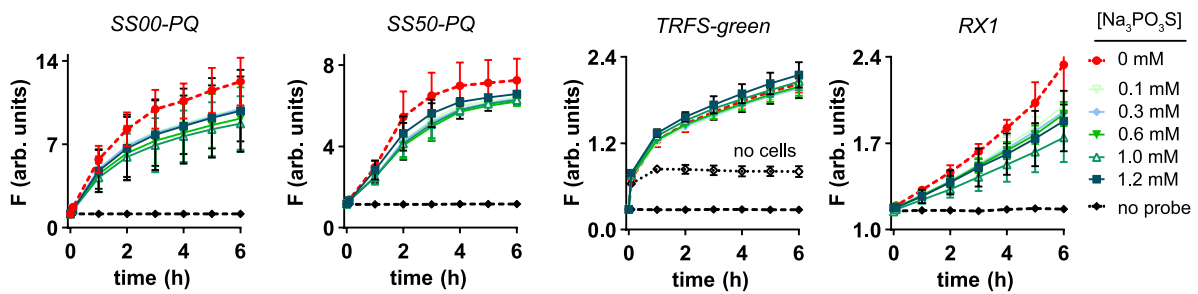
Supplementary Fig 7 Dose-response plots of **SS50-PQ** and **TRFS-green** (both at 10 μM) cross-evaluated against increasing redox effector protein concentrations (0.01-10 μM) at timepoint $t = 6$ h. TRP14*: TRP14 was titrated without the addition of $\beta\text{-NADPH}$ and/or a reductase, as it can only be recycled efficiently by TrxR1 and TrxR1 has itself fast kinetics in reduction of both **SS50-PQ** and **TRFS-green**. *Representative example out of 3 independent experiments.*

1.5 Cellular TrxR suppression, knockdown, knockout and knockin

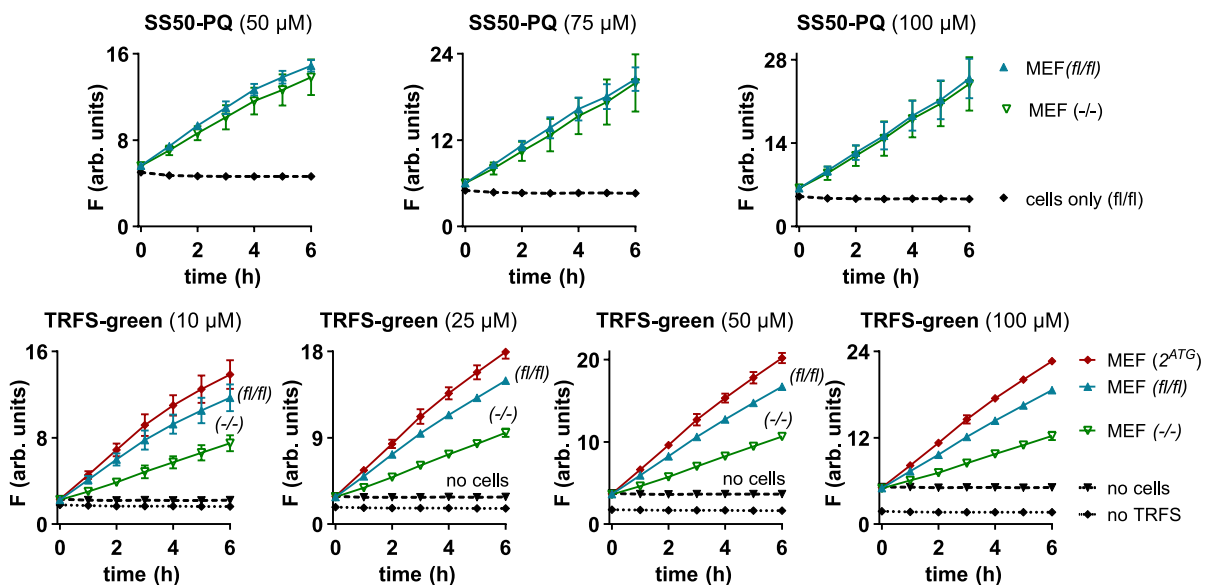
a Selenium supplementation/starvation - A549 cells



b chemical knockdown (Sec to Cys - A549 cells)



c genetic knockdown - MEF TrxR knockout cells



Supplementary Fig 8 Cellular tests of the TrxR-dependency of **SS50-PQ** and **TRFS-green**, with comparisons to the performance of positive control probe **SS00-PQ** and the TrxR1-selective probe **RX1**². (a) A549 cells were supplemented with (a) Na_2SeO_3 (25-100 nM) (b) with $\text{Na}_3\text{PO}_3\text{S}$ (0.1-1.2 mM) for 48 h, before treated with **SS00-PQ**, **SS50-PQ**, **TRFS-green** and **RX1** (all at 100 μM) and fluorescence was monitored (ex/em 355bp10/520lp or 390bp10/520lp) for 6 h. (c) Assay comparing fluorescence (ex/em 355bp10/520lp or 440bp10/520lp) timecourses in MEF cells with TrxR1 knockout (-/-)¹⁵, to the precursor MEF cell line from which knockout was not performed (fl/fl), as well as to the 2^{ATG} cell line¹⁶ where TrxR1 is knocked in. All graphs in Supplementary Figure 8 show Mean+SD calculated from 3 independent experiments.

Summary of TrxR modulation results

TrxR1 functional suppression (**Supplementary Figure 8a**), knockdown (**Supplementary Figure 8b**), or knockout (**Supplementary Figure 8c**), do not prevent signal generation from either probe. It should also be noted that all these TrxR1 modulations will also affect the redox status of all its downstream targets, both direct targets such as Trx1 and indirect ones (targets of Trx1); that membrane-bound Trx1¹⁷ is a significant species in cell-surface thiol chemistry; and that the fact that the **TRFS-green** signal saturates above 10 μ M is consistent with the presence of a limiting mechanism for signal generation, such as rate of thiol-mediated uptake and concentration into water-excluded environment, being a determinant of cellular signal: but is not consistent with the linearity of dose-response seen for the faster-releasing environment-independent probe **SS50-PQ**. The interested reader can also revisit the discussion following **Supplementary Figure 3**, in which we argue based on rates of reaction with 10-fold excess of TCEP that the very slow release-based signal generation of **TRFS-green** makes it to our understanding impossible that this probe can hope to report cleanly on TrxR activity in cells, instead of giving a signal that is entirely dominated by environment-dependent effects.

1.6 Supplementary Note 1: 1,2-dithiolanes; and PAINS

Specific dithiol/disulfide-exchange reactions are central to biology, and engineered disulfides exploiting these reaction manifolds have applications from chemical biology probes to biophysics and materials chemistry. 1,2-dithiolanes have emerged as substrates of interest in chemical biology^{8,11,12} (**Supplementary Figure 2**), although it has remained contentious whether its reduction is enzyme-selective, or nonspecific. In this paper we answered this question by studying the biochemical and biological performance of the novel 1,2-dithiolane-based redox probe **SS50-PQ**. The disulfide was integrated in a stable, modular design that can be adapted to release arbitrary phenols: in this case, a release-activated fluorescent cargo, that we could even use in flow cytometry studies and for cell-resolved imaging in live embryos.

A rigorous methodology of reductant titrations, enzyme panel screenings, and inhibitor/knockout cell experiments has here demonstrated the nonspecific reduction-based cleavage of the 1,2-dithiolane. While 1,2-dithiolane can indeed be rapidly opened by TrxR, particularly TrxR1 (**Supplementary Figure 4**), it is also rapidly opened by GSH at sub physiological concentrations (**Supplementary Figure 3**) as well as by many thiol protein reductants (**Supplementary Figures 5-7**). Therefore, inside cells, it is highly unlikely to selectively report on TrxR, instead of on more abundantly present reductants. The cellular data also show that neither TrxR1 knockdown, knockout, nor TrxR inhibition by recently developed Au-free inhibitors (**Supplementary Figures 8, 10-15**), greatly modulate the cellular signal obtained from the 1,2-dithiolane-based probes.

Note 1.1: Comparisons between the different cargo-releasing dithiolane probe designs

The same nonselectivity conclusions outlined above for **SS50-PQ** apply also to the other tested dithiolane probes. Particularly, for the irreversible cyclisation-driven-release probe **TRFS-green**:

(1) It is significant to show which reductants are capable of triggering fluorophore release in the cell-free setting. **Figure 3c-d** shows that the aniline-eliminating probe **TRFS-green** is kinetically labile to all tested redox effector proteins Trx1, Trx2, Grx1, Grx2 and TRP14, with very similar dose-response as the phenol-eliminating **SS50-PQ**, just with an apparent shift to higher reductant doses: although this shift arises not because of any difference of intrinsic reducibility (selectivity) of their 1,2-dithiolanes, but simply because anilines are poorer leaving groups. Therefore, we consider that the post-reduction-expulsion kinetics of **SS50-PQ** and **TRFS-green** are predictably different according to the nature of the chemical cargo (TCEP challenge half-life ca. 3 hours for aniline expulsion of **TRFS-green**, but only ca. 5 minutes for phenolate expulsion from the more sensitive and easier to interpret **SS50-PQ**). This similarity is supported by **Supplementary Figures 5-6**, and particularly by the full dose-responses and tabulated EC₅₀ values of **SS50-PQ** compared to **TRFS-green** for all protein effectors (**Supplementary Figure 7**) showing there is a consistent 3-to-5-fold difference of the 6 hour fluorescence dose-response across all effectors. This seems a compelling reiteration that redox structure-activity relationships do exist: the 1,2-dithiolane is the reducible motif constant across both probes, the distant aniline/phenol cargo is the leaving group kept constant between probe series, the only way that reduction rates between the series can maintain the same ratios across different reductants is if the dithiolane motif itself dictates reactivity (i.e. the disulfide plays the key role in selectivity, not the cargo).

(2) We also take **TRFS-green** through cellular signal generation studies to show that its signal generation is independent from its claimed reductase TrxR, supporting our general conclusion that 1,2-dithiolane-based probes are not capable of cellular selectivity:

(2a) TrxR1 knockdown does not prevent **TRFS-green** signal generation in cells (**Figure 5, Supplementary Figure 8**) but only reduces it by ca. 40%. TrxR2, the other isozyme of TrxR, is only present in mitochondria, and is not expected to have a comparable expression level to TrxR1. Additionally, TrxR2 is also known to have lower turnover of small molecule substrates in general, and cell-free data show (**Supplementary Figure 5**) that it is almost entirely incapable of **TRFS-green** reduction. Therefore, at least ca. 60% of signal generation in cells by **TRFS-green** cannot

be directly related to TrxR activity. Regarding the 40% drop, this can arise straightforwardly in probes that are partially processed by downstream reductants dependent on TrxR, such as Trxs, without this change indicating any direct reduction of the probe specifically by TrxR. By comparison, **SS50-PQ** is entirely unresponsive to TrxR1 knockout. The similarity of cellular behaviour of the two probe systems, which in cell-free settings are strikingly similarly reducible by the same broad range of redox effectors, should be kept in mind: it strongly suggests that results from **SS50-PQ** should also apply to **TRFS-green**. We believe this indicates that the **SS50-PQ** environment-independent release-based probe has more straightforwardly revealed, that 1,2-dithiolane probe activation is not significantly due to direct reduction by TrxR1 in the cellular context.

(2b) Selenium supplementation/depletion has no effect on **TRFS-green** signal generation in cells, even though this controls the amount of active site selenolthiol TrxR (**Figure 5, Supplementary Figure 8**). Thiophosphate supplementation (**Figure 5, Supplementary Figure 8**) which likewise prevents selenocysteine incorporation, is also ineffective at reducing **TRFS-green** signal. Unsurprisingly to us, **SS50-PQ** performs identically in both these respects i.e. is similarly nonresponsive to changes in the amount of functional cellular TrxR. It can again be concluded that cellular reduction of 1,2-dithiolane-based probes does not depend on correctly-expressed UC-containing TrxR. For comparison to how a TrxR-dependent probe should perform, **Figure 5** references results of the redox probe candidate RX1², that data indicate to be near-exclusively directly activated by TrxR1: e.g. the >90% signal suppression by TrxR1 knockout, the signal enhancement by selenium supplementation, and the signal reduction by thiophosphate treatment.

(3) We also introduce new comparisons between several probes to show how assay interpretation requires combining independent experiments. For example:

(3a) 1,2-dithiolane **SS50-PQ** is unaffected by cellular TrxR knockout (**Figure 5, Supplementary Figure 8**): so it is not significantly cellularly activated by TrxR: yet its signal is mildly suppressed by cellular treatment with chalcophilic S_NAr-based electrophiles such as TRi-1 and TRi-3 (**Figure 5**), and strongly suppressed by cellular treatment with the lipophilic Au(I)-based Lewis acid auranofin (AF), which has more than 20 attested targets (new **Supplementary Figure 10-15**). Thus, treating cells with these thiol/selenol-affine electrophiles and observing this suppression of cellular signal from a dithiolane probe, cannot be cited as a proof that that 1,2-dithiolane-based probe is a selective reporter of TrxR, since **SS50-PQ** provides a clear counterexample. Relevant to this, Matile's studies⁴ have showed that 1,2-dithiolanes substantially rely on *free* exofacial thiols for cellular uptake. This uptake is inhibited by general thiol-reactive species of all tested chemotypes (including even other disulfides) typically even suppressing uptake to only 10% of normal. This provides a coherent explanation: these lipophilic electrophiles can suppress cellular 1,2-dithiolane signal generation by reacting with thiols on the cell surface, so substantially blocking the otherwise strain-promoted enhanced cellular uptake that dithiolanes can experience.

(3b) Next, the electrophile treatment data for 1,2-dithiolane **TRFS-green**, show almost identical signal suppression as **SS50-PQ** (**Figure 5, Supplementary Figure 11**). Having shown that the electrophile assay does not test *TrxR selectivity* (see above), it is still supported by literature that one would expect that these electrophiles should inhibit strain-promoted cellular uptake of the dithiolane **TRFS-green** very similarly as for the dithiolane **SS50-PQ**. The observation that the level of inhibition is so similar between **SS50-PQ** and **TRFS-green** again suggests that their chemical behaviour (rooted in their 1,2-dithiolane) is the same, i.e. that the signal of **TRFS-green** is likewise being inhibited by electrophilic blocking of cellular thiols, not from the effects those electrophiles also have by partially reacting with cellular TrxR (which is only one of their many cellular targets).

(3c) To counter-test these results, the linear disulfide probe **SS00-PQ** was used. This unstrained probe should not benefit from strain-promoted thiol-mediated uptake enhancement (which can be suppressed by electrophiles); and we as well as others have shown that linear disulfide probes are not selective for any particular cellular reductant - while they are reducible by TrxR, they are also reducible by the vastly more concentrated GSH, Trx, Grx, etc. The electrophile assay results are perfectly coherent with this expectation (**Figure 5, Supplementary Figure 12**): the electrophiles do not suppress signal from **SS00-PQ**, since the signal from this non-dithiolane probe is not limited by strain-promoted uptake.

This coherent intercomparison of results across multiple probes (**Supplementary Figure 13**), and the unity of results between the releasing probe **SS50-PQ** and the alternative releasing design **TRFS-green**, delivers strong evidence for the generality of the nonselectivity of 1,2-dithiolane as a reducible motif, and for the other effects we report.

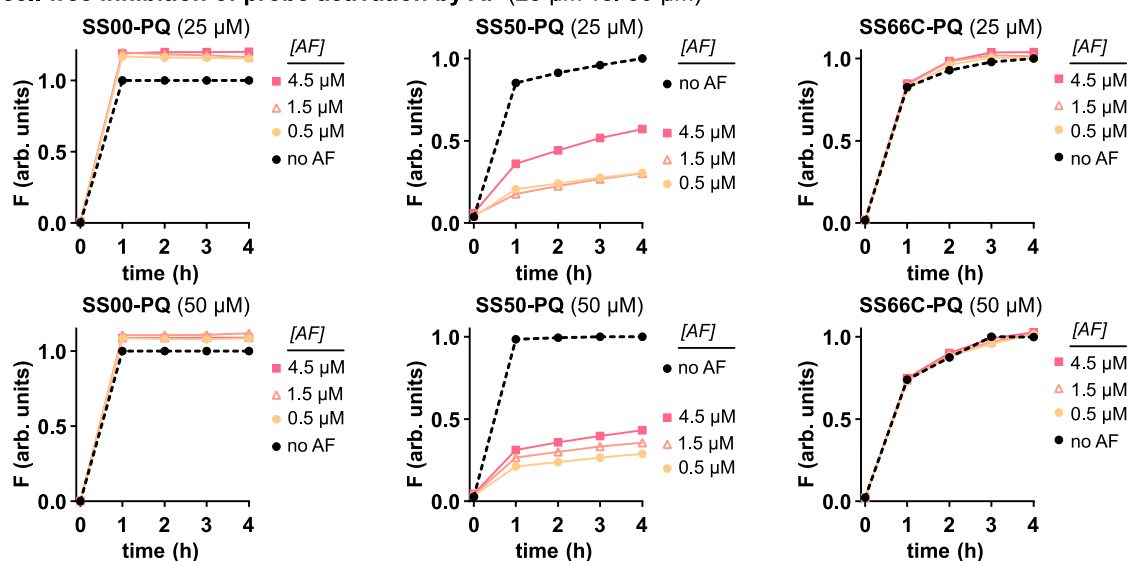
Taken together, we conclude that 1,2-dithiolane is a nonspecifically reduced motif, that is not a TrxR-specific substrate. Beyond the dithiolane-relevant references in the introduction to this paper, we also refer the interested reader to excellent work by Lothrop, Ruggles and Hondal¹⁸, which shows that even when the unique selenothiol *N*-terminal reaction centre of TrxR is deleted, 1,2-dithiolane can still be reduced, further weakening the argument that dithiolane has any intrinsic selectivity for TrxR.

Note 1.2: Misinterpreting Dithiolanes can lead to PAINS

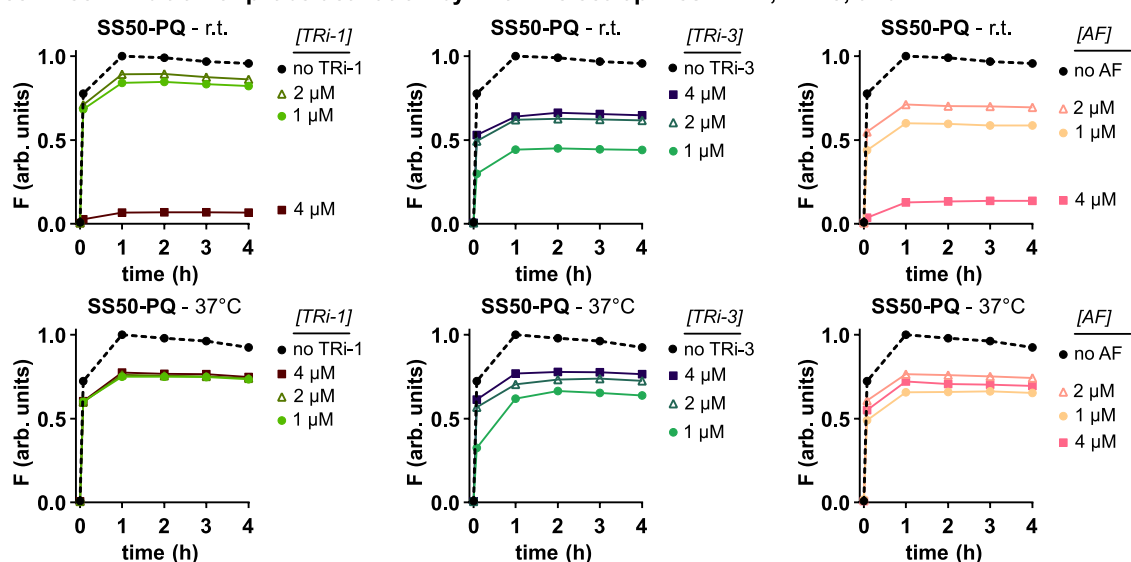
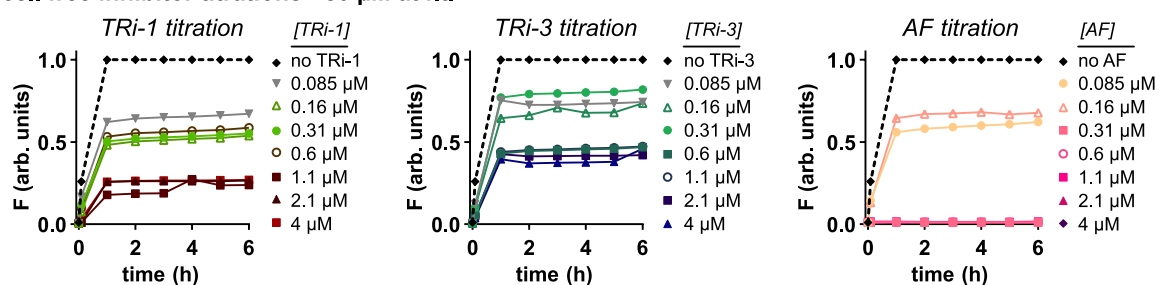
In recent years, a range of 1,2-dithiolane-based TRFS probes have been reported as TrxR-specific substrates; they have been used as such for mechanistic validations during screening¹² and in disease characterisation.^{9,19} These reports interpret cellular 1,2-dithiolane probe readouts as monitoring TrxR activity; but we contend that these reports may benefit from re-evaluation for alternative interpretation and application. We also caution that since 1,2-dithiolane-based probes such as **TRFS-green** are commercialised, they may continue to be used in assays without appreciation that their *cellular* readouts do not uniquely monitor TrxR-activity: however, research that assumes they are TrxR-selective, risks false outcomes in the same ways that have been reviewed for pan-assay interference compounds.²⁰

Indeed, the set of 13 compounds that was reported to be "validated" as TrxR inhibitors on the basis of comparison to a 1,2-dithiolane-based probe¹², consists entirely of hydrophobic PAINS compounds (9 Michael acceptors, 2 naphthoquinones, and 2 polyphenolic flavones) including the archetypical PAINS, curcumin²¹ and myricetin²²; while the 20 new inhibitors also reported included no single compound that is not a typical or known PAINS candidate (ortho- or para-quinones, Michael acceptors, catecholic polyphenols/flavonoids, and the known thiol-reactive PAINS disulfiram²³). The cautionary results and stepwise methodology we report can also prevent mistakes in the future. Both will be useful for systematising redox probe development.

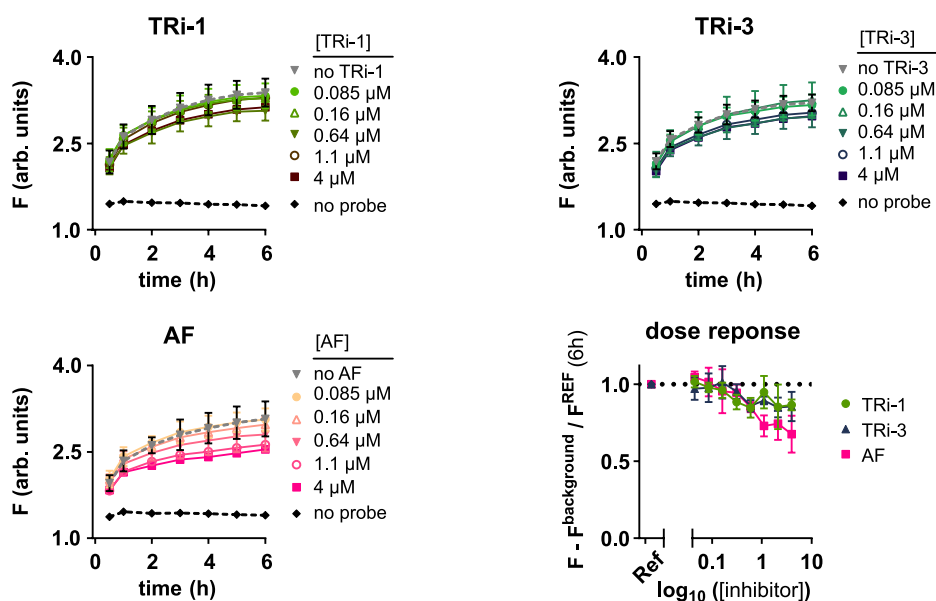
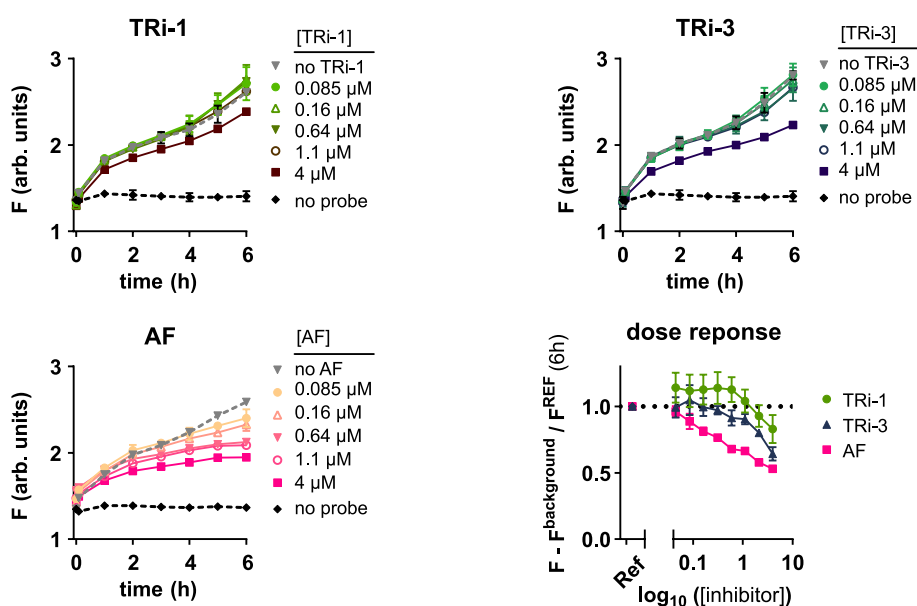
1.7 Cell-free and cellular studies with electrophilic inhibitors

a cell-free inhibition of probe activation by AF (25 μ M vs. 50 μ M)

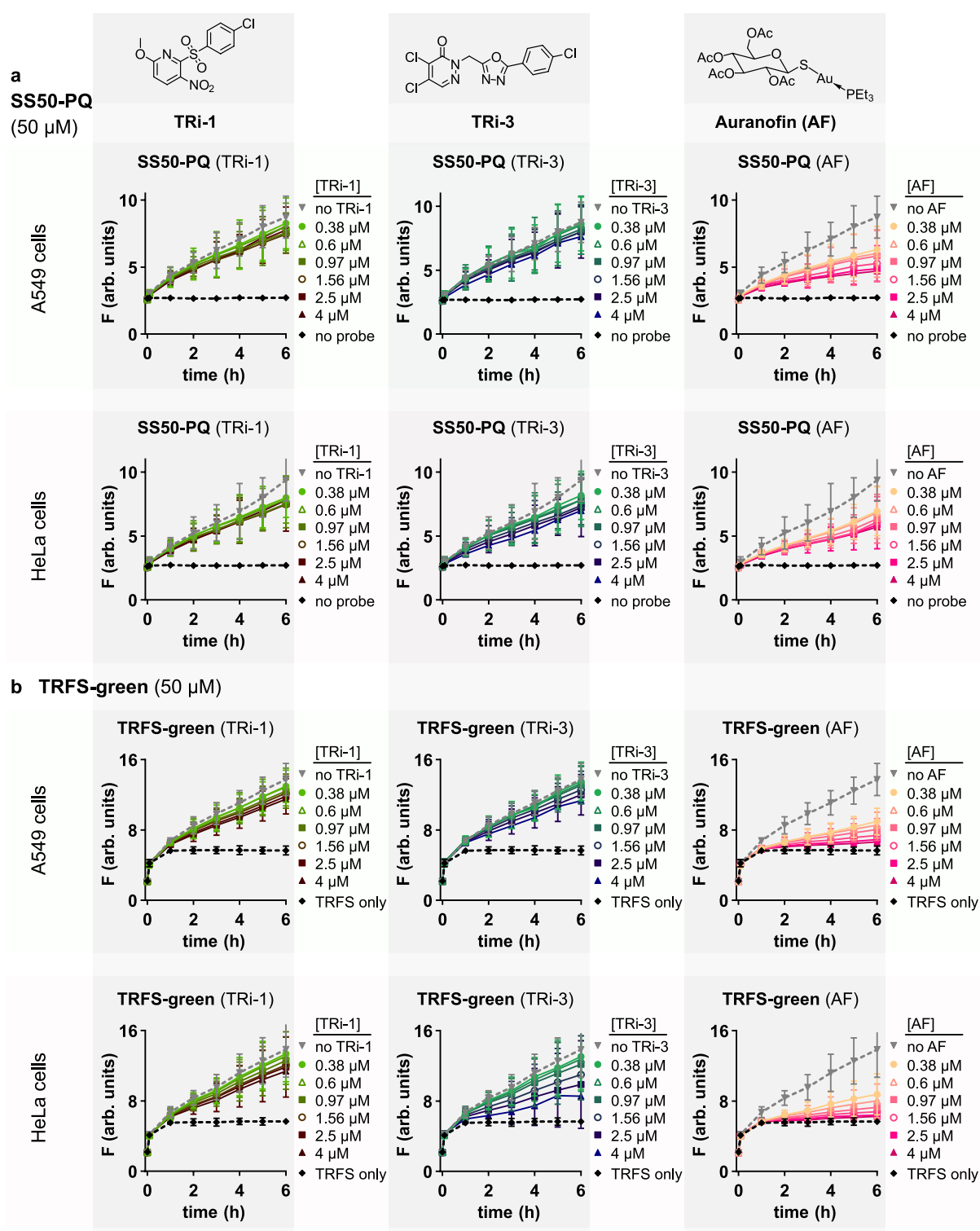
b cell-free inhibition of probe activation by known electrophiles TRI-1, TRI-3, and AF

c cell free inhibitor titrations - 50 μ M at r.t.

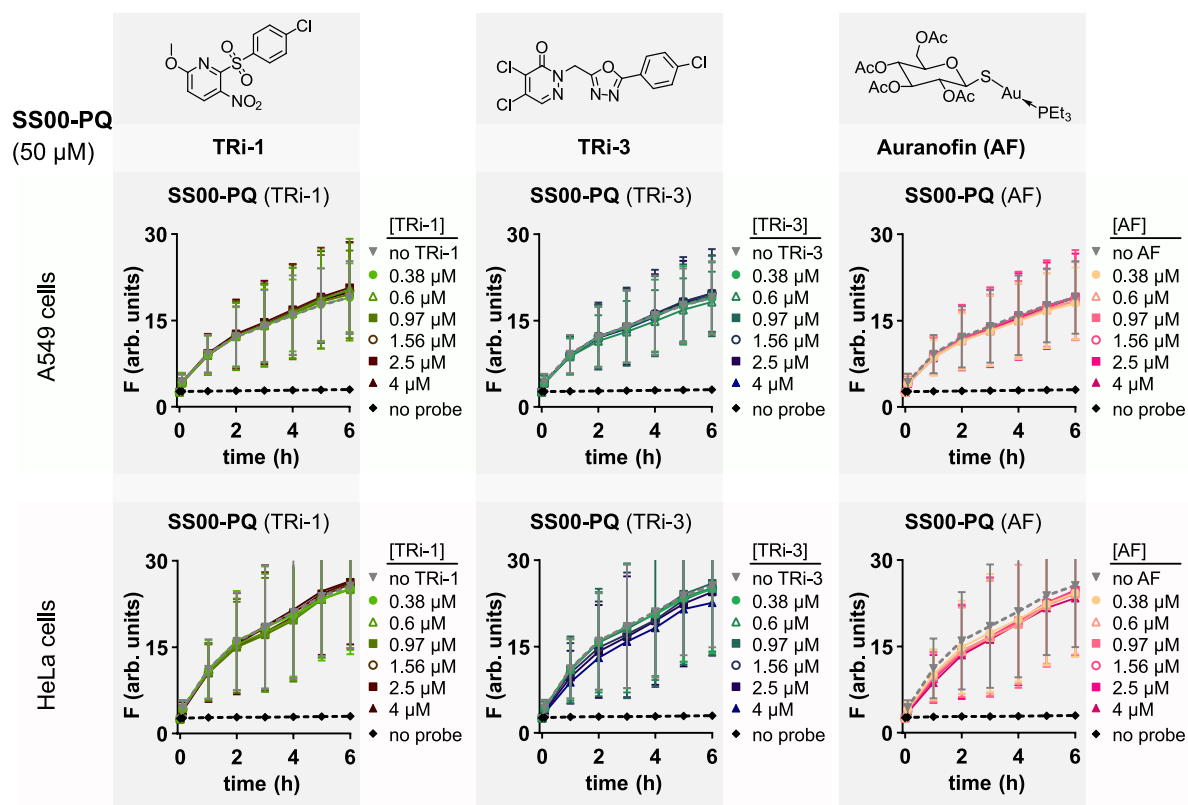
Supplementary Fig 9 Cell-free inhibition of potential reductive probe activation by electrophilic known TrxR-inhibitors was tested for **SS50-PQ** and referenced to non-cyclic **SS00-PQ** and non-strained **SS66C-PQ**¹⁴ reference probes. Fluorescence timecourses for (a) **SS50-PQ**, **SS00-PQ** and **SS66C-PQ** (at 25 μ M or 50 μ M as indicated) pre-treated with AF (0.5–4.5 μ M) for 2 h at r.t.; then treated with TCEP (at 100 μ M). (b) **SS50-PQ** (at 50 μ M) pre-treated with TRI-1, TRI-3 or AF (1.0–4.0 μ M) for 2 h at r.t. or 37 °C (as indicated); then treated with TCEP (at 100 μ M) (c) **SS50-PQ** (at 50 μ M) pre-treated with TRI-1, TRI-3 or AF (0.085–4.0 μ M) for 2 h at r.t.; then treated with TCEP (at 100 μ M). (a–c) show single experiments with technical replicates.

a SS50-PQ (25 μ M) - inhibitor studies - A549 cells**b SS50-PQ (25 μ M) - inhibitor studies - HeLa cells**

Supplementary Fig 10 Preliminary evaluation of cellular response of SS50-PQ under cellular treatment with known Au(I)-free TrxR inhibitors TRI-1 and TRI-3, and with the Au(I)-based inhibitor auranofin (AF). Conditions differ slightly from those used in the final evaluation (**Supplementary Figure 10**). Cellular fluorescence (ex/em 355bp10/520lp) and dose-response plots for (a) A549 cells pre-treated with TRI-1, TRI-3 and AF (25 μ M SS50-PQ, 3 h pre-treatment). (b) HeLa cells were pre-treated (3 h pre-treatment) TRI-1, TRI-3 and AF and then treated with 25 μ M SS50-PQ. (a-b) show graphs representing Mean+SD calculated from 3 independent experiments.

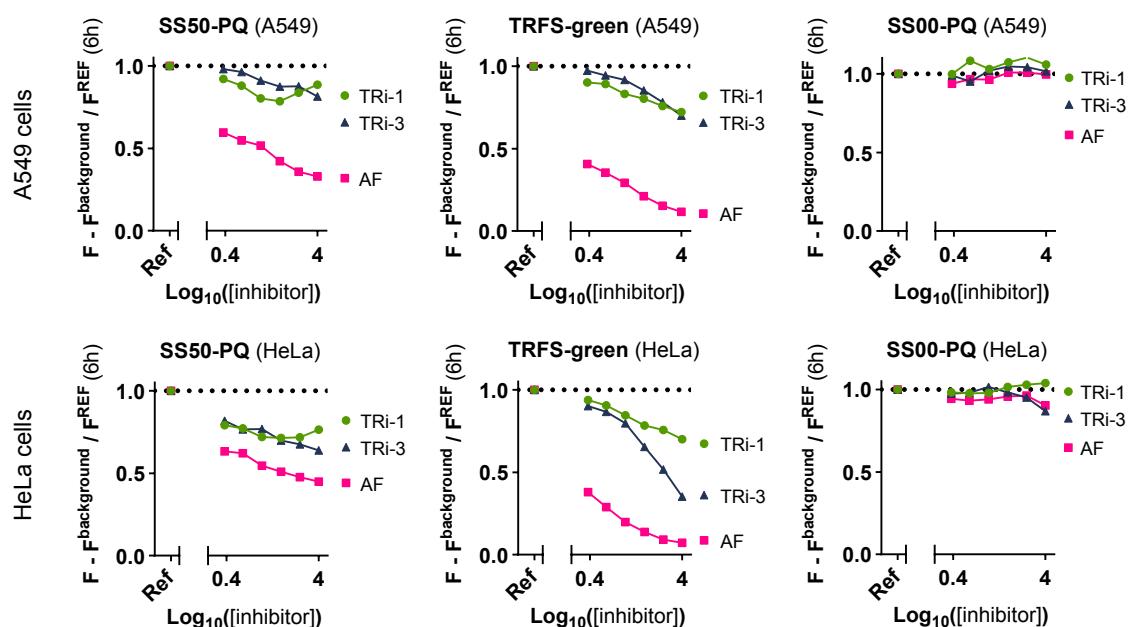


Supplementary Fig 11 Final comparison of **SS50-PQ** and **TRFS-green** cross-evaluated with TRi-1, TRi-3 and AF. Fluorescence timecourse upon cellular processing in (a) A549 cells pre-treated with TRi-1, TRi-3 and AF (50 μ M **SS50-PQ** or **TRFS-green**, 2 h pre-treatment) and (b) HeLa cells pre-treated with TRi-1, TRi-3 and AF (50 μ M **SS50-PQ** or **TRFS-green**, 2 h pre-treatment). Note that micromolar concentrations of these electrophiles are also cytotoxic.²⁴ (a-b) show graphs representing Mean+SD calculated from 3 independent experiments.

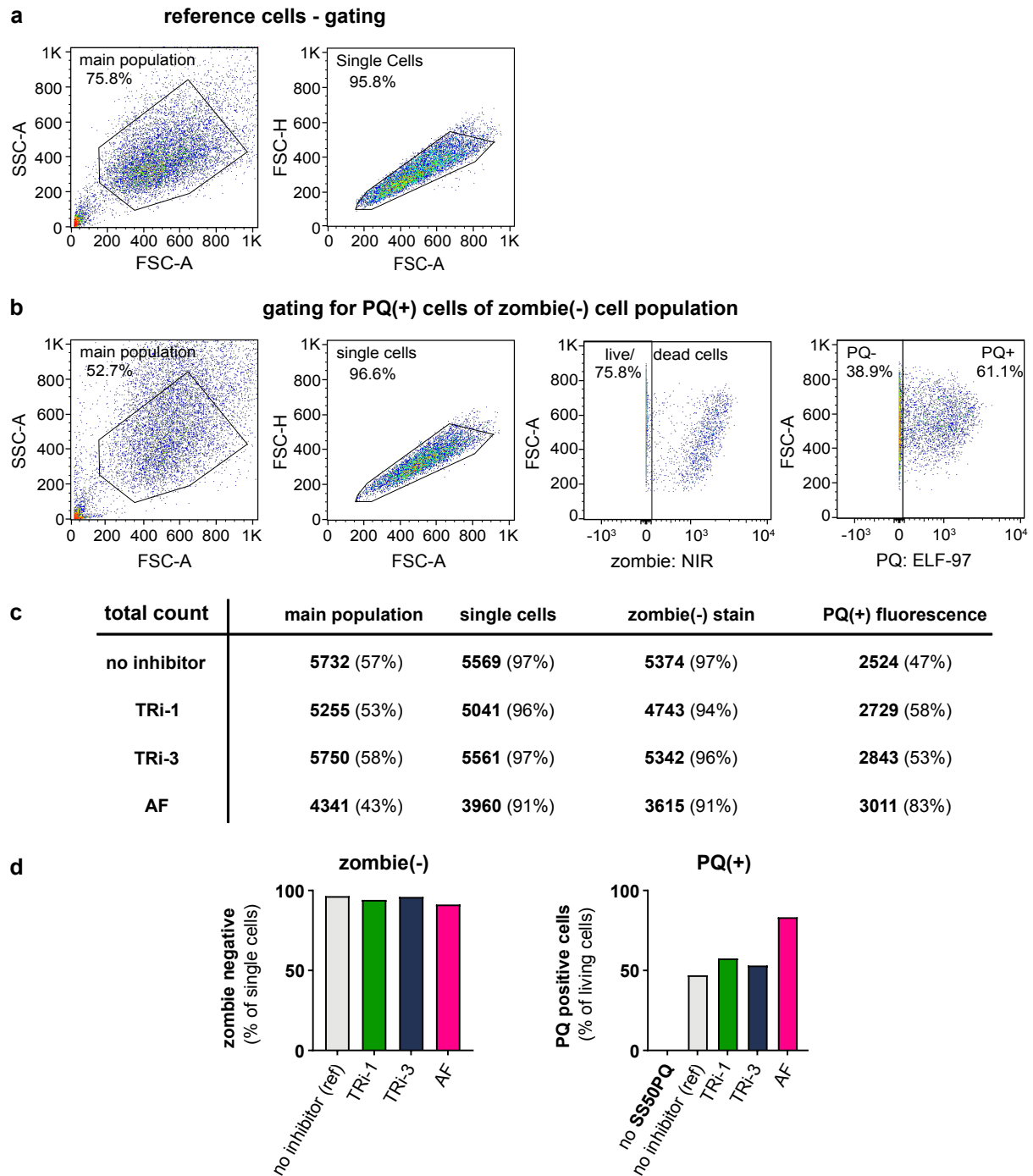


Supplementary Fig 12 Results of reference compound **SS00-PQ** cross-evaluated with TRI-1, TRI-3 and AF. Cellular fluorescence time-courses for A549 cells pre-treated with TRI-1, TRI-3 and AF (50 μ M **SS00-PQ**, 2 h pre-treatment). Graphs represent Mean+SD calculated from 3 independent experiments.

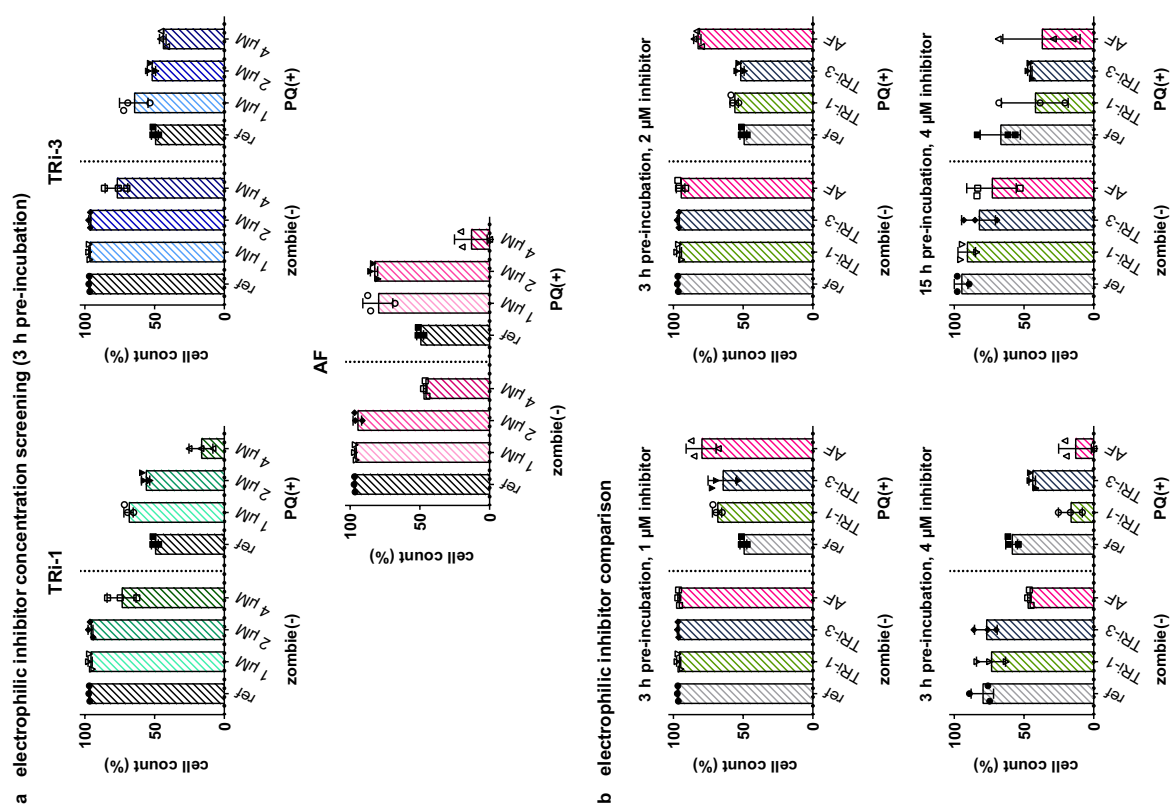
inhibitor dose-response (50 μ M)



Supplementary Fig 13 Dose-response plots for **SS50-PQ**, **TRFS-green** and **SS00-PQ** cross-evaluated with TRI-1, TRI-3 and AF as specified above (timepoint t = 6 h). Graphs show the data also presented in **Supplementary Figure 11-12** representing Mean calculated from 3 independent experiments.



Supplementary Fig 14 Flow cytometry-based workflow for data processing, used to collect single cell statistics of Jurkat T-cells treated with **SS50-PQ**. **(a)** Untreated reference cells: (1) exclusion of debris in FSC-A/SSC-A, (2) selection of single cells in FSC-A/FSC-H. **(b)** Jurkat T-cells treated only with **SS50-PQ** (25 μ M) gated according to (1) and (2), followed by (3) live/dead selection applying zombie-staining (ex/em 647laser/780bp60), (4) PQ(+) cells out of the zombie(-) cell populations by detecting ELF-97 fluorescence (ex/em: 365laser/520lp). **(c)** Flow cytometry-related total count for an example inhibitor screening experiment: Jurkat T-cells treated with **SS50-PQ** (25 μ M) optionally after 3 h of pre-incubation with TRi-1, TRi-3 or AF (2 μ M). **(d)** Results from **(c)** in bar chart representation: plot of live cells (Zombie-negative) as a percentage of all gated single cells; and PQ(+) live cells as a percentage of all live cells. **(c-d)** show representative examples out of >3 independent experiments.



Supplementary Fig 15 (a) Flow cytometry-based single-cell statistics of Jurkat T-cells treated with **SS50-PQ** (25 μM) optionally after 3 h of pre-incubation with TRI-1, TRI-3 or AF (1–4 μM) to determine the onset of toxicity with each inhibitor. Comparison of live cells (Zombie-negative) as a percentage of all gated single cells; and PQ(+) live cells as a percentage of all live cells. (b) Results with TRI-1, TRI-3 or AF used at nontoxic concentrations (1 μM and 2 μM for all inhibitors) and at moderately toxic concentration (4 μM), with pre-incubations of cells with inhibitor either for 3 h (all concentrations) or 15 h (only 4 μM). Graphs show barchart representation using Mean+SD calculated from 3 independent experiments including individual datapoints for each experiment.

1.8 Supplementary Note 2: Auranofin's polypharmacology

Our cell-free and cellular assays had shown that 1,2-dithiolane is not selective for TrxR. However, previous studies of 1,2-dithiolane-based probes have claimed excellent TrxR selectivity. This claim was substantially based on assays where exposure of cells or lysates to the chalcophilic Au(I) complex auranofin (AF) dose-dependently reduced fluorescence signals as compared to untreated controls.⁹ We were intrigued to study AF more closely, to understand if/why it may have led to misinterpretation of selectivity for 1,2-dithiolane-based probes.

AF is a chalcophilic Au(I) species that is popularly used as an inhibitor of TrxR. AF does bind TrxR in cell-free assays and in cells. However, AF is a broadly “potent thiol-reactive species”²⁵ that is **also** reported to bind at least 20 other thiol protein targets. Its therapeutic mechanism/s of action are widely accepted to be unresolved.²⁶ Although it is clear that TrxR is one of its major targets,²⁶ it is also noted that AF is a particularly strong binder of membrane thiols, likely driven by its lipophilicity.²⁷

We confirmed that cells pre-treated with AF (0.1 to 4 μM) had decreased probe processing, seen by both single-cell (**Supplementary Figure 14-15**) and population average (**Supplementary Figure 10-13**) measurements. However, this *does not* indicate that probe processing occurs through TrxR. Given AF's polypharmacology, the dithiolane's cell-free nonselectivity, and the minor effects of non-Au-based TrxR modulation on probe activation (TRI results in **Supplementary Figure 11 and 13**), we were motivated to look more critically into this result. Conclusively, even in a fully cell- and enzyme-free setting, AF catalytically suppressed the fluorescence generated upon TCEP treatment, without a clear dose-dependence (**Supplementary Figure 9**). Therefore, signal suppression in the cellular assay cannot be used to argue that TrxR, or any other cellular target of auranofin, might be a selective reductant of 1,2-dithiolane.

We present two hypotheses that plausibly explain why AF suppresses signal from **SS50-PQ**, that are consistent with 1,2-dithiolane being a nonspecific thiol probe for which TrxR is not a significant cellular reductant. (1) The strained disulfide probe usually benefits from dynamic covalent exchange enhancement of cellular delivery, therefore AF's binding to membrane thiols²⁷ suppresses cellular delivery and signal. Similar suppression of delivery of strained disulfide substrates has been achieved by thiophilic organic alkylators of exofacial thiols.⁴ This delivery inhibition is consistent with literature findings and our data showing that 1,2-dithiolanes are nonspecifically opened by thiols (**Fig 3**), and it could be responsible for some or most of the cellular signal suppression by auranofin. (2) AF also reacts both directly and catalytically with 1,2-dithiolane-based probes to suppress signal by diminishing their reducibility. Literature reports indeed show that Au(I)-(thiolate)(phosphine) complexes react with disulfides, initially forming triethylphosphine oxide and the thioglucose-gold-thiolate complex.^{28,29} Since Au(I)-bis(thiolate) complexes undergo facile net ligand exchange with disulfides, they mediate thiol-disulfide exchange reactions³⁰, which in the case of 1,2-dithiolane triggers ring-opening polymerisation,³¹ which is discussed and demonstrated extensively for Fast-TRFS (**Figure 6, Supplementary Note 4**, etc). Polymerisation of the 1,2-dithiolane-based **SS50-PQ** would generate hydrophobic polymeric products, which (as we observed and as literature suggests³²) are not reducible by even such strong aqueous reductants as TCEP, thus suppressing fluorescent signal generation. This would explain auranofin's cell-free signal suppression (**Supplementary Figure 9**), and could even be sufficient to explain the cellular signal suppression, that we and others have observed.

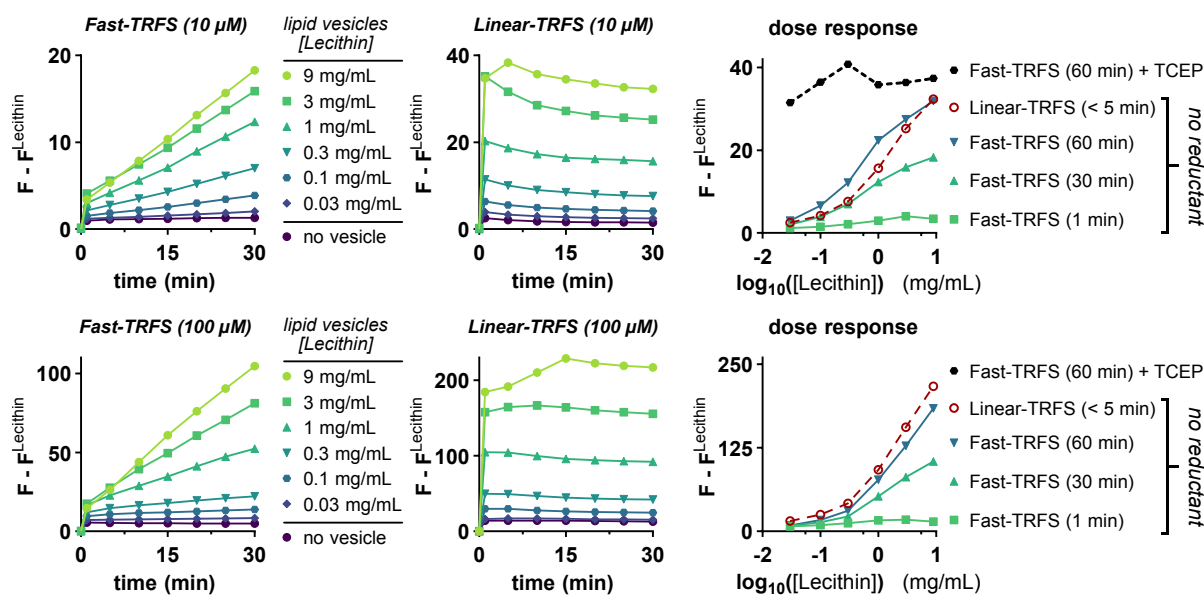
Motivated by the known broad spectrum of auranofin's targets and effects, it would be beneficial to at least take design precautions (e.g. cell-free controls testing AF-probe interactions, or using TRi inhibitors for competition assays) to identify likely confounding factors before advancing targets of strained disulfide probes based on AF experiments. However, we think it would be best to avoid interpreting Au-based reagent studies with strained disulfides altogether, due to the high chance of any assay result being misinterpreted based on a populous literature of AF targets with no clear consensus. These may be valuable guides for analysis of cellular redox probe selectivities in the future.

Conclusion and Outlook for Auranofin: We have pooled literature references with our data to show that inhibition of cellular activation of probes based on 5-membered cyclic disulfides by treatment with auranofin can result from at least two plausible, precedented processes that do not involve TrxR: i.e., delivery inhibition by binding exofacial thiols, and suppressing probe bioavailability and reducibility by catalysing dithiolane ring-opening polymerisation in extracellular medium. This calls generally for caution when claiming cellular mechanisms of probe activity based on inhibitor studies with the potential for direct inhibitor-probe interactions, spontaneous probe degradation, and known non-specific probe-activating mechanisms (such as 1,2-dithiolane exofacial thiolysis). In general, most biological literature using auranofin interprets AF assays in light of TrxR inhibition. Here, we have drawn attention to the thiol/disulfide reactivities of AF to caution that it cannot be used for mechanistic evaluation of cellular targets of strained disulfides, whereas recent gold-free TrxR inhibitors¹ may be better suited for this purpose. With a nuanced view of AF, a more promising avenue of research is suggested. If the FDA-approved auranofin shows substantial inhibition of disulfide-mediated uptake not only in monolayer cell culture but also in 3D models and *in vivo*, this could make it interesting for repurposing, or as a therapeutic lead. The cellular uptake of some viruses and toxins is mediated by thiols, and inhibitors of this process are valuable targets, with the most potent inhibitors reported³³ apparently being comparable to what we have observed with auranofin. In an illustrative recent example, AF was reported to slow SARS-COV-2 replication by 95%, although inhibition of thiol-mediated uptake was not considered as a potential basis for this inhibition³⁴.

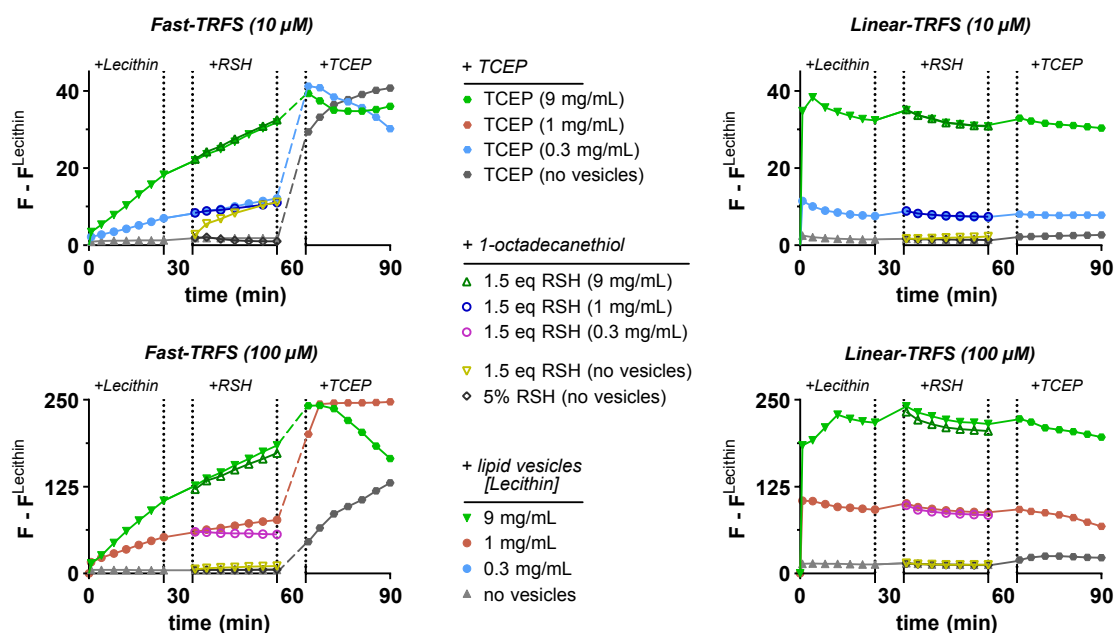
Separately, the interesting question has been raised in review, of whether a probe is likely to enter the cell, get reduced to the (di)thiol form, and only then coordinate with AF (as a monothiol, since the Au(I) prefers a linear coordination geometry that a 6-membered ring cannot permit) so reducing its cyclisation - which could be an alternative mechanism for cellular signal suppression. We do not think this is relevant. We consider that the intracellular background thiol concentration (5 mM GSH, up to 50 mM protein thiols) is much higher than the instantaneous reduced intracellular probe reduction (di)thiol intermediate is ever likely to be, particularly for the rapidly-cyclising **SS50-PQ**, and since we see no basis for selective AF reaction with the reduced (di)thiol intermediate, we do not imagine that intracellular reaction can be significant for suppression of signal generation - particularly since AF is applied at max. 4 μM and typically we are using probe at up to 50-100 μM .

1.9 Lipid vesicle-mediated ROP of Fast-TRFS

a lipid vesicle-mediated ROP-based activation of Fast-TRFS



b spike of cat./excess thiol nucleophiles vs. quantitative reduction



Supplementary Fig 16 (a) Fluorescence timecourse (355bp10/460bp20) monitored for **Fast-TRFS** and **Linear-TRFS** (both at 10 μM and 100 μM as indicated) incubated at 37°C with solubilised lipid vesicles (prepared from commercial lecithin at 0.03-9 mg/mL in deionised water according to Fromherz *et al.*³⁵ Background fluorescent signal (concentration-dependent scatter from lecithin) has been subtracted. (b) After 30 min of fluorescence monitoring, 1-octadecanethiol (RSH) was spiked at catalytic amounts (0.05 eq.) or in excess (1.5 eq. vs. probe concentration) and compared to an untreated reference experiment. After 30 min of further fluorescence monitoring, the potential for additional, *reduction-mediated* fluorescence increase was tested by treatment with excess TCEP (at 100 μM) and fluorescence was further monitored for 30 min. (a-b) show graphs representing single experiments with technical replicates. (1) The **Linear-TRFS** model compound's fluorescence turn-on *instantly reaching plateaus that depend on lecithin concentration* illustrates the environment-dependence of fluorescence of the intact aminocoumarin-urea disulfide; (2) **Fast-TRFS** turn-on is, without reduction required, concentration-dependently initiated in the presence of a lipid environment resulting from surface-initiated strain-promoted ring-opening polymerisation of the vesicle-partitioned proportion of probe.

1.10 Supplementary Note 3: Fast-TRFS' *TrxR*-independent fluorogenicity

Cell-free experiments with the known **non-cargo-releasing** 1,2-dithiolane-based probe **Fast-TRFS**¹² could show important conclusions, through comparison to results for its novel linear disulfide analogue **Linear-TRFS** we report here.

Fast-TRFS was intended to be fluorescence-quenched in its intact cyclic 1,2-dithiolane state, and was reported to be "a specific and superfast fluorogenic probe of mammalian thioredoxin reductase" that should act in cells by increasing in fluorescence upon "reduction [to **Dithiol-TRFS**, see **Fig 6**]"¹² We now show that there are at least three hitherto unreported confounding aspects to this **Fast-TRFS** probe system, and discuss how these combine with each other to give misleading results: and in doing so we support our thesis that 1,2-dithiolane is not a viable redox sensor for selective probes.

Firstly, in our hands, **Fast-TRFS** performs with poor reproducibility that matches entirely to Whitesides' characterisation of polymerisation-prone dithiolanes,³⁶ and to the observations we report about polymerisation-prone **SS50-PQ** and its precursors (see main text).

Secondly, we show that a ring-opened species resulting from strain-promoted thiol attack on the **Fast-TRFS** 1,2-dithiolane [model compound **Linear-TRFS**] will be *just as fluorescent, as the fully-reduced Dithiol-TRFS* (e.g. on the dose-response panel in **Fig 6d**, at 9 mg/mL lecithin, ca. 36 fluorescence units). This means that any of several likely *TrxR*-independent ring-opening mechanisms will generate *TrxR*-independent fluorescence signal from **Fast-TRFS** (**Fig 6**, **Supplementary Figure 16**). These mechanisms include but are not limited to: (a) strain-promoted oligomerisation, that should be particularly relevant if high local concentrations of **Fast-TRFS** are created, resulting in all ring-opened probe molecules becoming fluorescent (see below and shown in **Fig 6c**); (b) strain-promoted cellular uptake is via the known mechanism of exofacial thiol attack on the dithiolane and so will likewise activate fluorescence before it ever reaches the intracellular environment; (c) opening of the dithiolane by any cellular thiol.

Thirdly, we show that the fluorescence signal from **Fast-TRFS** and from its oligomerisation and its reduction products, also have strong environment dependence which creates additional problems. For example, oxidised **Fast-TRFS** fluorescence is instantly ca. 3-fold enhanced just by moving from aqueous to apolar environment (at the first minute of **Fig 6d**, the fluorescence intensity without vesicles is 0.99, but rises to ca. 3.4 as the lipid concentration increases - i.e. already 1/10 of the total potential fluorescence signal) - and this is before *non-reductive* strain-promoted ring-opening has significantly taken place (which it then does, reaching 50% of completion within the next 29 minutes). We also show that the environment-dependence of the **Fast-TRFS** system entirely rules the fluorescence behaviour of the model compound **Linear-TRFS**, which is up to 17-fold enhanced just by exposure to lipids (**Fig 6d**: from 2.0 to 35) but is *almost entirely unaffected by reduction* (irrespective of which environment the probe is in - see TCEP spike at the end of its incubation, **Supplementary Figure 16**). Therefore, the faster that a **Fast-TRFS** probe of any redox status accumulates into (intracellular) lipid environments, the more quickly that the cellular fluorescence will rise.

The combination of these three effects provides a unified model rationalising the published "superfast" cellular fluorescence turn-on of **Fast-TRFS** without recourse to *TrxR*, which depending on the situation under testing may be relevant or dominant.

We propose that in cells, a local-concentration-dependent ring-opening-oligomerisation can be activated by partitioning the dithiolane **Fast-TRFS** from a relatively large volume of aqueous medium into a relatively smaller volume of apolar environment (ideally, of high surface area for rapidity), with subsequent need only for catalytic activation by a nucleophile that may or may not be a membrane-associated reductase. Then **Fast-TRFS** fluorescence (which already jumped threefold upon entering the apolar medium) would rapidly rise as increasing amounts of the more fluorescent oligomer would be formed. We predicted that this could allow even maximal theoretical fluorescence signal to be reached either with catalytic, or even zero, added reductants. We tested this experimentally with the series of vesicle assays (**Fig 6** and **Supplementary Figure 16**), simply sonicating commercial soybean lecithin (Sigma, P5638, ca. 60% phospholipids and 35% oils; zero content of *TrxR* or NADPH) in water to form a lipid vesicle stock,^{35,37} diluting it to various concentrations and mixing with **Fast-TRFS**. Surpassing our expectations, in just one hour, the **Fast-TRFS** signal in 0.9%wt vesicle mixture without any reductants reached *full maximal signal plateau, corresponding to that seen with full TCEP reduction to Dithiol-TRFS*. This can only be understood as local-concentration-dependent oligomerisation to the poly-(disulfido-TRFS), that is just as fluorescent as **Linear-TRFS** or **Dithiol-TRFS** when they are compared in the vesicle system (**Supplementary Figure 16**). This shows the confounding influence of redox-independent, strain-promoted processes on 1,2-dithiolane chemical behaviour: and illustrates how the environment-dependent readout of the **Fast-TRFS** compounds expands this complexity by generating a false positive signal.

1.11 Supplementary Note 4: TRFS-green's *TrxR*-independent fluorogenicity

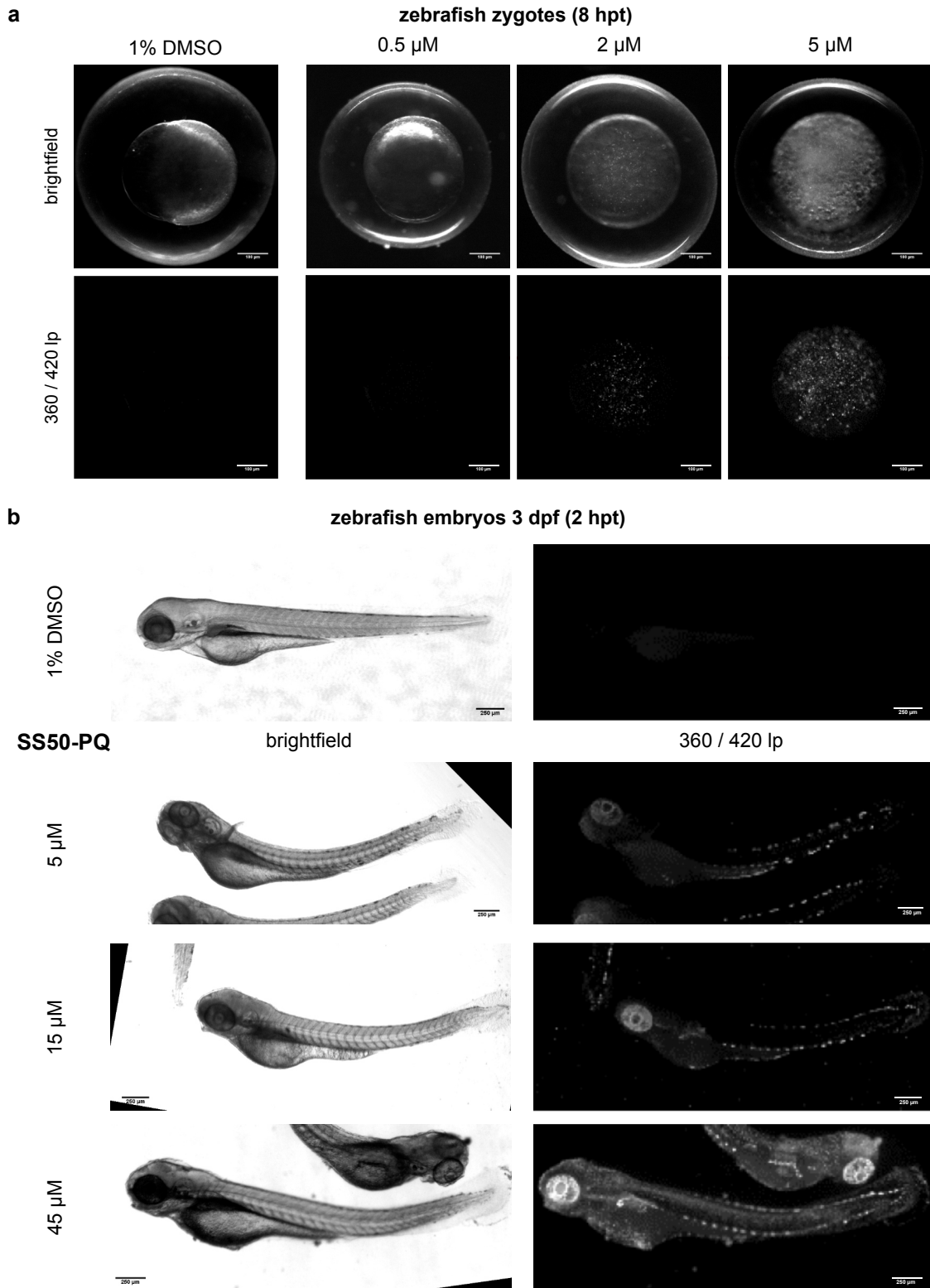
In the discussion following Supplementary Figure 3, we have argued based on rates of reaction with 10-fold excess of TCEP, that the very slow release-based signal generation of TRFS-green makes it to our understanding impossible that this probe can hope to report cleanly on TrxR activity in cells, instead of giving a signal that is entirely dominated by environment-dependent effects.

As the aminonaphthylimide core of **TRFS-green** is also a classic environment-dependent fluorophore we looked in the literature to see if this might be a similarly confounding issue as environment effects were shown to be for **Fast-TRFS**. We note that recently published results from the Fang group³⁸ show that their naphthylimide-based compound S1, which is similar to **TRFS-green**, experiences an instantaneous 45-fold enhancement of fluorescence intensity upon leaving all-aqueous environment and noncovalently associating to albumin in a cell-free experiment (their paper's Figure 3; note too that their aminocoumarin compound S3, which is similar to **Fast-TRFS**, has a ca. 4-fold fluorescence enhancement in the same experiment, matching our vesicle results with **Fast-TRFS**).

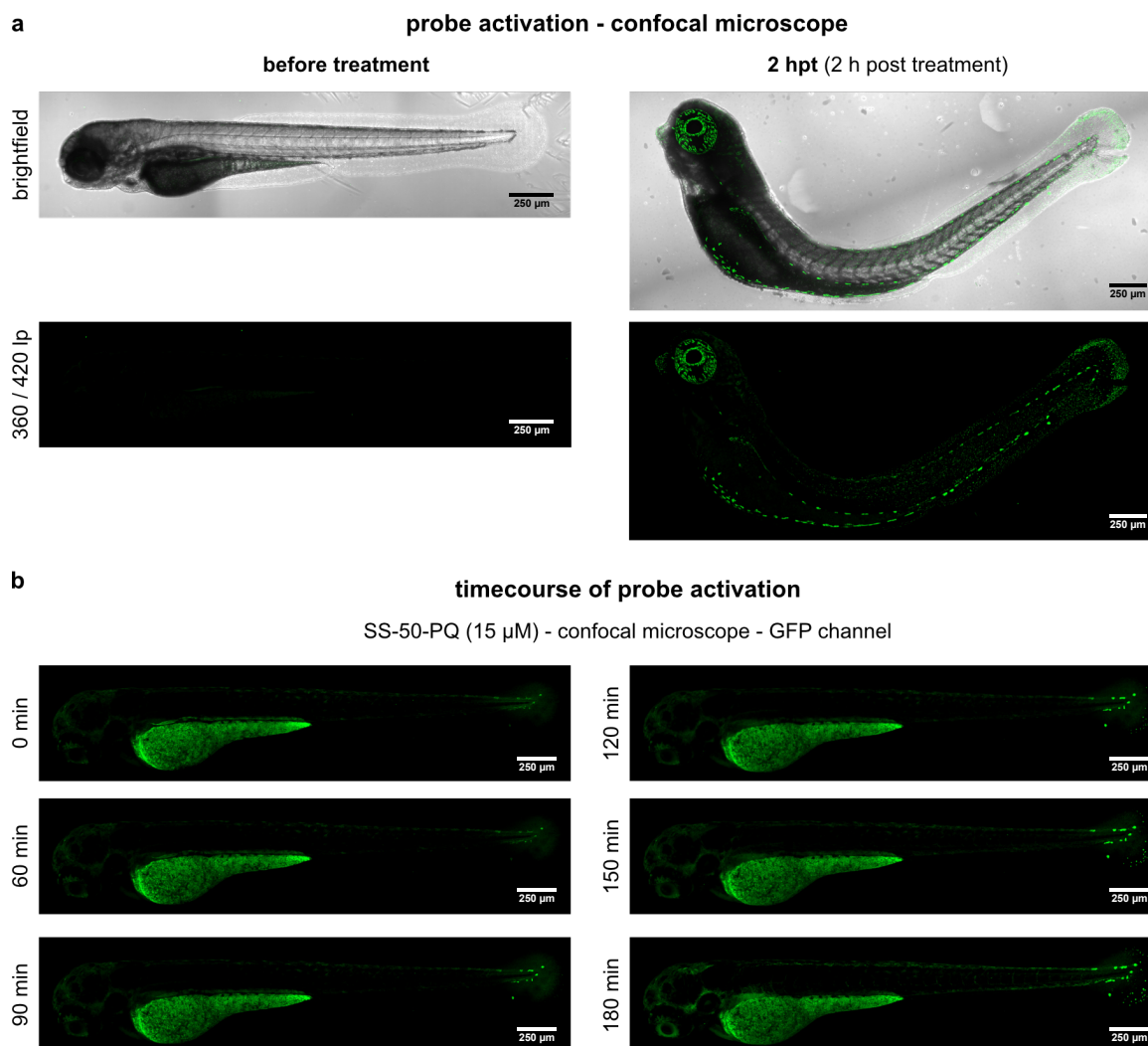
Paralleling our experimental investigation of TrxR-independent signal generation in the **Fast-TRFS** system, this literature report of environment-dependent-signal highlights how interpreting fluorescence increases with the **TRFS-green** probe may similarly not be straightforward since (1) in any context, even just leaving the aqueous (extracellular) environment will trigger a fluorescence increase, that can be entirely independent of any reaction on its 1,2-dithiolane motif; (2) in the cellular context, all TrxR-independent strain-promoted thiol-mediated uptake at the cell surface will covalently associate the **TRFS-green** probe onto membrane proteins and into membranes, thereby giving cell-uptake-driven signal independent of molecular encounter of the **TRFS-green** probe with intracellular TrxR, let alone cyclisation-driven release of the cargo. It is therefore consistent with these hypotheses that the same factors as we advanced for the dithiolane **Fast-TRFS** (concentration into membranes aided by membrane-thiol-based opening of the strained dithiolane, which gives an environment-dependent signal turn-on) will apply to **TRFS-green**, permitting it to generate signal based on cellular exofacial thiol status, without even encountering TrxR.

These suggestions could particularly be considered, in light of the demonstrations that cellular signal from **TRFS-green** is manifestly independent of TrxR and saturates at low concentrations (see legend to **Supplementary Figure 8**).

1.12 *In vivo* animal model, zebrafish: results and impact



Supplementary Fig 17 *in vivo* animal model for reduction-responsive imaging. Representative epifluorescence stereomicroscopy images of (a) zebrafish zygotes incubated **SS50-PQ** (8 hpt) (representative image of 3 independent experiments with similar results); (b) zebrafish embryos (3 dpf) treated with **SS50-PQ** (2 hpt) (representative image of 3 independent experiments with similar results).



Supplementary Fig 18 (a) Overlay of representative transmission microscope and confocal fluorescence microscope images of zebrafish embryos (3 dpf) incubated with **SS50-PQ** (15 μ M) before treatment and 2 hpt (representative image of 3 independent experiments with similar results). (b) Timecourse fluorescence increase recorded using a confocal microscope (ex/em 405 nm/520bp20 "GFP" filter) at 0 min, 60 min, 90 min, 120 min, 150 min and 180 min after treatment. Fluorescence channel images (green overlay) are maximum projections (representative image of 2 independent experiments with similar results).

Discussion of *in vivo* imaging in zebrafish

Activation of fluorescence, as compared to untreated control experiments, was already observed in zebrafish embryos at low **SS50-PQ** concentrations (5 μ M). Aggregation of solid, fluorescent particles with high brightness inside the living cells was observed. Connected to the release of solid particles, death was subsequently observed.

When embryos already at a mobile development stage (3 dpf) were incubated with **SS50-PQ**, signal was observed after short treatment time (2 hpt) at very low concentration. A clear response of the animals to the formation of the solid was observed leading to deformation, limitation of mobility and death. At 8 hpt no live animals were observed. Maximum projection images were taken for the off-to-on signal switch when zebrafish embryos (3 dpf) were incubated with **SS50-PQ** (15 μ M) and solid particles could be resolved on a single-cell level and localized due to transparency of the organism. Release of solid, fluorescent particles was observed time-dependently after incubation with **SS50-PQ**. Presumably, due to aggregation of release solid, the particles itself grow over time. Note that time-resolved confocal microscopy was possible because embryos were immobilized by embedding in gel. The PQ probe system design is responsible for the irreversible and non-diffusive accumulation of the bright, photostable signal inside cells, allowing for cellularly-resolved imaging, with the high Stokes shift delivering excellent signal to noise ratios, which are beneficial for further use with other trigger systems.

1.13 Supplementary Movie Caption

Supplementary Movie 1: Representative confocal time lapse microscopy of live HeLa cells treated with **SS50-PQ** (50 μ M) and immediately imaged for one hour at ex/em: 405/530bp20; fluorescence channel (green) overlaid on brightfield transmission image.

2 Supplementary methods Methods for *in vitro* evaluation

2.1.1 Cell-free chemoreductant assays

Cell-free *in vitro* assays were performed to evaluate the activation of **SS50-PQ** and **TRFS-green** upon reduction-mediated release of the water-insoluble dye **PQ-OH_(s)** (precipitation-based induction of ESIPT-based fluorescence monitored with ex/em 355bp10/520lp) or of 1-butyl-6-amino-naphthalimide (fluorescence monitored with ex/em 445bp10/520lp). The molecular process was monitored by fluorescence intensity increase based on the off-to-on mechanism. For **TRFS-green** subtraction of background fluorescence was conducted as indicated. We noted that upon standing **SS50-PQ** probe stocks had reduced capacity to generate fluorescence in reductant assays. Consequently, probe of **SS50-PQ** stocks were prepared freshly from the solids for all assays.

In a black 96-well plate with black bottom, 80 μ L of a diluted solution (12.5 μ M in aq. TE, pH 7.4, 1.25% DMSO) of **SS50-PQ** (final concentration 10 μ M) was mixed with a solution of selected chemical reductants (20 μ L of a solution (50 μ M to 50 mM in aq. TE, pH 7.4). As reductants were used tris(carboxyethyl)phosphine (TCEP) at 100 μ M final concentration; dithiothreitol (reduced, DTT), glutathione (reduced, GSH), L-glutathione (oxidized, GSSG), L-Cysteine (Cys), L-Serine (Ser), mercaptoethyl-dimethylamine (MEDA), cysteamine (CA) and N-acetyl L-Cysteine (NAC) all at 1 mM final concentration. For cell-free inhibition experiments 80 μ L of a diluted solution (62.5 μ M in aq. TE, pH 7.4, 1.25% DMSO) of **SS50-PQ** (final concentration 25 μ M or 50 μ M as indicated) was pre-treated with 2-((4-chlorophenyl)sulfonyl)-6-methoxy-3-nitropyridine (TRi-1), 4,5-dichloro-2-((5-(4-chlorophenyl)-1,3,4-oxadiazol-2-yl)methyl)pyridazine-3(2H)-one (TRi-3)¹ (from DMSO stock solutions) or auranofin (AF) (from ethanolic stock solutions) with final concentrations from 0.1 μ M to 4.5 μ M 2 h before maximum reduction was induced by addition of 20 μ L TCEP (at 100 μ M final concentration).

The reaction mixtures were incubated at 37 °C and 100% humidity for 6 h. Time-course measurements were conducted to determine kinetics of the reduction-mediated release. Data was interpreted by calculating the absolute, time-dependent fluorescence intensity **F(t)** normalised to the plateau signal observed in a reference maximum-fluorescence experiment **F^{TCEP}(t)** that used incubation with 100 μ M of TCEP. For monothiol-reductant concentration-dependent **SS50-PQ** was challenged with increased concentrations of glutathione (reduced, GSH) at 10 μ M, 30 μ M, 100 μ M, 300 μ M, 1 mM, 3 mM and 10 mM and the dose-response relation was later calculated from data representation on a \log_{10} [GSH/probe] vs. **F/F^{TCEP}(t = 6h)** graph. Dose-reponse curves were fitted using GraphPad Prism version 8.0.2. for windows from GraphPad Software, San Diego (USA).

2.1.2 Cell-free bioreductant assays

Cell-free *in vitro* enzyme specificity assays (bioreductants) were performed to evaluate the specificity and reaction kinetics of **SS50-PQ** and **TRFS-green** to enzymatic reduction based on the reduction-mediated release of **PQ-OH_(s)** or of 1-butyl-6-amino-naphthalimide after incubation with bioreductant cascade model systems. The molecular process was equally monitored by fluorescence intensity increase (ex/em 355bp10/520lp or 440bp10/520lp). In a black 96-Well Plate with black bottom, 50 μ L of a diluted solution (20 μ M in aq. TE, pH 7.4, 2% DMSO) of **SS50-PQ** or **TRFS-green** (final concentration 10 μ M) was mixed with 40 μ L of the selected oxidoreductase enzyme (TrxR1, TrxR2, GR to reach final concentrations of 20 nM) and/or its respective native substrate (Trx1, Trx2, TRP14, Grx1, Grx2 to reach final concentrations of 10 nM to 10 μ M respectively), including 100 μ M final concentration of GSH in case of GR-Grx-GSH system. The biochemical reaction was started by addition of 10 μ L of a solution of β -NADPH (1 mM in aq. TE, pH 7.4 to reach 100 μ M final concentration). The reaction mixtures were incubated at 37 °C and 100% humidity for 6 h.

Human recombinant thioredoxin (Trx1 and Trx2) (lyophilized) human recombinant glutaredoxin (Grx1 and Grx2) (lyophilized from 10 μ L TE-buffer, pH 7.5), human recombinant thioredoxin-related protein of 14 kDa (TRP14), human thioredoxin reductase (TrxR1 and TrxR2) (1.5 mg/mL in 50% glycerol/TE-buffer, pH 7.5) and human recombinant glutathione reductase (GR) (100 μ M in 50% glycerol/TE-buffer, pH 7.5) were obtained from *IMCO Corp.*, Stockholm (Sweden) or produced and purified as previously described.^{39–42}

The reaction mixtures were incubated at 37 °C and 100% humidity for 6 h. Time course measurements were conducted to determine kinetics of the enzyme-mediated release. Data was interpreted by calculating the *absolute, time-dependent* fluorescence intensity **F(t)** corrected by the *absolute, time-dependent* background fluorescence **F^{NADPH}(t)** caused by autofluorescence of reduced β -NADPH normalised to the plateau signal observed in a reference maximum-fluorescence experiment **F^{max}(t)** with 100 μ M of TCEP. Dose-reponse curves were fitted using GraphPad Prism version 8.0.2. for windows from GraphPad Software, San Diego (USA).

2.1.3 Cell-free environment-dependent polymerisation assay

Commercial *L*- α -lecithin (CAS 8002-43-5, derived from Sigma-Aldrich P5638) was hydrated with ultrapure water (Milli-Q, Reptile Bioscience Ltd., Boston, MA) to a final concentration of 9 mg/mL. The suspension was gently vortexed to achieve a homogeneous phase, which was then subjected to one freeze/thaw cycle. The stock solution was extruded through a polycarbonate membrane with a pore diameter of 400 nm, 21 times, using a Mini Extruder (Avanti Polar Lipids, Inc., Alabama, United States) according to Fromherz *et al.*³⁵ The stock was then diluted with deionised water to the indicated concentrations and treated with DMSO-stock solutions of **Fast-TRFS** and **Linear-TRFS** to final probe concentrations of 10 μ M or 100 μ M with maximum 1 % DMSO content. Fluorescence intensity (355bp10/460bp20) was recorded overtime and 1-octadecanethiol (RSH) was optionally spiked at catalytic amounts (0.05 eq.) or in excess (1.5 eq. vs. probe concentration) and compared to an untreated reference experiment. The potential for additional, *reduction-mediated* fluorescence increase was tested by treatment of the system with excess TCEP (0.1 mM, i.e. 1-10 eq.) and fluorescence was further monitored for 30 min.

2.2 Cell culture methods

2.2.1 General cell cultivation methods

HeLa, A549 or MEF cells were grown in Dulbecco's modified Eagle's medium (DMEM: L-glucose (4.5 g/L), L-glutamine, L-pyruvate, phenol-red, NaHCO₃ (2.7 g/L)) purchased from PAN Biotech, Aidenbach (Germany). Jurkat cells were grown in RPMI-1640 medium (L-glutamine, sodium bicarbonate) purchased from Sigma-Aldrich Life Science by Merck KGaA, Darmstadt (Germany). Media were supplemented with 10% heat-inactivated fetal bovine serum, penicillin (100 U/mL), streptomycin (100 μ g/mL) and optionally with Na₂SeO₃ (0-100 nM) or Na₃PO₃S (0-1.2 mM). For washing and resuspending steps PBS Dulbecco buffer from Merck GmbH, Darmstadt (Germany) was used and for trypsination, TrypLE™ Express from gibco Life Technologies Inc., Massachusetts (USA) was used. Centrifugation steps were conducted using a centrifuge 5810R from Eppendorf GmbH, Hamburg (Germany) was used. Cells were grown at 37 °C under 5% CO₂ atmosphere and cell growth was confirmed using a Nikon Eclipse Ti microscope from Nikon Corp., Minato (Japan).

2.2.2 Cell lines

HeLa (DSMZ; ACC57), A549 (DSMZ; ACC107) and Jurkat (ATCC; TIB-152) cell lines were purchased from the German Collection of Microorganisms and Cell Cultures. TrxR1 knockout and reference mouse embryonic fibroblasts (MEF) are a kind gift from Marcus Conrad. Briefly, MEFs isolated from conditional TrxR1 knockout mouse embryos, were immortalised by lentiviral transduction. In vitro deletion of TrxR1 was achieved by Tat-Cre induced recombination and verified by PCR and Immunoblotting for TrxR1.¹⁵ All cell lines are tested regularly for mycoplasma contamination and only mycoplasma negative cells are used in assays.

2.2.3 Cellular activation and inhibition assays

For evaluation of cellular processing of **SS50-PQ** and **TRFS-green** cells were seeded in 96-well plates (Microplates, 96-Well, F-Bottom, black, Fluotrack, high binding) from Greiner bio-one GmbH, Kremsmünster (Austria) at a medium level of 100 μ L. Cell medium was treated with **SS50-PQ**, **TRFS-green** or respective reference compounds **SS00-PQ** or **RX1** (from stock solution in 100% DMSO) to reach final concentrations of 1 μ M to 100 μ M at maximum final levels of 1% DMSO. For inhibition experiments cells were pre-treated with the selected TrxR inhibitors TRI-1 and TRI-3¹ (from DMSO stock solutions) and AF (from ethanolic stock solution), 3 h or 15 h before probe treatment.

Treated cell plates were incubated at 37 °C under 5 % CO₂ atmosphere and timecourse fluorescence measurements were conducted to determine kinetics of cellular processing. Fluorescence readout of cell-free activity and/or cell assays was performed either using a *FluoStar Omega* plate reader from BMG Labtech, Ortenburg (Germany) (ex/em 355bp10/520lp or 440bp10/520lp) or a Tecan Infinite M200 plate reader from Tecan, Maennedorf (Switzerland) (ex/em 355bp10/520lp or 440bp10/520lp) recording fluorescence intensity. Data was interpreted by representing the absolute, time-dependent fluorescence intensity **F(t)** or representing time-dependent background-corrected fluorescence intensity $F(t) - F_{\text{Background}}(t)$ where indicated.

2.2.4 Fluorescence microscopy

Intracellular formation of solid green-fluorescent particles corresponding to a time-dependent increase **F(t)** was confirmed using a Nikon Eclipse Ti2 upright microscope from Nikon Instruments Europe BV, Amsterdam (Netherlands) (ex/em 355bp50/410lp; or transmitted light, as appropriate). Images were processed using Fiji version 1.51 (ImageJ)⁴³ open-source image processing software.

Confocal time lapse microscopy was performed on live HeLa cells seeded in 8-well ibiTreat μ ibidi slides from ibidi GmbH, Martinsried (Germany). Dishes were placed on the motorized stage of a Leica SP8 laser-scanning confocal microscope (Wetzlar, Germany), treated with **SS50-PQ** at 50 μ M on stage and immediately imaged for one hour at ex/em: 405laser/530bp20 comparing the fluorescence and the brightfield image. Acquired images were processed using Fiji version 1.51 (ImageJ)⁴³ open-source software.

2.2.5 Flow cytometry-based single-cell statistics

For single-cell resolved statistical analysis of intracellular solid green-fluorescent particles resulted from reduction-mediated activation/release of **SS50-PQ** a flow cytometry-based method was developed and implemented.

After respective treatment with TrxR inhibitors and/or **SS50-PQ**, cells were harvested and stained with a fixable viability dye according to manufacturer's recommendations (zombie NIR™ Fixable Viability Kit, BioLegend). Cells were fixed in 4% paraformaldehyde (PFA) in PBS for 30 min and either stored in PBS or immediately resuspended in a wash buffer containing PBS with 1% bovine serum albumin (BSA) and 1 mM EDTA Disodium salt (0.1 mol/L or 0.2 N).

Flow cytometry was conducted at the BioMedical Centre Core Facility of the LMU Munich on a BD LSRFortessa instrument (BD Bioscience) using the BD FACS Diva Software. The following excitation/detection settings were used: zombie (ex/em 647laser/780bp60) and PQ fluorescence (ex/em: 355laser/530bp30). Data was processed using FlowJo v.10.7.1(BD).

An unstained sample was used to exclude cell debris and doublets. Zombie dye was used to exclude dead cells. PQ-positive gate was set, so that 0% of cells were PQ positive in an unstained sample. Cell debris, singlets, Zombie and PQ gates were set on an appropriate sample in each experiment and applied to all samples. General gating strategy is shown **Supplementary Figure 6**.

2.3 Methods for *in vivo* animal model

2.3.1 Animal model

Danio rerio (8 hpf or 3 dpf, sex undetermined) were housed in groups of 20-40 individuals in a fish facility (Aquanearing) maintaining approx. 700 mS, pH 6.9 – 7.1 and 28 °C with a 14/10 h light/dark cycle as outlined by common zebrafish handling guidelines.⁴⁴ All experiments used fertilized eggs from *ab* wild-type parents, grown in 30% Danieau medium (0.12 mM MgSO₄, 0.21 mM KCl, 0.18 mM Ca(NO₃)₂, 17.4 mM NaCl, 1.5 mM HEPES, pH 7.2) at 28 °C, again with a 14/10 h light/dark cycle. To suppress melanin pigmentation, 150 µM phenylthiourea (PTU) was added to the 30% Danieau medium at 8-10 hpf when needed.

All procedures involving animals were carried out according to EU guidelines and German legislation (EU Directive 2010_63, licence number AZ 325.1.53/56.1-TU-BS). As all zebrafish embryos in this study were analysed at ages below 5 dpf, hence no approval by an ethics board was required. The study adhered to ARRIVE guidelines.

2.3.2 *In vivo* activation experiments

SS50-PQ was prepared as stock solutions (10 mM in DMSO) and stored at 4 °C and briefly warmed to 37 °C before use. 5 µM, 15 µM and 45 µM dilutions were freshly prepared in 30% Danieau supplemented with DMSO to 1% (final concentration). At 8 hpf or 3 dpf, embryos were transferred to each well of a 6-well plate, and the 30% Danieau medium exchanged for the test dilutions (5 ml per well). Embryos were incubated at 28 °C until the formation of solid green-fluorescent particles was observed.

2.3.3 Imaging

Signal development was initially monitored on a stereofluorescence microscope (Leica M205FA or MDG41, from Leica Microsystems, Wetzlar, Germany) equipped with a UV filter (ex/em: 360bp40/420lp). Then for confocal imaging, the embryos were embedded in lateral position in 1.2% ultra-low gelling agarose (type IX-A), overlaid with the test solution. The embryos were transferred to a confocal microscope (Zeiss Airyscan from Carl Zeiss microscopy, Jena, Germany) equipped with a 405 nm diode and several laser lines, with a Life Imaging Services heating chamber set to 28 °C. Whole embryos were recorded using a 10× objective and the 405 nm diode for excitation, with subsequent tile/grid stitching using the Fiji version 1.51 (ImageJ) open-source software.^{43,45} Image acquisition was controlled by the Zen Black software from Carl Zeiss microscopy, Jena, Germany.

2.4 Laboratory techniques

All solvents, reagents and building blocks were purchased from standard commercial sources. Anhydrous solvents obtained in septum-capped bottles and analytical grade or higher quality solvents were used without purification. Industrial grade solvents were distilled prior to use. Unless otherwise stated, reactions were performed at room temperature without precautions regarding air or moisture and were stirred using a magnetic Teflon[®]-coated stir bars. Air or moisture sensitive reactions were conducted in dry Schlenk glassware.

Flash column chromatography was performed on *Geduran*[®] Si 60 silica gel from *Merck GmbH*, Darmstadt (Germany) an optionally conducted using a *Biotage*[®] *Select* automated column chromatography system from *Biotage GmbH*, Uppsala (Sweden). Unless stated otherwise, and thin layer chromatography to monitor reactions and determine R_f -values was performed on silica coated aluminium sheets with fluorescent indicator (*TLC Silica gel 60 F254* from *Merck GmbH*, Darmstadt, Germany) with visualisation by UV irradiation (254 nm/360 nm) or staining with KMnO_4 solution (3.0 g KMnO_4 , 20 g K_2CO_3 , 0.30 g KOH, 0.30 L H_2O).

2.4.1 Mass spectrometry

High resolution mass spectrometry (**HRMS**) was conducted either using a *Thermo Finnigan LTQ FT Ultra FourierTransform* ion cyclotron resonance spectrometer from *ThermoFisher Scientific GmbH*, Dreieich (Germany) applying electron spray ionisation (ESI) with a spray capillary voltage of 4 kV at temperature 250 °C with a method dependent range from 50 to 2000 u or a *Finnigan MAT 95* from *Thermo Fisher Scientific*, Dreieich (Germany) applying electron ionisation (EI) at a source temperature of 250 °C and an electron energy of 70 eV with a method dependent range from 40 to 1040 u. All reported m/z values refer to positive ionization mode, unless stated otherwise.

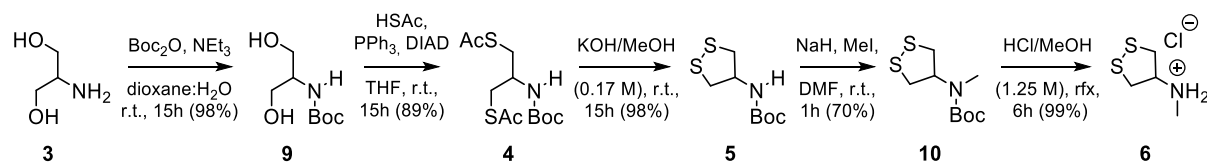
2.4.1 NMR spectroscopy

Nuclear magnetic resonance (**NMR**) spectroscopy was performed using a *Bruker Avance* (600/150 MHz, with *TCI cryoprobe*) or a *Bruker Avance III HD Biospin* (400/100 MHz, with BBFO cryoprobeTM) from *Bruker Corp.*, Billerica (USA) either at 400 MHz or 500 MHz. ¹⁹F-NMR spectra were recorded on a *Bruker Avance III* spectrometer (400 MHz for ¹H; 377 MHz for ¹⁹F). NMR-spectra were measured at 298 K, unless stated otherwise, and were analysed with the program *MestrelNova 12* developed by *Mestrelab Ltd.*, Santiago de Compostela (Spain). ¹H-NMR spectra chemical shifts (δ) in parts per million (ppm) relative to tetramethylsilane ($\delta = 0$ ppm) are reported using the residual protic solvent (CHCl_3 in CDCl_3 : $\delta = 7.26$ ppm, DMSO-d_5 in DMSO-d_6 : $\delta = 2.50$ ppm, CHD_2OD in CD_3OD : $\delta = 3.31$ ppm) as an internal reference. For ¹³C-NMR spectra, chemical shifts in ppm relative to tetramethylsilane ($\delta = 0$ ppm) are reported using the central resonance of the solvent signal (CDCl_3 : $\delta = 77.16$ ppm, DMSO-d_6 : $\delta = 39.52$ ppm, CD_3OD : $\delta = 49.00$ ppm) as an internal reference. For ¹H-NMR spectra in addition to the chemical shift the following data is reported in parenthesis: multiplicity, coupling constant(s), number of hydrogen atoms and, if available, assignment. The abbreviations for multiplicities and related descriptors are s = singlet, d = doublet, t = triplet, q = quartet, p = pentuplet or combinations thereof, m = multiplet and br = broad. The numbering scheme used for the assignments is specified in each case in a figure depicting the respective molecular structure and does not follow any convention. The reported assignments are supported by 2D-NMR experiments (HMBC, HSQC, COSY). Where known products matched literature analysis data, only selected data acquired are reported.

2.4.1 HPLC(-MS) analysis

Analytical high pressure liquid chromatography (**HPLC**) analysis was conducted either using an *Agilent 1100* system from *Agilent Technologies Corp.*, Santa Clara (USA) equipped with a DAD detector and a *Hypersil Gold* HPLC column from *ThermoFisher Scientific GmbH*, Dreieich (Germany) or a *Agilent 1200 SL* system *Agilent Technologies Corp.*, Santa Clara (USA) equipped with a DAD detector, a *Hypersil Gold* HPLC column from *ThermoFisher Scientific GmbH*, Dreieich (Germany) and consecutive low-resolution mass detection using a *HCT ultra PTM discovery* system applying ESI from *Bruker Corp.*, Billerica (USA). For both systems mixtures of water (analytical grade, 0.1% formic acid) and MeCN (analytical grade, 0.1% formic acid) were used as eluent systems.

3 Synthetic Procedures



N-Boc serinol (9)¹²

2-amino-1,3-diol **3** (2.50 g, 27.4 mmol) was dissolved in a 1:1-mixture of dioxane:H₂O (200 mL, 0.13 M) and NEt₃ (4.85 mL, 35 mmol) was added. The mixture was cooled to 0 °C and a solution of Boc₂O (7.04 g, 32.2 mmol) dissolved in 1,4-dioxane (35 mL) was added, the reaction mixture was allowed to warm to r.t. and was then further stirred for 15 h. The solution was acidified to pH 4 using 2 M aq. HCl, then saturated with potassium sodium tartrate and extracted with EtOAc (3×200 mL). The combined organic layers were dried over Na₂SO₄, filtered and concentrated under reduced pressure to give **9** (5.03 g, 26.3 mmol, 96%) as a colourless solid and used without further purification.¹²

TLC R_f = 0.50 (EtOAc). The product matched literature analysis data¹². Selected data acquired: **HRMS** (EI): C₈H₁₅NO₃⁺ [M-e]: calc. 173.1046, found 173.1046. **¹H-NMR** (400 MHz, CDCl₃): δ (ppm) = 5.29 (d, *J* = 6.7 Hz, 1H), 3.81 (dd, *J* = 11.1, 4.4 Hz, 2H), 3.74 (dd, *J* = 11.1, 4.5 Hz, 2H), 3.67 (s, 1H, NH), 2.89 (s, 2H, OH), 1.44 (s, 9H).

N-Boc 2-amino-1,3-bis(acetylthio)propane (4)⁴⁶

Protocol A:

To a solution of PPh₃ (13.50 g, 51.5 mmol) in anhydrous THF (300 mL) under N₂-atmosphere at 0 °C was dropwise added DIAD (10.0 mL, 50.8 mmol). The mixture was stirred for 30 min and precipitation of a colourless crystalline solid was observed. Then, a solution of N-Boc serinol **9** (4.70 g, 24.3 mmol) in anhydrous THF (25 mL) and HSAc (3.8 mL, 53.5 mmol) were added under vigorous stirring. The reaction mixture was stirred at 0 °C for 1 h, was then allowed to warm to r.t. and further stirred for 16 h, before being concentrated under reduced pressure. The residue was dry-loaded on activation silica gel (Ceduran®) and purified by flash column chromatography (isohexane:EtOAc, 90:10 to 0:100) to give and compound **4** (6.63 g, 21.6 mmol, 88%) as a colourless solid.⁴⁶

Protocol B:

Step 1: To a solution of N-Boc serinol (77 mg, 0.40 mmol), and pyridine (157 μL, 1.95 mmol) in anhydrous DCM (10 mL) under N₂-atmosphere at 0 °C was added MsCl (31 μL, 0.40 mmol). The mixture was stirred for 30 min, then warmed to r.t. and stirred further for 1.5 h. After diluting with DCM (20 mL), the mixture was washed with sat. aq. NaCl (2×20 mL) and the aq. washings were extracted with DCM (2×10 mL). The combined organic layers were dried over Na₂SO₄ and concentrated under reduced pressure to N-Boc 2-aminopropane-1,3-diyl dimethanesulfonate as a colourless oil, which was used without further purification.

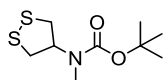
Step 2: The material obtained in step 1 was dissolved in acetone (5 mL), potassium thioacetate (recrystallized from EtOH, 137 mg, 1.20 mmol) was added and the mixture was heated to reflux for 2 h. Then the volatiles were removed under reduced pressure and DCM (10 mL) and H₂O (10 mL) were added. The layers were separated and the aq. layer was extracted with DCM (2×10 mL). The combined organic layers were dried over Na₂SO₄, filtered over a short layer of silica gel and concentrated under reduced pressure to give compound **4** (110 mg, 0.36 mmol, 89%) as a colourless solid.

TLC R_f = 0.36 (*n*-pentane:Et₂O, 3:1). **HRMS** (ESI⁺): C₁₂H₂₁NNaO₄S₂⁺ [M+Na]⁺: calc. 330.08042, found 330.08039. **¹H-NMR** (400 MHz, CDCl₃): δ (ppm) = 4.88 – 4.62 (m, 1H), 3.99 – 3.80 (m, 1H), 3.07 (d, *J* = 7.0 Hz, 4H), 2.35 (s, 6H), 1.42 (s, 9H).¹²

N-Boc 1,2-dithiolan-4-amine (5)¹²

Bis-thioacetate **4** (4.59 g, 14.9 mmol) was dissolved in a 0.17 M solution of KOH in methanol (500 mL). The mixture was stirred at r.t. open to air for 15 h, concentrated under reduced pressure (at <40 °C) and the remaining yellow oil was dissolved in EtOAc (200 mL). The solution was washed with aq. NaCl (2×50 mL) and H₂O (100 mL), dried over Na₂SO₄, filtered and concentrated under reduced pressure (at T < 40 °C) to afford compound **5** (3.22 g, 14.6 mmol, 98%) as a yellow solid.¹²

TLC R_f = 0.49 (isohexane:EtOAc, 10:1). **HRMS** (ESI⁻): C₈H₁₄NO₂S₂⁻ [M-H]⁻: calc. 220.04714, found 220.04718. **¹H-NMR** (400 MHz, CDCl₃): δ (ppm) = 5.06 (d, *J* = 3.9 Hz, 1H, NH), 4.95 (s, 1H, CH), 3.21 (dd, *J* = 11.6, 4.8 Hz, 2H), 3.09 (dd, *J* = 11.6, 2.0 Hz, 2H), 1.44 (s, 9H).

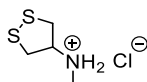
N-Boc N-methyl-1,2-dithiolan-4-amine (10)

To a mixture of 60% NaH suspension in mineral oil (434 mg, 10.8 mmol), anhydrous DMF (180 mL) and iodomethane (731 μ L, 11.7 mmol) under N_2 -atmosphere at 0 °C was added dithiolane **5** (2.00 g, 9.04 mmol) in one portion. After stirring at 0 °C for 40 min, H_2O (500 mL) was added and the mixture was extracted with EtOAc (3 \times 250 mL). The extracts were washed with H_2O (200 mL) and aq. NaCl (2 \times 200 mL), dried over Na_2SO_4 and concentrated under reduced pressure.

The remaining yellow oil (3.41 g) was dissolved in methanol (250 mL) and KOH (2.10 g, 37.5 mmol) was added. This "depolymerization mixture" was stirred open to air for 6 days and was extracted four times (after 1 day, 2 days, 4 days and 6 days) to obtain compound **10** (507 + 587 + 307 + 90 mg = 1.49 g, 6.33 mmol, 70%) according to the following procedure:

The depolymerization mixture was extracted with hexanes (2 \times 350 mL). The extracts were washed with half-saturated aq. NaCl (300 mL), dried over Na_2SO_4 and filtered over a plug of silica gel (32 g). The filtrate was discarded and compound **10** was eluted with a 1:8-mixture of EtOAc:hexanes (360 mL). After evaporating the eluent, compound **10** was obtained as a yellow oil. Additionally, the silica was washed with ethyl acetate (200 mL), the washings were evaporated, the remainder was dissolved in small amount of methanol and added back into the depolymerization mixture.

TLC R_f = 0.49 (iso-hexane:EtOAc 10:1). **HRMS** (EI): $C_9H_{17}NO_2S_2$: [M-e] calc. 235.0696, found 235.0677. **¹H-NMR** (400 MHz, $CDCl_3$): δ (ppm) = 5.49 – 4.73 (m, 1H), 3.30 (dd, J = 12.0, 7.8 Hz, 2H), 3.03 (dd, J = 12.0, 5.9 Hz, 2H), 2.82 (s, 3H), 1.47 (s, 9H). **¹³C-NMR** (101 MHz, $CDCl_3$): δ (ppm) = 155.3 (C=O), 80.5 ($C(CH_3)_3$), 61.2 (CH), 40.5 (CH_2), 29.5 (CH_3), 28.5 (CH_3).

N-methyl-1,2-dithiolan-4-amine hydrochloride (6)

Dithiolane **10** (118 mg, 0.501 mmol) was dissolved in anhydrous MeOH (0.033 M, 15 mL) and stirred open to air for 1 h before a 1.25 M solution of HCl in MeOH (5 mL, 6.25 mmol) was added. The resulting mixture was heated to reflux for 6 h and then evaporated under reduced pressure to yield hydrochloride **6** (85 mg, 0.50 mmol, quant.) as a colourless solid.

¹H-NMR (400 MHz, $DMSO-d_6$): δ (ppm) = 8.49 (s, 2H), 3.35 (p, J = 5.1 Hz, 1H), 2.58 (dd, J = 5.2, 1.7 Hz, 4H), 1.74 (s, 3H). **¹³C-NMR** (101 MHz, $DMSO-d_6$): δ (ppm) = 63.3 (CH), 40.4 (CH_2), 31.1 (CH_3).

1,2-dithiolan-4-ol (13)

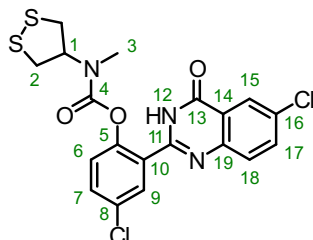
Step 1: To a solution of 4-dimethylaminopyridine (189 mg, 1.55 mmol, 0.1 eq.), pyridine (1.25 mL, 15.5 mmol, 1.0 eq.) and benzoyl chloride (1.98 mL, 17.1 mmol, 1.1 eq.) in anhydrous DCM (40 mL) at 0 °C was dropwise added 1,3-dichloropropan-2-ol **11** (1.48 mL, 15.5 mmol, 1.0 eq.). The mixture was stirred with warming to r.t. for 15 h, diluted with DCM (40 mL), washed with 2 M aq. HCl (40 mL), water (40 mL) and sat. aq. $NaHCO_3$ (40 mL) and dried over $MgSO_4$. The volatiles were evaporated under reduced pressure and the remaining colourless oil was directly used in the next step.

Step 2: The material obtained in step 1 was dissolved in acetone (150 mL) and potassium thioacetate (4.43 g, 38.8 mmol, 2.5 eq.) was added. The mixture was stirred at r.t. for three days, and then at reflux for six more days. While stirring at reflux, more KSAc was added on day four (2.66 g, 23.5 mmol, 1.5 eq.) and day five (2.66 g, 23.5 mmol, 1.5 eq.). After cooling to r.t., the mixture was filtered, the solids were discarded and the filtrate was evaporated under reduced pressure. The residue was suspended in DCM (50 mL), the suspension was filtered, the solids were discarded and the filtrate was evaporated under reduced pressure. The residue was purified by FCC (silica, DCM/iso-hexane) to afford a dark red oil containing O-benzoyl-bis(thioacetate) **12** (1.38 g, 4.42 mmol, 29%).

Step 3: The material obtained in step 2 was dissolved in MeOH (150 mL), KOH (1.24 g, 22.1 mmol, 5.0 eq.) was added and the mixture was stirred at r.t. under air for seven days. Then, the mixture was filtered and the solids were discarded. The filtrate was diluted with diethyl ether (200 mL), washed with water (200 mL), 2 M aq. NaOH

(150 mL) and sat. aq. NaCl (100 mL) and dried over MgSO₄. The volatiles were removed under reduced pressure and the remaining crude 1,2-dithiolan-4-ol **13** (60 mg, 0.49 mmol, 11%) was used without further purification.

4-chloro-2-(6-chloro-4-oxo-3,4-dihydroquinazolin-2-yl)phenyl (1,2-dithiolan-4-yl) (methyl)carbamate (SS50-PQ, 1)



Step 1: To a solution of **PQ-OH (2)** (Prepared according to procedures reported in Felber *et al.*¹⁴) (57.2 mg, 0.187 mmol) in anhydrous DCM (5 mL) under nitrogen atmosphere at 0 °C was added a solution of triphosgene (60.5 mg, 0.204 mmol) in anhydrous DCM (1 mL), followed by a solution of DIPEA (38 μ L, 0.221 mmol) in anhydrous DCM (2 mL). The resulting mixture was stirred at 0 °C for 30 min, then warmed to r.t. and stirred further for 30 min, before being evaporated under high vacuum (the volatiles were condensed in a liquid nitrogen trap and treated with 2M aq. NaOH as well as piperidine to discharge residual phosgene). The remainder was dissolved in anhydrous DCM (12.5 mmol) and this solution of **PQ-OH**-chloroformate was directly used in the next reaction.

Step 2: To a suspension of compound **6** (29.2 mg, 0.170 mmol) in anhydrous DCM (2 mL) was added DIPEA (34 μ L, 0.20 mmol), the resulting solution was added dropwise at 0 °C to the solution of **PQ-OH** chloroformate obtained in step 1 and the mixture was stirred at 0 °C for 15 min. Then, additional DIPEA (29 μ L, 0.17 mmol) was added, before the mixture was warmed to ambient temperature. After stirring for 30 min, the mixture was concentrated under reduced pressure and the residue was purified by FCC (isohexane:EtOAc, 90:10 to 0:100) to give compound **1** (39.0 mg, 0.083 mmol, 49%) as a colourless solid.

Only weak, blue residual fluorescence was observed upon irradiation with UV-light, confirming that the obtained material was not contaminated with **PQ-OH**.

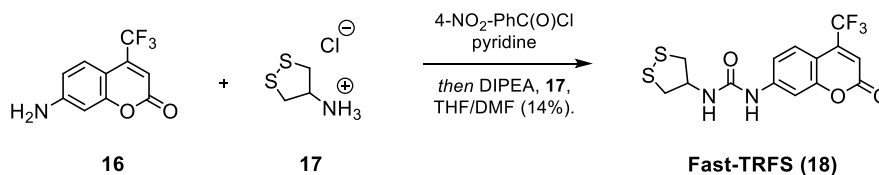
TLC R_f = 0.26 (isohexane:EtOAc, 3:1).

HRMS (ESI⁺): C₁₉H₁₆Cl₂N₃O₃S₂⁺ [M+H]⁺: calc. 468.00046, found 468.00049.

Individual rotamers were observed by NMR spectroscopy at 298 K (ratio \approx 2/1) and time-averaged spectra were obtained at 373 K.

¹H-NMR (400 MHz, tetrachlorethan-*d*₂, 373 K): δ (ppm) = 8.24 – 8.22 (m, 1H, **15-H**), 7.95 (d, J = 2.6 Hz, 1H, **9-H**), 7.71 (d, J = 1.9 Hz, 2H, **17-H**; **18-H**), 7.50 (dd, J = 8.7, 2.7 Hz, 1H, **7-H**), 7.20 (d, J = 8.7 Hz, 1H, **6-H**), 5.09 (p, J = 6.7 Hz, 1H, **1-H_{ax}**), 3.32 (dd, $^2J_{2'-2}$ = 12.1 Hz, $^3J_{2'-1}$ = 7.6 Hz, 2H, **2-H_{ax}**), 3.10 (dd, $^2J_{2'-2}$ = 12.1 Hz, $^3J_{2'-1}$ = 5.6 Hz, 2H, **2'-H_{eq}**), 3.04 (s, 3H, **3-H**).

¹³C-NMR (101 MHz, tetrachlorethan-*d*₂, 373 K): δ (ppm) = 160.1 (C=O, **C13**), 153.7 (C=O, **C4**), 149.0 (C=N, **C11**), 147.6 (C_{Ar}, **C5**), 147.4 (C_{Ar}, **C14**), 135.3 (C_{Ar}H, **C18**), 133.6 (C_{Ar}, **C19**), 132.3 (C_{Ar}H, **C7**), 132.1 (C_{Ar}, **C8**), 130.4 (C_{Ar}H, **C9**), 129.7 (C_{Ar}H, **C17**), 128.0 (C_{Ar}, **C10**), 126.1 (C_{Ar}H, **C15**), 125.2 (C_{Ar}H, **C6**), 122.4 (C_{Ar}, **C16**), 62.9 (CH, **C1**), 40.7 (CH₂, **C2**), 30.6 (CH₃, **C3**).

1-(1,2-dithiolan-4-yl)-3-(2-oxo-4-(trifluoromethyl)-2H-chromen-7-yl)urea (Fast-TRFS) (18)

To a solution of 4-nitrophenyl chloroformate (78 mg, 0.39 mmol, 1.1 eq.) in anhydrous tetrahydrofuran (3 mL) under nitrogen atmosphere at 0 °C was dropwise added a solution of compound 7-amino-4-(trifluoromethyl)-2H-chromen-2-one **16** (prepared according to Sun *et al.*⁴⁹ (80 mg, 0.35 mmol, 1.0 eq.) and pyridine (42 μ L, 0.52 mmol, 1.5 eq.) in anhydrous THF (3 mL). The mixture was stirred with warming to r.t. for 4 h. Then, a suspension consisting of 1,2-dithiolan-4-amine hydrochloride **17** (prepared according to Felber *et al.*¹⁴) (66 mg, 0.42 mmol, 1.2 eq.), DIPEA (245 μ L, 1.4 mmol, 4.0 eq.) and anhydrous DMF (1.5 mL) was added. The mixture was stirred at r.t. overnight and concentrated under reduced pressure. The residue was taken up in EtOAc (40 mL), washed with water (30 mL) and sat. aq. NaCl (30 mL) and dried over MgSO₄. The volatiles were removed under reduced pressure and the residue was subjected to FCC (silica, isohexane/EtOAc), which afforded a yellowish solid (51 mg) that consisted of **Fast-TRFS** and minor impurities. This solid was dissolved in warm (approx. 50 °C) MeCN, the solution was cooled to -20 °C overnight and the resulting precipitate was collected to afford pure **Fast-TRFS (18)** (18 mg, 0.048 mmol, 14%) as a faint yellow solid.

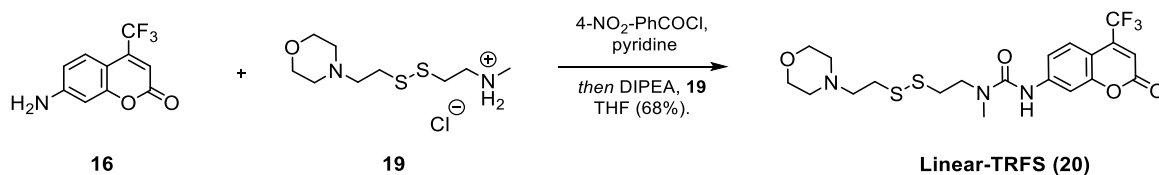
TLC R_f = 0.6 (isohexane:EtOAc, 1:1).

HRMS (ESI+): C₁₄H₁₂F₃N₂O₃S₂ [M+H]⁺ calc. 377.0236, found 377.0237.

¹H-NMR (400 MHz, DMSO-d₆): 9.37 (s, 1H), 7.75 (d, J = 2.1 Hz, 1H), 7.59 (dd, J = 8.9, 2.0 Hz, 1H), 7.27 (dd, J = 8.9, 2.2 Hz, 1H), 6.81 (s, 1H), 6.68 (d, J = 8.1 Hz, 1H), 4.96 (dtt, J = 7.8, 5.1, 2.7 Hz, 1H), 3.30 (dd, J = 11.5, 4.9 Hz, 2H), 3.16 (dd, J = 11.5, 2.7 Hz, 2H).

¹³C-NMR (100 MHz, DMSO-d₆): 158.9, 155.2, 153.7, 144.8, 139.4 (q, J = 32.2 Hz), 125.4, 121.8 (q, J = 275.6 Hz), 114.8, 113.0 (q, J = 5.7 Hz), 106.6, 104.2, 55.6, 44.1.

The previously reported spectroscopic data by Li *et al.*¹² contained significant errors, which complicated a comparison with our spectroscopic data. Upon close inspection of the ¹H-NMR spectral data, we noticed that the values provided by Li *et al.* did not correspond to DMSO-d₆ as specified, but instead were based on a measurement in CDCl₃. We did not further characterize our material in CDCl₃, as the reported ¹H-NMR spectrum in CDCl₃ by Li *et al.* was clearly not pure and we already had obtained a high quality ¹H-NMR spectrum in DMSO-d₆, which confirmed that our batch of **Fast-TRFS** was pure. Furthermore, the ¹³C-NMR spectrum in DMSO-d₆ was in agreement with the previously reported values. However, regarding the ¹³C-NMR spectrum, Li *et al.* have ignored the splitting of several signals that resulted from the presence of fluorine in the molecule and consequently several chemical shifts were incorrectly reported. Additionally, the ¹³C-NMR signals were shifted in an absolute, but not in a relative manner, which we suspect to be the result of incorrect referencing. Despite these issues, we were able to match all the signal that had been reported by Li *et al.* and thereby confirmed that we had indeed prepared the same compound.

1-methyl-1-(2-((2-morpholinoethyl)disulfaneyl)ethyl)-3-(2-oxo-4-(trifluoromethyl)-2H-chromen-7-yl)urea (Linear-TRFS) (20)

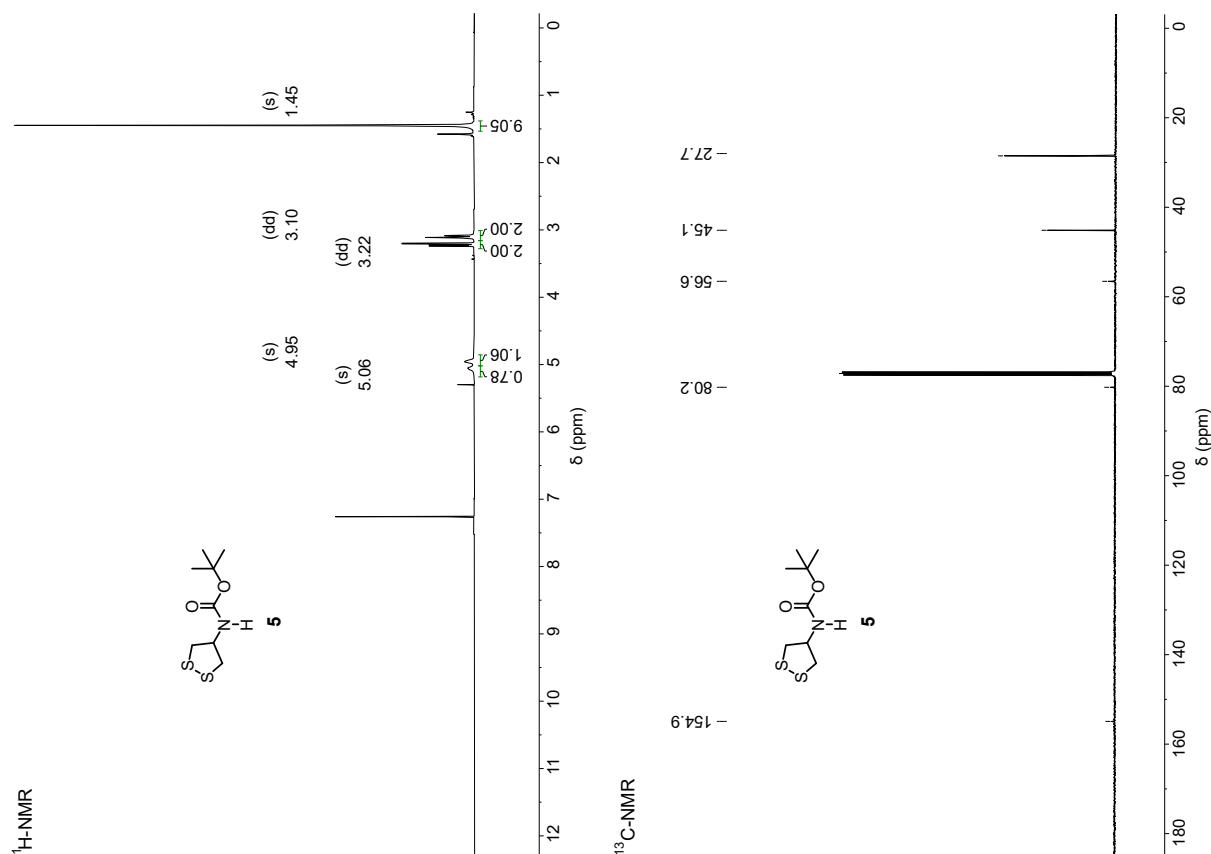
To a solution of 4-nitrophenyl chloroformate (97 mg, 0.48 mmol, 1.1 eq.) in anhydrous tetrahydrofuran (4 mL) under nitrogen atmosphere at 0 °C was dropwise added a solution of compound 7-amino-4-(trifluoromethyl)-2H-chromen-2-one **16** (100 mg, 0.44 mmol, 1.0 eq.) and pyridine (53 μL , 0.66 mmol, 1.5 eq.) in anhydrous THF (4 mL). The mixture was stirred with warming to r.t. for 4 h. Then, solid *N*-methyl-2-((2-morpholinoethyl)disulfaneyl)ethan-1-amine dihydrochloride (prepared according to Felber *et al.*¹⁴) **19** (162 mg, 0.52 mmol, 1.2 eq.) and DIPEA (608 μL , 3.5 mmol, 8.0 eq.) were added. The mixture was stirred at r.t. overnight, diluted with 30 mL of sat. aq. NaHCO_3 and extracted with DCM (3 \times 30 mL). The combined organic phases were dried over MgSO_4 , the volatiles were removed under reduced pressure and the residue was subjected to FCC (silica, isohexane/EtOAc) to afford pure **Linear-TRFS (20)** (145 mg, 0.30 mmol, 68%) as a faint yellow solid.

TLC R_f = 0.33 (acetone:EtOAc, 1:9).

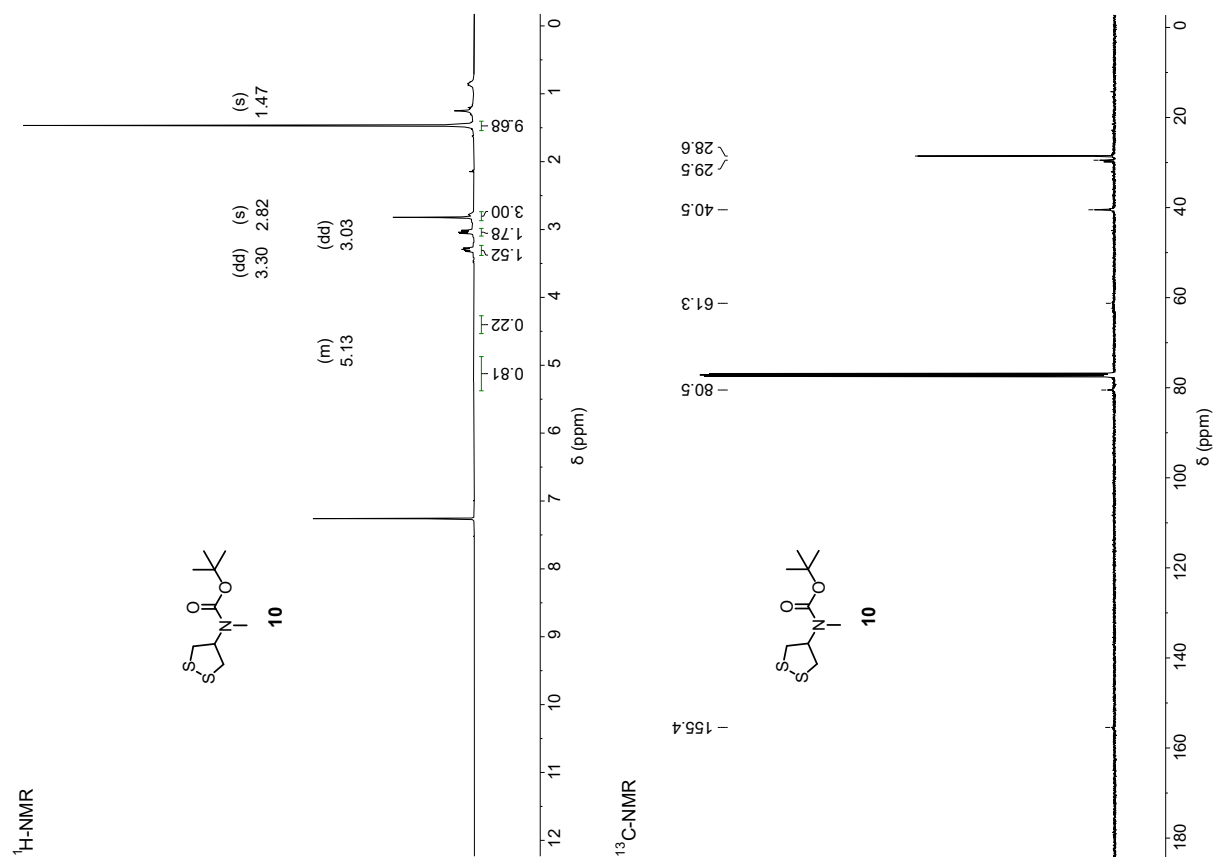
HRMS (ESI⁺): $\text{C}_{20}\text{H}_{25}\text{F}_3\text{N}_3\text{O}_4\text{S}_2$ [M+H]⁺ calc. 492.1233, found 492.1234.

¹H-NMR (400 MHz, CDCl_3): 7.65 (s, 1H), 7.61 (dq, J = 8.9, 2.0 Hz, 1H), 7.44 (d, J = 8.9 Hz, 1H), 7.11 (s, 1H), 6.64 (s, 1H), 3.80 – 3.68 (m, 6H), 3.12 (s, 3H), 3.01 – 2.85 (m, 4H), 2.75 (s, 2H), 2.54 (s, 4H).

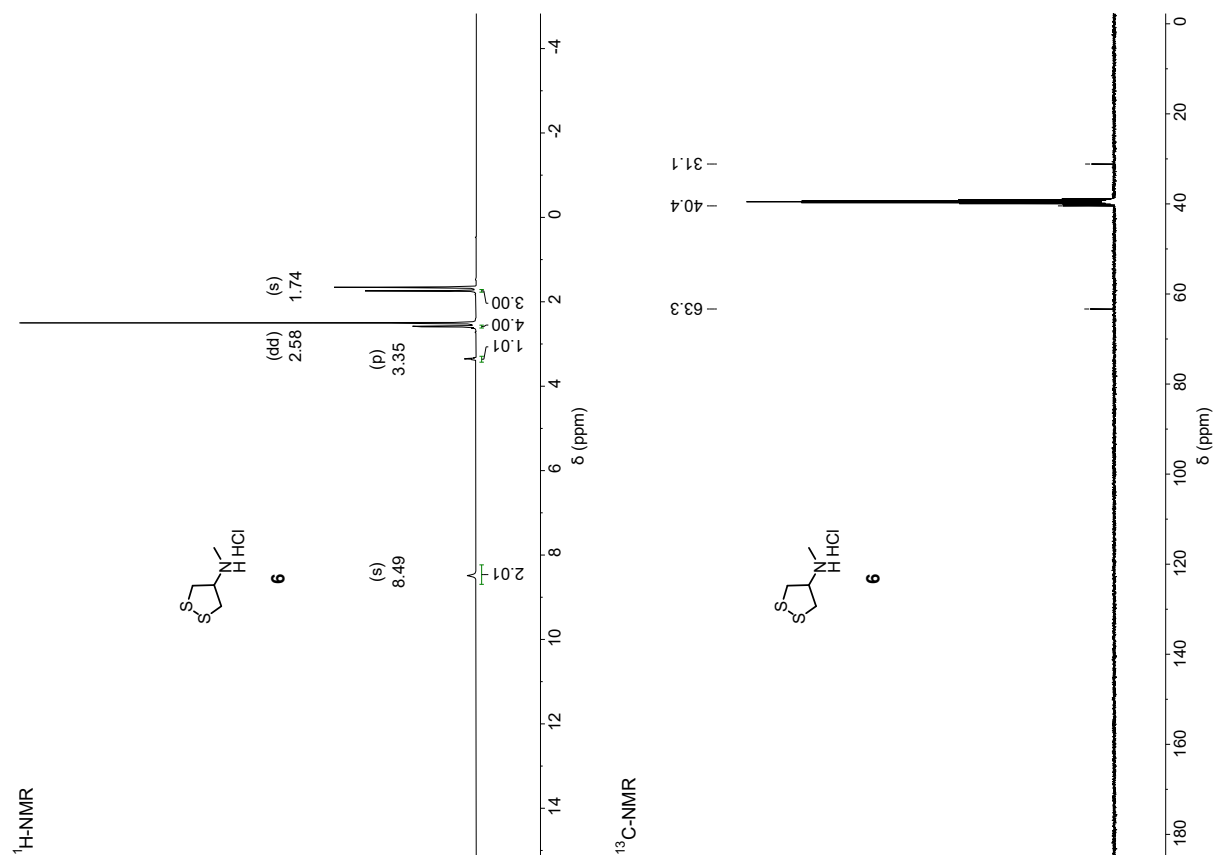
¹³C-NMR (100 MHz, CDCl_3): 159.7, 155.5, 154.5, 144.5, 141.64 (q, J = 32.9 Hz), 125.89 (q, J = 2.1 Hz), 121.70 (q, J = 275.5 Hz), 116.2, 112.96 (q, J = 5.7 Hz), 108.3, 106.8, 66.6, 57.9, 53.5, 48.7, 36.6, 35.7, 35.3.

4 NMR Spectra***N*-Boc 1,2-dithiolan-4-amine (5)**

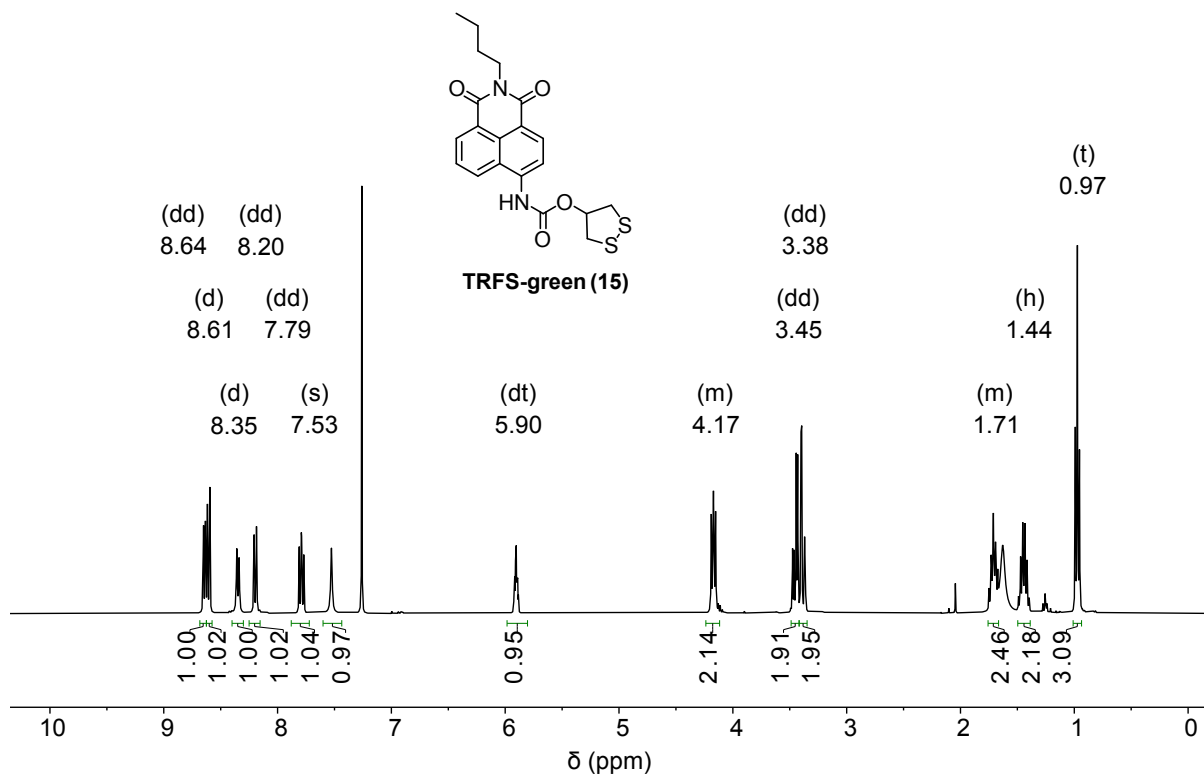
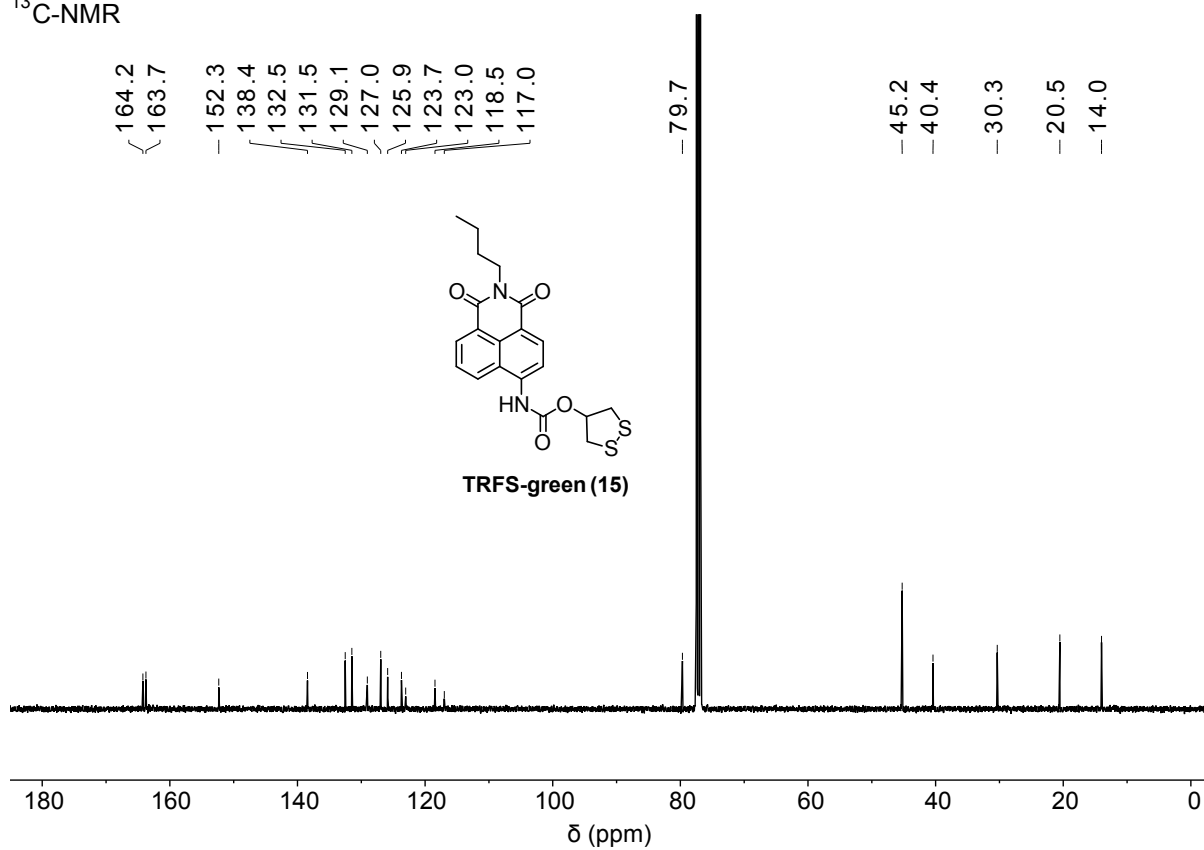
***N*-Boc *N*-methyl-1,2-dithiolan-4-amine (10)**



***N*-methyl-1,2-dithiolan-4-amine hydrochloride (6)**

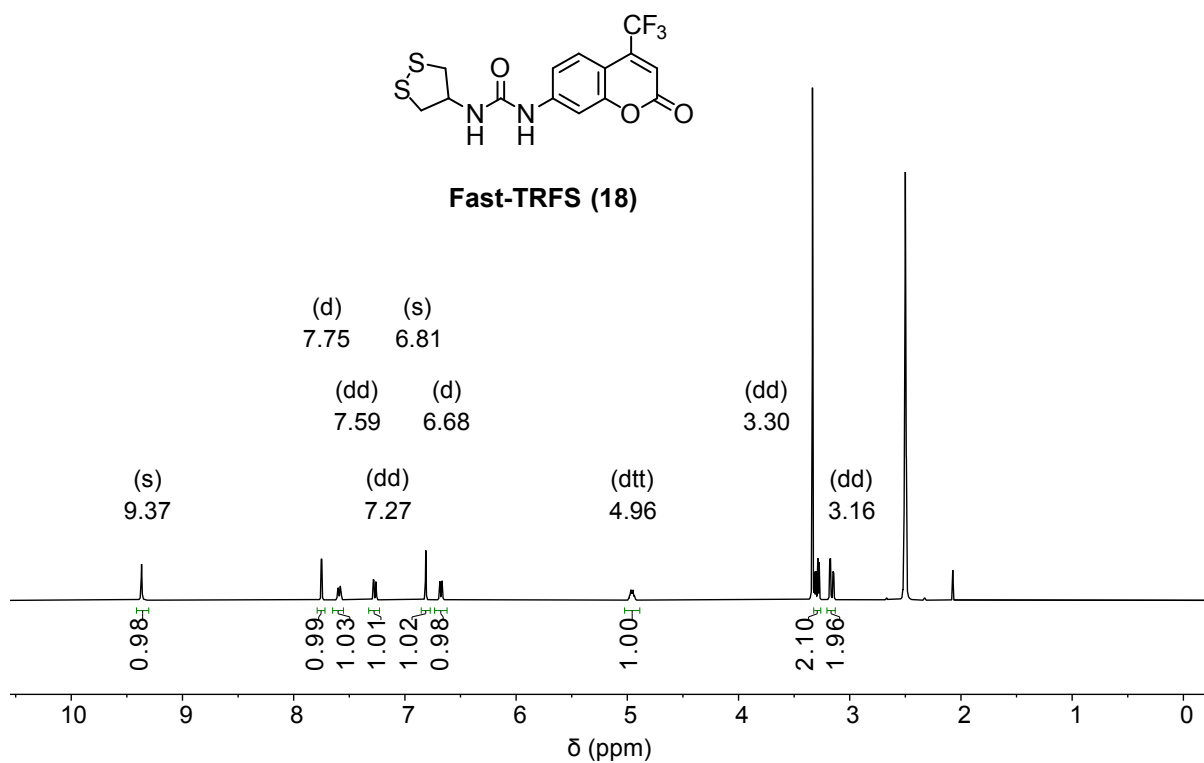


TRFS-green (15)

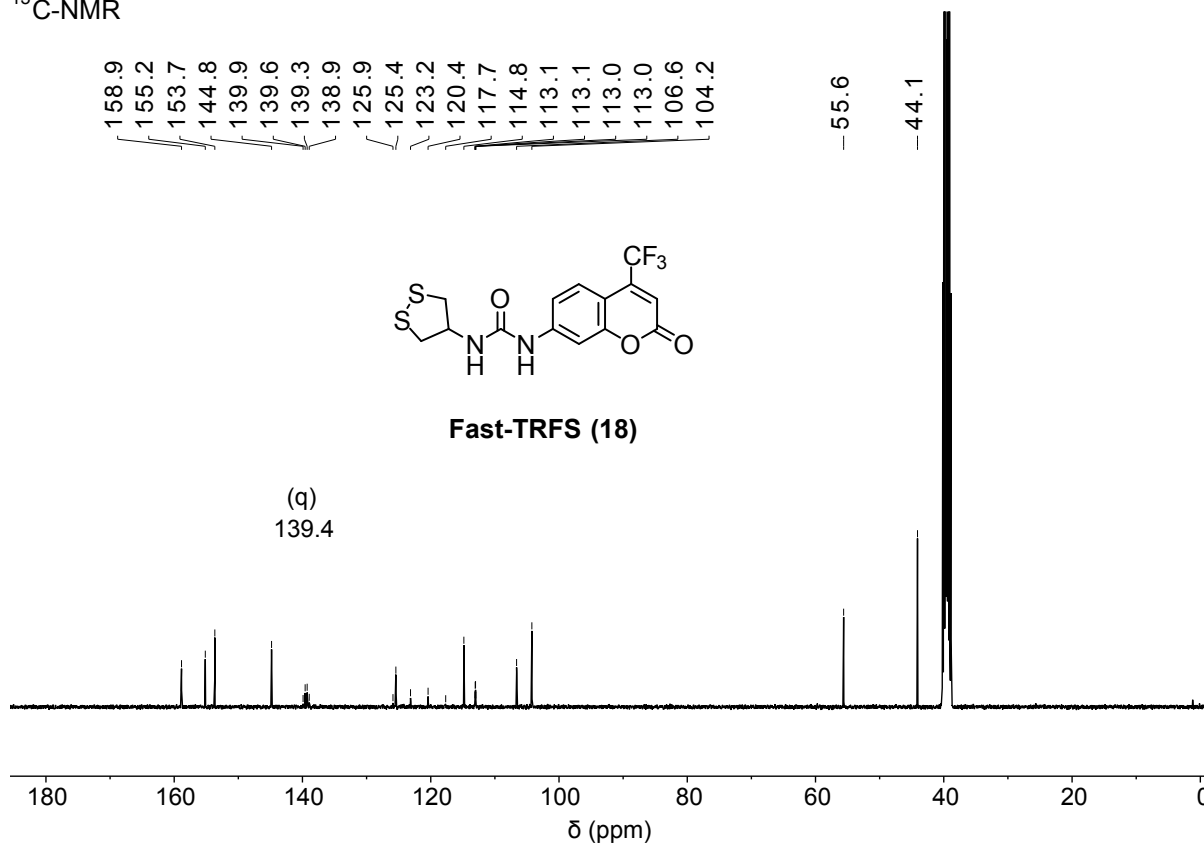
 $^1\text{H-NMR}$  $^{13}\text{C-NMR}$ 

Fast-TRFS (18)

¹H-NMR

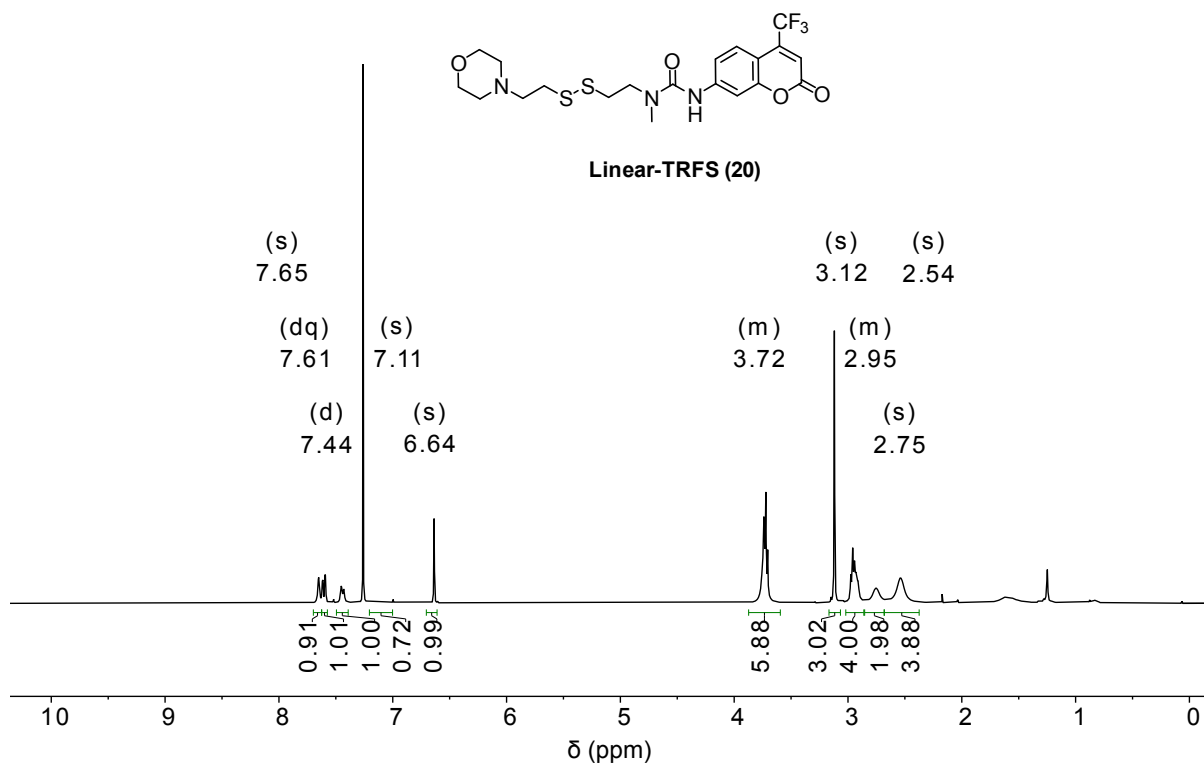


¹³C-NMR

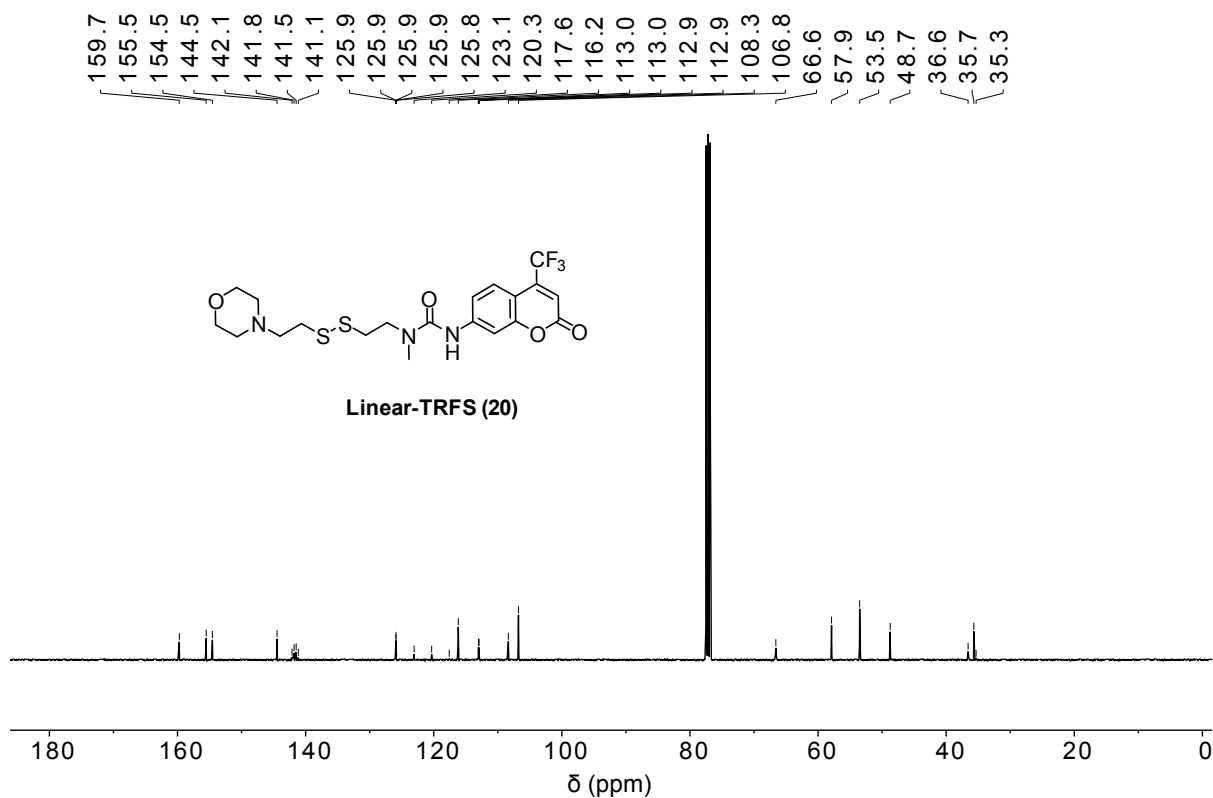


Linear-TRFS (20)

¹H-NMR



¹³C-NMR



5. Supplementary References

1. Busker, S. *et al.* Irreversible TrxR1 inhibitors block STAT3 activity and induce cancer cell death. *Sci. Adv.* **6**, eaax7945 (2020). <https://doi.org/10.1126/sciadv.aax7945>.
2. Zeisel, L. *et al.* Selective cellular probes for mammalian thioredoxin reductase TrxR1: rational design of RX1, a modular 1,2-thiaselenane redox probe. *ChemRxiv* (2021). <https://doi.org/10.33774/chemrxiv-2021-52kwx>.
3. Carmine, A., Domoto, Y., Sakai, N. & Matile, S. Comparison of Lipoic and Asparagusic Acid for Surface-Initiated Disulfide-Exchange Polymerization. *Chem.-Eur. J.* **19**, 11558–11563 (2013). <https://doi.org/10.1002/chem.201301567>.
4. Gasparini, G., Sargsyan, G., Bang, E.-K., Sakai, N. & Matile, S. Ring Tension Applied to Thiol-Mediated Cellular Uptake. *Angew. Chem. Int. Ed.* **54**, 7328–7331 (2015). <https://doi.org/10.1002/anie.201502358>.
5. Abegg, D. *et al.* Strained Cyclic Disulfides Enable Cellular Uptake by Reacting with the Transferrin Receptor. *J. Am. Chem. Soc.* **139**, 231–238 (2017). <https://doi.org/10.1021/jacs.6b09643>.
6. Chuard, N. *et al.* Strain-Promoted Thiol-Mediated Cellular Uptake of Giant Substrates: Liposomes and Polymersomes. *Angew. Chem. Int. Ed.* **56**, 2947–2950 (2017). <https://doi.org/10.1002/anie.201611772>.
7. Martinet, R., Du, D., López-Andarias, J., Sakai, N. & Matile, S. Oligomers of Cyclic Oligochalcogenides for Enhanced Cellular Uptake. *ChemBioChem* **21**, 1–8 (2020). <https://doi.org/10.1002/cbic.202000630>.
8. Zhang, L. *et al.* Highly Selective Off-On Fluorescent Probe for Imaging Thioredoxin Reductase in Living Cells. *J. Am. Chem. Soc.* **136**, 226–233 (2014). <https://doi.org/10.1021/ja408792k>.
9. Liu, Y. *et al.* A small molecule probe reveals declined mitochondrial thioredoxin reductase activity in a Parkinson's disease model. *Chem. Commun.* **52**, 2296–2299 (2016). <https://doi.org/10.1039/C5CC09998F>.
10. Ma, H., Zhang, J., Zhang, Z., Liu, Y. & Fang, J. A fast response and red emission probe for mammalian thioredoxin reductase. *Chem. Commun.* **52**, 12060–12063 (2016). <https://doi.org/10.1039/C6CC04984B>.
11. Li, X. *et al.* Selective Activation of a Prodrug by Thioredoxin Reductase Providing a Strategy to Target Cancer Cells. *Angew. Chem. Int. Ed.* **57**, 6141–6145 (2018). <https://doi.org/10.1002/anie.201801058>.
12. Li, X. *et al.* A fast and specific fluorescent probe for thioredoxin reductase that works via disulphide bond cleavage. *Nat. Commun.* **10**, 1–12 (2019). <https://doi.org/10.1038/s41467-019-10807-8>.
13. Zhao, J. *et al.* Loss of thioredoxin reductase function in a mouse stroke model disclosed by a two-photon fluorescent probe. *Chem. Commun.* **56**, 14075–14078 (2020). <https://doi.org/10.1039/D0CC05900E>.
14. Felber, J. G. *et al.* Selective, Modular Probes for Thioredoxins Enabled by Rational Tuning of a Unique Disulfide Structure Motif. *J. Am. Chem. Soc.* **143**, 8791–8803 (2021). <https://doi.org/10.1021/jacs.1c03234>.
15. Mandal, P. K. *et al.* Loss of Thioredoxin Reductase 1 Renders Tumors Highly Susceptible to Pharmacologic Glutathione Deprivation. *Cancer Res.* **70**, 9505–9514 (2010). <https://doi.org/10.1158/0008-5472.CAN-10-1509>.
16. Mandal, P. K. Complex Redundancy between the Mammalian Thioredoxin and Glutathione Systems in Cell Proliferation and Tumorigenesis. (Ludwig-Maximilian-University Munich, 2009).
17. Karlenius, T. C., Shah, F., Di Trapani, G., Clarke, F. M. & Tonissen, K. F. Cycling hypoxia up-regulates thioredoxin levels in human MDA-MB-231 breast cancer cells. *Biochem. Biophys. Res. Commun.* **419**, 350–355 (2012). <https://doi.org/10.1016/j.bbrc.2012.02.027>.
18. Lothrop, A. P., Ruggles, E. L. & Hondal, R. J. No Selenium Required: Reactions Catalyzed by Mammalian Thioredoxin Reductase That Are Independent of a Selenocysteine Residue. *Biochemistry* **48**, 6213–6223 (2009). <https://doi.org/10.1021/bi802146w>.
19. Zhao, J. *et al.* Loss of thioredoxin reductase function in a mouse stroke model disclosed by a two-photon fluorescent probe. *Chem. Commun.* **56**, 14075–14078 (2020). <https://doi.org/10.1039/D0CC05900E>.
20. Baell, J. B. & Nissink, J. W. M. Seven Year Itch: Pan-Assay Interference Compounds (PAINS) in 2017—Utility and Limitations. *ACS Chem. Biol.* **13**, 36–44 (2018). <https://doi.org/10.1021/acscchembio.7b00903>.
21. Nelson, K. M. *et al.* The Essential Medicinal Chemistry of Curcumin. *J. Med. Chem.* **60**, 1620–1637 (2017). <https://doi.org/10.1021/acs.jmedchem.6b00975>.
22. Bisson, J. *et al.* Can Invalid Bioactives Undermine Natural Product-Based Drug Discovery? *J. Med. Chem.* **59**, 1671–1690 (2016). <https://doi.org/10.1021/acs.jmedchem.5b01009>.
23. Thorne, N., Auld, D. S. & Ingles, J. Apparent activity in high-throughput screening: origins of compound-dependent assay interference. *Mol. Divers.* **14**, 315–324 (2010). <https://doi.org/10.1016/j.cbpa.2010.03.020>.
24. Stafford, W. C. *et al.* Irreversible inhibition of cytosolic thioredoxin reductase 1 as a mechanistic basis for anticancer therapy. *Sci. Transl. Med.* **10**, eaaf7444 (2018). <https://doi.org/10.1126/scitranslmed.aaf7444>.
25. Cassini, A. & Messori, L. Molecular Mechanisms and Proposed Targets for Selected Anticancer Gold Compounds. *Curr. Top. Med. Chem.* **11**, 2647–2660 (2011). <https://doi.org/10.2174/156802611798040732>.
26. Saei, A. A. *et al.* Comprehensive chemical proteomics for target deconvolution of the redox active drug auranofin. *Redox Biol.* **32**, 101491 (2020). <https://doi.org/10.1016/j.redox.2020.101491>.
27. Snyder, R. M., Mirabelli, C. K. & Crooke, S. T. Cellular interactions of auranofin and a related gold complex with raw 264.7 macrophages. *Biochem. Pharmacol.* **36**, 647–654 (1987). [https://doi.org/10.1016/0006-2952\(87\)90715-5](https://doi.org/10.1016/0006-2952(87)90715-5).
28. Albert, A. *et al.* Speciation analysis of the antirheumatic agent Auranofin and its thiol adducts by LC/ESI-MS and LC/ICP-MS. *J. Anal. At. Spectrom.* **27**, 975–981 (2012). <https://doi.org/10.1039/C2JA30109A>.
29. Coffey, M. T., Shaw, C. F., Hormann, A. L., Mirabelli, C. K. & Crooke, S. T. Thiol competition for Et3PAuS-albumin: a nonenzymatic mechanism for Et3PO formation. *J. Inorg. Biochem.* **30**, 177–187 (1987). [https://doi.org/10.1016/0162-0134\(87\)80062-4](https://doi.org/10.1016/0162-0134(87)80062-4).
30. Bachman, R. E., Bodolosky-Bettis, S. A., Pyle, C. J. & Gray, M. A. Reversible Oxidative Addition and Reductive Elimination of Fluorinated Disulfides at Gold(I) Thiolate Complexes: A New Ligand Exchange Mechanism. *J. Am. Chem. Soc.* **130**, 14303–14310 (2008). <https://doi.org/10.1021/ja805266r>.
31. Reglinski, J., Hoey, S. & Smith, W. E. Exchange reactions between disulphides and myocristin: An in vitro model for a mechanism in chrysotherapy. *Inorganica Chim. Acta* **152**, 261–264 (1988). [https://doi.org/10.1016/S0020-1693\(00\)91479-8](https://doi.org/10.1016/S0020-1693(00)91479-8).
32. Thomas, R. C. & Reed, L. J. Disulfide Polymers of DL- α -Lipoic Acid. *J. Am. Chem. Soc.* **78**, 6148–6149 (1956). <https://doi.org/10.1021/ja01604a053>.
33. Cheng, Y. *et al.* Inhibitors of thiol-mediated uptake. *Chem. Sci.* (2021). doi:10.1039/D0SC05447J. <https://doi.org/10.1039/D0SC05447J>.
34. Rothan, H. A. *et al.* The FDA-approved gold drug Auranofin inhibits novel coronavirus (SARS-COV-2) replication and attenuates inflammation in human cells. *bioRxiv* 2020.04.14.041228 (2020). doi:10.1101/2020.04.14.041228. <https://doi.org/10.1101/2020.04.14.041228>.
35. Fromherz, P. & Ruppel, D. Lipid vesicle formation: the transition from open disks to closed shells. *FEBS Lett.* **179**, 155–159 (1985). [https://doi.org/10.1016/0014-5793\(85\)80211-8](https://doi.org/10.1016/0014-5793(85)80211-8).
36. Burns, J. A. & Whitesides, G. M. Predicting the stability of cyclic disulfides by molecular modeling: effective concentrations in thiol-disulfide interchange and the design of strongly reducing dithiols. *J. Am. Chem. Soc.* **112**, 6296–6303 (1990). <https://doi.org/10.1021/ja00173a017>.
37. Blaschke, B. M., Böhm, P., Drieschner, S., Nickel, B. & Garrido, J. A. Lipid Monolayer Formation and Lipid Exchange Monitored by a Graphene Field-Effect Transistor. *Langmuir* **34**, 4224–4233 (2018). <https://doi.org/10.1021/acs.langmuir.8b00162>.
38. Hu, G. *et al.* Fluorescent Probes for Imaging Protein Disulfides in Live Organisms. *ACS Sens.* **6**, 1384–1391 (2021). <https://doi.org/10.1021/acssensors.1c00049>.
39. Dóka, É. *et al.* A novel persulfide detection method reveals protein persulfide- and polysulfide-reducing functions of thioredoxin and glutathione systems. *Sci. Adv.* **2**, e1500968 (2016). <https://doi.org/10.1126/sciadv.1500968>.
40. Cheng, Q. & Arnér, E. S. J. Selenocysteine Insertion at a Predefined UAG Codon in a Release Factor 1 (RF1)-depleted *Escherichia coli* Host Strain Bypasses Species Barriers in Recombinant Selenoprotein Translation. *J. Biol. Chem.* **292**, 5476–5487 (2017). <https://doi.org/10.1074/jbc.M117.776310>.
41. Xu, J., Cheng, Q. & Arnér, E. S. J. Details in the catalytic mechanism of mammalian thioredoxin reductase 1 revealed using point mutations and juglone-coupled enzyme activities. *Free Radic. Biol. Med.* **94**, 110–120 (2016). <https://doi.org/10.1016/j.freeradbiomed.2016.02.013>.
42. Pader, I. *et al.* Thioredoxin-related protein of 14 kDa is an efficient L-cysteine reductase and S-denitrosylase. *Proc. Natl. Acad. Sci. U. S. A.* **111**, 6964–6969 (2014). <https://doi.org/10.1073/pnas.1317320111>.
43. Schindelin, J. *et al.* Fiji: an open-source platform for biological-image analysis. *Nat. Methods* **9**, 676–682 (2012). <https://doi.org/10.1038/nmeth.2019>.
44. Westerfield, M. *The Zebrafish Book. A Guide for the Laboratory Use of Zebrafish (Danio rerio)*. (University of Oregon Press).
45. Preibisch, S., Saalfeld, S. & Tomancak, P. Globally optimal stitching of tiled 3D microscopic image acquisitions. *Bioinformatics* **25**, 1463–1465 (2009). <https://doi.org/10.1093/bioinformatics/btp184>.
46. Lukesh, J. C., Palte, M. J. & Raines, R. T. A Potent, Versatile Disulfide-Reducing Agent from Aspartic Acid. *J. Am. Chem. Soc.* **134**, 4057–4059 (2012). <https://doi.org/10.1021/ja211931f>.
47. Zhou, P., Yao, J., Hu, G. & Fang, J. Naphthalimide Scaffold Provides Versatile Platform for Selective Thiol Sensing and Protein Labeling. *ACS Chem. Biol.* **11**, 1098–1105 (2016). <https://doi.org/10.1021/acscchembio.5b00856>.
48. Ao, X., Bright, S. A., Taylor, N. C. & Elmes, R. B. P. 2-Nitroimidazole based fluorescent probes for nitroreductase; monitoring reductive stress in cellulose. *Org. Biomol. Chem.* **15**, 6104–6108 (2017). <https://doi.org/10.1039/C7OB01406F>.
49. Sun, Q. *et al.* Non-Peptide-Based Fluorogenic Small-Molecule Probe for Elastase. *Anal. Chem.* **85**, 11304–11311 (2013). <https://doi.org/10.1021/acs402097g>.

Supporting Information to:

Selective, modular probes for thioredoxins enabled by rational tuning of a unique disulfide structure motif

Jan G. Felber¹, Lukas Zeisel¹, Lena Poczka¹, Karoline Scholzen², Sander Busker², Martin S. Maier¹, Ulrike Theisen³, Christina Brandstädter⁴, Katja Becker⁴, Elias S. J. Arnér^{2,5}, Julia Thorn-Seshold¹, Oliver Thorn-Seshold¹

¹ Department of Pharmacy, Ludwig Maximilians University Munich, Butenandtstr. 5-13, 81377 Munich, DE.

² Department of Medical Biochemistry, Karolinska Institutet, Solnavägen 9, 17177 Stockholm, SE.

³ Institute of Pharmacology and Toxicology, Medical Center, University of Rostock, Schillingallee 70, 18057 Rostock, DE.

⁴ Interdisciplinary Research Centre (IFZ), Justus Liebig University Giessen, Heinrich-Buff-Ring 26-32, 35392 Giessen, DE.

⁵ Department of Selenoprotein Research, National Institute of Oncology, 1122 Budapest, HU.

Author Contributions

J.G.F. performed synthesis, analysis, chemoreductant and enzyme studies, coordinated data assembly and wrote the manuscript. L.Z. performed synthesis, analysis, and chemoreductant assays. L.P. and K.S. performed enzyme titration assays. S.B. and C.B. performed enzyme selectivity screenings. M.S.M. performed synthesis and analysis. U.T. performed early biological evaluations. K.B., E.S.J.A. and J.T.-S. supervised enzymatic selectivity screenings. O.T.-S. designed the concept and experiments, supervised all other experiments, coordinated data assembly and wrote the manuscript, with input from all co-authors.

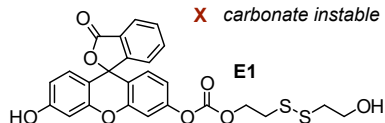
Table of contents

1.	Disulfide-based bioimaging and prodrug approaches.....	S2
2.	Fluorescence properties	S3
3.	Relative kinetics of cyclisation.....	S5
4.	Evaluation of redox potentials using the SS-Bz series.....	S6
5.	Evaluation of reduction mediated release.....	S7
6.	Enzyme specificity/activity study.....	S12
7.	General methods.....	S19
8.	Synthetic Procedures	S21
8.1.	General protocols	S21
8.2.	Trigger synthesis	S23
8.3.	Cargo synthesis	S37
8.4.	Probe synthesis	S39
9.	NMR Spectra.....	S52
10.	X-ray crystallographic data.....	S78
11.	Supporting Information Bibliography	S83

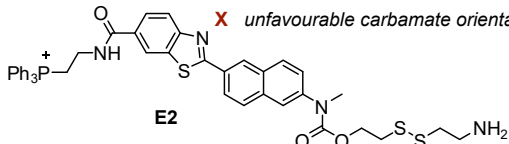
1. Disulfide-based bioimaging and prodrug approaches

a imaging agents: linear trigger

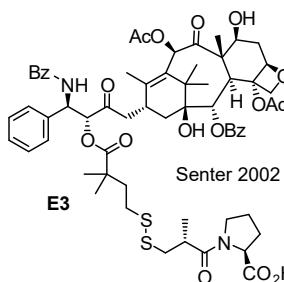
- Kim 2014
- ✓ simple thiol sensor
 - ✗ fluorescence quenching insufficient
 - ✗ carbonate instable to hydrolysis



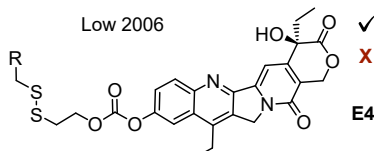
- Cho 2011
- ✓ mitochondria targeted thiol sensor
 - ✗ aniline is a poor leaving group
 - ✗ unfavourable carbamate orientation



b prodrugs: linear trigger



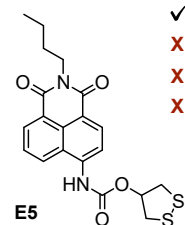
- Senter 2002
- ✓ paclitaxel-releasing prodrug
 - ✓ Thorpe-Ingold spacer
 - ✗ alcohol is a poor leaving group
 - ✗ ester linkage



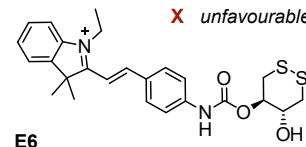
- ✓ camptothecin prodrug
- ✗ carbonate instable to hydrolysis

c imaging agents: cyclic trigger

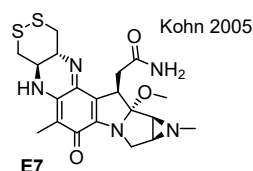
- Fang 2014
- ✓ first cyclic disulfide
 - ✗ fluorescence quenching insufficient
 - ✗ unfavourable release kinetics
 - ✗ aniline is a poor leaving group



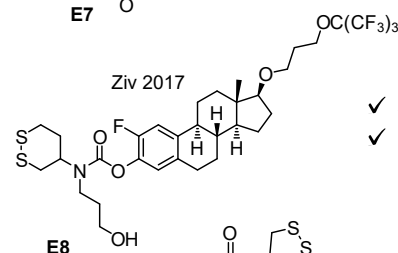
- Tang 2017
- ✓ in vivo compatible NIR dye
 - ✗ aniline is a poor leaving group
 - ✗ unfavourable carbamate orientation



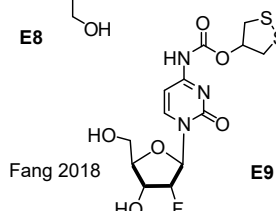
d prodrugs: cyclic trigger



- ✓ mytomycin prodrug
- ✓ resistant disulfide approach
- ✓ unique activation mechanism



- ✓ resistant disulfide approach
- ✓ phenolic cargo

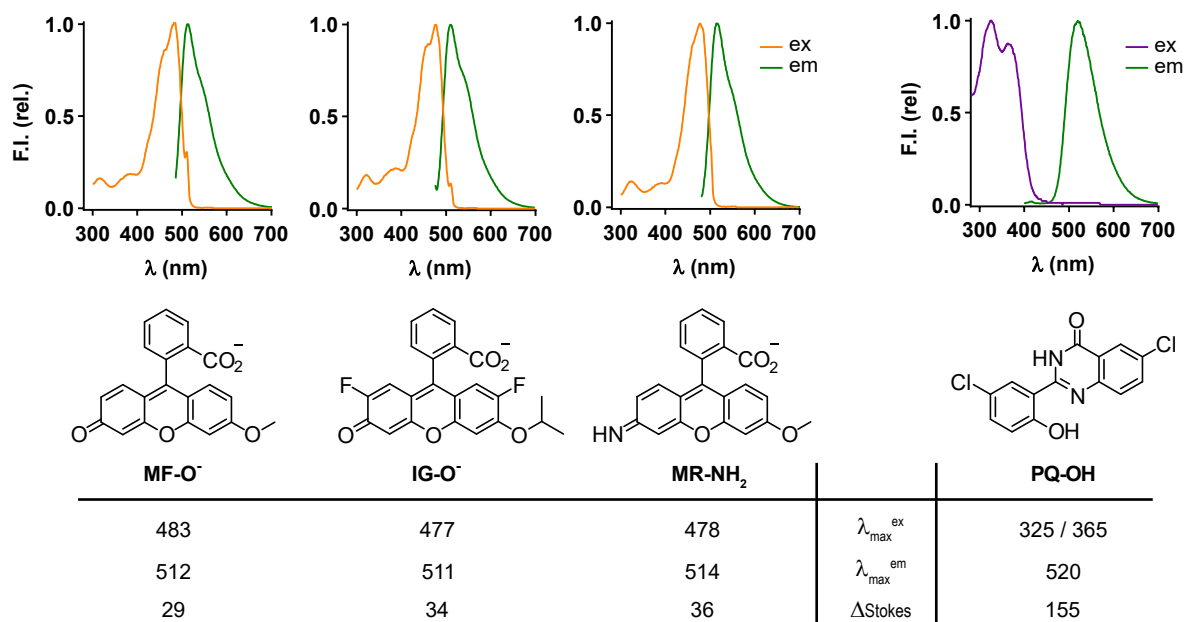


- ✓ cyclic disulfide approach
- ✗ aniline is a poor leaving group

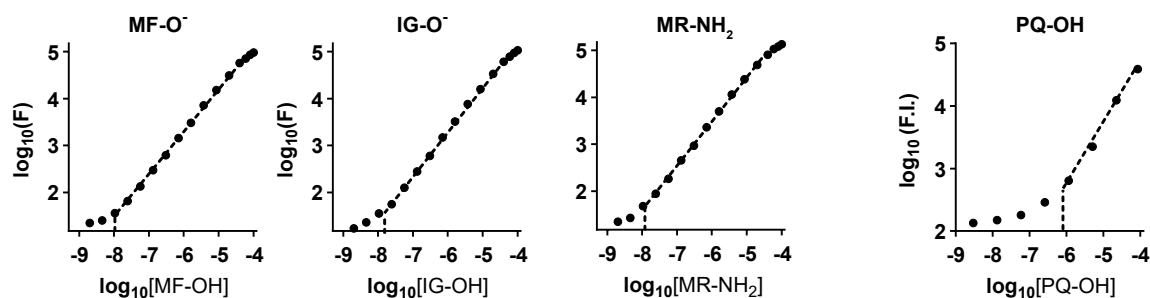
Figure S1 Disulfide-based bioimaging and prodrug approaches: representative recent examples from the literature. **(a)** linear disulfide based imaging agents for thiol sensing from Kim¹ and Cho². **(b)** linear disulfide based prodrug approaches from Senter³ and Low⁴. **(c)** cyclic disulfide based bioimaging from Fang⁵ and Tang⁶. **(d)** cyclic disulfide based prodrug approaches from Kohn⁷, Ziv⁸ and Fang⁹.

2. Fluorescence properties

a fluorescence properties



b calibration - linearity of fluorescence



c fluorogenic probe activation - cargo release

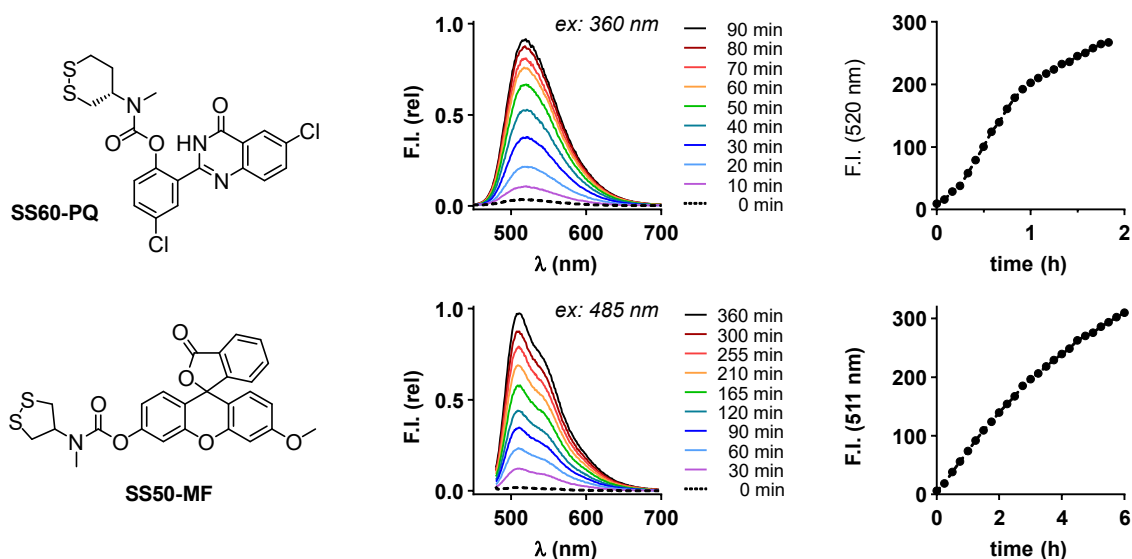


Figure S2 Photophysical properties of **MF-O⁻**, **IG-O⁻**, **MR-NH₂** and **PQ-OH** (a) Excitation and emission spectra (1 μM in TE-buffer, 1 % DMSO).; (b) Calibration: concentration-dependent fluorescence intensity (logarithmic scale 10^{-6} -1 mM in TE-buffer, 1 % DMSO. (c) Off-to-on fluorescence switch-on of **SS60-PQ** and **SS50-MF** (2 μM incubated with 1 mM DTT): raw fluorescence intensities: no baseline subtraction (for intact probe).

Fluorophore selection

Fluorogenic probes based on the soluble dyes **MF-OH**, **IG-OH** or **MR-NH₂** should linearly release fluorescent signal upon release, by thiol cyclisation following trigger disulfide reduction. As substitutions of xanthene-based dyes only mildly affect fluorescence properties, **MF-OH**, **IG-OH** and **MR-NH₂** have similar fluorescence properties, with excitation maximum of 480 nm and emission band maximum of 510 nm and small Stokes shift of 30 nm (**Fig. S2a**), and they display a consistent linear response range (ca. 15 nM - 100 μ M) on a standard platereader with substantially lower detection limit and linear range possible on a fluorimeter. **PQ-OH** is fluorescent only in the solid state, with excitation maximum 365 nm and emission band maximum of 520 nm (**Fig. S2b**). **PQ**-based probes therefore generate signal only after local accumulation of released **PQ-OH** passes its solubility limit, and their fluorescence signal timecourse additionally depends on kinetics of precipitation of **PQ-OH**. Since fluorescence in the assay is inhomogenous (suspended/sedimented solid) there is potential that the probes' fluorescence signal does not necessarily correspond to released **PQ-OH** concentration (e.g. up to solubility limit, no signal seen (can be corrected for in analysis, but we found this not necessary and did not do it); past the solubility limit, size-and-morphology-dependent Lambert-Beer shielding by variable optical path length through a solid particle or stack of particles can add nonlinearity - see discussion in¹⁰; etc). However, we cross-checked a variety of conditions and confirmed precise linear response from ca. 1 - 100 μ M (**Fig S2b**) on a standard fluorescence platereader, matching the cell-free **PQ-OH** precipitation threshold of just under 1 μ M.

Properties of cargo release of fluorogenic probes

We next confirmed the true off-to-on switch character of **SS60-PQ** and **SS50-MF** as two model representatives and investigated their signal increase kinetics. At low concentrations (1 μ M in buffered aq. solution) fluorescence intensity (at 511 nm and 520 nm respectively) was close to zero, whereas a constant increase of intensity in the spectra were measured upon incubation with a strong model reductant (1 mM DTT). Signal increase at the emission maximum matched expectations (**Fig S2b**), as a short delay of steep increase at the very start was observed only for the **PQ-OH** releasing probe (while the released amount reaches the precipitation threshold), whereas a linear increase with definite slope was detected for the **MF-OH** releasing probe due to continuous liberation of the dye. Significant differences on the release kinetics were visible as similar fluorescence intensities were accessible after 2 h for the **PQ-OH** releasing probe and after 6 h for the **MF-OH** releasing probe.

3. Relative kinetics of cyclisation

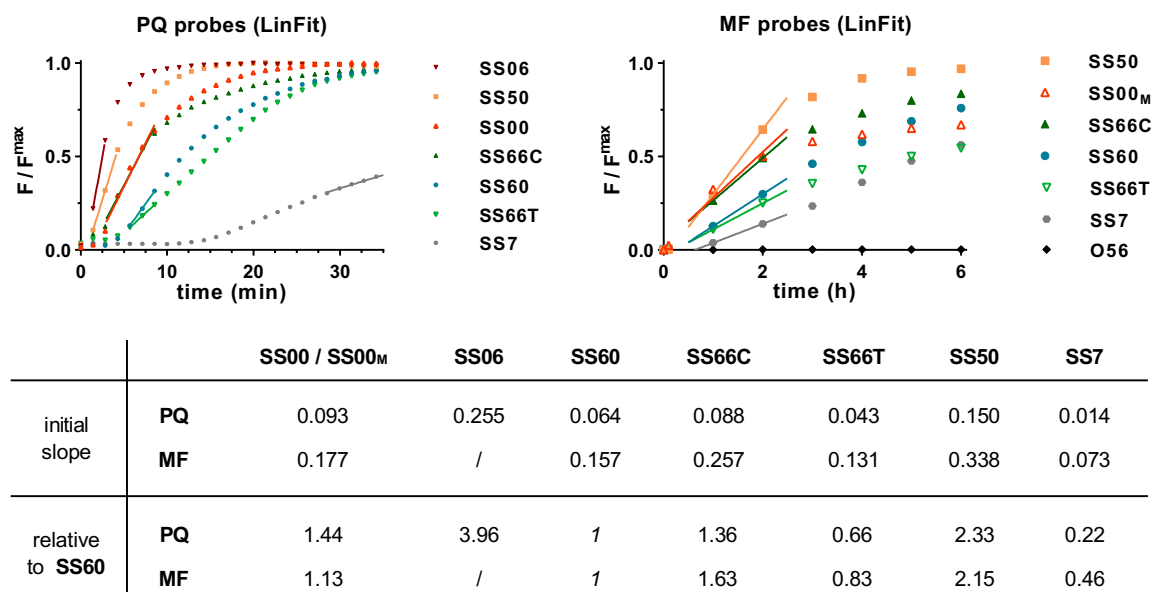


Figure S3: Linear fitting to initial release rates for relative rate comparison between triggers (see Fig 6b).

Approximate comparison of the cyclisation rates between different triggers (Fig 6b) was performed by linear fitting to the earliest linear region of initial signal generation timecourses upon treatment with excess of quantitative reductant tris(2-carboxyethyl)phosphine (TCEP) (Fig S3). The logic is that excess of TCEP should rapidly, quantitatively and irreversibly reduce the monomeric disulfide probes; and within a series, all elimination rates from the tetrahedral thiol cyclisation intermediate will be identical; so the relative linear fits should report on the relative rates of thiol cyclisation as long as the initial reduction is indeed rapid.

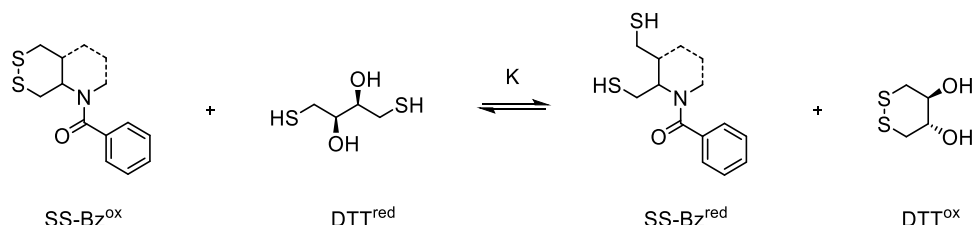
Relative trigger rates: (a) excellent agreement between the determined from each series of probes was found (Fig 6b, Fig S3) despite the very different actual release rates (that are modified by cargo elimination rate: faster for PQ, slower for MF). Other features of the relative rates that are of design interest include: (b) the rate of cyclisation of the SS50-type trigger is almost exactly twice that of SS00-type triggers, matching expectations as it has two rather than one cyclisable groups, but is otherwise identically disposed for cyclisation. The SS7-type trigger also has two cyclisable groups, but it is much slower than either SS50- or SS00-type trigger. We take this to reflect poor kinetics of TCEP reduction of the probe (note very slow reaction with DTT also in the equilibration tests); by analogy to previous work on SS50-type motifs¹¹ we assign this to oligomerised probe with poor reductant access. (c) Annelation-preorganised SS06-type trigger cyclisation is 3 times faster than that of linear SS00-type triggers. (d) The post-reduction intermediates (C in Fig 2b) of SS06-, SS66C-, and SS66T-type motifs should be roughly similar in their speed to cyclise; so do the post-reduction intermediates of SS60- and SS00-type. As significant differences are seen between these sets, we conclude that SS66T- and SS66C-type triggers are ca. 3-6-fold slower to be reduced by TCEP than SS06-type; while the SS60-type trigger is only ca. 20% slower to be reduced by TCEP than linear SS00-type triggers.

Relevance to Mechanism: With TCEP, SS60-PQ has ca. 12 min release half-time and SS60-MF ca. 200 min. The other triggers similarly have a ca. 16-fold faster rate as PQ-conjugates across all triggers. We conclude that the major rate-limiting aspect for signal generation with TCEP is thiol cyclisation and cargo elimination; and that this takes minutes to hours. Therefore we are confident that on-reductant cyclisation of the intermediates B and D (if either would directly cyclise to release PhOH before full reduction to C; Fig 2) is not a major contributor to released cargo quantities under expected lifetimes of the transthiolated intermediates (while we cannot estimate those lifetimes from our data, we note the work of Matile¹² measuring half-times of just 7 ms at 25 °C of a comparable intramolecular thiol/disulfide transthiolation as would be needed to regenerate A by retroaddition of B/D).

4. Evaluation of redox potentials using the SS-Bz series

General protocols

HPLC-grade MeOH and TE buffer (50 mM Tris-HCl, 1 mM EDTA, pH 7.4) were separately degassed by bubbling inert gas for 1 h. Solutions of **SS-Bz**^{ox} (2 mM or 5 mM in degassed MeOH) and DTT^{red} (2 mM, 5 mM or 10 mM in degassed TE) were prepared freshly, then in a pre-dried HPLC vial 75 μ L of the **SS-Bz**^{ox} solution was mixed with 75 μ L of DTT^{red} solution. Several HPLC based measurements were conducted with 10 μ L injecting volume at different timepoints. Relative ratio of **SS-Bz**^{ox} and **SS-Bz**^{red}, as well as DTT^{red} and DTT^{ox} calculated from the HPLC chromatogram areas.



The HPLC-based measurement of relative reduction potentials is based on the fully reversible bimolecular reaction equilibrium between oxidized disulfide-type probes tagged with a UV active tracer (**Bz**-Series) and the dithiol-type reducing agent DTT. Due to strong polarity differences disulfide and dithiol species can easily be separated by standard HPLC methods and well quantified by integration of the peaks' UV absorption traces at 210 nm for DTT or 230 nm for **SS-Bz** derivatives. Absorption spectra and intensities of oxidized/reduced species of DTT and the **SS-Bz** derivative were compared at the respective wavelength to ensure the suitability of the measurement for quantification. The method can only be applied if no other reaction products or UV active species are detected.

$$\text{(eq. 1)} \quad [\text{SS-Bz}^{\text{ox}}] + [\text{SS-Bz}^{\text{red}}] = [\text{SS-Bz}^{\text{start}}] \quad \text{and} \quad [\text{DTT}^{\text{ox}}] + [\text{DTT}^{\text{red}}] = [\text{DTT}^{\text{start}}]$$

$$\text{(eq. 2) for equimolar amounts:} \quad [\text{DTT}^{\text{ox}}] = [\text{SS-Bz}^{\text{red}}] \quad \text{and} \quad [\text{DTT}^{\text{red}}] = [\text{SS-Bz}^{\text{ox}}]$$

for equimolar amounts:

$$\text{with (eq. 2)} \quad E_{[\text{SS-Bz}]}^0 = E_{[\text{DTT}]}^0 - \frac{R \cdot T}{n \cdot F} \ln \frac{[\text{DTT}^{\text{red}}] = [\text{SS-Bz}^{\text{ox}}]}{[\text{DTT}^{\text{ox}}] = [\text{SS-Bz}^{\text{red}}]}$$

$$\text{with (eq. 1)} \quad E_{[\text{SS-Bz}]}^0 = E_{[\text{DTT}]}^0 - \frac{R \cdot T}{n \cdot F} \ln \frac{[\text{SS-Bz}^{\text{ox}}]^2}{[\text{SS-Bz}^{\text{red}}]^2}$$

$$\begin{aligned} \text{thus (eq. 3)} \quad E_{[\text{SS-Bz}]}^0 &= E_{[\text{DTT}]}^0 - \frac{R \cdot T}{n \cdot F} \ln \frac{\% \text{SS-Bz}^{\text{ox}} \cdot [\text{SS-Bz}^{\text{start}}]^2}{\% \text{SS-Bz}^{\text{red}} \cdot [\text{SS-Bz}^{\text{start}}]^2} \\ &= E_{[\text{DTT}]}^0 - \frac{R \cdot T}{n \cdot F} \ln \frac{\% \text{SS-Bz}^{\text{ox}}}{\% \text{SS-Bz}^{\text{red}}} \end{aligned}$$

for non-equimolar amounts:

$$\text{with (eq. 1)} \quad E_{[\text{SS-Bz}]}^0 = E_{[\text{DTT}]}^0 - \frac{R \cdot T}{n \cdot F} \ln \frac{\% \text{SS-Bz}^{\text{ox}} \cdot [\text{SS-Bz}^{\text{start}}] \cdot \% \text{DTT}^{\text{red}} \cdot [\text{DTT}^{\text{start}}]}{\% \text{SS-Bz}^{\text{red}} \cdot [\text{SS-Bz}^{\text{start}}] \cdot \% \text{DTT}^{\text{ox}} \cdot [\text{DTT}^{\text{start}}]}$$

$$\text{thus (eq. 4)} \quad E_{[\text{SS-Bz}]}^0 = E_{[\text{DTT}]}^0 - \frac{R \cdot T}{n \cdot F} \ln \frac{\% \text{SS-Bz}^{\text{ox}} \cdot \% \text{DTT}^{\text{red}}}{\% \text{SS-Bz}^{\text{red}} \cdot \% \text{DTT}^{\text{ox}}}$$

5. Evaluation of reduction mediated release

General protocol

Cell-free *in vitro* assays were performed to evaluate the fluorogenic probes' performance based on reduction-mediated (chemical reductants) release of their fluorescent cargo. The molecular process was monitored by fluorescence intensity increase based on the off-to-on mechanism both for **PQ-OH_(s)** (precipitation-based induction of ES IPT fluorescence monitored with ex/em 355bp10/520lp) and for **MF-OH_(aq)**, **IG-OH_(aq)** and **MR-NH_{2(aq)}** (conjugation-based induction of long-wavelength absorption and fluorescence monitored with ex/em 485bp10/520lp).

In a black 96-well plate with black bottom, 80 μ L of a diluted solution (12.5 μ M in aq. TE, pH 7.4, 1.25% DMSO) of the **PQ-**, **MF-**, **IG-** or **MR-**based fluorogenic probe (to reach a final concentration of 10 μ M) was mixed with 20 μ L of a solution of selected chemical reductants (50 μ M to 50 mM in aq. TE, pH 7.4 to reach 10 μ M to 10 mM). The reaction mixtures were incubated at 37 °C and 100% humidity for 6 h.

Timecourse measurements were conducted to determine kinetics of the reduction-mediated release. Data was interpreted by calculating the *absolute, time-dependent* fluorescence intensity normalised to the plateau signal observed in a reference maximum-fluorescence experiment **F^{max}(t)** that used incubation with an excess of tris(carboxyethyl)phosphine (TCEP) for **PQ**-probes. For **MF-**, **IG-** and **MR-**based probes the *absolute, time-dependent* fluorescence intensity was normalized according to a separate calibration experiment using the free, soluble fluorophores **MF-OH**, **IG-OH** and **MR-NH₂**.

Notes

Since small differences in assay setup affect the kinetics in the early phase, for each graph we report TCEP control reduction assays that were run on the same plate under the same conditions, rather than averaged behaviour from other runs. The TCEP run kinetics thus differ slightly between different reduction series tests, but can be used to more accurately compare to outcomes in the series reported. Further, we noted that upon standing, both **SS-50**-type and **SS-7**-type probe stocks had reduced capacity to generate fluorescence in reductant assays. This may be attributed to the formation of ring-opened and relatively hydrophobic polymer species with reduced accessibility to aqueous reductants, upon standing in concentrated solutions, as Houk and Whitesides observed for similar species.¹³ Consequently, their probe stocks were prepared freshly from the solids for all later assays. The linear or 6-membered disulfide probes did not display this instability.

Chemoreductants

reductant	c (mM)	eq. (reductant/probe)
TCEP	0.1 – 3	10 – 300
DTT	0.01 – 10	1 – 1000
DTT ^{ox}	1	100
GSH	0.01 – 10	1 – 1000
GSSG, Ser	1	100
Cys, NAC	1	100
MEDA, CA	1	100

TCEP: tris(carboxyethyl)phosphine, DTT: dithiothreitol (reduced), DTT^{ox}: dithiothreitol (oxidized), GSH: glutathione (reduced), GSSG: glutathione (oxidized), Cys: L-Cysteine, Ser: L-Serine, MEDA: mercaptoethyl-dimethylamine, CA: cysteamine and NAC: N-acetyl L-Cysteine.

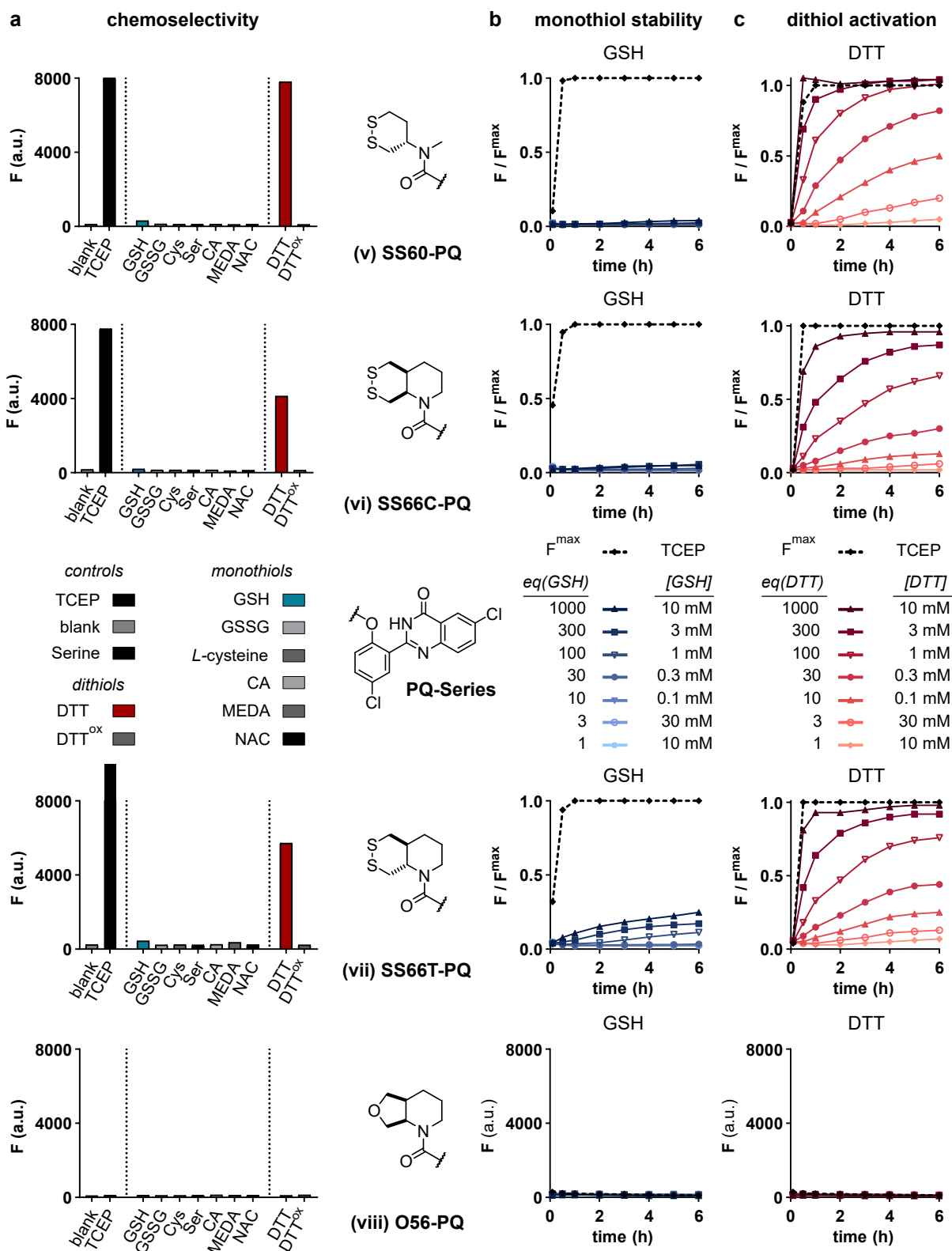


Fig. S5 Evaluation of reduction mediated cargo release of **(v) SS60-PQ**, **(vi) SS66C-PQ**, **(vii) SS66T-PQ** and **(viii) O56-PQ** (10 μ M in TE-buffer). **(a)** Fluorescence signal after 2 h upon incubation with the following reductants: TCEP (100 μ M), DTT (1 mM), DTT^{ox} (1 mM), GSH (1 mM), GSSG (1 mM), Cys (1 mM), Ser (1 mM), MEDA (1 mM), CA (1 mM) and NAC (1 mM) **(b)** Relative fluorescence signal 0-6 h upon incubation with **(c)** GSH and **(d)** DTT with increasing concentrations (10 μ M, 30 μ M, 100 μ M, 300 μ M, 1 mM, 3 mM and 10 mM) with respect to TCEP (100 μ M).

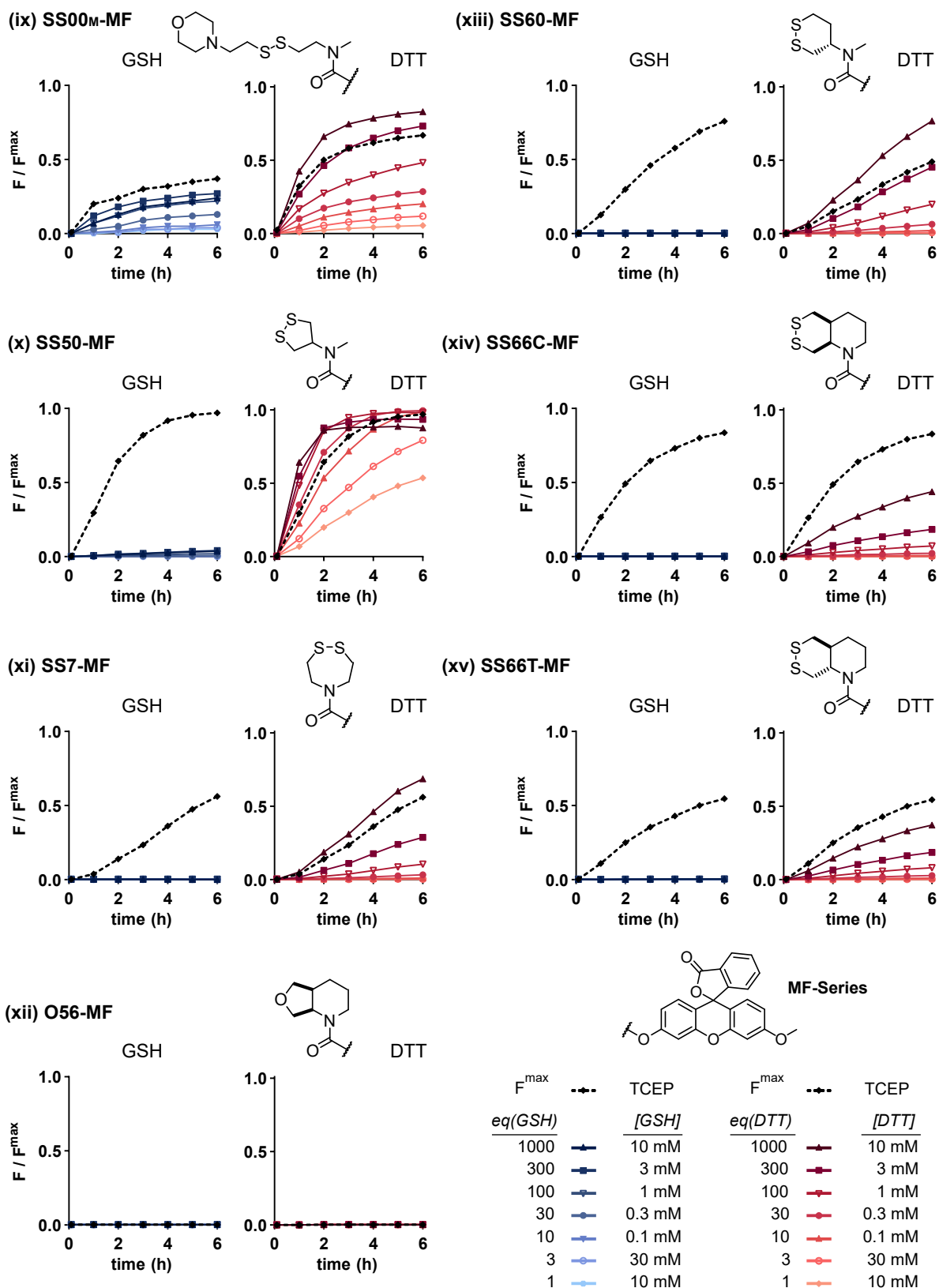
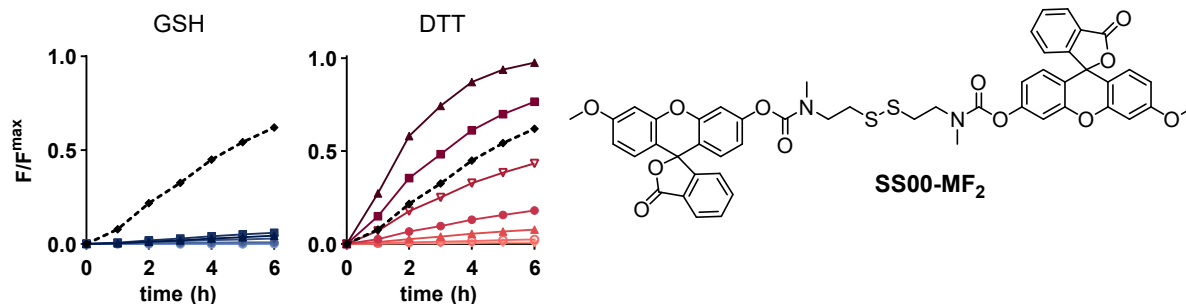
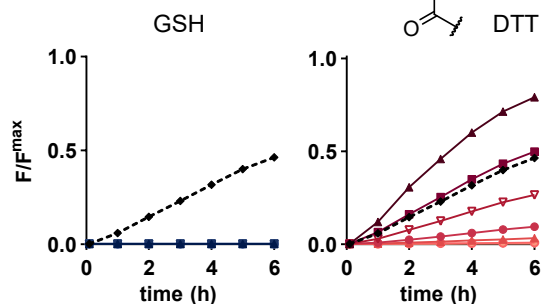


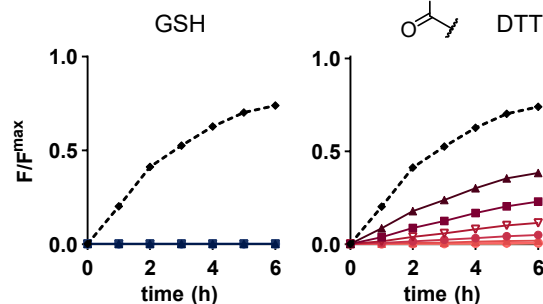
Fig. S6 Evaluation of reduction mediated cargo release of (ix) SS00M-MF, (x) SS50-MF, (xi) SS7-MF, (xii) O56-MF, (xiii) SS60-MF, (xiv) SS66C-MF and (xv) SS66T-MF (10 μ M in TE-buffer). Relative fluorescence signal (timecourse: 0-6 h) upon incubation with GSH and DTT with increasing concentrations (10 μ M, 30 μ M, 100 μ M, 300 μ M, 1 mM, 3 mM and 10 mM) with respect to TCEP (100 μ M) and normalized according to the calibration shown in Fig S2.

(xvi) SS00-MF₂


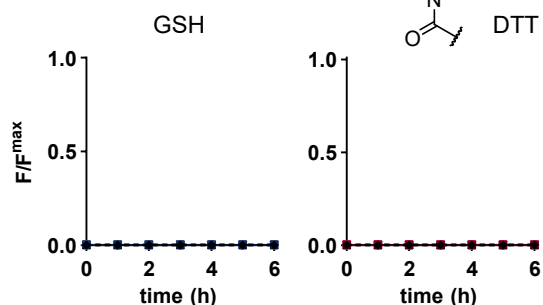
(xvii) SS60-IG



(xviii) SS66C-IG



(xix) O56-IG



(xx) SS60-MR

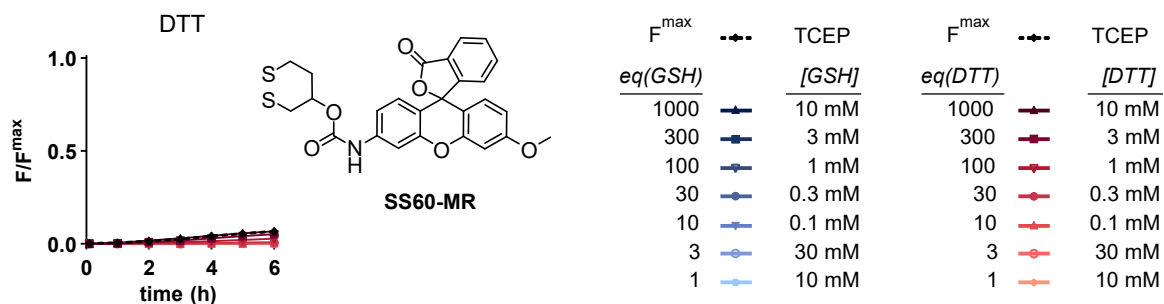


Fig. S7 Evaluation of reduction mediated cargo release of (xvi) SS00-MF₂, (xvii) SS60-IG, (xviii) SS66C-IG, (xix) O56-IG and (xx) SS60-MR (10 μ M in TE-buffer). Relative fluorescence signal (timecourse: 0-6 h) upon incubation with GSH and DTT with increasing concentrations (10 μ M, 30 μ M, 100 μ M, 300 μ M, 1 mM, 3 mM and 10 mM) with respect to TCEP (100 μ M) and normalized according to the calibration shown in Fig S2.

6. Enzyme specificity/activity study

General protocol

Cell-free *in vitro* enzyme specificity assays (bioreductants) were performed to evaluate the fluorogenic probes based on the reduction-mediated release of their fluorescent cargo after incubation with bioreductant cascade model systems. The molecular process was monitored by fluorescence intensity increase based on the off-to-on mechanism for **PQ-OH_(s)** (precipitation-based induction of ES IPT fluorescence monitored with ex/em 355bp10/520lp) or **MF-OH** (ex/em 485bp10/520lp).

In a black 96-Well Plate with black bottom, 50 μ L of a diluted solution (20 μ M or 2 μ M in aq. TE, pH 7.4, 2% DMSO to reach final concentrations of 1 μ M and 10 μ M respectively) of the fluorogenic probe was mixed with 40 μ L of the selected oxidoreductase enzyme (TrxR1, TrxR2, GR to reach final concentrations of 20 nM) and/or its respective native substrate (Trx1, Trx2, TRP14, Grx1, Grx2 to reach final concentrations of 10 nM to 10 μ M respectively). The biochemical reaction was started by addition of 10 μ L of a solution of β -NADPH (1 mM in aq. TE, pH 7.4 to reach final concentrations of 100 μ M). The reaction mixtures were incubated at 37 °C and 100% humidity for 6-12 h.

Timecourse measurements were conducted to determine kinetics of the reduction-mediated release. Data was interpreted by calculating the *absolute, time-dependent* fluorescence intensity **F (t)** (a.u.), that was (optionally for **PQ**-type probes) corrected by the background fluorescence **F^{NADPH} (t)** (a.u.) caused by autofluorescence of reduced β -NADPH. Results were compared to the expected maximum-fluorescence during a reference experiment **F^{max}(t)** that used incubation with an excess of tris(carboxyethyl)phosphine (200 μ M TCEP) for internal control.

Bioreductants

assay factor	c (μ M)	eq. (reductant/Probe)
NADPH	100	10
GSH	100	10
TrxR1, TrxR2	0.02	0.002
Trx1, Trx2, TRP14	0.01 – 10	0.001 - 1
GR	0.02	0.002
Grx1, Grx2	0.01 - 10	0.001 – 1

NADPH: β -Nicotinamide adenine dinucleotide phosphate, GSH: glutathione (reduced), TrxR1: recombinant human cytosolic TrxR, TrxR2: recombinant human mitochondrial isoform of TrxR, Trx1: recombinant human cytosolic thioredoxin (Trx), Trx2: recombinant human mitochondrial isoform of Trx, TRP14: recombinant human cytosolic thioredoxin-related protein of 14 kDa (TRP14), GR: recombinant human glutathione reductase (GR), Grx1: recombinant human cytosolic glutaredoxin (Grx1), Grx2: recombinant human cytosolic isoform of Grx.

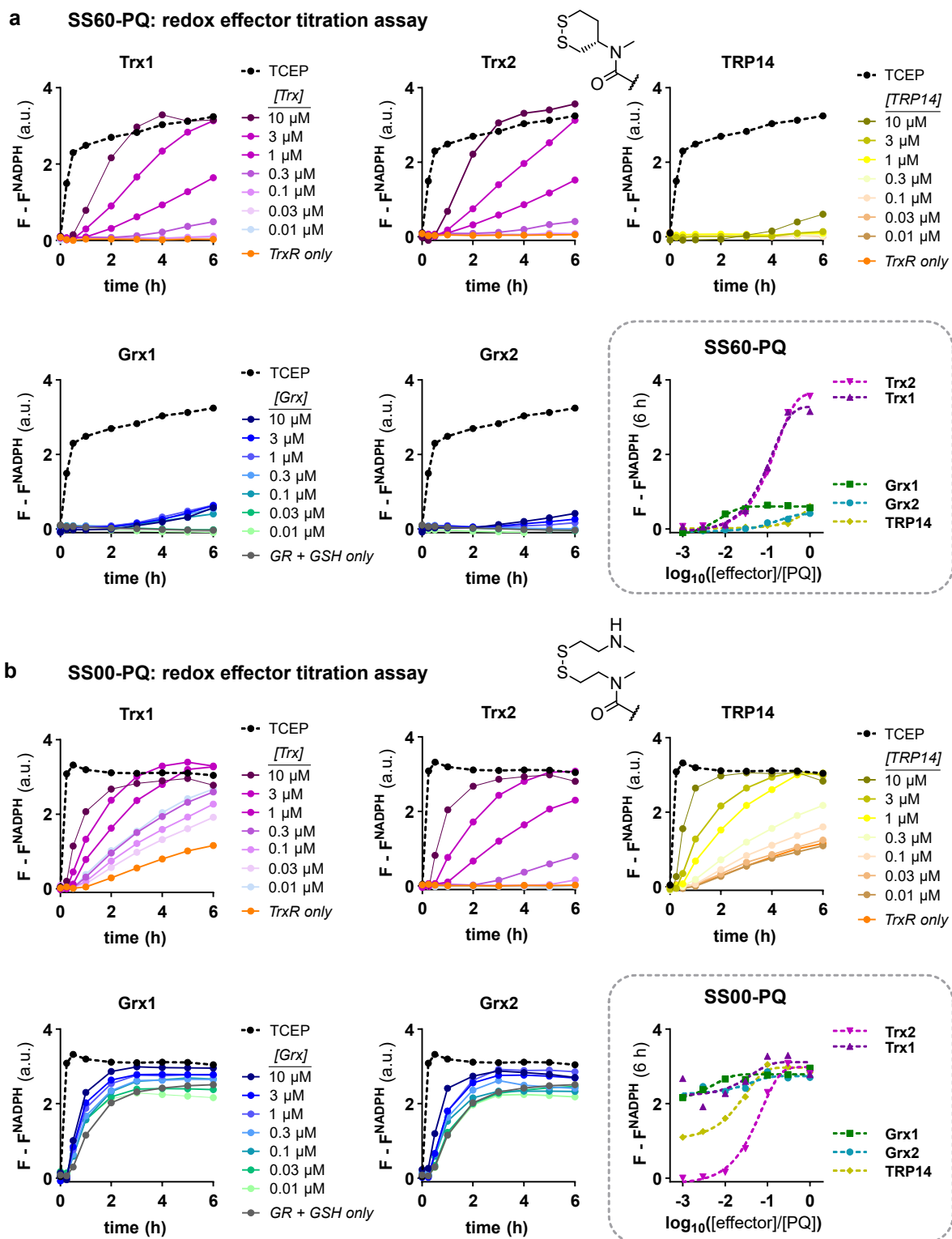


Fig. S8 Redox effector titration assay: **(a)** Timecourse fluorescence intensity ($t = 0-6$ h) of **SS60-PQ** (10 μM) upon incubation with Trx1, Trx2, TRP14, Grx1 or Grx2 (0.01-10 μM) as compared to a reference experiment: TCEP (200 μM). All mixtures additionally containing β -NADPH (100 μM) and the respective upstream system TrxR1, TrxR2 (20 nM) or GR (20 nM) + GSH (100 μM). **(b)** Same evaluation for **SS00-PQ** (10 μM).

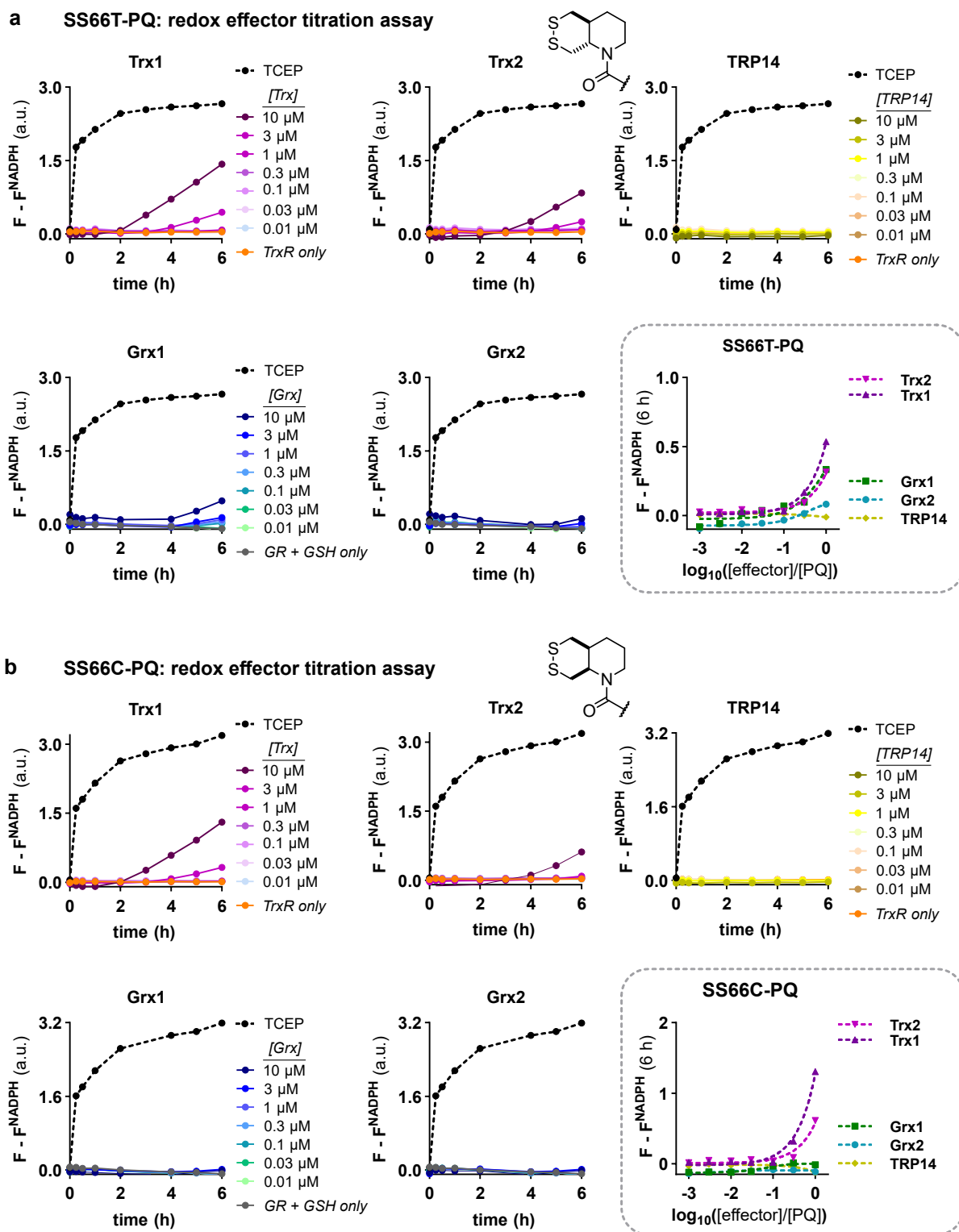
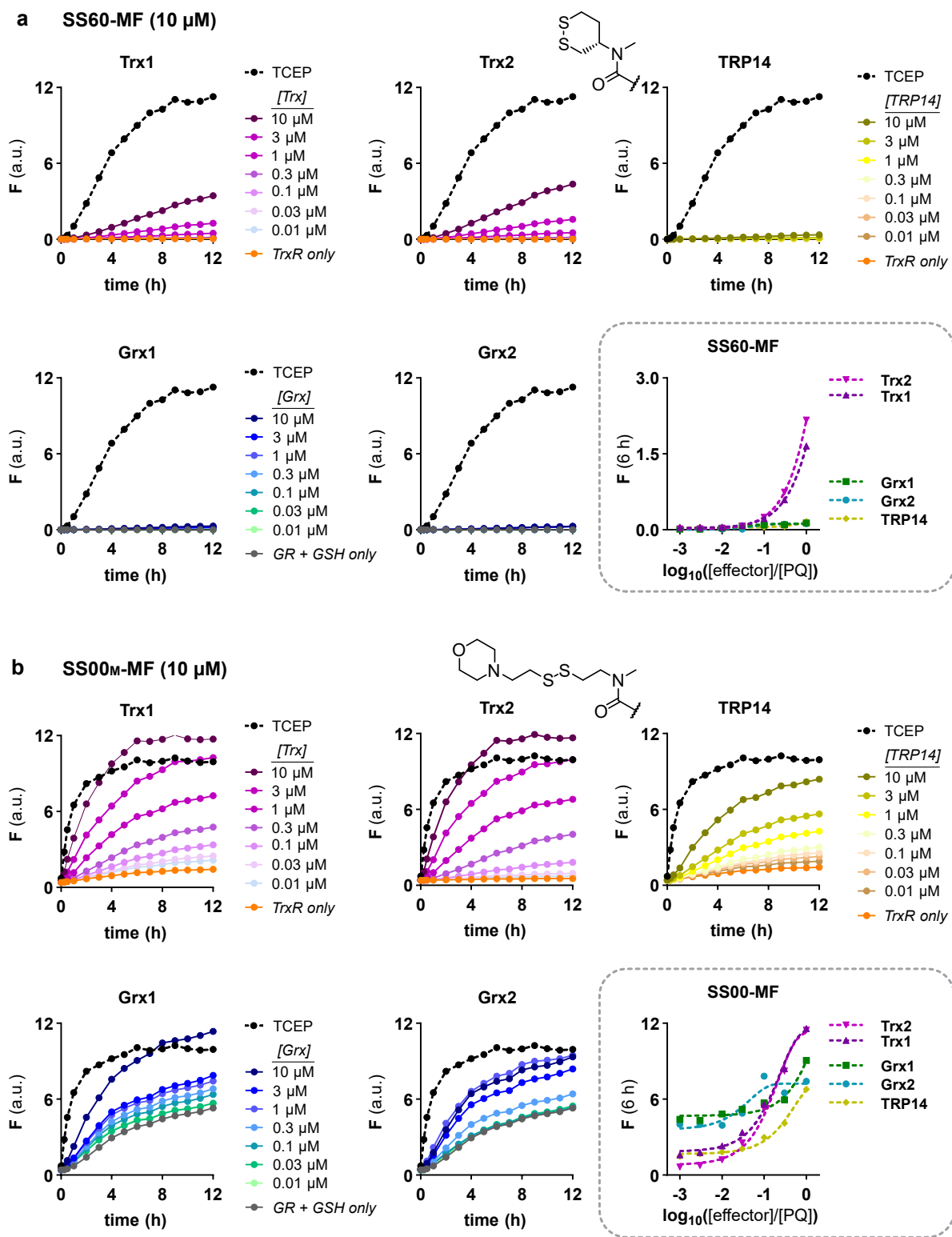
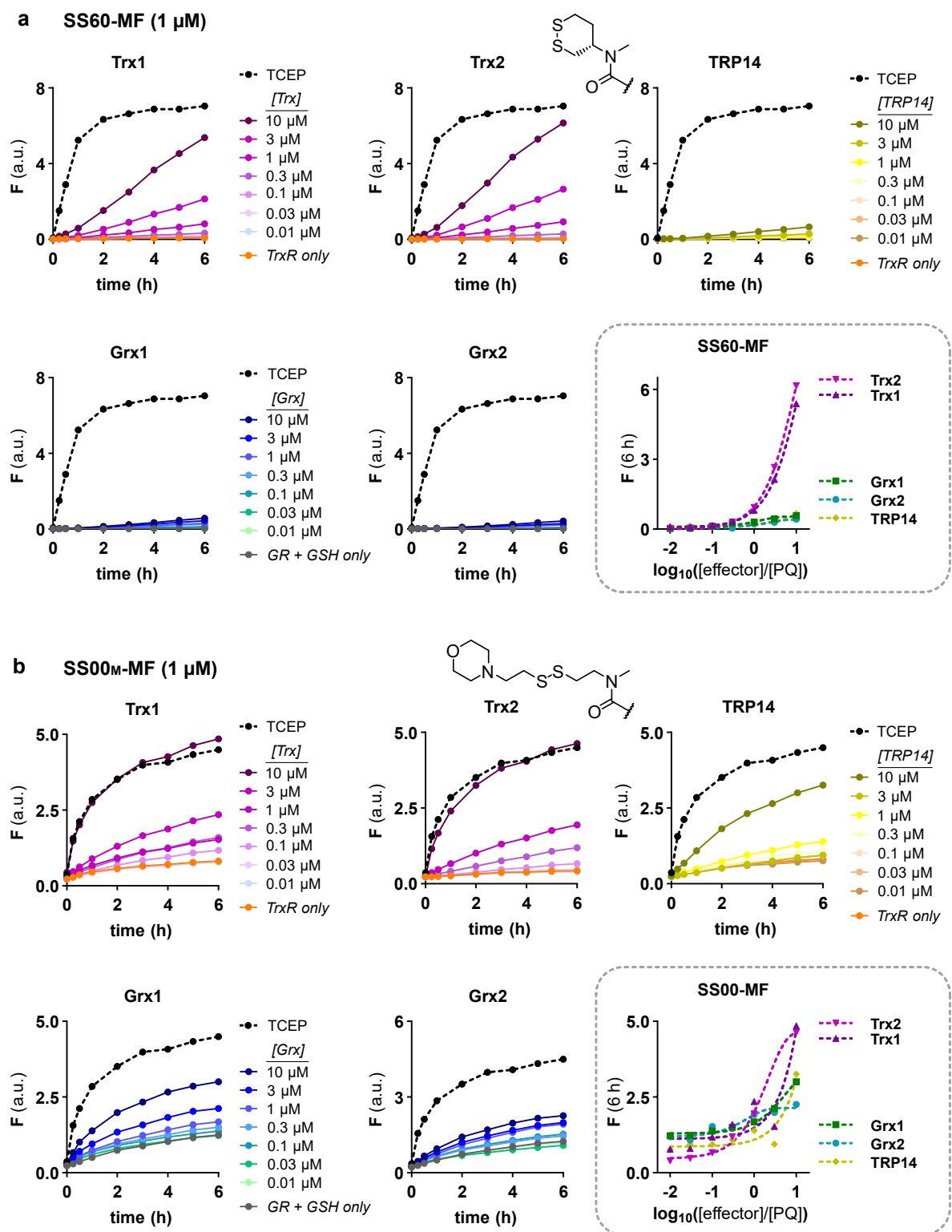
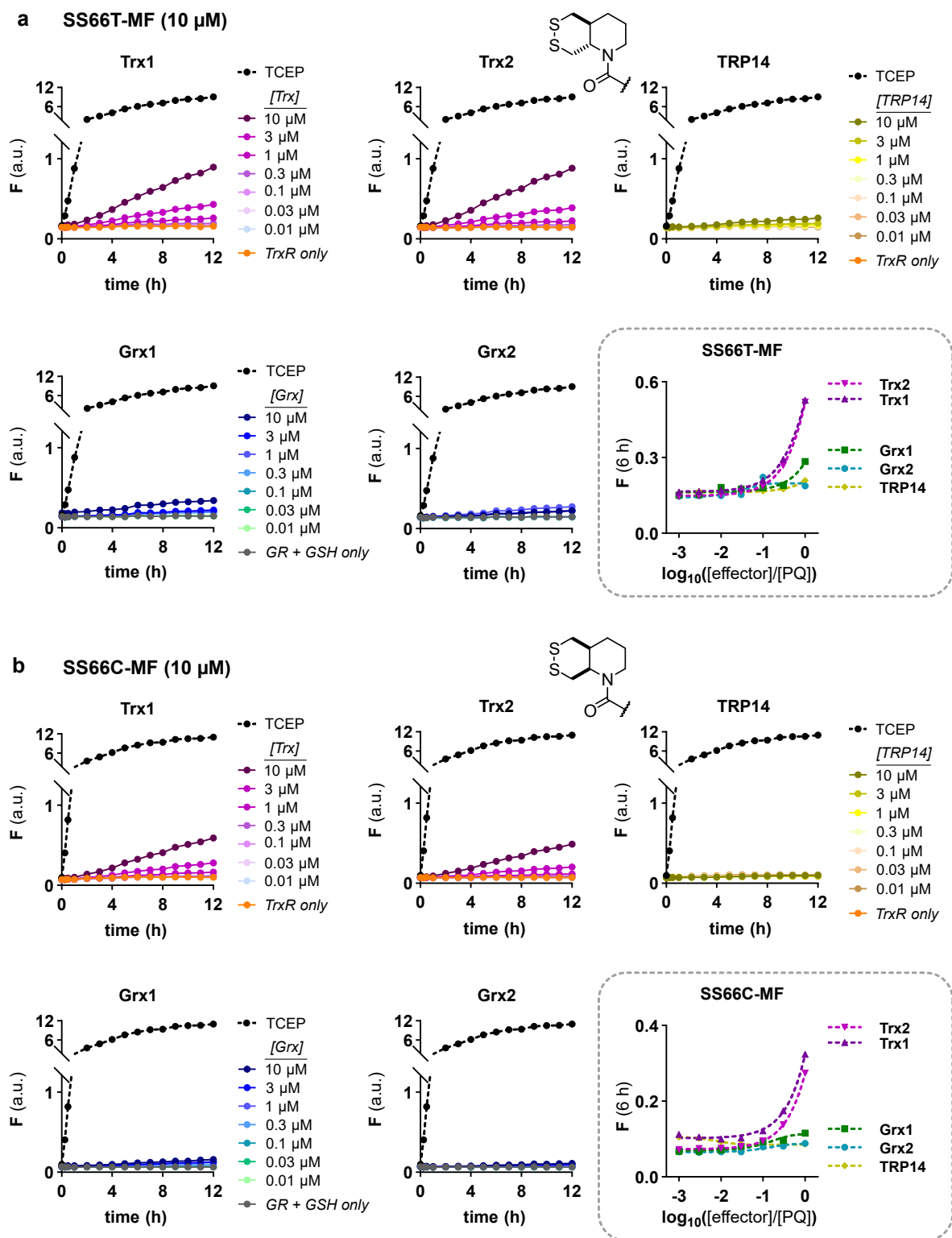


Fig. S9 Redox effector titration assay: **(a)** Timecourse fluorescence intensity ($t = 0-6$ h) of **SS66T-PQ** (10 μ M) upon incubation with Trx1, Trx2, TRP14, Grx1 or Grx2 (0.01-10 μ M) as compared to a reference experiment: TCEP (200 μ M). All mixtures additionally containing β -NADPH (100 μ M) and the respective upstream system TrxR1, TrxR2 (20 nM) or GR (20 nM) + GSH (100 μ M). **(b)** Same evaluation of **SS66C-PQ** (10 μ M).







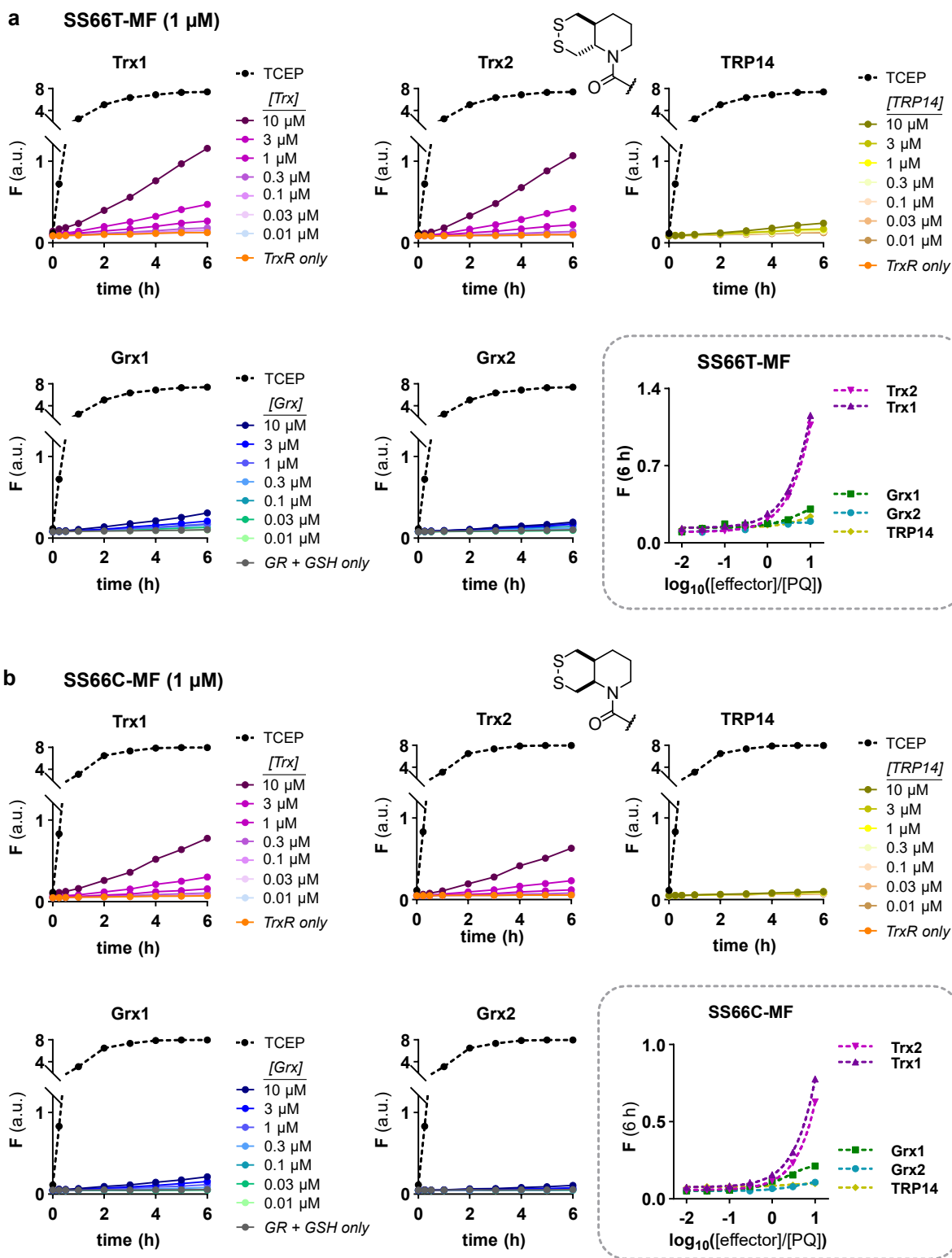


Fig. S13 Redox effector titration assay: **(a)** Timecourse fluorescence intensity ($t = 0-6$ h) of **SS66T-MF** (1 μ M) upon incubation with Trx1, Trx2, TRP14, Grx1 or Grx2 (0.01-10 μ M) as compared to a reference experiment: TCEP (200 μ M). All mixtures additionally containing β -NADPH (100 μ M) and the respective upstream system TrxR1, TrxR2 (20 nM) or GR (20 nM) + GSH (100 μ M). **(b)** Same evaluation of **SS66C-MF** (1 μ M).

7. General methods

6.1 Enzyme biochemistry

For early enzymatic activation profiling we used human natively isolated cytosolic thioredoxin 1 (hTrx1), native thioredoxin reductase 1 (hTrxR1) natively isolated from human placenta,¹⁴ recombinant human thioredoxin reductase 1 point mutant (U498C mutant – hTrxRU498C)¹⁵ and recombinant human glutathione reductase (hGR).¹⁶

For early redox effector titrations we used human recombinant thioredoxin 1 (Trx1) (lyophilized), recombinant human glutaredoxin 1 (Grx1) (lyophilized from 10 μ L TE-buffer, pH 7.5), human thioredoxin reductase (TrxR1) (0.6 mg/mL in 50% glycerol/TE-buffer, pH 7.5) and baker's yeast glutathione reductase (GR) (100 μ M in 50% glycerol/TE-buffer, pH 7.5) as obtained from *IMCO Corp.*, Stockholm (Sweden).

For final redox effector titrations (including **Fig 7**, **Fig S8-S13**) we used recombinant human proteins expressed in *E. coli*: thioredoxin 1 (Trx1) in 50 mM Tris, 2 mM EDTA, pH 7.5, recombinant thioredoxin 2 (Trx2) in 100 mM Tris, 500 mM NaCl, 2 mM EDTA, 30% glycerol, pH 7.5, thioredoxin-related protein 14 (TRP14) in 100 mM Tris, 300 mM NaCl, 2 mM EDTA, 30% glycerol, pH 7.5, glutaredoxin 1 (Grx1) in TES buffer, 30% glycerol, pH 7.5 and recombinant human glutaredoxin 2 (Grx2) in 100 mM Tris, 2 mM EDTA, pH 7.5, enabled by the upstream reductases selected from thioredoxin reductase 1 (TrxR1) in 100 mM Tris, 2 mM EDTA, 50% glycerol, pH 7.5, thioredoxin reductase 2 (TrxR2) in 100 mM Tris, 2 mM EDTA, 50% glycerol, pH 7.5 or glutathione reductase (GR) in 50 mM Tris, 100 mM NaCl 2 mM EDTA, 50% glycerol, pH 7.5.

6.2 Fluorescence spectroscopy and detection

Fluorescence spectroscopy measurements were conducted using a *Varian Cary Eclipse* fluorescence spectrophotometer from *Agilent Technologies Inc.*, Santa Clara (USA) at 298 K either using a constant excitation mode (e.g. ex 355 nm) with emission fluorescence intensity screening or alternatively a constant emission mode (e.g. em 520 nm) with excitation efficiency screening mode. For exemplary timecourse measurements of emission spectra a constant excitation mode (355 nm for **SS60-PQ** and 485 nm for **SS50-MF**) was used.

Raw fluorescence readout of cell-free activity was performed either using a *FluoStar Omega* plate reader from *BMG Labtech*, Ortenburg (Germany), a *Tecan Infinite M200Pro* plate reader from Tecan, Maennedorf, Switzerland, set to exc: 355bp10 and em: 520lp or to ex: 485bp10 and em: 520lp recording fluorescence intensity.

6.3 Laboratory techniques

All solvents, reagents and building blocks were purchased from standard commercial sources. Anhydrous solvents obtained in septum-capped bottles and analytical grad or higher quality solvents were used without purification. Industrial grade solvents were distilled prior to use. Unless otherwise stated, reactions were performed at room temperature without precautions regarding air or moisture and were stirred using a magnetic Teflon[®]-coated stir bars. Air or moisture sensitive reactions were conducted in dry Schlenk glassware.

Flash column chromatography (FCC) was performed on *Geduran[®] Si 60* silica gel from *Merck GmbH*, Darmstadt (Germany) an optionally conducted using a *Biotage[®] Select* automated column chromatography system from *Biotage GmbH*, Uppsala (Sweden). Unless stated otherwise, and thin layer chromatography (TLC) to monitor reactions and determine R_f values was performed on silica coated aluminium sheets with fluorescent indicator (*TLC Silica gel 60 F254* from *Merck GmbH*, Darmstadt, Germany) with visualisation by UV irradiation (254 nm/360 nm) or staining with KMnO_4 solution (3.0 g KMnO_4 , 20 g K_2CO_3 , 0.30 g KOH, 0.30 L H_2O).

6.4 Analytical methods

High resolution mass spectrometry (**HRMS**) was conducted either using a *Thermo Finnigan LTQ FT Ultra FourierTransform* ion cyclotron resonance spectrometer from *ThermoFisher Scientific GmbH*, Dreieich (Germany) applying electron spray ionisation (ESI) with a spray capillary voltage of 4 kV at temperature 250 °C with a method dependent range from 50 to 2000 u or a *Finnigan MAT 95* from *Thermo Fisher Scientific*, Dreieich (Germany) applying electron ionisation (EI) at a source temperature

of 250 °C and an electron energy of 70 eV with a method dependent range from 40 to 1040 u. All reported m/z values refer to positive ionization mode, unless stated otherwise.

Nuclear magnetic resonance (**NMR**) spectroscopy was performed using a *Bruker Avance* (600/150 MHz, with *TCl cryoprobe*) or a *Bruker Avance III HD Biospin* (400/100 MHz, with BBFO cryoprobeTM) from Bruker Corp., Billerica (USA) either at 400 MHz or 500 MHz. ¹⁹F-NMR spectra were recorded on a *Bruker Avance III* spectrometer (400 MHz for ¹H; 377 MHz for ¹⁹F). NMR-spectra were measured at 298 K, unless stated otherwise, and were analysed with the program *Mestrelab Nova 12* developed by *Mestrelab Ltd.*, Santiago de Compostela (Spain). ¹H-NMR spectra chemical shifts (δ) in parts per million (ppm) relative to tetramethylsilane ($\delta = 0$ ppm) are reported using the residual protic solvent (CHCl₃ in CDCl₃: $\delta = 7.26$ ppm, DMSO-d₅ in DMSO-d₆: $\delta = 2.50$ ppm, CHD₂OD in CD₃OD: $\delta = 3.31$ ppm) as an internal reference. For ¹³C-NMR spectra, chemical shifts in ppm relative to tetramethylsilane ($\delta = 0$ ppm) are reported using the central resonance of the solvent signal (CDCl₃: $\delta = 77.16$ ppm, DMSO-d₆: $\delta = 39.52$ ppm, CD₃OD: $\delta = 49.00$ ppm) as an internal reference. For ¹H-NMR spectra in addition to the chemical shift the following data is reported in parenthesis: multiplicity, coupling constant(s), number of hydrogen atoms and, if available, assignment. The abbreviations for multiplicities and related descriptors are s = singlet, d = doublet, t = triplet, q = quartet, p = pentuplet, hept = heptet or combinations thereof, m = multiplet and br = broad. The numbering scheme used for the assignments is specified in each case in a figure depicting the respective molecular structure and does not follow any convention. The reported assignments are supported by 2D-NMR experiments (HMBC, HSQC, COSY). Where known products matched literature analysis data, only selected data acquired are reported.

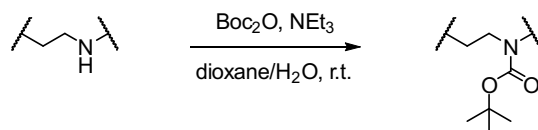
Analytical high pressure liquid chromatography (**HPLC**) analysis was conducted either using an *Agilent 1100* system from *Agilent Technologies Corp.*, Santa Clara (USA) equipped with a DAD detector and a *Hypersil Gold* HPLC column from *ThermoFisher Scientific GmbH*, Dreieich (Germany) or a *Agilent 1200 SL* system *Agilent Technologies Corp.*, Santa Clara (USA) equipped with a DAD detector, a *Hypersil Gold* HPLC column from *ThermoFisher Scientific GmbH*, Dreieich (Germany) and consecutive low-resolution mass detection using a LC/MSD IQ mass spectrometer applying ESI from *Agilent Technologies Corp.*, Santa Clara (USA). For both systems mixtures of water (analytical grade, 0.1% formic acid) and MeCN (analytical grade, 0.1% formic acid) were used as eluent systems.

Single crystal **X-Ray** crystallography was conducted using a *Bruker D8 Venture TXS* system from *Bruker Corp.*, Billerica (USA) equipped with a multilayer mirror monochromator and a Mo K α rotating anode X-ray tube ($\lambda = 0.71073$ Å). The frames were integrated with the *Bruker SAINT* software package (Bruker, 2012. SAINT. Bruker AXS Inc., Madison, Wisconsin, USA). Data were corrected for absorption effects using the Multi-Scan method (SADABS) (Sheldrick, G. M., 1996. SADABS. University of Goettingen, Germany). The structures were solved and refined using the *Bruker SHELXTL* Software Package.¹⁷ The figures have been drawn at the 50% ellipsoid probability level.¹⁸ Crystallographic data have been deposited with the *Cambridge Crystallographic Data Centre, CCDC*, 12 Union Road, Cambridge CB21EZ, UK. Copies of the data can be obtained free of charge on quoting the depository numbers CCDC 2072440 (**5**), 2072441 (**66**), 2072442 (**65**), 2072438 (**67**), 2072439 (**75**). (<https://www.ccdc.cam.ac.uk/structures/>).

8. Synthetic Procedures

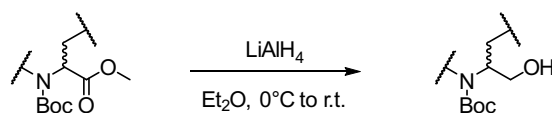
8.1. General protocols

General protocol A: Amine protection with di-*tert*-butyl dicarboxylate. (*N*-Boc protection)



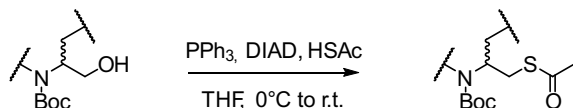
To a 0.25–0.5 M solution of the primary or secondary amine (1.0 eq.) in a mixture of dioxane/water (1:1) was added NEt₃ (1.3 eq per amino group) and a 0.5 M solution of di-*tert*-butyl dicarbonate (1.0 eq. per amino group) in 1,4-dioxane and the resulting biphasic solution was stirred at r.t. for 15 h. The reaction mixture was acidified to pH < 4 with 2 M aq. HCl and diluted with EtOAc. The organic phase was separated, washed with sat. aq. NaCl and the combined aqueous layers were extracted with EtOAc (3×). The combined organic layers were dried over Na₂SO₄ and concentrated to afford the desired *N*-Boc protected amine. If necessary, the crude product was further purified by FCC or recrystallization.^{19,20}

General protocol B: Reduction of dicarboxylic acid diesters with LiAlH₄.



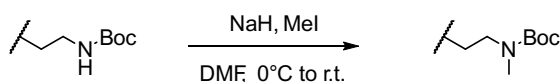
To a 0.2 M suspension of LiAlH₄ (3.0 eq.) in anhydrous Et₂O or THF under nitrogen atmosphere at 0 °C was dropwise added a 0.2 M solution of dimethyl dicarboxylate (1.0 eq.) in anhydrous Et₂O with vigorous stirring. The reaction mixture was stirred for 30 min at 0 °C, was then allowed to warm to r.t. and was further stirred at r.t. for 1 h, before water (1 mL per 1 mmol substrate) was carefully added at 0 °C. This was followed by addition of 2 M aq. NaOH until the grey suspension cleared and a colourless solid formed. Then, Na₂SO₄ (20 g per 1 mmol substrate) was added, the mixture was filtered and the solids were washed with EtOAc. The filtrate was concentrated under reduced pressure to afford the desired product, which was used without further purification.

General protocol C: Thioacetate formation by Mitsunobu reaction.

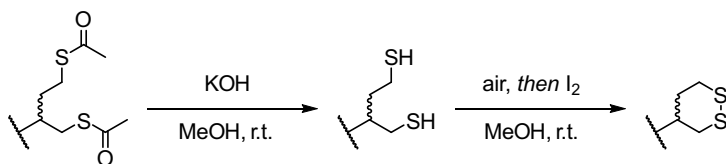


To PPh₃ (1.2 eq. per hydroxy group) in anhydrous THF (0.25 M) under nitrogen atmosphere was dropwise added DIAD (1.25 eq. per hydroxy group) at 0 °C. After the reaction mixture had stirred for 30 min, a 0.3 M solution of the alcohol or diol (1.0 eq.) in anhydrous THF and successively neat HSAC (1.25 eq. per hydroxy group) were added dropwise and immediate change of colour was observed. The reaction mixture was further stirred at 0 °C for 1 h, was then allowed to warm to r.t. and was further stirred for 15 h. All volatiles were removed under reduced pressure and the residue was purified by FCC.

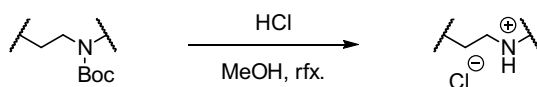
General protocol D: Monomethylation of *N*-Boc protected amines.



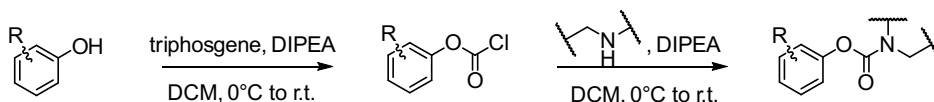
To a 0.02 M solution of the *N*-Boc amine (1.0 eq.) in anhydrous DMF under nitrogen atmosphere at 0 °C was portionwise added 60% NaH dispersion in mineral oil (1.1 eq. per amino group), followed by iodomethane (1.2 eq. per amino group). The reaction mixture was stirred at 0 °C for 30 min, was then allowed to warm to r.t. and stirred until complete reaction turnover was confirmed by thin layer chromatography. The mixture was diluted with EtOAc and washed with sat. aq. NaCl (2×). The combined aqueous layers were extracted with EtOAc (3×) and the combined organic layers were dried over Na₂SO₄, filtered and concentrated under reduced pressure to afford the crude product as a colourless oil/solid, which was further purified by FCC.²¹

General protocol E: Thioester cleavage and dithiol oxidation.

The (bis-)ethanthioate (1.0 eq.) was dissolved in a 0.17 M methanolic KOH solution (4.0 eq.) and mixture was stirred open to air for 15 h. Then, the mixture was concentrated under reduced pressure, diluted with water and extracted with EtOAc (3×). The combined organic layers were dried over Na₂SO₄ and concentrated under reduced pressure to afford the desired product, which was used without further purification. In case of incomplete oxidation of the intermediate thiol/dithiol, a 0.5 M solution of I₂ in MeOH was added dropwise until a permanently coloured solution was observed, before the reaction mixture was concentrated. Dilute aq. Na₂S₂O₃ was used to quench excess of I₂ during the aq. workup.²²

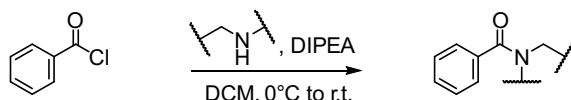
General protocol F: Amine deprotection.

To a 0.05 M solution of the *N*-Boc amine (1.0 eq.) in anhydrous MeOH was added a 1.25 M methanolic solution of HCl (10 eq.) and the mixture was heated to reflux for 2 h. Then, all volatiles were removed under reduced pressure and the remaining hydrochloride salt was used without further purification.

General protocol G: Chloroformate formation with triphosgene and carbamate coupling.

Step 1: To a 0.04 M solution of the phenol (1.0 eq.) in anhydrous DCM under nitrogen atmosphere at 0 °C was added a 0.2 M solution of triphosgene (BTC) (1.2 eq.) in anhydrous DCM, followed by a 0.1 M solution of DIPEA (4 eq.) in anhydrous DCM. The resulting mixture was stirred at 0 °C for 30 min, was then allowed to warm to r.t. and was further stirred for 1.5 h. All volatiles were evaporated by applying high vacuum to afford the corresponding chloroformate derivative was redissolved in anhydrous DCM to obtain a 0.015 M solution of the corresponding chloroformate intermediate (assuming quantitative conversion of the phenol substrate). The volatiles were collected in a liquid nitrogen trap and residual phosgene was discharged by subsequently adding a 2 M aq. NaOH and piperidine.

Step 2: To a 0.1 M suspension of the secondary amine or its hydrochloride salt (1.0 eq.) in anhydrous DCM was added DIPEA (1.2 eq.). The resulting solution was added dropwise at 0 °C to the 0.015 M chloroformate solution (1.0 eq.) obtained in step 1 and the mixture was stirred at 0 °C for 15 min before additional DIPEA (1.0 eq.) was added, then mixture was then allowed to warm to r.t. and was further stirred for 1.5 h. After stirring at r.t. for 45 min, sat. aq. NaHCO₃ was added. The mixture was diluted with DCM and the layers were separated. The organic layer was washed with sat. aq. NaCl and the combined aq. layers were extracted with DCM (2×). The combined organic layers were dried over Na₂SO₄, filtered and concentrated under reduced pressure to afford the crude product as a coloured solid. The residue was purified by FCC.

General protocol H: Amide coupling with benzoyl chloride.

To a 0.1 M suspension of the secondary amine or its hydrochloride (1.0 eq.) in anhydrous DCM were added NEt₃ (2.0 eq.) and benzoyl chloride (2.0 eq.). The mixture was stirred for 2 h, concentrated under reduced pressure and the residue was purified by FCC.

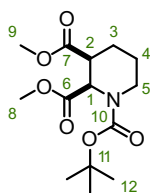
8.2. Trigger synthesis

Annulated SS66-type precursor**dimethyl *cis*-piperidine-2,3-dicarboxylate (13)**

To a solution of dimethyl pyridine-2,3-dicarboxylate **1** (8.00 g, 41.0 mmol) in MeOH (35 mL) was added 96% H₂SO₄ (0.22 mL, 4.1 mmol) and 10% Pd/C (250 mg, 0.235 mmol). The mixture was stirred under hydrogen atmosphere (40 bar) for 15 h, filtered over Celite® and concentrated to afford **13** (8.09 g, 40.2 mmol 98%) as a colourless oil.²³

TLC R_f = 0.50 (DCM:MeOH, 50:1). **HRMS** (ESI): C₉H₁₆NO₄⁺: [M+H]⁺ calc. 202.10738, found 202.10734.

¹H-NMR (400 MHz, CDCl₃): δ (ppm) = 3.73 (s, 3H), 3.68 (s, 3H), 3.63 (d, *J* = 3.5 Hz, 1H), 3.10 – 2.95 (m, 2H), 2.76 – 2.62 (m, 1H), 2.22 – 2.11 (m, 1H), 2.07 (s, 1H), 1.84 – 1.71 (m, 1H), 1.61 – 1.41 (m, 2H). **¹³C-NMR** (101 MHz, CDCl₃) δ (ppm) = 173.3 (C=O), 172.6 (C=O), 59.5 (CH), 52.2 (CH₃), 52.0 (CH₃), 45.4 (CH₂), 42.3 (CH), 26.1 (CH₂), 23.5 (CH₂).

dimethyl *cis*-*N*-Boc-piperidine-2,3-dicarboxylate (2)

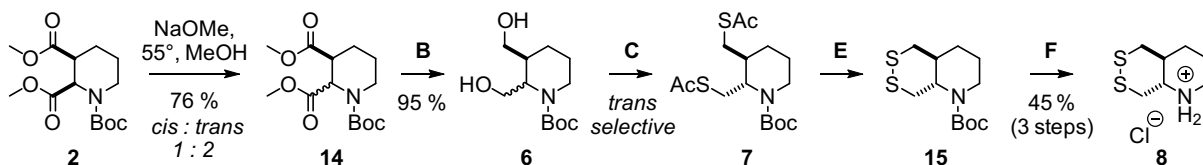
Prepared from **13** (3.00 g, 14.9 mmol) according to **general protocol A**. Compound **2** (4.43 g, 14.7 mmol, 99%) was obtained as a colourless solid after FCC (isohexane/EtOAc).

TLC R_f = 0.35 (isohexane:EtOAc, 2:1). **HRMS** (ESI⁺): C₁₄H₂₃NNaO₆⁺ [M+Na]⁺: calc. 324.14176, found 324.14165.

Individual rotamers were observed by NMR spectroscopy at 298 K and time-averaged spectra were obtained at 373 K.

¹H-NMR (400 MHz, tetrachlorethane-*d*₂, 373 K): δ (ppm) = 5.32 (s, 1H, 1-H), 4.05 – 3.87 (m, 1H, 5-H_A), 3.68 (s, 3H, 8-H), 3.66 (s, 3H, 9-H), 2.85 – 2.71 (m, 1H, 5-H_B), 2.59 (ddd, *J* = 12.7, 5.0, 3.6 Hz, 1H, 2-H), 2.11 – 1.92 (m, 1H, 3-H_A), 1.74 – 1.66 (m, 1H, 4-H_A), 1.61 (td, *J* = 13.3, 3.9 Hz, 1H, 3-H_B), 1.45 (s, 9H, 12-H), 1.44 – 1.36 (m, 1H, 4-H_B).

¹³C-NMR (101 MHz, tetrachlorethane-*d*₂, 373 K): δ (ppm) = 171.7 (C=O, C6), 170.3 (C=O, C7), 155.0 (C=O, C10), 80.5 (C(CH₃)₃, C11), 55.9 (CH, C1), 51.9 (CH₃, C9), 51.7 (CH₃, C8), 43.5 (CH, C2), 41.3 (CH₂, C5), 28.5 (C(CH₃)₃, C12), 24.3 (CH₂, C4), 22.6 (CH₂, C3).

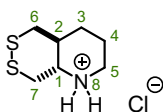
SS66T-type precursor***trans*-hexahydro-[1,2]dithiino[4,5-*b*]pyridine hydrochloride (8)**

Step 1: A mixture of **2** (5.33 g, 17.7 mmol, 1.0 eq.), anhydrous MeOH (50 mL) and NaOMe (1.15 g, 21.2 mmol, 1.2 eq.) was stirred under nitrogen atmosphere at 55 °C for 15 h, before AcOH (1.52 mL, 26.5 mmol, 1.5 eq.) was added and all volatiles were removed under reduced pressure. The residue was suspended in DCM and filtered. The solids were rinsed with a small amount of DCM and discarded. The filtrate was diluted with hexane and directly purified by FCC (isohexane:EtOAc, 4:1) to afford a *cis/trans* mixture of *N*-Boc dimethyl piperidine-2,3-dicarboxylate **14** (4.08 g, 13.5 mmol, 76%; 62% *trans*) as a yellowish oil. The *cis/trans* ratio was determined to be 0.6 (*cis*):1.0 (*trans*) by ¹H-NMR spectroscopy (CDCl₃) at 298 K based on the intensity of the signals at 5.50 and 5.26 ppm (*cis*) and the signal at 5.40 ppm (*trans*).

Step 2: To a suspension of LiAlH₄ (1.54 g, 40.6 mmol, 3.0 eq.) in anhydrous THF (80 mL) at 0 °C under nitrogen atmosphere was dropwise added a solution of the material obtained in step 1 (4.08 g, 13.5 mmol, 1.0 eq.) in anhydrous THF (5.5 mL). The mixture was stirred for 30 min, the cooling bath was removed and stirring continued for 2 h at r.t.. The mixture was again cooled to 0 °C, then EtOAc (5 mL), MeOH (5 mL), water (10 mL) and 2 M aq. NaOH (10 mL) were added carefully in the specified order. The cooling bath was removed and the mixture was stirred at r.t. for 1 h, before being filtered. The solids were washed with a small amount of THF and discarded. The filtrate was evaporated under reduced pressure, Et₂O (50 mL) and Na₂SO₄ (30 g) were added and the mixture was filtered. The solids were washed with Et₂O and discarded. The filtrate was evaporated under reduced pressure and remaining yellowish oil containing **6** (3.16 g, 12.9 mmol, 95%) was used in the next step without further purification.

Step 3: The material obtained in step 2 (2.35 g, 9.58 mmol) was treated according to **general protocol C**. The diol solution and the HSAc were premixed and added to the reaction mixture simultaneously instead of successively. Instead of purification by FCC the residue obtained after removal of the volatiles was suspended in a mixture of Et₂O/isohexane (1:2, 150 mL) and filtered. The solids were washed with additional Et₂O/hexane (1/2, 60 mL) and discarded. The filtrate was evaporated under reduced pressure, isohexane (50 mL) was added and the mixture was filtered again. The solids were washed with a small amount of isohexane and discarded. The filtrate was evaporated under reduced pressure and the remaining yellow oil containing **7** (4.93 g) was used in the next step without purification.

Step 4: The material obtained in step 3 was dissolved in MeOH (200 mL) and KOH (1.68 g, 29.9 mmol) was added. The mixture was stirred open to air for 15 h, before AcOH (1.72 mL, 30.1 mmol) was added and all volatiles were removed under reduced pressure. The residue was suspended in EtOAc (40 mL) and filtered. The solids were washed with additional EtOAc (2×20 mL) and discarded. The filtrate was evaporated under reduced pressure and the residue was partially purified by FCC (isohexane:EtOAc, 10:1) to remove tetrahydrofuran **5**, which afforded a yellowish oil (1.50 g) containing **15**.

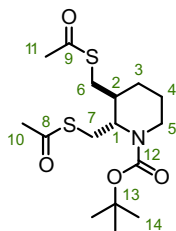


Step 5: To the impure **15** obtained in step 4 was added a 4 M solution of HCl in dioxane (6.0 mL, 24 mmol). The mixture was stirred for 2 h, before Et₂O (50 mL) was added and stirring was continued for several minutes. The precipitate was collected, washed with additional Et₂O and dried to afford **8** (908 mg, 4.29 mmol, 45% over 3 steps) as a white solid.

¹H-NMR (400 MHz, DMSO-*d*₆): 9.34 (d, *J* = 20.9 Hz, 2H, 8-H), 3.29 – 3.16 (m, 2H, 1-H; 5-H_A), 3.11 (dd, *J* = 13.0, 3.1 Hz, 1H, 7-H_A), 3.00 (dd, *J* = 12.9, 11.3 Hz, 1H, 7-H_B), 2.97 – 2.84 (m, 2H, 5-H_B; 6-H_A), 2.82 (dd, *J* = 13.8, 10.9 Hz, 1H, 6-H_B), 2.01 (tdd, *J* = 10.9, 7.4, 3.3 Hz, 1H, 2-H), 1.82 – 1.69 (m, 2H, 4-H), 1.64 (d, *J* = 13.1 Hz, 1H, 3-H_A), 1.34 (dt, *J* = 21.0, 12.4 Hz, 1H, 3-H_B).

¹³C-NMR (101 MHz, DMSO-*d*₆): 59.4 (CH, C1), 43.9 (CH₂, C5), 40.2 (CH, C2) 38.6 (CH₂, C6), 34.2 (CH₂, C7), 28.8 (CH₂, C3), 21.9 (CH₂, C4).

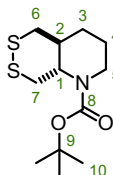
During the experiments that were performed while establishing the synthetic sequence described above, pure samples of **7** and **15** have been obtained. The analytical data for these compounds is reported in the following.

trans-N-Boc 2,3-bis((acetylthio)methyl)piperidine (7)

TLC R_f = 0.50 (isohexane:EtOAc, 3:1). HRMS (ESI⁺): C₁₆H₂₇NNaO₄S₂⁺ [M+Na]⁺: calc. 384.12737, found 384.12765.

¹H-NMR (400 MHz, CDCl₃): δ (ppm) = 4.26 (s, 1H, 1-H), 4.15 – 3.80 (m, 1H, 7-H_A), 3.33 – 3.13 (m, 1H, 6-H_A), 3.06 (s, 1H, 6-H_B), 2.99 (dd, J = 13.7, 6.4 Hz, 1H, 5-H_A), 2.88 (dd, J = 13.7, 8.4 Hz, 1H, 5-H_B), 2.73 (s, 1H, 7-H_B), 2.33 (s, 3H, 10-H), 2.32 (s, 3H, 11-H), 1.89 – 1.74 (m, 2H, 2-H; 3-H_A), 1.70 – 1.52 (m, 2H, 3-H_B; 4-H_A), 1.45 (s, 9H, 14-H), 1.44 – 1.39 (m, 1H, 4-H_B).

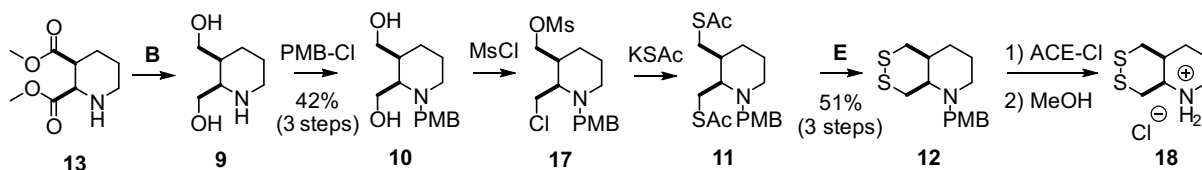
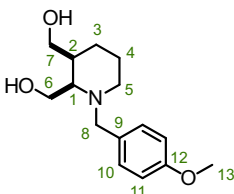
¹³C-NMR (101 MHz, CDCl₃): δ (ppm) = 195.7 (C=O, C8), 195.3 (C=O, C9), 155.4 (C=O, C12), 80.0 ((C(CH₃)₃, C13), 52.6 (CH, C1), 37.7 (CH₂, C7), 36.3 (CH, C2), 31.4 (CH₂, C5), 30.8 (CH₃, C10), 30.7 (CH₃, C11), 29.8 (CH₂, C6), 28.5 (CH₃, C14), 23.1 (CH₂, C3), 19.9 (CH₂, C4).

trans-N-Boc hexahydro-[1,2]dithiino[4,5-b]pyridine (15)

TLC R_f = 0.72 (isohexane:EtOAc, 4:1). HRMS (ESI⁺): C₁₂H₂₂NNaO₂S₂⁺ [M-C₄H₈]⁺: calc. 220.04605, found 220.04617.

¹H-NMR (500 MHz, CDCl₃): δ (ppm) = 3.75 (ddd, J = 14.0, 7.4, 2.0 Hz, 1H, 5-H_A), 3.64 (ddd, J = 10.9, 7.7, 5.6 Hz, 1H, 1-H), 3.06 (ddd, J = 14.0, 11.2, 5.8 Hz, 1H, 5-H_B), 2.98 (d, J = 2.1 Hz, 1H, 7-H_A), 2.97 (s, 1H, 7-H_B), 2.88 (dd, J = 13.5, 10.8 Hz, 1H, 6-H_A), 2.75 (dd, J = 13.5, 2.8 Hz, 1H, 6-H_B), 2.03 (dtt, J = 13.7, 10.8, 2.9 Hz, 1H, 2-H), 1.84 (dddd, J = 13.0, 11.3, 9.3, 7.4, 1.7 Hz, 1H, 4-H_A), 1.70 – 1.63 (m, 1H, 4-H_B), 1.56 (dddd, J = 12.8, 9.7, 2.9, 1.9 Hz, 1H, 3-H_A), 1.45 (s, 9H, 10-H), 1.35 – 1.19 (m, 1H, 3-H_B).

¹³C-NMR (126 MHz, CDCl₃): δ (ppm) = 155.1 (C=O, C8), 80.1 (C(CH₃)₃, C9), 62.4 (CH, C1), 41.2 (CH₂, C6), 40.7 (CH, C2), 38.2 (CH₂, C5), 37.3 (CH₂, C7), 28.6 (CH₃, C10), 27.1 (CH₂, C3), 23.1 (CH₂, C4).

SS66C-type precursor***cis*-N-(4-methoxybenzyl)-2,3-bis(hydroxymethyl)piperidine (**10**)**

Step 1: To dimethyl pyridine-2,3-dicarboxylate **1** (4.11 g, 21.1 mmol) in MeOH (30 mL) was added 96% H₂SO₄ (0.11 mL, 2.1 mmol) and 10% Pd/C (125 mg, 0.105 mmol). The mixture was stirred under hydrogen atmosphere (85 bar) for 15 h, filtered over Celite® and concentrated to afford **13** as a colourless oil, which was used in the next step without purification.

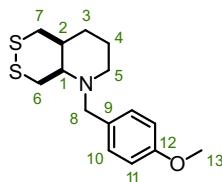
Step 2: The material obtained in step 1 was mixed with anhydrous THF (20 mL), which dissolved most material. The solution was added dropwise to a suspension of LiAlH₄ (2.40 g, 63.3 mmol, 3.0 eq.) in anhydrous THF (125 mL) at 0 °C under nitrogen atmosphere. Then, the remaining undissolved material from step 1 (a THF-insoluble, viscous mass) was added neat to the LiAlH₄ suspension. The mixture was allowed to warm to r.t. and was further stirred at r.t. for 15 h, was then cooled to 0 °C and EtOAc (5 mL), MeOH (5 mL), water (10 mL) and 2 M aq. NaOH (10 mL) were added carefully in the specified order. The cooling bath was removed and the mixture was stirred at r.t. for 1 h, before being filtered. The solids were washed with THF (2×30 mL) and discarded. The filtrate was evaporated under reduced pressure. The residue as taken up in THF (30 mL) and MeOH (10 mL). After drying over Na₂SO₄ all volatiles were removed under reduced pressure and the residue containing **9** was directly used in the next step without further purification.

Step 3: To the material obtained in step 2 were added EtOH (45 mL), K₂CO₃ (7.29 g, 52.8 mmol, 2.5 eq.) and PMB-Cl (4.29 mL, 31.7 mmol, 1.5 eq.). After the mixture had stirred at r.t. for 15 h, the solids were filtered off, washed with EtOH and discarded. The filtrate was evaporated under reduced pressure, 2 M aq. HCl (60 mL) was added and the mixture was washed with DCM (3×30 mL). The organic washings were discarded, the aqueous solution was basified with 2 M aq. NaOH (70 mL) and extracted with DCM (2×60 mL). The extracts were dried over Na₂SO₄ and evaporated under reduced pressure. The residue was purified by FCC (DCM:MeOH:conc. NH₃, 95:5:0.5 to 90:10:1) to afford **10** (2.36 g, 8.89 mmol, 42% over 3 steps) as a faint orange oil.

TLC R_f = 0.20 (EtOAc). **HRMS** (ESI⁺): C₁₅H₂₄NO₃⁺ [M+H]⁺: calc. 266.17507, found 266.17468.

¹H-NMR (400 MHz, CDCl₃): δ (ppm) = 7.24 (d, *J* = 8.5 Hz, 2H, **10-H**), 6.86 (d, *J* = 8.6 Hz, 2H, **11-H**), 3.86 (d, *J* = 13.1 Hz, 1H, **8-H_A**), 3.81 (t, *J* = 9.5 Hz, 1H, **6-H_A**), 3.79 (s, 3H, **13-H**), 3.71 (d, *J* = 13.1 Hz, 1H, **8-H_B**), 3.67 – 3.52 (m, 3H, **6-H_B**; **7-H**), 2.98 – 2.90 (m, 1H, **1-H**), 2.74 (ddd, *J* = 13.6, 10.6, 3.3 Hz, 1H, **5-H_A**), 2.49 (dd, *J* = 13.5, 3.9 Hz, 1H, **5-H_B**), 2.17 (dd, *J* = 10.5, 4.4 Hz, 1H, **2-H**), 1.74 – 1.60 (m, 2H, **3-H**), 1.54 – 1.37 (m, 2H, **4-H**).

¹³C-NMR (101 MHz, CDCl₃): δ (ppm) = 159.0 (C_{Ar}, **C9**), 130.8 (C_{Ar}, **C12**), 130.1 (C_{Ar}H, **C10**), 114.0 (C_{Ar}H, **C11**), 64.9 (CH₂, **C8**), 60.8 (CH, **C1**), 57.5 (CH₂, **C6**), 57.3 (CH₂, **C7**), 55.4 (CH₂, **C13**), 46.4 (CH₂, **C5**), 36.4 (CH, **C2**), 25.0 (CH₂, **C3**), 20.9 (CH₂, **C4**).

cis-N-(4-methoxybenzyl)-octahydro-[1,2]dithiino[4,5-b]pyridine (12)

Step 1: To a solution of **10** (1.11 g, 4.18 mmol, 1.0 eq.) and Et₃N (2.92 mL, 20.9 mmol, 5.0 eq.) in anhydrous DCM (45 mL) at 0 °C under nitrogen atmosphere, was dropwise added MsCl (0.664 mL, 8.58 mmol, 2.05 eq.). The mixture was stirred for 1 h, then the cooling bath was removed. After the mixture had stirred at r.t. for 1 h, it was washed with water (50 mL) and the aqueous washings were extracted with DCM (2×20 mL). The combined organic layers were dried over Na₂SO₄, evaporated under reduced pressure and the residue containing **17** was directly used in the next step without purification.

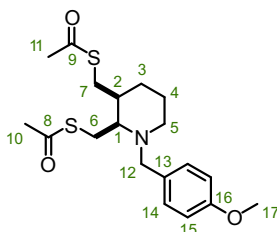
Step 2: The material obtained in step 1 was dissolved in anhydrous DMF (85 mL), KSAc (1.43 g, 12.5 mmol, 3.0 eq.) was added and the mixture was stirred at r.t. for 15 h. Then, the mixture was evaporated under reduced pressure and the residue was suspended in Et₂O (50 mL). The solids were filtered off, washed with additional Et₂O (4×10 mL) and discarded. The filtrate was evaporated under reduced pressure and the residue was partially purified by FCC (isohexane:EtOAc, 4:1), which afforded an orange oil (922 mg) containing **11** that was used in the next step without further purification.

Step 3: The material obtained in step 2 was dissolved in MeOH (50 mL), KOH (420 mg) was added and the mixture was stirred open to air for 72 h. Then, AcOH (0.5 mL) was added, all volatiles were removed under reduced pressure and the residue was suspended in EtOAc (20 mL). The solids were filtered off, washed with additional EtOAc (2×10 mL) and discarded. The filtrate was evaporated under reduced pressure and the residue was purified by FCC (isohexane:EtOAc, 6:1) to afford **12** (629 mg, 2.13 mmol, 51% over 3 steps) as a yellowish oil.

TLC R_f = 0.47 (isohexane:EtOAc, 4:1). HRMS (ESI⁺): C₁₅H₂₂NOS₂⁺ [M+H]⁺: calc. 296.11373, found 296.11341.

¹H-NMR (400 MHz, DMSO-d₆): δ (ppm) = 7.22 (d, *J* = 8.2 Hz, 2H, 10-H), 6.87 (d, *J* = 8.5 Hz, 2H, 11-H), 3.73 (s, 3H, 13-H), 3.66 (d, *J* = 12.5 Hz, 1H, 8-H_A), 3.52 (d, *J* = 12.8 Hz, 1H, 8-H_B), 3.40 – 3.31 (m, 1H, 6-H_A), 3.25 (d, *J* = 13.0 Hz, 1H, 5-H_A), 2.94 (d, *J* = 9.6 Hz, 1H, 1-H), 2.84 (d, *J* = 12.9 Hz, 1H, 5-H_B), 2.70 (dd, *J* = 12.3, 7.1 Hz, 1H, 6-H_B), 2.49 – 2.32 (m, 2H, 7-H), 2.25 – 2.14 (m, 1H, 2-H), 2.09 (d, *J* = 10.9 Hz, 1H, 4-H_A), 1.69 – 1.56 (m, 1H, 3-H_A), 1.56 – 1.48 (m, 1H, 3-H_B), 1.34 (d, *J* = 11.8 Hz, 1H, 4-H_B). **¹³C-NMR** (101 MHz, DMSO-d₆): δ (ppm) = 158.2 (C_{Ar}, C9), 131.1 (C_{Ar}, C12), 129.5 (C_{Ar}H, C10), 113.6 (C_{Ar}H, C11), 58.2 (CH, C1), 56.5 (CH₂, C8), 55.0 (CH₃, C13), 45.0 (CH₂, C7), 41.8 (CH₂, C5), 36.8 (CH, C2), 25.0 (CH₂, C3; 6-H), 22.6 (CH₂, C4).

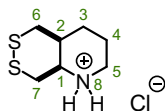
During the experiments that were performed while establishing the synthetic sequence described above, a pure sample of **11** has been obtained and the analytical data for this compound is reported in the following.

cis-N-((1-(4-methoxybenzyl)piperidine-2,3-diyl)bis(methylene)) diethanethioate (11)

TLC R_f = 0.36 (isohexane:EtOAc, 4:1). HRMS (ESI⁺): C₁₉H₂₈NO₃S₂⁺ [M+H]⁺: calc. 382.15051, found 382.15002.

¹H-NMR (400 MHz, CDCl₃): δ (ppm) = 7.24 (d, *J* = 8.4 Hz, 2H, 14-H), 6.84 (d, *J* = 8.6 Hz, 2H, 15-H), 3.80 (s, 3H, 17-H), 3.67 (s, 2H, 12-H), 3.25 (dd, *J* = 13.6, 8.0 Hz, 1H, 6-H_A), 2.99 (dd, *J* = 13.6, 5.4 Hz, 1H, 6-H_B), 2.91 (dt, *J* = 8.5, 4.5 Hz, 1H, 1-H), 2.88 – 2.77 (m, 2H, 7-H_A), 2.60 (td, *J* = 12.3, 11.3, 3.2 Hz, 1H, 5-H_A), 2.44 (d, *J* = 13.3 Hz, 1H, 5-H_B), 2.33 (s, 3H, 10-H), 2.33 (s, 3H, 11-H), 2.13 – 2.00 (m, 1H, 2-H), 1.75 – 1.65 (m, 1H, 3-H_A), 1.63 – 1.53 (m, 1H, 4-H_A), 1.48 – 1.40 (m, 1H, 4-H_B), 1.40 – 1.30 (m, 1H, 3-H_B).

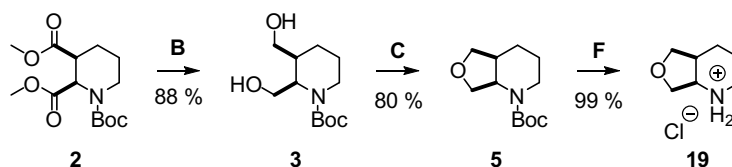
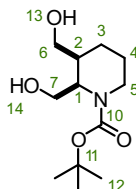
¹³C-NMR (101 MHz, CDCl₃): δ (ppm) = 196.4 (C=O, C8), 195.8 (C=O, C9), 158.7 (C_{Ar}, C13), 131.8 (C_{Ar}, C16), 129.8 (C_{Ar}H, C14), 113.7 (C_{Ar}H, C15), 61.0 (CH, C1), 57.8 (CH₂, C12), 55.4 (CH₃, C17), 45.3 (CH₂, C5), 37.6 (CH, C2), 32.0 (CH₂, C7), 30.8 (CH₃, C10), 30.7 (CH₃, C11), 26.0 (CH₂, C6), 25.5 (CH₂, C3), 22.3 (CH₂, C4).

cis-octahydro-[1,2]dithiino[4,5-b]pyridine hydrochloride (18)

To a solution of **12** (494 mg, 1.67 mmol, 1.0 eq.) in anhydrous THF (5 mL) at 0 °C was dropwise added 1-chloroethyl chloroformate (ACE-Cl) (362 μ L, 3.34 mmol, 2.0 eq.). The mixture was warmed to r.t. and stirred for three days, before Et₂O (30 mL) was added and the mixture was washed with 2 M aq. HCl (25 mL). The aq. washings were extracted with Et₂O (2 \times 30 mL), basified by addition of 2 M aq. NaOH (30 mL) and unreacted **12** (89 mg, 0.30 mmol, 18%) was recovered after extracting the basified extracts with Et₂O, drying over MgSO₄ and removal of the solvent under reduced pressure. The extracts that were obtained before basifying the aq. washings were dried over MgSO₄ and evaporated under reduced pressure. The residue was purified by FCC (DCM/isohehexane), collecting a fraction with R_f = 0.5 (DCM). To the resulting colourless oil was added anhydrous MeOH (50 mL), the mixture was stirred at reflux for 1 h and evaporated under reduced pressure. The residue was washed with Et₂O to obtain **18** (207 mg, 0.977 mmol, 58%) as an off-white solid.

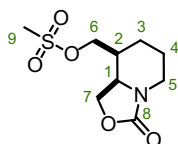
Broad signals were observed by NMR spectroscopy at 298 K, which was attributed to a slow interconversion between conformers, and sharp signals were observed by measurements at 373 K.

¹H-NMR (400 MHz, DMSO-d₆, 373 K): δ (ppm) = 9.55 (s, 2H), 3.66 (dt, J = 6.7, 3.2 Hz, 1H), 3.51 (dd, J = 13.9, 7.6 Hz, 1H), 3.29 (s, 1H), 3.14 (d, J = 12.9 Hz, 2H), 3.04 – 2.85 (m, 1H), 2.35 (s, 1H), 1.91 (s, 1H), 1.82 (ddq, J = 12.6, 8.4, 4.3 Hz, 1H), 1.76 – 1.65 (m, 1H), 1.61 (td, J = 9.2, 4.5 Hz, 1H).

O56-type precursor and side products**cis-N-Boc 2,3-bis(hydroxymethyl)piperidine (3)**

Prepared from **2** (10.7 g, 35.5 mmol) according to **general protocol B**. Compound **3** (7.7 g, 31.4 mmol, 88%) was obtained as a colourless oil and used without further purification.

TLC R_f = 0.30 (EtOAc). **HRMS** (EI): C₁₁H₂₀NO₃⁺ [M-CH₃O-e]⁺; calc. 214.1438, found 214.1435. **¹H-NMR** (400 MHz, CDCl₃): δ (ppm) = 4.41 (s, 1H, 1-H), 3.93 (s, 1H, 5-H_A), 3.86 (dd, J = 11.1, 7.3 Hz, 1H, 7-H_A), 3.69 – 3.52 (m, 3H, 6-H; 7-H_B), 3.08 (s, 2H, 13-H; 14-H), 2.73 (s, 1H, 5-H_B), 1.93 (dq, J = 7.9, 3.7 Hz, 1H, 2-H), 1.92 – 1.80 (m, 1H, 2-H), 1.69 (m, 1H, 4-H_A), 1.63 – 1.52 (m, 1H, 3-H_A), 1.45 (s, 9H, 12-H), 1.40 (m, 2H, 3-H_B; 4-H_B). **¹³C-NMR** (101 MHz, CDCl₃): δ (ppm) = 156.0 (C=O, C10), 80.1 (C(CH₃)₃, C11), 68.1 (CH₂, C5), 64.6 (CH₂, C7), 59.6 (CH₂, C6), 54.0 (CH, C1), 40.7 (CH, C2), 28.6 (C(CH₃)₃, C12), 25.3 (CH₂, C4), 22.7 (CH₂, C3).

cis-(3-oxohexahydro-3H-oxazolo[3,4-a]pyridin-8-yl)methyl methanesulfonate (4)

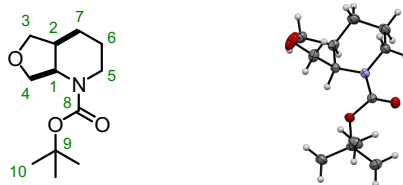
To a solution of **3** (372 mg, 1.51 mmol, 1.0 eq.) in anhydrous DCM (38 mL) at 0 °C under nitrogen atmosphere were added Et₃N (1.05 mL, 7.57 mmol, 5.0 eq.) and MsCl (0.29 mL, 3.79 mmol, 2.5 eq.). The mixture was stirred for 1 h, then warmed to r.t. and stirred for further 12 h, before washing with water (50 mL). The aqueous washings were extracted with DCM (2 \times 50 mL) and the combined organic layers were dried over Na₂SO₄ and evaporated under reduced pressure. The residue was purified by FCC (isohehexane/EtOAc) to afford **4** (336 mg, 1.35 mmol, 89%) as a colourless oil.

TLC R_f = 0.26 (isohehexane:EtOAc, 2:1).

¹H-NMR (400 MHz, CDCl₃): δ (ppm) = 4.42 (dd, *J* = 10.6, 7.1 Hz, 1H, 6-H_A), 4.35 (t, *J* = 9.0 Hz, 1H, 7-H_A), 4.32 – 4.25 (m, 2H, 6-H_B; 7-H_B), 3.94 – 3.87 (m, 2H, 1-H; 5-H_A), 3.05 (s, 3H, 9-H), 2.90 (ddd, *J* = 13.1, 10.9, 5.4 Hz, 1H, 5-H_B), 2.30 (tq, *J* = 6.8, 3.6 Hz, 1H, 2-H), 2.14 – 2.02 (m, 1H, 4-H_A), 1.76 – 1.48 (m, 3H, 3-H; 4-H_B).

¹³C-NMR (101 MHz, CDCl₃): δ (ppm) = 157.3 (C=O, C8), 67.3 (CH₂, C6), 64.5 (CH₂, C7), 56.4 (CH, C1), 41.6 (CH₂, C5), 37.6 (CH₃, C9), 34.9 (CH, C2), 26.0 (CH₂, C4), 19.1 (CH₂, C3).

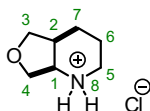
cis-*N*-Boc hexahydrofuro[3,4-*b*]pyridine (**5**)



Prepared from **3** (1.77 g, 7.14 mmol) according to **general protocol C**. Different concentrations than in the general protocol were employed: 0.11 M for the PPh₃ solution and 0.36 M for the substrate solution. Before being concentrated, the reaction mixture was filtered to remove precipitated S=PPh₃ and O=PPh₃. **5** (1.3 g, 5.72 mmol, 80%) was obtained as a colourless oil after FCC (isohexane/EtOAc). Crystals suitable for single crystal X-Ray crystallography were prepared by slow evaporation of a solution in DCM.

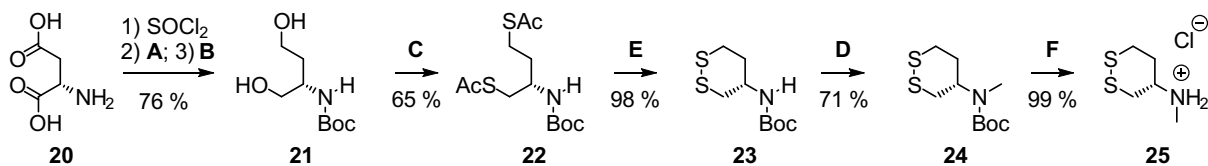
TLC *R*_f = 0.43 (isohexane:EtOAc, 2:1). **HRMS** (ESI⁺): C₇H₁₄NO⁺ [M+H]⁺: calc. 128.10699, found 128.10700. **¹H-NMR** (400 MHz, CDCl₃): δ (ppm) = 4.65 (s, 1H, 1-H), 4.03 – 3.78 (m, 3H, 3-H_A; 4-H_A; 5-H_A), 3.64 (dd, *J* = 8.7, 1.3 Hz, 1H, 5-H_B), 3.65 (t, *J* = 8.6 Hz, 1H, 4-H_B), 2.74 (t, *J* = 12.1 Hz, 1H, 3-H_B), 2.20 – 2.07 (m, 1H, 2-H), 1.80 – 1.72 (m, 1H, 7-H_A), 1.69 (s, 1H, 6-H_A), 1.45 (s, 9H, 10-H), 1.43 – 1.39 (m, 2H, 6-H_B; 7-H_B). **¹³C-NMR** (101 MHz, CDCl₃): δ (ppm) = 155.5 (C=O, C8), 79.9 (C(CH₃)₃, C9), 73.4 (CH₂, C5), 66.2 (CH₂, C4), 53.5 (CH, C1), 39.7 (CH₂, C3), 36.0 (CH, C2), 28.5 (C(CH₃)₃, C10), 25.3 (CH₂, C7), 23.7 (CH₂, C6).

cis-octahydrofuro[3,4-*b*]pyridine hydrochloride (**19**)



Prepared from **5** (145 mg, 0.64 mmol) according to **general protocol F** using a larger amount of HCl (15 eq.) to afford **19** (104 mg, 0.64 mmol, quant.) as a colourless crystalline solid.

¹H-NMR (500 MHz, DMSO-*d*₆): δ (ppm) = 9.95 (s, 1H, 8-H_A), 8.63 (s, 1H, 8-H_B), 3.89 – 3.78 (m, 3H, 3-H; 4-H_A), 3.71 (q, *J* = 5.0, 4.6 Hz, 1H, 1-H), 3.66 (dd, *J* = 9.7, 8.3 Hz, 1H, 4-H_B), 3.07 (d, *J* = 11.9 Hz, 1H, 5-H_A), 2.83 (d, *J* = 11.3 Hz, 1H, 5-H_B), 2.57 – 2.51 (m, 1H, 2-H), 1.83 – 1.72 (m, 1H, 6-H_A), 1.64 (dddd, *J* = 17.8, 15.5, 12.8, 7.6 Hz, 3H, 6-H_B; 7-H). **¹³C-NMR** (126 MHz, DMSO-*d*₆): δ (ppm) = 69.9 (CH₂, C3), 68.1 (CH₂, C4), 55.3 (CH, C1), 41.5 (CH₂, C5), 35.0 (CH, C2), 19.5 (CH₂, C6), 17.1 (CH₂, C7).

SS60-type precursor: initial Mitsunobu route**(S)-N-Boc-2-aminobutane-1,4-diol (21)²²**

Step 1: To a solution of *L*-aspartic acid **20** (10.0 g, 75.1 mmol) in anhydrous MeOH (150 mL) at 0 °C was dropwise added SOCl₂ (16.2 mL, 223.3 mmol). The mixture was warmed to 50 °C and stirred at that temperature for 2 h, before the volatiles were removed under reduced pressure. The residue was used in the next step without purification.

Step 2: The material obtained in step 1 was treated according to **general protocol A**. Different reaction conditions than in the general procedure were used: the reaction mixture was heated to 50 °C for 5 h instead of stirring at room temperature overnight. Dimethyl *N*-Boc-*L*-aspartate (16.4 g, 62.8 mmol, 84% over 2 steps) was obtained as a colourless solid after recrystallization from MeOH.

Step 3: The material obtained in step 2 (5.00 g, 19.1 mmol) was treated according to **general protocol B**. Compound **21** (3.55 g, 17.3 mmol, 91%) was obtained as a colourless solid after recrystallization from Et₂O.²²

TLC R_f = 0.29 (isohexane:EtOAc, 1:1). **HRMS** (ESI⁺): C₉H₂₀NO₄⁺ [M+H]⁺: calc. 206.1387, found 206.1384. **¹H-NMR** (400 MHz, CDCl₃): δ (ppm) = 5.10 (d, *J* = 8.6 Hz, 1H, -NH), 3.83 (q, *J* = 5.0 Hz, 1H), 3.71 (d, *J* = 11.9 Hz, 3H), 3.62 (dd, *J* = 11.0, 4.6 Hz, 1H), 3.51 (s, 1H, OH), 3.05 (s, 1H, OH), 1.80 (ddt, *J* = 13.9, 9.3, 4.7 Hz, 1H), 1.61 (tt, *J* = 9.0, 7.3, 5.6 Hz, 1H), 1.44 (s, 9H).

(S)-N-Boc-2-amino-1,4-bis(acetylthio)butane(22)²²

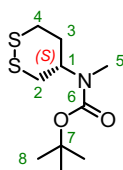
Prepared from **21** (2.00 g, 9.7 mmol) according to **general protocol C**. Compound **22** (2.01 g, 6.3 mmol, 65%) was obtained as a colourless solid after FCC (*n*-pentane/Et₂O).²²

TLC R_f = 0.13 (isohexane:EtOAc, 1:1). **HRMS** (ESI⁺): C₁₃H₂₃NNaO₄S₂⁺ [M+Na]⁺: calc. 344.09607, found 344.09613. **¹H-NMR** (400 MHz, CDCl₃): δ (ppm) = 4.58 (d, *J* = 9.0 Hz, 1H, -NH), 3.89 – 3.74 (m, 1H), 3.08 (td, *J* = 16.5, 15.2, 6.0 Hz, 2H), 2.98 (ddd, *J* = 14.0, 8.6, 5.5 Hz, 1H), 2.82 (ddd, *J* = 13.7, 8.6, 7.0 Hz, 1H), 2.35 (s, 3H), 2.32 (s, 3H), 1.79 (dddd, *J* = 13.5, 8.6, 7.0, 4.7 Hz, 1H), 1.74 – 1.63 (m, 1H), 1.43 (s, 9H).

(S)-N-Boc-1,2-dithian-4-amine (23)²²

Prepared from **22** (501 mg, 1.56 mmol) according to **general protocol E**. Compound **23** (360 mg, 1.53 mmol, 98%) was obtained as a colourless solid.²²

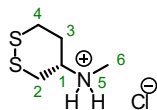
TLC R_f = 0.57 (*n*-pentane:Et₂O, 2:1). **HRMS** (ESI⁺): C₉H₁₇NO₂S₂⁺ [M+H]⁺: calc. 235.0701, found 235.0694. **¹H-NMR** (500 MHz, DMSO-*d*₆): δ (ppm) = 7.08 (d, *J* = 8.1 Hz, 1H), 3.56 – 3.44 (m, 1H), 3.11 – 3.01 (m, 1H), 2.95 (t, *J* = 12.3 Hz, 1H), 2.87 (dd, *J* = 12.9, 3.2 Hz, 1H), 2.60 (dd, *J* = 13.0, 10.5 Hz, 1H), 2.06 (dd, *J* = 13.3, 3.7 Hz, 1H), 1.64 (dd, *J* = 14.4, 11.2 Hz, 1H), 1.38 (s, 9H).

(S)-N-Boc-N-methyl-1,2-dithian-4-amine (24)

Prepared from **23** (400 mg, 1.70 mmol) according to **general protocol D**. Compound **24** (301 mg, 1.21 mmol, 71%) was obtained as a colourless solid after purification by FCC (isohexane/EtOAc).

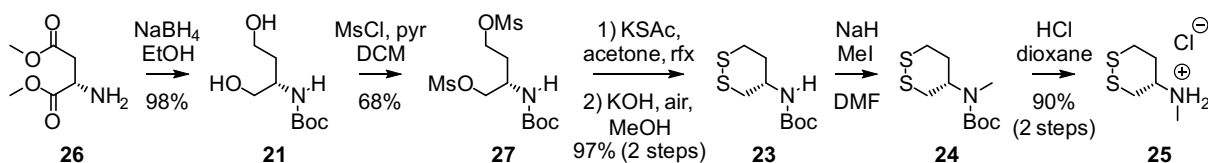
TLC R_f = 0.74 (*n*-pentane:Et₂O, 2:1). **HRMS** (EI): C₁₀H₁₉NO₂S₂ [M-e]: calc. 249.0852, found 249.0867.

¹H-NMR (400 MHz, CDCl₃): δ (ppm) = 4.48 – 3.88 (m, 1H, 1-H), 3.18 (t, *J* = 13.0 Hz, 1H, 3-H_A), 2.99 (t, *J* = 15.4 Hz, 2H, 2-H_A; 3-H_B), 2.76 (s, 3H, 5-H), 2.66 (dd, *J* = 12.8, 3.2 Hz, 1H, 2-H_B), 2.09 (d, *J* = 13.1 Hz, 1H, 4-H_A), 2.05 – 1.92 (m, 1H, 4-H_B), 1.46 (s, 9H, 8-H). **¹³C-NMR** (101 MHz, CDCl₃): δ (ppm) = 155.2 (C=O, C6), 80.2 (C(CH₃)₃, C7), 55.9, 53.3 (CH, C1), 36.4 (CH₂, C3), 36.1 (CH₂, C2), 32.9 (CH₂, C4), 29.3 (CH₃, C5), 28.6 (C(CH₃)₃, C8).

(S)-N-methyl-1,2-dithian-4-amine hydrochloride (25)

Prepared from **24** (92 mg, 0.37 mmol) according to **general protocol F** using a larger amount of HCl (15 eq.). **25** (68 mg, 0.37 mmol, quant.) was obtained as a colourless solid.

¹H-NMR (500 MHz, DMSO-*d*₆): δ (ppm) = 9.34 (s, 2H, 5-H), 3.32 – 3.25 (m, 2H, 1-H; 2-H), 3.16 (ddd, *J* = 13.9, 5.4, 3.2 Hz, 1H, 2-H_B), 3.03 – 2.90 (m, 2H, 3-H), 2.53 (s, 3H, 6-H), 2.45 – 2.37 (m, 1H, 4-H_A), 1.86 (q, *J* = 11.7 Hz, 1H, 4-H_B). **¹³C-NMR** (126 MHz, DMSO-*d*₆): δ (ppm) = 55.8 (CH, C1), 33.0 (CH₂, C2), 32.9 (CH₂, C3), 30.0 (CH₂, C4), 28.9 (CH₃, C6).

SS60-type precursor: Scale-up route**(S)-N-Boc 2-aminobutane-1,4-diol (21)**

To a solution of *N*-Boc *L*-aspartic acid dimethyl ester **26** (17.4 g, 66.6 mmol, 1.0 eq.) in anhydrous EtOH (260 mL) at 0 °C was carefully added NaBH₄ (20.2 g, 533 mmol, 8 eq.) in portions, the resulting mixture was allowed to warm to r.t. and further stirred for 15 h. Then, the mixture was heated to reflux for 3 h. After cooling to r.t., sat. aq. NaCl (250 mL) was added, the mixture was stirred for several minutes and filtered. The solids were washed with Et₂O (4×50 mL) and discarded. The layers were separated and the aq. layer was extracted with additional Et₂O (2×75 mL). The combined organic layers were dried over MgSO₄, filtered and the solvent was removed under reduced pressure. After azeotropic drying of the residue with toluene, **21** (13.4 g, 65.3 mmol, 98%) was obtained as a white solid.

(S)-N-Boc 2-aminobutane-1,4-diyl dimethanesulfonate (27)

To a mixture of **21** (4.86 g, 23.7 mmol, 1.0 eq.), anhydrous DCM (50 mL) and pyridine (9.56 mL, 118 mmol, 5.0 eq.) at 0 °C was dropwise added MsCl (4.03 mL, 52.1 mmol, 2.2 eq.). The mixture was warmed to r.t. and was further stirred at r.t. for 15 h, was then diluted with DCM (25 mL), washed with 2 M aq. HCl (100 mL and 50 mL) and water (50 mL), dried over MgSO₄, filtered and concentrated under reduced pressure. The residue was suspended in DCM (50 mL) and filtered. The solids were dried to obtain **27** (3.30 g, 8.85 mmol, 37%) as a white solid. The filtrate was diluted with toluene (25 mL), the DCM was evaporated under reduced pressure and the remainder kept at r.t. for 1 h. The resulting precipitate was collected, washed with toluene (25 mL and 10 mL) followed by a small amount of hexane and dried to afford additional **27** (2.64 g, 7.30 mmol, 31%) as an off-white solid.

(S)-N-Boc 1,2-dithian-4-amine (23)

Step 1: A mixture of **27** (3.00 g, 8.30 mmol, 1.0 eq.), KSAc (2.84 g, 24.9 mmol, 3.0 eq.) and acetone (85 mL) was heated to reflux for 2 h. Then, all volatiles were evaporated under reduced pressure. DCM (75 mL) and sat. aq. NaHCO₃ (75 mL) were added to the residue, the layers were separated and the aqueous layer was extracted with additional DCM (2×25 mL). The combined organic layers were washed with water (100 mL), dried over MgSO₄, filtered and the solvent was removed under reduced pressure. The residue was directly used without purification in the next step.

Step 2: The material obtained in step 1 was dissolved in a 0.15 M solution of KOH in MeOH (170 mL). After stirring open to air for 15 h, AcOH (1.53 mL, 26.8 mmol) was added, all volatiles were evaporated under reduced pressure and the residue was taken up in EtOAc (100 mL) and sat. aq. NaCl (60 mL). The layers were separated and the aq. layer was extracted with EtOAc (30 mL). The combined organic layers were dried over MgSO₄, filtered and evaporated under reduced pressure. The residue was dissolved in EtOAc (10 mL) and hexane (30 mL) was added. The solution was filtered over silica (6 g) and the silica was washed with additional isohexane/EtOAc (3:1, 80 mL). Removal of the solvent under reduced pressure afforded **23** (1.89 g, 8.03 mmol, 97% over 2 steps) as a faint yellow solid.

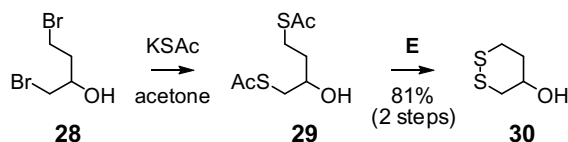
(S)-N-methyl-1,2-dithian-4-amine hydrochloride (25)

Step 1: To a mixture of 60% NaH mineral oil suspension (0.408 mg, 10.2 mmol, 1.5 eq.) and anhydrous DMF (25 mL) at 0 °C under nitrogen atmosphere was dropwise added a solution of **23** (1.60 g, 6.8 mmol, 1.0 eq.) in anhydrous DMF (5 mL). After stirring for 30 min, MeI (635 μL, 10.2 mmol, 1.5 eq.) was added and stirring was continued for 4 h with warming to r.t., before the mixture was carefully poured into sat. aq. NH₄Cl (60 mL) and extracted with EtOAc (3×40 mL). The organic extracts were washed with water (2×60 mL) and sat. aq. NaCl

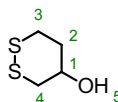
(60 mL), dried over MgSO₄, filtered and the solvent was removed under reduced pressure. The residue containing **24** was directly used without purification in the next step.

Step 2: To the material obtained in step 1 was added a 4 M solution of HCl in dioxane (7.5 mL). The mixture was stirred for 3.5 h, before Et₂O (30 mL) was added and the mixture was filtered. The solids were washed with Et₂O (2×15 mL) and dried to afford **25** (1.20 g, 6.46 mmol, 90% over 2 steps) as a faint brownish-grey solid.

Inverted SS60-type precursor



1,2-dithian-4-ol (30)

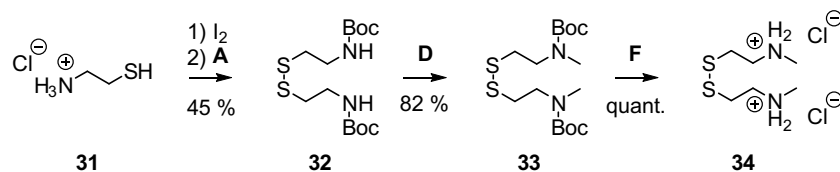


Step 1: To a mixture of KSAc (2.95 g, 25.9 mmol, 3.0 eq.) and acetone (85 mL) under nitrogen atmosphere was added 1,4-dibromo-2-butanol **28** (2.00 g, 8.62 mmol, 1.0 eq.). The mixture was stirred in the dark for 15 h, then filtered. The solids were washed with acetone and discarded. The filtrate was evaporated under reduced pressure and the residue was taken up in DCM (75 mL) and sat. aq. NaHCO₃ (75 mL). The layers were separated and the aq. layer was extracted with DCM (2×25 mL). The combined organic layers were washed with water (100 mL), dried over MgSO₄, filtered and the solvent was removed under reduced pressure. The residue containing **29** was directly used without purification in the next step.

Step 2: To the material obtained in step 1 were added MeOH (170 mL) and KOH (1.43 g, 25.5 mmol). The mixture was stirred open to air for 15 h, before AcOH (1.53 mL, 26.8 mmol) was added and all volatiles were removed under reduced pressure. The residue was suspended in DCM (10 mL) and filtered. The solids were washed with additional DCM (2×10 mL) and discarded. The filtrate was evaporated under reduced pressure and the residue was purified by FCC (isohexane:EtOAc, 2:1) to afford **30** (951 mg, 6.98 mmol, 81%) as an off-white solid.

TLC R_f = 0.41 (isohexane:EtOAc, 1:1). **HRMS** (ESI⁻): C₄H₇OS₂⁻ [M-H]⁻ calc. 134.99438, found 134.99247.

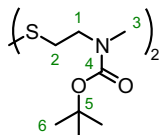
¹H-NMR (400 MHz, DMSO-d₆): δ (ppm) = 5.18 (d, *J* = 5.0 Hz, 1H, 5-H), 3.54 (td, *J* = 10.0, 5.4 Hz, 1H, 1-H), 3.05 (dt, *J* = 13.8, 4.1 Hz, 1H, 2-H_A), 2.98 – 2.85 (m, 2H, 2-H_B, 4-H_A), 2.56 (dd, *J* = 12.9, 10.0 Hz, 1H, 4-H_B), 2.16 (d, *J* = 13.4 Hz, 1H, 3-H_B), 1.60 – 1.44 (m, 1H, 3-H_A). **¹³C-NMR** (101 MHz, DMSO-d₆): δ (ppm) = 67.1 (CH, C1), 39.2 (CH₂, C2), 36.8 (CH₂, C4), 34.3 (CH₂, C3).

Symmetric linear disulfide SS00-type probe precursor**N-Boc, N'-Boc 2,2'-disulfanediybis(ethan-1-amine) (32)²⁴**

Step 1: To a solution of cysteamine hydrochloride **31** (1.00 g, 8.80 mmol) and KOH (1.16 g, 17.6 mmol) in MeOH (30 mL) was dropwise added a 0.5 M solution of I₂ in MeOH until a permanently coloured solution was obtained. The volatiles were removed under reduced pressure and sat. aq. NaCl and a small amount of aq. Na₂S₂O₃ were added. The mixture was extracted with DCM, dried over Na₂SO₄, filtered and concentrated under reduced pressure. The residue was directly in the next step without further purification.

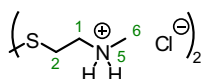
Step 2: The material obtained in step 1 was treated according to **general protocol A**. Compound **32** with minor impurities (0.70 g, 2.00 mmol, 45%) was obtained as colourless solid after FCC (*n*-pentane/Et₂O). A pure sample of **32** was obtained by recrystallization from methanol.²⁴

TLC R_f = 0.29 (isohexane:EtOAc, 3:1). **HRMS** (ESI⁺): C₁₄H₂₈NNa₂O₄S₂⁺ [M+Na]⁺: calc. 375.13827, found 375.13825. **¹H-NMR** (400 MHz, CDCl₃): δ (ppm) = 5.01 (s, 2H), 3.45 (q, *J* = 6.3 Hz, 4H), 2.79 (t, *J* = 6.4 Hz, 4H), 1.45 (s, 18H). **¹³C-NMR** (101 MHz, CDCl₃): δ (ppm) 155.8 (C=O), 79.6 (C(CH₃)₃), 39.3 (CH₂), 38.5 (CH₂), 28.4 (C(CH₃)₃).

N-Boc, N'-Boc 2,2'-disulfanediybis(N-methylethan-1-amine) (33)

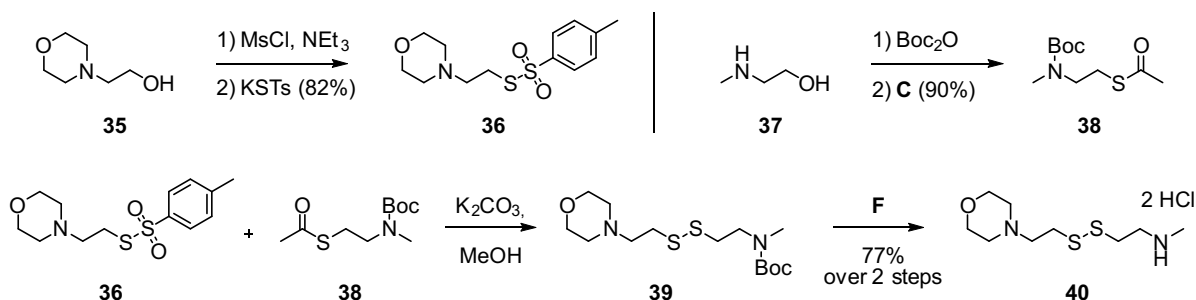
Prepared from **32** (0.78 g, 2.21 mmol) according to **general protocol D**. Compound **33** (0.69 g, 1.82 mmol, 82%) was obtained as a colourless solid after FCC (isohexane/EtOAc).

TLC R_f = 0.5 (isohexane:EtOAc, 3:1). **HRMS** (ESI⁺): C₁₆H₃₂N₂O₄S₂Na⁺: [M+Na]⁺ calc. 403.16957, found 403.16964. **¹H-NMR** (400 MHz, CDCl₃): δ (ppm) = 3.50 (t, *J* = 7.2 Hz, 4H, 1-H), 2.89 (s, 6H, 3-H), 2.81 (s, 4H, 2-H), 1.46 (s, 18H, 6-H). **¹³C-NMR** (101 MHz, CDCl₃): δ (ppm) = 155.4 (C=O, C4), 79.6 (C(CH₃)₃, C5), 48.3 (CH₂, C1), 36.1 (CH₂, C2), 34.5 (CH₃, C3), 28.3 (C(CH₃)₃, C6).

2,2'-disulfanediybis(N-methylethan-1-amine) dihydrochloride (34)

Prepared from **33** (0.69 mg, 1.82 mmol) according to **general protocol F** using a larger amount of HCl (15 eq.). **34** (0.46 mg, 1.82 mmol, quant.) was obtained as a colourless solid.

¹H-NMR (400 MHz, DMSO-*d*₆): δ (ppm) = 9.27 (s, 4H, 5-H), 3.19 (d, *J* = 7.4 Hz, 4H, 1-H), 3.09 (dd, *J* = 8.1, 5.7 Hz, 4H, 2-H), 2.56 (s, 6H, 6-H). **¹³C-NMR** (101 MHz, DMSO-*d*₆): δ (ppm) = 47.0 (CH₂, C1), 32.4 (CH₂, C2), 32.3 (CH₃, C6).

Unsymmetric linear disulfide SS00M-type precursor

S-(2-morpholinoethyl) 4-methylbenzenesulfonothioate (36)

Step 1: Et₃N (5.58 mL, 40.0 mmol) was added to a solution of 2-morpholinoethanol **35** (3.50 g, 26.7 mmol) in anhydrous DCM (100 mL) under N₂-atmosphere. The mixture was cooled to 0 °C and MsCl (2.48 mL, 32.0 mmol) was added dropwise. After stirring for 15 min, the mixture was washed with sat. aq. NaHCO₃ (100 mL) and dried over Na₂SO₄ and filtered. The volatiles were evaporated under reduced pressure and the residue was used in the next step without purification.

Step 2: To the material obtained in step 1 were added acetone (100 mL) and potassium *p*-toluenethiosulfonate (KSTs) (6.04 g, 26.7 mmol). The mixture was warmed to reflux for 1.25 h, cooled to r.t., further stirred for 15 h and before being filtered. The solids were washed with additional acetone and discarded. The filtrate was concentrated under reduced pressure to remove all acetone and the residue was taken up in EtOAc (50 mL). The mixture was filtered over silica (15 g) and the silica was washed with additional EtOAc (75 mL). The volatiles were removed under reduced to obtain thiosulfonate **36** as a yellowish oil (6.59 g, 21.9 mmol, 82% over 2 steps), which was used without further purification.

¹H-NMR (400 MHz, CDCl₃): δ (ppm) = 7.81 (d, *J* = 8.4 Hz, 2H), 7.34 (d, *J* = 8.2 Hz, 2H), 3.67 – 3.62 (m, 4H), 3.13 (t, *J* = 6.9 Hz, 2H), 2.61 (t, *J* = 6.9 Hz, 2H), 2.45 (s, 3H), 2.42 – 2.36 (m, 4H).

The spectroscopic data matched previously reported values.²⁵

S-(2-((*tert*-butoxycarbonyl)(methyl)amino)ethyl) ethanethioate (38)

Step 1: 2-methylaminoethanol **37** (2.82 g, 37.6 mmol) was dissolved in THF (20 mL) and placed in water bath at r.t.. Boc₂O (8.21 g, 37.6 mmol) was weighed into in a vial, molten and dropwise added to the solution of 2-methylaminoethanol. Then, the remaining material in the vial was dissolved in THF (5 mL) and also added to the reaction mixture. After stirring at r. t. for 1.5 h, the volatiles were evaporated and the residue was taken forward to the next step without purification.

Step 2: A solution of material obtained in step 1 (37.6 mmol) was treated according to **general procedure C**. The volatiles were removed under reduced pressure and the residue was suspended in Et₂O (50 mL), followed by the addition of isohexane (100 mL). The mixture was filtered, the solids were discarded, the filtrate was concentrated under reduced pressure and hexanes (100 mL) were added to the residue. The mixture was again filtered and the solids were discarded. Finally, the filtrate was concentrated under reduced pressure and the residue was purified by FCC (isohexane:EtOAc) to obtain compound **38** as a faint yellow oil (7.50 g, 32.1 mmol, 90%).

TLC *R_f* = 0.39 (isohexane:EtOAc, 6:1). **¹H-NMR** (400 MHz, CDCl₃): δ (ppm) = 3.35 (t, *J* = 7.1 Hz, 2H), 3.00 (t, *J* = 6.9 Hz, 2H), 2.89 (s, 3H), 2.34 (s, 3H), 1.46 (s, 9H).

The spectroscopic data matched previously reported values.²⁶

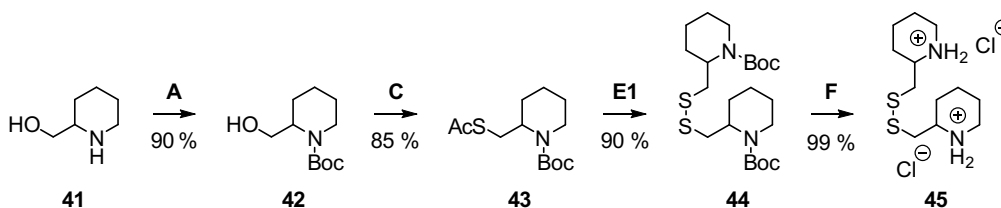
N-methyl-2-((2-morpholinoethyl)disulfaneyl)ethan-1-amine dihydrochloride (40)

Step 1: A degassed solution of thiosulfonate **36** (5.68 g, 18.9 mmol) and thioacetate **38** (4.00 g, 17.1 mmol) in anhydrous MeOH (160 mL) under N₂-atmosphere was added K₂CO₃ (2.37 g, 17.1 mmol) and mixture was degassed again. After stirring for 2.5 h, the volatiles were evaporated under reduced pressure, the residue was suspended in EtOAc (40 mL) and the mixture was filtered. The solids were washed with a small amount additional EtOAc and discarded. The filtrate was concentrated under reduced pressure and the residue was partially purified by FCC (isohexane:EtOAc, *R_f* = 0.37). Two fractions of disulfide **39** (*R_f* = 0.37 (EtOAc)) were obtained. Both fractions contained small amounts of unidentified impurities and one fraction additionally a significant contamination by remaining excess thiosulfonate **36**. The two fractions were carried forward separately without further purification.

Step 2: To the almost pure fraction (2.54 g) of disulfide **39** from the preceding step was added a 4 M solution of HCl in 1,4-dioxane (8 mL). The mixture was stirred for 1 h, diluted with Et₂O (40 mL) and filtered. The solids were washed with additional Et₂O and the filtrate was discarded. The solids were suspended in isopropanol (30 mL) and the mixture was warmed to reflux. After cooling back to r.t., the mixture was diluted with isohexane (60 mL) and filtered again. The filtrate was discarded and the solids were dried to obtain dihydrochloride **40** (2.11 g, 6.82 mmol, 40% over two steps) as a white powder. The second fraction (2.66 g) of disulfide **39** was treated identically to afforded additional **40** (1.97 g, 6.37 mmol, 37% over two steps), also in the form of a white powder.

The material that was obtained did not consist only of dihydrochloride **X56**, but also contained a fraction of the corresponding monohydrochloride. This was observed during NMR spectroscopy, as several signals in the ¹H-NMR spectrum were significantly broadened. To obtain pure dihydrochloride **X56** for characterization by NMR spectroscopy, a sample was dissolved in a solution of HCl in methanol (1.25 M solution), the solution was evaporated and the residue was dissolved in deuterium oxide. Acetonitrile was added and the signal of the methyl group was used as an internal reference (¹H-NMR: 2.06 ppm, ¹³C-NMR: 1.47).²⁷

HRMS (ESI⁺): C₉H₂₁N₂OS₂⁺: [M+H]⁺ calc. 237.10898, found 237.10918. **¹H-NMR** (400 MHz, D₂O): δ (ppm) = 4.13 (dd, *J* = 13.2, 3.4 Hz, 2H), 3.86 (ddd, *J* = 13.7, 11.8, 2.2 Hz, 2H), 3.70 – 3.52 (m, 4H), 3.49 – 3.40 (m, 2H), 3.28 (td, *J* = 12.6, 3.7 Hz, 2H), 3.22 – 3.11 (m, 2H), 3.07 (t, *J* = 6.5 Hz, 2H), 2.77 (s, 3H). **¹³C-NMR** (100 MHz D₂O): δ (ppm) = 64.2, 56.0, 52.4, 47.6, 33.4, 32.7, 30.1.

Symmetric linear disulfide SS06-type precursor**N-Boc piperidin-2-ylmethanol (42)¹⁹**

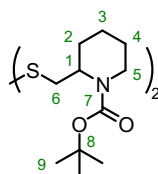
Prepared from 2-piperidinylmethanol **41** (1.00 g, 8.68 mmol) according to **general protocol A**. Instead of a dioxane and water mixture the reaction was performed in a 4/3 mixture of THF/water at a concentration of 0.025 M and with K_2CO_3 (3.0 eq.) replacing Et_3N as the base. **42** (1.69 g, 7.85 mmol, 90%) was obtained as a crystalline solid after recrystallization from MeOH:Et₂O (1:3).¹⁹

TLC R_f = 0.50 (isohexane:EtOAc, 1:1). **HRMS** (EI): C₁₁H₂₁NO₃ [M-e]: calc. 215.1516, found 215.1513. **¹H-NMR** (400 MHz, CDCl₃): δ (ppm) = 4.25 (dq, J = 6.0, 3.1 Hz, 1H), 3.91 (d, J = 13.6 Hz, 1H), 3.76 (dd, J = 10.9, 8.8 Hz, 1H), 3.58 (dd, J = 11.0, 6.2 Hz, 1H), 2.83 (t, J = 12.2 Hz, 1H), 2.47 (s, 1H), 1.71 – 1.63 (m, 1H), 1.62 – 1.51 (m, 3H), 1.46-1.32 (m, 2H), 1.43 (s, 9H).

N-Boc (S)-(piperidin-2-ylmethyl) ethanethioate (43)²⁸

Prepared from **42** (1.62 g, 7.45 mmol) according to **general protocol C**. A different concentration than in the general protocol was employed: 0.18 M for the PPh₃ solution. **43** (1.74 g, 6.35 mmol, 85%) was obtained as a colourless solid after FCC (isohexane/EtOAc).²⁸

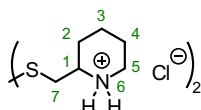
TLC R_f = 0.59 (isohexane:EtOAc, 2:1). **HRMS** (ESI⁺): C₁₃H₂₃NNaO₃S⁺: [M+Na]⁺ calc. 296.12909, found 296.12909. **¹H-NMR** (400 MHz, CDCl₃): δ (ppm) = 4.35 (s, 1H), 4.00 (d, J = 13.8 Hz, 1H), 3.18 (dd, J = 13.5, 8.5 Hz, 1H), 3.09 (dd, J = 13.6, 7.2 Hz, 1H), 2.77 (t, J = 13.5 Hz, 1H), 2.34 (s, 3H), 1.76 – 1.53 (m, 4H), 1.47 (s, 9H), 1.47 – 1.32 (m, 2H).

N-Boc, N'-Boc 1,2-bis(piperidin-2-ylmethyl)disulfane (44)

Prepared from **43** (1.050 g, 3.84 mmol) according **general protocol E** using a methanolic solution of KOH (1.00 mL, 0.015 M). **44** (801 mg, 1.74 mmol, 91%) was obtained as a colourless solid.

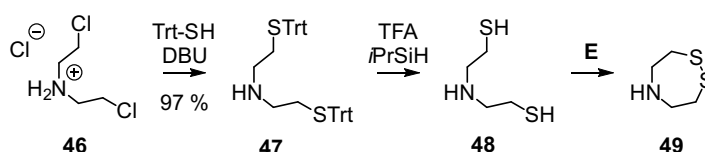
TLC R_f = 0.46 (isohexane:EtOAc, 5:1). **HRMS** (ESI⁺): C₂₂H₄₁N₂O₂S₂⁺: [M+H]⁺: calc. 461.25023, found 461.25020.

¹H-NMR (400 MHz, CDCl₃): δ (ppm) = 4.47 (s, 2H, 1-H), 4.01 (d, J = 13.6 Hz, 2H, 5-H_A), 3.00 – 2.79 (m, 4H, 6-H), 2.72 (t, J = 12.5 Hz, 2H, 5-H_B), 1.85 (dd, J = 13.7, 3.1 Hz, 2H, 4-H_A), 1.67 – 1.58 (m, 6H, 2-H, 4-H_B), 1.46 (s, 18H, 9-H), 1.39 (m, 4H, 3-H). **¹³C-NMR** (101 MHz, CDCl₃): δ (ppm) = 155.0 (C=O, C7), 79.7 (C(CH₃)₃, C8), 49.9 (CH, C1), 39.3 (CH₂, C5), 38.9 (CH₂, C6), 28.6 (C(CH₃)₃, C9), 26.8 (CH₂, C4), 25.5 (CH₂, C2), 19.1 (CH₂, C3).

1,2-bis(piperidin-2-ylmethyl)disulfane dihydrochloride (45)

Prepared from **44** (714 mg, 1.55 mmol) according to **general protocol F**. A larger amount of HCl (15 eq.) than in the general protocol was employed. **45** (513 mg, 1.54 mmol, 99%) was obtained as a colourless crystalline solid.

¹H-NMR (400 MHz, DMSO-*d*₆): δ (ppm) = 9.37 (s, 4H, 6-H), 3.33 – 3.29 (m, 2H, 1-H), 3.28 – 3.17 (m, 4H, 5-H_A; 7-H_A), 3.01 (ddd, J = 19.4, 13.8, 7.7 Hz, 2H, 7-H_B), 2.91 (d, J = 10.9 Hz, 2H, 5-H_B), 2.00 (d, J = 7.6 Hz, 2H, 2-H_A), 1.82 – 1.58 (m, 6H, 2-H_B; 4-H), 1.59 – 1.44 (m, 4H, 3-H). **¹³C-NMR** (101 MHz, DMSO-*d*₆): δ (ppm) = 54.5 (CH, C1), 54.3 (CH, C1'), 43.9 (CH₂, C5), 39.1 (CH₂, C7), 27.0 (CH₂, C2), 21.7 (CH₂, C4), 21.4 (CH₂, C3).

SS7-type precursor**bis((2-(triphenylmethyl)sulfanyl)ethyl)amine (47)²⁹**

To bis-(chloroethyl)amine hydrochloride **46** (1.46 g, 8.00 mmol, 1.0 eq.) in anhydrous DMF (24 mL) under nitrogen atmosphere at 0 °C were added triphenylmethanethiol (4.79 g, 16.80 mmol, 2.1 eq.) and DBU (4.78 mL, 32.0 mmol, 4.0 eq.). The cooling bath was removed and the mixture was stirred at room temperature for 3 h, before being concentrated under reduced pressure. The residue was purified by FCC (isohexane/EtOAc) to afford **47** (4.82 g, 7.75 mmol, 97%) as a colourless powder.²⁹

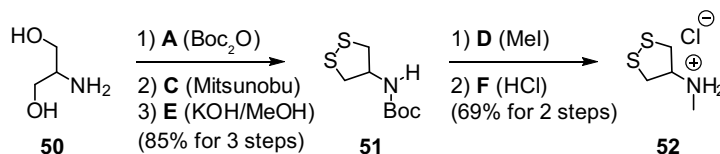
TLC R_f = 0.42 (isohexane:EtOAc; 4:1; 1% NEt₃). HRMS (EI): C₄₂H₄₀NS₂ [M-e] calc. 622.25967, found 622.25967.

¹H-NMR (500 MHz, CDCl₃): δ (ppm) = 7.36 – 7.28 (m, 12H), 7.17 (dd, J = 8.6, 7.0 Hz, 12H), 7.12 – 7.07 (m, 6H), 2.27 (t, J = 6.8 Hz, 4H), 2.17 (t, J = 6.7 Hz, 4H). ¹³C-NMR (126 MHz, CDCl₃): δ (ppm) = 144.9 (C_{Ar}), 129.6 (C_{Ar}H), 127.9 (C_{Ar}H), 126.7 (C_{Ar}H), 66.6 (C_{trityl}), 47.8 (CH₂), 32.2 (CH₂).

1,2-dithi-5-azepane (49)

Step 1: To a 0.16 M solution of **47** (1.0 eq.) in anhydrous DCM at 0 °C were added TFA (10 eq.) and triisopropylsilane (2.0 eq.). The mixture was stirred at 0 °C for 15 min, the mixture was warmed to r.t., further was stirred for further 4 h and evaporated under reduced pressure. The residue containing **48** was directly used in the next step without purification.

Step 2: To a 0.1 M solution in MeOH of the material obtained in step 1 (assuming quantitative conversion of compound **47**) was dropwise added a 0.5 M solution of I₂ in MeOH until a permanently coloured solution was observed (**general protocol E**). All volatiles were removed and the remaining crude **49** was directly used without purification.

SS50-type precursor¹¹**N-Boc 1,2-dithiolan-4-amine (51)^{11,30}**

Step 1: 2-amino-1,3-diol **50** (2.50 g, 27.4 mmol) was treated according to **general protocol A** to give *N*-Boc 2-amino-1,3-diol (5.03 g, 26.3 mmol, 96%) as a colourless solid and used without further purification.

Step 2: A solution of *N*-Boc 2-amino-1,3-diol (4.70 g, 24.3 mmol) obtained in step 1 was treated according to **general protocol C** to give *N*-Boc 2-amino-1,3-bis(thioacetate) (6.63 g, 21.6 mmol, 88%) as a colourless solid.

Step 3: *N*-Boc 2-amino-1,3-bis(thioacetate) (4.59 g, 14.9 mmol) obtained in step 2 was treated according to **general protocol E** to afford **51** (3.22 g, 14.6 mmol, 98%) as a yellow solid.

TLC R_f = 0.49 (isohexane:EtOAc, 10:1). HRMS (ESI⁻): C₈H₁₄NO₂S₂⁻ [M-H]⁻: calc. 220.04714, found 220.04718. ¹H-NMR (400 MHz, CDCl₃): δ (ppm) = 5.06 (d, J = 3.9 Hz, 1H, NH), 4.95 (s, 1H, CH), 3.21 (dd, J = 11.6, 4.8 Hz, 2H), 3.09 (dd, J = 11.6, 2.0 Hz, 2H), 1.44 (s, 9H).

N-methyl-1,2-dithiolan-4-amine hydrochloride (52)¹¹

Step 1: **51** (2.00 g, 9.04 mmol) was treated according to **general protocol D** to give *N*-Boc *N*-methyl 1,2-dithiolan-4-amine as a yellow oil.

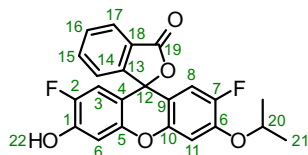
Step 2: *N*-Boc *N*-methyl 1,2-dithiolan-4-amine (118 mg, 0.501 mmol) obtained in step 1 was treated according to **general protocol F** to give hydrochloride **52** (85 mg, 0.50 mmol, quant.) as a colourless solid.

¹H-NMR (400 MHz, DMSO-*d*₆): δ (ppm) = 8.49 (s, 2H), 3.35 (p, J = 5.1 Hz, 1H), 2.58 (dd, J = 5.2, 1.7 Hz, 4H), 1.74 (s, 3H). ¹³C NMR (101 MHz, DMSO-*d*₆): δ (ppm) = 63.3 (CH), 40.4 (CH₂), 31.1 (CH₃).

32.1 mmol and the mixture was stirred for 15 h, before all volatiles were removed under reduced pressure. The residue was directly used in the next step without purification.

Step 3: To the material obtained in step 2 in MeOH (20 mL) was added 2 M aq. NaOH (1.6 mL) and the mixture was stirred for 15 h before the MeOH was evaporated under reduced pressure. Et₂O (50 mL) and diluted aq. HCl (100 mL, pH 2) were added. The organic layer was separated and the aq. layer was extracted with Et₂O (3×50 mL). The combined organic layers were dried over Na₂SO₄, filtered and evaporated under reduced pressure. The residue was purified by FCC (isohexane/EtOAc) to afford **IG-OH (62)** (0.25 g, 0.61 mmol, 19%) as an orange solid.

Bright green fluorescence was observed, when an aqueous solution of **IG-OH (62)** was exposed to UV light.

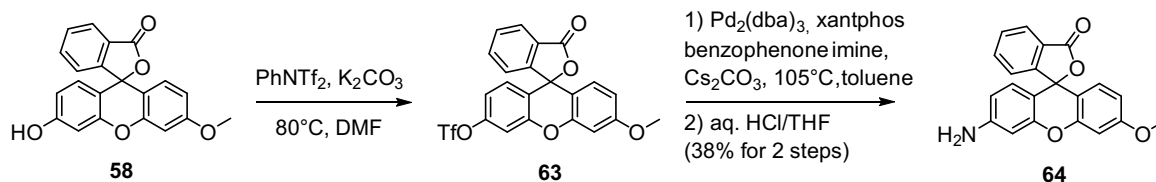


TLC R_f = 0.47 (isohexane:EtOAc; 1:1). **HRMS** (ESI⁺): C₂₃H₁₇F₂O₅⁺ [M+H]⁺: calc. 411.10386, found 411.10356.

¹H-NMR (400 MHz, DMSO-*d*₆): δ (ppm) = 10.77 (s, 1H, 22-H), 8.00 (d, *J* = 7.5 Hz, 1H, 17-H), 7.80 (t, *J* = 7.5 Hz, 1H, 15-H), 7.74 (t, *J* = 7.4 Hz, 1H, 16-H), 7.30 (d, *J* = 7.6 Hz, 1H, 14-H), 7.20 (d, *J* = 7.3 Hz, 1H, 6-H), 6.90 (d, *J* = 7.5 Hz, 1H, 3-H), 6.55 (d, *J* = 11.5 Hz, 1H, 11-H), 6.51 (d, *J* = 11.3 Hz, 1H, 8-H), 4.79 (p, *J* = 6.0 Hz, 1H, 20-H), 1.32 (dd, *J* = 5.8, 4.1 Hz, 6H, 21-H).

¹³C-NMR (101 MHz, CDCl₃): δ (ppm) = 169.2 (C=O, C19), 152.1, 151.0, 149.0, 148.6, 148.5, 148.5, 148.4, 148.1 (d, *J* = 2.0 Hz, C_{Ar}, C2), 146.7, 135.5 (C_{Ar}H, C15), 130.4 (C_{Ar}H, C16), 126.7 (C_{Ar}H, C17), 125.6, 124.1 (C_{Ar}H, C14), 114.1 (d, *J* = 21.4 Hz, C_{Ar}H, C3), 113.7 (d, *J* = 20.8 Hz, C_{Ar}H, C8), 110.4 (d, *J* = 6.0 Hz, C_{Ar}, C2), 109.5 (d, *J* = 6.1 Hz, C_{Ar}, C7), 105.4 (C_{Ar}H, C6), 104.1 (C_{Ar}H, C11), 72.5 (C_{spiro}, C12), 29.8 (CH, C20), 22.0 (CH₃, C21).

3'-amino-6'-methoxy-3H-spiro[isobenzofuran-1,9'-xanthen]-3-one (MR-NH₂, 64)



Step 1: A mixture of **58** (800 mg, 2.31 mmol, 1.0 eq.), K₂CO₃ (479 mg, 3.46 mmol, 1.5 eq.), bis(trifluoromethane sulfonyl)aniline (908 mg, 2.54 mmol, 1.1 eq.) and anhydrous DMF (10 mL) was stirred at 80 °C for 1.5 h. Then, the solvent was evaporated under reduced pressure. The residue was taken up in DCM (10 mL), the mixture was filtered over silica (6 g) and the silica was washed with additional DCM (60 mL). The solvent was removed under reduced pressure and the residue containing **63** was directly used for further steps without purification.

Step 2: To the material obtained in step 1 were added Pd₂(dba)₃ (212 mg, 0.231 mmol, 0.1 eq.), Xantphos (200 mg, 0.346 mmol, 0.15 eq.), Cs₂CO₃ (1.05 g, 3.23 mmol, 1.4 eq.) and toluene (25 mL). The mixture was degassed by evacuating under sonication and refilling with nitrogen, before benzophenone imine (465 μL, 2.77 mmol, 1.2 eq.) was added. Then, the mixture was again degassed and warmed to 105 °C. After stirring at 105 °C for 15 h, the mixture was cooled to r.t. and filtered over Celite®. The Celite® was washed with DCM until the filtrate turned colourless. The filtrate was evaporated under reduced pressure, then THF (30 mL) and 1 M aq. HCl (3 mL) were added. After stirring for 1 h, water (40 mL) was added and the mixture was extracted with EtOAc (3×40 mL). The extracts were washed with sat. aq. NaCl (40 mL), dried over Na₂SO₄, filtered and evaporated under reduced pressure. The residue was purified by FCC (0 to 30% EtOAc in DCM) to afford compound **MR-OH (64)** (302 mg, 0.874 mmol, 38%) as an orange solid.

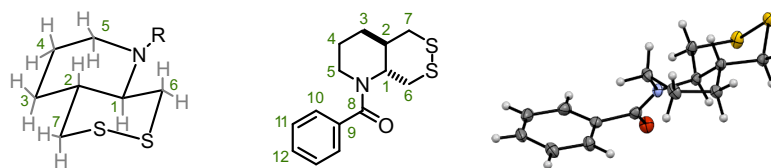
Bright green fluorescence was observed, when an aqueous solution of **MR-NH₂ (64)** was exposed to UV light.

TLC R_f = 0.43 (30% EtOAc in DCM).

¹H-NMR (400 MHz, DMSO-*d*₆): δ (ppm) = 7.97 (dd, *J* = 7.6, 1.2 Hz, 1H), 7.78 (td, *J* = 7.5, 1.2 Hz, 1H), 7.70 (td, *J* = 7.4, 1.0 Hz, 1H), 7.25 (d, *J* = 7.7 Hz, 1H), 6.90 (d, *J* = 2.5 Hz, 1H), 6.67 (dd, *J* = 8.8, 2.5 Hz, 1H), 6.59 (d, *J* = 8.8 Hz, 1H), 6.43 (d, *J* = 2.1 Hz, 1H), 6.37 (d, *J* = 8.5 Hz, 1H), 6.34 (s, 1H), 5.68 (s, 2H), 3.80 (s, 3H).

The spectroscopic data agrees with previously reported values.³³

8.4. Probe synthesis

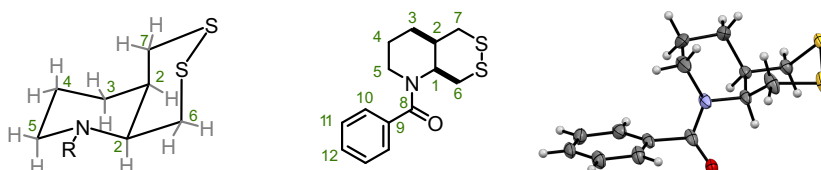
Bz-Series**trans-(hexahydro-[1,2]dithiino[4,5-b]pyridin-1(2H)-yl)benzamide (SS66T-Bz, 65)**

Prepared from **8** (16.7 mg, 0.079 mmol) and BzCl (15.0 μ L, 0.128 mmol) according to **general protocol H**. Purification by FCC (isohehexane/EtOAc) gave **65** (14.5 mg, 0.052 mmol, 66%) as a colourless solid. Unambiguous confirmation of the absolute configuration was derived from a single-crystal X-Ray analysis.

TLC R_f = 0.59 (isohehexane:EtOAc, 2:1). **HRMS** (EI): $C_{14}H_{17}NOS_2$ [M-e] calc. 279.0747, found 279.0747.

1H -NMR (500 MHz, $CDCl_3$): δ (ppm) = 7.42 – 7.38 (m, 3H, 10-H; 12-H), 7.38 – 7.34 (m, 2H, 11-H), 4.13 (td, $^3J_{1-6}$ = 10.7 Hz, $^3J_{1-6'}$ = 2.9 Hz, 1H, 1-H), 3.48 (ddd, $^2J_{5-5}$ = 14.2 Hz, $^3J_{5-4}$ = 7.3 Hz, $^3J_{5-4'}$ = 2.0 Hz, 1H, 5'-H), 3.32 (ddd, $^2J_{5-5'}$ = 14.1 Hz, $^3J_{5-4}$ = 11.2 Hz, $^3J_{5-4'}$ = 5.4 Hz, 1H, 5-H), 3.22 (dd, $^2J_{6-6}$ = 12.7 Hz, $^3J_{6-1}$ = 2.9 Hz, 1H, 6'-H), 3.08 (dd, $^2J_{6-6'}$ = 12.7 Hz, $^3J_{6-1}$ = 10.4 Hz, 1H, 6-H), 2.96 (dd, $^2J_{7-7'}$ = 13.4 Hz, $^3J_{7-2}$ = 10.9 Hz, 1H, 7-H), 2.80 (dd, $^2J_{7-7'}$ = 13.5 Hz, $^3J_{7-2}$ = 2.6 Hz, 1H, 7'-H), 2.20 (dt, J = 13.5 Hz, $^3J_{2-7}$ = 11.0 Hz, $^3J_{2-7'}$ = 2.7 Hz, 1H, 2-H), 1.83 – 1.72 (m, 1H, 4-H), 1.70 – 1.59 (m, 2H, 4-H; 3-H), 1.46 – 1.34 (m, 1H, 3-H).

^{13}C -NMR (126 MHz, $CDCl_3$): δ (ppm) = 171.6 (C=O, C8), 136.8 (C_{Ar} , C9), 129.8 (C_{ArH} , C10), 128.7 (C_{ArH} , C12), 126.8 (C_{ArH} , C11), 61.6 (CH, C1), 42.0 (CH_2 , C5), 41.1 (CH_2 , C7), 40.5 (CH, C2), 36.3 (CH_2 , C6), 26.7 (CH_2 , C3), 23.8 (CH_2 , C4).

cis-(hexahydro-[1,2]dithiino[4,5-b]pyridin-1(2H)-yl)benzamide (SS66C-Bz, 66)

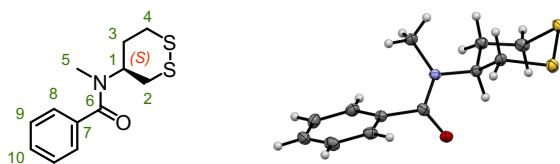
Prepared from crude **18** (corresponding to 20.0 mg, 0.068 mmol of compound **12**) and BzCl (16 μ L, 0.135 mmol) according to **general protocol H**. Compound **66** (7.8 mg, 0.028 mmol, 41%) was obtained as a colourless solid after FCC (isohehexane/EtOAc). Unambiguous confirmation of the absolute configuration was derived from a single-crystal X-Ray analysis.

TLC R_f = 0.48 (isohehexane:EtOAc, 2:1). **HRMS** (EI): $C_{14}H_{17}NOS_2$ [M-e] calc. 279.0747, found 279.0744.

Individual rotamers were observed by NMR spectroscopy at 298 K (ratio ca. 2:1) and measurements at 373 K were not sufficient to obtain time-averaged spectra. The following data refers to the major rotamer and is supported by 2D-NMR and TOCSY experiments.

1H -NMR (400 MHz, $CDCl_3$): δ (ppm) = 7.52 – 7.30 (m, 5H, 10-H; 11-H; 12-H), 5.07 (d, J = 12.0 Hz, 1H, 1-H), 3.70 – 3.44 (m, 3H, 5- H_A ; 6- H_A ; 7- H_A), 3.03 (t, J = 13.3 Hz, 1H, 5- H_B), 2.81 (d, J = 14.1 Hz, 1H, 7- H_B), 2.56 (d, J = 12.9 Hz, 1H, 6- H_B), 2.37 (t, J = 13.4 Hz, 1H, 4- H_A), 2.27 (d, J = 13.7 Hz, 1H, 2-H), 1.80 – 1.68 (m, 1H, 3- H_A), 1.64 (br-s, 1H, 3- H_B), 1.53 (d, J = 13.7 Hz, 1H, 4- H_B).

^{13}C -NMR (101 MHz, $CDCl_3$): δ (ppm) = 170.8 (C=O, C8), 136.2 (C_{Ar} , C9), 129.8 (C_{ArH} , C12), 128.7 (C_{ArH} , C10), 126.9 (C_{ArH} , C11), 50.8 (CH, C1), 43.8 (CH_2 , C7), 42.1 (CH_2 , C5), 35.8 (CH, C2), 29.5 (CH_2 , C6), 26.1 (CH_2 , C3), 23.9 (CH_2 , C4).

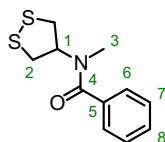
(S)-N-methyl-N-(1,2-dithian-4-yl)benzamide (SS60-Bz, 67)

Prepared from **25** (74 mg, 0.40 mmol) and BzCl (2.7 eq.) according to **general protocol H**. Purification by FCC (isohexane/EtOAc) gave **67** (80 mg, 0.31 mmol, 79%) a colourless solid. Unambiguous confirmation of the absolute configuration was derived from a single-crystal X-Ray analysis.

TLC R_f = 0.28 (isohexane:EtOAc, 2:1). **HRMS** (EI): $C_{12}H_{15}NOS_2$ [M-e] calc. 253.0590, found 253.0587.

1H -NMR (400 MHz, DMSO- d_6 , 373 K): δ (ppm) = 7.48 – 7.41 (m, 3H, 8-H; 10-H), 7.39 – 7.33 (m, 2H, 9-H), 4.19 (s, 1H, 1-H), 3.19 (dd, J = 12.9, 11.2 Hz, 1H, 2- H_A), 3.11 (dt, J = 13.7, 4.0 Hz, 1H, 3- H_A), 3.02 (d, J = 11.0 Hz, 1H, 2- H_B), 2.91 – 2.82 (m, 1H, 3- H_B), 2.84 (s, 3H, 5-H), 2.21 – 2.04 (m, 2H, 4-H).

^{13}C -NMR (101 MHz, DMSO- d_6 , 373 K): δ (ppm) = 169.7 (C=O, 6-H), 136.4 (C_{Ar} , 7-H), 128.6 (C_{Ar} , 8-H), 127.8 (C_{Ar} , 9-H), 125.9 (C_{Ar} , 10-H), 54.9 (CH, 1-H), 35.1 (CH $_2$, 2-H), 34.7 (CH $_2$, 3-H), 31.5 (CH $_2$, 4-H), 30.0 (CH $_3$, 5-H).

N-methyl-N-(1,2-dithiolan-4-yl)benzamide (SS50-Bz, 68)

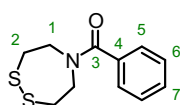
Prepared from **52** (43.0 mg, 0.250 mmol) and BzCl (4.0 eq.) according to **general protocol H**. Purification by FCC (isohexane/EtOAc) gave **67** (21.7 mg, 0.091 mmol, 36%) as a colourless solid.

TLC R_f = 0.44 (isohexane:EtOAc, 2:1). **HRMS** (EI): for $C_{11}H_{13}NOS_2$ [M-e] calc. 239.0434, found 239.0432.

Individual rotamers were observed by NMR spectroscopy at 298 K (ratio ca. 1:1) and time-averaged spectra were obtained at 373 K.

1H -NMR (400 MHz, DMSO- d_6 , 373 K): δ (ppm) = 7.50 – 7.43 (m, 3H, 6-H; 8-H), 7.43 – 7.37 (m, 2H, 7-H), 5.03 (s, 1H, 1-H), 3.37 (dd, $^2J_{2A-2B}$ = 11.9 Hz, $^3J_{2A-1}$ = 7.4 Hz, 2H, 2- H_A), 3.28 (dd, $^2J_{2B-2A}$ = 11.9 Hz, $^3J_{2B-1}$ = 6.4 Hz, 2H, 2- H_B), 2.92 (s, 3H, 3-H).

^{13}C -NMR (101 MHz, DMSO- d_6 , 373 K): δ (ppm) = 170.2 (C=O, C4), 136.1 (C_{Ar} , C5), 128.8 (C_{Ar} , C8), 127.8 (C_{Ar} , C6), 126.1 (C_{Ar} , C7), 61.7 (CH $_2$, C1), 39.0 (CH $_2$, C2), 30.1 (CH $_2$, C3).

(1,2,5-dithiazepan-5-yl)(phenyl)methanone (SS7-Bz, 69)

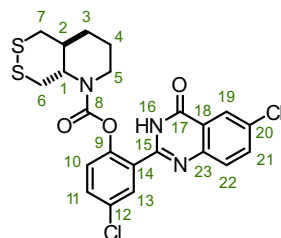
Prepared from crude **49** (corresponding to 200 mg, 0.321 mmol of compound **47**) and BzCl (2.0 eq.) according to **general protocol H**. Purification by FCC (isohexane/EtOAc) gave **68** (6.4 mg, 0.027 mmol, 8%) as a solid.

TLC R_f = 0.33 (isohexane:EtOAc, 2:1). **HRMS** (EI): $C_{11}H_{13}NOS_2$ [M-e] calc. 239.0434, found 239.0432.

Individual rotamers were observed by NMR spectroscopy at 298 K (ratio ca. 1:1) and measurements at 373 K were not sufficient to obtain time-averaged spectra.

1H -NMR (400 MHz, $CDCl_3$): δ (ppm) = 7.32 (br-s, 5H, 5-H; 6-H, 7-H), 4.01 (t, J = 5.7 Hz, 2H, 1-H), 3.61 (t, J = 5.7 Hz, 2H, 1'-H), 3.11 (t, J = 5.7 Hz, 2H, 2-H), 2.63 (t, J = 5.7 Hz, 2H, 2'-H).

^{13}C -NMR (101 MHz, $CDCl_3$): δ (ppm) = 172.2 (C=O, C3), 136.8 (C_{Ar} , C4), 129.6 (C_{Ar} , C7), 128.8 (C_{Ar} , C5), 126.2 (C_{Ar} , C6), 53.6 (CH $_2$, C1), 49.7 (CH $_2$, C1'), 40.2 (CH $_2$, C2), 25.4 (CH $_2$, C2').

PQ-Series***trans*-chloro-2-(chloro-4-oxo-3,4-dihydroquinazolin-2-yl)phenyl *trans*-hexahydro-[1,2]dithiino [4,5-*b*]pyridine-1(2*H*)-carboxylate (SS66T-PQ, 70)**

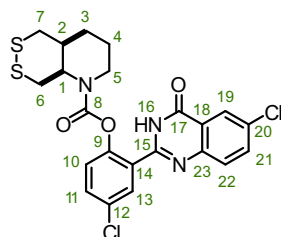
Prepared from **8** (57.9 mg, 0.273 mmol) and **55** (70.0 mg, 0.228 mmol) according to **general protocol G**. Purification by FCC (isohexane/EtOAc) gave **70** (75.0 mg, 0.148 mmol, 65%) as a colourless solid.

TLC R_f = 0.44 (isohexane:EtOAc, 2:1). **HRMS** (ESI⁺): for C₂₂H₂₀Cl₂N₃O₃S₂⁺ [M+H]⁺: calc. 508.03176, found 508.03187.

Individual rotamers were observed by NMR spectroscopy at 298 K (ratio ca. 1:1) and time-averaged spectra were obtained at 373 K.

¹H-NMR (400 MHz, tetrachlorethane-*d*₂, 373 K): δ (ppm) = 8.23 (t, ⁴ J_{19-21} = 1.5 Hz, 1H, **19-H**), 7.95 (d, J_{13-11} = 2.6 Hz, 1H, **13-H**), 7.76 – 7.67 (m, 1H, **21-H; 22-H**), 7.49 (dd, ³ J_{11-10} = 8.7 Hz, ⁴ J_{11-13} = 2.6 Hz, 1H, **11-H**), 7.15 (d, ³ J_{10-11} = 8.7 Hz, 1H, **10-H**), 3.77 (ddd, ² J_{5A-5B} = 13.6 Hz, ³ J_{5A-4} = 6.8 Hz, ³ J_{5A-4B} = 3.3 Hz, 1H, **5-H_A**), 3.72 (ddd, ³ J_{1-2} = 11.0 Hz, ³ J_{1-6A} = 10.5 Hz, ³ J_{1-6B} = 3.2 Hz, 1H, **1-H**), 3.38 (ddd, ² J_{5B-5A} = 14.0 Hz, ³ J_{5B-4} = 10.2 Hz, ³ J_{5-4B} = 5.5 Hz, 1H, **5-H_B**), 3.11 (dd, ² J_{6A-6B} = 12.9 Hz, ³ J_{6A-1} = 10.3 Hz, 1H, **6-H_A**), 3.03 (dd, ² J_{6B-6A} = 13.0 Hz, ³ J_{6B-1} = 3.3 Hz, 1H, **6-H_B**), 2.87 (dd, ² J_{7A-7B} = 13.6 Hz, ³ J_{7A-2} = 10.7 Hz, 1H, **7-H_A**), 2.75 (dd, ² J_{7B-7A} = 13.5 Hz, ³ J_{7B-2} = 3.0 Hz, 1H, **7-H_B**), 2.07 (ddd, ³ J_{2-1} = 13.5 Hz, ³ J_{2-7A} = 10.7 Hz, 1H, **2-H**), 1.86 (ddd, ² J_{4A-4B} = 11.3 Hz, ³ J_{4A-5B} = 7.6 Hz, 1H, **4-H_A**), 1.70 (ddd, ² J_{4B-4A} = 12.4 Hz, ³ J_{4B-5B} = 3.4 Hz, 1H, **4-H_B**), 1.66 – 1.55 (m, 1H, **3-H_A**), 1.39 – 1.22 (m, 1H, **3-H_B**).

¹³C-NMR (101 MHz, tetrachlorethane-*d*₂, 373 K): δ (ppm) = 160.4 (C=O, **C17**), 153.3 (C=O, **C8**), 149.0 (C=N, **C15**), 147.1 (C_{Ar}, **C18**), 135.3 (C_{Ar}H, **C22**), 133.2 (C_{Ar}, **C23**), 132.3 (C_{Ar}H, **C11**), 131.9 (C_{Ar}, **C12**), 130.3 (C_{Ar}H, **C13**), 129.5 (C_{Ar}H, **C21**), 128.0 (C_{Ar}, **C14**), 125.8 (C_{Ar}H, **C19**), 125.3 (C_{Ar}H, **C10**), 121.9 (C_{Ar}, **C20**), 63.1 (CH, **C1**), 40.7 (CH₂, **C7**), 40.2 (CH, **C2**), 39.5 (CH₂, **C5**), 36.2 (CH₂, **C6**), 26.9 (CH₂, **C3**), 23.1 (CH₂, **C4**).

***cis*-chloro-2-(chloro-4-oxo-3,4-dihydroquinazolin-2-yl)phenyl-hexahydro-[1,2]dithiino [4,5-*b*]pyridine-1(2*H*)-carboxylate (SS66C-PQ, 71)**

Prepared from crude **18** (corresponding to 41.5 mg, 0.140 mmol of **12**) and **55** (51.6 mg, 0.168 mmol) according to **general protocol G**. Purification by FCC (isohexane/EtOAc) gave **71** (28.4 mg, 0.056 mmol, 40%) as a colourless solid.

TLC R_f = 0.40 (isohexane:EtOAc, 2:1). **HRMS** (ESI⁺): C₂₂H₂₀Cl₂N₃O₃S₂⁺ [M+H]⁺: calc. 508.03176, found 508.03186.

Individual rotamers were observed by NMR spectroscopy at 298 K (ratio ca. 1.2:1). The following data refers to the major rotamer, as indicated based on 2D-NMR analysis.

¹H-NMR (500 MHz, CDCl₃): δ (ppm) = 10.15 (s, 1H, 16-H), 8.26 (t, ⁴J₁₉₋₂₁ = 2.3 Hz, 1H, 19-H), 7.99 (d, ⁴J₁₃₋₁₁ = 2.6 Hz, 1H, 13-H), 7.80 – 7.67 (m, 2H, 21-H; 22-H), 7.51 (dt, ³J₁₁₋₁₀ = 8.8 Hz, ⁴J₁₁₋₁₃ = 2.7 Hz, 1H, 11-H), 7.17 (d, ³J₁₀₋₁₁ = 6.8 Hz, 1H, 10-H), 4.50 (dt, ³J_{1-6A} = 12.1 Hz, ³J_{1-6B} = 4.2 Hz, 1H, 1-H), 4.15 (dd, ²J_{5A-5B} = 13.9 Hz, ³J_{5A-4A} = 4.6 Hz, 1H, 5-H_A), 3.47 (dd, ²J_{7A-7B} = 13.9 Hz, ³J_{7A-2} = 6.2 Hz, 1H, 7-H_A), 3.41 (t, ²J_{6A-6B} = 13.0 Hz, ³J_{6A-1} = 12.1 Hz, 1H, 6-H_A), 3.07 (td, ²J_{5B-5A} = 13.5 Hz, ³J_{5B-4A} = 3.1 Hz, 1H, 5-H_B), 2.79 (td, ²J_{7B-7A} = 13.9 Hz, ³J_{7B-2} = 13.2 Hz, 1H, 7-H_B), 2.39 (dd, ²J_{6B-6A} = 13.1 Hz, ³J_{6B-1} = 3.9 Hz, 1H, 6-H_B), 2.30 (dd, ²J_{3A-3B} = 12.9 Hz, ³J_{3A-2} = 4.0 Hz, 1H, 3-H_A), 2.20 (dt, ³J_{2-7B} = 12.5 Hz, ³J_{2-7A} = 3.7 Hz, 1H, 2-H), 1.83 (t, ²J_{4A-4B} = 13.6 Hz, 1H, 4-H_A), 1.68 – 1.55 (m, 1H, 4-H_B), 1.49 (d, ²J_{3B-3A} = 13.3 Hz, 1H, 3-H_B).

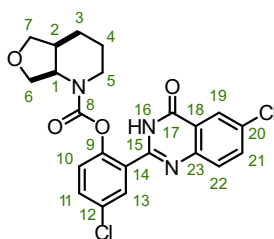
¹³C-NMR (101 MHz, CDCl₃): δ (ppm) = 160.7 (C=O, C17), 153.3 (C=O, C8), 149.3 (C=N, C15), 147.6 (C_{Ar}, C9), 147.5 (C_{Ar}, C18), 135.5 (C_{Ar}, C22), 133.6 (C_{Ar}, C23), 132.5 (C_{Ar}H, C11), 132.4 (C_{Ar}, C12), 130.7 (C_{Ar}H, C13), 129.8 (C_{Ar}H, C21), 128.1 (C_{Ar}, C14), 126.2 (C_{Ar}H, C19), 125.3 (C_{Ar}H, C10), 122.3 (C_{Ar}, C20), 53.3 (CH, C1), 42.1 (CH₂, C7), 40.7 (CH₂, C5), 35.2 (CH, C2), 29.3 (CH₂, C6), 26.3 (CH₂, C3), 23.4 (CH₂, C4).

Time-averaged spectra were obtained at 373 K.

¹H-NMR (400 MHz, tetrachlorethan-*d*₂, 373 K): δ (ppm) = 9.72 (s, 1H, 16-H), 8.23 (t, ⁴J₁₉₋₂₁ = 1.5 Hz, 1H, 19-H), 7.99 (d, ⁴J₁₃₋₁₁ = 2.6 Hz, 1H, 13-H), 7.73 (m, 2H, 21-H; 22-H), 7.50 (dd, ³J₁₁₋₁₀ = 8.7 Hz, ⁴J₁₁₋₁₃ = 2.6 Hz, 1H), 7.17 (d, ³J₁₀₋₁₁ = 8.7 Hz, 1H, 10-H), 4.48 (d, ³J_{1-6A} = 11.7 Hz, 1H, 1-H), 4.07 (d, ²J_{5A-5B} = 12.5 Hz, 1H, 5-H_A), 3.53 – 3.33 (m, 2H, 6-H_A; 7-H_A), 3.18 – 2.88 (m, 1H, 5-H_A), 2.77 (dd, ²J_{7B-7A} = 14.0 Hz, *J* = 3.0 Hz, 1H, 7-H_B), 2.43 (d, ²J_{6B-6A} = 12.7 Hz, 1H, 6-H_B), 2.28 (dd, ²J_{3A-3B} = 12.7 Hz, *J* = 4.0 Hz, 1H, 3-H_A), 2.25 – 2.17 (m, 1H, 2-H), 1.81 (d, ²J_{4A-4B} = 13.6 Hz, 1H, 4-H_A), 1.70 – 1.54 (m, 1H, 4-H_B), 1.47 (d, ²J_{3B-3A} = 13.1 Hz, 1H, 3-H_B).

¹³C-NMR (101 MHz, tetrachlorethan-*d*₂, 373 K): δ (ppm) = 160.2 (C=O, C17), 154.9 (C=O, C8), 149.1 (C=N, C15), 147.7 (C_{Ar}, C19), 147.5 (C_{Ar}, C18), 135.3 (C_{Ar}H, C22), 133.5 (C_{Ar}, C23), 132.4 (C_{Ar}H, C11), 132.3 (C_{Ar}, C12), 130.5 (C_{Ar}H, C13), 129.9 (C_{Ar}H, C21), 128.0 (C_{Ar}, C14), 126.1 (C_{Ar}H, C18), 125.4 (C_{Ar}H, C10), 122.4 (C_{Ar}, C20), 54.6 (CH, C1), 42.2 (CH₂, C7), 41.3 (CH₂, C5), 36.0 (CH, C2), 29.7 (CH₂, C6), 25.3 (CH₂, C3), 23.1 (CH₂, C4).

cis-chloro-2-(chloro-4-oxo-3,4-dihydroquinazolin-2-yl)phenyl-hexahydrofuro-[3,4-*b*]pyridine-1(2*H*)-carboxylate (O56-PQ, 72)



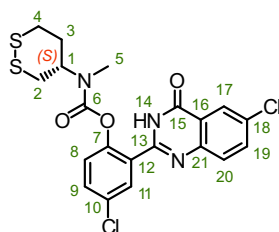
Prepared from **19** (92 mg, 0.56 mmol) and **55** (345 mg, 1.12 mmol) according to **general protocol G**. Purification by FCC (Et₂O) gave **72** (199 mg, 0.432 mmol, 77%) as a colourless solid.

TLC R_f = 0.51 (Et₂O). **HRMS** (ESI⁺): C₂₂H₂₀Cl₂N₃O₄⁺ [M+H]⁺: calc. 460.08254, found 460.08240.

Individual rotamers were observed by NMR spectroscopy at 298 K (ratio ca. 1.2:1) and time-averaged spectra were obtained at 373 K.

¹H-NMR (400 MHz, tetrachlorethane-*d*₂, 373 K): δ (ppm) = 9.65 (s, 1H, 16-H), 8.23 (t, *J* = 1.5 Hz, 1H, 19-H), 7.96 (d, *J* = 2.6 Hz, 1H, 13-H), 7.78 – 7.63 (m, 2H, 21-H; 22-H), 7.48 (dd, *J* = 8.7, 2.6 Hz, 1H, 11-H), 7.17 (d, *J* = 8.7 Hz, 1H, 10-H), 4.69 (q, *J* = 8.0 Hz, 1H, 1-H), 3.99 (dd, *J* = 13.7, 4.4 Hz, 1H, 5-H_A), 3.90 (t, *J* = 8.5 Hz, 1H, 6-H_A), 3.83 (dd, *J* = 8.8, 5.4 Hz, 1H, 7-H_A), 3.63 (dd, *J* = 8.8, 1.9 Hz, 1H, 7-H_B), 3.63 (dd, *J* = 9.0, 8.5 Hz, 1H, 6-H_B), 3.07 (t, *J* = 12.9 Hz, 1H, 5-H_B), 2.25 (tq, *J* = 7.4, 2.8, 2.1 Hz, 1H, 2-H), 1.86 – 1.69 (m, 2H, 3-H_A; 4-H_A), 1.57 – 1.44 (m, 2H, 3-H_B; 4-H_B).

¹³C-NMR (101 MHz, tetrachlorethan-*d*₂, 373 K): δ (ppm) = 160.1 (C=O, C17), 153.7 (C=O, C8), 149.1 (C=N, C15), 147.8 (C_{Ar}, C9), 147.5 (C_{Ar}, C18), 135.1 (C_{Ar}H, C22), 133.4 (C_{Ar}, C23), 132.2 (C_{Ar}H, C11), 132.1 (C_{Ar}, C12), 130.4 (C_{Ar}H, C13), 129.8 (C_{Ar}H, C21), 128.0 (C_{Ar}, C14), 126.0 (C_{Ar}H, C19), 125.1 (C_{Ar}H, C10), 122.4 (C_{Ar}, C20), 73.2 (CH₂, C7), 67.1 (CH₂, C6), 54.8 (CH, C1), 41.3 (CH₂, C5), 36.0 (CH, C2), 24.6 (CH₂, C3), 22.8 (CH₂, C4).

chloro-2-(chloro-4-oxo-3,4-dihydroquinazolin-2-yl)phenyl ((S)-1,2-dithian-4-yl) (methyl) carbamate (SS60-PQ, 73)

Prepared from **25** (56 mg, 0.30 mmol) and **55** (180 mg, 0.586 mmol) according to **general protocol G**. Purification by FCC (Et₂O) gave **73** (108 mg, 0.224 mmol, 75%) as a colourless solid.

TLC R_f = 0.31 (isohexane:EtOAc, 2:1). **HRMS** (ESI⁺): C₂₀H₁₈Cl₂N₃O₃S₂⁺ [M+H]⁺ calc. 482.01611, found 482.01592.

Individual rotamers were observed by NMR spectroscopy at 298 K (ratio ca. 1.5:1) and time-averaged spectra were obtained at 373 K.

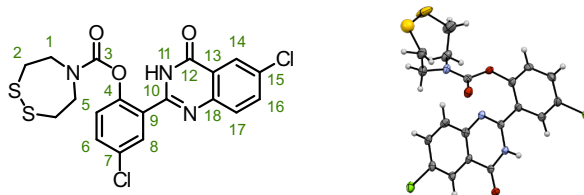
¹H-NMR (400 MHz, tetrachlorethane-*d*₂, 373 K): δ (ppm) = 9.56 (s, 1H, **14-H**), 8.22 (t, *J* = 1.5 Hz, 1H, **17-H**), 7.97 (d, *J* = 2.6 Hz, 1H, **11-H**), 7.78 – 7.66 (m, 2H, **19-H**; **20-H**), 7.49 (dd, *J* = 8.7, 2.6 Hz, 1H, **9-H**), 7.17 (d, *J* = 8.8 Hz, 1H, **8-H**), 4.17 (d, *J* = 12.1 Hz, 1H, **1-H**), 3.15 (ddd, *J* = 13.8, 11.8, 2.8 Hz, 1H, **3-H_B**), 3.10 (dd, *J* = 12.9, 11.4 Hz, 1H, **2-H_A**), 2.97 (s, 3H, **5-H**), 2.93 (t, *J* = 3.8 Hz, 1H, **3-H_B**), 2.72 (dd, *J* = 12.8, 3.2 Hz, 1H, **2-H_B**), 2.17 – 2.01 (m, 2H, **4-H**).

¹³C-NMR (101 MHz, tetrachlorethan-*d*₂, 373 K): δ (ppm) = 160.0 (C=O, **C15**), 153.4 (C=O, **C6**), 149.0 (C=N, **C13**), 147.7 (C_{Ar}, **C7**), 147.5 (C_{Ar}, **C16**), 135.2 (C_{Ar}H, **C20**), 133.5 (C_{Ar}, **C21**), 132.3 (C_{Ar}H, **C9**), 132.3 (C_{Ar}, **C10**), 130.4 (C_{Ar}H, **C11**), 129.8 (C_{Ar}H, **C19**), 128.0 (C_{Ar}, **C12**), 126.0 (C_{Ar}H, **C17**), 125.2 (C_{Ar}H, **C8**), 122.5 (C_{Ar}, **C18**), 57.1 (CH, **C1**), 36.1 (CH₂, **C2**), 35.9 (CH₂, **C3**), 32.6 (CH₂, **C4**), 30.5 (CH₃, **C5**).

4-chloro-2-(6-chloro-4-oxo-3,4-dihydroquinazolin-2-yl)phenyl (1,2-dithiolan-4-yl) (methyl)carbamate (SS50-PQ, 74)¹¹

Prepared from **52** (56 mg, 0.30 mmol) and **55** (180 mg, 0.586 mmol) according to **general protocol G**. Purification by FCC (isohexane/EtOAc) gave **74** (39.0 mg, 0.083 mmol, 49%) as a colourless solid.

TLC R_f = 0.26 (isohexane:EtOAc, 3:1). **HRMS** (ESI⁺): C₁₉H₁₆Cl₂N₃O₃S₂⁺ [M+H]⁺: calc. 468.00046, found 468.00049. **¹H-NMR** (400 MHz, tetrachlorethan-*d*₂, 373 K): δ (ppm) = 8.24 – 8.22 (m, 1H), 7.95 (d, *J* = 2.6 Hz, 1H), 7.71 (d, *J* = 1.9 Hz, 2H), 7.50 (dd, *J* = 8.7, 2.7 Hz, 1H), 7.20 (d, *J* = 8.7 Hz, 1H), 5.09 (p, *J* = 6.7 Hz, 1H), 3.32 (dd, *J* = 12.1, 7.6 Hz, 2H), 3.10 (dd, *J* = 12.1, 5.6 Hz, 2H), 3.04 (s, 3H). **¹³C-NMR** (101 MHz, tetrachlorethan-*d*₂, 373 K): δ (ppm) = 160.1, 153.7, 149.0, 147.6, 147.4, 135.3, 133.6, 132.3, 132.1, 130.4, 129.7, 128.0, 126.1, 125.2, 122.4, 62.9, 40.7, 30.6.

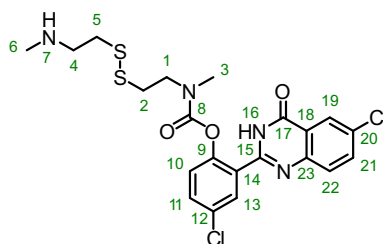
chloro-2-(chloro-4-oxo-3,4-dihydroquinazolin-2-yl)phenyl 1,2,5-dithiazepane-carboxylate (SS7-PQ, 75)

Prepared from crude **49** (corresponding to 400 mg, 0.642 mmol of **47**) and an excess of **55** (237 mg, 0.771 mmol) according to **general protocol G** to give **75** (23 mg, 0.049 mmol, 7%) as a colourless solid after FCC (isohexane/EtOAc). Unambiguous confirmation of the absolute configuration was derived from a single-crystal X-Ray analysis.

TLC R_f = 0.32 (isohexane:EtOAc, 2:1). **HRMS** (ESI⁺): C₁₉H₁₆Cl₂N₃O₃S₂⁺ [M+H]⁺: calc. 466.9932, found 466.9930.

¹H-NMR (400 MHz, CDCl₃): δ (ppm) = 10.04 (s, 1H, **11-H**), 8.28 (dd, *J* = 2.1, 0.9 Hz, 1H, **14-H**), 7.90 (d, *J* = 2.6 Hz, 1H, **8-H**), 7.80 – 7.65 (m, 2H, **16-H**; **17-H**), 7.53 (dd, *J* = 8.7, 2.6 Hz, 1H, **6-H**), 7.19 (d, *J* = 8.7 Hz, 1H, **5-H**), 3.91 (dt, *J* = 5.8 Hz, 4H, **1-H**), 3.02 (dt, *J* = 30.7, 5.7 Hz, 4H, **2-H**).

¹³C-NMR (126 MHz, CDCl₃): δ (ppm) = 160.6 (C=O, **C12**), 154.4 (C=O, **C3**), 149.4 (C=N, **C10**), 147.4 (C_{Ar}, **C4**), 147.3 (C_{Ar}, **C13**), 135.4 (C_{Ar}H, **C17**), 133.6 (C_{Ar}, **C18**), 132.6 (C_{Ar}H, **C6**), 132.5 (C_{Ar}, **C7**), 130.7 (C_{Ar}H, **C8**), 129.7 (C_{Ar}H, **C16**), 128.9 (C_{Ar}, **C9**), 126.2 (C_{Ar}H, **C14**), 125.3 (C_{Ar}H, **C5**), 122.7 (C_{Ar}, **C15**), 52.5 (CH, **C1**), 51.8 (CH, **C1'**), 37.9 (CH₂, **C2**), 36.4 (CH₂, **C2'**).

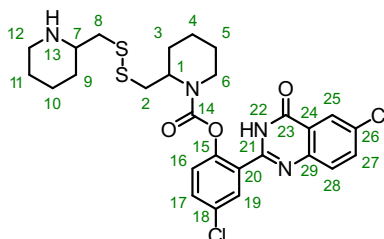
chloro-2-(chloro-4-oxo-3,4-dihydroquinazolin-2-yl)phenyl methyl(2-((2-(methylamino)ethyl)disulfaneyl)ethyl)carbamate (SS00-PQ, 76)

Prepared from **34** (715 mg, 2.82 mmol) and **55** (333 mg, 1.08 mmol) according to **general protocol G** to give **76** (245 mg, 0.477 mmol, 44%) as a colourless solid FCC (EtOAc/MeOH). Precipitation of the hydrochloride salt was achieved by adding HCl (1 M in Et₂O) to a solution of the residue in Et₂O, followed by filtration to **76**·HCl as a colourless solid.

TLC R_f = 0.22 (DCM:MeOH, 19:1). **HRMS** (ESI⁺): C₂₁H₂₃Cl₂N₄O₃S₂⁺ [M+H]⁺: calc. 513.05831, found 513.05886.

¹H-NMR (400 MHz, DMSO-*d*₆): δ (ppm) = 9.03 (s, 1H, 7-H_A), 8.97 (s, 1H, 7-H_B), 8.10 (d, *J* = 2.5 Hz, 1H, 13-H), 7.89 (dd, *J* = 8.7, 2.2 Hz, 1H, 11-H), 7.81 (d, *J* = 2.1 Hz, 1H, 19-H), 7.70 (t, *J* = 8.2 Hz, 1H, 10-H), 7.66 (dd, *J* = 8.7, 2.5 Hz, 1H, 21-H), 7.38 (dd, *J* = 11.6, 8.8 Hz, 1H, 22-H), 3.61 (t, *J* = 6.7 Hz, 1H, 4-H_A), 3.37 (t, *J* = 6.8 Hz, 1H, 4-H_B), 3.10 (m, 2H, 1-H), 2.99 (s, 2H, 3-H_A), 2.97 – 2.86 (m, 3H, 2-H; 5-H_A), 2.78 (s, 1H, 3-H), 2.60 (t, *J* = 6.8 Hz, 1H, 5-H_B), 2.53 (t, *J* = 5.3 Hz, 3H, 6-H). **¹H-NMR** (400 MHz, tetrachlorethan-*d*₂, 373 K): δ (ppm) = 8.20 (t, *J* = 1.5 Hz, 1H, 19-H), 7.87 (d, *J* = 2.6 Hz, 1H, 13-H), 7.71 (d, *J* = 1.5 Hz, 2H, 21-H; 22-H), 7.48 (dd, *J* = 8.7, 2.6 Hz, 1H, 11-H), 7.24 (d, *J* = 8.7 Hz, 1H, 10-H), 3.62 (s, 2H, 4-H), 3.23 (d, *J* = 6.2 Hz, 2H, 1-H), 3.18 (d, *J* = 6.1 Hz, 2H, 2-H), 3.03 (s, 3H, 6-H), 2.88 (s, 2H, 5-H), 2.66 (s, 3H, 3-H).

¹³C-NMR (101 MHz, DMSO-*d*₆): δ (ppm) = 160.8 (C=O, C17), 153.1 (C=O, C8), 150.6 (C=N, C15), 147.9 (C_{Ar}, C9), 147.2 (C_{Ar}, C18), 134.9 (C_{Ar}H, C11), 131.5 (C_{Ar}, C12), 131.4 (C_{Ar}H, C21), 130.1 (C_{Ar}H, C19), 129.6 (C_{Ar}, C23), 129.4 (C_{Ar}H, C10), 128.5 (C_{Ar}, C14), 125.2 (C_{Ar}H, C22), 125.0 (C_{Ar}H, C13), 122.4 (C_{Ar}, C20), 47.7 (CH₂, C4), 47.0 (CH₂, C1), 35.1 (CH₂, C5), 34.6 (CH₃, C3), 32.4 (CH₃, C6), 32.3 (CH₂, C2).

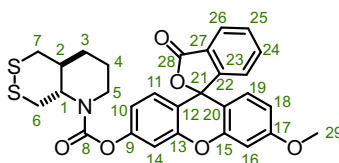
chloro-2-(chloro-4-oxo-3,4-dihydroquinazolin-2-yl)phenyl 2-(((piperidin-2-ylmethyl)disulfaneyl)methyl)piperidine-carboxylate (SS06-PQ, 77)

Prepared from **45** (150 mg, 0.45 mmol) and **55** (138 mg, 0.45 mmol) according to **general protocol G** to give **77** (90 mg, 0.15 mmol, 33%) as a colourless solid after FCC (EtOAc/MeOH).

TLC R_f = 0.15 (DCM:MeOH, 19:1). **HRMS** (ESI⁺): C₂₇H₃₁Cl₂N₄O₃S₂⁺ [M+H]⁺: calc. 593.12091, found 593.12024.

¹H-NMR (400 MHz, tetrachlorethan-*d*₂, 373 K): δ (ppm) = 8.27 – 8.16 (m, 1H, 25-H), 7.91 (t, *J* = 2.8 Hz, 1H, 19-H), 7.75 – 7.66 (m, 2H, 27-H; 28-H), 7.52 – 7.44 (m, 1H, 17-H), 7.38 – 7.21 (m, 1H, 16-H), 4.57 (s, 1H, NH, 13-H), 4.05 (d, *J* = 14.5 Hz, 1H, 1-H), 3.65 – 3.42 (m, 1H), 3.39 – 3.27 (m, 2H), 3.20 (dd, *J* = 13.5, 7.0 Hz, 1H), 3.11 (s, 1H), 3.01 (dd, *J* = 14.0, 6.7 Hz, 1H), 2.96 – 2.68 (m, 3H), 2.09 – 1.90 (m, 2H), 1.90 – 1.82 (m, 2H), 1.81 – 1.73 (m, 2H), 1.65 (t, *J* = 9.7 Hz, 2H), 1.46 (dd, *J* = 22.1, 10.9 Hz, 4H).

¹³C-NMR (400 MHz, tetrachlorethan-*d*₂, 373 K): δ (ppm) = 160.5 (C=O, C23), 152.5 (C=O, C14), 149.4 (C=N, C21), 147.9 (C_{Ar}, C15), 147.6 (C_{Ar}, C24), 135.0 (C_{Ar}H, C28), 133.2 (C_{Ar}, C29), 131.9 (C_{Ar}H, C17), 131.7 (C_{Ar}, C18), 130.4 (C_{Ar}H, C19), 129.7 (C_{Ar}H, C27), 128.2 (C_{Ar}, C20), 126.0 (C_{Ar}H, C25), 124.9 (C_{Ar}H, C16), 122.5 (C_{Ar}, C26), 56.8 (CH, C7), 55.7 (CH, C1), 45.3 (CH₂), 41.2 (CH₂), 40.7 (CH₂), 28.2 (CH₂), 27.5 (CH₂), 25.0 (CH₂), 22.5 (CH₂), 22.0 (CH₂), 18.7 (CH₂).

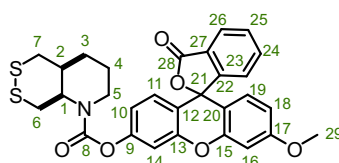
MF-Series***trans*-3'-methoxy-3-oxo-3*H*-spiro[isobenzofuran-1,9'-xanthen]-6'-yl hexahydro-[1,2]dithiino [4,5-*b*]pyridine-1(2*H*)-carboxylate (SS66T-MF, 78)**

Prepared from **8** (21.2 mg, 0.100 mmol) and **58** (38.1 mg, 0.110 mmol) according to **general protocol G** to give **78** (27.1 mg, 0.049 mmol, 49%) as a colourless solid after FCC (isohexane/EtOAc).

TLC R_f = 0.33 (isohexane:EtOAc, 3:1). **HRMS** (ESI⁺) C₂₉H₂₆NO₆S₂⁺ [M+H]⁺: calc. 548.11961, found 548.11973.

¹H-NMR (500 MHz, CDCl₃): δ (ppm) = 8.02 (d, J = 7.1 Hz, 1H, 26-H), 7.67 (tt, J = 7.5, 1.4 Hz, 1H, 24-H), 7.62 (t, J = 7.3 Hz, 1H, 25-H), 7.15 (d, J = 7.4 Hz, 1H, 23-H), 7.09 (dd, J = 3.7, 1.7 Hz, 1H, 14-H), 6.84 – 6.77 (m, 2H, 10-H; 11-H), 6.76 (d, J = 2.5 Hz, 1H, 16-H), 6.70 (d, J = 8.8 Hz, 1H, 19-H), 6.62 (dd, J = 8.8, 2.5 Hz, 1H, 18-H), 3.94 – 3.84 (m, 1H, 5-H_A), 3.84 (s, 3H, 29-H), 3.80 (dd, J = 10.1, 3.4 Hz, 1H, 6-H_A), 3.35 (d, J = 15.2 Hz, 1H, 1-H), 3.20 – 3.06 (m, 2H, 5-H_B, 6-H_B), 2.94 (dd, J = 13.5, 10.8 Hz, 1H, 7-H_A), 2.81 (dd, J = 13.5, 2.7 Hz, 1H, 7-H_B), 2.23 – 2.09 (m, 1H, 2-H), 1.96 (dt, J = 19.0, 8.5 Hz, 1H, 3-H_A), 1.84 – 1.72 (m, 1H, 4-H_A), 1.72 – 1.60 (m, 1H, 3-H_B), 1.48 – 1.36 (m, 1H, 4-H_B).

¹³C-NMR (101 MHz, CDCl₃): δ (ppm) = 169.5 (C=O, C28), 161.5 (C_{Ar}, C17), 153.4 (C=O, C8), 153.2 (C_{Ar}, C27), 152.6 (C_{Ar}, C13), 152.4 (C_{Ar}, C20), 152.0 (C_{Ar}, C15), 135.2 (C_{Ar}H, C23), 130.0 (C_{Ar}H, C25), 129.2 (C_{Ar}H, C10), 129.1 (C_{Ar}H, C19), 126.6 (C_{Ar}, C22), 125.2 (C_{Ar}H, C26), 124.2 (C_{Ar}H, C23), 117.6 (C_{Ar}H, C11), 116.4 (C_{Ar}, C12), 112.0 (C_{Ar}H, C18), 111.0 (C_{Ar}, C9), 110.4 (C_{Ar}H, C14), 101.0 (C_{Ar}H, C16), 82.7 (C_{spiro}, C21), 63.1 (CH, C1), 55.7 (CH₃, C29), 41.1 (CH₂, C6), 40.7 (CH₂, C7), 37.0 (CH₂, C5), 34.3 (CH, C2), 27.2 (CH₂, C3), 23.1 (CH₂, C4), 22.8, 22.5, 20.6.

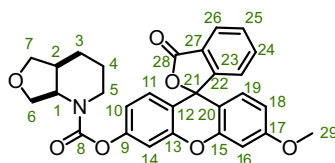
***cis*-3'-methoxy-3-oxo-3*H*-spiro[isobenzofuran-1,9'-xanthen]-6'-yl hexahydro-[1,2]dithiino [4,5-*b*]pyridine-1(2*H*)-carboxylate (SS66C-MF, 79)**

Prepared from **18** (14.0 mg, 0.066 mmol) and **58** (25.1 mg, 0.073 mmol) according to **general protocol G** to give **79** (11.0 mg, 0.002 mmol, 30%) as a colourless solid after FCC (isohexane/EtOAc).

TLC R_f = 0.34 (isohexane:EtOAc, 3:1). **HRMS** (ESI⁺) C₂₉H₂₆NO₆S₂⁺ [M+H]⁺: calc. 548.11961, found 548.11996.

¹H-NMR (500 MHz, CDCl₃): δ (ppm) = 8.02 (d, J = 7.4 Hz, 1H, 26-H), 7.67 (t, J = 7.3 Hz, 1H, 24-H), 7.62 (t, J = 7.3 Hz, 1H, 25-H), 7.16 (d, J = 7.5 Hz, 1H, 23-H), 7.12 – 7.01 (m, 1H, 14-H), 6.82 – 6.77 (m, 2H, 10-H; 11-H), 6.76 (d, J = 2.4 Hz, 1H, 16-H), 6.70 (d, J = 8.8 Hz, 1H, 19-H), 6.62 (dd, J = 8.8, 2.4 Hz, 1H, 18-H), 4.56 (t, J = 10.9 Hz, 1H, 1-H), 4.14 (t, J = 12.5 Hz, 1H, 5-H_A), 3.84 (s, 3H, 29-H), 3.62 – 3.42 (m, 2H, 6-H_A; 7-H_A), 2.97 (dt, J = 44.8, 12.0 Hz, 1H, 5-H_B), 2.83 (t, J = 15.1 Hz, 1H, 7-H_B), 2.51 (ddt, J = 10.9, 7.0, 4.1 Hz, 1H, 2-H), 2.39 – 2.21 (m, 2H, 3-H_A; 6-H_B), 1.86 (d, J = 13.4 Hz, 1H, 4-H_A), 1.74 – 1.59 (m, 1H, 3-H_B), 1.52 (d, J = 11.9 Hz, 1H, 4-H_B).

¹³C-NMR (101 MHz, CDCl₃): δ (ppm) = 169.5 (C=O, C28), 161.5 (C_{Ar}, C17), 153.2 (C=O, C8), 153.0 (C_{Ar}, C27), 152.7 (C_{Ar}, C13), 152.4 (C_{Ar}, C20), 152.0 (C_{Ar}, C15), 135.2 (C_{Ar}H, C23), 130.0 (C_{Ar}H, C25), 129.2 (C_{Ar}H, C10), 129.0 (C_{Ar}H, C19), 126.6 (C_{Ar}, C22), 125.2 (C_{Ar}H, C26), 124.2 (C_{Ar}H, C23), 117.6 (C_{Ar}H, C11), 116.3 (C_{Ar}, C12), 112.0 (C_{Ar}H, C18), 111.0 (C_{Ar}, C9), 110.4 (C_{Ar}H, C14), 101.0 (C_{Ar}H, C16), 82.7 (C_{spiro}, C21), 55.7 (CH₃, C29), 54.1 (CH, C1; minor), 53.3 (CH, C1; major), 42.3 (CH₂, C6; major), 42.2 (CH₂, C6; minor), 40.7 (CH₂, C7; major), 40.2 (CH₂, C7; minor), 36.2 (CH₂, C5; minor), 35.9 (CH₂, C5; major), 30.1 (CH, C2; minor), 29.4 (CH, C2; major), 25.5 (CH₂, C3; major), 25.0 (CH₂, C3; minor), 23.6 (CH₂, C2).

***cis*-3'-methoxy-3-oxo-3*H*-spiro[isobenzofuran-1,9'-xanthen]-6'-yl hexahydrofuro[3,4-*b*]pyridine-1(2*H*)-carboxylate (O56-MF, 80)**

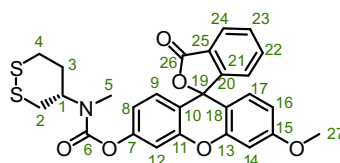
Prepared from **19** (65 mg, 0.40 mmol) and **58** (208 mg, 0.601 mmol) according to **general protocol G** to give **80** (158 mg, 0.316 mmol, 79%) as a colourless solid after FCC (Et₂O).

TLC R_f = 0.29 (isohexane:EtOAc, 1:1). **HRMS** (ESI): C₂₉H₂₆NO₇⁺ [M+H]⁺: calc. 500.17038, found 500.17059.

¹H-NMR (400 MHz, CDCl₃): δ (ppm) = 8.02 (d, *J* = 7.6 Hz, 1H, 26-H), 7.67 (tt, *J* = 7.5, 1.2 Hz, 1H, 24-H), 7.62 (td, *J* = 7.3 Hz, 1H, 25-H), 7.16 (dt, *J* = 7.5, 0.9 Hz, 1H, 23-H), 7.09 (s, 1H, 14-H), 6.84 – 6.78 (m, 2H, 10-H; 11-H), 6.76 (d, *J* = 2.4 Hz, 1H, 16-H), 6.70 (d, *J* = 8.8 Hz, 1H, 19-H), 6.62 (dd, *J* = 8.8, 2.5 Hz, 1H, 18-H), 4.85 (s, 1H, 1-H), 4.12 (s, 1H, 5-H_A), 4.03 (t, *J* = 8.4 Hz, 1H, 6-H_A), 3.92 (s, 1H, 7-H_A), 3.84 (s, 3H, 29-H), 3.72 (d, *J* = 8.6 Hz, 2H, 6-H_B; 7-H_B), 3.13 – 2.83 (m, 1H, 5-H_B), 2.35 – 2.16 (m, 1H, 2-H), 1.93 – 1.74 (m, 2H, 3-H_A; 4-H_A), 1.57 – 1.49 (m, 2H, 3-H_B; 4-H_B).

¹³C-NMR (101 MHz, CDCl₃): δ (ppm) = 169.5 (C=O, C28), 161.6 (C_{Ar}, C17), 153.9 (C=O, C8), 153.2 (C_{Ar}, C27), 152.7 (C_{Ar}, C13), 152.5 (C_{Ar}, C20), 152.0 (C_{Ar}, C15), 135.2 (C_{Ar}H, C23), 130.0 (C_{Ar}H, C25), 129.2 (C_{Ar}H, C10), 129.0 (C_{Ar}H, C19), 126.6 (C_{Ar}, C22), 125.2 (C_{Ar}H, C26), 124.2 (C_{Ar}H, C23), 117.6 (C_{Ar}H, C11), 116.6 (C_{Ar}, C12), 112.0 (C_{Ar}H, C18), 111.1 (C_{Ar}, C9), 110.5 (C_{Ar}H, C14), 101.0 (C_{Ar}H, C16), 82.7 (C_{spiro}, C21), 73.4 (CH₂, C7), 66.3 (CH₂, C6), 55.7 (CH₃, C29), 54.4 (CH, C1), 41.0 (CH₂, C5), 36.1 (CH, C2), 25.1 (CH₂, C3), 23.6 (CH₂, C4).

3'-methoxy-3-oxo-3H-spiro[isobenzofuran-1,9'-xanthen]-6'-yl ((S)-1,2-dithian-4-yl)(methyl)carbamate (SS60-MF, 81)



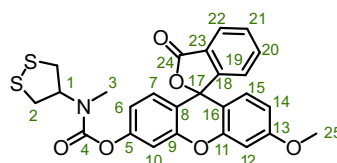
Prepared from **25** (74 mg, 0.40 mmol) and **58** (213 mg, 0.62 mmol) according to **general protocol G** to give **81** (133 mg, 0.26 mmol, 65%) as a colourless solid after FCC (Et₂O).

TLC R_f = 0.35 (isohexane:EtOAc, 2:1). **HRMS** (ESI⁺): C₂₇H₂₄NO₆S₂⁺ [M+H]⁺: calc. 522.10396, found 482.10438.

Individual rotamers were observed by NMR spectroscopy at 298 K (ratio ca. 1.5:1). The following data refers to all signals observed at 298 K.

¹H-NMR (400 MHz, CDCl₃): δ (ppm) = 8.02 (dd, *J* = 8.0, 1.1 Hz, 1H, 24-H), 7.67 (td, *J* = 7.4, 1.4 Hz, 1H, 22-H), 7.62 (td, *J* = 7.4, 1.2 Hz, 1H, 23-H), 7.16 (dt, *J* = 7.7, 1.0 Hz, 1H, 21-H), 7.09 (d, *J* = 1.8 Hz, 1H, 12-H), 6.83 – 6.78 (m, 2H, 8-H; 9-H), 6.76 (d, *J* = 2.4 Hz, 1H, 14-H), 6.70 (d, *J* = 8.8 Hz, 1H, 17-H), 6.62 (dd, *J* = 8.8, 2.5 Hz, 1H, 16-H), 4.33 (t, *J* = 11.3 Hz, 1H, 1-H), 3.84 (s, 3H, 27-H), 3.24 (t, *J* = 13.1 Hz, 1H, 3-H), 3.14 (t, *J* = 12.3 Hz, 1H, 2-H), 3.07 – 2.97 (m, 3H, 3'-H; 5-H), 2.94 (s, 1H, 5'-H), 2.80 (t, *J* = 16.4 Hz, 1H, 2'-H), 2.23 (dd, *J* = 25.0, 14.0 Hz, 1H, 4-H), 2.09 (dd, *J* = 11.7, 10.6 Hz, 1H, 4'-H). **¹³C-NMR** (101 MHz, CDCl₃): δ (ppm) = 169.5 (C=O, C26), 161.6 (C_{Ar}, C15), 153.7 (C=O, C6), 153.2 (C_{Ar}, C25), 152.7 (C_{Ar}, C11), 152.6 (C_{Ar}, C11'), 152.4 (C_{Ar}, C18), 152.0 (C_{Ar}, C13), 135.2 (C_{Ar}H, C21), 130.0 (C_{Ar}H, C23), 129.2 (C_{Ar}H, C8), 129.0 (C_{Ar}H, C17), 126.6 (C_{Ar}, C20), 125.2 (C_{Ar}H, C24), 124.2 (C_{Ar}H, C21), 117.6 (C_{Ar}H, C9), 116.6 (C_{Ar}, C10), 112.0 (C_{Ar}H, C16), 111.1 (C_{Ar}, C7), 110.5 (C_{Ar}H, C12), 101.0 (C_{Ar}H, C14), 82.7 (C_{spiro}, C19), 56.1 (CH, C1), 55.7 (CH₃, C27), 36.3 (CH₂, C3), 36.2 (CH₂, C3'), 36.1 (CH₂, C2), 35.7 (CH₂, C2'), 33.2 (CH₂, C4), 32.5 (CH₂, C4'), 30.1 (CH₃, C5).

3'-methoxy-3-oxo-3H-spiro[isobenzofuran-1,9'-xanthen]-6'-yl (1,2-dithiolan-4-yl) (methyl)carbamate (SS50-MF, 82)



Prepared from **52** (75.0 mg, 0.319 mmol) and **58** (221.0 mg, 0.637 mmol) according to **general protocol G** to give **82** (32.0 mg, 0.063 mmol, 20%) as a colourless solid after FCC (aluminium oxide, isohexane/EtOAc).

TLC R_f = 0.43 (silica, isohexane:EtOAc, 2:1); R_f = 0.40 (aluminium oxide, isohexane:EtOAc, 5:2).

HRMS (ESI⁺) C₂₆H₂₂NO₆S₂⁺ [M+H]⁺: calc. 508.08831, found 508.08862.

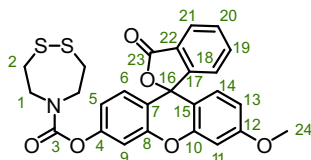
Individual rotamers were observed by NMR spectroscopy at 298 K (ratio ca. 1.2:1). The following data refers to all signals observed at 298 K.

¹H-NMR (400 MHz, CDCl₃): δ (ppm) = 8.03 (dt, *J* = 7.3, 1.2 Hz, 1H, 22-H), 7.67 (td, *J* = 7.4, 1.4 Hz, 1H, 20-H), 7.62 (td, *J* = 7.4, 1.2 Hz, 1H, 21-H), 7.16 (d, *J* = 7.7 Hz, 1H, 19-H), 7.10 (d, *J* = 1.8 Hz, 1H, 10-H), 6.84 – 6.79 (m, 2H, 6-H; 7-H), 6.77 (d, *J* = 2.4 Hz, 1H, 12-H), 6.70 (d, *J* = 8.9 Hz, 1H, 15-H), 6.63 (dd, *J* = 8.9, 2.5 Hz, 1H, 14-H), 5.27

(ddd, $J = 13.3, 7.8, 5.6$ Hz, 1H, **1-H**), 3.84 (s, 3H, **25-H**), 3.51 – 3.33 (m, 2H, **2-H_A**), 3.24 – 3.11 (m, 2H, **2-H_B**), 3.09 (s, 2H, **3-H**; major), 3.00 (s, 1H, **3-H**; minor).

¹³C-NMR (101 MHz, CDCl₃): δ (ppm) = 169.5 (C=O, **C24**), 161.6 (C_{Ar}, **C13**), 153.2 (C=O, **C4**), 153.1 (C_{Ar}, **C23**), 152.6 (C_{Ar}, **C9**), 152.4 (C_{Ar}, **C16**), 152.0 (C_{Ar}, **C11**), 135.2 (C_{Ar}H, **C19**), 130.0 (C_{Ar}H, **C21**), 129.2 (C_{Ar}H, **C6**), 129.1 (C_{Ar}H, **C15**), 126.7 (C_{Ar}, **C18**), 125.2 (C_{Ar}H, **C22**), 124.2 (C_{Ar}H, **C19**), 117.6 (C_{Ar}H, **C7**), 116.6 (C_{Ar}, **C8**), 112.0 (C_{Ar}H, **C14**), 111.1 (C_{Ar}, **C5**), 110.4 (C_{Ar}H, **C10**), 101.0 (C_{Ar}H, **C12**), 82.7 (C_{spiro}, **C17**), 62.0 (CH, **C1**), 55.8 (CH₃, **C25**), 40.9 (CH₂, **C2**), 30.2 (CH₃, **C3**).

3'-methoxy-3-oxo-3H-spiro[isobenzofuran-1,9'-xanthen]-6'-yl 1,2,5-dithiazepane-carboxylate
(SS7-MF, **83**)



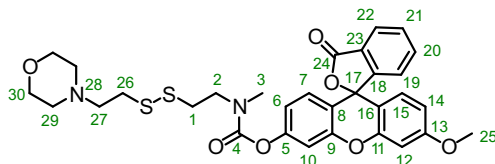
Prepared from crude **49** (corresponding to 400 mg, 0.642 mmol of compound **47**) and an excess of **58** (267 mg, 0.771 mmol) according to **general protocol G** to give **83** (43 mg, 0.085 mmol, 13%) as a colourless solid after FCC (aluminium oxide, isohehexane/EtOAc).

TLC $R_f = 0.29$ (isohehexane:EtOAc, 2:1). **HRMS** (ESI⁺): C₂₆H₂₂NO₆S₂⁺ [M+H]⁺: calc. 507.0810, found 507.0815.

¹H-NMR (400 MHz, CDCl₃): δ (ppm) = 8.02 (dd, ³ $J_{21-20} = 7.3$ Hz, ⁴ $J_{21-19} = 1.1$ Hz, 1H, **21-H**), 7.66 (td, ³ $J_{19-18} = 7.4$ Hz, ⁴ $J_{19-21} = 1.4$ Hz, 1H, **19-H**), 7.62 (td, ³ $J_{20-21} = 7.4$ Hz, ⁴ $J_{20-18} = 1.2$ Hz, 1H, **20-H**), 7.16 (dt, ³ $J_{18-19} = 7.5$ Hz, ⁴ $J_{18-20} = 1.0$ Hz, 1H, **18-H**), 7.11 (d, ⁴ $J_{9-5} = 2.2$ Hz, 1H, **9-H**), 6.82 (dd, ³ $J_{5-6} = 8.7$ Hz, ⁴ $J_{5-9} = 2.2$ Hz, 1H, **5-H**), 6.79 (d, ³ $J_{6-5} = 8.4$ Hz, 1H, **6-H**), 6.77 (d, ⁴ $J_{11-13} = 2.6$ Hz, 1H, **11-H**), 6.70 (d, ³ $J_{14-13} = 8.8$ Hz, 1H, **14-H**), 6.62 (dd, ³ $J_{13-14} = 8.8$ Hz, ⁴ $J_{13-11} = 2.5$ Hz, 1H, **13-H**), 3.96 (t, ³ $J_{1A-2} = 5.8$ Hz, 2H, **1-H_A**), 3.88 (t, ³ $J_{1B-2} = 5.7$ Hz, 2H, **1-H_B**), 3.84 (s, 3H, **24-H**), 3.08 (t, ³ $J_{2-1} = 5.9$ Hz, 4H).

¹³C-NMR (101 MHz, CDCl₃): δ (ppm) = 169.5 (C=O, **C23**), 161.6 (C_{Ar}, **C12**), 153.8 (C=O, **C3**), 153.2 (C_{Ar}, **C22**), 152.6 (C_{Ar}, **C8**), 152.4 (C_{Ar}, **C15**), 152.0 (C_{Ar}, **C10**), 135.2 (C_{Ar}H, **C19**), 130.0 (C_{Ar}H, **C20**), 129.2 (C_{Ar}H, **C5**; **C14**), 126.6 (C_{Ar}, **C17**), 125.2 (C_{Ar}H, **C21**), 124.2 (C_{Ar}H, **C18**), 117.6 (C_{Ar}H, **C6**), 116.6 (C_{Ar}, **C7**), 112.0 (C_{Ar}H, **C13**), 111.1 (C_{Ar}, **C4**), 110.5 (C_{Ar}H, **C9**), 101.0 (C_{Ar}H, **C11**), 82.7 (C_{spiro}, **C16**), 55.7 (CH₃, **C24**), 52.1 (CH₂, **C1**), 51.6 (CH₂, **C1'**), 38.3 (CH₂, **C2**), 37.0 (CH₂, **C2'**).

3'-methoxy-3-oxo-3H-spiro[isobenzofuran-1,9'-xanthen]-6'-yl methyl(2-((2-morpholinoethyl) disulfaneyl) ethyl)carbamate (SS00M-MF, **84**)

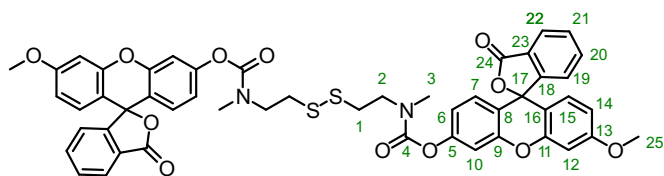


Prepared from **40** (25.0 mg, 0.09 mmol) and **58** (213 mg, 0.10 mmol) according to **general protocol G** to give **84** (133 mg, 0.26 mmol, 65%) as solid after FCC (isohehexane/EtOAc). The solid was taken into DCM (0.5 mL) and added to 10 mL of a diluted solution of HCl in Et₂O, the solid precipitate was separated and dried under reduced pressure to yield **84**·HCl (28.0 mg, 0.05 mmol, 56%) as a colourless solid.

TLC $R_f = 0.16$ (EtOAc). **HRMS** (EI⁻): C₃₁H₃₃N₂O₄S₂⁻: [M-e]⁻ calc. 608.1651, found 608.1636.

¹H-NMR (400 MHz, CDCl₃): δ (ppm) = 13.65 – 12.97 (m, 1H, **NH**, **28-H**), 8.02 (d, $J = 7.3$ Hz, 1H, **22-H**), 7.68 (t, $J = 7.2$ Hz, 1H, **20-H**), 7.62 (t, $J = 7.0$ Hz, 1H, **21-H**), 7.17 (d, $J = 7.1$ Hz, 1H, **19-H**), 7.14 – 7.08 (m, 1H, **10-H**), 6.87 – 6.74 (m, 3H, **6-H**; **7-H**; **12-H**), 6.69 (dd, $J = 8.8, 2.3$ Hz, 1H, **15-H**), 6.62 (dd, $J = 8.8, 2.0$ Hz, 1H, **14-H**), 4.30 – 4.21 (m, 1H, **29-H_A**), 4.17 (d, $J = 12.0$ Hz, 1H, **29-H_B**), 3.97 (d, $J = 12.8$ Hz, 1H, **29-H_C**), 3.90 – 3.86 (m, 1H, **29-H_D**), 3.84 (s, 3H, **25-H**), 3.78 (t, $J = 6.5$ Hz, 1H, **1-H_A**), 3.69 (dq, $J = 19.9, 7.2$ Hz, 1H, **1-H_B**), 3.40 (d, $J = 10.7$ Hz, 2H, **30-H**), 3.34 – 3.21 (m, 4H, **26-H**; **27-H**), 3.12 (s, 2H, **3-H**, major rotamer), 3.04 (s, 1H, **3-H**, minor rotamer), 2.99 (dd, $J = 11.9, 5.4$ Hz, 2H, **2-H**), 2.86 (dd, $J = 19.5, 10.6$ Hz, 2H, **30-H**).

¹³C-NMR (101 MHz, CDCl₃): δ (ppm) = 169.0 (C=O, **C24**), 161.6 (C_{Ar}, **C13**), 153.8 (C=O, **C4**), 153.0 (C_{Ar}, **C23**), 152.7 (C_{Ar}, **C9**), 152.4 (C_{Ar}, **C16**), 151.9 (C_{Ar}, **C11**), 135.3 (C_{Ar}H, **C20**), 130.0 (C_{Ar}H, **C21**), 129.2 (C_{Ar}H, **C6**), 129.0 (C_{Ar}H, **C15**), 126.7 (C_{Ar}, **C18**), 125.2 (C_{Ar}H, **C22**), 124.1 (C_{Ar}H, **C19**), 117.7 (C_{Ar}H, **C7**), 116.5 (C_{Ar}, **C8**), 112.1 (C_{Ar}H, **C14**), 111.0 (C_{Ar}, **C5**), 110.5 (C_{Ar}H, **C10**), 100.9 (C_{Ar}H, **C12**), 82.7 (C_{spiro}, **C17**), 63.7 (CH₂, **C29**), 57.2 (CH₂, **C27**), 55.8 (CH₃, **C25**), 52.3 (CH₂, **C30**), 52.2 (CH₂, **C30**), 48.6 (CH₂, **C1**, major rotamer), 48.0 (CH₂, **C1**, major rotamer), 36.3 (CH₂, **C2**), 35.5 (CH₃, **C3**, minor rotamer), 35.3 (CH₃, **C3**, major rotamer), 30.2 (CH₂, **C26**).

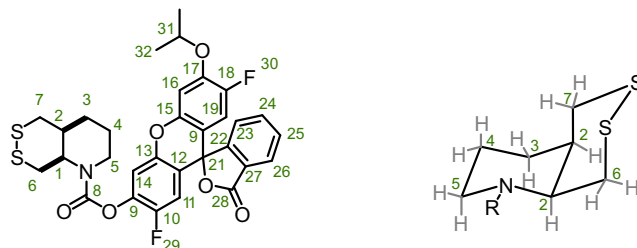
bis(3'-methoxy-3-oxo-3H-spiro[isobenzofuran-1,9'-xanthen]-6'-yl) (disulfanediy)bis(ethane-2,1-diyl)bis(methylcarbamate) (SS00-MF₂, 85)

Prepared from **34** (96.8 mg, 0.382 mmol) and **58** (221.0 mg, 0.637 mmol) according to **general protocol G** to give **85** (27.3 mg, 0.026 mmol, 23%) as a colourless solid after FCC (isohexane/EtOAc).

TLC R_f = 0.39 (isohexane:EtOAc, 1:2). **HRMS** (ESI⁺): C₅₀H₄₁N₂O₁₂S₂⁺ [M+H]⁺: calc. 925.20954, found 925.21066.

¹H-NMR (400 MHz, CDCl₃): δ (ppm) = 8.02 (d, J = 7.4 Hz, 2H, **22-H**), 7.66 (t, J = 7.4 Hz, 2H, **20-H**), 7.61 (t, J = 7.4 Hz, 2H, **21-H**), 7.15 (dd, J = 7.5, 3.2 Hz, 2H, **19-H**), 7.10 (t, J = 1.9 Hz, 2H, **10-H**), 6.85 – 6.79 (m, 2H, **6-H**), 6.79 – 6.74 (m, 4H, **7-H**; **12-H**), 6.69 (dd, J = 8.8, 1.4 Hz, 2H, **15-H**), 6.62 (dd, J = 8.8, 2.3 Hz, 2H, **14-H**), 3.83 (d, J = 3.4 Hz, 6H, **25-H**), 3.75 (t, J = 7.0 Hz, 2H, **1-H**), 3.66 (t, J = 7.1 Hz, 2H, **1'-H**), 3.13 (d, J = 3.6 Hz, 3H, **3-H, major**), 3.04 (s, 3H, **3-H, major**), 2.94 (q, J = 6.9 Hz, 4H, **2-H**).

¹³C-NMR (101 MHz, CDCl₃): δ (ppm) = 169.5 (C=O, **C24**), 161.6 (C_{Ar}, **C13**), 153.9 (C=O, **C4**), 153.2 (C_{Ar}, **C23**), 152.7 (C_{Ar}, **C9**), 152.5 (C_{Ar}, **C16**), 152.0 (C_{Ar}, **C11**), 135.2 (C_{Ar}H, **C20**), 130.0 (C_{Ar}H, **C21**), 129.2 (C_{Ar}H, **C6**), 129.0 (C_{Ar}H, **C15**), 126.7 (C_{Ar}, **C18**), 125.2 (C_{Ar}H, **C22**), 124.2 (C_{Ar}H, **C19**), 117.7 (C_{Ar}H, **C7**), 116.3 (C_{Ar}, **C8**), 112.0 (C_{Ar}H, **C14**), 111.1 (C_{Ar}, **C5**), 110.4 (C_{Ar}H, **C10**), 101.0 (C_{Ar}H, **C12**), 82.7 (C_{spiro}, **C17**), 55.7 (CH₃, **C25**), 49.2 (CH₂, **C1**), 48.6 (CH₂, **C1'**), 36.4 (CH₂, **C2**), 35.8 (CH₂, **C2'**), 35.6 (CH₃, **C3**).

IG-Series**cis-2',7'-difluoro-3'-isopropoxy-3-oxo-3H-spiro[isobenzofuran-1,9'-xanthen]-6'-yl-hexahydro-[1,2]dithiino[4,5-b]pyridine-1(2H)-carboxylate (SS66C-IG, 86)**

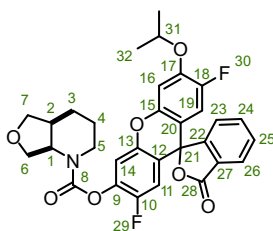
Prepared from crude **12** (corresponding to 41 mg, 0.14 mmol of **18**) and **62** (48 mg, 0.12 mmol) according to **general protocol G** to give **86** (26 mg, 0.043 mmol, 36%) as a colourless solid FCC (isohexane/EtOAc).

TLC R_f = 0.67 (isohexane:EtOAc, 2:1). **HRMS** (ESI⁺) $C_{31}H_{38}F_2NO_6S_2^+$ [M+H]⁺: calc. 612.13206, found 612.13221.

Individual rotamers were observed by NMR spectroscopy at 298 K (ratio ca. 1:1). The following data refers to all signals observed at 298 K.

¹H-NMR (400 MHz, CDCl₃): δ (ppm) = 8.04 (d, J = 7.4 Hz, 1H, **26-H**), 7.72 (tt, J = 7.5, 1.5 Hz, 2H, **24-H**), 7.66 (t, J = 7.4 Hz, 1H, **25-H**), 7.19 (d, J = 7.5 Hz, 1H, **23-H**), 7.15 (dd, J = 6.5, 4.1 Hz, 1H, **14-H**), 6.83 (d, J = 7.1 Hz, 1H, **16-H**), 6.53 (dd, J = 10.1, 3.3 Hz, 1H, **11-H**), 6.44 (d, J = 11.2 Hz, 1H, **19-H**), 4.62 (hept, J = 6.5 Hz, 1H, **31-H**), 4.58 – 4.47 (m, 1H, **1-H**), 4.12 (dd, J = 27.8, 13.8 Hz, 1H, **5-H_A**), 3.61 – 3.41 (m, 2H, **6-H_A**; **7-H_A**), 3.15 – 2.89 (m, 1H, **5-H_B**), 2.88 – 2.75 (m, 1H, **6-H_B**), 2.62 – 2.45 (m, 1H, **7-H_B**), 2.41 – 2.22 (m, 2H, **2-H**; **3-H_A**), 1.86 (d, J = 11.5 Hz, 1H, **4-H_A**), 1.76 – 1.64 (m, 1H, **4-H_B**), 1.52 (dd, J = 9.3, 5.4 Hz, 1H, **3-H_B**), 1.41 (d, J = 6.0 Hz, 6H, **32-H**).

¹³C-NMR (101 MHz, CDCl₃): δ (ppm) = 168.8 (C=O, **C28**), 152.2 (C_{Ar}, **C27**), 152.1 (C=O, **C8**), 150.8 (C_{Ar}, **C17**), 148.7 (C_{Ar}, **C20**), 148.4 (d, J_{C-F} = 12.5 Hz, C_{Ar}, **C18**), 147.7 (d, J_{C-F} = 27.0 Hz, C_{Ar}, **C10**), 140.7 (C_{Ar}, **C9**), 135.6 (C_{Ar}H, **C25**), 130.5 (C_{Ar}H, **C24**), 126.4 (C_{Ar}, **C22**), 125.6 (C_{Ar}H, **C26**), 124.6 (C_{Ar}H, **C23**), 116.2 (C_{Ar}, **C12**), 114.7 (d, J_{C-F} = 21.6 Hz, C_{Ar}H, **C19**), 114.1 (d, J_{C-F} = 21.6 Hz, C_{Ar}H, **C11**), 112.9 (d, J_{C-F} = 18.0 Hz, C_{Ar}H, **C14**), 109.3 (C_{Ar}, **C17**), 104.0 (C_{Ar}H, **C19**), 82.6 (C_{spiro}, **C21**), 72.4 (CH, **C31**), 54.6 (CH, **C1**; major), 53.9 (CH, **C1**; minor), 42.3 (CH₂, **C6**; minor), 42.1 (CH₂, **C6**; major), 41.0 (CH₂, **C5**; minor), 40.5 (CH₂, **C5**; major), 36.4 (CH, **C2**; minor), 36.1 (CH, **C2**; minor), 30.0 (CH₂, **C7**; minor), 29.4 (CH₂, **C7**; minor), 25.4 (CH₂, **C4**; minor), 25.0 (CH₂, **C4**; major), 23.5 (CH₂, **C3**), 22.0 (CH₃, **C32**), 21.9 (CH₃, **C32**).

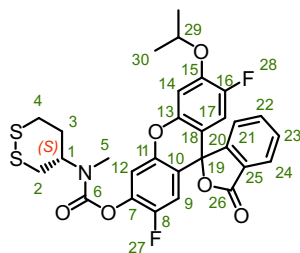
cis-2',7'-difluoro-3'-isopropoxy-3-oxo-3H-spiro[isobenzofuran-1,9'-xanthen]-6'-yl hexahydrofuro[3,4-b]pyridine-1(2H)-carboxylate (O56-IG, 87)

Prepared from **19** (25 mg, 0.15 mmol) and **62** (48 mg, 0.12 mmol) according to **general protocol G** to give **87** (35 mg, 0.062 mmol, 52%) as a colourless solid after FCC (isohexane/EtOAc).

TLC R_f = 0.26 (isohexane:EtOAc, 2:1). **HRMS** (ESI⁺): $C_{31}H_{28}F_2NO_7^+$ [M+H]⁺: calc. 564.1829, found 564.1825.

¹H-NMR (400 MHz, CDCl₃): δ (ppm) = 8.04 (d, J = 7.4 Hz, 1H, **26-H**), 7.72 (t, J = 7.4 Hz, 1H, **24-H**), 7.67 (t, J = 7.4 Hz, 1H, **25-H**), 7.22 – 7.12 (m, 2H, **23-H**; **14-H**), 6.83 (d, J = 7.1 Hz, 1H, **16-H**), 6.53 (d, J = 10.1 Hz, 1H, **11-H**), 6.44 (dd, J = 11.3, 1.1 Hz, 1H, **19-H**), 4.95 – 4.75 (m, 1H, **1-H**), 4.62 (hept, J = 6.0 Hz, 1H, **31-H**), 4.19 – 4.08 (m, 1H, **5-H_A**), 4.10 – 4.01 (m, 1H, **6-H_A**), 3.92 (s, 1H, **7-H_A**), 3.73 (d, J = 6.4 Hz, 2H, **6-H_B**; **7-H_B**), 3.16 – 2.85 (m, 1H, **5-H_B**), 2.38 – 2.20 (m, 1H, **2-H**), 1.94 – 1.76 (m, 2H, **3-H_A**; **4-H_A**), 1.61 – 1.49 (m, 2H, **3-H_B**; **4-H_B**), 1.41 (d, J = 6.0 Hz, 6H, **32-H**).

¹³C-NMR (101 MHz, CDCl₃): δ (ppm) = 167.5 (C=O, **C28**), 152.1 (C=O, **C8**), 151.2 (C_{Ar}, **C17**), 148.7 (C_{Ar}, **C20**), 148.4 (d, J_{C-F} = 12.5 Hz, C_{Ar}, **C18**), 147.7 (d, J_{C-F} = 32.2 Hz, C_{Ar}, **C10**), 140.7 (C_{Ar}, **C9**), 135.6 (C_{Ar}H, **C25**), 130.5 (C_{Ar}H, **C24**), 126.4 (C_{Ar}, **C22**), 125.6 (C_{Ar}H, **C26**), 124.1 (C_{Ar}H, **C23**), 115.9 (C_{Ar}, **C12**), 114.7 (d, J_{C-F} = 21.5 Hz, C_{Ar}H, **C19**), 114.1 (d, J_{C-F} = 21.5 Hz, C_{Ar}H, **C11**), 112.9 (C_{Ar}H, **C14**), 109.3 (C_{Ar}, **C17**), 104.0 (C_{Ar}H, **C19**), 82.1 (C_{spiro}, **C21**), 73.4 (CH₂, **C7**), 72.4 (CH, **C31**), 66.3 (CH₂, **C6**), 54.5 (CH, **C1**), 41.4 (CH₂, **C5**), 35.9 (CH, **C2**), 26.5 (CH₂, **C3**), 23.9 (CH₂, **C4**), 22.0 (CH₃, **C32**).

2',7'-difluoro-3'-isopropoxy-3-oxo-3H-spiro[isobenzofuran-1,9'-xanthen]-6'-yl ((S)-1,2-dithian-4-yl)(methyl)carbamate (SS60-IG, 88)

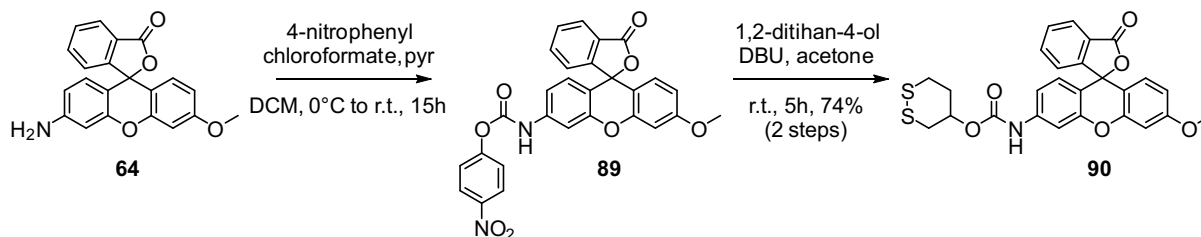
Prepared from **25** (28.0 mg, 0.150 mmol) and **62** (48.0 mg, 0.12 mmol) according to **general protocol G** to give **88** (38.0 mg, 0.065 mmol, 54%) as a colourless solid after FCC (isohexane/EtOAc).

TLC R_f = 0.57 (isohexane:EtOAc, 2:1). **HRMS** (ESI⁺): C₂₉H₂₆F₂NO₆S₂⁺ [M+H]⁺: calc. 586.11641, found 586.11609.

Individual rotamers were observed by NMR spectroscopy at 298 K (ratio ca. 1.5:1). The following data refers to all signals observed at 298 K.

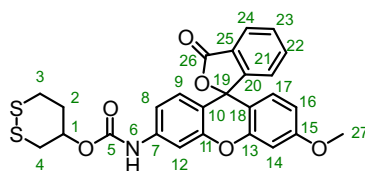
¹H-NMR (400 MHz, CDCl₃): δ (ppm) = 8.04 (d, J = 7.4 Hz, 1H, **24-H**), 7.72 (td, J = 7.4, 1.2 Hz, 1H, **22-H**), 7.66 (t, J = 7.4 Hz, 1H, **23-H**), 7.15 (t, J = 6.0 Hz, 1H, **21-H**), 7.15 (dd, J = 6.5, 4.1 Hz, 1H, **12-H**), 6.83 (d, J = 7.1 Hz, 1H, **14-H**), 6.53 (dd, J = 10.1, 2.8 Hz, 1H, **9-H**), 6.44 (d, J = 11.2 Hz, 1H, **17-H**), 4.62 (hept, J = 6.1 Hz, **29-H**), 4.30 (ddd, J = 17.7, 10.5, 4.7 Hz, 1H, **1-H**), 3.22 (ddd, J = 14.1, 8.7, 2.5 Hz, 1H, **2-H_A**), 3.14 (dd, J = 12.1, 2.5 Hz, 1H, **3-H_A**), 3.07 – 2.97 (m, 3H, **2-H_B**; **5-H**), 2.95 (s, 1H, **5'-H**), 2.89 – 2.74 (m, 1H, **3-H_B**), 2.24 (dd, J = 29.3, 13.2 Hz, 1H, **4-H_A**), 2.14 – 2.06 (m, 1H, **4-H_B**), 1.41 (d, J = 6.1 Hz, 6H, **30-H**).

¹³C-NMR (101 MHz, CDCl₃): δ (ppm) = 168.8 (C=O, **C26**), 152.8 (C=O, **C6**), 152.6 (C=O, **6'-C**), 152.2 (C_{Ar}, **C25**), 149.6 (C_{Ar}, **C15**), 148.7 (C_{Ar}, **C18**), 148.4 (d, J_{C-F} = 12.5 Hz, C_{Ar}, **C16**), 147.7 (d, J_{C-F} = 28.2 Hz, C_{Ar}, **C8**), 140.7 (C_{Ar}, **C7**), 135.6 (C_{Ar}H, **C23**), 130.5 (C_{Ar}H, **C22**), 126.4 (C_{Ar}, **C20**), 125.6 (C_{Ar}H, **C24**), 124.1 (C_{Ar}H, **C21**), 116.5 (C_{Ar}, **C10**), 114.7 (d, J_{C-F} = 21.4 Hz, C_{Ar}H, **C17**), 114.1 (d, J_{C-F} = 21.5 Hz, C_{Ar}H, **C9**), 112.9 (d, J_{C-F} = 18.0 Hz, C_{Ar}H, **C12**), 109.3 (C_{Ar}, **C15**), 104.0 (C_{Ar}H, **C17**), 82.1 (C_{spiro}, **C19**), 72.4 (CH, **C29**), 56.4 (CH, **C1**; minor), 56.0 (CH, **C1**; major), 36.2 (CH₂, **C2**, major), 36.1 (CH₂, **C2**, minor), 35.6 (CH₂, **C3**), 33.0 (CH₂, **C4**, major), 32.4 (CH₂, **C4**, minor), 30.3 (CH₃, **C5**), 21.9 (CH₃, **C30**).

MR-Series**1,2-dithian-4-yl (3'-methoxy-3-oxo-3H-spiro[isobenzofuran-1,9'-xanthen]-6'-yl)carbamate**
(SS60-MR, 90)

Step 1: To a solution of **64** (50.0 mg, 0.145 mmol, 1.0 eq.) and pyridine (23.5 μ L, 0.291 mmol, 2.0 eq.) in anhydrous DCM (3 mL) at 0 °C was added 4-nitrophenyl chloroformate (35.0 mg, 0.174 mmol, 1.2 eq.) and the mixture was allowed to warm to r.t. and was further stirred for 15 h. Then, the reaction mixture was directly subjected to FCC (0 to 5% EtOAc in DCM), which afforded partially purified **89** (62 mg) as a yellow solids. This material still contaminated a significant amount 4-nitrophenol and was used without further purification in the next step.

Step 2: The material obtained in step 1 (20 mg) containing **89** and **30** (7.5 mg, 0.055 mmol) were dissolved in anhydrous acetone (0.4 mL). DBU (7 μ L, 0.05 mmol) was added and the mixture was stirred for 5 h, before the volatiles were removed under reduced pressure. The residue was dissolved in DCM (5 mL), washed with half-sat. aq. K_2CO_3 until the aqueous layer stayed colourless. Then, the organic layers were dried over Na_2SO_4 , filtered and again evaporated under reduced pressure. The residue was purified by FCC (EtOAc:isohexane:DCM = 1:4:4) to afford **90** (17.5 mg, 0.035 mmol, 74% over two steps) as a colourless solid.



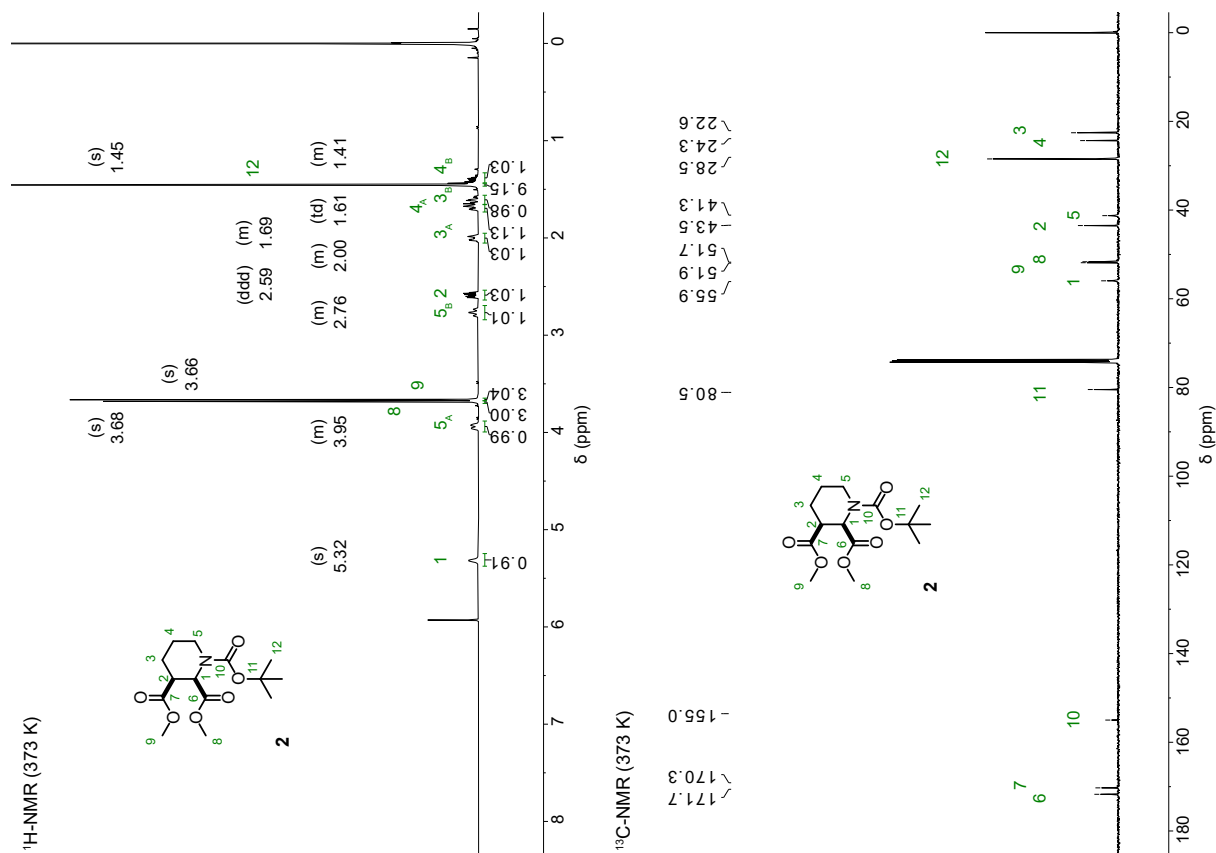
TLC R_f = 0.27 (EtOAc:hexane:DCM, 1:4:4). **HRMS** (ESI): $C_{22}H_{26}NO_6S_2^+$ $[M+H]^+$ calc. 508.08831, found 508.08880.

1H -NMR (400 MHz, $DMSO-d_6$): δ (ppm) = 10.13 (s, 1H, 6-H), 8.02 (d, J = 7.7 Hz, 1H, 24-H), 7.80 (td, J = 7.5, 1.3 Hz, 1H, 22-H), 7.73 (td, J = 7.4, 1.0 Hz, 1H, 23-H), 7.58 (s, 1H, 13-H), 7.28 (d, J = 7.6 Hz, 1H, 21-H), 7.20 (dt, J = 8.8, 1.5 Hz, 1H, 17-H), 7.00 (d, J = 2.5 Hz, 1H, 12-H), 6.76 – 6.70 (m, 2H, 8-H; 16-H), 6.67 (d, J = 8.8 Hz, 1H, 9-H), 4.87 (td, J = 9.8, 8.9, 4.1 Hz, 1H, 1-H), 3.82 (s, 3H, 27-H), 3.25 – 3.14 (m, 2H, 2- H_A ; 4- H_A), 3.08 (t, J = 12.1 Hz, 1H, 2- H_B), 2.86 (dd, J = 13.0, 9.6 Hz, 1H, 4- H_B), 2.40 – 2.27 (m, 1H, 3- H_A), 1.84 (q, J = 11.3, 10.6 Hz, 1H, 3- H_B).

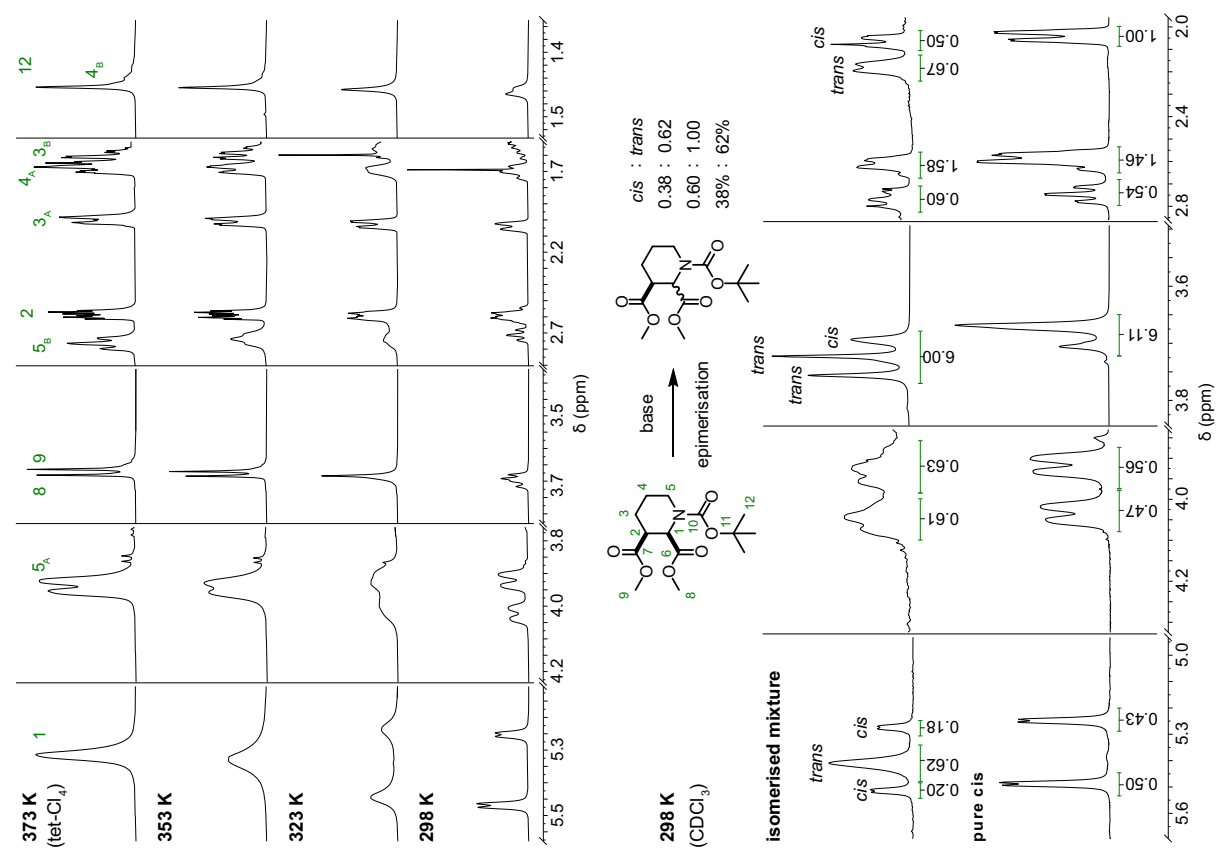
^{13}C -NMR (101 MHz, $DMSO-d_6$): δ (ppm) = 169.1 (C=O), 161.6 (C=O), 153.0 (C_{Ar}), 152.7 (C_{Ar}), 152.2 (C_{Ar}), 151.4 (C_{Ar}), 141.8 (C_{Ar}), 136.2 (C_{Ar} , C-22), 130.7 (C_{Ar} , C-23), 129.4 (C_{Ar} , C-9), 129.1 (C_{Ar} , C-8), 126.3 (C_{Ar}), 125.2 (C_{Ar} , C-25), 124.4 (C_{Ar} , C-21), 115.0 (C_{Ar} , C-17), 113.0 (C_{Ar}), 112.6 (C_{Ar} , C-16), 111.2 (C_{Ar}), 105.6 (C_{Ar} , C-13), 101.3 (C_{Ar} , C-12), 82.6 (C_{spiro} , C-19), 70.9 (CH, C-1), 56.2 (CH_3 , C-27), 36.8 ($2 \times CH_2$, C-2; C-4), 33.8 (CH_2 , C-3).

9. NMR Spectra

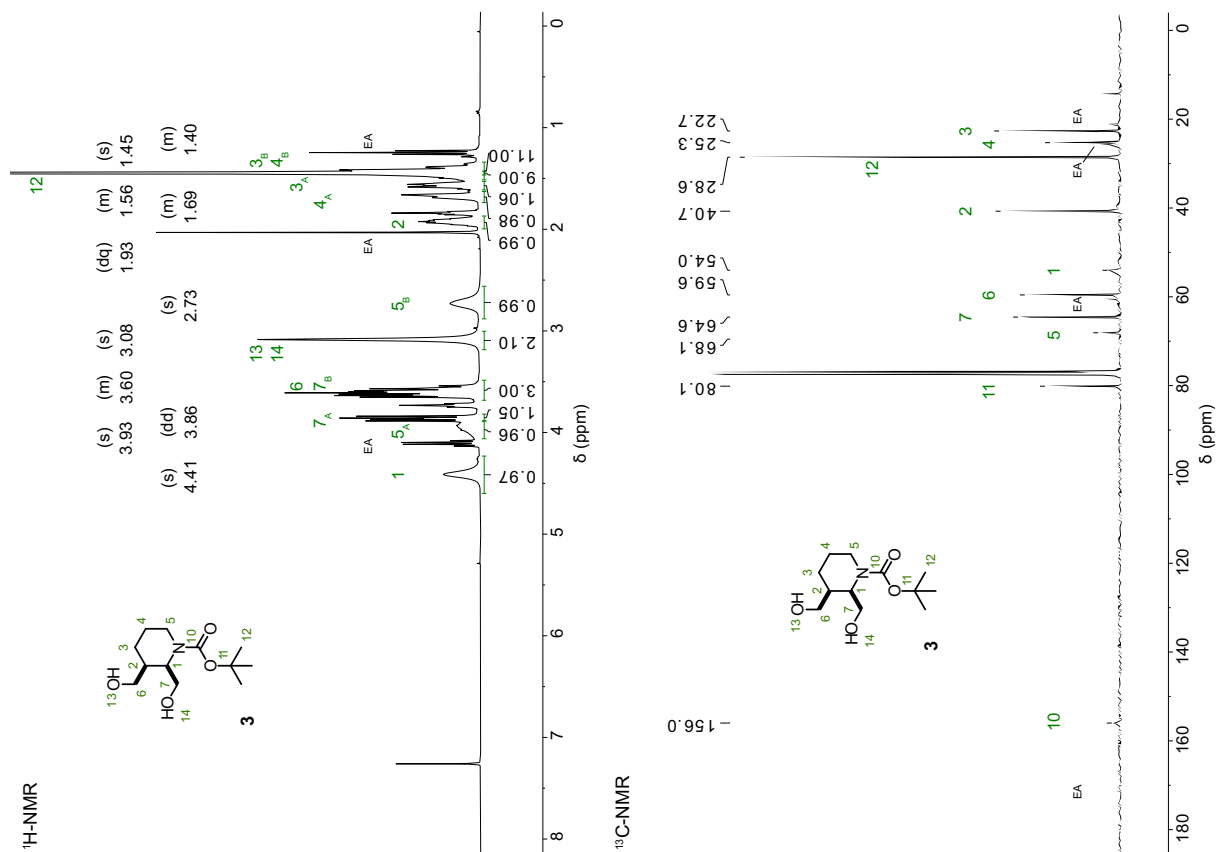
dimethyl *cis*-*N*-Boc-piperidine-2,3-dicarboxylate (**2**)



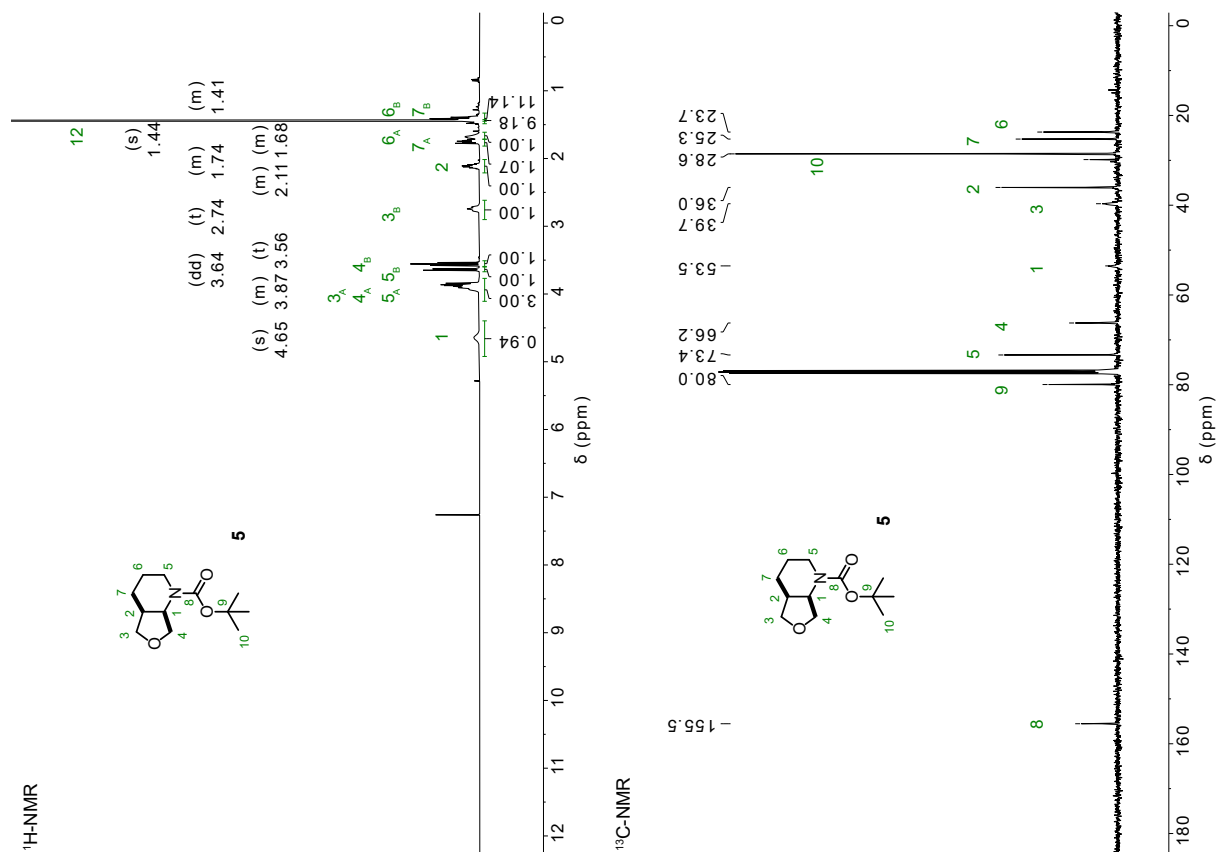
cis/trans-epimerisation: dimethyl *N*-Boc-piperidine-2,3-dicarboxylate (**14**)



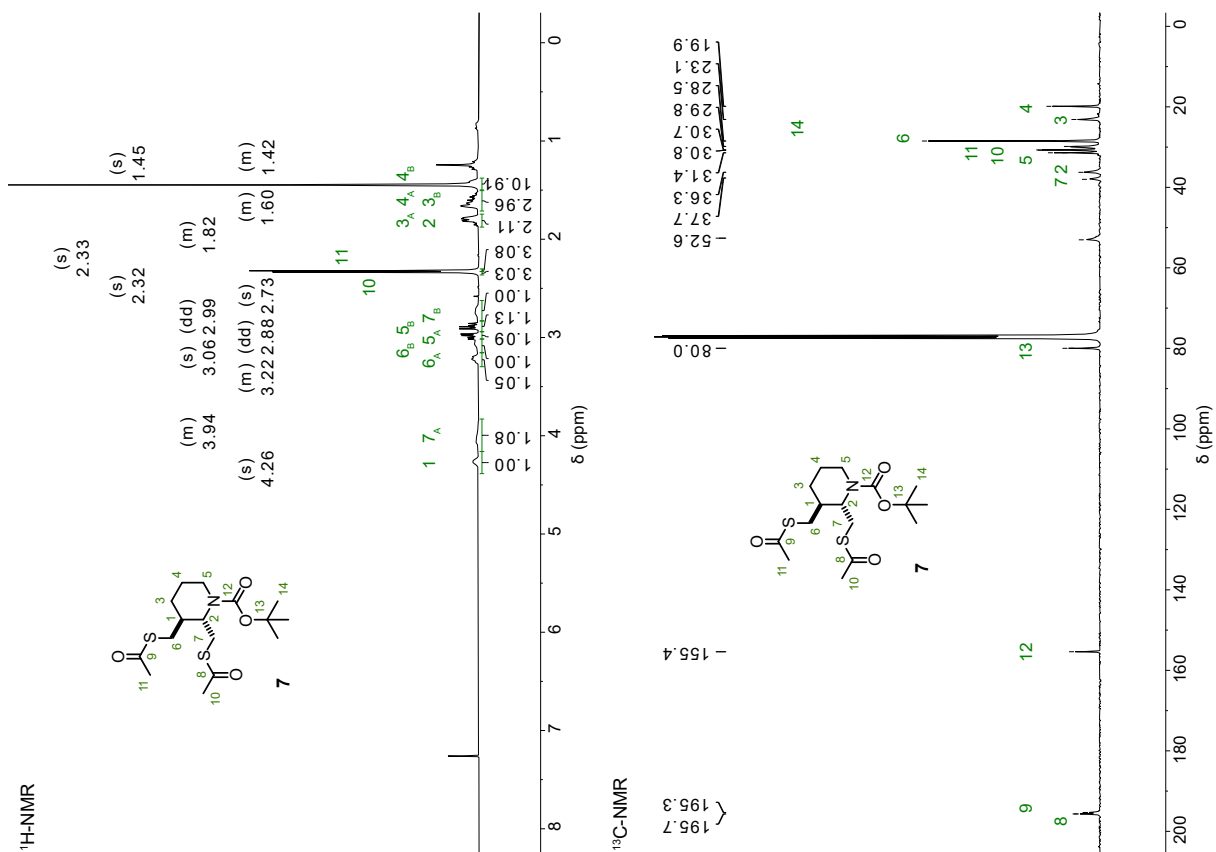
cis-N-Boc 2,3-bis(hydroxymethyl)piperidine (3)



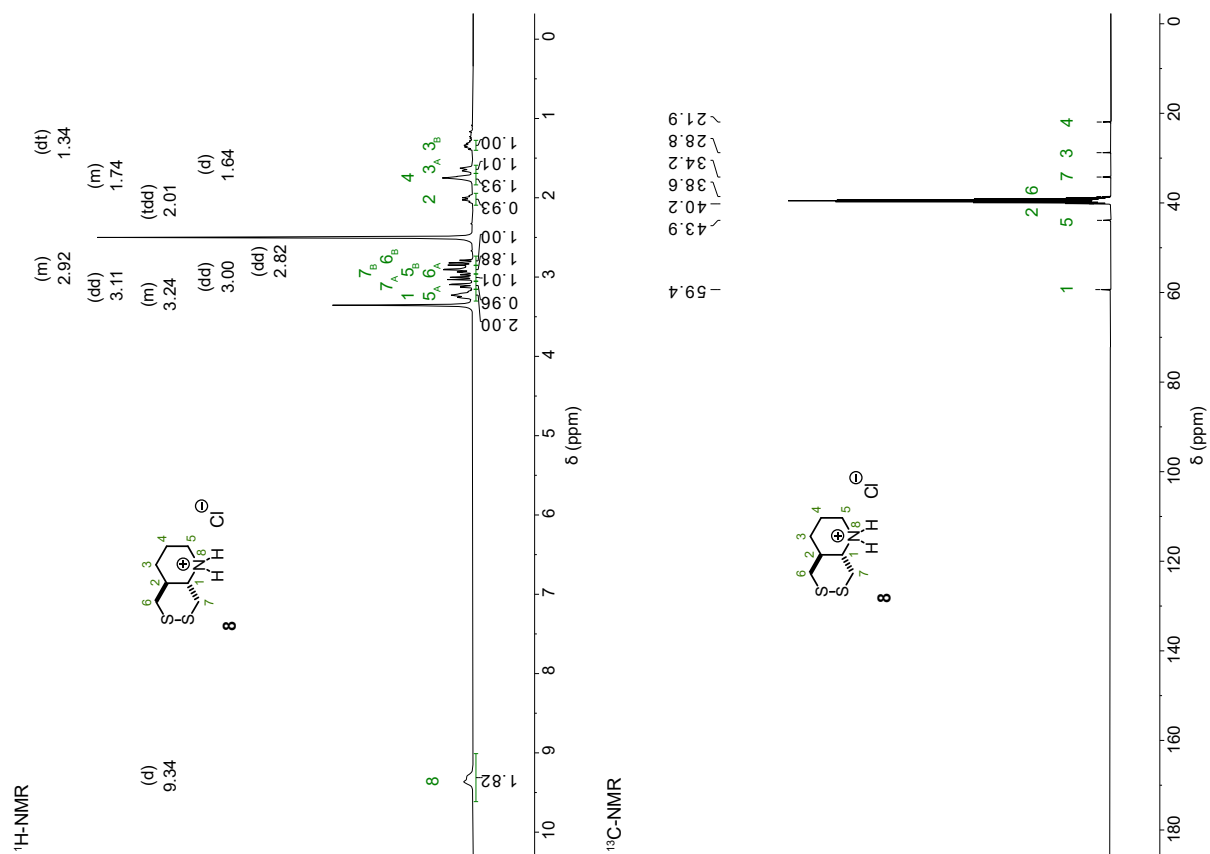
cis-N-Boc hexahydrofuro[3,4-b]pyridine (5)



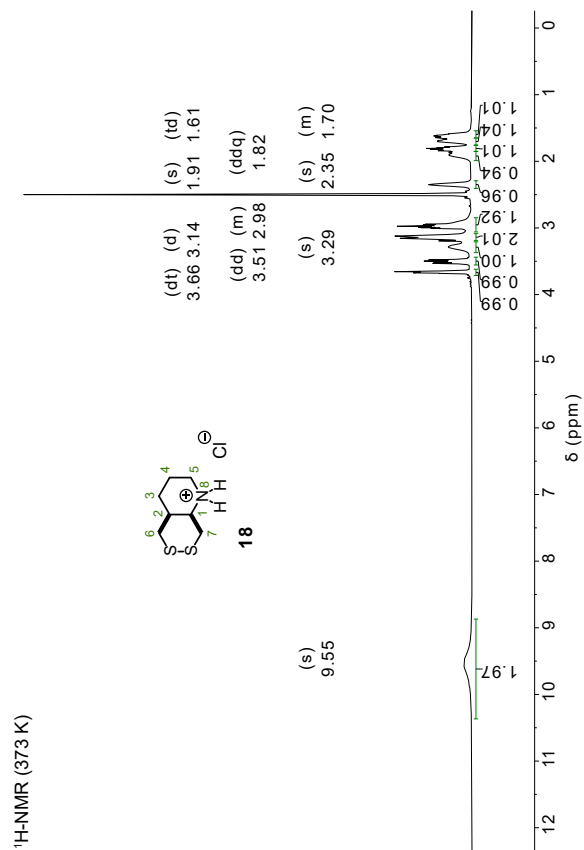
trans-N-Boc 2,3-bis((acetylthio)methyl)piperidine (7)



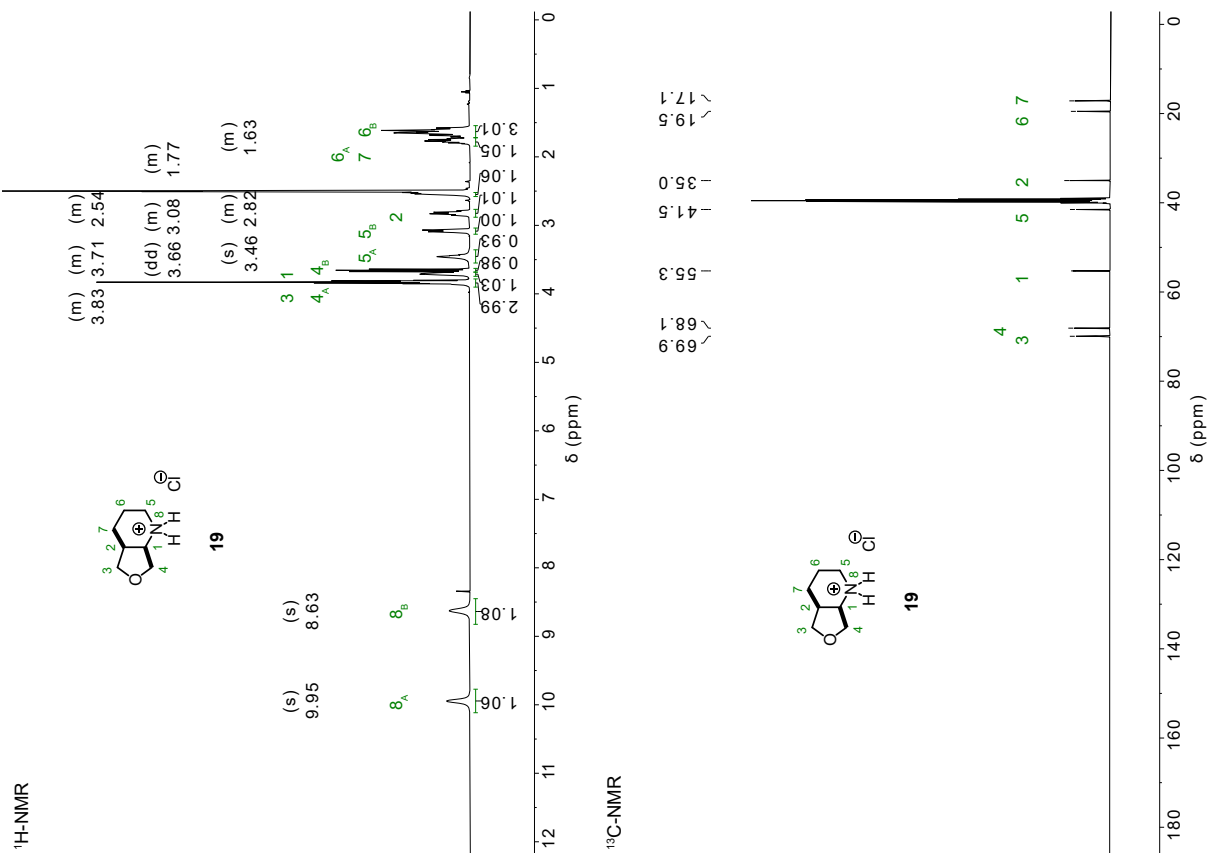
trans-hexahydro-[1,2]dithiino[4,5-b]pyridine hydrochloride (8)



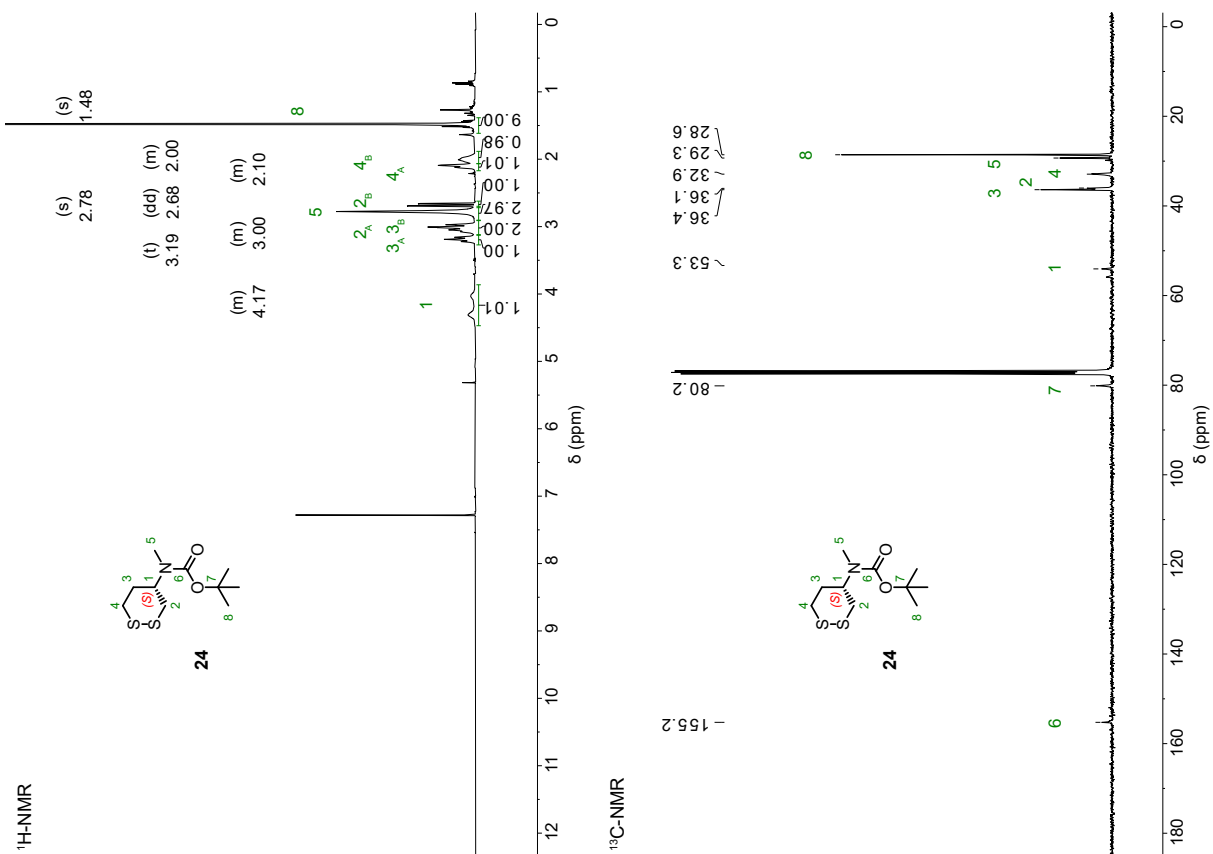
cis-octahydro-[1,2]dithiino[4,5-b]pyridine hydrochloride (18)



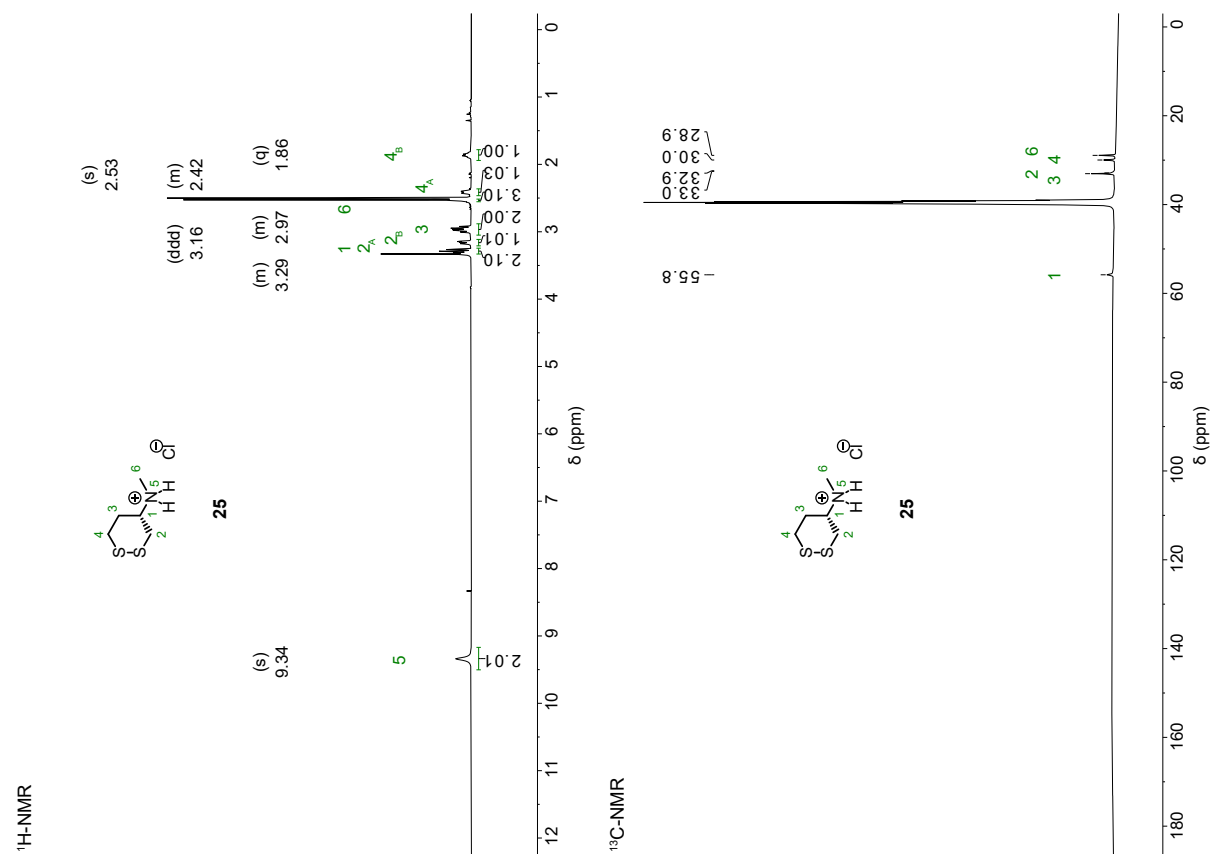
cis-octahydrofuro[3,4-b]pyridine hydrochloride (19)



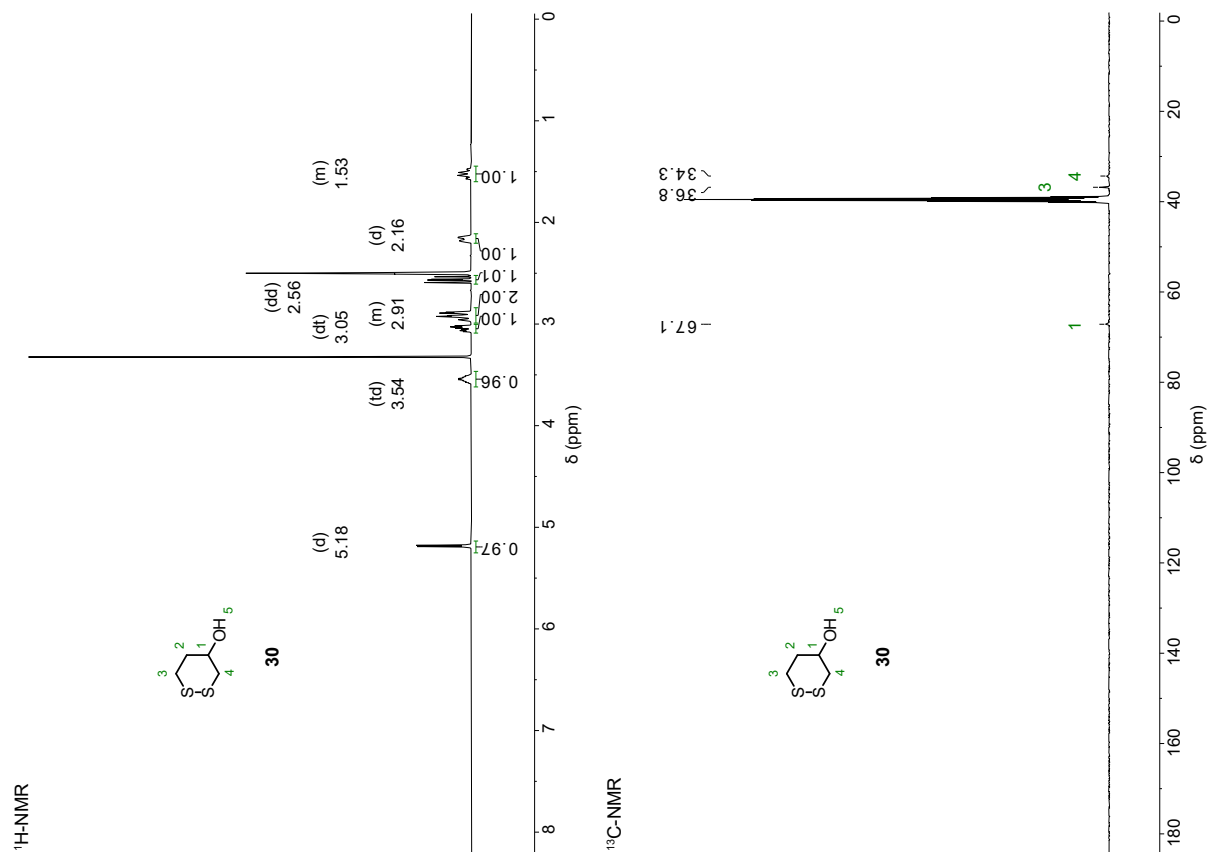
(S)-N-Boc-N-methyl-1,2-dithian-4-amine (24)



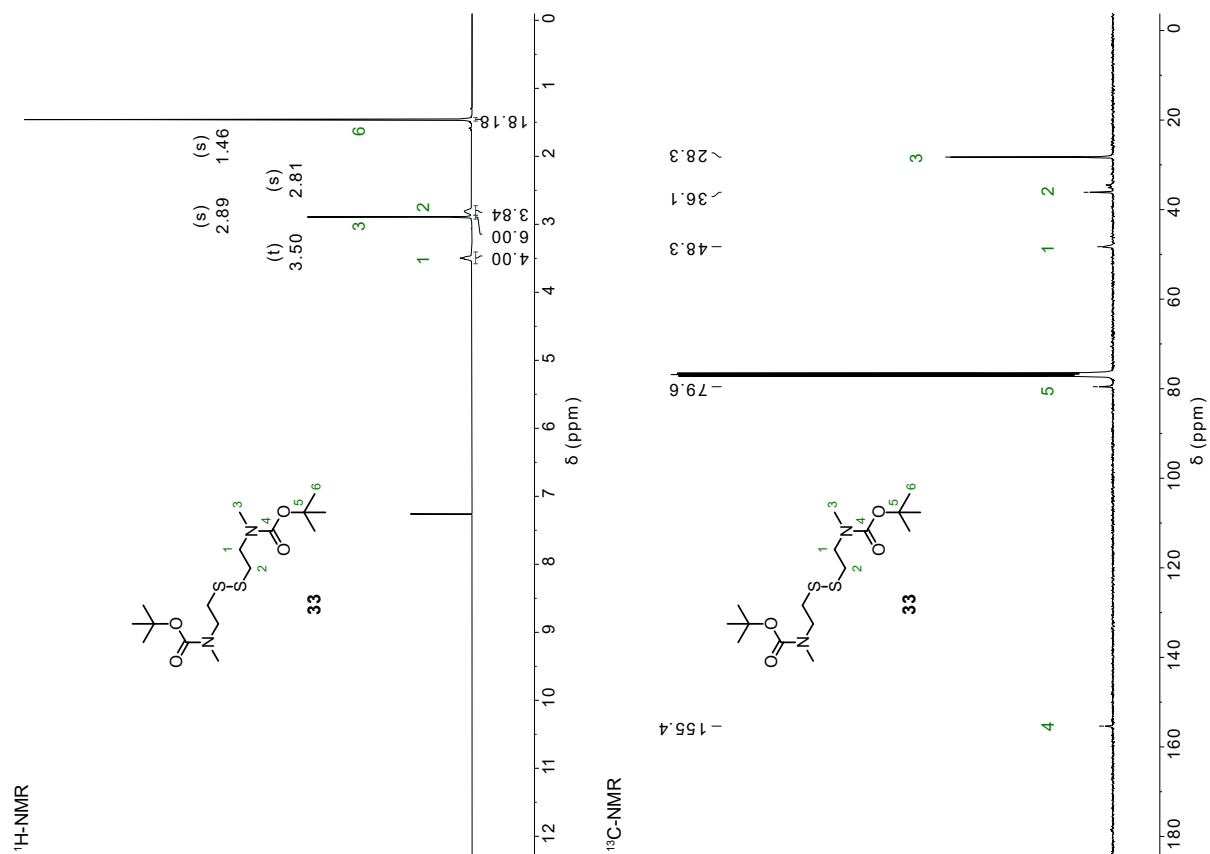
(S)-N-methyl-1,2-dithian-4-amine hydrochloride (25)



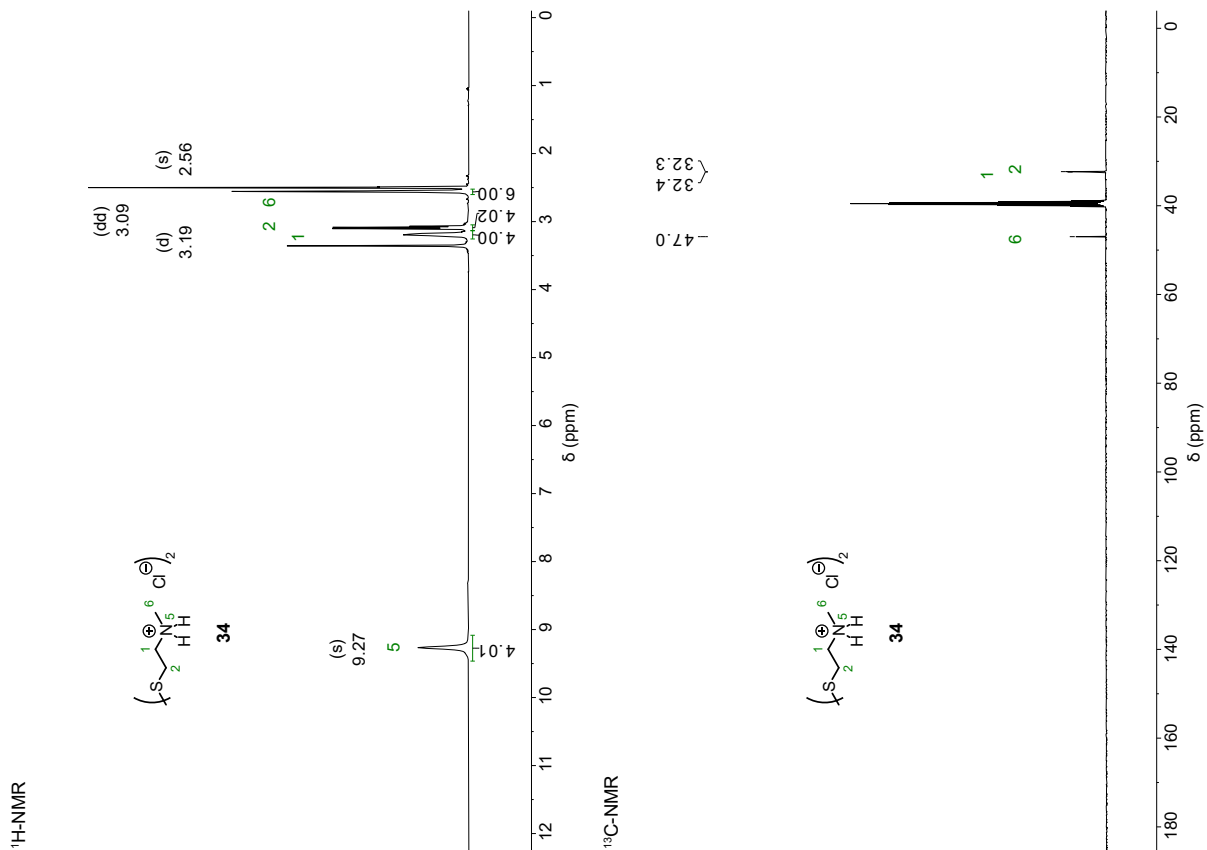
1,2-dithian-4-ol (30)



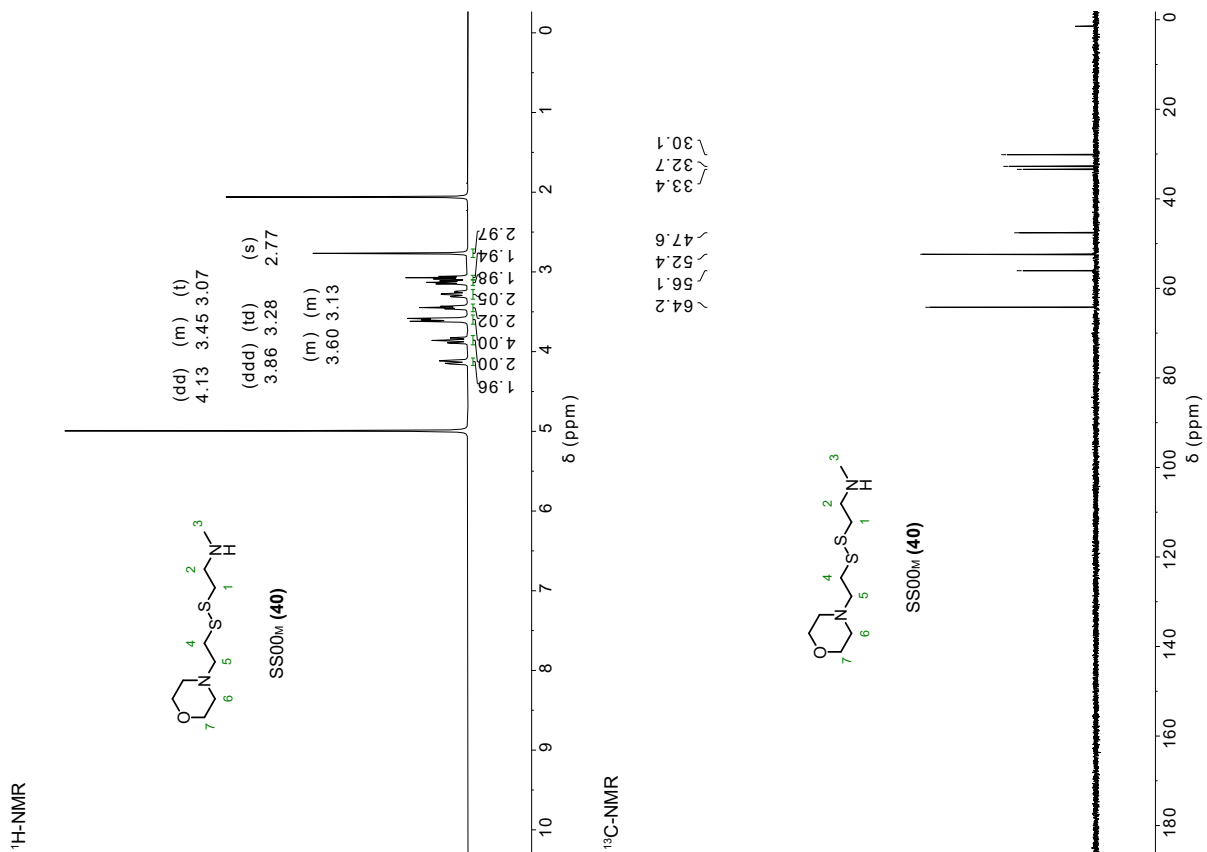
***N*-Boc, *N'*-Boc 2,2'-disulfanediybis(*N*-methylethan-1-amine) (33)**

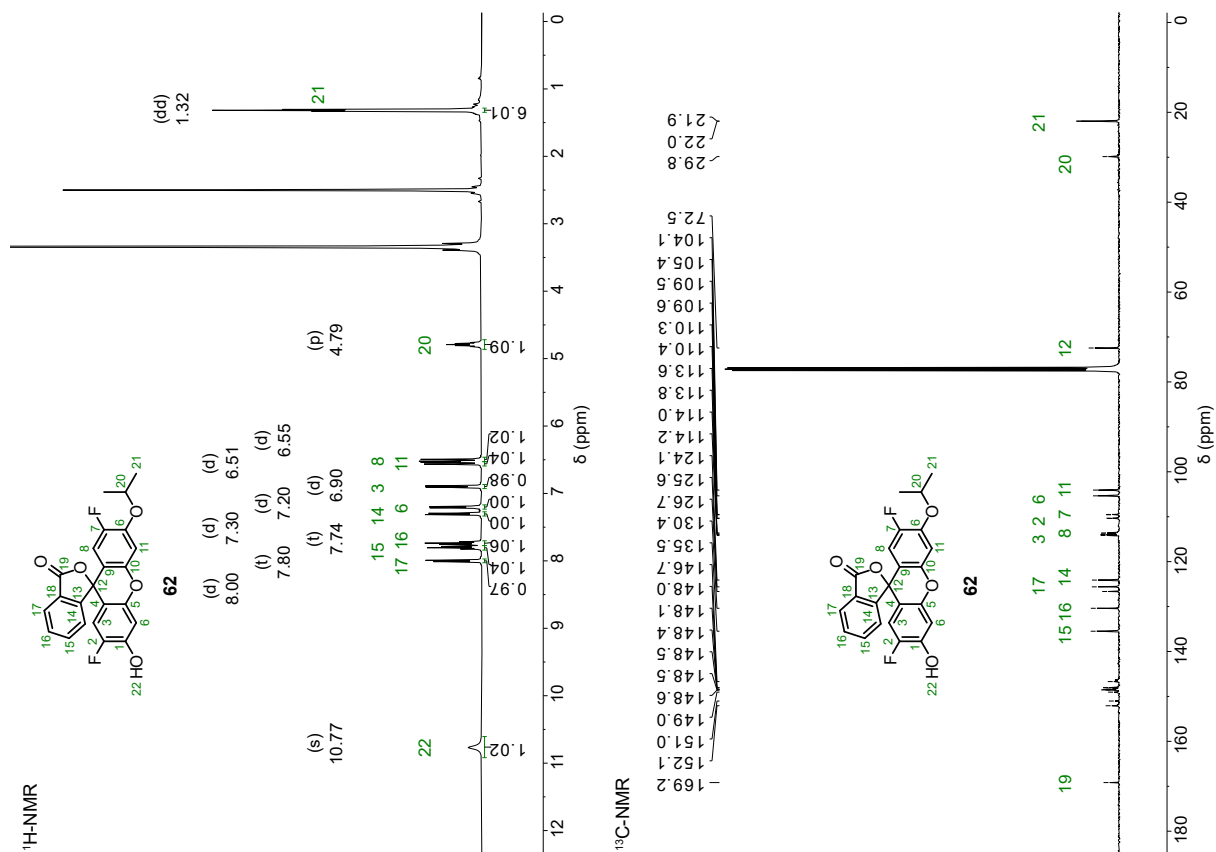
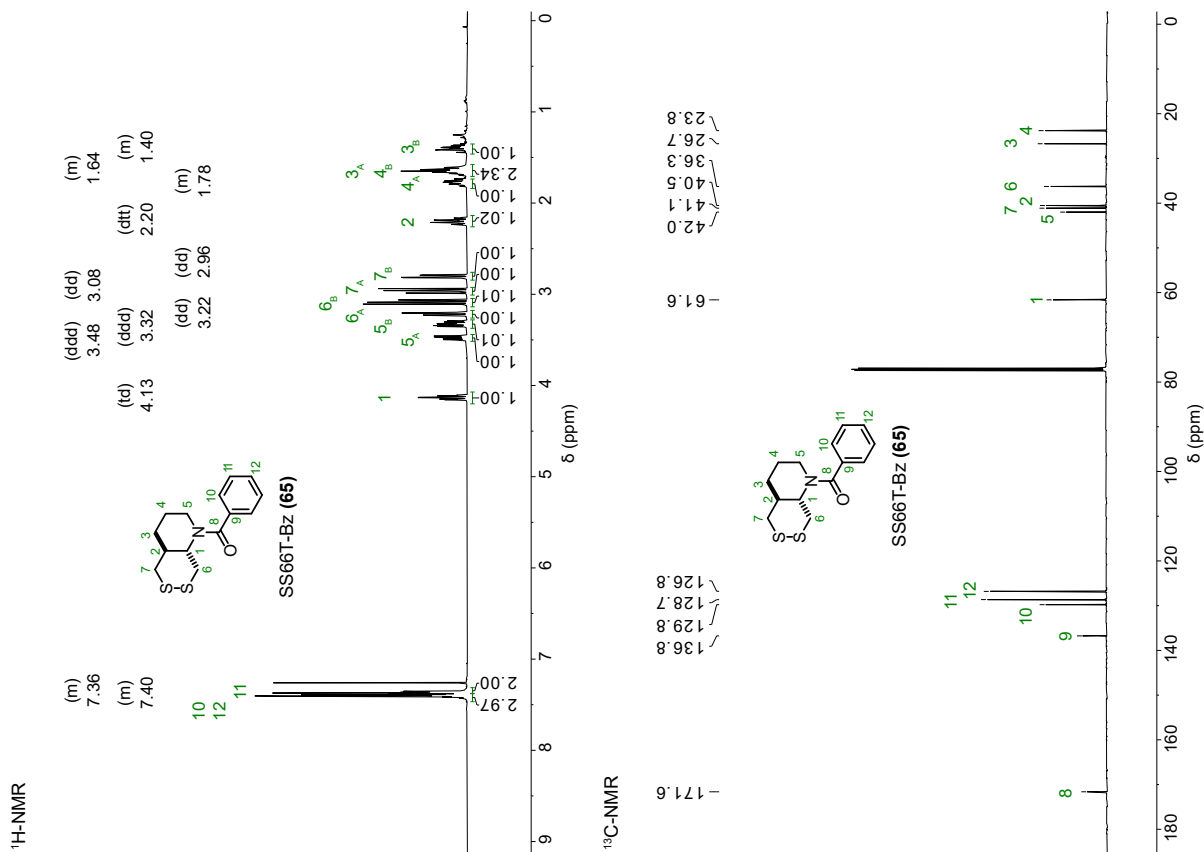


2,2'-disulfanediylbis(*N*-methylethan-1-amine) dihydrochloride (34)

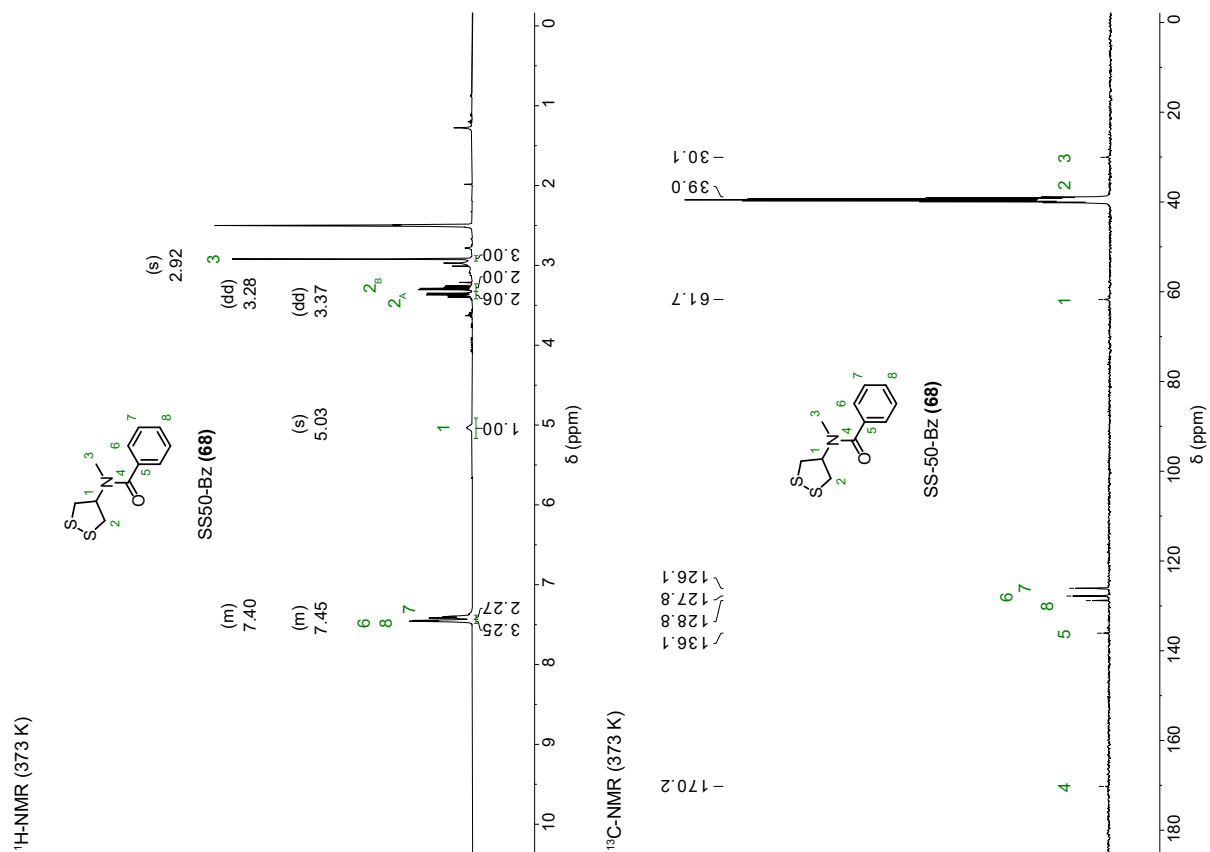


***N*-methyl-2-((2-morpholinoethyl)disulfaneyl)ethan-1-amine dihydrochloride (40)**

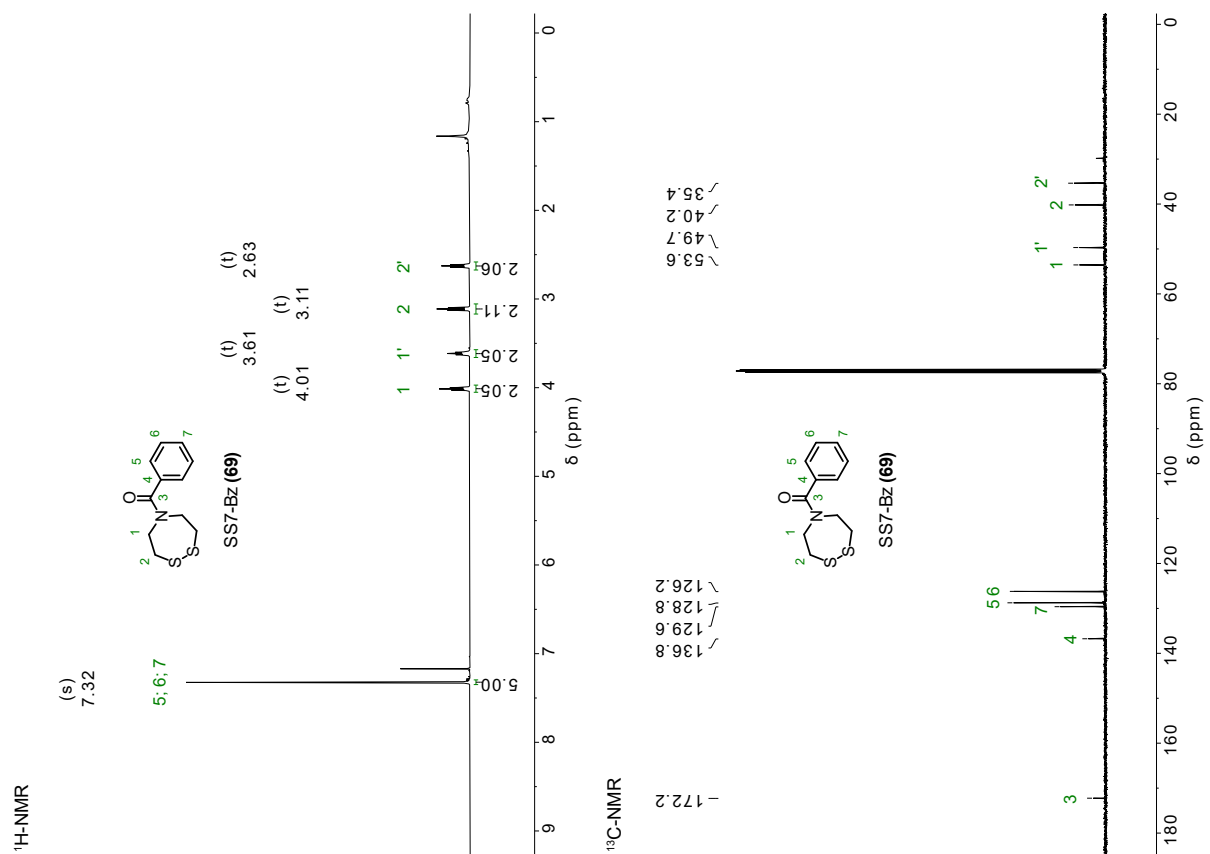


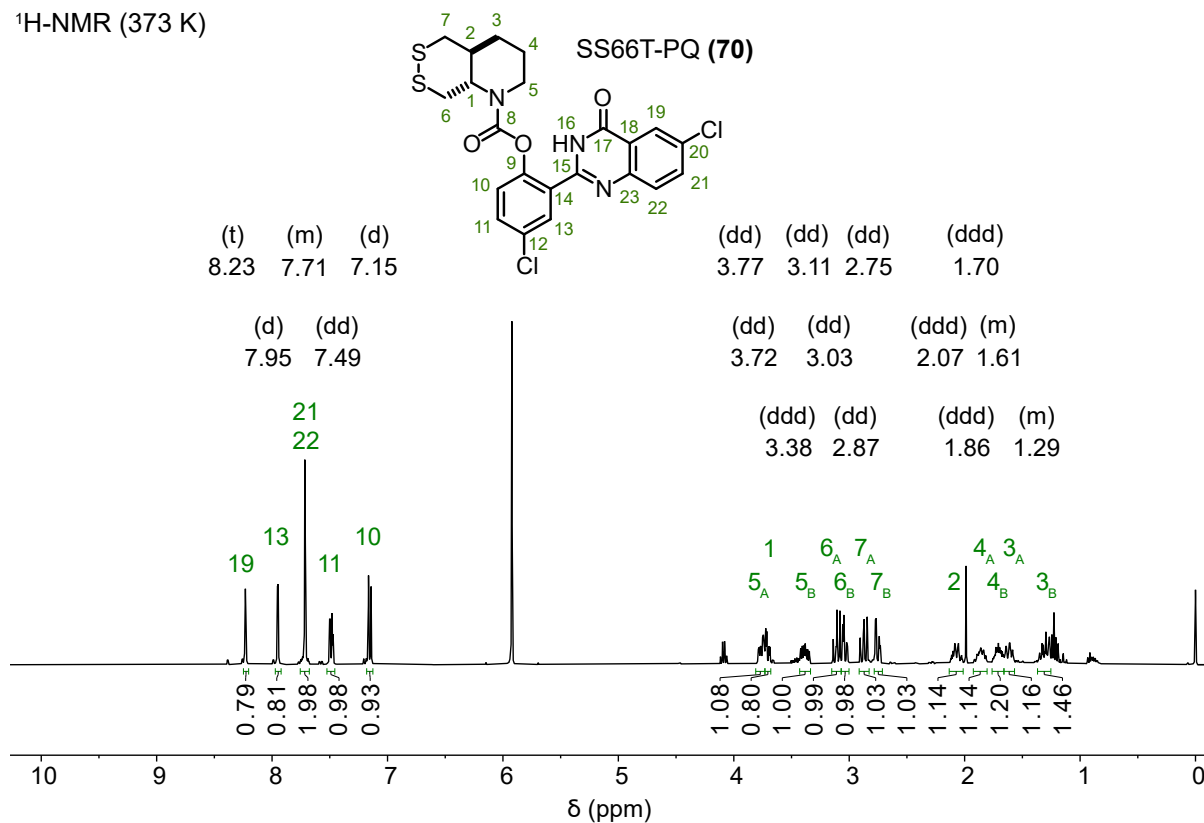
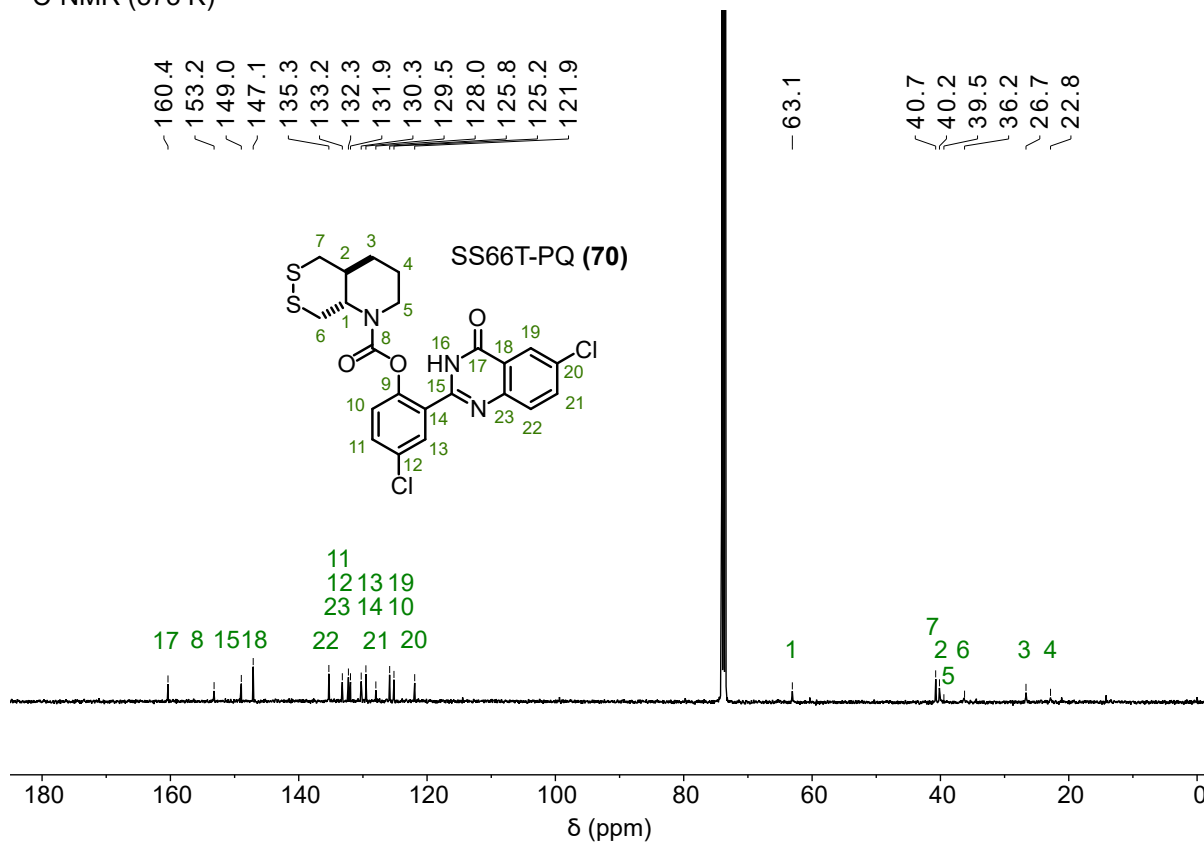
2',7'-difluoro-3'-hydroxy-6'-isopropoxy-3H-spiro[isobenzofuran-1,9'-xanthen]-3-one (IG-OH, 62)**trans-(hexahydro-[1,2]dithiino[4,5-b]pyridin-1(2H)-yl)benzamide (SS66T-Bz, 65)**

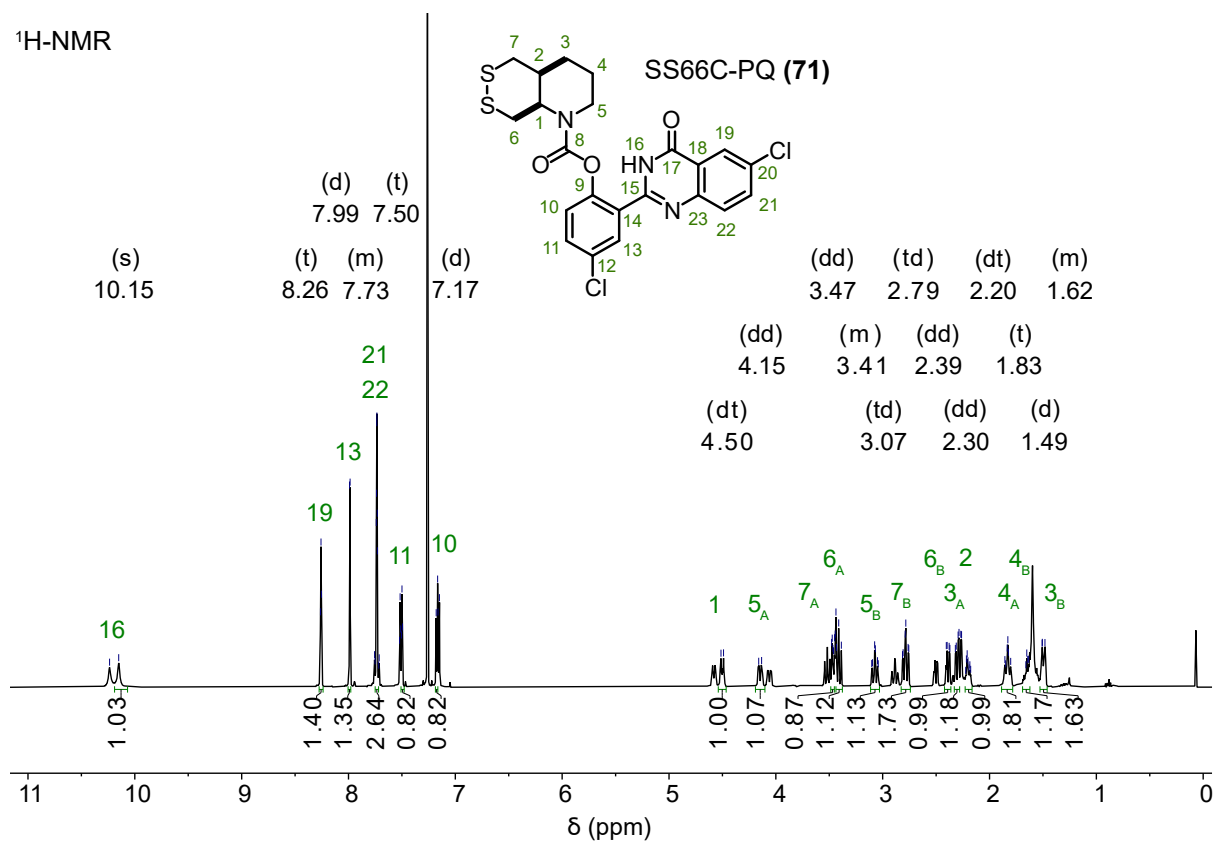
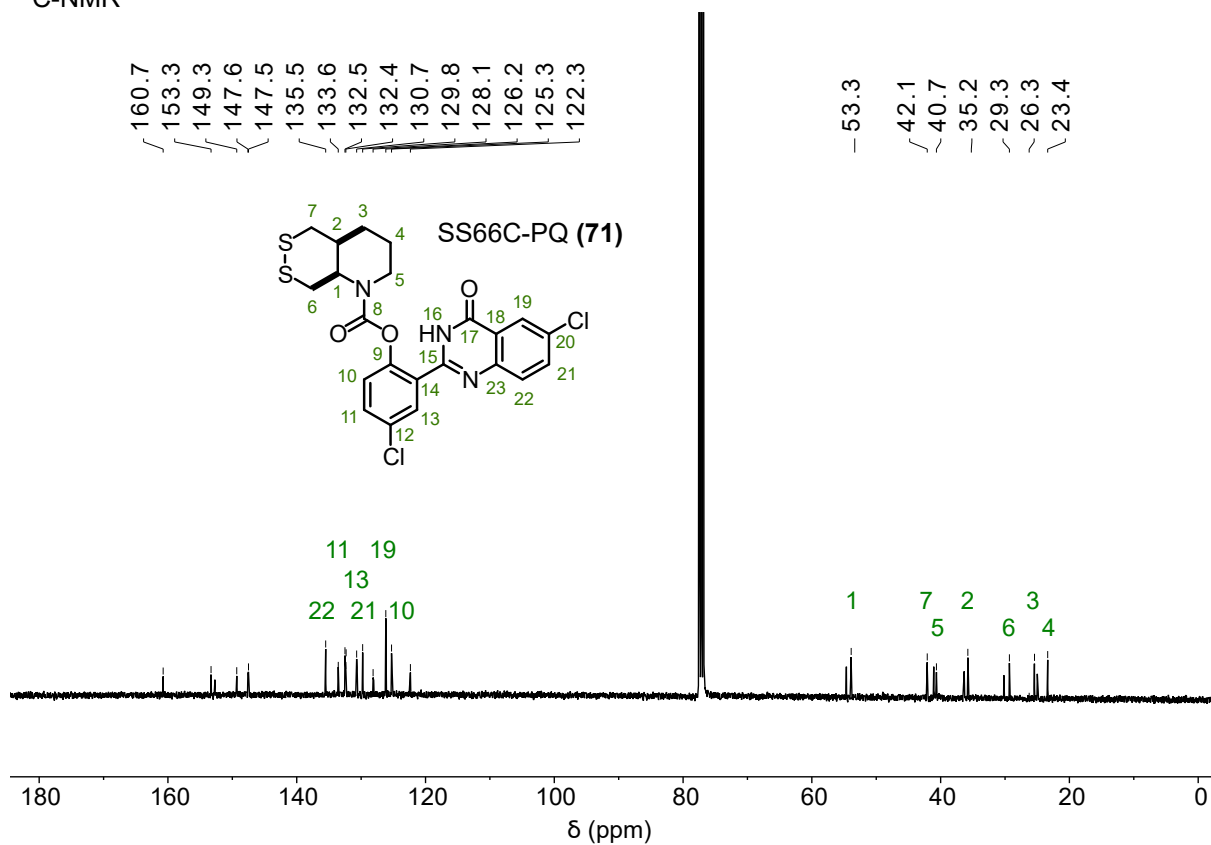
***N*-methyl-*N*-(1,2-dithiolan-4-yl)benzamide (SS50-Bz, 68)**



(1,2,5-dithiazepan-5-yl)(phenyl)methanone (SS7-Bz, 69)

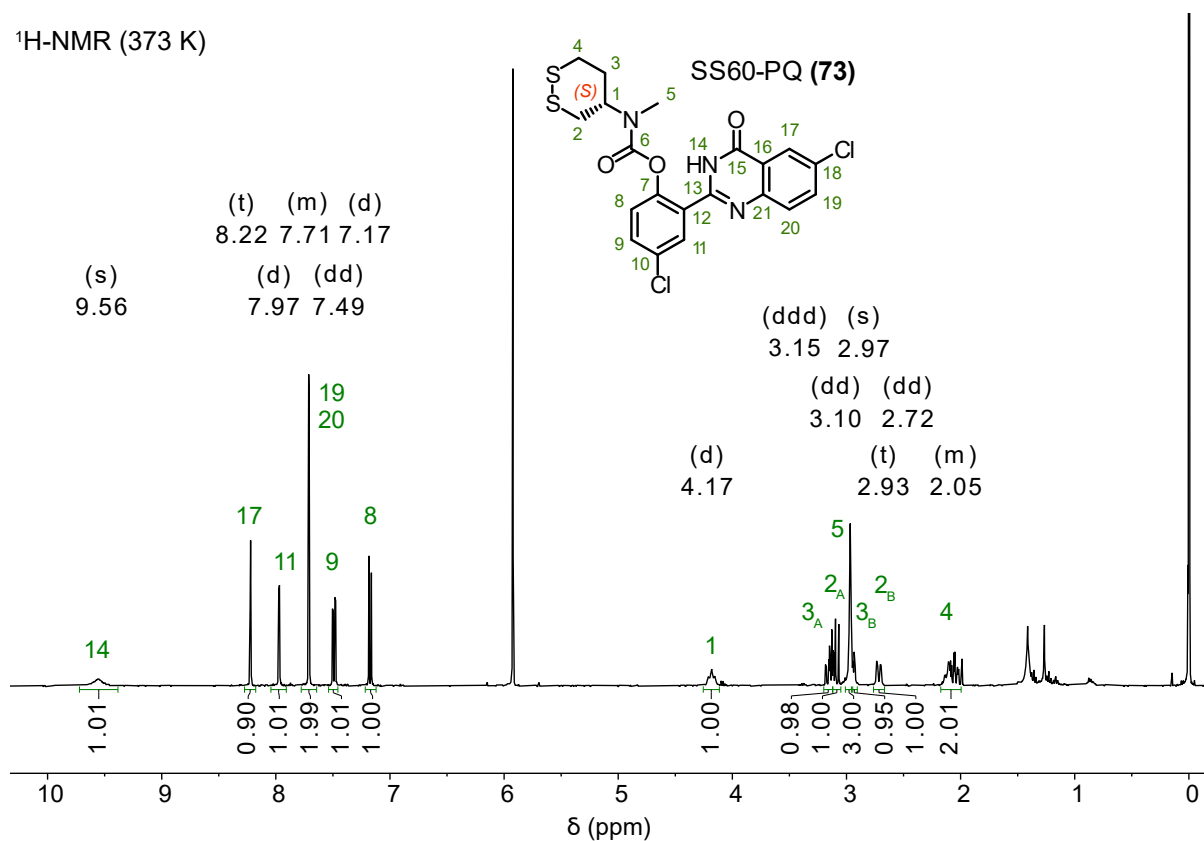


***trans*-chloro-2-(chloro-4-oxo-3,4-dihydroquinazolin-2-yl)phenyl *trans*-hexahydro-[1,2]dithiino [4,5-*b*]pyridine-1(2*H*)-carboxylate (SS66T-PQ, 70)**¹H-NMR (373 K)¹³C-NMR (373 K)

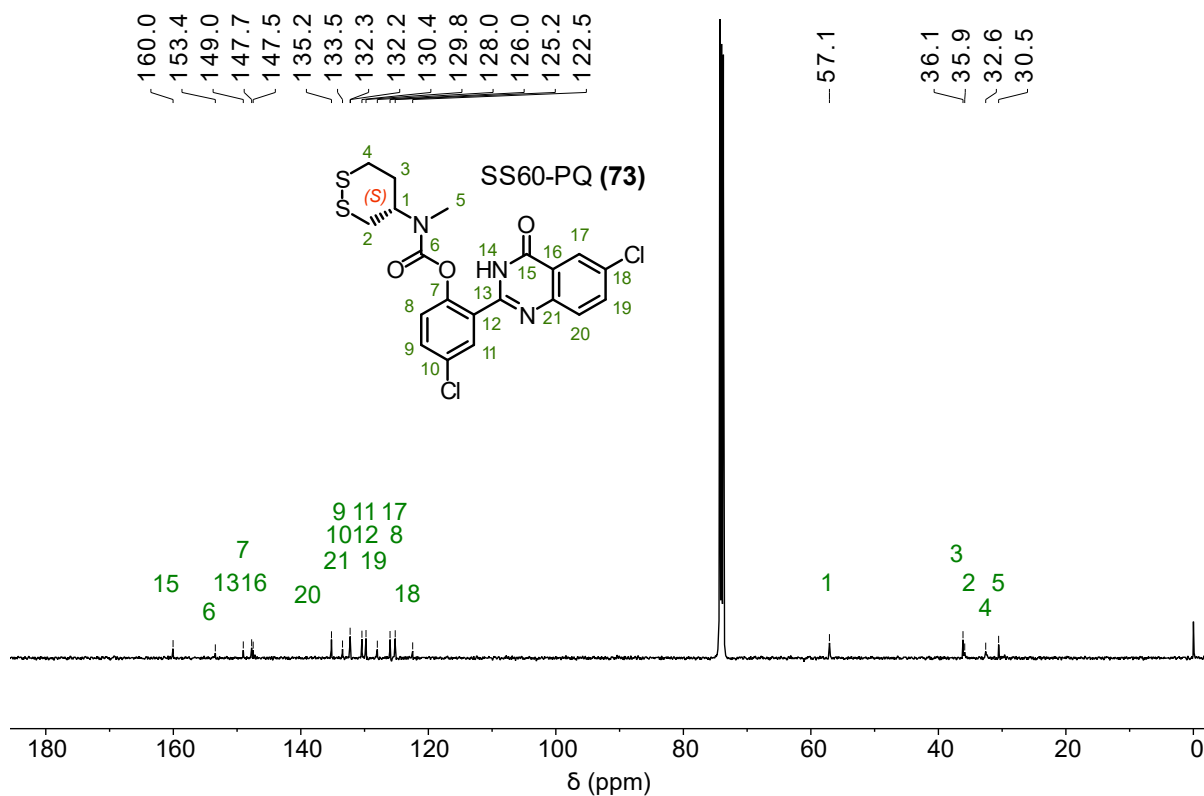
cis-chloro-2-(chloro-4-oxo-3,4-dihydroquinazolin-2-yl)phenyl-hexahydro-[1,2]dithiino [4,5-b]pyridine-1(2H)-carboxylate (SS66C-PQ, 71)¹H-NMR¹³C-NMR

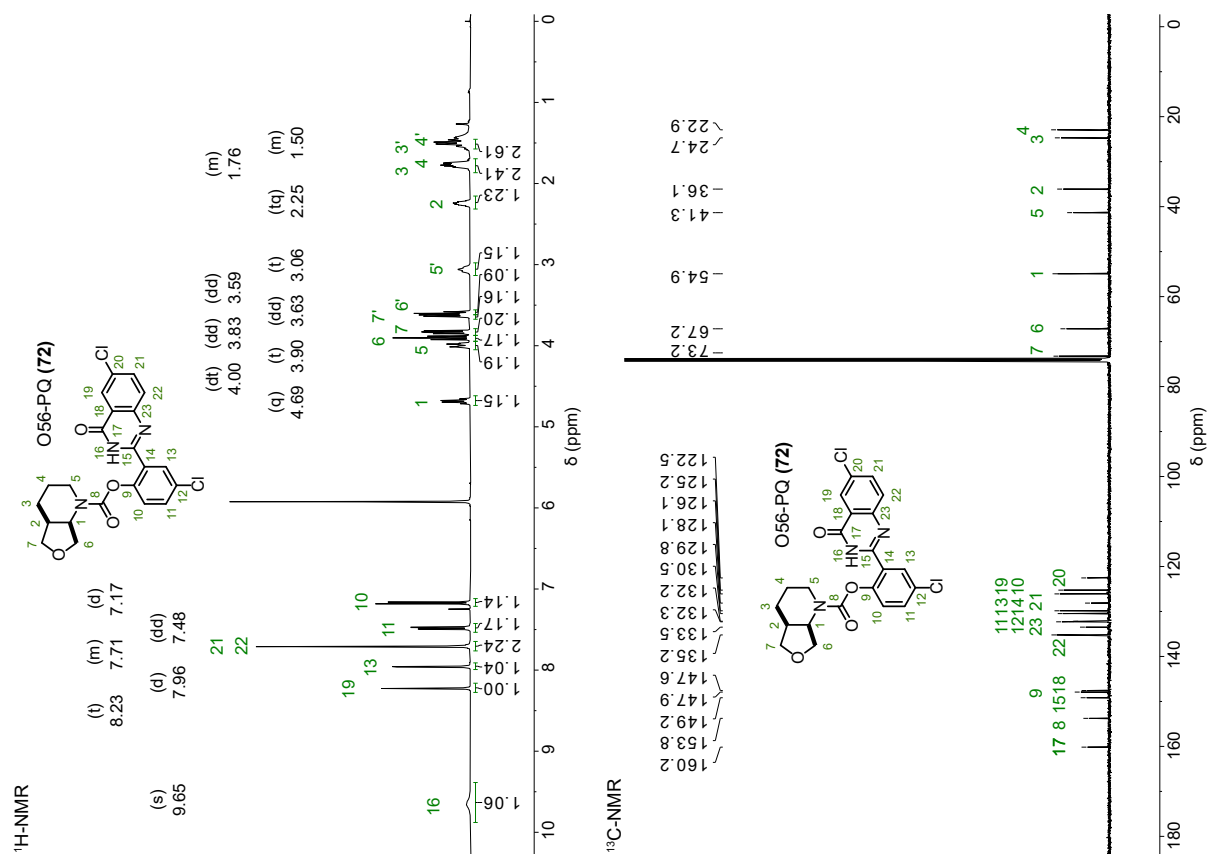
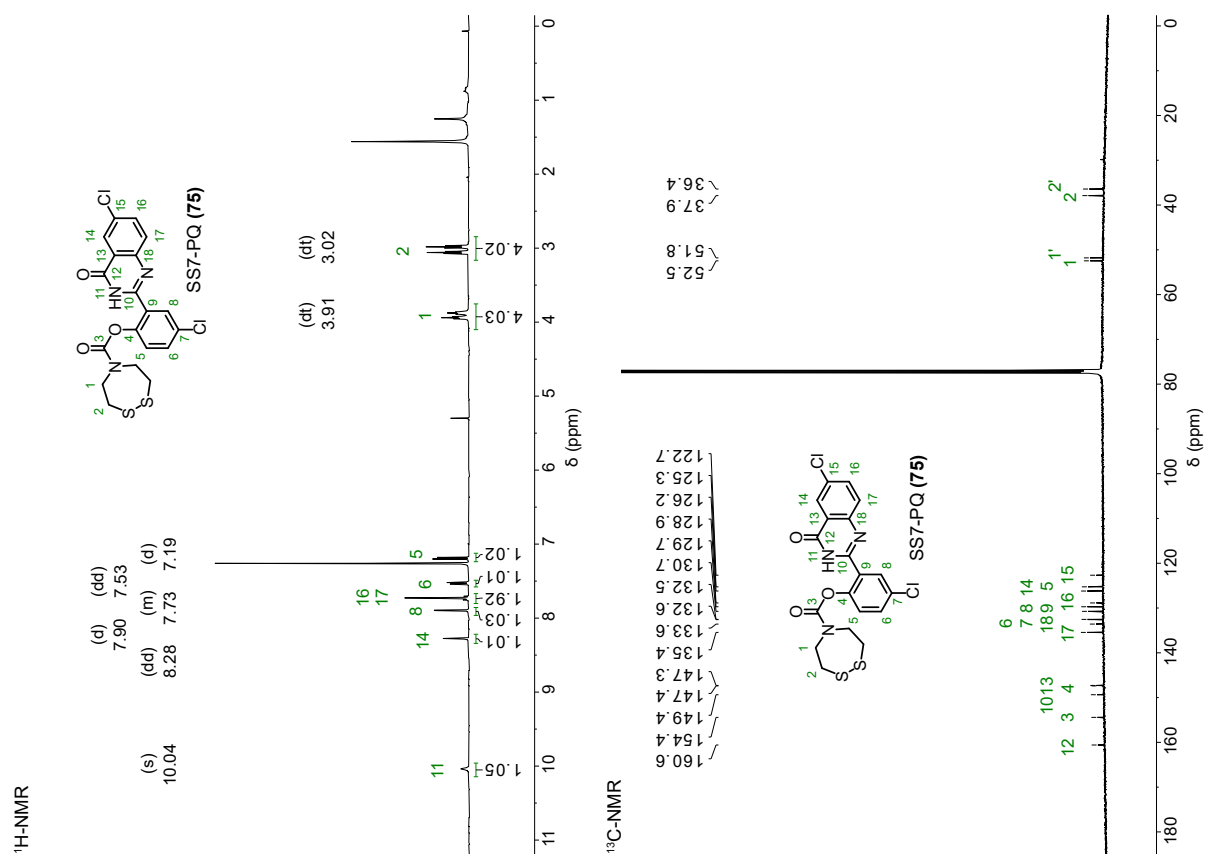
chloro-2-(chloro-4-oxo-3,4-dihydroquinazolin-2-yl)phenyl ((S)-1,2-dithian-4-yl) (methyl) carbamate (SS60-PQ, 73)

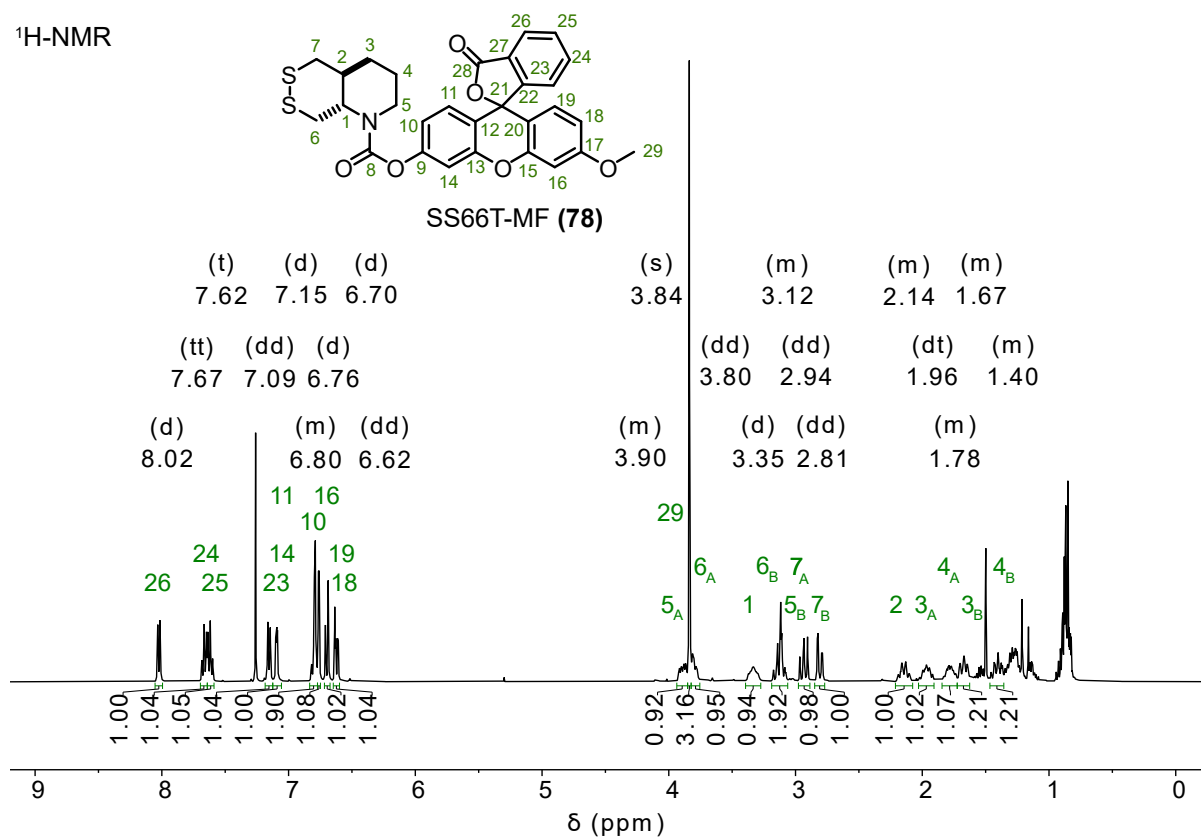
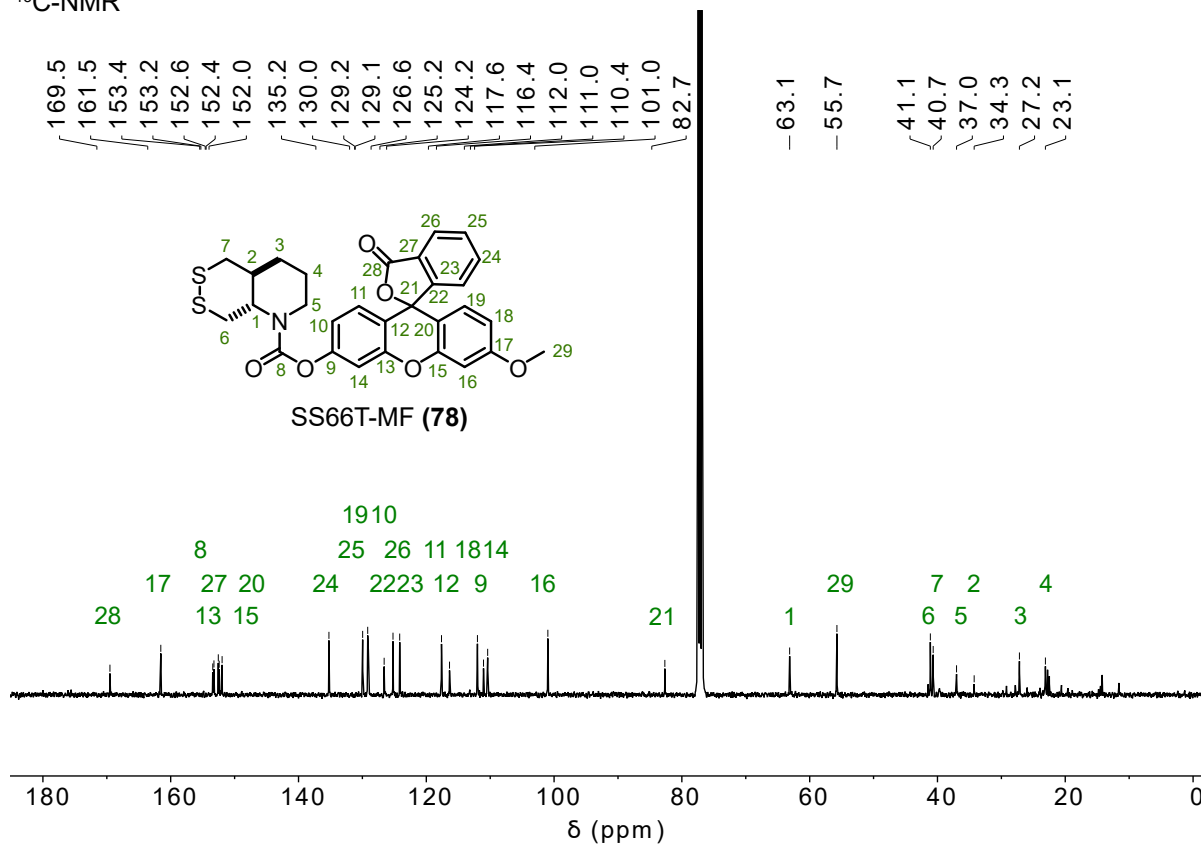
¹H-NMR (373 K)

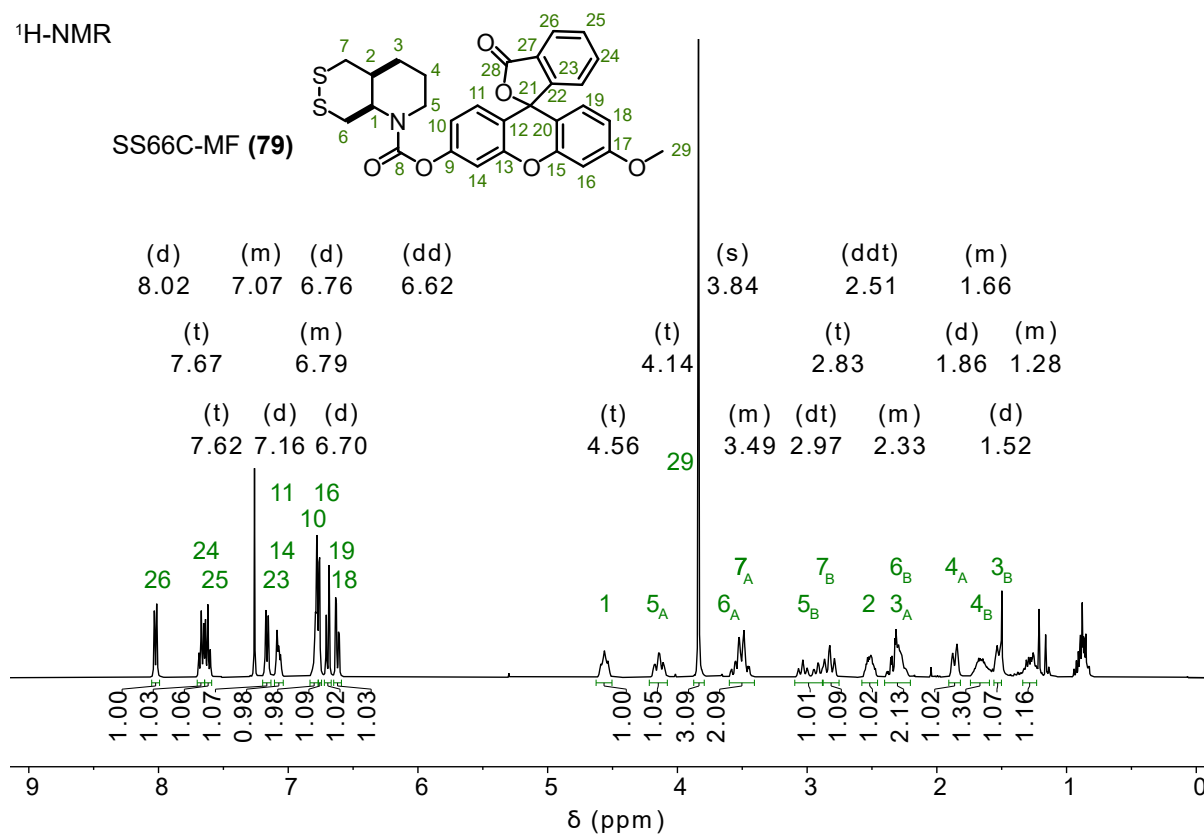
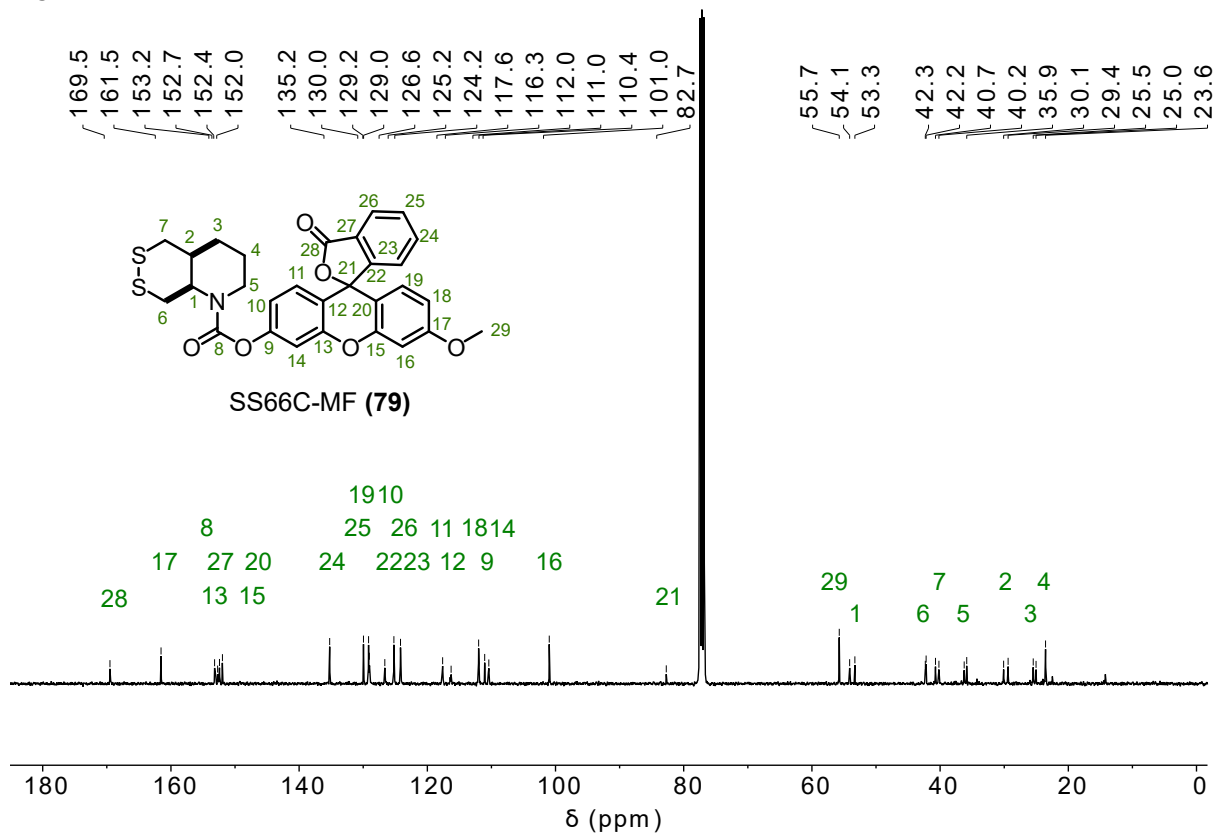


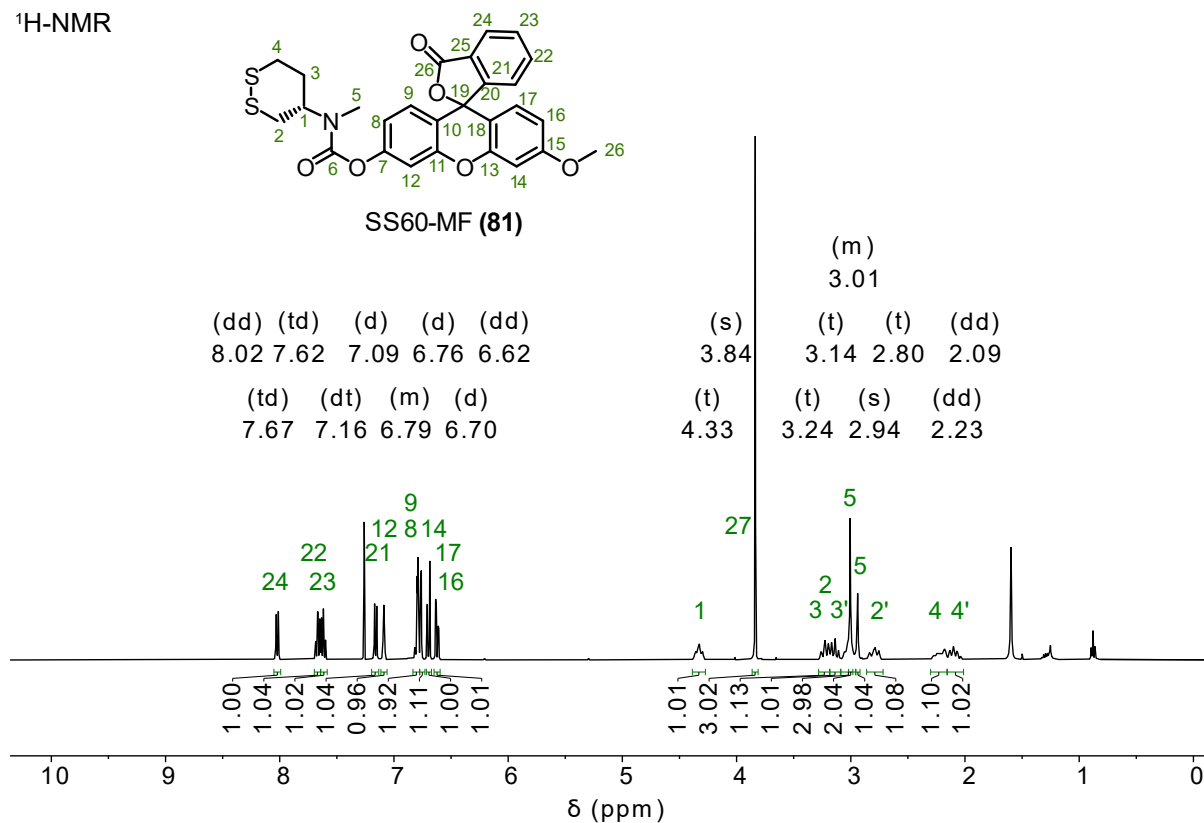
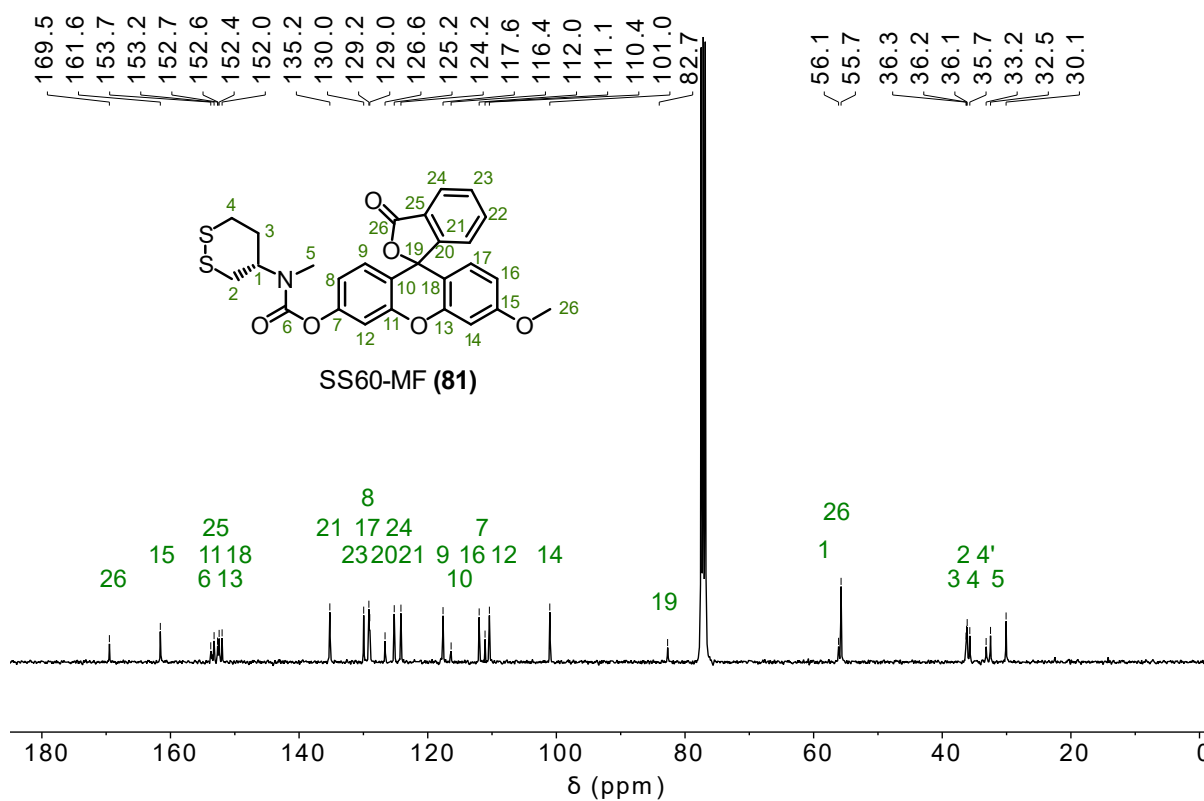
¹³C-NMR (373 K)

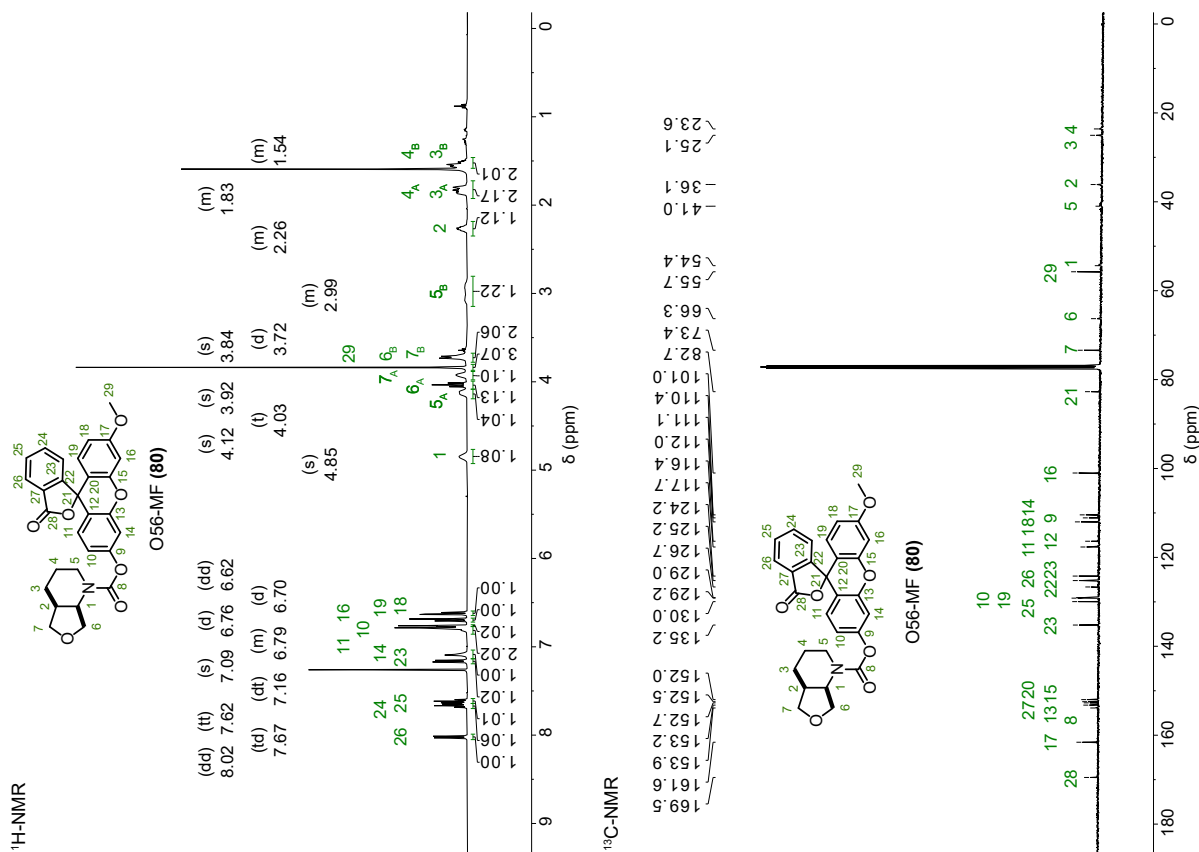
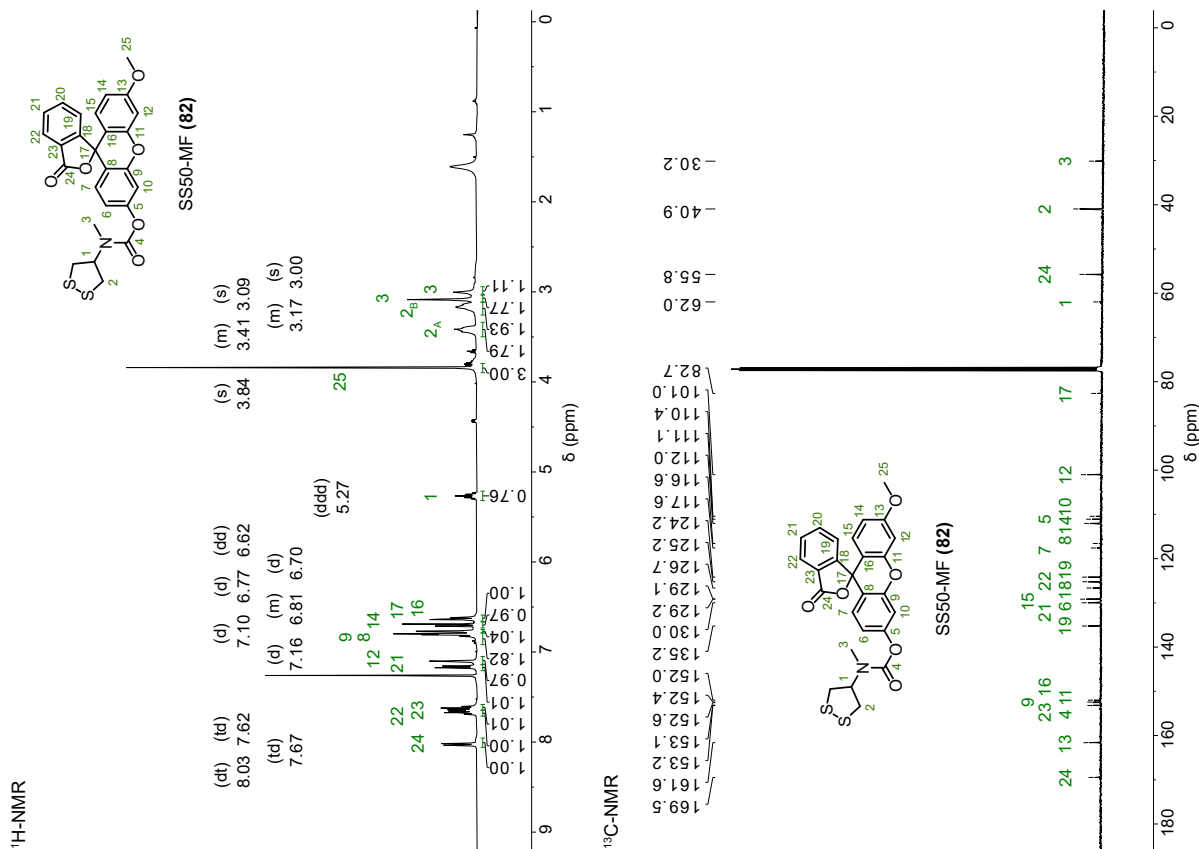


cis-chloro-2-(chloro-4-oxo-3,4-dihydroquinazolin-2-yl)phenyl-hexahydrofuro-[3,4-b]pyridine-1(2H)-carboxylate (O56-PQ, 72)**chloro-2-(chloro-4-oxo-3,4-dihydroquinazolin-2-yl)phenyl 1,2,5-dithiazepane-carboxylate (SS7-PQ, 75)**

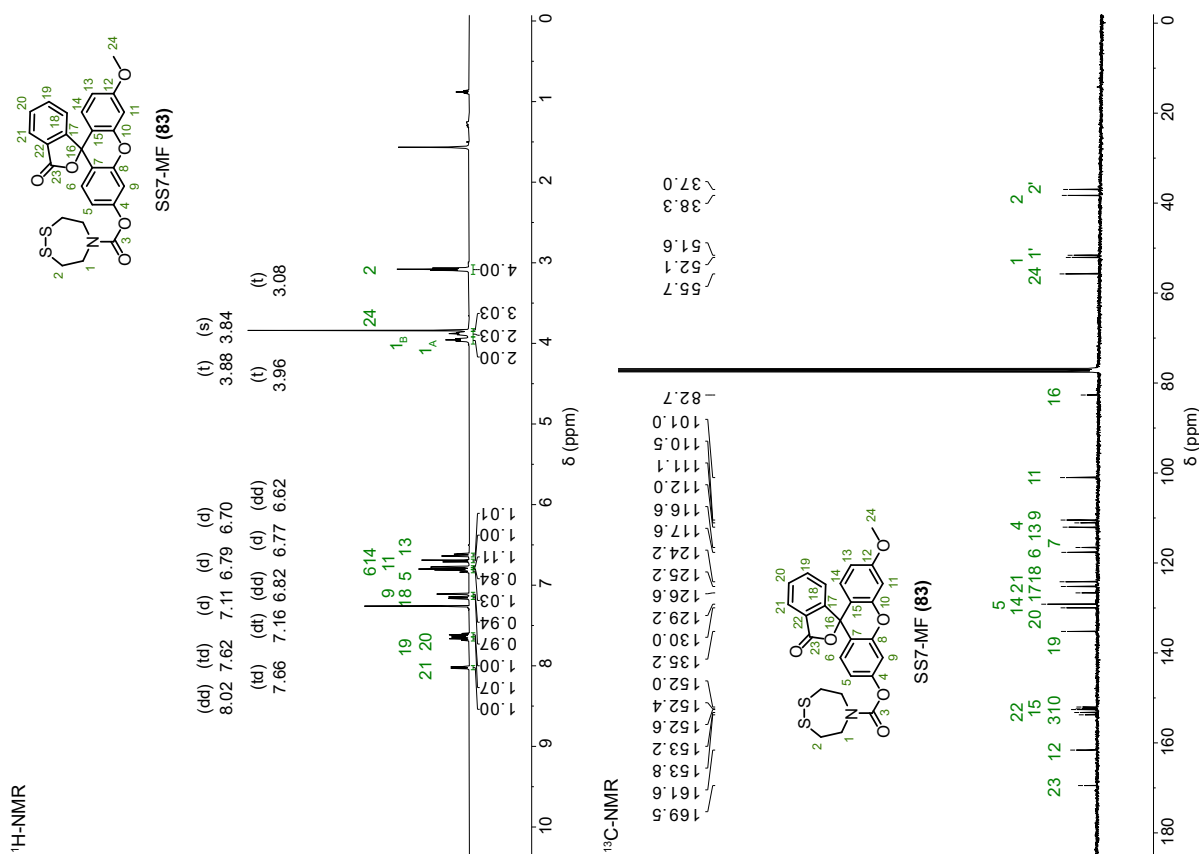
***trans*-3'-methoxy-3-oxo-3*H*-spiro[isobenzofuran-1,9'-xanthen]-6'-yl hexahydro-[1,2]dithiino [4,5-*b*]pyridine-1(2*H*)-carboxylate (SS66T-MF, 78)**¹H-NMR¹³C-NMR

cis-3'-methoxy-3-oxo-3H-spiro[isobenzofuran-1,9'-xanthen]-6'-yl hexahydro-[1,2]dithiino [4,5-b]pyridine-1(2H)-carboxylate (SS66C-MF, 79)¹H-NMR¹³C-NMR

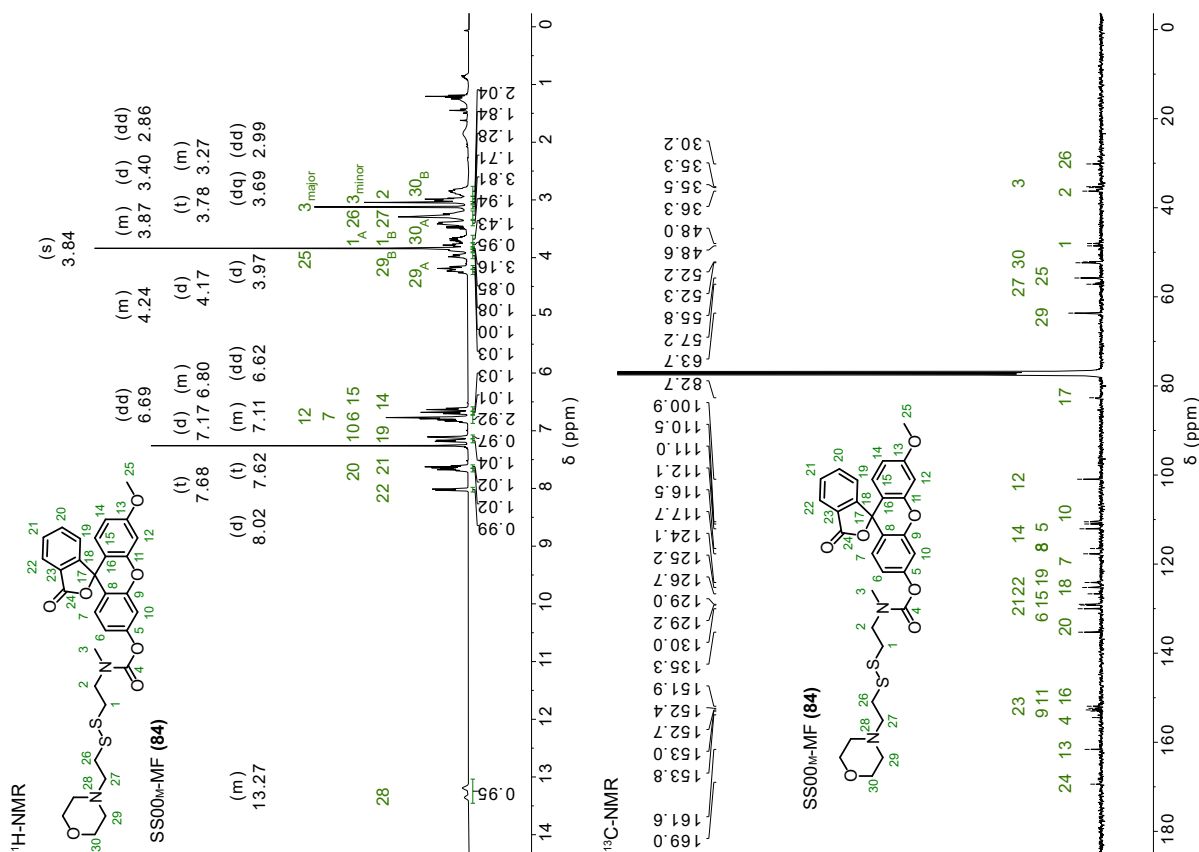
3'-methoxy-3-oxo-3H-spiro[isobenzofuran-1,9'-xanthen]-6'-yl ((S)-1,2-dithian-4-yl)(methyl)carbamate (SS60-MF, 81)¹H-NMR¹³C-NMR

cis-3'-methoxy-3-oxo-3H-spiro[isobenzofuran-1,9'-xanthen]-6'-yl hexahydrofuro[3,4-b]pyridine-1(2H)-carboxylate (O56-MF, 80)**3'-methoxy-3-oxo-3H-spiro[isobenzofuran-1,9'-xanthen]-6'-yl (1,2-dithiolan-4-yl) (methyl)carbamate (SS50-MF, 82)**

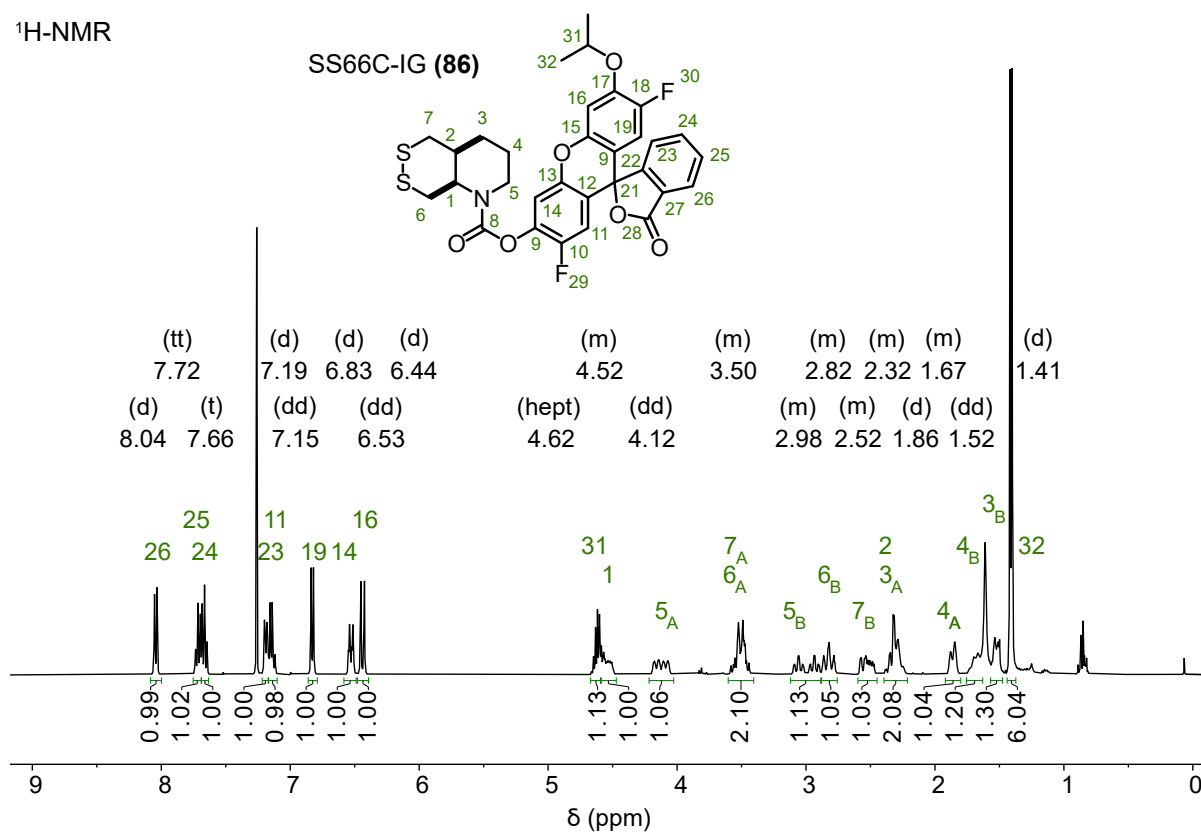
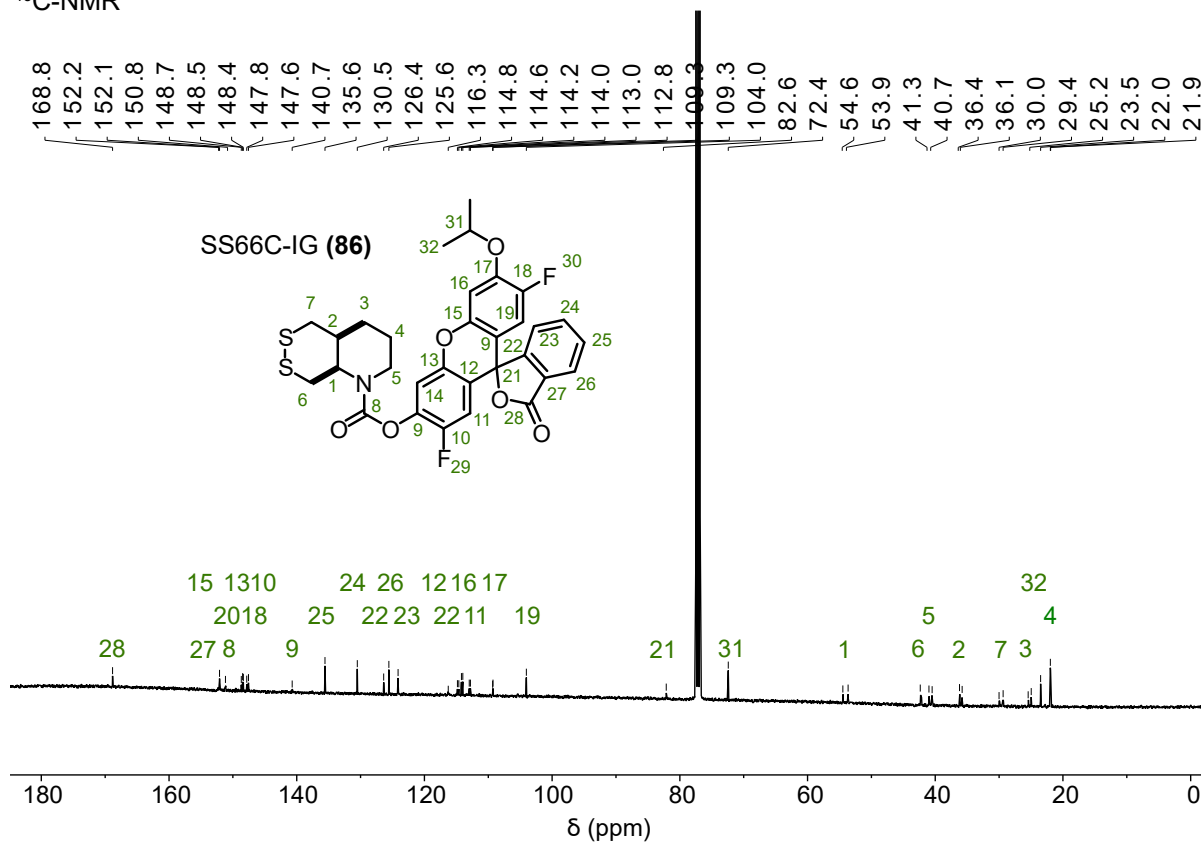
3'-methoxy-3-oxo-3H-spiro[isobenzofuran-1,9'-xanthen]-6'-yl 1,2,5-dithiazepane-carboxylate (SS7-MF, 83)



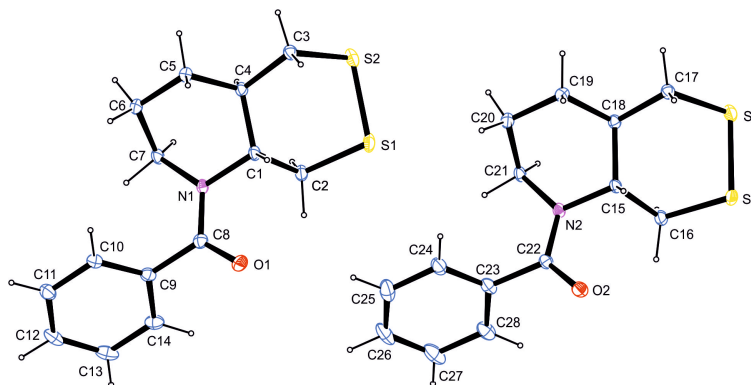
3'-methoxy-3-oxo-3H-spiro[isobenzofuran-1,9'-xanthen]-6'-yl disulfaneyl ethyl)carbamate (SS00_M-MF, 84)



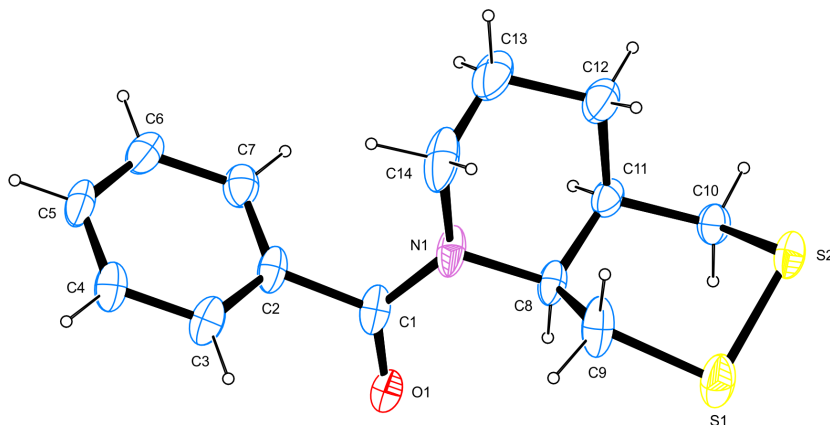
methyl(2-((2-morpholinoethyl) disulfaneyl ethyl)carbamate (SS00_M-MF, 84))

cis-2',7'-difluoro-3'-isopropoxy-3-oxo-3H-spiro[isobenzofuran-1,9'-xanthen]-6'-yl-hexahydro-[1,2]dithiino[4,5-b]pyridine-1(2H)-carboxylate (SS66C-IG, 86)¹H-NMR¹³C-NMR

10. X-ray crystallographic data

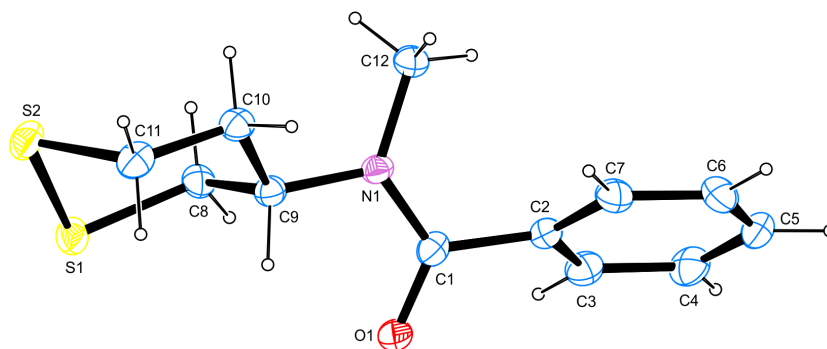
***trans*-(hexahydro-[1,2]dithiino[4,5-*b*]pyridin-1(2*H*)-yl)benzamide (SS66T-Bz, 65)**

compound	65
CCDC number	2072442
net formula	C ₁₄ H ₁₇ NOS ₂
<i>M_r</i> /g mol ⁻¹	279.40
crystal size/mm	0.080 × 0.060 × 0.040
<i>T</i> /K	102.(2)
radiation	MoKα
diffractometer	'Bruker D8 Venture TXS'
crystal system	monoclinic
space group	'P 1 c 1'
<i>a</i> /Å	12.6211(6)
<i>b</i> /Å	10.9095(5)
<i>c</i> /Å	10.2423(5)
α/°	90
β/°	106.629(2)
γ/°	90
<i>V</i> /Å ³	1351.28(11)
<i>Z</i>	4
calc. density/g cm ⁻³	1.373
μ/mm ⁻¹	0.381
absorption correction	Multi-Scan
transmission factor range	0.95–0.98
refls. measured	26059
<i>R</i> _{int}	0.0297
mean σ(<i>I</i>)/ <i>I</i>	0.0252
θ range	3.369–27.101
observed refls.	5745
<i>x</i> , <i>y</i> (weighting scheme)	0.0314, 0.2724
hydrogen refinement	constr
Flack parameter	0.036(18)
refls in refinement	5929
parameters	325
restraints	2
<i>R</i> (<i>F</i> _{obs})	0.0252
<i>R</i> _w (<i>F</i> ²)	0.0614
<i>S</i>	1.056
shift/error _{max}	0.001
max electron density/e Å ⁻³	0.328
min electron density/e Å ⁻³	-0.230

cis-(hexahydro-[1,2]dithiino[4,5-b]pyridin-1(2H)-yl)benzamide (SS66C-Bz, 66)

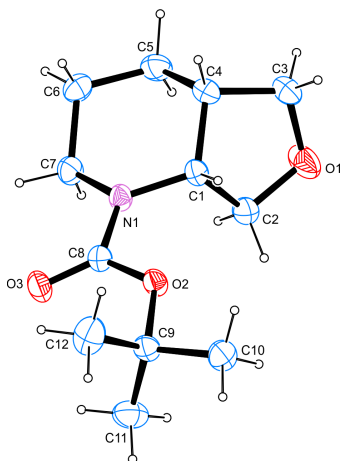
compound	66
CCDC number	2072441
net formula	C ₁₄ H ₁₇ NOS ₂
<i>M_r</i> /g mol ⁻¹	279.40
crystal size/mm	0.080 × 0.050 × 0.030
<i>T</i> /K	102.(2)
radiation	MoKα
diffractometer	'Bruker D8 Venture TXS'
crystal system	monoclinic
space group	'C 1 2/c 1'
<i>a</i> /Å	18.5223(5)
<i>b</i> /Å	6.4668(2)
<i>c</i> /Å	24.1601(8)
α /°	90
β /°	109.8500(10)
γ /°	90
<i>V</i> /Å ³	2721.96(14)
<i>Z</i>	8
calc. density/g cm ⁻³	1.364
μ /mm ⁻¹	0.378
absorption correction	Multi-Scan
transmission factor range	0.92–0.99
refls. measured	20433
<i>R</i> _{int}	0.0360
mean $\sigma(I)/I$	0.0249
θ range	3.360–26.730
observed refls.	2543
<i>x</i> , <i>y</i> (weighting scheme)	0.0236, 7.1329
hydrogen refinement	constr
refls in refinement	2865
parameters	163
restraints	18
<i>R</i> (<i>F</i> _{obs})	0.0468
<i>R</i> _w (<i>F</i> ²)	0.1059
<i>S</i>	1.179
shift/error _{max}	0.001
max electron density/e Å ⁻³	0.336
min electron density/e Å ⁻³	-0.354

ISOR applied in order to improve the anisotropic displacement parameters of C12, C13 and C14.

(S)-N-methyl-N-(1,2-dithian-4-yl)benzamide (SS60-Bz, 67)

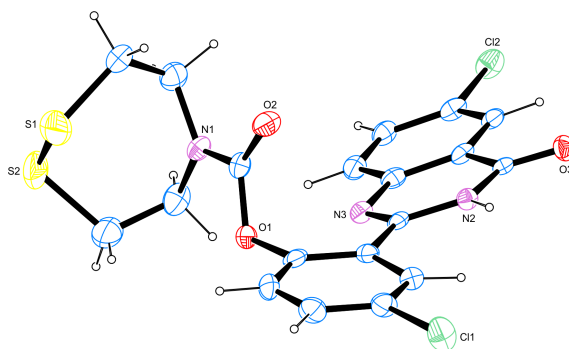
compound	67
CCDC number	2072438
net formula	C ₁₂ H ₁₅ NOS ₂
<i>M_r</i> /g mol ⁻¹	253.37
crystal size/mm	0.100 × 0.100 × 0.090
<i>T</i> /K	107.(2)
radiation	MoKα
diffractometer	'Bruker D8 Venture TXS'
crystal system	triclinic
space group	'P 1'
<i>a</i> /Å	5.4422(8)
<i>b</i> /Å	5.9216(9)
<i>c</i> /Å	10.5764(15)
<i>α</i> /°	88.173(5)
<i>β</i> /°	79.770(5)
<i>γ</i> /°	65.997(4)
<i>V</i> /Å ³	306.11(8)
<i>Z</i>	1
calc. density/g cm ⁻³	1.374
<i>μ</i> /mm ⁻¹	0.413
absorption correction	Multi-Scan
transmission factor range	0.85–0.96
refls. measured	6796
<i>R</i> _{int}	0.0356
mean <i>σ</i> (<i>I</i>)/ <i>I</i>	0.0398
<i>θ</i> range	3.770–27.099
observed refls.	2479
<i>x</i> , <i>y</i> (weighting scheme)	0, 0.4159
hydrogen refinement	constr
Flack parameter	0.09(14)
refls in refinement	2538
parameters	147
restraints	3
<i>R</i> (<i>F</i> _{obs})	0.0399
<i>R</i> _w (<i>F</i> ²)	0.0949
<i>S</i>	1.150
shift/error _{max}	0.001
max electron density/e Å ⁻³	0.442
min electron density/e Å ⁻³	-0.336

Refined as inversion twin, BASF 0.09.

cis-N-Boc-hexahydrofuro[3,4-b]pyridine (5)

compound	5
CCDC number	2072440
net formula	C ₁₂ H ₂₁ NO ₃
<i>M_r</i> /g mol ⁻¹	227.30
crystal size/mm	0.100 × 0.060 × 0.050
<i>T</i> /K	102.(2)
radiation	MoKα
diffractometer	'Bruker D8 Venture TXS'
crystal system	monoclinic
space group	'P 1 21/c 1'
<i>a</i> /Å	8.8168(4)
<i>b</i> /Å	17.0374(7)
<i>c</i> /Å	8.4751(3)
α/°	90
β/°	98.0550(10)
γ/°	90
<i>V</i> /Å ³	1260.53(9)
<i>Z</i>	4
calc. density/g cm ⁻³	1.198
μ/mm ⁻¹	0.085
absorption correction	Multi-Scan
transmission factor range	0.96–1.00
refls. measured	21814
<i>R</i> _{int}	0.0394
mean σ(<i>I</i>)/ <i>I</i>	0.0230
θ range	2.706–27.097
observed refls.	2396
<i>x</i> , <i>y</i> (weighting scheme)	0.0358, 0.5700
hydrogen refinement	constr
refls in refinement	2772
parameters	148
restraints	0
<i>R</i> (<i>F</i> _{obs})	0.0395
<i>R</i> _w (<i>F</i> ²)	0.1024
<i>S</i>	1.060
shift/error _{max}	0.001
max electron density/e Å ⁻³	0.254
min electron density/e Å ⁻³	-0.203

Racemate due to centrosymmetric space group.

chloro-2-(chloro-4-oxo-3,4-dihydroquinazolin-2-yl)phenyl 1,2,5-dithiazepane-carboxylate (SS7-PQ, 75)

compound	75
CCDC number	2072439
net formula	C ₁₉ H ₁₅ Cl ₂ N ₃ O ₃ S ₂
<i>M_r</i> /g mol ⁻¹	468.36
crystal size/mm	0.100 × 0.060 × 0.020
<i>T</i> /K	102.(2)
radiation	MoKα
diffractometer	'Bruker D8 Venture TXS'
crystal system	monoclinic
space group	'P 1 21/c 1'
<i>a</i> /Å	18.2066(9)
<i>b</i> /Å	6.1995(3)
<i>c</i> /Å	18.0583(10)
α /°	90
β /°	102.270(2)
γ /°	90
<i>V</i> /Å ³	1991.71(18)
<i>Z</i>	4
calc. density/g cm ⁻³	1.562
μ /mm ⁻¹	0.563
absorption correction	Multi-Scan
transmission factor range	0.84–0.99
refls. measured	3611
<i>R</i> _{int}	0.0763
mean $\sigma(I)$ / <i>I</i>	0.0366
θ range	2.290–25.346
observed refls.	3374
<i>x</i> , <i>y</i> (weighting scheme)	0, 4.3669
hydrogen refinement	constr
refls in refinement	3611
parameters	272
restraints	0
<i>R</i> (<i>F</i> _{obs})	0.0492
<i>R</i> _w (<i>F</i> ²)	0.0992
<i>S</i>	1.172
shift/error _{max}	0.001
max electron density/e Å ⁻³	0.283
min electron density/e Å ⁻³	-0.329

Refined as a 2-component twin. BASF 0.35. C2 along (100). S2 moiety disordered, split model applied, sof ratio refined to 0.95/0.05, minor part refined isotropically. Minor part not depicted in figure above.

11. Supporting Information Bibliography

- (1) Hong, K.-H.; Kim, D. I.; Kwon, H.; Kim, H.-J. A Fluoresceinylcarbonate-Based Fluorescent Probe for the Sensitive Detection of Biothiols in a HEPES Buffer and Its Cellular Expression. *RSC Advances* **2014**, *4* (2), 978–982. <https://doi.org/10.1039/C3RA42935K>.
- (2) Lim, C. S.; Masanta, G.; Kim, H. J.; Han, J. H.; Kim, H. M.; Cho, B. R. Ratiometric Detection of Mitochondrial Thiols with a Two-Photon Fluorescent Probe. *Journal of the American Chemical Society* **2011**, *133* (29), 11132–11135. <https://doi.org/10.1021/ja205081s>.
- (3) Vrudhula, V. M.; MacMaster, J. F.; Li, Z.; Kerr, D. E.; Senter, P. D. Reductively Activated Disulfide Prodrugs of Paclitaxel. *Bioorganic & Medicinal Chemistry Letters* **2002**, *12*, 3591–3594.
- (4) Henne, W. A.; Doornweerd, D. D.; Hilgenbrink, A. R.; Kularatne, S. A.; Low, P. S. Synthesis and Activity of a Folate Peptide Camptothecin Prodrug. *Bioorganic & Medicinal Chemistry Letters* **2006**, *16* (20), 5350–5355. <https://doi.org/10.1016/j.bmcl.2006.07.076>.
- (5) Zhang, L.; Duan, D.; Liu, Y.; Ge, C.; Cui, X.; Sun, J.; Fang, J. Highly Selective Off-On Fluorescent Probe for Imaging Thioredoxin Reductase in Living Cells. *Journal of the American Chemical Society* **2014**, *136* (1), 226–233. <https://doi.org/10.1021/ja408792k>.
- (6) Kong, F.; Zhao, Y.; Liang, Z.; Liu, X.; Pan, X.; Luan, D.; Xu, K.; Tang, B. Highly Selective Fluorescent Probe for Imaging H₂Se in Living Cells and in Vivo Based on the Disulfide Bond. *Analytical Chemistry* **2017**, *89* (1), 688–693. <https://doi.org/10.1021/acs.analchem.6b03136>.
- (7) Lee, S. H.; Kohn, H. 7-N,7'-N'-(1",2"-Dithianyl-3",6"-Dimethylenyl)Bismitomycin C: Synthesis and Nucleophilic Activation of a Dimeric Mitomycin. *Organic & Biomolecular Chemistry* **2005**, *3* (3), 471–482. <https://doi.org/10.1039/B414806A>.
- (8) Ziv, I. Pro-Drugs and Related Methods. WO2017017669A1, 2017.
- (9) Li, X.; Hou, Y.; Meng, X.; Ge, C.; Ma, H.; Li, J.; Fang, J. Selective Activation of a Prodrug by Thioredoxin Reductase Providing a Strategy to Target Cancer Cells. *Angewandte Chemie International Edition* **2018**, *57* (21), 6141–6145. <https://doi.org/10.1002/anie.201801058>.
- (10) Zeisel, L.; Felber, J. G.; Poczka, L.; Scholzen, K.; Maier, M. S.; Arnér, E. S. J.; Thorn-Seshold, J.; Thorn-Seshold, O. Selective Cellular Probes for Mammalian Thioredoxin Reductase TrxR1: Rational Design of Modular 1,2-Thiaselenane-Based "RX1" Redox Probes. *paper in submission* **2021**.
- (11) Felber, J. G.; Poczka, L.; Busker, S.; Theisen, U.; Zeisel, L.; Maier, M. S.; Brandstädter, C.; Scholzen, K.; Becker, K.; Arnér, E. S. J.; Ahlfeld, J.; Thorn-Seshold, O. Cyclic 5-Membered Disulfides Are Not Selective Substrates of Thioredoxin Reductase, but Are Opened Nonspecifically by Thiols. *ChemRxiv* **2020**. <https://doi.org/10.26434/chemrxiv.13483155.v1>.
- (12) Laurent, Q.; Sakai, N.; Matile, S. The Opening of 1,2-Dithiolanes and 1,2-Diselenolanes: Regioselectivity, Rearrangements, and Consequences for Poly(Disulfide)s, Cellular Uptake and Pyruvate Dehydrogenase Complexes. *Helvetica Chimica Acta* **2019**, *102* (2), e1800209. <https://doi.org/10.1002/hlca.201800209>.
- (13) Houk, J.; Whitesides, G. M. Structure-Reactivity Relations for Thiol-Disulfide Interchange. *Journal of the American Chemical Society* **1987**, *109* (22), 6825–6836. <https://doi.org/10.1021/ja00256a040>.
- (14) Gromer, S.; Arcsott, L. D.; Williams, C. H.; Schirmer, R. H.; Becker, K. Human Placenta Thioredoxin Reductase: Isolation of the Selenoenzyme, Steady State Kinetics, and Inhibition by Therapeutic Gold Compounds. *Journal of Biological Chemistry* **1998**, *273* (32), 20096–20101. <https://doi.org/10.1074/jbc.273.32.20096>.
- (15) Urig, S.; Lieske, J.; Fritz-Wolf, K.; Irmeler, A.; Becker, K. Truncated Mutants of Human Thioredoxin Reductase 1 Do Not Exhibit Glutathione Reductase Activity. *FEBS Letters* **2006**, *580* (15), 3595–3600. <https://doi.org/10.1016/j.febslet.2006.05.038>.
- (16) Nordhoff, A.; Buecheler, U. S.; Werner, D.; Schirmer, R. H. Folding of the Four Domains and Dimerization Are Impaired by the Gly446Glu Exchange in Human Glutathione Reductase. Implications for the Design of Antiparasitic Drugs. *Biochemistry* **1993**, *32* (15), 4060–4066. <https://doi.org/10.1021/bi00066a029>.
- (17) Sheldrick, G. M. SHELXT – Integrated Space-Group and Crystal-Structure Determination. *Acta Crystallographica Section A Foundations and Advances* **2015**, *71* (1), 3–8. <https://doi.org/10.1107/S2053273314026370>.
- (18) Farrugia, L. J. WinGX and ORTEP for Windows: An Update. *Journal of Applied Crystallography* **2012**, *45* (4), 849–854. <https://doi.org/10.1107/S0021889812029111>.
- (19) Liéby-Muller, F.; Marion, F.; Schmitt, P.; Annereau, J.-P.; Kruczynski, A.; Guilbaud, N.; Bailly, C. Synthesis and Biological Evaluation of (–)-6-O-Desmethylcryptopleurine and Analogs. *Bioorganic & Medicinal Chemistry Letters* **2015**, *25* (2), 184–187. <https://doi.org/10.1016/j.bmcl.2014.11.086>.
- (20) Sánchez-Sancho, F.; Herradón, B. Short Syntheses of (S)-Pipelicolic Acid, (R)-Coniine, and (S)-δ-Coniceine Using Biocatalytically-Generated Chiral Building Blocks. *Tetrahedron: Asymmetry* **1998**, *9* (11), 1951–1965. [https://doi.org/10.1016/S0957-4166\(98\)00178-5](https://doi.org/10.1016/S0957-4166(98)00178-5).
- (21) Niphakis, M. J.; Turunen, B. J.; Georg, G. I. Synthesis of 6- and 7-Membered Cyclic Enaminones: Scope and Mechanism. *The Journal of Organic Chemistry* **2010**, *75* (20), 6793–6805. <https://doi.org/10.1021/jo100907u>.
- (22) Lukesh, J. C.; Palte, M. J.; Raines, R. T. A Potent, Versatile Disulfide-Reducing Agent from Aspartic Acid. *Journal of the American Chemical Society* **2012**, *134* (9), 4057–4059. <https://doi.org/10.1021/ja211931f>.
- (23) Moss, N.; Beaulieu, P.; Duceppe, J.-S.; Ferland, J.-M.; Gauthier, J.; Ghire, E.; Goulet, S.; Guse, I.; Llinas-Brunet, M.; Plante, R.; Plamondon, L.; Wernic, D.; Déziel, R. Ureido-Based Peptidomimetic Inhibitors of Herpes Simplex Virus Ribonucleotide Reductase: An Investigation of Inhibitor Bioactive Conformation. *Journal of Medicinal Chemistry* **1996**, *39* (11), 2178–2187. <https://doi.org/10.1021/jm950825x>.
- (24) Baugh, S. D. P.; Yang, Z.; Leung, D. K.; Wilson, D. M.; Breslow, R. Cyclodextrin Dimers as Cleavable Carriers of Photodynamic Sensitizers. *Journal of the American Chemical Society* **2001**, *123* (50), 12488–12494. <https://doi.org/10.1021/ja011709o>.
- (25) Butler, D.; Iwamoto, N.; Meena, M.; Svrzikapa, N.; Verdine, G. L.; Zlatev, I. Chiral Control. WO 2014/012081 A2.
- (26) Batisse, C.; Dransart, E.; Ait Sarkouh, R.; Brulle, L.; Bai, S.-K.; Godefroy, S.; Johannes, L.; Schmidt, F. A New Delivery System for Auristatin in STxB-Drug Conjugate Therapy. *European Journal of Medicinal Chemistry* **2015**, *95*, 483–491. <https://doi.org/10.1016/j.ejmech.2015.03.047>.
- (27) Fulmer, G. R.; Miller, A. J. M.; Sherden, N. H.; Gottlieb, H. E.; Nudelman, A.; Stoltz, B. M.; Bercaw, J. E.; Goldberg, K. I. NMR Chemical Shifts of Trace Impurities: Common Laboratory Solvents, Organics, and Gases in Deuterated Solvents Relevant to the Organometallic Chemist. *Organometallics* **2010**, *29* (9), 2176–2179. <https://doi.org/10.1021/om100106e>.
- (28) Na, Y.; Kohn, H. Quinone-Cyclized Porfiriomycins. *Heterocycles* **2001**, *55* (7), 1347–1364. <https://doi.org/10.3987/COM-01-9215>.
- (29) Ollivier, N.; Dheur, J.; Mhidia, R.; Blanpain, A.; Melnyk, O. Bis(2-Sulfanylethyl)Amino Native Peptide Ligation. *Organic Letters* **2010**, *12* (22), 5238–5241. <https://doi.org/10.1021/ol102273u>.
- (30) Li, X.; Zhang, B.; Yan, C.; Li, J.; Wang, S.; Wei, X.; Jiang, X.; Zhou, P.; Fang, J. A Fast and Specific Fluorescent Probe for Thioredoxin Reductase That Works via Disulphide Bond Cleavage. *Nature Communications* **2019**, *10* (2745), 1–12. <https://doi.org/10.1038/s41467-019-10807-8>.
- (31) Aw, J.; Shao, Q.; Yang, Y.; Jiang, T.; Ang, C.; Xing, B. Synthesis and Characterization of 2-(2'-Hydroxy-5'-Chlorophenyl)-6-Chloro-4(3 H)-Quinazolinone-Based Fluorogenic Probes for Cellular Imaging of Monoamine Oxidases. *Chemistry - An Asian Journal* **2008**, NA-NA. <https://doi.org/10.1002/asia.201000025>.
- (32) More, K. N.; Lim, T.-H.; Kim, S.-Y.; Kang, J.; Inn, K.-S.; Chang, D.-J. Characteristics of New Bioreductive Fluorescent Probes Based on the Xanthene Fluorophore: Detection of Nitroreductase and Imaging of Hypoxic Cells. *Dyes and Pigments* **2018**, *151*, 245–253. <https://doi.org/10.1016/j.dyepig.2018.01.008>.
- (33) Fu, Q.; Li, H.; Duan, D.; Wang, C.; Shen, S.; Ma, H.; Liu, Z. External-Radiation-Induced Local Hydroxylation Enables Remote Release of Functional Molecules in Tumors. *Angewandte Chemie International Edition* **2020**, *59* (48), 21546–21552. <https://doi.org/10.1002/anie.202005612>.

Supplementary Information to:

Selective cellular probes for mammalian thioredoxin reductase TrxR1: Rational design of RX1, a modular 1,2-thiaselenane redox probe

Lukas Zeisel¹, Jan G. Felber¹, Karoline C. Scholzen², Lena Poczka¹, Dorian Cheff³, Martin S. Maier¹, Qing Cheng², Min Shen³, Matthew D. Hall³, Elias S. J. Arnér^{2,4}, Julia Thorn-Seshold¹, Oliver Thorn-Seshold^{1,5*}

¹ Department of Pharmacy, Ludwig-Maximilians University of Munich, Butenandtstr. 5-13, 81377 Munich, DE.

² Division of Biochemistry, Department of Medical Biochemistry and Biophysics, Karolinska Institutet, Solnavägen 9, 17177 Stockholm, SE.

³ National Center for Advancing Translational Sciences, NIH, 9800 Medical Center Drive, Rockville, Maryland 20850, USA.

⁴ Department of Selenoprotein Research, National Institute of Oncology, 1122 Budapest, HU.

⁵ Lead contact; * correspondence to: oliver.thorn-seshold@cup.lmu.de

Supplemental Experimental Procedures	S2
1 Supporting Notes	S2
Supporting Note 1: Prior art in the development of dichalcogenide probes for redox biology	S2
Supporting Note 2: Considerations for dichalcogenide triggers in irreversibly-activated probes:	S4
Supporting Note 3: Full proposed mechanism of activation for A- and G-type probes	S5
Supporting Note 4: Advantages, Drawbacks and Properties of PQ-OH as a fluorogenic cargo	S7
Supporting Note 5: How quantitatively comparable is PQ signal from different reductants?	S8
Supporting Note 6: Other Selenoproteins?	S8
Supporting Note 7: Additional synthetic efforts towards selenenyl sulfide triggers	S9
2 (Bio)chemical reduction assays	S11
2.1 General protocols.....	S11
2.2 Probe activation with chemical reductants.....	S12
2.3 Probe activation with reducing dithiol/disulfide-type proteins and enzymes	S15
3 Cellular assays	S28
3.1. General protocols.....	S28
4 High-throughput screening	S33
4.1 Materials and methods.....	S33
4.2 LOPAC HTS-screen using RX1, and comparison to prior art enzymatic screen	S35
5 Organic synthesis	S39
5.1 General methods	S39
5.2 General procedures	S40
5.3 Linear and five-membered dichalcogenide triggers	S41
5.4 Cyclic, six-membered dichalcogenide-amines.....	S47
5.5 Trigger functionalisation.....	S51
5.6 Probe assembly	S56
6 Mechanistic analysis of probe activation	S63
6.1 Inhibition of probe release quantified through fluorescence	S63
6.2 Qualitative analysis of the probe activation mechanism by LCMS	S65
7 NMR spectra	S69
8 Supplemental References	S97

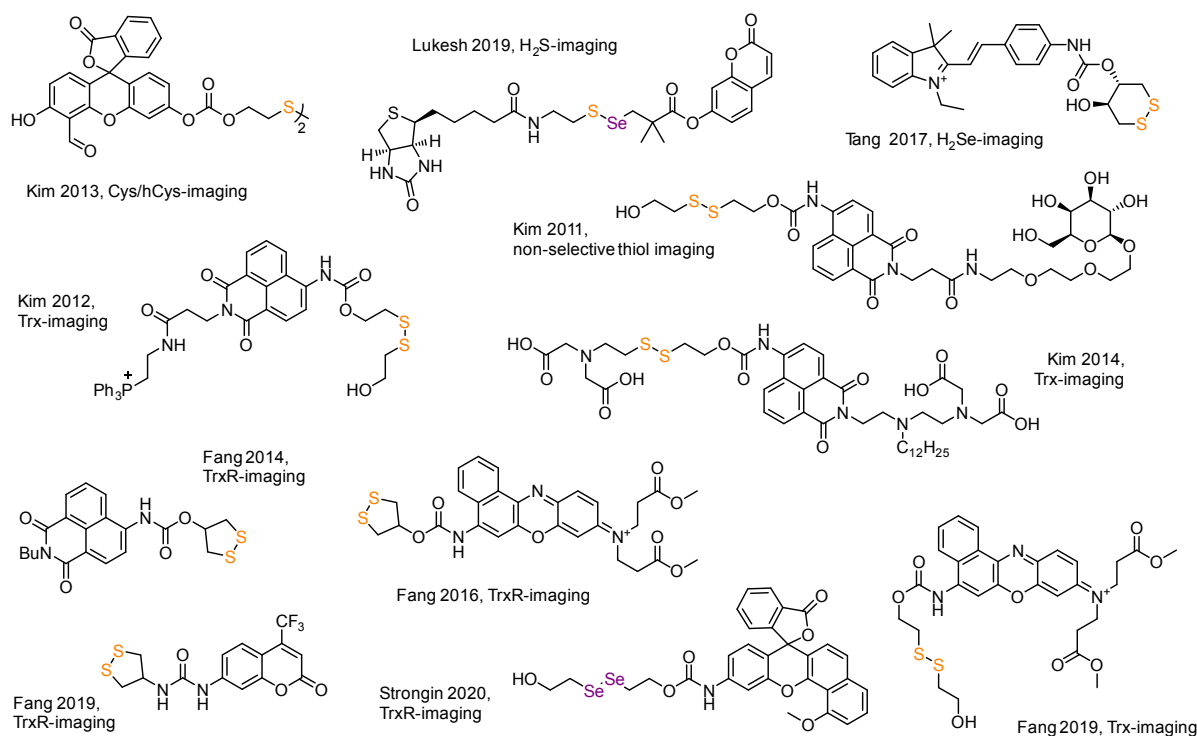
Supplemental Experimental Procedures

1 Supporting Notes

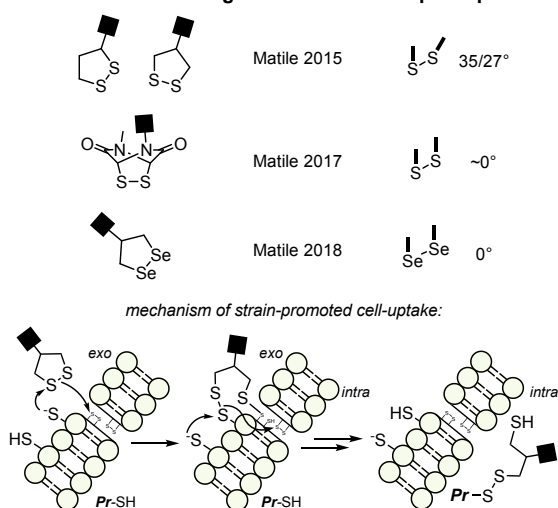
Preamble: the fascinating (bio)chemistries of selenium, selenenylsulfides, and TrxR have inspired much devotion.¹ The interested reader is referred to the computational studies of Bachrach,^{2,3} practical investigations of Iwaoka,^{4,5} and biochemical and mechanistic analyses of Holmgren⁶ and Honda⁷ for much useful information that cannot be given here.

Supporting Note 1: Prior art in the development of dichalcogenide probes for redox biology

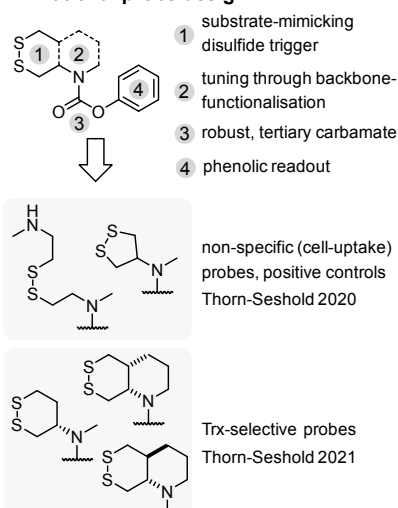
a chemical probes for redox biology



b strained dichalcogenides as cellular uptake probes



c rational probe design



d precedents on cyclic selenenyl sulfides

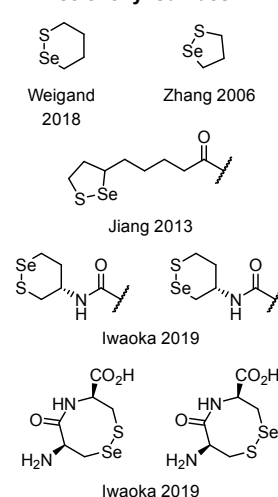


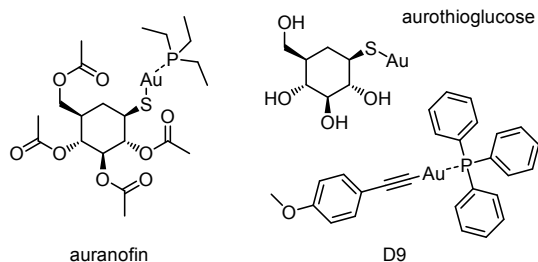
Figure S1 Prior art in the development of dichalcogenide probes for redox biology. **(a)** Chemical probes reported in prior art as being selective for imaging key players in cellular redox processes. **(b)** Matile's cellular uptake probes based on strained disulfides and their proposed mechanism of cell internalisation.⁸⁻¹¹ **(c)** Rational design of dichalcogenide fluorogenic probes introduced by Thorn-Seshold^{12,13}. **(d)** Selected synthetic precedents for cyclic selenenylsulfides.

In **Figure S1**, redox probe designs, and the behaviour of redox-active motifs related to the current work, are depicted. Hydrogen chalcogenide imaging was reported for H₂S by Lukesh¹⁴ and for H₂Se by Tang.¹⁵ Linear disulfides were used as redox triggers both in thiol probes reported to be non-selective, as well as probes reported to be cysteine- or Trx-selective.¹⁶⁻

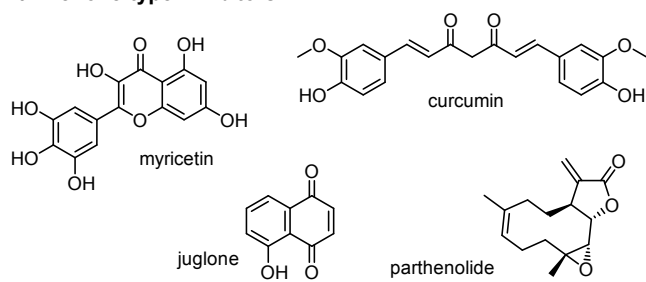
²⁰ The literature reports of TrxR-selective imaging in cells are dominated by Fang's 1,2-dithiolane-based probes,^{21–24} recently supplemented by Strongin's linear diselenide-based design;²⁵ although we have recently published experimental critiques of the 1,2-dithiolanes as being monothiol reporters,¹³ Fang has shown experimentally that linear diselenides are monothiol-labile²⁶ (see Supporting Note 2), and very recently Fang and coworkers published two reports stating that contrary to their initial papers, the cyclic 5-membered disulfide TRFS compounds are actually not cellular reporters of TrxR but are instead responding to (at least) Trx and Grx^{27,28} (other reductants not tested, yet a retraction of the previous data interpretations was also not offered). We maintain that these dithiolanes are in reality not cellularly selective for *any* given set of reductants but are simply pan-reactive and should not be misinterpreted as selective for any particular protein/s (further discussion in ref.¹³), leaving the situation of the prior art as being, that there are no working cellular probes for TrxR.

Note too the predominance of aniline-releasing designs, whose ease of design and synthesis comes at the cost of very sluggish to impractical kinetics,¹³ and which can be compared with the performance of our phenolate-releasing systems. (Note however the exception of Fang's urea "FastTRFS" which has a non-release-based fluorogenic mechanism relying on alleviating disulfide ring strain either by linearisation or by ring-opening: although its cellular spectrum of targets and even its auto-activation by exposure to non-living lipid membranes does not let it act as a cellular probe for any given species)^{13,27}.

a gold-based inhibitors



b enone-type inhibitors



c S_NAr-type inhibition

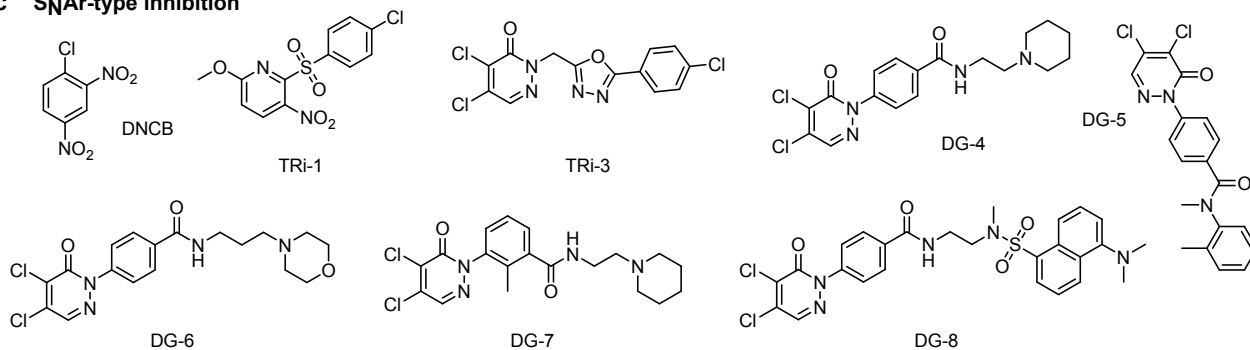


Figure S2 Some compounds that have been reported as inhibiting TrxR at least in purified-enzyme assays in cell-free conditions, based on (a) gold complexes; (b) reactive organics / Michael acceptors (note: known PAINS molecules, unlikely to be valuable as selective inhibitors in the cellular context); (c) electrophiles undergoing S_NAr reaction with selenols.

In this paper, we build on previous research that evaluated TrxR inhibitor strategies for use with chalcogen-based redox probes,¹³ and accordingly we avoid using auranofin (AF, **Fig S2a**) in our studies. AF is a thiophilic Au(I) complex that has been widely used as an inhibitor of TrxR. AF does bind TrxR in cell-free assays and also in cells. However, in cells, it *also* binds at least 20 other known and defined thiol protein targets, as well as known but undefined ones such as membrane thiols that can be highly relevant to probe uptake and processing (cf. Matile's uptake probes²⁹).³⁰ Worse still, the thiophilic inhibitor AF directly interacts with and can destroy disulfide- or thiol-containing small molecule probes, such that assay results are not meaningful. Therefore, we have avoided using AF and other gold-based inhibitors altogether in this study.

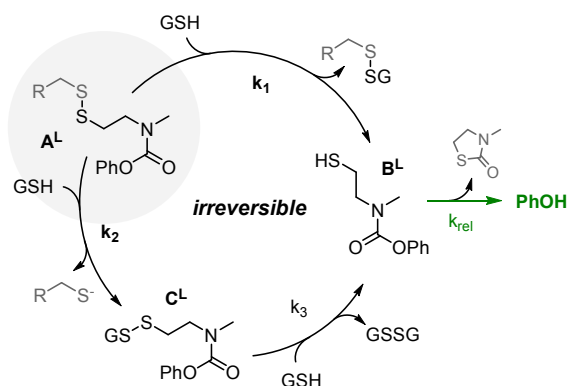
Another class of small molecules which have been reported as TrxR-selective inhibitors are α,β -unsaturated carbonyls such as enones, enamides, acrylates or quinones (**Fig S2b**).^{31–33} While these highly reactive electrophiles are indeed very potent inhibitors of TrxR in cell-free settings and can efficiently react with the active site selenol, these compounds' exceptional reactivity is problematic for cellular studies since actual selectivity for TrxR as a nM enzyme is hard to achieve in a cellular context - and indeed, our data support that the vast majority of the dose of Michael acceptor inhibitors that are applied to cells are actually, and predictably, lost to reactions with non-TrxR targets (discussion at Fig S31). Indeed, compounds of the "enone-type"-class have increasingly been identified as PAINS compounds (Pan Assay INterference compounds)^{34–36} that should only be used very cautiously, and only in cell-free assays. Additionally, Hondal recently published an interesting *in vitro* study on TrxR's ability to circumvent irreversible inhibition by enones through a selenoxide-type elimination.³⁷

Based on the exceptionally high nucleophilicity of TrxR's selenocysteine, a third class of inhibitors based on nucleophilic aromatic substitution (S_NAr) has gained momentum (**Fig S2c**). Already in 1995, 1-chloro-2,4-dinitrobenzene (DNCB) was identified as a covalent inhibitor for TrxR, which possesses a strong kinetic advantage compared to thiol-nucleophile S_NAr reactions.^{38,39} In order to address selectivity issues, Arnér and coworkers recently optimised selective inhibitors of TrxR through extensive screening efforts.^{40,41} The two most potent and selective inhibitors rely on electron-deficient nitropyridines and dichloropyridazinones, which alkylate TrxR by S_NAr. We believe that these scaffolds provide a more useful basis for

selective TrxR inhibition particularly in the context of chalcogenide-based probe development, and have thus selected the most promising member from each compound class (TRi-1 and TRi-3) for our study.

Supporting Note 2: Considerations for dichalcogenide triggers in irreversibly-activated probes:

a mechanism of activation for linear disulfide probes



b mechanism of activation for cyclic disulfide probes

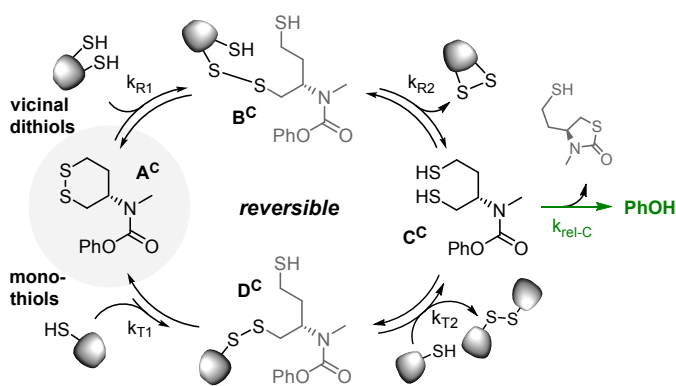


Figure S3 Irreversible and reversible stages of linear (L) and cyclic (C) topology dichalcogenide probe commitment (shown: disulfides). Linear topology probes are irreversible with any reductant, while cyclic topology probes are reversible with either mono-thiol- or dithiol-type reductants, regardless of initial attack site (shown: attack at proximal chalcogen). Importantly, cyclic topology probes offer the possibility of post-reduction re-oxidation ($C^C \rightarrow D^C$) by chemocompatible dichalcogenides in their environment.

GENERAL: for irreversibly-activated probes to resist a given reductive challenge, **their kinetic rate** of sampling/reaching the reduced signal-generating intermediate (B^L or C^C ; Fig S3) must be vanishingly small: otherwise the irreversible step will pull the pseudoequilibrium through to give substantial signal-release: i.e. non-resistance to the challenge.

Therefore we must consider kinetics of sampling the signal-generating intermediate C^C for reversible, i.e. cyclic topology species; or the kinetics of committing irreversibly towards the signal-generating intermediate B^L (for linear topology species).

Given this emphasis on kinetics, we can anticipate cases where even challenge agents that would give strongly thermodynamically disfavoured reductions (i.e. those which would give very low amounts of C^C or B^L at a hypothetical equilibrium, if no irreversible activation step would later take place) can cause substantial probe activation. This is indeed the case that we postulated for the reduction of linear diselenides, and which Fang later corroborated experimentally²⁶: although it has been clear since the 1960s⁴² that **full** reduction of linear diselenides by monothiols under equilibrium conditions requires a 1000-fold excess of the monothiol [which, for a linear diselenide probe applied to a cell with ca. 3-5 mM glutathione is almost certainly a requirement that is met], the additional kinetic trapping consideration for probes (aggravated no doubt by the selenolate's rapid immolation kinetics) makes the linear diselenide probe devastatingly sensitive to even subphysiological GSH levels (see below).

As an aside, it may be interesting to consider by what reductant linear diselenide (selenocystine) reduction in cells is *actually* performed. Considering cell-free conditions: (1) physiological, millimolar GSH levels *could* achieve substantial reduction of the likely $\ll \mu\text{M}$ selenocystine at equilibrium by Le Chatelier's principle;⁴² with this becoming especially relevant to cells since (as was raised by constructive comment of reviewer 1) downstream selenocystine-beta-lyase acts effectively as an irreversible "sink" for selenocystine upon its production; or on the other end of the scale of likely reductants, (2) nanomolar TrxR has the selenolate nucleophile needed to perform kinetically much faster attack and reduction on selenocystine, and likewise has been shown to use NADPH to reduce selenocystine efficiently in cell-free settings⁴³ - again, in a driven situation (e.g. constant supply of NADPH, or a selenocystine sink) this could be highly relevant.

However, considering cellular reality: whether, and to what degree, either of these reductants (or any of the other likely thiol-type reducing species) actually carries out selenocystine cleavage/reduction in live cells, is as far as we know a matter open to speculation. It seems reasonable to assume that reduction can and does occur by redundant pathways (much as we outline for strained disulfide probes) as we see no basis to exclude any given, reasonable reductant from being at least *theoretically* capable of splitting the linear dichalcogenide. An interested reader may also pursue research works of Koppenool, Hilvert, and Moroder in addition to those of the scientists cited here.

Linear disulfides (cf. **SS00**) have no kinetic basis to resist any thiol-disulfide or selenol-disulfide exchange, which are both irreversible steps due to the expulsion of a thiolate. Therefore they should be labile to all reductants, with rates that depend only on their nucleophilicity and concentration: i.e. no meaningful selectivity in the complex cellular environment (compare **Supporting Note 1** and **Fig S1**).

Linear diselenides are thermodynamically more stable, but conceptually they too access the irreversible pathway (cf. **Fig S3a**), so in our analysis they ought to be monothiol-labile at relevant reductant concentrations and therefore in no way selective - in the sense that they cannot resist the monothiol background. An aniline carbamate linear diselenide was recently reported by Strongin (**Fig S1**); however, we consider that there are several areas in which the linear diselenide is

either not selective for TrxR, or else was not conclusively evaluated with respect to this question. (1) Challenge of the linear diselenide for 20 min with 1 mM GSH reached 1/6 of TrxR (100 nM) turn-on levels. 1 mM GSH is on the low side of what is often considered a physiological value (upwards of 3 mM) while 100 nM TrxR is rather higher (20 nM); if the GSH/TrxR comparison had been performed with 3 mM GSH / 20 nM TrxR, the probe would have been reported as 2 times more activated by GSH than by TrxR. GSH is not the only monothiol in cells and we consider it unlikely that such a probe can resist the overall monothiol background so much that it reports meaningfully on TrxR in a way that can be quantitatively attributed to TrxR reduction. (2) No reducing proteins (Trx1, Trx2, Grx1, Grx2, TrxR2, etc: their *Figure 4*) were tested; these are highly reducing species which are likely reductive competitors to TrxR, but have much higher expression levels, and it would be instructive to test these before concluding on cellular selectivity.

In the days preceding submission of this paper, Fang also published a study including a linear diselenide prodrug (Cpt-Se4)²⁶ showing ca. 60 s half-life for cleavage of 10 μ M diselenide with 1 mM GSH (their *Figure 2B*), confirmed by the ca. 120 s half-life for its cyclisation-based elimination of the active drug Cpt (their *Figure 2F*) and other careful studies (their *Figure 3A,C,D*). Their paper does not take the view that the linear diselenide could be selective for reduction by TrxR in the cellular context. Our view is that linear diselenides were actively shown to be not capable of cellular TrxR reporting.

A **linear selenenylsulfide** phenolic ester probe was reported by Lukesh as being selective for H₂S sensing (**Fig S1**).¹⁴ However, in our analysis, this linear dichalcogenide too should access the irreversible pathway (cf. **Fig S3a**). In the event, the reported probe was not tested against any redox enzymes, nor were controls run for thiolysis of the phenolic ester by 50 μ M Na₂S; so in the absence of such data we do not consider that such linear dichalcogenides can be selective in cells.

We have already evaluated **cyclic 6-membered disulfide** SS60¹² and found it to be well selective for Trx, so we expected the same profile for the similar but solubilised **S1**.

We expected that a stable **cyclic 6-membered diselenide (Se3)** would strongly resist exchange with either thiol or selenol nucleophiles; that if ring-opened it would rapidly re-close the ring; and if it were reduced, it would tend to rapidly react with any oxidised dichalcogenide species encountered: therefore it would be very poorly activated by any thiol or selenol reductant (a "dead probe"); perhaps high concentrations of vicinal dithiol might force some probe activation by thermodynamic equilibration. We also expected that its reaction with phosphine TCEP might give some useful upper limit estimate for the combined 5- and 6-*exo*-trig selenolate cyclisation kinetics. Finally, in this cyclic diselenide there is no preference for which atom should be attacked; this would allow it to suffer the same mechanistic problem (on-reductant cyclisation) as outlined for G-type selenenylsulfides, which if anything might make it somewhat labile to transthioation-mediated cargo release (though we note that Matile's careful studies of diselenolane opening by thiols, in which the kinetic product of transthioation rearranges to the thermodynamic selenenylsulfide within 4 ms at 25 °C,¹¹ reinforce our view informed by the thermodynamic stability to be expected of *cyclic* 6-membered diselenides, that diselenide re-closure by 6-*exo*-tet cyclisation would likely be fast enough to minimise the concentration of the on-reductant intermediate).

Interestingly, this "dead by design" diselenide **Se3** fulfils a second control function related to oxidation. Selenium species are excellent reducing agents for peroxides; it might be questioned whether selenium oxidation in cells in a diselenide or selenenylsulfide probe could ultimately sensitise the probe towards cargo release (the sulfur analogues, "thiosulfates", are an exciting topic of current research for us and for other groups⁴⁴). While this deceptively simple mechanistic question will be addressed in a forthcoming paper, in brief, we noted here that no probe release was evidenced, so we concluded that there is no basis to suspect that the cyclic selenenylsulfide probes release their cargo in cells by mechanisms involving other oxidation states than the -1 and -2 involved in transthioation/full reduction.

Supporting Note 3: Full proposed mechanism of activation for A- and G-type probes

Ensuring that only ca. 20 nM TrxR catalyses cargo release, while highly reducing dithiol proteins e.g. Trx and Grx (10 μ M) or GSH (up to 8 mM) do not, is a challenge that cannot be met with thermodynamics alone. For example, Trx-reducible 1,2-dithianes are reduced only slowly by even 10 μ M Trx, while kinetically resisting the more powerful reductant TrxR¹². Selectivity requires specificity either in binding or in the reductive mechanism: and in our analysis, it requires methods to *exclude undesired reactivity* (more than it requires methods to promote desired reaction).

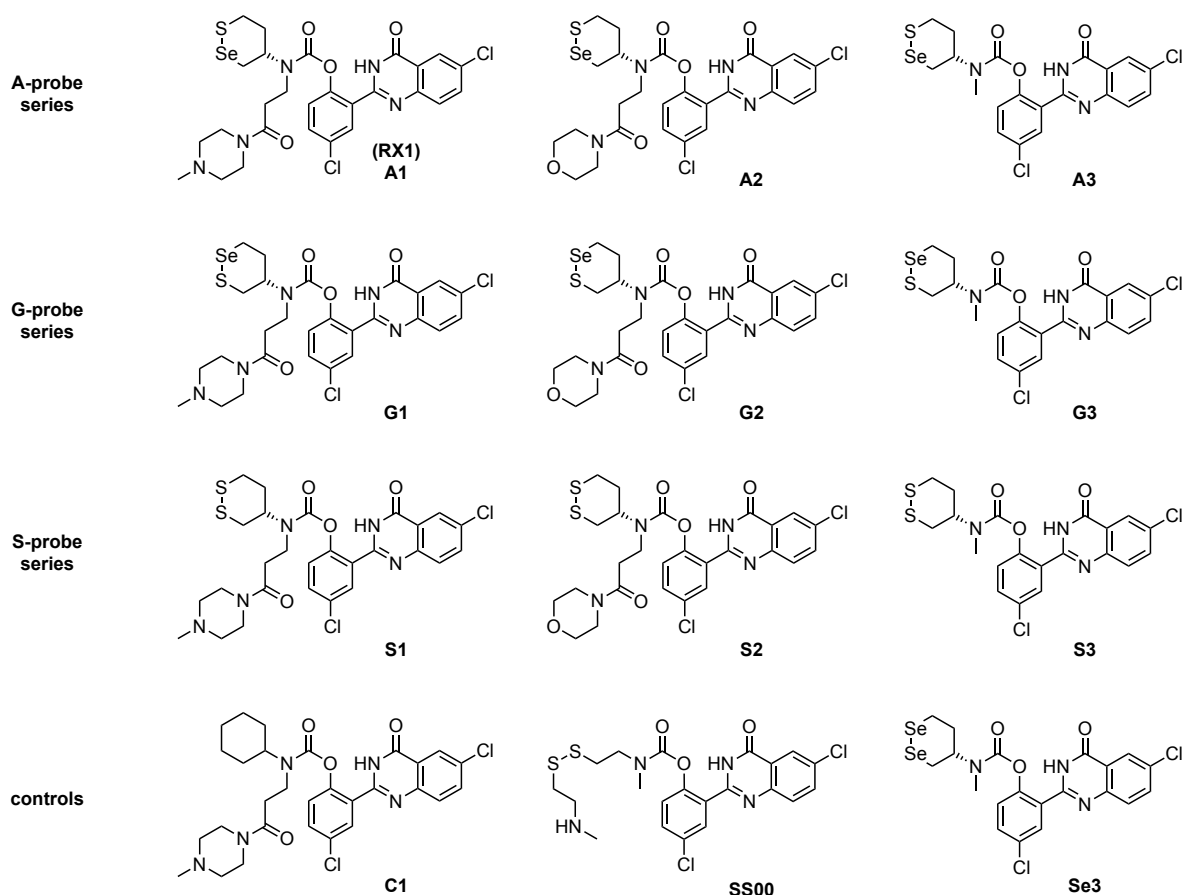


Figure S5 Overview of all probes synthesised and evaluated in this work.

Supporting Note 4: Advantages, Drawbacks and Properties of PQ-OH as a fluorogenic cargo

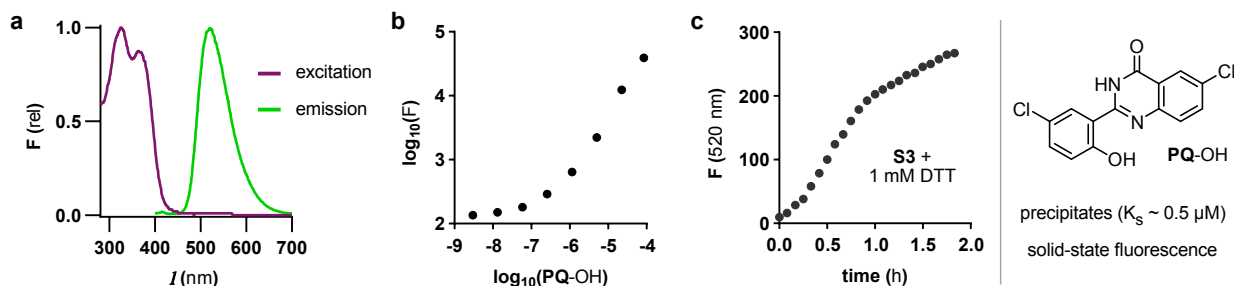


Figure S6 Properties of **PQ-OH** as a fluorophore. **(a)** Excitation/emission spectra of **PQ-OH**. $\lambda_{\text{max}}(\text{ex}) = 325/365$ nm. $\lambda_{\text{max}}(\text{em}) = 520$ nm. **(b)** Solid-state fluorescence of **PQ-OH** increases linearly with concentration once the precipitation limit of ca. $0.5 \mu\text{M}$ is reached **(c)** Kinetics of **PQ-OH** fluorescence increase when activating **S3** (2 μM) with DTT (1 mM).

We selected Haugland's precipitating fluorophore **PQ-OH** (Fig 2d-e)⁴⁵ as our proof-of-concept fluorogenic phenolic cargo.^{46,47} Acylating its phenol completely mechanistically quenches its high-quantum-yield, large-Stokes-shift fluorescence (ex/em 360/520 nm, Fig S6a), since this depends on excited state intramolecular proton transfer (ESIPT) of the phenolic hydrogen; therefore (1) the probes can operate as true turn-on systems, with zero self-background.⁴⁸ **PQ-OH** precipitates after its released concentration passes its low aqueous solubility limit (ca. $0.5 \mu\text{M}$; Fig 2e, Fig S6b-c), which is critical for its performance. While ESIPT fluorescence is blocked by hydrogen bonding and conformational flexibility in solution, it is very strong in the crystalline precipitate: precipitation is therefore the turn-on mechanism for fluorescence.^{49,50} (2) The large Stokes shift avoids any self-quenching, making it a rare example of a solid-state fluorophore with a linear relationship of amount released to intensity measured (Fig S6b). The solid state is an entirely reproducible matrix which is also protected from the environment: so (3) this **PQ-OH** fluorescence has no environment- or pH-dependency, and (4) has extraordinary resistance to photobleaching. Combined with its 160 nm Stokes shift (Fig S6a) that avoids biological autofluorescence (typically ca. 20-30 nm Stokes shift), (5) these properties permit longterm imaging at low excitation intensity giving excellent signal-to-noise (S/N): we typically observe S/N ratios above 300 without even requiring background subtraction. **PQ-OH** precipitates (6) are retained inside activating cells⁴⁵ even after fixation, which permits quantitative and unbiased flow cytometry-based statistical analysis (this is highly unusual for small molecule probes, but is extremely beneficial); it also avoids

the "leach-out" of fluorescence that prevents cell-precise imaging with soluble fluorophores like fluoresceins.⁴⁸ Finally, (7) the **PQ-OH** 2,4-electron-withdrawn substitution pattern promotes ca. 10-fold faster release kinetics than seen with typical phenols,⁴⁸ for good kinetic response. Indeed, there are very few drawbacks of **PQ-OH** for cell-free and cellular proof-of-concept studies (see below). In these ways, all our **PQ**-releasing probes would feature a true off-to-on mechanistic activation of fluorescence signal upon carbamate cleavage-based release of **PQ** past its solubility limit, which would irreversibly mark individual releasing cells with a bright, photostable, reliably quantifiable fluorophore, with outstanding signal-to-noise ratios.

Considerations and/or drawbacks for translating **PQ** beyond cellular proof of concept studies include: (1) if excitation at 360 nm is not possible, 405 nm excitation must be used; this yields ca. 1% of maximal **PQ** fluorescence intensity but for similar cost of photodamage to the sample, which limits bioimaging. (2) **PQ** crystals can be anticipated to cause cellular damage as well as damage responses; at high released **PQ**, cells are eventually killed. (3) In settings where less than the precipitation threshold concentration of **PQ** is released, no signal is observed; and kinetic analysis at low turnover (< 2 μM released) is sensitive to data treatment and choice of model.

Supporting Note 5: How quantitatively comparable is **PQ** signal from different reductants?

Reductant Stability: In practice, the cell-free TrxR assay underestimates the probes' TrxR sensitivity, since (i) TrxR loses its functionality during the cell-free assay (low TrxR concentrations do not approach full probe conversion even at longer assay times, presumably due to a limit on catalytic cycles before irreversible oxidative damage); and (ii) due to the precipitation-based turn-on mechanism, no signal is seen for the release of the first ca. 1 μM of probe (see **Supporting Note 3**). These effects disproportionately suppress signal generation in low-TrxR conditions. For example, 5 nM TrxR1 plateaus at less than one third of the maximal signal, whereas 20 nM TrxR1 reaches this level in 24 min; TrxR2 shows similar features although its much lower **RX1** processing rate should be noted (**Fig S10**). Similarly, degradation of any other cell-free reductant during an assay will suppress signal generation in its cell-free assay and this will particularly affect low-reductant-concentration assays. In the cellular context, reductant repair and resupply mechanisms are anticipated to substantially take care of this problem and provide a steady state supply of reductant in cellular assays.

Effects of **PQ crystallisation on signal:** The signal resulting from net precipitation of a fixed concentration of **PQ-OH** is dependent on the crystal size and morphology (even assuming identical liquid-volume-to-precipitate-settling-surface area, such as in a reproducible assay format like in 96 well plates). On a basic level, the greater the excitation optical path length in the crystal/s, the more optical shielding by surface layers will absorb the incoming excitation light and prevent full-crystal fluorescence, so larger crystals should have less signal per fluorophore than small ones. This is classic Lambert-Beer shielding, which is most significant at strongly-absorbed wavelengths (360 nm), and much less so at more weakly-absorbed ones (e.g. 385 - 400 nm). Additionally, light scattering at crystal-solvent boundaries (which is nearly wavelength independent) should tend to reduce the excitation of samples of crystals with high surface area to volume ratio, meaning that larger and more regular crystals may appear brighter than irregular powders of the same total mass.

Crystal size and morphology depend among other factors on the supersaturation profile experienced during precipitation: so fluorescence signal intensity is quantitatively comparable only with similar time-profiles of **PQ-OH** release. For example, excess-TCEP-controls (100 μM for 10 μM probe) cause quasi-instant **PQ-OH** release by second-order kinetics and probably large supersaturation. Enzymatic release by e.g. 5 nM TrxR (steadily incrementing the **PQ-OH** concentration by 5 nM per turnover cycle) should not be expected to reach the same supersaturation, so will probably give gradual and more optimal crystal growth. The precise chemistry in a given solution will also affect the profile, not only by cosolvent concentration or by hydrophobe-adsorbant proteins, but also by tending to adsorb species onto crystal surfaces to different degrees, all of which will further modifying crystal growth kinetics. The real relationship of crystal growth to fluorescence signal is probably further complicated by anisotropic crystal growth and by defect incorporation (scattering surface).

This long list of potential complicating factors has to be viewed through the lens of experimental results across very different assay conditions, showing that different probes (different release profiles and rates), challenged with reductants of different kinetic profiles (TCEP, catalysts, stoichiometric dithiols, etc), in different environments (cell-free, cellular, buffers), *all gave approximately similar* total maximal fluorescence values: usually within about 50% from a central value. Considering the difficulties outlined above this is excellent reproducibility. While "50%" may seem inaccurate, it should be remembered that our purpose throughout the paper is to determine sensitivity profiles on *logarithmic scales* of challenge reductant concentrations: therefore a difference of 0.5-fold (corresponding to 0.3 log units) is negligible compared to typical 1000-fold sensitivity shifts between the probes or their reductants (e.g. >3.5 log units difference between nonselective **SS00**'s sensitivity to monothiol GSH and that of TrxR-selective **RX1**; compare **Fig 4a**).

Supporting Note 6: Other Selenoproteins?

We had asked the question: what biological species other than TrxR might cause **A/G**-type probe activation? As well as the mono/dithiols we assessed here, we were most worried about other selenol proteins: because initial exchange by any RSeH could have similar thermodynamics and kinetics as the initial exchange by TrxR (there are no low-molecular-weight selenol bioreductants at significant concentrations in cells). Luckily, the human proteome codes for just 25 selenol-bearing proteins, of which many have restricted and/or low expression (much information is to be found in Gladyshev *et al*⁵¹).

Of these, we considered that two monoselenol glutathione peroxidases (GPx1/4) had sufficiently broad expression at significant levels, to potentially confound TrxR-selectivity; and their ability to react with e.g. cumene hydroperoxide (GPx1) and cholesterol hydroperoxide (GPx4) indicates that they can accept hydrophobic small molecules as substrates.⁵¹ However,

they are monoselenol enzymes, so they would require on-protein cyclisation to cause signal generation (**Fig 2a-b**). If on-protein cyclisation would be possible, then e.g. on-GPx1 5-*exo*-trig cyclisation of the diselenide adduct of the **G**-type probes in particular could be thought to result in signal generation. We therefore challenged both **RX1** and **G1** with GPx1 in a titration assay (100-1000 nM) using GSH (200 μ M, 20 equiv.) as the native upstream component to recover oxidised GPx1 (**Fig S15a**). None of the applied conditions resulted in measurable probe activation classifying both thiaselenane-probes inert to this monoselenol enzyme. Although it is likely that GPx1 is simply not able to react with larger molecules due to its sterically confined active site,⁵² this clearly excludes GPx1 as potential bioreductant of **RX1** and **G1**. The relative contributions of GPx1's specificity for its native substrate, or of the general inhibition of polar cyclisation of a charged chalcogenide (more difficult for the less acidic thiol of the **G** series, rather than the selenide of the **A** series), remain open for further testing - as does the possibility of profiling all other GPxs and all other monoselenols. Focusing instead on selenolthiol enzymes, there are only very few other than TrxR, at any expression level. The enzyme methionine-*R*-sulfoxide reductase (MsrB1) is one selenolthiol-active-site enzyme, however it has very high substrate specificity for methionine-*R*-sulfoxide residues in proteins. SelW is another. It is the fond hope of the authors to find possibilities to screen the **RX1**-series probes in cell-free and cellular conditions against these, and any or all other selenoproteins, towards still more comprehensively profiling the biochemical performance of this unique small molecule approach. Taking a practical perspective on performance in the cellular context however, the results with TrxR knock-out, knock-in, inhibition, and Sec disfavouring/favouring by thiophosphate/selenite, all point strongly to a probe that is selective in cells, to a very high degree at least, for TrxR1.

Supporting Note 7: Additional synthetic efforts towards selenenyl sulfide triggers

Cyclic 5-membered dichalcogenide triggers

Ultimately, we succeeded in synthesising 1,2-diselenolananes and -thiaselenolananes starting from commercially available serinol (**Fig S9**). Boc-protection of the starting material followed by dimesylation gave **S1** in good yield and enabled a double S-acetylation-selenocyanation sequence to introduce both dichalcogens towards **S2**. Similarly, the dimesylate **S1** could be charged with an excess of KSeCN giving diselenocyanate **S4**. Ring closure towards **S3** and **S5** was achieved in dilute solution under basic conditions, and afforded both heterocycles in excellent yield. Matching the synthetic difficulties we observed for 3-amino-1,2-dithiolanes,¹³ neither the selenenylsulfide nor the diselenide were tractable for NH deprotonation and alkylation, presumably due to polymerisation as well as irreversible degradations. This contrasts to the tractable cyclic 6-membered systems. While future researchers wishing to access these compounds could likely do so by early-stage *N*-alkylation, we discontinued any further attempts as the instability observed during attempted alkylation did not qualify these dichalcogenides as selective triggers for reliable use in cellular probes.

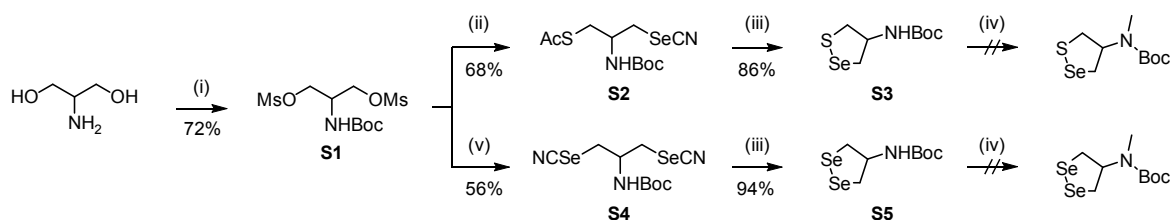


Figure S7 Synthesis of 1,2-thiaselenolananes and – diselenolananes. (i) Boc₂O, NEt₃, H₂O/dioxane, 16 h, r.t.; MsCl, NEt₃, DCM, 3 h, 0 °C, 72% over two steps. (ii) KSAc, 18-crown-6, DMF, 12 h, r.t.; KSeCN, NaI, 18-crown-6, THF, 14 h, 50 °C, 68% over two steps. (iii) KOH, THF/MeOH, 10 min, r.t., 86%. (iv) NaH, Mel, DMF, 2 h, 0 °C→r.t.. (v) KSeCN, NaI, 18-crown-6, THF, 14 h, 50 °C, 56%.

Linear selenenyl sulfide triggers

With a reliable methodology in hand, we next targeted linear selenenylsulfide triggers. Our strategy again involved the use of nucleophilic thiols (**S9**, **S12**) and electrophilic selenocyanates (**S7**, **S13**) as building blocks, and Boc-protected amines as future cargo coupling sites. As dummy fragments distal to the cargo, we used thiocarbamates due to their decent solubility and chemical inertness. Starting from cysteine, we could isolate key dimesyl-intermediate **S11** in 4 steps passing via **S10**, then could install either sulfur (**S12**) or selenium (**S13**) in good yields. Dichalcogen coupling was conducted in neutral methanolic solution and yielded defined, desymmetrised Boc-protected selenenyl sulfides **S14** and **S15** in excellent yield. The use of base as in the synthesis of cyclic dichalcogenides gave concomitant formation of diselenide side products and is thus not recommended. This route to desymmetrised dichalcogenides is, we feel, superior to others we have found in the literature, however we leave it to the interested reader to pursue such kinetically labile triggers further if desired.

2 (Bio)chemical reduction assays

2.1 General protocols

In vitro assays determining the **PQ** probes' redox properties are based on reduction-induced fluorophore release. In practice, this turn-on of fluorescence was quantified using a plate reader ($\lambda_{\text{ex}} = 355 \text{ nm}$, $\lambda_{\text{em}} = 520 \text{ nm}$).

Probes were dissolved in DMSO and stored as 10 mM stocks at 4 °C for at least 3 months. LC/MS analysis of DMSO stock solutions revealed that several rounds of freezing and thawing, and even storage at r.t. over several months were well tolerated and did not result in measurable decomposition of the probe.

To prevent precipitation of the **PQ** conjugates (particularly for non-solubilised probes), DMSO stock solutions (10 mM) were diluted to 1 mM in DMSO before ultimate dissolution in TE buffer (Tris-HCl (50 mM), EDTA (1 mM), pH = 7.4). A black 96-well plate with black bottom was charged with probe (final concentration: 10 μM , 1% DMSO in TE buffer) and subjected to a variety of chemo- and bioreductants. The PQ-release kinetics were monitored at set time points (1 min, 15 min, 30 min, 1 h, 2 h, 3 h, 4 h, 5 h, 6 h, 15 h). In between measurements, the 96-well plates were incubated in a regular heating oven at 37 °C and in a H₂O-saturated atmosphere. Every experiment was run with *blank* control wells to estimate residual fluorescence of non-activated probe or potential decomposition during incubation in TE buffer.

Reduction resistance assays

Initial proof-of-concept experiments were conducted according to the following protocol: 80 μL of **PQ** probe (12.5 μM in TE buffer/1.25% DMSO) were placed into the 96-well plate and the solution was charged with 20 μL of the respective reductant. The resulting 100 μL -reaction mixture thus contained 10 μM of probe and varying concentrations of chemoreductant. The strongest reductant of the experimental set up (TCEP, 10 equiv. 100 μM) was added last, followed by an immediate first (time point zero) measurement on the plate reader. Raw data were processed using *Microsoft Excel* and *GraphPad Prism*, the former serving as platform for data assembly, organisation and calculation of mean values for each data point. Consecutively, obtained values $F(t)$ were further processed by normalising each data point to $F^{\text{TCEP}}(t)$, using TCEP as an estimated reference for fast, quantitative probe reduction and activation. Data plotting was conducted using *Prism*.

Resistance assays with key players in cellular redox

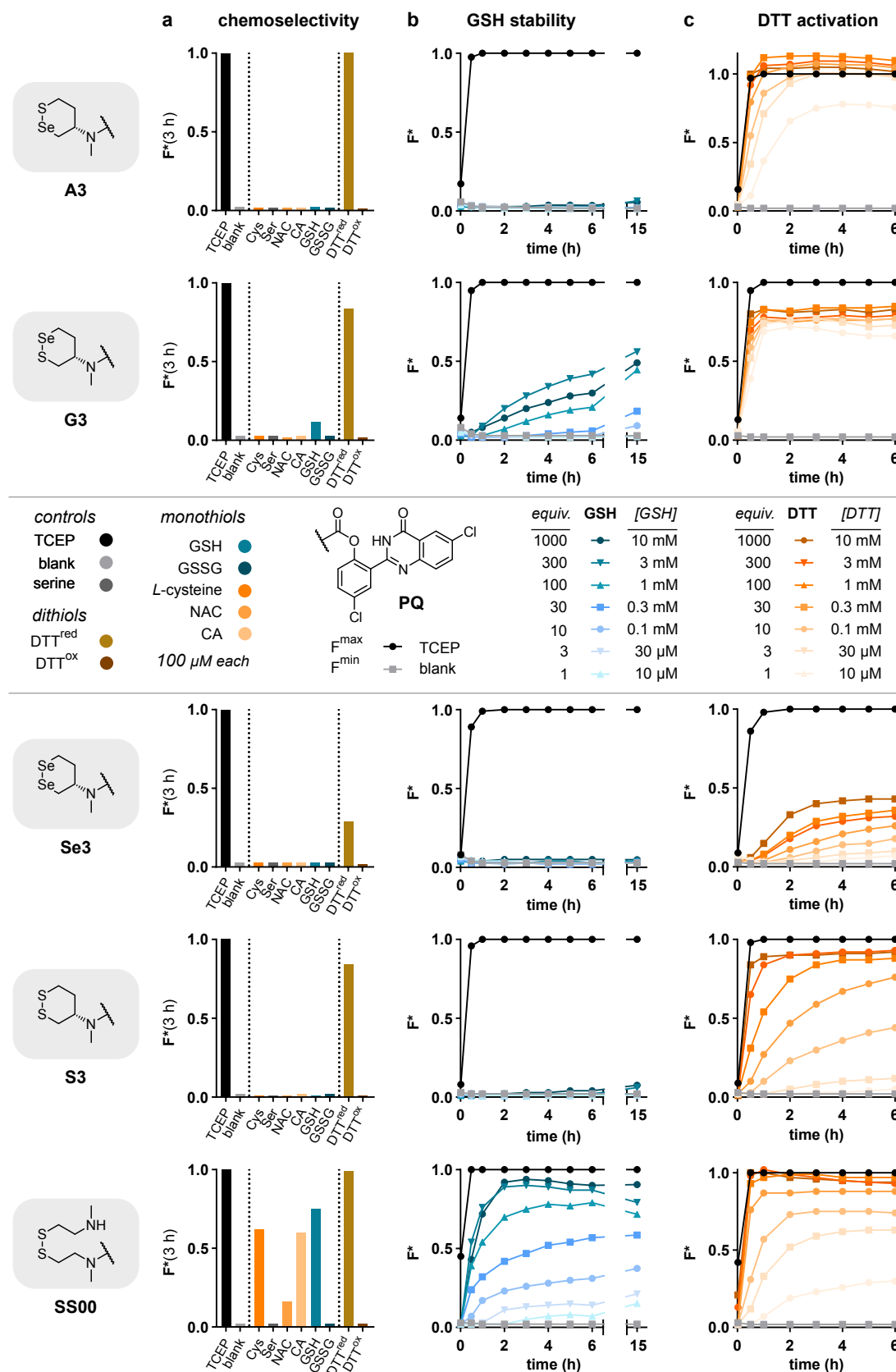
Redox stability of the designed probes towards key cellular reductants was conducted as follows: in case of two-component systems, the respective bioreductant (40 μL in TE) was placed into the corresponding wells and was subsequently charged with 50 μL of probe (20 μM in TE buffer/2% DMSO, to result in a final concentration of 10 μM and 1% respectively). The reaction was started by addition of 10 μL of the reductive driving force, (NADPH or GSH; 10 μL , 1 mM in TE, 10 equiv) and the following, time point zero measurement was conducted.

Closely related to that, three-component experiments were prepared by first adding 40 μL of the reductant (TrxR/GR in TE (50 mM Tris-HCl, 1 mM EDTA, pH 7.5) to reach final concentration of 2 to 50 nM) and/or the corresponding native substrate (Trxs/Grxs in TE, to reach final concentrations of 0.01 to 10 μM). Consecutively, 50 μL probe (20 μM in TE buffer/2% DMSO, to reach final concentrations of 10 μM and 1% respectively) was added and the reaction was started by addition of 10 μL of 1 mM NADPH. TCEP (40 μL , 5 mM in TE, 20 equiv., final concentration of 200 μM) was added to a control-row for maximum activation and a first measurement (time point zero) was conducted right away.

Raw data was processed using *Microsoft Excel* and *GraphPad Prism*. As before, *Excel* was used for data assembly and calculation of mean values for each data point. In contrast to previous experiments, application of NADPH required an additional processing step to eliminate its background fluorescence, which interferes with the readout of the fluorescent PQ cargo.⁵³ Absolute fluorescence values $F(t)$ were therefore simply subtracted by $F^{\text{NADPH}}(t)$; NADPH control wells were run on every plate under the same conditions, rather than averaging values from other runs. NADPH-corrected absolute values were then further processed by normalising each data point to $F^{\text{TCEP}}(t)$, using TCEP as an estimated reference for fast, quantitative probe reduction and activation. Ultimate data visualisation in graphs was conducted in *Prism*.

Human recombinant thioredoxin 1 (Trx 1) (lyophilized), human recombinant glutaredoxin 1 (Grx 1) (lyophilized from 10 μL TE-buffer, pH 7.5), human thioredoxin reductase (TrxR) (1.5 mg/mL in 50% glycerol/TE-buffer, pH 7.5) and baker's yeast glutathione reductase (GR) (100 μM in 50% glycerol/TE-buffer, pH 7.5) were obtained from IMCO Corp., Stockholm (Sweden). The rat TrxR1 mutant rTrxR1^{U498C} used in this study was previously produced by Cheng *et al.*⁵⁴

2.2 Probe activation with chemical reductants



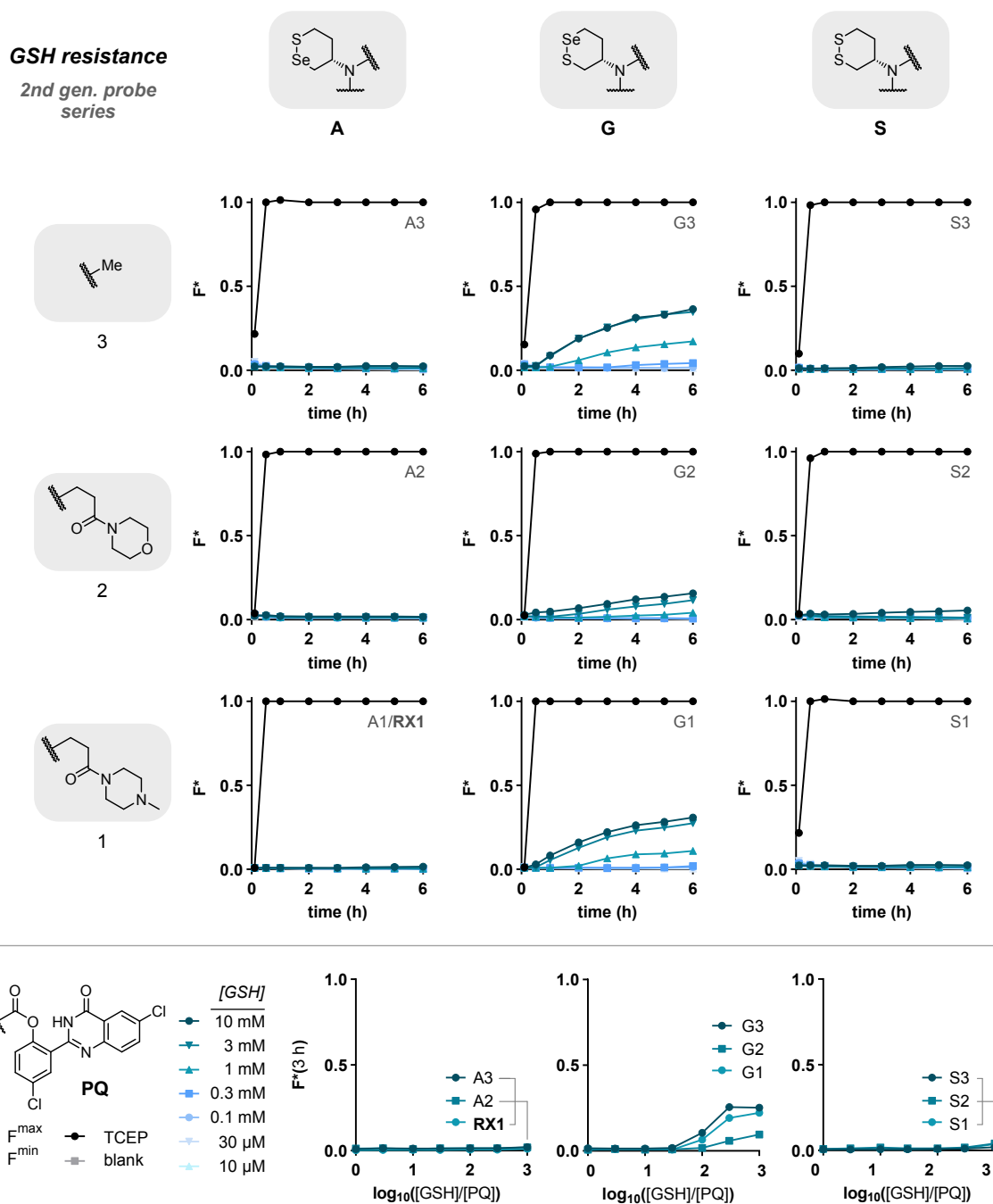


Figure S10 GSH-titration assay of the “second generation” probe series including (i) **A3**, (ii) **A2**, (iii) **RX1**, (iv) **G3**, (v) **G2**, (vi) **G1**, (vii) **S3**, (viii) **S2**, and (ix) **S1** (10 μ M in TE-buffer). F^* represents the relative fluorescence signal F/F^{TCEP} using TCEP (10 equiv., 100 μ M) as estimated reference for fast, quantitative probe reduction and activation. Reduction mediated cargo release is evaluated after 0-6 h of incubation with a range of GSH-concentrations (10 μ M, 30 μ M, 100 μ M, 300 μ M, 1 mM, 3 mM and 10 mM).

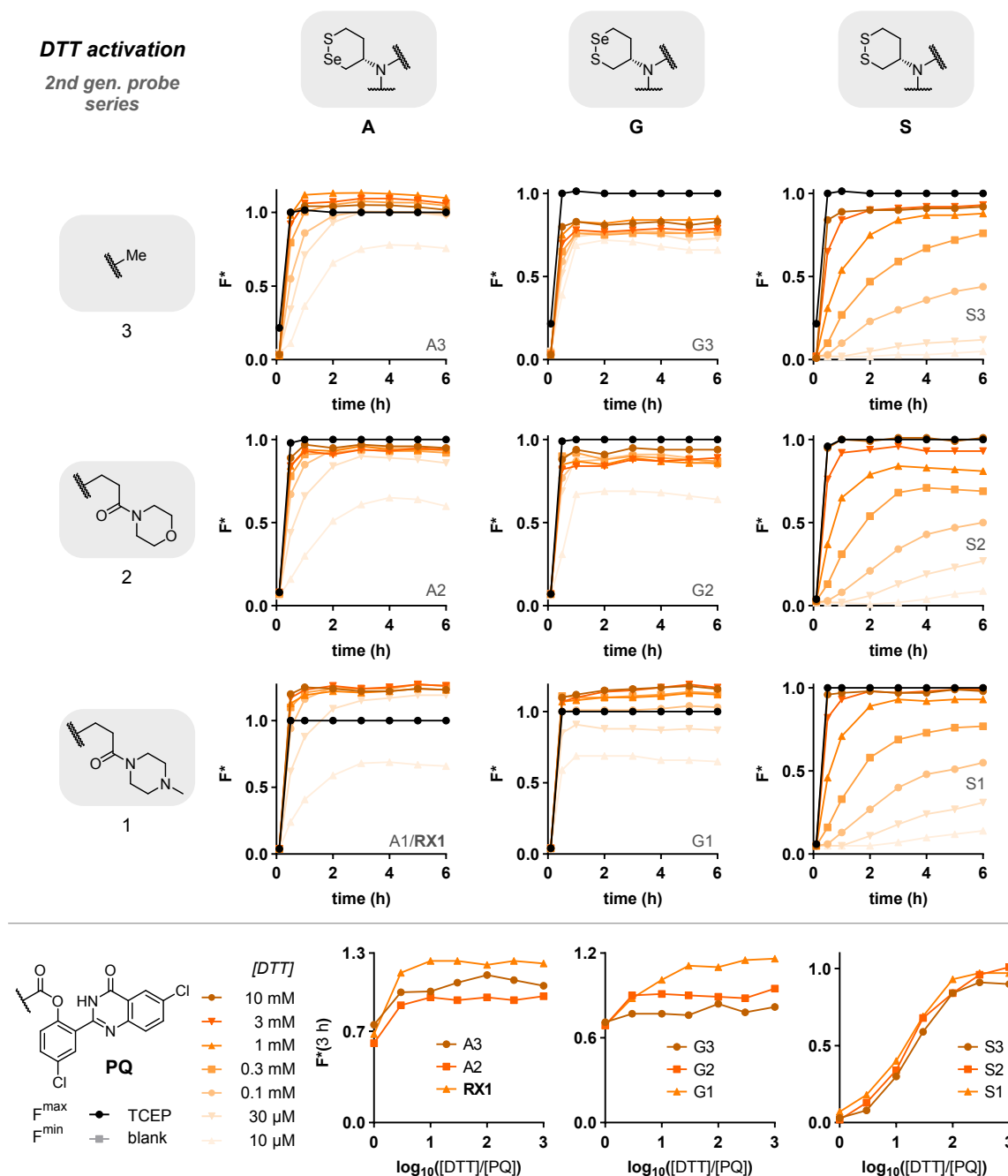


Figure S11 DTT-titration assay of the “second generation” probe series including (i) **A3**, (ii) **A2**, (iii) **RX1**, (iv) **G3**, (v) **G2**, (vi) **G1**, (vii) **S3**, (viii) **S2**, and (ix) **S1** (10 μ M in TE-buffer). F^* represents the relative fluorescence signal F/F^{TCEP} using TCEP (10 equiv., 100 μ M) as estimated reference for fast, quantitative probe reduction and activation. Reduction mediated cargo release is evaluated after 0-6 h of incubation with a range of DTT-concentrations (10 μ M, 30 μ M, 100 μ M, 300 μ M, 1 mM, 3 mM and 10 mM).

2.3 Probe activation with reducing dithiol/disulfide-type proteins and enzymes

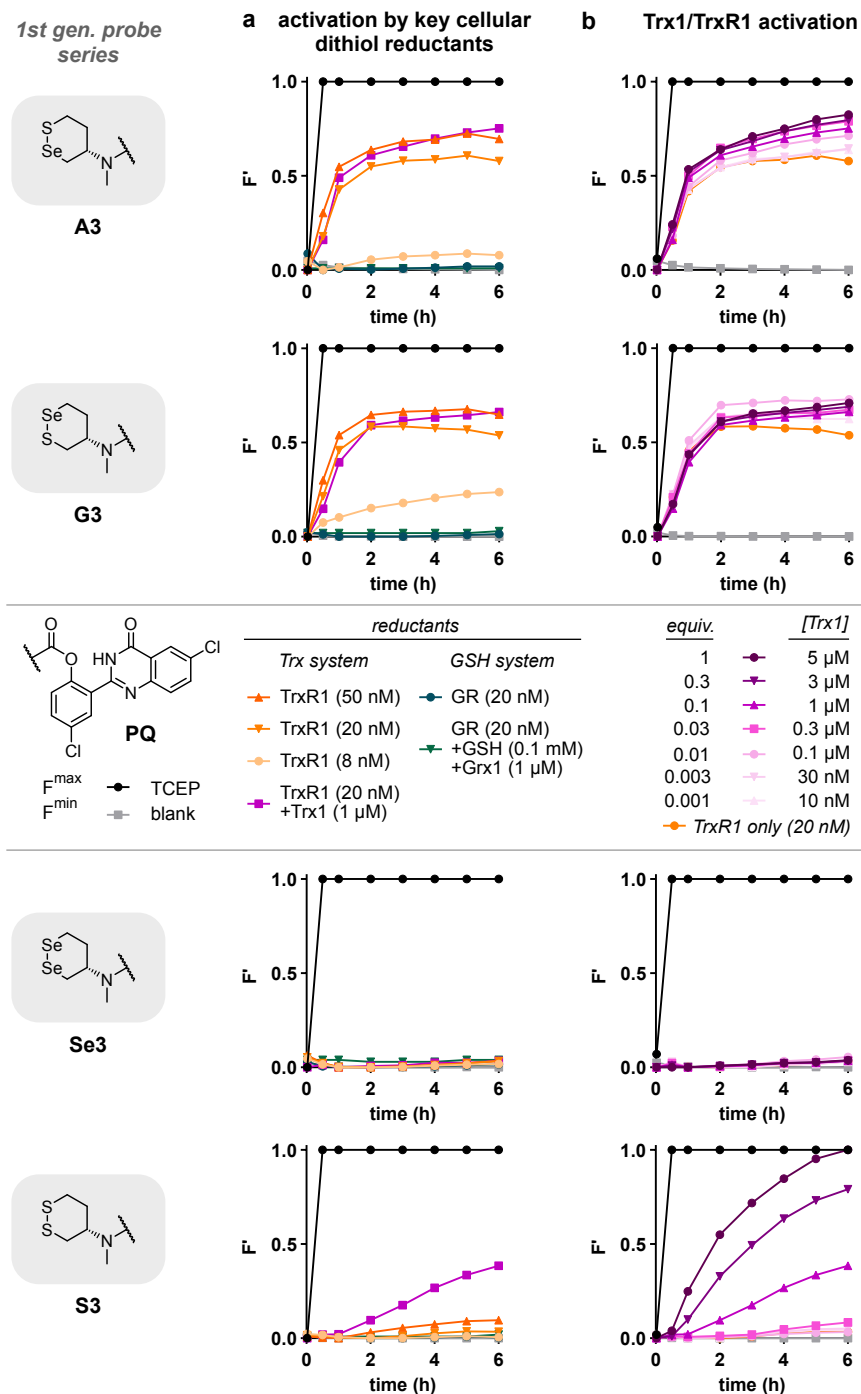
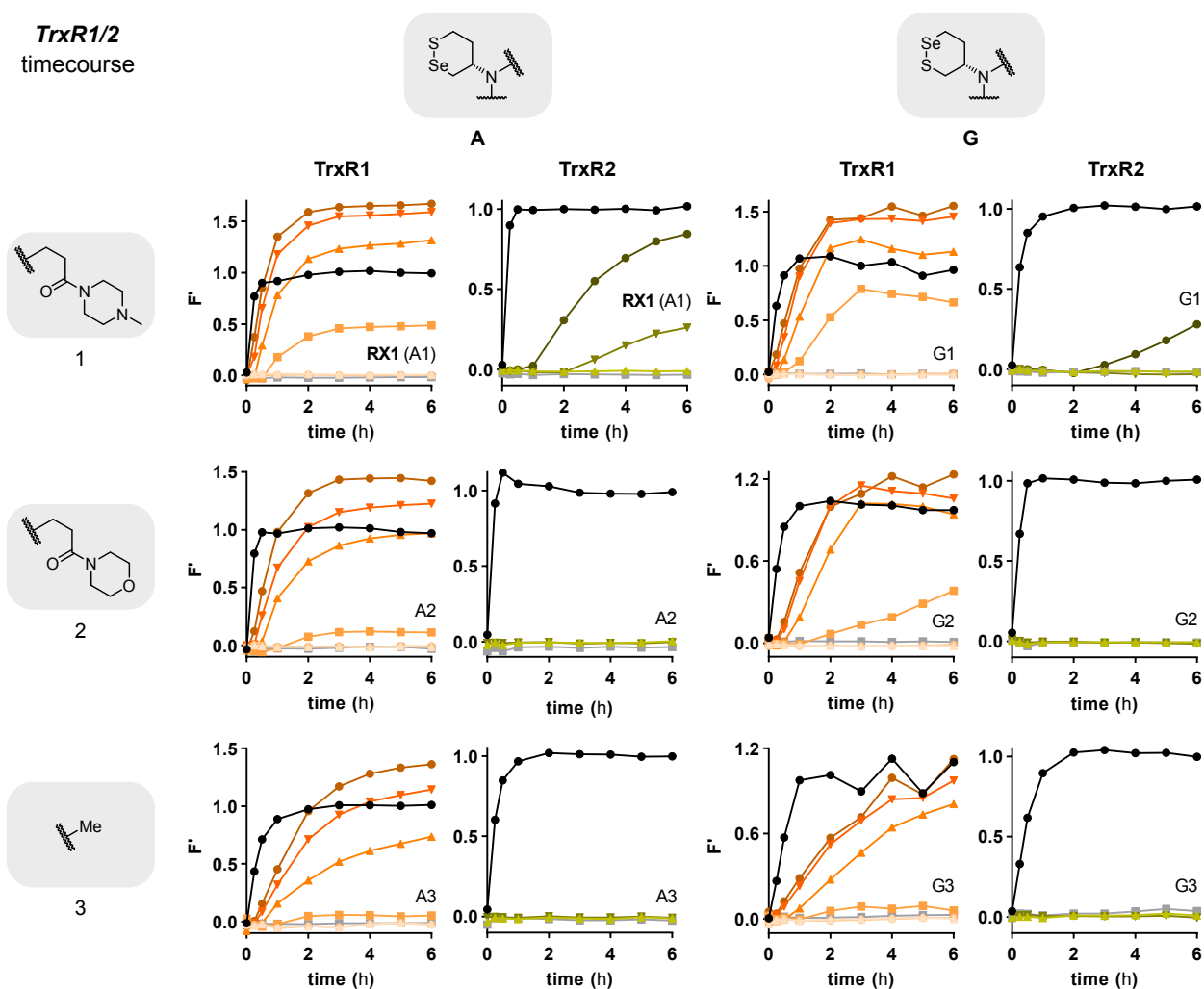


Figure S12 Biochemical evaluation of the “first generation” probe series including (i) **A3**, (ii) **G3**, (iii) **Se3** and (iv) **S3** (10 μ M in TE-buffer). F' represents the relative, NADPH-corrected fluorescence signal F/F^{TCEP} using TCEP (10 equiv., 100 μ M) as estimated reference for fast, quantitative probe reduction and activation. **(a)** Relative fluorescence signal after 0-6 h of incubation with key players of cellular redox biology, including GR, Grx1, Trx1 and TrxR1 at different concentrations. **(b)** Trx1-titration assay using NADPH (100 μ M) and TrxR1 (20 nM) as native upstream components. Trx1 is applied at a broad range of concentrations (0 nM, 10 nM, 30 nM, 0.1 μ M, 0.3 μ M, 1 μ M, 3 μ M, 5 μ M). Probe activation is evaluated as the time-dependent increase of the relative fluorescence signal from 0-6 h of incubation.

a *TrxR1/2*
timecourse



b *TrxR1/2*
dose-response

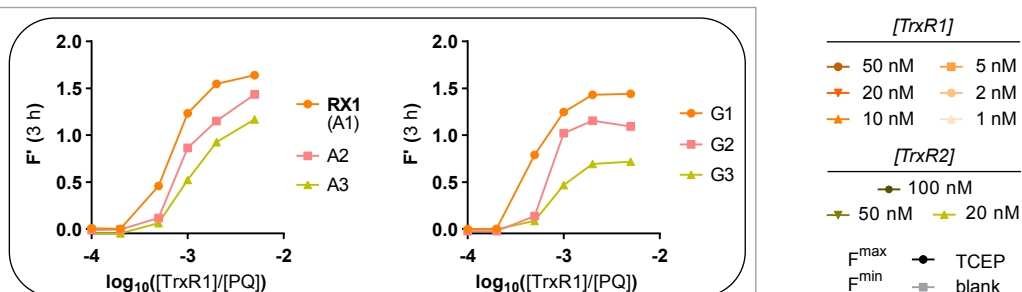


Figure S13 TrxR-activation assays for (i) **A3**, (ii) **A2**, (iii) **RX1** and (iv) **G3**, (v) **G2** and (vi) **G1** (10 μ M in TE-buffer). F' represents the relative, NADPH-corrected fluorescence signal F/F^{TCEP} using TCEP (10 equiv., 100 μ M) as estimated reference for fast, quantitative probe reduction and activation. TrxR1 and TrxR2 applied at a broad range of concentrations and assayed using NADPH (200 μ M) as native upstream component. Probe activation is evaluated as the time-dependent increase of the relative fluorescence signal from 0-6 h and as dose-response curves after 3 h of incubation.

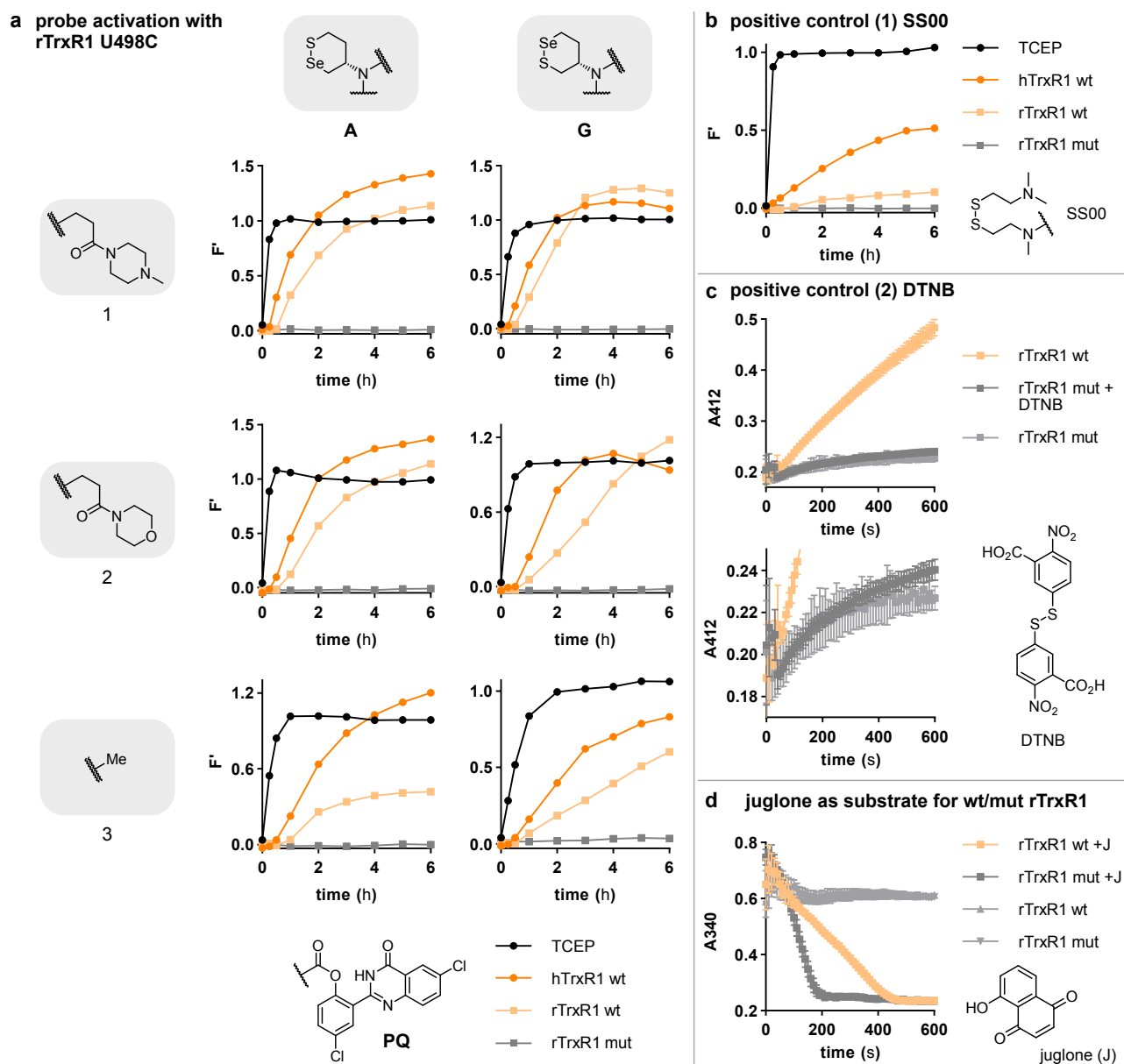
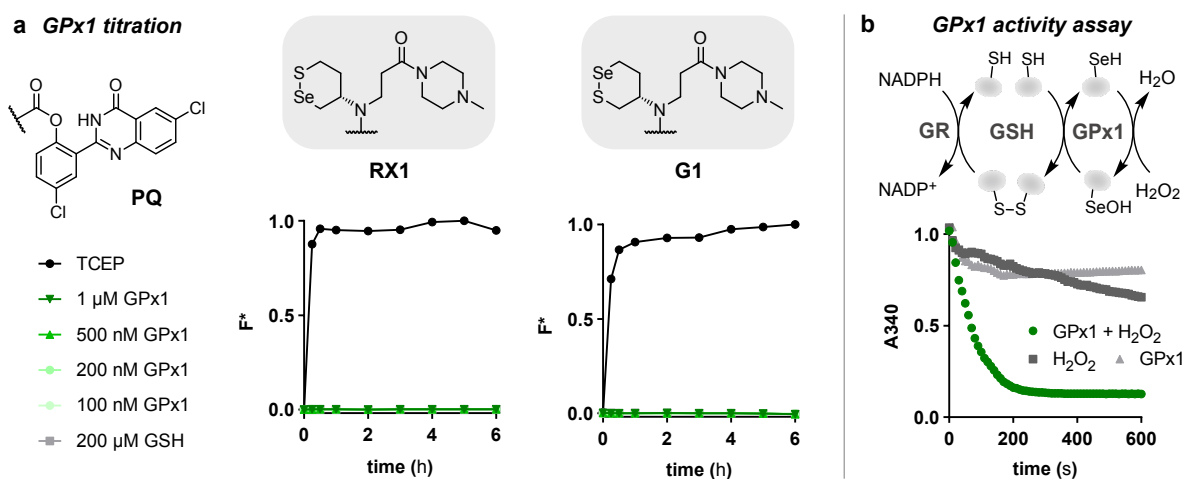


Figure S14 Probe activation by wildtype hTrxR and rTrxR (both U498, C497) compared to mutant rTrxR^{U498C.4454}. Assays were performed at 20 nM enzyme and 100 μ M NADPH in TE buffer. **(a)** Activation of **A1-3** (including **RX1**) and **G1-3** as the time-dependent increase of the relative fluorescence signal from 0-6 h; **(b)** Activation of **SS00** as the time-dependent increase of the relative fluorescence signal from 0-6 h; **(c)** Reduction of DTNB as time-dependent increase of absorbance at 412 nm indicative for accumulation of 2-nitro-5-thiobenzoate. As reported by Rackham⁵⁵, rTrxR^{U498C} showed to retain 5% activity as compared to the wildtype; **(d)** TrxR1-processing of juglone (J) as decrease of absorbance at 340 nm indicative for reduction of the benzoquinone-core. Retained reductase activity as seen for rTrxR^{U498C} indicates the presence of TrxR with a functional N-terminal active site.⁵⁶



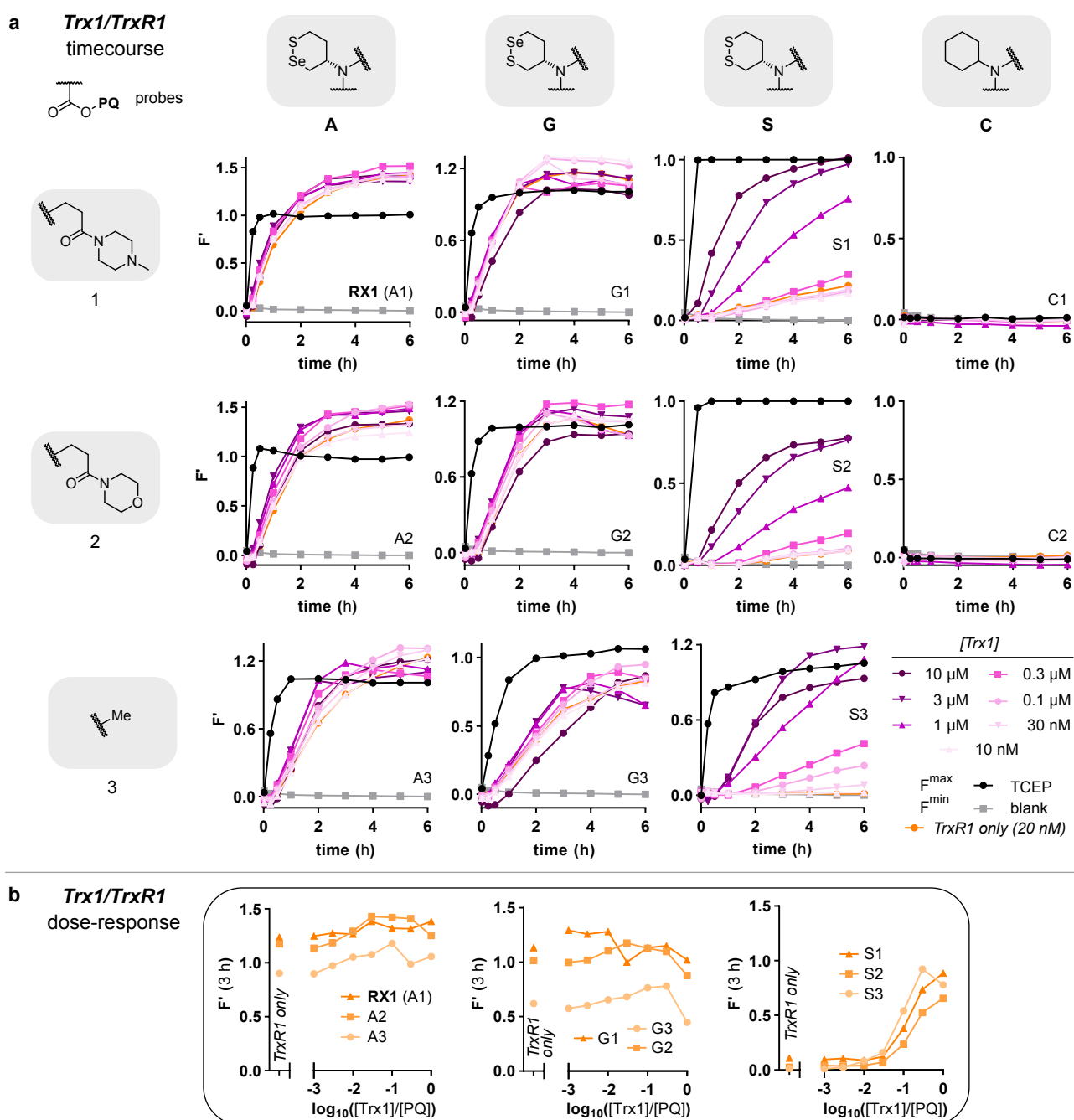


Figure S16 *Trx1*-titration assays for **A1-3** (including **RX1**), **G1-3**, **S1-3** and **C1-2** (10 μ M in TE-buffer). F' represents the relative, NADPH-corrected fluorescence signal F/F^{TCEP} using TCEP (10 equiv., 100 μ M) as estimated reference for fast, quantitative probe reduction and activation. *Trx1* is applied at a broad range of concentrations (0 nM, 10 nM, 30 nM, 0.1 μ M, 0.3 μ M, 1 μ M, 3 μ M, 10 μ M), NADPH (200 μ M) and *TrxR1* (20 nM) were applied as native upstream components. Probe activation is evaluated as the time-dependent increase of the relative fluorescence signal from 0-6 h and as dose-response curves after 2 h of incubation.

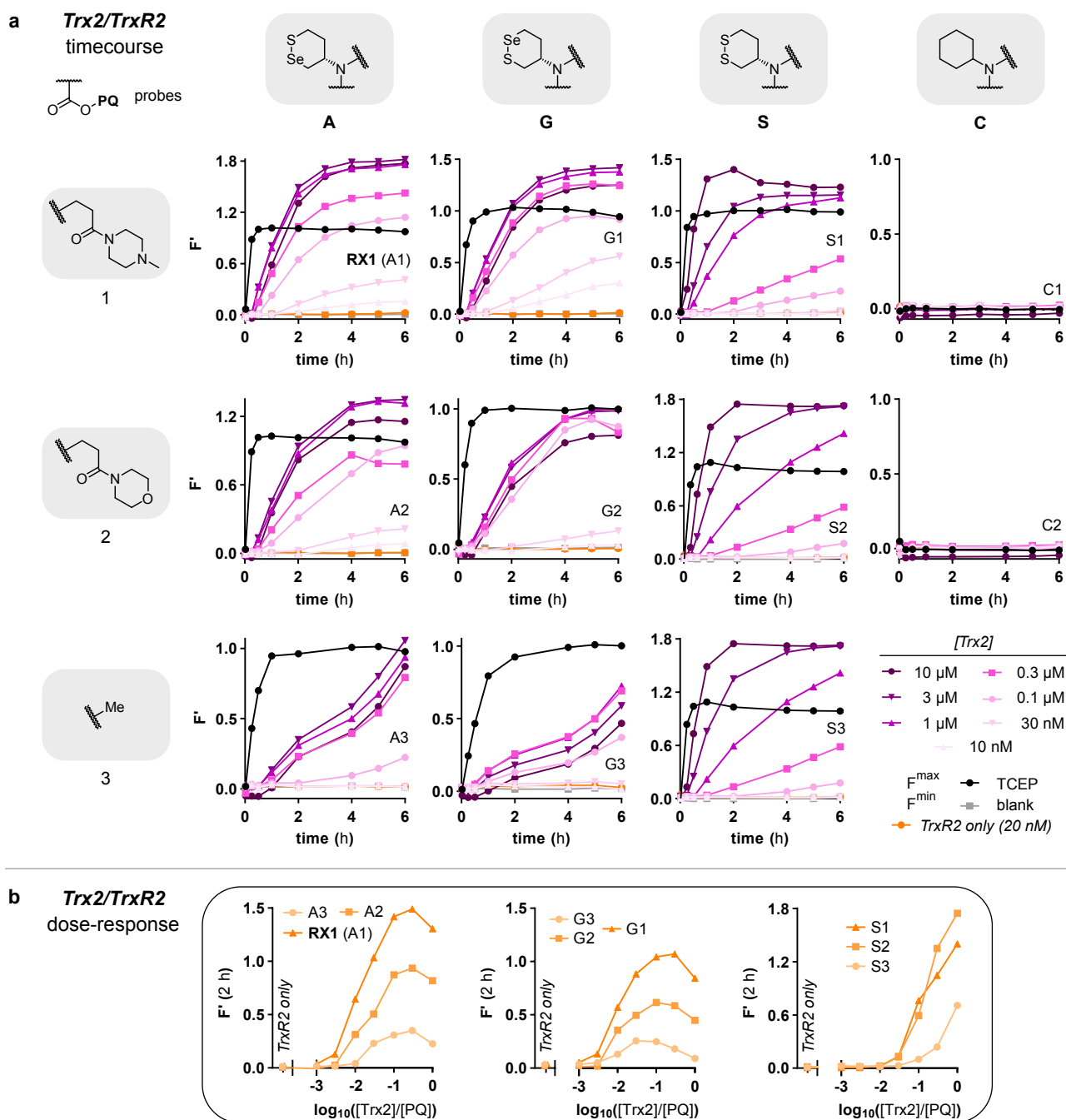


Figure S17 Trx2-titration assays for **A1-3** (including **RX1**), **G1-3**, **S1-3** and **C1-2** (10 μM in TE-buffer). F' represents the relative, NADPH-corrected fluorescence signal F/F^{TCEP} using TCEP (10 equiv., 100 μM) as estimated reference for fast, quantitative probe reduction and activation. Trx2 is applied at a broad range of concentrations (0 nM, 10 nM, 30 nM, 0.1 μM , 0.3 μM , 1 μM , 3 μM , 10 μM), NADPH (200 μM) and TrxR2 (20 nM) were applied as native upstream components. Probe activation is evaluated as the time-dependent increase of the relative fluorescence signal from 0-6 h and as dose-response curves after 2 h of incubation.

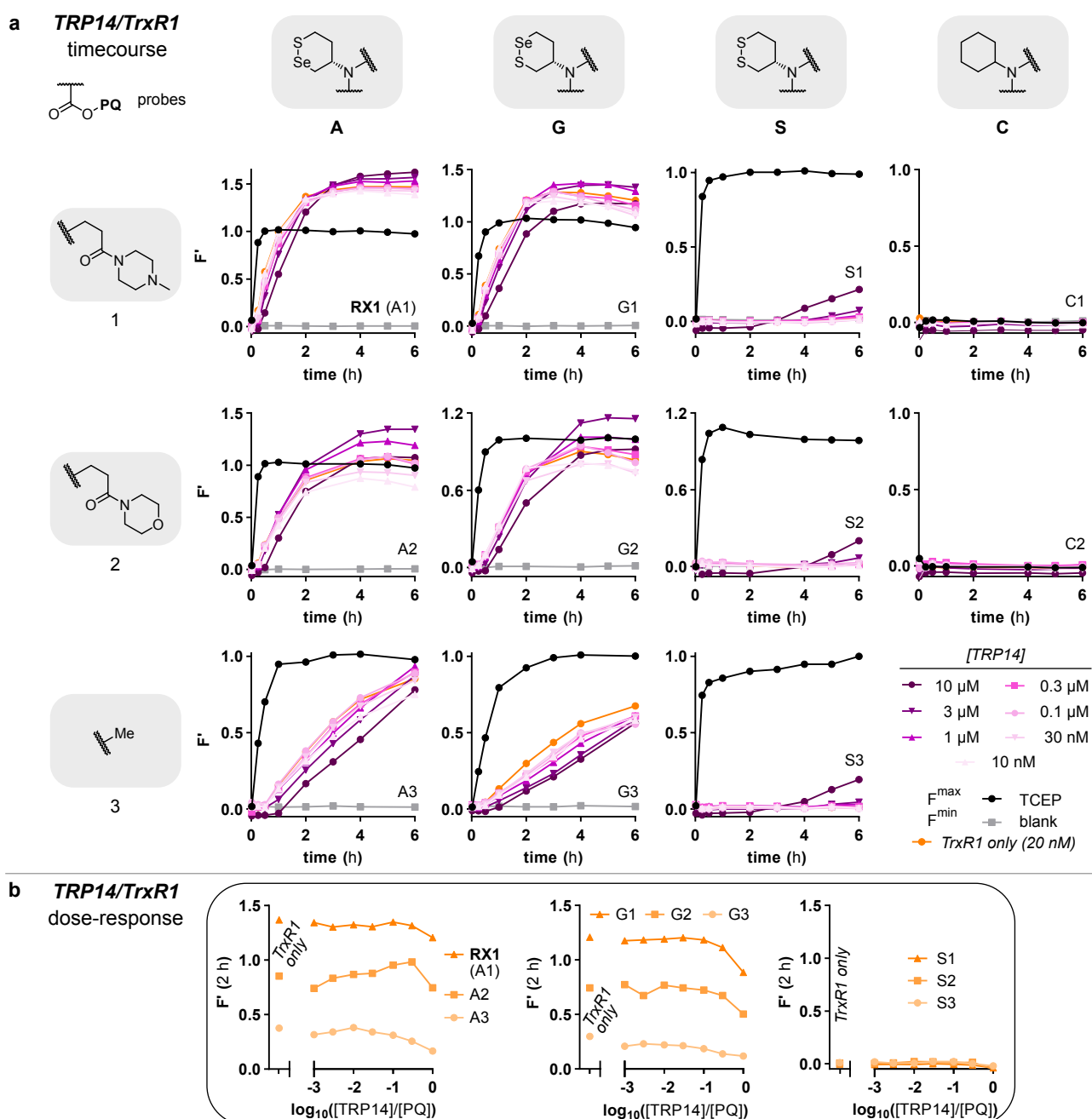


Figure S18 TRP14-titration assays for **A1-3** (including **RX1**), **G1-3**, **S1-3** and **C1-2** (10 μ M in TE-buffer). F' represents the relative, NADPH-corrected fluorescence signal F/F^{TCEP} using TCEP (10 equiv., 100 μ M) as estimated reference for fast, quantitative probe reduction and activation. TRP14 is applied at a broad range of concentrations (0 nM, 10 nM, 30 nM, 0.1 μ M, 0.3 μ M, 1 μ M, 3 μ M, 10 μ M), NADPH (200 μ M) and TrxR1 (20 nM) were applied as native upstream components. Probe activation is evaluated as the time-dependent increase of the relative fluorescence signal from 0-6 h and as dose-response curves after 2 h of incubation.

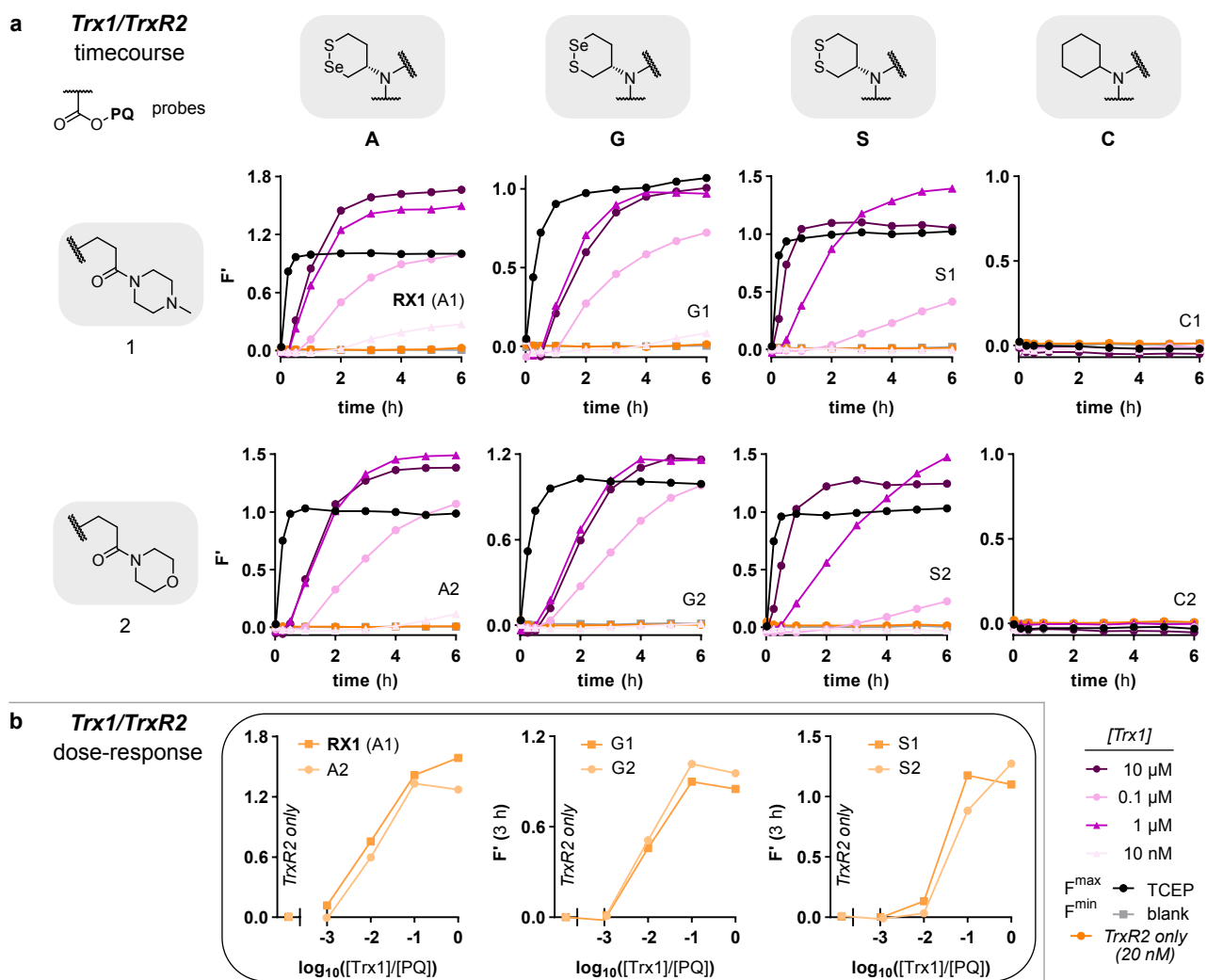


Figure S19 Cross-system Trx1-titration assays for **A1-3** (including **RX1**), **G1-3**, **S1-3** and **C1-2** (10 μM in TE-buffer). F' represents the relative, NADPH-corrected fluorescence signal F/F^{TCEP} using TCEP (10 equiv., 100 μM) as estimated reference for fast, quantitative probe reduction and activation. Trx1 is applied at a broad range of concentrations (10 nM, 0.1 μM , 1 μM , 10 μM), NADPH (200 μM) and TrxR2 (20 nM) were applied as upstream components. Probe activation is evaluated as the time-dependent increase of the relative fluorescence signal from 0-6 h and as dose-response curves after 3 h of incubation.

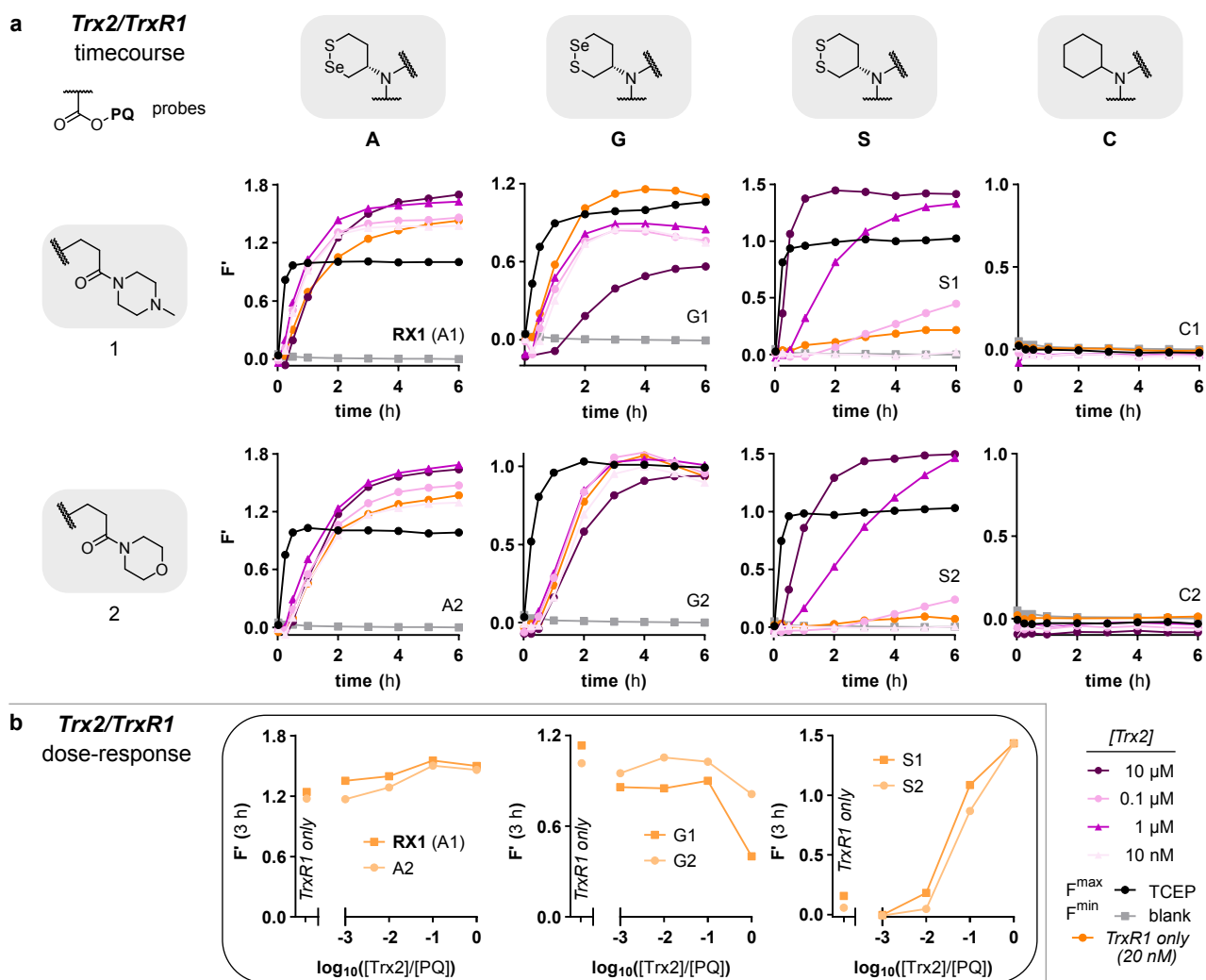
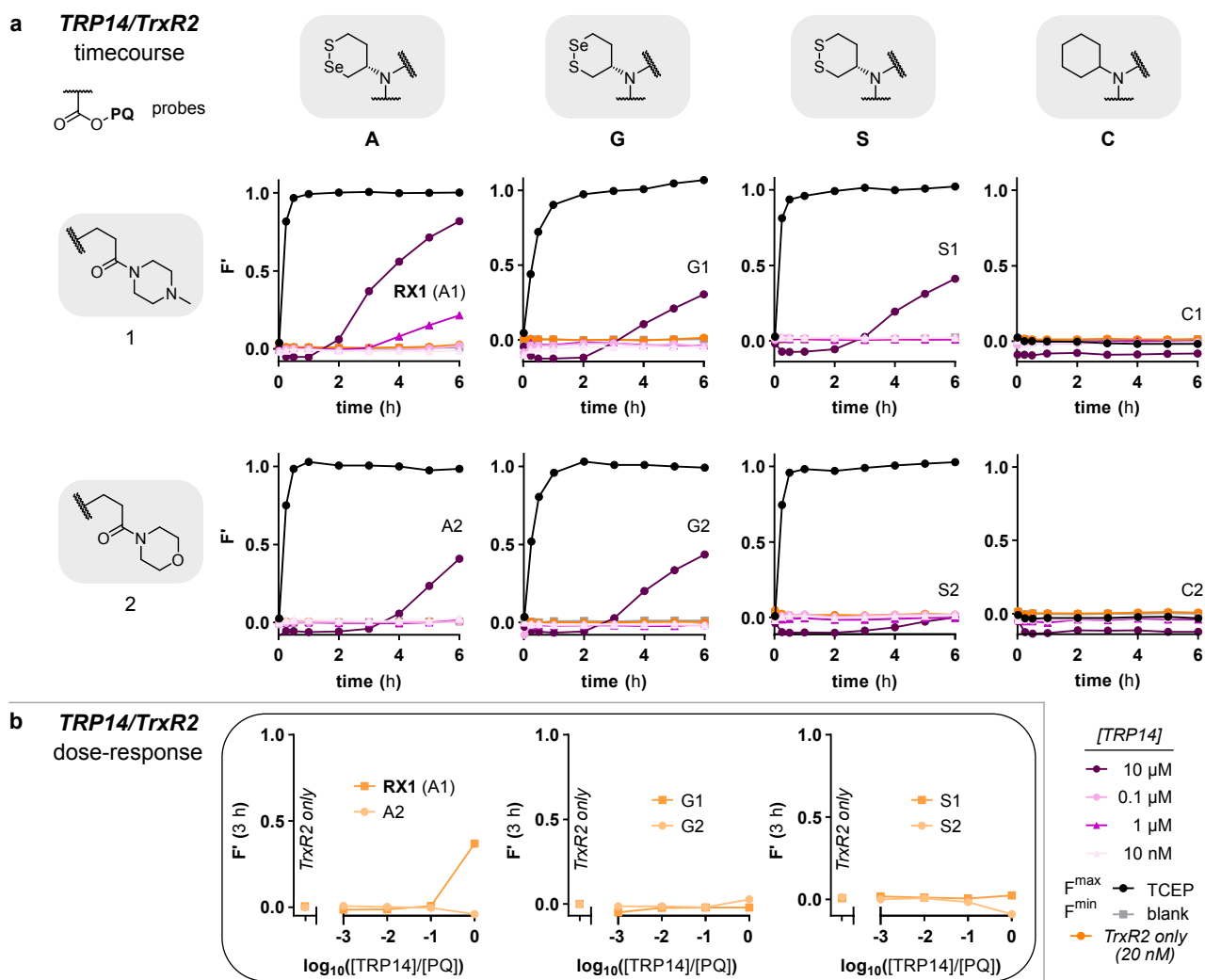


Figure S20 Cross-system Trx2-titration assays for **A1-3** (including **RX1**), **G1-3**, **S1-3** and **C1-2** (10 μM in TE-buffer). F' represents the relative, NADPH-corrected fluorescence signal F/F^{TCEP} using TCEP (10 equiv., 100 μM) as estimated reference for fast, quantitative probe reduction and activation. Trx2 is applied at a broad range of concentrations (10 nM, 0.1 μM , 1 μM , 10 μM), NADPH (200 μM) and TrxR1 (20 nM) were applied as upstream components. Probe activation is evaluated as the time-dependent increase of the relative fluorescence signal from 0-6 h and as dose-response curves after 3 h of incubation.



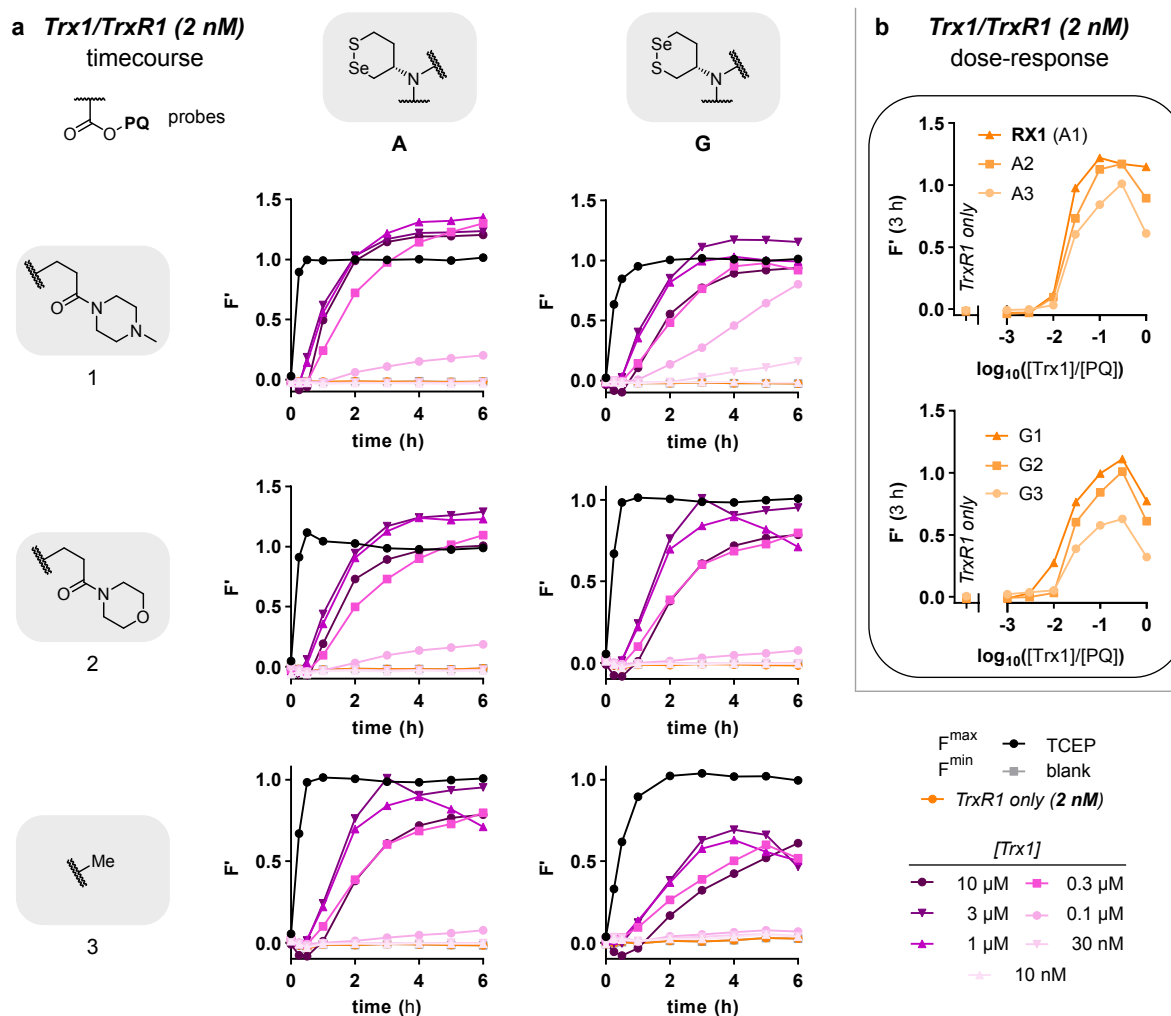


Figure S22 Low-*TrxR1* Trx1-titration assays for **A1-3** (including **RX1**) and **G1-3** (10 μ M in TE-buffer). F' represents the relative, NADPH-corrected fluorescence signal F/F^{TCEP} using TCEP (10 equiv., 100 μ M) as estimated reference for fast, quantitative probe reduction and activation. Trx1 is applied at a broad range of concentrations (10 nM, 30 nM, 0.1 μ M, 0.3 μ M, 1 μ M, 3 μ M, 10 μ M), NADPH (200 μ M) and TrxR1 (2 nM) were applied as native upstream components. Probe activation is evaluated as the time-dependent increase of the relative fluorescence signal from 0-6 h and as dose-response curves after 3 h of incubation.

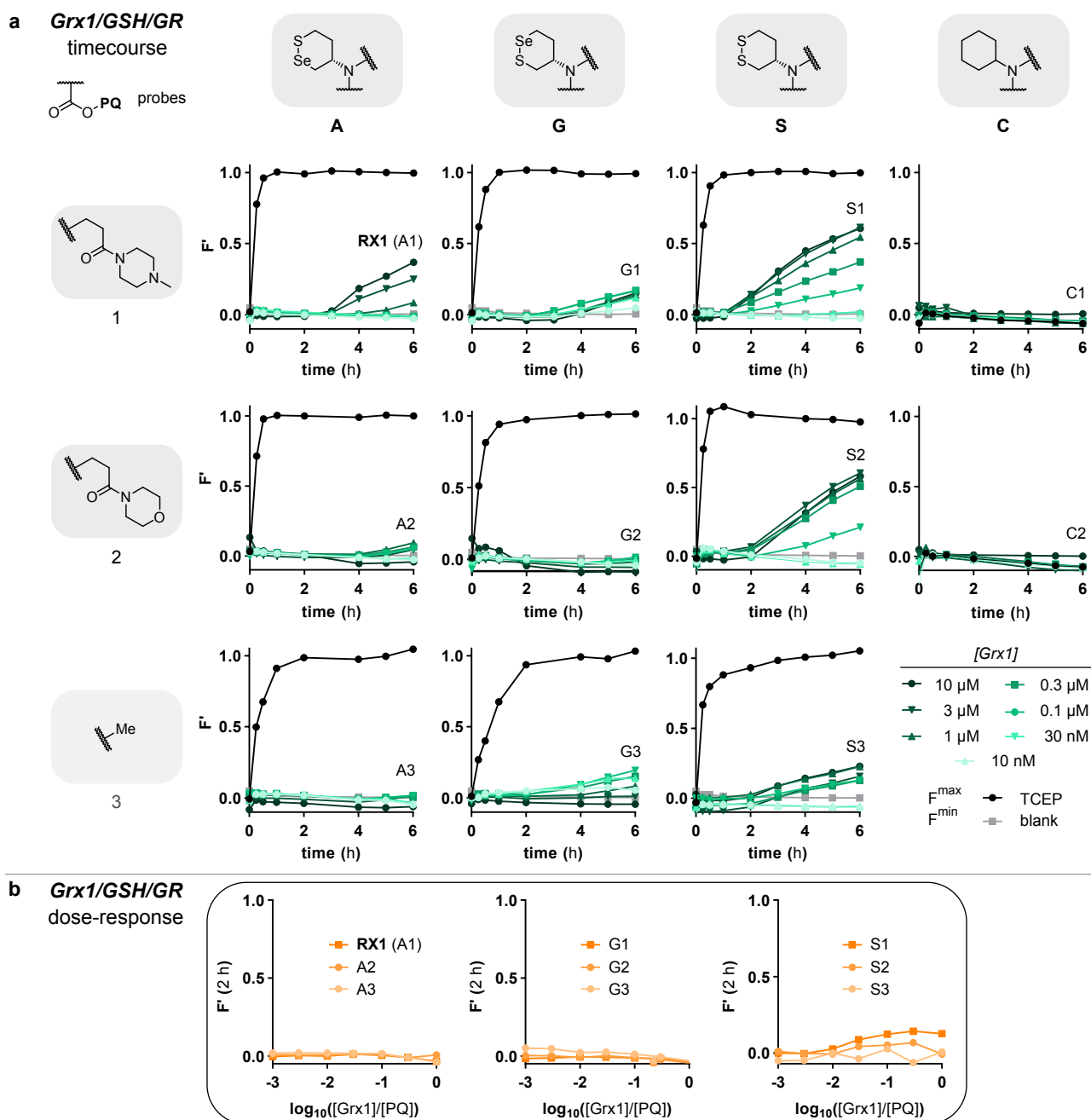


Figure S23 Grx1-titration assays for **A1-3** (including **RX1**), **G1-3**, **S1-3** and **C1-2** (10 μM in TE-buffer). F' represents the relative, NADPH-corrected fluorescence signal F/F^{TCEP} using TCEP (10 equiv., 100 μM) as estimated reference for fast, quantitative probe reduction and activation. Trx1 is applied at a broad range of concentrations (10 nM, 30 nM, 0.1 μM , 0.3 μM , 1 μM , 3 μM , 10 μM), NADPH (200 μM), GSH (100 μM) and GR (20 nM) were applied as native upstream components. Probe activation is evaluated as the time-dependent increase of the relative fluorescence signal from 0-6 h and as dose-response curves after 2 h of incubation.

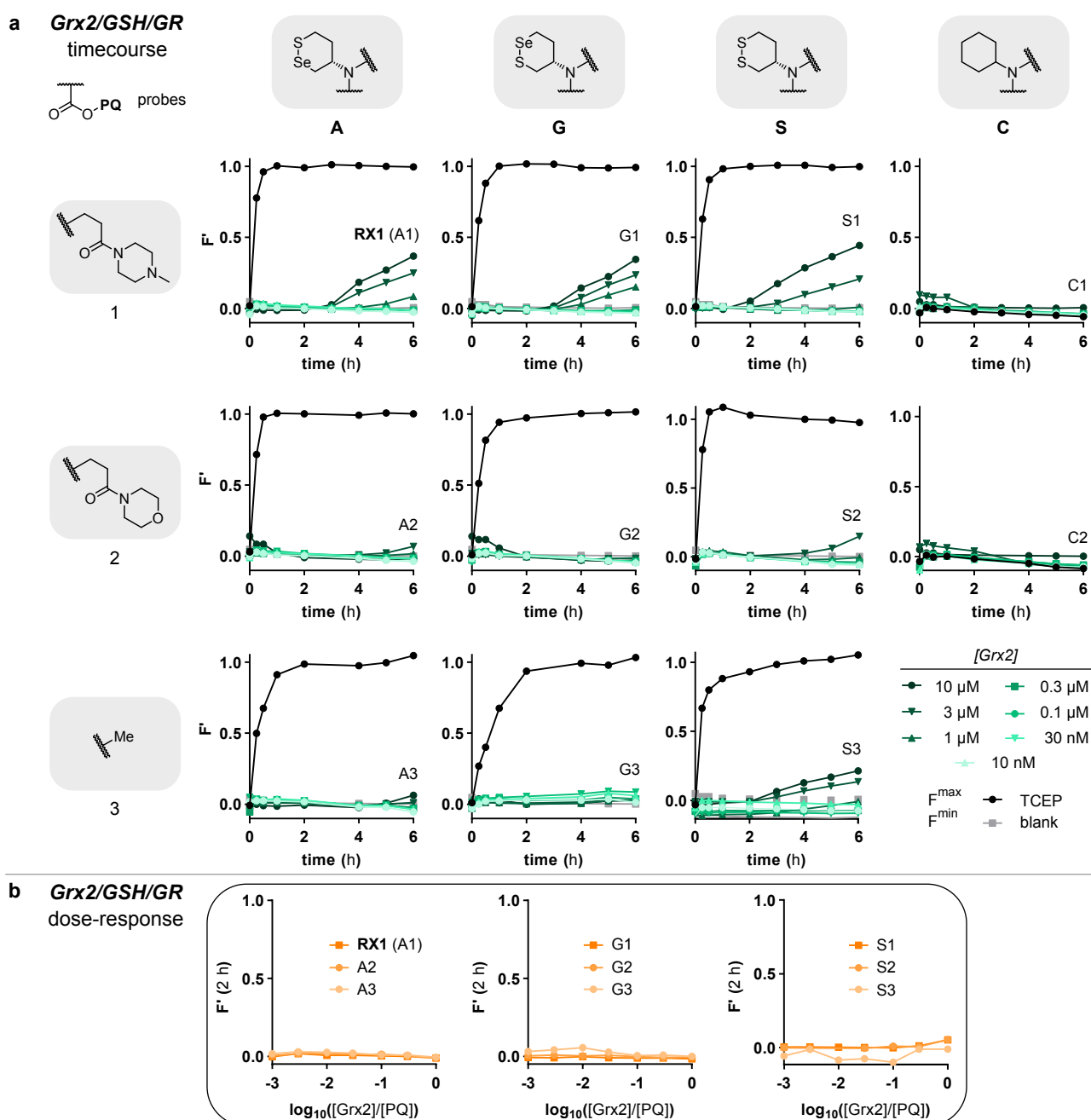


Figure S24 Grx2-titration assays for A1-3 (including RX1), G1-3, S1-3 and C1-2 (10 μ M in TE-buffer). F' represents the relative, NADPH-corrected fluorescence signal F/F^{TCEP} using TCEP (10 equiv., 100 μ M) as estimated reference for fast, quantitative probe reduction and activation. Trx1 is applied at a broad range of concentrations (10 nM, 30 nM, 0.1 μ M, 0.3 μ M, 1 μ M, 3 μ M, 10 μ M), NADPH (200 μ M), GSH (100 μ M) and GR (20 nM) were applied as native upstream components. Probe activation is evaluated as the time-dependent increase of the relative fluorescence signal from 0-6 h and as dose-response curves after 2 h of incubation.

3 Cellular assays

3.1. General protocols

General cell cultivation methods

Cells were grown in Dulbecco's modified Eagle's medium (DMEM: L-glucose (4.5 g/L), L-glutamine, L-pyruvate, phenol-red, NaHCO₃ (2.7 g/L); PAN Biotech) at 37 °C under 5% CO₂ atmosphere. Media were supplemented with 10% heat-inactivated fetal bovine serum, penicillin (100 U/mL), streptomycin (100 µg/mL) and Na₂SeO₃ (100 nM) unless stated otherwise. Selenium supplementation changes were always followed by at least 7 days of culturing the cells in the newly supplemented media before performing any experiments. Washing steps were performed in DPBS (Merck GmbH, Darmstadt, Germany), cell detachment was performed using TrypLE™ Express (gibco Life Technologies Inc.). Cell growth was monitored using a Nikon Eclipse Ti microscope (Nikon Corp.).

Cell lines

HeLa (DSMZ; ACC 57) and A549 (DSMZ; ACC 107) cell lines were purchased from the German Collection of Microorganisms and Cell Cultures. TrxR knockout and reference mouse embryonic fibroblasts (MEF) were a kind gift from Marcus Conrad. MEFs isolated from conditional TrxR1 knockout mouse embryos, were immortalised by lentiviral transduction. *In vitro* deletion of TrxR1 was achieved by *Tat-Cre* induced recombination and verified by PCR and immunoblotting for TrxR1.⁵⁷ The knock-in cell line emerged from the knockout cells through lentiviral transduction, encoding wildtype TrxR1.⁵⁸ The successful stable expression of TrxR1 was validated by western blot and TrxR1 activity assays. All cell lines are tested regularly for mycoplasma contamination and only mycoplasma negative cells are used in assays.

Cellular activation and inhibition assays

Cells were seeded in 96-well plates (microplates, 96-well, F-bottom, black, Fluotrack, high binding; Greiner bio-one GmbH) in 100 µL medium. Cells were treated with the respective probe (in 100% DMSO) to reach 25, 50, 75 or 100 µM final probe concentrations (1% DMSO final concentration) using a D300e digital dispenser (Tecan). For inhibition experiments, HeLa and cells were pre-treated with TrxR inhibitors TRi-1 and TRi-3⁴⁰ (from DMSO stock solutions) 16 h prior to probe treatment. A549 cell lines were preincubated with TRi-1 (4, 8, 16 µM from DMSO stock solutions, 50 µL medium) 3 h prior to probe addition or untreated as non-inhibited internal control. Inhibitor concentrations given in the following refer to *final* concentrations (100 µL medium after probe addition).

Time-course fluorescence measurements were conducted to determine kinetics of cellular processing. Fluorescence readout of cell-free activity and/or cell assays was performed either using a *FluoStar Omega* plate reader from BMG Labtech (ex/em 355bp20/520lp) or a Tecan Infinite M200 plate reader (ex/em 355bp10/520lp recording fluorescence intensity). Data was interpreted by representing the absolute, time-dependent fluorescence intensity *F*. Cells were kept at 37 °C under 5 % CO₂ atmosphere between measurements.

Fluorescence microscopy

Intracellular formation of solid green-fluorescent precipitates corresponding to a time-dependent increase *F* was confirmed using a Nikon Eclipse Ti2 upright microscope (ex/em 355bp50/410lp; or transmitted light, as appropriate). Images were processed using FIJI (ImageJ)⁵⁹ open-source image processing software.

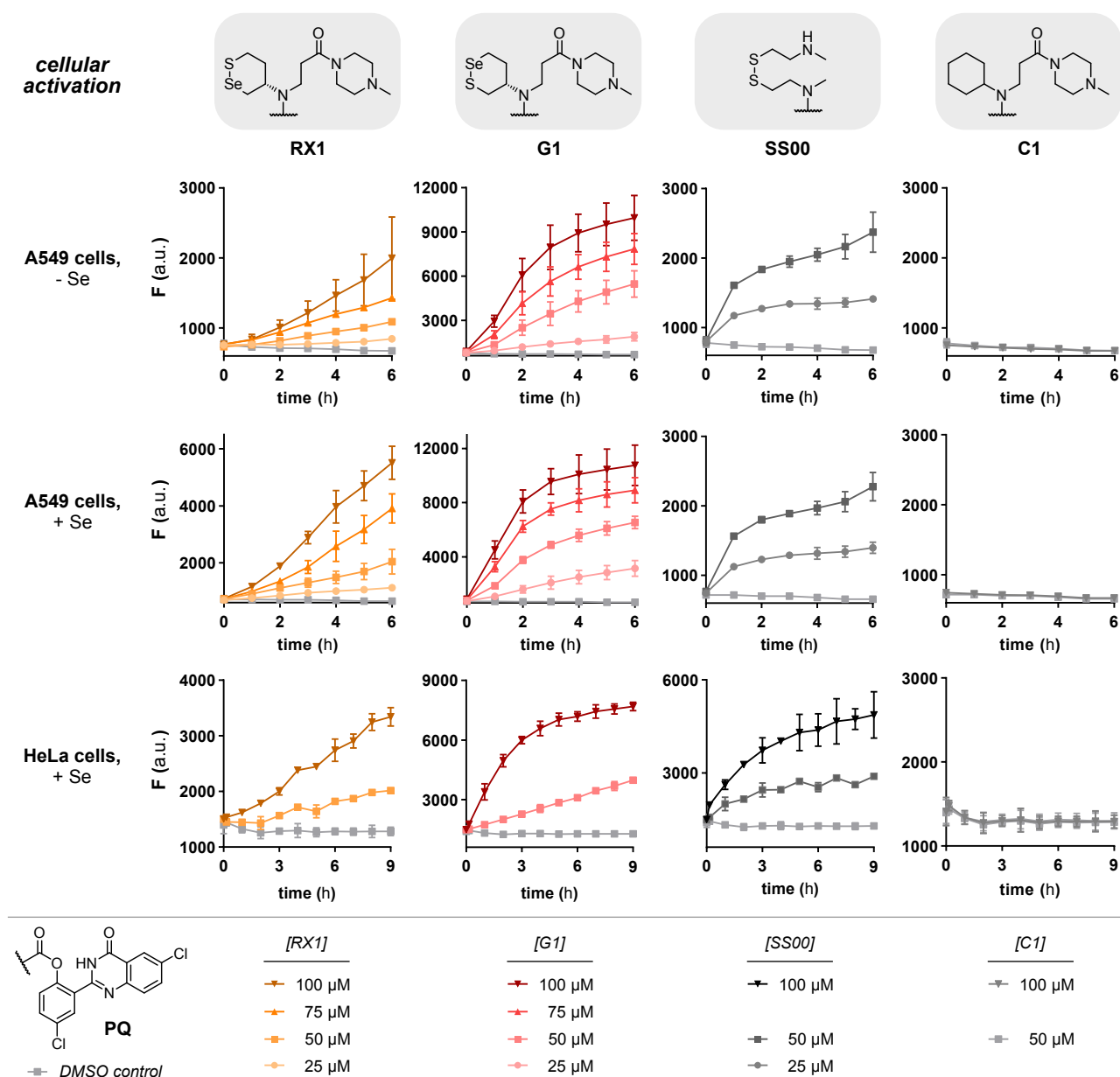


Figure S25 Time- and dose-dependent probe activation in HeLa and A549 cell lines (three independent experiments, mean of raw fluorescence values uncorrected for background baseline signal, therefore including all sources of technical or biological variations) over 6-9 h of incubation. In A549 cell lines, the effect of selenium-supplementation (in form of Na_2SeO_3) is evaluated. Absolute fluorescence signal increase of TrxR1-probe **RX1** is compared to design control **G1**, linear disulfide **SS00** as positive control and non-reducible **C1** as negative/probe-hydrolysis control.

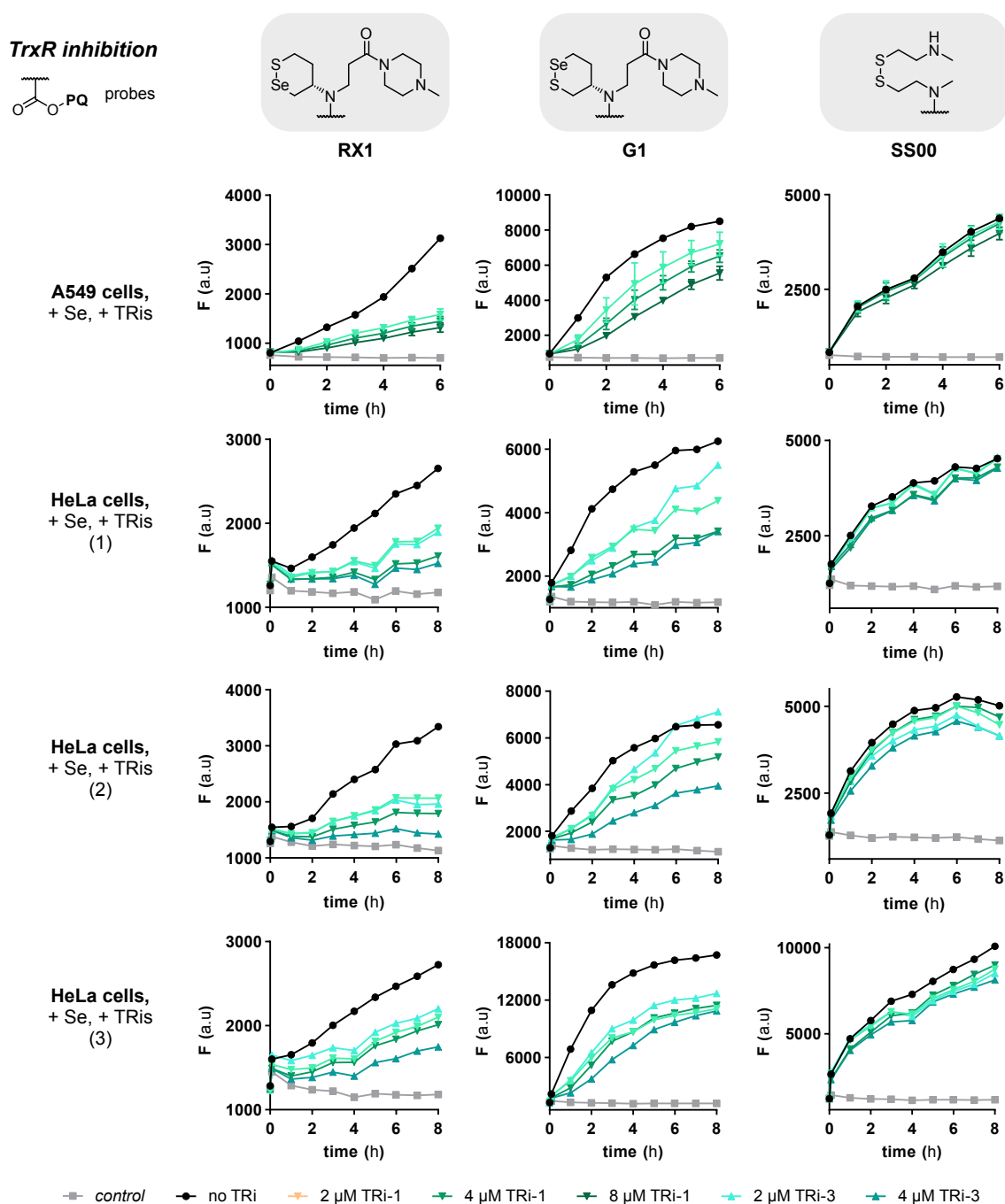


Figure S26 Inhibition of probe activation in HeLa (single experiments are shown) and A549 (three independent experiments, mean of raw fluorescence values uncorrected for background baseline signal, therefore including all sources of technical or biological variations) cell lines using TrxR1-inhibitors TRi-1 and TRi-3 at different concentrations (2, 4 and 8 μ M). HeLa cells were supplied with TRi-inhibitors 16 h before probe treatment, A549 cells were preincubated with inhibitors for 3 h. Absolute fluorescence signal increase of TrxR1-probe **RX1** is compared to design control **G1** and linear disulfide **SS00** as positive control. Experiments in HeLa cells were conducted with 100 μ M, 75 μ M were used in A549. "control" refers to DMSO background in HeLa and **C1**-probe background in A549 cell lines.

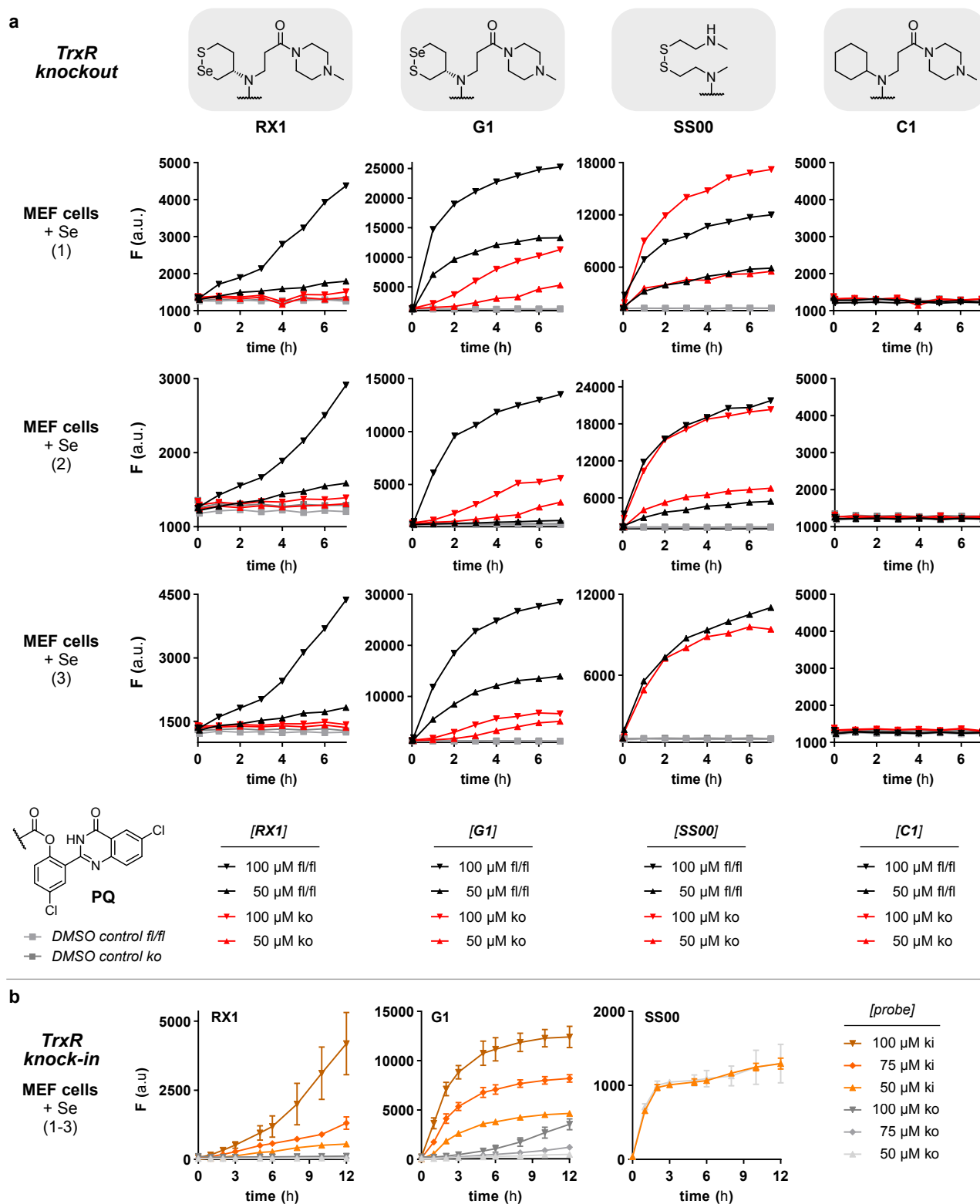


Figure S27 Time- and dose-dependent probe activation (three independent experiments, mean of raw fluorescence values uncorrected for background baseline signal, therefore including all sources of technical or biological variations) in selenium-supplemented (in form of Na_2SeO_3) cell lines with altered TrxR1-availability. Absolute fluorescence signal increase of TrxR1-probe **RX1** is compared to design control **G1**, linear disulfide **SS00** as positive control and non-reducible **C1** as negative/probe-hydrolysis control. **(a)** TrxR1-knockout MEF and fl/fl MEF cell lines over 7 h of incubation. **(b)** TrxR1-knockout and -knock-in MEF cell lines over 12 h of incubation. Reconstitution of TrxR1 expression was achieved through a lentivirus-based approach.⁵⁸

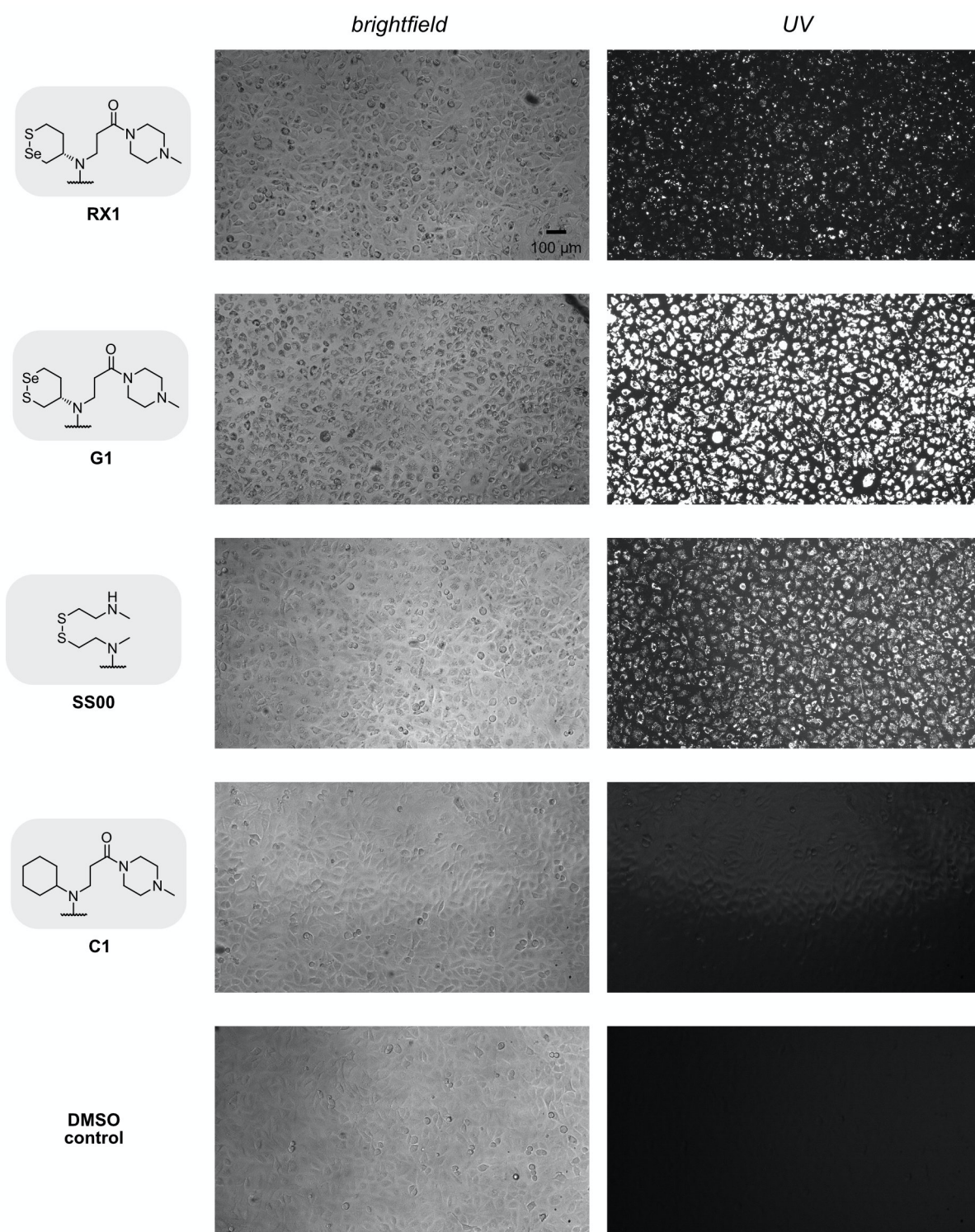


Figure S28 Fluorescence microscopy images in brightfield and UV showing cell-marking performance of the TrxR probes **RX1**, **G1** and non-selective positive control **SS00**. **C1** and DMSO-treated cells are given as negative control reference.

4 High-throughput screening

Comments on HTS requirements

A HTS-suitable probe must be TrxR-selective; but it must also pass many additional criteria for automatic operation, including (a) broad dynamic range (negligible background and cellular crosstalk, yet high signal-to-noise after activation); (b) linear response across the full dynamic range (so that results are quantifiable without compensation); (c) can be monitored noninvasively with a minimum of error-prone steps (no additional reagents, lysis, cosubstrates); (d) requires no tailoring of conditions or manual results compensation no matter the test compound being used; (e) returns consistently high-quality data: stable signal of high technical precision (small experimental error) and high biological accuracy (high confidence of TrxR quantification, minimum interference from test compounds of different classes).

The data quality is particularly important: since the higher the data quality, the fewer technical replicates are needed to obtain a single data point, which scales the assay time & requirements as well as the confidence in the conclusions.

4.1 Materials and methods

A549 human lung cells were purchased from ATCC (CCL-185, Manassas, VA). Cell media was purchased from Thermo Fisher (Pittsburgh, PA), Fetal bovine serum and trypsin were from GIBCO (Gaithersburg, MD). The Library of 1,280 Pharmacologically Active Compounds (LOPAC1280) was procured from Sigma-Aldrich (St. Louis, MO) and the compound plates were prepared as described previously.⁶⁰ CellTiter-Glo® Luminescent Cell Viability Assay was purchased from Promega (Madison, Wisconsin). Microplates were purchased from Corning.

Cell culture

A549 cells were cultured in DMEM/F-12, no phenol red media (ThermoFisher Scientific, Pittsburgh, PA) supplemented with 10% FBS (Millipore Sigma) and 100 nM sodium selenite (Millipore Sigma, St. Louis, MO). Cells were grown until reaching 80% confluence and split using 0.05% Trypsin-EDTA (GIBCO) before being passaged or plated for experiments. If plated, cells were pelleted in a centrifuge, and resuspended in media twice to remove remnant trypsin prior to conducting experiments. Cells were tested for mycoplasma contamination prior to every experiment using the MycoAlert Mycoplasma Detection Kit (Lonza).

Optimisation

Initial optimisation of cell density, probe concentration, and incubation time were tested together. A549 cells were split and prepared as described above. 5 μ L of cell mixtures at varying concentrations (0-3000 cells/well) were dispensed into six columns each of a 1536-well black/clear flat bottom TC-treated microplate (Corning) using a Multidrop™ Combi Reagent Dispenser (ThermoFisher Scientific). Following a 4 h incubation period at 37 °C, 1 μ L of several concentrations of **RX1** diluted in media (final concentrations ranging from 0-200 μ M) were dispensed into six rows each of the plate using a BioRAPTR 2 Flying Reagent Dispenser (Beckman Coulter), resulting in a grid of conditions (n=36). This plate was imaged at 1 h time intervals and remained at 37 °C between readings. Fluorescence at each time point was measured using an Envision plate reader ($\lambda_{\text{ex}} = 340/25$ nm, $\lambda_{\text{em}} = 520/25$ nm, 10 flashes). Average signal for each condition was plotted and assessed for best signal-to-noise ratio in a linear range. 100 μ M **RX1** at 4 h produced a robust signal above no-probe and was used for the following optimisation experiments.

To assess signal-to-noise of cell vs. no cell controls, varying cell concentrations were plated again in columns of 1536-well black/clear flat bottom TC-treated microplate, as above, and treated after a 4 h incubation period with **RX1** to a final concentration of 100 μ M. After 4 h at 37 °C, fluorescence at 525 nm was measured on the Envision, and average signal was calculated. Finally, a Z' was determined by plating half of a microplate with 1,250 A549 cells/well in media, and the other half with 5 μ L media. The plate was incubated at 37 °C for 4 h, 1 μ L of **RX1** in media was dispensed across the plate, and the plate was incubated again for 4 h. The plate was imaged, and fluorescence was measured using an Envision plate reader, and average signal and standard deviation of the cell and no cell conditions was used to determine the Z' value.

Probe concentrations showed suitable increases in signal that plateaued at 3-5 hours; 100 μ M **RX1** and 1,250 cells/ well at the 4-hour timepoint were selected such that a robust signal-to-noise ratio (7.2-fold) was produced while staying within the linear signal range (0-200 μ M). Whole-plate cell vs. no cell activity was conducted and yielded a promising Z' of 0.642, and a signal-to-noise of 7.0-fold, suggesting adequate reproducibility and suitable performance for high-throughput screening.

Known TrxR1 inhibitors Auranofin, TRi-1, and TRi-2, were then screened in dose-response to further validate the assay. Assay was completed as optimised, in triplicate with final compound concentrations ranging from 703 pM to 41.5 μ M. Data from this prior art screen was normalised to cell/no cell conditions, and dose-response curves were generated. The assay yielded an average Z' of 0.654 and a signal-to-noise of 7.6-fold (**Figure S29**). All three inhibitors showed a complete reduction of **RX1** signal at top dose, with average IC_{50} 0.52 μ M for Auranofin, 0.18 μ M for TRi-1, and 2.31 μ M for TRi-2.

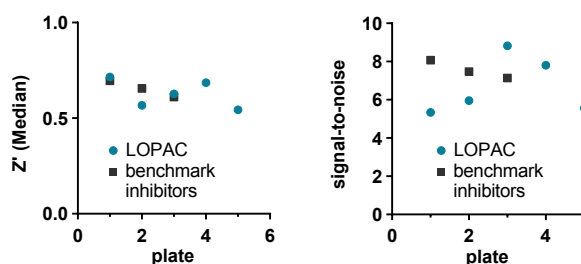


Figure S29 Determination of average Z' and S/N ratio.

Optimised assay conditions

Table S1 Protocol sequence for **RX1**/TrxR1 probe assay.

Step	Parameter	Value	Description
1	Cells	5 μ L	A549 cells
2	Incubation 1	4 h	37 °C incubation
3	Library Compounds	25 nL	Compounds added
4	Incubation 2	1 h	37 °C incubation
5	Reagent	1 μ L	RX1 probe
6	Incubation 3	4 h	37 °C incubation
7	Detection	Fluorescence	Fluorescence Read, Envision bottom read

Step	Notes
1	5 μ L A549 cells; 500 cells/well, DMEM/F-12, no phenol red + 10% FBS + 100 nM sodium selenite
2	Incubation 1; 37 °C, covered, 4 h (allow cells to adhere)
3	25 nL LOPAC1280 compounds and controls (1:3 5-point dilution, in DMSO) spotted into each well of black solid bottom Greiner 1536-well plate using Echo 525 Acoustic liquid handler
4	Incubation 1; 37 °C, covered, 1 h
5	Reagent Dispense; 1 μ L RX1 in media [final concentration ~100 μ M] dispensed into each well using BioRaprtr 2 FRD Dispenser (LGR)
6	Incubation 2; 37°C, covered, 4 h
7	Fluorescence Read; λ_{ex} = 340/25 nm, λ_{em} = 520/25 nm. EnVision bottom read.

High-throughput cellular screen of the LOPAC¹²⁸⁰ library

Cells were split and prepared as described above, before being resuspended to a concentration of 100,000 cells/well in fresh DMEM/F-12K supplemented media. 5 μ L of cell mixture was dispensed into columns 3-48 of a 1536-well black/clear flat bottom TC-treated microplate (Corning) using a MultidropTM Combi Reagent Dispenser (ThermoFisher Scientific). 5 μ L of media was dispensed in column 1-2 as a no-cell control. Plates were covered and incubated at 37 °C for 4 h to allow attachment prior to treatment with compounds. 25 nL of LOPAC₁₂₈₀ library compounds in 5-point dose-response were transferred into each well using either a pintool (Kalypsys) or an Echo 525 Acoustic Liquid Handler (Beckman Coulter), for primary screening and follow-up, respectively. All compounds were dissolved in DMSO and 25 nL of DMSO was transferred into columns 1-4 for the controls, and final compound concentrations ranged from 0.512 μ M to 41.5 μ M. The cells were incubated with the compounds for one hour before 1 μ L of **RX1** diluted in media was added to a final concentration of 100 μ M using a BioRAPTR 2 Flying Reagent Dispenser (Beckman Coulter). After four hours of incubation at 37 °C, the fluorescence at 525 nm was measured on an EnVision plate reader (λ_{ex} = 340/25 nm, λ_{em} = 520/25 nm, 10 flashes). To identify compounds that could interfere with the fluorescent reading, compounds were pinned into 6 μ L DMEM/F-12, no phenol red media, and were read as above on the EnVision plate reader; likely due to the large Stokes shift of the probe, no compounds were identified as interfering with fluorescence.

The **RX1** screen performed well, yielding an average Z' of 0.628 and a signal-to-noise ratio of 6.7-fold. Percent activity was computed after normalisation using the median values for the DMSO-treated uninhibited cell control (64 wells per plate) as 100%, and the DMSO-treated, no-cell control (64 wells per plate) as 0%. Dose-response curves were fitted to the normalised data using a Hill equation in GraphPad Prism (version 9.0) software (GraphPad Software, Inc., La Jolla, CA), constrained to plateaus of 100% and 0%: thus IC₅₀ values represent true 50% of maximal theoretical inhibition and are comparable across all compounds.

Short-term cytotoxicity counterscreen

Potential for cytotoxicity during the 4 h HTS assay was assessed after 4 h exposure to test compounds using CellTiter-Glo viability assay (Promega). Briefly, 5 μ L of A549 cells in DMEM/F-12, no phenol red supplemented media was dispensed into columns 3-48 of a 1536-well white solid bottom TC treated microplate (Corning) using a Multidrop. 5 μ L of media was dispensed into columns 1-2. Plates were covered and incubated at 37 $^{\circ}$ C for 4 h, and then 25 nL of top-dose LOPAC compounds were pinned into each well, with 25 nL of DMSO pinned into control columns 1-4. After an additional 4 h incubation at 37 $^{\circ}$ C, 2.5 μ L of CellTiter-Glo solution was dispensed into each well using a Multidrop, and the plates were covered at room temperature for 10 min. Plates were read for luminescence to determine any compound effects on growth inhibition during the **RX1** assay timing. Data was normalised to the cell/no cell controls and library compounds showing >50% cell killing at this dose would have been eliminated from further study. However, no such compounds were identified so none were excluded in this way.

4.2 LOPAC HTS-screen using RX1, and comparison to prior art enzymatic screen**"Hit" definitions**

Two compounds of LOPAC, Cisplatin (high-quality RX1 performance) and Carboplatin (inconclusive RX1), were removed from further analysis due to known interference with DMSO used in the HTS.⁶¹

Compounds were then classified based on potency and curve fit (**Fig S30**):

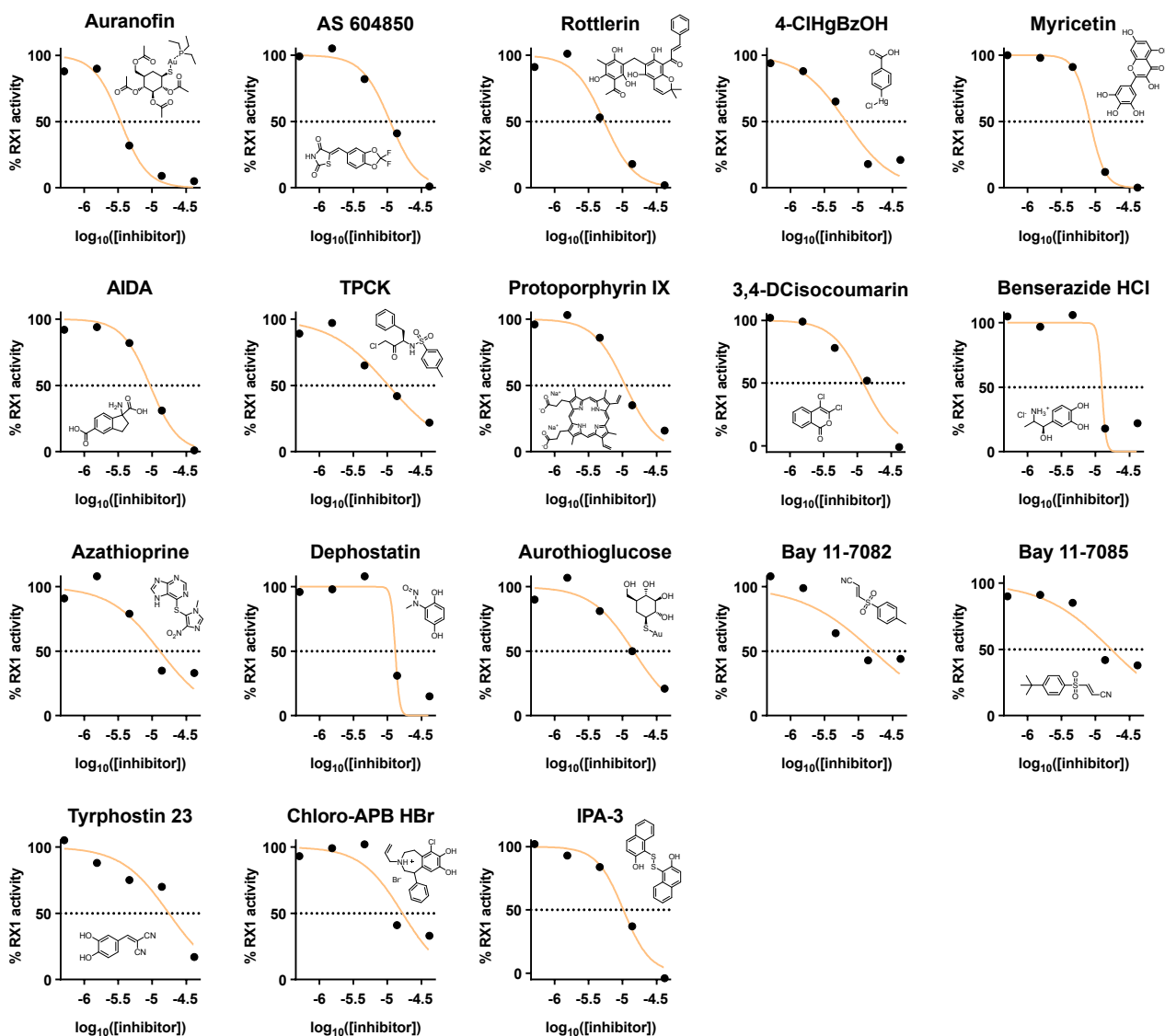


Figure S30 Dose-response curves and chemical structures for the 18 high-quality hits of the cellular **RX1** LOPAC screen.

We define a **"high-quality hit"** as a compound with an IC_{50} that can be reliably determined as $<20 \mu\text{M}$ ($\text{pIC}_{50} \geq 4.7$) and a well-formed sigmoidal inhibition curve, which is typically reflected in three criteria: (1) >50% reduction of fluorescence at the

second highest concentration (14 μM), (2) >60% reduction of fluorescence at the highest concentration (41 μM), (3) signal values at the second highest and highest concentrations should not both lie within the range 0.50-0.35, i.e. no "partial inhibitors" as these are not expected to be true hits for TrxR. These criteria gave a total of 18 high-quality LOPAC hits in the cellular assay, which corresponds to a <1.5% hit rate (18/1275 compounds; **Fig S30, Supporting Datafile**). The top 9 high-quality hits as ranked by IC_{50} passed all three criteria; the 9 bottom-ranked (dichloroisocoumarin, benserazide, azathioprine, dephostatin, aurothioglucose, Bay 11-7082, chloro-APB, Bay 11-7085, and Tyrphostin 23) typically failed one criterion but their IC_{50} values were deemed to be robust enough for further use.

We define "**borderline hits**" as those for which IC_{50} values cannot confidently be assessed (and which are therefore not used in the IC_{50} comparisons) but lie roughly within the range 15-30 μM , indicating **probable inhibitor leads** that could be followed up (4/1275 compounds in the cellular assay, all likely Michael acceptors: a chromenone, static, parthenolide, and tyrphostin A9). Typically, such compounds failed criterion 1 by a significant margin.

We define "**disqualified hits**" as low-quality hits with poor sigmoidal fits (typically, pass criterion 1 but significantly fail criterion 2 and/or 3, indicating 'weak partial inhibitor' curve form) that **cannot reliably be interpreted** either as weak hits or as interferences: and should therefore not be used either in hit or no-hit lists (1/1275 compounds in the cellular assay).

We define true "**inactive**" or "**not hit**" compounds as those which significantly fail all criteria 1-3 and which we are therefore **confident** are not good leads for TrxR inhibitors (1252/1275 compounds in the cellular assay).

Borderlines or disqualifieds are NOT used in IC_{50} comparison of hits in the context of on-target results; nor are they counted as "inactives" in the context of false negative results (see Section 4.2).

Encouraged by the good compatibility of our cellular HTS-screen, we reassessed the only known LOPAC screen for TrxR1: an enzymatic, cell-free screen performed in 2011.⁶² This enzymatic qHTS-assay relied on NADPH-consumption as fluorescent readout for TrxR1-activity. In brief, NADPH and purified rat TrxR1 were treated with the library compound, then selenite was added as a TrxR1 substrate, and NADPH concentration decrease over time was followed by fluorescence. Reduced NADPH consumption in comparison to non-treated controls, indicated inhibitory action by the treated compound. Re-assessing the enzymatic screen⁶² using our moderate cutoff criteria (detailed above) then resulted in 21 high-quality hits, 3 borderline hits, 39 disqualified hits, and 1213 inactives (**Table S2, Table S3, Supporting Datafile spreadsheet**).

Table S2 - Repartition of LOPAC test compounds into hit classes. See **Supporting Datafile** spreadsheet for compound listing, annotation, data, and filters. rTrxR enzymatic qHTS analysis is given in grey text since that data were not acquired in the context of this study, but only post-hoc analysed.

<i>Individual Screens Summary</i>	
RX1 hit	18
RX1 Borderline	4
RX1 Disqualified	1
RX1 Not Hit	1252
<i>subtotal</i>	1275
rTrxR1 Disqualified	39
rTrxR1 Hit	21
rTrxR1 Borderline	3
rTrxR1 Not Hit	1213
<i>subtotal</i>	1276
Cross-Test Compounds	1047

To compare hit compounds for both cellular (2021) and cell-free (2011) LOPAC assays (*note: total compounds screened in each are just under the 1280 total compounds in the libraries due to selected compound removal*), the compound libraries had to be examined manually to link identical compounds named with different NGC and PubChem identifiers in each library, as SMILES code crosschecking did not identify salt/free base formulation overlaps. A total of 1047 compounds were assessed in both screens. Full combined data for both screens are given and annotated in the **Supporting Datafile** (spreadsheet) and compounds of interest are listed in **Table S3**.

Table S3 – Repartition of LOPAC test compounds according to cross-assay performance. See **Supporting Datafile** spreadsheet for compound listing, annotation, data, and filters.

<i>LOPAC Cross-Hit Summary</i>		
RX1 Hit/rTrxR1 Hit	7	4-Chloromercuribenzoic acid, Protoporphyrin IX disodium, 3,4-dichloroisocoumarin, Dephostatin, Aurothioglucose, Bay 11-7082, Bay 11-7085
RX1 Hit/rTrxR1 Borderline	2	Azathioprine, Tyrphostin 23
RX1 Hit/rTrxR1 Disqualified	5	Rottlerin, Myricetin, AIDA, TPCK, Benserazide hydrochloride
RX1 Hit/rTrxR1 Not Hit	2	IPA-3, (μ)-Chloro-APB-hydrochloride
RX1 Hit/rTrxR1 Not Tested	1	AS 604850
RX1 Borderline/rTrxR1 Hit	1	Stattic
RX1 Borderline/rTrxR1 Borderline	1	Parthenolide
RX1 Borderline/rTrxR1 Disqualified	1	Tyrphostin A9
RX1 Borderline/rTrxR1 Not Hit	1	LY-294,002 hydrochloride
RX1 Borderline/rTrxR1 Not Tested	0	
RX1 Disqualified/rTrxR1 Hit	0	
RX1 Disqualified/rTrxR1 Borderline	0	
RX1 Disqualified/rTrxR1 Disqualified	1	(-)-alpha-Methylnorepinephrine
RX1 Disqualified/rTrxR1 Not Hit	0	
RX1 Disqualified/rTrxR1 Not Tested	0	
RX1 Not Hit/rTrxR1 Hit	9	Me-3,4-Dephostatin, BBMP, SB-415286, 6-Hydroxy-DL-DOPA, Pifithrin- μ , 3,4-Dihydroxyphenylacetic acid, MNS, Z-L-Phe chloromethyl ketone, Wortmannin
RX1 Not Hit/rTrxR1 Borderline	0	
RX1 Not Hit/rTrxR1 Disqualified	24	<i>see Supporting Datafile</i>
RX1 Not Hit/rTrxR1 Not Hit	993	<i>see Supporting Datafile</i>
RX1 Not Hit/rTrxR1 Not Tested	226	<i>see Supporting Datafile</i>
RX1 Not Tested/rTrxR1 Hit	4	R(-)-N-Allylnorapomorphine hydrobromide, NSC-724771, ZM-39923, Masoprocol
RX1 Not Tested/rTrxR1 Borderline	0	
RX1 Not Tested/rTrxR1 Disqualified	8	<i>see Supporting Datafile</i>
RX1 Not Tested/rTrxR1 Not Hit	217	<i>see Supporting Datafile</i>
Other entries	8	<i>see Supporting Datafile</i>
Total	1511	

High-quality hits identified in the cellular assay which were not part of the cell-free LOPAC are shown in **Figure S31a**; ones that hit in the cell-free assay, but are not part of the current LOPAC are shown in **Figure S31b**.

We next examined those compounds tested in both assays, aiming **towards evaluating cases where both assays returned confident results (either "Hit" or "No Hit")**, and neglecting all compounds for which one or both assays had a "disqualified" result.

(A) Of the 17 cell-free high-quality hits that are still part of the current LOPAC, 7 were shared cellular/cell-free hits, while 9 were cellularly inactive (**Fig S31c**; only 1 cell-free high-quality hit, stattic, was cellularly borderline; and pleasingly, no high-quality cell-free hit gave poor data in the cellular assay that would have required disqualification).

(B) Of the 16 high-quality cellular hits that had been tested in the cell-free assay, 7 [as above] were shared cellular/cell-free hits, 2 were borderline hits in the cell-free assay (azathioprine and tyrphostin 23, each a likely selenol-reactive species), 5 were disqualified from comparative analysis due to poor curve form in the cell-free assay, and 2 had been cell-free non-hits: IPA-3 (redox-active chelator/catechol precursor) and Chloro-APB (catechol).

(C) Most pleasingly, of the 1011 compounds that were not disqualified or borderline in one or both assays, 1000 return the same confident result in both assays (either hit/hit or inactive/inactive): only the aforementioned 11 compounds "switch results" between assays, of which only the mechanistically likely IPA-3 and Chloro-APB were unique results to the cellular assay. This 99% overall agreement between the cell-free purified rTrxR1 enzyme assay, and the cellular **RX1** assay, is a powerful argument that **RX1** behaves as a reliable TrxR1-selective probe in the complex cellular environment.

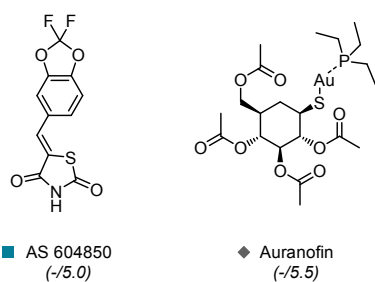
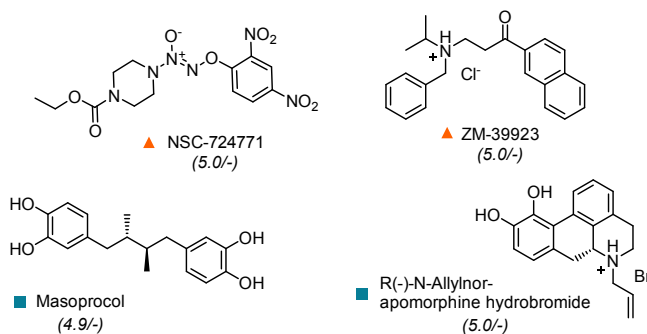
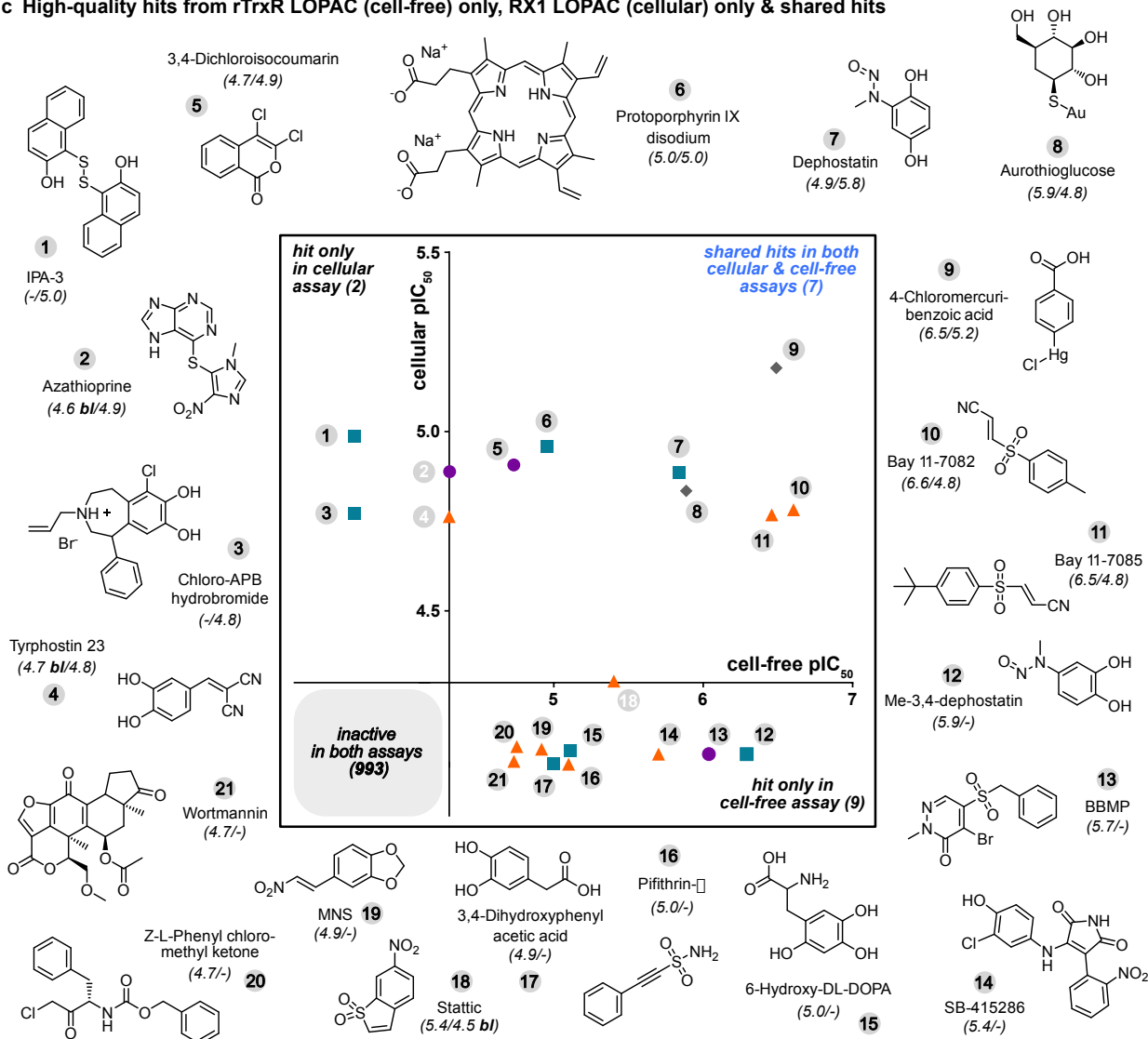
a Compounds, which were not in the old LOPAC (cell-free, 2011), but are hits in the RX1 LOPAC (cellular, 2021)**b Hits from rTrxR LOPAC (cell-free, 2011), which were not in the current RX1-LOPAC (cellular, 2021)****c High-quality hits from rTrxR LOPAC (cell-free) only, RX1 LOPAC (cellular) only & shared hits**

Figure S31 Comparison of cellular RX1 LOPAC hits and cell-free, enzymatic LOPAC hits (only compounds present in the purchased LOPAC libraries are shown; i.e. Tri-1 and Tri-2 are not shown, and auranofin is classed as 'not in old LOPAC'). pIC₅₀ values (*cellular/cell-free*) for either assay are given below the compound name. **(a)** Cellular hits, which were not included in the 2011 LOPAC. **(b)** Cell-free hits, which were not included in the 2021 LOPAC. **(c)** Non-disqualified compounds applied in both cellular and cell-free LOPAC (1011), separated into shared hits (7), cellular-hits-that-are-cell-free-borderlines (2) plus azathioprine and tyrphostin 23 that are cellular-hits-and-cell-free-borderlines (shown greyed out for information); cell-free-hits-that-are-cellular-inactives (9) plus static that is cell-free-hit-and-cellularly-borderline (shown greyed out for information); and the 993 compounds that were non-hits in both assays (structures not shown). Graph axes are pIC₅₀ values, with the graph origin set to (4.3, 4.3) to be offset below the IC₅₀ cutoffs, for better legibility.

An important question though beyond the scope of this paper, is, why do some inhibitor classes (e.g. the Michael acceptors) seem to lose so much potency in going from cell-free to cellular assays? An intriguing possibility was raised by Hondal, that Michael acceptors can undergo not only the known retro-Michael reaction but also can undergo selenium-redox-based selenoxide elimination specifically on TrxR.³⁷ This is undoubtedly relevant to TrxR's physiological role and behaviour. However, we suspect retro-reaction or elimination-based escape are not the problem - we rather read the potency loss as reflecting that most of the cell-permeating portion of these electrophiles are soaked up indiscriminately by other cellular thiol nucleophiles when alternative targets are provided at hundreds/thousands of times higher concentration (cysteines, GSH, and particularly other redox-active / highly nucleophilic cysteines) and just do not reach TrxR - therefore, giving a lower apparent potency. Inhibitors that would be more poorly reactive with these thiol nucleophiles (e.g. tempered electrophiles, albeit by definition), would in this picture have higher cellularly-intact proportions available to still react with TrxR: thus suffering less loss of potency.

5 Organic synthesis

5.1 General methods

Analytical methods

High resolution mass spectrometry (**HRMS**) was conducted either using a *Thermo Finnigan LTQ FT Ultra FourierTransform* ion cyclotron resonance spectrometer from *ThermoFisher Scientific GmbH*, Dreieich (Germany) applying electron spray ionisation (ESI) with a spray capillary voltage of 4 kV at temperature 250 °C with a method dependent range from 50 to 2000 u or a *Finnigan MAT 95* from *Thermo Fisher Scientific*, Dreieich (Germany) applying electron ionisation (EI) at a source temperature of 250 °C and an electron energy of 70 eV with a method dependent range from 40 to 1040 u. All reported *m/z* values refer to positive ionization mode, unless stated otherwise.

Nuclear magnetic resonance (**NMR**) spectroscopy was performed using a *Bruker Avance* (600/150 MHz, with *TCI cryoprobe*) or a *Bruker Avance III HD Biospin* (400/100 MHz, with *BBFO cryoprobe*TM) from *Bruker Corp.*, Billerica (USA) either at 400 MHz or 500 MHz. NMR-spectra were measured at 298 K, unless stated otherwise, and were analysed with the program *Mestrelab Nova 12* developed by *Mestrelab Ltd.*, Santiago de Compostela (Spain). ¹H-NMR spectra chemical shifts (δ) in parts per million (ppm) relative to tetramethylsilane ($\delta = 0$ ppm) are reported using the residual protic solvent (CHCl₃ in CDCl₃: $\delta = 7.26$ ppm, DMSO-d₅ in DMSO-d₆: $\delta = 2.50$ ppm, CHD₂OD in CD₃OD: $\delta = 3.31$ ppm) as an internal reference. For ¹³C-NMR spectra, chemical shifts in ppm relative to tetramethylsilane ($\delta = 0$ ppm) are reported using the central resonance of the solvent signal (CDCl₃: $\delta = 77.16$ ppm, DMSO-d₆: $\delta = 39.52$ ppm, CD₃OD: $\delta = 49.00$ ppm) as an internal reference. For ¹H-NMR spectra in addition to the chemical shift the following data is reported in parenthesis: multiplicity, coupling constant(s) and number of hydrogen atoms. The abbreviations for multiplicities and related descriptors are s = singlet, d = doublet, t = triplet, q = quartet, or combinations thereof, m = multiplet and br = broad. Where known products matched literature analysis data, only selected data acquired are reported.

Analytical high performance liquid chromatography (**HPLC**) analysis was conducted either using an *Agilent 1100* system from *Agilent Technologies Corp.*, Santa Clara (USA) equipped with a DAD detector and a *Hypersil Gold* HPLC column from *ThermoFisher Scientific GmbH*, Dreieich (Germany) or a *Agilent 1200 SL* system *Agilent Technologies Corp.*, Santa Clara (USA) equipped with a DAD detector, a *Hypersil Gold* HPLC column from *ThermoFisher Scientific GmbH*, Dreieich (Germany) and consecutive low-resolution mass detection using a LC/MSD IQ mass spectrometer applying ESI from *Agilent Technologies Corp.*, Santa Clara (USA). For both systems mixtures of water (analytical grade, 0.1 % formic acid) and MeCN (analytical grade, 0.1 % formic acid) were used as eluent systems.

Laboratory techniques

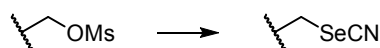
Unless stated otherwise, all reactions were performed without precautions in regard of potential air- and moisture-sensitivity and were stirred with Teflon-coated magnetic stir bars. For work under inert gas (nitrogen) atmosphere, a Schlenk apparatus equipped with a liquid nitrogen trap and a high vacuum pump from *Vacuubrand GmbH*, Wertheim (Germany) were used. For solvent evaporation a *Laborota 400* from *Heidolph GmbH*, Schwabach (Germany) equipped with a vacuum pump was used. Flash column chromatography was conducted under positive nitrogen pressure using *Ceduran® Si 60 silica gel* from *Merck GmbH*, Darmstadt (Germany) as stationary phase. Reactions were monitored by thin layer chromatography (TLC) on TLC plates (*Si 60 F254 on aluminium sheets*) provided by *Merck GmbH* and visualised by UV irradiation and/or KMnO₄ (3.0 g KMnO₄, 20 g K₂CO₃, 0.30 g KOH, 0.30 L H₂O).

Chemicals

All chemicals, which were obtained from *Sigma-Aldrich*, *TCI*, *Alfa Aesar*, *Acros*, *abcr* or *carbolution* were used as received and without purification. Tetrahydrofuran (THF), dichloromethane (DCM) and dimethylformamide (DMF) were provided by *Acros* and were stored under argon atmosphere and dried over molecular sieves. TLC control, extractions and column chromatography were conducted using distilled, technical grade solvents. Whenever it is referred to the term *hexanes*, the applied solvent actually comprised isomeric mixtures of hexane (2-methylpentane, 3-methylpentane, 2,2-dimethylbutane, 2,3-dimethylbutane).

5.2 General procedures

General procedure A: selenocyanation of alkyl mesylates



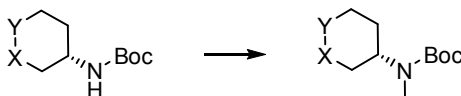
Selenocyanation was conducted based on a modified procedure from Block et al.⁶³. The respective mesylate was dissolved in THF (0.1 M) and sequentially charged with NaI (3.0 equiv.), 18-crown-6 (1.1 equiv.) and KSeCN (2.2 equiv.). The resulting, colourless suspension was heated to 50 °C for 16 h. The reaction mixture was diluted with brine and DCM, the organic layer was removed, and the aqueous layers was extracted with DCM (three times). The combined organic phases were dried over MgSO₄, filtered and concentrated *in vacuo*. Purification of the orange, oily crude product by flash column chromatography afforded targeted alkyl selenocyanates as colourless/pale yellow solids.

General procedure B: base-mediated selenosulfide/diselenide formation⁶³



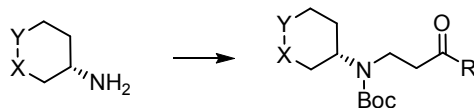
A solution of selenocyanate starting material (1.0 equiv.) in THF (0.05 M), was charged with a methanolic solution of KOH (0.2 M, 2.0 equiv.) in a dropwise manner. Within a few seconds, the reaction mixture turned from colourless to yellow and TLC control indicated full conversion of the starting material. The reaction was quenched with NaHCO₃ (sat. aq.), and the aqueous layer was extracted with DCM (three times). The combined organic layers were dried over MgSO₄, filtered and concentrated *in vacuo*. The targeted selenenylsulfide was received as a deeply coloured solid and without further purification.

General procedure C: methylation of *N*-Boc protected amines⁶⁴



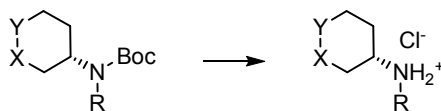
In a flame-dried Schlenk flask, *N*-Boc protected amine (1.0 equiv.) was dissolved in dry DMF (20 mM) under a nitrogen atmosphere. The solution was cooled to 0 °C and charged with first iodomethane (1.1 equiv.) then NaH (60%, 1.1 equiv.). The reaction was allowed to slowly warm to r.t. and was stirred for 5-7 h, until TLC control confirmed full conversion of the starting material. The reaction was quenched with NaHCO₃ (aq. sat.) and diluted with DCM. The aqueous layer was extracted with DCM (three times) and the combined organic layers were dried over MgSO₄ and concentrated under reduced pressure. The crude product was purified by flash column chromatography to yield the target species as colourless or yellow oil.

General procedure D: Monoalkylation of primary amines by 3-bromo-propionyl derivatives.

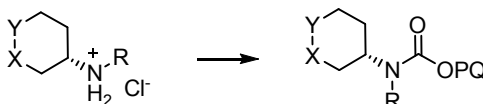


Step 1: To a solution of the primary amine (1.5 equiv.) in MeOH (0.3 M) was added the respective *N*-substituted 3-bromo-propanamide (1.0 eq). In case the starting amine was used as an HCl salt, DIPEA (1.5 equiv.) was added for neutralisation. The clear solution was heated in a sealed tube using a laboratory microwave (120 °C, 25 W, 60 min), was then cooled to r.t. and concentrated under reduced pressure.

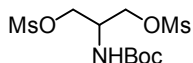
Step 2: The material obtained in step 1 was suspended in DCM (0.1 M) and charged with NEt₃ (3.0 equiv.) and Boc₂O (1.8 equiv., 1 M in DCM) at r.t., and the mixture was stirred at retained temperature for 15 h. The reaction was then concentrated under reduced pressure. Purification by flash column chromatography yielded the *N*-Boc protected alkylation product of the primary amine.

General procedure E: Boc-deprotection of primary amines

Boc-protected amine (1.0 equiv.) was dissolved in DCM (0.1 M), and HCl (4 M in dioxane, 10 equiv.) was added at r.t.. In most cases and within minutes, formation of a precipitate was observed. Full conversion of the starting material was checked by TLC and observed within 4-12 hours. Excessive HCl and DCM were removed under reduced pressure, yielding targeted amines as HCl salts.

General procedure F: Carbamate formation with primary amine hydrochlorides and PQ-chloroformate⁶⁵

An amine hydrochloride was suspended in DCM (50 mM) and solubilised by addition of NEt₃ (3.0 equiv.), regenerating the free amine. Subsequently, a suspension of preformed PQCl₂-OC(O)Cl **S33** in DCM (0.25 M) was slowly charged with the respective secondary amines and the resulting reaction mixture was stirred for 1 h. Once LCMS-control indicated full conversion of the starting material, the reaction mixture was concentrated *in vacuo* yielding pale yellow crude oils. In most cases, flash column chromatography provided the target carbamates in excellent purity and ensured no residual fluorescence of unreacted fluorophore. For the solubilised 2nd-generation probe series, additional purification by preparative HPLC was conducted.

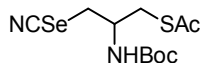
5.3 Linear and five-membered dichalcogenide triggers***N*-Boc-2-aminopropane-1,3-diyl dimethanesulfonate (**S1**)**

Step 1: Serinol (8.00 g, 87.8 mmol, 1.0 equiv.) was dissolved in a mixture of water (80 mL) and dioxane (80 mL) before being subjected to NEt₃ (30.4 mL, 220 mmol, 2.5 equiv.) and Boc₂O (23.0 g, 105 mmol, 1.2 equiv.). Within 5 h, full conversion to the desired product was achieved according to LCMS. The reaction mixture was acidified to pH < 3 using 2 M aqueous HCl. Upon dilution with DCM, the organic layer was separated, and the aqueous layer was further extracted with DCM (three times). The combined organic extracts were washed with brine, dried over MgSO₄, and concentrated under reduced pressure. The Boc-protected diol was received as a pure, colourless solid without further purification (16.6 g, 86.9 mmol, 99%). NMR data of **S1** match spectra provided by Serna et al.⁶⁶

¹H NMR (400 MHz, CDCl₃): δ (ppm) = 5.23 (s, 1H), 3.83 (dd, *J* = 11.0, 4.4 Hz, 2H), 3.77 (dd, *J* = 11.1, 4.4 Hz, 2H), 3.71 – 3.64 (m, 1H), 1.45 (s, 9H). **¹³C NMR** (101 MHz, CDCl₃): δ (ppm) = 156.6, 80.1, 63.4, 53.2, 28.5. **HRMS** (EI+): *m/z* calc. for C₈H₁₇NO₄ [M]⁺ 191.1152, found 191.1153.

Step 2: The diol intermediate (3.00 g, 15.7 mmol, 1.0 equiv.) was dissolved in anhydrous DMF (0.05 M, 300 mL) and charged with NEt₃ (10.9 mL, 78.4 mmol, 5.0 equiv.) and MsCl (2.79 mL, 36.1 mmol, 2.3 equiv.) at 0 °C. After having been stirred for 3 h at retained temperature, acidic workup and column chromatography (SiO₂, h = 6 cm, d = 6 cm, hexanes/EtOAc 1:1, 200 mL dead volume, 20 mL tubes, Fr11-42) gave target species **50** as a colourless solid (3.93 g, 11.3 mmol, 72%). NMR data of **S1** closely match reported data.⁶⁷

TLC R_f = 0.10 (hexanes/EtOAc 1:1) **¹H NMR** (400 MHz, CDCl₃): δ (ppm) = 4.99 (d, *J* = 8.5 Hz, 1H), 4.35 (dd, *J* = 10.2, 4.5 Hz, 2H), 4.29 (dd, *J* = 10.3, 5.4 Hz, 2H), 4.26 – 4.19 (m, 1H), 3.07 (s, 6H), 1.45 (s, 9H). **HRMS** (EI+): *m/z* calc. for C₉H₁₈NO₈S₂ [M-CH₃]⁺ 332.0468, found 332.0445.

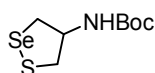
N-Boc-2-amino-3-selenocyanatopropyl ethanethioate (S2)

Step 1: In anhydrous DMF (0.2 M, 100 mL), **S1** (6.90 g, 19.9 mmol, 1.0 equiv.) was charged with 18-crown-6 (6.30 g, 23.8 mmol, 1.2 equiv.) and KSAc (2.27 g, 19.9 mmol, 1.0 equiv.) at room temperature and stirred for 12 h. All volatiles were removed, and the residue was purified by flash column chromatography (SiO₂, h = 10 cm, d = 6 cm, hexanes/EtOAc 2:1, 300 mL dead volume, 100 mL tubes, Fr2-651) giving the mono-S-acetylation product as a colourless solid (4.75 g, 14.5 mmol, 73%).

TLC R_f = 0.15 (hexanes/EtOAc 2:1) **¹H NMR** (400 MHz, CDCl₃): δ (ppm) = 4.89 (s, 1H), 4.32 – 4.22 (m, 2H), 4.02 (s, 1H), 3.12 (dd, J = 6.7, 3.4 Hz, 2H), 3.06 (s, 3H), 2.38 (s, 3H), 1.44 (s, 9H). **HRMS** (EI+): m/z calc. for C₁₁H₂₁NO₆S₂ [M]⁺ 327.0805, found 327.0813.

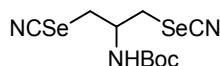
Step 2: Selenocyanation was achieved following general procedure A: the starting material (0.50 g, 1.5 mmol, 1.0 equiv.) was dissolved in THF (0.1 M, 15 mL), subjected to NaI (0.69 g, 4.6 mmol, 3.0 equiv.), 18-crown-6 (330 mg, 0.916 mmol, 0.6 equiv.) and KSeCN (0.48 g, 3.4 mmol, 2.2 equiv.) and heated to 50 °C for 21 h. Aqueous work up followed by column chromatography (SiO₂, h = 8 cm, d = 4 cm, hexanes/EtOAc 3:1, 170 mL dead volume, 20 mL tubes, Fr19-51) provided the product as a pale yellow solid and in excellent purity (0.46 g, 1.4 mmol, 93%).

TLC R_f = 0.30 (hexanes/EtOAc 3:1) **¹H NMR** (400 MHz, CDCl₃): δ (ppm) = 4.93 (s, 1H), 4.03 (dp, J = 8.1, 6.2 Hz, 1H), 3.34 – 3.12 (m, 4H), 2.39 (s, 3H), 1.45 (s, 9H). **¹³C NMR** (101 MHz, CDCl₃) δ (ppm) = 196.0, 155.2, 102.1, 80.7, 51.3, 33.4, 32.5, 30.7, 28.4. **HRMS** (EI+): m/z calc. for C₁₁H₁₆N₂O₃SSe [M-H]⁺ 336.0041, found 336.0044.

N-Boc-1,2-thiaselenolan-4-amine (S3)

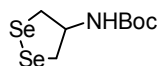
Selenosulfide formation was conducted in analogy to general procedure B: selenocyanide **S2** (900 mg, 2.67 mmol, 1.0 equiv.) was dissolved in THF (0.05 M, 50 mL) and immediately after KOH (0.167 M in MeOH, 19.0 mL, 3.20 mmol, 1.2 equiv.) was added, the reaction mixture turned deeply orange. Aqueous workup gave the title compound alongside traces of its reduced form as an orange oil (616 mg, 2.30 mmol, 86%). *Note:* Isolation of **S3** was unreliable, especially when keeping the compound in solution and at elevated temperatures. Therefore, **S3** should be kept dry, under nitrogen-atmosphere and used for further transformations as quickly as possible.

TLC R_f = 0.62 (hexanes/EtOAc 3:1) **¹H NMR** (400 MHz, CDCl₃): δ (ppm) = 5.16 (s, 2H), 3.55 – 3.31 (m, 2H), 3.16 (d, J = 11.9 Hz, 1H), 3.03 (dt, J = 11.8, 1.5 Hz, 1H), 1.44 (s, 9H). **¹³C NMR** (101 MHz, CDCl₃) δ (ppm) = 155.0, 80.2, 57.5, 45.7, 37.5, 28.5. **HRMS** (EI+): m/z calc. for C₈H₁₅NO₂SSe [M]⁺ 268.9983, found 268.9982.

N-Boc-1,3-diselenocyanatopropan-2-amine (S4)

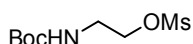
S3 (0.60 g, 1.7 mmol, 1.0 equiv.) with NaI (0.78 g, 5.2 mmol, 3.0 equiv.) was reacted with 18-crown-6 (1.0 g, 3.8 mmol, 2.2 equiv.) and an excess of KSeCN (0.62 g, 4.3 mmol, 2.5 equiv.) according to general procedure A. Aqueous workup and subsequent purification by column chromatography (SiO₂, h = 7 cm, d = 3 cm, hexanes/EtOAc 3:1 → hexanes/EtOAc 1:1, 100 mL dead volume, 20 mL tubes, Fr21-39) gave **S4** as a colourless solid (0.12 g, 0.31 mmol, 56%).

TLC R_f = 0.48 (hexanes/EtOAc 1:1) **¹H NMR** (400 MHz, CDCl₃): δ (ppm) = 5.07 (s, 1H), 4.24 – 4.08 (m, 1H), 3.57 – 3.26 (m, 4H), 1.46 (s, 9H). **¹³C NMR** (101 MHz, CDCl₃) δ (ppm) = 154.9, 101.1 (2C), 81.5, 52.0, 32.4 (2C), 28.4. **HRMS** (EI+): m/z calc. for C₁₀H₁₅N₃O₂Se₂ [M]⁺ 368.9489, found 369.0019.

N-Boc-1,2-diselenolan-4-amine (S5)

According to general procedure A, **S4** (0.33 g, 0.90 mmol, 1.0 equiv.) was reacted with KOH (0.17 M in MeOH, 8.1 mL, 1.4 mmol, 1.5 equiv.) in THF (0.1 M, 8 mL). Within seconds, the colourless reaction mixture turned deeply red and TLC control indicated full conversion of the starting material. Following aqueous work up, the title compound was received as an intensely coloured, red solid (0.27 g, 0.85 mmol, 94%). Data provided by Fang closely match obtained NMR.²¹

TLC R_f = 0.68 (hexanes/EtOAc 3:1) **¹H NMR** (400 MHz, CDCl₃): δ (ppm) = 5.51 (s, 1H), 5.40 – 4.99 (m, 1H), 3.43 – 3.22 (m, 4H), 1.45 (s, 9H). **¹³C NMR** (101 MHz, CDCl₃) δ (ppm) = 155.0, 80.2, 58.4, 38.3, 28.5, 21.2. **HRMS** (EI+): m/z calc. for C₈H₁₅NO₂Se₂ [M]⁺ 316.9428, found 316.9430.

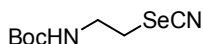
N-Boc-2-aminoethyl methanesulfonate (S6)

Step 1: Ethanolamine (2.4 mL, 40 mmol, 1.0 equiv.) was dissolved in a biphasic 1:1-mixture of dioxane (40 mL) and water (40 mL) and was subsequently charged with NEt₃ (14 mL, 0.10 mol, 2.5 equiv.) and Boc₂O (11 g, 48 mmol, 1.2 equiv.) at 0 °C. The reaction was allowed to warm to room temperature and stirred for 3 h. The reaction mixture was acidified to pH < 3 using 2 M aqueous HCl. Upon dilution with DCM, the organic layer was separated, and the aqueous layer was further extracted with DCM (three times). The combined organic extracts were washed with brine, dried over MgSO₄, and concentrated under reduced pressure giving the *N*-Boc alcohol as a colourless oil (6.4 g, 40 mmol, 100%) in excellent purity and without further purification. NMR data for 1 match previously published reports.⁶⁸

¹H NMR (400 MHz, CDCl₃): δ (ppm) = 4.94 (s, 1H), 3.70 (dd, J = 5.6, 4.5 Hz, 2H), 3.28 (t, J = 5.0 Hz, 2H), 2.14 (s, 1H), 1.44 (s, 9H). **¹³C NMR** (101 MHz, CDCl₃) δ (ppm) = 157.0, 79.9, 62.9, 43.3, 28.5. **HRMS** (EI+): m/z calc. for C₃H₅NO₂ [M-C₄H₁₀O]⁺ 87.0320, found 87.0317.

Step 2: The alcohol intermediate (2.00 g, 12.4 mmol, 1.0 equiv.) was dissolved in DCM (0.05 M, 250 mL) and charged with NEt₃ (4.30 mL, 31.0 mmol, 2.5 equiv.) and MsCl (1.10 mL, 14.3 mmol, 1.15 equiv.) at 0 °C. After stirring at retained temperature for 3 h, the reaction was quenched with sat. aq. NH₄Cl and the organic layer was removed. The aqueous phase was extracted with DCM (two times) and the combined organic layers were dried over MgSO₄, filtered and concentrated. Column chromatography (SiO₂, h = 5 cm, d = 6 cm, hexanes/EtOAc 2:1, 100 mL dead volume 20 mL tubes, Fr10-36) gave the title compound as a colourless solid (2.65 g, 11.1 mmol, 90%). NMR chemical shifts of **S6** match literature data.⁶⁹ **Note S6** will decompose within days if stored on air and at room temperature. It is best used directly for subsequent transformations.

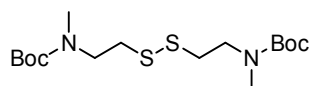
TLC R_f = 0.14 (hexanes/EtOAc 2:1) **¹H NMR** (400 MHz, CDCl₃): δ (ppm) = 4.90 (s, 1H), 4.28 (t, J = 5.1 Hz, 2H), 3.47 (q, J = 5.6, 5.0, 4.6 Hz, 2H), 3.03 (s, 3H), 1.45 (s, 9H) **LRMS** (ESI+): m/z calc. for C₈H₁₇NO₅S [M]⁺ 239.08, found 239.26.

N-Boc-2-selenocyanatoethanamine (S7)

According to general procedure A, **S6** (1.00 g, 4.18 mmol, 1.0 equiv.) was dissolved in THF (0.1 M, 40 mL) and subjected to NaI (1.88 g, 12.5 mmol, 3.0 equiv.), 18-crown-6 (1.22 g, 4.60 mmol, 1.1 equiv.) and KSeCN (1.32 g, 9.19 mmol, 2.2 equiv.). After having reached full conversion within 2 days at 50 °C, aqueous workup and removal of the organic solvent gave an orange crude oil. Purification by flash chromatography (SiO₂, h = 4 cm, d = 6 cm, hexanes/EtOAc 3:1, 100 mL dead volume, 20 mL tubes, Fr11-31) gave the title compound as a pale yellow oil, which crystallized over time (959 mg, 3.84 mmol, 92%).

TLC R_f = 0.10 (hexanes/EtOAc 3:1) **¹H NMR** (400 MHz, CDCl₃): δ (ppm) = 5.01 (s, 1H), 3.57 (q, J = 6.2 Hz, 2H), 3.20 (t, J = 6.4 Hz, 2H), 1.45 (s, 9H). **¹³C NMR** (101 MHz, CDCl₃) δ (ppm) = 155.9, 101.3, 80.4, 41.1, 29.8, 28.5. **HRMS** (ESI+): m/z calc. for C₈H₁₅N₂O₂Se [M+H]⁺ 251.03, found 251.04.

Di-tert-butyl (disulfanediy)bis(ethane-2,1-diy)bis(methylcarbamate) (S8)



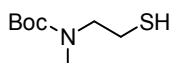
Step 1: A solution of the cystamine dihydrochloride (7.00 g, 31.1 mmol, 1.0 equiv.) in a 1:1-mixture of dioxane (30 mL) and water (30 mL) was cooled to 0 °C and NEt₃ (19.8 mL, 143 mmol, 4.6 equiv.) and Boc₂O (16.3 g, 74.6 mmol, 2.4 equiv.) were added sequentially. After stirring for 3 h, the reaction was acidified to pH = 2-3 using hydrochloric acid (2 M aqueous solution). The aqueous layer was extracted with EtOAc (three times) and the combined organic layers were washed with brine, dried over MgSO₄ and filtered. Concentration of the filtrate gave the title compound as a colourless solid and (10.8 g, 30.8 mmol, 99%) and without further purification. NMR data match spectra by Feng and coworkers.⁷⁰

¹H NMR (400 MHz, CDCl₃): δ (ppm) = 5.02 (s, 2H), 3.44 (q, *J* = 6.3 Hz, 4H), 2.79 (t, *J* = 6.3 Hz, 4H), 1.44 (s, 18H). **¹³C NMR** (101 MHz, CDCl₃): δ (ppm) = 156.0, 45.9, 39.4, 38.6, 28.5. **HRMS** (ESI⁺): *m/z* calc. for C₁₄H₂₉N₂O₄S₂ [M+H]⁺ 353.1563, found 353.1567.

Step 2: In similarity to general procedure C, di-*N*-Boc cystamine (4.0 g, 11 mmol, 1.0 equiv.) in DMF (0.1 M, 110 mL) was reacted with NaH (1.0 g, 25 mmol, 2.2 equiv.) and MeI (1.7 mL, 27 mmol, 2.4 equiv.) at 0 °C. After aqueous work-up and purification by flash column chromatography (SiO₂, h = 5 cm, d = 6 cm, hexanes/EtOAc 6:1, 100 mL dead volume, 20 mL tubes, Fr13-47), the title compound was isolated as a colourless oil (3.9 g, 10 mmol, 90%). NMR data for **S8** match previously published reports.¹²

TLC R_f = 0.18 (hexanes/EtOAc 6:1). **¹H NMR** (400 MHz, CDCl₃): δ (ppm) = 3.50 (s, 4H), 2.89 (s, 6H), 2.81 (s, 4H), 1.46 (s, 18H). **¹³C NMR** (101 MHz, CDCl₃): δ (ppm) = 155.7, 79.9, 48.7, 36.5, 28.6. **HRMS** (EI⁺): *m/z* calc. for C₁₆H₃₂N₂O₄S₂ [M]⁺ 380.1798, found 380.1779.

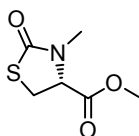
***N*-Boc-*N*-methylcysteamine (**S9**)⁶⁹**



S8 (1.0 g, 2.6 mmol, 1.0 equiv.) was dissolved in DCM (0.1 M, 20 mL) and DIPEA (0.55 mL, 3.2 mmol, 1.2 equiv.) and *D,L*-dithiothreitol (0.49 g, 3.2 mmol, 1.2 equiv.) were added. The reaction mixture was stirred at room temperature for 4 h before being washed with HCl (aq., 1 M), NaHCO₃ (sat. aq.) and water. The organic layer was dried over MgSO₄, filtered and concentrated *in vacuo* providing a colourless crude product. Flash chromatography (SiO₂, h = 20 cm, d = 4 cm, hexanes/EtOAc 9:1, 150 mL dead volume, 20 mL tubes, Fr18-32) enabled isolation of pure thiol **S9** as a colourless oil (0.75 g, 4.0 mmol, 77%). NMR data for **S9** match data from Chalker and coworkers.⁶⁹

TLC R_f = 0.32 (hexanes/EtOAc 9:1) **¹H NMR** (400 MHz, CDCl₃): δ (ppm) = 3.42 – 3.32 (m, 2H), 2.88 (s, 3H), 2.65 (q, *J* = 7.7 Hz, 2H), 1.30 (t, *J* = 6.8 Hz, 1H). **¹³C NMR** (101 MHz, CDCl₃): δ (ppm) = 155.8, 79.8, 52.4, 35.2, 28.6, 22.9. **HRMS** (EI⁺): *m/z* calc. for C₈H₁₆NO₂S [M-H]⁺ 190.0896, found 190.0910.

***Methyl*-(3-*methyl*-2-oxothiazolidine)-4-carboxylate (**S10**)**



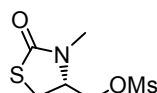
Step 1: *L*-Cysteine (2.0 g, 17 mmol, 1.0 equiv.) was added to a solution of NaOH (2.6 g, 66 mmol) in water (20 mL). A solution of phenyl chloroformate (4.2 mL, 33 mmol, 2.0 equiv.) in toluene (14 mL) was added dropwise to this mixture at room temperature. To prevent the reaction temperature exceeding 30 °C, the reaction vessel was placed in a water bath. After having stirred the reaction mixture at 25 °C for 2 h, the aqueous layer was separated and washed with toluene (three times) to afford the sodium salt of 2-oxothiazolidine-4-carboxylic acid in aqueous solution. Adjusting the pH to 1 allowed extraction of the carboxylic acid with EtOAc (4 times). Drying of the organic extracts over MgSO₄, filtration and removal of the solvent gave a colourless crude which was further washed with toluene and hexanes to remove residual apolar impurities. As a result, the carboxylic acid intermediate was obtained as a pure, colourless powder (1.7 g, 12 mmol, 71%). The NMR matches data from Seki et al.⁷¹

TLC R_f = 0.12 (EtOAc) **¹H NMR** (400 MHz, DMSO-*d*₆): δ (ppm) = 13.21 (s, 1H), 8.44 (s, 1H), 4.39 (ddd, *J* = 8.6, 3.5, 1.4 Hz, 1H), 3.72 (dd, *J* = 11.4, 8.6 Hz, 1H), 3.45 (dd, *J* = 11.4, 3.4 Hz, 1H). **¹³C NMR** (101 MHz, DMSO-*d*₆): δ (ppm) = 173.1, 172.5, 55.4, 31.8. **HRMS** (ESI⁻): *m/z* calc. for C₄H₄NO₃S [M-H]⁻ 145.9917, found 145.9915.

Step 2: Oxothiazolidine-intermediate (2.7 g, 18 mmol, 1.0 equiv.) was dissolved in water (0.2 M, 100 mL) and sodium hydroxide (2.2 g, 54 mmol, 3.0 equiv.) was added in small batches. The resulting solution was cooled to 0 °C and dimethyl sulfate (5.1 mL, 54 mmol, 3.0 equiv.) was slowly added in a dropwise manner. The reaction mixture was allowed to warm to room temperature and was stirred for 12 h. The aqueous phase was extracted with EtOAc (three times) and the combined organic layers were dried over MgSO₄, filtered and the solvent was removed in vacuo to yield *N*-methylated oxothiazolidine as a mixture of its free carboxylic acid and the corresponding methyl ester. The crude product was then subjected to thionyl chloride (1.3 mL, 18 mmol, 1.0 equiv.) in methanolic solution (50 mL) yielding a pale yellow crude solid, which, after removal of the solvent was purified by column chromatography (SiO₂, h = 4 cm, d = 6 cm, hexanes/EtOAc 2:1, 20 mL tubes, Fr16-35) to give **S10** as a colourless solid (2.0 g, 12 mmol, 67%).

TLC R_f = 0.18 (hexanes/EtOAc 2:1) **¹H NMR** (400 MHz, CDCl₃): δ (ppm) = 4.30 (dd, *J* = 8.6, 3.1 Hz, 1H), 3.83 (s, 3H), 3.62 (dd, *J* = 11.4, 8.6 Hz, 1H), 3.37 (dd, *J* = 11.4, 3.1 Hz, 1H), 2.95 (s, 3H). **¹³C NMR** (101 MHz, CDCl₃) δ (ppm) = 171.7, 170.50, 62.5, 53.1, 31.7, 29.1. **HRMS** (ESI⁺): *m/z* calc. for C₆H₁₀NO₃S [M+H]⁺ 176.0376, found 176.0378.

(3-Methyl-2-oxothiazolidin-4-yl)methyl methanesulfonate (**S11**)



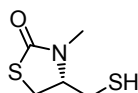
Step 1: To a stirred solution of **S10** (0.20 g, 1.1 mmol, 1.0 equiv.) in MeOH (1 M, 1 mL) at 0 °C was added NaBH₄ (48 mg, 1.3 mmol, 1.1 equiv.) in portions, and the solution was stirred at retained temperature for 30 min and 2.5 h at r.t.. Once TLC control indicated full conversion of the starting material, the reaction was quenched with water and diluted with EtOAc. The aqueous phase was extracted with EtOAc (three times) and the combined organic layers were washed with brine and dried over Na₂SO₄. Filtration and removal of the solvent gave a colourless oil as crude product which was purified by column chromatography (SiO₂, h = 2.5 cm, d = 6 cm, hexanes/EtOAc 1:3, 20 mL tubes, Fr12-45). As a result, the alcohol intermediate was obtained as a colourless oil (0.14 g, 0.97 mmol, 85%).

TLC R_f = 0.15 (hexanes/EtOAc 1:3) **¹H NMR** (400 MHz, CDCl₃): δ (ppm) = 3.87 (dd, *J* = 10.6, 5.2 Hz, 1H), 3.83 – 3.75 (m, 2H), 3.40 (dd, *J* = 11.0, 8.0 Hz, 1H), 3.26 (dd, *J* = 11.0, 4.9 Hz, 1H), 2.93 (s, 3H), 2.17 (s, 1H). **¹³C NMR** (101 MHz, CDCl₃) δ (ppm) = 172.6, 62.2, 61.5, 31.0, 27.9. **HRMS** (ESI⁺): *m/z* calc. for C₅H₁₀NO₂S [M+H]⁺ 148.0427, found 148.0428.

Step 2: 4-(hydroxymethyl)thiazolidin-2-one (0.13 g, 0.88 mmol, 1.0 equiv.) was dissolved in dry DCM (0.05 M, 20 mL) and subjected to NEt₃ (0.61 mL, 4.4 mmol, 5.0 equiv.) and MsCl (82 μL, 1.1 mmol, 1.2 equiv.) at 0 °C. After stirring at retained temperature for 3 h, the reaction was quenched with sat. aq. NH₄Cl and the organic layer was removed. The aqueous phase was extracted with DCM (two times) and the combined organic layers were dried over MgSO₄, filtered and concentrated. The crude oil was purified by flash chromatography (SiO₂, h = 4 cm, d = 6 cm, hexanes/EtOAc 1:2, 50 mL dead volume 20 mL tubes, Fr11-32) to yield the title compound as a colourless oil, which crystallized over time (0.17 g, 0.76 mmol, 86%).

TLC R_f = 0.15 (hexanes/EtOAc 1:2) **¹H NMR** (400 MHz, CDCl₃): δ (ppm) = 4.38 (dd, *J* = 10.7, 6.2 Hz, 1H), 4.32 (dd, *J* = 10.7, 4.3 Hz, 1H), 4.03 (dddd, *J* = 8.0, 6.2, 4.3, 3.6 Hz, 1H), 3.53 (dd, *J* = 11.5, 8.1 Hz, 1H), 3.17 (dd, *J* = 11.5, 3.6 Hz, 1H), 3.09 (s, 3H), 2.97 (s, 3H). **¹³C NMR** (101 MHz, CDCl₃) δ (ppm) = 171.4, 66.0, 59.5, 38.0, 31.1, 28.0. **HRMS** (ESI⁺): *m/z* calc. for C₆H₁₂NO₄S₂ [M+H]⁺ 226.0202, found 226.0205.

4-(Mercaptomethyl)-3-methylthiazolidin-2-one (**S12**)



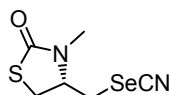
Step 1: Mesylate **S11** (3.0 g, 13 mmol, 1.0 equiv.) was dissolved in anhydrous DMF (0.1 M, 100 mL), 18-crown-6 (3.9 g, 15 mmol, 1.1 equiv.) and potassium thioacetate (1.7 g, 15 mmol, 1.1 equiv.) were sequentially added and the reaction was stirred at room temperature for 24 h. Column chromatography (SiO₂, h = 10 cm, d = 6 cm, hexanes/EtOAc 2:1 → hexanes/EtOAc 1:1, 150 mL dead volume 20 mL tubes, Fr30-49) gave *S*-((2-oxothiazolidin-4-yl)methyl) ethanethioate as a colourless solid (2.5 g, 12 mmol, 92%).

TLC R_f = 0.50 (hexanes/EtOAc 1:1) **¹H NMR** (400 MHz, CDCl₃): δ (ppm) = 3.81 – 3.75 (m, 1H), 3.45 (ddd, *J* = 11.4, 7.8, 0.9 Hz, 1H), 3.32 (ddd, *J* = 13.9, 3.1, 0.9 Hz, 1H), 3.02 – 2.97 (m, 2H), 2.95 (s, 3H), 2.39 (s, 3H). **¹³C NMR** (101 MHz, CDCl₃) δ (ppm) = 194.8, 171.3, 60.6, 30.8, 30.6, 30.2, 29.8. **HRMS** (EI⁺): *m/z* calc. for C₇H₁₁NO₂S₂ [M]⁺ 205.0226, found 205.0226.

Step 2: The thioacetate-intermediate (2.0 g, 9.5 mmol, 1.0 equiv.) was dissolved in MeOH (0.1 M, 100 mL) and KOH (1.3 g, 19 mmol, 2.0 equiv.) was added in one batch. After stirring at room temperature for 10 min, TLC control indicated full conversion of the starting material. The reaction was quenched with HCl (aqueous, 2 M), MeOH was removed *in vacuo*, and the aq. layer was extracted with DCM (three times). After drying the combined organic layers over MgSO₄, filtration and concentration, the crude product was purified by column chromatography (SiO₂, h = 6 cm, d = 5 cm, hexanes/EtOAc 1:1, 20 mL tubes, Fr12-22) to yield **S12** as a colourless oil (1.5 g, 9.3 mmol, 98%).

TLC R_f = 0.41 (hexanes/EtOAc 1:1) **¹H NMR** (400 MHz, CDCl₃): δ (ppm) = 3.78 (ddt, *J* = 7.8, 6.5, 4.8 Hz, 1H), 3.45 (dd, *J* = 11.3, 7.8 Hz, 1H), 3.27 (dd, *J* = 11.3, 4.6 Hz, 1H), 2.88 (s, 3H), 2.84 – 2.78 (m, 2H), 1.39 (t, *J* = 8.5 Hz, 1H). **¹³C NMR** (101 MHz, CDCl₃) δ (ppm) = 171.7, 62.7, 30.5, 29.2, 25.6. **HRMS** (EI+): *m/z* calc. for C₅H₉NOS₂ [M]⁺ 163.0120, found 163.0113.

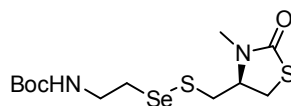
3-Methyl-4-(selenocyanatomethyl)thiazolidin-2-one (S13)



Selenocyanation was achieved according to general procedure A. Mesylate **S11** (500 mg, 2.22 mmol, 1.0 equiv.) was dissolved in THF (0.3 M, 10 mL) and 18-crown-6 (80.0 mg, 0.222 mmol, 0.1 equiv.), as well as KSeCN (352 mg, 2.44 mmol, 1.1 equiv.) were added sequentially. The resulting, colourless suspension was refluxed for 3 days after which LCMS analysis indicated clean conversion of the starting material. After aqueous workup, the orange crude oil was purified by column chromatography (SiO₂, h = 4.5 cm, d = 6 cm, hexanes/EtOAc 2:1 → hexanes/EtOAc 1:2, 80 mL dead volume 20 mL tubes, Fr18-32) to yield **S13** as a colourless solid (415 mg, 1.76 mmol, 79%).

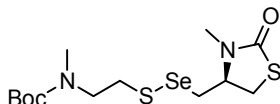
TLC R_f = 0.45 (hexanes/EtOAc 1:2) **¹H NMR** (400 MHz, CDCl₃): δ (ppm) = 4.07 (ddt, *J* = 8.7, 7.7, 3.0 Hz, 1H), 3.65 (ddd, *J* = 11.7, 7.7, 1.0 Hz, 1H), 3.40 (ddd, *J* = 12.6, 2.9, 0.9 Hz, 1H), 3.26 – 3.19 (m, 2H), 2.96 (s, 3H). **¹³C NMR** (101 MHz, CDCl₃) δ (ppm) = 171.0, 100.2, 60.8, 30.8, 30.4, 29.2. **HRMS** (EI+): *m/z* calc. for C₆H₈N₂OSSe [M]⁺ 235.9517, found 235.9519.

4-((N-Boc-2-aminoethylselanyl)thiomethyl)-3-methylthiazolidin-2-one (S14)



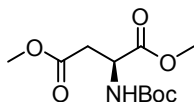
Based on general procedure B, selenocyanide **S7** (0.60 g, 2.4 mmol, 1.0 equiv.) was dissolved in MeOH (0.1 M, 25 mL) and was slowly charged with thiol **S12** (0.39 g, 2.4 mmol, 1.0 equiv.) at room temperature. After stirring vigorously for 30 min, LCMS control indicated full conversion of both starting materials and the formation of the desired product. The reaction was concentrated and the crude solids were purified by flash chromatography (SiO₂, h = 15 cm, d = 4 cm, hexanes/EtOAc 3:1 → hexanes/EtOAc 2:1, 500 mL dead volume, 20 mL tubes, Fr11-42), ultimately yielding selenenyl sulfide **S14** as a pale yellow oil (0.94 g, 2.4 mmol, 100%).

TLC R_f = 0.35 (hexanes/EtOAc 1:1) **¹H NMR** (400 MHz, CDCl₃): δ (ppm) = 4.88 (s, 1H), 3.90 (tdd, *J* = 7.7, 4.7, 3.2 Hz, 1H), 3.51 (ddd, *J* = 11.3, 7.9, 4.6 Hz, 3H), 3.26 (dd, *J* = 11.3, 3.3 Hz, 1H), 3.10 – 2.96 (m, 4H), 2.91 (s, 3H), 1.44 (s, 9H). **¹³C NMR** (101 MHz, CDCl₃) δ (ppm) = 171.4, 155.8, 79.9, 61.6, 40.2, 38.1, 31.7, 30.6, 29.9, 28.5. **HRMS** (ESI+): *m/z* calc. for C₁₂H₂₃N₂O₃S₂Se [M]⁺ 387.0310, found 387.0319.

4-((N-Boc-N-methyl-cysteaminy)selamethyl)-3-methylthiazolidin-2-one (S15)

To a vigorously stirred solution of selenocyanide **S13** (62 mg, 0.26 mmol, 1.0 equiv.) in MeOH (0.1 M, 2.5 mL), thiol **S9** (50 mg, 0.26 mmol, 1.0 equiv.) was added. Within 1 min, TLC control indicated full conversion of both reactants. Removal of the solvent and purification by column chromatography (SiO₂, h = 20 cm, d = 2 cm, hexanes/EtOAc 3:1 → hexanes/EtOAc 2:1, 75 mL dead volume, 20 mL tubes, Fr29-42) gave **S15** as a colourless oil (0.10 g, 0.25 mmol, 96%). *Note:* **S15** proved to be unstable when being stored at room temperature and on air. Therefore, storage under inert gas and in a freezer is recommended.

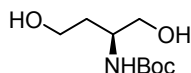
TLC R_f = 0.19 (hexanes/EtOAc 3:1) **¹H NMR** (400 MHz, CDCl₃): δ (ppm) = 3.98 (ddt, *J* = 9.3, 7.6, 3.4 Hz, 1H), 3.53 (dd, *J* = 11.3, 7.6 Hz, 2H), 3.47 (s, 2H), 3.24 (dd, *J* = 11.4, 3.6 Hz, 1H), 3.22 – 3.10 (m, 1H), 3.05 (dd, *J* = 12.8, 9.4 Hz, 1H), 2.97 – 2.91 (m, 2H), 2.90 (s, 3H), 2.88 (s, 3H), 1.45 (s, 9H). **¹³C NMR** (101 MHz, CDCl₃) δ (ppm) = 171.4, 155.8, 80.0, 61.2, 49.4, 35.8, 35.1, 31.8, 30.7, 30.5, 28.6. **HRMS** (ESI⁺): *m/z* calc. for C₁₃H₂₅N₂O₃SSe₂ [M]⁺ 401.0466, found 401.0467.

5.4 Cyclic, six-membered dichalcogenide-amines**N-Boc-dimethylaspartate (S16)**

Step 1: A suspension of aspartic acid (10.0 g, 75.1 mmol, 1.0 equiv.) in MeOH (0.3 M, 200 mL) was cooled to 0 °C and carefully charged with SOCl₂ (21.8 mL, 301 mmol, 4.0 equiv.). After 3 h, all volatiles were removed yielding dimethylaspartate hydrochloride as a colourless solid.

Step 2: Without further purification, the dimethyl ester obtained in step 1 was dissolved in a 1:1-mixture of water (75 mL) and dioxane (75 mL), cooled to 0 °C and was charged with NEt₃ (26.0 mL, 188 mmol, 2.5 equiv.) and Boc₂O (19.7 g, 90.1 mmol, 1.2 equiv.). The reaction was stirred for 14 h, then acidified to pH = 2-3 using hydrochloric acid (2 M aqueous solution). The aqueous layer was extracted with EtOAc (three times) and the combined organic layers were washed with brine, dried over MgSO₄, filtered and concentrated. The crude solids were purified via flash column chromatography (SiO₂, h = 3 cm, d = 6 cm, hexanes/EtOAc 3:1, 50 mL tubes, Fr8-20) giving target species **S16** as a colourless solid (18.7 g, 71.6 mmol, 95%). NMR data of **S16** match spectra reported by Raines.⁷²

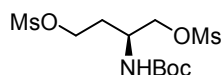
TLC R_f = 0.39 (hexanes/EtOAc 3:1). **¹H NMR** (400 MHz, CDCl₃): δ (ppm) = 5.48 (d, *J* = 8.7 Hz, 1H), 4.57 (dt, *J* = 9.2, 4.7 Hz, 1H), 3.75 (s, 3H), 3.69 (s, 3H), 2.99 (dd, *J* = 16.9, 4.7 Hz, 1H), 2.81 (dd, *J* = 16.9, 4.7 Hz, 1H), 1.44 (s, 9H). **¹³C NMR** (101 MHz, CDCl₃): δ (ppm) = 171.7, 171.5, 155.5, 80.3, 52.8, 52.1, 50.0, 36.8, 28.4. **HRMS** (EI⁺): *m/z* calc. for C₁₁H₁₉NO₆ [M]⁺ 261.1207, found 261.1206.

N-Boc-2-aminobutane-1,4-diol (S17)

Diester **S16** (7.00 g, 26.8 mmol, 1.0 equiv.) in anhydrous THF (0.2 M, 135 mL) was carefully added to a suspension of LAH (3.05 g, 80.4 mmol, 3.0 equiv.) in dry THF (0.2 M, 135 mL) at 0 °C. After 3 h, Fieser-type work-up gave crude **S17** as a colourless crude oil. Flash column chromatography (SiO₂, h = 12 cm, d = 6 cm, hexanes/EtOAc 1:1 → EtOAc, 150 mL dead volume, 20 mL tubes, Fr68-105) ultimately provided the target diol as a colourless solid (4.00 g, 19.5 mmol, 73%). NMR spectra of **S17** match reported data.⁷²

TLC R_f = 0.30 (EtOAc). **¹H NMR** (400 MHz, CDCl₃): δ (ppm) = 4.99 (s, 1H), 3.91 – 3.82 (m, 1H), 3.78 – 3.62 (m, 4H), 2.24 (s, 2H), 1.81 (ddt, *J* = 14.1, 9.3, 4.6 Hz, 1H), 1.63 (tt, *J* = 10.1, 4.2 Hz, 1H), 1.45 (s, 9H). **¹³C NMR** (101 MHz, CDCl₃): δ (ppm) = 157.2, 80.2, 65.6, 58.9, 49.5, 35.0, 28.5. **HRMS** (EI⁺): *m/z* calc. for C₈H₁₆NO₃ [M-CH₃O]⁺ 174.1125, found 174.1122.

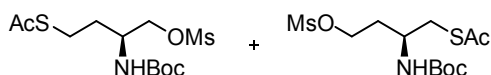
N-Boc-2-aminobutane-1,4-diyl dimethanesulfonate (1)



A solution of diol **S17** (0.18 g, 0.87 mmol, 1.0 equiv.) in anhydrous DCM (0.05 M, 20 mL) was charged with NEt_3 (0.61 mL, 4.3 mmol, 5.0 equiv.) and MsCl (0.15 mL, 2.0 mmol, 2.3 equiv.) at 0 °C. The reaction was allowed to warm to r.t. and further stirred for 2 h. Once TLC indicated full conversion of the starting material, the reaction was quenched with NH_4Cl (sat. aq.) and the aqueous phase was extracted with DCM (three times). The combined organic layers were dried over MgSO_4 , filtered and concentrated. Purification by flash column chromatography (SiO_2 , h = 6 cm, d = 4 cm, hexanes/EtOAc 1:1 → hexanes/EtOAc 1:2, 50 mL dead volume, 20 mL tubes, Fr12-26) gave the desired product as a colourless solid (0.30 g, 0.82 mmol, 94%). NMR spectra published by Raines and coworkers closely resemble received data for **1**.⁷²

TLC R_f = 0.37 (hexanes/EtOAc 1:2) **¹H NMR** (400 MHz, CDCl_3): δ (ppm) = 4.78 (d, J = 8.7 Hz, 1H), 4.39 – 4.23 (m, 4H), 4.10 – 4.02 (m, 1H), 3.05 (s, 3H), 3.04 (s, 3H), 2.11 – 2.04 (m, 1H), 2.02 – 1.93 (m, 1H), 1.45 (s, 9H). **¹³C NMR** (101 MHz, CDCl_3): δ (ppm) = 155.3, 80.5, 71.0, 66.3, 46.9, 37.5 (2C), 31.0, 28.4 (3C). **HRMS** (EI+): m/z calc. for $\text{C}_{11}\text{H}_{23}\text{NO}_8\text{S}_2$ [M]⁺ 361.0860, found 361.0861.

***N*-Boc-(3-amino-4-(methanesulfonyl)oxybutyl)ethanethioate (2) & *N*-Boc-(2-amino-4-(methanesulfonyl)oxybutyl)ethanethioate (3)**

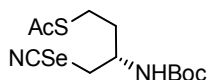


18-crown-6 (0.12 g, 0.33 mmol, 1.2 equiv.) and KSac (32 mg, 0.277 mmol, 1.0 equiv.) were sequentially added to a solution of **1** (0.10 g, 0.28 mmol, 1.0 equiv.) in dry DMF (0.05 M, 27 mL) at r.t.. After 15 h, the solvent was removed and the obtained crude was purified by flash column chromatography (SiO_2 , h = 6 cm, d = 4 cm, hexanes/EtOAc 1:1, 75 mL dead volume, 20 mL tubes, Fr4-9) yielding **2** as a colourless solid (55 mg, 0.16 mmol, 57%) along with its regioisomeric form **3** (21 mg, 87 μmol , 31%). NMR data of **2** closely match data by Iwaoka and coworkers.⁷³

(2): **TLC** R_f = 0.47 (hexanes/EtOAc 1:1) **¹H NMR** (400 MHz, CDCl_3): δ (ppm) = 4.75 (s, 1H), 4.31 – 4.20 (m, 2H), 3.91 (br s, 1H), 3.04 (s, 3H), 3.03 – 2.95 (m, 1H), 2.89 – 2.81 (m, 1H), 2.34 (s, 3H), 1.85 (dt, J = 13.7, 6.9 Hz, 2H), 1.45 (s, 9H). **¹³C NMR** (101 MHz, CDCl_3): δ (ppm) = 195.8, 155.4, 71.0, 49.1, 37.5, 31.6, 30.8, 28.5, 25.6. **HRMS** (EI+): m/z calc. for $\text{C}_{12}\text{H}_{23}\text{NO}_6\text{S}_2$ [M]⁺ 341.0961, found 341.0957.

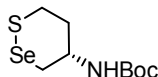
(3): **TLC** R_f = 0.44 (hexanes/EtOAc 1:1) **¹H NMR** (400 MHz, CDCl_3): δ (ppm) = 4.59 (d, J = 8.9 Hz, 1H), 4.33 – 4.25 (m, 2H), 3.90 (s, 1H), 3.08 (dd, J = 6.2, 2.9 Hz, 2H), 3.04 (s, 3H), 2.37 (s, 3H), 2.07 – 1.99 (m, 1H), 1.90 – 1.80 (m, 1H), 1.43 (s, 9H). **¹³C NMR** (101 MHz, CDCl_3): δ (ppm) = 195.7, 155.6, 66.9, 47.9, 37.5, 33.8, 30.7, 28.5. **HRMS** (EI+): m/z calc. for $\text{C}_{12}\text{H}_{23}\text{NO}_6\text{S}_2$ [M]⁺ 341.0961, found 341.0930.

***N*-Boc-(2-amino-4-selenocyanatobutyl)ethanethioate (4)**



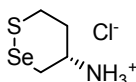
Selenocyanation was conducted based on general procedure A. Mesylate **2** (0.60 g, 1.8 mmol, 1.0 equiv.) was dissolved in THF (0.1 M, 20 mL), and subjected to NaI (0.79 mg, 5.3 mmol, 3.0 equiv.), 18-crown-6 (5.1 g, 1.9 mmol, 1.1 equiv.) and KSeCN (557 mg, 3.87 mmol, 2.2 equiv.). Purification via flash column chromatography (SiO_2 , h = 7 cm, d = 4 cm, hexanes/EtOAc 4:1 → hexanes/EtOAc 3:1, 150 mL dead volume, 20 mL tubes, Fr21-42) after aqueous work-up provided **4** as a pale yellow solid (552 mg, 1.57 mmol, 89%). *Note*: **4** proved to be rather unstable being stored at ambient temperature and on air and turned purple within a few weeks.

TLC R_f = 0.20 (hexanes/EtOAc 3:1) **¹H NMR** (400 MHz, CDCl_3): δ (ppm) = 4.82 (s, 1H), 3.88 (h, J = 7.8, 7.3, 6.3, 6.3, 5.1 Hz, 1H), 3.44 – 3.31 (m, 1H), 3.31 – 3.22 (m, 1H), 3.04 – 2.97 (m, 1H), 2.85 (dt, J = 13.9, 7.7 Hz, 1H), 2.35 (s, 3H), 1.88 (q, J = 7.3 Hz, 2H), 1.46 (s, 9H). **¹³C NMR** (101 MHz, CDCl_3): δ (ppm) = 196.0, 155.5, 80.6, 50.3, 41.0, 35.1, 34.2, 30.8, 28.5, 25.7. **HRMS** (EI+): m/z calc. for $\text{C}_{12}\text{H}_{20}\text{N}_2\text{O}_3\text{SSe}$ [M]⁺ 352.0354, found 352.0365.

N-Boc-1,2-thiaselenan-4-amine (5)

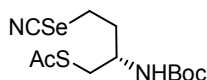
Thiaselenane-formation was achieved according to general procedure B. **4** (0.70 g, 2.0 mmol, 1.0 equiv.) was dissolved in THF (0.05 M, 40 mL) and KOH was added (0.17 M in MeOH, 16 mL, 2.7 mmol, 1.4 equiv.). Within seconds, the colourless reaction mixture turned yellow and TLC control indicated full conversion of the starting material. Aqueous work-up gave pure **5** as a pale yellow solid (0.55 mg, 2.0 mmol, 100%). NMR data of **5** match data by Iwaoka and coworkers.⁷³

TLC R_f = 0.61 (hexanes/EtOAc 3:1) **¹H NMR** (400 MHz, CDCl₃): δ (ppm) = 4.93 (s, 1H), 3.94 (s, 1H), 3.23 (ddd, J = 14.3, 7.8, 2.8 Hz, 2H), 3.00 (d, J = 13.2 Hz, 1H), 2.87 – 2.78 (m, 1H), 2.16 (d, J = 13.1 Hz, 1H), 1.77 (s, 1H), 1.45 (s, 9H). **¹³C NMR** (101 MHz, CDCl₃): δ (ppm) = 154.7, 80.0, 47.4, 35.1, 32.2, 30.1, 28.5. **HRMS** (EI⁺): m/z calc. for C₉H₁₇NO₂SSe [M]⁺ 283.0140, found 283.0136.

1,2-thiaselenan-4-aminium chloride (6)

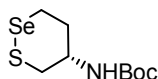
Deprotection of thiaselenane **5** was conducted according to general procedure E. Starting material (0.89 g, 3.1 mmol, 1.0 equiv.) in DCM (30 mL, 0.1 M) was charged with HCl (7.9 mL, 4 M in dioxane, 10 equiv.) and stirred overnight. The organic phase was discarded, and the precipitates were washed twice with Et₂O giving the title compound as a yellow solid (0.66 g, 3.0 mmol, 97%).

¹H NMR (400 MHz, D₂O): δ (ppm) = 3.64 (tt, J = 10.8, 3.3 Hz, 1H), 3.26 (ddd, J = 14.4, 5.8, 3.0 Hz, 1H), 3.17 – 3.04 (m, 3H), 2.31 (ddt, J = 13.8, 5.5, 2.7 Hz, 1H), 1.80 (dtd, J = 13.9, 10.9, 3.0 Hz, 1H). **HRMS** (ESI⁺): m/z calc. for C₄H₁₀NSSe [M+H]⁺ 183.9694, found 183.9695.

N-Boc-(2-amino-5-selenocyanatobutyl)ethanethioate (7)

Following selenocyanation protocol A, mesylate **3** (0.44 g, 1.3 mmol, 1.0 equiv.) was dissolved in THF (0.1 M, 13 mL) and subjected to NaI (0.58 g, 3.9 mmol, 3.0 equiv.), 18-crown-6 (0.38 g, 1.4 mmol, 1.1 equiv.) and KSeCN (0.41 g, 2.8 mmol, 2.2 equiv.) in a consecutive manner. Subsequent aqueous work-up gave an orange crude product which was purified by column (SiO₂, h = 10 cm, d = 5 cm, hexanes/EtOAc 3:1, 150 mL dead volume, 20 mL tubes, Fr21-38). **7** was received as a pale yellow solid (0.43 g, 1.2 mmol, 92%).

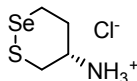
TLC R_f = 0.55 (hexanes/EtOAc 1:1) **¹H NMR** (400 MHz, CDCl₃): δ (ppm) = 4.60 (d, J = 9.0 Hz, 1H), 3.91 (s, 1H), 3.19 (ddd, J = 12.6, 7.8, 5.1 Hz, 1H), 3.07 (d, J = 6.2 Hz, 2H), 2.99 (dt, J = 12.3, 7.9 Hz, 1H), 2.38 (s, 3H), 2.18 – 2.07 (m, 1H), 2.06 – 1.97 (m, 1H), 1.43 (s, 9H). **¹³C NMR** (101 MHz, CDCl₃): δ (ppm) = 195.8, 156.0, 80.3, 50.5, 41.0, 36.4, 33.6, 30.7, 28.5, 26.6. **HRMS** (EI⁺): m/z calc. for C₁₂H₂₀N₂O₃SSe [M]⁺ 352.0354, found 352.0352.

N-Boc-1,2-thiaselenan-5-amine (8)

According to general procedure B, **7** (0.40 g, 1.1 mmol, 1.0 equiv.) was dissolved in THF (0.05 M, 20 mL) and potassium hydroxide (0.17 M in MeOH, 10 mL, 1.7 mmol, 1.5 equiv.) was slowly added. The reaction mixture immediately changed from colourless to yellow and, within 5 min, full conversion of the starting material was indicated by TLC. Aqueous work-up and concentration of the combined organic extracts gave the desired product as a pale yellow solid (0.32 g, 1.1 mmol, 100%). NMR spectra match previously reported data by Iwaoka.⁷⁴

TLC R_f = 0.64 (hexanes/EtOAc 3:1) **$^1\text{H NMR}$** (400 MHz, CDCl_3): δ (ppm) = 5.02 (s, 1H), 3.96 – 3.83 (m, 1H), 3.30 – 3.13 (m, 2H), 2.97 (s, 1H), 2.80 (dd, J = 13.5, 7.7 Hz, 1H), 2.25 (t, J = 11.8 Hz, 1H), 2.04 (s, 1H), 1.45 (s, 9H). **$^{13}\text{C NMR}$** (101 MHz, CDCl_3): δ (ppm) = 154.8, 79.9, 47.2, 37.7, 28.5, 23.1. **HRMS** (EI+): m/z calc. for $\text{C}_9\text{H}_{17}\text{NO}_2\text{SSe}$ $[\text{M}]^+$ 283.0140, found 283.0133.

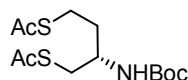
1,2-thiaselenan-5-aminium chloride (9)



Thiaselenane **8** was deprotected according to general procedure E. **8** (1.5 g, 5.2 mmol, 1.0 equiv.) in DCM (50 mL, 0.1 M) was charged with HCl (13 mL, 4 M in dioxane, 10 equiv.) and stirred overnight. The organic phase was discarded, and the precipitates were washed twice with Et_2O giving the title compound as a yellow solid (1.1 g, 5.2 mmol, 100%).

$^1\text{H NMR}$ (400 MHz, D_2O): δ (ppm) = 3.57 – 3.46 (m, 1H), 3.17 (dd, J = 14.6, 7.5 Hz, 3H), 2.98 (dd, J = 13.8, 9.6 Hz, 1H), 2.42 (dq, J = 13.5, 4.3 Hz, 1H), 2.05 (td, J = 14.3, 6.5 Hz, 1H). **HRMS** (ESI+): m/z calc. for $\text{C}_4\text{H}_{10}\text{NSSe}$ $[\text{M}+\text{H}]^+$ 183.9694, found 183.9695.

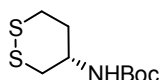
N-Boc-(2-aminobutane-1,4-diyl)diethanethioate (S18)



1 (2.1 g, 5.9 mmol, 1.0 eq.) was dissolved in acetone (60 mL, 1 M) and charged with KSAc (2.1 g, 18 mmol, 3.0 eq.). The resulting mixture was heated to reflux for 4 h. All volatiles were evaporated under reduced pressure. DCM and NaHCO_3 (sat. aq.) were added to the residue, the layers were separated and the aqueous layer was extracted twice with additional DCM. The combined organic layers were washed with brine, dried over MgSO_4 , filtered and the solvent was removed under reduced pressure. The obtained, red crude oil was purified by flash column chromatography (hexanes/EtOAc 1:1→1:2), yielding the title compound as a colourless solid (2.3 g, 5.3 mmol, 90%).

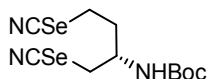
TLC R_f = 0.13 (hexanes/EtOAc, 1:1). **$^1\text{H NMR}$** (400 MHz, CDCl_3): δ (ppm) = 4.58 (d, J = 9.0 Hz, 1H), 3.89 – 3.74 (m, 1H), 3.08 (td, J = 16.5, 15.2, 6.0 Hz, 2H), 2.98 (ddd, J = 14.0, 8.6, 5.5 Hz, 1H), 2.82 (ddd, J = 13.7, 8.6, 7.0 Hz, 1H), 2.35 (s, 3H), 2.32 (s, 3H), 1.79 (dddd, J = 13.5, 8.6, 7.0, 4.7 Hz, 1H), 1.74 – 1.63 (m, 1H), 1.43 (s, 9H). **HRMS** (ESI+): $\text{C}_{13}\text{H}_{23}\text{NNaO}_4\text{S}_2^+$ $[\text{M}+\text{Na}]^+$: calc. 344.09607, found 344.09613.

N-Boc-1,2-dithian-4-amine (10)



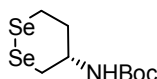
S18 (0.17 g, 0.52 mmol, 1.0 equiv.) was dissolved in a methanolic solution of KOH (10 mL, 0.2 M, 2.1 mmol, 4.0 equiv.) and vigorously stirred at room temperature for 14 h, while being exposed to air. All volatiles were evaporated under reduced pressure and the residue was taken up in EtOAc and sat. aq. NaCl. The layers were separated and the aqueous layer was extracted twice with EtOAc. The combined organic layers were dried over MgSO_4 , filtered and evaporated under reduced pressure, giving the title compound as a colourless solid and in excellent purity (0.12 g, 0.51 mmol, 98%).

TLC R_f = 0.57 (*n*-pentane/ Et_2O 2:1). **$^1\text{H NMR}$** (500 MHz, $\text{DMSO}-d_6$): δ (ppm) = 7.08 (d, J = 8.1 Hz, 1H), 3.56 – 3.44 (m, 1H), 3.11 – 3.01 (m, 1H), 2.95 (t, J = 12.3 Hz, 1H), 2.87 (dd, J = 12.9, 3.2 Hz, 1H), 2.60 (dd, J = 13.0, 10.5 Hz, 1H), 2.06 (dd, J = 13.3, 3.7 Hz, 1H), 1.64 (dd, J = 14.4, 11.2 Hz, 1H), 1.38 (s, 9H). **HRMS** (ESI+): m/z calc. for $\text{C}_9\text{H}_{17}\text{NO}_2\text{S}_2^+$ $[\text{M}+\text{H}]^+$: 235.0701, found 235.0694.

N-Boc-1,4-diselenocyanatobutan-2-amine (S19)

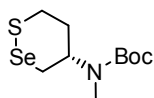
According to general procedure A, NaI (83 mg, 0.55 mmol, 1.0 equiv.), 18-crown-6 (0.32 g, 1.2 mmol, 2.2 equiv.) and KSeCN (0.20 g, 1.4 mmol, 2.5 equiv.) were added to a THF-solution (0.1 M, 6 mL) of dimesylate **1** (0.20 g, 0.55 mmol, 1.0 equiv.). Aqueous work-up followed by flash column chromatography (SiO₂, h = 8 cm, d = 4 cm, hexanes/EtOAc 3:1 → hexanes/EtOAc 1:1, 250 mL dead volume, 20 mL tubes, Fr13-25) provided the title compound as a colourless solid (0.18 g, 0.46 mmol, 83%).

TLC R_f = 0.50 (hexanes/EtOAc 1:1) **¹H NMR** (400 MHz, CDCl₃): δ (ppm) = 4.74 (s, 1H), 4.06 (h, J = 7.5, 6.6 Hz, 1H), 3.43 – 3.13 (m, 3H), 3.01 (dt, J = 12.4, 7.8 Hz, 1H), 2.31 – 2.11 (m, 2H), 1.45 (s, 9H). **¹³C NMR** (101 MHz, CDCl₃): δ (ppm) = 155.5, 101.5, 101.4, 81.0, 50.7, 35.8, 34.5, 28.4, 25.8. **HRMS** (EI+): m/z calc. for C₁₀H₁₆N₂O₂Se₂ [M-CH₂N]⁺ 355.9537, found 355.9537.

N-Boc-1,2-diselenan-4-amine (11)

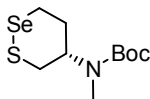
Diselenide formation was achieved in analogy to general protocol B: di-selenocyanate **S19** (0.50 g, 1.3 mmol, 1.0 equiv.) was provided in THF-solution (0.03 M, 30 mL) and KOH (0.17 M in MeOH, 9.4 mL, 1.6 mmol, 1.2 equiv.) was added. Within seconds, a deeply yellow species formed in the reaction vessel and full conversion was achieved according to TLC control. Subsequently conducted aqueous work-up provided the title compound as a yellow solid (0.35 mg, 1.1 mmol, 85%). NMR data of **11** match spectra provided by Fang.²¹

TLC R_f = 0.58 (hexanes/EtOAc 3:1) **¹H NMR** (400 MHz, CDCl₃): δ (ppm) = 5.03 (s, 1H), 4.00 – 3.81 (m, 1H), 3.30 (tdd, J = 15.4, 9.1, 2.0 Hz, 2H), 3.10 – 3.00 (m, 1H), 2.89 (dd, J = 12.3, 8.2 Hz, 1H), 2.22 (ddt, J = 14.2, 8.8, 2.9 Hz, 1H), 2.03 – 1.91 (m, 1H), 1.43 (s, 9H). **¹³C NMR** (101 MHz, CDCl₃): δ (ppm) = 154.6, 79.8, 47.5, 35.0, 28.5, 28.5, 22.2. **HRMS** (EI+): m/z calc. for C₉H₁₇NO₂Se₂ [M]⁺ 330.9584, found 330.9588.

5.5 Trigger functionalisation**N-Boc-N-methyl-1,2-thiaselenan-4-amine (S20)**

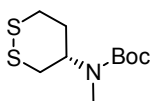
Following general protocol C, MeI (79 μL, 1.3 mmol, 1.2 equiv.) then NaH (47 mg, 1.2 mmol, 1.1 equiv.) were added to a solution of **5** (0.30 g, 1.1 mmol, 1.0 equiv.) in dry DMF (0.02 M, 60 mL). After 5 h, basic, aqueous work-up was followed by flash column chromatography (SiO₂, h = 23 cm, d = 2 cm, hexanes/EtOAc 93:7, 100 mL dead volume, 10 mL tubes, Fr7-11) yielding **S20** as a pale yellow oil (88 mg, 0.30 mmol, 28%). *Note*: the title compound was observed as a mixture of rotameric species. Reported NMR data refer to the major rotamer.

TLC R_f = 0.30 (hexanes/EtOAc 93:7) **¹H NMR** (400 MHz, CDCl₃): δ (ppm) = 4.42 (s, 0.6H, major rotameric species), 4.12 (s, 0.4H, minor rotameric species), 3.37 – 3.15 (m, 3H), 2.75 (s, 3H), 2.69 (ddd, J = 11.7, 3.1, 1.3 Hz, 1H), 2.09 (d, J = 13.2 Hz, 1H), 1.95 (m, 1H), 1.46 (s, 9H). **¹³C NMR** (101 MHz, CDCl₃): δ (ppm) = 155.2, 80.1, 54.4, 36.3, 34.0, 29.0, 28.6 (3C), 27.0. **HRMS** (ESI-): m/z calc. for C₁₀H₁₈NO₂SSe [M-H]⁻ 296.0229, found 296.0230.

***N*-Boc-*N*-methyl-1,2-thiaselenan-5-amine (S21)**

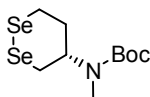
Methylation of 1,2-thiaselenan **8** was achieved following general procedure C: **8** (0.20 g, 0.71 mmol, 1.0 equiv.) was dissolved in dry DMF (0.03 M, 25 mL) and charged with MeI (53 μ L, 0.85 mmol, 1.2 equiv.) and NaH (60%, 31 mg, 0.78 mmol, 1.1 equiv.) at 0 °C. After 5SiO₂, h = 21 cm, d = 2 cm, hexanes/EtOAc 93:7, 150 mL dead volume, 10 mL tubes, Fr1-13/Note: the title compound was observed as a mixture of rotameric species. Reported NMR data refer to the major rotamer.

TLC R_f = 0.30 (hexanes/EtOAc 9:1) **¹H NMR** (400 MHz, CDCl₃): δ (ppm) = 4.17 (s, 1H), 3.42 (t, *J* = 12.3 Hz, 1H), 3.14 (t, *J* = 12.5, 10.6 Hz, 1H), 3.04 (td, *J* = 12.8, 3.2 Hz, 1H), 2.79 (d, *J* = 3.0 Hz, 1H), 2.76 (s, 3H), 2.15 (d, *J* = 26.2 Hz, 2H), 1.46 (s, 9H). **¹³C NMR** (101 MHz, CDCl₃): δ (ppm) = 155.4, 80.2, 57.4 (minor), 55.5 (major), 35.5, 33.8, 29.4, 28.6, 28.2. **HRMS** (EI⁺): *m/z* calc. for C₁₀H₁₉NO₂SSe [M]⁺ 297.0296, found 297.0303.

***N*-Boc-*N*-methyl-1,2-dithian-4-amine (S22)**

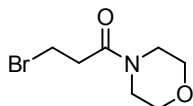
According to general procedure C, **10** (0.40 g, 1.7 mmol, 1.0 equiv.) in DMF (0.02 M, 85 mL) was sequentially charged with MeI (0.13 mL, 2.0 mmol, 1.2 equiv.) and NaH (77 mg, 1.9 mmol, 1.1 equiv.) at 0 °C. Following basic, aqueous work-up, flash column chromatography (hexanes/EtOAc 20:1) enabled isolation of pure **S22** as a colourless solid (0.30 g, 1.2 mmol, 71%). Note: the title compound was observed as a mixture of rotameric species. Reported NMR data refer to the major rotamer.

TLC R_f = 0.74 (*n*-pentane/Et₂O 2:1). **¹H-NMR** (400 MHz, CDCl₃): δ (ppm) = 4.48 – 3.88 (m, 1H), 3.18 (t, *J* = 13.0 Hz, 1H), 2.99 (t, *J* = 15.4 Hz, 2H), 2.76 (s, 3H), 2.66 (dd, *J* = 12.8, 3.2 Hz, 1H), 2.09 (d, *J* = 13.1 Hz, 1H), 2.05 – 1.92 (m, 1H), 1.46 (s, 9H). **¹³C-NMR** (101 MHz, CDCl₃): δ (ppm) = 155.2, 80.2, 55.9, 53.3, 36.4, 36.1, 32.9, 29.3, 28.6. **HRMS** (EI⁺): *m/z* calc. for C₁₀H₁₉NO₂S₂ [M]⁺ 249.0852, found 249.0867.

***N*-Boc-*N*-methyl-1,2-diselenane-4-amine (S23)**

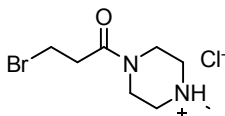
11 was methylated according to general procedure C: starting material (200 mg, 0.608 mmol, 1.0 equiv.) in DMF (0.02 M, 40 mL) was sequentially charged with MeI (45 μ L, 0.729 mmol, 1.2 equiv.) and NaH (27 mg, 0.668 mmol, 1.1 equiv.) at 0 °C. Following basic, aqueous work-up, flash column chromatography (SiO₂, h = 23 cm, d = 2 cm, hexanes/EtOAc 20:1, 200 mL dead volume, 10 mL tubes, Fr2-8) gave pure **S23** as a yellow solid (80 mg, 0.232 mmol, 38%). Note: the title compound was observed as a mixture of rotameric species. Reported NMR data refer to the major rotamer.

TLC R_f = 0.29 (hexanes/EtOAc 9:1) **¹H NMR** (400 MHz, CDCl₃): δ (ppm) = 4.37 (s, 1H), 3.52 – 3.42 (m, 1H), 3.30 (d, *J* = 13.0 Hz, 2H), 2.84 – 2.68 (m, 4H), 2.21 (d, *J* = 13.3 Hz, 1H), 2.16 – 2.05 (m, 1H), 1.46 (s, 9H). **¹³C NMR** (101 MHz, CDCl₃): δ (ppm) = 155.2, 80.1, 55.7, 34.6, 29.1, 28.6, 27.2, 25.6. **HRMS** (ESI⁻): *m/z* calc. for C₁₀H₁₈NO₂Se₂ [M-H]⁻ 343.9674, found 343.9677.

3-Bromo-1-morpholinopropan-1-one (S24)

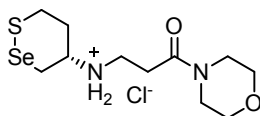
To a solution of morpholine (0.81 mL, 9.4 mmol, 1.0 eq) and NEt_3 (2.0 mL, 14 mmol, 1.5 eq) in DCM (100 mL, 0.1 M) was carefully added a solution of 3-bromo-propionyl chloride (1.0 mL, 9.4 mmol, 1.0 eq, 1.0 M in DCM) at 0°C. The mixture was stirred for 15 min, was allowed to warm to r.t. and was further stirred for 15 min. The mixture was quenched by addition of brine, the aqueous layer was extracted with EtOAc (three times) and the combined organic layers were washed with brine, dried with Na_2SO_4 , filtered and concentrated under reduced pressure to yield **S24** as a colourless oil (1.5 g, 6.8 mmol, 72%).

TLC R_f = 0.48 (EtOAc). **$^1\text{H NMR}$** (400 MHz, $\text{DMSO-}d_6$): δ (ppm) = 3.64 (t, J = 6.7 Hz, 2H), 3.54 (dd, J = 10.1, 5.2 Hz, 4H), 3.43 (q, J = 5.0 Hz, 4H), 2.95 (t, J = 6.7 Hz, 2H). **$^{13}\text{C NMR}$** (101 MHz, $\text{DMSO-}d_6$): δ (ppm) = 168.2, 66.1, 66.1, 45.2, 41.6, 35.2, 28.9. **HRMS** (ESI+): m/z calc. for $\text{C}_7\text{H}_{13}\text{N}_2\text{OBr}$: $[\text{M}+\text{H}]^+$ 222.01242, found 222.01256.

3-Bromo-1-(4-methylpiperazin-1-yl)propan-1-one hydrochloride (12)

3-bromo-propionyl chloride (3.0 mL, 28 mmol, 1.0 equiv.) was dissolved in dry DCM (30 mL, 1 M), and cooled to 0°C. *N*-methyl-piperazine (3.1 mL, 28 mmol, 1.0 equiv.) in DCM (90 mL, 0.3 M), was added and the reaction was stirred at retained temperature for 1 h. The colourless precipitates formed during the reaction were filtered, washed with Et_2O and dried on air to give the target as a colourless solid (7.2 g, 26 mmol, 93%)

$^1\text{H NMR}$ (400 MHz, $\text{DMSO-}d_6$): δ (ppm) = 11.25 (s, 1H), 4.41 (s, 1H), 4.03 (s, 1H), 3.63 (t, J = 6.7 Hz, 2H), 3.54 – 3.27 (m, 3H), 3.11 – 2.82 (m, 5H), 2.74 (s, 3H). **$^{13}\text{C NMR}$** (101 MHz, $\text{DMSO-}d_6$): δ (ppm) = 168.7, 52.7, 52.5, 42.5, 42.1, 38.5, 35.5, 29.0. **HRMS** (ESI+): m/z calc. for $\text{C}_8\text{H}_{16}\text{N}_2\text{OBr}$: $[\text{M}+\text{H}]^+$ 235.04405, found 235.04418.

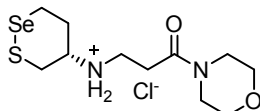
(S)-3-((1,2-Thiaselenan-4-yl)amino)-1-morpholinopropan-1-one hydrochloride (S25)

(*S*)-1,2-thiaselenan-4-amine hydrochloride (0.10 g, 0.52 mmol, 1.2 equiv.), DIPEA (0.25 mL, 0.52 mmol, 1.2 equiv.) and **S24** (86 mg, 0.40 mmol, 1.0 equiv.) were reacted in MeOH (1.2 mL, 0.3 M) according to general procedure D. Boc-protection using Boc_2O (0.13 g, 0.60 mmol, 1.5 equiv.) and DIPEA (0.58 mL, 1.2 mmol, 3 equiv.) in DCM (2 mL, 0.2 M) gave Boc-protected **S25** (49 mg, 0.12 mmol, 30%) after purification by flash column chromatography (DCM→DCM/MeOH 9:1).

TLC R_f = 0.56 (EtOAc). **HRMS** (ESI+): m/z calc. for $\text{C}_{16}\text{H}_{28}\text{NaN}_2\text{O}_4\text{SSe}$: $[\text{M}+\text{Na}]^+$ 447.08272, found 447.08310.

Following general procedure E, hydrochloric acid (0.30 mL, 4 M in dioxane, 1.2 mmol, 10 equiv.) enabled Boc-deprotection in DCM (1.2 mL, 0.1 M). HCl-salt **S25** (42 mg, 0.12 mmol, 30% over 3 steps) was obtained as a solid after filtration from the reaction mixture.

$^1\text{H NMR}$ (400 MHz, $\text{MeOD-}d_4$): δ (ppm) = 3.68 (dt, J = 10.6, 4.7 Hz, 6H), 3.62 – 3.57 (m, 2H), 3.54 – 3.46 (m, 3H), 3.44 – 3.34 (m, 3H), 3.26 – 3.14 (m, 2H), 2.85 (t, J = 5.9 Hz, 2H), 2.48 (d, J = 11.3 Hz, 1H), 1.94 (d, J = 10.9 Hz, 1H). **HRMS** (ESI+): m/z calc. for $\text{C}_{11}\text{H}_{21}\text{N}_2\text{O}_4\text{SSe}$: $[\text{M}+\text{H}]^+$ 325.04835, found 325.04865.

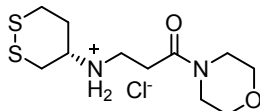
3-((1,2-Thiaselenan-5-yl)amino)-1-morpholinopropan-1-one hydrochloride (S26)

(S)-1,2-thiaselenan-5-amine hydrochloride (0.11 g, 0.52 mmol, 1.3 equiv.), DIPEA (0.25 mL, 0.52 mmol, 1.3 equiv.) and **S24** (89 mg, 0.40 mmol, 1.0 equiv.) were dissolved in MeOH (1.2 mL, 0.3 M) and reacted under microwave irradiation (120 °C, 60 min) according to general procedure D. Subsequent protection using Boc₂O (0.13 g, 0.60 mmol, 1.5 equiv.) and DIPEA (0.58 mL, 1.2 mmol, 3 equiv.) in DCM (2 mL, 0.2 M) gave **S26a** (49 mg, 0.12 mmol, 29%) after isolation from flash column chromatography (DCM→DCM/MeOH 9:1).

TLC R_f = 0.59 (EtOAc). **HRMS** (ESI⁺): m/z calc. for C₁₆H₂₈NaN₂O₄S₂: [M+Na]⁺ 447.08272, found 447.08318.

Boc-deprotection using HCl (0.30 mL, 4 M in dioxane, 1.2 mmol, 10 equiv.) in DCM (1.2 mL, 0.1 M) according to general procedure E gave **S26** (41 mg, 0.12 mmol, 29% over 3 steps) as a colourless solid.

¹H NMR (400 MHz, MeOD-*d*₄): δ (ppm) = 3.71 – 3.64 (m, 6H), 3.62 – 3.58 (m, 2H), 3.55 (d, *J* = 9.7 Hz, 1H), 3.54 – 3.49 (m, 2H), 3.42 – 3.33 (m, 3H), 3.31 – 3.25 (m, 1H), 3.14 (dd, *J* = 13.8, 9.4 Hz, 1H), 2.86 (t, *J* = 6.0 Hz, 2H), 2.61 (d, *J* = 14.3 Hz, 1H), 2.25 (s, 1H). **¹³C NMR** (101 MHz, MeOD-*d*₄): δ (ppm) = 170.4, 68.1, 67.6, 67.5, 46.9, 43.3, 42.2, 41.8, 35.1, 34.6, 29.8. **HRMS** (ESI⁺): m/z calc. for C₁₁H₂₁N₂O₄S₂: [M+H]⁺ 325.04835, found 325.04859.

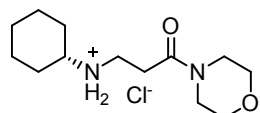
(S)-3-((1,2-Dithian-4-yl)amino)-1-morpholinopropan-1-one hydrochloride (S27)

According to general procedure D, (S)-1,2-dithian-4-amine hydrochloride (95 mg, 0.55 mmol, 1.5 equiv.), DIPEA (0.26 mL, 0.55 mmol, 1.5 equiv.) and **S24** (82 mg, 0.37 mmol, 1.0 equiv.) were dissolved in MeOH (1.5 mL, 0.3 M) and reacted in a microwave at 120 °C for 60 min. The crude oil was then resuspended in DCM (2 mL, 0.2 M) and charged with DIPEA (0.48 mL, 1.0 mmol, 3.0 equiv.) and Boc₂O (0.12 g, 0.55 mmol, 1.5 equiv.). After having been stirred overnight, the reaction was concentrated and the crude product was purified by flash column chromatography (DCM→DCM/MeOH 9:1) to yield **S27a** as a colourless solid (25 mg, 0.065 mmol, 18%).

TLC R_f = 0.54 (EtOAc).

Boc-deprotection in analogy to general procedure E using **S27a** in DCM (1 mL, 0.1 M) and hydrochloric acid (0.18 mL, 4 M in dioxane, 0.7 mmol, 10 equiv.) gave the title compound as a colourless solid after filtration from the reaction mixture (20 mg, 0.064 mmol, 17% over 3 steps).

¹H NMR (400 MHz, MeOD-*d*₄): δ (ppm) = 3.72 – 3.64 (m, 6H), 3.64 – 3.58 (m, 2H), 3.53 – 3.45 (m, 3H), 3.35 (t, *J* = 6.4 Hz, 2H), 3.29 – 3.24 (m, 1H), 3.21 – 3.07 (m, 1H), 3.02 (dd, *J* = 13.4, 10.0 Hz, 1H), 2.84 (t, *J* = 6.0 Hz, 2H), 2.49 (d, *J* = 13.9 Hz, 1H), 2.02 (d, *J* = 9.7 Hz, 1H). **¹³C NMR** (101 MHz, MeOD-*d*₄): δ (ppm) = 169.3, 68.1, 67.6, 67.5, 46.9, 43.3, 42.2, 35.4, 30.4. **HRMS** (ESI⁺): m/z calc. for C₁₁H₂₁N₂O₄S₂: [M+H]⁺ 277.10390, found 277.10402.

3-(Cyclohexylamino)-1-morpholinopropan-1-one hydrochloride (S28)

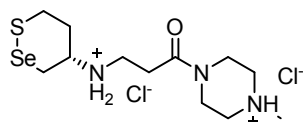
Following general procedure D, cyclohexylamine (0.17 mL, 1.5 mmol, 1.5 equiv.), and **S24** (0.22 g, 1.0 mmol, 1.0 equiv.) were dissolved in MeOH (3 mL, 0.3 M) and reacted in a microwave at 120 °C for 60 min. The crude mixture was then resuspended in DCM (5 mL, 0.2 M) and charged with DIPEA (0.54 mL, 3.0 mmol, 3.0 equiv.) and Boc₂O (0.33 g, 1.5 mmol, 1.5 equiv.). After 15 h, all volatiles were removed and the crude product was purified by flash column chromatography (DCM→DCM/MeOH 9:1) to yield *N*-Boc protected **S28** as a colourless solid (0.13 g, 0.38 mmol, 38%).

TLC R_f = 0.70 (EtOAc). **HRMS** (ESI⁺): m/z calc. for C₁₈H₃₂NaN₂O₄: [M+Na]⁺ 363.22543, found 363.22575.

According to general procedure E, Boc-deprotection in DCM (4 mL, 0.1 M) using hydrochloric acid (1.0 mL, 4 M in dioxane, 4.0 mmol, 10 equiv.) gave **S28** as a colourless solid, which precipitated from the reaction mixture and was collected by filtration (71 mg, 0.26 mmol, 26% over 3 steps).

¹H NMR (400 MHz, DMSO-*d*₆): δ (ppm) = 8.92 (s, 2H), 3.57 (dt, *J* = 16.1, 4.8 Hz, 4H), 3.43 (dt, *J* = 12.3, 4.8 Hz, 4H), 3.09 (p, *J* = 6.8 Hz, 2H), 3.03 – 2.90 (m, 1H), 2.80 (t, *J* = 7.0 Hz, 2H), 2.02 (d, *J* = 10.2 Hz, 2H), 1.74 (d, *J* = 12.8 Hz, 2H), 1.59 (d, *J* = 12.5 Hz, 1H), 1.40 – 1.28 (m, 2H), 1.22 (q, *J* = 12.5 Hz, 2H), 1.15 – 1.04 (m, 1H). **¹³C NMR** (101 MHz, DMSO-*d*₆): δ (ppm) = 168.1, 66.0, 66.0, 55.9, 45.2, 41.6, 28.8, 28.5, 24.8, 23.9. **HRMS** (ESI+): *m/z* calc. for C₁₃H₂₅N₂O₄: [M+H]⁺ 241.19105, found 241.19110.

(S)-3-((1,2-Thiaselenan-4-yl)amino)-1-(4-methylpiperazin-1-yl)propan-1-one dihydrochloride (14)



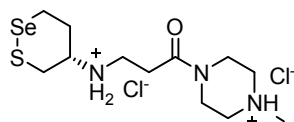
(S)-1,2-thiaselenan-4-amine hydrochloride (0.31 g, 1.4 mmol, 1.4 equiv.), DIPEA (0.24 mL, 1.3 mmol, 1.3 equiv.) and **12** (0.28 g, 1.0 mmol, 1.0 equiv.) were reacted in MeOH (3 mL, 0.3 M) according to general procedure D. Boc-protection was implemented using Boc₂O (0.34 g, 1.5 mmol, 1.5 equiv.) and DIPEA (0.55 mL, 3.1 mmol, 3 equiv.) in DCM (10 mL, 0.2 M). Purification by flash column chromatography (DCM→DCM/MeOH 9:1) gave **13** as a colourless solid (0.15 g, 0.35 mmol, 35%).

TLC R_f = 0.54 (DCM/MeOH 9:1). **HRMS** (ESI+): *m/z* calc. for C₁₇H₃₂N₃O₃S₂Se: [M+H]⁺ 438.13241, found 438.13276.

Using hydrochloric acid (0.88 mL, 4 M in dioxane, 3.5 mmol, 10 equiv.) in DCM (3.5 mL, 0.1 M), Boc-deprotection of **13** according to general procedure E, gave **14** (0.13 g, 0.32 mmol, 91%) as a pale yellow solid after filtration of the reaction mixture.

¹H NMR (400 MHz, MeOD-*d*₄): δ (ppm) = 4.69 (d, *J* = 10.9 Hz, 1H), 4.15 (d, *J* = 15.8 Hz, 1H), 3.71 – 3.62 (m, 2H), 3.55 (dd, *J* = 18.0, 7.9 Hz, 3H), 3.39 (dd, *J* = 11.5, 5.8 Hz, 2H), 3.28 – 3.16 (m, 2H), 3.10 (d, *J* = 9.1 Hz, 2H), 3.06 – 2.98 (m, 1H), 2.95 (s, 3H), 2.91 – 2.80 (m, 1H), 2.51 (d, *J* = 8.9 Hz, 1H), 2.03 – 1.84 (m, 1H). **¹³C NMR** (101 MHz, MeOD-*d*₄): δ (ppm) = 170.5, 54.1, 51.2, 43.7, 43.6, 43.4, 42.0, 39.9, 34.5, 30.0. **HRMS** (ESI+): *m/z* calc. for C₁₁H₂₁N₂O₄S₂Se: [M+H]⁺ 338.07998, found 338.08022.f

3-((1,2-Thiaselenan-5-yl)amino)-1-(4-methylpiperazin-1-yl)propan-1-one dihydrochloride (S29)

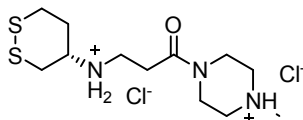


Following general procedure D, (S)-1,2-thiaselenan-5-amine hydrochloride (0.44 g, 2.0 mmol, 1.35 equiv.), DIPEA (0.35 mL, 1.9 mmol, 1.3 equiv.) and **12** (0.40 g, 1.5 mmol, 1.0 equiv.), were dissolved in MeOH (5 mL, 0.3 M) and reacted under microwave irradiation (120 °C, 60 min). Boc-protection of the crude diamine was conducted using Boc₂O (0.48 g, 2.2 mmol, 1.5 equiv.) and DIPEA (0.79 mL, 4.4 mmol, 3 equiv.) in DCM (7.5 mL, 0.2 M). **S29a** was received as a colourless solid (0.17 g, 0.38 mmol, 25%) after purification via flash column chromatography (DCM→DCM/MeOH 9:1).

TLC R_f = 0.40 (DCM/MeOH 9:1). **HRMS** (ESI+): *m/z* calc. for C₁₇H₃₂N₃O₃S₂Se: [M+H]⁺ 438.13241, found 438.13263.

Deprotection of **S29a** was achieved according to general procedure E. Starting material (0.17 g, 0.38 mmol, 1.0 equiv.) in DCM (4 mL, 0.1 M) was charged with HCl (0.95 mL, 4 M in dioxane, 3.8 mmol, 10 equiv.) and the title compound was collected through filtration of the reaction mixture (0.15 g, 0.36 mmol, 95%).

¹H NMR (400 MHz, MeOD-*d*₄): δ (ppm) = 4.68 (d, *J* = 11.2 Hz, 1H), 4.15 (d, *J* = 15.4 Hz, 1H), 3.71 – 3.65 (m, 1H), 3.63 – 3.49 (m, 5H), 3.38 (t, *J* = 5.7 Hz, 3H), 3.27 (d, *J* = 11.0 Hz, 2H), 3.18 – 3.04 (m, 4H), 2.95 (s, 3H), 2.61 (d, *J* = 9.1 Hz, 1H), 2.24 (d, *J* = 8.1 Hz, 1H). **¹³C NMR** (101 MHz, MeOD-*d*₄): δ (ppm) = 170.5, 54.3, 54.1, 43.7, 43.7, 43.4, 42.0, 41.7, 39.9, 33.4, 30.0, 25.7. **HRMS** (ESI+): *m/z* calc. for C₁₁H₂₁N₂O₄S₂Se: [M+H]⁺ 338.04835, found 338.08024.

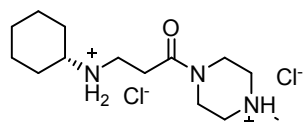
(S)-3-((1,2-Dithian-4-yl)amino)-1-(4-methylpiperazin-1-yl)propan-1-one dihydrochloride (S30)

According to general procedure D, (S)-1,2-dithian-4-amine hydrochloride (0.14 g, 0.80 mmol, 1.5 equiv.), DIPEA (0.39 mL, 0.80 mmol, 1.5 equiv.) and **12** (0.11 g, 0.54 mmol, 1.0 equiv.) were dissolved in MeOH (1.6 mL, 0.3 M) and reacted in a microwave (120 °C, 60 min). Treating the crude product with Boc₂O (0.13 g, 0.60 mmol, 1.5 equiv.) and DIPEA (0.58 mL, 1.2 mmol, 3 equiv.) in DCM (2 mL, 0.2 M) gave **S30a** (66 mg, 0.17 mmol, 32%) as a colourless solid after purification by flash column chromatography (DCM→DCM/MeOH 9:1).

TLC R_f = 0.50 (DCM/MeOH 9:1). **¹H NMR** (400 MHz, CDCl₃): δ (ppm) = 4.31 – 3.51 (m, 2H), 3.38 (s, 1H), 3.13 (q, *J* = 7.3 Hz, 4H), 3.06 – 2.83 (m, 1H), 2.80 – 2.36 (m, 5H), 2.19 (s, 2H), 1.53 – 1.40 (m, 9H). **HRMS** (ESI+): *m/z* calc. for C₁₇H₃₂N₃O₃S₂: [M+H]⁺ 390.18796, found 390.18852.

A portion (51 mg, 0.13 mmol) of the material obtained above was deprotected via general procedure E. After being reacted with HCl (0.33 mL, 4 M in dioxane, 1.3 mmol, 10 equiv.) in DCM (1.3 mL, 0.1 M), compound **S30** (46 mg, 0.13 mmol, 31% over 3 steps) precipitated from the reaction mixture and was obtained as a colourless solid after filtration. Obtained solids were used without further purification or analysis.

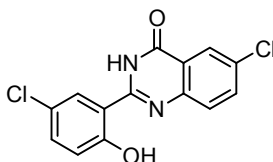
HRMS (ESI+): *m/z* calc. for C₁₂H₂₄N₃O₂: [M+H]⁺ 290.13553, found 290.13569.

3-(Cyclohexylamino)-1-(4-methylpiperazin-1-yl)propan-1-one dihydrochloride (S31)

According to general procedure D, cyclohexylamine (57 μL, 0.50 mmol, 1.25 eq) and **12** (77 mg, 0.40 mmol, 1.0 equiv.) were reacted in MeOH (1.2 mL, 0.3 M) under microwave irradiation (120 °C, 60 min). Boc-protection using Boc₂O (0.13 g, 0.60 mmol, 1.5 equiv.) and DIPEA (0.58 mL, 1.2 mmol, 3 equiv.) in DCM (2 mL, 0.2 M) gave **S31a** (0.12 g, 0.32 mmol, 81%) upon isolation by flash column chromatography (DCM→DCM/MeOH 9:1).

TLC R_f = 0.45 (DCM/MeOH 9:1). **¹H NMR** (400 MHz, CDCl₃) δ (ppm) = 3.98 – 3.50 (m, 3H), 3.36 (s, 2H), 3.13 (q, *J* = 7.3 Hz, 2H), 2.55 (s, 2H), 2.44 (s, 2H), 2.36 (s, 2H), 1.76 (d, *J* = 11.8 Hz, 1H), 1.66 (d, *J* = 10.7 Hz, 1H), 1.60 (d, *J* = 13.1 Hz, 1H), 1.49 – 1.40 (m, 9H), 1.36 – 1.17 (m, 2H), 1.19 – 0.92 (m, 1H). **¹³C NMR** (101 MHz, CDCl₃) δ (ppm) = 169.9, 155.5, 79.6, 56.7, 55.1, 54.6, 46.1, 46.0, 45.2, 41.2, 39.7, 34.2, 31.4, 31.1, 28.7, 26.1, 25.5. **HRMS** (ESI+): *m/z* calc. for C₁₉H₃₆N₃O₃: [M+H]⁺ 354.27512, found 354.27544.

Boc-deprotection was conducted following general procedure E. Intermediate **S31a** (46 mg, 0.13 mmol, 1.0 equiv.) was dissolved in DCM (1.3 mL, 0.1 M) and reacted with HCl (0.33 mL, 4 M in dioxane, 1.3 mmol, 10 equiv.). Filtration of the precipitates formed during the reaction gave compound **S31** (42 mg, 0.13 mmol, 80% over 3 steps) as a colourless solid which was used without further analysis or purification.

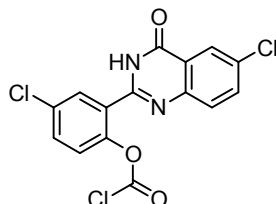
5.6 Probe assembly**6-Chloro-2-(5-chloro-2-hydroxyphenyl)quinazolin-4(3H)-one (PQ-OH, S32)**

To a solution of 5-chloro-salicylaldehyde (5.00 g, 31.9 mmol, 1.0 equiv.) in anhydrous ethanol (0.05 M, 620 mL), 2-amino-5-chlorobenzamide (5.45 g, 31.9 mmol, 1.0 equiv.) and *p*-toluene sulfonic acid (607 mg, 3.19 mmol, 0.1 equiv.) were added and the resulting suspension was heated to 90 °C for 1 h. The reaction mixture was cooled to 0 °C and 2,3-dichloro-5,6-dicyano-1,4-benzoquinone (DDQ, 7.25 g, 31.9 mmol, 1.0 equiv.) was added in small batches. The reaction was further stirred at retained temperature for 1 h upon which a yellow precipitate occurred. The solid was filtered, washed with ice-cold ethanol

and dried to afford the title compound as a beige solid (8.40 g, 27.3 mmol, 86%). When excited with UV-light, **S32** exhibited bright green fluorescence. NMR spectra match reported data.⁶⁵

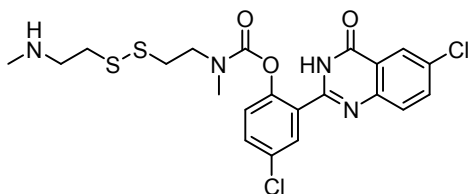
¹H NMR (400 MHz, DMSO-*d*₆): δ (ppm) = 13.34 (s, 1H), 12.74 (s, 1H), 8.29 (d, *J* = 2.6 Hz, 1H), 8.09 (d, *J* = 2.4 Hz, 1H), 7.90 (dd, *J* = 8.7, 2.5 Hz, 1H), 7.84 (d, *J* = 8.7 Hz, 1H), 7.49 (dd, *J* = 8.9, 2.6 Hz, 1H), 7.04 (d, *J* = 8.8 Hz, 1H). **HRMS** (ESI-): *m/z* calc. for C₁₄H₇Cl₂N₂O₂ [M-H]⁻ 304.9890, found 304.9891.

4-Chloro-2-(6-chloro-4-oxo-3,4-dihydroquinazolin-2-yl)phenyl chloroformate (**PQ-OCOCI**, **S33**)



Under a nitrogen atmosphere, 6-chloro-2-(5-chloro-2-hydroxyphenyl) quinazolin-4-one (**S32**, 1.44 g, 4.70 mmol, 1.0 equiv.) was suspended in dry dichloromethane (0.04 M, 125 mL). Triphosgene (1.53 g, 5.17 mmol, 1.1 equiv.) in dry DCM (1.0 M, 5 mL) was added and the mixture was cooled to 0 °C. The mixture was then slowly charged with NEt₃ (1.07 mL, 6.11 mmol, 1.3 equiv.) in dry DCM (1.0 M, 6 mL). The reaction was stirred at retained temperature for 30 min, was then allowed to warm to r.t. and was further stirred for 30 min. Exposure of the reaction mixture to 366 nm UV light allowed assessment of the reaction progress: starting material **S32** shows bright green fluorescence under these conditions, while the target species exhibits weak, blue fluorescence. Upon full conversion was indicated by LCMS, all volatile compounds were removed using two serially connected, external liquid nitrogen traps while carefully exposing the reaction vessel to reduced pressure. Excess phosgene which was caught in either of the liquid nitrogen traps was quenched when still cold by carefully adding an excess of piperidine. Chloroformate **S33** was received as a beige solid and was used without further purification. For following carbamate coupling reactions, the crude solid was resuspended in dry DCM (0.04 M, 118 mL).

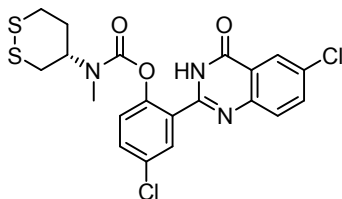
SS00



Deprotection of **S8** was executed according to general procedure E. **S8** (1.9 mmol, 1.7 equiv.) in DCM (0.2 M, 10 mL) was reacted with HCl (5 mL, 4 M in dioxane, 20 mmol, 17 equiv.), giving *N,N'*-dimethyl cystamine dihydrochloride as a colourless solid after filtration. The diamine was then coupled to **S33** (0.72 g, 1.1 mmol, 1.0 equiv.) according to general procedure F. Purification by flash column chromatography (DCM/MeOH) gave **SS00** as a colourless powder (0.25 g, 0.48 mmol, 44%).

R_f = 0.22 (DCM/MeOH 9:1). **¹H NMR** (400 MHz, tetrachlorethane-*d*₂, 373 K): δ (ppm) = 8.20 (t, *J* = 1.5 Hz, 1H), 7.87 (d, *J* = 2.6 Hz, 1H), 7.71 (d, *J* = 1.5 Hz, 2H), 7.48 (dd, *J* = 8.7, 2.6 Hz, 1H), 7.24 (d, *J* = 8.7 Hz, 1H), 3.62 (s, 2H), 3.23 (d, *J* = 6.2 Hz, 2H), 3.18 (d, *J* = 6.1 Hz, 2H), 3.03 (s, 3H), 2.88 (s, 2H), 2.66 (s, 3H). **¹³C NMR** (101 MHz, DMSO-*d*₆): δ (ppm) = 160.8, 153.1, 150.6, 147.9, 147.2, 134.9, 131.5, 131.4, 130.1, 129.6, 129.4, 128.5, 125.2, 125.0, 122.4, 47.7, 47.0, 35.1, 34.6, 32.4, 32.3. **HRMS** (ESI+) *m/z* calc. for C₂₁H₂₃Cl₂N₄O₃S₂ [M+H]⁺ 513.05831, found 513.05886.

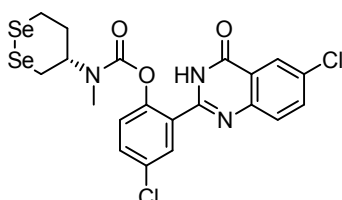
S3



Prepared from **S22** (56 mg, 0.30 mmol) and **S33** (180 mg, 0.586 mmol) according to general protocols E and F. Purification by flash column chromatography (Et₂O) gave the title compound as a colourless solid (108 mg, 0.224 mmol, 75%). *Note:* Individual rotamers were observed by NMR spectroscopy at 298 K (ratio ca. 1.5:1) and time-averaged spectra were obtained at 373 K.

TLC R_f = 0.31 (hexanes/EtOAc 2:1). **¹H NMR** (400 MHz, tetrachlorethane-*d*₂, 373 K): δ (ppm) = 9.56 (s, 1H), 8.22 (t, *J* = 1.5 Hz, 1H), 7.97 (d, *J* = 2.6 Hz, 1H), 7.78 – 7.66 (m, 2H), 7.49 (dd, *J* = 8.7, 2.6 Hz, 1H), 7.17 (d, *J* = 8.8 Hz, 1H), 4.17 (d, *J* = 12.1 Hz, 1H), 3.15 (ddd, *J* = 13.8, 11.8, 2.8 Hz, 1H), 3.10 (dd, *J* = 12.9, 11.4 Hz, 1H), 2.97 (s, 3H), 2.93 (t, *J* = 3.8 Hz, 1H), 2.72 (dd, *J* = 12.8, 3.2 Hz, 1H), 2.17 – 2.01 (m, 2H). **¹³C NMR** (101 MHz, tetrachlorethane-*d*₂, 373 K): δ (ppm) = 160.0, 153.4, 149.0, 147.7, 147.5, 135.2, 133.5, 132.3, 132.3, 130.4, 129.8, 128.0, 126.0, 125.2, 122.5, 57.1, 36.1, 35.9, 32.6, 30.5. **HRMS** (ESI⁺): *m/z* calc. for C₂₀H₁₈Cl₂N₃O₃S₂⁺ [M+H]⁺ 482.01611, found 482.01592.

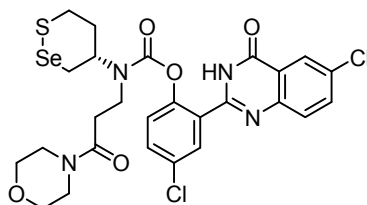
Se3



HPQ-coupling of **S23** was conducted according to general protocols E and F. Following deprotection of the starting material (70 mg, 0.20 mmol, 1.0 equiv.) by HCl (4 M in dioxane, 0.51 mL, 2.0 mmol, 10 equiv.), a solution of the amine-HCl salt in DCM (0.05 M, 6 mL) and NEt₃ (85 μL, 0.61 mmol, 3.0 equiv.) was reacted with chloroformate **XX** (0.25 M in DCM, 1.7 mL, 0.44 mmol, 2.0 equiv.). Upon completion, aqueous work-up and flash column chromatography (SiO₂, h = 22 cm, d = 2 cm, hexanes/EtOAc 3:1, 200 mL dead volume, 10 mL tubes, Fr6-16) gave **Se3** as a yellow solid (67 mg, 0.116 mmol, 57%). *Note:* the title compound was observed as a mixture of rotameric species. Reported NMR data refer to the major rotamer.

TLC R_f = 0.18 (hexanes/EtOAc 3:1) **¹H NMR** (400 MHz, CDCl₃): δ (ppm) = 10.11 (s, 1H), 8.26 (dd, *J* = 2.1, 0.9 Hz, 1H), 7.99 (dd, *J* = 6.0, 2.6 Hz, 1H), 7.77 – 7.70 (m, 2H), 7.54 – 7.49 (m, 1H), 7.18 (d, *J* = 8.7 Hz, 1H), 4.33 (t, *J* = 11.8 Hz, 1H), 3.46 (t, *J* = 12.9 Hz, 1H), 3.42 – 3.24 (m, 2H), 3.02 (s, 3H), 2.78 (d, *J* = 11.9 Hz, 1H), 2.25 – 2.09 (m, 2H). **¹³C NMR** (101 MHz, CDCl₃): δ (ppm) = 160.7, 153.8, 149.3, 147.6, 147.5, 135.5, 133.6, 132.5, 132.4, 130.7, 129.8, 128.1, 126.2, 125.3, 122.4, 58.1, 34.2, 30.1 **HRMS** (ESI⁺): *m/z* calc. for C₂₀H₁₈Cl₂N₃O₃Se₂⁺ [M+H]⁺ 577.9050, found 577.9048.

A2

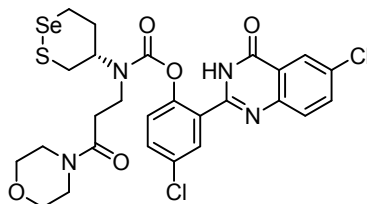


Prepared from **S25** (40 mg, 0.11 mmol, 1.0 equiv.) and **S33** (3.0 mL, 0.04 M in DCM, 0.12 mmol, 1.1 equiv.) according to general protocol F. Purification by flash column chromatography (isohexane/EtOAc) gave **A2** as a colourless solid (43 mg, 0.065 mmol, 59%). Light blue solid-state fluorescence was observed under UV-light. NMR spectroscopy of the title compound revealed the presence of two rotameric species. Individual signals could not be clearly identified at 298 K.

TLC R_f = 0.48 (EtOAc). **¹H NMR** (400 MHz, CDCl₃): δ (ppm) = 10.46 (d, *J* = 64.1 Hz, 1H), 8.22 (d, *J* = 3.0 Hz, 1H), 7.92 (dd, *J* = 16.2, 2.3 Hz, 1H), 7.78 – 7.68 (m, 2H), 7.56 – 7.47 (m, 1H), 7.17 (dd, *J* = 8.6, 2.7 Hz, 1H), 4.49 – 4.12 (m, 1H), 3.73 (s,

1H), 3.68 (dd, $J = 8.5, 3.7$ Hz, 3H), 3.66 – 3.58 (m, 5H), 3.52 (d, $J = 12.7$ Hz, 3H), 3.50 – 3.46 (m, 1H), 3.43 – 3.35 (m, 1H), 3.33 (d, $J = 13.5$ Hz, 1H), 3.30 – 3.17 (m, 2H), 2.82 – 2.67 (m, 1H), 2.64 – 2.58 (m, 1H), 2.58 – 2.47 (m, 1H), 2.22 – 2.01 (m, 2H). $^{13}\text{C NMR}$ (101 MHz, CDCl_3): δ (ppm) = 168.9, 168.5, 160.8, 153.7, 149.6, 147.5, 147.1, 135.5, 133.6, 132.5, 130.7, 129.8, 128.6, 126.0, 125.1, 124.9, 122.3, 67.2, 67.0, 66.7, 66.5, 58.6, 46.0, 45.8, 42.2, 42.0, 40.0, 36.2, 36.0, 34.8, 33.6, 32.6, 27.4. **HRMS** (ESI+): m/z calc. for $\text{C}_{26}\text{H}_{27}\text{Cl}_2\text{N}_5\text{O}_4\text{SSe}$: $[\text{M}+\text{H}]^+$ 657.02389, found 657.02417.

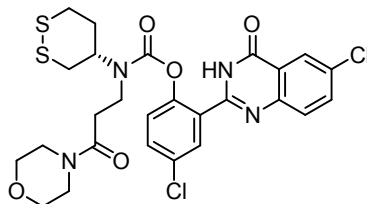
G2



Prepared from **S26** (40 mg, 0.11 mmol, 1.0 equiv.) and **S33** (3.0 mL, 0.04 M in DCM, 0.12 mmol, 1.1 equiv.) according to general protocol F. Purification by flash column chromatography (isohexane/EtOAc) gave **G2** as a colourless solid (58 mg, 0.088 mmol, 80%). Light blue solid-state fluorescence was observed under UV-light. NMR spectroscopy of the title compound revealed the presence of two rotameric species. Individual signals could not be clearly identified at 298 K.

TLC $R_f = 0.46$ (EtOAc). $^1\text{H NMR}$ (400 MHz, CDCl_3): δ (ppm) = 10.48 (d, $J = 52.1$ Hz, 0H), 8.25 – 8.18 (m, 1H), 7.91 (dd, $J = 24.5, 2.5$ Hz, 1H), 7.80 – 7.68 (m, 2H), 7.51 (td, $J = 7.9, 7.0, 2.5$ Hz, 1H), 7.21 – 7.11 (m, 1H), 4.33 – 3.88 (m, 1H), 3.77 – 3.71 (m, 1H), 3.71 – 3.66 (m, 4H), 3.66 – 3.58 (m, 5H), 3.53 (d, $J = 14.5$ Hz, 4H), 3.50 – 3.45 (m, 2H), 3.43 – 3.20 (m, 4H), 3.07 – 2.98 (m, 1H), 2.88 (d, $J = 10.6$ Hz, 1H), 2.78 (d, $J = 7.0$ Hz, 1H), 2.59 (t, $J = 7.3$ Hz, 1H), 2.51 (q, $J = 7.2$ Hz, 1H), 2.40 – 2.27 (m, 2H), 2.21 (s, 1H). **HRMS** (ESI+): m/z calc. for $\text{C}_{26}\text{H}_{27}\text{Cl}_2\text{N}_5\text{O}_4\text{SSe}$: $[\text{M}+\text{H}]^+$ 657.02389, found 657.02401.

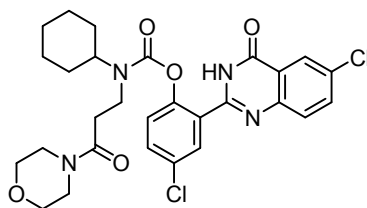
S2



Prepared from **S27** (20 mg, 0.064 mmol) and **S33** (1.8 mL, 0.04 M in DCM, 0.070 mmol, 1.1 equiv.) according to general procedure F. Purification by flash column chromatography (isohexane/EtOAc) gave **S2** as a colourless solid (26 mg, 0.043 mmol, 67%). Light blue solid-state fluorescence was observed under UV-light. NMR spectroscopy of the title compound revealed the presence of two rotameric species. Individual signals could not be clearly identified at 298 K.

TLC $R_f = 0.45$ (EtOAc). $^1\text{H NMR}$ (400 MHz, CDCl_3): δ (ppm) = 10.43 (d, $J = 60.3$ Hz, 1H), 8.27 – 8.15 (m, 1H), 7.91 (dd, $J = 23.0, 2.5$ Hz, 1H), 7.78 – 7.68 (m, 2H), 7.52 (td, $J = 7.5, 6.4, 2.5$ Hz, 1H), 7.21 – 7.13 (m, 1H), 4.38 – 3.95 (m, 1H), 3.74 (d, $J = 3.9$ Hz, 1H), 3.68 (dd, $J = 8.3, 3.7$ Hz, 3H), 3.66 – 3.58 (m, 5H), 3.58 – 3.50 (m, 3H), 3.50 – 3.45 (m, 2H), 3.36 – 3.32 (m, 1H), 3.26 – 3.20 (m, 1H), 3.20 – 3.10 (m, 2H), 3.01 – 2.90 (m, 1H), 2.80 – 2.73 (m, 1H), 2.70 – 2.63 (m, 1H), 2.59 (t, $J = 7.4$ Hz, 1H), 2.52 (q, $J = 8.0$ Hz, 1H), 2.25 – 2.04 (m, 2H). $^{13}\text{C NMR}$ (101 MHz, CDCl_3): δ (ppm) = 168.9, 168.5, 160.8, 153.8, 149.6, 147.5, 147.1, 135.6, 133.6, 132.5, 130.7, 129.8, 128.7, 126.0, 125.1, 124.9, 122.3, 67.0, 66.9, 66.7, 66.5, 58.3, 46.0, 45.8, 42.2, 42.0, 40.0, 36.7, 36.3, 36.0, 33.6, 33.5, 32.7, 32.6, 29.8, 28.7. **HRMS** (ESI+): m/z calc. for $\text{C}_{26}\text{H}_{27}\text{Cl}_2\text{N}_5\text{O}_4\text{S}_2$: $[\text{M}+\text{H}]^+$ 609.07944, found 609.08006.

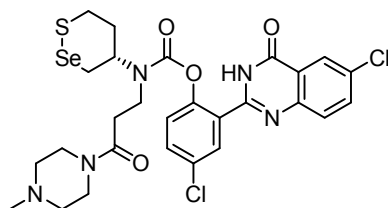
C2



Prepared from **S28** (55 mg, 0.20 mmol, 1.0 equiv.), and **S33** (5.5 mL, 0.04 M in DCM, 0.22 mmol, 1.1 equiv.) according to general procedure F. Purification by flash column chromatography (isohexane/EtOAc) gave **C2** as a colourless solid (91 mg, 0.16 mmol, 79%). Light blue solid-state fluorescence was observed under UV-light. NMR spectroscopy of the title compound revealed the presence of two rotameric species. Individual signals could not be clearly identified at 298 K.

TLC R_f = 0.50 (EtOAc). **¹H NMR** (400 MHz, CDCl₃): δ (ppm) = 10.44 (d, J = 73.9 Hz, 1H), 8.23 (d, J = 11.4 Hz, 1H), 7.91 (dd, J = 19.8, 2.5 Hz, 1H), 7.77 – 7.69 (m, 2H), 7.50 (dt, J = 8.6, 3.4 Hz, 1H), 7.21 – 7.11 (m, 1H), 3.91 (dt, J = 37.2, 11.9 Hz, 1H), 3.66 (dt, J = 8.3, 4.9 Hz, 3H), 3.54 (ddd, J = 16.0, 8.7, 4.7 Hz, 5H), 3.48 – 3.41 (m, 1H), 3.29 – 3.16 (m, 1H), 2.57 (dt, J = 8.4, 4.7 Hz, 2H), 1.76 (q, J = 14.8, 14.1 Hz, 4H), 1.63 (s, 2H), 1.57 – 1.41 (m, 3H), 1.37 – 1.22 (m, 4H), 1.15 – 1.02 (m, 1H). **¹³C NMR** (101 MHz, CDCl₃): δ (ppm) = 169.4, 160.8, 160.6, 154.6, 154.0, 149.9, 147.5, 147.5, 135.4, 133.4, 132.5, 132.4, 132.3, 132.0, 130.7, 129.8, 128.9, 128.4, 126.0, 125.2, 125.0, 122.4, 66.9, 66.8, 66.5, 57.5, 45.9, 45.7, 41.9, 40.6, 40.1, 33.8, 32.7, 31.4, 30.7, 29.8, 25.8, 25.3, 25.2, 22.8. **HRMS** (ESI⁺): m/z calc. for C₂₈H₃₁Cl₂N₅O₄: [M+H]⁺ 573.16660, found 573.16724.

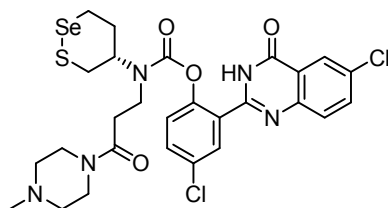
RX1



Prepared from **14** (20 mg, 0.049 mmol, 1.0 equiv.) and **S33** (1.4 mL, 0.04 M in DCM, 0.054 mmol, 1.1 equiv.) according to general protocol F. Purification by flash column chromatography (DCM→DCM/MeOH 9:1) gave **RX1** as a colourless solid (20 mg, 0.030 mmol, 61%). Further purification by preparative HPLC (MeCN/H₂O, 0.1% FA) yielded **RX1** as a colourless solid. Light blue solid-state fluorescence was observed under UV-light. NMR spectroscopy of the title compound revealed the presence of two rotameric species. Individual signals could not be clearly identified at 298 K.

TLC R_f = 0.45 (DCM/MeOH 9:1). **¹H NMR** (400 MHz, MeOD-*d*₄): δ (ppm) = 8.21 (t, J = 2.4 Hz, 1H), 7.87 (dt, J = 8.8, 3.1 Hz, 1H), 7.83 (d, J = 2.6 Hz, 1H), 7.76 (dd, J = 8.8, 4.4 Hz, 1H), 7.65 (dt, J = 8.9, 2.8 Hz, 1H), 7.39 (dd, J = 8.8, 4.3 Hz, 1H), 4.47 (s, 0.5H), 3.90 (t, J = 11.6 Hz, 0.5H), 3.75 – 3.47 (m, 4H), 3.39 (m, 2H), 3.27 (m, 2H), 3.13 (m, 1H), 2.89 (d, J = 11.6 Hz, 0.5H), 2.78 (t, J = 8.0 Hz, 1H), 2.66 – 2.49 (m, 4.5H), 2.44 (d, J = 4.7 Hz, 3H), 2.36 (q, J = 7.2 Hz, 1H), 2.25 – 2.16 (m, 0.6H), 2.08 – 1.96 (m, 1H), 1.88 (d, J = 13.3 Hz, 0.4H). **¹³C NMR** (101 MHz, MeOD-*d*₄): δ (ppm) = 171.4, 171.0, 154.0, 152.7, 149.0, 148.8, 148.7, 136.5, 136.4, 134.1, 133.0, 132.4, 132.4, 131.9, 131.0, 130.5, 130.4, 126.6, 126.5, 126.1, 126.0, 123.6, 123.5, 60.5, 55.6, 55.5, 55.2, 55.0, 45.6, 45.5, 43.7, 41.8, 41.6, 37.2, 35.8, 34.6, 34.4, 33.5, 28.3, 27.3. **HRMS** (ESI⁺): m/z calc. for C₂₇H₃₀Cl₂N₅O₄SSe: [M+H]⁺ 670.05553, found 670.05587.

G1

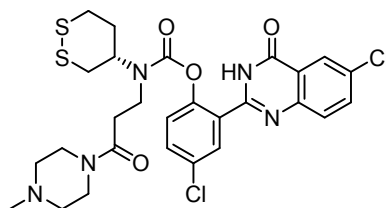


Prepared from **S29** (12 mg, 0.030 mmol, 1.0 equiv.) and **S33** (0.83 mL, 0.04 M in DCM, 0.033 mmol, 1.1 equiv.) according to general protocol F. Purification by flash column chromatography (DCM→DCM/MeOH 9:1) gave **G1** as a colourless solid (13 mg, 0.020 mmol, 66%). Further purification by preparative HPLC (MeCN/H₂O, 0.1% FA) yielded **G1** as a colourless

solid. Light blue solid-state fluorescence was observed under UV-light. NMR spectroscopy of the title compound revealed the presence of two rotameric species. Individual signals could not be clearly identified at 298 K.

TLC R_f = 0.44 (DCM/MeOH 9:1). **$^1\text{H NMR}$** (400 MHz, MeOD- d_4): δ (ppm) = 8.20 (t, J = 2.6 Hz, 1H), 7.86 (dt, J = 8.8, 2.3 Hz, 1H), 7.83 – 7.79 (m, 1H), 7.74 (dd, J = 8.7, 2.8 Hz, 1H), 7.63 (dt, J = 8.7, 3.1 Hz, 1H), 7.37 (dd, J = 8.7, 2.2 Hz, 1H), 4.23 (s, 0.5H), 3.66 (s, 3.5H), 3.56 (s, 1H), 3.38 (m, 3H), 3.22 (m, 1H), 3.07 (d, J = 13.1 Hz, 0.5H), 2.93 (d, J = 13.0 Hz, 1H), 2.87 – 2.65 (m, 5H), 2.56 (d, J = 8.4 Hz, 3H), 2.42 – 2.14 (m, 3H), 2.00 – 1.91 (m, 0.5H). **$^{13}\text{C NMR}$** (101 MHz, MeOD- d_4): δ (ppm) = 171.4, 171.1, 154.2, 152.6, 148.9, 148.8, 148.6, 136.4, 134.2, 133.0, 131.0, 130.4, 126.6, 126.1, 123.6, 123.5, 61.6, 55.3, 55.1, 55.0, 54.7, 45.1, 45.0, 41.2, 41.0, 36.9, 35.9, 35.5, 34.3, 33.5, 29.0. **HRMS** (ESI+): m/z calc. for $\text{C}_{27}\text{H}_{30}\text{Cl}_2\text{N}_5\text{O}_4\text{SSe}$: $[\text{M}+\text{H}]^+$ 670.05553, found 670.05587.

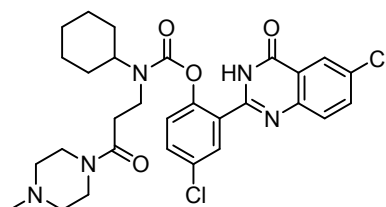
S1



Prepared from **S30** (47 mg, 0.13 mmol, 1.0 equiv.) and **S33** (3.5 mL, 0.04 M in DCM, 0.14 mmol, 1.1 equiv.) according to general protocol F. Purification by flash column chromatography (DCM→DCM/MeOH 9:1) gave **S1** as a colourless solid (36 mg, 0.061 mmol, 47%). Further purification by preparative HPLC (MeCN/H₂O, 0.1% FA) yielded **S1** as a colourless solid. Light blue solid-state fluorescence was observed under UV-light.

TLC R_f = 0.55 (DCM/MeOH 9:1). **$^1\text{H NMR}$** (400 MHz, DMSO- d_6): δ (ppm) = 12.75 (s, 1H), 8.07 (s, 1H), 7.89 – 7.80 (m, 2H), 7.75 – 7.60 (m, 2H), 7.42 – 7.32 (m, 1H), 3.90 (d, J = 195.7 Hz, 1H), 3.53 (s, 1H), 3.37 (s, 1H), 3.25 (d, J = 15.3 Hz, 2H), 3.15 – 3.02 (m, 2H), 3.01 – 2.92 (m, 3H), 2.69 – 2.53 (m, 2H), 2.33 (s, 1H), 2.16 (s, 2H), 2.15 (d, J = 2.2 Hz, 5H), 1.98 (s, 1H). **HRMS** (ESI+): m/z calc. for $\text{C}_{27}\text{H}_{30}\text{Cl}_2\text{N}_5\text{O}_4\text{S}_2$: $[\text{M}+\text{H}]^+$ 622.11108, found 622.11171.

C1



Prepared from **S31** (42 mg, 0.13 mmol, 1.0 equiv.) and **S33** (3.5 mL, 0.04 M in DCM, 0.14 mmol, 1.1 equiv.) according to general protocol F. Purification by flash column chromatography (DCM→DCM/MeOH 9:1) gave **C1** as a colourless solid (55.0 mg, 0.088 mmol, 68%). Further purification by preparative HPLC (MeCN/H₂O, 0.1% FA) yielded **C1** as a colourless solid. Light blue solid-state fluorescence was observed under UV-light. NMR spectroscopy of the title compound revealed the presence of two rotameric species. Individual signals could not be clearly identified at 298 K.

TLC R_f = 0.55 (DCM/MeOH 9:1). **$^1\text{H NMR}$** (400 MHz, MeOD- d_4): δ (ppm) = 8.18 (dd, J = 4.1, 2.4 Hz, 1H), 7.84 (td, J = 7.9, 7.1, 2.5 Hz, 1H), 7.79 (dd, J = 4.6, 2.6 Hz, 1H), 7.72 (dd, J = 8.7, 3.3 Hz, 1H), 7.61 (dd, J = 8.8, 2.5 Hz, 1H), 7.34 (dd, J = 8.7, 2.2 Hz, 1H), 4.04 (t, J = 11.5 Hz, 0.6H), 3.57 (m, 4H), 3.34 (s, 0.4H), 3.26 (m, 1H), 2.74 (t, J = 7.9 Hz, 1H), 2.55 (m, 2H), 2.49 (t, J = 5.0 Hz, 2H), 2.40 (d, J = 3.4 Hz, 3H), 2.34 – 2.21 (m, 1H), 1.87 – 1.51 (m, 4.5H), 1.51 – 1.28 (m, 4.5H), 1.28 – 0.97 (m, 1H). **$^{13}\text{C NMR}$** (101 MHz, MeOD- d_4): δ (ppm) = 171.5, 171.2, 154.7, 136.4, 134.1, 133.0, 132.9, 132.3, 131.0, 130.9, 130.9, 130.4, 130.4, 126.5, 126.1, 126.1, 63.1, 58.9, 58.1, 55.3, 55.2, 55.1, 55.0, 54.8, 45.1, 44.9, 41.7, 41.1, 37.7, 34.6, 34.4, 33.6, 32.2, 31.3, 26.8, 26.3. **HRMS** (ESI+): m/z calc. for $\text{C}_{29}\text{H}_{34}\text{Cl}_2\text{N}_5\text{O}_4$: $[\text{M}+\text{H}]^+$ 586.19824, found 586.19933.

6 Mechanistic analysis of probe activation

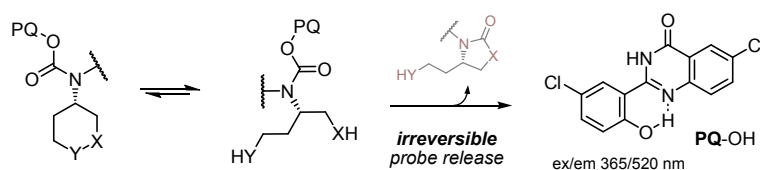


Figure S32 Generalised mechanism of dichalcogenide probe activation.

6.1 Inhibition of probe release quantified through fluorescence

Experimental procedure

For a detailed description of the *in vitro* reduction assay see section 4.2. Probes (**RX1**, **G1**, **SS00**, **C1**, 10 μM) were incubated with 5, 10 and 20 μM (0.5, 1.0 and 2.0 equiv.) of alkylating agents TRi-1 and iodoacetamide at 37 $^{\circ}\text{C}$ for 1 h. Immediately after treatment with TCEP (100 μM , 10 equiv.), fluorescence turn-on was followed on the plate reader in two-minute intervals.

Results

To test our mechanistic proposal for probe activation (Fig 2a-b), particularly the difference between TrxR-selective probe **RX1** and design control **G1**, we hoped to irreversibly intercept the intermediary chalcogenol and thus inhibit the release of fluorescent **PQ-OH** (Fig 2e, Fig S31). We therefore used the widely applied, non-selective thiol-alkylating agent iodoacetamide (IA) as well as selenol-reactive TrxR inhibitor TRi-1 in varying concentrations (0.5, 1.0 and 2.0 equiv.). The non-selective release probe **SS00** and non-reducible **C1** were used as controls (Fig S31).

By design, **RX1** features a 1,2-thiaselenane motif where the amino-functionality is in a 1,4-relationship to selenium and only 1,5- to sulfur. Upon reduction, the intermediary selenolthiol can then perform **PQ-OH**-release through chalcogenol-cyclisation onto the linking carbamate under either a 5-*exo*-trig (Se) or a 6-*exo*-trig cyclisation (S). Based on our hypothesis, the 5-*exo*-trig reaction dominates regardless of the chalcogenol (full discussion in the main text), successful **RX1**-activation thus requires a functional selenol-intermediate. Consequently, when incubating **RX1** with selenol-selective alkylator TRi-1, fluorescence signal generation is efficiently suppressed. The dose-dependent inhibition of probe release indicates an exceptionally fast and selective selenol-alkylation by this TrxR-inhibitor, outpacing 5-*exo*-trig cyclisation and classifying TRi-1 as a general tool for selenol-alkylation. In line with these experiments, IA similarly succeeded in dose-dependently suppressing probe activation, but to a significantly lesser degree. Since even 2.0 equiv. of IA only lead to a ~50% decrease in fluorescence intensity, we expect selenol-alkylation by IA in much bigger competition with 5-*exo*-trig cyclisation than for TRi-1.

In line with our mechanistic proposal and in contrast to **RX1**, **G1** undergoes **PQ-OH** release under a 5-*exo*-trig cyclisation from sulfur instead of selenium, a 6-*exo*-trig cyclisation from selenium is considered unlikely. Supporting this rationale, treatment of **G1** with TRi-1 (which proved highly selenol-selective in the case of **RX1**) did not have a significant effect at 0.5 and 1.0 equiv. Only when applying 2.0 equiv. of inhibitor, a decrease in fluorescence by 50% was observed. This supports although kinetically favoured, not only selenols, but also thiols can be alkylated with an excess of TRi-1 and in the absence of selenols (here: already alkylated with 1.0 equiv. TRi-1). In addition, incubation with IA did not result in a measurable decrease in probe activation regardless of the applied concentration. We again expect alkylation at Se to be kinetically favoured over S and iodoacetamide as a weaker alkylating agent than TRi-1. Therefore, only a selenol-dependant activation mechanism as seen for **RX1** would be affected by IA. Since this does not apply, the experiments support the “irrelevance” of **G1**'s intermediary selenol for **PQ-OH** release.

As a comparative example for a selenium-independent probe activation mechanism, we additionally examined **SS00**, which upon reduction commits to a thiol-5-*exo*-trig cyclisation. Treatment with both TRi-1 and IA did not lead in considerable inhibition of fluorescence at any of the applied concentrations. This supports the above findings that within the 15 min-timeframe, only selenols are significantly alkylated with the applied agents. The proposed 50% alkylation of **G1**'s intermediary thiol with 20 μM TRi-1 might thus after all result from a higher local basicity/ thiol-reactivity due to the appended piperazinamide sidechain or a slower 5-*exo*-trig cyclisation.

In conclusion, the interception of the reduced selenolthiol intermediates of **RX1** and **G1** provided strong support for our mechanistic rationale. Successful inhibition with alkylators not only proved the presence of a reduced selenolthiol intermediate, but also indicates an activation mechanism through 5-*exo*-trig cyclisation onto the linker carbamate regardless of the chalcogenol. As a final remark, it is worth noting that following incubation with TCEP alone, **RX1** reaches the plateau of maximum fluorescence after roughly 15 min, while **G1** and **SS00** do not plateau within the timeframe of this experiment. This again is in line with a selenium-5-*exo*-trig reaction being faster than for sulfur.

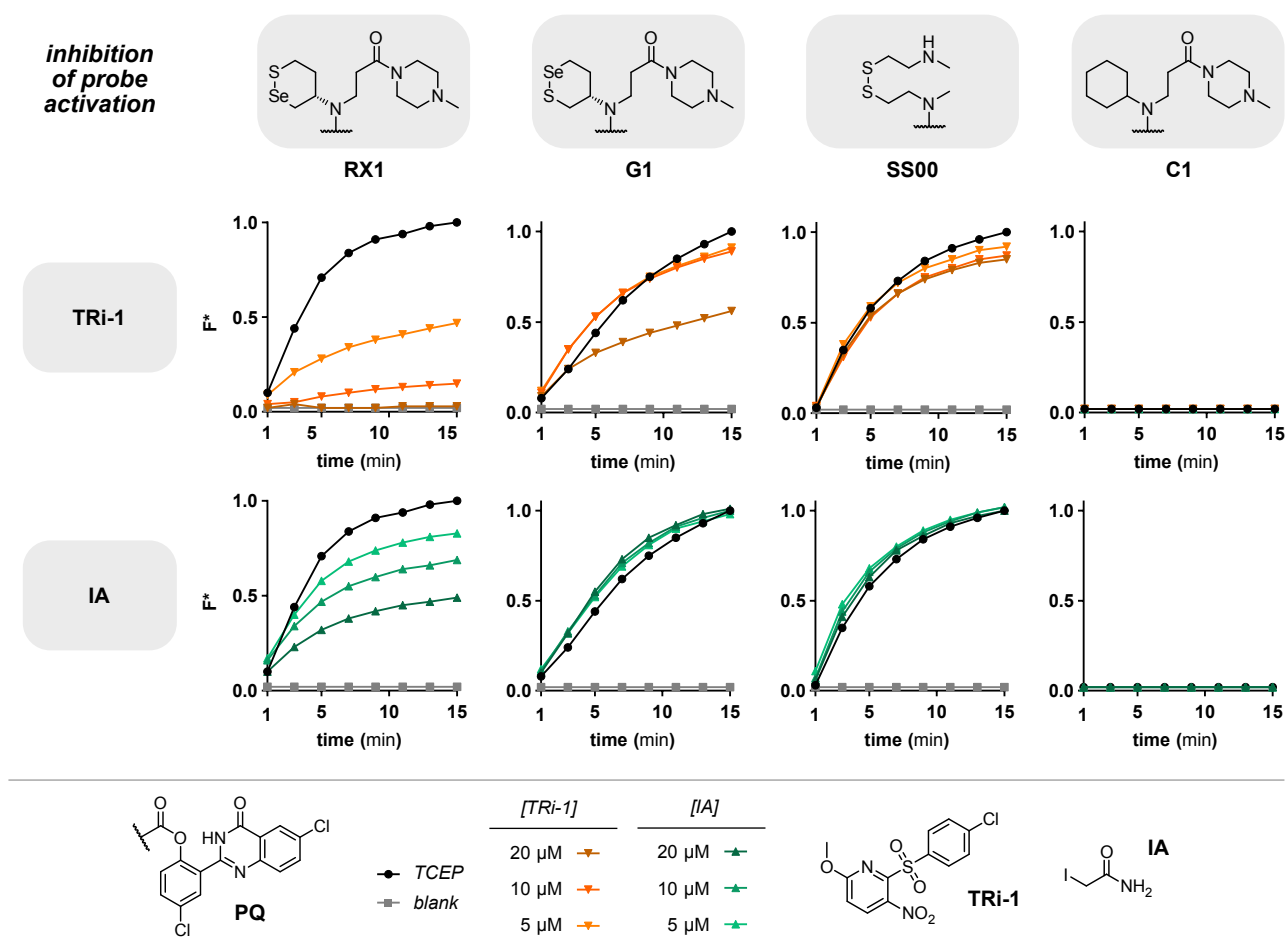


Figure S33 Inhibition of probe activation with chalcogenol-reactive alkylating agents TRi-1 and iodoacetamide (IA). Probes (**RX1**, **G1**, **SS00**, **C1**) were preincubated with inhibitors (0.5, 1.0 and 2.0 equiv.) and activated with TCEP (10 equiv.). Fluorescence turn-on was monitored in two-minute intervals for 15 min.

6.2 Qualitative analysis of the probe activation mechanism by LCMS

Experimental procedure

In an LCMS vial, 10 μ L probe (**RX1**, **G1**, **SS00** or **C1**, 1 mM in DMSO) were spiked into 190 μ L TE buffer and optionally treated with 10 μ L of chalcogen alkylator (TRi-1 or IA, 1.0 equiv., 1 mM in DMSO). The mixture was incubated at 37 °C for 1 h and then optionally charged with 20 μ L of TCEP (10 equiv., 5 mM in TE buffer). After another hour of incubation, samples were analysed by HPLC-MS.

Results

As a complementary experiment to inhibition of fluorescence readout, we analysed inhibited TCEP-mediated probe activation by HPLC-MS. In doing so, we hoped to identify side products and intercepted intermediates of our postulated release mechanism, while ruling out alternative pathways of **PQ-OH** release. We analysed our probes (**RX1**, **G1**, **SS00**, **C1**) incubated under five different conditions: (1) pure probe in buffer, (2) probe activated with TCEP, (3) probe incubated with TRi-1, (4) probe pre-incubated with TRi-1, then activated with TCEP, (5) probe pre-incubated with IA, then activated with TCEP. Results are depicted in Fig S34-37, the outcomes of each experiment are represented by the DAD trace at 254 nM (black) and the total ion current (TIC, ESI+, blue). The HPLC-MS trace is cut off before 2 min, since only buffer components (EDTA, Tris) and TCEP (reduced and oxidised forms) eluted until this retention time. The results presented should only be interpreted *qualitatively*, since varying absorbance and ionizability of the observed species do not allow quantification.

Incubation of **RX1** with TCEP for 1 h fully consumes the probe and cleanly yields free **PQ-OH** and the 5-exo-trig cyclisation selenocarbamate product. Based on these LCMS-data alone, a 6-exo-trig thiocarbamate species would also appear feasible. Incubation of **RX1** with TRi-1 provided clean traces of the unreacted species, proving inhibition effects observed above (section 5.1) as a result of alkylation of the post-reduction selenolthiol intermediate. When challenging pre-treated (with equimolar amounts of TRi-1) **RX1** with TCEP, the probe is fully consumed – but neither resulting in free **PQ-OH** or the corresponding selenocarbamate byproduct. Instead, the presence of TRi-1 efficiently provides the mono-alkylated, reduced intermediate of **RX1**. This, as well as the observed sulfinic acid byproduct clearly proves both the S_NAr -type mechanism of action of the TrxR-inhibitor TRi-1 and the diminished fluorescence observed in section 5.1. Matching these observations, IA-inhibition of **RX1**-activation similarly gave significant amounts of the mono-alkylated intermediate alongside **PQ-OH** – now fully corresponding to the inhibition-efficiency seen during fluorescence measurements.

G1 in comparison, exhibited a remarkable difference in the species observed upon activation. When treated with TCEP, **G1** cleanly provides the free PQ-fluorophore and the cyclisation byproduct, although not under full conversion of the probe. The decisive distinction to **RX1** is the nature of the carbamate byproduct which now possesses an m/z as well as the isotope pattern of the diselenide dimer. This clearly suggests the thiol-5-exo-trig cyclisation as the dominant mechanism of activation for **G1**, and the selenol-5-exo-trig for **RX1**. Incubation of **G1** with TRi-1 again did not result in any reactivity, while TCEP-mediated probe reduction in this mixture efficiently generated **PQ-OH**. Going in line with the above observations, the cyclisation byproduct now exhibits an alkylated rather than a dimerised selenol. In case for **G1**, the cyclisation mechanism can not be inhibited with IA, matching the fluorescence read-out given in section 5.1.

Control probes **SS00** and **C1** ran as expected, with the linear disulfide reacting fully to thiocarbamate and **PQ-OH** upon treatment with TCEP. Both TRi-1 and IA could not inhibit TCEP-mediated probe activation. The presence of a TRi-1-alkylated cysteamine-byproduct gives indication for the rates of thiol-5-exo-trig versus alkylation by TRi-1, the former being faster due to the absence of an intercepted, reduced **SS00**. Since **C1** remained unaffected by treatment with TCEP, no further experiments were run for this probe.

In conclusion, HPLC-MS results underline observations made in section 5.1 and validate our mechanistic proposal for probe activation and design rationale for TrxR-selective probe **RX1**. 5- rather than 6-exo-trig cyclisation occurs regardless of the initiating chalcogenol and is supported through the nature of the observed cyclisation byproducts (**RX1**: thiol, **G1**: diselenide) and the fact that equimolar selenolate alkylators almost entirely block **PQ-OH** release from **RX1**, but only slightly from **G1**. This latter observation also suggests our proposed “on-reductant cyclisation” (e.g. with GSH) may be significant for **G1** but not **RX1**: so matching the third design consideration in section 2.1.

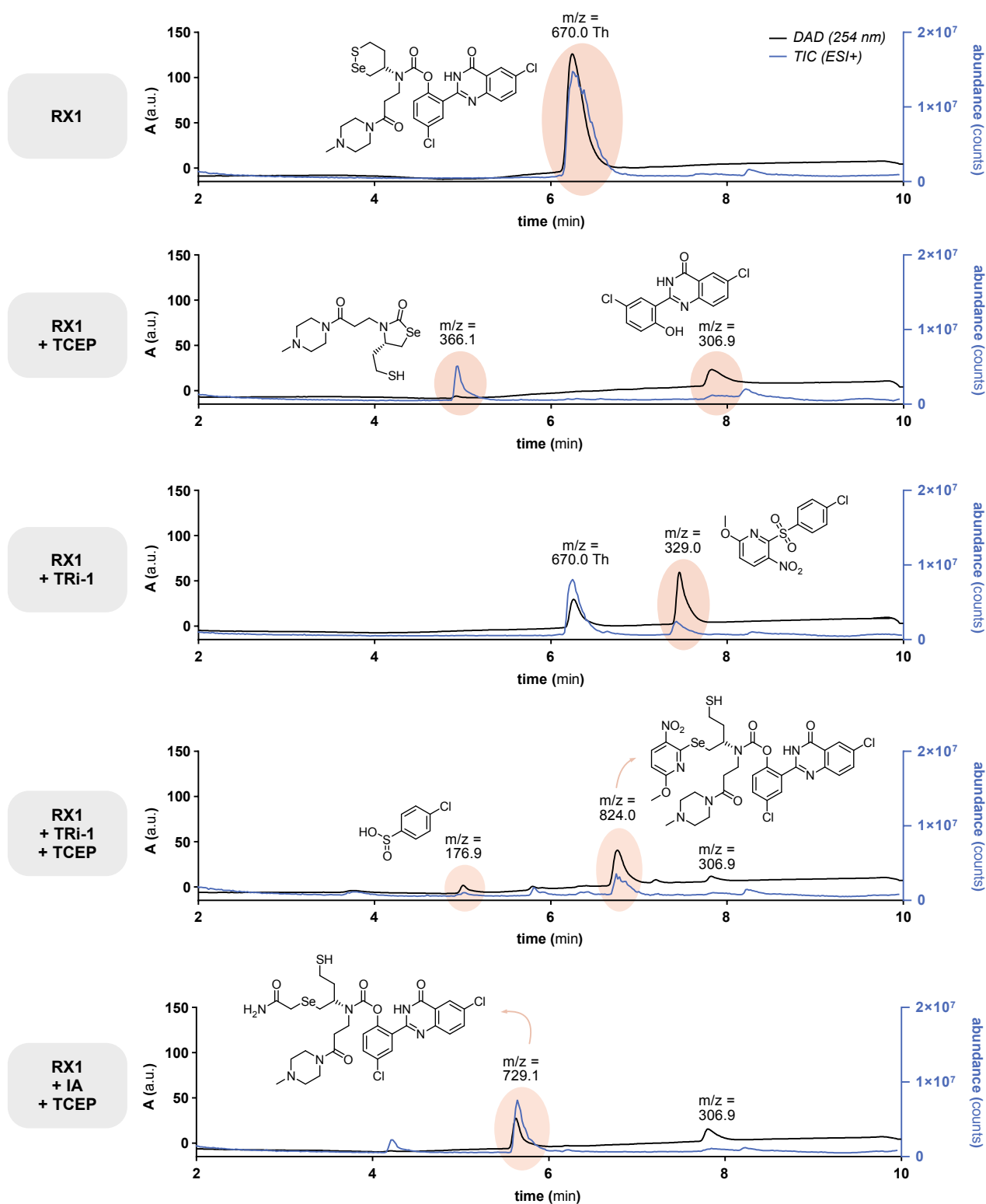


Figure S34 HPLC-MS experiments assessing **RX1**-probe activation, release products and reactivity with TRi-1/IA (1.0 equiv.) with and without TCEP-mediated (10 equiv.) reduction. After each treatment with an additive, the reaction vial was incubated at 37 °C for 1 h.

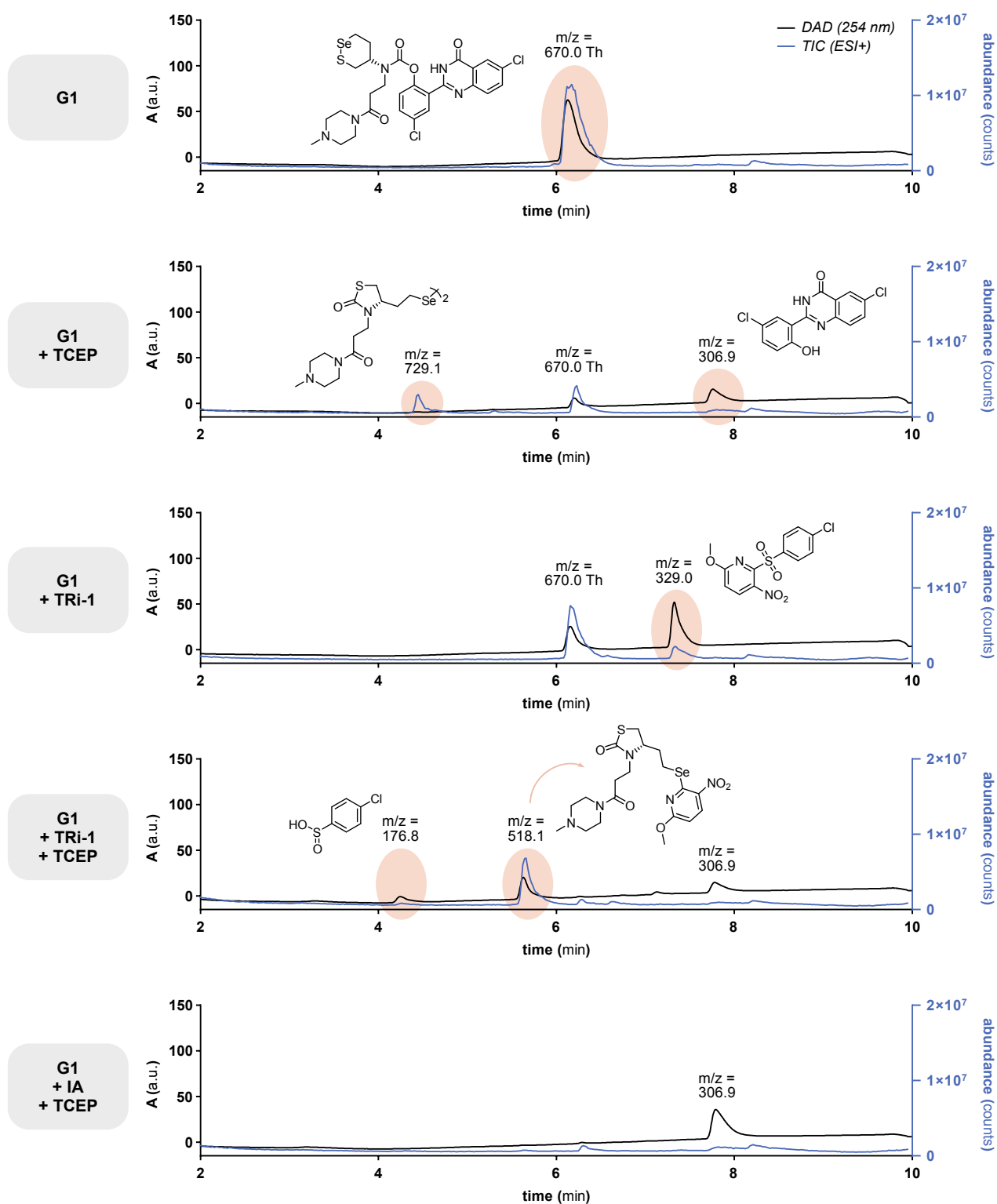


Figure S35 HPLC-MS experiments assessing **G1**-probe activation, release products and reactivity with TRi-1/IA (1.0 equiv.) with and without TCEP-mediated (10 equiv.) reduction. After each treatment with an additive, the reaction vial was incubated at 37 °C for 1 h.

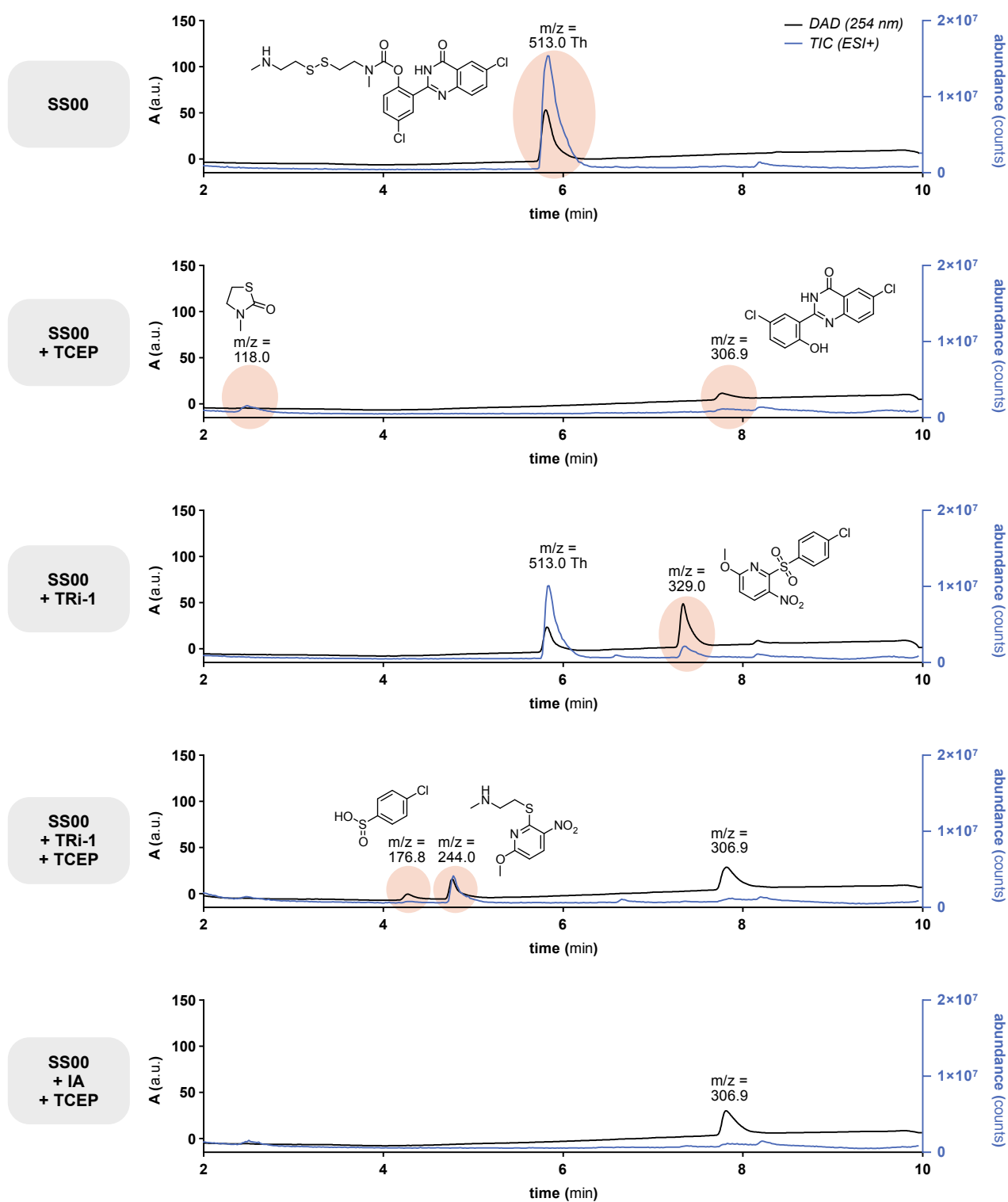


Figure S36 HPLC-MS experiments assessing **SS00**-probe activation, release products and reactivity with TRi-1/IA (1.0 equiv.) with and without TCEP-mediated (10 equiv.) reduction. After each treatment with an additive, the reaction vial was incubated at 37 °C for 1 h.

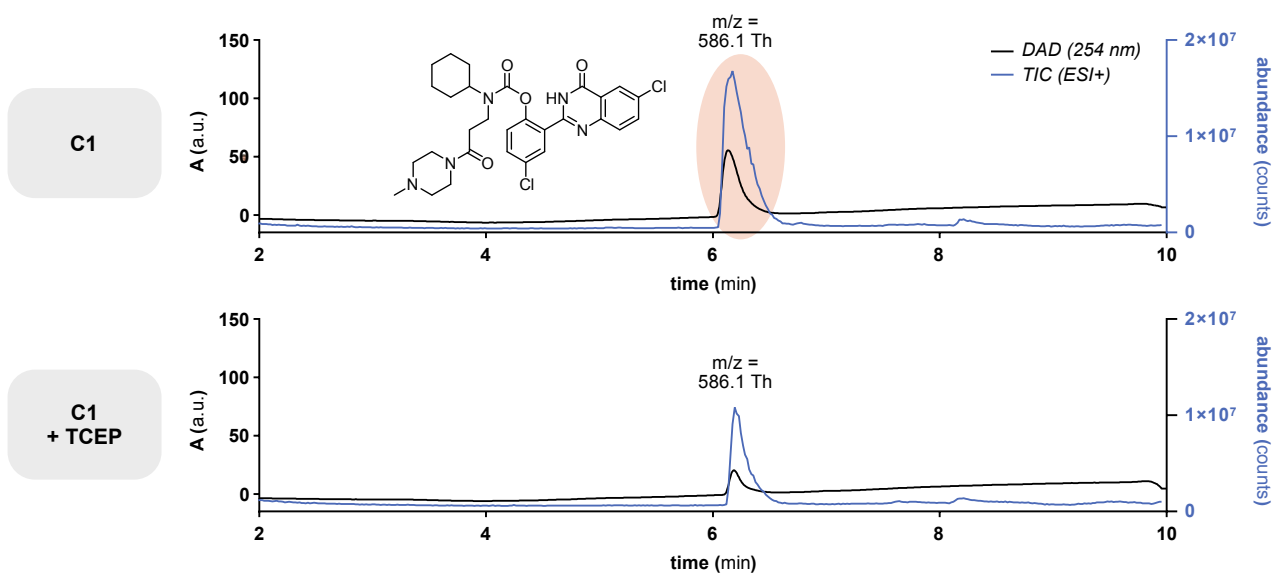


Figure S37 HPLC-MS experiments assessing **C1**-probe activation, release products and reactivity with TRi-1/IA (1.0 equiv.) with and without TCEP-mediated (10 equiv.) reduction. After each treatment with an additive, the reaction vial was incubated at 37 °C for 1 h.

7 NMR spectra

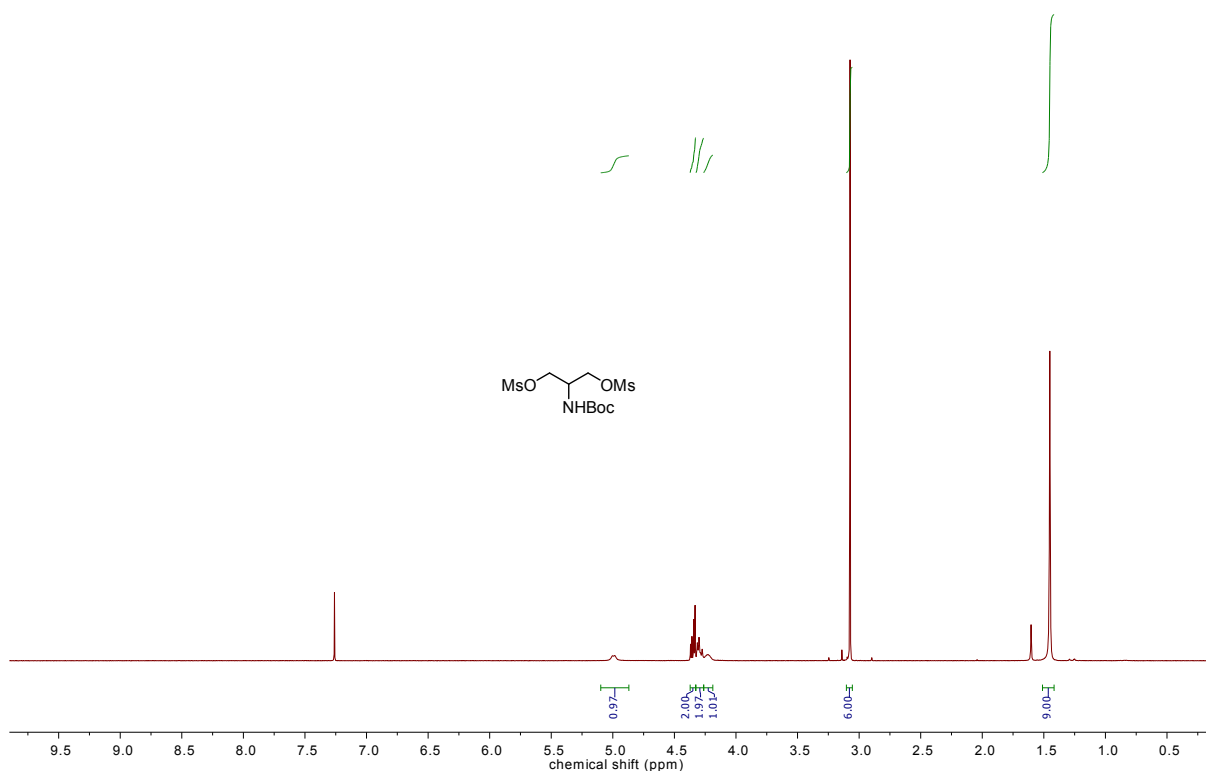


Figure S38 ¹H NMR of *N*-Boc-2-aminopropane-1,3-diyl dimethanesulfonate (**S1**).

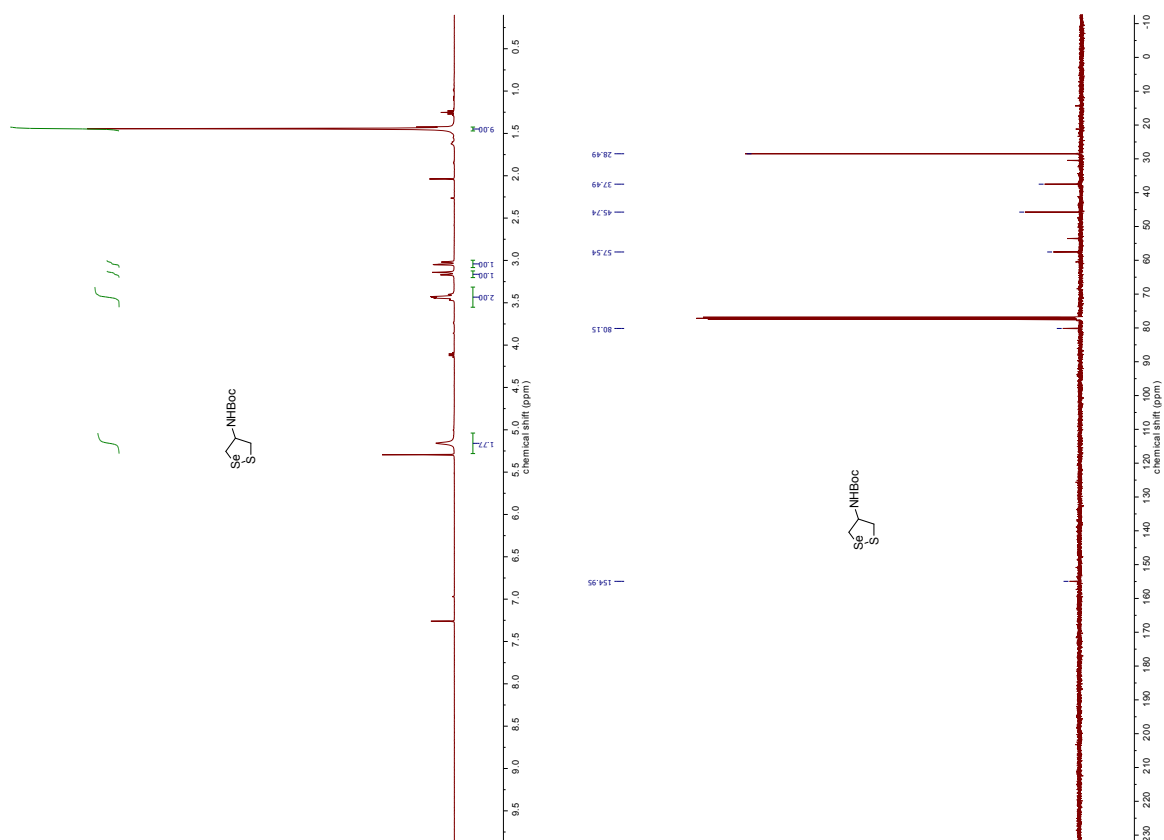


Figure S43, S44 ^1H NMR and ^{13}C NMR of *N*-Boc-1,3-diselenocyanatopropan-2-amine (S4).

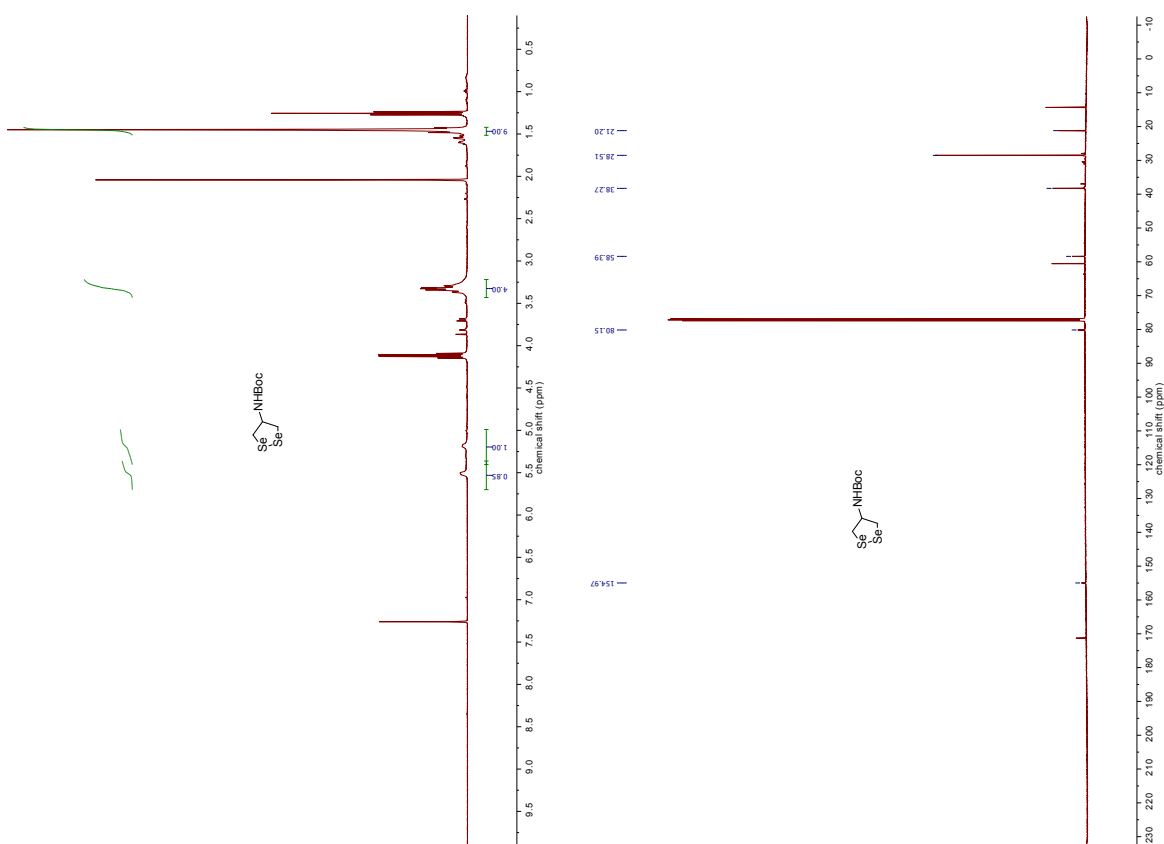


Figure S45, S46 ^1H NMR and ^{13}C NMR of *N*-Boc-1,2-diselenolan-4-amine (S5).

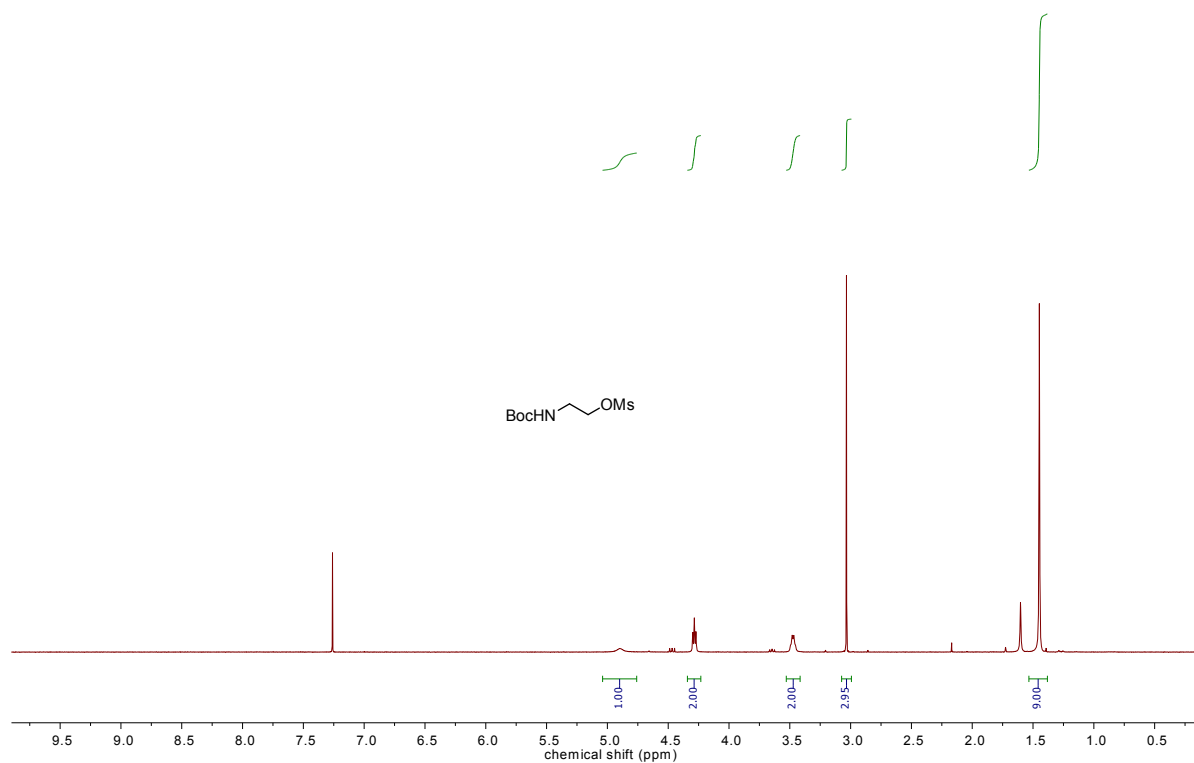


Figure S47 ¹H NMR of *N*-Boc-2-aminoethyl methanesulfonate (**S6**).

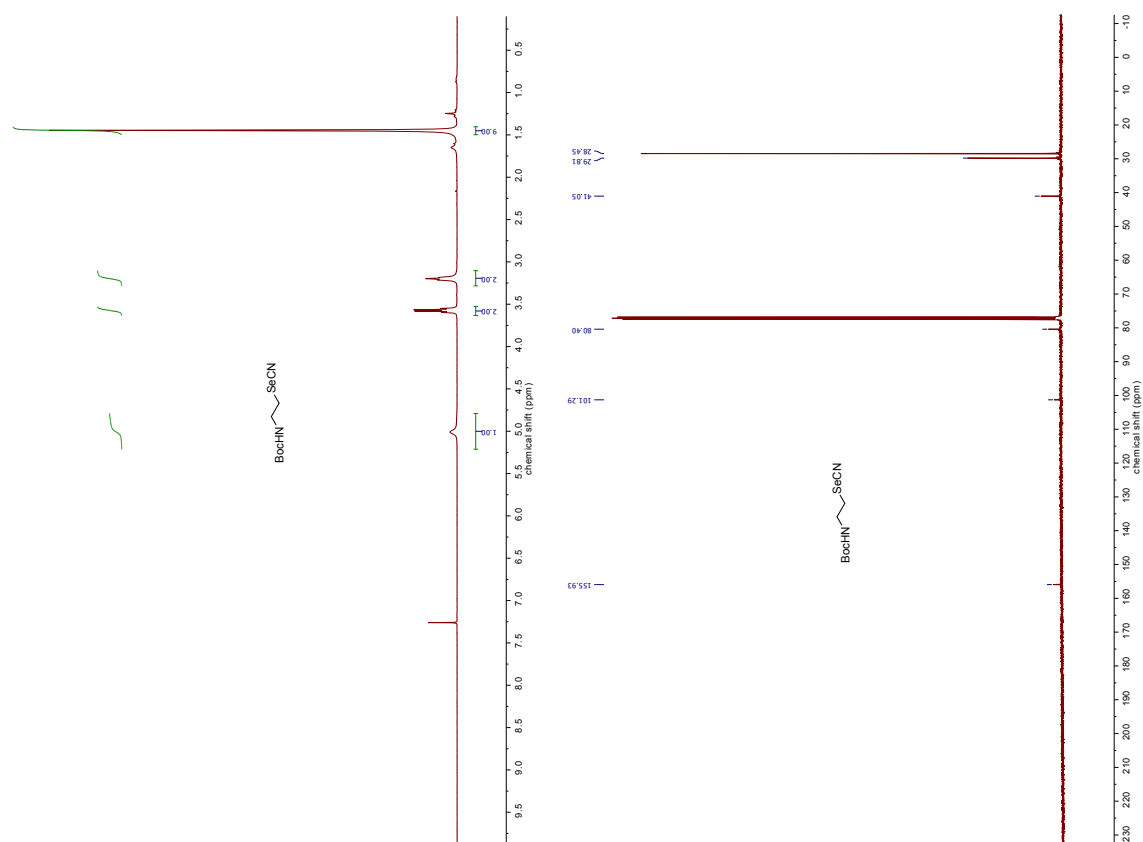


Figure S48, S49 ¹H NMR and ¹³C NMR of *N*-Boc-2-selenocyanatoethanamine (**S7**).

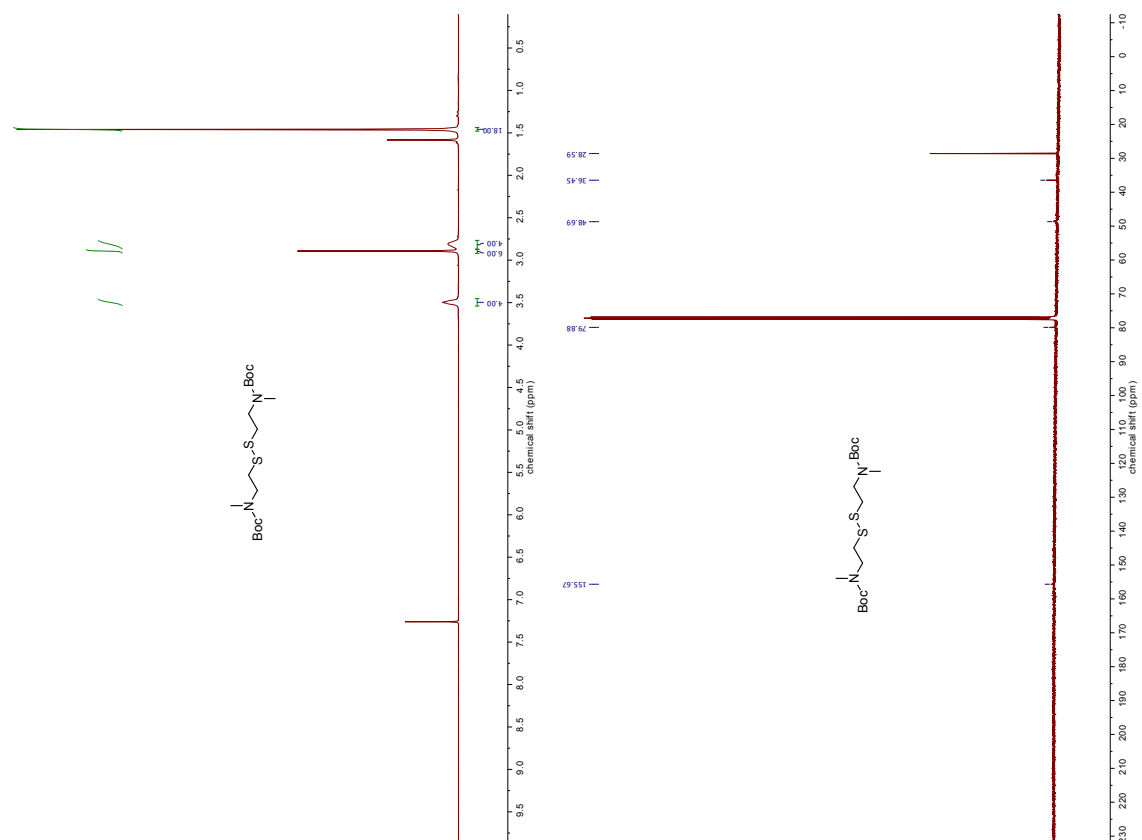


Figure S50 ¹H NMR and ¹³C NMR of di-tert-butyl (disulfanediybis(ethane-2,1-diyl))bis(methylcarbamate) (**S8**).

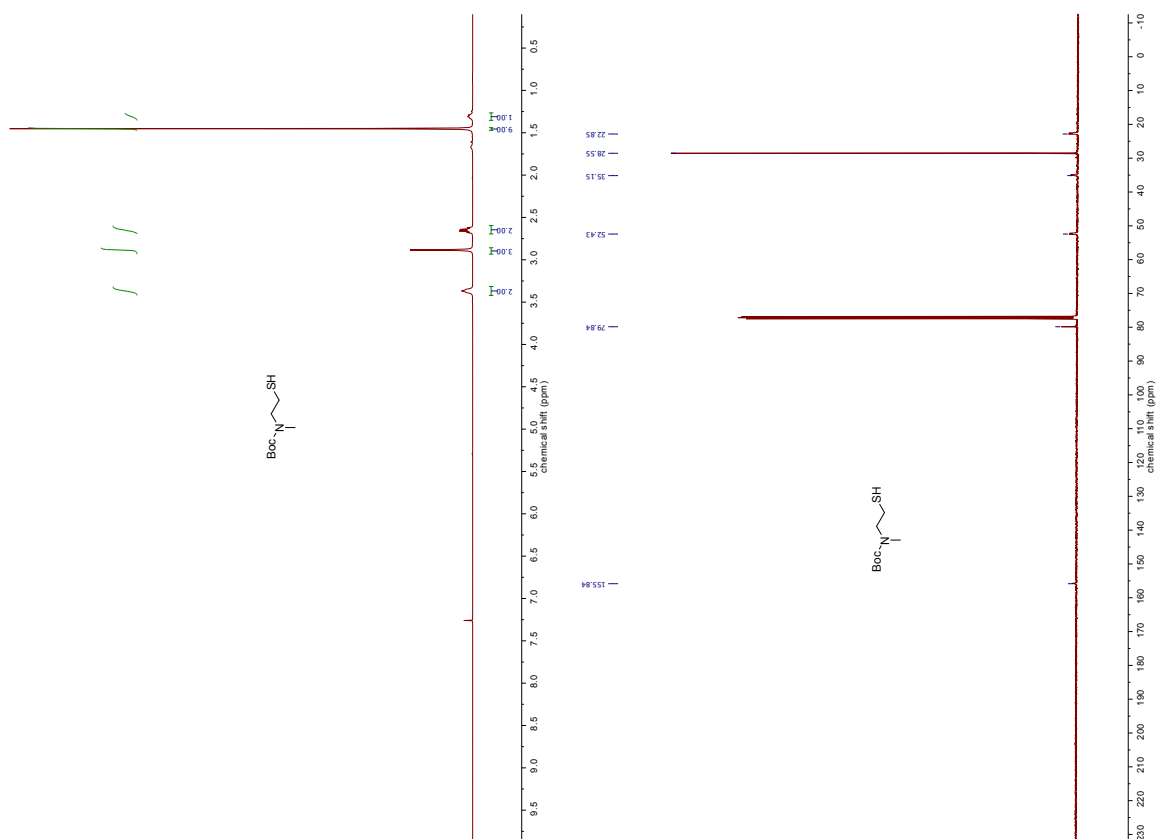


Figure S51, S52 ¹H NMR and ¹³C NMR of *N*-Boc-*N*-methylcysteamine (**S9**).

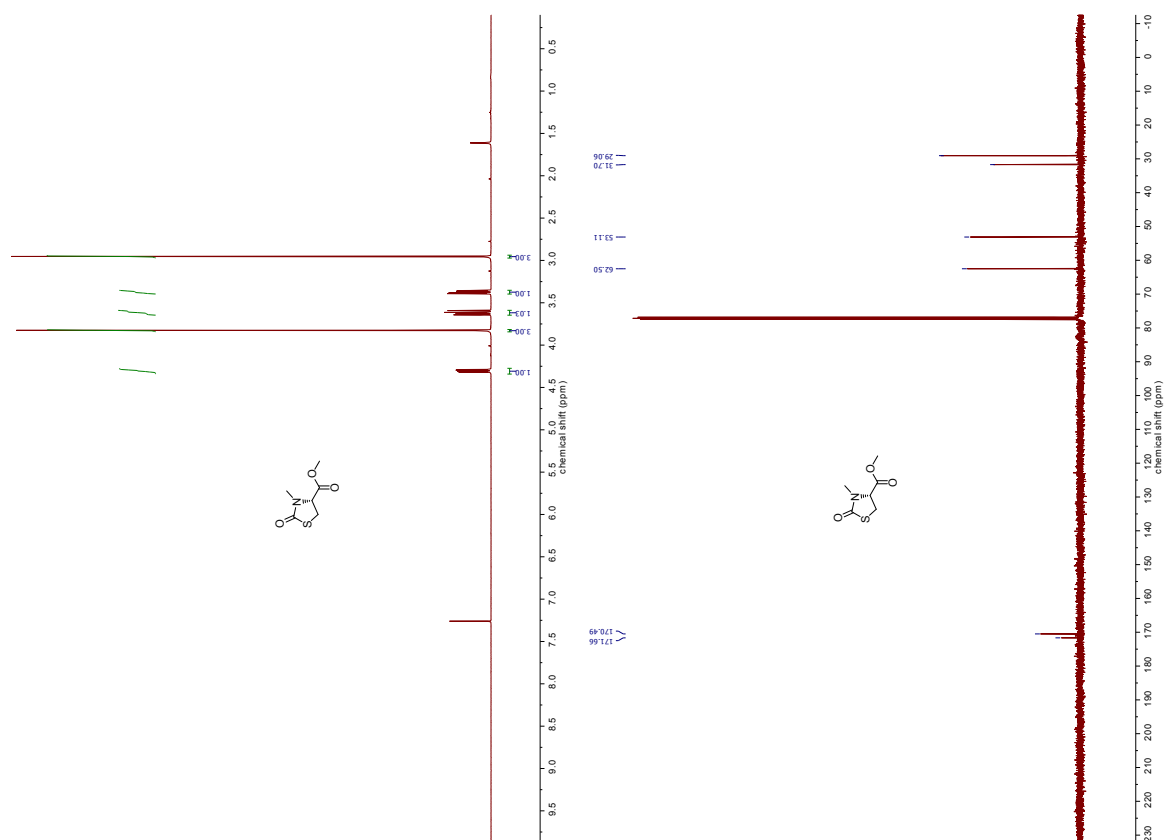


Figure S53, S54 ¹H NMR and ¹³C NMR of methyl-(3-methyl-2-oxothiazolidine)-4-carboxylate (**S10**).

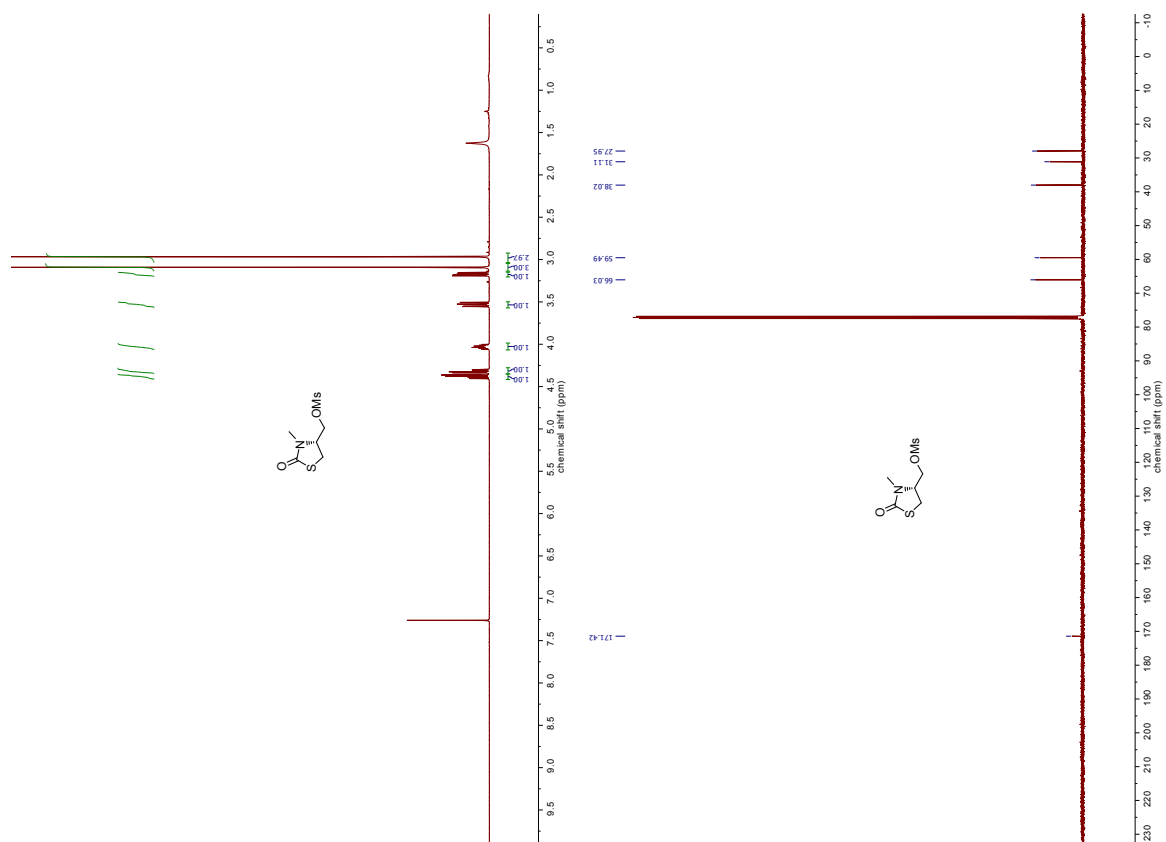


Figure S55, S56 ¹H NMR and ¹³C NMR of (3-methyl-2-oxothiazolidin-4-yl)methyl methanesulfonate (**S11**).

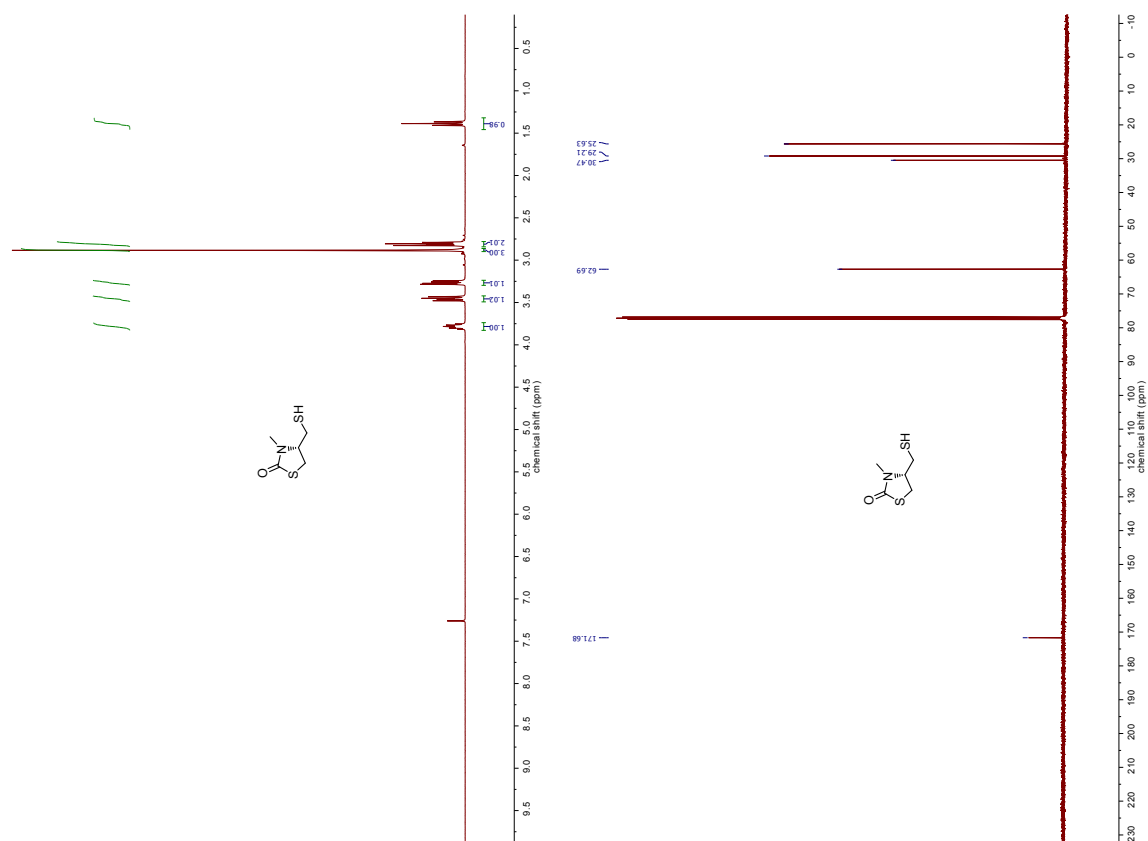


Figure S57, S58 ^1H NMR and ^{13}C NMR of 4-(mercaptomethyl)-3-methylthiazolidin-2-one (**S12**).

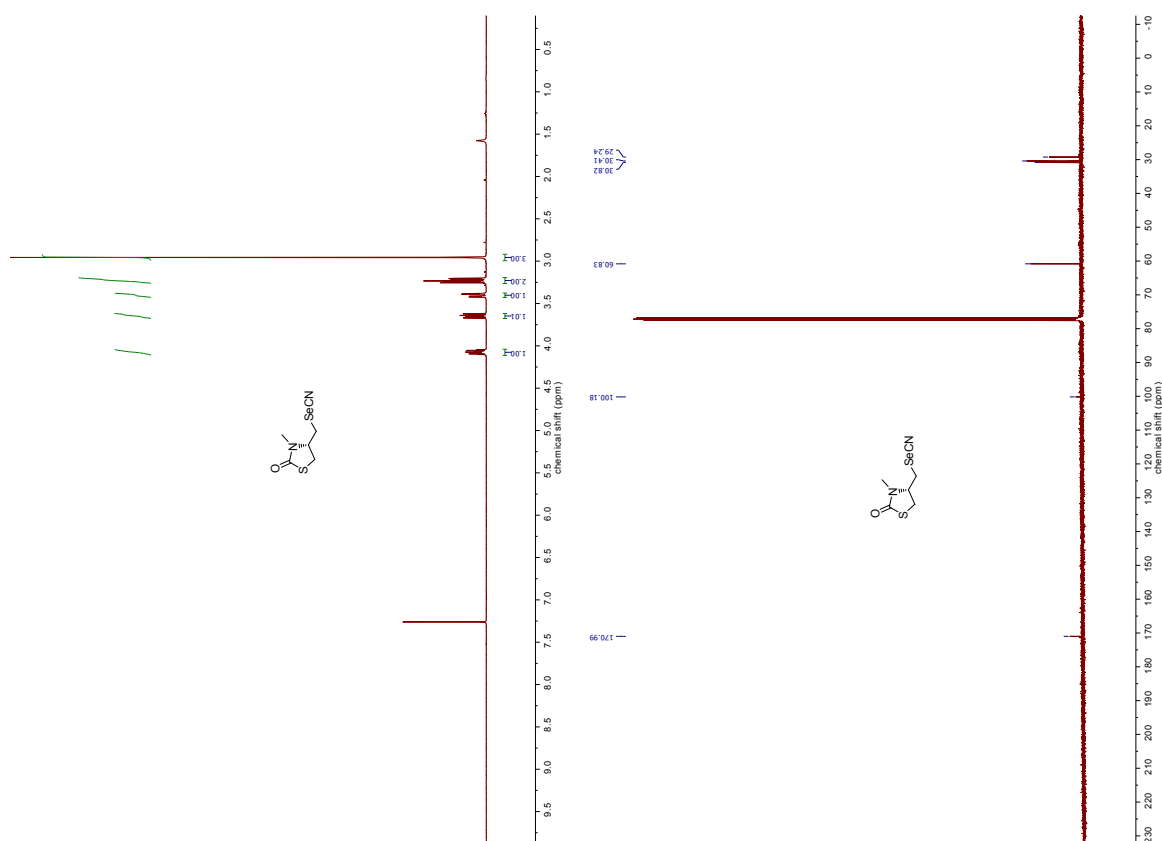


Figure S59, S60 ^1H NMR and ^{13}C NMR of 3-methyl-4-(selenocyanatomethyl)thiazolidin-2-one (**S13**).

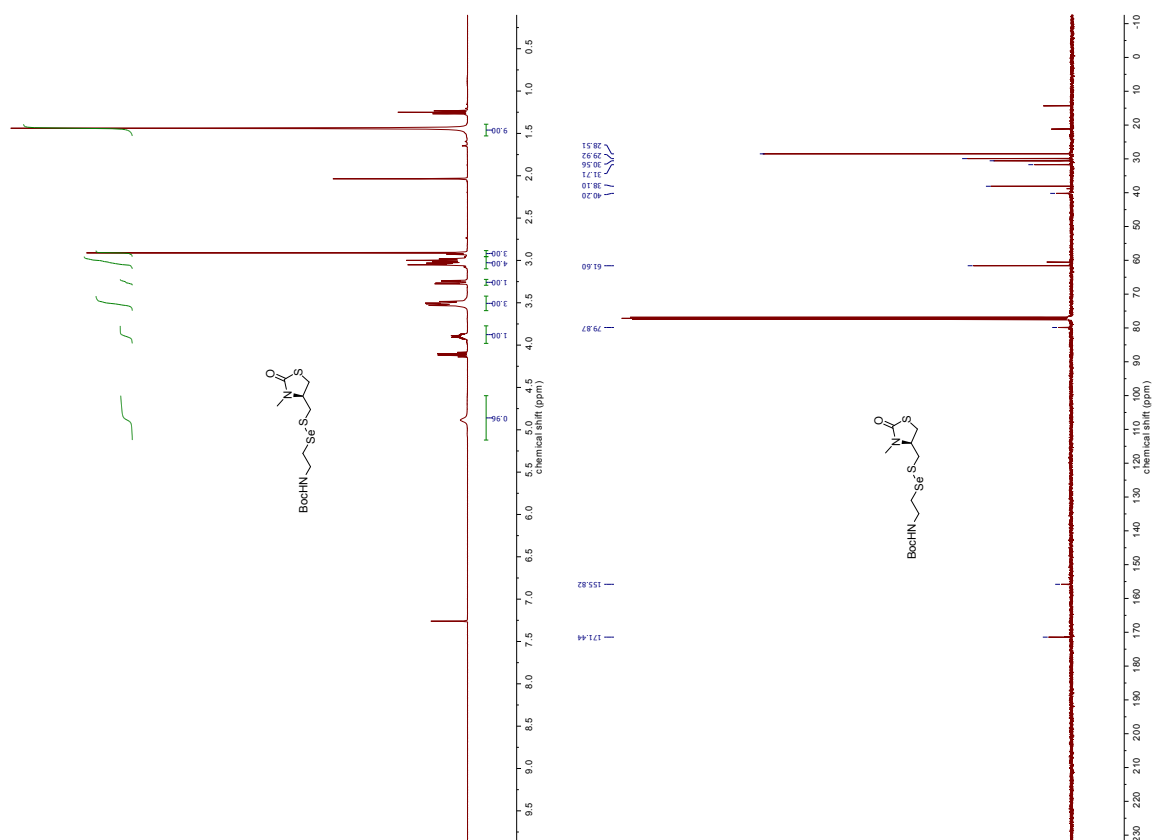


Figure S61, S62 ¹H NMR and ¹³C NMR of 4-((N-Boc-2-aminoethylselanyl)thiomethyl)-3-methylthiazolidin-2-one (S14).

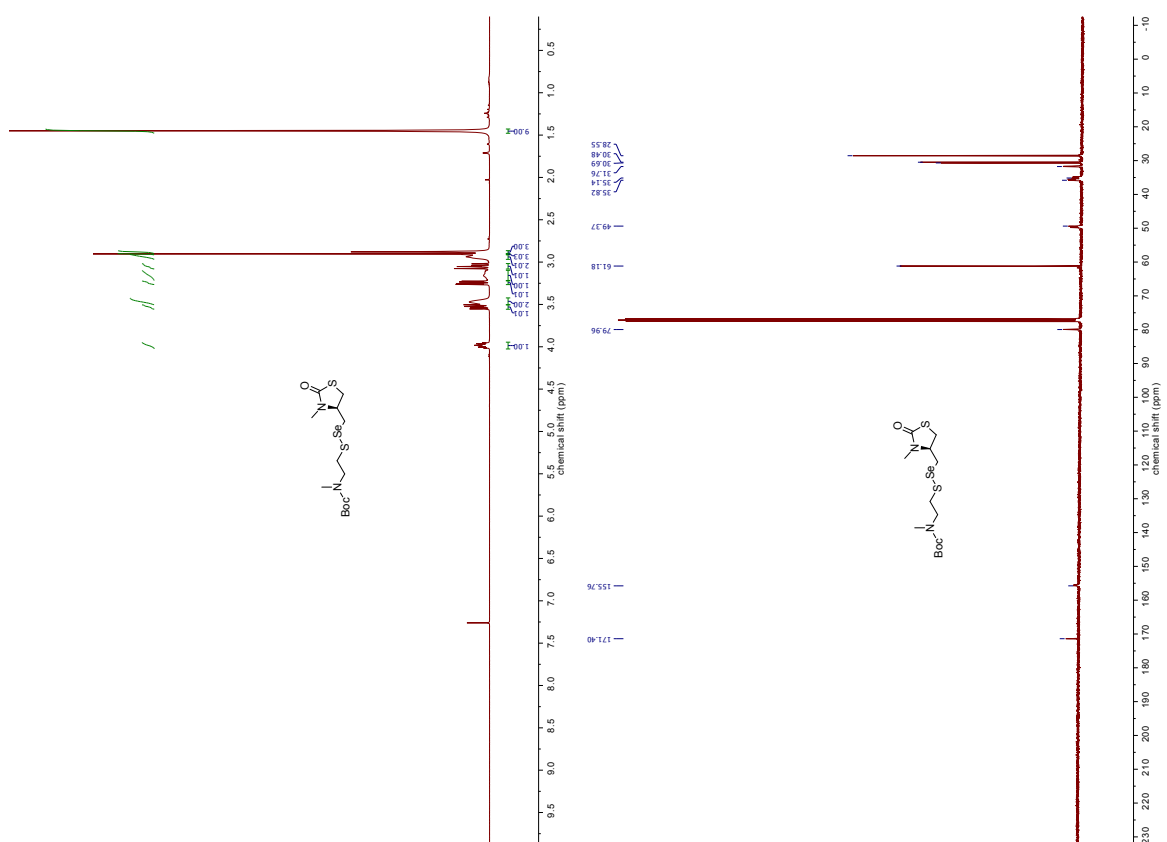


Figure S63, S64 ¹H NMR and ¹³C NMR of 4-((N-Boc-N-methyl-cysteaminy)selamethyl)-3-methylthiazolidin-2-one (S15).

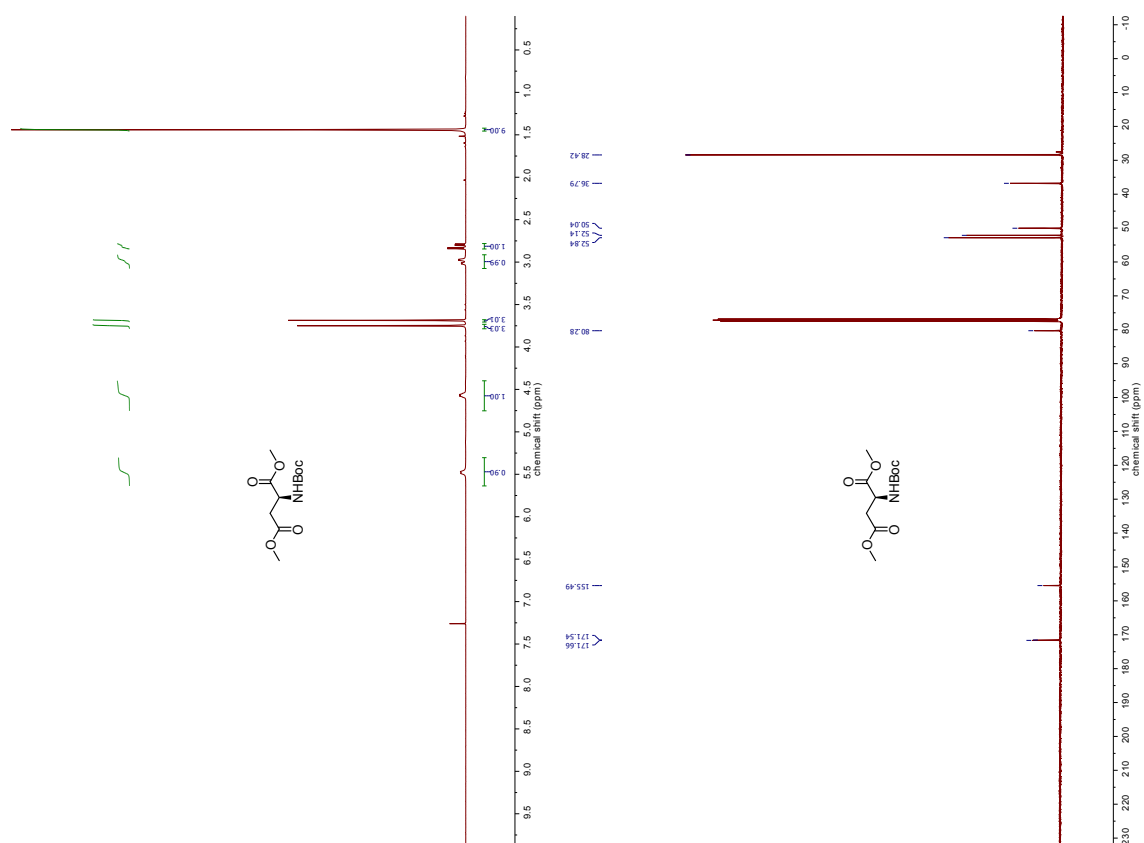


Figure S65, S66 ¹H NMR and ¹³C NMR of *N*-Boc-dimethylaspartate (S16).

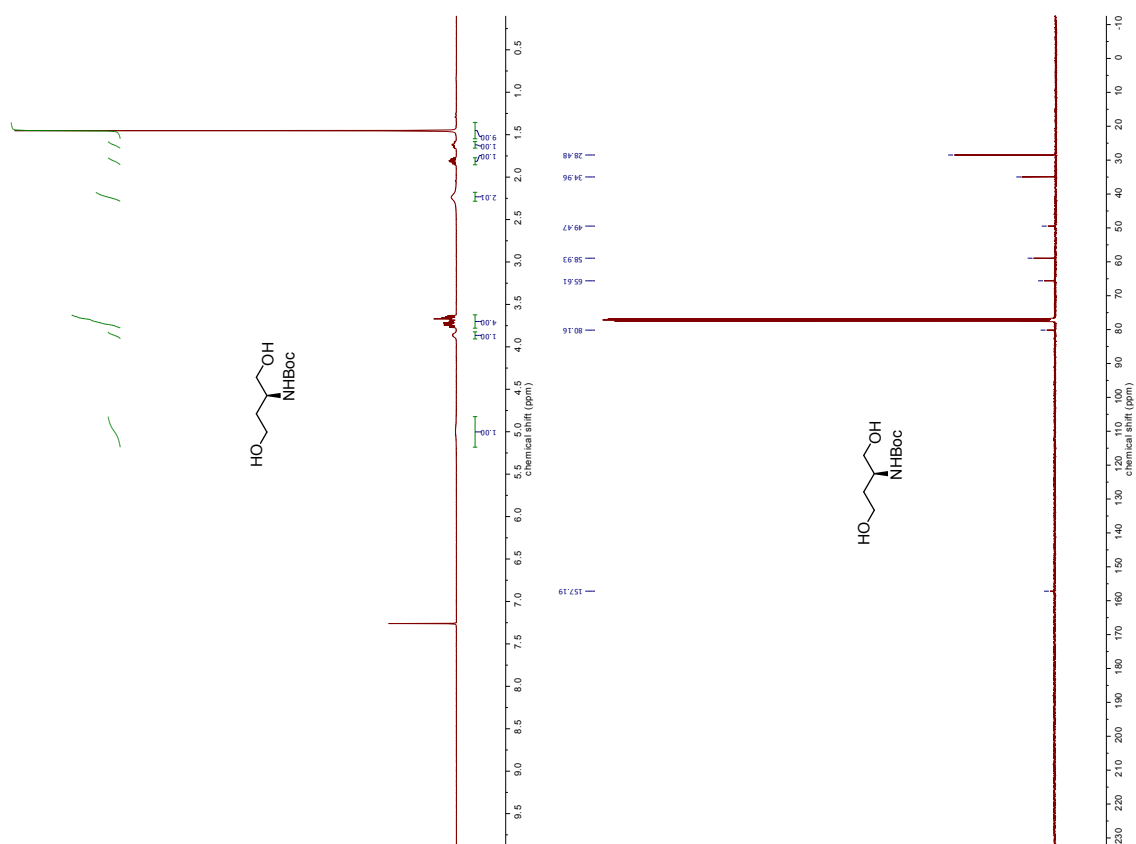


Figure S67, S68 ¹H NMR and ¹³C NMR of *N*-Boc-2-aminobutane-1,4-diol (S17).

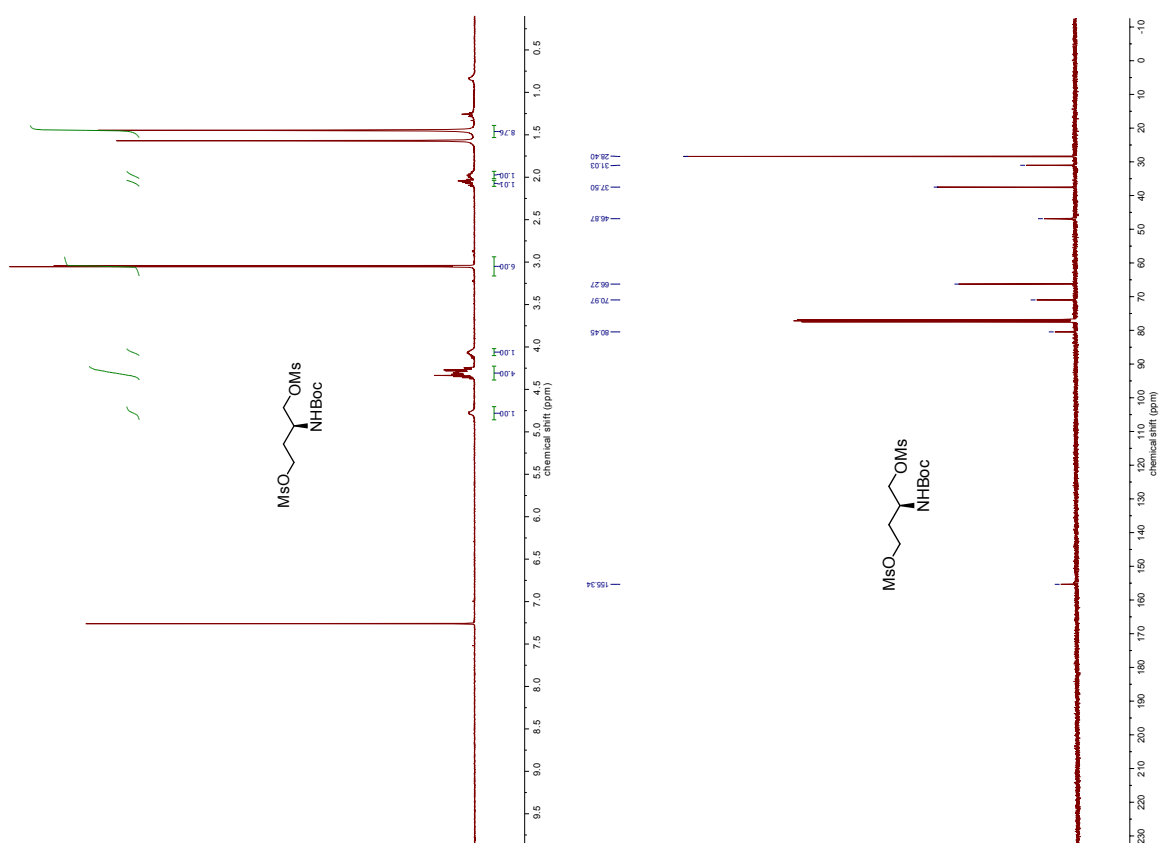


Figure S69, S70 ¹H NMR and ¹³C NMR of *N*-Boc-2-aminobutane-1,4-diyl dimethanesulfonate (1).

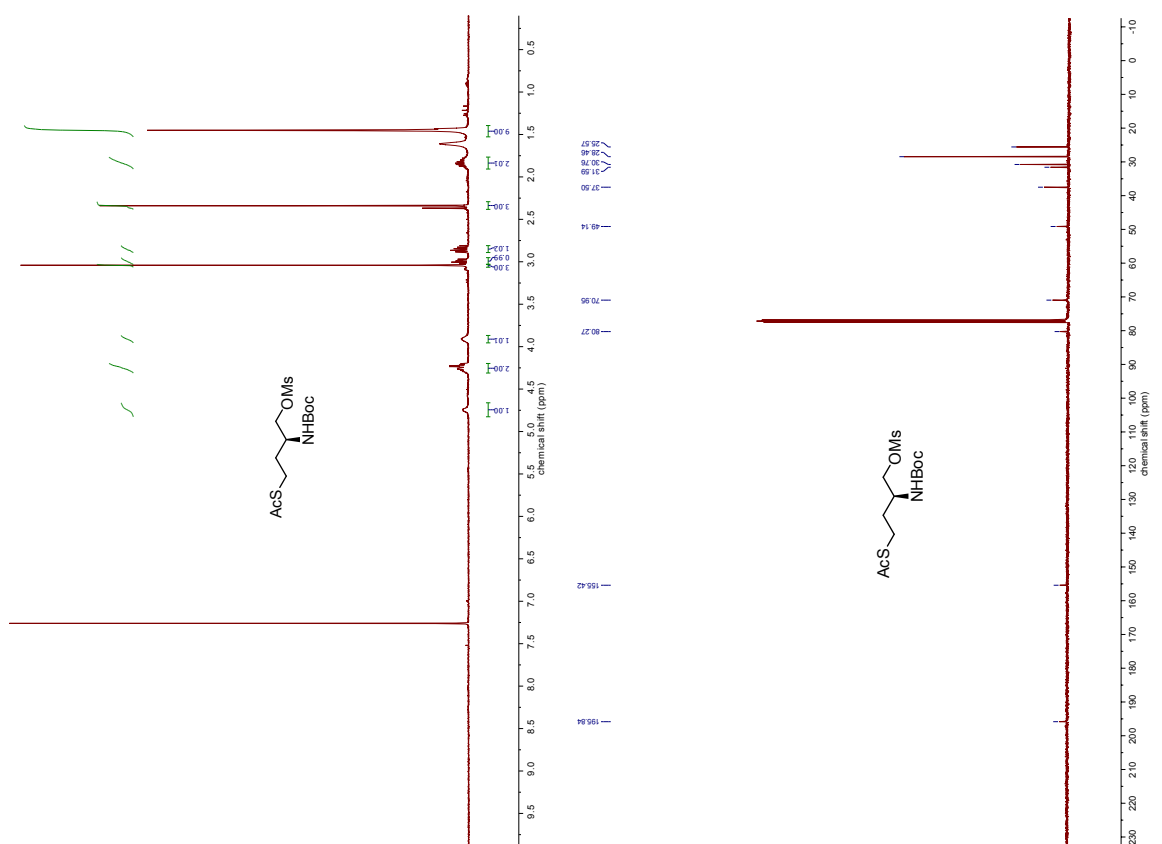


Figure S71, S72 ¹H NMR and ¹³C NMR of *N*-Boc-(3-amino-4-(methanesulfonyl)oxybutyl)ethanethioate (2).

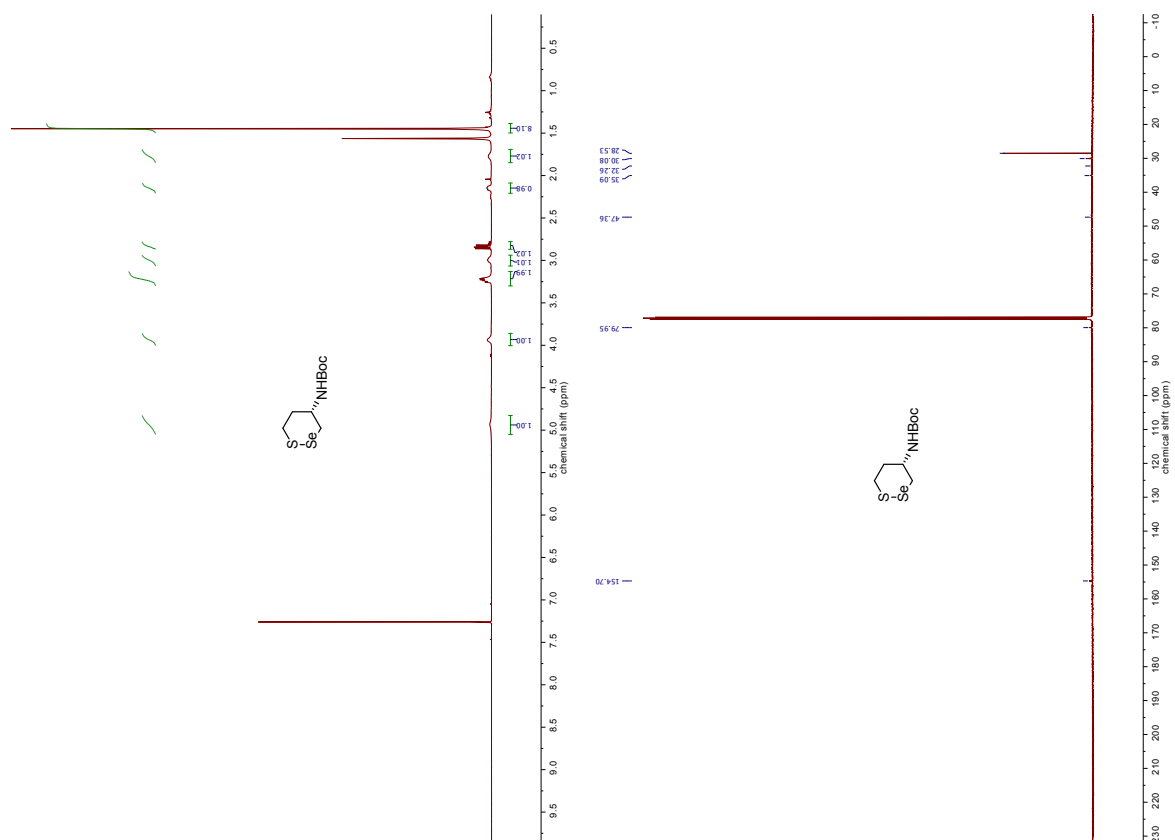


Figure S77, S78 ¹H NMR and ¹³C NMR of *N*-Boc-1,2-thiaselenan-4-amine (5).

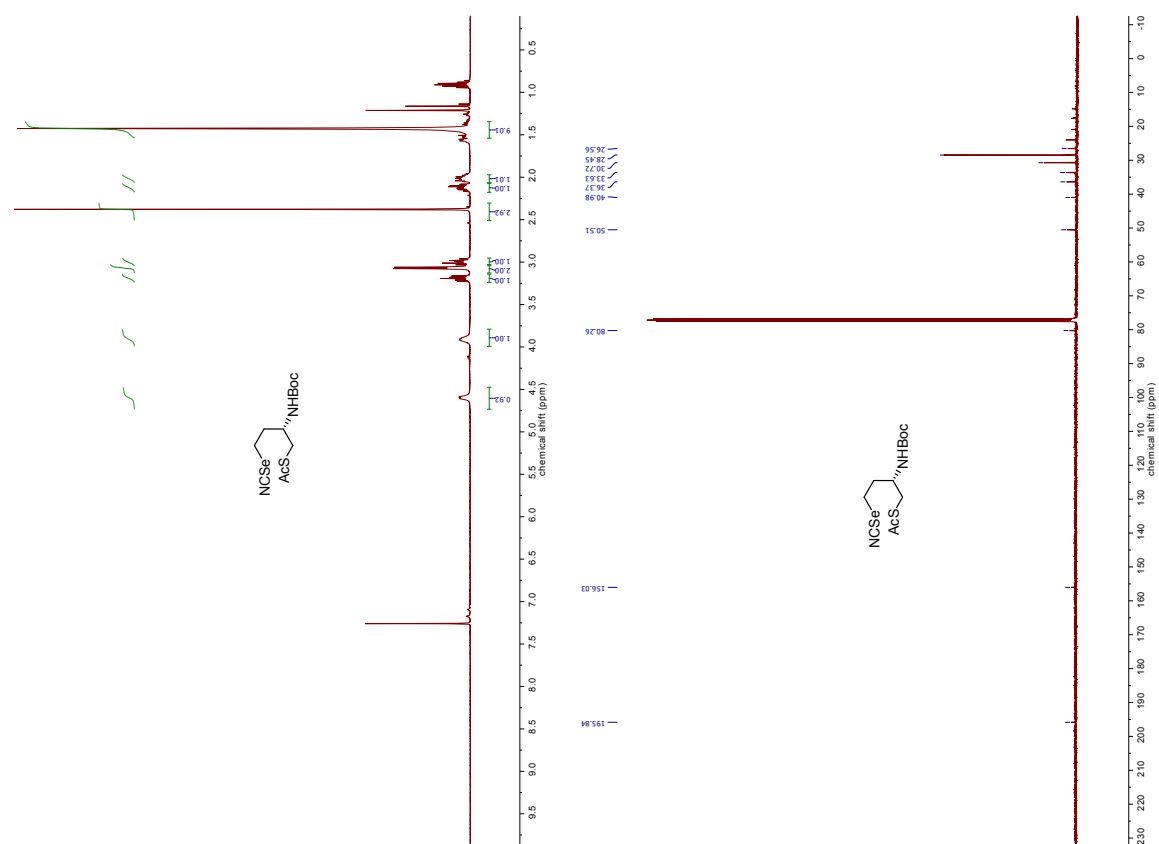


Figure S80, S81 ¹H NMR and ¹³C NMR of *N*-Boc-(2-amino-5-selenocyanatobutyl)ethanethioate (7).

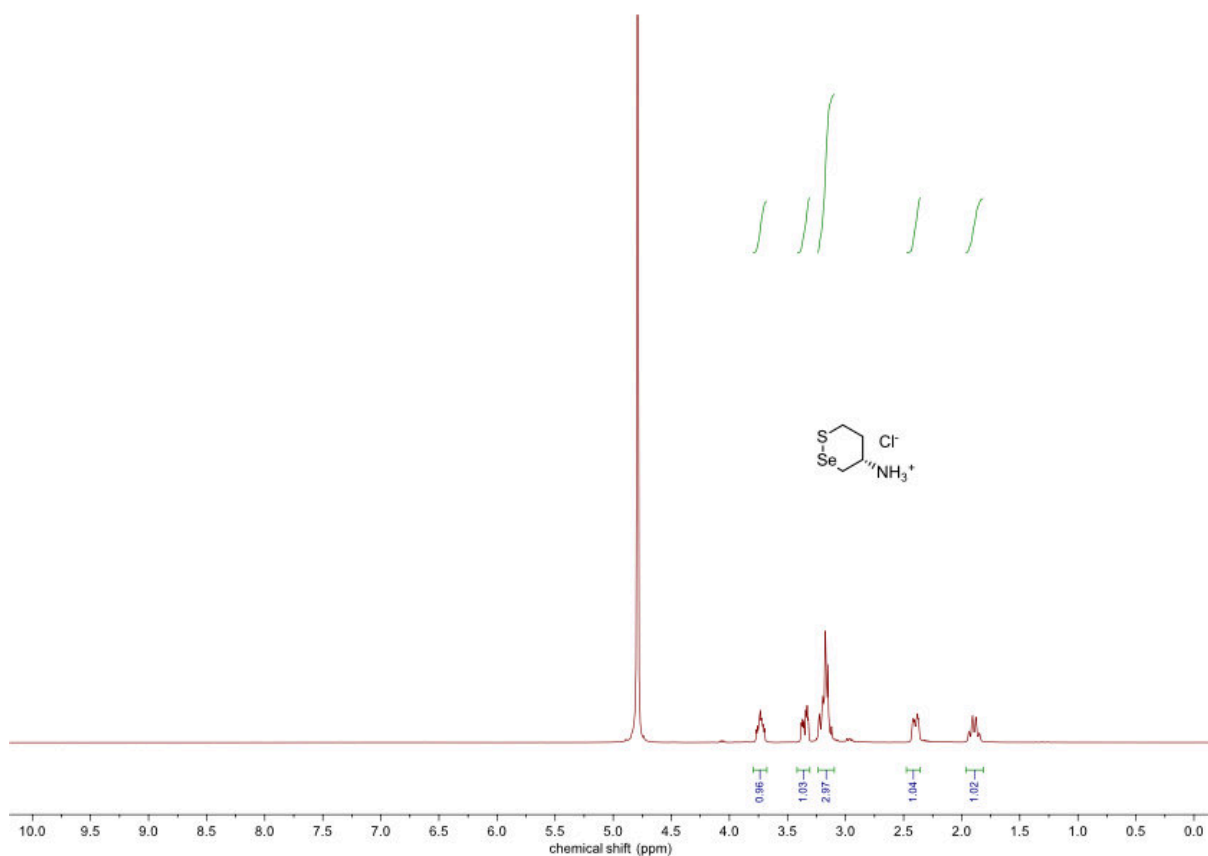


Figure S79 ^1H NMR of 1,2-thiaselenan-4-aminium chloride (**6**).

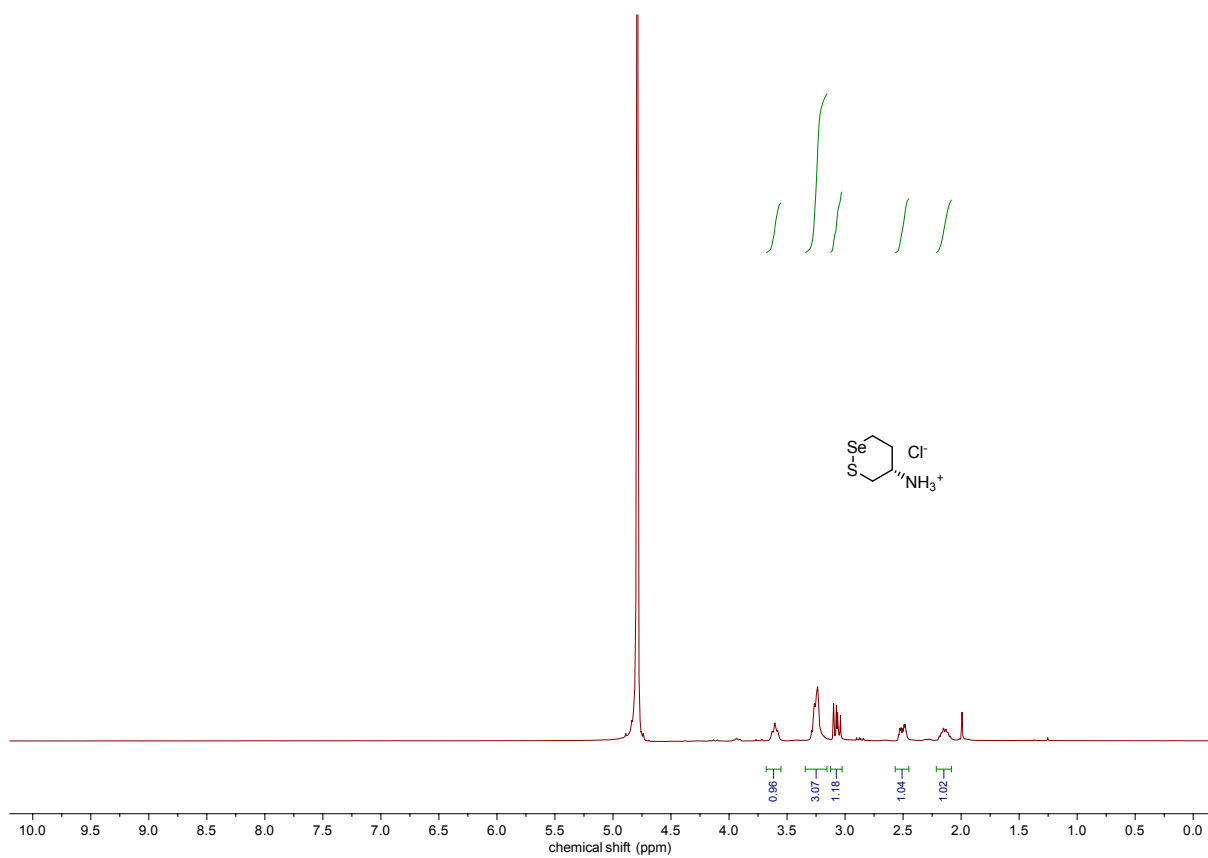


Figure S84 ^1H NMR of 1,2-thiaselenan-5-aminium chloride (**9**).

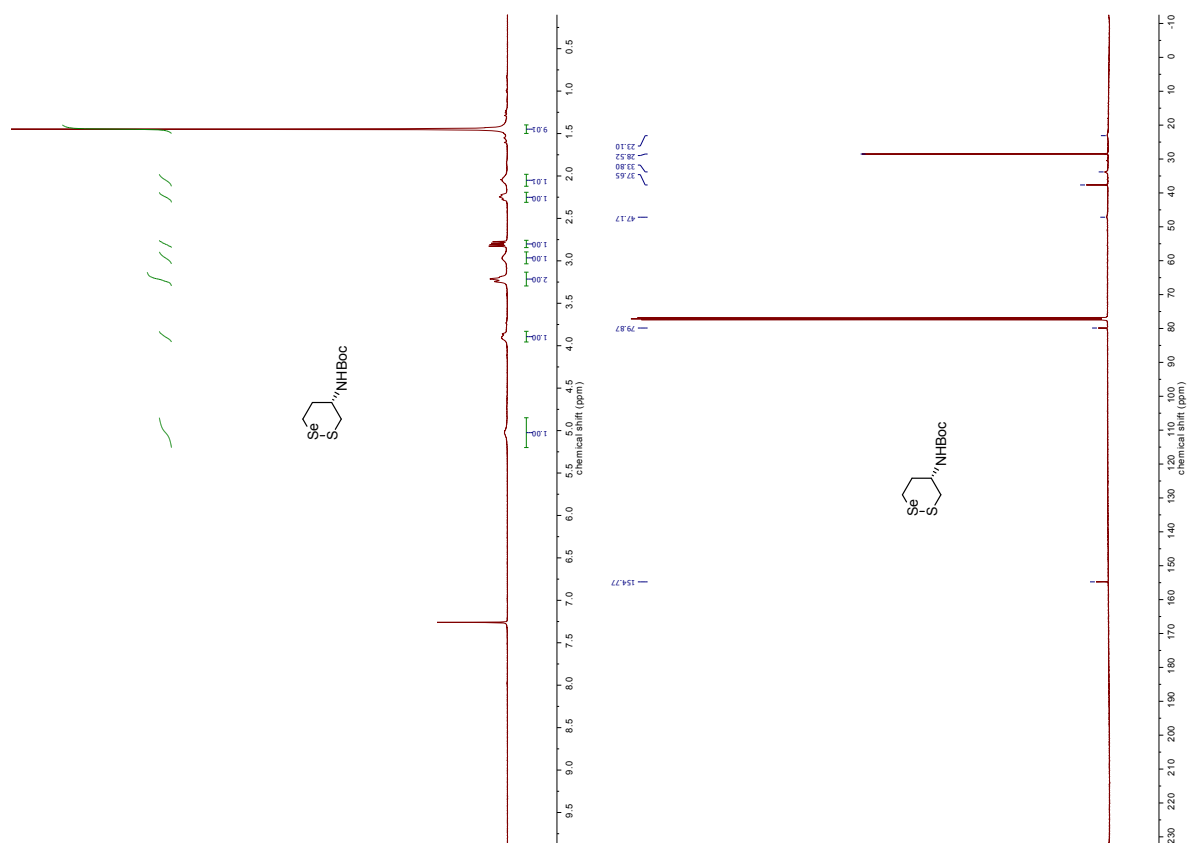


Figure S82, S83 ^1H NMR and ^{13}C NMR of *N*-Boc-1,2-thiaselenan-5-amine (**8**).

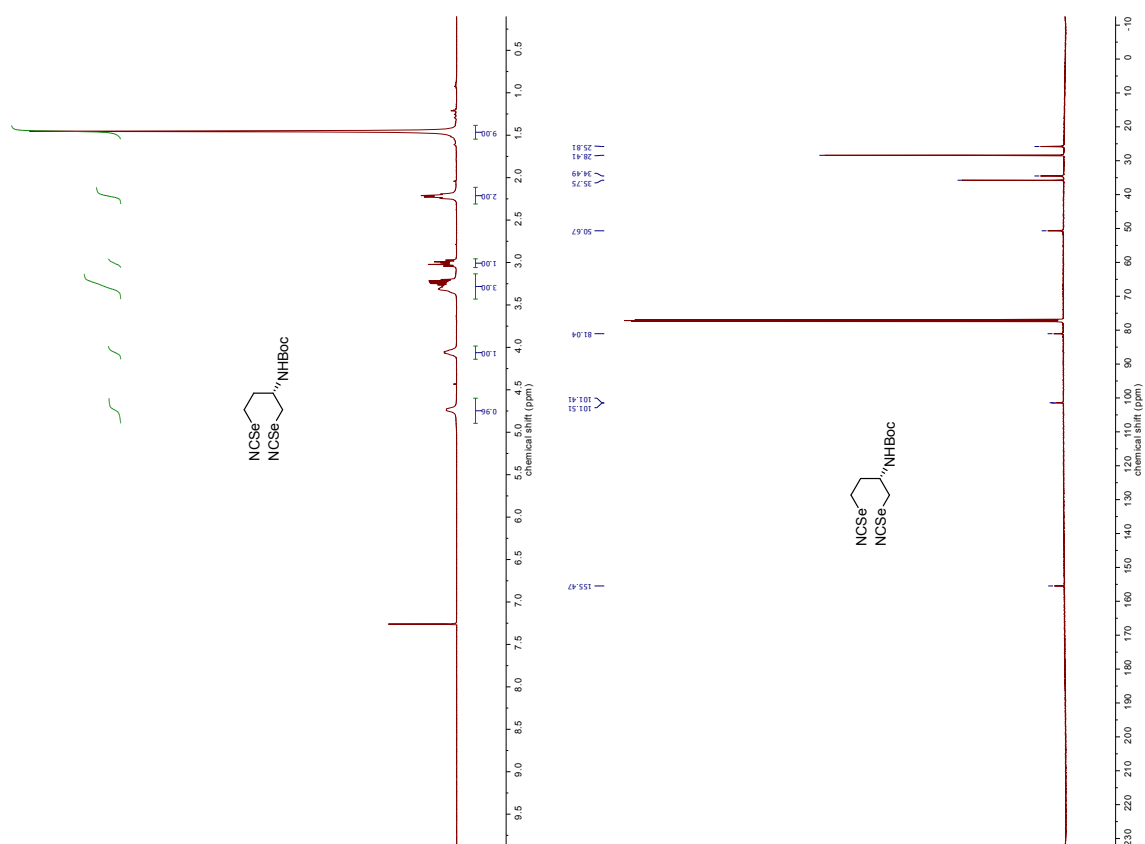


Figure S85, S86 ^1H NMR and ^{13}C NMR of *N*-Boc-1,4-diselenocyanatobutan-2-amine (**S19**).

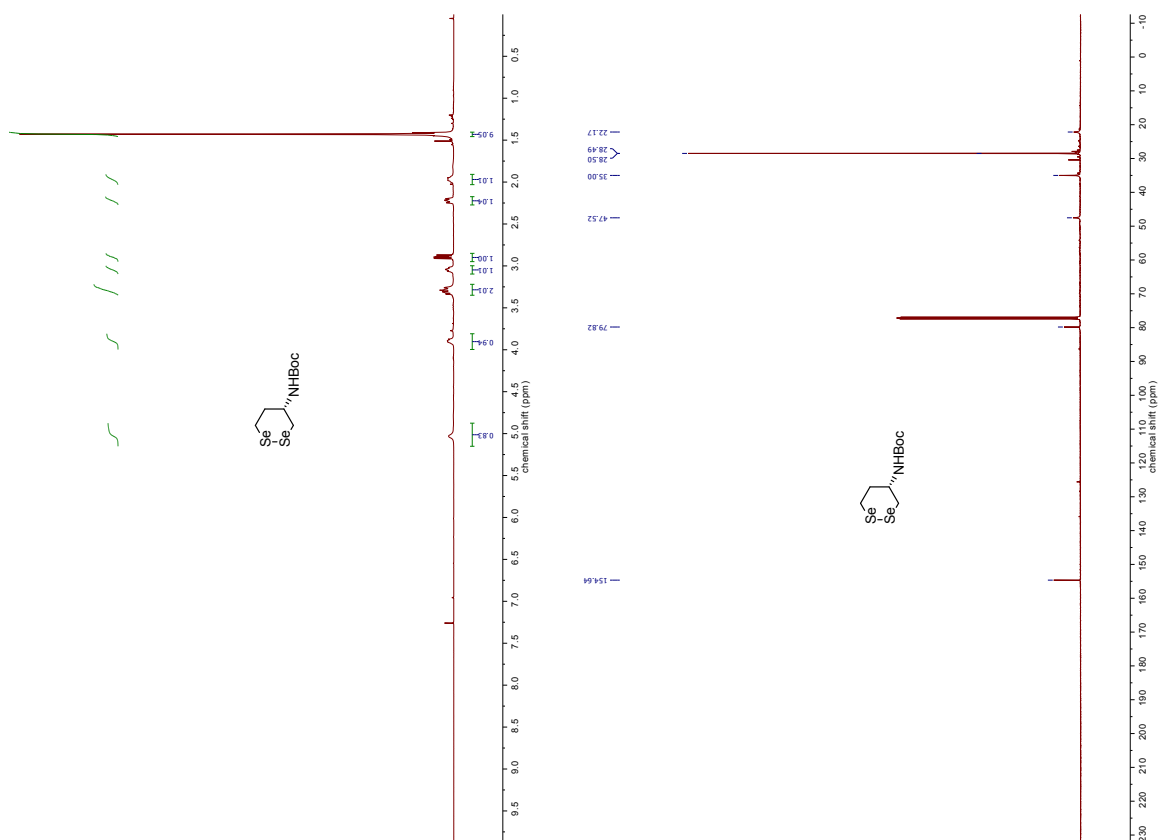


Figure S87, S88 ¹H NMR and ¹³C NMR of *N*-Boc-1,2-diselenan-4-amine (**11**).

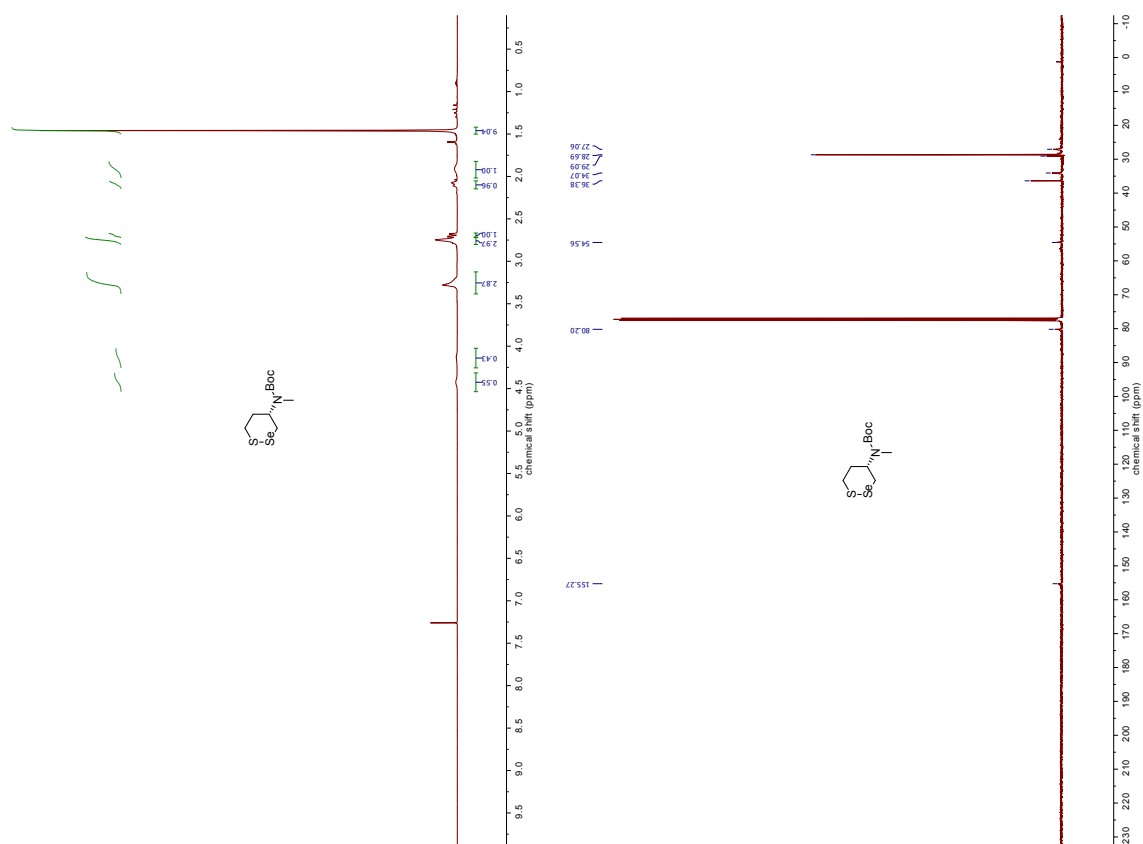


Figure S89, S90 ¹H NMR and ¹³C NMR of *N*-Boc-*N*-methyl-1,2-thiaselenan-4-amine (**S20**).

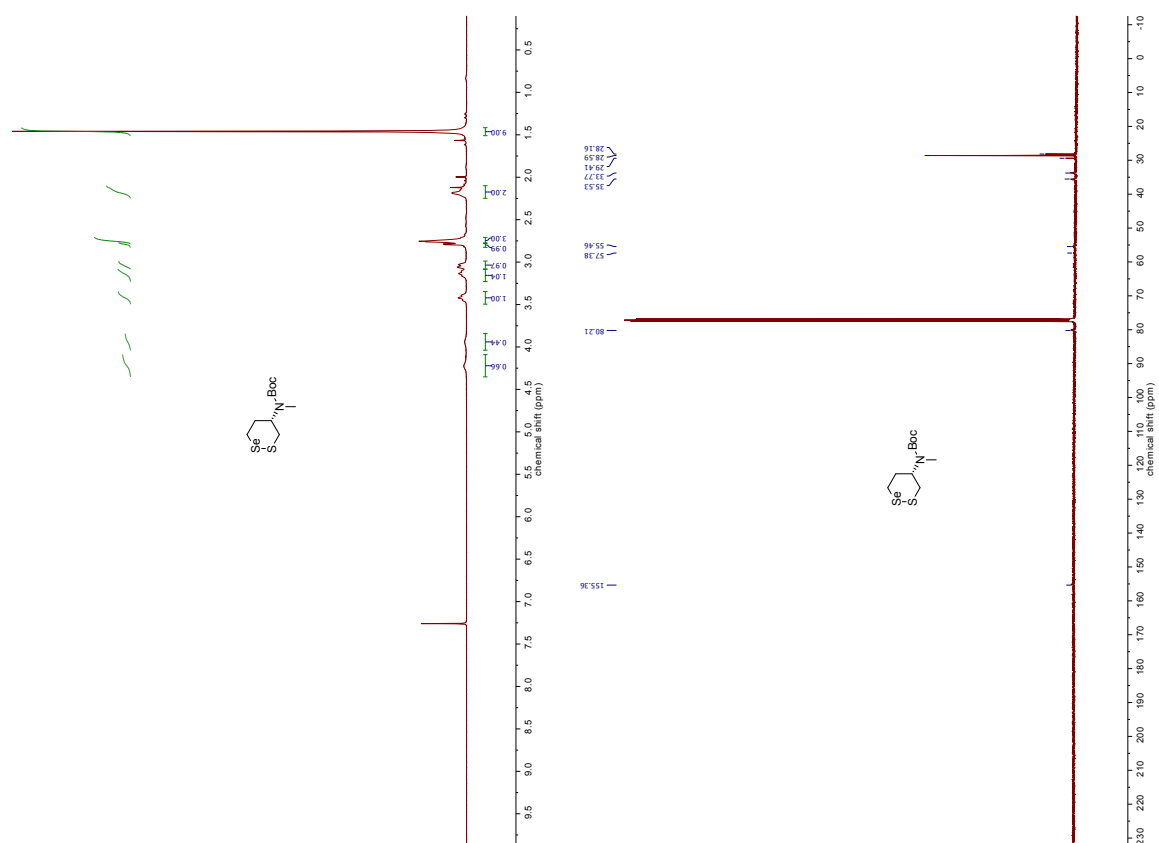


Figure S91, S92 ¹H NMR and ¹³C NMR of *N*-Boc-*N*-methyl-1,2-thiaselenan-5-amine (S21).

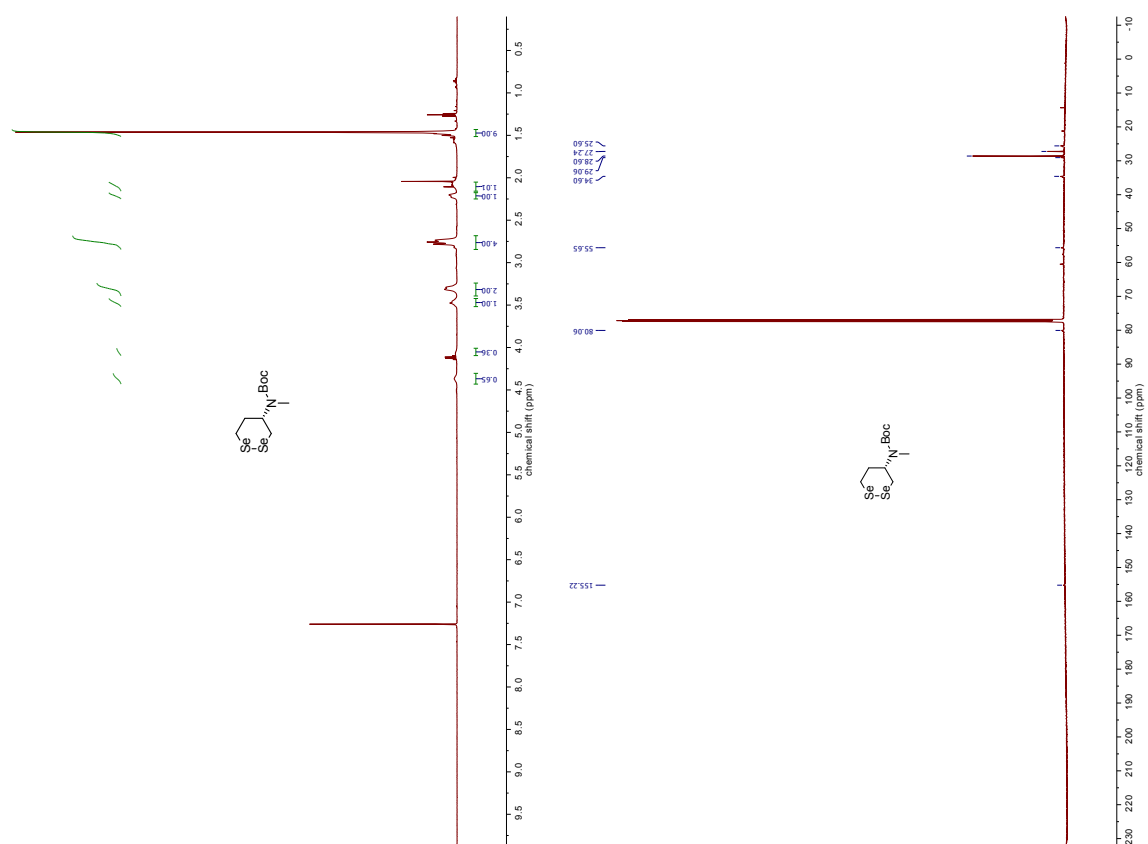


Figure S93, S94 ¹H NMR and ¹³C NMR of *N*-Boc-*N*-methyl-1,2-diselenan-4-amine (S23).

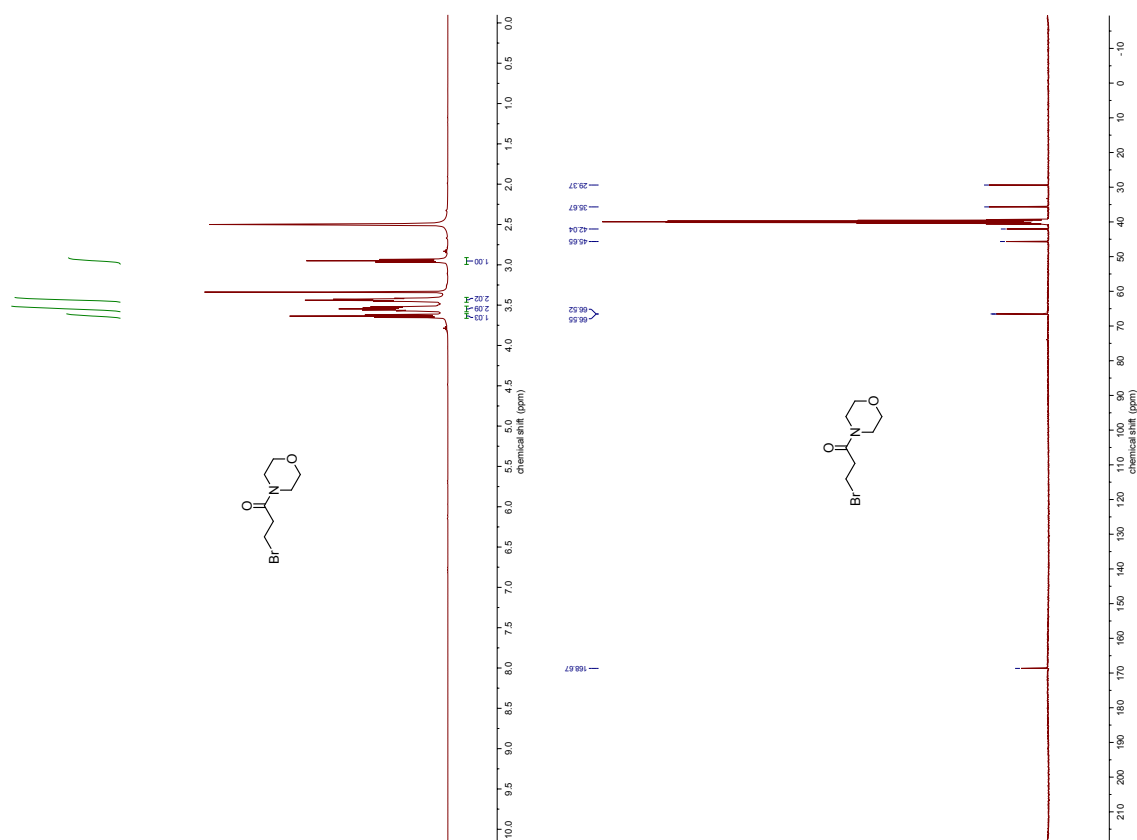


Figure S95, S96 ^1H NMR and ^{13}C NMR of 3-bromo-1-morpholinopropan-1-one (**S24**).

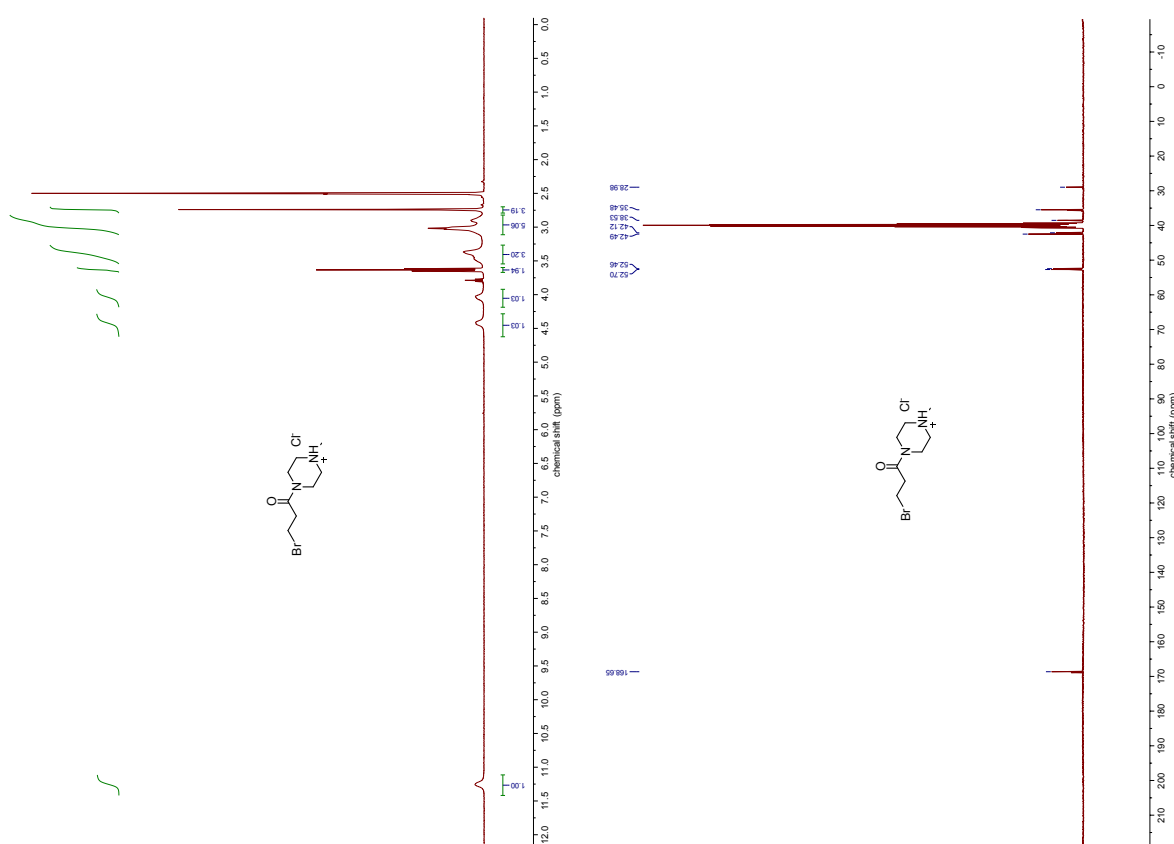


Figure S97, S98 ^1H NMR and ^{13}C NMR of 3-bromo-1-(4-methylpiperazin-1-yl)propan-1-one hydrochloride (**12**).

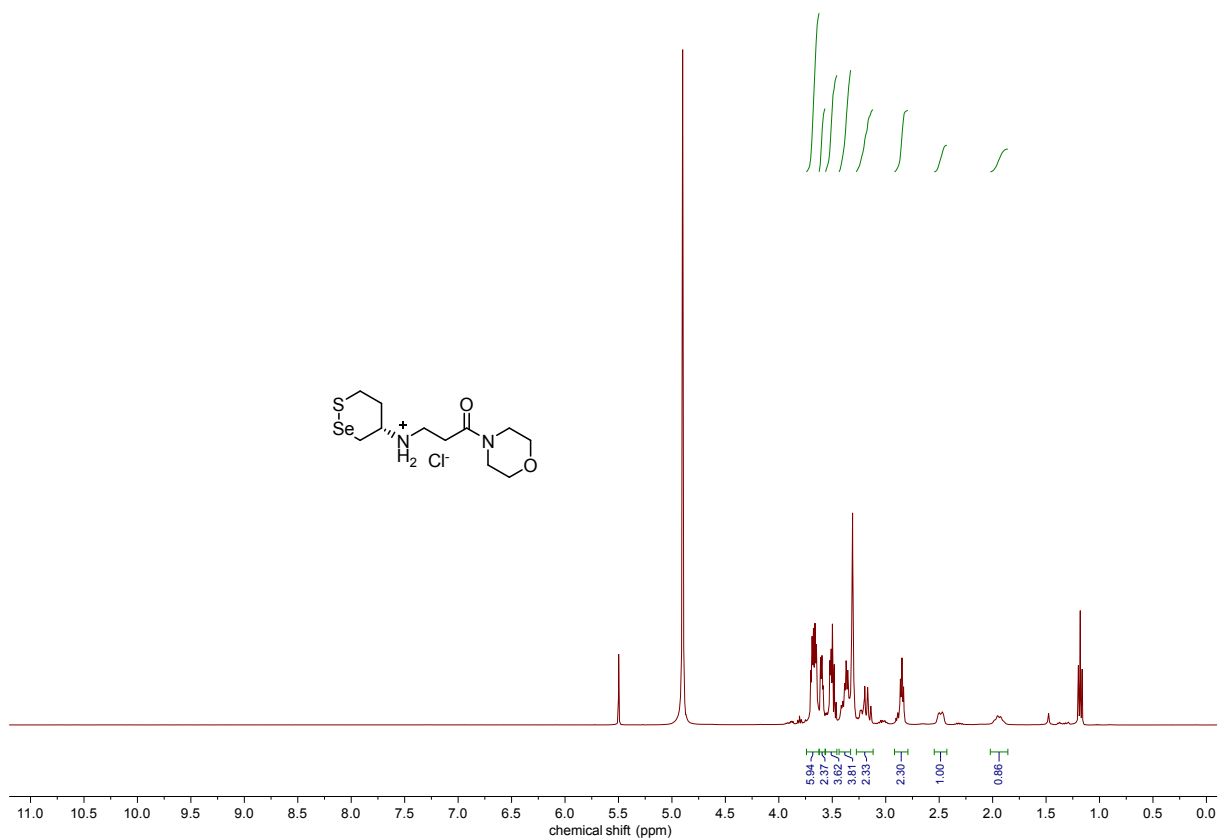


Figure S99 ¹H NMR of (S)-3-((1,2-thiaselenan-4-yl)amino)-1-morpholinopropan-1-one hydrochloride (S25).

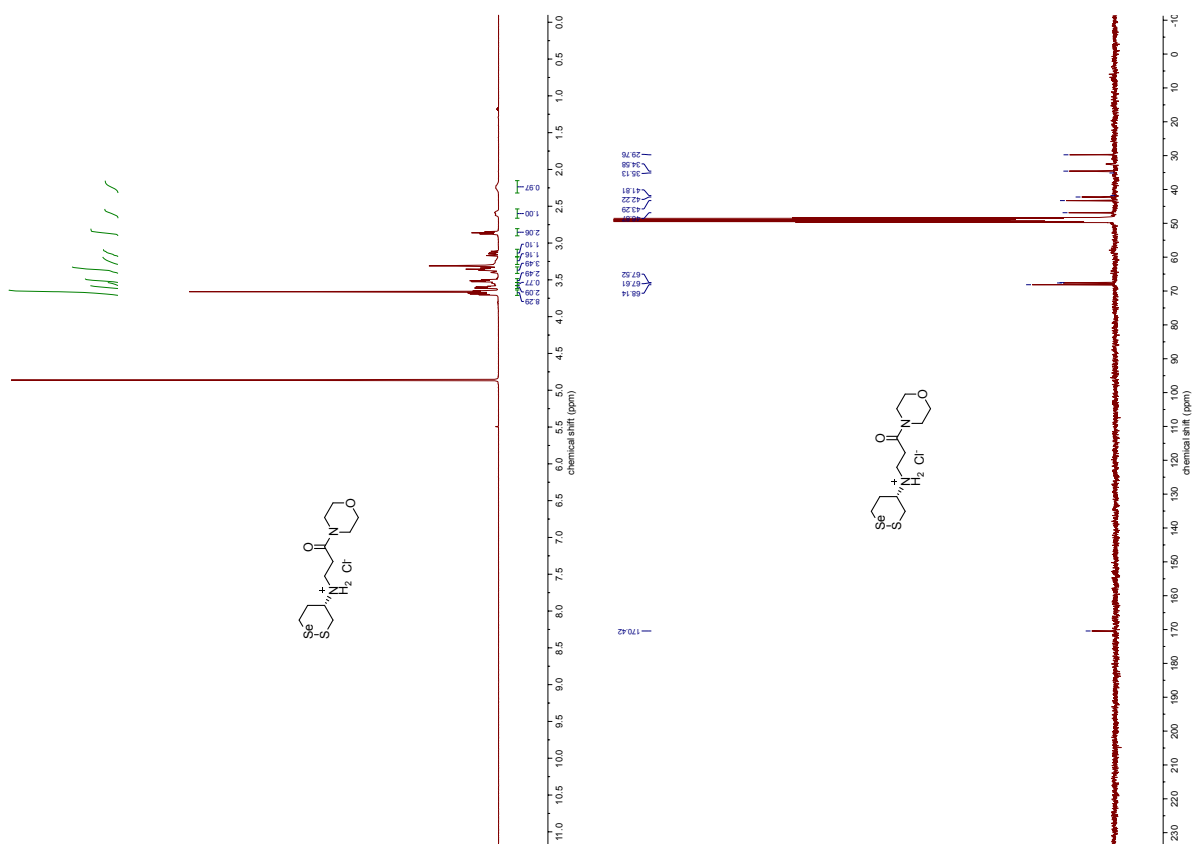


Figure S100, S101 ¹H NMR and ¹³C NMR of (S)-3-((1,2-thiaselenan-5-yl)amino)-1-morpholinopropan-1-one hydrochloride (S26).

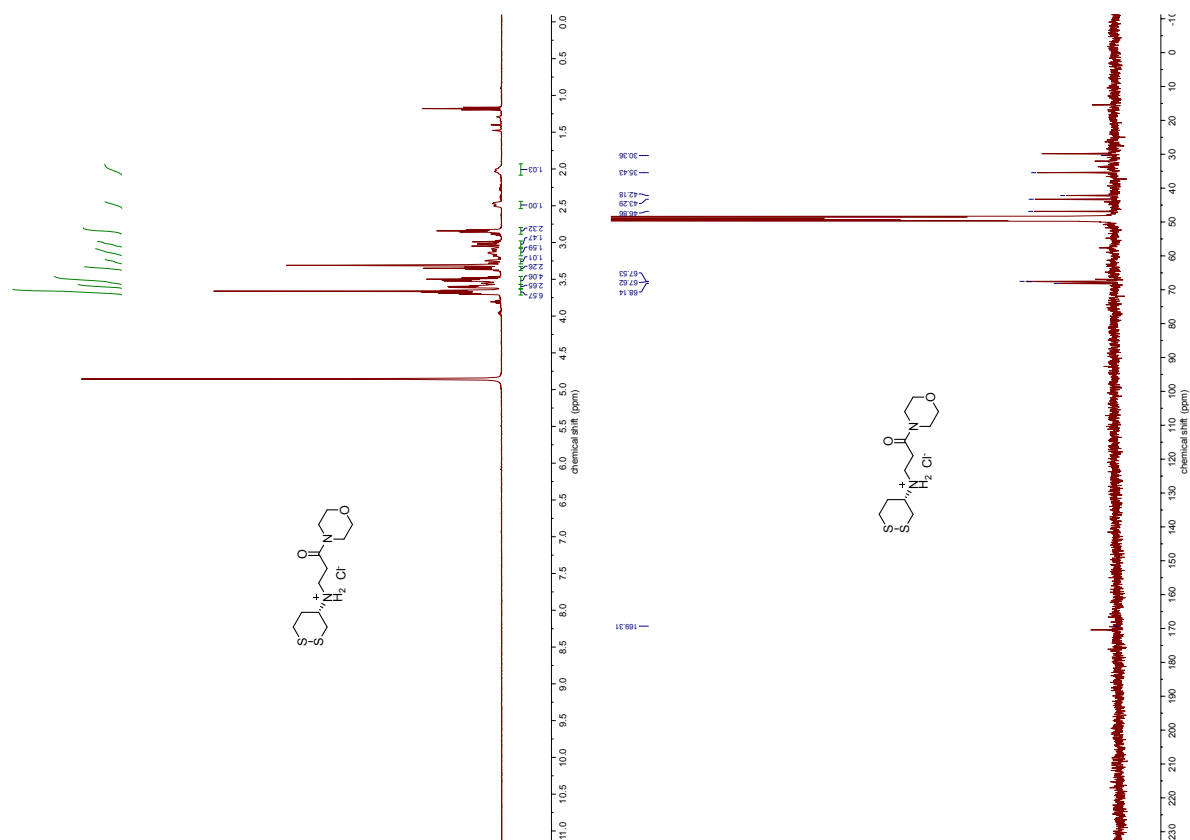


Figure S102, S103 ¹H NMR and ¹³C NMR of (S)-3-((1,2-dithian-4-yl)amino)-1-morpholinopropan-1-one hydrochloride (S27).

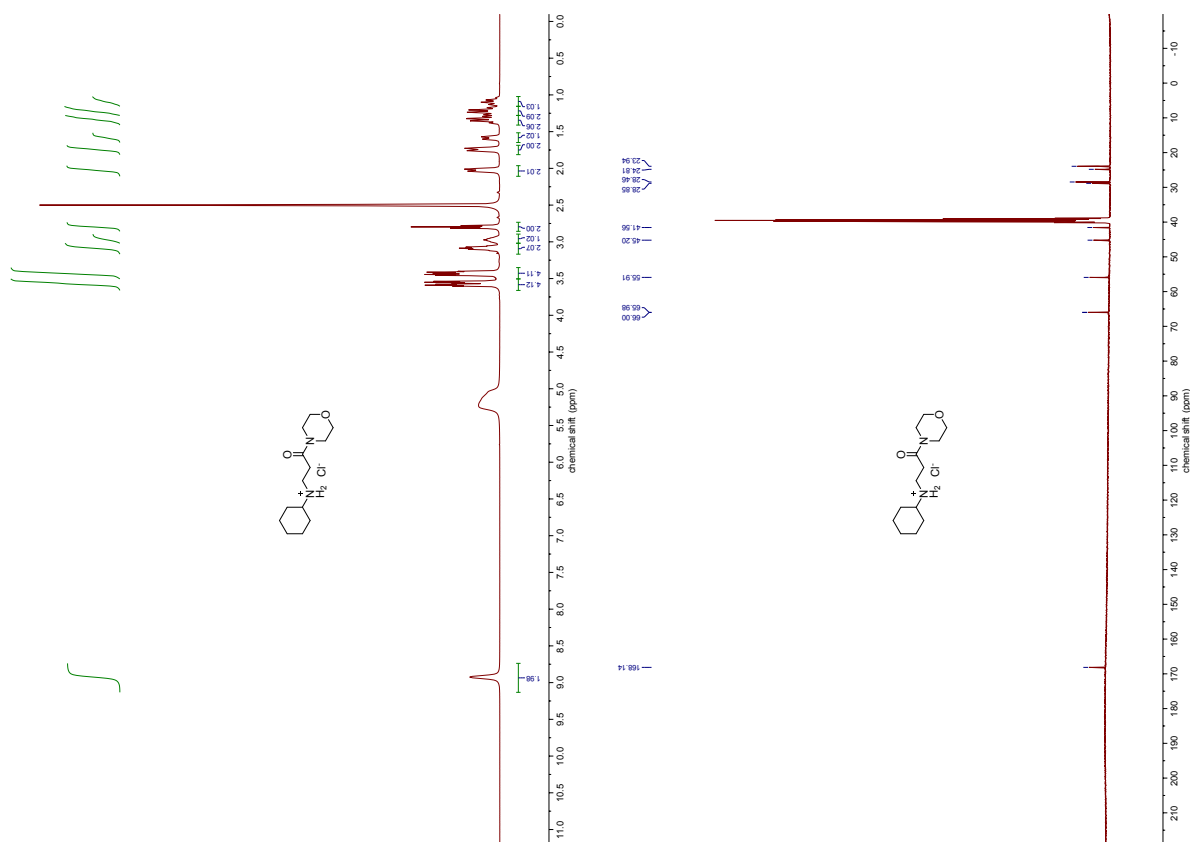


Figure S104, S105 ¹H NMR and ¹³C NMR of 3-(cyclohexylamino)-1-morpholinopropan-1-one hydrochloride (S28).

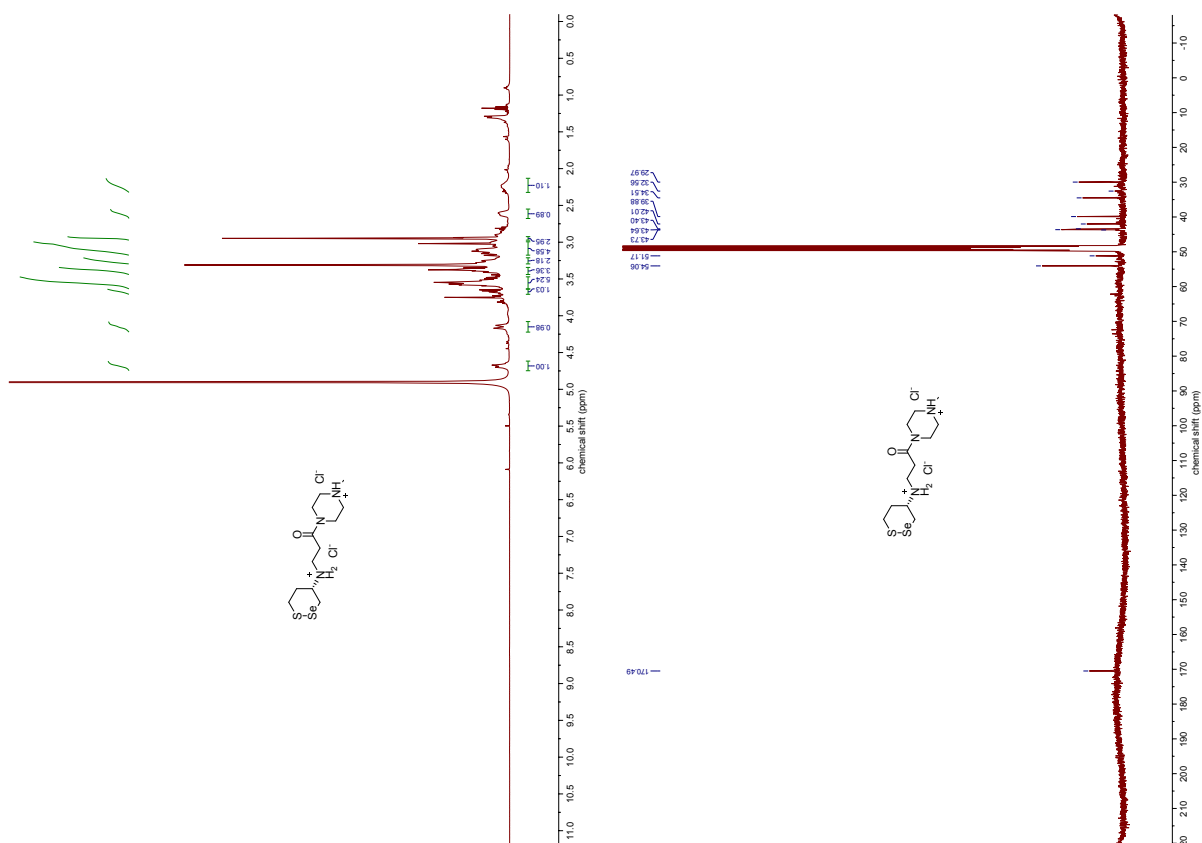


Figure S106, S107 ^1H NMR and ^{13}C NMR of (S)-3-((1,2-thiaselenan-4-yl)amino)-1-(4-methylpiperazin-1-yl)propan-1-one dihydrochloride (**14**).

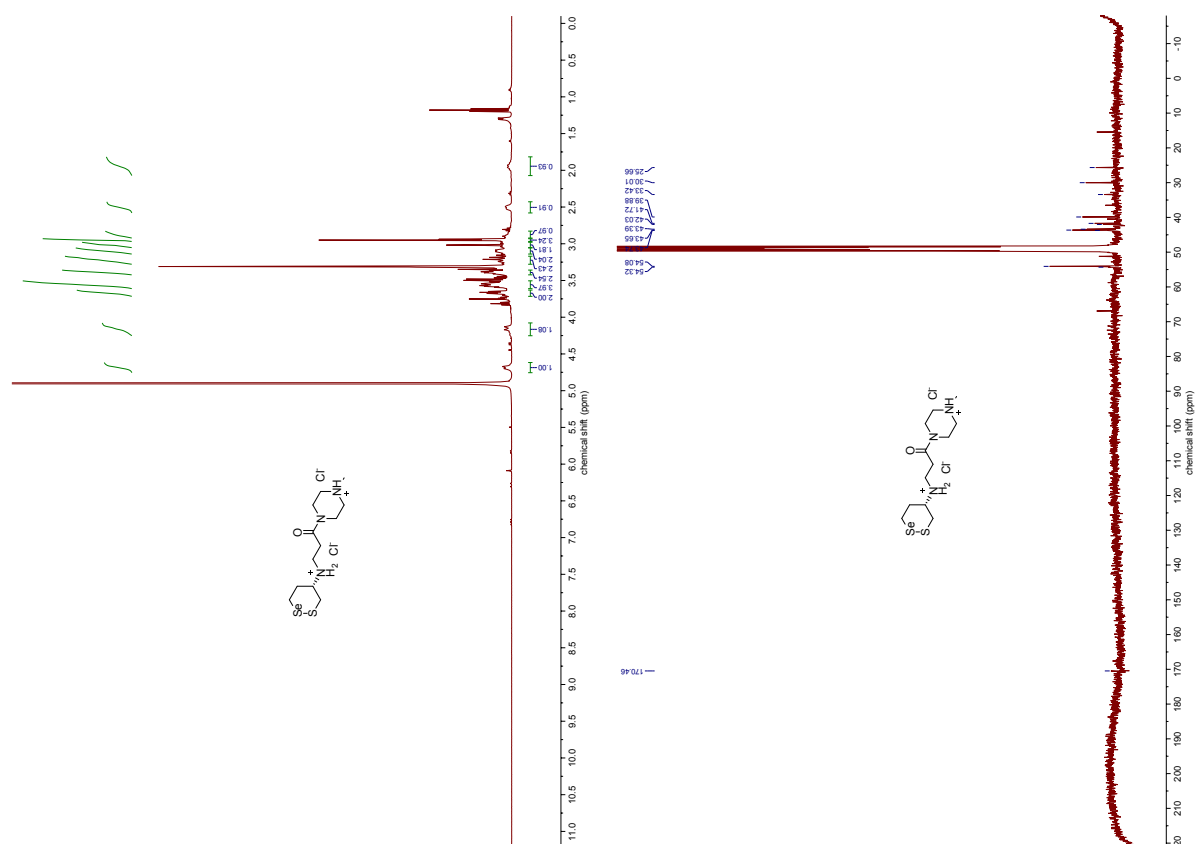


Figure S108, S109 ^1H NMR and ^{13}C NMR of (S)-3-((1,2-thiaselenan-5-yl)amino)-1-(4-methylpiperazin-1-yl)propan-1-one dihydrochloride (**S29**).

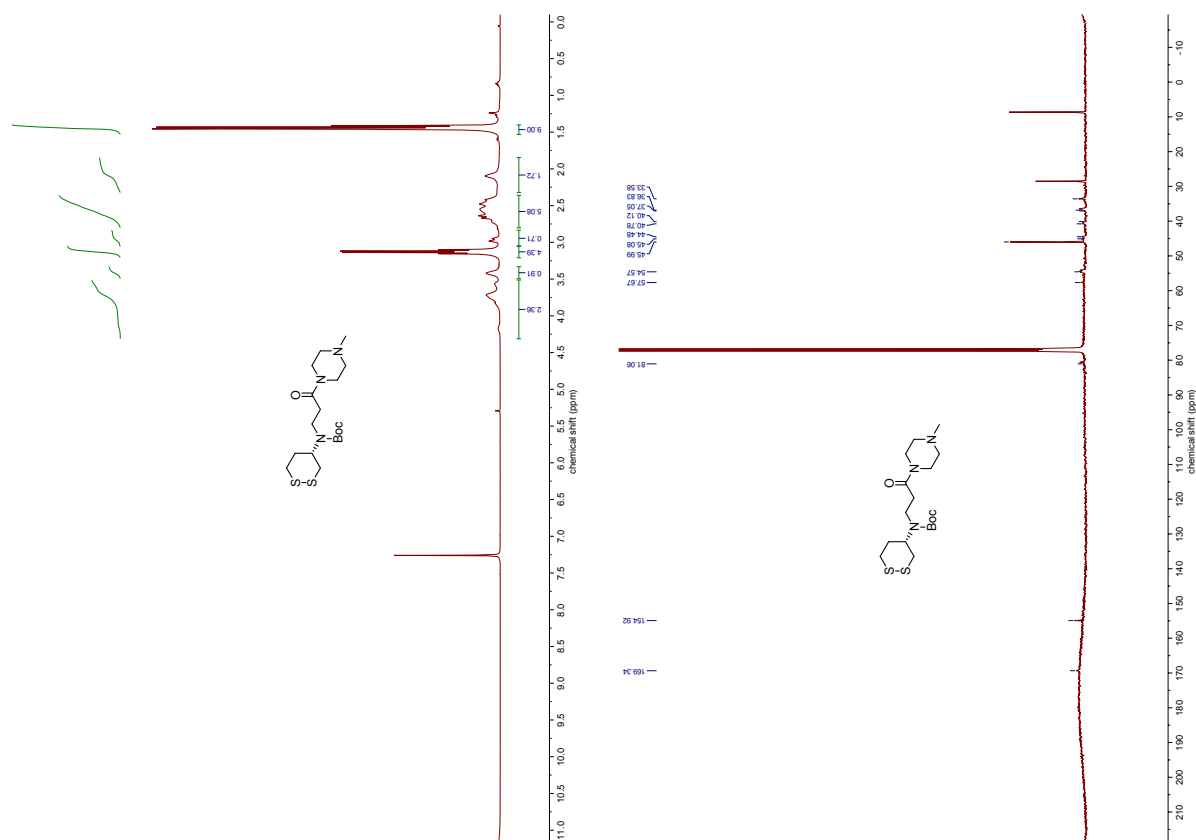


Figure S110, S111 ¹H NMR and ¹³C NMR of (S)-3-((1,2-dithian-5-yl)amino)-1-(4-methylpiperazin-1-yl)propan-1-one dihydrochloride (**S30a**).

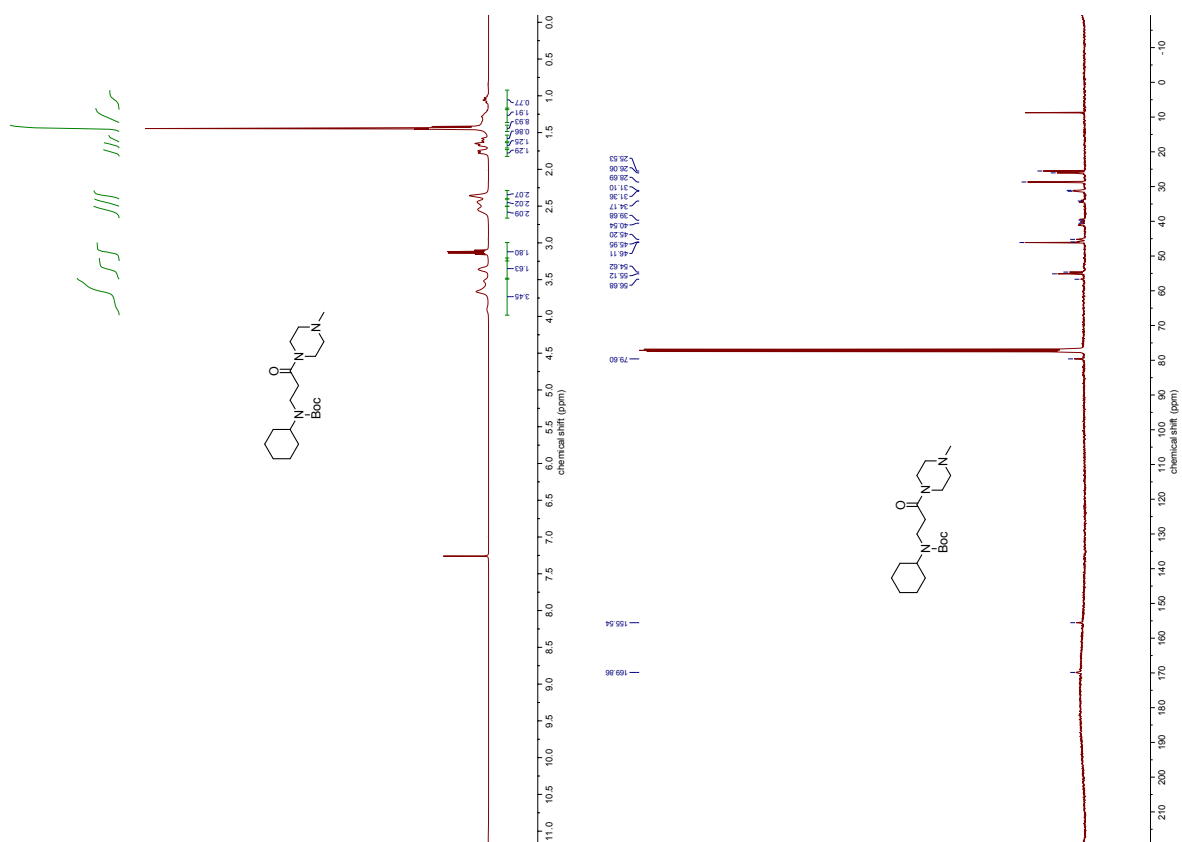


Figure S112, S113 ¹H NMR and ¹³C NMR of 3-(cyclohexylamino)-1-(4-methylpiperazin-1-yl)propan-1-one dihydrochloride (**S31a**).

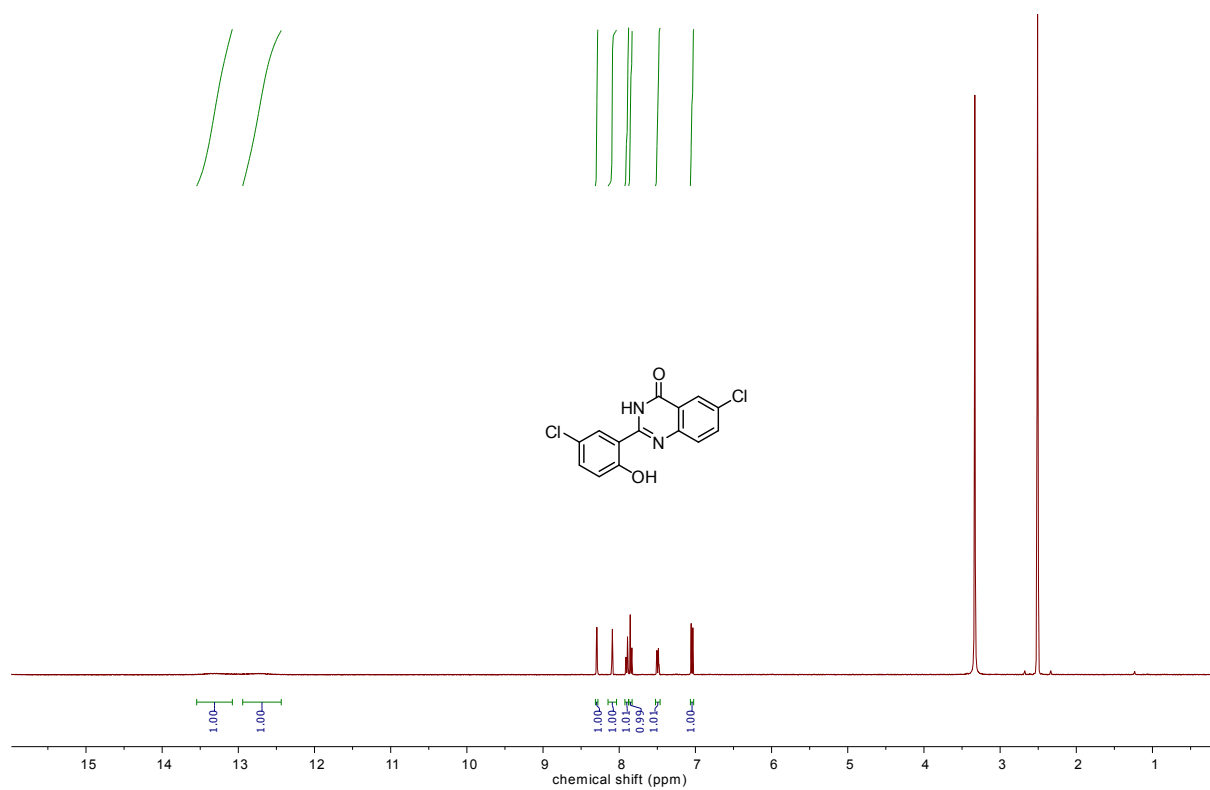


Figure S114 ¹H NMR of 6-chloro-2-(5-chloro-2-hydroxyphenyl)quinazolin-4(3H)-one (S32).

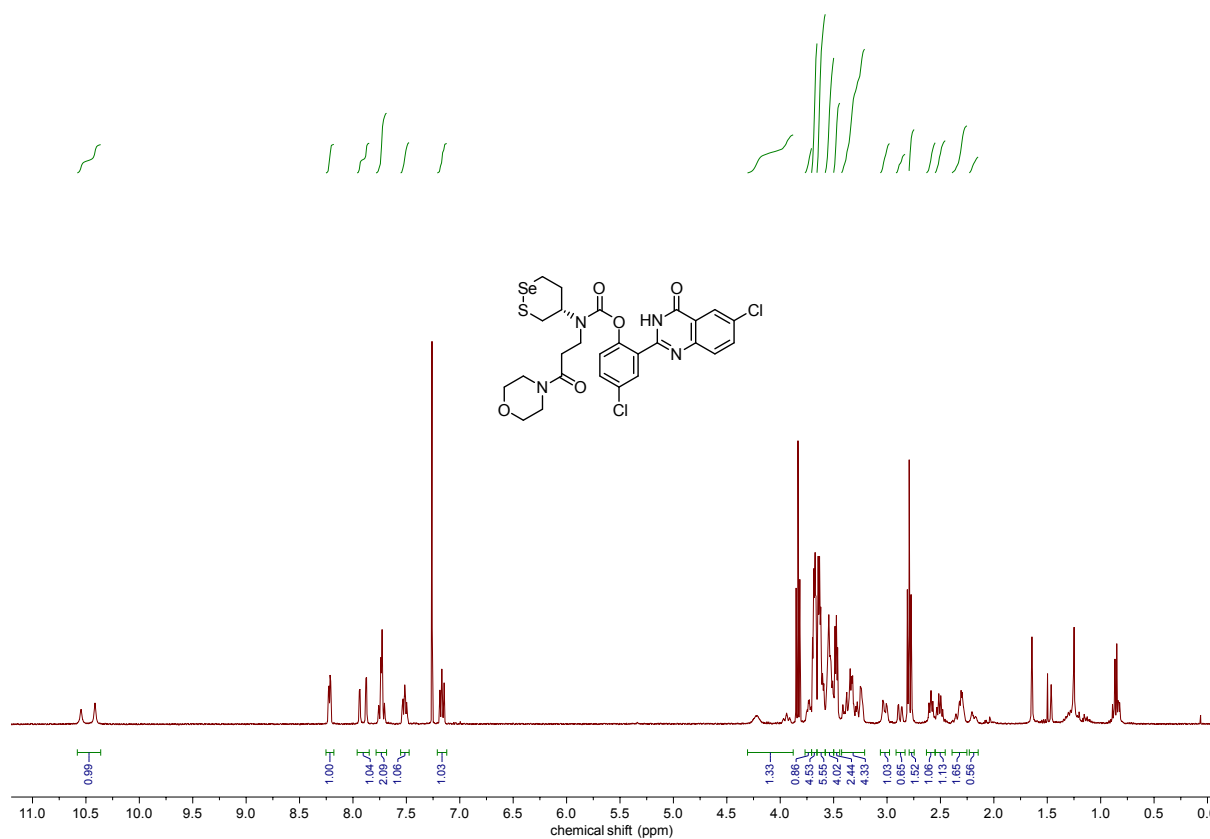


Figure S123 ¹H NMR of G2.

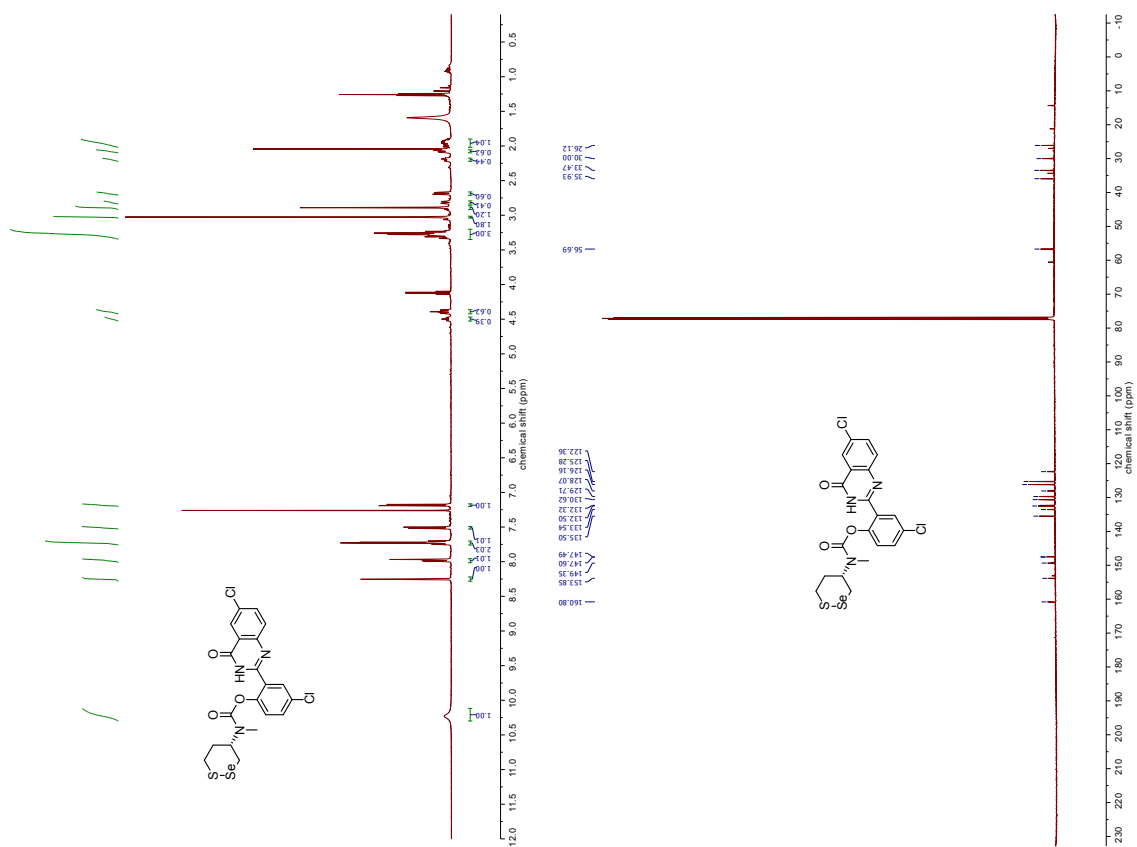


Figure S115, S116 ^1H NMR and ^{13}C NMR of **A3**.

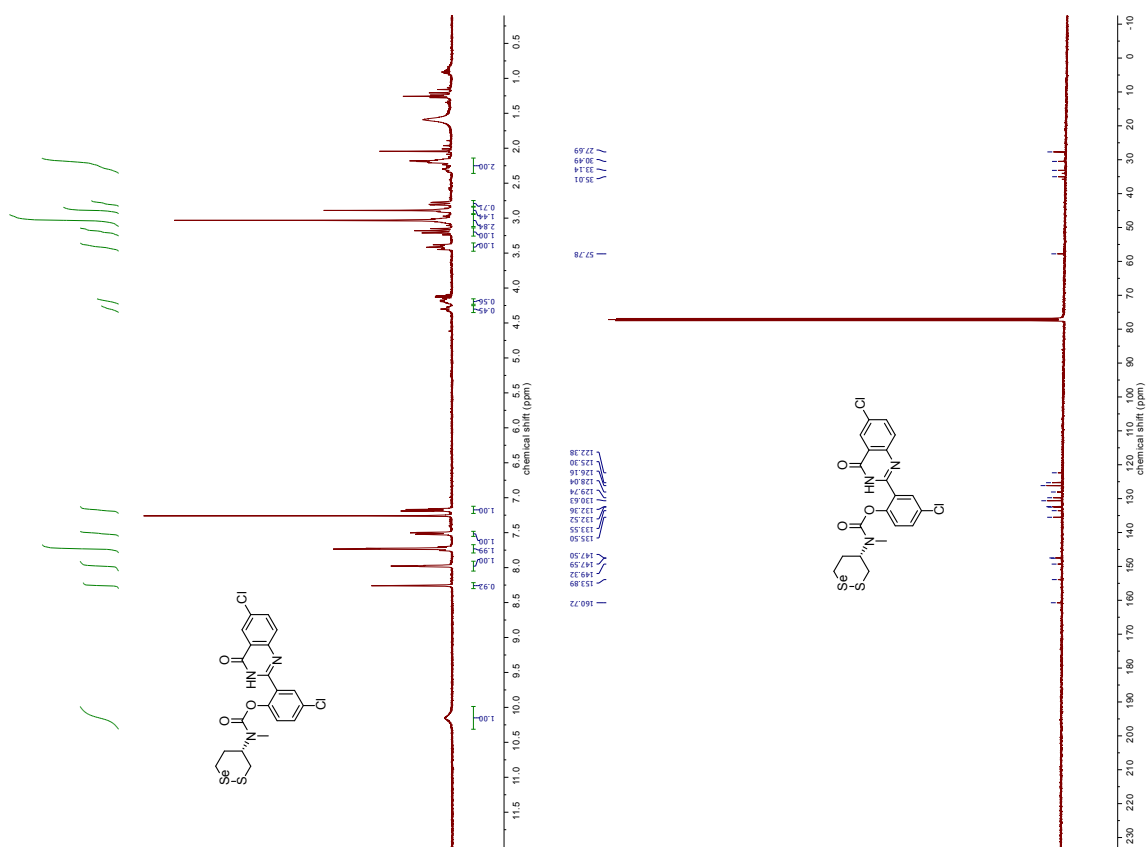


Figure S117, S118 ^1H NMR and ^{13}C NMR of **G3**.

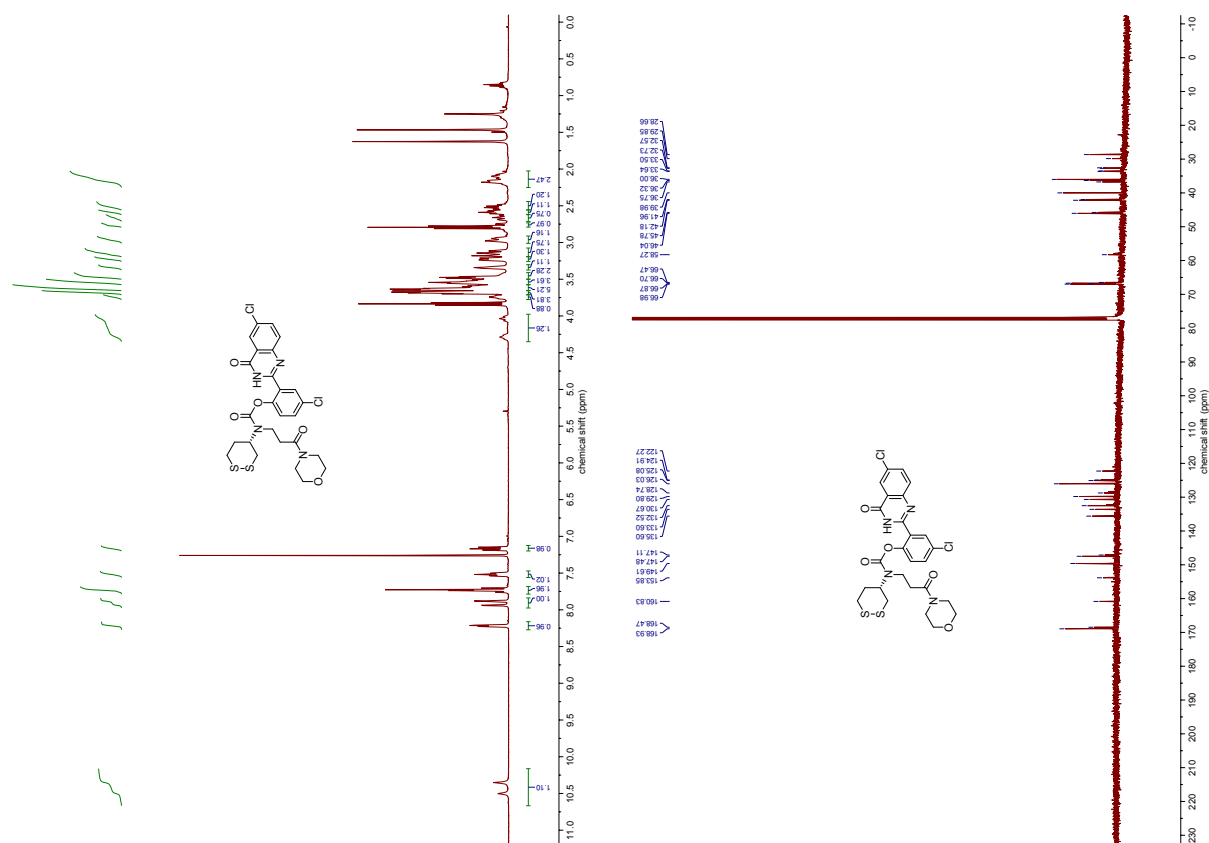


Figure S124, S125 ^1H NMR and ^{13}C NMR of S2.

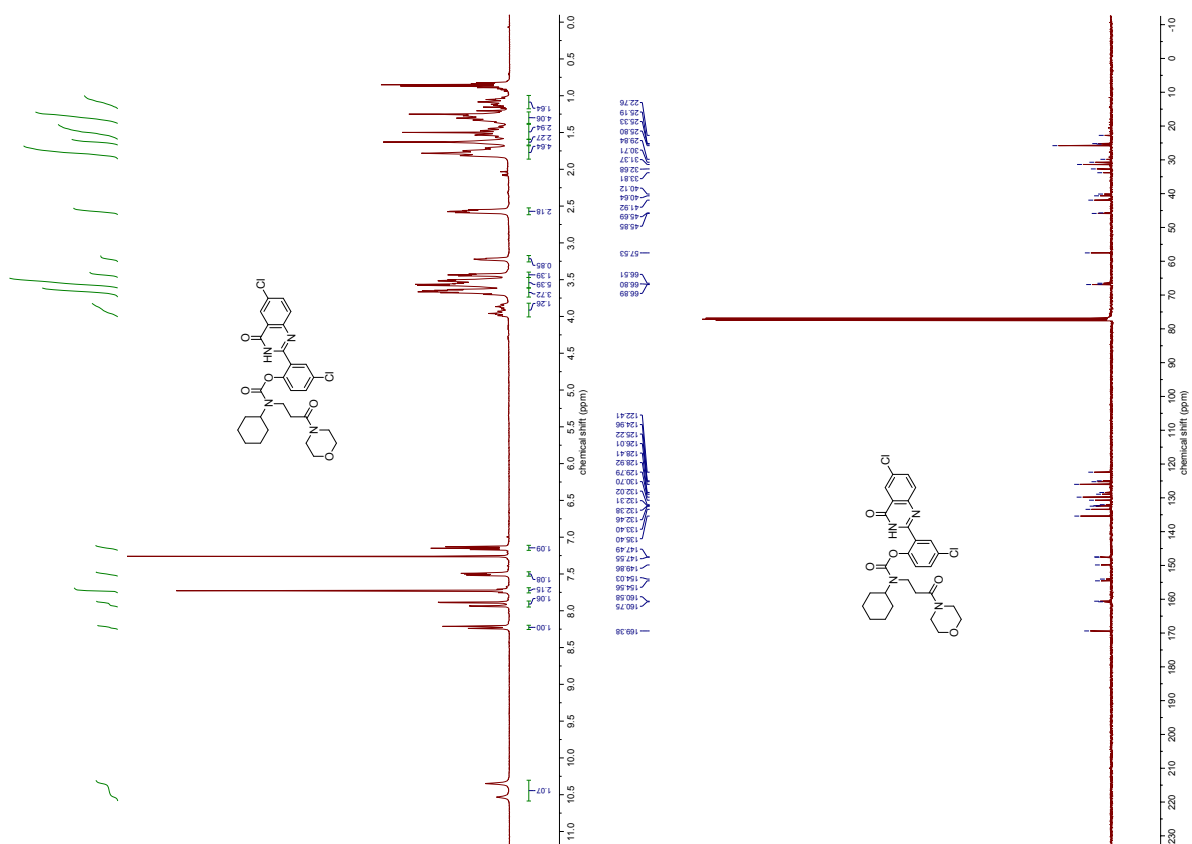


Figure S126, S127 ^1H NMR and ^{13}C NMR of C2.

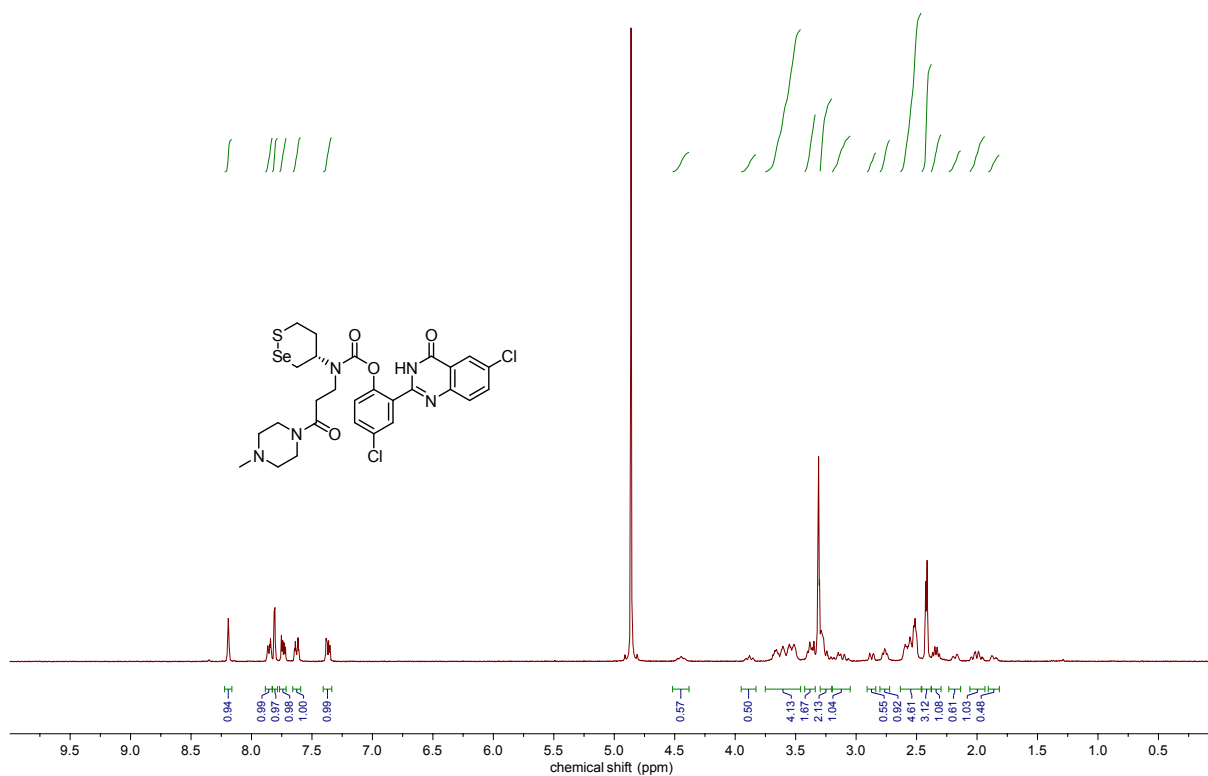


Figure S128 ^1H NMR of RX1.

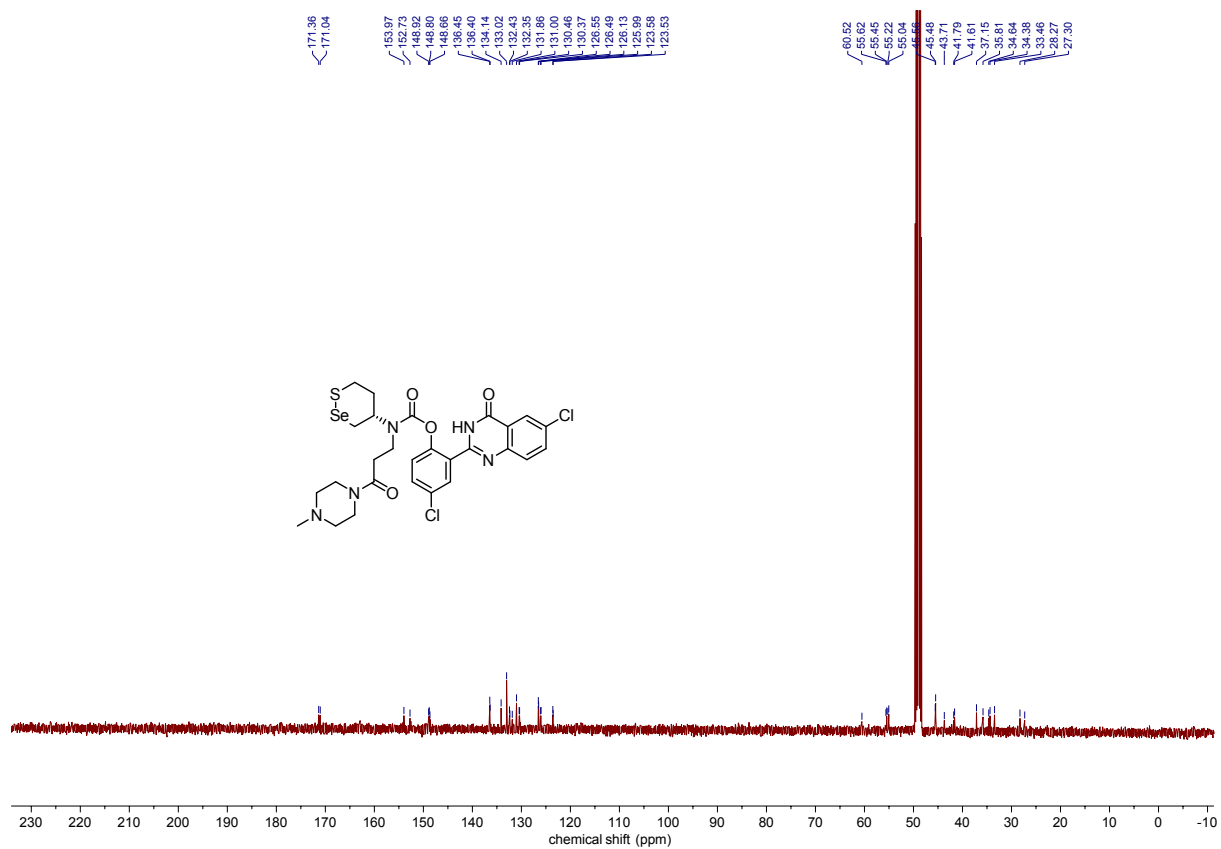


Figure S129 ^{13}C NMR of RX1.

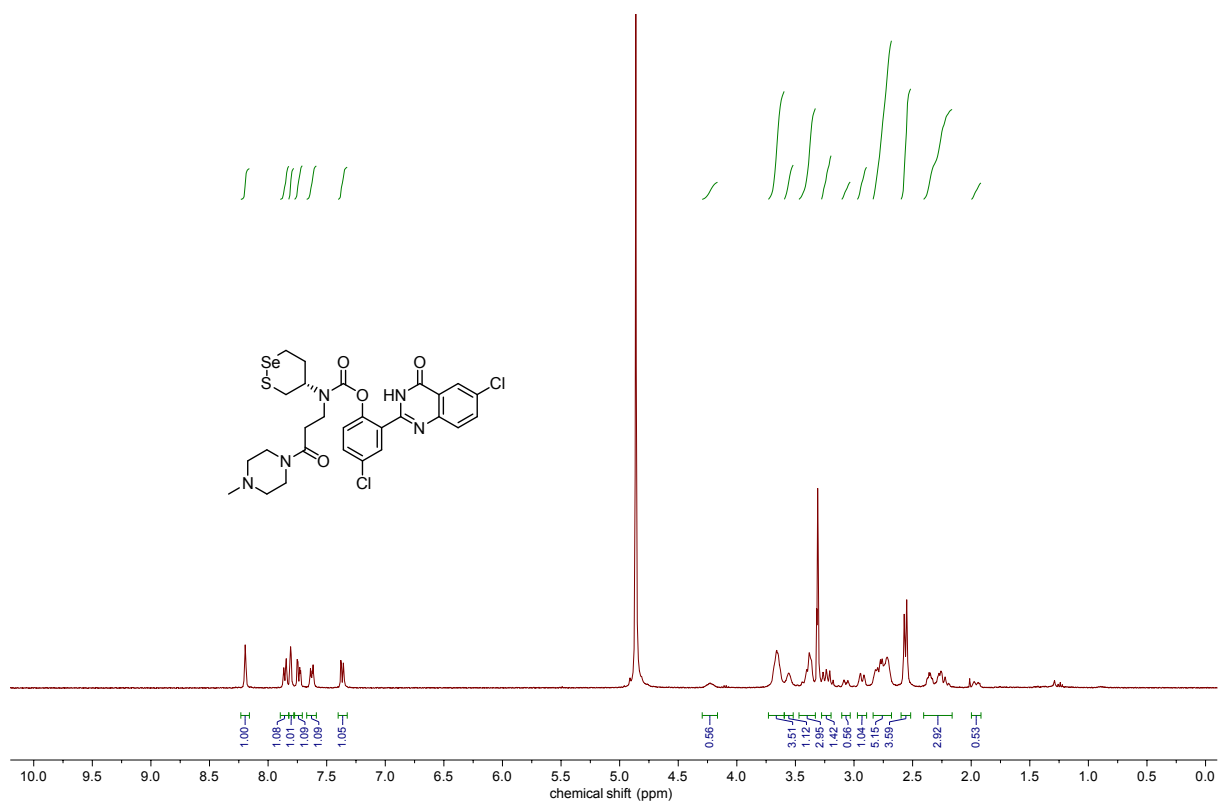


Figure S130 ¹H NMR of G1.

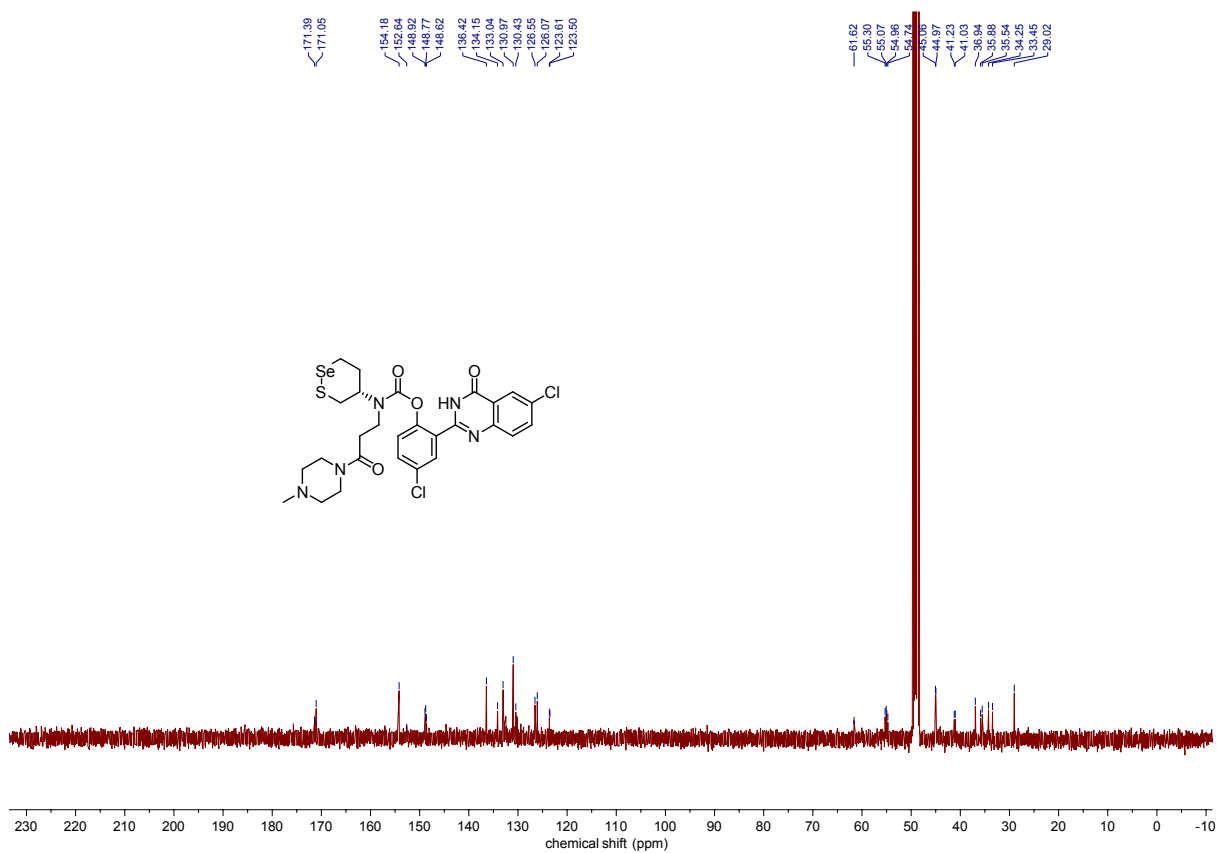


Figure S131 ¹³C NMR of G1.

8 Supplemental References

- Wessjohann, L.A., Schneider, A., Abbas, M., and Brandt, W. (2007). Selenium in chemistry and biochemistry in comparison to sulfur. *388*, 997–1006.
- Bachrach, S.M., Demoin, D.W., Luk, M., and Miller, J.V. (2004). Nucleophilic Attack at Selenium in Diselenides and Selenosulfides. A Computational Study. *J. Phys. Chem. A* *108*, 4040–4046.
- Bachrach, S.M., Walker, C.J., Lee, F., and Royce, S. (2007). Effect of Ring Strain on Nucleophilic Substitution at Selenium: A Computational Study of Cyclic Diselenides and Selenenyl Sulfides. *J. Org. Chem.* *72*, 5174–5182.
- Arai, K., Matsunaga, T., Ueno, H., Akahoshi, N., Sato, Y., Chakrabarty, G., Mughes, G., and Iwaoka, M. (2019). Modeling Thioredoxin Reductase-Like Activity with Cyclic Selenenyl Sulfides: Participation of an NH...Se Hydrogen Bond through Stabilization of the Mixed Se–S Intermediate. *Chem. – Eur. J.* *25*, 12751–12760.
- Arai, K., Sato, Y., Nakajima, I., Saito, M., Sasaki, M., Kanamori, A., and Iwaoka, M. (2020). Glutathione peroxidase-like functions of 1,2-diselenane-4,5-diol and its amphiphilic derivatives: Switchable catalytic cycles depending on peroxide substrates. *Bioorg. Med. Chem.*, 115866.
- Zhong, L., Arner, E.S.J., and Holmgren, A. (2000). Structure and mechanism of mammalian thioredoxin reductase: The active site is a redox-active selenothiol/selenenylsulfide formed from the conserved cysteine-selenocysteine sequence. *Proc. Natl. Acad. Sci.* *97*, 5854–5859.
- Lothrop, A.P., Ruggles, E.L., and Hondal, R.J. (2009). No Selenium Required: Reactions Catalyzed by Mammalian Thioredoxin Reductase That Are Independent of a Selenocysteine Residue. *Biochemistry* *48*, 6213–6223.
- Gasparini, G., Sargsyan, G., Bang, E.-K., Sakai, N., and Matile, S. (2015). Ring Tension Applied to Thiol-Mediated Cellular Uptake. *Angew. Chem. Int. Ed.* *54*, 7328–7331.
- Zong, L., Bartolami, E., Abegg, D., Adibekian, A., Sakai, N., and Matile, S. (2017). Epithiodiketopiperazines: Strain-Promoted Thiol-Mediated Cellular Uptake at the Highest Tension. *ACS Cent. Sci.* *3*, 449–453.
- Abegg, D., Gasparini, G., Hoch, D.G., Shuster, A., Bartolami, E., Matile, S., and Adibekian, A. (2017). Strained Cyclic Disulfides Enable Cellular Uptake by Reacting with the Transferrin Receptor. *J. Am. Chem. Soc.* *139*, 231–238.
- Laurent, Q., Sakai, N., and Matile, S. (2019). The Opening of 1,2-Dithiolanes and 1,2-Diselenolanes: Regioselectivity, Rearrangements, and Consequences for Poly(disulfide)s, Cellular Uptake and Pyruvate Dehydrogenase Complexes. *Helv. Chim. Acta* *102*, e1800209.
- Felber, J.G., Zeisel, L., Poczka, L., Scholzen, K., Busker, S., Maier, M.S., Theisen, U., Brandstädter, C., Becker, K., Arnér, E.S.J., et al. (2021). Selective, Modular Probes for Thioredoxins Enabled by Rational Tuning of a Unique Disulfide Structure Motif. *J. Am. Chem. Soc.* *143*, 8791–8803.
- Felber, J.G., Poczka, L., Scholzen, K.C., Zeisel, L., Maier, M.S., Busker, S., Theisen, U., Brandstädter, C., Becker, K., Arnér, E.S.J., et al. (2022). Cyclic 5-membered disulfides are not selective substrates of thioredoxin reductase, but are opened nonspecifically. *Nat. Commun.* *10.1038/s41467-022-29136-4*.
- Suarez, S.I., Ambrose, R., Kalk, M.A., and Lukesh III, J.C. (2019). Selenosulfides Tethered to gem-Dimethyl Esters: A Robust and Highly Versatile Framework for H₂S Probe Development. *Chem. – Eur. J.* *25*, 15736–15740.
- Kong, F., Zhao, Y., Liang, Z., Liu, X., Pan, X., Luan, D., Xu, K., and Tang, B. (2017). Highly Selective Fluorescent Probe for Imaging H₂Se in Living Cells and in Vivo Based on the Disulfide Bond. *Anal. Chem.* *89*, 688–693.
- Lee, H., and Kim, H.-J. (2013). Fluorescein aldehyde with disulfide functionality as a fluorescence turn-on probe for cysteine and homocysteine in HEPES buffer. *Org. Biomol. Chem.* *11*, 5012.
- Lee, M.H., Han, J.H., Kwon, P.-S., Bhuniya, S., Kim, J.Y., Sessler, J.L., Kang, C., and Kim, J.S. (2012). Hepatocyte-Targeting Single Galactose-Appended Naphthalimide: A Tool for Intracellular Thiol Imaging in Vivo. *J. Am. Chem. Soc.* *134*, 1316–1322.
- Lee, M.H., Han, J.H., Lee, J.-H., Choi, H.G., Kang, C., and Kim, J.S. (2012). Mitochondrial Thioredoxin-Responding Off–On Fluorescent Probe. *J. Am. Chem. Soc.* *134*, 17314–17319.
- Lee, M.H., Jeon, H.M., Han, J.H., Park, N., Kang, C., Sessler, J.L., and Kim, J.S. (2014). Toward a Chemical Marker for Inflammatory Disease: A Fluorescent Probe for Membrane-Localized Thioredoxin. *J. Am. Chem. Soc.* *136*, 8430–8437.
- Jia, H., Hu, G., Shi, D., Gan, L., Zhang, H., Yao, X., and Fang, J. (2019). Fluorophore-Dependent Cleavage of Disulfide Bond Leading to a Highly Selective Fluorescent Probe of Thioredoxin. *Anal. Chem.* *91*, 8524–8531.
- Li, X., Zhang, B., Yan, C., Li, J., Wang, S., Wei, X., Jiang, X., Zhou, P., and Fang, J. (2019). A fast and specific fluorescent probe for thioredoxin reductase that works via disulfide bond cleavage. *Nat. Commun.* *10*, 2745.
- Ma, H., Zhang, J., Zhang, Z., Liu, Y., and Fang, J. (2016). A fast response and red emission probe for mammalian thioredoxin reductase. *Chem. Commun.* *52*, 12060–12063.
- Liu, Y., Ma, H., Zhang, L., Cui, Y., Liu, X., and Fang, J. (2016). A small molecule probe reveals declined mitochondrial thioredoxin reductase activity in a Parkinson's disease model. *Chem. Commun.* *52*, 2296–2299.
- Zhang, L., Duan, D., Liu, Y., Ge, C., Cui, X., Sun, J., and Fang, J. (2014). Highly Selective Off–On Fluorescent Probe for Imaging Thioredoxin Reductase in Living Cells. *J. Am. Chem. Soc.* *136*, 226–233.
- Mafireyi, T.J., Laws, M., Bassett, J.W., Cassidy, P.B., Escobedo, J.O., and Strongin, R.M. (2020). A Diselenide Turn-On Fluorescent Probe for the Detection of Thioredoxin Reductase. *Angew. Chem. Int. Ed.* *59*, 15147–15151.
- Zhao, J., Wang, Z., Zhong, M., Xu, Q., Li, X., Chang, B., and Fang, J. (2021). Integration of a Diselenide Unit Generates Fluorogenic Camptothecin Prodrugs with Improved Cytotoxicity to Cancer Cells. *J. Med. Chem.*
- Zhao, Y., Zuo, X., Liu, S., Qian, W., Tang, X., and Lu, J. (2022). A Fluorescent Probe to Detect Quick Disulfide Reductase Activity in Bacteria. *Antioxidants* *11*.
- Zuo, X., Zhao, Y., Zhao, J., Ouyang, Y., Qian, W., Hou, Y., Yu, C., Ren, X., Zou, L., Fang, J., et al. (2022). A fluorescent probe for specifically measuring the overall thioredoxin and glutaredoxin reducing activity in bacterial cells. *Analyst* *147*, 834–840.
- Cheng, Y., Pham, A.-T., Kato, T., Lim, B., Moreau, D., López-Andarias, J., Zong, L., Sakai, N., and Matile, S. (2021). Inhibitors of thiol-mediated uptake. *Chem. Sci.*
- Snyder, R.M., Mirabelli, C.K., and Crooke, S.T. (1987). Cellular interactions of auranofin and a related gold complex with raw 264.7 macrophages. *Biochem. Pharmacol.* *36*, 647–654.
- Zhang, J., Zhang, B., Li, X., Han, X., Liu, R., and Fang, J. (2019). Small molecule inhibitors of mammalian thioredoxin reductase as potential anticancer agents: An update. *Med. Res. Rev.* *39*, 5–39.
- Fulvio, S., Francesco, A., Giovanna, B., Daniela, C., Gianni, D., Adriana, E.M., and Andrea, B. (2014). Thioredoxin Reductase and its Inhibitors. *Curr. Protein Pept. Sci.* *15*, 621–646.
- Duan, D., Zhang, J., Yao, J., Liu, Y., and Fang, J. (2016). Targeting Thioredoxin Reductase by Parthenolide Contributes to Inducing Apoptosis of HeLa Cells. *J. Biol. Chem.* *291*, 10021–10031.
- Aldrich, C., Bertozzi, C., Georg, G.I., Kiessling, L., Lindsley, C., Liotta, D., Merz, K.M., Schepartz, A., and Wang, S. (2017). The Ecstasy and Agony of Assay Interference Compounds. *ACS Med. Chem. Lett.* *8*, 379–382.
- Sun, J., Zhong, H., Wang, K., Li, N., and Chen, L. (2021). Gains from no real PAINS: Where 'Fair Trial Strategy' stands in the development of multi-target ligands. *Acta Pharm. Sin. B*, S221138352100071X.
- Baell, J., and Walters, M.A. (2014). Chemistry: Chemical con artists foil drug discovery. *Nature* *513*, 481–483.
- Sté. Marie, E.J., Wehrle, R.J., Haupt, D.J., Wood, N.B., van der Vliet, A., Previs, M.J., Masterson, D.S., and Hondal, R.J. (2020). Can Selenoenzymes Resist Electrophilic Modification? Evidence from Thioredoxin Reductase and a Mutant Containing α-Methylselenocysteine. *Biochemistry* *59*, 3300–3315.
- Arnér, E.S.J., Björnstedt, M., and Holmgren, A. (1995). 1-Chloro-2,4-dinitrobenzene Is an Irreversible Inhibitor of Human Thioredoxin Reductase: loss of thioredoxin disulfide reductase activity is accompanied by a large increase in nadph oxidase activity (*). *J. Biol. Chem.* *270*, 3479–3482.
- Nordberg, J., Zhong, L., Holmgren, A., and Arnér, E.S. (1998). Mammalian thioredoxin reductase is irreversibly inhibited by dinitrohalobenzenes by alkylation of both the redox active selenocysteine and its neighboring cysteine residue. *J. Biol. Chem.* *273*, 10835–10842.
- Busker, S., Qian, W., Haraldsson, M., Espinosa, B., Johansson, L., Attarha, S., Kolosenko, I., Liu, J., Dagnell, M., Grandér, D., et al. (2020). Irreversible TrxR1 inhibitors block STAT3 activity and induce cancer cell death. *Sci. Adv.* *6*, eaax7945.
- Stafford, W.C., Peng, X., Olofsson, M.H., Zhang, X., Luci, D.K., Lu, L., Cheng, Q., Trésaugues, L., Dexheimer, T.S., Coussens, N.P., et al. (2018). Irreversible inhibition of cytosolic thioredoxin reductase 1 as a mechanistic basis for anticancer therapy. *Sci. Transl. Med.* *10*, eaaf7444.
- Dickson, R.C., and Tappel, A.L. (1969). Reduction of selenocysteine by cysteine or glutathione. *Arch. Biochem. Biophys.* *130*, 547–550.
- Björnstedt, M., Kumar, S., Björkhem, L., Spyrou, G., and Holmgren, A. (1997). Selenium and the thioredoxin and glutaredoxin systems. *Biomed. Environ. Sci. BES* *10*, 271–279.
- Donnelly, D.P., Dowgiallo, M.G., Salisbury, J.P., Aluri, K.C., lyengar, S., Chaudhari, M., Mathew, M., Miele, I., Auclair, J.R.,

- Lopez, S.A., et al. (2018). Cyclic Thiosulfonates and Cyclic Disulfides Selectively Cross-Link Thiols While Avoiding Modification of Lone Thiols. *J. Am. Chem. Soc.* *140*, 7377–7380.
45. Huang, Z., Terpetschnig, E., You, W., and Haugland, R.P. (1992). 2-(2'-Phosphoryloxyphenyl)-4(3H)-quinazolinone derivatives as fluorogenic precipitating substrates of phosphatases. *Anal. Biochem.* *207*, 32–39.
46. Liu, H.-W., Li, K., Hu, X.-X., Zhu, L., Rong, Q., Liu, Y., Zhang, X.-B., Hasserodt, J., Qu, F.-L., and Tan, W. (2017). In Situ Localization of Enzyme Activity in Live Cells by a Molecular Probe Releasing a Precipitating Fluorochrome. *Angew. Chem. Int. Ed.* *56*, 11788–11792.
47. Prost, M., Canaple, L., Samarut, J., and Hasserodt, J. (2014). Tagging Live Cells that Express Specific Peptidase Activity with Solid-State Fluorescence. *ChemBioChem* *15*, 1413–1417.
48. Thorn-Seshold, O., Vargas-Sanchez, M., McKeon, S., and Hasserodt, J. (2012). A robust, high-sensitivity stealth probe for peptidases. *Chem. Commun.* *48*, 6253–6255.
49. Machida, T., Dutt, S., and Winssinger, N. (2016). Allosterically Regulated Phosphatase Activity from Peptide-PNA Conjugates Folded Through Hybridization. *Angew. Chem. Int. Ed.* *55*, 8595–8598.
50. Rando, G., Winssinger, N., Lindberg, E., and Anzola, M. New compounds and uses thereof for detection of target molecules in a sample.
51. Labunsky, V.M., Hatfield, D.L., and Gladyshev, V.N. (2014). Selenoproteins: Molecular Pathways and Physiological Roles. *Physiol. Rev.* *94*, 739–777.
52. Dimastrogiovanni, D., Anselmi, M., Miele, A.E., Boumis, G., Peterson, L., Angelucci, F., Nola, A.D., Brunori, M., and Bellelli, A. (2010). Combining crystallography and molecular dynamics: The case of *Schistosoma mansoni* phospholipid glutathione peroxidase. *Proteins Struct. Funct. Bioinforma.* *78*, 259–270.
53. Patterson, G.H., Knobel, S.M., Arkhammar, P., Thastrup, O., and Piston, D.W. Separation of the glucose-stimulated cytoplasmic and mitochondrial NAD(P)H responses in pancreatic islet β cells. 5.
54. Cheng, Q., Antholine, W.E., Myers, J.M., Kalyanaraman, B., Arnér, E.S.J., and Myers, C.R. (2010). The Selenium-independent Inherent Pro-oxidant NADPH Oxidase Activity of Mammalian Thioredoxin Reductase and Its Selenium-dependent Direct Peroxidase Activities*. *J. Biol. Chem.* *285*, 21708–21723.
55. Rackham, O., Shearwood, A.-M.J., Thyer, R., McNamara, E., Davies, S.M.K., Callus, B.A., Miranda-Vizuete, A., Berners-Price, S.J., Cheng, Q., Arnér, E.S.J., et al. (2011). Substrate and inhibitor specificities differ between human cytosolic and mitochondrial thioredoxin reductases: Implications for development of specific inhibitors. *Free Radic. Biol. Med.* *50*, 689–699.
56. Xu, J., Cheng, Q., and Arnér, E.S.J. (2016). Details in the catalytic mechanism of mammalian thioredoxin reductase 1 revealed using point mutations and juglone-coupled enzyme activities. *Free Radic. Biol. Med.* *94*, 110–120.
57. Mandal, P.K., Schneider, M., Kolle, P., Kuhlencordt, P., Forster, H., Beck, H., Bornkamm, G.W., and Conrad, M. (2010). Loss of Thioredoxin Reductase 1 Renders Tumors Highly Susceptible to Pharmacologic Glutathione Deprivation. *Cancer Res.* *70*, 9505–9514.
58. Peng, X., Mandal, P.K., Kaminsky, V.O., Lindqvist, A., Conrad, M., and Arnér, E.S.J. (2014). Sec-containing TrxR1 is essential for self-sufficiency of cells by control of glucose-derived H₂O₂. *Cell Death Dis.* *5*, e1235.
59. Schindelin, J., Arganda-Carreras, I., Frise, E., Kaynig, V., Longair, M., Pietzsch, T., Preibisch, S., Rueden, C., Saalfeld, S., Schmid, B., et al. (2012). Fiji: an open-source platform for biological-image analysis. *Nat. Methods* *9*, 676–682.
60. Inglese, J., Auld, D.S., Jadhav, A., Johnson, R.L., Simeonov, A., Yasgar, A., Zheng, W., and Austin, C.P. (2006). Quantitative high-throughput screening: A titration-based approach that efficiently identifies biological activities in large chemical libraries. *Proc. Natl. Acad. Sci.* *103*, 11473–11478.
61. Hall, M.D., Telma, K.A., Chang, K.-E., Lee, T.D., Madigan, J.P., Lloyd, J.R., Goldlust, I.S., Hoeschele, J.D., and Gottesman, M.M. (2014). Say No to DMSO: Dimethylsulfoxide Inactivates Cisplatin, Carboplatin, and Other Platinum Complexes. *Cancer Res.* *74*, 3913–3922.
62. Prast-Nielsen, S., Dexheimer, T.S., Schultz, L., Stafford, W.C., Cheng, Q., Xu, J., Jadhav, A., Arnér, E.S.J., and Simeonov, A. (2011). Inhibition of thioredoxin reductase 1 by porphyrins and other small molecules identified by a high-throughput screening assay. *Free Radic. Biol. Med.* *50*, 1114–1123.
63. Block, E., Dikarev, E.V., Glass, R.S., Jin, Li, B., Li, X., and Zhang, S.-Z. (2006). Synthesis, Structure, and Chemistry of New, Mixed Group 14 and 16 Heterocycles: Nucleophile-Induced Ring Contraction of Mesocyclic Dications. *J. Am. Chem. Soc.* *128*, 14949–14961.
64. He, C., Stratton, T.P., and Baran, P.S. (2019). Concise Total Synthesis of Herquelines B and C. *J. Am. Chem. Soc.* *141*, 29–32.
65. Thorn-Seshold, O., Vargas-Sanchez, M., McKeon, S., and Hasserodt, J. (2012). A robust, high-sensitivity stealth probe for peptidases. *Chem. Commun.* *48*, 6253–6255.
66. Morales-Serna, J.A., Garcia-Rios, E., Bernal, J., Paleo, E., Gaviño, R., and Cárdenas, J. (2011). Reduction of Carboxylic Acids Using Esters of Benzotriazole as High-Reactivity Intermediates. *Synthesis* *2011*, 1375–1382.
67. Busto, E., Gotor-Fernández, V., Montejo-Bernardo, J., Garcia-Granda, S., and Gotor, V. (2009). Development of a chemoenzymatic strategy for the synthesis of optically active and orthogonally protected polyamines. *Tetrahedron* *65*, 8393–8401.
68. Cho, Y.-J., Kim, H.-Y., Huang, H., Slutsky, A., Minko, I.G., Wang, H., Nechev, L.V., Kozekov, I.D., Kozekova, A., Tamura, P., et al. (2005). Spectroscopic Characterization of Interstrand Carbinolamine Cross-Links Formed in the 5'-CpG-3' Sequence by the Acrolein-Derived γ -OH-1,N2-Propano-2'-deoxyguanosine DNA Adduct. *J. Am. Chem. Soc.* *127*, 17686–17696.
69. Sato, M., Kawakami, H., Motomura, T., Aramaki, H., Matsuda, T., Yamashita, M., Ito, Y., Matsuzaki, Y., Yamataka, K., Ikeda, S., et al. (2009). Quinolone Carboxylic Acids as a Novel Monoketo Acid Class of Human Immunodeficiency Virus Type 1 Integrase Inhibitors. *J. Med. Chem.* *52*, 4869–4882.
70. Wang, Y., Liu, D., Zheng, Q., Zhao, Q., Zhang, H., Ma, Y., Fallon, J.K., Fu, Q., Haynes, M.T., Lin, G., et al. (2014). Disulfide Bond Bridge Insertion Turns Hydrophobic Anticancer Prodrugs into Self-Assembled Nanomedicines. *Nano Lett.* *14*, 5577–5583.
71. Seki, M., Hatsuda, M., Mori, Y., Yoshida, S., Yamada, S., and Shimizu, T. (2004). A Practical Synthesis of (+)-Biotin from L-Cysteine. *Chem. – Eur. J.* *10*, 6102–6110.
72. Lukesh, J.C., Palte, M.J., and Raines, R.T. (2012). A Potent, Versatile Disulfide-Reducing Agent from Aspartic Acid. *J. Am. Chem. Soc.* *134*, 4057–4059.
73. Arai, K., Matsunaga, T., Ueno, H., Akahoshi, N., Sato, Y., Chakrabarty, G., Mughesh, G., and Iwaoka, M. (2019). Modeling Thioredoxin Reductase-Like Activity with Cyclic Selenenyl Sulfides: Participation of an NH...Se Hydrogen Bond through Stabilization of the Mixed Se–S Intermediate. *Chem. – Eur. J.* *25*, 12751–12760.
74. Shimodaira, S., and Iwaoka, M. (2019). Synthesis of selenocysteine-containing dipeptides modeling the active site of thioredoxin reductase. *Phosphorus Sulfur Silicon Relat. Elem.* *194*, 750–752.

Supporting Information to:

Bifunctional, piperazine-fused cyclic disulfides for oxidoreductase-activated cellular proagentsLukas Zeisel^{1.#}, Jan G. Felber^{1.#}, Karoline C. Scholzen², Carina Schmitt¹, Alexander J. Wiegand¹, Leonid Komissarov³, Elias S.J. Arnér^{2,4}, Oliver Thorn-Seshold^{1.*}¹ Department of Pharmacy, Ludwig Maximilians University Munich, Butenandtstr. 5-13, 81377 Munich.² Department of Medical Biochemistry, Karolinska Institutet, Solnavägen 9, 171 65 Solna, Sweden.³ Center for Molecular Modeling (CMM), Ghent University, Technologiepark-Zwijnaarde 46, 9052 Ghent, Belgium.⁴ Department of Selenoprotein Research, National Institute of Oncology, 1122 Budapest, Hungary.#The two first authors contributed equally to this work. *Corresponding author: oliver.thorn-seshold@cup.lmu.de**Author Contributions**

Lukas Zeisel developed the synthetic access to diastereomerically pure piperazine-fused 1,2-dithianes and 1,2-diselenanes, performed synthesis and analysis, chemoreductant assays and mechanistic analysis. Jan G. Felber performed synthesis and analysis and developed strategies for functional diversification, performed chemoreductant, enzymatic specificity screening and DFT-based calculations. The two first authors contributed equally to the design of the experiments, data assembly and visualisation, conceptual analysis of the scientific outcomes and writing the manuscript. Karoline C. Scholzen performed biochemical screenings, cellular inhibitor and knockout studies. Carina Schmitt and Alexander J. Wiegand performed synthesis and analysis. Leonid Komissarov performed DFT-based calculations. Elias S. J. Arnér supervised biochemical studies and cell biology. Oliver Thorn-Seshold designed the concept and experiments, coordinated data assembly, and wrote the manuscript with input from all co-authors.

Table of contents

1 Supporting Notes	S2
1.1 Synthetic optimisations for scalable assembly of the dichalcogenide piperazine scaffolds	S2
1.2 Probe overview	S3
2 Do thermodynamics still matter?	S4
2.1 Experimental redox potentials of piperazine-fused 1,2-dithianes	S4
2.2 DFT-calculation of bicyclic 1,2-dithiane energetics	S5
3 Kinetic analyses of TCEP, GSH and DTT probe activation	S11
4 Enzymatic specificity assays	S16
5 Cellular assays	S23
6 Materials and methods	S28
6.1 Determination of reduction potentials	S28
6.2 DFT calculations	S28
6.3 (Bio)chemical probe activation assays	S28
6.4 Cellular assays	S29
6.5 Synthesis	S30
7 Synthetic Procedures	S31
7.1 General protocols	S31
7.2 Final short trigger synthesis	S33
7.3 Probe synthesis	S46
7.4 Initial synthetic route	S57
8. Supporting Information references	S66
9. NMR spectra	S67

1 Supporting Notes

1.1 Synthetic optimisations for scalable assembly of the dichalcogenide piperazine scaffolds

Our retrosynthetic approach for dichalcogenide piperazines was guided by the following key aspects: (1) We intended to apply our established methodologies for the synthesis of dithianes and diselenanes, which proceed via alcohol activation, chalcogenide introduction via S_N2 , and ultimate formation of the heterocycle. (2) In earlier work, we have shown that the redox properties, i.e. reduction potential and release kinetics of piperidine-annellated dithianes fundamentally rely on the architecture of the bicyclic core (cis- or trans-fused). Therefore, high diastereomeric purity is needed. Based on our synthetic endeavours on the disulfide piperidines, we wanted to develop routes which fully circumvent conditions that can lead to epimerisation, particularly the use of strong base. (3) We envisioned a unified and scalable synthetic route that can provide all four dichalcogenide piperazines from the same starting material. In an initial effort, we identified 1,4-dithioerythritol (cis) and 1,4-dithiothreitol (trans) as seemingly ideal starting materials towards dichalcogenide piperazines; both would solely require oxidation and subsequent piperazine assembly. Unfortunately, for both DTE^{ox}/DTT^{ox} mesylates and triflates, C-N bond formation was unsuccessful regardless of the N-nucleophile (Fig S2, top right).

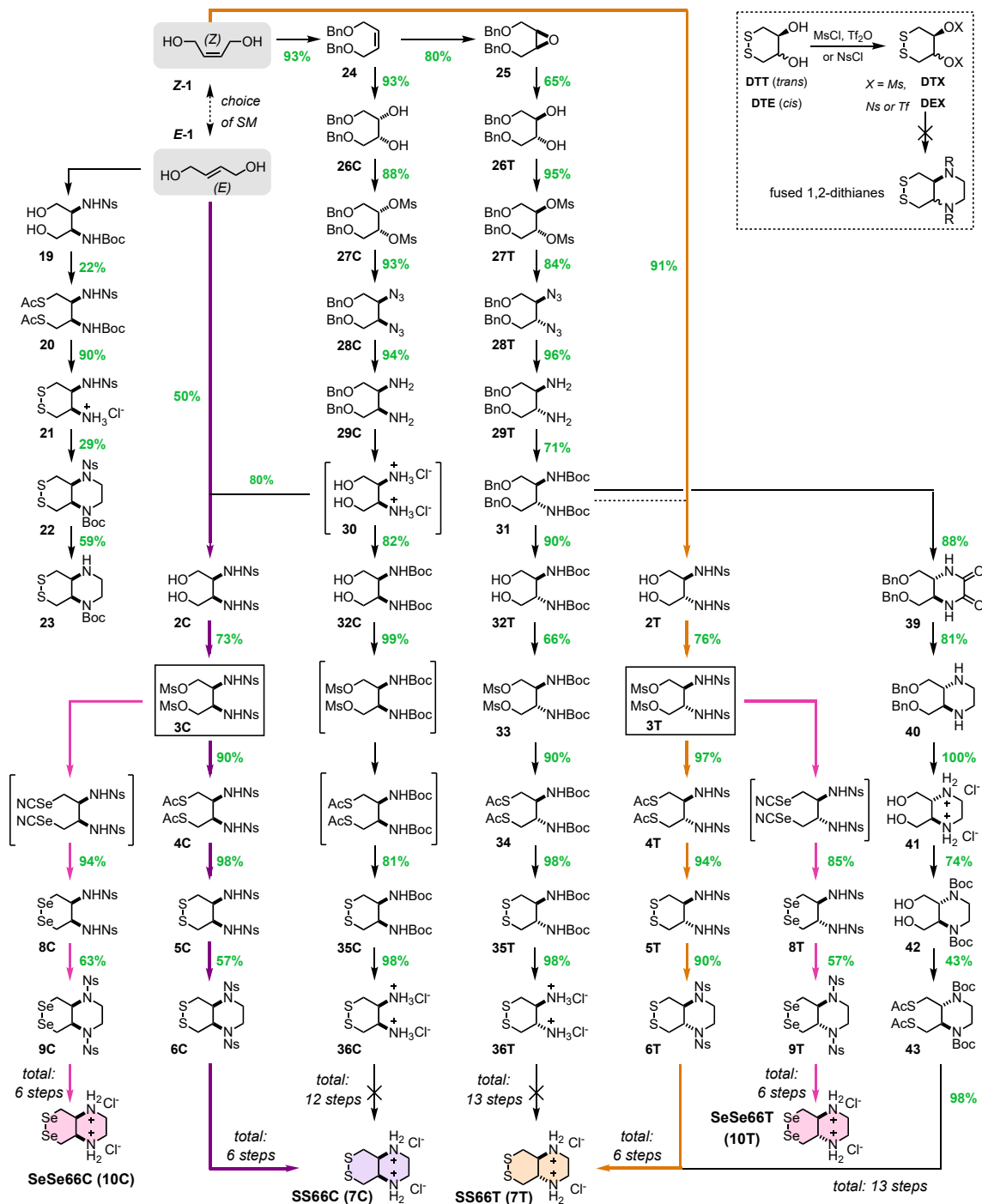
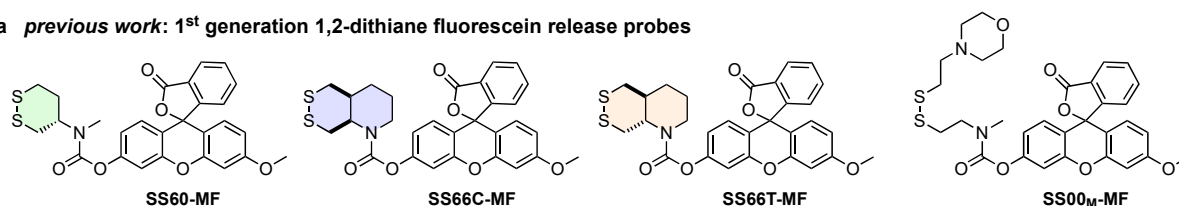
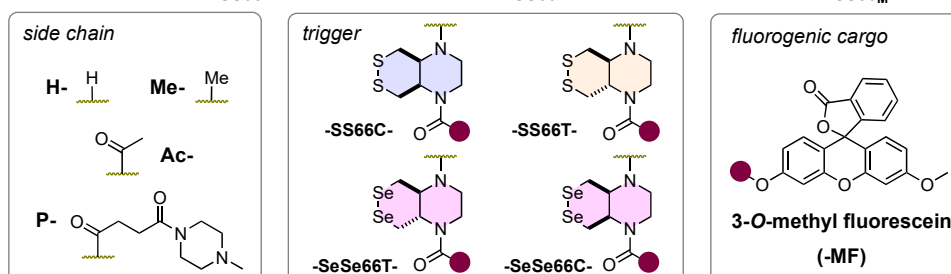
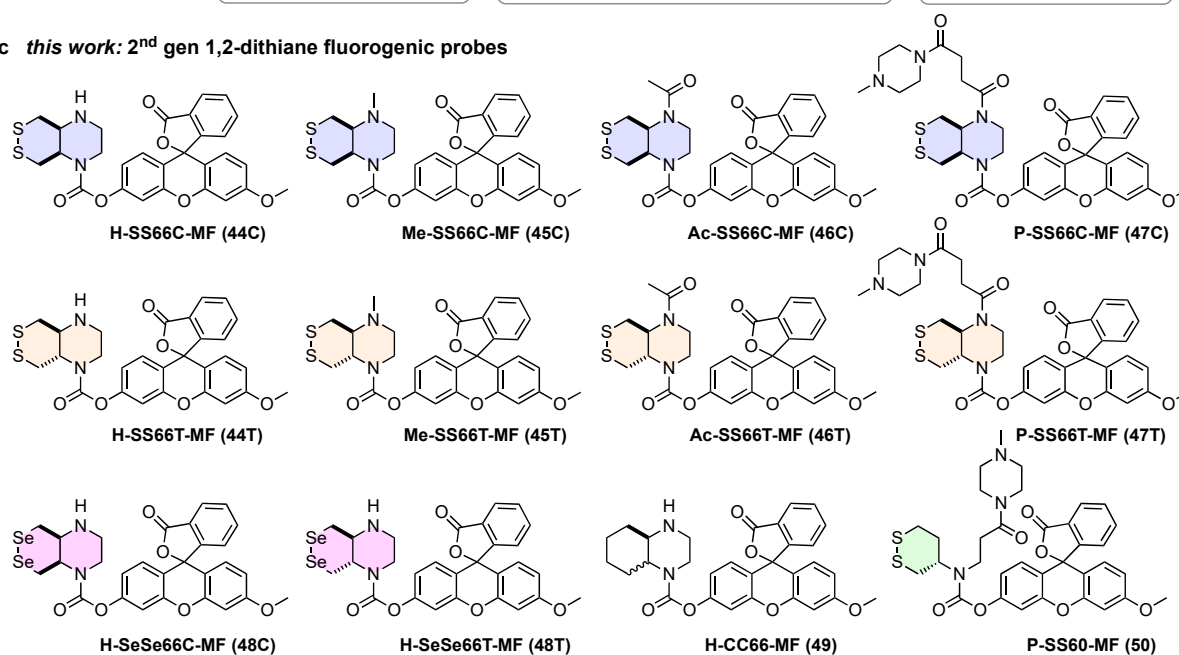


Figure S1 Overview of synthetic routes towards piperazine dichalcogenides starting from butene-diol Z-1 and E-1.

1.2 Probe overview

a *previous work*: 1st generation 1,2-dithiane fluorescein release probes

b modular design & nomenclature

c *this work*: 2nd gen 1,2-dithiane fluorogenic probes

d diversification platform probes

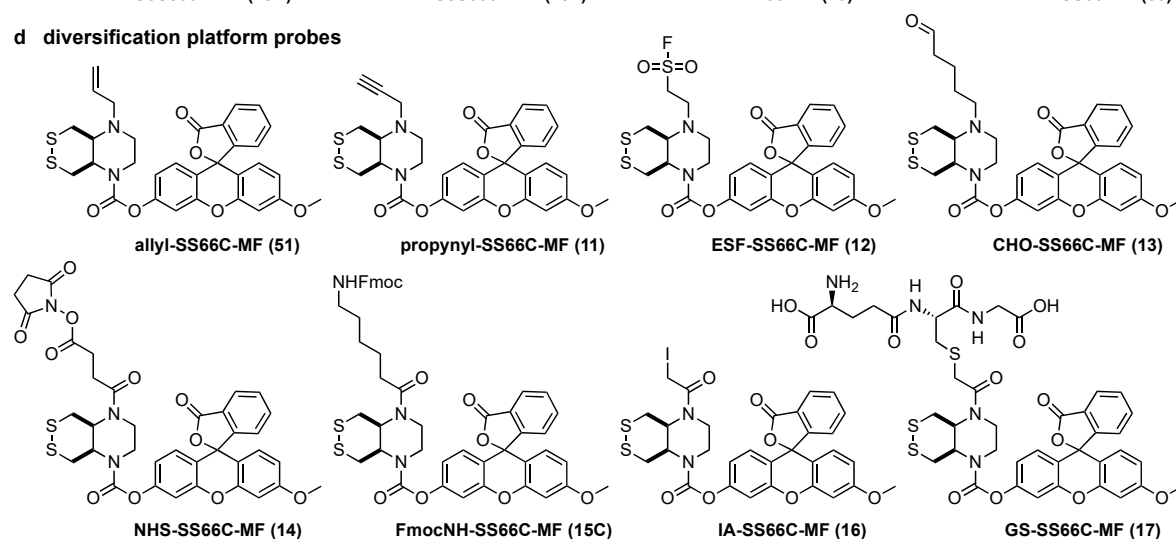


Figure S2 Overview of 3-O-methyl fluorescein (MF) conjugates. (a) Previous MF-series.¹ (b) Design and nomenclature. Probes used for (c) kinetic/cellular evaluation and (d) as models for functional derivatisation.

2 Do thermodynamics still matter?

2.1 Experimental redox potentials of piperazine-fused 1,2-dithianes

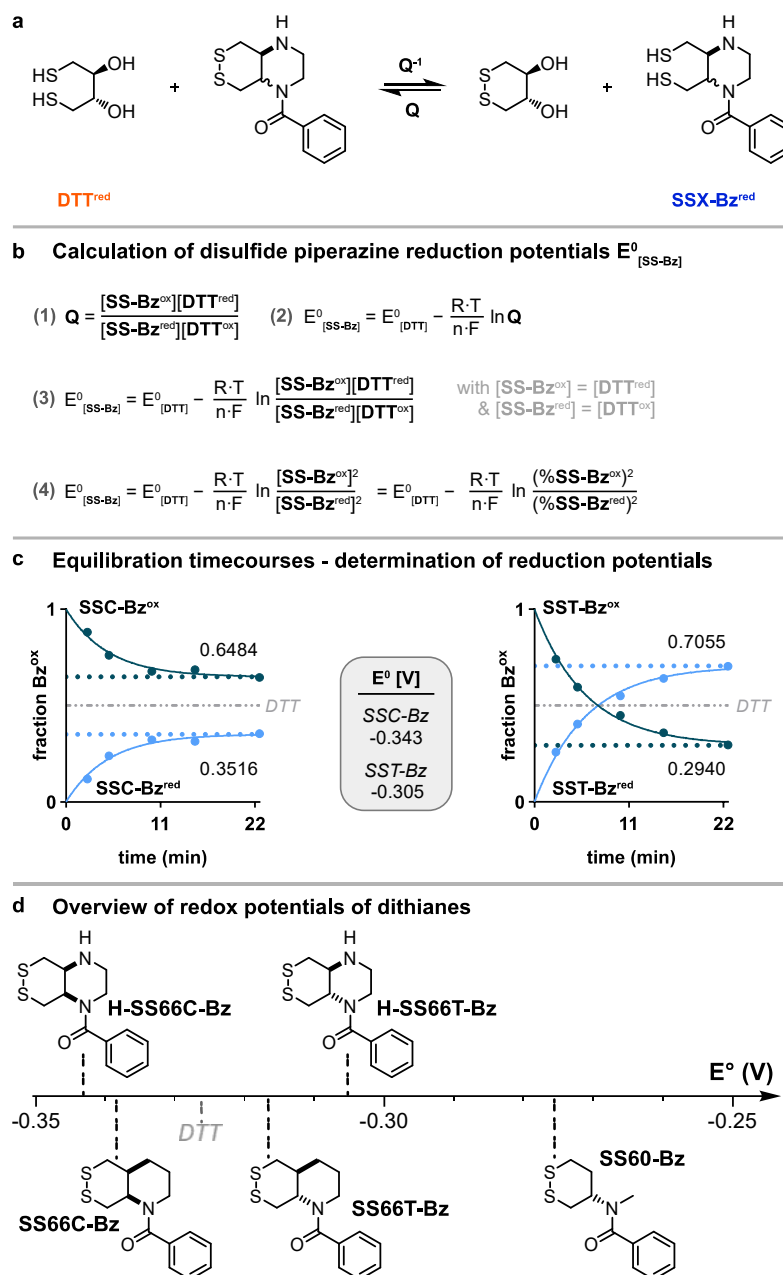


Figure S3 Experimental reduction potential for the benzamide model compounds **H-SS66C-Bz** (**52C**) and **H-SS66T-Bz** (**52T**) (a) Reaction formula for equilibration with dithiol-type reductant 1,4-dithiothreitol (DTT). (b) Calculation of the relative reduction potential according to Nernst's equation. (c) Equilibration timecourses determined by HPLC for equimolar ratios of benzamide and DTT. Note that the fitted plateaus for the oxidized and reduced forms of each compound add up to 1.00, indicating validation of the 210 nm integral use (see also Methods section). Note too that the plateaus are reached in ca. 25 min, which is > 10-fold faster than observed for benzamide of the piperidine-fused 1,2-dithianes described earlier. (d) Overview of relative reduction potentials for benzamides **52C** and **52T** of this work and previous **SS66C-Bz**, **SS66T-Bz** and monocyclic **SS60-Bz**.^{1,2}

2.2 DFT-calculation of bicyclic 1,2-dithiane energetics

Table S1 – part 1/3. DFT calculation of fused dichalcogenide ring energies. *Continues the following page.*

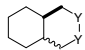
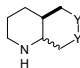
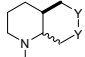
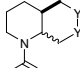
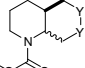
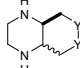
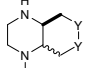
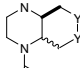
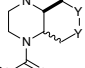
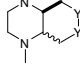
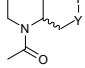
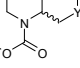
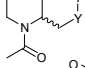
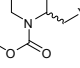
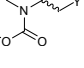
raw data (part 1)	disulfides (SS66)			diselenides (SeSe66)			
		E[kJ/mol]	ZPE[kJ/mol]		E[kJ/mol]	ZPE[kJ/mol]	
	H ₂	-7.44E+02	2.62E+01	H ₂	-7.44E+02	2.62E+01	
C-C 	<i>cis</i> ox	C-SS66C-C	-1.44E+04	5.49E+02	C-SeSe66C-C	-1.43E+04	5.43E+02
		red	C-SS66C-C	-1.52E+04	5.91E+02	C-SeSe66C-C	-1.50E+04
	<i>trans</i> ox	C-SS66T-C	-1.44E+04	5.49E+02	C-SeSe66T-C	-1.43E+04	5.43E+02
		red	C-SS66T-C	-1.52E+04	5.90E+02	C-SeSe66T-C	-1.50E+04
C-H 	<i>cis</i> ox	C-SS66C-H	-1.40E+04	5.20E+02	C-SeSe66C-H	-1.38E+04	5.14E+02
		red	C-SS66C-H	-1.48E+04	5.61E+02	C-SeSe66C-H	-1.45E+04
	<i>trans</i> ox	C-SS66T-H	-1.40E+04	5.19E+02	C-SeSe66T-H	-1.38E+04	5.14E+02
		red	C-SS66T-H	-1.48E+04	5.61E+02	C-SeSe66T-H	-1.46E+04
C-Me 	<i>cis</i> ox	C-SS66C-Me	-1.57E+04	5.91E+02	C-SeSe66C-Me	-1.56E+04	5.86E+02
		red	C-SS66C-Me	-1.65E+04	6.33E+02	C-SeSe66C-Me	-1.63E+04
	<i>trans</i> ox	C-SS66T-Me	-1.57E+04	5.92E+02	C-SeSe66T-Me	-1.56E+04	5.86E+02
		red	C-SS66T-Me	-1.65E+04	6.34E+02	C-SeSe66T-Me	-1.63E+04
C-Ac 	<i>cis</i> ox	C-SS66C-Ac	-1.76E+04	6.19E+02	C-SeSe66C-Ac	-1.74E+04	6.13E+02
		red	C-SS66C-Ac	-1.84E+04	6.63E+02	C-SeSe66C-Ac	-1.82E+04
	<i>trans</i> ox	C-SS66T-Ac	-1.76E+04	6.18E+02	C-SeSe66T-Ac	-1.74E+04	6.12E+02
		red	C-SS66T-Ac	-1.84E+04	6.60E+02	C-SeSe66T-Ac	-1.82E+04
C-MC 	<i>cis</i> ox	C-SS66C-MC	-1.84E+04	6.31E+02	C-SeSe66C-MC	-1.82E+04	6.25E+02
		red	C-SS66C-MC	-1.92E+04	6.75E+02	C-SeSe66C-MC	-1.90E+04
	<i>trans</i> ox	C-SS66T-MC	-1.84E+04	6.34E+02	C-SeSe66T-MC	-1.83E+04	6.26E+02
		red	C-SS66T-MC	-1.92E+04	6.73E+02	C-SeSe66T-MC	-1.90E+04
H-H 	<i>cis</i> ox	H-SS66C-H	-1.35E+04	4.89E+02	H-SeSe66C-H	-1.33E+04	4.84E+02
		red	H-SS66C-H	-1.43E+04	5.31E+02	H-SeSe66C-H	-1.41E+04
	<i>trans</i> ox	H-SS66T-H	-1.35E+04	4.90E+02	H-SeSe66T-H	-1.34E+04	4.84E+02
		red	H-SS66T-H	-1.43E+04	5.32E+02	H-SeSe66T-H	-1.41E+04
H-Me 	<i>cis</i> ox	H-SS66C-Me	-1.52E+04	5.61E+02	H-SeSe66C-Me	-1.51E+04	5.57E+02
		red	H-SS66C-Me	-1.60E+04	6.03E+02	H-SeSe66C-Me	-1.58E+04
	<i>trans</i> ox	H-SS66T-Me	-1.53E+04	5.62E+02	H-SeSe66T-Me	-1.51E+04	5.57E+02
		red	H-SS66T-Me	-1.61E+04	6.04E+02	H-SeSe66T-Me	-1.59E+04
H-Ac 	<i>cis</i> ox	H-SS66C-Ac	-1.71E+04	5.90E+02	H-SeSe66C-Ac	-1.69E+04	5.84E+02
		red	H-SS66C-Ac	-1.79E+04	6.33E+02	H-SeSe66C-Ac	-1.77E+04
	<i>trans</i> ox	H-SS66T-Ac	-1.71E+04	5.89E+02	H-SeSe66T-Ac	-1.70E+04	5.83E+02
		red	H-SS66T-Ac	-1.79E+04	6.32E+02	H-SeSe66T-Ac	-1.77E+04
H-MC 	<i>cis</i> ox	H-SS66C-MC	-1.79E+04	6.03E+02	H-SeSe66C-MC	-1.78E+04	5.97E+02
		red	H-SS66C-MC	-1.87E+04	6.45E+02	H-SeSe66C-MC	-1.85E+04
	<i>trans</i> ox	H-SS66T-MC	-1.79E+04	6.01E+02	H-SeSe66T-MC	-1.78E+04	5.96E+02
		red	H-SS66T-MC	-1.87E+04	6.45E+02	H-SeSe66T-MC	-1.85E+04
Me-Me 	<i>cis</i> ox	Me-SS66C-Me	-1.70E+04	6.34E+02	Me-SeSe66C-Me	-1.68E+04	6.28E+02
		red	Me-SS66C-Me	-1.78E+04	6.75E+02	Me-SeSe66C-Me	-1.76E+04
	<i>trans</i> ox	Me-SS66T-Me	-1.70E+04	6.35E+02	Me-SeSe66T-Me	-1.69E+04	6.28E+02
		red	Me-SS66T-Me	-1.78E+04	6.77E+02	Me-SeSe66T-Me	-1.76E+04
Me-Ac 	<i>cis</i> ox	Me-SS66C-Ac	-1.89E+04	6.61E+02	Me-SeSe66C-Ac	-1.87E+04	6.55E+02
		red	Me-SS66C-Ac	-1.97E+04	7.03E+02	Me-SeSe66C-Ac	-1.95E+04
	<i>trans</i> ox	Me-SS66T-Ac	-1.89E+04	6.60E+02	Me-SeSe66T-Ac	-1.87E+04	6.55E+02
		red	Me-SS66T-Ac	-1.97E+04	7.03E+02	Me-SeSe66T-Ac	-1.95E+04
Me-MC 	<i>cis</i> ox	Me-SS66C-MC	-1.97E+04	6.75E+02	Me-SeSe66C-MC	-1.96E+04	6.68E+02
		red	Me-SS66C-MC	-2.05E+04	7.17E+02	Me-SeSe66C-MC	-2.03E+04
	<i>trans</i> ox	Me-SS66T-MC	-1.97E+04	6.74E+02	Me-SeSe66T-MC	-1.96E+04	6.70E+02
		red	Me-SS66T-MC	-2.05E+04	7.16E+02	Me-SeSe66T-MC	-2.03E+04
Ac-Ac 	<i>cis</i> ox	Ac-SS66C-Ac	-2.07E+04	6.87E+02	Ac-SeSe66C-Ac	-2.06E+04	6.82E+02
		red	Ac-SS66C-Ac	-2.15E+04	7.30E+02	Ac-SeSe66C-Ac	-2.13E+04
	<i>trans</i> ox	Ac-SS66T-Ac	-2.08E+04	6.87E+02	Ac-SeSe66T-Ac	-2.06E+04	6.84E+02
		red	Ac-SS66T-Ac	-2.16E+04	7.29E+02	Ac-SeSe66T-Ac	-2.13E+04
Ac-MC 	<i>cis</i> ox	Ac-SS66C-MC	-2.16E+04	6.99E+02	Ac-SeSe66C-MC	-2.14E+04	6.94E+02
		red	Ac-SS66C-MC	-2.24E+04	7.42E+02	Ac-SeSe66C-MC	-2.22E+04
	<i>trans</i> ox	Ac-SS66T-MC	-2.16E+04	7.00E+02	Ac-SeSe66T-MC	-2.14E+04	6.96E+02
		red	Ac-SS66T-MC	-2.24E+04	7.42E+02	Ac-SeSe66T-MC	-2.22E+04
MC-MC 	<i>cis</i> ox	MC-SS66C-MC	-2.24E+04	7.13E+02	MC-SeSe66C-MC	-2.22E+04	7.17E+02
		red	MC-SS66C-MC	-2.32E+04	7.56E+02	MC-SeSe66C-MC	-2.30E+04
	<i>trans</i> ox	MC-SS66T-MC	-2.24E+04	7.16E+02	MC-SeSe66T-MC	-2.22E+04	7.08E+02
		red	MC-SS66T-MC	-2.32E+04	7.56E+02	MC-SeSe66T-MC	-2.30E+04

Table S1 – part 2/3. DFT calculation of fused dichalcogenide ring energies. *Continues on following page.*

processed data (part 2)		disulfides (SS66)				diselenides (SeSe66)						
		$E^{\text{ox}*} = E(\text{SS}^{\text{ox}}) + E(\text{H}_2); E^{\text{red}*} = E(\text{SS}^{\text{red}})$				$E^{\text{ox}*} = E(\text{SeSe}^{\text{ox}}) + E(\text{H}_2); E^{\text{red}*} = E(\text{SeSe}^{\text{red}})$						
		E^* [kJ/mol]	ZPE* [kJ/mol]	$E^{\text{total}} = E^* + \text{ZPE}^*$	E^{rel} [kJ/mol]	E^* [kJ/mol]	ZPE* [kJ/mol]	$E^{\text{total}} = E^* + \text{ZPE}^*$	E^{rel} [kJ/mol]			
C-C 	cis	ox	-15170.04	575.27	-14594.77		31.0	-15009.88	568.90	-14440.98		5.6
		red	-15211.50	590.73	-14620.77		5.0	-15007.69	582.56	-14425.13		21.5
	trans	ox	-15177.89	574.70	-14603.19		22.5	-15015.32	568.74	-14446.59		0
		red	-15216.01	590.28	-14625.73		0	-15012.27	582.19	-14430.08		16.5
C-H 	cis	ox	-14710.32	546.01	-14164.31		31.7	-14551.26	540.65	-14010.61		5.6
		red	-14751.82	561.20	-14190.62		5.4	-14548.59	553.22	-13995.37		20.8
	trans	ox	-14717.84	545.42	-14172.42		23.6	-14555.98	539.78	-14016.20		0
		red	-14756.86	560.84	-14196.02		0	-14552.14	552.53	-13999.61		16.6
C-Me 	cis	ox	-16477.74	617.53	-15860.21		26.9	-16318.43	612.48	-15705.95		0
		red	-16520.50	633.37	-15887.13		0	-16316.71	625.01	-15691.70		14.3
	trans	ox	-16473.38	618.10	-15855.28		31.8	-16311.29	612.37	-15698.92		7.0
		red	-16515.28	633.79	-15881.49		5.6	-16311.29	625.20	-15686.09		19.9
C-Ac 	cis	ox	-18309.75	645.05	-17664.70		62.9	-18148.11	638.93	-17509.18		30.7
		red	-18367.11	662.75	-17704.36		23.2	-18160.84	652.35	-17508.49		31.4
	trans	ox	-18339.44	644.21	-17695.23		32.4	-18178.25	638.37	-17539.88		0
		red	-18388.07	660.47	-17727.60		0	-18182.00	651.02	-17530.98		8.9
C-MC 	cis	ox	-19141.42	657.34	-18484.08		54.1	-18981.53	651.57	-18329.96		20.1
		red	-19183.00	675.03	-18507.97		30.2	-18991.17	664.95	-18326.22		23.9
	trans	ox	-19160.55	659.78	-18500.77		37.4	-19002.29	652.22	-18350.07		0
		red	-19211.54	673.39	-18538.15		0	-19005.85	664.55	-18341.30		8.8
H-H 	cis	ox	-14222.41	515.43	-13706.98		59.4	-14064.67	510.48	-13554.19		31.9
		red	-14262.86	531.05	-13731.81		34.6	-14067.84	524.24	-13543.60		42.5
	trans	ox	-14257.37	516.15	-13741.22		25.2	-14096.16	510.09	-13586.07		0
		red	-14298.45	532.04	-13766.41		0	-14092.78	523.67	-13569.11		17.0
H-Me 	cis	ox	-15988.03	587.66	-15400.37		49.7	-15829.42	582.75	-15246.67		20.2
		red	-16028.93	603.35	-15425.58		24.5	-15836.18	597.22	-15238.96		27.9
	trans	ox	-16011.12	588.60	-15422.52		27.6	-15849.60	582.71	-15266.90		0
		red	-16054.19	604.08	-15450.11		0	-15850.27	595.68	-15254.59		12.3
H-Ac 	cis	ox	-17850.47	615.84	-17234.63		60.2	-17690.01	609.72	-17080.29		14.8
		red	-17905.85	632.60	-17273.25		21.5	-17692.63	622.57	-17070.06		25.0
	trans	ox	-17874.62	614.96	-17259.66		35.1	-17704.60	609.52	-17095.08		0
		red	-17926.47	631.67	-17294.80		0	-17710.50	622.60	-17087.90		7.2
H-MC 	cis	ox	-18681.26	628.73	-18052.53		30.7	-18522.42	623.36	-17899.07		6.7
		red	-18728.24	645.03	-18083.21		0	-18538.28	634.98	-17903.30		2.5
	trans	ox	-18673.40	626.88	-18046.52		36.7	-18528.44	622.64	-17905.80		0
		red	-18724.75	644.87	-18079.88		3.3	-18518.50	635.71	-17882.79		23.0
Me-Me 	cis	ox	-17750.38	659.73	-17090.65		46.7	-17591.25	654.48	-16936.77		18.4
		red	-17797.75	675.37	-17122.38		15.0	-17597.77	667.34	-16930.43		24.7
	trans	ox	-17773.88	661.05	-17112.83		24.6	-17609.62	654.48	-16955.14		0
		red	-17814.41	677.02	-17137.39		0	-17609.31	668.25	-16941.06		14.1
Me-Ac 	cis	ox	-19618.49	686.91	-18931.58		47.6	-19457.19	681.62	-18775.57		17.4
		red	-19667.81	703.17	-18964.64		14.6	-19463.18	694.87	-18768.31		24.6
	trans	ox	-19636.73	686.67	-18950.06		29.2	-19473.70	680.74	-18792.96		0
		red	-19681.85	702.64	-18979.21		0	-19477.97	696.45	-18781.52		11.4
Me-MC 	cis	ox	-20475.31	701.35	-19773.96		28.9	-20316.97	694.48	-19622.50		0
		red	-20519.60	716.75	-19802.85		0	-20318.88	711.05	-19607.83		14.7
	trans	ox	-20456.72	699.99	-19756.73		46.1	-20299.28	696.13	-19603.15		19.3
		red	-20506.47	716.28	-19790.19		12.7	-20295.02	707.39	-19587.63		34.9
Ac-Ac 	cis	ox	-21492.13	713.67	-20778.46		49.3	-21332.53	708.06	-20624.47		2.7
		red	-21549.68	729.67	-20820.01		7.7	-21336.60	720.20	-20616.40		10.8
	trans	ox	-21509.79	713.03	-20796.76		31.0	-21295.24	709.81	-20585.44		41.8
		red	-21556.81	729.07	-20827.74		0	-21347.50	720.28	-20627.22		0
Ac-MC 	cis	ox	-22322.80	725.09	-21597.71		37.0	-22164.63	720.44	-21444.19		10.1
		red	-22376.90	742.23	-21634.67		0	-22187.34	733.05	-21454.29		0
	trans	ox	-22325.96	726.02	-21599.94		34.7	-22121.14	721.75	-21399.39		54.9
		red	-22373.53	742.46	-21631.07		3.6	-22171.55	734.29	-21437.26		17.0
MC-MC 	cis	ox	-23136.77	739.13	-22397.65		33.4	-22977.95	742.83	-22235.12		13.5
		red	-23187.03	755.96	-22431.07		0	-22974.88	746.94	-22227.94		20.6
	trans	ox	-23139.97	742.28	-22397.69		33.4	-22983.06	734.48	-22248.58		0
		red	-23186.48	755.68	-22430.80		0.3	-22980.97	745.83	-22235.14		13.4

Table S1 – part 3/3. DFT calculation of fused dichalcogenide / dichalcogenol free energies.

part 3	oxidized: $E^{\text{total}}(\text{cis}) - E^{\text{total}}(\text{trans})$		$E^{\text{total}}(\text{red}) - E^{\text{total}}(\text{ox})$		$[E_{\text{red}}^{\text{total}} - E_{\text{ox}}^{\text{total}}]_{\text{trans}} - [E_{\text{red}}^{\text{total}} - E_{\text{ox}}^{\text{total}}]_{\text{cis}}$	
[kJ/mol]	Positive value = <i>trans</i> more stable than <i>cis</i>		Positive value = <i>reduced</i> form preferred		Positive value = energy gain upon reduction for <i>cis</i> is higher than for <i>trans</i>	
	SS66	SeSe66	SS66	SeSe66	SS66	SeSe66
C-C	8.4	5.6	<i>cis</i> 26.0 <i>trans</i> 22.5	-15.9 -16.5	-3.5	-0.6
C-H	8.1	5.6	<i>cis</i> 26.3 <i>trans</i> 23.6	-15.2 -16.6	-2.7	-1.3
C-Me	-4.9	-7.0	<i>cis</i> 26.9 <i>trans</i> 26.2	-14.3 -12.8	-0.7	1.4
C-Ac	30.5	30.7	<i>cis</i> 39.7 <i>trans</i> 32.4	-0.7 -8.9	-7.3	-8.2
C-MC	16.7	20.1	<i>cis</i> 23.9 <i>trans</i> 37.4	-3.7 -8.8	13.5	-5.0
H-H	34.2	31.9	<i>cis</i> 24.8 <i>trans</i> 25.2	-10.6 -17.0	0.4	-6.4
H-Me	22.2	20.2	<i>cis</i> 25.2 <i>trans</i> 27.6	-7.7 -12.3	2.4	-4.6
H-Ac	25.0	14.8	<i>cis</i> 38.6 <i>trans</i> 35.1	-10.2 -7.2	-3.5	3.1
H-MC	-6.0	6.7	<i>cis</i> 30.7 <i>trans</i> 33.4	4.2 -23.0	2.7	-27.2
Me-Me	22.2	18.4	<i>cis</i> 31.7 <i>trans</i> 24.6	-6.3 -14.1	-7.2	-7.7
Me-Ac	18.5	17.4	<i>cis</i> 33.1 <i>trans</i> 29.2	-7.3 -11.4	-3.9	-4.2
Me-MC	-17.2	-19.3	<i>cis</i> 28.9 <i>trans</i> 33.5	-14.7 -15.5	4.6	-0.8
Ac-Ac	18.3	-39.0	<i>cis</i> 41.6 <i>trans</i> 31.0	-8.1 41.8	-10.6	49.9
Ac-MC	2.2	-44.8	<i>cis</i> 37.0 <i>trans</i> 31.1	10.1 37.9	-5.8	27.8
MC-MC	0.0	13.5	<i>cis</i> 33.4 <i>trans</i> 33.1	-7.2 -13.4	-0.3	-6.3

Supporting Note for DFT-based calculation of bicyclic dichalcogenide ring energies

The DFT calculations performed for this section have the following aims: (i) to compare bicyclic ring energies of *cis*-fused vs. *trans*-fused dichalcogenides to conclude on their tendency for ring opening based on thermodynamics; (ii) to compare fused 1,2-dithianes and 1,2-diselenanes with respect to their reduction/oxidation; (iii) to conclude on the influence of modifications in the backbone ring.

The following conditions apply: (i) calculate the total energy ($E^{\text{total}} = E^* + \text{ZPE}^*$) from the electronic energy E (kJ/mol) and the ZPE (zero point vibrational energy) for oxidized or reduced bicyclic dichalcogenide species. (ii) For the oxidized isomers we correct E^{total} with one equivalent of H_2 for comparison of absolute energies [ox: $E^*(\text{RS}_2) = E(\text{RS}_2) + E(\text{H}_2)$; $\text{ZPE}^*(\text{RS}_2) = \text{ZPE}(\text{RS}_2) + \text{ZPE}(\text{H}_2)$ and red: $E^*(\text{R}(\text{SH})_2) = E(\text{R}(\text{SH})_2)$; $\text{ZPE}^*(\text{R}(\text{SH})_2) = \text{ZPE}(\text{R}(\text{SH})_2)$] with $\text{RS}_2 + \text{H}_2 \rightarrow \text{R}(\text{SH})_2$ as the underlying redox reaction.

Table S1 - part 1 shows the calculated raw data. The exact energies are provided in the downloadable archive as part of the Supporting Information. **Part 2** shows the calculated E^{total} with diastereomeric pairs and oxidized/reduced pairs referenced each to the lowest number in the series (E^{rel}). **Figure S4a** represents all these referenced values on a single scale for intercomparison.

Table S1 - part 3 shows characteristic values, that allow conclusions on relative stabilities between ring isomers, oxidation states and side chain attachments. The *relative energies between cis vs. trans* (left columns) show if, depending on the side chain attachment, the *cis*-fused or the *trans*-fused dichalcogenide is thermodynamically more stable. For 1,2-dithianes and 1,2-diselenanes mostly the *trans*-fused bicyclic systems are preferred.

The *relative energies between oxidized vs. reduced* species (middle columns) show that for 1,2-dithianes, the reduced form is thermodynamically more preferred, whereas for 1,2-diselenanes the oxidized form is more stable (which in a probe setting could translate to either re-oxidation to the cyclic diselenide after reduction, or else the formation of linear diselenides by ring-opening polymerisation).

Lastly, overall, *the relative gain of energy upon reduction for cis vs. for trans stereoisomers with the same substituents* (right columns) shows no clear preference trends.

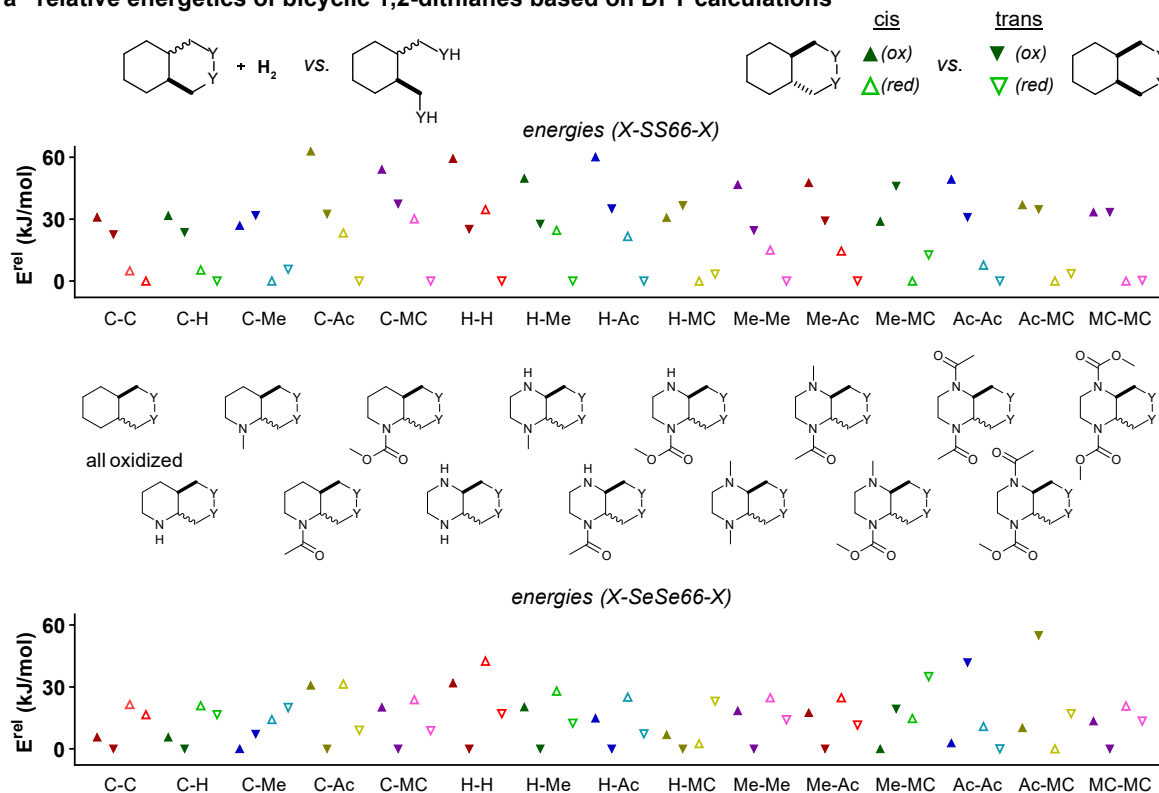
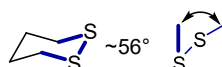
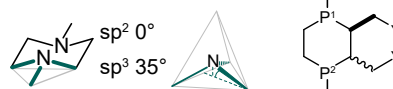
a relative energetics of bicyclic 1,2-dithianes based on DFT calculations**b geometric analysis** $\Delta(\text{SS}/\text{SeSe})$ bond distance $\varphi(\text{CSSC})$ dihedral angle $\theta(\text{CCC-P})$ C/N-pyramidal angle

Figure S4 (a) DFT-based calculation of relative energies for bicyclic cyclohexane-, piperidine- or piperazine-fused 1,2-dithianes and 1,2-diselenanes with optional substitution with $-\text{CH}_2-$ (**C**), $-\text{NH}-$ (**H**), $-\text{NMe}-$ (**Me**), $-\text{NC(O)Me}-$ (**Ac**), $-\text{NC(O)OMe}-$ (**MC**) (see **Table S1**). **(b)** Ring strain parameters for 1,2-dithianes and 1,2-diselenanes (**Table S2**).

Table S2 Analysis of ring strain parameters of piperazine-fused 1,2-dithianes and 1,2-diselenanes with optional substitution. $\Delta(X-X)$: S-S or Se-Se bond distance, $\varphi(CXXC)$: Dihedral angle of the CSSC or CSeSeC motif; $\theta(\text{CCC-P}^1/\text{P}^2)$: pyramidal (out-of-CCC plane) angle for the central substituent atom P¹ and P².

geometric analysis (part 2)			$\Delta(X-X)$	$\varphi(CXXC)$	$\theta(\text{CCC-P}^1)$	$\theta(\text{CCC-P}^2)$	$\Delta^{\text{rel}}(X-X)$	$\varphi^{\text{rel}}(CXXC)$	$\theta^{\text{rel}}(\text{CCC-P}^1)$	$\theta^{\text{rel}}(\text{CCC-P}^2)$	
C-C	<i>cis</i>	ox	C-SS66C-C	2.09	56.7	34.4	36.0	100	101	98	100
	<i>trans</i>	ox	C-SS66T-C	2.09	56.1	35.8	35.8	100	99	102	100
	<i>cis</i>	ox	C-SeSe66C-C	2.37	53.8	35.0	36.7	100	100	99	102
	<i>trans</i>	ox	C-SeSe66T-C	2.37	54.1	35.6	34.9	100	100	101	98
C-H	<i>cis</i>	ox	C-SS66C-H	2.07	57.3	36.4	34.8	99	102	104	97
	<i>trans</i>	ox	C-SS66T-H	2.09	56.4	35.5	31.2	100	100	101	87
	<i>cis</i>	ox	C-SeSe66C-H	2.37	54.4	37.1	35.3	100	101	105	99
	<i>trans</i>	ox	C-SeSe66T-H	2.37	54.3	35.5	36.9	100	101	100	103
C-Me	<i>cis</i>	ox	C-SS66C-Me	2.09	57.2	36.5	29.3	100	101	104	81
	<i>trans</i>	ox	C-SS66T-Me	2.09	58.0	35.5	29.7	100	103	101	83
	<i>cis</i>	ox	C-SeSe66C-Me	2.37	54.2	36.7	29.2	100	100	104	81
	<i>trans</i>	ox	C-SeSe66T-Me	2.37	55.6	35.3	30.1	100	103	100	84
C-Ac	<i>cis</i>	ox	C-SS66C-Ac	2.08	54.9	35.4	15.5	100	97	101	43
	<i>trans</i>	ox	C-SS66T-Ac	2.09	60.9	29.6	19.4	100	108	84	54
	<i>cis</i>	ox	C-SeSe66C-Ac	2.37	52.1	36.5	16.8	100	97	103	47
	<i>trans</i>	ox	C-SeSe66T-Ac	2.37	59.2	34.0	18.5	100	110	96	52
C-MC	<i>cis</i>	ox	C-SS66C-MC	2.09	56.6	35.2	10.6	100	100	100	29
	<i>trans</i>	ox	C-SS66T-MC	2.09	54.8	36.3	5.5	100	97	103	15
	<i>cis</i>	ox	C-SeSe66C-MC	2.37	54.2	36.3	11.7	100	101	103	33
	<i>trans</i>	ox	C-SeSe66T-MC	2.38	51.7	36.1	3.8	100	96	102	11
H-H	<i>cis</i>	ox	H-SS66C-H	2.09	55.8	36.3	35.0	100	99	103	97
	<i>trans</i>	ox	H-SS66T-H	2.09	56.7	37.2	31.5	100	100	106	88
	<i>cis</i>	ox	H-SeSe66C-H	2.37	52.6	34.8	36.0	100	98	98	101
	<i>trans</i>	ox	H-SeSe66T-H	2.37	54.5	37.1	37.3	100	101	105	104
H-Me	<i>cis</i>	ox	H-SS66C-Me	2.09	56.9	34.7	31.8	100	101	99	89
	<i>trans</i>	ox	H-SS66T-Me	2.09	58.1	36.8	29.6	100	103	105	82
	<i>cis</i>	ox	H-SeSe66C-Me	2.38	54.1	34.9	32.0	100	100	99	89
	<i>trans</i>	ox	H-SeSe66T-Me	2.37	55.8	30.4	29.5	100	104	86	82
H-Ac	<i>cis</i>	ox	H-SS66C-Ac	2.08	55.7	36.2	13.7	100	99	103	38
	<i>trans</i>	ox	H-SS66T-Ac	2.09	61.1	35.5	15.1	100	108	101	42
	<i>cis</i>	ox	H-SeSe66C-Ac	2.37	52.5	37.0	17.9	100	97	105	50
	<i>trans</i>	ox	H-SeSe66T-Ac	2.37	59.5	30.5	18.7	100	110	86	52
H-MC	<i>cis</i>	ox	H-SS66C-MC	2.09	57.0	35.8	16.1	100	101	102	45
	<i>trans</i>	ox	H-SS66T-MC	2.09	56.2	34.3	17.6	100	100	98	49
	<i>cis</i>	ox	H-SeSe66C-MC	2.37	54.9	36.2	13.2	100	102	102	37
	<i>trans</i>	ox	H-SeSe66T-MC	2.37	59.4	35.7	18.2	100	110	101	51
Me-Me	<i>cis</i>	ox	Me-SS66C-Me	2.09	61.7	30.4	28.5	100	109	87	79
	<i>trans</i>	ox	Me-SS66T-Me	2.08	57.7	31.7	29.7	100	102	90	83
	<i>cis</i>	ox	Me-SeSe66C-Me	2.37	59.2	28.3	29.8	100	110	80	83
	<i>trans</i>	ox	Me-SeSe66T-Me	2.37	55.7	33.4	29.7	100	103	94	83
Me-Ac	<i>cis</i>	ox	Me-SS66C-Ac	2.08	55.2	30.6	18.2	100	98	87	51
	<i>trans</i>	ox	Me-SS66T-Ac	2.06	61.0	32.4	15.3	99	108	92	43
	<i>cis</i>	ox	Me-SeSe66C-Ac	2.37	52.9	30.7	19.0	100	98	87	53
	<i>trans</i>	ox	Me-SeSe66T-Ac	2.37	58.5	32.2	15.4	100	109	91	43
Me-MC	<i>cis</i>	ox	Me-SS66C-MC	2.09	56.9	33.2	6.4	100	101	95	18
	<i>trans</i>	ox	Me-SS66T-MC	2.09	56.1	29.8	4.2	100	100	85	12
	<i>cis</i>	ox	Me-SeSe66C-MC	2.37	54.8	33.2	8.9	100	102	94	25
	<i>trans</i>	ox	Me-SeSe66T-MC	2.37	53.5	29.6	2.8	100	99	84	8
Ac-Ac	<i>cis</i>	ox	Ac-SS66C-Ac	2.08	56.1	14.1	2.2	100	99	40	6
	<i>trans</i>	ox	Ac-SS66T-Ac	2.09	58.0	17.3	3.6	100	103	49	10
	<i>cis</i>	ox	Ac-SeSe66C-Ac	2.37	53.6	15.4	6.1	100	99	43	17
	<i>trans</i>	ox	Ac-SeSe66T-Ac	2.37	67.2	20.5	15.3	100	125	58	43
Ac-MC	<i>cis</i>	ox	Ac-SS66C-MC	2.09	57.7	2.7	13.2	100	102	8	37
	<i>trans</i>	ox	Ac-SS66T-MC	2.09	57.4	5.9	22.3	100	102	17	62
	<i>cis</i>	ox	Ac-SeSe66C-MC	2.37	55.4	1.7	14.7	100	103	5	41
	<i>trans</i>	ox	Ac-SeSe66T-MC	2.37	66.1	18.5	24.9	100	123	52	70
MC-MC	<i>cis</i>	ox	MC-SS66C-MC	2.09	57.9	13.1	4.5	100	103	37	13
	<i>trans</i>	ox	MC-SS66T-MC	2.09	57.8	17.2	5.1	100	102	49	14
	<i>cis</i>	ox	MC-SeSe66C-MC	2.37	56.0	13.7	6.7	100	104	39	19
	<i>trans</i>	ox	MC-SeSe66T-MC	2.37	55.6	20.8	3.9	100	103	59	11

Supporting Note: Ring strain, torsion angles and pyramidal angles

We looked at factors that might indicate ring strain in the bicyclic 1,2-dichalcogenide systems: The bond distance $\Delta(X-X)$ (S-S or Se-Se) would show significant ring strain in the 1,2-disulfide/diselenane ring; the dihedral angle $\varphi(CXXC)$ (CSSC or CSeSeC) would indicate low to significant ring strain in the dichalcogenide ring; the pyramidal (out-of-CCC plane) angles $\theta(CCC-P)$ around the two substitution points would indicate ring strain in the backbone rings (see **Figure S3b**).

Bond distance. We did not observe the dichalcogenide bond distance to be very stable throughout the series of substituted bicyclic systems. $\Delta(S-S)$ usually 2.085 Å, $\Delta(S-Se)$ usually 2.373 Å.

Dihedral CXXC angle. 56° is the dihedral angle found for preferred conformations of simple 1,2-disulfides and 1,2-diselenanes. We did observe angles around this value ($\pm 5\%$) for substitutions with -CH₂- (**C**), -NH- (**H**), -NMe- (**Me**) on both sides, while significant deviations ($>5\%$) for some combinations that included e.g. -NAc- (**Ac**) or -NC(O)OMe- (**MC**) were found.

Pyramidal angle around the backbone substituents. For substitutions with **C**, **H** and **Me** we expected pyramidal angles of ca. 35°, whereas angles of 0-30° were expected for substitutions with **Ac** and **MC**. We would interpret these effects as reflecting the sp²- and sp³-character of these substituents. Having one or two sp²-type substitutions in the backbone ring would significantly increase the ring strain of the whole bicyclic system. We indeed observed perfect chair-like conformations with torsion angles of 30-37° for combinations of two substitutions from **C**, **H** and **Me**. In contrast, around the substitutions with **Ac** and **MC** significantly lower pyramidal angles of 5-20° were found. If two of these substitutions were combined **Ac-Ac**, **Ac-MC** or **MC-MC**, near planar backbone rings with high ring strains were found. This had also an effect on the dihedral CXXC angle in some cases.

Overall, these results reflect the geometrical properties, that we expected. As the deviations for the dihedral CXXC angles and the X-X bond distances were not significantly changed even with highly strained backbone rings we conclude that the effect of backbone substitutions on the stability of the dichalcogenide and ultimately on the reducibility is not predominant.

3 Kinetic analyses of TCEP, GSH and DTT probe activation

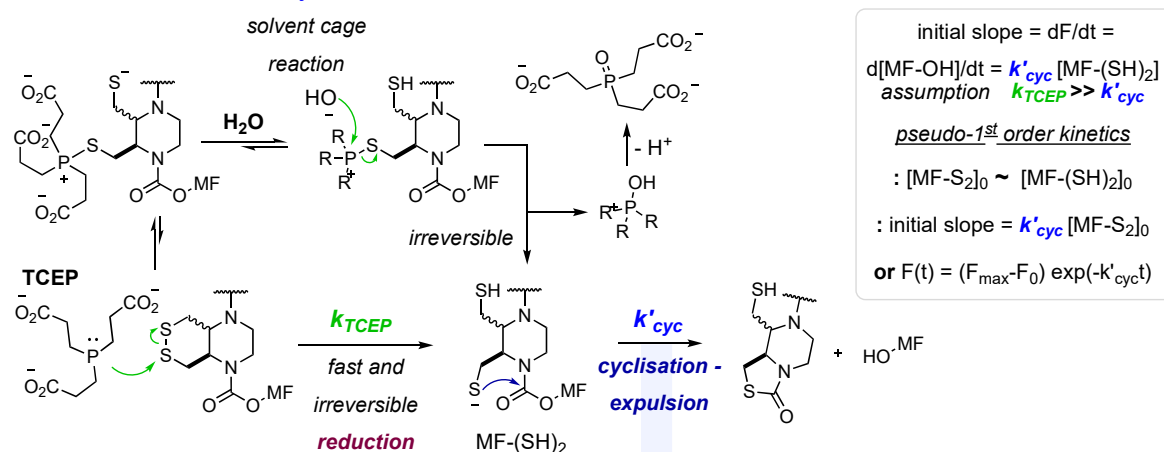
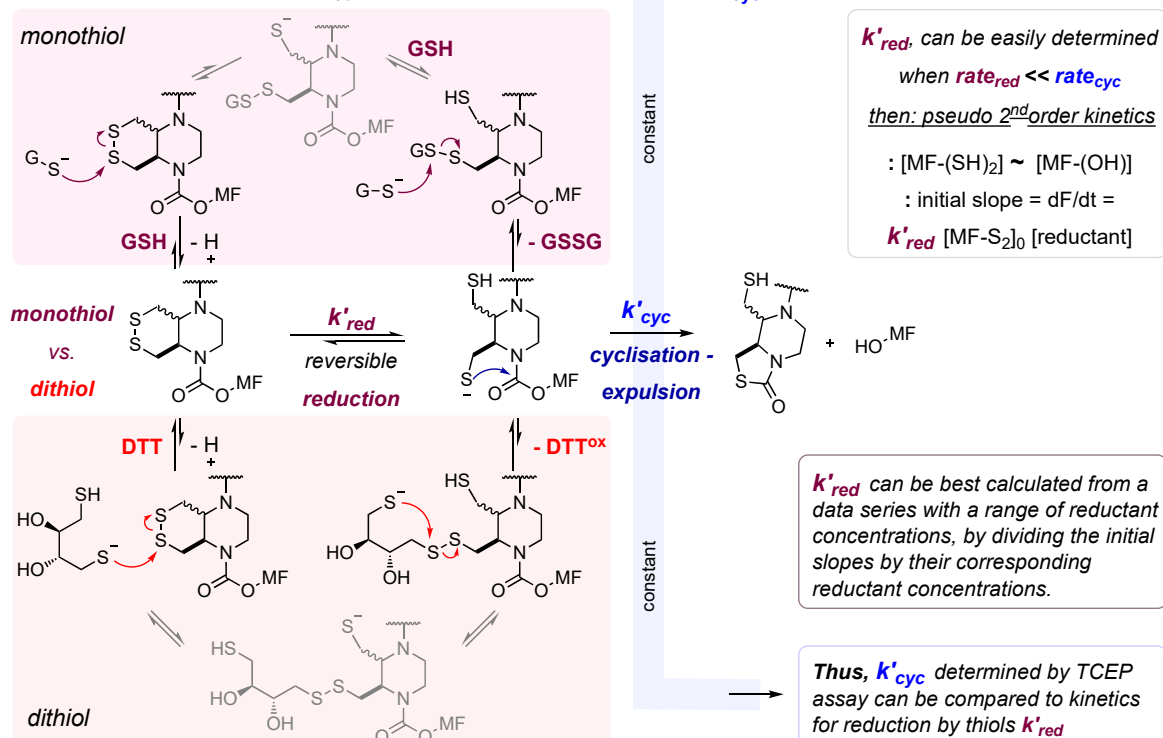
a cyclisation kinetics k'_{cyc} - derived by assuming fast and irreversible disulfide reduction with TCEPb thiol reduction kinetics k'_{red} - can be fitted if is slower than k'_{cyc} 

Figure S5 Reduction mechanism considerations for kinetic evaluation. (a) TCEP-mediated disulfide reduction follows a nucleophilic attack at $MF-S_2$ that leads to (i) reversible phosphonium-adduct formation; (ii) aqueous environment allows proton exchange equilibrium even below the diffusion rates, followed by (iii) nucleophilic S_N2 -type replacement at the phosphonium expels the reduced thiolate and the (iv) aq. environment proton exchange irreversibly forms phosphorus(V)oxide as the thermodynamic sink. The reduced $MF-(SH)_2$ then cyclises to generate $MF-OH$ with k'_{cyc} (pseudo 1st order kinetics) for the assumption that $k_{TCEP} \gg k'_{cyc}$. (b) Mono (GSH)- or dithiol (DTT)-mediated disulfide reduction of $MF-S_2$ follows 4 sequential reversible steps: (i) initial thiol deprotonation, (ii) nucleophilic attack at either of one disulfide sulfur atoms, (iii) proton equilibrium and (iv) inter-(monothiol) or intramolecular (dithiol) thiol resolution giving reduced $MF-(SH)_2$. To determine k'_{red} , only cases for $rate_{red} \ll rate_{cyc}$ should be considered (= low concentrations of thiol-reductant). Initial slopes of $MF-S_2$ activation give k'_{red} when referenced to reductant concentrations. Referencing k'_{red} to k'_{cyc} allows intercomparison of reduction kinetics for each probe.

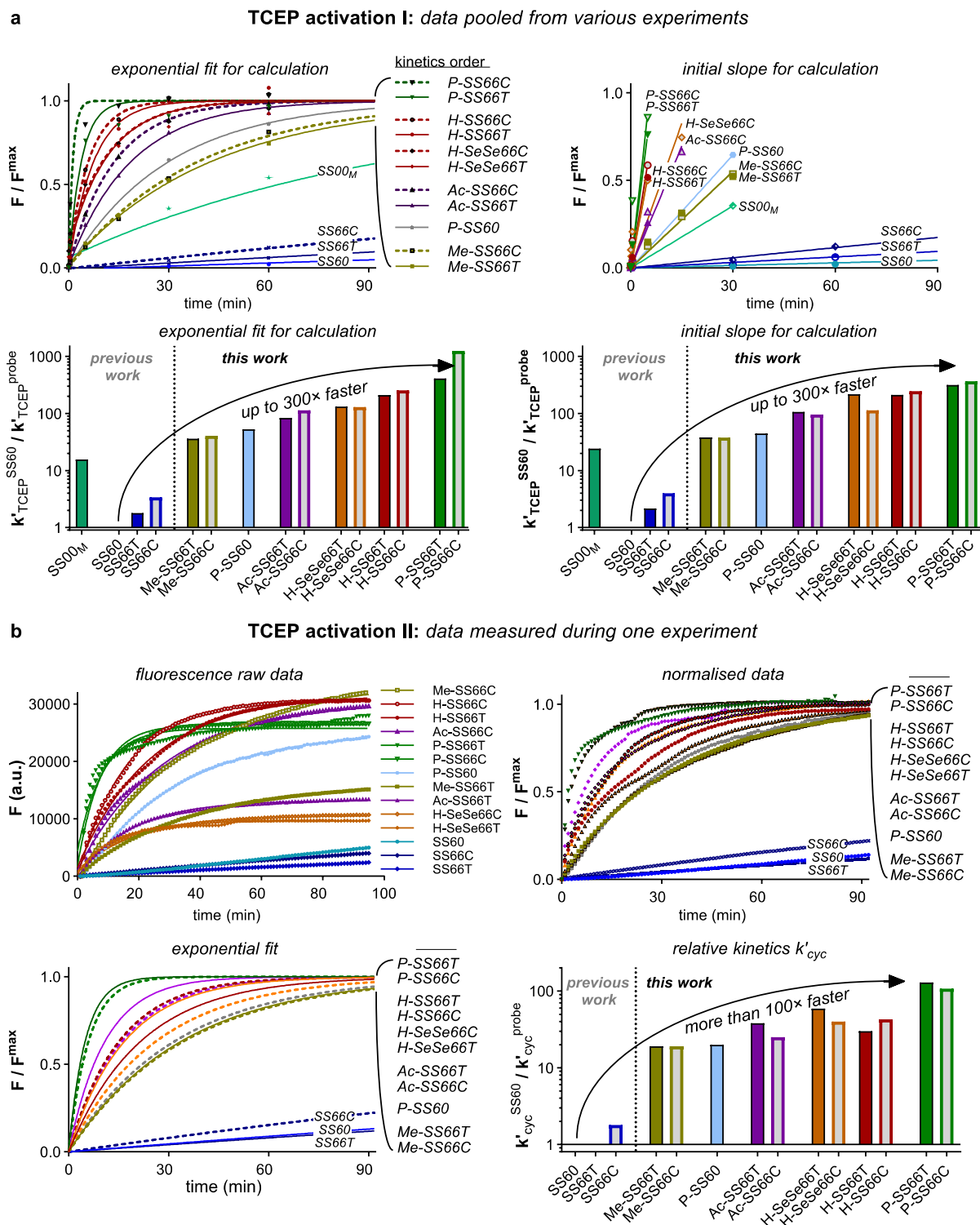


Figure S6 Determination of k'_{cyc} from TCEP-mediated probe fluorescence response. (a) Data pooled from various experiments with timepoints 0 min, 5 min, 15 min, 30 min, 60 min, 120 min. Calculation of k'_{cyc} via either exponential fit with $F(t) = (F_{max} - F_0) \cdot \exp(-k'_{cyc} \times t)$ or from initial slope calculations. Comparison of the kinetics with reference compound **SS60-MF** for both calculations. (b) Data measured during one experiment with timepoints every minute for 100 min. Calculations from raw data to normalised and with an exponential fit giving the referenced cyclisation kinetics.

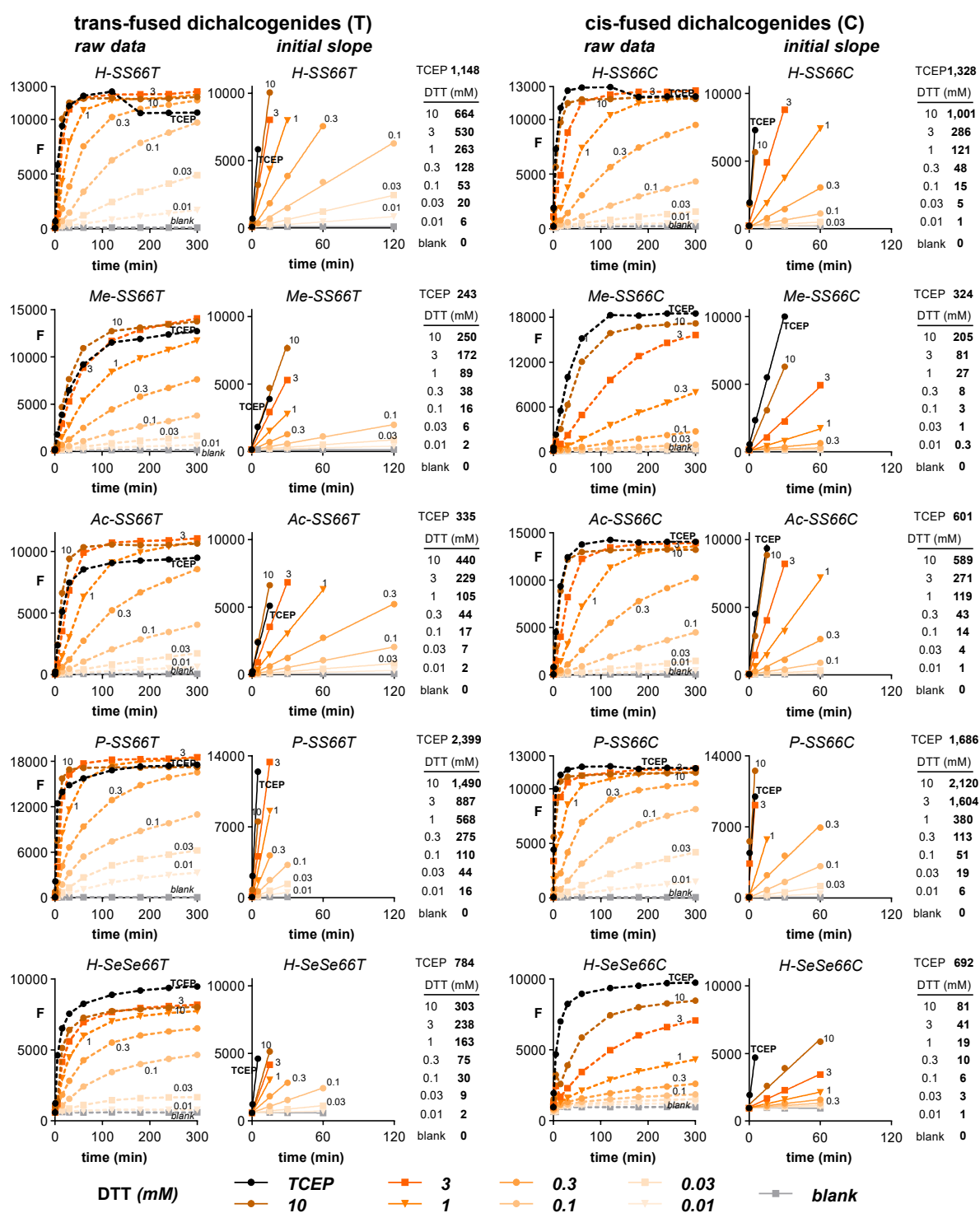


Figure S7 – part 1/2. Dithiol-based reduction. MF-conjugates of **X-SS66-MF** each substituted by either **-H**, **-Me**, **-Ac** or **-P** and **H-SeSe66-MF** (probe at 10 μ M in aq. TE buffer, pH 7.4) were challenged with increasing concentration of DTT (from 0.01-10 mM) at 37 $^{\circ}$ C for 300 min. For both the *trans*-fused 1,2-dichalcogenides (**T**) and the *cis*-fused 1,2-dichalcogenides (**C**) each the raw data time course (0-300 min) and the initial time window of 120 min are shown. For kinetic analysis the initial rates were calculated by fitting the linear phase of fluorescence increase at the beginning of the measurement. *Continues the following page.*

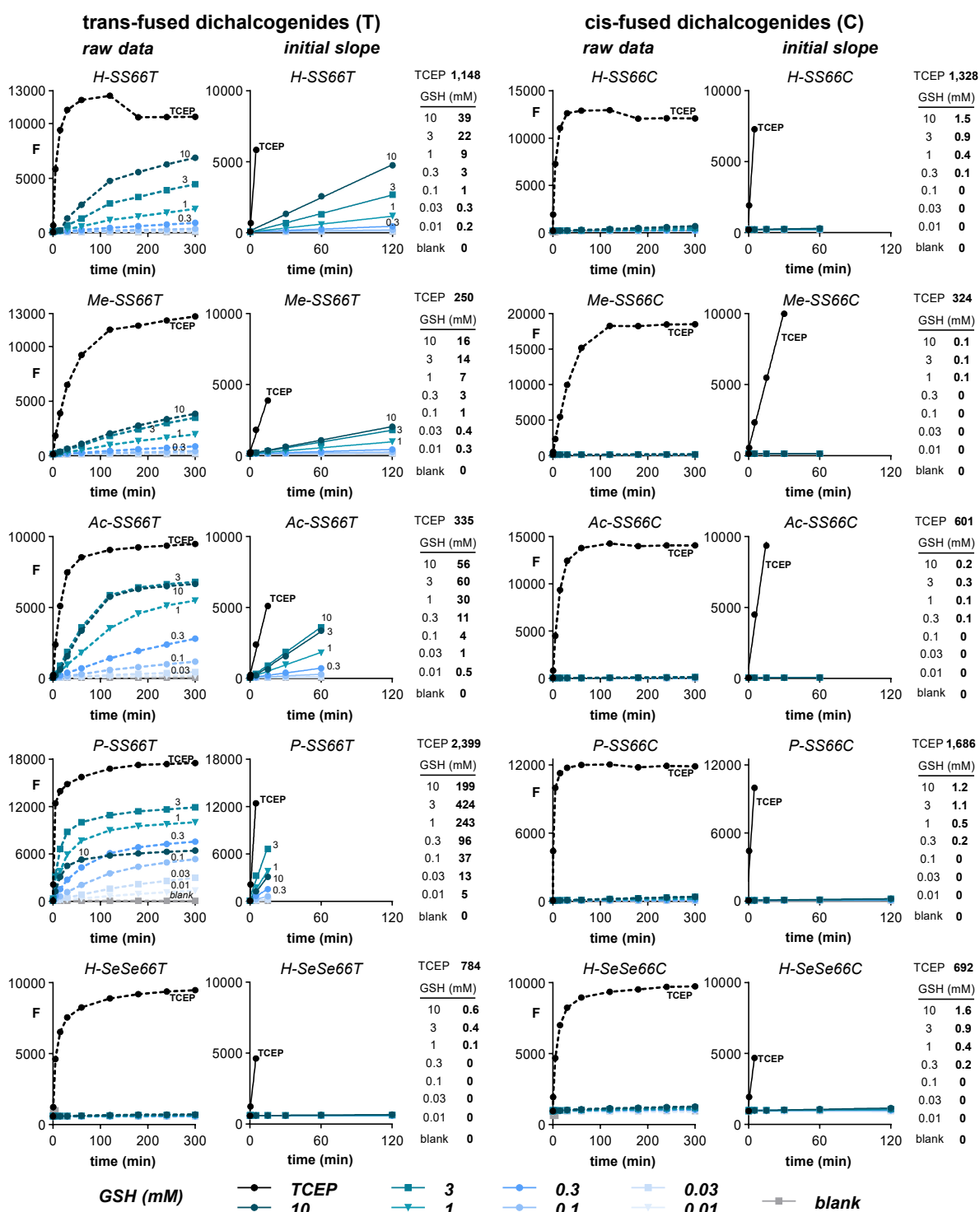


Figure S7 – part 2/2. Monothiol-based reduction. MF-conjugates of X-SS66-MF each substituted by either -H, -Me, -Ac or -P and H-SeSe66-MF (probe at 10 μ M in aq. TE buffer, pH 7.4) are challenged with increasing concentration of GSH (from 0.01-10 mM) at 37 $^{\circ}$ C for 300 min. For both the *trans*-fused 1,2-dichalcogenides (T) and the *cis*-fused 1,2-dichalcogenides (C) each the raw data time course (0-300 min) and the initial time window of 120 min are shown. For kinetic analysis the initial rates were calculated by fitting the linear phase of fluorescence increase at the beginning of the measurement.

a raw initial slopes

	DTT (mM)							TCEP			GSH (mM)				
	10	3	1	0.3	0.1	0.03	0.01	0.1	10	3	1	0.3	0.1	0.03	0.01
H-SS66T	664	530	263	128	53	20	6.5	1148	39	22	9.3	3.2	1.1	0.3	0.2
Me-SS66T	250	172	89	38	16	6.2	2.3	250	16	14	7.0	2.5	1.0	0.4	0.3
Ac-SS66T	440	229	105	44	17	6.6	2.2	335	56	60	30	11	4.2	1.4	0.5
P-SS66T	1490	887	568	275	110	44	16	2399	199	424	243	96	37	13	4.5
H-SeSe66T	303	238	163	75	30	8.9	2.1	784	0.6	0.4	0.1	-0.1	-0.1	-0.1	-0.1
H-SS66C	1001	286	121	48	15	4.6	1.3	1328	1.5	0.9	0.4	0.2	0.01	0.04	-0.03
Me-SS66C	205	81	27	8.5	2.7	0.9	0.3	324	0.1	0.1	0.1	-0.02	-0.03	0.01	0.03
Ac-SS66C	589	271	119	43	14	4.4	1.3	601	0.2	0.3	0.1	0.1	0.02	0.02	-0.02
P-SS66C	2120	1604	380	113	51	19	6	1686	1.2	1.1	0.5	0.2	0.04	-0.01	0.01
H-SeSe66C	81	41	19	10	5.9	3.2	1.4	692	1.6	0.9	0.4	0.2	-0.01	-0.1	-0.1
P-SS60	285	247	129	57	21	6.1	1.5	285	1.3	0.9	0.3	0.4	0.4	0.3	0.2

b initial slope divided by reductants concentrations extracting the rate constant k'_{red} for pseudo 2nd order kinetics

	10	3	1	0.3	0.1	0.03	0.01		10	3	1	0.3	0.1	0.03	0.01
H-SS66T	66	177	263	425	527	669	646	/	4	7	9	11	11	11	24
Me-SS66T	25	57	89	128	156	208	231	/	2	5	7	8	10	12	26
Ac-SS66T	44	76	105	146	170	219	224	/	6	20	30	38	42	45	47
P-SS66T	149	296	568	917	1097	1464	1570	/	20	141	243	321	373	421	451
H-SeSe66T	30	79	163	249	303	295	211	/	0	0	0	0	-1	-4	-15
H-SS66C	100	95	121	160	154	155	131	/	0	0	0	1	0	1	-3
Me-SS66C	21	27	27	28	27	30	26	/	0	0	0	0	0	0	3
Ac-SS66C	59	90	119	143	141	146	128	/	0	0	0	0	0	1	-2
P-SS66C	212	535	380	377	514	625	594	/	0	0	1	1	0	0	1
H-SeSe66C	8	14	19	34	59	105	136	/	0	0	0	1	0	-3	-10
P-SS60	28	82	129	190	214	205	145	/	0	0	0	1	4	9	20

c reductant initial slope divided by TCEP-derived initial slope

	10	3	1	0.3	0.1	0.03	0.01	0.1	10	3	1	0.3	0.1	0.03	0.01
H-SS66T	0.578	0.461	0.229	0.111	0.046	0.017	0.006	1	0.034	0.019	0.008	0.003	0.001	0.000	0.000
Me-SS66T	1.003	0.689	0.355	0.153	0.063	0.025	0.009	1	0.064	0.055	0.028	0.010	0.004	0.002	0.001
Ac-SS66T	1.312	0.684	0.314	0.131	0.051	0.020	0.007	1	0.167	0.178	0.088	0.034	0.013	0.004	0.001
P-SS66T	0.621	0.370	0.237	0.115	0.046	0.018	0.007	1	0.083	0.177	0.101	0.040	0.016	0.005	0.002
H-SeSe66T	0.387	0.304	0.209	0.095	0.039	0.011	0.003	1	0.001	0.000	0.000	0.000	0.000	0.000	0.000
H-SS66C	0.754	0.215	0.091	0.036	0.012	0.004	0.001	1	0.001	0.001	0.000	0.000	0.000	0.000	0.000
Me-SS66C	0.634	0.249	0.083	0.026	0.008	0.003	0.001	1	0.000	0.000	0.000	0.000	0.000	0.000	0.000
Ac-SS66C	0.980	0.451	0.198	0.072	0.023	0.007	0.002	1	0.000	0.000	0.000	0.000	0.000	0.000	0.000
P-SS66C	1.257	0.951	0.225	0.067	0.030	0.011	0.004	1	0.001	0.001	0.000	0.000	0.000	0.000	0.000
H-SeSe66C	0.117	0.059	0.028	0.015	0.008	0.005	0.002	1	0.002	0.001	0.001	0.000	0.000	0.000	0.000
P-SS60	0.998	0.866	0.453	0.200	0.075	0.022	0.005	1	0.005	0.003	0.001	0.001	0.001	0.001	0.001

d summary k'_{red} dithiol (DTT) vs. monothiol (GSH)

	k'_{red} (DTT)	k'_{red} (GSH)	$\log_{10}[k'_{red}$ (DTT)]	$\log_{10}[k'_{red}$ (GSH)]
H-SS66T	658	11	2.8	1.0
Me-SS66T	219	10	2.3	1.0
Ac-SS66T	221	45	2.3	1.7
P-SS66T	1517	415	3.2	2.6
H-SeSe66T	299	0.10	2.5	-1.0
H-SS66C	156	0.27	2.2	-0.6
Me-SS66C	28	0.04	1.4	-1.3
Ac-SS66C	140	0.09	2.1	-1.1
P-SS66C	578	0.34	2.8	-0.5
H-SeSe66C	120	0.29	2.1	-0.5
P-SS60	210	0.26	2.3	-0.6

Figure S8 Calculation of k'_{red} summary. (a) Initial slopes calculated from the fluorescence timecourse data (see **Figure S7**) for TCEP (0.1 mM) or DTT and GSH (both from 0.01-10 mM). (b) Pseudo-rate constants calculated from the initial slopes at each of the applied concentrations, according to $dF/dt \propto k'_{red} \times [\text{reductant}]_0$ (giving k'_{red} in units of $(\text{min}^{-1} \cdot \text{mM}^{-1}_{\text{reductant}})$). The datasets for which the overall $\text{rate}_{red} \ll \text{rate}_{cyc}(\text{TCEP})$ used for calculation are highlighted in green; and the apparent rate constant k'_{red} given for each reductant/probe pair was calculated as the mean of the corresponding green-highlighted values. The selection of these highlighted values is done as follows: in reality, the fitted rates should approach a maximum at low reductant concentration which corresponds to the true rate, although due to experimental error the fitted rates may drop below this if the reductant concentration is further diminished. Our selections of which data best reflects these true rates are then checked for plausibility in panel (c) by dividing the (raw) initial slopes for the reductants by the initial slopes for TCEP activation: a rough criterion for plausibility is that the raw reductant rates should not exceed 5% of the TCEP rates (related to assuming that overall reduction rate is substantially slower than cyclisation rate), while the raw initial slopes should still be large enough to be reliable (see panel i - this particularly limits the selection of GSH data). (d) The tabulated best-selection-averaged k'_{red} values for each probe/reductant pair.

4 Enzymatic specificity assays

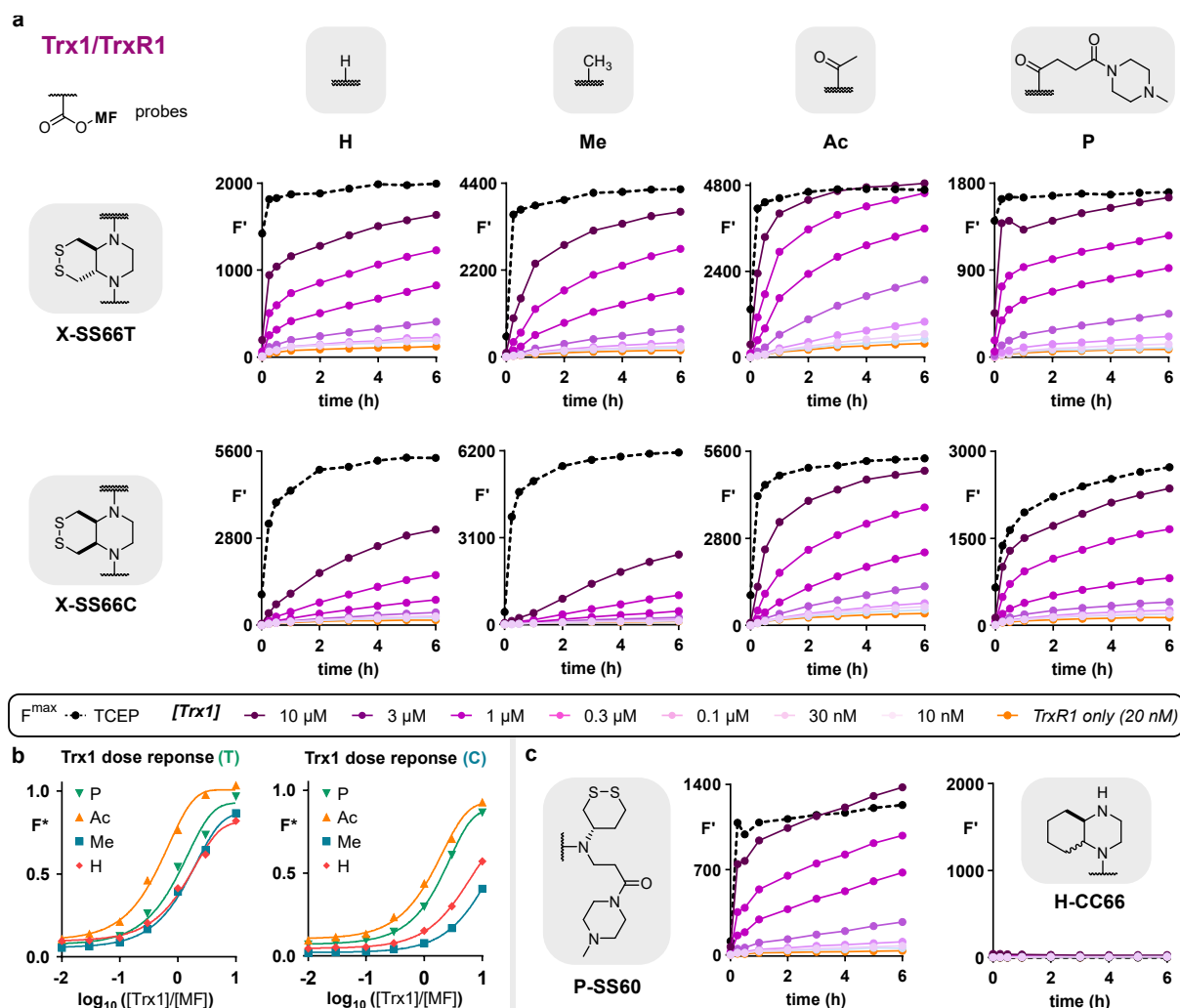


Figure S9 – part 1/5. Trx1-titration assays for H-/Me-/Ac-/P-SS66T-MF, H-/Me-/Ac-/P-SS66C-MF, P-SS60-MF and hydrolysis control H-CC66-MF (10 μ M in TE-buffer). F' represents the fluorescence signal $F - F^{\text{blank}}$. F^{blank} accounts for background fluorescence of enzyme-free samples containing just probe and NADPH in buffer. TCEP (10 equiv.,³ 100 μ M) is shown as estimated reference for fast, quantitative probe reduction and activation. Trx1 was applied at various concentrations (10 nM, 30 nM, 0.1 μ M, 0.3 μ M, 1 μ M, 3 μ M, 10 μ M), NADPH (200 μ M) and TrxR1 (20 nM) were applied as upstream components. Probe activation is evaluated as (a) the time-dependent increase of the relative fluorescence signal from 0-6 h and (b) as dose-response curves after 3 h of incubation. $F^* = F'/F_{\text{TCEP}}$. (c) Trx1-activation of reference compounds P-SS60-MF and hydrolysis control H-CC66-MF.

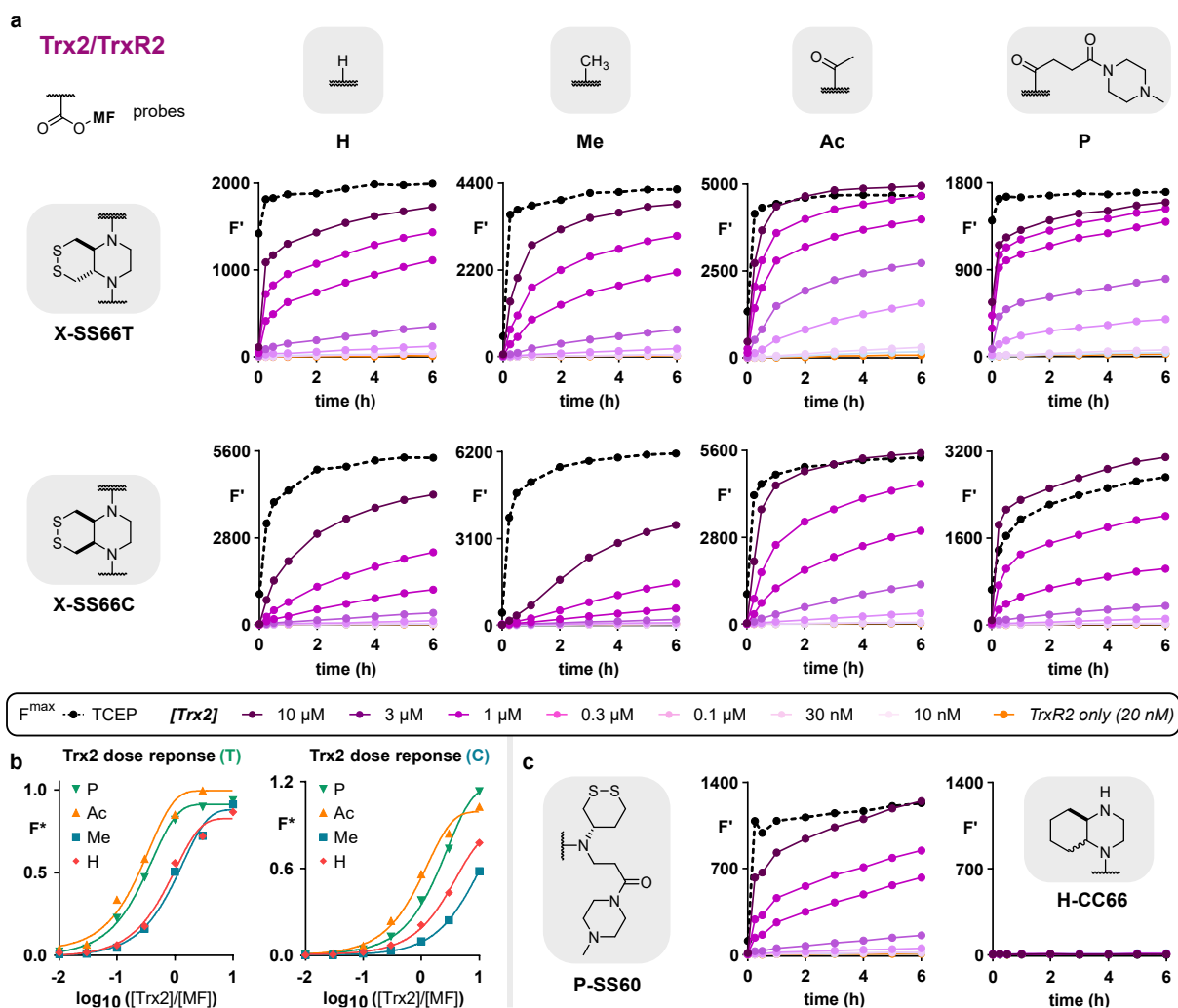


Figure S9 – part 2/5. Trx2-titration assays for H-/Me-/Ac-/P-SS66T-MF, H-/Me-/Ac-/P-SS66C-MF, P-SS60-MF and hydrolysis control H-CC66-MF (10 μ M in TE-buffer). F' represents the fluorescence signal $F - F^{\text{blank}}$. F^{blank} accounts for background fluorescence of enzyme-free samples containing just probe and NADPH in buffer. TCEP (10 equiv., 100 μ M) is shown as estimated reference for fast, quantitative probe reduction and activation. Trx2 is applied at various concentrations (10 nM, 30 nM, 0.1 μ M, 0.3 μ M, 1 μ M, 3 μ M, 10 μ M), NADPH (200 μ M) and TrxR2 (20 nM) were applied as upstream components. Probe activation is evaluated as (a) the time-dependent increase of the relative fluorescence signal from 0-6 h and (b) as dose-response curves after 3 h of incubation. $F^* = F'/F_{\text{TCEP}}$. (c) Trx2-activation of reference compounds P-SS60-MF and hydrolysis control H-CC66-MF.

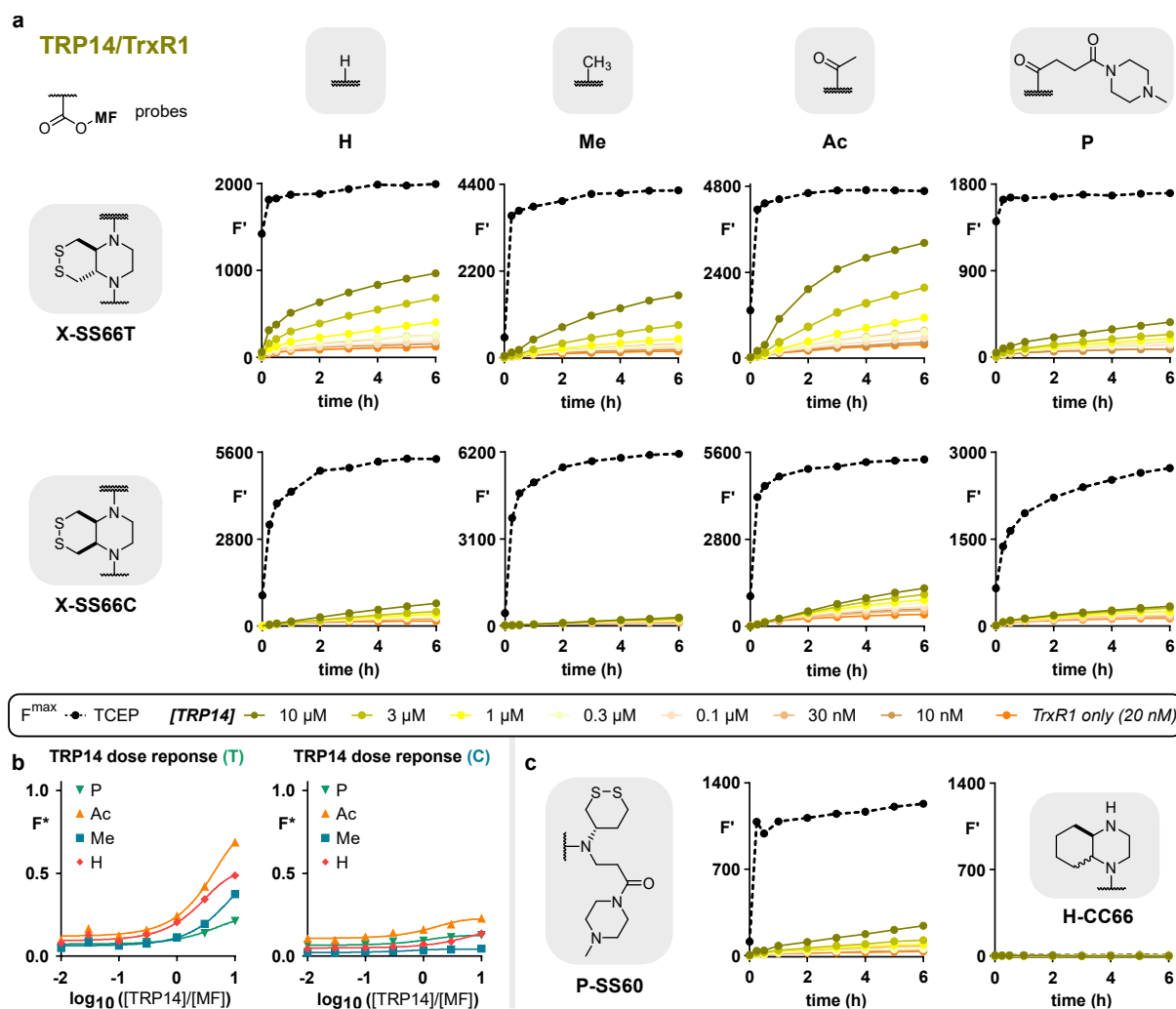


Figure S9 – part 3/5. TRP14-titration assays for H-/Me-/Ac-/P-SS66T-MF, H-/Me-/Ac-/P-SS66C-MF, P-SS60-MF and hydrolysis control H-CC66-MF (10 μ M in TE-buffer). F' represents the fluorescence signal $F - F^{\text{blank}}$. F^{blank} accounts for background fluorescence of enzyme-free samples containing just probe and NADPH in buffer. TCEP (10 equiv., 100 μ M) is shown as estimated reference for fast, quantitative probe reduction and activation. TRP14 is applied at various concentrations (10 nM, 30 nM, 0.1 μ M, 0.3 μ M, 1 μ M, 3 μ M, 10 μ M), NADPH (200 μ M) and TrxR1 (20 nM) were applied as upstream components. Probe activation is evaluated as (a) the time-dependent increase of the relative fluorescence signal from 0-6 h and (b) as dose-response curves after 3 h of incubation. $F^* = F'/F_{\text{TCEP}}$. (c) TRP14-activation of reference compounds P-SS60-MF and hydrolysis control H-CC66-MF.

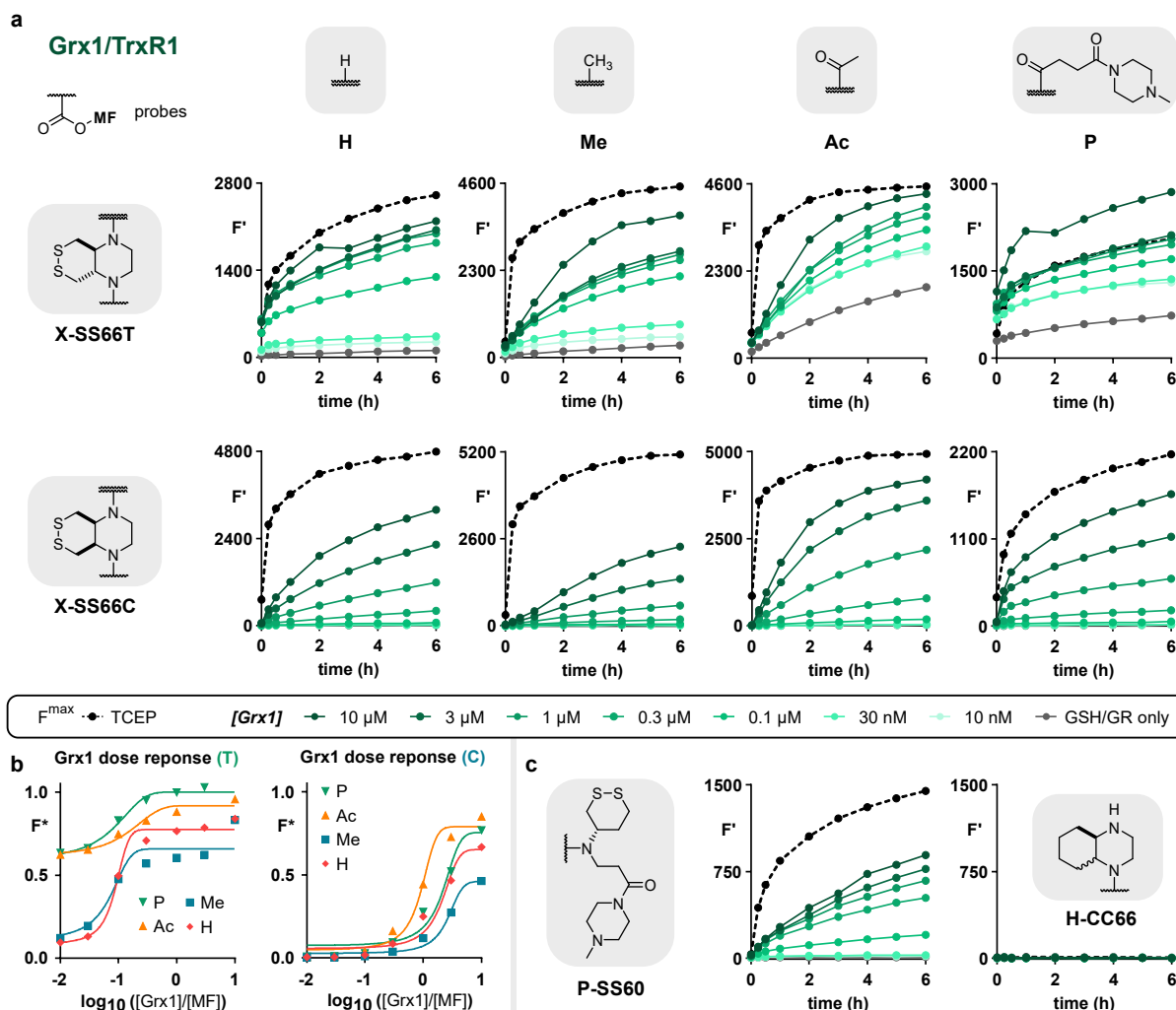


Figure S9 – part 4/5. Grx1-titration assays for H-/Me-/Ac-/P-SS66T-MF, H-/Me-/Ac-/P-SS66C-MF, P-SS60-MF and hydrolysis control H-CC66-MF (10 μ M in TE-buffer). F' represents the fluorescence signal $F-F^{blank}$. F^{blank} accounts for background fluorescence of enzyme-free samples containing just probe and NADPH in buffer. TCEP (10 equiv., 100 μ M) is shown as estimated reference for fast, quantitative probe reduction and activation. Grx1 is applied at various concentrations (10 nM, 30 nM, 0.1 μ M, 0.3 μ M, 1 μ M, 3 μ M, 10 μ M), NADPH (200 μ M), GSH (100 μ M) and GR (20 nM) were applied as upstream components. Probe activation is evaluated as (a) the time-dependent increase of the relative fluorescence signal from 0-6 h and (b) as dose-response curves after 3 h of incubation. $F^* = F'/F_{TCEP}$. (c) Grx1-activation of reference compounds **P-SS60-MF and hydrolysis control **H-CC66-MF**. Note that for **SS66T** probes, 100 μ M GSH itself can contribute to notable probe activation. Control experiments allow for an estimation of this baseline reactivity of the GSH/GR system.**

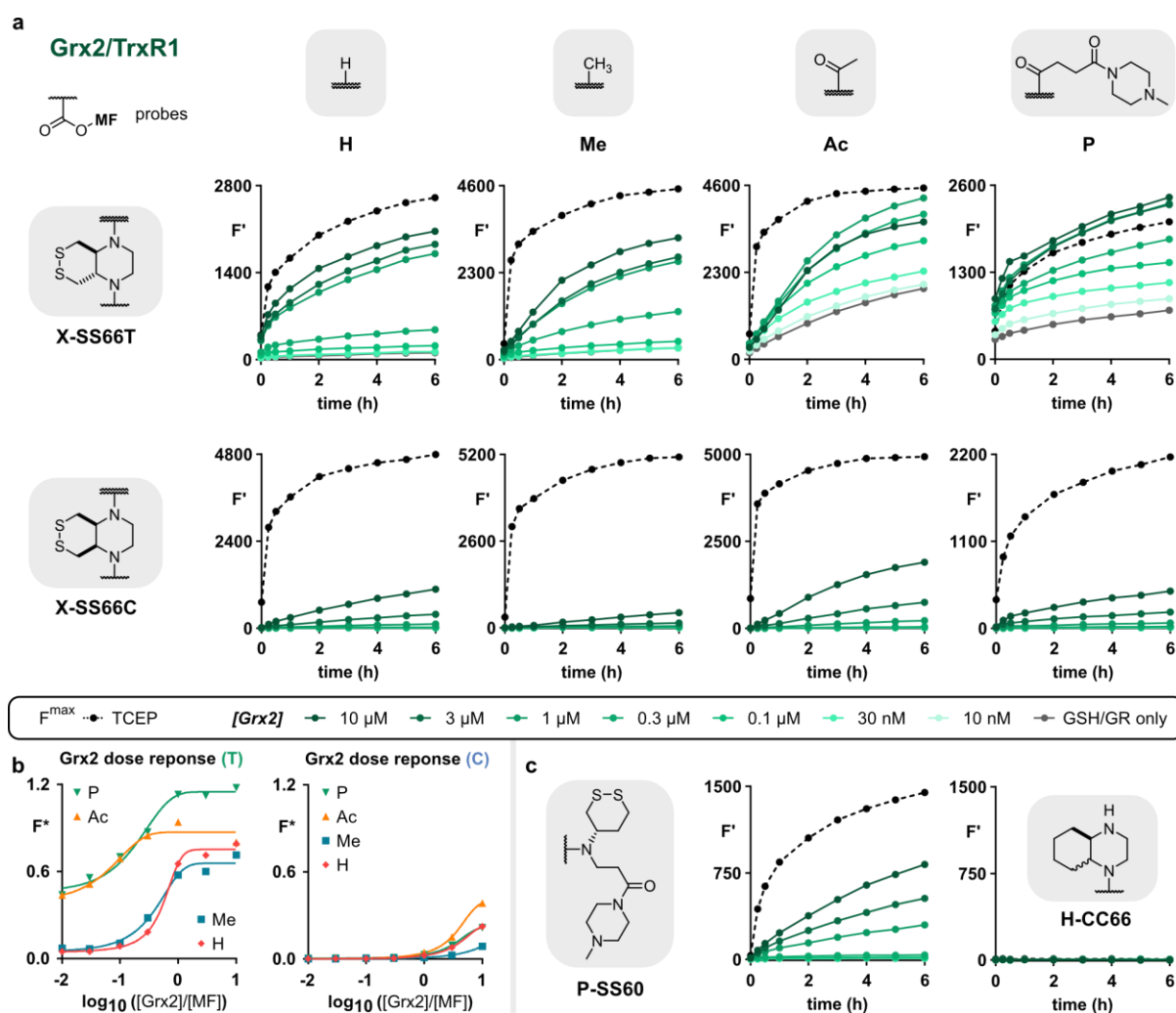


Figure S9– part 5/5. Grx2-titration assays for H-/Me-/Ac-/P-SS66T-MF, H-/Me-/Ac-/P-SS66C-MF, P-SS60-MF and hydrolysis control H-CC66-MF (10 μ M in TE-buffer). F' represents the fluorescence signal $F - F_{\text{blank}}$. F_{blank} accounts for background fluorescence of enzyme-free samples containing just probe and NADPH in buffer. TCEP (10 equiv., 100 μ M) is shown as estimated reference for fast, quantitative probe reduction and activation. Grx2 is applied at various concentrations (10 nM, 30 nM, 0.1 μ M, 0.3 μ M, 1 μ M, 3 μ M, 10 μ M), NADPH (200 μ M), GSH (100 μ M) and GR (20 nM) were applied as upstream components. Probe activation is evaluated as (a) the time-dependent increase of the relative fluorescence signal from 0-6 h and (b) as dose-response curves after 3 h of incubation. $F^* = F'/F_{\text{TCEP}}$. (c) Grx2-activation of reference compounds P-SS60-MF and hydrolysis control H-CC66-MF. Note that for SS66T probes, 100 μ M GSH itself can contribute to notable probe activation. Control experiments allow for an estimation of this baseline reactivity of the GSH/GR system.

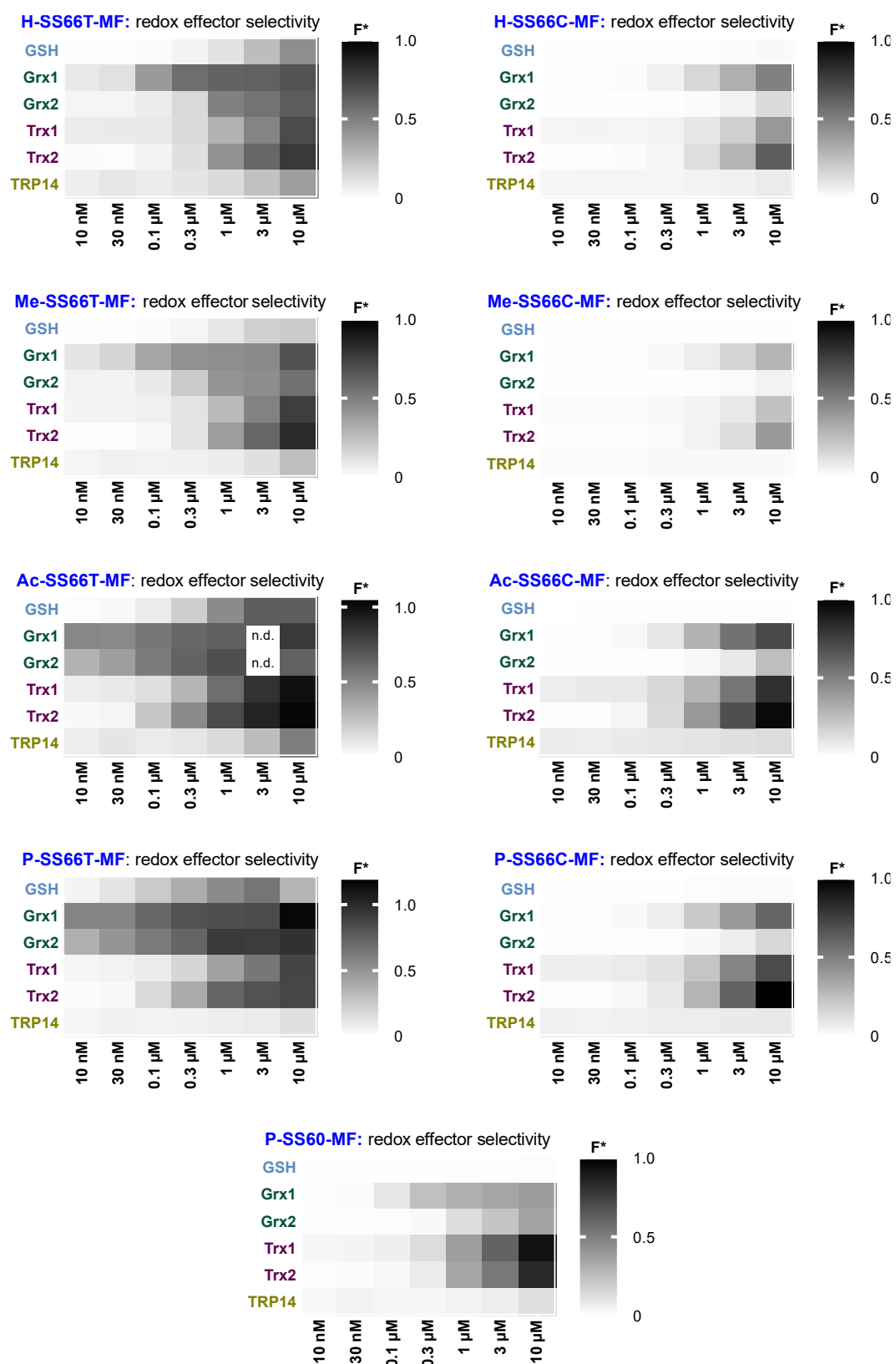


Figure S10 Overview of enzymatic selectivity screening across all reducible disulfide probes applied at 10 μM . F^* represents the relative, NADPH-corrected fluorescence signal F/F^{TCEP} using TCEP (10 equiv., 100 μM) as estimated reference for fast, quantitative probe reduction and activation.

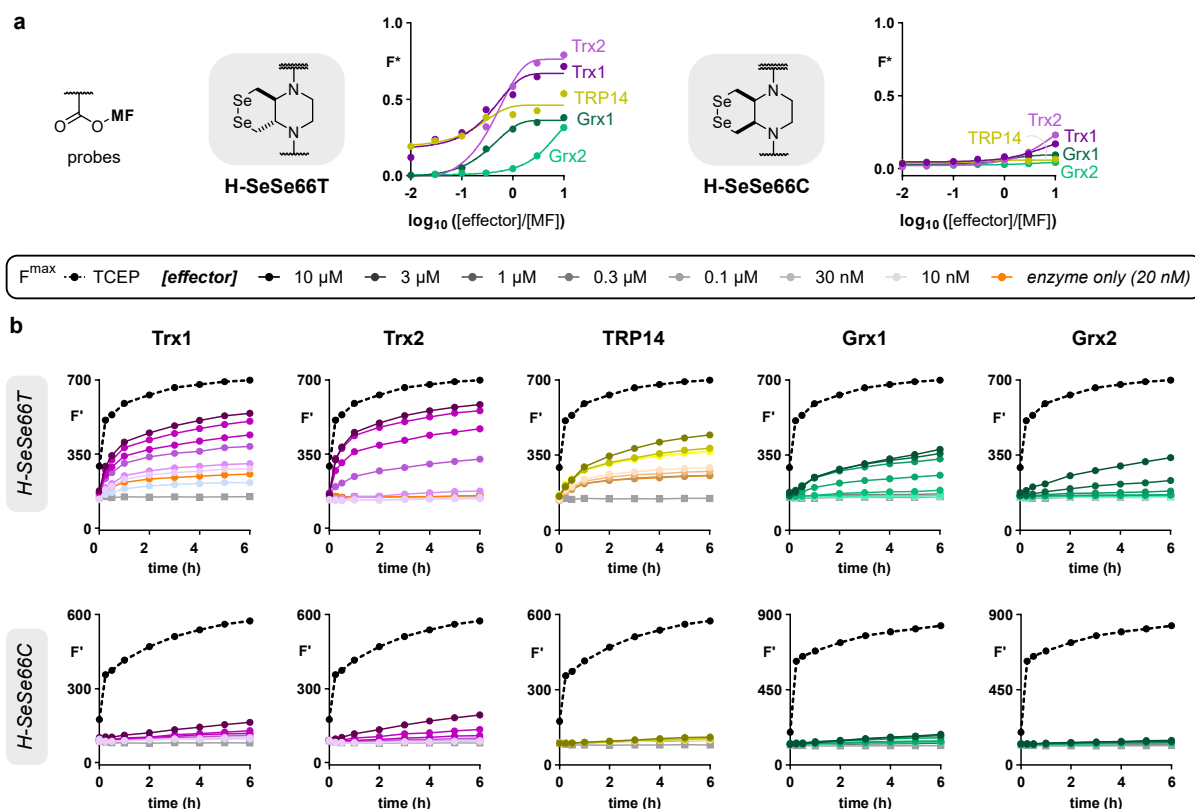


Figure S11 Overview of enzymatic selectivity screening for **H-SeSe66T-MF** and **H-SeSe66C-MF** applied at 10 μ M. *Note: We advise to only assess this biochemical data qualitatively, since both diselenane piperazines repeatedly degraded over time. We can thus not guarantee accurate probe stock dilutions.* Redox effector proteins are applied at various concentrations (10 nM, 30 nM, 0.1 μ M, 0.3 μ M, 1 μ M, 3 μ M, 10 μ M), NADPH (200 μ M), and/or GSH (100 μ M) and/or TrxR/GR (20 nM) were applied as upstream components. **(a)** Dose-response curves after 3 h of incubation. F^* represents the relative, NADPH-corrected fluorescence signal F/F^{TCEP} using TCEP (10 equiv., 100 μ M) as estimated reference for fast, quantitative probe reduction and activation. **(b)** Time-dependent increase of the relative fluorescence signal from 0-6 h. F' represents the fluorescence signal $F-F^{blank}$. F^{blank} accounts for background fluorescence of enzyme-free samples containing just probe and NADPH in buffer.

5 Cellular assays

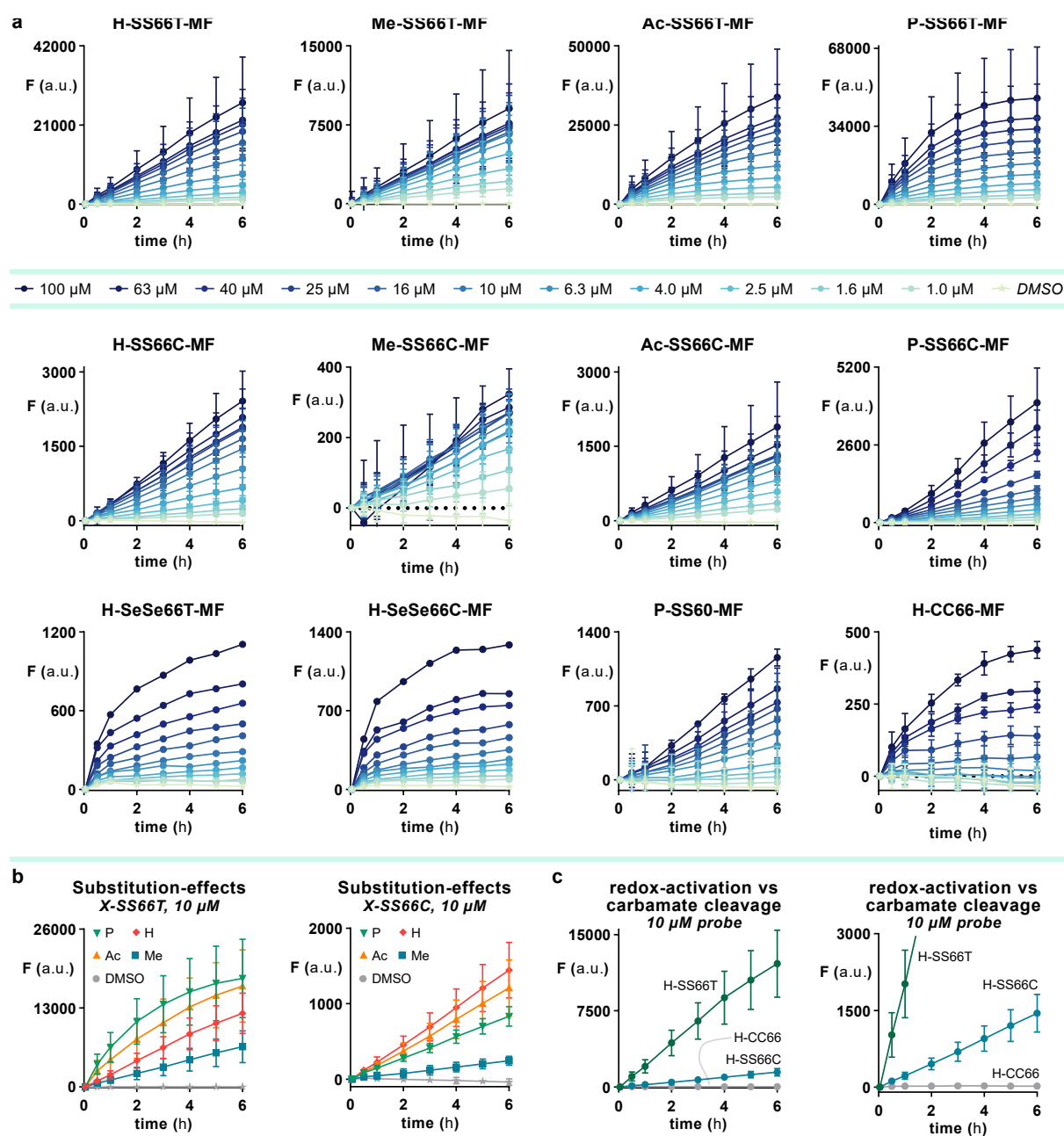


Figure S12 – part 1/2. Cellular evaluation of dichalcogenide fluorescein probes. **(a)** Dose-response assays (1–100 μM probe) in A549 cells (three independent experiments, mean of raw fluorescence values corrected for background baseline signal) over 6 h of incubation. For **H-SeSe66T/C-MF**, due to their instability, only single experiments were performed for a qualitative assessment of their cellular performance. **(b)** Evaluation of substitution effects on cellular probe activation. Probes were treated at 10 μM. **(c)** Example: comparison of cellular activation of **H-SS66T-MF**, **H-SS66C-MF** and their non-redox-active counterpart **H-CC66-MF**, which functions as a carbamate-hydrolysis control.

Cell viability and linearity of probe activation

Cellular dose-response assays revealed a non-linear activation for some probes. We were intrigued whether this could be attributed to cell death – an observation we have made in earlier work for probes releasing precipitating dyes.⁴ Therefore, we performed cell viability assays 6 h after probe treatment. Indeed, all probes which exhibit non-linearity in their activation timecourses were seen to be somewhat cytotoxic (**H-CC66**, **P-SS66T**, **P-SS66C**). For diselenide-based compounds, we assume that non-linearity could also arise from polymerisation/degradation of the probe, independent of cell uptake or of their intended reduction-dependent activation mechanism. However, it is beyond the scope of this work to further investigate these effects. Since cytotoxicity, particularly for **P-SS66T**, does not substantiate in the short-term (which is its intended use), we assessed efficiency of cellular probe activation based on the slope of fluorescent signal increase within the linear range of probe activation (avoiding time regions where non-linearity can be an indicator for cell death).

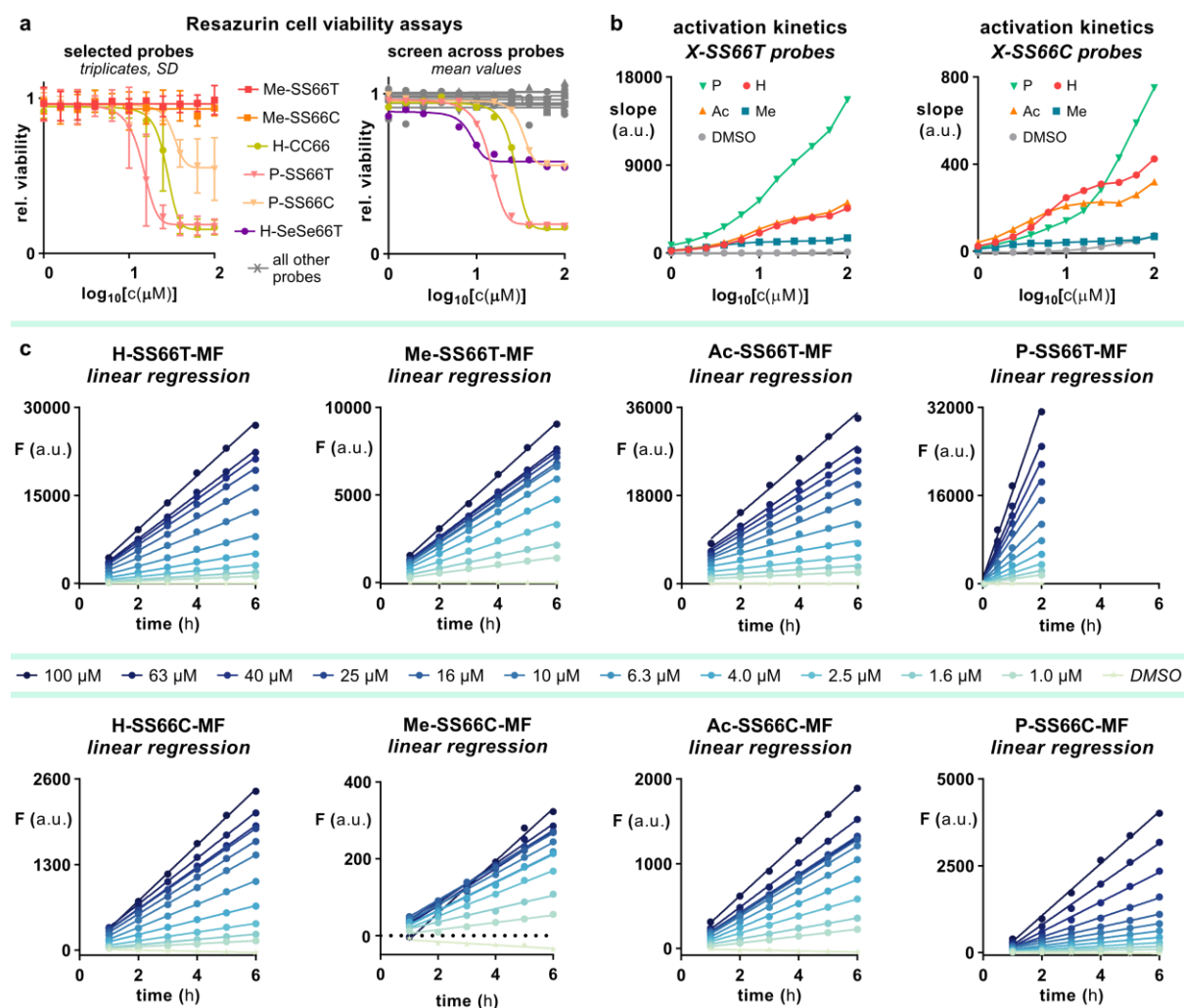


Figure S12 – part 2/2. Cell viability assays inform adjusted evaluation of activation kinetics. (a) Resazurin cell viability assays in A549 cells (three independent experiments, SD of raw fluorescence values corrected for background baseline signal) after 6 h of incubation with probe. Viability read-out after 15 h of incubation with resazurin. An initial set of probes (left), which appeared to suffer from non-linear activation over 6 h were assessed in triplicates. A qualitative, single-experiment assay was conducted across all probes (right). (b) Summary of cell death-, diffusion- and uptake-corrected probe activation kinetics across **SS66T** (left) and **SS66C** (right) probes. (c) Linear regression of probe activation for all disulfide-based probes from 1-100 μM .

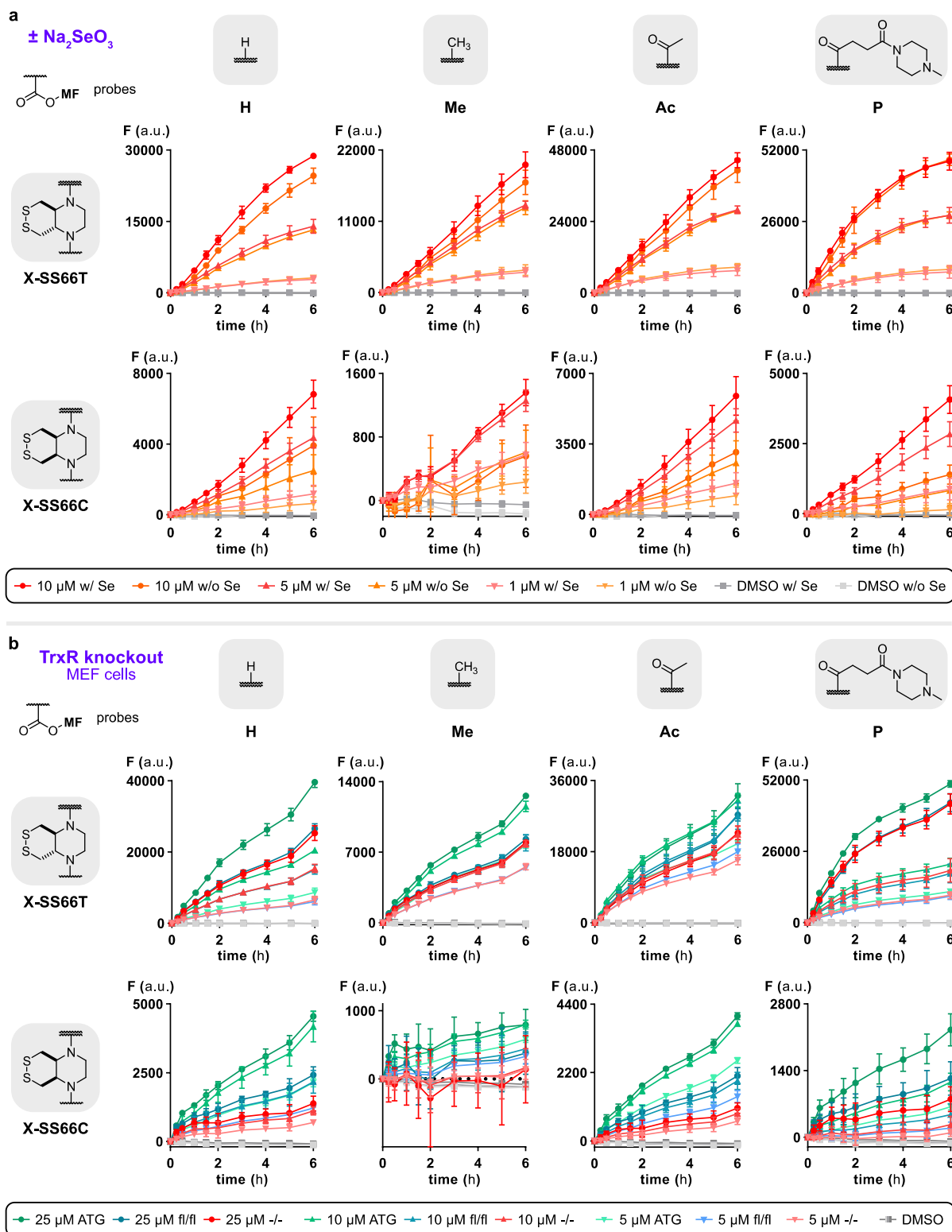
Modulation of the cellular Trx and GSH systems

Figure S13 (a) Effects of Na_2SeO_3 -supplementation on probe activation (three independent experiments, mean of raw fluorescence values corrected for background baseline signal). MF-probes were applied at 1, 5 or 10 μM . Selenite ensures sufficient Sec-incorporation into TrxR and thus correlates with Trx-system activity. **(b)** Time- and dose-dependent probe activation (three independent experiments, SD of raw fluorescence values corrected for background baseline signal) in selenium-supplemented (in form of Na_2SeO_3) MEF cell lines with altered TrxR1-availability. MF-probes were applied at 5, 10 or 25 μM . Reconstitution of TrxR1 expression (ATG) was achieved through a lentivirus-based approach.⁵

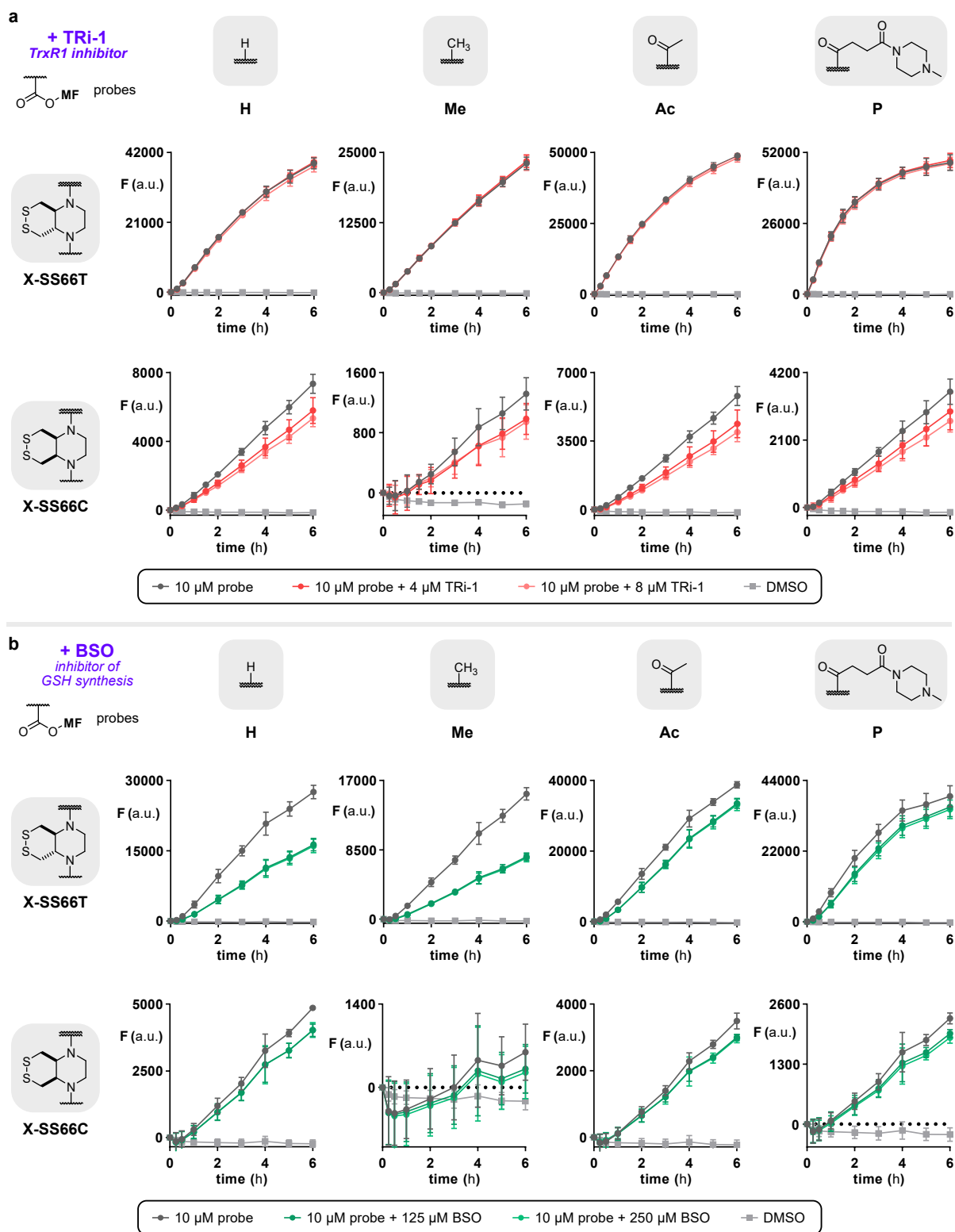


Figure S14 (a) Effects of TrxR1-inhibition (by means of the established inhibitor TRi-1) on probe activation (three independent experiments, mean of raw fluorescence values corrected for background baseline signal). MF-probes were applied 10 μ M. (b) Inhibition of cellular GSH-synthesis *via* BSO (buthioninsulfoximin, 125 and 250 μ M) and its effect on probe activation (three independent experiments, mean of raw fluorescence values corrected for background baseline signal). MF-probes were applied 10 μ M.

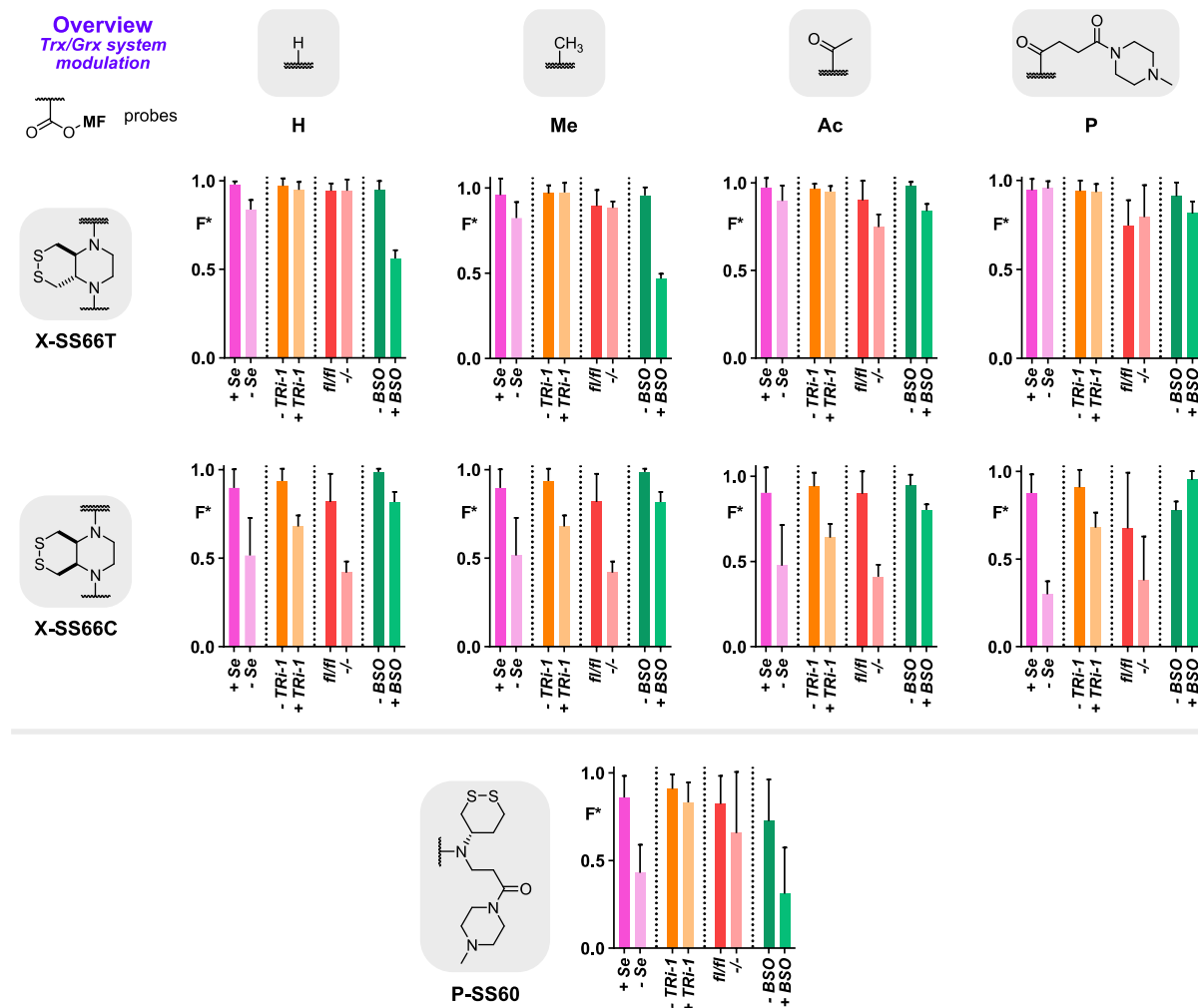


Figure S15 Overview of Trx- and Grx-system modulation and the effects on cellular probe activation across all dithiane probes.

6 Materials and methods

6.1 Determination of reduction potentials

Reduction potentials were determined using known protocols by Raines and Thorn-Seshold via HPLC.^{1,2}

In brief, first, TE buffer (50 mM Tris-HCl, 1 mM EDTA, pH 7.4) was degassed through bubbling with dry nitrogen for 1 h. Solutions of **H-SS66C/T-Bz^{ox}** (25 mM in DMSO) and DTT^{red} (5 mM in degassed TE buffer) were prepared freshly before each experiment. In an HPLC-vial with 100 μ L-micro insert, 2 μ L of **H-SS66C/T-Bz^{ox}** were diluted with 13 μ L TE buffer, giving a 5 mM probe solution. 15 μ L of DTT^{red} were added, and a sample was injected into the HPLC. The timepoints we measured (2.5 min, 5 min, 10 min, 15 min, 22.5 min) amounts the exact difference between reagent mixing and the HPLC needle drawing a 10 μ L sample from the reaction mixture. Integration of HPLC chromatogram areas at 210 nm allowed calculation of relative ratios of oxidised and reduced species. This method can only be applied if no other reaction products or UV active species are detected.

6.2 DFT calculations

All calculations were performed as geometry optimization tasks with the B3LYP functional⁶, a triple- ζ polarized (TZP) basis set, and Grimme's D3(BJ) dispersion correction⁷, as implemented in the Amsterdam Density Functional (ADF) software version 2022.201.⁸ Furthermore, to account for solvent effects in aqueous phase, the conductor-like screening model (COSMO)⁹ with the default Klamt cavity radii¹⁰ was applied. For Selenium, a radius of 190.8 pm was used.

6.3 (Bio)chemical probe activation assays

In vitro assays determining the **MF** probes' redox properties are based on reduction-induced fluorophore release. The turn-on of fluorescence was quantified using a plate reader ($\lambda_{\text{ex}} = 480$ nm, $\lambda_{\text{em}} = 520$ nm).

Probes were dissolved in DMSO and stored as 10 mM stocks at 4 °C for at least 3 months. LC/MS analysis of DMSO stock solutions revealed that several rounds of freezing and thawing, and even storage at r.t. over several months were well tolerated and did not result in measurable decomposition of the probe.

A black 96-well plate with black bottom was charged with probe (final concentration: 10 μ M, 1% DMSO in TE buffer: Tris-HCl (50 mM), EDTA (2 mM), pH = 7.5) and subjected to a variety of chemo- and bioreductants. The **MF**-release kinetics were monitored at set time points (1 min, 15 min, 30 min, 1 h, 2 h, 3 h, 4 h, 5 h, 6 h). In between measurements, the 96-well plates were incubated in a regular heating oven at 37 °C and in a H₂O-saturated atmosphere. Every experiment was run with *blank* control wells to estimate residual fluorescence of non-activated probe or potential decomposition during incubation in TE buffer.

Reduction resistance assays

Initial proof-of-concept experiments were conducted according to the following protocol: 80 μ L of **MF** probe (12.5 μ M in TE buffer/1.25% DMSO) were placed into the 96-well plate and the solution was charged with 20 μ L of the respective reductant. The resulting 100 μ L-reaction mixture thus contained 10 μ M of probe and varying concentrations of chemoreductant (TCEP, GSH or DTT). The strongest reductant of the experimental set up (TCEP, 10 equiv. 100 μ M) was added last, followed by an immediate first (time point zero) measurement on the plate reader. Raw data were processed using *Microsoft Excel* and *GraphPad Prism*, the former serving as platform for data assembly and calculation of mean values for each data point. Consecutively, obtained values $F(t)$ were further processed by normalising each data point to $F^{\text{TCEP}}(t)$, using TCEP as an estimated reference for fast, quantitative probe reduction and activation. Data plotting was conducted using *Prism*.

Resistance assays with key players in cellular redox

Redox stability of the designed probes toward key cellular reductants was conducted as follows: in case of two-component systems, the respective bioreductant (40 μ L in TE) was placed into the corresponding wells and was subsequently charged with 50 μ L of probe (20 μ M in TE buffer/2% DMSO, to result in a final concentration of 10 μ M and 1% respectively). The reaction was initiated by addition of 10 μ L of the reductive driving force, (NADPH or GSH; 10 μ L, 1 mM in TE, 10 equiv.) and the following, time point zero measurement was conducted.

Closely related to that, three-component experiments were prepared by first adding 40 μ L of the reductant (TrxR/GR in TE (50 mM Tris-HCl, 1 mM EDTA, pH 7.5) to reach final concentration of 2 to 50 nM) and/or the corresponding native substrate (Trxs/Grxs in TE, to reach final concentrations of 0.01 to 10 μ M). Consecutively, 50 μ L probe (20 μ M in TE buffer/2% DMSO, to reach final concentrations of 10 μ M and 1% respectively) was added and the reaction was started by addition of 10 μ L of 1 mM NADPH. TCEP (40 μ L, 5 mM in TE, 20 equiv., final concentration of 200 μ M) was added to a control-row for maximum activation and a first measurement (time point zero) was conducted right away.

Raw data was processed using *Microsoft Excel* and *GraphPad Prism*. As before, *Excel* was used for data assembly and calculation of mean values for each data point. In contrast to previous experiments, application of NADPH required an additional processing step to eliminate its background fluorescence, which interferes with the readout of the fluorescent PQ cargo.¹¹ Absolute fluorescence values $F(t)$ were therefore simply subtracted by $F^{\text{NADPH}}(t)$; NADPH control wells were run on every plate under the same conditions, rather than averaging values from other runs. NADPH-corrected absolute values were then further processed by normalising each data point to $F^{\text{TCEP}}(t)$, using TCEP as an estimated reference for fast, quantitative probe reduction and activation. Ultimate data visualisation in graphs was conducted in *Prism*.

Human recombinant thioredoxin 1 (Trx 1) (lyophilized), human recombinant glutaredoxin 1 (Grx 1) (lyophilized from 10 μL TE-buffer, pH 7.5), human thioredoxin reductase (TrxR) (1.5 mg/mL in 50% glycerol/TE-buffer, pH 7.5) and baker's yeast glutathione reductase (GR) (100 μM in 50% glycerol/TE-buffer, pH 7.5) were obtained from IMCO Corp., Stockholm (Sweden) or produced as previously described.^{12,13}

6.4 Cellular assays

General cell cultivation methods

Cells were grown in Dulbecco's modified Eagle's medium (DMEM: L-glucose (4.5 g/L), L-glutamine, L-pyruvate, phenol-red, NaHCO_3 (2.7 g/L); PAN Biotech) at 37 °C under 5% CO_2 atmosphere. Media were supplemented with 10% heat-inactivated fetal bovine serum, and Na_2SeO_3 (100 nM) unless stated otherwise. Selenium supplementation changes were always followed by at least 7 days of culturing the cells in the newly supplemented media before performing any experiments. Washing steps were performed in REcombinaDPBS (Merck GmbH, Darmstadt, Germany), cell detachment was performed using TrypLE™ Express (gibco Life Technologies Inc.). Cell growth was monitored using a Nikon Eclipse Ti microscope (Nikon Corp.).

Cell lines

A549 (DSMZ; ACC 107) cell lines were purchased from the German Collection of Microorganisms and Cell Cultures. TrxR knockout and reference mouse embryonic fibroblasts (MEF) were a kind gift from Marcus Conrad. MEFs isolated from conditional TrxR1 knockout mouse embryos, were immortalised by lentiviral transduction. *In vitro* deletion of TrxR1 was achieved by *Tat-Cre* induced recombination and verified by PCR and immunoblotting for TrxR1.¹⁴ The knock-in cell line emerged from the knockout cells through lentiviral transduction, encoding wildtype TrxR1.⁵ The stable expression of TrxR1 was validated by western blot and TrxR1 activity assays. All cell lines are tested regularly for mycoplasma contamination and only mycoplasma negative cells are used in assays.

Cellular activation and inhibition assays

A549 Cells were seeded in 96-well plates (20.000 each well) (microplates, 96 well, F-bottom, black, clear bottom, ViewPlate™-96 F TC, PerkinElmer) in 100 μL medium. After seeding, cells were incubated overnight and treated with probes (in 100% DMSO) to reach 1-100 μM final probe concentrations (1% final DMSO concentration) the next day. In brief: the media was removed and fresh media, containing the probes, was added to the cells. During the timecourse of the measurements, cells were kept at 37 °C under 5% CO_2 atmosphere and fluorescent signal was measured over 6 hours. For inhibition experiments, A549 cell lines were preincubated with TRi-1 (8, 16 μM from DMSO stock solutions, 50 μL medium, 0.23% DMSO) 3 h prior to probe addition or untreated (DMSO control), as non-inhibited internal control. After 3 hours of incubation, 10 μM probe (in 100% DMSO) was added in fresh media, to reach a final volume of 100 μL per well. Inhibitor concentrations given in the following refer to final concentrations (100 μL medium after probe addition). For buthionine sulfoximine (BSO) inhibitor studies, A549 cells were treated with 125 or 250 μM BSO in 100 μL for 24 h instead, with subsequent media change and addition of fresh media containing 10 μM probe and 125 or 250 μM BSO (1% DMSO) for the measurement. The BSO concentration was kept consistent throughout the experiment. MEF cells were seeded in 96-well plates (10.000 each well) in 100 μL DMEM with 10% FBS and 100 nM Na_2SeO_3 and incubated for 48 hours, before probe addition.

Time-course fluorescence measurements were conducted to determine kinetics of cellular processing. Fluorescence readout of cell-free activity and/or cell assays was performed either using a *FluoStar Omega* plate reader from BMG Labtech or a Tecan Infinite M200 plate reader (ex/em 480bp10/520lp recording fluorescence intensity). Data was interpreted by representing the absolute, time-dependent fluorescence intensity F . Cells were kept at 37 °C under 5 % CO_2 atmosphere between measurements.

Resazurin antiproliferation assays

Following up on a 6 h-cellular activation assay, wells were treated with Resazurin 150 mg/mL for 15 h. Fluorescence was measured at 590 nm (excitation 544 nm) using a *FluoStar Omega* plate reader (BMG Labtech). Absorbance data was averaged over the technical replicates, then normalised to viable cell count from the cosolvent control cells as 100%, where 0% viability was assumed to correspond to fluorescence signal in PBS only with no cells. Data were plotted against the log of MF-probe concentration ($\log_{10}[c(\mu\text{M})]$) with mean or SD.

6.5 Synthesis

Analytical methods

High resolution mass spectrometry (**HRMS**) was conducted either using a *Thermo Finnigan LTQ FT Ultra Fourier Transform* ion cyclotron resonance spectrometer from *ThermoFisher Scientific GmbH*, Dreieich (Germany) applying electron spray ionisation (ESI) with a spray capillary voltage of 4 kV at temperature 250 °C with a method dependent range from 50 to 2000 u or a *Finnigan MAT 95* from *Thermo Fisher Scientific*, Dreieich (Germany) applying electron ionisation (EI) at a source temperature of 250 °C and an electron energy of 70 eV with a method dependent range from 40 to 1040 u. All reported *m/z* values refer to positive ionisation mode, unless stated otherwise.

Nuclear magnetic resonance (**NMR**) spectroscopy was performed using a *Bruker Avance* (600/150 MHz, with *TCI cryoprobe*) or a *Bruker Avance III HD Biospin* (400/100 MHz, with *BBFO cryoprobe*) from *Bruker Corp.*, Billerica (USA) either at 400 MHz or 500 MHz. NMR-spectra were measured at 298 K, unless stated otherwise, and were analysed with the program *MestreNova 12* developed by *MestreLab Ltd.*, Santiago de Compostela (Spain). ¹H-NMR spectra chemical shifts (δ) in parts per million (ppm) relative to tetramethylsilane ($\delta = 0$ ppm) are reported using the residual protic solvent (CHCl₃ in CDCl₃: $\delta = 7.26$ ppm, DMSO-d₅ in DMSO-d₆: $\delta = 2.50$ ppm, CHD₂OD in CD₃OD: $\delta = 3.31$ ppm) as an internal reference. For ¹³C-NMR spectra, chemical shifts in ppm relative to tetramethylsilane ($\delta = 0$ ppm) are reported using the central resonance of the solvent signal (CDCl₃: $\delta = 77.16$ ppm, DMSO-d₆: $\delta = 39.52$ ppm, CD₃OD: $\delta = 49.00$ ppm) as an internal reference. For ¹H-NMR spectra in addition to the chemical shift the following data is reported in parenthesis: multiplicity, coupling constant(s) and number of hydrogen atoms. The abbreviations for multiplicities and related descriptors are s = singlet, d = doublet, t = triplet, q = quartet, or combinations thereof, m = multiplet and br = broad. Where known products matched literature analysis data, only selected data acquired are reported.

Analytical high performance liquid chromatography (**HPLC**) analysis was conducted either using an *Agilent 1100* system from *Agilent Technologies Corp.*, Santa Clara (USA) equipped with a DAD detector and a *Hypersil Gold* HPLC column from *ThermoFisher Scientific GmbH*, Dreieich (Germany) or a *Agilent 1200 SL* system *Agilent Technologies Corp.*, Santa Clara (USA) equipped with a DAD detector, a *Hypersil Gold* HPLC column from *ThermoFisher Scientific GmbH*, Dreieich (Germany) and consecutive low-resolution mass detection using a LC/MSD IQ mass spectrometer applying ESI from *Agilent Technologies Corp.*, Santa Clara (USA). For both systems mixtures of water (analytical grade, 0.1 % formic acid) and MeCN (analytical grade, 0.1 % formic acid) were used as eluent systems.

Laboratory techniques

Unless stated otherwise, all reactions were performed without precautions in regard of potential air- and moisture-sensitivity and were stirred with Teflon-coated magnetic stir bars. For work under inert gas (nitrogen) atmosphere, a Schlenk apparatus equipped with a liquid nitrogen trap and a high vacuum pump from *Vacuubrand GmbH*, Wertheim (Germany) were used. For solvent evaporation a *Laborota 400* from *Heidolph GmbH*, Schwabach (Germany) equipped with a vacuum pump was used. Flash column chromatography was conducted under positive nitrogen pressure using *Ceduran® Si 60 silica gel* from *Merck GmbH*, Darmstadt (Germany) as stationary phase. Reactions were monitored by thin layer chromatography (TLC) on TLC plates (*Si 60 F254 on aluminium sheets*) provided by *Merck GmbH* and visualised by UV irradiation and/or KMnO₄ (3.0 g KMnO₄, 20 g K₂CO₃, 0.30 g KOH, 0.30 L H₂O).

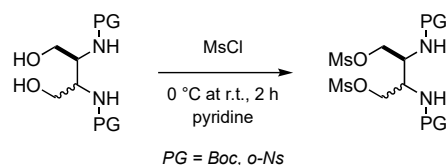
Chemicals

All chemicals, which were obtained from *Sigma-Aldrich*, *TCI*, *Alfa Aesar*, *Acros*, *abcr* or *carbolution* were used as received and without purification. Tetrahydrofuran (THF), dichloromethane (DCM) and dimethylformamide (DMF) were provided by *Acros* and were stored under argon atmosphere and dried over molecular sieves. TLC control, extractions and column chromatography were conducted using distilled, technical grade solvents. Whenever it is referred to the term *hexanes*, the applied solvent comprised isomeric mixtures of hexane (2-methylpentane, 3-methylpentane, 2,2-dimethylbutane, 2,3-dimethylbutane).

7 Synthetic Procedures

7.1 General protocols

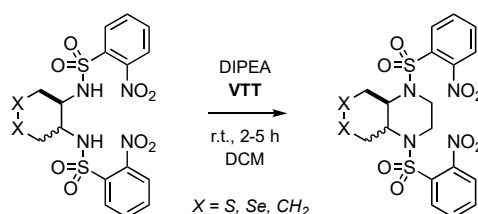
General protocol A: Mesylation of 1,4-diols



N,N-bis-protected 1,4-diol starting material (1.0 equiv.) was dissolved in pyridine (0.1 M) and cooled to 0 °C. The colourless solution was carefully charged with MsCl (2.2-3.5 equiv.), upon which an immediate colour change to bright yellow indicated the formation of activated methylsulfonyl-pyridinium chloride. The reaction was allowed to warm to r.t. and was stirred for 2 h. Once full conversion of the starting material was indicated by LCMS analysis, the reaction mixture was poured into ice-cold water, causing the formation of thick, colourless precipitates. The solids were filtered off and extensively washed with water, then ether. The solids were collected and dried under high vacuum, giving the target dimesylate as a colourless solid and without further purification.

Note: Boc-protected dimesylates generally exhibited better solubility in organic solvents than their nosyl-protected counterparts. Therefore, to ensure good yields, it is advised to wash the collected precipitates with water and only small amounts of ether. Alternatively, one could leave the wet filter cake to dry on air overnight or, azeotropically remove residual water with toluene or heptane.

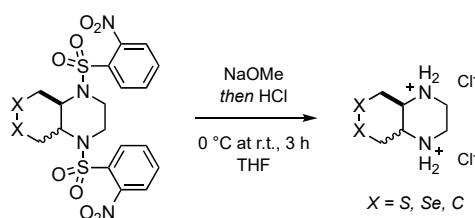
General protocol B: Synthesis of bicyclic piperazines



Monocyclic, bis-sulfonamides (1.0 equiv.) were suspended in DCM (0.05 M) and charged with DIPEA (3.5 equiv.). To the heterogeneous mixture was added vinyl thianthrenium triflate (**VTT**, 1.3 equiv.) in DCM (0.3 M) in a dropwise manner. The reaction was monitored by LCMS, and full conversion of the starting material was accompanied by formation of a fully homogeneous solution within 3-5 hours. The reaction was quenched by NH₄Cl (sat. aq.) and the aqueous layer was extracted with DCM (two times). The combined organic layers were dried over MgSO₄, filtered and concentrated, giving yellow crude solids. Purification by FCC (X = S, C: hexane/EtOAc, X = Se: hexane/DCM) gave the bicyclic piperazines as colourless (X = S, C) or yellow (X = Se) foams.

Note: The reaction proceeds cleanly, without formation of any side products. The only species that need to be removed during purification are DIPEA, traces of unreacted VTT and thiantrene, thus not requiring great care during purification. DIPEA and VTT stick to the baseline and TT, due to its apolarity, will elute within the first few fractions.

General protocol C: Piperazine deprotection

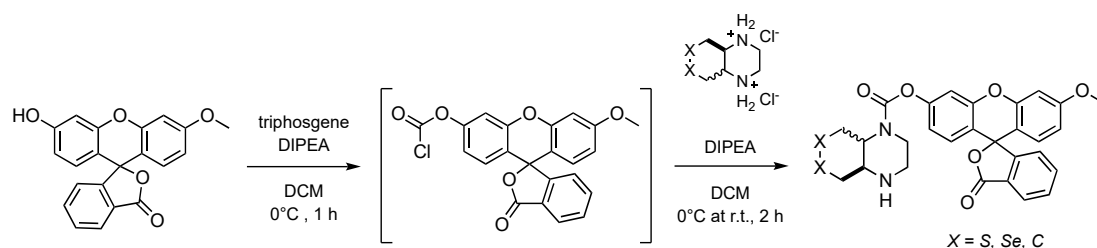


Bis(*o*-nosyl)piperazines (1.0 equiv.) were dissolved in THF (0.05 M), cooled to 0 °C and charged with NaOMe (5.4 M in MeOH, 2.5 equiv.) in THF (1 M). The orange solution was allowed to warm to r.t. and monitored by LCMS. Upon full deprotection of the starting material which occurred within 3 h, the reaction was directly charged with hydrochloric acid (4 M in dioxane, 10 equiv.), causing the title compound to precipitate from the reaction mixture.

The solids were filtered off and washed extensively with DCM and Et₂O, giving piperazine dihydrochlorides as colourless (X = S, C) or yellow solids (X = Se).

Note: As a consequence of the mechanism of deprotection, NaOMe can to some extent cause S_NAr to not occur at the sulfone, but at the adjacent nitro-group. In our case, this led to the formation of ca. 5-10% of singly protected 1-((2-methoxyphenyl)sulfonyl)piperazine, which equally precipitated after addition of HCl. Extensive washings with DCM could remove much of this side product, but traces usually remained. As a second note, the given procedure yields one equivalent of NaCl for every equivalent of NaOMe. Thus, the isolated product by default contains 2.5 equiv. NaCl, which we take into account for yield determination and purity of the target piperazines.

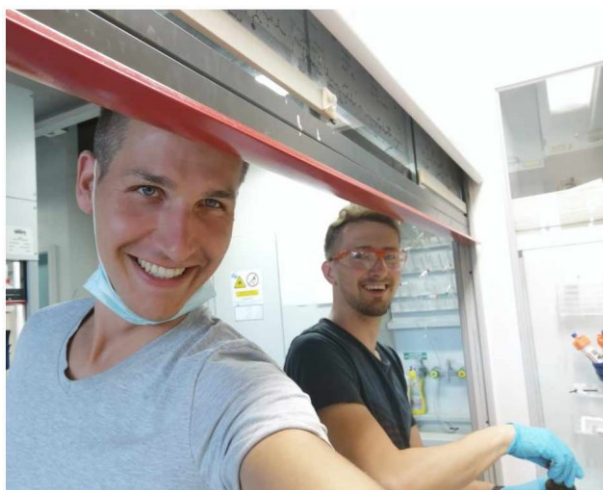
General protocol D: Assembly of fluorescein carbamates



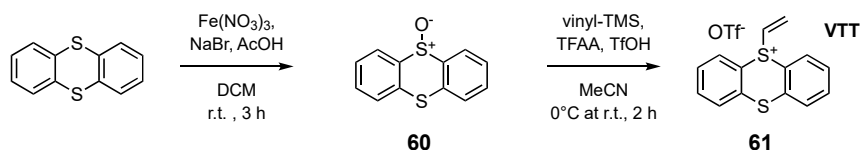
Methyl fluorescein (1.0 equiv.) was suspended in dry DCM (0.05 M) and sequentially charged with solutions of triphosgene (1.1 equiv.) and DIPEA (1.5 equiv.) in dry DCM (1.0 M) at 0 °C. Reaction progress was monitored by LCMS through *in situ* carbamate formation of a reaction aliquot with *N*-methylpiperazine. Upon full conversion, all volatile compounds were removed using two serially connected, external liquid nitrogen traps while carefully exposing the reaction vessel to reduced pressure. Excess phosgene which was caught in either of the liquid nitrogen traps was quenched when still cold by carefully adding an excess of piperidine. The chloroformate intermediate was received as a dark orange solid and was used without further purification.

For ensuing carbamate coupling reactions, the crude solid was resuspended in dry DCM (0.05 M) and slowly added to a solution of the respective bicyclic piperazine (1.4 equiv.) and DIPEA (2.8 equiv.) in DCM (0.05 M) at 0 °C. The reaction was allowed to warm to r.t. and stirred for 2 h. All volatiles were removed and the crude oil was purified by FCC (hexane/EtOAc) giving the title compounds as colourless to pale yellow solids. To fully remove traces of free fluorescein, each conjugate was additionally purified by preparative HPLC (H₂O/MeCN/FA).

Note: Fluorescein-chloroformate formation is accompanied by the *in-situ* formation of gaseous, highly toxic phosgene. Therefore, as an additional safety precaution, the reaction was exclusively performed in a separate fume hood to avoid exposure in the event of a leaky reaction setup.



7.2 Final short trigger synthesis

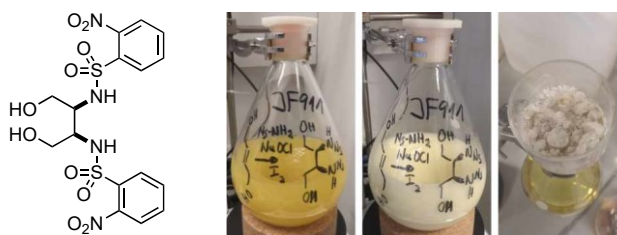
7.2.1 Ritter-VTT synthesis¹⁵

Step 1: Thiantrene (7.0 g, 32 mmol, 1.0 equiv.) was suspended in DCM (0.5 M, 65 mL) and sequentially charged with NaBr (0.17 g, 1.6 mmol, 0.05 equiv.), Fe(NO₃)₃ nonahydrate (13 g, 32 mmol, 1.0 equiv.) and AcOH (12.1 mL, 24 mmol, 0.75 equiv.), which was accompanied by a gradual colour change from colourless to orange and finally dark red. The heterogeneous mixture was stirred at r.t. for 3 h, upon which LCMS control indicated full conversion of the starting material. The reaction was diluted with water (50 mL), and the aqueous layer was extracted with DCM (three times). The combined organic layers were washed with brine, dried over MgSO₄, filtered and concentrated, giving the thiantrene-5-oxide **60** as a colourless solid (6.5 g, 28 mmol, 86%). Analytical data match literature values.¹⁵

HRMS (ESI): m/z C₁₂H₉OS₂⁺ [M+H]⁺: calc. 233.0089, found: 233.0091. **¹H-NMR** (400 MHz, CDCl₃) δ (ppm) = 7.92 (dd, J = 7.8, 1.4 Hz, 1H), 7.62 (dd, J = 7.7, 1.2 Hz, 1H), 7.54 (td, J = 7.6, 1.2 Hz, 1H), 7.42 (td, J = 7.6, 1.4 Hz, 1H). **¹³C-NMR** (101 MHz, CDCl₃) δ (ppm) = 141.5, 130.0, 129.1, 128.5, 124.6.

Step 2: **60** (5.0 g, 22 mmol, 1.0 equiv.) was suspended in MeCN (0.2 M, 200 mL), and vinyl-TMS (6.3 mL, 43 mmol, 2.0 equiv.) was added. The heterogeneous mixture was cooled to 0 °C, and carefully charged with TFAA (9.0 mL, 65 mmol, 3.0 equiv.), which resulted in an immediate colour change from colourless to bright pink. Next, TfOH (2.3 mL, 26 mmol, 1.2 equiv.) was added, and the reaction mixture turned dark purple. The reaction was allowed to warm to r.t., was stirred for 2 h and then concentrated to ~20% of its volume. The residue was diluted with DCM (200 mL) and the organic mixture was washed with NaHCO₃ (sat. aq., two times. *Caution:* add aqueous base very carefully. Vigorous gas formation occurs.). The organic layer was then dried over MgSO₄, filtered and concentrated to ~10% of its volume. The crude solution was then carefully added to vigorously stirred Et₂O (200 mL), resulting in the precipitation of off-white solids, which stuck to the wall of the flask. The liquid phase was removed, and the solid residues were washed with Et₂O (two times) and dried under high vacuum, giving vinyl thiantrenium triflate **61** (**VTT**) as an off-white solid (6.5 g, 20 mmol, 92%). Characterisation matches analytical data from Ritter et al.¹⁵

HRMS (ESI): m/z C₁₂H₈S₂⁺ [M]⁺: calc. 216.0062, found: 216.0064. **¹H-NMR** (400 MHz, CDCl₃) δ (ppm) = 8.33 – 8.22 (m, 2H), 7.83 (dd, J = 7.9, 1.3 Hz, 2H), 7.77 (td, J = 7.7, 1.4 Hz, 2H), 7.65 (td, J = 7.6, 1.4 Hz, 2H), 6.72 (dd, J = 16.0, 8.8 Hz, 1H), 6.30 (dd, J = 8.8, 2.8 Hz, 1H), 6.23 (dd, J = 16.0, 2.8 Hz, 1H). **¹³C-NMR** (101 MHz, CDCl₃) δ (ppm) = 136.1, 135.0, 134.7, 134.2, 130.3, 130.3, 119.5, 118.4.

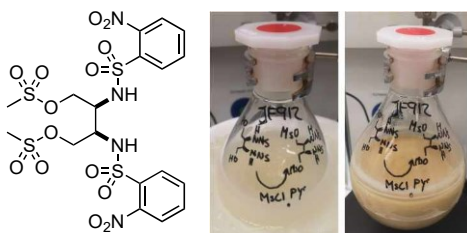
7.2.2 (*cis*)-dinosyl-Route*N,N'*-1,4-dihydrobutane-2,3-diyl)bis(2-nitrobenzenesulfonamide) (*cis*) **2C**

Protocol A: Following a procedure from Okumura and coworkers,¹⁶ trans-2-butene-1,4-diol (0.19 mL, 2.3 mmol, 1.0 equiv.) was dissolved in MeCN (12 mL, 0.2 M) and 2-nitrobenzenesulfonamide (1.0 g, 5.0 mmol, 2.2 equiv.), iodine (58 mg, 0.23 mmol, 0.1 equiv.) and sodium hypochlorite pentahydrate (822 mg, 5.0 mmol, 2.2 equiv.) were added at room temperature. The resulting, pale yellow heterogeneous mixture was stirred at r.t. for 3 h, then heated to 70 °C and further stirred for 15 h. To the reaction mixture was added 0.5 M aq. Na₂S₂O₃ (40 mL) and EtOAc (50 mL) and the organic layer was washed with aq. NaCl (2×20 mL), the aq. extracted with EtOAc (4×30 mL), the combined organic layers were dried over Na₂SO₄ and concentrated under reduced pressure to give **2C** as a colourless solid (562 mg, 1.1 mmol, 50%).

Protocol B: **30** (355 mg, 1.8 mmol, 1.0 equiv.) was suspended in pyridine (37 mL, 0.05 M) and cooled to 0 °C. TMS-Cl (1.2 mL, 9.2 mmol, 5.0 equiv.) was added in one portion and the resulting mixture was stirred at 0 °C for 15 min, was then allowed to warm to r.t. and was further stirred for 2 h, until a clear solution was observed. To the mixture was then added at 0 °C a solution of 2-nitrobenzenesulfonyl chloride (1222 mg, 5.5 mmol, 3.0 equiv.) and the resulting mixture was stirred at 0 °C for 15 min, was then allowed to warm to r.t. and was further stirred for 10 h. The mixture was portioned between 2 M aq. HCl (100 mL) and EtOAc (150 mL) for 5 min. The aq. layer was separated, and the organic layer was washed with 2 M aq. HCl (4×20 mL), the combined aq. layers were saturated with NaCl and extracted with EtOAc (3×20 mL). The combined organic layers were dried over Na₂SO₄ and concentrated under reduced pressure to give **2C** as a colourless solid (722 mg, 1.5 mmol, 80%).

HRMS (ESI): C₁₆H₁₇N₄O₁₀S₂⁻: [M-H]⁻ calc. *m/z* 489.03916, found 489.04007. **¹H-NMR** (400 MHz, DMSO-*d*₆): δ (ppm) = 8.08 – 8.02 (m, 2H), 8.00 – 7.93 (m, 2H), 7.85 – 7.78 (m, 4H), 7.63 – 7.51 (m, 2H, N-H), 4.40 (s, 2H), 3.55 (p, *J* = 5.3 Hz, 2H), 3.41 (h, *J* = 5.6 Hz, 4H). **¹³C-NMR** (101 MHz, DMSO-*d*₆): δ (ppm) = 147.2 (C_{Ar}), 133.8 (C_{ArH}), 133.7 (C_{Ar}), 132.7 (C_{ArH}), 130.0 (C_{ArH}), 124.5 (C_{ArH}), 60.3 (CH₂), 56.5 (CH).

2,3-bis((2-nitrophenyl)sulfonamido)butane-1,4-diyl dimethanesulfonate (*cis*) **3C**



Following **general procedure A**, **2C** (722 mg, 1.5 mmol, 1.0 equiv.) was dissolved in pyridine (10 mL, 0.15 M) and reacted with MsCl (356 μL, 4.6 mmol, 3.0 equiv.). After precipitation from water and washings with ether **3C** was received as a colourless solid and in excellent purity (694 mg, 1.1 mmol, 73%).

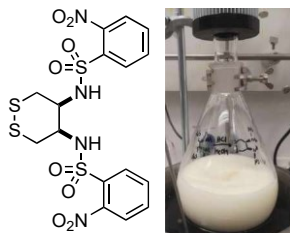
HRMS (ESI): C₁₈H₂₁N₄O₁₄S₄⁻: [M-H]⁻ calc. *m/z* 644.99426, found 644.99520. **¹H-NMR** (400 MHz, DMSO-*d*₆): δ (ppm) = 8.50 (d, *J* = 8.5 Hz, 2H), 8.06 – 7.95 (m, 4H), 7.92 – 7.78 (m, 4H), 4.19 (d, *J* = 8.4 Hz, 2H), 4.05 (dd, *J* = 10.2, 6.2 Hz, 2H), 3.89 (s, 2H), 2.87 (s, 6H). **¹³C-NMR** (101 MHz, DMSO-*d*₆): δ (ppm) = 147.0 (C_{Ar}), 134.4 (C_{ArH}), 133.3 (C_{Ar}), 133.1 (C_{ArH}), 130.0 (C_{ArH}), 124.8 (C_{ArH}), 68.0 (CH₂), 53.1 (CH), 36.3 (CH₃).

2-((2-nitrophenyl)sulfonamido)-3-((2-nitrophenylsulfonyl)methyl)butane-1,4-diyl diethanethioate (*cis*) **4C**



3C (694 mg, 1.1 mmol, 1.0 equiv.) was suspended in acetone (21 mL, 0.05 M) and KSAc (366 mg, 3.2 mmol, 3.0 equiv.) was added in one portion. The mixture was stirred at r.t. for 3 h, before being poured into water (50 mL). The solid was azeotropically dried using toluene to yield **4C** as a colourless solid (579 mg, 0.96 mmol, 90%).

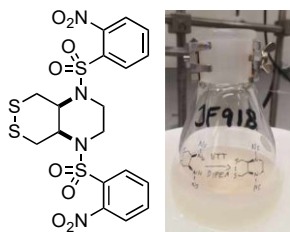
TLC *R*_f = 0.55 (isohexane:EtOAc, 1:2). **HRMS** (ESI): C₂₀H₂₁N₄O₁₀S₄⁻: [M-H]⁻ calc. *m/z* 605.01460, found 605.01597. **¹H-NMR** (400 MHz, DMSO-*d*₆): δ (ppm) = 8.17 (d, *J* = 8.3 Hz, 2H, N-H), 8.02 – 7.96 (m, 2H), 7.95 – 7.91 (m, 2H), 7.89 – 7.84 (m, 4H), 3.54 (t, *J* = 9.0 Hz, 2H), 3.20 (dd, *J* = 13.9, 3.6 Hz, 2H), 2.77 (dd, *J* = 13.9, 9.4 Hz, 2H), 2.03 (s, 6H). **¹³C-NMR** (101 MHz, DMSO-*d*₆): δ (ppm) = 194.3 (C=O), 147.1 (C_{Ar}), 134.1 (C_{ArH}), 133.5 (C_{Ar}), 132.6 (C_{ArH}), 130.1 (C_{ArH}), 124.4 (C_{ArH}), 57.4 (CH), 30.3 (CH₂), 30.1 (CH₃).

***N,N'*-1,2-dithiane-4,5-diyl)bis(2-nitrobenzenesulfonamide) (*cis*) 5C**

Protocol A: **4C** (572 mg, 0.95 mmol, 1.0 equiv.) was suspended in MeOH (35 mL, 0.03 M) and a solution of HCl (4.0 M in dioxane, 11.9 mL, 47.7 mmol, 50.0 equiv.) was added in one portion. The mixture was heated to 70 °C and was stirred for 15 h, before being cooled to r.t. and poured into water (50 mL). The solid was collected and azeotropically dried using toluene to yield **5C** as a colourless solid (484 mg, 0.93 mmol, 98%).

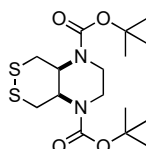
Protocol B: **36C** (144 mg, 0.64 mmol, 1.0 equiv.) was suspended in anhydrous DCM (18 mL, 0.05 M) and NEt₃ (268 μL, 1.9 mmol, 3.0 equiv.) was added. A clear solution was observed and a solution of 2-nitrobenzenesulfonyl chloride (343 mg, 1.6 mmol, 2.4 equiv.) in anhydrous DCM (0.3 M) was added dropwise at 0 °C. The mixture was stirred at 0 °C for 15 min, was then allowed to warm to r.t. and was further stirred for 4 h, before being concentrated under reduced pressure. Purification was achieved using FCC (isohexane:DCM 1:1 to DCM) to yield **5C** as a colourless solid (125 mg, 0.24 mmol, 38%).

TLC R_f = 0.25 (DCM). **HRMS** (ESI): C₁₆H₁₅N₄O₈S₄⁻: [M-H]⁻ calc. *m/z* 518.97782, found 518.97835. **¹H-NMR** (400 MHz, DMSO-*d*₆): δ (ppm) = 8.15 (d, *J* = 6.6 Hz, 2H, N-H), 8.06 (d, *J* = 5.4 Hz, 2H), 8.00 – 7.92 (m, 2H), 7.89 – 7.79 (m, 4H), 3.76 (br-s, 2H), 3.46 (br-s, 4H). **¹³C-NMR** (101 MHz, DMSO-*d*₆): δ (ppm) = 147.4 (C_{Ar}), 134.4 (C_{Ar}H), 132.9 (C_{Ar}H), 129.8 (C_{Ar}H), 124.5 (C_{Ar}H), 54.9 (CH₂), 53.6 (CH).

1,4-bis((2-nitrophenyl)sulfonyl)octahydro-[1,2]dithiino[4,5-*b*]pyrazine (*cis*) 6C

Following **general procedure B**, **5C** (484 mg, 0.93 mmol, 1.0 equiv.) was dissolved in anhydrous DCM (18 mL, 0.05 M) and reacted with DIPEA (576 μL, 3.25 mmol, 3.5 equiv.) and VTT (371 mg, 1.2 mmol, 1.2 equiv.). Purification by FCC (hexanes/DCM 1:1 → DCM) gave **6C** as a colourless solid (291 mg, 0.53 mmol, 57%).

TLC R_f = 0.56 (DCM). **HRMS** (ESI): C₁₉H₁₉N₄O₁₀S₄⁻: [M+HCO₂]⁻ calc. *m/z* 590.99895, found 590.99972. **¹H-NMR** (400 MHz, DMSO-*d*₆): δ (ppm) = 8.05 (d, *J* = 7.7 Hz, 2H), 7.93 (d, *J* = 7.0 Hz, 2H), 7.87 (t, *J* = 7.3 Hz, 2H), 7.76 (t, *J* = 7.6 Hz, 2H), 4.18 (d, *J* = 7.0 Hz, 2H, N-H), 3.74 – 3.58 (m, 4H), 3.57 – 3.46 (m, 2H), 3.07 (d, *J* = 13.9 Hz, 2H). **¹³C-NMR** (101 MHz, DMSO-*d*₆): δ (ppm) = 147.4 (C_{Ar}), 135.3 (C_{Ar}H), 132.7 (C_{Ar}H), 130.3 (C_{Ar}H), 124.5 (C_{Ar}H), 54.1 (CH), 42.3 (CH₂), 36.8 (CH₂).

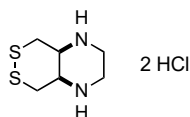
di-*tert*-butyl hexahydro-[1,2]dithiino[4,5-*b*]pyrazine-1,4-dicarboxylate (*cis*) 18C

A solution of NaOMe (25% in MeOH, 3.61 mL, 15.8 mmol, 10.0 equiv.) was added in one portion to a solution of **6C** (0.86 g, 1.6 mmol, 1.0 equiv.) in THF (32 mL, 0.05 M). The reaction mixture was stirred at r.t. for 1 h, before a solution of NaHCO₃ (1.59 g, 19.0 mmol, 12 equiv.) in water (32 mL) was added to the mixture. After 15 min, NEt₃ (1.10 mL, 7.9 mmol, 5 equiv.) and Boc₂O (3.45 g, 15.8 mmol, 10.0 equiv.) were added and the reaction mixture was then stirred at r.t. overnight. The reaction mixture was then diluted with EtOAc (100 mL) and washed with an

aq. NH₄Cl solution (1.5 M, 150 mL). The organic layer was dried over Na₂SO₄, concentrated and purified by FCC (hexanes:EtOAc: 20:1) to give **18C** (0.52 g, 1.38 mmol, 87%) as a clear brownish oil.

TLC R_f = 0.60 (hexanes:EtOAc, 5:1). **HRMS** (ESI): C₁₆H₂₉N₂O₄S₄⁺: [M+H]⁺ calc. *m/z* 377.15633, found 377.15666. **¹H-NMR** (400 MHz, CDCl₃): δ (ppm) = 4.27 – 4.21 (m, 2H), 3.84 (d, *J* = 7.8 Hz, 2H), 3.50 (dd, *J* = 12.6, 6.3 Hz, 4H), 2.97 (dd, *J* = 14.3, 2.9 Hz, 2H), 1.47 (s, 18H). **¹³C-NMR** (101 MHz, CDCl₃): δ (ppm) = 155.0 (C=O), 80.9 (C(CH₃)₃), 77.4 (CH), 51.1 (CH₂), 41.9 (CH₂), 28.5 (C(CH₃)₃).

SS66C·2HCl octahydro-[1,2]dithiino[4,5-*b*]pyrazine dihydrochloride (*cis*) **7C**

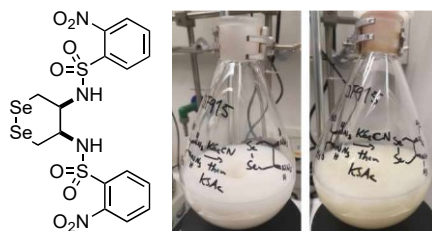


Protocol A: Closely following **general procedure C**, **6C** (1,192 mg, 2.18 mmol) in THF (45 mL, 0.05 M) was reacted with NaOMe (5.4 M in MeOH, 1.01 mL, 5.45 mmol, 2.5 equiv.) in THF (4.4 mL, 1 M). After quantitative deprotection, the dihydrochloride **7C** was precipitated from the reaction mixture using HCl (4 M in dioxane, 5.5 mL, 22 mmol, 10 equiv.). After filtration, **7C** was isolated as a pale-yellow solid (**SS66C·2 HCl·2.5 NaCl**, 851 mg, 1.08 mmol, 99%, 63 w% content of **SS66C·2 HCl**).

Protocol B: **X48** (782 mg, 2.08 mmol) was dissolved in anhydrous DCM (200 mL, 0.01 M), HCl (4 M in dioxane) was added at r.t. and the resulting solution was stirred for 6 h. Precipitation was observed and the mixture was poured into Et₂O (400 mL) and the solid was filtered off and dried under reduced pressure to yield **7C** (286 mg, 1.15 mmol, 55%, 100 w% content of **SS66C·2 HCl**) as a colourless solid.

HRMS (ESI): C₆H₁₃N₂S₂: [M-H]⁺ calc. *m/z* 177.05147, found 177.05176. **¹H-NMR** (400 MHz, DMSO-*d*₆): δ (ppm) = 10.01 (s, 4H), 4.02 (d, *J* = 7.0 Hz, 4H), 3.93 (d, *J* = 12.7 Hz, 2H), 3.60 (d, *J* = 15.0 Hz, 2H), 3.00 (d, *J* = 11.2 Hz, 2H). **¹³C-NMR** (101 MHz, DMSO-*d*₆): δ (ppm) = 50.9 (CH), 36.6 (CH₂), 26.8 (CH₂).

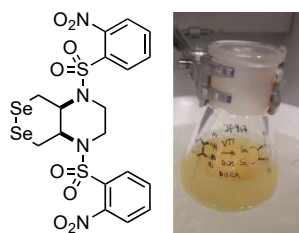
N,N'-(1,2-diselenane-4,5-diyl)bis(4-nitrobenzenesulfonamide) (*cis*) **8C**



3C (228 mg, 0.35 mmol, 1.0 equiv.) was suspended in acetone (21 mL, 0.05 M) and KSeCN (203 mg, 1.4 mmol, 4.0 equiv.) was added in one portion. The mixture was stirred at r.t. for 3 h, before KSAc (322 mg, 2.8 mmol, 8.0 equiv.) was added and the mixture was stirred for 1 h at r.t., before being poured into ice-cold water (30 mL). The solid was filtered off and azeotropically dried using toluene to yield **8C** as a colourless solid (203 mg, 0.33 mmol, 94%).

TLC R_f = 0.21 (DCM). **HRMS** (ESI): C₁₆H₁₅N₄O₈S₂Se₂⁻: [M-H]⁻ calc. *m/z* 614.86672, found 614.86817. **¹H-NMR** (400 MHz, CDCl₃): δ (ppm) = 8.21 – 8.01 (m, 2H), 7.97 – 7.83 (m, 2H), 7.83 – 7.68 (m, 4H), 6.13 (d, *J* = 8.2 Hz, 2H, *N-H*), 3.92 (t, *J* = 9.0 Hz, 2H), 3.28 – 2.99 (m, 4H). **¹³C-NMR** (101 MHz, CDCl₃) δ (ppm) = 147.9 (C_{Ar}), 134.3 (C_{Ar}H), 133.3 (C_{Ar}H), 130.8 (C_{Ar}H), 125.7 (C_{Ar}H), 55.0 (CH).

1,4-bis((2-nitrophenyl)sulfonyl)octahydro-[1,2]diselenino[4,5-*b*]pyrazine (*cis*) **9C**

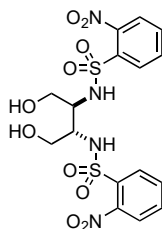


Following **general procedure B**, **8C** (181 mg, 0.30 mmol, 1.0 equiv.) was dissolved in anhydrous DCM (6 mL, 0.05 M) and reacted with DIPEA (209 μ L, 1.18 mmol, 4.0 equiv.) and (176 mg, 0.53 mmol, 1.8 equiv.). Purification by FCC (hexanes/DCM 1:1 \rightarrow DCM) gave **9C** as a colourless solid (119 mg, 0.19 mmol, 63%).

TLC R_f = 0.52 (DCM). **HRMS** (ESI): $C_{19}H_{19}N_4O_{10}S_2Se_2^-$: $[M+HCO_2]^-$ calc. m/z 686.88785, found 686.88953. **1H -NMR** (400 MHz, DMSO- d_6): δ (ppm) = 8.08 – 8.01 (m, 2H), 7.93 (dd, J = 8.0, 1.2 Hz, 2H), 7.87 (td, J = 7.7, 1.2 Hz, 2H), 7.76 (td, J = 7.9, 1.4 Hz, 2H), 4.22 (d, J = 8.1 Hz, 2H), 3.89 (dd, J = 13.4, 7.8 Hz, 2H), 3.72 – 3.60 (m, 2H), 3.58 – 3.46 (m, 2H), 3.23 (d, J = 12.9 Hz, 2H). **^{13}C -NMR** (101 MHz, DMSO- d_6): δ (ppm) = 147.4 (C_{Ar}), 135.3 (C_{ArH}), 132.7 (C_{ArH}), 130.3 (C_{ArH}), 124.4 (C_{ArH}), 55.5 (CH), 42.0 (CH_2), 28.2 (CH_2).

7.2.3 (*trans*)-dinosyl-Route

N,N'-1,4-dihydrobutane-2,3-diylbis(2-nitrobenzenesulfonamide) (*trans*) **2T**

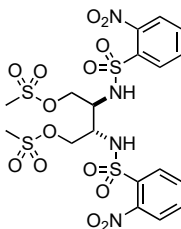


Closely following the procedure from Okumura and coworkers,¹⁶ *cis*-2-butene-1,4-diol (0.2 mL, 2.5 mmol, 1.0 equiv.) was dissolved in MeCN (15 mL, 0.2 M) and sequentially charged with 2-nitrobenzenesulfonamide (1.1 g, 5.3 mmol, 2.2 equiv.), iodine (62 mg, 0.24 mmol, 0.1 equiv.) and sodium hypochlorite pentahydrate (0.88 g, 5.3 mmol, 2.2 equiv.). The resulting, pale yellow heterogeneous mixture was stirred at r.t. for 12 h, then heated to 70 °C and stirred for another 12 h. Upon full conversion the reaction was quenched by adding $Na_2S_2O_3$ (1 M aq.) and the aqueous layer was extracted with EtOAc (3 \times 50 mL). The combined organic extracts were dried over anhydrous $MgSO_4$ and concentrated under reduced pressure, yielding **2T** in good purity and without further purification (1.1 g, 2.2 mmol, 91%).

Note: Once isolated in its solid form, the di-nosyl-diol target poorly redissolves in EtOAc or MeOH. Thus, if further purification of the crude product is required, we recommend recrystallisation from EtOAc instead of column chromatography (e.g. on >40 mmol scale, yield after purification: 65-75%).

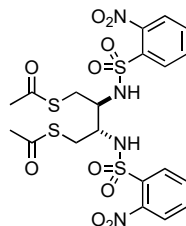
HRMS (ESI): $C_{16}H_{15}N_4O_9S_2^-$: $[M-H_2O-H]^-$ calc. m/z 471.0286, found 471.0295. **1H -NMR** (400 MHz, DMSO- d_6): δ (ppm) = 8.04 – 8.00 (m, 2H), 7.95 (ddd, J = 7.2, 3.4, 1.9 Hz, 2H), 7.88 – 7.78 (m, 4H), 4.56 (s, 2H), 3.57 (s, 2H), 3.38 – 3.29 (m, 2H), 3.24 (dd, J = 10.8, 6.2 Hz, 2H). **^{13}C -NMR** (101 MHz, DMSO- d_6): δ (ppm) = 147.2 (C_{Ar}), 133.9 (C_{ArH}), 133.6 (C_{Ar}), 132.5 (C_{ArH}), 130.2 (C_{ArH}), 124.4 (C_{ArH}), 60.2 (CH_2), 55.8 (CH).

2,3-bis((2-nitrophenyl)sulfonamido)butane-1,4-diyl dimethanesulfonate (*trans*) **3T**



Following **general procedure A**, **2T** (12 g, 25 mmol, 1.0 equiv.) was dissolved in pyridine (0.25 M, 0.16 L) and reacted with $MsCl$ (6.6 mL, 86 mmol, 3.5 equiv.). After precipitation from water and washings with ether **3T** was received as a colourless solid and in excellent purity (12 g, 19 mmol, 76%).

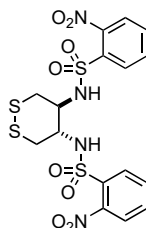
HRMS (ESI): $C_{18}H_{21}N_4O_{14}S_4^-$: $[M-H]^-$ calc. 644.99426, found 644.99637. **1H -NMR** (400 MHz, DMSO- d_6): δ (ppm) = 8.45 (d, J = 8.6 Hz, 2H), 8.04 – 7.97 (m, 4H), 7.92 – 7.82 (m, 4H), 4.20 (dd, J = 10.3, 4.1 Hz, 2H), 4.05 (dd, J = 10.3, 8.3 Hz, 2H), 3.88 (ddd, J = 10.5, 6.9, 3.7 Hz, 2H), 2.91 (s, 6H). **^{13}C -NMR** (101 MHz, DMSO- d_6): δ (ppm) = 147.1 (C_{Ar}), 132.9 (C_{ArH}), 132.8 (C_{Ar}), 130.2 (C_{ArH}), 124.7 (C_{ArH}), 67.7 (CH_2), 54.0 (CH), 36.5 (CH_3).

2-((2-nitrophenyl)sulfonamido)-3-((2-nitrophenylsulfonyl)methyl)butane-1,4-diyl diethanethioate (*trans*) 4T

3T (0.50 g, 0.77 mmol, 1.0 equiv.) was suspended in acetone (0.05 M, 20 mL) and charged with KSAc (0.27 g, 2.3 mmol, 3.0 equiv.) at r.t.. The reaction was stirred for 1 h, during which the heterogeneous mixture significantly thickened due to the formation of insoluble KOMs. Once LCMS-control indicated full conversion of the starting material, the reaction was concentrated to ca. 20% of its volume and the remaining mixture was partitioned between brine and EtOAc. The aqueous layer was extracted with EtOAc (three times), and the combined organic layers were washed with brine, dried over MgSO₄ and concentrated. The orange crude solid containing **4T** was directly used for further transformations (0.46 g, 0.75 mmol, 97%).

Notes: (1) In contrast to the thioacetylations of Boc-protected substrates, basic workup must be strictly avoided due to hydrolysis of the thioester and sequential intramolecular amine-deprotection through S_NAr of the liberated thiolate. (2) For large-scale syntheses (>20 mmol), the reaction does not always proceed as cleanly. After aqueous workup, the crude solids should be recrystallised from MeOH – several washings of the crude solids with hot MeOH usually suffice to receive a solid residue containing the target compound in excellent purity.

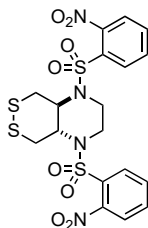
TLC R_f = 0.51 (hexanes:EtOAc, 1:2). **HRMS** (ESI): C₂₀H₂₁N₄O₁₀S₄⁻: [M-H]⁻ calc. *m/z* 605.01460, found 605.01622. **¹H-NMR** (400 MHz, DMSO-*d*₆): δ (ppm) = 8.20 (d, *J* = 8.6 Hz, 2H), 8.06 – 8.01 (m, 2H), 8.00 – 7.96 (m, 2H), 7.93 – 7.85 (m, 4H), 3.58 – 3.46 (m, 2H), 3.09 (dd, *J* = 13.9, 4.5 Hz, 2H), 2.79 (dd, *J* = 13.9, 9.4 Hz, 2H), 2.02 (s, 6H). **¹³C-NMR** (101 MHz, DMSO-*d*₆): δ (ppm) = 194.8 (C=O), 147.6 (C_{Ar}), 134.8 (C_{Ar}H), 133.5 (C_{Ar}), 133.2 (C_{Ar}H), 130.7 (C_{Ar}H), 125.3 (C_{Ar}H), 57.3 (CH), 30.6 (CH₂), 29.8 (CH₃).

***N,N'*-1,2-dithiane-4,5-diylbis(2-nitrobenzenesulfonamide) (*trans*) 5T**

4T (2.9 g, 4.8 mmol, 1.0 equiv.) was suspended in MeOH (0.1 M, 50 mL) and charged with HCl (4 M in dioxane, 24 mL, 20 equiv.) at r.t.. The reaction was stirred for 16 h, upon which the mixture turned homogeneous, and LCMS-control indicated full deprotection of the thioester. Next, a solution of iodine (1.2 g, 4.8 mmol, 1.0 equiv.) in MeOH (0.3 M, 17 mL) was slowly added to the reaction mixture, swiftly causing the formation of orange precipitates. TLC control confirmed full turnover to the dithiane **X54** within 5 min, which was followed by the addition of water (200 mL). The solid precipitates were filtered, washed with water and ether, and were dried on high vacuum overnight, giving **5T** as an orange solid (2.4 g, 4.5 mmol, 94%).

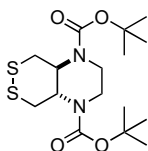
Note: (1) Basic hydrolysis of the thioester leads to rapid and quantitative intramolecular Ns-deprotection by the formed thiolate (2) Purification by flash column chromatography gives the target as a colourless solid and in excellent purity, but leads to significantly compromised yield due to its poor solubility.

TLC R_f = 0.26 (DCM). **HRMS** (ESI): C₁₆H₁₅N₄O₈S₄⁻: [M-H]⁻ calc. *m/z* 518.97782, found 518.9791. **¹H-NMR** (400 MHz, DMSO-*d*₆): δ (ppm) = 8.14 (s, 2H), 8.00 (dd, *J* = 6.0, 3.3 Hz, 2H), 7.94 – 7.89 (m, 2H), 7.88 – 7.78 (m, 4H), 3.53 (d, *J* = 7.8 Hz, 2H), 2.95 (s, 4H). **¹³C-NMR** (101 MHz, DMSO-*d*₆): δ (ppm) = 147.5 (C_{Ar}), 134.5 (C_{Ar}H), 133.4 (C_{Ar}), 130.2 (C_{Ar}H), 124.9 (C_{Ar}H), 56.9 (CH₂).

1,4-bis((2-nitrophenyl)sulfonyl)octahydro-[1,2]dithiino[4,5-*b*]pyrazine (*trans*) 6T

Following **general procedure B**, **5T** (0.24 g, 0.47 mmol, 1.0 equiv.) was dissolved in anhydrous DCM (20 mL, 0.05 M) and reacted with DIPEA (0.29 mL, 1.6 mmol, 3.5 equiv.) and VTT (0.20 g, 0.60 mmol, 1.3 equiv.). Purification by FCC (hexanes/DCM 1:1 → DCM) gave **6T** was obtained as a colourless foam (0.23 g, 0.42 mmol, 90%).

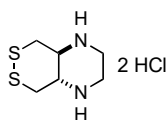
TLC R_f = 0.54 (DCM). **HRMS** (ESI): $C_{18}H_{22}N_5O_8S_4^-$: $[M+NH_4]^+$ calc. m/z 564.0351, found 564.0344. **1H -NMR** (400 MHz, $DMSO-d_6$): δ (ppm) = 8.11 – 8.04 (m, 2H), 8.02 – 7.93 (m, 2H), 7.90 – 7.78 (m, 4H), 4.28 – 4.14 (m, 2H), 3.98 – 3.83 (m, 2H), 3.77 – 3.59 (m, 2H), 3.54 – 3.42 (m, 2H), 3.00 (d, J = 13.0 Hz, 2H). **^{13}C -NMR** (101 MHz, $DMSO-d_6$): δ (ppm) = 147.1 (C_{Ar}), 134.7 (C_{ArH}), 133.0 (C_{ArH}), 129.9 (C_{ArH}), 124.5 (C_{ArH}), 60.8 (CH), 43.2 (CH_2), 38.5 (CH_2).

di-*tert*-butyl hexahydro-[1,2]dithiino[4,5-*b*]pyrazine-1,4-dicarboxylate (*trans*) 18T

Step 1: Following general procedure C, NaOMe (5.4 M in MeOH, 0.7 mL, 4.0 mmol, 2.5 equiv.) was added to a solution of **6T** (0.86 g, 1.6 mmol, 1.0 equiv.) in THF (32 mL, 0.05 M). The reaction mixture was stirred at r.t. for 3 h, and the deprotected amine was then precipitated from the reaction mixture using hydrochloric acid (4.0 M in dioxane, 4.0 mL, 16 mmol, 10 equiv.). The colourless precipitate was collected by filtration, washed with diethyl ether and dried on air.

Step 2: The solids received above were dissolved in a 1:1 mixture of THF (3.0 mL, 0.5 M) and H_2O (3.0 mL, 0.5 M), and triethylamine (1.5 mL, 11 mmol, 7.0 equiv.) was added. The reaction was cooled to 0 °C, Boc_2O (3.5 g, 16 mmol, 10 equiv.) was added and the reaction was allowed to warm to r.t. and stirred overnight. The reaction was quenched by addition of hydrochloric acid (1 M in H_2O), and the pH was adjusted to 3. The aqueous layer was extracted twice with DCM and the combined organic layers were dried over $MgSO_4$, filtered and concentrated. Purification by column chromatography (SiO_2 , hexanes/ $EtOAc$ 20:1 → 6:1) afforded **18T** (0.13 g, 0.36 mmol, 22%) as a colourless solid.

TLC R_f = 0.58 (hexanes: $EtOAc$, 5:1). **LRMS** (ESI): $C_{16}H_{29}N_2O_4S_4^+$: $[M+Na]^+$ calc. m/z 399.1, found 399.1. **1H -NMR** (400 MHz, $CDCl_3$): δ (ppm) = 3.85 (dt, J = 6.8, 1.7 Hz, 2H), 3.65 – 3.51 (m, 4H), 3.53 – 3.40 (m, 2H), 3.26 – 2.99 (m, 2H), 1.45 (s, 18H). **^{13}C -NMR** (101 MHz, $CDCl_3$): δ (ppm) = 155.4, 80.9, 59.6, 41.8, 39.3, 28.5.

SS66T·2 HCl octahydro-[1,2]dithiino[4,5-*b*]pyrazine dihydrochloride (*trans*) 7T

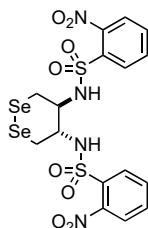
Protocol A: **43** (57 mg, 0.12 mmol, 1.0 equiv.) was dissolved in MeOH (1.0 mL, 0.1 M) and charged with HCl (4 M in dioxane, 0.62 mL, 2.5 mmol, 20 equiv.) at r.t.. The reaction was stirred overnight, upon which full amine- and thiol-deprotection was achieved according to LCMS analysis. The dithiol intermediate was oxidised through addition of a methanolic solution of iodine (0.25 M, 0.5 mL, 0.12 mmol, 1.0 equiv.). The reaction was concentrated to approximately 10% of its volume and was then added to a vigorously stirring solution of HCl in Et_2O (1.0 M, 0.25 mL, 0.25 mmol, 2.0 equiv.). The occurring precipitates were allowed to settle, and the solvent was removed.

The pale-yellow solids were washed with Et₂O giving **7T** without further purification (30 mg, 0.12 mmol, 98%, 100 w% content of **SS66T**·2 HCl).

Protocol B: Closely following **general procedure C**, **6T** (1.9 g, 3.4 mmol, 1.0 equiv.) in THF (40 mL, 0.05 M) was reacted with NaOMe (5.4 M in MeOH, 1.6 mL, 8.6 mmol, 2.5 equiv.) in THF (9.0 mL, 1 M). After quantitative deprotection, the dihydrochloride **7T** was precipitated from the reaction mixture using HCl (4 M in dioxane, 8.6 mL, 34 mmol, 10 equiv.). After filtration, **7T** was isolated as a pale-yellow solid (**SS66T**·2 HCl·2.5 NaCl, 0.83 g, 3.3 mmol, 97%, 63 w% content of **SS66T**·2 HCl).

HRMS (ESI): C₆H₁₃N₂S₂: [M-H]⁺ calc. *m/z* 177.0515, found 177.05162. **¹H-NMR** (400 MHz, D₂O): δ (ppm) = 3.83 – 3.72 (m, 1H), 3.72 – 3.61 (m, 1H), 3.50 – 3.33 (m, 1H), 3.26 – 3.07 (m, 2H). **¹³C-NMR** (101 MHz, D₂O): δ (ppm) = 56.6 (CH), 40.9 (CH₂), 35.6 (CH₂).

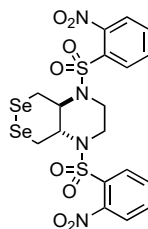
***N,N'*-(1,2-diselenane-4,5-diyl)bis(4-nitrobenzenesulfonamide) (trans) 8T**



3T (6.3 g, 9.7 mmol, 1.0 equiv.) was suspended in acetone (0.02 M, 500 mL) and charged with KSeCN (4.9 g, 34 mmol, 3.5 equiv.) at r.t.. The heterogeneous mixture thickened heavily during the reaction due to precipitation of KOMs, and thus had to be stirred vigorously. LCMS control indicated full conversion to the di-selenocyanate within 2 h, upon which an excess of KSAc (5.6 g, 49 mmol, 5.0 equiv.) was added. The thick, pale-yellow slurry intensified in colour, and full conversion to the diselenane **8T** was achieved within 4 h. The reaction was poured onto ice-cold water (500 mL) and the yellow precipitates were collected through filtration. The solids were washed with water and ether, giving **8T** in excellent purity (5.1 g, 8.3 mmol, 85%).

HRMS (ESI C₁₆H₁₅N₄O₈S₂Se₂⁻: [M-H]⁻ calc. *m/z* 614.86672, found 614.86722. **¹H-NMR** (400 MHz, CDCl₃): δ (ppm) = 8.13 (s, 2H), 8.02 – 7.97 (m, 2H), 7.95 – 7.90 (m, 2H), 7.86 – 7.77 (m, 4H), 3.54 (s, 2H), 3.46 – 3.30 (m, 2H), 3.07 (s, 2H). **¹³C-NMR** (101 MHz, CDCl₃) δ (ppm) = 147.6 (C_{Ar}), 134.6 (C_{Ar}H), 134.0 (C_{Ar}), 133.3 (C_{Ar}H), 130.1 (C_{Ar}H), 125.0 (C_{Ar}H), 55.4 (CH₂), 46.9 (CH₂).

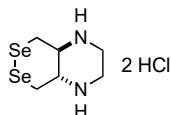
1,4-bis((2-nitrophenyl)sulfonyl)octahydro-[1,2]diselenino[4,5-*b*]pyrazine (trans) 9T



Following **general protocol B**, **8T** (1.0 g, 1.6 mmol, 1.0 equiv.) was dissolved in anhydrous DCM (0.05 M, 30 mL) and reacted with DIPEA (0.97 mL, 5.7 mmol, 3.5 equiv.) and VTT (0.83 g, 2.1 mmol, 1.3 equiv.). Purification by FCC (hexanes/DCM 1:1 → DCM) gave **9T** as a yellow solid (0.60 g, 0.93 mmol, 57%).

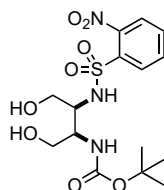
Note: Isolation of clean product proved to be challenging due to the recurring formation of a completely insoluble, yellow residue both during the reaction and after aqueous workup. We can only speculate that this might result from the formation of a diselenide polymer, but based on our practical experience, it is recommended to perform workup and purification, as well as the following deprotection step as quickly as possible.

TLC R_f = 0.45 (DCM). **HRMS** (EI): C₁₈H₁₈N₄O₈S₂Se₂⁺: [M]⁺ calc. *m/z* 641.8891, found 641.8868. **¹H-NMR** (400 MHz, CDCl₃): δ (ppm) = 8.09 – 7.99 (m, 2H), 7.72 – 7.66 (m, 4H), 7.63 (dd, *J* = 7.0, 2.3 Hz, 2H), 4.13 (d, *J* = 9.1 Hz, 2H), 4.03 – 3.90 (m, 2H), 3.83 (dd, *J* = 6.8, 3.9 Hz, 2H), 3.75 (t, *J* = 11.2 Hz, 2H), 3.32 (d, *J* = 12.2 Hz, 2H). **¹³C-NMR** (101 MHz, CDCl₃): δ (ppm) = 134.7, 133.9, 132.3, 131.1, 124.5, 63.8, 44.1, 29.2.

SeSe66T-2 HCl octahydro-[1,2]diselenino[4,5-*b*]pyrazine dihydrochloride (*trans*) 10T

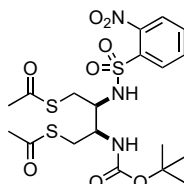
According to **general procedure C**, **9T** (0.59 g, 0.92 mmol, 1.0 equiv.) was dissolved in THF (0.05 M, 20 mL) and reacted with NaOMe (5.4 M in MeOH, 0.43 mL, 2.3 mmol, 2.5 equiv.) in THF (2.5 mL, 1 M). The target dihydrochloride was precipitated from the reaction mixture using HCl (4 M in dioxane, 2.3 mL, 9.2 mmol, 10 equiv.). After filtration, **10T** was isolated as a yellow solid (0.30 g, 0.86 mmol, 93%).

HRMS (ESI): C₆H₁₃N₂Se₂⁺: [M+H]⁺ calc. 270.9412, found 270.9415. **¹H-NMR** (400 MHz, D₂O): δ (ppm) = 3.98 – 3.90 (m, 2H), 3.80 (dd, *J* = 10.1, 2.5 Hz, 2H), 3.65 – 3.51 (m, 6H).

7.2.4 Desymmetrized synthesis of Boc-SS66C-*o*-nosyl***tert*-butyl(1,4-dihydroxy-3-((2-nitrophenyl)sulfonamido)butan-2-yl)carbamate (*cis*) 19**

To solution of 2-nitrobenzenesulfonamide (2.29 g, 11.4 mol, 1.0 equiv.) and iodine (0.29 g, 1.1 mmol, 0.1 equiv.) in MeCN (70 mL) at 0 °C was added *trans*-2-butene-1,4-diol (1.0 g, 11.4 mmol, 1.0 equiv.) and sodium hypochlorite pentahydrate (1.90 g, 11.4 mmol, 1.0 equiv.) with vigorous stirring. The reaction mixture was then allowed to warm to r.t. and was stirred for 16 h. After the solution was cooled down to 0 °C again, *tert*-butyl carbamate (1.99 g, 17.0 mmol, 1.5 equiv.) and sodium hypochlorite pentahydrate (2.80 g, 17.0 mmol, 1.5 equiv.) were added to the reaction mixture and stirring was continued for 2 h at 45 °C. The reaction mixture was washed with brine (100 mL) and the aq. layer was extracted with EtOAc (2×200 mL). The combined organic layers were dried over Na₂SO₄ and concentrated under reduced pressure. The residue was resuspended in DCM (20 mL), filtered and the filtrate was concentrated under reduced pressure to give **19** in satisfying purity as a brownish oil (3.98 g, 9.8 mmol, 86%).

TLC R_f = 0.68 (isohexane:EtOAc, 5:1). **HRMS** (ESI): C₁₅H₂₂N₃O₈S: [M+H]⁺ calc. *m/z* 404.11331, found 404.11311. **¹H-NMR** (400 MHz, CDCl₃): δ (ppm) = 8.16 – 8.03 (m, 1H), 7.96 – 7.82 (m, 1H), 7.82 – 7.65 (m, 2H), 6.36 (d, *J* = 8.9 Hz, 1H), 5.44 (d, *J* = 8.5 Hz, 1H), 4.27 (dd, *J* = 12.1, 2.1 Hz, 1H), 3.70 (dd, *J* = 12.1, 2.9 Hz, 1H), 3.67 – 3.53 (m, 2H), 3.51 – 3.35 (m, 1H), 3.08 (dd, *J* = 12.7, 2.7 Hz, 1H), 1.40 (s, 9H). **¹³C-NMR** (101 MHz, CDCl₃): δ (ppm) = 157.4 (C=O), 148.0 (C_{Ar}), 134.1 (C_{Ar}H), 134.0 (C_{Ar}H), 133.1 (C_{Ar}), 130.7 (C_{Ar}H), 125.8 (C_{Ar}H), 80.9 (C(CH₃)₃), 61.3 (CH₂), 61.0 (CH₂), 55.7 (CH), 51.7 (CH), 28.4 (C(CH₃)₃).

(2-((*tert*-butoxycarbonyl)amino)-3-((2-nitrophenyl)sulfonamido)butane-1,4-diyl) diethanesulfonate (*cis*) 20

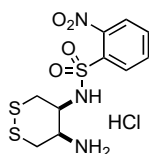
Step 1: Following **general procedure A**, **19** (278 mg, 0.69 mmol, 1.0 equiv.) was dissolved in pyridine (0.14 M, 5 mL) and reacted with MsCl (0.13 mL, 1.71 mmol, 2.5 equiv.). After precipitation from water and washings with Et₂O (*cis*)-2-((*tert*-butoxycarbonyl)amino)-3-((4-nitrophenyl)sulfonamido)butane-1,4-diyl dimethanesulfonate was received as a brownish solid (257 mg, 0.46 mmol, 67%). The intermediate was found to be instable and was directly used without further purification.

TLC R_f = 0.35 (isohexane:EtOAc, 1:2). **HRMS** (ESI): C₁₇H₂₆N₃O₁₂S: [M-H]⁻ calc. *m/z* 560.06841, found 560.06869.

Step 2: KSAc (50.8 mg, 0.45 mmol, 5.0 equiv.) was added to a solution of the material obtained in step 1 (50 mg, 0.09 mmol, 1.0 equiv.) in acetone (110 mL, 0.05 M) and the reaction mixture was stirred at r.t. for 4 h. The reaction mixture was then poured on water (250 mL), washed with brine, and extracted with EtOAc (2×300 mL). The combined organic layers were dried over Na₂SO₄, concentrated, and purified by FCC (isohexane/EtOAc: 4:1 to 0:1) to give **20** as a colourless solid (14.5 mg, 0.03 mmol, 33%).

TLC R_f = 0.34 (isohexane:EtOAc, 2:1). **HRMS** (ESI): C₁₉H₂₆N₃O₈S₃: [M-H]⁻ calc. *m/z* 520.08875, found 520.08891. **¹H-NMR** (400 MHz, CDCl₃): δ (ppm) = 8.17 – 8.10 (m, 1H), 7.96 – 7.87 (m, 1H), 7.85 – 7.70 (m, 2H), 5.98 (d, *J* = 9.2 Hz, 1H), 4.83 (d, *J* = 9.0 Hz, 1H), 3.84 (ddt, *J* = 14.0, 9.2, 5.1 Hz, 1H), 3.73 (tt, *J* = 9.4, 4.7 Hz, 1H), 3.22 (dd, *J* = 14.3, 4.2 Hz, 1H), 3.09 (dd, *J* = 14.2, 5.1 Hz, 1H), 2.99 (td, *J* = 15.5, 14.4, 8.6 Hz, 2H), 2.35 (s, 3H), 2.19 (s, 3H), 1.41 (s, 9H). **¹³C-NMR** (126 MHz, CDCl₃): δ (ppm) = 196.2 (C=O), 195.2 (C=O), 155.8 (C=O), 147.8 (C_{Ar}), 134.9 (C_{Ar}H), 133.7, 133.2 (C_{Ar}), 130.7 (C_{Ar}H), 125.7 (C_{Ar}H), 80.3 (C(CH₃)₃), 57.8 (CH), 54.3 (CH), 30.7 (CH₂), 30.6 (CH₃), 30.5 (CH₃), 30.2 (CH₂), 28.4 (C(CH₃)₃).

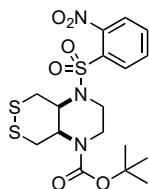
***N*-(5-amino-1,2-dithian-4-yl)-2-nitrobenzenesulfonamide (cis) 21**



20 (209 mg, 0.40 mmol, 1.0 equiv.) was dissolved in MeOH (40 mL, 0.01 M) and a solution of HCl in dioxane (4.0 M, 5.0 mL, 50 equiv.) was added in one portion. The reaction mixture was then stirred for 14 h at 50 °C. After reaching r.t., iodine (10 mg, 0.04 mmol, 0.1 equiv.) was added to the reaction mixture, which was then stirred for additional 4 h. The reaction mixture was concentrated, poured into Et₂O (200 mL), filtered and the precipitate was washed with Et₂O (100 mL) to give **21** as a brownish solid (135 mg, 0.36 mmol, 90%).

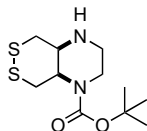
HRMS (ESI): C₁₀H₁₄N₃O₄S₃: [M+H]⁺ calc. *m/z* 336.01409, found 336.01448. **¹H-NMR** (400 MHz, MeOD-*d*₄): δ (ppm) = 8.20 (dt, *J* = 7.5, 3.2 Hz, 1H), 7.95 – 7.82 (m, 3H), 3.91 – 3.83 (m, 1H), 3.61 (dt, *J* = 8.5, 4.1 Hz, 1H), 3.35 (s, 1H), 2.99 (dd, *J* = 14.8, 4.0 Hz, 1H), 2.82 – 2.66 (m, 2H), 2.57 (dd, *J* = 14.5, 8.1 Hz, 1H). **¹³C-NMR** (101 MHz, MeOD-*d*₄): δ (ppm) = 148.0 (C_{Ar}), 134.3 (C_{Ar}H), 133.1 (C_{Ar}), 132.4 (C_{Ar}H), 130.9 (C_{Ar}H), 124.8 (C_{Ar}H), 57.8 (CH), 55.4 (CH), 24.6 (CH₂), 21.7 (CH₂).

***tert*-butyl 4-((2-nitrophenyl)sulfonyl)hexahydro-[1,2]dithiino[4,5-*b*]pyrazine-1(2*H*)-carboxylate (cis) 22**



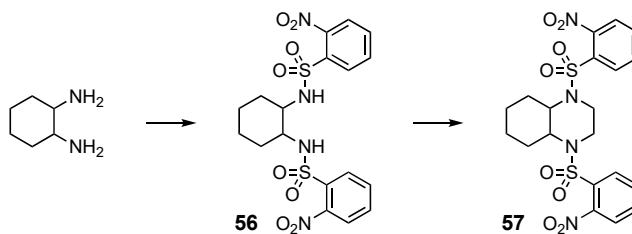
Following **general procedure B**, **21** (112 mg, 0.30 mmol, 1.0 equiv.) was dissolved in anhydrous DCM (60 mL, 0.005 M) and reacted with DIPEA (0.26 mL, 1.50 mmol, 5.0 equiv.) and VTT (178 mg, 0.45 mmol, 1.5 equiv.). Purification by FCC (hexanes/DCM 95:5 to 3:2) gave **22** as a brownish resin (41 mg, 0.09 mmol, 29%).

TLC R_f = 0.69 (isohexane:EtOAc, 1:1). **HRMS** (ESI): C₁₃H₁₆N₃O₆S₃: [M-*tert*-butyl+H]⁺ calc. *m/z* 406.01957, found 406.02012. **¹H-NMR** (400 MHz, CDCl₃): δ (ppm) = 7.84 – 7.77 (m, 1H), 7.55 – 7.41 (m, 3H), 4.01 – 3.91 (m, 2H), 3.63 (dt, *J* = 13.6, 5.6 Hz, 1H), 3.47 – 3.39 (m, 2H), 3.32 (tdd, *J* = 8.6, 7.3, 4.7 Hz, 2H), 3.26 – 3.15 (m, 1H), 2.81 (dd, *J* = 14.7, 2.8 Hz, 1H), 2.67 (dd, *J* = 14.2, 2.7 Hz, 1H), 1.16 (s, 9H). **¹³C-NMR** (101 MHz, CDCl₃): δ (ppm) = 154.4 (C=O), 148.1 (C_{Ar}), 134.3 (C_{Ar}H), 133.4 (C_{Ar}), 132.2 (C_{Ar}H), 130.8 (C_{Ar}H), 124.9 (C_{Ar}H), 81.2 (C(CH₃)₃), 54.2 (CH), 52.6 (CH), 44.2 (CH₂), 41.0 (CH₂), 38.3 (CH₂), 28.4 (C(CH₃)₃).

tert-butyl hexahydro-[1,2]dithiino[4,5-b]pyrazine-1(2H)-carboxylate (cis) 23

22 (41.0 mg, 0.087 mmol, 1.0 equiv.) was dissolved in THF (4.5 mL, 0.02 M). A solution of NaOMe in MeOH (25%, 0.2 mL, 0.88 mmol, 10 equiv.) was added in one portion and the resulting mixture was stirred at r.t. for 1.5 h. The reaction mixture was then concentrated under reduced pressure and purified by FCC (isohexane/EtOAc: 1:1 to 0:1) to yield **23** as a brownish resin (14.0 mg, 0.051 mmol, 59%).

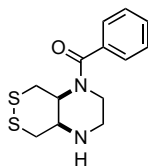
TLC R_f = 0.22 (EtOAc). **HRMS** (ESI): $C_{11}H_{21}N_2O_2S_2$: $[M+H]^+$ calc. m/z 277.10390, found 277.10432. *Two rotameric species with ca. 1:1 ratio were detected by NMR spectroscopy.* **1H -NMR** (800 MHz, MeOD- d_4): δ (ppm) = 4.47 (dd, J = 71.7, 12.0 Hz, 1H), 4.17 – 4.02 (m, 1H), 3.79 (dd, J = 15.3, 5.6 Hz, 1H), 3.62 (dd, J = 15.2, 2.4 Hz, 1H), 3.61 – 3.54 (m, 1H), 3.43 – 3.34 (m, 1H), 3.28 – 3.12 (m, 3H), 2.71 – 2.60 (m, 1H), 1.47 (d, J = 3.0 Hz, 9H). **^{13}C -NMR** (201 MHz, MeOD- d_4): δ (ppm) = 153.8 (C=O), 81.5 ($C(CH_3)_3$), 53.1 (CH), 52.9 (CH), 51.2 (CH), 49.7 (CH), 43.7 (CH₂), 37.9 (CH₂), 36.6 (CH₂), 35.3 (CH₂), 28.0 (CH₂), 27.2 ($C(CH_3)_3$), 27.0 ($C(CH_3)_3$).

7.2.5 reference compounds**1,4-bis((2-nitrophenyl)sulfonyl)decahydroquinoxaline (racemic) 57**

Step 1: Racemic 1,2-diaminocyclohexane (1.0 mL, 8.1 mmol, 1.0 equiv.) was dissolved in pyridine (0.2 M, 80 mL) and cooled to 0 °C. The colourless suspension was charged with *o*-NsCl (4.7 g, 21 mmol, 2.6 equiv.) and the bright yellow solution was stirred for 16 h. Once LCMS-control indicated full conversion of the starting material, the reaction mixture was poured onto ice-cold water (200 mL) and the bright orange precipitates were collected by filtration. The residue was washed with water and ether, giving **56** as an orange solid (3.0 g, 6.2 mmol, 76%) after drying on air.

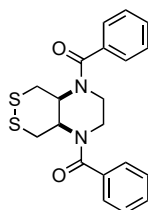
Step 2: Following general protocol B, protected **56** (1.5 g, 3.1 mmol, 1.0 equiv.) in DCM (0.05 M, 60 mL) was reacted with DIPEA (1.8 mL, 11 mmol, 3.5 equiv.) and **VTT** (1.6 g, 4.0 mmol, 1.3 equiv.). Aqueous workup of the dark red reaction mixture and purification via flash column chromatography (hexanes/DCM 1:1 → DCM) gave **57** as a yellow solid (1.2 g, 2.4 mmol, 76%). Deconvolution of NMR signals obtained for pure **57** is tedious due to the presence of rotamers and diastereomers. We therefore simply integrated 1H signals and did not assign protons.

TLC R_f = 0.56 (DCM). **HRMS** (ESI): $C_{14}H_{18}N_3O_4S^+$: $[M-Ns-H_2+H]^+$ calc. m/z 324.1013, found 324.0993. **1H -NMR** (400 MHz, $CDCl_3$): δ (ppm) = 8.16 – 7.91 (m, 2H), 7.91 – 7.48 (m, 6H), 3.99 – 3.87 (m, 1.3H), 3.73 – 3.58 (m, 1.3H), 3.51 – 3.42 (m, 1.4H), 3.42 – 3.24 (m, 2H), 2.30 (p, J = 6.4, 5.8 Hz, 0.6H), 1.96 – 1.85 (m, 1.4H), 1.66 – 1.33 (m, 3.5H), 11.33 – 1.08 (m, 2.5H). **^{13}C -NMR** (101 MHz, $CDCl_3$): δ (ppm) = 148.0 (C_{Ar}), 147.7 (C_{Ar}), 134.9 (C_{ArH}), 132.6 (C_{ArH}), 132.2 (C_{Ar}), 132.1 (C_{Ar}), 130.5 (C_{ArH}), 130.1 (C_{ArH}), 124.6 (C_{ArH}), 124.2 (C_{ArH}), 61.8 (CH), 60.4 (CH), 57.6 (CH₂), 45.7 (CH₂), 44.2 (CH₂), 29.9 (CH₂), 27.9 (CH₂), 24.8 (CH₂), 22.4 (CH₂), 14.2.

H-SS66C-Bz (hexahydro-[1,2]dithiino[4,5-*b*]pyrazin-1(*2H*)-yl)(phenyl)methanone (*cis*) **52C**

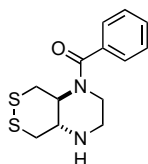
To a solution of **7C** (4.5 mg, 100 w%, 0.018 mmol, 1.0 equiv.) in anhydrous DCM (0.2 mL, 0.01 M) was added DIPEA (6 μ L, 0.04 mmol, 2 equiv.). The mixture was cooled down to 0 °C and a BzCl solution (0.1 M in DCM, 91 μ L, 0.009 mmol, 0.5 equiv.) was added. The reaction mixture was stirred for 15 min at 0 °C, warmed to r.t. and stirred for 45 min. The mixture was then concentrated under reduced pressure and directly purified by preparative HPLC (H₂O/MeCN/FA) to give **52C** (2.5 mg, 0.009 mmol, 50%) as a colourless solid.

TLC R_f = 0.08 (EtOAc). **HRMS** (ESI): C₁₃H₁₇N₂O₂S₂: [M+H]⁺ calc. m/z 281.07768, found 281.07804. *Two rotameric species with ca. 2:1 ratio were detected by NMR spectroscopy.* **¹H-NMR** (800 MHz, MeOD-*d*₄): δ (ppm) = 7.48 (dd, J = 17.6, 8.9 Hz, 3H), 7.40 (d, J = 7.5 Hz, 2H), 4.38 (d, J = 13.6 Hz, 0.3H), 3.91 – 3.82 (m, 0.7H), 3.78 (t, J = 12.7 Hz, 0.7H), 3.56 (d, J = 14.1 Hz, 0.7H), 3.51 – 3.44 (m, 0.7H), 3.38 (d, J = 12.5 Hz, 1H), 3.27 – 3.20 (m, 0.7H), 3.06 (t, J = 14.0 Hz, 1.7H), 2.95 (dd, J = 31.1, 12.5 Hz, 1.3H), 2.67 – 2.59 (m, 0.7H), 2.54 (d, J = 13.1 Hz, 0.3H). **¹³C-NMR** (201 MHz, MeOD-*d*₄): δ (ppm) = 171.5 (C=O), 135.2 (C_{Ar}), 129.9 (C_{Ar}H), 128.7 (C_{Ar}H), 128.4 (C_{Ar}H), 126.6 (C_{Ar}H), 126.1 (C_{Ar}H), 52.9, 52.3 (CH), 50.1 (CH), 44.8 (CH₂), 43.7 (CH₂), 42.9 (CH₂), 40.4 (CH₂), 36.9 (CH₂), 29.4 (CH₂), 28.2 (CH₂).

Bz-SS66C-Bz (hexahydro-[1,2]dithiino[4,5-*b*]pyrazine-1,4-diyl)bis(phenylmethanone) (*cis*) **53C**

To a solution of **7C** (10.0 mg, 0.04 mmol, 1.0 equiv.) in DCM (4.2 mL, 0.01 M) was added DIPEA (21 μ L, 0.12 mmol, 3.0 equiv.). The mixture was cooled down to 0 °C, before BzCl (23 μ L, 0.20 mmol, 5 equiv.) was added. The reaction mixture was stirred for 15 min at 0 °C, warmed to r.t. and stirred for 45 min. The mixture was concentrated under reduced pressure and purified by FCC (isohexane/EtOAc: 3:1 to 0:1) to give **53C** as a brown oil (5.4 mg, 0.014 mmol, 61%).

TLC R_f = 0.32 (isohexane:EtOAc, 1:1). **HRMS** (ESI): C₂₀H₂₁N₂O₂S₂: [M+H]⁺ calc. m/z 385.10390, found 385.10452. **¹H-NMR** (400 MHz, CDCl₃): δ (ppm) = 7.61 – 7.37 (m, 10H), 4.62 (s, 2H), 3.77 (s, 4H), 3.70 (dd, J = 14.3, 7.4 Hz, 2H), 3.23 – 2.97 (m, 2H). **¹³C-NMR** (101 MHz, CDCl₃): δ (ppm) = 172.2 (C=O), 135.4 (C_{Ar}), 130.7 (C_{Ar}H), 129.0 (C_{Ar}H), 127.2 (C_{Ar}H), 51.5 (CH), 45.0 (CH₂), 37.2 (CH₂).

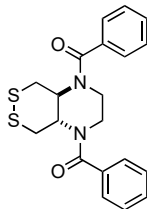
H-SS66T-Bz (hexahydro-[1,2]dithiino[4,5-*b*]pyrazin-1(*2H*)-yl)(phenyl)methanone (*trans*) **52T**

To a solution of **7T** (3.2 mg, 0.013 mmol, 1.0 equiv.) in DCM (0.2 mL, 0.01 M) was added DIPEA (5 μ L, 0.03 mmol, 2 equiv.). The mixture was cooled down to 0 °C and a BzCl solution (0.1 M in DCM, 65 μ L, 0.006 mmol, 0.5 equiv.) was added. The reaction mixture was stirred for 15 min at 0 °C, warmed to r.t. and stirred for 45 min. The mixture was then concentrated under reduced pressure and purified via by preparative HPLC (H₂O/MeCN/FA) to give **52T** as a colourless solid (3.5 mg, 0.013 mmol, 99%).

TLC R_f = 0.08 (EtOAc). **HRMS** (ESI): C₁₃H₁₇N₂O₂S₂: [M+H]⁺ calc. m/z 281.07768, found 281.07791. **¹H-NMR** (800 MHz, MeOD-*d*₄): δ (ppm) = 7.51 – 7.45 (m, 3H), 7.44 – 7.41 (m, 2H), 4.20 (ddd, J = 10.5, 9.2, 4.1 Hz, 1H),

3.64 (ddd, $J = 14.5, 10.9, 6.0$ Hz, 1H), 3.53 (ddd, $J = 14.5, 6.5, 2.0$ Hz, 1H), 3.36 – 3.32 (m, 1H), 3.26 – 3.21 (m, 2H), 3.04 (td, $J = 11.5, 6.6$ Hz, 1H), 3.01 (d, $J = 5.3$ Hz, 1H), 2.99 (s, 1H), 2.98 (d, $J = 1.5$ Hz, 1H). **¹³C-NMR** (201 MHz, MeOD-*d*₄): δ (ppm) = 172.6 (C=O), 135.8 (C_{Ar}), 129.9 (C_{Ar}H), 128.4 (C_{Ar}H), 126.4 (C_{Ar}H), 62.5 (CH), 55.5 (CH), 43.9 (CH₂), 41.1 (CH₂), 39.3 (CH₂), 36.1 (CH₂).

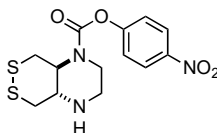
Bz-SS66T-Bz (hexahydro-[1,2]dithiino[4,5-*b*]pyrazine-1,4-diyl)bis(phenylmethanone) (*trans*) **53T**



TLC $R_f = 0.35$ (isohexane:EtOAc, 1:1). To a solution of **7T** (28 mg, 63 w%, 0.07 mmol, 1.0 equiv.) and DIPEA (60 μ L, 0.34 mmol, 4.8 equiv.) in anhydrous DCM (1 mL, 0.07 M) was added BzCl (13 μ L, 0.11 mmol, 1.6 equiv.) in one portion. The mixture was stirred at r.t. for 1 h, was then concentrated under reduced pressure. Purification by FCC (isohexane/EtOAc) gave **53T** as a colourless foam (15 mg, 0.04 mmol, 57%).

HRMS (ESI): C₂₀H₂₁N₂O₂S₂: [M+H]⁺ calc. m/z 385.10390, found 385.10391. **¹H-NMR** (400 MHz, CDCl₃): δ (ppm) = 7.50 – 7.35 (m, 10H), 4.32 (s, 2H), 3.74 (s, 2H), 3.53 (s, 2H), 3.19 (d, $J = 12.4$ Hz, 2H). **¹³C-NMR** (101 MHz, CDCl₃): δ (ppm) = 173.1 (C=O), 135.5 (C_{Ar}), 130.8 (C_{Ar}H), 128.9 (C_{Ar}H), 127.4 (C_{Ar}), 60.2 (CH), 45.9 (CH₂), 38.8 (CH₂).

4-nitrophenyl-hexahydro-[1,2]dithiino[4,5-*b*]pyrazine-1(2H)-carboxylate (*trans*) **54**

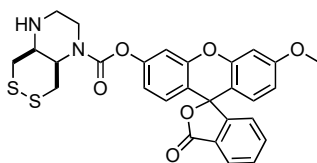


54 (4.3 mg, 0.013 mmol, 8%) was obtained as a side product from the preparation of **44T** (3.6 mg, 0.006 mmol, 4%) from **7T** (39 mg, 63 w%, 0.10 mmol), MF-OH (45 mg, 0.13 mmol) and 4-nitrophenyl chloroformate (39 mg, 0.20 mmol). A sample suitable for single crystal X-Ray spectroscopy was analysed.

TLC $R_f = 0.1$ (EtOAc). **HRMS** (ESI): C₁₃H₁₆N₂O₂S₂: [M+H]⁺ calc. m/z 342.05767, found 342.05779. **¹H-NMR** (400 MHz, CDCl₃): δ (ppm) = 8.26 (d, $J = 9.3$ Hz, 1H), 7.37 – 7.27 (m, 2H), 3.96 (s, 0H), 3.59 (t, $J = 14.7$ Hz, 1H), 3.41 – 3.20 (m, 5H), 3.03 (d, $J = 6.8$ Hz, 2H). **¹³C-NMR** (101 MHz, CDCl₃): δ (ppm) = 155.8 (C=O), 152.8 (C_{Ar}), 145.3 (C_{Ar}), 125.3 (C_{Ar}H), 122.5 (C_{Ar}H), 64.2 (CH), 56.9 (CH₂), 44.5 (CH₂), 40.2 (CH₂), 37.8 (CH₂).

7.3 Probe synthesis

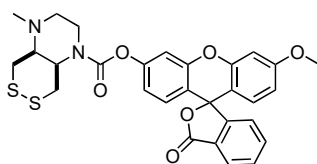
H-SS66C-MF (3'-methoxy-3-oxo-3*H*-spiro[isobenzofuran-1,9'-xanthen]-6'-yl) (*cis*)-hexahydro-[1,2]dithiino[4,5-*b*]pyrazine-1(2*H*)-carboxylate **44C**



Following **general protocol D**, MF-OC(O)Cl was prepared in situ from MF-OH (55.4 mg, 0.16 mmol, 1.0 equiv.). To a solution of **7C** (40.0 mg, 0.16 mmol, 100 w% **SS66C**·2 HCl) and DIPEA (79 μ L, 0.45 mmol, 2.8 equiv.) in anhydrous DCM (8 mL, 0.02 M), was added MF-OC(O)Cl (8 mL, 0.02 M). Purification by FCC (isohexanes:EtOAc 1:1 \rightarrow EtOAc) gave **44C** as a colourless powder (53.0 mg, 0.10 mmol, 62%).

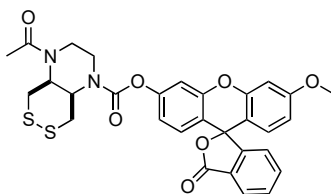
TLC R_f = 0.55 (DCM:MeOH, 9:1). **HRMS** (ESI): $C_{28}H_{25}N_2O_6S_2^+$: $[M+H]^+$ calc. m/z 549.11485, found 549.11458. **¹H-NMR** (400 MHz, $CDCl_3$): δ (ppm) = 8.03 (d, J = 7.4 Hz, 1H), 7.67 (td, J = 7.4, 1.2 Hz, 1H), 7.62 (t, J = 7.2 Hz, 1H), 7.16 (d, J = 7.5 Hz, 1H), 7.11 – 7.04 (m, 1H), 6.83 – 6.75 (m, 3H), 6.70 (d, J = 8.8 Hz, 1H), 6.62 (dd, J = 8.8, 2.5 Hz, 1H), 4.38 (ddt, J = 11.5, 7.9, 3.5 Hz, 1H), 4.08 – 3.92 (m, 1H), 3.64 (dtd, J = 32.4, 12.8, 12.2, 3.4 Hz, 1H), 3.50 (dt, J = 14.0, 2.3 Hz, 1H), 3.39 – 3.29 (m, 1H), 3.27 – 2.93 (m, 4H), 2.64 – 2.52 (m, 1H). **¹³C-NMR** (101 MHz, $CDCl_3$): δ (ppm) = 169.5 (C=O), 161.6 (C=O), 153.2 ($2 \times C_{Ar}$), 152.9 (C_{Ar}), 152.4 (C_{Ar}), 152.0 (C_{Ar}), 135.3 (C_{ArH}), 130.0 (C_{ArH}), 129.2 ($2 \times C_{ArH}$), 126.6 (C_{Ar}), 125.2 (C_{ArH}), 124.2 (C_{ArH}), 117.5 (C_{ArH}), 116.5 (C_{Ar}), 112.0 (C_{ArH}), 111.0 (C_{ArH}), 110.4 (C_{Ar}), 101.0 (C_{ArH}), 82.7 (C_{spiro}), 55.7 (CH_3), 52.9 (CH, *rotamer* 1), 52.6 (CH, *rotamer* 2), 52.4 (CH, *rotamer* 2), 51.9 (CH, *rotamer* 1), 45.3 (CH_2 , *rotamer* 1), 45.1 (CH_2 , *rotamer* 2), 42.2 (CH_2 , *rotamer* 2), 42.0 (CH_2 , *rotamer* 1), 40.9 (CH_2 , *rotamer* 1), 40.1 (CH_2 , *rotamer* 2), 29.8 (CH_2 , *rotamer* 2), 29.0 (CH_2 , *rotamer* 1).

Me-SS66C-MF 3'-methoxy-3-oxo-3*H*-spiro[isobenzofuran-1,9'-xanthen]-6'-yl (*cis*)-4-methylhexahydro-[1,2]dithiino[4,5-*b*]pyrazine-1(2*H*)-carboxylate **45C**



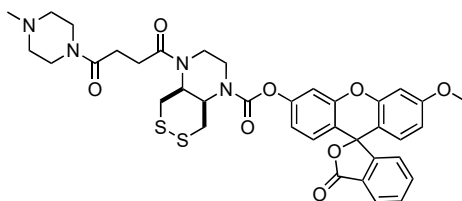
To **44C** (4.0 mg, 0.007 mmol, 1.0 equiv.) in MeOH (1.8 mL, 0.04 M) was added formaldehyde (189 μ L, from 0.88 M in MeOH:H₂O 9:1, 150 mmol, 30 equiv.) and the mixture was stirred at r.t. for 10 min, before NaCNBH₃ (44 μ L, from 0.5 M in MeOH, 3.0 equiv.) was added. The mixture was further stirred for 15 h. The mixture was concentrated under reduced pressure and purified using either FCC (DCM/MeOH) to yield **45C** as a colourless foam (3.3 mg, 0.006 mmol, 86%).

TLC R_f = 0.67 (DCM:MeOH, 9:1). **HRMS** (ESI): $C_{29}H_{27}N_2O_6S_2^+$: $[M+H]^+$ calc. 563.13050, found 563.13047. **¹H-NMR** (400 MHz, $CDCl_3$): δ (ppm) = 8.02 (d, J = 7.5 Hz, 1H), 7.67 (tt, J = 7.5, 1.3 Hz, 1H), 7.62 (t, J = 7.4 Hz, 1H), 7.16 (d, J = 7.6 Hz, 1H), 7.14 – 7.04 (m, 1H), 6.83 – 6.75 (m, 4H), 6.70 (d, J = 8.8 Hz, 1H), 6.63 (dd, J = 8.8, 2.5 Hz, 1H), 4.46 – 4.29 (m, 1H), 4.02 (dd, J = 23.5, 13.0 Hz, 1H), 3.97 – 3.86 (m, 1H), 3.84 (s, 3H), 3.52 – 3.41 (m, 1H), 3.33 (q, J = 14.1, 13.0 Hz, 2H), 2.95 (d, J = 7.7 Hz, 1H), 2.59 – 2.47 (m, 2H), 2.47 – 2.33 (m, 1H), 2.29 (s, 3H). **¹³C-NMR** (101 MHz, $CDCl_3$): δ (ppm) = 169.5 (C=O), 161.6 (C=O), 153.2 (C_{Ar}), 152.8 (C_{Ar}), 152.5 (C_{Ar}), 152.4 (C_{Ar}), 152.0 (C_{Ar}), 135.2 (C_{ArH}), 130.0 (C_{ArH}), 129.2 ($2 \times C_{ArH}$), 126.7 (C_{Ar}), 125.2 (C_{ArH}), 124.2 (C_{ArH}), 117.5 (C_{ArH}), 116.3 (C_{Ar}), 112.0 (C_{ArH}), 111.1 (C_{Ar}), 110.4 (C_{ArH}), 101.0 (C_{ArH}), 82.7 (C_{spiro}), 61.3 (CH), 56.1 (CH_2 , *rotamer* 1), 55.9 (CH_2 , *rotamer* 2), 55.8 (CH_3), 54.7 (CH, *rotamer* 2), 53.8 (CH, *rotamer* 2), 53.6 (CH, *rotamer* 3), 41.8 (CH_3), 40.9 (CH_2 , *rotamer* 1), 40.2 (CH_2 , *rotamer* 2), 39.1 (CH_2 , *rotamer* 1), 38.9 (CH_2 , *rotamer* 2), 30.5 (CH_2 , *rotamer* 1), 29.8 (CH_2 , *rotamer* 2).

Ac-SS66C-MF 3'-methoxy-3-oxo-3*H*-spiro[isobenzofuran-1,9'-xanthen]-6'-yl (*cis*)-4-acetylhexahydro-[1,2]dithiino [4,5-*b*]pyrazine-1(2*H*)-carboxylate **46C**

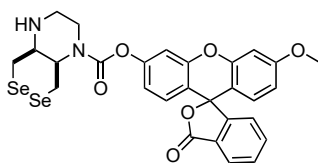
To **44C** (4.0 mg, 0.007 mmol, 1.0 equiv.) in anhydrous DCM (1.5 mL, 0.05 M) was added DIPEA (29 μ L from 0.5 M in DCM, 2.0 equiv.). The mixture was cooled to 0 °C and a solution of AcCl (146 μ L from 0.5 M in DCM, 20.0 equiv.) was added dropwise. The mixture was allowed to warm to r.t. and was further stirred for 1 h, before being concentrated under reduced pressure. Purification by FCC (EtOAc) gave **46C** (4.2 mg, 0.007 mmol, 99%).

TLC R_f = 0.29 (EtOAc). **HRMS** (ESI): $C_{30}H_{27}N_2O_7S_2^+$: $[M+H]^+$ calc. m/z 591.12542, found 591.12511. **1H -NMR** (400 MHz, $CDCl_3$): δ (ppm) = 8.03 (d, J = 7.4 Hz, 1H), 7.67 (t, J = 7.4 Hz, 1H), 7.62 (t, J = 7.3 Hz, 1H), 7.16 (d, J = 7.4 Hz, 1H), 7.11 (s, 1H), 6.85 – 6.74 (m, 3H), 6.70 (d, J = 8.8 Hz, 1H), 6.63 (dd, J = 8.8, 2.3 Hz, 1H), 4.71 (s, 1H), 4.40 (s, 1H), 4.22 (s, 1H), 3.93 – 3.80 (m, 5H), 3.81 – 3.66 (m, 2H), 3.50 (dd, J = 13.8, 9.1 Hz, 1H), 3.22 – 3.12 (m, 1H), 2.98 (d, J = 10.7 Hz, 1H), 2.16 (s, 3H). **^{13}C -NMR** (101 MHz, $CDCl_3$): δ (ppm) = 170.4 (C=O), 169.4 (C=O), 161.6 (C=O), 153.4 (C_{Ar}), 153.1 (C_{Ar}), 152.4 (C_{Ar}), 152.1 (C_{Ar}), 152.1 (C_{Ar}), 135.3 (C_{ArH}), 130.0 (C_{ArH}), 129.2 ($2 \times C_{ArH}$), 126.6 (C_{Ar}), 125.3 (C_{ArH}), 124.2 (C_{ArH}), 117.5 (C_{ArH}), 116.9 (C_{Ar}), 112.1 (C_{ArH}), 111.0 (C_{Ar}), 110.4 (C_{ArH}), 101.0 (C_{ArH}), 82.6 (C_{Spiro}), 55.2 (CH_3), 51.6 (CH), 47.0 (CH_2), 42.0 (CH_2), 37.0 (CH_2), 30.3 (CH_2), 22.0 (CH_3).

P-SS66C-MF 3'-methoxy-3-oxo-3*H*-spiro[isobenzofuran-1,9'-xanthen]-6'-yl (*cis*)-4-(4-(4-methylpiperazin-1-yl)-4-oxobutanoyl)hexahydro-[1,2]dithiino[4,5-*b*]pyrazine-1(2*H*)-carboxylate **47C**

4-(4-methylpiperazin-1-yl)-4-oxobutanoic acid hydrochloride (20.7 mg, 0.088 mmol, 12.0 equiv.) was suspended in anhydrous DCM (1.0 mL, 0.09 M), DIPEA (31 μ L, 0.175 mmol, 24.0 equiv.) and trimethylacetyl chloride (11 μ L, 0.088 mmol, 12.0 equiv.) were added sequentially. The resulting mixture was stirred at r.t. for 2 h, **44C** (4.0 mg, 0.007 mmol, 1.0 equiv.) in 1,2-dichloroethane (1.0 mL, 0.04 M) was added in one portion. The mixture was heated to 70 °C for 15 h, reaction progress was monitored by LCMS analysis. The mixture was concentrated under reduced pressure and purification by preparative HPLC ($H_2O/MeCN/FA$) gave **47C** as a colourless foam (3.4 mg, 0.005 mmol, 71%).

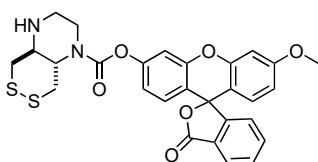
TLC R_f = 0.40 (DCM:MeOH, 9:1). **HRMS** (ESI): $C_{37}H_{39}N_4O_8S_2^+$: $[M+H]^+$ calc. m/z 731.22038, found 731.21939. **1H -NMR** (400 MHz, $CDCl_3$): δ (ppm) = 8.02 (d, J = 7.5 Hz, 1H), 7.71 – 7.65 (m, 1H), 7.62 (t, J = 7.4 Hz, 1H), 7.16 (d, J = 7.5 Hz, 1H), 7.11 (dd, J = 4.3, 2.0 Hz, 1H), 6.87 – 6.75 (m, 3H), 6.70 (dd, J = 8.8, 1.1 Hz, 1H), 6.63 (dd, J = 8.8, 2.5 Hz, 1H), 4.73 (s, 1H), 4.39 (s, 1H), 4.27 (s, 1H), 3.97 (s, 1H), 3.90 (d, J = 10.6 Hz, 1H), 3.84 (s, 3H), 3.77 (s, 2H), 3.63 (s, 2H), 3.59 – 3.50 (m, 2H), 3.52 – 3.41 (m, 1H), 3.17 (d, J = 13.3 Hz, 1H), 2.99 (d, J = 11.1 Hz, 1H), 2.80 – 2.60 (m, 4H), 2.50 – 2.36 (m, 4H), 2.31 (s, 3H). **^{13}C -NMR** (101 MHz, $CDCl_3$): δ (ppm) = 172.2 (C=O), 170.1 (C=O), 169.5 (C=O), 161.6 (C=O), 153.4 (C_{Ar}), 153.2 (C_{Ar}), 152.4 (C_{Ar}), 152.2 (C_{Ar}), 152.0 (C_{Ar}), 135.3 (C_{ArH}), 130.0 (C_{ArH}), 129.2 ($2 \times C_{ArH}$), 126.6 (C_{Ar}), 125.3 (C_{ArH}), 124.2 (C_{ArH}), 123.2 (C_{ArH}), 117.5 (C_{ArH}), 116.8 (C_{Ar}), 112.1 (C_{ArH}), 111.1 (C_{Ar}), 110.5 (C_{ArH}), 101.0 (C_{ArH}), 82.6 (C_{Spiro}), 55.8 (CH_3), 55.0 (CH_2), 54.7 (CH_2), 51.8 (CH), 46.0 (CH_3), 45.2 (CH_2), 41.8 (CH_2), 39.0 (CH), 35.8 (CH_2), 28.2 ($2 \times CH_2$).

H-SeSe66C-MF 3'-methoxy-3-oxo-3*H*-spiro[isobenzofuran-1,9'-xanthen]-6'-yl (*cis*)-hexahydro-[1,2]diselenino[4,5-*b*]pyrazine-1(2*H*)-carboxylate **48C**

Step 1: Closely following **general procedure C**, **9C** (110 mg, 0.171 mmol, 1.0 equiv.) in THF (4 mL, 0.05 M) was reacted with NaOMe (5.4 M in MeOH, 130 μ L, 0.69 mmol, 4.0 equiv.) in THF (0.7 mL, 1 M). After quantitative deprotection, the dihydrochloride was precipitated from the reaction mixture using HCl (4 M in dioxane, 1.4 mL, 1.37 mmol, 8.0 equiv.). After filtration, **SeSe66C-2 HCl** was isolated as a yellow solid (**SeSe66C-2 HCl**·4 NaCl, 99 mg, 0.170 mmol, quant, 65 w% content of **SeSe66C-2 HCl** expected).

Step 2: Following **general protocol D**, MF-OC(O)Cl was prepared *in situ* from MF-OH (56.0 mg, 0.16 mmol, 1.0 equiv.). To a solution of the material obtained in step 1 and DIPEA (57 μ L, 0.32 mmol, 2.0 equiv.) in anhydrous DCM (4 mL, 0.04 M), was added MF-OC(O)Cl (4 mL, 0.04 M). Purification by FCC (isohexanes:EtOAc 1:1 \rightarrow EtOAc) gave **48C** as a colourless powder (10.1 mg, 0.016 mmol, 9% over two steps).

TLC R_f = 0.69 (DCM:MeOH, 9:1). **HRMS** (ESI): $C_{28}H_{25}N_2O_6Se_2^+$: $[M+H]^+$ calc. m/z 645.00376, found 645.00393. **¹H-NMR** (400 MHz, $CDCl_3$): δ (ppm) = 8.02 (d, J = 7.4 Hz, 1H), 7.67 (t, J = 7.4 Hz, 1H), 7.62 (t, J = 7.2 Hz, 1H), 7.16 (d, J = 7.3 Hz, 1H), 7.11 – 7.05 (m, 1H), 6.83 – 6.74 (m, 3H), 6.70 (d, J = 8.8 Hz, 1H), 6.62 (dd, J = 8.8, 2.4 Hz, 1H), 4.41 (ddd, J = 12.3, 9.1, 3.2 Hz, 1H), 4.00 – 3.85 (m, 2H), 3.84 (s, 3H), 3.82 – 3.75 (m, 1H), 3.45 – 3.32 (m, 1H), 3.29 – 2.98 (m, 4H), 2.66 (ddd, J = 11.0, 8.4, 4.9 Hz, 1H). **¹³C-NMR** (101 MHz, $CDCl_3$): δ (ppm) = 169.5 (C=O), 161.6 (C=O), 153.2 (C_{Ar}), 153.0 (C_{Ar}), 152.4 ($2 \times C_{Ar}$), 152.0 (C_{Ar}), 135.2 (C_{ArH}), 130.0 (C_{ArH}), 129.2 ($2 \times C_{ArH}$), 126.6 (C_{Ar}), 125.2 (C_{ArH}), 124.2 (C_{ArH}), 117.5 (C_{ArH}), 116.5 (C_{Ar}), 112.0 (C_{ArH}), 111.0 (C_{Ar}), 110.4 (C_{ArH}), 101.0 (C_{ArH}), 82.7 (C_{spiro}), 55.7 (CH_3), 54.2 (CH, *rotamer 1*), 53.4 (CH, *rotamer 2*), 53.3 (CH, *rotamer 3*), 45.4 (CH_2 , *rotamer 1*), 45.2 (CH_2 , *rotamer 2*), 40.7 (CH_2 , *rotamer 1*), 39.9 (CH_2 , *rotamer 2*), 34.1 (CH_2 , *rotamer 2*), 33.9 (CH_2 , *rotamer 1*), 19.2 (CH_2 , *rotamer 2*), 18.6 (CH_2 , *rotamer 1*).

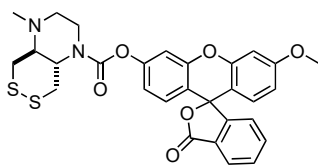
H-SS66T-MF 3'-methoxy-3-oxo-3*H*-spiro[isobenzofuran-1,9'-xanthen]-6'-yl (*trans*)-hexahydro-[1,2]dithiino[4,5-*b*]pyrazine-1(2*H*)-carboxylate **44T**

Following **general protocol D**, MF-OC(O)Cl was prepared *in situ* from MF-OH (0.2 M in DCM, 0.19 mmol, 0.7 equiv.). To a solution of **7T** (0.15 g, 0.28 mmol, 60 w% **SS66C-2 HCl** 5 NaCl) and DIPEA (97 μ L, 0.55 mmol, 2.0 equiv.) in anhydrous DCM (5 mL, 0.05 M), was added MF-OC(O)Cl (1.0 mL, 0.2 M). Purification by FCC (DCM \rightarrow DCM/MeOH 9:1), then preparative HPLC (MeCN/H₂O 10 \rightarrow 100%, 0.3% formic acid) gave **44T** as a colourless yellow powder (31 mg, 57 μ mol, 29%).

TLC R_f = 0.52 (DCM:MeOH, 9:1). **HRMS** (ESI): $C_{28}H_{25}N_2O_6S_2^+$: $[M+H]^+$ calc. m/z 549.11485, found 549.11466. **¹H-NMR** (400 MHz, $CDCl_3$): 8.05 – 8.00 (m, 1H), 7.70 – 7.58 (m, 2H), 7.19 – 7.13 (m, 1H), 7.12 – 7.08 (m, 1H), 6.84 – 6.75 (m, 3H), 6.70 (d, J = 8.8 Hz, 1H), 6.63 (dd, J = 8.8, 2.5 Hz, 1H), 3.91 (ddt, J = 13.1, 6.8, 3.5 Hz, 1H), 3.84 (s, 1H), 3.57 (ddd, J = 14.6, 9.6, 5.6 Hz, 1H), 3.30 – 3.14 (m, 5H), 2.97 – 2.92 (m, 2H). **¹³C-NMR** (101 MHz, $CDCl_3$): δ (ppm) = 169.5, 161.6, 153.5, 153.2, 152.4, 152.0, 135.2, 130.0, 129.2, 126.6, 125.2, 124.2, 117.6, 116.6, 112.1, 111.1, 110.4, 101.0, 82.6, 65.0, 56.9, 55.8, 44.8, 40.6, 37.8.

¹H-NMR (400 MHz, $DMSO-d_6$): δ (ppm) = 8.04 (d, J = 7.6 Hz, 1H), 7.81 (t, J = 7.5 Hz, 1H), 7.75 (td, J = 7.5, 0.8 Hz, 1H), 7.32 (d, J = 7.6 Hz, 1H), 7.27 (t, J = 2.5 Hz, 1H), 6.96 – 6.92 (m, 2H), 6.83 (d, J = 8.7 Hz, 1H), 6.75 (dd, J = 8.8, 2.5 Hz, 1H), 6.71 (dd, J = 8.8, 0.9 Hz, 1H), 3.83 (s, 3H), 3.81 – 3.70 (m, 2H), 3.58 – 3.46 (m, 1H), 3.24 (dd, J = 13.0, 10.7 Hz, 1H), 3.18 – 3.13 (m, 1H), 3.09 – 2.96 (m, 3H), 2.93 (dq, J = 8.2, 3.0 Hz, 1H), 2.83 (dd, J = 13.1, 10.6 Hz, 1H). **¹³C-NMR** (101 MHz, $DMSO-d_6$): δ (ppm) = 168.5 (C=O), 161.2 (C=O), 152.8 (C_{Ar}), 152.5 (C_{Ar}), 152.4 (C_{Ar}), 151.6 (C_{Ar}), 151.0 (C_{Ar}), 135.9 (C_{ArH}), 130.4 (C_{ArH}), 129.1 (C_{ArH}), 128.9 (C_{ArH}), 125.7 (C_{Ar}), 124.9 (C_{ArH}), 124.0 (C_{ArH}), 118.3 (C_{ArH}), 115.9 (C_{Ar}), 112.3 (C_{ArH}), 110.6 (C_{Ar}), 110.2 (C_{ArH}), 100.8 (C_{ArH}), 81.7 (C_{spiro}), 63.9 (CH), 55.8 (CH_3), 55.7 (CH), 43.8 (CH_3), 36.7 (CH_3).

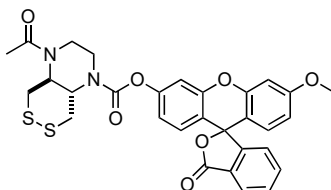
Me-SS66T-MF 3'-methoxy-3-oxo-3*H*-spiro[isobenzofuran-1,9'-xanthen]-6'-yl (trans)-4-methylhexahydro-[1,2]dithiino[4,5-*b*]pyrazine-1(2*H*)-carboxylate **45T**



To **44T** (4.0 mg, 0.007 mmol, 1.0 equiv.) in MeOH (1.5 mL, 0.05 M) was added formaldehyde (250 μ L, from 0.88 M in MeOH:H₂O 9:1, 219 mmol, 40 equiv.) and the mixture was stirred at r.t. for 10 min, before NaCNBH₃ (22 μ L, from 1.0 M in MeOH, 3.0 equiv.) was added. The mixture was further stirred for 1 h. The mixture was concentrated under reduced pressure and purified using either FCC (DCM/MeOH) to yield **45T** as a colourless foam (3.7 mg, 0.006 mmol, 86%).

TLC R_f = 0.53 (DCM:MeOH, 9:1). **HRMS** (ESI): C₂₉H₂₇N₂O₆S₂⁺: [M+H]⁺ calc. m/z 563.13050, found 563.13037. **¹H-NMR** (500 MHz, CDCl₃): δ (ppm) = 8.05 – 7.99 (m, 1H), 7.69 – 7.64 (m, 1H), 7.62 (t, J = 7.4 Hz, 1H), 7.18 – 7.14 (m, 2H), 7.13 – 7.06 (m, 1H), 6.83 – 6.79 (m, 2H), 6.77 (d, J = 2.5 Hz, 1H), 6.70 (d, J = 8.8 Hz, 1H), 6.62 (dd, J = 8.8, 2.5 Hz, 1H), 3.95 (t, J = 10.5 Hz, 1H), 3.91 – 3.86 (m, 1H), 3.84 (s, 3H), 3.68 – 3.53 (m, 1H), 3.41 (t, J = 12.2 Hz, 1H), 3.26 – 3.09 (m, 3H), 2.99 (dd, J = 13.2, 10.6 Hz, 1H), 2.91 – 2.76 (m, 1H), 2.74 – 2.56 (m, 1H), 2.35 (d, J = 1.2 Hz, 3H). **¹³C-NMR** (101 MHz, CDCl₃): δ (ppm) = 169.5 (C=O), 161.6 (C=O), 153.2 (C_{Ar}), 152.4 (C_{Ar}), 152.0 (C_{Ar}), 135.2 (C_{Ar}H), 130.0 (C_{Ar}H), 129.2 (C_{Ar}H), 129.1 (C_{Ar}H), 126.6 (C_{Ar}), 125.2 (C_{Ar}H), 124.2 (C_{Ar}H), 117.6 (C_{Ar}H), 116.6 (C_{Ar}), 112.0 (C_{Ar}H), 111.1 (C_{Ar}), 110.5 (C_{Ar}H), 110.4 (C_{Ar}H), 101.0 (C_{Ar}H), 82.6 (C_{spiro}), 63.5 (CH), 62.6 (CH), 55.7 (CH₃), 55.0 (CH₂), 40.8 (CH₃), 40.5 (CH₂), 38.9 (CH₂), 37.7 (CH₂).

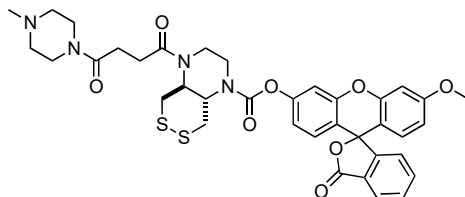
Ac-SS66T-MF 3'-methoxy-3-oxo-3*H*-spiro[isobenzofuran-1,9'-xanthen]-6'-yl (trans)-4-acetylhexahydro-[1,2]dithiino[4,5-*b*]pyrazine-1(2*H*)-carboxylate **46T**



To **44T** (4.0 mg, 0.007 mmol, 1.0 equiv.) in anhydrous DCM (1.5 mL, 0.05 M) was added DIPEA (29 μ L from 0.5 M in DCM, 2.0 equiv.). The mixture was cooled to 0 °C and a solution of AcCl (73 μ L from 0.5 M in DCM, 10.0 equiv.) was added dropwise. The mixture was allowed to warm to r.t. and was further stirred for 1 h, before being concentrated under reduced pressure. Purification by FCC (EtOAc) gave **46T** (4.1 mg, 0.007 mmol, 99%).

TLC R_f = 0.32 (EtOAc). **HRMS** (ESI): C₃₀H₂₇N₂O₇S₂⁺: [M+H]⁺ calc. m/z 591.12542, found 591.12516. **¹H-NMR** (500 MHz, CDCl₃): δ (ppm) = 8.02 (d, J = 7.4 Hz, 1H), 7.72 – 7.59 (m, 2H), 7.16 (d, J = 7.4 Hz, 1H), 7.06 (s, 1H), 6.84 – 6.76 (m, 3H), 6.70 (d, J = 8.7 Hz, 1H), 6.63 (d, J = 8.8 Hz, 1H), 4.75 – 3.98 (m, 4H), 3.84 (s, 3H), 3.73 (d, J = 38.2 Hz, 4H), 3.44 – 2.84 (m, 2H), 2.12 (s, 3H). **¹³C-NMR** (126 MHz, CDCl₃): δ (ppm) = 169.5 (C=O), 161.6 (C=O), 153.2 (C_{Ar}), 152.4 (C_{Ar}), 152.0 (C_{Ar}), 135.3 (C_{Ar}H), 130.0 (C_{Ar}H), 129.2 (C_{Ar}H), 129.2 (C_{Ar}H), 126.6 (C_{Ar}), 125.3 (C_{Ar}H), 124.2 (C_{Ar}H), 117.5 (C_{Ar}H), 116.9 (C_{Ar}), 112.1 (C_{Ar}H), 111.0 (C_{Ar}), 110.5 (C_{Ar}H), 101.0 (C_{Ar}H), 82.6 (C_{spiro}), 60.0 (CH), 55.8 (CH₃), 39.3 (CH₂), 29.8 (CH₂), 27.2 (CH₂), 22.5 (CH₃).

P-SS66T-MF 3'-methoxy-3-oxo-3*H*-spiro[isobenzofuran-1,9'-xanthen]-6'-yl (trans)-4-(4-(4-methylpiperazin-1-yl)-4-oxobutanoyl)hexahydro-[1,2]dithiino[4,5-*b*]pyrazine-1(2*H*)-carboxylate **47T**

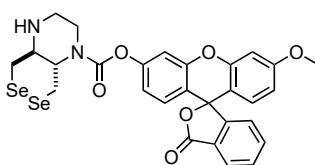


4-(4-methylpiperazin-1-yl)-4-oxobutanoic acid hydrochloride (17.3 mg, 0.073 mmol, 10.0 equiv.) was suspended in anhydrous DCM (1.0 mL, 0.07 M), DIPEA (26 μ L, 0.146 mmol, 20.0 equiv.) and trimethylacetyl chloride (9 μ L,

0.073 mmol, 10.0 equiv.) were added sequentially. The resulting mixture was stirred at r.t. for 2 h, **44T** (4.0 mg, 0.007 mmol, 1.0 equiv.) in 1,2-dichloroethane (1.0 mL, 0.04 M) was added in one portion. The mixture was heated to 70 °C for 15 h, reaction progress was monitored by LCMS analysis. The mixture was concentrated under reduced pressure and purification by preparative HPLC (H₂O/MeCN/FA) gave **47T** as a colourless foam (4.1 mg, 0.006 mmol, 86%).

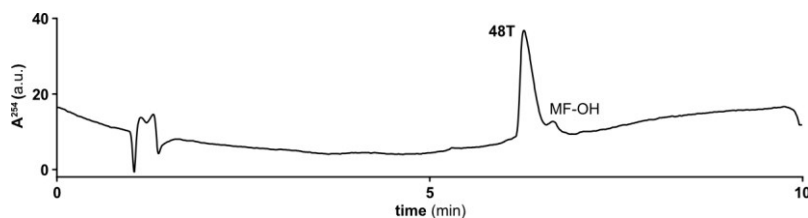
TLC R_f = 0.42 (DCM:MeOH, 9:1). **HRMS** (ESI): C₃₇H₃₉N₄O₈S₂⁺: [M+H]⁺ calc. *m/z* 731.22038, found 731.22017. **¹H-NMR** (500 MHz, CDCl₃): δ (ppm) = 8.02 (d, *J* = 7.5 Hz, 1H), 7.66 (t, *J* = 6.9 Hz, 1H), 7.62 (t, *J* = 7.2 Hz, 1H), 7.20 – 7.11 (m, 2H), 6.84 – 6.74 (m, 3H), 6.70 (d, *J* = 8.8 Hz, 1H), 6.62 (dd, *J* = 8.8, 2.5 Hz, 1H), 4.77 – 4.36 (m, 2H), 4.30 – 3.97 (m, 2H), 3.92 – 3.70 (m, 5H), 3.65 – 3.56 (m, 2H), 3.56 – 3.47 (m, 2H), 3.25 (d, *J* = 49.3 Hz, 3H), 2.94 (d, *J* = 96.9 Hz, 1H), 2.67 (s, 4H), 2.47 – 2.39 (m, 2H), 2.39 – 2.33 (m, 2H), 2.29 (s, 3H). **¹³C-NMR** (126 MHz, CDCl₃): δ (ppm) = 170.0 (C=O), 169.5 (C=O), 161.6 (C=O), 153.3 (C_{Ar}), 152.4 (C_{Ar}), 152.2 (C_{Ar}), 152.0 (C_{Ar}), 135.2 (C_{Ar}H), 130.0 (C_{Ar}H), 129.2 (C_{Ar}H), 129.1 (C_{Ar}H), 126.6 (C_{Ar}), 125.2 (C_{Ar}H), 124.2 (C_{Ar}H), 117.6 (C_{Ar}H), 116.7 (C_{Ar}H), 112.0 (C_{Ar}H), 111.1 (C_{Ar}), 110.5 (C_{Ar}H), 101.0 (C_{Ar}H), 82.6 (C_{spiro}), 59.8 (CH), 55.7 (CH₃), 55.0 (CH₂), 54.7 (CH₂), 46.1 (CH₃), 45.2 (CH₂), 41.8 (CH₂), 38.5 (CH₂), 28.3 (CH₂).

H-SeSe66T-MF 3'-methoxy-3-oxo-3H-spiro[isobenzofuran-1,9'-xanthen]-6'-yl (*trans*)-hexahydro-[1,2]diselenino[4,5-*b*]pyrazine-1(2H)-carboxylate **48T**



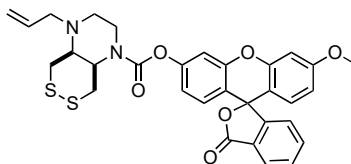
According to **general protocol D**, a solution of MF-OC(O)Cl in DCM (0.2 M, 0.86 mL, 0.17 mmol, 1.0 equiv.) was prepared from MF-OH. To this, a solution of **10T** (109 mg, 0.172 mmol, 65 w%) and DIPEA (60 μL, 0.34 mmol, 2.0 equiv.) in DCM (4 mL, 0.05 M), was added. Purification by first FCC (DCM → DCM/MeOH 9:1) then preparative HPLC (H₂O/MeCN/FA) gave **48T** as a pale yellow powder (10 mg, 0.016 mmol, 9% over two steps).

Note: 48T proved to be very unstable and readily degraded when kept in organic solution, presumably via strain-promoted polymerisation. We thus were not able to perform NMR characterisation and instead ran an HPLC measurement to confirm purity after preparative HPLC. We accepted remaining free MF-OH as "higher baseline" impurity in order to prevent further degradation during additional purification steps.



TLC R_f = 0.65 (DCM/MeOH 9:1). **HRMS** (ESI): C₂₈H₂₅N₂O₆Se₂⁺: [M+H]⁺ calc. *m/z* 645.00376, found 645.00382.

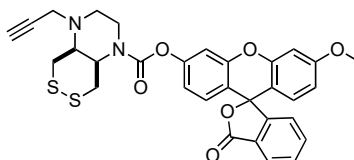
Allyl-SS66C-MF 3'-methoxy-3-oxo-3H-spiro[isobenzofuran-1,9'-xanthen]-6'-yl (*cis*)-4-allylhexahydro[1,2]dithiino[4,5-*b*]pyrazine-1(2H)-carboxylate **51**



A mixture of **44C** (26.5 mg, 0.048 mmol, 1.0 equiv.) and Na₂CO₃ (16.4 mg, 0.155 mmol, 3.2 equiv.) in THF (1 mL, 0.5 M) was cooled down to 0 °C. Allyl bromide (42 μL, 0.48 mmol, 10 equiv.) was added dropwise to the solution and the reaction mixture was stirred at r.t. for 44 h. After removing the solvent under reduced pressure, the residue was resuspended in DCM (5 mL), washed with brine and dried over Na₂SO₄. The organic layer was concentrated and purified by FCC (isohexane/EtOAc: 9:1 to 1:1) to give **51** (25.0 mg, 0.043 mmol, 90%) as a colourless oil.

TLC R_f = 0.80 (isohexane:EtOAc, 1:1). **HRMS** (ESI): $C_{31}H_{29}N_2O_6S_2^+$: $[M+H]^+$ calc. m/z 589.14615, found 589.14714. **1H -NMR** (400 MHz, CD_2Cl_2): δ (ppm) = 7.93 (d, J = 7.7 Hz, 1H), 7.67 – 7.60 (m, 1H), 7.57 (t, J = 7.5 Hz, 1H), 7.11 (dd, J = 7.6, 0.8 Hz, 1H), 7.01 (d, J = 9.3 Hz, 1H), 6.78 – 6.68 (m, 3H), 6.63 (d, J = 8.8 Hz, 1H), 6.56 (dd, J = 8.8, 2.5 Hz, 1H), 5.89 – 5.80 (m, 1H), 5.20 – 5.10 (m, 2H), 4.25 (dd, J = 73.2, 10.2 Hz, 1H), 3.98 – 3.78 (m, 2H), 3.41 – 3.26 (m, 2H), 3.21 (d, J = 15.1 Hz, 1H), 2.94 (dd, J = 14.2, 8.0 Hz, 1H), 2.89 (d, J = 11.9 Hz, 1H), 2.73 (d, J = 22.8 Hz, 1H), 2.48 – 2.34 (m, 1H). **^{13}C -NMR** (101 MHz, $CDCl_3$): δ (ppm) = 169.4 (C=O), 161.6 (C_{Ar}), 153.0 (C_{Ar}), 152.3 (C_{Ar}), 152.0 (C_{Ar}), 135.3 (C_{ArH}), 133.5 (C_{Ar}), 130.1 (C_{ArH}), 129.2 (C_{ArH}), 129.2 (C_{ArH}), 126.6 (C_{Ar}), 125.3 (C_{ArH}), 124.2 (C_{ArH}), 117.4 (C_{ArH}), 112.1 (C_{ArH}), 110.9 (C_{Ar}), 110.4 (C_{ArH}), 101.0 (C_{ArH}), 83.0, 82.6 (C_{spiro}), 79.9, 71.6, 55.8 (CH_3), 55.1, 55.0, 52.0, 46.5, 42.1, 40.9, 37.0, 35.5, 32.0, 29.8, 29.5, 29.3, 28.4, 27.2, 25.9, 25.1, 24.0, 22.8, 22.8, 20.9, 17.6, 17.4, 14.8, 14.3, 14.2.

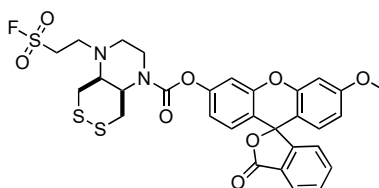
Propynyl-SS66C-MF 3'-methoxy-3-oxo-3*H*-spiro[isobenzofuran-1,9'-xanthen]-6'-yl (cis)-4-(prop-2-yn-1-yl)hexahydro-[1,2]dithiino[4,5-*b*]pyrazine-1(2*H*)-carboxylate **11**



To a mixture of **44C** (5.0 mg, 0.009 mmol, 1.0 equiv.) and K_2CO_3 (3.8 mg, 0.027 mmol, 3.0 equiv.) in DMF (0.25 mL, 0.04 M) was added allyl bromide (5 μ L, 0.05 mmol, 5 equiv.). The reaction mixture was stirred at r.t. for 4 h. Purification by preparative HPLC ($H_2O/MeCN/FA$) gave **11** (3.2 mg, 0.005 mmol, 56%) as a colourless solid.

TLC R_f = 0.68 (isohexane:EtOAc, 1:1). **HRMS** (ESI): $C_{31}H_{27}N_2O_6S_2^+$: $[M+H]^+$ calc. m/z 587.13050, found 587.13261. *Multiple rotameric species were observed by NMR spectroscopy at 298 K. All NMR signals are given without specific assignment to each of the rotamers.* **1H -NMR** (800 MHz, $CDCl_3$): δ (ppm) = 8.63 (s, 1H), 8.03 (d, J = 7.7 Hz, 1H), 7.74 – 7.65 (m, 1H), 7.62 (t, J = 7.5 Hz, 1H), 7.33 – 7.28 (m, 1H), 7.21 – 7.12 (m, 1H), 7.11 – 7.03 (m, 1H), 6.85 – 6.74 (m, 3H), 6.70 (d, J = 8.8 Hz, 1H), 6.63 (dd, J = 8.8, 2.1 Hz, 1H), 4.45 – 4.36 (m, 1H), 4.06 (dd, J = 40.9, 12.3 Hz, 1H), 3.94 – 3.77 (m, 4H), 3.76 – 3.68 (m, 1H), 3.49 – 3.27 (m, 4H), 3.02 – 2.93 (m, 1H), 2.88 (dqt, J = 16.0, 8.0, 3.4 Hz, 1H), 2.79 (t, J = 10.4 Hz, 1H), 2.55 – 2.47 (m, 1H), 2.32 – 2.23 (m, 1H). **^{13}C -NMR** (201 MHz, $CDCl_3$): δ (ppm) = 169.5 (C=O), 161.6 (C_{Ar}), 153.2 (C_{Ar}), 153.2 (C_{Ar}), 153.2 (C_{Ar}), 152.8 (C_{Ar}), 152.7 (C_{Ar}), 152.7 (C_{Ar}), 152.5 (C_{Ar}), 152.4 (C_{Ar}), 152.4 (C_{Ar}), 152.4 (C_{Ar}), 152.0 (C_{Ar}), 152.0 (C_{Ar}), 150.0 ($C\equiv CH$), 136.1 (C_{Ar}), 135.2 (C_{ArH}), 130.0 (C_{ArH}), 129.2 (C_{ArH}), 129.2 (C_{ArH}), 129.1 (C_{ArH}), 129.1 (C_{ArH}), 126.7, 126.6, 126.6, 125.2 (C_{ArH}), 124.2 (C_{ArH}), 123.9 (C_{ArH}), 117.6 (C_{ArH}), 117.5 (C_{ArH}), 117.5 (C_{ArH}), 117.5 (C_{ArH}), 116.7 (C_{Ar}), 116.6 (C_{Ar}), 116.5 (C_{Ar}), 116.5 (C_{Ar}), 112.0 (C_{ArH}), 111.1 (C_{Ar}), 110.5 (C_{ArH}), 110.4 (C_{ArH}), 110.4 (C_{ArH}), 110.4 (C_{ArH}), 110.3 (C_{ArH}), 101.0 (C_{ArH}), 82.7 (C_{spiro}), 82.6 (C_{spiro}), 76.1 (CH_2), 74.6 (CH_2), 56.4 (CH), 56.4 (CH), 56.2 (CH), 56.2 (CH), 55.8 (CH_3), 54.7 (CH), 53.7 (CH), 52.2 (CH_2), 52.1 (CH_2), 41.8 (CH_2), 41.8 (CH_2), 40.6 (CH_2), 39.9 (CH_2), 38.4 (CH_2), 38.2 (CH_2), 30.3 (CH_2), 29.5 (CH_2).

ESF-SS66C-MF 3'-methoxy-3-oxo-3*H*-spiro[isobenzofuran-1,9'-xanthen]-6'-yl (cis)-4-(2-(fluorosulfonyl)ethyl)hexahydro-[1,2]dithiino[4,5-*b*]pyrazine-1(2*H*)-carboxylate **12**

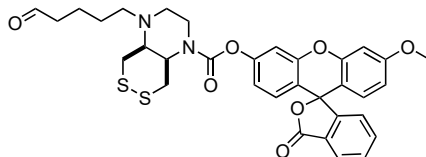


To a suspension of **44C** (5.0 mg, 0.009 mmol, 1.0 equiv.) in DCM (1.0 mL, 0.01 M) at r.t. was added ethenesulfonyl fluoride (42 μ L, 0.50 mmol, 55 equiv.) and DIPEA (7 μ L, 0.04 mmol, 4.5 equiv.). The reaction mixture was stirred at r.t. for 1 h, concentrated using a nitrogen stream, diluted with MeCN (2 mL) and directly purified preparative HPLC ($H_2O/MeCN/FA$) to give **12** (4.2 mg, 0.006 mmol, 67%) was obtained as a colourless solid.

TLC R_f = 0.43 (isohexane:EtOAc, 1:1). **HRMS** (ESI): $C_{30}H_{28}FN_2O_8S_3^+$: $[M+H]^+$ calc. m/z 659.09863, found 659.10126. **1H -NMR** (600 MHz, $CDCl_3$): δ (ppm) 8.03 (d, J = 7.6 Hz, 1H), 7.67 (tt, J = 7.5, 1.4 Hz, 1H), 7.65 – 7.59 (m, 1H), 7.16 (dd, J = 7.6, 1.1 Hz, 1H), 7.08 (d, J = 5.4 Hz, 1H), 6.82 – 6.75 (m, 3H), 6.70 (dd, J = 8.8, 1.0 Hz, 1H), 6.63 (dd, J = 8.8, 2.5 Hz, 1H), 4.41 (s, 1H), 4.08 (t, J = 20.5 Hz, 1H), 3.97 – 3.90 (m, 1H), 3.84 (s, 3H), 3.71 – 3.62 (m, 1H), 3.56 (ddt, J = 14.1, 9.0, 4.2 Hz, 1H), 3.44 – 3.35 (m, 2H), 3.31 (s, 2H), 3.05 (s, 1H), 3.01 (d, J = 11.5 Hz, 1H), 2.93 (s, 1H), 2.62 (s, 1H), 2.49 (dd, J = 12.9, 3.3 Hz, 1H). **^{13}C -NMR** (201 MHz, $CDCl_3$): δ (ppm) = 169.3 (C=O), 161.5 (C_{Ar}), 153.0 (C_{Ar}), 152.5 (C_{Ar}), 152.3 (C_{Ar}), 151.9 (C_{Ar}), 135.1 (C_{ArH}), 129.9 (C_{ArH}), 129.1 (C_{ArH}),

126.5, 125.1 (C_{Ar}H), 124.0 (C_{Ar}H), 117.3 (C_{Ar}H), 111.9 (C_{Ar}H), 110.9 (C_{Ar}), 110.2 (C_{Ar}H), 100.9 (C_{Ar}H), 82.5 (C_{spiro}), 58.1 (CH), 55.6 (CH₃), 54.9, 53.9 (CH), 52.0 (CH₂, *rotamer* 1), 51.8 (CH₂, *rotamer* 2), 47.1 (CH₂, *rotamer* 1), 47.0 (CH₂, *rotamer* 2), 45.3 (CH₂), 40.5 (CH₂), 39.8 (CH₂), 38.1 (CH₂), 30.2 (CH₂), 29.7 (CH₂).

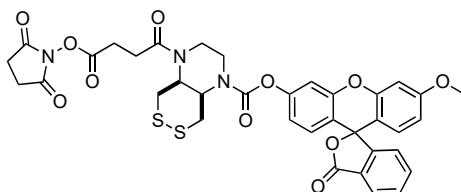
COH-SS66C-MF 3'-methoxy-3-oxo-3*H*-spiro[isobenzofuran-1,9'-xanthen]-6'-yl (*cis*)-4-(5-oxopentyl) hexahydro-[1,2]dithiino[4,5-*b*]pyrazine-1(2*H*)-carboxylate **13**



To a solution of aqueous glyoxal (24%, 0.36 mL, 0.91 mmol, 100 equiv.) and MeOH (3 mL) at r.t. was added dropwise a methanolic solution of **44C** (0.006 M, 1.5 mL, 0.009 mmol, 1.0 equiv.). After 15 min of stirring, a methanolic solution of NaCNBH₃ (0.06 M, 1.5 mL, 0.009 mmol, 1.0 equiv.) was added and the mixture was stirred for additional 30 min. The reaction mixture was concentrated using a nitrogen stream and directly purified preparative HPLC (H₂O/MeCN/FA) to give **13** (4.7 mg, 0.007 mmol, 78%) as a colourless solid.

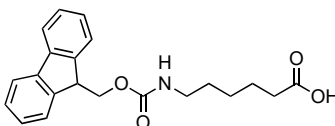
TLC R_f = 0.48 (isohexane:EtOAc, 3:1). **HRMS** (ESI): C₃₃H₃₃N₂O₇S₂⁺: [M+H]⁺ calc. *m/z* 633.17237, found 633.17456. *Multiple rotameric species were observed by NMR spectroscopy at 298 K. All NMR signals are given without specific assignment to each of the rotamers.* **¹H-NMR** (800 MHz, DMSO-*d*₆): δ (ppm) 9.68 (s, 1H), 9.67 – 9.64 (m, 1H), 8.04 (d, *J* = 7.7 Hz, 1H), 7.81 (t, *J* = 7.5 Hz, 1H), 7.75 (t, *J* = 7.5 Hz, 1H), 7.32 (d, *J* = 7.5 Hz, 1H), 7.28 (d, *J* = 39.2 Hz, 1H), 6.93 (d, *J* = 14.8 Hz, 2H), 6.82 (d, *J* = 8.7 Hz, 1H), 6.75 (dd, *J* = 8.8, 2.5 Hz, 1H), 6.70 (d, *J* = 9.4 Hz, 1H), 4.99 – 4.89 (m, 1H), 4.31 – 4.10 (m, 1H), 3.95 – 3.88 (m, 1H), 3.83 (s, 3H), 3.79 – 3.73 (m, 1H), 2.95 (t, *J* = 12.3 Hz, 1H), 2.69 (ddd, *J* = 12.8, 9.4, 6.4 Hz, 1H), 2.36 – 2.17 (m, 2H), 1.83 – 1.68 (m, 1H), 1.61 – 1.51 (m, 4H), 1.50 – 1.45 (m, 3H), 1.40 – 1.32 (m, 1H). **¹³C-NMR** (201 MHz, DMSO-*d*₆): δ (ppm) = 203.7 (C=O), 203.4 (C=O), 203.3 (C=O), 168.6 (C=O), 161.2 (C_{Ar}), 152.5 (C_{Ar}), 152.4 (C_{Ar}), 152.1 (C_{Ar}), 151.6 (C_{Ar}), 151.0 (C_{Ar}), 135.9 (C_{Ar}H), 130.4 (C_{Ar}H), 129.1 (C_{Ar}H), 128.8 (C_{Ar}H), 125.7 (C_{Ar}H), 124.9, 124.0 (C_{Ar}H), 118.6 (C_{Ar}H), 118.2 (C_{Ar}H), 116.0 (C_{Ar}), 115.9 (C_{Ar}), 112.4 (C_{Ar}H), 110.6 (C_{Ar}H), 110.1 (C_{Ar}H), 100.8 (C_{Ar}H), 100.2, 99.4, 97.0, 90.4, 81.8 (C_{spiro}), 68.1 (CH), 57.7 (CH), 57.7 (CH), 55.8 (CH₃), 54.6 (CH), 53.8 (CH), 50.5 (CH₂), 50.4 (CH₂), 50.2 (CH₂), 42.9 (CH₂), 40.6 (CH₂), 37.8 (CH₂), 33.8 (CH₂), 33.1 (CH₂), 33.0 (CH₂), 27.9 (CH₂), 26.8 (CH₂), 25.6 (CH₂), 23.1 (CH₂), 19.4 (CH₂), 18.3 (CH₂), 17.7 (CH₂), 15.9 (CH₂), 15.8 (CH₂).

NHS-SS66C-MF 3'-methoxy-3-oxo-3*H*-spiro[isobenzofuran-1,9'-xanthen]-6'-yl (*cis*)-4-(4-((2,5-dioxopyrrolidin-1-yl)oxy)-4-oxobutanoyl)hexahydro-[1,2]dithiino[4,5-*b*]pyrazine-1(2*H*)-carboxylate **14**



To a solution of **44C** (5.0 mg, 0.009 mmol, 1.0 equiv.) and DIPEA (8 μL, 0.05 mmol, 5 equiv.) in DMF (0.25 mL, 0.04 M) at r.t. was added DMAP (1 mg, 0.01 mmol, 1 equiv.) and a solution of succinic anhydride (20 μL, 0.05 mmol, 5.0 equiv., in DMF). After 2.5 h, the reaction mixture was heated to 60 °C and then stirred for 15 h. TSTU (34.2 mg, 0.11 mmol, 13 equiv.) in 1 mL DMF was added and the resulting mixture was stirred at 60 °C for 6 h. Purification of the reaction mixture by preparative HPLC (H₂O/MeCN/FA) gave **14** (1.7 mg, 0.002 mmol, 22%) as a colourless solid.

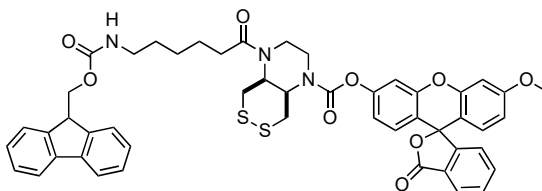
TLC R_f = 0.25 (DCM:MeOH, 98:2). **HRMS** (ESI): C₃₆H₃₂N₃O₁₁S₂⁺: [M+H]⁺ calc. *m/z* 746.14728, found 746.15118. **¹H-NMR** (800 MHz, CDCl₃): δ (ppm) 8.03 (dt, *J* = 7.6, 1.0 Hz, 1H), 7.67 (tdd, *J* = 7.5, 2.7, 1.2 Hz, 1H), 7.63 (tt, *J* = 7.4, 1.1 Hz, 1H), 7.18 – 7.15 (m, 1H), 7.11 (dd, *J* = 6.1, 1.9 Hz, 1H), 6.84 – 6.79 (m, 2H), 6.77 (dd, *J* = 2.5, 1.2 Hz, 1H), 6.70 (dd, *J* = 8.8, 1.7 Hz, 1H), 6.63 (dd, *J* = 8.8, 2.5 Hz, 1H), 4.40 (s, 1H), 4.25 (s, 1H), 3.89 (s, 2H), 3.84 (s, 3H), 3.81 – 3.63 (m, 3H), 3.17 (d, *J* = 14.5 Hz, 1H), 3.03 (qd, *J* = 6.6, 2.4 Hz, 2H), 2.98 (d, *J* = 13.0 Hz, 1H), 2.90 – 2.68 (m, 8H). **¹³C-NMR** (201 MHz, CDCl₃): δ (ppm) = 169.8 (C=O), 169.3 (C=O), 168.9 (C=O), 168.2 (C=O), 161.5 (C_{Ar}), 153.2 (C_{Ar}), 153.0 (C_{Ar}), 152.3 (C_{Ar}), 152.0 (C_{Ar}), 151.9 (C_{Ar}), 151.9 (C_{Ar}), 135.2 (C_{Ar}H), 129.9 (C_{Ar}H), 129.1 (C_{Ar}H), 129.1 (C_{Ar}H), 126.5 (C_{Ar}), 125.1 (C_{Ar}H), 124.0 (C_{Ar}H), 117.4 (C_{Ar}), 116.7 (C_{Ar}H), 112.0 (C_{Ar}H), 110.9 (C_{Ar}), 110.3 (C_{Ar}H), 100.9 (C_{Ar}H), 82.5 (C_{spiro}), 68.0 (CH₂), 55.6 (CH₃), 51.4 (CH), 42.6 (CH₂), 41.9 (CH₂), 36.0 (CH₂), 28.2 (CH₂), 26.7 (CH₂), 25.6 (CH₂).

6-((((9H-fluoren-9-yl)methoxy)carbonyl)amino)hexanoic acid (*N*-Fmoc-hexanoic acid) **58**

6-amino-hexanoic acid (1.06 g, 8.1 mmol) was dissolved in a dioxane:H₂O mixture (3:2, 20 mL, 0.1 M) and Na₂CO₃ (2.15 g, 20.3 mmol, 2.5 equiv.) was added as a solid. Fmoc-Cl (2.31 g, 8.9 mmol, 1.1 equiv.) was added portion-wise and the resulting mixture was stirred at r.t. for 12 h. The mixture was extracted with Et₂O (3×10 mL) and the aqueous phase was acidified using 6 M aq. HCl. A solid precipitate was observed, which was filtered off, washed with water (40 mL) and dried to obtain **58** as a colourless solid (2.79 g, 7.9 mmol, 98%). *The analytical data matched literature reports.*¹⁷

TLC R_f = 0.69 (EA). **¹H-NMR** (400 MHz, MeOD-*d*₄): δ (ppm) = 7.79 (d, *J* = 7.5 Hz, 1H), 7.64 (d, *J* = 7.4 Hz, 1H), 7.38 (t, *J* = 7.4 Hz, 1H), 7.30 (t, *J* = 7.3 Hz, 1H), 4.34 (d, *J* = 6.9 Hz, 1H), 4.19 (t, *J* = 6.8 Hz, 0H), 2.28 (td, *J* = 7.3, 4.1 Hz, 1H), 1.67 – 1.56 (m, 1H), 1.50 (p, *J* = 7.2 Hz, 1H), 1.34 (p, *J* = 7.4, 6.7 Hz, 1H). **¹³C-NMR** (101 MHz, MeOD-*d*₄): δ (ppm) = 176.9, 158.3, 144.7, 142.0, 128.1, 127.5, 125.5, 120.3, 66.9, 40.9, 34.2, 29.9, 26.7, 25.1.

FmocNH-SS66C-MF 3'-methoxy-3-oxo-3*H*-spiro[isobenzofuran-1,9'-xanthen]-6'-yl (*cis*)-4-(6-((((9*H*-fluoren-9-yl)methoxy)carbonyl)amino)hexanoyl)hexahydro-[1,2]dithiino[4,5-*b*]pyrazine-1(2*H*)-carboxylate **15C**

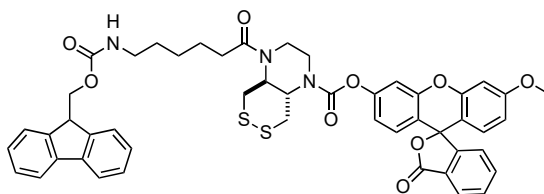


Step 1: *N*-Fmoc-hexanoic acid (105 mg, 0.297 mmol) was dissolved in anhydrous DCM (0.06 M, 6 mL) and oxalyl chloride (76 μL, 0.89 mmol, 3.0 equiv.) was added, followed by dimethylformamide (11.5 μL, 0.15 mmol, 0.5 equiv.). The mixture was stirred at r.t. for 1 h, was then concentrated under reduced pressure to obtain *N*-Fmoc-hexanoyl chloride as a colourless solid. The material was used for further coupling without further purification and analysis assuming quantitative activation. Yields were calculated referring to the *N*-Fmoc-hexanoic acid precursor.

Step 2: **44C** (10.0 mg, 18 μmol) was dissolved in anhydrous DCM (0.02 M, 0.9 mL) and DIPEA (15 μL, 91 μmol, 5.0 equiv.) was added at 0 °C. To the mixture was added a solution of *N*-Fmoc-hexanoyl chloride (0.04 M, 0.9 mL) activated from *N*-Fmoc-hexanoic acid **53** (12.9 mg, 36.5 μmol, 2.0 equiv.) using (COCl)₂/DMF and the reaction mixture was warmed and further stirred at r.t. for 1 h. Purification was achieved using FCC (isohexane/EtOAc) to give **15C** as a colourless solid (6.0 mg, 6.8 μmol, 37%).

TLC R_f = 0.79 (EA). **¹H-NMR** (400 MHz, CDCl₃): δ (ppm) = 9.06 (s, 1H), 8.03 (d, *J* = 7.5 Hz, 1H), 7.78 (d, *J* = 7.6 Hz, 2H), 7.67 (t, *J* = 7.4 Hz, 1H), 7.62 (t, *J* = 7.3 Hz, 1H), 7.54 (d, *J* = 7.4 Hz, 2H), 7.42 (t, *J* = 7.4 Hz, 2H), 7.33 (t, *J* = 7.4 Hz, 2H), 7.16 (d, *J* = 7.4 Hz, 1H), 7.10 (s, 1H), 6.80 (s, 2H), 6.77 (s, 1H), 6.70 (d, *J* = 8.8 Hz, 1H), 6.63 (dd, *J* = 8.8, 2.3 Hz, 1H), 4.72 (d, *J* = 5.6 Hz, 2H), 4.38 (s, 1H), 4.29 (t, *J* = 5.5 Hz, 1H), 4.19 (s, 1H), 3.86 (s, 1H), 3.84 (s, 3H), 3.73 (s, 1H), 3.57 – 3.37 (m, 3H), 3.21 – 2.91 (m, 1H), 2.43 – 2.20 (m, 2H), 1.71 (s, 1H), 1.68 – 1.54 (m, 2H), 1.45 – 1.30 (m, 2H), 1.26 – 1.03 (m, 4H). **¹³C-NMR** (101 MHz, CDCl₃): δ (ppm) = 169.5 (C=O), 162.7 (C=O), 161.6 (C=O), 154.1 (C_{Ar}), 153.2 (C_{Ar}), 152.4 (C_{Ar}), 152.2 (C_{Ar}), 143.2 (C_{Ar}), 141.6 (C_{Ar}), 135.3 (C_{Ar}H), 130.0 (C_{Ar}H), 129.2 (C_{Ar}H), 128.2 (C_{Ar}H), 127.5 (C_{Ar}H), 126.6 (C_{Ar}), 125.3 (C_{Ar}H), 124.7 (C_{Ar}H), 124.2 (C_{Ar}H), 120.4 (C_{Ar}H), 117.5 (C_{Ar}H), 116.9 (C_{Ar}), 112.1 (C_{Ar}H), 111.0 (C_{Ar}), 110.4 (C_{Ar}H), 101.0 (C_{Ar}H), 68.5 (CH₂), 55.8 (CH₃), 51.3 (CH), 47.0 (CH), 42.4 (CH₂), 40.7 (CH₂), 33.4 (CH₂), 29.9 (CH₂), 27.9 (CH₂), 26.4 (CH₂), 24.5 (CH₂).

FmocNH-SS66T-MF 3'-methoxy-3-oxo-3*H*-spiro[isobenzofuran-1,9'-xanthen]-6'-yl (*trans*)-4-(6-((((9*H*-fluoren-9-yl)methoxy)carbonyl)amino)hexanoyl)hexahydro-[1,2]dithiino[4,5-*b*]pyrazine-1(2*H*)-carboxylate **15T**

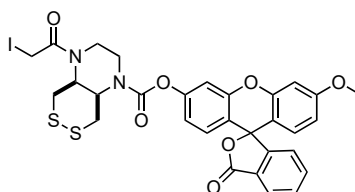


Step 1: See preparation of *N*-Fmoc-hexanoyl chloride above (**15C**).

Step 2: **44T** (12.0 mg, 22 μ mol) was dissolved in anhydrous DCM (0.02 M, 1.1 mL) and DIPEA (19 μ L, 109 μ mol, 5.0 equiv.) was added at 0 °C. To the mixture was added a solution of *N*-Fmoc-hexanoyl chloride (0.04 M, 0.9 mL) activated from *N*-Fmoc-hexanoic acid **53** (15.4 mg, 43.7 μ mol, 2.0 equiv.) using (COCl)₂/DMF and the reaction mixture was warmed and further stirred at r.t. for 1 h. Purification was achieved using FCC (isohexane/EtOAc) to give **15T** as a colourless solid (11.6 mg, 13.1 μ mol, 60%).

TLC R_f = 0.61 (EA). **¹H-NMR** (400 MHz, CDCl₃): δ (ppm) = 8.02 (d, J = 7.1 Hz, 1H), 7.76 (d, J = 7.5 Hz, 2H), 7.69 – 7.60 (m, 2H), 7.58 (d, J = 7.2 Hz, 2H), 7.39 (t, J = 7.4 Hz, 2H), 7.30 (t, J = 7.4 Hz, 2H), 7.14 (d, J = 7.3 Hz, 1H), 7.05 (s, 1H), 6.82 – 6.72 (m, 3H), 6.69 (d, J = 8.8 Hz, 1H), 6.61 (dd, J = 8.8, 2.3 Hz, 1H), 4.90 (s, 1H), 4.76 – 4.54 (m, 1H), 4.36 (d, J = 6.9 Hz, 2H), 4.27 – 4.15 (m, 2H), 3.82 (s, 3H), 3.78 – 3.50 (m, 4H), 3.29 (d, J = 10.8 Hz, 1H), 3.16 (s, 3H), 2.44 – 2.18 (m, 2H), 1.76 – 1.47 (m, 8H). **¹³C-NMR** (101 MHz, CDCl₃): δ (ppm) = 161.6 (C=O), 156.6 (C=O), 155.0 (C_{Ar}), 152.3 (C_{Ar}), 152.0 (C_{Ar}), 144.1 (C_{Ar}), 141.4 (C_{Ar}), 135.3 (C_{Ar}H), 130.0 (C_{Ar}H), 129.2 (C_{Ar}H), 127.8 (C_{Ar}H), 127.2 (C_{Ar}H), 126.6 (C_{Ar}), 125.2 (C_{Ar}H), 124.1 (C_{Ar}H), 120.1 (C_{Ar}H), 117.5 (C_{Ar}H), 112.1 (C_{Ar}H), 111.0 (C_{Ar}H), 110.6 (C_{Ar}), 101.0 (C_{Ar}H), 66.7 (CH₂), 54.9 (CH₃), 47.4 (CH), 40.8 (CH₂), 38.7 (CH₂), 34.1 (CH₂), 32.4 (CH₂), 29.9 (CH₂), 26.8 (CH₂), 26.1 (CH₂), 24.6 (CH₂), 22.8 (CH₂).

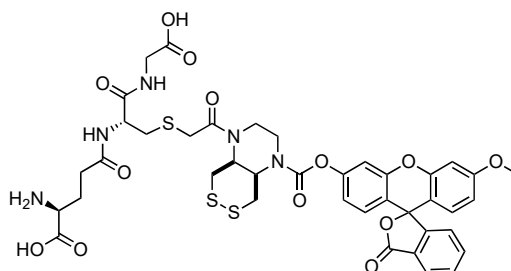
IA-SS66C-MF 3'-methoxy-3-oxo-3*H*-spiro[isobenzofuran-1,9'-xanthen]-6'-yl (*cis*)-4-(2-iodoacetyl)hexahydro-[1,2]dithiino[4,5-*b*]pyrazine-1(2*H*)-carboxylate **16**



To a suspension of **44C** (26.5 mg, 0.048 mmol, 1.0 equiv.) in DCM (5.0 mL, 0.05 M) was added NEt₃ (10 μ L, 0.07 mmol, 1.5 equiv.) and the resulting solution was cooled to 0 °C. A solution of chloroacetyl chloride (1.26 M in DCM, 77 μ L, 0.097 mmol, 2.0 equiv.) was added and the reaction mixture was stirred for 15 min at 0 °C, was then allowed to warm to r.t. and stirred further for 1 h. The solvent was removed under reduced pressure and the residue was resuspended in acetone (5 mL). NaI (112 mg, 0.75 mmol, 16 equiv.) was added and the mixture was stirred at r.t. for 15 h. The reaction mixture was diluted with EtOAc (15 mL), washed with brine, then with aq. sat. NH₄Cl solution and the aq. layer was extracted with EtOAc (2×20 mL). The combined organic layers were dried over Na₂SO₄ and concentrated under reduced pressure. Purification by FCC (isohexane:EtOAc, 7:3 to 1:1) gave **16** (30.0 mg, 0.042 mmol, 88%) as a colourless oil.

TLC R_f = 0.72 (EtOAc). **HRMS** (ESI): C₃₀H₂₆N₂O₇S₂⁺: [M+H]⁺ calc. m/z 717.02206, found 717.02336. **¹H-NMR** (800 MHz, CDCl₃): δ (ppm) = 8.03 (dt, J = 7.7, 1.0 Hz, 1H), 7.67 (tdd, J = 7.5, 2.3, 1.2 Hz, 1H), 7.63 (tt, J = 7.5, 1.0 Hz, 1H), 7.16 (ddd, J = 7.6, 1.7, 0.9 Hz, 1H), 7.14 – 7.06 (m, 1H), 6.85 – 6.79 (m, 2H), 6.77 (dd, J = 2.5, 1.5 Hz, 1H), 6.70 (dd, J = 8.8, 1.6 Hz, 1H), 6.63 (dd, J = 8.8, 2.5 Hz, 1H), 4.79 – 4.59 (m, 1H), 4.43 (s, 1H), 4.27 (s, 1H), 3.93 – 3.85 (m, 2H), 3.86 – 3.82 (m, 4H), 3.79 – 3.74 (m, 2H), 3.73 – 3.67 (m, 1H), 3.55 (d, J = 10.4 Hz, 1H), 3.17 (d, J = 14.4 Hz, 1H), 3.02 (dd, J = 14.2, 4.1 Hz, 1H). **¹³C-NMR** (201 MHz, CDCl₃): δ (ppm) = 169.4 (C=O), 161.6 (C=O), 153.3 (C_{Ar}), 153.1 (C_{Ar}), 152.4 (C_{Ar}), 152.1 (C_{Ar}), 152.0 (C_{Ar}), 135.3 (C_{Ar}H), 130.0 (C_{Ar}H), 129.3 (C_{Ar}H), 129.2 (C_{Ar}H), 126.6 (C_{Ar}), 125.3 (C_{Ar}H), 124.2 (C_{Ar}H), 117.5 (C_{Ar}H), 116.9 (C_{Ar}), 112.1 (C_{Ar}H), 111.0 (C_{Ar}H), 110.4 (C_{Ar}H), 101.0 (C_{Ar}H), 82.6 (C_{spiro}), 62.5 (CH), 55.8 (CH₃), 51.2 (CH), 44.0 (CH₂), 41.9 (CH₂), 35.4 (CH₂).

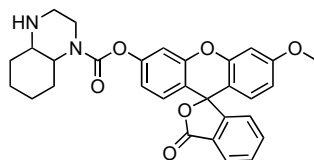
GS-SS66C-MF N^5 -((2S)-1-((carboxymethyl)amino)-6-((*cis*)-4-(((3'-methoxy-3-oxo-3*H*-spiro[isobenzofuran-1,9'-xanthen]-6'-yl)oxy)carbonyl)hexahydro-[1,2]dithiino[4,5-*b*]pyrazin-1(2*H*)-yl)-1,6-dioxohexan-2-yl)-*L*-glutamine **17**



To a solution of **16** (28.0 mg, 0.039 mmol, 1.0 equiv.) in MeCN (4.0 mL, 0.01 M) at r.t. was added dropwise a solution of aq. reduced. *L*-glutathione (0.015 M, 4.0 mL, 0.06 mmol, 5.0 equiv., 0.1 M PBS, pH 7.45). The mixture was stirred at r.t. for 1 h. The reaction mixture was directly purified by preparative HPLC (H₂O/MeCN/FA) to give **17** (1.6 mg, 0.002 mmol, 5%) was obtained as a colourless solid.

HRMS (ESI): C₄₀H₄₂N₅O₁₃S₃⁺: [M+H]⁺ calc. *m/z* 896.19357, found 896.19570. **¹H-NMR** (800 MHz, DMSO-*d*₆): δ (ppm) 8.58 – 8.32 (m, 2H), 8.04 (d, *J* = 7.7 Hz, 1H), 7.81 (tt, *J* = 7.5, 1.3 Hz, 1H), 7.78 – 7.72 (m, 1H), 7.37 – 7.29 (m, 2H), 6.99 (dt, *J* = 8.7, 2.2 Hz, 1H), 6.96 (d, *J* = 2.5 Hz, 1H), 6.83 (d, *J* = 8.7 Hz, 1H), 6.74 (dd, *J* = 8.8, 2.5 Hz, 1H), 6.70 (dd, *J* = 8.8, 1.7 Hz, 1H), 4.56 (s, 1H), 4.51 – 4.41 (m, 1H), 4.35 (s, 1H), 4.06 – 3.89 (m, 1H), 3.83 (s, 3H), 3.73 – 3.47 (m, 8H), 3.29 – 3.13 (m, 6H), 3.00 (dt, *J* = 13.9, 4.0 Hz, 1H), 2.71 (dt, *J* = 13.5, 9.4 Hz, 1H), 2.36 (s, 1H), 2.33 – 2.25 (m, 1H), 1.92 (s, 1H), 1.85 (s, 1H). **¹³C-NMR** (201 MHz, DMSO-*d*₆): δ (ppm) = 172.0 (C=O), 170.9 (C=O), 170.3 (C=O), 170.1 (C=O), 168.5 (C=O), 161.2 (C_{Ar}), 152.8 (C_{Ar}), 152.4 (C_{Ar}), 152.4 (C_{Ar}), 152.3 (C_{Ar}), 151.6 (C_{Ar}), 150.9 (C_{Ar}), 135.9 (C_{Ar}H), 130.4 (C_{Ar}H), 129.6 (C_{Ar}), 129.0 (C_{Ar}H), 128.8 (C_{Ar}H), 125.7 (C_{Ar}), 124.9 (C_{Ar}H), 124.0 (C_{Ar}H), 118.4 (C_{Ar}H), 116.0 (C_{Ar}H), 112.3 (C_{Ar}H), 110.5 (C_{Ar}), 110.4 (C_{Ar}H), 100.8 (C_{Ar}H), 81.7 (C_{spiro}), 55.7 (CH₃), 53.2 (CH), 52.4 (CH), 42.1 (CH₂), 41.8 (CH₂), 33.7 (CH₂), 33.4 (CH₂), 31.7 (CH₂), 26.9 (CH₂).

H-CC66-MF 3'-methoxy-3-oxo-3*H*-spiro[isobenzofuran-1,9'-xanthen]-6'-yl -octahydroquinoxaline-1(2*H*)-carboxylate (*racemic*) **49**

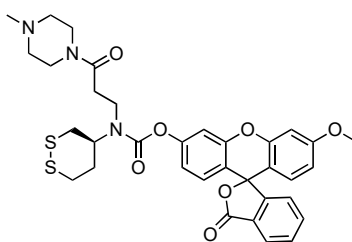


Step 1: 1,2-cyclohexyldiamine (*racemic*) (49 μL, 0.40 mmol, 1.0 equiv.) was dissolved in anhydrous DCM (5 mL, 0.05 M), DIPEA (350 μL, 2.0 mmol, 5.0 equiv.) was added at 0°C and a solution of VTT (140 mg, 0.42 mmol, 1.05 equiv.) in anhydrous DCM (2 mL) was added dropwise at 0°C.

Step 2: Following **general protocol D**, MF-OC(O)Cl was prepared *in situ* from MF-OH (138 mg, 0.40 mmol, 1.0 equiv.). To the solution obtained in step 1 was added MF-OC(O)Cl (2 mL, 0.2 M). Purification by FCC (isohexanes:EtOAc 1:1 → EtOAc) gave **49** as a colourless powder (7.2 mg, 0.014 mmol, 3%).

TLC R_f = 0.45 (DCM:MeOH, 9:1). **HRMS** (ESI): C₃₀H₂₉N₂O₆⁺: [M+H]⁺ calc. *m/z* 513.20201, found 513.20181. **¹H-NMR** (400 MHz, CDCl₃): δ (ppm) = 8.02 (d, *J* = 7.2 Hz, 1H), 7.67 (t, *J* = 7.4 Hz, 1H), 7.62 (td, *J* = 7.5, 0.9 Hz, 1H), 7.17 (d, *J* = 7.5 Hz, 1H), 7.08 (d, *J* = 8.4 Hz, 1H), 6.83 – 6.74 (m, 3H), 6.69 (d, *J* = 8.8 Hz, 1H), 6.62 (dd, *J* = 8.8, 2.5 Hz, 1H), 4.10 (d, *J* = 4.9 Hz, 1H), 4.05 – 3.89 (m, 1H), 3.84 (s, 3H), 3.35 – 3.02 (m, 3H), 2.91 (dd, *J* = 12.7, 3.7 Hz, 1H), 2.25 – 1.93 (m, 1H), 1.89 – 1.54 (m, 4H), 1.55 – 1.40 (m, 2H), 1.36 (dt, *J* = 16.1, 5.4 Hz, 1H). **¹³C-NMR** (101 MHz, CDCl₃): δ (ppm) = 169.5 (C=O), 161.5 (C=O), 153.2 (2×C_{Ar}), 152.9 (C_{Ar}), 152.5 (C_{Ar}), 152.0 (C_{Ar}), 135.2 (C_{Ar}H), 129.9 (C_{Ar}H), 129.2 (C_{Ar}H), 129.0 (C_{Ar}H), 126.7 (C_{Ar}), 125.2 (C_{Ar}H), 124.2 (C_{Ar}H), 117.7 (C_{Ar}H), 116.0 (C_{Ar}), 112.0 (C_{Ar}H), 111.1 (C_{Ar}), 110.5 (C_{Ar}H), 101.0 (C_{Ar}H), 82.8 (C_{spiro}), 55.7 (CH₃), 54.0 (CH), 53.2 (CH), 46.0 (CH₂), 39.5 (CH₂), 31.6 (CH₂), 25.3 (CH₂), 24.2 (CH₂, rotamer 1), 23.2 (CH₂ rotamer 2), 19.7 (CH₂).

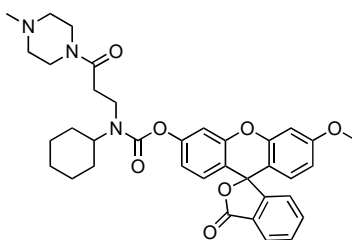
P-SS60-MF 3'-methoxy-3-oxo-3*H*-spiro[isobenzofuran-1,9'-xanthen]-6'-yl ((*S*)-1,2-dithian-4-yl)(3-(4-methylpiperazin-1-yl)-3-oxopropyl)carbamate **50**



Following **general protocol D**, MF-OC(O)Cl was prepared in situ from MF-OH (12.1 mg, 0.035 mmol, 1.5 equiv.). To a solution of (*S*)-3-((1,2-Dithian-4-yl)amino)-1-(4-methylpiperazin-1-yl)propan-1-one dihydrochloride (8.3 mg, 0.023 mmol, 1.0 equiv.) and DIPEA (12 μ L, 0.07 mmol, 3.0 equiv.) in anhydrous DCM (1 mL, 0.03 M), was added MF-OC(O)Cl (0.9 mL, 0.04 M). Purification by FCC (isohexanes:EtOAc 1:1 \rightarrow EtOAc) gave **50** as a colourless powder (4.3 mg, 0.007 mmol, 30%).

TLC R_f = 0.68 (DCM:MeOH, 9:1). **HRMS** (ESI): $C_{34}H_{36}N_3O_7S_2^+$: $[M+H]^+$ calc. m/z 662.19892, found 662.19902. **1H -NMR** (400 MHz, $CDCl_3$): δ (ppm) = 8.03 (d, J = 7.4 Hz, 1H), 7.67 (d, J = 7.3 Hz, 1H), 7.62 (t, J = 7.3 Hz, 1H), 7.15 (d, J = 5.9 Hz, 1H), 7.09 (s, 1H), 6.80 (d, J = 5.5 Hz, 2H), 6.77 (d, J = 2.3 Hz, 1H), 6.70 (d, J = 8.8 Hz, 1H), 6.63 (dd, J = 8.8, 2.3 Hz, 1H), 4.19 (d, J = 27.8 Hz, 2H), 3.84 (s, 3H), 3.64 (t, J = 18.8 Hz, 4H), 3.49 (d, J = 13.7 Hz, 2H), 3.28 (t, J = 12.2 Hz, 1H), 3.21 (t, J = 12.5 Hz, 1H), 3.03 (t, J = 12.0 Hz, 1H), 2.79 (dd, J = 20.4, 13.1 Hz, 1H), 2.73 – 2.63 (m, 2H), 2.39 (d, J = 4.7 Hz, 4H), 2.30 (s, 3H), 2.24 (d, J = 21.9 Hz, 2H). **^{13}C -NMR** (101 MHz, $CDCl_3$): δ (ppm) = 169.5 (C=O), 169.0 (C=O), 168.6 (C=O), 161.6 (C_{Ar}), 153.5 (C_{Ar}), 153.2 (C_{Ar}), 152.4 (C_{Ar}), 152.0 (C_{Ar}), 135.2 (C_{ArH}), 130.0 (C_{ArH}), 129.2 (C_{ArH}), 126.6 (C_{Ar}), 125.3 (C_{ArH}), 124.1 (C_{ArH}), 117.6 (C_{ArH}), 117.5 (C_{ArH}), 116.7 (C_{Ar}), 112.0 (C_{ArH}), 111.1 (C_{Ar}), 110.4 (C_{ArH}), 101.1 (C_{ArH}), 82.6 (C_{spiro}), 58.0 (CH, rotamer 2), 57.8 (CH, rotamer 1), 55.8 (CH₃), 55.3 (CH₂), 55.1 (CH₂), 54.7 (CH₂), 46.1 (CH₂), 45.5 (CH₂, rotamer 1), 45.4 (CH₂, rotamer 2), 42.0 (CH₂, rotamer 2), 41.6 (CH₂, rotamer 1), 36.9 (CH₂, rotamer 1), 36.5 (CH₂, rotamer 2), 36.4 (CH₂, rotamer 1), 36.3 (CH₂, rotamer 2), 34.1 (CH₂, rotamer 1), 33.8 (CH₂, rotamer 2), 33.2 (CH₂, rotamer 1), 33.0 (CH₂, rotamer 1).

P-CC60-MF 3'-methoxy-3-oxo-3*H*-spiro[isobenzofuran-1,9'-xanthen]-6'-yl ((*R/S*)-1,2-dithian-4-yl)(3-(4-methylpiperazin-1-yl)-3-oxopropyl)carbamate **59**



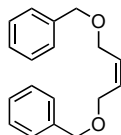
Step 1: To a solution of 4-nitrophenyl chloroformate (18.5 mg, 0.09 mmol, 1.0 equiv.) and MF-OH (39.8 mg, 0.12 mmol, 1.3 equiv.) in anhydrous THF (1.8 mL, 0.05 M) was added DIPEA (20 μ L, 0.12 mmol, 1.3 equiv.), the resulting mixture was stirred at r.t. for 4 h and was then concentrated under reduced pressure.

Step 2: To a solution of (3-(cyclohexylamino)-1-(4-methylpiperazin-1-yl)propan-1-one dihydrochloride (33.0 mg, 0.10 mmol, 1.1 equiv.) in anhydrous DMF (2 mL, 0.05 M), was added the material obtained in step 1 (2.0 mL of a 0.05 M solution in DMF, 0.09 mmol, 1.0 equiv.) at 0 $^{\circ}C$, then DIPEA (41 μ L, 0.23 mmol, 2.5 equiv.) was added and the resulting mixture was allowed to warm to r.t. and stirred for 1 h. The mixture was directly purified by preparative HPLC ($H_2O/MeCN/FA$) to yield **59** as a colourless powder (19 mg, 0.03 mmol, 33%).

TLC R_f = 0.55 (DCM:MeOH, 9:1). **HRMS** (ESI): $C_{36}H_{40}N_3O_7^+$: $[M+H]^+$ calc. m/z 626.28608, found 626.28569. **1H -NMR** (400 MHz, $CDCl_3$): δ (ppm) = 8.02 (d, J = 7.3 Hz, 1H), 7.70 – 7.57 (m, 2H), 7.15 (t, J = 6.4 Hz, 1H), 7.09 (s, 1H), 6.86 – 6.73 (m, 3H), 6.70 (d, J = 8.8 Hz, 1H), 6.62 (dd, J = 8.8, 2.3 Hz, 1H), 3.95 (s, 1H), 3.84 (s, 3H), 3.72 – 3.57 (m, 3H), 3.57 – 3.38 (m, 3H), 2.80 – 2.62 (m, 2H), 2.47 – 2.32 (m, 4H), 2.29 (s, 3H), 1.98 – 1.62 (m, 8H), 1.62 – 1.49 (m, 2H), 1.35 (q, J = 13.0 Hz, 2H), 1.18 – 1.02 (m, 1H). **^{13}C -NMR** (101 MHz, $CDCl_3$): δ (ppm) = 169.5 (C=O), 169.1 (C=O), 161.6 (C=O), 153.3 ($2 \times C_{Ar}$), 152.8 (C_{Ar}), 152.5 (C_{Ar}), 152.0 (C_{Ar}), 135.2 (C_{ArH}), 130.0 (C_{ArH}), 129.2 (C_{ArH}), 129.1 (C_{ArH}), 126.7 (C_{Ar}), 125.2 (C_{ArH}), 124.2 (C_{ArH}), 117.8 (C_{ArH}), 116.3 (C_{Ar}), 112.0 (C_{Ar}), 111.1 (C_{ArH}), 110.5 (C_{ArH}), 101.0 (C_{ArH}), 82.7 (C_{spiro}), 57.3 (CH, rotamer 1), 56.9 (CH, rotamer 2), 55.7 (CH₂, rotamer 1), 55.4 (CH₂, rotamer 1), 55.2 (CH₂, rotamer 2), 54.8 (CH₂, rotamer 2), 46.1 (CH₃), 45.6 (CH₂, rotamer 1), 45.3 (CH₂, rotamer 2), 41.5 (CH₂), 40.9 (CH₂, rotamer 1), 40.2 (CH₂, rotamer 2), 33.5 (CH₂), 31.5 (CH₂, rotamer 1), 30.8 (CH₂, rotamer 2), 26.0 (CH₂), 25.4 (CH₂).

7.4 Initial synthetic route

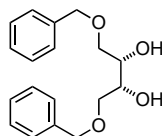
7.4.1 (cis)-Boc-Route

(Z)-1,4-bis(benzyloxy)but-2-ene 24

To a solution of (Z)-but-2-ene-1,4-diol (3.8 g, 42 mmol, 1.0 equiv.) in dry DMF (150 mL, 0.3 M), NaH (60 % in mineral oil, 4.3 g, 0.11 mol, 2.5 equiv.) was added at 0 °C and the reaction mixture was stirred for 20 minutes. Benzyl bromide (18 mL, 0.15 mol, 3.5 equiv.) was added dropwise and the resulting mixture stirred vigorously overnight. The reaction was quenched with a 1:1 mixture of NaHCO₃ (sat. aq.) and NaCl (sat. aq.) and the aqueous layer was extracted with DCM (three times). The combined organic layers were washed with brine, dried over MgSO₄. After filtration and removal of the solvent, a yellow crude oil was received. Purification *via* column chromatography (hexanes/EtOAc 20:1 → 10:1) gave **24** as a colourless oil (11 g, 39 mmol, 93%).

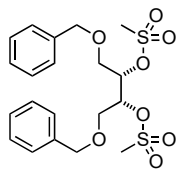
Note: After addition of benzyl bromide, the reaction mixture needed to be stirred vigorously to prevent formation of a thick slurry which will impede sufficient stirring.

TLC R_f = 0.44 (hexanes/EtOAc 9:1). **¹H-NMR** (400 MHz, CDCl₃) δ (ppm): 7.38 – 7.27 (m, 10H), 5.80 (ddd, J = 4.9, 3.7, 1.1 Hz, 2H), 4.49 (s, 4H), 4.07 (dd, J = 4.6, 1.1 Hz, 4H). **¹³C-NMR** (101 MHz, CDCl₃) δ (ppm): 138.3, 129.7, 128.6, 127.9, 127.8, 72.4, 65.9.

1,4-bis(benzyloxy)butane-2,3-diol (cis) 26C

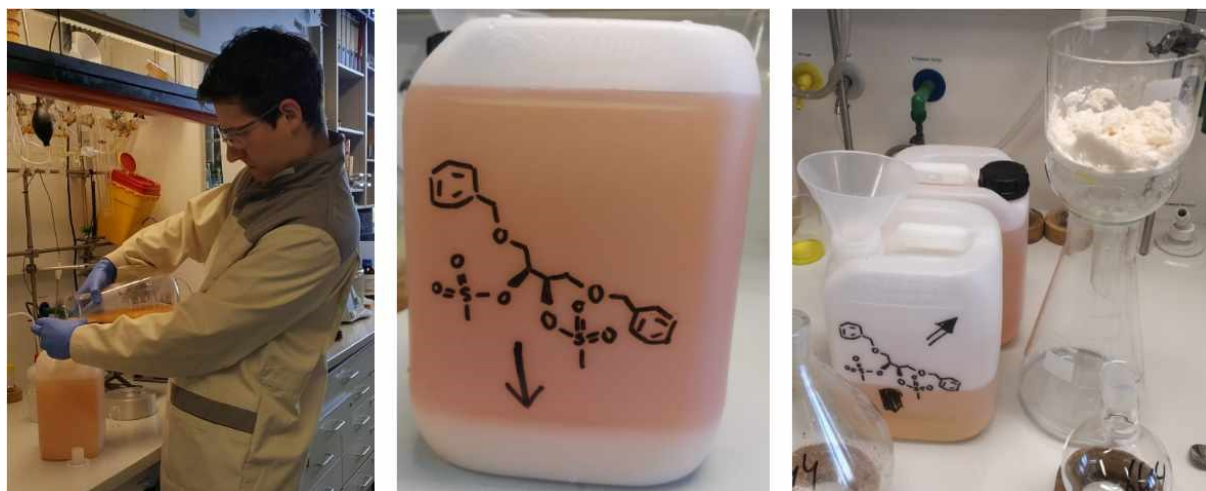
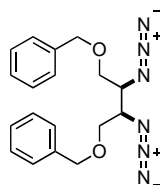
To a solution of **24** (15.8 g, 59 mmol, 1.0 equiv.) acetone:H₂O (3:1, 260 mL) were added 4-methylmorpholine *N*-oxide (19.9 g, 0.15 mol, 2.5 equiv.) and K₂[OsO₂(OH)₄] (141 mg, 0.38 mmol, 0.0065 equiv.). The reaction mixture was stirred at r.t. for 15 h, before being poured into sat. aq. sodium bisulfite solution. The aq. layer was extracted with EtOAc (3×200 mL), and the combined organic layers were washed with sat. aq. NaCl, dried over Na₂SO₄ and concentrated under reduced pressure to give **26C** as a colourless solid (16.5 g, 55 mmol, 93%) without further purification.

TLC R_f = 0.33 (iso-hexane:EtOAc, 1:1). **HRMS** (ESI): C₁₈H₂₂O₄⁺ [M+H]⁺: calc. m/z 302.1518, found: 302.1523. **¹H-NMR** (400 MHz, CDCl₃): δ (ppm) = 7.43 – 7.28 (m, 10H), 4.55 (s, 4H), 3.84 (dq, J = 4.2, 1.8 Hz, 2H), 3.73 – 3.57 (m, 4H), 2.68 (s, 2H). **¹³C-NMR** (101 MHz, CDCl₃) δ (ppm) = 137.9, 128.6, 128.0, 127.9, 73.7, 71.5, 71.2.

1,4-bis(benzyloxy)butane-2,3-diyl dimethanesulfonate (*cis*) 27C

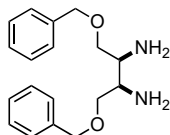
Following **general procedure A**, **26C** (16.5 g, 55 mmol, 1.0 equiv.) was dissolved in pyridine (600 mL, 0.1 M) and reacted with MsCl (10.0 mL, 0.13 mmol, 2.4 equiv.). After precipitation from water and washings with ether **27C** was received as a colourless solid and in excellent purity (22.1 g, 48.2 mmol, 88%).

HRMS (ESI): $C_{20}H_{26}ClO_8S_2^-$: $[M+Cl]^-$ calc. m/z 493.07619, found 493.07631. **1H -NMR** (400 MHz, $CDCl_3$): δ (ppm) = 7.42 – 7.28 (m, 10H), 5.04 (td, J = 4.2, 2.0 Hz, 2H), 4.54 (d, J = 1.4 Hz, 4H), 3.85 – 3.68 (m, 4H), 3.06 (s, 6H). **^{13}C -NMR** (101 MHz, $CDCl_3$) δ (ppm) = 137.1, 128.7, 128.2, 128.0, 79.4, 73.7, 68.0, 38.7.

**((2,3-diazidobutane-1,4-diyl)bis(oxy))bis(methylene)dibenzene (*cis*) 28C**

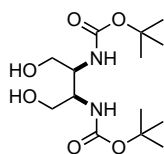
A mixture of **27C** (22.1 g, 48 mmol, 1.0 equiv.) and sodium azide (7.21 g, 0.11 mol, 2.3 equiv.) in DMSO (140 mL, 0.3 M) was stirred at 80°C for 96 h, cooled to r.t., and the colourless suspension was diluted with water/aq. NaCl (1:1, 300 mL). The aq. layer was extracted with EtOAc (3×150 mL) and the combined organic layers were dried over Na_2SO_4 , filtered and concentrated under reduced pressure. The yellow crude oil was purified by FCC (hexane/EtOAc 9:1) giving **28C** as a colourless liquid (15.8 g, 44.8 mmol, 93%).

TLC R_f = 0.45 (isohexane:EtOAc, 9:1). **1H -NMR** (400 MHz, $CDCl_3$): δ (ppm) = 7.43 – 7.28 (m, 10H), 4.58 (s, 4H), 3.93 – 3.44 (m, 6H). **^{13}C -NMR** (101 MHz, $CDCl_3$) δ (ppm) = 137.9, 128.6, 128.0, 127.9, 73.7, 71.5, 71.2.

1,4-bis(benzyloxy)butane-2,3-diamine (cis) 29C

To a solution of **28C** (15.7 g, 44.6 mmol) in MeOH (400 mL, 0.1 M) was added Pd/C (10%, 634 mg). The mixture was stirred at r.t. under H₂-atmosphere at 1 bar for 15 h. The catalyst was removed by filtration over Celite® and the filtrate was concentrated under reduced pressure giving **29C** as a colourless oil (12.6 g, 41.9 mmol, 94%).

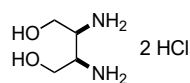
HRMS (ESI): C₁₈H₂₅N₂O₂⁺: [M+H]⁺ calc. *m/z* 301.19105, found 301.19139. **¹H-NMR** (400 MHz, CDCl₃): δ (ppm) = 7.31 (qd, *J* = 8.4, 7.8, 2.2 Hz, 10H), 4.55 – 4.47 (m, 4H), 3.58 (dd, *J* = 9.3, 3.1 Hz, 2H), 3.49 (ddt, *J* = 6.3, 4.8, 3.3 Hz, 2H), 3.04 – 2.96 (m, 2H). **¹³C-NMR** (101 MHz, CDCl₃) δ (ppm) = 138.3, 128.6, 127.8, 73.5, 73.1, 53.9.

di-tert-butyl (1,4-dihydroxybutane-2,3-diyl)dicarbamate (cis) 32C

Step 1: **29C** (12.6 g, 41.9 mmol, 1.0 equiv.) was charged with concentrated aq. HCl (186 mL, 2.2 mol, 50.0 equiv.) and was heated to 80°C for 8 h, was then further stirred at r.t. for 15 h. The reaction mixture was concentrated under reduced pressure and the residue was dried by azeotropic evaporation using toluene (2×200 mL), was then washed with Et₂O (300 mL) and dried under reduced pressure to give crude 2,3-diaminobutane-1,4-diol dihydrochloride **30** as a brown solid without further purification.

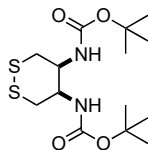
Step 2: The material obtained in step 1 was dissolved in H₂O:1,4-dioxane (0.2 M, 220 mL) and was reacted with Boc₂O (23.4 g, 107 mmol, 2.4 equiv.) and NEt₃ (50 mL, 357 mmol, 8.0 equiv.) at r.t. for 15 h. The reaction mixture was then acidified to pH < 4 using aq. HCl (2 M), EtOAc was added, and the organic phase was separated and washed with a sat. aq. NaCl. The combined aq. layers were extracted with EtOAc (3×), then the combined organic layers were dried over Na₂SO₄ and concentrated to afford **32C** as a colourless solid (11.1 g, 34.7 mmol, 83% over 2 steps). No further purification was required.

TLC R_f = 0.32 (EtOAc). **HRMS** (EI): C₁₈H₂₂O₄⁺: [M]⁺ calc. *m/z* 320.1947, found 320.1946. **¹H-NMR** (400 MHz, DMSO-*d*₆): δ (ppm) = 6.41 (d, *J* = 7.3 Hz, 2H), 4.48 (t, *J* = 5.6 Hz, 2H), 3.51 (q, *J* = 5.2 Hz, 2H), 3.40 (t, *J* = 5.1 Hz, 4H), 1.38 (s, 18H). **¹³C-NMR** (101 MHz, DMSO-*d*₆) δ (ppm) = 155.5, 77.7, 60.8, 52.9, 28.2.

2,3-diaminobutane-1,4-diol dihydrochloride (cis) 30

32C (3.90 g, 12.20 mmol, 1.0 equiv.) was suspended in DCM (0.1 M, 120 mL) and HCl (4 M in dioxane, 46 mL, 183 mmol, 15 equiv.) was added in one portion. The mixture was stirred at r.t. for 15 h and was then poured into Et₂O (200 mL). The precipitate was filtered off and washed with Et₂O (100 mL), the filtrate was dried under reduced pressure to give **30** as a colourless solid (2.3 g, 12.1 mmol, 99%).

¹H-NMR (400 MHz, DMSO-*d*₆): δ (ppm) = 8.53 (s, 6H), 5.58 (s, 2H), 3.95 – 3.66 (m, 4H), 3.45 (s, 2H). **¹³C-NMR** (101 MHz, DMSO-*d*₆) δ (ppm) = 57.8, 51.0.

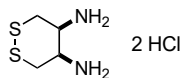
di-tert-butyl (1,2-dithiane-4,5-diyl)dicarbamate (cis) 35C

Step 1: Following **general procedure A**, **30** (3.44 g, 10.7 mmol, 1.0 equiv.) was dissolved in pyridine (40 mL, 0.3 M) and reacted with MsCl (1.83 mL, 23.6 mmol, 2.2 equiv.). After precipitation from water and washings with ether (*cis*)-2,3-bis((*tert*-butoxycarbonyl)amino)butane-1,4-diyl dimethanesulfonate was received as a colourless solid (5.07 g, 10.6 mmol, 99%). **TLC** R_f = 0.38 (hexanes/EtOAc 1:1). **¹H-NMR** (400 MHz, CDCl₃): δ (ppm) = 5.03 (s, 2H), 4.32 (t, J = 12.4 Hz, 4H), 4.06 (s, 2H), 3.08 (s, 6H), 1.45 (s, 18H).

Step 2: The material obtained in step 1 (5.07 g, 10.6 mmol, 1.0 equiv.) was dissolved in acetone (75 mL, 0.15 M) and treated with KSAc (2.7 g, 23.6 mmol, 2.2 equiv.). The reaction mixture was heated to 75 °C and was stirred for 56 h, before being cooled to r.t. and taken into EtOAc (200 mL). The organic layer was washed with sat. aq. NaCl (3×200 mL), dried over Na₂SO₄ and concentrated under reduced pressure to give (*cis*)-*S,S'*-(2,3-bis((*tert*-butoxycarbonyl)amino)butane-1,4-diyl) diethanethioate as a colourless solid, which was directly taken for the next reaction step without further purification or characterisation.

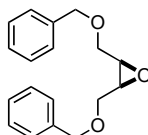
Step 3: The material obtained in step 2 was dissolved in MeOH (0.05 M, 250 mL) and solid KOH (2.83 g, 42.9 mmol, 4.0 equiv.) was added. The mixture was stirred at r.t. open to air for 15 h, before being concentrated under reduced pressure and taken into a mixture of H₂O:Et₂O (1:1, 300 mL). The aq. layer was extracted with Et₂O (3×50 mL), the combined organic layers were dried over Na₂SO₄ and concentrated under reduced pressure to give **35C** as a colourless solid (3.03 g, 8.64 mmol, 81% over 3 steps).

TLC R_f = 0.45 (isohexanes:EtOAc, 6:1). **HRMS** (ESI): C₁₄H₂₆N₂O₄S₂⁺: [M+H]⁺ calc. m/z 351.14068, found 351.14104. **¹H-NMR** (400 MHz, CDCl₃): δ (ppm) = 5.55 – 5.20 (br-s, 2H), 4.42 – 3.72 (br-m, 2H), 3.54 – 3.08 (br-m, 2H), 2.88 (br-dd, J = 13.4, 7.9 Hz, 2H), 1.45 (s, 18H). **¹³C-NMR** (101 MHz, CDCl₃) δ (ppm) = 155.5 (C=O), 80.3 (C(CH₃)₃), 53.2 (CH), 41.7 (CH₂), 28.4 (C(CH₃)₃).

1,2-dithiane-4,5-diamine dihydrochloride (cis) 36C

35C (3.00 g, 8.56 mmol, 1.0 equiv.) was suspended in DCM (0.3 M, 30 mL) and HCl/dioxane (10.7 mL of a 4 M solution, 42.8 mmol, 5.0 equiv.) was added in one portion. The mixture was stirred at r.t. for 4 h and was then poured into Et₂O (100 mL). The precipitate was filtered off and washed with Et₂O (20 mL), the filtrate was dried under reduced pressure to give **36C** as a colourless solid (1.87 g, 8.38 mmol, 98%).

HRMS (EI): C₄H₁₀N₂S₂⁺: [M-e]⁺ calc. m/z 150.0285, found 150.0282. **¹H-NMR** (400 MHz, DMSO-*d*₆): δ (ppm) = 8.95 (s, 6H), 4.07 – 3.77 (m, 2H), 3.51 – 2.89 (m, 4H). **¹³C-NMR** (101 MHz, DMSO-*d*₆) δ (ppm) = 53.7, 30.0.

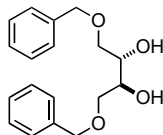
7.4.2 (trans)-Boc-Route**2,3-bis((benzyloxy)methyl)oxirane 25**

To a solution of **24** (30 g, 0.12 mol, 1.0 equiv.) in DCM (120 mL, 1.0 M), *m*-CPBA (77 %, 33 g, 0.15 mol, 1.2 equiv.) was added in batches at 0 °C. The reaction mixture was allowed to warm to r.t. and stirred overnight, during which a thick, colourless suspension formed. The reaction was quenched with NaHCO₃ (sat. aq.) and the aqueous layer

was extracted with DCM (3×300 mL). The combined organic layers were washed with brine, dried over MgSO₄, concentrated and purified by FCC (hexanes/EtOAc 9:1 → 5:1) to give **25** as a colourless oil (28 g, 0.1 mol, 80%).

TLC R_f = 0.21 (hexane:EtOAc, 9:1). **HRMS** (ESI): C₁₈H₂₁O₃⁺ [M+H]⁺: calc. m/z 285.1485, found: 285.1488. **¹H-NMR** (400 MHz, CDCl₃) δ (ppm) = 7.38 – 7.27 (m, 10H), 4.62 (d, J = 11.9 Hz, 2H), 4.52 (d, J = 11.9 Hz, 2H), 3.69 (dd, J = 11.3, 4.0 Hz, 2H), 3.53 (ddm, J = 11.3, 6.5 Hz, 2H), 3.31 – 3.22 (m, 2H). **¹³C-NMR** (101 MHz, CDCl₃) δ (ppm) = 137.8, 128.6, 127.9, 127.9, 73.4, 68.2, 54.5.

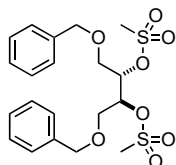
1,4-bis(benzyloxy)butane-2,3-diol (*trans*) **26T**



To a solution of **25** (37 g, 0.13 mol, 1.0 equiv.) in a 6:1 mixture of THF (240 mL) and water (40 mL), concentrated H₂SO₄ (35 mL, 0.65 mol, 5.0 equiv.) was added at 0 °C. The reaction was allowed to warm to r.t. and was stirred overnight. The reaction was diluted with water and EtOAc, and the aqueous layer was extracted with EtOAc (two times). The combined organic layers were washed with NaCl (sat. aq.), dried over MgSO₄, filtered and concentrated. The colourless crude oil was purified by FCC (hexanes/EtOAc 3:1) giving **26T** as a colourless oil (26 g, 85 mmol, 65%).

TLC R_f = 0.38 (hexanes:EtOAc, 1:1). **HRMS** (ESI): C₁₈H₂₃O₄⁺ [M+H]⁺: calc. m/z 303.1591, found: 303.1595. **¹H-NMR** (400 MHz, CDCl₃) δ (ppm) = 7.39 – 7.27 (m, 10H), 4.66 – 4.47 (m, 4H), 3.88 (t, J = 4.3 Hz, 2H), 3.71 – 3.53 (m, 4H), 2.74 (s, 2H). **¹³C-NMR** (101 MHz, CDCl₃) δ (ppm) = 137.9, 128.6, 128.0, 127.9, 73.8, 72.1, 70.7.

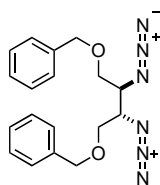
1,4-bis(benzyloxy)butane-2,3-diyl dimethanesulfonate (*trans*) **27T**



Following **general procedure A**, **26T** (6.6 g, 22 mmol, 1.0 equiv.) was dissolved in pyridine (8.8 mL, 0.11 mol, 5.0 equiv.) and reacted with MsCl (3.7 mL, 48 mmol, 2.2 equiv.). After precipitation from water and washings with ether **27T** was received as a colourless solid and in excellent purity (9.8 g, 21 mmol, 95%).

¹H-NMR (400 MHz, CDCl₃) δ (ppm) = 7.41 – 7.27 (m, 10H), 5.05 – 4.97 (m, 2H), 4.57 (d, J = 11.6 Hz, 2H), 4.47 (d, J = 11.5 Hz, 2H), 3.76 (dt, J = 3.4, 1.3 Hz, 4H), 3.04 (s, 6H). **¹³C-NMR** (101 MHz, CDCl₃) δ (ppm) = 137.1, 128.7, 128.3, 128.2, 78.9, 73.8, 68.8, 38.9.

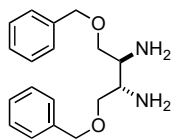
((2,3-diazidobutane-1,4-diyl)bis(oxy))bis(methylene)dibenzene (*trans*) **28T**



27T (2.3 g, 5.0 mmol, 1.0 equiv.) was dissolved in DMSO (15 mL, 0.3 M) and charged with sodium azide (0.82 g, 13 mmol, 2.50 equiv.). The colourless suspension was stirred at 80 °C for 36 h and was then diluted with a 1:1 mixture of water and NaHCO₃ (sat. aq.). The aqueous layer was extracted with ethyl acetate (three times), and the combined organic layers were washed with NaCl (sat. aq.), dried over MgSO₄ and concentrated *in vacuo*. The pale-yellow crude oil was purified by FCC (isohexanes/EtOAc 20:1 → 9:1), giving **28T** as a colourless oil (1.5 g, 4.2 mmol, 84%).

TLC R_f = 0.46 (hexanes:EtOAc, 9:1). **HRMS** (ESI): $C_{18}H_{20}ClN_6O_2^-$ [M+Cl] $^-$: calc. m/z 387.13418, found: 387.13420. **1H -NMR** (400 MHz, $CDCl_3$) δ (ppm) = 7.44 – 7.28 (m, 10H), 4.55 (s, 4H), 3.74 (ddt, J = 7.7, 4.0, 2.0 Hz, 2H), 3.70 – 3.62 (m, 4H). **^{13}C -NMR** (101 MHz, $CDCl_3$) δ (ppm) = 137.5, 128.7, 128.1, 127.9, 73.7, 69.8, 61.1.

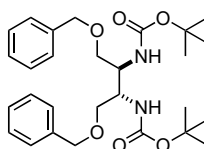
1,4-bis(benzyloxy)butane-2,3-diamine (*trans*) **29T**



Pd/C (10 %, 39 mg, 33 μ mol, 0.05 equiv.) was added to a hydrogenation tube and wetted with ca. 0.5 mL DCM. Next, a solution of **28T** (0.20 g, 0.57 mmol, 1.0 equiv.) in methanol (6 mL, 0.1 M) was carefully added. The reaction vessel was sealed, and the heterogeneous mixture was hydrogenated at 7 bar for 16 h. The catalyst was removed by filtration over Celite, and the filter cake was extensively washed with MeOH and then disposed of in a separate hydrogenation waste container while still wet. The filtrate was concentrated to give **29T** as a colourless oil (0.16 g, 0.55 mmol, 96%).

1H -NMR (400 MHz, $CDCl_3$) δ (ppm) = 7.36 – 7.28 (m, 10H), 4.51 (s, 4H), 3.51 (dd, J = 9.2, 4.1 Hz, 2H), 3.42 (dd, J = 9.2, 6.3 Hz, 2H), 3.06 – 2.95 (m, 2H). **^{13}C -NMR** (101 MHz, $CDCl_3$) δ (ppm) = 138.4, 128.6, 127.8, 73.6, 73.4, 52.8.

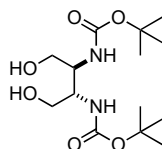
di-*tert*-butyl (1,4-bis(benzyloxy)butane-2,3-diyl)dicarbamate (*trans*) **31**



To a solution of **29T** (1.2 g, 4.0 mmol, 1.0 equiv.) in a 1:1 mixture of dioxane/water (8 mL, 0.5 M), NEt_3 (2.8 mL, 20 mmol, 5.0 equiv.), di-*tert*-butyl dicarbonate (2.1 g, 9.6 mmol, 2.4 equiv.) and DMAP (98 mg, 0.80 mmol, 0.2 equiv.) were added at 0 °C. The reaction mixture was allowed to warm to r.t. while stirring overnight. The reaction mixture was diluted with DCM, acidified to pH < 3 using aqueous HCl (2 M) and extracted with DCM (three times). The combined organic layers were washed with NaCl (sat. aq.), dried over $MgSO_4$ and concentrated *in vacuo*. Purification by FCC (isohexanes/EtOAc 8:1 \rightarrow 4:1) gave **31** as a colourless solid (1.4 g, 2.8 mmol, 71%).

TLC R_f = 0.33 (isohexanes:EtOAc, 4:1). **HRMS** (ESI): $C_{28}H_{41}N_2O_6^+$ [M+H] $^+$: calc. m/z 501.2959, found: 501.2963. **1H -NMR** (400 MHz, $CDCl_3$) δ (ppm) = 7.37 – 7.27 (m, 10H), 5.24 (s, 2H), 4.48 (d, J = 11.9 Hz, 2H), 4.38 (d, J = 12.0 Hz, 2H), 3.98 (s, 2H), 3.55 – 3.42 (m, 4H), 1.43 (s, 18H). **^{13}C -NMR** (101 MHz, $CDCl_3$) δ (ppm) = 138.0, 128.5, 127.9, 79.5, 73.4, 69.8, 51.8, 28.5.

di-*tert*-butyl (1,4-dihydroxybutane-2,3-diyl)dicarbamate (*trans*) **32T**

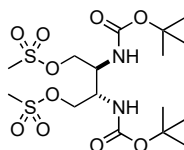


Pd/C (10 %, 21 mg, 20 μ mol, 0.1 equiv.) was added to a hydrogenation tube and wetted with ca. 0.2 mL DCM. The black slurry was charged with a solution of **31** (0.1 g, 0.2 mmol, 1.0 equiv.) in MeOH (2 mL, 0.1 M) and the reaction vessel was sealed. The heterogeneous reaction mixture was hydrogenated at 40 bar for 2 d, upon which the catalyst was removed by filtration over Celite. The filter cake was extensively washed with MeOH and then disposed of in a separate hydrogenation waste container while still wet. The filtrate was concentrated and the crude product was purified by FCC (hexanes/EtOAc 4:1 \rightarrow 1:1) to give **32T** as a colourless solid (59 mg, 0.18 mmol, 90%).

Notes: (1) The title compound exhibited poor solubility in both DCM and EtOAc, which resulted in the compound eluting over many fractions during purification. (2) As an alternative, the two-step protocol from **29C** to **32C** can also be applied here to avoid the high pressure and prolonged reaction time needed for hydrogenation.

TLC R_f = 0.38 (EtOAc). **HRMS** (ESI): $C_{14}H_{29}N_2O_6^+$ $[M+H]^+$: calc. m/z 321.2020, found: 321.2029. **1H -NMR** (400 MHz, $CDCl_3$) δ (ppm) = 4.85 (s, 2H), 3.86 (s, 2H), 3.74 (d, J = 9.5 Hz, 4H), 3.50 (s, 2H), 1.45 (s, 18H). **^{13}C -NMR** (101 MHz, $CDCl_3$) δ (ppm) = 157.3, 80.4, 62.9, 52.6, 28.4.

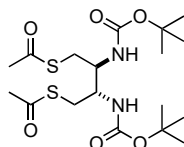
2,3-bis((tert-butoxycarbonyl)amino)butane-1,4-diyl dimethanesulfonate (trans) 33



Following **general protocol A**, **32T** (0.32 g, 1.0 mmol, 1.0 equiv.) in pyridine (10 mL, 0.1 M), was reacted with $MsCl$ (0.18 mL, 2.3 mmol, 2.3 equiv.) giving **33** as a colourless solid (0.31 g, 0.66 mmol, 66%) after precipitation from water and ensuing filtration and washings.

HRMS (EI): $C_{16}H_{32}N_2NaO_{10}S_2^+$ $[M+Na]^+$: calc. m/z 499.1491, found: 499.1496, **1H -NMR** (400 MHz, $CDCl_3$) δ (ppm): 5.23 (s, 2H), 4.33 (s, 4H), 4.08 (d, J = 4.4 Hz, 2H), 3.07 (s, 6H), 1.45 (s, 18H). **^{13}C -NMR** (101 MHz, $CDCl_3$) δ (ppm): 156.1, 80.8, 68.0, 50.4, 37.7, 28.4.

2,3-bis((tert-butoxycarbonyl)amino)butane-1,4-diyl dimethanesulfonate (trans) 34

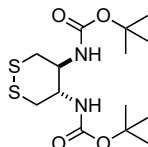


A solution of **33** (0.28 g, 0.59 mmol, 1.0 equiv.) and $KSAc$ (0.20 g, 1.8 mmol, 3.0 equiv.) in acetone (6 mL, 0.1 M) was stirred at 50 °C for 2 h. The reaction was diluted with DCM and $NaHCO_3$ (sat. aq.), and the aqueous layer was extracted with DCM (three times). The combined organic layers were washed with $NaCl$ (sat. aq.), dried over $MgSO_4$, filtered, and concentrated, giving a dark red crude solid. Purification by FCC (isohexanes/EtOAc 3:1) gave **34** as a colourless solid (0.23 g, 0.59 mmol, 90%).

Note: The reaction of $KSAc$ with alkyl mesylates in acetone quickly leads to the formation of insoluble KOMs which, especially on a larger scale, can prevent proper stirring of the reaction mixture. Whenever stirring is impeded, dilution down to a 0.02 M suspension in acetone is advisable.

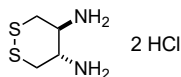
TLC R_f = 0.33 (isohexanes:EtOAc, 3:1). **HRMS** (ESI): $C_{18}H_{33}N_2O_6S_2^+$ $[M+H]^+$: calc. m/z 437.1775, found: 437.1780. **1H -NMR** (400 MHz, $CDCl_3$) δ (ppm) = 4.87 (s, 2H), 3.80 (s, 2H), 3.09 (d, J = 6.0 Hz, 4H), 2.35 (s, 6H), 1.43 (s, 18H). **^{13}C -NMR** (101 MHz, $CDCl_3$) δ (ppm) = 196.0, 156.4, 80.0, 54.1, 31.8, 30.7, 28.5.

di-tert-butyl (1,2-dithiane-4,5-diyl)dicarbamate (trans) 35T



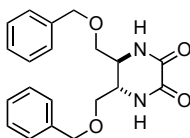
To a solution of **34** (0.23 g, 0.52 mmol, 1.0 equiv.) in MeOH (10 mL, 0.05 M), a methanolic solution of KOH (0.2 M, 10 mL, 2.1 mol, 4.0 equiv.) was added. The reaction was continuously purged with air and stirred overnight. The colourless solution was diluted with water and the aqueous layer was extracted with EtOAc (two times). The combined organic layers were dried over $MgSO_4$ and concentrated, giving **35T** as a colourless solid and without further purification (0.18 g, 0.51 mmol, 98%).

TLC R_f = 0.29 (isohexanes:EtOAc, 9:1). **HRMS** (EI): $C_{14}H_{26}N_2O_4S_2^+$ $[M]^+$: calc. m/z 350.1334, found: 350.1331. **1H -NMR** (400 MHz, $CDCl_3$) δ (ppm) = 5.04 (s, 2H), 3.91 – 3.57 (m, 2H), 3.12 (s, 2H), 2.85 (s, 2H), 1.43 (s, 18H). **^{13}C -NMR** (101 MHz, $CDCl_3$) δ (ppm) = 156.0, 80.2, 55.4, 40.5, 28.5.

1,2-dithiane-4,5-diamine dihydrochloride (*trans*) 36T

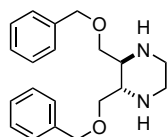
35T (170 mg, 0.485 mmol, 1.0 equiv.) was suspended in DCM (0.15 M, 3 mL) and HCl/dioxane (3.65 mL of a 4 M solution, 14.6 mmol, 30 equiv.) was added in one portion. The mixture was stirred at r.t. for 2 h and was then poured into Et₂O (100 mL). The precipitate was filtered off and washed with Et₂O (10 mL), the filtrate was dried under reduced pressure to give **36T** as a colourless solid (106 mg, 0.475 mmol, 98%).

¹H-NMR (400 MHz, DMSO-*d*₆): δ (ppm) = 8.82 (s, 6H), 3.65 (d, *J* = 6.5 Hz, 2H), 3.58 (d, *J* = 13.6 Hz, 2H), 3.08 (dd, *J* = 13.8, 6.9 Hz, 2H).

5,6-bis((benzyloxy)methyl)piperazine-2,3-dione (*trans*) 39

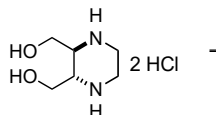
A solution of **29T** (0.50 g, 1.7 mmol, 1.0 equiv.) and dimethyloxalate (0.22 g, 1.8 mmol, 1.1 equiv.) in toluene (30 mL, 0.06 M) was stirred at 110 °C for 22 h. Once LCMS control indicated full conversion of the starting material, the reaction was diluted with NaHCO₃ (sat. aq.) and the aqueous layer was extracted with DCM (three times). The combined organic layers were dried over MgSO₄ and concentrated giving **39** as a yellow solid and without further purification (0.53 g, 1.5 mmol, 88%).

HRMS (ESI): C₂₀H₂₃N₂O₄ [M+H]⁺: calc. *m/z* 355.16523, found: 355.16571. **¹H-NMR** (400 MHz, CDCl₃) δ (ppm) = 7.54 (d, *J* = 3.1 Hz, 2H), 7.45 – 7.26 (m, 10H), 4.58 – 4.42 (m, 4H), 3.81 (dt, *J* = 6.4, 3.7 Hz, 2H), 3.57 (dd, *J* = 9.6, 5.8 Hz, 2H), 3.51 (dd, *J* = 9.5, 5.8 Hz, 2H). **¹³C-NMR** (101 MHz, CDCl₃) δ (ppm) = 158.0, 137.1, 128.8, 128.3, 128.0, 73.7, 70.0, 51.4.

2,3-bis((benzyloxy)methyl)piperazine (*trans*) 40

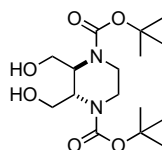
39 (0.30 g, 0.85 mmol, 1.0 equiv.) was dissolved in dry THF (10 mL, 0.1 M) and carefully charged with LAH (0.32 g, 8.5 mmol, 10 equiv.). The mixture was heated to 65 °C and stirred for 6 h. The reaction was monitored by LCMS analysis, and once full conversion was achieved, the reaction was quenched with NaOH (2 M in water) and diluted with EtOAc. The organic layer was extracted with HCl (2 M in water, two times) and the combined aqueous layers were basified with NaOH (6 M in water) and back-extracted with EtOAc (three times). The combined organic layers were dried over MgSO₄, filtered and concentrated to yield **40** as a yellow oil (0.22 g, 0.68 mmol, 81%).

HRMS (ESI): C₂₀H₂₇N₂O₂⁺ [M+H]⁺: calc. *m/z* 327.2067, found: 327.2069. **¹H-NMR** (400 MHz, CDCl₃) δ (ppm) = 7.41 – 7.23 (m, 10H), 4.48 (dd, *J* = 11.6, 6.5 Hz, 4H), 3.52 (dd, *J* = 9.1, 2.4 Hz, 2H), 3.42 – 3.31 (m, 2H), 2.95 (d, *J* = 8.2 Hz, 2H), 2.79 (d, *J* = 8.1 Hz, 2H), 2.77 – 2.68 (m, 2H), 2.45 (s, 2H). **¹³C-NMR** (101 MHz, CDCl₃) δ (ppm) = 138.18, 128.56, 127.91, 127.87, 73.64, 71.57, 57.45, 46.47.

piperazine-2,3-diyl)dimethanol dihydrochloride (*trans*) 41

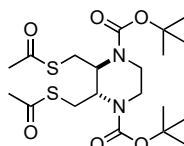
A mixture of **40** (3.6 g, 11 mmol, 1.0 equiv.) was suspended in concentrated hydrochloric acid (30 mL) and the mixture was heated to 80 °C and stirred for 4 h. The solvent was removed *in vacuo*, and the residue was repeatedly washed with EtOH to giving **41** as an off-white solid (2.6 g, 11 mmol, 100%).

HRMS (ESI): C₆H₁₅N₂O₂⁺ [M+H]⁺: calc. *m/z* 147.1128, found: 147.1129. **¹H-NMR** (400 MHz, D₂O) δ (ppm) = 3.99 (dt, *J* = 13.2, 1.3 Hz, 1H), 3.92 (dt, *J* = 13.2, 2.1 Hz, 1H), 3.79 (d, *J* = 9.9 Hz, 1H), 3.73 (q, *J* = 1.8 Hz, 1H), 3.50 (d, *J* = 9.9 Hz, 1H). **¹³C-NMR** (101 MHz, D₂O) δ (ppm) = 57.3, 55.0, 40.0.

di-*tert*-butyl 2,3-bis(hydroxymethyl)piperazine-1,4-dicarboxylate (*trans*) 42

41 (50 mg, 0.23 mmol, 1.0 equiv.) was dissolved in a 1:1 mixture of water and dioxane (1 mL, 0.25 M) and cooled to 0 °C. The solution was charged with DIPEA (0.25 mL, 1.4 mmol, 6.0 equiv.) and Boc₂O (0.15 g, 0.69 mmol, 3.0 equiv.) and was allowed to warm to r.t. overnight. The reaction was quenched with NH₄Cl (sat. aq.) and the aqueous layer was extracted with DCM (three times). The combined organic layers were washed with water, dried over MgSO₄ and concentrated giving a yellow crude oil. Purification by FCC (hexanes/EtOAc 1:1 → EtOAc) gave the **42** as a colourless oil (60 mg, 0.17 mmol, 74%). **42** gives a mixture of rotameric species in NMR analysis. Signals are not deconvoluted.

TLC R_f = 0.40 (EtOAc). **LRMS** (ESI): C₁₆H₃₁N₂O₆⁺ [M+H]⁺: calc. *m/z* 347.22, found 347.25. **¹H-NMR** (400 MHz, CDCl₃) δ (ppm) = 4.27 (dt, *J* = 15.2, 7.6 Hz, 1H), 4.17 – 4.05 (m, 1H), 3.95 – 3.81 (m, 1H), 3.77 – 3.49 (m, 4H), 2.97 (q, *J* = 10.3, 7.5 Hz, 2H), 2.83 (ddd, *J* = 16.4, 12.1, 6.1 Hz, 1H), 1.39 (s, 18H). **¹³C-NMR** (101 MHz, CDCl₃) δ (ppm) = 156.8, 156.4, 155.6, 81.1, 80.9, 60.6, 60.0, 52.6, 51.4, 51.1, 39.5, 39.4, 38.2, 28.5.

di-*tert*-butyl 2,3-bis((acetylthio)methyl)piperazine-1,4-dicarboxylate (*trans*) 43

To PPh₃ (0.95 g, 3.6 mmol, 2.4 equiv.) in anhydrous THF (15 mL, 0.25 M) under nitrogen atmosphere was added DIAD (40% in toluene, 1.9 mL, 3.8 mmol, 2.5 equiv.) in a dropwise manner at 0 °C. After the reaction mixture had stirred for 30 min, a solution of **42** (0.52 g, 1.5 mmol, 1.0 equiv.) in anhydrous THF (5 mL, 0.3 M) and neat HSAC (0.27 mL, 3.8 mmol, 2.5 equiv.) were added sequentially. The reaction mixture was stirred at 0 °C for 1 h, was then allowed to warm to r.t. and was stirred for another 15 h. All volatiles were removed, and the crude oil was purified by FCC (hexanes/EtOAc 6:1 → 4:1), giving **43** as a colourless solid (0.3 g, 0.65 mmol, 43%). **43** gives a mixture of rotameric species in NMR analysis. Signals are not deconvoluted.

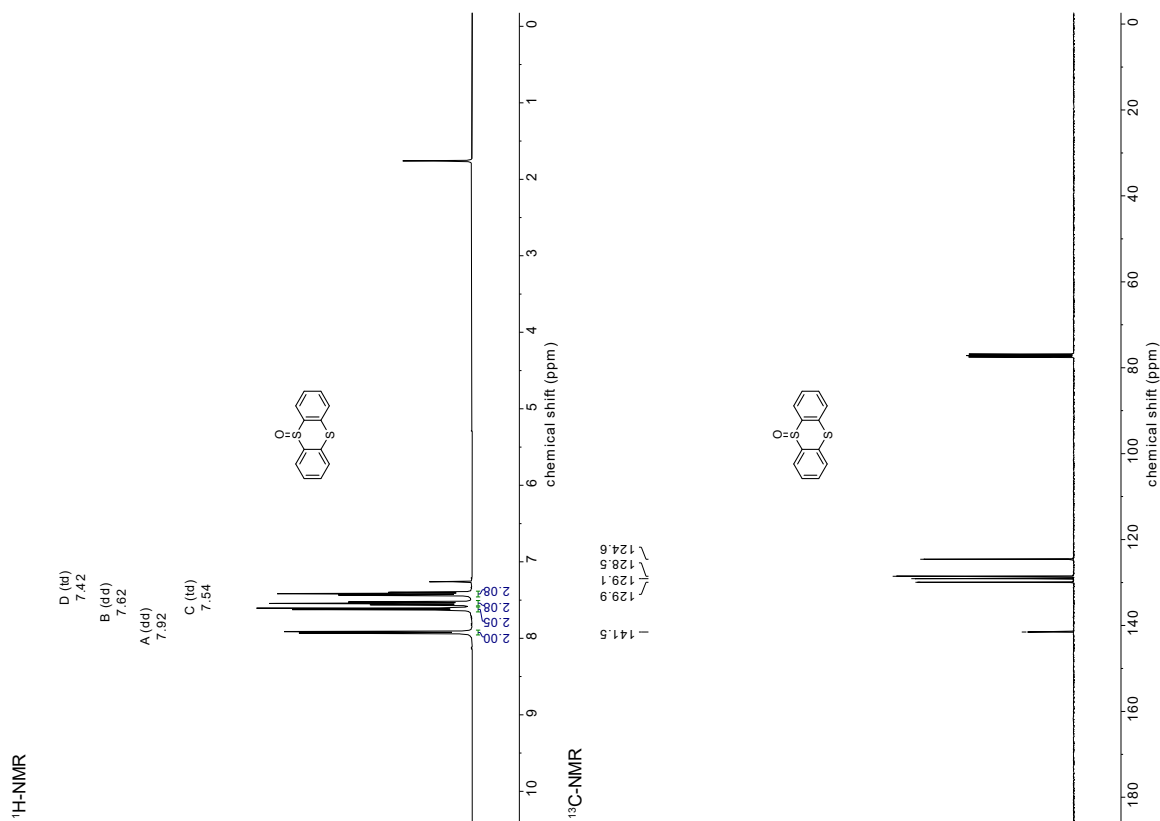
TLC R_f = 0.63 (hexanes/EtOAc 3:1). **LRMS** (ESI): C₂₀H₃₅N₂O₆S₂⁺ [M+H]⁺: calc. *m/z* 463.19, found: 463.25. **¹H-NMR** (400 MHz, CDCl₃) δ (ppm) 4.43 – 4.11 (m, 2H), 4.04 – 3.67 (m, 2H), 3.27 – 2.72 (m, 6H), 2.50 – 2.18 (m, 6H), 1.43 (s, 18H).

8. Supporting Information Bibliography

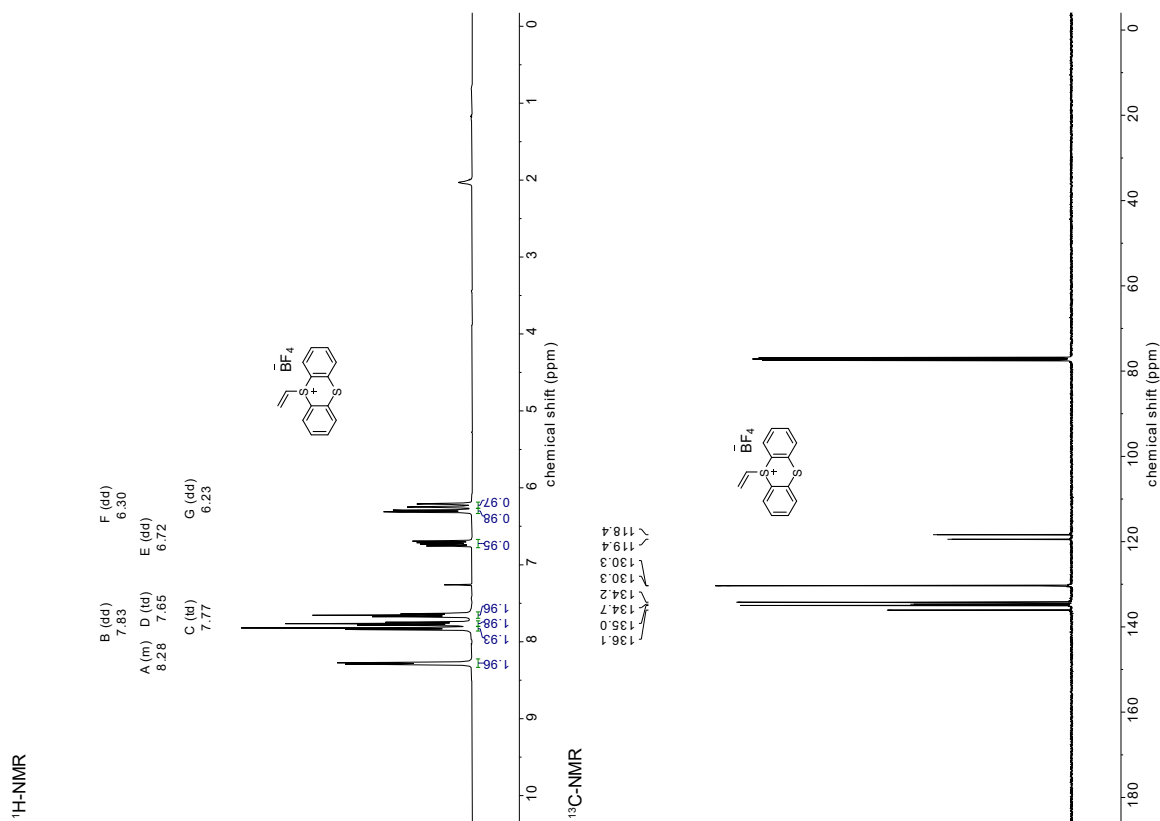
- (1) Felber, J. G.; Zeisel, L.; Poczka, L.; Scholzen, K.; Busker, S.; Maier, M. S.; Theisen, U.; Brandstädter, C.; Becker, K.; Arnér, E. S. J.; Thorn-Seshold, J.; Thorn-Seshold, O. Selective, Modular Probes for Thioredoxins Enabled by Rational Tuning of a Unique Disulfide Structure Motif. *J. Am. Chem. Soc.* **2021**, *143* (23), 8791–8803. <https://doi.org/10.1021/jacs.1c03234>.
- (2) Lukesh, J. C.; Palte, M. J.; Raines, R. T. A Potent, Versatile Disulfide-Reducing Agent from Aspartic Acid. *J. Am. Chem. Soc.* **2012**, *134* (9), 4057–4059. <https://doi.org/10.1021/ja211931f>.
- (3) Equivalent (Chemistry). *Wikipedia*; 2022.
- (4) Zeisel, L.; Felber, J. G.; Scholzen, K. C.; Poczka, L.; Cheff, D.; Maier, M. S.; Cheng, Q.; Shen, M.; Hall, M. D.; Arnér, E. S. J.; Thorn-Seshold, J.; Thorn-Seshold, O. Selective Cellular Probes for Mammalian Thioredoxin Reductase TrxR1: Rational Design of RX1, a Modular 1,2-Thiaselenane Redox Probe. *Chem* **2022**, *8* (5), 1493–1517. <https://doi.org/10.1016/j.chempr.2022.03.010>.
- (5) Peng, X.; Mandal, P. K.; Kaminsky, V. O.; Lindqvist, A.; Conrad, M.; Arnér, E. S. J. Sec-Containing TrxR1 Is Essential for Self-Sufficiency of Cells by Control of Glucose-Derived H₂O₂. *Cell Death Dis* **2014**, *5*, e1235. <https://doi.org/10.1038/cddis.2014.209>.
- (6) Stephens, P. J.; Devlin, F. J.; Chabalowski, C. F.; Frisch, M. J. Ab Initio Calculation of Vibrational Absorption and Circular Dichroism Spectra Using Density Functional Force Fields. *J. Phys. Chem.* **1994**, *98* (45), 11623–11627. <https://doi.org/10.1021/j100096a001>.
- (7) Grimme, S.; Ehrlich, S.; Goerigk, L. Effect of the Damping Function in Dispersion Corrected Density Functional Theory. *Journal of Computational Chemistry* **2011**, *32* (7), 1456–1465. <https://doi.org/10.1002/jcc.21759>.
- (8) te Velde, G.; Bickelhaupt, F. M.; Baerends, E. J.; Fonseca Guerra, C.; van Gisbergen, S. J. A.; Snijders, J. G.; Ziegler, T. Chemistry with ADF. *Journal of Computational Chemistry* **2001**, *22* (9), 931–967. <https://doi.org/10.1002/jcc.1056>.
- (9) Klamt, A. Conductor-like Screening Model for Real Solvents: A New Approach to the Quantitative Calculation of Solvation Phenomena. *J. Phys. Chem.* **1995**, *99* (7), 2224–2235. <https://doi.org/10.1021/j100007a062>.
- (10) Andreas Klamt, *; Volker Jonas, †; Thorsten Bürger, and; Lohrenz, J. C. W. *Refinement and Parametrization of COSMO-RS*. ACS Publications. <https://doi.org/10.1021/jp980017s>.
- (11) Patterson, G. H.; Knobel, S. M.; Arkhammar, P.; Thastrup, O.; Piston, D. W. Separation of the Glucose-Stimulated Cytoplasmic and Mitochondrial NAD(P)H Responses in Pancreatic Islet β Cells. *5*.
- (12) Dóka, É.; Pader, I.; Bíró, A.; Johansson, K.; Cheng, Q.; Ballagó, K.; Prigge, J. R.; Pastor-Flores, D.; Dick, T. P.; Schmidt, E. E.; Arnér, E. S. J.; Nagy, P. A Novel Persulfide Detection Method Reveals Protein Persulfide- and Polysulfide-Reducing Functions of Thioredoxin and Glutathione Systems. *Sci Adv* **2016**, *2* (1), e1500968. <https://doi.org/10.1126/sciadv.1500968>.
- (13) Cheng, Q.; Arnér, E. S. J. Overexpression of Recombinant Selenoproteins in E. Coli. In *Selenoproteins: Methods and Protocols*; Chavatte, L., Ed.; Methods in Molecular Biology; Springer: New York, NY, 2018; pp 231–240. https://doi.org/10.1007/978-1-4939-7258-6_17.
- (14) Mandal, P. K.; Schneider, M.; Kolle, P.; Kuhlencordt, P.; Forster, H.; Beck, H.; Bornkamm, G. W.; Conrad, M. Loss of Thioredoxin Reductase 1 Renders Tumors Highly Susceptible to Pharmacologic Glutathione Deprivation. *Cancer Research* **2010**, *70* (22), 9505–9514. <https://doi.org/10.1158/0008-5472.CAN-10-1509>.
- (15) Juliá, F.; Yan, J.; Paulus, F.; Ritter, T. Vinyl Thianthrenium Tetrafluoroborate: A Practical and Versatile Vinylating Reagent Made from Ethylene. *J. Am. Chem. Soc.* **2021**, *jacs.1c06632*. <https://doi.org/10.1021/jacs.1c06632>.
- (16) Minakata, S.; Miwa, H.; Yamamoto, K.; Hirayama, A.; Okumura, S. Diastereodivergent Intermolecular 1,2-Diamination of Unactivated Alkenes Enabled by Iodine Catalysis. *J. Am. Chem. Soc.* **2021**, *143* (11), 4112–4118. <https://doi.org/10.1021/jacs.1c00228>.
- (17) Ellison, A. J.; Raines, R. T. A Pendant Peptide Endows a Sunscreen with Water-Resistance. *Org. Biomol. Chem.* **2018**, *16* (39), 7139–7142. <https://doi.org/10.1039/C8OB01773E>.

9. NMR spectra

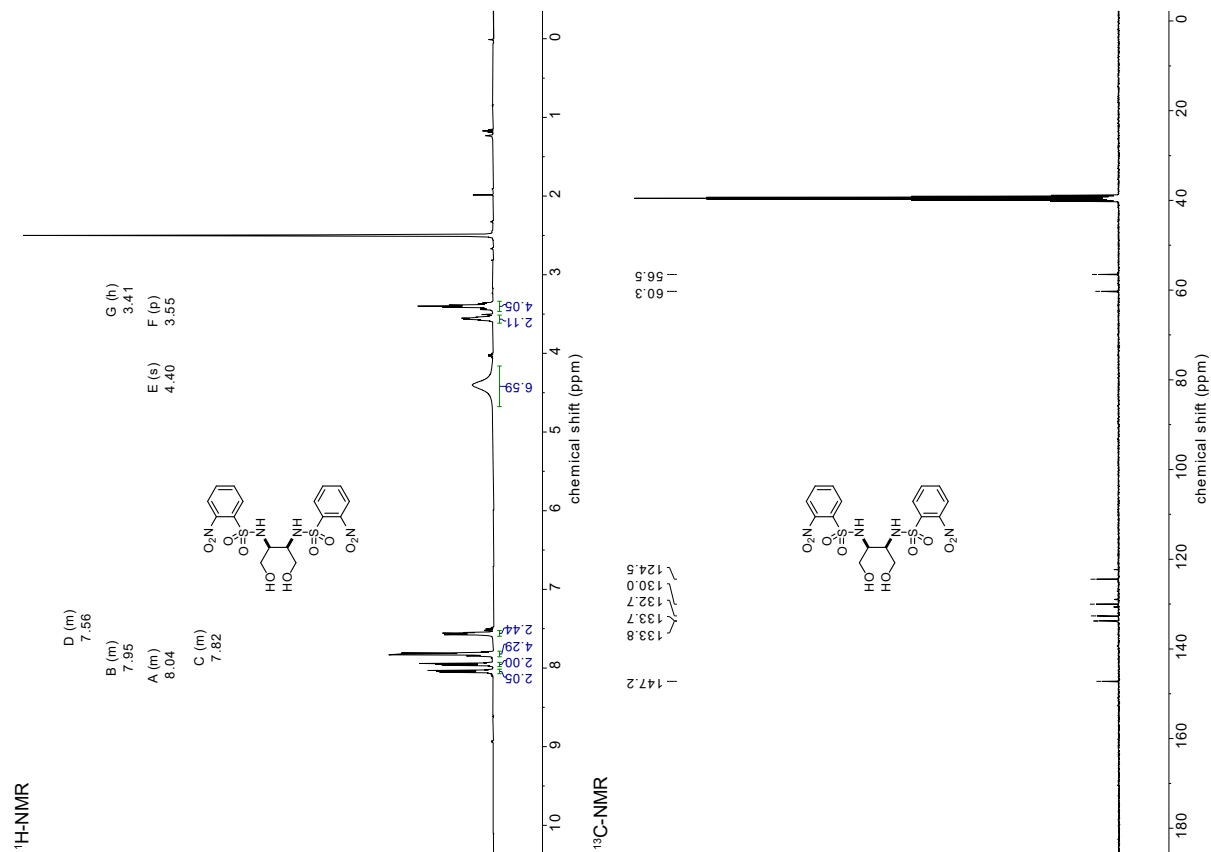
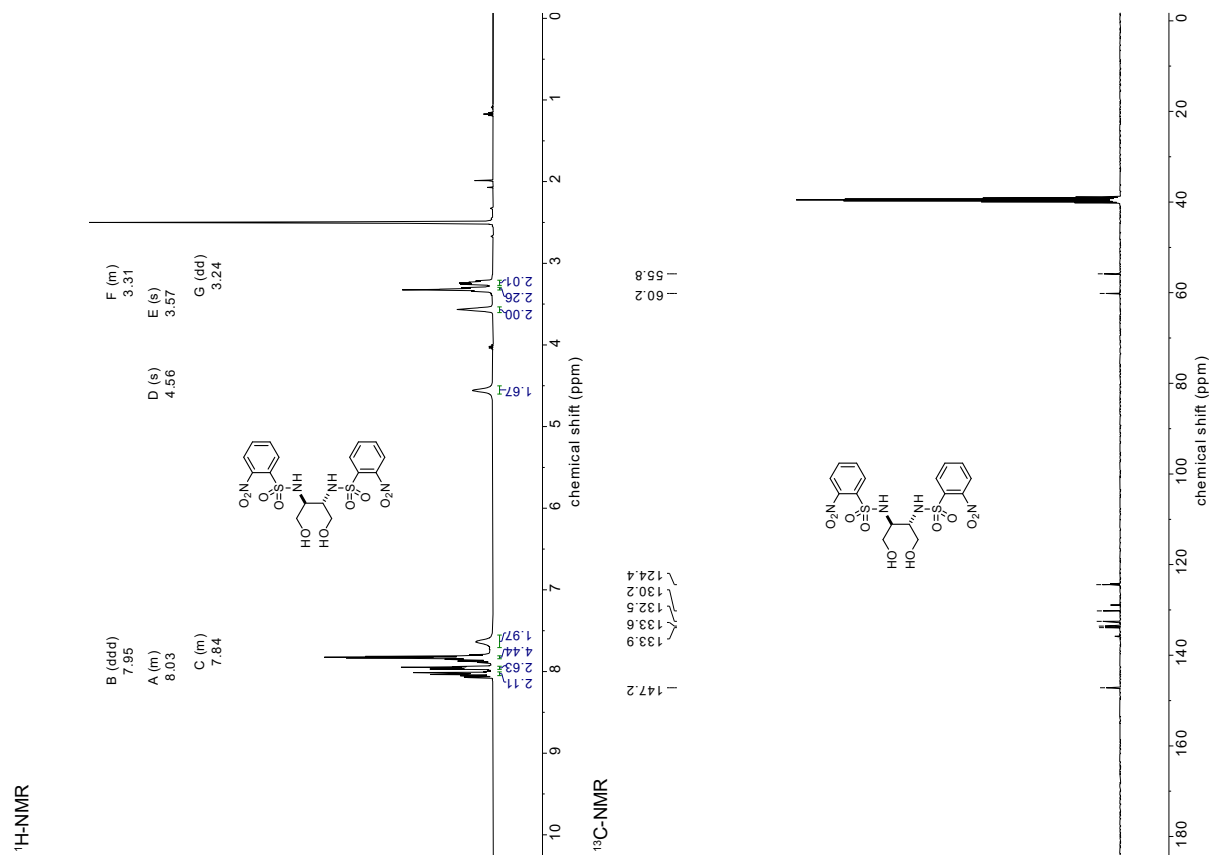
60

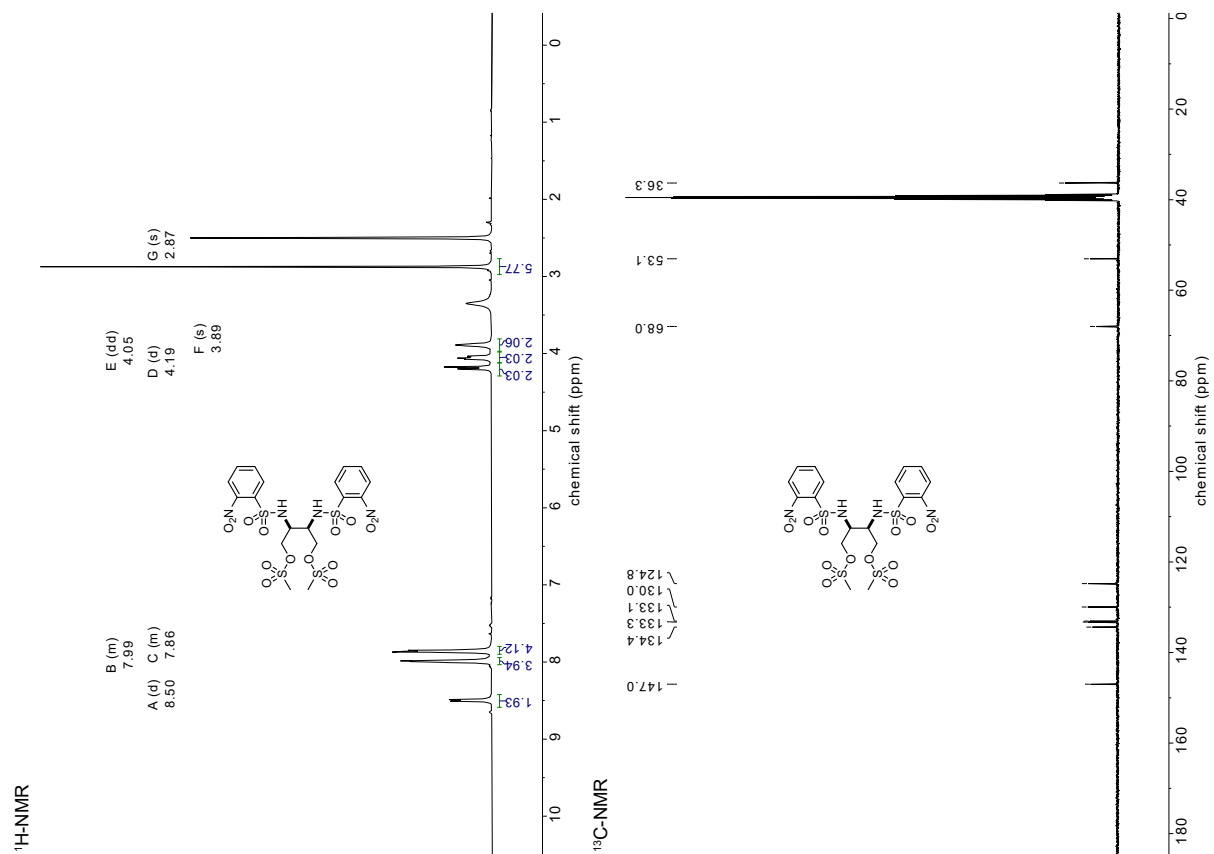
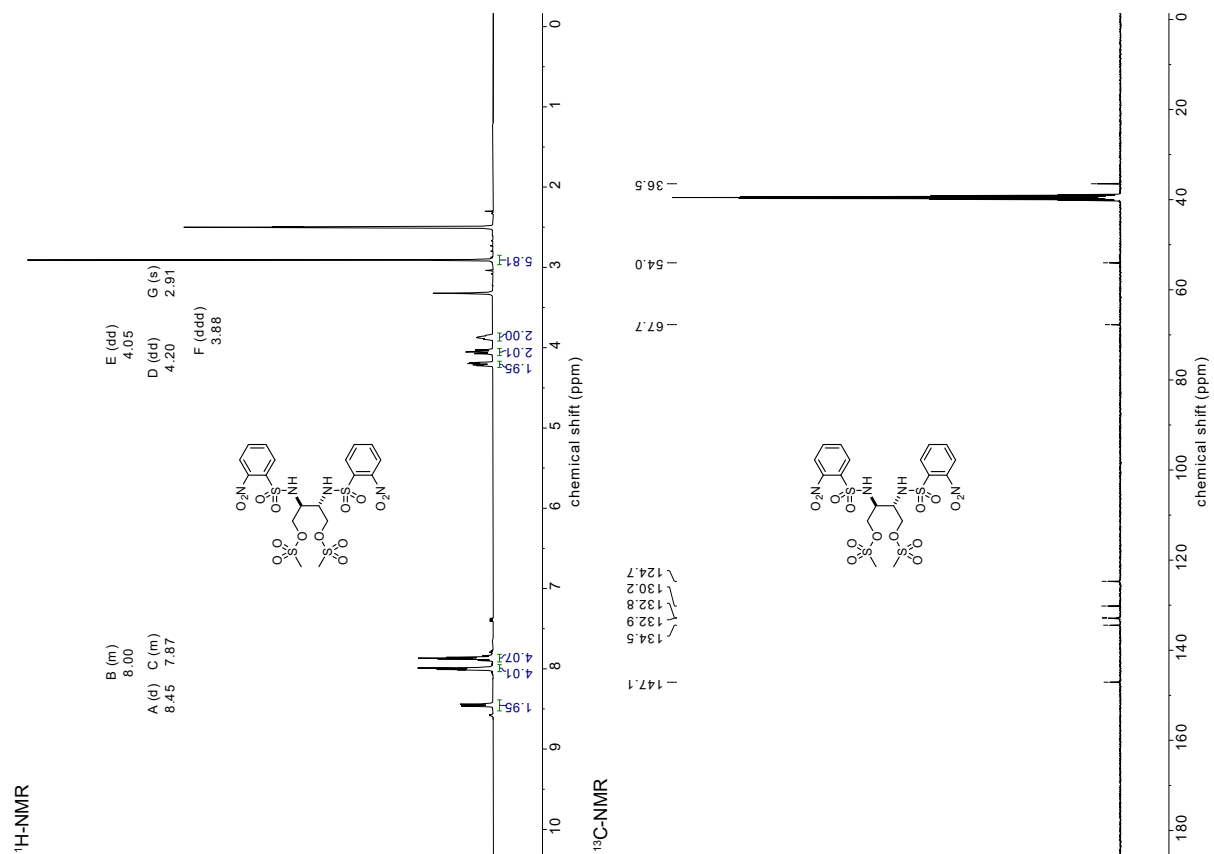


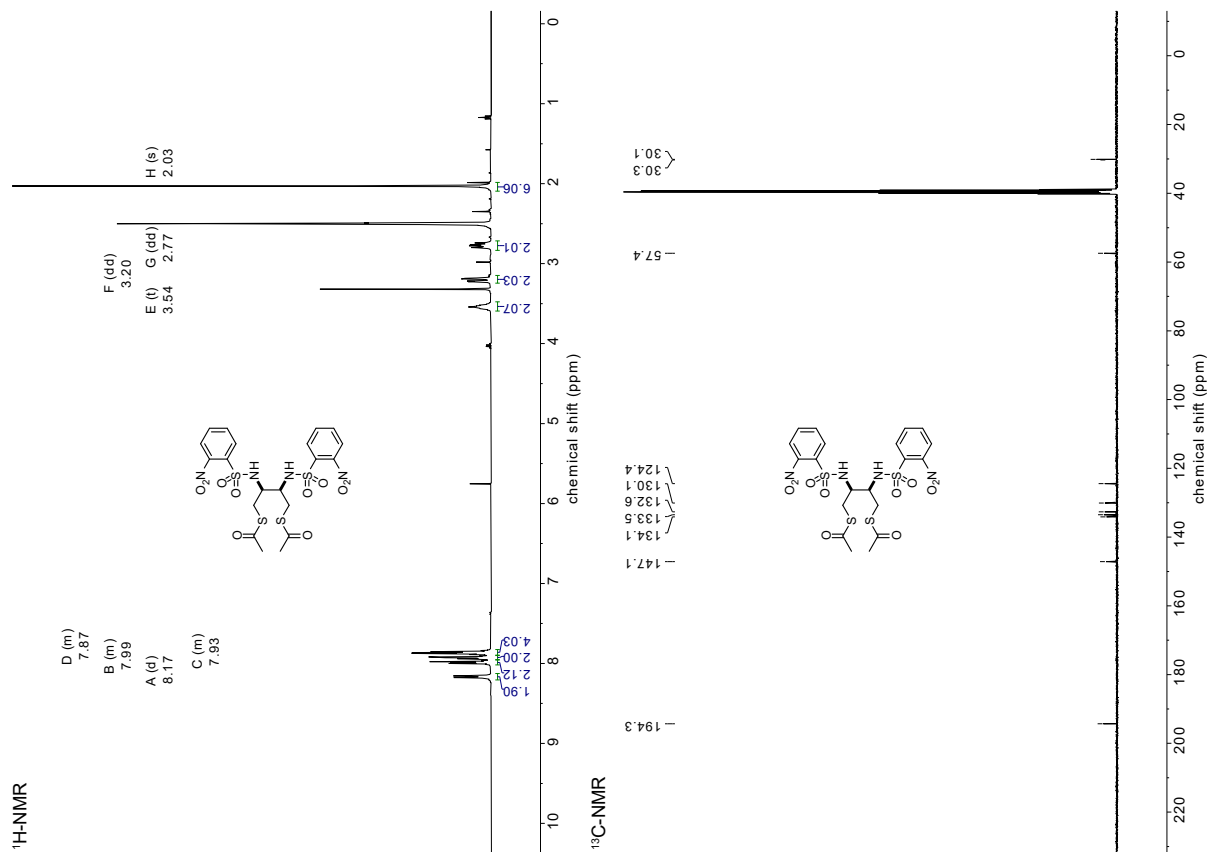
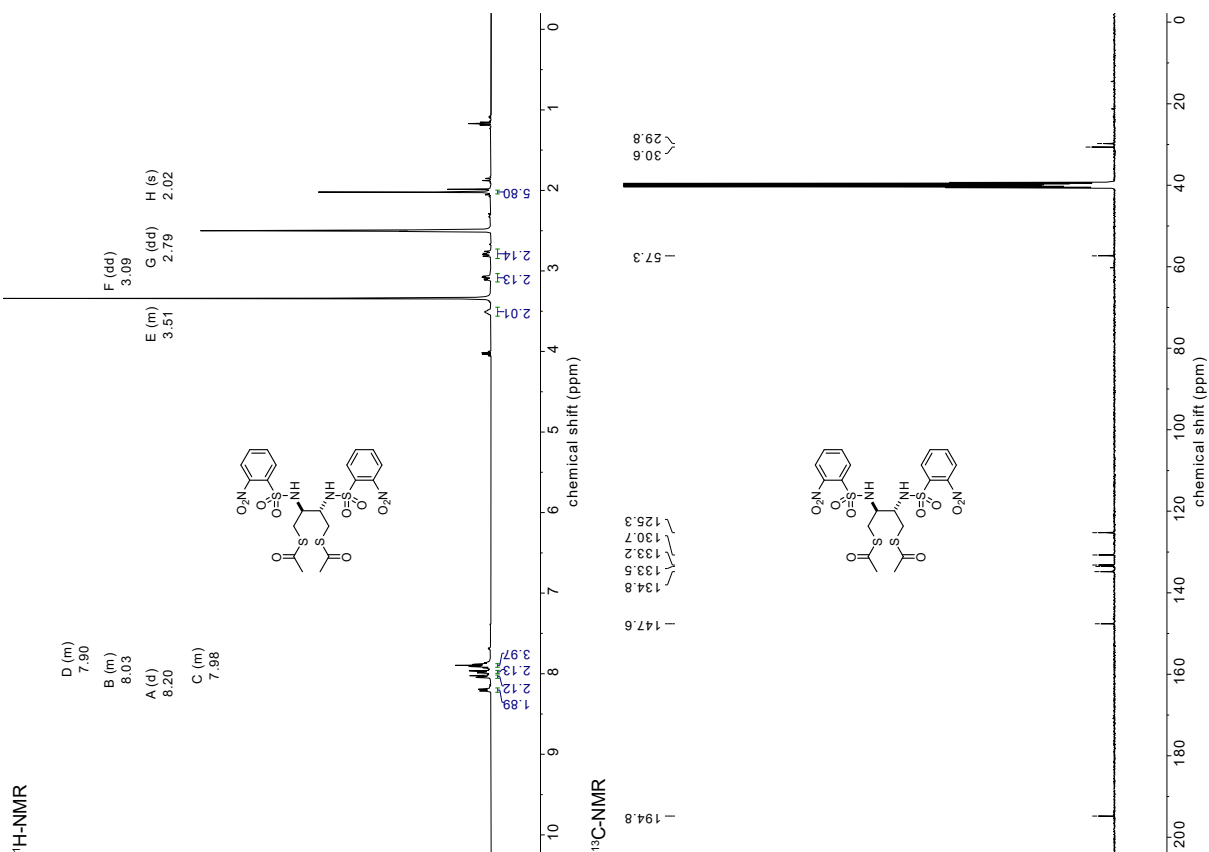
VTT 61

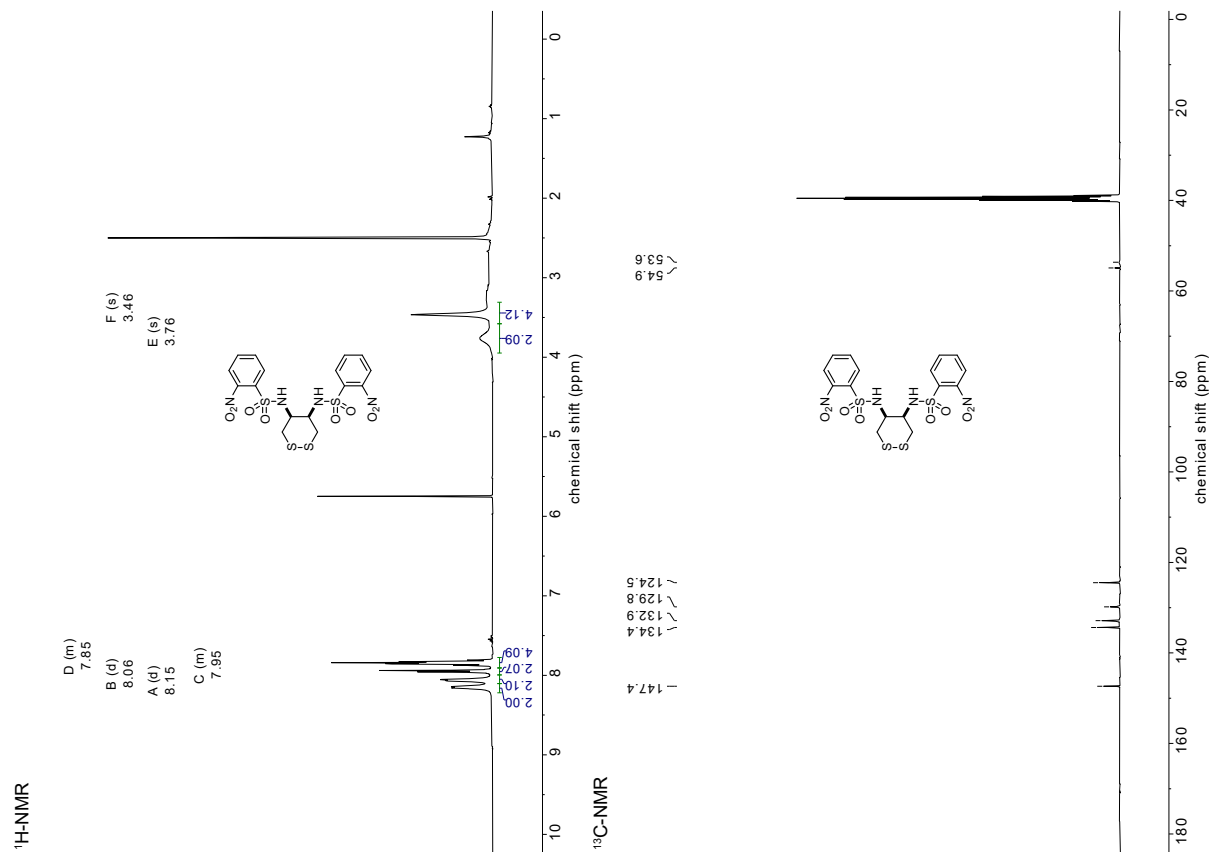
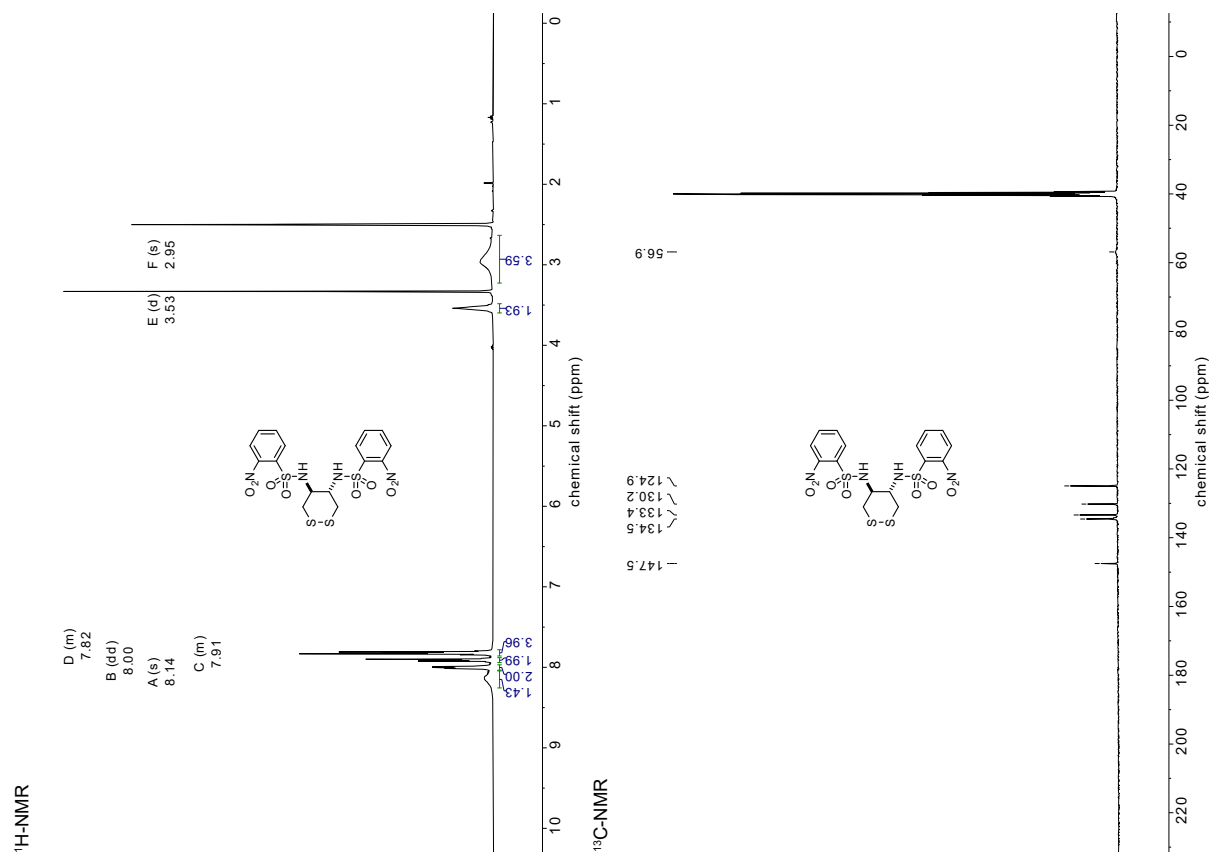


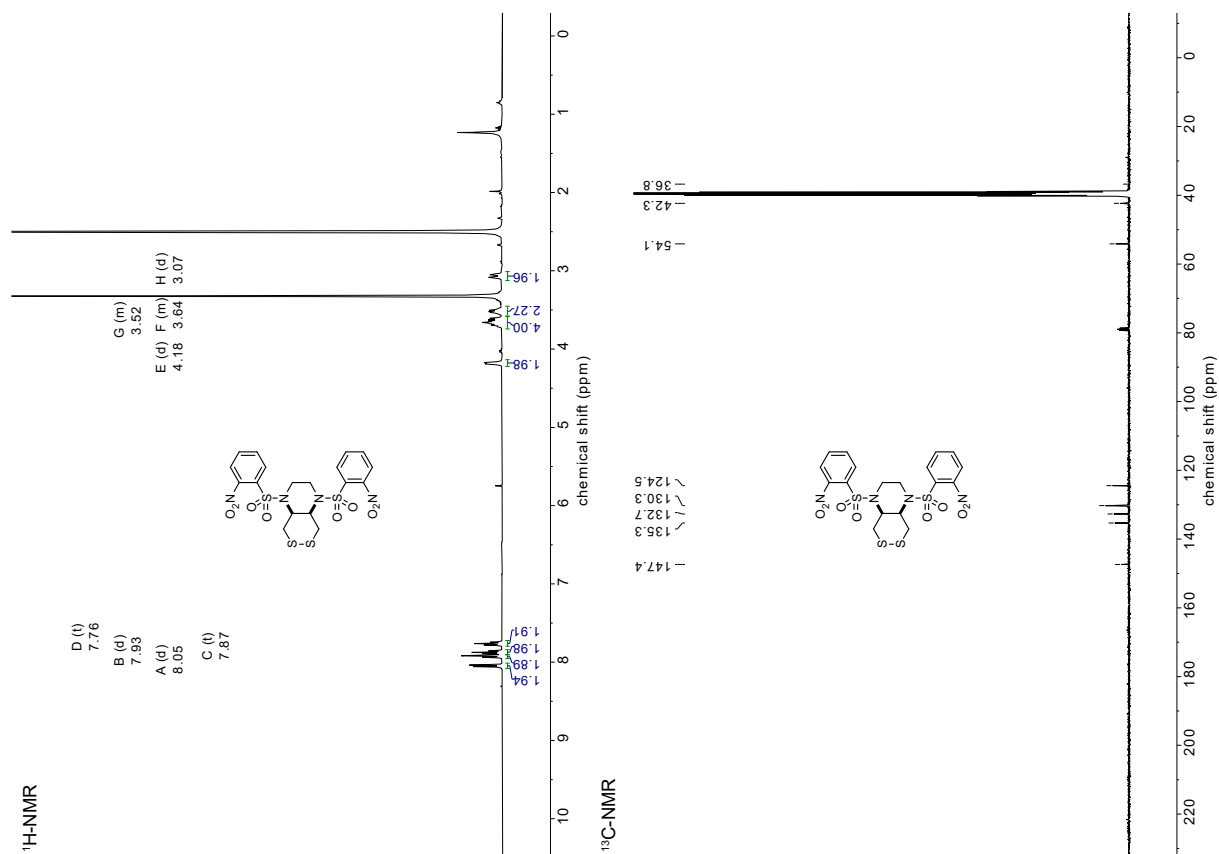
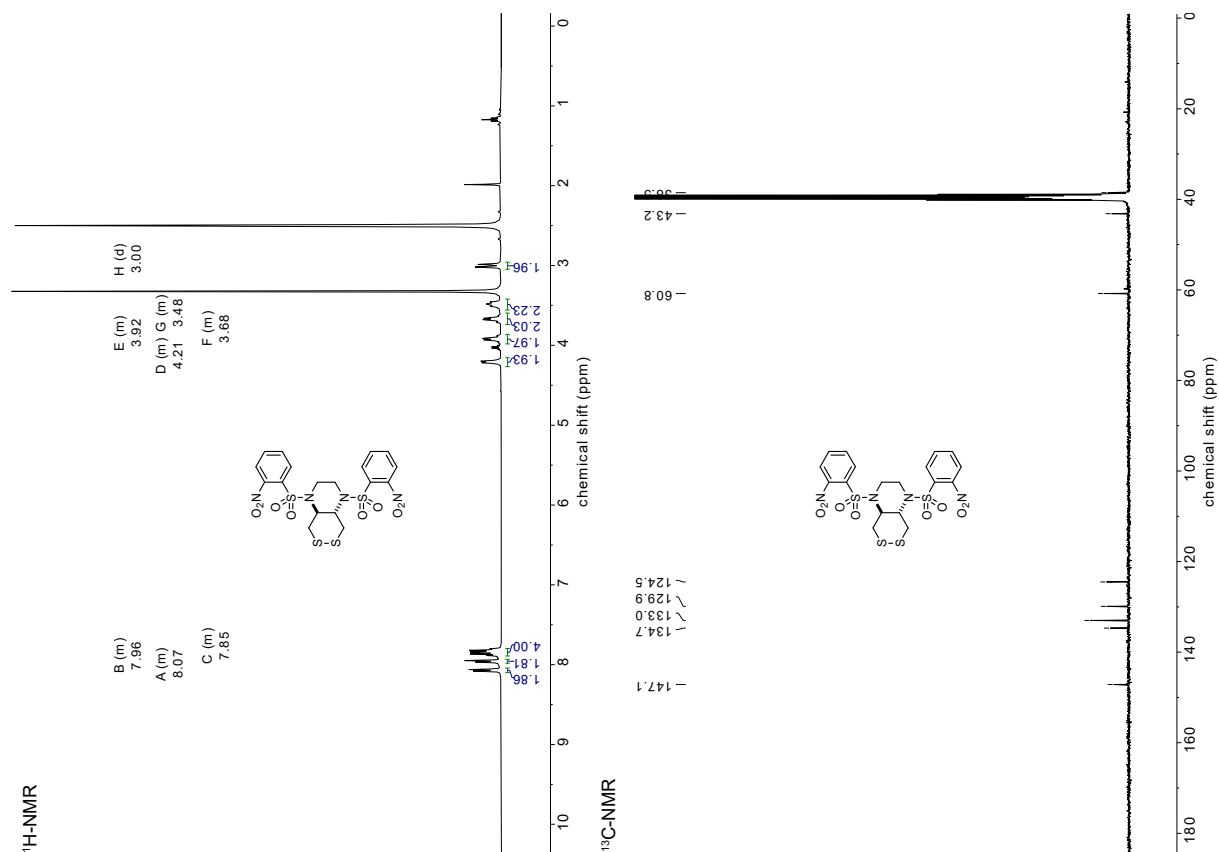
S67

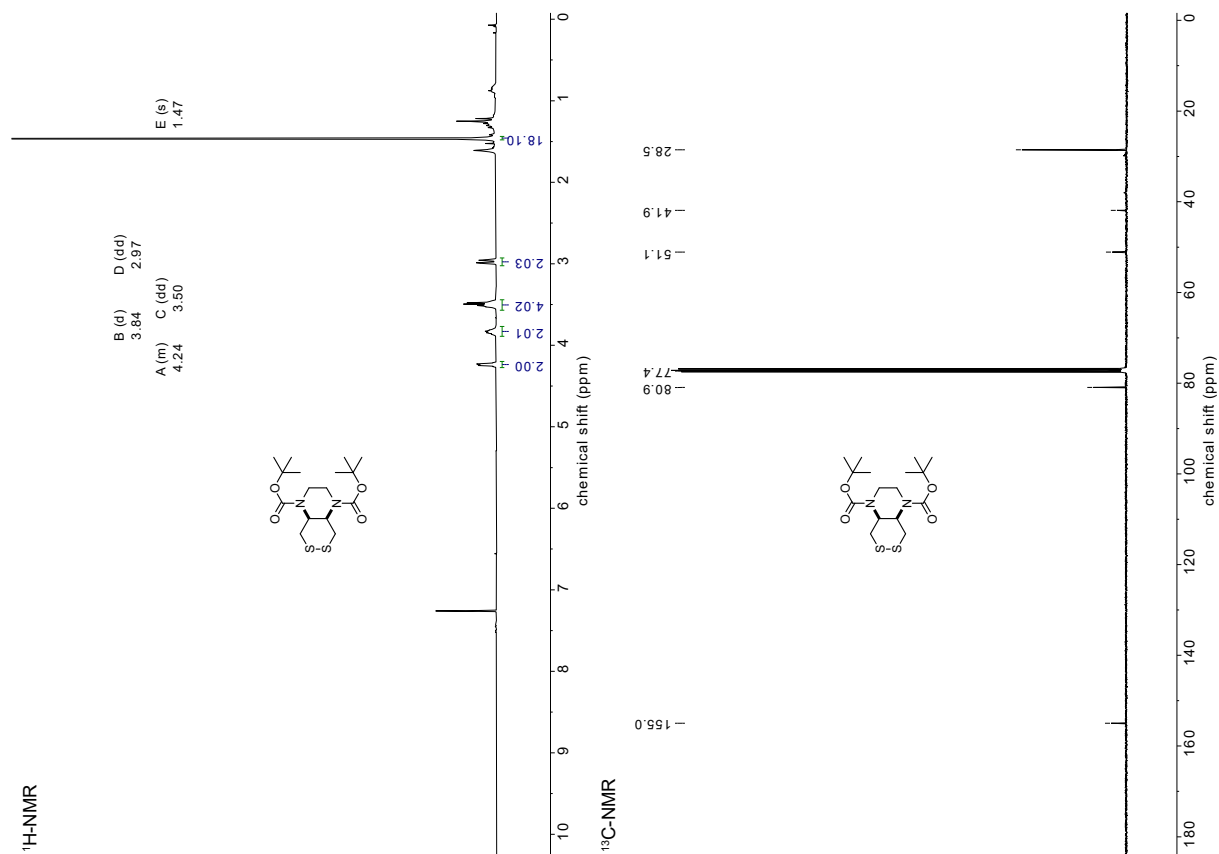
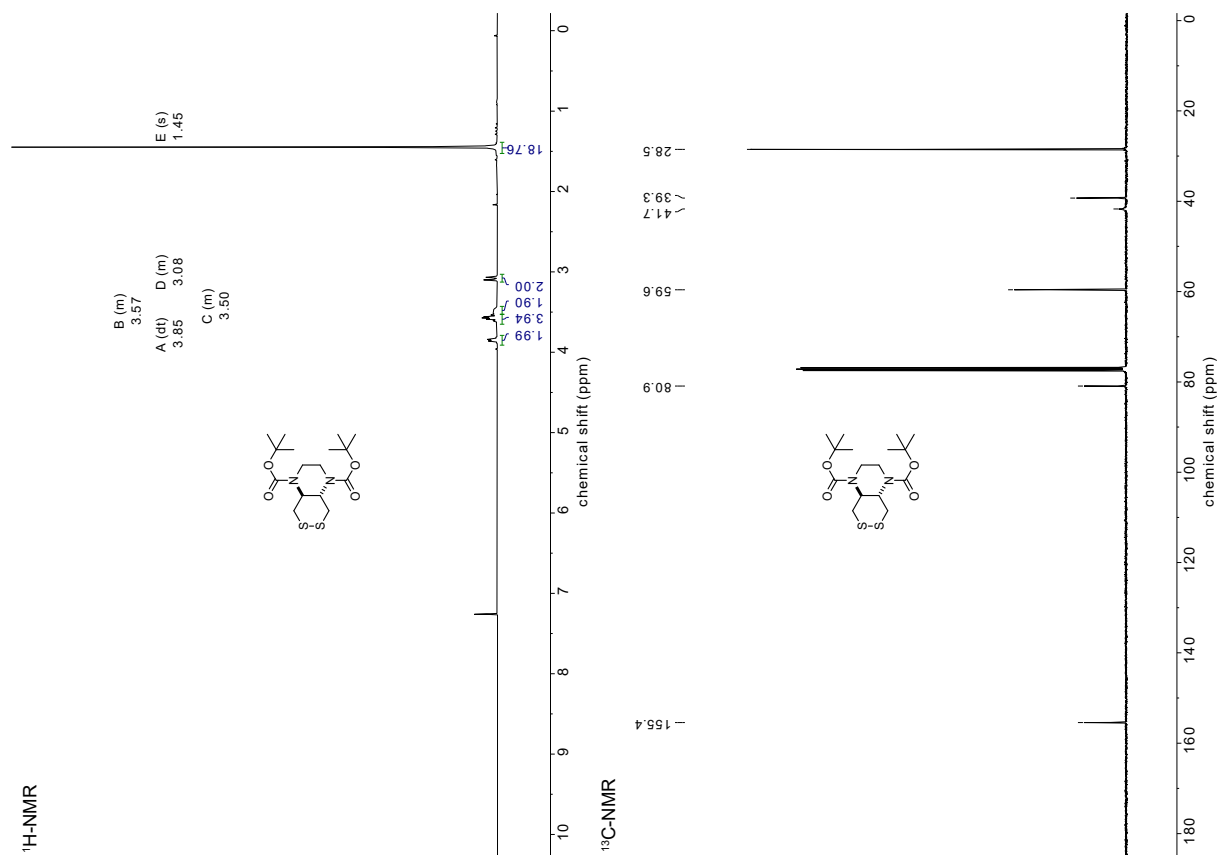
N,N'*-1,4-dihydrobutane-2,3-diylbis(2-nitrobenzenesulfonamide) (*cis*) 2C**N,N'*-1,4-dihydrobutane-2,3-diylbis(2-nitrobenzenesulfonamide) (*trans*) 2T**

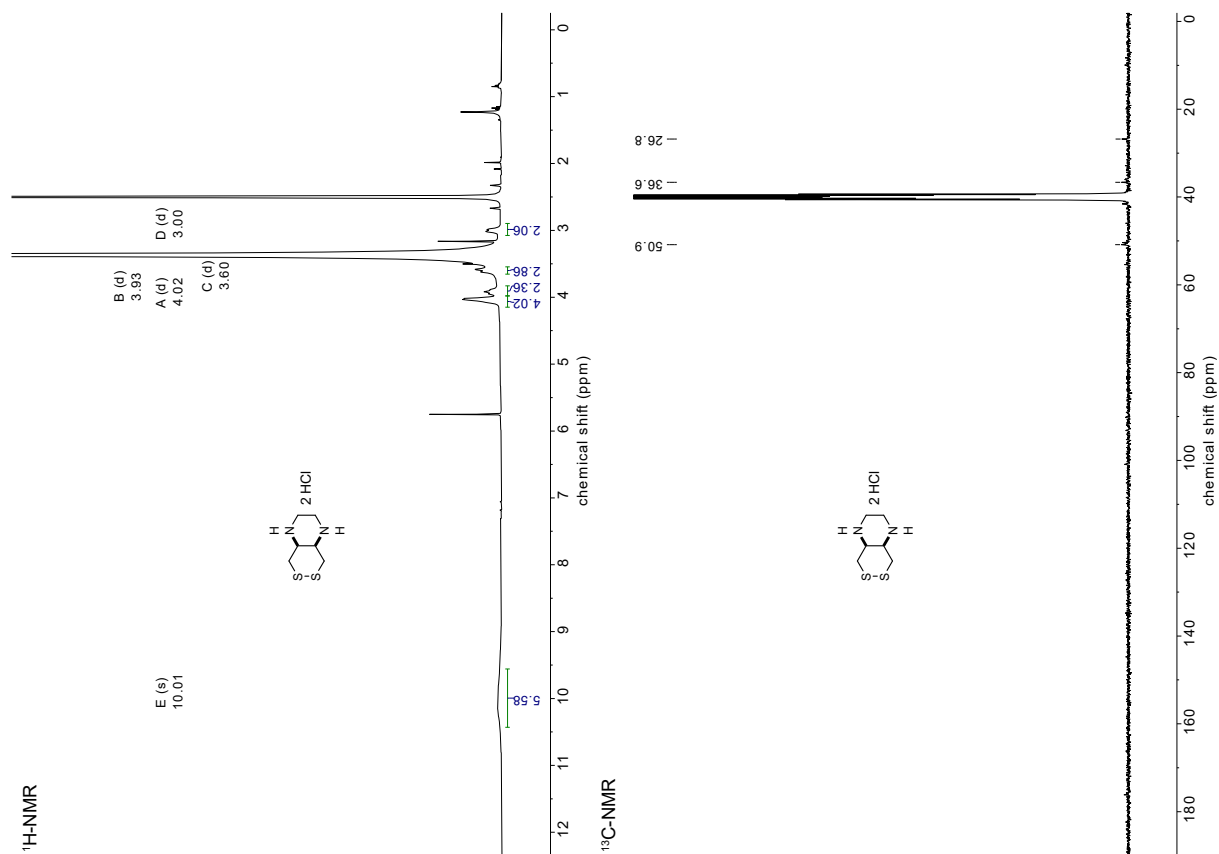
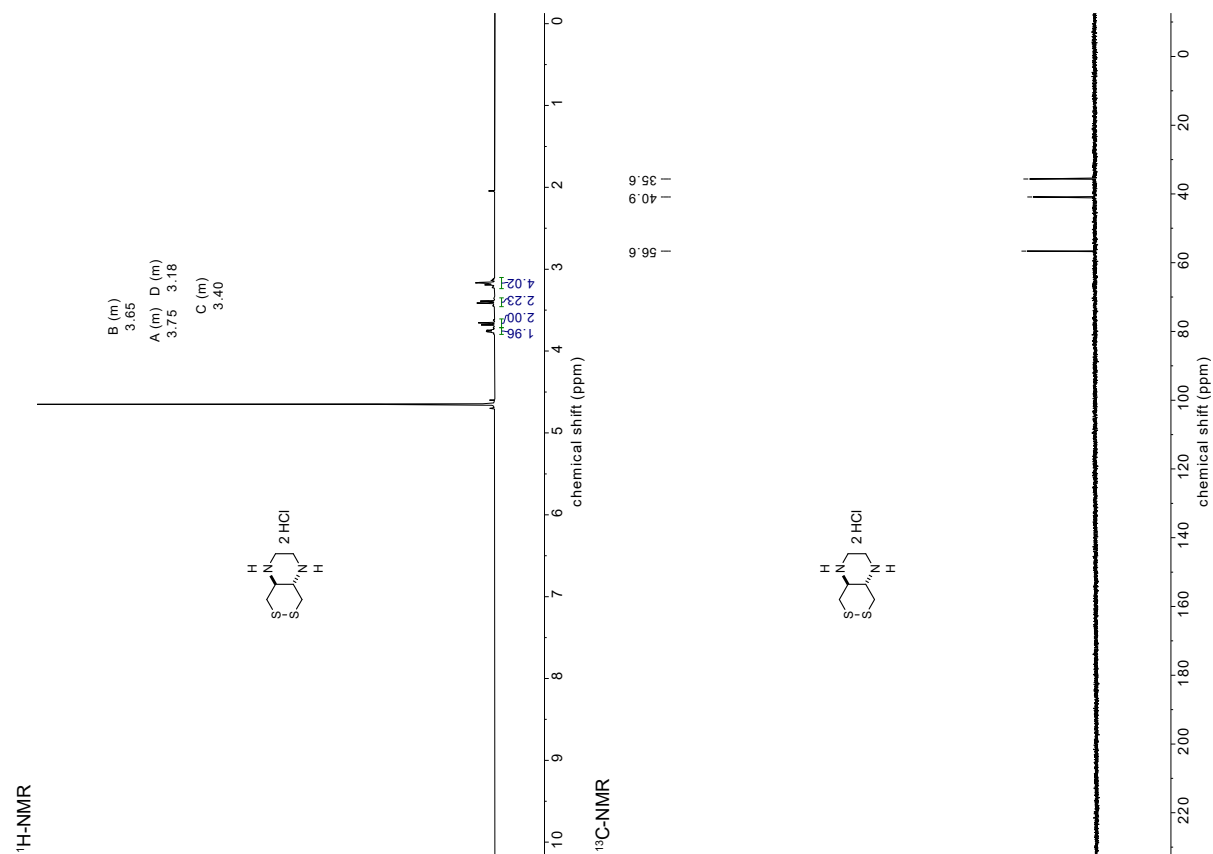
2,3-bis((2-nitrophenyl)sulfonamido)butane-1,4-diyl dimethanesulfonate (*cis*) 3C**2,3-bis((2-nitrophenyl)sulfonamido)butane-1,4-diyl dimethanesulfonate (*trans*) 3T**

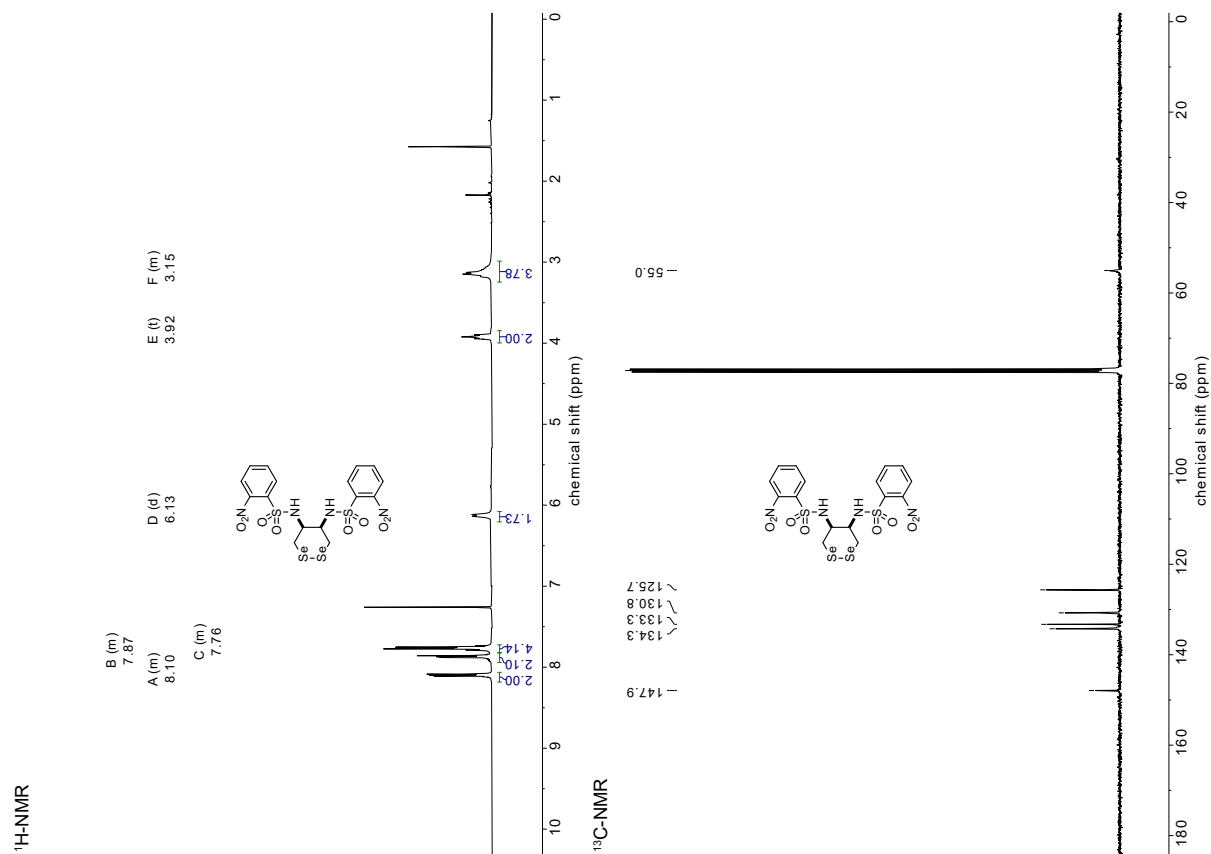
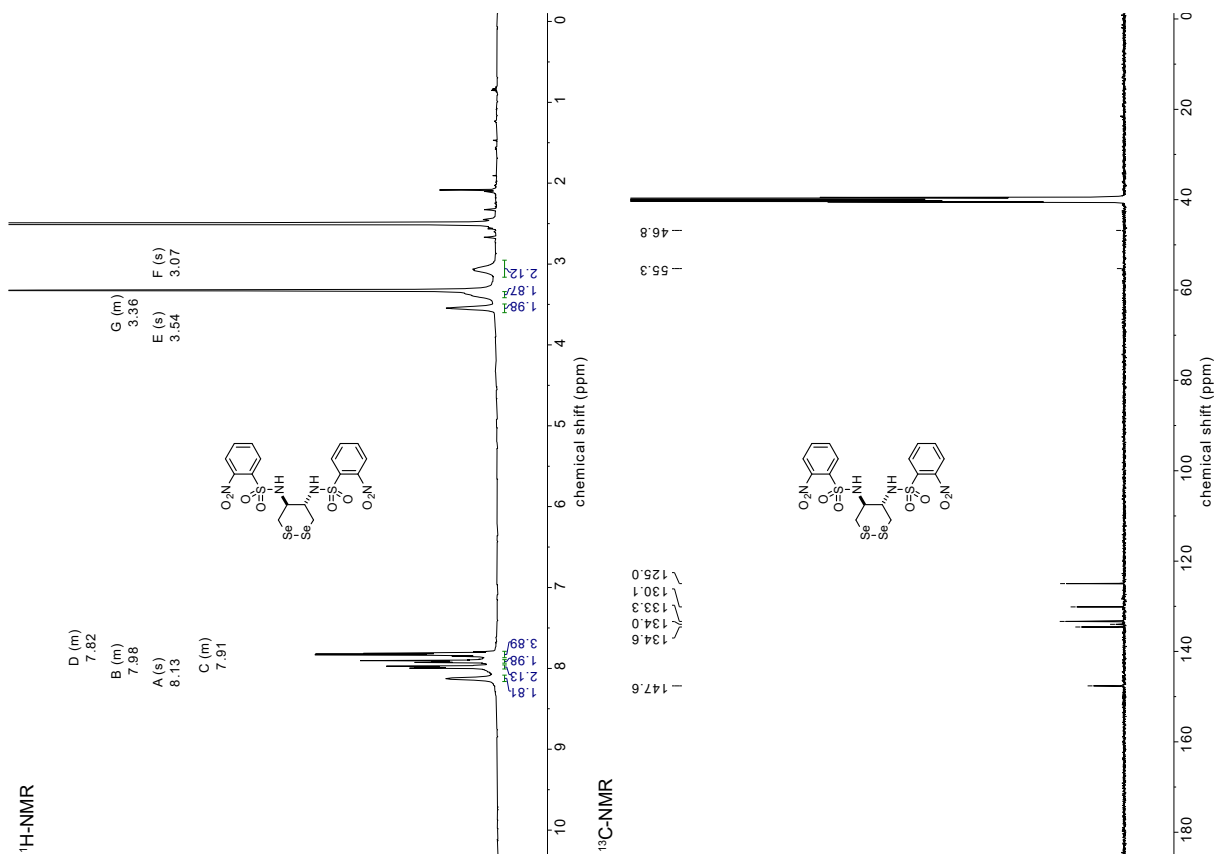
2-((2-nitrophenyl)sulfonamido)-3-((2-nitrophenylsulfonyl)methyl)butane-1,4-diyl diethanethioate (*cis*) 4C**2-((2-nitrophenyl)sulfonamido)-3-((2-nitrophenylsulfonyl)methyl)butane-1,4-diyl diethanethioate (*trans*) 4T**

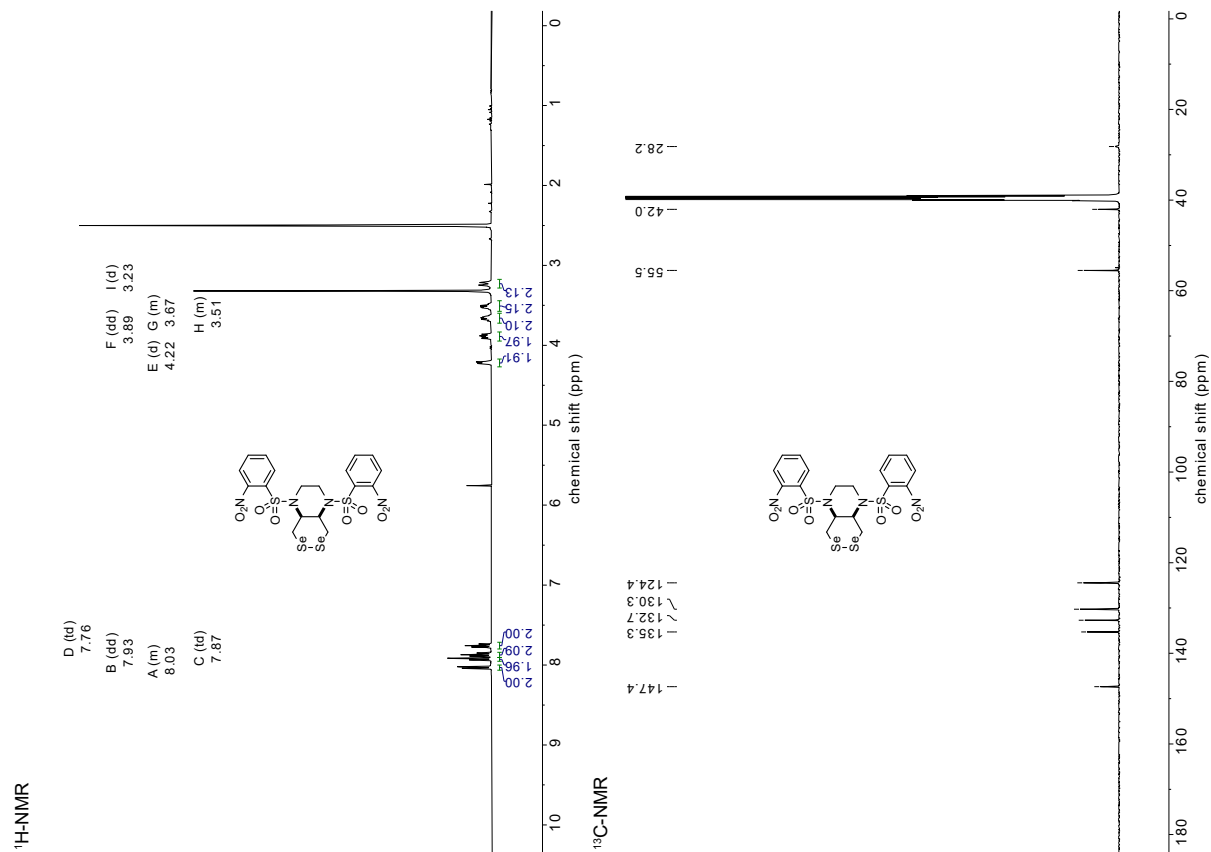
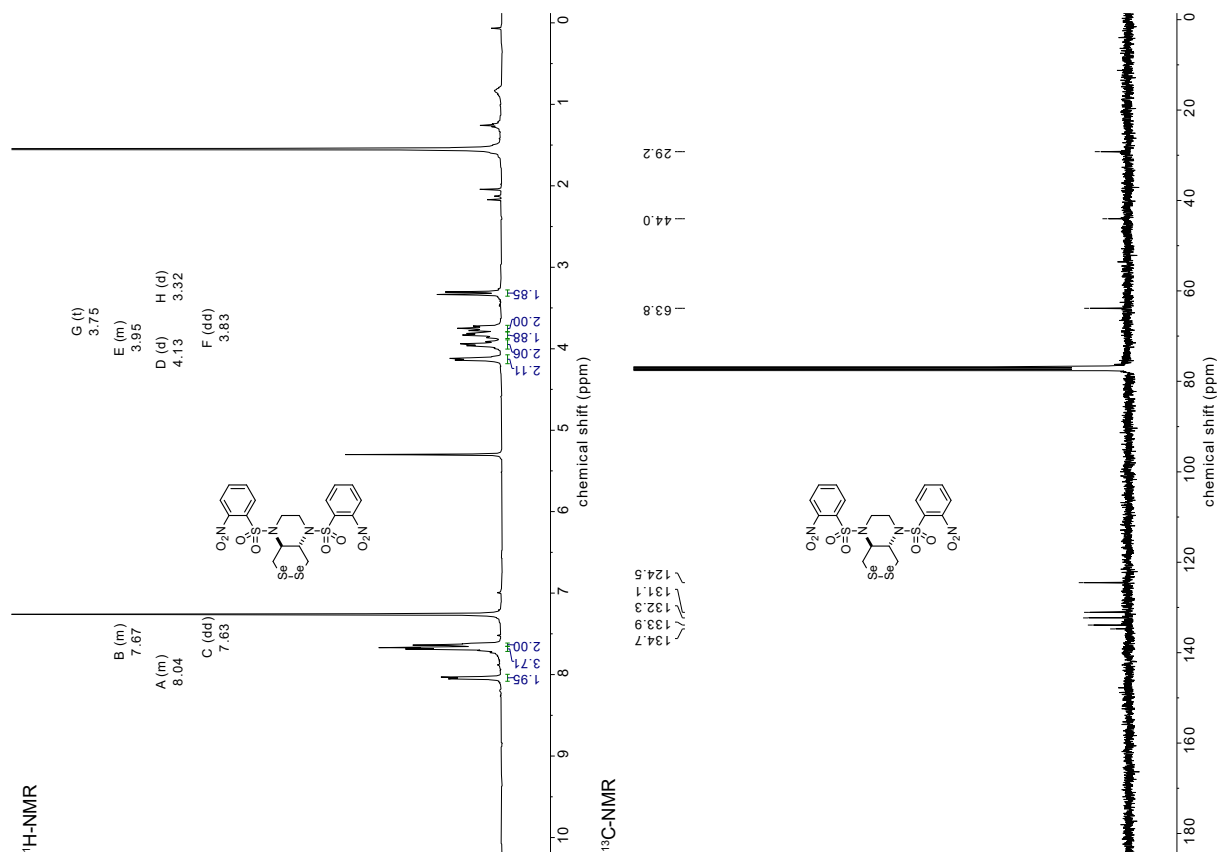
N,N'*-1,2-dithiane-4,5-diyl)bis(2-nitrobenzenesulfonamide) (*cis*) 5C**N,N'*-1,2-dithiane-4,5-diyl)bis(2-nitrobenzenesulfonamide) (*trans*) 5T**

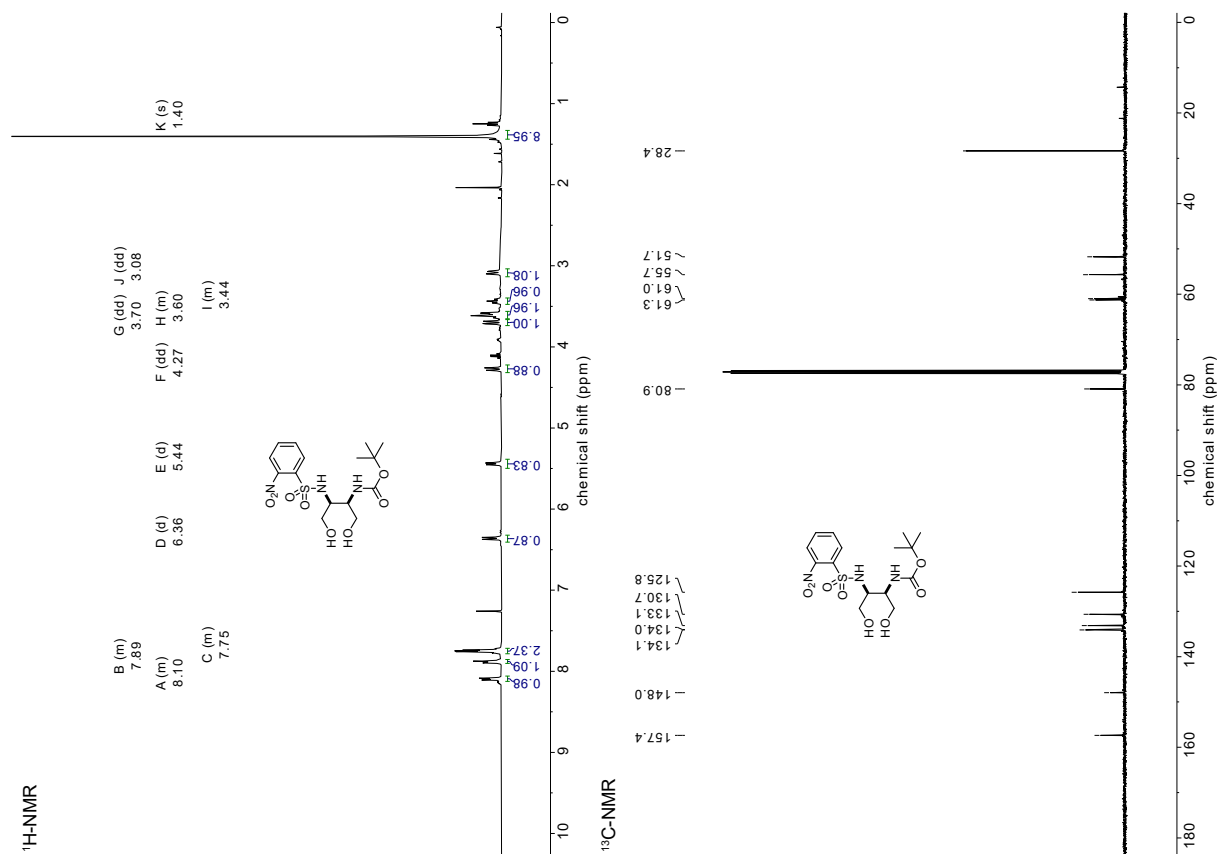
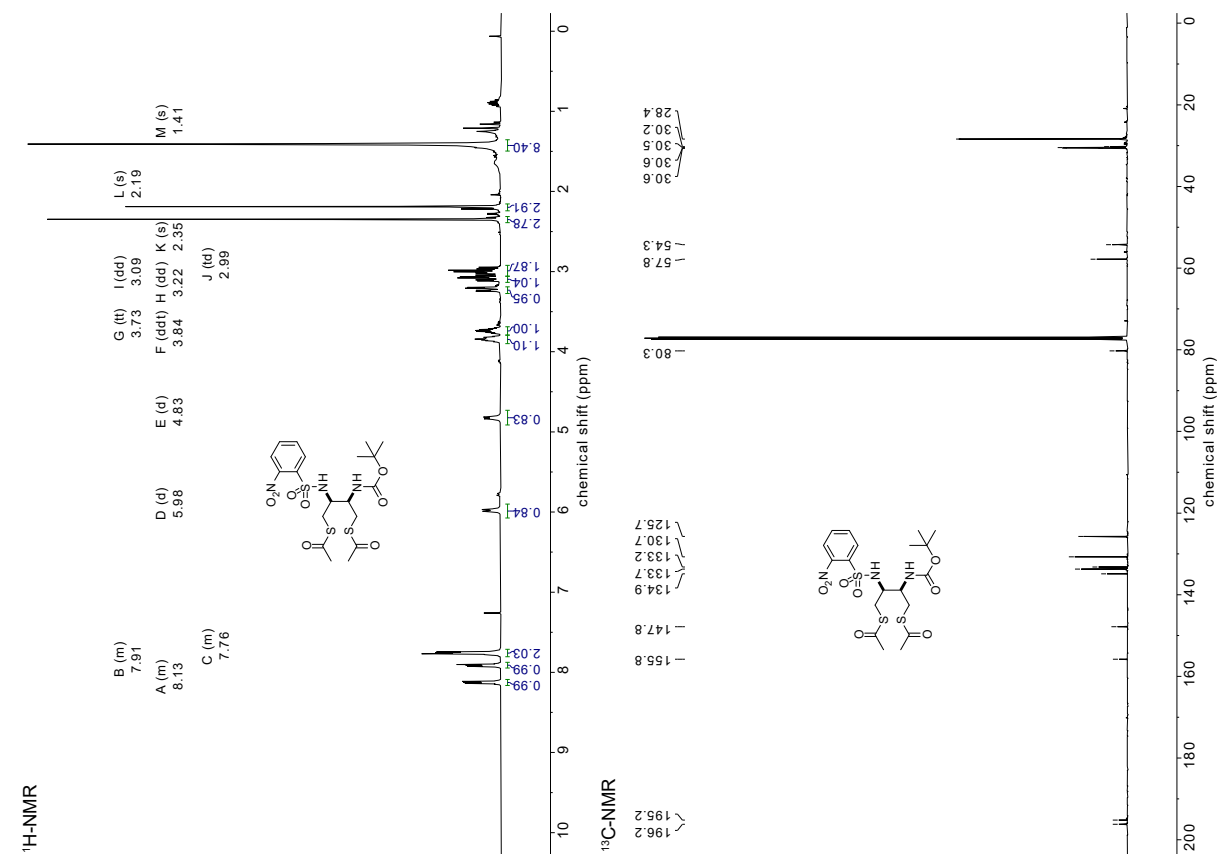
1,4-bis((2-nitrophenyl)sulfonyl)octahydro-[1,2]dithiino[4,5-b]pyrazine (*cis*) 6C**1,4-bis((2-nitrophenyl)sulfonyl)octahydro-[1,2]dithiino[4,5-b]pyrazine (*trans*) 6T**

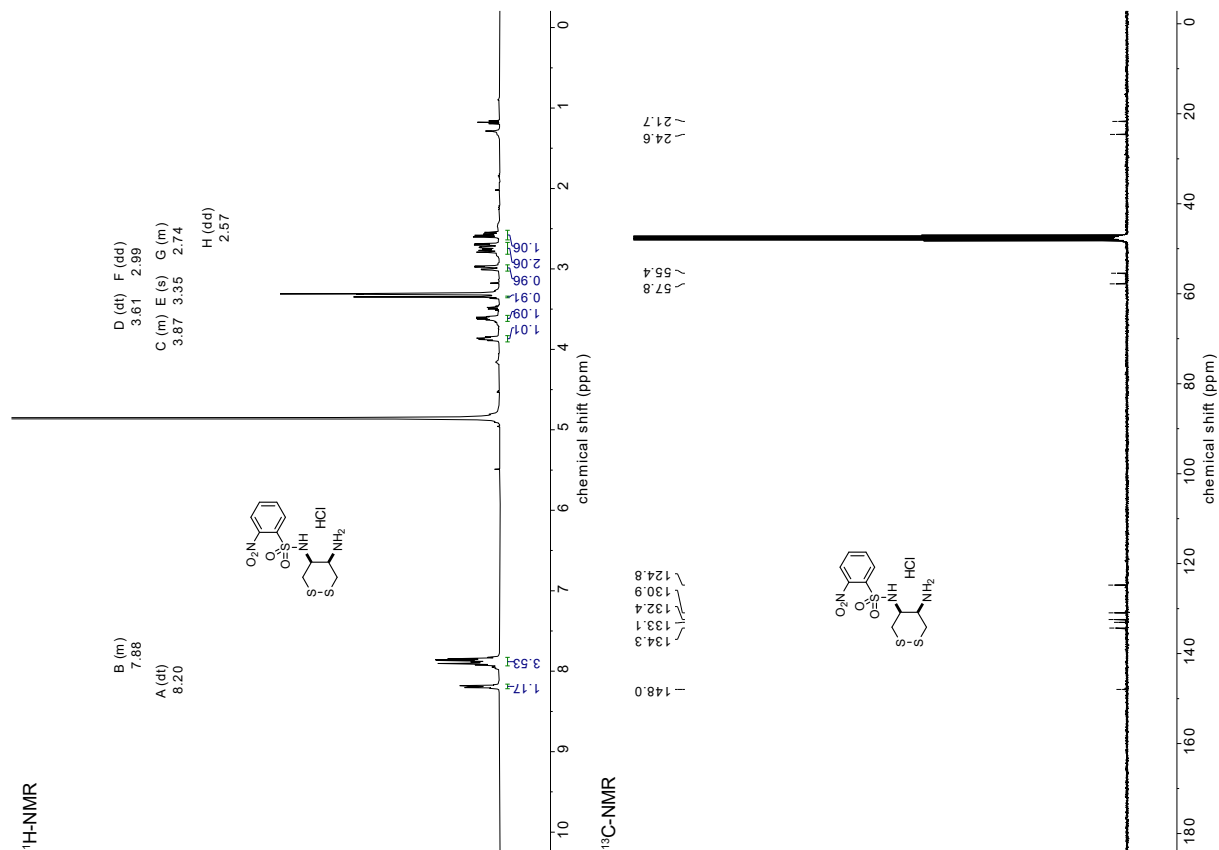
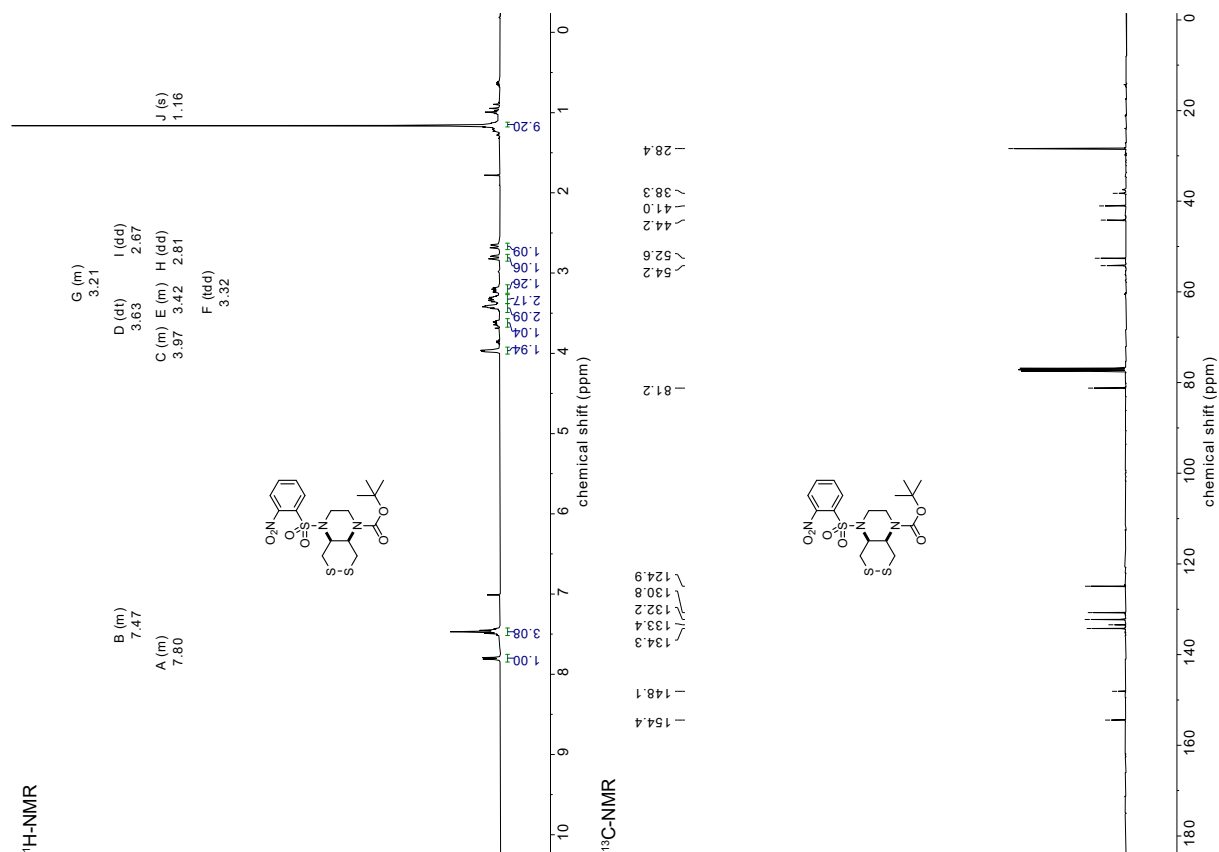
di-*tert*-butyl hexahydro-[1,2]dithiino[4,5-*b*]pyrazine-1,4-dicarboxylate (*cis*) 18C**di-*tert*-butyl hexahydro-[1,2]dithiino[4,5-*b*]pyrazine-1,4-dicarboxylate (*trans*) 18T**

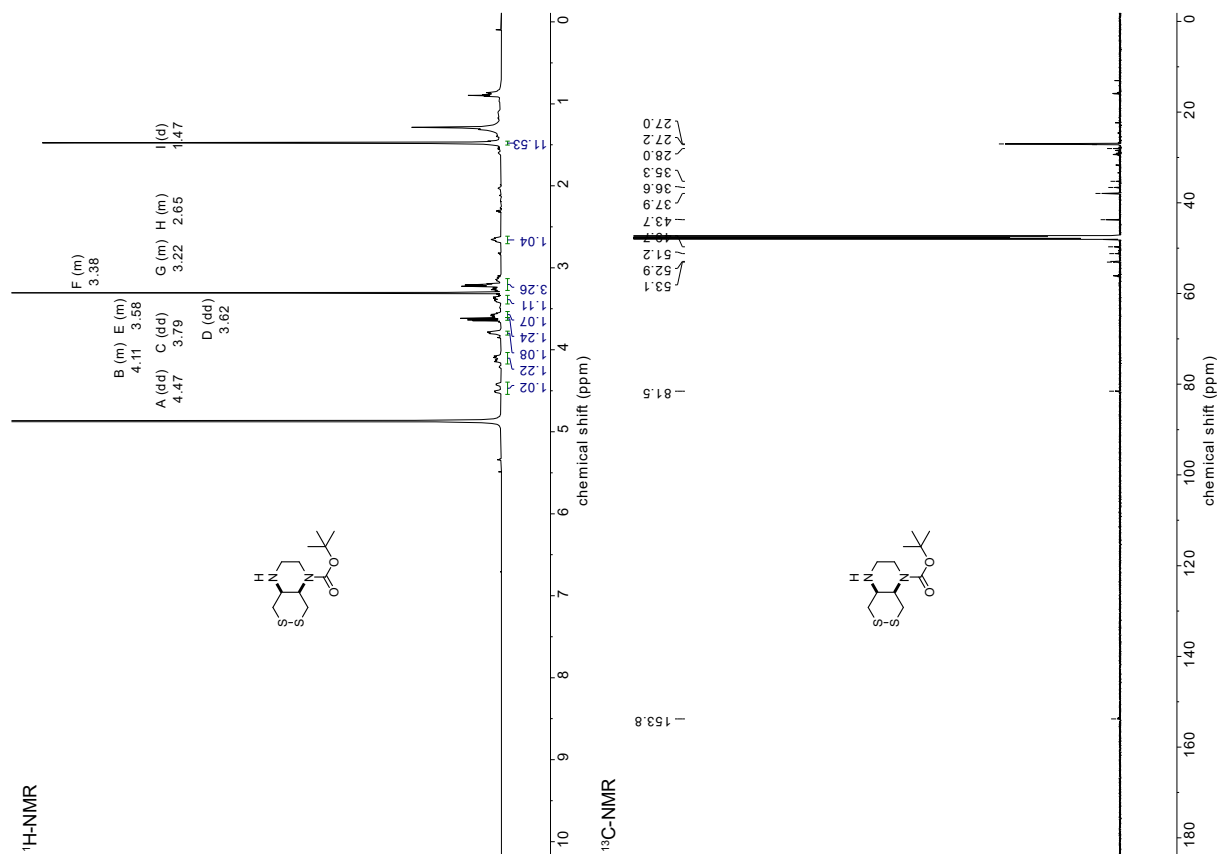
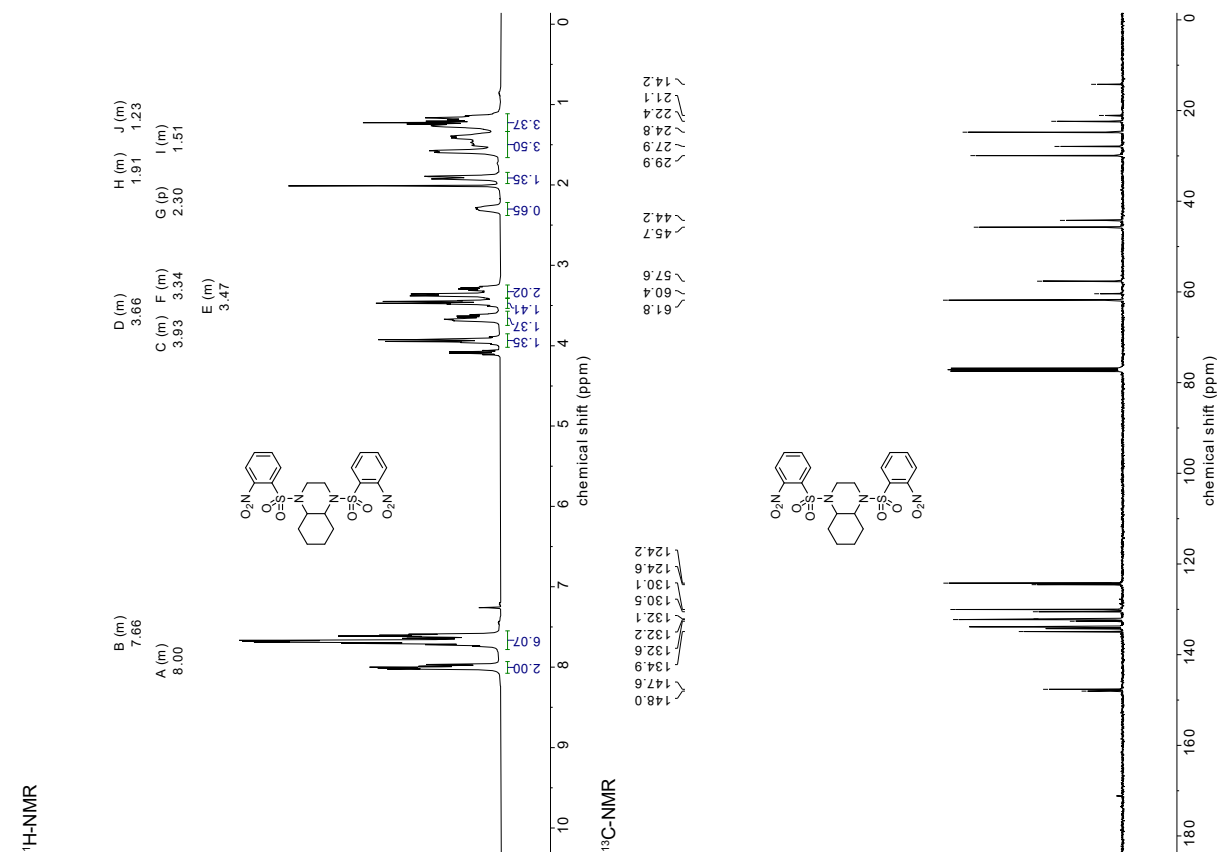
SS66C·2HCl octahydro-[1,2]dithiino[4,5-*b*]pyrazine dihydrochloride (*cis*) **7C****SS66T·2 HCl** octahydro-[1,2]dithiino[4,5-*b*]pyrazine dihydrochloride (*trans*) **7T**

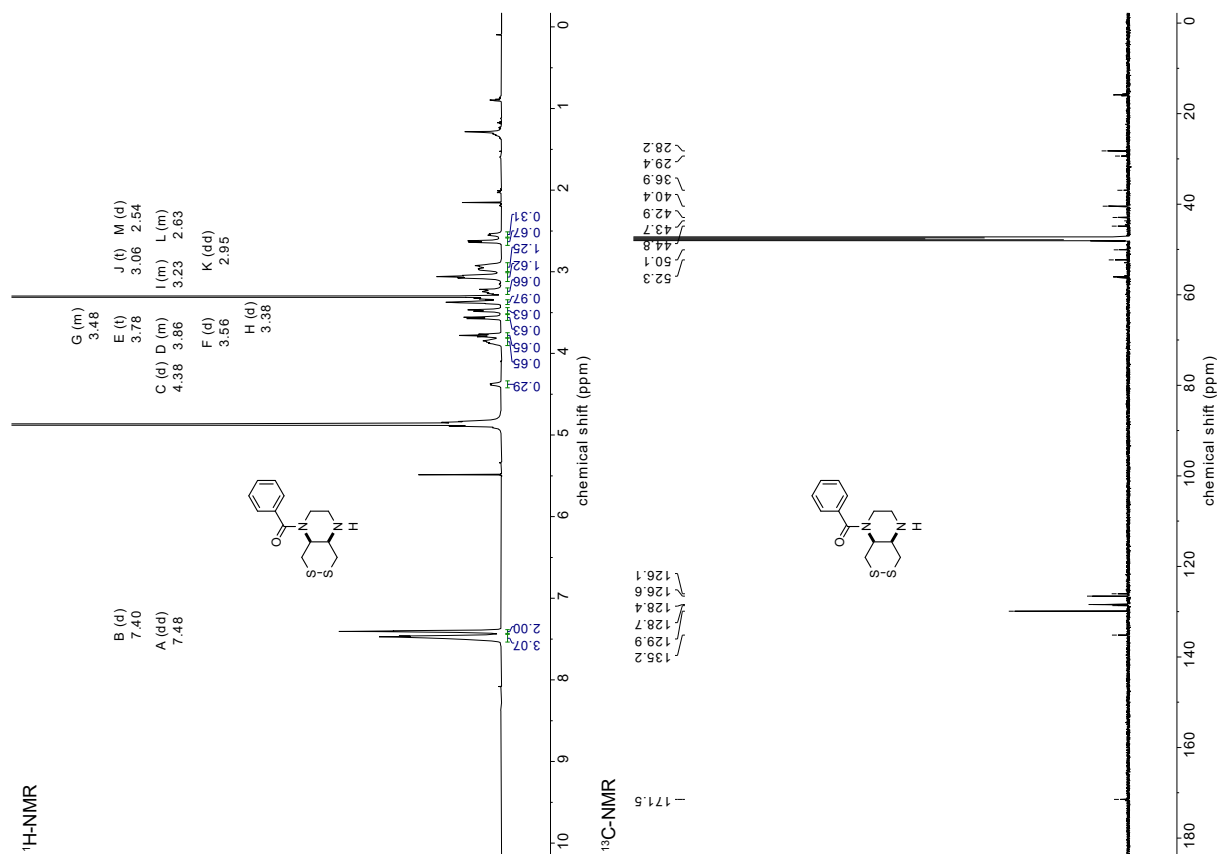
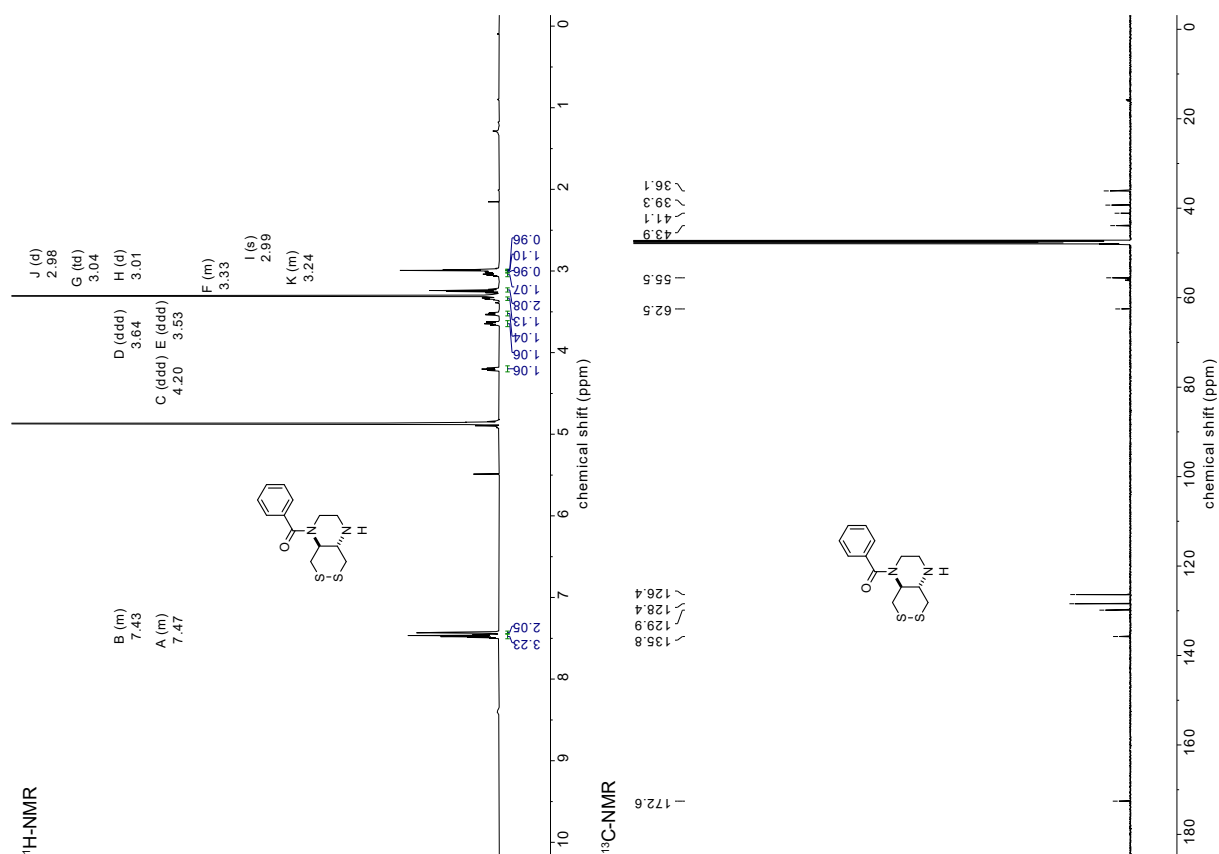
N,N'*-(1,2-diselenane-4,5-diyl)bis(4-nitrobenzenesulfonamide) (cis) 8C**N,N'*-(1,2-diselenane-4,5-diyl)bis(4-nitrobenzenesulfonamide) (trans) 8T**

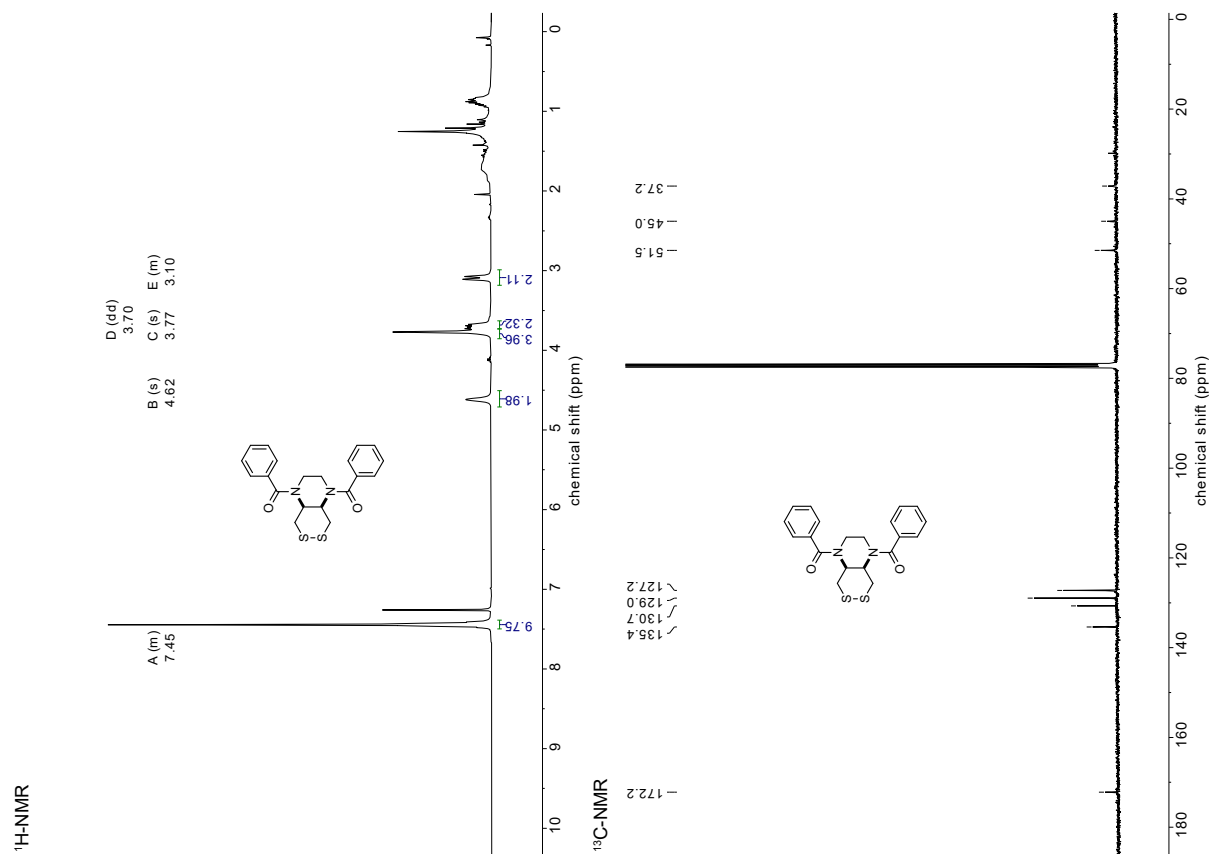
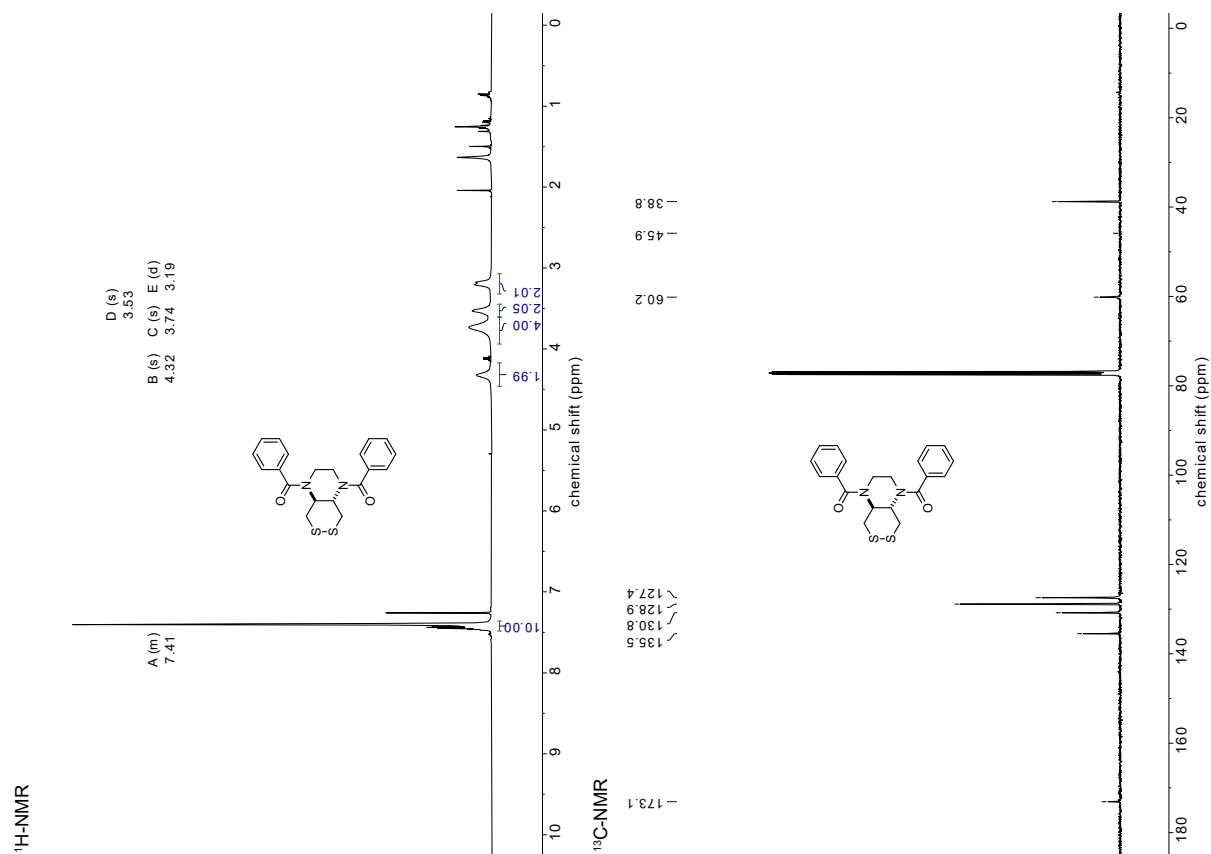
1,4-bis((2-nitrophenyl)sulfonyl)octahydro-[1,2]diselenino[4,5-b]pyrazine (*cis*) 9C**1,4-bis((2-nitrophenyl)sulfonyl)octahydro-[1,2]diselenino[4,5-b]pyrazine (*trans*) 9T**

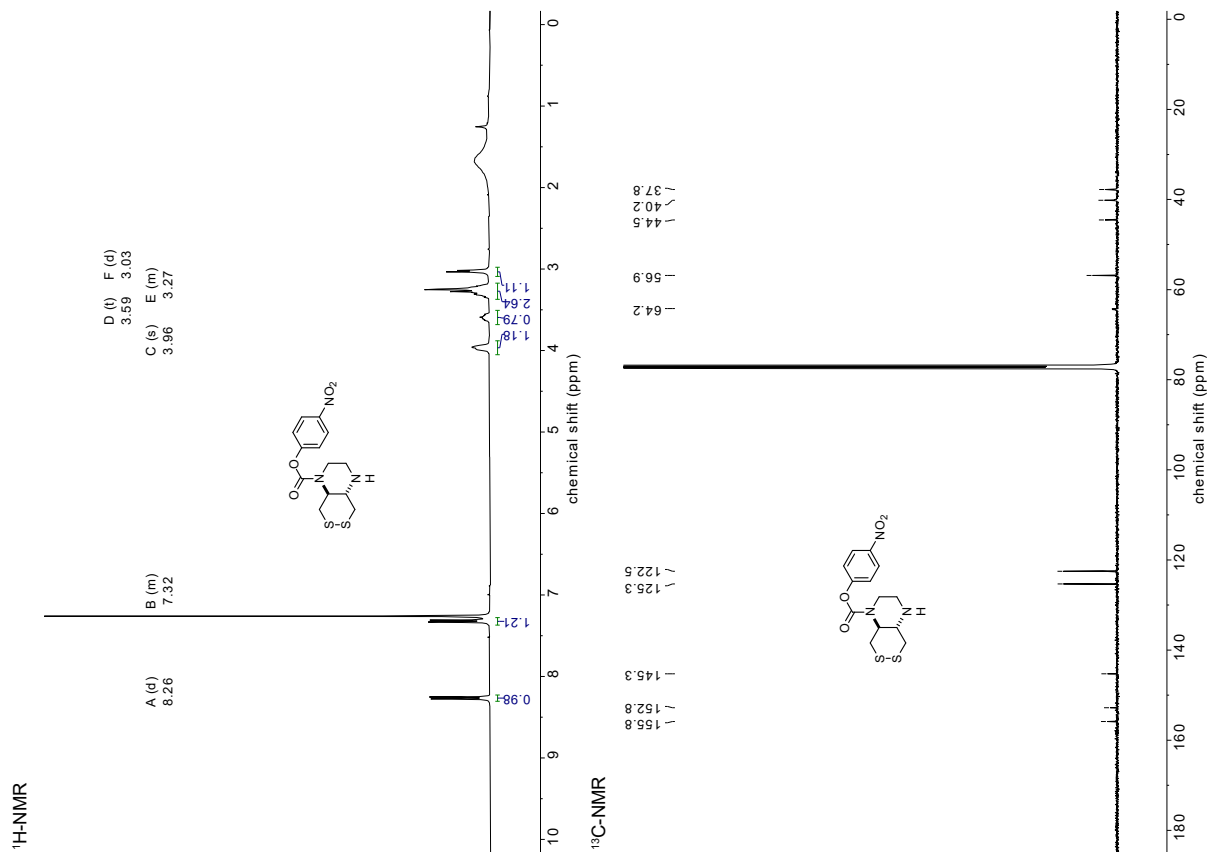
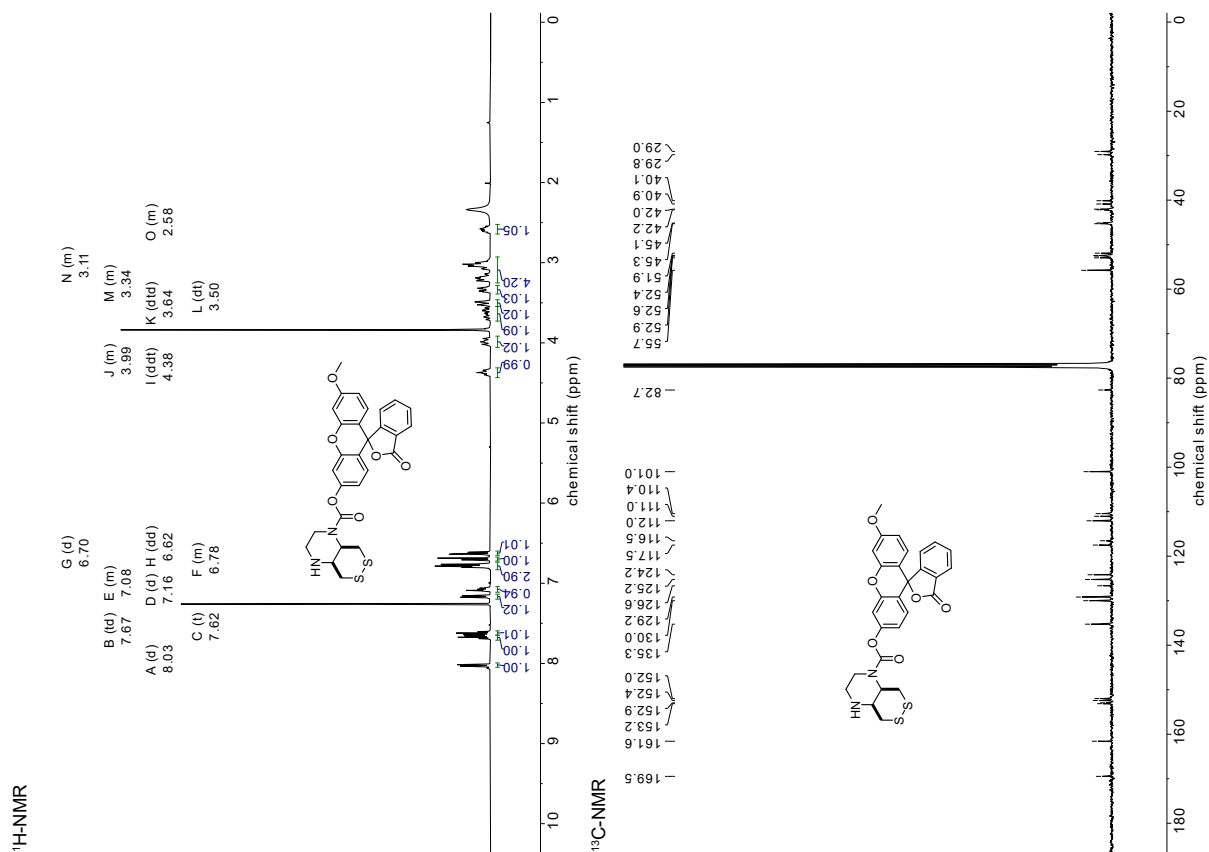
tert-butyl(1,4-dihydroxy-3-((2-nitrophenyl)sulfonamido)butan-2-yl)carbamate (*cis*) 19**(2-((tert-butoxycarbonyl)amino)-3-((2-nitrophenyl)sulfonamido)butane-1,4-diyl) diethanethioate (*cis*) 20**

N*-(5-amino-1,2-dithian-4-yl)-2-nitrobenzenesulfonamide (cis) 21**tert*-butyl 4-((2-nitrophenyl)sulfonyl)hexahydro-[1,2]dithiino[4,5-*b*]pyrazine-1(2*H*)-carboxylate (cis) 22**

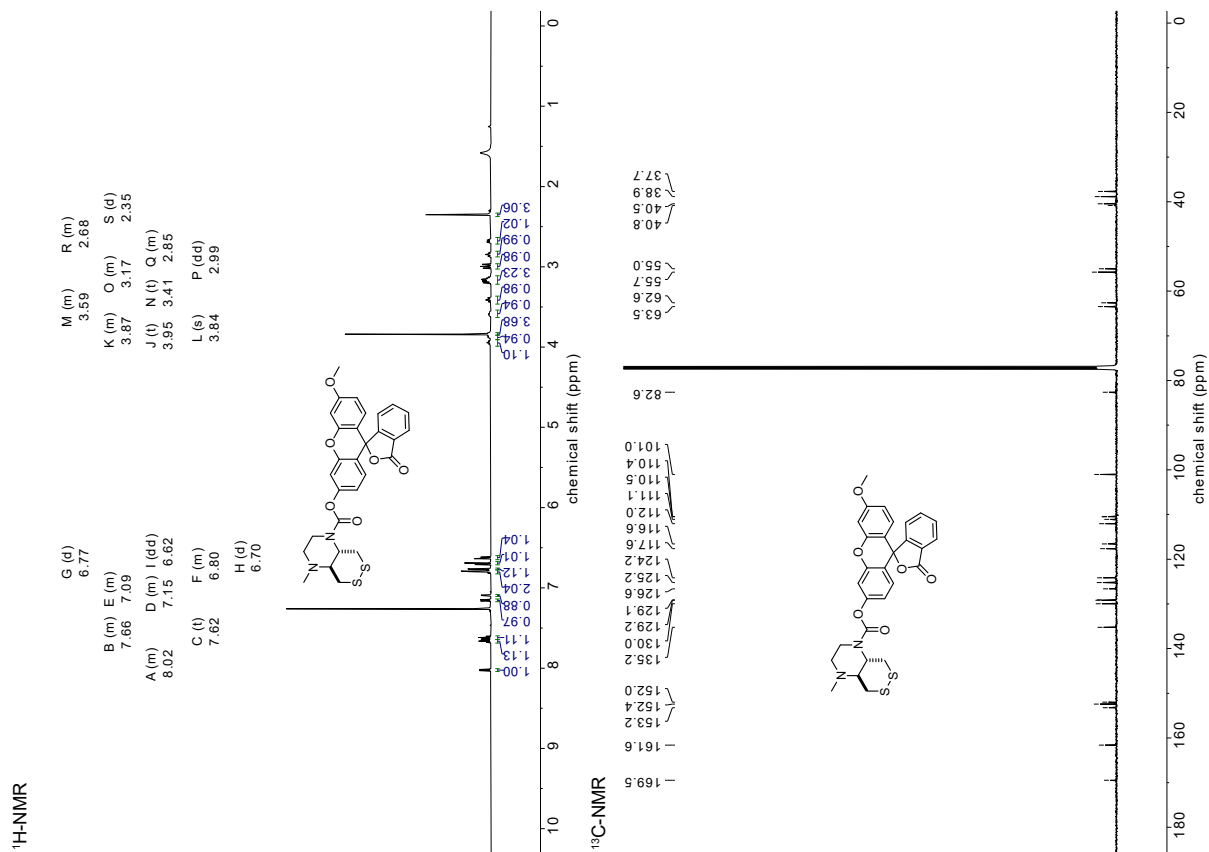
tert-butyl hexahydro-[1,2]dithiino[4,5-b]pyrazine-1(2H)-carboxylate (*cis*) 23**1,4-bis((2-nitrophenyl)sulfonyl)decahydroquinoline (*racemic*) 57**

H-SS66C-Bz (hexahydro-[1,2]dithiino[4,5-*b*]pyrazin-1(2*H*)-yl)(phenyl)methanone (*cis*) **52C****H-SS66T-Bz** (hexahydro-[1,2]dithiino[4,5-*b*]pyrazin-1(2*H*)-yl)(phenyl)methanone (*trans*) **52T**

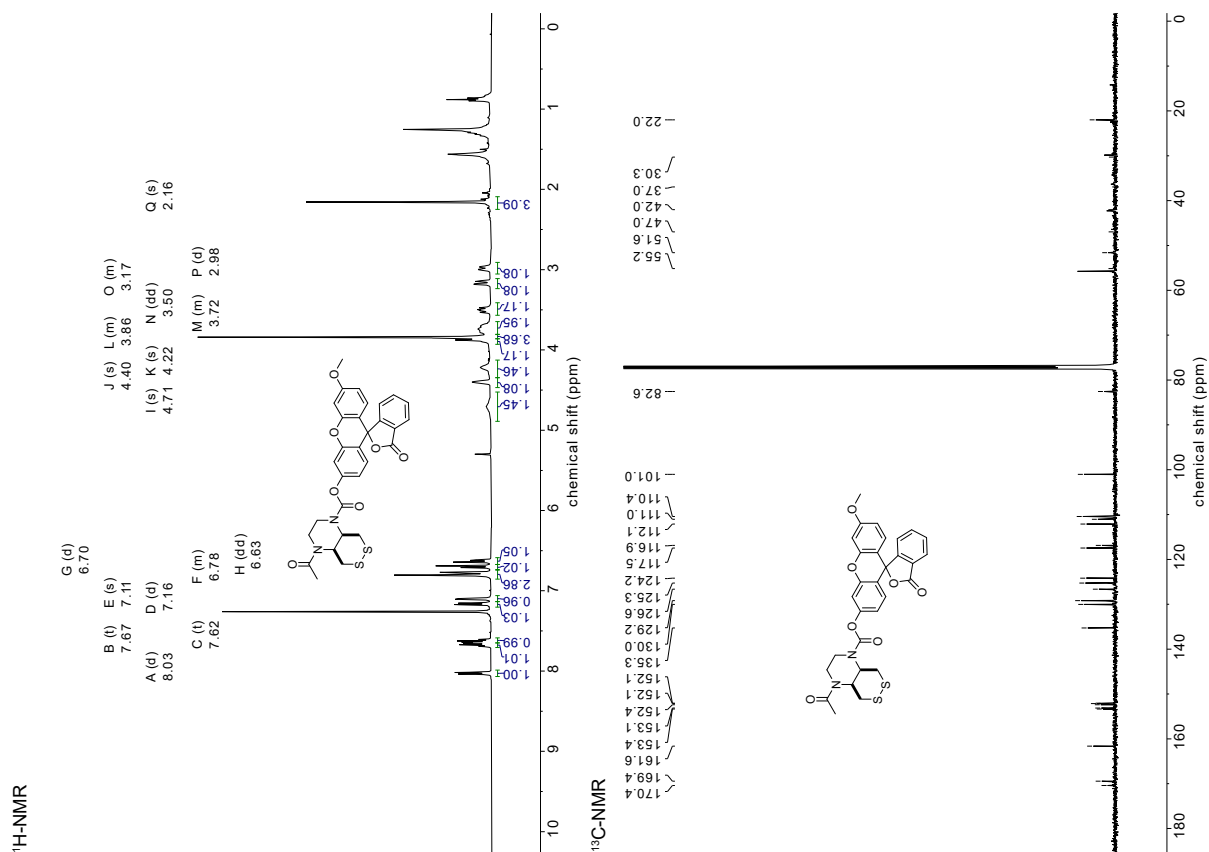
Bz-SS66C-Bz (hexahydro-[1,2]dithiino[4,5-*b*]pyrazine-1,4-diyl)bis(phenylmethanone) (*cis*) **53C****Bz-SS66T-Bz** (hexahydro-[1,2]dithiino[4,5-*b*]pyrazine-1,4-diyl)bis(phenylmethanone) (*trans*) **53T**

4-nitrophenyl-hexahydro-[1,2]dithiino[4,5-*b*]pyrazine-1(2*H*)-carboxylate (*trans*) 54**H-SS66C-MF (44C)**

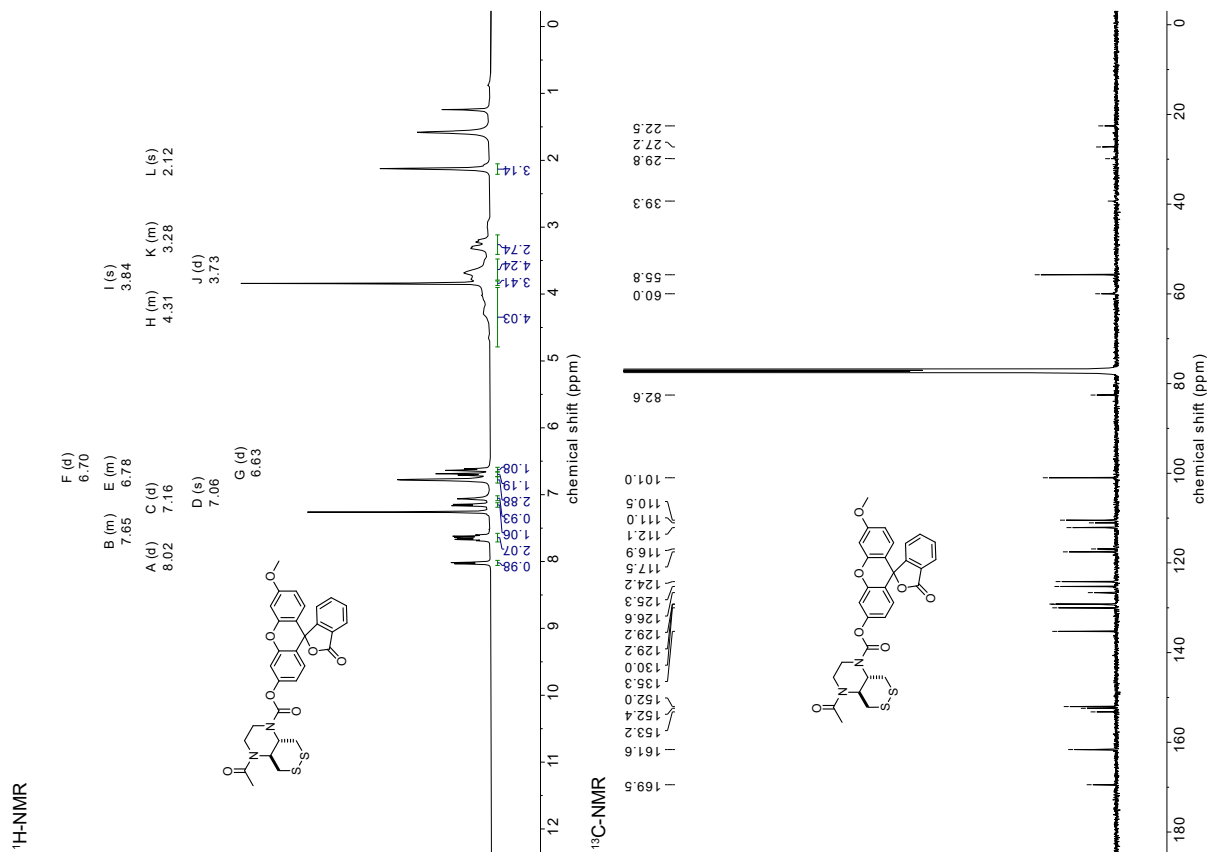
Me-SS66T-MF (45T)



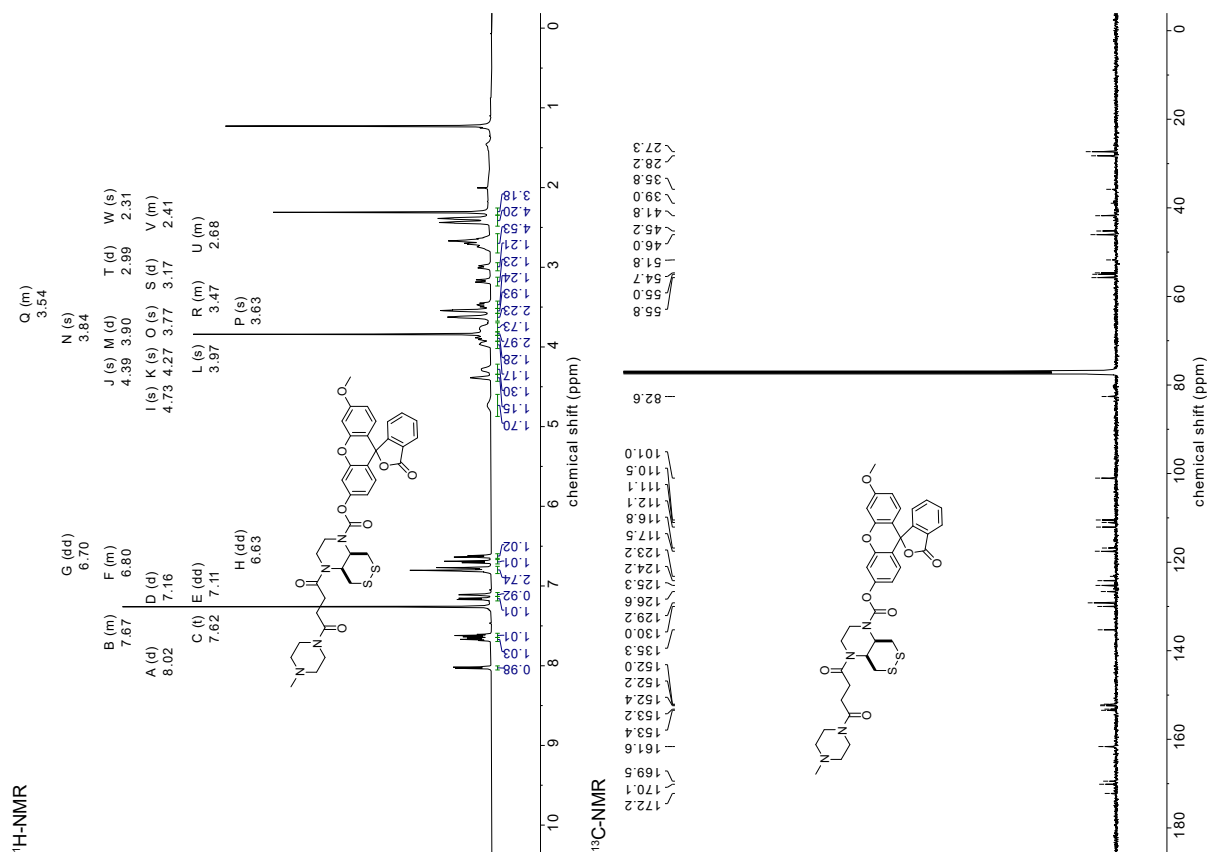
Ac-SS66C-MF (46C)

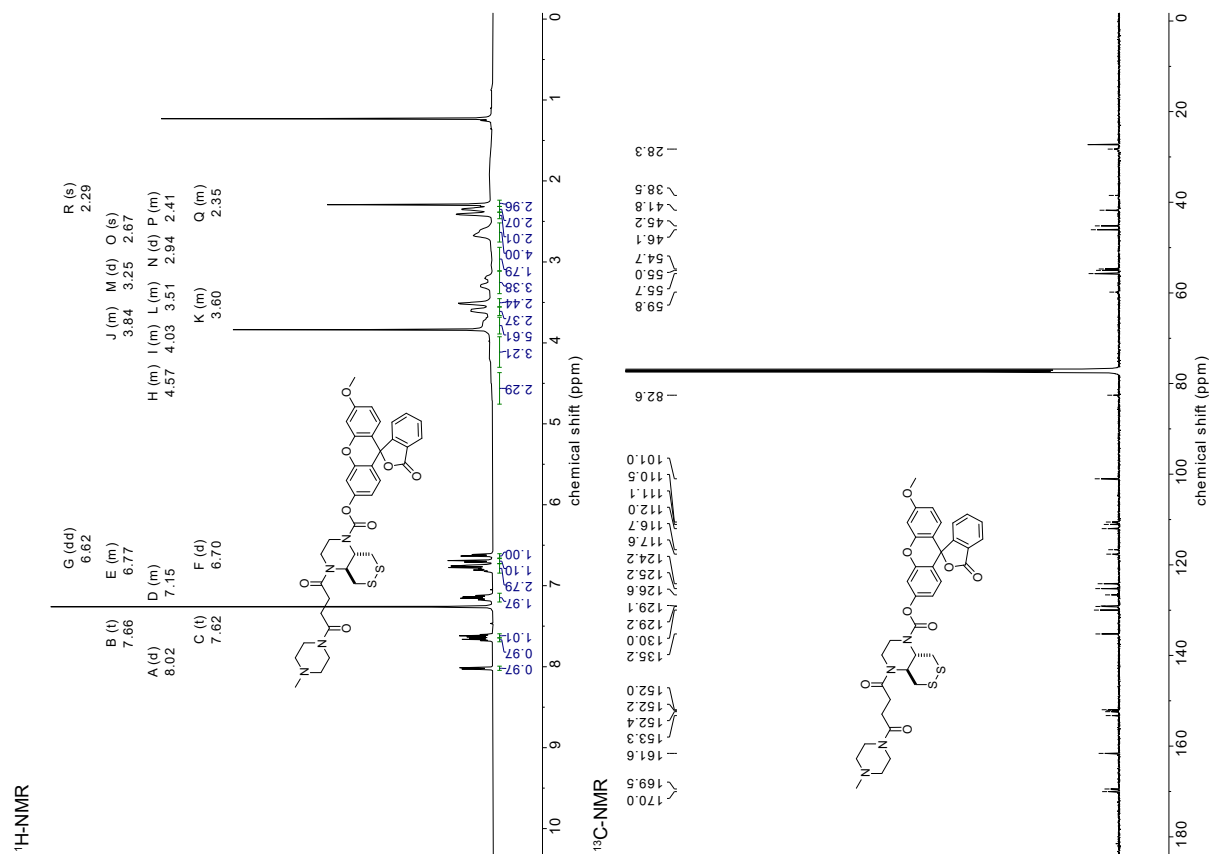
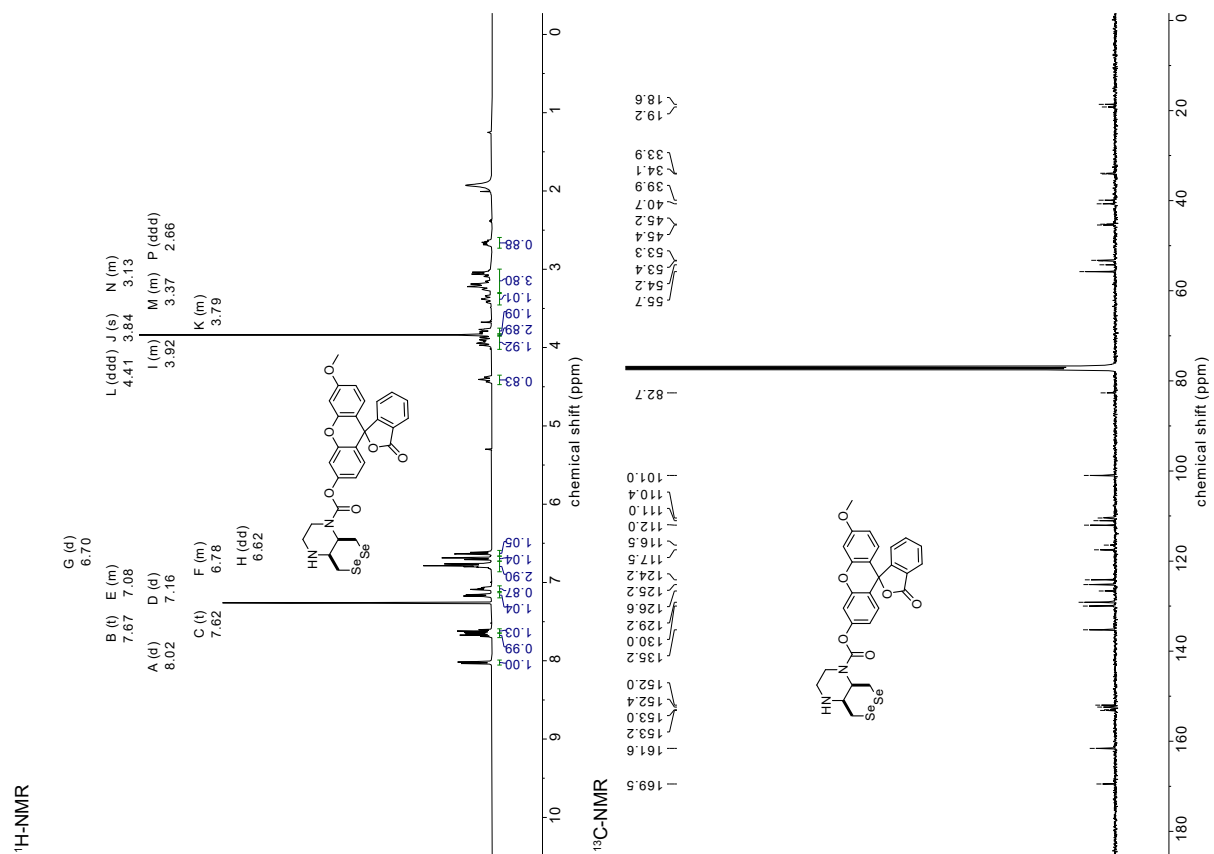


Ac-SS66T-MF (46T)

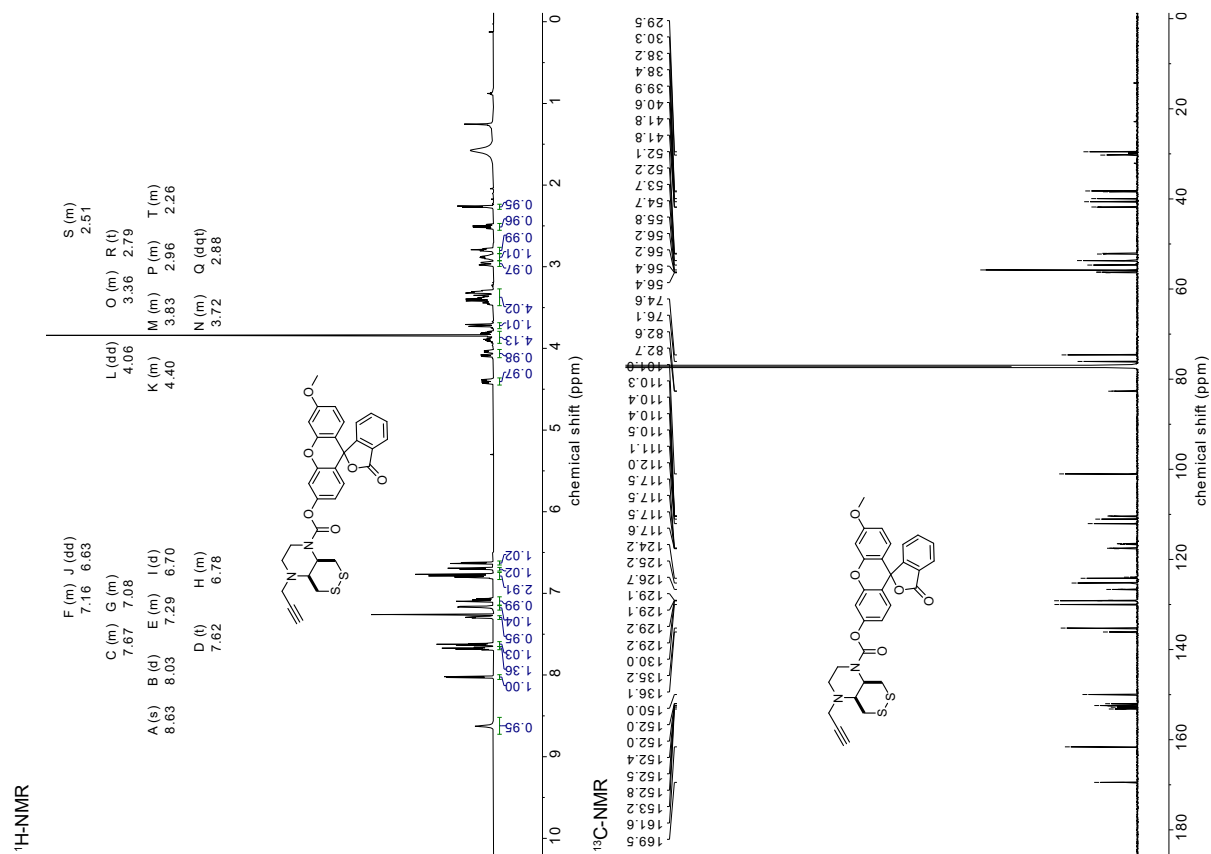


P-SS66C-MF (47C)

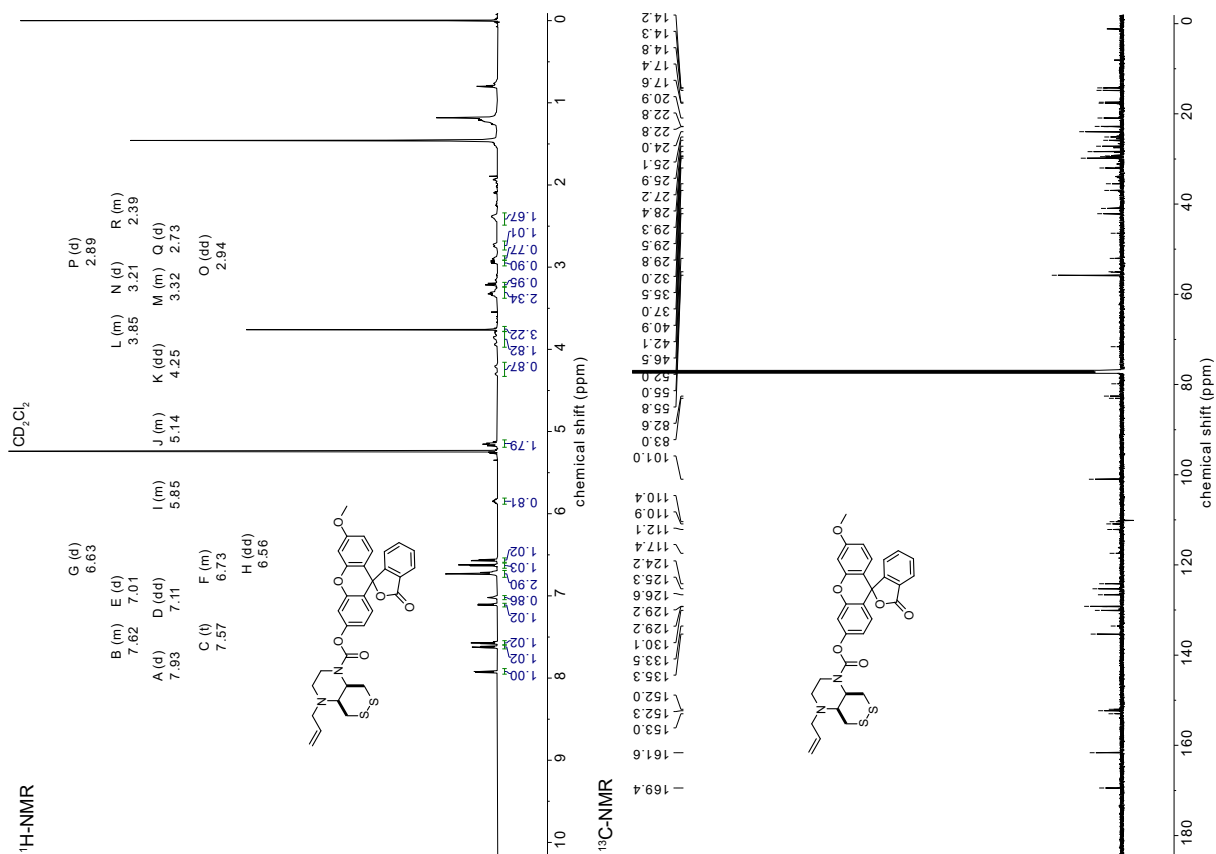


P-SS66T-MF (47T)**H-SeSe66C-MF (48C)**

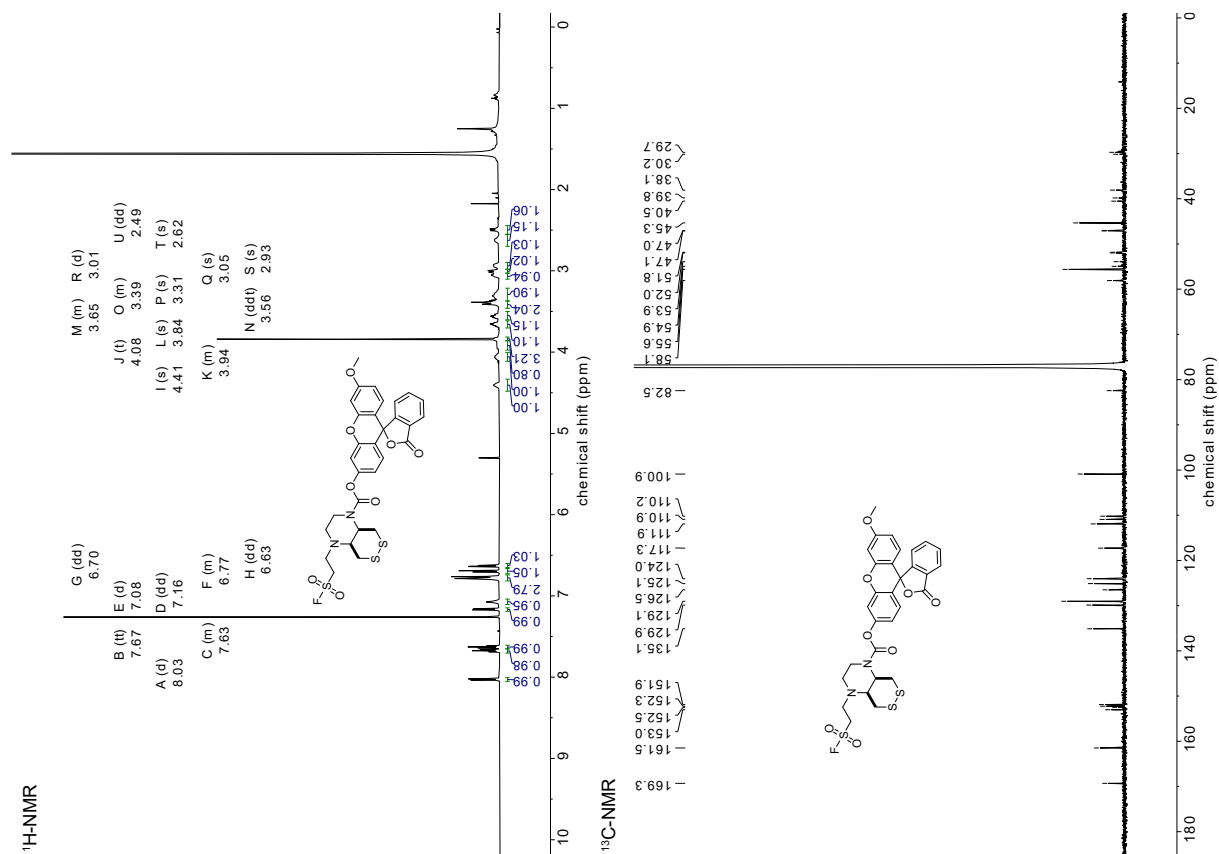
Propargyl-SS66C-MF (11)



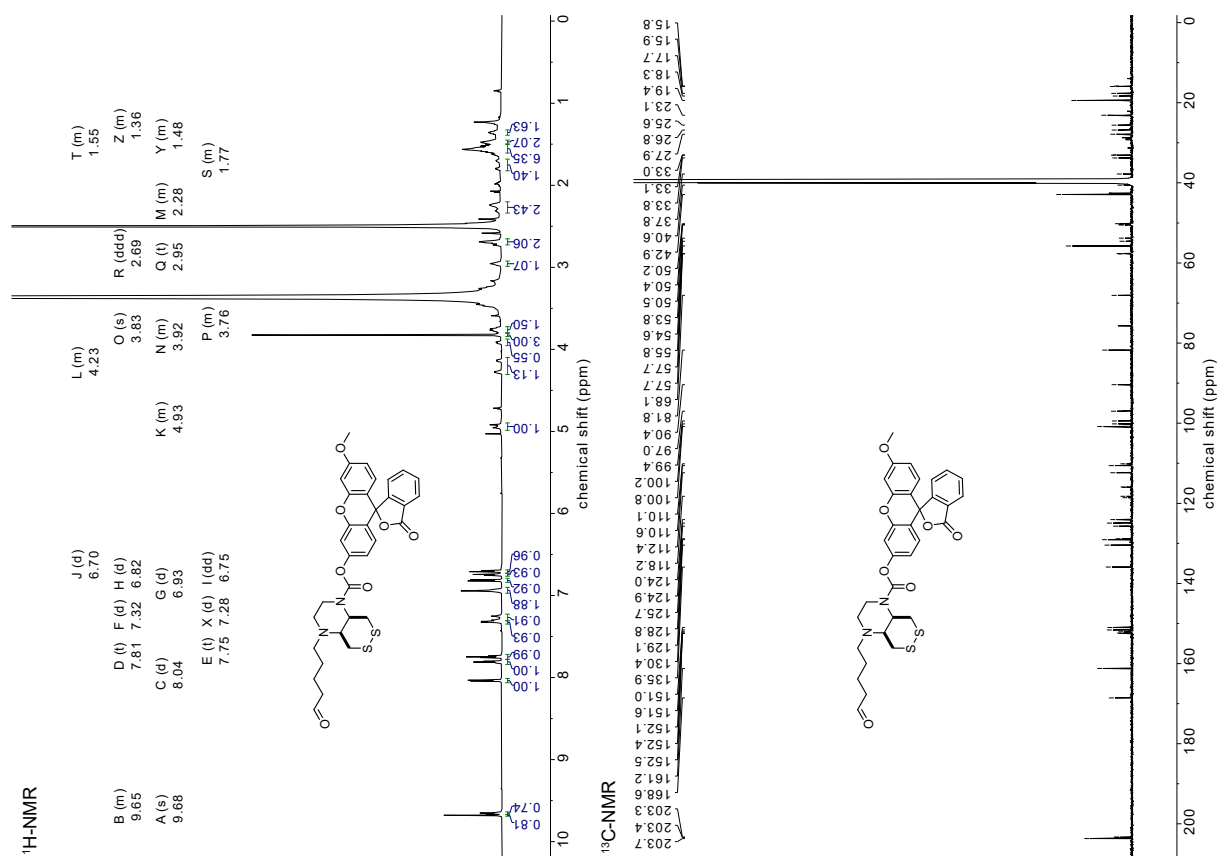
Allyl-SS66C-MF (51)

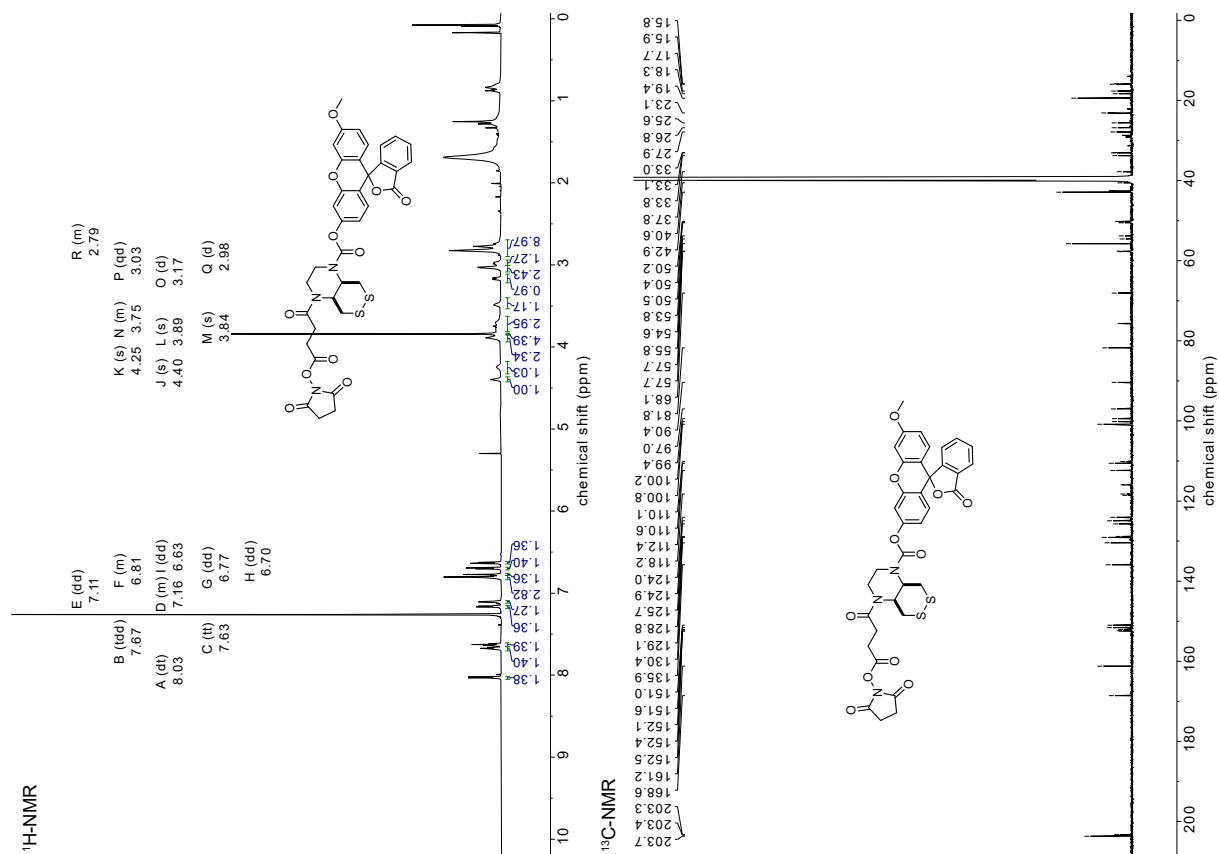
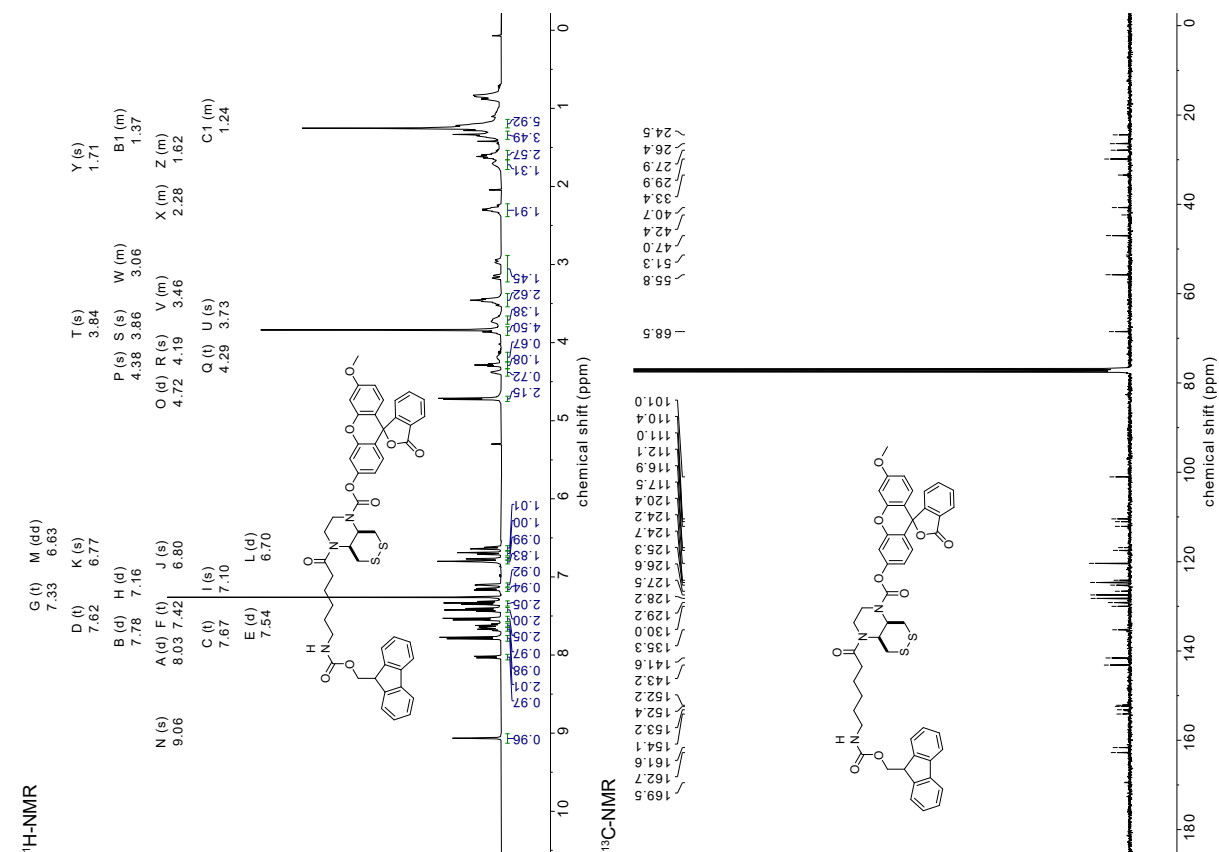


ESF-SS66C-MF (12)

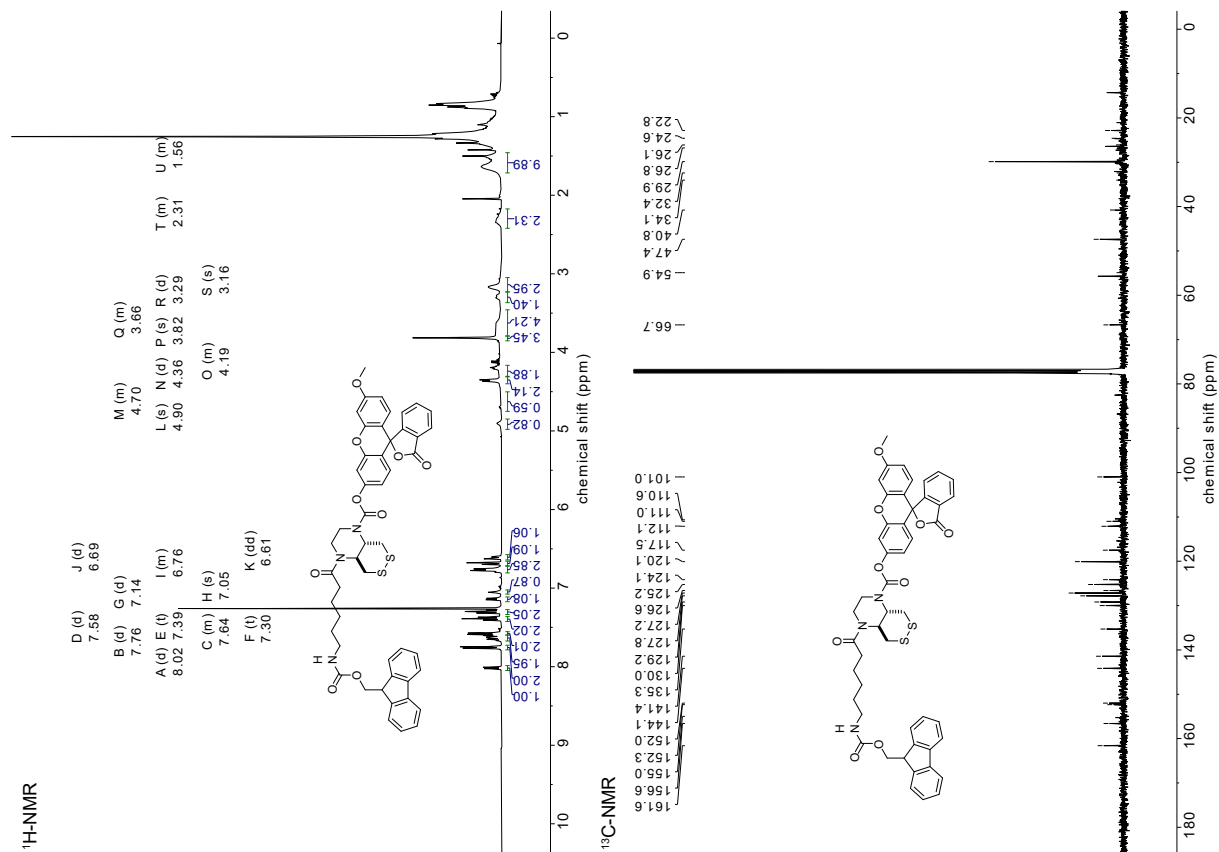


COH-SS66C-MF (13)

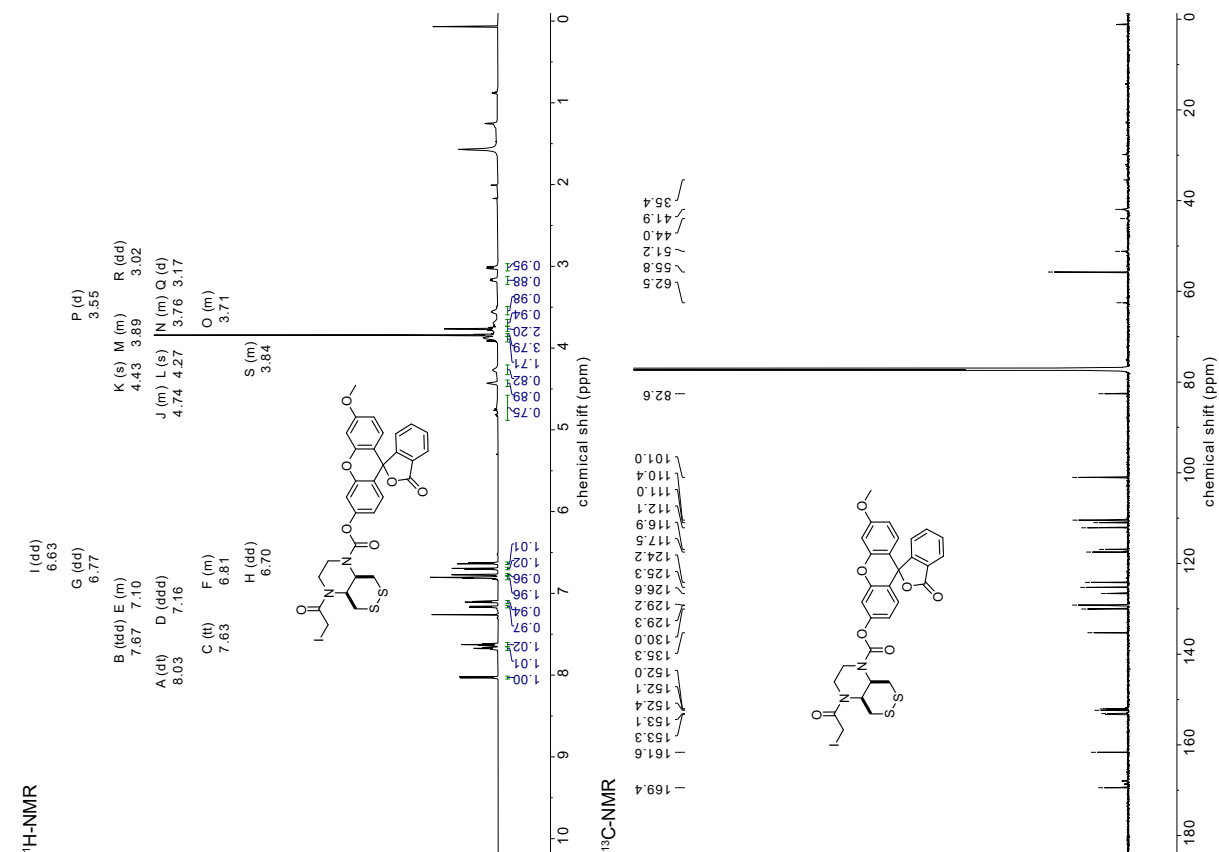


NHS-SS66C-MF (14)

FmocNH-SS66C-MF (15C)


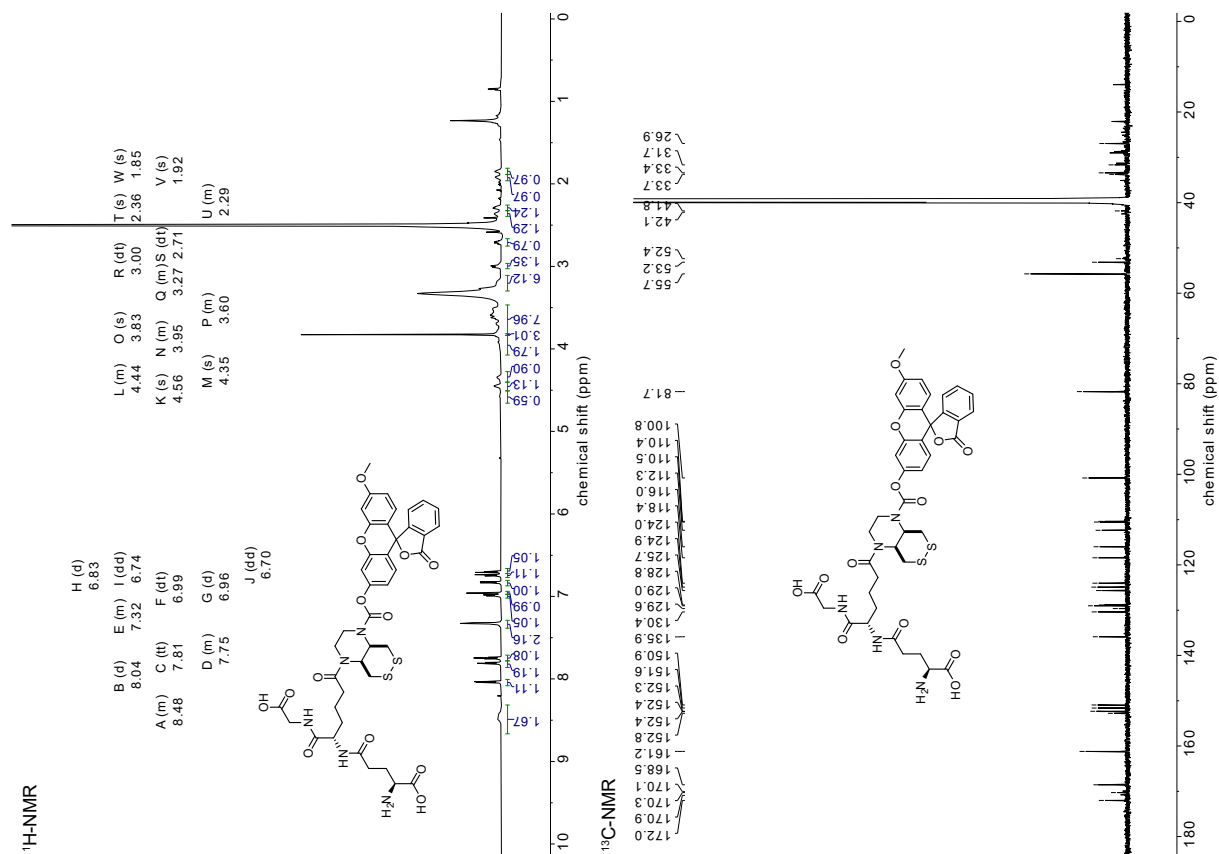
FmocNH-SS66T-MF (15T)



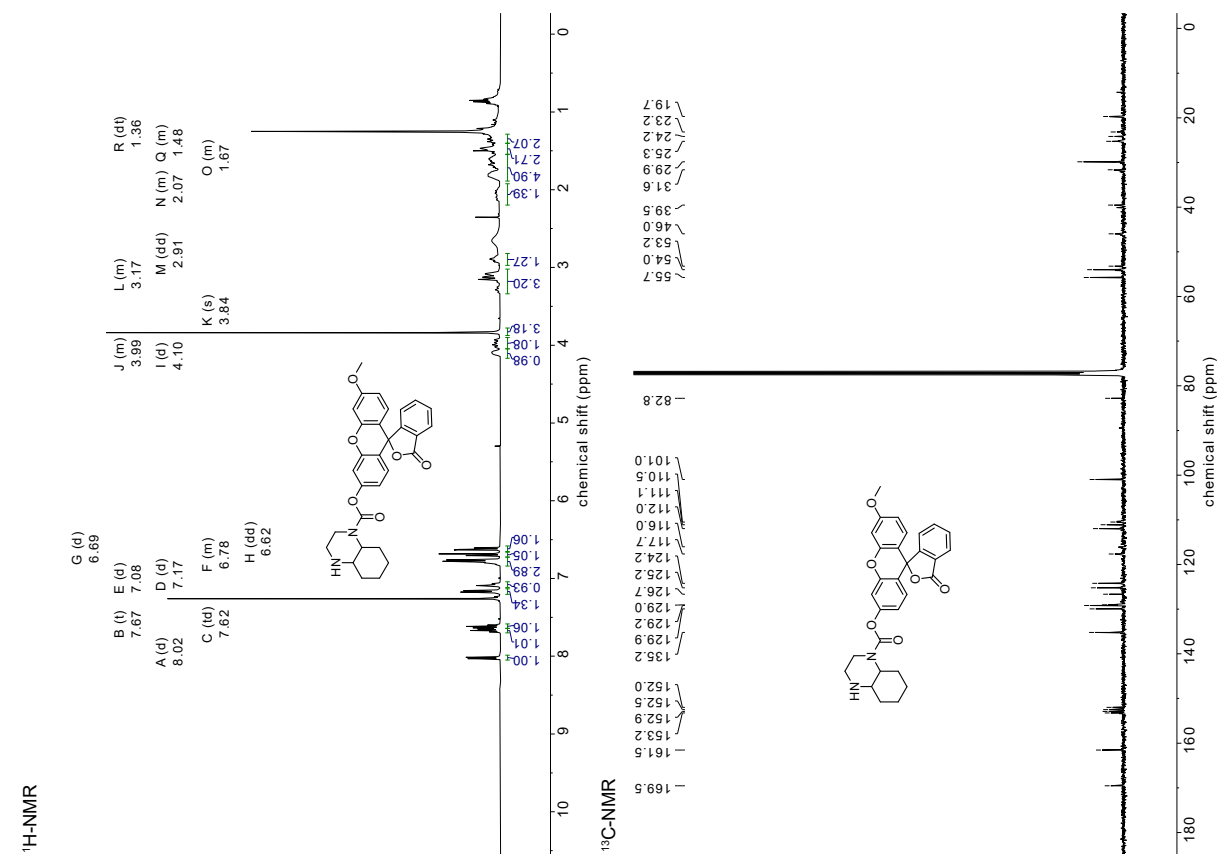
IA-SS66C-MF (16)

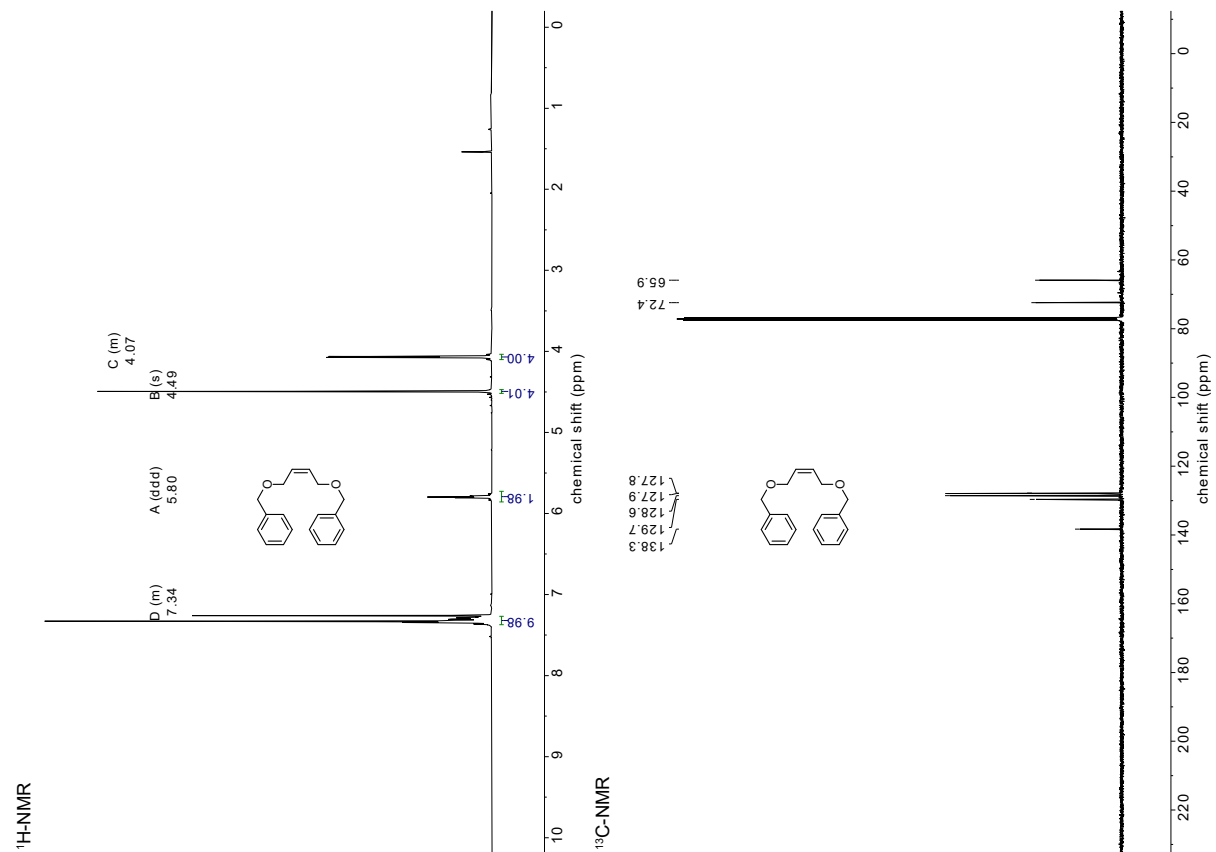
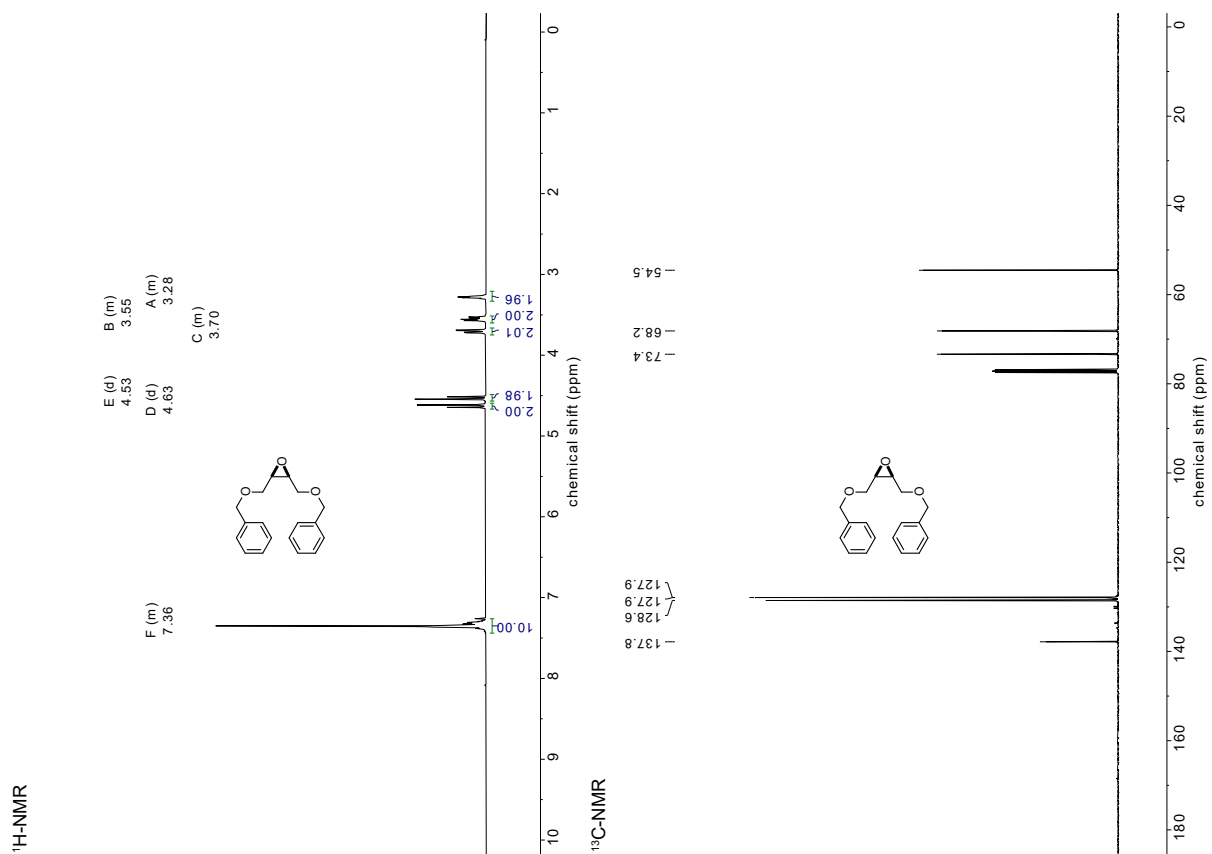


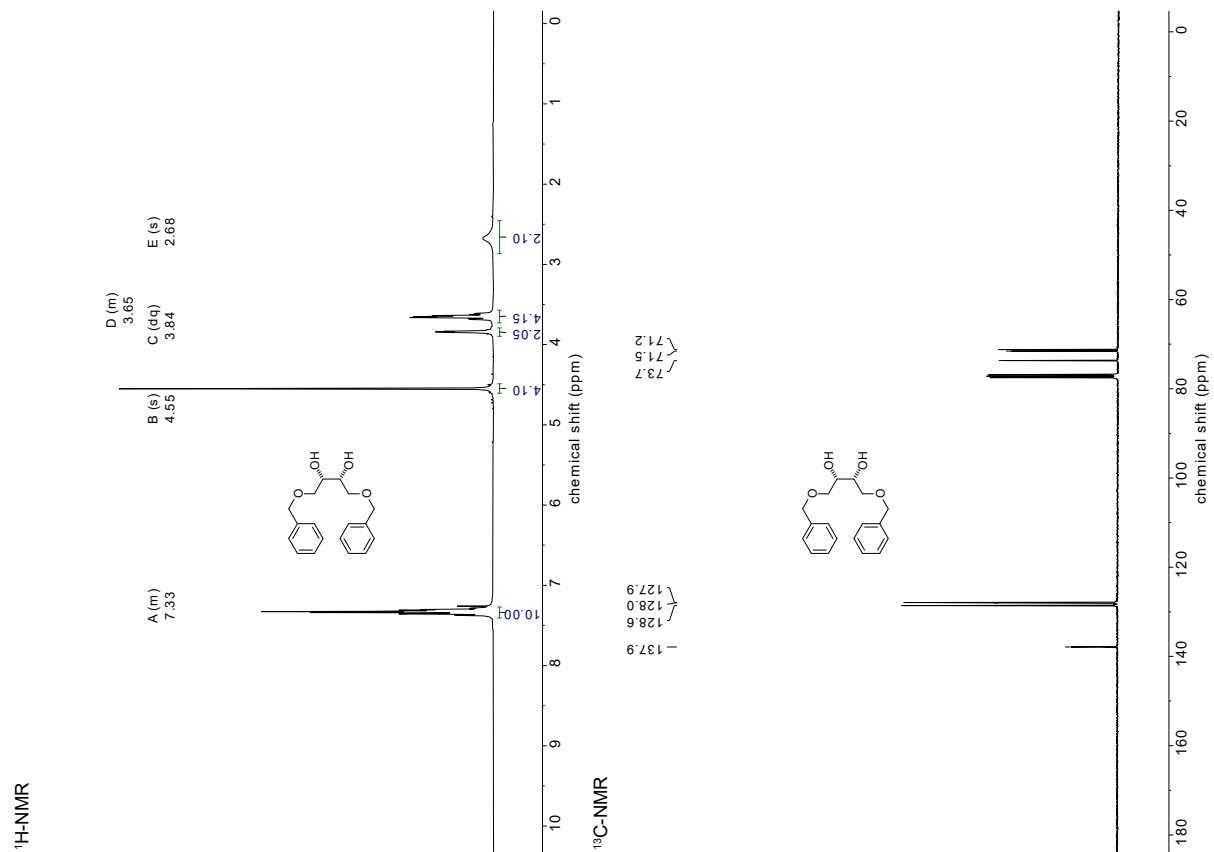
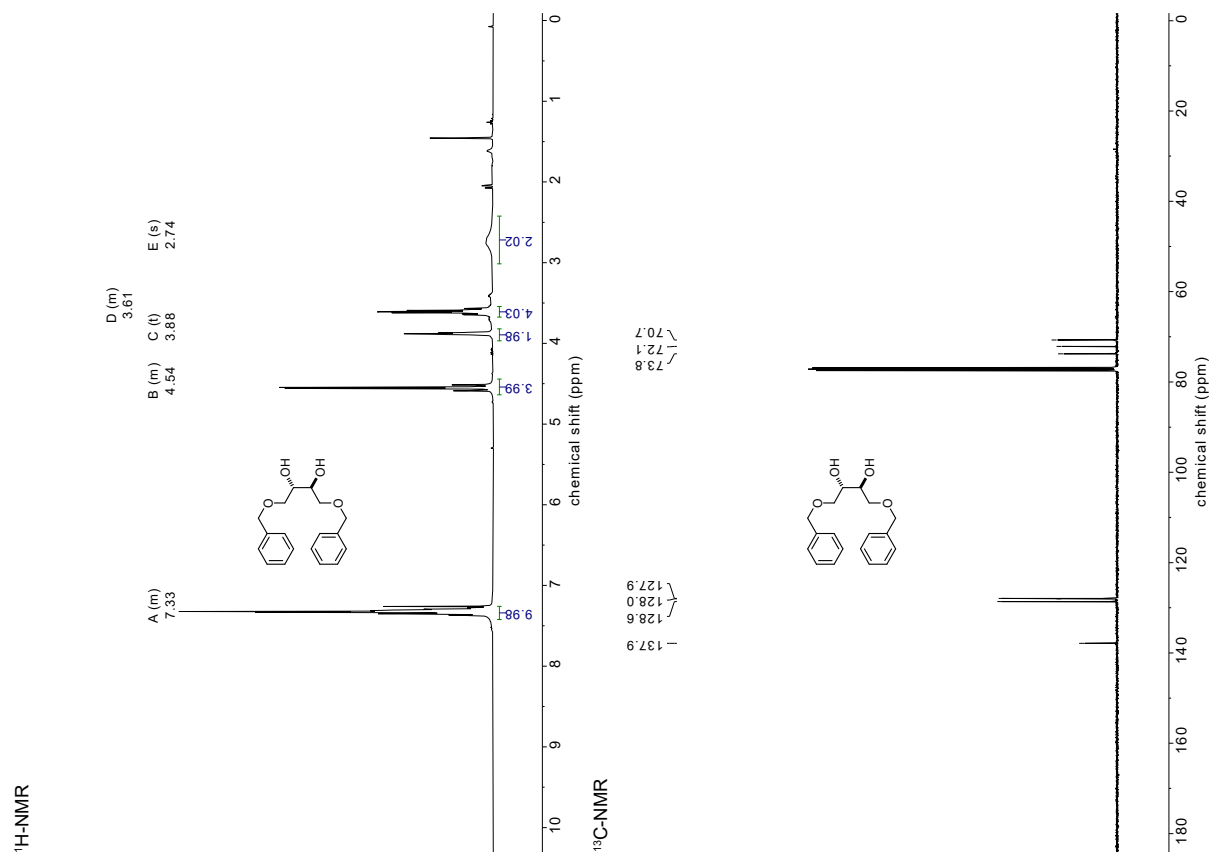
GS-SS66C-MF (17)

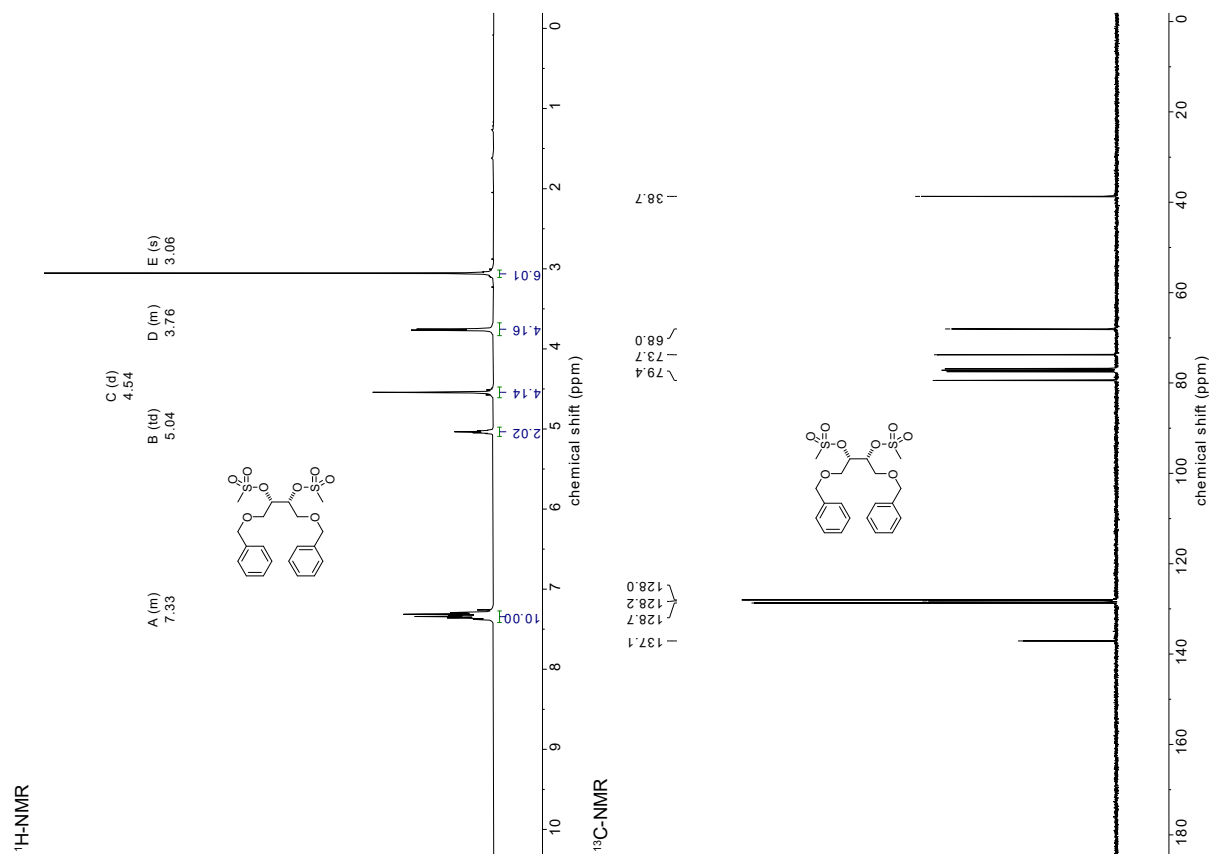
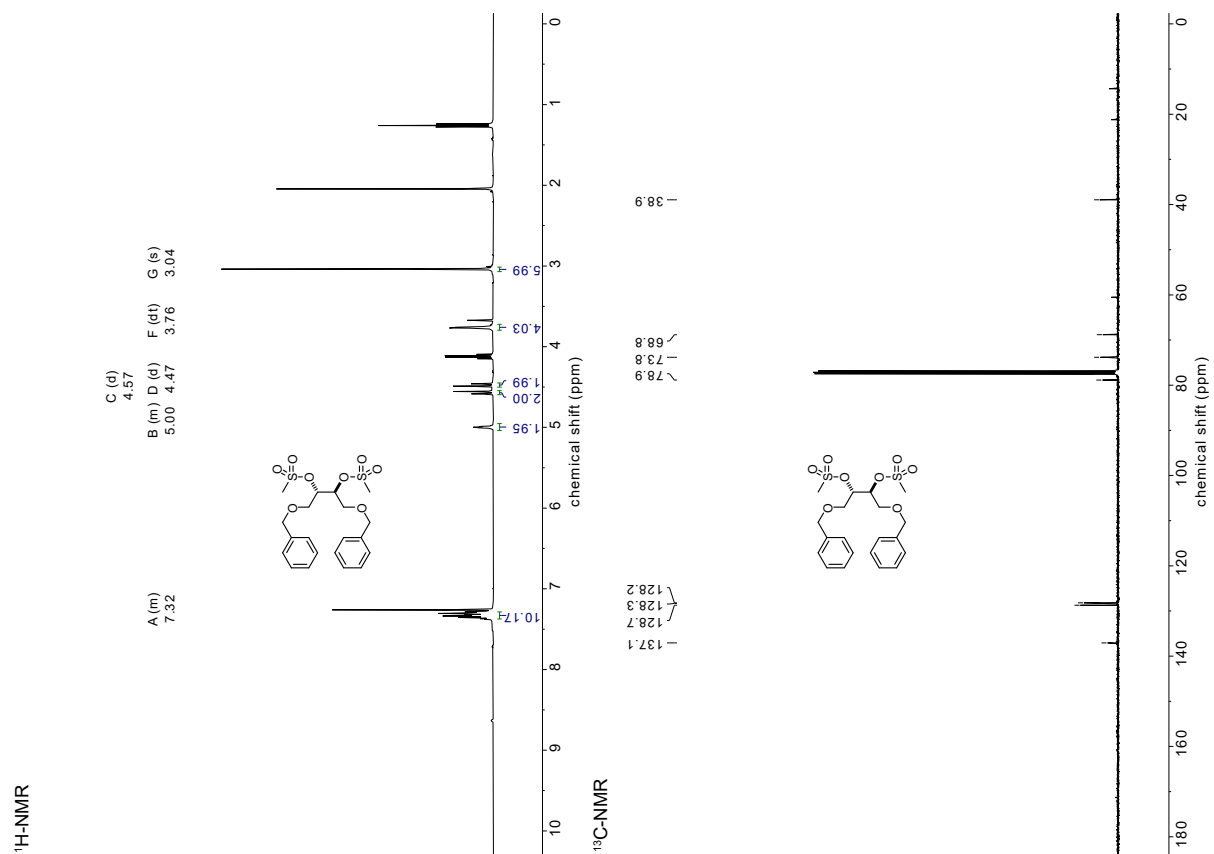


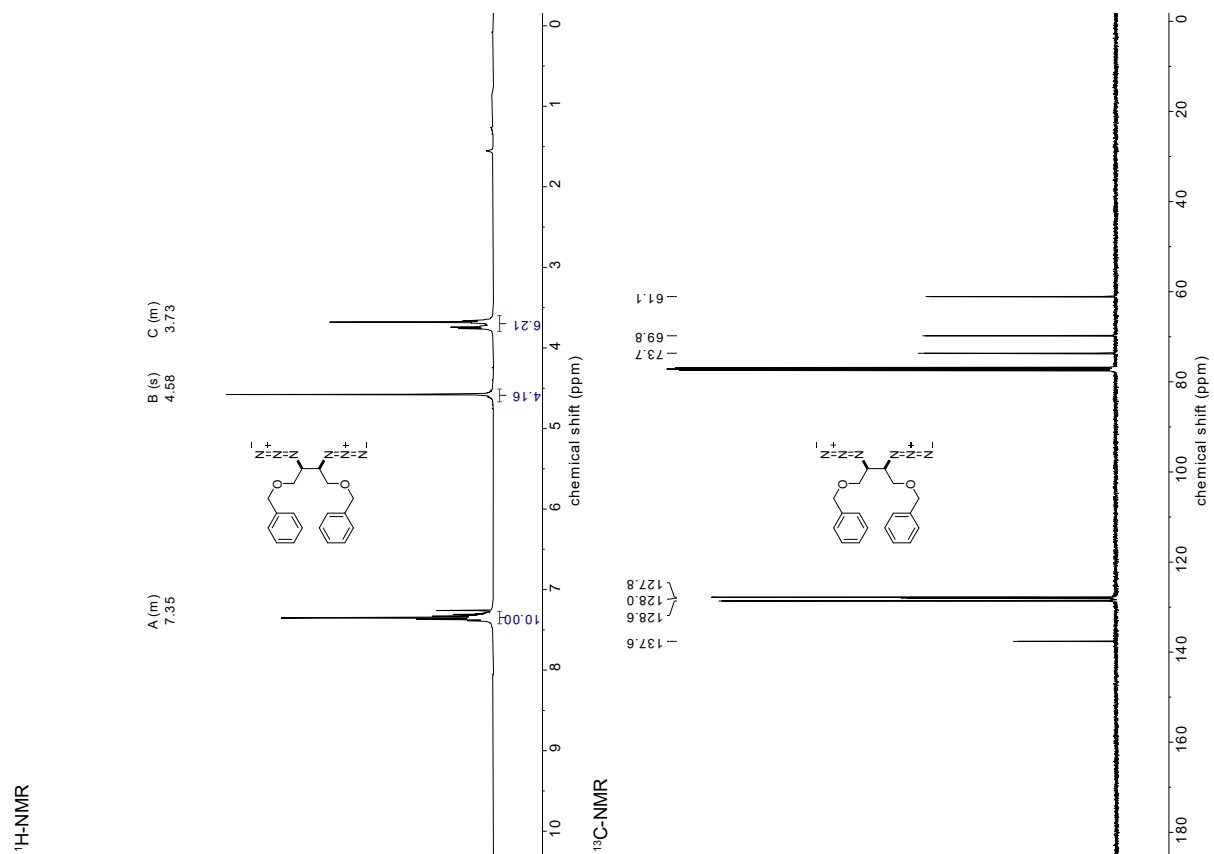
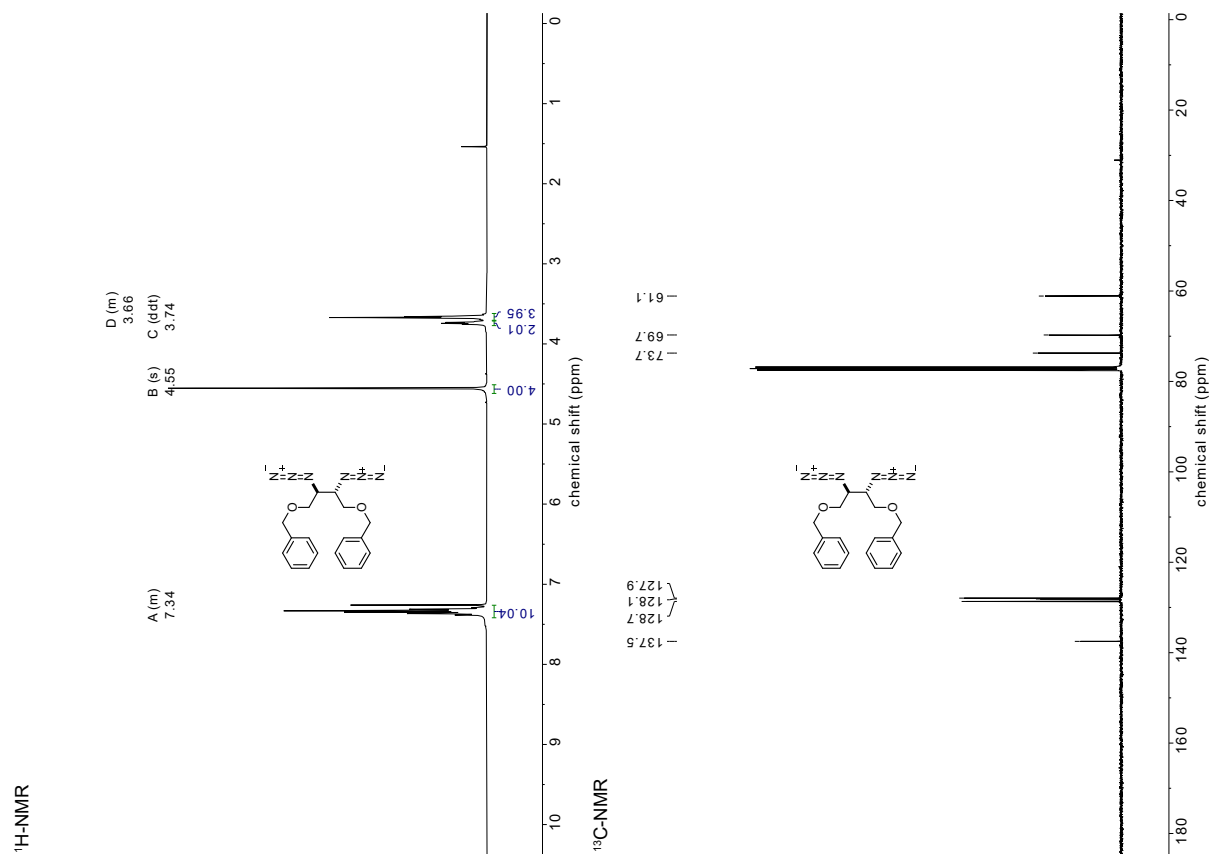
H-CC66-MF (49)

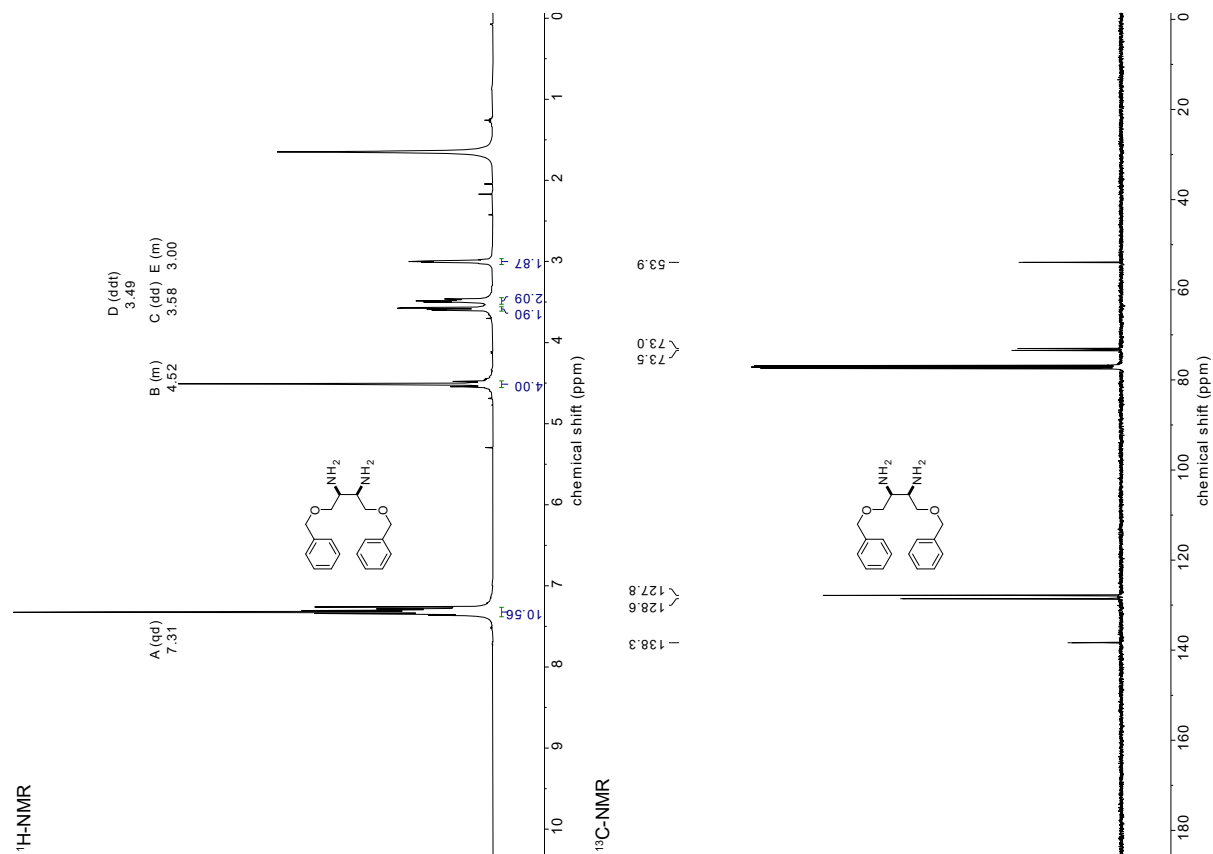
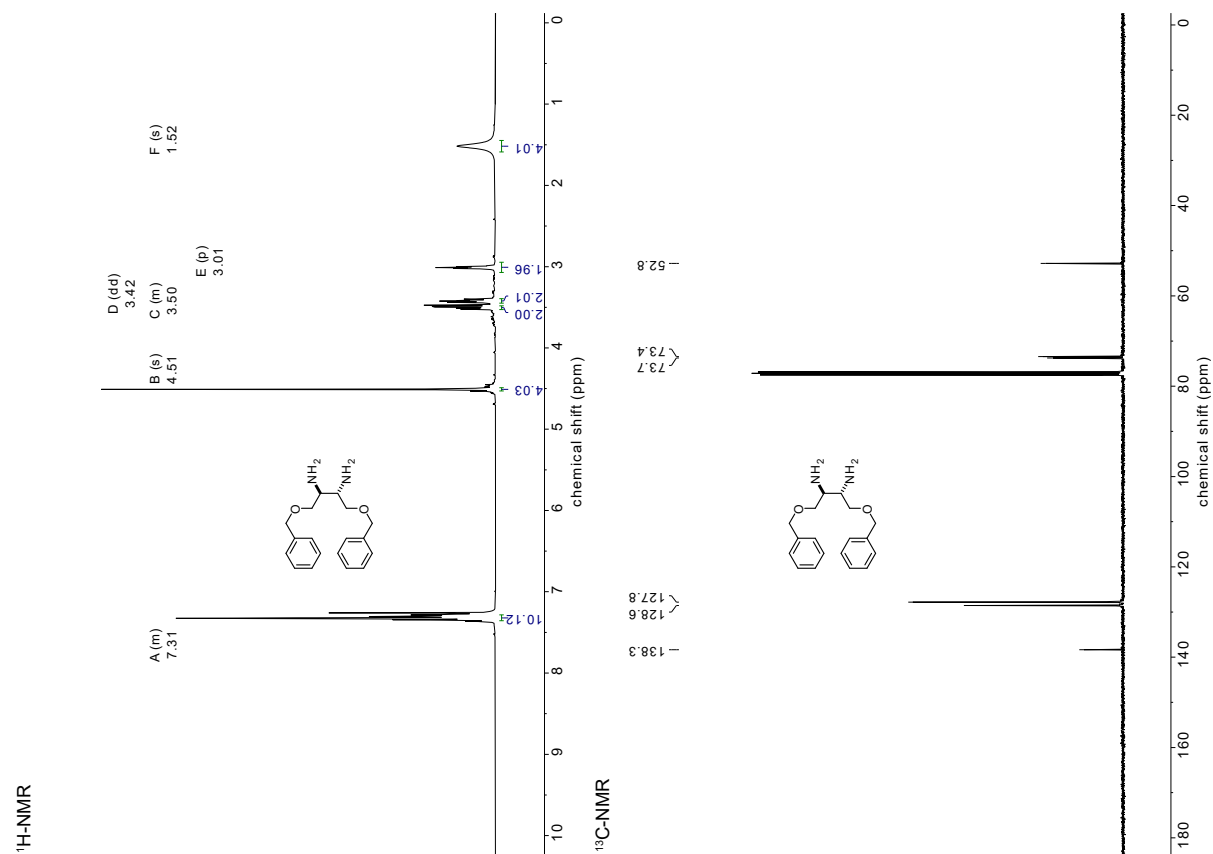


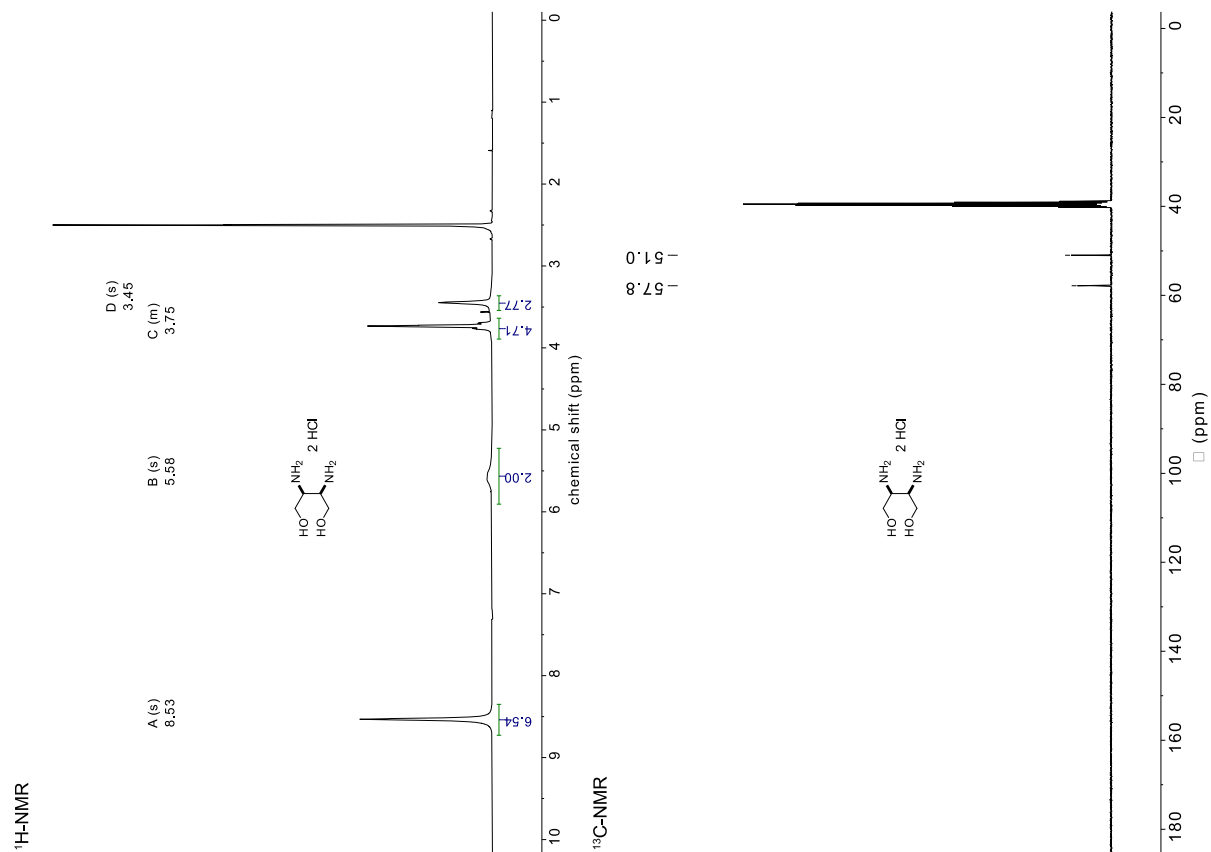
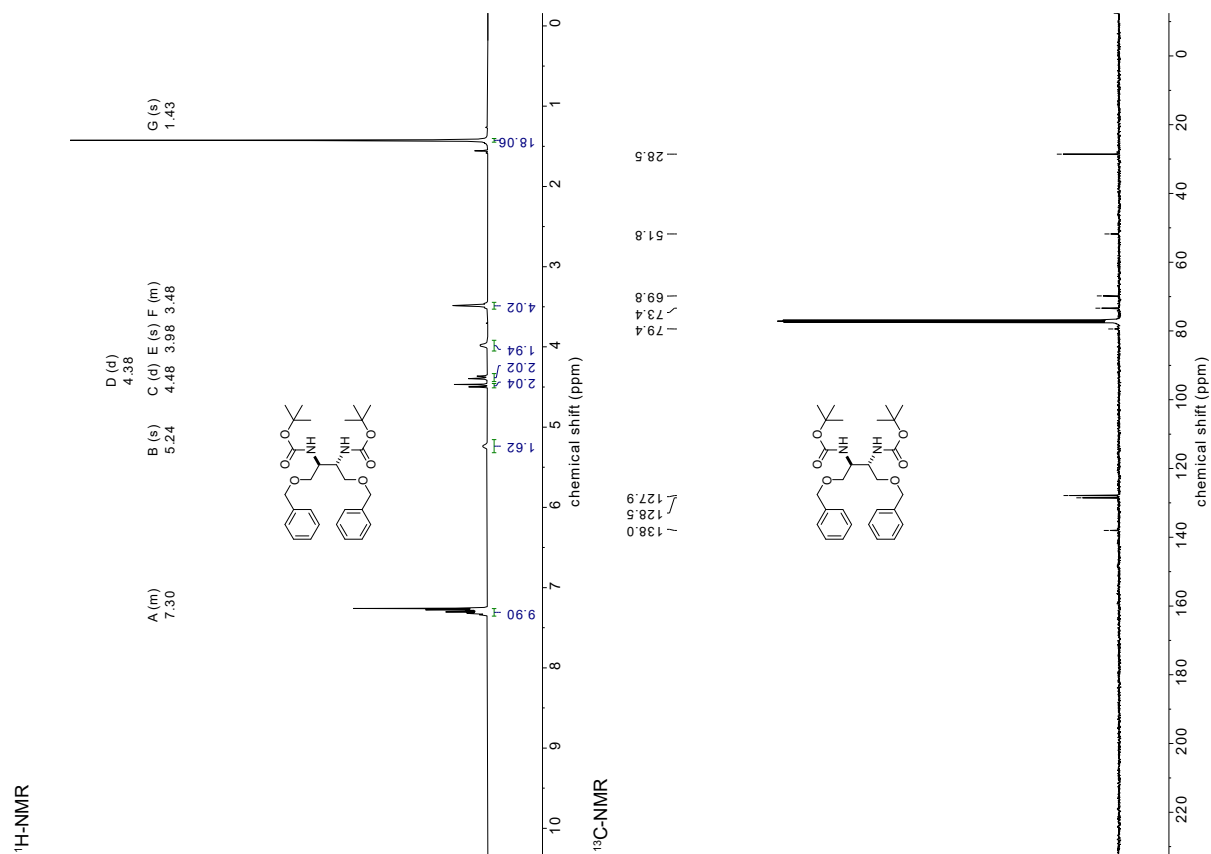
(Z)-1,4-bis(benzyloxy)but-2-ene 24**2,3-bis((benzyloxy)methyl)oxirane 25**

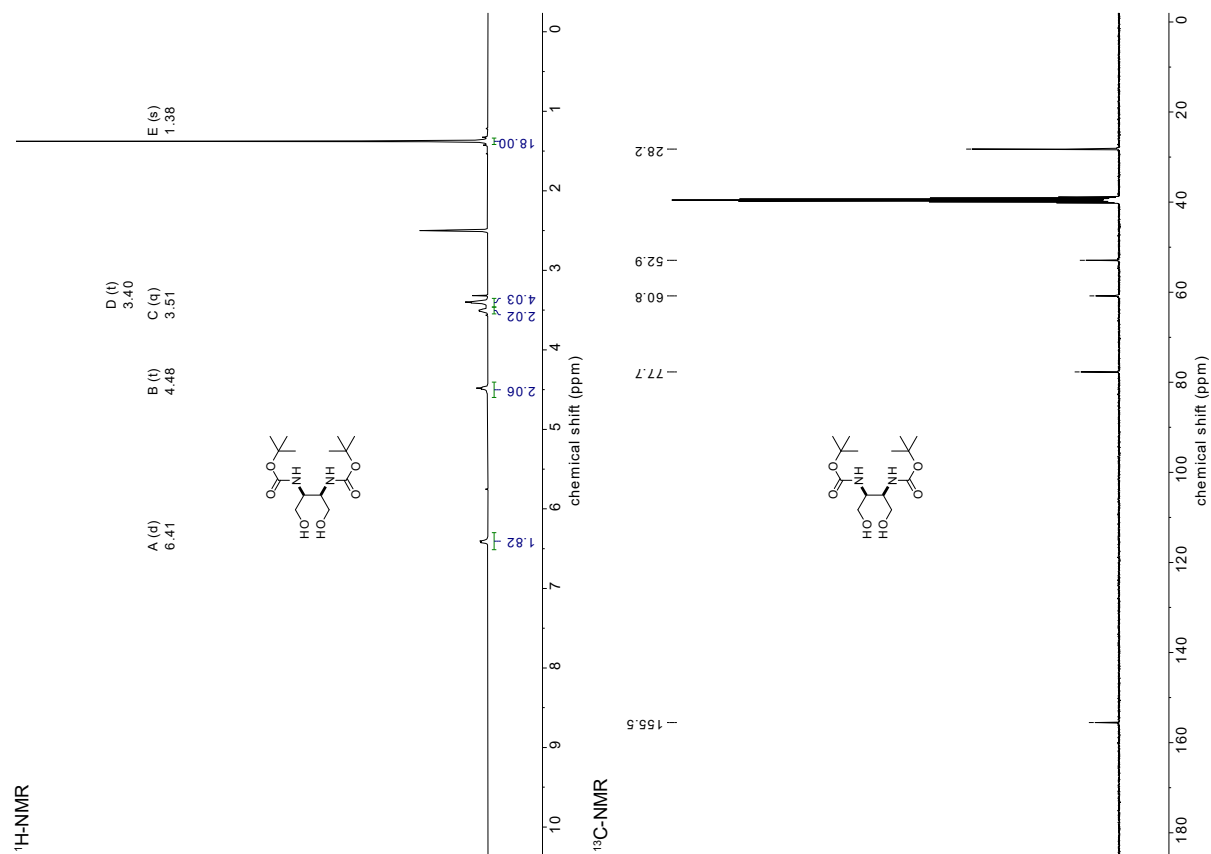
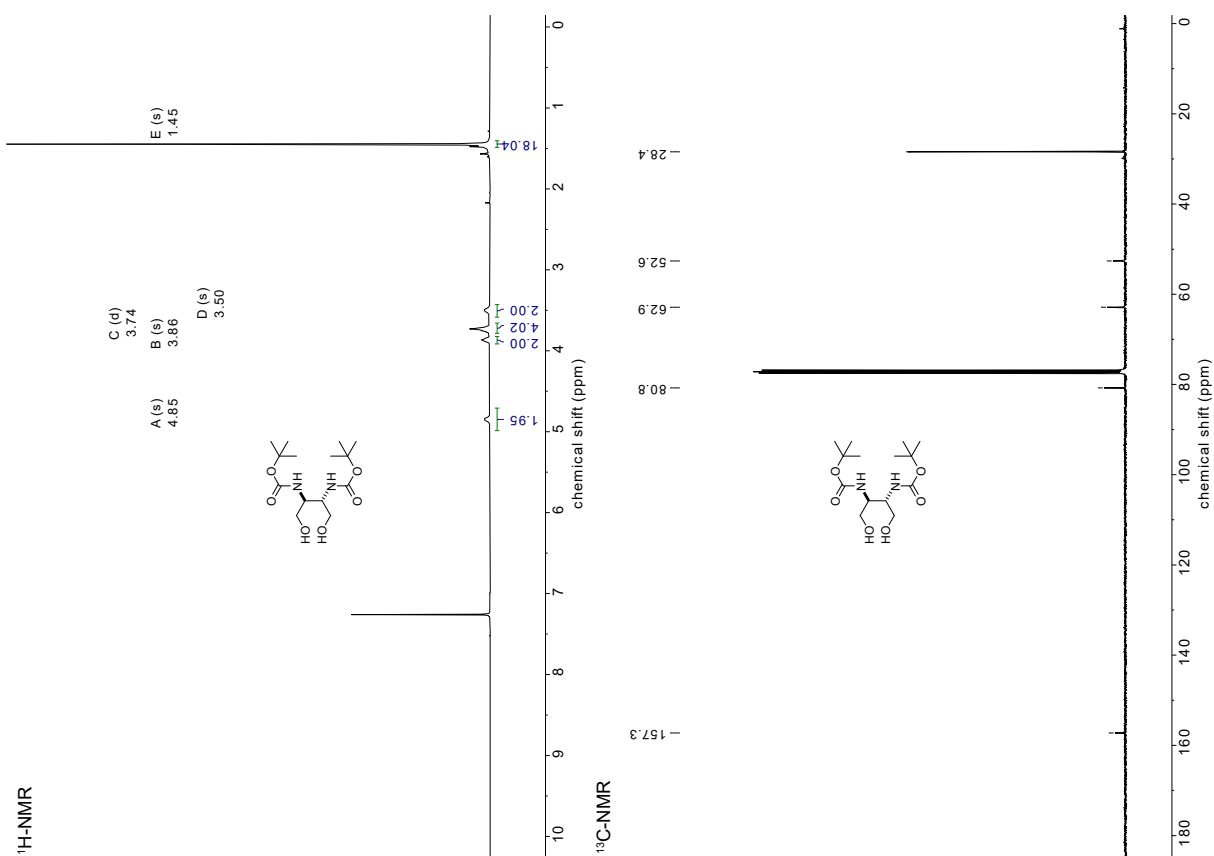
1,4-bis(benzyloxy)butane-2,3-diol (*cis*) 26C**1,4-bis(benzyloxy)butane-2,3-diol (*trans*) 26T**

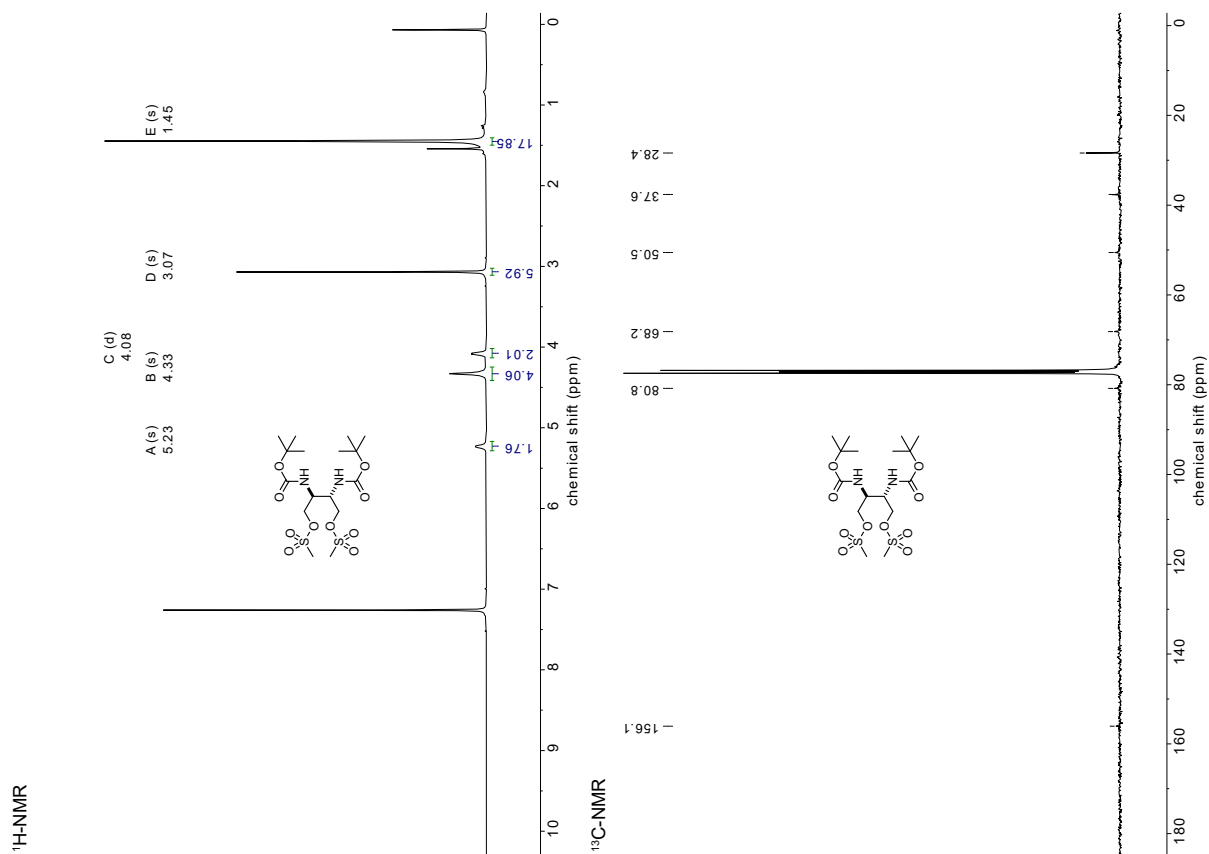
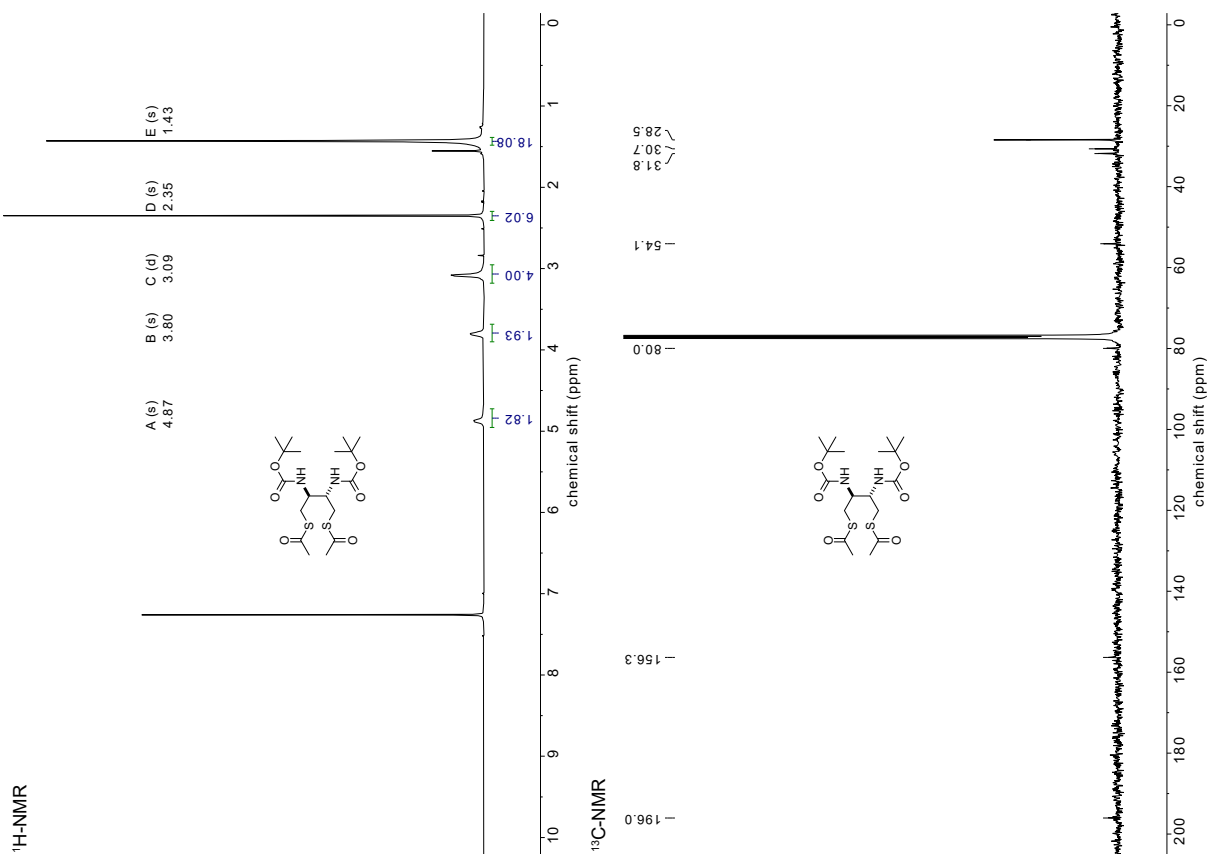
1,4-bis(benzyloxy)butane-2,3-diyl dimethanesulfonate (*cis*) 27C**1,4-bis(benzyloxy)butane-2,3-diyl dimethanesulfonate (*trans*) 27T**

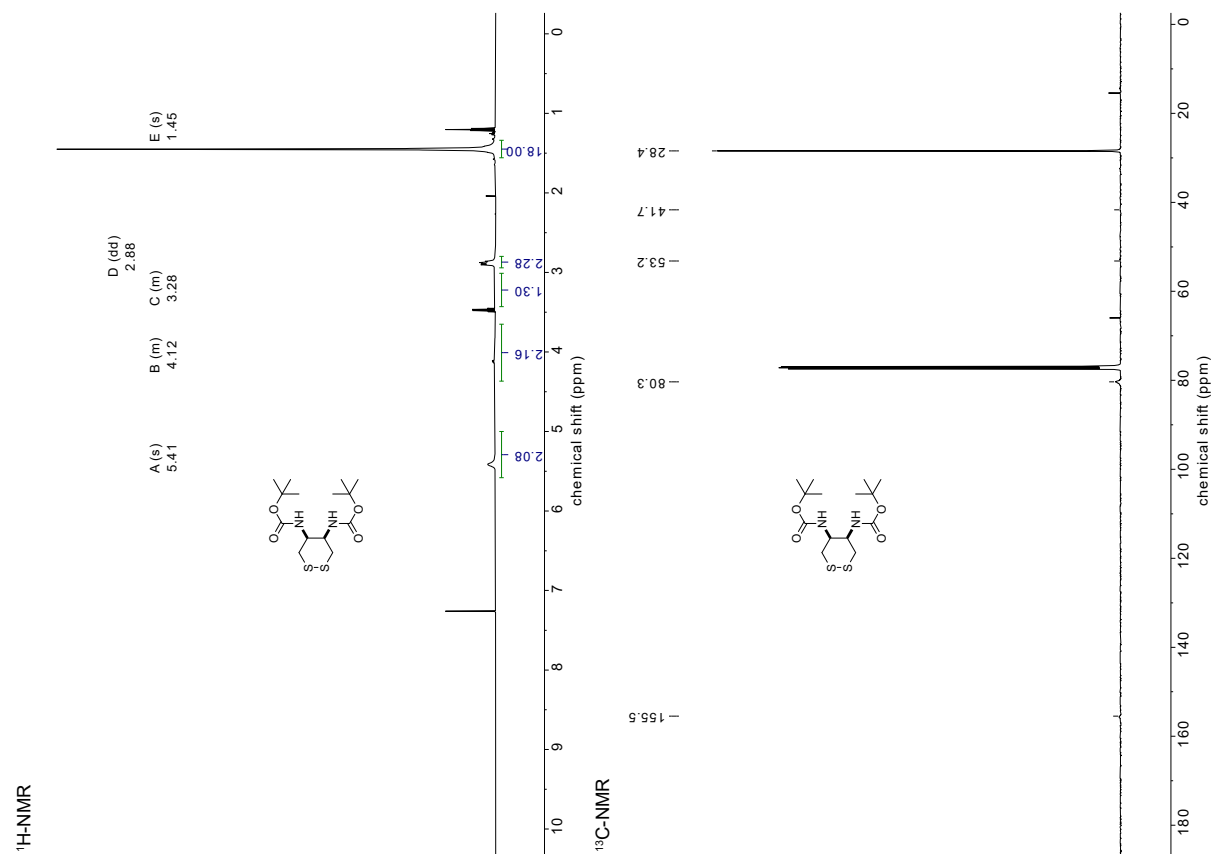
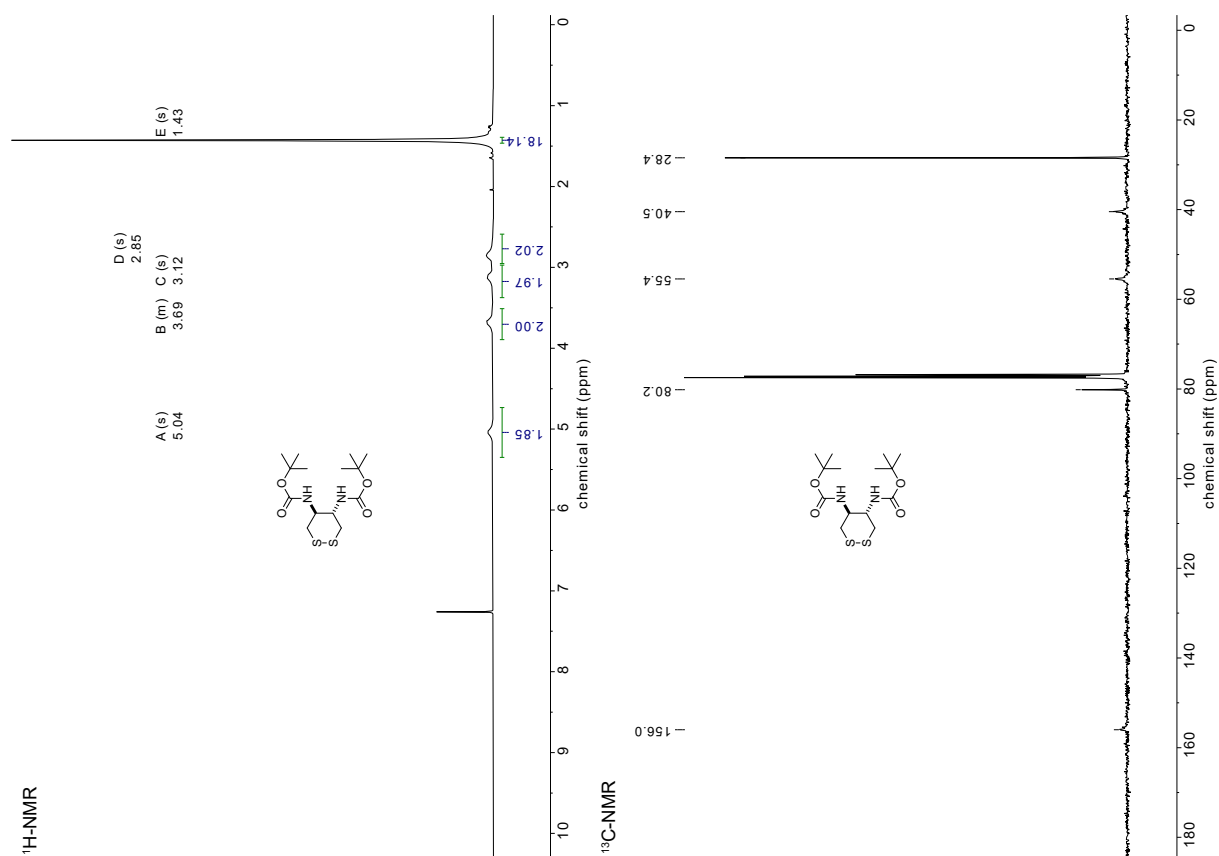
(((2,3-diazidobutane-1,4-diyl)bis(oxy))bis(methylene))dibenzene (*cis*) 28C**(((2,3-diazidobutane-1,4-diyl)bis(oxy))bis(methylene))dibenzene (*trans*) 28T**

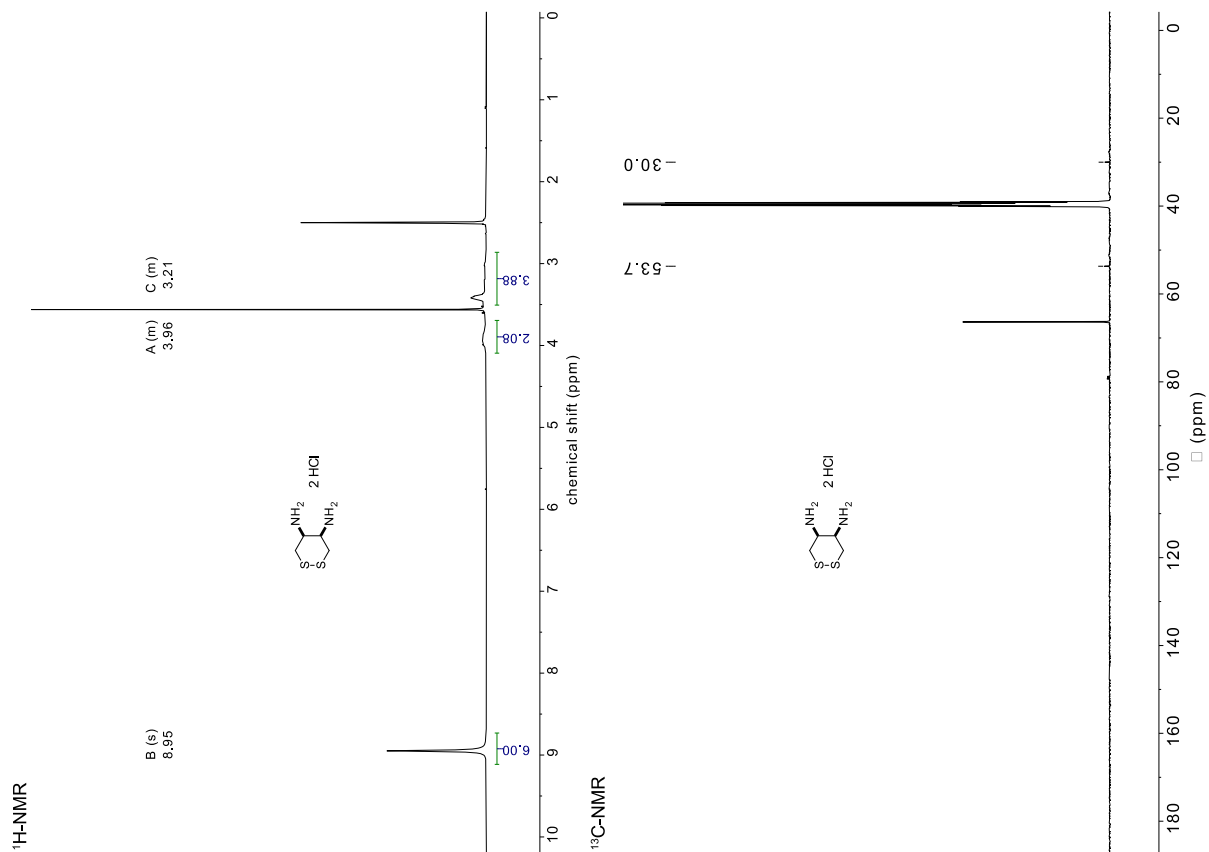
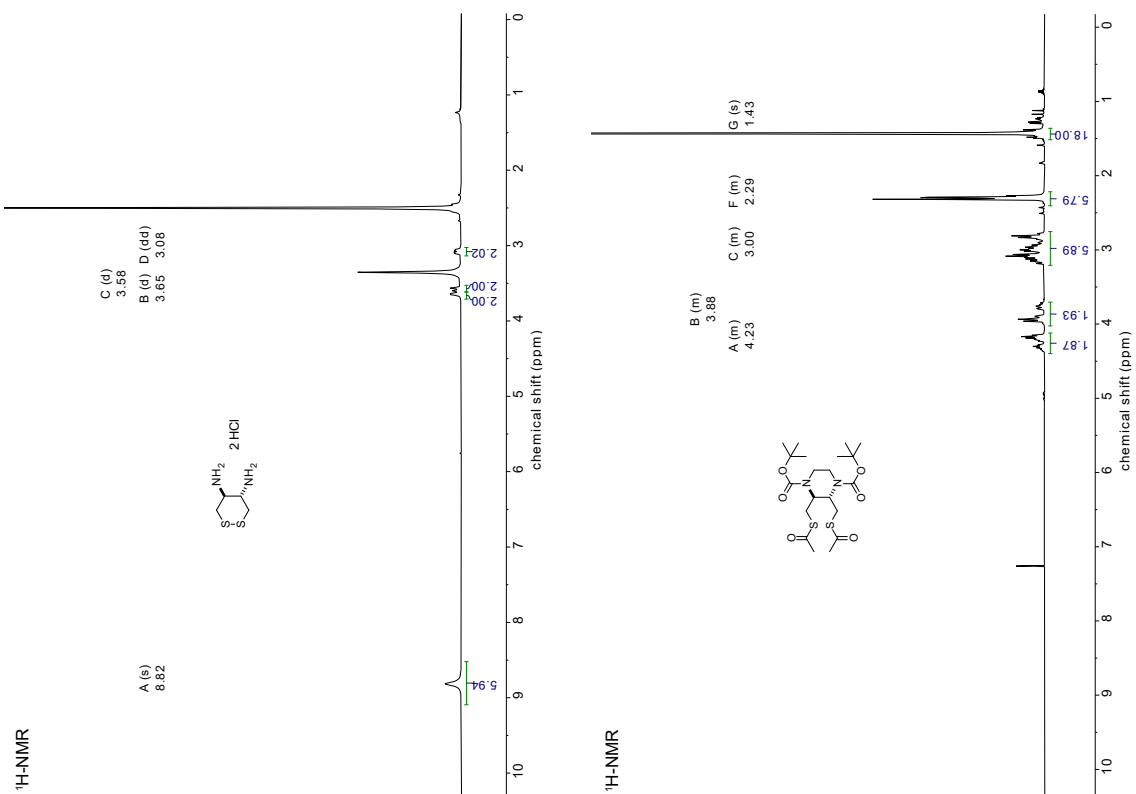
1,4-bis(benzyloxy)butane-2,3-diamine (*cis*) 29C**1,4-bis(benzyloxy)butane-2,3-diamine (*trans*) 29T**

2,3-diaminobutane-1,4-diol dihydrochloride (*cis*) 30**di-*tert*-butyl (1,4-bis(benzyloxy)butane-2,3-diyl)dicarbamate (*trans*) 31**

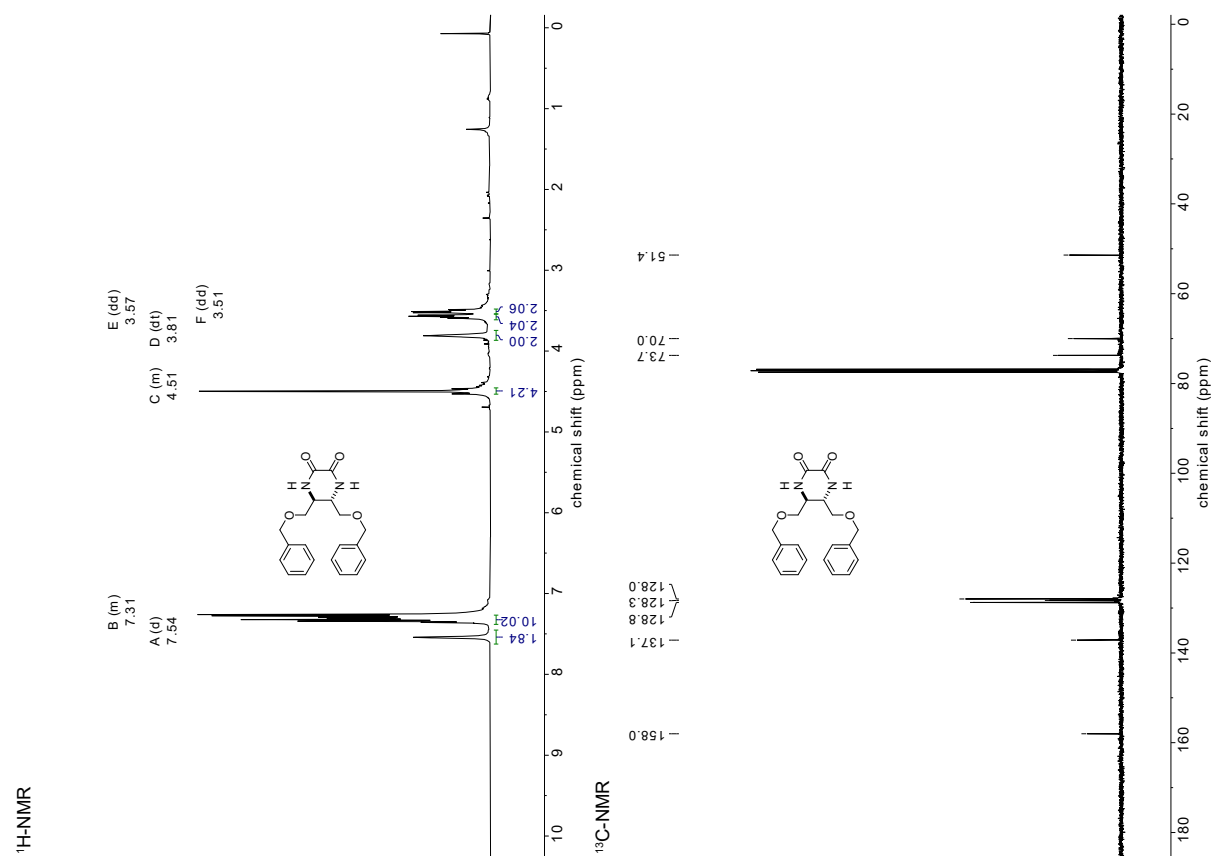
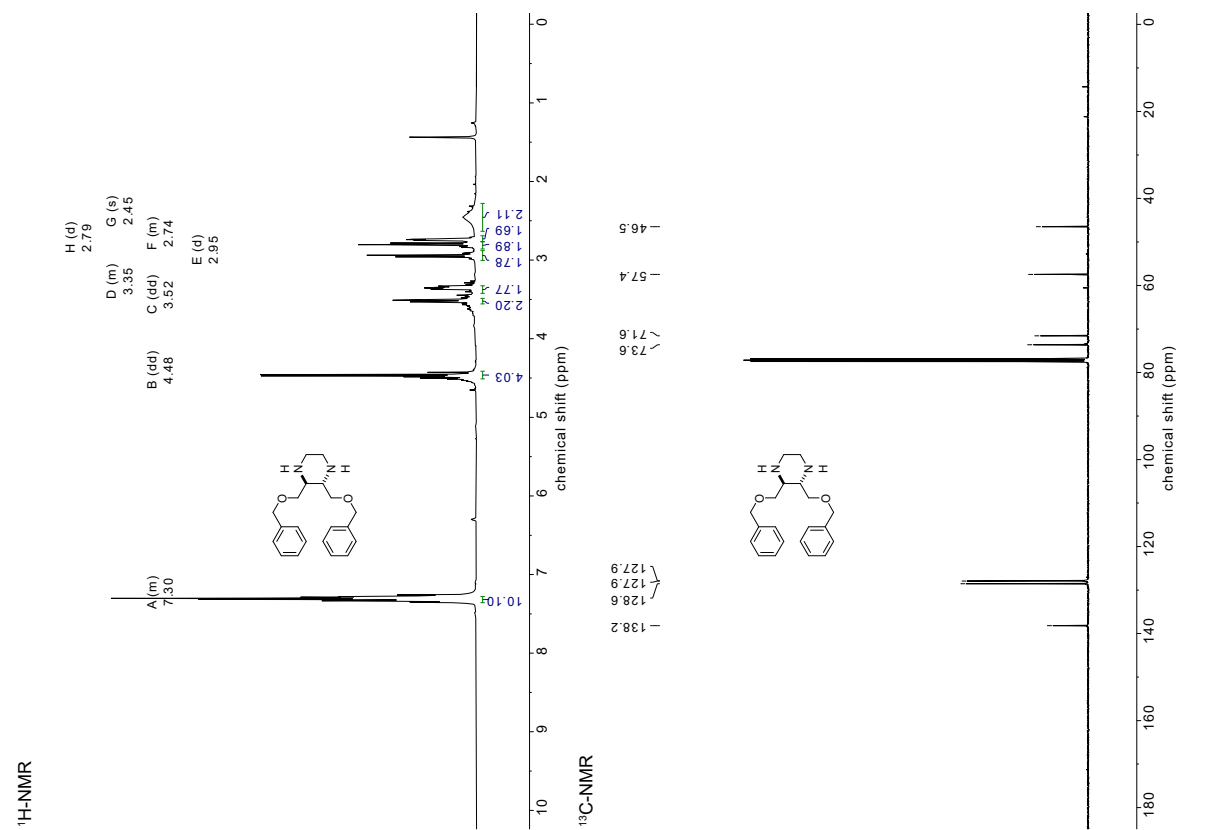
di-*tert*-butyl (1,4-dihydroxybutane-2,3-diyl)dicarbamate (*cis*) 32C**di-*tert*-butyl (1,4-dihydroxybutane-2,3-diyl)dicarbamate (*trans*) 32T**

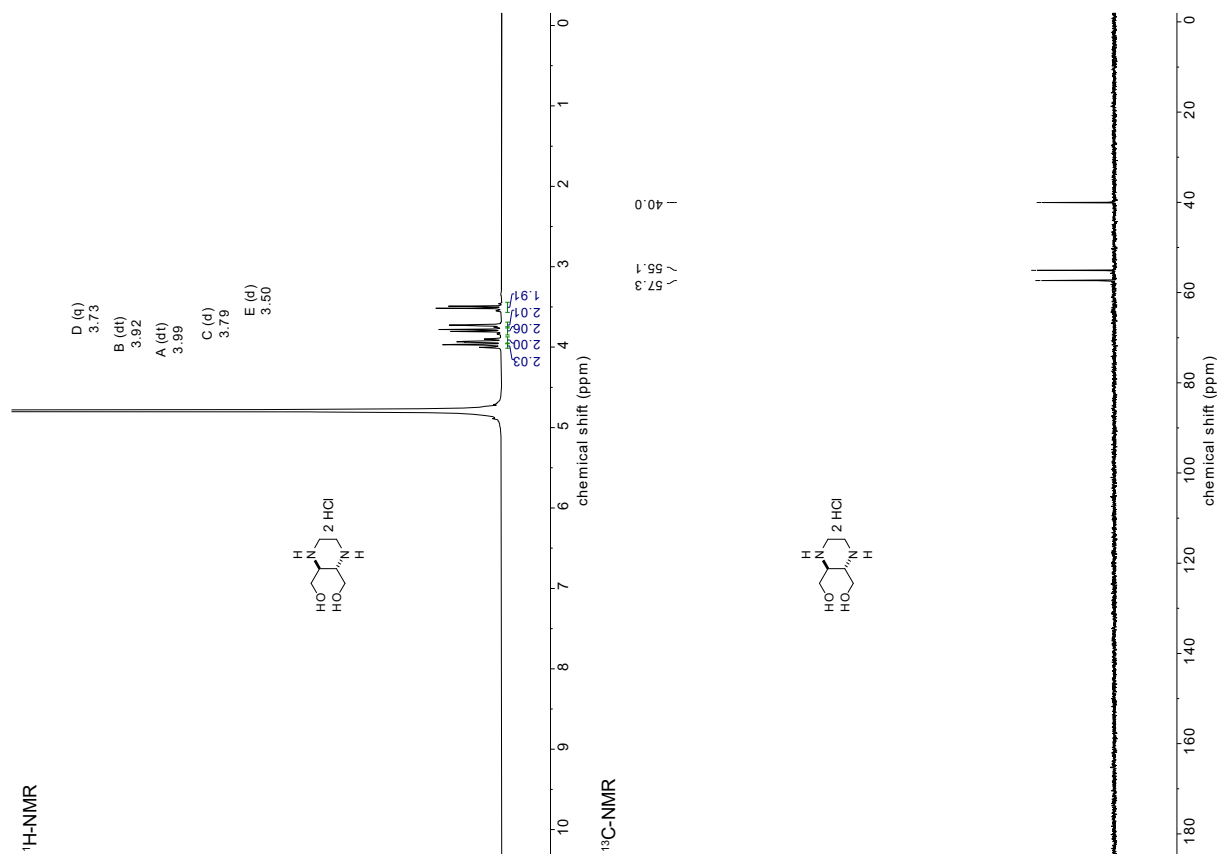
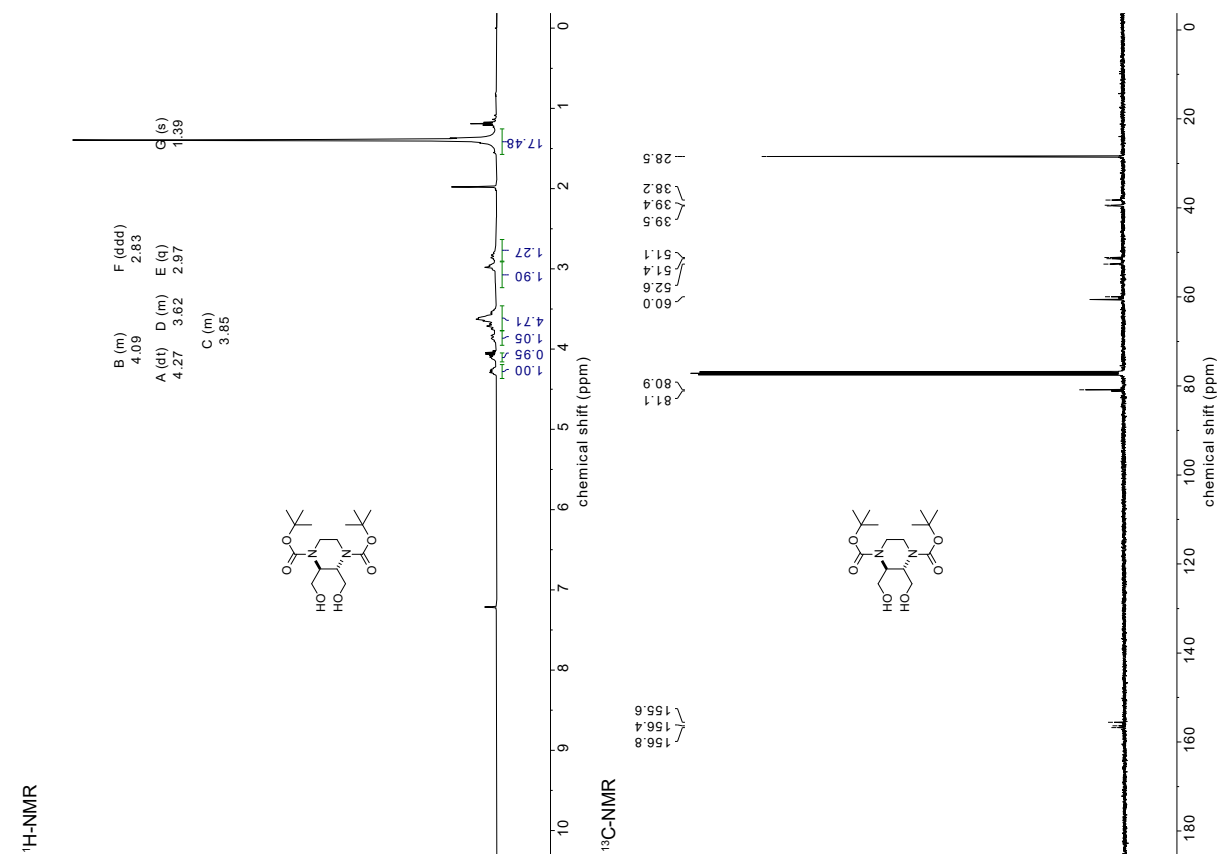
2,3-bis((tert-butoxycarbonyl)amino)butane-1,4-diyl dimethanesulfonate (*trans*) 33**2,3-bis((tert-butoxycarbonyl)amino)butane-1,4-diyl dimethanesulfonate (*trans*) 34**

di-*tert*-butyl (1,2-dithiane-4,5-diyl)dicarbamate (*cis*) 35C**di-*tert*-butyl (1,2-dithiane-4,5-diyl)dicarbamate (*trans*) 35T**

1,2-dithiane-4,5-diamine dihydrochloride (*cis*) 36C**1,2-dithiane-4,5-diamine dihydrochloride (*trans*) 36T and di-*tert*-butyl 2,3-bis((acetylthio)methyl)piperazine-1,4-dicarboxylate (*trans*) 43**

S102

5,6-bis((benzyloxy)methyl)piperazine-2,3-dione (*trans*) 39**2,3-bis((benzyloxy)methyl)piperazine (*trans*) 40**

piperazine-2,3-diyl)dimethanol dihydrochloride (*trans*) **41**di-*tert*-butyl 2,3-bis(hydroxymethyl)piperazine-1,4-dicarboxylate (*trans*) **42**

Supplementary Information to:

40 years of duocarmycins: a graphical structure/function review of their chemical evolution, from SAR to prodrugs and ADCs

Jan G. Felber* and Oliver Thorn-Seshold*

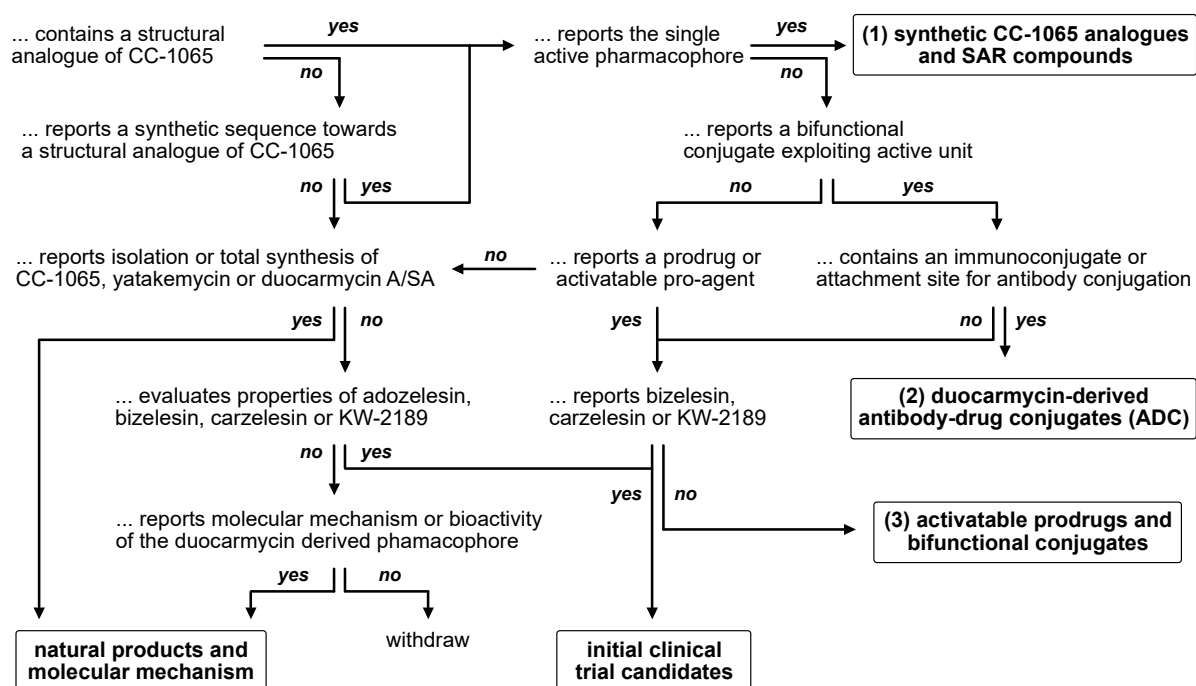
Department of Pharmacy, Ludwig Maximilians University of Munich
Butenandtstr. 5-13, D-81377 Munich, Germany.

E-mail: jan.felber@cup.lmu.de, oliver.thorn-seshold@cup.lmu.de

1. Systematic literature review (SLR) – extended	S2
2. List of main contributors and their co-authors (≥3 authorships)	S3
3. Bibliography	S4
(a) molecular mechanism (146 items – 145 journal publications, 1 patent)	S4
(b) early clinical trials (49 journal publications).....	S8
(1) SAR studies (191 items - 182 journal publications, 9 patents)	S10
(2) prodrugs/bifunctionals (102 items - 84 journal publications, 18 patents).....	S16
(3) duocarmycin ADCs (72 items - 39 journal publications, 33 patents)	S20
(x) duocarmycin reviews (23 items).....	S23

*The accompanying hyperlinked **A0 Poster** of the 200 Duocarmycins is actively curated; the current version is downloadable from the [authors' website](#). Please inform us of any errors with the Poster. We are happy to acknowledge substantial suggestions by a cloth print of the updated poster, valued at 2.56 San Serriffe dollars.*

1. Systematic literature review (SLR) – extended



Supplementary Figure S1 Strategy and methods applied to collect and sort primary research items referring to duocarmycins according to systematic literature review (SLR).

The goal of this literature search was to collate the vast majority of references, that (a) report the isolation, molecular mechanism and use of natural products that structurally relate to CC-1065, that (b) report the results of early clinical trial compounds or their synthesis, evaluation or clinical results, that (1) report syntheses and/or evaluation of bioactivity of synthetic CC 1065 analogues or their respective seco-analogues, that (2) report synthesis, evaluation of bioactivity and/or therapeutic use in vivo of activatable proagents or bifunctional conjugates employing a synthetic CC 1065 analogue or its seco-version or that (3) report conjugation/assembly and/or therapeutic efficacy of (multi)functional antibody-drug conjugates incorporating a synthetic CC 1065 analogue or its seco version. This literature collection should be exploited as a database that allows a systematic analysis of both primary reports and metadata to decipher the chemical evolution of structure that the duocarmycin/CC-1065 derived alkylating unit has undergone over the last 40 years.

The search for this systematic literature review (SLR) has gone through many cycles using PubMed, ResearchGate, Google Scholar and Google for journal publications and review articles and FreePatentsOnline and Google Patents for related patents. During a first phase the phrases ["CC 1065" or "duocarmycin"] in combination with ["analogue" or "prodrug" or "derivative" or "review"] have been used and related references have been categorised according to (a1) isolation, early reports or total syntheses of CC-1065 related natural product and (a2) mechanism of action; (b) early small molecule based clinical trial compounds and related articles; (1a) synthetic derivatives that allow to conclude on structure-activity-relationship (SAR) and (1b) reports of synthons that allow are relevant for synthetic duocarmycin-analogues; (2a) functional proagents based on the seco-duocarmycin/cyclobenz[e]indole (CBI) functional unit or (2b) bifunctional conjugates that bear at least one duocarmycin analogue or its seco-version or (3) antibody-drug conjugates that employ a duocarmycin-type alkylating unit as pharmacophore for therapeutic use. More specifically, reports have been collected that refer to the natural products "duocarmycin A", "duocarmycin SA", "yatakemycin", the specific clinical trial compounds "adozelesin", "bizelesin", "carzelesin" or "pibrozelesin/KW 2189", the ADC-related research items ["duocarmycin" or "CBI" or "CPI"] in combination with ["ADC" or "antibody-drug conjugate"] and the clinical trial candidates "SYD985", "MDX-1302" or "MGC018".

Secondly, the major driving scientific groups behind each area of research have been identified (L. H. Hurley, D. L. Boger, M. Lee, H. Sugiyama, L. F. Tietze, H. Saito and W. A. Denny/M. Tercel, Byondis BV). For each group all references that report aspects related to the duocarmycin-derived pharmacophore have been collected and categorized accordingly. The major scientific research groups or pharmaceutical companies, that drive CBI-based ADCs recently, have been identified (Byondis B.V./Syntarga B.V., Medarex Inc., Genentech Inc., Immunogen Inc. and others) and journal publications have been searched at Google Scholar, whereas patents have been search at FreePatentsOnline and Google Patents. Lastly, recent review articles (Wang 2021, Pors 2020, Lee 2015, Tietze 2011, Pors 2011 and Tietze 2009) have been screened and references have been cross-compared to collate a conclusive library.

2. List of main contributors and their co-authors (≥3 authorships)

(1) Dale Boger: Prof. of Chemistry, The Scripps Research Institute (TSRI), La Jolla:

<https://www.scripps.edu/boger/> - 125 Publications:

Paul S. Kitos (14), Douglas S. Johnson (12), Ishizaki Takayoshi (11), Inkyu Hwang (10), Hamideh Zarrinmayeh (10), Robert M. Garbaccio (9), Weiya Yun (9), Christopher W. Boyce (8), Karen MacMillan (8), Stephan A. Munk (8), Qing Jin (7), David B. Kastrinsky (7), James P. Lajiness (7), Jeffrey A. McKie (7), Hui Cai (6), Nianhe Han (6), Michael P. Hedrick (6), Oranart Suntornwat (6), Scott E. Wolkenberg (6), Robert S. Coleman (5), Jay P. Parrish (5), Mark Searcey (5), Mark S. Tichenor (5), George A. Vielhauer (5), Pier G. Baraldi (4), Takahide Nishi (4), Philippe Mesini (4), Thomas J. Rayl (4), William M. Robertson (4), Christine M. Tarby (4), John D. Trzupke (4), Amanda L. Wolfe (4), Bernd Bollinger (3), Kristopher E. Boyle (3), Katherine K. Duncan (3), Joel Goldberg (3), Donald L. Hertzog (3), Nikhil K. Parekar (3), Winston C. Tse (3), Philip Turnbull (3), Scott J. Weir (3), Ronald Wysocki (3).

(2) Hiroshi Sugiyama: Prof. Chemical Biology, Kyoto University:

<http://kuchem.kyoto-u.ac.jp/chembio/> - 58 Publications:

Toshikazu Bando (45), Ken-Ichi Shinohara (18), Masafumi Minoshima (14), Isao Saito (12), Shunta Sasaki (12), Gengo Kashiwaza (10), Kaori Hashiya (9), Akihiko Narita (9), Rhys Dylan Taylor (6), Tsuyoshi Fujiwara (5), Zhi-Fu Tao (5), Jun Fujimoto (4), Hiroki Nagase (4), Tatsuhiro Shimizu (4), Anandhakumar Chandran (3), Yusuke Kawamoto (3), Rina Maeda (3), Gadesh N. Pandian (3), Toshiki Takagaki (3).

(3) William A. Denny: Prof. Medicinal Chemistry, Auckland University and Dr. Moana Tercel, Senior Research Fellow, Auckland University:

<https://unidirectory.auckland.ac.nz/profile/b-denny/>
<https://unidirectory.auckland.ac.nz/profile/m-tercel/>

49 publications with authorship of either William A. Denny or Moana Tercel:

Moana Tercel (38), William A. Denny (35), William R. Wilson (24), Graham Atwell (15), Frederik B. Pruijn (15), Ralph J. Stevenson (10), Sarath H. D. Liyanage (8), Thomas H. Pillow (8), Shangjin Yang (7), Jane Botting (6), Ho H. Lee (6), Adam V. Patterson (6), Jared Milbank (6), Amir Ashoorzadeh (4), Sarah P. McManaway (4), Sunali Mehta (4), Robert F. Anderson (3), Michael P. Hay (3), Eileen Smith (3).

(4) Lutz Tietze: Prof. Organic and biomolecular Chemistry, University of Goettingen:

Laboratory Website: <http://www.tietze.chemie.uni-goettingen.de/ewelcome.php> - 35 Publications:

Ingrid Schuberth (17), Birgit Krewer (13), Felix Major (8), Kianga Schmuck (7), J. Marian von Hof (6), Heiko J. Schuster (6), Frauke Alves (4), Tim Feuerstein (4), Frank Haurert (4), Tobias Herzig (4), Michael Müller (4), Olaf Panknin (3), Stephan A. Sieber (3).

(5) Laurence H. Hurley: Prof. Medicinal Chemistry, Arizona - 28 publications:

Daekyu Sun (11), Chong-Soon Lee (5), Paul A. Aristoff (4), Hsiung Chin Lin (4), Vincent L. Reynolds (4), David H. Swenson (4), Donald R. Needham-VanDev (3), Patrick J. McGovern (3), Gary L. Petzold (3), William C. Krueger (1), Li H. Li (1).

Related researchers and/or groups with independent publications and at least 3 authorships:

William C. Krueger (17), David H. Swenson (13), Mark D. Prairie (12), Gary L. Petzold (12), Patrick J. McGovern (11), Bijoy K. Bhuyan (10), Robert C. Kelly (10), Li H. Li (10), Paul A. Aristoff (7), Martha A. Warpehoski (7), Thomas F. DeKoning (5), Tanya L. Wallace (4), Ilse Gebhard (3).

(6) Moses Lee, Furman University, Greenville/Georgia State University:

<https://www.researchgate.net/scientific-contributions/Moses-Lee-38856864> - 25 Publications:

John A. Hartley (14), Konstantinos Kiakos (14), Stephen J. Hudson (7), Carlie A. Price (6), Kaitlin Summerville (6), Heather L. Handl (5), Bethany Purnell (5), Heather Townes (5), Tetsuji Asao (4), Phillip Bowen (4), Brian Lingerfelt (4), Pravil Patil (4), Atsushi Sato (4), Adrienne E. Scott (4), James Toth (4), Tiffany T. Howard (3), LuAnne McNulty (3).

(7) Hiromitsu Saito, Kyowa Hakko Kogyo Co Ltd., Tokyo and Pharm. Res. Laboratories, Shimotogari:

<https://www.researchgate.net/scientific-contributions/Hiromitsu-Saito-20136372> - 23 publications:

Satoru Nagamura (19), Katsushige Gomi (14), Eiji Kobayashi (13), Akira Asai (10), Nobuyoshi Amishiro (7), Akihiko Okamoto (7), Masami Okabe (6), Yutaka Kanda (3).

(8) Synthron Biopharmaceuticals/Byondis B.V., Nijmegen: www.byondis.com - 22 publications:

Patrick H. Beusker (13), Franciscus M. H. de Groot (10), Rudy G. E. Coumans (8), Willem Dokter (8), Henri J. Sprijker (8), Albertus F. Joosten (7), Ronald C. Elgersma (6), Miranda van der Lee (6), Wiro M. P. B. Menge (6), David Egging (5), Marco Timmers (5), Peter Goedings (4), Patrick Groothuis (4), Tjil Huijbregts (4), Alessandro D. Santin (4), Ruud Ubink (4), Gijs Verheijden (4), Tanja van Achterberg (3), Masoud Azodi (3), Elena Bonazzoli (3), Stefania Bellone (3), Jonathan Black (3), Natalia Buza (3), Diels van den Dobbelsteen (3), Pei Hui (3), Eline M. Loosveld (3), Gulden Menderes (3), Babak Litkouhi (3), Elena Ratner (3), Dan-Arin Silasi (3), Peter E. Schwartz (3), Monique van der Vleuten (3), Serena Wong (3).

3. Bibliography

(a) molecular mechanism (146 items – 145 journal publications, 1 patent)

- (1) Hanka, L. J.; Dietz, A.; Gerpheide, S. A.; Kuentzel, S. L.; Martin, D. G. CC-1065 (NSC-298223), A New Antitumor Antibiotic. Production, In Vitro Biological Activity, Microbiological Assays and Taxonomy of the Producing Microorganism. *J. Antibiot.* **1978**, *31* (12), 1211–1217. <https://doi.org/10.7164/antibiotics.31.1211>.
- (2) Martin, D. G.; Chidester, C. G.; Duchamp, D. J.; Mizsak, S. A. Structure of CC-1065 (NSC-298223), A New Antitumor Antibiotic. *J. Antibiot.* **1980**, *33* (8), 902–903. <https://doi.org/10.7164/antibiotics.33.902>.
- (3) Martin, D. G.; Biles, C.; Gerpheide, S. A.; Hanka, L. J.; Krueger, W. C.; McGovren, J. P.; Mizsak, S. A.; Neil, G. L.; Stewart, J. C.; Visser, J. CC-1065 (NSC 298223), a Potent New Antitumor Agent. Improved Production and Isolation, Characterization and Antitumor Activity. *J. Antibiot.* **1981**, *34* (9), 1119–1125. <https://doi.org/10.7164/antibiotics.34.1119>.
- (4) Li, L. H.; Swenson, D. H.; Schpok, S. L. F.; Kuentzel, S. L.; Dayton, B. D.; Krueger, W. C. CC-1065 (NSC-298223), a Novel Antitumor Agent That Interacts Strongly with Double-Stranded DNA. *Cancer Res.* **1982**, *42*, 999–1994.
- (5) Swenson, D. H.; Li, L. H.; Hurley, L. H.; Rokem, J. S.; Petzold, G. L.; Dayton, B. D.; Wallace, T. L.; Krueger, W. C. Mechanism of Interaction of CC-1065 (NSC-298223) with DNA. *Cancer Res.* **1982**, *42*, 2821–2828.
- (6) Bhuyan, B. K.; Crampton, S. L.; Adams, E. G. Cell Cycle Effects of CC-1065. *Cancer Res.* **1983**, *43*, 4227–4232.
- (7) Hurley, L. H.; Rokem, J. S. Biosynthesis of the Antitumor Antibiotic CC-1065 by *Streptomyces Zelenis*. *J. Antibiot.* **1983**, *36* (4), 383–390. <https://doi.org/10.7164/antibiotics.36.383>.
- (8) Hurley, L. H.; Reynolds, V. L.; Swenson, D. H.; Petzold, G. L.; Scahill, T. A. Reaction of the Antitumor Antibiotic CC-1065 with DNA: Structure of a DNA Adduct with DNA Sequence Specificity. *Science* **1984**, *226* (4676), 843–844. <https://doi.org/10.1126/science.6494915>.
- (9) McGovren, J. P.; Clarke, G. L.; Pratt, E. A.; DeKoning, T. F. Preliminary Toxicity Studies with the DNA-Binding Antibiotic CC-1065. *J. Antibiot.* **1984**, *37* (1), 63–70. <https://doi.org/10.7164/antibiotics.37.63>.
- (10) Krueger, W. C.; Li, L. H.; Moscovitz, A.; Prairie, M. D.; Petzold, G.; Swenson, D. H. Binding of CC-1065 to Poly- and Oligonucleotides. *Biopolymers* **1985**, *24* (8), 1549–1572. <https://doi.org/10.1002/bip.360240811>.
- (11) Martin, D. G.; Mizsak, S. A.; Krueger, W. C. CC-1065 Transformations. *J. Antibiot.* **1985**, *38* (6), 746–752. <https://doi.org/10.7164/antibiotics.38.746>.
- (12) Reynolds, V. L.; Molineux, I. J.; Kaplan, D. J.; Swenson, D. H.; Hurley, L. H. Reaction of the Antitumor Antibiotic CC-1065 with DNA. Location of the Site of Thermally Induced Strand Breakage and Analysis of DNA Sequence Specificity. *Biochemistry* **1985**, *24* (22), 6228–6237. <https://doi.org/10.1021/bi00343a029>.
- (13) Harbach, P. R.; Trzos, R. J.; Zimmer, D. M.; Petzold, G. L.; Bhuyan, B. K. Genotoxicity of the Antitumor Antibiotic CC-1065. *Mutagenesis* **1986**, *1* (6), 407–410. <https://doi.org/10.1093/mutage/1.6.407>.
- (14) Jacobson, M. K.; Twehous, D.; Hurley, L. H. Depletion of Nicotinamide Adenine Dinucleotide in Normal and Xeroderma Pigmentosum Fibroblast Cells by the Antitumor Drug CC-1065. *Biochemistry* **1986**, *25* (20), 5929–5932. <https://doi.org/10.1021/bi00368a014>.
- (15) Krueger, W. C.; Duchamp, D. J.; Li, L. H.; Moscovitz, A.; Petzold, G. L.; Prairie, M. D.; Swenson, D. H. The Binding of CC-1065 to Thymidine and Deoxyadenosine Oligonucleotides and to Poly(DA) · Poly(DT). *Chem.-Biol. Int.* **1986**, *59*, 55–72. [https://doi.org/10.1016/S0009-2797\(86\)80055-2](https://doi.org/10.1016/S0009-2797(86)80055-2).
- (16) Needham-VanDevanter, D. R.; Hurley, L. H. Construction and Characterization of a Site-Directed CC-1065-N3-Adenine Adduct within a 117 Base Pair DNA Restriction Fragment. *Biochemistry* **1986**, *25* (26), 8430–8436. <https://doi.org/10.1021/bi00374a016>.
- (17) Reynolds, V. L.; McGovren, J. P.; Hurley, L. H. The Chemistry, Mechanism of Action and Biological Properties of CC-1065, a Potent Antitumor Antibiotic. *J. Antibiot.* **1986**, *39* (3), 319–333. <https://doi.org/10.7164/antibiotics.39.319>.
- (18) Wierenga, W.; Bhuyan, B. K.; Kelly, R. C.; Krueger, W. C.; Li, L. H.; McGovren, J. P.; Swenson, D. H.; Warpehoski, M. A. Antitumor Activity and Biochemistry of Novel Analogs of the Antibiotic CC-1065. *Adv. Enz. Reg.* **1986**, *25*, 141–155. [https://doi.org/10.1016/0065-2571\(86\)90012-9](https://doi.org/10.1016/0065-2571(86)90012-9).
- (19) Hurley, L. H.; Needham-Vandevanter, D.; Lee, C.-S. Demonstration of the Asymmetric Effect of CC-1065 on Local DNA Structure Using a Site-Directed Adduct in a 117-Base-Pair Fragment from M13mpl. *Proc. Natl. Acad. Sci. USA* **1987**, *84*, 6412–6416. <https://doi.org/10.1073/pnas.84.18.6412>.
- (20) Krueger, W. C.; Prairie, M. D. A Circular Dichroism Study of the Binding of CC-1065 to B and Z Form Poly(DI-5BrdC)-poly(DI-5BrdC). *Chem.-Biol. Int.* **1987**, *62* (3), 281–295. [https://doi.org/10.1016/0009-2797\(87\)90028-7](https://doi.org/10.1016/0009-2797(87)90028-7).
- (21) Zakrzewska, K.; Randrianarivelo, M.; Pullman, B. Theoretical Study of the Sequence Specificity in the Covalent Binding of the Antitumor Drug CC-1065 to DNA. *Nucl. Acid Res.* **1987**, *15* (14), 5775–5785. <https://doi.org/10.1093/nar/15.14.5775>.
- (22) Adams, E. G.; Badiner, G. J.; Bhuyan, B. K. Effects of U-71,184 and Several Other CC-1065 Analogues on Cell Survival and Cell Cycle of Chinese Hamster Ovary Cells. *Cancer Res.* **1988**, *48*, 109–116.
- (23) Boger, D. L.; Coleman, R. S. Total Synthesis of (+)-CC-1065 and Ent(-)-CC-1065. *J. Am. Chem. Soc.* **1988**, *110* (4), 1321–1323. <https://doi.org/10.1021/ja00212a067>.
- (24) Harbach, P. R.; Zimmer, D. M.; Mazurek, J. H.; Bhuyan, B. K. Mutagenicity of the Antitumor Antibiotic CC-1065 and Its Analogues in Mammalian (V79) Cells and Bacteria. *Cancer Res.* **1988**, *48*, 32–36.
- (25) Hurley, L. H.; Lee, C. S.; McGovren, J. P.; Warpehoski, M. A.; Mitchell, M. A.; Kelly, R. C.; Aristoff, P. A. Molecular Basis for Sequence-Specific DNA Alkylation by CC-1065. *Biochemistry* **1988**, *27* (10), 3886–3892. <https://doi.org/10.1021/bi00410a054>.
- (26) Selby, C. P.; Sancar, A. ABC Excinuclease Incises Both 5' and 3' to the CC-1065-DNA Adduct and Its Incision Activity Is Stimulated by DNA Helicase II and DNA Polymerase I. *Biochemistry* **1988**, *27* (19), 7184–7188. <https://doi.org/10.1021/bi00419a004>.
- (27) Swenson, D. H.; Petzold, G. L.; Williams, M. G.; Li, L. H.; Prairie, M. D.; Krueger, W. C. Evaluation of DNA Binding Characteristics of Some CC-1065 Analogs. *Chem.-Biol. Int.* **1988**, *67* (3–4), 199–213. [https://doi.org/10.1016/0009-2797\(88\)90058-0](https://doi.org/10.1016/0009-2797(88)90058-0).
- (28) Takahashi, I.; Takahashi, K.-I.; Ichimura, M.; Morimoto, M.; Asano, K.; Kawamoto, I.; Tomita, F.; Nakano, H. Duocarmycin A, a New Antitumor Antibiotic from *Streptomyces*. *J. Antibiot.* **1988**, *41* (12), 1915–1917. <https://doi.org/10.7164/antibiotics.41.1915>.
- (29) Tang, M. S.; Lee, C. S.; Doisy, R.; Ross, L.; Needham-Vandevanter, D. R.; Hurley, L. H. Recognition and Repair of the CC-1065-(N3-Adenine)-DNA Adduct by the UVRABC Nucleases. *Biochemistry* **1988**, *27* (3), 893–901. <https://doi.org/10.1021/bi00403a009>.
- (30) Thériault, N. Y.; Krueger, W. C.; Prairie, M. D. Studies on the Base Pair Binding Specificity of CC-1065 to Oligomer Duplexes. *Chem.-Biol. Int.* **1988**, *65* (2), 187–201. [https://doi.org/10.1016/0009-2797\(88\)90054-3](https://doi.org/10.1016/0009-2797(88)90054-3).
- (31) Warpehoski, M. A.; Gebhard, I.; Kelly, R. C.; Krueger, W. C.; Li, L. H.; McGovren, J. P.; Prairie, M. D.; Wicnienski, N. A.; Wierenga, W. Stereoelectronic Factors Influencing the Biological Activity and DNA Interaction of Synthetic Antitumor Agents Modeled on CC-1065. *J. Med. Chem.* **1988**, *31* (3), 590–603. <https://doi.org/10.1021/jm00398a017>.

- (32) Moy, B. C.; Prairie, M. D.; Krueger, W. C.; Bhuyan, B. K. Interaction of CC-1065 and Its Analogues with Mouse DNA and Chromatin. *Cancer Res.* **1989**, *49*, 1983–1988.
- (33) Boger, D. L.; Invergo, B. J.; Coleman, R. S.; Zarrinmayeh, H.; Kitos, P. A.; Thompson, S. C.; Leong, T.; McLaughlin, L. A. Demonstration of the Intrinsic Importance of Stabilizing Hydrophobic Binding and Non-Covalent Van-Der-Waals Contacts Dominant in the Non-Covalent CC-1065/DNA Binding. *Chem.-Biol. Int.* **1990**, *73*, 29–52. [https://doi.org/10.1016/0009-2797\(90\)90107-x](https://doi.org/10.1016/0009-2797(90)90107-x).
- (34) Boger, D. L.; Zarrinmayeh, H. Regiocontrolled Nucleophilic Addition to Selectively Activated P-Quinone Diimines: Alternative Preparation of a Key Intermediate Employed in the Preparation of the CC-1065 Left-Hand Subunit. *J. Org. Chem.* **1990**, *55* (4), 1379–1390. <https://doi.org/10.1021/jo00291a059>.
- (35) Ichimura, M.; Ogawa, T.; Takahashi, K.-I.; Kobayashi, E.; Kawamoto, I.; Yasuzawa, T.; Takahashi, I.; Nakano, H. Duocarmycin SA, a New Antitumor Antibiotic from *Streptomyces* Sp. *J. Antibiot.* **1990**, *43* (8), 1037–1038. <https://doi.org/10.7164/antibiotics.43.1037>.
- (36) Moy, B. C.; Petzold, G. L.; Badiner, G. J.; Kelly, R. C.; Aristoff, P. A.; Adams, E. G.; Li, L. H.; Bhuyan, B. K. Characterization of B16 Melanoma Cells Resistant to the CC-1065 Analogue. *Cancer Res.* **1990**, *50*, 2485–2492. <https://doi.org/PMID:2317831>.
- (37) Nakano, H.; Takahashi, I.; Ichimura, M.; Isao, K.; Asasno, F.; Sano, H.; Yasuzawa, T.; Morimoto, M.; Fujimoto, K. Duocarmycin A Antibiotics Derived from Certain *Streptomyces* Culture. US004923990 A, May 8, 1990.
- (38) Scahill, T. A.; Jensen, R. M.; Swenson, D. H.; Hatzenbuehler, N. T.; Petzold, G.; Wierenga, W.; Brahme, N. D. An NMR Study of the Covalent and Noncovalent Interactions of CC-1065 and DNA. *Biochemistry* **1990**, *29* (11), 2852–2860. <https://doi.org/10.1021/bi00463a031>.
- (39) Sugiyama, H.; Hosoda, M.; Saito, I. Covalent Alkylation of DNA with Duocarmycin A. Identification of Abasic Site Structure. *Tet. Lett.* **1990**, *31* (49), 7197–7200.
- (40) Boger, D. L.; Zarrinmayeh, H.; Munk, S. A.; Kitos, P. A.; Suntorawat, O. Demonstration of a Pronounced Effect of Noncovalent Binding Selectivity on the (+)-CC-1065 DNA Alkylation and Identification of the Pharmacophore of the Alkylation Subunit. *Proc. Natl. Acad. Sci. USA* **1991**, *88* (4), 1431–1435. <https://doi.org/10.1073/pnas.88.4.1431>.
- (41) Boger, D. L.; Ishizaki, T.; Zarrinmayeh, H. Isolation and Characterization of the Duocarmycin-Adenine DNA Adduct. *J. Am. Chem. Soc.* **1991**, *113* (17), 6645–6649. <https://doi.org/10.1021/ja00017a042>.
- (42) Ichimura, M.; Ogawa, T.; Katsumata, S.; Takahashi, K.-I.; Takahashi, I.; Nakano, H. Duocarmycins, New Antitumor Antibiotics Produced by *Streptomyces*; Producing Organisms and Improved Production. *J. Antibiot.* **1991**, *44* (10), 1045–1053. <https://doi.org/10.7164/antibiotics.44.1045>.
- (43) Krueger, W. C.; Hatzenbuehler, N. T.; Prairie, M. D.; Shea, M. H. DNA Sequence Recognition by the Antitumor Antibiotic CC-1065 and Analogs of CC-1065. *Chem.-Biol. Int.* **1991**, *79* (3), 265–286. [https://doi.org/10.1016/0009-2797\(91\)90109-K](https://doi.org/10.1016/0009-2797(91)90109-K).
- (44) Krueger, W. C.; Prairie, M. D. The Origin of the DNA Induced Circular Dichroism of CC-1065 and Analogs. *Chem.-Biol. Int.* **1991**, *79* (2), 137–149. [https://doi.org/10.1016/0009-2797\(91\)90078-L](https://doi.org/10.1016/0009-2797(91)90078-L).
- (45) Lee, C. S.; Sun, D.; Kizu, R.; Hurley, L. H. Determination of the Structural Features of (+)-CC-1065 That Are Responsible for Bending and Winding of DNA. *Chem. Res. Toxicol.* **1991**, *4* (2), 203–213. <https://doi.org/10.1021/tx00020a013>.
- (46) Lee, C.-S.; Gibson, N. W. DNA Damage and Differential Cytotoxicity Produced in Human Carcinoma Cells by CC-1065 Analogues, U-73,975 and U-77,779. *Cancer Res.* **1991**, *51*, 6586–6591. <https://doi.org/PMID1742731>.
- (47) Lin, C. H.; Beale, J. M.; Hurley, L. H. Structure of the (+)-CC-1065-DNA Adduct: Critical Role of Ordered Water Molecules and Implications for Involvement of Phosphate Catalysis in the Covalent Reaction. *Biochemistry* **1991**, *30* (15), 3597–3602. <https://doi.org/10.1021/bi00229a002>.
- (48) Lin, C. H.; Sun, D.; Hurley, L. H. (+)-CC-1065 Produces Bending of DNA That Appears to Resemble Adenine/Thymine Tracts. *Chem. Res. Toxicol.* **1991**, *4*, 21–26. <https://doi.org/10.1021/TX00019A003>.
- (49) Yasuzawa, T.; Saitoh, Y.; Ichimura, M.; Takahashi, I.; Sano, H. Structure of Duocarmycin SA, a Potent Antitumor Antibiotic. *J. Antibiot.* **1991**, *44* (4), 445–447. <https://doi.org/10.7164/antibiotics.44.445>.
- (50) Zsido, T. J.; Woynarowski, J. M.; Baker, R. M.; Gawron, L. S.; Beerman, T. A. Induction of Heat-Labile Sites in DNA of Mammalian Cells by the Antitumor Alkylating Drug CC-1065. *Biochemistry* **1991**, *30* (15), 3733–3738. <https://doi.org/10.1021/bi00229a021>.
- (51) Boger, D. L.; Machiya, K. Total Synthesis of (+)-Duocarmycin SA. *J. Am. Chem. Soc.* **1992**, *114* (25), 10056–10058. <https://doi.org/10.1021/ja00051a045>.
- (52) Boger, D. L.; Munk, S. A. DNA Alkylation Properties of Enhanced Functional Analogs of CC-1065 Incorporating the 1,2,9,9a-Tetrahydrocyclopropa[1,2-c]Benz[1,2-e]Indol-4-One (CBI) Alkylation Subunit. *J. Am. Chem. Soc.* **1992**, *114* (14), 5487–5496. <https://doi.org/10.1021/ja00040a001>.
- (53) Boger, D. L.; Yun, W.; Terashima, S.; Fukuda, Y.; Nakatani, K.; Kitos, P. A.; Jin, Q. DNA Alkylation Properties of the Duocarmycins: (+)-Duocarmycin A, Epi-(+)-Duocarmycin A, Ent-(-)-Duocarmycin A and E&Ent-(-)-Duocarmycin A. *Bioorg. Med. Chem. Lett.* **1992**, *2* (7), 759–765. [https://doi.org/10.1016/S0960-894X\(00\)80407-2](https://doi.org/10.1016/S0960-894X(00)80407-2).
- (54) Gomi, K.; Kobayashi, E.; Miyoshi, K.; Ashizawa, T.; Okamoto, A.; Ogawa, T.; Katsumata, S.; Mihara, A.; Okabe, M.; Hirata, T. Anticellular and Antitumor Activity of Duocarmycins, Novel Antitumor Antibiotics. *Jpn. J. Cancer Res.* **1992**, *83*, 113–120. <https://doi.org/10.1111/j.1349-7006.1992.tb02360.x>.
- (55) Krueger, W. C.; Prairie, M. D. Calf Thymus DNA Binding/Bonding Properties of CC-1065 and Analogs as Related to Their Biological Activities and Toxicities. *Chem.-Biol. Int.* **1992**, *82* (1), 31–46. [https://doi.org/10.1016/0009-2797\(92\)90012-A](https://doi.org/10.1016/0009-2797(92)90012-A).
- (56) Lin, C. H.; Patel, D. J. Site-Specific Covalent Duocarmycin A: Intramolecular DNA Triplex Complex. *J. Am. Chem. Soc.* **1992**, *114* (26), 10658–10660. <https://doi.org/10.1021/ja00052a085>.
- (57) Lin, C. H.; Hill, G. C.; Hurley, L. H. Characterization of a 12-Mer Duplex d(GCGGAGTTAGG).Cnntdot.d(CCTAACTCCGCC) Containing a Highly Reactive (+)-CC-1065 Sequence by Proton and Phosphorus-31 NMR, Hydroxyl-Radical Footprinting, and NOESY Restrainted Molecular Dynamics Calculations. *Chem. Res. Toxicol.* **1992**, *5* (2), 167–182. <https://doi.org/10.1021/tx00026a005>.
- (58) Maine, I. P.; Sun, D.; Hurley, L. H.; Kodadek, T. The Antitumor Agent CC-1065 Inhibits Helicase-Catalyzed Unwinding of Duplex DNA. *Biochemistry* **1992**, *31* (16), 3968–3975. <https://doi.org/10.1021/bi00131a012>.
- (59) Sun, D.; Hurley, L. H. Effect of the (+)-CC-1065-(N3-Adenine)DNA Adduct on in Vitro DNA Synthesis Mediated by *Escherichia Coli* DNA Polymerase. *Biochemistry* **1992**, *31* (10), 2822–2829. <https://doi.org/10.1021/bi00125a025>.
- (60) Sun, D.; Hurley, L. H. Structure-Activity Relationships of (+)-CC-1065 Analogs in the Inhibition of Helicase-Catalyzed Unwinding of Duplex DNA. *J. Med. Chem.* **1992**, *35* (10), 1773–1782. <https://doi.org/10.1021/jm00088a012>.
- (61) Warpehoski, M. A.; Harper, D. E.; Mitchell, M. A.; Monroe, T. J. Reversibility of the Covalent Reaction of CC-1065 and Analogs with DNA. *Biochemistry* **1992**, *31* (9), 2502–2508. <https://doi.org/10.1021/bi00124a009>.
- (62) Zsido, T. J.; Beerman, T. A.; Meegan, R. L.; Woynarowski, J. M.; Baker, R. M. Resistance of CHO Cells Expressing P-Glycoprotein to Cyclopropylpyrrolindole (CPI) Alkylating Agents. *Biochem. Pharm.* **1992**, *43* (8), 1817–1822. [https://doi.org/10.1016/0006-2952\(92\)90715-U](https://doi.org/10.1016/0006-2952(92)90715-U).
- (63) Boger, D. L.; Machiya, K.; Hertzog, D. L.; Kitos, P. A.; Holmes, D. Total Synthesis and Preliminary Evaluation of (+)- and Ent-(-)-Duocarmycin SA. *J. Am. Chem. Soc.* **1993**, *115* (20), 9025–9036. <https://doi.org/10.1021/ja00073a019>.
- (64) Boger, D. L.; Yun, W. Reversibility of the Duocarmycin A and SA DNA Alkylation Reaction. *J. Am. Chem. Soc.* **1993**, *115* (21), 9872–9873. <https://doi.org/10.1021/ja00074a093>.

- (65) Ding, Z.-M.; Harshey, R. M.; Hurley, L. H. (+)-CC-1065 as a Structural Probe of Mu Transposase- Induced Bending of DNA: Overcoming Limitations of Hydroxyl-Radical Footprinting. *Nucl. Acid Res.* **1993**, *21* (18), 4281–4287. <https://doi.org/10.1093/nar/21.18.4281>.
- (66) Sugiyama, H.; Ohmori, K.; Chan, K. L.; Hosoda, M.; Asai, A.; Saito, H.; Saito, I. A Novel Guanine N3 Alkylation by Antitumor Antibiotic Duocarmycin A. *Tet. Lett.* **1993**, *34* (13), 2179–2182.
- (67) Sun, D.; Lin, C. H.; Hurley, L. H. A-Tract and (+)-CC-1065-Induced Bending of DNA. Comparison of Structural Features Using Non-Denaturing Gel Analysis, Hydroxyl-Radical Footprinting, and High-Field NMR. *Biochemistry* **1993**, *32* (17), 4487–4495. <https://doi.org/10.1021/bi00068a003>.
- (68) Yamamoto, K.; Sugiyama, H.; Kawanishi, S. Concerted DNA Recognition and Novel Site-Specific Alkylation by Duocarmycin A with Distamycin A. *Biochemistry* **1993**, *32* (4), 1059–1066. <https://doi.org/10.1021/bi00055a010>.
- (69) Asai, A.; Nagamura, S.; Saito, H. A Novel Property of Duocarmycin and Its Analogs for Covalent Reaction with DNA. *J. Am. Chem. Soc.* **1994**, *116* (10), 4171–4177. <https://doi.org/10.1021/ja00089a004>.
- (70) Asai, A.; Nagamura, S.; Saito, H.; Takahashi, I.; Nakano, H. The Reversible DNA-Alkylating Activity of Duocarmycin and Its Analogues. *Nucl. Acid Res.* **1994**, *22* (1), 88–93. <https://doi.org/10.1093/nar/22.1.88>.
- (71) Boger, D. L.; Johnson, D. S.; Yun, W. (+)- and Ent(-)-Duocarmycin SA and (+)- and Ent(-)-N-Boc-DSA DNA Alkylation Properties. Alkylation Site Models That Accommodate the Offset AT-Rich Adenine N3 Alkylation Selectivity of the Enantiomeric Agents. *J. Am. Chem. Soc.* **1994**, *116* (5), 1635–1656. <https://doi.org/10.1021/ja00084a004>.
- (72) Boger, D. L.; Johnson, D. S.; Yun, W.; Tarby, C. M. Molecular Basis for Sequence Selective DNA Alkylation by (+)- and Ent(-)-CC-1065 and Related Agents: Alkylation Site Models That Accommodate the Offset AT-Rich Adenine N3 Alkylation Selectivity. *Bioorg. Med. Chem.* **1994**, *2* (2), 115–135. [https://doi.org/10.1016/s0968-0896\(00\)82007-6](https://doi.org/10.1016/s0968-0896(00)82007-6).
- (73) Chiang, S.-Y.; Welch, J.; Rauscher, F. J.; Beerman, T. A. Effects of Minor Groove Binding Drugs on the Interaction of TATA Box Binding Protein and TFIIA with DNA. *Biochemistry* **1994**, *33* (23), 7033–7040. <https://doi.org/10.1021/bi00189a003>.
- (74) McHugh, M. M.; Woynarowski, J. M.; Mitchell, M. A.; Gawron, L. S.; Weiland, K. L.; Beerman, T. A. CC-1065 Bonding to Intracellular and Purified SV40 DNA: Site Specificity and Functional Effects. *Biochemistry* **1994**, *33*, 9158–9168. <https://doi.org/10.1021/bi00197a019>.
- (75) Sugiyama, H.; Fujiwara, T.; Ura, A.; Tashiro, T.; Yamamoto, K.; Kawanishi, S.; Saito, I. Chemistry of Thermal Degradation of Abasic Sites in DNA. Mechanistic Investigation on Thermal DNA Strand Cleavage of Alkylated DNA. *Chem. Res. Toxicol.* **1994**, *7* (5), 673–683. <https://doi.org/10.1021/tx00041a013>.
- (76) Tang, M. S.; Qian, M.; Pao, A. Formation and Repair of Antitumor Antibiotic CC-1065-Induced DNA Adducts in the Adenine Phosphoribosyltransferase and Amplified Dihydrofolate Reductase Genes of Chinese Hamster Ovary Cells. *Biochemistry* **1994**, *33* (9), 2726–2732. <https://doi.org/10.1021/bi00175a048>.
- (77) Wrasidlo, W.; Johnson, D. S.; Boger, D. L. Induction of Endonucleolytic DNA Fragmentation and Apoptosis by the Duocarmycins. *Bioorg. Med. Chem. Lett.* **1994**, *4* (4), 631–636. [https://doi.org/10.1016/S0960-894X\(01\)80168-2](https://doi.org/10.1016/S0960-894X(01)80168-2).
- (78) Boger, D. L.; Johnson, D. S. Second Definitive Test of Proposed Models for the Origin of the CC-1065 and Duocarmycin DNA Alkylation Selectivity. *J. Am. Chem. Soc.* **1995**, *117* (4), 1443–1444. <https://doi.org/10.1021/ja00109a035>.
- (79) Boger, D. L.; Mesini, P. DNA Alkylation Properties of CC-1065 and Duocarmycin Analogs Incorporating the 2,3,10,10a-Tetrahydrocyclopropa[d]Benzo[f]Quinol-5-One Alkylation Subunit: Identification of Subtle Structural Features That Contribute to the Regioselectivity of the Adenine N3 Alkylation Reaction. *J. Am. Chem. Soc.* **1995**, *117* (47), 11647–11655. <https://doi.org/10.1021/ja00152a004>.
- (80) Boger, D. L.; Yun, W.; Han, N.; Johnson, D. S. CC-1065 CBI Analogs: An Example of Enhancement of DNA Alkylation Efficiency through Introduction of Stabilizing Electrostatic Interactions. *Bioorg. Med. Chem.* **1995**, *3* (6), 611–621. [https://doi.org/10.1016/0968-0896\(95\)00048-L](https://doi.org/10.1016/0968-0896(95)00048-L).
- (81) Kim, D.-Y.; Shih, D. S.; Cho, D.-Y.; Swenson, D. H. Helix-Stabilizing Compounds CC-1065 and U-71,184 Bind to RNA-DNA and DNA-DNA Duplexes Containing Modified Internucleotide Linkages and Stabilize Duplexes Against Thermal Melting. *Antisense Res. Dev.* **1995**, *5* (1), 49–57. <https://doi.org/10.1089/ard.1995.5.49>.
- (82) Kim, D.-Y.; Swenson, D. H.; Cho, D.-Y.; Taylor, H. W.; Shih, D. S. Helix-Stabilizing Agent, CC-1065, Enhances Suppression of Translation by an Antisense Oligodeoxynucleotide. *Antisense Res. Dev.* **1995**, *5* (2), 149–154. <https://doi.org/10.1089/ard.1995.5.149>.
- (83) Linsemann, D. A.; Branstetter, D. G.; Yu, R. L.; Aaron, C. S. Lung Tumor Induction in A/J Mice and Clastogenic Effects in CD-1 Mice of the Sequence-Selective DNA Alkylating Agent (+)-CC-1065 and (-)-CC-1065. *Natural Toxins* **1995**, *3*, 32–40. <https://doi.org/10.1002/nt.2620030108>.
- (84) Muratake, H.; Matsumura, N.; Natsume, M. Total Synthesis of Natural (+)-Duocarmycin SA. *Chem. Pharm. Bull.* **1995**, *43* (6), 1064–1066. <https://doi.org/10.1248/cpb.43.1064>.
- (85) Boger, D. L.; Goldberg, J.; McKie, J. A. A Comparative Study of the Solvolysis Reactivity, Regioselectivity, and Stereochemistry of the Duocarmycin a and Sa Alkylation Subunits. *Bioorg. Med. Chem. Lett.* **1996**, *6* (16), 1955–1960. [https://doi.org/10.1016/0960-894X\(96\)00346-0](https://doi.org/10.1016/0960-894X(96)00346-0).
- (86) Boger, D. L.; Johnson, D. S. CC-1065 and the Duocarmycins: Understanding Their Biological Function through Mechanistic Studies. *Angew. Chem. Int. Ed.* **1996**, *35* (1314), 1438–1474. <https://doi.org/10.1002/anie.199614381>.
- (87) Boger, D. L.; McKie, J. A.; Nishi, T.; Ogiku, T. Enantioselective Total Synthesis of (+)-Duocarmycin A, Epi-(+)-Duocarmycin A, and Their Unnatural Enantiomers. *J. Am. Chem. Soc.* **1996**, *118* (9), 2301–2302. <https://doi.org/10.1021/ja953777e>.
- (88) Boger, D. L.; Zhou, J.; Cai, H. Demonstration and Definition of the Noncovalent Binding Selectivity of Agents Related to CC-1065 by an Affinity Cleavage Agent: Noncovalent Binding Coincidental with Alkylation. *Bioorg. Med. Chem.* **1996**, *4* (6), 859–867. [https://doi.org/10.1016/0968-0896\(96\)00073-9](https://doi.org/10.1016/0968-0896(96)00073-9).
- (89) Gunz, D.; Hess, M. T.; Naegeli, H. Recognition of DNA Adducts by Human Nucleotide Excision Repair. *J. Biol. Chem.* **1996**, *271* (41), 25089–25098. <https://doi.org/10.1074/jbc.271.41.25089>.
- (90) Gunz, D.; Naegeli, H. A Noncovalent Binding-Translocation Mechanism for Site-Specific CC-1065-DNA Recognition. *Biochem. Pharm.* **1996**, *52* (3), 447–453. [https://doi.org/10.1016/0006-2952\(96\)00247-X](https://doi.org/10.1016/0006-2952(96)00247-X).
- (91) Henderson, D.; Hurley, L. H. Specific Targeting of Protein-DNA Complexes by DNA-Reactive Drugs (+)-CC-1065 and Pluramycins. *J. Mol. Recog.* **1996**, *9*, 75–87. [https://doi.org/10.1002/\(sici\)1099-1352\(199603\)9:2<75::aid-jmr247>3.0.co;2-4](https://doi.org/10.1002/(sici)1099-1352(199603)9:2<75::aid-jmr247>3.0.co;2-4).
- (92) Lukhtanov, E. A.; Podyminogin, M. A.; Kutuyavin, I. V.; Meyer, R. B.; Gamper, H. B. Rapid and Efficient Hybridization-Triggered Crosslinking Within a DNA Duplex by an Oligodeoxyribonucleotide Bearing a Conjugated Cyclopropapyrrolindole. *Nucl. Acid Res.* **1996**, *24* (4), 683–687. <https://doi.org/10.1093/nar/24.4.683>.
- (93) Muratake, H.; Abe, I.; Natsume, M. Preparation of Alkyl-Substituted Indoles in the Benzene Portion. Part 14. Synthesis of (+)-Duocarmycin SA, Natural (+)-Duocarmycin SA and Non-Natural (-)-Duocarmycin SA. *Chem. Pharm. Bull.* **1996**, *44* (1), 67–79. <https://doi.org/10.1248/cpb.44.67>.
- (94) Muratake, H.; Toneygawa, M.; Natsume, M. Alternative Synthesis of Duocarmycin SA Using a Tricyclic Heteroaromatic Intermediate Prepared by Palladium-Catalyzed Coupling Reactions. *Chem. Pharm. Bull.* **1996**, *44* (8), 1631–1633. <https://doi.org/10.1248/cpb.44.1631>.
- (95) Sugiyama, H.; Lian, C.; Isomura, M.; Saito, I.; Wang, A. H.-J. Distamycin A Modulates the Sequence Specificity of DNA Alkylation by Duocarmycin A. *Proc. Natl. Acad. Sci. USA* **1996**, *93* (25), 14405–14410. <https://doi.org/10.1073/pnas.93.25.14405>.

- (96) Sun, D.; Hurley, L. H.; Harshey, R. M. Structural Distortions Induced by Integration Host Factor (IHF) at the H' Site of Phage λ Probed by (+)-CC-1065, Pluramycin, and KMnO_4 and by DNA Cyclization Studies. *Biochemistry* **1996**, *35* (33), 10815–10827. <https://doi.org/10.1021/bi952786x>.
- (97) Turner, P. R.; Denny, W. A. The Mutagenic Properties of DNA Minor-Groove Binding Ligands. *Mut. Res.* **1996**, *355*, 141–169. [https://doi.org/10.1016/0027-5107\(96\)00027-9](https://doi.org/10.1016/0027-5107(96)00027-9).
- (98) Boger, D. L.; Boyce, C. W.; Johnson, D. S. PH Dependence of the Rate of DNA Alkylation for (+)-Duocarmycin SA and (+)-CCBI-TMI. *Bioorg. Med. Chem. Lett.* **1997**, *7* (2), 233–238. [https://doi.org/10.1016/S0960-894X\(96\)00605-1](https://doi.org/10.1016/S0960-894X(96)00605-1).
- (99) Boger, D. L.; Garbaccio, R. M. Catalysis of the CC-1065 and Duocarmycin DNA Alkylation Reaction: DNA Binding Induced Conformational Change in the Agent Results in Activation. *Bioorg. Med. Chem.* **1997**, *5* (2), 263–276. [https://doi.org/10.1016/S0960-896\(96\)00238-6](https://doi.org/10.1016/S0960-896(96)00238-6).
- (100) Boger, D. L.; McKie, J. A.; Nishi, T.; Ogiku, T. Total Synthesis of (+)-Duocarmycin A, *Epi*-(+)-Duocarmycin A and Their Unnatural Enantiomers: Assessment of Chemical and Biological Properties. *J. Am. Chem. Soc.* **1997**, *119* (2), 311–325. <https://doi.org/10.1021/ja962431q>.
- (101) Eis, P. S.; Smith, J. A.; Ryzewski, J. M.; Case, D. A.; Boger, D. L.; Chazin, W. J. High Resolution Solution Structure of a DNA Duplex Alkylated by the Antitumor Agent Duocarmycin SA. *J. Mol. Biol.* **1997**, *272* (2), 237–252. <https://doi.org/10.1006/jmbi.1997.1223>.
- (102) Park, H.-J.; Hurley, L. H. Covalent Modification of N3 of Guanine by (+)-CC-1065 Results in Protonation of the Cross-Strand Cytosine. *J. Am. Chem. Soc.* **1997**, *119* (3), 629–630. <https://doi.org/10.1021/ja9632264>.
- (103) Hurley, L. H.; Lee, C. S.; McGovern, J. P.; Warpehoski, M. A.; Mitchell, M. A.; Kelly, R. C.; Aristoff, P. A. Reaction of CC-1065 and Select Synthetic Analogs with DNA. *Biochem. Pharm.* **1998**, *37* (9), 1795–1796. [https://doi.org/10.1016/0006-2952\(88\)90450-9](https://doi.org/10.1016/0006-2952(88)90450-9).
- (104) Asai, A.; Yano, K.; Mizukami, T.; Nakano, H. Characterization of a Duocarmycin-DNA Adduct-Recognizing Protein in Cancer Cells. *Cancer Res.* **1999**, *59*, 5417–5420. <https://doi.org/PMID10554008>.
- (105) Boger, D. L.; Garbaccio, R. M. Are the Duocarmycin and CC-1065 DNA Alkylation Reactions Acid-Catalyzed? Solvolysis PH-Rate Profiles Suggest They Are Not. *J. Org. Chem.* **1999**, *64* (15), 5666–5669. <https://doi.org/10.1021/jo990762g>.
- (106) Fujiwara, T.; Tao, Z.-F.; Ozeki, Y.; Saito, I.; Wang, H.-J.; Lee, M.; Sugiyama, H. Modulation of Sequence Specificity of Duocarmycin-Dependent DNA Alkylation by Pyrrole-Imidazole Triamides. *J. Am. Chem. Soc.* **1999**, *121* (33), 7706–7707. <https://doi.org/10.1021/ja991331i>.
- (107) Muratake, H.; Matsumura, N.; Natsume, M. Preparation of Alkyl-Substituted Indoles in the Benzene Portion. Part 15. Asymmetric Synthesis of (+)-Duocarmycin SA Using Novel Procedure for Preparation of Hydroxyindoles. *Chem. Pharm. Bull.* **1999**, *46* (4), 559–571. <https://doi.org/10.1248/cpb.46.559>.
- (108) Reddy, B. S. P.; Sondhi, S. M.; Lown, J. W. Synthetic DNA Minor Groove-Binding Drugs. *Pharm. & Ther.* **1999**, *84*, 1–111. [https://doi.org/10.1016/s0163-7258\(99\)00021-2](https://doi.org/10.1016/s0163-7258(99)00021-2).
- (109) Schnell, J. R.; Ketchum, R. R.; Boger, D. L.; Chazin, W. J. Binding-Induced Activation of DNA Alkylation by Duocarmycin SA: Insights from the Structure of an Indole Derivative–DNA Adduct. *J. Am. Chem. Soc.* **1999**, *121* (24), 5645–5652. <https://doi.org/10.1021/ja983556j>.
- (110) Tercel, M.; Gieseg, M. A.; Milbank, J. B.; Boyd, M.; Fan, J.-Y.; Tan, L. K.; Wilson, W. R.; Denny, W. A. Cytotoxicity and DNA Interaction of the Enantiomers of 6-Amino-3-(Chloromethyl)-1-[[5,6,7-Trimethoxyindol-2-Yl]Carbonyl]Indoline (Amino- Seco -Cl-TMI). *Chem. Res. Toxicol.* **1999**, *12* (8), 700–706. <https://doi.org/10.1021/tx990069o>.
- (111) Tokoro, Y.; Isoe, T.; Shindo, K. Gilvusmycin, a New Antitumor Antibiotic Related to CC-1065. *J. Antibiot.* **1999**, *52* (3), 263–268. <https://doi.org/10.7164/antibiotics.52.263>.
- (112) Kirschner, K. N.; Lee, M.; Stanley, R. C.; Bowen, J. P. Density Functional and Ab Initio Studies on N -Acetyl-Duocarmycin SA: Insight into Its DNA Interaction Properties. *Bioorg. Med. Chem.* **2000**, *8* (2), 329–335. [https://doi.org/10.1016/S0960-896\(99\)00278-3](https://doi.org/10.1016/S0960-896(99)00278-3).
- (113) Nazimiec, M.; Lee, C.-S.; Tang, Y.-L.; Ye, X.; Case, R.; Tang, M. Sequence-Dependent Interactions of Two Forms of UvrC with DNA Helix-Stabilizing CC-1065–N3-Adenine Adducts. *Biochemistry* **2001**, *40* (37), 11073–11081. <https://doi.org/10.1021/bi010953p>.
- (114) Skladanowski, A.; Koba, M.; Konopa, J. Does the Antitumor Cyclopropylpyrroloindole Antibiotic CC-1065 Cross-Link DNA in Tumor Cells? *Biochem. Pharm.* **2001**, *61* (1), 67–72. [https://doi.org/10.1016/S0006-2952\(00\)00528-1](https://doi.org/10.1016/S0006-2952(00)00528-1).
- (115) Ambrose, Y.; Boger, D. L. The DNA Phosphate Backbone Is Not Involved in Catalysis of the Duocarmycin and CC-1065 DNA Alkylation Reaction. *Bioorg. Med. Chem. Lett.* **2002**, *12* (3), 303–306. [https://doi.org/10.1016/S0960-894X\(01\)00740-5](https://doi.org/10.1016/S0960-894X(01)00740-5).
- (116) Kiakos, K.; Howard, T. T.; Lee, M.; Hartley, J. A.; McHugh, P. J. Saccharomyces Cerevisiae RAD5 Influences the Excision Repair of DNA Minor Groove Adducts. *J. Biol. Chem.* **2002**, *277* (46), 44576–44581. <https://doi.org/10.1074/jbc.M208169200>.
- (117) Park, H.-J. Evidence for a Common Molecular Basis for Sequence Recognition of N3-Guanine and N3-Adenine DNA Adducts Involving the Covalent Bonding Reaction of (+)-CC-1065. *Arch. Pharm. Res.* **2002**, *25* (1), 11–24. <https://doi.org/10.1007/BF02975255>.
- (118) Igarashi, Y.; Futamata, K.; Fujita, T.; Sekine, A.; Senda, H.; Naoki, H.; Furumai, T. Yatakemycin, a Novel Antifungal Antibiotic Produced by Streptomyces Sp. TP-A0356. *J. Antibiot.* **2003**, *56* (2), 107–113. <https://doi.org/10.7164/antibiotics.56.107>.
- (119) Kuwabara, T.; Noda, T.; Ohtake, H.; Ohtake, T.; Toyama, S.; Ikariyama, Y. Classification of DNA-Binding Mode of Antitumor and Antiviral Agents by the Electrochemiluminescence of Ruthenium Complex. *Anal. Biochem.* **2003**, *314* (1), 30–37. [https://doi.org/10.1016/S0003-2697\(02\)00651-6](https://doi.org/10.1016/S0003-2697(02)00651-6).
- (120) Parrish, J. P.; Kastrinsky, D. B.; Wolkenberg, S. E.; Igarashi, Y.; Boger, D. L. DNA Alkylation Properties of Yatakemycin. *J. Am. Chem. Soc.* **2003**, *125* (36), 10971–10976. <https://doi.org/10.1021/ja035984h>.
- (121) Tietze, L. F.; Haunert, F.; Feuerstein, T.; Herzog, T. A Concise and Efficient Synthesis of Seco-Duocarmycin SA. *Eur. J. Org. Chem.* **2003**, *2003* (3), 562–566. <https://doi.org/10.1002/ejoc.200390094>.
- (122) LaBarbera, D. V.; Skibo, E. B. Solution Kinetics of CC-1065 A-Ring Opening: Substituent Effects and General Acid/Base Catalysis. *J. Am. Chem. Soc.* **2006**, *128* (11), 3722–3727. <https://doi.org/10.1021/ja057289a>.
- (123) Okano, K.; Tokuyama, H.; Fukuyama, T. Total Synthesis of (+)-Yatakemycin. *J. Am. Chem. Soc.* **2006**, *128* (22), 7136–7137. <https://doi.org/10.1021/ja0619455>.
- (124) Spiegel, K.; Rothlisberger, U.; Carloni, P. Duocarmycins Binding to DNA Investigated by Molecular Simulation. *J. Phys. Chem. B* **2006**, *110* (8), 3647–3660. <https://doi.org/10.1021/jp0548265>.
- (125) Tichenor, M. S.; Trzuppek, J. D.; Kastrinsky, D. B.; Shiga, F.; Hwang, I.; Boger, D. L. Asymmetric Total Synthesis of (+)- and *Ent* -(-)-Yatakemycin and Duocarmycin SA: Evaluation of Yatakemycin Key Partial Structures and Its Unnatural Enantiomer. *J. Am. Chem. Soc.* **2006**, *128* (49), 15683–15696. <https://doi.org/10.1021/ja064228j>.
- (126) Trzuppek, J. D.; Gottesfeld, J. M.; Boger, D. L. Alkylation of Duplex DNA in Nucleosome Core Particles by Duocarmycin SA and Yatakemycin. *Nat. Chem. Biol.* **2006**, *2* (2), 79–82. <https://doi.org/10.1038/nchembio761>.
- (127) Hirota, M.; Fujiwara, T.; Mineshita, S.; Sugiyama, H.; Teraoka, H. Distamycin A Enhances the Cytotoxicity of Duocarmycin A and Suppresses Duocarmycin A-Induced Apoptosis in Human Lung Carcinoma Cells. *Int. J. Biochem. Cell Biol.* **2007**, *39* (5), 988–996. <https://doi.org/10.1016/j.biocel.2007.01.019>.

- (128) MacMillan, K. S.; Boger, D. L. An Additional Spirocyclization for Duocarmycin SA. *J. Am. Chem. Soc.* **2008**, *130* (49), 16521–16523. <https://doi.org/10.1021/ja806593w>.
- (129) Tichenor, M. S.; Boger, D. L. Yatakemycin: Total Synthesis, DNA Alkylation, and Biological Properties. *Nat. Prod. Rep.* **2008**, *25* (2), 220–226. <https://doi.org/10.1039/B705665F>.
- (130) Zhong, H.; Kirschner, K. N.; Lee, M.; Bowen, J. P. Binding Free Energy Calculation for Duocarmycin/DNA Complex Based on the QPLD-Derived Partial Charge Model. *Bioorg. Med. Chem. Lett.* **2008**, *18* (2), 542–545. <https://doi.org/10.1016/j.bmcl.2007.11.090>.
- (131) MacMillan, K. S.; Boger, D. L. Fundamental Relationships between Structure, Reactivity, and Biological Activity for the Duocarmycins and CC-1065. *J. Med. Chem.* **2009**, *52* (19), 5771–5780. <https://doi.org/10.1021/jm9006214>.
- (132) Huang, W.; Xu, H.; Li, Y.; Zhang, F.; Chen, X.-Y.; He, Q.-L.; Igarashi, Y.; Tang, G.-L. Characterization of Yatakemycin Gene Cluster Revealing a Radical S-Adenosylmethionine Dependent Methyltransferase and Highlighting Spirocyclopropane Biosynthesis. *J. Am. Chem. Soc.* **2012**, *134* (21), 8831–8840. <https://doi.org/10.1021/ja211098r>.
- (133) Yoshidome, T.; Endo, M.; Kashiwazaki, G.; Hidaka, K.; Bando, T.; Sugiyama, H. Sequence-Selective Single-Molecule Alkylation with a Pyrrole-Imidazole Polyamide Visualized in a DNA Nanoscaffold. *J. Am. Chem. Soc.* **2012**, *134* (10), 4654–4660. <https://doi.org/10.1021/ja209023u>.
- (134) Terce, M.; McManaway, S. P.; Leung, E.; Liyanage, H. D. S.; Lu, G.-L.; Pruij, F. B. The Cytotoxicity of Duocarmycin Analogues Is Mediated through Alkylation of DNA, Not Aldehyde Dehydrogenase 1: A Comment. *Angew. Chem. Int. Ed.* **2013**, *52* (21), 5442–5446. <https://doi.org/10.1002/anie.201208373>.
- (135) Chandran, A.; Syed, J.; Taylor, R. D.; Kashiwazaki, G.; Sato, S.; Hashiya, K.; Bando, T.; Sugiyama, H. Deciphering the Genomic Targets of Alkylating Polyamide Conjugates Using High-Throughput Sequencing. *Nucl. Acid Res.* **2016**, *44* (9), 4014–4024. <https://doi.org/10.1093/nar/gkw283>.
- (136) Lin, J.; Hiraoka, K.; Watanabe, T.; Kuo, T.; Shinozaki, Y.; Takatori, A.; Koshikawa, N.; Chandran, A.; Otsuki, J.; Sugiyama, H.; Horton, P.; Nagase, H. Identification of Binding Targets of a Pyrrole-Imidazole Polyamide KR12 in the LS180 Colorectal Cancer Genome. *PLoS ONE* **2016**, *11* (10), e0165581. <https://doi.org/10.1371/journal.pone.0165581>.
- (137) Zou, T.; Kizaki, S.; Pandian, G. N.; Sugiyama, H. Nucleosome Assembly Alters the Accessibility of the Antitumor Agent
- Duocarmycin B₂ to Duplex DNA. *Chem. Eur. J.* **2016**, *22* (26), 8756–8758. <https://doi.org/10.1002/chem.201600950>.
- (138) Mullins, E. A.; Shi, R.; Eichman, B. F. Toxicity and Repair of DNA Adducts Produced by the Natural Product Yatakemycin. *Nat. Chem. Biol.* **2017**, *13* (9), 1002–1008. <https://doi.org/10.1038/nchembio.2439>.
- (139) Wu, S.; Jian, X.-H.; Yuan, H.; Jin, W.-B.; Yin, Y.; Wang, L.-Y.; Zhao, J.; Tang, G.-L. Unified Biosynthetic Origin of the Benzopyrrole Subunit in CC-1065. *ACS Chem. Biol.* **2017**, *12*, 1603–1610. <https://doi.org/10.1021/acscchembio.7b00302>.
- (140) Yuan, H.; Zhang, J.; Cai, Y.; Wu, S.; Yang, K.; Chan, H. C. S.; Huang, W.; Jin, W.-B.; Li, Y.; Yin, Y.; Igarashi, Y.; Yuan, S.; Zhou, J.; Tang, G.-L. GyrI-like Proteins Catalyze Cyclopropanoid Hydrolysis to Confer Cellular Protection. *Nat. Comm.* **2017**, *8* (1), 1485. <https://doi.org/10.1038/s41467-017-01508-1>.
- (141) Boyle, K. E.; Boger, D. L.; Wroe, A.; Vazquez, M. Duocarmycin SA, a Potent Antitumor Antibiotic, Sensitizes Glioblastoma Cells to Proton Radiation. *Bioorg. Med. Chem. Lett.* **2018**, *28* (16), 2688–2692. <https://doi.org/10.1016/j.bmcl.2018.04.008>.
- (142) Jin, W.-B.; Wu, S.; Jian, X.-H.; Yuan, H.; Tang, G.-L. A Radical S-Adenosyl-L-Methionine Enzyme and a Methyltransferase Catalyze Cyclopropane Formation in Natural Product Biosynthesis. *Nat. Comm.* **2018**, *9* (1), 2771. <https://doi.org/10.1038/s41467-018-05217-1>.
- (143) Kashiwazaki, G.; Maeda, R.; Kawase, T.; Hashiya, K.; Bando, T.; Sugiyama, H. Evaluation of Alkylating Pyrrole-Imidazole Polyamide Conjugates by a Novel Method for High-Throughput Sequencer. *Bioorg. Med. Chem. Lett.* **2018**, *26* (1), 1–7. <https://doi.org/10.1016/j.bmcl.2017.08.057>.
- (144) Schmidt, M. A.; Simmons, E. M.; Wei, C. S.; Park, H.; Eastgate, M. D. An Enantioselective Total Synthesis of (+)-Duocarmycin SA. *J. Org. Chem.* **2018**, *83* (7), 3928–3940. <https://doi.org/10.1021/acs.joc.8b00285>.
- (145) Wang, X.; Wu, S.; Jin, W.; Xu, B.; Tang, G.; Yuan, H. Bioinformatics-Guided Connection of a Biosynthetic Gene Cluster to the Antitumor Antibiotic Gilvusmycin. *Acta Biochim. Biophys. Sin.* **2018**, *50* (5), 516–518. <https://doi.org/10.1093/abbs/gmy030>.
- (146) Imaizumi, T.; Yamashita, Y.; Nakazawa, Y.; Okano, K.; Sakata, J.; Tokuyama, H. Total Synthesis of (+)-CC-1065 Utilizing Ring Expansion Reaction of Benzocyclobutenone Oxime Sulfonate. *Org. Lett.* **2019**, *21* (16), 6185–6189. <https://doi.org/10.1021/acs.orglett.9b01690>.

(b) early clinical trials (49 journal publications)

- (1) Li, L. H.; Kelly, Robert C.; Warpehoski, Martha A.; McGovren, J. P.; Gebhard, I.; DeKoning, Thomas F. Adozelesin, a Selected Lead among Cyclopropylpyrroloindole Analogs of the DNA-Binding Antibiotic, CC-1065. *Invest. New Drugs* **1991**, *9* (2). <https://doi.org/10.1007/BF00175081>.
- (2) Mitchell, M. A.; Kelly, R. C.; Wicnienski, N. A.; Hatzenbuehler, N. T.; Williams, M. G.; Petzold, G. L.; Slightom, J. L.; Siemieniak, D. R. Synthesis and DNA Crosslinking by a Rigid CPI Dimer. *J. Am. Chem. Soc.* **1991**, *113* (23), 8994–8995. <https://doi.org/10.1021/ja00023a085>.
- (3) Weiland, K. L.; Dooley, T. P. In Vitro and in Vivo DNA Bonding by the CC-1065 Analog U-73975. *Biochemistry* **1991**, *30* (30), 7559–7565. <https://doi.org/10.1021/bi00244a027>.
- (4) Bhuyan, B. K.; Smith, K. S.; Adams, E. G.; Petzold, G. L.; McGovren, J. P. Lethality, DNA Alkylation, and Cell Cycle Effects of Adozelesin (U-73975) on Rodent and Human Cells. *Cancer Res.* **1992**, *52*, 5687–5692.
- (5) Bhuyan, B. K.; Smith, K. S.; Adams, E. G.; Wallace, T. L.; Von Hoff, D. D.; Li, L. H. Adozelesin, a Potent New Alkylating Agent: Cell-Killing Kinetics and Cell-Cycle Effects. *Cancer Chemother. Pharmacol.* **1992**, *30* (5), 348–354. <https://doi.org/10.1007/BF00689961>.
- (6) Li, L. H.; DeKoning, T. F.; Kelly, R. C.; Krueger, W. C.; McGovren, J. P.; Padbury, G. E.; Petzold, G. L.; Wallace, T. L.; Ouding, R. J.; Prairie, M. D.; Gebhard, I. Cytotoxicity and Antitumor Activity of Carzelesin, a Prodrug Cyclopropylpyrroloindole Analogue. *Cancer Res.* **1992**, *52*, 4904–4913.
- (7) Nguyen, H. N.; Sevin, B.-U.; Averette, H.; Perras, J.; Ramos, R.; Donato, D. Spectrum of Cell-Cycle Kinetics of Alkylating Agent Adozelesin in Gynecological Cancer Cell Lines: Correlation with Drug-Induced Cytotoxicity. *J. Cancer Res. Clin. Oncol.* **1992**, *118* (7), 515–522. <https://doi.org/10.1007/BF01225266>.
- (8) Hightower, R. D.; Sevin, B.-U.; Perras, J.; Nguyen, H.; Angioli, R.; Untch, M.; Averette, H. In Vitro Evaluation of the Novel Chemotherapeutic Agents U-73, 975, U-77, 779, and U-80, 244 in Gynecologic Cancer Cell Lines. *Cancer Invest.* **1993**, *11* (3), 276–282. <https://doi.org/10.3109/07357909309024852>.
- (9) Monroe, T. J.; Mitchell, M. A. In Vivo Mutagenesis Induced by CC-1065 and Adozelesin DNA Alkylation in a Transgenic Mouse Model. *Cancer Res.* **1993**, *53*, 5690–5696.
- (10) Sun, D.; Park, H. J.; Hurley, L. H. Alkylation of Guanine and Cytosine in DNA by Bizelesin. Evidence for a Covalent Immobilization Leading to a Proximity-Driven Alkylation of Normally Unreactive Bases by a (+)-CC-1065 Cross-Linking Compound. *Chem. Res. Toxicol.* **1993**, *6* (6), 889–894. <https://doi.org/10.1021/tx00036a020>.
- (11) Fleming, G. F.; Ratain, M. J.; O'Brien, S. M.; Schilsky, R. L.; Hoffman, P. C.; Richards, J. M.; Vogelzang, N. J.; Kasunic, D. A.; Earhart, R. H. Phase I Study of Adozelesin Administered by 24-Hour Continuous Intravenous Infusion. *J. Natl. Cancer Inst.* **1994**, *86* (5), 368–372. <https://doi.org/10.1093/jnci/86.5.368>.

- (12) Kobayashi, E.; Okamoto, A.; Asada, M.; Okabe, M.; Nagamura, S.; Asai, A.; Saito, H.; Gomi, K.; Hirata, T. Characteristics of Antitumor Activity of KW-2189, a Novel Water-Soluble Derivative of Duocarmycin, against Murine and Human Tumors. *Cancer Res.* **1994**, *54*, 2404–2410.
- (13) Ogasawara, H.; Nishio, K.; Takeda, Y.; Ohmori, T.; Kubota, N.; Funayama, Y.; Ohira, T.; Kuraishi, Y.; Isogai, Y.; Saijo, N. A Novel Antitumor Antibiotic, KW-2189 Is Activated by Carboxyl Esterase and Induces DNA Strand Breaks in Human Small Cell Lung Cancer Cells. *Jpn. J. Cancer Res.* **1994**, *85*, 418–425. <https://doi.org/10.1111/j.1349-7006.1994.tb02375.x>.
- (14) Okamoto, A.; Asai, A.; Saito, H.; Okabe, M.; Gomi, K. Differential Effect of Duocarmycin A and Its Novel Derivative DU-86 on DNA Strand Breaks in HeLa S3 Cells. *Jpn. J. Cancer Res.* **1994**, *85*, 1304–1311. <https://doi.org/10.1111/j.1349-7006.1994.tb02944.x>.
- (15) Shamdas, G. J.; Alberts, D. S.; Modiano, M.; Wiggins, C.; Power, J.; Kasunic, D. A.; Elfring, G. L.; Earhart, R. H. Phase I Study of Adozelesin (U-73,975) in Patients with Solid Tumors. *Anti-Cancer Drugs* **1994**, *5*, 10–14. <https://doi.org/10.1097/00001813-199402000-00002>.
- (16) van Tellingen, O.; Pels, E. M.; Henrar, R. E. C.; Schaaf, L. J.; Padbury, G. E.; Beijnen, J. H.; Nooijen, W. J. Fully Automated High-Performance Liquid Chromatographic Method for the Determination of Carzelesin (U-80,244) and Metabolites (U-76,073 and U-76,074) in Human Plasma. *J. Chromat. B: Biomed. Sci. Appl.* **1994**, *652* (1), 51–58. [https://doi.org/10.1016/0378-4347\(93\)E0377-3](https://doi.org/10.1016/0378-4347(93)E0377-3).
- (17) Walker, D. L.; Reid, J. M.; Ames, M. M. Preclinical Pharmacology of Bizelesin, a Potent Bifunctional Analog of the DNA-Binding Antibiotic CC-1065. *Cancer Chemother. Pharmacol.* **1994**, *34*, 317–322.
- (18) Houghton, P. J.; Cheshire, P. J.; Hallman, J. D.; Houghton, J. A. Therapeutic Efficacy of the Cyclopropylpyrrolindole, Carzelesin, against Xenografts Derived from Adult and Childhood Solid Tumors. *Cancer Chemother. Pharmacol.* **1995**, *36*, 45–52. <https://doi.org/10.1007/BF00685731>.
- (19) Ogasawara, H.; Nishio, K.; Kanzawa, F.; Lee, Y.-S.; Funayama, Y.; Ohira, T.; Kuraishi, Y.; Isogai, Y.; Saijo, N. Intracellular Carboxyl Esterase Activity Is a Determinant of Cellular Sensitivity to the Antineoplastic Agent KW-2189 in Cell Lines Resistant to Cisplatin and CPT-11. *Jpn. J. Cancer Res.* **1995**, *86*, 124–129. <https://doi.org/10.1111/j.1349-7006.1995.tb02997.x>.
- (20) Smith, K. S.; Folz, B. A.; Adams, E. G.; Bhuyan, B. K. Synergistic and Additive Combinations of Several Antitumor Drugs and Other Agents with the Potent Alkylating Agent Adozelesin. *Cancer Chemother. Pharmacol.* **1995**, *35*, 471–482.
- (21) Carter, C. A.; Waud, W. R.; Li, L. H.; DeKoning, T. F.; McGovern, J. P.; Plowman, J. Preclinical Antitumor Activity of Bizelesin in Mice. *Clin. Cancer Res.* **1996**, *2*, 1143–1149.
- (22) Foster, B. J.; LoRusso, P. M.; Poplin, E.; Zalupski, M.; Valdivieso, M.; Wozniak, A.; Flaherty, L.; Kasunic, D. A.; Earhart, R. H.; Baker, L. H. Phase I Trial of Adozelesin Using the Treatment Schedule of Daily x 5 Every 3 Weeks. *Invest. New Drugs* **1996**, *13*, 321–326. <https://doi.org/10.1007/BF00873138>.
- (23) Jonkman-De Vries, J. D.; Doppenberg, W. G.; Henrar, R. E. C.; Bult, A.; Beijnen, J. H. Systematic Study on the Chemical Stability of the Prodrug Antitumor Agent Carzelesin (U-80,244). *J. Pharm. Sci.* **1996**, *85* (11), 1227–1233. <https://doi.org/10.1021/ls960005n>.
- (24) Nagamura, S.; Kobayashi, E.; Gomi, K.; Saito, H. Studies on the Active Metabolite (DU-86) of KW-2189, a Novel Derivative of Duocarmycin. *Bioorg. Med. Chem. Lett.* **1996**, *6* (17), 2147–2150. [https://doi.org/10.1016/0960-894X\(96\)00388-5](https://doi.org/10.1016/0960-894X(96)00388-5).
- (25) Volpe, D. A.; Tomaszewski, J. E.; Parchment, R. E.; Garg, A.; Flora, K. P.; Murphy, M. J.; Grieshaber, C. K. Myelotoxic Effects of the Bifunctional Alkylating Agent Bizelesin on Human, Canine and Murine Myeloid Progenitor Cells. *Cancer Chemother. Pharmacol.* **1996**, *39* (1–2), 143–149. <https://doi.org/10.1007/s002800050550>.
- (26) Wolff, I.; Bench, K.; Beijnen, J. H.; Brunsch, U.; Cavalli, F.; de Jong, J.; Groot, Y.; van Tellingen, O.; Wanders, J.; Sessa, C. Phase I Clinical and Pharmacokinetic Study of Carzelesin (U-80244) Given Daily for Five Consecutive Days. *Clin. Cancer Res.* **1996**, *2*, 1717–1723.
- (27) Burris, H. A.; Dieras, V. C.; Tunca, M.; Earhart, R. H.; Eckardt, J. R.; Rodriguey, G. I.; Shaffer, D. S.; Fields, S. M.; Campbell, E.; Schaaf, L.; Kasunic, D. A.; Von Hoff, D. D. Phase I Study with the DNA Sequence-Specific Agent Adozelesin. *Anti-Cancer Drugs* **1997**, *8*, 588–596. <https://doi.org/10.1097/00001813-199707000-00006>.
- (28) Nagamura, S.; Kinugawa, M.; Ogasa, T.; Saito, H. The Synthesis of [3H]KW-2189, a Novel Antitumor Antibiotic. *J. Lab. Comp. Radiopharm.* **1997**, *39* (6), 471–477.
- (29) Ogasawara, H.; Nishio, K.; Ishida, T.; Arioka, H.; Fukuoka, K.; Saijo, N. In Vitro Enhancement of Antitumor Activity of a Water-Soluble Duocarmycin Derivative, KW-2189, by Caffeine-Mediated DNA-Repair Inhibition in Human Lung Cancer Cells. *Jpn. J. Cancer Res.* **1997**, *88*, 1033–1037. <https://doi.org/10.1111/j.1349-7006.1997.tb00326.x>.
- (30) Alberts, S. R.; Erlichman, C.; Reid, J. M.; Sloan, J. A.; Ames, M. M.; Richardson, R. L.; Goldberg, R. M. Phase I Study of the Duocarmycin Semisynthetic Derivative KW-2189 given Daily for Five Days Every Six Weeks. *Clin. Cancer Res.* **1998**, *4*, 2111–2117.
- (31) Cristofanilli, M.; Bryan, W. J.; Miller, L. L.; Chang, A. Y.-C.; Gradishar, W. J.; Kufe, D. W.; Hortobagyi, G. N. Phase II Study of Adozelesin in Untreated Metastatic Breast Cancer. *Anti-Cancer Drugs* **1998**, *9*, 779–782. <https://doi.org/10.1097/00001813-199810000-00006>.
- (32) Kinugawa, M.; Nagamura, S.; Sakaguchi, A.; Masuda, Y.; Saito, H.; Ogasa, T.; Kasai, M. Practical Synthesis of the High-Quality Antitumor Agent KW-2189 from Duocarmycin B2 Using a Facile One-Pot Synthesis of an Intermediate. *Org. Process Res. Dev.* **1998**, *2* (6), 344–350. <https://doi.org/10.1021/op980038k>.
- (33) van Tellingen, O.; Punt, C. J. A.; Groot, Y.; Henrar, R. E. C.; Awada, A.; Wagener, D. J. T.; Piccart, M. J.; Schaaf, L. J.; Nooijen, W. J.; Beijnen, J. H. A Clinical Pharmacokinetics Study of Carzelesin given by Short-Term Intravenous Infusion in a Phase I Study. *Cancer Chemother. Pharmacol.* **1998**, *41* (5), 377–384. <https://doi.org/10.1007/s002800050754>.
- (34) van Tellingen, O.; Nooijen, W. J.; Schaaf, L. J.; Henrar, R. E. C.; Beijnen, J. H. Comparative Pharmacology of the Novel Cyclopropylpyrrolindole-Prodrug Carzelesin in Mice, Rats, and Humans. *Cancer Res.* **1998**, *58*, 2410–2416.
- (35) Awada, A.; Punt, C. J. A.; Piccart, M. J.; Tellingen, O. V.; Manen, L. V.; Kerger, J.; Groot, Y.; Wanders, J.; Verweij, J.; Wagener, D. J. T. Phase I Study of Carzelesin (U-80,244) given (4-Weekly) by Intravenous Bolus Schedule. *Br. J. Cancer* **1999**, *79* (9–10), 1454–1461. <https://doi.org/10.1038/sj.bjc.6690232>.
- (36) Hidalgo, M.; Izbicka, E.; Cerna, C.; Gomez, L.; Rowinsky, E. K.; Weitman, S. D.; Von Hoff, D. D. Comparative Activity of the Cyclopropylpyrrolindole Compounds Adozelesin, Bizelesin and Carzelesin in a Human Tumor Colony-Forming Assay. *Anti-Cancer Drugs* **1999**, *10*, 295–302. [https://doi.org/Comparative Activity of the Cyclopropylpyrrolindole Compounds Adozelesin, Bizelesin and Carzelesin in a human tumor colony-forming assay](https://doi.org/Comparative%20Activity%20of%20the%20Cyclopropylpyrrolindole%20Compounds%20Adozelesin,%20Bizelesin%20and%20Carzelesin%20in%20a%20human%20tumor%20colony-forming%20assay).
- (37) Cameron, L.; Thompson, A. S. Determination of the Structural Role of the Linking Moieties in the DNA Binding of Adozelesin. *Biochemistry* **2000**, *39* (17), 5004–5012. <https://doi.org/10.1021/bi9926532>.
- (38) Liu, J.-S.; Kuo, S.-R.; McHugh, M. M.; Beerman, T. A.; Melendy, T. Adozelesin Triggers DNA Damage Response Pathways and Arrests SV40 DNA Replication through Replication Protein A Inactivation. *J. Biol. Chem.* **2000**, *275* (2), 1391–1397. <https://doi.org/10.1074/jbc.275.2.1391>.
- (39) Pavlidis, N.; Aamdal, S.; Awada, A.; Calvert, H.; Fumoleau, P.; Sorio, R.; Punt, C.; Verweij, J.; van Oosterom, A.; Morant, R.; Wanders, J.; Hanauske, A.-R. Carzelesin Phase II Study in Advanced Breast, Ovarian, Colorectal, Gastric, Head and Neck Cancer, Non-Hodgkin's Lymphoma and Malignant Melanoma: A Study of the EORTC Early Clinical Studies Group (ECSG). *Cancer Chemother. Pharmacol.* **2000**, *46* (2), 167–171. <https://doi.org/10.1007/s00280000134>.
- (40) Small, E. J.; Figlin, R.; Petrylak, D.; Vaughn, D. J.; Sartor, O.; Horak, I.; Pincus, R.; Kremer, A.; Bowden, C. A Phase II Pilot Study of KW-2189 in Patients with Advanced Renal Cell Carcinoma. *Invest. New Drugs* **2000**, *18*, 193–197.

- (41) Park, H.-J. DNA Structural Perturbation Induced by the CPI-Derived DNA Interstrand Cross-Linker: Molecular Mechanisms for the Sequence Specific Recognition. *Arch. Pharm. Res.* **2001**, *24* (5), 455–465. <https://doi.org/10.1007/BF02975194>.
- (42) Markovic, S. N.; Suman, V. J.; Vukov, A. M.; Fitch, T. R.; Hillman, D. W.; Adjei, A. A.; Alberts, S. R.; Kaur, J. S.; Braich, T. A.; Leitch, J. M.; Creagan, E. T. Phase II Trial of KW2189 in Patients With Advanced Malignant Melanoma. *Am. J. Clin. Oncol.* **2002**, *25* (3), 308–312. <https://doi.org/10.1097/0000421-200206000-00022>.
- (43) Pitot, H. C.; Reid, J. M.; Sloan, J. A.; Ames, M. M.; Adjei, A. A.; Rubin, J.; Bagniewski, P. G.; Atherton, P.; Rayson, D.; Goldberg, R. M.; Erlichman, C. A Phase I Study of Bizelesin (NSC 615291) in Patients with Advanced Solid Tumors. *Clin. Cancer Res.* **2002**, *8*, 712–717.
- (44) Cao, P.; McHugh, M. M.; Melendy, T.; Beerman, T. The DNA Minor Groove-Alkylating Cyclopropylpyrroloindole Drugs Adozelesin and Bizelesin Induce Different DNA Damage Response Pathways in Human Colon Carcinoma HCT116 Cells. *Mol. Cancer Ther.* **2003**, *2*, 651–659.
- (45) Schwartz, G. H.; Patnaik, A.; Hammond, L. A.; Rizzo, J.; Berg, K.; Von Hoff, D. D.; Rowinsky, E. K. A Phase I Study of Bizelesin, a Highly Potent and Selective DNA-Interactive Agent, in Patients with Advanced Solid Malignancies. *Ann. Oncol.* **2003**, *14* (5), 775–782. <https://doi.org/10.1093/annonc/mdg215>.
- (46) Taguchi, F.; Kusaba, H.; Asai, A.; Iwamoto, Y.; Yano, K.; Nakano, H.; Mizukami, T.; Saijo, N.; Kato, H.; Nishio, K. HnRNP L Enhances Sensitivity of the Cells to KW-2189. *Int. J. Cancer* **2004**, *108* (5), 679–685. <https://doi.org/10.1002/ijc.11616>.
- (47) Yanow, S. K.; Purcell, L. A.; Spithill, T. W. The A/T-Specific DNA Alkylating Agent Adozelesin Inhibits Plasmodium Falciparum Growth in Vitro and Protects Mice against Plasmodium Chabaudi Adami Infection. *Mol. Biochem. Parasit.* **2006**, *148* (1), 52–59. <https://doi.org/10.1016/j.molbiopara.2006.02.019>.
- (48) Alberts, S. R.; Suman, V. J.; Pitot, H. C.; Camoriano, J. K.; Rubin, J. Use of KW-2189, a DNA Minor Groove-Binding Agent, in Patients with Hepatocellular Carcinoma: A North Central Cancer Treatment Group (NCCTG) Phase II Clinical Trial. *J. Gastrointest. Cancer* **2007**, *38* (1), 10–14. <https://doi.org/10.1007/s12029-007-9007-6>.
- (49) Lee, S.-Y.; Pfeifer, G. P.; Lee, C.-S. Mutation Spectra Induced by Adozelesin in the SupF Gene of Human XP-A Fibroblasts. *Arch. Pharm. Res.* **2010**, *33* (4), 633–636. <https://doi.org/10.1007/s12272-010-0419-7>.

(1) SAR studies (191 items - 182 journal publications, 9 patents)

- (1) Sundberg, R. J.; Nishiguchi, T. Synthesis and Intramolecular Photoaddition of an Indole Quinonediazide. *Tet. Lett.* **1983**, *24* (44), 4773–4776. [https://doi.org/10.1016/S0040-4039\(00\)94004-8](https://doi.org/10.1016/S0040-4039(00)94004-8).
- (2) Boger, D. L.; Coleman, R. S.; Invergo, B. J. Studies on the Total Synthesis of CC-1065: Preparation of a Synthetic Simplified 3-Carbamoyl-1,2-Dihydro-3H-Pyrrolo[3,2-e]Indole Dimer/Trimer/Tetramer (CDPI Dimer/Trimer/Tetramer) and Development of Methodology for PDE-I Dimer Methyl Ester Formation. *J. Org. Chem.* **1987**, *52* (8), 1521–1530. <https://doi.org/10.1021/jo00384a026>.
- (3) Li, L. H.; Wallace, T. L.; DeKoning, T. F.; Warpehoski, M. A.; Kelly, R. C.; Prairie, M. D.; Krueger, W. C. Structure and Activity Relationship of Several Novel CC-1065 Analogs. *Invest. New Drugs* **1987**, *5* (4). <https://doi.org/10.1007/BF00169971>.
- (4) Boger, D. L.; Coleman, R. S. Total Synthesis of (+, -)-N2-(Phenylsulfonyl)-CPI, (+, -)-CC-1065, (+)-CC-1065, Ent-(-)-CC-1065, and the Precise, Functional Agents (+, -)-CPI-CDPI2, (+)-CPI-CDPI2, and (-)-CPI-CDPI2 [(+, -)-(3bR*, 4aS*)-, (+)-(3bR, 4aS)-, and (-)-(3bS, 4aR)-Deoxy-CC-1065]. *J. Am. Chem. Soc.* **1988**, *110* (14), 4796–4807. <https://doi.org/10.1021/ja00222a043>.
- (5) Boger, D. L.; Ishizaki, T.; Wysocki, R. J.; Munk, S. A.; Kitos, P. A.; Suntorwat, O. Total Synthesis and Evaluation of (+, -)-N-(Tert-Butoxycarbonyl)-CBI, (+, -)-CBI-CDPI1, and (+, -)-CBI-CDPI2: CC-1065 Functional Agents Incorporating the Equivalent 1,2,9,9a-Tetrahydrocyclopropa[1,2-c]Benz[e]Indol-4-One (CBI) Left-Hand Subunit. *J. Am. Chem. Soc.* **1989**, *111* (16), 6461–6463. <https://doi.org/10.1021/ja00198a089>.
- (6) Boger, D. L.; Wysocki, R. J. Total Synthesis of (+, -)-N-(Phenylsulfonyl)- and (+, -)-N-(Tert-Butoxycarbonyl)-CI, (+, -)-CI-CDPI1, and (+, -)-CI-CDPI2: CC-1065 Functional Analogs Incorporating the Parent 1,2,7,7a-Tetrahydrocycloprop[1,2-c]Indol-4-One (CI) Left-Hand Subunit. *J. Org. Chem.* **1989**, *54* (6), 1238–1240. <https://doi.org/10.1021/jo00267a004>.
- (7) Boger, D. L.; Ishizaki, T. Resolution of a CBI Precursor and Incorporation into the Synthesis of (+)-Cbi, (+)-CBI-CDPI1, (+)-CBI-CDPI2: Enhanced Functional Analogs of (+)-CC-1065. A Critical Appraisal of a Proposed Relationship between Electrophile Reactivity, DNA Binding Properties, and Cytotoxic Potency. *Tet. Lett.* **1990**, *31* (6), 793–796. [https://doi.org/10.1016/S0040-4039\(00\)94629-X](https://doi.org/10.1016/S0040-4039(00)94629-X).
- (8) Boger, D. L.; Coleman, R. S.; Invergo, B. J.; Sakya, S. M.; Ishizaki, T.; Munk, S. A.; Zarrinmayeh, H.; Kitos, P. A.; Thompson, S. C. Synthesis and Evaluation of Aborted and Extended CC-1065 Functional Analogs: (+) and (-)-CPI-PDE-I1, (+) and (-)-CPI-CDPI1, and (+, -), (+), and (-)-CPI-CDPI3. Preparation of Key Partial Structures and Definition of an Additional Functional Role of the CC-1065 Central and Right-Hand Subunits. *J. Am. Chem. Soc.* **1990**, *112* (12), 4623–4632. <https://doi.org/10.1021/ja00168a002>.
- (9) Boger, D. L.; Ishizaki, T.; Kitos, P. A.; Suntorwat, O. Synthesis of N-(Tert-Butoxycarbonyl)-CBI, CBI, CBI-CDPI1, and CBI-CDPI2: Enhanced Functional Analogs of CC-1065 Incorporating the 1,2,9,9a-Tetrahydrocyclopropa[1,2-c]Benz[e]Indol-4-One (CBI) Left-Hand Subunit. *J. Org. Chem.* **1990**, *55* (23), 5823–5832. <https://doi.org/10.1021/jo00310a013>.
- (10) Boger, D. L.; Ishizaki, T.; Zarrinmayeh, H.; Munk, S. A.; Kitos, P. A.; Suntorwat, O. Duocarmycin-Pyrindamycin DNA Alkylation Properties and Identification, Synthesis, and Evaluation of Agents Incorporating the Pharmacophore of the Duocarmycin-Pyrindamycin Alkylation Subunit. Identification of the CC-1065 Duocarmycin Common Pharmacophore. *J. Am. Chem. Soc.* **1990**, *112* (24), 8961–8971. <https://doi.org/10.1021/ja00180a048>.
- (11) Boger, D. L.; Ishizaki, T.; Zarrinmayeh, H.; Kitos, P. A.; Suntorwat, O. Synthesis and Preliminary Evaluation of Agents Incorporating the Pharmacophore of the Duocarmycin/Pyrindamycin Alkylation Subunit: Identification of the CC-1065/Duocarmycin Common Pharmacophore. *J. Org. Chem.* **1990**, *55* (15), 4499–4502. <https://doi.org/10.1021/jo00302a002>.
- (12) Boger, D. L.; Wysocki, R. J.; Ishizaki, T. Synthesis of N-(Phenylsulfonyl)-CI, N-(Tert-Butoxy)Carbonyl)-CI, CI-CDPI1, and CI-CDPI2: CC-1065 Functional Analog Incorporating the Parent 1,2,7,71-Tetrahydrocycloprop[1,2-c]Indol-4-One (CI) Left-Hand Subunit. *J. Am. Chem. Soc.* **1990**, *112* (13), 5230–5240. <https://doi.org/10.1021/ja00169a034>.
- (13) Boger, D. L.; Ishizaki, T.; Sakya, S. M.; Munk, S. A. Synthesis and Preliminary Evaluation of (+)-CBI-Indole2; An Enhanced Functional Analog of (+)-CC-1065. *Bioorg. Med. Chem. Lett.* **1991**, *1* (2), 115–120. [https://doi.org/10.1016/S0960-894X\(00\)80243-7](https://doi.org/10.1016/S0960-894X(00)80243-7).
- (14) Boger, D. L.; Ishizaki, T.; Zarrinmayeh, H.; Kitos, P. A.; Suntorwat, O. A Potent, Simple Derivative of an Analog of the CC-1065 Alkylation Subunit. *Bioorg. Med. Chem. Lett.* **1991**, *1* (1), 55–58. [https://doi.org/10.1016/S0960-894X\(01\)81090-8](https://doi.org/10.1016/S0960-894X(01)81090-8).
- (15) Boger, D. L.; Munk, S. A.; Ishizaki, T. (+)-CC-1065 DNA Alkylation: Observation of an Unexpected Relationship between Cyclopropane Electrophile Reactivity and the Intensity of DNA Alkylation. *J. Am. Chem. Soc.* **1991**, *113* (7), 2779–2780. <https://doi.org/10.1021/ja00007a077>.
- (16) Boger, D. L.; Munk, S. A.; Zarrinmayeh, H. (+)-CC-1065 DNA Alkylation: Key Studies Demonstrating a Noncovalent Binding Selectivity Contribution to the Alkylation Selectivity. *J. Am. Chem. Soc.* **1991**, *113* (10), 3980–3983. <https://doi.org/10.1021/ja00010a046>.
- (17) Aristoff, P. A.; Johnson, P. D. Synthesis of CBI-PDE-I-Dimer, the Benzannulated Analog of CC-1065. *J. Org. Chem.* **1992**, *57* (23), 6234–6239. <https://doi.org/10.1021/jo00049a035>.

- (18) Boger, D. L.; Sakya, S. M. CC-1065 Partial Structures: Enhancement of Noncovalent Affinity for DNA Minor Groove Binding through Introduction of Stabilizing Electrostatic Interactions. *J. Org. Chem.* **1992**, *57* (4), 1277–1284. <https://doi.org/10.1021/jo00030a042>.
- (19) Boger, D. L.; Yun, W.; Teegarden, B. R. An Improved Synthesis of 1,2,9,9a-Tetrahydrocyclopropa[c]Benz[e]Indol-4-One (CBI): A Simplified Analog of the CC-1065 Alkylation Subunit. *J. Org. Chem.* **1992**, *57* (10), 2873–2876. <https://doi.org/10.1021/jo00036a023>.
- (20) Aristoff, P. A.; Johnson, P. D.; Sun, D.; Hurley, L. H. Synthesis and Biochemical Evaluation of the CBI-PDE-I-Dimer, a Benzannulated Analog of (+)-CC-1065 That Also Produces Delayed Toxicity in Mice. *J. Med. Chem.* **1993**, *36* (14), 1956–1963. <https://doi.org/10.1021/jm00066a004>.
- (21) Boger, D. L.; Johnson, D. S.; Palanki, M. S. S.; Kitos, P. A.; Chang, J.; Dowell, P. Evaluation of Functional Analogs of CC-1065 and the Duocarmycins Incorporating the Cross-Linking 9a-Chloromethyl-1,2,9,9a-Tetrahydrocyclopropa[c]Benz[e]Indol-4-One (C2BI) Alkylation Subunit. *Bioorg. Med. Chem.* **1993**, *1* (1), 27–38. [https://doi.org/10.1016/S0968-0896\(00\)82100-8](https://doi.org/10.1016/S0968-0896(00)82100-8).
- (22) Wang, Y.; Gupta, R.; Huang, L.; Lown, J. W. CC-1065 Functional Analogs Possessing Different Electron-Withdrawing Substituents and Leaving Groups: Synthesis, Kinetics, and Sequence Specificity of Reaction with DNA and Biological Evaluation. *J. Med. Chem.* **1993**, *36* (26), 4172–4182. <https://doi.org/10.1021/jm00078a005>.
- (23) Boger, D. L.; Mesini, P. Design, Synthesis, and Evaluation of CC-1065 and Duocarmycin Analogs Incorporating the 2,3,10,10a-Tetrahydro-1H-Cyclopropa[d]Benzof[quinoxaline]-5-One (CBQ) Alkylation Subunit: Identification and Structural Origin of Subtle Stereoelectronic Features That Govern Reactivity and Regioselectivity. *J. Am. Chem. Soc.* **1994**, *116* (25), 11335–11348. <https://doi.org/10.1021/ja00104a013>.
- (24) Boger, D. L.; Mesini, P.; Tarby, C. M. Chemical and Structural Comparison of N-BOC-CBQ and N-BOC-CBI: Identification and Structural Origin of an Unappreciated but Productive Stability of the CC-1065 and Duocarmycin SA Alkylation Subunits. *J. Am. Chem. Soc.* **1994**, *116* (14), 6461–6462. <https://doi.org/10.1021/ja00093a067>.
- (25) Boger, D. L.; Nishi, T.; Teegarden, B. R. P-Quinonemethide Analog of the CC-1065 and Duocarmycin Alkylation Subunits. *J. Org. Chem.* **1994**, *59* (17), 4943–4949. <https://doi.org/10.1021/jo00096a043>.
- (26) Boger, D. L.; Yun, W. CBI-TMI: Synthesis and Evaluation of a Key Analog of the Duocarmycins. Validation of a Direct Relationship between Chemical Solvolytic Stability and Cytotoxic Potency and Confirmation of the Structural Features Responsible for the Distinguishing Behavior of Enantiomeric Pairs of Agents. *J. Am. Chem. Soc.* **1994**, *116* (18), 7996–8006. <https://doi.org/10.1021/ja00097a006>.
- (27) Mohamadi, F.; Spees, M. M.; Staten, G. S.; Marder, P.; Kipka, J. K.; Johnson, D. A.; Boger, D. L.; Zarrinmayeh, H. Total Synthesis and Biological Properties of Novel Antineoplastic (Chloromethyl)Furanoidolines: An Asymmetric Hydroboration Mediated Synthesis of the Alkylation Subunits. *J. Med. Chem.* **1994**, *37* (2), 232–239. <https://doi.org/10.1021/jm00028a005>.
- (28) Boger, D. L.; Johnson, D. S. CC-1065 and the Duocarmycins: Unraveling the Keys to a New Class of Naturally Derived DNA Alkylating Agents. *Proc. Natl. Acad. Sci. USA* **1995**, *92* (9), 3642–3649. <https://doi.org/10.1073/pnas.92.9.3642>.
- (29) Boger, D. L.; Yun, W.; Cai, H.; Han, N. CBI-CDPBO and CBI-CDPBII: CC-1065 Analogs Containing Deep-Seated Modifications in the DNA Binding Subunit. *Bioorg. Med. Chem.* **1995**, *3* (6), 761–767. [https://doi.org/10.1016/0968-0896\(95\)00066-p](https://doi.org/10.1016/0968-0896(95)00066-p).
- (30) Boger, D. L.; McKie, J. A. An Efficient Synthesis of 1,2,9,9a-Tetrahydrocyclopropa[c]Benz[e]Indol-4-One CBI: An Enhanced and Simplified Analog of the CC-1065 and Duocarmycin Alkylation Subunits. *J. Org. Chem.* **1995**, *60* (5), 1271–1275. <https://doi.org/10.1021/jo00110a034>.
- (31) Boger, D. L.; Nishi, T. Diastereoselective Dieckmann Condensation Suitable for Introduction of the Duocarmycin A C6 Center: Development of a Divergent Strategy for the Total Synthesis of Duocarmycins A and SA. *Bioorg. Med. Chem.* **1995**, *3* (1), 67–77. [https://doi.org/10.1016/0968-0896\(94\)00147-U](https://doi.org/10.1016/0968-0896(94)00147-U).
- (32) Boger, D. L.; Yun, W.; Han, N. 1,2,9,9a-Tetrahydrocyclopropa[c]Benz[e]Indol-4-One (CBI) Analogs of CC-1065 and the Duocarmycins: Synthesis and Evaluation. *Bioorg. Med. Chem.* **1995**, *3* (11), 1429–1453. [https://doi.org/10.1016/0968-0896\(95\)00130-9](https://doi.org/10.1016/0968-0896(95)00130-9).
- (33) Fregeau, N. L.; Wang, Y.; Pon, R. T.; Wylie, W. A.; Lown, J. W. Characterization of a CPI-Lexitropsin Conjugate-Oligonucleotide Covalent Complex by 1H NMR and Restrained Molecular Dynamics Simulation. *J. Am. Chem. Soc.* **1995**, *117* (35), 8917–8925. <https://doi.org/10.1021/ja00140a004>.
- (34) Nagamura, S.; Kanda, Y.; Kobayashi, E.; Gomi, K.; Saito, H. Synthesis and Antitumor Activity of Duocarmycin Derivatives. *Chem. Pharm. Bull.* **1995**, *49* (9), 1530–1535.
- (35) Boger, D. L.; Bollinger, B.; Johnson, D. S. Examination of the Role of the Duocarmycin SA Methoxy Substituents: Identification of the Minimum, Fully Potent DNA Binding Subunit. *Bioorg. Med. Chem. Lett.* **1996**, *6* (18), 2207–2210. [https://doi.org/10.1016/0960-894X\(96\)00401-5](https://doi.org/10.1016/0960-894X(96)00401-5).
- (36) Boger, D. L.; Han, N.; Tarby, C. M.; Boyce, C. W.; Cai, H.; Jin, Q.; Kitos, P. A. Synthesis, Chemical Properties, and Preliminary Evaluation of Substituted CBI Analogs of CC-1065 and the Duocarmycins Incorporating the 7-Cyano-1,2,9,9a-Tetrahydrocyclopropa[c]Benz[e]Indol-4-One Alkylation Subunit: Hammett Quantitation of the Magnitude of Electronic Effects on Functional Reactivity. *J. Org. Chem.* **1996**, *61* (15), 4894–4912. <https://doi.org/10.1021/jo9605298>.
- (37) Boger, D. L.; Jenkins, T. J. Synthesis, X-Ray Structure, and Properties of Fluorocyclopropane Analogs of the Duocarmycins Incorporating the 9,9-Difluoro-1,2,9,9a-Tetrahydrocyclopropa[c]Benzof[e]Indol-4-One (F₂ CBI) Alkylation Subunit. *J. Am. Chem. Soc.* **1996**, *118* (37), 8860–8870. <https://doi.org/10.1021/ja961888n>.
- (38) Boger, D. L.; McKie, J. A.; Cai, H.; Cacciari, B.; Baraldi, P. G. Synthesis and Properties of Substituted CBI Analogs of CC-1065 and the Duocarmycins Incorporating the 7-Methoxy-1,2,9,9a-Tetrahydrocyclopropa[c]Benz[e]Indol-4-One (MCBI) Alkylation Subunit: Magnitude of Electronic Substituents on the Functional Reactivity. *J. Org. Chem.* **1996**, *61* (5), 1710–1729. <https://doi.org/10.1021/jo952033g>.
- (39) Boger, D. L.; McKie, J. A.; Han, N.; Tarby, C. M.; Riggs, H. W.; Kitos, P. A. A Hammett Correlation for CC-1065 and Duocarmycin Analogs: Magnitude of Substituent Electronic Effects on Functional Reactivity. *Bioorg. Med. Chem. Lett.* **1996**, *6* (6), 659–664. [https://doi.org/10.1016/0960-894X\(96\)00093-5](https://doi.org/10.1016/0960-894X(96)00093-5).
- (40) Nagamura, S.; Kanda, Y.; Asai, A.; Kobayashi, E.; Gomi, K.; Saito, H. Wagner-Meerwein Rearrangement of Duocarmycins. *Chem. Pharm. Bull.* **1996**, *44* (5), 933–939.
- (41) Tercel, M.; Denny, W. A.; Wilson, W. R. Nitrogen and Sulfur Analogues of the SecoCl Alkylating Agent: Synthesis and Cytotoxicity. *Bioorg. Med. Chem. Lett.* **1996**, *6* (22), 2735–2740. [https://doi.org/10.1016/S0960-894X\(96\)00507-0](https://doi.org/10.1016/S0960-894X(96)00507-0).
- (42) Atwell, G. J.; Wilson, W. R.; Denny, W. A. Synthesis and Cytotoxicity of Amino Analogues of the Potent DNA Alkylating Agent Seco-CBI-TMI. *Bioorg. Med. Chem. Lett.* **1997**, *7* (12), 1493–1496. <https://doi.org/10.1021/jm990136b>.
- (43) Boger, D. L.; Bollinger, B.; Hertzog, D. L.; Johnson, D. S.; Cai, H.; Mesini, P.; Garbaccio, R. M.; Jin, Q.; Kitos, P. A. Reversed and Sandwiched Analogs of Duocarmycin SA: Establishment of the Origin of the Sequence-Selective Alkylation of DNA and New Insights into the Source of Catalysis. *J. Am. Chem. Soc.* **1997**, *119* (21), 4987–4998. <https://doi.org/10.1021/ja9637210>.
- (44) Boger, D. L.; Garbaccio, R. M.; Jin, Q. Synthesis and Evaluation of CC-1065 and Duocarmycin Analogues Incorporating the Iso-Cl and Iso-CBI Alkylation Subunits: Impact of Relocation of the C-4 Carbonyl. *J. Org. Chem.* **1997**, *62* (25), 8875–8891. <https://doi.org/10.1021/jo971686p>.
- (45) Boger, D. L.; Hertzog, D. L.; Bollinger, B.; Johnson, D. S.; Cai, H.; Goldberg, J.; Turnbull, P. Duocarmycin SA Shortened, Simplified, and Extended Agents: A Systematic Examination of the Role of the DNA Binding Subunit. *J. Am. Chem. Soc.* **1997**, *119* (21), 4977–4986. <https://doi.org/10.1021/ja9637208>.
- (46) Boger, D. L.; McKie, J. A.; Boyce, C. W. Asymmetric Synthesis of the CBI Alkylation Subunit of the CC-1065 and Duocarmycin'

- Analogs. *Synlett* **1997**, 515–517. <https://doi.org/10.1055/s-1997-6110>.
- (47) Boger, D. L.; Turnbull, P. Synthesis and Evaluation of CC-1065 and Duocarmycin Analogs Incorporating the 1,2,3,4,11,11a-Hexahydrocyclopropa[c]Naphtho[2,1- b]Azepin-6-One (CNA) Alkylation Subunit: Structural Features That Govern Reactivity and Reaction Regioselectivity. *J. Org. Chem.* **1997**, *62* (17), 5849–5863. <https://doi.org/10.1021/jo9707085>.
- (48) Muratake, H.; Hayakawa, A.; Natsume, M. A Novel Phenol-Forming Reaction for Preparation of Benzene, Furan, and Thiophene Analogs of CC-1065/Duocarmycin Pharmacophores. *Tet. Lett.* **1997**, *38* (43), 7577–7580. [https://doi.org/10.1016/S0040-4039\(97\)01786-3](https://doi.org/10.1016/S0040-4039(97)01786-3).
- (49) Shishido, K.; Haruna, S.; Yamamura, C.; Iitsuka, H.; Nemoto, H.; Shinohara, Y.; Shibuya, M. Synthesis and Evaluation of the Hybrid Molecules Possessing DNA-Cleaving Activity. *Bioorg. Med. Chem. Lett.* **1997**, *7* (20), 2617–2622. [https://doi.org/10.1016/S0960-894X\(97\)10030-0](https://doi.org/10.1016/S0960-894X(97)10030-0).
- (50) Atwell, G. J.; Tercel, M.; Boyd, M.; Wilson, W. R.; Denny, W. A. Synthesis and Cytotoxicity of 5-Amino-1-(Chloromethyl)-3-[(5,6,7-Trimethoxyindol-2-Yl)Carbonyl]-1,2-Dihydro-3 H -Benz[e]Indole (Amino- s Eco -CBI-TMI) and Related 5-Alkylamino Analogues: New DNA Minor Groove Alkylating Agents. *J. Org. Chem.* **1998**, *63* (25), 9414–9420. <https://doi.org/10.1021/jo981395w>.
- (51) Boger, D. L.; Boyce, C. W.; Garbaccio, R. M.; Searcey, M. Synthesis of CC-1065 and Duocarmycin Analogs via Intramolecular Aryl Radical Cyclization of a Tethered Vinyl Chloride. *Tet. Lett.* **1998**, *39* (16), 2227–2230. [https://doi.org/10.1016/S0040-4039\(98\)00232-9](https://doi.org/10.1016/S0040-4039(98)00232-9).
- (52) Boger, D. L.; Santillán, A.; Searcey, M.; Jin, Q. Critical Role of the Linking Amide in CC-1065 and the Duocarmycins: Implications on the Source of DNA Alkylation Catalysis. *J. Am. Chem. Soc.* **1998**, *120* (45), 11554–11557. <https://doi.org/10.1021/ja9818093>.
- (53) Boger, D. L.; Turnbull, P. Synthesis and Evaluation of a Carbocyclic Analogue of the CC-1065 and Duocarmycin Alkylation Subunits: Role of the Vinyllogous Amide and Implications on DNA Alkylation Catalysis. *J. Org. Chem.* **1998**, *63* (22), 8004–8011. <https://doi.org/10.1021/jo981698g>.
- (54) Fukuda, Y.; Furuta, H.; Kusama, Y.; Ebisu, H.; Oomori, Y.; Terashima, S. The Novel Cyclopropapyrroloindole (CPI) Bisalkylators Bearing Methoxycarbonyl and Trifluoromethyl Groups. *Bioorg. Med. Chem. Lett.* **1998**, *8* (11), 1387–1390. [https://doi.org/10.1016/S0960-894X\(98\)00235-2](https://doi.org/10.1016/S0960-894X(98)00235-2).
- (55) Fukuda, Y.; Seto, S.; Furuta, H.; Ebisu, H.; Oomori, Y.; Terashima, S. The Novel Cyclopropapyrroloindole (CPI) Bisalkylators Bearing 3,3'-(1,4-Phenylene)Diacyloyl Group as a Linker. *Bioorg. Med. Chem. Lett.* **1998**, *8* (15), 2003–2004. [https://doi.org/10.1016/S0960-894X\(98\)00346-1](https://doi.org/10.1016/S0960-894X(98)00346-1).
- (56) Nagamura, S.; Saito, H. Antitumor Antibiotics: Duocarmycins. *Chem. Heterocycl. Comp.* **1998**, *34* (12), 1386–1405. <https://doi.org/10.1007/BF02317808>.
- (57) Tercel, M.; Denny, W. A. Synthesis of Nitrogen and Sulfur Analogues of the Seco-CI Alkylating Agent. *J. Chem. Soc. Perkin Trans. 1* **1998**, No. 3, 509–520. <https://doi.org/10.1039/a706165j>.
- (58) Amishiro, N.; Nagamura, S.; Kobayashi, E.; Okamoto, A.; Gomi, K.; Saito, H. Synthesis and Antitumor Activity of Duocarmycin Derivatives: A-Ring Pyrrole Compounds Bearing 5-Membered Heteroarylacryloyl Groups. *Chem. Pharm. Bull.* **1999**, *47* (10), 1393–1403.
- (59) Amishiro, N.; Okamoto, A.; Murakata, C.; Tamaoki, T.; Okabe, M.; Saito, H. Synthesis and Antitumor Activity of Duocarmycin Derivatives: Modification of Segment-A of A-Ring Pyrrole Compounds. *J. Med. Chem.* **1999**, *42* (15), 2946–2960. <https://doi.org/10.1021/jm990094r>.
- (60) Atwell, G. J.; Milbank, J. J. B.; Wilson, W. R.; Hogg, A.; Denny, W. A. 5-Amino-1-(Chloromethyl)-1,2-Dihydro-3 H -Benz[e]Indoles: Relationships between Structure and Cytotoxicity for Analogues Bearing Different DNA Minor Groove Binding Subunits. *J. Med. Chem.* **1999**, *42* (17), 3400–3411. <https://doi.org/10.1021/jm990136b>.
- (61) Baraldi, P. G.; Cacciari, B.; Boyce, C. W.; Boger, D. L. Resolution of a CPZl Precursor, Synthesis and Biological Evaluation of (+) and (-)-N-Boc-CPZl: A Further Validation of the Relationship between Chemical Solvolytic Stability and Cytotoxicity. *Bioorg. Med. Chem. Lett.* **1999**, *9* (21), 3087–3092. [https://doi.org/10.1016/S0960-894X\(99\)00533-8](https://doi.org/10.1016/S0960-894X(99)00533-8).
- (62) Boger, D. L. CBI Prodrug Analogs of CC-1065 and the Duocarmycins. *Synthesis* **1999**, 1999 (S1), 1505–1509. <https://doi.org/10.1055/s-1999-3658>.
- (63) Boger, D. L. Iso-CBI and Iso-CI Analogs of CC-1065 and the Duocarmycins. WO 99/19298, April 22, 1999.
- (64) Boger, D. L.; Garbaccio, R. M. A Novel Class of CC-1065 and Duocarmycin Analogues Subject to Mitomycin-Related Reductive Activation. *J. Org. Chem.* **1999**, *64* (22), 8350–8362. <https://doi.org/10.1021/jo991301y>.
- (65) Boger, D. L.; Garbaccio, R. M. Shape-Dependent Catalysis: Insights into the Source of Catalysis for the CC-1065 and Duocarmycin DNA Alkylation Reaction. *Acc. Chem. Res.* **1999**, *32* (12), 1043–1052. <https://doi.org/10.1021/ar9800946>.
- (66) Fukuda, Y.; Furuta, H.; Kusama, Y.; Ebisu, H.; Oomori, Y.; Terashima, S. Novel Cyclopropapyrroloindole Derivative (AT-3510) Bearing Methoxycarbonyl and Trifluoromethyl Groups. *J. Med. Chem.* **1999**, *42* (8), 1448–1458. <https://doi.org/10.1021/jm980668c>.
- (67) Jia, G.; Iida, H.; William Lown, J. Synthesis of an Unsymmetrical Bis-Lexitropsin-1,2,9,9a-Tetrahydrocyclopropa[c]Benzo[e]Indol-4-One (CBI) Conjugate. *Chem. Commun.* **1999**, No. 2, 119–120. <https://doi.org/10.1039/a807884j>.
- (68) Milbank, J. B. J.; Tercel, M.; Atwell, G. J.; Wilson, W. R.; Hogg, A.; Denny, W. A. Synthesis of 1-Substituted 3-(Chloromethyl)-6-Aminoindoline (6-Amino- Seco -CI) DNA Minor Groove Alkylating Agents and Structure-Activity Relationships for Their Cytotoxicity. *J. Med. Chem.* **1999**, *42* (4), 649–658. <https://doi.org/10.1021/jm980545s>.
- (69) Tao, Z.-F.; Fujiwara, T.; Saito, I.; Sugiyama, H. Rational Design of Sequence-Specific DNA Alkylating Agents Based on Duocarmycin A and Pyrrole-Imidazole Hairpin Polyamides. *J. Am. Chem. Soc.* **1999**, *121* (21), 4961–4967. <https://doi.org/10.1021/ja983398w>.
- (70) Tao, Z.-F.; Fujiwara, T.; Saito, I.; Sugiyama, H. Sequence-Specific DNA Alkylation by Hybrid Molecules between Segment A of Duocarmycin A and Pyrrole-Imidazole Diamide. *Angew. Chem. Int. Ed.* **1999**, *38* (5), 650–653. [https://doi.org/10.1002/\(SICI\)1521-3773\(19990301\)38:5<650::AID-ANIE650>3.0.CO;2-O](https://doi.org/10.1002/(SICI)1521-3773(19990301)38:5<650::AID-ANIE650>3.0.CO;2-O).
- (71) Amishiro, N.; Nagamura, S.; Kobayashi, E.; Okamoto, A.; Gomi, K.; Okabe, M.; Saito, H. Synthesis and Antitumor Activity of Duocarmycin Derivatives: A-Ring Pyrrole Compounds Bearing β -(5H,6H,7H-Trimethoxy-2H-Indolyl)Acryloyl Group. *Bioorg. Med. Chem.* **2000**, *8*, 1637–1643. [https://doi.org/10.1016/S0968-0896\(00\)00086-9](https://doi.org/10.1016/S0968-0896(00)00086-9).
- (72) Amishiro, N.; Nagamura, S.; Murakata, C.; Okamoto, A.; Kobayashi, E.; Asada, M.; Gomi, K.; Tamaoki, T.; Okabe, M.; Yamaguchi, N.; Yamaguchi, K.; Saito, H. Synthesis and Antitumor Activity of Duocarmycin Derivatives: Modification at C-8 Position of A-Ring Pyrrole Compounds Bearing the Simplified DNA-Binding Groups. *Bioorg. Med. Chem.* **2000**, *8* (2), 381–391. [https://doi.org/10.1016/S0968-0896\(99\)00293-X](https://doi.org/10.1016/S0968-0896(99)00293-X).
- (73) Amishiro, N.; Okamoto, A.; Okabe, M.; Saito, H. Synthesis and Antitumor Activity of Duocarmycin Derivatives: Modification at the C-7 Position of Segment-A of A-Ring Pyrrole Compounds. *Bioorg. Med. Chem.* **2000**, *8*, 1195–1201.
- (74) Boger, D. L.; Boyce, C. W. Selective Metal Cation Activation of a DNA Alkylating Agent: Synthesis and Evaluation of Methyl 1,2,9,9a-Tetrahydrocyclopropa[c]Pyrido[3,2- e]Indol-4-One-7-Carboxylate (CPyl). *J. Org. Chem.* **2000**, *65* (13), 4088–4100. <https://doi.org/10.1021/jo000177b>.
- (75) Boger, D. L.; Fink, B. E.; Hedrick, M. P. A New Class of Highly Cytotoxic Diketopiperazines. *Bioorg. Med. Chem. Lett.* **2000**, *10* (10), 1019–1020. [https://doi.org/10.1016/S0960-894X\(00\)00152-9](https://doi.org/10.1016/S0960-894X(00)00152-9).
- (76) Boger, D. L.; Santillán, A.; Searcey, M.; Brunette, S. R.; Wolkenberg, S. E.; Hedrick, M. P.; Jin, Q. Synthesis and Evaluation of 1,2,8,8a-Tetrahydrocyclopropa[c]Pyrrolo[3,2- e]Indol-4(5 H)-One, the Parent Alkylation Subunit of CC-1065 and the Duocarmycins: Impact of the Alkylation Subunit Substituents and Its

- Implications for DNA Alkylation Catalysis. *J. Org. Chem.* **2000**, *65* (13), 4101–4111. <https://doi.org/10.1021/jo000297j>.
- (77) Boger, D. L.; Searcey, M.; Tse, W. C.; Jin, Q. Bifunctional Alkylating Agents Derived from Duocarmycin SA: Potent Antitumor Activity with Altered Sequence Selectivity. *Bioorg. Med. Chem. Lett.* **2000**, *10* (5), 495–498. [https://doi.org/10.1016/S0960-894X\(00\)00042-1](https://doi.org/10.1016/S0960-894X(00)00042-1).
- (78) Boger, D. L.; Wolkenberg, S. E.; Boyce, C. W. A New Method of In Situ Activation for a Novel Class of DNA Alkylating Agents: Tunable Metal Cation Complexation and Activation. *J. Am. Chem. Soc.* **2000**, *122* (26), 6325–6326. <https://doi.org/10.1021/ja000653f>.
- (79) Chang, A. Y.; Dervan, P. B. Strand Selective Cleavage of DNA by Diastereomers of Hairpin Polyamide- Seco -CBI Conjugates. *J. Am. Chem. Soc.* **2000**, *122* (20), 4856–4864. <https://doi.org/10.1021/ja994345x>.
- (80) Fukuda, Y.; Terashima, S. Intermediates for the Preparation of Duocarmycin SA and Derivatives Thereof, and Process for the Production of the Intermediates. US006066742A, May 23, 2000.
- (81) Jia, G.; Iida, H.; Lown, J. W. Solid-Phase Synthesis of 1-Chloromethyl-1,2-Dihydro-3 H -Benz[e]Indole (Seco -CBI) and a Polyamide Conjugate. *Synlett* **2000**, *2000* (05), 0603–0606. <https://doi.org/10.1055/s-2000-6631>.
- (82) Jia, G.; Lown, J. W. Design, Synthesis and Cytotoxicity Evaluation of 1-Chloromethyl-5-Hydroxy-1,2-Dihydro-3H -Benz[e]Indole (Seco-CBI) Dimers. *Bioorg. Med. Chem.* **2000**, *8* (7), 1607–1617. [https://doi.org/10.1016/S0968-0896\(00\)00088-2](https://doi.org/10.1016/S0968-0896(00)00088-2).
- (83) Muratake, H.; Hayakawa, A.; Natsume, M. Preparation of Benzene, Furan, and Thiophene Analogs of Duocarmycin SA Employing a Newly-Devised Phenol-Forming Reaction. *Chem. Pharm. Bull.* **2000**, *48* (10), 1558–1566. <https://doi.org/10.1248/cpb.48.1558>.
- (84) Tao, Z.-F.; Saito, I.; Sugiyama, H. Highly Cooperative DNA Dialkylation by the Homodimer of Imidazole–Pyrrole Diamide–CPI Conjugate with Vinyl Linker. *J. Am. Chem. Soc.* **2000**, *122* (8), 1602–1608. <https://doi.org/10.1021/ja9926212>.
- (85) Wang, Y.; Yuan, H.; Ye, W.; Wright, S. C.; Wang, H.; Larrick, J. W. Synthesis and Preliminary Biological Evaluations of CC-1065 Analogues: Effects of Different Linkers and Terminal Amides on Biological Activity. *J. Med. Chem.* **2000**, *43* (8), 1541–1549. <https://doi.org/10.1021/jm990514c>.
- (86) Bando, T.; Iida, H.; Saito, I.; Sugiyama, H. Sequence-Specific DNA Interstrand Cross-Linking by Imidazole–Pyrrole CPI Conjugate. *J. Am. Chem. Soc.* **2001**, *123* (21), 5158–5159. <https://doi.org/10.1021/ja003660c>.
- (87) Baraldi, P. G.; Balboni, G.; Pavani, M. G.; Spalluto, G.; Tabrizi, M. A.; Clercq, E. D.; Balzarini, J.; Bando, T.; Sugiyama, H.; Romagnoli, R. Design, Synthesis, DNA Binding, and Biological Evaluation of Water-Soluble Hybrid Molecules Containing Two Pyrazole Analogues of the Alkylating Cyclopropylpyrroloindole (CPI) Subunit of the Antitumor Agent CC-1065 and Polypyrrole Minor Groove Binders. *J. Med. Chem.* **2001**, *44* (16), 2536–2543. <https://doi.org/10.1021/jm0108404>.
- (88) Boger, D. L.; Brunette, S. R.; Garbaccio, R. M. Synthesis and Evaluation of a Series of C3-Substituted CBI Analogues of CC-1065 and the Duocarmycins. *J. Org. Chem.* **2001**, *66* (15), 5163–5173. <https://doi.org/10.1021/jo010309g>.
- (89) Boger, D. L.; Hughes, T. V.; Hedrick, M. P. Synthesis, Chemical Properties, and Biological Evaluation of CC-1065 and Duocarmycin Analogues Incorporating the 5-Methoxycarbonyl-1,2,9,9a-Tetrahydrocyclopropa[c]Benz[e]Indol-4-One Alkylation Subunit. *J. Org. Chem.* **2001**, *66* (7), 2207–2216. <https://doi.org/10.1021/jo001772g>.
- (90) Boger, D. L.; Schmitt, H. W.; Fink, B. E.; Hedrick, M. P. Parallel Synthesis and Evaluation of 132 (+)-1,2,9,9a-Tetrahydrocyclopropa[c]Benz[e]Indol-4-One (CBI) Analogues of CC-1065 and the Duocarmycins Defining the Contribution of the DNA-Binding Domain. *J. Org. Chem.* **2001**, *66* (20), 6654–6661. <https://doi.org/10.1021/jo010454u>.
- (91) Boger, D. L.; Stauffer, F.; Hedrick, M. P. Substituent Effects within the DNA Binding Subunit of CBI Analogues of the Duocarmycins and CC-1065. *Bioorg. Med. Chem. Lett.* **2001**, *11* (15), 2021–2024. [https://doi.org/10.1016/S0960-894X\(01\)00372-9](https://doi.org/10.1016/S0960-894X(01)00372-9).
- (92) Castedo, L.; Delamano, J.; Enjo, J.; Fernández, J.; Grávalos, D. G.; Leis, R.; López, C.; Marcos, C. F.; Ríos, A.; Tojo, G. Derivatives of Methyl 5-Methyl-4-Oxo-1,2,4,5,8,8a-Hexahydrocyclopropa[c]-Pyrrolo[3,2- e]Indole-7- Carboxylate: A Case of Inverse Electronic Effects on the Reactivity of CC-1065 Derivatives. *J. Am. Chem. Soc.* **2001**, *123* (21), 5102–5103. <https://doi.org/10.1021/ja005704n>.
- (93) Ellis, D. A.; Wolkenberg, S. E.; Boger, D. L. Metal Cation Complexation and Activation of Reversed CPyl Analogues of CC-1065 and Duocarmycin SA: Partitioning the Effects of Binding and Catalysis. *J. Am. Chem. Soc.* **2001**, *123* (38), 9299–9306. <https://doi.org/10.1021/ja010769f>.
- (94) Fukuda, Y.; Seto, S.; Furuta, H.; Ebisu, H.; Oomori, Y.; Terashima, S. Novel Seco Cyclopropa[c]Pyrrolo[3,2- e]Indole Bisalkylatrs Bearing a 3,3'-Arylenebisacryloyl Group as a Linker. *J. Med. Chem.* **2001**, *44*, 1396–1406. <https://doi.org/10.1021/jm000107x>.
- (95) Jennings, S. A.; Toth, J. L.; Roller, S. G.; Brooks, N.; O'Hare, C.; Kiakos, K.; Hartley, J. A.; Burke, P. J.; Lee, M. Efficient Synthesis of (+)-Seco-Cyclopropaneindoline Analogs of CC-1065. *Heterocyc. Commun.* **2001**, *7* (1). <https://doi.org/10.1515/HC.2001.7.1.7>.
- (96) Bando, T.; Narita, A.; Saito, I.; Sugiyama, H. Molecular Design of a Pyrrole–Imidazole Hairpin Polyamides for Effective DNA Alkylation. *Chem. Eur. J.* **2002**, *8* (20), 4781–4790. [https://doi.org/10.1002/1521-3765\(20021018\)8:20<4781::AID-CHEM4781>3.0.CO;2-J](https://doi.org/10.1002/1521-3765(20021018)8:20<4781::AID-CHEM4781>3.0.CO;2-J).
- (97) Boger, D. L. Synthesis of CC-1065/Duocarmycin Analogs. US 2002/0082424 A1, 2002.
- (98) Howard, T. T.; Lingerfelt, B. M.; Purnell, B. L.; Scott, A. E.; Price, C. A.; Townes, H. M.; McNulty, L.; Handl, H. L.; Summerville, K.; Hudson, S. J.; Bowen, J. P.; Kiakos, K.; Hartley, J. A.; Lee, M. Novel Furano Analogues of Duocarmycin C1 and C2: Design, Synthesis, and Biological Evaluation of Seco-Iso-Cyclopropylfuran[2,3- e]Indoline (Seco-Iso-CFI) and Seco-Cyclopropyltetrahydrofuran[2,3- f]Quinoline (Seco-CFQ) Analogues. *Bioorg. Med. Chem.* **2002**, *10* (9), 2941–2952. [https://doi.org/10.1016/S0968-0896\(02\)00157-8](https://doi.org/10.1016/S0968-0896(02)00157-8).
- (99) Kumar, R.; Lown, J. W. Design and Synthesis of Bis 1-Chloromethyl-5-Hydroxy-1,2-Dihydro-3 H -Benz[e]Indole (s Eco -CBI)-Pyrrole Polyamide Conjugates. *Org. Lett.* **2002**, *4* (11), 1851–1854. <https://doi.org/10.1021/ol020047k>.
- (100) Toth, J. L.; Price, C. A.; Madsen, E. C.; Handl, H. L.; Hudson, S. J.; Hubbard, III, R. B.; Bowen, J. P.; Kiakos, K.; Hartley, J. A.; Lee, M. Sequence Selective Recognition of DNA by Hairpin Conjugates of a Racemic Seco-Cyclopropaneindoline-2-Benzofurancarboxamide and Polyamides. *Bioorg. Med. Chem. Lett.* **2002**, *12*, 2245–2248. [https://doi.org/10.1016/s0960-894x\(02\)00341-4](https://doi.org/10.1016/s0960-894x(02)00341-4).
- (101) Yang, S.; Denny, W. A. A New Short Synthesis of 3-Substituted 5-Amino-1-(Chloromethyl)-1,2-Dihydro-3 H -Benzo[e]Indoles (Amino-CBIs). *J. Org. Chem.* **2002**, *67* (25), 8958–8961. <https://doi.org/10.1021/jo0263115>.
- (102) Bando, T.; Iida, H.; Tao, Z.-F.; Narita, A.; Fukuda, N.; Yamori, T.; Sugiyama, H. Sequence Specificity, Reactivity, and Antitumor Activity of DNA-Alkylating Pyrrole-Imidazole Diamides. *Chem. & Biol.* **2003**, *10* (8), 751–758. [https://doi.org/10.1016/S1074-5521\(03\)00160-1](https://doi.org/10.1016/S1074-5521(03)00160-1).
- (103) Bando, T.; Narita, A.; Saito, I.; Sugiyama, H. Highly Efficient Sequence-Specific DNA Interstrand Cross-Linking by Pyrrole/Imidazole CPI Conjugates. *J. Am. Chem. Soc.* **2003**, *125* (12), 3471–3485. <https://doi.org/10.1021/ja028459b>.
- (104) Kumar, R.; Lown, J. W. Synthesis and Cytotoxicity Evaluation of Novel C7–C7, C7–N3 and N3–N3 Dimers of 1-Chloromethyl-5-Hydroxy-1,2-Dihydro-3H-Benzo[e]Indole (Seco-CBI) with Pyrrole and Imidazole Polyamide Conjugates. *Org. Biomol. Chem.* **2003**, *1* (15), 2630–2647. <https://doi.org/10.1039/B303650M>.
- (105) Lee, M. Compositions and Methods of the Use Thereof Achiral Analogues of CC-1065 and the Duocarmycins. US20030073731A1, April 17, 2003.
- (106) Narita, A.; Bando, T.; Sugiyama, H. Molecular Design of Hairpin Pyrrole-Imidazole Polyamides Possessing Sequence Specific DNA Alkylating Moiety. *Nucl. Acid. Symp. Ser.* **2003**, *3* (1), 119–120. <https://doi.org/10.1093/nass/3.1.119>.

- (107) Oyoshi, T.; Kawakami, W.; Narita, A.; Bando, T.; Sugiyama, H. Inhibition of Transcription at a Coding Sequence by Alkylating Polyamide. *J. Am. Chem. Soc.* **2003**, *125* (16), 4752–4754. <https://doi.org/10.1021/ja029196v>.
- (108) Parrish, J. P.; Kastrinsky, D. B.; Hwang, I.; Boger, D. L. Synthesis and Evaluation of Duocarmycin and CC-1065 Analogues Incorporating the 1,2,9,9a-Tetrahydrocyclopropa[c]Benz[e]-3-Azaindol-4-One (CBA) Alkylation Subunit. *J. Org. Chem.* **2003**, *68* (23), 8984–8990. <https://doi.org/10.1021/jo035119f>.
- (109) Parrish, J. P.; Kastrinsky, D. B.; Stauffer, F.; Hedrick, M. P.; Hwang, I.; Boger, D. L. Establishment of Substituent Effects in the DNA Binding Subunit of CBI Analogues of the Duocarmycins and CC-1065. *Bioorg. Med. Chem.* **2003**, *11* (17), 3815–3838. [https://doi.org/10.1016/S0968-0896\(03\)00194-9](https://doi.org/10.1016/S0968-0896(03)00194-9).
- (110) Tietze, L. F.; Looft, J.; Feuerstein, T. Synthesis of Ring Size Seco-Analogs of the Antitumor Antibiotic CC-1065 by Two Consecutive Transition Metal-Initiated Transformations. *Eur. J. Org. Chem.* **2003**, *2003* (15), 2749–2755. <https://doi.org/10.1002/ejoc.200300077>.
- (111) Wang, Y.; Li, L.; Ye, W.; Tian, Z.; Jiang, W.; Wang, H.; Wright, S. C.; Larrick, J. W. CC-1065 Analogues Bearing Different DNA-Binding Subunits: Synthesis, Antitumor Activity, and Preliminary Toxicity Study. *J. Med. Chem.* **2003**, *46*, 634–637. <https://doi.org/10.1021/jm0203433>.
- (112) Bando, T.; Narita, A.; Asada, K.; Ayame, H.; Sugiyama, H. Enantioselective DNA Alkylation by a Pyrrole–Imidazole S -CBI Conjugate. *J. Am. Chem. Soc.* **2004**, *126* (29), 8948–8955. <https://doi.org/10.1021/ja049398f>.
- (113) Bando, T.; Narita, A.; Iwai, A.; Kihara, K.; Sugiyama, H. C–H to N Substitution Dramatically Alters the Sequence-Specific DNA Alkylation, Cytotoxicity, and Expression of Human Cancer Cell Lines. *J. Am. Chem. Soc.* **2004**, *126* (11), 3406–3407. <https://doi.org/10.1021/ja0387103>.
- (114) Boger, D. L. CBI Analogues of the Duocarmycins and CC-1065. WO 2004/101767 A2, 2004.
- (115) Cimino, P.; Improta, R.; Bifulco, G.; Riccio, R.; Gomez-Paloma, L.; Barone, V. Nucleophilic Cyclopropane Ring Opening in Duocarmycin SA Derivatives by Methanol under Acid Conditions: A Quantum Mechanical Study in the Gas-Phase and in Solution. *J. Org. Chem.* **2004**, *69* (8), 2816–2824. <https://doi.org/10.1021/jo0303517>.
- (116) Ham, Y.-W.; Boger, D. L. A Powerful Selection Assay for Mixture Libraries of DNA Alkylating Agents. *J. Am. Chem. Soc.* **2004**, *126* (30), 9194–9195. <https://doi.org/10.1021/ja0477930>.
- (117) Hiroya, K.; Matsumoto, S.; Sakamoto, T. New Synthetic Method for Indole-2-Carboxylate and Its Application to the Total Synthesis of Duocarmycin SA. *Org. Lett.* **2004**, *6* (17), 2953–2956. <https://doi.org/10.1021/ol0489548>.
- (118) Kastrinsky, D. B.; Boger, D. L. Effective Asymmetric Synthesis of 1,2,9,9a-Tetrahydrocyclopropa[c]Benzo[e]Indol-4-One (CBI). *J. Org. Chem.* **2004**, *69* (7), 2284–2289. <https://doi.org/10.1021/jo035465x>.
- (119) Kupchinsky, S.; Centioni, S.; Howard, T.; Trzupke, J.; Roller, S.; Carnahan, V.; Townes, H.; Purnell, B.; Price, C.; Handl, H.; Summerville, K.; Johnson, K.; Toth, J.; Hudson, S.; Kiakos, K.; Hartley, J. A.; Lee, M. A Novel Class of Achiral Seco-Analogs of CC-1065 and the Duocarmycins: Design, Synthesis, DNA Binding, and Anticancer Properties. *Bioorg. Med. Chem.* **2004**, *12* (23), 6221–6236. <https://doi.org/10.1016/j.bmc.2004.08.051>.
- (120) Pati, H.; Forrest, L.; Townes, H.; Lingerfelt, B.; McNulty, L.; Lee, M. Unexpected Syntheses of Seco-Cyclopropyltetrahydroquinolines >From a Radical 5-Exo-Trig Cyclization Reaction: Analogs of CC-1065 and the Duocarmycins. *Molecules* **2004**, *9* (3), 125–133. <https://doi.org/10.3390/90300125>.
- (121) Sugiyama, H.; Bando, T.; Saito, I. Novel Hairpin Polyamide. EP1491534A1, December 29, 2004.
- (122) Tichenor, M. S.; Kastrinsky, D. B.; Boger, D. L. Total Synthesis, Structure Revision, and Absolute Configuration of (+)-Yatakemycin. *J. Am. Chem. Soc.* **2004**, *126* (27), 8396–8398. <https://doi.org/10.1021/ja0472735>.
- (123) Al-Said, N.; Shawakfeh, K.; Abdullah, W. Cyclization of Free Radicals at the C-7 Position of Ethyl Indole-2-Carboxylate Derivatives: An Entry to a New Class of Duocarmycin Analogues. *Molecules* **2005**, *10* (12), 1446–1457. <https://doi.org/10.3390/10121446>.
- (124) Bando, T.; Narita, A.; Sasaki, S.; Sugiyama, H. Specific Adenine Alkylation by Pyrrole–Imidazole CBI Conjugates. *J. Am. Chem. Soc.* **2005**, *127* (40), 13890–13895. <https://doi.org/10.1021/ja052412l>.
- (125) Boger, D. L. CBI Analogues of CC-1065 and the Duocarmycins. US 20050014700A1, January 20, 2005.
- (126) Daniell, K.; Stewart, M.; Madsen, E.; Le, M.; Handl, H.; Brooks, N.; Kiakos, K.; Hartley, J. A.; Lee, M. Design, Synthesis, and Biological Evaluation of Achiral Analogs of Duocarmycin SA. *Bioorg. Med. Chem. Lett.* **2005**, *15* (1), 177–180. <https://doi.org/10.1016/j.bmcl.2004.10.021>.
- (127) Nelson, S. M.; Ferguson, L. R.; Denny, W. A. Demonstration by Real-Time Polymerase Chain Reaction That Cellular DNA Alkylation by Novel Aminindoline Compounds Affects Expression of the Protooncogene c-Myc. *Chem. Res. Toxicol.* **2005**, *18* (2), 239–248. <https://doi.org/10.1021/tx049852t>.
- (128) Price, C. A.; Lingerfelt, B. M.; Handl, H. L.; Kiakos, K.; Hartley, J. A.; Lee, M. Sequence Specific Recognition of DNA by Tailor-Made Hairpin Conjugates of Achiral Seco-Cyclopropaneindoline-2-Benzofurancarboxamide and Pyrrole–Imidazole Polyamides. *Bioorg. Med. Chem. Lett.* **2005**, *15* (12), 3151–3156. <https://doi.org/10.1016/j.bmcl.2005.04.006>.
- (129) Sato, A.; McNulty, L.; Cox, K.; Kim, S.; Scott, A.; Daniell, K.; Summerville, K.; Price, C.; Hudson, S.; Kiakos, K.; Hartley, J. A.; Asao, T.; Lee, M. A Novel Class of In Vivo Active Anticancer Agents: Achiral Seco -Amino- and Seco -Hydroxycyclopropylbenz[e]Indolone (Seco -CBI) Analogues of the Duocarmycins and CC-1065. *J. Med. Chem.* **2005**, *48* (11), 3903–3918. <https://doi.org/10.1021/jm050179u>.
- (130) Shinohara, K.-I.; Sasaki, S.; Bando, T.; Sugiyama, H. Sequence-Specific Gene Silencing by Alkylating Py-Im Polyamide. *Nucl. Acid. Symp. Ser.* **2005**, *49*, 75–76.
- (131) Toth, J.; Trzupke, J.; Flores, L.; Kiakos, K.; Hartley, J. A.; Pennington, W.; Lee, M. A Novel Achiral Seco-Amino-Cyclopropylindoline (CI) Analog of CC-1065 and the Duocarmycins: Design, Synthesis and Biological Studies. *Med. Chem.* **2005**, *1* (1), 13–19. <https://doi.org/10.2174/1573406053402523>.
- (132) Bando, T.; Sasaki, S.; Minoshima, M.; Dohno, C.; Shinohara, K.; Narita, A.; Sugiyama, H. Efficient DNA Alkylation by a Pyrrole–Imidazole CBI Conjugate with an Indole Linker: Sequence-Specific Alkylation with Nine-Base-Pair Recognition. *Bioconjugate Chem.* **2006**, *17* (3), 715–720. <https://doi.org/10.1021/bc060022w>.
- (133) Hartley, J.; Lee, M.; Kiakos, K.; Hudson, S.; Townes, H.; Summerville, K.; Scott, A.; Lingerfelt, B.; Purnell, B. Novel (S)-(-) and R-(+)-Seco-Iso-Cyclopropylfuran[e]Indoline-5,6,7-Trimethoxyindole-2-Carboxamide (Iso-CFI) Analogues of Duocarmycin C2: Synthesis and Biological Evaluation. *Med. Chem.* **2006**, *2* (2), 139–146. <https://doi.org/10.2174/157340606776056188>.
- (134) Minoshima, M.; Sasaki, S.; Shinohara, K.; Shimizu, T.; Bando, T.; Sugiyama, H. Molecular Design of DNA Alkylating Pyrrole–Imidazole Polyamides with Longer Recognition Sequence. *Nucl. Acid. Symp. Ser.* **2006**, *50* (1), 165–166. <https://doi.org/10.1093/nass/nrl082>.
- (135) Purnell, B.; Sato, A.; O'Kelley, A.; Price, C.; Summerville, K.; Hudson, S.; O'Hare, C.; Kiakos, K.; Asao, T.; Lee, M.; Hartley, J. A. DNA Interstrand Crosslinking Agents: Synthesis, DNA Interactions, and Cytotoxicity of Dimeric Achiral Seco-Amino-CBI and Conjugates of Achiral Seco-Amino-CBI with Pyrrolbenzodiazepine (PBD). *Bioorg. Med. Chem. Lett.* **2006**, *16* (21), 5677–5681. <https://doi.org/10.1016/j.bmcl.2006.08.005>.
- (136) Sasaki, S.; Bando, T.; Minoshima, M.; Shimizu, T.; Shinohara, K.; Takaoka, T.; Sugiyama, H. Sequence-Specific Alkylation of Double-Strand Human Telomere Repeat Sequence by Pyrrole–Imidazole Polyamides with Indole Linkers. *J. Am. Chem. Soc.* **2006**, *128* (37), 12162–12168. <https://doi.org/10.1021/ja0626584>.
- (137) Sato, A.; Scott, A.; Asao, T.; Lee, M. Efficient Synthesis of Achiral s Eco -Cyclopropylbenz[2,3- e]Indoline Analogues: [4-

- Amino-2-(5,6,7-Trimethoxyindole-2-Carboxamido)Naphthalen-1-Yl]Ethyl Chloride and [4-Hydroxy-2-(5,6,7-Trimethoxyindole-2-Carboxamido)Naphthalen-1-Yl]Ethyl Chloride. *J. Org. Chem.* **2006**, *71* (12), 4692–4695. <https://doi.org/10.1021/jo060501o>.
- (138) Shimizu, T.; Sasaki, S.; Minoshima, M.; Shinohara, K.; Bando, T.; Sugiyama, H. Synthesis and Evaluation of Sequence-Specific DNA Alkylating Agents: Effect of Alkylation Subunits. *Nucl. Acid. Symp. Ser.* **2006**, *50* (1), 155–156. <https://doi.org/10.1093/nass/nrl077>.
- (139) Shinohara, K. -i. Alkylation of Template Strand of Coding Region Causes Effective Gene Silencing. *Nucl. Acid Res.* **2006**, *34* (4), 1189–1195. <https://doi.org/10.1093/nar/gkl005>.
- (140) Shinohara, K.; Bando, T.; Sasaki, S.; Sakakibara, Y.; Minoshima, M.; Sugiyama, H. Antitumor Activity of Sequence-Specific Alkylating Agents: Pyrrole-Imidazole CBI Conjugates with Indole Linker. *Cancer Sci.* **2006**, *97* (3), 219–225. <https://doi.org/10.1111/j.1349-7006.2006.00158.x>.
- (141) Tietze, L. F.; Major, F. Synthesis of New Water-Soluble DNA-Binding Subunits for Analogues of the Cytotoxic Antibiotic CC-1065 and Their Prodrugs. *Eur. J. Org. Chem.* **2006**, *2006* (10), 2314–2321. <https://doi.org/10.1002/ejoc.200500060>.
- (142) Ganton, M. D.; Kerr, M. A. Aryl Amidation Routes to Dihydropyrrolo[3,2- e]Indoles and Pyrrolo[3,2- f]Tetrahydroquinolines: Total Synthesis of the (±)-CC-1065 CPI Subunit. *J. Org. Chem.* **2007**, *72* (2), 574–582. <https://doi.org/10.1021/jo062064j>.
- (143) Kiakos, K.; Sato, A.; Asao, T.; McHugh, M. M.; Lee, M.; Hartley, J. A. DNA Sequence Selection of Adenine Alkylation, Mechanism of Adduct Repair, and in Vivo Antitumor Activity of the Novel Achiral Seco-Amino-Cyclopropylbenz[e]Indolone Analogue of Duocarmycin AS-I-145. *Mol. Cancer Ther.* **2007**, *6* (10), 2708–2718. <https://doi.org/10.1158/1535-7163.MCT-07-0294>.
- (144) Minoshima, M.; Sasaki, S.; Fujimoto, J.; Shinohara, K. -i.; Bando, T.; Sugiyama, H. Synthesis and Biological Properties of Pyrrole-Imidazole Polyamide Conjugates. *Nucl. Acid. Symp. Ser.* **2007**, *51* (1), 35–36. <https://doi.org/10.1093/nass/nrm018>.
- (145) Minoshima, M.; Bando, T.; Sasaki, S.; Shinohara, K.; Shimizu, T.; Fujimoto, J.; Sugiyama, H. DNA Alkylation by Pyrrole-Imidazole Seco -CBI Conjugates with an Indole Linker: Sequence-Specific DNA Alkylation with 10-Base-Pair Recognition through Heterodimer Formation. *J. Am. Chem. Soc.* **2007**, *129* (17), 5384–5390. <https://doi.org/10.1021/ja065235a>.
- (146) Sasaki, S.; Minoshima, M.; Fujimoto, J.; Shinohara, K. -i.; Bando, T.; Sugiyama, H. Sequence-Specific Alkylation by a Tandem Motif of Pyrrole-Imidazole CBI Conjugate. *Nucl. Acid. Symp. Ser.* **2007**, *51* (1), 265–266. <https://doi.org/10.1093/nass/nrm133>.
- (147) Tichenor, M. S.; MacMillan, K. S.; Stover, J. S.; Wolkenberg, S. E.; Pavani, M. G.; Zanella, L.; Zaid, A. N.; Spalluto, G.; Rayl, T. J.; Hwang, I.; Baraldi, P. G.; Boger, D. L. Rational Design, Synthesis, and Evaluation of Key Analogues of CC-1065 and the Duocarmycins. *J. Am. Chem. Soc.* **2007**, *129* (45), 14092–14099. <https://doi.org/10.1021/ja073989z>.
- (148) Tichenor, M. S.; MacMillan, K. S.; Trzupke, J. D.; Rayl, T. J.; Hwang, I.; Boger, D. L. Systematic Exploration of the Structural Features of Yatakemycin Impacting DNA Alkylation and Biological Activity. *J. Am. Chem. Soc.* **2007**, *129* (35), 10858–10869. <https://doi.org/10.1021/ja072777z>.
- (149) Bando, T.; Minoshima, M.; Kashiwazaki, G.; Shinohara, K.; Sasaki, S.; Fujimoto, J.; Ohtsuki, A.; Murakami, M.; Nakazono, S.; Sugiyama, H. Requirement of β-Alanine Components in Sequence-Specific DNA Alkylation by Pyrrole-Imidazole Conjugates with Seven-Base Pair Recognition. *Bioorg. Med. Chem.* **2008**, *16* (5), 2286–2291. <https://doi.org/10.1016/j.bmc.2007.11.064>.
- (150) Kashiwazaki, G.; Bando, T.; Sugiyama, H. Sequence-Specific Alkylation of DNA by Pyrrole-Imidazole Polyamides through Cooperative Interaction. *Nucl. Acid. Symp. Ser.* **2008**, *52* (1), 365–366. <https://doi.org/10.1093/nass/nrm184>.
- (151) Minoshima, M.; Chou, J.; Lefebvre, S.; Bando, T.; Shinohara, K. -i.; Gottesfeld, J. M.; Sugiyama, H. Targeting Specific Gene by Alkylating Pyrrole-Imidazole Polyamides. *Nucl. Acid. Symp. Ser.* **2008**, *52* (1), 363–364. <https://doi.org/10.1093/nass/nrm183>.
- (152) Sasaki, S.; Bando, T.; Minoshima, M.; Shinohara, K.; Sugiyama, H. Sequence-Specific Alkylation by Y-Shaped and Tandem Hairpin Pyrrole-Imidazole Polyamides. *Chem. Eur. J.* **2008**, *14* (3), 864–870. <https://doi.org/10.1002/chem.200700571>.
- (153) Tietze, L. F.; Schuster, H. J.; Hampel, S. M.; Rühl, S.; Pfoh, R. Enantio- and Diastereoselective Synthesis of Duocarmycine-Based Prodrugs for a Selective Treatment of Cancer by Epoxide Opening. *Chem. Eur. J.* **2008**, *14* (3), 895–901. <https://doi.org/10.1002/chem.200700988>.
- (154) Gauss, C. M.; Hamasaki, A.; Parrish, J. P.; MacMillan, K. S.; Rayl, T. J.; Hwang, I.; Boger, D. L. Synthesis and Preliminary Evaluation of Duocarmycin Analogues Incorporating the 1,2,11,11a-Tetrahydrocyclopropa[c]Naphtho[2,3-e]Indol-4-One (CNI) and 1,2,11,11a-Tetrahydrocyclopropa[c]Naphtho[1,2-e]Indol-4-One (Iso-CNI) Alkylation Subunits. *Tetrahedron* **2009**, *65* (33), 6591–6599. <https://doi.org/10.1016/j.tet.2009.02.065>.
- (155) MacMillan, K. S.; Lajiness, J. P.; Cara, C. L.; Romagnoli, R.; Robertson, W. M.; Hwang, I.; Baraldi, P. G.; Boger, D. L. Synthesis and Evaluation of a Thio Analogue of Duocarmycin SA. *Bioorg. Med. Chem. Lett.* **2009**, *19* (24), 6962–6965. <https://doi.org/10.1016/j.bmcl.2009.10.063>.
- (156) MacMillan, K. S.; Nguyen, T.; Hwang, I.; Boger, D. L. Total Synthesis and Evaluation of Iso -Duocarmycin SA and Iso -Yatakemycin. *J. Am. Chem. Soc.* **2009**, *131* (3), 1187–1194. <https://doi.org/10.1021/ja808108g>.
- (157) Minoshima, M.; Bando, T.; Shinohara, K. -i.; Sugiyama, H. Molecular Design of Sequence Specific DNA Alkylating Agents. *Nucl. Acid. Symp. Ser.* **2009**, *53* (1), 69–70. <https://doi.org/10.1093/nass/nrp035>.
- (158) Neo, A. G.; Pérez, A.; López, C.; Castedo, L.; Tojo, G. Photocyclization of Tosylstilbenes as a Key Reaction in the Preparation of an Analogue of the Antitumor Agent CC-1065. *J. Org. Chem.* **2009**, *74* (8), 3203–3206. <https://doi.org/10.1021/jo900140i>.
- (159) Boyle, K. E.; MacMillan, K. S.; Ellis, D. A.; Lajiness, J. P.; Robertson, W. M.; Boger, D. L. Synthesis and Evaluation of Duocarmycin SA Analogs Incorporating the Methyl 1,2,8,8a-Tetrahydrocyclopropa[c]Oxazolo[2,3-e]Indol-4-One-6-Carboxylate (COI) Alkylation Subunit. *Bioorg. Med. Chem. Lett.* **2010**, *20* (6), 1854–1857. <https://doi.org/10.1016/j.bmcl.2010.01.145>.
- (160) Chavda, S.; Babu, B.; Yanow, S. K.; Jardim, A.; Spithill, T. W.; Kiakos, K.; Kluzza, J.; Hartley, J. A.; Lee, M. A Novel Achiral Seco-Cyclopropylpyrido[e]Indolone (CPyl) Analog of CC-1065 and the Duocarmycins: Synthesis, DNA Interactions, in Vivo Anticancer and Anti-Parasitic Evaluation. *Bioorg. Med. Chem.* **2010**, *18* (14), 5016–5024. <https://doi.org/10.1016/j.bmc.2010.05.078>.
- (161) Frecentese, F.; Fiorino, F.; Perissutti, E.; Severino, B.; Magli, E.; Esposito, A.; De Angelis, F.; Massarelli, P.; Nencini, C.; Viti, B.; Santagada, V.; Caliendo, G. Efficient Microwave Combinatorial Synthesis of Novel Indolic Arylpiperazine Derivatives as Serotonergic Ligands. *Eur. J. Med. Chem.* **2010**, *45* (2), 752–759. <https://doi.org/10.1016/j.ejmech.2009.11.023>.
- (162) Lajiness, J. P.; Boger, D. L. Synthesis and Characterization of a Cyclobutane Duocarmycin Derivative Incorporating the 1,2,10,11-Tetrahydro-9 H -Cyclobuta[c]Benzo[e]Indol-4-One (CbBI) Alkylation Subunit. *J. Am. Chem. Soc.* **2010**, *132* (39), 13936–13940. <https://doi.org/10.1021/ja106986f>.
- (163) Minoshima, M.; Bando, T.; Shinohara, K.; Kashiwazaki, G.; Nishijima, S.; Sugiyama, H. Comparative Analysis of DNA Alkylation by Conjugates between Pyrrole-Imidazole Hairpin Polyamides and Chlorambucil or Seco-CBI. *Bioorg. Med. Chem.* **2010**, *18* (3), 1236–1243. <https://doi.org/10.1016/j.bmc.2009.12.033>.
- (164) Minoshima, M.; Chou, J. C.; Lefebvre, S.; Bando, T.; Shinohara, K.; Gottesfeld, J. M.; Sugiyama, H. Potent Activity against K562 Cells by Polyamide-Seco-CBI Conjugates Targeting Histone H4 Genes. *Bioorg. Med. Chem.* **2010**, *18* (1), 168–174. <https://doi.org/10.1016/j.bmc.2009.11.005>.
- (165) Robertson, W. M.; Kastrinsky, D. B.; Hwang, I.; Boger, D. L. Synthesis and Evaluation of a Series of C5-Substituted Duocarmycin SA Analogs. *Bioorg. Med. Chem. Lett.* **2010**, *20* (9), 2722–2725. <https://doi.org/10.1016/j.bmcl.2010.03.078>.
- (166) Shinohara, K.-I.; Bando, T.; Sugiyama, H. Anticancer Activities of Alkylating Pyrrole-Imidazole Polyamides with Specific

- Sequence Recognition. *Anti-Cancer Drugs* **2010**, *21* (3), 228–242. <https://doi.org/10.1097/CAD.0b013e328334d8f9>.
- (167) Sugiyama, H.; Bando, T. Indole Derivative for Alkylating Specific Base Sequence of DNA and Alkylating Agent and Drug Containing the Derivative. US007745473B2, June 29, 2010.
- (168) Heinrich, D. M.; Youte, J.-J.; Denny, W. A.; Tercel, M. A New Enantioselective Approach to the Core Structure of Hypoxia Selective Prodrugs Related to the Duocarmycins. *Tet. Lett.* **2011**, *52* (51), 7000–7003. <https://doi.org/10.1016/j.tetlet.2011.10.105>.
- (169) Lajiness, J. P.; Boger, D. L. Asymmetric Synthesis of 1,2,9,9a-Tetrahydrocyclopropa[*c*]Benzo[*e*]Indol-4-One (CBI). *J. Org. Chem.* **2011**, *76* (2), 583–587. <https://doi.org/10.1021/jo102136w>.
- (170) Kashiwazaki, G.; Bando, T.; Yoshidome, T.; Masui, S.; Takagaki, T.; Hashiya, K.; Pandian, G. N.; Yasuoka, J.; Akiyoshi, K.; Sugiyama, H. Synthesis and Biological Properties of Highly Sequence-Specific-Alkylating *N*-Methylpyrrole-*N*-Methylimidazole Polyamide Conjugates. *J. Med. Chem.* **2012**, *55* (5), 2057–2066. <https://doi.org/10.1021/jm201225z>.
- (171) Rayburn, E.; Wang, W.; Li, M.; Zhang, X.; Xu, H.; Li, H.; Qin, J.-J.; Jia, L.; Covey, J.; Lee, M.; Zhang, R. Preclinical Pharmacology of Novel Indolecarboxamide ML-970, an Investigative Anticancer Agent. *Cancer Chemother. Pharmacol.* **2012**, *69* (6), 1423–1431. <https://doi.org/10.1007/s00280-012-1851-9>.
- (172) Takagaki, T.; Bando, T.; Sugiyama, H. Synthesis of Pyrrole-Imidazole Polyamide Seco-1-Chloromethyl-5-Hydroxy-1,2-Dihydro-3H-benz[*e*]Indole Conjugates with a Vinyl Linker Recognizing a 7 bp DNA Sequence. *J. Am. Chem. Soc.* **2012**, *134*, 13074–13081. <https://doi.org/10.1021/ja3044294>.
- (173) Neo, A. G.; López, C.; López, A.; Castedo, L.; Tojo, G. Studies on the Synthesis of a Hindered Analogue of the Antitumor Agent CC-1065. *Tetrahedron* **2013**, *69* (51), 11010–11016. <https://doi.org/10.1016/j.tet.2013.10.012>.
- (174) Patil, P.; Cousins, K.; Smith, M.; Wieskamp, S.; Ferrara, M.; Bruce, C. D.; Lee, M. Controlling the Radical 5-Exo-Trig Cyclization, and Selective Synthesis of Seco-Iso-Cyclopropylfurano[*e*]Indoline (Seco-Iso-CFI) and Seco-Cyclopropylthiophene[*e*]Indoline (Seco-CTI) DNA Alkylating Subunit of the Duocarmycins. *Tet. Lett.* **2013**, *54* (35), 4756–4759. <https://doi.org/10.1016/j.tetlet.2013.06.116>.
- (175) Wolfe, A. L.; Duncan, K. K.; Lajiness, J. P.; Zhu, K.; Duerfeldt, A. S.; Boger, D. L. A Fundamental Relationship between Hydrophobic Properties and Biological Activity for the Duocarmycin Class of DNA-Alkylating Antitumor Drugs: Hydrophobic-Binding-Driven Bonding. *J. Med. Chem.* **2013**, *56* (17), 6845–6857. <https://doi.org/10.1021/jm400665c>.
- (176) Patil, P. C.; Lee, M. An Efficient Synthesis of Furano Analogs of Duocarmycin C1 and C2: Seco-Iso-Cyclopropylfurano[*e*]Indoline-Trimethoxyindole and Seco-Cyclopropylfurano[*f*]Quinoline-Trimethoxyindole. *Tet. Lett.* **2014**, *55* (21), 3283–3285. <https://doi.org/10.1016/j.tetlet.2014.04.062>.
- (177) Taylor, R. D.; Asamitsu, S.; Takenaka, T.; Yamamoto, M.; Hashiya, K.; Kawamoto, Y.; Bando, T.; Nagase, H.; Sugiyama, H. Sequence-Specific DNA Alkylation Targeting for Kras Codon 13 Mutation by Pyrrole-Imidazole Polyamide Seco-CBI Conjugates. *Chem. Eur. J.* **2014**, *20* (5), 1310–1317. <https://doi.org/10.1002/chem.201303295>.
- (178) Taylor, R. D.; Kawamoto, Y.; Hashiya, K.; Bando, T.; Sugiyama, H. Sequence-Specific DNA Alkylation by Tandem Py-Im Polyamide Conjugates. *Chem. Asian J.* **2014**, *9* (9), 2527–2533. <https://doi.org/10.1002/asia.201402331>.
- (179) Tercel, M.; Pruijn, F. B.; O'Connor, P. D.; Liyanage, H. D. S.; Atwell, G. J.; Alix, S. M. Mechanism of Action of AminoCBIs: Highly Reactive but Highly Cytotoxic Analogues of the Duocarmycins. *ChemBioChem* **2014**, *15* (13), 1998–2006. <https://doi.org/10.1002/cbic.201402256>.
- (180) Yamamoto, M.; Bando, T.; Kawamoto, Y.; Taylor, R. D.; Hashiya, K.; Sugiyama, H. Specific Alkylation of Human Telomere Repeat Sequences by a Tandem-Hairpin Motif of Pyrrole-Imidazole Polyamides with Indole- Seco-CBI. *Bioconjugate Chem.* **2014**, *25* (3), 552–559. <https://doi.org/10.1021/bc400567m>.
- (181) Hiraoka, K.; Inoue, T.; Taylor, R. D.; Watanabe, T.; Koshikawa, N.; Yoda, H.; Shinohara, K.; Takatori, A.; Sugimoto, H.; Maru, Y.; Denda, T.; Fujiwara, K.; Balmain, A.; Ozaki, T.; Bando, T.; Sugiyama, H.; Nagase, H. Inhibition of KRAS Codon 12 Mutants Using a Novel DNA-Alkylating Pyrrole-Imidazole Polyamide Conjugate. *Nat. Comm.* **2015**, *6* (1), 6706. <https://doi.org/10.1038/ncomms7706>.
- (182) Stephenson, M. J.; Howell, L. A.; O'Connell, M. A.; Fox, K. R.; Adcock, C.; Kingston, J.; Sheldrake, H.; Pors, K.; Collingwood, S. P.; Searcey, M. Solid-Phase Synthesis of Duocarmycin Analogues and the Effect of C-Terminal Substitution on Biological Activity. *J. Org. Chem.* **2015**, *80* (19), 9454–9467. <https://doi.org/10.1021/acs.joc.5b01373>.
- (183) Taylor, R. D.; Chandran, A.; Kashiwazaki, G.; Hashiya, K.; Bando, T.; Nagase, H.; Sugiyama, H. Selective Targeting of the KRAS Codon 12 Mutation Sequence by Pyrrole-Imidazole Polyamide Seco-CBI Conjugates. *Chem. Eur. J.* **2015**, *21* (42), 14996–15003. <https://doi.org/10.1002/chem.201501870>.
- (184) Twum, E. A.; Nathubhai, A.; Wood, P. J.; Lloyd, M. D.; Thompson, A. S.; Threadgill, M. D. Initial Development of a Cytotoxic Amino-Seco-CBI Warhead for Delivery by Prodrug Systems. *Bioorg. Med. Chem.* **2015**, *23* (13), 3481–3489. <https://doi.org/10.1016/j.bmc.2015.04.034>.
- (185) Chanda, P. B.; Boyle, K. E.; Brody, D. M.; Shukla, V.; Boger, D. L. Synthesis and Evaluation of Duocarmycin SA Analogs Incorporating the Methyl 1,2,8,8a-Tetrahydrocyclopropa[*c*]imidazo[4,5-*e*]indol-4-One-6-Carboxylate (Ciml) Alkylation Subunit. *Bioorg. Med. Chem.* **2016**, *24* (20), 4779–4786. <https://doi.org/10.1016/j.bmc.2016.04.050>.
- (186) Guo, C.; Asamitsu, S.; Kashiwazaki, G.; Sato, S.; Bando, T.; Sugiyama, H. DNA Interstrand Crosslinks by H-Pin Polyamide (S)-Seco-CBI Conjugates. *ChemBioChem* **2017**, *18* (2), 166–170. <https://doi.org/10.1002/cbic.201600425>.
- (187) Stephenson, M. J.; Howell, L. A.; Searcey, M. Synthesis of Duocarmycin Analogues. US009765077B2, September 19, 2017.
- (188) Kiakos, K.; Englinger, B.; Yanow, S. K.; Wernitznig, D.; Jakupec, M. A.; Berger, W.; Keppler, B. K.; Hartley, J. A.; Lee, M.; Patil, P. C. Design, Synthesis, Nuclear Localization, and Biological Activity of a Fluorescent Duocarmycin Analog, HxTfA. *Bioorg. Med. Chem. Lett.* **2018**, *28* (8), 1342–1347. <https://doi.org/10.1016/j.bmcl.2018.03.016>.
- (189) Wang, S.; Chen, B.; Dragovich, P.; Pillow, T.; Staben, L.; Guo, J.; Su, D.; Zhang, C.; Bobba, S.; Ma, Y.; Wang, J.; Sangaraju, D.; Wei, B.; Phillips, G. L.; Khojasteh, C.; Zhang, D. A Novel Depurination Methodology to Assess DNA Alkylation of Chloro-Bis-Seco-Cyclopropylbenzoindoles Allowed for Comparison of Minor-Groove Reactivity. *Drug Metab Dispos* **2019**, *47* (5), 547–555. <https://doi.org/10.1124/dmd.118.085209>.
- (190) Maeda, R.; Ito, S.; Hashiya, K.; Bando, T.; Sugiyama, H. DNA Alkylation of the RUNX-Binding Sequence by CBI-PI Polyamide Conjugates**. *Chem. Eur. J.* **2020**, *26* (64), 14639–14644. <https://doi.org/10.1002/chem.202002166>.
- (191) Maeda, R.; Bando, T.; Sugiyama, H. Application of DNA-Alkylating Pyrrole-Imidazole Polyamides for Cancer Treatment. *ChemBioChem* **2021**, *22* (9), 1538–1545. <https://doi.org/10.1002/cbic.202000752>.

(2) prodrugs/bifunctionals (102 items - 84 journal publications, 18 patents)

- (1) Nagamura, S.; Asai, A.; Kanda, Y.; Kobayashi, E.; Gomi, K.; Saito, H. Synthesis and Antitumor Activity of Duocarmycin Derivatives: Modification of Segment A of Duocarmycin B2. *Chem. Pharm. Bull.* **1996**, *44* (9), 1723–1730. <https://doi.org/10.1248/cpb.44.1723>.
- (2) Nagamura, S.; Kobayashi, E.; Gomi, K.; Saito, H. Synthesis and Antitumor Activity of Duocarmycin Derivatives: A-Ring Pyrrole Analogues of Duocarmycin B2. *Bioorg. Med. Chem.* **1996**, *4* (8), 1379–1391. [https://doi.org/10.1016/0968-0896\(96\)00132-0](https://doi.org/10.1016/0968-0896(96)00132-0).

- (3) Boger, D. L.; Han, N. CC-1065/Duocarmycin and Bleomycin A2 Hybrid Agents: Lack of Enhancement of DNA Alkylation by Attachment to Noncomplementary DNA Binding Subunits. *Bioorg. Med. Chem.* **1997**, *5* (2), 233–243. [https://doi.org/10.1016/S0968-0896\(96\)00237-4](https://doi.org/10.1016/S0968-0896(96)00237-4).
- (4) Nagamura, S.; Asai, A.; Amishiro, N.; Kobayashi, E.; Gomi, K.; Saito, H. Synthesis and Antitumor Activity of Duocarmycin Derivatives: A-Ring Pyrrole Compounds Bearing Cinnamoyl Groups. *J. Med. Chem.* **1997**, *40* (6), 972–979. <https://doi.org/10.1021/jm9606094>.
- (5) Nagamura, S.; Asai, A.; Kobayashi, E.; Gomi, K.; Saito, H. Studies on Duocarmycin SA and Its Derivatives. *Bioorg. Med. Chem.* **1997**, *5* (3), 623–630. [https://doi.org/10.1016/S0968-0896\(96\)00276-3](https://doi.org/10.1016/S0968-0896(96)00276-3).
- (6) Powell, M. J. Cyclopropylindole Prodrugs. US005646298A, July 8, 1997.
- (7) Denny, W. A.; Tercel, M.; Atwell, G. J.; Milbank, J. B. J. Precursors of Cyclopropylindoles and Their Use as Prodrugs. AU199854192B2, March 9, 1998.
- (8) Larrick, J. W.; Wang, Y.; Wright, S. C. DNA-Binding Indole Derivatives, Their Prodrugs and Immunoconjugates as Anticancer Agents. US995843937A, December 1, 1998.
- (9) Amishiro, N.; Nagamura, S.; Kobayashi, E.; Gomi, K.; Saito, H. New Water-Soluble Duocarmycin Derivatives: Synthesis and Antitumor Activity of A-Ring Pyrrole Compounds Bearing β -Heteroarylacryloyl Groups. *J. Med. Chem.* **1999**, *42* (4), 669–676. <https://doi.org/10.1021/jm980559v>.
- (10) Asai, A.; Nagamura, S.; Kobayashi, E.; Gomi, K.; Saito, H. Synthesis and Antitumor Activity of Water-Soluble Duocarmycin B1 Prodrugs. *Bioorg. Med. Chem. Lett.* **1999**, *9* (20), 2995–2998. [https://doi.org/10.1016/S0960-894X\(99\)00518-1](https://doi.org/10.1016/S0960-894X(99)00518-1).
- (11) Denny, W. A.; Tercel, M. Cyclopropylindoles and Their Seco Precursors, and Their Use as Prodrugs. US005985909A, November 16, 1999.
- (12) Denny, W. A.; Tercel, M.; Atwell, G. J. Cyclopropylindole Compounds and Their Use as Prodrugs. EP0938474B1, September 1, 1999.
- (13) Hay, M. P.; Sykes, B. M.; Denny, W. A.; Wilson, W. R. A 2-Nitroimidazole Carbamate Prodrug of 5-Amino-1-(Chloromethyl)-3-[[5,6,7-Trimethoxyindol-2-yl]Carbonyl]-1,2-Dihydro-3H-Benz[e]Indole (Amino-Seco-CBI-TMI) for Use with ADEPT and GDEPT. *Bioorg. Med. Chem. Lett.* **1999**, *9*, 2237–2242. [https://doi.org/10.1016/S0960-894X\(99\)00381-9](https://doi.org/10.1016/S0960-894X(99)00381-9).
- (14) Tercel, M.; Gieseg, M. A.; Denny, W. A.; Wilson, W. R. Synthesis and Cytotoxicity of Amino-Seco-DISA: An Amino Analogue of the DNA Alkylating Agent Duocarmycin SA. *J. Org. Chem.* **1999**, *64*, 5946–5953. <https://doi.org/10.1021/jo990464j>.
- (15) Denny, W. A.; Tercel, M.; Atwell, G. J. Condensed N-Acylindoles as Antitumor Agents. US006130237A, Oc 2000.
- (16) Denny, W. A.; Tercel, M.; Atwell, G. J.; Milbank, J. B. Seco Precursors of Cyclopropylindolines and Their Use as Prodrugs. US006251933B1, June 26, 2001.
- (17) Tietze, L. F.; Herzig, T.; Fecher, A.; Hauernt, F.; Schuberth, I. Highly Selective Glycosylated Prodrugs of Cytostatic CC-1065 Analogues for Antibody-Directed Enzyme Tumor Therapy. *ChemBioChem* **2001**, *2* (10), 758. [https://doi.org/10.1002/1439-7633\(20011001\)2:10<758::AID-CBIC758>3.0.CO;2-G](https://doi.org/10.1002/1439-7633(20011001)2:10<758::AID-CBIC758>3.0.CO;2-G).
- (30) Yongxin, R.; Chari, R. V. J. CC-1065 Analogs Synthesis. US006534660B1, March 18, 2003.
- (31) Zhao, R. Y.; Chari, R. V. J. Prodrugs of CC-1065 Analogs. US007655660B2, June 29, 2004.
- (32) Ahn, G.-O.; Botting, K. J.; Patterson, A. V.; Ware, D. C.; Tercel, M.; Wilson, W. R. Radiolytic and Cellular Reduction of a Novel Hypoxia-Activated Cobalt(III) Prodrug of a Chloromethylbenzindoline DNA Minor Groove Alkylator. *Biochem. Pharm.* **2006**, *71* (12), 1683–1694. <https://doi.org/10.1016/j.bcp.2006.03.007>.
- (33) Tietze, L. F.; Krewer, B.; Frauendorf, H.; Major, F.; Schuberth, I. Investigation of Reactivity and Selectivity of DNA-Alkylating
- (18) Tietze, L. F.; Lieb, M.; Herzig, T.; Hauernt, F.; Schuberth, I. A Strategy for Tumor-Selective Chemotherapy by Enzymatic Liberation of Seco-Duocarmycin SA-Derivatives from Nontoxic Prodrugs. *Bioorg. Med. Chem.* **2001**, *9* (7), 1929–1939. [https://doi.org/10.1016/S0968-0896\(01\)00098-0](https://doi.org/10.1016/S0968-0896(01)00098-0).
- (19) Wang, Y.; Yuan, H.; Wright, S. C.; Wang, H.; Larrick, J. W. Synthesis and Preliminary Cytotoxicity Study of a Cephalosporin-CC-1065 Analogue Prodrug. *BMC Chem. Bio.* **2001**, *1*, 4–8.
- (20) Zhou, Q.; Duan, W.; Simmons, D.; Shayo, Y.; Raymond, M. A.; Dorr, R. T.; Hurley, L. H. Design and Synthesis of a Novel DNA–DNA Interstrand Adenine–Guanine Cross-Linking Agent. *J. Am. Chem. Soc.* **2001**, *123* (20), 4865–4866. <https://doi.org/10.1021/ja005658r>.
- (21) Tietze, L. F.; Feuerstein, T.; Fecher, A.; Hauernt, F.; Panknin, O.; Borchers, U.; Schuberth, I.; Alves, F. Proof of Principle in the Selective Treatment of Cancer by Antibody-Directed Enzyme Prodrug Therapy: The Development of a Highly Potent Prodrug. *Angew. Chem. Int. Ed.* **2002**, *41* (5), 759. [https://doi.org/10.1002/1521-3773\(20020301\)41:5<759::AID-ANIE759>3.0.CO;2-7](https://doi.org/10.1002/1521-3773(20020301)41:5<759::AID-ANIE759>3.0.CO;2-7).
- (22) Tietze, L. F.; Herzig, T.; Feuerstein, T.; Schuberth, I. Synthesis and Biological Evaluation of Novel Analogues and Prodrugs of the Cytotoxic Antibiotic CC-1065 for Selective Cancer Therapy. *Eur. J. Org. Chem.* **2002**, *2002* (10), 1634–1645. [https://doi.org/10.1002/1099-0690\(200205\)2002:10<1634::AID-EJOC1634>3.0.CO;2-Y](https://doi.org/10.1002/1099-0690(200205)2002:10<1634::AID-EJOC1634>3.0.CO;2-Y).
- (23) Townes, H.; Summerville, K.; Purnell, B. L.; Hooker, M.; Madsen, E. C.; Hudson, S.; Lee, M. Investigation of a Novel Reductively-Activatable Anticancer Prodrug of Seco -CBI-TMI, an Analog of Duocarmycin SA. *Med. Chem. Res.* **2002**.
- (24) Wang, Y.-D.; Dziegielewski, J.; Chang, A. Y.; Dervan, P. B.; Beerman, T. A. Cell-Free and Cellular Activities of a DNA Sequence Selective Hairpin Polyamide-CBI Conjugate. *Journal of Biological Chemistry* **2002**, *277* (45), 42431–42437. <https://doi.org/10.1074/jbc.M207179200>.
- (25) Wang, Y.; Yuan, H.; Wright, S. C.; Wang, H.; Larrick, J. W. Synthesis and Cytotoxicity of a Biotinylated CC-1065 Analogue. *BMC Chem. Bio.* **2002**, *2*, 1–4. <https://doi.org/10.1186/1472-6769-2-1>.
- (26) Hay, M. P.; Anderson, R. F.; Ferry, D. M.; Wilson, W. R.; Denny, W. A. Synthesis and Evaluation of Nitroheterocyclic Carbamate Prodrugs for Use with Nitroreductase-Mediated Gene-Directed Enzyme Prodrug Therapy. *J. Med. Chem.* **2003**, *46* (25), 5533–5545. <https://doi.org/10.1021/jm030308b>.
- (27) Hay, M. P.; Atwell, G. J.; Wilson, W. R.; Pullen, S. M.; Denny, W. A. Structure–Activity Relationships for 4-Nitrobenzyl Carbamates of 5-Aminobenz[e]Indoline Minor Groove Alkylating Agents as Prodrugs for GDEPT in Conjunction with *E. c Oll* Nitroreductase. *J. Med. Chem.* **2003**, *46* (12), 2456–2466. <https://doi.org/10.1021/jm0205191>.
- (28) Tercel, M.; Stribbling, S. M.; Sheppard, H.; Siim, B. G.; Wu, K.; Pullen, S. M.; Botting, K. J.; Wilson, W. R.; Denny, W. A. Unsymmetrical DNA Cross-Linking Agents: Combination of the CBI and PBD Pharmacophores. *J. Med. Chem.* **2003**, *46* (11), 2132–2151. <https://doi.org/10.1021/jm020526p>.
- (29) Wang, Y.; Yuan, H.; Wright, S. C.; Wang, H.; Larrick, J. W. Synthesis and Preliminary Cytotoxicity Study of Glucuronide Derivatives of CC-1065 Analogues. *Bioorg. Med. Chem.* **2003**, *11* (7), 1569–1575. [https://doi.org/10.1016/S0968-0896\(02\)00603-X](https://doi.org/10.1016/S0968-0896(02)00603-X).
- Duocarmycin Analogues by High-Resolution Mass Spectrometry. *Angew. Chem. Int. Ed.* **2006**, *45* (39), 6570–6574. <https://doi.org/10.1002/anie.200600935>.
- (34) Tietze, L. F.; Major, F.; Schuberth, I. Antitumor Agents: Development of Highly Potent Glycosidic Duocarmycin Analogues for Selective Cancer Therapy. *Angew. Chem. Int. Ed.* **2006**, *45* (39), 6574–6577. <https://doi.org/10.1002/anie.200600936>.
- (35) Wang, Y.; Li, L.; Tian, Z.; Jiang, W.; Larrick, J. W. Synthesis and Antitumor Activity of CBI-Bearing Ester and Carbamate Prodrugs of CC-1065 Analogue. *Bioorg. Med. Chem.* **2006**, *14* (23), 7854–7861. <https://doi.org/10.1016/j.bmc.2006.07.062>.

- (36) Jin, W.; Trzuppek, J. D.; Rayl, T. J.; Broward, M. A.; Vielhauer, G. A.; Weir, S. J.; Hwang, I.; Boger, D. L. A Unique Class of Duocarmycin and CC-1065 Analogues Subject to Reductive Activation. *J. Am. Chem. Soc.* **2007**, *129* (49), 15391–15397. <https://doi.org/10.1021/ja075398e>.
- (37) Tietze, L. F.; Major, F.; Schuberth, I.; Spiegl, D. A.; Krewer, B.; Maksimenka, K.; Bringmann, G.; Magull, J. Selective Treatment of Cancer: Synthesis, Biological Evaluation and Structural Elucidation of Novel Analogues of the Antibiotic CC-1065 and the Duocarmycins. *Chem. Eur. J.* **2007**, *13* (16), 4396–4409. <https://doi.org/10.1002/chem.200700113>.
- (38) Gangwar, S.; Thang, Q. Methods and Compounds for Preparing CC-1065 Analogs. US 20080281102A1, November 13, 2008.
- (39) Tietze, L. F.; Panknin, O.; Major, F.; Krewer, B. Synthesis of a Novel Pentagastrin-Drug Conjugate for a Targeted Tumor Therapy. *Chem. Eur. J.* **2008**, *14* (9), 2811–2818. <https://doi.org/10.1002/chem.200701521>.
- (40) Tietze, L. F.; Schuster, H. J.; Schmuck, K.; Schuberth, I.; Alves, F. Duocarmycin-Based Prodrugs for Cancer Prodrug Monotherapy. *Bioorg. Med. Chem.* **2008**, *16* (12), 6312–6318. <https://doi.org/10.1016/j.bmc.2008.05.009>.
- (41) Tietze, L. F.; von Hof, J. M.; Krewer, B.; Müller, M.; Major, F.; Schuster, H. J.; Schuberth, I.; Alves, F. Asymmetric Synthesis and Biological Evaluation of Glycosidic Prodrugs for a Selective Cancer Therapy. *ChemMedChem* **2008**, *3* (12), 1946–1955. <https://doi.org/10.1002/cmdc.200800250>.
- (42) Tietze, L.; Panknin, O.; Krewer, B.; Major, F.; Schuberth, I. Synthesis and Biological Evaluation of a Novel Pentagastrin-Toxin Conjugate Designed for a Targeted Prodrug Monotherapy of Cancer. *Int. J. Mol. Sci.* **2008**, *9* (5), 821–837. <https://doi.org/10.3390/ijms9050821>.
- (43) Wang, Y.; Jiang, J.; Jiang, X.; Cai, S.; Han, H.; Li, L.; Tian, Z.; Jiang, W.; Zhang, Z.; Xiao, Y.; Wright, S. C.; Larrick, J. W. Synthesis and Antitumor Activity Evaluations of Albumin-Binding Prodrugs of CC-1065 Analog. *Bioorg. Med. Chem.* **2008**, *16* (13), 6552–6559. <https://doi.org/10.1016/j.bmc.2008.05.025>.
- (44) Milbank, J. B. J.; Stevenson, R. J.; Ware, D. C.; Chang, J. Y. C.; Tercel, M.; Ahn, G.-O.; Wilson, W. R.; Denny, W. A. Synthesis and Evaluation of Stable Bidentate Transition Metal Complexes of 1-(Chloromethyl)-5-Hydroxy-3-(5,6,7-Trimethoxyindol-2-Ylcarbonyl)-2,3-Dihydro-1H-Pyrrolo[3,2-f]Quinoline (Seco-6-Aza-CBI-TMI) as Hypoxia Selective Cytotoxins. *J. Med. Chem.* **2009**, *52* (21), 6822–6834. <https://doi.org/10.1021/jm9008746>.
- (45) Tercel, M.; Atwell, G. J.; Yang, S.; Stevenson, R. J.; Botting, K. J.; Boyd, M.; Smith, E.; Anderson, R. F.; Denny, W. A.; Wilson, W. R.; Pruijn, F. B. Hypoxia-Activated Prodrugs: Substituent Effects on the Properties of Nitro Seco-1,2,9,9a-Tetrahydrocyclopropa[*c*]Benz[e]Indol-4-One (NitroCBI) Prodrugs of DNA Minor Groove Alkylating Agents. *J. Med. Chem.* **2009**, *52* (22), 7258–7272. <https://doi.org/10.1021/jm901202b>.
- (46) Tietze, L. F.; Krewer, B. Novel Analogues of CC-1065 and the Duocarmycins for the Use in Targeted Tumour Therapies. *Anti-Cancer Agents in Med. Chem.* **2009**, *9* (3), 304–325. <https://doi.org/10.2174/1871520610909030304>.
- (47) Tietze, L. F.; Schuster, H. J.; Krewer, B.; Schuberth, I. Synthesis and Biological Studies of Different Duocarmycin Based Glycosidic Prodrugs for Their Use in the Antibody-Directed Enzyme Prodrug Therapy. *J. Med. Chem.* **2009**, *52* (2), 537–543. <https://doi.org/10.1021/jm8009102>.
- (48) Tietze, L.; Krewer, B.; Von Hof, J. M.; Frauendorf, H.; Schuberth, I. Determination of the Biological Activity and Structure Activity Relationships of Drugs Based on the Highly Cytotoxic Duocarmycins and CC-1065. *Toxins* **2009**, *1* (2), 134–150. <https://doi.org/10.3390/toxins1020134>.
- (49) Wilson, W. R.; Stribbling, S. M.; Pruijn, F. B.; Syddall, S. P.; Patterson, A. V.; Liyanage, H. D. S.; Smith, E.; Botting, K. J.; Tercel, M. Nitro-Chloromethylbenzindolines: Hypoxia-Activated Prodrugs of Potent Adenine N 3 DNA Minor Groove Alkylators. *Mol. Cancer Ther.* **2009**, *8* (10), 2903–2913. <https://doi.org/10.1158/1535-7163.MCT-09-0571>.
- (50) Denny, W. A.; Wilson, W. R.; Stevenson, R. J.; Tercel, M.; Atwell, G. J.; Yang, S.; Patterson, A. V.; Pruijn, F. B. Nitrobenzindoles and Their Use in Cancer Therapy. US007718688B2, May 18, 2010.
- (51) Lajiness, J. P.; Robertson, W. M.; Dunwiddie, I.; Broward, M. A.; Vielhauer, G. A.; Weir, S. J.; Boger, D. L. Design, Synthesis, and Evaluation of Duocarmycin O-Amino Phenol Prodrugs Subject to Tunable Reductive Activation. *J. Med. Chem.* **2010**, *53* (21), 7731–7738. <https://doi.org/10.1021/jm1010397>.
- (52) Schuster, H. J.; Krewer, B.; von Hof, J. M.; Schmuck, K.; Schuberth, I.; Alves, F.; Tietze, L. F. Synthesis of the First Spacer Containing Prodrug of a Duocarmycin Analogue and Determination of Its Biological Activity. *Org. Biomol. Chem.* **2010**, *8* (8), 1833. <https://doi.org/10.1039/b925070k>.
- (53) Tercel, M.; Yang, S.; Atwell, G. J.; Smith, E.; Gu, Y.; Anderson, R. F.; Denny, W. A.; Wilson, W. R.; Pruijn, F. B. Hypoxic Selectivity and Solubility—Investigating the Properties of A-Ring Substituted Nitro Seco-1,2,9,9a-Tetrahydrocyclopropa[*c*]Benz[e]Indol-4-Ones (NitroCBIs) as Hypoxia-Activated Prodrugs for Antitumor Therapy. *Bioorg. Med. Chem.* **2010**, *18* (14), 4997–5006. <https://doi.org/10.1016/j.bmc.2010.06.001>.
- (54) Tietze, L. F.; Behrendt, F.; Major, F.; Krewer, B.; von Hof, J. M. Synthesis of Fluorescence-Labelled Glycosidic Prodrugs Based on the Cytotoxic Antibiotic Duocarmycin. *Eur. J. Org. Chem.* **2010**, *2010* (36), 6909–6921. <https://doi.org/10.1002/ejoc.201000966>.
- (55) Tietze, L. F.; von Hof, J. M.; Müller, M.; Krewer, B.; Schuberth, I. Glycosidic Prodrugs of Highly Potent Bifunctional Duocarmycin Derivatives for Selective Treatment of Cancer. *Angew. Chem. Int. Ed.* **2010**, *49* (40), 7336–7339. <https://doi.org/10.1002/anie.201002502>.
- (56) Ashoorzadeh, A.; Atwell, G. J.; Pruijn, F. B.; Wilson, W. R.; Tercel, M.; Denny, W. A.; Stevenson, R. J. The Effect of Sulfonate Leaving Groups on the Hypoxia-Selective Toxicity of Nitro Analogs of the Duocarmycins. *Bioorg. Med. Chem.* **2011**, *19* (16), 4851–4860. <https://doi.org/10.1016/j.bmc.2011.06.073>.
- (57) Boger, D. L. CBI Derivatives Subject to Reductive Activation. US 20110112163A1, May 12, 2011.
- (58) Lu, G.-L.; Stevenson, R. J.; Chang, J. Y.-C.; Brothers, P. J.; Ware, D. C.; Wilson, W. R.; Denny, W. A.; Tercel, M. N-Alkylated Cyclen Cobalt(III) Complexes of 1-(Chloromethyl)-3-(5,6,7-Trimethoxyindol-2-Ylcarbonyl)-2,3-Dihydro-1H-Pyrrolo[3,2-f]Quinolin-5-Ol DNA Alkylating Agent as Hypoxia-Activated Prodrugs. *Bioorg. Med. Chem.* **2011**, *19* (16), 4861–4867. <https://doi.org/10.1016/j.bmc.2011.06.076>.
- (59) Park, S.; Bando, T.; Shinohara, K.; Nishijima, S.; Sugiyama, H. Photocontrollable Sequence-Specific DNA Alkylation by a Pyrrole-Imidazole Polyamide Seco-CBI Conjugate. *Bioconjugate Chem.* **2011**, *22* (2), 120–124. <https://doi.org/10.1021/bc100352y>.
- (60) Pors, K.; Loadman, P. M.; Shnyder, S. D.; Sutherland, M.; Sheldrake, H. M.; Guino, M.; Kiakos, K.; Hartley, J. A.; Searcey, M.; Patterson, L. H. Modification of the Duocarmycin Pharmacophore Enables CYP1A1 Targeting for Biological Activity. *Chem. Commun.* **2011**, *47* (44), 12062. <https://doi.org/10.1039/c1cc15638a>.
- (61) Seubert, C. M.; Stritzker, J.; Hess, M.; Donat, U.; Sturm, J. B.; Chen, N.; Von Hof, J. M.; Krewer, B.; Tietze, L. F.; Gentschev, I.; Szalay, A. A. Enhanced Tumor Therapy Using Vaccinia Virus Strain GLV-1h68 in Combination with a β -Galactosidase-Activatable Prodrug Seco-Analog of Duocarmycin SA. *Cancer Gene Ther.* **2011**, *18* (1), 42–52. <https://doi.org/10.1038/cgt.2010.49>.
- (62) Stevenson, R. J.; Denny, W. A.; Ashoorzadeh, A.; Pruijn, F. B.; van Leeuwen, W. F.; Tercel, M. The Effect of a Bromide Leaving Group on the Properties of Nitro Analogs of the Duocarmycins as Hypoxia-Activated Prodrugs and Phosphate Pre-Prodrugs for Antitumor Therapy. *Bioorg. Med. Chem.* **2011**, *19* (20), 5989–5998. <https://doi.org/10.1016/j.bmc.2011.08.045>.
- (63) Takagaki, T.; Bando, T.; Kitano, M.; Hashiya, K.; Kashiwazaki, G.; Sugiyama, H. Evaluation of PI Polyamide Conjugates with Eight-Base Pair Recognition and Improvement of the Aqueous Solubility by PEGylation. *Bioorg. Med. Chem.* **2011**, *19*, 5896–5902. <https://doi.org/10.1016/j.bmc.2011.08.009>.
- (64) Tercel, M.; Atwell, G. J.; Yang, S.; Ashoorzadeh, A.; Stevenson, R. J.; Botting, K. J.; Gu, Y.; Mehta, S. Y.; Denny, W. A.; Wilson, W. R.; Pruijn, F. B. Selective Treatment of Hypoxic Tumor Cells In Vivo: Phosphate Pre-Prodrugs of Nitro Analogues of the Duocarmycins.

- Angew. Chem. Int. Ed.* **2011**, *50* (11), 2606–2609. <https://doi.org/10.1002/anie.201004456>.
- (65) Tercel, M.; Lee, H. H.; Yang, S.; Liyanage, H. D. S.; Mehta, S. Y.; Boyd, P. D. W.; Jaiswal, J. K.; Tan, K. L.; Pruijn, F. B. Preparation and Antitumour Properties of the Enantiomers of a Hypoxia-Selective Nitro Analogue of the Duocarmycins. *ChemMedChem* **2011**, *6* (10), 1860–1871. <https://doi.org/10.1002/cmdc.201100271>.
- (66) Tietze, L. F.; Schmuck, K.; Schuster, H. J.; Müller, M.; Schuberth, I. Synthesis and Biological Evaluation of Prodrugs Based on the Natural Antibiotic Duocarmycin for Use in ADEPT and PMT. *Chem. Eur. J.* **2011**, *17* (6), 1922–1929. <https://doi.org/10.1002/chem.201002798>.
- (67) Stevenson, R. J.; Denny, W. A.; Tercel, M.; Pruijn, F. B.; Ashoorzadeh, A. Nitro Seco Analogues of the Duocarmycins Containing Sulfonate Leaving Groups as Hypoxia-Activated Prodrugs for Cancer Therapy. *J. Med. Chem.* **2012**, *55* (6), 2780–2802. <https://doi.org/10.1021/jm201717y>.
- (68) Tietze, L. F.; Behrendt, F.; Pestel, G. F.; Schuberth, I.; Mitkovski, M. Synthesis, Biological Evaluation, and Live Cell Imaging of Novel Fluorescent Duocarmycin Analogs. *Chem. & Biodiv.* **2012**, *9* (11), 2559–2570. <https://doi.org/10.1002/cbdv.201200289>.
- (69) Wirth, T.; Schmuck, K.; Tietze, L. F.; Sieber, S. A. Duocarmycin Analogues Target Aldehyde Dehydrogenase 1 in Lung Cancer Cells. *Angew. Chem. Int. Ed.* **2012**, *51* (12), 2874–2877. <https://doi.org/10.1002/anie.201106334>.
- (70) Wolfe, A. L.; Duncan, K. K.; Parelkar, N. K.; Weir, S. J.; Vielhauer, G. A.; Boger, D. L. A Novel, Unusually Efficacious Duocarmycin Carbamate Prodrug That Releases No Residual Byproduct. *J. Med. Chem.* **2012**, *55* (12), 5878–5886. <https://doi.org/10.1021/jm300330b>.
- (71) Boger, D. L. Cyclic Prodrugs of Duocarmycin Analogs. WO 2013/148631 A1, October 3, 2013.
- (72) Chang, J. Y.-C.; Lu, G.-L.; Stevenson, R. J.; Brothers, P. J.; Clark, G. R.; Botting, K. J.; Ferry, D. M.; Tercel, M.; Wilson, W. R.; Denny, W. A.; Ware, D. C. Cross-Bridged Cyclen or Cyclam Co(III) Complexes Containing Cytotoxic Ligands as Hypoxia-Activated Prodrugs. *Inorg. Chem.* **2013**, *52* (13), 7688–7698. <https://doi.org/10.1021/ic4006967>.
- (73) Chen, K.-C.; Schmuck, K.; Tietze, L. F.; Roffler, S. R. Selective Cancer Therapy by Extracellular Activation of a Highly Potent Glycosidic Duocarmycin Analogue. *Mol. Pharm.* **2013**, *10* (5), 1773–1782. <https://doi.org/10.1021/mp300581u>.
- (74) Sheldrake, H. M.; Travica, S.; Johansson, I.; Loadman, P. M.; Sutherland, M.; Elsalem, L.; Illingworth, N.; Cresswell, A. J.; Reuillon, T.; Shnyder, S. D.; Mkrtchian, S.; Searcey, M.; Ingelman-Sundberg, M.; Patterson, L. H.; Pors, K. Re-Engineering of the Duocarmycin Structural Architecture Enables Bioprecursor Development Targeting CYP1A1 and CYP2W1 for Biological Activity. *J. Med. Chem.* **2013**, *56* (15), 6273–6277. <https://doi.org/10.1021/jm4000209>.
- (75) Tietze, L. F.; Müller, M.; Dufert, S.-C.; Schmuck, K.; Schuberth, I. Photoactivatable Prodrugs of Highly Potent Duocarmycin Analogues for a Selective Cancer Therapy. *Chem. Eur. J.* **2013**, *19* (5), 1726–1731. <https://doi.org/10.1002/chem.201202773>.
- (76) Tietze, L. F.; Sieber, S. A. Duocarmycin Analogues without a DNA-Binding Indole Unit Associate with Aldehyde Dehydrogenase 1A1 and Not DNA: A Reply. *Angew. Chem. Int. Ed.* **2013**, *52* (21), 5447–5449. <https://doi.org/10.1002/anie.201301923>.
- (77) Travica, S.; Pors, K.; Loadman, P. M.; Shnyder, S. D.; Johansson, I.; Alandas, M. N.; Sheldrake, H. M.; Mkrtchian, S.; Patterson, L. H.; Ingelman-Sundberg, M. Colon Cancer-Specific Cytochrome P450 2W1 Converts Duocarmycin Analogues into Potent Tumor Cytotoxins. *Clin. Cancer Res.* **2013**, *19* (11), 2952–2961. <https://doi.org/10.1158/1078-0432.CCR-13-0238>.
- (78) Vielhauer, G. A.; Swink, M.; Parelkar, N. K.; Lajiness, J. P.; Wolfe, A. L.; Boger, D. L. Evaluation of a Reductively Activated Duocarmycin Prodrug against Murine and Human Solid Cancers. *Cancer Biol. & Ther.* **2013**, *14* (6), 527–536. <https://doi.org/10.4161/cbt.24348>.
- (79) Wolfe, A. L.; Duncan, K. K.; Parelkar, N. K.; Brown, D.; Vielhauer, G. A.; Boger, D. L. Efficacious Cyclic N -Acyl O -Amino Phenol Duocarmycin Prodrugs. *J. Med. Chem.* **2013**, *56* (10), 4104–4115. <https://doi.org/10.1021/jm400413r>.
- (80) Hunter, F. W.; Jaiswal, J. K.; Hurley, D. G.; Liyanage, H. D. S.; McManaway, S. P.; Gu, Y.; Richter, S.; Wang, J.; Tercel, M.; Print, C. G.; Wilson, W. R.; Pruijn, F. B. The Flavoprotein FOXRED2 Reductively Activates Nitro-Chloromethylbenzindolines and Other Hypoxia-Targeting Prodrugs. *Biochemical Pharmacology* **2014**, *89* (2), 224–235. <https://doi.org/10.1016/j.bcp.2014.03.001>.
- (81) Krall, N.; Pretto, F.; Decurtins, W.; Bernardes, G. J. L.; Supuran, C. T.; Neri, D. A Small-Molecule Drug Conjugate for the Treatment of Carbonic Anhydrase IX Expressing Tumors. *Angew. Chem. Int. Ed.* **2014**, *53* (16), 4231–4235. <https://doi.org/10.1002/anie.201310709>.
- (82) Tercel, M.; McManaway, S. P.; Liyanage, H. D. S.; Pruijn, F. B. Preparation and Properties of Clickable Amino Analogues of the Duocarmycins: Factors That Affect the Efficiency of Their Fluorescent Labelling of DNA. *ChemMedChem* **2014**, *9* (9), 2193–2206. <https://doi.org/10.1002/cmdc.201402169>.
- (83) Uematsu, M.; Boger, D. L. Asymmetric Synthesis of a CBI-Based Cyclic N -Acyl O -Amino Phenol Duocarmycin Prodrug. *J. Org. Chem.* **2014**, *79* (20), 9699–9703. <https://doi.org/10.1021/jo501839x>.
- (84) Beusker, P. H. Water-Soluble CC-1065 Analogs and Their Conjugates. US008940784B2, January 27, 2015.
- (85) Koch, M. F.; Harteis, S.; Blank, I. D.; Pestel, G.; Tietze, L. F.; Ochsenfeld, C.; Schneider, S.; Sieber, S. A. Structural, Biochemical, and Computational Studies Reveal the Mechanism of Selective Aldehyde Dehydrogenase 1A1 Inhibition by Cytotoxic Duocarmycin Analogues. *Angew. Chem. Int. Ed.* **2015**, *54* (46), 13550–13554. <https://doi.org/10.1002/anie.201505749>.
- (86) Uematsu, M.; Brody, D. M.; Boger, D. L. A Five-Membered Lactone Prodrug of CBI-Based Analogs of the Duocarmycins. *Tet. Lett.* **2015**, *56* (23), 3101–3104. <https://doi.org/10.1016/j.tetlet.2014.11.038>.
- (87) Giddens, A. C.; Lee, H. H.; Lu, G.-L.; Miller, C. K.; Guo, J.; Lewis Phillips, G. D.; Pillow, T. H.; Tercel, M. Analogues of DNA Minor Groove Cross-Linking Agents Incorporating AminoCBI, an Amino Derivative of the Duocarmycins: Synthesis, Cytotoxicity, and Potential as Payloads for Antibody–Drug Conjugates. *Bioorg. Med. Chem.* **2016**, *24* (22), 6075–6081. <https://doi.org/10.1016/j.bmc.2016.09.068>.
- (88) Spangler, B.; Fontaine, S. D.; Shi, Y.; Sambucetti, L.; Mattis, A. N.; Hann, B.; Wells, J. A.; Renslo, A. R. A Novel Tumor-Activated Prodrug Strategy Targeting Ferrous Iron Is Effective in Multiple Preclinical Cancer Models. *J. Med. Chem.* **2016**, *59* (24), 11161–11170. <https://doi.org/10.1021/acs.jmedchem.6b01470>.
- (89) Boger, D. L. Cyclic N-Acyl O-Amino Phenol CBI Derivative. US009586974B2, March 7, 2017.
- (90) Jiménez-Moreno, E.; Guo, Z.; Oliveira, B. L.; Albuquerque, I. S.; Kitowski, A.; Guerreiro, A.; Boutourel, O.; Rodrigues, T.; Jiménez-Osés, G.; Bernardes, G. J. L. Vinyl Ether/Tetrazine Pair for the Traceless Release of Alcohols in Cells. *Angew. Chem. Int. Ed.* **2017**, *129* (1), 249–253. <https://doi.org/10.1002/ange.201609607>.
- (91) Tercel, M.; Lee, H. H.; Mehta, S. Y.; Youte Tendoung, J.-J.; Bai, S. Y.; Liyanage, H. D. S.; Pruijn, F. B. Influence of a Basic Side Chain on the Properties of Hypoxia-Selective Nitro Analogues of the Duocarmycins: Demonstration of Substantial Anticancer Activity in Combination with Irradiation or Chemotherapy. *J. Med. Chem.* **2017**, *60* (13), 5834–5856. <https://doi.org/10.1021/acs.jmedchem.7b00563>.
- (92) Tietze, L. F.; Penchalaiah, K. Bifunctional Prodrugs. WO 2017/072295A1, May 4, 2017.
- (93) Beekman, A. M.; Cominetti, M. M. D.; Cartwright, O. C.; Boger, D. L.; Searcey, M. A Small Molecule Drug Conjugate (SMDC) of DIPA and a Duocarmycin Built on the Solid Phase. *Med. Chem. Commun.* **2019**, *10* (12), 2170–2174. <https://doi.org/10.1039/C9MD00279K>.
- (94) Lee, H. H.; Dickson, B. D.; Stevenson, R. J.; Yang, S.; Tercel, M. Optimised Synthesis of a NitroCBI Hypoxia-Activated Prodrug

with Substantial Anticancer Activity. *Tetrahedron* **2019**, *75* (22), 3001–3007. <https://doi.org/10.1016/j.tet.2019.04.027>.

(95) Cartwright, O. C.; Beekman, A. M.; Cominetti, M. M. D.; Russell, D. A.; Searcey, M. A Peptide–Duocarmycin Conjugate Targeting the Thomsen–Friedenreich Antigen Has Potent and Selective Antitumor Activity. *Bioconjugate Chem.* **2020**, *31* (7), 1745–1749. <https://doi.org/10.1021/acs.bioconjchem.0c00282>.

(96) Guerrero, A.; Guiho, R.; Herranz, N.; Uren, A.; Withers, D. J.; Martínez-Barbera, J. P.; Tietze, L. F.; Gil, J. Galactose-modified Duocarmycin Prodrugs as Senolytics. *Aging Cell* **2020**, *19* (4). <https://doi.org/10.1111/acel.13133>.

(97) Hong, C. R.; Mehta, S. Y.; Liyanage, H. D. S.; McManaway, S. P.; Lee, H. H.; Jaiswal, J. K.; Bogle, G.; Tercel, M.; Puijn, F. B.; Wilson, W. R.; Hicks, K. O. Spatially-Resolved Pharmacokinetic/Pharmacodynamic Modelling of Bystander Effects of a Nitrochloromethylbenzindoline Hypoxia-Activated Prodrug. *Cancer Chemother. Pharmacol.* **2021**, *88* (4), 673–687. <https://doi.org/10.1007/s00280-021-04320-3>.

(3) duocarmycin ADCs (72 items - 39 journal publications, 33 patents)

(1) Chari, R. V. J.; Jacket, K. A.; Bourret, L. A.; Pullen, S. M.; Tadayoni, B. M.; Mattocks, K. M.; Shah, S. A.; Liu, C.; Blaettler, W. A.; Goldmacher, V. S. Enhancement of the Selectivity and Antitumor Efficacy of a CC-1065 Analogue through Immunoconjugate Formation. *Cancer Res.* **1995**, *55*, 4079–4084.

(2) Chari, R. V. J.; Goldmacher, V. S.; Blaettler, W. A. Cell Binding Agent Conjugates of Analogues and Derivatives of CC-1065. US005475092A, December 12, 1995.

(3) Chari, R. V. J.; Goldmacher, V. S.; Blaettler, W. A. Cyclopropylbenzindole-Containing Cytotoxic Drugs. US005585499A, December 17, 1996.

(4) Chari, R. V. J.; Goldmacher, V. S.; Blaettler, W. A. Targeted Delivery of Cyclopropylbenzindole-Containing Cytotoxic Drugs. US005846545A, December 8, 1998.

(5) Kelly, R. C.; Mitchell, M. A.; Aristoff, P. A. CC-1065 Analogs. US005739350A, April 14, 1998.

(6) Suzawa, T.; Nagamura, S.; Saito, H.; Ohta, S.; Hanai, N.; Yamasaki, M. Synthesis and HPLC Analysis of Enzymatically Cleavable Linker Consisting of Poly(Ethylene Glycol) and Dipeptide for the Development of Immunoconjugate. *J. Control. Rel.* **2000**, *69* (1), 27–41. [https://doi.org/10.1016/S0168-3659\(00\)00282-0](https://doi.org/10.1016/S0168-3659(00)00282-0).

(7) Suzawa, T.; Nagamura, S.; Saito, H.; Ohta, S.; Hanai, N.; Yamasaki, M. Synthesis of a Novel Duocarmycin Derivative DU-257 and Its Application to Immunoconjugate Using Poly(Ethylene Glycol)-Dipeptidyl Linker Capable of Tumor Specific Activation. *Bioorg. Med. Chem.* **2000**, *8*, 2175–2184. [https://doi.org/10.1016/s0968-0896\(00\)00157-7](https://doi.org/10.1016/s0968-0896(00)00157-7).

(8) Lillo, A. M.; Sun, C.; Gao, C.; Ditzel, H.; Parrish, J.; Gauss, C.-M.; Moss, J.; Felding-Habermann, B.; Wirsching, P.; Boger, D. L.; Janda, K. D. A Human Single-Chain Antibody Specific for Integrin Alpha1beta2 Capable of Cell Internalization and Delivery of Antitumor Agents. *Chem. & Biol.* **2004**, *11*, 897–906. <https://doi.org/10.1016/j.chembiol.2004.04.018>.

(9) Jeffrey, S. C.; Torgov, M. Y.; Andreyka, J. B.; Boddington, L.; Cerveny, C. G.; Denny, W. A.; Gordon, K. A.; Gustin, D.; Haugen, J.; Kline, T.; Nguyen, M. T.; Senter, P. D. Design, Synthesis, and in Vitro Evaluation of Dipeptide-Based Antibody Minor Groove Binder Conjugates. *J. Med. Chem.* **2005**, *48* (5), 1344–1358. <https://doi.org/10.1021/jm040137q>.

(10) Boyd, S. E.; Chen, L.; Gangwar, S.; Guerlavais, V.; Horgan, K.; Sufi, B.; Cardarelli, J. M.; Pan, C.; Huang, H.; King, D. J. Conjugates of Duocarmycin and Anti-CD70 or Anti-PSMA Antibodies. EP 2354163A2, September 26, 2006.

(11) Gangwar, S.; Sufi, B. Cytotoxic Compounds and Conjugates with Cleavable Substrates. US 20060247295A1, November 2, 2006.

(12) Janda, K. D.; Wirsching, P.; Boger, D. L. Compositions and Methods for Delivery of Antitumor Agents. WO 2006/002895A2, January 12, 2006.

(98) Sharrock, A. V.; McManaway, S. P.; Rich, M. H.; Mumm, J. S.; Hermans, I. F.; Tercel, M.; Puijn, F. B.; Ackerley, D. F. Engineering the Escherichia Coli Nitroreductase *fnsA* to Create a Flexible Enzyme-Prodrug Activation System. *Front. Pharmacol.* **2021**, *12*.

(99) Thorn-Seshold, O.; Felber, J.; Thorn-Seshold, J.; Zeisel, L. Disulfide-Based Prodrug Compounds. PCT/EP2022/057483, 2021.

(100) Thorn-Seshold, O.; Zeisel, L.; Felber, J. G. Dichalcogenide Prodrugs. PCT/EP2022/059280, 2021.

(101) Bart, A. G.; Morais, G.; Vangala, V. R.; Loadman, P. M.; Pors, K.; Scott, E. E. Cytochrome P450 Binding and Bioactivation of Tumor-Targeted Duocarmycin Agents. *Drug Metab Dispos* **2022**, *50* (1), 49–57. <https://doi.org/10.1124/dmd.121.006642>.

(102) Felber, J. G.; Kitowski, A.; Zeisel, L.; Maier, M. S.; Heise, C.; Thorn-Seshold, J.; Thorn-Seshold, O. Cancer Prodrug Activation through Trx/TrxR-Selective Bioreduction of Monothiol-Stable Seco-Duocarmycins in Vivo. *in preparation* **2022**.

(13) Boyd, S. E.; Chen, L.; Gangwar, S.; Guerlavais, V.; Horgan, K.; Sufi, B.; Huang, H.; King, D. J.; Pan, C.; Cardarelli, J. M. Antibody-Drug Conjugates and Methods of Use. US20080279868A1, November 13, 2008.

(14) Chen, L.; Gangwar, S.; Guerlavais, V.; Lonberg, N.; Zhang, Q. Chemical Linkers with Single Amino Acids and Conjugates Thereof. US20100113476A1, May 6, 2010.

(15) Sufi, B.; Guerlavais, V.; Chen, L.; Gangwar, S.; Zhang, Q.; Passmore, D. B. Chemical Linkers and Cleavable Substrates and Conjugates Thereof. US20100145036A1, June 10, 2010.

(16) Gangwar, S.; Sufi, B. Cytotoxic Compounds and Conjugates. US 007968586B2, June 28, 2011.

(17) Zhao, R. Y.; Erickson, H. K.; Leece, B. A.; Reid, E. E.; Goldmacher, V. S.; Lambert, J. M.; Chari, R. V. J. Synthesis and Biological Evaluation of Antibody Conjugates of Phosphate Prodrugs of Cytotoxic DNA Alkylators for the Targeted Treatment of Cancer. *J. Med. Chem.* **2012**, *55* (2), 766–782. <https://doi.org/10.1021/jm201284m>.

(18) Beusker, P. H.; Coumans, R. G. E.; Elgersma, R. C.; Menge, W. M. P. B.; Joosten, A. F.; Spijker, H. J.; de Groot, F. M. H. Novel Conjugates of CC-1065 Analogs and Bifunctional Linkers. US20130224227A1, August 29, 2013.

(19) Thevanayagam, L.; Bell, A.; Chakraborty, I.; Sufi, B.; Gangwar, S.; Zang, A.; Rangan, V.; Rao, C.; Wang, Z.; Pan, C.; Chong, C.; Cardarelli, P.; Deshpande, S.; Srinivasan, M. Novel Detection of DNA-Alkylated Adducts of Antibody–Drug Conjugates with Potentially Unique Preclinical and Biomarker Applications. *Bioanalysis* **2013**, *5* (9), 1073–1081. <https://doi.org/10.4155/bio.13.57>.

(20) Beusker, P. H.; Coumans, R. G. E.; Elgersma, R. C.; Menge, W. M. P. B.; Joosten, A. F.; Spijker, H. J.; de Groot, F. M. H. CC-1065 Analogs and Their Conjugates. US008889868B2, November 18, 2014.

(21) Beusker, P. H.; Spijker, H. J.; Joosten, A. F.; Huijbregts, T.; de Groot, F. M. H. Substituted CC-1065 Analogs and Their Conjugates. US008680293B2, March 25, 2014.

(22) Dokter, W.; Ubink, R.; van der Lee, M.; van der Vleuten, M.; van Achterberg, T.; Jacobs, D.; Loosveld, E.; van den Dobbels, D.; Egging, D.; Matlaar, E.; Groothuis, P.; Beusker, P.; Coumans, R.; Elgersma, R.; Menge, W.; Joosten, J.; Spijker, H.; Huijbregts, T.; de Groot, V.; Eppink, M.; de Roo, G.; Verheijden, G.; Timmers, M. Preclinical Profile of the HER2-Targeting ADC SYD983/SYD985: Introduction of a New Duocarmycin-Based Linker-Drug Platform. *Mol. Cancer Ther.* **2014**, *13* (11), 2618–2629. <https://doi.org/10.1158/1535-7163.MCT-14-0040-T>.

(23) Perrino, E.; Steiner, M.; Krall, N.; Bernardes, G. J. L.; Pretto, F.; Cusi, G.; Neri, D. Curative Properties of Noninternalizing Antibody–Drug Conjugates Based on Maytansinoids. *Cancer Res.* **2014**, *74* (9), 2569–2578. <https://doi.org/10.1158/0008-5472.CAN-13-2990>.

- (24) Elgersma, R. C.; Coumans, R. G. E.; Huijbregts, T.; Menge, W. M. P. B.; Joosten, J. A. F.; Spijker, H. J.; de Groot, F. M. H.; van der Lee, M. M. C.; Ubink, R.; van den Dobbelsteen, D. J.; Egging, D. F.; Dokter, W. H. A.; Verheijden, G. F. M.; Lemmens, J. M.; Timmers, C. M.; Beusker, P. H. Design, Synthesis, and Evaluation of Linker-Duocarmycin Payloads: Toward Selection of HER2-Targeting Antibody-Drug Conjugate SYD985. *Mol. Pharmaceutics* **2015**, *12* (6), 1813–1835. <https://doi.org/10.1021/mp500781a>.
- (25) Flygare, J. A.; Pillow, T. H.; Safina, B.; Verma, V.; Wei, B.; Denny, W. A.; Giddens, A. C.; Lee, H.; Lu, G.-L.; Miller, C.; Rewcastle, G.; Tercel, M.; Bonnet, M. 1-(Chloromethyl)-2,3-Dihydro-1H-Benzo[e]Indole Dimer Antibody-Drug Conjugate Compounds, and Methods of Use and Treatment. US20150165063A1, June 18, 2015.
- (26) Maderma, A.; Doroski, M. D.; Chen, Z.; Risley, H. L.; Casavant, J. M.; O'Donnell, C. J.; Porte, A. M.; Subramanyam, C. Bifunctional Cytotoxic Agents. US20150209445A1, July 30, 2015.
- (27) van der Lee, M. M. C.; Groothuis, P. G.; Ubink, R.; van der Vleuten, M. A. J.; van Achterberg, T. A.; Loosveld, E. M.; Dammig, D.; Jacobs, D. C. H.; Rouwette, M.; Egging, D. F.; van den Dobbelsteen, D.; Beusker, P. H.; Goedings, P.; Verheijden, G. F. M.; Lemmens, J. M.; Timmers, M.; Dokter, W. H. A. The Preclinical Profile of the Duocarmycin-Based HER2-Targeting ADC SYD985 Predicts for Clinical Benefit in Low HER2-Expressing Breast Cancers. *Mol. Cancer Ther.* **2015**, *14* (3), 692–703. <https://doi.org/10.1158/1535-7163.MCT-14-0881-T>.
- (28) Beusker, P. H.; Coumans, R. G. E.; Elgersma, R. C.; Menge, W. M. P. B.; Joosten, A. F.; Spijker, H. J.; de Groot, F. M. H. Novel CC-1065 Analogs and Their Conjugates. US20160052880A1, February 25, 2016.
- (29) Black, J.; Menderes, G.; Bellone, S.; Schwab, C. L.; Bonazzoli, E.; Ferrari, F.; Predolini, F.; De Haydu, C.; Cocco, E.; Buza, N.; Hui, P.; Wong, S.; Lopez, S.; Ratner, E.; Silasi, D.-A.; Azodi, M.; Litkouhi, B.; Schwartz, P. E.; Goedings, P.; Beusker, P. H.; van der Lee, M. M. C.; Timmers, C. M.; Dokter, W. H. A.; Santin, A. D. SYD985, a Novel Duocarmycin-Based HER2-Targeting Antibody-Drug Conjugate, Shows Antitumor Activity in Uterine Serous Carcinoma with HER2/Neu Expression. *Mol. Cancer Ther.* **2016**, *15* (8), 1900–1909. <https://doi.org/10.1158/1535-7163.MCT-16-0163>.
- (30) Chen, X.; Dennis, M.; Junutula, J. R.; Phillips, G. L.; Pillow, T. H.; Sliwkowski, M. X. Anti-Her2 Antibodies and Immunoconjugates. US20160096893A1, April 7, 2016.
- (31) Dokter, W.; Goedings, P. J.; Verheijden, G. F. M.; Beusker, P. H. Duocarmycin ADCs Showing Improved In Vivo Antitumor Activity. US20160008486A1, January 14, 2016.
- (32) Lin, R.-H.; Lin, S.-Y.; Hsieh, Y.-C.; Huang, C.-C.; Lee, S.-H.; Tsai, Y.-Y. Her2 Antibody-Drug Conjugates. US20160051695A1, February 25, 2016.
- (33) Maderma, A.; Subramanyam, C.; Tumey, L. N.; Chen, Z.; Casavant, J. M. Bifunctional Cytotoxic Agents Containing the CTI Pharmacophore. WO 2016/151432A1, September 29, 2016.
- (34) Owonikoko, T. K.; Hussain, A.; Stadler, W. M.; Smith, D. C.; Kluger, H.; Molina, A. M.; Gulati, P.; Shah, A.; Ahlers, C. M.; Cardarelli, P. M.; Cohen, L. J. First-in-Human Multicenter Phase I Study of BMS-936561 (MDX-1203), an Antibody-Drug Conjugate Targeting CD70. *Cancer Chemother. Pharmacol.* **2016**, *77* (1), 155–162. <https://doi.org/10.1007/s00280-015-2909-2>.
- (35) Santin, A. D.; Goedings, P. Duocarmycin ADCs for Use in Treatment of Endometrial Cancer. 009427480B2, August 30, 2016.
- (36) Wang, H.; Rangan, V. S.; Sung, M.-C.; Passmore, D.; Kempe, T.; Wang, X.; Thevanayagam, L.; Pan, C.; Rao, C.; Srinivasan, M.; Zhang, Q.; Gangwar, S.; Deshpande, S.; Cardarelli, P.; Marathe, P.; Yang, Z. Pharmacokinetic Characterization of BMS-936561, an Anti-CD70 Antibody-Drug Conjugate, in Preclinical Animal Species and Prediction of Its Pharmacokinetics in Humans: PHARMACOKINETICS OF α CD70-MED-A. *Biopharm. Drug Dispos.* **2016**, *37* (2), 93–106. <https://doi.org/10.1002/bdd.1953>.
- (37) Capone, E.; Piccolo, E.; Fichera, I.; Ciufici, P.; Barcaroli, D.; Sala, A.; De Laurenzi, V.; Iacobelli, S.; Iacobelli, S.; Sala, G. Generation of a Novel Antibody-Drug Conjugate Targeting Endosialin: Potent and Durable Antitumor Response in Sarcoma. *Oncotarget* **2017**, *8* (36), 60368–60377. <https://doi.org/10.18632/oncotarget.19499>.
- (38) Egging, D.; Beusker, P. H.; Mattaar, E.; Bos, E. S. Pan-Reactive Antibodies to Duocarmycins. US20170320965A1, November 9, 2017.
- (39) Huijbregts, T.; Elgersma, R. C.; Beusker, P. H.; Joosten, A. F.; Coumans, R. G. E.; Spijker, H. J.; Menge, W.; de Groot, F. M. H. Process for Making Duocarmycin Prodrugs. US20170145006A1, May 25, 2017.
- (40) Iacobelli, S.; Di Risio, A.; Piccolo, E.; Sala, G.; Capone, E. Endosialin-Binding Antibody. WO 2017/134234A1, August 10, 2017.
- (41) Menderes, G.; Bonazzoli, E.; Bellone, S.; Black, J.; Altwerger, G.; Masserdotti, A.; Pettinella, F.; Zammataro, L.; Buza, N.; Hui, P.; Wong, S.; Litkouhi, B.; Ratner, E.; Silasi, D.-A.; Huang, G. S.; Azodi, M.; Schwartz, P. E.; Santin, A. D. SYD985, a Novel Duocarmycin-Based HER2-Targeting Antibody-Drug Conjugate, Shows Promising Antitumor Activity in Epithelial Ovarian Carcinoma with HER2/Neu Expression. *Gynecologic Oncology* **2017**, *146* (1), 179–186. <https://doi.org/10.1016/j.ygyno.2017.04.023>.
- (42) Menderes, G.; Bonazzoli, E.; Bellone, S.; Black, J.; Predolini, F.; Pettinella, F.; Masserdotti, A.; Zammataro, L.; Altwerger, G.; Buza, N.; Hui, P.; Wong, S.; Litkouhi, B.; Ratner, E.; Silasi, D.-A.; Azodi, M.; Schwartz, P. E.; Santin, A. D. SYD985, a Novel Duocarmycin-Based HER2-Targeting Antibody-Drug Conjugate, Shows Antitumor Activity in Uterine and Ovarian Carcinosarcoma with HER2/Neu Expression. *Clin. Cancer Res.* **2017**, *23* (19), 5836–5845. <https://doi.org/10.1158/1078-0432.CCR-16-2862>.
- (43) Nani, R. R.; Gorka, A. P.; Nagaya, T.; Yamamoto, T.; Ivanic, J.; Kobayashi, H.; Schnermann, M. J. In Vivo Activation of Duocarmycin-Antibody Conjugates by Near-Infrared Light. *ACS Cent. Sci.* **2017**, *3* (4), 329–337. <https://doi.org/10.1021/acscentsci.7b00026>.
- (44) Osinga, N. J.; Boxmeer Van, E. J. B. Composition Comprising Antibody-Duocarmycin Drug Conjugates. WO 2017/009255A1, January 19, 2017.
- (45) Pillow, T. H.; Sadowsky, J. D.; Zhang, D.; Yu, S.-F.; Del Rosario, G.; Xu, K.; He, J.; Bhakta, S.; Ohri, R.; Kozak, K. R.; Ha, E.; Junutula, J. R.; Flygare, J. A. Decoupling Stability and Release in Disulfide Bonds with Antibody-Small Molecule Conjugates. *Chem. Sci.* **2017**, *8* (1), 366–370. <https://doi.org/10.1039/C6SC01831A>.
- (46) FDA Updates. Fast Track Designation Granted for Breast Cancer Treatment. *Oncology Times* **2018**, *40* (5), 16. <https://doi.org/10.1097/01.COT.0000531194.80509.6d>.
- (47) Helin, J.; Saarinen, J.; Satomaa, T.; Ekholm, F. S. Saccaride Derivative of a Toxic Payload and Antibody Conjugates Thereof. US20180228906A1, August 16, 2018.
- (48) Jin, J.; Park, G.; Park, J. B.; Kim, S.; Kim, H.; Chung, J. An Anti-EGFR \times Cytinine Bispecific Antibody Complexed with Cytinine-Conjugated Duocarmycin Inhibits Growth of EGFR-Positive Cancer Cells with KRAS Mutations. *Exp. Mol. Med.* **2018**, *50* (5), 1–14. <https://doi.org/10.1038/s12276-018-0096-z>.
- (49) Junutula, J. R.; Smith, S. W.; Borkin, D.; Degrad, S. Isoquinolidinobenzodiazepine (ICQ) - 1-(Chloromethyl)-2,3-Dihydro-1H-Benzo[e]indole (CBI) Dimers. WO 2018/071455 A1, April 19, 2018.
- (50) Lütje, S.; Gerrits, D.; Molkenboer-Kuening, J. D.; Herrmann, K.; Fracasso, G.; Colombatti, M.; Boerman, O. C.; Heskamp, S. Characterization of Site-Specifically Conjugated Monomethyl Auristatin E- and Duocarmycin-Based Anti-PSMA Antibody-Drug Conjugates for Treatment of PSMA-Expressing Tumors. *J. Nucl. Med.* **2018**, *59* (3), 494–501. <https://doi.org/10.2967/jnumed.117.196279>.
- (51) Nagaya, T.; Gorka, A. P.; Nani, R. R.; Okuyama, S.; Ogata, F.; Maruoka, Y.; Choyke, P. L.; Schnermann, M. J.; Kobayashi, H. Molecularly Targeted Cancer Combination Therapy with Near-Infrared Photoimmunotherapy and Near-Infrared Photorelease with Duocarmycin-Antibody Conjugate. *Mol. Cancer Ther.* **2018**, *17* (3), 661–670. <https://doi.org/10.1158/1535-7163.MCT-17-0851>.
- (52) Ubink, R.; Dirksen, E. H. C.; Rouwette, M.; Bos, E. S.; Janssen, I.; Egging, D. F.; Loosveld, E. M.; van Achterberg, T. A.; Berentsen, K.; van der Lee, M. M. C.; Bichat, F.; Raguin, O.; van der Vleuten, M. A. J.; Groothuis, P. G.; Dokter, W. H. A. Unraveling the Interaction between Carboxylesterase 1c and the Antibody-Drug

- Conjugate SYD985: Improved Translational PK/PD by Using Ces1c Knockout Mice. *Mol. Cancer Ther.* **2018**, *17* (11), 2389–2398. <https://doi.org/10.1158/1535-7163.MCT-18-0329>.
- (53) Yu, L.; Lu, Y.; Yao, Y.; Liu, Y.; Wang, Y.; Lai, Q.; Zhang, R.; Li, W.; Wang, R.; Fu, Y.; Tao, Y.; Yi, S.; Gou, L.; Chen, L.; Yang, J. Promiximab-Duocarmycin, a New CD56 Antibody-Drug Conjugates, Is Highly Efficacious in Small Cell Lung Cancer Xenograft Models. *Oncotarget* **2018**, *9* (4), 5197–5207. <https://doi.org/10.18632/oncotarget.23708>.
- (54) Zhang, D.; Le, H.; Cruz-Chuh, J. dela; Bobba, S.; Guo, J.; Staben, L.; Zhang, C.; Ma, Y.; Kozak, K. R.; Lewis Phillips, G. D.; Vollmar, B. S.; Sadowsky, J. D.; Vandlen, R.; Wei, B.; Su, D.; Fan, P.; Dragovich, P. S.; Khojasteh, S. C.; Hop, C. E. C. A.; Pillow, T. H. Immobilization of *p*-Aminobenzyl Ether Linker and Payload Potency and Stability Determine the Cell-Killing Activity of Antibody–Drug Conjugates with Phenol-Containing Payloads. *Bioconjugate Chem.* **2018**, *29* (2), 267–274. <https://doi.org/10.1021/acs.bioconjugchem.7b00576>.
- (55) Ariaans, G. J. A.; Coumans, R. G. E. Site-Specific Conjugation of Linker Drugs to Antibodies and Resulting ADCs. US010407743B2, September 10, 2019.
- (56) Banerji, U.; van Herpen, C. M. L.; Saura, C.; Thistlethwaite, F.; Lord, S.; Moreno, V.; Macpherson, I. R.; Boni, V.; Rolfo, C.; de Vries, E. G. E.; Rottey, S.; Geenen, J.; Eskens, F.; Gil-Martin, M.; Mommers, E. C.; Koper, N. P.; Aftimos, P. Trastuzumab Duocarmazine in Locally Advanced and Metastatic Solid Tumours and HER2-Expressing Breast Cancer: A Phase 1 Dose-Escalation and Dose-Expansion Study. *The Lancet Oncology* **2019**, *20* (8), 1124–1135. [https://doi.org/10.1016/S1470-2045\(19\)30328-6](https://doi.org/10.1016/S1470-2045(19)30328-6).
- (57) Fu, Y.; Urban, D. J.; Nani, R. R.; Zhang, Y.-F.; Li, N.; Fu, H.; Shah, H.; Gorka, A. P.; Guha, R.; Chen, L.; Hall, M. D.; Schnermann, M. J.; Ho, M. Glypican-3-Specific Antibody Drug Conjugates Targeting Hepatocellular Carcinoma. *Hepatology* **2019**, *70* (2), 563–576. <https://doi.org/10.1002/hep.30326>.
- (58) Jackson, P. M. J.; Thurston, D. E.; Rahman, K. M. Asymmetric Conjugate Compounds. US2019014443A1, May 16, 2019.
- (59) Kim, S.; Kim, H.; Jo, D. H.; Kim, J. H.; Kim, S. R.; Kang, D.; Hwang, D.; Chung, J. Bispecific Anti-MPDGFR β x Cotinine ScFv-Ck-ScFv Fusion Protein and Cotinine-Duocarmycin Can Form Antibody-Drug Conjugate-like Complexes That Exert Cytotoxicity against MPDGFR β Expressing Cells. *Methods* **2019**, *154*, 125–135. <https://doi.org/10.1016/j.ymeth.2018.10.002>.
- (60) Loo, D. T.; Huang, L.; Johnson, L. S.; Son, T.; Scribner, J. A.; Bonvini, E. Novel B7-H3 Binding Molecules, Antibody Drug Conjugates Thereof and Methods of Use Thereof. US2019012471A1, May 2, 2019.
- (61) Rinnerthaler, G.; Gampenrieder, S.; Greil, R. HER2 Directed Antibody-Drug-Conjugates beyond T-DM1 in Breast Cancer. *Int. J. Mol. Sci.* **2019**, *20* (5), 1115. <https://doi.org/10.3390/ijms20051115>.
- (62) Su, D.; Chen, J.; Cosino, E.; dela Cruz-Chuh, J.; Davis, H.; Del Rosario, G.; Figueroa, I.; Goon, L.; He, J.; Kamath, A. V.; Kaur, S.; Kozak, K. R.; Lau, J.; Lee, D.; Lee, M. V.; Leopold, D.; Liu, L.; Liu, P.; Lu, G.-L.; Nelson, C.; Ng, C.; Pillow, T. H.; Polakis, P.; Polson, A. G.; Rowntree, R. K.; Saad, O.; Safina, B.; Stagg, N. J.; Tercel, M.; Vandlen, R.; Vollmar, B. S.; Wai, J.; Wang, T.; Wei, B.; Xu, K.; Xue, J.; Xu, Z.; Yan, G.; Yao, H.; Yu, S.-F.; Zhang, D.; Zhong, F.; Dragovich, P. S. Antibody–Drug Conjugates Derived from Cytotoxic Seco -CBI-Dimer Payloads Are Highly Efficacious in Xenograft Models and Form Protein Adducts *In Vivo*. *Bioconjugate Chem.* **2019**, *30* (5), 1356–1370. <https://doi.org/10.1021/acs.bioconjugchem.9b00133>.
- (63) Tietze, L. F. Method for the Synthesis of Monoprotected Bifunctional Prodrugs and Antibody Drug Conjugates Based Thereon as Well as a Method for Preparing Antibody Drug Conjugates. WO 2019/030367A1, February 14, 2019.
- (64) Tong, X.-M.; Feng, L.; Sutte, S. R.; Weng, T.-H.; Hu, C.-Y.; Liu, Y.-Z.; Wu, Z.-G.; Wang, M.-H.; Yao, H.-P. Therapeutic Efficacy of a Novel Humanized Antibody-Drug Conjugate Recognizing Plexin-Semaphorin-Integrin Domain in the RON Receptor for Targeted Cancer Therapy. *J. Immunotherapy Cancer* **2019**, *7* (1), 250. <https://doi.org/10.1186/s40425-019-0732-8>.
- (65) Coumans, R. G. E.; Ariaans, G. J. A.; Spijker, H. J.; Renart Verkerk, P.; Beusker, P. H.; Kokke, B. P. A.; Schouten, J.; Blomenröhr, M.; van der Lee, M. M. C.; Groothuis, P. G.; Ubink, R.; Dokter, W. H. A.; Timmers, C. M. A Platform for the Generation of Site-Specific Antibody–Drug Conjugates That Allows for Selective Reduction of Engineered Cysteines. *Bioconjugate Chem.* **2020**, *31* (9), 2136–2146. <https://doi.org/10.1021/acs.bioconjugchem.0c00337>.
- (66) Hackshaw, M. D.; Danysh, H. E.; Singh, J.; Ritchey, M. E.; Ladner, A.; Taitt, C.; Camidge, D. R.; Iwata, H.; Powell, C. A. Incidence of Pneumonitis/Interstitial Lung Disease Induced by HER2-Targeting Therapy for HER2-Positive Metastatic Breast Cancer. *Breast Cancer Res. Treat.* **2020**, *183* (1), 23–39. <https://doi.org/10.1007/s10549-020-05754-8>.
- (67) Nadal-Serrano, M.; Morancho, B.; Escrivá-de-Romaní, S.; Bernadó Morales, C.; Luque, A.; Escorihuela, M.; Espinosa Bravo, M.; Peg, V.; Dijcks, F. A.; Dokter, W. H. A.; Cortés, J.; Saura, C.; Arribas, J. The Second Generation Antibody-Drug Conjugate SYD985 Overcomes Resistances to T-DM1. *Cancers* **2020**, *12* (3), 670. <https://doi.org/10.3390/cancers12030670>.
- (68) Scribner, J. A.; Brown, J. G.; Son, T.; Chiechi, M.; Li, P.; Sharma, S.; Li, H.; De Costa, A.; Li, Y.; Chen, Y.; Easton, A.; Yee-Toy, N. C.; Chen, F. Z.; Gorlatov, S.; Barat, B.; Huang, L.; Wolff, C. R.; Hooley, J.; Hotaling, T. E.; Gaynutdinov, T.; Ciccarone, V.; Tamura, J.; Koenig, S.; Moore, P. A.; Bonvini, E.; Loo, D. Preclinical Development of MGC018, a Duocarmycin-Based Antibody–Drug Conjugate Targeting B7-H3 for Solid Cancer. *Mol. Cancer Ther.* **2020**, *19* (11), 2235–2244. <https://doi.org/10.1158/1535-7163.MCT-20-0116>.
- (69) Voortman, G.; Koper, N. P. SYD985 Treatment of T-DM1 Refractory Cancer Patients. US010821191B2, November 3, 2020.
- (70) Jang, S.; Powderly, J. D.; Spira, A. I.; Bakkacha, O.; Loo, D.; Bohac, G. C.; Sharma, M. Phase 1 Dose Escalation Study of MGC018, an Anti-B7-H3 Antibody-Drug Conjugate (ADC), in Patients with Advanced Solid Tumors. *J. Clin. Onc.* **2021**, *39* (15 suppl), 2631–2631. https://doi.org/10.1200/JCO.2021.39.15_suppl.2631.
- (71) Ferhati, X.; Jiménez-Moreno, E.; Hoyt, E. A.; Salluce, G.; Cabeza-Cabrero, M.; Navo, C. D.; Compañón, I.; Akkapeddi, P.; Matos, M. J.; Salaverri, N.; Garrido, P.; Martínez, A.; Laserna, V.; Murray, T. V.; Jiménez-Osés, G.; Ravn, P.; Bernardes, G. J. L.; Corzana, F. Single Mutation on Trastuzumab Modulates the Stability of Antibody–Drug Conjugates Built Using Acetal-Based Linkers and Thiol-Maleimide Chemistry. *J. Am. Chem. Soc.* **2022**. <https://doi.org/10.1021/jacs.1c07675>.
- (72) Hyung, S.-J.; Leopold, D. D.; Lee, D. W.; Kaur, S.; Saad, O. M. Multiplexed Quantitative Analysis of Antibody–Drug Conjugates with Labile CBI-Dimer Payloads *In Vivo* Using Immunoaffinity LC-MS/MS. *Anal. Chem.* **2022**, *94* (2), 1158–1168. <https://doi.org/10.1021/acs.analchem.1c04338>.

(x) duocarmycin reviews (23 items)

- (1) Hurley, L. H.; Sun, D. (+)-CC-1065 as a Probe for Intrinsic and Protein-Induced Bending of DNA. *J. Mol. Recognit.* **1994**, *7* (2), 123–132. <https://doi.org/10.1002/jmr.300070209>.
- (2) Boger, D. L. The Duocarmycins: Synthetic and Mechanistic Studies. *Acc. Chem. Res.* **1995**, *28* (1), 20–29. <https://doi.org/10.1021/ar00049a004>.
- (3) Boger, D. L.; Boyce, C. W.; Garbaccio, R. M.; Goldberg, J. A. CC-1065 and the Duocarmycins: Synthetic Studies. *Chem. Rev.* **1997**, *97* (3), 787–828. <https://doi.org/10.1021/cr960095g>.
- (4) Cacciari, B.; Romagnoli, R.; Baraldi, P. G.; Ros, T. D.; Spalluto, G. CC-1065 and the Duocarmycins: Recent Developments. *Exp. Op. Ther. Patents* **2000**, *10* (12), 1853–1871. <https://doi.org/10.1517/13543776.10.12.1853>.
- (5) Denny, W. A. DNA Minor Groove Alkylating Agents. *Curr. Med. Chem.* **2001**, *8*, 533–544. <https://doi.org/10.2174/0929867003373283>.
- (6) Sharma, S.; Jia, G.; Lown, J. Novel Cyclopropylindole Conjugates and Dimers: Synthesis and Anti-Cancer Evaluation. *Curr. Med. Chem.* **2001**, *1* (1), 27–45. <https://doi.org/10.2174/1568011013354831>.
- (7) Denny, W. Nitroreductase-Based GDEPT. *Curr. Pharm. Des.* **2002**, *8* (15), 1349–1361. <https://doi.org/10.2174/1381612023394584>.
- (8) Searcey, M. Duocarmycins - Natures Prodrugs? *Curr. Pharm. Des.* **2002**, *8* (15), 1375–1389. <https://doi.org/10.2174/1381612023394539>.
- (9) Wolkenberg, S. E.; Boger, D. L. Mechanisms of in Situ Activation for DNA-Targeting Antitumor Agents. *Chem. Rev.* **2002**, *102* (7), 2477–2496. <https://doi.org/10.1021/cr010046g>.
- (10) Baraldi, P. G.; Bovero, A.; Fruttarolo, F.; Preti, D.; Tabrizi, M. A.; Pavani, M. G.; Romagnoli, R. DNA Minor Groove Binders as Potential Antitumor and Antimicrobial Agents. *Med. Res. Rev.* **2004**, *24* (4), 475–528. <https://doi.org/10.1002/med.20000>.
- (11) Bando, T.; Sugiyama, H. Synthesis and Biological Properties of Sequence-Specific DNA-Alkylating Pyrrole-Imidazole Polyamides. *Acc. Chem. Res.* **2006**, *39* (12), 935–944. <https://doi.org/10.1021/ar030287f>.
- (12) Ghosh, N.; Sheldrake, H.; Searcey, M.; Pors, K. Chemical and Biological Explorations of the Family of CC-1065 and the Duocarmycin Natural Products. *Curr. Top. Med. Chem.* **2009**, *9* (16), 1494–1524. <https://doi.org/10.2174/156802609789909812>.
- (13) Tietze, L. F.; Krewer, B. Antibody-Directed Enzyme Prodrug Therapy: A Promising Approach for a Selective Treatment of Cancer Based on Prodrugs and Monoclonal Antibodies. *Curr. Biol. Drug Des.* **2009**, *74* (3), 205–211. <https://doi.org/10.1111/j.1747-0285.2009.00856.x>.
- (14) Denny, W. A.; Wilson, W. R. The Design of Selectively-Activated Anti-Cancer Prodrugs for Use in Antibody-Directed and Gene-Directed Enzyme-Prodrug Therapies. *J. Pharm. Pharmacol.* **2011**, *50* (4), 387–394. <https://doi.org/10.1111/j.2042-7158.1998.tb06878.x>.
- (15) F. Tietze, L.; Schmuck, K. Prodrugs for Targeted Tumor Therapies: Recent Developments in ADEPT, GDEPT and PMT. *Curr. Pharm. Des.* **2011**, *17* (32), 3527–3547. <https://doi.org/10.2174/138161211798194459>.
- (16) Patil, P.; Satam, V.; Lee, M. A Short Review on the Synthetic Strategies of Duocarmycin Analogs That Are Powerful DNA Alkylating Agents. *Anti-Cancer Agents in Med. Chem.* **2015**, *15* (5), 616–630. <https://doi.org/10.2174/1871520615666141216144116>.
- (17) Beekman, A. M.; Cominetti, M. M. D.; Searcey, M. Duocarmycins as Antibody – Drug Conjugate (ADC) Payloads. In *Drug Discovery Series No. 71; Cytotoxic Payloads for Antibody-Drug Conjugates; The Royal Society of Chemistry, 2019; pp 187–208*.
- (18) Pillow, T. H.; Terce, M. Duocarmycin-PBD Dimers as Antibody-Drug Conjugate (ADC) Payloads. In *Drug Discovery Series No. 71; Cytotoxic Payloads for Antibody-Drug Conjugates; The Royal Society of Chemistry, 2019; pp 241–258*.
- (19) Procopiou, G.; O'Donnell, C. J. CXI Dimers as Antibody-Drug Conjugate (ADC) Payloads. In *Drug Discovery Series No. 71; Cytotoxic Payloads for Antibody-Drug Conjugates; The Royal Society of Chemistry, 2019; pp 209–240*.
- (20) Yu, Z.; Pandian, G. N.; Hidaka, T.; Sugiyama, H. Therapeutic Gene Regulation Using Pyrrole-Imidazole Polyamides. *Adv. Drug. Del. Rev.* **2019**, *147*, 66–85. <https://doi.org/10.1016/j.addr.2019.02.001>.
- (21) Jukes, Z.; Morais, G. R.; Loadman, P. M.; Pors, K. How Can the Potential of the Duocarmycins Be Unlocked for Cancer Therapy? *Drug Discovery Today* **2021**, *26* (2), 577–584. <https://doi.org/10.1016/j.drudis.2020.11.020>.
- (22) Yao, H.-P.; Zhao, H.; Hudson, R.; Tong, X.-M.; Wang, M.-H. Duocarmycin-Based Antibody-Drug Conjugates as an Emerging Biotherapeutic Entity for Targeted Cancer Therapy: Pharmaceutical Strategy and Clinical Progress. *Drug Discovery Today* **2021**, *26* (8), 1857–1874. <https://doi.org/10.1016/j.drudis.2021.06.012>.
- (23) Denny, W. A. Nitroaromatic Hypoxia-Activated Prodrugs for Cancer Therapy. *Pharmaceuticals* **2022**, *15* (2), 187. <https://doi.org/10.3390/ph15020187>.

Supporting Information to:

Cyclic dichalcogenides extend the reach of bioreductive prodrugs to harness the thioredoxin system: applications to seco-duocarmycins

Jan G. Felber, Annabel Kitowski, Lukas Zeisel, Martin S. Maier, Constanze Heise, Julia Thorn-Seshold, Oliver Thorn-Seshold*

Department of Pharmacy, Ludwig Maximilians University Munich, Butenandtstr. 5-13, 81377 Munich, DE.

* oliver.thorn-seshold@cup.lmu.de

Author Contributions

J.G.F. performed synthesis, analysis, cell-free prodrug activation and cellular assays; coordinated screening, analysed screening data, performed data assembly, and wrote the manuscript. A.K. performed cell-free prodrug activation, cellular assays, coordinated screening and *in vivo* studies, and performed data analysis. L.Z. and M.S.M. performed synthesis and analysis. C.H. performed cell-free prodrug activation and cellular assays. J.T.-S. designed, coordinated, and analysed *in vivo* studies, and performed data assembly. O.T.-S. designed the concept and experiments, supervised experiments, performed screening data analysis, coordinated data assembly, and wrote the manuscript, with input from all co-authors.

Table of contents

1.	Previous chemical tuning of dichalcogenide-based units and prodrug design	S2
2.	CBI-based redox prodrug assembly overview	S3
3.	Reduction-mediated prodrug release monitored by HPLC	S6
4.	Cellular proliferation assays	S9
5.	Prolifer-140 cancer cell screening	S13
5.1.	Prolifer-140 cancer cell screening: cellular cytotoxicity (IC ₅₀ values)	S13
5.2.	Prolifer-140 cancer cell screen: Summary and population analysis	S21
6.	NCI-60 cancer cell screening	S22
6.1.	NCI-60 growth inhibition results (GI ₅₀ values)	S22
6.2.	Comparison of NCI-60 and Prolifer-140 results for potency, and for reductive index	S23
6.3.	Test for correlation of oxidoreductase expression levels, to potency or reductive index	S24
7.	<i>in vivo</i> studies	S25
7.1.	<i>in vivo</i> PK and prodrug tolerance (mouse studies)	S25
7.2.	<i>in vivo</i> efficacy mouse studies	S27
8.	General methods	S28
8.1.	Cell-free HPLC protocols	S28
8.2.	Cell culture methods	S28
8.3.	Methods for <i>in vivo</i> animal studies	S28
8.4.	Synthetic techniques	S30
9.	Chemical synthesis	S32
9.1.	General synthetic protocols	S32
9.2.	Precursor syntheses	S35
9.3.	CBI-AZI prodrug series	S43
9.4.	CBI-TMI prodrug series	S48
10.	NMR Spectra	S53
11.	Supporting References	S77

1. Previous chemical tuning of dichalcogenide-based units and prodrug design

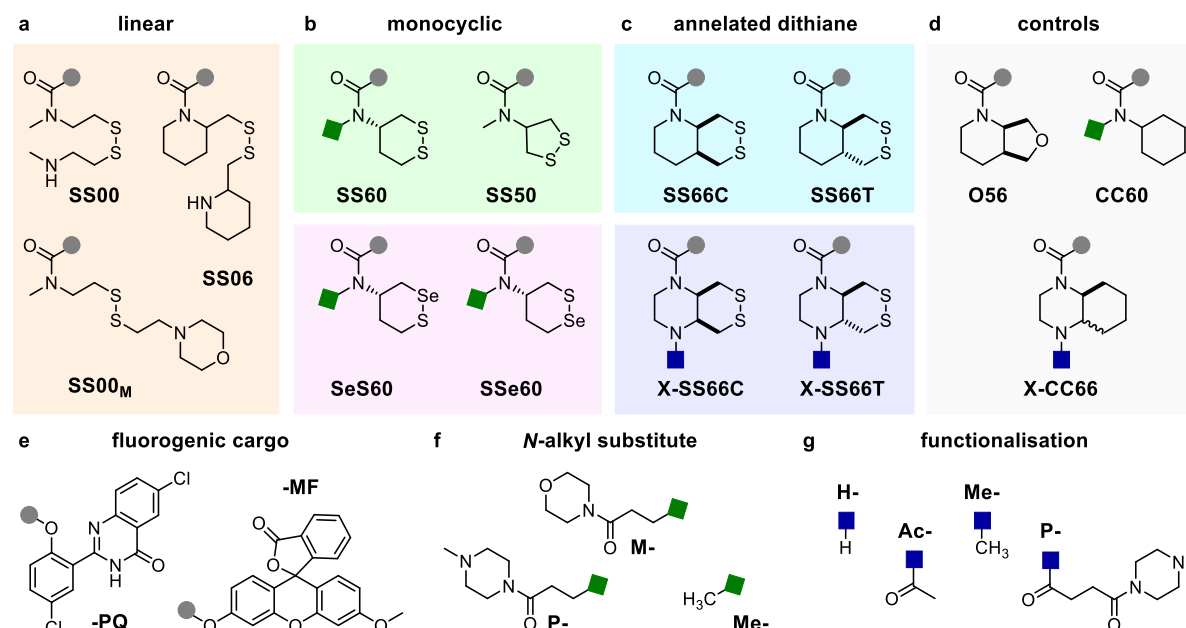


Figure S1: Summary of previous studies. Overview of redox triggers, molecular designs and fluorescent cargos to create fluorogenic probe systems.

(a) Linear disulfide-based redox trigger benchmark the basal thiol-mediated reduction in a system: The simple freely-rotatable **SS00**, the preorganised piperidine-derivative **SS06** and the asymmetric morpholino **SS00_M**.¹

(b) Monocyclic dichalcogenides show the impact of ring-strain and redox potential and the impact of a heterogenous S-Se bond at either of both positions. These studies revealed that 1,2-dithiolane **SS50** is labile under any thiol-mediated reduction and sensitive to ring-opening polymerisation, while 1,2-dithiane **SS60** is highly reduction resistant and activated only by strong bioreductants as e.g. the redox effector protein Thioredoxin.² 1,2-thiaselenanes **SeS60** and **SSe60** are highly reactive with selenol nucleophiles (Sec) as e.g. found in the active site of the selenoenzyme TrxR with kinetic reversibility being the key factor to differentiate both regioisomers.³

(c) Annelating 1,2-dithianes to create more complex ring structures of the **SS66**-type, with the trans-fused **SS66T**, against expectations, being thermodynamically less stable and labile to monothiol reduction as compared to the cis-fused **SS66C** being the most reduction-resistant motif of the whole series.¹ Fused **SS66**-type piperazine triggers instead gave **X-SS66C** and **X-SS66T** with similar selectivity profiles, but highly improved release kinetics optional diverse functionalisation.⁴

(d) Control motifs show the robustness of the molecular designs: **O56** to control for unspecific degradation or hydrolysis of the **SS66**-type annelated dithianes; **CC60** to control for **SS60**, **SeS60** and **SSe60** with optional *N*-alkyl substitution; and the annelated cyclohexane motif **X-CC66** to control for **X-SS66**-type annelated dithianes with optional functionalisation attached.

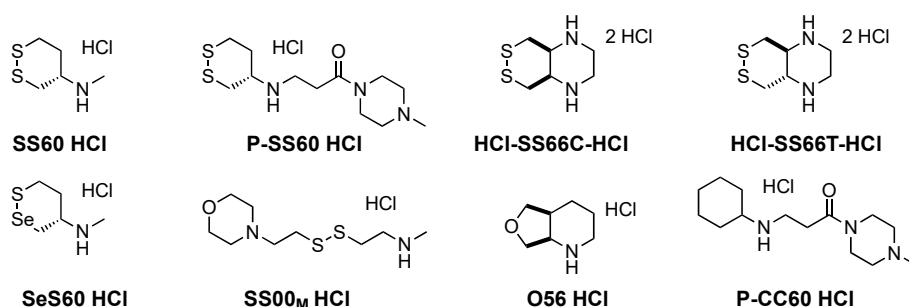
(e) Fluorescence of the molecular cargos **PQ-OH** (hydroxyphenylquinazolines) and **MF-OH** (3-*O*-methyl-fluorescein) was masked by freely combining trigger and cargo by mono-*O*-carbamoylation creating fluorogenic probes. Probes are activated by reduction of the dichalcogenide leading to 5-*exo*-trig cyclisation, that expels the cargo and re-establishes the molecular features key to its fluorescence properties.¹

(f) Several different monocyclic trigger designs have been improved by *N*-alkyl substitution with either *N*-methylpiperazinamide (**P**) or morpholinamide (**M**) instead of the simple methyl (**Me**)-derivatives.³

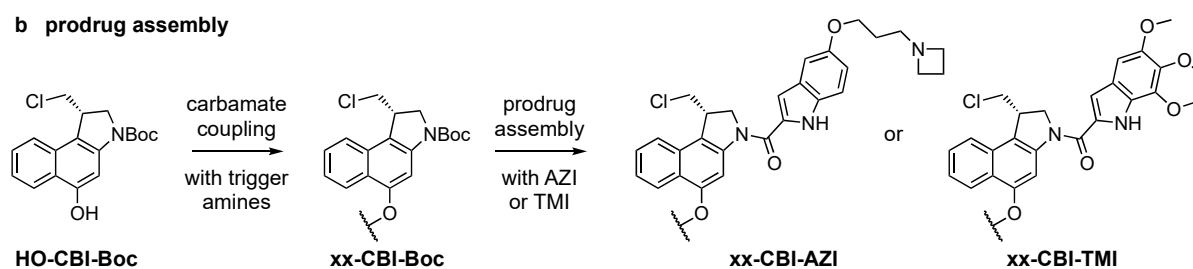
(g) Annelated 1,2-dithianes of the **X-SS66C**-type were optionally substituted by methyl (**Me**) instead of primary amines (**H**), acetyl (**Ac**) to differentiate *N*-alkylated vs. *N*-acylated versions and *N*-methylpiperazinamide (**P**) attached by acylation. Functionalisation did not affect the redox resistance and enzyme-selectivity profiles.⁴

2. CBI-based redox prodrug assembly overview

a trigger amine precursor



b prodrug assembly



<i>synthetic scales and yields</i>	carbamate coupling		amide coupling (AZI)	amide coupling (TMI)
SS60	123 mg (96%)		44 mg (49%)	<i>not made</i>
P-SS60	191 mg (58%)		17 mg (65%)	42 mg (82%)
H-SS66C <i>precursors</i>	97 mg (67%) $\xrightarrow[\text{additional derivatisation step}]{}$	Me-SS66C	2 mg (8%)	16 mg (44%)
		P-SS66C	<i>not made</i>	11 mg (65%)
H-SS66T	42 mg (35%) $\xrightarrow{\text{Me-SS66T}}$	Me-SS66T	2 mg (14%)	19 mg (78%)
SeS60	85 mg (65%)		27 mg (51%)	<i>not made</i>
SS00_M	206 mg (99%)		30 mg (21%)	9 mg (37%)
MC	72 mg (99%)		21 mg (75%)	8 mg (15%)
O56	116 mg (95%)		50 mg (20%)	<i>not made</i>
P-CC60	72 mg (63%)		<i>not made</i>	29 mg (78%)
OBn	commercial		90 mg (57%)	<i>not made</i>

Figure S2: (a) Trigger amine precursor used in this study. For synthetic procedures see 8.1. General synthetic protocols. (b) Prodrug assembly: synthetic steps and isolated yields. Carbamate coupling of **HO-CBI-Boc** was accomplished using *in situ* amine-activated triphosgene via chloroformate **Cl(CO)O-CBI-Boc** that was quenched with the various trigger amine HCl salts to give **xx-CBI-Boc** intermediates in good to excellent yields (35-99%). See General Procedure A and synthetic procedures for further details. Prodrug assembly of **xx-CBI-Boc** intermediates with **AZI-OH** or **TMI-OH** was accomplished either using EDCI (General Procedure B, Method D) or else **TMI-OH** pre-activated with oxalyl chloride/DMF (General Procedure B, Method E). The final 16 prodrugs and control compounds were prepared in mostly good yields (8-78%).

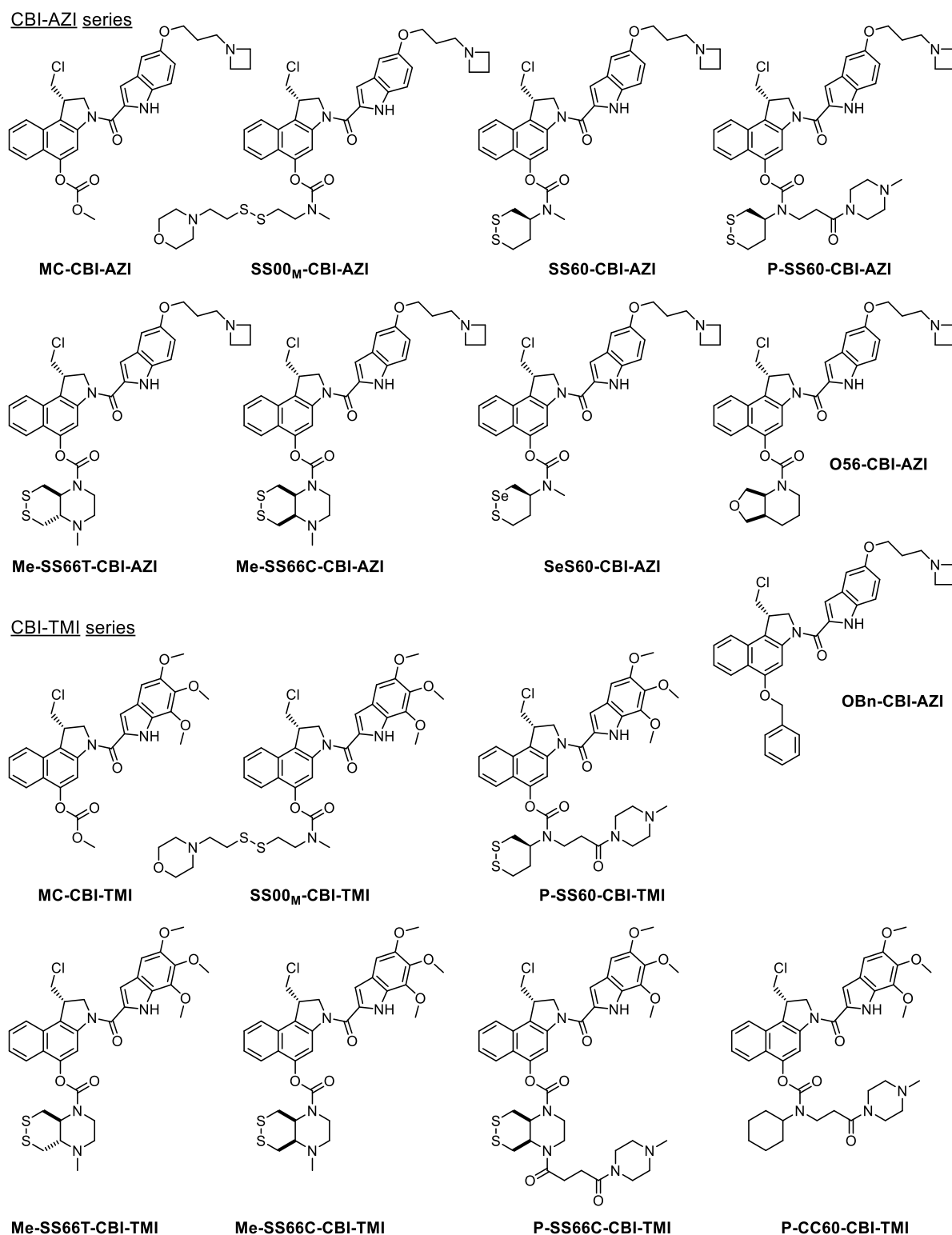
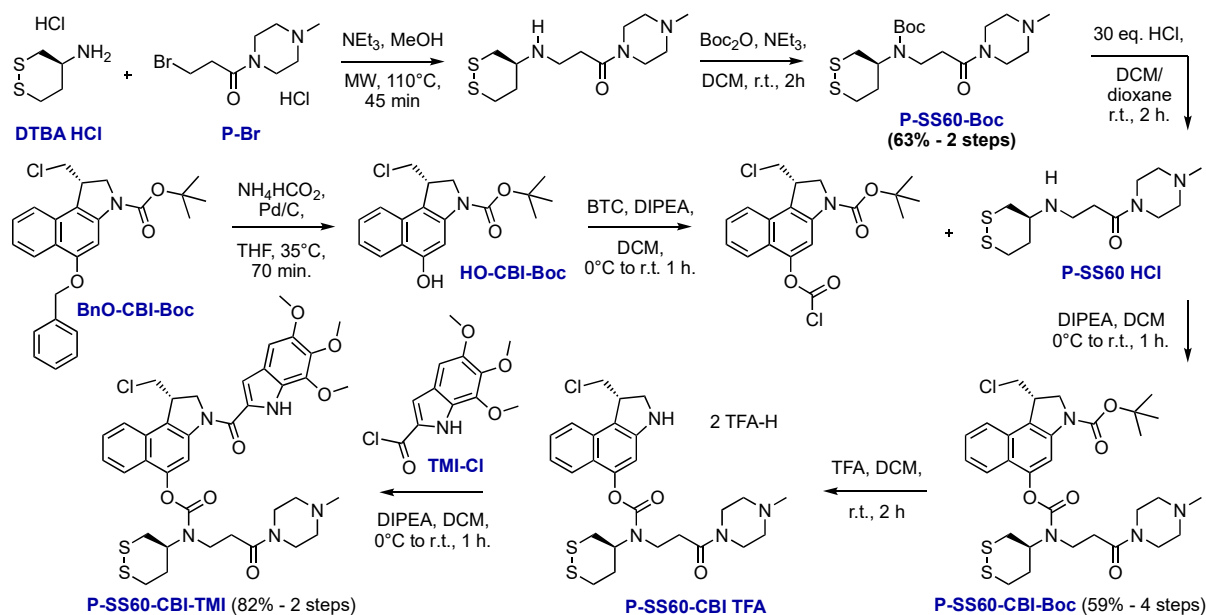


Figure S3: Prodrug overview. The **CBI-AZI series** consists of the monocyclic 1,2-dithiane-based redox prodrugs **SS60-CBI-AZI** and **P-SS60-CBI-AZI**, the 1,2-thiaselenane-based redox prodrug **SeS60-CBI-AZI**, the two annellated 1,2-dithiane-based prodrugs **Me-SS66C-CBI-AZI** and **Me-SS66T-CBI-AZI** controlled by methylcarbonate **MC-CBI-AZI**, linear disulfide reduction control **SS00_M-CBI-AZI**, and non-reducible stable carbamate **O56-CBI-AZI** and benzylether **OBn-CBI-AZI**. The **CBI-TMI series** contains the monocyclic 1,2-dithiane-based redox prodrug **P-SS60-CBI-TMI**, and the three annellated dithiane-based prodrugs **Me-SS66C-CBI-TMI** and **Me-SS66T-CBI-TMI** and **P-SS66C-CBI-TMI** controlled by methylcarbonate **MC-CBI-AZI**, linear disulfide reduction control **SS00_M-CBI-TMI** and the non-reducible **P-CC60-CBI-TMI**.

Example: Full Synthesis of P-SS60-CBI-TMI



Step 1: To a solution of the **DTBA-HCl** (335 mg, 1.95 mmol, 1.3 eq.) in MeOH (0.3 M) was added **P-Br** (407 mg, 1.50 mmol, 1.0 eq.) and NEt_3 (281 μL , 2.03 mmol, 1.35 eq.). The clear solution was heated in a sealed tube using a laboratory microwave (110 °C, 25 W, 45 min), was then cooled to r.t. and concentrated under reduced pressure.

Step 2: The material obtained in step 1 was suspended in DCM (0.1 M) and charged with NEt_3 (520 μL , 3.75 mmol, 2.5 eq.) and Boc_2O (655 mg, 3.00 mmol, 2.0 eq.) at r.t., and the mixture was stirred at for 2h. The reaction was then concentrated under reduced pressure. Purification by flash column chromatography yielded **P-SS60-Boc** as a crystalline, colourless solid (367 mg, 0.94 mmol, 63%).

Step 3: **P-SS60-Boc** (234 mg, 0.60 mmol) was dissolved in DCM (0.1 M), and HCl (3.0 ml of 4 M in dioxane, 20 equiv.) was added at r.t.. The reaction mixture was stirred at r.t. for 2h, precipitation was observed and all volatiles were removed under reduced pressure to obtain **P-SS60-HCl** as a colourless solid.

Step 4: **OBn-CBI-Boc** (424 mg, 1.00 mmol, 1.0 eq.) and dissolved in THF (60 mL, 0.02 M). The mixture was heated to 35 °C and Pd/C (118 mg, 10% on charcoal, 1.0 eq.) and NH_4HCO_2 (1.0 mL of 4 M aq. Solution, 4.0 eq.) were added. The mixture was stirred for 70 min at 35 °C until quantitative turnover was confirmed by TLC, was then filtered through Celite, the filter cake was washed with ethyl acetate (40 mL), and the combined filtrates were concentrated under reduced pressure to obtain **HO-CBI-Boc** as a colourless solid.

Step 5: The material obtained in step 4 was dissolved in anhydrous DCM (0.016 M) and the resulting solution was cooled to 0 °C. Triphosgene (350 mg, 1.18 mmol, 1.18 eq., 0.05 M solution in anhydrous DCM) and DIPEA (212 μL , 1.2 mmol 1.2 eq, 0.05 M solution in anhydrous DCM) were added. The resulting mixture was stirred at 0 °C for 15 min, was then allowed to warm to r.t. and was further stirred for 1 h. All volatiles were removed using an external liquid nitrogen trap to afford the corresponding chloroformate derivative as a colourless solid.

Step 6: The material obtained in step 3 containing **P-SS60-HCl** was suspended in anhydrous DCM (0.05 M) and DIPEA (239 μL , 1.35 mmol, 2.7 eq) was added to yield a colourless solution. To the mixture was added dropwise at 0 °C a solution of the material obtained in step 5 (0.05 M in anhydrous DCM). The resulting mixture was further stirred at 0 °C for 15 min, was then allowed to warm to r.t. and was further stirred for 1 h before being concentrated under reduced pressure. Purification by flash column chromatography yielded **P-SS60-CBI-Boc** as a crystalline, colourless solid (191 mg, 0.29 mmol, 59%).

Step 7: **P-SS60-CBI-Boc** (43.0 mg, 0.066 mmol, 1.0 eq.) was dissolved in anhydrous DCM (0.1 M), trifluoroacetic acid (230 μL , 3.91 mmol, 60.0 eq.) was added and the resulting mixture stirred at r.t. for 2 h. All volatiles were removed under reduced pressure to yield **P-SS60-CBI-TFA** as a colourless solid.

Step 8: The material obtained in step 7 was dissolved in anhydrous DCM (0.05 M), cooled to 0 °C and DIPEA (90 μL , 0.53 mmol 8.0 eq.) was added to give a clear solution. Then, a solution of **TMI-Cl** (pre-activated from **TMI**-0.2 M in DCM, 6.0 eq.) was added sequentially until full conversion of the aniline confirmed. The mixture was diluted with DCM, washed with water (2 \times) and the aq. layer was extracted with DCM (2 \times). The combined organic layers were dried over Na_2SO_4 and concentrated to give a coloured solid. Purification was achieved by FCC (DCM/MeOH) to give **P-SS60-CBI-TMI** (42.0 mg, 0.054 mmol, 82%) as a colourless solid.

3. Reduction-mediated prodrug release monitored by HPLC

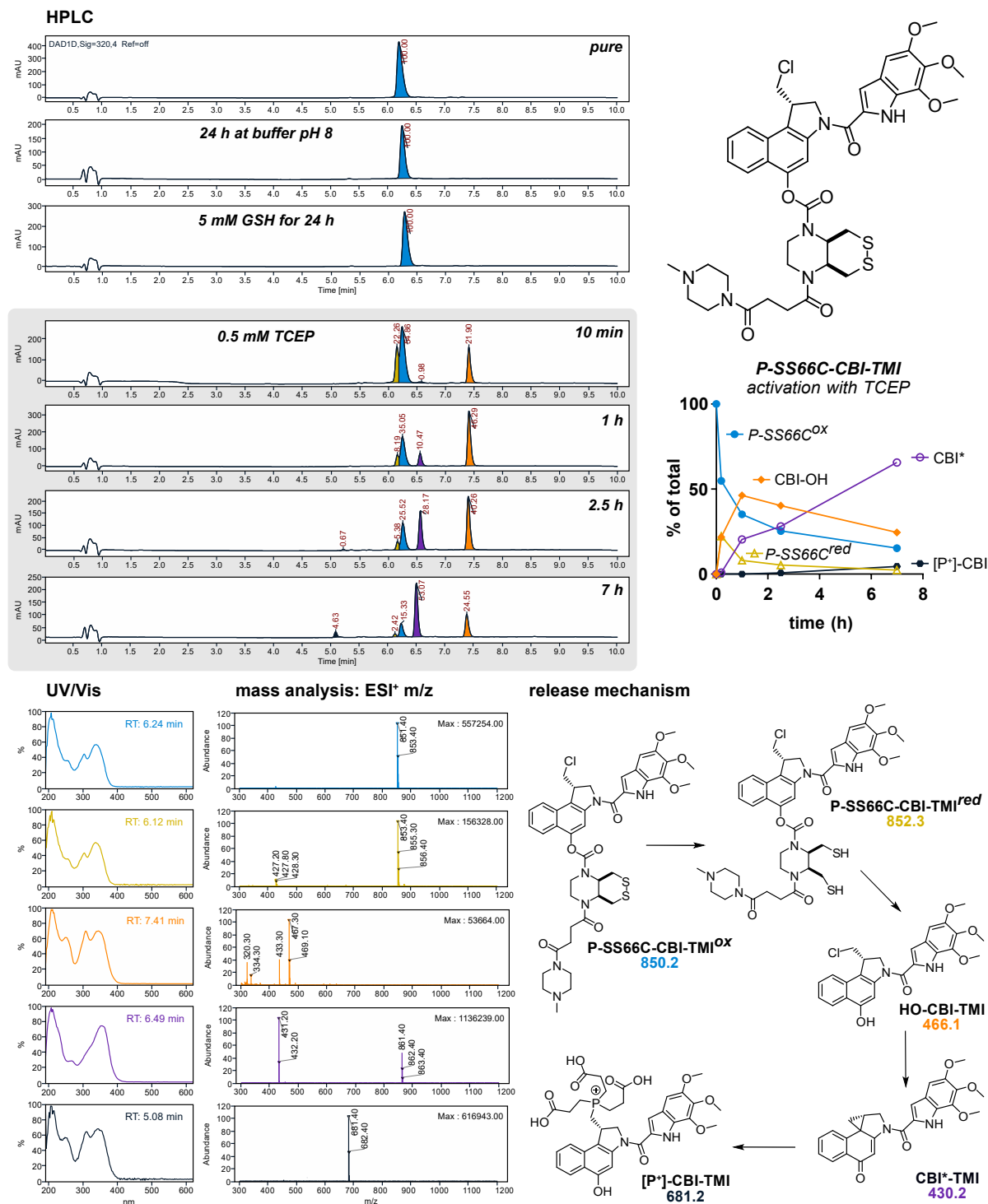


Figure S4: Reduction mediated prodrug activation - HPLC-based reduction assay. Phosphine-reductant-mediated cargo release of **P-SS66C-CBITMI^{ox}** monitored in cell-free buffer over 7 h showing: Reduction to **P-SS66C-CBI-TMI^{red}**, then intramolecular cargo expulsion giving **HO-CBI-TMI**, then formation of the biologically active species **CBI*-TMI**. With an excess of phosphine-based reduction-agent tris(2-carboxyethyl)-phosphine (TCEP) the corresponding adduct **[P*]-CBI-TMI** was detected. Compare the very slow kinetics of phosphine-reduction of this particular prodrug, to the much faster kinetics of phosphine-reduction of e.g. **P-SS60-CBI-AZI** (see next page).

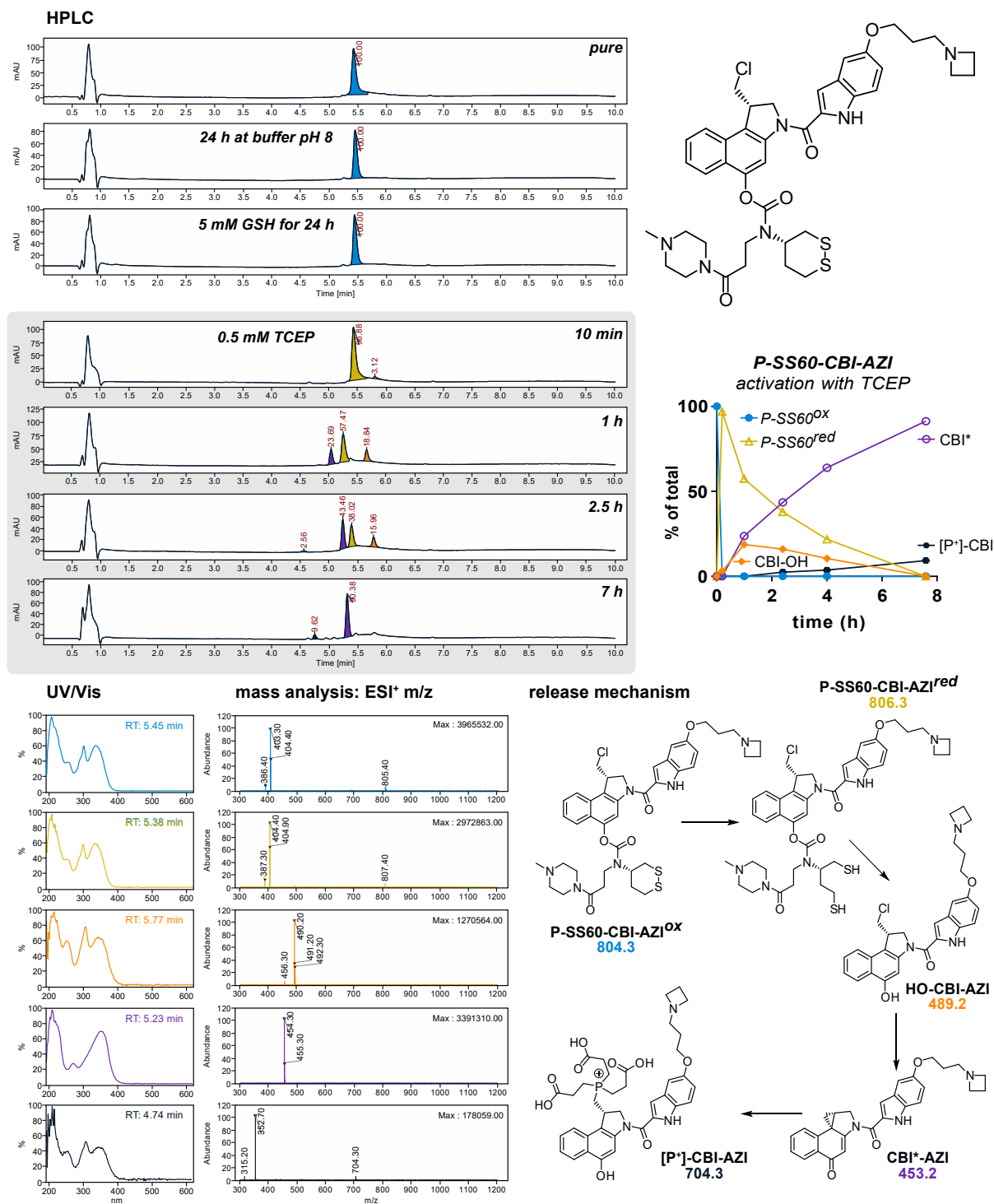
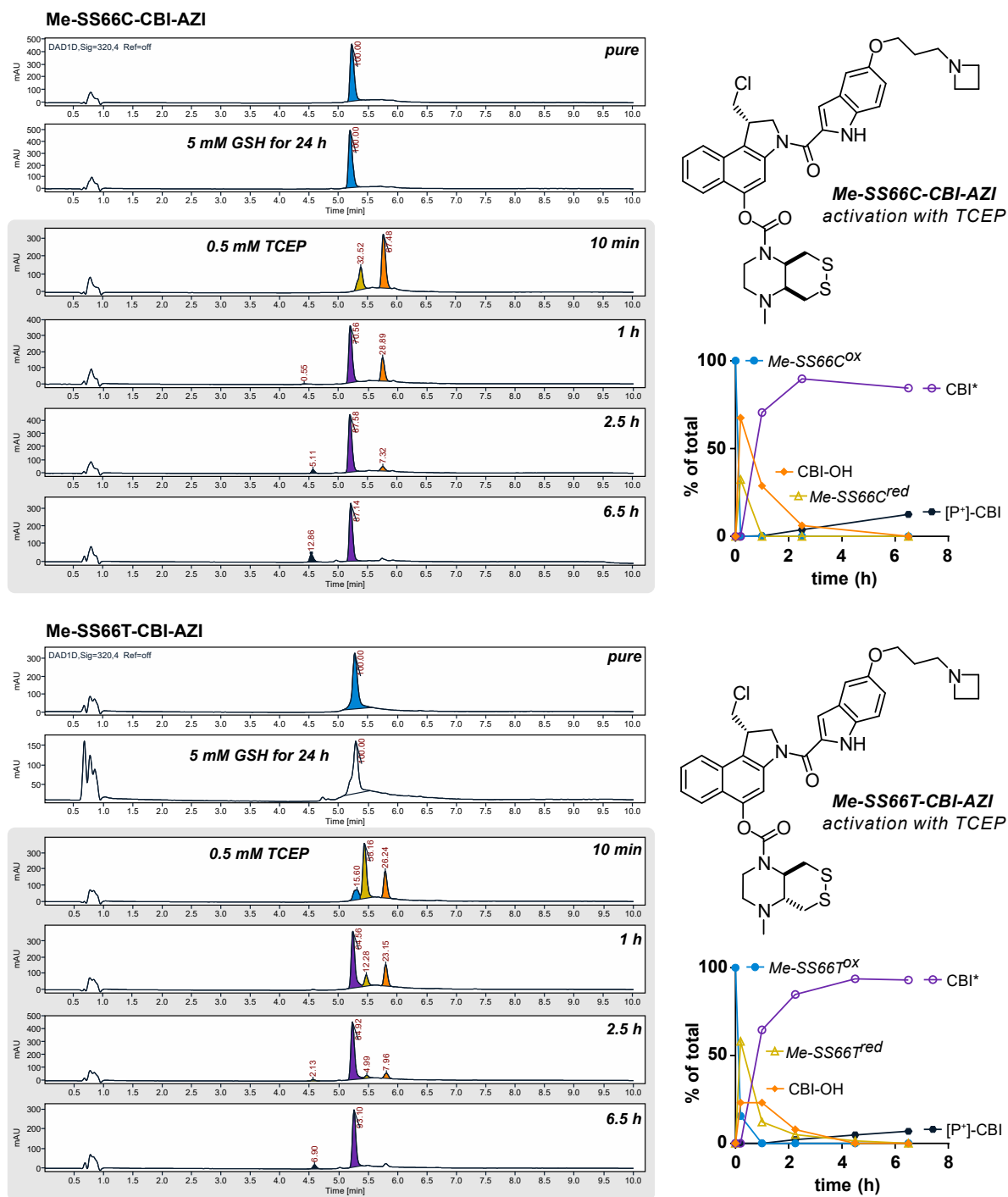


Figure S5: Reduction mediated prodrug activation - HPLC-based reduction assay. Phosphine-reductant-mediated cargo release of **P-SS60-CBI-AZI^{ox}** has been monitored at over 7 h showing: Reduction to **P-SS60-CBI-AZI^{red}** then intramolecular cargo expulsion giving **HO-CBI-AZI**, then formation of the biologically active species **CBI*-AZI**. Again, the phosphine adduct with TCEP **[P*]-CBI-AZI** was detected. Compare the relatively slow cargo expulsion rate for this prodrug, to the fast rates for annelated bicyclic Me-SS66C/T prodrugs (see next page).



4. Cellular proliferation assays

a cellular potencies in HeLa-HRE vs. A549

cellular response	HeLa-HRE			A549			IC ₅₀ (H*)/IC ₅₀ (A*)	log ₁₀ [IC ₅₀ (H*)/IC ₅₀ (A*)]
	mean	SD	n	mean	SD	n		
MC-CBI-AZI	8.09E-10	1.4E-10	3	1.13E-09	1.2E-09	3 (1)	0.7	-0.145
SS00 _M -CBI-AZI	6.85E-09	5.6E-09	4	4.12E-09	1.6E-10	5	1.7	0.427
SeS60-CBI-AZI	4.89E-08	2.9E-08	3	6.02E-08	6.5E-08	4	0.8	-0.090
Me-SS66T-CBI-AZI	4.88E-08	1.2E-08	3 (1)	5.06E-08	1.3E-08	3	1.0	-0.016
Me-SS66C-CBI-AZI	3.95E-07	2.0E-07	2 (1)	1.23E-08	3.5E-09	3	32.2	1.508
SS60-CBI-AZI	9.56E-08	5.0E-08	5	1.20E-07	1.1E-07	4	0.8	-0.097
P-SS60-CBI-AZI	8.88E-07	5.1E-07	3	1.04E-07	2.1E-08	2 (1)	8.6	0.933
O56-CBI-AZI	4.62E-07	5.5E-07	3	6.02E-08	6.5E-08	3	1.1	
OBn-CBI-AZI	7.45E-07	1.7E-07	2 (1)	4.16E-07	8.6E-08	4	1.8	0.253
MC-CBI-TMI	4.32E-09	1.8E-09	3	2.89E-09	1.5E-09	4	1.5	0.174
SS00 _M -CBI-TMI	1.25E-07	1.4E-08	3	3.51E-08	1.7E-08	4	3.6	0.551
Me-SS66T-CBI-TMI	5.89E-08	1.6E-08	3	5.92E-09	2.6E-09	3	10.0	0.998
Me-SS66C-CBI-TMI	2.19E-07	5.7E-08	3	1.72E-08	1.0E-08	3	12.7	1.105
P-SS60-CBI-TMI	4.19E-07	1.3E-07	5	1.84E-07	1.2E-08	3	2.3	0.357
P-SS66C-CBI-TMI	1.99E-07	7.0E-08	4	1.17E-08	6.9E-09	3	17.0	1.230
P-CC60-CBI-TMI	1.35E-06	3.9E-07	3 (2)	~1.6E-06	/	3	0.8	-0.075

b Trx/TrxR-dependent activity: MEF TrxR1 ko vs. wt

MEF dose response	ko			wt			IC ₅₀ (ko)/IC ₅₀ (wt)	log ₁₀ [IC ₅₀ (ko)/IC ₅₀ (wt)]
	mean	SD	n	mean	SD	n		
SeS60-CBI-AZI	1.73E-07	2.5E-08	3	1.26E-07	1.3E-08	3	1.4	0.137
Me-SS66T-CBI-AZI	2.82E-07	5.2E-08	2 (1)	1.05E-07	4.2E-08	3	2.7	0.429
Me-SS66C-CBI-AZI	1.36E-06	8.6E-07	2 (2)	3.86E-07	1.6E-07	4	3.5	0.547
SS60-CBI-AZI	3.29E-07	4.6E-08	3	4.09E-07	7.2E-08	3	0.8	-0.094
P-SS60-CBI-AZI	>1E-06		4	>1E-06		4	1	0
O56-CBI-AZI	>1E-06		2 (1)	>1E-06		2 (1)	1	0
OBn-CBI-AZI	>1E-06		2	>1E-06		2	1	0
MC-CBI-TMI	6.02E-09	1.6E-10	3	6.10E-09	1.1E-09	3	1.0	-0.006
SS00 _M -CBI-TMI	1.23E-07	4.1E-08	3	1.69E-07	4.8E-08	2	0.7	-0.137
Me-SS66T-CBI-TMI	6.42E-08	5.2E-09	3	2.58E-08	3.1E-09	3	2.5	0.396
Me-SS66C-CBI-TMI	3.00E-07	2.2E-08	3	6.20E-08	9.3E-09	3	4.8	0.684
P-SS60-CBI-TMI	1.92E-07	1.9E-08	3	1.30E-07	5.4E-08	3	1.5	0.171
P-SS66C-CBI-TMI	2.44E-07	2.4E-08	6	9.30E-08	7.0E-09	6	2.6	0.419
P-CC60-CBI-TMI	9.11E-07	7.3E-08	3	1.13E-06	2.6E-07	3	0.8	-0.095

Table S1: Summary of cellular resazurin-based cytotoxicity assays. (a) Tabulated IC₅₀ (SD, n) values calculated from independent assays. HeLa-HRE (4 h resazurin after 48 h treatment) and A549 (4 h resazurin after 72 h treatment). Potency was compared between A549 and HeLa-HRE by fold difference: IC₅₀(A549)/IC₅₀(HeLa-HRE) and log₁₀[IC₅₀(A549)/IC₅₀(HeLa-HRE)]. Compounds with a >10× fold-difference are highlighted in yellow. (b) Tabulated IC₅₀ (SD, n) values calculated from independent assays using MEF cells (fl/fl vs. -/-) (4 h resazurin after 72 h treatment). Potency was compared between fl/fl (wild type - wt) and -/- (knockout - ko) by fold difference: IC₅₀(ko)/IC₅₀(wt) and log₁₀[IC₅₀(ko)/IC₅₀(wt)]. Compounds with a >2.5× fold-difference are highlighted in yellow.

cellular potency I: HeLa-HRE cells (48 h treatment)

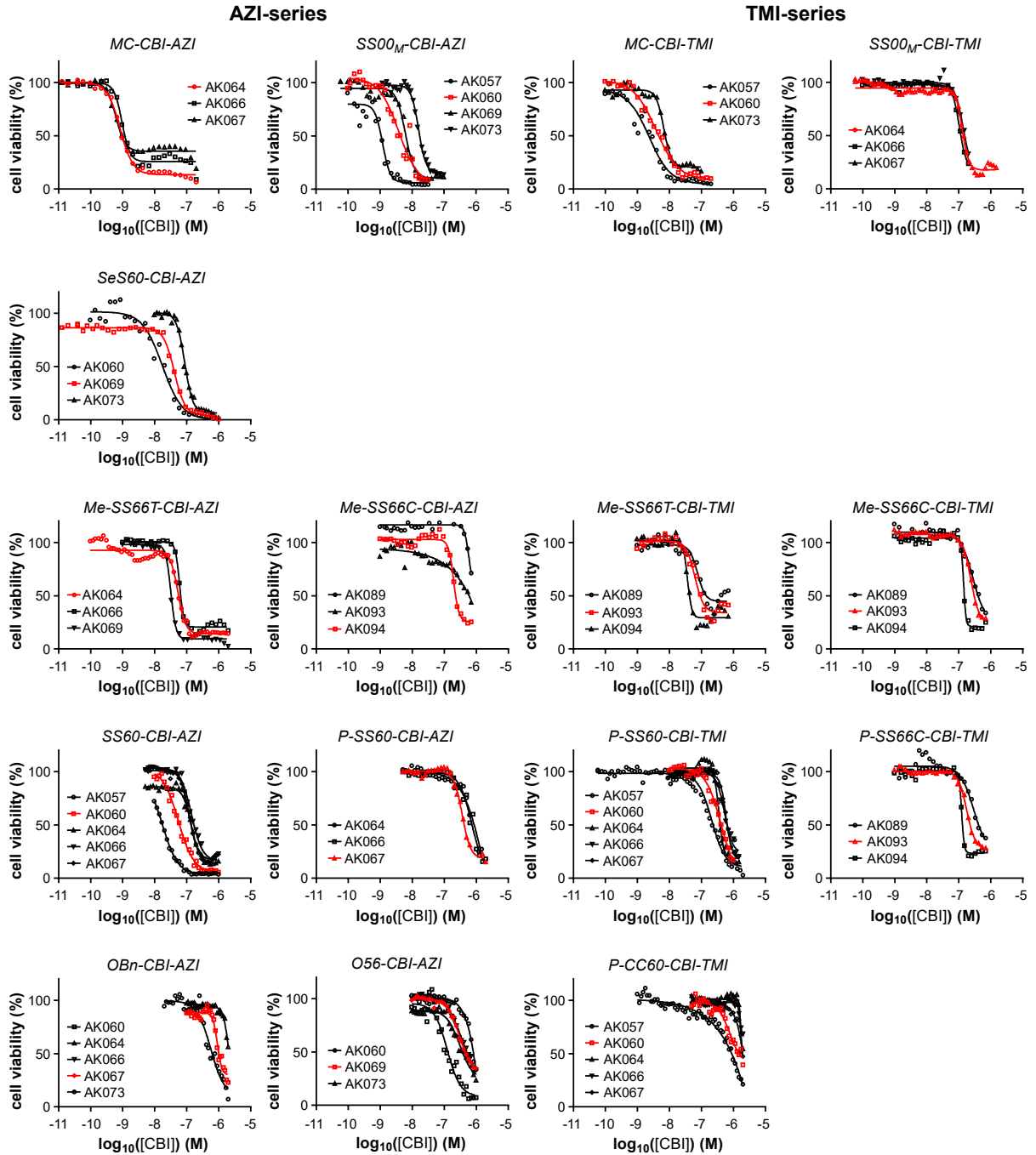


Figure S7: Cellular resazurin-based cytotoxicity assay. HeLa-HRE cells were treated with prodrugs of the CBI-TMI and CBI-AZI series for 48 h at concentrations from 10 pm to 30 μM depending on expected potencies of the constructs. Dose-response curves were calculated from at least 27 incremental single concentrations over a range of at least three log units. Individual experiments with annotated experiment numbers are shown for each prodrug with the representative example shown in **Figure 6** highlighted in red. IC₅₀ values are tabulated and correlated to dose response in A549 cells in **Table S1**.

cellular potency II: A549 cells (72 h treatment)

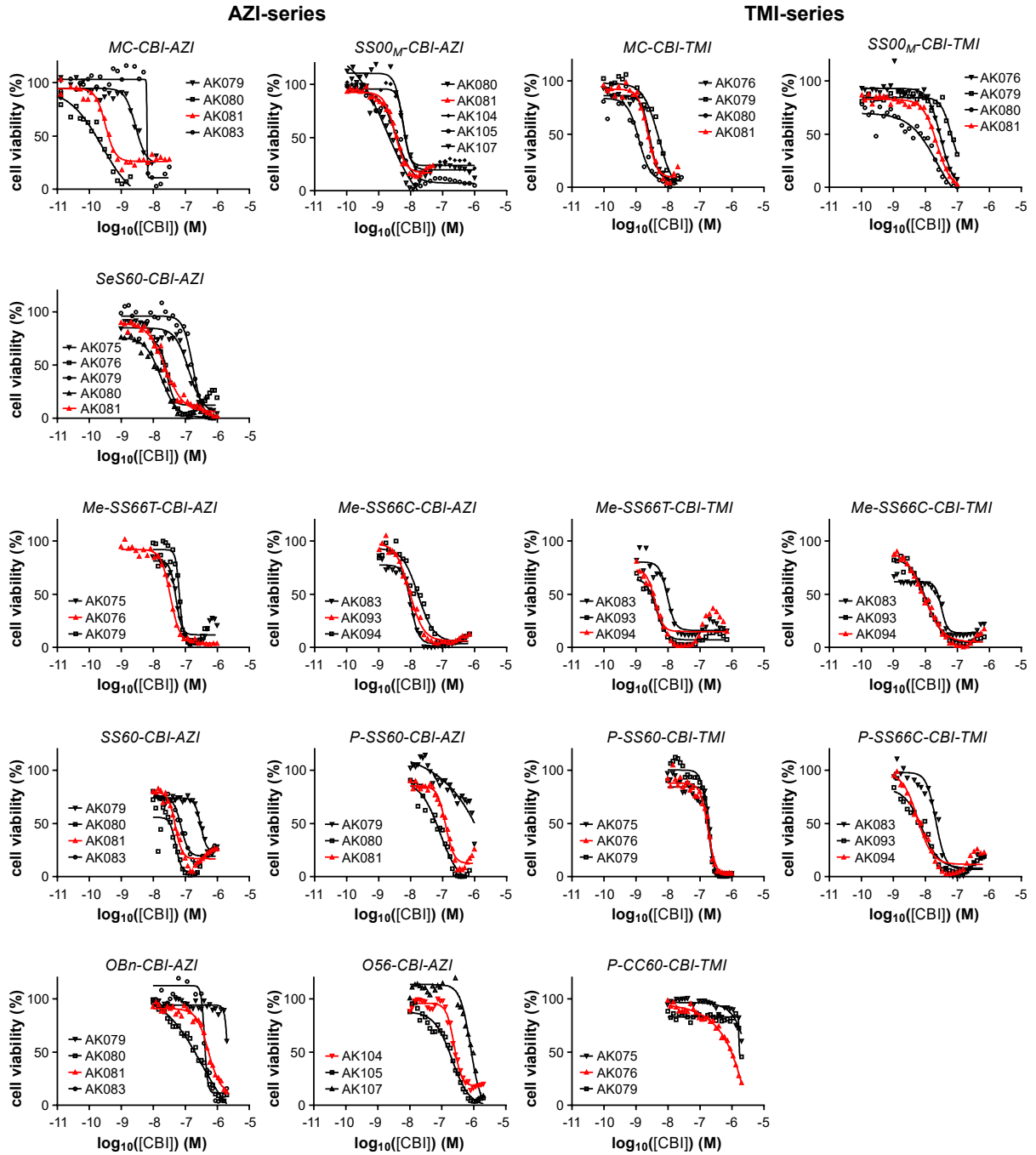


Figure S8: Cellular resazurin-based cytotoxicity assay. A549 cells were treated with prodrugs of the **CBI-TMI** and **CBI-AZI** series for 72 h at concentrations from 10 pm to 30 μM depending on expected potencies of the constructs. Dose-response curves were calculated from at least 27 incremental single concentrations over a range of at least three log units. Individual experiments with annotated experiment numbers are shown for each prodrug with the representative example shown in **Figure 6** highlighted in red. IC_{50} values are tabulated and correlated to dose response in HeLa-HRE cells in **Table S1**.

TrxR1/Trx1-dependent activation: MEF TrxR1 ko vs. wt cells (72 h treatment)

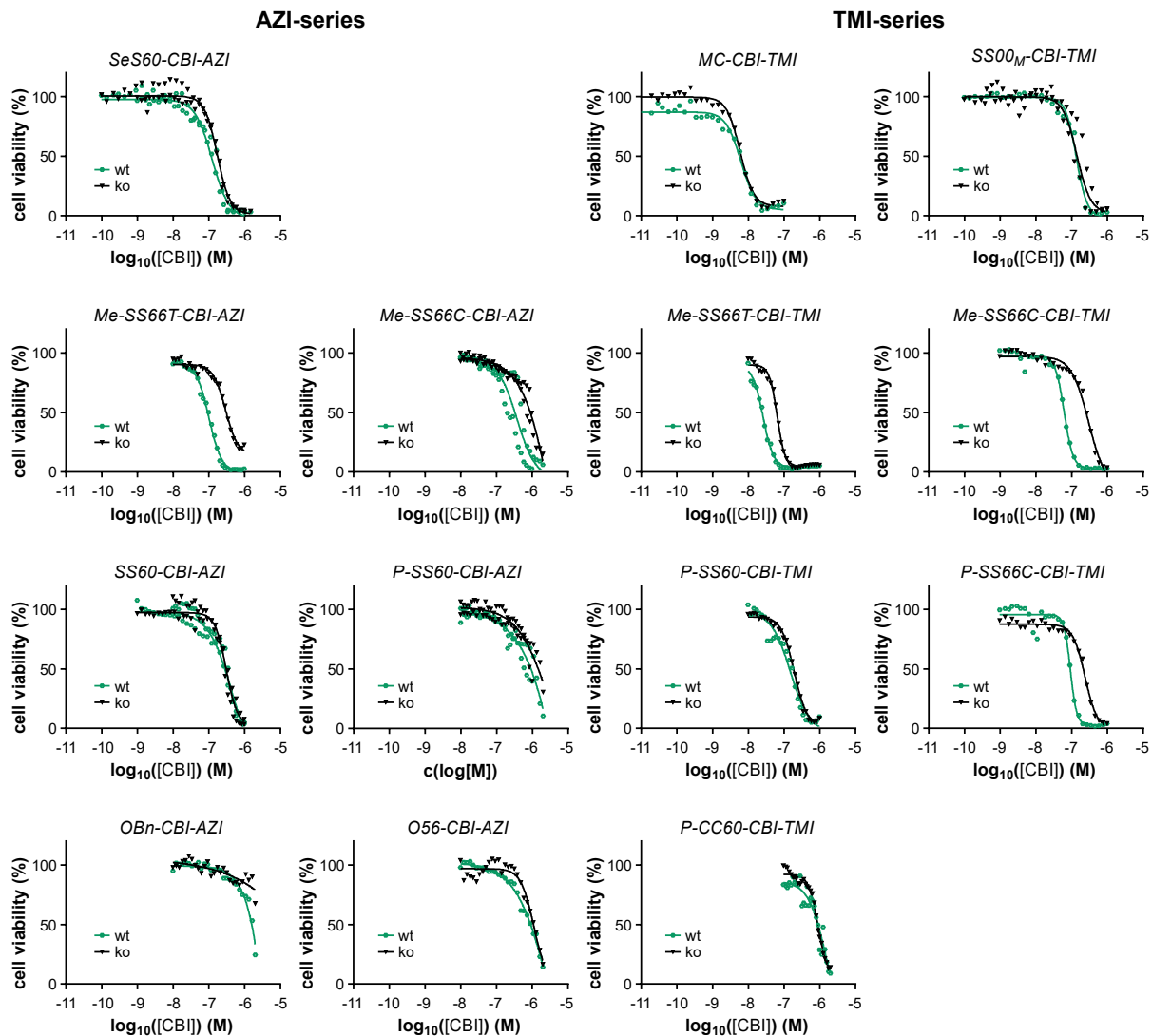


Figure S9: Evaluation of reduction-activated prodrugs – Resazurin-based cytotoxicity assay in stable TrxR1 knockout cells. MEF cells (*ko* vs. *wt*) were treated with prodrugs of the **CBI-TMI** and **CBI-AZI** series for 72 h at concentrations from 10 pm to 30 μ M at 27 incremental single concentrations depending on expected potencies of the constructs. Data from at least 3 individual experiments was combined (no error bars shown for clarity) for each cell line. Representative compounds with strong cellular TrxR1-dependence are shown in **Figure 7**. IC₅₀ values (SD, n) are tabulated and correlated in **Table S1**.

5. Prolifer-140 cancer cell screening

5.1. Prolifer-140 cancer cell screening: cellular cytotoxicity (IC_{50} values)

Nr.	Entity	Cell line	IC_{50} [M]				Reductive Activation Index			
			P-SS66C	P-SS60	P-CC60	Dox	P-SS66C	P-SS60	P-CC60	
76	Blood	MV4-11	1.5E-09	2.8E-09	1.2E-08	4.3E-09		7.7	4.3	1
119	Brain	SK-N-MC	1.6E-09	2.7E-09	1.3E-08	1.5E-08		8.3	4.9	1
95	Blood	OCI-LY19	2.8E-09	4.1E-09	1.5E-08	5.5E-09		5.4	3.7	1
48	Endometrium	Ishikawa	3.8E-09	7.1E-09	2.6E-08	7.7E-08		6.8	3.7	1
52	Blood	JVM-3	3.4E-09	8.7E-09	3.1E-08	3.0E-08		9.3	3.6	1
115	Bone	SK-ES-1	2.7E-09	5.7E-09	3.4E-08	2.6E-08		12	5.9	1
94	Blood	OCI-AML5	6.0E-09	8.6E-09	3.4E-08	3.1E-08		5.7	3.9	1
126	Blood	SU-DHL-5	2.6E-09	7.8E-09	5.0E-08	9.1E-09		19	6.4	1
31	Lung	H460	5.5E-09	7.1E-09	5.1E-08	2.6E-08		9.3	7.2	1
47	Duodenum	Hutu 80	9.6E-09	9.9E-09	5.4E-08	1.9E-08		5.6	5.4	1
77	Blood	NALM-6	2.5E-09	9.8E-09	5.6E-08	2.3E-08		23	5.7	1
78	Lung	NCI-H1048	4.0E-09	8.0E-09	5.9E-08	3.2E-08		15	7.4	1
74	Blood	MOLM-13	5.3E-09	9.1E-09	6.1E-08	2.1E-08		12	6.6	1
125	Ovary	SNU840	6.3E-08	3.8E-08	7.0E-08	1.3E-07		1.1	1.8	1
18	Lung	COR-L279	7.2E-09	1.4E-08	7.4E-08	7.9E-08		10	5.1	1
139	Blood	U-937	1.2E-08	1.6E-08	7.4E-08	2.6E-08		6.4	4.5	1
75	Blood	MOLT-4	8.6E-09	1.3E-08	7.6E-08	2.6E-08		8.8	5.9	1
30	Brain	H4	1.4E-08	1.5E-08	8.1E-08	8.2E-08		5.8	5.4	1
70	Blood	MEC-1	1.1E-08	1.5E-08	8.9E-08	7.3E-08		8.2	5.9	1
4	Ovary	A2780	8.1E-09	1.2E-08	8.9E-08	1.8E-08		11	7.4	1
23	Lung	DV90	1.2E-08	1.3E-08	9.0E-08	1.9E-08		7.8	6.9	1
51	Blood	Jurkat	6.2E-09	1.6E-08	9.4E-08	4.0E-08		15	5.7	1
42	Blood	HL-60	1.5E-08	1.8E-08	1.0E-07	2.6E-08		6.7	5.6	1
3	Skin	A2058	1.1E-08	1.5E-08	1.0E-07	3.7E-08		9.4	6.8	1
103	Lung	PC-9	1.4E-08	1.7E-08	1.1E-07	1.9E-07		8.1	6.7	1
19	Ovary	COV434	1.5E-08	2.2E-08	1.1E-07	7.0E-08		7.7	5.1	1
1	Kidney	786-O	2.9E-08	2.3E-08	1.2E-07	1.1E-07		4.1	5.2	1
87	Lung	NCI-H2286	1.7E-08	1.9E-08	1.2E-07	4.4E-08		7.5	6.5	1
137	Bone	U2OS	3.2E-08	2.4E-08	1.3E-07	1.1E-07		4.1	5.4	1
93	Blood	OCI-AML3	1.3E-08	3.3E-08	1.3E-07	7.6E-08		10	4.0	1
64	Blood	M07e	3.2E-08	1.6E-08	1.4E-07	4.6E-08		4.3	8.6	1
136	Blood	U-266	9.4E-09	2.2E-08	1.4E-07	1.1E-07		15	6.3	1
86	Lung	NCI-H2110	1.8E-08	2.7E-08	1.4E-07	3.6E-08		8.0	5.4	1
69	Breast	MDA-MB-468	1.9E-08	3.1E-08	1.5E-07	4.7E-08		7.9	4.8	1
111	Lung	SCLC-21H	2.6E-08	3.2E-08	1.6E-07	2.9E-07		6.2	4.9	1
116	Lung	SK-LU-1	2.3E-08	2.7E-08	1.6E-07	2.7E-07		7.1	6.0	1
5	Skin	A375	5.5E-08	3.2E-08	1.6E-07	4.8E-08		3.0	5.1	1
34	Breast	HCC38	1.4E-08	1.9E-08	1.7E-07	5.2E-08		12	8.7	1
22	Prostate	DU-145	1.6E-08	3.6E-08	1.8E-07	1.5E-07		11	5.1	1
100	Blood	P31/FUJ	2.3E-08	3.7E-08	1.9E-07	1.0E-07		8.3	5.1	1
99	Ovary	OVK18	4.6E-08	4.3E-08	2.0E-07	3.4E-08		4.4	4.7	1
97	Ovary	OV56	7.2E-08	6.5E-08	2.0E-07	2.0E-07		2.8	3.1	1
66	Breast	MCF-7	3.1E-08	4.5E-08	2.1E-07	2.3E-07		7.0	4.8	1
62	Colon	LOVO	1.9E-08	3.4E-08	2.2E-07	1.1E-07		12	6.6	1
122	Stomach	SNU-1	2.3E-08	3.0E-08	2.3E-07	5.9E-08		10	7.6	1
109	Bone	Saos-2 EC	6.6E-08	3.9E-08	2.3E-07	2.0E-07		3.5	6.0	1
40	Ovary	HeLa	9.9E-09	1.7E-08	2.4E-07	8.0E-08		24	14	1
88	Lung	NCI-H292	3.8E-08	4.8E-08	2.6E-07	7.2E-08		6.9	5.4	1
7	Skin	A431	2.0E-08	4.0E-08	2.6E-07	1.7E-07		13	6.5	1
89	Lung	NCI-H441	5.1E-08	5.4E-08	2.9E-07	3.5E-07		5.8	5.4	1
106	Colon	RKO	2.1E-08	4.5E-08	3.0E-07	9.9E-08		14	6.6	1

Start of Table S2 (part 1 of 3): Prolifer-140 potencies and reductive index. Table continues on next page.

Nr.	Entity	Cell line	IC ₅₀ [M]				Reductive Activation Index			
			P-SS66C	P-SS60	P-CC60	Dox	P-SS66C	P-SS60	P-CC60	
8	Kidney	A498	9.4E-08	5.0E-08	3.0E-07	3.2E-07	3.2	6.0	1	
79	Lung	NCI-H1437	1.8E-08	5.2E-08	3.0E-07	1.4E-07	16	5.8	1	
61	Lung	LOU-NH91	3.5E-08	7.5E-08	3.1E-07	2.9E-07	8.9	4.1	1	
20	Head/Neck	Detroit562	1.9E-08	4.3E-08	3.2E-07	1.5E-07	17	7.4	1	
44	Fibrosarcoma	HT-1080	2.1E-08	5.0E-08	3.2E-07	7.6E-08	15	6.4	1	
14	Kidney	Caki-1	6.3E-08	6.3E-08	3.3E-07	3.4E-07	5.2	5.2	1	
128	Colon	SW480	5.5E-08	6.5E-08	3.3E-07	1.2E-07	6.0	5.1	1	
108	Blood	RPMI 8226	1.2E-08	3.9E-08	3.4E-07	8.8E-08	28	8.8	1	
16	Lung	Calu-6	5.9E-08	5.2E-08	3.4E-07	7.7E-07	5.8	6.6	1	
58	Blood	KMS-12-BM	3.3E-08	6.6E-08	3.4E-07	1.6E-07	10	5.2	1	
114	Breast	SK-BR-3	4.2E-08	7.4E-08	3.7E-07	1.3E-07	8.8	5.0	1	
71	Pancreas	Mia PaCA 2	8.6E-08	6.8E-08	3.8E-07	7.4E-08	4.4	5.5	1	
113	Bone	SJSA-1	9.8E-08	2.4E-08	3.8E-07	4.0E-07	3.9	16	1	
110	Stomach	SCH	1.5E-08	5.2E-08	3.9E-07	1.4E-07	25	7.5	1	
134	Brain	U118MG	1.9E-07	1.4E-07	3.9E-07	2.6E-07	2.1	2.8	1	
29	Lung	H2228	4.5E-08	5.7E-08	4.0E-07	5.7E-08	8.8	7.0	1	
85	Lung	NCI-H2009	2.7E-08	6.2E-08	4.2E-07	1.4E-07	16	6.8	1	
82	Lung	NCI-H1581	4.7E-08	4.2E-08	4.3E-07	1.5E-07	9.3	10	1	
121	Ovary	SK-OV3	3.7E-08	6.2E-08	4.4E-07	1.8E-07	12	7.1	1	
36	Colon	HCT116	3.2E-08	6.9E-08	4.4E-07	1.1E-07	14	6.4	1	
105	Lung	RERF-LC-MS	3.1E-08	6.4E-08	4.6E-07	1.7E-07	15	7.1	1	
127	Brain	SW-1783	4.8E-08	6.7E-08	4.8E-07	3.0E-07	9.9	7.2	1	
73	Stomach	MKN-45	8.2E-08	9.1E-08	4.9E-07	3.2E-07	5.9	5.4	1	
27	Lung	EPLC-272H	4.6E-08	7.9E-08	5.1E-07	2.0E-07	11	6.4	1	
102	Prostate	PC3	4.0E-08	5.8E-08	5.2E-07	7.4E-07	13	8.9	1	
37	Colon	HCT-15	1.4E-07	1.0E-07	5.5E-07	6.4E-07	3.9	5.2	1	
57	Blood	KG-1 a	1.1E-07	1.0E-07	5.5E-07	4.9E-07	5.2	5.3	1	
2	Brain	A172	1.1E-07	1.2E-07	5.7E-07	9.4E-08	5.3	4.9	1	
112	Ovary	SiHa	1.1E-07	1.1E-07	6.1E-07	1.5E-07	5.4	5.5	1	
56	Blood	KG-1	1.9E-07	1.3E-07	6.2E-07	1.2E-06	3.2	4.7	1	
46	Liver	HuH7	1.0E-07	1.1E-07	6.5E-07	2.1E-07	6.5	5.7	1	
133	Brain	T98G	8.1E-08	8.6E-08	6.6E-07	1.2E-06	8.2	7.6	1	
96	Blood	OPM-2	2.6E-08	1.2E-07	6.6E-07	2.4E-07	25	5.4	1	
13	Pancreas	BxPC-3	4.6E-08	1.1E-07	6.6E-07	2.8E-07	14	6.1	1	
130	Colon	SW948	1.4E-07	1.3E-07	6.8E-07	3.5E-07	4.8	5.3	1	
118	Brain	SK-N-FI	1.4E-07	1.2E-07	6.8E-07	1.4E-06	4.9	5.7	1	
129	Colon	SW620	1.5E-07	1.4E-07	7.0E-07	3.1E-07	4.6	5.0	1	
54	Blood	KARPAS 299	1.1E-07	1.6E-07	7.1E-07	7.3E-08	6.5	4.4	1	
123	Stomach	SNU-16	6.2E-08	1.2E-07	7.1E-07	1.4E-07	11	5.8	1	
63	Blood	LP-1	1.0E-07	1.7E-07	7.2E-07	6.6E-07	6.9	4.2	1	
49	Bladder	J82	9.6E-08	9.9E-08	7.2E-07	8.0E-07	7.5	7.3	1	
59	Brain	LN229	1.3E-07	1.4E-07	7.2E-07	2.2E-07	5.4	5.2	1	
28	Lung	H1299	5.4E-08	7.9E-08	7.3E-07	2.2E-07	14	9.3	1	
67	Breast	MDA MB 231	1.4E-07	1.7E-07	7.4E-07	2.8E-07	5.4	4.2	1	
107	Endometrium	RL95-2	1.3E-07	1.5E-07	7.4E-07	2.0E-07	5.9	4.8	1	
120	Brain	SK-N-SH	1.1E-07	1.5E-07	7.5E-07	9.8E-08	6.5	5.1	1	
90	Lung	NCI-H82	8.8E-08	1.5E-07	7.5E-07	6.2E-07	8.5	5.0	1	
91	Lung	NCI-H838	7.4E-08	1.2E-07	7.5E-07	1.5E-07	10	6.2	1	
17	Colon	Colo 205	8.6E-08	1.6E-07	7.6E-07	1.5E-07	8.8	4.9	1	
9	Lung	A549	3.0E-08	1.2E-07	7.7E-07	3.1E-07	25	6.4	1	
104	Lung	RERF-LC-Ad2	1.4E-07	1.9E-07	7.8E-07	4.6E-07	5.5	4.2	1	
21	Colon	DLD-1	1.3E-07	1.7E-07	7.9E-07	1.4E-07	6.3	4.7	1	
83	Lung	NCI-H1703	5.1E-08	1.2E-07	8.1E-07	9.2E-08	16	6.7	1	
65	Ovary	MCAS	1.4E-07	1.3E-07	8.2E-07	1.1E-07	5.9	6.5	1	
84	Lung	NCI-H1838	7.7E-08	8.5E-08	8.2E-07	2.5E-07	11	9.6	1	

Middle of Table S2 (part 2 of 3): Proliferator-140 potencies and reductive index. Table continues on next page.

Nr.	Entity	Cell line	IC ₅₀ [M]				Reductive Activation Index			
			P-SS66C	P-SS60	P-CC60	Dox	P-SS66C	P-SS60	P-CC60	
6	Lung	A427	4.4E-08	1.6E-07	8.2E-07	6.6E-08	19	5.0	1	
60	Prostate	LnCap	2.7E-08	1.1E-07	8.9E-07	1.9E-07	33	8.0	1	
33	Breast	HCC202	9.1E-08	1.3E-07	9.0E-07	7.6E-07	9.8	7.1	1	
26	Ovary	EFO-27	6.2E-08	1.6E-07	9.0E-07	2.9E-07	15	5.7	1	
132	Colon	T84	1.6E-07	1.8E-07	9.1E-07	1.4E-06	5.7	5.1	1	
24	Breast	EFM-19	3.1E-07	2.3E-07	9.6E-07	4.7E-07	3.1	4.2	1	
43	Stomach	Hs 746T	7.5E-08	1.3E-07	9.9E-07	4.0E-07	13	7.7	1	
32	Breast	HCC 1569	3.6E-08	1.2E-07	9.9E-07	7.0E-07	28	8.2	1	
45	Colon	HT-29	1.1E-07	1.9E-07	1.0E-06	3.7E-07	9.5	5.3	1	
98	Ovary	OVCAR-3	7.9E-08	1.2E-07	1.0E-06	3.7E-07	13	8.7	1	
117	Skin	SK-MEL-3	1.6E-07	1.8E-07	1.0E-06	5.1E-07	6.6	5.8	1	
131	Breast	T-47D	9.8E-08	2.3E-07	1.0E-06	4.3E-07	11	4.5	1	
81	Lung	NCI-H1573	9.0E-08	1.8E-07	1.1E-06	3.0E-06	12	6.1	1	
68	Skin	MDA MB 435	1.3E-07	1.8E-07	1.1E-06	4.8E-07	8.6	6.1	1	
53	Blood	K562	1.3E-07	2.1E-07	1.1E-06	4.4E-07	8.6	5.3	1	
12	Breast	BT-20	1.2E-07	2.4E-07	1.1E-06	2.3E-07	9.1	4.6	1	
92	Stomach	NCI-N87	7.5E-08	1.4E-07	1.1E-06	2.0E-07	15	8.1	1	
138	Brain	U87MG	1.5E-07	2.3E-07	1.2E-06	1.6E-07	8.0	5.4	1	
41	Liver	Hep3B2.1-7	1.7E-07	2.4E-07	1.3E-06	5.3E-07	7.8	5.6	1	
101	Pancreas	PANC-1	2.0E-07	2.5E-07	1.4E-06	8.0E-07	6.9	5.4	1	
35	Lung	HCC827	9.1E-08	1.9E-07	1.4E-06	3.5E-07	15	7.3	1	
140	Breast	ZR-75-1	3.1E-07	2.2E-07	1.4E-06	1.3E-06	4.6	6.4	1	
11	Lung	BEN	5.3E-08	1.1E-07	1.4E-06	4.1E-06	27	13	1	
15	Kidney	Caki-2	2.7E-07	2.1E-07	1.5E-06	1.0E-06	5.6	7.2	1	
72	Stomach	MKN-1	1.4E-07	2.1E-07	1.5E-06	5.2E-08	11.1	7.3	1	
50	Breast	JIMT-1	1.0E-07	1.9E-07	1.6E-06	1.3E-06	15	8.4	1	
55	Stomach	Kato III	2.2E-07	3.7E-07	1.6E-06	9.0E-07	7.4	4.3	1	
80	Lung	NCI-H1563	1.1E-07	2.0E-07	1.7E-06	5.4E-07	15	8.6	1	
25	Breast	EFM-192A	2.7E-07	3.0E-07	1.8E-06	7.3E-07	6.6	5.9	1	
38	Endometrium	HEC-1-A	1.0E-07	2.8E-07	1.8E-06	3.3E-07	18	6.5	1	
124	Stomach	SNU-216	9.2E-08	2.7E-07	1.8E-06	3.9E-07	20	6.8	1	
135	Brain	U251MG	1.2E-07	1.9E-07	2.0E-06	7.8E-07	17	11	1	
10	Pancreas	AsPC-1	2.6E-07	2.6E-07	2.1E-06	1.2E-06	8.2	8.2	1	
39	Endometrium	HEC-1-B	4.0E-07	8.3E-07	3.3E-06	2.4E-06	8.3	4.0	1	

End of Table S2 (part 3 of 3): Prolifer-140 potencies and reductive index.

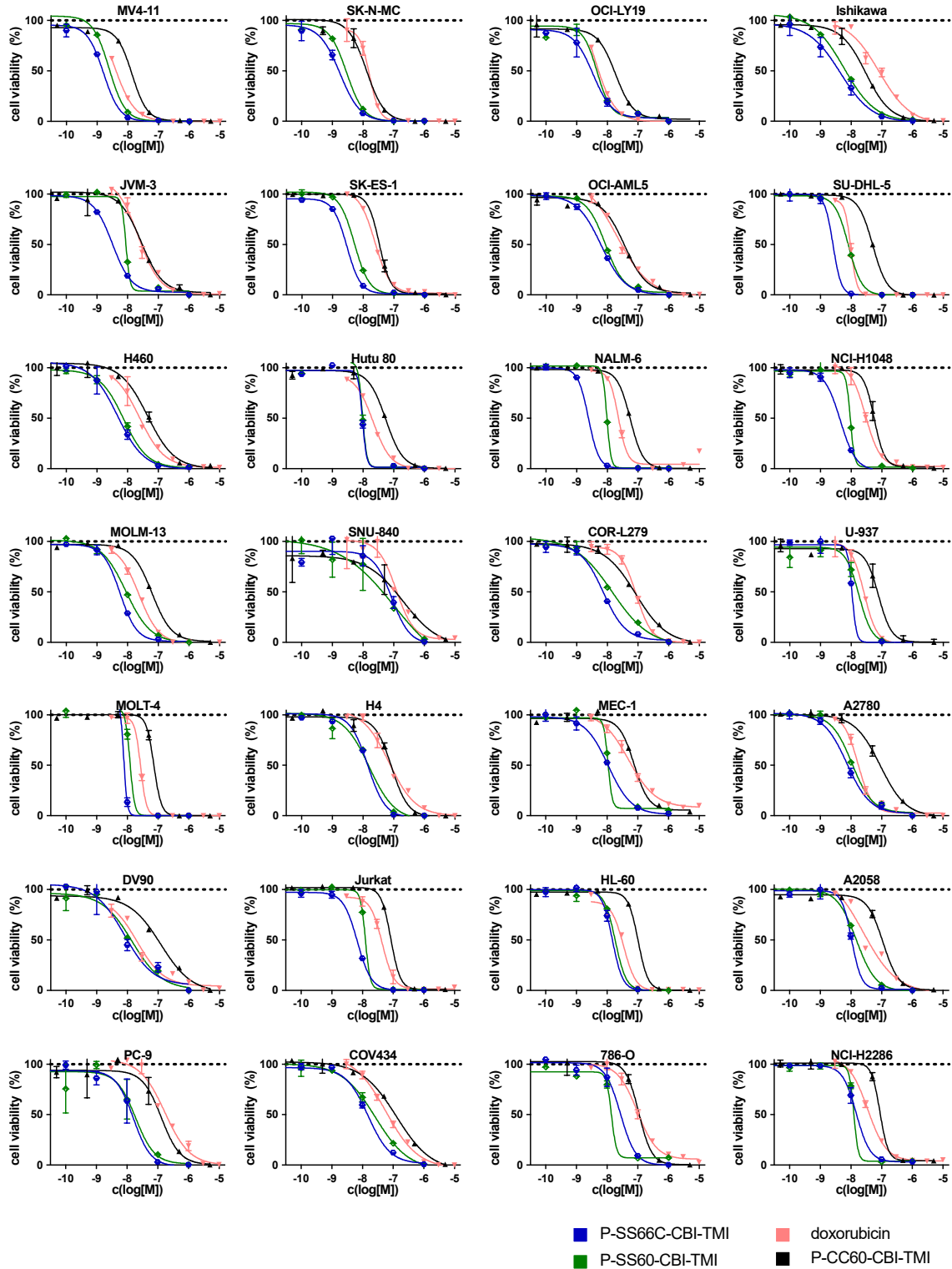
The first four data columns show the sensitivities of 140 cancer cell lines to bioreductive prodrugs **P-SS60-CBI-TMI** and **P-SS66C-CBI-TMI**, and to **P-CC60-CBI-TMI** (hydrolysis control) and doxorubicin (assay control, reference compound). Cell lines were sorted by increasing IC₅₀ values for **P-CC60-CBI-TMI**.

The final four columns show the ratios for the IC₅₀ values divided by those of **P-CC60-CBI-TMI** (**reductive activation index**): aiming to identify in which lines one or both prodrugs show significantly higher potency than in others, which may reflect greater degrees of reductive rather than only hydrolytic activation in those lines. *Cell lines with a >10× fold-index for P-SS66C-CBI-TMI are highlighted in yellow.*

For both mathematical and biological reasons, the index itself is not a quantitative measurement of bioreduction, and directly comparing indices across very different situations (e.g. for one prodrug in one cell line, compared to a different prodrug in a different cell line) is not an appropriate way to quantify differences in bioreductive activation. Quantitative analysis of bioreduction would instead require screening with a direct absolute readout - such as fluorogenic probes - not with the indirect and cell-line-dependent readout of cell death given here. We believe that such quantitative data would also be more appropriate for testing whether biological features (e.g. tissues of origin, gene expression patterns) might correlate usefully to reductive activation.

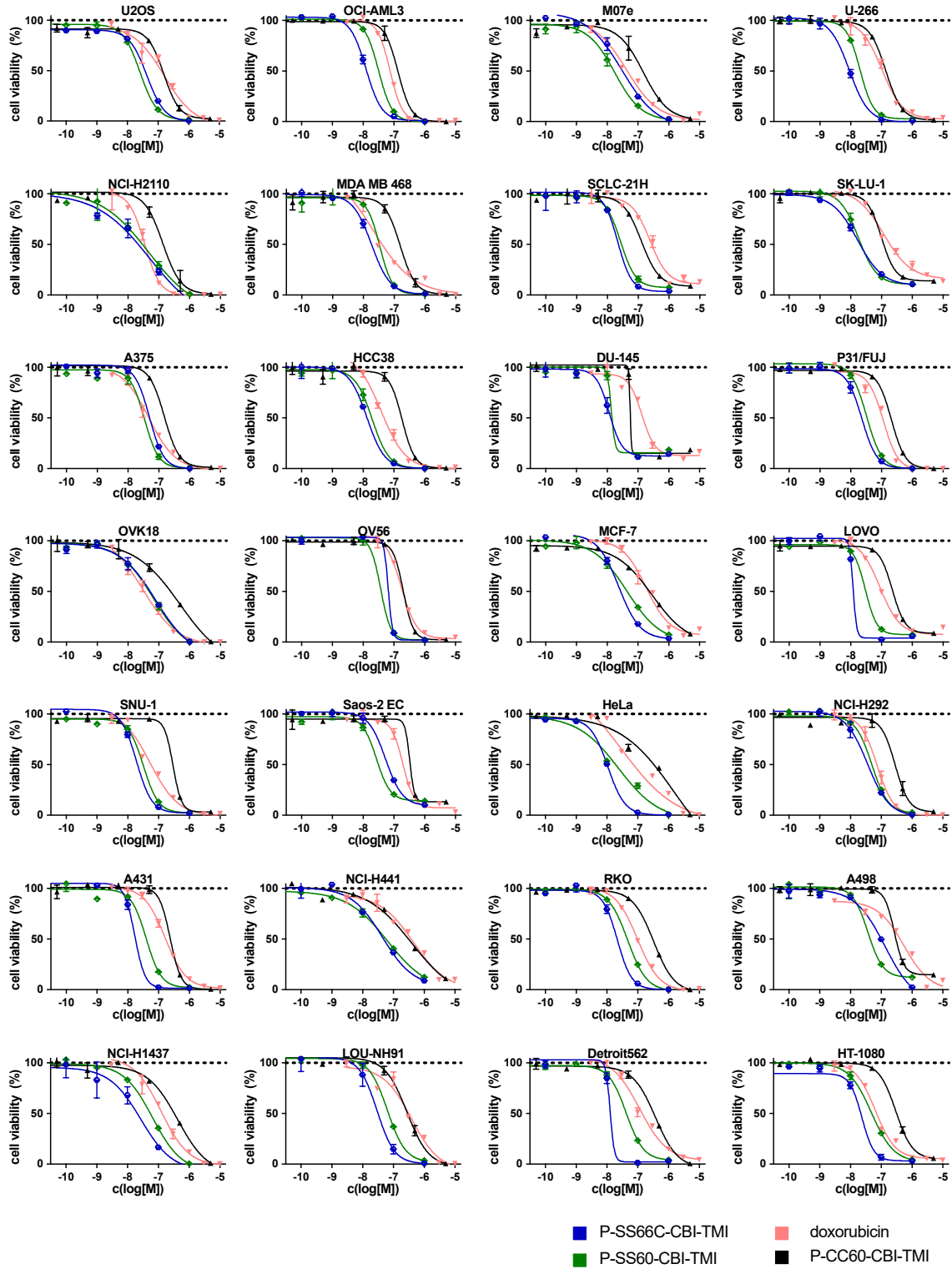
A simplistic, unbiased test of the correlation across all cell lines of each prodrug's potencies to gene expression (mRNA transcript levels, from Affymetrix HGU133 Plus 2.0) was carried out as a commercial service by 4HF Biotec GmbH. None of the correlations below a p < 0.05 cutoff for reductive prodrug sensitivity without similar CC60 control sensitivity were for genes we consider related to reductive activation. If similar investigations would be desired with future datasets, it could be informative to test reductive index correlation directly (rather than unbiased correlation of drug potencies then comparison of the results lists) but this possibility was not available.

Prolifer-140 cell line panel part I (lines 1-28)



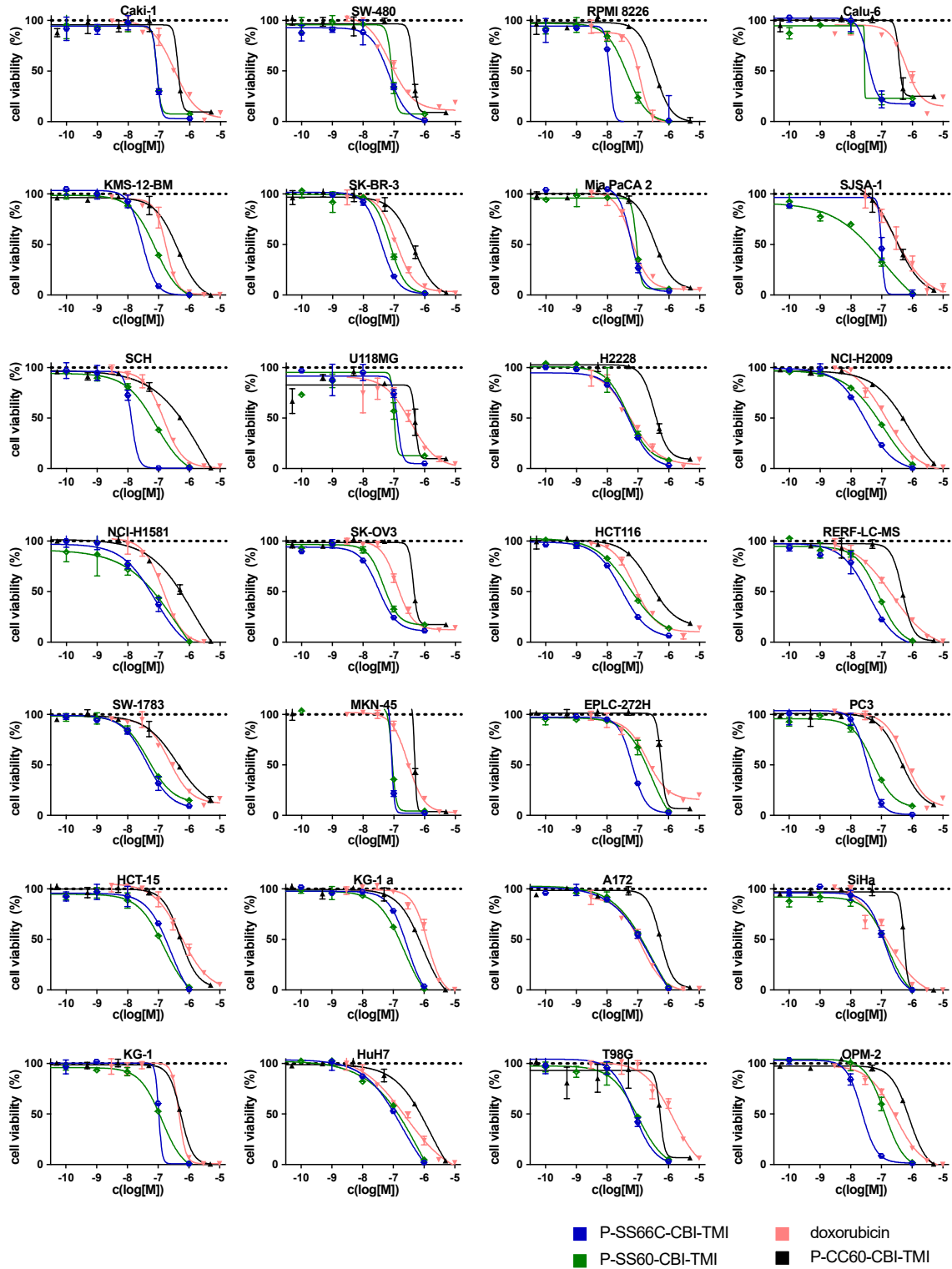
Start of Fig S10 (part 1 of 5: figure continues on next page): Prolifer-140 screen for cytotoxicities

Prolifer-140 cell line panel part II (lines 29-56)



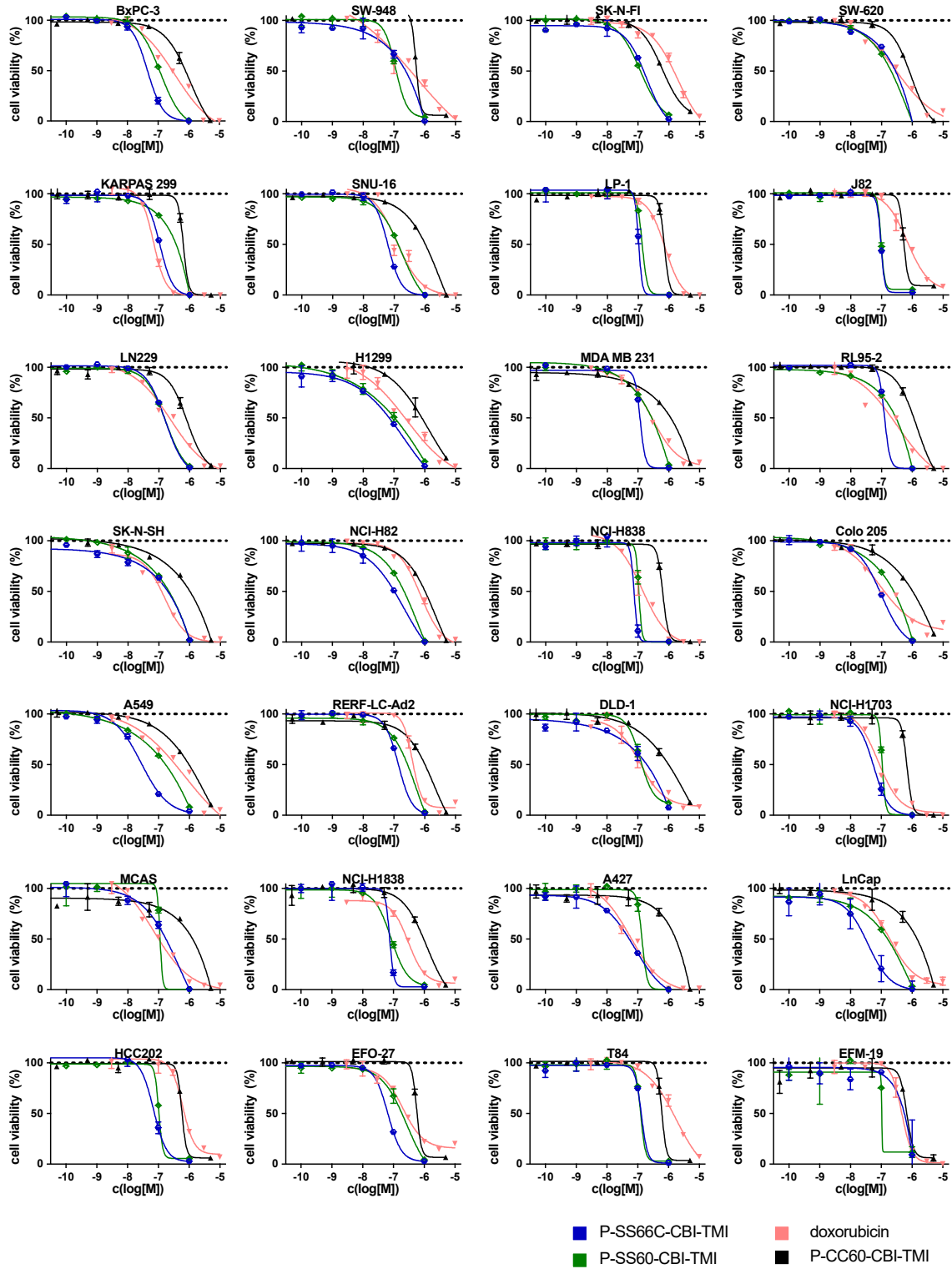
Continuation of Fig S10 (part 2 of 5: figure continues on next page): Prolifer-140 screen for cytotoxicities

Prolifer-140 cell line panel part III (lines 57-84)



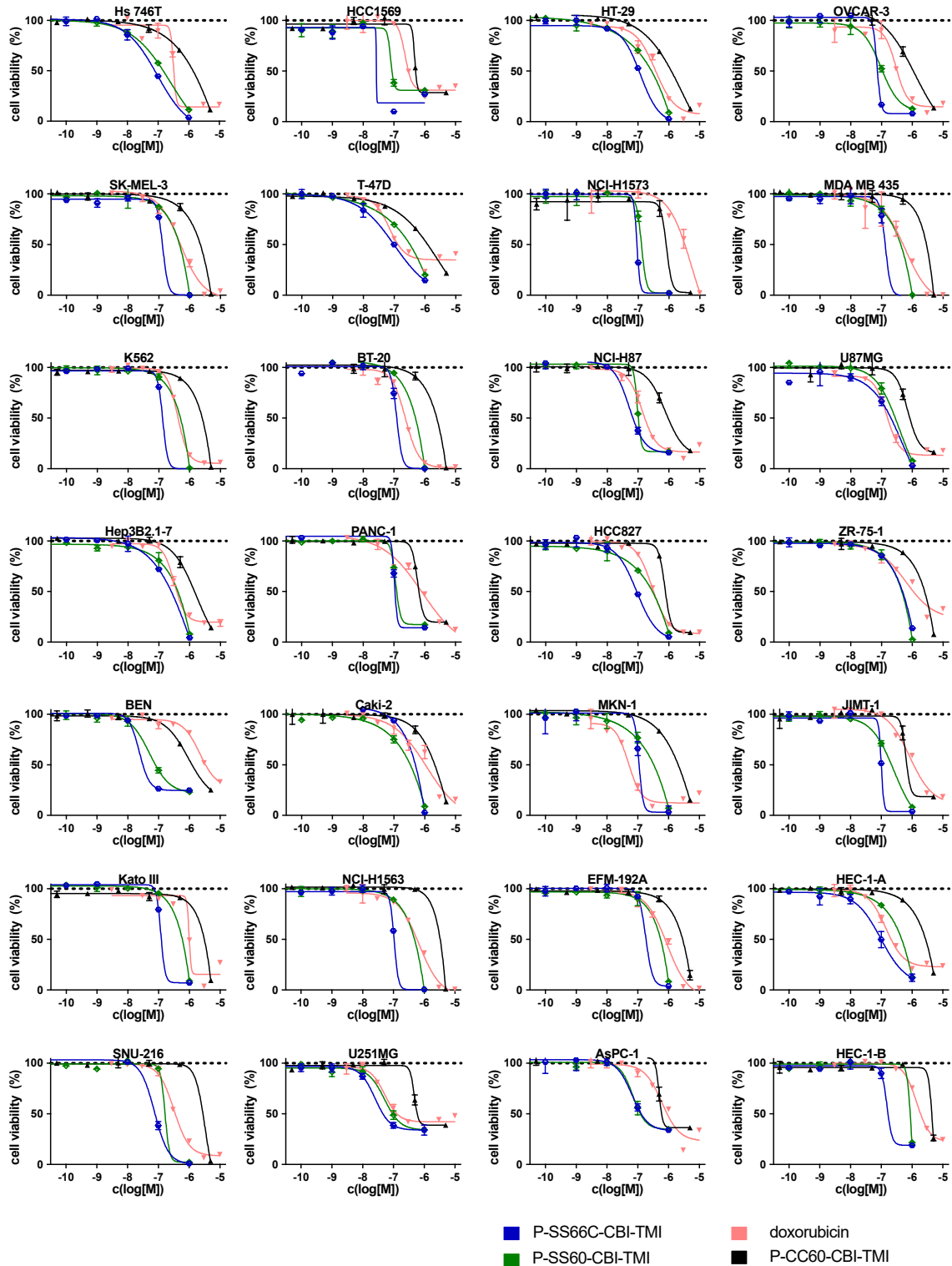
Continuation of Fig S10 (part 3 of 5: figure continues on next page): Prolifer-140 screen for cytotoxicities

Prolifer-140 cell line panel part IV (lines 85-112)



Continuation of Fig S10 (part 4 of 5: figure continues on next page): Prolifer-140 screen for cytotoxicities

Prolifer-140 cell line panel part V (lines 113-140)



End of Fig S10 (part 5 of 5): Prolifer-140 cancer cell line screening for cytotoxicity of the prodrugs. 8-data-point dose response curves from CellTiter-Glo® viability readout. All graphs within this figure have been presented in order of decreasing potency of **P-CC60-CBI-TMI**.

5.2. *Proliferator-140 cancer cell screen: Summary and population analysis*

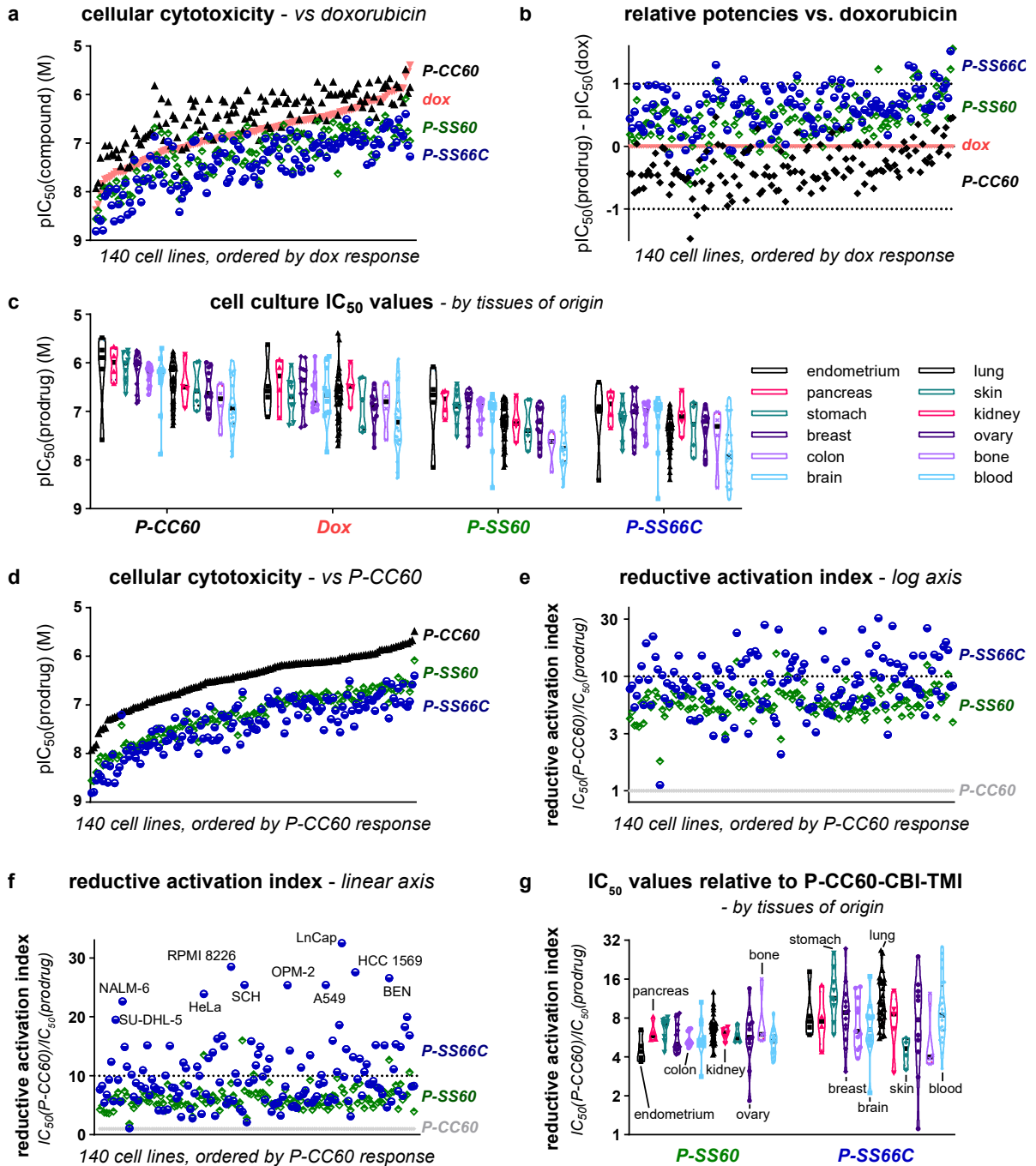


Figure S11: Proliferator-140 cancer cell screening – population analysis. (a) IC_{50} values for P-SS60-CBI-TMI (P-SS60), P-SS66C-CBI-TMI (P-SS66C) and P-CC60-CBI-TMI (P-CC60) are shown for 140 cell lines sorted by decreasing response to doxorubicin (dox). (b) pIC_{50} values ($= -\log_{10}(IC_{50})$ (M)) compared to those for dox, sorted by decreasing response to dox. (c) IC_{50} values sorted by tissue of origin. (d) IC_{50} values sorted by decreasing response to P-CC60. (e,f) Reductive activation index ($= IC_{50}(P-CC60)/IC_{50}(\text{prodrug})$) values, sorted by decreasing response to P-CC60. (g) Reductive activation index values for P-SS66C and P-SS60, grouped by tissues of origin.

6. NCI-60 cancer cell screening

6.1. NCI-60 growth inhibition results (GI_{50} values)

Cell line	GI_{50} [M]					Reductive Activation Index				
	P-CC60	P-SS60	P-SS66C	Me-SS66C	Me-SS66T	P-SS60	P-SS66C	Me-SS66C	Me-SS66T	
SR	2.8E-07	3.4E-08	2.0E-08	3.7E-08	4.0E-09	8	14	7	69	
MCF7	3.2E-07	3.5E-08	1.5E-08	2.8E-08	5.2E-09	9	21	11	61	
DU-145	4.6E-07	5.9E-08	2.5E-08	6.3E-08	3.5E-09	8	19	7	131	
NCI-H23	4.7E-07	5.5E-08	1.9E-08	4.5E-08	9.5E-09	9	25	10	49	
ACHN	4.9E-07	5.6E-08	4.2E-08	2.8E-08	9.6E-09	9	12	17	52	
NCI-H460	5.1E-07	5.6E-08	2.2E-08	4.1E-08	4.8E-09	9	23	12	107	
MOLT-4	5.9E-07	9.0E-08	6.3E-08	7.0E-08	9.9E-09	7	9	9	60	
HOP-62	5.9E-07	1.1E-07	4.1E-08	2.1E-07	1.2E-08	5	14	3	48	
K-562	6.8E-07	1.6E-07	8.9E-08	4.0E-07	2.5E-08	4	8	2	28	
MDA-MB-468	6.9E-07	1.7E-07	3.7E-08	1.6E-07	1.2E-08	4	18	4	60	
HL-60(TB)	7.5E-07	1.2E-07	4.8E-08	5.2E-08	1.2E-08	6	16	14	63	
CCRF-CEM	9.9E-07	2.2E-07	2.7E-07	1.1E-07	2.6E-08	5	4	9	38	
RXF 393	1.1E-06	1.5E-07	3.5E-08	1.3E-07	9.5E-09	7	31	8	111	
LOX IMVI	1.1E-06	2.1E-07	6.9E-08	1.7E-07	1.2E-08	5	16	7	90	
SN12C	1.2E-06	2.9E-07	4.5E-08	2.0E-07	1.7E-08	4	27	6	70	
SF-539	1.3E-06	1.7E-07	3.9E-08	1.7E-07	1.0E-08	8	34	8	131	
COLO 205	1.4E-06	3.4E-07	1.5E-07	3.3E-07	4.9E-08	4	9	4	28	
NCI-H226	1.4E-06	4.3E-07	2.5E-07	1.0E-06	9.5E-08	3	6	1	15	
RPMI-8226	1.5E-06	2.2E-07	1.4E-07	1.6E-07	3.4E-08	7	10	9	43	
CAKI-1	1.5E-06	2.7E-07	1.7E-07	2.5E-07	2.7E-08	5	9	6	55	
HCT-116	1.5E-06	1.6E-07	1.5E-07	1.9E-07	1.8E-08	9	10	8	83	
U251	1.5E-06	1.6E-07	8.1E-08	1.4E-07	1.1E-08	9	19	11	139	
HCC-2998	1.5E-06	1.6E-07	5.4E-08	1.4E-07	1.5E-08	10	28	11	99	
HT29	1.5E-06	2.7E-07	1.4E-07	2.3E-07	3.4E-08	6	11	7	45	
M14	1.5E-06	1.9E-07	1.2E-07	2.5E-07	1.1E-08	8	12	6	145	
UACC-62	1.5E-06	2.7E-07	1.4E-07	1.5E-07	1.5E-08	6	11	10	101	
SF-268	1.5E-06	1.9E-07	5.8E-08	1.8E-07	1.5E-08	8	26	9	104	
NCI-H322M	1.6E-06	2.4E-07	5.0E-08	2.4E-07	2.3E-08	7	31	6	66	
SF-295	1.6E-06	1.5E-07	1.1E-07	1.3E-07	9.7E-09	11	14	12	160	
MALME-3M	1.6E-06	2.8E-07	1.3E-07	2.1E-07	1.4E-08	6	12	7	115	
BT-549	1.6E-06	2.3E-07	1.4E-07	1.7E-07	1.5E-08	7	11	10	103	
SK-MEL-5	1.6E-06	1.7E-07	1.1E-07	1.7E-07	1.3E-08	10	15	10	124	
OVCAR-8	1.7E-06	1.9E-07	9.2E-08	1.5E-07	8.6E-09	9	18	11	193	
NCI-H522	1.7E-06	2.6E-07	5.6E-08	1.5E-07	1.2E-08	6	31	12	137	
HCT-15	1.7E-06	2.6E-07	2.4E-07	2.5E-07	2.2E-08	7	7	7	79	
786-0	1.7E-06	1.6E-07	1.1E-07	2.0E-07	1.6E-08	11	16	9	106	
MDA-MB-435	1.8E-06	2.1E-07	1.5E-07	8.4E-07	2.7E-08	8	12	2	65	
SW-620	1.9E-06	2.2E-07	1.3E-07	2.6E-07	5.8E-08	9	14	7	33	
T-47D	1.9E-06	7.0E-07	2.3E-07	2.9E-07	5.0E-08	3	8	7	38	
EKVX	2.0E-06	3.2E-07	2.1E-07	2.3E-07	1.8E-08	6	9	8	107	
A549/ATCC	2.0E-06	1.5E-07	9.0E-08	1.8E-07	1.2E-08	13	22	11	166	
UACC-257	2.0E-06	6.3E-07	2.7E-07	5.0E-07	2.4E-08	3	7	4	83	
KM12	2.1E-06	2.7E-07	1.3E-07	1.1E-06	4.4E-08	8	16	2	47	
OVCAR-3	2.1E-06	2.4E-07	1.4E-07	4.9E-07	5.3E-08	9	15	4	40	
SK-OV-3	2.2E-06	2.6E-07	7.2E-08	3.4E-08	1.2E-08	8	30	64	173	
SNB-19	2.2E-06	2.5E-07	9.1E-08	2.2E-07	1.6E-08	9	24	10	135	
IGROV1	2.3E-06	5.0E-07	2.0E-07	1.5E-06	5.8E-08	5	12	2	40	
OVCAR-4	2.3E-06	4.6E-07	1.9E-07	1.6E-06	1.6E-07	5	12	1	15	
HS 578T	2.4E-06	1.4E-06	2.9E-07	2.3E-06	1.6E-07	2	8	1	15	
HOP-92	2.5E-06	3.5E-07	1.8E-07	2.4E-07	2.7E-08	7	14	11	94	
A498	2.8E-06	2.5E-07	2.2E-07	1.2E-06	1.3E-07	11	13	2	22	
TK-10	2.9E-06	3.4E-06	1.1E-06	1.3E-06	1.3E-07	1	3	2	22	
PC-3	3.1E-06	7.2E-07	4.8E-07	3.6E-07	2.5E-08	4	7	9	128	
SK-MEL-28	3.6E-06	2.9E-07	1.6E-07	2.6E-07	1.5E-08	12	23	14	247	
OVCAR-5	5.1E-06	3.1E-07	2.6E-07	2.8E-07	3.6E-08	16	20	18	141	

Table S3: NCI-60 cancer cell screening. 55 standard cancer cell lines, tested for growth inhibition (GI) caused by **-CBI-TMI** redox prodrugs (controlled by the **P-CC60-** hydrolytic prodrug), screened by the National Cancer Institute (NCI) developmental therapeutics program (DTP). Cell lines were sorted by increasing GI_{50} values for **P-CC60-CBI-TMI**. Final four columns plot the reductive indices, i.e. potencies referenced against **P-CC60-CBI-TMI**, to reveal qualitatively where reductive activation occurs at significantly higher levels than hydrolysis.

6.2. Comparison of NCI-60 and Proliferator-140 results for potency, and for reductive index

Cell line	NCI-60			Proliferator			NCI-60			Proliferator		
	IC ₅₀ [M] P-CC60	GI ₅₀ [M] P-CC60	GI ₅₀ /IC ₅₀	IC ₅₀ [M] P-SS60	GI ₅₀ [M] P-SS60	GI ₅₀ /IC ₅₀	IC ₅₀ [M] P-SS66C	GI ₅₀ [M] P-SS66C	GI ₅₀ /IC ₅₀			
MCF7	2.1E-07	3.2E-07	1.5	4.5E-08	3.5E-08	0.8	3.1E-08	1.5E-08	0.5			
DU-145	1.8E-07	4.6E-07	2.5	3.6E-08	5.9E-08	1.6	1.6E-08	2.5E-08	1.5			
MOLT-4	7.6E-08	5.9E-07	7.8	1.3E-08	9.0E-08	6.9	8.6E-09	6.3E-08	7.3			
MDA-MB-468	1.5E-07	6.9E-07	4.6	3.1E-08	1.7E-07	5.4	1.9E-08	3.7E-08	2.0			
HL-60	1.0E-07	7.5E-07	7.4	1.8E-08	1.2E-07	6.5	1.5E-08	4.8E-08	3.2			
COLO 205	7.6E-07	1.4E-06	1.8	1.6E-07	3.4E-07	2.2	8.6E-08	1.5E-07	1.7			
RPMI-8226	3.4E-07	1.5E-06	4.4	3.9E-08	2.2E-07	5.8	1.2E-08	1.4E-07	12.0			
CAKI-1	3.3E-07	1.5E-06	4.5	6.3E-08	2.7E-07	4.3	6.3E-08	1.7E-07	2.7			
HCT-116	4.4E-07	1.5E-06	3.4	6.9E-08	1.6E-07	2.3	3.2E-08	1.5E-07	4.8			
HT29	1.0E-06	1.5E-06	1.5	1.9E-07	2.7E-07	1.4	1.1E-07	1.4E-07	1.3			
HCT-15	5.5E-07	1.7E-06	3.2	1.0E-07	2.6E-07	2.5	1.4E-07	2.4E-07	1.7			
786-0	1.2E-07	1.7E-06	14.7	2.3E-08	1.6E-07	7.3	2.9E-08	1.1E-07	3.7			
SW-620	7.0E-07	1.9E-06	2.7	1.4E-07	2.2E-07	1.6	1.5E-07	1.3E-07	0.9			
T-47D	1.0E-06	1.9E-06	1.8	2.3E-07	7.0E-07	3.0	9.8E-08	2.3E-07	2.3			
A549	7.7E-07	2.0E-06	2.6	1.2E-07	1.5E-07	1.3	3.0E-08	9.0E-08	3.0			
OVCAR-3	1.0E-06	2.1E-06	2.1	1.2E-07	2.4E-07	2.0	7.9E-08	1.4E-07	1.8			
SK-OV-3	4.4E-07	2.2E-06	4.9	6.2E-08	2.6E-07	4.2	3.7E-08	7.2E-08	1.9			
A498	3.0E-07	2.8E-06	9.2	5.0E-08	2.5E-07	5.0	9.4E-08	2.2E-07	2.3			
PC-3	5.2E-07	3.1E-06	6.1	5.8E-08	7.2E-07	12.4	4.0E-08	4.8E-07	11.9			
Mean			4.6			4.0			3.5			
SD			3.2			2.8			3.3			

Cell line	Reductive activation index			Reductive Activation Indices		
	NCI-60 P-SS60	Proliferator P-SS60	ratio	NCI-60 P-SS66C	Proliferator P-SS66C	ratio
MCF7	9	6.1	1.5	21	7.0	3.0
DU-145	8	3.1	2.5	19	11.3	1.6
MOLT-4	7	0.8	7.8	9	8.8	1.1
MDA-MB-468	4	0.9	4.6	18	7.9	2.3
HL-60	6	0.9	7.4	16	6.7	2.3
COLO 205	4	2.2	1.8	9	8.8	1.1
RPMI-8226	7	1.5	4.4	10	28.5	0.4
CAKI-1	5	1.2	4.5	9	5.2	1.7
HCT-116	9	2.8	3.4	10	13.6	0.7
HT29	6	3.7	1.5	11	9.5	1.1
HCT-15	7	2.1	3.2	7	3.9	1.8
786-0	11	0.7	14.7	16	4.1	4.0
SW-620	9	3.2	2.7	14	4.6	3.1
T-47D	3	1.5	1.8	8	10.7	0.8
A549	13	5.1	2.6	22	25.4	0.9
OVCAR-3	9	4.3	2.1	15	12.9	1.1
SK-OV-3	8	1.7	4.9	30	11.8	2.5
A498	11	1.2	9.2	13	3.2	4.0
PC-3	4	0.7	6.1	7	12.9	0.5
Mean			4.6			1.8
SD			3.2			1.1

Table S4: Comparison of absolute potencies and “Reductive Activation Indices” in the 19 overlapping cell lines between NCI-60 and Proliferator-140 screens.

6.3. Test for correlation of oxidoreductase expression levels, to potency or reductive index

We wanted to perform the first, even if simplistic, test of: whether the absolute bioactivity or the reductive index (or both) of a redox-triggered drug that seems substantially cellularly activated by specific reductases (e.g. SS66C by Trx1 as fuelled by TrxR1), will correlate to easily measured readouts such as protein expression levels that are commonly presented as proxies for the (unknown and so far unmeasurable) actual activity of those reductases, in a way that might indicate causation ("more protein triggers more drug causing more potent bioactivity").

The NCI "Cellminer" analysis portal (<https://discover.nci.nih.gov/cellminer/>) makes available a large amount of data concerning the properties of the NCI-60 cell lines: including features of epigenetics, mRNA transcript levels, protein levels, and drug sensitivity. The most desirable protein level quantifications are antibody-based assessment but that has only been reported for ca. 160 proteins which do not include reductases. We therefore exported the NCI's "SWATH proteomics data", which we thought is the best compromise protein level data covering many of our proteins of interest. We pulled expression profiles for 18 reductases across the 60-line-panel: including TrxR1 (TXNRD1), Trx1 (TXN), Trx2 (TXN2), GR (GSR), as well as GPxs, Prdxs, and a range of thioredoxin-domain proteins including TRP32 which is also called TXNL1 (a prominent redox effector with many roles including with the proteasome and in inflammation); some potential proteins of interest such as TrxR2 and Gpx4 are not featured in the SWATH data. We then performed Spearman correlation tests between the datasets of (i) each compound's potency profile, (ii) each compound's reductive index profile, (iii) each reductase's expression profile, where "profile" indicates that each dataset is defined as the value across all NCI panel cell lines. Results are in **Figure S12**.

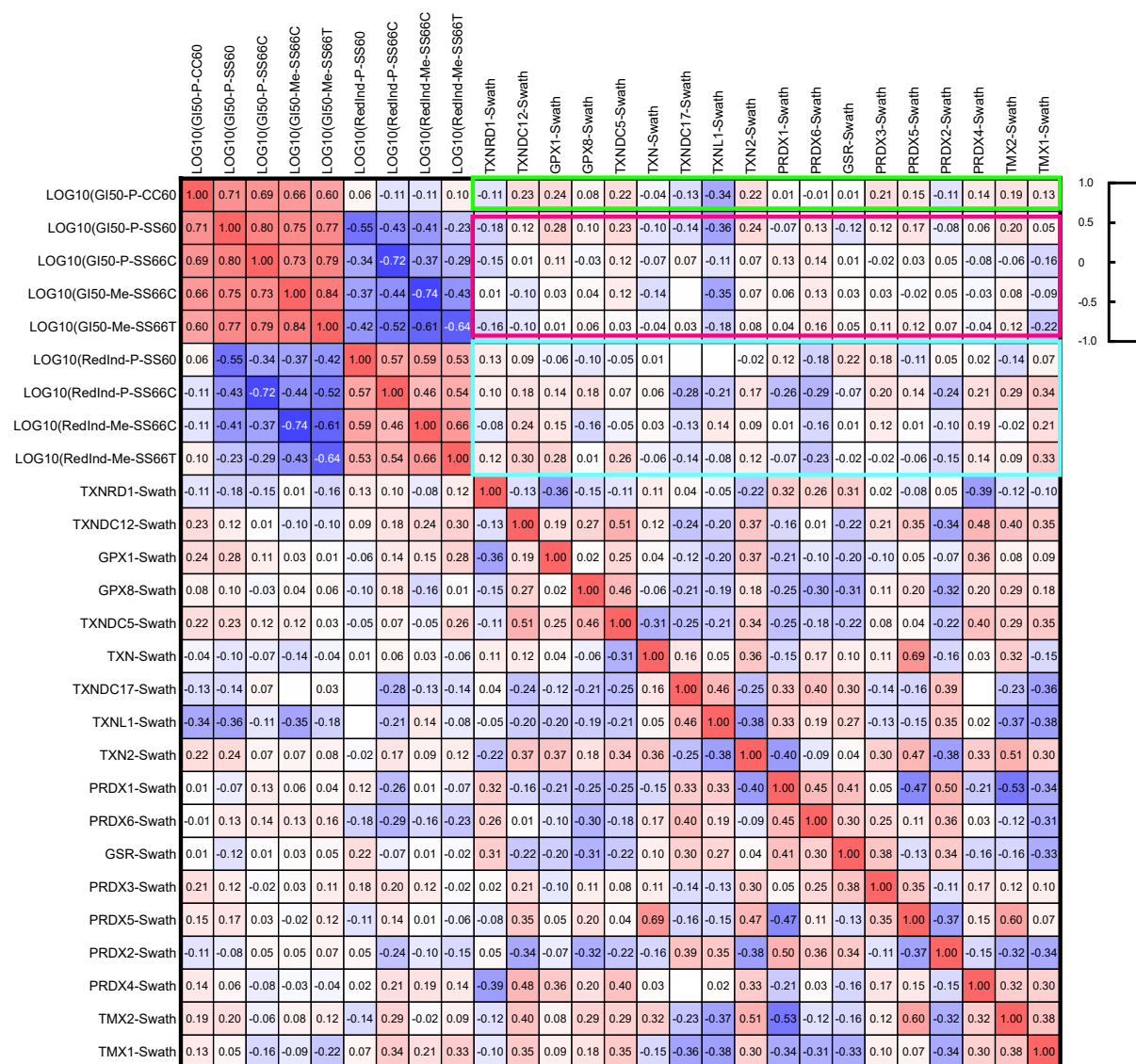


Fig S12: Spearman r correlation matrix for the sets of each compound's absolute potencies or reductive indices across the NCI-60 panel (as logarithms), with the sets of expression levels of individual oxidoreductases across those cell lines (as logarithmic peak areas for the distinctive peptide fragments, as determined in SWATH MS). No striking correlations are seen for the absolute potencies (red boxed region) or reductive indices (blue boxed region).

We were pleased to see that there are no correlations between the absolute potencies of the **P-CC60** control, and the reductive indices of the prodrugs ($|r| < 0.11$): which can support that analysing by reductive index meaningfully removes the influences of baseline levels of hydrolysis as well as of the intrinsic sensitivity of the cell lines.

Our expectations for potential correlations to protein SWATH had been that (i) absolute bioactivity *should not* correlate: bioactivity should depend more on baseline hydrolysis and cell line sensitivity to the drug class; and (ii) reductive release should be based on turnover/activity, which *need not* correlate to protein expression level (since regulation by PTMs, binding partners, upstream reductant throttling, compartmentalisation, and/or modulation by competition with native substrates, are just some of the likely mechanisms decoupling activity from expression). (Note also, that SWATH protein levels are best considered as qualitative reflections of true protein expression, with several potential sources of systematic bias for proteins in one cell line or for one protein between cell lines.)

We were therefore not surprised to see no significant correlations in our analysis (**Fig S12**). (i) The only moderate correlations of absolute potencies [in the red boxed region] are to TXNL1 ($r \sim 0.34$); but note that this also correlates for the **P-CC60** control [in the green boxed region], indicating it is not connected to reductive activation. (ii) No substantial correlations are indicated for the reductive indices [blue boxed region]. Considering the many layers of post-translational regulation of redox activity, we find this unsurprising. We rather argue, that the lack of mRNA (Proliferator) and protein level (NCI) correlations probably highlights a need for the redox field to move away from reporting gene/protein expression levels as if they are suitable data to support proposing either pathological mechanisms or therapeutic opportunities: at least for those oxidoreductases whose primary function is in electron transfer, their roles or validity as targets may be better understood by their activity.

7. *in vivo* studies

7.1. *in vivo* PK and prodrug tolerance (mouse studies)

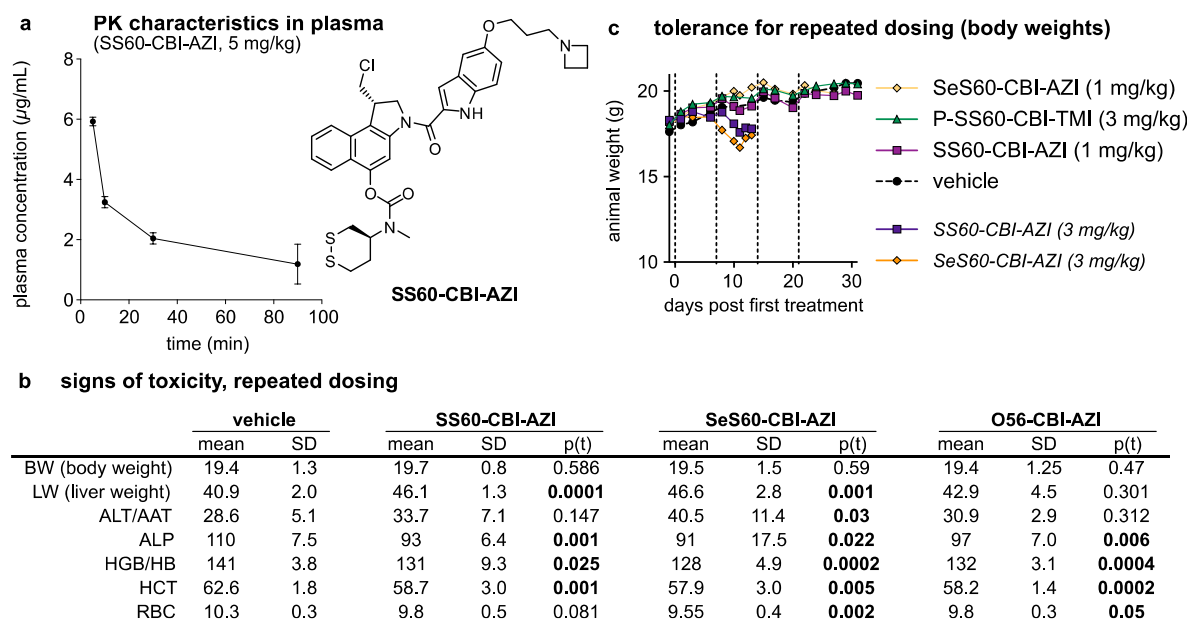


Fig S13: (a) plasma pharmacokinetics of initial (non-solubilised) prodrug **SS60-CBI-AZI** following *i.v.* injection in 100 μ L of 20:80 DMSO:saline [3 mice per timepoint; see Section 8.3]. (b) investigation of potential toxicity parameters for initial prodrugs [seven mice per group; see Section 8.3]. Dosing regimes: three injections, once per week; **SS60-CBI-AZI**: 0.3 then 0.1 then 0.1 mg/kg; **SeS60-CBI-AZI**: 0.3 then 0.2 then 0.2 mg/kg; **O56-CBI-AZI**: 0.3 then 0.2 then 0.2 mg/kg. (c) bodyweights during repeated dosing [3 mice per group; weekly injections in 10:90 DMSO:saline repeated up to up to three times; see Section 8.3]. BW: animal body weight (g). LW: liver weight (mg/g body weight). ALT/AAT: alpha-1 antitrypsin (U/L). ALP: alkaline phosphatase (U/L). HGB/HB: hemoglobin (g/L). HCT: hematocrit (%). RBC: red blood cell count ($\times 10^{12}/L$). p(t): p value compared to the vehicle group; Mann-Whitney U-test without correction for multiple comparisons.

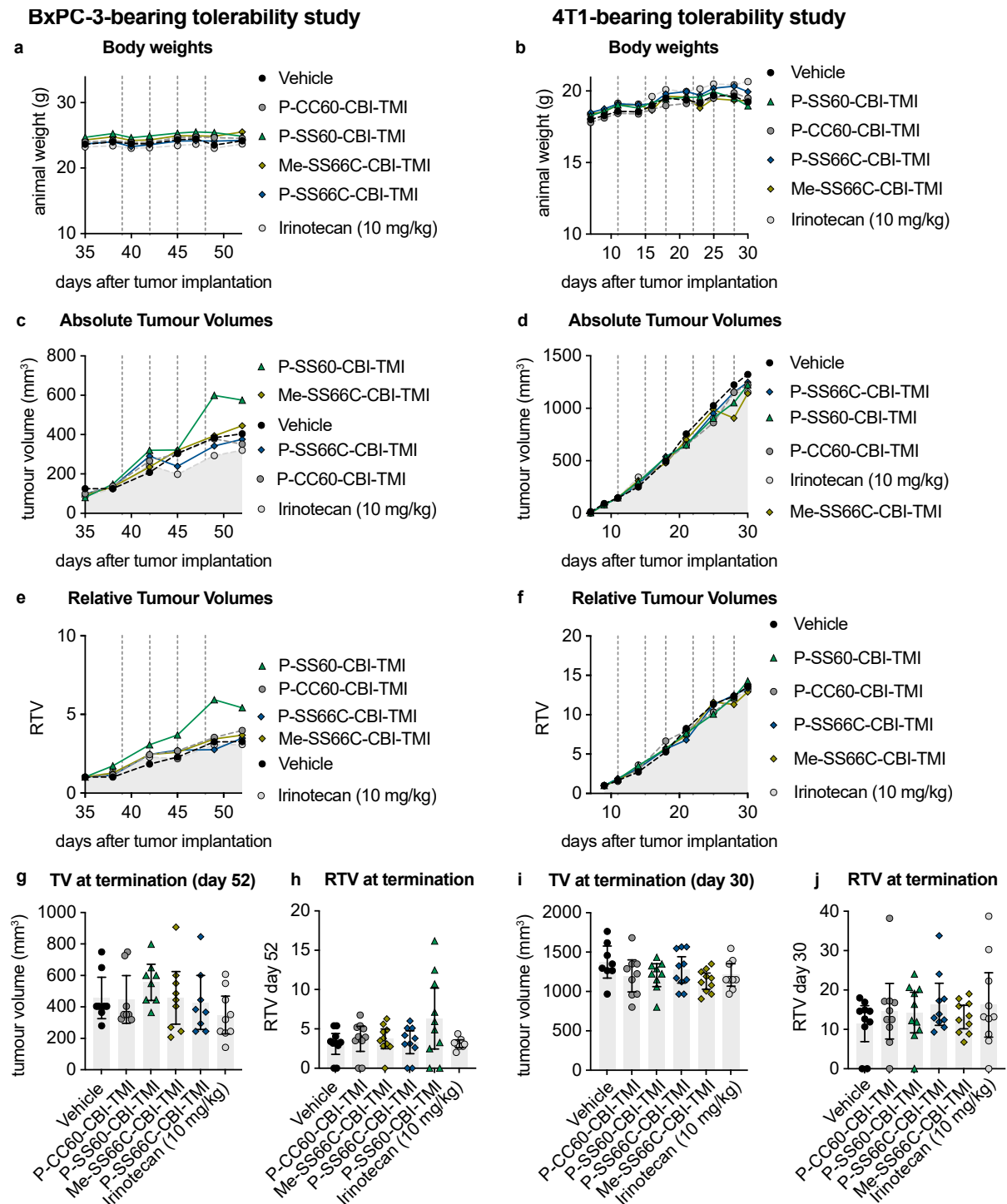


Fig S14: Repeated dosing studies in tumor-bearing mice. (a,c,e,g,h): BxPC-3 subcutaneous xenograft in NMRI mice, 10 mice per group; (b,d,f,i,j): 4T1 murine breast cancer syngeneic orthotopic implant in Balb/c mice, 10 mice per group. Note that reference therapeutic irinotecan failed to slow tumor growth in either model, indicating that these studies are not to be interpreted as efficacy assays but only for tolerability. (a,b) Bodyweights (means); (c,d) absolute tumor volumes (medians); (e,f) tumor volumes relative to individual volumes at start of treatment (medians); (g,h,i,j) absolute and relative tumor volumes at final day of study (datapoints with means and 95% confidence interval). All tumor measurements are *in vivo* caliper measurements. Dotted vertical lines indicate days of treatment. All CBI groups dosed at 3 mg/kg *i.v.*, ca. 100 μ L injection volume in vehicle (10:90 DMSO:saline).

7.2. *in vivo* efficacy mouse studies

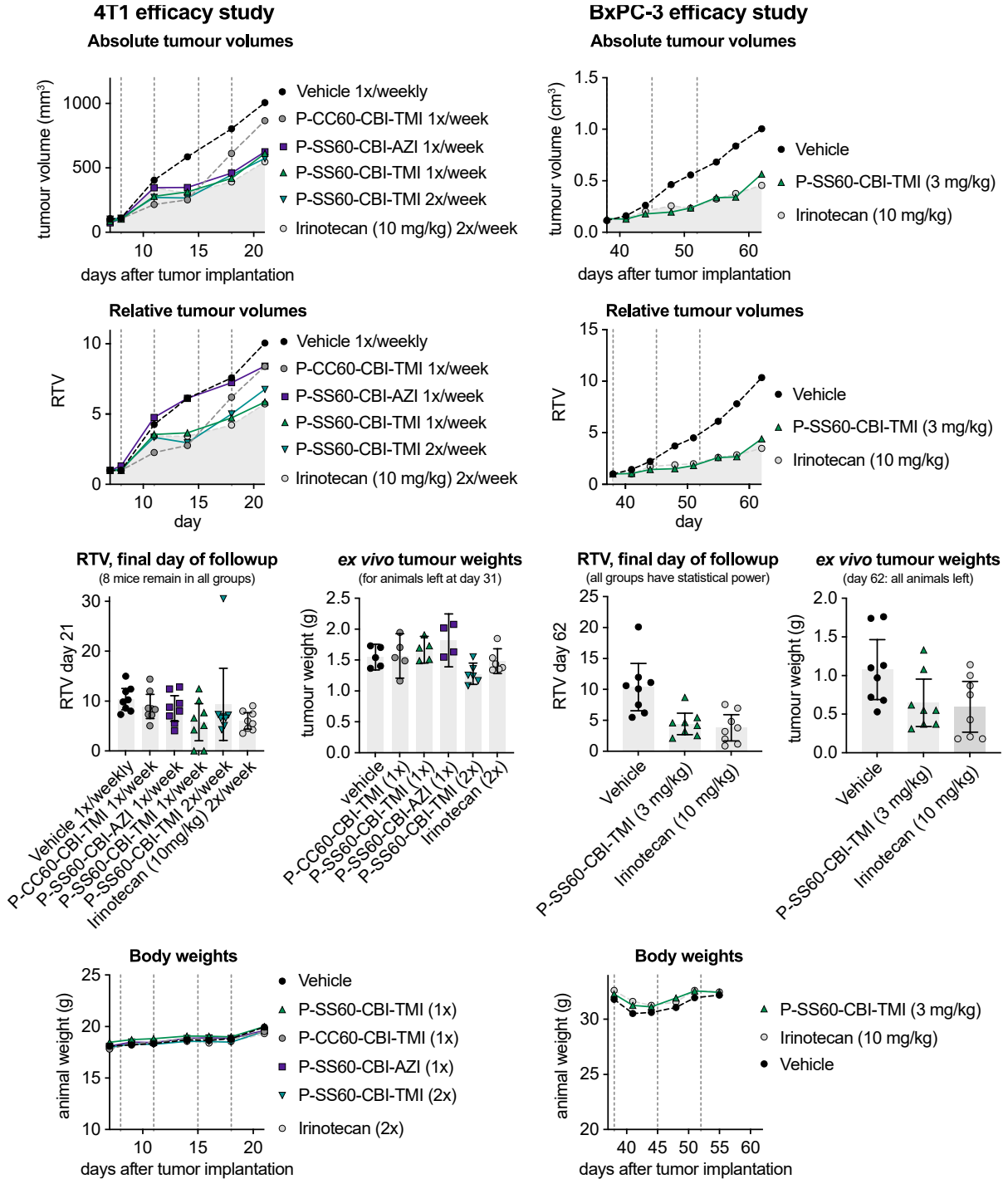


Fig S15: Efficacy studies in tumor-bearing mice. (a,c,e,f,i): 4T1 murine breast cancer syngeneic orthotopic implant in Balb/c mice, 8 mice per group; (b,d,g,h,j): BxPC-3 subcutaneous xenograft in NMR1 mice, 8 mice per group. (a,b) absolute tumor volumes (median); (c,d) tumor volumes relative to individual volumes at start of treatment (median); (e,g) *in vivo* caliper measurement of relative tumor volumes at final day of followup [last day when all mice in all groups remain in the study] (datapoints with means and 95% confidence interval); (f,h) *ex vivo* tumor weights at termination of study (only mice not terminated on ethical grounds before the indicated days were harvested); (i,j) Bodyweights (means). All tumor measurements are *in vivo* caliper measurements except panels f and h. All CBI groups dosed at 3 mg/kg *i.v.* either once or twice weekly as annotated (4T1 study), or once weekly (BxPC-3 study); dotted vertical lines indicate days of [potential] treatment.

8. General methods

8.1. Cell-free HPLC protocols

HPLC studies were conducted on an *Agilent 1200 SL* system *Agilent Technologies Corp.*, Santa Clara (USA) equipped with a DAD detector, a *Hypersil Gold* HPLC column from *ThermoFisher Scientific GmbH*, Dreieich (Germany) and consecutive low-resolution mass detection using a LC/MSD IQ mass spectrometer applying ESI from *Agilent Technologies Corp.*, Santa Clara (USA). The mobile phase consists of eluent A: water (analytical grade, 0.1% formic acid) and eluent B: MeCN (analytical grade, 0.1% formic acid). The analysis was performed using a gradient of 10% B to 90% B over 10 min.

Reduction assay using TCEP and GSH

10 μ L of a solution of the prodrug (1 mM in DMSO) was added to 80 μ L of TE-buffer (50 mM Tris-HCl, 20 mM EDTA, pH = 8) in HPLC vials with micro-insert, followed by addition of either 10 μ L of a solution of tris(2-carboxyethyl)phosphine (TCEP, 5 mM in TE-buffer), or reduced glutathione (GSH, 50 mM in TE-buffer) or else blank TE-buffer. Final concentrations: Prodrug (0.1 mM), TCEP (0.5 mM), GSH (5 mM). The blank sample was measured after 10 min ("pure") and 24 h ("OH⁻") to control for basic hydrolysis. The GSH sample was measured after 24 h to control for monothiol-based reductive release. The TCEP sample was measured at several timepoints (e.g. 10 min, 1 h, 2.5 h, 4 h, 7 h) to control for release kinetics of irreversible reduction-based activation. Individual species were identified using ESI-MS analysis. Separate UV/Vis spectra and mass spectra were extracted for each of the intermediate species and final release products. Peak areas were calculated relative to the sum of all peak areas at 320 nm to quantify individual species at each timepoints. As UV/Vis absorption at 320 nm is not equal for all species (especially CBI*-TMI/CBI*-AZI have slightly different absorption profiles) we expect the accuracy of this calculation within an error of $\pm 5\%$, which is sufficient for the purpose of this experiment.

8.2. Cell culture methods

General cell cultivation

HeLa, A549 or MEF cells were cultured in Dulbecco's modified Eagle's medium (DMEM: L-glucose (1 g/L), L-pyruvate, phenol-red, NaHCO₃ (2.7 g/L), purchased from *Merck GmbH*, Darmstadt, Germany), which was supplemented with 10% heat-inactivated fetal bovine serum, penicillin (100 U/mL), streptomycin (100 μ g/mL), L-glutamine and Na₂SeO₃ (100 nM). Dulbecco PBS buffer (*Merck GmbH*, Darmstadt, Germany) was used for washing and resuspension steps, TrypLE™ Express (*gibco Life Technologies Inc.*, Massachusetts, USA) was used for trypsination. Centrifugation steps were performed for 5 min at a speed of 500 \times g, by using an *Eppendorf centrifuge 5810R* (*Eppendorf GmbH*, Hamburg, Germany). Cells were maintained at 37 °C under 5% CO₂ and cell growth and morphology was monitored using a *Nikon Eclipse Ti* microscope from *Nikon Corp.*, Minato (Japan).

HeLa cells used in this study were HeLa-HRE (14-118ACL) cells, purchased from *abeomics Inc.* (Antibodies & Engineered Cell Lines™, San Diego, USA). Briefly, HeLa-HRE is a stably transfected HeLa cell line that expresses the renilla luciferase reporter gene under the transcriptional control of the hypoxia response element (HRE), which can be used in reporter studies of hypoxic response. A549 cells (DSMZ ACC107) were purchased from the German Collection of Microorganisms and Cell Cultures. TrxR1 knockout (*TrxR^{-/-}* or *TrxR-ko*) and reference (*TrxR^{fl/fl}* or *TrxR-wt*) mouse embryonic fibroblasts (MEF) are a kind gift from Marcus Conrad. Briefly, MEFs isolated from conditional TrxR1 knockout mouse embryos, were immortalised by lentiviral transduction. *In vitro* deletion of TrxR1 was achieved by Tat-Cre induced recombination and verified by PCR and Immunoblotting for TrxR1.⁵ All cell lines are tested regularly for mycoplasma contamination and only mycoplasma negative cells were used in assays.

Cellular toxicity assays – resazurin-based cell viability assay

For evaluation of cellular toxicity, HeLa-HRE, A549 or MEF cells were seeded in 96-well plates (Microplates, 96-well; F-bottom, transparent, *Greiner bio-one GmbH*, Kremsmünster, Austria), with a density of 10⁴ cells/well and in 100 μ L (HeLa-HRE, MEF) or 150 μ L (A549) of medium. Cells were allowed to attach over night before compound treatment was initiated the next morning. In general, compounds were applied from DMSO stock solutions, with a maximum final DMSO level of 2% per well and covering concentration ranges from 0.01 nM up to 30 μ M. All compounds were measured at least three times in independent experiments.

After treatment, cell plates were incubated at 37 °C under 5% CO₂ atmosphere for 48 h (HeLa-HRE) or 72 h (A549, MEF), before a resazurin solution (150 mg/L resazurin sodium salt in PBS) was added. Resazurin was left on cells for 4 h at 37 °C and 5% CO₂, before fluorescence of its metabolite resorufin was measured at 590 nm (excitation 544 nm) using a *FLUOstar Omega* microplate reader (*BMG Labtech GmbH*, Ortenburg, Germany). Data were normalized to data from DMSO treated control cells, as "100% viability", whereas signal from wells without cells served as "0% viability" control. Three different concentrations of the linear disulfide-based control compound **SS00_M-CBI-AZI** served as interrun controls on every plate. A minimum of three experiments was performed per compound. Analysis and visualization were performed in *GraphPad Prism 8.4.2* using a nonlinear regression curve (log (inhibitor) vs. response – variable slope, four parameter) to calculate "cellular IC₅₀ values".

8.3. Methods for *in vivo* animal studies

All *in vivo* studies were conducted as contract research together with *ReactionBiology Europe GmbH* (Freiburg, Germany), *EPO – Experimental Pharmacology & Oncology GmbH* (Berlin, Germany); *Bienta/Enamine Ltd.* (Kyiv, Ukraine) and *Leitat – Managing Technologies* (Barcelona, Spain), adhering to the respective animal welfare protocols.

Mice were kept in individually ventilated cages at constant temperature (22 ± 2 °C, air-conditioned) and humidity (45 – 65%), under optimum hygienic conditions with 10 – 15 air changes per hour. A cycle of 12 h artificial fluorescent lightning and 12 h darkness was applied, and animal behavior was monitored daily throughout the studies. The animals received food and water *ad libitum*.

Toxicity studies

To evaluate toxicity of selected compounds, dose level selection studies within dose range from 0.1 mg/kg to 10 mg/kg were performed by intravenous administration into Balb/c mice. Each dose for each tested compound was administered in one mouse. After drug administration, the animals were observed for mortality, body weight changes and clinical signs of gross toxicity three times per week for 21 consecutive days of post-dosing period. After the first week of observation without adverse events, two doses for each test compound were selected as tolerated. These two doses were tested in two additional mice for confirmation of tolerability. Additional animals were observed for mortality, body weight changes, and clinical signs of gross toxicity three times per week for 21 consecutive days of post-dosing period. Toxicity of repeated administrations was tested with three repeated pre-selected doses at a dosing interval of 7 days. Mortality, body weight changes, and clinical signs of gross toxicity were monitored after each drug administration and three times per week for 21 consecutive days after the first compound administration. Bleeding with subsequent hematological tests, clinical chemistry parameters analysis (ALT, AST, ALP, LDH, creatine kinase, creatinine, urea, cholesterol, and triglycerides), and necropsy with macroscopic inspection were performed on the terminal day of the repeated dosing-regime.

Pharmacokinetics of **SS60-CBI-AZI**

Following single dose intravenous administration, levels of **SS60-CBI-AZI** in blood plasma over time were determined by HPLC-MS/MS. Treatment groups were three Balb/c mice (randomly assigned) per time point (total: four termination time points, at 5, 10, 30 and 90 min). Blood collection was performed from the orbital sinus in microtainers containing K₂EDTA. All samples were immediately processed, flash-frozen and stored at -70 °C until analysis. Briefly, plasma samples (50 µL) were mixed with 200 µL of internal standard (**IS**) solution (IS-7639, 400 ng/mL in ethanol). After mixing by pipetting and centrifuging for 4 min at 6000 rpm, 2 µL of each supernatant was injected into LC-MS/MS (Shimadzu LC: 2 isocratic pumps LC-10ADvp, autosampler SIL-20AC, sub-controller FCV-14AH, degasser DGU-14A; AB Sciex MS: API 3000 (triple-quadrupole), ESI). The data acquisition and system control was performed using *Analyst 1.5.2 software* (AB Sciex Ltd., Canada).

Chromatographic Conditions:

Column: Discovery HS C18 (50 x 2.1 mm, 5 µm)

Mobile phase A: Acetonitrile : Water : Formic acid = 50 : 950 : 1

Mobile phase B: Acetonitrile : Formic acid = 100 : 0.1

Linear gradient: 0 min 5 % B, 1.1 min 100% B, 1.11 min 5 % B, 2.5 min stop.

Elution rate: 400 µL/min. A divert valve directed the flow to the detector from 1.2 to 2.3 min.

Column temperature: 30 °C

MS/MS Detection:

Scan type: Positive MRM, Ion source: Turbo spray, Ionization mode: ESI

Nebulizer gas: 15 L/min, Curtain gas: 8 L/min, Collision gas: 4 L/min.

Ion spray voltage: 5000 V, Temperature: 400 °C

Tolerability studies

To test tolerability of selected compounds *in vivo*, female BALB/c mice were randomized by weight into seven groups of three animals. On days 0 and 7, the first 3 groups were treated with 3 mg/kg of either **SS60-CBI-AZI**, **SeS60-CBI-AZI** or **P-SS60-CBI-TMI** and mice were inspected 30 min, 1 h, 2 h, 3 h and 4 h after the first treatment. If a treatment was well tolerated, it was taken into a confirmation cycle with another set of three mice; if a treatment was not tolerated, the applied dose was reduced and tested again in three mice. **P-SS60-CBI-TMI** was tolerated at 3 mg/kg over two weeks and 4 treatments, which was further confirmed by another group of 3 animals. Severe adverse effects (weight loss and signs of inflammation at injection site) were observed for both groups treated with 3 mg/kg **SS60-CBI-AZI** or **SeS60-CBI-AZI**, which led to a dose reduction to 1 mg/kg in a second cohort of each 3 mice (treated twice a week). 1 mg/kg **SS60-CBI-AZI** was tolerated in two groups of each three mice with only mild adverse effects, while **SeS60-CBI-AZI** still caused adverse effects leading to discontinuation of this compound.

Efficacy studies**Syngeneic breast cancer model: Balb/c:**

4T1 murine breast cancer cells were cultured in RPMI-1640 high Glutamax1 with 10 % fetal calf serum, 100 units penicillin/mL and 100 µg streptomycin/mL, until they reach a confluency of 70 – 90 %, before being split routinely using trypsin/EDTA. 100 µL 10⁵ 4T1 tumor cell suspension was orthotopically injected into the left mammary fat pad of each mouse.

Pancreatic cancer xenograft model in NMRI:nu/nu or athymic nude (crl: NU(NCr)-Foxn1^{nu}):

BxPC-3 human pancreas carcinoma cells were cultured in RPMI-1640 high Glutamax1 with 10 % fetal calf serum, 100 units penicillin/mL and 100 µg streptomycin/mL, until they reach a confluency of 70 – 90 %, before being split routinely using trypsin/EDTA. 100 µL 5 x 10⁶ BxPC-3 tumor cell suspension was subcutaneously injected into the left flank of each mouse.

Mice were randomized after a mean tumor volume of ~100 mm³ was reached, and treatment was started on the same day. In general, compounds were dissolved in DMSO to obtain a 10× stock solution, from which all further working solutions in 0.9% NaCl with a final concentration of 1% DMSO were prepared freshly. Treatment was performed in the indicated dosages, once or twice weekly, by intravenous injection. After start of the therapy, animal weight was determined three times weekly and tumor monitoring twice weekly by caliper. Deviation of the health status of the animals were documented and animals were euthanized individually before study termination when ethical abortion criteria were reached (e.g., body weight loss ≥ 20%, signs of sickness; after s.c. implantation: tumor diameter ≥ 2 cm, tumor ulceration). Single groups were terminated early if four animals of the group reached ethical abortion criteria.

8.4. Synthetic techniques

All solvents, reagents and building blocks were purchased from standard commercial sources. Anhydrous solvents obtained in septum-capped bottles and analytical grade, or higher quality solvents were used without purification. Industrial grade solvents were distilled prior to use. Unless otherwise stated, reactions were performed at room temperature without precautions regarding air or moisture and were stirred using a magnetic Teflon[®]-coated stir bars. Air or moisture sensitive reactions were conducted in dry Schlenk glassware.

The term “column chromatography” refers to either (a) manual flash column chromatography conducted under positive nitrogen pressure using *Ceduran® Si 60* silica gel (40–63 µm) from *Merck GmbH* as stationary phase, or (b) purification on the automated column chromatography system *Biotage® Select* using prepacked silica cartridges purchased from *Biotage GmbH*, Uppsala (Sweden). All eluent and solvent mixtures are given as volume ratios unless otherwise specified. Unless stated otherwise, and thin layer chromatography (TLC) to monitor reactions and determine R_f values was performed on silica coated aluminium sheets with fluorescent indicator (*TLC Silica gel 60 F254* from *Merck GmbH*, Darmstadt, Germany) with visualisation by UV irradiation (254 nm/360 nm) or staining with KMnO₄ solution (3.0 g KMnO₄, 20 g K₂CO₃, 0.30 g KOH, 0.30 L H₂O).

Analytical methods for chemical synthesis

High resolution mass spectrometry (HRMS) was conducted either using a *Thermo Finnigan LTQ FT Ultra FourierTransform* ion cyclotron resonance spectrometer from *ThermoFisher Scientific GmbH*, Dreieich (Germany) applying electron spray ionisation (ESI) with a spray capillary voltage of 4 kV at temperature 250 °C with a method dependent range from 50 to 2000 u or a *Finnigan MAT 95* from *Thermo Fisher Scientific*, Dreieich (Germany) applying electron ionisation (EI) at a source temperature of 250 °C and an electron energy of 70 eV with a method dependent range from 40 to 1040 u. All reported *m/z* values refer to positive ionization mode, unless stated otherwise.

Nuclear magnetic resonance (NMR) spectroscopy was performed using a *Bruker Avance* (600/150 MHz, with *TCI cryoprobe*) or a *Bruker Avance III HD Biospin* (400/100 MHz, with BBFO cryoprobeTM) from *Bruker Corp.*, Billerica (USA) either at 400 MHz or 500 MHz. ¹⁹F-NMR spectra were recorded on a *Bruker Avance III* spectrometer (400 MHz for ¹H; 377 MHz for ¹⁹F). NMR-spectra were measured at 298 K, unless stated otherwise, and were analysed with the program *MestreNova 12* developed by *MestreLab Ltd.*, Santiago de Compostela (Spain). ¹H-NMR spectra chemical shifts (δ) in parts per million (ppm) relative to tetramethylsilane (δ = 0 ppm) are reported using the residual protic solvent (CHCl₃ in CDCl₃: δ = 7.26 ppm, DMSO-d₅ in DMSO-d₆: δ = 2.50 ppm, CHD₂OD in CD₃OD: δ = 3.31 ppm) as an internal reference. For ¹³C-NMR spectra, chemical shifts in ppm relative to tetramethylsilane (δ = 0 ppm) are reported using the central resonance of the solvent signal (CDCl₃: δ = 77.16 ppm, DMSO-d₆: δ = 39.52 ppm, CD₃OD: δ = 49.00 ppm) as an internal reference. For ¹H-NMR spectra in addition to the chemical shift the following data is reported in parenthesis: multiplicity, coupling constant(s), number of hydrogen atoms and, if available, assignment. The abbreviations for multiplicities and related descriptors are s = singlet, d = doublet, t = triplet, q = quartet, p = pentuplet, hept = heptet or combinations thereof, m = multiplet and br = broad. The numbering scheme used for the assignments is specified in each case in a figure depicting the

respective molecular structure and does not follow any convention. The reported assignments are supported by 2D-NMR experiments (HMBC, HSQC, COSY). Where known products matched literature analysis data, only selected data acquired are reported.

Analytical high-performance liquid chromatography (**HPLC**) analysis was conducted either using an *Agilent 1100* system from *Agilent Technologies Corp.*, Santa Clara (USA) equipped with a DAD detector and a *Hypersil Gold* HPLC column from *ThermoFisher Scientific GmbH*, Dreieich (Germany) or a *Agilent 1200 SL* system *Agilent Technologies Corp.*, Santa Clara (USA) equipped with a DAD detector, a *Hypersil Gold* HPLC column from *ThermoFisher Scientific GmbH*, Dreieich (Germany) and consecutive low-resolution mass detection using a LC/MSD IQ mass spectrometer applying ESI from *Agilent Technologies Corp.*, Santa Clara (USA). For both systems mixtures of water (analytical grade, 0.1% formic acid) and MeCN (analytical grade, 0.1% formic acid) were used as eluent systems.

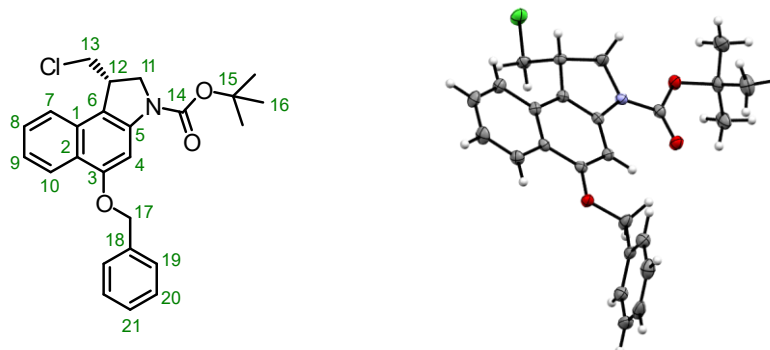
Single crystal **X-Ray** crystallography was conducted using a *Bruker D8 Venture TXS* system from *Bruker Corp.*, Billerica (USA) equipped with a multilayer mirror monochromator and a Mo K α rotating anode X-ray tube ($\lambda = 0.71073$ Å). The frames were integrated with the *Bruker SAINT software package* (Bruker, 2012. SAINT. Bruker AXS Inc., Madison, Wisconsin, USA). Data were corrected for absorption effects using the Multi-Scan method (SADABS) (Sheldrick, G. M., 1996. SADABS. University of Goettingen, Germany). The structures were solved and refined using the *Bruker SHELXTL Software Package*.⁶ The figures have been drawn at the 50% ellipsoid probability level.⁷ Crystallographic data have been deposited with the *Cambridge Crystallographic Data Centre*, CCDC, 12 Union Road, Cambridge CB21EZ, UK. Copies of the data can be obtained free of charge on quoting the depository number CCDC 2214471 (<https://www.ccdc.cam.ac.uk/structures/>).

9. Chemical synthesis

9.1. General synthetic protocols

BnO-CBI-Boc

N-Boc-(5-(benzyloxy)-(S)-1-(chloromethyl)-1,2-dihydro-3*H*-benzo[*e*]indole

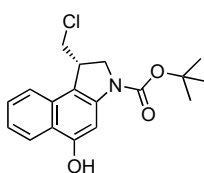


For the synthesis of *seco*-CBI derived prodrugs commercial **BnO-CBI-Boc** was purchased as a colourless, crystalline solid from *ArchBioscience Inc.*, West Chester, PA (USA). The identity and purity of the material was determined by NMR spectroscopy, MS and X-ray crystallography; in particular, the (*S*)-configuration at C1 which is fundamental for high-potency activity was confirmed by determination of the specific rotation⁸, and by acquiring an X-Ray crystallography structure (**Table S5**) matching literature⁹. Analytical data matched literature reports.

TLC R_f = 0.38 (isohexane:EtOAc, 5:1). **HRMS** (ESI⁺) for C₁₈H₂₁ClNO₃⁺: calcd. m/z 334.12045, found m/z 334.12068. $[\alpha]^{25}_D$ = -15.2 (c = 4.66 g/L, CH₂Cl₂). Unambiguous confirmation of the absolute configuration was derived from a single-crystal X-Ray analysis. **¹H-NMR** (500 MHz, CDCl₃): δ (ppm) = 8.30 (dd, J = 8.7, 1.2 Hz, 1H, 10-H), 7.88 (br-s, 1H, 4-H), 7.65 (d, J = 8.3 Hz, 1H, 7-H), 7.55 (d, J = 7.5 Hz, 2H, 19-H), 7.51 (ddd, J = 8.2, 6.8, 1.3 Hz, 1H, 9-H), 7.46 – 7.41 (m, 2H, 20-H), 7.39 – 7.36 (m, 1H, 21-H), 7.34 (ddd, J = 8.2, 6.8, 1.2 Hz, 1H, 8-H), 5.27 (s, 2H, 17-H), 4.27 (s, 1H, 11-H), 4.20 – 4.10 (m, 1H, 11'-H), 4.05 – 3.89 (m, 2H, 12-H+13-H), 3.44 (t, J = 10.4 Hz, 1H, 13'-H), 1.62 (s, 9H, 16-H). **¹³C-NMR** (126 MHz, CDCl₃): δ (ppm) = 156.2 (C3), 152.8 (C=O, C14), 142.0 (C_{Ar}, C5), 136.9 (C_{Ar}, C18), 130.4 (C_{Ar}, C2), 128.7 (C_{Ar}H, C20), 128.2 (C_{Ar}H, C21), 127.8 (C_{Ar}H, C9), 127.7 (C_{Ar}H, C19), 123.8 (C_{Ar}H, C10), 123.3 (C_{Ar}H, C8), 122.6 (C_{Ar}, C6), 121.9 (C_{Ar}H, C7), 114.5 (C_{Ar}, C1), 96.6 (C_{Ar}, C4), 81.5 (C(CH₃)₃, C15), 71.7 (CH₂, C17), 54.9 (CH₂, C13), 48.3 (CH₂, C11), 41.3 (CH, C12), 29.2 (C(CH₃)₃, C16).

HO-CBI-Boc

N-Boc-(S)-1-(chloromethyl)-5-hydroxy-1,2-dihydro-3*H*-benzo[*e*]indole

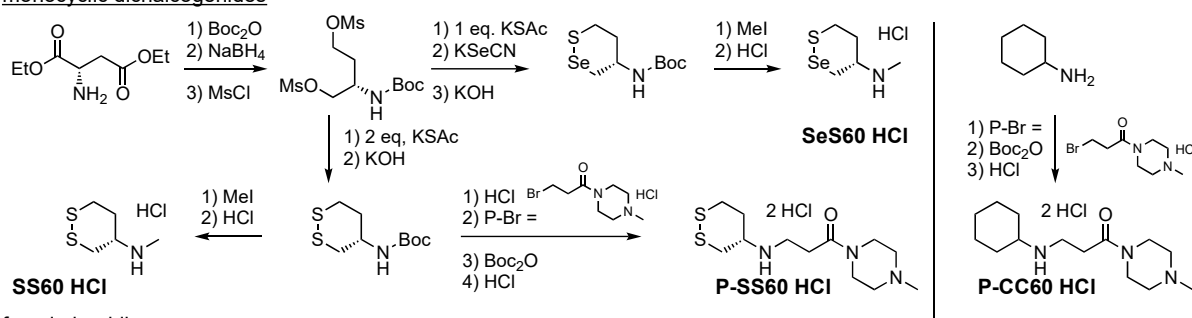


Commercial **BnO-CBI-Boc** (591 mg, 1.39 mmol) was dissolved in THF (75 mL, 0.02 M). The mixture was heated to 35 °C and Pd/C (297 mg, 10% on charcoal) and NH₄HCO₂ (1.4 mL of 4 M aq. solution) were added. The mixture was stirred for 70 min at 35 °C until quantitative turnover was confirmed by TLC, was then filtered through Celite and the filter cake was washed with EtOAc (40 mL). The combined filtrates were concentrated under reduced pressure to obtain **HO-CBI-Boc** as a colourless solid (460 mg, 1.38 mmol, 99%). Optional purification by FCC (isohexane/EtOAc) gave **HO-CBI-Boc** as a colourless solid. Analytical data matched literature reports.^{10,11}

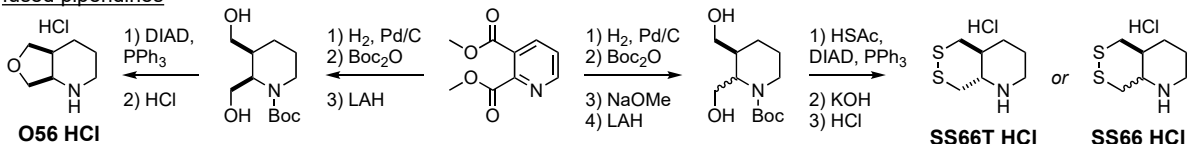
TLC R_f = 0.59 (isohexane:EtOAc, 10:1). **HRMS** (ESI⁻) for C₁₈H₂₁ClNO₃⁻: calcd. m/z 332.10589, found m/z 332.10639. **¹H-NMR** (400 MHz, CDCl₃): δ (ppm) = 8.18 (d, J = 8.4 Hz, 1H), 7.74 (s, 1H), 7.63 (d, J = 8.4 Hz, 1H), 7.50 (ddd, J = 8.3, 6.8, 1.3 Hz, 1H), 7.34 (ddd, J = 8.1, 6.8, 1.1 Hz, 1H), 6.32 (s, 1H), 4.24 (d, J = 11.9 Hz, 1H), 4.15 – 4.06 (m, 1H), 4.03 – 3.88 (m, 2H), 3.51 – 3.38 (m, 1H), 1.61 (s, 9H).

Summary of trigger precursor HCl salt syntheses

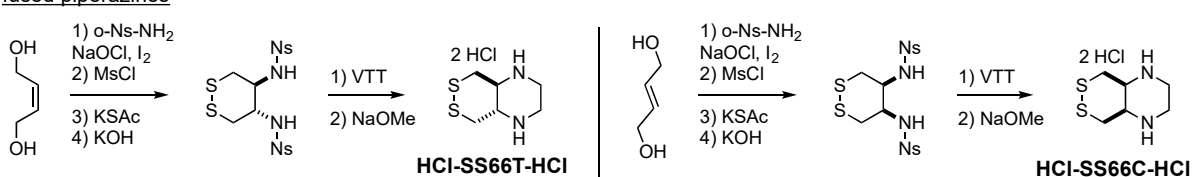
monocyclic dichalcogenides



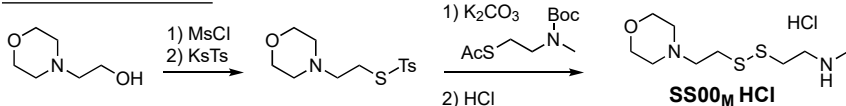
fused piperidines



fused piperazines

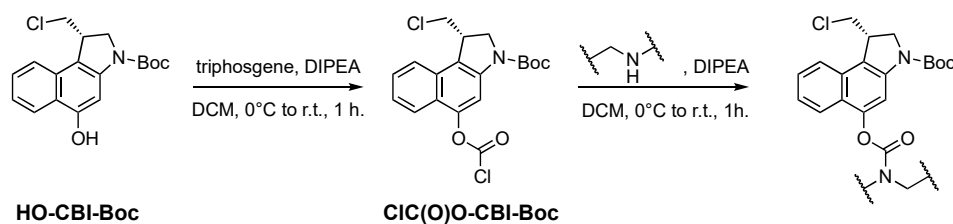


mixed linear disulfides



Scheme 1 Trigger Synthesis. (a) monocyclic dichalcogenides were prepared according to *JACS* 2021¹, *Chem* 2022³ and *ChemRxiv* 2022¹²; (b) fused piperidines according to *JACS* 2021¹; (c) fused piperazines according to *WO* 2022/200347¹³ and *paper in preparation* 2022⁴; (d) mixed linear disulfides according to *JACS* 2021.¹

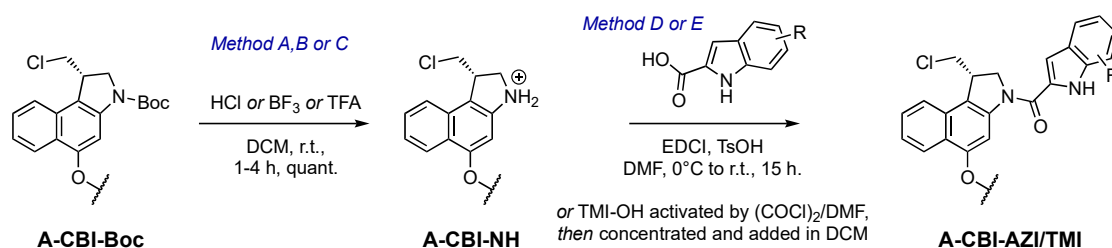
General protocol A: Carbamate coupling using triphosgene



Step 1: **HO-CBI-Boc** (1 eq.) was dissolved in anhydrous DCM (0.1 M) and the resulting solution was cooled to 0 °C. Triphosgene (1.2 eq., 0.2 M solution in anhydrous DCM) and DIPEA (4.0 eq, 0.4 M solution in anhydrous DCM) were subsequently added dropwise. The resulting mixture was stirred at 0 °C for 0.5 h, was then allowed to warm to r.t. and was further stirred for 0.5 h. All volatile compounds were removed under reduced pressure to afford the corresponding chloroformate **ClC(O)O-CBI-Boc** as a solid.

Note: Residual phosgene was collected using an external liquid nitrogen trap. The trapped mixture was carefully thawed and quenched by addition of an aq. solution of NaOH (2 M) and diisopropylamine (10 eq.).

Step 2: A secondary trigger amine hydrochloride (1.2 eq.) was suspended in anhydrous DCM (0.02 M). DIPEA (2.4 eq., 0.2 M solution in anhydrous DCM) was added to afford a clear solution of the corresponding free amine. A solution (0.02 M in anhydrous DCM) of **ClC(O)O-CBI-Boc** (1.0 eq) was added dropwise to the reaction flask at 0 °C and the resulting mixture was further stirred for 0.5 h, then allowed to warm to r.t. and further stirred for 0.5 h. Purification was achieved using FCC to give the title compounds as colourless solids.

General protocol B: Prodrug assembly (Amide coupling)**Step 1:**

Method A: The *N*-Boc protected *O*-alkyl or *O*-acyl *seco*-CBI derivative **A-CBI-Boc** (1.0 eq.) was dissolved in anhydrous DCM (0.05 M). The solution was cooled to 0 °C and a solution of HCl (80 eq., 4 M in dioxane) was added. The mixture was stirred at r.t. for 4 h. All volatiles were removed under reduced pressure to afford the corresponding aniline **A-CBI-NH** without further purification as a coloured solid.

Method B: The *N*-Boc protected *O*-alkyl or *O*-acyl *seco*-CBI derivative **A-CBI-Boc** (1.0 eq.) was dissolved in anhydrous DCM (0.05 M). The solution was cooled to 0 °C and BF₃·OEt₂ (5.0 eq.) was added in one portion. The mixture was stirred at 0 °C for 1 h. All volatiles were removed under reduced pressure to afford the corresponding aniline **A-CBI-NH** without further purification as a coloured solid.

Method C: The *N*-Boc protected *O*-alkyl or *O*-acyl *seco*-CBI derivative **A-CBI-Boc** (1.0 eq.) was dissolved in anhydrous DCM (0.1 M). To the solution was added trifluoroacetic acid (60 eq.) and the resulting mixture was stirred at r.t. for 2 h. All volatiles were removed under reduced pressure, the residue was co-evaporated with toluene (1×) to afford the corresponding aniline **A-CBI-NH** without further purification as a coloured solid.

Step 2:

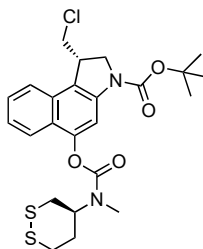
Method D: The free aniline *O*-alkyl or *O*-acyl *seco*-CBI derivative **A-CBI-NH** (1.0 eq.) was dissolved in anhydrous DMF (0.03 M). The solution was cooled to 0 °C and **AZI-OH** (1.1 eq., 68 wt%) or **TMI-OH**, EDCI (4.0 eq.) and *p*-TsOH (1.1 eq.) were added as solids. The mixture was stirred for 0.5 h, then allowed to warm to r.t. and further stirred for 15 h. All volatile compounds were removed under reduced pressure after co-evaporation with *n*-heptane to afford the crude mixture as a coloured solid. Purification by preparative HPLC (H₂O/MeCN/HCO₂H) afforded the title compounds **A-CBI-AZI** or **A-CBI-TMI** as colourless solids.

Method E: **TMI-OH** (2.0 eq.) was dissolved in anhydrous DCM (0.05 M), oxalyl chloride (6.0 eq.) was added and the mixture was cooled to 0 °C. A catalytic amount of DMF (1.0 eq.) was added and the mixture was allowed to warm to r.t. and was further stirred for 1.5 h. All volatiles were removed under reduced pressure, the residue was co-evaporated with toluene (1×) to afford the corresponding **TMI-Cl** without further purification as a brown solid. (Comment: Full conversion to the carbonyl chloride was detected by trapping with piperazine; the carbonyl chloride can be stored as a solid at r.t. for 1-2 weeks). The free aniline *O*-alkyl or *O*-acyl *seco*-CBI derivative **A-CBI-NH** (1.0 eq.) was dissolved in anhydrous DCM (0.05 M), cooled to 0 °C and DIPEA (8.0 eq.) was added to give a clear solution. Then, a solution of **TMI-Cl** (0.2 M in DCM, 2.0 eq.) was added dropwise, the mixture was allowed to warm to r.t. and was further stirred for 30 min. Conversion of the aniline was checked by LC-MS and further carbonyl chloride equivalents were added if required to ensure full conversion to the desired amide. The mixture was diluted with DCM, washed with water (2×) and the aq. layer was extracted with DCM (2×). The combined organic layers were dried over Na₂SO₄ and concentrated to give a coloured solid. Purification was achieved by FCC (DCM/MeOH or isohexane/EtOAc) to give the title compounds **A-CBI-TMI** as colourless solids. Further purification for cellular and *in vivo* application was achieved by preparative HPLC (H₂O/MeCN/0.1% formic acid).

9.2. Precursor syntheses

SS60-CBI-Boc

N-Boc (S)-5-(((S)-1,2-dithian-4-yl)(methyl)carbamoyloxy)-1-(chloromethyl)-1,2-dihydro-3*H*-benzo[*e*]indole

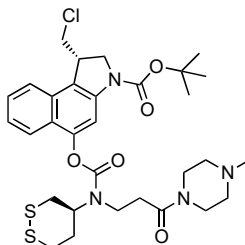


Carbamate coupling of **HO-CBI-Boc** (84 mg, 0.25 mmol) and (S)-*N*-methyl-1,2-dithian-4-amine hydrochloride (58 mg, 0.31 mmol) was accomplished according to the **General Protocol A** to give **SS60-CBI-Boc** as a colourless solid (123 mg, 0.24 mmol, 96%).

TLC R_f = 0.64 (isohexane:EtOAc, 2:1). **HRMS** (ESI⁺) for C₂₄H₃₀ClN₂O₄S₂⁺: calcd. m/z 526.15955, found m/z 526.15972. NMR experiments at r.t. showed two rotameric species: **¹H-NMR** (400 MHz, CDCl₃): δ (ppm) = 8.05 (*br-s*, 1H), 7.78 (dd, J = 15.2, 8.4 Hz, 1H), 7.70 (d, J = 8.4 Hz, 1H), 7.50 (t, J = 7.6 Hz, 1H), 7.41 – 7.32 (m, 1H), 4.61 – 4.31 (m, 1H), 4.27 (d, J = 10.9 Hz, 1H), 4.13 (dd, J = 11.7, 8.8 Hz, 1H), 4.08 – 3.97 (m, 1H), 3.86 (dd, J = 11.2, 3.2 Hz, 1H), 3.47 (t, J = 10.8 Hz, 1H), 3.32 – 3.16 (m, 2H), 3.18 – 2.91 (m, 4H), 2.88 – 2.76 (m, 1H), 2.44 – 2.02 (m, 2H), 1.58 (s, 9H). **¹³C-NMR** (101 MHz, CDCl₃): δ (ppm) = 154.3 (C=O, major rotamer), 154.1 (C=O, minor rotamer), 152.5 (C=O), 148.6 (C_{Ar}), 141.3 (C_{Ar}), 130.3 (C_{Ar}), 127.7 (C_{Ar}H), 124.4 (C_{Ar}H), 124.2 (C_{Ar}), 122.7 (C_{Ar}H), 122.5 (C_{Ar}H), 120.2 (C_{Ar}), 109.4 (C_{Ar}H), 81.7 (C(CH₃)₃), 56.3 (CH, minor rotamer), 55.3 (CH, major rotamer), 53.1 (CH₂), 46.0 (CH₂), 42.2 (CH), 36.5 (CH₂, minor rotamer), 36.3 (CH₂, minor rotamer), 36.2 (CH₂, major rotamer), 35.8 (CH₂, major rotamer), 33.4 (CH₂, minor rotamer), 32.6 (CH₂, major rotamer), 30.1 (CH₃), 28.6 (C(CH₃)₃).

P-SS60-CBI-Boc

N-Boc (S)-5-(((1,2-dithian-4-yl)(3-(4-methylpiperazin-1-yl)-3-oxopropyl)carbamoyloxy)-1-(chloromethyl)-1,2-dihydro-3*H*-benzo[*e*]indole

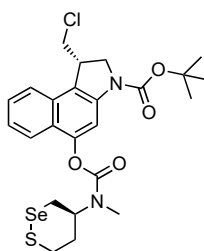


Carbamate coupling of **HO-CBI-Boc** (168 mg, 0.50 mmol) and (S)-3-((1,2-dithian-4-yl)amino)-1-(4-methylpiperazin-1-yl)propan-1-one dihydrochloride (199 mg, 0.55 mmol) was accomplished according to the **General Protocol A** to give **P-SS60-CBI-Boc** as a colourless solid (191 mg, 0.29 mmol, 58%).

TLC R_f = 0.47 (DCM:MeOH, 9:1). **HRMS** (ESI⁺) for C₃₁H₄₂ClN₄O₅S₂⁺: calcd. m/z 649.22797, found m/z 649.22830. **¹H-NMR** (500 MHz, CDCl₃): δ (ppm) = 8.04 (s, 1H), 7.72 (dd, J = 16.5, 8.4 Hz, 2H), 7.51 (t, J = 7.1 Hz, 1H), 7.43 – 7.33 (m, 1H), 4.49 – 4.16 (m, 2H), 4.17 – 4.10 (m, 1H), 4.02 (t, J = 9.5 Hz, 1H), 3.93 (d, J = 11.1 Hz, 1H), 3.86 – 3.79 (m, 1H), 3.64 (s, 3H), 3.53 (d, J = 15.7 Hz, 2H), 3.50 – 3.44 (m, 1H), 3.35 (dt, J = 41.8, 12.0 Hz, 1H), 3.28 – 3.16 (m, 1H), 3.04 (dd, J = 31.0, 13.8 Hz, 1H), 2.96 (d, J = 12.3 Hz, 1H), 2.86 – 2.78 (m, 1H), 2.72 (ddt, J = 23.1, 14.7, 7.8 Hz, 1H), 2.40 (s, 5H), 2.30 (d, J = 3.6 Hz, 4H), 1.58 (s, 9H). **¹³C-NMR** (126 MHz, CDCl₃): δ (ppm) = 169.1 (C=O), 168.7 (C=O), 154.1 (C=O), 152.6 (C_{Ar}), 148.3 (C_{Ar}), 141.2 (C_{Ar}), 130.4 (C_{Ar}), 127.8 (C_{Ar}H), 124.6 (C_{Ar}H), 124.1, 122.6 (C_{Ar}H), 120.6 (C_{Ar}), 109.4 (C_{Ar}H), 81.5 (C(CH₃)₃), 58.2 (CH, minor rotamer), 57.8 (CH, major rotamer), 55.1 (CH₂), 54.6 (CH₂), 54.2 (CH), 53.1 (CH₂), 46.4 (CH₂), 46.0 (CH₃, minor rotamer), 45.9 (CH₃, major rotamer), 45.4 (CH₂), 42.4 (CH), 42.1 (CH₂), 41.5 (CH₂), 41.3 (CH₂), 37.1 (CH₂), 36.6 (CH₂), 36.4 (CH₂), 36.3 (CH₂), 34.3 (CH₂), 34.0 (CH₂), 33.4 (CH₂), 33.0 (CH₂), 28.6 (C(CH₃)₃).

SeS60-CBI-Boc

N-Boc (S)-1-(chloromethyl)-5-((methyl((S)-1,2-thiaselenan-4-yl)carbamoyl)oxy)-1,2-dihydro-3*H*-benzo[*e*]indole

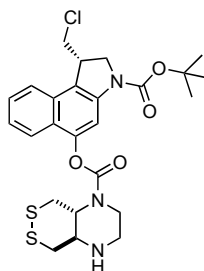


Carbamate coupling of **HO-CBI-Boc** (77 mg, 0.23 mmol) and (S)-*N*-methyl-1,2-thiaselenan-4-amine hydrochloride (56 mg, 0.24 mmol) was accomplished according to the **General Protocol A** to give **SeS60-CBI-Boc** as a colourless, crystalline solid (85 mg, 0.15 mmol, 65%).

TLC R_f = 0.79 (isohexane:EtOAc, 2:1). **HRMS** (ESI⁺) for C₂₄H₃₀ClN₂O₄SSe⁺: calcd. m/z 574.10400, found m/z 574.10383. NMR experiments at r.t. showed two rotameric species: **¹H-NMR** (500 MHz, CDCl₃): δ (ppm) = 8.05 (s, 1H), 7.78 (dd, J = 12.9, 8.6 Hz, 1H), 7.70 (d, J = 8.3 Hz, 1H), 7.50 (t, J = 7.3 Hz, 1H), 7.41 – 7.32 (m, 1H), 4.54 – 4.20 (m, 2H), 4.12 (dd, J = 13.8, 6.6 Hz, 1H), 4.01 (t, J = 9.5 Hz, 1H), 3.93 (d, J = 10.8 Hz, 1H), 3.46 (t, J = 10.9 Hz, 2H), 3.32 (dt, J = 33.0, 12.3 Hz, 1H), 3.20 – 3.05 (m, 3H), 2.95 (d, J = 16.8 Hz, 2H), 2.58 – 2.16 (m, 2H), 1.58 (s, 9H). **¹³C-NMR** (126 MHz, CDCl₃): δ (ppm) = 154.2 (C=O, major rotamer), 154.0 (C=O, minor rotamer), 152.5 (C=O), 148.5 (C_{Ar}), 141.2 (C_{Ar}), 130.3 (C_{Ar}), 127.7 (C_{Ar}H), 124.4 (C_{Ar}H), 122.6 (C_{Ar}H), 122.4 (C_{Ar}H), 120.3 (C_{Ar}), 109.4 (C_{Ar}H), 81.4 (C(CH₃)₃), 57.7 (CH, major rotamer), 57.1 (CH, minor rotamer), 53.0 (CH₂), 46.4 (CH₂), 42.2 (CH), 36.0 (CH₂), 35.3 (CH₂), 34.2 (CH₂), 33.4 (CH₂), 30.2 (CH₃), 28.5 (C(CH₃)₃), 28.0 (CH₂), 27.9 (CH₂).

H-SS66T-CBI-Boc

N-Boc (S)-1-(chloromethyl)-2,3-dihydro-1*H*-benzo[*e*]indol-5-yl (*trans*)-hexahydro-[1,2]dithiino[4,5-*b*]pyrazine-1(2*H*)-carboxylate

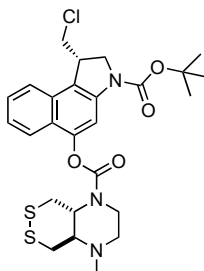


Carbamate coupling of **HO-CBI-Boc** (77.2 mg, 0.23 mmol) and *trans*-octahydro-[1,2]dithiino[4,5-*b*]pyrazine dihydrochloride (100.8 mg, 63 wt%, 0.35 mmol) was accomplished according to **General Protocol A** to give **H-SS66T-CBI-Boc** as a colourless solid (42.0 mg, 0.08 mmol, 35%).

TLC R_f = 0.32 (EtOAc). **HRMS** (ESI⁺) for C₂₅H₃₁ClN₃O₄S₂⁺: calcd. m/z 536.14390, found m/z 536.14431. **¹H-NMR** (500 MHz, CDCl₃) δ (ppm) = 8.06 (s, 1H), 7.86 – 7.77 (m, 1H), 7.71 (d, J = 8.4 Hz, 1H), 7.52 (t, J = 7.5 Hz, 1H), 7.46 – 7.32 (m, 1H), 4.25 (s, 1H), 4.19 – 4.12 (m, 1H), 4.09 – 3.98 (m, 3H), 3.93 (d, J = 10.8 Hz, 1H), 3.65 (s, 1H), 3.48 (td, J = 11.0, 1.9 Hz, 1H), 3.40 – 3.25 (m, 5H), 3.04 (dt, J = 13.8, 7.3 Hz, 2H), 2.94 – 2.74 (m, 1H), 1.58 (s, 9H). **¹³C-NMR** (126 MHz, CDCl₃) δ (ppm) = 154.0 (C=O), 152.6 (C=O), 148.1 (C_{Ar}), 141.2 (C_{Ar}), 130.3 (C_{Ar}), 127.8 (C_{Ar}H), 124.6 (C_{Ar}H), 124.0 (C_{Ar}), 122.7 (C_{Ar}H), 122.5 (C_{Ar}H), 120.6 (C_{Ar}), 109.3 (C_{Ar}H), 81.6 (C(CH₃)₃), 63.9 (CH), 56.7 (CH), 53.1 (CH₂), 46.4 (CH₂), 44.6 (CH₂), 42.2 (CH), 39.9 (CH₂), 38.0 (CH₂), 28.6 (C(CH₃)₃).

Me-SS66T-CBI-Boc

N-Boc (S)-1-(chloromethyl)-2,3-dihydro-1*H*-benzo[*e*]indol-5-yl (*trans*)-4-methylhexahydro-[1,2]dithiino[4,5-*b*]pyrazine-1(2*H*)-carboxylate

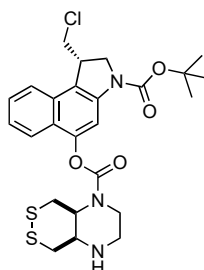


H-SS66T-CBI-Boc (20.0 mg, 0.037 mmol) was dissolved in MeOH (5 mM) and a solution of formaldehyde (424 μ L, 0.88 M in MeOH, 0.370 mmol) was added at r.t., followed by addition of a solution of NaCNBH₃ (40 μ L, 1 M in MeOH, 0.040 mmol). The reaction mixture was stirred at r.t. for 30 min, was then concentrated under reduced pressure; the residue was taken into DCM (10 mL) and washed with aq. NaCl (20 mL). The aq. layer was extracted with DCM (4 \times 10 mL), the combined organic layers were dried over Na₂SO₄, filtered and concentrated under reduced pressure. Purification was achieved by FCC (EtOAc) to give **Me-SS66T-CBI-Boc** (12.0 mg, 0.022 mmol, 59%) as a colourless solid.

TLC R_f = 0.53 (EtOAc). **HRMS** (ESI⁺) for C₂₆H₃₃ClN₃O₄S₂⁺: calcd. *m/z* 550.15955, found *m/z* 550.16002. **¹H-NMR** (500 MHz, CDCl₃): δ (ppm) = 8.06 (s, 1H), 7.81 (d, *J* = 8.6 Hz, 1H), 7.70 (d, *J* = 8.3 Hz, 1H), 7.55 – 7.48 (m, 1H), 7.42 – 7.35 (m, 1H), 4.27 (s, 1H), 4.13 (dd, *J* = 12.0, 8.9 Hz, 1H), 4.07 – 3.97 (m, 2H), 3.97 – 3.87 (m, 2H), 3.72 (s, 1H), 3.56 – 3.41 (m, 2H), 3.29 (d, *J* = 11.6 Hz, 1H), 3.19 (dt, *J* = 14.4, 4.8 Hz, 2H), 3.03 (ddd, *J* = 13.1, 10.6, 2.1 Hz, 1H), 2.90 (t, *J* = 10.1 Hz, 1H), 2.78 (dt, *J* = 10.8, 5.0 Hz, 1H), 2.41 (d, *J* = 0.9 Hz, 3H), 1.58 (s, 9H). **¹³C-NMR** (126 MHz, CDCl₃): δ (ppm) = 153.8 (C=O), 152.5 (C=O), 148.3 (C_{Ar}), 141.2 (C_{Ar}), 130.4 (C_{Ar}), 127.7 (C_{Ar}H), 124.5 (C_{Ar}H), 124.1 (C_{Ar}), 122.7 (C_{Ar}H), 122.5 (C_{Ar}H), 120.4 (C_{Ar}), 109.4 (C_{Ar}H), 81.4 (C(CH₃)₃), 63.6 (CH), 62.6 (CH), 55.1 (CH₃), 53.1 (CH₂), 46.4 (CH₂), 42.2 (CH), 40.6 (CH₂), 38.9 (CH₂), 37.9 (CH₂), 28.6 (C(CH₃)₃).

H-SS66C-CBI-Boc

N-Boc (S)-1-(chloromethyl)-2,3-dihydro-1*H*-benzo[*e*]indol-5-yl (*cis*)-hexahydro-[1,2]dithiino[4,5-*b*]pyrazine-1(2*H*)-carboxylate

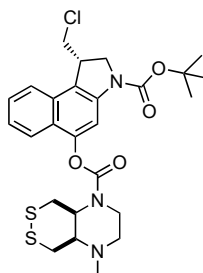


Carbamate coupling of **HO-CBI-Boc** (90.6 mg, 0.27 mmol) and *cis*-octahydro-[1,2]dithiino[4,5-*b*]pyrazine dihydrochloride (134.0 mg, 63 wt%, 0.34 mmol) was accomplished according to **General Protocol A**. **H-SS66C-CBI-Boc** was obtained as a colourless solid (97.1 mg, 0.18 mmol, 67%).

TLC R_f = 0.35 (EtOAc). **HRMS** (ESI⁺) for C₂₅H₃₁ClN₃O₄S₂⁺: calcd. *m/z* 536.14390, found *m/z* 536.14355. Individual rotamers were observed by NMR spectroscopy at 298 K (ratio ca. 1:1). **¹H-NMR** (600 MHz, CDCl₃) δ (ppm) = 8.05 (s, 2H), 7.80 – 7.72 (m, 2H), 7.70 (d, *J* = 8.4 Hz, 2H), 7.50 (t, *J* = 7.3 Hz, 2H), 7.37 (q, *J* = 7.3 Hz, 2H), 4.56 (d, *J* = 11.8 Hz, 1H), 4.37 (d, *J* = 11.6 Hz, 1H), 4.30 – 4.09 (m, 5H), 4.06 – 3.89 (m, 5H), 3.77 (td, *J* = 12.6, 7.6 Hz, 1H), 3.66 (t, *J* = 12.3 Hz, 1H), 3.58 – 3.44 (m, 4H), 3.42 (s, 1H), 3.40 – 3.33 (m, 1H), 3.31 – 3.19 (m, 3H), 3.13 – 2.98 (m, 6H), 1.93 (s, 2H), 1.58 (s, 18H). **¹³C-NMR** (151 MHz, CDCl₃) δ (ppm) = 153.6 (C=O, rotamer 1), 153.4 (C=O, rotamer 2), 152.5 (C=O), 148.3 (C_{Ar}), 141.2 (C_{Ar}), 130.3 (C_{Ar}), 127.7 (C_{Ar}H), 124.5 (C_{Ar}H, rotamer 1), 124.4 (C_{Ar}H, rotamer 2), 122.5 (2 \times C_{Ar}H), 120.6 (C_{Ar}, rotamer 1), 120.4 (C_{Ar}, rotamer 2), 109.4 (C_{Ar}H), 81.5 (C(CH₃)₃), 53.2 (CH, rotamer 1), 53.1 (CH₂), 52.9 (CH, rotamer 1), 52.6 (CH, rotamer 2), 52.0 (CH, rotamer 2), 46.4 (CH₂), 45.6 (CH₂, rotamer 1), 45.4 (CH₂, rotamer 2), 42.4 (CH₂, rotamer 1), 42.2 (CH, CH₂, rotamer 1), 41.1 (CH₂), 40.3 (CH₂), 30.0 (CH₂, rotamer 1), 29.8 (CH₂, rotamer 1), 29.2 (CH₂, rotamer 2), 29.1 (CH₂, rotamer 2), 28.5 (C(CH₃)₃).

Me-SS66C-CBI-Boc

N-Boc (S)-1-(chloromethyl)-2,3-dihydro-1*H*-benzo[*e*]indol-5-yl (cis)-4-methylhexahydro-[1,2]dithiino[4,5-*b*]pyrazine-1(2*H*)-carboxylate

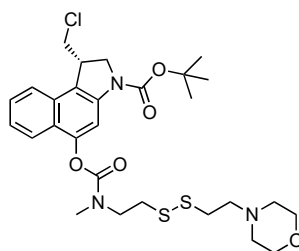


H-SS66C-CBI-Boc (78.0 mg, 0.145 mmol) was dissolved in MeOH (5 mM) and a solution of formaldehyde (4.96 mL, 0.88 M in MeOH, 4.36 mmol) was added at r.t., followed by addition of a solution of NaCNBH₃ (91.7 mg, 0.5 M solution in MeOH, 1.45 mmol). The reaction mixture was stirred at r.t. for 30 min, was then concentrated under reduced pressure; the residue was taken into DCM (10 mL) and washed with aq. NaCl (20 mL). The aq. layer was extracted with DCM (4×10 mL), the combined organic layer were dried over Na₂SO₄, filtered and concentrated under reduced pressure. Purification was achieved by FCC (isohexane/EtOAc) to give **Me-SS66C-CBI-Boc** (39.8 mg, 0.072 mmol, 50%) as a colourless solid. A fraction of unreacted starting material **H-SS66C-CBI-Boc** (32.7 mg, 0.061 mmol, 42 %) was recovered.

TLC R_f = 0.47 (isohexane:EtOAc, 1:1). **HRMS** (ESI⁺) for C₂₆H₃₃ClN₃O₄S₂⁺: calcd. *m/z* 550.15955, found *m/z* 550.15910. Individual rotamers were observed by NMR spectroscopy at 298 K (ratio ca. 1:1). **¹H-NMR** (800 MHz, CDCl₃): δ (ppm) = 8.05 (s, 2H), 7.78 – 7.75 (m, 1H), 7.75 – 7.72 (m, 1H), 7.70 (d, *J* = 8.2 Hz, 2H), 7.51 (t, *J* = 7.4 Hz, 2H), 7.37 (q, *J* = 7.2, 6.5 Hz, 2H), 4.57 (d, *J* = 10.2 Hz, 1H), 4.38 (d, *J* = 10.8 Hz, 1H), 4.30 – 4.20 (m, 3H), 4.19 – 4.07 (m, 2H), 4.09 – 3.96 (m, 4H), 3.96 – 3.89 (m, 3H), 3.57 (s, 1H), 3.55 – 3.45 (m, 2H), 3.45 – 3.26 (m, 5H), 3.10 – 2.93 (m, 2H), 2.69 (d, *J* = 7.8 Hz, 1H), 2.63 (s, 1H), 2.60 – 2.48 (m, 3H), 2.45 (t, *J* = 11.4 Hz, 1H), 2.32 (s, 6H), 1.57 (s, 18H). **¹³C-NMR** (201 MHz, CDCl₃): δ (ppm) = 153.3 (C=O, rotamer 1), 153.2 (C=O, rotamer 2), 152.5 (C=O), 148.3 (C_{Ar}), 141.3 (C_{Ar}), 130.3 (C_{Ar}), 127.7 (C_{Ar}H), 124.5 (C_{Ar}H, rotamer 1), 124.4 (C_{Ar}H, rotamer 2), 124.1 (C_{Ar}), 122.5 (2×C_{Ar}H), 120.5 (C_{Ar}), 109.4 (C_{Ar}H), 81.5 (C(CH₃)₃), 61.5 (CH, rotamer 1), 61.3 (CH, rotamer 2), 56.3 (CH₂, rotamer 1), 56.0 (CH₂, rotamer 2), 54.8 (CH, rotamer 1), 53.7 (CH, rotamer 2), 53.1 (CH₂), 46.4 (CH₂), 42.2 (CH), 41.9 (CH₃), 40.9 (CH₂, rotamer 1), 40.2 (CH₂, rotamer 2), 39.2 (CH₂, rotamer 1), 38.9 (CH₂, rotamer 2), 30.7 (CH₂, rotamer 1), 29.8 (CH₂, rotamer 2), 28.6 (C(CH₃)₃).

SS00M-CBI-Boc

N-Boc (S)-1-(chloromethyl)-5-((methyl(2-((2-morpholinoethyl)disulfaneyl)ethyl) carbamoyl)oxy)-1,2-dihydro-3*H*-benzo[*e*]indole

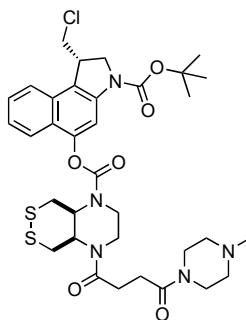


Carbamate coupling of **HO-CBI-Boc** (116.5 mg, 0.350 mmol) and *N*-methyl-2-((2-morpholinoethyl)disulfaneyl)ethan-1-amine dihydrochloride (130.0 mg, 0.42 mmol) was accomplished according to **General Protocol A** to give **SS00M-CBI-Boc** as a colourless solid (206.0 mg, 0.346 mmol, 99%).

TLC R_f = 0.58 (EtOAc:NEt₃, 30:1). **HRMS** (ESI⁺) for C₂₈H₃₉N₃O₅Cl⁺: calcd. *m/z* 596.20142, found *m/z* 596.20393. **¹H-NMR** (400 MHz, CDCl₃): δ (ppm) = 8.06 (s, 1H), 7.86 (d, *J* = 8.8 Hz, 1H), 7.70 (d, *J* = 8.4 Hz, 1H), 7.50 (t, *J* = 7.3 Hz, 1H), 7.41 – 7.34 (m, 1H), 4.25 (s, 1H), 4.13 (dd, *J* = 11.8, 8.7 Hz, 1H), 4.01 (t, *J* = 9.6 Hz, 1H), 3.93 (d, *J* = 11.1 Hz, 1H), 3.87 (t, *J* = 7.0 Hz, 1H), 3.74 – 3.59 (m, 5H), 3.46 (td, *J* = 10.9, 2.5 Hz, 1H), 3.28 (s, 2H, major rotamer), 3.10 (s, 1H, minor rotamer), 3.07 – 3.02 (m, 1H), 2.97 (t, *J* = 6.9 Hz, 1H), 2.90 – 2.83 (m, 2H), 2.68 (dd, *J* = 13.1, 7.0 Hz, 2H), 2.53 – 2.44 (m, 2H), 2.41 (s, 2H), 1.58 (s, 9H). **¹³C-NMR** (101 MHz, CDCl₃): δ (ppm) = 155.1 (C=O), 154.5 (C=O), 152.5 (C_{Ar}), 148.0 (C_{Ar}), 141.6 (C_{Ar}), 130.6 (C_{Ar}), 127.7 (C_{Ar}H), 126.8 (C_{Ar}), 124.4 (C_{Ar}H), 122.8 (C_{Ar}H), 122.4 (C_{Ar}H), 109.5 (C_{Ar}H), 81.5 (C(CH₃)₃), 66.9 (CH₂), 58.1 (CH₂), 53.6 (CH₂), 53.3 (CH₂), 49.2 (CH₂), 46.4 (CH₂), 42.2 (CH), 36.4 (CH₂), 35.9 (CH₃), 28.6 (C(CH₃)₃).

P-SS66C-CBI-Boc

N-Boc (S)-1-(chloromethyl)-2,3-dihydro-1*H*-benzo[*e*]indol-5-yl (*cis*)-4-(4-(4-methylpiperazin-1-yl)-4-oxobutanoyl)hexahydro-[1,2]dithiino[4,5-*b*]pyrazine-1(2*H*)-carboxylate

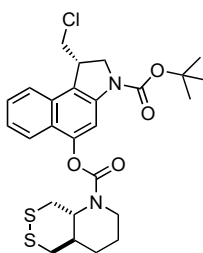


4-(4-methylpiperazin-1-yl)-4-oxobutanoic acid hydrochloride (68.0 mg, 0.29 μ mol, 7.0 eq.) was dissolved in anhydrous 1,2-dichloroethane (0.15 M) and DIPEA (98 μ L, 0.56 μ mol, 14.0 eq.) was added followed by trimethylacetyl chloride (35 μ L, 0.29 mmol, 7.0 eq.). The resulting mixture was stirred at r.t. for 2 h, before **H-SS66C-CBI-Boc** (22.0 mg, 0.041 mmol, 1.0 eq.) in 1,2-dichloroethane (0.1 M) was added in one portion. The mixture was heated to 70 $^{\circ}$ C for 15 h, was then concentrated under reduced pressure and taken into DCM (50 mL). The organic layer was washed with aq. NaCl (1 M, 4 \times 20 mL), was then dried over Na₂SO₄ and concentrated under reduced pressure. Purification was achieved using FCC (DCM/MeOH) to yield **P-SS66C-CBI-Boc** as a colourless solid (26.0 mg, 0.036 mmol, 88%).

TLC R_f = 0.53 (DCM:MeOH, 9:1). **HRMS** (ESI⁺) for C₃₄H₄₅ClN₅O₆S₂⁺: calcd. m/z 718.24943, found m/z 718.24928. **¹H-NMR** (400 MHz, CDCl₃): δ (ppm) = 8.06 (s, 1H), 7.77 (d, J = 8.5 Hz, 1H), 7.71 (d, J = 8.4 Hz, 1H), 7.51 (t, J = 7.2 Hz, 1H), 7.39 (t, J = 7.4 Hz, 1H), 4.75 (s, 1H), 4.44 (s, 2H), 4.35 – 4.21 (m, 1H), 4.20 – 4.09 (m, 1H), 4.01 (dd, J = 13.6, 8.1 Hz, 3H), 3.93 (d, J = 11.9 Hz, 1H), 3.89 – 3.62 (m, 6H), 3.57 – 3.40 (m, 2H), 3.20 (d, J = 14.1 Hz, 1H), 3.01 (d, J = 11.0 Hz, 1H), 2.81 – 2.54 (m, 8H), 2.46 (s, 3H), 1.57 (s, 9H). **¹³C-NMR** (151 MHz, CDCl₃): δ (ppm) = 172.1 (C=O), 170.4 (C=O), 154.0 (C=O), 152.5 (C=O), 148.0 (C_{Ar}), 141.2 (C_{Ar}), 130.4 (C_{Ar}), 127.8 (C_{Ar}H), 124.6 (C_{Ar}H), 123.9 (C_{Ar}), 122.5 (2 \times C_{Ar}H), 120.6 (C_{Ar}), 109.4 (C_{Ar}H), 81.5 (C(CH₃)₃), 54.6 (CH₂), 54.4 (CH₂), 53.1 (CH₂), 51.9 (CH), 46.4 (CH₂), 45.4 (CH), 44.6 (CH₂), 42.2 (CH), 42.0 (CH₂), 41.0 (CH₂), 36.0 (CH₂), 28.5 (C(CH₃)₃), 28.0 (CH₂).

SS66T-CBI-Boc

N-Boc (S)-1-(chloromethyl)-2,3-dihydro-1*H*-benzo[*e*]indol-5-yl (*trans*)-hexahydro-[1,2]dithiino[4,5-*b*]pyridine-1(2*H*)-carboxylate

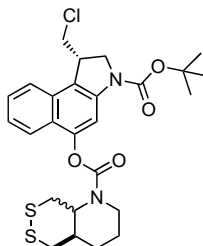


Carbamate coupling of **HO-CBI-Boc** (117.0 mg, 0.35 mmol) and *trans*-octahydro-[1,2]dithiino[4,5-*b*]pyridine hydrochloride (88.9 mg, 0.42 mmol) was accomplished according to the **General Protocol A** to give **SS66T-CBI-Boc** as a colourless, crystalline solid (162 mg, 0.30 mmol, 86%). *This compound was not further used for prodrug assembly in this study, but it is added to this report for comparison.*

TLC R_f = 0.44 (isohexane:EtOAc, 3:1). **HRMS** (ESI⁺) for C₂₆H₃₅ClN₃O₃S₂⁺: calcd. m/z 552.17520, found m/z 552.17594. **¹H-NMR** (500 MHz, CDCl₃) δ (ppm) = 8.06 (s, 1H), 7.78 (d, J = 8.4 Hz, 1H), 7.70 (d, J = 8.4 Hz, 1H), 7.51 (t, J = 7.3 Hz, 1H), 7.38 (t, J = 7.6 Hz, 1H), 4.26 (d, J = 10.8 Hz, 1H), 4.13 (t, J = 10.2 Hz, 1H), 4.05 – 3.96 (m, 2H), 3.96 – 3.82 (m, 2H), 3.57 – 3.40 (m, 2H), 3.21 (d, J = 5.9 Hz, 2H), 3.03 – 2.91 (m, 1H), 2.83 (dd, J = 13.5, 2.6 Hz, 1H), 2.28 – 2.14 (m, 1H), 2.12 – 1.99 (m, 1H), 1.93 – 1.78 (m, 1H), 1.77 – 1.67 (m, 1H), 1.58 (s, 9H), 1.54 – 1.43 (m, 1H). **¹³C-NMR** (126 MHz, CDCl₃) δ (ppm) = 154.0 (C=O), 152.5 (C=O), 148.4 (C_{Ar}), 141.5 (C_{Ar}), 130.3 (C_{Ar}), 128.1 (C_{Ar}), 127.7 (C_{Ar}H), 124.5 (C_{Ar}H), 122.6 (C_{Ar}H), 122.5 (C_{Ar}H), 120.4 (C_{Ar}), 109.4 (C_{Ar}H), 81.9 (C(CH₃)₃), 63.3 (CH), 53.0 (CH₂), 46.4 (CH₂), 42.2 (CH), 41.2 (CH₂), 40.8 (CH), 39.7 (CH₂), 37.2 (CH₂), 28.5 (C(CH₃)₃), 27.3 (CH₂), 23.3 (CH₂).

SS66-CBI-Boc (racemate; *cis:trans* 1:1)

N-Boc (S)-1-(chloromethyl)-2,3-dihydro-1*H*-benzo[*e*]indol-5-yl hexahydro-[1,2]dithiino[4,5-*b*]pyridine-1(2*H*)-carboxylate

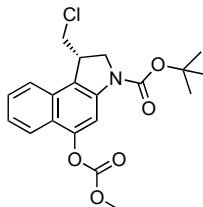


Carbamate coupling of **HO-CBI-Boc** (269 mg, 0.68 mmol) and octahydro-[1,2]dithiino[4,5-*b*]pyridine hydrochloride (racemate; *cis:trans* 1:1) (144 mg, 0.68 mmol) was accomplished according to the **General Protocol A** to give **SS66-CBI-Boc** as a colourless, crystalline solid (245 mg, 0.46 mmol, 68%). *This compound was not further used for prodrug assembly in this study, but it is added to this report for comparison.*

TLC R_f = 0.44 (isohexane:EtOAc, 3:1, two isomers indistinguishable on TLC). **HRMS** (ESI⁺) for C₂₆H₃₅ClN₃O₃S₂⁺: calcd. *m/z* 552.17520, found *m/z* 552.17531. **¹H-NMR** (400 MHz, CDCl₃): δ (ppm) = 8.05 (s, 1H), 7.77 (dd, *J* = 10.9, 7.8 Hz, 1H), 7.70 (d, *J* = 8.5 Hz, 1H), 7.50 (tt, *J* = 8.9, 1.7 Hz, 1H), 7.41 – 7.32 (m, 1H), 4.84 – 4.50 (m, 0.5H, *cis*), 4.35 (d, *J* = 13.6 Hz, 0.5H, *cis*), 4.27 (d, *J* = 11.4 Hz, 1H, *trans*), 4.21 – 4.09 (m, 1.5H), 4.06 – 3.98 (m, 1.5H), 3.97 – 3.89 (m, 1.5H), 3.64 (td, *J* = 12.7, 3.3 Hz, 0.5H, *cis*), 3.59 – 3.36 (m, 2H), 3.21 (d, *J* = 6.9 Hz, 1H, *trans*), 3.13 (d, *J* = 13.4 Hz, 0.5H, *cis*), 3.02 – 2.92 (m, 1H), 2.92 – 2.78 (m, 1H), 2.76 – 2.50 (m, 1H, *cis*), 2.46 – 2.27 (m, 1H, *cis*), 2.27 – 2.13 (m, 0.5H, *trans*), 2.12 – 1.98 (m, 0.5H, *trans*), 1.96 – 1.80 (m, 1H), 1.77 – 1.67 (m, 1H), 1.58 (s, 9H), 1.54 – 1.43 (m, 1H). **¹³C-NMR** (126 MHz, CDCl₃): δ (ppm) = 154.2 (C=O, *cis*), 154.0 (C=O, *trans*), 153.7 (C=O, *cis*), 153.5 (C=O, *cis*), 152.8 (C=O, *cis*), 152.5 (C=O, *trans*), 148.5 (C_{Ar}, *trans*), 147.3 (C_{Ar}, *cis*), 141.3 (C_{Ar}), 130.3 (C_{Ar}), 127.7 (C_{Ar}H, *trans*), 126.9 (C_{Ar}H, *cis*), 124.4 (C_{Ar}H), 122.6 (C_{Ar}H), 122.5 (C_{Ar}H), 120.2 (C_{Ar}), 109.4 (C_{Ar}H, *trans*), 109.3 (C_{Ar}H, *cis*), 81.4 (C(CH₃)₃), 63.3 (CH, *trans*), 57.0 (CH, *cis*), 54.3 (CH₂, *cis*), 53.3 (CH₂, *cis*), 53.1 (CH₂, *trans*), 46.4 (CH₂), 42.4 (CH, *cis*), 42.2 (CH, *trans*), 41.5 (CH₂, *cis*), 41.2 (CH₂, *trans*), 40.8 (CH, *trans*), 40.3 (CH, *cis*), 37.2 (CH₂, *trans*), 36.5 (CH₂, *cis*), 36.0 (CH₂, *cis*), 33.8 (CH₂), 30.3 (CH₂), 29.5 (CH₂), 28.6 (C(CH₃)₃), 27.4 (CH₂, *trans*), 25.7 (CH₂, *cis*), 25.2 (CH₂, *cis*), 23.6 (CH₂, *cis*), 23.3 (CH₂, *trans*).

MC-CBI-Boc

(S)-1-(chloromethyl)-5-((methoxycarbonyl)oxy)-1,2-dihydro-3*H*-benzo[*e*]indole-3-carboxylate

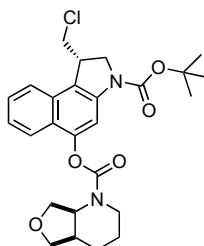


To a solution of **HO-CBI-Boc** (62.0 mg, 0.186 mmol) in anhydrous DCM (0.05 M) was added a solution of pyridine (75 μL, 0.56 mmol) and methyl chloroformate (43 μL, 0.56 mmol) at 0 °C. The mixture was stirred at r.t. for 1h, was then concentrated under reduced pressure to remove all volatiles. Purification by FCC (isohexane/EtOAc) afforded **MC-CBI-Boc** as a colourless solid (72.0 mg, 0.184 mmol, 99%).

TLC R_f = 0.56 (isohexane:EtOAc, 6:1). **HRMS** (ESI⁺) for C₂₀H₂₂NNaO₅Cl⁺: calcd. *m/z* 414.10787, found *m/z* 414.10871. **¹H-NMR** (400 MHz, CDCl₃): δ (ppm) = 8.15 (s, 1H), 7.92 (d, *J* = 8.4 Hz, 1H), 7.71 (d, *J* = 8.4 Hz, 1H), 7.59 – 7.45 (m, 1H), 7.40 (ddd, *J* = 8.1, 6.9, 1.0 Hz, 1H), 4.27 (s, 1H), 4.15 (t, *J* = 10.2 Hz, 1H), 4.07 – 3.98 (m, 1H), 3.96 (s, 3H), 3.92 (s, 1H), 3.48 (t, *J* = 10.8 Hz, 1H), 1.59 (s, 9H). **¹³C-NMR** (101 MHz, CDCl₃): δ (ppm) = 154.4 (C=O), 152.5 (C=O), 148.1 (C_{Ar}), 141.0 (C_{Ar}), 130.3 (C_{Ar}), 127.9 (C_{Ar}H), 124.6 (C_{Ar}H), 123.3 (C_{Ar}H), 122.5 (C_{Ar}H), 108.9 (C_{Ar}H), 81.6 (C(CH₃)₃), 56.6 (CH), 53.0 (CH₂), 47.0 (CH₂), 42.6 (CH₃), 28.6 (C(CH₃)₃).

O56-CBI-Boc

N-Boc (S)-1-(chloromethyl)-2,3-dihydro-1*H*-benzo[*e*]indol-5-yl (*cis*)-hexahydrofuro[3,4-*b*]pyridine-1(2*H*)-carboxylate

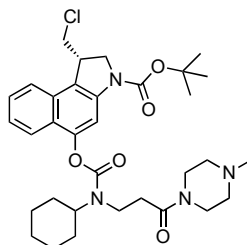


Carbamate coupling of **HO-CBI-Boc** (84 mg, 0.25 mmol) and *cis*-octahydrofuro[3,4-*b*]pyridine hydrochloride (51 mg, 0.31 mmol) was accomplished according to the **General Protocol A** to give **O56-CBI-Boc** as a colourless solid (116 mg, 0.24 mmol, 95%).

TLC R_f = 0.32 (isohexane:EtOAc, 2:1). **HRMS** (ESI⁺) for C₂₆H₃₂ClN₂O₅⁺: calcd. m/z 504.22598, found m/z 504.22598. NMR experiments at r.t. showed two rotameric species. A dynamic equilibrium between both rotameric species in the ¹H-NMR spectrum was induced at 323 K. **¹H-NMR** (400 MHz, CDCl₃, 323 K): δ (ppm) = 7.98 (s, 1H), 7.81 (d, J = 8.5 Hz, 1H), 7.70 (dt, J = 8.5, 1.0 Hz, 1H), 7.50 (ddd, J = 8.3, 6.8, 1.2 Hz, 1H), 7.36 (ddd, J = 8.2, 6.8, 1.1 Hz, 1H), 4.96 (s, 1H), 4.37 – 4.07 (m, 4H), 4.02 (ddd, J = 12.1, 7.7, 2.8 Hz, 1H), 3.98 – 3.91 (m, 2H), 3.87 – 3.78 (m, 1H), 3.74 (d, J = 8.7 Hz, 1H), 3.48 (t, J = 10.7 Hz, 1H), 3.10 (s, 1H), 2.44 – 2.24 (m, 1H), 1.96 – 1.79 (m, 2H), 1.59 (s, 9H), 1.56 – 1.51 (m, 2H). **¹³C-NMR** (126 MHz, CDCl₃, 298 K): δ (ppm) 154.4 (C=O), 152.5 (C=O), 148.5 (C_{Ar}), 141.3 (C_{Ar}), 130.3 (C_{Ar}), 127.7 (C_{Ar}H), 124.4 (C_{Ar}H), 122.7 (C_{Ar}H), 122.4 (C_{Ar}H), 120.2 (C_{Ar}), 109.4 (C_{Ar}H), 81.4 (C(CH₃)₃), 73.4 (CH₂), 66.5 (CH₂), 54.5 (CH, major rotamer), 54.1 (CH, minor rotamer), 53.1 (CH₂), 42.2 (CH), 40.9 (CH₂, major rotamer), 40.5 (CH₂, minor rotamer), 36.3 (CH, major rotamer), 36.1 (CH, minor rotamer), 28.6 (C(CH₃)₃), 25.1 (CH₂), 23.9 (CH₂, major rotamer), 23.6 (CH₂, minor rotamer).

P-CC60-CBI-Boc

N-Boc (S)-1-(chloromethyl)-5-((cyclohexyl(3-(4-methylpiperazin-1-yl)-3-oxopropyl)carbamoyl)oxy)-1,2-dihydro-3*H*-benzo[*e*]indole



Carbamate coupling of **HO-CBI-Boc** (62.9 mg, 0.189 mmol) and 3-(cyclohexylamino)-1-(4-methylpiperazin-1-yl)propan-1-one dihydrochloride (92.6 mg, 0.284 mmol) was accomplished according to the **General Protocol A** to give **P-CC60-Boc** as a colourless solid (71.9 mg, 0.117 mmol, 63%).

TLC R_f = 0.47 (DCM:MeOH, 9:1). **HRMS** (ESI⁺) for C₃₃H₄₆ClN₄O₅⁺: calcd. m/z 613.31512, found m/z 613.31534. **¹H-NMR** (600 MHz, MeOD-*d*₄): δ (ppm) = 7.94 (s, 1H), 7.91 – 7.83 (m, 2H), 7.58 (t, J = 7.4 Hz, 1H), 7.50 – 7.41 (m, 1H), 4.27 (t, J = 7.8 Hz, 1H), 4.20 (d, J = 7.1 Hz, 2H), 4.00 (d, J = 10.3 Hz, 1H), 3.91 (t, J = 12.5 Hz, 1H), 3.85 (d, J = 4.5 Hz, 1H), 3.78 – 3.67 (m, 3H), 3.66 – 3.61 (m, 1H), 2.95 (s, 1H), 2.88 (s, 1H), 2.84 – 2.77 (m, 2H), 2.74 – 2.62 (m, 2H), 2.57 (s, 2H), 2.44 (s, 1H), 2.08 (d, J = 10.8 Hz, 1H), 1.95 (d, J = 13.2 Hz, 1H), 1.90 (d, J = 10.6 Hz, 2H), 1.82 – 1.74 (m, 1H), 1.75 – 1.68 (m, 3H), 1.62 (s, 9H), 1.49 (q, J = 13.2 Hz, 1H), 1.28 – 1.19 (m, 1H). **¹³C-NMR** (151 MHz, MeOD-*d*₄): δ (ppm) = 171.7 (C=O, rotamer 1), 171.5 (C=O rotamer 2), 156.3 (C=O), 153.8 (C=O), 149.5 (C_{Ar}), 131.7 (C_{Ar}), 128.8 (C_{Ar}H), 125.6 (C_{Ar}H), 125.4 (C_{Ar}), 123.8 (C_{Ar}H), 123.5 (C_{Ar}H), 122.2 (C_{Ar}), 121.4 (C_{Ar}), 110.0 (C_{Ar}H), 82.5 (C(CH₃)₃), 59.0 (CH, major rotamer), 58.8 (CH, minor rotamer), 55.3 (CH₂, rotamer 1), 55.1 (CH₂, rotamer 2), 54.9 (CH₂, rotamer 3), 54.8 (CH₂, rotamer 4), 54.7 (CH₂, rotamer 5), 54.0 (CH₂), 47.7 (CH₂), 45.2 (CH₂), 45.1 (CH₃, minor rotamer), 44.8 (CH₃, major rotamer), 42.0 (CH), 41.7 (CH₂), 41.4 (CH₂), 35.2 (CH₂), 34.2 (CH₂), 32.6 (CH₂), 31.7 (CH₂), 28.7 (CH₃), 27.1 (CH₂), 26.5 (C(CH₃)₃), (CH₂).

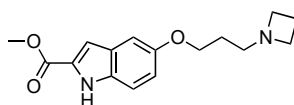
Methyl 5-hydroxy-1*H*-indole-2-carboxylate

5-hydroxy-1*H*-indole-2-carboxylic acid (1.27 g, 7.15 mmol) was dissolved in MeOH (14 mL) and cooled to 0 °C. SOCl₂ (0.78 mL, 1.28 g, 10.7 mmol) was added dropwise and the resulting mixture was heated to 75 °C for 2h, then cooled to 25 °C and diluted with EtOAc (100 mL). The organic layer was washed with sat. aq. NaHCO₃ (1×) and sat. aq. NaCl (1×) and the combined aqueous layers extracted with EtOAc (3×50 mL). The combined organic layers were dried over Na₂SO₄, filtered, and concentrated under reduced pressure to give an orange crude mixture. Purification by FCC (isohexane/EtOAc) gave methyl 5-hydroxy-1*H*-indole-2-carboxylate as a colourless powder (1.32 g, 6.9 mmol, 97%).

TLC R_f = 0.38 (isohexane:EtOAc, 5:1). **HRMS** (ESI⁺) for C₁₀H₁₀NO₃⁺: calcd. *m/z* 191.0582, found *m/z* 191.0578. **¹H-NMR** (500 MHz, CDCl₃): δ (ppm) = 8.75 (br-s, 1H), 7.30 (dd, *J* = 8.8, 0.8 Hz, 1H), 7.09 (dd, *J* = 2.1, 1.0 Hz, 1H), 7.06 (d, *J* = 2.4 Hz, 1H), 6.93 (dd, *J* = 8.8, 2.4 Hz, 1H), 4.60 (s, 1H), 3.93 (s, 3H). **¹³C-NMR** (126 MHz, CDCl₃): δ (ppm) = 162.4 (C=O), 150.3 (C_{Ar}), 132.5 (C_{Ar}), 128.3 (C_{Ar}), 128.1 (C_{Ar}), 116.3 (C_{Ar}H), 112.9 (C_{Ar}H), 108.1 (C_{Ar}H), 106.1 (C_{Ar}H), 52.2 (CH₃). Analytical data matched literature reports.¹⁴

AZI-OMe

Methyl 5-(3-(azetidine-1-yl)propoxy)-1*H*-indole-2-carboxylate



Route A:

Step 1: To methyl 5-hydroxy-1*H*-indole-2-carboxylate (190 mg, 1.00 mmol) in butanone (15 mL) was added K₂CO₃ (208 mg, 1.51 mmol) and 1-bromo-3-chloropropane (129 μL, 1.31 mmol). The mixture was stirred at 70 °C for 24 h, then cooled to 25 °C and poured into sat. aq. NaCl and diluted with EtOAc (50 mL). The layers were separated and the aqueous layer was extracted with EtOAc (3×50 mL). The combined organic layers were dried over Na₂SO₄ and concentrated under reduced pressure. Purification by FCC (isohexane/EtOAc) gave methyl 5-(3-chloropropoxy)-1*H*-indole-2-carboxylate as a colourless, crystalline solid (190 mg, 0.71 mmol, 71%).

Intermediate: methyl 5-(3-chloropropoxy)-1*H*-indole-2-carboxylate

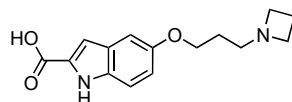
TLC R_f = 0.30 (isohexane:EtOAc, 4:1). **HRMS** (ESI⁻) for C₁₃H₁₃NO₂Cl⁻: calcd. *m/z* 266.05894, found *m/z* 266.05929. **¹H-NMR** (400 MHz, CDCl₃): δ (ppm) = 8.81 (br-s, 1H), 7.32 (dt, *J* = 8.9, 0.8 Hz, 1H), 7.13 (dd, *J* = 2.1, 1.0 Hz, 1H), 7.10 (d, *J* = 2.4 Hz, 1H), 7.00 (dd, *J* = 8.9, 2.4 Hz, 1H), 4.15 (t, *J* = 5.8 Hz, 2H), 3.94 (s, 3H), 3.78 (t, *J* = 6.4 Hz, 2H), 2.27 (p, *J* = 6.1 Hz, 2H). **¹³C-NMR** (101 MHz, CDCl₃): δ (ppm) = 162.4 (C=O), 153.9 (C_{Ar}), 132.4 (C_{Ar}), 128.0 (C_{Ar}), 127.8 (C_{Ar}), 117.5 (C_{Ar}H), 112.9 (C_{Ar}H), 108.5 (C_{Ar}H), 104.0 (C_{Ar}H), 65.1 (CH₂), 52.1 (CH₃), 41.8 (CH₂), 32.5 (CH₂).

Step 2: To methyl 5-(3-chloropropoxy)-1*H*-indole-3-carboxylate (154 mg, 0.58 mmol) in MeCN (20 mL) was added K₂CO₃ (318 mg, 2.30 mmol), NaI (43 mg, 0.29 mmol), 15-crown-5 (76 mg, 0.35 mmol) and azetidine hydrochloride (161 mg, 1.73 mmol). The mixture was stirred at 70 °C for 120 h, cooled to 25 °C, filtered and washed with EtOAc (20 mL). The filtrate was concentrated giving a brown oil. Purification by FCC (EtOAc/MeOH) gave **AZI-OMe** as a colourless solid (177 mg, 0.62 mmol, 93%).

Route B:

PPh₃ (1.25 g, 4.78 mmol, 1.1 eq) was dissolved in anhydrous THF (0.25 M) under inert gas atmosphere, the resulting solution was cooled to 0 °C and DIAD (0.95 mL, 4.78 mmol, 1.1 eq) was added. The mixture was stirred for 30 min and precipitation of a yellow solid was observed. A solution of methyl 5-hydroxy-1*H*-indole-2-carboxylate (0.99 g, 5.21 mmol, 0.5 M in anhydrous THF) and a solution of 3-(azetidine-1-yl)propanol (0.50 g, 4.34 mmol, 0.5 M in anhydrous THF) was added at 0 °C. The mixture was allowed to warm to r.t. and was further stirred at r.t. for 15 h, before being concentrated under reduced pressure. Purification by FCC (EtOAc/MeOH) gave **AZI-OMe** as a colourless solid (0.98 g, 3.39 mmol, 78%).

TLC R_f = 0.30 (isohexane:EtOAc, 4:1). **HRMS** (ESI⁻) for C₁₆H₂₁N₂O₂⁻: calcd. *m/z* 289.15467, found *m/z* 289.15478. **¹H-NMR** (400 MHz, CDCl₃): δ (ppm) = 8.89 (br-s, 1H), 7.29 (dt, *J* = 8.9, 0.8 Hz, 1H), 7.11 (dd, *J* = 2.1, 1.0 Hz, 1H), 7.06 (d, *J* = 2.4 Hz, 1H), 6.98 (dd, *J* = 8.9, 2.4 Hz, 1H), 4.02 (t, *J* = 6.4 Hz, 2H), 3.23 (t, *J* = 7.0 Hz, 4H), 2.61 (t, *J* = 7.2 Hz, 2H), 2.09 (p, *J* = 7.0 Hz, 2H), 1.93 – 1.79 (m, 2H). **¹³C-NMR** (101 MHz, CDCl₃): δ (ppm) = 162.5 (C=O), 154.2 (C_{Ar}), 132.4 (C_{Ar}), 128.0 (C_{Ar}), 127.6 (C_{Ar}), 117.6 (C_{Ar}H), 112.8 (C_{Ar}H), 108.5 (C_{Ar}H), 103.8 (C_{Ar}H), 66.7 (CH₂), 56.6 (CH₂), 55.4 (CH₂), 52.1 (CH₃), 27.7 (CH₂), 17.7 (CH₂).

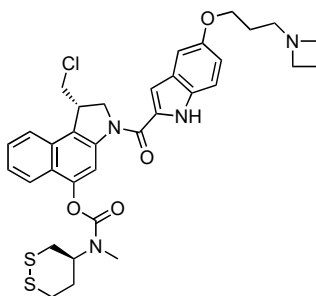
AZI-OH5-(3-(azetidine-1-yl)propoxy)-1*H*-indole-2-carboxylic acid

AZI-OMe (607 mg, 2.11 mmol) was dissolved in MeOH (100 mL) and solid KOH (167 mg, 2.53 mmol) was added. The resulting solution was heated to 75 °C for 15h, was cooled to r.t. and a solution of HCl (2.0 mL, 1.25 M in MeOH) was added. The resulting heterogenous mixture was concentrated under reduced pressure to obtain the product as a pure organic compound (quant., 68 w% calc. purity) contaminated with KCl. Purification of a fraction by RP chromatography (H₂O/MeCN) gave **AZI-OH** as a colourless powder (15 mg, 0.05 mmol).

HRMS (ESI⁺) for C₁₃H₁₃NO₂Cl: calcd. *m/z* 275.13902, found *m/z* 275.13910. **¹H-NMR** (400 MHz, DMSO-*d*₆): δ (ppm) = 11.14 (br-s, 1H), 7.25 (d, *J* = 8.8 Hz, 1H), 7.08 (d, *J* = 2.4 Hz, 1H), 6.75 (dd, *J* = 8.8, 2.3 Hz, 2H), 4.02 (t, *J* = 6.8 Hz, 2H), 3.63 (t, *J* = 7.5 Hz, 4H), 2.91 (t, *J* = 6.5 Hz, 2H), 2.20 (p, *J* = 7.5 Hz, 2H), 1.86 (p, *J* = 6.7 Hz, 2H). **¹³C-NMR** (101 MHz, DMSO-*d*₆): δ (ppm) = 165.1 (C=O), 152.6 (C_{Ar}), 134.1 (C_{Ar}), 131.7 (C_{Ar}H), 127.6 (C_{Ar}), 114.3 (C_{Ar}H), 112.9 (C_{Ar}H), 104.3 (C_{Ar}H), 102.6 (C_{Ar}H), 65.3 (CH₂), 53.2 (CH₂), 53.0 (CH₂), 25.4 (CH₂), 16.2 (CH₂).

9.3. CBI-AZI prodrug series**SS60-CBI-AZI**

(*S*)-3-(5-(3-(azetidin-1-yl)propoxy)-1*H*-indole-2-carbonyl)-1-(chloromethyl)-2,3-dihydro-1*H*-benzo[*e*]indol-5-yl ((*S*)-1,2-dithian-4-yl)(methyl)carbamate

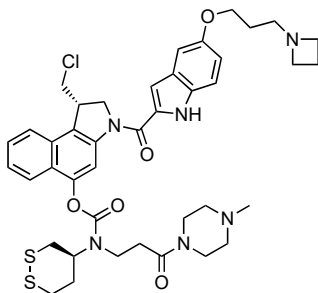


Amide coupling and was accomplished according to the **General Protocol B**. HCl (4 M in dioxane) (*Method A*) was applied for *N*-Boc deprotection of **SS60-CBI-Boc** (68.0 mg, 0.134 mmol) and **AZI-OH** (64.7 mg, 68 w%, 0.160 mmol) was activated for final prodrug assembly using EDCl (*Method D*). **SS60-CBI-AZI** was obtained as a colourless solid (43.6 mg, 0.655 mmol, 49%).

TLC R_f = 0.50 (DCM:MeOH, 4:1). **HRMS** (ESI⁺) for C₃₄H₃₈ClN₄O₄S₂⁺: calcd. *m/z* 665.20175, found *m/z* 665.20156. **¹H-NMR** (400 MHz, DMSO-*d*₆): δ (ppm) = 11.59 (s, 1H), 8.21 (s, 1H), 8.04 (d, *J* = 8.3 Hz, 1H), 7.84 (d, *J* = 8.5 Hz, 1H), 7.66 – 7.58 (m, 1H), 7.55 – 7.48 (m, 1H), 7.39 (d, *J* = 8.9 Hz, 1H), 7.22 – 7.08 (m, 2H), 6.91 (dd, *J* = 8.9, 2.3 Hz, 1H), 4.88 (t, *J* = 10.1 Hz, 1H), 4.62 (d, *J* = 10.9 Hz, 1H), 4.48 – 4.36 (m, 1H), 4.20 – 4.05 (m, 2H), 4.05 – 3.92 (m, 3H), 3.26 – 3.17 (m, 3H), 3.16 (s, 2H), 3.09 (t, *J* = 6.9 Hz, 4H), 2.99 – 2.89 (m, 2H), 2.23 – 2.07 (m, 1H), 1.95 (p, *J* = 6.9 Hz, 2H), 1.71 (p, *J* = 6.6 Hz, 2H). **¹³C-NMR** (126 MHz, DMSO-*d*₆): δ (ppm) = 160.2 (C=O), 153.4 (C=O), 153.1 (C_{Ar}), 147.3 (C_{Ar}), 141.5 (C_{Ar}), 131.7 (C_{Ar}), 130.6 (C_{Ar}), 129.5 (C_{Ar}), 127.6 (C_{Ar}), 127.5 (C_{Ar}H), 125.1 (C_{Ar}H), 124.3 (C_{Ar}), 123.4 (C_{Ar}H), 122.3 (C_{Ar}H), 116.0 (C_{Ar}H), 113.2 (C_{Ar}H), 110.7 (C_{Ar}H), 105.6 (C_{Ar}H), 103.1 (C_{Ar}H), 65.8 (CH₂), 55.7 (CH), 55.3 (CH₂), 55.0 (CH₂), 54.4 (CH₂), 47.7 (CH₂), 41.2 (CH), 35.6 (CH₂), 34.6 (CH₂), 31.7 (CH₂), 30.2 (CH₃), 26.7 (CH₂), 16.9 (CH₂).

P-SS60-CBI-AZI

(S)-3-(5-(3-(azetidin-1-yl)propoxy)-1*H*-indole-2-carbonyl)-1-(chloromethyl)-2,3-dihydro-1*H*-benzo[*e*]indol-5-yl ((S)-1,2-dithian-4-yl)(3-(4-methylpiperazin-1-yl)-3-oxopropyl)carbamate

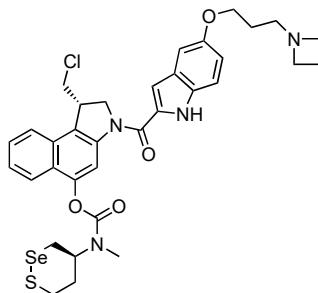


Amide coupling was accomplished according to the **General Protocol B**. $\text{BF}_3 \cdot \text{OEt}_2$ (*Method B*) was applied for *N*-Boc deprotection of **P-SS60-CBI-Boc** (22.0 mg, 0.034 mmol) and **AZI-OH** (26.5 mg, 68 w%, 0.051 mmol) was activated for final prodrug assembly using EDCI (*Method D*). **P-SS60-CBI-AZI** was obtained as a colourless solid (17.3 mg, 0.022 mmol, 65%).

TLC $R_f = 0.07$ (DCM:MeOH, 5:1). **HRMS** (ESI⁺) for $\text{C}_{41}\text{H}_{50}\text{ClN}_6\text{O}_5\text{S}_2^+$: calcd. m/z 805.29671, found m/z 805.29632. **¹H-NMR** (500 MHz, DMSO-*d*₆): δ (ppm) = 11.58 (s, 1H), 8.25 (s, 1H), 8.22 (s, 1H), 8.08 – 8.00 (m, 1H), 7.84 (t, $J = 8.1$ Hz, 1H), 7.66 – 7.59 (m, 1H), 7.56 – 7.48 (m, 1H), 7.40 (d, $J = 8.9$ Hz, 1H), 7.17 – 7.12 (m, 2H), 6.92 (dd, $J = 8.9, 2.3$ Hz, 1H), 4.87 (t, $J = 10.0$ Hz, 1H), 4.62 (d, $J = 10.9$ Hz, 1H), 4.41 (s, 1H), 4.09 (d, $J = 11.1$ Hz, 1H), 4.03 – 3.97 (m, 3H), 3.92 (s, 1H), 3.82 – 3.74 (m, 1H), 3.21 (t, $J = 7.0$ Hz, 3H), 3.15 – 3.11 (m, 1H), 3.01 (d, $J = 10.9$ Hz, 1H), 2.85 (dq, $J = 16.0, 8.2$ Hz, 1H), 2.67 (d, $J = 12.8$ Hz, 1H), 2.58 (t, $J = 7.0$ Hz, 1H), 3.33 – 3.27 (m, 2H), 2.31 – 2.21 (m, 5H), 2.21 – 2.08 (m, 5H), 2.00 (p, $J = 7.0$ Hz, 2H), 1.74 (p, $J = 6.5$ Hz, 2H). **¹³C-NMR** (126 MHz, DMSO-*d*₆): δ (ppm) = 169.8 (C=O), 164.9 (C=O), 160.5 (C=O), 152.7 (C_{Ar}), 148.1 (C_{Ar}), 141.9 (C_{Ar}), 132.2 (C_{Ar}), 131.0 (C_{Ar}), 130.2 (C_{Ar}), 128.0 (C_{Ar}H), 125.8 (C_{Ar}H), 125.0 (C_{Ar}), 123.9 (C_{Ar}H), 122.8 (C_{Ar}H), 116.9 (C_{Ar}H), 115.1 (C_{Ar}), 113.7 (C_{Ar}H), 111.4 (C_{Ar}H), 106.7 (C_{Ar}H), 103.6 (C_{Ar}H), 66.3 (CH₂), 58.5 (CH), 55.7 (CH₂), 55.4 (CH₂), 55.2 (CH₂), 54.9 (CH₂), 54.7 (CH₂), 48.3 (CH₂), 46.5 (CH₃), 45.9 (CH₂), 42.9 (CH₂), 41.7 (CH), 41.3 (CH₂), 36.6 (CH₂), 35.6 (CH₂), 33.8 (CH₂), 32.5 (CH₂), 28.5 (CH₂), 22.5, 18.0 (CH₂).

SeS60-CBI-AZI

(S)-3-(5-(3-(azetidin-1-yl)propoxy)-1*H*-indole-2-carbonyl)-1-(chloromethyl)-2,3-dihydro-1*H*-benzo[*e*]indol-5-yl methyl((S)-1,2-thiaselenan-4-yl)carbamate



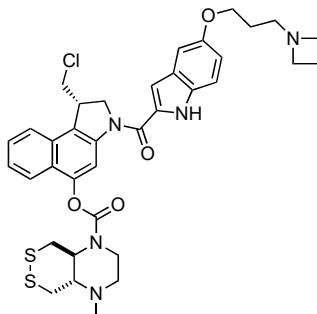
Amide coupling was accomplished according to the **General Protocol B**. HCl (4 M in dioxane) (*Method A*) was applied for *N*-Boc deprotection of **SeS60-CBI-Boc** (41.0 mg, 0.074 mmol) and **AZI-OH** (35.7 mg, 68 w%, 0.088 mmol) was activated for final prodrug assembly using EDCI (*Method D*). **SeS60-CBI-AZI** was obtained as a colourless solid (27.0 mg, 0.038 mmol, 51%).

TLC $R_f = 0.57$ (DCM:MeOH, 4:1). **HRMS** (ESI⁺) for $\text{C}_{34}\text{H}_{38}\text{ClN}_4\text{O}_4\text{SSe}^+$: calcd. m/z 713.14520, found m/z 713.14594. **¹H-NMR** (400 MHz, DMSO-*d*₆): δ (ppm) = 11.64 (s, 1H), 9.86 (s, 1H), 8.21 (s, 1H), 8.04 (d, $J = 8.5$ Hz, 1H), 7.84 (d, $J = 8.8$ Hz, 1H), 7.61 (q, $J = 7.3$ Hz, 1H), 7.52 (t, $J = 7.8$ Hz, 1H), 7.47 (d, $J = 7.9$ Hz, 1H, TsO⁻), 7.43 (d, $J = 9.0$ Hz, 1H), 7.18 (s, 1H), 7.14 (s, 1H), 7.11 (d, $J = 8.0$ Hz, 1H, TsO⁻), 6.95 (dd, $J = 8.9, 2.6$ Hz, 1H), 4.96 – 4.78 (m, 1.5H, major rotamer), 4.61 (d, $J = 9.8$ Hz, 1H), 4.56 – 4.51 (m, 0.5H, minor rotamer), 4.41 (s, 1H), 4.33 – 4.22 (m, 1H), 4.14 – 3.97 (m, 6H), 3.56 – 3.39 (m, 1H), 3.25 – 2.95 (m, 1H), 3.15 (s, 2H, major rotamer), 2.92 (s, 1H, minor rotamer), 2.41 – 2.30 (m, 2H), 2.28 (s, 1.5H, TsO⁻), 2.23 – 2.00 (m, 2H), 1.95 (p, $J = 6.5$ Hz, 2H). **¹³C-NMR** (126 MHz, DMSO-*d*₆): δ (ppm) = 160.2 (C=O), 152.7 (C=O), 150.7 (C_{Ar}), 147.3 (C_{Ar}), 145.8 (C_{Ar}, TsO⁻), 142.8 (C_{Ar}), 141.4 (C_{Ar}), 137.5 (C_{Ar}), 135.6 (C_{Ar}, TsO⁻), 131.8 (C_{Ar}), 130.8 (C_{Ar}), 129.5 (C_{Ar}), 128.0 (C_{Ar}H, TsO⁻), 127.7 (C_{Ar}), 127.5 (C_{Ar}H), 125.5 (C_{Ar}H, TsO⁻), 124.3 (C_{Ar}H), 123.7 (C_{Ar}H), 122.4 (C_{Ar}H), 117.3 (C_{Ar}), 115.9 (C_{Ar}H), 113.3 (C_{Ar}H), 110.4 (C_{Ar}H), 105.5 (C_{Ar}H), 103.4 (C_{Ar}H), 64.9 (CH₂), 56.0 (CH), 54.8 (CH₂), 54.0 (CH₂), 51.8 (CH₂).

47.2 (CH₂), 41.1 (CH), 32.9 (CH₂), 30.0 (CH₂), 26.6 (CH₂), 24.3 (CH₂), 20.8 (CH₃, TsO⁻), 15.9 (CH₂). 0.5 eq. TsO⁻: counter ion, 0.5 eq identified by NMR.

Me-SS66T-CBI-AZI

(S)-3-(5-(3-(azetidino-1-yl)propoxy)-1*H*-indole-2-carbonyl)-1-(chloromethyl)-2,3-dihydro-1*H*-benzo[*e*]indol-5-yl (*trans*)-4-methylhexahydro-[1,2]dithiino[4,5-*b*]pyrazine-1(2*H*)-carboxylate

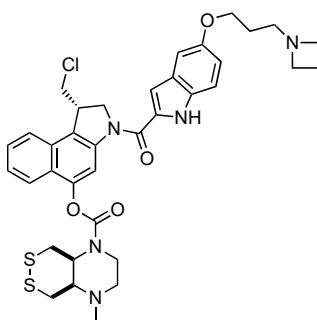


Amide coupling was accomplished according to the **General Protocol B**. BF₃·OEt₂ (*Method B*) was applied for *N*-Boc deprotection of **Me-SS66T-CBI-Boc** (12.0 mg, 0.021 mmol) and **AZI-OH** (17.0 mg, 68 w%, 0.033 mmol) was activated for final prodrug assembly using EDCI (*Method D*). **Me-SS66T-CBI-AZI** was obtained as a colourless solid (2.0 mg, 0.003 mmol, 14%).

.TLC R_f = 0.1 (DCM:MeOH 5:1). **HRMS** (ESI⁺) for C₃₆H₄₁ClN₅O₄S₂⁺: calcd. *m/z* 706.22830, found *m/z* 706.22814. **¹H-NMR** (800 MHz, DMSO-*d*₆): δ (ppm) = 11.61 (s, 1H), 8.21 (s, 1H), 8.05 (d, *J* = 8.3 Hz, 1H), 7.84 (d, *J* = 8.4 Hz, 1H), 7.65 – 7.60 (m, 1H), 7.58 – 7.51 (m, 1H), 7.47 (d, *J* = 8.0 Hz, 1H), 7.39 (d, *J* = 8.8 Hz, 1H), 7.16 – 7.12 (m, 2H), 7.11 (d, *J* = 7.8 Hz, 1H), 6.91 (dd, *J* = 8.8, 2.4 Hz, 1H), 4.87 (t, *J* = 9.4 Hz, 1H), 4.62 (dd, *J* = 10.6, 2.0 Hz, 1H), 4.42 (d, *J* = 2.7 Hz, 1H), 4.10 (dt, *J* = 11.2, 3.0 Hz, 1H), 4.00 (dt, *J* = 15.4, 6.6 Hz, 4H), 3.93 (s, 1H), 3.53 – 3.46 (m, 2H), 3.22 – 3.17 (m, 5H), 3.01 – 2.94 (m, 1H), 2.89 (d, *J* = 8.6 Hz, 1H), 2.71 – 2.65 (m, 2H), 2.58 – 2.55 (m, 1H), 2.33 – 2.27 (m, 3H), 1.99 (p, *J* = 7.0 Hz, 2H), 1.74 (p, *J* = 6.6 Hz, 2H). **¹³C-NMR** (201 MHz, DMSO-*d*₆): δ (ppm) = 163.6 (C=O), 160.3 (C=O), 153.1 (C_{Ar}), 147.0 (C_{Ar}), 145.9 (C_{Ar}), 141.5 (C_{Ar}), 137.5 (C_{Ar}), 131.7 (C_{Ar}), 130.6 (C_{Ar}), 129.6 (C_{Ar}), 128.0 (C_{Ar}), 127.7 (C_{Ar}H), 127.5 (C_{Ar}H), 125.5 (C_{Ar}H), 125.2 (C_{Ar}H), 124.3 (C_{Ar}), 123.5 (C_{Ar}H), 122.5 (C_{Ar}), 122.1 (C_{Ar}H), 116.1 (C_{Ar}H), 113.2 (C_{Ar}H), 110.6 (C_{Ar}H), 105.6 (C_{Ar}H), 103.1 (C_{Ar}H), 65.8 (CH₂), 62.2 (CH), 61.9 (CH), 55.4 (CH₂), 54.9 (CH₂), 54.5 (2×CH₂), 47.7 (CH₂), 43.5 (CH₂), 41.2 (CH), 38.2 (CH₂), 36.7 (CH₂), 26.8 (CH₂), 20.8 (CH₃), 17.0 (CH₂).

Me-SS66C-CBI-AZI

(S)-3-(5-(3-(azetidino-1-yl)propoxy)-1*H*-indole-2-carbonyl)-1-(chloromethyl)-2,3-dihydro-1*H*-benzo[*e*]indol-5-yl (*cis*)-4-methylhexahydro-[1,2]dithiino[4,5-*b*]pyrazine-1(2*H*)-carboxylate



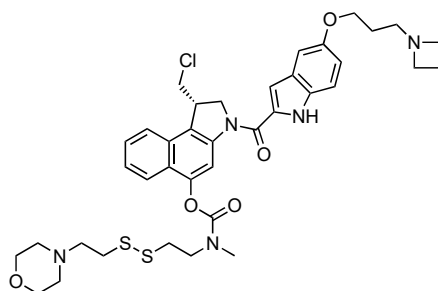
Amide coupling was accomplished according to the **General Protocol B**. BF₃·OEt₂ (*Method B*) was applied for *N*-Boc deprotection of **Me-SS66C-CBI-Boc** (21.0 mg, 0.038 mmol) and **AZI-OH** (36.6 mg, 68 w%, 0.105 mmol) was activated for final prodrug assembly using EDCI (*Method D*). **Me-SS66C-CBI-AZI** was obtained as a colourless solid (2.0 mg, 0.003 mmol, 8%).

TLC R_f = 0.1 (DCM:MeOH 5:1). **HRMS** (ESI⁺) for C₃₆H₄₁ClN₅O₄S₂⁺: calcd. *m/z* 706.22830, found *m/z* 706.22798. **¹H-NMR** (800 MHz, DMSO-*d*₆): δ (ppm) = 11.58 (s, 1H), 8.29 (s, 1H), 8.20 (s, 1H), 8.04 (d, *J* = 8.3 Hz, 1H), 7.87 – 7.80 (m, 1H), 7.62 (t, *J* = 7.5 Hz, 1H), 7.55 – 7.50 (m, 1H), 7.39 (d, *J* = 8.8 Hz, 1H), 7.16 – 7.11 (m, 2H), 6.91 (dd, *J* = 8.8, 2.4 Hz, 1H), 4.87 (t, *J* = 9.4 Hz, 1H), 4.62 (d, *J* = 10.6 Hz, 1H), 4.41 (s, 0H), 4.16 (dd, *J* = 30.6, 12.1 Hz, 1H), 4.09 (d, *J* = 11.2 Hz, 1H), 4.02 – 3.96 (m, 3H), 3.94 – 3.89 (m, 1H), 3.87 – 3.78 (m, 2H), 3.64 – 3.55 (m, 1H), 3.51 – 3.43 (m, 1H), 3.11 (t, *J* = 6.9 Hz, 4H), 2.96 (dd, *J* = 26.2, 10.8 Hz, 1H), 2.86 – 2.78 (m, 1H), 2.41 (dt, *J* = 3.6,

1.8 Hz, 2H), 2.34 – 2.25 (m, 1H), 2.21 (s, 3H), 1.99 – 1.92 (m, 2H), 1.72 (p, $J = 6.7$ Hz, 2H), 1.28 – 1.23 (m, 2H). **¹³C-NMR** (201 MHz, DMSO-*d*₆): δ (ppm) = 160.8 (C=O), 153.1 (C=O), 147.1 (C_{Ar}), 141.5 (C_{Ar}), 131.7 (C_{Ar}), 130.6 (C_{Ar}), 129.5 (C_{Ar}), 127.7 (C_{Ar}H, rotamer 1), 127.5 (C_{Ar}H, rotamer 2), 125.2 (C_{Ar}H), 124.2 (C_{Ar}H), 123.3 (C_{Ar}), 122.5 (C_{Ar}H, rotamer 1), 122.2 (C_{Ar}H, rotamer 2), 116.0 (C_{Ar}H), 113.2 (C_{Ar}H), 110.7 (C_{Ar}H), 105.6 (C_{Ar}H), 103.1 (C_{Ar}H), 65.9 (CH₂), 60.6 (CH, rotamer 1), 60.4 (CH, rotamer 2), 55.7 (CH₂), 55.4 (CH₂), 55.2 (CH₂, rotamer 1), 55.0 (CH₂, rotamer 2), 54.5 (CH₂), 54.3 (CH), 53.5 (CH), 47.7 (CH₂), 41.2 (CH₃), 40.5 (CH₂), 38.1 (CH₂), 29.0 (CH₂), 27.0 (CH₂), 17.0 (CH₂).

SS00_M-CBI-AZI

(S)-3-(5-(3-(azetidin-1-yl)propoxy)-1*H*-indole-2-carbonyl)-1-(chloromethyl)-2,3-dihydro-1*H*-benzo[e]indol-5-yl methyl(2-((2-morpholinoethyl)disulfaneyl)ethyl)carbamate

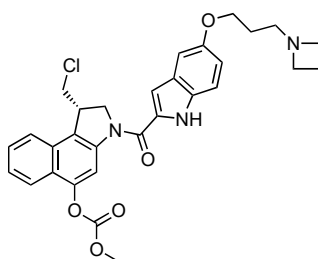


Amide coupling was accomplished according to the **General Protocol B**. HCl (4 M in dioxane) (*Method A*) was applied for *N*-Boc deprotection of **SS00_M-CBI-Boc** (112.0 mg, 0.188 mmol) and **AZI-OH** (90.9 mg, 68 w%, 0.225 mmol) was activated for final prodrug assembly using EDCl (*Method D*). **SS00_M-CBI-AZI** was obtained as a colourless solid (30 mg, 0.040 mmol, 21%).

TLC $R_f = 0.23$ (DCM:MeOH, 5:1). **HRMS** (ESI⁺) for C₃₈H₄₇ClN₅O₅S₂⁺: calcd. m/z 752.27037, found m/z 752.27017. **¹H-NMR** (400 MHz, DMSO-*d*₆): δ (ppm) = 11.61 (s, 1H), 8.38 (s, 1H), 8.23 (s, 1H), 8.04 (d, $J = 8.3$ Hz, 1H), 8.01 – 7.82 (m, 1H), 7.62 (t, $J = 7.5$ Hz, 1H), 7.55 – 7.47 (m, 1H), 7.39 (d, $J = 8.9$ Hz, 1H), 7.18 – 7.08 (m, 2H), 6.91 (dd, $J = 8.9, 2.4$ Hz, 1H), 4.87 (t, $J = 9.9$ Hz, 1H), 4.62 (d, $J = 11.0$ Hz, 1H), 4.41 (s, 1H), 4.10 (dd, $J = 11.0, 2.9$ Hz, 1H), 3.99 (q, $J = 6.5$ Hz, 3H), 3.89 (s, 1H), 3.64 (d, $J = 6.9$ Hz, 1H), 3.51 (d, $J = 4.4$ Hz, 2H), 3.47 – 3.42 (m, 2H), 3.26 (s, 2H), 3.15 (t, $J = 6.9$ Hz, 1H), 3.10 (t, $J = 6.9$ Hz, 4H), 3.07 – 2.98 (m, 3H), 2.90 (t, $J = 8.8$ Hz, 2H), 2.56 (dd, $J = 14.7, 5.5$ Hz, 2H), 2.39 – 2.32 (m, 2H), 2.28 (d, $J = 9.7$ Hz, 2H), 1.95 (p, $J = 6.9$ Hz, 2H), 1.71 (p, $J = 6.6$ Hz, 2H). **¹H/¹³C-HSQC** (400 MHz/101 MHz, DMSO-*d*₆): δ (ppm) = 127.2 (C_{Ar}H), 124.6 (C_{Ar}H), 123.3 (C_{Ar}H), 122.0 (C_{Ar}H), 115.9 (C_{Ar}H), 113.0 (C_{Ar}H), 110.4 (C_{Ar}H), 105.2 (C_{Ar}H), 102.6 (C_{Ar}H), 65.7 (CH₂), 65.4 (CH₂), 57.0 (CH₂), 55.4 (CH₂), 54.7 (CH₂), 54.1 (CH₂), 52.8 (CH₂), 47.6 (CH₂), 47.3 (CH₂), 40.8 (CH), 35.0 (CH₂), 43.3 (CH₃), 26.6 (CH₂), 16.5 (CH₂).

MC-CBI-AZI

(S)-3-(5-(3-(azetidin-1-yl)propoxy)-1*H*-indole-2-carbonyl)-1-(chloromethyl)-2,3-dihydro-1*H*-benzo[e]indol-5-yl methyl carbonate



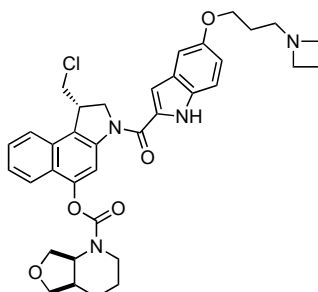
Amide coupling was accomplished according to the **General Protocol B**. BF₃·OEt₂ (*Method B*) was applied for *N*-Boc deprotection of **MC-CBI-Boc** (20.0 mg, 0.051 mmol) and **AZI-OH** (31.3 mg, 68 w%, 0.077 mmol) was activated for final prodrug assembly using EDCl (*Method D*). **MC-CBI-AZI** was obtained as a colourless solid (21.0 mg, 0.038 mmol, 75%).

TLC $R_f = 0.27$ (DCM:MeOH, 5:1). **HRMS** (ESI⁺) for C₃₀H₃₁ClN₃O₅⁺: calcd. m/z 548.19468, found m/z 548.19519. **¹H-NMR** (500 MHz, DMSO-*d*₆): δ (ppm) = 11.64 (s, 1H), 8.34 (s, 1H), 8.26 (s, 1H), 8.07 (d, $J = 8.3$ Hz, 1H), 7.89 (d, $J = 8.4$ Hz, 1H), 7.70 – 7.61 (m, 1H), 7.58 – 7.51 (m, 1H), 7.41 (d, $J = 8.8$ Hz, 1H), 7.19 – 7.12 (m, 2H), 6.93 (d, $J = 8.7$ Hz, 1H), 4.88 (t, $J = 10.0$ Hz, 2H), 4.63 (d, $J = 10.5$ Hz, 2H), 4.43 (s, 2H), 4.10 (d, $J = 8.9$ Hz, 1H), 4.05 – 3.97 (m, 2H), 3.92 (s, 4H), 3.46 – 3.34 (m, 4H), 2.74 (d, $J = 6.6$ Hz, 2H), 2.15 – 2.01 (m, 2H), 1.89 – 1.69 (m, 2H).

¹³C-NMR (101 MHz, DMSO-*d*₆): δ (ppm) = 164.2 (C=O), 160.3 (C=O), 153.7 (C_{Ar}), 153.0 (C_{Ar}), 146.6 (C_{Ar}), 141.5 (C_{Ar}), 131.8 (C_{Ar}), 130.5 (C_{Ar}), 129.6 (C_{Ar}), 127.9 (C_{Ar}), 127.5 (C_{Ar}H), 125.5 (C_{Ar}H), 123.6 (C_{Ar}), 123.5 (C_{Ar}H), 121.8 (C_{Ar}H), 116.1 (C_{Ar}H), 113.2 (C_{Ar}H), 110.2 (C_{Ar}H), 105.7 (C_{Ar}H), 103.2 (C_{Ar}H), 65.6 (CH₂), 55.9 (CH₃), 55.0 (CH₂), 54.4 (CH₂), 54.2 (CH₂), 47.6 (CH₂), 41.3 (CH), 26.1 (CH₂), 16.6 (CH₂).

O56-CBI-AZI

(S)-3-(5-(3-(azetidin-1-yl)propoxy)-1*H*-indole-2-carbonyl)-1-(chloromethyl)-2,3-dihydro-1*H*-benzo[*e*]indol-5-yl (*cis*)-hexahydrofuro[3,4-*b*]pyridine-1(2*H*)-carboxylate



Amide coupling was accomplished according to the **General Protocol B**. HCl (4 M in dioxane) (*Method A*) was applied for *N*-Boc deprotection of **O56-CBI-Boc** (189 mg, 0.388 mmol) and **AZI-OH** (167 mg, 68 w%, 0.407 mmol) was activated for final prodrug assembly using EDCI (*Method D*). **O56-CBI-AZI** was obtained as a colourless solid (50.0 mg, 0.078 mmol, 20%).

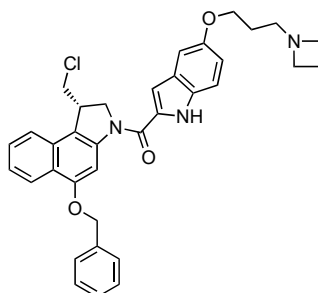
TLC R_f = 0.32 (DCM:MeOH, 5:1). **HRMS** (ESI⁺) for C₃₆H₄₀ClN₄O₅⁺: calcd. *m/z* 643.26817, found *m/z* 643.26776.

¹H-NMR (400 MHz, DMSO-*d*₆): δ (ppm) = 11.65 (m, 1H), 9.95 (s, 1H), 8.20 (s, 1H), 8.04 (d, *J* = 8.4 Hz, 1H), 7.87 – 7.77 (m, 1H), 7.67 – 7.58 (m, 1H), 7.52 (t, *J* = 7.8 Hz, 1H), 7.47 (d, *J* = 7.9 Hz, 1H, TsO⁻), 7.43 (d, *J* = 8.9 Hz, 1H), 7.18 (d, *J* = 2.4 Hz, 1H), 7.14 (d, *J* = 2.4 Hz, 1H), 7.11 (d, *J* = 8.0 Hz, 1H, TsO⁻), 6.95 (dt, *J* = 8.9, 2.9 Hz, 1H), 5.02 (s, 0.5H, major rotamer), 4.94 – 4.79 (m, 1H), 4.68 (s, 0.5H, major rotamer), 4.62 (dd, *J* = 10.9, 2.3 Hz, 1H), 4.41 (s, 1H), 4.34 – 4.17 (m, 1H), 4.05 (m, 8H), 3.85 (s, 3H), 3.62 (d, *J* = 8.5 Hz, 2H), 3.32 – 3.27 (m, 2H), 3.00 (s, 1H), 2.39 – 2.30 (m, 3H), 2.28 (s, 1.5H, TsO⁻), 1.95 (p, *J* = 6.5 Hz, 2H), 1.87 – 1.75 (m, 2H), 1.67 – 1.42 (m, 2H).

¹³C-NMR (101 MHz, DMSO-*d*₆): δ (ppm) = 160.2 (C_{Ar}), 153.7 (C_{Ar}), 152.7 (C_{Ar}), 147.3 (C_{Ar}), 145.8 (C_{Ar}, TsO⁻), 141.5 (C_{Ar}), 137.6 (C_{Ar}, TsO⁻), 132.5 (C_{Ar}), 131.9 (C_{Ar}), 131.6 (C_{Ar}), 130.8 (C_{Ar}), 129.5 (C_{Ar}), 128.1 (C_{Ar}H, TsO⁻), 127.7 (C_{Ar}), 127.5 (C_{Ar}H), 125.9 (C_{Ar}H, TsO⁻), 124.8 (C_{Ar}H), 123.6 (C_{Ar}H), 122.4 (C_{Ar}H), 116.0 (C_{Ar}H), 113.3 (C_{Ar}H), 110.4 (C_{Ar}H), 105.6 (C_{Ar}H), 103.3 (C_{Ar}H), 72.5 (CH₂), 65.1 (CH₂), 64.9 (CH₂), 55.0 (CH₂), 53.9 (CH₂), 53.4 (CH), 51.8 (CH₂), 47.7 (CH₂), 41.3 (CH), 40.2 (CH₂), 35.0 (CH), 24.4 (CH₂), 24.3 (CH₂), 23.1 (CH₂), 20.8 (CH₃, TsO⁻), 15.9 (CH₂). TsO⁻: counter ion, 0.5 eq identified by NMR.

OBn-CBI-AZI

(S)-5-(3-(azetidin-1-yl)propoxy)-1*H*-indol-2-yl(5-(benzyloxy)-1-(chloromethyl)-1,2-dihydro-3*H*-benzo[*e*]indol-3-yl)methanone



Amide coupling was accomplished according to the **General Protocol B**. HCl (4 M in dioxane) (*Method A*) was applied for *N*-Boc deprotection of **OBn-CBI-Boc** (116.0 mg, 0.274 mmol) and **AZI-OH** (110.0 mg, 68 w%, 0.274 mmol) was activated for final prodrug assembly using EDCI (*Method D*). **OBn-CBI-AZI** was obtained as a colourless solid (90.0 mg, 0.155 mmol, 57%).

TLC R_f = 0.32 (DCM:MeOH, 5:1). **HRMS** (ESI⁺) for C₃₅H₃₅ClN₃O₃⁺: calcd. *m/z* 580.23615, found *m/z* 580.23615.

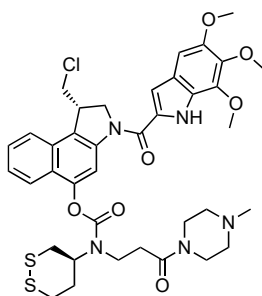
¹H-NMR (400 MHz, DMSO-*d*₆): δ (ppm) = 11.70 (s, 1H), 10.39 (br-s, 1H), 8.22 (d, *J* = 8.4 Hz, 1H), 8.12 (br-s, 1H), 7.94 (d, *J* = 8.4 Hz, 1H), 7.65 – 7.53 (m, 3H), 7.49 – 7.31 (m, 5H), 7.18 (d, *J* = 2.4 Hz, 1H), 7.12 (d, *J* = 2.1 Hz, 1H), 6.94 (dd, *J* = 8.9, 2.4 Hz, 1H), 5.32 (s, 2H), 4.82 (t, *J* = 10.1 Hz, 1H), 4.58 (dd, *J* = 10.9, 2.2 Hz, 1H), 4.30 (td, *J* = 6.9, 3.0 Hz, 1H), 4.13 – 3.96 (m, 7H), 3.92 (dd, *J* = 11.1, 7.1 Hz, 1H), 3.28 (t, *J* = 7.5 Hz, 2H), 2.37 – 2.29 (m,

2H), 2.03 – 1.89 (m, 2H). **¹³C-NMR** (101 MHz, DMSO-*d*₆): δ (ppm) = 160.2 (C_{Ar}), 154.4 (C=O), 153.2 (C_{Ar}), 142.0 (C_{Ar}), 136.8 (C_{Ar}), 131.8 (C_{Ar}), 131.0 (C_{Ar}), 129.7 (C_{Ar}), 128.6 (C_{Ar}H), 128.0 (C_{Ar}), 127.7 (C_{Ar}H), 127.5 (C_{Ar}H), 125.5 (C_{Ar}), 124.1 (C_{Ar}), 123.0 (C_{Ar}), 122.7 (C_{Ar}H), 122.6 (C_{Ar}H), 116.7 (C_{Ar}), 116.0 (C_{Ar}H), 113.2 (C_{Ar}H), 105.9 (C_{Ar}H), 103.2 (C_{Ar}H), 98.3 (C_{Ar}H), 70.5 (CH₂), 64.9 (CH₂), 54.9 (CH₂), 53.8 (CH₂), 51.7 (CH₂), 47.7 (CH₂), 41.2 (CH), 25.9 (CH₂), 15.6 (CH₂).

9.4. CBI-TMI prodrug series

P-SS60-CBI-TMI

(S)-1-(chloromethyl)-3-(5,6,7-trimethoxy-1*H*-indole-2-carbonyl)-2,3-dihydro-1*H*-benzo[*e*]indol-5-yl (1,2-dithian-4-yl)(3-(4-methylpiperazin-1-yl)-3-oxopropyl)carbamate

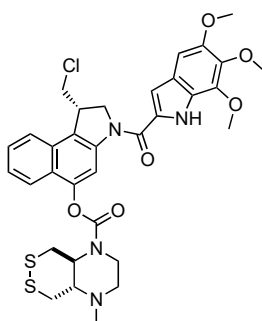


Amide coupling and was accomplished according to the **General Protocol B**. TFA (*Method C*) was applied for *N*-Boc deprotection of **P-SS60-CBI-Boc** (43.0 mg, 0.066 mmol) and **TMI-OH** (77.9 mg, 0.310 mmol) was activated for final prodrug assembly using oxalylchloride/DMF (*Method E*). **P-SS60-CBI-TMI** was obtained as a colourless solid (42.0 mg, 0.054 mmol, 82%).

TLC *R*_f = 0.58 (DCM:MeOH, 9:1). **HRMS** (ESI⁺) for C₃₈H₄₅ClN₅O₇S₂⁺: calcd. *m/z* 782.24434, found *m/z* 782.24486. **¹H-NMR** (800 MHz, MeOD-*d*₄): δ (ppm) = 8.17 (s, 1H), 7.95 (dd, *J* = 8.5, 3.4 Hz, 1H), 7.89 (dd, *J* = 27.3, 8.4 Hz, 1H), 7.61 (t, *J* = 7.4 Hz, 1H), 7.56 – 7.46 (m, 1H), 7.10 (s, 1H), 6.99 (s, 1H), 4.74 (d, *J* = 7.6 Hz, 2H), 4.62 (s, 1H), 4.30 (tt, *J* = 7.5, 3.3 Hz, 1H), 4.07 (d, *J* = 3.5 Hz, 3H), 4.05 – 4.02 (m, 1H), 3.92 – 3.90 (m, 8H), 3.80 (ddt, *J* = 16.3, 12.5, 6.0 Hz, 1H), 3.72 – 3.65 (m, 1H), 3.62 (s, 4H), 3.49 – 3.38 (m, 2H), 3.29 – 3.04 (m, 2H), 2.99 – 2.90 (m, 2H), 2.84 – 2.75 (m, 1H), 2.54 – 2.49 (m, 2H), 2.48 – 2.43 (m, 2H), 2.40 – 2.34 (m, 2H), 2.34 – 2.22 (m, 3H). **¹³C-NMR** (201 MHz, MeOD-*d*₄): δ (ppm) = 171.5 (C=O), 171.4 (C=O), 162.7 (C=O), 155.7 (C=O), 155.5 (C=O), 155.1 (C=O), 151.2 (C_{Ar}), 148.9 (C_{Ar}), 142.6 (C_{Ar}), 141.7 (C_{Ar}), 140.4 (C_{Ar}), 131.4 (C_{Ar}), 128.9 (C_{Ar}H), 127.4 (C_{Ar}), 126.4 (C_{Ar}), 126.3 (C_{Ar}H), 125.2 (C_{Ar}), 124.4 (C_{Ar}), 124.3 (C_{Ar}H), 123.6 (C_{Ar}H), 112.1 (C_{Ar}H), 108.2 (C_{Ar}), 107.9 (C_{Ar}H), 99.3 (C_{Ar}H), 61.9 (CH₃), 61.7 (CH₃), 60.1 (CH), 56.8 (CH₃), 56.7 (CH₂), 55.8 (CH₂), 55.3 (CH₂), 47.5 (CH₂), 46.3 (CH₂), 45.8 (CH₂), 44.0 (CH₂), 43.5 (CH), 42.2 (CH₂), 37.6 (CH₂), 36.9 (CH₂), 35.1 (CH₂), 33.9 (CH₂).

Me-SS66T-CBI-TMI

(S)-1-(chloromethyl)-3-(5,6,7-trimethoxy-1*H*-indole-2-carbonyl)-2,3-dihydro-1*H*-benzo[*e*]indol-5-yl (*trans*)-4-methylhexahydro-[1,2]dithiino[4,5-*b*]pyrazine-1(2*H*)-carboxylate



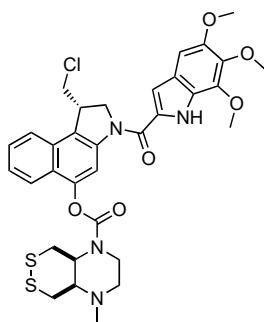
Amide coupling and was accomplished according to the **General Protocol B**. BF₃·OEt₂ (*Method B*) was applied for *N*-Boc deprotection of **Me-SS66T-CBI-Boc** (20.0 mg, 0.036 mmol) and **TMI-OH** (22.8 mg, 0.091 mmol) was activated for final prodrug assembly using oxalylchloride/DMF (*Method E*). **Me-SS66T-CBI-TMI** was obtained as a colourless solid (19.2 mg, 0.028 mmol, 78%).

TLC *R*_f = 0.32 (DCM:MeOH, 20:1). **HRMS** (ESI⁺) for C₃₃H₃₆ClN₄O₆S₂⁺: calcd. *m/z* 683.17593, found *m/z* 683.17534. **¹H-NMR** (400 MHz, CDCl₃): δ (ppm) = 9.41 (s, 1H), 8.39 (s, 1H), 7.87 (dd, *J* = 8.3, 4.6 Hz, 1H), 7.77 (d, *J* = 8.3 Hz, 1H), 7.55 (t, *J* = 7.4 Hz, 1H), 7.50 – 7.41 (m, 1H), 7.01 (d, *J* = 2.1 Hz, 1H), 6.88 (s, 1H), 4.81 (dd,

$J = 10.7, 1.6 \text{ Hz, 1H}$, 4.67 (t, $J = 9.5 \text{ Hz, 1H}$), 4.18 (dd, $J = 10.8, 5.9 \text{ Hz, 1H}$), 4.08 (s, 3H), 4.02 – 3.96 (m, 2H), 3.95 (s, 3H), 3.92 (s, 3H), 3.92 – 3.86 (m, 1H), 3.75 (d, $J = 10.4 \text{ Hz, 1H}$), 3.57 – 3.45 (m, 2H), 3.31 (d, $J = 12.2 \text{ Hz, 1H}$), 3.28 – 3.17 (m, 2H), 3.12 – 3.01 (m, 1H), 2.96 (t, $J = 10.0 \text{ Hz, 1H}$), 2.84 (dt, $J = 10.3, 4.6 \text{ Hz, 1H}$), 2.44 (s, 3H). $^{13}\text{C-NMR}$ (126 MHz, CDCl_3): δ (ppm) = 160.4 (C=O), 153.6 (C=O), 150.4 (C_{Ar}), 148.0 (C_{Ar}), 141.5 (C_{Ar}), 140.7 (C_{Ar}), 139.0 (C_{Ar}), 129.9 (C_{Ar}), 129.6 (C_{Ar}), 127.9 (C_{ArH}), 125.8 (C_{Ar}), 125.4 (C_{ArH}), 125.2 (C_{Ar}), 123.7 (C_{Ar}), 122.8 (C_{ArH}), 122.8 (C_{ArH}), 122.2 (C_{Ar}), 122.1 (C_{Ar}), 111.4 (C_{ArH}), 106.7 (C_{ArH}), 97.7 (C_{ArH}), 63.5 (CH), 61.6 (CH_3), 61.3 (CH_3), 56.4 (CH_3), 55.2 (CH_2), 55.2 (CH_2), 46.0 (CH_2), 43.5 (CH), 40.5 (CH_3), 38.7 (CH_2), 37.9 (CH_2).

Me-SS66C-CBI-TMI

(S)-1-(chloromethyl)-3-(5,6,7-trimethoxy-1*H*-indole-2-carbonyl)-2,3-dihydro-1*H*-benzo[*e*]indol-5-yl (*cis*)-4-methylhexahydro-[1,2]dithiino[4,5-*b*]pyrazine-1(2*H*)-carboxylate

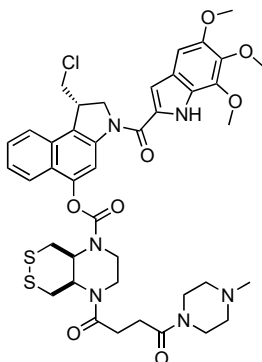


Amide coupling and was accomplished according to the **General Protocol B**. $\text{BF}_3 \cdot \text{OEt}_2$ (*Method B*) was applied for *N*-Boc deprotection of **Me-SS66C-CBI-Boc** (28.5 mg, 0.052 mmol) and **TMI-OH** (26.1 mg, 0.104 mmol) was activated for final prodrug assembly using oxalylchloride/DMF (*Method E*). **Me-SS66C-CBI-TMI** was obtained as a colourless solid (15.5 mg, 0.023 mmol, 44%).

TLC $R_f = 0.36$ (DCM:MeOH, 20:1). **HRMS** (ESI⁺) for $\text{C}_{33}\text{H}_{36}\text{ClN}_4\text{O}_6\text{S}_2^+$: calcd. m/z 683.17593, found m/z 683.17527. Individual rotamers/conformers were observed by NMR spectroscopy at 298 K (ratio ca. 1:1). $^1\text{H-NMR}$ (600 MHz, CDCl_3): δ (ppm) = 9.37 (s, 2H), 8.38 (s, 2H), 7.90 – 7.81 (m, 2H), 7.78 (d, $J = 8.3 \text{ Hz, 2H}$), 7.55 (t, $J = 7.5 \text{ Hz, 2H}$), 7.45 (t, $J = 7.5 \text{ Hz, 2H}$), 7.01 (d, $J = 2.1 \text{ Hz, 2H}$), 6.88 (s, 2H), 4.81 (d, $J = 10.6 \text{ Hz, 2H}$), 4.75 – 4.65 (m, 2H), 4.62 (dd, $J = 11.0, 3.3 \text{ Hz, 1H}$), 4.40 (d, $J = 11.6 \text{ Hz, 1H}$), 4.32 – 4.25 (m, 1H), 4.19 (t, $J = 8.4 \text{ Hz, 2H}$), 4.09 (s, 6H), 4.04 (d, $J = 11.7 \text{ Hz, 2H}$), 4.03 – 3.98 (m, 2H), 3.95 (s, 6H), 3.92 (s, 6H), 3.61 (t, $J = 13.0 \text{ Hz, 1H}$), 3.51 (t, $J = 11.0 \text{ Hz, 2H}$), 3.43 – 3.27 (m, 5H), 3.02 (dd, $J = 19.7, 11.7 \text{ Hz, 2H}$), 2.72 (dt, $J = 13.0, 3.1 \text{ Hz, 1H}$), 2.66 (s, 1H), 2.55 (dd, $J = 23.5, 13.2 \text{ Hz, 3H}$), 2.47 (t, $J = 11.7 \text{ Hz, 1H}$), 2.33 (s, 6H). $^{13}\text{C-NMR}$ (151 MHz, CDCl_3): δ (ppm) = 160.4 (C=O), 153.3 (C=O, rotamer 1), 153.3 (C=O, rotamer 2), 153.2 (C_{Ar} , rotamer 1), 153.1 (C_{Ar} , rotamer 2), 150.3 (C_{Ar}), 148.1 (C_{Ar}), 148.0 (C_{Ar} , rotamer 1), 148.0 (C_{Ar} , rotamer 2), 141.5 (C_{Ar} , rotamer 1), 141.5 (C_{Ar} , rotamer 2), 140.7 (C_{Ar} , rotamer 1), 139.0 (C_{Ar}), 129.9 (C_{Ar} , rotamer 1), 129.9 (C_{Ar} , rotamer 2), 129.6 (C_{Ar} , rotamer 1), 129.6 (C_{Ar} , rotamer 2), 128.0 (C_{ArH} , rotamer 1), 127.9 (C_{ArH} , rotamer 2), 125.7 (C_{Ar}), 125.4 (C_{ArH} , rotamer 1), 125.3 (C_{ArH} , rotamer 2), 125.2 (C_{Ar} , rotamer 1), 125.1 (C_{Ar} , rotamer 1), 123.7 (C_{Ar}), 122.9 (C_{ArH} , rotamer 1), 122.8 (C_{ArH} , rotamer 2), 122.6 (C_{ArH} , rotamer 1), 122.6 (C_{ArH} , rotamer 2), 122.2 (C_{Ar} , rotamer 1), 122.2 (C_{Ar} , rotamer 2), 122.1 (C_{Ar} , rotamer 1), 122.1 (C_{Ar} , rotamer 2), 111.4 (C_{ArH} , rotamer 1), 111.3 (C_{ArH} , rotamer 2), 106.7 (C_{ArH} , rotamer 2), 97.6 (C_{ArH} , rotamer 2), 61.6 (CH_3), 61.4 (CH, rotamer 1), 61.3 (CH_3), 61.3 (CH, rotamer 2), 56.4 (CH_3), 56.2 (CH_2 , rotamer 1), 56.2 (CH_2 , rotamer 2), 56.0 (CH_2), 55.2 (CH_2 , rotamer 1), 55.1 (CH_2 , rotamer 2), 54.8 (CH, rotamer 1), 54.7 (CH, rotamer 2), 53.7 (CH, rotamer 3), 53.6 (CH, rotamer 4), 46.0 (CH_2), 43.5 (CH), 42.0 (CH_3 , rotamer 1), 41.9 (CH_3 , rotamer 2), 40.9 (CH_2 , rotamer 1), 40.9 (CH_2 , rotamer 2), 40.2 (CH_2), 39.1 (CH_2), 38.8 (CH_2).

P-SS66C-CBI-TMI

(S)-1-(chloromethyl)-3-(5,6,7-trimethoxy-1*H*-indole-2-carbonyl)-2,3-dihydro-1*H*-benzo[*e*]indol-5-yl (*cis*)-4-(4-methylpiperazin-1-yl)-4-oxobutanoyl)hexahydro-[1,2]dithiino[4,5-*b*]pyrazine-1(2*H*)-carboxylate

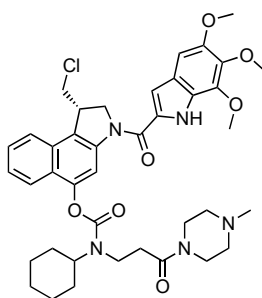


Amide coupling and was accomplished according to the **General Protocol B**. $\text{BF}_3 \cdot \text{OEt}_2$ (*Method B*) was applied for *N*-Boc deprotection of **P-SS66C-CBI-Boc** (14.5 mg, 0.020 mmol) and **TMI-OH** (10.0 mg, 0.040 mmol) was activated for final prodrug assembly using oxalylchloride/DMF (*Method E*). **P-SS66C-CBI-TMI** was obtained as a colourless solid (10.9 mg, 0.013 mmol, 65%).

TLC $R_f = 0.36$ (DCM:MeOH, 20:1). **HRMS** (ESI⁺) for $\text{C}_{41}\text{H}_{48}\text{ClN}_6\text{O}_8\text{S}_2^+$: calcd. m/z 851.26581, found m/z 851.26421. **¹H-NMR** (400 MHz, CDCl_3): δ (ppm) = 9.37 (s, 1H), 8.40 (d, $J = 3.8$ Hz, 1H), 7.89 – 7.82 (m, 1H), 7.78 (d, $J = 8.3$ Hz, 1H), 7.57 (t, $J = 7.6$ Hz, 1H), 7.51 – 7.43 (m, 1H), 7.01 (d, $J = 2.2$ Hz, 1H), 6.88 (s, 1H), 4.81 (d, $J = 10.7$ Hz, 1H), 4.68 (t, $J = 9.6$ Hz, 1H), 4.47 (s, 1H), 4.19 (t, $J = 9.4$ Hz, 1H), 4.09 (s, 3H), 4.07 – 3.96 (m, 3H), 3.95 (s, 3H), 3.92 (s, 3H), 3.90 – 3.82 (m, 2H), 3.64 (d, $J = 4.7$ Hz, 2H), 3.60 – 3.46 (m, 4H), 3.21 (d, $J = 14.1$ Hz, 1H), 3.04 (d, $J = 11.2$ Hz, 1H), 2.74 (d, $J = 8.9$ Hz, 4H), 2.45 (dd, $J = 144.7, 4.7$ Hz, 2H), 2.39 (t, $J = 4.9$ Hz, 2H), 2.32 (s, 3H). **¹³C-NMR** (101 MHz, CDCl_3): δ (ppm) = 172.2 (C=O), 170.2 (C=O), 160.5 (C=O), 154.0 (C_{Ar}), 150.4 (C_{Ar}), 147.9 (C_{Ar}), 141.5 (C_{Ar}), 140.8 (C_{Ar}), 139.0 (C_{Ar}), 130.0 (C_{Ar}), 129.6 (C_{Ar}), 128.0 (C_{ArH}), 125.8 (C_{Ar}), 125.6 (C_{ArH}), 125.1 (C_{Ar}), 123.7 (C_{Ar}), 122.9 (C_{ArH}), 122.7 (C_{ArH}), 122.3 (C_{Ar}), 111.4 (C_{ArH}), 106.8 (C_{ArH}), 97.7 (C_{ArH}), 61.6 (CH_3), 61.3 (CH_3), 56.4 (CH_3), 55.2 (CH_2), 55.1 (CH_2), 54.8 (CH_2), 52.0 (CH), 46.1 (CH_3), 46.0 (CH_2), 45.3 (CH_2), 43.5 (CH), 42.3 (CH_2), 41.8 (CH_2), 28.3 (CH_2).

P-CC60-CBI-TMI

(S)-1-(chloromethyl)-3-(5,6,7-trimethoxy-1*H*-indole-2-carbonyl)-2,3-dihydro-1*H*-benzo[*e*]indol-5-yl cyclohexyl(3-(4-methylpiperazin-1-yl)-3-oxopropyl)carbamate

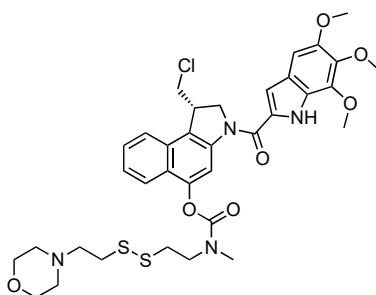


Amide coupling and was accomplished according to the **General Protocol B**. TFA (*Method C*) was applied for *N*-Boc deprotection of **P-CC60-CBI-Boc** (31.0 mg, 0.050 mmol) and **TMI-OH** (76.3 mg, 0.303 mmol) was activated for final prodrug assembly using oxalylchloride/DMF (*Method E*). **P-CC60-CBI-TMI** was obtained as a colourless solid (29.0 mg, 0.039 mmol, 78%).

TLC $R_f = 0.58$ (DCM:MeOH, 9:1). **HRMS** (ESI⁺) for $\text{C}_{40}\text{H}_{49}\text{ClN}_5\text{O}_7^+$: calcd. m/z 746.33150, found m/z 746.33220. **¹H-NMR** (800 MHz, MeOD-d_4): δ (ppm) = 8.29 – 8.09 (m, 1H), 7.93 – 7.82 (m, 2H), 7.56 (t, $J = 7.5$ Hz, 1H), 7.52 – 7.43 (m, 1H), 7.06 (s, 1H), 6.97 (s, 1H), 4.66 (q, $J = 11.5, 10.9$ Hz, 2H), 4.30 – 4.13 (m, 2H), 4.05 (s, 3H), 4.00 (dd, $J = 11.3, 3.2$ Hz, 1H), 3.89 (s, 6H), 3.83 (dd, $J = 13.8, 7.5$ Hz, 1H), 3.79 – 3.71 (m, 1H), 3.67 – 3.56 (m, 4H), 2.92 (s, 1H), 2.83 – 2.73 (m, 1H), 2.45 (d, $J = 18.6$ Hz, 2H), 2.36 (d, $J = 21.5$ Hz, 2H), 2.30 – 2.18 (m, 3H), 2.04 (d, $J = 10.2$ Hz, 1H), 2.00 – 1.91 (m, 1H), 1.88 (d, $J = 9.2$ Hz, 2H), 1.72 (dd, $J = 31.7, 12.9$ Hz, 3H), 1.54 – 1.18 (m, 4H). **¹³C-NMR** (201 MHz, MeOD-d_4): δ (ppm) = 171.8 (C=O), 171.5 (C=O), 162.6 (C=O), 151.2 (C_{Ar}), 149.1 (C_{Ar}), 142.7 (C_{Ar}), 141.7 (C_{Ar}), 140.4 (C_{Ar}), 131.4 (C_{Ar}), 128.9 (C_{ArH}), 127.3 (C_{Ar}), 126.4 (C_{Ar} , C_{ArH}), 125.2 (C_{Ar}), 124.3 (C_{ArH}), 123.6 (C_{ArH}), 112.1 (C_{ArH}), 108.2 (C_{ArH}), 99.3 (C_{ArH}), 61.8 (CH_3), 61.7 (CH_3), 58.9 (CH), 58.8 (CH), 56.7 (CH_2), 55.8 (CH_3), 55.3 (CH_2), 47.5 (CH_2), 46.3 (CH_2), 45.8 (CH_3), 43.5 (CH), 42.2 (CH_2), 41.9 (CH_2), 35.4 (CH_2), 34.1 (CH_2), 32.6 (CH_2), 31.7 (CH_2), 30.4 (CH_2), 27.1 (CH_2), 26.4 (CH_2).

SS00_M-CBI-TMI

(S)-1-(chloromethyl)-3-(5,6,7-trimethoxy-1*H*-indole-2-carbonyl)-2,3-dihydro-1*H*-benzo[*e*]indol-5-yl methyl(2-((2-morpholinoethyl)disulfaneyl)ethyl)carbamate

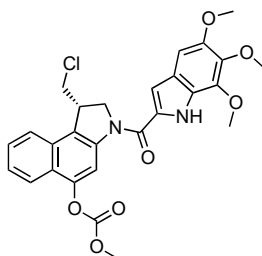


Amide coupling and was accomplished according to the **General Protocol B**. $\text{BF}_3 \cdot \text{OEt}_2$ (*Method B*) was applied for *N*-Boc deprotection of **SS00_M-CBI-Boc** (18.7 mg, 0.031 mmol) and **TMI-OH** (15.8 mg, 0.063 mmol) was activated for final prodrug assembly using EDCI (*Method D*). **SS00_M-CBI-TMI** was obtained as a colourless solid (8.5 mg, 0.012 mmol, 37%).

TLC R_f = 0.65 (EtOAc). **HRMS** (ESI⁺) for $\text{C}_{35}\text{H}_{41}\text{ClN}_4\text{O}_7\text{S}_2^+$: calcd. m/z 728.20942, found m/z 729.21892. **¹H-NMR** (500 MHz, $\text{DMSO}-d_6$): δ (ppm) = 11.47 (d, J = 1.6 Hz, 1H, N-H), 8.16 (s, 1H), 8.02 (d, J = 8.4 Hz, 1H), 7.91 (dd, J = 17.8, 8.5 Hz, 1H), 7.65 – 7.57 (m, 1H), 7.50 (t, J = 7.6 Hz, 1H), 7.10 (d, J = 2.1 Hz, 1H), 6.97 (s, 1H), 4.82 (t, J = 10.1 Hz, 1H), 4.54 (dd, J = 11.0, 2.1 Hz, 1H), 4.37 (s, 1H), 4.08 (dd, J = 11.2, 3.2 Hz, 1H), 3.99 – 3.95 (m, 1H), 3.94 (s, 3H), 3.91 – 3.86 (m, 1H), 3.82 (s, 3H), 3.80 (s, 3H), 3.67 – 3.61 (m, 1H), 3.54 – 3.49 (m, 2H), 3.46 – 3.42 (m, 2H), 3.25 (s, 2H), 3.14 (t, J = 6.9 Hz, 1H), 3.03 (t, J = 6.8 Hz, 1H), 3.00 (s, 1H), 2.89 (q, J = 6.6 Hz, 2H), 2.57 (t, J = 7.1 Hz, 1H), 2.54 (d, J = 7.6 Hz, 1H), 2.36 (d, J = 1.8 Hz, 2H), 2.27 (s, 2H). **¹³C-NMR** (126 MHz, $\text{DMSO}-d_6$): δ (ppm) = 160.3 (C=O), 153.9 (C_{Ar}), 153.7 (C_{Ar}), 149.2 (C_{Ar}), 147.5 (C_{Ar}), 147.3 (C_{Ar}), 141.5 (C_{Ar}), 140.0 (C_{Ar}), 139.1 (C_{Ar}), 130.6 (C_{Ar}), 129.6 (C_{ArH}), 127.6 (C_{Ar}), 125.5 (C_{Ar}), 125.0 (C_{Ar}), 124.4 (C_{ArH}), 123.4 (C_{ArH}), 123.2, 122.4 (C_{Ar}), 122.2 (C_{ArH}), 110.6 (C_{Ar}), 110.4 (C_{Ar}), 106.4 (C_{ArH}), 98.0 (C_{ArH}), 66.1 (CH_2 , rotamer 1), 66.0 (CH_2 , rotamer 2), 61.1 (CH_3), 61.0 (CH_3), 57.4 (CH_2), 56.0 (CH_3), 55.0 (CH_2), 53.0 (CH_2), 52.9 (CH_2), 48.2 (CH_2), 47.9 (CH_2), 47.6 (CH_2), 41.1 (CH), 35.6 (CH_2), 35.2 (CH_2), 34.9 (CH_3 , rotamer 1), 34.8 (CH_3 , rotamer 2).

MC-CBI-TMI

(S)-1-(chloromethyl)-3-(5,6,7-trimethoxy-1*H*-indole-2-carbonyl)-2,3-dihydro-1*H*-benzo[*e*]indol-5-yl methyl carbonate

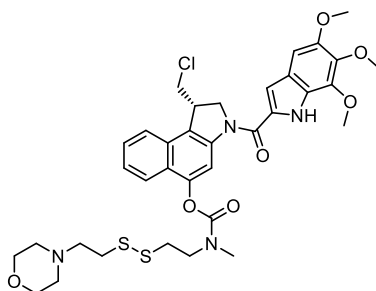


Amide coupling and was accomplished according to the **General Protocol B**. $\text{BF}_3 \cdot \text{OEt}_2$ (*Method B*) was applied for *N*-Boc deprotection of **MC-CBI-Boc** (39.2 mg, 0.100 mmol) and **TMI-OH** (25.1 mg, 0.010 mmol) was activated for final prodrug assembly using EDCI (*Method D*). **MC-CBI-TMI** was obtained as a colourless solid (7.9 mg, 0.015 mmol, 15%).

TLC R_f = 0.55 (isohexane:EtOAc, 1:1). **HRMS** (ESI⁺) for $\text{C}_{27}\text{H}_{26}\text{ClN}_2\text{O}_7^+$: calcd. m/z 525.14231, found m/z 525.14229. **¹H-NMR** (500 MHz, CDCl_3): δ (ppm) = 9.39 (s, 1H), 8.49 (s, 1H), 7.99 (d, J = 8.4 Hz, 1H), 7.79 (d, J = 8.3 Hz, 1H), 7.58 (t, J = 7.2 Hz, 1H), 7.47 (t, J = 7.3 Hz, 1H), 7.01 (d, J = 2.2 Hz, 1H), 6.88 (s, 1H), 4.83 (dd, J = 10.8, 1.7 Hz, 1H), 4.74 – 4.65 (m, 1H), 4.20 (t, J = 9.4 Hz, 2H), 4.09 (s, 3H), 4.03 – 3.99 (m, 2H), 3.98 (s, 3H), 3.95 (s, 3H), 3.92 (s, 3H), 3.52 (t, J = 11.0 Hz, 1H). **¹³C-NMR** (126 MHz, CDCl_3): δ (ppm) = 160.5 (C=O), 154.3 (C_{Ar}), 150.4 (C_{Ar}), 147.9 (C_{Ar}), 141.5 (C_{Ar}), 140.8 (C_{Ar}), 139.0 (C_{Ar}), 130.0 (C_{Ar}), 129.7 (C_{Ar}), 128.1 (C_{ArH}), 125.8 (C_{Ar}), 125.5 (C_{ArH}), 124.5 (C_{Ar}), 123.7 (C_{Ar}), 122.8 (C_{ArH}), 122.7 (C_{ArH}), 122.5 (C_{Ar}), 110.9 (C_{ArH}), 106.7 (C_{ArH}), 97.8 (C_{ArH}), 61.6 (CH_3), 61.3 (CH_3), 56.4 (CH_3), 55.9 (CH_3), 55.2 (CH_2), 45.9 (CH_2), 43.6 (CH).

SS00_M-CBI-TMI

(S)-1-(chloromethyl)-3-(5,6,7-trimethoxy-1*H*-indole-2-carbonyl)-2,3-dihydro-1*H*-benzo[*e*]indol-5-yl methyl(2-((2-morpholinoethyl)disulfaneyl)ethyl)carbamate

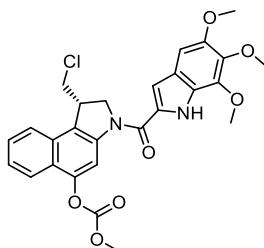


Amide coupling and was accomplished according to the **General Protocol B**. $\text{BF}_3 \cdot \text{OEt}_2$ (*Method B*) was applied for *N*-Boc deprotection of **SS00_M-CBI-Boc** (18.7 mg, 0.031 mmol) and **TMI-OH** (15.8 mg, 0.063 mmol) was activated for final prodrug assembly using EDCl (*Method D*). **SS00_M-CBI-TMI** was obtained as a colourless solid (8.5 mg, 0.012 mmol, 37%).

TLC R_f = 0.65 (EtOAc). **HRMS** (ESI⁺) for $\text{C}_{35}\text{H}_{41}\text{ClN}_4\text{O}_7\text{S}_2^+$: calcd. m/z 728.20942, found m/z 729.21892. **¹H-NMR** (500 MHz, $\text{DMSO}-d_6$): δ (ppm) = 11.47 (d, J = 1.6 Hz, 1H, *N-H*), 8.16 (s, 1H), 8.02 (d, J = 8.4 Hz, 1H), 7.91 (dd, J = 17.8, 8.5 Hz, 1H), 7.65 – 7.57 (m, 1H), 7.50 (t, J = 7.6 Hz, 1H), 7.10 (d, J = 2.1 Hz, 1H), 6.97 (s, 1H), 4.82 (t, J = 10.1 Hz, 1H), 4.54 (dd, J = 11.0, 2.1 Hz, 1H), 4.37 (s, 1H), 4.08 (dd, J = 11.2, 3.2 Hz, 1H), 3.99 – 3.95 (m, 1H), 3.94 (s, 3H), 3.91 – 3.86 (m, 1H), 3.82 (s, 3H), 3.80 (s, 3H), 3.67 – 3.61 (m, 1H), 3.54 – 3.49 (m, 2H), 3.46 – 3.42 (m, 2H), 3.25 (s, 2H), 3.14 (t, J = 6.9 Hz, 1H), 3.03 (t, J = 6.8 Hz, 1H), 3.00 (s, 1H), 2.89 (q, J = 6.6 Hz, 2H), 2.57 (t, J = 7.1 Hz, 1H), 2.54 (d, J = 7.6 Hz, 1H), 2.36 (d, J = 1.8 Hz, 2H), 2.27 (s, 2H). **¹³C-NMR** (126 MHz, $\text{DMSO}-d_6$): δ (ppm) = 160.3 (C=O), 153.9 (C_{Ar}), 153.7 (C_{Ar}), 149.2 (C_{Ar}), 147.5 (C_{Ar}), 147.3 (C_{Ar}), 141.5 (C_{Ar}), 140.0 (C_{Ar}), 139.1 (C_{Ar}), 130.6 (C_{Ar}), 129.6 (C_{ArH}), 127.6 (C_{Ar}), 125.5 (C_{Ar}), 125.0 (C_{Ar}), 124.4 (C_{ArH}), 123.4 (C_{ArH}), 123.2, 122.4 (C_{Ar}), 122.2 (C_{ArH}), 110.6 (C_{Ar}), 110.4 (C_{Ar}), 106.4 (C_{ArH}), 98.0 (C_{ArH}), 66.1 (CH_2 , *rotamer 1*), 66.0 (CH_2 , *rotamer 2*), 61.1 (CH_3), 61.0 (CH_3), 57.4 (CH_2), 56.0 (CH_3), 55.0 (CH_2), 53.0 (CH_2), 52.9 (CH_2), 48.2 (CH_2), 47.9 (CH_2), 47.6 (CH_2), 41.1 (CH), 35.6 (CH_2), 35.2 (CH_2), 34.9 (CH_3 , *rotamer 1*), 34.8 (CH_3 , *rotamer 2*).

MC-CBI-TMI

(S)-1-(chloromethyl)-3-(5,6,7-trimethoxy-1*H*-indole-2-carbonyl)-2,3-dihydro-1*H*-benzo[*e*]indol-5-yl methyl carbonate

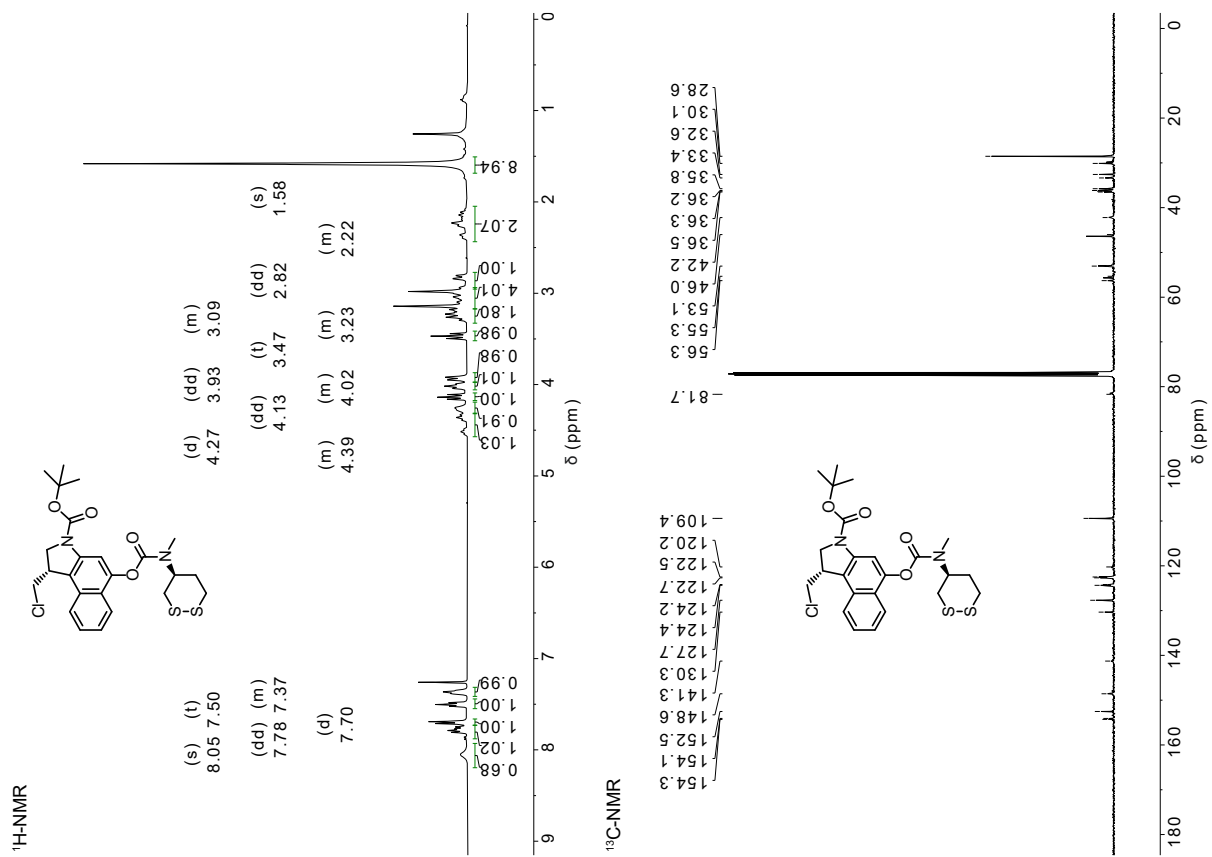


Amide coupling and was accomplished according to the **General Protocol B**. $\text{BF}_3 \cdot \text{OEt}_2$ (*Method B*) was applied for *N*-Boc deprotection of **MC-CBI-Boc** (39.2 mg, 0.100 mmol) and **TMI-OH** (25.1 mg, 0.010 mmol) was activated for final prodrug assembly using EDCl (*Method D*). **MC-CBI-TMI** was obtained as a colourless solid (7.9 mg, 0.015 mmol, 15%).

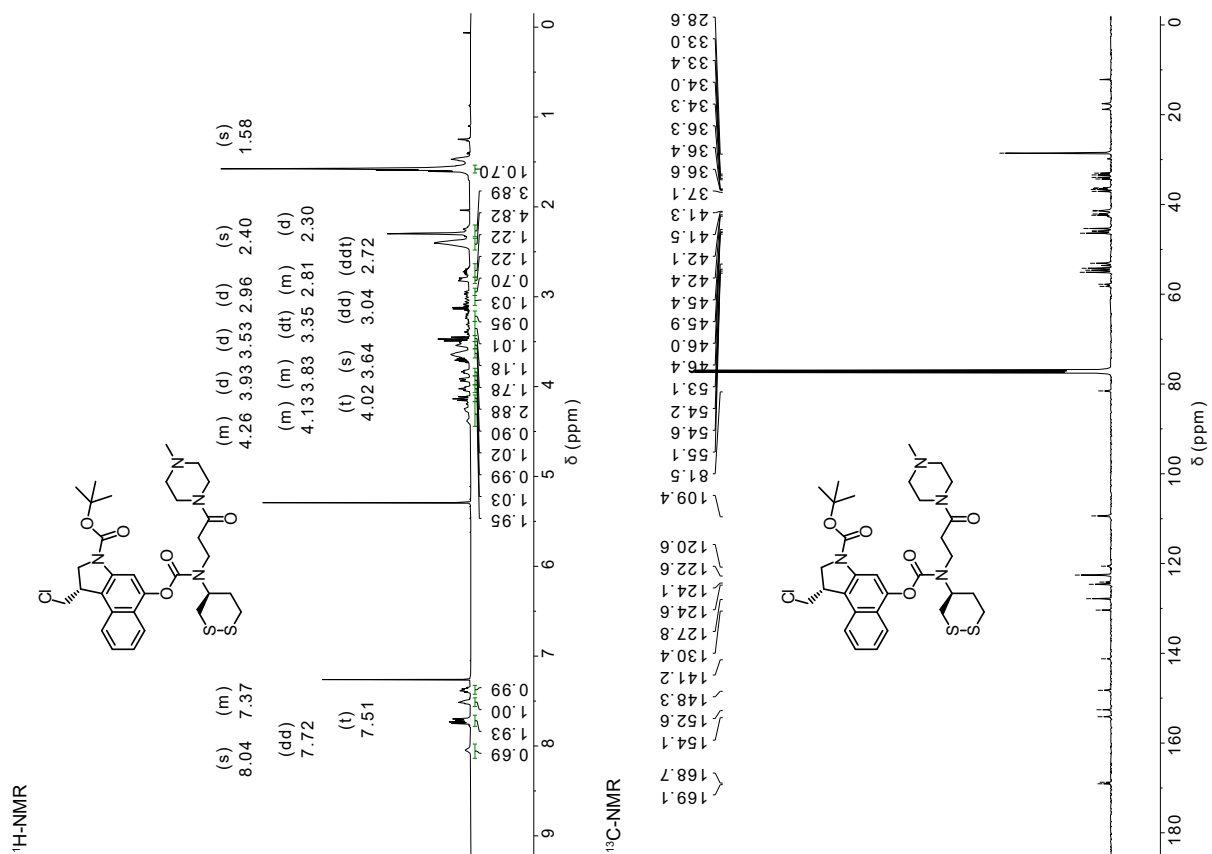
TLC R_f = 0.55 (isohexane:EtOAc, 1:1). **HRMS** (ESI⁺) for $\text{C}_{27}\text{H}_{26}\text{ClN}_2\text{O}_7^+$: calcd. m/z 525.14231, found m/z 525.14229. **¹H-NMR** (500 MHz, CDCl_3): δ (ppm) = 9.39 (s, 1H), 8.49 (s, 1H), 7.99 (d, J = 8.4 Hz, 1H), 7.79 (d, J = 8.3 Hz, 1H), 7.58 (t, J = 7.2 Hz, 1H), 7.47 (t, J = 7.3 Hz, 1H), 7.01 (d, J = 2.2 Hz, 1H), 6.88 (s, 1H), 4.83 (dd, J = 10.8, 1.7 Hz, 1H), 4.74 – 4.65 (m, 1H), 4.20 (t, J = 9.4 Hz, 2H), 4.09 (s, 3H), 4.03 – 3.99 (m, 2H), 3.98 (s, 3H), 3.95 (s, 3H), 3.92 (s, 3H), 3.52 (t, J = 11.0 Hz, 1H). **¹³C-NMR** (126 MHz, CDCl_3): δ (ppm) = 160.5 (C=O), 154.3 (C_{Ar}), 150.4 (C_{Ar}), 147.9 (C_{Ar}), 141.5 (C_{Ar}), 140.8 (C_{Ar}), 139.0 (C_{Ar}), 130.0 (C_{Ar}), 129.7 (C_{Ar}), 128.1 (C_{ArH}), 125.8 (C_{Ar}), 125.5 (C_{ArH}), 124.5 (C_{Ar}), 123.7 (C_{Ar}), 122.8 (C_{ArH}), 122.7 (C_{ArH}), 122.5 (C_{Ar}), 110.9 (C_{ArH}), 106.7 (C_{ArH}), 97.8 (C_{ArH}), 61.6 (CH_3), 61.3 (CH_3), 56.4 (CH_3), 55.9 (CH_3), 55.2 (CH_2), 45.9 (CH_2), 43.6 (CH).

10. NMR Spectra

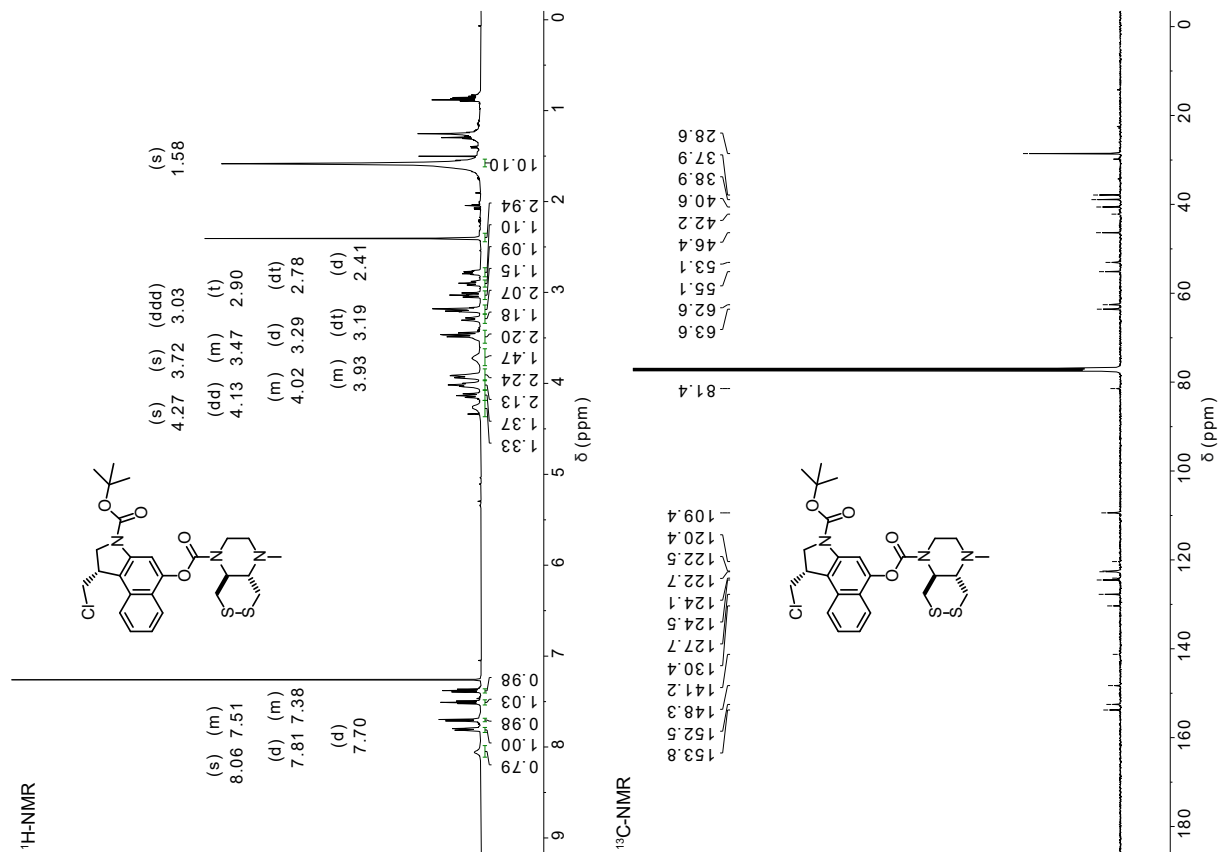
SS60-CBI-Boc



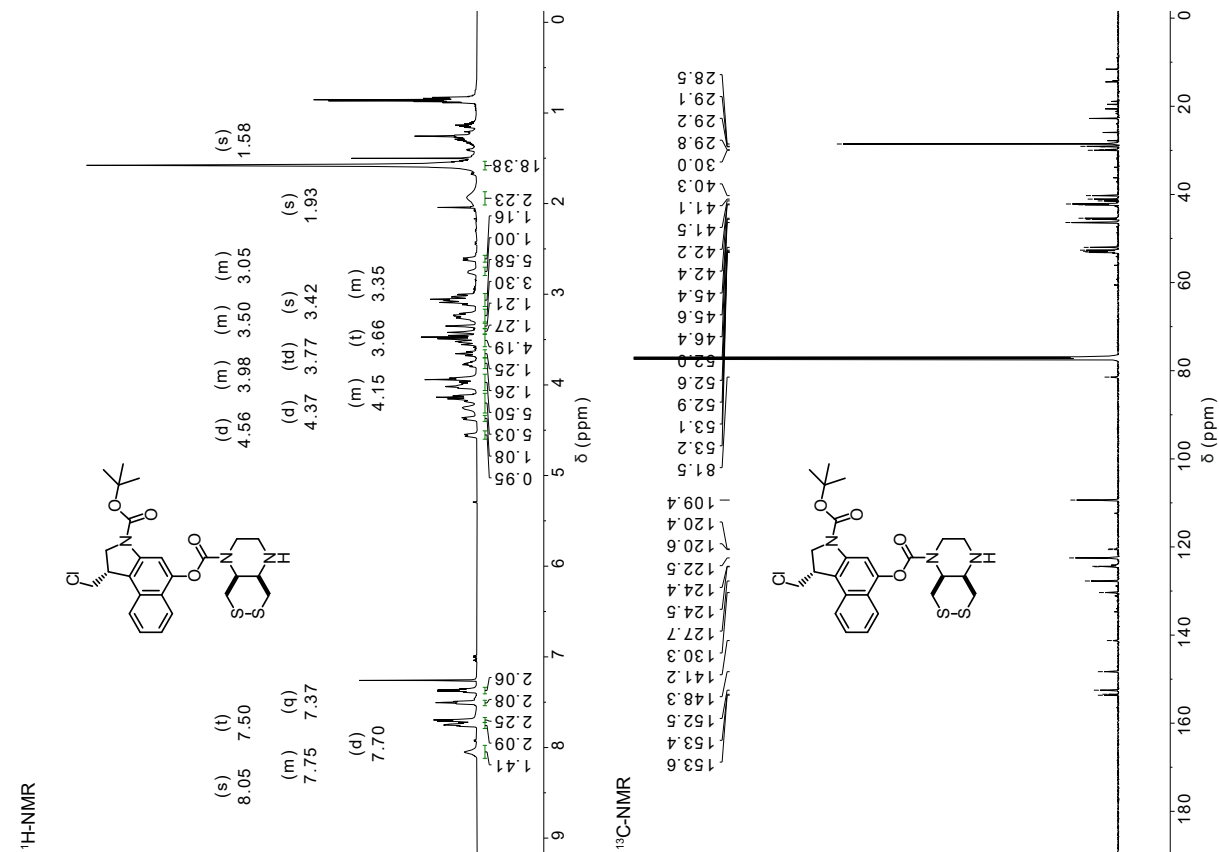
P-SS60-CBI-Boc



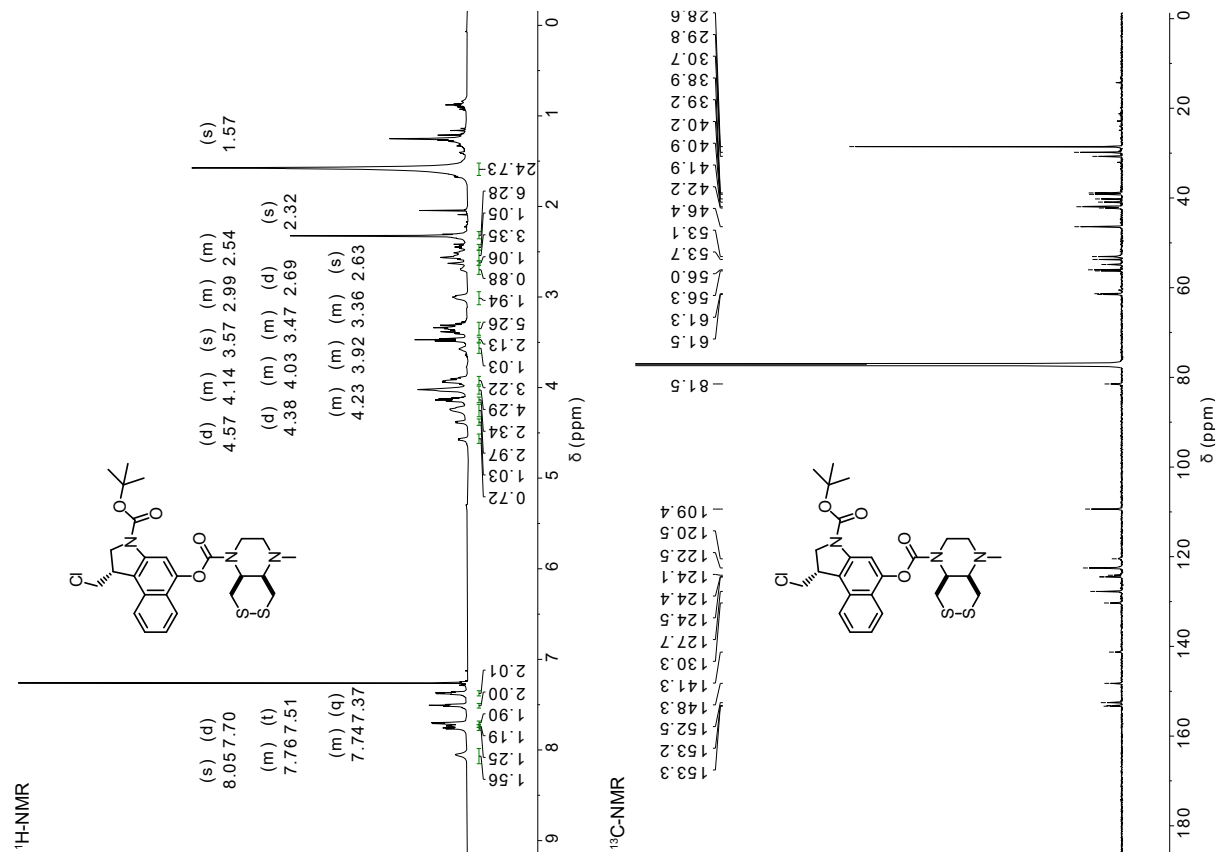
Me-SS66T-CBI-Boc



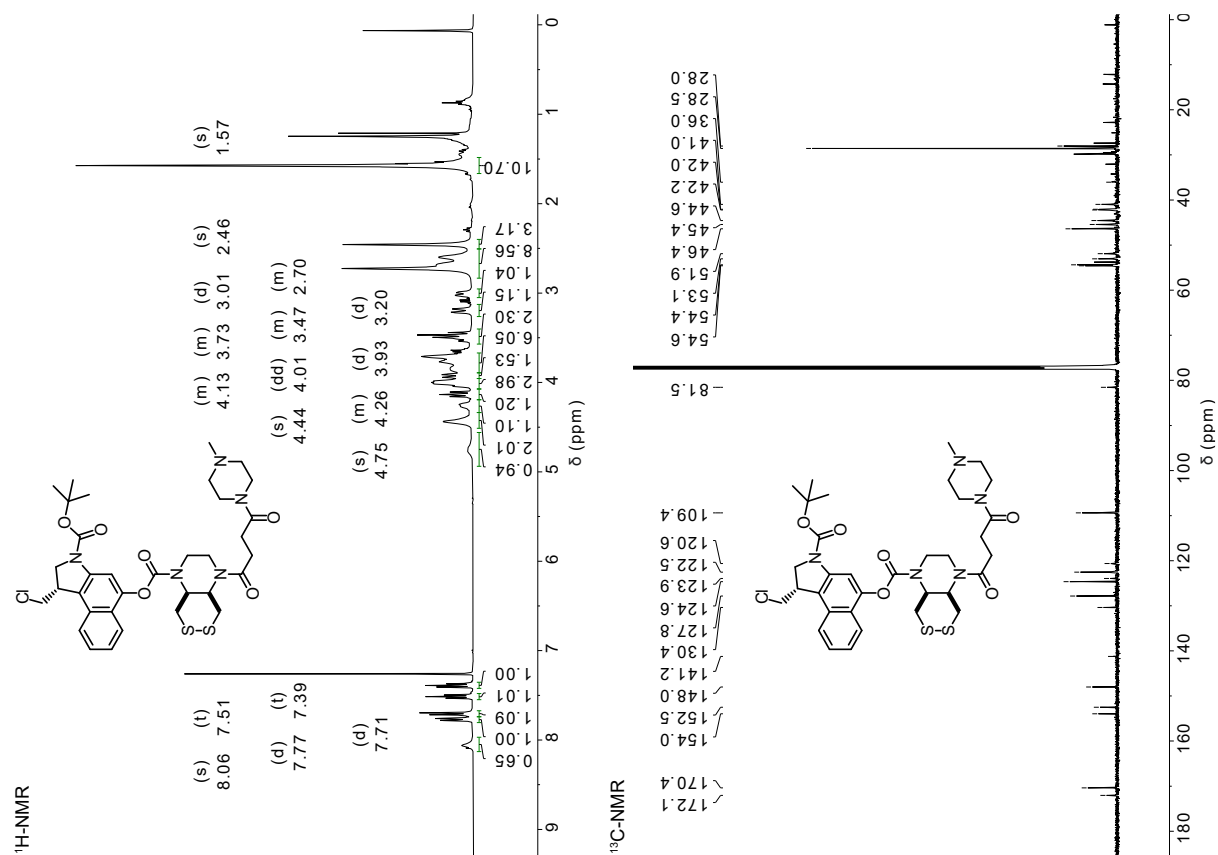
H-SS66C-CBI-Boc



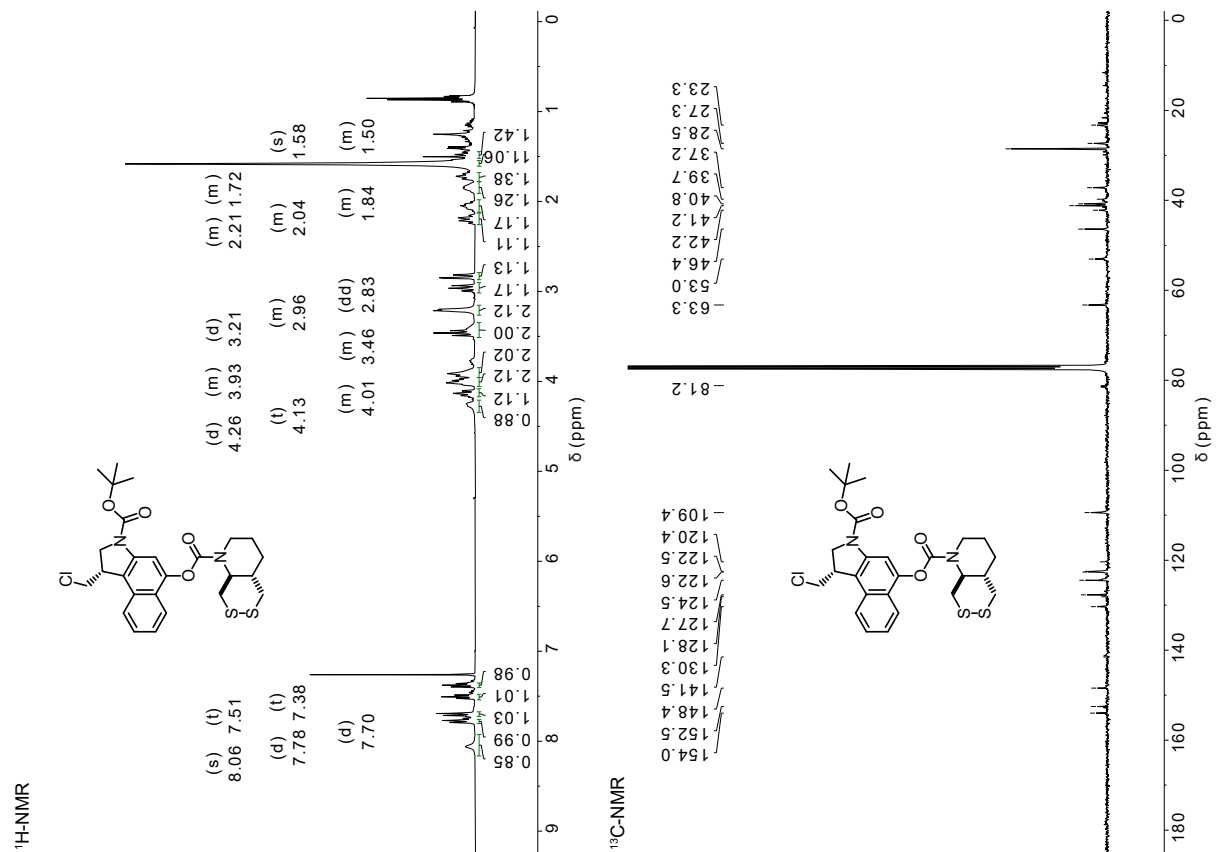
Me-SS66C-CBI-Boc



P-SS66C-CBI-Boc



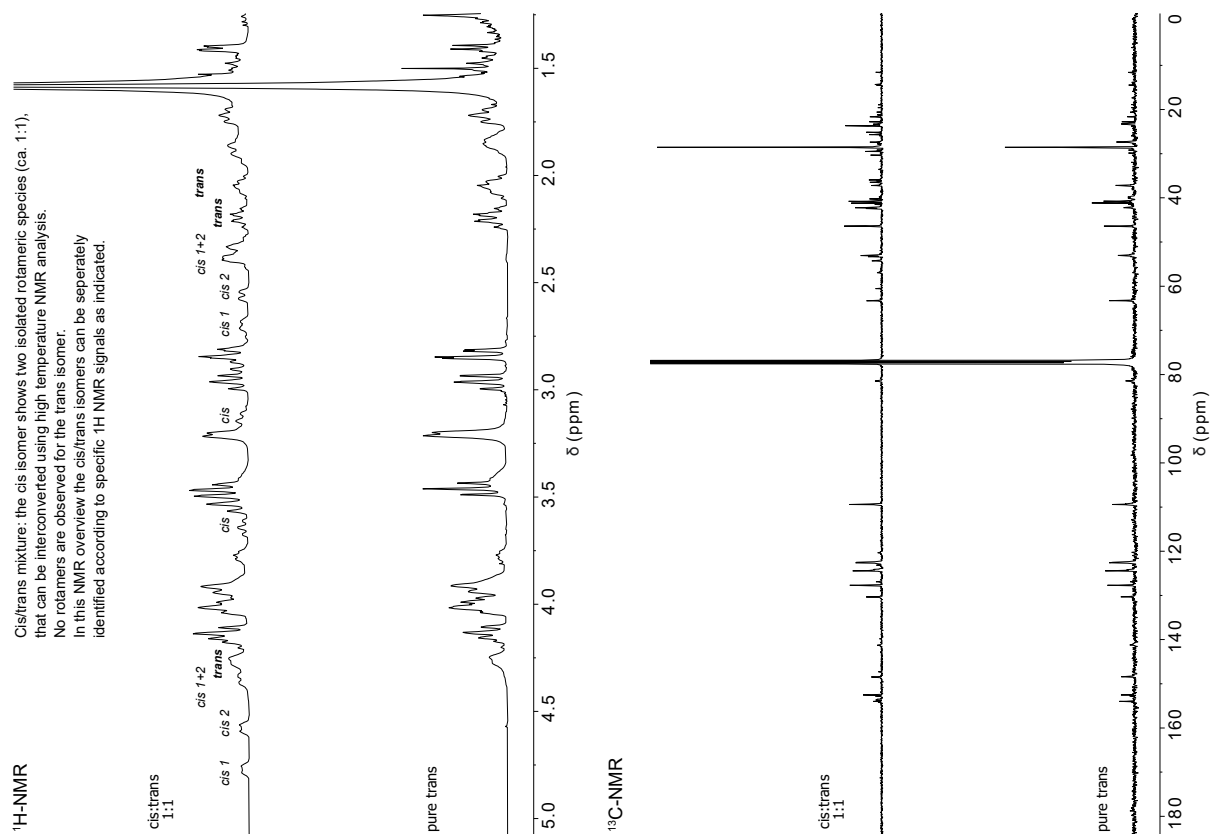
SS66T-CBI-Boc



SS00_M-CBI-Boc

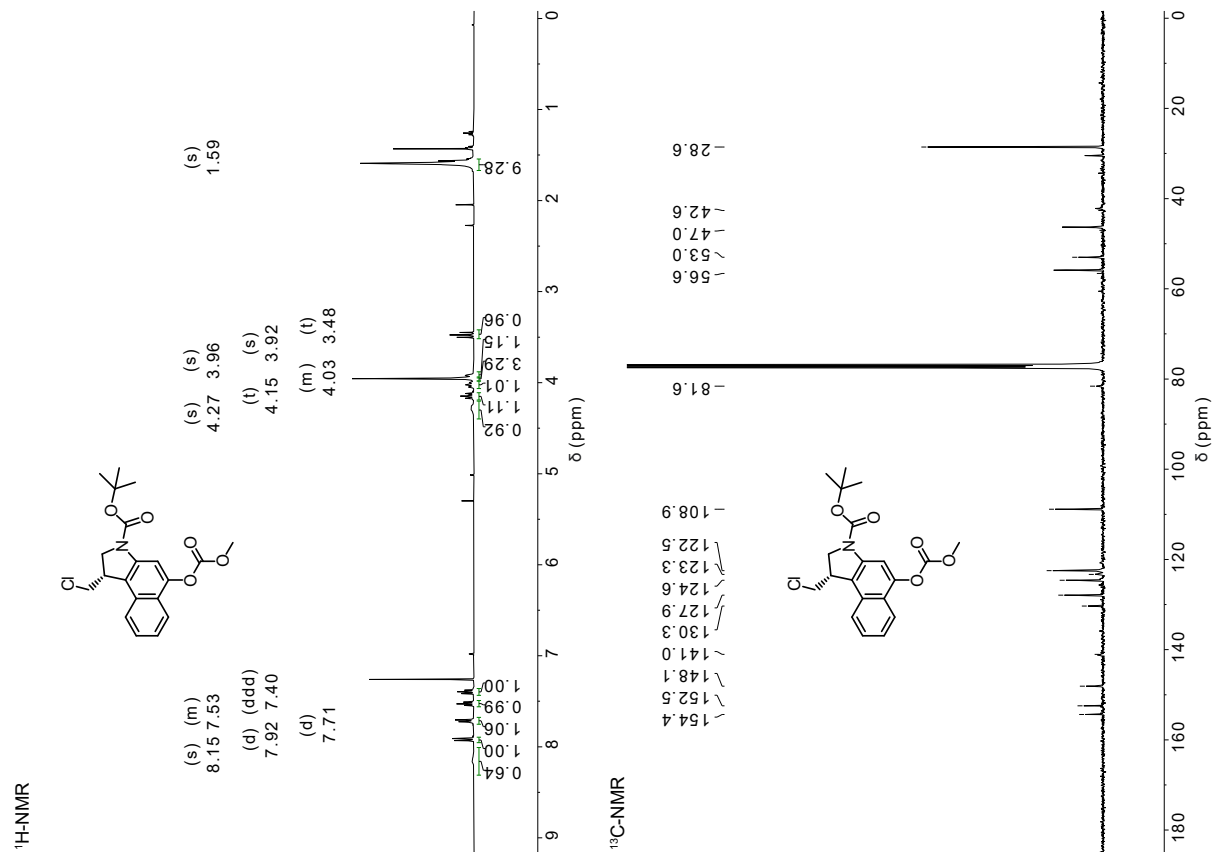


SS66-CBI-Boc (1:1 mixture cis:trans)

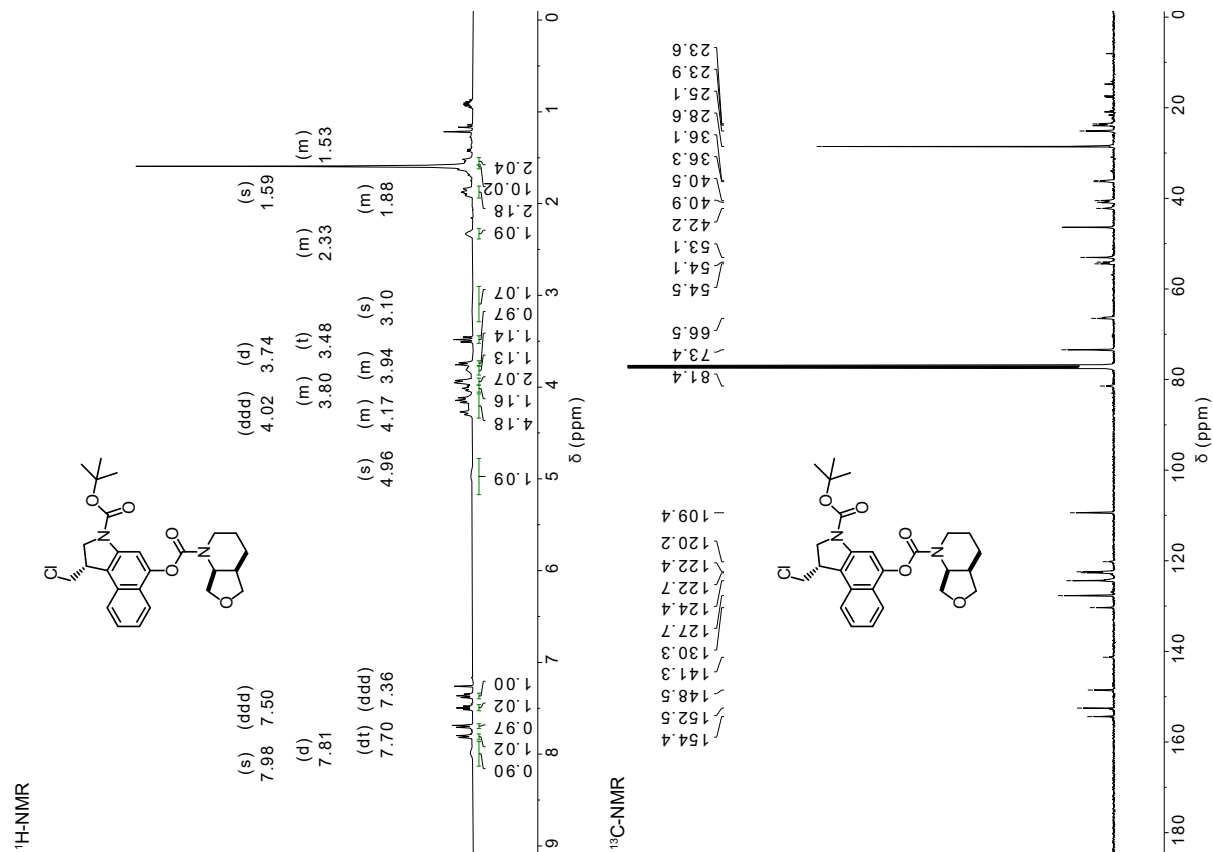


Cis/trans mixture: the cis isomer shows two isolated rotameric species (ca. 1:1), that can be interconverted using high temperature NMR analysis. No rotamers are observed for the trans isomer. In this NMR overview the cis/trans isomers can be separately identified according to specific ¹H NMR signals as indicated.

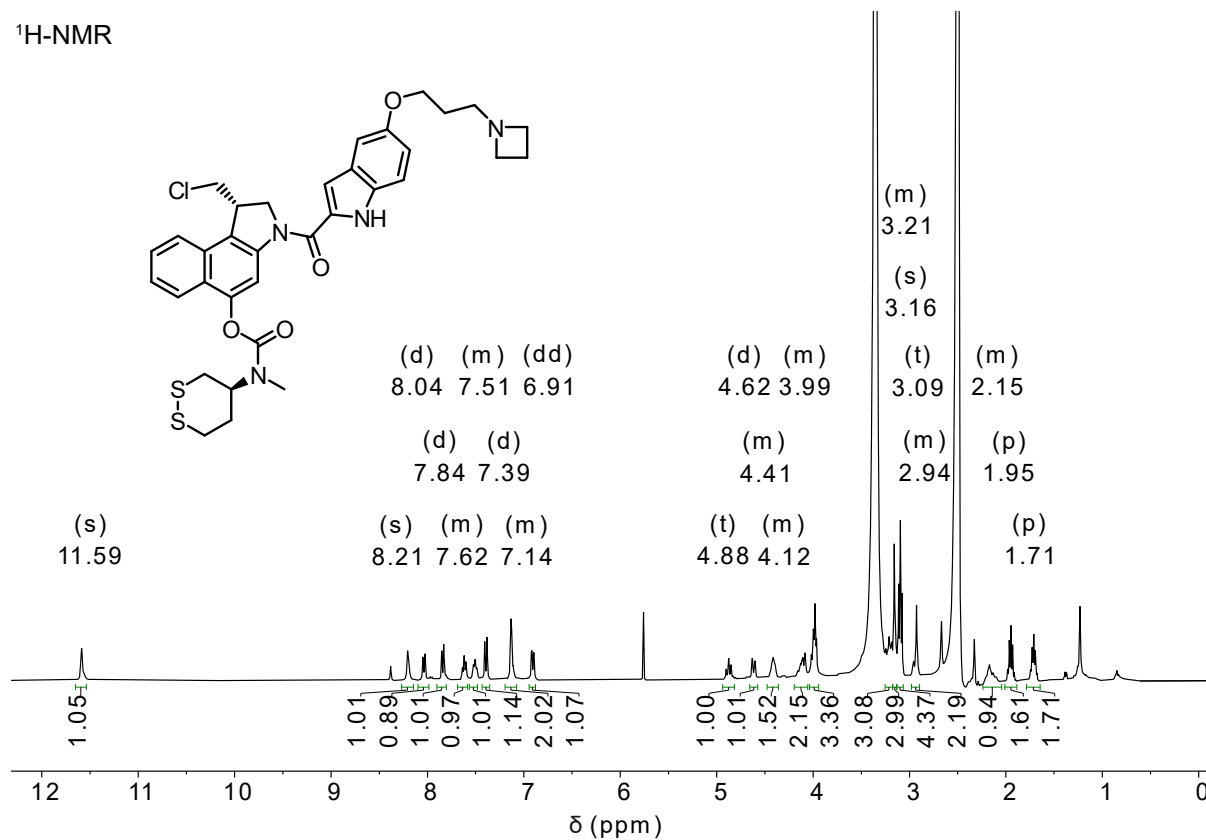
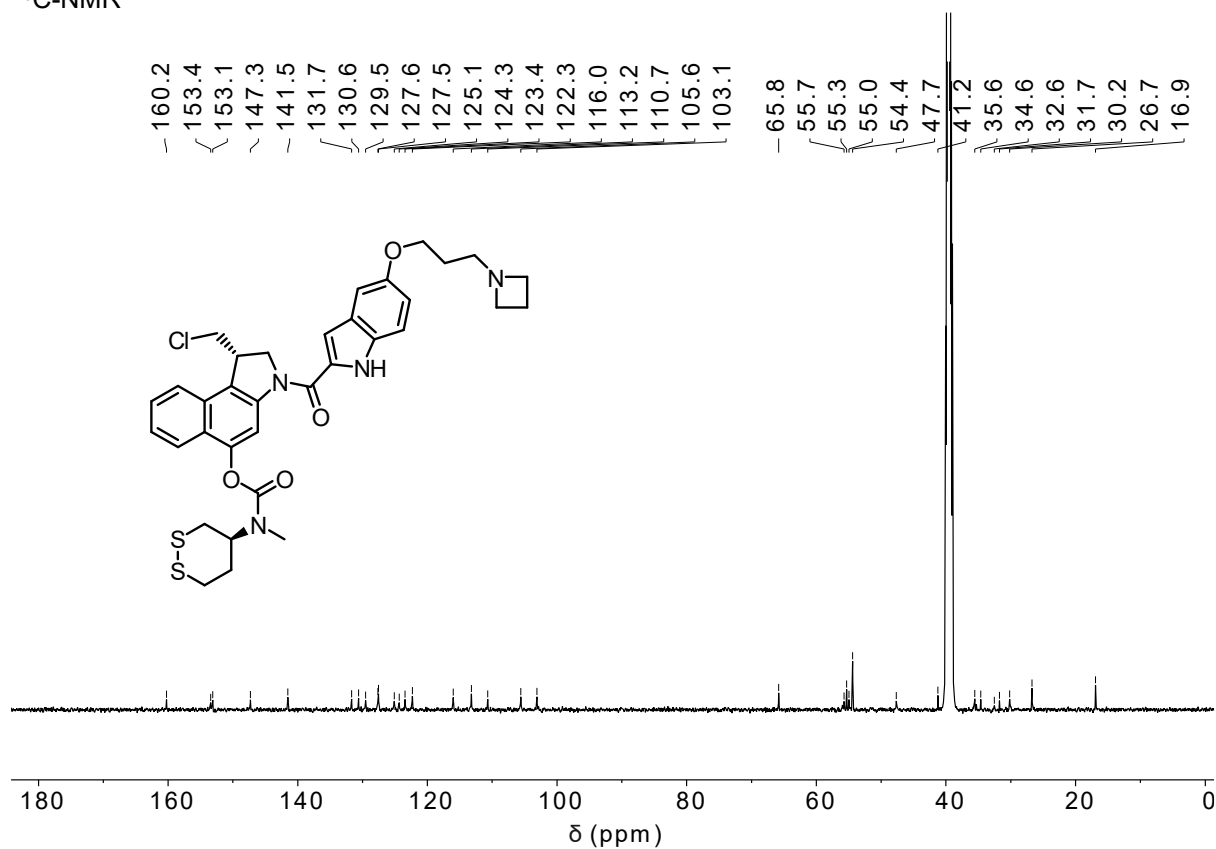
MC-CBI-Boc

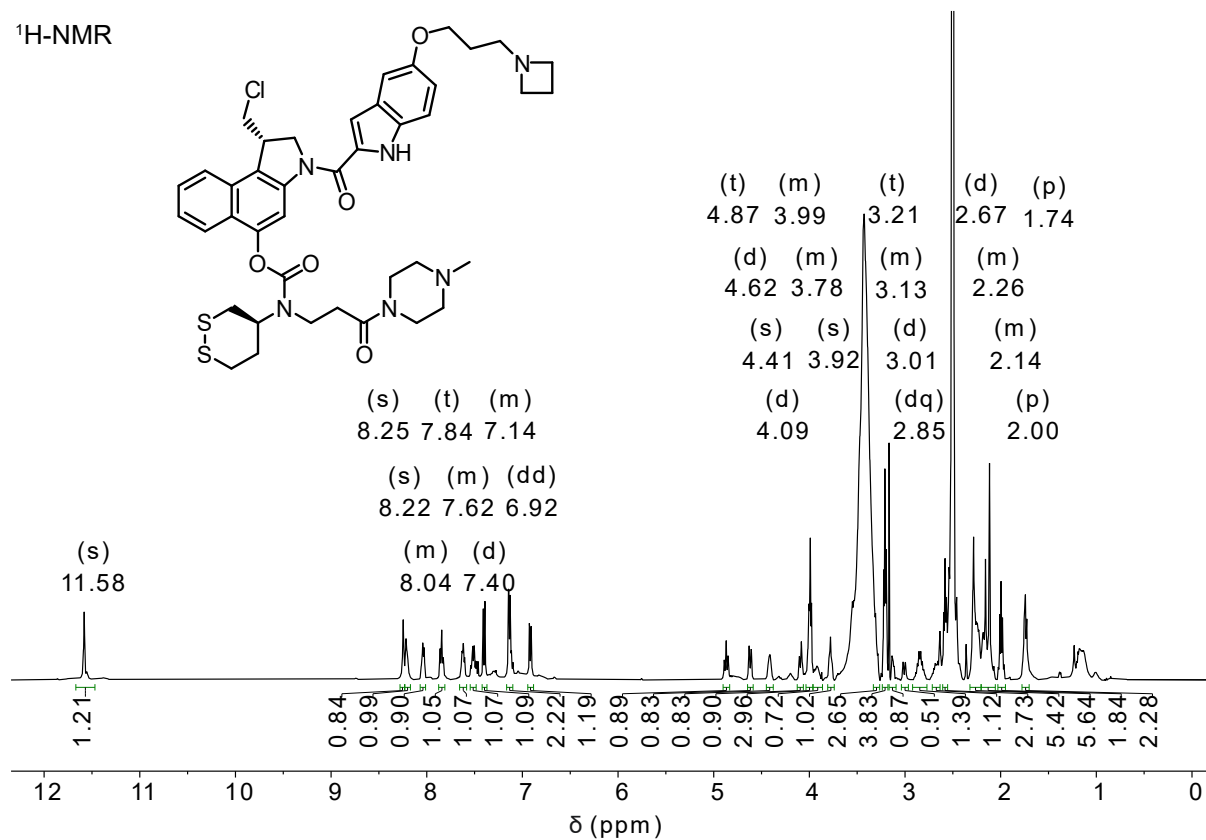
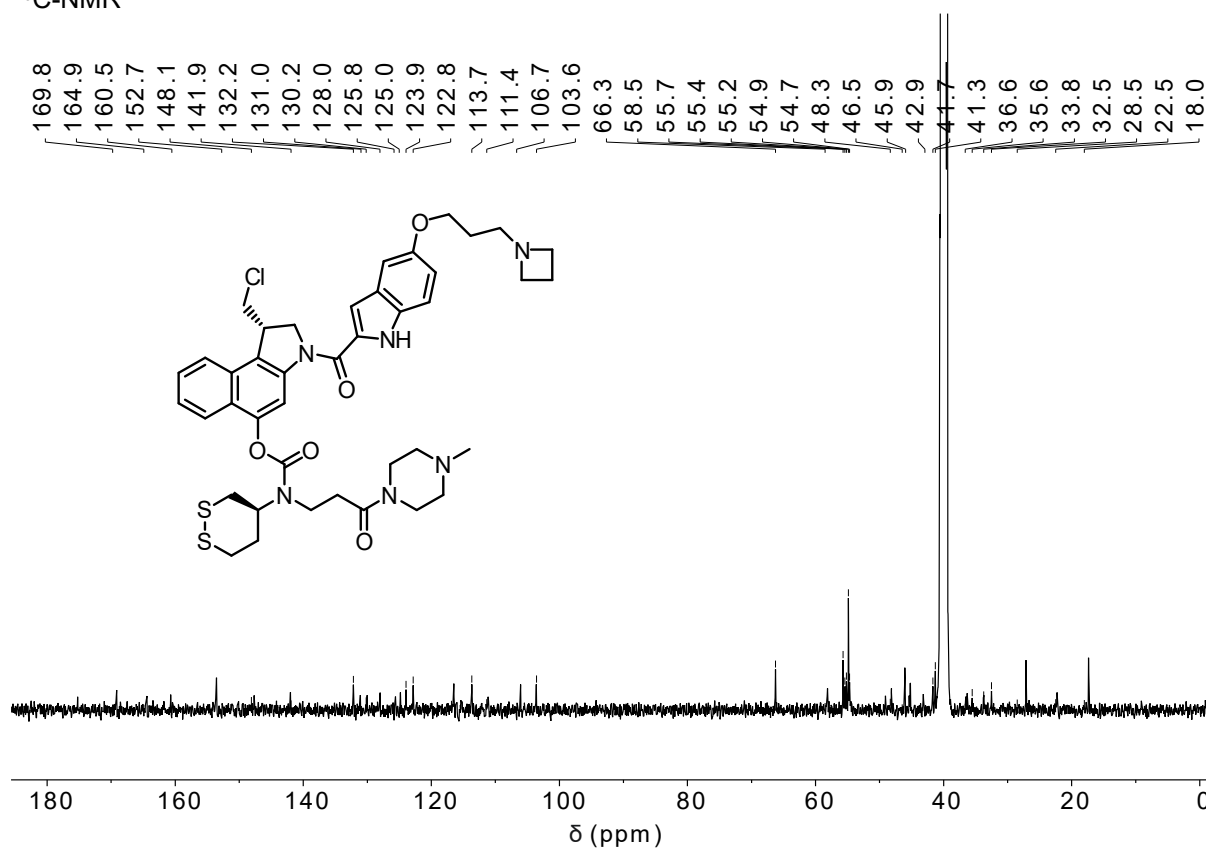


O56-CBI-Boc

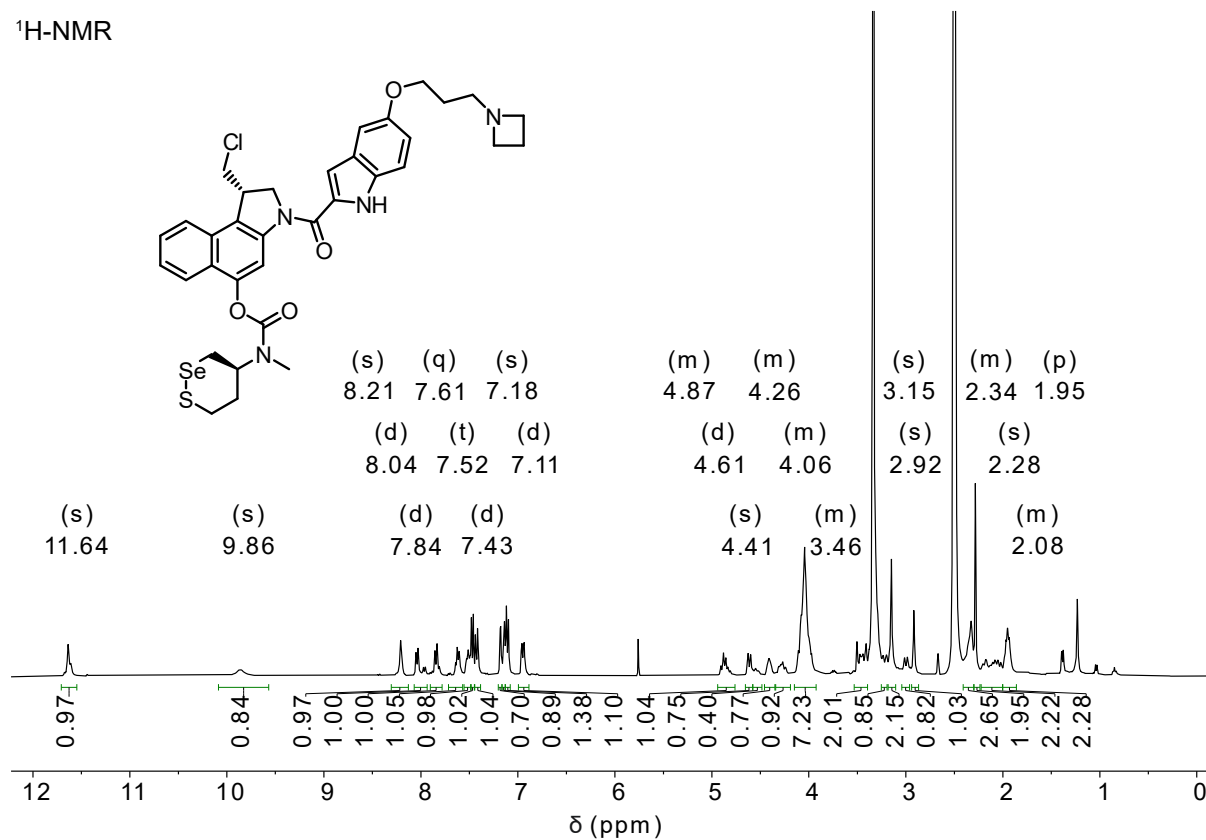
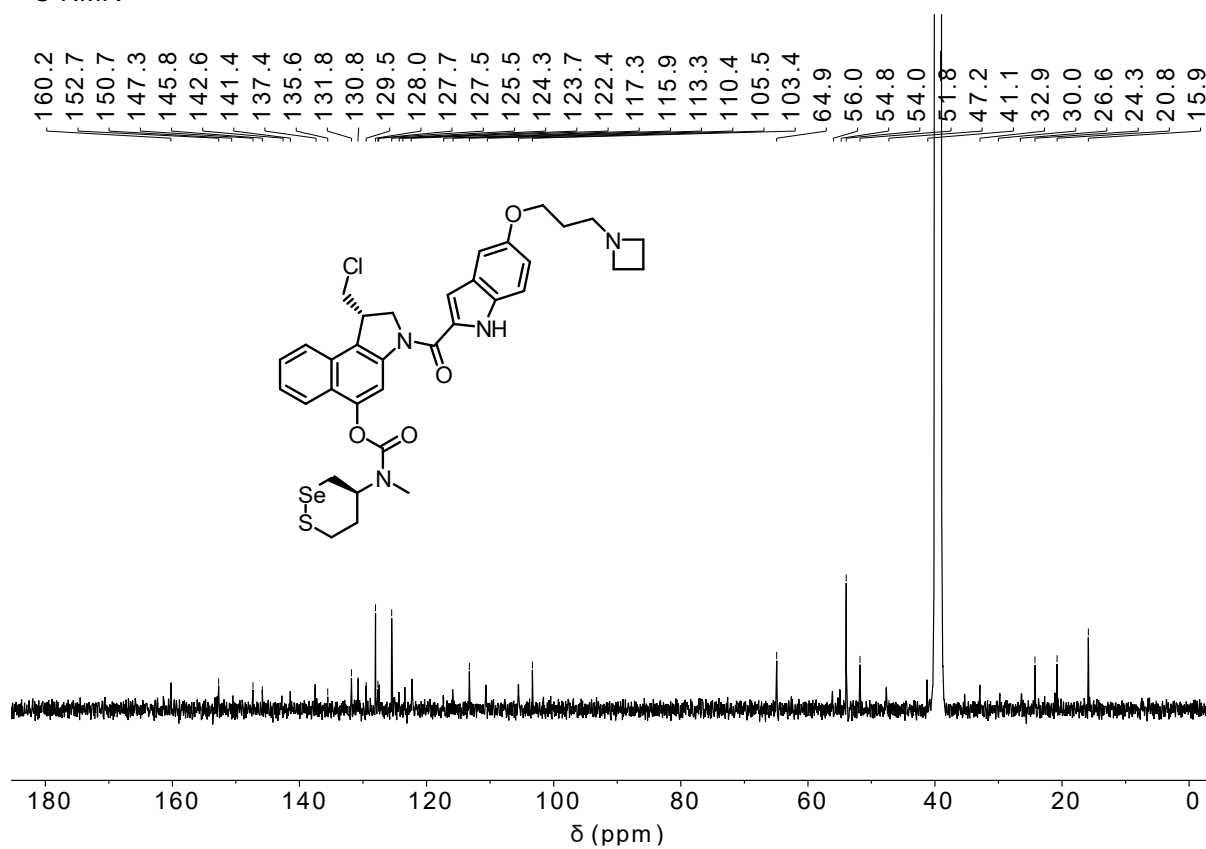


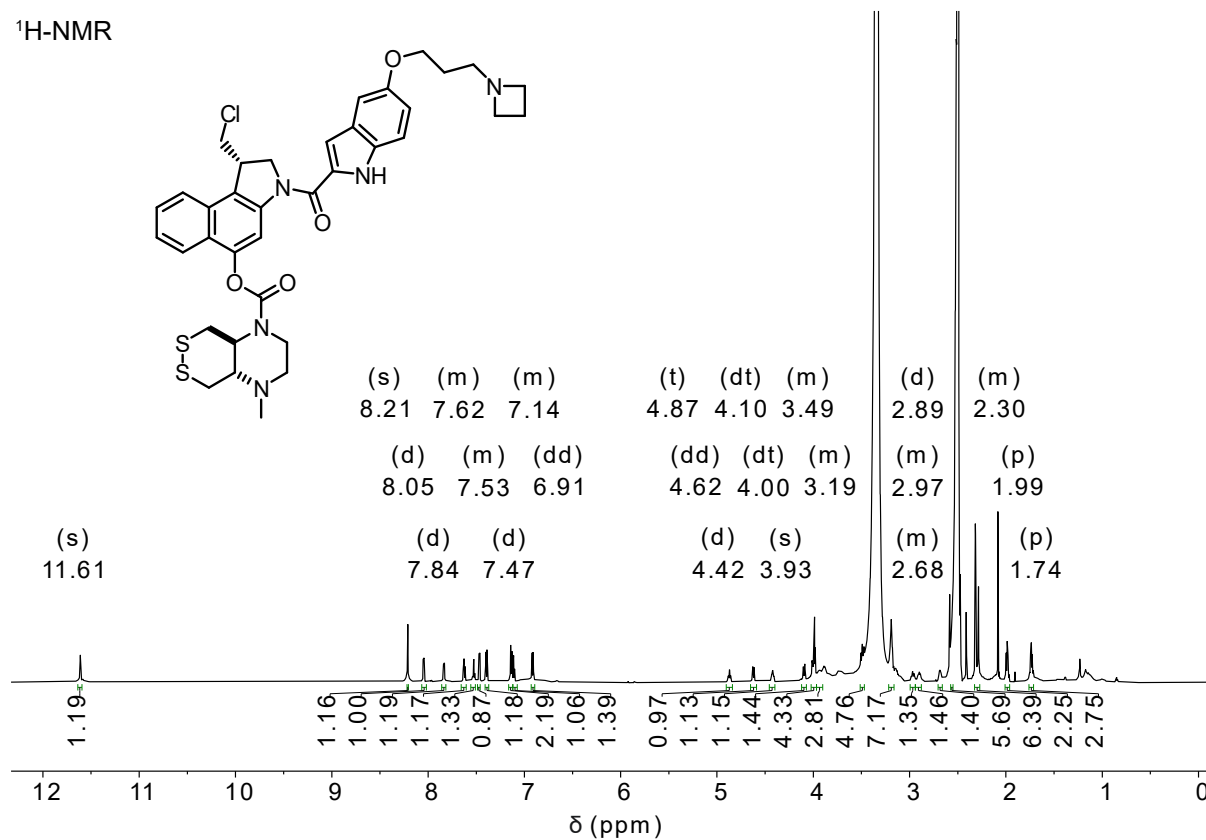
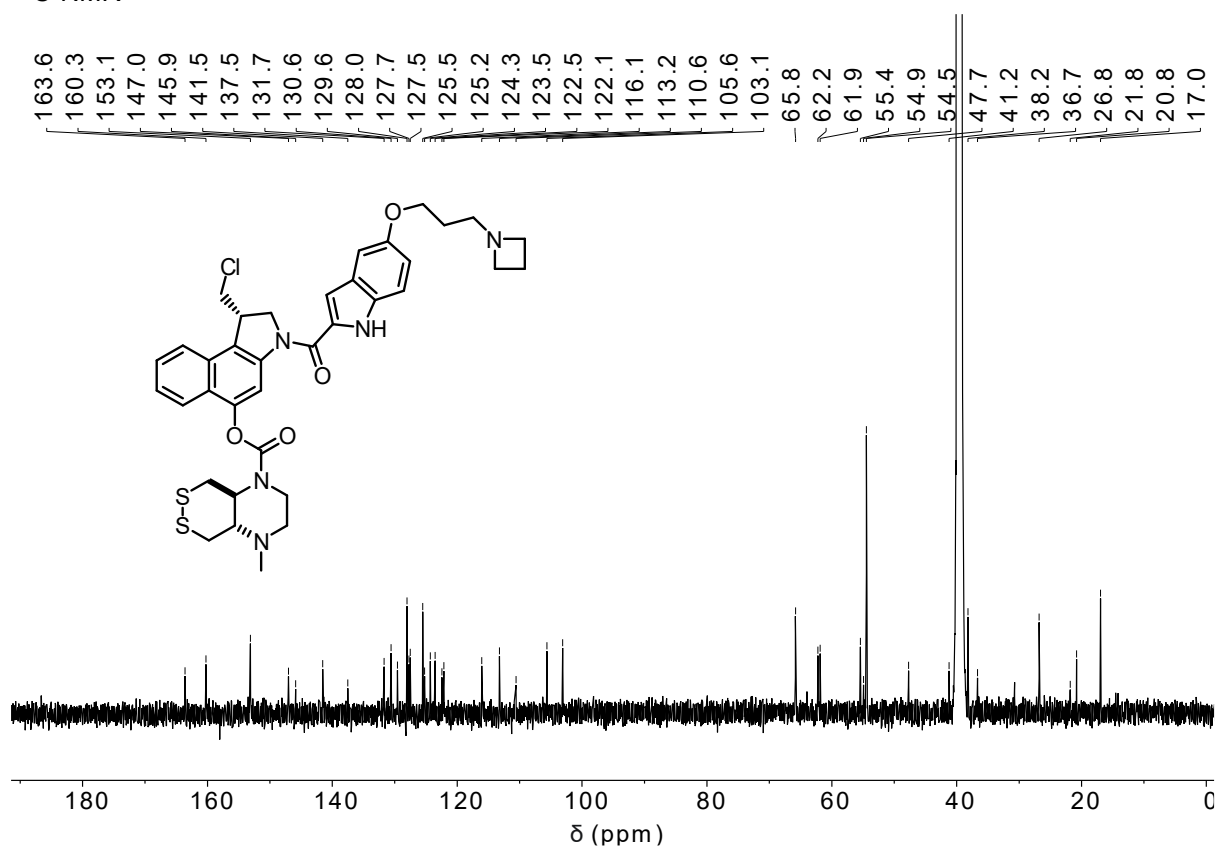
SS60-CBI-AZI

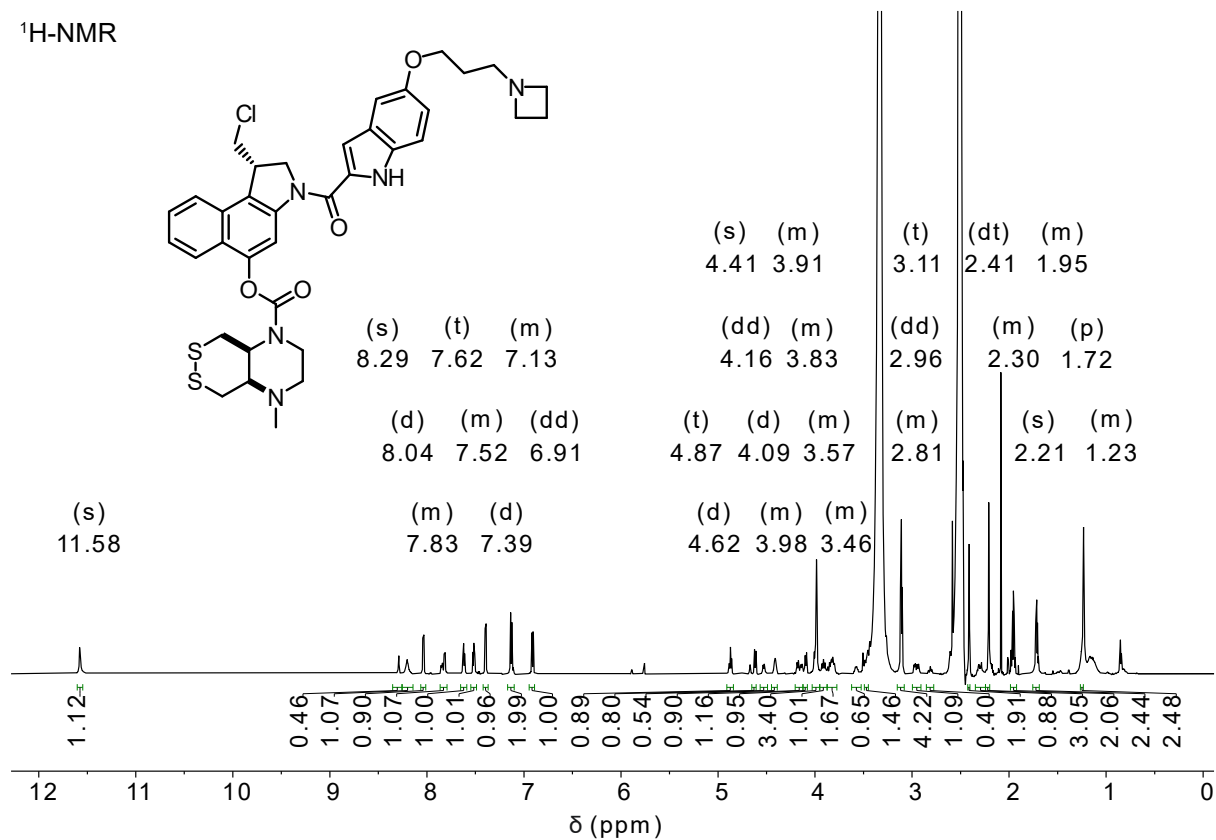
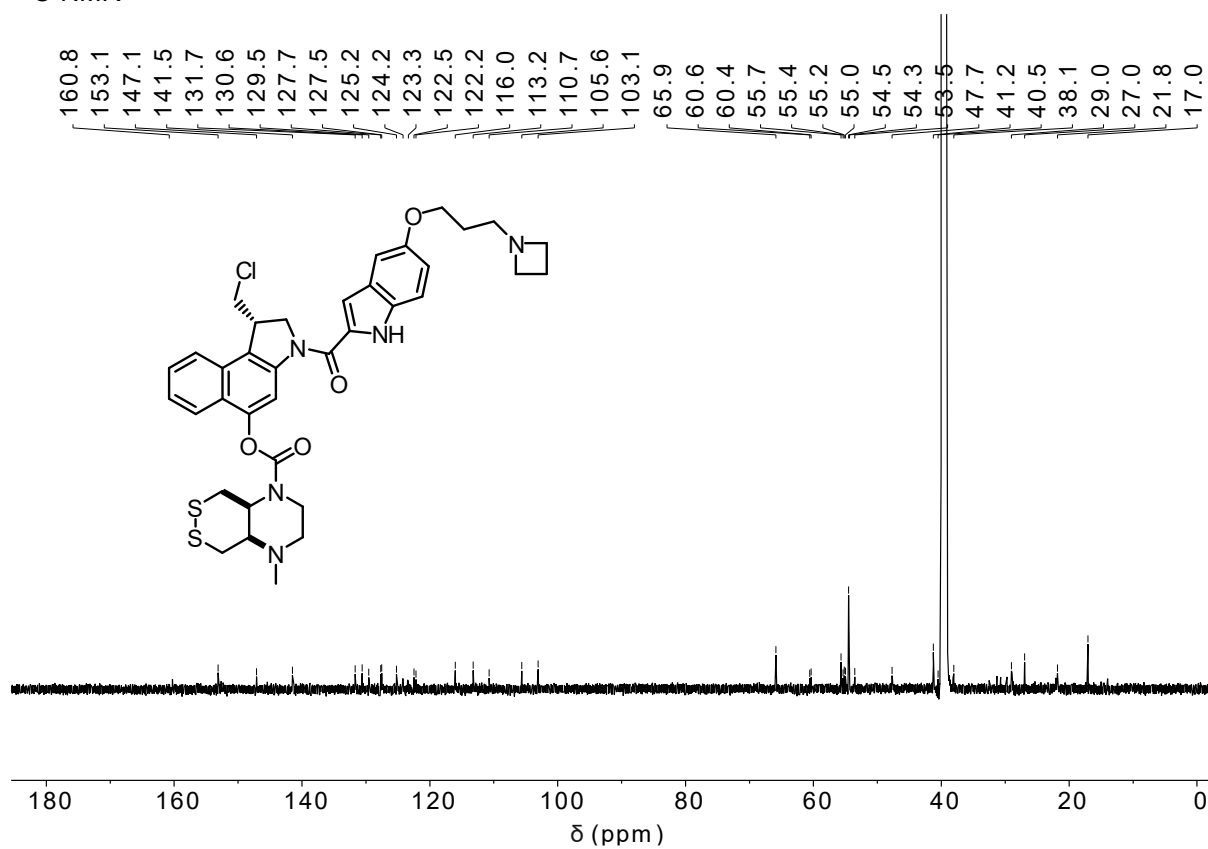
¹H-NMR¹³C-NMR

P-SS60-CBI-AZI¹H-NMR¹³C-NMR

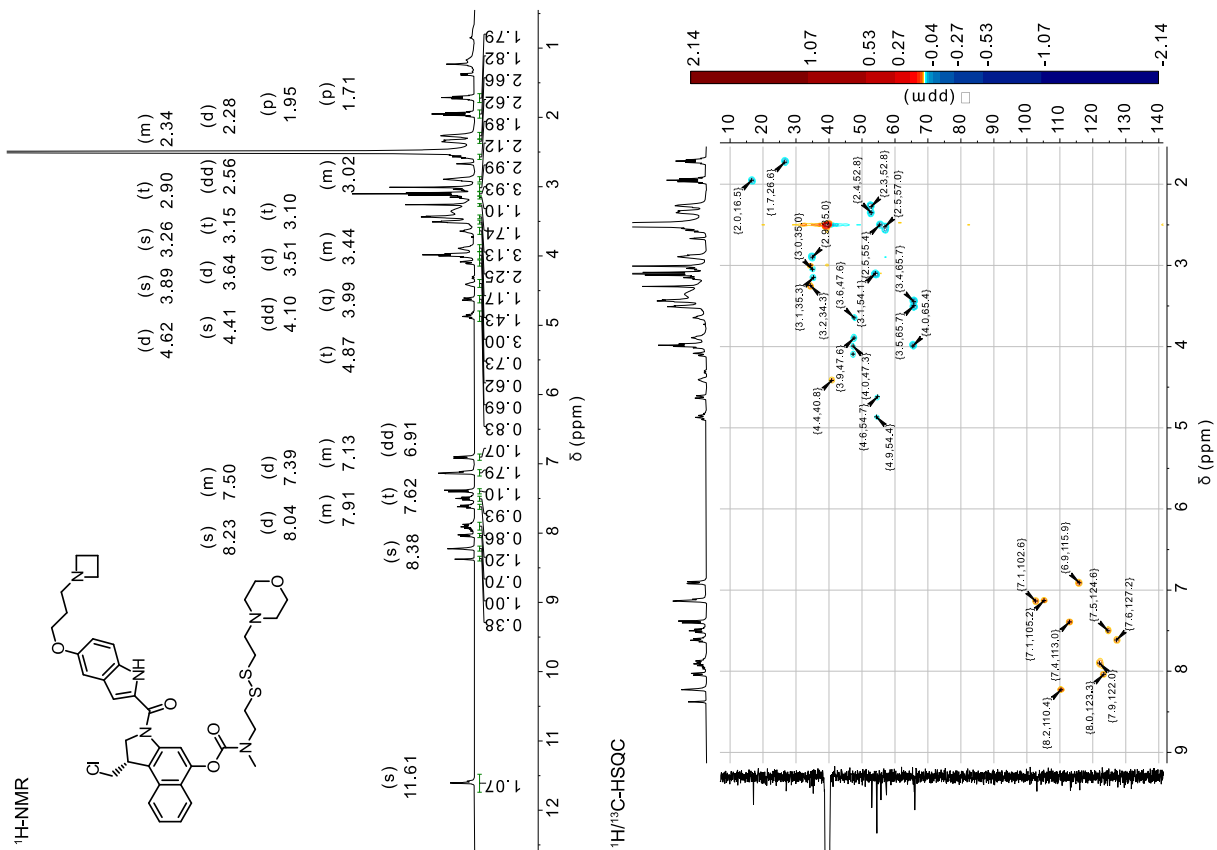
SeS60-CBI-AZI

¹H-NMR¹³C-NMR

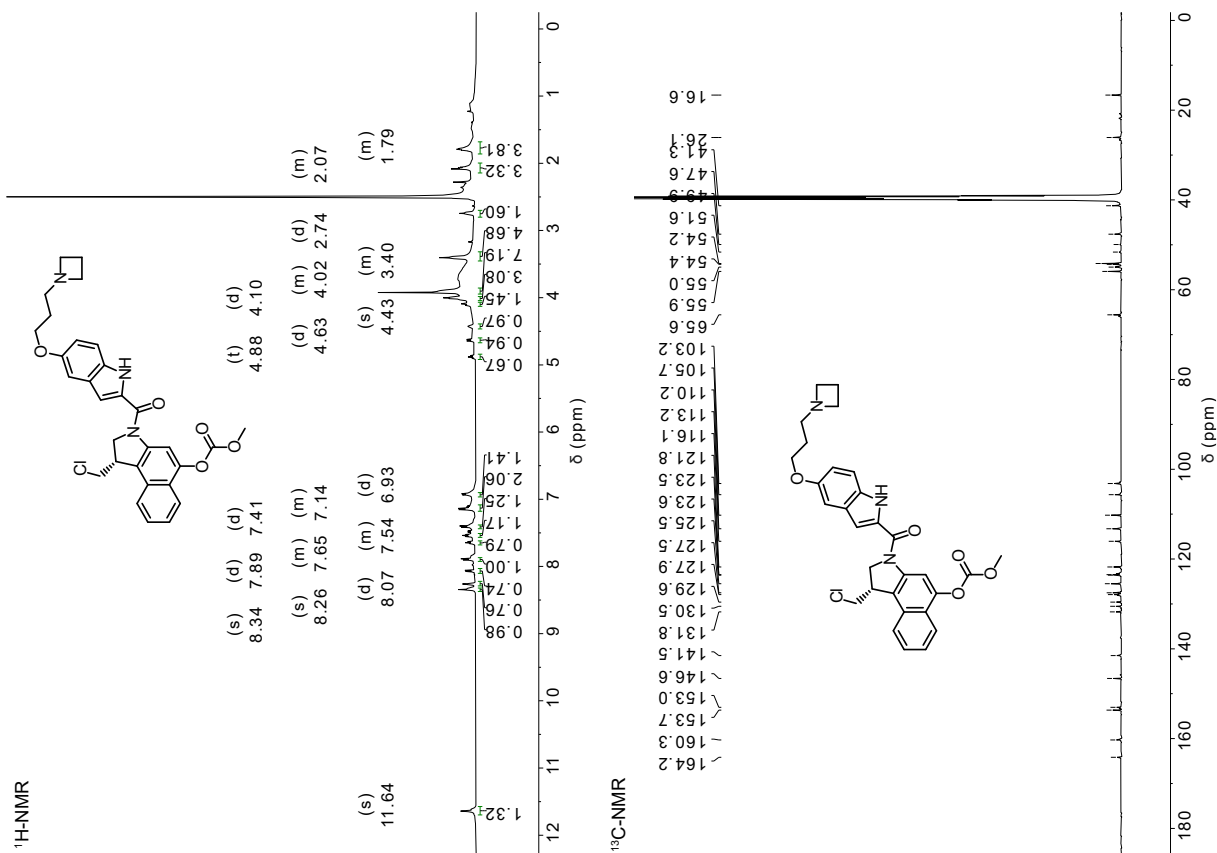
Me-SS66T-CBI-AZI¹H-NMR¹³C-NMR

Me-SS66C-CBI-AZI¹H-NMR¹³C-NMR

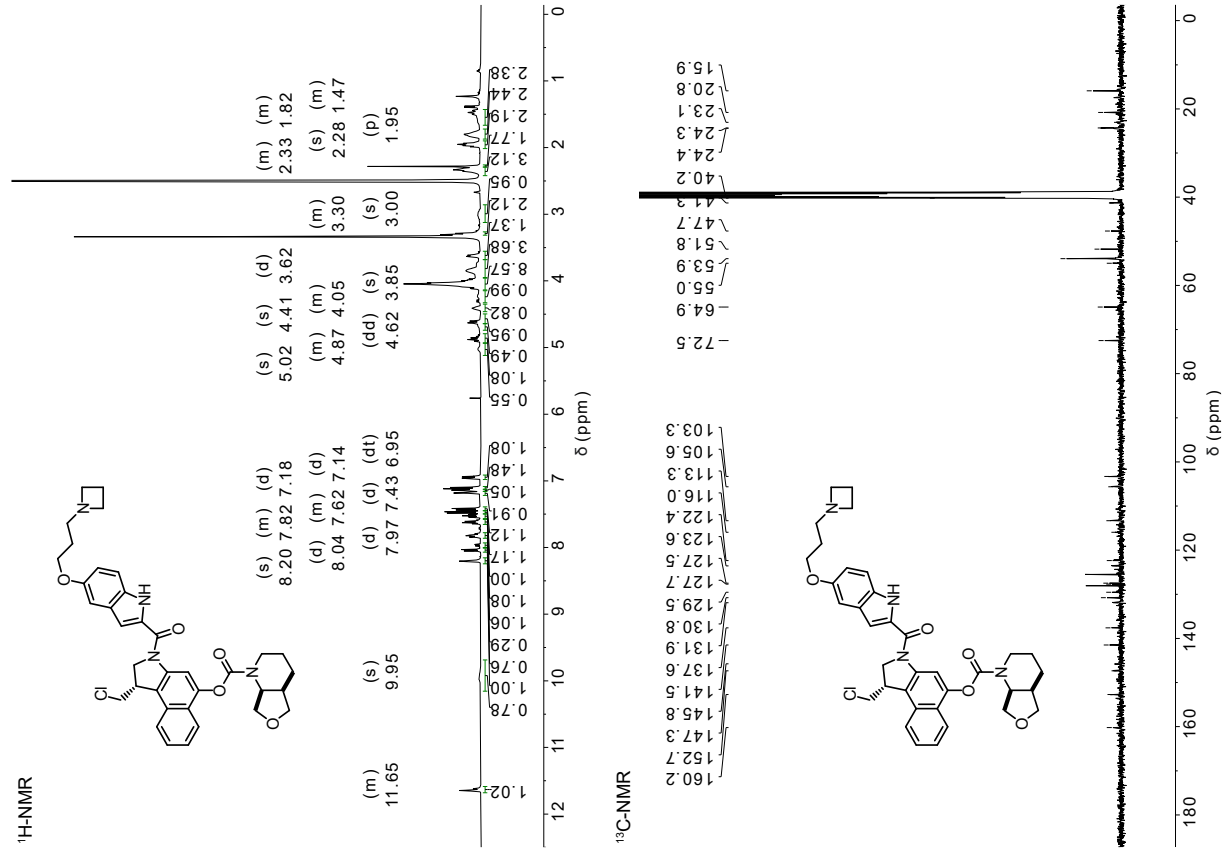
SS00_M-CBI-AZI



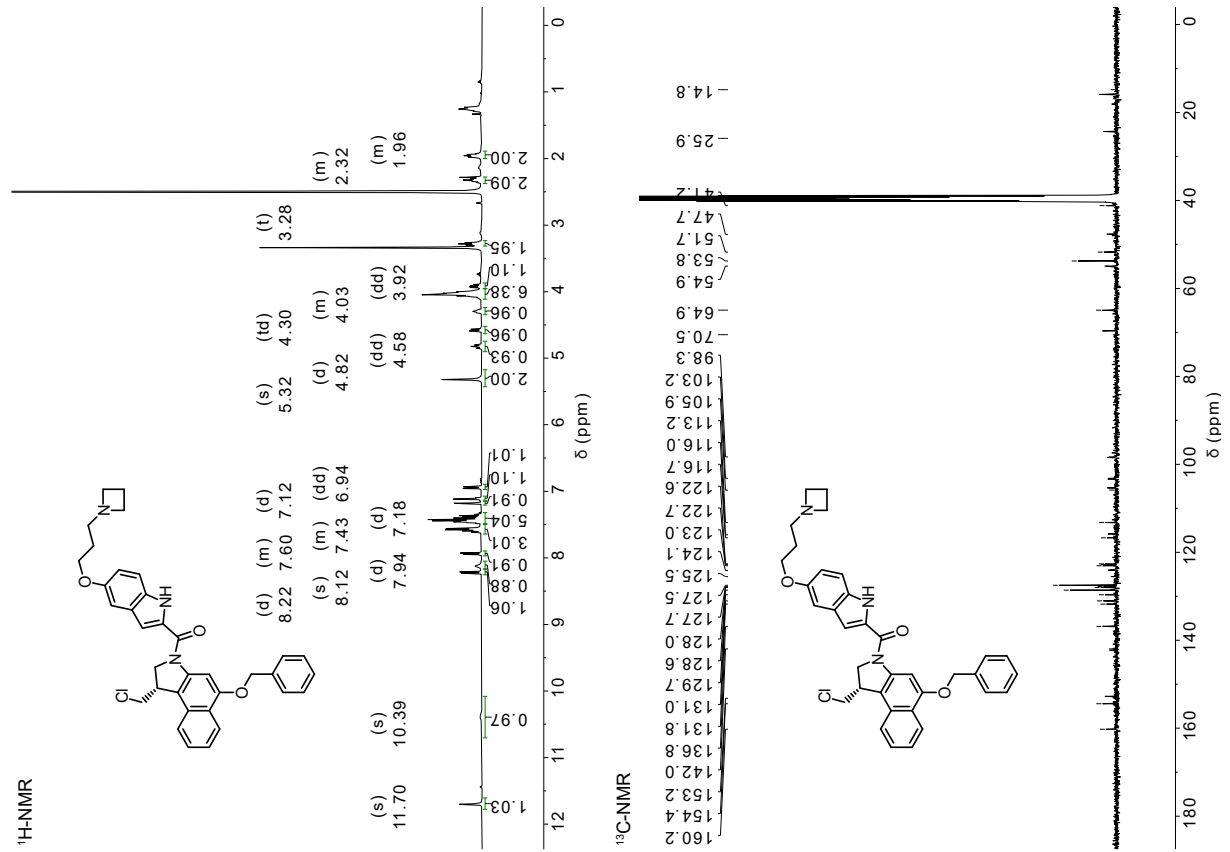
MC-CBI-AZI

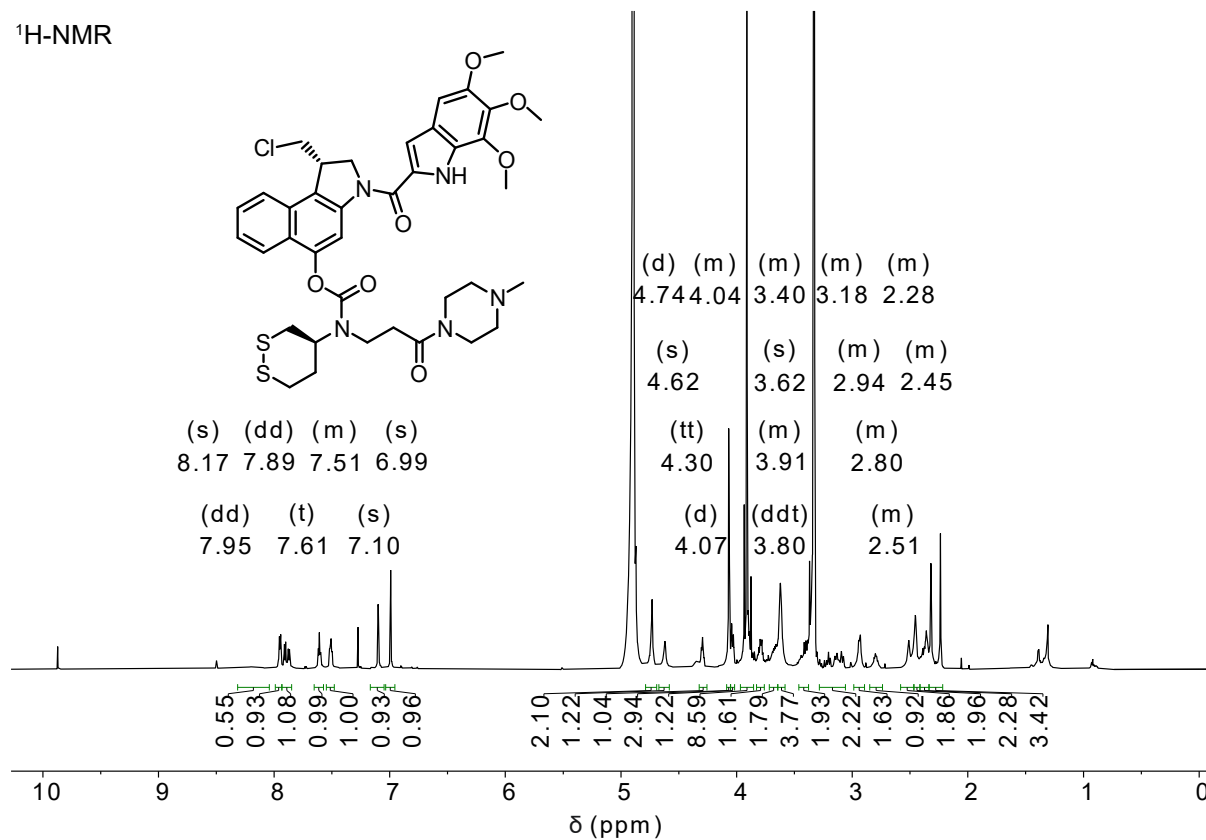
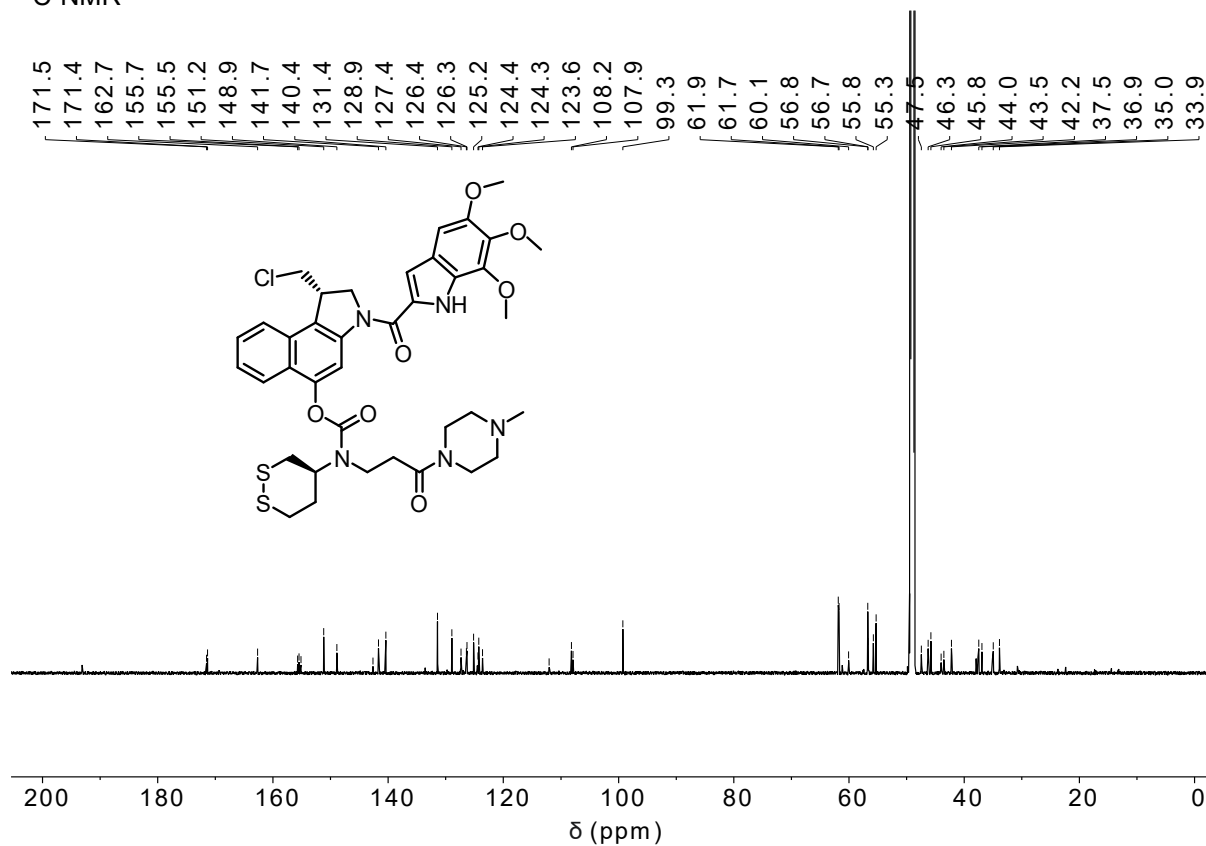


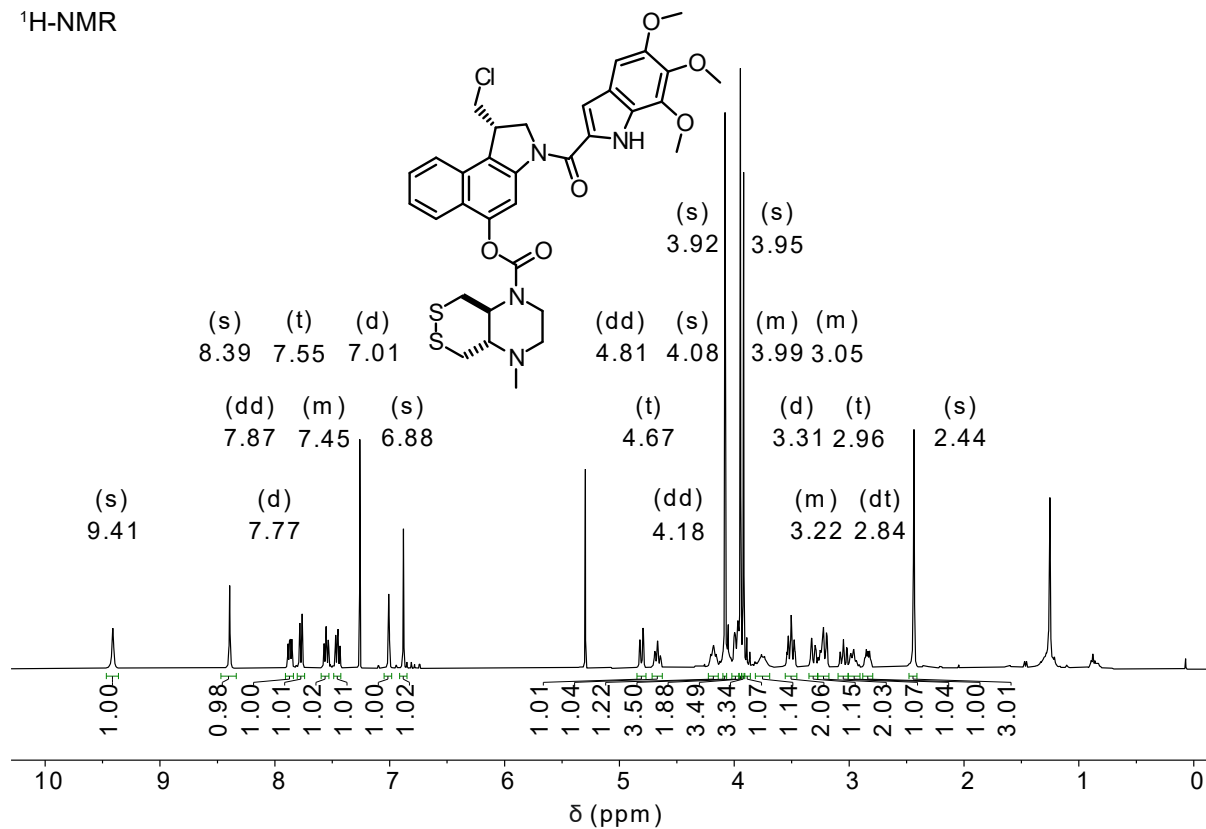
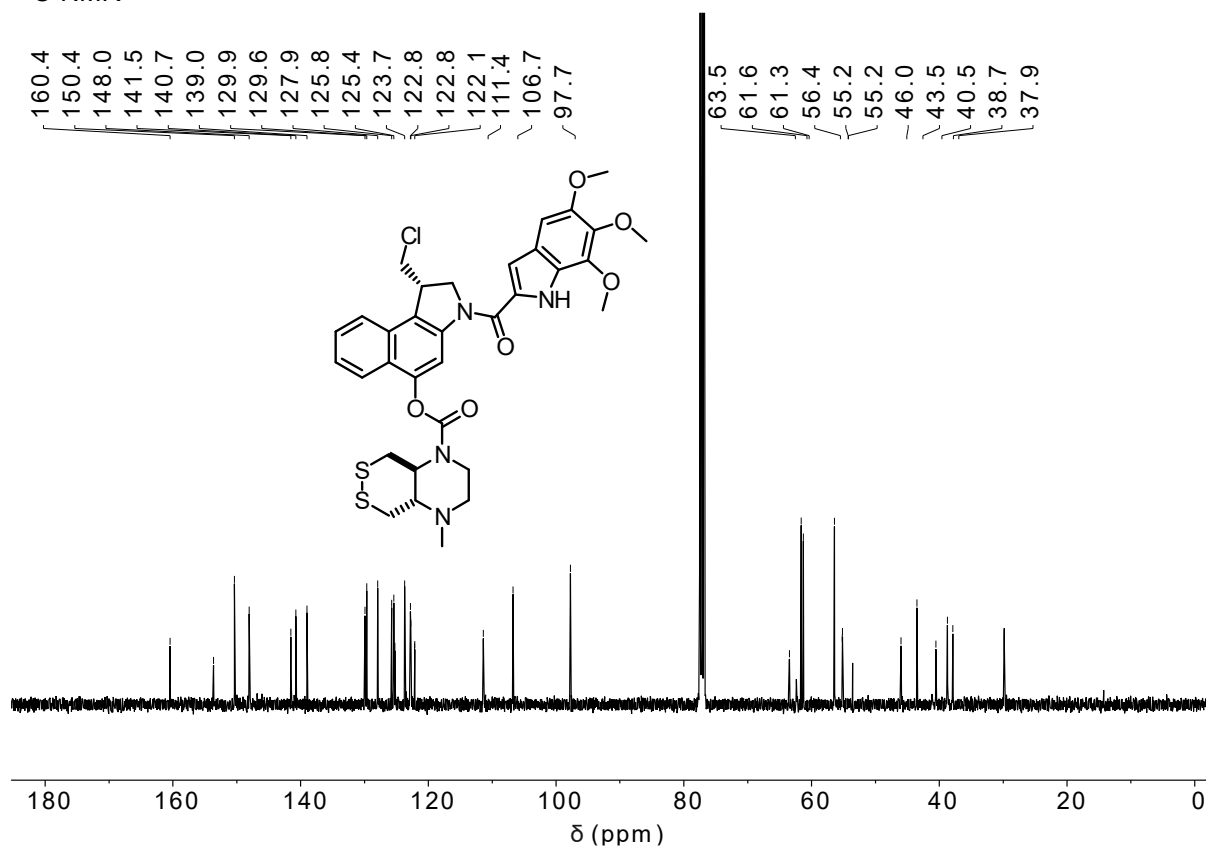
O56-CBI-AZI



OBn-CBI-AZI

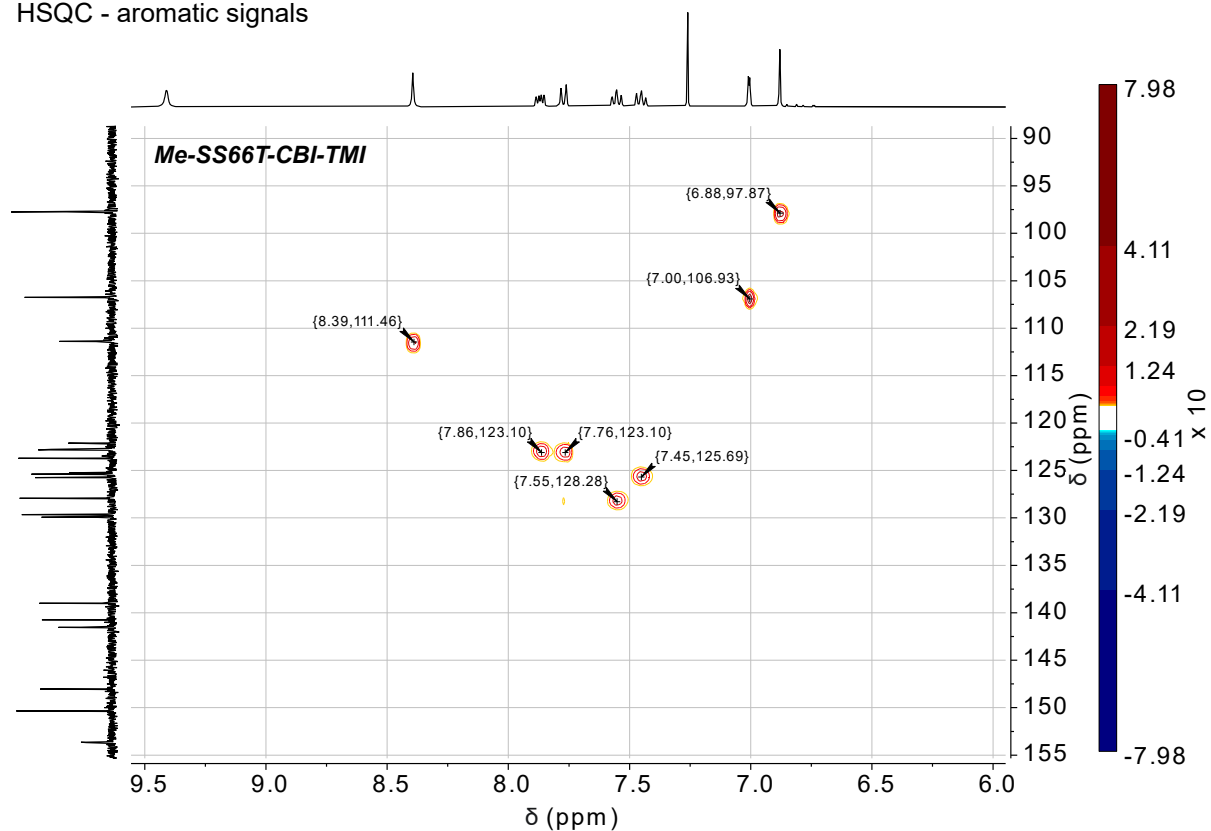


P-SS60-CBI-TMI¹H-NMR¹³C-NMR

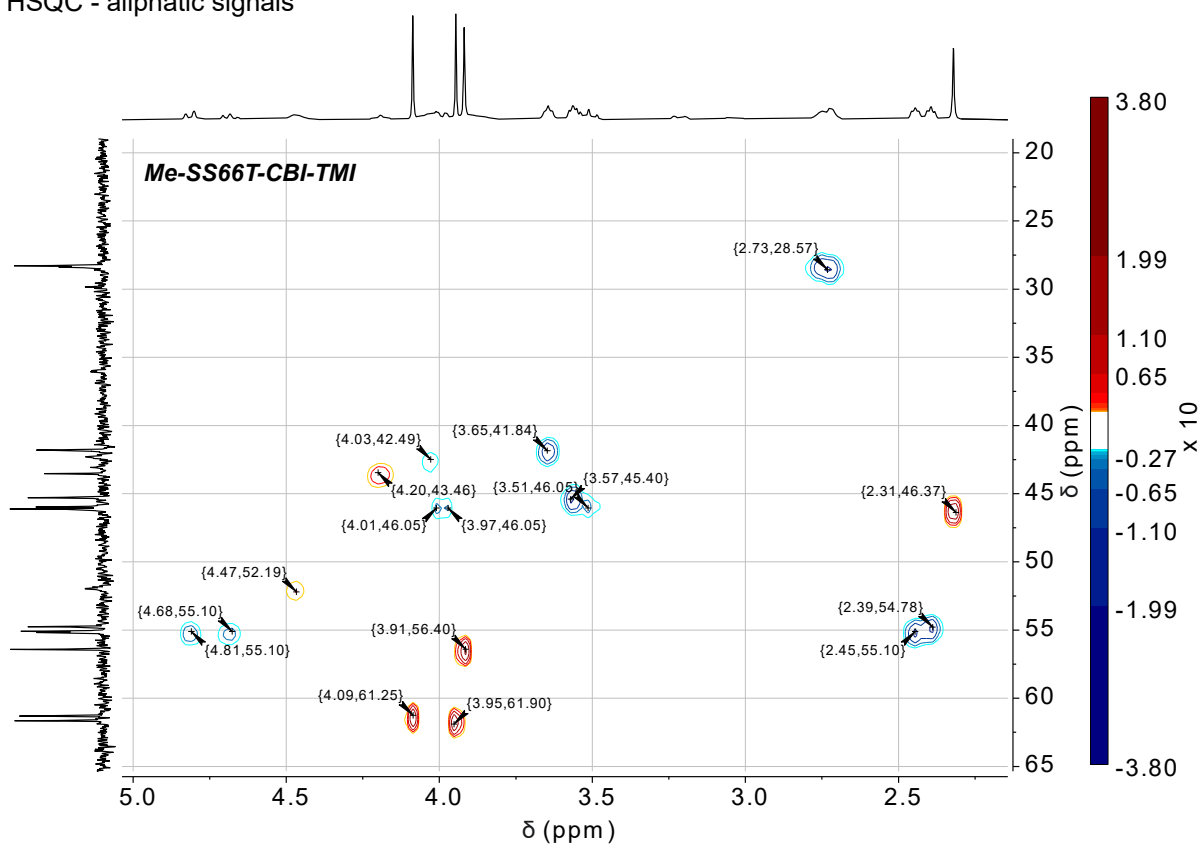
Me-SS66T-CBI-TMI¹H-NMR¹³C-NMR

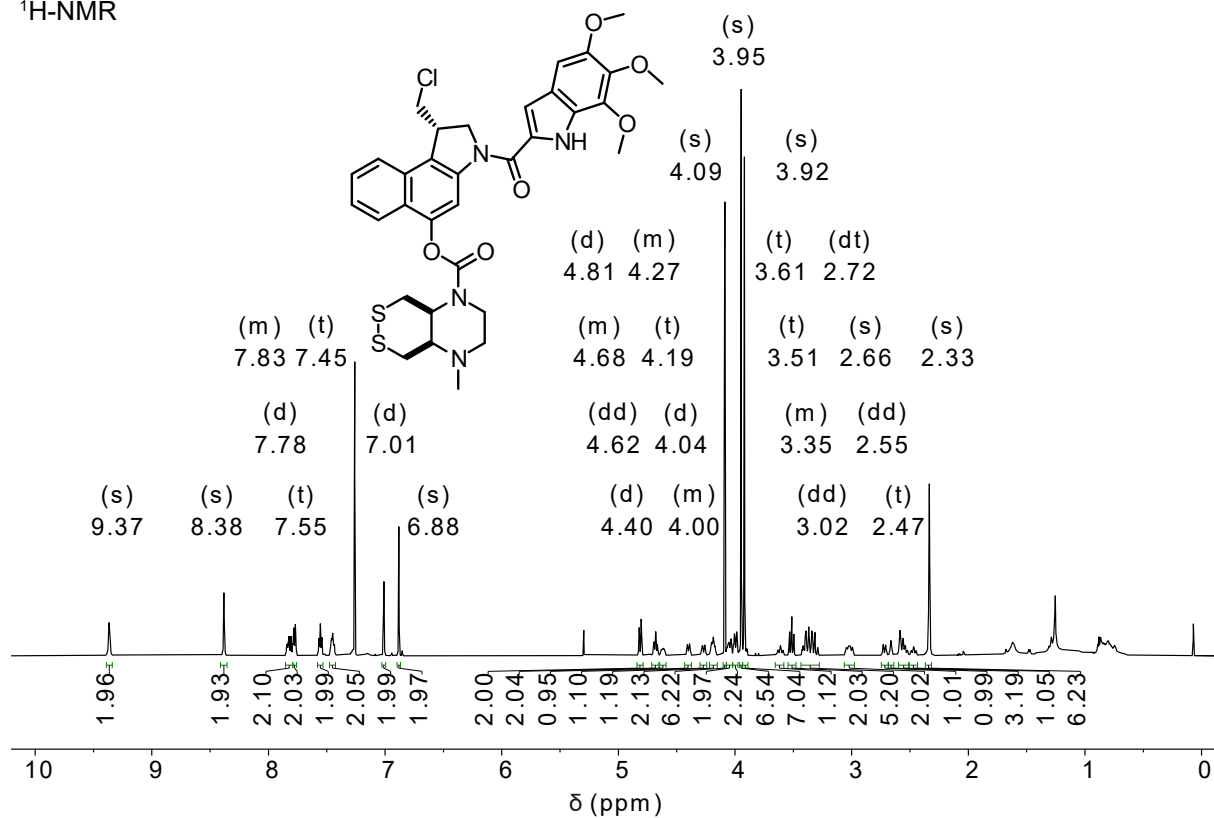
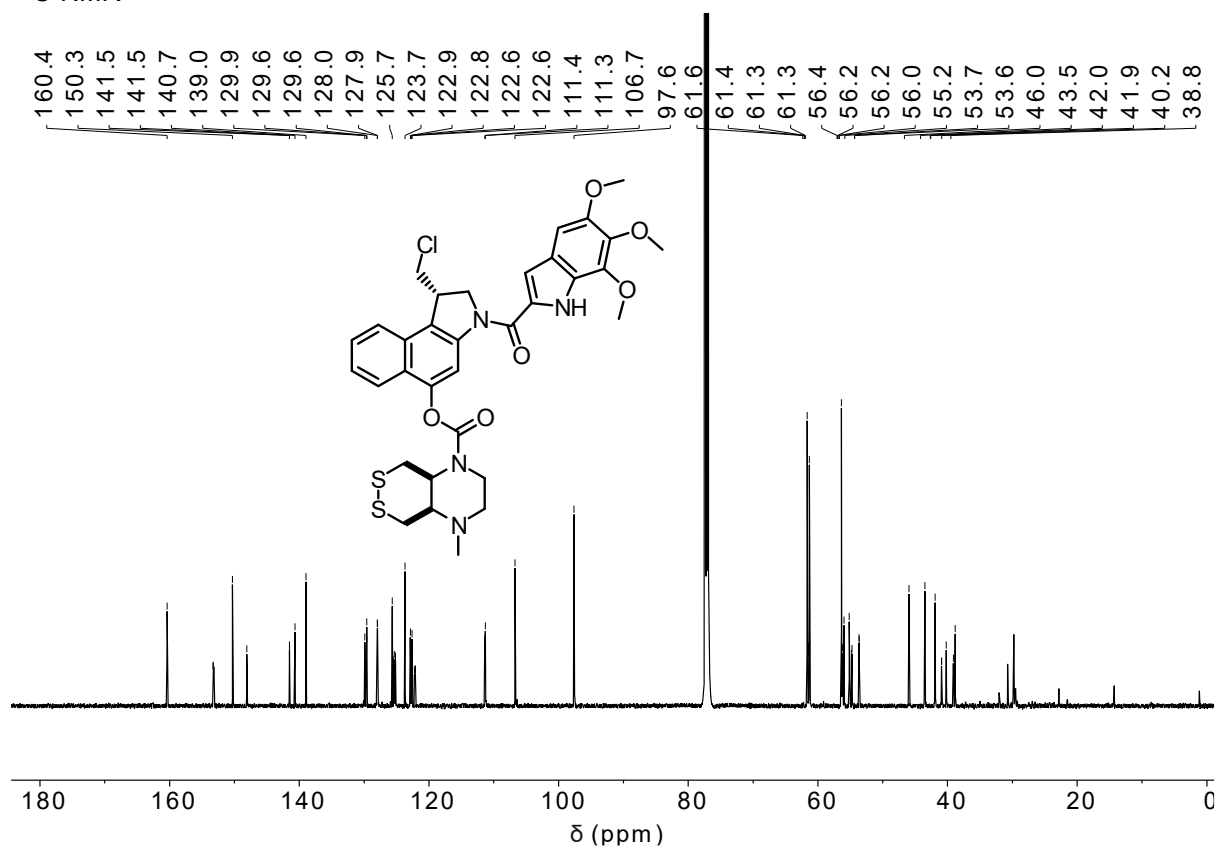
Me-SS66T-CBI-TMI

HSQC - aromatic signals



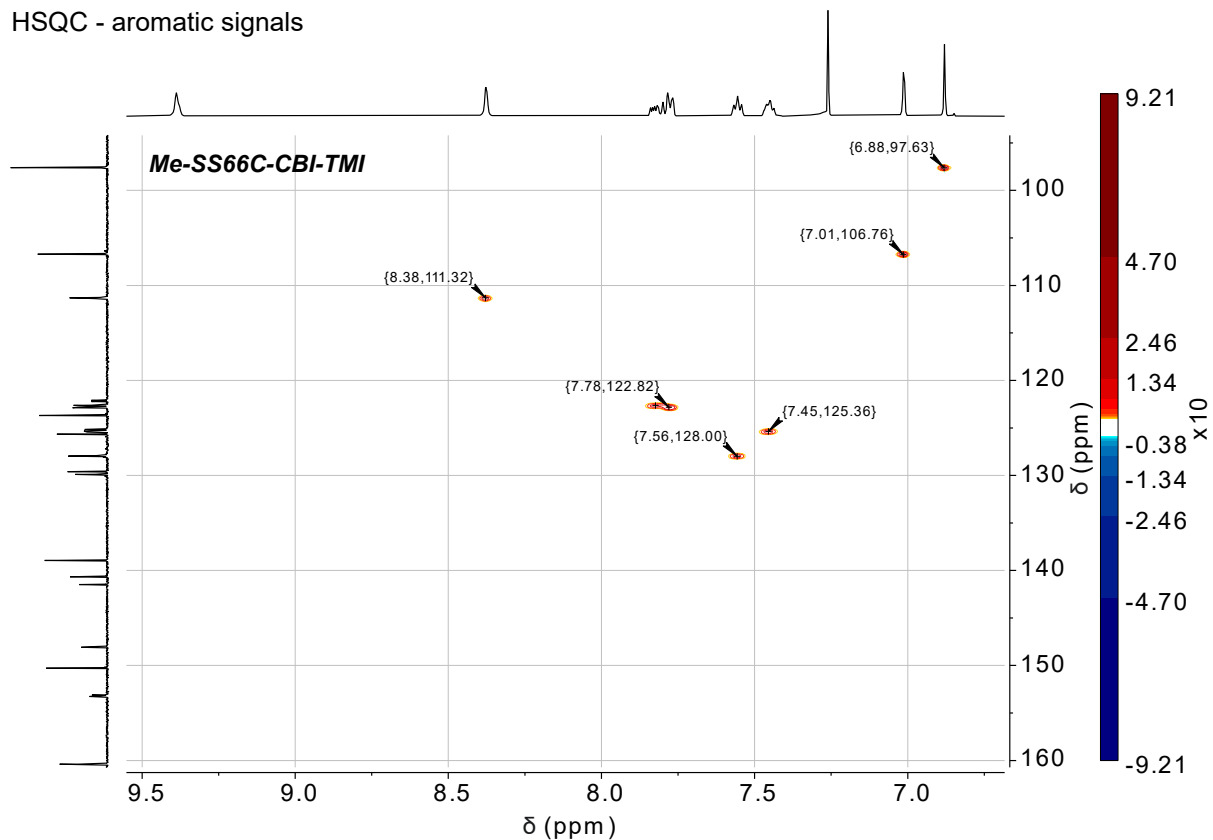
HSQC - aliphatic signals



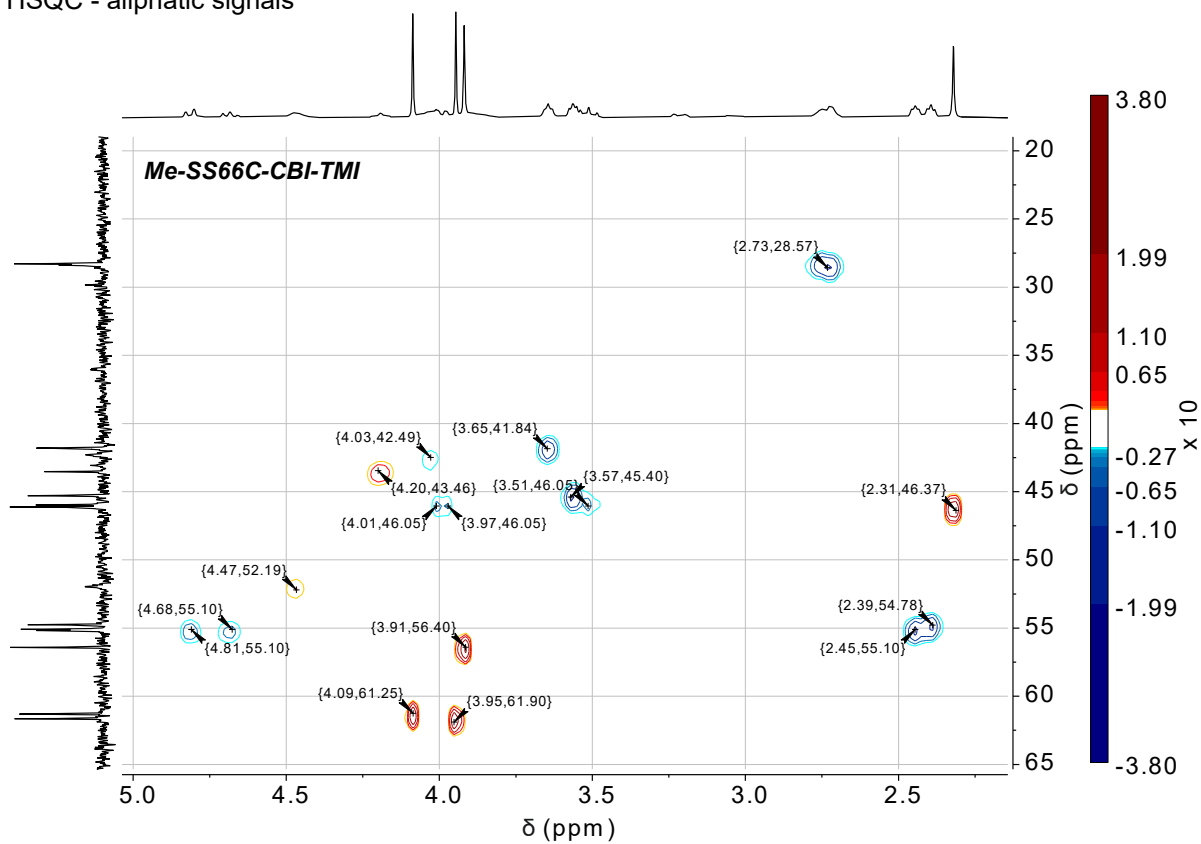
Me-SS66C-CBI-TMI¹H-NMR¹³C-NMR

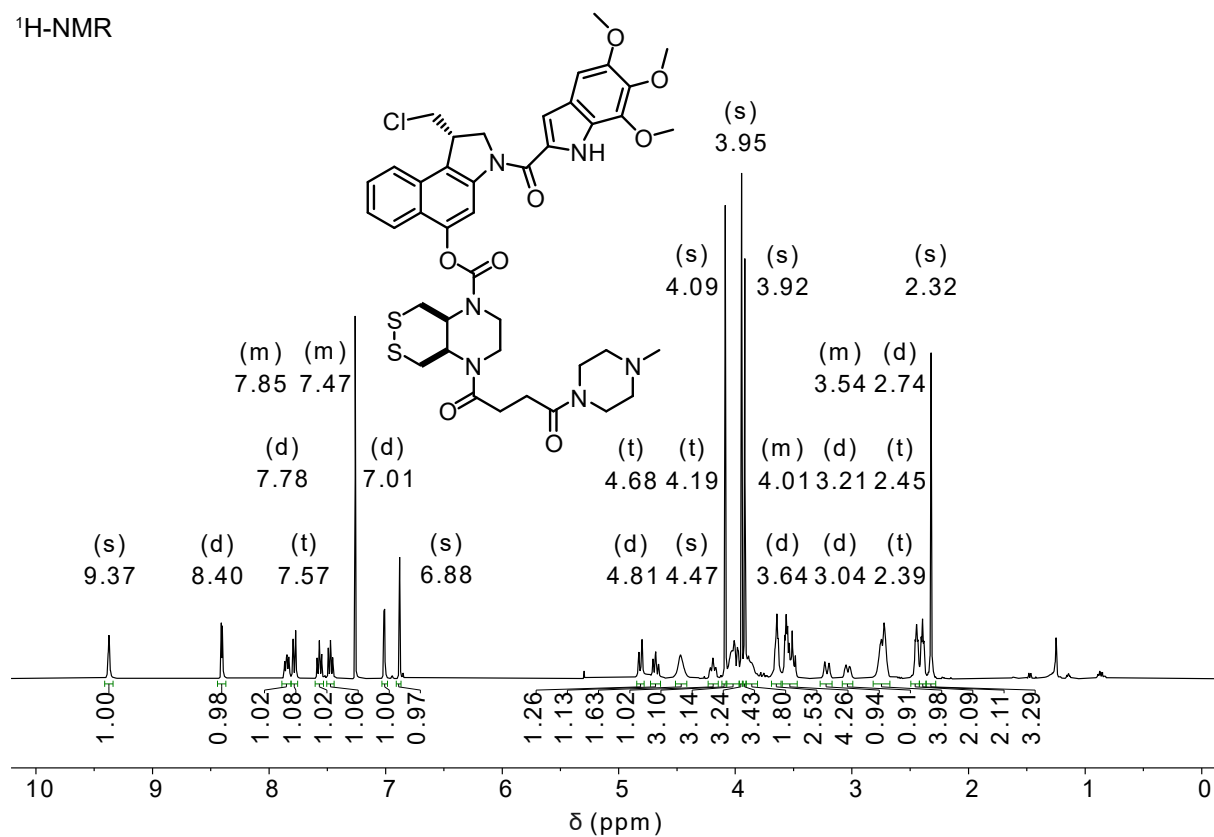
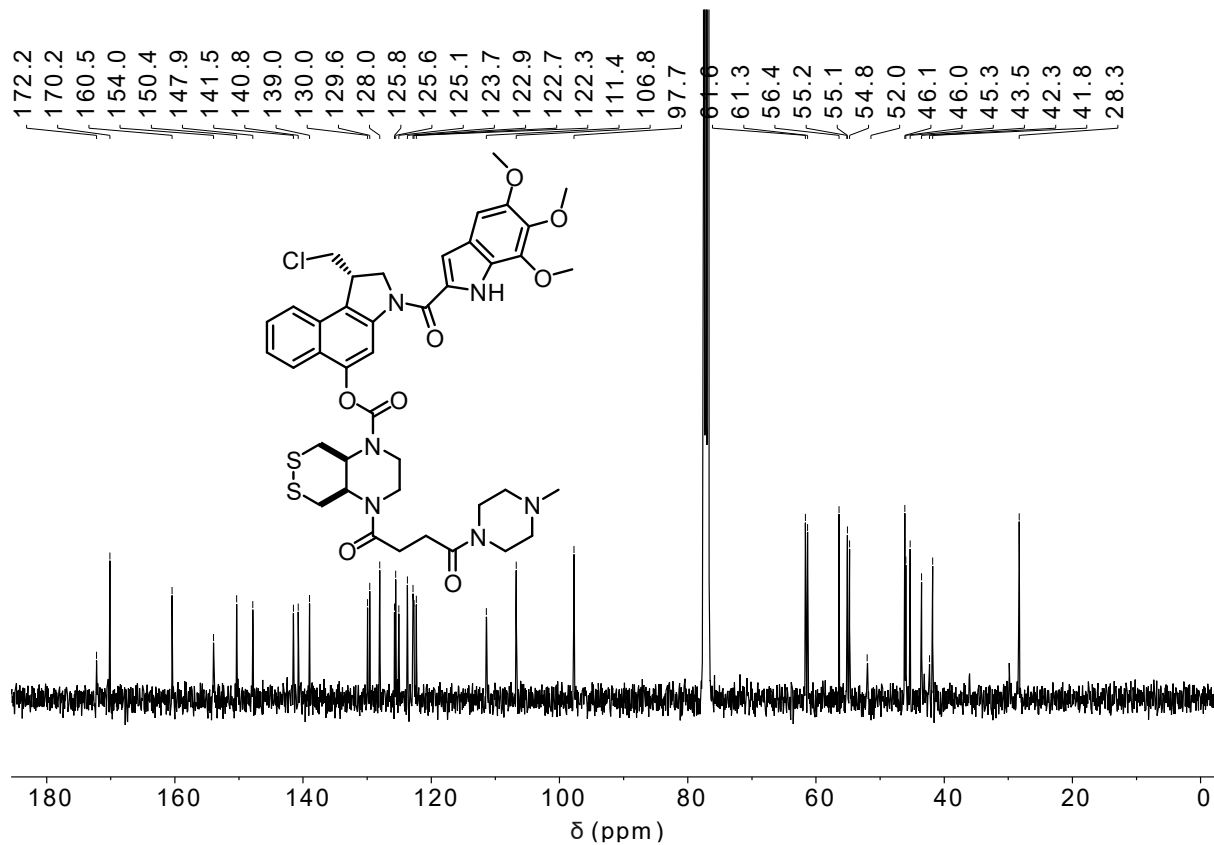
Me-SS66C-CBI-TMI

HSQC - aromatic signals

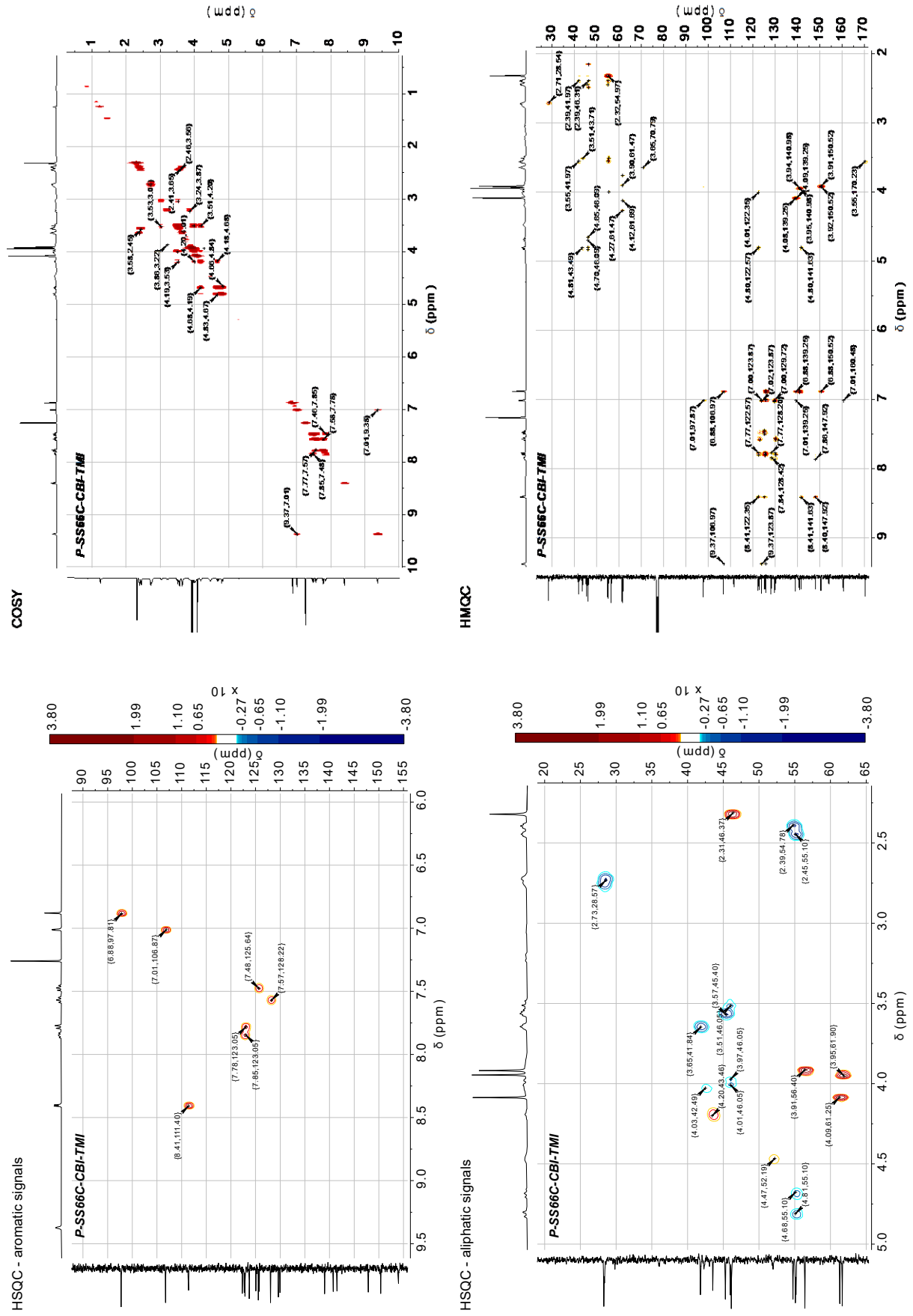


HSQC - aliphatic signals



P-SS66C-CBI-TMI¹H-NMR¹³C-NMR

P-SS66C-CBI-TMI



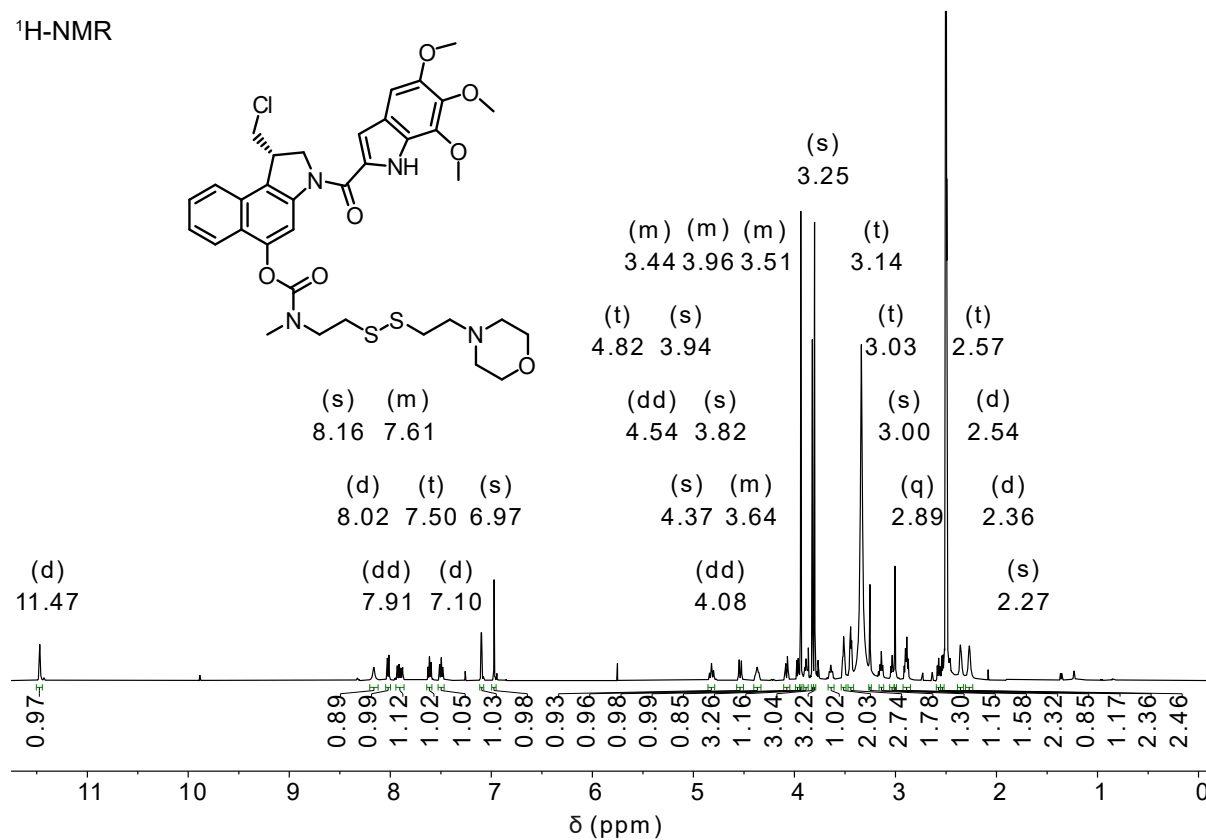
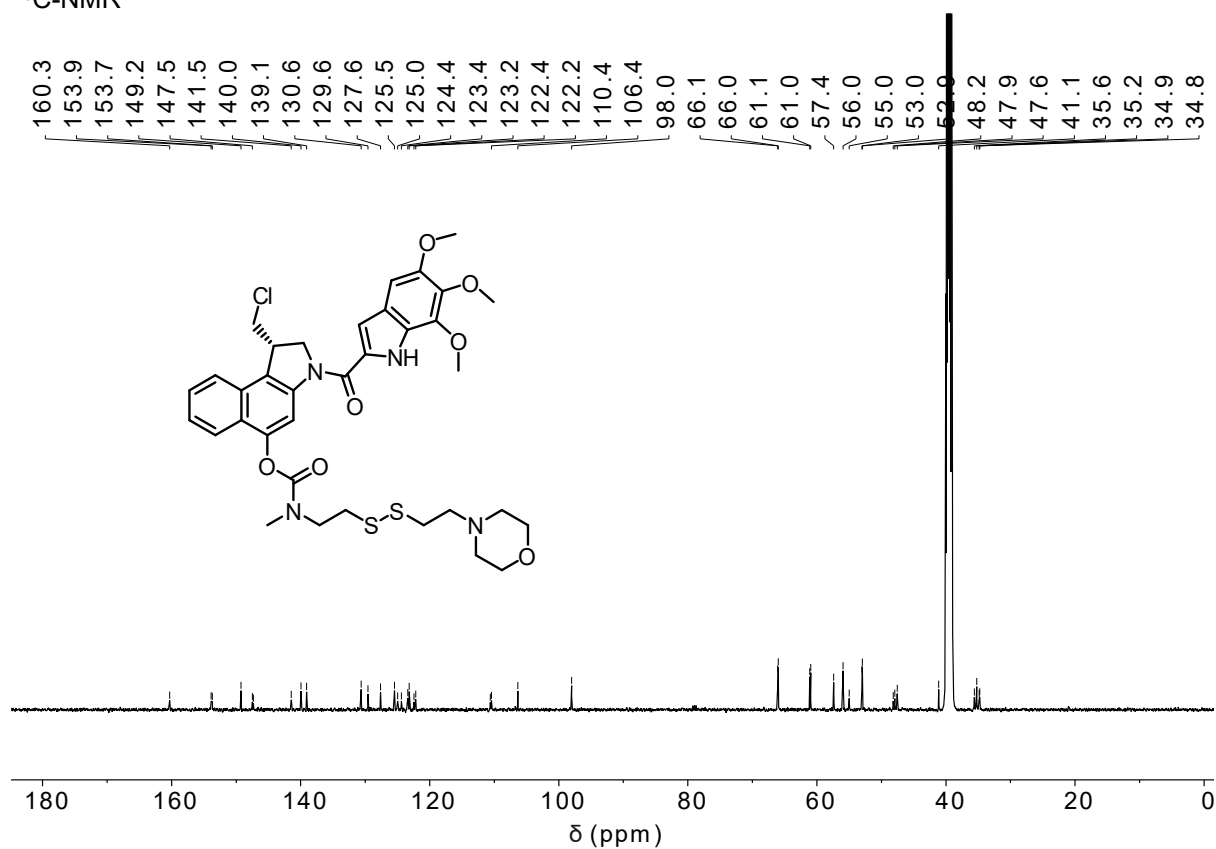
SS00_M-CBI-TMI¹H-NMR¹³C-NMR

Table S5. Crystallographic data. **BnO-CBI-Boc**

	1
net formula	C ₂₅ H ₂₆ ClNO ₃
<i>M_r</i> /g mol ⁻¹	423.92
crystal size/mm	0.080 × 0.050 × 0.030
<i>T</i> /K	102.(2)
radiation	MoKα
diffractometer	'Bruker D8 Venture TXS'
crystal system	orthorhombic
space group	'P 21 21 21'
<i>a</i> /Å	7.8910(4)
<i>b</i> /Å	12.8528(6)
<i>c</i> /Å	21.6817(11)
α/°	90
β/°	90
γ/°	90
<i>V</i> /Å ³	2198.99(19)
<i>Z</i>	4
calc. density/g cm ⁻³	1.280
μ/mm ⁻¹	0.200
absorption correction	Multi-Scan
transmission factor range	0.97–0.99
refls. measured	39132
<i>R</i> _{int}	0.0394
mean σ(<i>I</i>)/ <i>I</i>	0.0261
θ range	3.029–28.275
observed refls.	5214
<i>x</i> , <i>y</i> (weighting scheme)	0.0401, 0.5584
hydrogen refinement	constr
Flack parameter	0.012(15)
refls in refinement	5446
parameters	274
restraints	0
<i>R</i> (<i>F</i> _{obs})	0.0324
<i>R</i> _w (<i>F</i> ²)	0.0838
<i>S</i>	1.094
shift/error _{max}	0.001
max electron density/e Å ⁻³	0.248
min electron density/e Å ⁻³	-0.199

Anomalous dispersion effects (Flack test) applied in order to determine the correct structure.

11. Supporting References

- (1) Felber, J. G.; Zeisel, L.; Poczka, L.; Scholzen, K.; Busker, S.; Maier, M. S.; Theisen, U.; Brandstädter, C.; Becker, K.; Arnér, E. S. J.; Thorn-Seshold, J.; Thorn-Seshold, O. Selective, Modular Probes for Thioredoxins Enabled by Rational Tuning of a Unique Disulfide Structure Motif. *J. Am. Chem. Soc.* 2021, 143 (23), 8791–8803. <https://doi.org/10.1021/jacs.1c03234>.
- (2) Felber, J. G.; Poczka, L.; Scholzen, K. C.; Zeisel, L.; Maier, M. S.; Busker, S.; Theisen, U.; Brandstädter, C.; Becker, K.; Arnér, E. S. J.; Thorn-Seshold, J.; Thorn-Seshold, O. Cyclic 5-Membered Disulfides Are Not Selective Substrates of Thioredoxin Reductase, but Are Opened Nonspecifically. *Nat. Commun.* 2022, 13 (1), 1754. <https://doi.org/10.1038/s41467-022-29136-4>.
- (3) Zeisel, L.; Felber, J. G.; Scholzen, K. C.; Poczka, L.; Cheff, D.; Maier, M. S.; Cheng, Q.; Shen, M.; Hall, M. D.; Arnér, E. S. J.; Thorn-Seshold, J.; Thorn-Seshold, O. Selective Cellular Probes for Mammalian Thioredoxin Reductase TrxR1: Rational Design of RX1, a Modular 1,2-Thiaselenane Redox Probe. *Chem* 2022, 8 (5), 1493–1517. <https://doi.org/10.1016/j.chempr.2022.03.010>.
- (4) Zeisel, L.; Felber, J. G.; Scholzen, K. C.; Wiegand, A. J.; Schmitt, C.; Komissarov, L.; Arnér, E. S. J.; Thorn-Seshold, O. Bifunctional, piperazine-fused cyclic disulfides for oxidoreductase-activated cellular proagents. in preparation. 2022.
- (5) Mandal, P. K.; Schneider, M.; Kollé, P.; Kuhlencordt, P.; Forster, H.; Beck, H.; Bornkamm, G. W.; Conrad, M. Loss of Thioredoxin Reductase 1 Renders Tumors Highly Susceptible to Pharmacologic Glutathione Deprivation. *Cancer Res.* 2010, 70 (22), 9505–9514. <https://doi.org/10.1158/0008-5472.CAN-10-1509>.
- (6) Sheldrick, G. M. SHELXT – Integrated Space-Group and Crystal-Structure Determination. *Acta Crystallogr. Sect. Found. Adv.* 2015, 71 (1), 3–8. <https://doi.org/10.1107/S2053273314026370>.
- (7) Farrugia, L. J. WinGX and ORTEP for Windows: An Update. *J. Appl. Crystallogr.* 2012, 45 (4), 849–854. <https://doi.org/10.1107/S0021889812029111>.
- (8) Boger, D. L.; Ishizaki, T.; Kitos, P. A.; Suntornwat, O. Synthesis of N-(Tert-Butyloxycarbonyl)-CBI, CBI, CBI-CDPI1, and CBI-CDPI2: Enhanced Functional Analogs of CC-1065 Incorporating the 1,2,9,9a-Tetrahydrocyclopropa[c]Benz[e]Indol-4-One (CBI) Left-Hand Subunit. *J. Org. Chem.* 1990, 55 (23), 5823–5832. <https://doi.org/10.1021/jo00310a013>.
- (9) Boger, D. L.; Yun, W. CBI-TMI: Synthesis and Evaluation of a Key Analog of the Duocarmycins. Validation of a Direct Relationship between Chemical Solvolytic Stability and Cytotoxic Potency and Confirmation of the Structural Features Responsible for the Distinguishing Behavior of Enantiomeric Pairs of Agents. *J. Am. Chem. Soc.* 1994, 116 (18), 7996–8006. <https://doi.org/10.1021/ja00097a006>.
- (10) Tietze, L. F.; von Hof, J. M.; Krewer, B.; Müller, M.; Major, F.; Schuster, H. J.; Schuberth, I.; Alves, F. Asymmetric Synthesis and Biological Evaluation of Glycosidic Prodrugs for a Selective Cancer Therapy. *ChemMedChem* 2008, 3 (12), 1946–1955. <https://doi.org/10.1002/cmdc.200800250>.
- (11) Boger, D. L.; Ishizaki, T.; Zarrinmayeh, H.; Kitos, P. A.; Suntornwat, O. Synthesis and Preliminary Evaluation of Agents Incorporating the Pharmacophore of the Duocarmycin/Pyrindamycin Alkylation Subunit: Identification of the CC-1065/Duocarmycin Common Pharmacophore. *J. Org. Chem.* 1990, 55 (15), 4499–4502. <https://doi.org/10.1021/jo00302a002>.
- (12) Zeisel, L.; Maier, M. S.; Thorn-Seshold, O. Regioselective, Efficient and Scalable Syntheses of 1,2-Thiaselenanes. *ChemRxiv* 2022. <https://doi.org/10.26434/chemrxiv-2022-99slz>.
- (13) Thorn-Seshold, O.; Felber, J.; Thorn-Seshold, J.; Zeisel, L. Disulfide-Based Prodrug Compounds. *WO* 2022/200347, 2021.
- (14) Frecentese, F.; Fiorino, F.; Perissutti, E.; Severino, B.; Magli, E.; Esposito, A.; De Angelis, F.; Massarelli, P.; Nencini, C.; Viti, B.; Santagada, V.; Caliendo, G. Efficient Microwave Combinatorial Synthesis of Novel Indolic Arylpiperazine Derivatives as Serotonergic Ligands. *Eur. J. Med. Chem.* 2010, 45 (2), 752–759. <https://doi.org/10.1016/j.ejmech.2009.11.023>.

9.2 Additional experimental sections

9.2.1 Experimental Part for chapter 5.2.2: Chemical proteomics probes for cysteine profiling

A. Proteomics platform: Cysteine site of labeling

Cell culture. Cells were grown in Dulbecco's modified Eagle's medium (DMEM) supplemented with glutamine, 10% heat-inactivated fetal bovine serum (FBS), streptomycin (100 U/mL), and penicillin (100 U/mL) at 37 °C under 5% CO₂ atmosphere and were monitored using an Olympus CK2 light microscope. HEK293T cells were grown to 80-90% confluency, then the cell medium was removed, and 0.25 % Trypsin was added. After 3-5 min incubation at r.t, fresh DMEM was added, and the cells were suspended and replated in a fresh DMEM medium.

Cellular treatment. HEK293T cells (3 million cells in 10 mL DMEM) were seeded 15 h prior to use, and experiments were performed at ca. 80% confluency. Cells were treated with a competitor (**CJF252-CJF260** from 50 mM DMSO stock solutions) at final concentrations of 50 μM at 0.1% DMSO content and incubated at 37 °C for 3 h. The medium was taken off, 0.25 % Trypsin was added (0.5 mL per well, 1 mL per dish), after 3-5 min of incubation at r.t. the equal amount of fresh DMEM was added, and the cell suspension was transferred to 1.5 mL Eppendorf tubes. The cells were centrifuged at 500 × g for 5 min, the supernatant was taken off, and the cells were resuspended 2 × in cold Dulbecco's. After centrifugation at 500 × g for 5 min, the supernatant was taken off, and the cell palette was shock-frozen in liquid nitrogen and stored at -80 °C for further use.

Protein labeling. To the cell palette, 550 μL of cold PBS was added, and cell lysis was achieved by sonication (2 × 8 pulses). Total protein quantification was performed using Pierce™ BCA protein assay kit from Thermo Scientific, and samples were normalized by dilution with PBS to a final concentration of 1,250 μg/mL in 500 μL. To the cell lysates iodoacetamide-PEG₃-desthiobiotin (5 μL of a 10 mM DMSO solution, purchased from WuXi Biology) was added, the samples were shaken vigorously and incubated for 1 h at r.t. Protein precipitation was observed. 600 μL of MeOH, 100 μL of CHCl₃ and 100 μL of MQ-water were added, and the samples were vortexed and centrifuged at 16,000 × g at 4 °C for 15 min. A protein disk was observed at the interphase, and the liquid layers were discarded. 600 μL of MeOH was added, the samples were mixed, centrifuged at 16,000 × g at 4 °C for 15 min, and the liquid layer was discarded. The protein palette was air-dried for 15 h and stored at -80 °C.

Peptide enrichment and TMT labeling. The protein palette was resuspended in 90 μL of a reduction buffer (9 M urea, 10 mM 1,4-dithiothreitol (DTT), 50 mM tetramethylammonium bicarbonate (TEAB)) at pH 8.5, and the mixture was shaken at 65 °C for 20 min. At r.t., the samples were treated with 10 μL of iodoacetamide (500 mM in MQ-water), shaken at 37 °C for 30 min, and then diluted with 300 μL 50 mM TEAB. To each sample, 4 μL of trypsin (1 μg modified trypsin purchased from Promega Corp, resuspended in 3 μL of trypsin resuspension buffer and 1 μL of 100 mM CaCl₂) were added, and the samples were incubated under shaking at 37 °C for 15 h. 50 μL of streptavidin agarose beads (50% aq. slurry purchased from Thermo Scientific) were washed with a wash buffer (50 mM TEAB, 150 mM NaCl, 0.2% IGEPAL® CA-630 (NP-40) purchased from Sigma Aldrich), resuspended in 300 μL of that wash buffer and then added to the samples. The samples were rotated at 37 °C for 2 h, then filtered on a Micro Bio-Spin™ column (purchased from BioRad Laboratories), and the beads were washed with 3 × 1 mL of a second wash buffer (50 mM TEAB, 150 mM NaCl, 0.1% NP-40), 3 × 1 mL of PBS and 3 × 1 mL of MQ-water. The peptides were eluted by the addition of 300 μL of an elution buffer (50% MeCN, 50% MQ-water, 0.1% formic acid, purchased from Fisher Scientific) and concentrated to dryness using a Speedvac SPD2030 from Thermo Scientific. The samples were resuspended in 70 μL 200 mM of (4-(2-hydroxyethyl)-1-piperazine propanesulfonic acid (EPPS) at pH 8, in MQ-water) and 30 μL MeCN, mixed and incubated at 37 °C for 15 min. 3 μL of the corresponding TMT tag (solution in MeCN; TMT10plex™ isobaric label reagent purchased from ThermoFisher) were added, and the samples were mixed and incubated at r.t. for 75 min. Then, 5 μL of 50 % hydroxylamine in H₂O were added, and the samples were incubated at r.t. for a further 15 min. 5 μL of formic acid was added, and all samples of one 10-plex were combined and concentrated using a Speedvac SPD2030.

Peptide fractionation The dry sample was resuspended in 0.5 mL of buffer A (95% H₂O, 5% MeCN, 0.1% FA), and 40 μL of formic acid was added. The sample was sonicated in a water bath for 5 min. Acidic pH (pH < 3) was tested using pH paper. For de-salting the sample, a SepPak® C18 column from Waters, pre-conditioned with 100% MeCN and equilibrated with 3 × 1 mL buffer A was used. Then, the sample was added dropwise (1 drop/sec), and the flow-through was reloaded dropwise. The column was washed with 3 × 1 mL buffer A, and the peptides were eluted with 1 mL buffer B (80% MeCN, 20% H₂O, 0.1% FA) and concentrated using the Speedvac SPD2030. The dry sample was resuspended in 0.5 mL of buffer A and sonicated in a water bath for 5 min. A preparative HPLC system was used for fractionation. The C18 column was conditioned with 80% MeCN, 20% aq. 10 mM (NH₄)₂CO₃ for 15 min, then equilibrated in 100% aq. 10 mM (NH₄)₂CO₃, and the sample was injected. A gradient from 100% aq. 10 mM (NH₄)₂CO₃ to 80% MeCN, 20% aq. 10 mM (NH₄)₂CO₃ was applied over 115 min total run time, and 96 fractions were collected in a 96-well plate pre-treated with 20 μL of 20% FA, 80% H₂O in each well. The fractions on the plates were concentrated using the Speedvac SPD2030. Using a 12-channel multi pipette, 100 μL of buffer B was added to the first row of the 96-well plates, and wells of one column (e.g. wells 1,13,25,37,49,61,73,85) were subsequently washed. The procedure was repeated three times to combine the fractions in a final volume of 300 μL. The fractions were concentrated and directly used for mass analysis.

B. Synthesis**(*cis*)-1,4-bis((2-nitrophenyl)sulfonyl)decahydroquinoxaline (CJF263)**

Step 1: (*Cis*)-1,2-diaminocyclohexane (1.0 mL, 8.34 mmol, 1.0 eq.) was dissolved in pyridine (0.2 M, 45 mL) and cooled to 0 °C. The colorless suspension was charged with *o*-NsCl (4.62 g, 20.8 mmol, 2.5 eq.), and the bright yellow solution was stirred for 16 h. The reaction mixture was poured onto ice-cold water (200 mL), and the bright orange precipitates were collected by filtration. The residue was washed with water and Et₂O, subsequently giving (*cis*)-*N,N'*-(cyclohexane-1,2-diyl)bis(2-nitrobenzenesulfonamide) as an orange solid (5.15 g crude mixture).

Step 2: The material obtained in step 1 was dissolved in anhydrous DCM (0.05 M, 170 mL) and reacted with DIPEA (4.0 mL, 29 mmol, 3.5 eq.) and 5-vinyl-5*H*-thianthren-5-ium tetrafluoroborate (1.6 g, 11.7 mmol, 1.4 eq.). Aqueous workup of the dark red reaction mixture and purification by FCC (isohexane/DCM 1:1 → DCM) gave the title compound a yellow solid (3.35 g, 6.6 mmol, 79%).

HRMS (ESI): C₂₁H₂₃N₄O₁₀S₂: [M+HCO₂]⁺ calc. 555.08611, found 555.08652. **¹H-NMR** (500 MHz, CD₂Cl₂): δ (ppm) = 7.98 (dd, *J* = 7.6, 1.6 Hz, 2H), 7.78 – 7.68 (m, 4H), 7.65 (dd, *J* = 7.5, 1.6 Hz, 2H), 3.72 – 3.60 (m, 4H), 3.35 – 3.26 (m, 2H), 2.33 (dt, *J* = 13.9, 6.3 Hz, 2H), 1.51 (dq, *J* = 11.4, 3.9 Hz, 2H), 1.32 (dtd, *J* = 16.6, 9.5, 4.0 Hz, 4H). **¹³C-NMR** (126 MHz, CD₂Cl₂): δ (ppm) = 148.6 (C_{Ar}), 134.7 (C_{Ar}H), 133.0 (C_{Ar}), 132.6 (C_{Ar}H), 130.9 (C_{Ar}H), 125.0 (C_{Ar}H), 58.2 (CH), 44.8 (CH₂), 28.4 (CH₂), 22.9 (CH₂).

Step 3: The material obtained in step 2 (3.30 g, 6.5 mmol) was reacted with NaOMe (5.4 M in THF, 3.04 mL, 16.4 mmol, 2.5 eq.) in THF (0.05 M, 130 mL). Upon full deprotection, precipitation from the reaction mixture was achieved using HCl (4 M in dioxane, 8.2 mL, 32.8 mmol, 5.0 eq.). The precipitate was isolated by filtration, giving (*cis*)-decahydroquinoxaline dihydrochloride (·2.5 NaCl, 52% purity) as a colorless solid (1.85 g, 2.57 mmol, 78%). The material was used for coupling reaction without further purification or characterization.

***tert*-butyl (*cis*)-4-acryloyloctahydroquinoxaline-1(2*H*)-carboxylate (CJF 257)**

(*cis*)-decahydroquinoxaline dihydrochloride (·2.5 NaCl, 52% purity) (1.25 g, 3.5 mmol) was suspended in anhydrous DCM (0.04 M, 90 mL) and NEt₃ (1.2 mL, 8.73 mmol, 2.5 eq.) was added. The suspension did not fully dissolve. At 0 °C a solution of Boc₂O (762 mg, 3.5 mmol, 1.0 eq.) in anhydrous DCM was added dropwise, and the solution was stirred for 30 min, was then warmed to r.t. and further stirred for 2 h. A solution of acryloyl chloride (425 μL, 5.25 mmol, 1.5 eq.) was added dropwise, and the solution was further stirred for 30 min before being concentrated. Purification was achieved using FCC (isohexane/EtOAc) to give the title compound as a colorless solid (86 mg, 0.29 mmol, 8%). As a side product di-*tert*-butyl (*cis*)-octahydroquinoxaline-1,4-dicarboxylate was obtained as a colorless solid (440 mg, 1.19 mmol, 34%).

TLC R_f = 0.53 (isohexane:EtOAc; 1:1). **¹H-NMR** (400 MHz, CDCl₃): δ (ppm) = 6.50 (dd, *J* = 16.7, 10.3 Hz, 1H), 6.34 (dd, *J* = 16.7, 2.1 Hz, 1H), 5.70 (dd, *J* = 10.3, 2.1 Hz, 1H), 4.30 – 4.18 (m, 1H), 3.98 (q, *J* = 5.6 Hz, 1H), 3.95 – 3.87 (m, 1H), 3.83 (ddd, *J* = 14.5, 8.9, 5.4 Hz, 1H), 3.59 (dddd, *J* = 19.5, 12.4, 8.0, 4.0 Hz, 2H), 2.21 (dd, *J* = 13.6, 4.1 Hz, 1H), 2.00 – 1.85 (m, 1H), 1.83 – 1.67 (m, 2H), 1.65 – 1.54 (m, 2H), 1.46 (s, 9H), 1.46 – 1.39 (m, 2H). **¹³C-NMR** (101 MHz, CDCl₃): δ (ppm) = 166.3 (C=O), 155.5 (C=O), 128.4 (C=CH₂), 128.0 (C=CH-), 80.3 (C(CH₃)₃), 52.0 (CH), 51.3 (CH), 42.4 (CH₂), 41.1 (CH₂), 30.8 (CH₂), 29.8 (CH₂), 28.6 (C(CH₃)₃), 23.4 (CH₂), 21.6 (CH₂).

Di-*tert*-butyl (*cis*)-octahydroquinoxaline-1,4-dicarboxylate (CJF262): **TLC** R_f = 0.66 (isohexane:EtOAc; 6:1). **¹H-NMR** (400 MHz, CDCl₃): δ (ppm) = 3.93 (p, *J* = 5.2 Hz, 2H), 3.77 – 3.65 (m, 2H), 3.54 – 3.39 (m, 2H), 2.03 (ddt, *J* = 10.5, 7.0, 3.5 Hz, 2H), 1.61 (ddd, *J* = 13.2, 7.5, 3.6 Hz, 2H), 1.50 (dt, *J* = 10.0, 4.0 Hz, 2H), 1.45 (s, 18H), 1.36 (dtd, *J* = 15.1, 8.1, 3.4 Hz, 2H). **¹³C-NMR** (101 MHz, CDCl₃): δ (ppm) = 155.5 (C=O), 80.0 (C(CH₃)₃), 52.2 (CH), 41.7 (CH₂), 30.6 (CH₂), 28.6 (CH₂), 22.7 (CH₂).

(*cis*)-decahydroquinoxaline dihydrochloride (CJF262)

Di-*tert*-butyl (*cis*)-octahydroquinoxaline-1,4-dicarboxylate (400 mg, 1.17 mmol) was dissolved in anhydrous DCM (0.1 M, 15 mL) and HCl (4 M in dioxane, 1.76 mL, 6.0 eq) was added dropwise at r.t. The solution was stirred for 15 h, and a solid precipitate was observed. Et₂O (30 mL) was added, and the mixture was filtered, washed with Et₂O (10 mL), and the solid was dried under reduced pressure to obtain the title compound as a colorless solid (186 mg, 0.87 mmol, 75%).

¹H-NMR (400 MHz, DMSO-*d*₆): δ (ppm) = 10.21 (s, 1H), 9.81 (s, 1H), 3.77 – 3.55 (m, 2H), 3.29 (s, 4H), 2.09 (s, 2H), 1.86 – 1.64 (m, 4H), 1.40 (s, 2H).

General protocol

(*cis*)-decahydroquinoxaline dihydrochloride (CJF262) ($\cdot 2.5$ NaCl, 52% purity) (1.0 eq.) was suspended in anhydrous DCM (0.015 M) and NEt_3 (3.0 eq.) was added. A solution of a benzoyl chloride/sulfonyl chloride (1.1 eq.) in anhydrous DCM was added dropwise, and the solution was stirred for 1 h before a solution of acryloyl chloride (2.0 eq.) was added dropwise, and the solution was further stirred for 30 min, before being concentrated. Purification was achieved using preparative TLC to give the title compounds.

1-((*cis*)-4-(4-methoxybenzoyl)octahydroquinoxalin-1(2H)-yl)prop-2-en-1-one (CJF 255)

Prepared according to the general protocol using CJF262 (35 mg, 0.047 mmol), NEt_3 (25 μL , 0.141 mmol), 4-methoxybenzoyl chloride (8.8 mg, 0.052 mmol), acryloyl chloride (8 μL , 0.10 mmol). Purification by preparative TLC (EtOAc) gave the title compound as a colorless oil (11.1 mg, 0.034 mmol, 72%).

TLC R_f = 0.38 (EtOAc). **HRMS** (ESI): $\text{C}_{19}\text{H}_{25}\text{N}_2\text{O}_3^+$: $[\text{M}+\text{H}]^+$ calc. 329.1865, found 329.1861. **$^1\text{H-NMR}$** (500 MHz, CDCl_3): δ (ppm) = 7.47 (d, J = 8.8 Hz, 2H), 6.92 (d, J = 8.8 Hz, 2H), 6.50 (dd, J = 16.7, 10.3 Hz, 1H), 6.37 (dd, J = 16.7, 2.0 Hz, 1H), 5.72 (dd, J = 10.3, 2.0 Hz, 1H), 4.33 (q, J = 4.7 Hz, 1H), 4.31 – 4.21 (m, 1H), 3.87 – 3.81 (m, 5H), 3.76 – 3.62 (m, 2H), 2.58 – 2.49 (m, 1H), 2.00 – 1.91 (m, 1H), 1.85 (qd, J = 10.6, 5.5 Hz, 1H), 1.76 – 1.68 (m, 1H), 1.65 (s, 1H), 1.57 – 1.39 (m, 4H). **$^{13}\text{C-NMR}$** (126 MHz, CDCl_3): δ (ppm) = 173.4 (C=O), 165.9 (C=O), 161.5 (C_{Ar}), 129.8 (C_{ArH}), 128.7 (C=CH₂), 127.4 (C=CH-), 114.0 (C_{ArH}), 55.5 (CH₃), 52.9 (CH), 52.2 (CH), 45.1 (CH₂), 42.8 (CH₂), 32.3 (CH₂), 29.1 (CH₂), 23.9 (CH₂), 21.3 (CH₂).

1-((*cis*)-4-(4-(dimethylamino)benzoyl)octahydroquinoxalin-1(2H)-yl)prop-2-en-1-one (CJF 259)

Prepared according to the general protocol using CJF262 (39 mg, 0.052 mmol), NEt_3 (28 μL , 0.157 mmol), *N,N*-dimethyl 4-aminobenzoyl chloride (10.5 mg, 0.058 mmol), acryloyl chloride (10.5 mg, 0.058 mmol). Purification by preparative TLC (EtOAc) gave the title compound as a colorless oil (4.2 mg, 0.012 mmol, 24%).

TLC R_f = 0.42 (EtOAc). **HRMS** (ESI): $\text{C}_{20}\text{H}_{28}\text{N}_3\text{O}_2^+$: $[\text{M}+\text{H}]^+$ calc. 342.2182, found 342.2177. **$^1\text{H-NMR}$** (500 MHz, CDCl_3): δ (ppm) = 7.48 – 7.44 (m, 2H), 6.67 (d, J = 8.9 Hz, 2H), 6.50 (dd, J = 16.7, 10.3 Hz, 1H), 6.37 (dd, J = 16.7, 2.1 Hz, 1H), 5.72 (dd, J = 10.3, 2.1 Hz, 1H), 4.34 (t, J = 4.0 Hz, 1H), 4.23 (s, 1H), 3.89 (dd, J = 5.9, 3.3 Hz, 2H), 3.72 (dt, J = 13.2, 3.9 Hz, 1H), 3.61 (ddd, J = 13.3, 9.0, 6.5 Hz, 1H), 3.01 (s, 6H), 2.61 (d, J = 12.9 Hz, 1H), 1.98 (d, J = 12.9 Hz, 1H), 1.88 – 1.78 (m, 1H), 1.74 (d, J = 10.2 Hz, 1H), 1.52 – 1.38 (m, 4H). **$^{13}\text{C-NMR}$** (126 MHz, CDCl_3): δ (ppm) = 174.0 (C=O), 165.8 (C=O), 152.2 (C_{Ar}), 130.0 (C_{ArH}), 128.6 (C=CH₂), 127.5 (C=CH-), 122.7 (C_{Ar}), 111.3 (C_{ArH}), 52.8 (CH), 52.0 (CH), 48.8 (CH₂), 45.7 (CH₃), 40.3 (CH₂), 29.0 (CH₂), 24.3 (CH₂), 21.1 (CH₂).

1-((*cis*)-4-(3-fluoro-4-(trifluoromethyl)benzoyl)octahydroquinoxalin-1(2H)-yl)prop-2-en-1-one (CJF 258)

Prepared according to the general protocol using CJF262 (40 mg, 0.054 mmol), NEt_3 (28 μL , 0.161 mmol), 3-fluoro-4-(trifluoromethyl)benzoyl chloride (13.3 mg, 0.059 mmol), acryloyl chloride (9 μL , 0.11 mmol). Purification by preparative TLC (isohexane/EtOAc) gave the title compound as a colorless oil (9.0 mg, 0.023 mmol, 44%).

TLC R_f = 0.57 (EtOAc). **HRMS** (ESI): $\text{C}_{19}\text{H}_{21}\text{F}_4\text{N}_2\text{O}_2^+$: $[\text{M}+\text{H}]^+$ calc. 385.1539, found 385.1534. **$^1\text{H-NMR}$** (500 MHz, CDCl_3): δ (ppm) = 7.69 (t, J = 7.5 Hz, 1H), 7.36 – 7.28 (m, 2H), 6.56 – 6.47 (m, 1H), 6.38 (dd, J = 16.7, 2.0 Hz, 1H), 5.75 (dd, J = 10.3, 2.0 Hz, 1H), 4.28 (d, J = 4.3 Hz, 2H), 3.86 – 3.68 (m, 4H), 2.43 (d, J = 11.5 Hz, 1H), 1.90 (d, J = 4.7 Hz, 2H), 1.69 (d, J = 4.5 Hz, 1H), 1.64 – 1.60 (m, 1H), 1.56 – 1.40 (m, 3H). **$^{13}\text{C-NMR}$** (126 MHz, CDCl_3): δ (ppm) = 169.7 (C=O), 166.1 (C=O), 142.2 (C_{Ar}), 129.1 (C=CH₂), 128.0 (C_{ArH}), 127.4 (C=CH-), 123.1 (C_{ArH}), 120.3 (C_{Ar}), 116.24 (d, J = 22.0 Hz, C_{ArH}), 52.5 (CH), 51.9 (CH), 44.4 (CH₂), 42.3 (CH₂), 31.6 (CH₂), 29.3 (CH₂), 23.3 (CH₂), 21.6 (CH₂). **$^{19}\text{F-NMR}$** (376 MHz, CDCl_3) δ (ppm) = -64.3 (d, J = 12.1 Hz), -114.9 (q, J = 12.6 Hz).

1-((*cis*)-4-(2-(3,5-bis(trifluoromethyl)phenyl)acetyl)octahydroquinoxalin-1(2H)-yl)prop-2-en-1-one (CJF 254)

Prepared according to the general protocol using CJF262 (37 mg, 0.050 mmol), NEt_3 (26 μL , 0.149 mmol), 2-(3,5-bis(trifluoromethyl)phenyl)acetyl chloride (15.8 mg, 0.055 mmol), acryloyl chloride (8 μL , 0.10 mmol). Purification by preparative TLC (EtOAc) gave the title compound as a colorless oil (2.7 mg, 0.006 mmol, 12%).

TLC R_f = 0.25 (isohexane;EtOAc, 1:1). **HRMS** (ESI): $\text{C}_{21}\text{H}_{23}\text{F}_6\text{N}_2\text{O}_2^+$: $[\text{M}+\text{H}]^+$ calc. 449.1664, found 449.1658. **$^1\text{H-NMR}$** (500 MHz, CDCl_3): δ (ppm) = 7.79 (s, 1H), 7.71 (s, 2H), 6.49 (dd, J = 16.8, 10.3 Hz, 1H), 6.36 (dd, J = 16.8, 2.0 Hz, 1H), 5.74 (dd, J = 10.3, 2.0 Hz, 1H), 4.29 (d, J = 4.8 Hz, 1H), 4.13 (dd, J = 11.9, 6.4 Hz, 1H), 3.88 – 3.75 (m, 3H), 3.69 (ddt, J = 17.0, 11.7, 5.8 Hz, 2H), 2.16 (s, 1H), 1.96 (dt, J = 13.6, 7.0 Hz, 1H), 1.85 – 1.77 (m, 1H), 1.74 – 1.59 (m, 2H), 1.52 – 1.41 (m, 3H). **$^{13}\text{C-NMR}$** (126 MHz, CDCl_3): δ (ppm) = 177.4 (C=O), 169.4 (C=O), 137.0 (C_{Ar}), 132.4 (C_{Ar}), 130.0 (C_{ArH}), 128.9 (C=CH₂), 127.9 (C=CH-), 120.8 (C_{ArH}), 50.9 (CH), 42.4 (CH₂), 40.1 (CH₂), 30.6 (CH₂), 22.6 (CH₂), 21.5 (CH₂). **$^{19}\text{F-NMR}$** (376 MHz, CDCl_3) δ (ppm) = -65.5.

5-((*cis*)-4-acryloyloctahydroquinoxalin-1(2*H*)-yl)-5-oxopentanoic acid (CJF 256)

Prepared according to the general protocol using CJF262 (40 mg, 0.054 mmol), NEt₃ (28 μ L, 0.161 mmol), glutaric anhydride (6.7 mg, 0.059 mmol), acryloyl chloride (9 μ L, 0.11 mmol). Purification by preparative TLC (EtOAc) gave the title compound as a colorless oil (3.5 mg, 0.011 mmol, 21%).

TLC R_f = 0.20 (EtOAc, 5% formic acid). **HRMS** (ESI): C₁₆H₂₃N₂O₄: [M+H]⁺ calc. 309.1814, found 309.1815. **¹H-NMR** (500 MHz, CDCl₃): δ (ppm) = 6.50 (dd, J = 16.8, 10.4 Hz, 1H), 6.35 (dd, J = 16.8, 1.9 Hz, 1H), 5.73 (dd, J = 10.4, 1.9 Hz, 1H), 4.27 (s, 2H), 4.16 – 4.02 (m, 1H), 3.79 (s, 1H), 3.74 – 3.65 (m, 1H), 3.65 – 3.57 (m, 1H), 2.50 – 2.35 (m, 4H), 2.15 (s, 1H), 1.98 (p, J = 7.1 Hz, 2H), 1.92 (d, J = 9.0 Hz, 1H), 1.80 (s, 1H), 1.72 – 1.56 (m, 2H), 1.53 – 1.37 (m, 3H). **¹³C-NMR** (126 MHz, CDCl₃): δ (ppm) = 176.5 (C=O), 172.2 (C=O), 167.1 (C=O), 129.3 (C=CH₂), 128.6 (C=CH-), 51.9 (CH), 41.4 (CH₂), 33.1 (CH₂), 32.3 (CH₂), 22.7 (CH₂), 21.8 (CH₂), 20.2 (CH₂).

1-((*cis*)-4-(dibenzo[*b,d*]furan-2-ylsulfonyl)octahydroquinoxalin-1(2*H*)-yl)prop-2-en-1-one (CJF 252)

Prepared according to the general protocol using CJF262 (7.5 mg, 0.010 mmol), NEt₃ (6 μ L, 0.032 mmol), dibenzo[*b,d*]furan-2-sulfonyl chloride (3.0 mg, 0.011 mmol), acryloyl chloride (2 μ L, 0.020 mmol). Purification by preparative TLC (EtOAc) gave the title compound as a colorless oil (3.6 mg, 0.008 mmol, 78%).

TLC R_f = 0.51 (isohexane:EtOAc, 1:1). **HRMS** (ESI): C₂₃H₂₅N₂O₄S⁺: [M+H]⁺ calc. 425.1535, found 425.1536. **¹H-NMR** (500 MHz, CDCl₃): δ (ppm) = 8.39 (dd, J = 2.0, 0.5 Hz, 1H), 8.01 (ddd, J = 7.7, 1.3, 0.6 Hz, 1H), 7.87 (dd, J = 8.7, 2.0 Hz, 1H), 7.71 (dd, J = 8.7, 0.5 Hz, 1H), 7.64 (dt, J = 8.3, 0.8 Hz, 1H), 7.56 (ddd, J = 8.4, 7.3, 1.3 Hz, 1H), 7.44 (td, J = 7.7, 1.0 Hz, 1H), 6.38 (dd, J = 16.8, 10.5 Hz, 1H), 6.19 (dd, J = 16.8, 1.8 Hz, 1H), 5.63 (dd, J = 10.5, 1.8 Hz, 1H), 4.04 (dt, J = 12.0, 3.5 Hz, 1H), 3.46 – 3.36 (m, 1H), 2.97 – 2.82 (m, 2H), 2.77 – 2.60 (m, 1H), 2.26 – 2.09 (m, 1H), 1.94 – 1.78 (m, 2H), 1.58 – 1.38 (m, 4H). **¹³C-NMR** (128 MHz, CDCl₃): δ (ppm) = 165.1 (C=O), 158.4 (C_{Ar}), 157.2 (C_{Ar}), 130.8 (C_{Ar}), 128.9 (C_{Ar}H), 128.7 (C=CH₂), 127.2 (C=CH-), 126.7 (C_{Ar}H), 125.3 (C_{Ar}), 123.9 (C_{Ar}H), 121.4 (C_{Ar}H), 121.3 (C_{Ar}H), 112.6 (C_{Ar}H), 112.3 (C_{Ar}H), 57.8 (CH), 48.6 (CH₂), 31.2 (CH₂), 26.3 (CH₂), 25.2 (CH₂), 20.3 (CH₂).

1-((*cis*)-4-((5-chloro-3-methylbenzo[*b*]thiophen-2-yl)sulfonyl)octahydroquinoxalin-1(2*H*)-yl)prop-2-en-1-one (CJF 253)

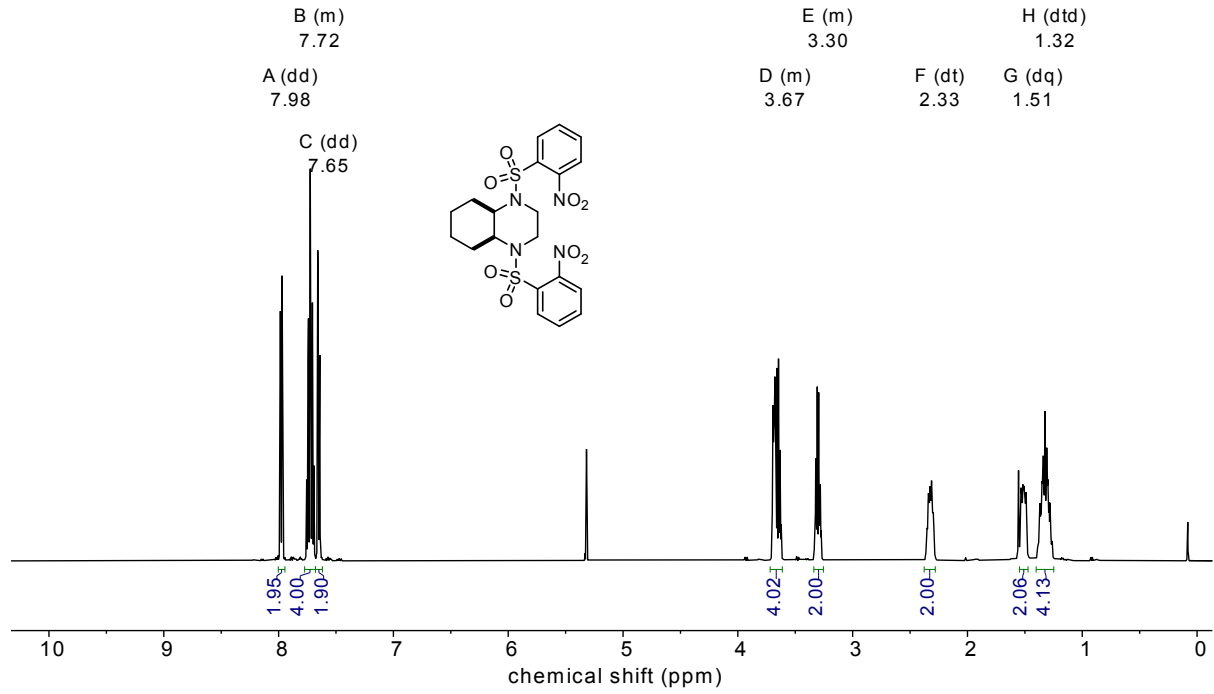
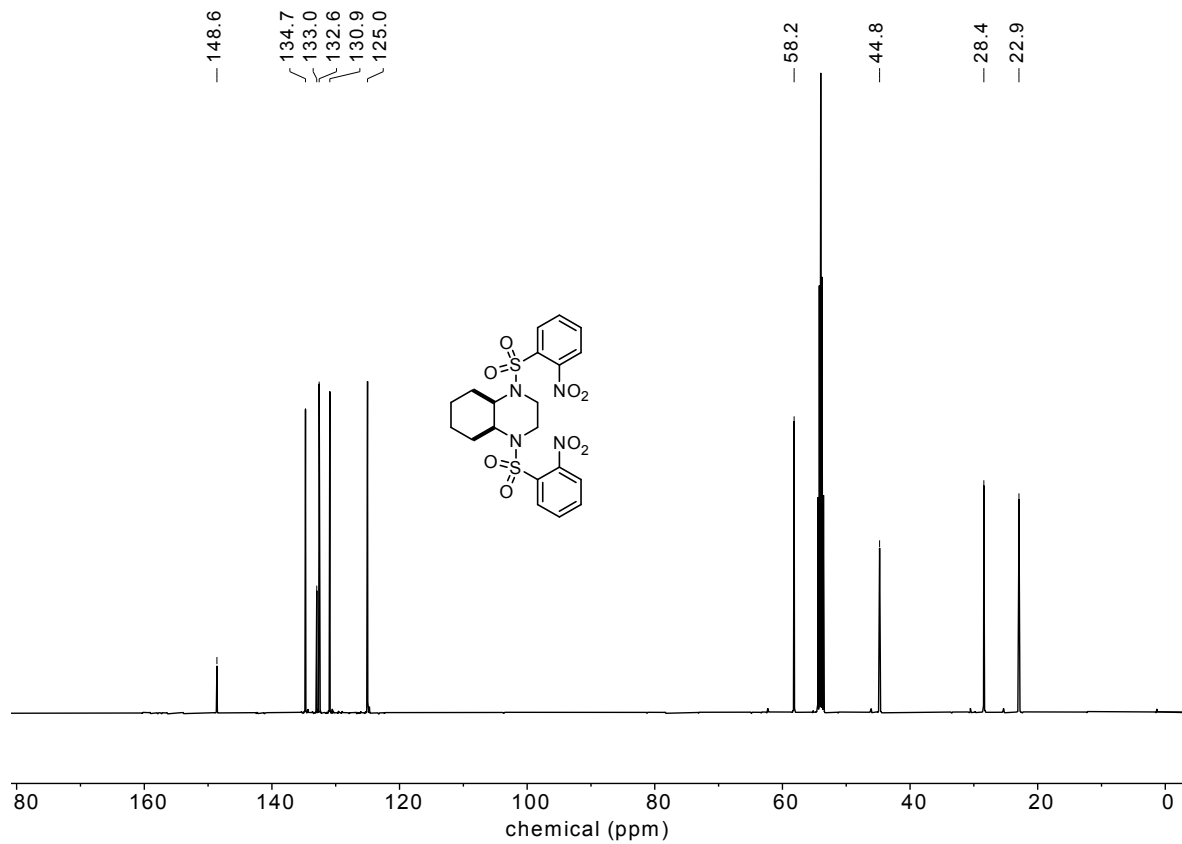
Prepared according to the general protocol using CJF262 (15 mg, 0.020 mmol), NEt₃ (11 μ L, 0.064 mmol), 5-chloro-3-methylbenzo[*b*]thiophene-2-sulfonyl chloride (6.6 mg, 0.023 mmol), acryloyl chloride (4 μ L, 0.040 mmol). Purification by preparative TLC (EtOAc) gave the title compound as a colorless oil (7.4 mg, 0.008 mmol, 80%).

TLC R_f = 0.58 (isohexane:EtOAc, 1:1). **HRMS** (ESI): C₂₀H₂₄ClN₂O₃S₂⁺: [M+H]⁺ calc. 439.0917, found 439.0910. **¹H-NMR** (500 MHz, CDCl₃): δ (ppm) = 7.81 (d, J = 1.9 Hz, 1H), 7.75 (d, J = 8.6 Hz, 1H), 7.47 (dd, J = 8.6, 2.0 Hz, 1H), 6.40 (dd, J = 16.8, 10.5 Hz, 1H), 6.23 (dd, J = 16.8, 1.8 Hz, 1H), 5.65 (dd, J = 10.5, 1.9 Hz, 1H), 4.25 – 3.99 (m, 1H), 3.96 (dt, J = 12.3, 3.5 Hz, 1H), 3.43 (t, J = 10.3 Hz, 1H), 3.36 – 3.30 (m, 1H), 3.04 – 2.93 (m, 1H), 2.84 (d, J = 12.8 Hz, 1H), 2.70 (s, 3H), 2.13 – 1.99 (m, 1H), 1.87 – 1.80 (m, 1H), 1.75 – 1.64 (m, 1H), 1.61 – 1.40 (m, 4H). **¹³C-NMR** (128 MHz, CDCl₃): δ (ppm) = 165.3 (C=O), 140.7 (C_{Ar}), 137.7 (C_{Ar}), 137.3 (C_{Ar}), 131.9 (C_{Ar}), 128.8 (C=CH₂), 128.3 (C_{Ar}H), 127.1 (C=CH-), 123.8 (C_{Ar}H), 123.7 (C_{Ar}H), 57.8 (CH), 47.4 (CH₂), 31.0 (CH₂), 24.9 (CH₂), 20.3 (CH₂), 13.1 (CH₃).

1-((*cis*)-4-((5-methyl-3-(trifluoromethyl)furan-2-yl)sulfonyl)octahydroquinoxalin-1(2*H*)-yl)prop-2-en-1-one (CJF 260)

Prepared according to the general protocol using CJF262 (21.3 mg, 0.10 mmol), NEt₃ (42 μ L, 0.30 mmol), 5-methyl-3-(trifluoromethyl)furan-2-sulfonyl chloride (24.9 mg, 0.10 mmol), acryloyl chloride (16 μ L, 0.20 mmol). Purification by preparative TLC (isohexane/EtOAc) gave CJF260 as a colorless oil (12.0 mg, 0.03 mmol, 30%).

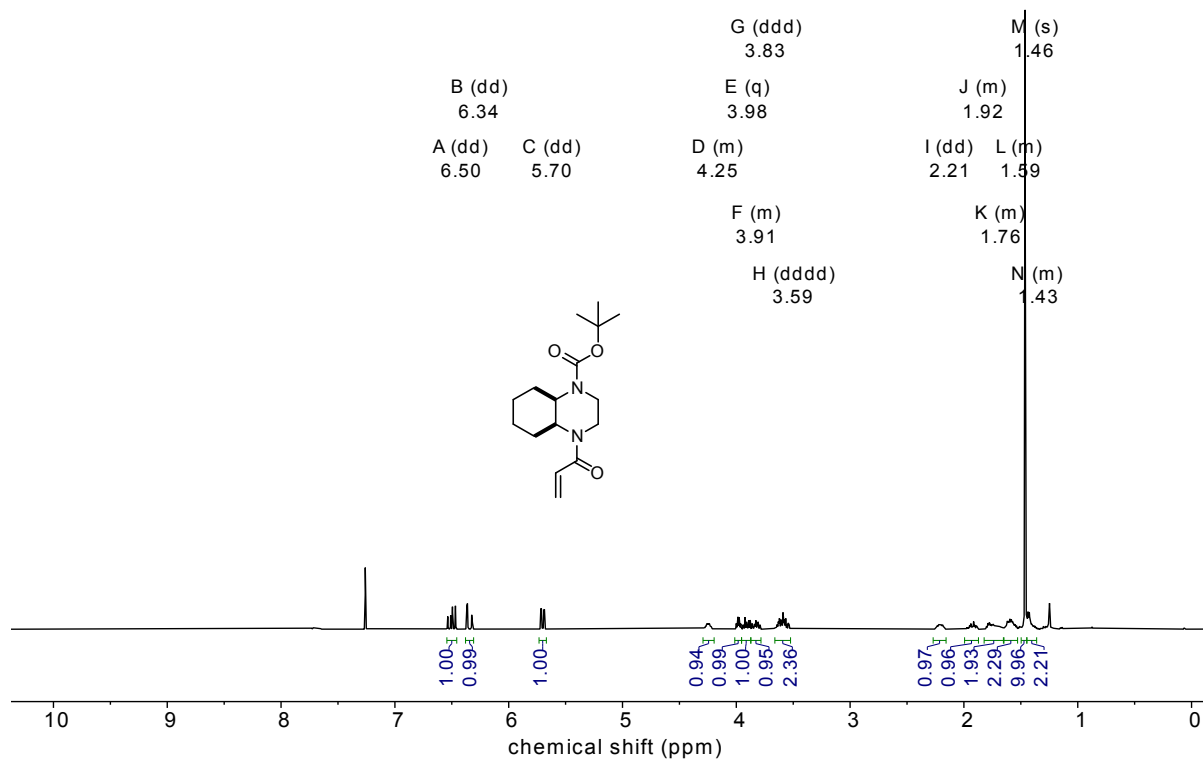
TLC R_f = 0.55 (isohexane:EtOAc, 1:1). **HRMS** (ESI): C₁₇H₂₂F₃N₂O₄S⁺: [M+H]⁺ calc. 407.1252, found 407.1260. **¹H-NMR** (500 MHz, CDCl₃): δ (ppm) = 6.86 (d, J = 0.7 Hz, 1H), 6.46 (dd, J = 16.8, 10.5 Hz, 1H), 6.29 (dd, J = 16.8, 1.9 Hz, 1H), 5.72 (dd, J = 10.4, 1.9 Hz, 1H), 4.20 (s, 1H), 4.13 – 4.04 (m, 1H), 3.93 (dt, J = 11.9, 3.5 Hz, 1H), 3.45 – 3.36 (m, 1H), 3.10 – 3.02 (m, 1H), 2.78 – 2.65 (m, 2H), 2.63 (s, 3H), 2.16 – 2.01 (m, 1H), 1.85 (d, J = 12.8 Hz, 1H), 1.79 – 1.65 (m, 1H), 1.59 – 1.49 (m, 3H), 1.46 (dt, J = 12.6, 3.8 Hz, 1H). **¹³C-NMR** (128 MHz, CDCl₃): δ (ppm) = 166.1 (C=O), 142.2 (C_{Ar}), 129.1 (C=CH₂), 128.0 (C_{Ar}H), 127.4 (C=CH-), 123.1 (C_{Ar}H), 120.3 (C_{Ar}), 116.24 (d, J = 22.0 Hz, C_{Ar}H), 52.5 (CH), 51.9 (CH), 44.4 (CH₂), 42.3 (CH₂), 31.6 (CH₂), 29.3 (CH₂), 23.3 (CH₂), 21.6 (CH₂). **¹⁹F-NMR** (376 MHz, CDCl₃) δ (ppm) = -67.1.

(*cis*)-1,4-bis((2-nitrophenyl)sulfonyl)decahydroquinoxaline (CJF263)¹H-NMR¹³C-NMR

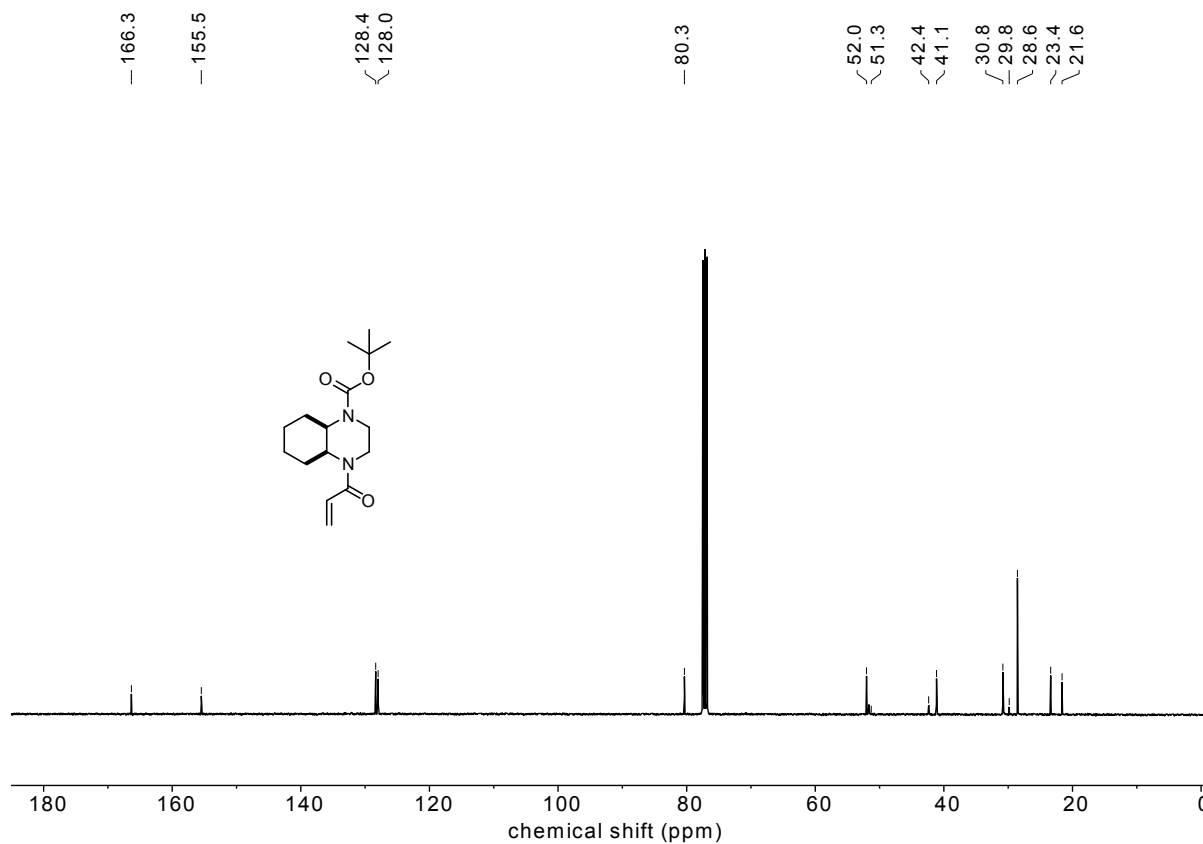
Appendix

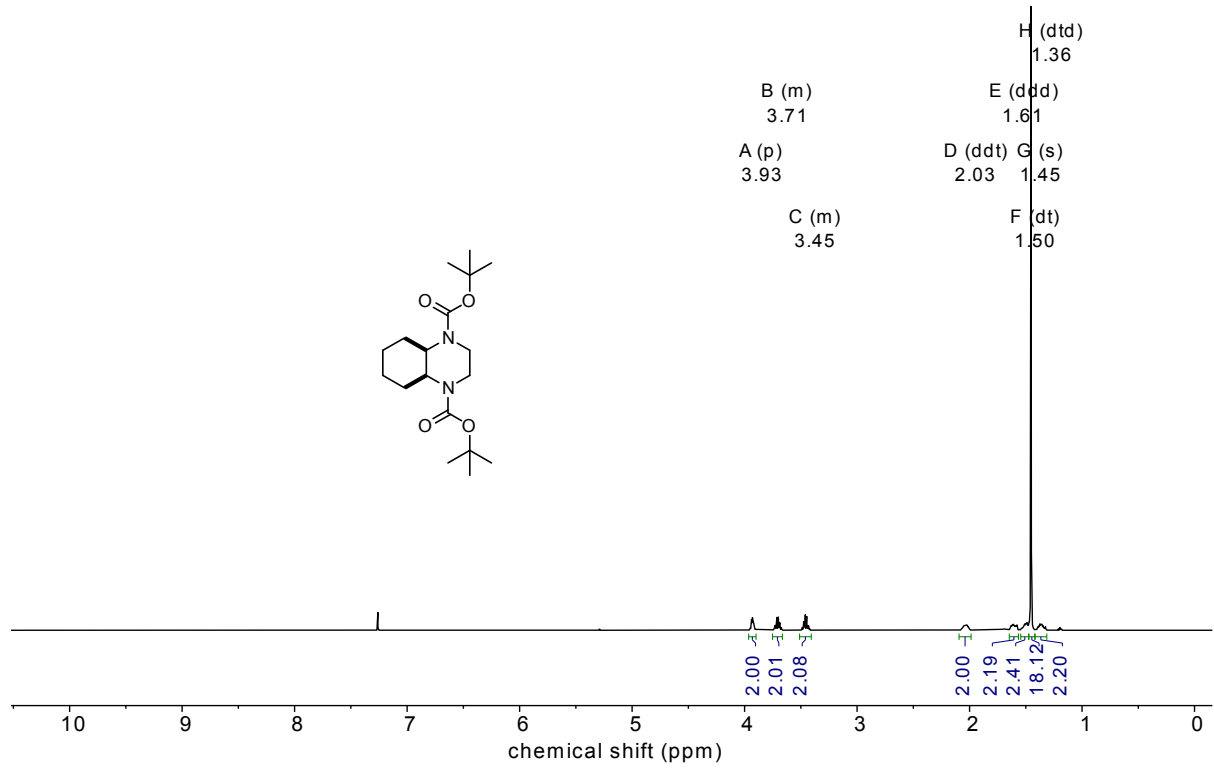
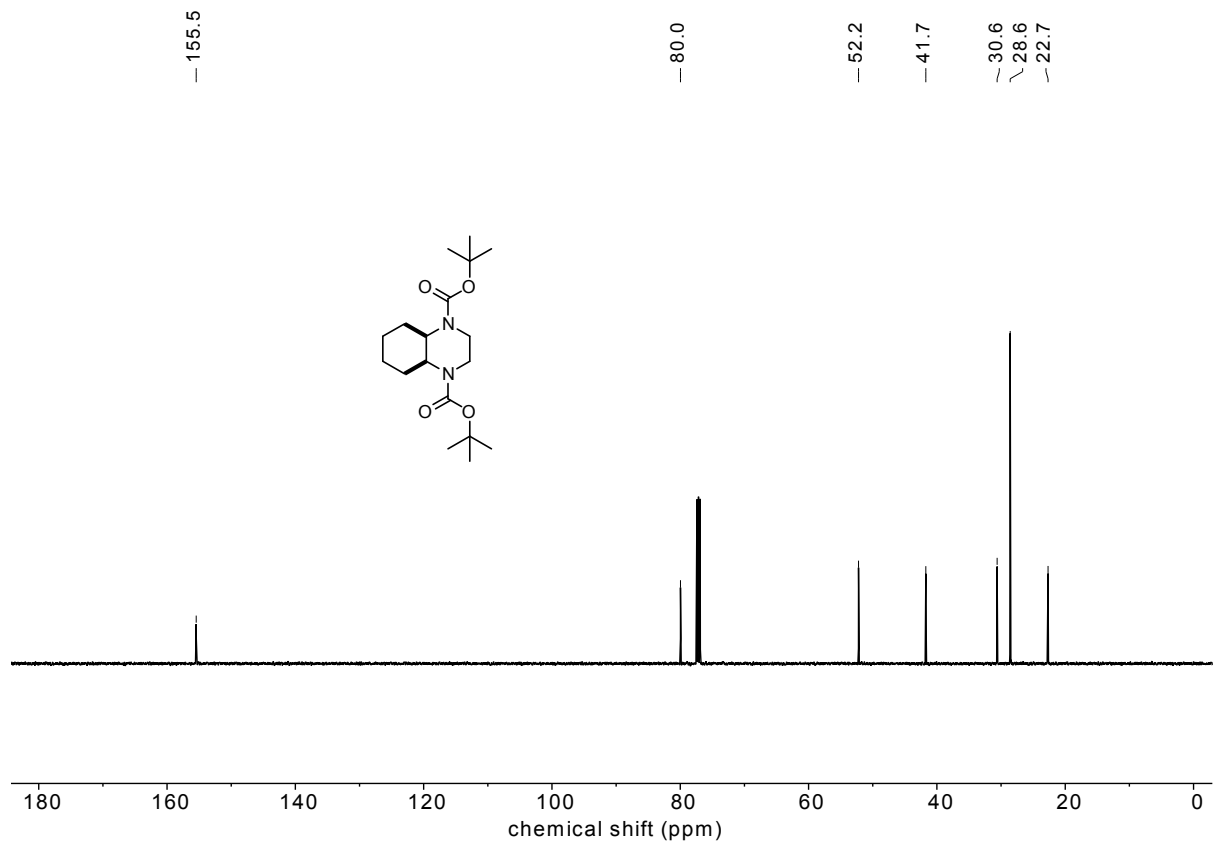
***tert*-butyl (*cis*)-4-acryloyloctahydroquinoxaline-1(2*H*)-carboxylate (CJF 257)**

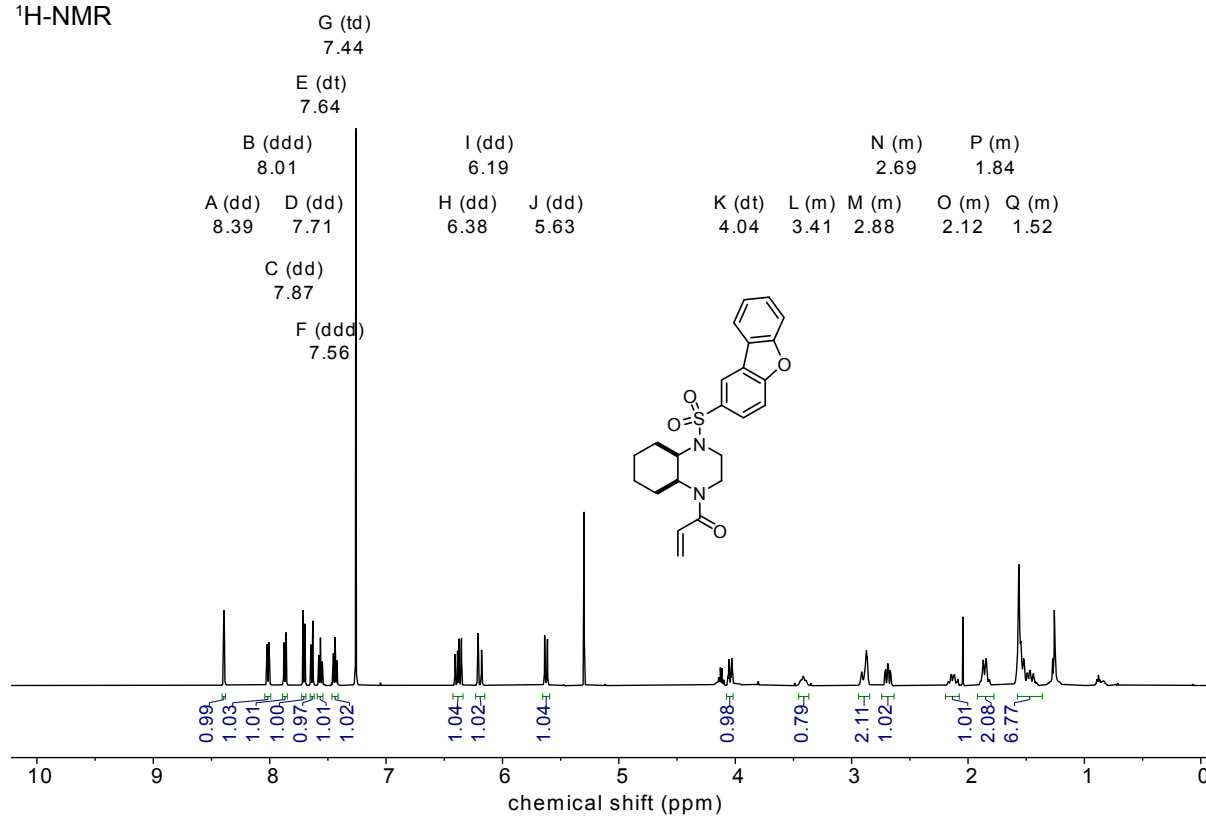
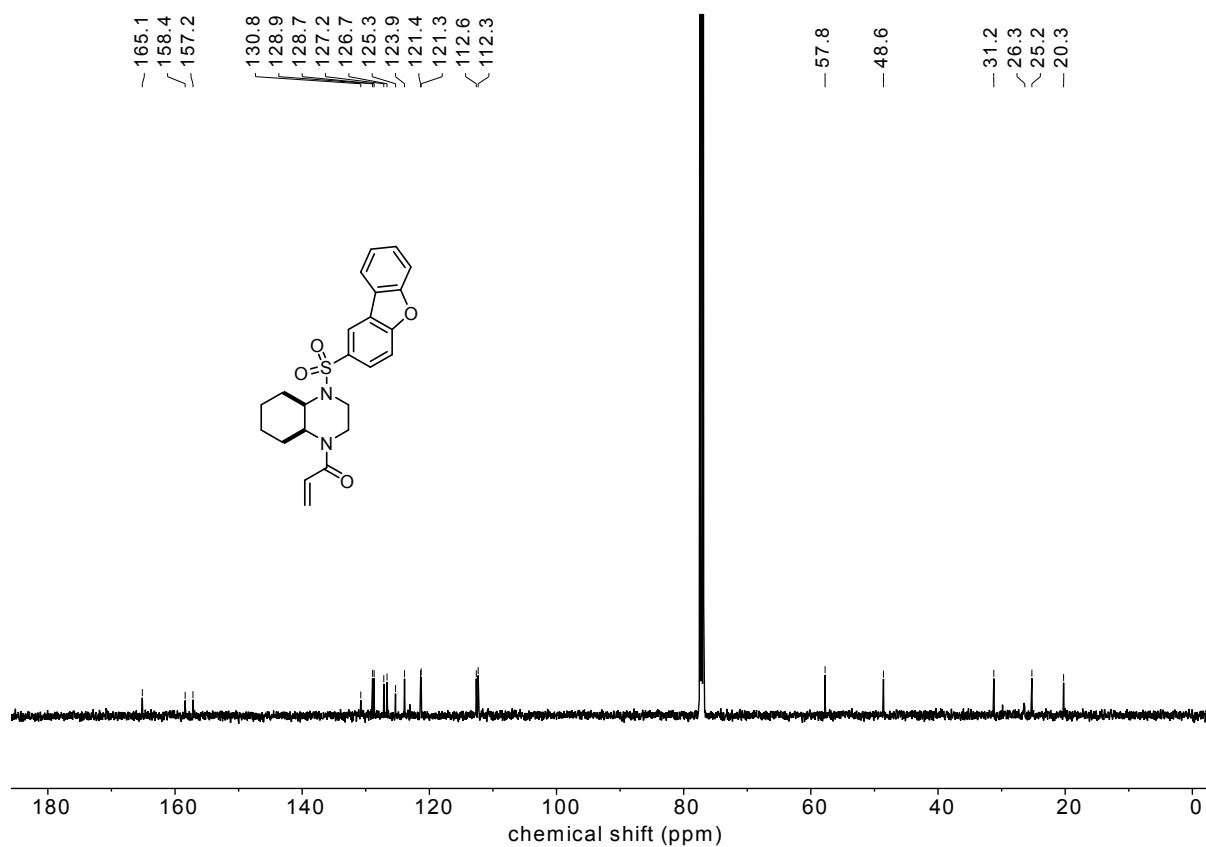
¹H-NMR



¹³C-NMR

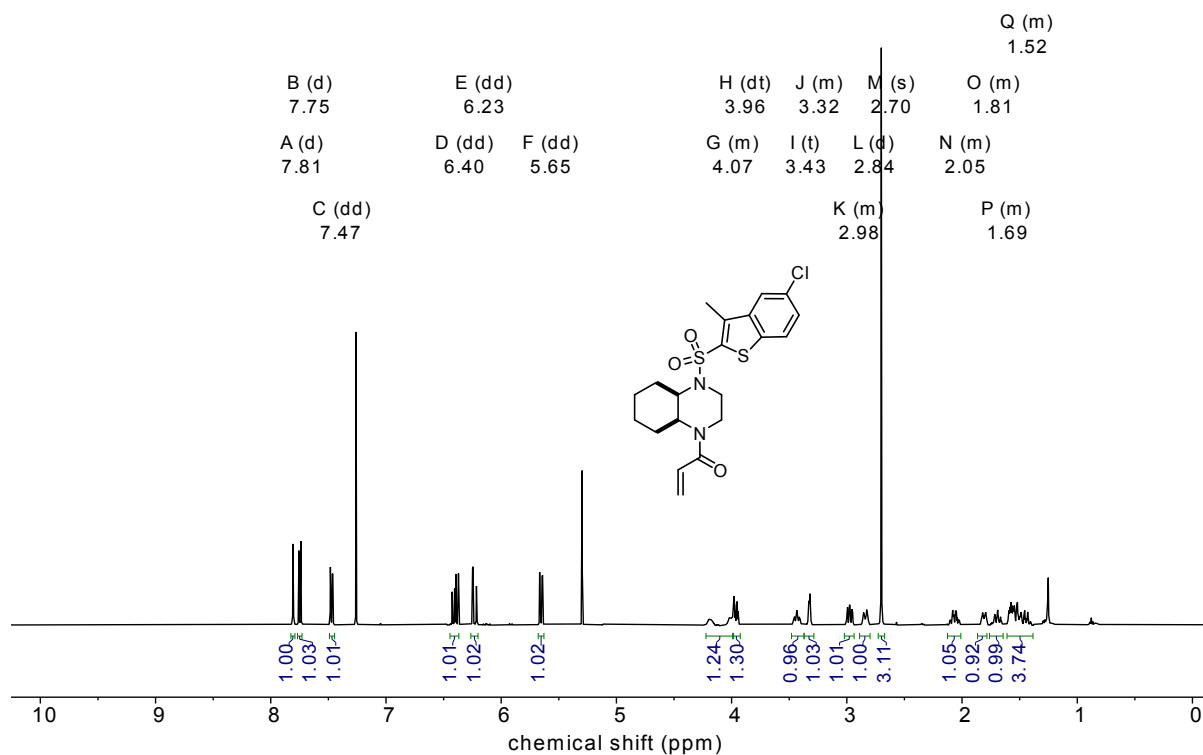


Di-*tert*-butyl (*cis*)-octahydroquinoxaline-1,4-dicarboxylate (CJF 262)¹H-NMR¹³C-NMR

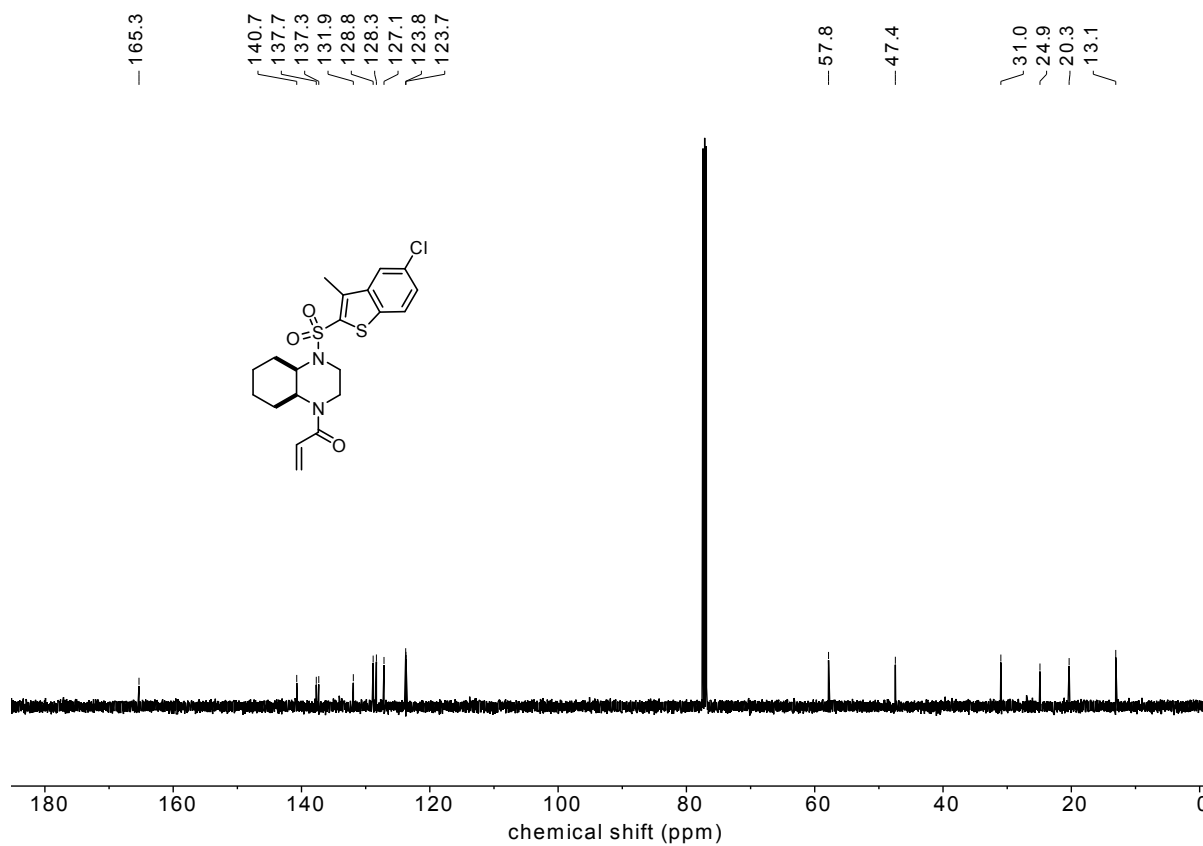
1-((*cis*)-4-(dibenzo[*b,d*]furan-2-ylsulfonyl)octahydroquinoxalin-1(2*H*)-yl)prop-2-en-1-one (CJF 252)¹H-NMR¹³C-NMR

1-((*cis*)-4-((5-chloro-3-methylbenzo[*b*]thiophen-2-yl)sulfonyl)octahydroquinoxalin-1(2*H*)-yl)prop-2-en-1-one (CJF 253)

¹H-NMR



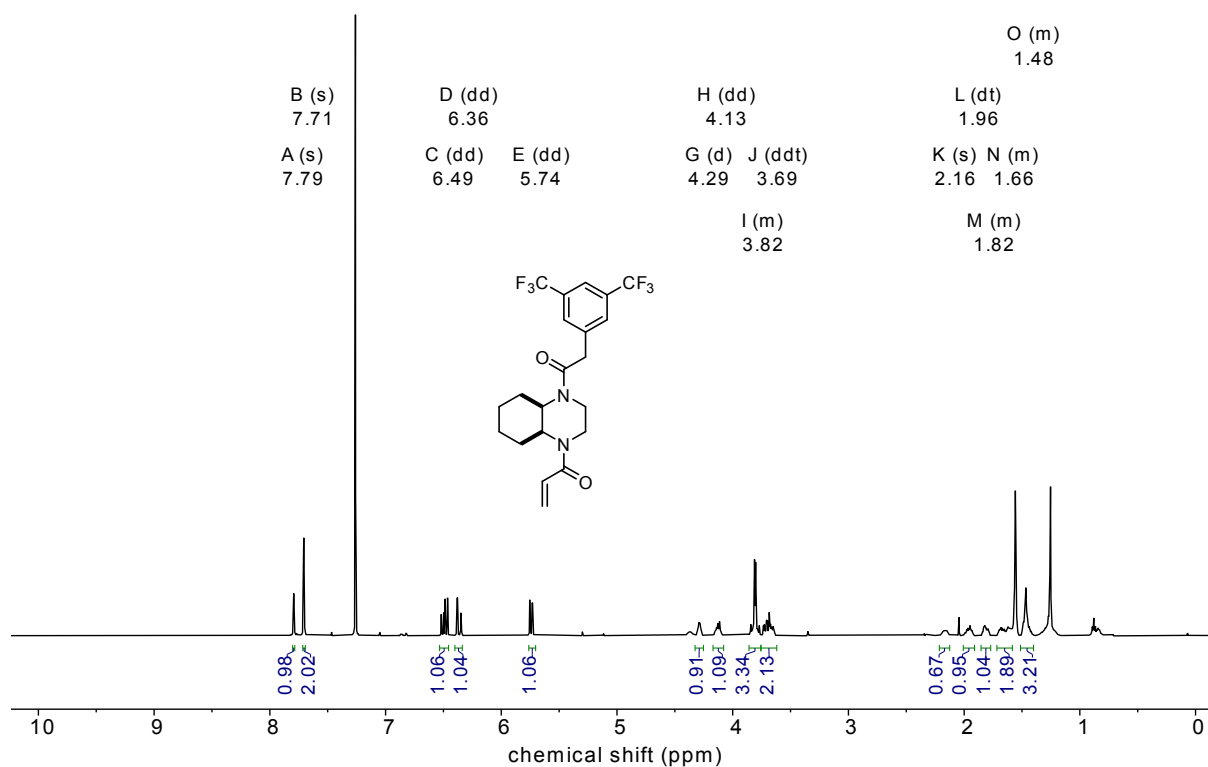
¹³C-NMR



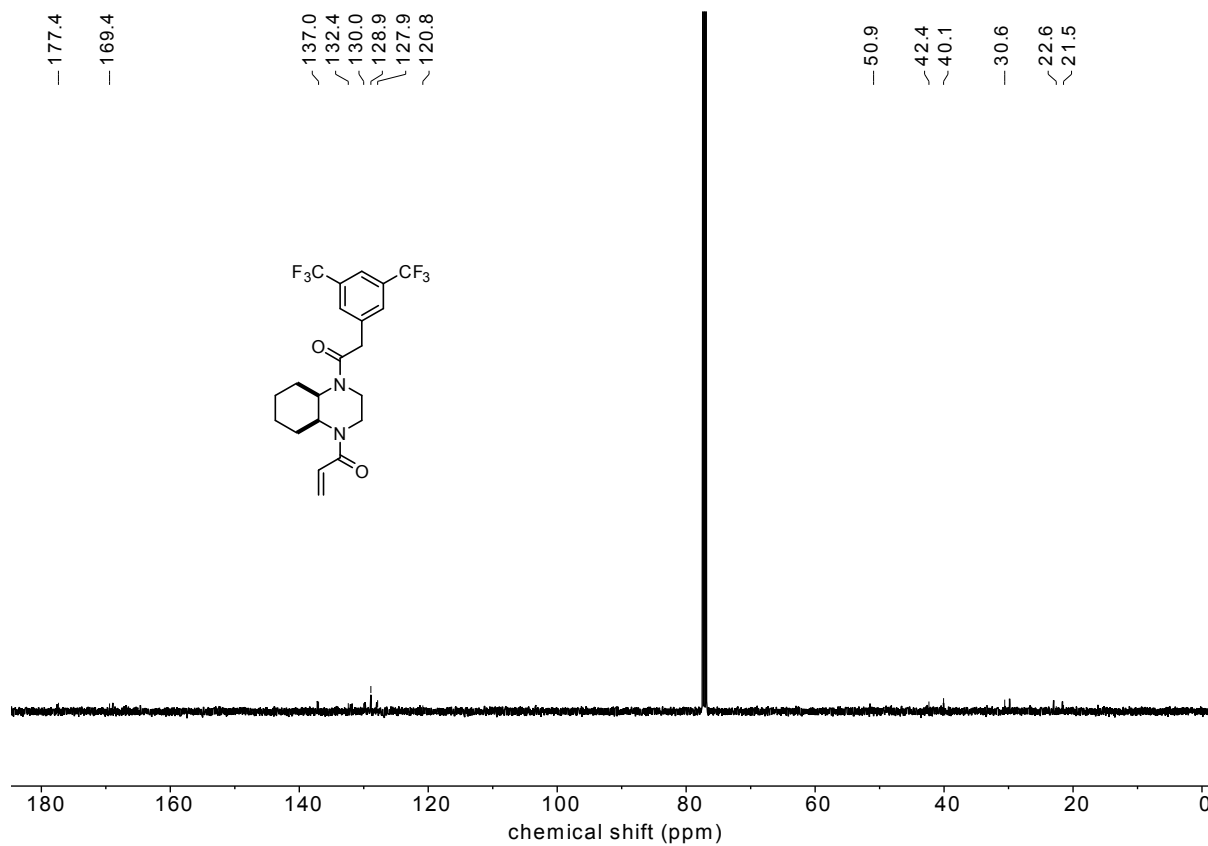
Appendix

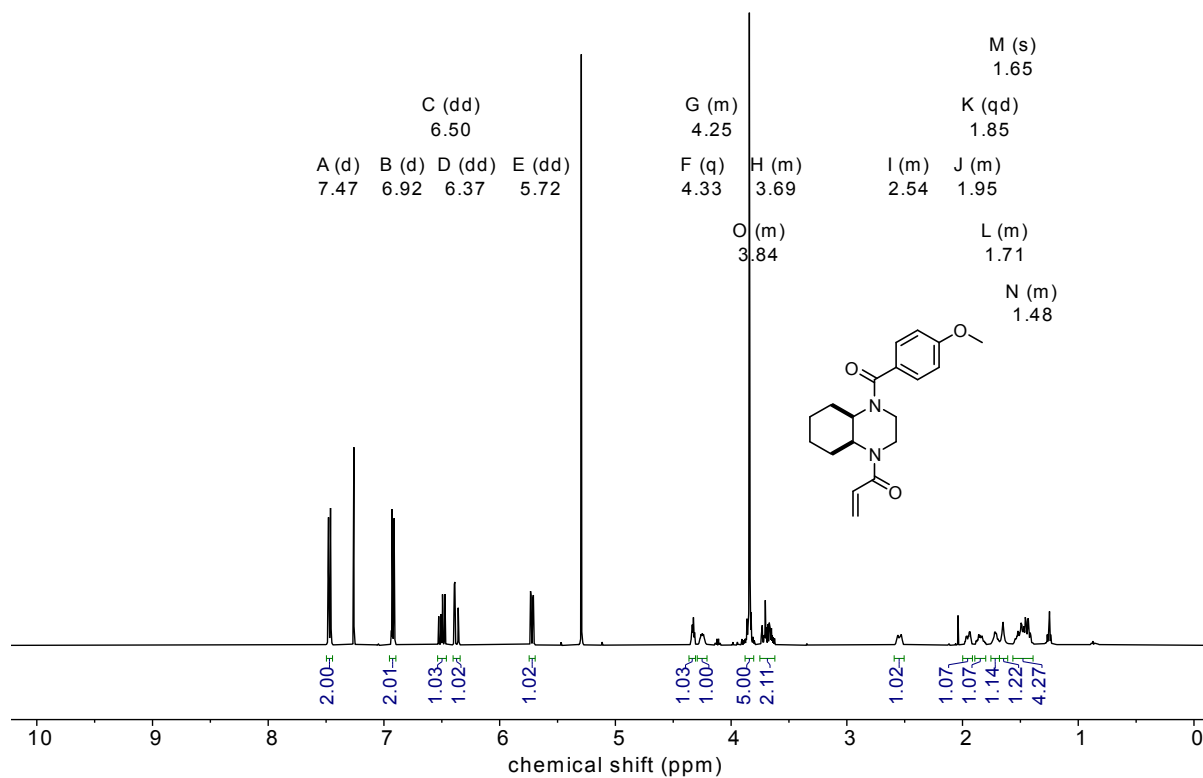
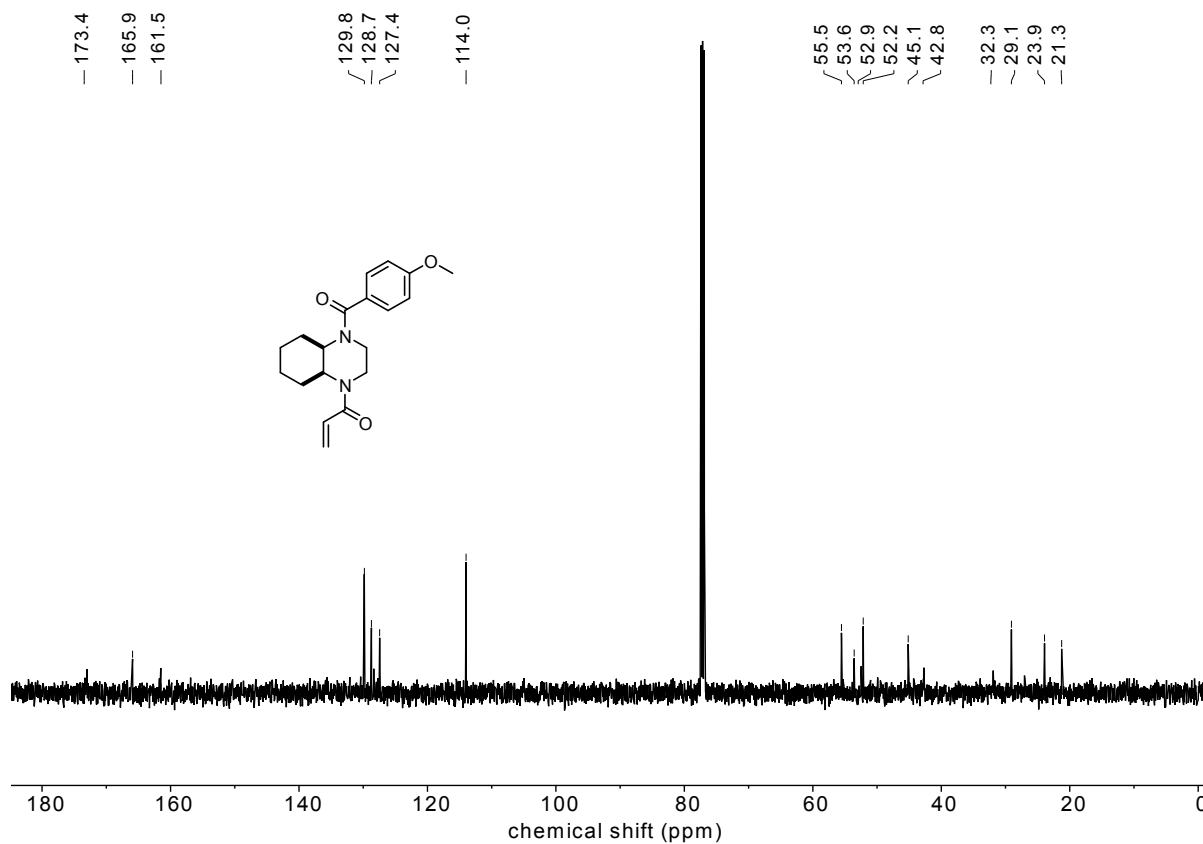
1-((*cis*)-4-(2-(3,5-bis(trifluoromethyl)phenyl)acetyl)octahydroquinoxalin-1(2*H*)-yl)prop-2-en-1-one
(CJF 254)

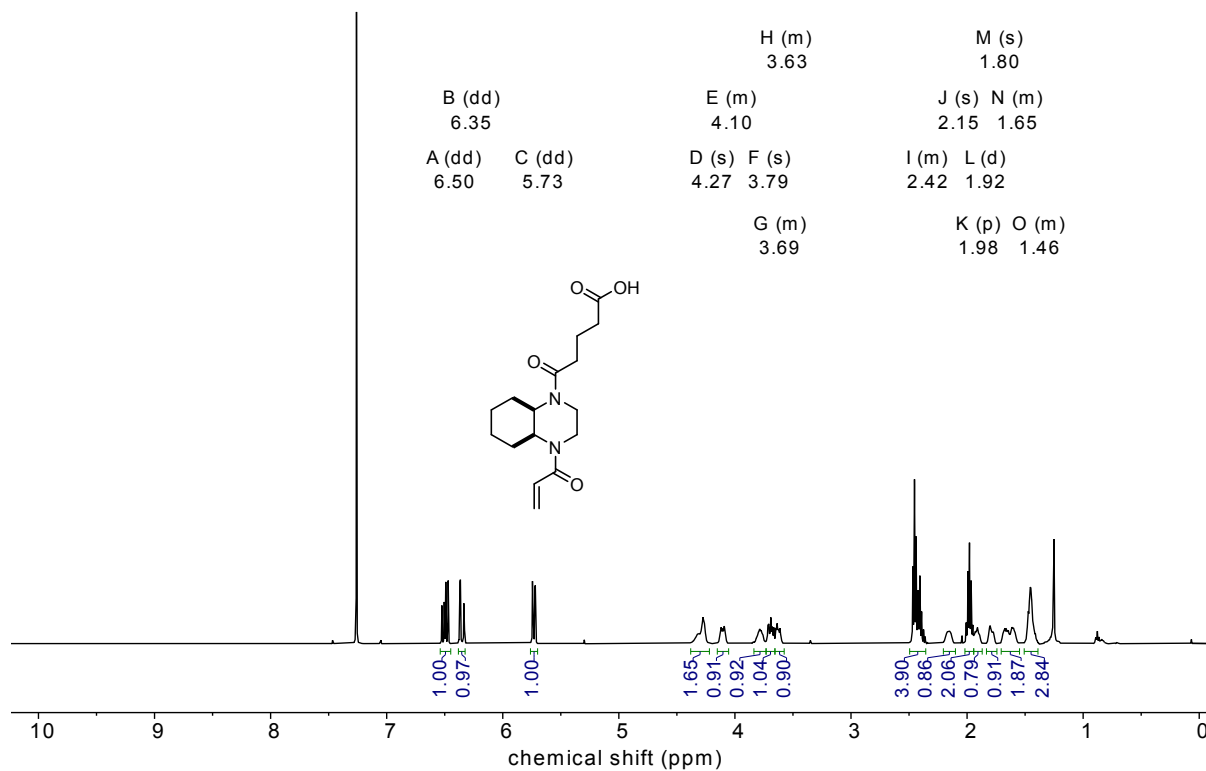
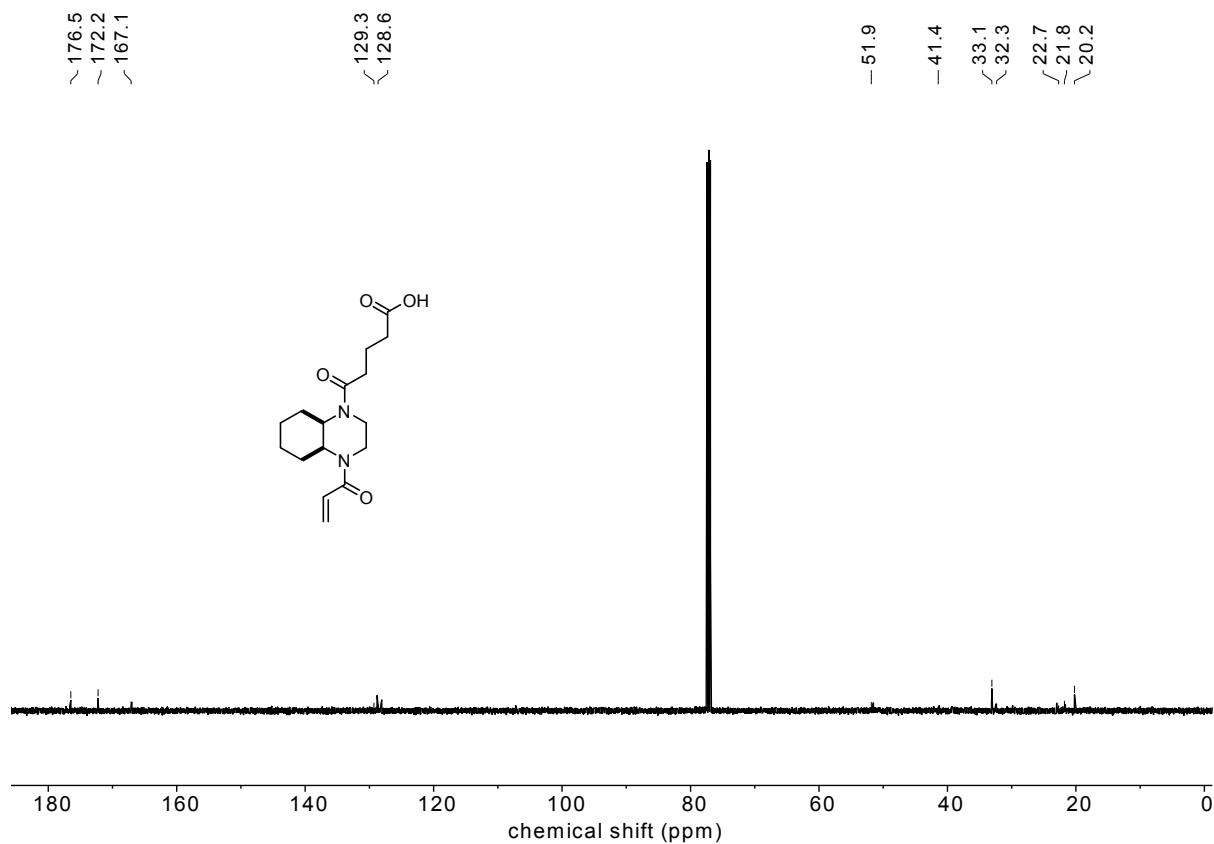
¹H-NMR

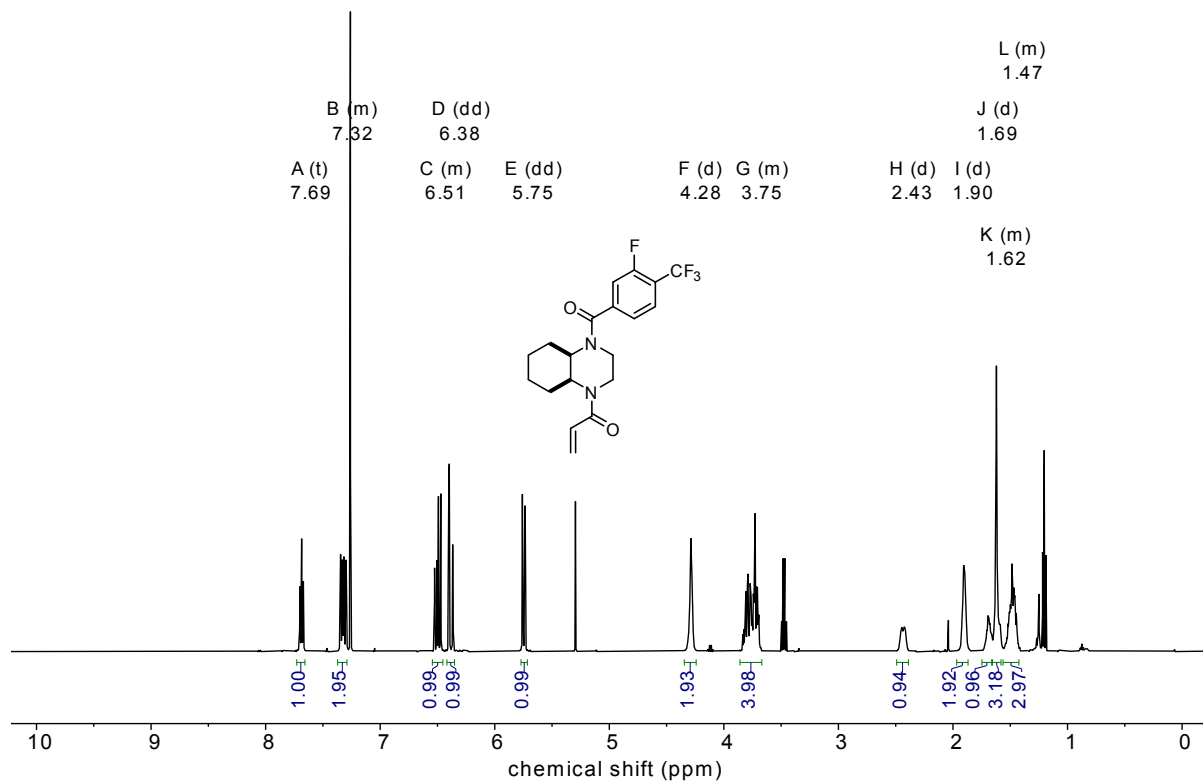
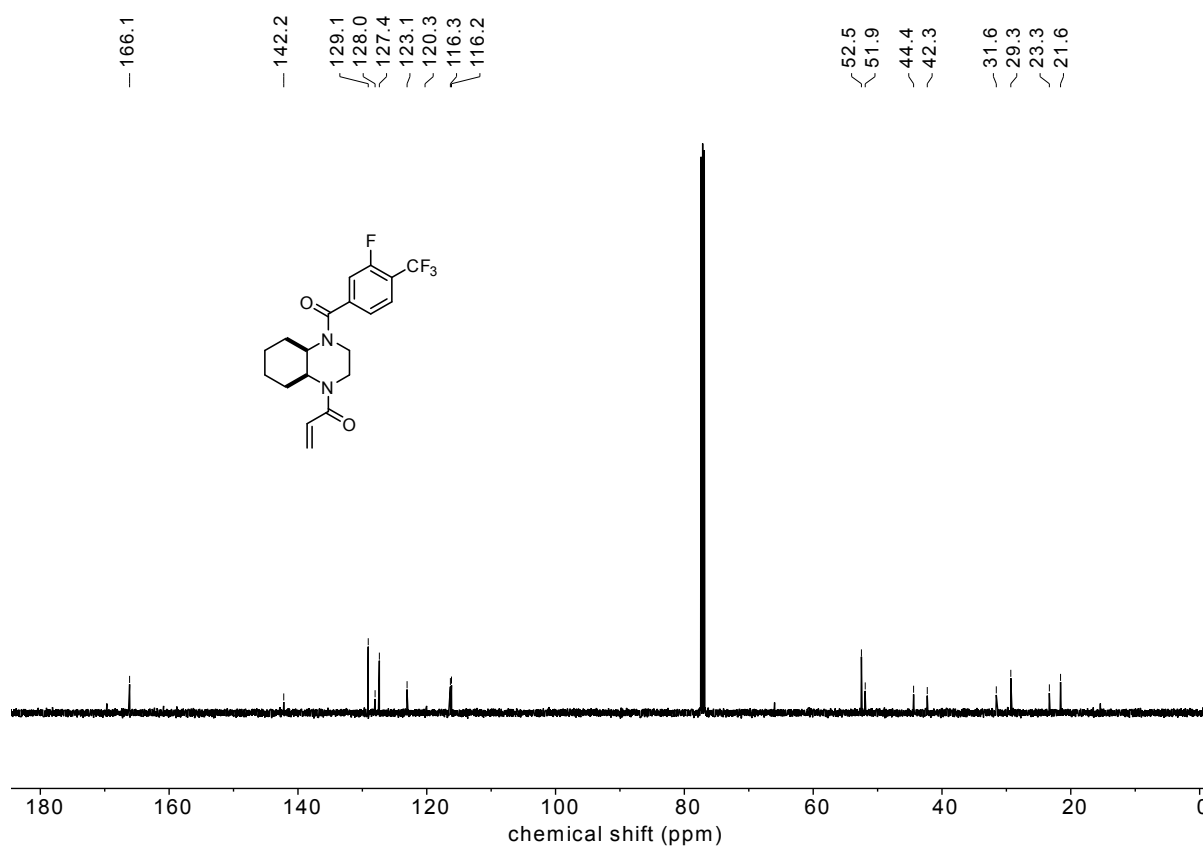


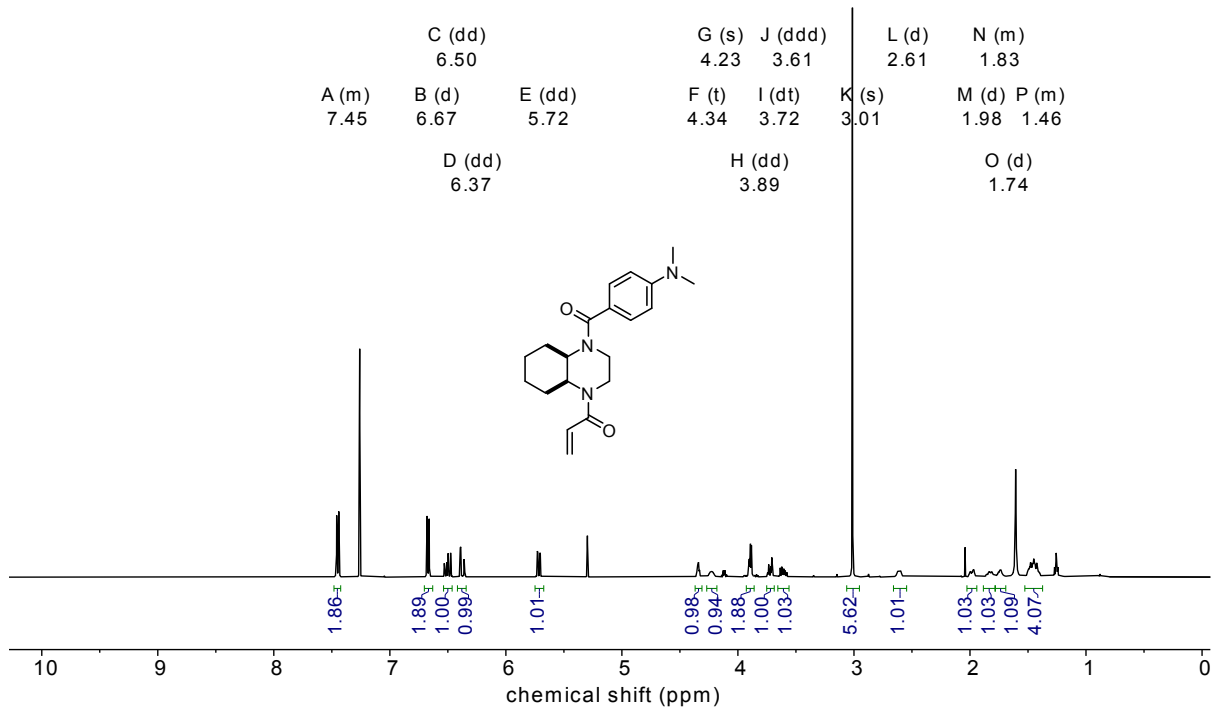
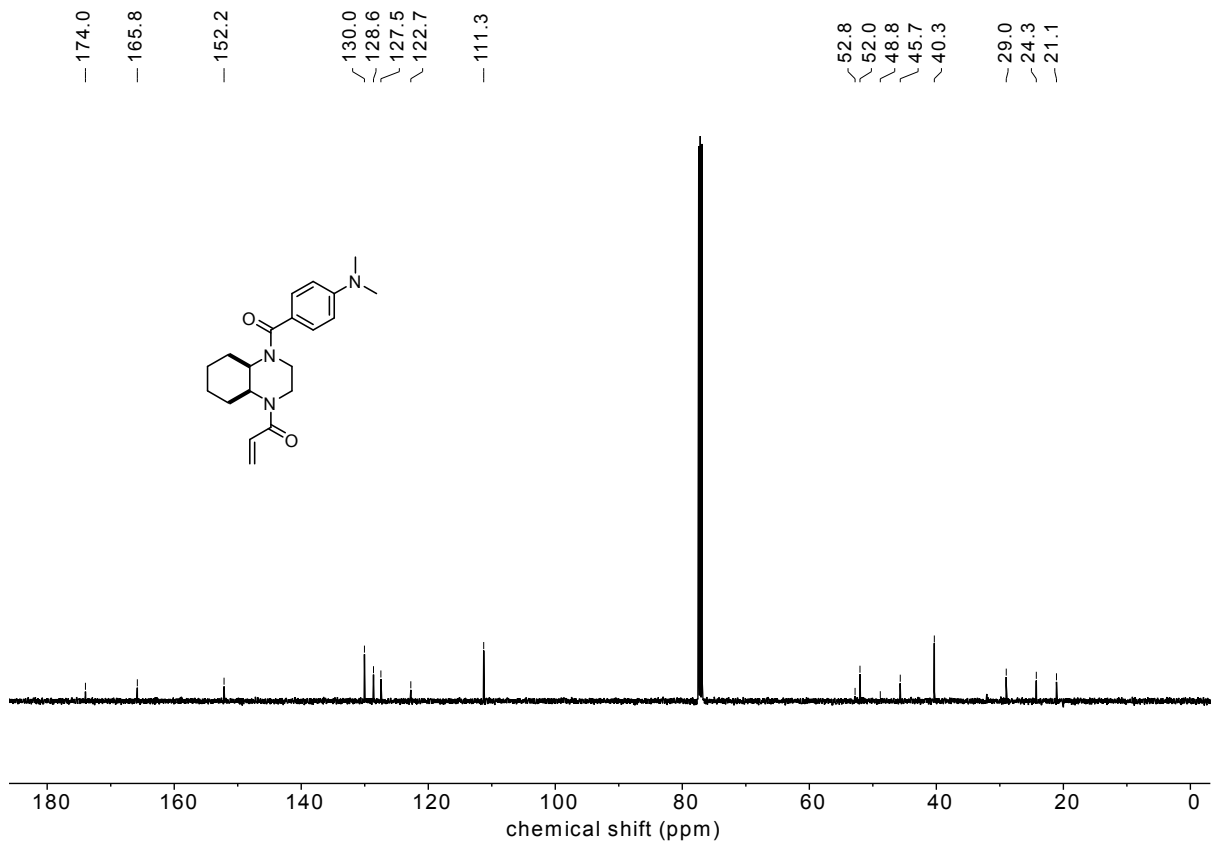
¹³C-NMR



1-((*cis*)-4-(4-methoxybenzoyl)octahydroquinoxalin-1(2H)-yl)prop-2-en-1-one (CJF 255)¹H-NMR¹³C-NMR

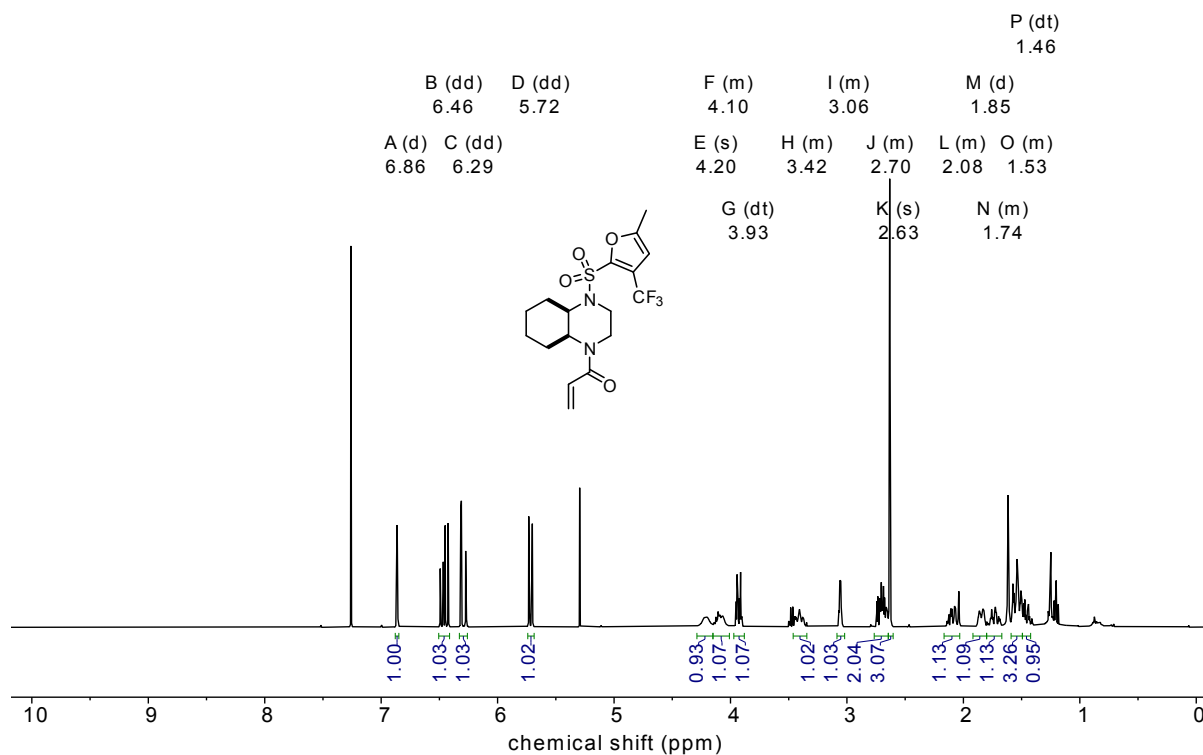
5-((*cis*-4-acryloyloctahydroquinolin-1(2*H*)-yl)-5-oxopentanoic acid (CJF 256)¹H-NMR¹³C-NMR

1-((*cis*)-4-(3-fluoro-4-(trifluoromethyl)benzoyl)octahydroquinoxalin-1(2H)-yl)prop-2-en-1-one (CJF 258)¹H-NMR¹³C-NMR

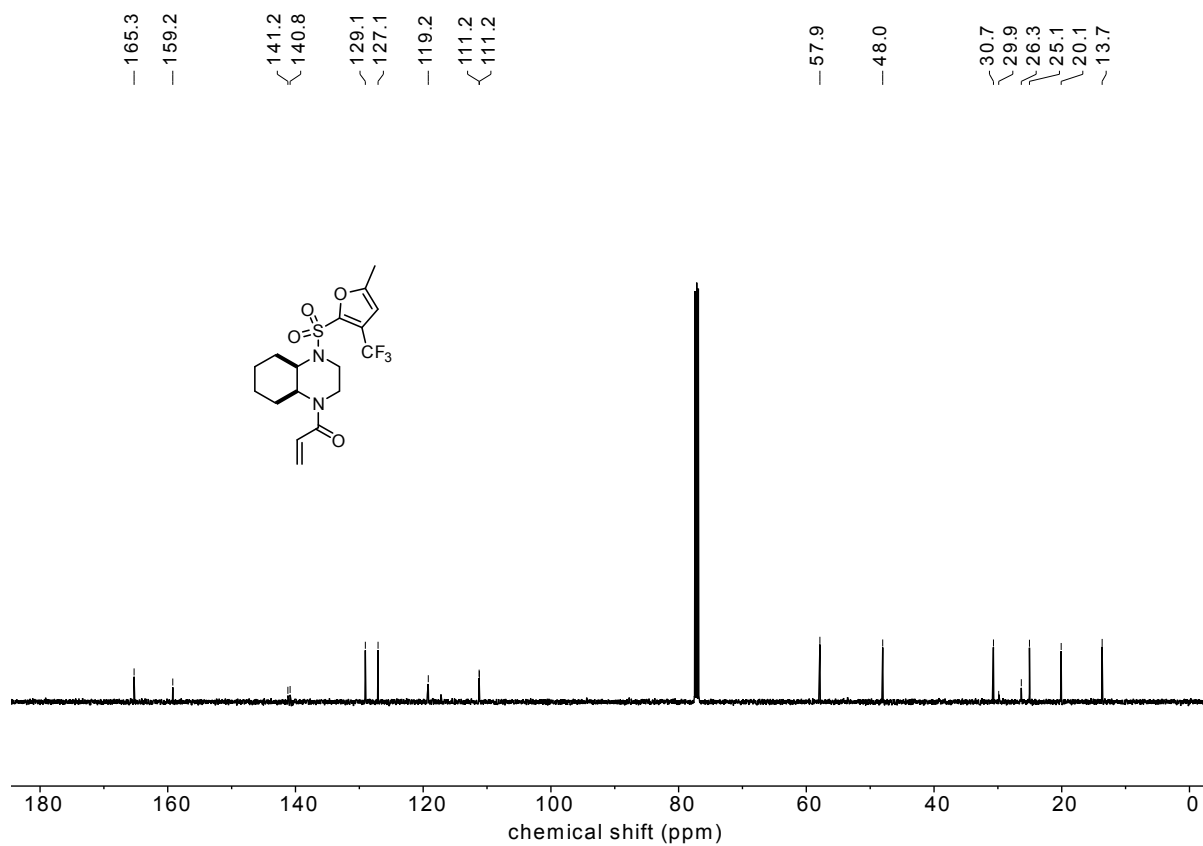
1-((*cis*)-4-(4-(dimethylamino)benzoyl)octahydroquinoxalin-1(2H)-yl)prop-2-en-1-one (CJF 259)¹H-NMR¹³C-NMR

1-((*cis*)-4-((5-methyl-3-(trifluoromethyl)furan-2-yl)sulfonyl)octahydroquinoxalin-1(2*H*)-yl)prop-2-en-1-one
(CJF 260)

¹H-NMR

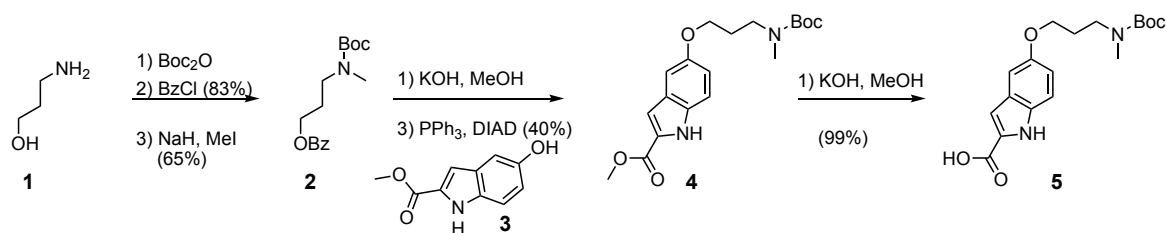


¹³C-NMR



9.2.2 Experimental Part for chapter 5.4: A new disulfide linker for ADCs

(A) precursor syntheses

**3-((*tert*-butoxycarbonyl)(methyl)amino)propyl benzoate (2)**

Step 1: To a solution of Boc_2O (6.4 g, 28.3 mmol) in DCM (1 M) was added dropwise at 0 °C a solution of 3-amino-1-propanol **1** (2.0 mL, 26.6 mmol) in anhydrous DCM (3 M). The reaction mixture was allowed to warm to r.t. and further stirred for 15 h, before a solution of BzCl (3.7 mL, 32 mmol) in DCM (3 M) was added, and the resulting mixture was further stirred for 4 h, before being poured into a mixture of sat. aq. $\text{NH}_4\text{Cl}/\text{H}_2\text{O}$ (1:1, 100 mL). The organic layer was separated, and the aq. layer was extracted with DCM (3×50 mL), the combined organic layers were dried over Na_2SO_4 , concentrated under reduced and purified by FCC (isohexane/ EtOAc) to yield 3-((*tert*-butoxycarbonyl)amino)propyl benzoate as a colorless oil (6.2 g, 22.2 mmol, 83%).

Step 2: To the material obtained in step 1 (1.87 g, 6.69 mmol) in anhydrous DMF (0.02 M) at 0 °C was added iodomethane (0.5 mL, 8.03 mmol), directly followed by the addition of solid NaH (60%, 0.295 g, 7.36 mmol), the mixture was then allowed to warm to r.t. and was further stirred for 2 h, before being poured into a mixture of sat. aq. $\text{NaCl}/\text{H}_2\text{O}$ (1:1, 100 mL). The organic layer was separated, and the aq. layer was extracted with DCM (3×50 mL), the combined organic layers were dried over Na_2SO_4 , filtered, concentrated under reduced pressure, and purified by FCC (isohexane/ EtOAc) to yield **2** as a colorless oil (1.28 g, 4.36 mmol, 65%).

TLC R_f = 0.47 (isohexane: EtOAc , 3:1). **HRMS** (ESI^+) for $\text{C}_{16}\text{H}_{24}\text{NNaO}_4$: calc 316.15193, found 316.15250. **$^1\text{H-NMR}$** (400 MHz, CDCl_3): δ (ppm) = 8.04 (d, J = 7.1 Hz, 2H), 7.55 (t, J = 7.4 Hz, 1H), 7.43 (t, J = 7.6 Hz, 2H), 4.34 (t, J = 6.3 Hz, 2H), 3.39 (t, J = 6.9 Hz, 2H), 2.88 (s, 3H), 1.99 (p, J = 6.5 Hz, 2H), 1.43 (s, 9H). **$^{13}\text{C-NMR}$** (101 MHz, CDCl_3): δ (ppm) = 166.6, 155.8, 133.1, 130.3, 129.7, 128.5, 79.6, 62.8, 46.2, 33.9, 28.5, 27.5.

methyl 5-(3-((*tert*-butoxycarbonyl)(methyl)amino)propoxy)-1H-indole-2-carboxylate (4)

Step 1: To a solution of compound **2** (1.06 g, 3.61 mmol) in MeOH (11 mL) at 0 °C was added a freshly prepared solution of KOH in MeOH (1 M, 5.4 mL, 5.4 mmol), the reaction mixture was allowed to warm to r.t. and was further stirred for 3 h, before being concentrated under reduced pressure. The residue was taken into a mixture of sat. aq. $\text{NH}_4\text{Cl}/\text{H}_2\text{O}$ (1:1, 50 mL) and extracted with EtOAc (3×50 mL) at pH<5 to yield intermediate *tert*-butyl (3-hydroxypropyl)(methyl)carbamate as a colorless oil (0.68 g, 3.59 mmol, 99%).

Step 2: PPh_3 (911 mg, 3.47 mmol) was dissolved in THF (0.25 M) and cooled to 0 °C. DIAD (701 μL , 3.57 mmol) was added dropwise, and the mixture was stirred at r.t. for 30 min. A solution of the material obtained in step 1 containing *tert*-butyl (3-hydroxypropyl)(methyl)carbamate (632 mg, 3.31 mmol) in THF and a solution of the 5-methyl-1H-indole-2-carboxylate **3** (0.5 M) in THF were added subsequently. The mixture was allowed to warm to r.t. for 1 h, was then further stirred for 15 h, before being poured into a mixture of sat. aq. $\text{NaCl}/\text{H}_2\text{O}$ (1:1, 50 mL). The organic layer was separated, and the aq. layer was extracted with EtOAc (3×50 mL), the combined organic layers were dried over Na_2SO_4 , filtered, concentrated under reduced pressure, and purified by FCC (isohexane/ EtOAc) to yield **4** as a colorless solid (485 mg, 1.34 mmol, 40%).

TLC R_f = 0.56 (isohexane: EtOAc , 2:1). **HRMS** (ESI^+) for $\text{C}_{19}\text{H}_{27}\text{N}_2\text{NaO}_5$: calc 385.17339, found 385.17382. **$^1\text{H-NMR}$** (400 MHz, CDCl_3): δ (ppm) = 8.94 (s, 1H), 7.31 (d, J = 9.0 Hz, 1H), 7.14 – 7.10 (m, 1H), 7.05 (s, 1H), 6.99 (dd, J = 8.9, 2.3 Hz, 1H), 4.00 (t, J = 6.1 Hz, 2H), 3.93 (s, 3H), 3.43 (t, J = 6.8 Hz, 2H), 2.88 (s, 3H), 2.02 (s, 2H), 1.43 (s, 9H). **$^{13}\text{C-NMR}$** (101 MHz, CDCl_3): δ (ppm) = 162.5, 156.5, 156.0, 154.0, 132.4, 127.9, 127.6, 117.5, 112.9, 108.4, 103.5, 79.5, 65.6, 52.1, 46.2, 34.6, 29.7, 28.1.

5-(3-((*tert*-butoxycarbonyl)(methyl)amino)propoxy)-1H-indole-2-carboxylic acid (5)

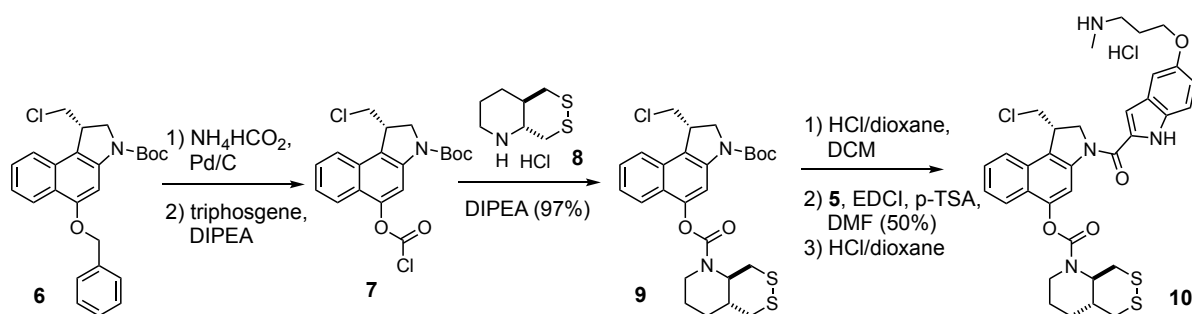
To a solution of compound **4** (403 mg, 1.11 mmol) in MeOH/ H_2O (2:1, 60 mL) at r.t. was added solid KOH (780 mg, 11.1 mmol), the reaction mixture was heated to 80 °C and stirred for 2 h, before being cooled to r.t. and concentrated under reduced pressure. The residue was taken into a mixture of sat. aq. $\text{NH}_4\text{Cl}/\text{H}_2\text{O}$ (1:1, 50 mL) and extracted with EtOAc (3×) at pH<5 to yield **5** as a colorless oil (384 mg, 1.1 mmol, 99%).

TLC R_f = 0.28 (DCM:MeOH, 9:1). **$^1\text{H-NMR}$** (400 MHz, CDCl_3) δ (ppm) = 8.92 (s, 1H), 7.20 (s, 1H), 7.01 (d, J = 9.9 Hz, 2H), 6.39 (s, 1H), 3.98 (s, 2H), 3.42 (s, 2H), 2.88 (s, 3H), 2.02 (s, 2H), 1.43 (s, 9H).

N-Fmoc-hexanoic acid: 6-(((9H-fluoren-9-yl)methoxy)carbonyl)amino)hexanoic acid (12)

6-amino-hexanoic acid (**11**) (1.06 g, 8.1 mmol) was dissolved in a dioxane:H₂O mixture (3:2, 20 mL, 0.1 M) and Na₂CO₃ (2.15 g, 20.3 mmol, 2.5 eq) was added as a solid. 9-fluorenylmethyl chloroformate (2.31 g, 8.9 mmol, 1.1 eq) was added portion-wise, and the resulting mixture was stirred at r.t. for 12 h. The mixture was extracted with Et₂O (3×10 mL), and the aqueous phase was acidified using 6 M aq. HCl. A solid precipitate was observed, which was filtered off, washed with water (40 mL), and dried to obtain the title compound **12** as a colorless solid (2.79 g, 7.9 mmol, 98%).

TLC R_f = 0.69 (EtOAc). **¹H-NMR** (400 MHz, MeOD-*d*₄): δ (ppm) = 7.79 (d, J = 7.5 Hz, 1H), 7.64 (d, J = 7.4 Hz, 1H), 7.38 (t, J = 7.4 Hz, 1H), 7.30 (t, J = 7.3 Hz, 1H), 4.34 (d, J = 6.9 Hz, 1H), 4.19 (t, J = 6.8 Hz, 0H), 2.28 (td, J = 7.3, 4.1 Hz, 1H), 1.67 – 1.56 (m, 1H), 1.50 (p, J = 7.2 Hz, 1H), 1.34 (p, J = 7.4, 6.7 Hz, 1H). **¹³C-NMR** (101 MHz, MeOD-*d*₄): δ (ppm) = 177.6 (C=O), 158.9 (C=O), 145.4 (C_{Ar}), 142.6 (C_{Ar}), 128.7 (C_{Ar}H), 128.1 (C_{Ar}H), 126.2 (C_{Ar}H), 120.9 (C_{Ar}H), 67.5 (CH₂), 41.6 (CH₂), 34.9 (CH₂), 30.6 (CH₂), 27.3 (CH₂), 25.8 (CH₂).

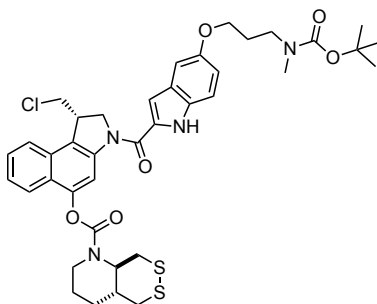
(B) duocarmycin-ADC precursor: design 1**CIC(O)O-CBI-Boc (S)-3-(Boc)-1-(chloromethyl)-5-(chlorocarbonyloxy)-1,2-dihydro-3H-benzo[e]indole 7**

Step 1: **OBn-CBI-Boc** (528 mg, 1.25 mmol, 1.0 eq.) and dissolved in THF (62 mL, 0.02 M). The mixture was heated to 35 °C and Pd/C (148 mg, 10% on charcoal, 1.0 eq.) and NH₄HCO₂ (1.25 mL of 4 M aq. Solution, 4.0 eq.) were added. The mixture was stirred at 35 °C for 70 min until quantitative turnover was confirmed by TLC, was then filtered through Celite, the filter cake was washed with ethyl acetate (40 mL), and the combined filtrates were concentrated under reduced pressure to obtain **HO-CBI-Boc** as a colourless solid. *Analytical data matched our previous reports: TLC* R_f = 0.59 (isohexane:EtOAc, 10:1).

Step 2: The material obtained in step 1 was dissolved in anhydrous DCM (62 mL, 0.02 M) and the resulting solution was cooled to 0 °C. Triphosgene (370 mg, 1.25 mmol, 1.0 eq., 0.1 M solution in anhydrous DCM) and DIPEA (212 μL, 1.25 mmol 1.0 eq, 0.1 M solution in anhydrous DCM) were added. The resulting mixture was further stirred at 0 °C for 15 min, was then allowed to warm to r.t. and was further stirred for 1 h. All volatiles were removed using an external liquid nitrogen trap to afford the corresponding chloroformate derivative **CIC(O)O-CBI-Boc (7)** as a colourless solid without further purification. A stock solution in anhydrous DCM was prepared at 0.1 mol/L referring to the initial amount of material, that was used for further coupling reactions.

SS66T-CBI-Boc (CJF128) (*S*)-3-(*tert*-butoxycarbonyl)-1-(chloromethyl)-2,3-dihydro-1*H*-benzo[*e*]indol-5-yl (*trans*)-hexahydro-[1,2]dithiino[4,5-*b*]pyridine-1(2*H*)-carboxylate (**9**)

(*trans*)-octahydro-[1,2]dithiino[4,5-*b*]pyridine (**8**) (88.9 mg, 0.42 mmol) was suspended in anhydrous DCM (10 mL) and DIPEA (200 μ L, 1.13 mmol) was added. To the clear solution, a solution of **CIC(O)O-CBI-Boc (7)** (139 mg, 0.35 mmol) in anhydrous DCM (10 mL) was added dropwise at 0 $^{\circ}$ C. The mixture was stirred for 20 min, was then allowed to warm to r.t. and further stirred for 1 h. The mixture was concentrated and directly purified by FCC (isohehexane/EtOAc) to give **9** as a colorless, crystalline solid (162 mg, 0.30 mmol, 86%). *This compound was reported by us earlier and analytical data is provided elsewhere.*



SS66T-CBI-NBocPI (CJF136) (*S*)-3-(5-(3-((*tert*-butoxycarbonyl)(methyl)amino)propoxy)-1*H*-indole-2-carbonyl)-1-(chloromethyl)-2,3-dihydro-1*H*-benzo[*e*]indol-5-yl (*trans*)-hexahydro-[1,2]dithiino[4,5-*b*]pyridine-1(2*H*)-carboxylate

Step 1: Compound **9** (22.0 mg, 0.04 mmol) was dissolved in anhydrous DCM (0.05 M). The solution was cooled to 0 $^{\circ}$ C and a solution of HCl (80 eq., 4 M in dioxane) was added. The mixture was stirred at r.t. for 4 h. All volatiles were removed under reduced pressure to afford the corresponding aniline (*S*)-1-(chloromethyl)-2,3-dihydro-1*H*-benzo[*e*]indole-5-yl (*trans*)-hexahydro-[1,2]dithiino [4,5-*b*]pyridine a colorless solid.

Step 2: The material obtained in step 1 was dissolved in DMF (0.03 M). Compound **5** (23.2 mg, 0.05 mmol), EDCl (31 mg, 0.16 mmol), and *p*-TSA (7 mg, 0.04 mmol) were added. The solution was stirred at r.t. for 15 h, before being poured into a mixture of sat. aq. NaCl/H₂O (1:1, 20 mL). The organic layer was separated, and the aq. layer was extracted with EtOAc (3 \times 15 mL), the combined organic layers were dried over Na₂SO₄, concentrated under reduced pressure and purified by FCC (isohehexane/EtOAc) to yield **SS66T-CBI-NBocPI** (12.6 mg, 0.02 mmol, 50%) as a colorless solid.

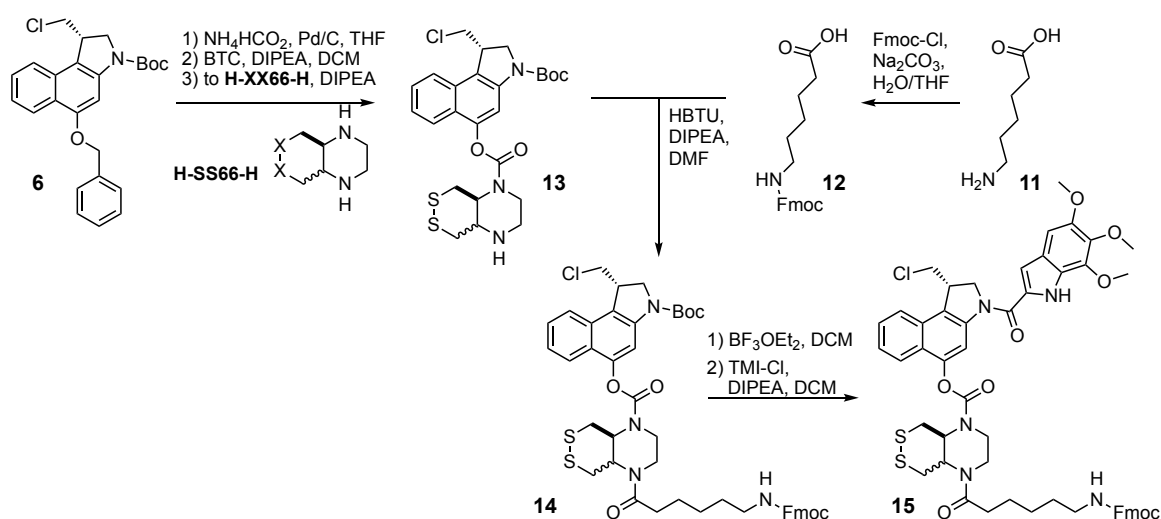
TLC R_f = 0.59 (isohehexane:EtOAc, 1:1). **HRMS** (ESI⁺) for C₃₉H₄₆N₄NaO₆S₂Cl: calc 787.23613, found 787.23632. **¹H-NMR** (400 MHz, CDCl₃): δ (ppm) = 9.47 (s, 1H), 8.40 (s, 1H), 7.85 (d, J = 8.4 Hz, 1H), 7.76 (dd, J = 8.2, 2.2 Hz, 1H), 7.55 (t, J = 7.6 Hz, 1H), 7.49 – 7.43 (m, 1H), 7.36 – 7.27 (m, 1H), 7.11 (s, 1H), 7.05 – 7.00 (m, 1H), 6.97 (ddd, J = 8.9, 3.8, 2.4 Hz, 1H), 4.82 (d, J = 10.7 Hz, 1H), 4.67 (t, J = 9.6 Hz, 1H), 4.15 (dd, J = 11.4, 8.2 Hz, 1H), 4.08 – 3.97 (m, 4H), 3.97 – 3.88 (m, 2H), 3.54 – 3.48 (m, 1H), 3.45 (t, J = 7.0 Hz, 3H), 3.22 (d, J = 6.8 Hz, 2H), 3.03 – 2.92 (m, 1H), 2.90 (s, 3H), 2.83 (dd, J = 13.4, 2.3 Hz, 1H), 2.27 – 2.14 (m, 1H), 2.06 (dt, J = 13.6, 3.6 Hz, 3H), 1.85 (d, J = 6.3 Hz, 1H), 1.78 – 1.68 (m, 1H), 1.64 (s, 3H), 1.45 (s, 9H). **¹³C-NMR** (101 MHz, CDCl₃): δ (ppm) = 160.6, 156.0, 154.0, 148.2, 147.0, 141.5, 131.5, 130.4, 129.9, 128.4, 127.9, 127.2, 125.4, 125.0, 123.5, 122.9, 122.7, 122.5, 122.1, 117.4, 112.9, 111.4, 106.2, 103.4, 79.5, 65.6, 63.2, 55.2, 46.2, 46.0, 43.5, 41.1, 40.7, 39.8, 37.1, 34.7, 29.8, 28.6, 28.2, 27.7, 27.3, 23.3.

SS66T-CBI-NHPI (CJF138) (*S*)-1-(chloromethyl)-3-(5-(3-(methylamino)propoxy)-1*H*-indole-2-carbonyl)-2,3-dihydro-1*H*-benzo[*e*]indol-5-yl (*trans*)-hexahydro-[1,2]dithiino[4,5-*b*]pyridine-1(2*H*)-carboxylate (**10**)

SS66T-CBI-NBocPI (5.1 mg, 0.007 mmol) was dissolved in anhydrous DCM (0.05 M). The solution was cooled to 0 $^{\circ}$ C, and a solution of HCl (80 eq., 4 M in dioxane) was added. The mixture was stirred at r.t. for 4 h. All volatiles were removed under reduced pressure, and the residue was purified by preparative HPLC (H₂O/MeCN, 0.1% FA) to afford compound **10** as a colorless solid.

TLC R_f = 0.15 (DCM:MeOH, 5:1). **¹H-NMR** (600 MHz, DMSO-*d*₆): δ (ppm) = 11.65 (s, 1H), 8.49 (s, 2H), 8.21 (s, 1H), 8.04 (d, J = 8.3 Hz, 1H), 7.86 – 7.79 (m, 1H), 7.63 (t, J = 7.7 Hz, 1H), 7.57 – 7.51 (m, 1H), 7.42 (d, J = 8.9 Hz, 1H), 7.18 (d, J = 1.9 Hz, 1H), 7.17 – 7.10 (m, 1H), 6.95 (dd, J = 8.9, 2.3 Hz, 1H), 4.88 (t, J = 10.0 Hz, 1H), 4.61 (d, J = 10.8 Hz, 1H), 4.42 (s, 1H), 4.13 – 4.06 (m, 3H), 4.00 (dd, J = 11.2, 6.8 Hz, 1H), 3.30 (t, J = 11.3 Hz, 1H), 3.08 (dt, J = 14.5, 7.6 Hz, 3H), 3.01 (d, J = 11.1 Hz, 1H), 2.95 (d, J = 12.5 Hz, 1H), 2.63 – 2.59 (m, 3H), 2.50 (dd, J = 3.9, 2.0 Hz, 2H), 2.38 (s, 1H), 2.21 (q, J = 11.1 Hz, 1H), 2.08 (p, J = 6.3 Hz, 2H), 1.94 (s, 1H), 1.81 (s, 1H), 1.69 (t, J = 10.8 Hz, 1H), 1.45 (p, J = 12.3, 10.8 Hz, 1H). **¹³C-NMR** (151 MHz, DMSO-*d*₆): δ (ppm) = 160.2, 153.2, 152.8, 147.2, 141.5, 139.3, 131.8, 130.8, 129.5, 127.7, 127.5, 125.2, 124.3, 123.5, 122.3, 122.2, 115.9, 113.3, 110.6, 109.5, 105.5, 103.3, 67.8, 65.0, 62.5, 54.9, 47.7, 46.0, 41.2, 33.7, 32.7, 26.3, 25.6, 21.9.

(C) duocarmycin-ADC precursor: design 2



FmocHex-SS66C-CBI-Boc (CJF243) (*S*)-3-(*tert*-butoxycarbonyl)-1-(chloromethyl)-2,3-dihydro-1*H*-benzo[*e*]indol-5-yl (*cis*)-4-(6-(((9*H*-fluoren-9-yl)methoxy)carbonyl)amino)hexanoyl)hexahydro-[1,2]dithiino[4,5-*b*]pyrazine-1(2*H*)-carboxylate (**14a**)

Step 1: H-SS66C-H-2 HCl·2.5 NaCl (139 mg, 64% content, 0.351 mmol, 1.2 eq.) was suspended in anhydrous DCM (20 mL, 0.015 M), DIPEA (149 μL , 0.878 mmol, 3.0 eq) was added at r.t. and the resulting mixture was stirred for 30 min. A solution of **CIC(O)O-CBI-Boc (7)** (2.9 mL, 0.1 M in anhydrous DCM, 0.293 mmol, 1.0 eq.) was added dropwise at 0 °C, and the resulting mixture was stirred at 0 °C for 30 min, was then allowed to warm to r.t. and was further stirred for 1 h, before being concentrated under reduced pressure. Purification of the intermediate was achieved by FCC (EtOAc) to elute **H-SS66C-CBI-Boc (13a)** (153 mg) with satisfying purity. *Analytical data matched our previous reports: TLC R_f = 0.35 (EtOAc).*

Step 2: *N*-Fmoc-hexanoic acid (**12**) (61.7 mg, 0.175 mmol, 1.2 eq.) was dissolved in anhydrous DMF (3 mL, 0.05 M) and HBTU (66.2 mg, 0.175 mmol, 1.2 eq.) and DIPEA (75 μL , 0.582 mmol, 4.0 eq) were added, and the resulting mixture was stirred at r.t. for 10 min. A solution of **H-SS66C-CBI-Boc (13a)** (78 mg, 50 w% of the material obtained in step 1) in 0.7 mL of anhydrous DMF was added dropwise, and the resulting mixture was stirred for 15 h before being concentrated under reduced pressure. Purification by FCC (iso-hexane/EtOAc) gave title compound **14a** as a colorless solid (29.3 mg, 0.034 mmol, 23% over 4 steps).

TLC R_f = 0.87 (EtOAc); 0.23 (iso-hexane:EtOAc, 1:1). **HRMS** (ESI): C₄₆H₅₅ClN₅O₇S₂⁺: [M+NH₄]⁺ calc. 888.32259, found 888.32234. **¹H-NMR** (500 MHz, CDCl₃) δ (ppm) = 8.07 (s, 1H), 7.76 (d, *J* = 7.5 Hz, 3H), 7.71 (d, *J* = 8.4 Hz, 1H), 7.59 (d, *J* = 7.4 Hz, 2H), 7.54 – 7.48 (m, 1H), 7.39 (q, *J* = 6.5, 5.7 Hz, 3H), 7.31 (t, *J* = 7.4 Hz, 2H), 4.89 (s, 1H), 4.83 – 4.57 (m, 1H), 4.45 (s, 1H), 4.39 (d, *J* = 6.9 Hz, 2H), 4.35 – 4.26 (m, 1H), 4.21 (t, *J* = 6.8 Hz, 1H), 4.18 – 4.11 (m, 1H), 4.02 (t, *J* = 8.4 Hz, 1H), 3.93 (d, *J* = 10.0 Hz, 2H), 3.85 – 3.74 (m, 2H), 3.60 – 3.50 (m, 1H), 3.50 – 3.43 (m, 1H), 3.29 – 3.16 (m, 3H), 2.99 (d, *J* = 12.1 Hz, 1H), 2.39 (s, 2H), 1.80 – 1.67 (m, 2H), 1.58 (s, 9H), 1.47 – 1.38 (m, 2H). **¹³C-NMR** (126 MHz, CDCl₃): δ (ppm) = 172.7, 156.6, 153.9, 152.5, 148.0, 144.1, 141.5, 130.4, 127.8, 127.8, 127.2, 125.2, 124.7, 122.6, 122.5, 120.1, 109.4, 66.7, 53.1, 51.8, 47.4, 46.4, 42.9, 42.3, 40.9, 36.3, 33.5, 29.9, 29.8, 28.6, 28.3, 26.5, 24.5.

FmocHex-SS66T-CBI-Boc (CJF244) (*S*)-3-(*tert*-butoxycarbonyl)-1-(chloromethyl)-2,3-dihydro-1*H*-benzo[*e*]indol-5-yl (*trans*)-4-(6-(((9*H*-fluoren-9-yl)methoxy)carbonyl)amino)hexanoyl)hexahydro-[1,2]dithiino[4,5-*b*]pyrazine-1(2*H*)-carboxylate (**14b**)

Step 1: H-SS66T-H-2 HCl·2.5 NaCl (139 mg, 64% content, 0.351 mmol, 1.2 eq.) was suspended in anhydrous DCM (20 mL, 0.015 M), DIPEA (149 μL , 0.878 mmol, 3.0 eq) was added at r.t. and the resulting mixture was stirred for 30 min. A solution of **CIC(O)O-CBI-Boc (7)** (2.9 mL, 0.1 M in anhydrous DCM, 0.293 mmol, 1.0 eq.) was added dropwise at 0 °C, and the resulting mixture was stirred at 0 °C for 30 min, was then allowed to warm to r.t. and was further stirred for 1 h, before being concentrated under reduced pressure. Purification of the intermediate was achieved by FCC (EtOAc) to elute **H-SS66T-CBI-Boc (13b)** (215 mg) with satisfying purity. *Analytical data matched our previous reports: TLC R_f = 0.53 (EtOAc).*

Step 2: *N*-Fmoc-hexanoic acid (**12**) (61.7 mg, 0.175 mmol, 1.2 eq.) was dissolved in anhydrous DMF (3 mL, 0.05 M) and HBTU (66.2 mg, 0.175 mmol, 1.2 eq.) and DIPEA (75 μL , 0.582 mmol, 4.0 eq) were added, and the resulting mixture was stirred at r.t. for 10 min. A solution of **H-SS66T-CBI-Boc (13b)** (107 mg, 50 w% of the material obtained in step 1 with estimated content of 73%) in 1.0 mL of anhydrous DMF was added dropwise, and the resulting mixture was stirred for 15 h before being concentrated under reduced pressure. Purification by FCC (iso-hexane/EtOAc) gave the title compound **14b** as a colorless solid (51.5 mg, 0.059 mmol, 41% over 4 steps).

TLC R_f = 0.83 (EtOAc); 0.16 (isohehexane:EtOAc, 1:1). **HRMS** (ESI): $C_{46}H_{55}ClN_5O_7S_2^+$: $[M+NH_4]^+$ calc. 888.32259, found 888.32231. **1H -NMR** (500 MHz, $CDCl_3$) δ (ppm) = 8.01 (d, J = 8.3 Hz, 1H), 7.75 (t, J = 7.5 Hz, 3H), 7.71 – 7.65 (m, 2H), 7.57 (d, J = 7.3 Hz, 2H), 7.53 – 7.47 (m, 1H), 7.38 (q, J = 7.3 Hz, 3H), 7.29 (t, J = 7.4 Hz, 2H), 4.37 (s, 2H), 4.27 (d, J = 39.5 Hz, 2H), 4.17 (d, J = 12.3 Hz, 1H), 4.16 – 4.08 (m, 2H), 4.00 (d, J = 9.6 Hz, 1H), 3.90 (d, J = 11.2 Hz, 1H), 3.73 (s, 4H), 3.45 (t, J = 10.8 Hz, 1H), 3.36 (d, J = 12.0 Hz, 1H), 3.26 – 3.19 (m, 1H), 3.19 – 3.03 (m, 2H), 2.41 (s, 2H), 1.72 – 1.66 (m, 2H), 1.57 (s, 9H), 1.53 – 1.44 (m, 2H). **^{13}C -NMR** (126 MHz, $CDCl_3$): δ (ppm) = 156.6, 152.5, 147.9, 144.1, 142.6, 141.4, 130.3, 127.8, 127.2, 127.2, 125.2, 125.0, 124.7, 124.0, 122.5, 120.1, 110.6, 109.4, 81.3, 66.7, 60.5, 59.5, 53.0, 50.2, 47.4, 47.2, 46.3, 44.4, 42.0, 40.8, 34.6, 33.9, 32.1, 30.5, 29.8, 29.7, 29.5, 28.5, 26.4, 24.8, 24.3, 22.8, 21.2.

FmocHex-SS66C-CBI-TMI (CJF251) (S)-1-(chloromethyl)-3-(5,6,7-trimethoxy-1*H*-indole-2-carbonyl)-2,3-dihydro-1*H*-benzo[e]indol-5-yl (cis)-4-(6-(((9*H*-fluoren-9-yl)methoxy)carbonyl)amino)hexanoyl hexahydro-[1,2]dithiino[4,5-*b*]pyrazine-1(2*H*)-carboxylate (**15a**)

Step 1: FmocHex-SS66C-CBI-Boc (14a) (20.0 mg, 0.023 mmol) was dissolved in anhydrous DCM (0.02 M) and $BF_3 \cdot OEt_2$ (15 μ L, 0.12 mmol, 5.0 eq.) was added dropwise at r.t. and the mixture was stirred at r.t. for 30 min, before being concentrated under reduced pressure to yield the intermediate **FmocHex-SS66C-CBI-NH** as a brown solid, that was used without further purification.

Step 2: The material obtained in step 1 was suspended in anhydrous DCM (0.05 M), DIPEA (12 μ L, 0.07 mmol, 3.0 eq.) was added, and a clear solution was observed. The mixture was then added dropwise at r.t. to a solution of TMI-Cl (9.3 mg, 0.034 mmol, 1.5 eq.) (TMI-OH pre-activated with $(COCl)_2/DMF$), the resulting mixture was stirred at r.t. for 1 h. Complete turnover as indicated by TLC. The mixture was poured into 5 mL sat. aq. NaCl and 5 mL water was added. The mixture was extracted with DCM (4 \times 10 mL). The combined organic layers were dried over Na_2SO_4 and concentrated under reduced pressure. Purification by FCC (isohehexane:EtOAc, 1:1 to 0:1) gave **FmocHex-SS66C-CBI-TMI (15a)** as a colorless solid (17.7 mg, 0.018 mmol, 78%).

TLC R_f = 0.61 (EtOAc). **HRMS** (ESI): $C_{53}H_{53}ClN_5O_9S_2^-$: $[M-H]^-$ calc. 1002.29787, found 1002.29657. **1H -NMR** (400 MHz, $CDCl_3$) δ (ppm) = 9.37 (s, 1H), 8.46 – 8.34 (m, 1H), 7.82 (dd, J = 13.4, 5.7 Hz, 1H), 7.76 (d, J = 7.5 Hz, 5H), 7.59 (d, J = 7.4 Hz, 4H), 7.56 – 7.50 (m, 1H), 7.50 – 7.44 (m, 1H), 7.39 (t, J = 7.5 Hz, 4H), 7.30 (t, J = 7.3 Hz, 4H), 7.03 – 6.99 (m, 1H), 6.90 – 6.87 (m, 1H), 4.99 – 4.87 (m, 1H), 4.82 (d, J = 10.7 Hz, 1H), 4.76 – 4.64 (m, 1H), 4.54 – 4.45 (m, 1H), 4.39 (d, J = 6.6 Hz, 4H), 4.36 – 4.29 (m, 1H), 4.26 – 4.14 (m, 2H), 4.08 (s, 3H), 4.02 – 3.96 (m, 2H), 3.95 (s, 3H), 3.92 (s, 3H), 3.85 – 3.72 (m, 2H), 3.64 – 3.43 (m, 2H), 3.30 – 3.11 (m, 5H), 3.00 (d, J = 11.9 Hz, 1H), 2.47 – 2.31 (m, 3H), 1.80 – 1.67 (m, 4H), 1.65 – 1.52 (m, 4H), 1.52 – 1.37 (m, 4H). **^{13}C -NMR** (101 MHz, $CDCl_3$): δ (ppm) = 173.2, 156.6, 153.9, 150.4, 147.8, 144.1, 141.4, 141.0, 138.8, 130.0, 128.1, 127.8, 127.2, 125.6, 125.2, 123.7, 122.9, 122.6, 120.1, 111.4, 106.8, 97.7, 66.7, 61.6, 61.3, 56.4, 55.0, 51.9, 47.4, 46.0, 43.5, 40.9, 36.3, 33.5, 31.3, 29.8, 26.5, 24.5, 22.5, 14.3.

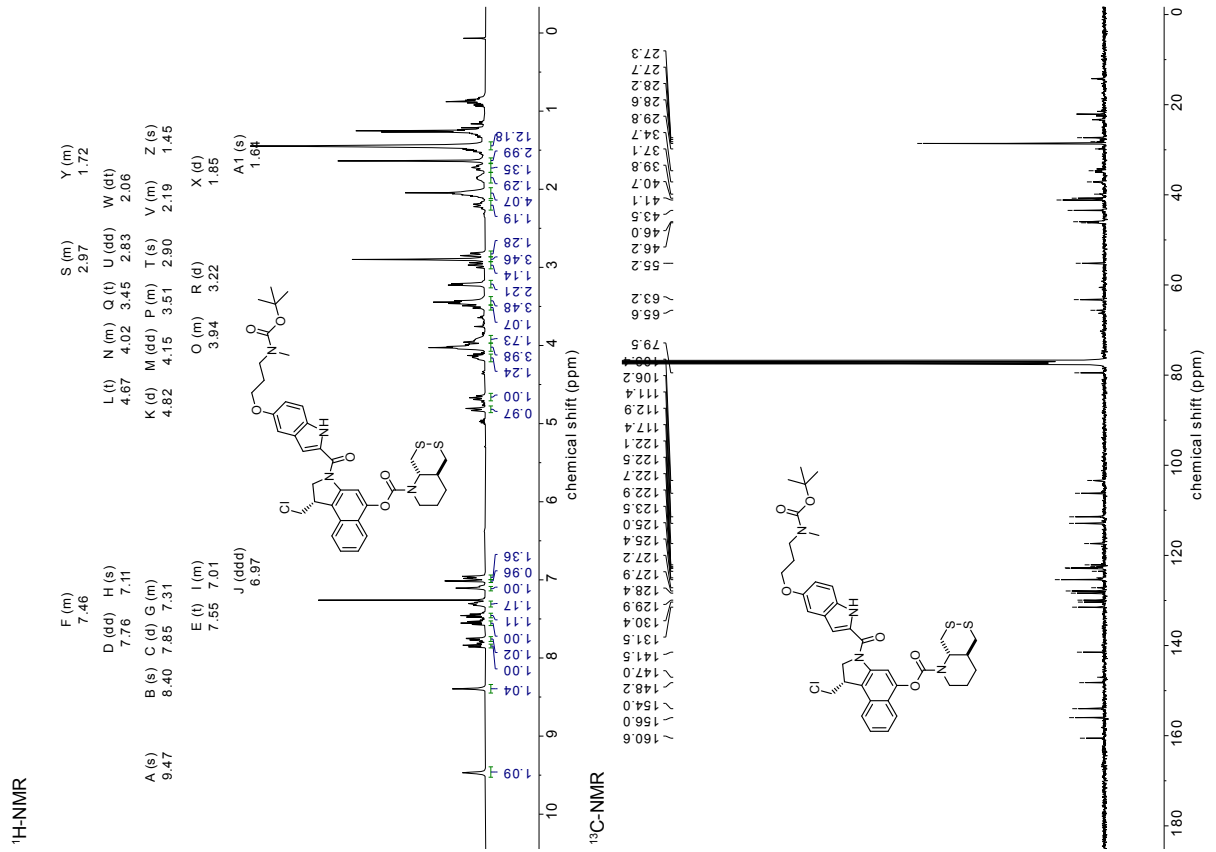
FmocHex-SS66T-CBI-TMI (CJF247) (S)-1-(chloromethyl)-3-(5,6,7-trimethoxy-1*H*-indole-2-carbonyl)-2,3-dihydro-1*H*-benzo[e]indol-5-yl (trans)-4-(6-(((9*H*-fluoren-9-yl)methoxy)carbonyl)amino)hexanoyl hexahydro-[1,2]dithiino[4,5-*b*]pyrazine-1(2*H*)-carboxylate (**15b**)

Step 1: FmocHex-SS66T-CBI-Boc (14b) (25.0 mg, 0.029 mmol) was dissolved in anhydrous DCM (0.02 M) and $BF_3 \cdot OEt_2$ (18 μ L, 0.14 mmol, 5.0 eq.) was added dropwise at r.t. and the mixture was stirred at r.t. for 30 min, before being concentrated under reduced pressure to yield the intermediate **FmocHex-SS66T-CBI-NH** as a brown solid, that was used without further purification.

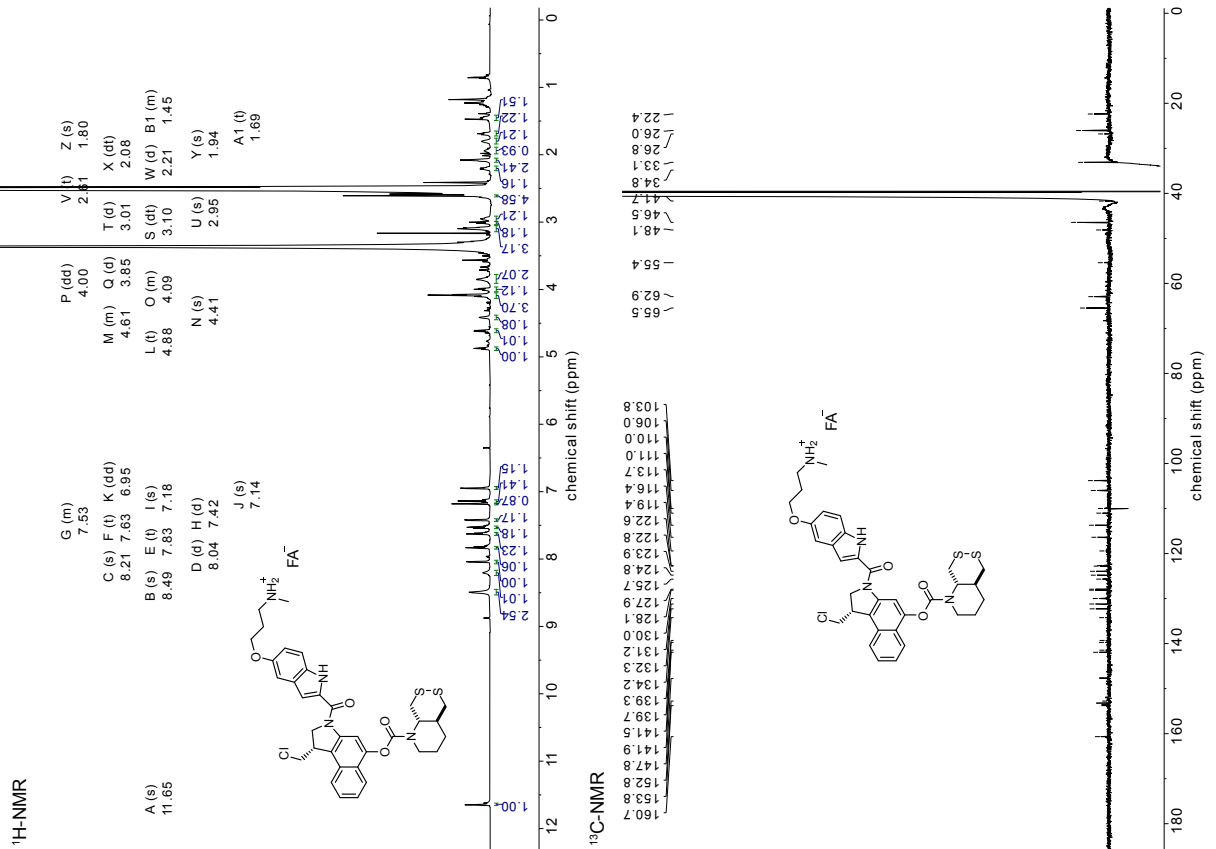
Step 2: The material obtained in step 1 was suspended in anhydrous DCM (0.05 M), DIPEA (15 μ L, 0.09 mmol, 3.0 eq.) was added, and a clear solution was observed. The mixture was then added dropwise at r.t. to a solution of TMI-Cl (11.6 mg, 0.043 mmol, 1.5 eq.) (TMI-OH pre-activated with $(COCl)_2/DMF$), and the resulting mixture was stirred at r.t. for 1 h. Complete turnover as indicated by TLC. The mixture was poured into 5 mL sat. aq. NaCl and 5 mL water was added. The mixture was extracted with DCM (4 \times 10 mL). The combined organic layers were dried over Na_2SO_4 and concentrated under reduced pressure. Purification by FCC (Hex:EtOAc, 1:1 to 0:1) gave **FmocHex-SS66T-CBI-TMI (15b)** as a colorless solid (21.6 mg, 0.022 mmol, 76%).

TLC R_f = 0.59 (EA). **HRMS** (ESI): $C_{53}H_{53}ClN_5O_9S_2^-$: $[M-H]^-$ calc. 1002.29787, found 1002.29730. **1H -NMR** (800 MHz, $CDCl_3$) δ (ppm) = 9.44 (s, 1H), 8.35 (s, 1H), 7.76 (d, J = 8.1 Hz, 2H), 7.74 – 7.70 (m, 2H), 7.55 (s, 3H), 7.45 (s, 1H), 7.37 (d, J = 18.8 Hz, 2H), 7.31 – 7.21 (m, 2H), 6.98 (s, 1H), 6.87 (s, 1H), 5.10 (s, 1H), 4.79 (d, J = 10.2 Hz, 1H), 4.70 – 4.62 (m, 1H), 4.53 – 4.28 (m, 4H), 4.17 (d, J = 29.1 Hz, 2H), 4.07 (s, 3H), 4.05 – 4.01 (m, 1H), 3.99 – 3.92 (m, 5H), 3.91 (s, 3H), 3.82 – 3.63 (m, 3H), 3.48 (t, J = 10.9 Hz, 1H), 3.43 – 2.87 (m, 5H), 2.42 (s, 2H), 1.70 (d, J = 43.0 Hz, 3H), 1.63 – 1.24 (m, 6H). **^{13}C -NMR** (201 MHz, $CDCl_3$): δ (ppm) = 160.5, 156.6, 150.4, 150.3, 147.8, 144.1, 141.5, 141.4, 140.7, 140.6, 139.0, 130.1, 129.9, 129.6, 128.0, 127.7, 127.3, 127.1, 125.8, 125.6, 125.2, 123.7, 122.9, 122.4, 120.0, 111.4, 106.8, 97.8, 97.7, 67.1, 66.6, 61.6, 61.3, 60.0, 56.4, 55.2, 47.4, 45.9, 43.5, 40.8, 39.1, 35.0, 34.3, 33.9, 29.7, 26.3, 24.8.

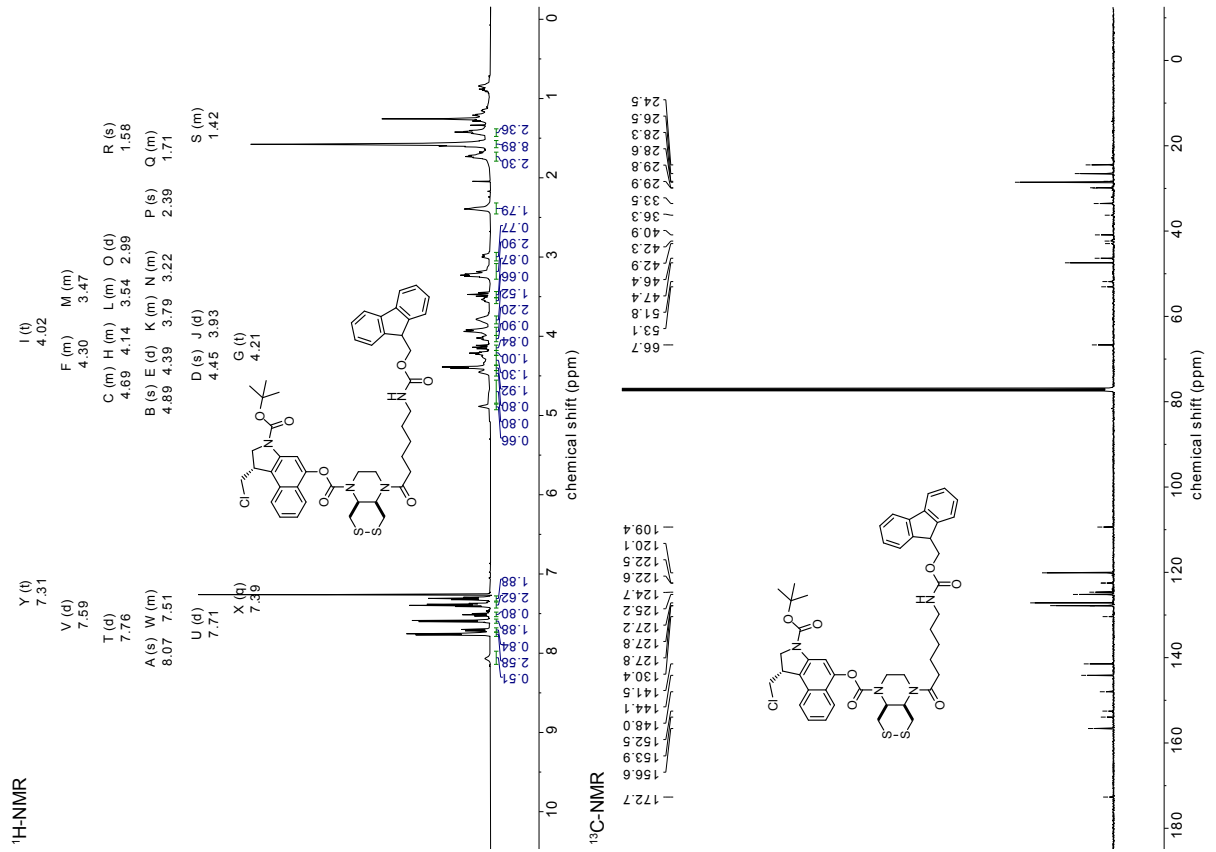
SS66T-CBI-NBocPI (CJF136)



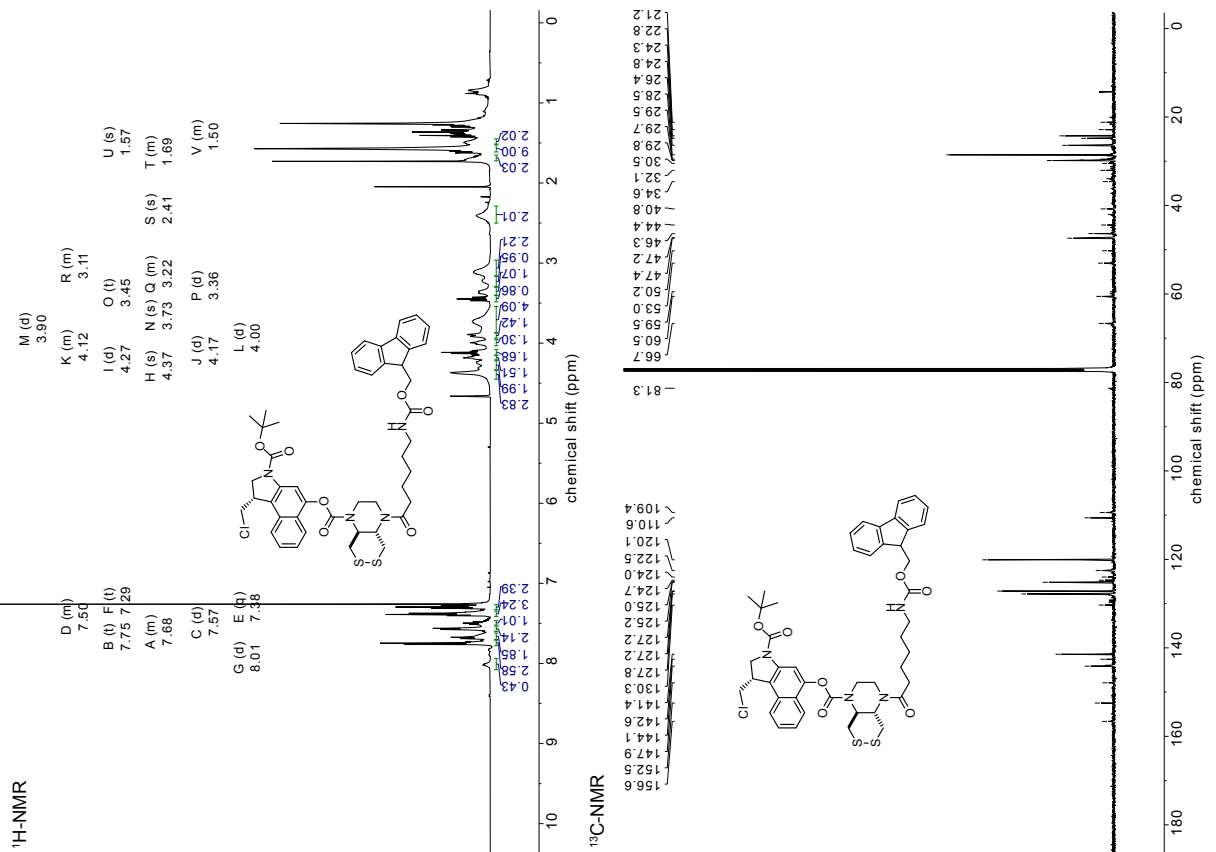
SS66T-CBI-NHPI (CJF138)



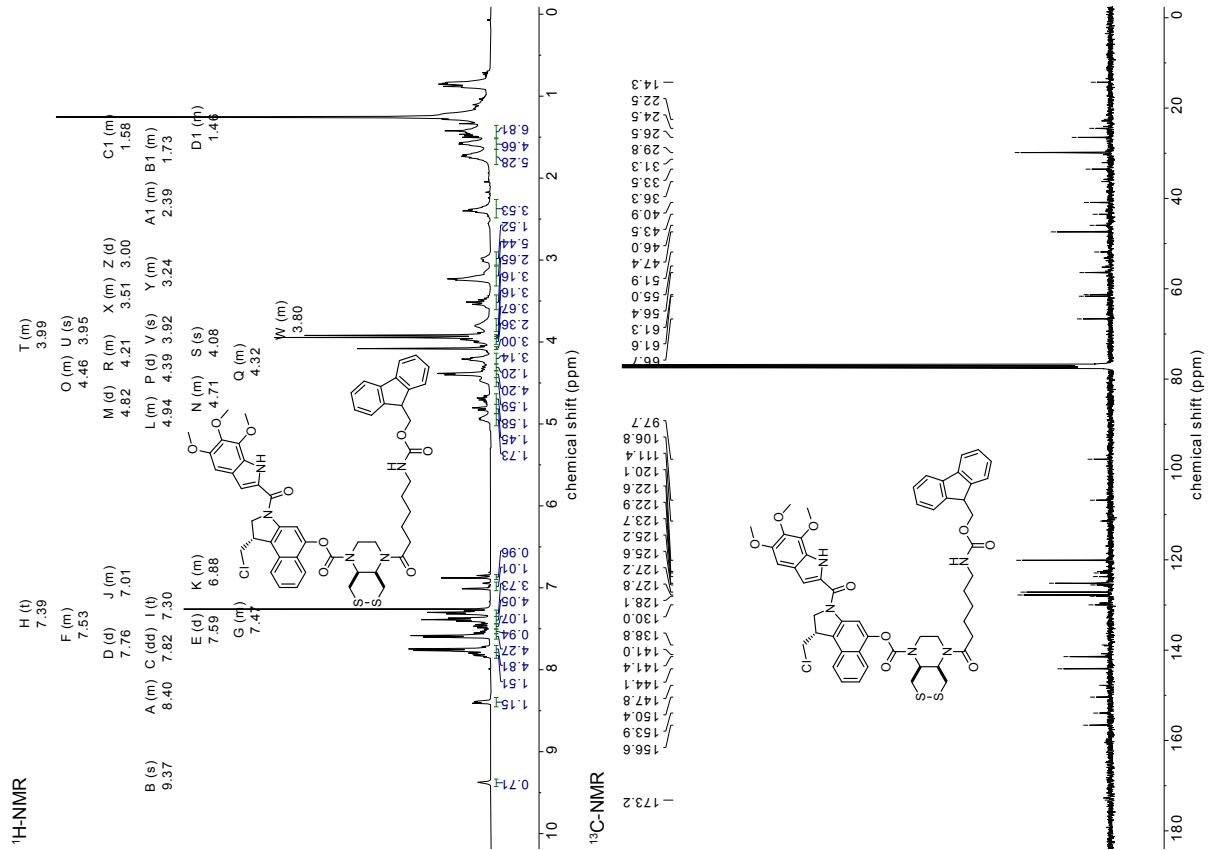
FmocHex-SS66C-CBI-Boc (CJF243)



FmocHex-SS66T-CBI-Boc (CJF244)



FmocHex-SS66C-CBI-TMI (CJF251)



FmocHex-SS66T-CBI-TMI (CJF247)

